

TRANSACTIONS
OF THE
AMERICAN SOCIETY
OF
MECHANICAL ENGINEERS

1950

VOLUME 72



PUBLISHED BY
THE AMERICAN SOCIETY OF MECHANICAL ENGINEERS
29 WEST THIRTY-NINTH STREET, NEW YORK, N. Y.

Engineering Lib.

73

1

.AG

T8

Copyright, 1951, by
THE AMERICAN SOCIETY OF MECHANICAL ENGINEERS

Printed in the United States of America by
The Mack Printing Co., Easton, Pa.

Engin Lib
84
Duesel
3-29-21

Foreword

VOLUME 72 of the Transactions of The American Society of Mechanical Engineers contains the individual papers published during 1950 under the sponsorship of the Society's professional divisions and technical committees, including the contributions of the Applied Mechanics Division, issued originally in a quarterly known as *Journal of Applied Mechanics*, and the 1950 Society Records and Index. The technical papers and reports that make up this volume represent the Society's annual contribution to the permanent record of mechanical-engineering achievement. Most of these papers and reports were presented at meetings of the Society and its professional divisions and sections and were published in monthly issues, eight being distributed as the Transactions of The American Society of Mechanical Engineers and four as the *Journal of Applied Mechanics*. These indexes will be found at the end of this volume; an index to *Mechanical Engineering*, an index to the eight issues published as Transactions, and an index to the four issues published as the *Journal of Applied Mechanics*. Indexes to other ASME papers and publications will be found on page SR-59 at the end of this volume.

In view of the fact that the material of which this volume is composed was originally issued periodically as the Transactions, *Journal of Applied Mechanics*, and Society Records, three sets of page numbers will be found. Numbers without letter symbols are those of the eight issues of Transactions, and the *Journal of Applied Mechanics*, and those with letter symbol SR to the Society Records and Index section, which concludes the volume.

All sections of the Transactions are bound together at the end of the year for the convenience of libraries and of engineers who wish all of the papers in permanent form. Copies of the bound Transactions will be found in depositories located in selected engineering, university, and public libraries throughout the world. A complete list of these depositories will be found on pages SR-55 to SR-58 of the Society Records and Index. Copies of the Transactions have also been set aside for sale.

PUBLICATIONS COMMITTEE

e
li
je
in
m
in
of
al
T
of
th
In
pa
Di
wa
cor
tic
C
Me
Am
N
for
S
as in
Pap

Solid-Type Journal Bearings in High-Speed Freight Service

By E. S. PEARCE,¹ R. J. SHOEMAKER,² AND I. E. COX³

This paper encompasses the operating conditions involved in the selection of the bearing equipment used in high-speed freight service. Consideration is given to the performance of the solid-type bearing, as well as the potentials of future development, and the superior adaptability of the solid-type bearing to the economics of railroad operation.

INTRODUCTION

THE term "high-speed freight" implies the shortening of elapsed time between terminals. This would require higher top speeds and more rapid acceleration.

The public has been led to picture freight equipment operating continuously at sustained speeds of 50, 60, 80, and 100 mph. To achieve this result, it would be necessary to have less gross tons per train; less resistance per train; or more power per train; or a combination of all three.

In the final analysis, high-speed freight must be obtained within the practical limits of cost and over-all economies of railroad operation. If high-speed freight is not to be restricted as to interchange, special equipment, and special movements, then all freight equipment must be equally adaptable to high-speed operation as and when the occasion arises.

For high-speed freight, bearings are involved in the elements of the following:

- Less resistance per train.
- Dependability and safety.
- Economy in first cost, maintenance, and weight.

There are listed, for freight-train service operation, 1,902,265 cars under railroad ownership, and 263,747 cars under private-line ownership.⁴ There are, therefore, in excess of 17,000,000 journals with companionate bearings in operation today. The investment in these journals and bearings, and the operation and maintenance of them are the common responsibility of all interchanging rolling-stock operators.

Six railroads have been selected as representing a cross section of certain operating conditions upon which an analysis of the over-all bearing problem for high-speed freight must be predicated. These six roads represent an operating ownership of 25 per cent of all freight equipment. Basic data are given in Table 1⁵ for the year 1947.

¹ President, Railway Service and Supply Corporation, Indianapolis, Ind. Fellow ASME.

² Chief Engineer, Magnus Metal Division, National Lead Company, Chicago, Ill. Fellow ASME.

³ Vice-President in Charge of Engineering, National Bearing Division, American Brake Shoe Company, St. Louis, Mo.

⁴ "The Pocket List," Third Quarter 1948, published by The Railway Equipment and Publication Company, New York, N. Y.

⁵ "Freight Operating Statistics of Large Steam Railways," data compiled monthly by the Bureau of Transport Economic and Statistics, Interstate Commerce Commission.

Contributed by the Railroad Division and presented at the Annual Meeting, New York, N. Y., November 27-December 2, 1948, of THE AMERICAN SOCIETY OF MECHANICAL ENGINEERS.

NOTE: The authors constitute the Research Advisory Committee for Railroad Journal Bearing Manufacturers.

Statements and opinions advanced in papers are to be understood as individual expressions of their authors and not those of the Society. Paper No. 48-A-128.

TABLE 1 AVERAGE NUMBER OF CARS IN EACH 100 CARS OPERATED BY EACH RESPECTIVE ROAD WHICH ARE OF OWNERSHIP OTHER THAN ITS OWN^a

Road	No. foreign cars per 100 cars operated
A	55.2
B	68.7
C	72.8
D	83.8
E	72.2
F	69.0

The basic elements of facility and economy of maintenance, repair, and replacement must be recognized as the first requirement of the bearing equipment.

Gross tons per train in high-speed freight will be made up in units of weights given in Table 2.⁵ It is the rolling resistance

TABLE 2 AVERAGE GROSS TONS PER LOADED CAR

Road	Gross tons per car		
	Average	Minimum	Maximum
A	58.4	57.0	59.1
B	55.6	54.9	57.8
C	55.5	54.1	56.3
D	52.8	52.2	54.0
E	53.7	52.7	54.2
F	69.7	69.0	70.4

of units of these weights that will determine train resistance. It is units of these weights that will determine the required bearing-load carrying capacity. It is under such bearing loads at the contemplated operating speeds, that bearing resistance in pounds per ton, in relation to total resistance, must be determined as a relative factor in high-speed freight.

Table 3⁵ gives the distance that the average car on line, which was in movement or subject to movement, traveled per day. It

TABLE 3 AVERAGE DISTANCE IN MILES PER DAY OF ALL CARS IN MOVEMENT OR SUBJECT TO MOVEMENT

Road	Distance per day, miles		
	Average	Minimum	Maximum
A	34.5	32.1	37.2
B	30.0	26.9	33.2
C	40.6	37.2	44.0
D	61.9	56.2	67.6
E	47.7	42.1	52.3
F	48.4	39.1	59.6

is only in movement that the function of the journal bearing assumes any relative and significant importance. It is in this distance that the functional advantages of the bearing are utilized and the investment justified.

Table 4 reflects the factor of dependability under the operating conditions as obtained in 1947.

TABLE 4 AVERAGE JOURNAL BEARINGS IN SERVICE PER DAY ON ALL CARS IN MOVEMENT OR SUBJECT TO MOVEMENT PER BEARING FAILURE

Road	Number of bearings for one failure		
	Yearly avg	Minimum	Maximum
A	37432	20288	113480
B	86948	48464	204984
C	32304	15992	97104
D	19424	9376	55304
E	33624	17576	69856
F	45560	20968	147072

A minimum average of one failure for 9376 bearings to a maximum of one failure for 204,984 bearings is equivalent to one failure for 526,931 bearing-miles as a minimum to 6,805,469 bearing-miles as a maximum. Since this reflects the actual performance of the solid unit-type bearing under existing operating conditions, this measure of dependability is an outstanding factor to consider.

UNIT SOLID-TYPE-BEARING TESTS

To determine the potential possibilities of the unit solid-type bearing under the more accelerated rate of operation of high-speed freight, it is necessary to turn to the laboratory test plant. Such tests are required since there are no road-test data available; nor is there ever likely to be, due to the inability to separate journal resistance from other elements which go to make up total car resistance. Likewise, extended operation under high speeds, effect of temperature, and other factors to give controlled conditions so that journal-bearing operation alone may be evaluated, are available only in the laboratory test plant.

In evaluating laboratory bearing-performance data, it must be recognized that laboratory operation is purposely "controlled accelerated service experience." Failure is the objective in order that the cause and effect may be determined and improvement devised and evaluated. A construction which may operate successfully on the railroad may fail under the adverse conditions in the test plant. These adverse test-plant factors are as follows:

- 1 Laboratory tests are conducted in still air, as against a high-velocity flow of air around journal-box contained parts in service.
- 2 The load on a journal bearing in a laboratory test is a maximum "dead" static load; whereas, in service, the load is "alive" and varying.
- 3 In a laboratory test there is no benefit of lateral motion of the axle in distribution of lubricant between the journal and the bearing; whereas, in actual service, the axle is constantly moving laterally, enhancing distribution of lubricant.
- 4 Speeds can be high and for extended periods of time not obtainable in practice. Rates of acceleration and deceleration, to and from high speeds, are attained that are not obtainable in practice.

Fig. 1 represents the data obtained with a $5\frac{1}{2}$ -in. \times 10-in. conventional solid-type journal-box assembly operated under the foregoing conditions, augmented by, subzero temperatures. The total bearing load was 16,375 lb, equivalent to a 70-ton car. The bearing, being nonfitted to the journal, had a crown area of only 22.5 sq in. The resulting unit loading was 735 psi. With a full or fitted bearing area of 45.7 sq in., the unit loading would have been reduced to 358 psi. The operation was one of constant speed at 50 mph for 66 hr. The run started in an atmosphere of +80 F, with temperature reducing, as the run progressed, to a minimum of -12 F. The operation was equivalent to a continuous run of 3300 miles. Ambient temperature, journal temperature, and journal resistance in pounds per ton are shown in Fig. 1.

To evaluate these results properly, some comparison should be made with total car resistance under like conditions of load, speed, and ambient temperature. This is true also for bearing resistance only of other types of bearings, such as those of multiple-unit design, of which type the roller bearing is a sample. However, such data apparently have not been developed.

As some measure of relative comparison, it is interesting to note that the distance of 3300 miles is 3 times the distance from New York to Chicago. The speed of 50 mph is 10 miles under the average speed of the 20th Century Limited.

Fig. 2 represents data obtained from tests using the same journal-box assembly and loading as used in the test covered in

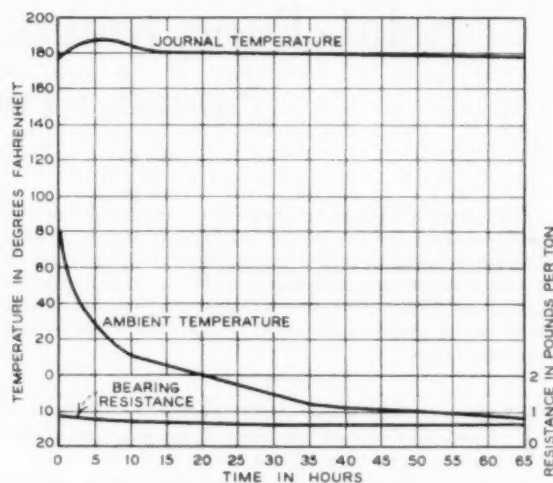


FIG. 1 TEST DATA WITH $5\frac{1}{2}$ -IN. \times 10-IN. CONVENTIONAL SOLID-TYPE JOURNAL-BOX ASSEMBLY

Fig. 1, but operating in an atmosphere of -14 F to -10 F at speeds of 20, 60, 80, and 100 mph. On the speed-cycle curve are reflected acceleration, sustained speeds, deceleration, reversal of movement, ambient temperature, journal temperature, and resistance in pounds per ton.

SIGNIFICANCE OF JOURNAL RESISTANCE

It is in order to explore the potential significance of journal resistance in high-speed freight. For this purpose we have such basic data as shown in Figs. 1 and 2; and for available drawbar pull, motive power of the characteristics shown in Fig. 3.⁶ It is assumed that operation will take place on tangent level track with trains made up of 70-ton cars, at speeds of 50 and 80 mph.

Total car resistance for 70-ton cars at 80 mph is 10.5 lb per ton; at 50 mph, 6.7 lb per ton.⁷ Journal resistance only at 50 mph, Fig. 2, is 0.71 lb per ton. From Fig. 3, journal resistance after accelerating to 80 mph is 0.96 and 0.86 lb per ton. After running at 80 mph, it is 0.69 and 0.73 lb per ton. The average of these is 0.81 lb per ton. Drawbar pull of the S-1 locomotive at 50 mph is 36,000 lb and at 80 mph, 22,000 lb.

With bearing resistance entirely eliminated, the resistance of the 70-ton car at 50 mph is 5.99 lb per ton, and at 80 mph, 9.69 lb per ton on tangent level track. At 50 mph the available drawbar pull of the S-1 locomotive is equivalent to 86 cars of 70 tons each per train, and at 80 mph 32 cars of 70 tons each per train.

Speed has been increased 60 per cent to achieve high-speed freight at a sacrifice of 63.5 per cent in the number of cars per train for factors other than bearing resistance.

At 80 mph the bearing resistance for a train of 70-ton cars if entirely eliminated is the difference between a train of 30 cars as compared to 32 cars.

In freight service, under the prevailing conditions of railroad operation in the last 20 years, with the unit solid-type bearing, the average freight car has increased its average daily production as shown in Table 5.

Transportation service by the railroads, as required in this

⁶ "Railroad Motive Power," by P. W. Kiefer, published by Steam Locomotive Research Institute, Inc., New York, N. Y., June, 1947, chart B, p. 52.

⁷ "The Steam Locomotive," by R. P. Johnson, Simmons-Boardman Publishing Corporation, New York, N. Y., 1942, p. 188, table 31.

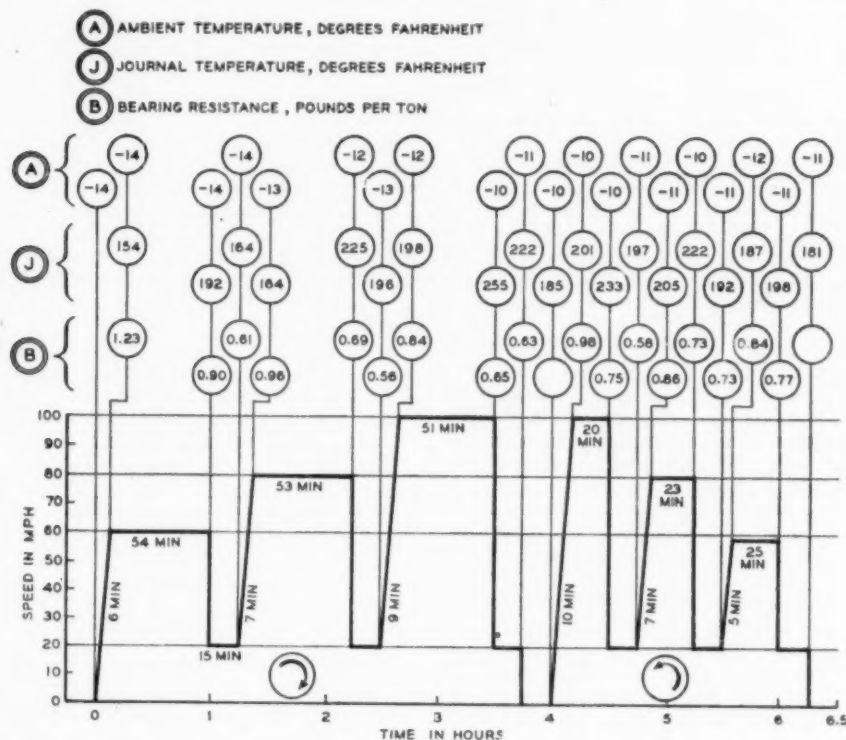


FIG. 2 TEST DATA WITH 5 1/2-IN. X 10-IN. CONVENTIONAL SOLID-TYPE JOURNAL-BOX ASSEMBLY OPERATING IN ATMOSPHERE OF -14 F TO -10 F

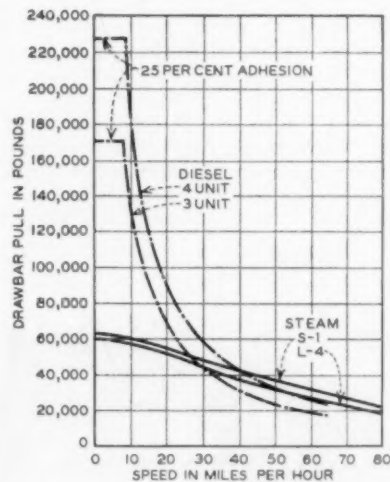


FIG. 3 POWER CHARACTERISTIC CURVES FOR RECIPROCATING-STEAM AND DIESEL-ELECTRIC FREIGHT LOCOMOTIVES

country, makes necessary the highest degree of unrestricted movement of equipment over the railroad mileage of the continent regardless of territorial extent and ownership of any one railroad. Obviously, uniform and universal facility of maintenance is a basic necessity; hence there has developed a high degree of standardization and interchange of parts. This imposes severe

TABLE 5 TWENTY-YEAR INCREASE IN DAILY FREIGHT-CAR PRODUCTION

	1926	1946	Per cent increase
Average car miles per day ^a	32.6	45.2	38.6
Average freight-car capacity, tons ^b	45.1	51.3	13.8
Average net ton-miles per car per day ^a	569	948	66.5

^a "Year Book of Railroad Information," Eastern Railroad Presidents Conference, Committee of Public Relations, 1948, p. 72.

^b Ibid., p. 12.

limitations on improvements in design, restricting changes to those not incompatible with maintaining standards.

It is recognized that improvements in design, materials, and practice relating to the unit solid-type-journal bearing-box assembly, can be made within the confines of the foregoing limitations of standardization.

THE JOURNAL BOX

There is general recognition of the necessity for a properly sealed and vented journal box to keep dirt, water, and other foreign matter out and to retain the lubricant in the journal box. Likewise, it is equally evident that lateral, in its ultimate reaction on lading and wear on mechanical parts, must be flexibly controlled and not rigidly opposed. These objectives are obtainable.

THE AXLE JOURNAL

Journals are finished by roller-burnishing, a practice which is scarcely conducive to a geometrically perfect surface. It requires considerable bearing-lining life and many miles of running to lap a rolled car journal to a satisfactory bearing surface. The permissible tolerances of journals, both diametrically and axially, are not only limiting factors in performance, but greatly

restrict the latitude in future bearing design and construction.

To illustrate, the $5\frac{1}{2}$ -in. \times 10-in. journal bearing is bored to $5\frac{9}{16}$ -in., but it is applied to a journal that will vary from a minimum of 5 in. to a maximum of $5\frac{1}{2}$ in.; and it is expected to perform equally well on either. Paradoxically, it does surprisingly well. Likewise, the length of the journal may vary as much as $\frac{11}{16}$ in. from maximum to minimum; and, at the same time, the bearing can vary in length $\frac{3}{8}$ in. due to wear, so that there is a total of $1\frac{1}{16}$ in. possible difference in the length of the bearing and length of the journal. Coupled with this is the further fact that these variations apply to only one journal on one end of the axle, whereas there may be a different combination of dimensional tolerances on the opposite end of the axle. A renewable journal sleeve will overcome these objections.

BEARINGS

The loads imposed on car journal bearings are well within the safe load limits of lead-base bearing lining. The low elastic modulus of bearing babbitt is the only reason that we have been able to operate successfully under the constant fluctuation of alignment, the widespread diametral tolerance, improper bearing and journal surfaces, and the great spread in both the quality and quantity of lubrication. It is the high plastic yield of lead-base lining which relieves the localized pressure caused by these conditions, thereby avoiding seizure and failure. This plastic condition of lining performs the important function of absorbing and removing abrasive materials from the journal surface.

Shock loads, caused by improper dimensional conditions of the wedge and bearing, are the cause of spread linings. This is in no sense a reason for condemning or changing the lining metal, as closer tolerances of the collateral journal-box parts will solve this problem. It is necessary to continue to use $\frac{1}{4}$ -in.-thick bearing linings, as this dimension is controlled by the journal diametral tolerance. This journal-bearing clearance has made necessary the design of the present bearing designated as the "no clearance type." The present journal collar fixes the bearing are at approximately 120 deg.

In considering improvements in design and materials of the present unit solid-type bearing per se, the low but widely fluctuating incidence of failure, shown in Table 4, presents an economic element for consideration. There is the question as to the relative improvement in performance that would accrue through proper maintenance practices, as compared to improved design and materials, although it is obvious that combination of both is the ultimate goal.

The economic value of relatively simple facilities of repair and maintenance of the solid-type bearing and journal-box assembly, wheels, and trucks must be recognized in considering improvements in design and materials. Likewise, changes in design and/or materials must be consistent with the economies of the present numerous sources of bearing supply with the added element of protection in time of national emergencies when railroad transportation is the backbone of defense.

The solid-type-bearing journal-box assembly, by virtue of its extreme simplicity, is victimized by unsubstantiated opinions and deprived of the benefits of facts. As an example, the derogatory misnomer, "friction bearing," established by advertising is now popularly accepted as descriptive of the standard AAR car journal bearing. The use of the term "friction type," applying to solid bearings, and the term "antifriction" to roller and ball bearings is erroneous and misleading, implying that friction is created in the operation of the solid type, and no friction in the operation of the roller and ball-bearing types. This is far from the true fact. Nonperformance in the proper functioning of any component parts of the journal-box assembly and truck manifests itself ultimately in a bearing failure. This results in promoting

the false idea that the bearing is deficient because it fails to overcome the detrimental influences introduced by the other component parts of the journal box and truck.

CONCLUSION

In its broadest aspect, the problems of bearing performance are not peculiar to the railroad industry alone. A co-ordinated, factual, aggressive, persistent, and effective approach to their economic solution has been far less evident in the railroad industry than in such other fields as aircraft, marine, automotive, and Diesel. This fact has been aptly described as an example of "What is everybody's business is nobody's business." Quoting Dr. Hersey:⁴ "The fact should not be overlooked, that in many applications where improvement has been reported as the result of the substitution of some novel type of bearing, equally good or better performance may be obtained from the simple oil-film bearing if properly designed and lubricated."

The Mechanical Division of the Association of American Railroads has facilities for the investigation of all elements of bearing performance. It now has under consideration an all-inclusive research and development program on this subject. Developments in design, materials, and practices, which are directed toward improvement in dependability, economy, and safety of the unit solid-type-bearing journal-box assembly, have been submitted to the AAR for investigation and evaluation.

APPENDIX A

The potential developments in the conventional solid-type-bearing journal-box assembly, without disturbing the standards of basic design and preserving the most essential facility of maintenance in unrestricted interchange, are shown by the composite illustration, Fig. 4.

The conventional journal box is cut away in section showing the axle journal, packing, bearing, and wedge, on the right or rear of the box, the oil-seal dust guard; and, on the left or front of the journal box, the water and dustproof lid. The small mirror in the front of the box is used to reflect the appearance of the end of the axle journal for purposes of illustration.

The dust guard and lid are to meet the requirement for a properly sealed journal box to keep dirt, water, and other foreign matter out and retain the lubricant in the journal box.

The axle journal, as shown, has had the conventional collar removed, and shows in place on the journal one form of sleeve. The use of the sleeve is to eliminate the use of journals varying

⁴ "Theory of Lubrication," by Mayo D. Hersey, John Wiley & Sons, Inc., New York, N. Y., 1936, p. 13.

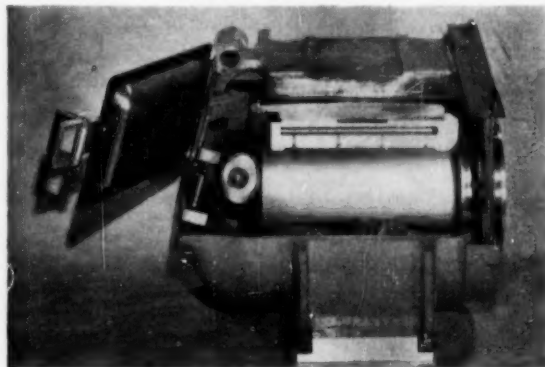


FIG. 4 SOLID-TYPE-BEARING JOURNAL-BOX ASSEMBLY

$\frac{1}{2}$ in. in diam; and, as in the case of the illustration, a $5\frac{1}{2}$ -in. \times 10-in. journal, maintaining the diameter at $5\frac{1}{2}$ in. instead of a variation from 5 in. to $5\frac{1}{2}$ in. occasioned by the necessity for turning journals to repair surface conditions. The sleeve is $\frac{1}{8}$ -in. straight-wall tubing fitting over a $5\frac{1}{4}$ -in. journal with a very light shrink fit of 0.005 in. at 380 F. This provides a retaining force of 60,000 lb. Maintenance of axle-journal surface is accomplished by the renewal of the sleeve, no machining of the axle journal being necessary. To remove a damaged sleeve, simply split with a chisel and apply a new sleeve by heating to 380 F and rapidly slipping on the journal. The journal bearing is that described in a previous paper by E. S. Pearce.⁹

The journal-box wedge is the conventional wedge with a downwardly projecting ledge or lug welded to the existing wedge. This lug is to replace the function of the axle-journal collar to retain the journal bearing in place laterally. This eliminates the troublesome limitations introduced by the presence of the conventional journal collar, that is, service difficulties, as well as those pertaining to future bearing design.

The reflection of the end of the axle shows in the centering hole a plastic plug. This plug is made of a temperature-responsive material, whose liquid point and softening point are identical. The material can be made to respond within 2 deg F to any desired temperature. When the predetermined temperature is reached, the plug liquefies and by centrifugal force is spread over the end of the axle marking it a yellow color. The predetermined temperature is known as the "potential failure temperature." This temperature is an indication before a journal heating exists that attention should be given; and, if given, a road delay due to a journal heating will be avoided. The objective is to eliminate the personal equation in inspecting and servicing journal boxes by indicating positively those that need attention and, conversely, by the absence of the indication those that do not need attention.

Journal-box packing is of conventional material (waste and oil), applied, however, in the form of machine-made pads of oil-saturated waste. This insures uniform packing of boxes and prevents displacement of the packing in whole or in part from the normal position in contact with the bottom of the journal.

APPENDIX B

NATIONAL BEARING DIVISION—AMERICAN BRAKE SHOE COMPANY

The renewable axle sleeve and the compound bore bearing as hereinafter described, have been submitted to the Mechanical Division of the Association of American Railroads as two of our developments in design, material, and practice directed toward improvement in dependability, economy, and safety of the unit solid-type bearing and its assembly.

The Renewable Axle Sleeve. A renewable axle sleeve has been developed after several years of study and investigation, as illustrated in Figs. 5 and 6.

It consists of a rigid type of bushing made of high-carbon low-alloy steel, heat-treated to 480–520 Bhn, with ground journal and dust-guard-fit surfaces. This sleeve bushing is provided with a ground-finished taper bore $\frac{1}{4}$ in. to the foot, and is arranged to be locked in place by a nut screwed on the end of the axle.

Axle preparation for the use of this sleeve consists of turning either new or worn axles with a taper to fit the sleeve bore, and threading the end of the axle for the axle nut.

The renewable axle sleeve should be induction-heated or immersion-heated in oil to 200 F, and assembled on the axle, tightening the axle nut immediately so the sleeve will have a shrink fit in place.

⁹ "Locomotive and Car Journal Lubrication," by E. S. Pearce, Trans. ASME, vol. 58, 1936, pp. 37–45.

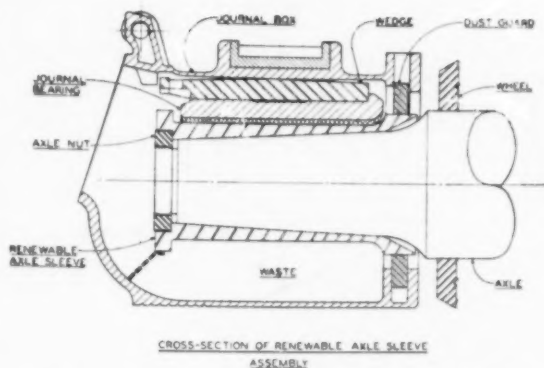


FIG. 5 CROSS SECTION OF RENEWABLE AXLE-SLEEVE ASSEMBLY

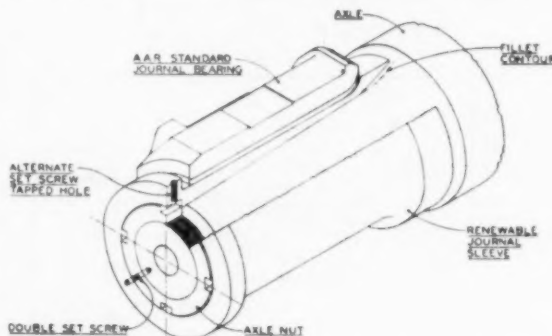
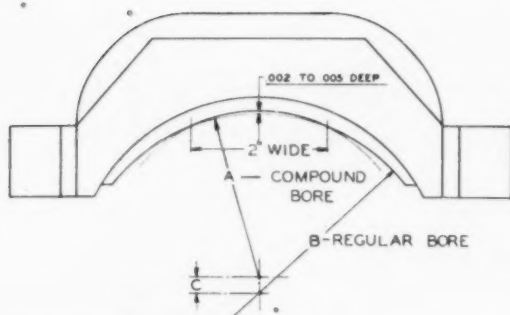


FIG. 6 PHANTOM VIEW OF RENEWABLE AXLE-SLEEVE ASSEMBLY

It can be removed readily by use of a hydraulic jack mounted in a stirrup with lugs to fit over the renewable axle sleeve collar so the jacking pressure can be applied against the end of the axle. The axle nut should be unscrewed only a turn or two so it will act as an arrester when the shrink fit is broken. A thin coating of white lead and oil swabbed on the axle before driving the heated sleeve in place will prevent galling of the sleeve on the axle.

The advantages claimed for the renewable bearing-axle sleeve are as follows:

- 1 The provision of a hardened and accurately ground journal, journal collar, and journal fillet will eliminate excessive wear and enable the use of full-size journals throughout axle life.
- 2 The use of the renewable axle sleeve will enable the continued use of worn axles that would otherwise have to be scrapped.
- 3 Axle life will be limited only by fatigue defects that are detected by magnafluxing.
- 4 By maintenance of proper journal size, the tendency of forming waste grabs will be reduced greatly because of the reduction in clearance between the bearing and the journal, adjacent to the contact area.
- 5 Both starting and running friction will be reduced due to improved fit between axle and journal, and by better and harder journal surface.
- 6 Bearing failures due to spread and distorted lining will be reduced since, with full-sized journal, component contained parts of the journal box will not be displaced from their intended position. This displacement of parts which occurs on undersize journal, also causes interruption to lubrication and packing down of waste away from the journal, two troubles that will be greatly reduced.



SIZE	A - DIA.	B - DIA.	C
5 x 9	5.004	5 1/8	1/32
5 1/2 x 10	5.504	5 7/8	1/32
6 x 11	6.004	6 1/2	1/32
6 1/2 x 12	6.504	6 3/4	1/32

FIG. 7 COMPOUND-BORE JOURNAL BEARING

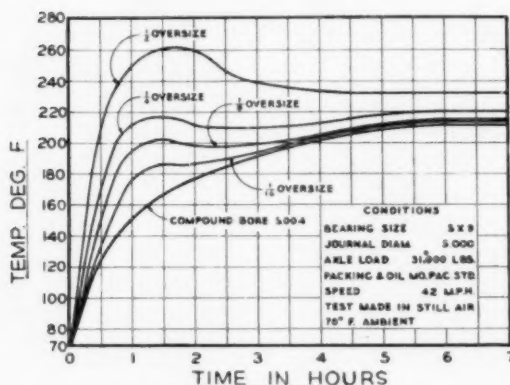


FIG. 8 TIME-TEMPERATURE CURVE FOR AAR JOURNAL BEARING AS AFFECTED BY VARIATION BETWEEN JOURNAL DIAMETER AND BEARING BORE

Compound-Bore Journal Bearing. The compound-bore journal bearing has a secondary bore superimposed on the standard or primary bore, providing a precision fit 0.004 in. in diam over the nominal axle diameter approximately 2 in. wide, parallel to and in the center of the standard bore, as shown in Fig. 7.

The compound-bore bearing provides the equivalent to precision hand-scraped fit on a full-size axle. Where it is applied on undersized axles there is much less conformation of bearing required in initial operation. Comparative breaks in temperature characteristics are shown in Fig. 8.

The advantages claimed for the compound-bore car journal bearing are:

- 1 Possibility of waste grabs and lint burns is decreased during initial operation, which are invited by larger clearances adjacent to contact area between journal and a standard bore bearing.
- 2 Due to reduced conformation of bearing lining to journal surface, there is a reduction of pulling and cracking of the babbit lining.
- 3 Hot boxes are reduced by the reduction of both the severity and duration of high-temperature "break-in" period experienced initially on all bearings applied.
- 4 Lubrication is improved by insurance of a larger initial contact area under load, reducing the initial fluid-film pressure per unit of area. Frequently, initial fluid-film pressures com-

bined with high initial operating temperature, and relatively small initial contact areas causes oil film to fail, and in extreme cases fluid-film cannot even be established.

The compound-bore journal bearing is now in use by several leading railroads in both freight and passenger service.

The compound-bore journal bearing has been submitted to the AAR, requesting its approval as an alternate standard for interchange use and is on the test program. However, there will be no objection to its interchange use pending this approval since in no way does it conflict with specifications now in force, under which hand scraping of bearing bore is condoned and practiced.

APPENDIX C

MAGNUS METAL CORPORATION

Some of the improvements in designs and materials developed and recommended by the Magnus Metal Corporation in connection with the service of solid-type bearings and their assemblies in high-speed freight service, are herein described. These improved products have been developed as a result of many years research and they have a background of millions of miles of successful service in railroad operation.

Satco Bearing Metal. Satco bearing metal has been used very successfully for many years past as a lining for various types of railway bearings in place of lead and tin-base babbitts, antimonial lead, etc. This alloy was made an alternate for babbit metal in linings of freight-car bearings by the Association of American Railroads.¹⁰

Satco metal is a lead-base alloy composed of approximately 95-98 per cent lead with balance calcium and other hardeners. The composition of the alloy is varied according to the service in which the bearings are used. One of the mixtures used by the railroads as a general-purpose bearing metal contains approximately 97-98 per cent lead, with balance calcium and other hardeners.

Graphs showing the physical properties of Satco metal at normal and elevated temperatures, as compared with AAR lead-base babbit, tin-base babbit, and antimonial lead are shown in Figs. 9 and 10.

Satco metal has a melting point approximately 150 deg F higher than that of babbit metals with a correspondingly higher hardness at elevated temperatures. These are very important advantages as they are a measure of the heat resistance to spalling and melting of the bearing lining in service. This is particularly important in protecting the bearing against the effects of "waste grabs." Satco-lined bearings are said to function perfectly at temperatures where babbit-lined bearings fail by melting.

Satco can be bonded firmly to brass, bronze, steel, and aluminum, the bond strength between lining and brass being 20-40 per cent greater than that obtained with babbit-lined material. Consequently, bearings lined with Satco metal are more resistant to cracking and loosening of the lining and resist oil penetration to a much greater degree than with babbit-lined bearings.

Illustrations showing some of the various types of bearings lined with Satco metal used by the railroads for passenger cars and locomotives are shown in Figs. 11, 12, and 13.

"Twinplex" Satco-Lined Alarm Journal Bearings. The "Twinplex" Satco-lined alarm journal bearing shown in Fig. 11 is an AAR emergency-type bearing equipped with two brass tubes, each having a small orifice sealed with fusible metal which melts at 350 F. If the temperature of the bearing reaches that point, one of the tubes releases a distinctive and penetrating odor and the other a large volume of dense white smoke. The discharge continues until both tubes are empty, which requires

¹⁰ Circular DV-905, May 15, 1937.

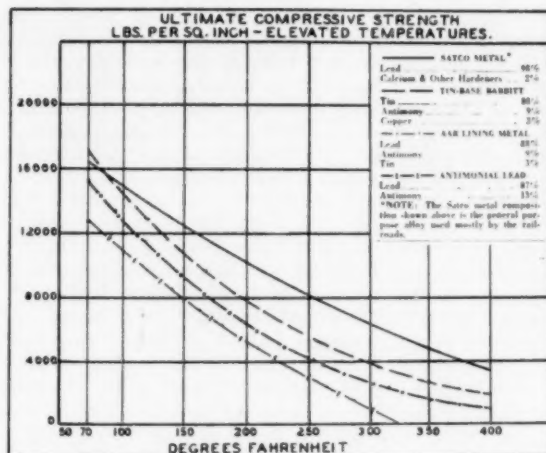


Fig. 9

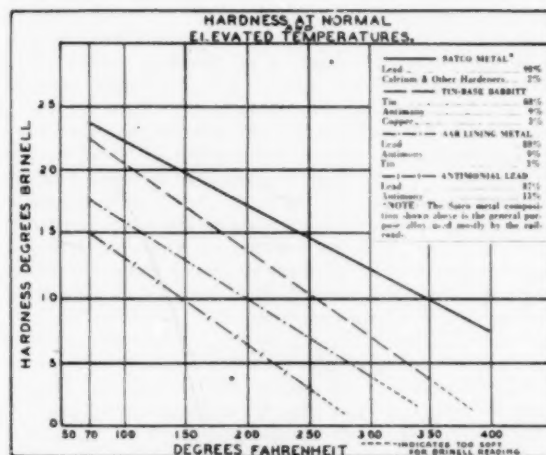


Fig. 10

about 8 min. This device has had wide application for several years past on main-line high-speed passenger cars and locomotives of an important Eastern trunk line railroad. Experience has shown that the odor can be detected in any car in a passenger train, regardless of whether it is a tightly sealed, air-conditioned car or not. This odor is noticeable in the train for from 4 to 8 min.

"Magsafe" Satco-Lined Journal Bearing. The Magsafe Satco-lined journal bearing shown in Fig. 12 is a standard AAR type bearing equipped with a special device to prevent lint wipers and "waste grabs."

This device consists of two T-section brass comb strips one on either side of the crown of the bearing, positioned in longitudinal grooves milled in the brass. In running position, the comb strips drop down of their own weight and contact the journal at all times, regardless of whether the journal is new or turned down to the limit of wear, thus preventing lint and strands of waste from climbing the journal.

The comb strips are stopped off 1 in. from the hub end of the bearing to prevent end leakage of oil and to maintain full bearing contact at the hub end of the wheel.

The comb and slots are T-shaped to prevent combs from falling out of the bearing when being applied or removed from the jour-

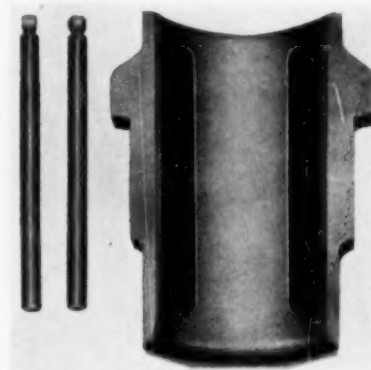


Fig. 11 SATCO-LINED "TWINPLEX" ALARM JOURNAL BEARING

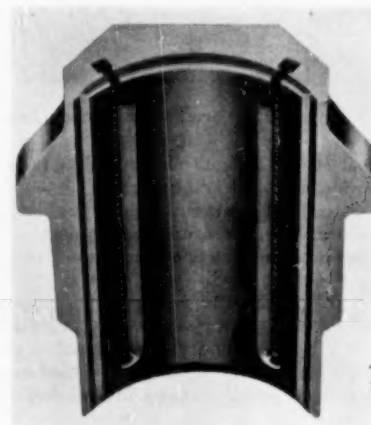


Fig. 12 "MAGSAFE" SATCO-LINED JOURNAL BEARING

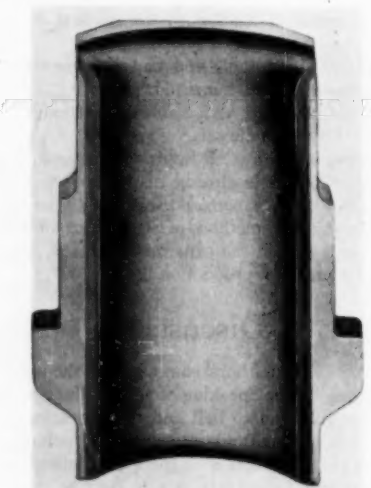


Fig. 13 STANDARD AAR PREWAR OR EMERGENCY SATCO-LINED JOURNAL BEARING

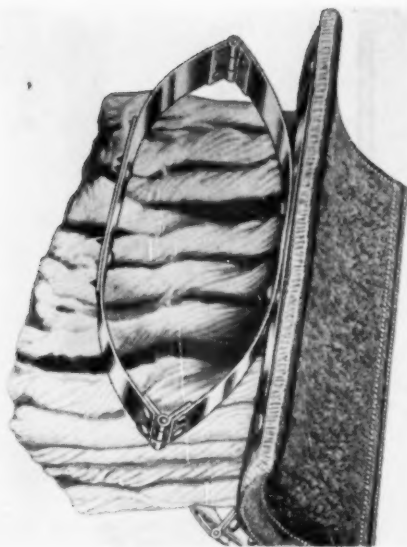


Fig. 14 MAGNUS "R.B." SPRING-PAD JOURNAL LUBRICATOR

nal.* The comb strips distribute oil evenly along the journal, and they also provide oil storage in the bearing.

Magsafe Satco-lined journal bearings are being used as standard for main-line passenger-car equipment and regularly assigned Pullman cars on one of our important transcontinental railroads.

Magnus "R.B." Spring-Pad Lubricator. A recent Magnus development is the R.B. spring-pad journal lubricator shown in photograph in Fig. 14. This device is adapted to the standard round-bottom AAR type of box and is being used successfully in place of conventional packing in locomotive-tender, engine-truck, and trailer boxes.

The R.B. lubricator pad is inserted easily or removed without being necessary to jack up the box or remove the bearing and wedge. It is recommended for use in journal boxes of freight-car equipment in high-speed service in place of conventional packing, as a means of obtaining more efficient and dependable lubrication.

In addition to the designs and materials described, Magnus has also developed improved methods of casting, machining, and broaching of the standard AAR babbitt-lined freight-car bearing now being used by the railroads.

One new development is an improved method of casting the lining metal. From tests already made, the bond strength between lining and brass is increased from 20-40 per cent, as compared with the standard methods of casting heretofore used. This special process is still in the experimental stage, but it is being developed on a practical production basis.

Discussion

S. J. NEEDS.¹¹ The authors' comments on the use of the terms "friction bearing" when speaking of the oil-film type, and "antifriction" when referring to ball and roller bearings, are indeed timely. All bearings are fundamentally antifriction, since one of their functions is to operate with the least friction possible; but taken together, the foregoing terms do seem to imply that some

inherent friction miracle is to be found in ball and roller bearings. However, it is questionable whether many users of bearings are misled by this propaganda. Ball and roller bearings have been highly developed. They fill many important needs and have become vital parts of many mechanical structures. The methods by which they are produced form an outstanding part of our production achievements. It is unfortunate that they have been given a name that they cannot hope to live up to.

The company with which the writer is associated has been building thrust and journal bearings of the oil-film type for many years. Regarding load-carrying capacity, we generally think of the oil-film bearing as beginning where the ball and roller bearings leave off. This is seen in the many instances where we have replaced overloaded ball and roller bearings with oil-film bearings. As far as bearing life is concerned there is no room for comparison. A properly designed and lubricated oil-film bearing suffers no wear except at the moments of starting and stopping, hence will last practically forever. It is generally recognized, however, that ball and roller bearings, even though lubricated and cared for properly, are limited by an uncertain span of life.

There are instances where the two types are not in competition and fall into well-defined fields. For example it is almost certain that a majority of our automobiles would be stalled along the roads if sleeve bearings were substituted for roller bearings in the wheels without some complicated, and doubtless expensive, oiling system to insure their lubrication. The same crippled condition of the automobiles probably would also follow from substituting ball or roller bearings for oil-film bearings on motor crankshafts.

Both oil-film and ball and roller bearings have their inherent advantages. The latter have the definite advantage of holding a shaft in approximately the same relative position whether running or not. A pivoted-pad oil-film journal bearing will accomplish the same result, but that is not possible with a complete cylindrical bearing which must have running clearance. It may be that ball and roller types more properly could be called "anticlearance" bearings rather than antifriction bearings.

It is noteworthy that much theoretical treatment and many test results are to be found in the literature regarding friction in oil-film bearings. Similar data on ball and roller bearings are very few indeed and these fail to substantiate the term antifriction. In 1945 the writer published a paper,¹² in which an attempt was made to analyze friction in railway-car journal bearings of the oil-film type. Some tests were run later with roller bearings under similar conditions. These studies were sponsored by the Association of American Railroads. If the data on roller bearings were also published, they might throw some light on the relative frictions of the two types, and the quantitative value of the term antifriction could then be established for railway-car roller bearings.

AUTHORS' CLOSURE

To whatever extent or particular the operation of the conventional solid-type journal-box assembly per se may be factually deficient in meeting present-day requirements, it is evident that:

- 1 Economic improvement does not lie in replacement or substitution of the unit as a whole.
- 2 Improvement does lie in the proper evaluation of the nature, cause, and extent of presumed deficiencies.
- 3 With such factual evaluation available, the testing and selection of materials, practices, and designs of the elements of the journal-box assembly already developed will lead to the most dependable and economic operation.

¹¹ Service Manager, Kingsbury Machine Works, Inc., Philadelphia, Pa. Mem. ASME.

¹² "Tests of Oil-Film Journal Bearings for Railroad Cars," by S. J. Needs, Trans. ASME, vol. 68, 1946, pp. 337-353.

The Development of a Design of Smokeless Stove for Bituminous Coal

By B. A. LANDRY¹ AND R. A. SHERMAN,² COLUMBUS, OHIO

This paper presents an account of an extended systematic investigation which resulted in the development of a method for burning bituminous coals in nonmechanical hand-fired heaters or stoves with substantially smokeless operation. The research was sponsored by Bituminous Coal Research, Inc., and a group of stove manufacturers. An experimental investigation of the three principles of combustion in fuel beds led to the adoption of the cross-feed principle. The design of a special grate and the research to prevent puffing, a difficulty often encountered with magazine heaters, are described. The principles of a calorimeter room in which the output of a space heater can be directly measured are presented. Data given show the thermal efficiency of a manufacturer's model of the heater, which had an output of 41,000 Btu per hr, to be 65 per cent.

THE United States leads the world in the number and proportion of residences that are heated from a central plant, and a high percentage of these use automatic firing of coal, oil, or gas. However, the Census of 1940 showed that 16,000,000, or about 47 per cent of the dwelling units of the country were being heated by some type of stove. Some 40 per cent of these dwellings use coal as a fuel. Because many dwellings use more than one stove, it can be estimated that there are probably about 8,000,000 coal-burning stoves in the United States today and several hundred thousand are sold each year. Estimates have been made that 25 to 30 million tons of coal are used annually in stoves.

Because these stoves operate on the simple surface-burning principle and because they are usually connected to low chimneys, the charge that stoves are important contributors to the smoke problem of cities where bituminous coal is used is probably not without some justification.

As a part of its program to develop improved equipment for the utilization of bituminous coal, Bituminous Coal Research, Inc. (BCR), the research agency of the bituminous-coal industry, initiated at Battelle late in 1940 a research project aimed at the development of stoves that would burn bituminous coal without the emission of objectionable smoke. In July, 1941, a group of manufacturers of stoves joined BCR in support of the program.

This paper presents an account of the steps that were followed in the investigation which has now culminated in the design of smokeless stoves which are in commercial production and are being sold and used. The design principles developed are applicable also to warm-air furnaces and residential boilers, and are now in process of being applied to these types of equipment.

¹ Supervisor, Fuels Research, Battelle Memorial Institute. Mem. ASME.

² Assistant Director, Battelle Memorial Institute. Mem. ASME.

Contributed by the Fuels Division and presented at the Annual Meeting, New York, N. Y., November 28-December 3, 1948, of THE AMERICAN SOCIETY OF MECHANICAL ENGINEERS.

NOTE: Statements and opinions advanced in papers are to be understood as individual expressions of their authors and not those of the Society. Paper No. 48-A-119.

GENERAL PRINCIPLES OF COMBUSTION OF BITUMINOUS COAL

As do all other natural solid fuels, and some processed ones, bituminous coals, when heated, release gaseous products composed of water vapor, hydrocarbons, hydrogen, and sometimes carbon monoxide, and carbon dioxide. The weight of these products is approximately directly related to the volatile-matter content of the coal. Following the process of distillation or devolatilization of the coal, there still remains an appreciable portion of the fixed carbon to burn. Hence, the complete burning of bituminous coals involves, usually in two steps, the burning of gases and the burning of solids.

When bituminous coal is burned in pulverized form, the single process of mixing air with coal particles is effective in carrying out the burning requirements of both gases and solids. However, when the coal is burned in fuel beds other than exceptionally thin overfeed beds, two distinct processes are needed to burn satisfactorily the two fuel forms. One, of course, simply involves passing air through the fuel bed to burn the coke; the other, requires (1) that air be mixed thoroughly with the gases, as they are released from the portion of the bed where devolatilization takes place, and (2) that temperatures be maintained high enough for completion of the combustion reactions. Failure to satisfy these two requirements results in the formation of smoke.

If no air is provided for mixing with the gases, and temperatures in the furnace are low, smoke consists mainly of a tar fog which is condensed hydrocarbons. If air is supplied but mixing is incomplete, and furnace temperatures are high enough to cause ignition, there will be regions of intense burning wherever oxygen is available, and other regions where, because of the absence of oxygen, the hydrocarbons simply will be heated by radiation to temperatures high enough to cause cracking, with formation of carbon or soot which will appear as smoke. Actually, both tar and soot may be emitted simultaneously with the gases from different parts of the furnace.

In mechanically fired industrial furnaces with good control of the air/fuel ratio, streams of gases rich in hydrocarbons may arise from certain portions of the fuel bed while other streams of gases, in which excess air is present, may arise from other portions. The mixing of these two streams may take place rapidly enough to avoid smoke formation if mixing arches are provided or if a large furnace volume gives time for mixing by diffusion. With smaller furnace volumes or higher rates of operation, which decrease time available for diffusion, smoke is of common occurrence unless overfire jets are used to establish turbulence where stratification otherwise would prevail. Even overfire jets, however, may not be completely effective if furnace volumes are too small or control of the air/fuel ratio is lost as a result of large intermittent firings.

Smoke emission from hand-fired heating equipment results from causes similar to those described, with considerable exaggeration of some of them, particularly in regard to the relatively large intermittent firings that are made, as is necessitated by the impracticality of frequent attention, and in regard to the low furnace temperatures usually maintained, which are unfavorable for ignition of the mixture but which are required to prevent overheating. The palliative of overfire-airjets is not available

for this type of equipment because furnace conditions would render them ineffective. Elimination of smoke from hand-fired heating equipment must depend primarily, therefore, on the selection and application of such combustion principles that will be effective purely as a result of design arrangements. The difficulties associated with following such a course have long been considered as affording little chance of success.

STAGES OF INVESTIGATION

The stages followed in the investigation were as follows:

- 1 A test survey of all those commercially available heaters, for which differences could be recognized in the principles used for combustion, in order not to overlook any promising feature of design. This period was also of value in the development of methods of test, including the use of a light-sensitive smoke meter, to insure reproducibility of results and the drawing of assured conclusions.

- 2 The selection of the cross-feed principle of burning, so disposed that the fuel moved downward from a magazine toward a horizontal grate above which cross-feed air and gases moved horizontally across the bed, and the addition of an arch of special construction to provide for the intimate mixing of secondary air with the gases escaping from the bed for complete combustion.

- 3 The introduction of air above the fuel fired in the magazine in order to alter the caking properties of the fuel and convert strongly caking coals to a free-burning form for gravity feeding to the "hearth" or cross-feed burning portion of the bed.

- 4 The development of special grates to insure horizontal flow of air above them, without danger of short-circuiting through the ashpit, and to provide a dumping arrangement to dispose of larger pieces of ash, especially laminated material.

- 5 The translation from the laboratory type of construction to a commercial design.

- 6 The development of a calorimeter room to measure directly the output of heaters and to make possible the evaluation of the various heat losses including the saving in fuel from smoke elimination.

RESULTS OF TEST SURVEY

Method of Test. The method of test used in making the survey, which remained essentially unchanged during the course of the investigation, consisted in placing the heater or stove on scales to observe the rate of weight loss during the burning, and providing flexible connections to the points where drafts were measured, temperatures taken by means of thermocouples, and gas samples obtained by means of water-cooled samplers. Imposed conditions to evaluate performance and to permit duplication of tests, to insure reproducibility of results, were either (1) to maintain constant flue-gas temperature, at some preassigned value, or (2) to maintain constant applied draft, again at some preassigned value. The first type of operation is valuable to show the frequency and type of attention required to maintain approximately constant output; the second type of operation serves to relate burning rate and output to applied draft to ascertain whether the burning process is under control. Both types of test were usually required for complete evaluation of the heaters.

Heaters Tested. Figs. 1 to 6, inclusive, show in diagrammatic form the burning principles of heaters on which tests were conducted during the survey stage preceding the development of the smokeless stove. In these diagrams the diagonally hatched areas represent solid fuel, whether freshly fired or at various degrees of devolatilization, except for Fig. 5 where the rectangular hatching represents freshly fired coal. Comments which follow refer to the performance of these heaters when burning bituminous coal.

Fig. 1 represents the conventional "surface-fired" heater with primary air admitted through the grates, and secondary air admitted either through the firing-door slots or through a "down-blast" pipe. This type of heater produces abundant smoke, because of poor mixing with secondary air, or low temperatures during devolatilization, or both; the period between attentions is short, but the average CO_2 is acceptable and draft requirements are well within the capacity of a small chimney.

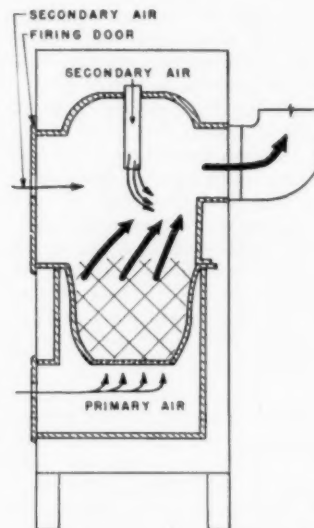


FIG. 1 CONVENTIONAL SURFACE-FIRED STOVE WITH TWO ALTERNATE FORMS OF SECONDARY-AIR ADMISSION

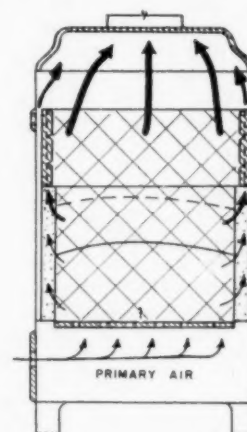


FIG. 2 "MAGAZINE-TYPE" HEATER WITH DEEP FIRE POT

Fig. 2 represents a version of the so-called magazine-type heater having a deep fire pot, primary air passing through the grates and gases leaving the fuel bed at various heights through side channels or ducts, or at the top of the bed, the type of flow depending on the extent of caking in the fuel bed. The devolatilization of the charge is more rapid in this type of heater so that the smoking period, because of poor mixing with secondary air at low temperatures, is more intense although of relatively shorter duration than in the conventional heater, in view of the larger firing possible. The period between attentions is long, the

average CO_2 is acceptable, but the draft requirements are so low that the rate of burning may easily become excessive and control of heat output may be lost.

Fig. 3 represents a downdraft heater with part of the air supply passing through a rear slot to burn the gases at the outlet which is small in comparison with the size of heater. Because high temperatures are not maintained at the throat, owing to excessive air flow in comparison to the flow through the bed, smoke from this heater is abundant, rates of burning are low, and draft requirements high unless frequent poking is done to break the cake and prevent short-circuiting of primary air to the slot.

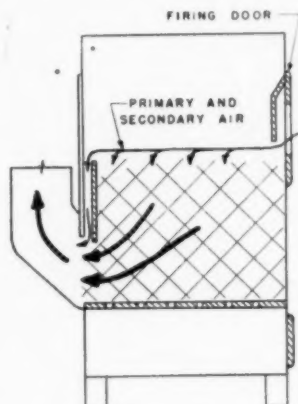


FIG. 3 DOWNDRAFT HEATER

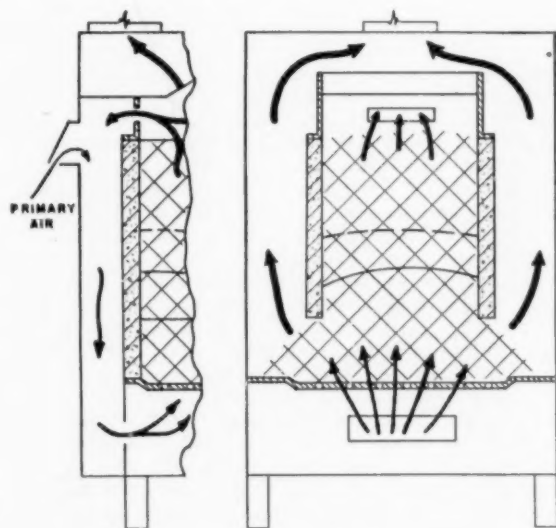


FIG. 4 DUAL-SIDE HEATER

Fig. 4 represents a dual-side heater in which devolatilization takes place, because of lateral heating, in the fuel magazine; the volatile gases escape at the top and are allowed to mix with primary air which serves also as secondary air when passing through the edges of the bed. Because of poor mixing, abundant smoke is produced, rates of burning are low, with low CO_2 , unless frequent poking replenishes the fuel supply at the two sides, which also tend to burn at uneven rates.

Fig. 5 represents a divided heater with a half-circular lid which is pivoted on the partition. As the fuel in one half burns, the fuel in the other half devolatilizes by heat transfer, the gaseous products leaving through a hole in the partition to pass into the burning side; after refiring, the lid is rotated over the freshly fired side. Nearly smokeless operation can be obtained, with acceptable average CO_2 and low-draft requirements, if the heater is as small as a 14-in.-diam cylinder. With a further increase in diameter, heat transfer is not high enough to devolatilize all of the fresh fuel during the burning of the residual fuel, and with increase in diameter of heater, progressively more abundant smoke is produced after rotation of the lid.

Fig. 6 represents a type of cross-feed unit in which air is admitted at two levels, at the side (1) at the lower level, to burn the residual coke, and (2) at the upper level, to act as secondary air for mixing with the gases leaving the bed. Air is admitted also at the top of the magazine to alter the caking properties of the fuel in the magazine. Because of the unequal flow of the lower air, owing to its tendency to make a short curvature bend immediately after entering the heater, and thus escape contact with the fuel, the rate of burning can be maintained only by frequent poking to fill cavities formed, and smoke is produced in objectionable

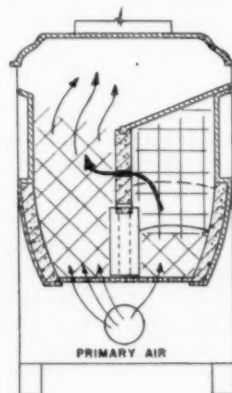


FIG. 5 DIVIDED HEATER WITH PIVOTED LID

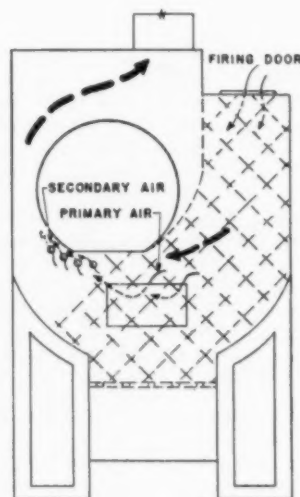


FIG. 6 SIDE-FEED HEATER

quantity because of poor mixing of the secondary air with the gases for the same reason. With frequent poking, average CO_2 is acceptable and the draft required is low.

Discussion of Results of Survey. Consideration of the results obtained during the survey led to a number of conclusions. One of these was that if the products of combustion, as they emerge from the fuel bed, contain smoke-forming constituents, the casual introduction of secondary air into the combustion space will not eliminate smoke. This results from the stratification of the gas and air streams, owing to their low velocities, at all rates of operation, in addition to the impossibility of attainment of temperatures high enough for ignition at the lower rates. Hence, a positive means of insuring mixing of gases with air in a region of high temperature, at all rates of burning, was indicated as a requisite for smoke elimination. This conclusion made it appear that a bed fired from above with air admitted through the grates was not a promising principle for the smokeless heater.

Another conclusion was that burning by means of admission of air at the top of the charge, as attempted in the heater shown in Fig. 3, could not be depended upon to prevent caking of bituminous coals rapidly enough to maintain air flow at the higher burning rates, and hence offered little promise.

By elimination, therefore, only the cross-feed principle remained as one upon which further investigation appeared to be warranted. None of the heaters tested in the survey could be considered as embodying true cross-feed burning; however, to the extent that the heater shown in Fig. 6 represented an attempt at cross-feed burning, to the same extent it could be concluded that this type of burning was not one which would give smokeless burning purely by virtue of the relative directions of flow of air and fuel.

BASIS FOR SELECTION OF CROSS-FEED PRINCIPLE FOR SMOKELESS HEATER

Although the cross-feed bed is used to advantage in so-called "underfeed-stoker" beds, yet, for this type of application, mechanical action is required to move the fuel from the retorts laterally across the tuyeres. Thus, if cross-feed burning were to be used in heaters, in the absence of mechanical means of feeding, the motion of the fuel relative to the air stream could only be so directed as to result in a downward flow under the action of gravity, the air movement being at right angles, or in a horizontal direction. This arrangement provided for the following distinct advantages:

- 1 Horizontal flow of the gaseous products of combustion across the bed would require the use of a vertical arch descending to a level adjacent to the grate to confine the bed while permitting the outflow of gases under the edge of the structure. Admission of secondary air in this region was indicated because the gases would be at their maximum temperature at all times to favor sustained ignition.

- 2 Generation of heat over the entire volume of hearth subject to cross-feed burning would favor transfer of heat through the upper boundary of the hearth for devolatilization of the fresh fuel fired in the magazine space above, and thus insure eventual minimum release of hydrocarbons during the cross-feed burning.

- 3 Constancy in the thickness of bed between the arch and the opposite wall would favor sustained combustion efficiency during the burning cycle.

In carrying out the development of a smokeless stove using the cross-feed principle of burning, there were two main stages, namely (1) stoves that required poking to bring the caked fuel down from the magazine into the hearth, and (2) stoves for which the necessity to poke was eliminated by providing oxidizing conditions during devolatilization to prevent caking.

FIRST STAGE IN DEVELOPMENT OF SMOKELESS STOVE

Fig. 7 is a diagrammatic view of the heater that was built to test in a preliminary way whether the advantages described would accrue from cross-feed burning. All of the primary air was admitted through louvers set in a wall opening opposite to the arch. Secondary air was admitted at the bottom of the passage under the arch through similar louvers, and a combustion chamber was provided on the other side of the arch to give time for the completion of the reactions. Results showed that, as compared with smoke emission from conventional heaters, much improvement had been obtained; however, observation showed that the stream of products of combustion, usually containing combustible

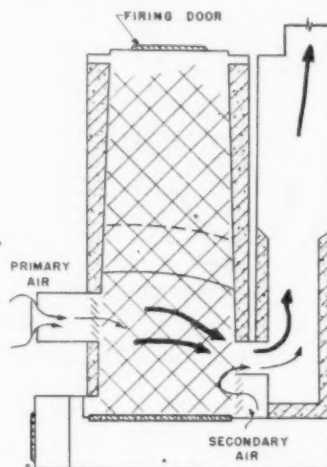


FIG. 7 PRELIMINARY CROSS-FEED HEATER

gases, passed closely under the bottom of the arch as they left the fuel bed and did not mix well with the stream of secondary air coming from below, and that the stratification thus set up did not disappear in the combustion chamber.

Fig. 8 shows the next design in which provision was made for the admission of secondary air through a flattened metal pipe, approximately 3 in. wide, set above a 7-in. refractory-lined duct serving as gas outlet. A 1-in. pipe vent was also provided to relieve the gas pressure that otherwise would build up at the top of the magazine owing to the formation of a hard and impervious layer of coke at the lower boundary of the fresh charge. The vent was so disposed as to make the gases mix with primary air before passage through the fuel bed.

Results were immediately so promising from the point of view of smoke elimination that there was no doubt that the proper method of introduction of secondary air had been provided to give complete mixing of air and gases as both streams moved along the bottom of the arch, that is, the top of the gas outlet or throat. The heat-exchanger section, attached to the outlet, no longer served as combustion chamber, but solely to dissipate heat. In the form sketched in Fig. 8, the heater could be placed in one room, adjacently to a wall, and the heat exchanger placed in the adjoining room, the connection outlet passing through a hole in the wall. Operation of the heater disclosed, however, that the rate of burning was definitely limited to low values under the maximum allowable draft; it was reasoned that the restricted outlet limited the flow of air to a small cross section of the bed in addition to offering rather high resistance to the flow of gases.

Fig. 9 represents the next important development. For this heater, a generally rectangular construction was adopted to

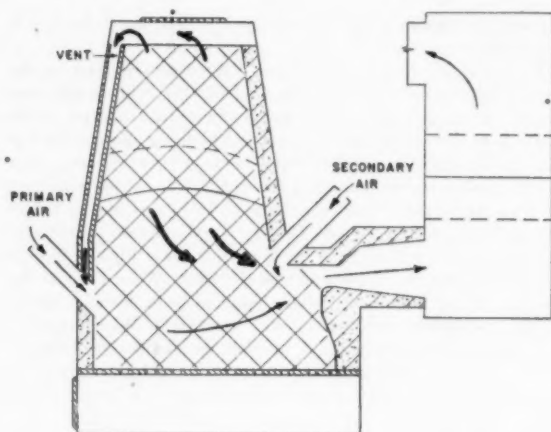


FIG. 8 SECOND VERSION OF THE SMOKELESS HEATER

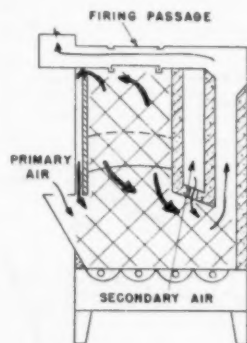


FIG. 9 A THIRD VERSION OF THE SMOKELESS HEATER

provide a combustion-gas outlet as wide as the heater, and the heat exchanger was, so to speak, wrapped around the side and top of the heater for compactness. Secondary air, introduced through the ends of a refractory arch, was admitted above the gas passage, but the error was made of admitting the air through eight $\frac{1}{4}$ -in. holes spaced about 2 in. apart, whereas in the heater of Fig. 8 the secondary-air slot had extended continuously over the gas outlet. It was found that smoke was not completely eliminated, and it was verified that lateral stratification of streams of gases occurred, owing to lack of side mixing with air. An investigation was carried out whereby the individual holes were first replaced by four 4-in. divided slots having 1-in. closed spacing between them, and then by a continuous slot extending over the entire length of arch.

Table 1 summarizes average results obtained from four successive tests under each of the conditions listed. The advantage of replacing individual holes by a continuous slot, to prevent lateral stratification, is shown by the decrease obtained in recorded durations of smoke, indicated by the inclusive minutes above each of the conventional Ringelmann numbers. The average percentage of carbon dioxide obtained in these tests was also of interest in showing that, by standards of low-duty, hand-fired heating equipment, acceptable and rather constant combustion efficiency was being obtained with decrease in smoke.

In this connection, tests made with the four 4-in-slot arrangement had shown a distinct relation between the area of opening

TABLE 1 COMPARISON OF RESULTS OF SMOKE EMISSION FROM USE OF HOLES, OF DIVIDED SLOTS, AND OF A CONTINUOUS SLOT IN SECONDARY-AIR ARCH. AVERAGE RESULTS FROM FOUR TESTS OF HEATER SHOWN IN FIG. 9

(Ohio No. 6 coal, size 2 in. \times 1 in.)			
Secondary-air openings in arch...	Eight, $\frac{1}{4}$ -in. holes	Four, 4-in. slots	Continuous 20-in. slot
Average applied draft, in. water.....	0.059	0.056	0.060
Combustible gasified, lb.....	19.25	19.10	23.75
Duration, hr.....	3.5	4.0	4.0
Combustible gasified, lb per hr.....	5.5	4.8	6.0
Average flue-gas temperature, deg F.....	875	850	880
Smoke, Ringelmann No., minutes (inclusive) in test period			
Above No. 1.....	26	16	15
Above No. 2.....	12	4	2
Above No. 3.....	8	2	1
Above No. 4.....	6	1	0
Average flue-gas composition, per cent			
CO ₂	9.6	9.2	10.0
O ₂	9.7	10.2	9.2
CO.....	0.1	0.1	0.3

provided for the admission of secondary air to the interior plenum of the arch, the smoke emission, and the excess air. Table 2 illustrates the relation determined by the average of four tests in each series with the stated areas of opening. The table shows that with a small area the CO₂ was high at 13.5 per cent and also the smoke emission. With increase in area and, consequently,

TABLE 2 RELATION OF SMOKE EMISSION AND OF AVERAGE CO₂ TO AREA OF SECONDARY-AIR OPENING IN HEATER SHOWN IN FIG. 9

(Ohio No. 6 Coal, size 2 in. \times 1 in.)			
Area of opening for secondary air, sq in...	1.77	3.53	5.30
Average CO ₂	13.5	10.0	9.2
Smoke, Ringelmann No., minutes (inclusive) in test period of 4 hr			
Above No. 1.....	80	18	16
Above No. 2.....	62	5	4
Above No. 3.....	37	3	2
Above No. 4.....	6	2	1

increase of secondary air, both CO₂ and smoke decreased, but the reduction in smoke obtained with a CO₂ content as low as 9.2 per cent was not so large as that obtained by replacing the partial slots by a continuous slot, in further view of the fact that an average CO₂ of 10 per cent was obtained with the latter arrangement.

Discussion of Results of First Stage of Development. Although the evolution described in the design of the cross-feed heater properly could be considered to have solved the problems of smoke emission and of compactness of design, yet there remained the serious difficulty that the heater required poking to bring devolatilized fuel into the hearth. To minimize the labor of poking, successive heaters had been made smaller, with a firing door at the top, to permit more advantageous use of the poker in breaking the hard coke layer formed above the hearth section. Such small heaters had the disadvantage of a short interval between firings, of approximately 4 hr, as shown in Tables 1 and 2, and could not be construed as magazine heaters. This was confirmed in field trials of some twenty units of a jacketed heater based upon the heater shown in Fig. 9, for which the principal complaint was precisely the difficulty of poking. Hence, it was indicated that means had to be found to prevent caking in the magazine if a smokeless heater with true magazine feed was to be developed to give users the very tangible advantage of a long period between refirings, at rating, in addition to smokeless operation. This was the objective of the second stage.

SECOND STAGE IN THE DEVELOPMENT OF THE SMOKELESS STOVE

One of the simplest ways to prevent the caking of bituminous coal is to provide oxidizing conditions around pieces, as tar exudes from them while the coal is being heated. Little air is required to prevent caking in this manner when the rate of heating is low but the reverse is true at higher rates. The application of this principle to the smokeless stove appeared promising enough that

trials were made in a deep-magazine heater built for this purpose. As soon as confirmation had been obtained that caking could be prevented, a number of units were built for field tests.

Fig. 10 is a diagrammatic cross section of this second field-test unit which embodied a means of admission of magazine air, under controlled conditions, for self-feeding. The air was admitted through an external duct and entered near the top of the firing space above the magazine charge. Flow of this air through the fresh charge of caking fuel induced upward travel of ignition of the tarry substances, against the flow of air. Meanwhile, cross-feed burning, in the hearth, maintained heat output and provided the heat source from which the upward travel of ignition could start; thus the time was provided that is required to convert the caking coal to the free-burning stage to permit its

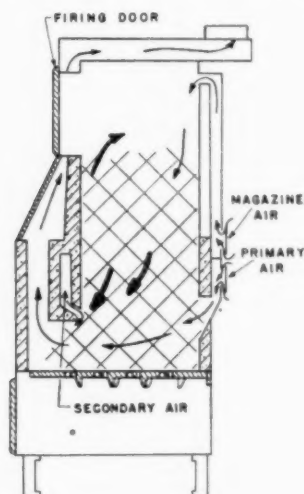


Fig. 10 SECOND FIELD-TEST MODEL OF SMOKELESS HEATER

descent into the hearth. This combination of principles was found to correct, in the manner described, for the operating deficiencies of the heater shown in Fig. 3, which depended entirely on downdraft burning to sustain the burning rate. Because of air admission to the magazine, the vent formerly used to lead fumes from the magazine to the point of entry of cross-feed air was no longer required and was not provided in the heater shown in Fig. 10, and in other heaters subsequently built.

Occurrence and Cure of Puffing. At this stage of the development, laboratory and field experience showed that, as a result of the admission of air to the magazine, "puffing" was introduced during operation, particularly following an adjustment in the rate of air supply. The puffing was normally inaudible but manifested itself by the emission of visible smoke puffs at one or more of the various air inlets to the heater, the smoke having the characteristic odor of incompletely burned gases from bituminous coal. This occurrence led to a rather long investigation to obtain a cure; the fact that puffs might appear at any of the air openings made it difficult to understand their exact cause.

Final conclusions reached were that puffing could occur as a result of two types of actions, namely, (1) formation of an ignitable mixture within the fuel-bed voids, in the vicinity of the secondary-air arch, when these voids were large enough to yield appreciable kinetic effects upon ignition of the mixture, and (2) formation of an ignitable mixture of combustible gases and air in the firing space above the magazine charge, followed by ignition of the

mixture, as a result of the upward travel of ignition to the top of the charge.

Fig. 11 shows the general design of three heaters used for the experimental work on which the first of these conclusions was based. In these heaters the magazine air was introduced within the charge rather than near the top of the firing space as in Fig. 10. The three heaters were similar in every respect, except that the dimension corresponding to the distance from the refractory arch to the opposite wall was only 11.75 in., as in the heater shown in Fig. 10, for the first heater; for the second heater, this dimension was 14.75 in. as in the heater shown in Fig. 11; and in the third heater this dimension was 18.25 in. When burning the weakly caking Illinois or Indiana coals in these heaters, under steady conditions, no puffing was observed. When burning the strongly caking Pittsburgh coal, however, puffs were observed, under steady operation, with the first of these heaters, but not with the other two having the longer dimensions from arch to wall.

The explanation for this behavior was that the residual-coke pieces formed with the more strongly caking coal were much larger than those formed with the weakly caking coals; hence the void spaces between pieces were also correspondingly larger, and appreciable kinetic effects could be developed, in the vicinity

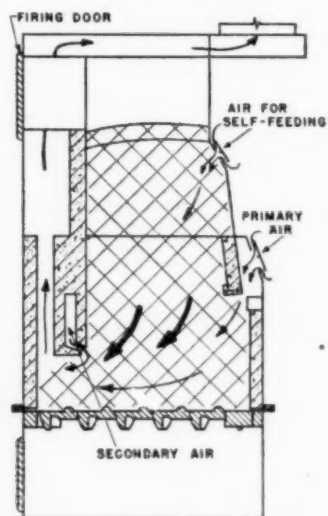


Fig. 11 SMOKELESS HEATER WITH ADMISSION OF MAGAZINE AIR BELOW TOP OF CHARGE OF COAL

of the arch, provided there was enough residual oxygen brought into the void spaces to mix with the combustible gases also entering into them in their flow downward from the fresh fuel in the magazine. Since combustion efficiency would increase, with increase in the hearth dimension described, and also with decrease in size of coke pieces, it was apparent that only in the heater with the shortest hearth dimension were the two conditions both fulfilled, when burning a caking coal, of large voids and of enough residual oxygen to give an explosive mixture. This was confirmed by a flue-gas analysis which gave averages of 9.3 and 9.4 per cent CO_2 , over an 8-hr period, for the two larger heaters, but only 6.7 per cent CO_2 for the smallest when burning Pittsburgh coal without smoke formation. The net result was that freedom from puffing from this cause required that the arch-to-wall dimension be at least 14 in., with little gain in combustion efficiency from any further increase in this dimension.

The second process mentioned, in which a mixture of combustible gases and air could form in the space above the magazine fuel is illustrated in Fig. 10 by the arrow, showing the tendency for gases to leave the top of the charge in opposition to the downward flow of air. That such a process existed was demonstrated by the arrangement shown in Fig. 11 whereby the air required to induce self-feeding of the coal was introduced within the charge, through a narrow slot as wide as the heater, at a level some 2 in. below the top of the charge. Because little or none of the air passed to the space above, no puffing was experienced with this arrangement under steady or variable operation. However, a layer of hard coke was formed above the level of the air entry, and this layer remained in place even after the free-burning fuel below had fed down, thus giving a deceptive appraisal of the quantity of fuel in the magazine. Raising the level of self-feeding air admission to the level of the top of a normal firing was successful in avoiding the formation of the coke arch, but reintroduced occasional puffing following partial closure of the cross-feed air inlet to reduce heat output.

Fig. 12 illustrates how the change in level of air admission was carried out and shows also the next change made which was to provide a sloping roof in the magazine to halve, approximately, the volume available for the mixture and reduce the kinetic effects, following ignition.

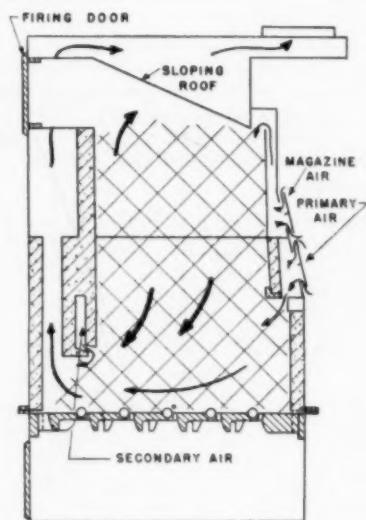


FIG. 12 SMOKELESS HEATER WITH SLOPING ROOF OF MAGAZINE

The final arrangement designed to make it practically impossible for any slight puff to manifest itself outside of the heater was to provide a common plenum duct covering both the magazine-air and the cross-feed air inlets, and extending enough downwardly so that the duct opening would be approximately at the grate level.

GRATES OF THE SMOKELESS STOVE

Throughout the development of the smokeless stove, a great deal of attention had to be devoted to the development of a grate design that would (1) insure no short-circuiting of air through the ashpit in order to maintain the flow of cross-feed air above the grate, and (2) provide a dumping element for disposal of unburned refuse.

Fig. 13 shows the design of the final type of grate developed. The close-fitting fingered portion is intended to offer enough re-

sistance to the flow of air to prevent short-circuiting while effectively serving to shake the bed and remove the fine ash released. Unburnable refuse is transferred by the motion of the grate into the troughlike end grate, under the vertical gas passage, for periodic removal by turning a crank attached to the trunnion support and thereby dumping the accumulation. The dump grate is counterbalanced to return automatically to a sealing position under the frame. A special re-entrant at the wall adja-

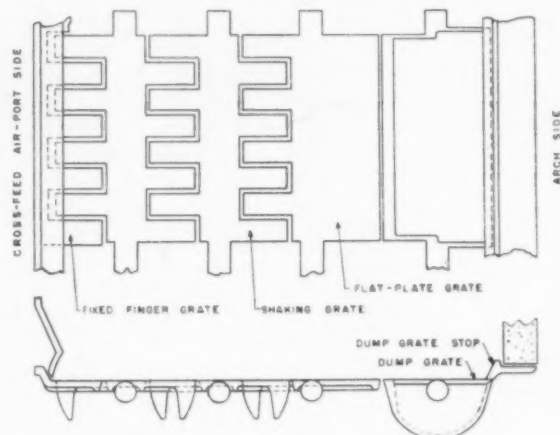


FIG. 13 PLAN AND SIDE VIEW OF SPECIAL GRATE FOR SMOKELESS STOVE

cent to the first rocking finger grate serves to prevent wedging of hard coke against this grate element.

CHARACTERISTICS OF PRESENT COMMERCIAL SMOKELESS HEATER

Fig. 14 shows in diagrammatic form the design of one of the present commercial smokeless stoves on which the plenum duct described earlier is visible. A feature of this design is the replacement by alloyed metal of the refractory portion of the arch, formerly on the fuel-bed side, to give longer life under existing

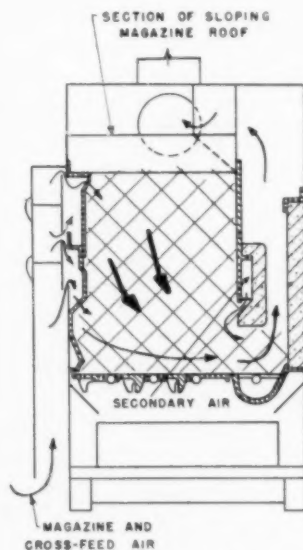


FIG. 14 DIAGRAMMATIC VIEW OF BCR SMOKELESS STOVE

TABLE 3 TYPICAL TEST RESULTS, HEATER BCR-2A: CONSECUTIVE FIRING CYCLES

(Pittsburgh coal, size 2 in. \times 1 1/4 in.)				
Air openings:				
Magazine, position.....	4	4	4	4
Cross-feed, position.....	1 and 4	4	4	4
Secondary, in.....	1/4	1/4	1/4	1/4
Average stack draft (natural), in. water	0.047	0.054	0.045	0.042
Weight of fuel fired, lb.....	43.5	47.0	43.0	45.0
Duration of test, hr.....	8.00	8.00	8.08	8.16
Average fuel gasified, lb per hr.....	3.94	5.13	4.46	4.04
Average flue-gas temperature, deg F.....	863	876	859	859
Flue-gas composition, per cent				
CO ₂	9.1	8.2	8.3	8.8
O ₂	9.5	10.9	10.7	10.5
CO.....	0.0	0.0	0.0	0.0
Smoke, Ringelmann No., min (inclusive) in 24 hr ^a				
Above No. 1.....	20 $\frac{1}{2}$	7	5	11
Above No. 2.....	9 $\frac{1}{2}$	5	0	6
Above No. 3.....	5 $\frac{1}{2}$	3	0	0
Above No. 4.....	3 $\frac{1}{2}$	0	0	0

^a Smoke data include 8-hr burning test and 16-hr banking period.^b Smoke data include start of a new fire.

stresses. Table 3 summarizes typical test data obtained with this heater on a 24-hr firing cycle, 8 hr at rating and 16 under bank. The smoke-emission data are for 24 hr; those given in the first column include the start of a new fire, which by comparison even with the smoke normally emitted following a re-firing, as shown in the other columns, would not be considered excessive.

The user of the smokeless stove regulates the heat output by adjustment of the cross-feed air damper only, except when chimney draft is excessive, when adjustment by means of a turn damper in the flue, or a barometric damper, may also be required. The magazine-air damper and the secondary-air dampers are adjusted by the coal dealer as follows: The magazine-air damper is set at the wide-open position for strongly caking coals (all Appalachian coals), at the mid-open point for mildly caking coals (Midwestern coals), and at the closed position for anthracite, coke, or the free-burning subbituminous coals and lignite. The secondary-air damper is set at the full opening for high-volatile coals, at the mid-opening for low-volatile coals, and at the closed position for anthracite and coke. A double-screened coal within the size range 3 to 1 in. is best-suited to the heater; smaller sizes have been found to give caking difficulty and larger sizes may contain impurities difficult to discharge through the dump grate. Run-of-mine coal is not recommended.

CALORIMETER-ROOM TESTS

A not inconsiderable part of the investigation for the development of the smokeless stove had to do with the design and construction of a calorimeter room in which the heat output of heaters could be measured directly. Fig. 15 is a cutaway view of the structure that was built for this purpose. On a simple

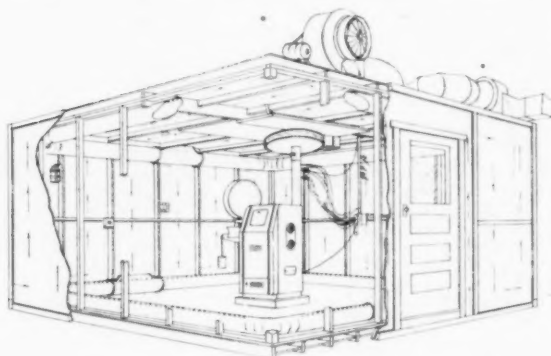


FIG. 15 CUTAWAY VIEW OF CALORIMETER ROOM

stud-and-joint framework 12 ft \times 12 ft \times 8 ft, were attached sheets of 1/2-in. rigid fiber insulating board provided with differential thermocouples to indicate the average temperature difference between the inside and outside of the wall. Two blowers were mounted on the roof to force air in and withdraw air through constricted ducts for measurement of both (1) the quantity of air flow by means of Pitot tubes, and (2) the temperature of the air by means of thermocouple grids. A highly insulated floor was used. The room was calibrated by use of an electric heater, the unknown being the average thermal conductivity of the walls and ceiling which was obtained by subtracting from the known heat input the heat corresponding to the temperature rise of measured air flow and dividing by the indicated average temperature difference between the inside and outside wall and ceiling thermocouples.

Otherwise, the room was provided with all facilities for running burning tests of heaters from which heat losses in the dry flue gases, in the steam, and in the refuse could be determined directly. Knowledge of the heat input from the weight of coal burned and of the output as given by the room data thus made it possible to evaluate normally unaccountable heat losses due to tar and soot in the gases. By such tests it was shown that a conventional heater, such as shown in Fig. 1, gave a heat loss, due to smoke, of the order of 12 per cent of the heat input. By comparison, smokeless heater BCR-2 gave an unaccounted-for loss of less than 3 per cent.

Table 4 summarizes the heat-balance results from a typical test run in the calorimeter room on a 12-hr firing cycle with a commercial model of the BCR smokeless heater, using Illinois No. 6 coal. The rating output obtained of 41,000 Btu per hr with an applied draft of 0.05 in. of water and with firings every 12 hr, was also obtained with Island Creek and with Pittsburgh bed coals with this heater.

TABLE 4 SUMMARY HEAT-BALANCE RESULT, CALORIMETER ROOM TEST OF A COMMERCIAL MODEL OF THE BCR HEATER, 12-HR FIRING PERIOD

(Illinois No. 6 coal, size 2 in. \times 1 1/4 in.)		
Measured heat output, Btu per hr:		
Heat gained by room air.....		32350
Heat loss through wall.....		11140
Heat from flue pipe.....		2560
Rating output of heater (12-hr basis).....		40930
Heat balance		
	Btu/lb	Percent
Heat utilized (efficiency).....	7649	64.6
Losses:		
Steam.....	656	5.5
Dry flue gas.....	2539	21.4
CO.....	70	0.6
Ashpit.....	591	5.0
Unaccounted for.....	335	2.9
Calorific value of fuel.....	11,840	100.0

For the 5 ft of pipe in the calorimeter room, Table 4 shows that 2560 Btu per hr corresponding to a 4 per cent gain in efficiency was transferred to the room. In a residential installation, additional recovery of heat and gain in efficiency may be realized from the flue pipe and chimney. However, because this is so variable with different installations and is uncontrollable after the installation is made, the efficiencies are reported here, as in usual practice, only on the output of the heater, including the first 20 in. of the metal flue pipe.

Under average winter-load conditions, firing would be expected to be required about once in 18 to 24 hr, and banking periods as long as 72 hr, followed by good pickup, have been obtained.

Fig. 16 is an exterior view of a circulator-type commercial version of the BCR smokeless heater. Fig. 17 is an exterior view of a radiant-type commercial version, the performance of which is similar to that of the circulator type.

A smaller-size radiant unit has also been developed and is in



FIG. 16 FULL-SIZE, CIRCULATOR TYPE, COMMERCIAL VERSION OF BCR SMOKELESS HEATER



FIG. 17 FULL-SIZE, RADIANT TYPE, COMMERCIAL VERSION OF BCR SMOKELESS HEATER



FIG. 18 SMALL-SIZE, RADIANT TYPE, COMMERCIAL VERSION OF BCR SMOKELESS HEATER

commercial production. Fig. 18 illustrates this heater which has a rated output of 25,000 Btu per hr, under a 12-hr firing period, at an applied draft of 0.040 in. of water. The indicated efficiency of this unit is 67 per cent when burning bituminous coal.

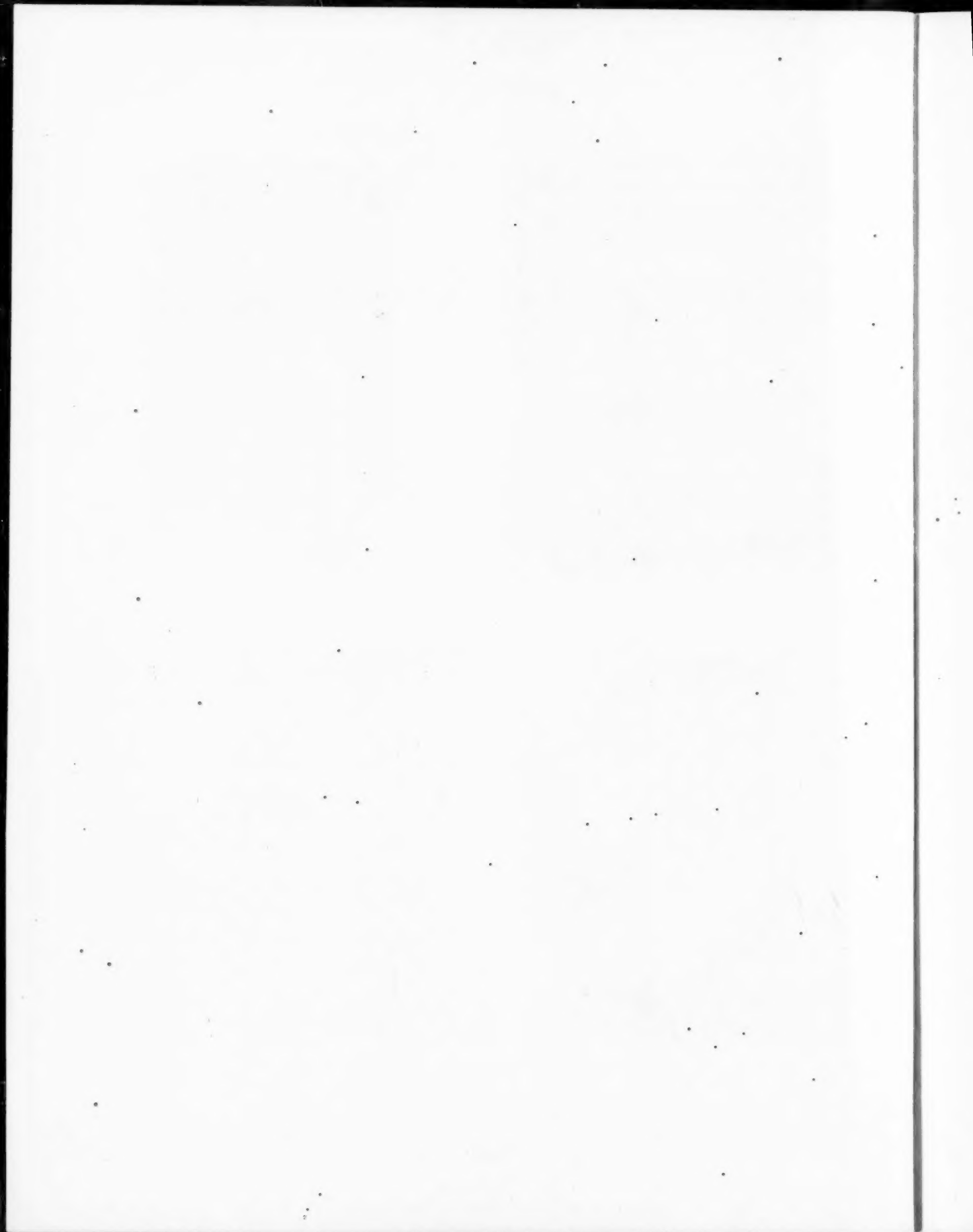
Patent applications have been filed in the United States and Great Britain and various claims allowed for the developments described in this paper. A Canadian patent has been issued.

ACKNOWLEDGMENTS

Acknowledgment is made of the significant contributions during the early stages of the work of Howard Limbacher, Henry Ostborg, and Robert Mattox; in the development of the calorimeter room, of the work of Paul Vyff; and of the contributions of Edward Erickson and John Tieman, all former or present research engineers at Battelle Memorial Institute.

Especial mention is made of the contributions of Elmer R. Kaiser, assistant director of research, and James R. Garvey, development engineer, Bituminous Coal Research, Inc., and of King Ehret, president, Oakland Foundry Company, Belleville, Ill., in the translation of laboratory design to finished commercial design.

Finally, thanks are due to H. J. Rose, vice-president and director of research, Bituminous Coal Research, Inc., to the Hand-Fired Heating Committee of the Technical Advisory Board of BCR, to other members of the Board, and to the members of the Stove Manufacturers Research Group, for their helpful suggestions and sustained interest and support during the long program.



Corrosion-Erosion of Boiler Feed Pumps and Regulating Valves at Marysville, Second Test Program

By J. M. DECKER,¹ H. A. WAGNER,² AND J. C. MARSH,³ DETROIT, MICH.

Corrosion-erosion tests at 320 and 385 F indicated that, at these temperatures, carbon steel is attacked to a lesser extent than at 250 F, whereas the reverse is true of the chromium-bearing steels. However, the rate of attack of the chromium steels is still only a fraction of that of carbon steels, so that use of the alloy steels for boiler-feed-pump parts is warranted at the higher temperatures also. Increasing the pH of the feedwater from 7.6 to 8.4 doubled the corrosion-erosion attack on carbon steel in the Marysville boiler feedwater at 250 F, as compared with previous tests at the lower pH. Of two bronzes tested, Navy M material appeared satisfactory at temperatures up to 320 F; a leaded bronze was unsatisfactory at all test temperatures in this program.

INTRODUCTION

IN a previous paper,⁴ the authors dealt with tests made at the Marysville plant of The Detroit Edison Company to determine the relative resistance of 18 different materials to the corrosion-erosion type of attack commonly experienced in boiler feed pumps and regulating valves. Feedwater at 250 F was used for these tests. Shortly after the paper was presented, plans were started for a 200-mw extension to the company's Trenton Channel plant. The plan adopted requires a cycle in which the feedwater temperature is 315 F at the boiler feed pumps. Initially, temperatures as high as 425 F were considered.

In order to obtain corrosion-erosion data for feedwater at the higher temperatures commonly found in newer power plants, a second test program was conducted at the Marysville plant. Temperatures of approximately 320 F and 385 F were chosen for the tests because they were within the range that was considered for the Trenton Channel and Connors Creek plant extensions, and because feedwater at those temperatures was available from the 7th and 4th stage heaters, respectively, of No. 7 turbogenerator. Since feedwater at 250 F from the boiler-feed-pump discharge of this same turbogenerator had been used in the earlier tests, the tests at higher temperatures should therefore evaluate the effect of the higher temperatures rather than some other variable.

Early in the test program it was noted that when the evaporator was taken from service, the pH of the feedwater increased from an average of about 7.3 to 8.3. Advantage was taken of

this situation to determine in one series of tests the influence of pH in this range on the corrosion-erosion resistance of cast carbon steel. Included in this series of tests was one specimen each of 1.25 per cent chromium, 0.5 per cent molybdenum steel and leaded bronze.

The purpose of this paper is to present (1) the results obtained in the second test program; and (2) a comparison of the information thus obtained with corresponding data from the original tests.

MATERIALS TESTED

Nine different materials were tested. The materials, with their chemical compositions and physical properties, are listed in Table I.

Six of the materials: Navy M (a bronze); 5 per cent Cr, 0.5 per cent Mo; 12 per cent Cr; 18 per cent Cr, 8 per cent Ni; Cr-Ni-Mo; and carbon steel, had been tested earlier at 250 F. With the exception of the carbon steel, which was used for control specimens, all of these materials had shown good corrosion-erosion resistance. They were selected, therefore, for testing at the higher temperatures. The other three materials were selected for the following reasons:

1 Lead bronze had been suggested by a pump manufacturer for wearing-ring material in boiler feed pumps for the Trenton Channel plant extension.

2 An alloy steel containing 1.25 per cent chromium, 0.5 per cent molybdenum is being used frequently for high-temperature steam lines, and, if found to have good corrosion-erosion resistance, could be used advantageously for boiler-feedwater service because it is readily available. Previous tests also had indicated that steels of low chromium content would be satisfactory.

3 Chromium plating was included because it might be useful for protecting existing cast-carbon-steel equipment from attack, if it possessed the corrosion-erosion resistance common to iron-chromium alloys.

Four specimens of cast carbon steel were used in the test to determine the effect of increased pH on the corrosion-erosion rate. Cast carbon steel was chosen because any effect which changing the pH might have would be more readily observed on cast carbon steel than on the materials possessing greater corrosion-erosion resistance. This test was made at 250 F, as more data for comparative purposes were available for that test temperature than for other temperatures.

Specimens of 1.25 per cent chromium, 0.5 per cent molybdenum steel and of leaded bronze were included with the four cast-carbon-steel specimens because no tests of these materials had been made previously at 250 F.

DESCRIPTION OF TEST

The test method and equipment used for determining the corrosion-erosion resistance of the metals have been described in detail in the earlier paper⁴ on this subject. Briefly it consists in exposing specimens of the material to be tested to the action of

¹ Research Department, The Detroit Edison Company. Jun. ASME.

² Engineering Department, The Detroit Edison Company. Mem. ASME.

³ Production Department, The Detroit Edison Company.

⁴ "Corrosion-Erosion of Boiler Feed Pumps and Regulating Valves," by H. A. Wagner, J. M. Decker, and J. C. Marsh, Trans. ASME, vol. 69, 1947, pp. 389-397.

Contributed by the Joint Research Committee on Boiler Feedwater Studies and the Power Division and presented at the Annual Meeting, New York, N. Y., November 29-December 3, 1948, of THE AMERICAN SOCIETY OF MECHANICAL ENGINEERS.

NOTE: Statements and opinions advanced in papers are to be understood as individual expressions of their authors, and not those of the Society. Paper No. 48-A-118.

TABLE 1 CHEMICAL COMPOSITIONS AND PHYSICAL PROPERTIES OF TEST SPECIMENS

Specimen Designation	Material	Heat No.	Chemical Composition, per cent										Physical Properties							
			C	Si	Mn	Cr	Ni	Mo	P	S	Cu	Sn	Pb	Zn	Fe	Tensile Strength, psi	Yield Strength, psi	Elongation, per cent	Reduction of Area, per cent	Brinell [†]
10, 13A, B, C, D, E and F	Carbon steel	3208	0.25	0.44	0.55				0.024	0.028						65,000 [‡]	35,000	24	35	102
17†, 18, 19	"	3191	0.24	0.45	0.69				0.028	0.027						65,000 [‡]	35,000	24	35	102
20, 20A, B, C	5% Cr, 0.5% Mo	4-6947	0.20	0.42	0.44	5.84		0.41								90,000 [‡]	60,000	18	30	224
21A, B, C, D	12% Chromium	9121-AW	0.09	0.75	0.68	12.17	0.62	0.13								110,000 [‡]	85,000	24	55	241
22A, B, C, D	18% Chromium-8% Nickel	9122-AW	0.11	1.15	0.72	18.84	8.95									75,000 [‡]	56,000	45		144
23A, B, C, D	1-1/4% Chromium-1/2% Niobium		0.16	0.32	0.70	1.35	0.09	0.55	0.030	0.019	0.21					70,000 [‡]	46,000	22	35	169
24	Cr-Ni-Mo	9120-AW	0.30	0.41	0.75	0.79	0.65	0.25								85,000 [‡]	53,000	22	35	185
25A, B, C, D, E	Navy M				0.49				0.01	0.03	87.50	5.39	0.05	4.14	1.64	40,000	22,000	30		52
26, 27A, B, C	Leaded bronze										70.0	4.0		26.0		21,650		15		40

† Base metal of chromium-plated specimen. ‡ Approximate physical properties. § Brinell hardness mostly by test. □ Specified minimum.

high-velocity turbulent feedwater under conditions similar to those encountered in boiler feed pumps and regulating valves. The two parts of a test specimen with the mating faces upward are shown in Fig. 1.

During test, a weighed specimen is held in a corrosion-erosion tester as shown in Fig. 2. For 500 hr a differential pressure of 300 psi is maintained across the specimen. This pressure forces feedwater through the center hole in the bottom part of the specimen to impinge on the plain face of the top part, causing the flow of feedwater to change direction and leave the specimen at a velocity of about 200 fps through the slot openings in the lower part of the specimen.

At the end of the 500-hr period, the specimen is cleaned, reweighed, and the loss in weight calculated.

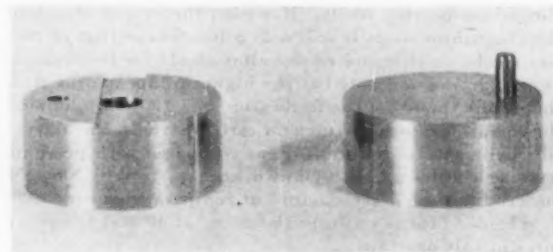


FIG. 1 TYPICAL CORROSION-EROSION TEST SPECIMEN BEFORE TEST

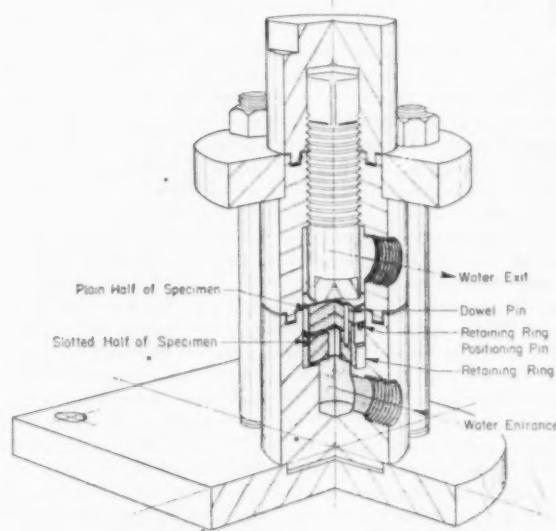


FIG. 2 SECTIONAL VIEW, CORROSION-EROSION TESTER

PROCEDURE AND RESULTS

At Marysville, six specimens were tested simultaneously. The six corrosion-erosion testers, pressure-measuring equipment, and pressure-regulating valves used are shown in Fig. 3.

Six series of 500-hr tests (tests No. 8 to 13, inclusive) were conducted in this program. As in previous tests, continuous records of pH, specific conductance, and dissolved oxygen concentration, were made with recording instruments, and were supplemented by spot tests made with indicating instruments to check the accuracy of the recorded values.

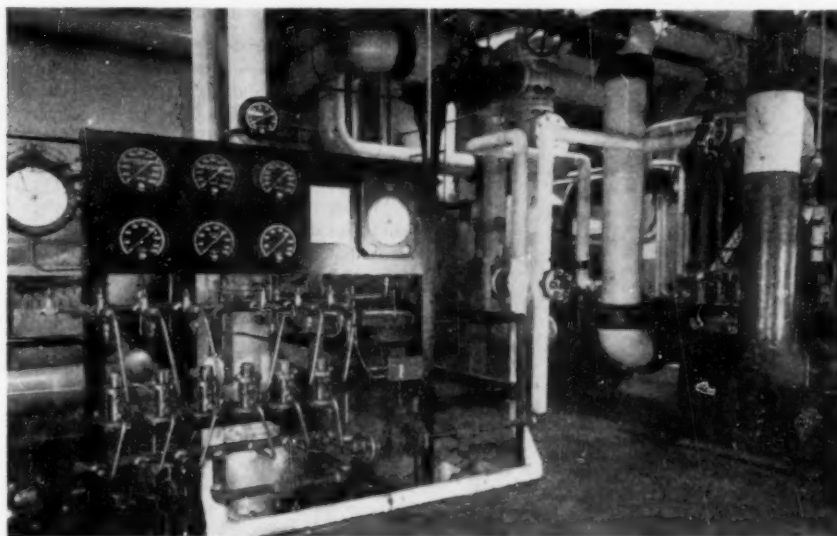


FIG. 3 GENERAL VIEW OF TEST SETUP

TABLE 2 BOILER FEEDWATER PRESSURE DIFFERENTIALS, TEMPERATURES, TEST RESULTS, AND WEIGHT LOSSES OF SPECIMENS

Test No.	Specimen & No.	Average Pressure Differential, psi	Average Water Temp. F	Avg. pH	Average Conductivity, Micromhos	Average Dissolved Oxygen, ppm	Total Weight Loss, 500 Hr, Grams
8	Carbon steel 18	299.7	381	7.3	0.43	0.008	0.6822
	5% Cr 20						0.0427
	12% Cr 3A						0.0447
	18-8 5A						0.0230
	Navy M 13A						0.0265
	Leaded bronze 19						0.2490
9	Carbon steel 18A	299.9	318	7.4	0.48	0.007	3.4673*
	5% Cr 20A						0.0641
	12% Cr 3B						0.0406
	18-8 5B						0.0348
	Navy M 13B						0.0473
	Leaded bronze 19A						0.2878
10	Carbon steel 18B	299.6	384	7.2	0.39	0.008	0.3915
	5% Cr 20B						0.0587
	12% Cr 3C						0.0606
	Navy M 13C						0.2304
	Leaded bronze 19B						0.4699
	1-1/4 Cr-1/2 Mo 21A						0.0770
11	Carbon steel 18C	300.1	323	7.2	0.39	0.007	1.3638
	5% Cr 20C						0.0614
	12% Cr 3D						0.0953
	18-8 5C						0.0208
	Navy M 13D						0.0394
	1-1/4 Cr-1/2 Mo 21B						0.0670
12	Carbon steel 18D	299.9	388	7.5	0.41	0.004	0.1978
	Cr-Mo 9A						0.0609
	1-1/4 Cr-1/2 Mo 21C						0.0570
	18-8 5D						0.0171
	Navy M 13E						0.2678
	Cr Plated C steel 1F						0.3266
13	Carbon steel, 1G	297.8	255	8.4	0.66	0.007	4.6179
	" " 1H						5.2467**
	" " 18E						4.0695
	" " 18F						4.1394
	1-1/4 Cr-1/2 Mo, 21A						0.1678
	Leaded bronze, 19C						0.3822

* Loss corresponding to 447-hour test.

** Loss corresponding to 439-hour test.

In Table 2 the specimens are identified and averages of pressure differential, temperature, pH, specific conductance, and dissolved oxygen concentration, and specimen weight losses are given for each test. Weight losses are shown graphically in Figs. 5 and 6, along with data obtained in earlier tests at 250 F.

In Fig. 5 the weight losses obtained at 250, 320, and 385 F for

each material are grouped together to show readily the effect of temperature on the corrosion-erosion rate of the various metals tested.

The weight losses obtained for cast carbon steel at 250 F are plotted in Fig. 6 to show the effect of the pH on the corrosion-erosion rate.

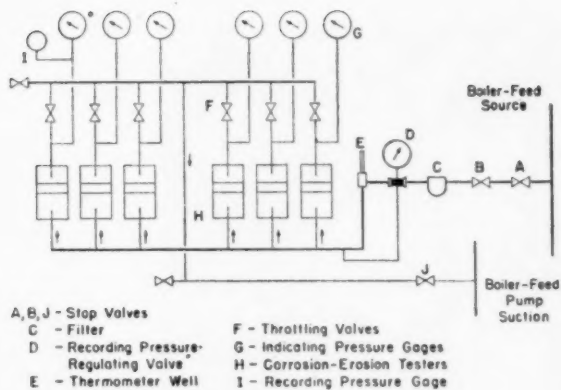


FIG. 4 SCHEMATIC DIAGRAM, CORROSION-EROSION TEST SETUP

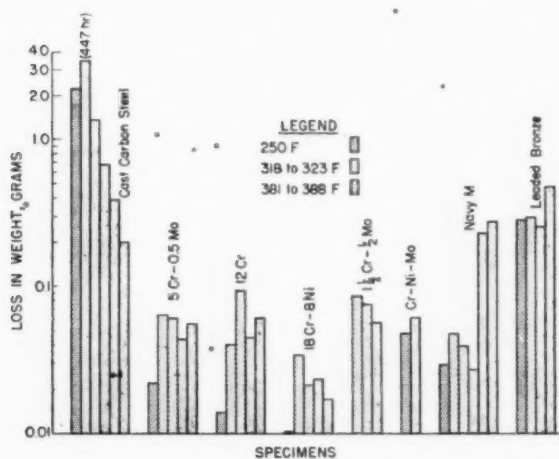


FIG. 5 RESULTS OF 500-Hr CORROSION-EROSION TESTS OF CAST-METAL SPECIMENS AT VARIOUS TEMPERATURES (Pressure differential 300 psi.)

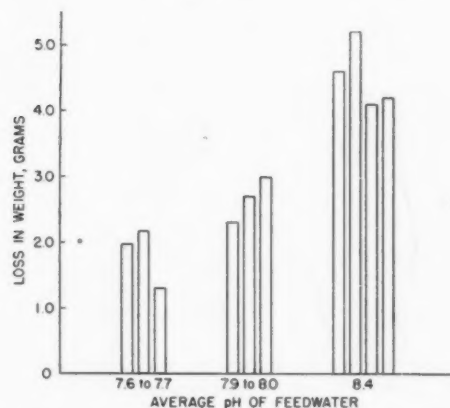


FIG. 6 RESULTS OF 500-Hr CORROSION-EROSION TESTS OF CAST-CARBON-STEEL SPECIMENS AT VARIOUS pH VALUES (Temperature 250 F, pressure differential 300 psi.)

DISCUSSION OF RESULTS

In general, test results indicate that cast carbon steel is more resistant to corrosion-erosion attack at high temperatures than at low (See Table 2 and Fig. 5). At 388 F, for example, the loss in weight (0.1978 g) is less than $1/10$ that of the average (2.2582 g) of six specimens at 250 F. An exception to this generalization was observed, however. At 318 F, Specimen 18A (test No. 9) was attacked so extensively that the 300-psi differential across the specimen could not be maintained after 447 hr of test. A careful analysis of test and water conditions revealed no variations that would account for the accelerated attack. Specimen 18C, which was made from the same bar, lost much less weight under similar conditions. Microscopic examination of the metal structure of the two specimens revealed no significant differences that would account for the variation in weight losses. There may have been some slight variations in specimen dimensions or surface finish, although it is difficult on this basis to account for the great difference in attack.

The indication that cast carbon steel has higher corrosion-erosion resistance at 385 F than at 250 F is substantiated to some extent by actual experience at Marysville. Recently a check valve at the discharge of No. 7 boiler feed pump, where the feed-water temperature is 250 F, was found to be badly damaged. An identical valve located in the same line at the discharge of the 4th-stage heater, where the temperature is 385 F, however, showed little attack after the same number of service hours.

Inasmuch as water is more highly ionized at 320 F and 385 F than at 250 F (see Fig. 7), it would seem likely that metals would be more rapidly attacked at the higher temperatures. In the case of cast carbon steel, however, it seems that a more tenacious oxide coating forms on the surface of the metal at the high temperatures than at the low ones, and actually causes a reduction in rate of attack.

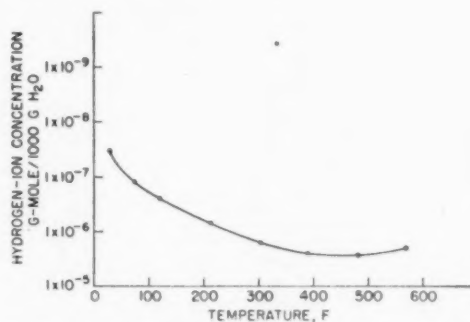


FIG. 7 CHANGE OF HYDROGEN-ION CONCENTRATION WITH TEMPERATURE IN PURE WATER

(From "Properties of Ordinary Water Substance," by N. E. Dorsey, Reinhold Publishing Corporation, New York, N. Y., 1940, Table 182, page 378.)

During the series of tests that composed this study, it was observed that the color of the coating on the specimens depended on the temperature at which they were tested. At 320 and 385 F the coatings were black, indicating them to be magnetic iron oxide, and at 250 F they were red, indicating ferric oxide. The black coatings were more tenaciously bonded to the specimens and were more difficult to remove than the red coatings.

In all cases the chromium-bearing steels were much more corrosion-erosion resistant than the carbon steel. As would be expected, the 18 per cent chromium-8 per cent nickel had the highest resistance. At 250 F the corrosion-erosion resistances of the chromium-bearing steels were roughly proportional to their chromium contents. At the higher temperatures, the relative

advantage of the high-chromium alloys was greatly reduced. For example, at 385 F the corrosion-erosion resistances of the Cr-Ni-Mo steel containing 0.79 per cent chromium, and of the 1.25 per cent chromium, 0.5 per cent molybdenum steel were about equal to that of 5 per cent and 12 per cent chromium steels.⁶

The test results indicate that Navy M bronze should be satisfactory for service in feed pumps operating at temperatures up to 320 F. Two of three tests indicated that the rate of attack would be too high at 385 F for satisfactory service, the rate being about 10 times that found at 250 F. The rate of attack in the third test at 385 F was abnormally low, so much so that it was disregarded in evaluating this metal.

Test results obtained for leaded bronze indicated that it is not well suited for corrosion-erosion service at temperatures from 250 to 400 F. Experience with a coil-drains pump on an evaporator at the Trenton Channel plant corroborates these results. After operating for 6-months at approximately 400 F, the leaded-bronze wearing rings in the pump were badly damaged and had to be renewed, whereas other parts of the pump made of 12 per cent chromium steel were only slightly attacked.

Since even a small amount of chromium imparted a pronounced resistance to corrosion-erosion attack, it seemed that a thin chromium plate on the interior surface of carbon-steel pump casings might provide excellent protection for pumps already in service. It was determined that pumps could be plated at a reasonable cost. However, results of a test at 388 F of a chromium-plated (0.001-in. plate directly on steel⁶), cast carbon-steel specimen showed that the chromium plating was porous or cracked, which allowed the unprotected base metal to be attacked. The weight loss given for the specimen (see Table 2, test No. 12) is much too high as it includes part of the chromium plating which was stripped from the specimen during the cleaning treatment that preceded weighing. The view of the specimen, Fig. 8, shows that the chromium plating had broken down in spots and that the base metal had been attacked.

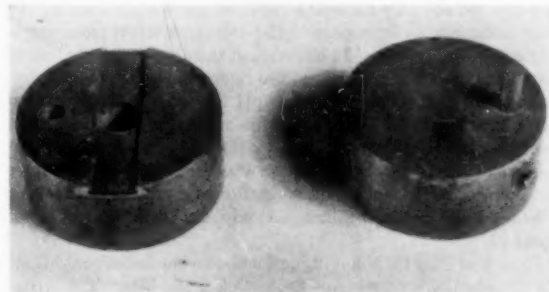


FIG. 8 TEST SPECIMEN NO. 1F; CHROMIUM-PLATED CAST CARBON STEEL AFTER 500-HR TEST AT 388 F

The results of the tests of cast carbon-steel specimens indicate that at 250 F the rate of corrosion-erosion-attack increases with pH between 7.6 and 8.4, the rate at 8.4 being about double that at 7.6 (see Fig. 6). This is contrary to what is usually expected. However, in a different type of corrosion-erosion test, conducted at Ohio State University on similar material, using distilled water at 122 F, the rate at pH 8 was about 10 times that at pH 6, (see Fig. 9). These data tend to substantiate results obtained at Marysville, although no direct comparison is justified because of differences in test conditions. However, it is indicated that in-

⁶ Chrome-plating directly on the steel instead of on an intermediate plate of copper and nickel was recommended by the plater as a superior wear-resistant coating.

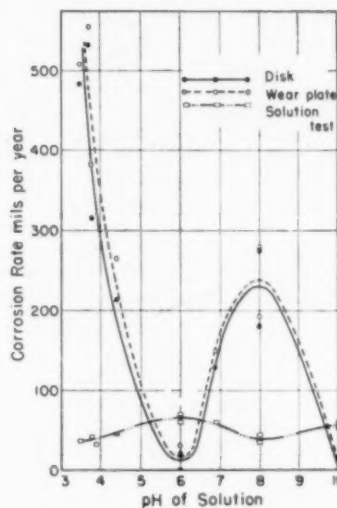


FIG. 9 EFFECT OF pH ON CORROSION-EROSION OF STEEL
(W. A. Luce, Engineering Experiment Station News, Ohio State University vol. 19, no. 5, pages 29-32.)

creases in feedwater pH for the purpose of reducing corrosion-erosion attack should be made with caution.

The attack on the 1.25 per cent chromium, 0.5 per cent molybdenum-steel specimen at 250 F and pH 8.4 (test No. 13, Table 2) was about twice that measured in the other tests at higher temperature and lower pH (test Nos. 10 and 11, Table 2). No direct comparison to show the effect of pH on this alloy could be made, however, as no tests had been made at 250 F and the lower pH. Although it seems that the higher pH had little effect on the corrosion-erosion resistance of the leaded bronze, here again comparable data were not available.

It was noted at the end of the test at 250 F and pH 8.4 (test No. 13), that the specimens were exceptionally clean. There was very little, if any, of the red iron oxide which formed heavy coatings on the specimens during earlier tests at 250 F and lower pH. This seemed to indicate that the higher pH retarded the formation of protective oxide films on the specimens, thereby promoting metal wastage.

CONCLUSIONS

The rate of corrosion-erosion attack on carbon steel decreased with increase in temperature of Marysville feedwater, whereas the rate of attack increased for chromium-iron alloys. There is some indication that attack of the chromium alloys is greatest at some point between 250 and 385 F. At all temperatures at which tests were made, the chromium alloys were much more resistant to corrosion-erosion attack than cast carbon steel, and therefore they are considered to be satisfactory for service in boiler feed pumps and regulating valves up to 400 F in all Detroit Edison plants where the feedwater has similar characteristics.

The 1.25 per cent chromium, 0.5 per cent molybdenum steel and the Cr-Ni-Mo steel were not attacked to a significantly greater extent than the 5 and 12 per cent chromium steels at the higher temperatures. Because of greater weldability and lower cost, it appears that the low-chromium alloys might be used advantageously in feedwaters having similar or less corrosive characteristics.

Leaded bronze is not a good material for use at 250 to 400 F under conditions where corrosion-erosion attack can be expected. Navy M bronze is satisfactory at temperatures up to about 320 F.

Chromium plating as a means of protecting existing carbon-steel pump casings is not satisfactory.

As in the previous tests,⁴ the authors have not been able to deduce the underlying causes for corrosion-erosion attack, nor to determine which of the many variables is the most important. Increasing the pH of feedwater at Marysville from about 7.6 to 8.4, however, approximately doubled the rate at which cast carbon steel was attacked. This indicated that, for the Marysville feedwater, the lower pH is more desirable from the corrosion-erosion standpoint. While in some quarters higher pH values have been advocated as a panacea for all corrosion-erosion troubles, these results would seem to indicate that some caution should be exercised in increasing pH of feedwater indiscriminately.

Discussion

T. W. BIGGER.⁶ The Detroit Edison Company is to be warmly commended for making the investigation which is so ably reported in this and the original paper. The work has been carefully done and the information which is reported is usable and valuable to the industry.

Corrosion-erosion to an abnormal degree occurs only occasionally in a steam turbine, but is similar to that in feedwater pumps, in that it does not follow a set pattern as to the apparent conditions under which it does occur. Corrosion-erosion will be quite severe in a turbine in one plant, and an identical turbine in another with the same pressure and temperature conditions will be virtually free of damage. The erosion occurs principally on the low-carbon-steel parts, the high-chromium steels being but little affected by this type of attack.

Corrosion-erosion is not a serious problem in the superheat region of steam turbines, nor in the coldest stages at the exhaust end. However, it does occur in some machines in the so-called wet region, principally in the range where the steam contains up to about 5 per cent moisture. One turbine did not erode appreciably during the early months of operation when on base load, but corrosion-erosion became quite noticeable when the machine was changed to variable and intermittent operation. This can be construed as indicating that oxygen is a contributing factor.

Some time ago the writer's company studied the problem of determining the best method of making tests to solve the erosion problem. Moisture which is freshly formed within a turbine in a modern station is of a very high degree of purity, containing less impurities than the average distilled water. It was determined that the production of steam of sufficient purity in a laboratory would be extremely difficult and almost prohibitive in cost. It seemed that steam extracted from a turbine where erosion had occurred would be representative, and the Boston Edison Company kindly agreed to let us run the tests with steam extracted from such a turbine in its Mystic station.

About that time the original paper⁴ by the present authors was published. Since the arrangement of specimens which they used simulated closely the condition of a leak between a turbine diaphragm and a shell ledge, and it seemed desirable for purposes of comparison to use a specimen which had been agreed upon in the industry, our specimens are dimensionally identical with theirs. To make possible a clean job of heat insulation we mounted our specimens in a recess in a solid block of steel and covered them with a small flange containing a jackscrew for clamping the specimens together.

Saturated steam for testing is taken from the 14th-stage extraction line and fed to eight specimens at 25 to 28 psig through a well-drained header. The supply laterals are short and receive

steam from the top of the header. Several inches of each lateral are left bare to supply equal amounts of fresh moisture for the specimens. All inlet piping is stainless steel to minimize contamination. The exhaust goes to the main condenser where the pH of the condensate in the hot well is in the order of 6.5.

Tests of 1000 hr duration for a total of 16 specimens have been completed. Many of the specimens were of turbine materials commonly known as corrosion-resistant. They were run for purposes of comparison and of course stood up very well. A few specimens of cast low-carbon ferrous materials have been tried. From these essentially preliminary runs, we have been able to learn that 2 per cent chromium improves low-carbon cast steel for use under these conditions more than 4 to 1, a good check of the results reported in the paper under discussion. Cast iron was not benefited by the addition of up to 1.5 per cent nickel, but was improved nearly 50 per cent by the addition of 3 per cent nickel and 1 per cent silicon. Specimens of sprayed corrosion-resistant metals over cast iron are in test and in preparation.

A study is being made of the use of small amounts of alloying elements in carbon cast steel and cast iron with the object of producing useful low alloys at a reasonable cost. Samples of these alloys will be tested as rapidly as possible.

C. E. BRUNE.⁷ Evidence from operating results in several stations of the American Gas and Electric System seems to indicate that plain carbon steel is subjected to greater attack under higher temperature or lower pH. Attack was evident sooner and more severe in stations with feed pumps handling water over 400 F than in a station where pumping temperature was less than 400 F. At one station a set of pumps with feedwater pH of 7.5 experienced severe attack while another set with feedwater pH of 8.5 experienced none. Feedwater temperature for both sets was 450 F. When the low pH was brought up to 8.5, the attack ceased.

Another phenomenon was experienced whereby deposits of corrosion products on sides of impellers, causing increase of motor horsepower, apparently, were reduced when feedwater temperature was reduced, by removing from service the last heater. In some instances, at least part of the deposit resulted from corrosion within the pumps. In one station the deposits started when ammonia content went down in the river from which evaporated make-up originates, and feedwater pH fell from above 8 progressively to as low as 6. When ammonia content of river water and feedwater pH rose to normal values, the deposits apparently disappeared. There may be a question whether lowered temperature and increased pH lessened the formation of corrosion products or whether these changes influenced only the deposition of those products.

From test No. 13, the authors incline to the belief that higher pH retards the formation of protective oxide film. The writer wonders whether the slightly more complete deaeration in test No. 13, as compared with earlier tests reported in the previous paper,⁴ might not also have been a factor in retarding film formation.

While the authors consider the tests to justify use of the chromium alloys under test up to 400 F in deaerated feedwater, it is believed this limit can be raised, at least for some of those alloys, since no attack is evident on a 5.5 per cent chrome alloy in several stations on the A. G. & E. system after years of operation with deaerated feedwater at 450-460 F.

F. P. FAIRCHILD.⁸ This paper is a useful addition to the information presented by the authors in their first paper.⁴ Our

⁷ Mechanical Engineering Division, American Gas and Electric Service Corporation, New York, N. Y.

⁸ Chief Engineer, Electric Engineering Department, Public Service Electric and Gas Company, Newark, N. J. Mem. ASME.

⁶ Development Engineer, General Electric Company, Schenectady, N. Y. Mem. ASME.

corrosion-erosion tests on steel specimens with varying pH values indicate just the opposite of the findings of this paper, as reported in discussion of the paper on the first test program. We found that a higher pH results in less corrosion-erosion attack at both 90 and 205 F water temperatures.

Recently we made some corrosion-erosion tests in an attempt to determine why high-pressure boiler-feed-pump parts of nickel cast steel had a longer service life at Essex Station than similar parts under similar conditions at Marion Station. Detectors made from diffusers of the Essex and Marion pumps were tested side by side under similar conditions in the Marion feedwater. Contrary to expectations, the detector made from the shorter-lived Marion pump had the smaller weight loss in 500 hr by 12 per cent. Thus difference in materials was eliminated as an answer to the problem.

Having eliminated material as a cause of longer life, we next investigated the effect of condenser leakage, because the Essex condensate comes from condensers with packed tubes whereas the Marion condenser tubes are rolled at both ends. A tank and a variable-stroke proportioning pump were arranged to permit the injection of fluid from the tank into the line carrying feedwater to one of the detectors. Thus we were able to make concurrent corrosion-erosion tests comparing normal with polluted feedwater, using detectors of like material (cold-rolled steel).

Three tests simulating condenser leakage were run; two at Essex (4th and 5th) and one at Marion (11th), as shown in Fig. 10 of this discussion. In all of these tests a solution of condenser cir-

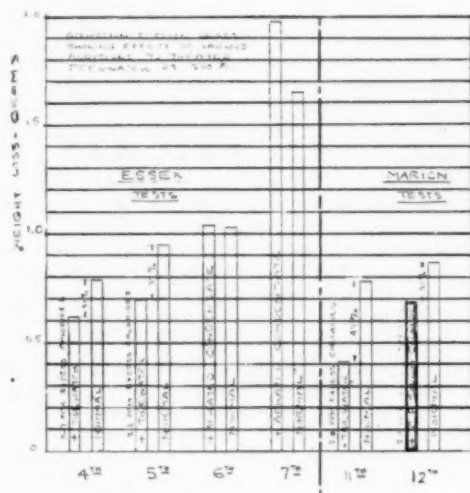


FIG. 10 CORROSION-EROSION TESTS SHOWING EFFECT OF VARIOUS ADDITIONS TO TREATED FEEDWATER AT 200 F

culating water was injected into the line feeding one detector while normal feedwater flowed through the second detector. At Essex 0.7 ppm excess chlorides reduced the corrosion-erosion weight loss 21 per cent in 335 hr; and in the next run 2.2 ppm excess chlorides reduced the weight loss 37 per cent in 525 hr. At Marion the same test resulted in a reduction of weight loss of 47 per cent with 2 ppm excess chlorides in 500 hr.

Since the tank containing the injection water was an open tank, there was the possibility that oxygen in the water might be the cause of the unexpected results of pollution. Therefore, at Essex we repeated the test, polluting with undeaerated, pure condensate instead of raw water. The test shown as the 6th in Fig. 10, showed practically no effect of such pollution and very little dif-

ference in oxygen content of the two effluents. Another similar test (the 7th) was run in which air was bubbled through the condensate in order to increase the amount of oxygen in the injected condensate. In this case the corrosion-erosion of the polluted water was about 20 per cent greater than that of normal water. Thus oxygen was eliminated as a contributing factor.

The 12th test at Marion used a solution of chemically pure sodium chloride for pollution. In this case 2 ppm excess chlorides resulted in a reduction of corrosion-erosion weight loss of 21 per cent, about one half that resulting from the same excess chlorides with raw-water pollution.

In all of the foregoing tests, the degree of pollution was so small that there was no measurable difference between the pH of the normal and polluted water. This would seem to indicate that pH alone may not be the best criterion for controlling corrosion-erosion.

J. B. GODSHALL.⁹ The reported unexpected effects of raising the pH value and the temperature of the feedwater are of considerable academic interest. The major consideration, however, is the confirmation of the earlier conclusions regarding the vast superiority of the chromium-bearing steels over carbon steels.

It is particularly interesting to note that 12 per cent chromium has virtually no advantage over 5 per cent chromium, 0.5 per cent molybdenum stainless steel. Furthermore, the lower-chromium steel has certain advantages. For example, it is less susceptible to galling in pump service.

Still lower-chromium steels, such as the 1.25 per cent chromium, 0.5 per cent molybdenum steel, may be practical for the feedwater at Marysville. Caution will be required if this material is considered for use in the many central-station feedwaters that are more aggressive toward carbon steel than the Marysville water appears to be.

These considerations, plus the impossibility of maintaining absolute control of the many variables affecting feedwater quality from a corrosion standpoint, indicate that the pump materials always should be selected for their ability to withstand any of the conditions likely to be encountered. Then, nominal fluctuation of the pH value or conductivity, or even a change in the water temperature, will be of no practical importance from the standpoint of corrosion-erosion.

The failure of the chromium-plated specimen probably was not unexpected. This failure, however, should not eliminate chromium plating from consideration for all feed-pump applications. Shaft sleeves are relatively easy to plate, and have very good resistance to corrosion-erosion by the feedwater. In addition, they provide an extremely hard, excellent wearing surface.

A. L. PENNIMAN.¹⁰ The writer believes there is a strong probability that some of the factors assumed to have been insignificant in effect as to rate of metal loss were perhaps actually significant. This comment applies particularly to the first paragraph under "Discussion of Results."

Since the average velocity is quite high and is accompanied by a sharp change in the direction of water flow, it is considered likely that there will be considerable variation in filament velocities with respect to both time and cross section which can result in some cavitation effect with material acceleration of metal loss, depending upon characteristics of metal and water. Under such conditions, it is believed that minor surface variations could influence the results materially.

⁹ Metallurgist, Cameron Division, Ingersoll-Rand Company, Phillipsburg, N. J.

¹⁰ General Superintendent, Electrical Operations, Consolidated Gas, Electric Light & Power Company of Baltimore, Md. Fellow ASME.

While it is recognized that maintenance of a constant differential pressure tends to maintain the average velocity of flow constant and thereby hinder large progressive changes in rate of loss, it is believed that the static pressure is also of importance and should be recorded since it, as well as temperature, affects cavitation.

It is noted that to obtain water at different temperatures, water was taken from different parts of the cycle. It is our opinion that such waters may differ in effect because of factors other than temperature which may have been assumed to be insignificant, e.g., suspended matter, metal and gas content. A filter is shown in Fig. 4 of the paper which obviously was intended to remove suspended matter. It would be of interest to learn the type and construction of this filter, since our experience in filtering-out suspended matter from boiler feedwater has not been considered satisfactory.

While the use of an evaporator may have been a convenient means of varying the pH content of the water, it is our opinion that there were influences other than pH which were brought into the picture, e.g., evaporator carry-over of solids and gases. Also, can we consider that it makes no difference whether or not the alkaline source is ammonia, ferrous hydroxide, or a solid like caustic soda?

Reference is made to Mr. Luce's work at Ohio State University, with Fig. 9 given as an illustration. While the statement is made that distilled water was used, the oxygen content was not mentioned. Since it is extremely difficult to obtain zero content of oxygen and other oxidizing influences, it is recommended that some statement be made about this. It would also be of interest to know about how the pH variation was obtained, and how the hydraulic conditions varied. Was only one point obtained at pH 10 where a negligible loss is shown?

If Mr. Luce's work is used as a criterion, it would appear that quite a number of plants in attempting to improve conditions have made them worse in maintaining the pH in the range of 8 to 9. However, maintenance of a pH of 6 does not fit in well with the use of sodium sulphite to react with remanent oxygen in the feedwater.

AUTHORS' CLOSURE

The work being done by the General Electric Company at the Boston Edison Company's Mystic station should produce some worth-while information. Inasmuch as the tests are being made with wet steam instead of water, information on a new phase of metal wastage will be obtained. It is interesting that results of tests of 2 per cent chromium cast steel obtained at Mystic station are similar to those obtained at Marysville with water. Information to be obtained on corrosion-resistant metals sprayed over cast carbon steel also will be valuable.

Experiences of the American Gas and Electric Company do not agree with the test results obtained at Marysville. The authors cannot explain this discrepancy. There is a possibility, however, that at 450 F corrosion-erosion might be much more severe than at 388 F, the maximum temperature used in the tests at Marysville. Because of the many variables involved, comparison of experiences on pumps operating on different feedwaters can be most misleading.

At the Detroit Edison Company's Connors Creek Plant where the feedwater temperature is approximately 250 F, severe corrosion-erosion of the feed pumps occurred when the pH of the feedwater was about 8.5. In this case, at least, the relatively high pH apparently did not protect the pumps.

A few years ago the source of feedwater for the evaporators producing make-up for the Connors Creek plant was changed. The new supply is practically free from ammonia whereas the old supply contained an appreciable amount. This caused a lowering of the pH from about 8.5 to about 8. Unfortunately, a change to corrosion-resistant metals for pump repairs was made at about the same time. This made it impossible accurately to gage the effect of the pH change. Results indicate, however, that the rate of corrosion-erosion is no higher than it was previously, and perhaps lower.

The experience of the American Gas and Electric Company indicates that the chromium alloys will give satisfactory service at temperatures 60 to 70 deg F higher than the test temperatures used at Marysville. This is a valuable supplement to the data submitted by the authors.

Results of the test presented by Mr. Fairchild indicate that the salts present in feedwater may have a very profound effect on the rate of corrosion-erosion attack of metals. Previously it was commonly believed that pH and dissolved oxygen were the most important factors. If the concentration of sodium chloride in the tests at Marion and Essex stations influenced the test results so greatly, it is conceivable that the presence of other salts may also greatly influence corrosion-erosion rates. This opens a whole new field the investigation of which would provide valuable information, particularly where salt water is used for condenser cooling.

At Marysville the salt concentrations in the feedwater were very low and specific conductance records indicated that variations were small. Therefore it is doubtful if variations in concentrations from one test to another had much effect on the results obtained. Inasmuch as concentrations in many plants cannot be controlled closely, Mr. Godshall's statement that "... pump materials always should be selected for their ability to withstand any of the conditions likely to be encountered" is a good one.

The filter about which Mr. Penniman inquired was placed in the circuit to remove suspended iron oxide from the feedwater used in the test. The filter element is made of a spool wound with cotton cord. The authors have found these filters to be quite effective for this purpose in this and similar installations.

The authors have no data nor have they seen any which would prove or disprove that one alkali is better than another for increasing the pH for corrosion prevention. The authors are inclined to agree, however, that the means for varying this pH may be most important.

The static pressure at the inlet to the test specimens was maintained at 700 psi, and the outlet pressure was, correspondingly, 400 psi. The saturation pressure corresponding to 388 F is about 200 psi gage. It is the authors' opinion that cavitation was not a factor under these conditions, which is supported by the fact that the type of metal wastage resulting from cavitation was not found.

When referring to Mr. Luce's work at Ohio State University the authors neglected to state that it was done in aerated distilled water. The type of corrosion-erosion equipment used by Mr. Luce, and the conditions under which his tests were made were so different from the tests conducted by the authors that no valid comparison can be drawn between them. The authors merely wished to point out that some evidence exists tending to support the unexpected increase in corrosion-erosion attack secured on increasing the pH. These results were reported solely to indicate that changes in the pH should be made with caution.

The authors wish to express their appreciation to all those who submitted comments and discussion on the paper.

The Forces and Moments in the Leg During Level Walking

By B. BRESLER¹ AND J. P. FRANKEL²

The mechanism of normal level walking is presented in this paper in terms of the displacements of and the force systems at the leg joints. The data on four normal subjects were obtained from simultaneous recording of the positions of the leg in space and the floor reactions during level walking. The mass moments of inertia of the lower extremity were determined experimentally and the effects of gravity and inertia were included in the analysis. The forces and moments are presented in terms of the space components referred to a system of horizontal and vertical orthogonal axes.

INTRODUCTION

AS a locomotive mechanism the human body is extremely complex. In order to perform the various operations of locomotion such as walking, running, climbing slopes and stairs, man has been provided with an articulating system of levers (the arms, torso, and legs) connected by "superuniversal" joints (the shoulder, hip, knee, and ankle joints, for example). These levers are powered with a multitude of motor units (the muscle fibers) and operated by an elaborate network of controls (the nervous system).

The human mechanism is one that operates in three dimensions—further complicating its analysis. It is true that the main effects of locomotion are evidenced in a single plane (the plane of progression), but this should not lead one to neglect the effect of lateral displacement on the mechanics of locomotion. This omission has been made by some previous investigators in order to simplify the mechanical aspects of the problem, but does not seem to be justified by the results of this investigation.

Unlike the inanimate machines, one human body varies greatly from another in build (mass distribution), musculature (power supply), and mannerisms of motion (controlled by the nervous system). The effect of these variables on the displacement and forces involved in the locomotion process introduces an additional complication into the analysis of the experimental data.

Before attempting to correct any mechanical deficiencies in the human body, the surgeon, limb and brace maker, and physiotherapist must be well-acquainted with the mechanical functions of the affected parts of the body. The techniques and scope of orthopedic treatment and surgery, limb and brace fitting, and the like are seriously limited by the force and displacement characteristics normally involved in the damaged or missing members. Recognizing the need for a scientific analysis of the mechanical functions of the legs in walking, the Advisory Committee on Artificial Limbs of the National Research Council and the Veteran's

Administration sponsored a research program of fundamental studies of locomotion at the University of California at Berkeley.

In view of the range of variables involved in the mechanics of human locomotion, a complete analysis of the problem is not possible at this time. Various phases of this problem have already been reported (1),³ others are now under investigation at the University of California Artificial Limbs Research Project. The material presented herein is based upon the investigations carried out at the University of California, and will deal primarily with the force systems in and the displacements of the lower extremities during level walking of normal subjects.

HISTORICAL BACKGROUND

The present-day knowledge of the mechanism of locomotion is due to the contributions of many scientists. Only a few of these contributions will be mentioned here to introduce to the reader the state of present-day knowledge in this field.

In 1836, Wilhelm and Eduard Weber (2) presented a theory of walking and running based on measurements on cadavers and tests on living bodies. From studies of pendulum motions of the leg in both living and anatomical specimens the brothers Weber reached the conclusion that leg motion during the swinging phase of gait, that is, the time when the leg is off the ground, is a pure pendulum motion and does not depend upon muscular action. The Weber pendulum theory gave rise to much discussion by subsequent investigators and was later repudiated by Fischer and others. The Weber book contains also a great deal of information on other various aspects of gait, including a mathematical analysis of the data collected. In another publication Eduard Weber discusses some fundamental aspects of muscle physiology wherein the tension that a muscle can develop is compared to the shortening it undergoes. The importance of muscles as the prime movers of the articulating levers of the body focuses great attention on the work of Eduard Weber in this regard.

E. J. Marey, Professor at the College of France, reported in 1873, and on later dates (3, 4, 5, 6, 7) tests performed to determine the locus of the center of pressure on the sole of the foot and the vertical displacement of the body during walking. In addition, his computations of energy output during locomotion are worthy of mention in any bibliography however brief it may be. Marey's greatest contribution to the study of locomotion is no doubt his development of chronophotography. Successive exposures were made on the same photographic plate by means of a rotating disk in front of the camera. The subject was dressed entirely in black on which brilliant metal buttons and shining bands were attached to represent joints and bony segments. The subject, illuminated by the sun, was photographed as he walked in front of a black screen. This method is known as geometric photography, since the pictures obtained show points and lines only. Variations of this method have been used in practically all subsequent investigations, including that reported herein.

Otto Fischer, whose six volumes of research (8) were published from 1894 to 1904, is best-known for his studies on human gait.

³ Numbers in parentheses refer to the Bibliography at the end of the paper.

¹ Assistant Professor of Civil Engineering, University of California, Berkeley, Calif.

² Instructor in Engineering, University of California, Los Angeles, Calif.

Contributed by the Applied Mechanics Division, co-sponsored with Management and Aviation Divisions, and presented at the Annual Meeting, New York, N. Y., November 28–December 3, 1948, of THE AMERICAN SOCIETY OF MECHANICAL ENGINEERS.

NOTE: Statements and opinions advanced in papers are to be understood as individual expressions of their authors and not those of the Society. Paper No. 48–A-62.

These were based upon chronophotographic studies similar to that employed by Marey but with some improvements. Fischer, a mathematician, in co-operation with Braune, an anatomist, made detailed studies (9) of the kinetic properties of the different segments of the human body. To these men belongs the credit for the first rational scientific investigation of the problems in human locomotion; so detailed was their treatment of the subject that no later publication has superseded the works of Braune and Fischer and that of Fischer himself as the classical works on gait.

In Moscow, in 1935, was published a comprehensive volume (10) on research in the biodynamics of locomotion performed by N. A. Bernstein and his associates. In this study the accuracy obtained by Fischer was questioned and techniques were developed to improve on his accuracy. In all, the gait of 65 subjects was investigated. Many more photographs were taken of the subject during one complete cycle of walking. Further, the curves were not smoothed out, since Bernstein felt that the complexity of locomotion would preclude the smoothing out of any curves. Fischer's data for locations of the centers of gravity of the various segments, their radii of gyration, and their relative masses were used in this study. The experiments included investigation of normal walking of men both carrying weights, and unburdened, as well as an analysis of fatigue effects due to these conditions. Mention is made of a volume on the determination of the masses and centroids of the segments of the human body on live subjects, but at the time of this writing such information has not become available to the authors. Mention is made, however, of the fact that differences from Fischer's data were found.

Most recently, Elftman has reported in articles from 1934 to the present, investigations on locomotion including studies of the distribution of pressure in the human foot (11), the function of the arms in walking (12), the force exerted by the ground in

walking (13), the rotation of the body (14), the forces and energy changes in walking (15), the function of the muscles in locomotion (16), and the action of muscles in the body (17).

Elftman has made a valuable contribution to the analysis of problems of locomotion even though he had a limited amount of experimental data at his disposal. Some of the results and conclusions presented were based partly on Fischer's classical experiments and partly on Elftman's direct measurements. The present investigation of locomotion, considered as a three-dimensional process, was undertaken at the suggestion of Elftman.

THEORETICAL ANALYSIS

It has been felt by the authors that a knowledge of the positions of the joints of the lower part of the body and the internal force systems at these joints offer an adequate introductory description of the locomotive process of man.⁴

Fig. 1 is a free-body diagram of the leg during the stance phase of walking, i.e., when the foot is in contact with the ground. The reference (co-ordinate) axes are taken with the origin at the center of the force plate (described in the next section), and are designated by the lower-case letters x , y , and z . Postive co-ordinates denote inward (with respect to the leg investigated), forward, and upward directions. To define the position of a particular point of the leg, appropriate subscripts are used, e.g., x_A , y_A , and z_A are the three space co-ordinates of the ankle joint. The following subscripts are used throughout the paper

F = foot	A = ankle
S = shank	K = knee
T = thigh	H = hip
O = center of pressure on the foot	

The external forces acting on the body during walking are of only two types; (a) gravitational, due to the weights of the various parts of the body; and, (b) reactional, representing the ground forces acting on one or both feet.

The gravitational forces are considered acting at the centers of gravity of the leg segments, and are denoted by W with an appropriate subscript. Thus W_F denotes the weight of the foot, W_S denotes the weight of the shank of the leg, etc.

The ground reactions on the foot are obtained experimentally from a force-plate record and are considered to be applied to the foot at the center of pressure, which is also defined by the force-plate record. As shown in Fig. 1, X_0 , Y_0 , and Z_0 are the components of the ground reaction, and M_{0z} is the torque in the plane of the force plate between the foot and the plate.

The internal forces acting at the leg joints are resolved into components parallel to the xyz reference axes and are denoted by X , Y , and Z , respectively. To define the force acting at a particular joint appropriate subscripts are used, e.g., Z_A denotes a vertical force at the ankle joint, Y_A denotes forward force at the ankle, etc. The sign convention used in the calculations of the joint forces is as follows:

- X = inward force with respect to part of leg below joint.
- Y = forward force with respect to part of leg below joint.
- Z = compressive force (acting downward on part of leg below joint).

The internal moments acting at the leg joints are denoted by M_A , M_K , and M_H , at the ankle, knee, and hip, respectively. These moments are resolved into components about the xyz reference axes and are defined by appropriate subscripts, e.g., M_{Ax} denotes an internal moment at the ankle about the x -axis (a fore-and-aft moment), M_{Ay} denotes an internal moment at the ankle about the y -axis (inward-outward moment), etc. The sign

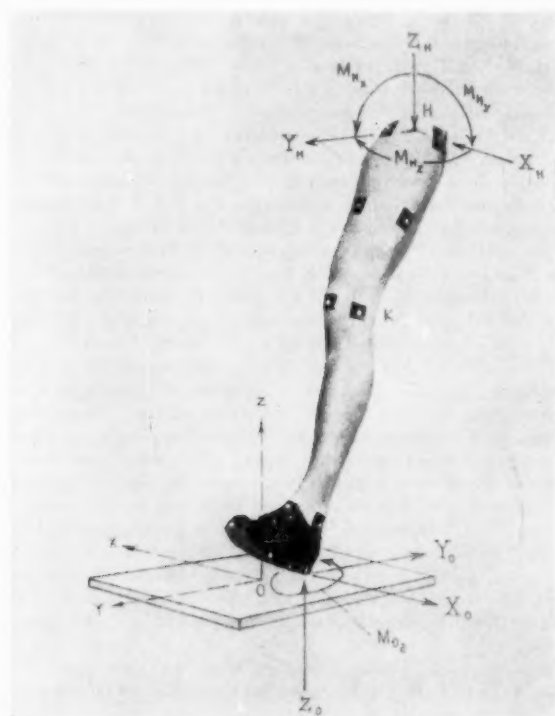


FIG. 1 FREE-BODY DIAGRAM; LEFT LEG

⁴ A paper describing the energy and power aspects of locomotion is now in preparation.

convention used in the calculation of the internal moments is based upon the "screw" rule, the right-hand rule being used for the right leg, while, for the left leg, the left-hand rule is used, see Fig. 1.

By considering a free-body diagram of the leg below a section cut at a joint, one may state the equations of motion for the free body in terms of forces and accelerations. Using D'Alembert's principle of "equilibrium" of bodies in motion, the internal forces (or moments) at the joints can be expressed directly in terms of reaction forces (R), gravity forces (G), and "inertia forces" (I). Thus may be obtained the relations shown in Table 1. This table shows the reaction, gravity, and inertia terms in summary form for all force components at the joints of the leg. The symbols used in Table 1 and not previously explained are as follows:

- g = acceleration due to gravity
 $\ddot{x}, \ddot{y}, \ddot{z}$ = components of linear acceleration of centroid of segment
 $\alpha_x, \alpha_y, \alpha_z$ = components of angular acceleration of segment
 J_x, J_y, J_z = mass moments of inertia of segment about three axes through its center of mass

EXPERIMENTAL METHODS AND REDUCTION OF DATA

For a complete description of the behavior of the legs of the

human mechanism in walking a knowledge of the forces and moments at the joints is essential. The determination of these forces and moments requires either measurement or calculation of the mass distribution of the leg, displacements and accelerations of the leg segments through one complete cycle, and the reactional forces of the ground on the foot.

Mass Distribution of Leg. The mass distribution of the leg is defined in terms of the weight (or mass), the location of the center of mass, and the mass moment of inertia about the center of mass. To date no adequate method has been presented whereby the numerical values of mass and inertia can be measured accurately from living subjects.⁵ The most commonly used methods are the use of Fischer's coefficients and the Weinbach graphical method (19). Braune and Fischer (8, 9) established coefficients for expressing the relative masses of the segments as compared to the body as a whole, and the position of centers of mass and radii of gyration of the segments as proportional parts of the length of the segment. Although Braune and Fischer worked on a few frozen corpses their results have been accepted and used in most subsequent investigations. According to Fischer, the weight

⁵ A reference to a Russian publication dealing with this subject has come to the attention of the authors, but this is not available in the United States at this time. The reference is given in the Bibliography as item (18).

TABLE 1 FORMULAS FOR JOINT FORCES AND MOMENTS

EFFECT OF:		FLOOR REACTIONS— R	GRAVITY— G	INERTIA— I
COLUMN:	(1)	(2)	(3)	(4)
ANKLE	FORCES	X_A	X_0	0
		Y_A	Y_0	0
		Z_A	Z_0	$-W_F$
	MOMENTS	M_{Ax}	$Z_0(y_0 - y_A) - Y_0(z_A)$	$-W_F(y_F - y_A)$
		M_{Ay}	$-Z_0(x_0 - x_A) + X_0(z_A)$	$W_F(x_F - x_A)$
		M_{Az}	$M_{0x} - Y_0(x_0 - x_A) + X_0(y_0 - y_A)$	0
KNEE	FORCES	X_K	X_0	0
		Y_K	Y_0	0
		Z_K	Z_0	$-W_F - W_S$
	MOMENTS	M_{Kx}	$Z_0(y_0 - y_K) - Y_0(z_K)$	$-W_F(y_F - y_K) - W_S(y_S - y_K)$
		M_{Ky}	$-Z_0(x_0 - x_K) + X_0(z_K)$	$W_F(x_F - x_K) + W_S(x_S - x_K)$
		M_{Kz}	$M_{0x} - Y_0(x_0 - x_K) + X_0(y_0 - y_K)$	0
HIP	FORCES	X_H	X_0	0
		Y_H	Y_0	0
		Z_H	Z_0	$-W_F - W_S - W_T$
	MOMENTS	M_{Hx}	$Z_0(y_0 - y_H) - Y_0(z_H)$	$-W_F(y_F - y_H) - W_S(y_S - y_H) - W_T(y_T - y_H)$
		M_{Hy}	$-Z_0(x_0 - x_H) + X_0(z_H)$	$W_F(x_F - x_H) + W_S(x_S - x_H) + W_T(x_T - x_H)$
		M_{Hz}	$M_{0x} - Y_0(x_0 - x_H) + X_0(y_0 - y_H)$	0

NOTE: COLUMN (1) = (2) + (3) + (4)

of a segment divided by the weight of the body is a constant C_1 ; the distance of the center of mass from the proximal joint divided by the length of a segment is a constant C_2 , and the radius of gyration of the segment about the mediolateral centroidal axis divided by the length of segment is also a constant C_3 . Thus

- (a) Weight of segment = $C_1 \times$ weight of body
- (b) Distance from proximal joint to center of mass of segment = $C_2 \times$ length of segment
- (c) Radius of gyration, $\rho_x = C_3 \times$ length of segment; hence mass moment of inertia $J_x = \text{mass of segment} \times (\rho_x)^2$

The method proposed by Weinbach is based on the assumption that any cross section of a segment is elliptical and that the density of the body is uniform throughout. The masses, the locations of the centers of mass, and the radii of gyration of the leg segments may be determined by numerical or graphical integration of data obtained from front and side-view photographs of the leg. This method, proposed by Weinbach, is so tedious that in view of the questionable assumptions of ellipticity and uniform density, it was deemed adequate for the purpose of this paper to use Fischer's coefficients of location of centers of gravity, weights and masses, and the radii of gyration.

Calculations for the mass, centroid location, and moment of inertia of the combined shank and foot of one normal subject were made using both Fischer's and Weinbach's methods. All values as determined by Weinbach's methods were less than those by Fischer's method by about 10 per cent of the latter.

In the case of the location of the center of mass of the foot, Fischer's laborious graphical construction was replaced by an arbitrary coefficient. Table 2 shows the coefficients used in the calculations.

TABLE 2 ASSUMED COEFFICIENTS

Member	C_1	C_2	C_3
Body.....	1.0000		
Thigh.....	0.1158	0.44	0.31
Shank.....	0.0527	0.42	0.25
Foot.....	0.0179	0.35	0.30

In order to check the accuracy of the coefficients listed in Table 2, a simple experiment was performed at the University of California.

A subject was seated so that one leg was supported only by a chair, as in Fig. 2. A cable connected to a proving ring was attached to the ankle. Mounted on the same ankle was an electrical accelerometer. The subject, by extending his knee joint, created a tension in the cable which was measured by the proving ring and a recording oscillograph. The moment of this force about the knee was thus determinable from the recorded force and the known distance of the cable from the knee joint. The cable was then cut, with the result that the shank and foot swung upward rapidly. The acceleration of the ankle was recorded on an oscillograph actuated by the accelerometer, and the angular acceleration of the foot and shank about the knee computed.

By assuming that the knee moment (M) supplied by the musculature was equal to the external moment before the cable was cut, the moment of inertia of the foot and shank about the knee J_x' was computed from the relationship

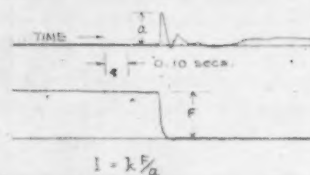
$$J_x' = \frac{M}{\alpha_x}$$

The results of the experiments on three subjects are presented in Table 3.

The fair agreement between the theoretical and experimental values shown in Table 3, together with the small effect of inertia



A. TEST APPARATUS



B. TYPICAL OSCILLOGRAPH RECORD

FIG. 2 MOMENT OF INERTIA DETERMINATION

(see "Results"), would seem to indicate that use of the coefficients shown in Table 2 is sufficiently accurate for purposes of comparison of several subjects.

TABLE 3 COMPARISON OF EXPERIMENTAL AND THEORETICAL VALUES OF MOMENT OF INERTIA OF LOWER LEG PLUS SHOE, ABOUT KNEE

Subject	Experimental J_x' , slug-ft ²	Theoretical J_x' , (from Table 2), slug-ft ²
1	0.28	0.274
2	0.20	0.265
3	0.24	0.258

Displacements and Accelerations. Several methods of defining the displacements, velocities, and accelerations of the joints of the leg were tried. The chronophotographic method of Marey, as improved by Fischer, was improved still further by substituting continuously lighted ophthalmoscope bulbs at significant points on the leg, and taking all pictures in a darkened room. By exposing the film to the lights 30 times each second, a photograph containing many points of light was obtained. With the application of a suitable scale factor the co-ordinates of the lighted joints could be plotted, and graphic or arithmetic methods used to calculate velocities and accelerations. This method was useful only for the side view of the walking operation, since there was no gradual displacement of the body when viewed from the front to preclude overlapping of the point images on the film. In addition, the allowable magnification of the film was too limited to allow of accurate convenient reduction of the data.

For these reasons 35-mm motion-picture photography taken at 40 frames per sec from the front and side, while the subject was walking over a force plate, was used to obtain joint displacements. Targets were placed as close as possible to the most probable locations of the centers of the joints at the toe, ankle, knee, and hip of the leg nearest the side camera. Fig. 3 shows the positions of these targets. The use of targets taped to the skin involves

several limitations, namely, the movement of the skin over the bone causes some slight error in location, and due to the definite thickness of the limbs, the front and side targets will not be at the same elevation when the member is inclined. Since the elevation in the frontal view figures in the determination of lateral movement, while that in the lateral view determines the fore-and-aft

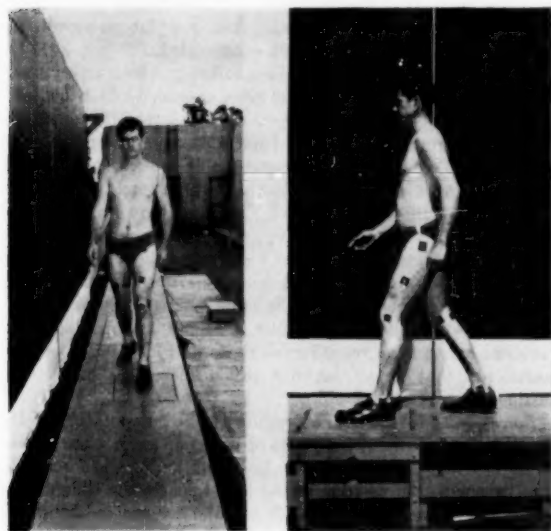


FIG. 3. SUBJECT 4 ON FORCE PLATE

moment, small discrepancies will exist in a comparison of the two components of moment. The resulting film was projected to about one-half actual size and the co-ordinates plotted to a convenient scale. The origin of co-ordinates was taken as the center of the wearing surface of the force plate; the co-ordinate axes were z , positive upward; x , positive inward; and y , positive forward. Figs. 4 to 6, inclusive, show the displacements of the leg joints as obtained from the motion-picture records.

The x , y , z -components of the linear accelerations of the joints were obtained by differentiating twice the curves of the joint displacements with respect to time. In view of the accuracy of the motion-picture data, it was found that graphical differentiation was the best and quickest method and hence was used for determining accelerations.

The co-ordinates of the center of mass of each segment were obtained on the basis of the coefficients given by means of simple equations, for example (referring to Fig. 1 and Table 2)

$$x_S = x_R + 0.42(x_A - x_R) = 0.58x_R + 0.42x_A$$

where

x_S = x -co-ordinate of shank center of mass

x_R = x -co-ordinate of knee joint

x_A = x -co-ordinate of ankle joint

The linear accelerations of the center of mass of each segment were obtained in a similar manner, using the same form as the equations for center-of-mass location, but substituting accelerations for displacements in the foregoing equation.

In order to facilitate the calculations of the location of center of mass and corresponding linear accelerations simple nomograms were used.

The α_x and α_y components of the angular accelerations of each

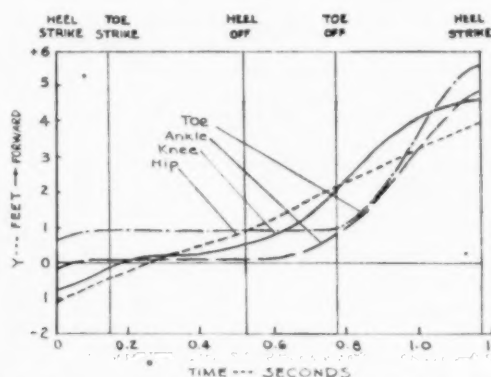


FIG. 4. FORE-AND-AFT DISPLACEMENT OF JOINTS OF LEG; SUBJECT 1

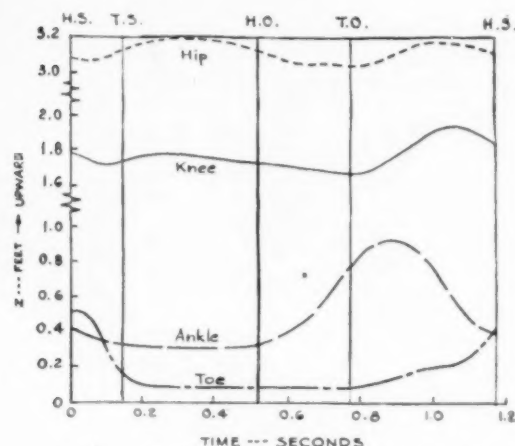


FIG. 5. VERTICAL DISPLACEMENT OF JOINTS OF LEG; SUBJECT 1

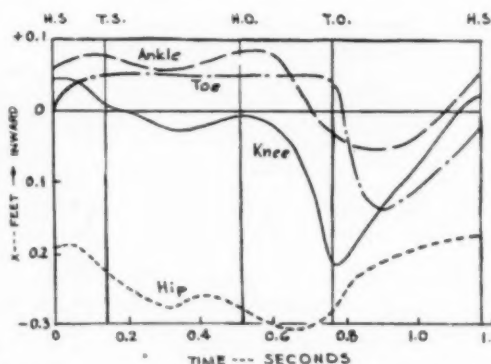


FIG. 6. LATERAL DISPLACEMENT OF JOINTS OF LEG; SUBJECT 1

segment were calculated from the linear accelerations of the two end points of the respective segment, as follows:

The tangential component of the relative acceleration of the upper joint with respect to the lower joint of a particular leg segment is equal to the product of the distance between the joints and the angular acceleration of the segment. The sign convention for the angular acceleration is the same "screw" rule convention as used for the moments.

The effect of the angular acceleration about the z -axis on the moments about the z -axis is very small, and hence was neglected in the calculations. Further, the angular accelerations about the z -axis could not be computed without the aid of measurements of the twists of the segments (21).

Reaction Forces. The reaction forces on the foot were measured on a force plate designed and manufactured under the supervision of Don M. Cunningham at the Artificial Limbs Research Project of the University of California. The lack of moving parts, and the recording of all measurements on an oscillograph tape made this force plate ideal for the problem at hand. The force plate determined the location of the center of pressure, the torque about z -axis, and the vertical and horizontal forces applied to the foot. A paper dealing with the details of the equipment and experimental procedures is now in preparation.

Data Reduction. The computations were set up in a tabular form but, nevertheless, constituted long and tedious procedure. The extent of the work involved in calculating the quantities for only one stride is indicated by the fact that approximately 14,000 numerical calculations were performed, 72 curves were plotted, and 24 curves were subjected to graphic differentiation. This work required approximately 500 man-hours at first but due to increased experience of the reduction personnel the computations for the fourth subject were completed in 250 man-hours.

RESULTS

Displacements. While the subject is walking forward in a relaxed automatic manner, various segments of the body undergo displacements during different phases of a stride. The integrated result of these displacements is a stable, uniform, and mechanically efficient process of locomotion. Some displacements have a definite function in the process of locomotion—such as stabilizing the body during support on one foot, improving efficiency of muscle action, etc. Other displacements have no definite apparent function. A complete description of the kinematics of human locomotion will not be given here, since it is not necessary for analysis of the force system in locomotion. A few brief remarks about the displacement data used for force calculations are, however, in order.

Figs. 4, 5, and 6 show the components of the linear joint displacement of one subject in graphical form. A typical stride shown in these figures consists of a complete cycle of stance (foot in contact with the ground) and swing (foot off the ground) starting at heel strike of the left foot and ending at the next heel strike of the same foot. This cycle takes 1.18 sec, during which the subject moves forward through a distance of 5 ft.

It is apparent from examination of Fig. 4 that the hip moves through 5 ft at about a uniform rate during the entire cycle, while the toe and the ankle move through 5 ft only during 0.4 sec of the swing phase; thus the foot and ankle have larger accelerations than the hip.

Fig. 5 shows the vertical displacements of the leg joints. The rapid toe descent following heel strike, and the toe pickup during the swing phase are clearly apparent. The ankle starts rising just preceding toe-off, and starts descending just after toe-off. Little vertical motion takes place at the knee. The hip joint has a displacement pattern which is typical of joints lying closely to the torso; it has a period half that of the complete stride—the hip rises and falls twice during one complete stride.

The mediolateral displacements of the leg joints are shown in Fig. 6. These displacements are of relatively small magnitude but are of great importance for the stability of the body during normal walking. As the weight is transferred from one leg to the other, the body shifts toward the weight-bearing side. The lateral displacements of the hip joint, shown in Fig. 6, clearly indicate this motion. These data exhibited a large amount of

scatter and the smooth curves representing joint-displacement variation are the best approximations. While the forward and vertical displacement patterns, shown in Figs. 4 and 5, are also represented by smooth curves, the amount of scatter for these data are definitely negligible. In comparing the character of data in Figs. 4, 5, and 6, however, it must be remembered that the displacement scales in these figures vary a great deal. The relative scales of the displacements are 20:4:1 for the forward, vertical, and lateral movements; thus any inaccuracy in the lateral-displacement data is much exaggerated.

It must be emphasized that locomotion involves a very sensitive balance on one foot—it has been previously described as a continuous process of fall and recovery—and therefore small displacements from the position of unstable equilibrium are to be expected. The stability of locomotion is preserved by muscle actions (controlled by nerve impulses) which tend to return the body to the equilibrium position. This results in minute jerkiness of motion which is not ordinarily apparent, but contributes to the scatter of the data. This "jerky" characteristic of locomotion is not reproducible, and the small deviations from the smooth process vary in each step even for the same subject. Since the purpose of this analysis is to consider the forces and displacements involved in a general reproducible pattern of locomotion, it was considered that smoothing out the displacement curves was justified.

Forces and Moments. The results of the computation of the forces and moments at the joints of the same subject are plotted in Figs. 7 and 8. To correlate the variation of the forces and moments with the position of the leg in space, the time of heel strike, toe strike, heel-off, toe-off, and the heel strike of the next stride are shown in the figures.

In order to obtain the over-all system of forces acting on the body, the forces acting on both legs must be considered. The total force on the body can be obtained by superposition of two curves, adjusting the time of beginning of each curve to correspond to the proper phase sequence of motion. This places the heel strike of the opposite leg little less than halfway between heel-off and toe-off of the given leg. (An accurate analysis of the forces acting on the body has been carried out at the University of California using data from two force plates. This analysis has not been included here).

The X -(lateral) components of joint forces shown in Fig. 7 have very small magnitudes. These forces are important, however, in providing the lateral stability in walking and contribute a large share of the lateral hip moment (M_H). As the body weight is shifted from one leg to the other the lateral force must be directed inward with respect to the body (negative X_H), in order to prevent the subject from falling sidewise. The magnitude of this force will depend largely upon the amount of lateral hip motion.

The Y -(fore-and-aft) components of joint forces shown in Fig. 7 have a typical shape approximating a full sine wave during the stance phase. During swing phase, the Y -forces are small and their variations are somewhat irregular. With the sign convention adopted in this analysis, a positive Y -force indicates an external force tending to retard the forward motion of the body. Thus it is apparent that the variation in Y -component of the force on the leg is due to the fact that upon heel strike the leg first must retard the forward motion of the body, and then a fraction of a second later must provide the "push-off" or forward acceleration necessary to continue the motion.

The Z -(vertical) components of joint forces shown in Fig. 7 have a typical double-peak shape; this is due to vertical upward and downward accelerations of the body. The difference between the vertical component of floor reaction Z_0 (very nearly equal to Z_A), and the body weight is proportional to the vertical accelera-

tion of the body. The first peak occurs shortly after heel strike, when the body rolls over the supporting leg, and the other peak occurs when the leg "pushes" the body up just before the other leg strikes the floor.

The differences between the forces at the ankle, knee, and hip joints indicate the effect of gravity and inertia at these joints. Thus the maximum vertical compressive force occurs at the ankle joint, while at the hip joint this force is reduced by the gravity and inertia effects of the shank and thigh. The variation in the X-

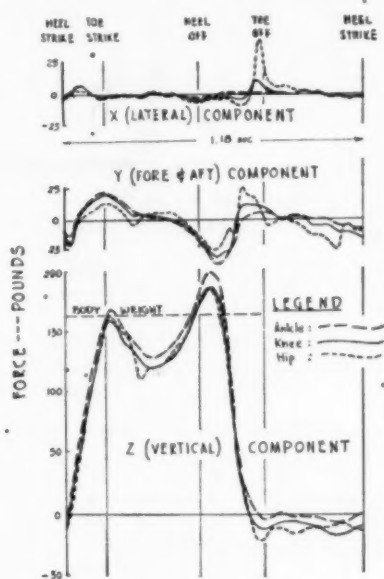


FIG. 7 JOINT FORCES; SUBJECT 1
(Time for one complete stride, 1.18 sec.)

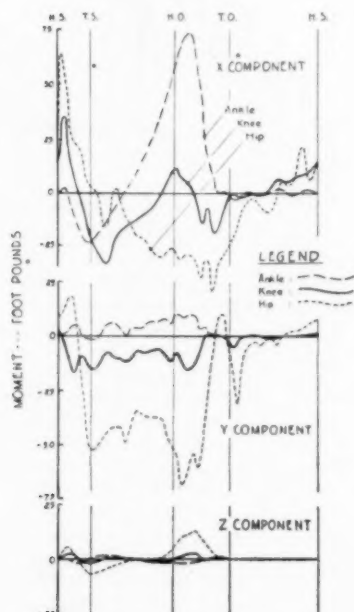


FIG. 8 JOINT MOMENTS; SUBJECT 1

and Y-components of forces at the ankle, knee, and hip joints are due to inertia effects only, since gravity does not affect these components.

The X-component of moment shown at the top of Fig. 8 is that component tending to extend or flex the foot. From the adopted sign convention, a positive X-moment would be produced by the resultant force passing in front of the joint. Thus the negative X-moment occurring just after heel strike indicates that the resultant force passes behind the ankle at this time, when the toe is still being lowered. When the foot is flat the load shifts so as to pass ahead of the ankle, yielding positive moment which increases rapidly, reaching a maximum value at the time the subject pushes off on the foot. It is to be expected that the magnitude and timing of the negative moment, occurring when the foot is being lowered, would be a definite aid in diagnosis of such pathological conditions, as, for example, *talus dorsalis* where the foot is allowed to slap down, possibly registering less negative moment over a shorter time than normal.

The X-component of the knee moment registers quite clearly a phenomenon of gait found in nearly all normal subjects to date. The sign of this component of the knee moment is such that, when negative, the resultant force passes behind the knee, tending to flex it (and therefore render it unstable), while a positive moment indicates that the knee is being moved into or held in a "locked" position (stable). Thus, from the curve, one may conclude that at heel strike the leg is quickly stabilized, then unlocked; and once again locked for the push-off phase of the step. This "double-locking" action permits the subject to move forward with a minimum raising of his center of gravity, and therefore with less expenditure of work.

The location of the resultant of the forces at the hip, as partially indicated by the sign and magnitude of the X-component of the hip moment, serves to demonstrate the precept of continual rotation of the body pointed out so clearly by Elftman (14). The initial positive moment at the hip indicates that the forward rotation of the torso is being retarded, while the later change to negative moment indicates the renewal of forward torso rotation.

The lateral components of moment reflect the requirements of bipedal walking on the joints of the leg. In shifting from leg to leg, the torso is shoved first one way then the other, and moments somewhat proportional to the elevation of the joint above the ground are recorded. This points out the relatively large magnitude of the Y-(lateral) component of moment at the hip, a factor beyond the analysis of investigations which have their attention confined to the plane of progression.

The Z-components of moment reflect the positioning of the shears in the leg, and therefore may be associated largely with the twist of the body as well as that of the segments of the leg. Of interest is the fact that the results of pin studies (21) on twist of the segments agree quite consistently in phasic nature with the M_z -curves in Fig. 8.

Fig. 9 illustrates the significance of inertial and gravitational effects on the fore-and-aft moments at the ankle, knee, and hip. The contributions of reactions to these moments at the ankle, knee, and hip are compared to the total computed moments, so that the difference in ordinate between the total moment and the reactional moment represents the effect of gravity and inertia of the segments below the indicated joint. It is apparent from Fig. 9 that the effect of gravity and inertia on fore-and-aft moments is very small for the ankle and knee moments, and relatively small on the hip moments throughout most of the stance phase.

Since the computations of the moments about the joints due to these effects are the bulk of the calculations, a rapid first approximation to the magnitudes of moment and force may be made by considering only the moment due to the floor reactions. In

the case of the hip, however, considerable error may be introduced in such an approximation.

To serve as an indication of the general value of the results for one subject, comparisons of several characteristic joint forces and

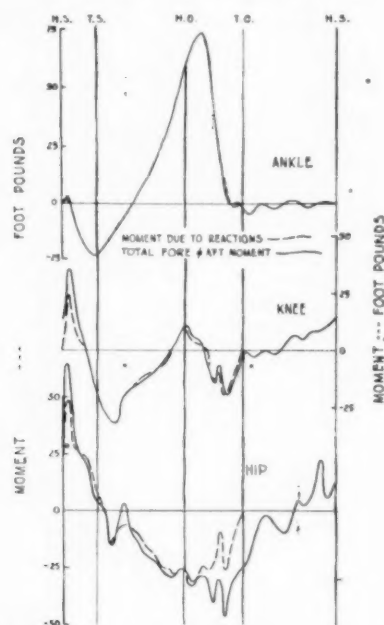


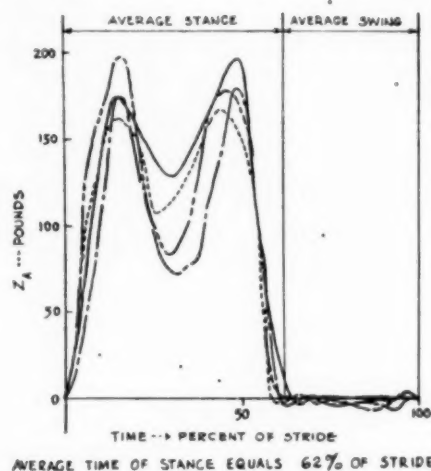
FIG. 9 CONTRIBUTION OF REACTIONS: FORE-AND-AFT MOMENTS; SUBJECT 1

moments, computed for four subjects, are shown in Figs. 10 to 14, inclusive. The values plotted are the vertical force at the ankle (Fig. 10), fore-and-aft moments at the ankle, knee, and hip (Figs. 11, 12, and 13), and lateral moments at the hip (Fig. 14). These curves were selected as the most important ones, particularly from the point of view of magnitude. In these figures the time scale is plotted as per cent of the time for one complete stride, in order that the phasic activity of the four subjects can be most closely compared.

The examination of the comparison curves for four subjects illustrates the degree of variation between the individual subjects. Notwithstanding the large variations in magnitudes of the peak values and their phases relative to heel strike, the general patterns of the curves discussed with reference to Figs. 7 and 8 are apparent.

The curves shown are but one way of plotting the results of the calculations. If one chooses to ignore the inertial effects and the weight of the segments of the leg, a very convenient method of representing the results would be that employed by Elftman and his co-workers at New York University. This consists in plotting the positions of the segments in space as lines, and showing the accompanying floor reactions as vectors with the proper magnitude, direction, and point of application. By prolonging the line of action of this force vector, one may note by inspection the orientation of the joints of the leg with respect to the line of action of the ground force. One of the limitations of this method is that the walking cycle must be broken into many small intervals if one is to obtain a reasonable picture of the gait of the individual—a procedure of dubious economy, compared to the instantaneous indications of such curves as are presented herein.

No study of the mechanics of locomotion would be complete



SUBJECT	CODE	HEIGHT	WEIGHT
1	---	5'-11"	165 lbs.
2	---	5'-8"	153
3	---	5'-8"	140
4	---	5'-11"	161

FIG. 10 VERTICAL ANKLE FORCE; FOUR SUBJECTS

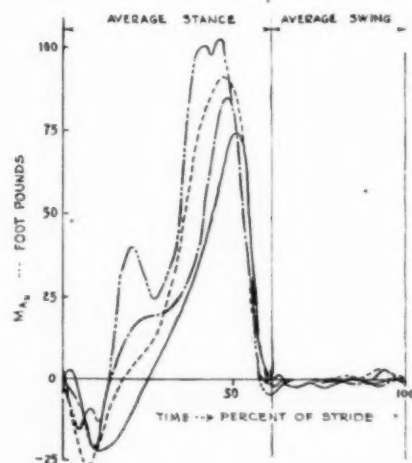


FIG. 11 FORE-AND-AFT ANKLE MOMENT; FOUR SUBJECTS

without the mention of the bone forces. Only the muscles at a joint can provide the moments, and since they act only in tension, the resultant force at a joint at the times when moment is evidenced can be compressive only if the bone forces are very high compressions themselves. Since muscles may also act to oppose each other at a joint so that there is no resultant moment, high compressive bone forces may be expected at times when there is no moment. It is not unreasonable to expect that at such times as push-off the bone forces may easily exceed twice the body weight. Inman (20) has investigated forces acting on the femur at the hip joint under several static conditions. He found that under these conditions the force on the femoral head is 2.4 to 2.6 times as great as the body weight, while the tension in the abductor muscles is 1.4 to 1.9 times the body weight. The magnitudes of the lateral hip moment used in Inman's investigation approach closely the peak values computed

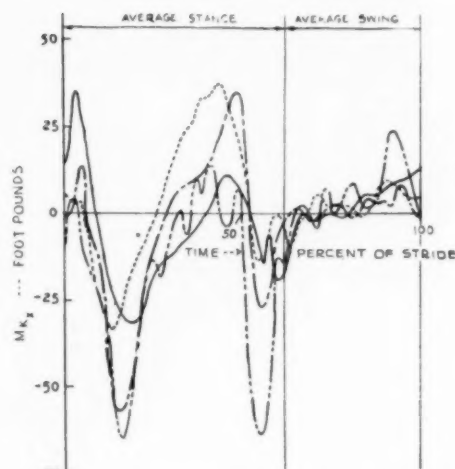


FIG. 12 FORE-AND-AFT KNEE MOMENT: FOUR SUBJECTS

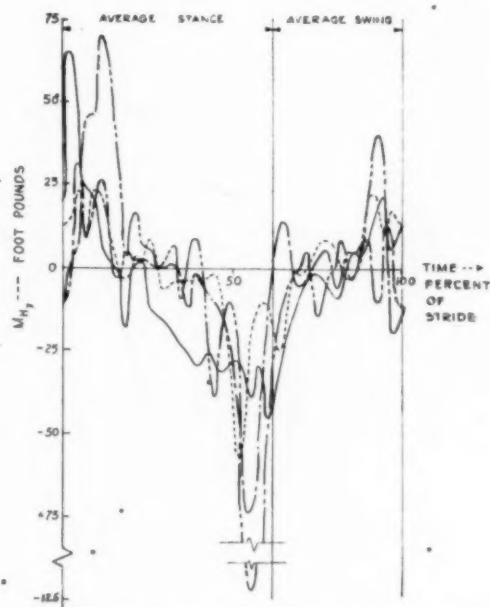


FIG. 13 FORE-AND-AFT HIP MOMENT: FOUR SUBJECTS

during level walking, and hence his results are indicative of forces acting at the hip joint during normal locomotion. Eiftman (15) has made some computations of this nature, using such simplifying assumptions as the moment arms of the different muscles, and their time of action. Auxiliary studies of phasic activity of the muscles have shown, however, that any such calculations at this time would be, at best, first approximations.

It is apparent from the foregoing discussion that the variations of forces and moments in the leg joints are closely related to the mechanical functions of the leg in walking. These relationships, in addition to the studies of energy of human locomotion, investigations of the activity of different muscles of the leg, and the anatomical studies of leg-joint mechanisms (1) are necessary in order to solve the problems confronting the orthopedic surgeon and the designer of artificial legs and braces.

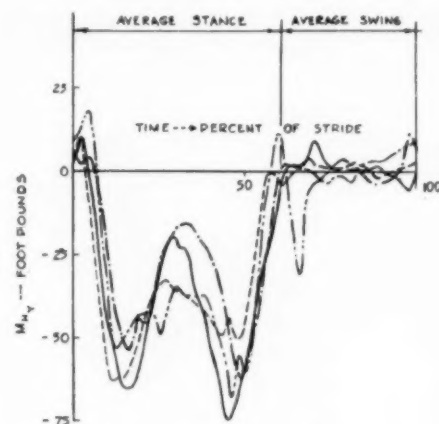


FIG. 14 LATERAL HIP MOMENT, FOUR SUBJECTS

BIBLIOGRAPHY

- 1 "Fundamental Studies of Human Locomotion and Other Information Relating to Artificial Limbs," Report to National Research Council, Advisory Committee on Artificial Limbs, vols. 1 and 2, June, 1947.
- 2 "Mechanik der menschlichen Gehwerkzeuge" ("Mechanics of Human Locomotion"), by Wilhelm and Eduard Weber, Göttingen, Germany, 1836.
- 3 "De la locomotion terrestre chez les bipèdes et les quadrupèdes" ("Terrestrial Locomotion of Biped and Quadruped"), by E. J. Marey, *Journal de l'Anat. et de la Physiol.*, vol. 9, 1873, pp. 42-80.
- 4 "Animal Mechanism: A Treatise on Terrestrial and Aerial Locomotion," by E. J. Marey, Appleton-Century-Crofts, Inc., New York, N. Y., 1874.
- 5 "La methode graphique dans les sciences experimentales" ("The Graphic Method in Experimental Sciences"), by E. J. Marey, G. Masson, Paris, France, 1885.
- 6 "Etudes experimentales de la locomotion humaine" ("Experimental Studies on Human Locomotion"), by E. J. Marey and G. Demy, *Comptes Rendus Acad. des Sciences*, vol. 105, 1887, pp. 544-552.
- 7 "Movement," by E. J. Marey, D. Appleton Co., New York, N. Y., 1895.
- 8 "Der Gang des Menschen" ("Human Gait"), by O. Fischer, *Abhandlungen der Saechs. Gesellschaft der Wissenschaften*, vol. 21-28, 1898-1904.
- 9 "Über den Schwerpunkt des menschlichen Körpers mit Rücksicht auf die Ausrüstung des deutschen Infanteristen" ("Concerning the Center of Gravity of the Human Body With Reference to the Equipment of the German Infantryman"), by W. Braune and O. Fischer, *Abhandlungen der Königl. Saechs. Gesellschaft der Wissenschaften*, vol. 15, 1872.
- 10 "Biodynamics of Locomotion," by N. A. Bernstein, et al, VIEM, Moscow, USSR, vol. 1, 1935.
- 11 "A Cinematic Study of the Distribution of Pressure in the Human Foot," by Herbert Eiftman, *Anatomical Record*, vol. 59, 1934, pp. 481-490.
- 12 "The Function of the Arms in Walking," by Herbert Eiftman, *Human Biol.*, vol. 2, 1939, pp. 529-535.
- 13 "The Force Exerted by the Ground in Walking," by Herbert Eiftman, *Arbeitsphysiologie*, vol. 10, 1939, pp. 485-491.
- 14 "The Rotation of the Body in Walking," by Herbert Eiftman, *Arbeitsphysiologie*, vol. 10, 1939, pp. 477-483.
- 15 "Forces and Energy Changes in the Leg During Walking," by Herbert Eiftman, *American Journal of Physiology*, vol. 125, 1939, pp. 339-356.
- 16 "The Function of the Muscles in Locomotion," by Herbert Eiftman, *American Journal of Physiology*, vol. 125, 1939, pp. 357-366.
- 17 "The Action of the Muscles in the Body," by Herbert Eiftman, *Biol. Symposia*, vol. 3, 1941, pp. 191-209.
- 18 "Determination of Masses and Centroids of Segments of Human Body on Live Subjects," by N. A. Bernstein, et al, VIEM, Moscow, USSR, 1936.

19 "Contour Maps, Center of Gravity, Moment of Inertia and Surface Area of the Human Body," by A. P. Weinbach, *Human Biology*, vol. 10, Sept., 1938, pp. 356-371.

20 "Functional Aspects of the Abductor Muscles of the Hip," by

V. T. Inman, *Journal of Bone and Joint Surgery*, vol. 29, July, 1947.

21 "Transverse Rotation of the Segments of the Lower Extremity in Locomotion," by A. S. Levens, V. T. Inman, and J. H. Blosser, *Journal of Bone and Joint Surgery*, October, 1948, pp. 859-872.

Report on Graphitization Studies on High-Temperature Welded Piping of The Philadelphia Electric Company

By J. B. ABELE¹ AND A. E. WHITE²

Summaries of the work which has been done by and for the Philadelphia Electric Company in ascertaining the degree of graphitization in the piping system in the Chester, Schuylkill, and Richmond Stations since the fall of 1946, are reported in this paper. The results of a full-size pipe tension test on a graphitized weld section are reported. Solution treatment for removal of graphitization is described with some physical test results.

SECTION 1 By J. B. ABELE

THIS report is a supplement to one presented in 1946, by Hopping and White,³ and gives results of further studies and investigations covering a period of approximately 2 years. The conclusions of the previous report, based upon the work done up to that time, led to a decision to continue the use of the pipe, and periodically to examine the welds further as a means of comparison and determination of increases, if any, in the formation of graphite. Such findings were to be used as a basis for a decision either to continue the use of the piping in its existing condition or to take appropriate steps to remedy this condition. The piping under investigation was as follows:

Chester Station. Operating since 1941 at a pressure of 1250 psi and 925 F; carbon-moly pipe, killed with $\frac{1}{2}$ lb of aluminum per ton of steel.

Schuylkill Station. Operating since 1938 at a pressure of 1250 psi and 900 F; carbon-moly pipe, killed with 1.8 lb of aluminum per ton of steel.

Richmond Station. Operating since July, 1943, at a pressure of 400 psi and 850 F; carbon-steel pipe. From 1935 to July, 1943, the operating temperature was 875 F with occasional swings to 900 F.

OPERATING RESULTS AT CHESTER AND SCHUYLKILL STATION

Since the previous report, samples have been removed from all three stations for investigation.

At Chester Station, where approximately 20,000 service-hours have been added since the previous report, no appreciable amount of graphite has formed on either side of the welds in the heat-affected zones or in the pipe metal. Previous examinations of

samples from the same welds showed no graphite in either the heat-affected zones or the pipe metal. Samples, however, have been removed from other welds where small amounts of nodular graphite were found. The conclusion, therefore, up to the present time and after 50,000 hr of service, is that very little graphite will form in the welds at Chester Station; however, occasional check examinations will be made in the future.

At Schuylkill Station the situation is somewhat different. Since the previous report, additional samples have been removed. They were taken from welds previously sampled and represent an additional 25,000 hr of service. In two of the samples examined, the amount of graphite in the heat-affected zones appeared to be somewhat greater and more continuous than was found in samples previously examined from the same welds. In another sample, the graphite did not appear to be quite as severe as that found in the sample previously examined from the same weld. In view of these findings, it is intended to remove completely one of these welds for mechanical tests, since metallographic examination does not give a quantitative measure of the degree of deterioration of the properties due to the presence of graphite.

The indicated increase in severity of graphite may be evidence of increased graphitization since the last examination, but this is not conclusive because previous work has shown that the amount of graphite varies considerably around the circumference of the weld. It can be stated, however, that the added graphite, if any, is quite small for the added service period of approximately 25,000 hr. At present, therefore, it is believed that, while there are indications of a slight increase in graphite in the welds at Schuylkill Station, it has not progressed to a point where continued use of the pipe in its present condition would be unwise. The results of future examinations will determine the action to be taken at Schuylkill Station.

It is thought that the small amount of aluminum used in killing the steel for the piping at Chester Station, as contrasted with the larger amount used for the Schuylkill Station piping, is the reason for the difference in the amount of graphite found in the welds at the two stations.

DETAILS OF TESTS AT RICHMOND STATION

At Richmond Station a full section of 20-in.-OD carbon-steel pipe was removed for a tension test. The section was approximately 3 ft long with a weld in the center and was tested on the 4,000,000-lb tension testing machine at the shops of the American Bridge Company, Ambridge, Pa. Fig. 1 shows the specimen before testing. It consisted of the section of pipe, two internally tapered transition rings, and two massive pulling heads. Twelve Baldwin Southwark SR-4 strain gages were used to measure strain. Four gages were placed on the weld, 90 deg apart and 4 gages were placed on the pipe 90 deg apart on each side of the weld.

The cross-sectional dimensions of the pipe, the data developed from the test loading and the strains measured with the SR-4 gages are given in Table 1. Yielding of the steel in the pipe metal on one side of the weld occurred at a load of 1,200,000 lb, which is

¹ Senior Engineer, Philadelphia Electric Company, Philadelphia, Pa.

² Director of Engineering Research Institute, University of Michigan, Ann Arbor, Mich. Fellow ASME.

³ "Report on Graphitization Studies in High-Temperature Welded Piping of the Philadelphia Electric Company," by E. L. Hopping and A. E. White, Trans. ASME, vol. 69, 1947 (see "Graphitization of Steel Piping," special pamphlet).

Contributed by the Joint Committee on Effect of Temperature on the Properties of Metals and Power and Metals Engineering Divisions and presented at the Annual Meeting, November 28-December 3, 1948, of THE AMERICAN SOCIETY OF MECHANICAL ENGINEERS.

NOTE: Statements and opinions advanced in papers are to be understood as individual expressions of their authors and not those of the Society. Paper No. 48-A-94.

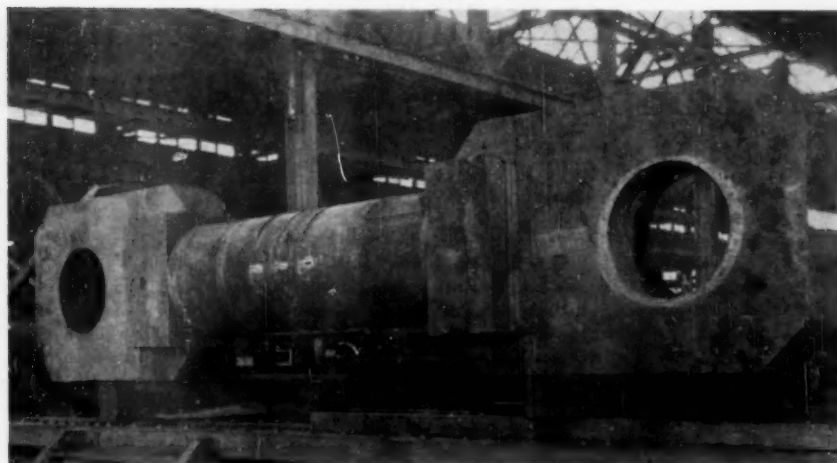


FIG. 1 SPECIMEN BEFORE TESTING

TABLE 1 DIMENSIONS, TEST LOADING, AND MEASURED STRAINS FOR WELDED JOINT IN 20-IN. PIPE FOR PHILADELPHIA ELECTRIC COMPANY

		Outside diameter of pipe	20.00 in. Nominal
		Inside diameter of pipe	18.188 in. Nominal
		Wall thickness	.906 in. Nominal
		Cross-sectional area of pipe	54.35 sq. in. Nominal

Total Load	Load Stress on Nominal Cross-sectional Area of Pipe (psi)	Strains Measured with SR-4 Gauges (Micro-inches per inch)											
		Gauges on Weld				Gauges on Pipe							
		BT	BB	BE	BU	Northerly Half				Southerly Half			
AT	AB					AE	AW	CT	CB	CE	CW		
0	0	0	0	0	0	0	0	0	0	0	0	0	0
250 000	4 600	73	51	90	64	108	89	90	74	102	95	143	90
500 000	9 200	206	118	213	160	283	211	258	253	246	262	305	189
1 000 000	18 400	487	251	460	412	616	491	583	501	575	578	687	470
1 200 000	22 080	Yield point in weld				Yield point in south half							
1 250 000	23 000	636	339	594	532	774	641	766	581	763	767	1 139	600
1 500 000	27 600	948	571	811	717	765	818	988	791	3 617	3 397	*	1 061
1 750 000	32 200	1 761	924	1 463	1 302	970	977	1 155	881	*	*	*	*
						Yield point in north half							
2 000 000	36 800	2 746	1 496	2 561	2 529	1 149	1 141	1 352	1 101				
2 250 000	41 400	4 085	3 550	*	*	*	1 443	*	1 486				
2 545 000	46 830	Pipe fractured at heat affected zone along south side of weld.											

* Gage yielding or fractured.

TABLE 2 ELONGATION MEASUREMENTS FOR WELDED JOINT IN 20-IN. PIPE FOR PHILADELPHIA ELECTRIC COMPANY^a

Gauge Lines		Northerly Half				Southerly Half			
		1	2	3	Av.	4	5	6	Av.
Length before test	(ft)	.998	1.001	1.000	-	1.000	1.001	1.000	-
Length after test	(ft)	1.018	1.018	1.010	-	1.044	1.041	1.045	-
Elongation after fracture	(%)	.020	.017	.010	-	.044	.040	.045	-
	(%)	2.0	1.7	1.0	1.6	4.4	4.0	4.5	4.3

^a Fracture was outside both sets of gage lines.

equivalent to a stress of 22,080 psi. The strains measured by the SR-4 strain gages on the weld indicate that the weld metal also yielded at this load which is equivalent to a stress of about 19,280 psi in the weld metal. The yielding of the steel in the pipe metal on the other side of the weld occurred at a load of 1,750,000 lb which is equivalent to a stress of 32,200 psi. The elongation measurements are listed in Table 2. It is to be noted that neither set of measurements listed in Table 2 encompass the fracture of the specimen.

The fracture occurred in the weld-heat-affected zone and had three zones of distinctly different appearance; an outer zone of black and gray conchoidal fracture which is identified as graphitized steel extending in varying widths all around the fracture; a zone of a dark fine granular fracture extending around one-quarter of the pipe; and an inner zone, the largest, of a normal-appearing white fine granular fracture. Fig. 2 is a general view of the fracture, and Figs. 3 and 4 are detail views of a portion of the fracture.

From Table 1 it will be noted that the specimen broke in the weld at a load of 2,545,000 lb, equivalent to a fiber stress of 46,830 psi. The original tensile strength of the steel as reported by the mill was 70,900 psi. Probably half of the reduction in strength is due to the annealing effect from a service of 92,000 hr at temperatures ranging from 850 to 875 F, with occasional swings to 900 F. The balance of the reduction to 46,830 psi is due, without doubt, to graphitization. While a stress of 46,830 psi provides an ample factor of safety in a sound weld, resistance to thermal shock is of great importance and provision for this in a weld of this kind is none too good.

The appearance and nature of this fracture led to a decision to correct the condition at the earliest convenient time. Consideration was given to replacement of all the affected piping. An investigation, however, of the steel a short distance from the welds showed that the mechanical properties and the structure of the steel had not been unduly impaired, although the tensile strength had dropped to about 54,000 psi through normal service conditions but with no loss in ductility. It seemed inadvisable therefore to remove the pipe, and consideration was given to the

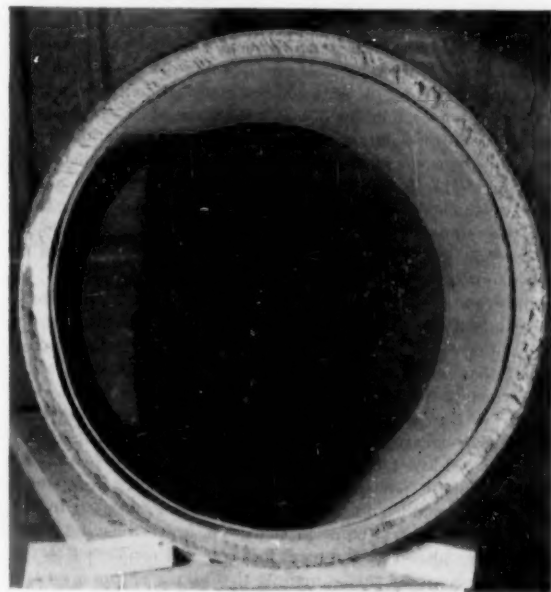


FIG. 2 GENERAL VIEW OF TEST SPECIMEN AFTER FRACTURE

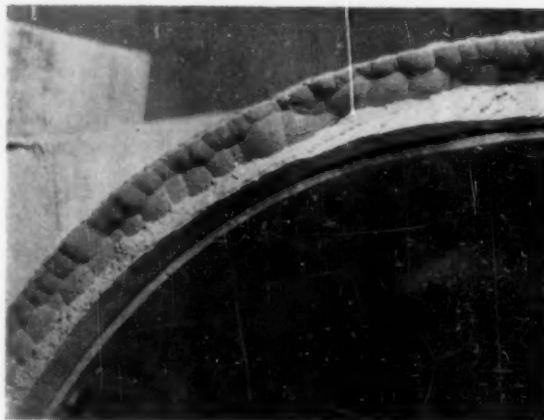


FIG. 3 DETAILED VIEW OF TEST SPECIMEN AFTER FRACTURE

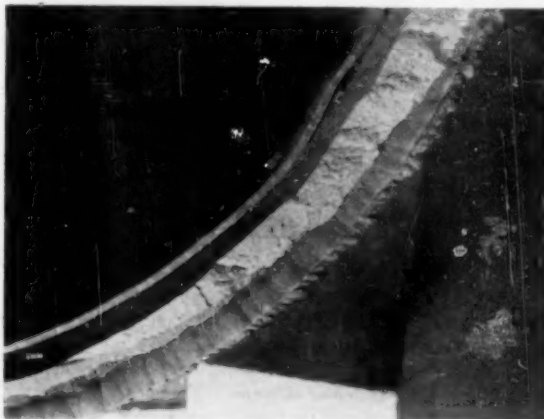


FIG. 4 DETAILED VIEW OF TEST SPECIMEN AFTER FRACTURE

replacement of the welds or to a solution treatment of the welds to disperse the graphite.

Earlier work in normalizing at 1700 F at the University of Michigan together with more recent work at the same institution convinced us that this method offered a possible effective means of restoring graphitized welds.

SOLUTION TREATMENT TO DISPERSE GRAPHITE

Investigation by A. E. White at the University of Michigan, discussed later on, disclosed the fact that solution treatment, followed by proper stress relief placed the graphitized metal in a safe state of strength and ductility. Therefore, it was decided to repair the pipe by this method rather than replace the welds. The latter method would require more time and involve greater cost.

A careful investigation of the practical application of solution treatment of welds in the field also indicated that the work could be speedily and successfully done.

The procedure finally agreed upon was as follows: Heat to 1700 F at a rate not to exceed 300 deg per hr from 1000 F to 1700 F. Hold at 1700 F for 2 hr. Control cooling from 1700 F to 1200 F at a rate not to exceed 100 deg per hr. Allow to cool, uncontrolled, from 1200 F to approximately 700 F. Stress-relieve by raising temperature to 1275 F at a rate of 400 deg per hr. Hold at

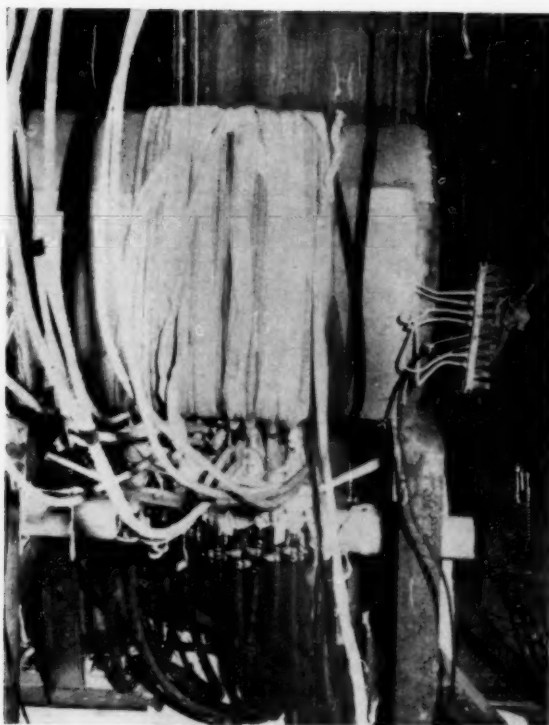


FIG. 5 HEATING ARRANGEMENT ON EXPERIMENTAL PIECE

1275 F for 1 hr per in. of thickness. Cool to 700 F at a rate of 200 deg per hr. Allow to cool uncontrolled from 700 F.

A method of electronic heating was discussed with the engineers of the Radio Corporation of America. This method, however, was not practical because of the mass of metal involved. Calculations indicated that approximately 40 kw of radio-frequency power would be required to maintain a band 6 in. wide at 1700 F in the 20-in.-OD pipe. While it is true that their 75-kw generator would produce enough heat to perform the normalizing treatment, it was felt that the portability and the relatively great expense of the equipment made its use impractical.

Heating with gas was considered, but this too was thought to be impractical since it was felt that it would be difficult to maintain a uniform heat around the entire circumference unless an oven or muffle was built around the pipe. Because of insufficient clearances and other interferences in many cases, such a muffle could not be used.

Induction Method of Heating Pipe. It was finally decided that the induction method was the most logical one to use and, accordingly, experimental tests were run on a short length of 20-in.-OD pipe. Because of the extreme temperature and high amperage required, water-cooled coils were used.

Twelve turns of $\frac{3}{8}$ -in.-OD 0.035-in.-wall copper tubing were used on each side of the welded joint (24 turns total). The turns were arranged so that the cooling water was discharged and fresh water was admitted for each 3 turns around the pipe. Four 60-kva stress-relieving transformers were used, making a total of 240 kva available. They were connected, two in series, to each heating coil with a separate control cabinet for each set of transformers. A water relay was used with each cabinet to shut the power off automatically in case the cooling-water supply failed. The leads between the transformers and heating coils were made up of

four welding leads in parallel 100 ft long. Fig. 5 shows the setup on the experimental piece.

Experiments were also conducted in an effort to determine whether or not scale formation could be prevented or at least minimized. The amounts of scale formed were compared for (1) open-ended pipe with a free circulation of air, (2) dead air by blanking each end of the pipe, and (3) by the use of inhibitors such as helium, nitrogen, and CO_2 . While the amount of scale varied between methods, the total in no case was considered great enough to warrant the use of any of the special methods; the conclusion being that there would be no more scale than is found in the welded joints of a new installation.

Formulating the Solution Treatment. In formulating a program for the solution treatment of the welds at Richmond Station, it was decided to remove additional boat samples from welds representing the various materials and combinations of materials. Samples were removed from pipe to pipe joints both in the 16-in. and 20-in. seamless pipe, and from pipe to pipe joints as well as from longitudinal welds in the 24-in. fabricated pipe. While graphite was found in the 16-in. and 20-in. welds, no graphite was found in the 24-in. fabricated piping, due, we believe, to the high silicon content of the plate material.

In passing, it will be of interest to note that a gas shop weld in the 20-in. pipe was examined and no graphite or other detrimental structural alterations were found in it. It would be unwise, however, to draw too general conclusions from the examination of a single weld.

Material for the castings for the gate and nonreturn valves contained approximately 1.00 per cent nickel, 0.70 per cent chrome and 0.50 per cent molybdenum. No samples were removed from the welds at these valves since it was reasonable to assume that little or no graphite exists on the valve side because of their high chromium content. Also, these welds were to be safeguarded by a solution treatment.

Valve Tests. It was feared that some valve distortion might occur with the 1700 F temperature heat, making it necessary to repair or reseat the valves; therefore, temperature measurements were taken in the castings to provide data for future temperature applications to valve welds. The nonreturn valves are Schutte & Koerting 16-in. double inlet, 20-in. single outlet. Thermocouples placed on the body at the center of the valves during solution treatment of the weld on the 20-in.-diam outlet, which was 28 in. away from the center line of the weld, indicated a temperature of approximately 575 F. Removal of the bonnets of these valves after solution treatment and an examination of the trim, and a subsequent pressure test, showed that there had been no distortion of the seating surfaces. Similarly, thermocouples placed on the body of the 20-in. gate valves, 12 in. from the weld showed a temperature of 800 F. It is evident, therefore, that a temperature of 1700 F at the welding ends of valves of comparable size will not affect the trim of valves adversely.

Some thought was given to adequate bracing of the piping during solution treatment because of the plastic condition of the weld metal and of possible strain in the piping. It was finally decided that no elaborate means of bracing need be used, a decision which proved to be correct.

Electrical Energy for Solution Treatment. Electrical energy for the solution treatment at Richmond Station was delivered through a 600-kva temporary power bank, installed to provide 440-volt 3-phase power from the 2300-volt bus. Temporary feeders were installed to the distribution center located in the vicinity of the work to be performed. The stress-relieving transformers were placed at a central location and connected to the distribution center in such a manner that all transformers on any one joint were all on the same phase. The data in Table 3 show the requirements for heat-treatment.

TABLE 3 HEAT-TREATMENT DATA

Actual kva required to normalize 20-in. pipe.....	175
Average primary voltage required.....	445-450
Average secondary voltage required at pipe.....	62-65
Average secondary voltage required at transformer.....	70-72
Average secondary amperage.....	1100-1200
Water flow through 1 coil (3 turns), gpm, approx.....	1-1/4
Water flow through 8 coils (24 turns), gpm, approx.....	15
Water pressure at header, psi.....	24
24 turns of 3/8-in.-OD, 0.035-in.-wall, copper tubing insulated with woven asbestos.....	
Pipe insulated with 4 layers of 1/8-in. X 10-in. asbestos paper.....	

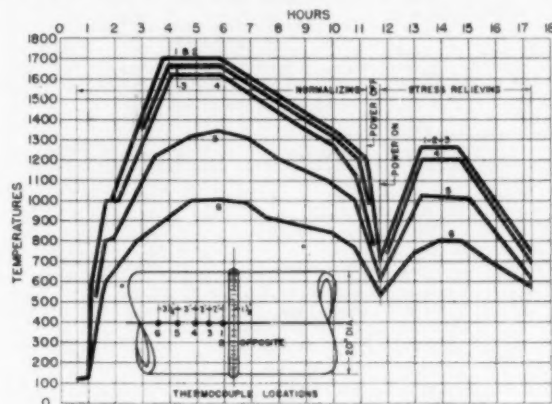


FIG. 6 TYPICAL NORMALIZING & STRESS-RELIEVING CHART

FIG. 6 TYPICAL NORMALIZING AND STRESS-RELIEVING CHART SHOWING TEMPERATURE AT WELD AND AT VARIOUS DISTANCES FROM WELD

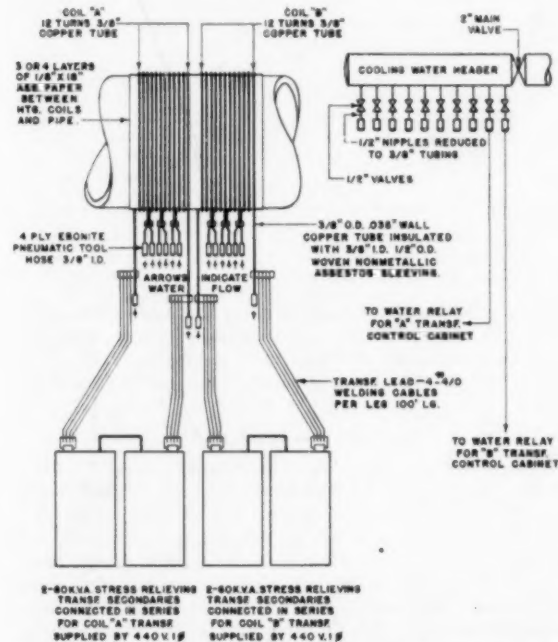


FIG. 7 DIAGRAM OF NORMALIZING AND STRESS-RELIEVING EQUIPMENT

Fig. 6 is a typical time-temperature chart showing the temperatures at the weld and at various distances from the weld during the solution and stress-relieving treatment. Fig. 7 is a schematic layout of the equipment used.

All welds in the high-pressure piping system at Richmond Station were solution-treated with the following exception: The 24-in. fabricated pipe where no graphite was found, and the pipe from the superheater header to the nonreturn valve on one boiler, which was replaced with one-half chrome and one-half moly pipe left over from Southwark Station.

Twenty-Nine Welds Treated. Twenty-nine welds were solution-treated and the work was completed in nineteen 24-hr working days, thus effecting a material time-saving over and above that which would be required were the graphitized welds cut out and replaced with new welds. It is felt, however, that the treatment has removed a latent critical condition, either temporarily or permanently, and substantially prolonged the useful life of this pipe, although it is not necessarily to be construed that this method should be used if graphitization has advanced to an undue degree.

Later samples will be removed from time to time and a future course of action will depend upon the findings.

SECTION 2 By A. E. WHITE

RESTORATION OF PROPERTIES OF GRAPHITIZED WELD SECTIONS BY HEAT-TREATMENT

Mr. Abele has pointed out that this author would deal with the subject of the restoration of the properties of graphitized weld sections by heat-treatment at the Richmond Station of the Philadelphia Electric Company.

The restoration of graphitized weld sections was advanced by the author in 1943, and a report covering some preliminary work in this field was given to the Philadelphia Electric Company on February 5, 1944. The restoration procedure, from a laboratory standpoint, is simple. It merely involves heating graphitized sections above the upper critical temperature for a sufficient time so that all of the graphite will go back into solution, with a time interval at this temperature sufficient to provide for the best possible dispersion of the resultant carbide. In this connection, a temperature of 1700 F continued over a period of 2 hr has been found adequate for graphitized-pipe weld sections.

No claim is advanced that the restoration of graphitized welds by solution treatment, which is the term commonly used to describe the heat-treatment, can be employed successfully in all cases. If the graphitization is too pronounced, some claim small disconnected sections or cavities might remain where the graphite had been, even though the conversion of graphite to carbon was complete. Also, there is a possibility that, due to location, not all types of graphitized welds might lend themselves to a solution treatment. A weld adjacent to a valve might be a case in point. However, as the technique of solution treatment advances, it is expected that less and less difficulty will be encountered in this respect.

With this background, serious consideration was given to restoration of the graphitized welds at the Richmond Station by solution treatment. This was because of the marked degree of graphitization found in a full-size pipe section that was broken at Ambridge, as well as the evidence of considerable graphitization obtained from boat samples and full-size pipe sections which had been removed from service for purposes of investigation.

Prior to the adoption of the solution treatment for the removal of graphite from many of the welded pipe sections, numerous solution treatments were run on small samples to show that the graphite could be put into solution. This was then followed by laboratory solution treatments on tensile specimens, accompanied, in some cases, by stress relief.

A summary of some of the most important of these tests is given in Table 4. It should be noted that the test sections removed early in 1948, for which figures are given in this table, were

TABLE 4 ROOM-TEMPERATURE TENSILE PROPERTIES FROM PREVIOUS TESTS ON 20-IN-DIAM WELDED CARBON-STEEL PIPE FROM RICHMOND STATION

Location of Test Section	Heat Treatment	Tensile Strength (psi)	0.2% Offset Yield Strength (psi)	Elongation in 2 In. (%)	Reduction of Area (%)	Location of Fracture	Year of Removal of Weld Section
(The Gage Section of the Samples Was 0.750-Inch Thick, 1.25-Inches wide and 3-Inches Long)							
Across weld	As removed from service	51,300	—	12.0	11.4	Graphite concentration	1945
Across weld	As removed from service	57,700	—	12.0	17.5	Graphite concentration	1945
Across weld	As removed from service	48,900	—	10.0	5.4	Graphite concentration	1945
Across weld	As removed from service	51,900	—	11.0	6.5	Graphite concentration	1945
Pipe metal	As removed from service	51,650	—	41.0	66.1	—	1945
Pipe metal	As removed from service	51,125	—	35.5	58.3	—	1945
Across weld	As removed from service	57,140	37,700	34.0	50.5	Pipe metal	1948
Across weld	As removed from service	60,000	37,900	29.4	47.1	Weld metal	1948
Across weld	As removed from service	58,200	35,400	14.0	16.6	Graphite concentration	1948
Across weld	As removed from service	60,600	36,000	17.0	16.0	Graphite concentration	1948
Across weld	1600°F, 2 hr, A.C.	66,600	44,000	23.5	32.8	Weld metal	1948
Across weld	1700°F, 2 hr, A.C.	65,760	41,600	19.0	28.8	Weld metal	1948
Across weld	1700°F, 2 hr, A.C.	64,630	40,800	13.0	22.0	Weld metal	1948
Across weld	1700°F, 2 hr, A.C. + 1 hr at 1200°F	62,700	39,400	31.0	39.2	Weld metal	1948
Across weld	1700°F, 2 hr, A.C. + 1 hr at 1200°F	55,200	39,300	29.0	47.5	Weld metal	1948
Across weld	1700°F, 2 hr, A.C. + 2 hr at 1275°F	58,500	36,000	33.5	56.8	Weld metal	1948
Across weld	1700°F, 2 hr, A.C. + 2 hr at 1275°F	58,100	34,800	33.0	54.6	Weld metal	1948

* Yield strengths were not obtained on these samples because at the time the tests were made interest centered only on tensile strength, elongation, and reduction of area.

NOTE: A.C. = air cooled.

from a weld which was graphitized to approximately the same degree as existed in the weld broken at Ambridge, which is illustrated in Figs. 2, 3, and 4. These results, together with the complete lack of evidence of graphite in the solution-treated samples, showed this treatment to be so promising that it was adopted as a method of restoring many of the graphitized sections in the carbon-steel pipe at the Richmond Station. The word "many" is used because a few of the graphitized welds, due to location, or some other cause, were removed and replaced by new welded sections.

It will be noted that greater ductility was found in the sample solution-treated at 1600 F than in the samples solution-treated at 1700 F. It was felt, however, that a solution treatment at 1700 F would be preferable to a solution treatment at 1600 F because of greater assurance of a more complete dispersion of the carbides. However, the greater ductility found with a 1600 F solution treatment led this author to suspect that a stress relief would improve the ductility of the metal which had undergone a 1700 F solution treatment. When tried, this proved to be the case and, because a stress relief of 1275 F gave superior ductility to the metal to a stress relief of 1200 F, the former was adopted. The procedure finally adopted, therefore, was to give the graphitized welds a solution treatment at 1700 F for 2 hr, followed by a stress relief of 1275 F for 1 hr per in. of metal thickness.

In the investigation weld-prober samples were taken from two graphitized weld sections and examined at the University to determine which one of the two sections contained the greater amount of graphite. These sections were designated as weld A and weld B. From the graphitization standpoint, little difference was found in the two sections and was less than had been found in other sections previously examined, although weld A appeared to have slightly more graphite than weld B. Weld A, therefore, was the section selected for a solution treatment, with a subsequent stress relief. Both sections were removed from the pipe line and, after weld A was given the solution treatment, followed by stress relief, at the Richmond Station, they were shipped to the University of Michigan for examination.

TEST MATERIAL

The pipe was purchased to ASTM Specification A-106-33T Grade B. The samples were 16 in. diam with wall thickness of 0.745 in. and were 18 in. long with the weld in the center.

The mill analysis was reported as follows:

	Per cent
Carbon.....	0.23
Manganese.....	0.93
Phosphorus.....	0.014
Sulphur.....	0.03
Silicon.....	Not given

The physical properties, as reported by the mill, are as follows:

Tensile strength, psi.....	70900
Elongation in 2 in., per cent.....	35

The average operating temperature of the pipe sections since July, 1943, was 850 F, although from 1935, to July, 1943, the operating temperature was 875 F, with momentary swings to as high as 900 F. The pipe sections had been in service 92,000 hr.

PROPERTIES OF WELD B PIPE

The room-temperature tensile properties of the welded carbon-steel pipe known as weld B are given in Table 5. It will be noted that, although the test specimens included the weld sections and the heat-affected zone sections wherein the most graphite would be found, the specimens all broke in the unaffected-pipe-metal sections. The values in the table, therefore, are more indicative of the values that would be found in the pipe metal than of the values that would be found in the metal in the weld or in the heat-affected zone. Attention is called to the fact that, although the pipe metal was reported as having a tensile strength of 70,900 psi, the tensile strength of the pipe metal after 92,000 hr of service averaged 56,375 psi.

PROPERTIES OF WELD A—SOLUTION-TREATED

By far the larger amount of this particular investigation re-

TABLE 5 ROOM-TEMPERATURE TENSILE PROPERTIES OF WELDED CARBON-STEEL PIPE FROM THE RICHMOND STATION AS REMOVED FROM SERVICE
(Intermediate field weld between pieces MS-12 and MS-43 in the 16-inch down-river superheater piping of No. 66 boiler. Weld probe samples 16R, 17R, 21R, and 22R had previously been removed from this weld.^a)

Sample	Location of Gage Section	Tensile Strength (psi)	0.2% Offset Yield Strength (psi)	Elongation in 2 In. (%)	Reduction of Area (%)	Location of Fracture
(The gage section of the samples was 0.50-inch thick, 1.25-inch wide, and 3-inches long.)						
H-1	Across weld	56,200	35,500	40.0	68.0	Unaffected pipe metal
H-1	Across weld	56,800	35,200	40.0	67.0	Unaffected pipe metal
H-1	Across weld	56,400	36,000	39.0	67.0	Unaffected pipe metal
H-2	Across weld	56,100	32,900	38.0	69.1	Unaffected pipe metal

^a The degree of graphitization was not severe as is shown in Report No. 39.
NOTE: The samples were taken from four quadrants of the pipe, 90 deg apart.

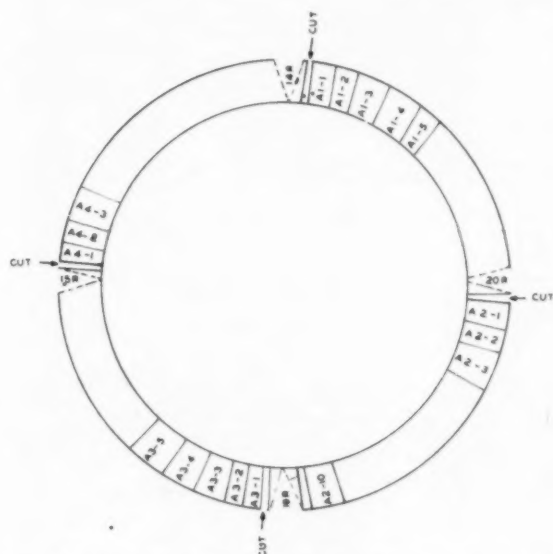


FIG. 8 SKETCH SHOWING LOCATION OF TEST SAMPLES IN PIPE CIRCUMFERENCE
(Weld-prober samples had been removed from locations labeled 14R, 15R, 19R, and 20R.)

lated to the studies which were made on the section of the welded carbon-steel pipe which was given a solution treatment, followed by a stress relief, at the Richmond Station of the Philadelphia Electric Company. Details with regard to the heat-treatment given this pipe section are covered in the portion of the paper by Mr. Abele.

Test Procedure. The test procedure which was followed in the examination of this pipe at the University was as follows:

- 1 The section of the pipe was cut into longitudinal strips to supply samples for macro- and microexaminations and for tensile tests, as indicated in Figs. 8, 9(a), and 9(b).
- 2 Strips from four quadrants were macroetched the full length of the pipe sample to check the structure at the weld and at the heat-affected zone resulting from the solution treatment.
- 3 Metallographic examinations were made to determine if the graphite at the heat-affected zone of the original weld had been dissolved and to show the microstructure resulting from heat-treatment.
- 4 Tensile tests were conducted at room temperature to establish the physical properties of the metal in the weld area and through the adjacent pipe metal following the solution treatment.

The locations of the tensile test sections are shown in Fig. 9(b). Attempts to force fracture at the outside of the original weld-heat-affected zone, where the concentrated graphite had dissolved, were not successful.

Wherever possible, rectangular test specimens with a gage section 0.50 in. \times 1.25 in. \times 3 in. were used. The pipe sample was so short that it was necessary to use 0.505-in.-diam test specimens when testing the material heated between the critical temperatures during the solution treatment.

GENERAL RESULTS OF STUDY

Physical Tests. The results of the tensile tests on the solution-treated pipe given in Table 6 indicate that the solution treatment and stress relief produced a material with satisfactory strength and ductility. The following additional comments are offered:

1 When the gage section of the test specimens was placed across the weld, the weld-deposited metal was the weakest, and fracture occurred at that point. The area where graphite had originally been concentrated, the coarse-grained area, had the higher strength.

2 When samples were machined (A2-10D and A3-3U) which covered the zone from the weld to a point where the temperature reached the upper critical temperature during solution treatment, the strength and ductility were both higher than that in the weld metal. It was not possible to force fracture at the region of graphite concentration before solution treatment in order to determine the ductility at that point.

3 The metal heated between the critical temperatures had strength about the same as the weld metal and somewhat lower elongation. This comparison is not to be interpreted too literally because, in order to test this section, it was necessary to use 0.505-in. test bars, whereas the other test bars were 0.50-in. \times 1.25 in. \times 3 in. The important point is that this portion of the solution-treated pipe had adequate strength and ductility.

4 Test data are not available for pipe metal heated at the lower critical temperature or the pipe metal not affected by the solution treatment, as the length of pipe supplied was cut just beyond the point where the temperature reached the lower critical.

As removed from service, there was very little difference in the amount of graphite in the two weld sections submitted for this investigation. Weld A had, at most, only slightly more graphite than weld B. Therefore the graphitization in weld A before solution treatment can be inferred to be about the same as that in weld B. The results of the tensile tests as given in Table 5 for weld B, therefore, can be assumed to be representative of what the tensile tests would show for weld A before solution treatment.

Although none of the samples broke in the heat-affected zone in any of the tests reported in Tables 5 and 6, it is evident

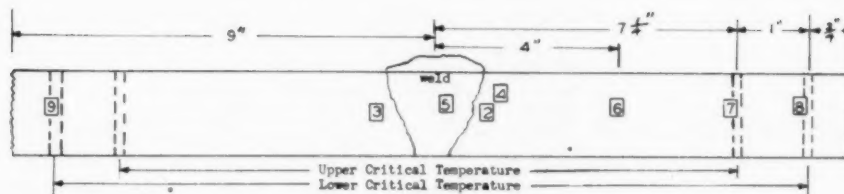


FIG. 9(a) LOCATION OF PHOTOMICROGRAPHS OF PIPE SECTION
(□ Refers to plate numbers)

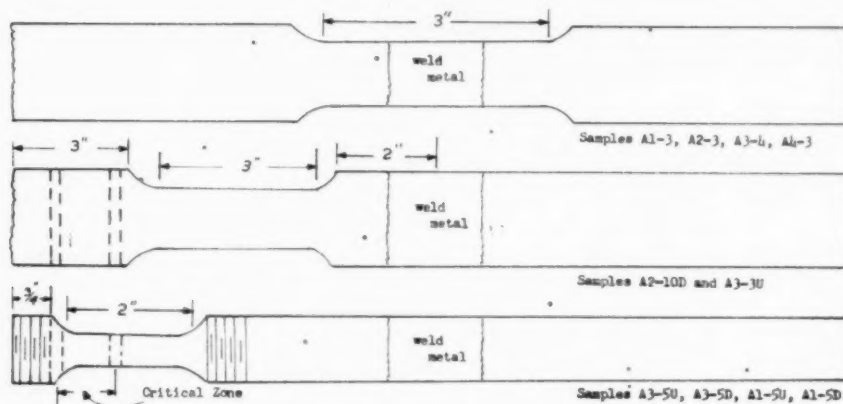


FIG. 9(b) LOCATION OF GAGE SECTION OF TENSILE SPECIMENS OF PIPE SECTION

TABLE 6 ROOM-TEMPERATURE TENSILE PROPERTIES OF WELDED CARBON-STEEL STEAM PIPE FROM THE RICHMOND STATION AFTER FIELD HEAT-TREATMENT TO DISSOLVE GRAPHITE
(Center of weld heated to 1700 F for 2 hr, slowly cooled, and stream-relieved at 1275 F. Fig. 2 shows location of test coupons with position of gage section shown in Fig. 3.)

Sample	Location of Gage Section	Tensile Strength (psi)	0.2% Offset Yield Strength (psi)	Elongation in 2 In. (%)	Reduction of Area (%)	Location of Fracture
(The gage section of the samples below was 0.50-inch thick, 1.25-inch wide, and 3-inches long.)						
A1-3	Across weld including original weld heat-affected zones	56,700	30,100	33.0	60.9	Weld metal
A2-3	Across weld including original weld heat-affected zones	54,700	32,100	31.0	56.5	Weld metal
A3-4	Across weld including original weld heat-affected zones	56,700	34,300	27.0*	36.1*	Weld metal
A4-3	Across weld including original weld heat-affected zones	55,900	31,300*	32.0	54.9	Weld metal
A2-10D	Downstream pipe metal heated above upper critical temperature	58,000	37,500	43.0	59.9	—
A3-3U	Upstream pipe metal heated above upper critical temperature	59,600	35,300	43.0	59.8	—
(The gage section of the samples below was 0.505-inch diameter and 2-inches long.)						
A3-5U	Upstream pipe metal across upper critical temperature zone	56,400	30,000	30.5	64.5	Pipe metal heated to temperature between upper and lower critical temperature during solution treatment.
A3-5D	Downstream pipe metal across upper critical temperature zone	56,900	30,500	28.0	64.0	
A1-5U	Upstream pipe metal across upper critical temperature zone	54,300	27,900	28.0	65.2	
A1-5D	Downstream pipe metal across upper critical temperature zone	56,800	30,500	29.5	64.0	

* Sample A3-4 fractured through a flaw in the weld metal.

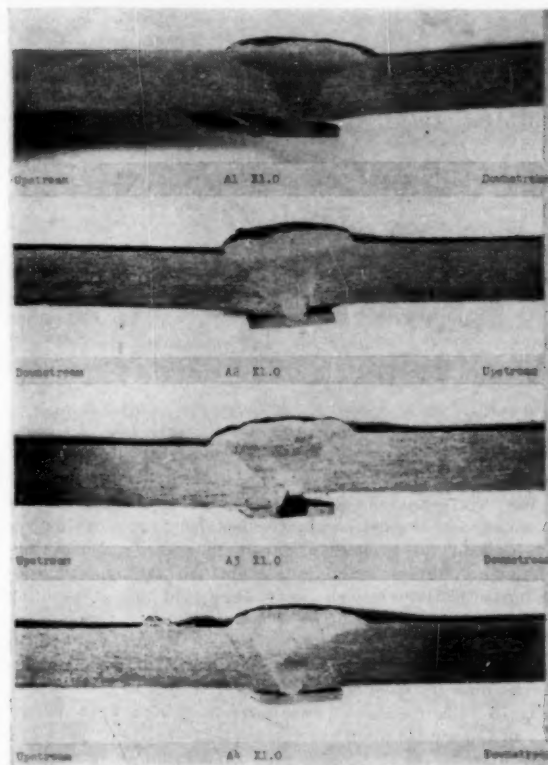
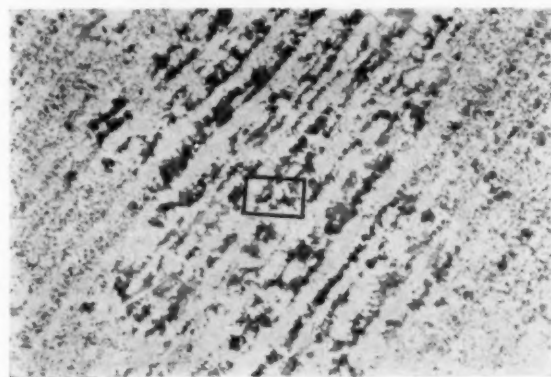
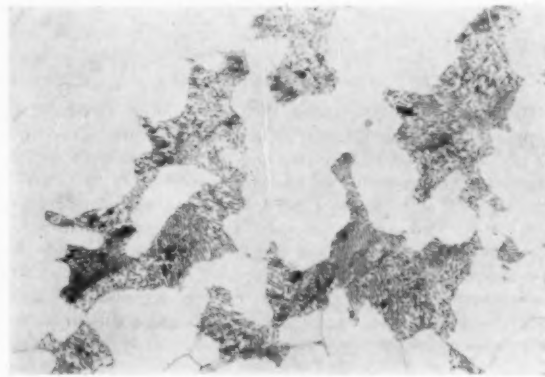


FIG. 10 PHOTOMACROGRAPH OF WELD SECTION OF MACROETCHED SAMPLES FROM FOUR QUADRANTS OF PIPE SECTION A



×100



×1000

FIG. 11 REPRESENTATIVE PHOTOMICROGRAPHS OF UPSTREAM AND DOWNSTREAM WELD-HEAT-AFFECTED ZONE OF ALL FOUR QUADRANTS OF SOLUTION-TREATED PIPE SECTION

that the solution treatment did not affect the properties of the metal adversely in the weld areas as a result of the conversion of the graphite in the heat-affected zone. This statement is made in spite of the rather large grains found in the heat-affected zones, which resulted from the very slow cooling of the metal during the solution treatment, as shown in Fig. 11.

It is believed that if a more rapid rate of cooling from the solution-treatment temperature had been adopted, a fine-grained

structure would have resulted as has been the case in all of the samples which were laboratory solution-treated.

Macrographic and Metallographic Studies. Macroetching of samples from quadrants of the pipe section known as weld A give the results shown in Fig. 10.

Metallographic examination of this same weld area gave the following results:

1 No graphite could be found at the location of the original heat-affected zone. Slow cooling during the solution treatment produced annealed types of structures.

2 A band of comparatively coarse grains was located parallel to the weld and at a location believed to be that of the outside edges of the heat-affected zones of the original weld where the more concentrated graphite had formed during service. Fig. 11 is representative of both the upstream and downstream weld-heat-affected zones of all four quadrants of the solution-treated pipe. Fig. 12 is fairly representative of all of these sections before solution treatment.

The band of comparatively coarse grains shown in Fig. 11 is believed to be due to the slow cooling to which this pipe was subjected following its heating to 1700 F. Had the rate of cooling been more rapid, equivalent to that used in normalizing, it is believed that a normal fine-grained structure would have resulted.

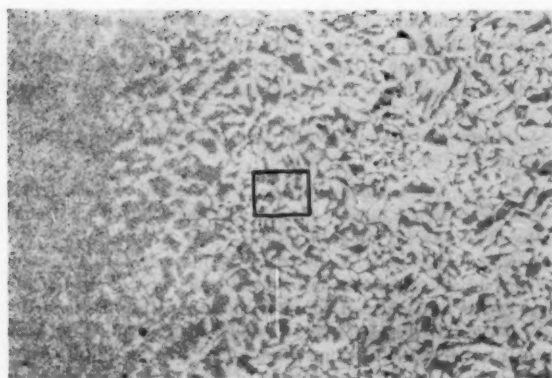
Naturally, during the solution treatment, a temperature gradient would exist from the center of the weld along the pipe in both directions. The zones in these different gradients were examined but nothing of moment was found, although mention is made of a graphitelike substance found about 1 in. from the heat-affected zone which showed slight discontinuities.

CONCLUSIONS

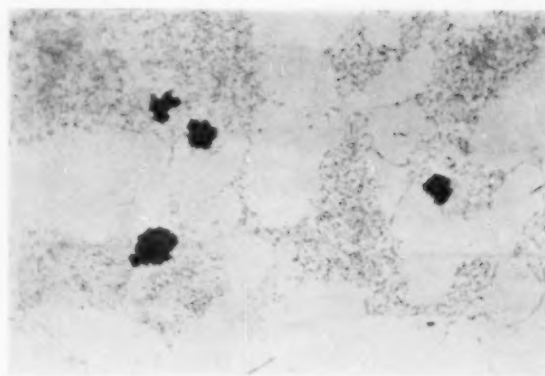
The field solution treatment resulted in the metal in the weld zone having the same strength and ductility at room temperatures as was found in the original pipe metal after it had been subjected to service for 92,000 hr. As was expected, the weld-

deposited metal was the weakest. The strength values were somewhat lower than those which previously have resulted from laboratory normalized samples because the heat cycle of the field solution treatment involved cooling rates slow enough to anneal the metal.

Graphitization during service had not been severe enough to affect the strength of the welded section given a solution treatment.



×100



×1000

FIG. 12 MICROSTRUCTURE OF UPSTREAM AND DOWNSTREAM HEAT-AFFECTED ZONE OF WELD-PROBER SAMPLE 15R
(Sample removed prior to field solution treatment. Sample fairly representative of all four quadrants.)

No evidence was observed to indicate that the solution treatment had increased the amount of graphite in the pipe metal.

Finally, although the physical properties of the solution-treated weld section were not materially different from those in the untreated weld section, because the amount of graphite in the untreated weld section was not sufficiently great to have any influence on the properties of the sections in question, yet, it is believed that the treatment was worth while in that it converted any possible concentrated graphite to a carbide, with a resultant good dispersion of the carbide, and thus would restore any badly graphitized sections to a serviceable condition.

In conclusion, it should be pointed out that this treatment is not one which will effect a cure, but one which will permit the continued use of the pipe for possibly as long as it had been used previously. As stated by Mr. Abele, however, in his portion of the paper, these solution-treated sections, as well as all welded sections, should undergo inspection at suitable intervals in the interest of safety.

ACKNOWLEDGMENTS

The authors wish to express their appreciation to Mr. E. L. Hopping, Consulting Engineer, Philadelphia Electric Company, for his counsel, encouragement, and continued support to this program. Also, grateful acknowledgment is made to the field organizations of both the United Engineers and Constructors Inc., and the Philadelphia Electric Company for the constructive work done in the development of field methods which made the heat-treatment procedure so successful. Acknowledgment is further made to Dr. J. W. Freeman, research engineer, Mr. J. J. Heller, and others of the Engineering Research Institute, for their co-operative services.

Discussion

F. EBERLE.⁴ This paper is of considerable practical importance in that it shows a possibly effective procedure of solution-heat-treating weld joints which are not too severely graphitized, thereby giving them, so to speak, a new lease on life. The authors used room-temperature tensile tests in conjunction with microscopic examination to evaluate the existing degree or extent of graphitization, low elongation and reduction of area plus failure in the zone of graphite concentration being the in-

⁴ Chief Metallurgist, Research and Development Department, The Babcock & Wilcox Company, Alliance, Ohio.

indicator of a potentially hazardous condition. This method of examination undoubtedly will reveal whether there is any danger to be expected due to shock, as illustrated by the original Springdale failure; but one may question whether it will also indicate the further behavior of such a graphitized weld joint at operating temperature when it is not exposed to shock. Therefore, it may be of interest to present here the result of a creep test which was made with a specimen containing a graphitized carbon-molybdenum pipe weld in the center of the gage length.

Fig. 13 of this discussion shows the condition in the weld-affected zone of the sample prior to creep testing. This pipe joint had been in service for 5½ years at a temperature of 930–950 F. Graphitization, though discontinuous, was considered at that

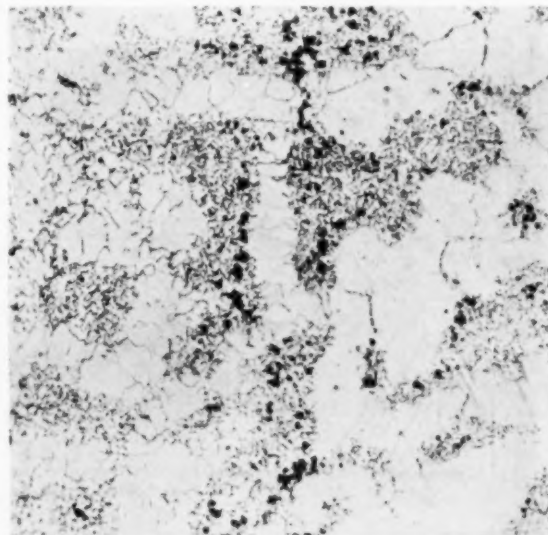


FIG. 13 WELD-HEAT-AFFECTED ZONE OF CREEP-TEST SPECIMEN
PRIOR TO CREEP TESTING
(Nital etch; ×100)

time severe enough to remove this joint from service. The specimen prepared from it was tested at 1000 F under a load of 5000 psi, which is the maximum allowable working stress given by the

Boiler Code. We kept this specimen under test for 40,200 hr, during which it displayed the following rates of creep, expressed in per cent per 100,000 hr:

	Per Cent
0 to 15000 hr.....	0.7
15000 to 31000 hr.....	0.8
31000 to 40200 hr.....	0.5

Fig. 14 shows the condition of the weld-affected zone after termination of the test. It will be observed that the manner and extent of graphitization is now in every respect as severe as it was in the original failed Springdale pipe. The graphite is seen to be almost totally concentrated in the grain boundaries, forming

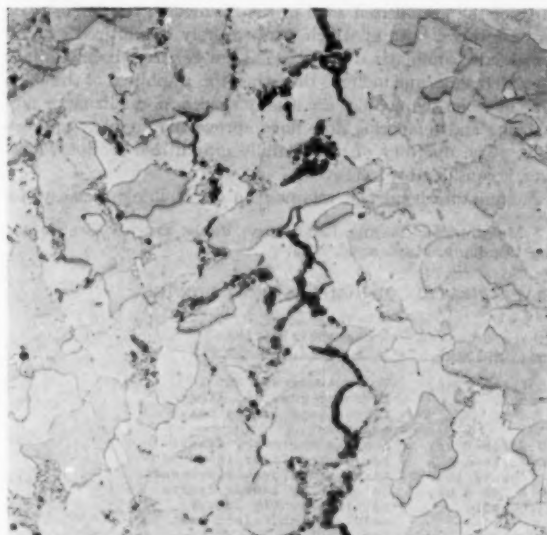


FIG. 14 WELD-HEAT-AFFECTED ZONE OF CREEP-TEST SPECIMEN AFTER 40,200 HR AT 1000 F UNDER 5000 PSI (Nital etch; $\times 100$.)

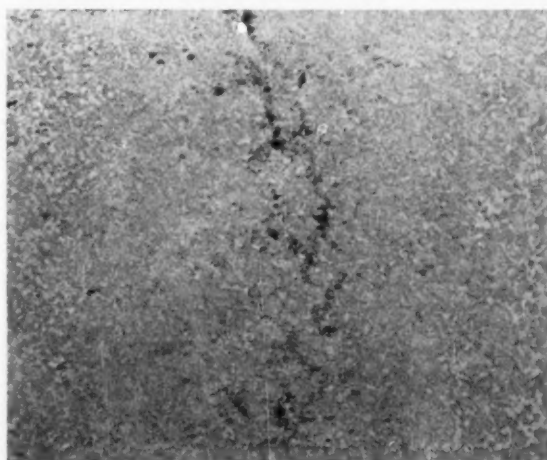
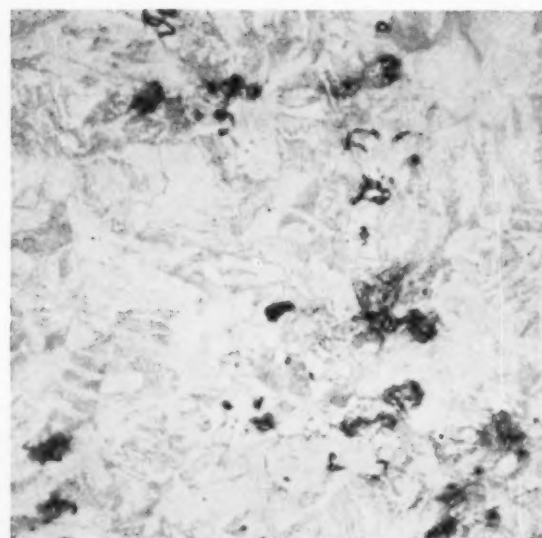


FIG. 15 WELD-HEAT-AFFECTED ZONE OF CREEP-TEST SPECIMEN AFTER 2-HR SOLUTION TREATMENT AT 1700 F, FOLLOWING TERMINATION OF CREEP TEST (Light nital etch; $\times 100$.)



(a)



(b)

FIG. 16 UNDISSOLVED GRAPHITE AND MICROFISSURES IN WELD-AFFECTED ZONE OF SOLUTION-TREATED CREEP-TEST SPECIMEN (a, Unetched section; $\times 500$. b, Lightly etched section; nital etch, $\times 500$.)

a continuous chain through the entire cross section of the specimen. One cannot help wondering why the latter did not rupture. It certainly would appear from this example that there is little likelihood of immediate danger at operating temperatures for weld joints in which graphite is present in a discontinuous manner, provided of course that they are not exposed to shock.

It may be necessary sometimes to make a decision as to whether a weld joint may be permitted to continue in service for a certain length of time before remedial measures are taken. To our knowledge, there are no means or methods of predicting safely if and within what length of time a discontinuously graphitized weld-affected metal will develop dangerous graphite concentration

or continuous grain-boundary chain graphite. The authors of the paper have observed that graphitization in some field welds was found to have increased very little, if at all, when checked again after 25,000 hr.

Our own graphitization studies have led us to believe that stress is one of the most important factors in promoting graphitization, and the outstanding factor in causing the formation of grain-boundary chain graphite. We are of the opinion that the graphitized weld from which the previously discussed creep-test specimen was prepared would not have deteriorated to the same extent as the latter if it had been exposed to the same temperature and for the same length of time in the unstressed condition. Elimination of stress concentrations in the weld-heat-affected metal, therefore, appears to be of paramount importance if the formation of dangerous graphite concentration or of grain-boundary chain graphite is to be avoided. A normalizing treatment followed by thorough stress-relieving would appear to be a step in this direction.

It seems to us that the effectiveness of restoring graphitized weld joints by this method will depend not only upon the complete solution of the existing graphite but also upon the effective dispersion of the locally dissolved carbon by diffusion.

Figs. 15 and 16 show the weld-heat-affected zone of the previously described creep-test specimen after a 2-hr solution heat-treatment at 1700 F, following termination of the creep test.

It will be noted that some graphite remained undissolved throughout the entire cross section and, more important yet, that microfissures formed at locations where massive graphite went into solution. These microfissures were identified as such by the seepage of drying alcohol, and the resulting staining during microscopic examination. We are presenting this extreme case as a matter of general interest only.

H. J. ROBAR.⁵ Early in the investigation of graphitization of welded pipe sections we, among many others, considered solution of the graphite by heat-treatment as a means of restoring ductility to severely graphitized zones in the C-Mn pipe and castings. In 1944 H. Weisberg reported that normalizing at temperatures up to 2200 F did not materially improve the ductility of the graphitized zone in the Springdale pipe or in a 12-in. cast valve, both of which were severely graphitized. Additional data, summarized in Table 7 (page 49), have been obtained since that time, and indicate that when the graphite is of the chain type or when the nodules are closely spaced, normalizing or normalizing and tempering does not improve the ductility appreciably. The ductility of more mildly graphitized sections, however, is considerably improved.

A miniature bend test was used in determining ductility, for

⁵ Metallurgist, Testing Laboratory, Public Service Electric and Gas Company, Maplewood, N. J.

TABLE 8 SOLUTION HEAT-TREATMENT AND REGRAPHITIZATION OF SAMPLES FROM SERVICE

Spec. No.	C-Mn Material	Service Hr	Degree of Graphitization in Service	Graphite Solution Heat Treatment	Degree of Regraphitization in 6000 hr at 1000 F
28DN	Pipe	24636	Medium	1700 F for 2 hr, air cool.	To same degree, but in narrower zone and larger flakes than before heat treatment.
28DA	"	"	"	1700 F for 2 hr, furnace cool	Zone is narrower, flakes larger and fewer in number than before heat treatment.
47UN	"	45972	Mild	300 F/hr to 1000 F, 1700 F for 2 hr, air cooled.	To slightly lesser degree but in slightly larger nodules than before heat treatment.
48DA	"	"	"	1700 F for 2 hr, furnace cool at 300 F/hr to 1000 F.	To slightly greater degree than before heat treatment.
50.1DN	Casting	29000	Heavy	1700 F for 2 hr, air cooled.	To same degree as before heat treatment.
50.1DA	"	"	"	1700 F for 2 hr, furnace cool at 300 F/hr to 1000 F.	To same degree, but in slightly larger nodules than before heat treatment.

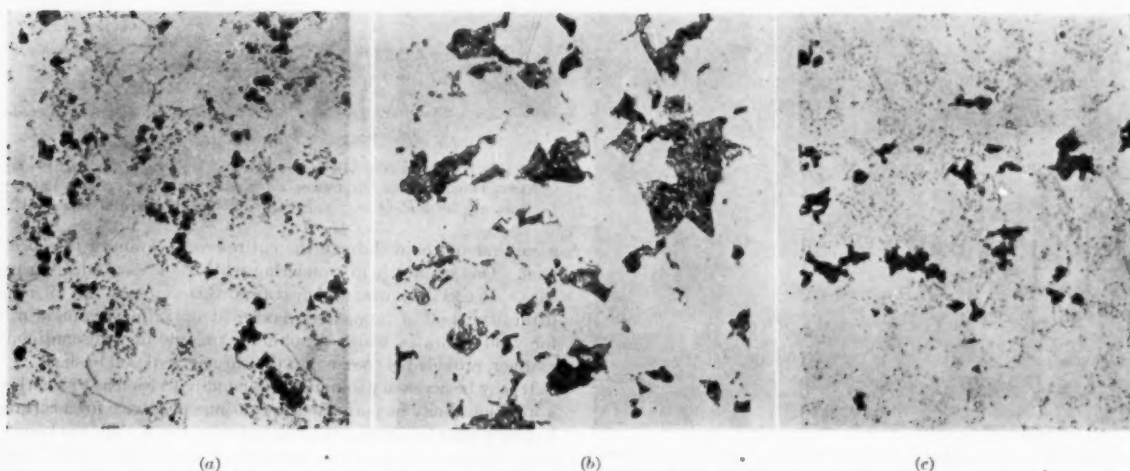


FIG. 17 REGRAPHITIZATION OF CARBON-MOLY STEEL, $\times 500$

(a, Graphite formed in service; b, same as a after normalizing at 1700 F for 2 hr; c, regraphitization of b after 6000 hr at 1000 F.)

TABLE 7 EFFECT OF SOLUTION HEAT-TREATMENT ON DUCTILITY OF GRAPHITIZED WELDED JOINTS

Spec. No.	C-Mn Material	Degree and Type of Graphitization	Graphite Solution Heat Treatment	Bend Test Results
4-C AR	Pipe (Springdale)	Heavy chain	None	Cracking started at 1% elongation.
4-C NA	"	" "	1700 F for 2 hr in N ₂ , furnace cooled 300 F/hr in N ₂ to 1000 F.	Cracking started at 1% elongation.
4-C X9	"	" "	2200 F for 5 min., air cooled.	Cracking started at no measurable elongation.
4-C X 10	"	" "	2200 F, compressed 4%, held 5 min. at 2200 F, air cooled.	1/2" long crack at 6% elongation.
50.3D	Valve casting	Heavy; closely spaced large nodules.	None.	Cracking started at 7.7% elongation, at 11.5% elongation crack was 0.3" long.
50.3DNA	" "	Same as 50.3D.	1700F for 2 hr in N ₂ , furnace cooled 300 F/hr in N ₂ to 1000 F.	Cracking started at 16% elongation, at 20% elongation crack was 0.3" long.
50.1D	" "	" " "	None	Cracking started at 1.98% elongation.
50.1DN	" "	" " "	1700 F for 2 hr, air cooled.	0.18" long crack at 6% elongation.
50.2D	" "	" " "	None	Cracking started at 3.8% elongation, at 5.7% elongation crack was 0.25" long.
50.2DA	" "	" " "	1700 F for 2 hr, furnace cooled 300 F/hr to 1000 F.	0.06" long crack at 14.3% elongation.
99.2U	Pipe (Essex)	Medium; scattered medium size nodules.	None	Three small fissures at 20% elongation.
99.2UN	"	Same as 99.2U	1700 F for 2 hr, air cooled.	No cracking at 24% elongation.
99.2D	"	Medium; medium size nodules, scattered and in short chains.	None	0.3" long crack at 8% elongation, at 16% elongation crack was 0.6" long.
99.2DN	"	Same as 99.2D.	1700 F for 2 hr, air cooled.	No cracking at 30% elongation.
102.2U	"	Heavy; medium size nodules, scattered and in short chains.	None	0.58" long crack at 4% elongation.
102.2UN	"	Same as 102.2U	1700 F for 2 hr, air cooled.	0.1" long crack at 11.5% elongation, 0.5" long crack at 17.3% elongation.
102.2D	"	Medium; scattered medium size nodules.	None	0.05" long crack at 21.6% elongation, no change at 32.3% elongation.
102.2DN	"	Same as 102.2D	1700 F for 2 hr, air cooled.	No cracking at 32% elongation.
106.2U	"	Medium; scattered medium size nodules	None	Slight fissures at 6% elongation, no change at 31% elongation.
106.2UN	"	Same as 106.2U	1700 F for 2 hr, air cooled.	No cracking at 32% elongation.
106.2D	"	Medium to heavy; scattered medium size nodules.	None	0.2" long crack at 8% elongation, 0.34" long crack at 16% elongation.
106.2DN	"	Same as 106.2D	1700 F for 2 hr, air cooled.	No cracking at 30% elongation.
138.2U	"	Medium; scattered medium size nodules in narrow zone.	None	At 7% elongation specimen was cracked completely across its width.
138.2UN	"	Same as 138.2U	1700 F for 2 hr, air cooled.	Cracking started at 11% elongation, at 22% elongation crack was 0.3" long.
138.2UNT	"	Same as 138.2U	1700 F for 2 hr, air cooled, 1275 F for 2 hr, air cooled.	Cracking started at 6% elongation, at 20% elongation crack was 0.08" long, no further cracking.
138.2D	"	Heavy; medium size nodules as short chains and aggregates.	None	0.3" long crack at 6% elongation.
138.2DN	"	Same as 138.2D.	1700 F for 2 hr, air cooled.	Cracking started at 11.8% elongation, at 15.4% elongation crack was 0.38" long.
138.2DNT	"	Same as 138.2D.	1700 F for 2 hr, air cooled, 1275 F for 2 hr, air cooled.	Cracking started at 10% elongation, further bending increased extent of cracking.

the only available material was small boat-shaped probes cut out of pipe joints. The test specimens, $\frac{1}{8}$ -in.-thick center sections of the probes, were bent in a guided-bend test jig along the zone of graphitization. Fiber elongation was measured on a $\frac{1}{2}$ -in. gage length.

Heat-treatment does not restore ductility to all graphitized zones, because a residue of unknown composition remains after the solution of the graphite. When the graphite is of the chain type, the residue exists as an irregular fine line; if the graphite is nodular, the residue is nodular, annular, and/or crescent-shaped. It is because of this similarity in form between the residue and the graphite that the ductility of severely graphitized sections is not restored by solution heat-treatment.

Concomitant with the foregoing study, the possibility of re-graphitization after solution heat-treatment was investigated. Specimens of varying degrees of graphitization were solution-heat-treated, as shown in Table 8 (page 48) of this discussion, and then maintained in an oven at a temperature of 1000 F for 6000 hr. Subsequent metallographic examination disclosed that all specimens had graphitized again and to approximately the same degree that existed before solution treatment. Fig. 17 herewith illustrates the degree of graphitization before heat-treatment, after solution treatment and degree of re-graphitization in the 6000-hr period:

Based upon these results, we have not resorted to solution heat-treatment as a means of rehabilitating graphitized welded sections. Our practice has been to cut out and reweld those joints that are severely graphitized and of poor ductility. All welded sections in old specification pipe and all castings are of course probed at suitable intervals.

I. A. ROHRIG.⁶ The authors are to be commended for the information they have contributed on the subject of heat-treatment of welded joints in high-temperature main steam piping. Their method of accomplishing the heat-treatment has been outlined clearly, and their test data show that graphitized welded joints can be reconditioned suitably for further service, provided the graphitization has not become critical.

Work of the same nature has been done by the writer's company, and the results are in general agreement with those presented by the authors. An account of this study has been given by D. H. Corey and the writer.⁷ By the use of this method normalizing of graphitized welded pipe joints while in position has been carried out by the writer's company since early in 1947.

The tensile-test data given in the paper show that the ductility of the graphitized welded joints used for test was improved markedly by heat-treatment. The data, however, apparently do not reveal the ductility of that part of the sample which is of greatest importance, namely, the graphitized zone. The paper states, "Attempts to force fracture at the outside of the original weld-heat-affected zone where the concentrated graphite had dissolved were not successful." What is required, therefore, is a test that can be applied to the graphitized zone.

The bend test mentioned by Mr. Weisberg in his discussion of an earlier paper⁸ meets this requirement reasonably well. That test indicates in a quick and simple manner the relative bend ductility of the graphitized zone. It has been used in the Research Department of The Detroit Edison Company with satis-

factory results in evaluating the condition of graphitized welded joints. The apparatus used in the Research Department in performing the bend test consists of two dies, similar to those

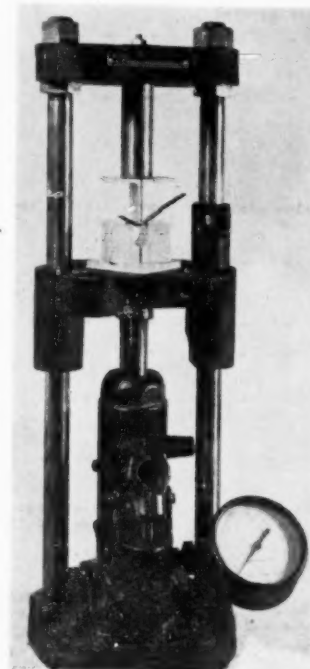


FIG. 18 BEND-TEST DIES IN USE IN METALLOGRAPHIC SPECIMEN-MOUNT PRESS

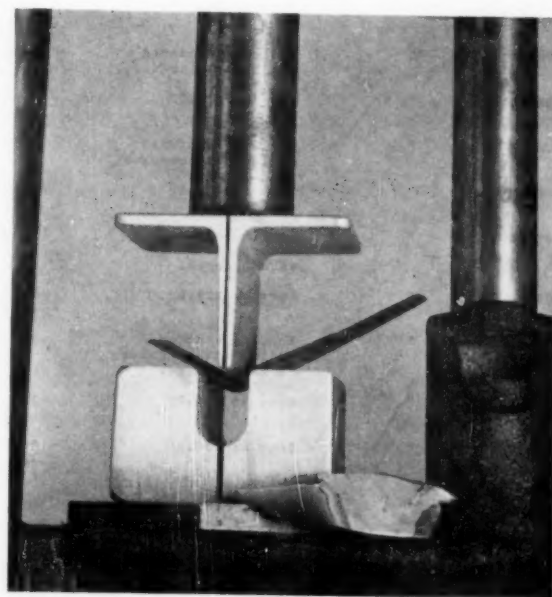


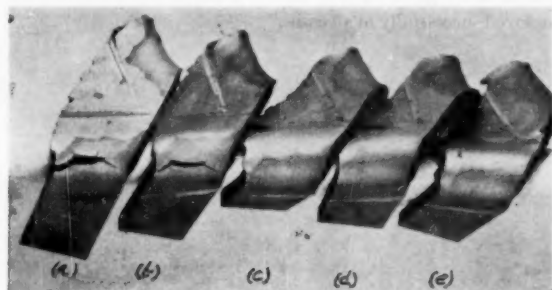
FIG. 19 CLOSE-UP VIEW OF BEND TEST DIES IN USE IN METALLOGRAPHIC SPECIMEN-MOUNT PRESS AND OF GRAPHITIZED WELD SAMPLE AFTER BENDING

⁶ Research Dept., The Detroit Edison Company, Detroit, Mich.

⁷ "Normalizing of Welds in Carbon-Molybdenum Steel Pipe by 60-Cycle Induction Heating," by D. H. Corey and I. A. Rohrig, Welding Research Supplement of *The Welding Journal*, vol. 24, January, 1945, pp. 1-6-8.

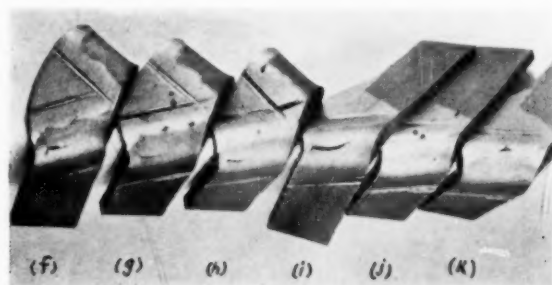
⁸ See pamphlet, "Graphitization of Low-Carbon and Low-Carbon-Molybdenum Steels," by H. J. Kerr and F. Eberly, bound with *Trans. ASME*, vol. 67, 1945, pp. 1-45; discussion by H. Weisberg, pp. 35-39.

used by Mr. Weisberg, and mounted in a metallographic specimen-mount press, as shown in Fig. 18 of this discussion. A close-up view is shown in Fig. 19. Pressure is applied by a hydraulic jack, manually operated. A specimen after bending is



Specimen (a) As removed from service after 64,000 hr at 825 F
(b) Heated at 1700 F for 2 hr, cooled in still air
(c) Heated at 1700 F for 2 hr, furnace-cooled to 800 F, then cooled in still air to room temperature
(d) Same as (c), followed by a draw at 1200 F for 1 hr
(e) Same as (c) followed by a draw at 1275 F for 1 hr

FIG. 20 BEND-TEST SPECIMENS FROM A WELDED JOINT IN MEDIUM-CARBON-STEEL PIPE



Specimen (f) As removed from service after 59,000 hr at 825 F
(g) Heated at 1700 F for 2 hr, cooled in still air
(h) Heated at 1700 F for 2 hr, furnace-cooled to 800 F, then cooled in still air to room temperature
(i) Same as (h), followed by a draw at 1100 F for 1 hr
(j) Same as (h), followed by a draw at 1200 F for 1 hr
(k) Same as (h), followed by a draw at 1275 F for 1 hr

FIG. 21 BEND-TEST SPECIMENS FROM WELDED JOINT IN MEDIUM-CARBON-STEEL PIPE

shown adjacent to the lower die in Fig. 19. Note that the specimen which was cut from a weld-prober sample removed from a graphitized welded joint has cracked badly in the graphitized zone.

The specimens shown are $\frac{1}{8}$ in. thick and are finish-ground on both faces. Slight etching before test readily reveals the outline of the weld and facilitates positioning of the specimens in the dies so that the bending can be made to occur in the graphitized zone. The results obtained by means of the bend test may be stated in terms such as, length and width of cracks after bending, angle of bend, elongation of the bent area, or gage pressure. Some of the results obtained from this test may be of interest. Bend-test specimens of medium-carbon steel representing various conditions of heat-treatment are shown in Fig. 20.

Severe cracking occurred in the graphitized zone of specimen (a) and in the formerly graphitized zone of specimen (b), when bent. Specimen (c) which had been furnace-cooled, exhibited

satisfactory ductility as did specimens (d) and (e), which had been drawn at 1200 F and 1275 F, respectively.

The bend-test specimens shown in Fig. 21 also were taken from a medium-carbon-steel welded joint removed from service.

Although specimen (h), which had been furnace-cooled after 2 hr at 1700 F, had much better bend ductility than specimens (f) and (g), it exhibited a crack in the formerly graphitized zone. Specimen (i), which had been drawn at 1100 F, cracked badly in the affected zone. This fact indicates that a draw treatment at 1100 F may cause brittleness in the formerly graphitized zone. Samples (j) and (k), which had been drawn at 1200 F and 1275 F, respectively, did not crack even when bent 110 deg. The single heat-treatment, consisting in heating at 1700 F for 2 hr, followed by slow cooling, produced good improvement in ductility as determined by the bend test. Further improvement in ductility of joints so treated could be expected as a result of the annealing effect of service at 800 to 900 F.

The results of the bend test, which was made on the samples described herein, are in agreement with the tensile-test results given in the paper, in that the best ductility was obtained by employing a draw treatment at 1275 F, following the 1700 F solution treatment.

The primary purpose of this discussion, however, is to point out that the bend test has the advantage in that the testing force can be applied to the significant area, i.e., the graphitized zone.

AUTHORS' CLOSURE

The authors are grateful to Messrs. Eberle, Robar, and Rohrig for the contributions made to their paper through their discussions.

They are in agreement with the thought expressed by Mr. Eberle, that stress concentration in weld-heat-affected zones appears to be of paramount importance in the formation of dangerous graphite concentrations or of grain-boundary chain graphite. They have never found in their examinations of graphitized metal, after a solution treatment, as large an amount of what we may speak of as "constituent X"—that is, voids, graphite, inclusions, or occlusions, as shown in Fig. 15. As a matter of fact, they have not found any evidence of constituent X in any of the heat-affected zones following solution treatment in the plain carbon steel reported in this paper. They have found constituent X in the carbon-moly steel, in the heat from which the 12-inch pipe was made in the main steam line in the Schuylkill Station, though it was smaller in amount and in particle size than that shown in the photomicrographs in Fig. 16 of Mr. Eberle's discussion. The evidence of constituent X at the time the paper was given was not pronounced. Also, the constituent X was not of a chain-like type.⁹

The authors are grateful for the valuable contribution of Mr. Robar. They recognize that solution treatments would not materially improve the ductility of graphitized zones in pipe as severely graphitized as was the case with the Springdale pipe. Also, they have found that the graphite has a tendency to return to the locations in which it was found after several thousand hours of heating. They have never held that solution treating was a cure, but a method which might be employed for prolonging the useful life of graphitized pipe, provided the graphitization has not developed to too great a degree.

The authors also appreciate the contribution of Mr. Rohrig which so completely described the bend test procedure used by The Detroit Edison Company.

⁹ A recent further examination of carbon-moly welded pipe which had been solution treated, that was made nine months after this paper was presented, shows in one of the quadrants of a heat-affected zone a constituent X somewhat similar to that shown in Fig. 16 of Mr. Eberle's discussion.

The authors' feeling with regard to the solution treatment is summed up by Mr. Abele in his statement to the effect that "The treatment has removed a latent critical condition, either temporarily or permanently, and substantially prolonged the useful life of the pipe." This statement, of course, relates to the pipe that had undergone graphitization at the Richmond Station. It

does not necessarily hold, however, for all graphitized plain carbon pipe.

Also, the feeling of the authors is covered in the statement by A. E. White to the effect that "No claim is advanced that the restoration of graphitized welds by solution treatment can be employed successfully in all cases."

Development of the Hydraulic Design for the Grand Coulee Pumps

By CARL BLOM,¹ LOS ANGELES, CALIF.

The Grand Coulee pumping plant has been the subject of an extensive hydraulic research program. The first part of this program was conducted at The California Institute of Technology for the Bureau of Reclamation from January, 1938, to July, 1940. Some of the results of this program have already been published (1 to 4),² and other papers (5, 6) describe the different features of this project. This paper presents some of the results of continued experimental research of the author's company from 1943 to 1946. The investigation covered the effects of various diffuser-type pump cases and impellers on the pump characteristics of the Grand Coulee model. The paper concludes with the description of the final test of the contractor's model completed in July, 1947.

PRELIMINARY INVESTIGATIONS AND OPERATING REQUIREMENTS

IN a paper by E. B. Moses (5) is described the development of the Grand Coulee Project in detail. A brief summary of the pumping plant will be reviewed here for ready reference. The pumping plant is situated at the Grand Coulee Dam on the Columbia River in the State of Washington. This huge pumping plant will consist of twelve vertical single-stage pumping units. Each unit will be driven by a 65,000-hp motor, or a total of 780,000 hp for the complete pumping plant. The pumps will have a wide operating head range, from 365 to 270 ft, with a corresponding capacity of 1100 cfs to 1650 cfs, when operating at the constant speed of 200 rpm. The pumps will be of the vertical single-stage single-suction type, with 12-ft-diam discharge, and a 14-ft-diam suction.

The Grand Coulee Project makes one feel the daring of its conception, the overwhelming grandeur of its size and power, and last but not least the painstaking care given to the investigation of all its details. In order to obtain strict and exacting final specifications, a research program lasting 2½ years was conducted at the Hydraulic Machinery Laboratory of the California Institute of Technology (later called Cal Tech), sponsored by the Bureau of Reclamation (later called The Bureau), and carried through with the co-operation of three pump manufacturers.

The foregoing program was considered necessary even though the investigations and test results of the large pumping units (7, 8) for the Metropolitan Water District of Southern California were available. No part of the research program mentioned would have been effective in detail without the development of Cal Tech Hydraulic Machinery Laboratory (9), with its precision instruments and exact measurements to aid in securing the effect of small design changes.

The final specifications called for a minimum flow rate of 1350 cfs at a rated total dynamic head of 310 ft, and a minimum war-

ranted pump efficiency of 87 per cent at this point. Furthermore the specifications require a minimum flow rate of 800 cfs at a total dynamic head of 365 ft, and a maximum load not to exceed 65,000 hp at 270 ft total dynamic head. The great variations of head and flow rate had to be obtained at a constant speed of 200 rpm. The specifications also prescribe that the head-capacity curve shall be relatively steep, and the pump efficiency as high as possible over the entire range of operation. The pump shall have stable operation free from cavitation within the full range of operating heads.

PUMPING-PLANT LAYOUT AND HEAD VARIATION

Each pumping unit will pump through separate piping systems (see Fig. 1). Each system consists of the trash rack, intake structure, a 90-ft-long 14-ft-diam suction pipe and elbow, and an 850-ft-long 12-ft-diam discharge pipe. The water surface at the intake to the pumping plant will fluctuate from a maximum elevation of 1290 to a minimum of 1208, that is, a total difference of 82 ft. At the same time the water surface at the outlet will vary between the elevations of 1571 and 1557, a difference of 14 ft.

The foregoing head variations, and the pipe-friction loss, also shown in Fig. 1, and the static water-surface elevation from the intake to the outlet lead to a variation of total dynamic heads from a minimum of 270 ft to a maximum of 365 ft, or an operating range from 100 to 135 per cent. The most severe suction conditions occur at low capacities when the water surface at the intake is at an elevation of 1208. The center line of the pump is located at an elevation of 1203, which provides only a 5-ft submersion for pumping heads from 365 ft down to 350 ft.

NEED FOR FURTHER INVESTIGATIONS

Difficulties were encountered when the former test results were applied to our investigation of a pumping unit of minimum weight and cost. Early weight calculations eliminated the most attractive case type, that is, the double-volute case. This type satisfied all the requirements of the specifications. However, the weight became excessive because of the heavy reinforcing needed to maintain permissible stresses in the open section. Unlike this, the diffuser-type case, in which the diffuser vanes act as connecting members between the two side walls, leads to a lighter pump case and thereby to the most economical unit.

In the original model study, pumps with diffuser cases gave a very unstable performance near the 365-ft operating head. The problem therefore was to design a diffuser-type case which would meet all the hydraulic requirements and particularly have stability of performance near the high operating head. This unstable portion of the pump characteristics was greatly affected by the pump-case design and had not been overcome satisfactorily by the preliminary experiments with diffuser-type cases.

Further investigation was also necessary owing to the wider operating head range given in the final specifications. The original model study conducted at Cal Tech from 1938 to 1940, was based upon a total head variation from 295 to 365 ft, or a total operating range from 100 to 125 per cent, while the final specifications call for an operating range of from 100 to 135 per cent.

¹ Chief Engineer of Byron Jackson Co. Mem. ASME.

² Numbers in parentheses refer to the Bibliography at the end of the paper.

Contributed by the Hydraulic Division and presented at the Semi-Annual Meeting, San Francisco, Calif., June 27-30, 1949, of THE AMERICAN SOCIETY OF MECHANICAL ENGINEERS.

NOTE: Statements and opinions advanced in papers are to be understood as individual expressions of their authors and not those of the Society. Paper No. 49-SA-8.

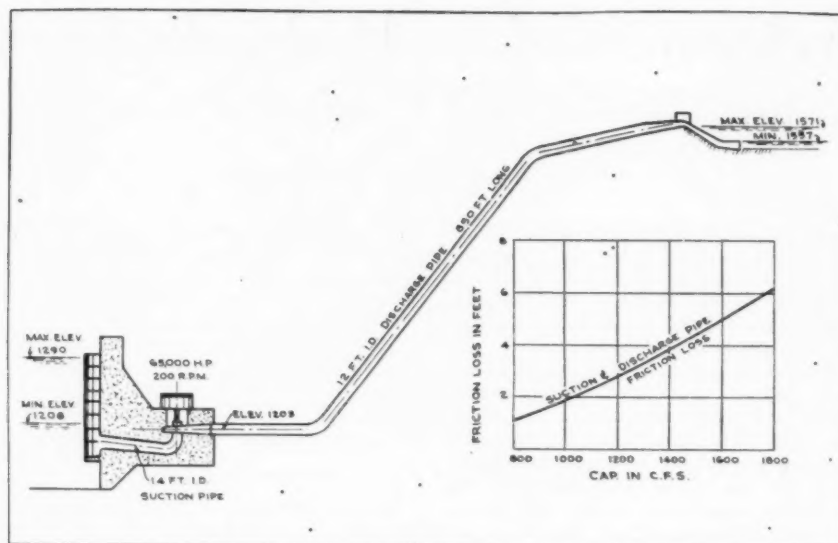


FIG. 1 SECTIONAL ELEVATION OF GRAND COULEE PUMPING PLANT

As these and other problems became more evident soon after Byron Jackson Co. and The Pelton Water Wheel Company decided to make a joint bid, they initiated in 1943, a program of development. This program assigned to Byron Jackson Co. the task to design, build, and test models in order to develop the final hydraulic lines of the pump. The investigation was conducted at Byron Jackson Co.'s plant from 1943 to 1946, and carried to a successful completion in spite of war and postwar difficulties.

At the end of the investigation a bid was submitted and resulted in the award of a contract to build six pumping units. After the award the research program was continued at Byron Jackson Company's plant and, at the same time, it was decided to conduct the final acceptance test at Cal Tech. It was deemed advisable to take advantage of the precision test facilities at Cal Tech because of the magnitude of the project and the desirability of having impartial observers. Also, the big prototype-to-model ratio of 13 to 1 made it imperative that tests should be conducted with the greatest possible accuracy.

PRESENTATION OF TEST DATA

Before going into the details and comparisons of test results at the different stages of development, the following differences of presentation are noted. The preliminary tests at Cal Tech and some of the tests by the author's company were made with model units of greater size than the final ones used for acceptance tests. The reason for this was that the horsepower available at Cal Tech was not sufficient to run the original model at speeds corresponding to the operating heads in the field. The specifications called for tests at field heads. Furthermore, in the final model the casing was built with sectional breaks in curvature, corresponding to the welded structure of the prototype case. This was a deviation from the earlier models which were all furnished with smooth pump cases and were of a larger size. Unfortunately, time did not permit us to duplicate the final model with a smooth casing so that the friction losses in the two cases might have been compared.

In the original testing program from 1938 to 1940, the suction-head reading was taken at the suction flange, and the discharge head reading 10 diam beyond the end of the discharge

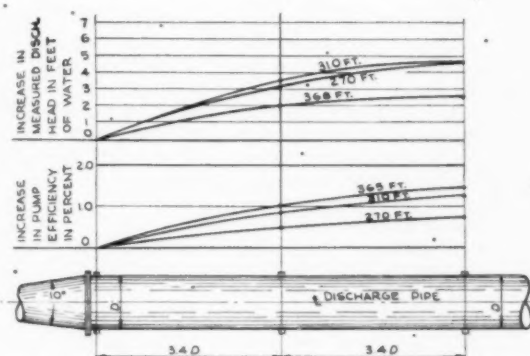


FIG. 2 HEAD-RECOVERY AND DISCHARGE PIPE BEYOND CONE

cone of the volute, giving afterward a credit for the friction loss in the 10-diam-long pipe. In the final specifications, however, the suction-pressure readings were to be taken at the extreme end of the suction elbow, thus charging the pump with the loss through the elbow.

Another change in the specifications calls for measurements of the discharge head at the end of the diffuser-case cone where the velocity distribution is far from uniform, while the velocity head is figured from a uniform velocity arrived at by dividing the capacity with the area. That there is an apparent gain in discharge head further downstream figured on this basis is shown in Fig. 2.

To determine the amount of this gain in discharge head, a set of readings was taken on a model with a 10-deg-discharge cone at the end of the cone, and 3.4 and 6.8 diam beyond the cone. These readings showed a substantial gain at 6.8 diam beyond the end of the cone, and so justify the Hydraulic Institute's recommendation of measuring the head at a point 10 diam beyond the cone. However, the specifications permitted lengthening of the discharge cone by reducing the total cone angle, thereby obtaining much more uniform velocity distribution at the end of the cone.

In the last models a discharge cone with a 3-deg total cone

angle was used, and head readings obtained at the end of this cone were slightly lower than readings obtained with a 10-deg cone at a point 6.8 diam beyond the end of the cone.

Owing to these different definitions and measurements of total head, the different performance curves are not directly comparable. No attempt was made to recalculate the performance curves and bring them to the same basis, but performance curves shown on any one figure were obtained with the same test procedure and are directly comparable.

For convenience of comparison, most of the model test data were converted into prototype values at an operating speed of 200 rpm. Also, it was found most practical to compare the pump characteristics at an operating point of 1450 cfs at 310 ft. This point gave the same percentage of safety above the minimum required capacity of 1350 cfs at 310 ft as the power percentage safety below the maximum permissible power requirement of 65,000 hp at 270 ft.²

For better understanding of the various performance curves, the main dimensions for the various model impellers and pump cases referred to in the various figures are given in Table 1. All models were mounted horizontally and were of a construction as shown in Fig. 15.

Following is a description of the step-by-step development of various pump cases and impellers to arrive at the smallest pump size and highest pump efficiency unit having a stable noncavitating performance curve under all operating conditions.

PUMP-CASING STUDY

The pump casing represents a high percentage of the total pump weight and, as previously mentioned, the diffuser-type casing proved to be lighter than the single- and double-volute case. However, the pump characteristics with a 12-vane diffuser-type case had not proved satisfactory. Therefore, a continued study of various types of diffuser cases was necessary.

The effect of the pump-casing type on the head-capacity characteristics is shown in Fig. 3. Here the same impeller was tested in two pump cases, a double-volute case with a volute area of 21 sq in. and a 12-fixed-vane diffuser case with a diffuser entrance area of 20.8 sq in. The double-volute-case performance meets all the requirements with a stable head-capacity curve over the operating range, and also exceeds the minimum pump efficiency of 87 per cent at the 310-ft operating point. The 12-vane diffuser case, however, has an abrupt drop in head near the 365-ft head, and the pump efficiency at the 310-ft operating point is

² To permit simplified test procedure and also to eliminate the possibility of cavitation, all performance tests were run with a constant net positive suction head of 115 ft.

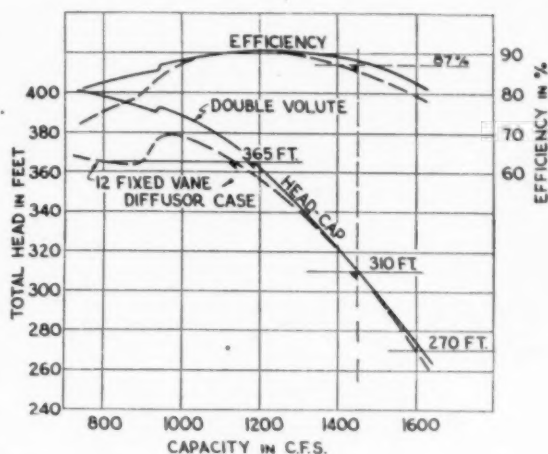


FIG. 3 EFFECTS OF CASING TYPE ON PUMPING CHARACTERISTICS

below the minimum 87 per cent required. This drop in head also affected the brake horsepower, and this unstable portion of the performance curve was considered too close to the 365-ft head for safe operation. The foregoing performance curves indicate that the lower number of diffuser vanes would give a more stable and, in general, a more satisfactory performance.

In order to determine the influence of diffuser-case entrance area on the pump characteristics, a series of tests were run with a gradual increase of diffuser-case entrance areas, using the same impeller for all tests. In Fig. 4 is shown the effect of diffuser-vane inlet area on pump characteristics for model pumps using the same impeller and the same 12-fixed-vane diffuser case as described and illustrated in Fig. 3. The diffuser-case inlet area was changed from A to B, which latter is 18 per cent larger than A. Alternating the diffuser-vane inlet area also affects the diffuser-vane entrance angle, but experiments have shown that the area affects the pump performance to a much greater degree than the diffuser-vane angle. The increased diffuser-vane entrance area improved by several points the pump efficiency at 310-ft head, but the head-capacity curve dropped below the 365-ft head. Therefore this performance curve was not acceptable, and further study of the 12-fixed-vane diffuser case was abandoned.

Next a design study was made of fixed-vane diffuser cases with 3, 4, 5, and 6 diffuser vanes, in order to analyze the practical

TABLE 1 IMPELLER AND CASING DIMENSIONS OF MODELS

	Fig. 3	Fig. 4	Fig. 5	Fig. 6 Fig. 8 Fig. 9	Fig. 10	Figs. 11, 12, 13 Final model— A B	
Impeller	Outlet diam, in.....	14 1/8	14 1/8	12 1/2	14 1/8	12 1/2	12 1/2
	Outlet width, in.....	1 1/2	1 1/2	1 1/2	1 1/2	1 1/2	1 1/2
	Eye diam, in.....	7 1/2	7 1/2	6 1/2	7 1/2	6 1/2	6 1/2
	Outlet vane angle, deg	23 1/2	23 1/2	24	Fig. 10	23 1/2	24
	Number of vanes.....	8	8	7	8 6	8	7
Diffuser case	Entrance area, sq in....	21 (volute) 20.8	20.8	20.8 21.0	18.7	22.0	18.7
	Outlet area, sq in.....	44.0	44.0	44.0	28.0	36.0	28.0
	Vane lip diam, in.....	15.5	15.5	15.5	13 1/2	15.6	13 1/2
	Vane lip width, in.....	2 1/2 (volute) 1 1/2	1 1/2	1 1/2	1 1/2	1 1/2	1 1/2
	Number of vanes.....	12	12	12 6	6	6 with rib	6 with rib
	Model size.....	11.5	11.8	11.8	13.0	Fig. 10	13.1
Factor.....	11.8	11.5				13.1	13.0

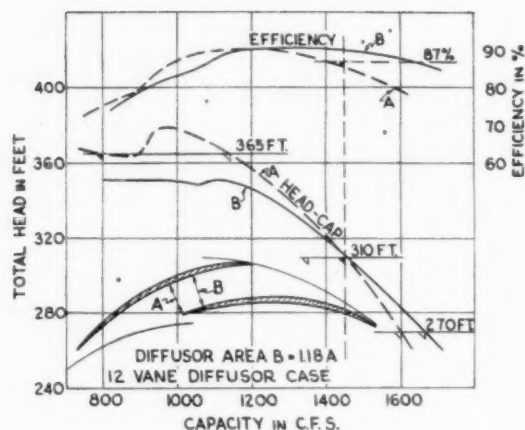


FIG. 4 EFFECTS OF DIFFUSER-INLET AREA ON PUMP CHARACTERISTICS

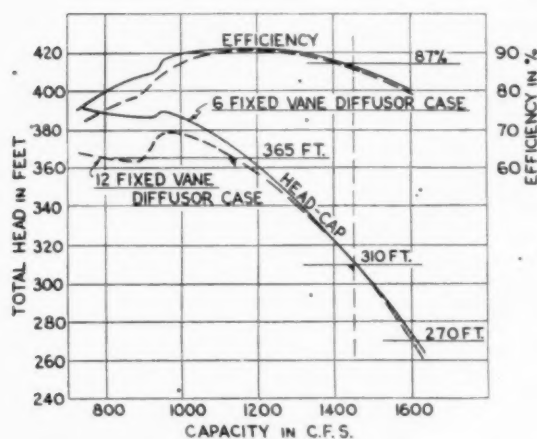


FIG. 5 EFFECTS OF NUMBER OF DIFFUSER VANES ON PUMP CHARACTERISTICS

minimum number of vanes which would give sufficient strength and allow a substantial weight saving and still meet all requirements. This study proved that the 6-vane diffuser case was the most satisfactory.

Fig. 5 shows comparison of pump characteristics for 6 and 12-fixed-vane diffuser cases. Here the same impeller was tested in the two diffuser cases, both having practically the same diffuser-vane inlet area but different diffuser-vane outlet areas as shown in Table 1. The 6-vane diffuser case improved noticeably the head-capacity performance near the 365-ft head and materially reduced the dip in the unstable range. The pump efficiency at the 310-ft operating point for the 6-vane diffuser case showed only a slight gain over the 12-vane diffuser case. However, the pump efficiency at that point was later improved. This was accomplished partly by increasing the diffuser-case inlet area which was permissible with the 6-vane diffuser casing, as this casing still gave a stable characteristic at the 365-ft head.

Next, the change of performance with increased outlet area of the diffuser cases was determined. As might be expected, the larger diffuser cases with lower velocities permitted a greater head recovery at the end of the diffuser vanes and therefore showed

some improvement in the pump efficiency. However, this would have resulted in too large a pump case, and therefore further study was continued in order to improve the pump efficiency with the small diffuser case.

New-Type Diffuser Case. By studying the flow distribution in the outlet of the pump-discharge cone for a 6-vane diffuser case, it was found that the higher velocities crowded toward the outside of the pump casing. To obtain a more uniform flow at the end of the discharge cone, several ribs were tried in the pump casing. The best result was obtained when using one rib dividing the flow in a diffuser case into two separate streams similar in principle to a double-volute case. This rib design is shown in Fig. 6. The location of the dividing rib may also be seen in Fig. 7 which shows the final model on its base in the laboratory with the front half of the case removed but with impeller diffuser ring and dividing rib in place.

The velocity distribution at the end of a 3-deg discharge cone for a 6-vane diffuser case, with and without a dividing rib, is shown in Fig. 8. The effect of this dividing rib on the pump characteristics, resulting in increased head and higher efficiency, is shown in Fig. 9.

The same tests were repeated on 6-vane diffuser cases, with and without dividing rib, the cases having a total cone angle of 10 deg, and the results were relatively the same. In the two sets of tests, the gain in pump efficiency and head for the case, with a dividing rib as against the case without this rib, was greater than the energy difference calculated by the integration of the velocity heads corresponding to the different velocity distributions, Fig. 8.

It will be noted that the first three diffuser vanes remain the same in the two pump cases with and without the dividing rib. The difference in performance obtained by these two pump cases therefore can only be the result of what happens beyond the outlet of the third diffuser vane. From this point on, in the case without the dividing rib, the streams from the 4th, 5th, and 6th diffuser vanes flowing into the stream from the first three diffuser vanes must introduce shock and mixing losses which are greater than the friction loss from the two separate streams in the case with a dividing rib. This result was somewhat surprising, since the dividing rib decreases the hydraulic radius of the case.

By continued use of this reasoning, the best results should perhaps be obtained by separating all the streams coming from the diffuser vanes. But such a diffuser case would become impractical to manufacture and, undoubtedly, the further decrease of the hydraulic radius would result in greater friction losses which would offset the gain in reduced mixing and shock losses.

No further tests were made to clear up this point. The improved efficiency in the larger diffuser case previously mentioned, undoubtedly was the result of longer diffuser vanes, although in that case we dealt with diffuser cases with lower velocities. Hence the results are not directly comparable.

EFFECTS OF IMPELLER-DISCHARGE VANE ANGLE ON PUMP CHARACTERISTICS AND PUMP SIZE

Three impellers, having the same profile but with $26\frac{1}{2}$, $23\frac{1}{2}$, and $18\frac{1}{2}$ deg discharge vane angles were tested in a 6-fixed-vane diffuser case. The pump characteristics of these three impellers are shown in Fig. 10. In this particular case, it was more advantageous to present the actual model performance curves, as they more clearly indicate the spread in the head-capacity performance.

The impeller with the $26\frac{1}{2}$ -deg discharge vane angle will require a multiplying factor of 11.4, while the impeller with an $18\frac{1}{2}$ -deg angle requires a multiplying factor of 12.3 of this larger model, or, converted into weight, the impeller with the lower

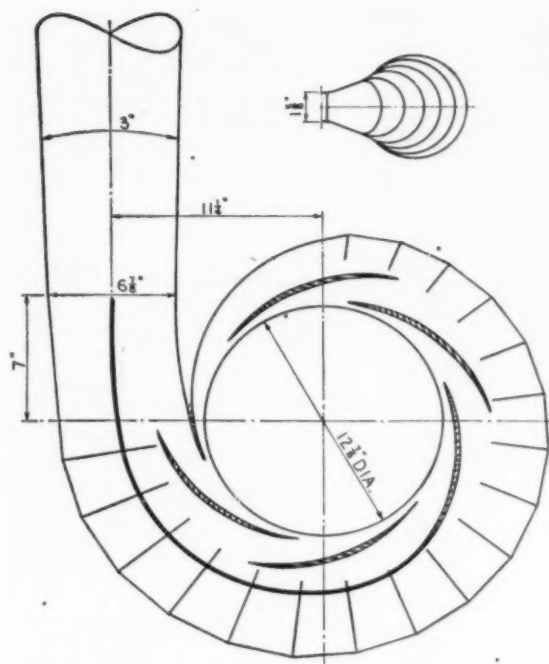


FIG. 6 DIFFUSER CASE WITH SEPARATING RIB FOR GRAND COULEE MODEL PUMP

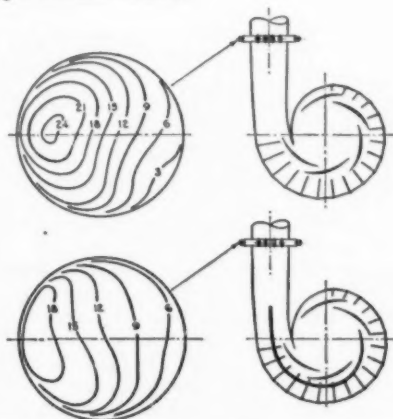
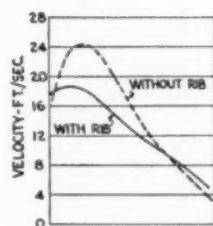


FIG. 8 VELOCITY DISTRIBUTION IN PUMP DISCHARGE FOR 6-VANE DIFFUSER CASE WITH AND WITHOUT SEPARATING RIB

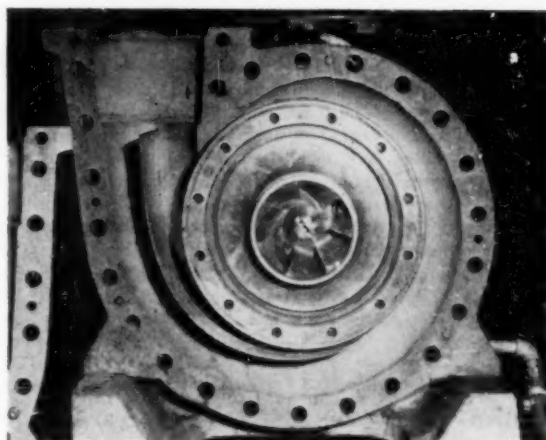


FIG. 7 GRAND COULEE MODEL PUMP WITH HALF OF CASING REMOVED SHOWING IMPELLER, DIFFUSER RING, AND SEPARATING RIB

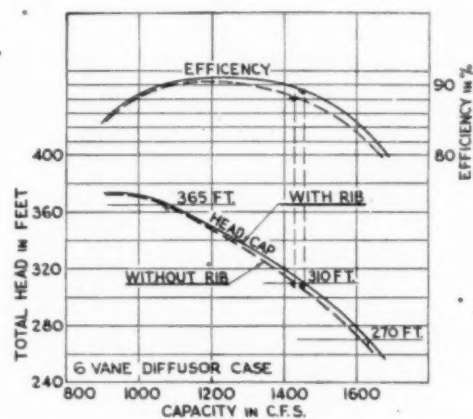


FIG. 9 EFFECTS OF CASING SEPARATING RIB ON PUMP CHARACTERISTICS

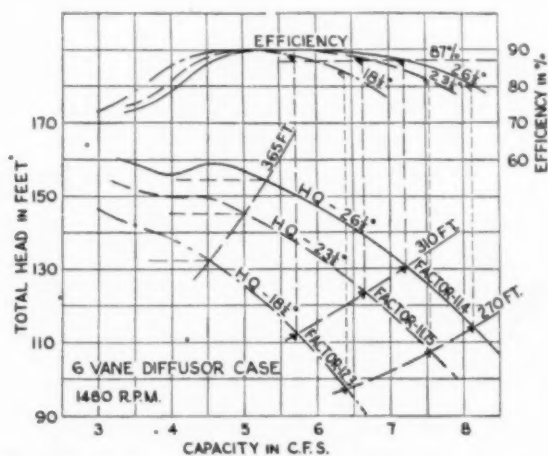


FIG. 10 EFFECTS OF IMPELLER-OUTLET VANE ANGLE ON PUMP CHARACTERISTICS

angle would result in a 25 per cent heavier pump case than an impeller with the steeper angle.

However, the head-capacity performance near the 365-ft head became more unstable for impellers with steeper vane angles. The unstable part of the curve for the $26\frac{1}{2}$ -deg vane angle was considered the upper safe limit for an impeller with this profile. Therefore, to allow for a certain margin of safety in the unstable range, the final model pump was designed with impellers having outlet discharge vane angles of 24 deg. Also, impellers with wider profiles were tested in wider diffuser cases, but these casings had the same diffuser inlet area as the narrow diffuser casings. The wide-profile impeller gave the same type of performance as a narrow-profile impeller with steeper vane angle. No noticeable gain in pump efficiency was obtained with the wider impellers.

EFFECTS OF IMPELLER-VANE ENTRANCE ANGLE ON CAVITATION PERFORMANCE AND PUMP CHARACTERISTICS

Impellers with different impeller-eye profiles were designed and tested to determine the effect of the ratio between radial and peripheral eye velocities on the cavitation performance. In this study it was found that the information given in C. A. Gongwer's paper (2) was very useful, and the best cavitation performance was obtained with an impeller-eye profile which agreed with the formula recommended in that paper.

The effect of the impeller-entrance vane angle on the cavitation performance and pump characteristics is demonstrated by two impellers, A and B, tested in the same 6-vane diffuser case with a separating rib. The two impellers have practically the same profile and outlet vane angle (see Table 1). The main differences in design are the impeller-entrance vane angles as shown on the diagrams in Fig. 11.

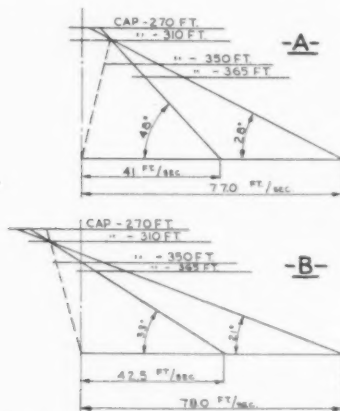


FIG. 11 ENTRANCE VELOCITY TRIANGLES FOR IMPELLERS A AND B

Impeller A, with entrance vane angles 28 deg at the eye and 48 deg at the hub, favor shock-free operation at the larger capacity, while impeller B, with vane entrance angles of 21 deg at the eye and 33 deg at the hub, will give shock-free operation at lower capacities.

Fig. 12 shows the result of cavitation tests for these two impellers. Impeller A does not satisfy the minimum σ requirement for the lower capacities at 365 and 350-ft head but, as expected, gives ample safety at the larger capacities, particularly for the capacity at 270 ft. Impeller B, however, satisfies all requirements, but the amount of safety of course is less at the larger capacities.

The pump characteristics of the two impellers are shown in

Fig. 13. A comparison of these two pump characteristics shows that the impeller-vane entrance angle also has an amazingly great effect on the pump performance. The lower impeller-vane en-

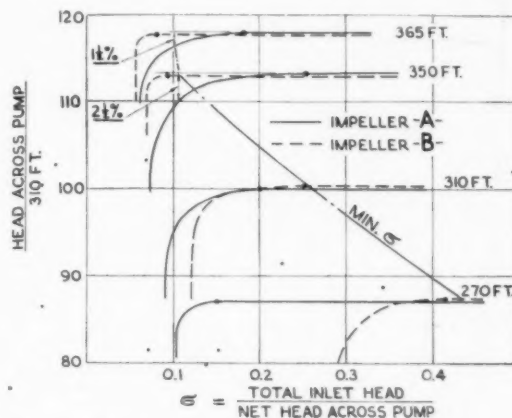


FIG. 12 EFFECTS OF IMPELLER-ENTRANCE VANE ANGLE ON CAVITATION CHARACTERISTICS

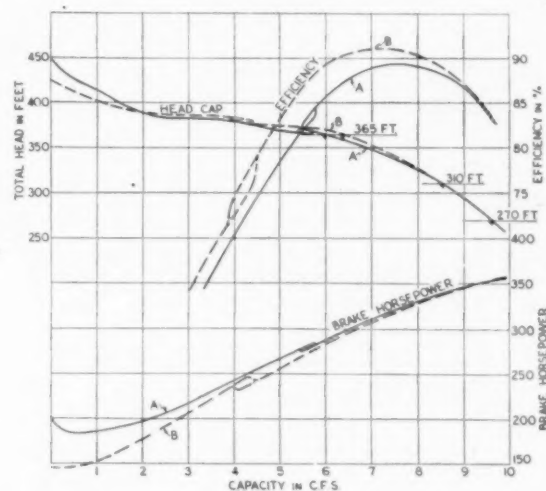


FIG. 13 EFFECTS OF IMPELLER-ENTRANCE VANE ANGLE ON PUMP CHARACTERISTICS

trance angles on impeller B have also several beneficial results on the pump characteristics, as follows:

- 1 Lower head and brake horsepower at the closed valve, which latter would result in less starting-torque requirement for the motor if started under shutoff conditions. The lower head may be the result of less back pressure created by the lower vane angle at zero and low capacities.

- 2 The unstable portion of the head-capacity curve and brake horsepower moves to a lower capacity with a flatter impeller-entrance vane angle and allows for greater safety of stable operation near the 365-ft head. It is interesting to note in the previous figures shown that the unstable performance caused by the pump casing remains at the same capacity from one type of pump case to the next, and the case design affected only the magnitude of the dip in the head-capacity curves. This also held true in the unstable portion of the brake-horsepower curve. As the lowering

of the impeller-entrance vane angles moved the unstable portion of the head-capacity curve as well as the brake-horsepower curve to a lower capacity, this would indicate that the unstable portion in the performance is the result of flow conditions in the impeller eye.

3 The improved pump efficiency over the operating range, particularly at the lower capacities, gives a strong indication that for pumps designed for a definite operating point, in this case, for instance, 310 ft, the impeller should have vane entrance angles giving a velocity diagram similar to impeller B, rather than the conventional diagram as obtained by impeller A. The suction approach and the NPSH available must of course also be given consideration in the selection of the impeller-entrance vane angles. For commercial pumps, however, which must cover a wide range of capacities it probably will be found necessary to use impellers with vane entrance angles similar to those used in impeller A, as this steeper vane entrance angle has a greater safety against cavitation at the larger capacities.

The final model used for acceptance tests incorporated all the improvements mentioned, and the following résumé will give the results of the final acceptance tests.

MODEL-PUMP TESTS

Final model tests were conducted by the Cal Tech Hydrodynamics Laboratory. Laboratory equipment, except for slight modifications, was the same as previously described in detail (9).

Specifications No. 1128 of the United States Department of the

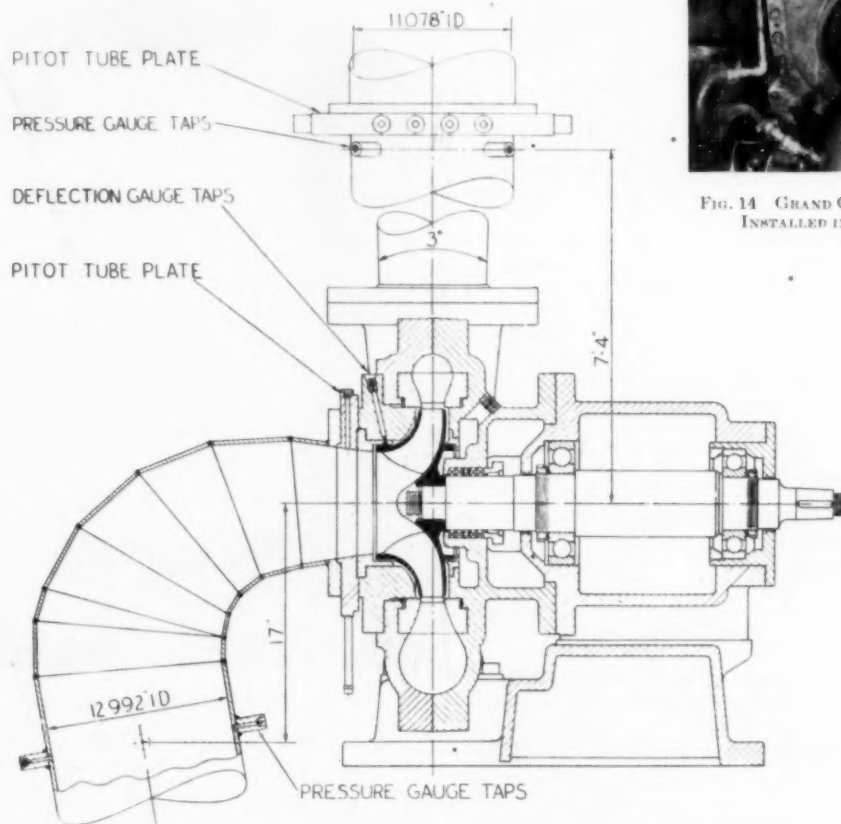


FIG. 15 ASSEMBLY, GRAND COULEE MODEL PUMP

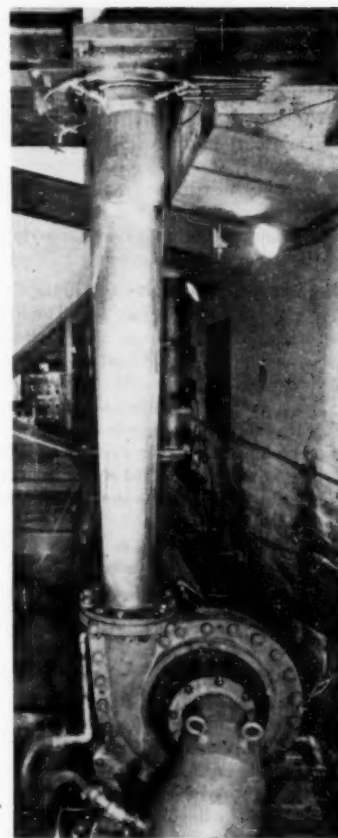


FIG. 14 GRAND COULEE MODEL PUMP
INSTALLED IN CAL TECH LAB

Interior, Bureau of Reclamation, under which the contract for the six 65,000-hp pumps was awarded, required, in addition to characteristic and cavitation tests, the determination of the following:

- 1 Amount of unbalanced side thrust on the impeller.
- 2 Distribution of flow and amount of prerotation at the eye of the impeller.
- 3 Velocity distribution at the end of the casing extension diffuser.
- 4 Pressure variations near the periphery of the impeller in both the top and bottom covers.

The final model, set up for test in the Cal Tech Hydrodynamics Laboratory, is shown in Fig. 14. The long stainless-steel casing extension diffuser is shown, with discharge piezometer connections at the upper end. A portion of the converging-cone suction elbow, together with one of the balance lines from the back of the impeller to suction pressure, also will be noted in this illustration.

Fig. 15, the model pump assembly, shows the location of both suction and discharge piezometer connections and also the Pitot-tube plates used in the determination of velocity distribution. Piezometer connections, as shown, are located in accordance with the specifications.

From Figs. 14 and 15 it may be seen that the heads and efficiencies obtained in these tests, and reported herein, are not those of the model pump alone but include losses in the suction and discharge piping between the piezometer connections and the pump.

CHARACTERISTIC AND CAVITATION TESTS

All testing was performed at heads equal to those of the prototype, necessitating operation at 2600 rpm, i.e., prototype speed of 200 rpm multiplied by the model ratio of 13. Results of characteristic tests are plotted in Fig. 16 on which a scale has been added for prototype capacity, obtained by multiplying model capacity by the cube of the model ratio, and the inverse ratio of the operating speeds. In accordance with the specifications, the efficiencies shown are those obtained by the model and include losses in suction and discharge piping between piezometer connections. Furthermore, model efficiencies are shown as applying to the prototype, unlike turbine practice wherein an increase is permitted due to decreased relative roughness and clearances.

The test installation included a scale model of the trash rack and inlet structure of the prototype, enclosed in a pressure tank to permit varying the suction pressure (see Fig. 17). The width of the channel ahead of this trash rack was restricted by side plates to that equivalent to one bay in the Grand Coulee wing dam. Water flowing into this channel was passed through a gravel-bed filter having sufficient resistance to insure uniform flow, in an effort to duplicate, as nearly as possible, suction conditions obtaining in the prototype. The entire suction from the trash-rack structure to the pump duplicated that of the prototype to a model ratio scale of 1 to 13.

Table 2 is a comparison of model test results with specification requirements.

The minor discontinuity in the head-capacity curve, indicating unstable operation, falls well outside the operating range of the prototype.

The test results show the model ratio of 13 to be ideal in that it permits minor variations, either smaller or larger, due to manu-

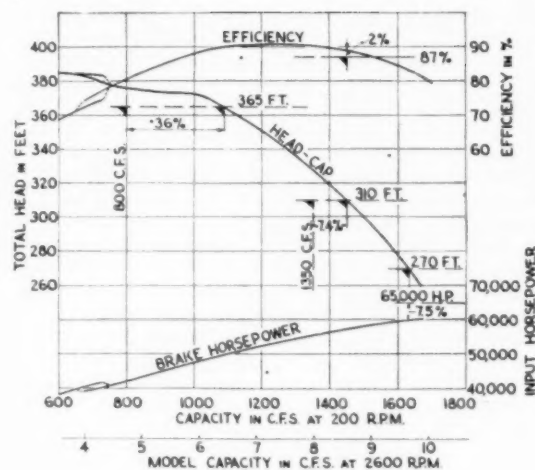


FIG. 16 MODEL PUMP CHARACTERISTICS

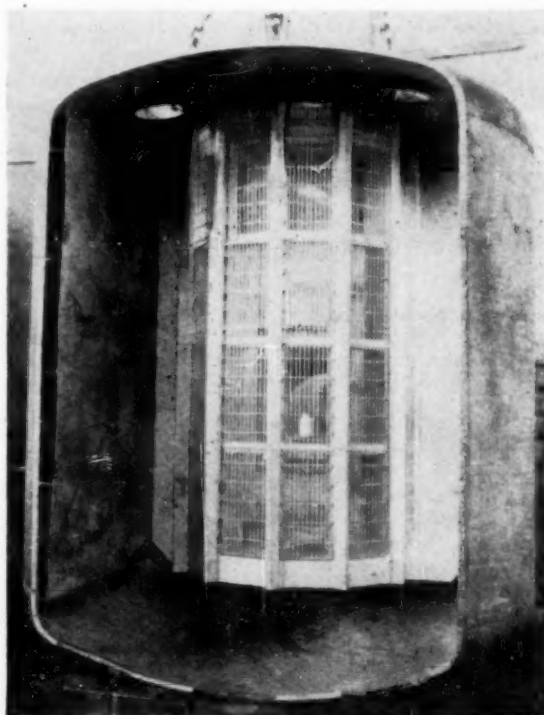


FIG. 17 MODEL OF INLET TRASH RACK

TABLE 2 COMPARISON OF MODEL TEST RESULTS WITH SPECIFICATION REQUIREMENTS

	From Fig. 16	Required by specifications	Safety above requirements, per cent
Cap. at 365-ft head.....	1087 cfs	800 cfs (min)	36
Cap. at 310-ft head.....	1450 cfs	1350 cfs (min)	7.4
Eff. at 310-ft head.....	88.9 per cent	87 per cent (min)	2
Bhp at 270-ft head.....	60100	65000 max	7.5

facturing tolerances in the prototype, without falling short of the minimum required capacities or exceeding the maximum permissible horsepower.

Cavitation performance is shown in Fig. 18 for each of four operating conditions, i.e., the maximum head, the minimum head, the normal (or warranted) head, and a head corresponding to low water in both the lake and the discharge canal. The operating range shown is based on prototype performance, lake levels on the suction side, discharge canal levels, and anticipated conduit and entrance and exit losses. Upper and lower limits of this operating-range area are based upon high and low water

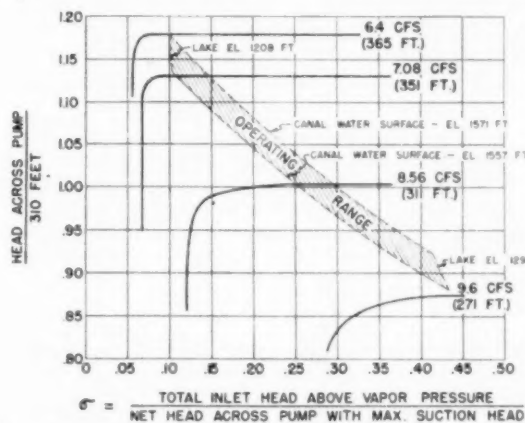


FIG. 18. CAVITATION CHARACTERISTICS OF FINAL MODEL

in the discharge canal, and right and left limits are based on high and low water in Lake Roosevelt. These tests show a margin of safety between the operating range and the inception of cavitation sufficient to exclude the possibility of cavitation damage.

UNBALANCED SIDE THRUST ON IMPELLER

The direct measurement of the amount of unbalanced side thrust on the impeller of a pump, operating at 2600 rpm and 355 bhp, presents numerous difficulties, aggravated by the requirement to make the measurements on a model which in its final form had only 0.007-in. diametral clearance between the rotating and stationary seal rings. Therefore it was decided that the deflections of the pump shaft during operation would be measured; which, combined with the spring constant of the shaft determined at rest, would permit accurate calculation of the forces causing the deflection.

To measure the deflection of the shaft during operation, two insulated metal probes were inserted at points 90 deg apart through holes in the suction cover. A suitable bracket was provided for each probe to hold it in position and at the same time permit fine control of its movement, toward or away from the impeller seal ring. A dial indicator reading to 0.0001 in. was rigidly mounted on each bracket and used to determine the location of each probe. Contact with the impeller seal ring was determined by neon bulbs operated by transformers through a low-voltage trip circuit (see Fig. 19).

It was possible accurately to locate the center position of the impeller with the pump filled with water and slowly rotating so that side thrust was negligible. Then, with the model operating at full speed, deflection readings were taken at various capacities. The resultants of these readings, at the proper angle with the model center lines, are plotted in Fig. 20.

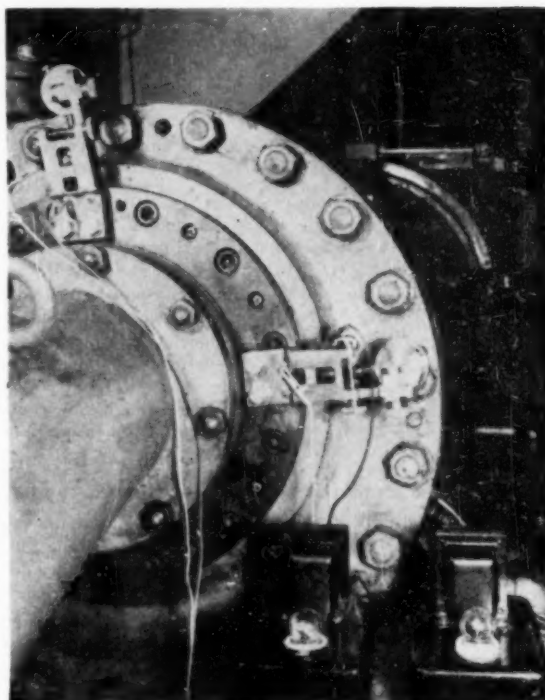


FIG. 19. SETUP FOR MEASURING DEFLECTION AT IMPELLER, GRAND COULEE MODEL

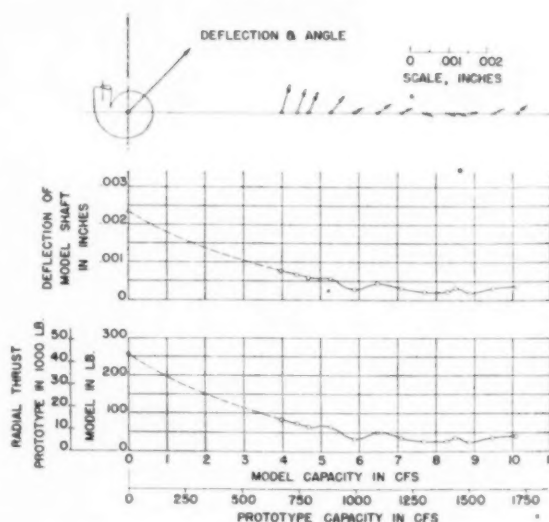


FIG. 20. DEFLECTION AND RADIAL THRUST OF FINAL MODEL

Determination of the spring constant of the model shaft, while at rest, with a beam and weights, permitted the calculation and plotting of the lower curve in Fig. 20, radial thrust versus capacity. The radial-thrust scale for the prototype was obtained by multiplying the model thrust scale by the ratio of areas, that is, the square of the model ratio.

From this curve it may be seen that the maximum radial

thrust under any operating condition, to be encountered in the prototype, is less than 9000 lb and the maximum at shutoff head is only 43,000 lb. This is considered insignificant in a unit of this size having a shaft nearly $2\frac{1}{2}$ ft diam and an impeller which weighs nearly 30 tons.

DISTRIBUTION OF FLOW AND AMOUNT OF PREROTATION AT EYE OF IMPELLER

The velocity and direction of flow of the water entering the impeller were determined by a direction-finding Pitot tube inserted into a plate located approximately 2 in. ahead of the impeller, as shown in Fig. 15. Five traverses were made in each direction. Readings were taken through the entire cross section and results plotted. Numbers on the isovelocity diagrams in Fig. 21 indicate velocity in feet per second.

Velocities on these diagrams are unusually uniform and corroborate the wisdom of The Bureau in the choice of a converging-cone elbow for the pump suction. There is no backflow and consequently no prerotation within the normal operating range for the prototype.

VELOCITY DISTRIBUTION AT END OF CASING-EXTENSION DIFFUSER

Velocity and direction of flow of the water leaving the casing-extension diffuser were determined by a direction-finding Pitot tube inserted in a plate similar to that used on the suction side, except that four traverses instead of five were made in each of two directions at 90 deg. The plate used is illustrated in Fig. 22 with a Pitot tube inserted through one of the holes. Note the cir-

cular scale with a vernier to determine accurately the direction in which the impact hole in the tube is pointed. A scale on the mounting head permits determination of the location of the impact- and static-pressure holes with respect to the center of the pipe. This plate may be seen installed in the discharge line at the end of the upper casing-extension diffuser in Fig. 14.

Results of readings taken at the highest head, normal or guaranteed head, and lowest head, are shown in Fig. 21. Numbers indicate velocity in feet per second.

At the guaranteed point of 310-ft head, the unit produces approximately 0.6 ft more head than it can be credited with owing to additional kinetic energy available in excess of that based on uniform velocity. This may be proved by integration of the velocity-distribution chart for 310-ft head.

PRESSURE VARIATION NEAR PERIPHERY OF IMPELLER IN BOTH COVERS

Pressures were taken at 12 piezometer connections in each cover (see Fig. 23), at operating heads of 365 ft, 310 ft, and 270 ft, and results plotted in Fig. 24. Velocity and direction of flow were not measured. However, the result of the change in the absolute angle of the water leaving the impeller is clearly indicated by the reversal of high- and low-pressure points between the maximum and minimum head conditions.

CONCLUSIONS

The pump-casing type has a great influence on the pump performance, as pumps with single-volute, double-volute, and

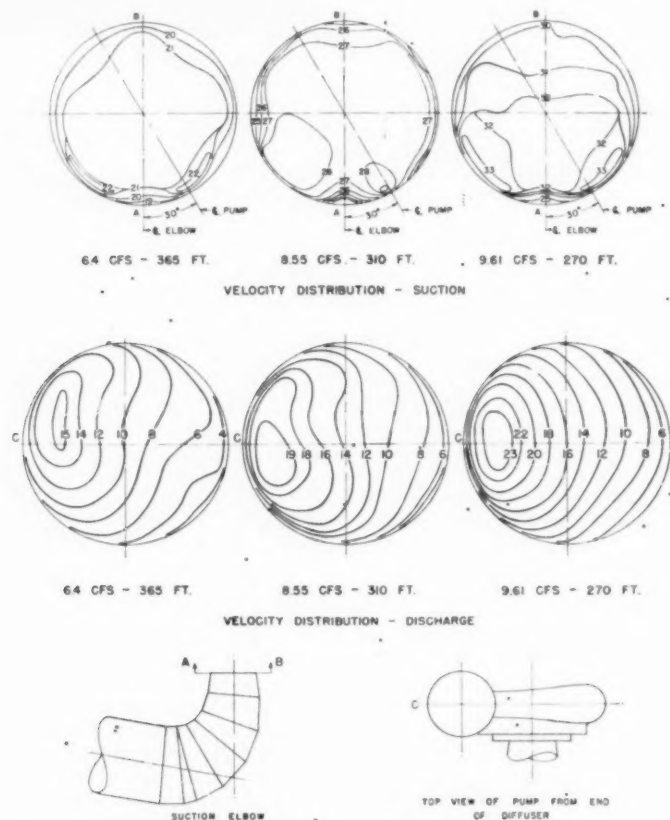


FIG. 21 VELOCITY DISTRIBUTION IN SUCTION AND DISCHARGE OF FINAL MODEL

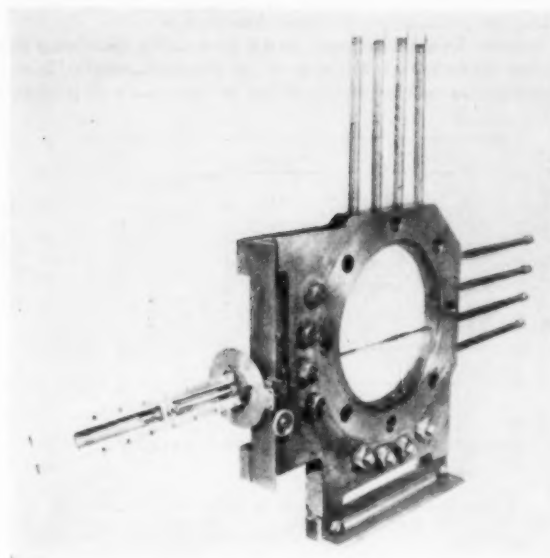


FIG. 22 PITOT-TUBE PLATE FOR DISCHARGE PIPE

diffuser casing designed on the same basis will give different performances. Furthermore, the number of diffuser vanes in the diffuser case has a definite influence on the unstable portion of the performance curve. Fewer diffuser vanes reduce the magnitude of the dip in the head-capacity curve. The diffuser-case inlet area affects the shape of the head-capacity curve and also the pump-efficiency curve. Six diffuser vanes seem to be the minimum number for practical design of a welded pump-diffuser-casing structure, which will give the casing sufficient strength and also allow a substantial reduction in weight. A dividing rib in the diffuser case gives better velocity distribution and improves the pump efficiency.

Impellers with the same profile, but with different impeller-outlet vane angles, materially affect the pump size and weight. The steeper vane angle gives a flatter performance curve and produces a more pronounced dip in the unstable head-capacity range.

The impeller-inlet vane design has a great influence on the cavitation characteristics and also affects the unstable portion of the head-capacity and horsepower curves. A flat entrance vane angle reduces the head and horsepower at closed valve and also improves the pump efficiency at lower capacity.

The unusual performance of the Grand Coulee pumps was a challenge to existing knowledge and techniques. To obtain the desired results, careful testing was required, and the use of the latest testing equipment was necessary. It is hoped that the work presented will be useful and will be followed by detailed disclosures in similar pump studies.

ACKNOWLEDGMENT

The Bureau of Reclamation started the Grand Coulee model test study which was conducted at The California Institute of Technology. Without this basic study the final results of the model would not have been possible.

The author is indebted to Mr. L. N. McClellan, Chief Electrical and Mechanical Engineer of the Bureau of Reclamation, and to Mr. I. A. Winter, Senior Engineer of the Bureau of Reclamation, for technical advice and assistance, as well as to Mr. E. B.

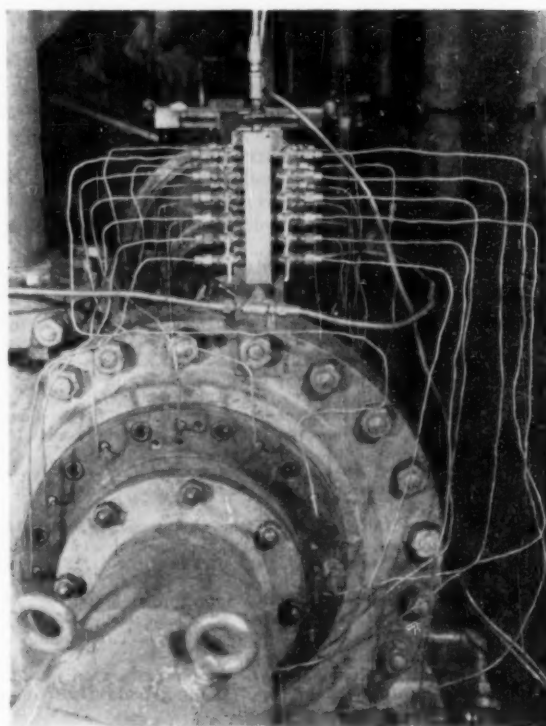


FIG. 23 SETUP FOR MEASURING PRESSURES AROUND PERIPHERY OF IMPELLER IN BOTH COVERS

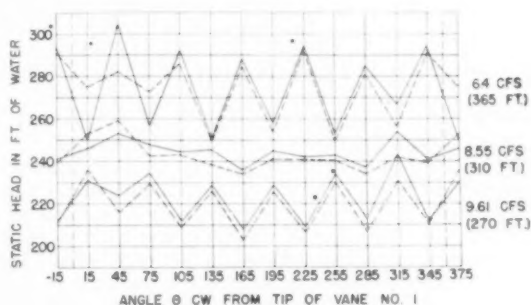


FIG. 24 PRESSURE DISTRIBUTION NEAR PERIPHERY OF IMPELLER OF FINAL MODEL

Moses, who represented The Bureau at the acceptance tests.

The close collaboration between Byron Jackson Co. and The Pelton Water Wheel Company, particularly the co-operation of Mr. M. White, its Chief Engineer, made the results presented possible.

Special acknowledgment is due Mr. A. Hollander, Associate Professor of Mechanical Engineering, California Institute of

Technology, who took an active part in the original model study and followed the design progress of the final model as technical consultant of Byron Jackson Co.

The final model testing was conducted at the California Institute of Technology under the direction of Prof. R. L. Daugherty and the Director of the Hydraulic Laboratory, R. T. Knapp, who also assisted with valuable suggestions.

The model testing technical staff was in charge of Mr. E. Lindros, Assistant Chief Engineer, Byron Jackson Co., who also worked out the data on the final model test presented in this paper.

BIBLIOGRAPHY

- 1 "Cavitation Characteristics of Centrifugal Pumps Described by Similarity Considerations," by G. F. Wislicenus, R. M. Watson, and I. J. Karassik, *Trans. ASME*, vol. 61, 1939, pp. 17-24.
- 2 "A Theory of Cavitation Flow in Centrifugal-Pump Impellers," by A. Gungwer, *Trans. ASME*, vol. 63, 1941, pp. 29-40.
- 3 "Centrifugal-Pump Performance as Affected by Design Features," by R. T. Knapp, *Trans. ASME*, vol. 63, April, 1941, pp. 251-260.
- 4 "Test Characteristics of a Combined Pump-Turbine Model With Wicket Gates," by R. V. Terry and F. E. Jaski, *Trans. ASME*, vol. 64, 1942, pp. 731-744.
- 5 "History and Development of the Grand-Coulee Pumping Plant," by E. B. Moses, for presentation at the Semi-Annual Meeting, San Francisco, Calif., June 27-30, 1949, of THE AMERICAN SOCIETY OF MECHANICAL ENGINEERS.
- 6 "The Mechanical Design and Manufacturing of the Grand Coulee Pumps," by I. M. White, for presentation at the Semi-Annual Meeting, San Francisco, Calif., June 27-30, 1949, of THE AMERICAN SOCIETY OF MECHANICAL ENGINEERS.
- 7 "Experimental Determinations of the Flow Characteristics in the Volute of Centrifugal Pumps," by R. C. Binder and R. T. Knapp, *Trans. ASME*, vol. 58, 1936, pp. 649-661.
- 8 "Complete Characteristics of Centrifugal Pumps and Their Use in the Prediction of Transient Behavior," by R. T. Knapp, *Trans. ASME*, vol. 59, 1937, pp. 683-689.
- 9 "The Hydraulic Machinery Laboratory at the California Institute of Technology," by R. T. Knapp, *Trans. ASME*, vol. 58, 1936, pp. 663-676.

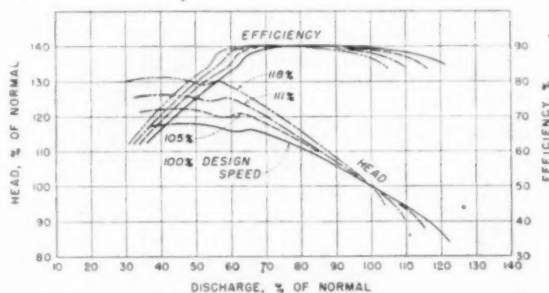
Discussion

I. A. WINTER.⁴ This paper presents some of the outstanding results of experimental research as applied to the development and construction of large centrifugal pumping units. It is of particular interest to the utility engineer since it presents basic research data on construction features related to the pump-impeller design. The importance of the hydraulic designs of the inlet and discharge to the pump casing, and to the casing itself, are presented in the text of the paper and in the comprehensive list of illustrations. The continuity of the presentation is excellent and the material selected is pertinent.

The difficulty of obtaining a satisfactory mechanical design of pump casing of the size and for the pressure required for the Grand Coulee development indicated that some form of diffuser casing would offer the most economical construction. The testing program of the Bureau was directed toward establishing the feasibility of such a design. It had been the general policy of the pump designers of this country to consider the turbine or diffuser casing detrimental to the performance of the pump, although, until recently, it had received wide application in important European installations. It was generally believed that the introduction of vanes in the line of flow opposite the impeller discharge would result in a loss of from 3 to 5 per cent in pumping efficiency. The initial tests at the California Institute of Technology on diffuser casings resulted in the development of designs which

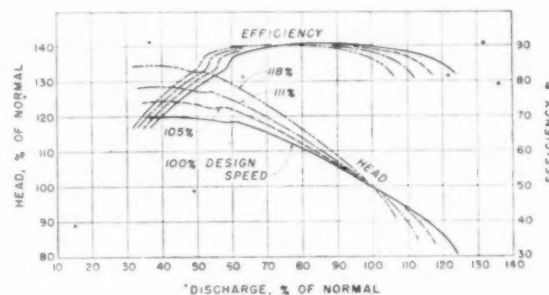
gave efficiencies and capacities equal to and exceeding, in some cases, the performance of single-volute casings.

Further development work, as will be noted by comparing the curves shown in Figs. 25 and 26 of this discussion, resulted in obtaining performance with the diffuser casing equal in all practical



FIXED-VANE DIFFUSER CASING

Fig. 25



DOUBLE VOLUTE CASING

Fig. 26

respects to the performance of the double-volute casing without the use of an auxiliary splitter as described by the author. The difference in performance between the double-volute casing and the 12-fixed-vane casing, as shown in Fig. 3 of the paper, undoubtedly could be considerably reduced by the use of a larger casing, which would provide for greater expansion in the first stage of diffusion. The author's study and development have been quite properly directed toward obtaining the maximum performance for the minimum mechanical equipment. It is likely that any appreciable improvement in pump performance above that presented by the author would be obtained at an increase in cost inherent with the construction of larger equipment.

The development of a satisfactory recovery of velocity head within a diffuser casing requires two separate and distinct stages. The first stage is developed within the diffusers opposite the periphery of the impeller and provides an outflow area 2.4 of the inflow area as described later. The second and final stage is in the conventional conical discharge nozzle also having an outflow area 2.4 of the inflow area for optimum performance. The casing channel at the end of the diffusers, because of the transfer of momentum opposite each diffuser, collects the fluid into a stream having a velocity distribution at the end of the last diffuser vane favorable to the recovery of pressure head in the expanding diffuser of the pump discharge nozzle. Experiments have indicated that the efficiency of a straight conical diffuser is greatly influenced by the distribution of flow at its inlet, and the best design of casing would have a well-distributed velocity relation.

⁴ Head, Hydraulic Machinery Division, Branch of Design and Construction, Bureau of Reclamation, Denver, Colo.

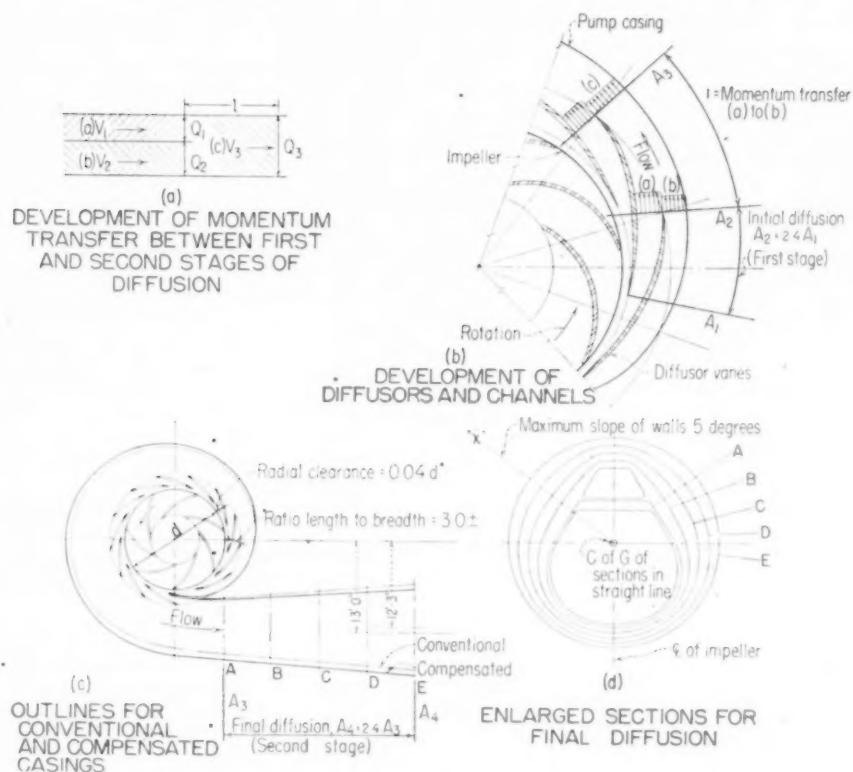


FIG. 27 DESIGN DETAILS

at this point. The diffuser-type casing offers the best possibilities in this regard.

The initial design of diffuser casing prepared by the Bureau was on the basis of turbine draft-tube practice utilizing the principle shown in (b) of Fig. 27 herewith. The basic diffuser for both casings had a nominal outflow area of 2.4 of the inflow area which represents the optimum amount of negative acceleration which can be obtained in a single stage of diffusion, as determined when the change in momentum of the stream within a closed conduit exactly equals the change in pressure. The number of vanes placed around the casing was selected to obtain an optimum ratio of height to breadth of water passage at the outflow in conformance with the best practice in fluid mechanics.

Two methods of balancing the pressure and discharge throughout the 360 deg of impeller periphery were investigated. The first casing provided for a variable amount of expansion in the diffuser ring with the greatest rate of expansion in the diffuser immediately following the tongue of the casing, because of the greater amount of friction head developed beyond this point. The estimated loss of pressure throughout the entire casing at rated capacity was approximately 2.20 ft, and therefore it was necessary to provide 2.20 ft greater recovery of velocity head in the first diffuser, as compared to the last diffuser. These adjustments were made on all vanes in a manner which would produce the same effective pressure around the periphery of the impeller thereby minimizing the amount of unbalanced hydraulic side thrust and creating substantially a uniform rate of flow through the various passages of the impeller.

It is possible that the sudden change in pressure within the passages of an impeller, as the vanes pass the tongue of the pump

casing, may be one of the contributing factors to excessive cavitation and vibration. A sudden change in velocity of flow through a pump impeller when created by a change in pressure would have a cavitation effect because of the presence of inertia similar to that of a vibrating column as used in commercial cavitation-testing apparatus. The favorable sigma value obtained with the 12-vane diffuser casing in the initial tests, where the pressure around the impeller was substantially uniform, lends support to this concept.

Further investigations of the optimum design of diffuser casings resulted in the development of the method shown in Fig. 27(a). The purpose of this design is also to compensate for the losses in pressure head around the periphery of the impeller due to friction. The equalizing effect is accomplished within the casing proper by the transfer of momentum from the relatively higher velocity jets issuing from each consecutive diffuser to the slower moving fluid having been discharged into the casing from previous diffusers. This method may be compared to the transfer of momentum and conversion to pressure of fluids as utilized in jet-pump designs whereby the momentum of one mass is transferred to a second mass having a lesser velocity in accordance with basic laws. The momentum theory states that $M_1 + M_2 = M_3$ or $Q_1 V_1 + Q_2 V_2 = Q_3 V_3$, that is, the velocity after mixing

$$V_3 = \frac{Q_1 V_1 + Q_2 V_2}{Q_3}$$

is illustrated in Fig. 27(a).

The momentum transfer design of casing requires that the difference in velocity head, as represented by the momentum and

pressure formula between each adjacent vane, will be equal to the friction head developed in the distance corresponding to f , as shown on the diagram of Fig. 27(a). This procedure differs from the one previously described in the respect that the recovery of velocity head required to compensate for the loss of friction head in the corresponding section is created in the casing, whereas in the first design, the recovery was effected within the first-stage diffuser ring.

After completion of the tests on the vanes with varying clearances between the impeller and diffuser entrances, the vanes were cut off at the discharge edge until the outflow area of all diffusers were equal. The test on the altered diffuser ring did not result in any noticeable change in pump performance, and it is concluded that the refinement resulting from variable length diffusers is not justified. The author has apparently come to the same conclusion as the illustrations indicate that all six diffusers of the final design are identical. Initial results did not indicate that the principle of the first design was important and the second lacks experimental confirmation. The proposed methods, however, serve the purpose of arriving at a design of casing based on sound engineering principles.

A casing designed to equalize the pressures around the pump impeller, independently of the friction developed within the casing, has been designated as a "compensated" casing and differs from the conventional casing without a diffuser ring approximately as shown in Fig. 27(c). Comparing the compensated casing, having an optimum amount of diffusion in the first stage with the casing described by the author, indicates that a proper design of 12-vane diffuser ring would require a somewhat larger casing than the conventional casing. It is likely that the difference in performance between the 6 and 12-vane diffusers, as shown in Fig. 5 of the paper, may be the result of an inadequate amount of diffusion in the first stage, and to the small hydraulic channels external to the diffusers. Early experiments with rings of various diameters would indicate this possibility.

The author refers to the difficulty of developing the desired pumping capacity under the wide range of effective heads required for the Grand Coulee development. During the early stages of the preliminary investigations conducted by the Bureau, it was realized that this objective may not have been possible of attainment. Accordingly, the prime movers for the Grand Coulee pumps were purchased with provisions for variations in speed of 15 per cent above and below normal so that the best speed for pump operation could be obtained. Results of the investigations made to determine the effect of a change in speed of the pumping unit on the steepness of the head-discharge curve are presented in Figs. 25 and 26 herewith. These data show that the steepness of the head-discharge curves may be affected appreciably by changing the speed of the unit.

On the basis of the preliminary experiments, the specifications for the pumps required that satisfactory operation be obtained at constant speed throughout the full range of pumping heads. It was contemplated that the successful bidder would select characteristics whereby the rated speed of the unit was increased above the normal optimum speed in an amount which would result in the desired operating characteristics within the specified range. It was realized that the required performance would be obtained at an increase in cost of the pumping equipment since the capacity of the pump is lessened as its speed is increased. This, however, was considered to be a proper approach to the problem since it offered means of operating the pumps at synchronous speeds from commercial electrical distribution systems at all times. This flexibility was highly desirable because of the possibility of utilizing excess energy for pumping which might be available from associated generating plants. It was also realized that some doubt would develop regarding the hydraulic performance ob-

tainable over such a wide range of head, and the minimum acceptable warranty of efficiency was lowered accordingly.

The author has further explored the possibility of increasing the steepness of the head-capacity curve, as shown in Fig. 4 of the paper, where it is evident that an adjustment at the entrance edge of the diffuser considerably affects the steepness of the head-capacity curve. Some of the differences shown in this curve may be due to an increase in radial clearance between the periphery of the impeller and the entering edge of the diffuser vanes.

In turbine practice it has been established that the clearance between the movable and stationary vanes should not be less than 4 per cent of the diameter of the runner at the vane tips. In the experiments conducted by the Bureau, a similar relation was found to exist for pumps. The first model tested used a diffuser vane having a clearance at the periphery of the impeller of approximately 3 per cent of the impeller diameter. The performance was erratic and generally unsatisfactory. The vanes were then cut back until a clearance of approximately 4 per cent of the impeller diameter was obtained, and satisfactory performance resulted. Further cutting of the vanes resulted in a loss in pump performance.

The difference in the slope of the head-capacity curves shown in Fig. 3 of the paper, may be due in part to the influence of the volute and diffuser vanes upon the characteristics of the flow as it leaves the pump impeller. It will be noted that the slope of the curve for the double-volute casing is somewhat more favorable than that of the fixed-vane diffuser casing. Best results are obtained with a fixed-vane diffuser if velocity traverses are first made to determine the exact angle of discharge from the impeller while it was being operated in a single-volute casing and the entrance to the diffusers designed to accommodate the actual measured angle of flow. It is not believed that the calculated angle is sufficiently accurate for the purpose of designing the entrance to the diffusers.

The wide range of development work described in the paper is the result of an interest in the Grand Coulee pumps and related engineering development work considerably beyond the requirement for the manufacture of adequate pumping equipment. The author and his associates are to be highly commended for the professional attitude manifested in this important undertaking and the industry, as a whole, is indebted to this symposium for the presentation of the engineering problems and their solution in connection with the world's outstanding pumping development.

R. T. KNAPP.⁵ This is an exceptional paper, not only because it presents the performance of an exceptionally good pump, but also because it gives in detail the steps taken and the reasons for taking them in the design and development program that led to this very successful result. Both the author and his company are to be congratulated on their achievement and their farsightedness in making this technical information available to the engineering profession. The writer is confident that this policy of free exchange of knowledge will prove to be of benefit not only to the engineering profession at large, but also to the individual organizations contributing to it.

The writer would like to emphasize one point brought out by the paper. It should be remembered that the diffuser-case design was selected for the Grand Coulee pumps, not for hydraulic reasons but to secure greater mechanical strength and lower cost of manufacture. These factors were of major importance in this installation, both because of the tremendous size of the pump units and also because of the exceptionally low cost of electric power for their operation. From an hydraulic point of view, it is nearly certain that if the double-volute design could have been

⁵ Director, Hydrodynamics Laboratory, California Institute of Technology, Pasadena, Calif. Mem. ASME.

used, somewhat better performance characteristics would have been obtained; specifically, the head-capacity characteristic would have been somewhat steeper, and the average efficiency would have been slightly higher. Therefore, although this design of the Grand Coulee pump represents a sizable step forward in the development of the diffuser-case volute pumps, it does not mean that it will now become the cure-all for all pump problems. Diffuser-case pumps now simply join the ranks of good design, superior for some applications, of equal merit with different types for other installations, and inferior to other designs for still other requirements.

It is interesting to note that the Grand Coulee pump departs quite radically from all previous diffuser-case designs employed in American and European practice. Although this design is described as a diffuser-case pump, it is truly a cross between the normal fixed-vane diffuser design and double-volute case. As such, it has some of the merits of both. One of the fundamental virtues of the double-volute type of design is that it establishes two symmetrical discharge zones around the periphery of the impeller, and thus creates automatically a balanced system of radial forces for all conditions of flow. The separating rib of the Grand Coulee pump divides the case very effectively into two symmetrical volutes, each containing two fixed diffuser vanes. This geometrical result is shown very clearly in Fig. 6 of the paper. Furthermore, Fig. 20 gives the measurements which show the effectiveness of this construction in securing low radial thrusts for all values of discharge.

There is another aspect of this pump that deserves emphasis. Up until very recently most pumps, large or small, have been purchased from specifications which required given performance characteristics at one operating point only. Specifications might also request a certain general shape of the head-capacity curve and describe other desirable operating characteristics. Contrast this to the requirements for the Grand Coulee machine. Here the minimum capacities are specified at two widely separated heads. The minimum efficiency is specified at one of these heads and the maximum brake horsepower is specified at still a third head. Furthermore, the pump must operate over this entire head range with complete freedom from cavitation. It would seem that this represents a definite trend for the future requirements which will be set up for large units. Such pumps are truly "tailor-made" to fit the measurements of the installation. The Grand Coulee pump is a fine example of how good a fit the manufacturer can obtain for his customer with the help of a well-planned and executed design and development program.

The writer must confess to some amusement concerning the dilemma in which both the manufacturer and the purchaser found themselves concerning the measurement of discharge head. The resulting solution might be called the triumph of specifications over good engineering judgment. As can be seen from the paper, the test results established quite clearly that for the velocity distribution existing in the diffuser a short 10-deg diffuser followed by a length of full-diameter pipe was a little more efficient energy converter than the long 3-deg diffuser. Nevertheless, to meet the specifications the manufacturer is required to furnish a long diffuser and the purchaser to install it even though he thereby secures a slightly less efficient installation than if he had accepted the original design. This minor incident does not detract from the remarkably fine co-operation between the purchaser, the manufacturer, and the laboratory that existed throughout this successful development program.

A. J. STEPANOFF.⁶ The testing program reported by the author

⁶ Development Engineer, Ingersoll-Rand Company, Phillipsburg, N. J. Mem. ASME.

was initiated with the intent to find a better type of pump to meet special conditions of one particular installation. However, the problems investigated are of general interest and deal with the most intimate design features for which it is possible to build up a theoretical background and in this way to make results applicable to different types.

The following points are of particular interest to the writer: The first deals with the moot question of the impeller-inlet conditions. In a great majority of existing designs the impeller-inlet angles are "exaggerated," or are considerably higher than those required for "shockless" entrance at the best efficiency point. The reason for such design can be traced to a quite common misconception that exaggerated inlet angles improve cavitation qualities of the impeller. Although a larger area for the relative flow accompanies higher inlet angles, this may not produce a greater flow for a fixed net positive suction head because a sizable portion of this area is not available to the flow on account of a bad (high) angle of attack. The author's tests prove this. This has been known for some time to the leading pump manufacturers.⁷

On the entrance-velocity triangles *A* and *B*, Fig. 11 of the paper, the author selects the vane-inlet angles for the impeller eye and hub diameters in such a way that the two lines intersect on figure *A* about 14 deg to the right and on figure *B*, 16 deg to the left of the vertical axis, both at capacities corresponding to the head of 310 ft. This latter is not a best efficiency or design point. The objection to such an arrangement is that by allowing the same linear prerotation or the same tangential component of the absolute velocity (c_{u1}) for two different diameters would require a different angular velocity for these two streamlines. Assuming the same pattern of flow will extend to the center of the eye, this would result in an infinite angular velocity there. This is hard to visualize in view of a constant angular velocity of impeller causing this prerotation.

A much simpler pattern of flow and a simpler rule for layout of impeller-inlet angles is obtained if the two lines representing the impeller vane angles are made to intersect on the vertical axis shown in Fig. 28 herewith. Then a desired degree of prerotation is obtained by moving point of intersection *D*, or changing the ratio P_{12}/c_{m1} , where c_{m1} is the meridional velocity at the best efficiency point. This ratio can be established experimentally for different suction-nozzle designs. Thus for horizontally split double-suction pumps, this ratio, being a measure of the degree of prerotation, is within the limits 1.25 to 1.42. For pumps with end suction nozzle, like the author's pumps, lower values should be used. If the velocity triangles in Fig. 11 of the paper are redrawn to comply with the foregoing method, and keeping the same angles at the impeller eye (28 deg for *A*, and 21 deg for *B*), the ratio $P_{12}/c_{m1} = 1.41$ for *A*, and 1.115 for *B* are obtained. The

⁷ The National Transit Pump and Machine Company, in its Bulletin 6000, 1947, p. 4, states that the minimum net positive suction-head requirement is accomplished by "using lowest practical impeller-vane inlet angles" and maximum impeller eye area.

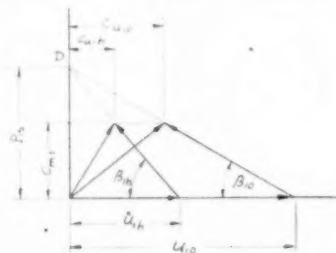


FIG. 28 INLET-VELOCITY TRIANGLE

angle at the hub will change from 48 to 44 deg for A , and from 33 to 34½ deg for B . The effect of such change on performance, if any, will be insignificant, but the method has the advantage of simplicity and a better theoretical reasoning.

The physical meaning of the ratio P_{12}/c_{m1} is the ratio of "shockless" capacity to the normal or design capacity Q_0/Q_n . The writer has shown in a previous publication⁸ that the best efficiency point always occurs at a capacity lower than the shockless capacity. The pattern of flow following from the described method of inlet-vane layout requires a constant angular velocity of prerotation at any capacity, which is the easiest thing to imagine and natural to expect.

It should be realized that the impeller-inlet conditions play only a minor part in comparison to the impeller discharge in locating the shockless and normal capacity of the pump.

A study of the discharge conditions from the impeller also is interesting and instructive. For this the writer has plotted the best efficiency points of the tests from Figs. 10 and 13, on the writer's chart of centrifugal-pump characteristics⁹ (Fig. 29 of this discussion). On this, heads and capacities appear in dimensionless form, (points E, F, G, H), and actual discharge-velocity triangles are obtained by joining these points with points A and O . All velocities appear on this chart as ratios to the impeller peripheral velocity at discharge. From inspection of this figure the following can be stated:

1 The points plot very closely on the respective lines of the discharge angle β_2 , the two high angle points fall slightly above

⁸ "Centrifugal and Axial Flow Pumps," by A. J. Stepanoff, John Wiley & Sons, Inc., New York, N. Y., 1948, p. 173.

⁹ Ibid., footnote 1, p. 184.

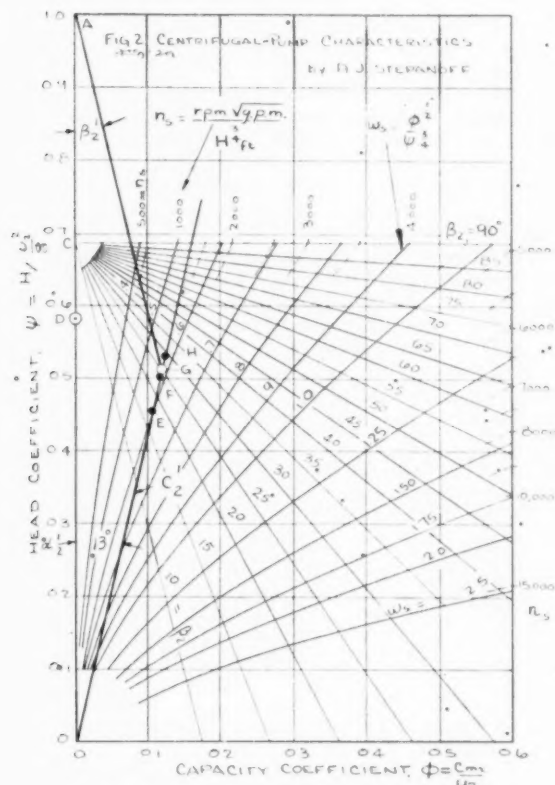


FIG. 29 CENTRIFUGAL-PUMP CHARACTERISTICS

their respective lines. The latter could be expected as the performance of the author's pumps is better than those for which the chart was intended (best commercial pumps).

2 The absolute discharge velocity angle α_2' measures 13 deg. As far as can be ascertained from the small-scale drawings of the paper, the angle of the mean line of the diffuser vanes in B of Fig. 4 is approximately 13 deg.

3 Note that all points fall on the same line of c_2' (13 deg from the axis of heads), indicating that the peak-efficiency point is determined by the pump casing, which was the same for three impellers. If the casing were to be changed to suit the impeller-discharge angles, points would follow the constant specific-speed line, which is associated with a given impeller profile.

4 The absolute velocity at the impeller discharge for the point G (test Fig. 13) scales 0.525, which corresponds to $0.525 \times 146.3 = 76.8$ fps absolute velocity ($u_2 = 146.3$ is the peripheral velocity at discharge). The average velocity at the diffuser inlet is calculated to be $c_3 = 54.8$ fps. Some time ago the writer had prepared a curve, reproduced in Fig. 30 herewith, of what was called "volute velocity distribution factor" $c_3/c_2' = R_{c3}$. For the point G this factor is $54.8/76.8 = 0.713$ which falls on the curve in Fig. 30.

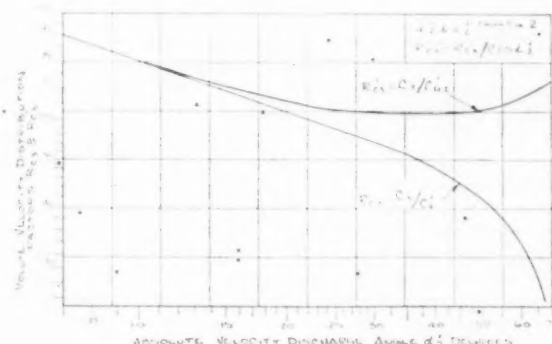


FIG. 30 VOLUTE VELOCITY-DISTRIBUTION FACTORS

The casing velocity-distribution factor represents the ratio of the average velocity in the volute or diffusion-vane casing to the maximum velocity at the impeller discharge. This latter is given approximately but very accurately by the writer's chart, Fig. 29.

The pump casing as finally adopted, with 6 vanes, was intended to provide mechanical strength to the casing and thus reduce its size and weight. Hydraulically the casing is equivalent to a double volute—with an addition of 4 guide vanes. With a diffusion angle of 40 deg in the radial plane (profile) and a small vane overlap, the 6-vane casing does not make a good diffuser.

The beneficial effect of the "rib" on the velocity distribution, Fig. 6(a), and efficiency, Fig. 7, can be observed on any double-volute pump as compared with single volute. In other words, hydraulically the 6-vane casing has no advantage over a double volute.

B. L. VANDERBOEGH.¹⁰ The extensive and painstaking research necessary to design pumps of this magnitude becomes evident when the testing-program results are released. The author is to be commended for his clear presentation of valuable data.

Comments by the author on several points would be enlightening. It would be interesting to compare tests made with the

¹⁰ Hydraulic Division, Newport News Shipbuilding and Dry Dock Company, Newport News, Va. Mem. ASME.

smooth pump casing with those of the segmented casing to learn of the degree of difference in frictional losses between the two.

It is noted the specifications permitted lengthening the pump-discharge nozzle beyond the original location, with a resulting gain in efficiency and head when pressure readings were taken farther downstream. This increased length was not allowed in testing the Granby pump models, and so, with due allowance for the difference in specific speeds and casing design, a comparison of test results is difficult. It is strongly urged that the recommendations of the Hydraulic Institute be followed in locating discharge piezometer connections. Pumps then would be allowed to develop their full heads and test results would be comparable.

In Fig. 6 of the paper the overlap of the diffuser vanes appears to be about 25 per cent of the vane length. This is a relatively short distance to allow for diffusion, and the reasoning that the water is more guided than diffused seems proper, for the figure also shows a rather rapid enlargement between vanes. Comments as to the percentage of velocity decrease in this diffusion area would be of interest.

It is noted in Fig. 16 of the paper that the point of discontinuity lies outside the operating range. This instability occurs at about 2 per cent above the high head condition and extends over a fairly broad range. A margin of 2 per cent appears relatively slight when it is considered that a surge of approximately 200 cfs is involved.

It is believed that data were taken well below the 270-ft head condition, but the H-Q test curves are not completely shown. Perhaps the author will describe the shape of the H-Q curve below 270 ft head and mention where cutoff occurred.

AUTHOR'S CLOSURE

The Bureau of Reclamation took an active part in the preliminary Grand Coulee model-testing program and also developed the first diffuser-type casing, so Mr. Winter's comments are therefore of particular interest and his discussion a valuable addition to this paper.

Mr. Winter suggests that a larger diffuser case with a greater diffuser expansion should reduce the unstable portion of the performance curve near the high-head condition shown in Fig. 3 of the paper. The author ran performance tests with the same impeller in two 6-vane diffuser cases, which had the same diffuser-vane entrance area but different ratio of the diffuser-vane inlet-to-outlet area. This ratio was 1.5 for a small case, the same as used in the final model for Grand Coulee, and 2.5 for a large case. The performance with the large case did not show any noticeable improvement in the unstable head-capacity range over the small case. The pump efficiency, however, as mentioned in the paper, was slightly higher for the pump with the large case than for the small case, and about equal to the pump efficiency obtained with the small case furnished with the separating rib. However, the weight of the large case was 25 per cent heavier than the small case.

The two types of diffuser-vane designs, investigated by Mr. Winter, to develop even pressure distribution around the impeller periphery have a great deal of merit. His reasoning, however, is based upon the assumption that the outlet velocity from the diffusers and the velocity in the volute sections are uniform. Actual measurements show uneven velocity distribution at the end of the volute discharge cone (see Fig. 8 of the paper), and the velocity distribution between the diffuser vanes shows a greater variation. It is therefore difficult to suggest a diffuser-vane design which will give balanced pressure distribution around the periphery before this uneven velocity type of flow has been further explored.

The effect of change of speed on the steepness of the performance curves, shown in Fig. 25 and Fig. 26, gives the mis-

leading impression that the slope of the performance curve could easily be changed. These curves are calculated from the same model performance by changing the size model ratio, which means operating the model at different speeds to meet the same operating point. This, in reality, is nothing more than moving the operating point up and down the same performance curve. The smaller pump at higher speed would move the operating point down on the performance curve and result in a steeper performance curve, but with reduced pump efficiency at the 310-ft operating point (see Fig. 16). A larger pump at lower speed would move the operating point up on the performance curve and improve the pump efficiency at the 310-ft operating point, but the high-head point would move closer to the unstable portion of the head-capacity curve.

The author agrees with Dr. Knapp that the Grand Coulee type diffuser casing has no hydraulic advantage over the double-volute case, but is hydraulically inferior. Unquestionably, the double-volute case will remain the practical and best solution in most pump designs, and the division line between it and the Grand Coulee type case will be determined by various factors, such as, size, test pressure, number of units involved, and others. Dr. Knapp's complimentary remarks, which clear up further some of the problems posed by the condition of operation of these pumps, are greatly appreciated.

Dr. Stepanoff shows a suction-vane layout, which has a better theoretical background than the one used by the author, if we suppose uniform radial velocity approach in the impeller eye at all capacities. In the design of entrance-velocity diagrams, consideration should be given to the uneven flow distribution in the impeller eye, which is of greater variation than measured at the suction flange, shown in Fig. 21 of the paper. The author agrees that the minor differences in vane angle arrived at by Stepanoff's and the author's procedure will have no significant effect on the performance.

The author feels gratified that the model-test results and pump proportions are in agreement with Stepanoff's excellent charts. The author objects to the quotation that the minimum suction-head requirements are obtained by using lowest practical impeller-vane inlet angles and maximum impeller-eye area. While the word, "practical" somewhat excuses the statement, it is well known to designers that the cavitation depends on the absolute inlet velocity which is the vector sum of peripheral and radial velocity, and that there is a ratio of these two velocities at which the cavitation will occur at the minimum head.

The pump casing as finally adopted is not equivalent to a double-volute case with additional guide vanes as claimed by Dr. Knapp and Dr. Stepanoff, but must be considered as a diffuser-type case with a dividing rib. The main purpose of a double-volute-case design is to balance the radial forces acting on the impeller, and therefore all volute sections 180 deg apart in a double-volute case are identical in area and shape. In the separating-rib-type case, however, the final volute sections 180 deg apart differ materially in shape with a half-circle shape in one, and a trapezoid shape in the other.

The last paragraph in Dr. Knapp's discussion is an excellent answer to Mr. VanderBoegh's remark regarding the length of the discharge cone. The author strongly supports Mr. VanderBoegh's recommendation that pump specifications should be based upon the Standards of the Hydraulic Institute and no deviations allowed.

The diffuser-vane length is determined by the chosen pump-case size or the ratio of diffuser-vane inlet-to-outlet area. A ratio of 1.5 was used in the diffuser-case design finally adopted, and the total diffuser-vane cone angle in the direction of flow was 12 deg, which is somewhat larger than the 8 deg recommended for uniform flow. In pump cases where the flow is far from uniform,

tests with cases having a total discharge-cone angle of 15 deg, have given the same pump efficiency as cases with 8 deg.

The instability in the head-capacity curve is admittedly close to the high-head operating point, but it is difficult to determine the percentage of safety required to guard against surges. The model development accomplished two major improvements in this respect: (1) It moved the unstable portion of the horsepower curve further away from the high-head point. (2) It eliminated the dip in the head-capacity curve, and thereby pre-

vented the pump from passing over a hump in the performance in case of a major surge.

Test data were taken for heads as low as 200 ft with 145 ft NPSH at the pump suction, and the head-capacity curve continued on the smooth curve without a sign of instability or cut-off.

In conclusion, the author wishes to thank the discussers for their encouraging comments and valuable contributions to this paper.

In
wh
rigi
be c
indi
for
men
in a
and
(wat
all
cuss
spon
nece
atta
conc

I
tions
In m
conn
attac
sensi
porti
cation
conv
than
twel
inter
from
Th
fer h
tive
requi
meas
vesse
the c
of th
The
stead
heat
In th
head
loss
temp
stalla

D
Cor
sion
May
NEER
Not
under
the So

Heat-Conduction Errors in Temperature Measurements

By L. E. SMITH,¹ WATERBURY, CONN.

In practical applications of temperature measurements where the temperature-sensitive bulb assembly is fastened rigidly to a containing vessel, heat-conduction errors must be considered in order to determine the accuracy of the indicated or recorded temperature. This paper presents for various thermometer-bulb assemblies, the experimental magnitude of the heat-conduction error possible in a medium with a low heat-transfer coefficient (air), and in a medium with a high heat-transfer coefficient (water). The effect of heat-conduction error on the overall response in simulated practical installations is discussed. It is shown that comparative information on response action of any type of temperature-sensitive element necessitates careful considerations of the condition of attaching the element to a wall or vessel, where heat-conduction effects are present.

PRACTICAL CONSIDERATIONS

IN practical applications of temperature-measuring instruments, it is desirable that the temperature of the medium be indicated or recorded accurately and promptly, despite variations of the temperature outside the vessel containing the medium. In many applications, the measuring bulb, by means of a union connection, is fastened rigidly into a threaded bushing which is attached permanently to the containing wall. A supporting non-sensitive extension for the bulb usually separates the sensitive portion from the union connection, Fig. 1. For other applications, the bulb is inserted into a protecting well, Fig. 2, and for convenience of removal it is necessary that the bulb be smaller than the inside diameter of the well, resulting in an air gap between the bulb and the well. A liquid or metallic filler may be interposed between them, but in all cases, the transfer of heat from the medium to the sensitive portion of the bulb is retarded.

The primary requirement in measuring temperature is to transfer heat from the measured medium to the fluid inside of the sensitive portion of the bulb in the shortest possible time. It is also required that a minimum amount of the heat available from the measured medium must be lost to the union connection and vessel walls by way of the bulb extension. Where a well is used, the condition is aggravated because heat will also escape by way of that portion of the well which surrounds the bulb extension. The accuracy of measurement for a given application under a steady state of heat flow will be dependent upon the amount of heat lost to the union connection and the well head in a unit time. In the majority of cases, the temperature around the thermometer head will change with time, causing a change in the rate of heat loss. This change in heat flow will also influence the indicated temperature reading, an effect particularly emphasized in installations where the measured medium has a low heat-transfer

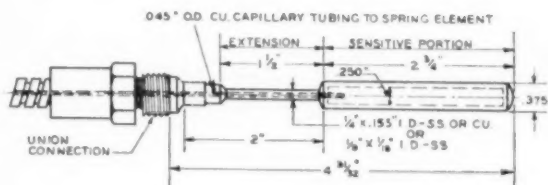


FIG. 1 UNION-CONNECTED BULB

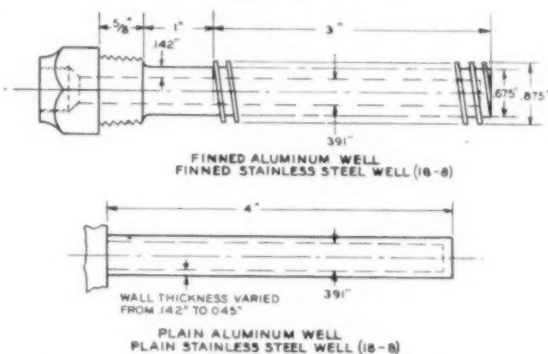


FIG. 2 VARIOUS WELLS USED WITH UNION-CONNECTED BULBS

value, such as flowing gas or air. Here, too, the over-all rate of response of the thermometer bulb will be seriously affected.

Others have written papers on response characteristics of thermometer elements (1, 2, 3)² and heat-conduction effects (4, 5). The object of this paper is to present experimental data simulating practical applications, to indicate the magnitude of heat-conduction errors, and to show how heat conduction influences the response time of thermometer bulbs. Means for improving the over-all performance of an installation are studied. Filled-system thermometer assemblies are utilized in this investigation, but similar results will be obtained with resistance-bulb or thermocouple assemblies.

TEST EQUIPMENT

The thermometer system used in the tests was liquid-filled, and consisted of a union-connected bulb, Fig. 1, which was connected to the recording Bourdon-spring element by 10 feet of capillary tubing. The spring element was installed in a regular recording-thermometer case, and readings recorded on a 12-in.-diam chart driven by a clock mechanism. This system was of the fully compensated variety, so that changes in ambient temperature of the capillary tubing or spring element had no effect on the recorded reading.

In the case of the union-connected bulb with bushing, all heat-conduction loss is through the extension, and the factors which affect the rate of heat loss from the sensitive portion of the bulb to the head and bushing for a given application are as follows:

² Numbers in parentheses refer to the Bibliography at the end of the paper.

¹ Development Engineer, The Bristol Company.

Contributed by the Industrial Instruments and Regulators Division and presented at the Spring Meeting, New London, Conn., May 2-4, 1949, of THE AMERICAN SOCIETY OF MECHANICAL ENGINEERS.

NOTE: Statements and opinions advanced in papers are to be understood as individual expressions of their authors and not those of the Society. Paper No. 49-8-35.

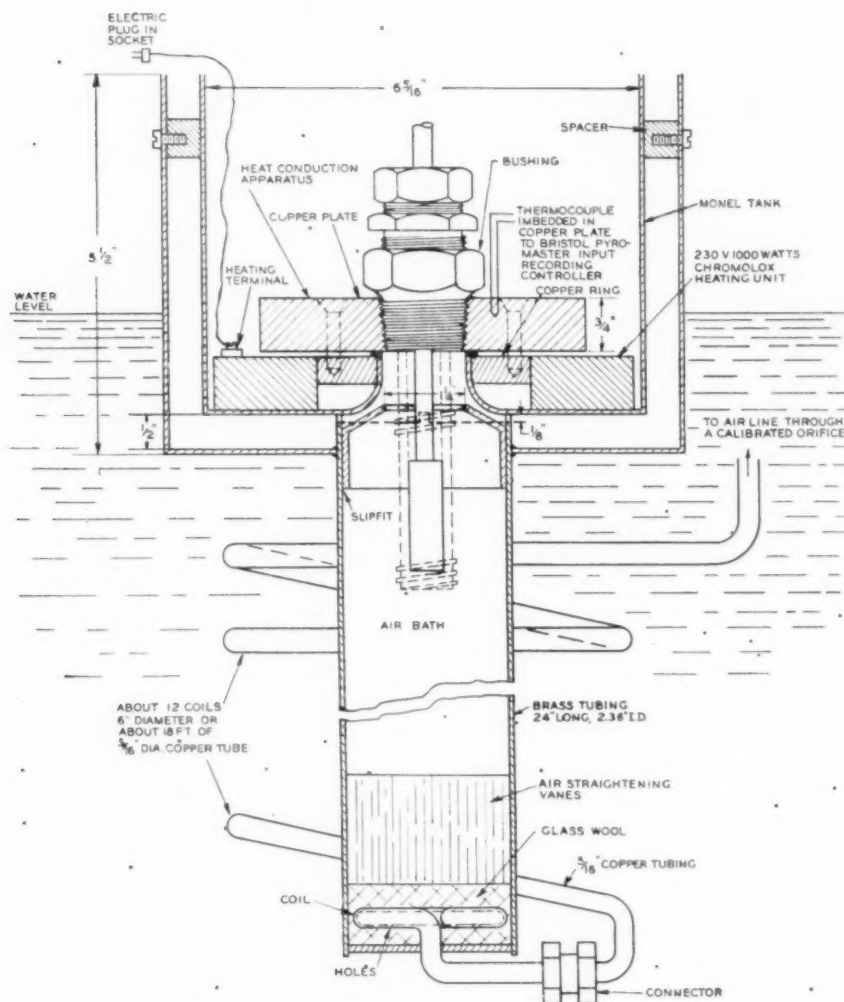


FIG. 3 HEAT-CONDUCTION APPARATUS INSTALLED IN AIR BATH

(a) The thermal conductivity of the material of the extension; (b) the cross-sectional area of the extension; (c) the length of the extension. In the tests, the following combinations of bulb and extension were used (extension was $1\frac{1}{2}$ in. long in all cases; see Fig. 1, for actual dimensions):

- 1 Copper bulb, with $\frac{1}{4}$ -in-OD \times 0.155-in-ID copper extension.
- 2 18-8 stainless-steel bulb, with $\frac{1}{4}$ -in-OD \times 0.155-in-ID 18-8 stainless-steel extension.
- 3 18-8 stainless-steel bulb, with $\frac{1}{8}$ -in-OD \times $\frac{1}{16}$ -in-ID 18-8 stainless-steel extension.

When the bulb is installed in a well, the heat loss is the total through the portion of well surrounding the extension, and that through the extension. The design factors which affect the rate of heat loss from the body of the well surrounding the sensitive portion of the bulb are the same as for the bulb extension. In the design of the well it is possible to increase the external area of the surface exposed to the medium to improve the rate of heat flow. The following combinations were used to determine the effect of the various factors (see Fig. 2 for well designs):

- 1 Copper bulb with $\frac{1}{4}$ -in-OD \times 0.155-in-ID copper extension in (a) a finned aluminum well with 0.142-in. wall; (b) a finned 18-8 stainless-steel well with 0.142-in. wall.
- 2 18-8 stainless-steel bulb with $\frac{1}{4}$ -in-OD \times 0.155-in-ID 18-8 stainless-steel extension in (a) a finned aluminum well with 0.142-in. wall; (b) a plain aluminum well with 0.142-in. wall; (c) a plain aluminum well with 0.045-in. wall; (d) a finned 18-8 stainless-steel well with 0.142-in. wall; (e) a plain 18-8 stainless-steel well with 0.142-in. wall; (f) a plain 18-8 stainless-steel well with 0.045-in. wall.
- 3 18-8 stainless-steel bulb with $\frac{1}{8}$ -in-OD \times $\frac{1}{16}$ -in-ID 18-8 stainless-steel extension in (a) a finned aluminum well with 0.142-in. wall; (b) a plain aluminum well with 0.142-in. wall; (c) a finned 18-8 stainless-steel well with 0.142-in. wall; (d) a plain 18-8 stainless-steel well with 0.142-in. wall; (e) a plain 18-8 stainless-steel well with 0.045-in. wall.

The heat-conduction apparatus used to determine the performance of the bulb and well assemblies is shown in Fig. 3. It consists essentially of a copper plate provided with a pipe thread for holding the well or the bushing for the union-connected bulb. A

thermocouple was imbedded in the copper plate, the temperature of which was recorded continuously and controlled by a recording-potentiometer input controller. Heat was supplied by a resistance coil, and the temperature of the plate was varied by adjusting the set point of the controller. The plate-and-coil assembly was fastened rigidly inside of a monel tank. The complete unit could be handled easily and moved from one water bath to another, or quickly placed in the air chamber, as shown in Fig. 3.

The air chamber was used for studying response action and heat-conduction errors of the various thermometer-bulb assemblies in a flowing air medium. It consisted of a long piece of brass pipe connected rigidly to an upper chamber which housed the heat-conduction apparatus. The air chamber was heated to a constant temperature by first passing the air through $\frac{3}{16}$ -in.-diam coiled copper tubing submerged in a controlled water bath and then bleeding it into the chamber through a number of small holes in the tubing. The flow rate was controlled by measuring the pressure drop across a calibrated orifice, and the velocity of air past the inserted bulb or well in the chamber was calculated.

Air chambers were installed in each of two adjacent water baths, one bath being held at 70 F, the second bath at 120 F.

EXPERIMENTAL PROCEDURE

The tests were conducted in water, a medium with high heat-transfer coefficient, and air, a medium with low heat-transfer coefficient. In the water-medium tests, the heat-conduction apparatus was placed in the cold bath with the monel tank partly submerged. Sufficient time was allowed for the heat-conduction plate and bulb to reach their equilibrium temperature conditions. The apparatus was then transferred quickly to the hot bath, and equilibrium conditions again reached. Time-temperature curves of the bulb-assembly response were obtained on the recording thermometer, and similar curves for the copper conduction plate were obtained on the recording-potentiometer controller. The temperature of the heat-conduction plate was then raised about 50 deg F by connecting the heating unit to the controller, and equilibrium conditions were again reached. The recorded change in the temperature of the bulb assembly was noted for the temperature change of the heat-conduction plate. The change in bulb temperature due to 1 deg change in plate temperature is called the "extension conduction error," a term which will be used throughout this paper.

In the air-medium tests, the heat-conduction-plate apparatus with bulb assembly, installed in the air-chamber unit, was located in the cold-water bath. Response of the bulb assembly in air at a given velocity was determined by transferring the heat-con-

duction-plate apparatus from the cold-air chamber to the hot-air chamber. The procedure was identical with that in the water-bath tests, except that the temperature of the heat-conduction plate was raised in 20 F intervals to provide additional points on the extension conduction-error curve.

In addition to the foregoing tests, the response of the various bulb and well combinations in the water bath and air bath was obtained in the usual way without the heat-conduction apparatus, that is, by moving the unattached bulb assembly from one bath to the other. In the air bath, a third method of obtaining response was utilized. The heat-conduction plate was heated up to the hot-air temperature prior to the insertion of the heat-conduction apparatus from the cold-air chamber to the hot-air chamber. It remained in the cold-air chamber until temperature equilibrium was obtained. Extension conduction effect on the response action was thus obtained from heat flowing into the sensitive portion of the bulb.

DATA DERIVED FROM TESTS

Water-Bath Tests. The response time for a 63.2 per cent change (1) (called time constant or time lag), a 90 per cent change, and the heat-conduction factor are tabulated in Table 1 for an agi-

TABLE 1 PERFORMANCE OF UNION-CONNECTED BULB ASSEMBLIES IN AGITATED WATER*

Well used	Response time, sec—		Extension conduction error	Heat-conduction apparatus
	63.2 Per cent change	90 Per cent change		
None.....	14	31	0.010	Yes
	14	31		No
Finned.....	63	132	0.050	Yes
aluminum.....	57	120		No
Plain.....	63	132	0.056	Yes
aluminum.....	57	120		No
0.045-in. wall				
Plain.....	78	175	0.059	Yes
stainless steel, 0.045-in. wall	71	152		No

* $\frac{1}{4}$ -in.-OD \times 0.155-in.-ID stainless-steel extension.

tated water-bath medium. The complete response actions of the bare bulb and the various bulb and well combinations are shown in Fig. 4. It should be noted that data include tests made both with the assembly attached and not attached to the heat-conduction plate. In all these tests a stainless-steel bulb with a $\frac{1}{4}$ -in.-OD \times 0.155-in.-ID stainless-steel extension was used.

It is seen that with a bulb assembly immersed in a fluid with a high heat-transfer coefficient such as water:

- 1 The heat-conduction plate has no effect on the response of

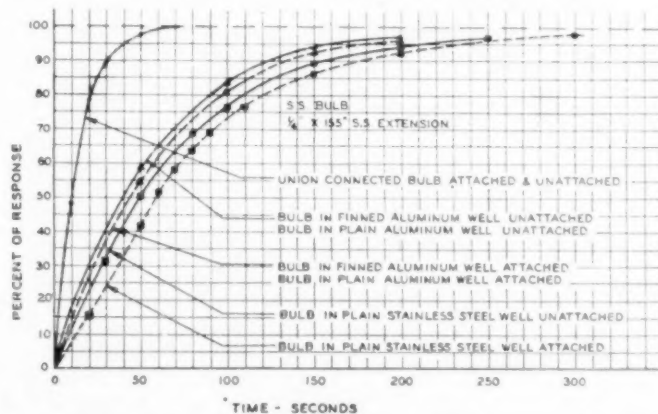


FIG. 4 RESPONSE IN WATER WITH AND WITHOUT HEAT-CONDUCTION APPARATUS

the union-connected bulb assembly with bushing whose extension-conduction error was very low.

2 The heat-conduction plate has only a small effect on the response of the union-connected bulb assembly with well. The response action is slowed down about 10 per cent when the heat-conduction apparatus is used.

3 The material of the well has some effect on the response, the response depending upon the thermal conductivity and heat capacity of the well material.

4 The use of fins on a well, as applied and designed here, does not improve the response or materially affect the conduction error.

5 The use of a well produces an extension conduction error which is practically independent of the material of the well.

6 Extension conduction errors are negligible for a bulb with a stainless-steel extension immersion of $1\frac{1}{2}$ in. installed in a bushing.

In order to check the extension conduction effects obtained with the heat-conduction apparatus, a separate installation was made by inserting the well in a bushing welded into the sheet-metal side of the water bath used for the tests. With the bulb installed in any of the listed wells, the recorded reading after equilibrium conditions were obtained was $\frac{3}{4}$ F lower than the reading with the bulb suspended at the same position in the bath, but not rigidly connected to the metal side. The temperature of the exposed head of the well was 105 F, while the water bath itself was 120 F. This gave an extension conduction error of 0.05, which agreed with the results obtained with the heat-conduction apparatus.

It is thus apparent that even in the best of heat-transfer media, the bulb assemblies must be considered carefully. In applications where the length of the extension is shorter, the cross-sectional area of the extension is greater, or the extension material has a higher heat conductivity than the design tested, the extension conduction error will be greatly increased. This condition will be greatly aggravated in poor heat-transfer media, as shown in the following discussion on results in the air bath.

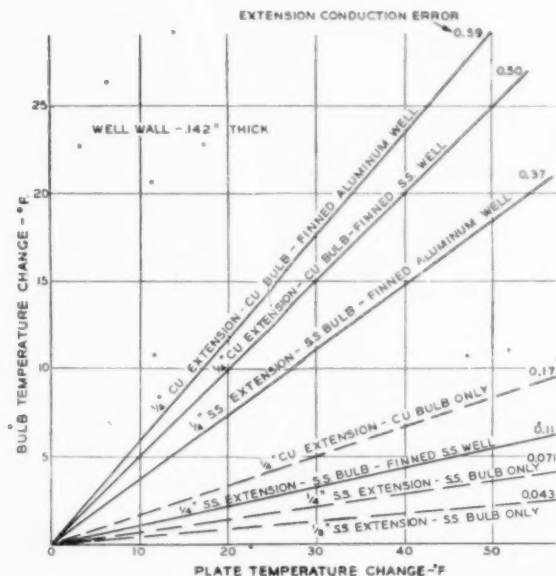


FIG. 5 EXTENSION CONDUCTION ERROR OF VARIOUS UNION-CONNECTED BULB ASSEMBLIES WITH BUSHING AND WITH WELLS (Air velocity, 250 fpm.)

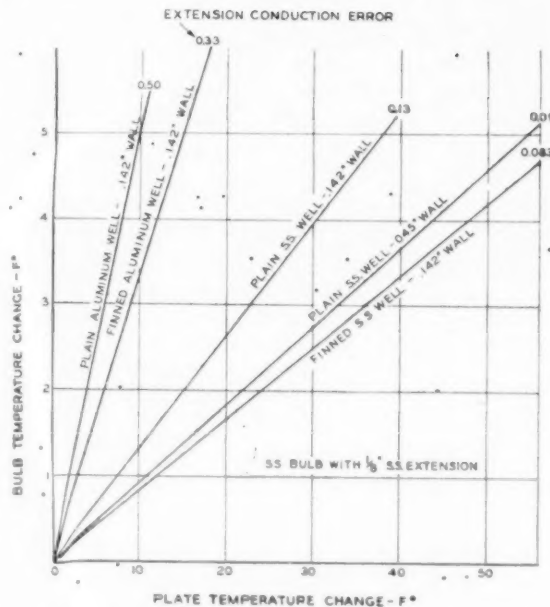


FIG. 6 EFFECT OF FINES ON WELL AND OF WELL THICKNESS (Air velocity, 250 fpm.)

Air Bath Tests. The extension conduction errors obtained with different union-connected bulb assemblies and varying plate temperatures are shown in Fig. 5, for an air velocity of 250 fpm. The relationship between plate temperature and extension conduction error is found to be linear. The following conclusions are possible for the various bulb assemblies with well:

1 The worst combination is a bulb with a good conducting extension (copper) and a good conducting well (aluminum). A 1.7 F change in the plate temperature causes a 1 F change in bulb reading, or 0.59 extension conduction error.

2 If the well material only is changed to a less conducting material (stainless steel) a small improvement is noted; 0.50 extension conduction error.

3 If the extension material is changed to a less conducting material, the improvement is more marked; 0.37 extension conduction error.

4 If both the extension and well materials are changed to less conducting materials, the improvement is outstanding, with the extension conduction error decreased to 0.11. This combination would be a desirable one for practical installations.

In considering bulb assemblies with bushing, in which the bulb is directly exposed to the air medium, the following is observed from Fig. 5:

1 With the $\frac{1}{8}$ -in. copper extension, the extension conduction error is 0.17. Thus this bulb alone produces a greater error than that obtained with the best bulb assembly with well combination in item 4 of the foregoing conclusions.

2 If the extension is changed to $\frac{1}{8}$ -in. stainless steel, the extension conduction error is decreased to 0.071.

3 If the cross-sectional area of the stainless-steel extension is decreased by use of $\frac{1}{8}$ -in-OD \times $\frac{1}{16}$ -in-ID instead of $\frac{1}{8}$ -in-OD \times 0.155-in-ID material (area ratios of 1 to 3), the extension conduction error can be reduced to 0.043.

A series of tests were made on wells to study the effect of fins, and also of the thickness of the well wall on the extension con-

ducti
can b

1

condu
sion o
less-s

2

from
from

It s
of the
 $\frac{1}{8}$ -in-
condu
the st

Res

bulb a
sion o
in all
appars
runs,
from t

In T
is the
with th
temper
test, an
to the
plate.

From

1 T

respons

2 T

the hea
pected,
unit tim

3 T

from on
can be
The div
action is

This p
necessity o

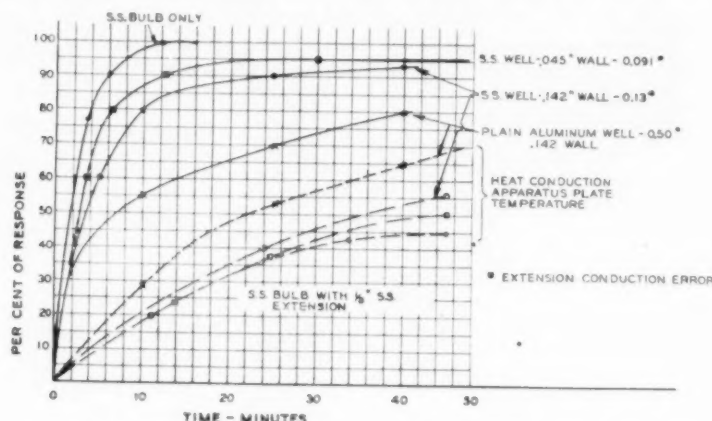


Fig. 7 RESPONSE OF UNION-CONNECTED BULB ASSEMBLY WITH BUSHING AND WITH WELL ATTACHED TO HEAT-CONDUCTION APPARATUS

duction errors (see Fig. 6, for data.). The following conclusions can be made:

1 Removal of the fins from the well increases the extension conduction error. In the case of the aluminum well, the extension conduction error is increased from 0.33 to 0.50; for the stainless-steel well, from 0.083 to 0.132.

2 A decrease in the wall thickness of the stainless-steel well from 0.142 to 0.045 in. decreased the extension conduction error from 0.132 to 0.091.

It should be mentioned that a change in the cross-sectional area of the stainless-steel extension from $\frac{1}{8}$ -in.-OD \times 0.155 in. ID to $\frac{1}{8}$ -in.-OD \times $\frac{1}{16}$ -in.-ID produces a decrease in the extension-conduction error from 0.11 to 0.083, when the bulb is used with the stainless-steel finned well.

Response in Air. In Fig. 7 the response of the union-connected bulb assembly with bushing and wells is shown. A bulb extension of $\frac{1}{8}$ -in.-OD \times $\frac{1}{16}$ -in.-ID stainless-steel material was used in all cases. The actual temperature of the heat-conduction-apparatus plate is also plotted with time for the given response runs. In this part of the test, the plate was allowed to heat up from the natural flow of heat from the well and bulb.

In Table 2, data taken from Fig. 7, are tabulated. Also shown is the 90 per cent response time of the same assemblies obtained with the heat-conduction-apparatus plate heated initially to the temperature of the hotter air bath before beginning the response test, and with the bulb assembly being moved from one chamber to the other without the use of the heat-conduction-apparatus plate.

From Fig. 7 and Table 2 it is seen that:

1 The less the extension conduction error, the better is the response action.

2 The greater the extension conduction error, the faster does the heat-conduction-apparatus plate heat up. This is to be expected, as more heat flows up the well wall and the extension per unit time.

3 The response of a bulb assembly when immersed directly from one bath to another is much better where heat conduction can be disregarded than where heat conduction can function. The divergence between the two methods of obtaining response action is more marked for a poorly designed bulb assembly.

CONCLUSION

This paper has attempted to show the advisability and the necessity of considering the complete design of any type of a tem-

TABLE 2 PERFORMANCE OF UNION-CONNECTED BULB ASSEMBLIES IN AIR AT 250 FPM*

Well used	Response time, min—		Extension conduction error	Heat-conduction apparatus
	63.2 per cent change	90 per cent change		
None.....	2.5	5.7	0.043	Yes
		6.0		Yes—Heated
		5.8		No
Plain aluminum, 0.142-in. wall	16	58	0.50	Yes
		5.6		Yes—Heated
		13		No
Plain stainless steel, 0.142-in. wall	5.3	25	0.13	Yes
		11		Yes—Heated
		15		No
Plain stainless steel, 0.045-in. wall	3.5	13	0.091	Yes
		9		No

* $\frac{1}{8}$ -in.-OD \times $\frac{1}{16}$ -in.-ID stainless-steel extension.

NOTE: Under heat-conduction apparatus, "Yes—heated" refers to the condition where the conduction apparatus was heated before moving the assembly from the cold bath to the hot bath.

perature-measuring bulb from the viewpoint of extension conduction errors, rather than from the response action of a bulb or bulb-and-well combination, as ordinarily obtained by simply moving the bulb or bulb assembly from one bath to another.

In the case of a measured medium with a good heat-transfer coefficient, this common way of obtaining the response characteristic is generally acceptable. However, designs are possible where there may be considerable heat transfer, resulting in large extension conduction errors. This is true in a design with no extension between the sensitive portion of the bulb and the union connection, or where a short extension has a large cross-sectional area and is composed of a good heat-conducting material.

In a poor heat-transfer medium, the usual way of obtaining the response characteristic is not advisable, unless one knows that heat-conduction effects are negligible. Extension conduction errors may be very large in many industrial applications, particularly where it is necessary to use a protecting well. Comparative response actions in practical applications may be entirely different from those obtained by the customary laboratory methods.

In general, it is recognized that the lowest extension-conduction error can be realized by the proper selection of material, a minimum cross-sectional area of the well and the connecting extension of the bulb, and a maximum length of the extension between the sensitive portion of the bulb and the union connection to the well.

Too often, a thermometer system is condemned as having calibration error, or not being properly compensated for ambient-temperature changes. This observation may be based upon a check with a mercury-in-glass test thermometer placed in another well with an extension conduction error which may be much differ-

ent from that of the recording thermometer bulb-and-well installation. The discrepancy noted may be the result of extension conduction errors, and will vary with the ambient temperature. On the other hand, an agreement between the mercury-in-glass thermometer and the tested thermometer system does not necessarily mean accurate calibration, as they may possess similar extension conduction errors. It is necessary to know the magnitude of the extension conduction error of the test thermometer in order to determine the exact performance of the measuring-thermometer system.

The best way to overcome the effects of heat conduction is the familiar method of covering the thermometer head and its containing vessel with insulation so that the head remains at the approximate temperature of the measured medium and will not change measurably with ambient-temperature changes.

This paper has touched upon the high lights of the variables which result in heat-conduction losses, and has not attempted to consider errors due to other effects such as radiation. Such errors

would be added to those from heat conduction to give the over-all errors. Also statements made are based upon a given immersion assembly; for a different immersion, the relative performance may be altered.

BIBLIOGRAPHY

- 1 "Thermometric Time Lag," by Rudolph Beck, Trans. ASME, vol. 63, 1941, pp. 531-543.
- 2 "Response Time and Lag of a Thermometer Element Mounted in a Protecting Case," by W. N. Goodwin, Trans. AIEE, vol. 64, 1945, pp. 665-670.
- 3 "Response Characteristics of Thermometer Elements," by A. J. Hornfeck, Trans. ASME, vol. 71, 1949, pp. 121-133.
- 4 "Heat-Flow Effects in a Resistance-Type Thermometer," by N. P. Millar, Trans. AIEE, vol. 64, 1945, pp. 678-685.
- 5 "Temperaturmessfehler in Gasen und überhitzten Dämpfen Durch Wärmeableitung von der Mass-stelle," by Von H. Reiher and K. Cleve, *Archiv. für Warmewirtschaft und Dampfkesselwesen*, vol. 7, October, 1926, pp. 273-279.

Qua
flange
their
or rati
engine
proble
streng
ternal
bendin
or tem
surrou
intend
latter
which
assembl
and h
calcula

O
made it
formati
has pro
stresses
the pipi
efforts o
Commit
common
their pre
The p
and inve
gasket o
applied
and, pe
forming
arises, n
subject
tions or

The in
the prob
pose of a
ing the
types, at
prehensi
undertak
which us
Cyclic
blies inv

1 Chief
2 Resea
Contrib
Meeting
SOCIETY O
NOTE:
understo
of the Soc

Fatigue Tests on Flanged Assemblies

By A. R. C. MARKL¹ AND H. H. GEORGE,² LOUISVILLE, KY.

Qualitative differences between the various types of pipe flanges in common use have long been recognized, but their quantitative evaluation in terms of rules, formulas, or ratings which could be used as a guide by the practicing engineer has been accomplished only partially. Two problems are involved, i.e., the determination of the strength and tightness of a flanged assembly under internal pressure, and the other the effects of the variable bending moments associated with mechanical vibrations or temperature fluctuations of the flowing medium or surrounding atmosphere. The present investigation is intended to contribute toward an understanding of the latter phase; stress-intensification factors are reported which have been obtained from fatigue tests of full-scale assemblies of 4-in. flanges of the 300-lb ASA pressure class and hence are directly applicable to piping flexibility calculations.

INTRODUCTION

OF LATE, a growing demand for a more complete understanding and detailed evaluation of the components entering into the design of pressure containers and piping has made itself felt. In the pressure-vessel field, this has led to the formation of the Pressure Vessel Research Council which already has produced valuable information on the magnitude of local stresses at shell-to-head junctions and other related problems. In the piping field, evidence of the same trend is to be found in the efforts of a special subgroup of Subcommittee 3 of ASA Sectional Committee B16 to define more closely the limitations of the commonly used types of pipe flanges and to differentiate between their pressure ratings.

The pressure-vessel flange problem is primarily one of statics and involves an evaluation of the interaction of bolt extension, gasket compression, and flange rotation under the effects of an applied bolt load and internal pressure, as it affects flange stress and, perhaps more significantly, joint tightness. For flanges forming part of a piping system, an additional, dynamic problem arises, namely, that of evaluating the useful life of assemblies subject to cyclic bending moments caused by mechanical vibrations or thermal changes.

SCOPE OF TESTS

The investigation reported herein relates to the latter aspect of the problem. While it has been initiated with the express purpose of assisting ASA Committee B16 in its difficult task of defining the proper uses, ratings, and limitations of different flange types, at the same time it is to be considered as part of a comprehensive fatigue-testing program on full-scale piping assemblies undertaken by the authors' company as a service to the industries which use its products.

Cyclically reversed bending tests were carried out on assemblies involving the following types of commonly used flanges:

- (A) Slip-on flanges.
- (B) Socket-welding flanges.
- (C) Welding-neck or butt-welding flanges.
- (D) Ring flanges.
- (E) Lap-joint flanges.
- (F) Threaded flanges.

Wherever different methods of attachment could be visualized, their influence on the life of the assembly was explored separately. For instance, in the case of slip-on flanges, not only were two types of double-welded designs tested, but separate runs were made with a hub weld only and a face weld only, to determine their relative contributions to the endurance strength of the assembly. In the case of socket welding flanges, similar investigations were carried out and, in addition, an attempt was made to evaluate the effect of the relative proximity of front and back welds; also to find out whether any significant differences in strength are evident where the pipe is butted against the bottom of the socket as compared with a loose assembly leaving a gap at the end of the pipe. In the case of threaded flanges, some assemblies were made up with normal thread engagement, and others with the pipe threaded through the flange and refaced. Every one of the basic variants is illustrated in Fig. 1.

All the assemblies involved in the main test series were made using 4-in. carbon-steel flanges of the 300-lb ASA pressure class and standard weight (Schedule 40) pipe, all welding being done by the Heat and Power Corporation, Baltimore, Md., employing welders qualified by The Hartford Inspection and Insurance Company.

Supplementary tests were run with some of the same types of assemblies, but using ordinary experienced welders who had been instructed expressly to deposit the minimum amount of welding which might be considered as passing the requirements of Section VIII of the ASME Boiler Construction Code, the express purpose being to widen the range of the test data and assure that any values derived for design use would be reasonably conservative.

A further supplementary test series, restricted to slip-on and welding neck flanges, was run with pipe of 0.080 in. wall thickness to obtain an idea of the size effect; this test series, besides providing direct information on assemblies involving 4-in. light-wall pipe, also might be considered as a model test of, say, a 12-in. flange attached to standard-weight pipe.

MATERIALS AND PREPARATION

All assemblies were of 4-in. nominal size, the flanges being made of forged steel and conforming to the 300-lb American Standard, and the pipe and lap-joint stub ends to standard weight (except for the supplementary tests on lightweight pipe referred to previously). Dimensional and materials information on these components is compiled in Table 1.

Through-threaded bolt studs of $\frac{1}{4}$ in. diam and SAE 4140 material were used to attach the test flanges to the mating flanges on the adapters, which were designed to be slightly stiffer to assure that flange failure, if encountered, would occur in the test specimen rather than the adapter. The physical properties of the studs conformed to the requirements of ASTM Specification A193, Grade BC. The semifinished hexagon nuts conformed to the heavy series of ASA Standard B18.2.

Gaskets were $\frac{1}{16}$ in. thick \times 4 in. ID \times $7\frac{1}{4}$ in. OD asbestos

¹ Chief Research Engineer, Tube Turns, Inc.

² Research Engineer, Tube Turns, Inc.

Contributed by the Power Division and presented at the Spring Meeting, New London, Conn., May 2-4, 1949, of THE AMERICAN SOCIETY OF MECHANICAL ENGINEERS.

NOTE: Statements and opinions advanced in papers are to be understood as individual expressions of their authors and not those of the Society. Paper No. 49-S-6.

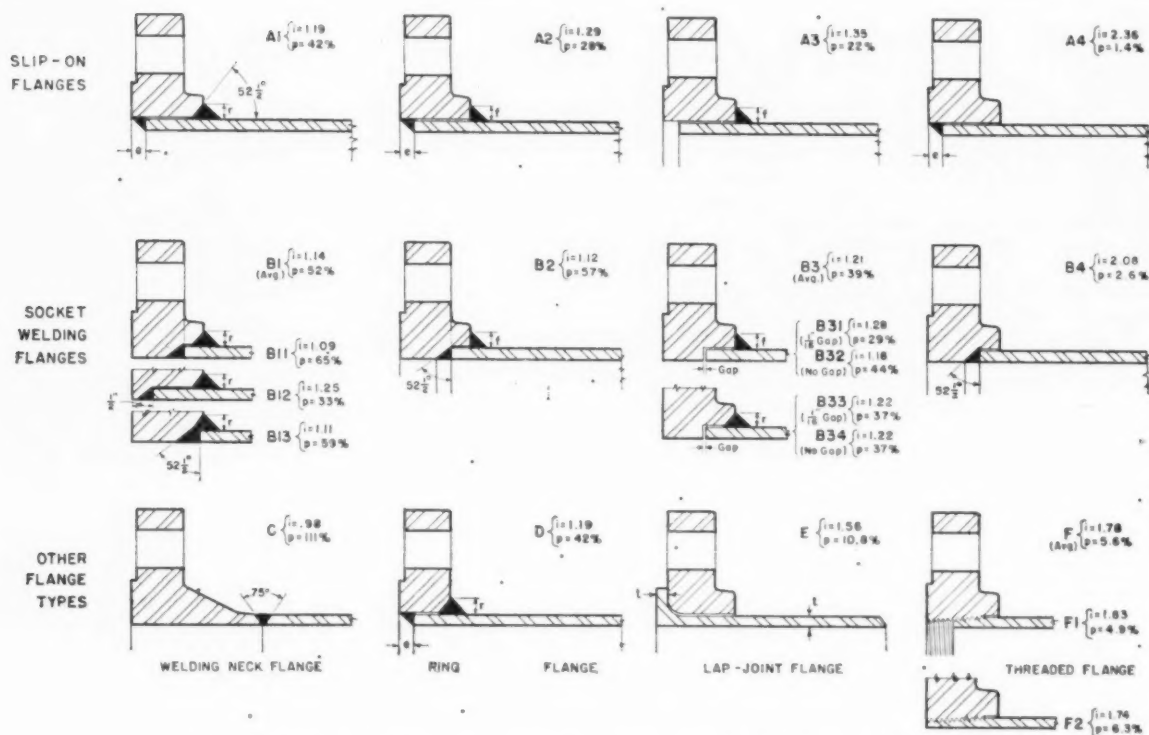


FIG. 1 DETAILS OF FLANGES AND VARIANTS OF FLANGE ATTACHMENT TESTED IN MAIN SERIES

The hub welds were specified to be $\frac{3}{16}$ -in. leg size or approximately 15 per cent heavier than required by the Code for Pressure Piping; the deposited welds actually ranged from $\frac{1}{4}$ to $\frac{11}{16}$ in. Symbol r denotes weld deposited against a $52\frac{1}{2}$ -deg recess, while symbol f denotes an ordinary fillet weld. The end welds for the slip-on flanges were full-fillet welds, the dimension e from the end of the pipe to the flange face being held to approximately $\frac{3}{8}$ in. The values i and p marked opposite each variant, respectively, denote the stress intensification factor and percentage of fatigue life in terms of that of straight pipe. The values noted opposite B1, B3, and F represent averages, weighted by the number of tests, of the subvariants shown thereunder.)

TABLE 1 DIMENSIONAL AND MATERIALS DATA

	Dimensional standard	Materials specifications	Range of physical properties, from tensile tests		
			Ultimate tensile strength, psi	Yield point, psi	Elongation per cent in 2 in.
Flanges ^a	ASA B16e	ASTM A-181, Gr. I	70250 to 74750	39500 to 41000	27.5 to 31.0
Pipe.....	ASA B36.10	ASTM A-106, Gr. B	69200 to 70600	39880 to 47500	37.0
Lap-joint stubs.....	ASA B16.9	ASTM A-106, Gr. B	62865	38600	39.0

^a The ring flanges were machined from forged flanges.

composition, manufacturer's designation "Tenax." A new gasket was used for each assembly; it was applied dry, without prior wetting or the use of a gasket compound.

The welds made in joining certain flange types, notably the slip-on and socket welding variants, were of two markedly different qualities. All the welding for the main test series was carried out by ASME Code qualified welders; while not strictly code welds (since they were not code-inspected or chipped to the extent customary when preparing for code inspection), the welds may be considered representative of good commercial practice; they were generously proportioned (the fillets attaching the flange hubs were practically full size) and presented a smooth, somewhat concave contour. By contrast, the welds prepared by welders of the research department of the authors' company for the supplementary tests, which were meant to represent the least weld size and quality compatible with code requirements, were small (the weld size on hub fillets was of the order of $\frac{5}{16}$ in. to $\frac{3}{8}$ in.) and of a beadlike, unfinished appearance.

Incidentally, no difficulties were encountered by the fabricator's welders in welding any of the flange types, except that the face welds on slip-on flanges were found to chill rather quickly,

resulting in an occasional poor weld which had to be machined out and redone.

The threaded flanges were made up with machine-threaded pipe to ASA Standard B2.1. In one set of tests, they were pulled up with 2000 ft-lb torque for normal thread engagement; in the second set, where the pipe was threaded through the flange and refaced, a 4000 ft-lb torque was applied. A liquid thread compound, sold under the name "Copaltite," was used on the threads in both cases.

TEST EQUIPMENT

A specially designed fatigue testing machine of the specific-strain reversed-bending type, as described in an earlier paper by the senior author,³ and illustrated in Fig. 2, was used. The test principle is a simple one, as becomes evident from the diagram in Fig. 3; the assembly presents a cantilever beam fixed at one end, with a cyclically reversed load being applied at the other. The specimen proper is located close to the fixed end, where the bend-

³ "Fatigue Tests of Welding Elbows and Comparable Double-Miter Bends," by A. R. C. Markl, Trans. ASME, vol. 69, 1947, pp. 869-879.

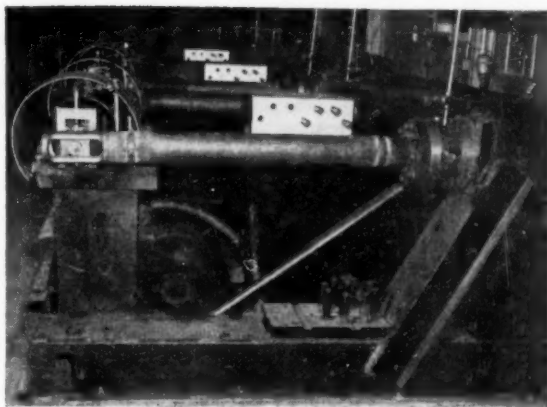


FIG. 2 FATIGUE-TESTING MACHINE

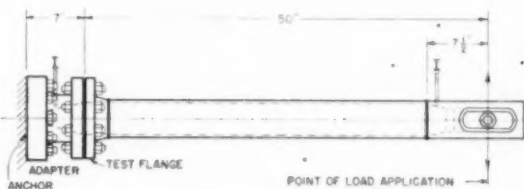


FIG. 3 DIAGRAM OF TEST ASSEMBLY

ing moment is a maximum. In the main test series, an adapter was used to approach the condition of two mating flanges of equal stiffness; in the supplementary tests no adapter was used, the test flanges being bolted directly to the anchor plate.

TEST PROCEDURE

Prior to mounting the specimens, each assembly was inspected and subjected to a pressure test of 600 psi, which is the service pressure at atmospheric temperature set up in ASA Standard B16e for flanges of the 300-lb-pressure class. Leakage was encountered in a single instance, this being a slip-on flange attached by a face weld only; the defective fillet was machined out, the specimen rewelded and retested with satisfactory results.

In mounting the specimens, careful attention was given to alignment and uniformity of bolt pull-up. The $\frac{3}{4}$ -in. bolts were pulled up incrementally with a torque wrench, using a predetermined sequence. The torque was set at 2000 in-lb, which corresponds to approximately 40,000 psi bolt stress, as determined with SR-4 strain gages. Originally it was planned to apply only 1200 in-lb, but this led to early gasket leakage of the specimens subjected to high deflections.

In the next step, each specimen was cycled at a low deflection amplitude about 20 times to "iron out" mounting irregularities; specimens were then realigned, where necessary, and the bolts rechecked with the torque wrench.

A load-deflection calibration of each specimen was next carried out, and the results were plotted as curves; the variation between individual specimens belonging to any one series being of the order of only a few per cent, an average or typical curve, such as is plotted in Fig. 4 for the welding neck type, was considered as adequate for all tests of one type. Using these data and the anticipated stress intensification factors, amplitudes of deflection were selected so as to spread failures evenly within the range from 1000 to 1,000,000 cycles.

Some of the large displacements required for the short-life

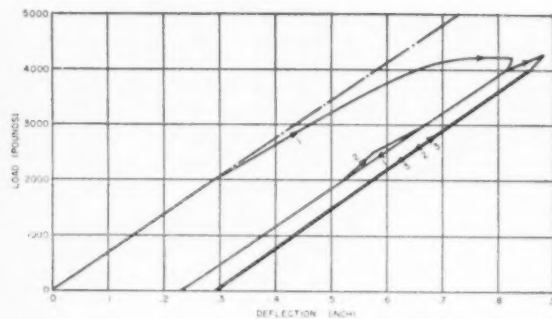


FIG. 4 TYPICAL LOAD-DEFLECTION CALIBRATION CURVE FOR WELDING-NECK FLANGE ASSEMBLIES

(Note that yielding occurs at appreciably higher load in the repeat calibration as compared with the first load application. The value S used in plotting the $S-N$ curves, Figs. 7, 8, and 9, is based upon the dash-dot extrapolation of the straight portion of the calibration curve.)

specimens fall onto the curved part of the load-deflection curve, denoting a stress high enough to produce more than local yielding. In the conversion of these displacements into loads, moments, and ultimately, stresses, the load-deflection curve, however, was considered as a straight line, i.e., the loads in the yield zone were obtained by an extrapolation from the elastic zone. A justification of this procedure, which, while not strictly correct, offers practical advantages, is given later under "Numerical Evaluation of Test Results."

In order to ascertain whether the originally applied load was maintained throughout the cyclic tests, a representative number of tests were interrupted for making check determinations of the load-deflection ratio. On flanges with wide gasket faces, no change in flexibility could be detected as the fatigue test progressed, and hence the stress conditions could be assumed as constant. The same was not true of the lap-joint flanges, specifically those under a high load. For example, in one specimen subjected to a load of 2350 lb (corresponding to failure in less than 3000 cycles), the load was reduced by about 3 per cent at 40 per cent of the total life of the assembly, by 10 per cent at 60 per cent, and by 16 per cent at 80 per cent of the life. After the stub end had cracked, the load was found to be 20 per cent lower than that originally applied. Inspection after disassembly led to the definite conclusion that the loss in load was attributable to progressive destruction of the gasket; the tops and bottoms at the inner circumference, which were alternately subjected to very high and low compressive stresses, were badly "chewed up." This was not the case for the lap-joint assemblies subjected to low moments, nor for any of the other assemblies, the gaskets invariably being found in good usable condition on taking the flange apart after failure.

All specimens were filled with water; a 25-in. head was held on those not under pressure to serve as a means for recognizing failure promptly. In order to find out whether the face weld cracked before the hub weld in double-welded slip-on or socket welding assemblies, a $\frac{1}{8}$ -in. hole was drilled through the hub at an angle of 45 deg from the bottom.

After all preliminaries were completed, the machine was started up and kept under constant observation. Where leakage appeared (or, in rare instances, a crack was noted shortly before leakage became apparent), the cycles which the unit had run were recorded. However, the test in nearly all cases was continued for at least 20 per cent more cycles to confirm failure and give information on the direction of crack propagation. Tests where no failure occurred within one or two million cycles were abandoned. In the case of threaded flanges, a slight seepage

along the threads, unaccompanied by a crack, often became evident early in the tests; by comparison, the later actual failure of threaded assemblies was always heralded by a sudden flow.

After completion of the test, the specimen was removed and photographed; a quarter section was cut out, with one of the saw cuts going through the center of the initial crack, and this was then etched and photomicrographed to record the type and location of failure. An occasional micrograph was made for more detailed study.

VISUAL TEST EVIDENCE

For various types of bolted flanged connections, tested with a given gasket and a uniform bolt pull-up, the tests established what type of failure is encountered under conditions of cyclic bending, where it occurs, and how many reversals are necessary to bring it about.

A joint could be rendered unsatisfactory by the occurrence of either of two things, i.e., it could leak, or some component could break. Leakage across the gasket to the outside of the flange or through the bolt holes did not occur in a single instance under the test conditions. A possibility of such leakage was approached, however, in the case of lap-joint assemblies where alternating overcompression of the gasket and release of most of its load resulted in deterioration of a large part of the gasket area in contact with the lap face. Another type of leakage, in the form of a persistent seepage along the threads, was encountered with threaded flanges. Even with only 25 in. head of water, this occurred long before structural failure, and with 600 psi pressure and some of the higher bending moments, around 100 reversals were enough to start a dribble of water.

In general, apart from the threaded joints, the usefulness of all

flange types was terminated by structural failure, not of the flange proper or the bolts, but invariably of the pipe, or, where a single attachment weld of small cross section or poor contour was used, the weld. All of these failures occurred as circumferential cracks and started on the outside of the pipe at or near the top or bottom of the assembly where bending stresses were highest. Fig. 5, reproducing representative photomicrographs taken of failed specimens of the main test series, will be used to comment more in detail on the nature of the failures.

The top line in Fig. 5 shows variants of slip-on flange attachment in the order of decreasing strength; the first three photographs, identification A1, A2, and A3, reveal identical failures, at the toe of the hub weld, whether a face weld was used in addition to it or not, and whether the hub weld was deposited against a square hub face or a reverse bevel or recess. In the last photograph, identification A4, which represents the obviously weak and hence unusual construction, where a face weld only is applied, failure occurred across the throat of the fillet weld. The middle line of photographs, in which the four basic variants of socket-welding flange attachment are assembled, presents almost identical evidence and requires no individual comment.

Referring to the bottom line, the butt-welding flange, shown at the left, designation C, shows failure at the edge of the weld overlay away from the flange, the crack remaining entirely within the pipe, as is also evident from the photomicrograph in Fig. 6. This is typical also of the cracks at the toes of fillet welds. The ring flange, designation D, failed at the extreme edge of the weld, as in the case of hub welds of slip-on or socket welding flanges. The lap-joint assembly, designation E, cracked across the stub end, close to the tangent point with the fillet radius. The threaded flange, designation F2 (and likewise F1, which is not shown)

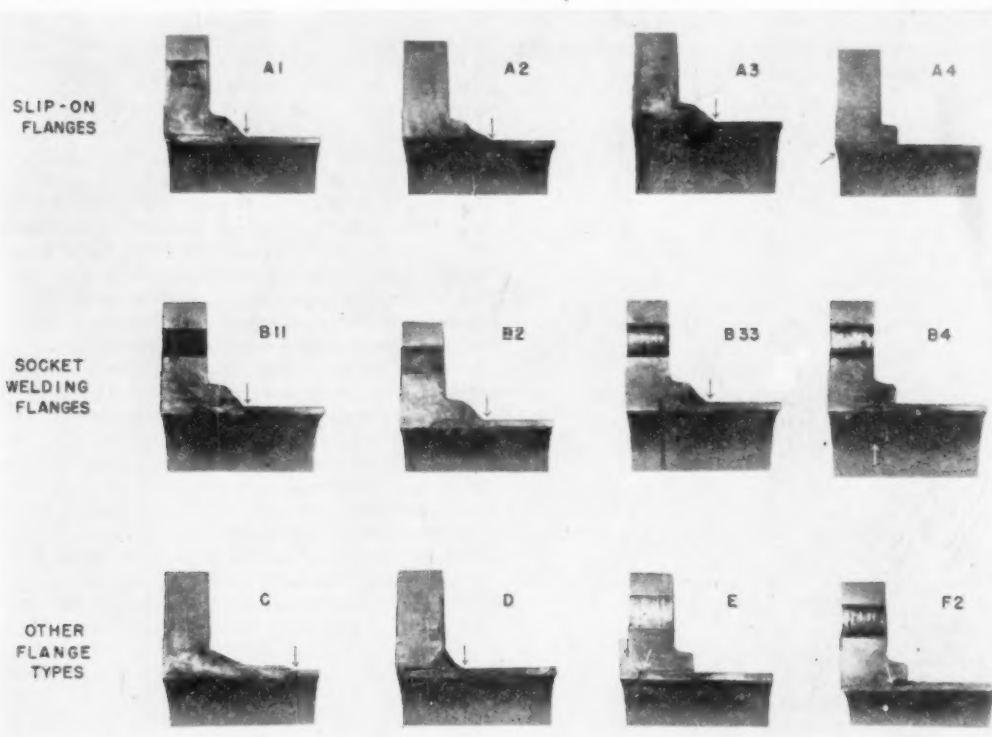


FIG. 5 PHOTOMICROGRAPHS OF REPRESENTATIVE FAILED SPECIMENS
(Arrows indicate location and approximate direction of cracks.)

Fig.

(Micro-
Crack

crack

Of
butt
pipe
other
with
flang
itself

The
tion

1
gask
in lin
acros
flang
super

2
are m
being
in thi
with
not b

3
a thic
bendi
on the

4
cyclic
ness,

5
the cr
section
of the
joints

Fat
curves
part i
undist
terms
For
the m
is stra
assemb
wall th
the sa

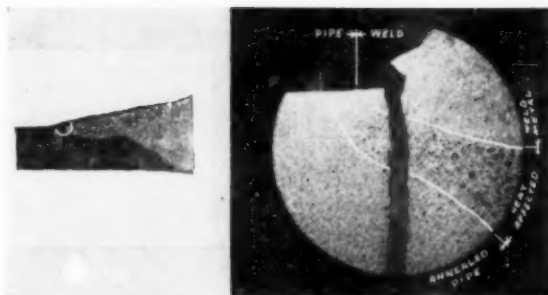


FIG. 6 PHOTOMACROGRAPH AND PHOTOMICROGRAPH OF CRACK IN WELDING NECK FLANGE ASSEMBLY
(Micrograph covers circled— $1/8$ -in. actual diam.—area of macrograph. Crack starts in edge of weld and propagates through pipe. Fracture is cross-crystalline.)

cracked through the root of one of the first three engaged threads.

Of the two supplementary series, the few exploratory runs of butt welding and double-welded slip-on flanges with lightweight pipe gave the same kinds of failure as the main test series. The other series, in which small and poorly contoured welds were used with standard-weight pipe, differed in only one respect; where flanges were attached by a single fillet weld at the hub, the weld itself failed in three out of four specimens.

The following conclusions can be drawn from visual observation during and after test:

1 Flanges of the size and types investigated, with the given gasket material and size, and using an amount of bolt pull-up in line with common practice, are stiff enough to avoid leakage across the gasket and strong enough to prevent failure of the flange proper under its maximum rated service pressure and a superimposed bending stress of appreciable magnitude.

2 The welds customarily deposited by experienced welders are more than adequate to prevent failure of welded joints, this being true even of single-fillet welded construction; not included in this statement, however, are slip-on and socket welding flanges with weld attachment of the pipe end only, these constructions not being found in common usage.

3 Caution is in order when using lap-joint flanges with laps of a thickness of the same order as the pipe wall in locations of high bending moments, since the lap apparently rocks back and forth on the gasket, and tends to destroy it.

4 Threaded flanges are unsatisfactory for any but the mildest cyclic services; the threads constitute not only a structural weakness, but are prone to open up under bending and cause leakage.

5 Structural failure appears associated entirely with contour, the crack invariably appearing at a location of marked change in section adjacent to the flange. For welded joints, this is the edge of the weld, for lap joints the start of the fillet, and for threaded joints the notch formed by the root of the thread.

NUMERICAL EVALUATION OF RESULTS

Fatigue data are usually reported in the form of so-called $S-N$ curves, and where the tests performed involve a comparison of a part in which a stress raiser is present with a similar part with undisturbed stress flow, it is convenient to interpret the results in terms of a stress-intensification factor.

For practical piping design, the properties of straight pipe offer the most satisfactory reference medium, since the bulk of piping is straight pipe. For this reason, the endurance strength of an assembly, involving a flange and straight pipe of a certain size and wall thickness, will herein be referred to the endurance strength of the same kind of straight pipe by itself. In an earlier paper by

the senior author,³ the endurance strength S of commercial straight Grade B carbon steel pipe between limits of 500 to 500,000 cycles of stress reversal was tentatively expressed in terms of cycles-to-failure N by the equation⁴

$$S = 245,000 N^{-0.2} \dots \dots \dots [1]$$

To make possible the construction of an $S-N$ curve for the recording of the present tests, it becomes necessary to translate the applied deflections into nominal stresses. In so far as the stresses caused by the deflections imposed upon the test cantilever remain within the elastic limit, the load-deflection calibrations of the different assemblies made preparatory to these tests serve to establish the loads corresponding to any specific deflection; by multiplication by the lever arm from the point of load application to the point of starting failure, the controlling moment is obtained, and this, divided by the section modulus of the pipe used, gives the nominal stress. In the present tests, however, the larger displacements applied in the short-life runs definitely caused more than local yielding. It would have been entirely possible to establish the corresponding load, and therewith the stresses, from the applicable load-deflection curve. However, in view of the fact that the results of this investigation are primarily intended for use in the flexibility analysis of piping systems (where the displacement is given and the loads or reactions are solved for), and since such calculations are commonly based upon the elastic theory, it has been considered preferable to extrapolate the straight-line portion of the load-deflection curves (see Fig. 4 for an example) and plot the cycles-to-failure against a fictitious stress thus obtained, which, obviously, is higher than the actual stress.

This last is the basis upon which the median lines given as the $S-N$ curves for different assemblies in Figs. 7, 8, and 9, have been derived. They are all drawn parallel to the $S-N$ curve for straight pipe expressed by Equation [1] and go through the computed center of the respective group of test points obtained from the main series; the results of the supplementary tests series (shown by symbols of reduced size, but otherwise identical with those used for recording the results of the main tests) have been ignored in drawing the median lines. The justification for using a constant slope for all median lines resides in the advantage this offers of representing the stress-intensification factor as a constant, which would not otherwise be possible. A study of the charts indicates that this arbitrary adjustment is accomplished without violating the test evidence seriously. To avoid undue reliance on the median lines in the low-cycle range, in view of the liberties taken in extrapolating the load-deflection curve beyond the elastic range, these median lines have been cut short at a stress level roughly corresponding to definite yielding.⁵

The test results as reduced to these median lines are readily interpreted in either of two ways. To derive the stress intensification factor i for any particular assembly, the nominal stresses applicable to straight pipe and the assembly in question are read at the intercepts of the two corresponding median lines with any one ordinate, and these divided by each other. To determine the comparable life of any assembly in relation to that of straight

⁴ Results obtained by this formula should not be confused with results of fatigue tests on polished bars, since commercial straight pipe involves certain inherent stress raisers in its surface condition, and additional stress raisers are introduced by any form of clamping or joining, mechanical or by welding, regardless of the amount of care taken to avoid notch effects. This should be well understood in view of possible future attempts at a rigorous mathematical analysis of the shapes involved in the present test.

⁵ It will be noted by reference to Fig. 4 that the departure from a straight-line law occurred much earlier in the first load application, as compared with subsequent retests; the latter only have been considered significant in the present investigation.

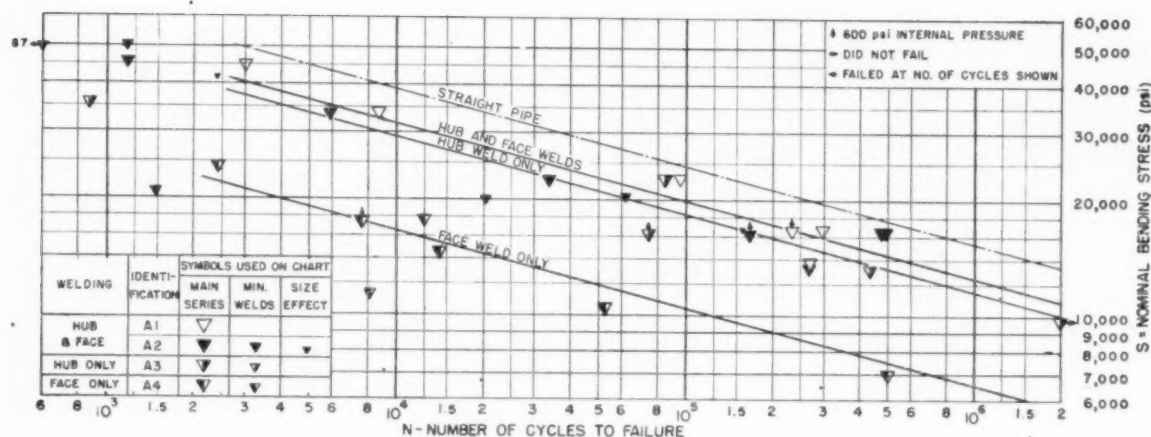


FIG. 7 S-N CURVES FOR SLIP-ON FLANGES

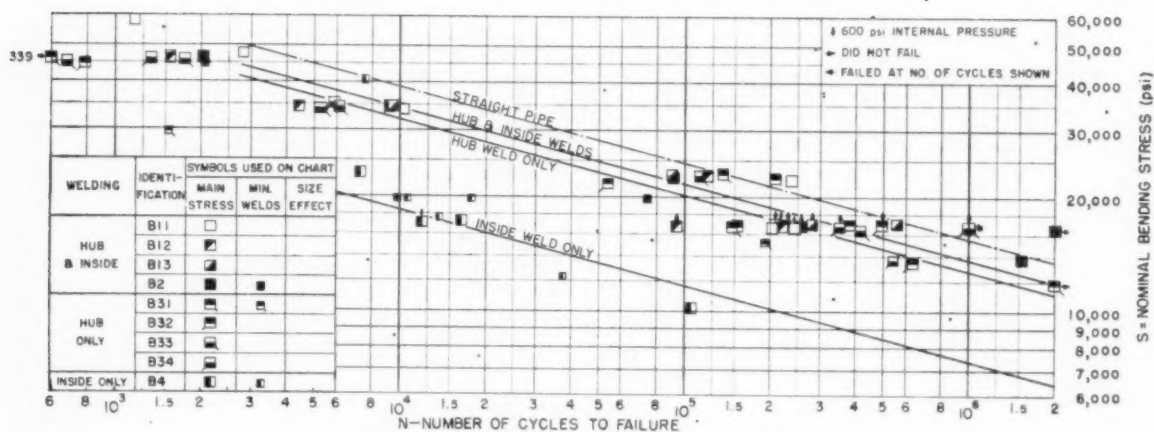


FIG. 8 S-N CURVES FOR SOCKET WELDING FLANGES

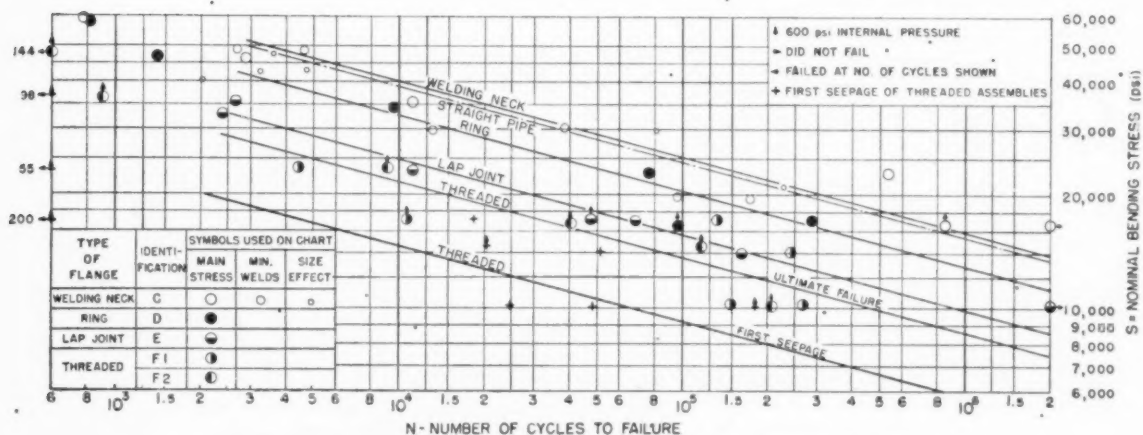


FIG. 9 S-N CURVES FOR FLANGES OTHER THAN SLIP-ON OR SOCKET WELDING

TABLE 2 DETAILED EVALUATION OF TEST RESULTS

Flanges and variants of flange attachment	Identification	Main series			Supplementary series					
		No. specimens	i	p , per cent	Minimum welds			Size effect		
					No. specimens	i	p , per cent	No. specimens	i	p , per cent
Slip-on flanges with double welds (average).....		12	1.24	34						
Recessed hub and fillet face welds.....	A1	6	1.19	42						
Fillet hub and face welds.....	A2	6	1.29	28						
Slip-on flanges with single fillet hub weld.....	A3	5	1.35	22	2	1.26	32	2	1.30	27
Slip-on flanges with single inside fillet face weld.....	A4	6	2.36	1.4	2	1.84	4.7			
Socket welding flanges with double welds (average).....		21	1.14	52						
Recessed hub and inside butt welds (average).....	B1	16	1.14	52						
Same with butt weld in line with back of flange.....	B11	6	1.09	65						
Same with butt weld 1/8 in. from face of flange.....	B12	5	1.25	33						
Same with butt weld made as through weld with hub weld.....	B13	5	1.11	59						
Fillet hub weld and inside butt weld.....	B2	5	1.12	57	2	1.25	33			
Socket welding flanges with single hub welds (average).....	B3	25	1.21	39						
Fillet welds (average).....		13	1.21	39						
Same with 1/8-in. gap between end of pipe and bottom of socket.....	B31	4	1.28	29	2	1.64	8.4			
Same with no gap: pipe bottomed in socket.....	B32	9	1.18	44						
Recessed welds (average).....		12	1.22	37						
Same with 1/8-in. gap between end of pipe and bottom of socket.....	B33	7	1.22	37						
Same with no gap—pipe bottomed in socket.....	B34	5	1.22	37						
Socket welding flanges with single inside butt weld.....	B4	4	2.08	2.6	6	1.78	5.6	6	1.06	75
Welding-neck flanges.....	C	5	0.98	111	6	1.09	65			
Ring flanges.....	D	6	1.19	42						
Lap-joint flanges.....	E	6	1.56	11						
		6	1.65 ^a	8.2 ^a						
Threaded flanges (average).....	F	12	1.78	5.6						
		12	2.65 ^b	0.8 ^b						
Same, with normal make-up.....	F1	6	1.83	4.9						
		6	2.48 ^b	1.1 ^b						
Same, with pipe threaded through and refaced.....	F2	6	1.74	6.3						
		6	2.83 ^b	0.6 ^b						

^a Value corrected for loss in load observed during course of test.

^b Value based upon first appearance of seepage whether accompanied by crack or not (i here is not strictly a stress-intensification factor, but may be applied as such for design purposes).

i = stress intensification relative to straight pipe.

p = life of assembly relative to straight pipe.

pipe, the cycles-to-failure are read for the assembly in question and for straight pipe along any abscissa denoting constant nominal stress, and the one is then expressed as a percentage p of the other. Both the i and p values for all variants tested in the main series are recorded against each type in Fig. 1 and compiled in Table 2 for ready comparison. The table also includes the results of the supplementary test series and gives the number of specimens tested of each variant.

It may be noted that a single median line has been drawn for all double-welded slip-on flanges, and the same has been done for the socket welding flanges. While these group averages are helpful in an over-all appraisal of the effect of the major design characteristics, a more detailed study of each individual variant in relation to others will be found worth while, inasmuch as it gives an idea of the contribution of minor details to the endurance strength of an assembly; while the differences between variants to be commented upon appear of a low order and well within the range of scatter of the test results, some of them are entirely too consistent and logical to be ignored, as will be shown. All comparisons will be made on the basis of the stress intensification factors developed, but it should be remembered that relatively small differences in this factor connote appreciable differences in fatigue life, i.e., the anticipated number of cycles to failure. As an example, a 10 per cent increase in stress-intensification factor is equivalent to a reduction in useful life under cyclic bending of over 40 per cent.

Single Welds. As expected, the butt weld used for attaching a welding-neck flange, test series C, was found vastly superior to any other form of attachment; it is equivalent to any butt weld between pipe, and practically as good as straight unwelded pipe. Even in an unfavorable location at the junction between two parts of greatly differing stiffness, as in socket welding variant B4, this form of weld gave a 13 per cent improvement over a similarly located fillet weld, as used in slip-on variant A4. As far as the two types of hub welds are concerned, i.e., the regular fillet weld and a weld deposited against a 52 1/2-deg reverse bevel or recess, neither the comparable single-welded variants (B31 versus B33,

and B32 versus B34), nor the double-welded ones (A2 versus A1 and B2 versus B11) show any consistent differences. Apparently, where both welds are of adequate size, the pipe failure is influenced solely by the contour at the toe of the weld, which is the same for both types.

Bottoming of Pipe in Socket. Having just mentioned variants B31, B32, B33, and B34, it may be opportune to cover briefly the second objective of this particular subproject, which was to discover whether butting the pipe solidly against the face of the recess in a socket-welding flange improved resistance to cyclic bending. From a comparison of the values of i , given for the condition with no gap with those for that with a 1/8-in. gap, it would appear that forcible contact of the end of the pipe with the socket face is helpful, but that the benefit is minor. Incidentally, the result of the slip-on flange series A3 would tend to confirm the results obtained on socket welding flanges with a definite gap.

Single Versus Double Welds. Three directly comparable groups of test series are available to evaluate the beneficial effect of the weld at the end of the pipe when used in conjunction with a hub fillet weld: Series A2 can be compared with series A3; series B31 and B32 with B2; and series B33 and B34 with B11. From such a study it may be concluded that the added welds produce an improvement in endurance strength of the order of 8 or 10 per cent.

Weld Proximity. There are indications that the distance between welds in double-welded flange attachments is not without significance: Below are listed the seven different variants of double-welded constructions tested, together with their stress-intensification factors; the order is from the closest spaced welds to those most widely separated:

B13:	1.11	} close (avg. 1.11)
B11:	1.09	
B2:	1.12	
D:	1.19	} intermediate
B12:	1.25	
A1:	1.19	} apart (avg. 1.24)
A2:	1.29	

Considering the two bracketed groups listed, it will be noted that a weld spacing not exceeding the height of the hub of a slip-on or socket welding flange on the average produces a 12 per cent higher endurance strength than a wider spacing, of the order of the flange thickness. Omitting test series B12 from the foregoing comparison, it will be seen that the two groups are directly representative of socket welding and slip-on flanges, and hence the former, when used with shallow sockets, can be pronounced about 12 per cent stronger against cyclic bending as compared with the latter.

The results for lap-joint and threaded-flange assemblies, as plotted in Fig. 9, and averaged in Fig. 1 and Table 2, require modification before they can be applied to piping design. It has been mentioned already that a slight loss in applied load was encountered in the case of lap-joint assemblies under high loadings; the plots are based on the initial loading (or strictly, the applied deflection), and adjustment to the approximate average loading over the test duration would raise the stress-intensification factor from 1.56 to 1.65, or reduce the life from about 11 per cent of that of straight pipe to only 8 per cent. In the case of threaded assemblies, seepage through the threads on the average occurred in one seventh of the time it took to produce structural failure. If we expand the definition of the "stress intensification factor" so that, for any given cyclic life, it expresses the relation between the stress producing fracture in a straight pipe and the stress producing failure from whatever cause in a comparative assembly (including the same kind of pipe), or in other words, if we consider leakage on equal terms with failure, this premature loss of serviceability of threaded flanges would have to be compensated by applying an "effective" stress intensification factor of 2.65 rather than 1.78 as obtained using cracking as the sole criterion of failure.

A few brief comments on the findings of the two supplementary test series included in Table 2 appear in order before going on to the conclusions. The one series, in which weld size effects were explored, indicated that it might be advisable for design purposes to increase the stress intensification factors obtained from the main test series somewhat for flanges involving attachment by fillet welding. The second series, involving thin-wall pipe, may be considered as providing a certain measure of assurance that, within the more common range of pipe sizes, the effect of the pipe-wall thickness and size or series of the flange is not overly significant.

CONCLUSIONS

The tests established that, even under unusually severe bending stresses, flange assemblies do not fail in the flange proper, or by fracture of the bolts, or by leakage across the joint face. Structural failure occurs almost invariably in the pipe adjacent to the flange, and in rare instances, across an unusually weak attachment weld; leakage well in advance of failure is observed only in the case of threaded flanges.

While it is the pipe that fails, the type of flange is influential in determining the endurance strength of the assembly, largely by the way in which it affects the stress transfer at the joint. The smooth tapering transition, afforded by a welding-neck flange, provides an endurance strength of the assembly equivalent to that of a butt-welded joint between two pieces of pipe, which itself is not greatly different from that of unwelded straight pipe to judge from indications obtained from tests in such pipe conducted by the authors. A fillet weld presents less favorable conditions owing to the sharp change in cross-section and stress-flow direction. In the case of lap-joint flanges, the transition would not appear unfavorable, but the lap apparently lends inadequate support to the neck of the stub end. Finally, in the case of threaded flanges, the reduced pipewall thickness and notch effect, caused by the threading, constitute weaknesses

which become even more apparent under cyclic loading than under static conditions.

In order to provide a quantitative measure of the relative endurance strength of different common flange assemblies, Table 3 has been prepared by the authors, using all the evidence produced in these tests, including the supplementary series and giving weight to any tendencies which may have been present of premature loss of serviceability prior to ultimate fracture. It is

TABLE 3 PROPOSED STRESS INTENSIFICATION FACTORS AND COMPARATIVE FATIGUE LIVES FOR DESIGN

Type of assembly	Stress-intensification factor, i	Relative fatigue life, p , per cent
Welding-neck flanges	1.00	100
Socket welding flanges (double-welded, with inside butt weld approximately in line with back of flange)	1.15	50
Double-welded slip-on or forged ring flanges	1.25	33
Single hub welded slip-on or socket welding flanges	1.30	27
Lap-joint flanges (with standard lap-joint stub ends)	1.60	10
Threaded flanges	2.30	1.5

thought that the stress-intensification factors given may find direct use in flexibility calculations following the rules of the Code for Pressure Piping, and that the parallel information on relative fatigue life, as more descriptive, may be helpful in setting limitations on flange types, depending upon the service involved.

ACKNOWLEDGMENT

The authors desire to acknowledge the co-operation of the management of Tube Turns, Inc., whose generosity in placing the facilities and personnel of its Research Department at their disposal made possible the investigation herein reported. The assistance in preparing the test assemblies, by welding the flanges to the pipe, rendered by Mr. John H. Zink, is also gratefully acknowledged. Mr. Zink, president of The Heat and Power Corporation of Baltimore, Md., is a member of the Subgroup on Flange Limitations of Subcommittee No. 3 of ASA B16, for the benefit of which the present investigation was conducted. Mr. Zink must also be given credit for proposing the design of the internally welded socket-weld flange which was included in the tests reported herein.

Discussion

H. F. MOORE.⁶ Full-size fatigue tests of structural and machine parts are always preferable to tests of small polished specimens when such full-size tests are feasible. Hence this paper is very welcome as it describes such full-size tests for flange-pipe assemblies.

The fatigue-testing machines used are of the simplest type—the type which measures directly the deflection of the specimen and the number of cycles of stress to cause fracture. The stress pattern, the load, and the bending moment are then measured from the deflection, using the specimen itself as the dynamometer. The authors determined the stress range from the deflection of the specimen, stopping the machine at various stages of the test to determine the steady value to which the stress range "settled down."

The authors carried out their tests to a maximum of about 2,000,000 cycles of reversed flexure. As is the case with railroad rails and with many structural parts, repeated-stress tests to 2,000,000 cycles are sufficiently long to cover the customary period of use. The results, plotted on log-log stress-cycle ($S-N$) diagrams show no sign of "flattening out," and show a con-

⁶ Research Professor of Engineering Materials, Emeritus, University of Illinois, Urbana, Ill. Mem. ASME.

siderable, although not too serious, scatter of test results. It is probable that longer tests would show a flattening out of the S-N diagrams. In that case extrapolation of the authors' results to 10,000,000, or even to 100,000,000 cycles might be expected to give results "on the safe side."

The writer is especially impressed by the poor showing made by the threaded flanges. Screw threads in any structural or machine part constitute one of the most dangerous of stress raisers, especially if the rod or pipe is screwed in as far as the thread will allow.

Attention is also called to the tabulation in Fig. 1 and Table 2 of both i , the effective stress-intensification factor, and to p , the ratio of length of endurance (number of cycles of stress) of a flanged assembly to that of the straight pipe. Thus the assembly can be judged on the basis either of comparison of stress range for a given endurance or of comparison of endurance for a given stress range of a straight-pipe specimen.

J. J. MURPHY.⁷ The authors are to be congratulated on having made a valuable contribution of test data on the performance of various flange types, on the organization of the tests, and presentation of the results for handy reference. There has been too little information available on this subject, and the paper is a fitting supplement to the senior author's previous paper.³

The role of fatigue-test data as an index to the relative serviceability of flange types is difficult to assess, and the authors have been careful not to draw any unwarranted conclusions. Data such as these are, nevertheless, quite valuable, and the order of performance of the various types fits in well with what would be expected, with the exception that the relatively poor performance of lap-joint flanges is somewhat surprising. While service experience with all types of flanges has been generally good, slip-on, lap, and threaded flanges are used normally only in the less severe services.

The tests provide excellent comparative data for the various weld details for slip-on and socket welding flanges. The ASME Boiler Code Subcommittee on Bolted Flanged Connections already has recognized a socket welding detail similar to B11 except that the inner weld is located at the mid-point of the flange thickness. The data here presented provide valuable information for permitting the weld to be located near the hub. The authors' opinion that the pipe failure is influenced solely by the contour at the toe of the weld appears logical, and it would be interesting to see if the performance of flange attachment B13 could be made to more closely approach butt-welded flange construction by modifying the fillet-weld contour as indicated in Fig. 10 of this discussion.

Also, it would be interesting to have comparative test data on threaded flanges with a seal weld, a construction which is widely used. The test data obtained in the supplementary tests provide valuable information on the possible effect of variations in weld quality and size to be expected in actual applications. It is

⁷ The M. W. Kellogg Company, Jersey City, N. J.

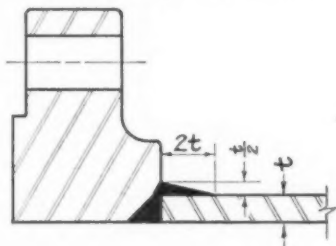


FIG. 10

noted that the performance of welding-neck flanges in the supplementary tests in Table 2 of the paper is the same as the main tests on flanges B11. The authors may wish to comment on this.

The bending moments applied in these tests simulate those which might be caused by mechanical vibrations or changes in temperature of the pipe line. Fluctuating pressures or cyclic temperature changes which cause the pipe locally to run cooler or hotter than the flange would impose a different-type loading on the attachment welds in that the shear and moment would be uniform around the circumference. It is possible that the performance of the various details would react somewhat differently to this type loading.

E. C. PETRIE.⁸ In interpreting the results of the authors' research investigations, the designer must consider the piping system as one integrated structure. In other words, it would be inconsistent to demand of a flanged assembly, resistance to fatigue of a much higher order than that required for another part of the piping system. Due precaution should be exercised, therefore, in attempting to draw all-inclusive conclusions from the results of a series of tests on only one size and class of product.

In order to illustrate this point, let us compare the test results obtained in the earlier Markl paper³ with those published in the present paper. The writer has combined these results in graph form in Fig. 11 of this discussion.

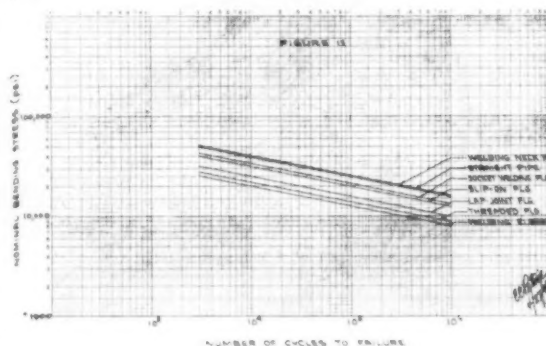


FIG. 11

It will be noted from this graph that the number of cycles to cause complete failure of the conventional and acceptable types of flange assemblies fall between those given for straight pipe and welding elbows. One exception is the welding-neck flange, which is slightly higher than that of straight pipe.

While it is a well-known fact that fatigue failures occur under certain conditions of severe stress in some threaded assemblies, there has been no indication, to the writer's knowledge, of failure in the side of a welding elbow due to fatigue as illustrated by the tests in the previous paper. The type of end fixation, notch effect in threads, clearances in flange assemblies, total resisting moment developed by bolting, are all important factors in an investigation of this type, and tests under various combinations may produce results which differ considerably from those presented in this paper. It is suggested, therefore, that more extensive investigations be made before arriving at any definite comparative values of fatigue life of elements which are component parts of a piping structure.

Another point mentioned in the paper being discussed is that the results obtained for lap-joint flanges indicate that "caution

⁸ Engineering and Research Division, Crane Company, Chicago, Ill. Mem. ASME.

is in order when using lap-joint flanges with laps of a thickness of the same order as the pipe wall in locations of high bending moments, since the lap apparently rocks back and forth on the gasket and tends to destroy it," but that "this was not the case for the lap-joint assemblies subject to low moments." Apparently the high moments referred to by the authors are not encountered in a properly designed piping system due to the fact that, to the writer's knowledge, this damage to the gasket has never been found under actual service conditions.

E. O. WATERS.⁹ Static stresses in piping and piping connections always have been given due respect. Somewhere along the road of acquiring knowledge of piping design, the effect of live loads caused by temperature differentials, and those due to rigid end connections and intermediate supports, were taken into account as a matter of course. However, even here the results of tests and theoretical analysis are mainly applicable to the pipe alone, and much still remains to be learned about the effect of live loads on flanged or other forms of piping connections, and on the vessels to which piping is attached. Most recently, the question of the endurance of piping systems subjected to dynamic loading has come to the fore, the chief reason for its importance doubtless being due to the substitution of welding for what might be termed "semipermeable" forms of pipe connection which always could be counted upon to leak profusely long before any structural failure took place.

The authors have made a factual statement of their findings without attempting any extensive analysis, and the question arises as to how best to interpret the results. In so far as the welding-neck type of joint is concerned, behavior was exactly as would be predicted; in this case, there are no sudden transitions in size of cross section, and no sharp re-entrant corners, the weld is inherently superior, and the flow of stress from flange to pipe follows comparatively straight lines and easy curves. At the other end of the scale, the poor showing of the single inside welds (series A4 and B4) was to be anticipated. However, there are several intermediate cases which give rather unexpected results, calling for further explanation. For example, the general setup in Fig. 1 of the paper would lead a superficial reader to conclude that socket-welded connections are, as a class, superior to slip-on connections. However, a closer inspection of the sketches in line 2 in Fig. 1 reveals that the quality of these connections is very sensitive to inside and outside weld proximity. In fact, the authors call attention to this point. This at once raises the question: If close proximity improves the performance of socket welds, would it not be possible to improve the slip-on group by inserting the pipe only part way into the flange? Also, from a comparison of series B11, B12, and B13, it appears that there is an optimum proximity beyond which a closer weld spacing impairs the fatigue life of the connection. This would seem to make further detailed study desirable, including if possible an investigation of the actual stresses at points of concentration, before truly quantitative conclusions can be drawn.

In conclusion, the writer would call attention to one feature wherein the tests showed remarkable consistency, namely, the location of the point or region of failure. This is consistent with static tests and theoretical stress analyses based on static loading, which always indicate a relatively high bending stress in the pipe that is intensified by a sudden transition from a comparatively thick flange to a thin-walled pipe. The inclusion of this stress as one of the criteria for the design of flanges has at times been a bone of contention among users of the ASME Unfired Pressure Vessel Code, on the ground that it imposed an unnecessarily severe restriction. However, the results of these fatigue

tests, as here reported, indicate that the existence of this stress, even though it is highly localized, cannot safely be ignored, at any rate when dynamic loads must be provided for.

AUTHORS' CLOSURE

The authors are appreciative of the lively interest exhibited in the tests reported by them, and value particularly those comments which raise the issue how the test data relate to service experience and what their significance is with respect to future piping design.

As has been pointed out in the discussion, there has been no published record of stress failures in service of the types shown in this and the senior author's earlier paper³, although failures in screwed joints, at branch connections and other points involving major stress raisers have been recognized as due to fatigue. One explanation, as inferred by Mr. Petrie, is that high sustained bending stresses, say, of 24,000 psi or over, are not encountered in properly designed piping systems; a second factor is that major stress cycles much in excess of 1000 over the life of a system are confined to the process industries, are not too frequent even there, and usually receive special consideration. Close inspection of Figs. 7, 8, and 9 reveals no stress failures of commonly used flanges within the quadrant defined by these limits, except in the case of threaded flanges, with lap-joint flanges coming close.

Accordingly it would seem that the tests and experience are in good accord. But, while experience proves that all but the two last-mentioned types of flanges will survive the conditions to which an average piping system is subjected, the tests are able to distinguish between the merits of the different types and thus offer an indication of how many more reversals at a given stress, or how much more stress at a given number of cycles, a welding-neck flange, for instance, can support with reference to any other variant. This is important in view of the trend toward more severe services in the process industries and the accompanying desire to liberalize allowable stresses; this latter objective can be accomplished, without reducing the true safety factor, only if our understanding of stresses improves so as to take part of the "ignorance component" out of the safety factor.

It is recognized that tests on a single size, class, and material of flange, with a specific type of gasket and bolting under a specific pull-up cannot be expected to form the basis for broad conclusions embracing the entire field of flanged connections. The authors, as some of the discussers noted, were careful to avoid such an impression. On the other hand, they feel that, considering the confirmation obtained from the supplementary test series, the results are suitable for engineering application to a somewhat broader range of conditions; in a way, there would seem to be no other alternative pending further experimental or analytical progress in this field.

A note of caution is in order with respect to comparisons of the type drawn by E. C. Petrie in Fig. 11. While the results of the flange tests might be applied with reasonable accuracy to a fairly wide range of sizes and thicknesses, those obtained for welding elbows are restricted to one specific size and thickness and can be extrapolated to other conditions only through the medium of a theoretical analysis, such as Beskin's development.¹⁰ Furthermore, moments due to expansion vary from zero to a maximum over the length of a line, so that a piping component with a lower stress-intensification factor situated at a location of high moment will often control even though other parts with higher factors are present in the line. The critical condition can only be properly evaluated by multiplying the stress at each significant location by the applicable stress-intensification factor.

⁹ Professor of Mechanical Engineering, Mason Laboratory, Yale University, New Haven, Conn. Mem. ASME.

¹⁰ "Bending of Curved Thin Tubes," by Leon Beskin, *Journal of Applied Mechanics*, Trans. ASME, vol. 67, 1945, p. A-1.

Many additional investigations have been proposed, and the authors would have wished to have been able to conduct these, but due to press of other work must confine themselves to giving answers which are no more than opinions.

J. J. Murphy's design, Fig. 10, might be expected to approach the welding-neck flange in performance, or at least equal the ring flange which behaved surprisingly well. A threaded flange with seal weld would probably be the equivalent of a single-hub-welded slip-on flange with minimum welding.

Professor Water's question, whether slip-on flanges would benefit from yield proximity to an equal extent as socket welding flanges is difficult to answer; the authors feel confident that they

would benefit, but perhaps not quite to the same extent as the socket welding type which can be reasoned to provide a somewhat better stress flow. No doubt there is an optimum distance between the front and back welds, but it is doubtful whether this can be determined from tests on commercially fabricated joints; a photoelastic analysis of models probably would furnish an answer.

Regarding J. J. Murphy's comment on the similarity in fatigue life of group B-11 and the supplementary welding-neck flange assemblies, no explanation can be offered except to point out that the results show a fair amount of scatter and hence overlapping between flange types of similar endurance strength.

c
u
u
is
o
sp
re
13
in
El
ta
fa
wa
Th
sin
pr
fu

T

who
thro
T
effi
per
boil
W
conc
atta

Fi
H
with
whic
rele
vapo
merc
heat
cury
merc
Th
-cury
steam

1 C
Schen
2 Su
Hartf
Con
Meet
SOCI
Not
unders
of the

Modern Mercury-Unit Power-Plant Design

By H. N. HACKETT¹ AND DWIGHT DOUGLASS²

This paper outlines briefly the general theory of mercury-binary cycle efficiency, how it works, and the more usual types of applications where it may be used. The use of the mercury-steam cycle as applied to topping plants is explained more completely with the relative capabilities of 140 psig mercury and 2300 psig steam for such service specifically compared. As a typical, as well as the most recent application of a mercury topping unit, the new 15,000-kw mercury-unit power-plant equipment recently installed at the South Meadow Station of the Hartford Electric Light Company is dealt with in considerable detail. In the manufacture of the mercury-boiler parts, factory prefabrication of relatively large mercury-furnace wall sections was successfully done for the first time. The new 15,000-kw mercury plant has been in operation since February 1, 1949, and for the month of February produced 20,000,000 kwhr of electric power at an average fuel rate of 10,200 Btu per net kwhr.

CYCLE EFFICIENCY

THE efficiency of a vapor cycle is determined largely by the saturated-temperature range through which it operates—the greater the range, the higher the efficiency of the cycle. This may be expressed by the equation, efficiency

$$E = \frac{T_1 - T_2}{T_1}$$

when T_1 and T_2 represent the saturated-temperature range through which the cycle operates, in degrees absolute.

The mercury cycle, superimposed on a steam cycle, boosts the efficiency of the resulting cycle because of the high boiling temperature of the mercury. For example, at 140 psig, mercury boils at 975 F, whereas at 1250 psig, water boils at 575 F.

With 975 F mercury and a proper selection of steam and fuel conditions, thermal efficiencies of from 34 to 38 per cent can be attained.

HOW THE MERCURY-STEAM POWER CYCLE WORKS

Fig. 1 shows a typical flow diagram of the mercury-steam cycle.

Heat from the burning fuel is absorbed by liquid mercury within the tubes of the mercury boiler to form mercury vapor, which passes from the boiler to the mercury turbine where it releases a portion of its energy to produce electric power. The vapor from the turbine is exhausted to the vacuum shell of the mercury-condenser boiler. There it condenses and releases its heat of vaporization to water within the tubes. The liquid mercury is returned from the sump, or hot well, to the boiler by a mercury feed pump, or by gravity, as the case may be.

The feedwater which absorbs heat from the condensing mercury vapor is boiled into steam at any desired pressure. This steam is then superheated in tubes located in gas passages of the

mercury boiler. This superheated steam is then available for driving a steam turbine, or may be put to other desired uses.

It is of interest to note that the steam thus produced by the binary cycle is only slightly less in amount than it would be if the equivalent fuel were burned directly in a steam boiler.

TYPES OF APPLICATION

A heat cycle or a power cycle upon which a higher-temperature heat cycle has been thermodynamically superposed may be said to have been topped. Hence a power plant composed of the higher-temperature cycle equipment may be known as a "topping plant." In reality, all power plants where binary cycles or superposed steam cycles are used, fall into the general class of topping applications. However, for the sake of simplicity, as well as for the purpose of easy identification, the types of applications for mercury-unit power plants have been divided into three general classes, i.e., topping plants, process or heating steam plants, and condensing plants.

A topping plant is one in which relatively high-pressure steam is desired, usually to be used in existing steam turbines.

A "process," or "heating steam plant" is one in which relatively low-pressure steam is required. If the steam is desired at a pressure below the minimum limit set for operation of the mercury-condenser boilers, it is then desirable to include a noncondensing steam turbine having its exhaust shell designed to exhaust the steam at a pressure suitable for the proposed application.

A "condensing plant" is one in which electric power only is produced. In this case, a condensing steam turbine of suitable size and design is included as a part of the mercury power plant.

The initial steam pressure and temperature for each of the three types of applications may be varied as dictated by existing steam conditions, or by the power-plant designer as he finds necessary in his effort to produce the most useful and economical over-all power plant.

RATIO OF MERCURY TOPPING KILOWATTS TO STEAM OUTPUT

A by-product kilowatt produced from a high-temperature topping cycle is obtained at nearly the mechanical equivalent of the thermal energy.³

Because of boiler and other machine efficiencies, by-product kilowatt output, as such, requires the expenditure of approximately 4000 Btu per hr from the fuel, regardless of whether the topping kilowatt-hour is produced by a steam topping turbine or a mercury topping unit.

Another way of indicating this situation might be to say, that whenever a heat power plant or a portion of a heat power plant is credited with heat rejected, then the net heat consumption of the kilowatts generated in that portion of the power plant is equal to heat put in minus heat rejected to the next portion or system, divided by the kilowatts produced; and that this is usually in the neighborhood of 4000 Btu per kwhr.

Mercury topping plants as generally applied, will produce about twice as many 4000-Btu kw per 1000 lb of high-pressure steam as can be secured from other topping cycles. Furthermore, a mercury topping plant, designed originally to produce, say, 400-psig steam, may be used if desired to top 850-psig steam, or higher, merely by altering the size of the steam superheater and changing the steam safety valves, if allowance has been made in the design

¹"Mercury for the Generation of Light, Heat, and Power," by H. N. Hackett, Trans. ASME, vol. 64, 1942, pp. 647-656.

¹Construction Engineering Division, General Electric Company, Schenectady, N. Y. Mem. ASME.

²Superintendent of Power, Hartford Electric Light Company, Hartford, Conn. Mem. ASME.

Contributed by the Power Division and presented at the Spring Meeting, New London, Conn., May 2-4, 1949, of THE AMERICAN SOCIETY OF MECHANICAL ENGINEERS.

NOTE: Statements and opinions advanced in papers are to be understood as individual expressions of their authors and not those of the Society. Paper No. 49-8-17.

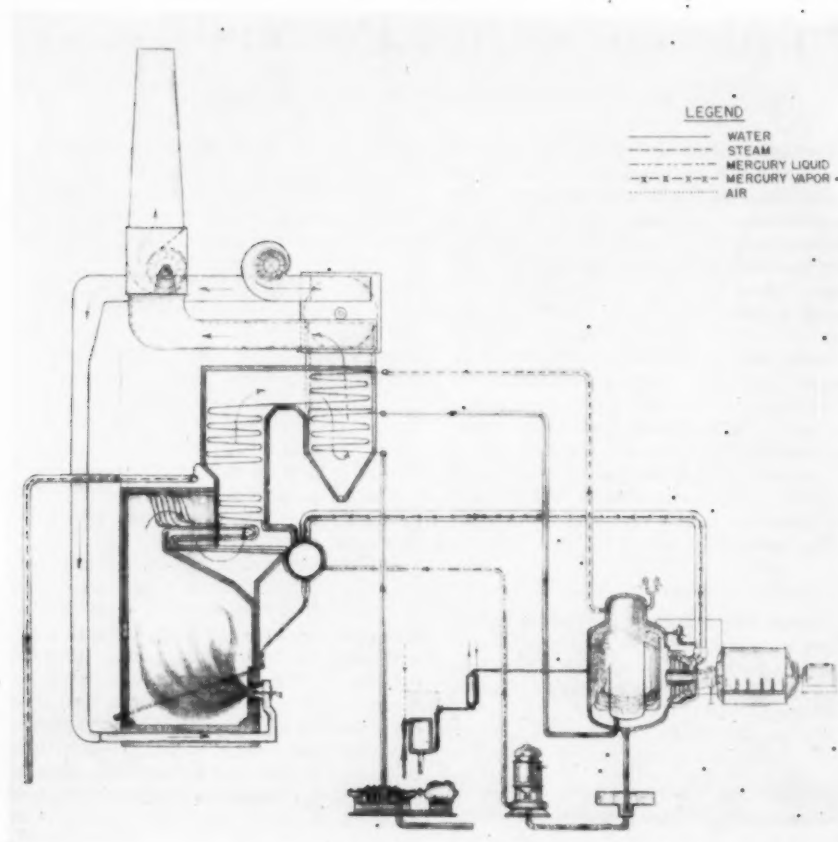


FIG. 1 TYPICAL FLOW DIAGRAM OF MERCURY-STEAM CYCLE

for the stresses which will be encountered at the desired pressure.

Fig. 2 gives a clue as to why mercury-topping power ratios are so high. In this comparison, the total heat of the mercury vapor and its competitor, high-pressure steam, have been corrected to the same total heat as is contained in 1 lb of 2300-psia 1050-F total temperature steam, or to 1497 Btu. For this total heat, 9.7 lb of mercury vapor must flow through a mercury turbine for each pound of 2300-psia steam flowing through a 2300-psi steam turbine.

As a basis for comparing the topping capabilities of these two cycles, the upper curve is a plot of the available energy of approximately 9.7 lb of mercury vapor when used to produce topping steam at various pressures in the mercury-condenser boilers. The lower curve is a plot of the available energy of 1 lb of 2300-psia steam used in a turbine, exhausting at the indicated back pressures. The steam pressures thus indicated by the abscissa are the back pressures of the steam expansion from the 2300-psi noncondensing steam turbine, or the pressure of the steam made in the mercury-condenser boilers. In keeping with present design practices, a 30-deg F terminal difference between the condensing mercury vapor from the mercury-turbine exhaust, and the boiling water was taken into account when establishing the mercury-vapor available-energy figures.

It will be noted on the chart that at 400-psia steam pressure, the available-energy ratio of mercury to steam is 442/220, or almost exactly 2 to 1, and, at 1250 psia, the ratio is 320/87 or almost 3.7 to 1.

The fact that the available energy of mercury vapor varies only some 27.5 per cent when generating steam in the mercury-condenser boilers at pressures varying from 400 psig to 1250 psig, makes it possible to design standard mercury units for wide ranges of by-product-steam pressures with a relatively small change in mercury-turbine output.

Over the same back-pressure range, the available energy of a 2300-psig noncondensing topping turbine varies about 60 per cent.

Further, the mercury power plant may be used effectively operating in conjunction with 850-psig or even 1250-psig steam turbines to increase greatly the over-all plant capacity and efficiency.

A steam-turbine plant capacity may be increased some 60 per cent for the same quantity of condensing water by mercury topping. For example, the new Schiller Station at Portsmouth includes a 25,000-kw steam turbine which, in effect, is topped with 15,000 kw of mercury capacity. For the 40,000 kw total capacity, only 25,000 kw are affected by the usual condenser losses. This saving in condenser-cooling-water requirements may become very important in localities where cooling water is scarce, although this was not the case at Portsmouth.

MERCURY TOPPING AT SOUTH MEADOW

The South Meadow Station of the Hartford Electric Light Company was the first steam-generating plant to use a mercury-vapor cycle to top existing steam-generating units as a commercial undertaking. This original 10,000-kw mercury topping plant was

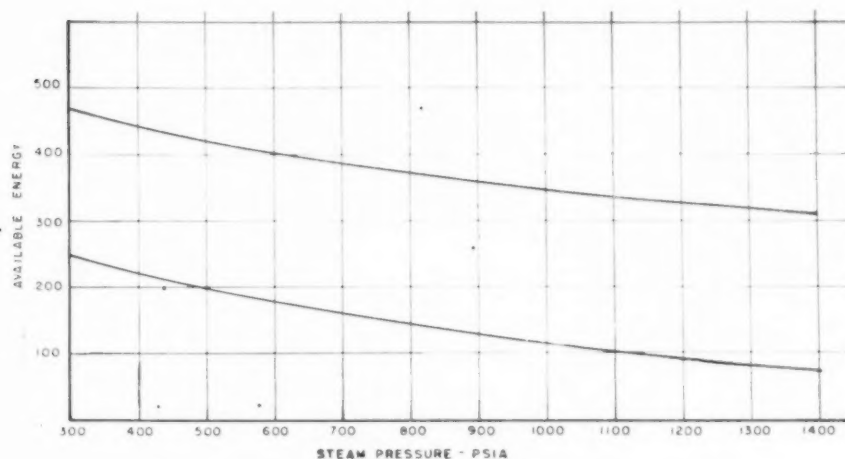


FIG. 2 AVAILABLE-ENERGY CURVES FOR MERCURY VAPOR AND STEAM

(The available energy of 155 psia 975 F total temperature mercury vapor and 2300 psia 1050 F total temperature steam have been corrected to the same total initial heat of 1497.1 Btu. The curves are then plotted with actual available energy of the two corrected fluids as the ordinate with the abscissa representing the back pressure of steam expansion of a 2300-psia noncondensing steam turbine, or the steam pressure generated in the mercury-condenser boilers. The mercury-turbine exhaust pressure has been corrected to include a designed drop of 30 deg F terminal difference in the mercury-condenser boilers.)

put into service in 1928, superposed on 250-psig 700 F total temperature steam-generating equipment installed in 1921. The design margin in the steam portion of this first mercury installation was ample to permit the raising of its operating pressure to 400 psig 700 F total temperature early in the 1930's simply by changing the safety valves.

In the 19 years between 1928 and 1947 this first commercial mercury topping plant operated on line for some 119,000 hr, producing a net output of more than 1.7 billion kwhr of electric power.

It was evident prior to 1946 that the original installation, constructed from materials available in 1927, was coming to the end of its economical life owing to the metal fatigue at the associated high operating temperatures. The Hartford Electric Light Company made an economic study of the value of a 50 per cent larger-capacity unit in the same building with the result that it was decided later in 1946, to proceed with active engineering of a modern replacement for the 1928 unit and its associated equipment.

The removal of the old equipment was started in the summer of 1947, to make the building area available for the installation of an entirely new design of mercury plant having a capacity at full load of 15,000 kw, and a steam output from the condenser boilers of 210,000 lb per hr at 400 psig 700 F total temperature.

NEW 15,000-KW MERCURY-UNIT POWER-PLANT EQUIPMENT

The mercury-unit power-plant equipment now in operation is entirely new except for the condenser-boiler steam drums and vacuum shells, the mercury-turbine generator, and a portion of the mercury-turbine exhaust shell. In order to assure reliable operation of the condenser boilers, new steam-generating tubes with water circulators were installed. Because of the ample size of the 10,000-kw generator stator frame and rotor, these parts were rewound to give maximum output of 15,000 kw at unity power factor.

Most of the existing building steel, as well as certain of the old boiler supporting members, were usable with the new equipment. However, as might be expected, the major portion of the equipment structural supports had to be replaced to meet the new design conditions.

Fig. 3 shows a schematic arrangement of the main equipment as it is now installed in the South Meadow Station.

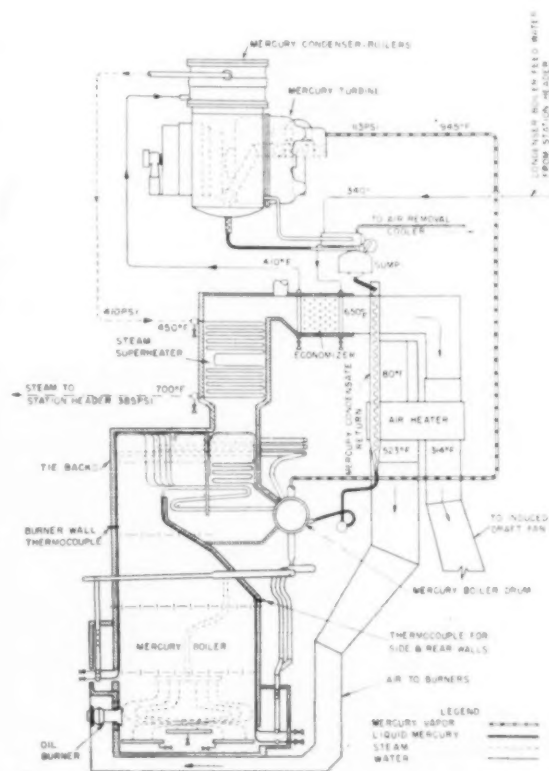


FIG. 3 SCHEMATIC ARRANGEMENT OF 15,000-KW MERCURY-UNIT POWER PLANT AT SOUTH MEADOW STATION

The oil-fired mercury boiler is of the latest design, having completely mercury-cooled furnace, slag screen, and mercury fog-convection surfaces. The steam superheater, water economizer,

and regenerative-type air preheater are of conventional design, as are the forced and induced-draft fans.

Mercury vapor is generated within the tubes of the mercury boiler at a pressure of 130 psig and at a saturated temperature of 964 F. The mercury vapor thus produced flows upward through four 12-in. vapor pipes to the five-stage single-flow mercury turbine located in the turbine room above the mercury boiler. Suitable mercury stop and throttle valves are attached directly to the mercury-turbine high-pressure shell for controlling the mercury-vapor flow to the turbine. Likewise, two 14-in. mercury-boiler relief valves are mounted out from the inlet end of the turbine stop valve to protect the mercury boiler from overpressure. When operating, these two relief valves discharge into the condenser-boiler vacuum shell where the energy from the overpressure mercury vapor is absorbed to produce steam which may then be used by the steam-turbine units, or exhausted to atmosphere through the condenser-boiler steam safety valves, depending upon the station load conditions.

The mercury turbine exhausts into two vertical-type side-mounted mercury-condenser boilers at an exhaust pressure of 1.5 psia 480 F. In condensing, the exhaust mercury vapor releases its heat of vaporization to water within the tubes of the condenser boilers to produce steam at 410 psig. The condensed mercury liquid then flows by gravity through a cleaning sump and suitable piping system to the mercury boiler where it is again evaporated at 130 psig.

The steam generated in the condenser-boiler tubes is superheated by the boiler flue gases to 700 F total temperature in the steam superheater mounted directly above the mercury boiler. The steam thus superheated is piped to the 385-psig station steam header for use in the 385-psig steam turbines.

When desired, steam may be generated for use with the 250-psig steam turbines. No equipment alterations are necessary as the change-over may be made from one station steam pressure to the other merely by valving the steam superheater-outlet pipe to the desired steam header.

The condenser-boiler feedwater is taken from the station feedwater header at 340 F, pumped through the cooling coils of the primary air-removal cooler and into the water economizer, where it is heated by the boiler flue gases to 410 F. The heated feedwater then flows into the condenser-boiler steam drums where it is boiled into steam by the condensing mercury vapor.

In order to assure satisfactory over-all power-plant combustion efficiency, a large regenerative-type air preheater heats the air used for combustion from 80 F to 523 F. The resulting exit-gas temperature with 15 per cent excess air leaving the furnace is expected to be 300 F, when corrected for air leakage through the air preheater.

MERCURY BOILER

A mercury-furnace tube operated with properly treated mercury is capable of pumping large quantities of liquid mercury and vapor through long flow circuits located considerably above the liquid level in the boiler drum. This action is produced by the relatively high pumping head of the down-flowing liquid column supplying the lower feed headers of the furnace tubes, as well as from the proportionately high available energy in the expanding mercury vapor as it flows upward through the boiler tube. The release of energy is brought about by the large change in pressure throughout the tube from where boiling first occurs in the lower portion of the furnace to where the tube enters the boiler drum at operating pressure. In a very high boiler this pressure head may be 100 psi or more.

As heat is applied to the boiler tube, generating more and more vapor, the theoretical density of the flowing mixture may change from solid liquid, weighing approximately 778 lb per cu ft, to a lean

mixture having a weight of approximately 2.5 lb per cu ft, before decrease in heat-absorbing ability of the tube occurs. In actual mercury-boiler designs, such as the 15,000-kw Hartford boiler, the mixture discharging into the boiler drum from the fog-convection tubes is designed to be in the order of 13 lb per cu ft for the heaviest loaded circuit. Such a mixture contains approximately 1 lb of vapor for each 7 lb of liquid mercury circulated, or may be said to have a circulation ratio of 7:1.

The economic advantage of such circuit design is immediately apparent as great savings in total boiler mercury are possible, since it is only necessary to fill the furnace tubes with mercury to a minimum depth with no liquid mercury in the fog-convection portions of the circuits at starting. The liquid portions of the tubes can be of small internal diameter while the fog section tubes may be much larger.

A mercury boiler usually requires some 70 to 80 per cent of the total heat-absorbing surface in the convection regions, and if it were necessary to use all liquid-filled tubes, the quantities of mercury required might be prohibitive. This theory of mercury-boiler design was first used successfully in 1940 in the 20,000-kw mercury boiler at Kearny where many of the fog circuits are some 250 ft long from end to end with approximately 40 ft of the furnace portion of the tubes liquid-filled at starting.^{3,4}

These simplifications and economies are possible because the titanium-magnesium-treated mercury in the boiler circuits produces intimate and perfect contact between the metal of the tubes and the flowing mercury. The treated mercury has lost its spheroidal properties and spreads in a tenacious film over the inside walls of the tubes, forming a "wetted" surface from which evaporation of the mercury occurs.⁵

The tenacity of the wetted film is such that it is not destroyed when superheated upward to 200 F above the temperature of the saturated-vapor-liquid mixture flowing in the circuit, as long as treated mercury is supplied to the heated film as rapidly as evaporation occurs. By maintaining suitable velocities of the flowing mixture in the tubes, the required "make-up" supply of mercury droplets is available over the extremely wide range from solid mercury liquid to the approximately low density of a 1.2 parts by weight of liquid mercury to 1 part-vapor.

The extensive use of mercury-fog-convection surface throughout the entire boiler reduces the maximum pressure at any point in the tube circuit, which subsequently reduces the boiling temperature of the mercury and the metal temperature of the tube steel. This allows added protection against oxidation of the tube metal on the fire side of the tubes, as well as increases the allowable working stress of the material.

Our standard-design, mercury-unit-power-plant mercury boilers, of which the 15,000-kw Hartford unit and the three 7500-kw units for Pittsfield and for the Schiller Station are typical examples, all utilize the well-proved principle of fog-circuit design.

THE HARTFORD MERCURY BOILER

Fig. 4 is a cross section of the Hartford boiler. The flow of mercury in the various boiler circuits is simple and direct. The operating liquid level is maintained at or near the inside bottom of the boiler drum. With the boiler in operation, the fluid mercury flows from the drum downward through suitable downcomer supply pipes to the various lower headers, and then upward to the drum, as required, to provide coolant for the furnace tubes and fog-convection circuits.

Owing to the simplicity of the mercury-boiler design, only four basic types of tube-flow circuits were required.

The tubes covering the two furnace side walls are simple

³ "The Mercury-Vapor Process," by A. R. Smith and E. S. Thompson, October, 1942.

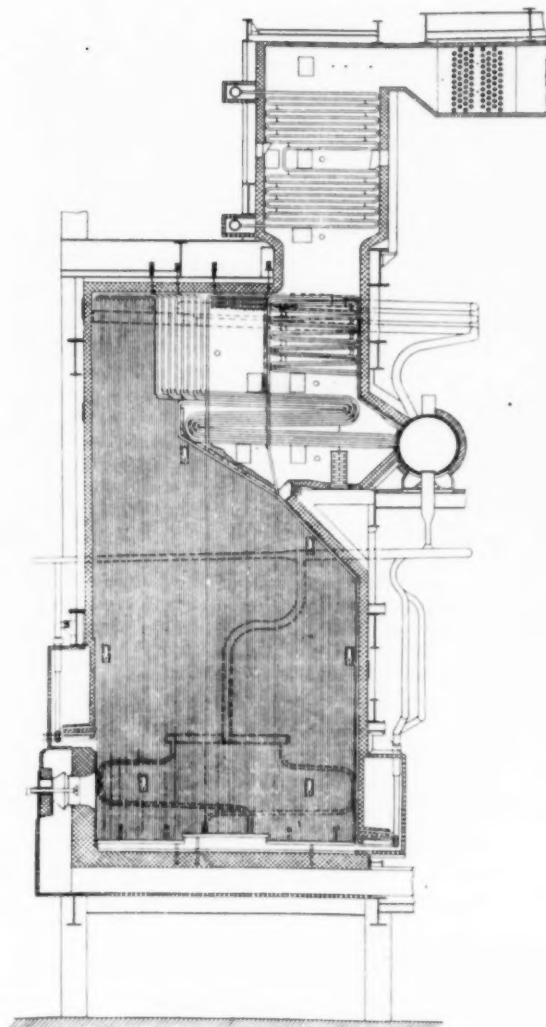


FIG. 4 CROSS SECTION OF 15,000-KW MERCURY BOILER
(Portion of furnace tubes, downflow slag screen, fog-convection tubes, drum and downcomer supply system, as well as steam superheater and water economizer are shown.)

straight-through elements receiving mercury from bottom headers and discharging into vapor headers at the top. Each of the six vapor headers connects to the mercury-boiler drum through a vapor discharge pipe. The side-wall furnace tubes are $1\frac{1}{2}$ in. OD \times $\frac{7}{8}$ in. ID for the lower 16 ft and are 1 in. ID for the remaining 30 ft of their length.

The burner-wall or front-wall tubes supply mercury to the roof section of the furnace vestibule, the vertical downflow slag-screen tubes, the first and second passes of the horizontal fog-convection tubes, and finally discharge into the drum. These tube circuits are stepped in size from $\frac{7}{8}$ in. ID, where they leave the lower headers, to $2\frac{1}{2}$ in. OD \times $1\frac{3}{4}$ in. ID, where they form the first-pass fog bank.

The rear-wall furnace tubes also form the sloping roof section under the fog-bank assemblies. A number of the roof tubes are directed upward and function as the two mercury-cooled supports for the fog circuits. These tubes then continue on to form the

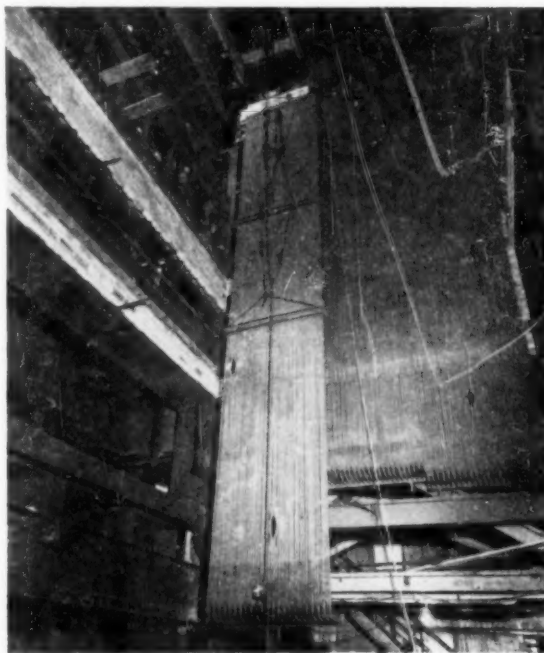


FIG. 5 15,000-KW MERCURY FURNACE SIDE-WALL ASSEMBLY BEING HOISTED INTO POSITION
(Showing sections already in place, a third section being hoisted into position to complete east furnace wall.)

third-pass fog circuits. The remainder of the roof tubes protect the nose of the furnace arch and then turn back and become a portion of the first and second-pass fog banks. The tube sizes vary from $1\frac{1}{2}$ in. OD \times $\frac{7}{8}$ in. ID at the bottom to $2\frac{1}{2}$ in. \times $1\frac{3}{4}$ in. where they form the fog circuits.

In an effort to reduce over-all costs as well as to reduce the time required to complete field assembly of the boiler units, factory fabrication of the furnace tubes with their liquid and vapor headers was tried for the first time. Fig. 5 shows one of the furnace-side-wall subassemblies of which there is a total of six, three for each side wall. These are approximately 7 ft wide \times 46 ft long. Some 47 tubes are completely assembled with their upper and lower headers, tiebacks, and supports ready for placing in position in the boiler-supporting steel. Similar but small subassemblies of the front and rear-wall tubes likewise were made at the factory and shipped ready for field erection. The fog tubes, slag-screen tubes, and the upper portions of the front and rear-wall tubes were handled as individual pieces in the field. However, the apparent savings in erection time and over-all cost seemed to be sufficient to warrant further development of factory prefabrication of mercury-boiler parts. Therefore similar but more complete subassemblies were manufactured for the three 7500-kw units now in the process of being erected.

Fig. 6 shows the upper portion of the completed Hartford furnace.

Fig. 7 shows the six horizontally mounted fuel-oil burners. These six burners are mounted under the front-wall tube headers near the bottom of the refractory furnace bottom.

MERCURY-BOILER DESIGN AND MANUFACTURE

The three 7500-kw boilers for Pittsfield and the Schiller Station are of identical design and are being manufactured by the Babcock & Wilcox Company from identical blueprints. The Hart-

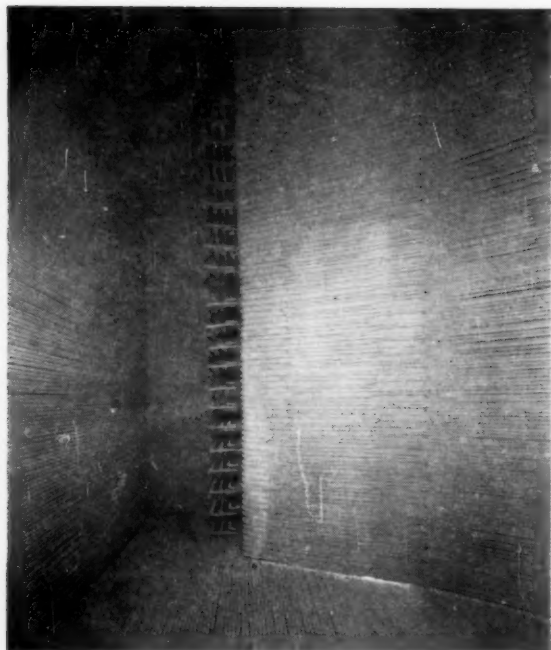


FIG. 6 VIEW TAKEN FROM INSIDE COMPLETED FURNACE OF THE 15,000-KW MERCURY BOILER, SOUTH MEADOW
(View shows upper portion of furnace walls, sloping arch and furnace roof. Downflow screen tubes are also shown above sloping roof sections.)

ford boiler, manufactured and installed by the Foster-Wheeler Corporation, differs somewhat from the 7500-kw boilers in that it was designed with a flat refractory-covered furnace floor for burning fuel oil only. The 7500-kw units have dry-ash mercury-cooled hopper-bottom furnaces for burning pulverized coal or fuel oil as desired.

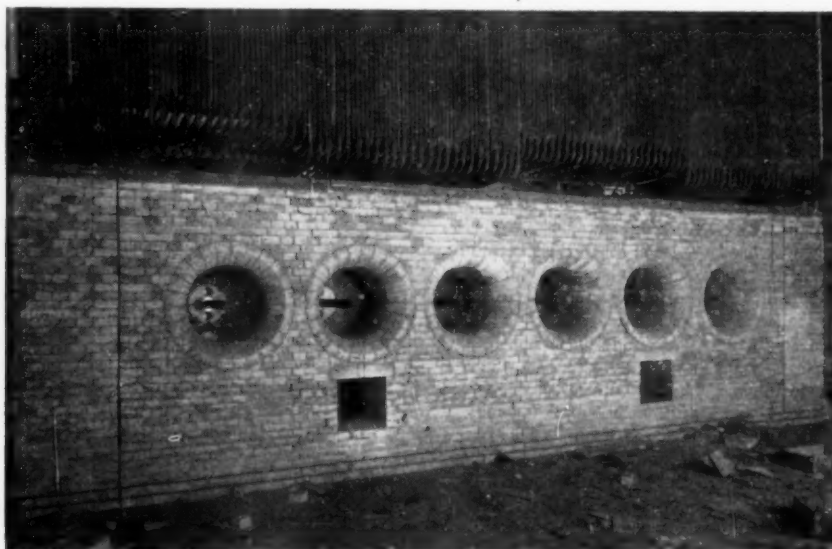


FIG. 7 SIX HORIZONTALLY MOUNTED FUEL-OIL BURNERS
(Lower end of front-wall furnace tubes, refractory burner wall, and refractory furnace bottom are shown.)

MERCURY-TURBINE GENERATOR

Fig. 8 shows the 10,000-kw Hartford turbine after 16 years' operation. This simple single-flow 720-rpm, five-stage turbine has run more than 116,000 hr since its last internal inspection. When finally dismantled in 1947 for replacement, the machine internals were found to be in unbelievably good condition for a unit that had operated without internal maintenance for such a period of time.

However, because of the design conditions at 15,000-kw output, requiring the use of higher pressure and temperature, it was necessary to replace the old mercury turbine completely, using the latest in materials and machine design. The new machine followed the general pattern of the original unit but included all of the modern improvements, such as mercury-sealed shaft seals, and vanadium-molybdenum alloy castings for the high-pressure turbine head, turbine control, and stop valves, and for the mercury-boiler relief valves. A complete new turbine-rotor assembly, having separately mounted split diaphragms, was provided. A new main bearing, incorporating a double-thrust-type thrust bearing, was also necessary. Because the unit was to be operated as a base-load machine, no speed governor was installed. Two emergency trips were provided, one on the hand-operated control valve, and one on the turbine stop valve.

Fig. 9 is a view of the mercury turbine with the four split diaphragms in place and the high-pressure head removed. The two wing-back-mounted condenser boilers have been placed in position ready for making the two large turbine-exhaust-shell welds.

Fig. 10 is a view of the exhaust opening of the east condenser boiler, showing the porcupine-type tube bundle.

Fig. 11 shows the completed assembly of the mercury turbine, condenser boilers, control and stop valves, and the mercury-boiler relief valves.

HARTFORD ELECTRIC LIGHT COMPANY OPERATING EXPERIENCE

Previous Designs. The Hartford Electric Light Company operating experience with the mercury cycle for power generation covers the period beginning in 1923 up to the present date.

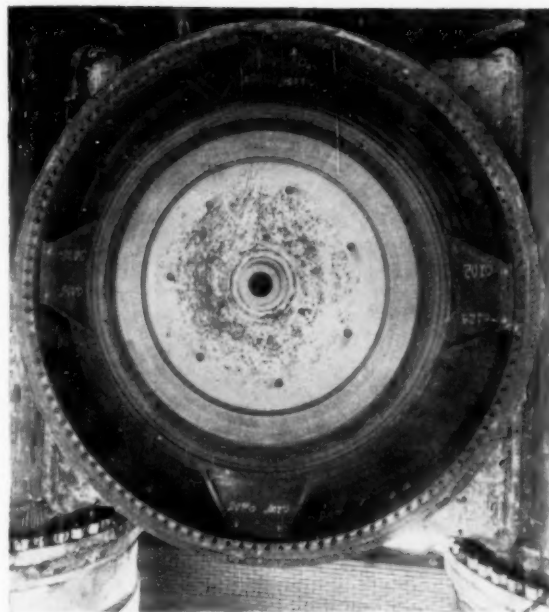


FIG. 8 10,000-KW MERCURY TURBINE BEING DISMANTLED IN 1947 AFTER 16 YEARS OF OPERATION IN SOUTH MEADOW STATION

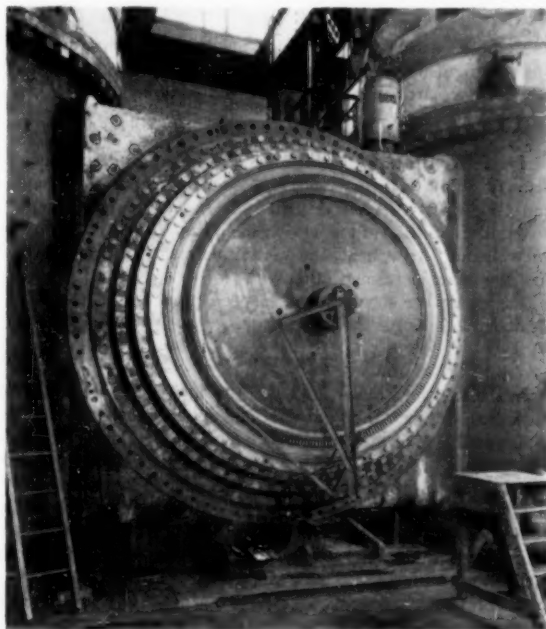


FIG. 9 15,000-KW MERCURY TURBINE BEING ASSEMBLED IN 1948, SOUTH MEADOW STATION

(View shows portion of original 10,000-kw turbine-exhaust shell, original but newly retubed condenser boilers, and partial assembly of new wheels and new built-up diaphragms. Split interstage diaphragms were used in new machine rather than the old shell-supported solid-disk type shown in Fig. 8)

During the first 4 years it was a joint venture with the General Electric Company for the purpose of developing a design that would meet all the requirements of a central station from the

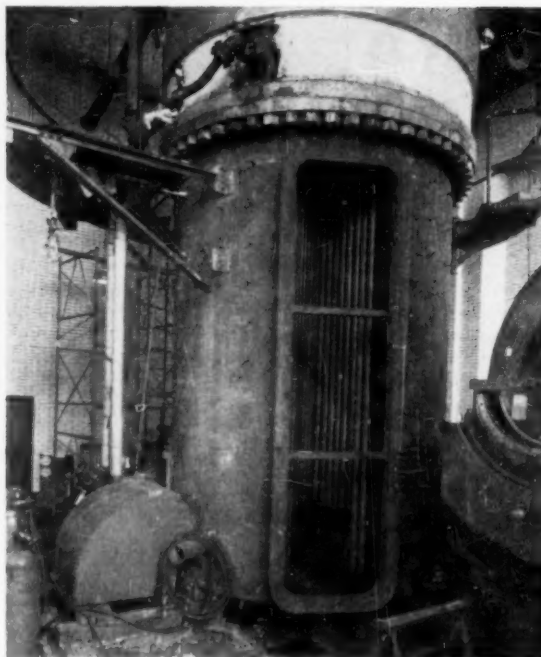


FIG. 10 MERCURY-CONDENSER BOILER SHOWING PORTION OF PORCUPINE-TYPE TUBE BUNDLE AND OPENING FOR ATTACHING TO MERCURY TURBINE-EXHAUST SHELL

(Downflow water circulators were installed in each steam-generating tube to improve circulation.)

point of flexibility, dependability, and economy. This first topping unit was installed in the Hartford Electric Light Company's Dutch Point plant and consisted of a 1500-kw generator, driven by a mercury-vapor turbine exhausting to a condenser-boiler operated at 200 psig and 540 F total temperature, the conditions of the main steam header in the plant. Five entirely different designs of boilers were covered in this experience cycle.

In 1927 a 10,000-kw mercury-vapor unit was contracted for as a plant extension at the South Meadow Plant to top an existing 250-psig, 700 F total temperature steam unit installed in 1921. This design was proved by the Dutch Point experience but in the larger size developed several faults. Consequently it was 1932 before all defects had been eliminated and the plant could be considered as dependable central-station equipment.

From 1932, until its removal in 1947, the 10,000-kw South Meadow unit operation was quite satisfactory even though it was necessary to reduce top operating load progressively as metal fatigue progressed. By thus reducing load, and consequently stresses, we were enabled to produce the results given in the first section of this paper at an over-all plant availability in excess of 85 per cent. This availability includes outage time for steam-cycle equipment as well as that for the mercury cycle.

Operation of 10,000-Kw Unit. Operation of this 10,000-kw unit was extremely simple: Liquid mercury was returned by gravity to the boiler; there was no treatment of the liquid-mercury charge; no treating of the boiler feedwater was required; there was no complicated feed-heating cycle, and the pressures were low.

Mercury replacement, due to all losses, was low, averaging less than 2000 lb per year from all causes both avoidable and unavoidable.

Maintenance was variable. General maintenance was usual for

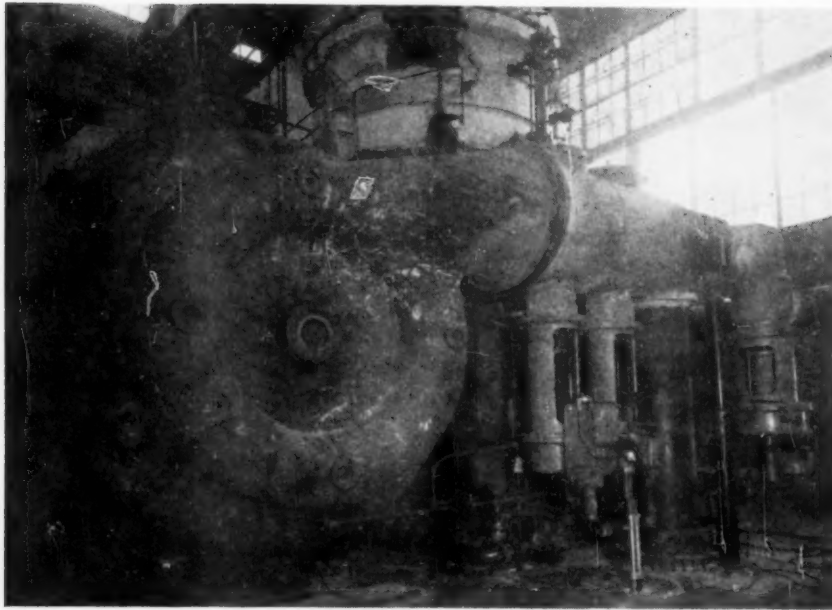


Fig. 11 ASSEMBLY OF 15,000-KW MERCURY TURBINE, SOUTH MEADOW STATION

(High-pressure shell control and stop-valve assembly with 26-in. mercury-vapor inlet pipe entering bottom of stop-valve casing. One of two 14-in. mercury-boiler-relief valves with their 18-in. vapor-relief pipe is shown attached beyond vapor-inlet pipe. Boiler relief valves discharge their vapor, when operating, into west condenser boiler.)

TABLE 1 15,000-KW SOUTH MEADOW MERCURY UNIT*

Oil burned, lb.....	12,281.169
Steam generated at 260 psig and 700 FTT, lb.....	126,118.000
Gross output from vapor-driven generator, kwhr.....	10,048.000
Gross generated from steam, kwhr.....	11,387.000
Total auxiliary usage, kwhr.....	565.000
Net total unit output, kwhr.....	20,870.000
Fuel rate, lb oil/net kwhr.....	0.588
Heat rate, Btu/net kwhr.....	10,200

* Twenty-eight consecutive days' operation at full load.

all associated equipment and there was no maintenance on the mercury turbine from 1931 until it was dismantled in 1947. The mercury boiler required a major internal cleaning approximately once a year using acid, and external cleaning at the same intervals as a steam boiler. As a general statement, it should be said that average maintenance costs for this unit were slightly in excess of those for a comparable steam unit.

NEW 15,000-KW MERCURY PLANT AT SOUTH MEADOW

While construction work had not been completed it had progressed to such a point that it was possible to light the first fire under the boiler on January 2, 1949. Preliminary operation consisting of boiling out, trying out all associated apparatus, and making indicated changes and adjustments had been completed by January 8, and the mercury-vapor-driven generator was phased in on the line. By February 1 construction work had been completed, the changes indicated by the first two runs had been made, and the unit phased for service the third time. The plant had been accepted for service with this third start and the results of this operating period are shown in Table 1.

All quantities shown in Table 1 are actual net figures, as all charges have been made to the mercury plant occurring from associated auxiliary equipment whether it is a part of the mercury plant directly or a part of the steam-turbine unit using the steam from the condenser boilers.

Shutdown of the unit at the end of 28 days of operation at full load was caused by a partial stoppage in the regenerative air

heater. Thorough inspection, during this shutdown, indicated that all parts of the mercury cycle were in as good condition as at time of the start-up.

CONCLUSION

From the Hartford Electric Light Company's experience to date, no serious difficulty is anticipated with any part of the equipment covered by the new design. The plant forces are adequate to handle all phases of the new problems introduced by the necessary chemical treatment, the special metals used in fabrication, and the novel instrumentation.

The operating economies have been proved, and the design demonstrated as generally adequate.

ACKNOWLEDGMENT

In the Hartford boiler, and also the three 7500-kw units, the basic boiler design, the treatment of the boiler mercury, and the design and size of the boiler flow circuits is by General Electric Company. However, such problems as structural supports, fuel burning, and over-all boiler performance, as well as actual detail designs, manufacturing, and erection of the complete boiler units could best be done by the boiler manufacturers. Joint responsibility was shared by the General Electric Company and the boiler companies with regard to the materials used in the tubes and other pressure parts.

This broad division of responsibility has offered no problems whatsoever of customer relations between either the General Electric Company as principal contractor and the boiler companies or operating companies in carrying out the several projects now under way. The relationship has been most cordial and all parties concerned have spared no efforts in promoting vigorously their various portions of the work. We particularly wish to congratulate at this time those of the Foster-Wheeler Corporation who have worked with such diligence and painstaking care in making the Hartford boiler such an outstanding success.

Discussion

WILLIAM KOWALSKY.⁵ Another step toward widespread commercial acceptance of the mercury-vapor steam cycle for power generation has been taken with the successful completion of the mercury power unit at the South Meadow Station of the Hartford Electric Light Company. The heat-rate data given in Table 1 of this paper will be a criterion against which other utilities may check their own plant performances.

For the writer's company, the work of planning, fabricating, and erecting the mercury boiler was an unusual and valuable experience. Each stage of development of the mercury boiler was preceded by exhaustive tests and investigations. No material or procedure was adopted until tried and proved. (It should be emphasized that this approach was used by General Electric Company from the very beginning of its experiments with the mercury-vapor process back in 1912. This step-by-step development can be pointed out as a classic example of the solution of an engineering problem in which there was no previous experience and where every item involved unknown elements.)

From a metallurgical standpoint, there were commercial alloys available for the furnace tubing which could withstand the 1100 F metal temperature and the 1000 F mercury temperature, but fabricating methods, welding, heat-treating, and stress-relieving procedures had to be developed. The difference between shop- and field-welding procedures had to be investigated. With the operating-temperature range mentioned, creep strength limited the design stresses, and considerable stress-analysis work was done to insure that the low permissible stresses were not exceeded. The boiler was designed to meet the requirements of the ASME Boiler Code in so far as possible.

Due to high metal temperature, it was necessary to select materials with high resistance to oxidation. High-silicon steels were selected. It is estimated that these superior materials give the mercury boiler the same economic life as a modern steam generator. The tube material for all of the furnace, slag screen, first-pass convection tubes, and eighteen rows of second-pass convection tubes, corresponded to SA-213-T13. The upper bank of second-pass convection tubes had a composition very similar to SA-213-T21. The mercury drum, downcomer system, upper and lower headers, conformed to SA-213-T12. Thus expensive alloys were used only where needed, as dictated by boiler conditions. Tube supports, fixed ties, and tie-back supports, when exposed to furnace or boiler temperatures, were normally of 25-20 alloy composition. The SA-213-T13 tubing (4 to 6 chrome, $\frac{1}{2}$ moly, 1 to 2 silicon) was welded by the atomic-hydrogen method, using a bare rod of the same composition as the tubing. The SA-213-T21 (2.75 to 3.25 chrome, 1 moly alloy) tubing was welded by electric arc with a 2 chrome 1 moly coated rod. The SA-213-T12 tubing (chrome-stabilized carbon-moly) was welded by electric arc with a $\frac{1}{2}$ chrome $\frac{1}{2}$ moly coated rod. Backing rings for all welded joints were of the integral type, machined right on the tube to form the male end, with a standard bevel machined in the matching tube for the female end. All welds in which SA-213-T13 material was involved, were ground and magnafluxed. Only random welds of the other compositions were ground and magnafluxed. A proof of the welding quality of the total volume under pressure or vacuum can be seen in the extremely low air leakage into the system.

The superheater is of the continuous-tube type of carbon-steel material. Because the superheater occupies the tail position in the boiler, and because of the variable mercury-pressure operation, the superheat characteristic drops very sharply as the load decreases. To get the maximum performance of the steam end at fractional loads, a group of parallel dampers have been installed

to by-pass the upper second-pass convection surface, and thereby increase the heat available for steam superheating.

In order to save time and expense in the field, and in order to accomplish as much of the welding as possible under shop conditions, the mercury-cooled walls were assembled in fourteen sections in the shop. The elements were fabricated, welded into the headers, and then stress-relieved as complete units. This was the first time a boiler had been shipped in such large flexible prefabricated assemblies. Necessarily, this procedure involved solving numerous problems, such as handling methods, assembly jigs, railroad clearances, erection clearances in the building, and so on.

The mercury boiler is supported across the front and rear at the level of the bottom of the mercury drum and is allowed to expand up and down from that point. The side walls are supported at the top of the furnace. Vertical expansions are of the order of 3 in. and require provision for flexibility in connecting downcomer piping to the riser side, a problem which was complicated by the much colder mercury on the downcomer side. Tie-backs are spaced at approximately 10-ft intervals and arranged for each tube to move laterally and vertically, independently of its neighboring tube.

During the initial start-up of the mercury boiler, when all concerned were crossing fingers, praying to the "gods of kilowatts," and trying hard to look unconcerned (even though we knew that every care and precaution possible had been taken), it was a source of wonderment to the writer to find how correctly the General Electric Company designers had predicted the behavior of this mercury boiler. When circulation of mercury was still erratic and efforts to induce some kick-over of hot mercury into the drum and downcomer system to try to equalize temperatures and expansions were being made, the prediction was offered that, starting at 4000 kw output, there would be some audible thumping of slugs of mercury in the vapor tubing, and that this would quiet down at 6500 kw. It worked exactly as predicted. We knew that untreated mercury did not "wet" the inside tube surfaces and that this caused erratic heat-transfer rates. We also knew that mercury with small amounts of magnesium and titanium did wet the inside tube surfaces and allow a uniform heat flow into the mercury. Nevertheless, we had to rub our eyes when we actually saw this happen. When circulation was established, our thermocouple readings indicated wide variations in first-pass convection-tube temperatures. Within a few minutes after the treating chemicals had been injected into the mercury feed lines, the temperature of these tubes dropped approximately 100 deg F, and all reached a more-or-less uniform level. It was obvious that the heat-transfer rates had suddenly become dependable.

The early mercury-boiler designs were complicated, but now it is just like any steam generator in appearance, both from the outside and from the inside of the furnace. The low position of the mercury drum with relation to the top of the furnace tubes strikes one as unorthodox at first glance; moreover, there is no level of mercury in the drum, a condition in which steam boilers are shut down promptly. The unit is specially developed and designed to run on minimum mercury content, which is possible because of the ability of mercury vapor to entrain substantial amounts of mercury mist or fog of tremendous cooling effect. It is necessary of course to supply a liquid mercury fog to the upper tubes to keep the film of mercury, which coats the inside tube surfaces, supplied with chemically treated mercury to replace that which has been evaporated. Provided reasonable mixture velocities are maintained, there is no limitation in size or shape of the tube circuits. The length of the tube circuit could be considerable, depending on the available mercury-circulating head and heat input. As long as treated liquid mercury mist is carried by the vapor, there can be no overheating of the tubes.

⁵ Project Engineer, Foster-Wheeler Corporation, New York, N. Y.

The Hartford mercury boiler was not built as another experimental attempt to improve the Emmet mercury-vapor process. It is just another boiler built on a purely commercial basis of sound economics, because the practicability of the system has been proved before.

H. WEISBERG.* At the Kearny Station, Public Service of N. J., there is installed a 20,000-kw superposed mercury-turbine generator which has been in operation since 1933. The combined mercury-steam capacity is 45,000 kw. For the first 6 years this unit was in service 51 per cent of the time, and generated over 750,000,000 kwhr; the average output being 32,000 kw.

In 1940 the boiler was replaced with a more modern design, somewhat similar to the new Hartford boiler. In the 9 years since then, the unit has been in service 72 per cent of the time. It has generated over 2,100,000,000 kwhr, and has had an average output of 38,000 kw. The total generation for both installations has been about 3,000,000,000 kwhr.

At the present time the unit is in regular operation on the system at loads up to full rated capacity. Early next year rather extensive repairs are planned to the furnace tubes owing to wastage on the gas side. Also, the vapor piping and control valves, which are plain-carbon steel and operate at 970 F, will be replaced with alloy-steel parts. It is expected that as a result of this work, along with other improvements which have been made in recent years, the availability of the unit will approach that of steam units, which is better than 90 per cent.

The heat rate of the unit, combined with 1925 design, 355-psi, 725-F steam capacity, compares favorably with the most efficient steam units which we are installing today, and as a result, with the inflation that has taken place since 1933, the value of the unit on the system is about double the original cost.

We are often asked whether we would install another mercury unit, or why we are not installing mercury units now rather than steam. The answer is that the availability up to the present time has not been as good as that of steam. It is our belief that the troubles we have had are not inherent in the mercury cycle and have been overcome by operating experience and development. With the present state of development, however, it seems inadvisable to build mercury boilers in capacities of 125,000 to 150,000 kw, which size steam units can be utilized safely on a system as large as that of the Public Service. This results in considerable disadvantage in the first cost of mercury units when compared with steam.

The mercury cycle when combined with modern steam capacity is more efficient than any steam cycle currently practicable, and therefore it is attractive where fuel costs are high and a unit not over 45,000 kw combined capacity is needed. Larger units would require two boilers and would be less economical. For superposition in sizes not over 20,000 to 30,000 kw, the mercury cycle is even more advantageous. Here again, if any of the Public Service units were to be superposed now, considerably larger units could be considered, and the mercury cycle would be at a disadvantage compared to steam. For these reasons we have not been able to justify additional mercury capacity on recent installations.

Summing up, 16 years of experience with the mercury cycle indicated definite and continuing progress. Additional installations appear to be justified at this time in limited sizes and for special applications.

O. L. WOOD.† There are many interesting details of the new

* Mechanical Engineer, Electric Engineering Department, Public Service Electric and Gas Company, Newark, N. J. Mem. ASME.

† Construction Engineering Division, General Electric Co., Schenectady, N. Y. Jun. ASME.

mercury installation at Hartford which might be used to supplement the comprehensive paper presented by the authors. The writer, however, will discuss only some of the phases of installing the new equipment, which is of 50 per cent greater capacity and operating pressure, within the space occupied by the original unit.

The original operating boiler pressure of 85 psig 908 F saturation was increased on the new unit to 130 psig 964 F. This was done, as explained in the paper to obtain (1) greater cycle efficiency by having the total heat available at a higher initial temperature, and (2) more available energy per pound of vapor.

The increase in capacity, requested by The Hartford Electric Light Company, was based upon its studies of a replacement and the real economies obtained on the original unit.

A new mercury-boiler design had been developed based upon considerable investigation of comparable steam-boiler experience. It required fewer types of circuits and bends, reducing circulation studies and manufacturing costs. This design fitted nicely between the main building columns at South Meadow. A 29-ft width and 20 1/2-ft depth of furnace were obtained to give the low heat-liberation rate of 18,150 Btu per cu ft at full load. Since the vertical cross section of the new boiler had been established, this fixed the location of the boiler drum 47 ft directly below the original turbine and condenser boiler-room floor.

It was decided to use four 12-in. schedule 80 vapor pipes of SA-280 material for the full-load flow of 1,640,000 lb per hr. This decision was based upon holding 15-psi pressure drop from the boiler drum through the double-disk stop and control valves to the turbine bowl. These pipes also had to be of sufficient length to take care of a vertical temperature expansion of 4 in. with stresses within code limits.

The turbine, generator, and condensers were rebuilt, rewound, and retubed, respectively, and placed in their original positions on the turbine-room floor.

The gravity mercury-return system, which carries the condensed mercury back to the boiler, was designed to have as a part of it a new type sealed sump. This sump, located 9 ft below the turbine-room floor, removes large foreign matter by flotation in a low-velocity section. In addition, by producing a better vacuum in the sump than that in the condenser boiler, a portion of the cascading mercury in the sump is flashed into vapor. This vapor passes through a short connection from the top of the sump to a cooler where it is condensed and run into the system through a trap. By means of this vapor carrier, the light magnesium-oxide dust, which is the only oxide residue in a chemically treated mercury system, is taken out of the returning mercury continuously and deposited in the cooler. The residue formation in Hartford is extremely small because of the all-welded mercury system, bellows-sealed valves, and leakproof turbine-shaft seal. The total air leakage of less than 1 cu ft per hr into the 3000-cu-ft operating vacuum space causes a metallic-magnesium loss in the treated boiler mercury of less than 1/2 lb per day.

Spiral ramps were designed to avoid shock from falling mercury in the gravity-return system. The largest of these ramps was calculated to carry the mercury down 24 ft vertically. The two elements required were to keep the mercury content in the flow circuit to a minimum and to hold the pressure drop within the limited head available. This head had been reduced by the increased boiler pressure of the new unit, which at 130 psi backs the liquid mercury 27 ft up the return line. Only a few feet are left above this to the sump outlet for additional pressure requirements for blowing the mercury safety valves and pressure drop through the return system at full load.

Other items, which were designed to a minimum size, but yet sufficiently large to meet the heat-balance requirements were (1) the water economizer, and (2) the air preheater. For the

economizer, the inlet water was increased 130 deg F over that used in the original unit by additional bleed-heating. A regenerative-type air heater was used instead of the tubular type used in the original installation.

AUTHOR'S CLOSURE

The modern-design fog-type mercury boilers such as the 15,000 kw Hartford Unit are in reality simple boilers offering no serious problems of design and manufacture although somewhat different procedures were necessary as compared to the present-day high-temperature steam generators. Operating problems appear to be quite similar particularly with regard to expansion and other temperature problems.

The problem of burning low-grade fuels may be somewhat more critical with the mercury units because of the higher metal temperatures encountered in the entire mercury boiler rather than in the high-temperature superheaters and their supports only.

As Mr. Weisberg mentioned in his discussion, furnace-tube wastage under certain conditions of coal or fuel-oil operation has been experienced in a greater or lesser degree at both Kearny and

Hartford as has also been the case in certain of the newer high-pressure, high-temperature steam boilers and superheaters.

Corrective measures for this annoying problem are being vigorously pursued with extremely encouraging results already reported from Kearny and elsewhere. Surface coatings of fused 25-20 weld metal as well as likely silicon coatings and paints are now under test in various mercury and steam plants while various tests are in progress using additives in the fuel as corrosion preventives.

Standard design mercury-unit power plants of extremely high over-all efficiency up to 80,000 kw combined mercury-steam capacity are now available for general power applications.

At the present time, only the plants larger than 50,000 kw total mercury-steam capacity require two mercury boilers per mercury turbine although a twin-boiler combination of mercury boilers and turbine may be had if desired in all but the smallest plant sizes.

For example, the new 40,000 kw Schiller Station of the Public Service Company of New Hampshire utilizes two standard-design 7500-kw mercury-unit power plants to supply steam to one 25,000-kw steam turbine.



FIG. 1 EXTERIOR VIEW OF COMMON MUSSEL, MATURE FORM

Some Biological Fundamentals of Marine Fouling

By WILLIAM F. CLAPP,¹ DUXBURY, MASS.

The common mussel is identified as the organism most important in the fouling of sea-water conduits and most difficult to control. Relevant features of its construction, living habits, rates of propagation and growth, and methods of locomotion and self-protection are described. While very young organisms, in general, are less resistant to unfavorable conditions than the mature of their respective kinds, and the mussel is probably no exception; in the case of the young mussel very high resistance is found very shortly after the permanent shell takes complete formation. Chlorination tests on mussels at Kure Beach, N. C., are described and results quoted.

CLASSIFICATION OF FOULING ORGANISMS

THERE are a number of different kinds of marine animals and plants which can be classed as fouling organisms. They can be divided into two important groups; those which are sessile or incapable of further movement after having become attached and those which can become secure or optionally motile. In the first group would be included such common fouling organisms as the barnacles, bryozoans, and algae; in the second, the common mussels and sea anemones.

Those in the first group are unable to escape from an environment which is no longer favorable. Those in the second group

are capable of migrating from an undesirable location and of locating again and becoming firmly attached where the surroundings are more suitable for the support of the organisms.

Among all of the organisms which might be classified as fouling,² the one group which generally appears to be most difficult to control is that of the mussels, typically shown in the mature form in Fig. 1. The various species in this group are frequently able to survive conditions which eliminate other groups of fouling organisms. Therefore the remarks following will be confined to the mussel, and it is believed safe to assume that in so far as organisms which are of real importance in the marine-fouling problem under discussion are concerned, methods or materials which will check fouling by mussels will be at least equally effective in controlling the other organisms.

Among the various species of mussel which are found commonly and plentifully in intake systems, the edible mussel, *Mytilus edulis*, is probably the worst offender. It has a very wide distribution along the Atlantic coasts of Europe and the United States, and also on the California coast. Other common species of fouling mussel are *Mytilus californicus*, *Mytilopsis leucophaea*, *Brachydontes exustus*, and *Brachydontes recurvus*.

USUAL HABITAT OF THE SEA MUSSEL, MYTILUS EDULIS

Mytilus edulis normally lives and thrives in enormous numbers in water with salinities varying between 15,000 ppm and the 30,000 ppm or more of normal sea water, in the between-tide

¹ President, William F. Clapp Laboratories, Inc.

Contributed by the Power Division and presented at the Spring Meeting, New London, Conn., May 2-4, 1949, and the Semi-Annual Meeting, San Francisco, Calif., June 27-30, 1949, of THE AMERICAN SOCIETY OF MECHANICAL ENGINEERS.

NOTE: Statements and opinions advanced in papers are to be understood as individual expressions of their authors and not those of the Society. Paper No. 49-8-15.

² "Macro-Organisms in Sea Water and Their Effect on Corrosion," by W. F. Clapp, The Corrosion Handbook, H. H. Uhlig, editor, John Wiley & Sons, Inc., New York, N. Y., 1948, p. 433.

"Fouling Organisms on Paints in Salt Water," by W. F. Clapp, Protective and Decorative Coatings, J. J. Matielo, editor, John Wiley & Sons, Inc., New York, N. Y., vol. 3, 1943, p. 401.

areas in more or less sheltered harbors and estuaries. The *Mytilus* also thrives, with appropriate conditions of environment, at considerable depths. Individuals may exist in water of lower salinity, but under such conditions comparatively few survive. Therefore those present under conditions of low salinity are so few in number that they contribute very little to fouling.

In harbors where conditions are favorable, *Mytilus edulis* frequently will form great "beds" several acres in extent on the mud flats which are exposed at low water. In these beds mussels of all ages and sizes are fastened together in clusters which may contain hundreds of individuals to the square foot.

While it is true that such mussel beds are also found below the mean low water and even at considerable depths in the open water outside of harbors, it seems probable that the heavy growths of mussels frequently found in intake tunnels are formed by the offspring of the parents living in the mussel beds in the shallow harbor water in the neighborhood of the intake tunnel.

PHYSIOLOGICAL FACTORS AND DEVELOPMENT OF *MYTILUS EDULIS*

The sexes are separate. The female *Mytilus edulis* may produce considerably more than 1,000,000 eggs in a single season. After fertilization, cell division and the development of the free-swimming embryo are rapid. The duration of this development of the *Mytilus* free-swimming larva, up to the appearance of the first embryonic shell, varies considerably. Some investigations have shown that this period of growth may be completed in as brief time as 12 days, while in other cases the same development requires more than 3 weeks. This variation appears to be normal and undoubtedly is due to favorable or unfavorable conditions of temperature and other factors.

During the period of larval development the embryos are not attached, in fact, are not sufficiently developed to have formed any organ which could be used for the purpose of obtaining a foothold. They may be carried back and forth by tides and currents and therefore may be widely distributed. When the embryo has formed the first protective shell it is approximately

0.25 mm in length. The shell is transparent and bears little resemblance to the second protective shell which the animal begins to form almost immediately beneath the original embryonic shell.

During the height of the breeding season these minute embryonic mussels, which have progressed to the shell form, may appear in great numbers on any material which provides a satisfactory foothold. Wooden panels placed in the water during the seasons when these larval forms are abundant frequently show great numbers of individuals which have arrived on the panels and are endeavoring to secure a firm foothold. While such "sets" generally occur during the late spring, summer, and early fall months, the past winter saw unusually heavy sets in December, January, and February, at Portland, Me., Atlantic Beach, N. Y., and other northern locations.

At Atlantic Beach, panels submerged for 30 days ending January 13, 1949, were found completely covered with the shelled embryos of *Mytilus edulis*. Many specimens had attained a length of 1 mm. The average number of individuals to the square inch was found to be more than 1000. Figs. 2, 3, and 4 are greatly enlarged views of mussels from the set at Atlantic Beach. These figures show young mussels in the two stages of development mentioned. The embryonic shell is clearly visible at the umbo of the larger specimens. Fig. 4 is of special interest showing juvenile mussels attached to a hydroid stock. It is possible that unusually favorable conditions during the past winter months have been responsible for the early development of embryo *Mytilus*. It is not known whether or not they are able to survive the unfavorable conditions of subsequent low temperatures and probably scanty food supply.

In the case of the normal mussel, 10 months after having become attached as a minute embryo 0.5 mm in length to any submerged object, an individual specimen of *Mytilus edulis* may grow to be more than 50 mm in length, 35 mm in width and 20 mm in thickness. Thus an individual may increase 1,000,000 times in bulk during a growing period of 10 months. It would also follow that if the majority of such embryos should

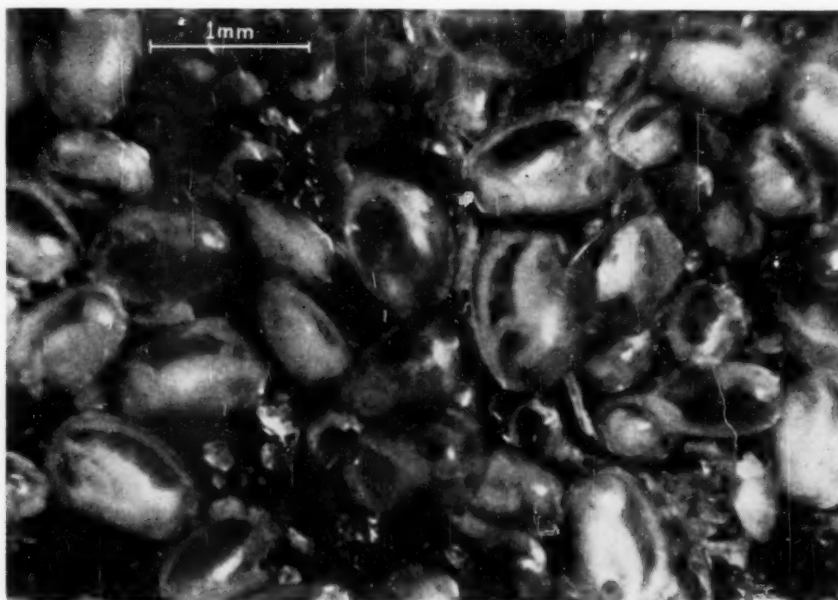


FIG. 2 EMBRYONIC AND JUVENILE MUSSEL, SHOWN CLUSTERED 8 TO 10 DEEP
(Collected at Atlantic Beach, N. Y., December 13, 1948-January 13, 1949.)

live, a
time,
or mo

RELAT

Fro
norma
rarely
Mytil
usuall

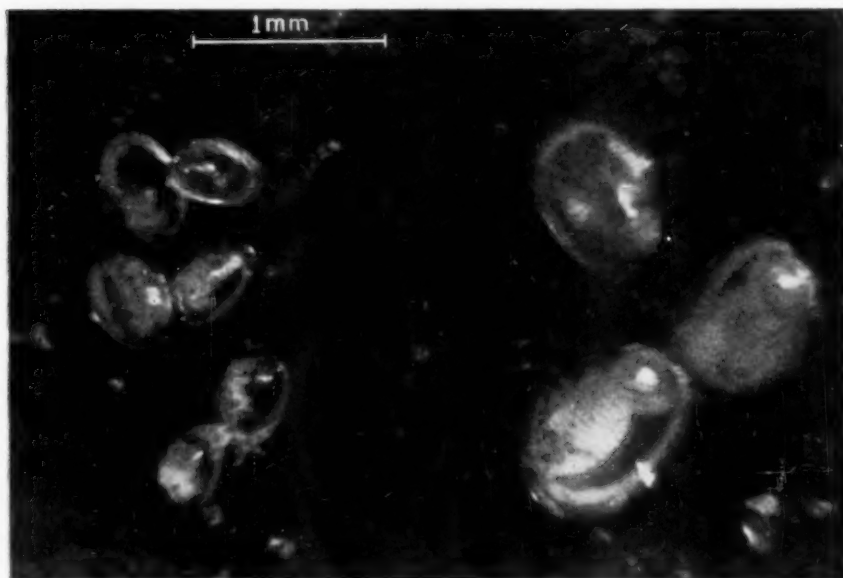


FIG. 3 EMBRYONIC AND JUVENILE MUSSELS—DETACHED INDIVIDUALS
(Collected at Atlantic Beach, N. Y., December 13, 1948-January 13, 1949.)



FIG. 4 EMBRYONIC AND JUVENILE MUSSELS, 1 MM LONG OR LESS, ATTACHED TO HYDROID STOCK, CLUSTERED 8 TO 10 DEEP
(Collected at Atlantic Beach, N. Y., December 13, 1948-January 13, 1949.)

live, a pint of *Mytilus* embryos might, in the same period of time, develop into a mass of mature specimens weighing 500 tons or more.

RELATIVE SUSCEPTIBILITY OF YOUNG *MYTILUS EDULIS* TO UNFAVORABLE ENVIRONMENT

From numerous observations it seems certain that under normal conditions embryonic and immature *Mytilus edulis*, rarely more than a few millimeters in size, are responsible for the *Mytilus* fouling in intake tunnels. The system of screens which usually is operated at the entrance of such intakes, would prevent

passage of large specimens, and certainly would prevent passage of individuals large enough to be breeders. Therefore the efforts of those who have attempted to control mussel fouling have been to prevent the attachment and survival of the embryonic and immature individuals which are carried into the tunnel.

It has been generally believed and undoubtedly is true that with all organisms the mortality is highest in the embryonic or immature stages. The mature organism is stronger and better adapted to survive unfavorable surroundings than the very young of the same species. This is probably true also with *Mytilus edulis*. However, apparently in the case of *Mytilus*

edulis a high degree of endurance is attained at a rather early age after acquiring the permanent shell. In certain studies made at the Kure Beach Test Station near Wilmington, N. C., and also in tests conducted by H. E. White,³ the very young of but few millimeters in size of at least some species of mussel are found as capable of surviving under the described unfavorable conditions as the mature animal. At this stage the bivalve shells can be closed tightly for long periods of time, thus completely excluding any obnoxious materials which may be present in the water.

LOCOMOTION AND GROUPING OF MYTILUS EDULIS

The *Mytilus*, like all other mollusks which are provided with such an organ, uses its single foot for locomotion. In young specimens 2 or 3 mm or less in length, the foot, when extruded, is of about the same length as the shell. Near the tip or outer end of the foot is a minute orifice through which the animal is able to extrude a very delicate filament quite similar to the strands of fine spider web. It is this web which provides the first "holdfast" for the immature mussel. By means of powerful muscles the foot can be moved in any direction, lengthened, or contracted at will. The motion of the foot in a mussel which is migrating from one location to another bears a striking resemblance to the motion of an elephant's trunk. When moving, the foot is extended to its full length, the tip end is arched, and the thread-spinning gland is touched to the surface of the material upon which the organism is moving. The thread is firmly cemented in the form of a minute pad to this spot, and it is sufficiently strong to support the weight of the entire animal and shell if suspended in the air. As soon as the thread is attached to the base, the foot is contracted and the shell is pulled forward until it is directly over the new point of attachment. Specimens which are as large as 5 mm in length are therefore capable of moving for a distance equal to the length of the shell at each time a new holdfast is formed. Since each forward movement may require only a few seconds, the total distance covered in an hour may be several feet. With still larger individuals, the length of the foot in proportion to the length of the entire shell tends to be smaller, progress so tends to be slower, and distance covered in a given period of time much less.

When the mussel has reached a spot where conditions are favorable, it remains stationary while the foot, waving around in all directions, exudes a large number of threads, known as the byssus, each of which is firmly cemented to whatever the gland of the

foot comes in contact with and provides an attachment which is exceptionally secure. Fig. 5 is a drawing of a mature mussel showing the foot extended and a number of byssus threads attached. Fig. 6, also a drawing, shows the internal anatomy. Many of the holdfasts may be upon the base upon which the mussel is traveling, or upon the shells of other mussels or other organisms near at hand. The mussels customarily come to rest in large clusters with a mass of weblike holdfasts attached to the base and to each other, as illustrated for small clusters in Fig. 7. When conditions, for one reason or another, become unsuitable, the organism can cut its cables and again endeavor to move on. However, in large clusters it is obviously necessary that all individuals have the same urge to separate one from an-

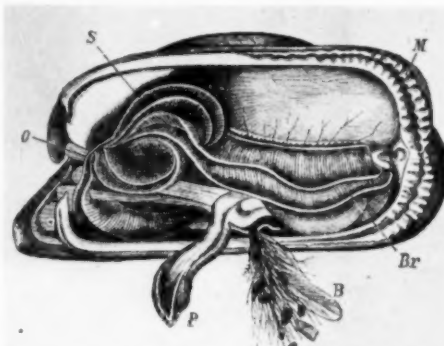


Fig. 5. — *Mytilus edulis*, Linné. Le lobe gauche du manteau est relevé. — O, bouche; S, palpe labiale externe; Br, branchie; P, pied; B, byssus; M, bord du manteau (de-haves).

FIG. 6 DIAGRAM OF INTERNALS OF MUSSEL

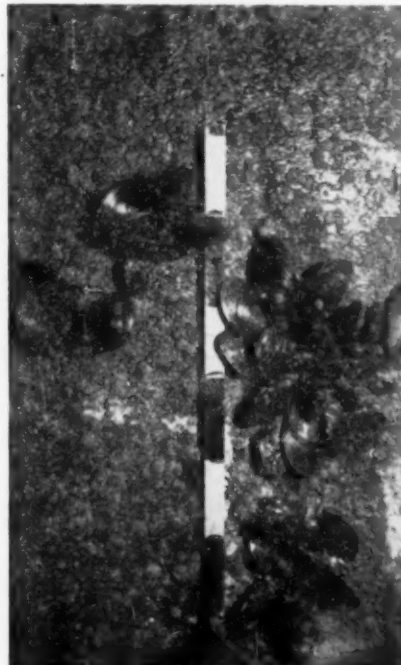


FIG. 7 CLUSTERS OF MUSSELS ON WALL OF INTAKE TUNNEL (Black and white scale divisions approximately 1 in.)

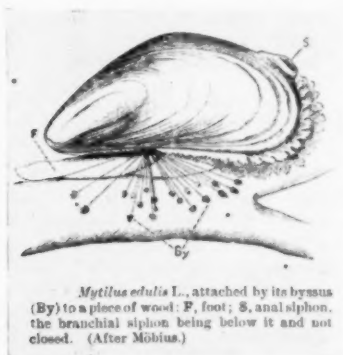


FIG. 5 SKETCH OF EXTERIOR OF MUSSEL, SHOWING MANTLE AND FOOT EXTENDED

³ "Control of Marine Fouling in Sea-Water Conduits Including Exploratory Tests on Killing Shelled Mussels," by H. E. White, published in this issue of the Transactions, pp. 117-126.

other and from the base. Tests have shown that complete severing of all holdfasts in a cluster can be and frequently is accomplished in the comparatively brief period of only an hour or two.

There is one other important method of locomotion of which the mussels are capable. Young individuals of 4 mm or 5 mm or less in length are able to sever their holdfasts and float away from their immediate environment. By means of tides, currents, and winds they may in this way be carried for long distances. Having no power to direct their movements, their ultimate landing spot is a matter of chance. Incidentally, during a migration of this type, many individuals up to 4 mm or 5 mm in diameter may be carried through the screens and then manage to secure a foothold in some portion of an intake tunnel or system. It is believed that such small mussels are capable of retaining inside of the shell a small bubble of air or gas which enables them to float at will in the water. If the mussel is disturbed while floating, the bubble disappears and the mussel sinks rapidly to the bottom.

KURE BEACH CHLORINATION TESTS

At the Kure Beach Station studies were undertaken to determine the comparative value of different schedules of chlorination in control of mussel growth. The procedure was to place a test tray in each group of identical weir boxes or compartments supplied with continuously flowing sea water. The general arrangement of the test equipment is shown in Fig. 8. Individual compartments were approximately 8 in. \times 10 in. \times 24 in. long. Turbulence was reduced by a perforated stilling baffle at the mid-length. Water entering the different compartments was chlorinated to selected residual concentrations by automatic feeders on predetermined schedules.

In order to determine the comparative value of various strengths of chlorine in the control of fouling organisms when added to the circulating water for varying periods of time, the following procedure was adopted:

The organisms used was the *Brachydontes exustus*, one of the mussels commonly found in intake systems in southern waters. The normal habitat of this mussel is in the between-tide area, where they grow in such abundance that they frequently completely encrust wharf piling, bulkheads, and other structures in the open sea. The individual specimens can become so firmly attached to steel, concrete, wood, or other materials, that they cannot be dislodged even by the heaviest surf. As in the case of other species of mussel, the young are incapable of attachment to any surface until they have developed to the stage at which the embryonic shell has been formed and the organism has reached a length of 0.25 mm or more.

Clusters of the mussels, containing from 50 to 100 specimens of lengths varying from 0.5 mm to 35 mm, obtained from the between-tide area of a sheet-steel bulkhead, were used in the test. Care was taken not to injure the specimens by rupturing the byssus gland in the foot. By means of a scalpel the byssus threads were cut as closely as possible to the pads on the tip ends of the threads. The clusters were then placed in separate porcelain dishes and the dishes submerged in clean flowing sea water. Within an hour or two the clusters had become sufficiently firmly attached to the extent that they could only be removed with difficulty. At the end of 24 hr the clusters could not be shaken loose from the containers. The dishes were then distributed in the various weir boxes as follows:

- Box No. 1—Nominal chlorine residual, 0.00 ppm...Control
- Box No. 2—Nominal chlorine residual, 0.25 ppm...Continuous
- Box No. 3—Nominal chlorine residual, 0.5 ppm...Continuous
- Box No. 4—Nominal chlorine residual, 1.5 ppm...2 hr on: 2 hr off
- Box No. 5—Nominal chlorine residual, 3.0 ppm...2 hr on: 2 hr off
- Box No. 6—Nominal chlorine residual, 1.5 ppm...2 hr on: 6 hr off
- Box No. 7—Nominal chlorine residual, 3.0 ppm...2 hr on: 6 hr off

It should be stated that the chlorine residuals given in the foregoing table were determined colorimetrically by the orthotolidine method with a disk-type comparator, instead of deter-

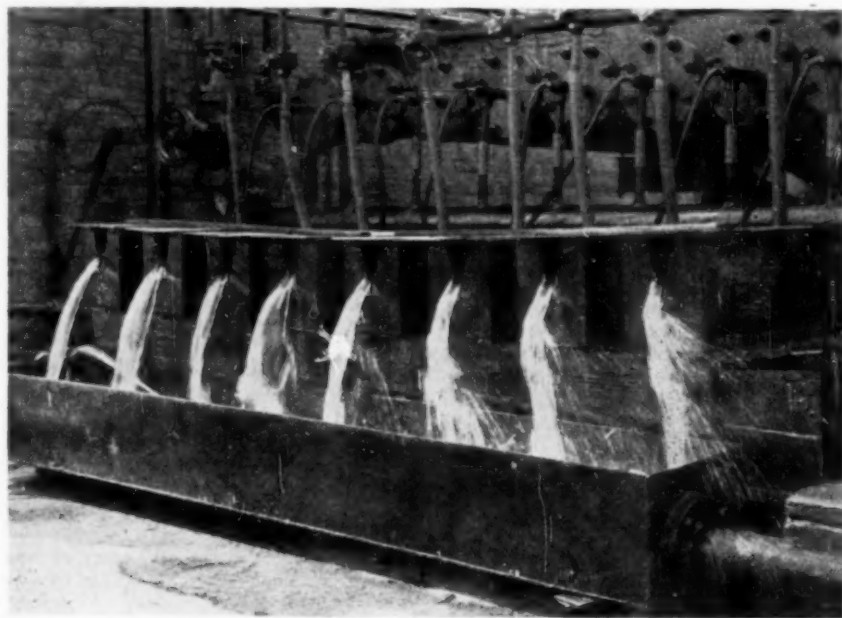


FIG. 8 ARRANGEMENT OF EQUIPMENT USED ON CHLORINATION STUDIES, KURE BEACH, N. C.

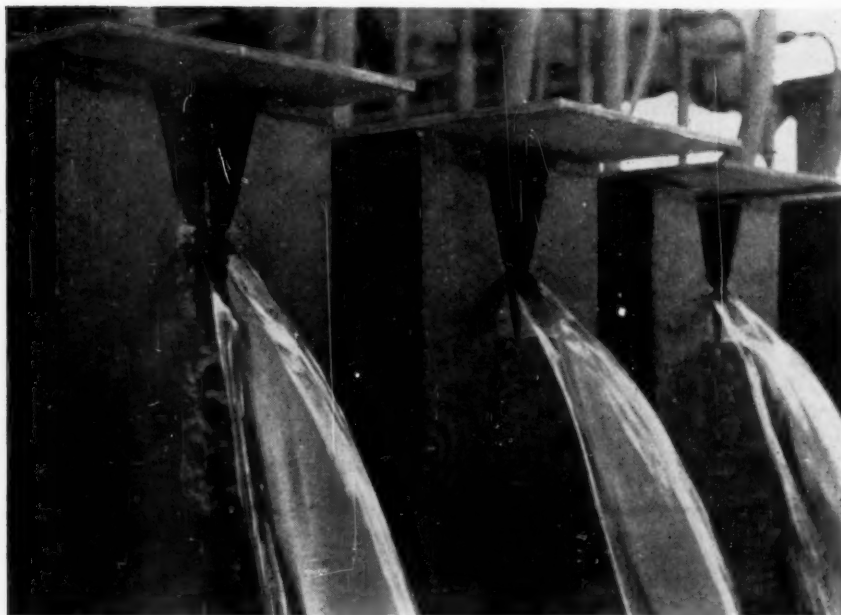


FIG. 9 CLOSE-UP VIEW OF WEIR BOXES, CHLORINATION TEST EQUIPMENT, KURE BEACH, SHOWING SLIME AT WEIR OF BOX NO. 1, ABSENCE OF SLIME AT OTHERS

mined by the starch-iodide method,⁴ or by the methyl orange method⁵ and accordingly are merely nominal values. It is possible that absolute values in the lower concentrations may have been as much as 100 per cent higher than shown in the tabulation. On the other hand, for comparison with figures secured by the orthotolidine method, of course no correction is required in these tabulated values.

At the end of 24 hr the clusters in the control-weir, box No. 1, with no treatment, were still firmly attached and no noticeable change had taken place. In all of the other weir boxes the mussels had begun to separate from the clusters and many were lying loose on the bottom of the containers with no attachment. At the end of 6 days no change had taken place in the control-weir, box No. 1. The clusters were still firmly attached, and the individuals in an apparently healthy condition. In the containers in weir boxes No. 2 and No. 3, which were being given continuous chlorine treatments with residuals of nominally 0.25 ppm and 0.5 ppm, respectively, the mussels had all lost their holdfasts. The shells of many were opened wide, and when the animal thus exposed was touched with a teasing needle the shells were not closed. The effect on slime-producing organisms from the continuous presence of chlorine in the sea water is shown in Fig. 9, a view of the weirs of boxes No. 1, No. 2, and No. 3, and the absence of mussel activity in water of 0.25-ppm chlorine concentration is shown in Fig. 10. The clusters in weir boxes Nos. 4, 5, 6, and 7 had also severed all attachments, but the majority of the specimens of all sizes had the shells tightly closed. Comparatively few had the shells open.

At this time, the end of 6 days, all of the containers were removed from the weir boxes and were submerged again in clear,

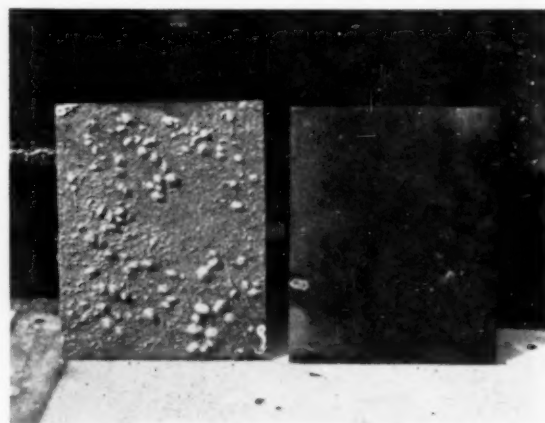


FIG. 10 GLASS PANELS FROM CHLORINATION TEST, KURE BEACH, COMPARING EFFECTS OF CONTINUOUS 0.25-PPM NOMINAL CHLORINE RESIDUAL AND UNTREATED SEA WATER USED FOR CONTROL

untreated, flowing salt water for 24 hr. All of the specimens in control container No. 1 appeared to be alive and in excellent condition. At the end of the 24 hours none of the specimens in containers Nos. 2 and 3 had revived, all shells were widely opened, and disintegration of the animals thus exposed had started. In containers Nos. 4, 5, 6, and 7, all of the specimens were still unattached but many still had the shells tightly closed and only 25 to 50 per cent had the shells open in any of these containers.

It should be noted here that many of the mussels which remained alive in container No. 6 (2 hr chlorination at 1.5 ppm, 6 hr no chlorination) extruded the foot and began to migrate within a few moments after having been submerged in clean salt water. Within 24 hr these individuals had again formed in two

⁴ "Residual Chlorine," Standard Methods for the Examination of Water and Sewage, American Public Health Association, 1936, pp. 164-165, and 228-232.

⁵ "Colorimetric Determination of Free Chlorine With Methyl Orange," by Michael Taras, *Analytical Chemistry*, American Chemical Society, vol. 19, 1947, pp. 342-343.

or three clusters and were firmly attached. This to a lesser degree was true in the case of the mussels in containers Nos. 4, 5, and 7. It was also noted that the very young specimens only 1 mm or less in size were as quick to recover and as agile in migrating as the larger specimens. This would tend to discount the belief that the shelled young are necessarily more susceptible to unfavorable conditions than the older individuals. Once this form has been reached the immature *Mytilus* is soon as resistant as the mature specimen. However, it is probable that the free-swimming larvae, without the protection of the shell, would succumb quickly to such severe conditions.

The mussels in containers Nos. 2 and 3 were discarded, and the dead mussels in containers Nos. 4, 5, 6, and 7 were removed and new specimens were added. The tests were then repeated for 5 consecutive weeks, following the same procedure and with approximately the same results. Since a considerable number of new healthy specimens were added to containers Nos. 4, 5, 6, and 7 at each weekly interval, the maximum period of individual survival under the intermittent treatment was not determined.

SUMMARY OF KURE BEACH TESTS

Continuous chlorination at 0.25 and 0.5 ppm resulted in a complete kill of *Brachydontes exustus*. In addition, no fouling organisms of any kind, or slime film, could be found in these weir boxes.

A varying number, probably averaging 50 per cent, of *Brachydontes exustus* were killed in the weir boxes which were provided with intermittent chlorination. In addition, living barnacles and Bryozoa were found in these weir boxes.

RELATED OBSERVATIONS AND DEDUCTIONS

Some organisms, generally those which are not provided with a protective shell or covering, are much more susceptible to unfavorable conditions than others. Among such organisms the sea anemones and hydroids probably belong. It is of importance in this connection to note that blocks of wood which were placed in the control weir box at Kure Beach Station were destroyed by teredo in a few weeks. Similar blocks placed in all of the other weir boxes showed no trace of any borer attack. It is evident that the embryonic teredo without the benefit of any shell for providing protection is unable to survive any of the

chlorine dosages used during this test. On the other hand, once having succeeded in entering the wood, the mature form of teredo would be well protected against all but the most severe unfavorable conditions.

Those marine mollusks which are accustomed to living exposed in the between-tide area are frequently provided not only with strong shells which can be closed very tightly, but also with very powerful muscles which enable the animals to keep the shells tightly closed for long periods of time. The scallops and mussels are of this type while the various species of burrowing soft clams, which are protected by the burrows they live in, frequently do not have tightly fitting shells or strong muscles for closing them.

The mussels living on our tidal flats are out of water and exposed to the rays of the hot sun during the summer for 2 hr or more during each low-tide period. For them to survive, it would be essential that they protect themselves by keeping the shells tightly closed during the period of exposure. It would appear to be a necessary adaptation. It would seem probable that the *Mytilus*, which can remain closed and survive exposure to the air and hot sun for 2 hr each day, could survive equivalent unfavorable conditions in an intake tunnel for equal periods of time.

It would seem from the tests described that continuously but comparatively slightly unfavorable conditions would eliminate the undeveloped and unprotected embryos of the fouling marine organisms. This would be the most desirable objective to attain. It would also seem that much more unfavorable conditions are necessary to produce a kill when the organisms have passed from the embryonic stage to the mature form.

On the other hand, the evidence seems to indicate that, with some *Mytilus*, even slight and intermittent chlorination would result in the mature specimens releasing the holdfasts. In this way it is conceivable that, if still small, they might then be carried through the system without causing further trouble. However, it is also possible that with sufficiently low velocities this might result in an accumulation on the bottom of the tunnel which, eventually, would have to be removed.

ACKNOWLEDGMENT

The author desires to express his appreciation to Mr. Frank L. LaQue of The International Nickel Company, for permission to reproduce the illustrations of test equipment used at Kure Beach Station, and to quote from results secured.

The
of aqua
years, l
the effe
mainte
on seve
neers a
Mytilus
résumé
program
cal.

IN, th
to n
Ele
program
tional 60
housed in

¹ Super
Contrib
Meeting,
Meeting,
SOCIETY

NOTE:
understo
of the Soc

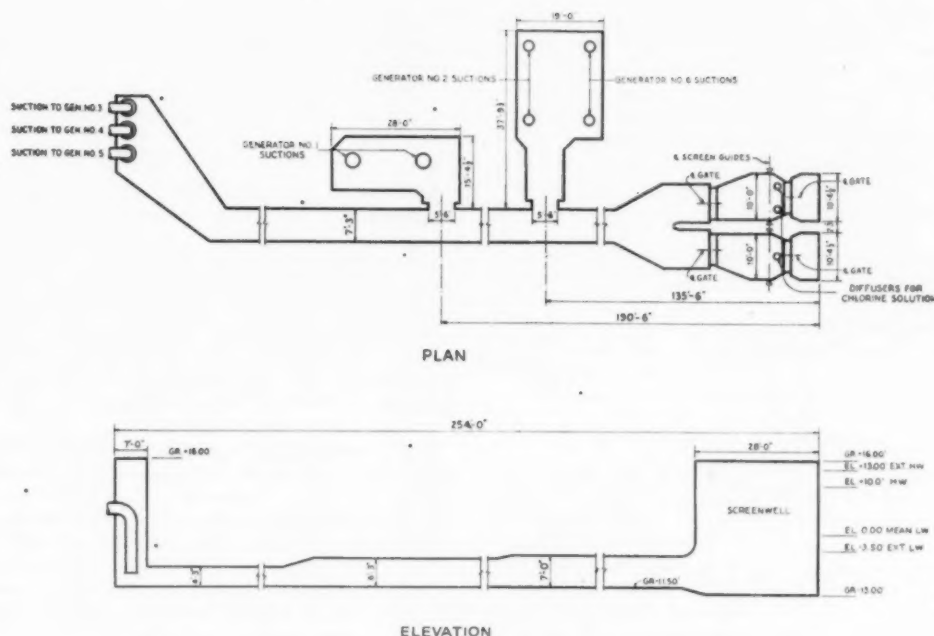


FIG. 1 ARRANGEMENT OF INTAKE TUNNEL, ELECTRIC GENERATING STATION

Project Study for the Mitigation of Marine Fouling

By I. A. PATTEN,¹ LYNN, MASS.

The growth of marine organisms with resultant fouling of aquatic vessels and tunnel structures, throughout the years, has presented the utility engineers with a problem the effect of which creates lower efficiencies and higher maintenance costs. Mitigation of such growth and fouling on several occasions has been studied by industrial engineers and biologists. The result of such studies indicates *Mytilus* are the most difficult to control. The paper is a résumé of experiments and the development of a chlorine program which to date has proved effective and economical.

INTAKE-TUNNEL ARRANGEMENT

IN the year 1927, fully realizing the necessity of expansion to meet the future supply of electricity, the Lynn Gas & Electric Company, Lynn, Mass., entered into a construction program the ultimate objective of which was to provide an additional 60,000-kw capacity. This entire development was to be housed in a new structure adjacent to the old generating station.

¹ Superintendent, Lynn Gas & Electric Company.

Contributed by the Power Division and presented at the Spring Meeting, New London, Conn., May 2-4, 1949, and the Semi-Annual Meeting, San Francisco, Calif., June 27-30, 1949, of THE AMERICAN SOCIETY OF MECHANICAL ENGINEERS.

NOTE: Statements and opinions advanced in papers are to be understood as individual expressions of their authors, and not those of the Society. Paper No. 49-8-20.

Included in the new development was a reinforced-concrete intake water tunnel for condenser-cooling purposes. The tunnel as designed provided for one concrete rectangular tube, 7 ft square near the intake and of progressively decreasing cross section, approximately 250 ft in length, as shown in Fig. 1. The intake end on the Lynn Harbor front, submerged to minus 13 ft relative to mean low-water datum, is equipped with inner and outer gates which permit unwatering and cleaning either screen well without interruption of service. The new tunnel, however, is a single-tube conduit; consequently, when tunnel cleaning becomes necessary, it can be accomplished only by shutting down the main tunnel and employing inadequate by-pass connections for circulating-water requirements. The maximum demand for total cooling water at this station is in the order of 9400 cfm. Due to the design and location of the suction chambers in the tunnel, the velocity of the water varies in its flow, but for all practical purposes the maximum rate is around 3 fps.

EARLY FOULING PROBLEMS—EQUIPMENT OUTAGES

The new station was put into operation in the fall of 1929, and, following approximately a year of satisfactory operation, condenser fouling due primarily to mussel and marine growths occurred. Within a relatively short time condenser outages were becoming very frequent, thus necessitating search for the cause of this trouble. A diver was sent into the tunnel to determine the marine-growth condition existing therein, and much to

the surprise of all concerned, a very heavy congestion of *Mytilus* (common mussels), *Tubularia* (sea moss), and *Metridia* (sea anemone) was found. These growths were firmly attached to the walls and roof of the tunnel and varied in amounts fairly consistent with the rate of flow; that is to say, the nearer to the intake, the more plentiful the attachment of the wall surfaces.

Now the handwriting was on the wall, so to speak, the operational problem of "condenser fouling" had a brother—"tunnel congestion," and these two factors were of grave concern as time passed.

It was a frequent occurrence for each turbine generator to be out once a week for condenser cleaning, and the deposits of slime, silt, and mussels in the tubes were very disheartening. The economics of such conditions in a modern generating station were embarrassing as outages necessitated purchasing power from a nearby utility, and operating efficiency was far below normal, primarily due to poor vacuum conditions in the turbine units.

MANUAL REMOVAL OF FOULING COSTLY

In the spring of 1931 it became necessary to unwater the tunnel and to do a thorough cleaning job, which was termed at the time the "clamming" expedition. This resulted in the removal of approximately 160 tons of mussels and other marine growths. Accompanying the marine growth, there was an accumulation on the floor of the tunnel to a depth of 18 to 24 in. of harbor silt, mussel excretion, and many dead-mussel shells.

From Fig. 1 it is obvious that an undertaking of this kind was costly and difficult to perform, as all debris must be raised from the tunnel through four manholes throughout the length. The temporary suction line was attached to the station's largest turbine generator (25,000 kva) and the deficiency of kilowatts was supplied from an adjacent system. The time consumed was approximately 20 hr, and the cost in the vicinity of \$6000 for equipment and labor. Yet, a tunnel-cleaning program had to be established for at least once every 12 months. The reality of this problem, plus the headache of condenser cleaning, the loss of station efficiency, and the accompanying high operating maintenance cost were factors which led to vigorous study and investigation of the mitigation of marine growth by means of agents not then too familiar to the utility industry.

INITIAL INVESTIGATION AND OBSERVATIONS

The investigation was begun by correspondence with other utility companies and a few industrial plants to gain knowledge of their experience. In a few cases, chlorine was mentioned favorably even though very little information was available that could be applied directly to the complete elimination of mussels by chlorination. The Department of Commerce, Bureau of Fisheries in Washington, supplied information relative to the spawning of mussels which they stated should cease about the first of August but added the cautionary comment that the free-floating larvae would exist in abundance for at least 2 weeks after the end of the spawning season and might be expected to attach themselves within the intake system during such period. They also advised that the use of chlorine gas for preventing the growth of mussels was being investigated by the Bureau.

During the interim two interesting facts were learned. The first was that the Atlantic seaboard during the seasons of 1930 and 1931, had produced what was termed in those days abnormal mussel years. While it seemed within reasonable prospect that future years would be more favorable, there still also seemed sufficient room for pessimistic doubt to warrant continuance of the investigation. The other, which was felt in part directly responsible for the mussel conditions in the immediate area, was the changed sea-water condition in Lynn harbor.

Up to 1929 the Lynn sewerage system had been flowing directly into the harbor, resulting in a fairly high concentration of pollution in the water. Subsequent to 1929 an outfall sewer system was laid, and the sewerage pollution was removed from the harbor waters, which was favorable to marine growth.

INITIAL TRIAL OF CHLORINATION

Further study, including reference of the problem to our engineers and to one of the country's most noted marine biologists, led to a decision to try chlorine as a preventive against mussel development. The equipment then available was not too elaborate or complete, and the installation and operation were equally in question as this process was still in its infancy. However, a voluntary committee was formed and, securing what equipment there was available, an operating schedule was set up on February 23, 1931. The recommended and trial cycle of operation consisted of $7\frac{1}{2}$ to 15-min injections once every 3 hr with a chlorine residual 0.4 to 0.8 ppm.

After a few months of operation there was found to be little if any improvement in the mussel situation. This, coupled with the fact that corrosion-erosion of condenser tubes and graphitization of condenser water boxes were noticed about the same time, aroused serious doubt as to the advisability of continuing chlorination. However, persistency prevailed and, in our endeavor to overcome these corrosion conditions, zinc plates were installed in the water boxes, ferrule extensions applied at inlet ends of condenser tubes, and the water-box surfaces treated with hot Apexior.

While these measures offered relief, it was apparent that they should be termed at best deterrents rather than cure. Chlorination was continued until May, 1932, and then discontinued, as everyone felt the objective, mussel mitigation, had not been reached and its attainment uncertain. While all felt chlorine had not failed completely, its continued use seemed unjustifiable until many of the unknown factors had been given further study and evaluation.

CORROSION NOT CAUSED BY CHLORINATION

Subsequent to discontinuing chlorination, the following became apparent:

1 The corrosion-erosion within the condenser tubes was being caused primarily by free oxygen in the circulating water, and the same cause seemed the primary factor in the attack on the ferrules, tube sheets, and water boxes. Tests showed that a considerable amount of entrapped air existed in our intake tunnel. This air, when passing through the circulating pumps and thence into the condenser, resulted in the liberation of large quantities of free oxygen. The first preventive step was to install a vent standpipe about midway of the intake tunnel. This procedure immediately showed favorable effects and was followed by installing air erosion eliminators in the condenser water boxes, in addition to the vent.

2 Stray-current electrolysis was also an important factor in the observed corrosion. In the process of investigation, tests were conducted for electrolytic action which discovered evidence of stray currents prevailing not only upon the condensers but the pump impellers and associated equipment. Preventive measures were taken, and it was soon learned that the foreign current extended out into the screen well and forebay. Finally, an open negative was discovered on an adjacent direct-current system ground submerged in the Saugus River. When repair to the negative was effected, the electrolytic condition was eliminated. These facts are mentioned to indicate how our thinking changed with reference to the effect of chlorine on this type of equipment.

ELECTROCUTION ATTEMPTED

One other experiment, worthy of mention in passing, was an attempt to electrocute various types of marine growth. Two framed wire grids were submerged in the forebay several feet outside the screen well. Low-voltage electric current was supplied to one grid and no energy to the other. The grids were withdrawn monthly for examination. The energized grid contained few if any mussels, and other types of marine growth, such as barnacles, etc. On the unenergized grid quantities of mussels and other marine growth were present. It seemed probable at the time that electric energy supplied through a properly designed screen or grid system of some kind would result in killing the mussels when in the embryonic or larval stage. However, due to lack of available equipment, after about 5 months of operation, the experiment was discontinued without actually determining the merit of the scheme.

DECISION TO RESUME CHLORINATION

From 1932 to 1944 little was accomplished in mussel mitigation, and the tunnel cleaning continued once each year. The season for cleaning was changed from spring to fall, however, and fall cleaning proved much more satisfactory than spring cleaning, that is, the tunnel was cleaned after the fall spawning season, say, in October, consequently eliminating a large proportion, by volume at least, of the mussels by not permitting them to remain in the tunnel and develop during the winter months. The majority of mussels then to be removed, consisting primarily of the current summer's breeding, were much smaller in size.

These last 10 years or so the clamming business was becoming tiresome, especially without a market for the product but, with renewed hope from several biologists, another vigorous attack was begun on the investigation and control of marine growth.

In June, 1945, thorough study for the elimination of marine growth, *Mytilus* especially, was resumed. All phases of the intake-tunnel conditions and condenser operations, all tests, and previous experiments were reviewed and analyzed. Several of the previous experiments were found inconclusive in the light of development and research through the intervening years, and a new tentative program finally was agreed on. Chlorination was decided upon as the weapon, and the greatest problem was the cycle of operation; intermittent chlorination with high residual, or continuous chlorination with much less residual. The burden of opinion from our consultants was in favor of intermittent chlorination. Accordingly it was decided again to try chlorine with intermittent injection. The installation of needed equipment was completed in November, 1945.

FOULING TEST PANELS

About this same time an investigation was undertaken to secure information on the current natural rate of marine fouling by the aid of a series of test panel boards, each 6 in. \times 12 in. and $\frac{1}{8}$ in. thick of black plastic composition, five of which were continuously active. The test panels were submerged within 3 ft of the bottom of the forebay and 5 ft in front of the intake tunnel at the rear of the screen house. Four of the test panels in use were given numerical identifications and the fifth serving as a control was designated X.

After the submersion of the test panels for 1 week, one of the numbered panels and the X control were removed and immediately wrapped with care in paper towels and sent to the biological laboratory for analysis. This was done on Monday of each succeeding week. A data sheet accompanying the panels listed tidal condition, sea-water temperature, and location from which the test panels were removed. After the first month, each numbered test panel should give a sample representative of potential

fouling development in the previous 4 weeks for comparison with the latest single week's record of the X-control panel.

Later in 1946 a test station was added about mid-length of the tunnel, directly in the flow of the chlorinated sea water to indicate the chlorination results. Test panels of different types of material including clear lucite and reinforced cement were tried, and Plexiglas supporting rods in place of flexible supporting cables. Widely varying results obtained from these panels led to the conclusion that they were not giving dependable indication of tunnel-fouling conditions.

CHLORINATION RESUMED

On November 3, 1945, the intake tunnel had been thoroughly cleaned. Chlorination on hand control was started November 4, 1945. Under this first schedule, from November, 1945, to April 3, 1946, chlorine was injected 1 hr, twice daily at 0.2 ppm residual. On April 3, 1946, time-clock automatic control was installed, and the chlorine-injection cycle was changed to 30 min each 8 hr with residual at 1 ppm. After 1 month of operation on this program, it was decided to increase the residual to 2 ppm and this was continued until about October 1, 1946.

On October 24, 1946, with approximately 1 year of experience with chlorination, the tunnel was inspected by a referee committee and subsequently cleaned. As compared with previous years, approximately as many mussels in number were found, but the average size was considerably smaller. The belief of all present was that, while chlorine had been instrumental in limiting the growth, it apparently had in no way affected the number present and adherence of the mussels to the walls of the tunnel. *Tubularia* and *Metridia*, on the other hand, had decreased materially.

Definite information was not available on how long a mussel can exist with the shell completely closed, without oxygen. Our biological consultants expressed belief that such a condition might prevail for many hours, and recommended longer periods of chlorination at lower residuals. This raised the question that if the length of the chlorine-injection period was increased sufficiently, what was the minimum residual concentration at which mussels could be killed.

From operating experiences and indecisions, the committee again conferred to determine whether or not sufficient improvement had been gained to warrant further experimental work and retention of the chlorinating equipment. From this conference the following was agreed:

- 1 Chlorination had brought no adverse results on condenser tubes, water boxes, or pump impellers.
- 2 *Tubularia* and *Metridia* had been practically eliminated from the tunnel, screen well, and suction chambers.

Even though the mussels were as numerous, they were smaller in size and apparently not so firmly attached to the surfaces. The chlorine plant had operated efficiently and satisfactorily. Thus, weighing the results, decision was reached to continue for another 12-month period. It seemed beyond doubt that by so doing operations would be improved, and the economics would justify chlorination, as materially better vacuum was then being secured owing to cleaner condenser tubes and less fouling of condensers.

PILOT TUNNEL

During the winter of 1946-1947 further efforts were made to determine the seasonal changes which should be made in the chlorination schedules to compensate for changes in water temperature and spawning season. System-load conditions prevented frequent inspections of the main tunnel. This, together with the misleading indications given by test panels, prompted

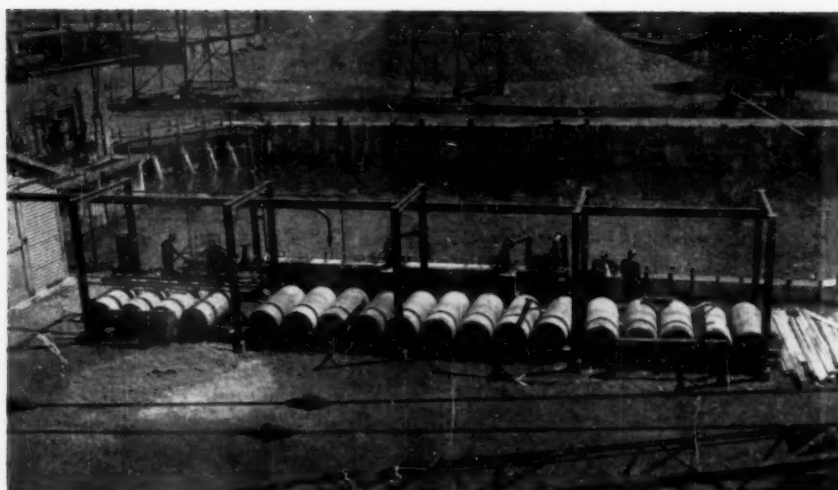


FIG. 2 PILOT TUNNEL AT INTAKE SLIP

the construction of a miniature tunnel which would allow as frequent inspections as desired. The pilot tunnel, which is shown in Fig. 2, is an exact reproduction of the main tunnel constructed on a scale of 1 to 7. Overflow ports of identical shape and proportions simulate entrances to the suction chambers of the various machines in the main tunnel. Water from the forebay is pumped through the pilot tunnel continuously, and chlorine is diffused at the same proportionate rate as used in the intake tunnel. In other words, chlorinating programs for the main and pilot tunnels are identical. Removable covers were installed at the top and end of the pilot tunnel, providing for intermittent inspection of inner surfaces of the tunnel.

In June, 1947, water was fed initially through the pilot tunnel and, from its subsequent inspections, establishment of more definite ideas relative to chlorination cycles and residuals became possible. In the section of the tunnel nearest the intake, which was designed to operate without chlorine injection, mass distribution of the mussels was obviously in inverse relation to local velocities, much as observed in the intake wells of the main tunnel. When chlorination was started in the pilot tunnel there had accumulated in the wooden discharge trough a considerable growth of sea moss and marine organisms which disappeared within a few days after chlorination.

PLANKTON NET

Coincident with operation of the pilot tunnel, an attempt was made to employ the Plankton net for trapping live organisms, the trapping equipment used consisting essentially of a closely woven silk sleeve of conical shape with a 6-in. opening at the entrance and a $1\frac{1}{2}$ -in. opening at the other end to which a sampling bottle is attached. Results were unsatisfactory even with the aid of a metal frame and rudder to hold the net submerged and parallel to the water flow. Very few mussels were trapped, although more numerous present as evidenced by infection of the pilot tunnel 20 ft away. No doubt the difficulty was due to the low velocity of flow in the forebay as such equipment has been effectively used at higher velocities.

THERMAL TREATMENT

Early in 1947 consideration was given to temperature treatment by steam or hot water for mussel elimination. The conclusion reached was that the procedure could be made effective

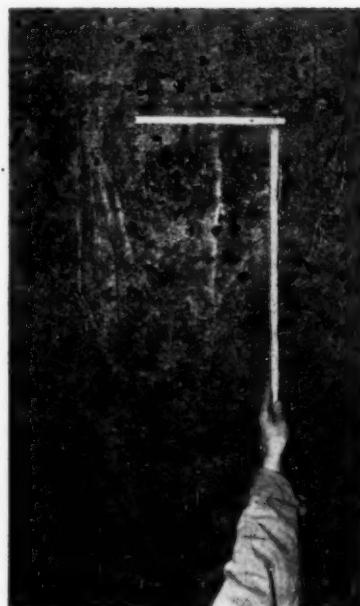


FIG. 3 EAST SIDE WALL OF TUNNEL, JULY 20, 1947

and, in some instances, possibly economical but, with the single main intake tunnel and the system demands, it was impractical for Lynn Station. Consequently the idea was abandoned.

INTERMITTENT CHLORINATION CONTINUED

On June 8 and on July 20, 1947, the main tunnel again was inspected by the referee committee and in comparison with inspections of October and November, 1946, a considerable area of concrete surface was visible, and the small clusters of mussels were scattered as shown in Fig. 3, taken on July 20, 1947. This was encouraging, as the previous inspections in the fall of 1946 showed continuous blanket formations from 2 in. to 4 in. thick on the walls as shown in Fig. 4 taken November 16, 1946. For

futu
were
Qu
1
infes
2
vent
3
slip"
4
is ou
TH
Whit
Co
summ
Nov
tons
How
short
was
30 m
No
equi
sider
no f
equi
and
The
The
equi
Expl
publ



FIG. 4 GENERAL VIEW IN TUNNEL, NOVEMBER 16, 1946
(Courtesy of Woods Hole Oceanographic Institution.)

future inspection comparisons, all metal and tunnel surfaces were zoned and their observed conditions recorded.

Questions raised from this 1947 inspection were as follows:

- 1 Why are certain areas free from mussels and other areas infested in such varying degrees?
- 2 Were chlorine diffusion nozzles designed properly to prevent streamlining of chlorine?
- 3 Due to irregularity in surface areas in concrete, did "water slip" lower chlorine concentration on the wall surface?
- 4 Are the survivors the "supermen" of the mussel family or is our chlorine program improperly designed?

These questions among others have been studied by H. E. White.²

Continuing the tests and tunnel examinations during the summer months of 1947, it was naturally gratifying when the November cleaning produced only 16 tons, compared with 107 tons in 1946, and 331 tons during 1945, as shown in Fig. 5. However, complete control was the goal sought, and anything short was not considered satisfactory; consequently, chlorination was continued during the winter of 1947-1948, on the basis of 30 min each 8 hr at 0.75 ppm residual.

November, 1947, being the second anniversary of the chlorine equipment, the question of its continued use had again been considered. Favorable factors included progress in mussel control, no further signs of corrosion-erosion of condenser and related equipment, reduced maintenance costs for condenser fouling, and cost for chlorine consumption had not exceeded the estimate. The single unfavorable factor was lack of full mussel control. The decision again was favorable for retaining the chlorination equipment.

² "Control of Marine Fouling in Sea-Water Conduits Including Exploratory Tests on Killing Shelled Mussels," by H. E. White, published in this issue of the Transactions, pp. 117-126.

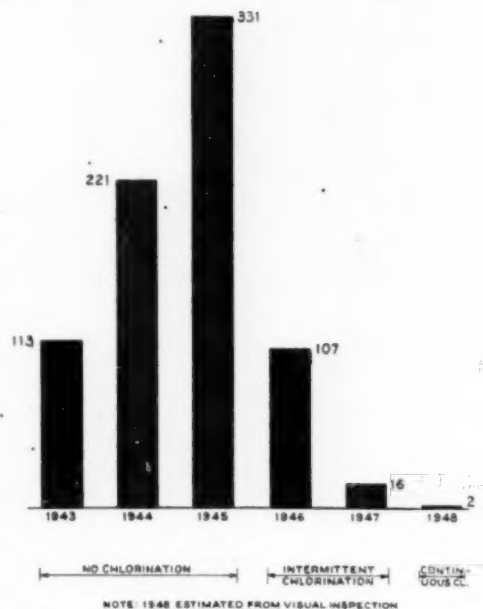


FIG. 5 TONS OF MUSSELS REMOVED ANNUALLY FROM INTAKE TUNNEL

On April 25, 1948, tunnel conditions were found about comparable with November, 1947, after cleaning. The few mussels present were small, ranging in size from 1 to 5 mm at approximately 2 to 5 per sq ft of area, even though chlorine injections were only three 20-min periods each 24 hr at 0.75 ppm residuals. On the other hand, elimination of mussels was not complete.

Decision was in favor of continuous chlorination at 1 ppm residual which was at once put into effect.

CONTINUOUS CHLORINATION

On June 27, 1948, after tunnel inspection which showed favorable results, a program of continuous chlorination at 0.5 ppm residual was set for the balance of the 1948 recognized propagating season, or until water temperatures dropped to 40 F, unless future inspections of the pilot tunnel indicated the necessity for change. Immediately after the inspection, new dual diffusion pipes were installed in one screen well at the tunnel intake, and apparently they are a decided improvement over the single diffuser.

The main tunnel was opened approximately each 6 weeks for the balance of the season, and results continued satisfactory. As shown in Fig. 6, the last seasonal inspection was made on October 17, 1948. All of the referee committee present agreed that a

of the tunnel. Grouping of large mussels is visible only near the base of the wall. The remainder of the wall and roof in this vicinity is devoid of any fouling.



FIG. 6 EAST WALL OF INTAKE TUNNEL NEAR INLET, OCTOBER 17, 1948, SHOWING BARE CONCRETE AFTER FULL SEASON OF OPERATION

decided improvement existed. Mussels where present were, in general, widely scattered, many wall areas completely void of any marine growth, mussels present were of miniature dimensions—some very small yet with completely formed shell. Attachment to the walls was rather weak with, it seemed, fewer byssus threads, while on the floor almost all the mussels were dead. From visual summation it was estimated, if the tunnel was thoroughly cleaned, the maximum in weight of all types of marine growth and silt would not exceed 2 tons, largely concentrated in the relatively less active north end of the tunnel where chlorination had not been continuous. Because of this small extent of the fouling, we decided not to clean the tunnel.

The view of the tunnel interior given in Fig. 6 is representative of the east side wall in the continuously active zone, photographed October 17, 1948. The man is standing in 3 to 4 in. of water about 20 ft from the inlet end of the 7-ft-square section

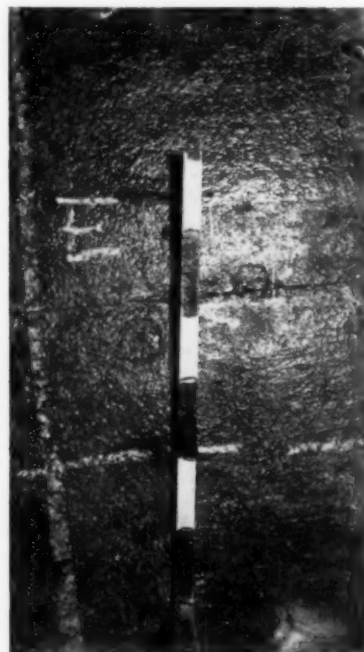


FIG. 7 CLOSE-UP OF EAST WALL, MID-LENGTH OF INTAKE TUNNEL, OCTOBER 17, 1948
(Black and white scale divisions approximately 1 in.)



FIG. 8 CLOSE-UP OF WEST WALL, MID-LENGTH OF INTAKE TUNNEL, OCTOBER 17, 1948
(Black and white scale divisions approximately 1 in.)

Figs. 7 and 8 show at close range views typical of the general area of the east and west walls, respectively, about 110-120 ft further from the inlet end of the tunnel where mussels were found in numbers of 1 and 11 per sq ft. Chlorine effectiveness observed in the main tunnel was reproduced closely in the pilot tunnel where walls in contact with chlorinated water were almost

completely free from fouling attachment. Contrast of areas respectively ahead of and following the point of chlorine introduction in the pilot tunnel is rather strikingly brought out in Figs. 9 and 10, views of the interior taken on October 20, 1948.

SUGGESTIONS

From the experience at Lynn Electric Generating Station the following suggestions are offered to those who have or are anticipating marine-growth control in forebays, tunnels, suction pipes, or other aquatic structures:

- 1 Acquire thorough familiarity to the last detail on items such as water analysis and water temperatures, especially during seasonal changes.
- 2 Determine as accurately as possible the hydraulic conditions and variants, including velocities in the structures in question.
- 3 Determine as accurately as possible the metallography of all equipment in the plant through which this water will pass.
- 4 Study as accurately as possible the amount of expenditure created directly by marine fouling in the plant equipment. There is now sufficient information available which at least will give a fair indication of the cost of elimination. In turn, this should establish wherein the economics of the problem lies.
- 5 Do not be impatient. Remember that the price of success is eternal vigilance, and problems not too readily solved are always to be expected.

CONCLUSIONS

In conclusion, the following are believed factual to at least the present degree of success attained at the Lynn plant:

- 1 Chlorine to the extent and magnitude of actual usage has not caused deterioration of condenser tubes, water boxes, pump impellers, or associated equipment although condenser tubes are of various alloys and makes.
- 2 Even in the days when success of marine-growth elimination by chlorine seemed doubtful, benefits were realized due to elimination of slime film on condenser tubes, which resulted in better vacuum and saving in the coal pile.
- 3 As the trial programs have progressed there have been direct and appreciable savings in labor for condenser cleaning, readily evaluated.
- 4 For the year 1948, what can be safely termed operating savings, which consist of avoiding the intake-tunnel cleaning, fewer condenser outages and cleanings, higher vacuum with a resultant reduction in coal usage, have been summarized, giving estimated gross operating savings of \$20,000. Deducting from this the gross operating cost of the chlorine plant, the direct cost for chlorine purchases, interest, taxes, and depreciation on the chlorine plant, the estimated net saving for the year is about \$12,000. It will be noted this estimate has been made on a conservative basis, applying only the recognized and tangible savings, and not including other variables which might be included by thorough analysis.

The author wishes to express his appreciation to Dr. William F. Clapp, his assistant Mr. Peter Richards, Dr. Louis W. Hutchins of Woods Hole Oceanographic Institution, Messrs. R. B. Martin and S. H. Newland of Wallace & Tiernan, and Messrs. E. B. Powell and H. E. White of Stone & Webster Engineering Corporation. Without their able assistance and determination we could not have succeeded to the present degree of mussel and marine-fouling control. While we shall continue to strive for perfection, even though we fall short, we feel assured that satisfactory operations can be continued and with a reasonable degree of economic success.



FIG. 9 CLOSE-UP OF MATTED MUSSELS INSIDE PILOT TUNNEL—NATURAL CONDITIONS AHEAD OF CHLORINE INJECTION, OCTOBER 20, 1948, AFTER ONE FOULING SEASON



FIG. 10 CLEAN CONCRETE WALL OF PILOT TUNNEL BEYOND CHLORINE INJECTION, OCTOBER 20, 1948, AFTER ONE FOULING SEASON

Hu
culati
in a si
deter
mina
mode
Gener
have
ate ch
nation
the re
usual
ment
positi
chlori
water
coasta
as ob
chart

M
tion.
tons o
power
nectio
some o
sels ha
plant
digging
Wit
contin
come i
liness
ing, th
eral y
nels a
condit

The
ble, a
would
der se

Me
Mem.
Con
Meetin
dual M
CAN SO
Not
unders
the So

Control of Marine Fouling in Sea-Water Conduits Including Exploratory Tests on Killing Shelled Mussels

By H. E. WHITE,¹ BOSTON, MASS.

Hundreds of tons of mussels may accumulate in the circulating-water tunnels of a large seaboard power station in a single season. Explicit practical procedures have been determined for meeting this problem by complete extermination of fully shelled mussels by chemical treatment, moderate temperature elevation, or combination of both. General results have broad application. Exploratory tests have demonstrated great practical influence of very moderate changes in temperature of the sea water in extermination of mussels. Any elevation of temperature reduces the required consumption of chlorine, which has been the usual killing agent. For plants with suitable arrangements and load conditions, it appears practical to achieve positive control of marine fouling in tunnels without chlorine or other chemicals by periodic increase of sea-water temperature to not more than 95 F for northeast coastal plants. Numerical results of various treatments as observed in the exploratory tests are summarized by charts.

CONDITIONS WHICH LED TO PROJECT

MARINE fouling develops at such a rate at some coastal sites that it can become a major factor in design of the circulating-water system of a steam-electric power station. In the absence of suitable control treatment, hundreds of tons of mussels may accumulate in the tunnel system of a large power station in a single season. Similar conditions arise in connection with sea-water systems of industrial plants. Even where some degree of control has been employed, accumulations of mussels have reached serious proportions. In some cases complete plant shutdowns have been required periodically for scraping and digging out mussels by hand labor.

With high plant investment and heavy demands for output and continuity of power supply, shutdowns for cleaning tunnels become increasingly objectionable. Continuous 100 per cent cleanliness of tunnels is desired in some plants to avoid periodic cleaning, though the normal intervals between cleanings may be several years. This view is prominent particularly (1) where tunnels are long, (2) where access is difficult, and (3) where labor conditions are unfavorable.

OBJECTIVES OF STUDIES

The objectives of the present project were to determine, if feasible, a practical procedure for control of marine fouling which would give full assurance of 100 per cent extermination at will, under severe conditions with minimum chlorine consumption, and

also, to determine the limitations of control treatments. Divergent opinion on questions of detail left no alternative but to make detailed observations. The specific objective, therefore, was to determine practical procedures which would give positive control of marine fouling based on more specific quantitative observations of actual results of treatments than had been available.

SCOPE OF INVESTIGATION

This paper relates particularly to control of marine fouling where sea water is used for cooling purposes. The primary emphasis is placed on extermination of shelled mussels because, as discussed later, these mussels are commonly the most troublesome element of fouling in circulating-water tunnels of power stations along the East Coast. Somewhat similar conditions are found on the West Coast. Results were needed as soon as possible; hence, although refined methods of tests were laid out, lack of time prevented adoption of most of these in the exploratory tests. The test procedures adopted are believed, nevertheless, to be adequate for the immediate engineering purposes.

OBSERVATIONS IN OPERATING PLANTS

In order to take full advantage of existing experience, personal inspections were made of circulating-water systems of power stations on the East Coast where fouling control treatments were in use, and results appeared reasonably satisfactory. Chlorination exclusively had been used at these stations. Continuous chlorination had been used in a few stations, but all tunnels which were available for internal inspection had been treated by intermittent chlorination.

While treatment had brought great improvement in all cases examined, nevertheless, in the tunnels which could be inspected visually, shelled mussels were found in various quantities regardless of the treatment, even where control treatment was applied conscientiously. In some cases, mussels reached 1½ in. in length. At a southern plant which had reported most successful control of mussels, it developed that the so-called "mussel" was an entirely different organism, which was much less resistant to killing treatments.

Fouling growths were removed by periodic manual cleaning. At one of the stations, fouling in the circulating-water tunnel had become so objectionable to the men who were to clean it that serious labor trouble was barely averted.

Various contingencies were found to occur which would permit mussels to enter and make attachment within the tunnels, for example:

Commercial shortage of chlorine temporarily interrupting chlorination.

Mechanical damage to chlorination equipment or piping, due to accident or unusual conditions such as a hurricane.

Deterioration of screens at the inlet of the circulating-water system from corrosion.

Wear of traveling-screen chains, resulting in sufficiently large openings between panels to permit passage of shelled mussels.

In all tunnels inspected, mussels were observed to attach in

¹ Mechanical Engineer, Stone & Webster Engineering Corporation. Mem. ASME.

Contributed by the Power Division and presented at the Spring Meeting, New London, Conn., May 2-4, 1949, and at the Semi-Annual Meeting, San Francisco, Calif., June 27-30, 1949, of THE AMERICAN SOCIETY OF MECHANICAL ENGINEERS.

NOTE: Statements and opinions advanced in papers are to be understood as individual expressions of their authors and not those of the Society. Paper No. 49-S-12.

greater numbers in corners between side walls and floor and roof, and in corners following a sudden enlargement of the cross section of the waterway. Any crevices or cracks in the flat surfaces afforded anchorage for mussels even where neighboring smooth surfaces of the wall were entirely free of mussels.

In the course of the investigation special equipment and technique were developed for sampling the sea water at a roof corner of the straight run of a main tunnel during normal commercial operation, in order to determine the reason for accumulation of mussels in corners. Prompt determination of residual chlorine showed full concentration at this location, even with intermittent chlorination, whenever chlorine was being fed. This suggested that the conformation of walls at the corners was more favorable for secure attachment of the mussels.

Another observation which seems of general application was that mussels occur in various arrangements: (1) In the absence of control treatment, all mussels are closely spaced. (2) If diffusion of chlorine is not uniform, localized accumulations occur. (3) Where control is partially effective, arrangements of mussels on the walls, generally develop in the following sequence after cleaning: initially, as individual scattered mussels; then, small groups; later, larger clusters; and, finally, continuous mats of mussels. Continuous mats of mussels may grow to a thickness of about 6 in. before tearing away from the wall and falling to the floor. The process is repeated and more fall to the floor. There they may form a stationary obstruction to the flowing water until removed manually.

Adhesion of clusters of mussels to the walls, in one instance, was found so strong that it was barely possible to pull them off with the fingers without use of metal scrapers. Under such conditions it seemed improbable that a brief application of any water velocity commonly used in a power-station tunnel would detach the mussels. The individual threads secreted by the mussels for attachment are comparatively strong, but the effective strength of the attachment of a cluster results from the great number of interconnected threads used by the group.

In most stations the object of fouling-control treatment was to kill the mussels when very young and most vulnerable, before they had developed shells. Tremendous numbers of these tiny young mussels, only a few hundredths of an inch in length, enter through the meshes of the usual screens during the summer season. Small shelled mussels would pass readily through the screens also. With the usual intermittent chlorination, attachment could be made between treatments.

Although the usual methods for fouling control resulted in great improvement, it was not apparent that any treatment in use in the stations where intake tunnels were inspected, could be relied upon to kill mussels with fully developed shells. Methods which appeared reasonably satisfactory at one site appeared inadequate when applied under other conditions.

From the observations of the survey it was concluded that where 100 per cent cleanliness is required under the ordinary conditions of practical operation, methods of control must be used which would kill shelled mussels and provide satisfactorily for their removal from the system.

GENERAL TEST PROGRAM

As correlation of field observations was not clear, it appeared that possibly some factors had not been evaluated fully. Uncertainties in attempting to apply results of the plant inspections to conditions at new sites, where full reliability and 100 per cent killing were desired, seemed to necessitate more detailed observations to answer conclusively immediate and essential questions. Tests on full-size circulating-water systems were of course desirable but were impractical at the time, not only from the viewpoint of attendance and expense involved, but also because the extensive

trial of new methods in commercial plants involved risk of more frequent shutdowns for cleaning. Therefore the possibility of testing at a small scale was reviewed.

The potential difficulties of reproducing natural conditions for maintaining mussels on a laboratory scale were recognized fully. However, to proceed effectively with the development of fouling-control treatment, it was essential that it be based upon the characteristics and protective measures of the individual mussel. These could be observed much more accurately in small-scale tests, if natural conditions could be simulated sufficiently well.

Uncertainty may arise in making observations in full-size circulating-water tunnels of power stations because small mussels may enter through the meshes of the screen, so that the time during which a given group of mussels has been subjected to treatment is uncertain. With intermittent treatment, mussels may move considerable distances along the interior walls of the tunnel during the intervals between inspections. Therefore, when the number of mussels in a particular zone changes, generally it is not known whether some have been killed, whether mussels have merely changed location, or whether some have been replaced by new mussels which have recently arrived. In small-scale tests, on the other hand, a fixed number of mussels can be kept isolated in separate receptacles and the period of treatment given each mussel may be determined definitely.

With small-scale tests, radical changes in control methods may be tried, because there is no need to proceed cautiously, as might be expedient in commercial stations. Hence, at least approximate results should be expected more quickly.

It had been concluded from inspection of plants in actual operation that the most resistant fouling organisms in circulating-water systems along the East Coast were the common mussel² and the barnacle.³ Also, these appeared to be important elsewhere. At stations where these organisms had been brought under control by chlorination, other forms of fouling became insignificant. Barnacles commonly do not grow to great thickness and hence, are not a direct source of difficulty in large tunnels. Therefore, study was concentrated on the common mussel.

Since no other quick approach to the general problem was immediately available, small-scale tests were attempted. The first step was to develop suitable procedure and then to determine its feasibility. When this had been demonstrated, tests of killing treatments were started. The project was continued except for minor interruptions for some 2 years, 24 hr per day. Several tests ordinarily were in progress simultaneously. Thus at different times, hundreds of mussels have been observed, not as masses of fouling, but as individuals, twice a day, often many more times, until dead.

INITIAL TESTS ON FEASIBILITY OF SMALL-SCALE TESTS

Maintenance of the mussels under reasonably normal conditions proved more successful in the small-scale tests than anticipated.³ Undoubtedly, further observations will dictate modification of details, but results have seemed reasonably consistent. In general, the mussels under test behaved similar to those in the tunnels. With minor exceptions, the specimens remained in groups and clusters as normally. The results in one test tray are shown by photographs.⁴ Fig. 1 shows the initial arrangement of the clusters maintained 2½ weeks after starting. Clusters had been formed and secure attachment made within one day of starting. Fig. 2 shows the conditions 6 weeks after placing the first specimens in the tray. No deaths had occurred. The final locations of the clusters are practically identical with the original, although the individual specimens had moved within the clus-

² Identified technically as *Mytilus edulis* and *Balanus*, respectively.

³ Detail procedure described in Appendix.

⁴ Photographs were taken after removing water from the trays.

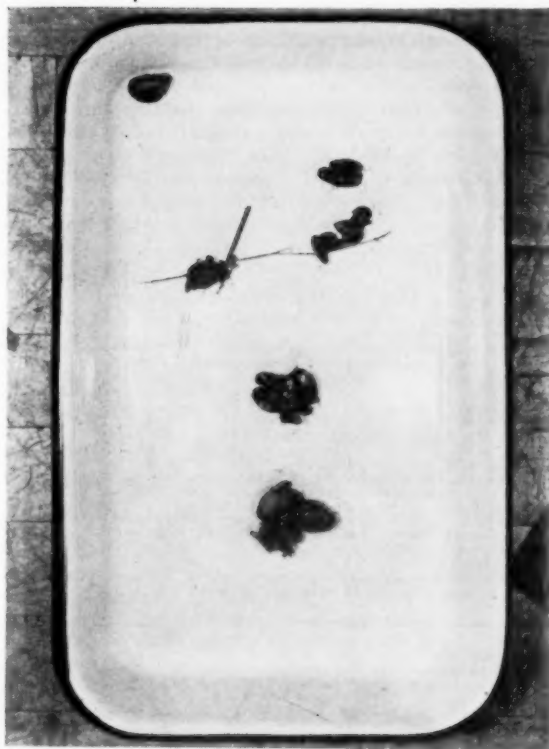


FIG. 1 LIVE MUSSELS IN TEST TRAY AFTER 2½ WEEKS

ters and even transferred from one to another. Two specimens wandered away and started to climb the side wall, but did not continue to the water line as customarily occurs when the condition of the water is unsatisfactory to the mussels. Attachment of the mussels was still firm after 6 weeks.

To illustrate the strength of attachment of the mussels, the entire tray was lifted by grasping the central cluster of mussels by the fingers. The weight lifted was 2¼ lb which was considered satisfactory for mussels of this size when maintained by batch replacement of the sea water. The specimens maintained mantles⁶ well extended throughout the test period and customarily "pumped"⁶ for continuous periods of several hours, although continuous flow of sea water in the tray had been used only for a few hours initially. Afterward the sea water in the tray was replaced only twice each 24 hr. The mussels remained alive for many days after the test was discontinued and no further replacement of water made. In another test the water had been taken from the ocean up to 4 days before use and, in general, was replaced only at average intervals of 1.3 days. With this adverse treatment only 2 mussels of the original 46 had died at the end of 12 weeks.

These preliminary tests were made at water temperatures of approximately 50 to 60 F. While this temperature range was favorable to longevity, subsequent tests at summer temperatures gave similar results. Although the preliminary trials showed that batch changes of sea water twice a day were adequate for the usual tests with 1-gal trays,⁷ containing approximately 50 mussels ranging in length from ½ to 1¼ in., flowing sea water was used

⁶ Mantles are fringed membranes between shells through which sea water is received.

⁷ The mussel pumps sea water through his system to obtain food and oxygen.



FIG. 2 LIVE MUSSELS IN TEST TRAY AFTER 6 WEEKS

as preferable for tests at the higher temperatures. It was concluded, therefore, that with simple precautions the common mussel could be maintained indoors in sea water satisfactorily to permit direct comparison of different control treatments.

CONTROL TESTS

Assurance of reasonably comparable results was obtained during the tests of killing treatments by maintaining simultaneously a segregated portion of the mussels of each batch in natural sea water, but otherwise under conditions as nearly similar to those of the test as feasible. Use of such control specimens is a customary procedure in zoological tests.

In the majority of tests no deaths whatever occurred among the untreated specimens. No more than one died from any group of 20 to 50 specimens used for individual tests. The few deaths among control specimens occurred within 1 or 2 days after removal from their natural habitat. No control specimen was lost at any later stage. Hence, the few random deaths of control specimens were not associated with the test manipulation but, rather, were considered the result of earlier natural conditions. The total number lost by deaths under control conditions were so few as to be negligible in comparison with the number killed by the treatment and thus have no significant effect on the conclusions.

PRELIMINARY TESTS OF MUSSEL-CONTROL TREATMENTS

In preliminary tests early in 1947, it was observed that it took more than 6 weeks to kill shelled mussels by continuous chlorination when the sea-water temperature was 50 F, in comparison with about 1 week at 71 F, as reported by Dobson.⁷ This markedly

⁷ "The Control of Fouling Organisms in Fresh- and Salt-Water Circuits," by J. G. Dobson, Trans. ASME, vol. 68, 1946, pp. 247-263.

longer killing time at the lower temperature drew attention abruptly to the great significance of moderate temperature changes in the atmospheric range. As early as June, 1947, a preliminary test indicated that at about 83 F, although complete killing occurred sooner with chlorination than without chlorination, the difference was scarcely noticeable. In another early test at the same period, it was found that at about 93 F, killing was only a matter of a day or two without any chlorine whatever. This led to further investigation of temperature effect.

IMPORTANT EFFECT OF TEMPERATURE OF WATER DURING CHLORINATION

Quantitative results on the effect of temperature of the sea water during chlorination are summarized in Table 1 and presented graphically in Fig. 3, showing the observed effect of various water temperatures on the rate at which shelled mussels are killed by continuous chlorination. The result of a test reported by Dobson⁷ at the single temperature of 71 F, approximately, for partial killing is shown for comparison and correlates satisfactorily. It will be noted that the time required for complete killing at 85 F is only 3 days, whereas at 55 F, the required time is something over 33 days, more than 11 times as great. This brings sharply to attention the very long time required to kill mussels of the Northeast Coast at natural sea-water temperature in winter and early spring.

All results obtained confirm the indication of the preliminary

tests that the temperature of the sea water during chlorination is the most important factor controlling the time required to kill normal shelled mussels. The deviation of results of individual tests from the curves suggests that other variable factors may be present, but subsequent tests to date indicate that they have far less effect than temperature of the water during the killing treatment.

Fig. 4 shows the data of Fig. 3 on "semilogarithmic" plotting paper. A straight-line "curve" appears to represent the data reasonably well. This is convenient because, when making tests under other conditions, a few reliable test points near the ends of

TABLE 1 EFFECT OF MODERATE TEMPERATURE CHANGE ON TIME FOR COMPLETE KILLING OF SHELLED MUSSELS BY CONTINUOUS CHLORINATION

Test no.	Temperature of sea water during test, deg F	Time to kill entire group of mussels, hr ^a	Number of specimens	Date of starting test	Notes
1	54.8	776	30	Nov. 28, 1948	(a)
2	74.8	240	32	June 12, 1948	(a)
3	88	42	25 ^b	June 18, 1947	(a)
4	89	57	38	Jan. 25, 1948	(b)
5	91.5	32	24	Feb. 7, 1948	(b)
6	105	19½	46	Mar. 20, 1948	(b)

^a Temperature was maintained continuously for time indicated as measured after temperature of water in test tray exceeded 70 F.

^b Approximate.

GENERAL DATA: All mussels and sea water for the tests were collected at Lynn Harbor, Mass. Range of temperature: 31 F to 70 F. Typical length of mussels: 1/4 to 1½ in.

NOTES:

(a) Sea water in test tray replaced twice daily in batch for this test.

(b) Continuous flow of sea water for this test.

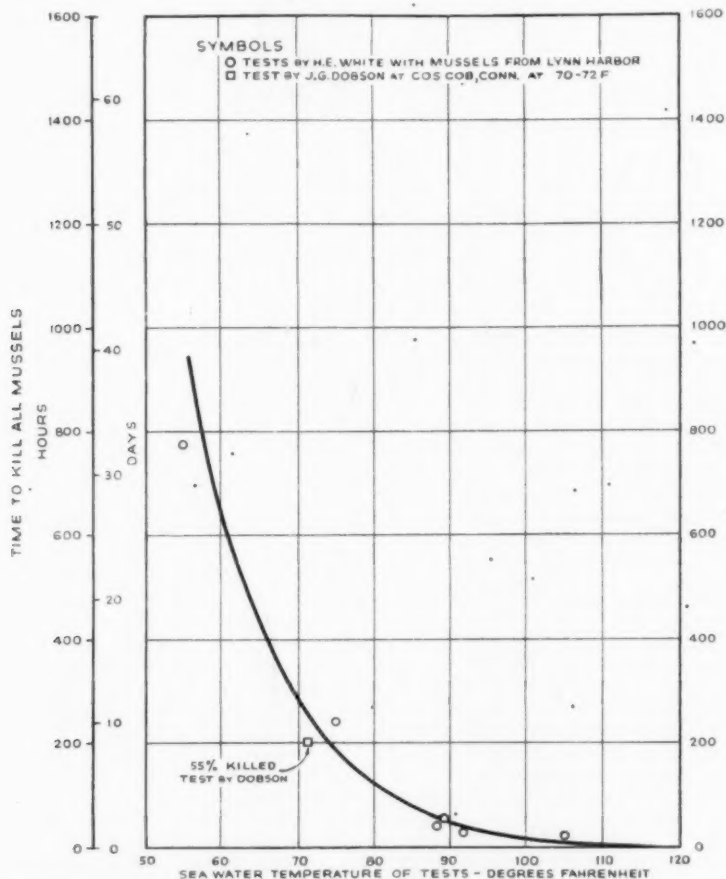


FIG. 3 EFFECT OF MODERATE TEMPERATURE CHANGE ON TIME FOR KILLING SHELLED MUSSELS BY CONTINUOUS CHLORINATION

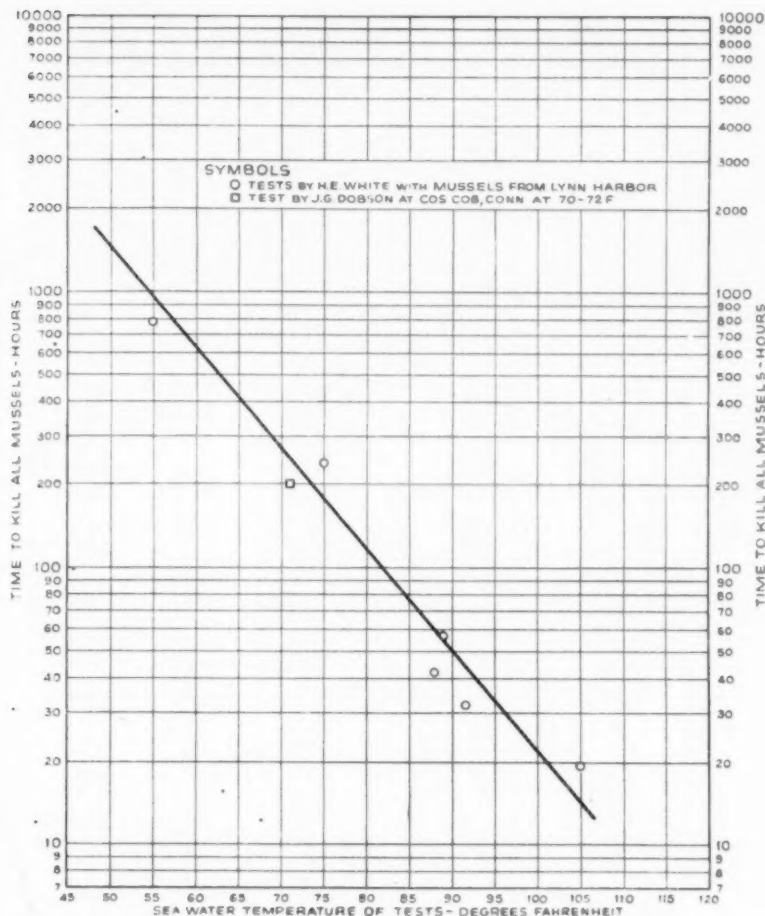


FIG. 4 EFFECT OF MODERATE TEMPERATURE CHANGE ON TIME FOR KILLING SHELLED MUSSELS BY CONTINUOUS CHLORINATION (Semilogarithmic co-ordinates.)

such a curve will establish a satisfactory basis for chlorination control.

During the tests with flowing sea water at the higher temperatures residual chlorine concentrations were maintained at 3 to 0.3 ppm. Hence at temperatures above 88 F the results closely approximate those to be expected in commercial operation. In the tests at lower temperatures the sea water was changed by complete replacement twice a day. The initial concentration of residual chlorine in these was high, but the chlorine was consumed progressively until restored with the next change of water. The average concentration was of the order of 10 to 15 ppm, and more at times. For these tests the resultant killing time probably is too low for the usual commercial concentrations, possibly by 20 per cent.⁸

RESULTS OF KILLING TESTS BY MODERATE HEATING ONLY—WITHOUT CHLORINATION

Preliminary tests had indicated that at temperatures approaching 90 F and higher there was very little difference in time required to kill shelled mussels, whether chlorine was used or not. To study this further a series of tests was conducted without any chlorine whatever. The tests with temperatures of 90 F and above

were made with continuous change of sea water and water-bath equipment.⁹

Obviously, in the absence of chlorine, or other chemical treatment, no killing could be expected at temperatures of 70 F or less, as these temperatures would approach those of natural sea water. However, under the conditions of test, shelled mussels from Lynn Harbor were killed without any chlorine whatever, at a temperature as low as 75 F, by maintaining that temperature continuously for a sufficient length of time. This proved to be more than 12 weeks (test No. 7). Also, observed results confirmed the preliminary conclusions that, at elevated sea-water temperature, chlorination does not reduce the time to kill.

The quantitative results of this series of killing tests without any chlorine or other chemical treatment are summarized in Table 2, presented graphically by the chart, Fig. 5, and plotted on semilogarithmic co-ordinate paper in Fig. 6. In this case a single straight line cannot be applied to the semilogarithmic relation of the data. An abrupt increase in time to kill East Coast mussels is apparent at temperatures slightly less than 85 F.

It will be noted further that above 85 F the time required to kill by continuous heat is approximately the same as when chlorine is used at these temperatures.

⁸ Rough estimate based on tests by Dobson at various concentrations at constant temperature.

⁹ See Appendix for test equipment.

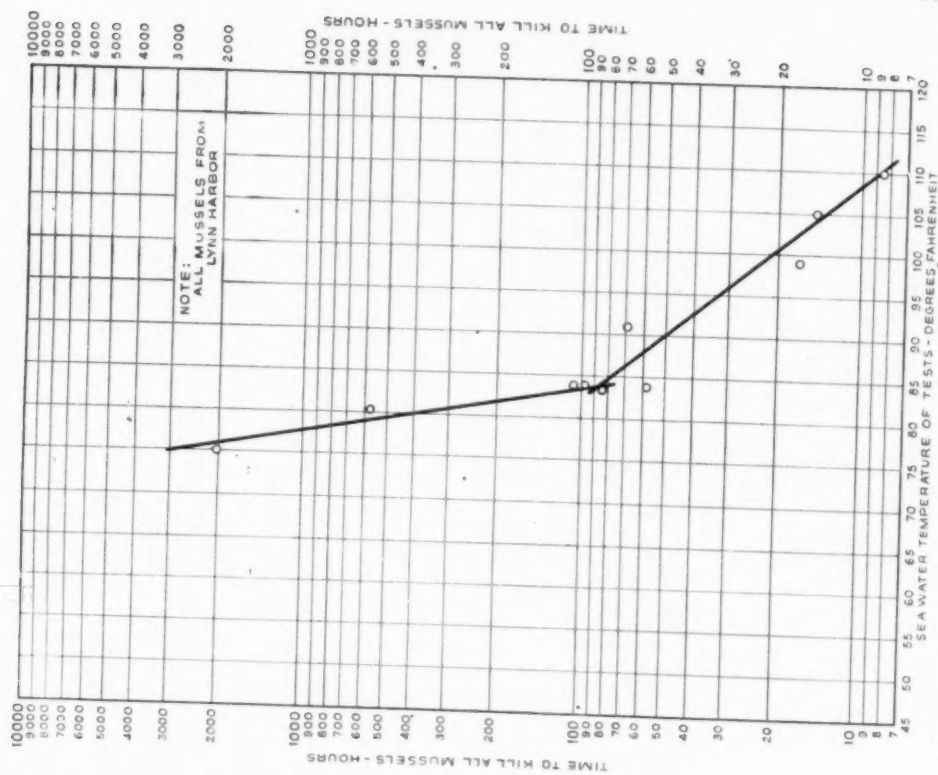


FIG. 5 EFFECT OF MODERATE TEMPERATURE CHANGE ONLY ON TIME FOR KILLING SHELLD MUSSELS—CONTINUOUS TREATMENT

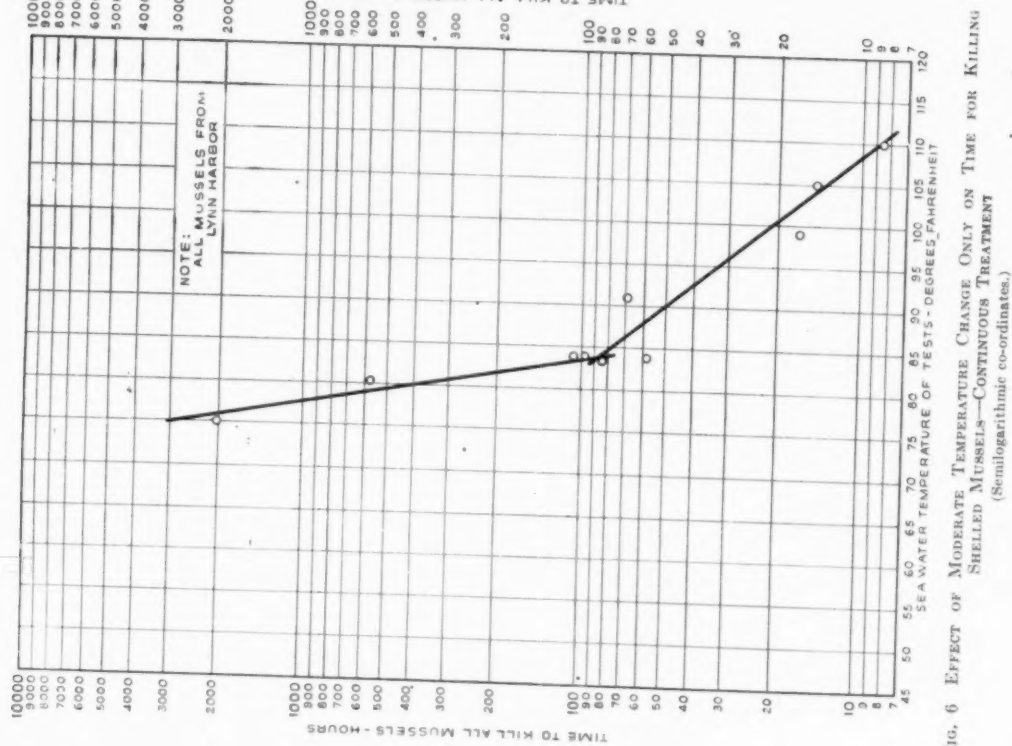


FIG. 6 EFFECT OF MODERATE TEMPERATURE CHANGE ONLY ON TIME FOR KILLING SHELLD MUSSELS—CONTINUOUS TREATMENT (Semilogarithmic co-ordinates.)

TABLE 2 EFFECT OF MODERATE TEMPERATURE CHANGE ONLY, ON TIME FOR COMPLETE KILLING OF SHELLED MUSSELS, NO CHEMICAL TREATMENT USED

Test no.	Temperature of sea water during test, deg F	Time to kill entire group of mussels, hr ^a	Number of specimens	Date of starting test	Notes
7	75	2016 + b	14	June 12, 1948	(a)
8	80.4	572	51	June 9, 1948	(a)
9	83.4	110	53	July 17, 1948	(a)
10	83.9	97	38	Sept. 6, 1948	(a)
11	83.9	58	32	Nov. 6, 1948	(a)
12	83.4	84	25 ^c	Nov. 11, 1948	(a)
13	91	69 1/4	13	Feb. 20, 1948	(b)
14	99	16 1/4	24	Feb. 26, 1948	(b)
15	105	14 1/2	51	Mar. 6, 1948	(b)
16	110	8 1/2	43	Mar. 14, 1948	(b)
17	115	1 1/4	19	Mar. 14, 1948	(b)

^a Temperature was maintained continuously for time indicated as measured after temperature of water in test tray exceeded 70 F.

^b One mussel still alive and recovered subsequently.

^c Approximate.

GENERAL DATA: All mussels and sea water for the tests were collected at Lynn Harbor, Mass. Range of temperature: 31 F to 70 F. Typical length of mussels: 1/4 to 1 1/4 in.

NOTES:

(a) Sea water in test tray replaced twice daily in batch for this test.

(b) Continuous flow of sea water for this test.

COMPARISON OF CHLORINATION, THERMAL TREATMENT, AND COMBINATIONS

Fig. 7 shows direct comparison of killing time, for continuous treatments with and without chlorine, for various water temperatures. Fig. 8 shows the same comparison with semilogarithmic co-ordinates.

From these charts it is obvious that at a temperature of 80 F or less the time required to kill was reduced greatly by chlorination as compared with no chlorination. At 70 F or lower, temperature alone will not give complete killing in any practical operating period, and use of chlorination or other treatment is required.

Conditions at an existing station may determine the most appropriate treatment or may preclude control of fouling by moderate heating alone. In the latter case chemical treatment may be desired. In the case of new construction, a choice may be available in the design stage. Where provisions in construction permit, moderate increase in temperature alone will give positive and complete killing in a predetermined period of 1 to 3 days with no chlorine or other chemical treatment.

If adequate temperature can be maintained at little cost as, for example, during light load periods at a power station, chemical treatment may offer little or no advantage for killing shelled mussels.

TECHNICAL CONCLUSIONS

The most troublesome form of marine fouling observed in stationary conduits was the common mussel.

For complete disposal of marine fouling, it is necessary under usual conditions of commercial operation to kill mussels after their shells are fully developed.

Under all conditions tested, a large proportion of the mussels

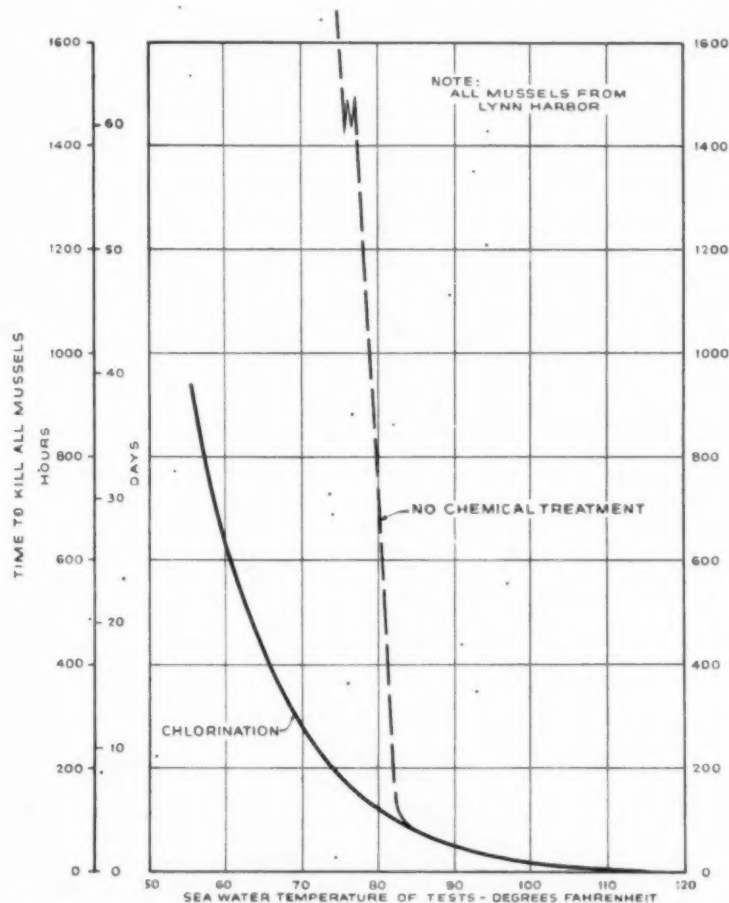


Fig. 7 COMPARATIVE TIME FOR KILLING SHELLED MUSSELS—CONTINUOUS TREATMENT

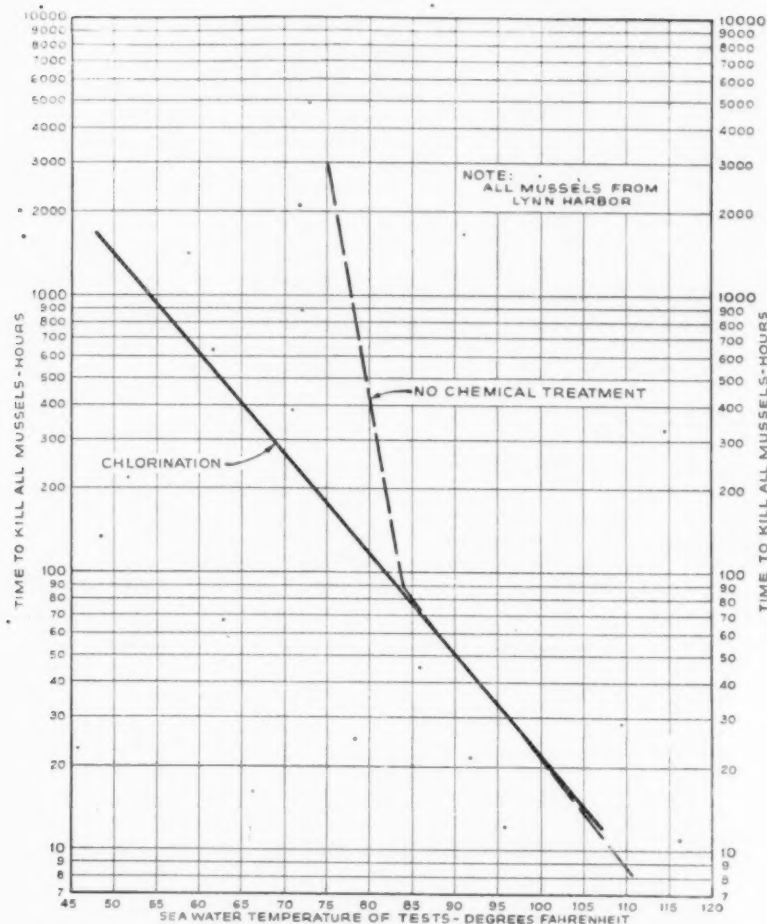


FIG. 8 COMPARATIVE TIME FOR KILLING SHELLED MUSSELS—CONTINUOUS TREATMENT
(Semilogarithmic co-ordinates.)

are killed within a fraction of the time required for killing all. This is significant because, in a power-station circulating-water tunnel, it is desirable, if mussels have accumulated, to remove them gradually so as to prevent clogging by sudden release and accumulation of uncontrolled masses of debris.

The chlorine consumption required to kill shelled mussels can be reduced greatly by increasing the temperature of the water moderately during chlorination.

The time required to kill shelled mussels by chlorination depends primarily upon the temperature of the water in which they are submerged at the time of chlorination. This is a much more significant factor than the variations of the concentration of the residual chlorine within the usual commercial range.

The most significant reduction in chlorine consumption by increasing the temperature of the sea water is obtained at the lower temperatures and for moderate temperature increases.

Complete killing of shelled mussels may be accomplished by the application of moderate increase in temperature alone, with no chlorine or other chemical agent, if applied continuously for sufficient periods.

There are logarithmic relationships between the time required for complete killing and temperature of sea water during killing treatments.

The following conclusions on killing of shelled mussels from Lynn Harbor apply specifically at that location only. They are significant, however, because, generally, similar results may be expected elsewhere, although at different temperature levels:

By increasing temperature of the sea water from 60 F to 70 F, the time required and the chlorine consumption for killing shelled mussels by continuous chlorination are reduced approximately 50 per cent.

With sea-water temperatures raised to 80 F or less, heat alone is quite inefficient for killing shelled mussels, and the use of chlorination or other treatment is indicated.

With sea-water temperatures increased to 85 F, continuous chlorination does not reduce the time for killing below that for continuous temperature without chemical treatment.

When the sea-water temperature is approximately 50 F, the time required for complete killing of shelled mussels by continuous chlorination is about 2 months.

The time required for complete killing of shelled mussels by temperature alone at 90 F was 80 per cent less than with chlorination at 70 F.

CONCLUSIONS ON TECHNIQUE OF SMALL-SCALE TEST PROCEDURE

It was demonstrated that with natural sea water at natural

temperatures, shelled mussels could be maintained in sea water in small receptacles indoors for many weeks in satisfactory condition for comparative tests of killing treatments if reasonable care was exercised in maintaining the natural condition of the sea water by replacing it periodically.

Many useful observations can be made by small-scale tests if the results are considered on a comparative basis, and if a few simple precautions are observed under the guidance of a qualified consultant. This is particularly convenient when it is considered impractical to try changes in the existing method for control of fouling in a commercial power station under heavy demands for power.

Because of the very large variation in the time periods required to kill individual specimen mussels of a given lot under the same treatment, it is important to use a reasonably large number of specimens for a given test in order to determine even approximately the time required to kill all the mussels under a given set of conditions. In general, a minimum of 50 specimens is suggested.

In many tests it was observed that mussels showing the greatest resistance were those of small size, $\frac{1}{2}$ in. long and less; hence these sizes should be included in each batch tested to assure determination of maximum killing time.

It appears desirable to establish a suitable criterion with respect to the varying physical condition of a mussel, or more specifically the resistance to killing. The time required to kill a representative group of 50 specimens by a standard procedure which would approximate a commercial control treatment has been used by the author.

APPLICATION

The small-scale tests have shown that mussels can be exterminated totally on various predetermined schedules of treatment.

The results of the tests are considered adequate for application to routine control of marine fouling of the Northeast Coast if used with liberal factors of safety. Such factors are required in any case because of the considerable variations in the condition of the natural water from time to time and the variations in the condition of the mussels at a given site. If, however, mats of mussels have been allowed to form in the tunnel, or other kinds of fouling must be removed first, it is expected that the time required for killing by continuous chlorination would be increased.

The results of a selected treatment may vary greatly with only moderate changes in conditions. Also, different degrees of control may be desired for different plants because of economic, constructional, or operating conditions. In order to set up a suitable schedule of control treatment at a given plant, therefore, specific quantitative information is desirable. Hence, local tests at the site for each season are recommended.

If for any reason initial treatment in the plant should prove inadequate, it would be necessary only to increase the duration of the treatment or possibly to increase the water temperature gradually, within the limitation of permissible differential temperature stress where massive concrete structures are involved.

The particular type of control for marine fouling to be selected as most appropriate for a given plant would depend on local conditions, including geographical location, fresh-water dilution, if present, industrial pollution, length of tunnel, access, operating conditions, station-load conditions, station design, and the like. This subject, however, is beyond the scope of the present paper.

General results have broad application. Although tests were carried out primarily in connection with the protection of circulating-water systems of power stations, corresponding problems of marine fouling may occur at any coastal plant where natural sea water is used, for example, in salt-water service pipe lines of industrial plants and salt-water fire lines. Salt-water piping systems aboard ships are not immune.

ACKNOWLEDGMENTS

This project has now extended over several years. Throughout we have had the most generous co-operation of a large number of people whose help is gratefully acknowledged. The advice of the following consulting marine biologists was particularly valuable: Dr. William F. Clapp, William F. Clapp Laboratories, Inc.; Dr. Denis L. Fox, Scripps Institution of Oceanography; Dr. Louis W. Hutchins, Woods Hole Oceanographic Institution.

Many power-station operating organizations on both the East and West Coasts have afforded us the advantage of inspection of circulating-water systems when feasible, and full discussion of operating techniques and results. We are particularly grateful to the executives and engineers of the Southern California Edison Company, Long Island Lighting Company, and Lynn Gas and Electric Company. Even from West Africa we received a most painstaking report on practical operating experience with a long submerged tunnel resting on the ocean floor.

The author wishes to express his personal appreciation of the continued interest and help of Mr. William F. Ryan, engineering manager, and Mr. E. B. Powell, consulting engineer, of Stone & Webster Engineering Corporation.

Appendix

TEST PROCEDURE

The general procedure developed in carrying out this series of tests was as follows:

Mussels, as collected from their ocean-shore surroundings, were first retained in trays of natural sea water at moderate room temperature until they functioned in an approximately normal manner before tests were started. The time required to kill the specimens by various treatments was then observed. During the winter, when specimens were taken from their natural habitat at temperatures between 31 F and 45 F, a period of gradual temperature rise of the sea water in the test vessel was allowed before starting the killing test.

For the tests at temperatures of 89 F and above, continuously flowing sea water was used. For other tests it was an essential detail of the technique to renew the sea water in the test receptacles twice daily by emptying and replacing completely so that the water in every part of the test receptacle would be changed.

Mussels for all tests reported were collected at the northeast end of Lynn Harbor on a rocky beach where rubble had been dumped. The harbor extends into an industrial area and has a typical range of tidal elevation of about 10 ft. Size of specimens varied from $\frac{1}{16}$ in. to $1\frac{1}{2}$ in.

Sea water used throughout the tests was taken from the same location in the harbor except on a few occasions when there appeared to be some local contamination. At these times other zones in the same harbor were used.

Sea water used for the control tests was collected from the same source and at the same time as that for the main tests.

Temperature of the sea water in the test receptacles was observed by glass-stem chemical thermometers.

Zonite was used as a convenient source of chlorine.

TEST EQUIPMENT USED

In the tests with water temperatures above 88 F, enameled trays of approximately 1 gal capacity were used with continuously flowing sea water. The arrangement of the equipment used for each test, however, was no more complex than that shown by preceding tests to be necessary. More refinement was required as the water temperature was increased. At approximately 30 deg F above room temperature it was necessary to minimize variations in water temperature during the test, and also to prevent

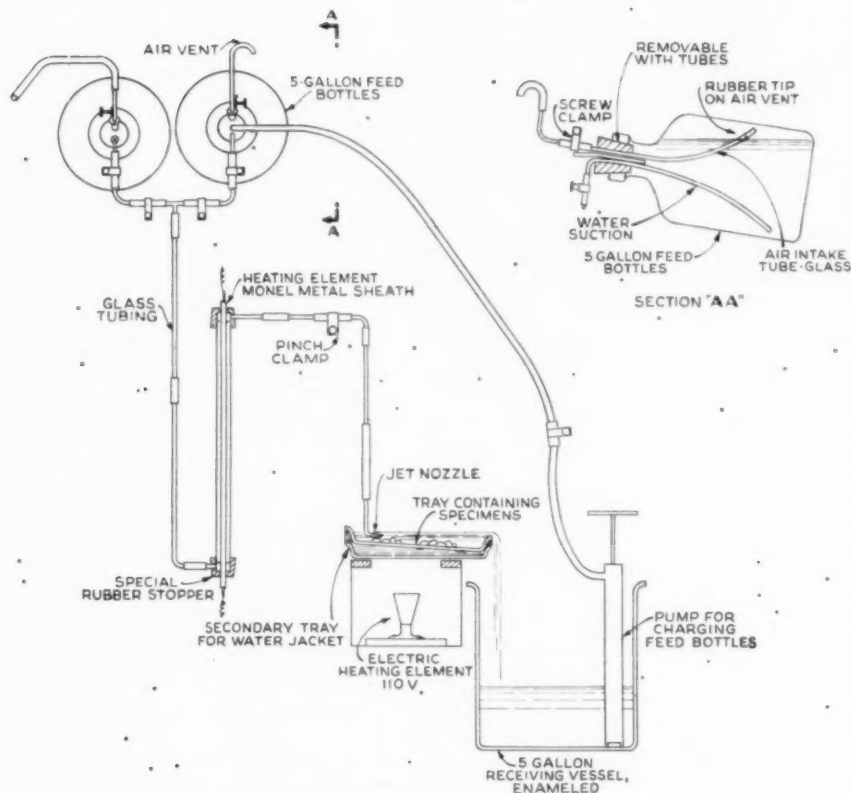


FIG. 9 DIAGRAM OF TEST EQUIPMENT

nonuniform distribution of temperature across the tray. The equipment adopted is shown in Fig. 9. Uniformity of temperature in the test tray containing the mussels was promoted by the use of a second tray of heated water directly below, acting as a water bath. The temperature of the water bath was controlled by adjusting the elevation of the radiant electric heating elements below the tray. Continuous replacement of the sea water was provided by a small jet supplied from overhead. It was found that the jet of incoming water was sufficient to maintain continual mixing of the water within the tray and thus assure uniform distribution of temperature throughout the test tray. The temperature of the sea water from the jet was raised to approximately that of the water in the test tray by first passing it through a tubular-type electric water heater of special design. The use of a small jet minimized the required capacity of the heater.

Even with a jet approximately 0.02 in. diam, mixing was entirely effective when the static head was only 2 ft, and, with a jet of this small size, it was possible to maintain the siphoning of sea water from the 5-gal bottles overhead for a period of several hours without refilling. No plugging of the small orifice occurred, as the large bottles permitted effective settling of suspended matter in the sea water.

The temperature of the water in the test tray has been shown to be a critical factor, and should be maintained nearly constant for a given test. Since manual adjustments required almost continual corrections at the higher temperatures, an automatic temperature

control is recommended to reduce the attendance and to improve precision.

PROGRESSIVE KILLING

In the earliest tests, it was apparent that the time required to kill shelled mussels by a given procedure varied over a wide range for the individual specimens of a single group in the same test tray and subjected to the same conditions. This is illustrated by the chart in Fig. 10 which shows the rate at which deaths occurred. All subsequent tests confirmed that individual mussels of a given group under test died in succession, suggesting significant differences between the resistance of individual mussels of a group, all of which had lived under the same natural conditions. It was shown, however, that if a considerable number of specimens were used for each test, the time required to kill the entire group gave reasonable correlation of results of various tests. This led to the conclusion that the work should proceed on a statistical basis. Because of the more consistent correlation of the "time to kill all mussels" of the vari-

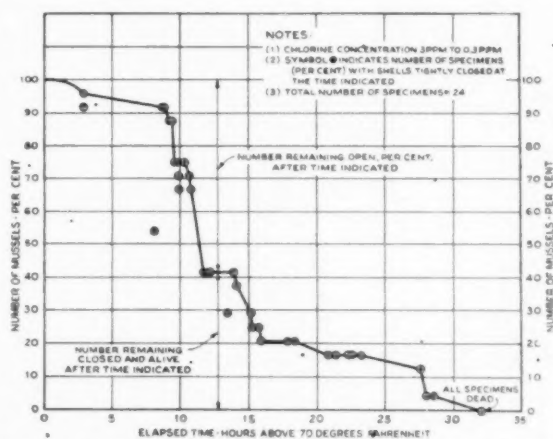


FIG. 10 RATE OF KILLING SHELLED MUSSELS AT GIVEN TEMPERATURE LEVEL

ous test groups, this measurement afforded a more satisfactory means of showing the fundamentals involved; therefore the time to kill, as reported in Tables 1 and 2, is that required to kill all mussels of the particular group under test by continuous treatment until dead.

Thermal Control of Marine Fouling at Redondo Steam Station of the Southern California Edison Company

By W. L. CHADWICK,¹ F. S. CLARK,² AND D. L. FOX³

The idea of controlling marine fouling by elevating the temperature of the sea water is not new, but it is felt that the application of this means of control in the cooling-water tunnels at the recently constructed Redondo Steam Station of the Southern California Edison Company at Redondo Beach, Calif., contains some features of interest. It is the object of this paper to describe the system employed and to present the results obtained during the first year of operation.

DESIGN CONSIDERATIONS

PRIOR to designing the Redondo Station, it had been observed at the company's Long Beach Station that, whereas heavy fouling growths occurred in the intake tunnels, no serious fouling growths occurred in the discharge tunnels, even though these had never been cleaned in the history of the plant. The only difference in the tunnels to which this freedom from growth could be attributed was the higher temperature of the water in the discharge lines. In designing the Redondo Station, it was decided to utilize this condition to the maximum extent practicable, and also to provide facilities for chlorinating the water in the lines should treatment by higher temperatures not be fully successful.

The Redondo Station is situated on a section of sea coast that is exposed to winter storms and resultant heavy wave action. Hence it was highly desirable to have no structure offshore which would rise above the water and be subjected to pounding by large waves. Also, the beach at the plant site is one of the most popular in Southern California, and consequently no structures could be used that would interfere with the recreational use of the beach by the public.

These considerations precluded the use of a trestle or other structure to support chlorinator lines and a tower at the seaward end to house the chlorine apparatus, but led to the suggestion that two separate submerged lines be constructed out into the sea each of which could be used alternately as an intake or discharge, controlled by flow-reversing gates located on the shore end of the lines.

THERMAL SENSITIVITY OF MARINE FOULING ANIMALS

Biochemical control measures are commonly employed in combating marine fouling. These may involve the application

of toxic paint surfaces to immersed structures such as ships' hulls, or the introduction of chlorine, organic chlorides, or other poisonous solutes into the moving streams of an enclosed system.

However, in an electric power-generating steam plant, utilizing flowing ocean water for cooling its condensers, a rather unique opportunity is offered for an introduction of a biophysical control feature, namely, heat. Two large tunnels at the Redondo plant of the Southern California Edison Company, each 10 ft ID, and extending for nearly 1900 ft into the open sea, are employed as intake and discharge channels, being alternated in these two functions at intervals of 2 to 4 weeks, depending upon the fouling season. Thus the periodic discharge of sea water through each tunnel at elevated temperatures has prevented the growth of fouling animals which have been observed in systems not accorded this treatment.

Experiments at the Scripps Institution of Oceanography reveal the fact that numerous sedentary marine invertebrate animals possess relatively sharp temperature-tolerance thresholds. Sedentary marine algae have not been investigated here, since they fail to colonize dark environments, and hence do not constitute a part of the fouling communities therein. Mussels, barnacles, sponges, tunicates, bryozoa, tube-worms, and anemones constitute the chief sources of trouble. In the Redondo and San Diego areas, the common mussel, *Mytilus edulis*, is the most prevalent member of fouling communities in sea-water tunnels. Barnacles, sponges, and tunicates are secondary foulers, while the large California mussel, *Mytilus californianus*, is an occasional invader at localities employing water from the open sea as distinguished from bays and estuaries which support only the other species, *Mytilus edulis*.

It has been found that the bay mussel, *Mytilus edulis*, is more resistant to exposures in warmed sea water than are *Mytilus californianus*, the barnacles *Balanus tintinnabulum*, *Balanus glandula*, the anemone *Cribrina xanthogrammica*, and other forms. *Mytilus edulis* is exceeded in this respect only by the small ribbed mussel, *Septifer bifurcatus*, but the latter species is so small and relatively sparse in numbers it does not constitute a serious threat.

In order to define working conditions which should hold promise for the practical thermal control of fouling, we therefore selected *Mytilus edulis* as representative of the most populous and relatively resistant fouling organisms common to these waters. Groups of young individuals (about 5-10 mm long, some 3-4 weeks old) were separated carefully and immersed in sea water at closely controlled temperatures for designated lengths of time. At the end of each experimental period, the animals were returned to running sea water and observed for possible survival. Survivors soon part their shells moderately, filter currents of sea water through their siphons, and attach themselves to solid surfaces by spinning the tough threads of adhesive byssus in the normal manner. Thermal casualties part their shells in a gaping fashion, die, and undergo decomposition of the flesh.

The following data have been collected relative to young specimens of *Mytilus edulis*:

¹ Manager, Engineering Department, Southern California Edison Company, Los Angeles, Calif. Mem. ASME.

² Consulting Engineer, Stone & Webster Engineering Corporation, Boston, Mass. Fellow ASME.

³ Professor of Marine Biochemistry, Scripps Institution of Oceanography, of the University of California, La Jolla, Calif.

Contributed by the Power Division and presented at the Spring Meeting, New London, Conn., May 2-4, 1949, and at the Semi-Annual Meeting, San Francisco, Calif., June 27-30, 1949, of THE AMERICAN SOCIETY OF MECHANICAL ENGINEERS.

NOTE: Statements and opinions advanced in papers are to be understood as individual expressions of their authors and not those of the Society. Paper No. 49-8-13.

Temperature, deg F	Thermal death time, hr
106	0.33 (20 min)
100	1
95	6-7
90	13
85	41
82	96
77	Survive indefinitely

A graph of the foregoing data yields a smooth exponential curve. It is believed that swimming or freshly settled mussel larvae, being without shells, metabolically active and relatively more sensitive to unfavorable environmental factors, doubtless succumb more readily than do the young individuals which have formed their shells and undergone growth. Thus plant practice, guided by the foregoing data in the Southern California area, provides a generous margin of safety, especially provided that (1) at the height of the marine reproductive season (i.e., from early spring to late fall), water flow is alternated sufficiently frequently (at least every 2 to 4 weeks) to affect the larval or juvenile animals before they have had time to become firmly established, and (2) that temperatures within the upper range are maintained for the periods correspondingly indicated.

Moribund mussels reveal their condition in several observable ways, e.g. (1) by gaping, (2) by failure to close their valves upon mechanical stimulation (tapping the shell), (3) by failure to spin byssus strands for attachment, and (4) by decomposition of their fleshy parts. Even if any or all of the first three diagnostic signs are observable in a treated lot of mussels, it is invariably essential to remove the batch of animals and place them in a container of running sea water at normal temperatures. This was always done in our procedure, by having each lot of ten animals in a large porcelain vessel with perforated bottom (a large Gooch crucible).

At the end of an experimental period, a crucible of experimental animals was removed, drained of water, and the mussels were transferred immediately into a container of fresh cool sea water. This latter container, covered by a screen, was then placed in a running sea-water aquarium, and the experimental animals thereafter were observed during periods of several days. Some heat-narcotized sluggish animals later revive under these conditions, spin byssus, and propel water normally through their valves. On

the other hand, some small mussels which fail to reveal their death by parting their valves, actually may be found to have died in this condition, the shell hinge being insufficiently rigid to operate conspicuously.

Observations always were continued on all animals given heat-treatment for a defined interval and then restored to natural conditions, until such time as we were able to determine that all died as a result of the heat, or that one or more survived. Thus sometimes the data are not all available for 3 or 4 days after the initial thermal treatment. Our data are all plotted on the basis of 100 per cent mortality.

With the use of this method of collecting reliable data, for example, we were able to obtain typical information relative to a series of mussels exposed to a temperature of 35 C or 95 F as shown in Table 1.

The time of 7 hr was manifestly the approximate period to be adopted as the lethal period for mussels of the indicated size and locality, exposed to a temperature of 95 F. Had we merely observed the condition of our animals in the experimental heating vessel, we should have been unable to collect reliable time data for lethality. The believed lethal period thus might exceed the actual lethal period by several or manyfold.

Manifestly the size range of experimental animals, the manner of heating and supplying reviving conditions, and clearly defined criteria of irreversible heat narcosis, leading to certain death, should all be standardized by experimenters in the field.

The definite possibility remains that mussels or other fouling species may vary somewhat in their thresholds of thermal tolerance, according to temperatures prevailing in their normal habitats. Marine animals living on the coast of the Pacific Northwest, for example, might be expected to manifest greater sensitivity, i.e., succumbing at less elevated temperatures and/or within shorter time intervals, than members of the same species, but possibly constituting a separate "physiological race," inhabiting Mexican waters. The sensitivity of races found at intermediate latitudes probably would lie between two such extremes. These matters should be borne in mind, and should be tested experimentally when contemplating the use of flowing sea water from any given region.

TABLE 1 THERMAL DEATH TIME OF MYTILUS EDULIS*

Date of start. <u>7-27-48</u>				Time of start. <u>2.00 P.M.</u>				Nominal temperature <u>35</u> °C. or <u>95</u> °F.									
Sample No.	Total No. per sample	Time heated		Temp °C.	Active			Indeterminate				Gaping				% Dead	
		Clock	Exp. hrs.		7/28	7/29	7/30	7/28	7/29	7/30	7/31	7/28	7/29	7/30	7/31		
1	10	5:00	3.0	34.7	1	10	10	9	0	0	0	0 (some sluggish)	0	0	0	0	
2	10	6:00	4.0	34.7	0	4	7	10	6	1		0 (sl)	0	2		20	
3	10	7:00	5.0	34.8	0	0	2	10	3			0 (sl)	7	1		80	
4	10	8:00	6.0	35.2	0	0	1	10	1			0 (9 sluggish)	9			90	
5	10	9:00	7.0	35.3	0	0	0	10				0 (all sluggish)	10			100	
6	10	10:00	8.0	35.3	0	0	0	10				0 (all sluggish)	10			100	

* From records of D. L. Fox.

DESCRIPTION OF CIRCULATING-WATER SYSTEM

Reference is made to Fig. 1 which shows the facilities for withdrawing water from the Pacific Ocean for the Redondo Station. Two 10-ft-ID precast concrete pipes are laid in the floor of the beach in trenches, having a minimum earth cover of 4 ft, and extend into the sea for a distance of about 1900 ft. The lines were constructed under water by the use of divers, and facilities for unwatering the lines are not provided. The terminal structures are vertical precast concrete towers 14 ft diam, extending about 10 ft above the sea floor and protected by a rock riprap. The top of these towers is about 20 ft below mean lower low water. They are separated laterally by 200 ft to avoid recirculation of the water.

The choice of pipe internal diameter was selected as 10 ft after considering such factors as cost, flow, and possible decrease in diameter by marine growths, with attendant increase in roughness factor. The present pipes will be adequate to handle all the circulating-water requirements for the plant when the latter is expanded to its present ultimate capacity of 264,000 kw. At this load the circulating-water requirement will be about 180,000 gpm.

The shore end of each concrete pipe is connected to a concrete structure in which there are four vertical steel gates which can be raised or lowered with electric motors. The gates are arranged and operated so that one of the concrete pipes acts as an intake and the other as a discharge conduit. At intervals, the position of the gates is changed so that flow is reversed in each conduit. In this way either conduit may be used alternately as a discharge or intake.

Other equipment in the shore structure includes a discharge chamber for warmed water returning from the main condensers in the power plant, a trash rack for collecting and removing seaweed and other trash, revolving screens for removing fish and other marine growth, a suction chamber for the main circulating-water pumps, and a pump house. Circulating water for the main condensers is conveyed from the pumps through 54-in-ID precast concrete pipes laid underground. The latter are not subjected to the antifouling treatment to be described later because it was possible to provide access to them for periodic cleaning by manual means whenever it becomes necessary to do so. Antifouling measures are applied to the two 10-ft-ID pipes under the ocean principally because of their inaccessibility for the usual methods of cleaning.

There is also provided in the pump house equipment for chlorinating the circulating water. Chlorine can be introduced into the water at two places and for two purposes as follows:

1 At the circulating-water pump intake as a desliming agent for the condensers.

2 At the shore end of the 10-ft-ID discharge pipes as a toxic agent for killing marine organisms in the pipe. So far the latter use of chlorine has not been necessary due to the success of the method to be described.

FLOW REVERSAL

The reversal of the circulating water is effected by four vertical gates, one located in each intake and two at the outlets of the transfer basin or reversing chamber. The gates normally will operate in pairs, one intake and one discharge opening, the other pair closing. Gates are 7 ft wide and 10 ft high, built of fabricated steel. They are provided with cast manganese-bronze guides with bronze sealing strips and with stainless-steel stems. The four gates normally operate together at uniform speed, 4 min being required for the complete stroke. The gate hoists are operated electrically, and the position of each is remotely indicated on both the circulating-water panel board in the steam station and the chlorination control panel on the second floor of the chlorination building.

During the 4-min period of reversal there will be a certain amount of recirculation of warmed water, from that gate which has been the discharge and which is now closing, to the intake, which has been closed and which is now opening. The flow in that tunnel, which has been the discharge, is gradually reversing, and some warmed circulating water will be drawn back into the intake. The effect of the reversal of the circulating water is shown in Fig. 2 in which the elevation of the free water level in the forebay has been plotted against elapsed time following the start of the gate movement. This curve sheet is based upon a circulating-water flow of 400 cfs and on a tide level of 0.0. It will be noted that the water level in the intake basin starts at approximately 3 ft below grade 0.0 (which is the head loss in the intake tunnel) and reaches a maximum low grade just after the gates have completed reversal. This lag is a result of the time required to decelerate and reverse the flow of water in the intake tunnel. Approximately 14 min are required for the re-establishment of equilibrium at a level of 3 ft below grade 0.0 (corresponding to the head loss in the discharge tunnel), and a peak water level of approximately 8.5 ft above grade 0.0 is reached just after the completion of the gate movement.

The foregoing maximum and minimum levels are based on an ocean grade of 0.0, corresponding to mean lower low water. When a low tide at -2.5 or a high tide at 7.0 ft occurs, these tide levels below and above grade 0.0 must be superimposed on the level variation shown in Fig. 2. Additional hydraulic data are shown in Table 2.

A weir has been provided at grade 16.0 in the top of the east wall of the transfer basin. Should simultaneous occurrence of

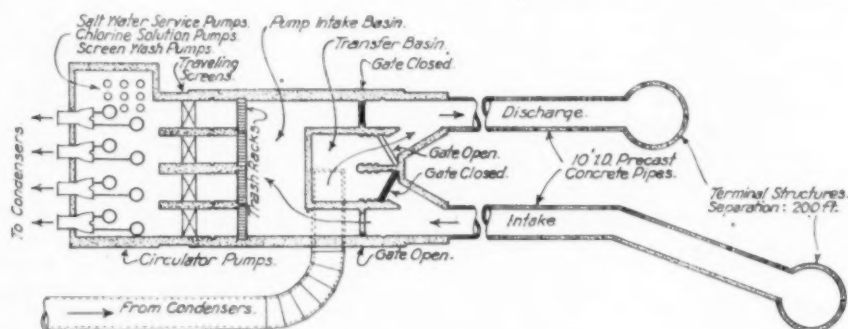


FIG. 1 FACILITIES FOR WITHDRAWING WATER FROM THE SEA FOR THE REDONDO STATION

TABLE 2 ELEVATIONS, HYDRAULIC GRADIENT, AND HEAD LOSSES OF CIRCULATING WATER SYSTEM, REDONDO STEAM STATION

Elevations:

(Mean lower low water = 0.0)

Top of intake and reversing-chamber structure	15.0 and 18.5
Bottom of intake and reversing-chamber structure	-19.0
Top of overflow weir reversing chamber	16.0
Bottom of screen well and pump well	-22.0
Pump-house floor	5.28 and 15.0
Circulating-pump intake bell	-19.16
Steam station basement floor	10.0
Center line of condenser intake	18.5
Top of condenser tail pipe	25.0
Center line of 10-ft discharge tunnel-condensers to reversing chamber	-2.5 and -2.0

Hydraulic gradient:

(Based on a flow of 400 cfs with allowance for marine growth on tunnel walls)

	High water (7.0)	Mean lower low water (0.0)	Low water (-2.5)
Level in intake basin	3.7	-3.3	-5.8
Minimum level of intake basin, during period of flow reversal			-9.8
Level in pump well	2.4	-4.6	-7.1
Minimum level in pump well, during period of flow reversal			-11.1
Level in reversing chamber	10.3	3.3	0.8
Maximum level in reversing chamber, during period of flow reversal	15.8		

Head losses:

(With allowance for marine growth on tunnel walls)

	Two units, 200 cfs	Four units, 400 cfs
Alternating intake and discharge tunnel ($L = 2007$ ft)	0.8 ft	3.3 ft
Screen wells	0.6	1.3
Inlet-pipe line, pumps to condenser	4.8	4.8
Condenser	16.9	16.9
Discharge pipe line, condenser to reversing chamber	7.9	9.8
Alternating intake and discharge tunnel ($L = 1825$ ft)	0.7	2.7
Total	31.7	38.8

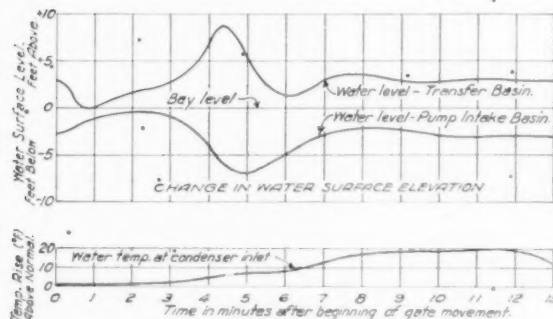


FIG. 2 EFFECT OF REVERSAL OF CIRCULATING WATER

maximum flow, flow reversal, and high tide cause this basin to overflow, the excess water will discharge into the intake basin.

For a short period following tunnel reversal, condensers will receive warmer than normal circulating water owing to the recirculation which occurred when all four gates were open and changing, and to the reversal of the flow in that tunnel which had been the discharge and which became the intake. Fig. 2 indicates that a temperature rise above normal may persist for some 12 min, with a peak rise of 19 deg F prevailing for 3 min. This calculated rise of inlet-water temperature above normal is based upon a heat rejection of 1720×10^6 Btu per hr to the circulating water corresponding to the extreme conditions of four units operating at 66,000 kw. For any lower station load, the magnitude of this temperature rise will be proportionally reduced. It has been found by experience that the reversal cycle does not affect the ability of the main units to carry full load.

ELECTRIC CONTROL OF REVERSING GATES

Each of the four gates is provided with an electric motor operator and means for automatic and manual position control.

Automatic control, under which all four gates operate in synchronism, two opening and two closing, is derived from the chlorination control panel. A manual switch for positioning the four gates synchronously is located on the chlorination panel, while local switches permit the positioning of individual gates. A position indicator for each gate is located on the chlorination control panel and the circulating-water panel in the steam station.

Indicating lights are provided at the chlorine control board and at the motors to show the position of the gates. Red indicates gate fully open. Green indicates gate fully closed. Red and green together indicate gate is either moving or stopped in an intermediate position.

After a gate-positioning operation has been initiated, should an obstruction or a power failure cause any one of the gates to stop before completion of one half of its travel, all gates reverse their travel and are restored to the same position as before operation was initiated. In case the gates have completed more than one half of their travel before one gate stops, all other gates complete the operation. An alarm will sound at the circulating-water gage board if gates go out of synchronism.

BASIS OF PRESENT TREATMENT

The marine fouling organisms which are particularly troublesome at this location are as follows:

- 1 Bay mussel (*Mytilus edulis*).
- 2 Large sea mussel (*Mytilus californianus*).
- 3 Barnacles (*Balanus tintinnabulum* and *Balanus glandula*).
- 4 Hydroids.

Laboratory investigations at the Scripps Institution of Oceanography, University of California, indicated that, of those organisms listed, *Mytilus edulis* is the most prolific and resistant to elevated temperatures, and therefore that any temperature found to be lethal for *Mytilus edulis* would also prove to be fatal for the others. Accordingly, further experimentation to determine the effect of temperature and time of exposure was confined to this mussel as it was abundant and convenient.

The result of the laboratory work is shown in Fig. 3. The curve indicates that this mussel can survive indefinitely at temperatures below 77 F. However, at temperatures above 82 F, survival is dependent upon the time of exposure and, after a temperature of 100 F is reached, the mussel dies within 1 hr.

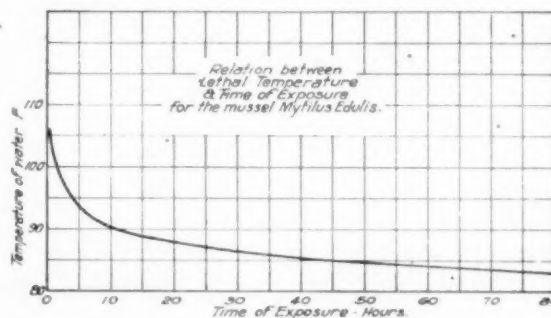


FIG. 3 RELATION BETWEEN LETHAL TEMPERATURE AND TIME OF EXPOSURE FOR THE MUSSEL, MYTILUS EDULIS

The reproductive cycle of this mussel practically ceases during the winter months when the ocean temperature drops below 60 F, and new mussels do not appear in troublesome numbers until the water temperature increases beyond 60 F in the late spring. Accordingly, it is believed that little or no treatment

will be required during the winter dormant period. Conclusive evidence on this point will not be available until further experience with the system has been obtained.

The information in Fig. 3 is applied to the problem of keeping the pipes free of marine organisms in the following way: During the months when the ocean water exceeds 60 F, the gate positions are reversed periodically, causing a reversal of flow in the two lines so that the line which acted as the intake line becomes the discharge line. As soon as this happens, the temperature of water in the line increases about 19 deg F if full load is being carried in the plant. Depending upon the ocean-water temperature, this is increased further by opening one of the gates partially to cause recirculation of the water to the condenser until the temperature of the water flowing in the discharge pipe is raised to about 102 F. As shown on the curve in Fig. 3, the mussels cannot survive this temperature for longer than 1 hr. To make certain that all mussels and other growths are killed, it has been the practice, during the first summer season that this method has been tried, to maintain this temperature for 4 hours before restoring the gate to normal position and stopping recirculation.

The function of the pipes has been reversed and the temperature of the water increased as just mentioned at varying intervals from 10 days to 3 weeks. It appears that once every 3 weeks may be sufficient and, as later experience with this method develops, it may be possible to increase the length of the interval between flow reversals.

RESULTS

During the summer of 1948 the pipes and terminal structures were treated as outlined, and during this time they remained completely free of any fouling organisms. To check upon the effectiveness of the method, a diver was employed to examine the interior of the pipes and terminal structures at least once a month and oftener during the initial phases of the operation. Also, removable concrete-test panels about 1 ft \times 3 ft were hung in the pipes to provide a spot sample for any growths which might have accumulated. These were removed periodically for examination above water, and likewise were found to be free of troublesome growths throughout the first summer period.

Effectiveness of the method also has been demonstrated in another way. Referring to Fig. 1, in the pump intake chamber there are located, in addition to the main circulator pumps, several small vertical pumps used for station salt-water service.

During the latter part of the first summer's operation, it was necessary to raise these for internal inspection, and it was found at that time that the external surface of the pump columns carried a layer of mussels about 6 to 8 in. thick below the water line. The water surrounding these pumps does not receive the full heat-treatment given to the main conduits, and therefore the mussels are not killed periodically but flourish instead in their unmolested environment. It is reasonable to expect that growths of similar magnitude might have accumulated in the main conduits during the same period had not the treatment described in the foregoing been used.

COST OF TREATMENT

The operating cost of the treatment is relatively small when the benefits derived are evaluated with it. It is also small when compared to the alternative method of using chlorine in lethal quantities to perform the same service. No exact data are available for the latter method because, so far, it has not been necessary to employ the method. However, an estimate has been made of the probable cost of using chlorine rather than heat and is reported here for comparison.

During the 4-hr period when the water temperature is elevated artificially at the expense of condenser vacuum and, consequently, fuel cost, the vacuum drops approximately 1 in. Hg. On an annual basis, it is estimated that the heat-treatment costs about \$800 for the two 66,000-kw turbine generators presently installed. Based upon the best available estimates rather than the actual use of chlorine to accomplish the same results, if such were possible, it is expected that the annual cost of chlorine would be about \$50,000.

While it is true that some additional capital expenditure was necessary to provide the facilities for reversing the flow of water periodically, it is judged that the fixed charges on these are considerably below the annual expense for chlorine as just estimated.

CONCLUSION

A system has been devised for controlling the troublesome growth of marine organisms in two concrete ocean-water conduits by elevating the temperature of the discharge water periodically for short periods to a value slightly in excess of 100 F. The scheme has worked well during the first year of plant operation and has done so at a cost believed to be much lower than with the use of chlorine.

S

T

Trans
will be
follow

1

W. F.

2

L. A.

3

cludin

E. W.

4

Static

Chad

He
offer a
foulin
indica
therm

The
ately
proble
localit

1

2

of chl
(prod

3

under

Spa
differ
nonpe
which
the Fu
month
third-d
initiat
low w
At Wa
Plyma
July,⁴
unusu
Atlant
ture fo

¹ Ass

Univer

² "L

ings of

523-55

³ "R

Mollus

and Fi

⁴ "M

⁵ "O

for Cil

vol. 67

⁶ "T

Miller,

1940.

Symposium on Marine Fouling—Discussion

THE following discussion is a composite of that given in connection with the symposium of papers on the subject of Marine Fouling which appears in this issue of the Transactions. References to individual papers of the Symposium will be given by numbers in parentheses as indicated in the following list, which also includes paper numbers.

- 1 "Some Biological Fundamentals of Marine Fouling," by W. F. Clapp, pages 101-107.
- 2 "Project Study for the Mitigation of Marine Fouling," by I. A. Patten, pages 109-115.
- 3 "Control of Marine Fouling in Sea-Water Conduits Including Exploratory Tests on Killing Shelled Mussels," by H. E. White, pages 117-126.
- 4 "Thermal Control of Marine Fouling at Redondo Steam Station of the Southern California Edison Company," by W. L. Chadwick, F. S. Clark, and D. L. Fox, pages 127-131.

DISCUSSION OF PAPERS

HELEN I. BATTLE.¹ The data presented in this symposium offer a definite contribution to the immediate problem of marine fouling and are particularly enlightening to the biologist as an indication of the paucity of specific knowledge regarding the thermal-tolerance ranges of many common organisms.

The possibility of the destruction of larvae prior to or immediately on settling would involve another type of approach to the problem, namely, an accurate determination for any given locality of the following:

- 1 Spawning characteristics of the adult.
- 2 Lethal temperatures and critical temperatures for duration of chlorination of the early larva (*trochophore*), straight hinge (*prodissoconch*) and calcareous shell stage of young (*dissococonch*).
- 3 Preparation of prediction curves for the actual settling time under any given temperature range.

Spawning in *Mytilus* is intermittent and varies considerably in different localities. For example, Fox² found a simultaneous nonperiodic spawning of *Mytilus* at Alexandria and Suez to which temperature apparently had no relationship. Battle,³ for the Fundy area, observed maximum spawning during the summer months at the time of first-quarter neaps, full-moon springs, and third-quarter neap tides, and suggested that spawning might be initiated by increased temperature of the littoral zone when the low water of the first-quarter neaps occurs during the midday. At Wood's Hole, spawning is usual from June to September, at Plymouth, England, from January to May, and in North Wales, in July.⁴ Dr. Clapp (1) has drawn attention to an apparently unusual spawning in December to February, off Portland and Atlantic Beach. Nelson⁵ placed a critical spawning temperature for *Mytilus* at 10-12°C. Miller⁶ found a minimum tempera-

ture of 11-13°C required to initiate spawning at Bideford, P. E. I.

A determination of lethal temperatures and critical temperatures for duration of chlorination of the larval, straight hinge, and young would lend itself readily to laboratory procedure. The eggs either can be fertilized in the laboratory and the young reared successfully on cultured diatoms, or can be obtained in plankton tows with No. 18 bolting silk net. Although it might be expected that the larvae will, in general, be more sensitive to unfavorable environmental factors than the young with shells, this cannot be taken as a generalization, and it would be necessary to determine the thermal death point experimentally.

Dr. J. C. Medcof⁷ has compiled composite curves for the prediction of oyster sets from growth-increment data at various constant temperatures. Such prediction curves would be of the greatest value in the instance of *Mytilus*. Conceivably, in certain localities, *Mytilus* will be subjected to a considerably greater temperature range than that of oysters, hence this will affect the duration of the free-swimming stage and present difficulties in the prediction of the actual settling time.

Further experimental work might be directed along the line of chemical control, possibly by the use of substances to dissolve or destroy the attachment of the byssus thread and not necessarily toxic to the organisms themselves. Such substances, no doubt would bring in the problems of upsetting the balance in nature since the effect might be widespread following their discharge into open water.

C. E. BLAIS.⁸ Paper (4) covering the control of marine fouling by temperature at the Redondo Steam Station is an excellent presentation of the basic treatment successfully carried out on a large-plant scale at this important public-utility station.

The planning, construction, and successful operation of the elevated heat-control method thus established brings into sharp focus the value of this system as compared to some of the other control methods which previously have been suggested and installed for preventing the settling of lava forms and the killing of adult forms of fouling organisms.

The fouling of both fresh and salt-water circulating systems is a common problem to many utility and industrial plants whether they be located on the Atlantic or the Pacific seaboard. The most prevalent source of trouble appears to be caused by those fouling organisms that are members of the *Phylum mollusca*, which includes the snails and other single-shelled *Gastropoda*; and clams, oysters, mussels, and other bivalves that are most troublesome. The *Mytilus edulis* identified as the black mussel on the Atlantic Coast and a similar bivalve that is closely related, known as the *Mytilus californianus*, common on the Pacific Coast, is the most common fouling mollusk throughout the world.

Control methods previously suggested and tried have been numerous, and today, due to the untiring efforts on the part of many eminent biologists and designing and operating engineers, the problem of control can be solved effectively. It is interesting to note that the design of the Redondo Steam Station's marine-fouling-control system was predicated on the two most popular known methods of combating the fouling of salt-water circulating systems: (a) The heating and the recirculating of circulating water, one of the earliest schemes used on a large-plant control

⁷ "Larval Life of the Oyster (*Ostrea virginica*) in Bideford River," by J. C. Medcof, *Journal of the Fisheries Research Board of Canada*, vol. 4, 1939, pp. 287-301.

⁸ Chief Engineer, PWD Power Plants, Quonset Naval Air Station, Quonset Point, R. I.

¹ Associate Professor, Department of Zoology and Applied Biology, University of Western Ontario, London, Canada.

² "Lunar Periodicity in Reproduction," by H. Munro Fox, *Proceedings of the Royal Society of London*, series B, vol. 95, 1924, pp. 523-550.

³ "Rhythmic Sexual Maturity and Spawning of Certain Bivalve-Molluscs," by Helen I. Battle, *Contributions to Canadian Biology and Fisheries*, vol. 7, 1932, pp. 257-276.

⁴ "Mytilus," by K. White, *LMBC Memoirs*, March, 1937.

⁵ "On the Distribution of Critical Temperatures for Spawning and for Ciliary Activity in Bi-Valve Molluscs," by T. C. Nelson, *Science*, vol. 67, 1928, pp. 220-221.

⁶ "The Larval Development of *Mytilus edulis*, L.," by M. M. Miller, Unpublished Report, Fisheries Research Board of Canada, 1940.

system; (b) chlorination control, probably the most extensively applied of all controlling systems in use today.

The design of the circulatory structure for the Redondo Station is novel and yet not radical. It does, however, contain certain features of much interest to future designers and operators of control installations. Of primary interest is the considered effort to construct, without in any manner interfering with or detracting from the natural recreational area, this necessary facility which otherwise might interfere with the future use of the beach by the public. The engineers are to be commended for the excellence of design, and the ultimate installation which so effectively overcame local difficulties.

The writer concurs with the type of control provided for combating effectively the fouling of the circulating-water lines. The system provides for control by elevated temperatures for primary elimination, and with chlorine injection as a safeguard or for secondary defouling and is worthy of mention. Even though complete and satisfactory results were achieved without the use of chlorine during the first year's run, it is quite within the realm of possibility that this method of prevention might be utilized if future conditions warrant. Experience in the Narragansett Bay area has shown considerable variation in the variety, volume, and the rate of growth of fouling organisms from year to year in any one part of the bay. It is therefore possible that the relatively short period upon which the report is based may not be entirely conclusive as to results.

The operating cost of the treatment for the first year of operation is exceptionally low considering the benefits resulting. A complete breakdown of the cost of the installation of the terminal structure, piping and pumping station would have been quite useful for comparative purposes with other installations, particularly for use in other contemplated studies made for the purpose of determining the specific type of equipment best fitted for the complete elimination of marine fouling in other areas.

The NAS main power plant at Quonset Point was designed and constructed during the duress of the last world war. A pumping station was constructed along the bulkhead south of the main plant, and no control equipment for marine fouling was installed in the initial building unit. The power plant was not long in operation, however, before it became apparent that the infiltration of bay mussels would affect seriously the operation of the turbogenerators. Within the first year of operation, serious clogging of the pump well and large intake and fouling of the condensers necessitated outages at opportune moments to facilitate the defouling of the condenser water boxes, tube sheets, pipes, and pump well. The matter of establishing a satisfactory control was given the highest priority. A survey of the physical features of the cooling-water system indicated that the close and compact arrangement of the prime operating equipment would preclude the possibility of installing the necessary piping for control of marine fouling by temperature. The survey, however, did bring to light the simplicity and feasibility of installing a complete chlorinating system that effectively would control the marine-fouling growth of bay mussels within the system.

An automatic vacuum chlorinator was procured and installed in the pumping station. Chlorine was injected on the lee side of the sluice operating gate before the rotary screen. The chlorinator was placed on automatic control for continuous operation during the warm-weather months, with the chlorine residual maintained at 1 ppm. During the early spring and early fall months up to about October 1, intermittent operation gives satisfactory results. During these periods, the residual is maintained at 0.5 ppm. This system of control treatment has continued to be effective and extremely flexible in meeting the

widely varying conditions, and the operation and maintenance are relatively inexpensive.

LOUIS ELLIOTT.⁹ While a steam plant is not as closely tied to nature as is a hydroelectric, there are still a number of reconciliations to make, of which the supply and handling of condensing water call for one of the most important. This condition obtains whether the station has an ocean, a lake, or a river to draw on for direct condensing, or whether in a dry country cooling towers must be used, with make-up from wells or other source.

The design adopted at the Redondo Station (4), with two 10-ft pipes laid under the sea bottom 1900 ft out from the shore, must presuppose a reasonably stable bottom—not subject to serious change of contour from waves and tides.

The paper (4) brings out the complications arising in a design of this kind—unexpected to one who has not tackled a similar problem. The 10-ft-diam pipes, to carry 400 cfs, give a moderate water velocity, e.g., 5.4 fps. This matter of pipe size was doubtless worked out with care, taking into account investment and fixed charges as against energy losses through friction, and complications arising from variation in head under various phases of operation.

Doubtless, also, the economics as to régime of changes in circulation have been worked out, taking into account necessities of temperature level to kill the mussels, loss of fuel resulting from higher water temperatures, and other elements.

Small-scale examples of similar conditions may be cited. At small steam plants on the Isthmus of Panama, difficulty arises from marine growths inside small pipes taking water from the ocean. These become clogged with mussels and other growths, in spite of the fact that according to Fig. 3 of the paper, the particular mussels encountered at Redondo would have been killed by the temperatures existing in these tropical waters. It is probable that the particular marine growths encountered at Panama are immune to the effect of temperatures that would kill *Mytilus edulis*.

Although no formal research has been conducted, certain approximate results may be compared with conditions in the north (3, 4).

South Avenue steam plant at Panama City has a capability of about 12 mw. There is an unusual condensing-water arrangement, worked out because of the wide shelving beach at the plant site, with the water receding a long distance from the plant at low tide. Circulating water is taken from the sea when the tide is high, and sufficient water is impounded in a basin to supply the cooling needs when the tide recedes beyond the suction line of the pumps. The storage basin is divided into two compartments, permitting certain control of circulation. Some surface cooling is effected during the period when tide is out.

Sea-water temperatures range from 70 F up, and condenser-inlet temperatures from 70 to over 110 F. Fouling by marine growths of pipes and other condensing-water works is experienced, particularly during the spring and early summer. This fouling has been minimized by heating the circulating water for brief periods. Arrangement can be made, daily if necessary, to raise water temperature to 115 F for a period of 20 to 30 min. This has been found effective in killing a great portion of the marine growth.

Data from southern California indicate that exposure of the mussels to 106 F kills them in 20 min. Corresponding data taken at Lynn shows a much longer time for killing all mussels with water at 105 F, and something over an hour with water at 115 F. As just stated, it has been determined at Panama that it is desirable to carry the water up to 115 F for approximately half

⁹ Consulting Mechanical Engineer, Ebasco Services Incorporated, New York, N. Y. Mem. ASME.

an hour. Because of the more general character of information from Panama no close comparison can be made with Redondo and Lynn.

A new plant under design for Panama takes advantage of this utilization of high temperatures, without use of chemicals, for killing marine growth. In this case, as at the South Avenue plant, there is to be a recirculation of warm water, 115 F maximum, through circulating-water conduits and condenser.

The circulating system for the new plant will have a siphon-type conduit 42 in. diam and 500 ft long, supplying water to the intake chamber of the circulating pumps at all stages of tide. This utilization of siphon action, permitting the placing of the intake chamber back on the shore in a protected location, has been made in a number of plants in Central and South America. At the new Panama station, a 12-in. recirculating line from the condenser discharge carries warm water, when required, to the pump-intake chamber and also to the intake siphon. The latter may be valved off, reversing the flow during the periods when high tide floods the intake chamber and the siphon feed is not required. Piping and valves are so arranged that flow can be reversed in each pass of the two-pass condenser, and any part of the circulating system subjected to a higher water temperature to kill mussels or other marine growth.

V. F. ESTCOURT.¹⁰ Although the effect of increased temperature in reducing the ability of mussels to remain attached to intake conduits has been known for many years, the experimental data which have been developed by the authors (4), demonstrating a definite correlation between time of exposure and various water temperatures beyond which specific types of mussels can survive or remain attached, is extremely valuable. This information should prove helpful in designing salt-water condensing systems in power plants for minimum trouble from this type of marine growth. Although the paper (4) relates to what was done to prevent such marine growth in a specific installation, it would appear appropriate to include in this discussion a few observations relative to the basic factors which enter into the problem.

Dr. Clapp (1) adequately describes some valuable research which has been conducted in connection with the chlorination of mussels, and H. E. White (3) correlates the effect of chlorination at different water temperatures in terms of the time required to kill the mussels. None of these papers is concerned with the influence of the basic layout of the salt-water intake system upon the economic application of other methods of control. Therefore some comments regarding this aspect of the problem may be helpful in suggesting a means of evaluating the various possible solutions in terms of how much capital investment can be justified economically for the various methods of control.

The control of marine fouling from the power-plant operator's viewpoint has as its objective the elimination of trouble from restrictions in the flow of cooling water in the various conduits and piping systems, and through the main condensers and other heat exchangers, resulting from the accumulation of mussels, and other fouling organisms at the tube inlets. Four important methods of control have been known for a number of years, i.e., (a) properly located revolving screens, (b) predetermined periodic increments in water velocity, (c) chlorination, (d) predetermined periodic increments in water temperature. Each of these methods is known to be effective in varying degrees, depending upon various local conditions and also upon whether one is used to the exclusion of the other three, or whether some optimum combination of two or more methods is applied. In so far as we are aware, the use of elevated temperatures prior to the Redondo job had

been confined to the process of increasing water velocities periodically, particularly during seasonal high water temperatures; and the effect of chlorination as a means of control had been somewhat inconclusive until the more recent tests at the Lynn Gas and Electric plant were completed (3).

Experience during the past 25 years in the San Francisco Bay area with salt-water cooling systems has indicated that the location of the screens in the intake system is a fundamental factor with respect to operating difficulties which will be encountered from fouling. We have examined intake tunnels up to the location of the revolving screens after many years of continuous operation and find that the accumulation of mussels on the walls of this section of conduit reaches a point of saturation which is determined by the apparent inability of the mussels under existing water velocities and temperatures to maintain a firm hold beyond a certain thickness. Although they may hang down in streamers for a while, eventually they will drop off and are then caught by the revolving screens. It is therefore extremely desirable to locate both the circulating pumps and the screens as close to the condenser as possible. What happens when there are large low-velocity conduits between the screens and the condenser is well illustrated in the paper by I. A. Patten (2).

In most instances there is little to fear from mussel accumulation in the intake conduits up to the point where the revolving screens are located. Absolutely no interruptions or curtailments of operation have resulted from mussel accumulations in this section of the intake tunnel in any of our San Francisco Bay area plants. However, as the authors point out, there were special considerations at Redondo which made it desirable to go to the expense of controlling marine growth in the unusually long intake conduits before the screens. They do not state specifically that smaller conduit cross sections were used in anticipation of an improved roughness factor, and larger effective cross-sectional area due to the absence of mussels. Sometimes other considerations dictate the economic size of the conduit, but it would be of interest to know whether there was any saving in reduced conduit sizes at the Redondo job due to mussel control.

On the other hand, there is a much greater fouling hazard in the section of tunnel or piping between the intake screens and the condensers. It is our understanding that the original design at Redondo for the control of temperature in the intake conduits up to the revolving screens has been extended in its application to the lengths of pipe between the screens and the condensers, in order to meet the problem which usually exists in these sections of conduit which are unprotected by screens. It would be of considerable interest if the authors (4) would describe the results obtained at this point in the system that is, between the circulating pumps and the condensers.

At our Moss Landing steam plant, because there were physical restrictions which made it difficult to bring the revolving screens close enough to the condenser, we not only have manifolded the individual circulating-water-pump discharges, but have arranged the condenser piping so that some or all of the water can be returned in reverse direction through one half of the condenser, thence continuing in reverse direction through one of the pump-discharge lines, thereby elevating the temperature of the cooling water and taking advantage of both increased temperature and velocity, if necessary, in order to remove any mussel accumulations. Had it been economically feasible to locate the revolving screens and pumps within, say, 25 ft or 50 ft of the condensers, these provisions probably would not have been necessary. Full reliance is being placed upon the ability of the revolving screens to prevent any trouble from mussel accumulations in the section of conduit up to this point.

This subject would not be complete without mentioning the

¹⁰ Engineer of Steam Operation, Pacific Gas & Electric Company, San Francisco, Calif. Mem. ASME.

special problem which sometimes develops in small salt-water pipes of, say, 3 in. diam or less. Mussels have been known to grow in these small lines until they are almost completely plugged. This has been eliminated in some instances by the substitution of heavy rubber hose and rubber-lined fittings. Apparently the mussels have difficulty in attaching themselves to rubber, and it would appear that the valuable investigations described in the papers of this Symposium might well be extended to include a further study with respect to the effect upon mussel accumulations of special linings and coatings on the inner surfaces of salt-water conduits.

GUSTAVE HEINEMANN.¹¹ At Corpus Christi plant of the writer's company, large volumes of sea water are used for process-cooling. Although it was planned to commence chlorination of the sea water at the time operations began in 1934, some delays were encountered in the installation of the chlorination equipment. This resulted in our operating the plant for several months with unchlorinated sea water before a chlorination program could be started. Drawing on the experience reported by others, in which it was claimed that shelled mussels could be killed after several days continuous chlorination, it was decided to chlorinate the water on a continuous basis, maintaining chlorine residual roughly 0.5-1.0 ppm for 4 days prior to commencing an intermittent chlorination program. At the end of the 4-day period the lines were flushed, resulting in the recovery of tremendous quantities of killed mussels. Although careful inspection of the lines was not possible, there were definite indications that the kill was essentially complete.

Following the initial continuous treatment, varying programs of intermittent chlorination were tried from 20 min each 8 hr to 40 min each 2 hr. Experimentation indicated that the latter heavier schedule appeared to be necessary for effective control in these waters. With a program of 40-min chlorination each 2 hr, and a residual approximating 0.5-1.5 ppm, essentially complete control is obtained. This experience has also been confirmed by a power plant in this area operating on water from the same source.

It appears evident that in any discussion of mussel control, a consideration of local conditions is of extreme importance. For example, H. E. White (3) shows that with mussels from Lynn Harbor, a complete kill is obtained at temperatures less than 85 F even without the use of any chlorine. W. L. Chadwick, F. S. Clark, and D. L. Fox (4) state that mussels in the Redondo Beach area of California are killed after the temperature of the water reaches 82 F. The growth of the mussels in the Texas Gulf Coast waters is extremely prolific, even during periods when the water temperature is as high as 90 F. This would indicate that the curves which have been presented cannot be applied to normally warm waters such as those in this area.

During the winter season when the water temperature is as low as approximately 60 F, and occasionally as low as 50 F, the rate of mussel growth is decreased tremendously. During the summer season, representing at least 4 or 5 months of the year when the water temperature will be in excess of 80 F, the rate of growth is very rapid. This would indicate that the mussels in this area will withstand temperatures considerably in excess of those at Lynn Harbor or at Redondo Beach.

We do not have any experience to show the effect of temperature on the length of time necessary to kill shelled mussels from waters in this area at varying temperatures using chlorination. Our experience along this line is confined principally to continuous chlorination for 3 to 4-day intervals, such as was employed when

chlorination was first begun, and at times when the water temperatures were in excess of 80 F.

It would appear desirable that further work be instituted to determine the length of time necessary to kill Gulf Coast mussels with chlorine under lower temperature conditions. It also would appear desirable that work be instituted to determine the thermal death temperature of these mussels under varying times of exposure.

B. G. HUME.¹² Marine fouling of circulating-water systems of steam plants on the West Coast has been particularly aggravating to the operating personnel. More trouble has been experienced from marine growth in plants located on open water, where fresh clean sea water is available, than in those located in harbors. Mussels in particular seem to like clean water. Undesirable as it is to have the circulating water contaminated with industrial wastes from a corrosion standpoint; it does discourage the growth of mussels and some other forms of marine life. Mussels are the most objectionable, as they break off from the tunnel walls, and frequently plug the condenser tubes completely or, worse still, lodge inside and cause tube failure from cavitation.

It has been found that chemical control of the circulating water is either too expensive or inadequate to prevent the growth of the more vigorous types of marine life. Therefore it has been necessary to resort to the very expensive method of cleaning tunnels by hand anywhere from one to three times a year. Chemical control still proves to be adequate and quite necessary to prevent the growth of the slimes that are so detrimental to a good heat-transfer rate in condensers, but the mussels protected by shells are highly resistant to chemicals.

The Department of Water and Power of Los Angeles Harbor steam plant uses water from the Los Angeles Harbor. The intake tunnels are about 1200 ft long, and no difficulty has been experienced from marine fouling during the 7 years these tunnels have been in use. In fact, they have been cleaned only once during this time. The sea water in the vicinity of the Seal Beach steam plant, however, is practically free from industrial contamination, hence considerable trouble is experienced with growth of marine life in the intake tunnels.

Mussels grow in great abundance in the inlet tunnels of this latter plant. They hang in festoons on tunnel walls, inlet pipes, and condenser water boxes. As this plant is now being used for hot stand-by service and is generally shut-down over week ends, attempts have been made to discourage the growth of mussels. This was done by injecting chlorine solution into the intake tunnels just before the week-end shutdown, thereby subjecting the growth therein to a "soaking," in water having a residual chlorine content of 2 to 4 ppm.

This procedure has failed to rid the tunnels of mussels, as they apparently close up tightly when the chlorine solution surrounds them and then open up when the danger has passed. Ordinary periodic chlorination for slime control seems to have little or no effect on them.

In designing the extension to the Seal Beach steam plant, the Department proposes to make use of the principles of recirculation in a slightly different manner from those adopted at Redondo. It is proposed that circulating water for the future units at Seal Beach will be taken from Alamitos Bay, as at present, by means of twin 8-ft-diam precast concrete tunnels and discharged to the San Gabriel River. When it is desired to raise the temperature of the water in the tunnels, a portion of the warm circulating water from the condensers will be discharged into one of the intake tunnels. By means of gates, the flow of water will be reversed in this tunnel and warm water will flow toward the

¹¹ Chief Chemist and Technical Director, Southern Alkali Corporation, Corpus Christi, Tex.

¹² Engineer of Steam Design, Department of Water and Power, The City of Los Angeles, Los Angeles, Calif.

intake structure where it will be recirculated and drawn into the other tunnel, and back into the condenser again. It is anticipated this reversal of flow will be done during week ends or other periods of light loads where one tunnel can be spared. In this fashion, the quantity of warm water recirculated can be varied, and the temperature of the water can be controlled to any desired degree. This scheme will permit raising the temperature of the water in the whole circulating-water system sufficiently to kill the marine life, thereby eliminating any parts of the system in which mussels could develop, break away, and get into the condenser tubes, causing tube failure.

The method of preventing growth in tunnels by raising periodically the temperature of the water to 100 F or thereabouts for a few hours, appears to be the answer to a very troublesome problem in this area. Those responsible for initiating and carrying out this very expensive and elaborate experimental work should be highly commended for their part in advancing the art of power-plant design and operation.

L. W. HUTCHINS.¹² The four papers of this Symposium provide a balanced, up-to-date account of most of the aspects of intake-tunnel fouling which are of practical importance, fanging from biological fundamentals to the two cases of plant-scale control.

The very rapid accumulation of fouling in intake tunnels and associated circulating systems is mentioned by several of the authors. Calculations show that the rate of growth in the Lynn tunnel in at least 2 years has exceeded the prodigious figure of 1000 tons per acre of surface per year. No figures remotely comparable are known to biologists from any other sources; thus under the most favorable conditions with the most productive crops, the best farm yields are only of the order of 10 tons per acre per year, for example. From our investigations in the Lynn tunnel, it appears both that the occurrence of large numbers of organisms and the growth of the individuals at unusually rapid rates are factors in the rate of accumulation of that fouling. On the one hand, as many as 6000 mussels have been found on a square foot of wall in the Lynn tunnel. Again, while Dr. Clapp (1) mentions a length of 50 mm being reached after 10 months, a figure which many authorities approximate as normal, in the Lynn tunnel this size may be reached after as little as 17 or 20 weeks.

Most of the common enemies of mussels are excluded from tunnels such as that at Lynn by the trash racks and screens, and probably this is responsible to an important degree for the large numbers of mussels occurring there. Darkness, continuous submergence, reasonably high salinities, adequate oxygen, moderate currents, and sufficient food are all factors which appear to promote mussel growth. It is obvious that an intake tunnel commonly will provide an ideal combination of these, which suggests an explanation of the rapid growth of the individual mussels. An intake tunnel, in short, is probably as close to a perfect environment for mussels as it would be possible to get.

Chlorination has certain effects on mussel growth which perhaps are worth mentioning. Measurements of several thousand mussels from the Lynn tunnel collected at various times over the last 5 years show conclusively that mussels subjected to chlorination are relatively fatter than those growing in unchlorinated water. The concentration of chlorine appears to have no effect in this connection, but the effect becomes more pronounced in mussels subjected to longer treatments in a given period, and it is most extreme in mussels subjected to continuous chlorination. With intermittent treatments of very short bursts, such as the 20 min per 8-hr shift used in 1946, there is no

killing and the over-all growth rate does not appear to be reduced. The result, therefore, due to the slight fattening induced by the chlorination, is to increase the actual bulk of fouling for equivalent numbers of mussels. Chlorination in short treatments thus not only achieves no control, but is actually detrimental in developing a larger bulk of fouling. This seems not to have been known previously.

All of the evidence now available indicates that chlorination, to be an effective control method, must be used in long doses. If intermittent chlorination is desired or necessary, as might be the case in a reversing tunnel system, the schedule apparently should be something on the order of a month on and a month off, rather than a short phase alternation.

Dr. Clapp's demonstration of mussel attachments on test panels at Atlantic Beach in midwinter shows that it is not entirely safe to schedule control methods only for normal fouling seasons. Usually, of course, it is the summer which is the critical time of year for fouling attachment, particularly in the temperate waters where *Mytilus edulis* is involved. Freak off-season sets do occur occasionally, however, and plants should be prepared to employ control methods at any time of year should inspection show that such an unusual set is taking place. It is essential to keep a continuous systematic watch over all installations and not to rely entirely on normal or average data about fouling seasons.

This is especially important in such an installation as the Redondo plant, where the tunnels cannot be cleaned manually and where, therefore, every possible precaution must be taken to maintain them in a clean condition. In this connection it may be noted that while the heavy set of mussels in the Redondo area normally does occur between spring and fall, some mussels are known to breed throughout the year.

Small-scale experiments or laboratory tests are always artificial to some degree and seldom if ever duplicate exactly the conditions obtaining in actual installations or in other tests. Discrepancies are to be expected, therefore, in comparing data from various sources, and it will be noted that there are some in these papers concerning the durations of exposure which are fatal at various temperatures for *Mytilus edulis*.

Thus the data in Mr. White's Fig. 5 (3) do not indicate that the Redondo treatment of 4 hr at 102 F would be adequate, nor do they support Ritchie's earlier use of 12 hr at 90 F at the Edinburgh Westbank Station, although satisfactory control seems to have been obtained at both plants. The differences are minor, however, and do not affect the general concept of control by heat.

Nearly all tests agree in indicating a critical temperature for *Mytilus edulis* in the vicinity of 84 F. Comparatively brief exposures to temperatures higher than this are fatal, while at temperatures below 84 F killing is achieved only by very much longer exposures or not at all. This agrees very closely with what can be inferred from the geographical distribution of *Mytilus edulis*. The southern limit of the species on all coasts throughout the world occurs just about where water temperatures in the hottest part of the summer can be expected to exceed 85 F for several days. Penetration of the species further into the tropics, in other words, would take it into water whose summer temperatures would be lethal. It is possible to make similar inferences about critical temperatures for many other fouling species from their geographical distributions.

Because the economics of fouling control have been debated widely with relatively little evidence, it is valuable to have two further cases in which control has been obtained economically. The Lynn case demonstrates that fouling dominated by *Mytilus edulis*, along with condenser sliming, can be controlled by continuous chlorination at a net saving to the company relative to the cost of maintenance and the less efficient operation without

¹² Marine Biologist, Woods Hole Oceanographic Institution, Woods Hole, Mass.

fouling control. The Redondo case provides a similar demonstration for the high-temperature method, although this is limited to the gross fouling and does not control sliming.

Since there has been considerable doubt of the practicality of fouling control by heat, the Redondo case is also interesting for the very close duplication and confirmation it affords of the experience at the Edinburgh Westbank station reported by Ritchie. Relative costs of chlorination and heat-treatment cannot be determined solely from the Lynn and Redondo data, as given, since neither includes figures for equipment, fixed charges on investment, etc., as well as because only one controls sliming. The Redondo estimates for chlorination there, however, seem high compared to the Lynn costs; solely on the basis of volumes of water handled, the Redondo cost estimate should not exceed about \$15,000 per year at present.

In any event, a final evaluation of the two methods cannot be obtained from only 1 or 2 years' experience at one or two installations; it is to be hoped that further reports on these plants will be forthcoming after the control methods have been in operation several years, and that additional data will be contributed by other units. Meanwhile, all who are concerned with this problem of fouling in circulating-water systems will be indebted to the present authors for their discussions of their experience.

F. L. LAQUE.¹⁴ It is evident that the attention being given the control of fouling in intake tunnels by the authors of papers (3) and (4) is providing a good technical basis for future progress.

At our Marine Test Station at the Ethyl Dow Chemical Company plant, Kure Beach, N. C., we have had opportunity to observe the growth of mussels under conditions which emphasize a point which is indicated also by a comparison of the results obtained in paper (3) as compared with those in paper (4). This point is that the heat that mussels can withstand is likely to be determined to a great extent by what they are accustomed to in their normal environment.

For example, the mussels exposed to the sun between tides on a steel bulkhead at Kure Beach are certainly able to survive combinations of time and temperature which the data of Chadwick, et al, indicate should kill them. Similarly, mussels there have survived the high temperature reached inside the upper surface of a partially buried 3/4-in-thick black steel pipe line which regularly remained full of stagnant sea water during daylight hours when pumps were not operated. Finally, the sea water itself at Kure Beach reaches temperatures during the summer months that may average 83 F with occasional peaks of 86 F. The only effect on the mussels appears to be to stimulate their growth instead of killing them in 80 hours or so, as indicated in Fig. 3 of the Chadwick paper (4).

Perhaps the absolute temperature is not as important as the extent and rate of increase in temperature above normal in determining the killing effect.

All this means, of course, is that the heat-treatment required to kill mussels will have to be established for each location, and results secured at any plant cannot be used as more than a rough guide as to what might be successful elsewhere.

Having in mind, also, the indications in Fig. 10 of Mr. White's paper (3), which show that some mussels are much harder than others, attention might be given the possibility that the offspring of the survivors of a killing treatment in its early stages may become conditioned to it. In time, as the number of survivors increases, it may be necessary to make the killing treatment progressively more severe.

In appraising the results of tests made in the laboratory, due

¹⁴ In Charge, Corrosion Engineering Section, Development and Research Division, The International Nickel Company, Inc., New York, N. Y.

consideration must be given to the possibility that the laboratory environment, in a general way, may be unhealthy. The mussels in the laboratory may, therefore, be more vulnerable to destruction. On this basis, therefore, the data indicating probable life at temperatures approaching normal may reflect largely the ability of the mussels to survive in the laboratory environment. It would be prudent to assume that in practice, killing treatments may need to be more drastic than indicated by laboratory studies.

In reports of the killing effects of chlorination it is necessary to define how the determination of residual chlorine content is made. It has been discovered¹⁵ that with sea water the common ortho-toluidine colorimetric method indicates a chlorine concentration which is about one half that shown by the standard starch-iodide method or by titration with methyl orange. For practical use of results, all that is required is that the method of measuring chlorine be defined or described so that it can be followed by anyone else.

With regard to effects of chlorination on corrosion, some recent tests at Kure Beach have shown that corrosion of 70:30 cupro-nickel alloy is reduced by continuous treatment with chlorine to a residual of 0.5 ppm (ortho-toluidine) and at water velocities up to 10 fps. Intermittent treatment with concentrations up to 3 ppm resulted in a slight increase in corrosion at the highest velocity, with the effect being greater with the longer the interruption of treatment. In general, the observations at Kure Beach, with respect both to killing effects on organisms and possible corrosion of metals, would favor continuous treatment at low chlorine concentrations (0.5 ppm ortho-toluidine) as compared with intermittent treatments at higher concentration.

R. B. MARTIN.¹⁶ During informal discussion following the meeting, particular attention was directed to the exceedingly high (\$50,000) estimate of annual chlorine requirements for the Redondo Steam Station (4) which appeared out of keeping with the chlorine rates and accomplishments discussed by Mr. Patten (2) for the Lynn Gas and Electric Company. The other papers and discussions also gave rise to the suggestion that moderate and economical combinations of chlorine with elevation of water temperatures to accelerate the life processes of the macroorganisms could be counted upon to produce equally good results at a probable saving in heat and in chlorine. Mention was made during the discussions of the continuing experimental work at Kure Beach, N. C., and elsewhere, wherein it is expected that extensive tests can be conducted to prove the value of combinations of low chlorine residuals and moderate elevations of temperatures.

As applied to the Redondo operating conditions, for example, the Lynn methods might call for an annual chlorine consumption for marine fouling of \$6000 for the two condensers now operating, to which might be added \$600 for 26 weeks of normal intermittent chlorination of the 90,000 gpm for slime control; whereas a combination of chlorination with the present use of \$800 of applied heat would use not more than \$70 of chlorine for the 13 annual periods of 4 hr of heating. This combination should show also some promise of alleviating the marine fouling in the pump-suction chamber, and in the discharge piping from the circulating pumps to the condenser-inlet water boxes.

S. T. POWELL.¹⁷ The growth of marine organisms in water-circulating tunnels is a serious problem in the operation of many

¹⁵ "Corrosion of Steel Pipe by Chlorinated Sea Water at Various Velocities," by V. B. Volkening, paper presented at NACE annual meeting, Cincinnati, Ohio, April 14, 1949.

¹⁶ Industrial Division, Wallace & Tiernan Products, Belleville, N. J.

¹⁷ Consulting Chemical Engineer, Baltimore, Md. Fellow ASME.

steam-generating plants using sea water for condenser cooling. This Symposium is most timely and should influence greatly the design of the intake tunnels in stations which are to be built in the future. These problems have been encountered and their importance recognized throughout the world, and it is surprising that control procedures merely by elevation of temperature have not been more universally practiced.

As early as 1903 an attempt was made to control the marine growth in tunnels by the addition of copper sulphate. This treatment was practiced by the Cargo Fleet Iron Company Ltd. of Middlesbrough on the northeast coast of Great Britain. Some beneficial results were obtained from the use of this chemical but the results were not wholly satisfactory. Subsequently, an extensive investigation was undertaken by Dr. James Ritchie of the Royal Scottish Museum in Edinburgh.

The investigation was made to develop a procedure for preventing the growth of mussels in submarine shafts and tunnels at the Westbank Electricity Station at Portobello. The earlier work was supplemented by an investigation to develop operating procedures to prevent blocking of the Portobello tunnels by seaweed. A number of forms of chemical treatment were studied, including the use of chlorine compounds, sulphuric acid, copper sulphate, and other chemicals. Other studies were carried out concurrently to determine the value of temperature variation for the control of mussels and other marine growth adhering to the walls of the tunnels and shafts.

It is most interesting to note the similarity of the findings of the present authors, and those of Dr. Ritchie reported more than twenty years ago. The recommendations made by Dr. Ritchie as a result of his comprehensive study are presented verbatim in the following:

1 "That a reversed current or outflow of heated sea water be passed down each tunnel, and that it be passed until all the water in tunnel and shafts has attained a minimum temperature of 110 F, by which time all the mussels will have been killed.

2 "That it is unnecessary to pass such heated water daily or even weekly, but that to prevent undue development of the mussels in the tunnels the heated current be passed once every four weeks during the spatting season.

3 "That, for all practical purposes, the spatting season and the season during which douching must be continued, may be reckoned from the beginning of March until the end of October.

4 "That immediately after the first application of the above recommendations control observations be made at the grid on the end of the sea-shaft to test the efficacy of the heated overflow."

The principal difference in the findings of the two groups of investigators appears to be the top limit of the temperature requirement for prevention of the growth and development of the marine organisms. However, at the Portobello investigation, it was definitely demonstrated that the temperatures below 100 F were very effective, but the higher temperature was recommended to insure as complete control as possible. It is conceivable, also, that there are different types of organisms encountered at the Portobello Station than those at Redondo and Lynn Harbor.

It would be interesting to evaluate the efficacy of the treatment on the different organisms found at the two stations. It is recognized of course that, as the temperature to which the water heated is increased, the cost of the treatment increases, and it is obvious from the standpoint of economy that the temperature should be raised only to the point at which the efficacy of the treatment is commensurate with the increased operating cost.

The writer was interested to note that the authors of these papers have drawn attention to the fact that this form of treat-

ment is not a substitute for control of bacterial slimes forming on condenser tubes, but the thermal treatment is a specific corrective measure for the control of shelled mussel growth. It would be interesting to evaluate the increased rate of growth of bacterial slimes resulting from the occasional increase in the temperature of the water. It is possible that the growth of bacteria responsible for slimes might increase because of the more favorable temperature of the water during the life cycle of the organisms. Other factors may be encountered because of the changing biology of organisms present in the water resulting from the elimination of the mussels.

LESTER RANDALL¹⁸ AND D. DOUGLASS.¹⁹ Favorable results in the control of marine fouling by intermittent chlorination at the steam station of Stamford Gas & Electric Company were obtained January, 1942, to August, 1945. The tests relate to a 25,000-kw installation which started operation in 1942. The circulating-water pipes carrying the sea water from the pumps at the screen well are 3 ft diam and have a total length of 262 ft. The load conditions have been such that the reported velocity of 5 fps has been maintained almost continuously. The present schedule of chlorination consists of feeding 60 min per 24 hr and maintaining a residual chlorine concentration of approximately 0.5 ppm at the condenser discharge.

The amounts of marine fouling removed annually from the circulating-water pipes were as follows:

Year	Marine fouling removed, cu ft
1945.....	3.7
1946.....	11.2
1947.....	12.5
1948.....	6.0

Continued accumulation of marine fouling at rates in excess of 200 cubic feet per year in the pits where chlorine had not yet dispersed, indicates corresponding accumulations would have continued in the pipes if chlorination had not been applied. The accompanying charts, Figs. 1 and 2 on the following page, show typical water temperatures in the intake, but it should be noted that these are in excess of natural sea-water temperatures for the locality because of partial recirculation of the heated circulating water.

G. K. SAURWEIN.²⁰ The Cannon Street Station of the New Bedford Gas and Edison Light Company is located on tide water at the mouth of the Acushnet River on Buzzards Bay. It was built by Stone & Webster in 1916. Several extensions have been added through the years and now the station has the following installed capacity:

- 1 10,000-kw unit at 210 psi, 500 F temperature
- 2 15,000-kw units at 210 psi, 500 F temperature
- 2 20,000-kw units at 210 psi, 500 F temperature
- 1 25,000-kw units at 875 psi, 900 F temperature
- 1 7500-kw topping unit at 875 psi and 850 F temperature

There is currently being installed a 30,000-kw 900-psi unit.

The units now in service require about 90,000 gpm supplied through a traveling screen house and an 11-ft-wide 6-ft-high intake tunnel running the length of the powerhouse, about 450 ft, with several suction wells each about 10 ft × 18 ft. This tunnel had no gate or other means for stopping off the water, and has never been cleaned.

About 20 years ago shell material began to get into the con-

¹⁸ Engineer, Ebasco Services, Inc., New York, N. Y.

¹⁹ Superintendent of Power, The Hartford Electric Light Company, Hartford, Conn. Mem. ASME.

²⁰ Mechanical Engineer, NEGEA Service Corporation, New Bedford Gas and Edison Light Company, Cambridge, Mass.

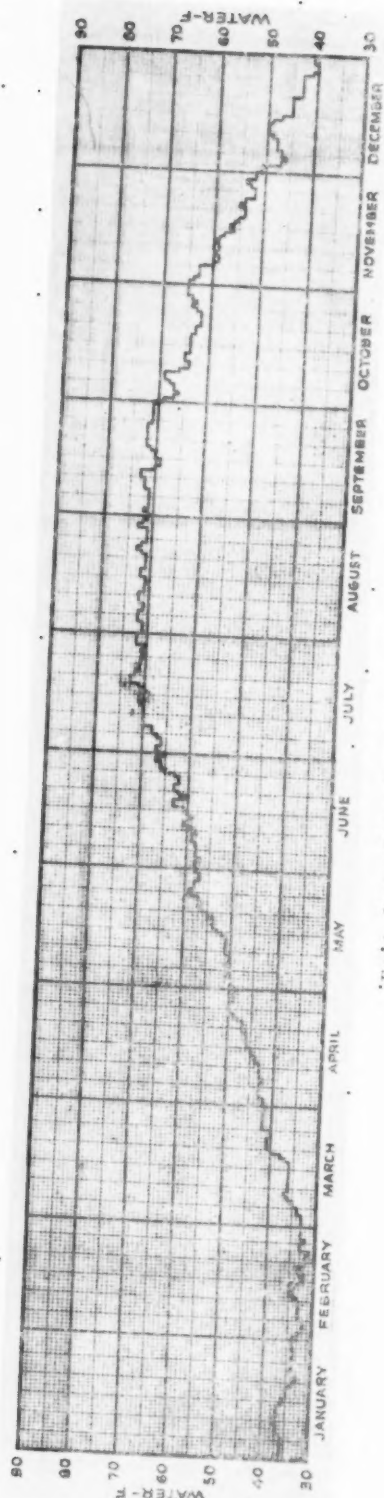


FIG. 1 INTAKE WATER TEMPERATURES—DAILY 1946

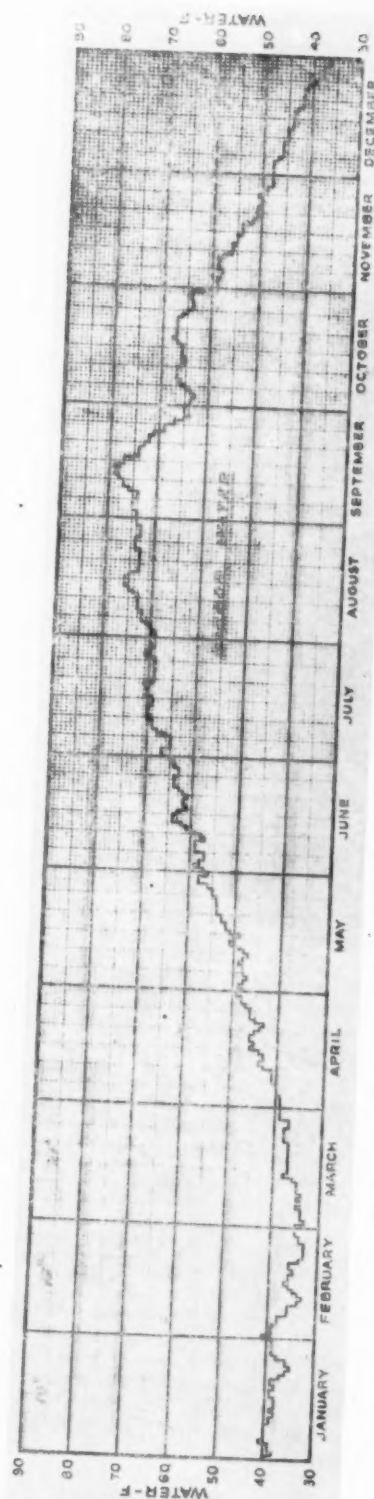


FIG. 2 INTAKE WATER TEMPERATURES—DAILY 1947

den
tro
wer
wa
ple
act
In
ceiv
at t
con
15,0
from
con
and
1943
seaw
tion
dept
De
this
warm
sels
tive
insta
water
carry
one o
The
necte
two 2
may
one sp
An
the so
venier
water
tunnel
tained
A c
rakes
will di
collect
have to
The
1937, v
replac
trols sh
Octobe
represe
tunnel
rates o
conden
has not
light int
heavier
mussel
chlorina
0.50 ppi
solids fr
Cost
cleaning
tions wil

The w
denced b

denser water boxes requiring shutdowns for cleaning. Shell trouble varied greatly from year to year; some seasons quantities were very large, and in others almost negligible. This trouble was not very disturbing during the 1930's when there was plenty of spare capacity in the station. However, when war activity began and load increased, these interruptions were serious. In 1939 R. D. Stauffer, chief engineer of the system, conceived the idea of providing a large-size blowdown connection at the bottom of the inlet water boxes. Twenty-inch "blow-down" connections were installed on the 20,000-kw units and 16 in. on the 15,000-kw units. These cut the time of cleaning water boxes from $1\frac{1}{2}$ hr to 7 min. This of course did not remedy the tunnel condition. More shell material was continually accumulating and obstructing the flow of water. Examination by diver in 1943 showed that the sides and roof were encrusted with matted seaweed and mussel shells to a depth of 6 in., and the accumulation of material on the floor varied from 1 ft to as much as 3 ft in depth. The discharge tunnel contains none of this material.

Due to the summer population of Cape Cod, the peak load on this plant occurs during the summer months, when the water is warm, use of condensing water greatest, and activity of the mussels at a maximum. To stop condenser plugging, it is imperative that the tunnel be cleaned. Therefore it was planned to install a gate in the tunnel, and to provide auxiliary condensing-water supply to the three largest units in the plant which will carry week-end loads. The tunnel may then be shut down over one or more week ends for the cleaning operation.

Three 15,000-gpm vertical pumps have been installed and connected by concrete and cast-iron piping to the 25,000-kw and the two 20,000-kw units. These pumps are so arranged that two may serve the new 30,000-kw unit now being installed, leaving one spare pump.

An 8-in. vertical dredge pump has been provided for handling the solid material. It will be lowered into the tunnel at convenient points along its length. When the auxiliary condensing-water pumps are in service, the tunnel gate will be closed and the tunnel pumped down to a 2-ft depth of water which will be maintained for flowage of the solids to the dredge pump.

A crew will then enter the tunnel with spades, scrapers, and rakes to move the solid material to the dredge pump. The pump will discharge through a pipe line laid with dresser couplings to a collection point at the dock. About 500 cu yd of material will have to be removed from the tunnel and the pump suction pockets.

The first chlorinating equipment was installed in the plant in 1937, when a 720-lb per day unit was put in. In 1940 this was replaced by two 2000-lb per day units. This equipment controls slime well but could not remedy the mussel condition. On October 3, 1943, officials of the company met at the plant with representatives of the Wm. F. Clapp Laboratories to examine the tunnel and discuss remedies. It was suggested then that higher rates of chlorination be used to give up to 3 ppm residual at the condenser tail pipes. However, larger chlorinating equipment has not been installed to date. A plan is now being considered of light intermittent dosing of about $3\frac{1}{2}$ ppm for slime control and a heavier continuous application during the summer months for mussel control. According to the Lynn experience, continuous chlorination during the summer with a residual of only 0.25 to 0.50 ppm will be effective. After removing the accumulation of solids from the tunnel it will be possible to keep it clean.

Cost of, auxiliary condensing-water installation and tunnel-cleaning equipment will approach \$100,000. Cleaning operations will be reported when completed.

CLOSURE TO PAPER (3) BY H. E. WHITE

The wide recognition of the importance of this project is evidenced by the breadth of discussion, which has significantly en-

hanced the value of the original papers. The specific appreciation of the background work expressed by Mr. Hume is particularly gratifying.

Dr. Battle's interesting discussion includes an outline of a rational procedure for studying the killing of mussels while very young, immediately upon arrival in an intake tunnel. Presumably, this would lead to continuous treatments at times determined by the active spawning periods. Certain of the proposals advanced might also bring improvement in existing methods of control:

- 1 Killing treatments for embryonic mussels can be successfully studied in the laboratory.

- 2 Spawning periods, although at some sites independent of water temperature, might be predictable with the aid of supplementary factors.

In case predictions were inaccurate, or unintended interruptions of the proposed treatments occurred, shelled mussels might develop and make necessary a return to types of treatment suitable for the adult form.

The possibility of destroying the mussels' attachment threads would make an interesting study, although preliminary trials were not encouraging for commercial application. The material resists long exposures to free chlorine approximating 100 ppm.

We are indebted to Mr. Elliott for extending the geographical range of observations to Panama where marine fouling organisms live at a minimum sea water temperature of 70 F, and 115 F is required for 30 minutes to give commercially acceptable control. It is striking that, where impounding basins may give temperatures of intake water exceeding 100 F during normal operation, the killing temperature may be only about 15 F higher.

Mr. Escourt's report further extends the range of data to San Francisco Bay. In that area, apparently, detached mussels are swept along the floor of the tunnel by the flowing water to the traveling screen and are there carried upward for disposal. Although somewhat similar action does occur on the East Coast with the lesser masses of small mussels, the typical thick mat in a zone ineffectively treated may merely fall to the floor and remain as a stationary obstruction. An accumulation from 1 ft to 3 ft deep of fouling debris in the tunnel at New Bedford was reported by Mr. Sauerwein. Greater depths have occurred elsewhere. Apparently, the volume of fouling carried along the tunnel to be lifted by a traveling screen would depend upon the effective water velocity and the size and effective specific gravity of the individual masses after detachment.

With reference to the use of rubber lining as a means of discouraging attachment of mussels, this might receive more detailed observation to determine the period for which the rubber surface would remain an effective retardant.

Mr. Heinemann reports that the typical winter temperature of the water at Corpus Christi is 60 F with continuing summer temperatures in excess of 80 F and that, in other Gulf Coast areas, growth of mussels is extremely prolific with natural water temperatures of 90 F. As these higher temperatures would kill mussels in the vicinity of Massachusetts in a few days, these Gulf Coast mussels obviously require higher temperatures for killing than those on the East Coast as he points out. It is also interesting that approximately complete killing is accomplished at Corpus Christi by continuous chlorination within four days at 80 F, suggesting that the resistance of mussels on the Gulf Coast to chlorination may not differ greatly from that of the mussels along the northern coast. The further studies which Mr. Heinemann suggests should add to the understanding of fouling control.

Mr. Hume's observations at Seal Beach Station on the ineffectiveness for mussel control of "soaking" chlorination over a week

end and the usual intermittent chlorination for slime control are in general accord with the test curves for chlorination. For accomplishing control within week-end intervals, killing may be accelerated by temperature rise.

Dr. Hutchins concludes that short, intermittent periods of chlorination are ineffective for killing shelled mussels and that longer periods of several weeks each would be much more efficient. This thesis is thoroughly supported by observations at Lynn, but variant cases reported in the symposium include stations at Stamford, Connecticut, and at Corpus Christi, Texas, although the partial recirculation may be a factor at Stamford.

Mr. LaQue's conclusion that conditions in tunnels of power stations may differ from those in small-scale tests is substantiated by specific observations. For example, mussels may have been permitted to gather into a continuous thick mat on the walls of the tunnel before the killing treatment is applied. This diverts the main current of water and may greatly extend the time required for the treatment to take effect on the organisms closest to the surface of the wall. In this case, the treatment required in the tunnel may be considerably longer than a laboratory test on individual mussels would indicate. Notwithstanding, it may be noted that the small-scale tests are generally applicable to the treatment actually reaching the individual mussel of a mat.

Another factor which may be important is the time of travel of the water through the tunnels. For a long tunnel this might be a half hour or more at light load. During such a period, the free chlorine initially available for killing at the point of introduction might be largely consumed by the accumulated organisms on the walls before reaching the farther end of the tunnel. Again, it may be noted that the small-scale tests indicate the concentration of chlorine which must actually reach the individual mussel in the commercial installation.

Mr. LaQue suggests that the second generation of mussels may have much more resistance to a given temperature treatment than the predecessors. This is probably so. Apparently, however, it is unnecessary to wait for a second generation, as limited observations indicate resistance of a given group of mussels to a given heat-treatment may increase within a few weeks.

Mr. Martin's suggestion as to possibilities of moderate temperature increase to minimize chlorine consumption may find application where moderate recirculation is already available, as for ice control.

Mr. Powell refers to the commendable pioneering work of Dr. James Ritchie. Dr. Ritchie showed that fouling could be controlled by heating without use of chlorine. As suggested by Mr. Powell and as clearly demonstrated by the present symposium, there is a wide variation in the required duration of a given killing treatment at different sites. It was, therefore, necessary to make specific tests at Lynn and Redondo to approximate reliable control schedules. The present paper includes, in addition, charts of specific effects of temperature on chlorination and approximate comparison of chlorination with control by temperature alone.

Messrs. Randall and Douglass report continued satisfactory commercial control of marine fouling at the steam station of Stamford Gas and Electric Company while using intermittent chlorination 60 minutes per 24 hours with a residual chlorine concentration of approximately 0.5 ppm at the condenser discharge. Possibly, the temperature rise from partial recirculation outside this station simulates to a degree the results at Panama where controlled external recirculation gives effective control by temperature alone.

Mr. Sauerwein's discussion illustrates limitations which develop where peak loads occur when growth of marine fouling is at a maximum. Possibly a contributing cause of the previous ineffectiveness of chlorination at Cannon Street station was an

insufficient period of treatment, particularly at the base of the thick mass of accumulated mussels.

Economics

Messrs. Blais, Elliott, Estcourt, Hume, Hutchins, Martin and Powell raise questions concerning the relative economic value of chlorination as compared with temperature rise alone or combinations. This was mentioned only briefly in the paper. Economic selection of treatment might be based logically on conditions at each individual station; particularly on (a) the steam consumption characteristics of the main turbine units, (b) the expected electrical load conditions, (c) the feasibility of reversing the flow of circulating water, and (d) the resistance of the local fouling organisms.

Where the temperature rise for control of marine fouling is obtained by partial recirculation of the circulating water, a reduction in vacuum on the main turbine generally occurs. For stations designed for stand-by service, the temperature rise of the circulating water through the condenser may reach approximately 20 F with no recirculation. Under these conditions the additional rise required for the desired killing treatment may be moderate. Many turbine generators recently installed are of the "preferred standard" type. As is well known, the effect of reduced vacuum on steam flow to the throttle for this type of turbine may be almost negligible at the high loads. In other words, for this particular design of turbine, under prevalent electrical loads water may be heated with very little increase in station fuel rate. For turbines of other designs and other loads, however, the costs might be considerably higher.

Where killing is desired within the minimum time from the beginning of treatment, as during a holiday shutdown, minimum elapsed time would be expected if treatment were continued until final death, as in the tests of the present paper. Where the cost of heating water is low, this may be a convenient practice. On the other hand, where heating cost is significant and time is available between treatment and delayed death, the cost of treatment may be significantly reduced, under some conditions at least, merely by reducing the duration of the treatment, as brought out by Dr. Fox.

Test Procedure

Dr. Hutchins and others were interested in details of test procedure used, particularly for possible comparison of reported results with those obtained by other procedures at widely separate sites. For reasons of space limitations, much detail was omitted from the original paper. The following amplifying comments may be helpful in interpreting the test procedure.

At the outset of the project the results of Dobson's²¹ test were the most specific published data found for mussels in the New England area. At least approximately comparable results seemed desirable. Fundamentally Dobson's procedure was adapted to indoor manipulation by the equipment described in the present paper. The principal deviation from Dobson's procedure was that the tests were continued until all specimens were considered dead. The reason for this was the considerable increment in the length of treatment required to kill the last survivors.

Specimens were retained in the trays under treatment until all were "dead." The criterion used to determine the time of death was the time when specimens no longer responded to a sharp needle applied to the soft tissues between the reopened shells.

When the killing treatment was discontinued before elapse of a substantial portion of the time required for final death of all mussels in the test tray, the following results were observed under New England conditions:

- 1 A few mussels had already reached final death.

²¹ The Control of Fouling Organisms in Fresh- and Salt-Water Circuits, by J. G. Dobson, Trans. ASME, vol. 68, 1946, pp. 247-265.

2 Some mussels which survived the treatment period died subsequently, even in sea water at atmospheric temperatures.

3 Other mussels which survived the treatment did not die subsequently when returned to sea water at atmospheric temperatures but instead recovered to various degrees.

Item 1 is as expected from the principle of progressive killing described in the paper. Item 2 is illustrated by data by Dr. Fox in the paper published on pages 127-132 of this issue. With respect to item 3, various degrees of recovery were evidenced by: voluntary closing of shells after water was poured from the test tray, voluntary opening of shells when water was replaced, voluntary extension of the mantle from between the shells and retraction, extension and retraction of the foot, movement of the mussel along the floor of the tray, climbing of side wall of tray, secretion and attachment of new byssus threads.

Recovery was very gradual, in some cases occupying weeks. Under such circumstances positive determination of the final condition of the specimens would have consumed much more time and attendance than was available. Therefore, to meet urgent engineering requirements, all treatments of the tests presented in the paper were continued until final death of all mussels in the test tray, to assure positive killing. The numerical values are specific only for the location, times, and treatment stated. Local tests are recommended for each individual site.

Several sources of uncertainty were observed to arise in a small percentage of cases under the procedure adopted. One possible source of error was the deferred opening of the shells after death had occurred. This delay was detected, in some cases at least, by flotation of the specimen. In cases where the shells were attached close to the bottom of the test pan, flotation was shown by carefully cutting the retaining threads. Delay in the opening of the shells was also indicated at times by the release of minute gas bubbles from between the shells of an individual mussel. Other possible sources of error were observed, but formal discussion would require more specific and detailed observation over a wide range of conditions. Where time of death was uncertain, specimens were eliminated from the tests. Since practical application of the small-scale tests would require observation of a given treatment under actual conditions of commercial operation and subsequent readjustment, the results were considered adequate for the purpose of the exploratory tests if applied with reasonable factors of safety.

While the immediate engineering objectives have been met, it is hoped that others will have opportunity to develop refinements which will lead to more precise control through more detailed observation. Data by Dr. Fox is a valuable contribution in this direction, as illustrating specifically the possible reduction in the duration of a treatment in the upper temperature range by taking advantage of delayed death. It is hoped that others may study the possibility of similar reduction in the lower temperature range, appropriate to chlorination.

It would appear necessary to have available more observational data on the reaction of the organisms under the various conditions of habitat and at various temperature levels before making direct comparison of results obtained at different sites by different procedures.

We concur with Dr. Hutchins that there would be great value in extending the observations of killing treatments at many more sites to show the maximum range of the reaction of the mussels in various geographical locations for different years and seasons. A rather simple test procedure might encourage wider participation by regular operating personnel of industrial plants.

Comparison of results obtained at different sites would be facilitated if test procedures could be standardized as originally proposed. In this Dr. Fox concurs. For the present, possibly two types of procedures might be set up:

1 A test, for adoption where opportunities permit, for more precise observation at a given site by a suitably equipped biologist.

2 A simpler procedure which might find wider use by personnel of industrial plants.

In any case, it would seem appropriate to examine further the procedure for determination of residual chlorine as proposed by Mr. LaQue.

CLOSURE TO PAPER (4) BY W. L. CHADWICK, F. S. CLARK,
AND D. L. FOX

The authors are grateful for the interesting and valuable comments contributed in the several discussions of their paper.

Mr. Elliot and Mr. Estcourt have asked about selection of pipe diameter for the sea lines. Several factors influenced the choice of diameter, the principal ones being cost and availability. The first units at Redondo Steam Station were constructed under an extremely close time schedule and many items were selected because of early delivery. In the early stages of design, consideration was given to the use of 9-ft-diam pipe, which would have given reasonable maximum velocities and friction losses, even allowing for a considerable accumulation of marine growth and debris. Flow calculations were based on Williams' and Hazen's formula for friction coefficients of 120 initially and of 90 for extreme allowable fouling. However, when contract bids were available and, hence, when construction costs and deliveries could be considered, it was found that one bidder had forms and equipment for handling 10-ft-diam pipe already available, and that the 10-ft-diam pipe was offered with earlier delivery at practically the same installed cost as the 9-ft-diam pipe. Accordingly, the choice was made on this basis.

Mr. Estcourt also inquired as to the effect of temperature control on the portion of the circulating-water system between the screens and the condenser. During the 1949 season, elevated temperatures have been employed throughout the entire salt-water circuit with beneficial results. The fouling has been greatly reduced in the condensers and in the lines between the condensers and the gates. Furthermore, a marked reduction in the amount of slime adhering to the condenser tubes has been noticed during this period. At this time (November, 1949), chlorine has not been used for 16 months, either for mussel or slime control.

Dr. Hutchins and Mr. Martin have questioned the estimated annual cost of chlorination. The estimate may seem high, but it was based on the rate of chlorination which experience in this area has indicated would be necessary to obtain satisfactory control of the severe fouling which would be expected at Redondo.

The authors would like to emphasize that at Redondo Steam Station provision for elevated-temperature control of the fouling did not involve a significant increase in cost. Since along the exposed coast at the plant site an accessible intake structure was not feasible, full provision for reversal of flow was necessary in order to provide for chlorination from the shore, hence only a small additional capital expenditure was required in order to permit raising the temperature of the discharge.

The authors are indebted to Mr. T. M. Hotchkiss for his able assistance in the preparation and presentation of the paper.

Mr. Blair mentions *Mytilus californianus* as the most common fouling mollusk on the Pacific Coast. In this connection it should be pointed out that *Mytilus edulis* likewise occurs on the Pacific Coast in vast numbers, and that it is, in fact, more tolerant toward both heterosmotic and thermal extremes than is *Mytilus californianus*. *Mytilus edulis* constitutes by far the most prominent fouling organism in sea-water conduits on the Southern California coast.

The point raised by Messrs. Elliott, Heinemann, LaQue, and Powell, regarding the relative thermal resistance of fouling organ-

isms as correlated with temperatures prevailing in their natural habitat, is very well made. This is indeed a recognized fact which applies to physiological races of the same species. *Mytilus edulis*, being a widely distributed form, is an outstanding example of thermal adaptability. This matter should always be kept in mind if construction of new sea-water tunnels is to be undertaken at contrasting latitudes.

Concerning the temperature and time thresholds for killing mussels at Lynn, it will be of great interest to learn exactly what kind of observational data were collected for the recognition of death or approaching death. A mussel which has received lethal

thermal treatment may not necessarily die on the same day¹ but may expire a day or two later, even after cool flowing sea-water has been restored.

Failure to spin new byssus threads, persistent gaping of the valves, even after mechanical stimulus, or "sulking" (i.e., remaining with valves continuously closed) for long periods, after the return from a warm environment to water of normal temperatures, are recognized signs of moribundity. Needless to say, such signs are of paramount importance if one is to make accurate determinations of the critical temperature and time required for lethality.

The
ous a
fixed
recen
funda
tween
behav
the m
norm
(c) th
tion.
retain
assur
tiona
plasti

C
shear

Thus
of σ_x ,
will be
The
the co
Consid
surface
rotate
P, Fig
tween
stresse
the ele
 σ_y , τ_{xy}
the su
sented
circle
maxim

1 Th
course
jointly
The p
ment
Applie
1948.
2 Th
3 Nu
the pag
4 See
Con
the Se
of THE
Not
unders
of the

Forming of a Plastic Sheet Between Fixed Cylindrical Guides With Coulomb Friction¹

By H. I. ANSOFF,² SANTA MONICA, CALIF.

The purpose of this investigation was to obtain a rigorous analysis of the drawing of a plastic sheet between two fixed cylindrical surfaces. A number of solutions have recently been given (1, 2, 3, 4, 5)³ in which the following fundamental assumptions are used: (a) The material between the cylinders is in a state of plane plastic flow and behaves according to the Saint Venant-Mises theory; (b) the normal stress in the direction of drawing σ_x and the normal stress at the boundary σ_y are the principal stresses, (c) the horizontal stress σ_x is constant over each cross section. In the present treatment only assumption (a) is retained. Shevchenko (4) has recently solved this problem assuming that the shearing stress at the walls is proportional to the relative velocity between the wall and the plastic material.

STRESS DISTRIBUTION IN PLANE PLASTIC FLOW

CONSIDER the plane flow of a plastic material in the x, y -plane and let σ_x, σ_y , and σ_z be the normal stresses in the x, y , and z -directions, respectively, and $\tau_{xy}, \tau_{yz}, \tau_{zx}$ the shearing stresses. For plane plastic flow

$$\tau_{xx} = \tau_{yy} = 0 \text{ and } \sigma_z = \frac{1}{2}(\sigma_x + \sigma_y)$$

Thus the state of stress can be described completely in terms of σ_x, σ_y , and τ_{xy} ; the latter stress component, for convenience, will be denoted by τ .

The dependence of the stress components on the orientation of the co-ordinate axes is easily described by means of Mohr's circle. Consider an arbitrary point P in the stressed medium and let a surface element through P and perpendicular to the x, y -plane be rotated continuously about the parallel to the z -axis through P , Fig. 1. Further, let α denote the counterclockwise angle between the element and the negative y -axis and σ_α and τ_α the stresses transmitted from the unshaded to the shaded side of the element. Thus, for example, $\sigma_0 = \sigma_x, \tau_0 = -\tau$ and $\sigma_{\pi/2} = \sigma_y, \tau_{\pi/2} = \tau$ as shown in Fig. 1. Now, for any given position of the surface element, the stresses transmitted across it are represented by the co-ordinates of a point on the circumference of a circle with center $[(\sigma_x + \sigma_y)/2, 0]$ and the radius equal to the maximum shearing stress

¹ The conclusions presented in this paper were obtained in the course of research conducted under Contract N7onr-358 sponsored jointly by the Office of Naval Research and the Bureau of Ships. The paper forms the first part of a thesis submitted in partial fulfillment of the requirements for the degree of Doctor of Philosophy in Applied Mathematics at Brown University, Providence, R. I., August, 1948.

² The Rand Corporation. Jun. ASME.

³ Numbers in parentheses refer to the Bibliography at the end of the paper.

⁴ See, for example, reference (8).

Contributed by the Metals Engineering Division and presented at the Semi-Annual Meeting, San Francisco, Calif., June 27-30, 1949, of THE AMERICAN SOCIETY OF MECHANICAL ENGINEERS.

NOTE: Statements and opinions advanced in papers are to be understood as individual expressions of their authors and not those of the Society. Paper No. 49-SA-22.

$$\tau_{\max} = \sqrt{\frac{1}{4}(\sigma_x - \sigma_y)^2 + \tau^2}$$

Fig. 2 shows this circle and, in particular, the points representing the stresses transmitted across the various surface elements shown in Fig. 1. It should be noted that the angle between any two points on the circumference is twice the angle between the corresponding elements of Fig. 1.

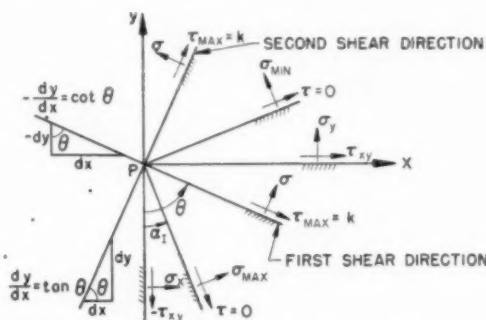


FIG. 1 STRESS DISTRIBUTION IN A PLANE

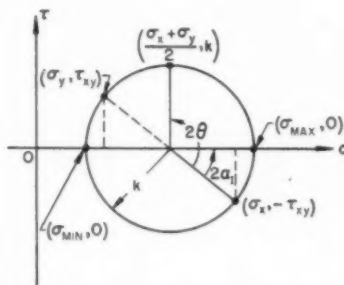


FIG. 2 MOHR'S CIRCLE

The following terminology will be used in the subsequent discussion. At two definite angles $\alpha = \alpha_1$ and $\alpha = \alpha_{11} = \alpha_1 + \pi/2$ the normal stress becomes maximum and minimum, respectively, and the shearing stress vanishes. The directions defined by α_1 and α_{11} , Fig. 1, are called the "first" and "second principal directions," respectively. The shearing stress becomes maximum for the angles $\alpha = \theta_1 = \alpha_1 + \pi/4$ and $\alpha = \theta_{11} = \alpha_{11} + \pi/4$. The corresponding directions are called the "first" and "second shear directions," respectively. Thus the first shear direction is along the bisector of the counterclockwise angle between the first and the second principal directions. In the following it will be convenient to omit the subscripts and to designate the angle between the negative y -axis and the first shear direction by θ .

The curves in the x, y -plane which are everywhere tangent to the first shear direction form the "first family of shear lines." The "second family of shear lines" is similarly defined as the

family of curves which is everywhere tangent to the second shear direction. Shear lines of different families intersect each other at right angles.

BASIC EQUATIONS

The discussion in the preceding section applies generally to the state of stress under conditions of plane strain. If the stressed material is elastic, then the radius of Mohr's circle varies with the position of the point P . If, on the other hand, the material is in the plastic state, then, according to the Saint Venant-Mises theory, the maximum shearing stress has a constant value k throughout the plastic region. Accordingly, Mohr's circle has the same radius k for any point P in the plastic region and the stresses in the plastic region are then related by

$$(\sigma_x - \sigma_y)^2 + 4\tau^2 = 4k^2 \quad [1]$$

If body and inertia forces are neglected, the equilibrium equations take the form

$$\left. \begin{aligned} \frac{\partial \sigma_x}{\partial x} + \frac{\partial \tau}{\partial y} &= 0 \\ \frac{\partial \sigma_y}{\partial y} + \frac{\partial \tau}{\partial x} &= 0 \end{aligned} \right\} \quad [2]$$

Under appropriate boundary conditions, Equations [1] and [2] completely determine the state of stress in the medium without reference to the stress-strain laws. The problem then is statically determinate.

With

$$\omega = (\sigma_x + \sigma_y)/4k \quad [3]$$

the stresses may be written in the following form, see Fig. 2

$$\left. \begin{aligned} \sigma_x/k &= 2\omega + \sin 2\theta \\ \sigma_y/k &= 2\omega - \sin 2\theta \\ \tau/k &= -\cos 2\theta \end{aligned} \right\} \quad [4]$$

In Equations [4], ω is one half of the mean normal stress divided by the yield stress in pure shear k , and θ is the angle between the negative y -axis and the first shear direction.

Substitution of Equations [4] into [1] yields an identity, and substitution into Equations [2] yields

$$\left. \begin{aligned} \omega_x + \theta_x \cos 2\theta + \theta_y \sin 2\theta &= 0 \\ \omega_y + \theta_x \sin 2\theta - \theta_y \cos 2\theta &= 0 \end{aligned} \right\} \quad [5]$$

where the subscripts x and y indicate differentiation with respect to these variables.

Let

$$\xi = \omega + \theta, \quad \eta = \omega - \theta \quad [6]$$

Substitution of Equations [6] into Equations [5], yields the canonic form of the partial differential equations of plane plastic flow (7)

$$\eta_x - \eta_y \cot \theta = 0 \quad [7a]$$

$$\xi_x + \xi_y \tan \theta = 0 \quad [7b]$$

From Equations [6], it follows that

$$\theta = \frac{1}{2} (\xi - \eta)$$

Equations [7] are, therefore, quasi-linear.

The characteristic equations of the system, Equations [7], are

$$\frac{dy}{dx} = -\cot \theta \quad [8a]$$

$$\frac{dy}{dx} = \tan \theta \quad [8b]$$

The characteristics satisfying Equation [8a] form the "first family of characteristics," and those satisfying Equation [8b] the "second family of characteristics."

Substitution of Equation [8a] into [7a] yields (9)

$$d\eta = \eta_x dx - \eta_y dy = 0 \quad [9]$$

Hence η is constant along each characteristic of the first family. Similarly, substitution of Equation [8b] into [7b] shows that ξ is constant along each characteristic of the second family.

Fig. 1 shows that the equations of the first and the second shear lines are identical to Equations [8a] and [8b], respectively. Hence the first and the second family of characteristics coincide with the first and the second family of shear lines.

BOUNDARY CONDITIONS

The proposed problem is indicated in Fig. 3. A sheet of material in the plastic state is drawn between two fixed cylindrical

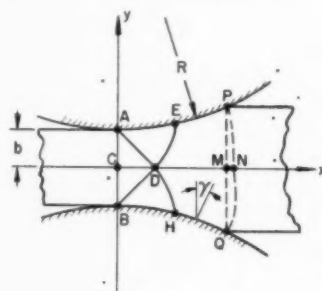


FIG. 3

surfaces of radius R . These surfaces are assumed to be rigid. The thickness of the sheet is $2b$, and the angle which the normal at any point of the boundary makes with the negative y -axis is denoted by γ . Along the surface of the upper cylinder, for instance

$$\left. \begin{aligned} x &= R \sin \gamma \\ y &= b + R(1 - \cos \gamma) \end{aligned} \right\} \quad [10]$$

In the industrial practice the ratio b/R is of the order $1/200$. In order to obtain a clearer idea of the stress distribution, however, the ratio $b/R = 1/5$ will be used in the major portion of this paper. (For purposes of comparison with the results obtained by Sachs (1), the problem has also been solved for $b/R = 1/160$. The results are discussed in the next to the last section.)

The following boundary conditions are now prescribed:

(a) The exit section AB is assumed free from lateral compression, i.e., it is assumed that $\sigma_y = 0$ along AB .

(b) A uniform normal stress is assumed to be applied along AB .

(c) It is assumed that the shearing stress exerted by the walls on the plastic material is directly proportional to the normal pressure and acts in the direction of the relative velocity of the walls with respect to the material. From Fig. 4 it is clear that in our case the normal pressure $p = -\sigma_n$, where σ_n is the normal stress at the walls. Since no tension can be transmitted by the

walls, $\sigma_n \leq 0$ at all times. According to the sign convention used in Fig. 1, the direction of the applied shearing stress is positive. Hence $\tau_n = -f\sigma_n$, where τ_n is the shearing stress along the walls, and f is the constant coefficient of friction.

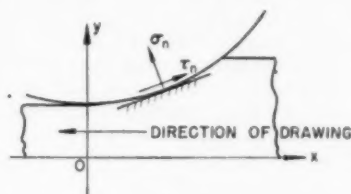


Fig. 4

On the other hand, according to the Saint Venant-Mises theory the shearing stress cannot exceed k , the yield stress in pure shear. The friction law at the walls should therefore be modified as follows

$$\left. \begin{aligned} \tau_n &= -f\sigma_n \text{ for } 0 < -f\sigma_n < k \\ \tau_n &= k \text{ for } -f\sigma_n \geq k \end{aligned} \right\} \dots\dots\dots [11]$$

From the definitions of θ and γ , it follows that the angle between the tangent to the boundary and the first shear direction is $\theta - \gamma + \pi/2$. The corresponding angle along Mohr's circle is $2(\theta - \gamma) + \pi$, and the stresses at the boundary are

$$\left. \begin{aligned} \sigma_n/k &= 2\omega - \sin 2(\theta - \gamma) \\ \tau_n/k &= -\cos 2(\theta - \gamma) \end{aligned} \right\} \dots\dots\dots [12]$$

Thus simultaneous solutions of Equations [11] and [12] determine the stresses at the boundary.

The state of stress at a boundary point is represented by a Mohr circle with the radius k . The location of the center of the circle depends upon the value of ω . Three representative positions of the circle are shown in Fig. 5.

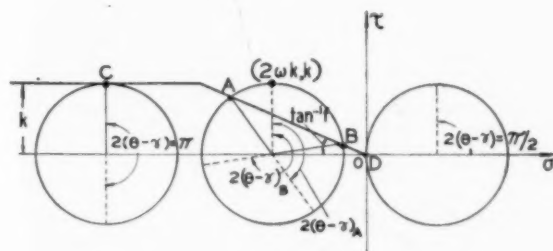


Fig. 5

The graph of τ_n versus σ_n satisfying Equations [11] consists of a straight line parallel to the σ_n -axis for $\sigma_n \leq -k/f$, and a straight line passing through the origin with a slope equal to $-f$ for $-k/f \leq \sigma_n < 0$, as shown in Fig. 5. The points which this graph has in common with the Mohr circle (such as A and B, C and D) represent the solutions of the system Equations [11] and [12]. As seen from Fig. 5, the angle $\theta - \gamma$ for point B is greater than $\pi/2$. When $\theta - \gamma$ reaches $\pi/2$, the characteristics of the first family become tangent to the boundary and further increase in $\theta - \gamma$ is physically meaningless. Therefore for any given value of ω , the point A represents the only solution which has physical meaning.

Examination of Fig. 5 now yields the following ranges of $\theta - \gamma$:

$$\text{If } 2\omega \leq -1/f, \text{ then } \theta - \gamma = \pi/2 \dots\dots\dots [13a]$$

$$\text{If } -1/f < 2\omega \leq 1, \text{ then } \pi/2 > \theta - \gamma \geq \pi/4 \dots\dots [13b]$$

Elimination of σ_n and τ_n from the first Equations [11] and [12] yields, with the aid of Equation [6]

$$\gamma - \xi = -\beta - \frac{1}{2} \sin 2\beta - \cos 2\beta \dots\dots\dots [14]$$

where $\beta = \theta - \gamma$ and the coefficient of friction f has been set equal to 0.5.

The angle γ is known at any point on the boundary (see Equations [10]). If ξ is also known, Equation [14] can be solved for β . The result will fall into one of two possible cases:

(a) If a real solution does not exist, or if $\beta > \pi/2$, Equation [13a] applies. In this case

$$\theta = \frac{\pi}{2} + \gamma \dots\dots\dots [15a]$$

(b) If the solution is in the range $\pi/2 > \beta > \pi/4$, Equation [13b] applies. In this case

$$\theta = \beta + \gamma \dots\dots\dots [15b]$$

With θ and ξ now known, σ_n and τ_n can be computed directly using Equations [6] and [12].

SOLUTION IN THE REGION ABD

In this paper the term "solution" of Equations [7] shall mean a determination of the families of characteristics defined by Equations [8] and the conditions at the boundary. It has been shown in the section "Basic Equations," that ξ and η are constant along characteristics of their respective families. Thus once the characteristic field is determined, the values of both ξ and η are known at the point of intersection of any two characteristics. The stresses at this point are then easily computed from these values by means of Equations [6] and [4].

It will be shown in the next three sections of this paper that the solution of Equations [7] can be carried out separately in three well-defined regions in the plastic material. The first region consists of the right triangle ADB, Fig. 3, the second region of two curvilinear triangles ADE and BDH, and the third region of the rest of the plastic material between the rolls. The solutions in the first two regions are trivial in nature and are called "lost" solutions for reasons to be pointed out in a later section.

According to conditions (a) and (b) given in the section "Boundary Conditions," $\sigma_x = \text{const}$ and $\sigma_y = 0$ along AB, Fig. 3. From the yield condition Equation [1], it follows that τ is also constant along AB. Furthermore, at A the shearing stress $\tau = \tau_n = 0$, according to Equations [11], Equation [1] yields

$$\left. \begin{aligned} \sigma_x &= 2k \\ \tau &= 0 \\ \sigma_y &= 0 \end{aligned} \right\} \text{ along AB} \dots\dots\dots [16]$$

This makes AB the first principal direction. Consequently, θ is constant along AB and is equal to $\pi/4$. Also from Equation [3]

$$\omega = \frac{\sigma_x + \sigma_y}{4k} = \frac{1}{2} \text{ along AB} \dots\dots\dots [17]$$

Then, by Equations [6], ξ and η are constant along AB and, in turn, ω and θ are constant throughout the region bounded by AB and two rectilinear characteristics AD and BD. Thus ABD is a "region of constant stress." The first family of characteristics, corresponding to the first shear lines, consists of straight

lines parallel to AD . The value of η is constant along the characteristics of this family. The second family is formed by straight lines parallel to BD . The value of ξ is constant along the characteristics of this family. From Equations [6] it follows that

$$\left. \begin{aligned} \xi_0 &= \frac{1}{2} + \frac{\pi}{4} = 1.285 \\ \eta_0 &= \frac{1}{2} - \frac{\pi}{4} = -0.285 \end{aligned} \right\} \text{in region } ABD \dots \dots [18]$$

Note that Equations [7] are identically satisfied in ABD .

SOLUTION IN REGION ADE

Because of the symmetry of the stress distribution with respect to the x -axis, the remainder of the solution will be obtained only for $y \geq 0$.

The region ADE is bounded by a portion of the boundary AE , a characteristic of the first family AD , and a characteristic of the second family DE . All of the characteristics crossing AD from region ADB have the same value of ξ_0 . Therefore ξ is constant throughout region ADE .

From Equations [6] it follows that $\eta = \xi_0 - 2\theta$. Hence θ is constant along any characteristic of the first family. The characteristics are straight lines and their equations are found by direct integration of Equation [8a]. Thus

$$y = -x \cot \theta + f(\theta) \dots \dots \dots [19]$$

where $f(\theta)$ is to be determined from the boundary values which are given by Equations [10], [14], and [15]. Because of the transcendental nature of these equations, the following procedure is used in determining $f(\theta)$:

A graph of $\gamma - \xi$ is plotted versus β for the full range of β allowed by Equations [15]. Then for any given value of x , the corresponding values γ and y are determined from Equations [10] and, using $\xi = \xi_0 = 1.285$, the appropriate value of β is read off from the graph. The angle θ is then determined from Equations [15], and the value of $f(\theta)$ from Equation [19]. The value of ξ is constant throughout the region ADE . Equation [7b] is satisfied identically, and it remains to determine only the characteristic DE which forms a boundary of the region. Equations [8a] and [19] form a system of simultaneous equations

$$\frac{dy}{dx} = \tan \theta, \text{ and } y = -x \cot \theta + f(\theta) \dots \dots \dots [20]$$

where $f(\theta)$ is now assumed known. It is possible to eliminate x from these equations and to obtain an integral for y in a closed form.⁵ In the present problem, however, $f(\theta)$ is transcendental and it is simpler to solve the system, Equations [20], by step-by-step integration. The resulting characteristic is shown in Fig. 6 together with a few characteristics of the first family plotted for equal steps in γ . A characteristic family (such as shown in Fig. 6), consisting of nonintersecting straight lines, is said to form a "noncentered fan."

SOLUTION IN REGION PEDM BY METHOD OF FINITE DIFFERENCES

The following boundary conditions are prescribed in this region.⁶ Along the boundary EP Equation [14] must be satisfied. Along the characteristic DE the values of ξ and η are given. Along the x -axis τ must be zero for reasons of symmetry and therefore from Equations [4]

$$\theta = \frac{\pi}{4} \text{ for } y = 0 \dots \dots \dots [21]$$

Since both ξ and η vary in this region, Equations [7] and [8] no longer simplify and must be solved by an approximate procedure. Two alternative methods of solution have been used in this problem. The first, discussed in this section, consists of reducing Equations [7] to a system of linear difference equations. The second consists of constructing the characteristic families, Equations [8], by using approximate radii of curvature; it is taken up in the next section.

Equations [7] can be linearized by interchanging dependent and independent variables provided the Jacobian of the transformation.

$$\frac{D(\xi, \eta)}{D(x, y)} = \xi_x \eta_y - \xi_y \eta_x \dots \dots \dots [22]$$

⁵ Reference (4), p. 5.

⁶ This type of problem, in which the boundary is composed in part of a characteristic and in part of a geometric contour with a reflection condition, is known as the "mixed problem" in the theory of partial differential equations.

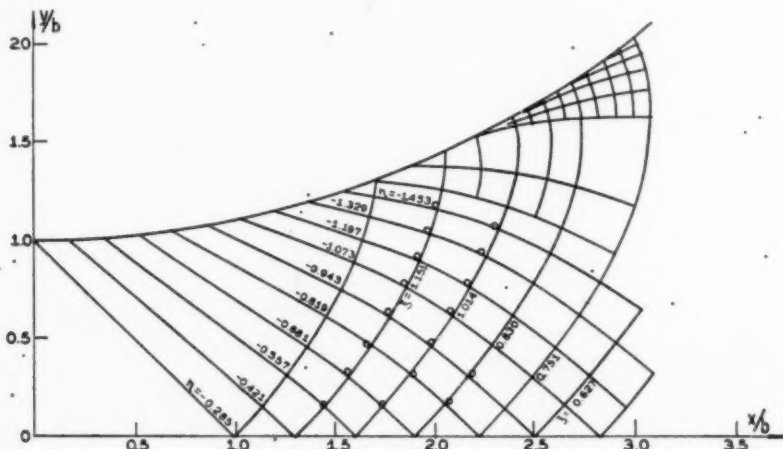


FIG. 6 GRAPHICAL SOLUTION USING APPROXIMATE RADIi OF CURVATURE FOR $b/R = 1/5$, $f = 0.5$

does not vanish identically in *PEDM*.⁷ Since ξ and η both vary in *PEDM*, this condition is clearly satisfied. The indicated transformation yields

$$y_{\eta} - x_{\eta} \tan \theta = 0, \quad y_{\xi} + x_{\xi} \cot \theta = 0, \dots [23]$$

where $\theta = (\xi - \eta)/2$.

To obtain the difference equations, assume that two intersecting characteristics have been determined completely, Fig. 7, and that from two arbitrary points $(k, l-1)$ and $(k-1, l)$, it is desired to construct two more characteristics up to their point of intersection at (k, l) . If points $(k, l-1)$ and $(k-1, l)$ are sufficiently close to $(k-1, l-1)$, Equations [23] can be replaced by the approximate expressions⁸

$$\frac{y_{k,l} - y_{k,l-1}}{\Delta \eta} - \frac{x_{k,l} - x_{k,l-1}}{\Delta \eta} \tan \frac{\theta_{k,l} + \theta_{k,l-1}}{2} = 0 \dots [24a]$$

$$\frac{y_{k,l} - y_{k-1,l}}{\Delta \xi} + \frac{x_{k,l} - x_{k-1,l}}{\Delta \xi} \cot \frac{\theta_{k,l} + \theta_{k-1,l}}{2} = 0 \dots [24b]$$

These equations are homogeneous in $\Delta \eta$ and $\Delta \xi$, respectively, and represent a system of two linear algebraic equations in three unknowns $x_{k,l}$, $y_{k,l}$, and $\theta_{k,l}$. The determination of these unknowns will differ somewhat depending upon the location of the point (k, l) . The following three cases have to be considered:

(a) Point (k, l) is on the line $y = 0$, Fig. 8. Then by Equa-

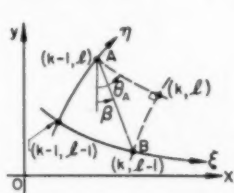


FIG. 7 A CELL OF CHARACTERISTICS

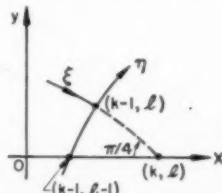


FIG. 8

tion [21], $y_{k,l} = 0$, $\theta_{k,l} = \pi/4$. Substitution of these values into Equation [24b] yields

$$x_{k,l} = x_{k-1,l} + y_{k-1,l} \tan \frac{\pi/4 + \theta_{k-1,l}}{2} = 0 \dots [25]$$

(b) Point (k, l) is inside the region, Fig. 7. From Equations [6]

$$\theta_{k,l} = \frac{\xi_{k,l} - \eta_{k,l}}{2} = \frac{\xi_{k,l-1} - \eta_{k-1,l}}{2} \dots [26]$$

Now let

$$\alpha_{l-1} = \frac{\theta_{k,l} + \theta_{k,l-1}}{2}, \text{ and } \alpha_{k-1} = \frac{\theta_{k,l} + \theta_{k-1,l}}{2}$$

Then Equation [24] yields

⁷ There are three distinct cases in which the Jacobian may vanish: (a), $\xi \equiv \text{const}$ in the region (b), $\eta \equiv \text{const}$. (c) ξ and η are both identically constant in the region. Cases (a) and (b) have been treated in the section "Solution in Region ADE;" (case b occurs in the region BDH and becomes identical to case a if ξ and η are interchanged in the equations). Case (c) has been treated in the section, "Solution in Region ABD." Since Equations [23] fail to provide solutions for these cases, they are termed "lost" solutions.

⁸ This procedure has been used by Sokolovsky (6) and Shevchenko (4).

$$x_{k,l} = \frac{x_{k-1,l} + x_{k,l-1} \tan \alpha_{k-1} \tan \alpha_{l-1} + (y_{k-1,l} - y_{k,l-1}) \tan \alpha_{k-1}}{1 + \tan \alpha_{k-1} \tan \alpha_{l-1}} \dots [27a]$$

$$y_{k,l} = \frac{y_{k-1,l} + y_{k,l-1} \tan \alpha_{k-1} \tan \alpha_{l-1} + (x_{k-1,l} - x_{k,l-1}) \tan \alpha_{l-1}}{1 + \tan \alpha_{l-1} \tan \alpha_{k-1}} \dots [27b]$$

(c) Point (k, l) is on the boundary, Fig. 9. There are now four unknowns: $x_{k,l}$, $y_{k,l}$, $\theta_{k,l}$ and γ ; and four Equations: [24a],

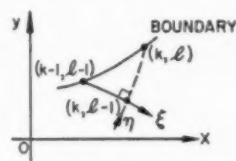


FIG. 9

two Equations [10], and [14]. Because of the transcendental nature of these equations, they are solved by the following procedure:

Starting from an arbitrarily selected point $(k, l-1)$, an estimate is made of $x_{k,l}$. Then γ and $y_{k,l}$ are computed from Equations [10], and $\theta_{k,l}$ is determined from the graph of Equation [14], with the aid of Equations [15]. Equation [24a] can be written

$$\tan \frac{\theta_{k,l} + \theta_{k,l-1}}{2} = \frac{y_{k,l} - y_{k,l-1}}{x_{k,l} - x_{k,l-1}} \dots [28]$$

The success of the approximation can now be checked by computing the r.h.s. of Equation [28], and comparing the resulting $\theta_{k,l}$ with the value obtained from the graph of Equation [14]. If the accuracy is insufficient, another estimate of $x_{k,l}$ is made and the entire procedure repeated.

Using the methods of solutions (a), (b), and (c), a network of points can now be plotted starting with the lower left corner of the region *PEDM* and extending as far as desired to the right. If continuous curves are now drawn through corresponding points, the two families of characteristics are obtained, and the solution is completed.

A running check on the accuracy of the computation is afforded by the orthogonal property of the characteristics (see Equations [8]). If at any stage the deviation from the 90-deg angle between two crossing characteristics is undesirably great, the size of the mesh can be decreased until the desired accuracy is reached.

The points computed by this procedure are indicated in Fig. 6 by small circles.

SOLUTION IN REGION *PEDM* BY USING APPROXIMATE RADII OF CURVATURE

The method used in the preceding section consists essentially of replacing the true curve of a characteristic by a sequence of straight-line segments. W. Prager (7) has recently suggested a method which approximates the characteristic by a sequence of circular arcs.⁹ This method improves the accuracy of the approximation and, in addition, represents a considerable saving in the computing time.

⁹ An alternative graphical method has been given by Prandtl (10). It has been used in parts of this problem where the curvature of the characteristics is small.

Again consider Fig. 7, and assume that the segment of the $\eta = \text{const}$ characteristic from point $(k-1, l)$ to point (k, l) is a circular arc. The length of the arc Δs and the radius R_η are related by

$$R_\eta = \frac{\Delta s}{\theta_{k,l} - \theta_{k-1,l}} \quad [29]$$

The arc length Δs is given approximately by

$$\Delta s = \overline{AB} \cos(\theta_A - \beta) \quad [30]$$

where \overline{AB} is the length of the straight line between A and B , and β is the angle between \overline{AB} and the negative y -axis. Also

$$\begin{aligned} \theta_{k,l} - \theta_{k-1,l} &= \frac{1}{2} [(\xi_{k,l} - \eta_{k,l}) - (\xi_{k-1,l} - \eta_{k-1,l})] \\ &= \frac{1}{2} (\xi_{k,l} - \xi_{k-1,l}) \end{aligned} \quad [31]$$

since

$$\eta_{k,l} = \eta_{k-1,l} \text{ and } \xi_{k,l} = \eta_{k,l-1}$$

Substitution of Equation [30] into [29] yields

$$R_\eta = \frac{2\overline{AB} \cos(\theta_A - \beta)}{\theta_{k,l} - \theta_{k-1,l}} \quad [32a]$$

and Equation [31] into [32a]

$$R_\eta = \frac{2\overline{AB} \cos(\theta_A - \beta)}{\xi_{k,l} - \xi_{k-1,l}} \quad [32b]$$

Identical procedure yields for the radius of curvature R_ξ of the $\xi = \text{const}$ characteristics

$$R_\xi = -\frac{\Delta s}{\theta_{k,l} - \theta_{k,l-1}} \quad [33a]$$

and

$$R_\xi = -\frac{2\overline{AB} \sin(\theta_A - \beta)}{\eta_{k,l} - \eta_{k,l-1}} \quad [33b]$$

In Equations [32] and [33] it is assumed that if ξ and η form a right-handed system of curvilinear co-ordinates, then positive values of R_η and R_ξ mean that the centers of curvature lie in the respective directions of increasing η and increasing ξ .

As in the previous section, computation will be different for the following cases:

(a) Point (k, l) is on the line $y = 0$, Fig. 8. In this case $\theta_{k,l} = \pi/4$, $\beta = 0$ and, because of symmetry with respect to the y -axis, $\overline{AB} = 2y_{k-1,l}$. The radius R_η is determined from Equation [32a].

(b) Point (k, l) falls inside the region. Equation [32b] and [33b] can be used directly.

(c) Point (k, l) falls on the boundary. Equation [33a] is used in conjunction with Equations [10] and [14]. A guess is made for the value of R_ξ and the corresponding arc is drawn to the boundary. Then Δs is measured, the co-ordinates (x_k, y_k) are read off, and $\theta_{k,l}$ is computed from Equations [10] and [14] as in the preceding section. Using Equation [33a], radius R_ξ is recomputed and the entire procedure is then repeated until satisfactory accuracy is obtained.

The field of characteristics for the region PEDM shown in Fig. 6 has been constructed by this method. At $x/b = 2.32$ the characteristics of the first family become tangent to the boundary, since β in Equations [15] reaches the value of $\pi/2$ and hence

$\theta - \gamma = \pi/2$. For $x/b > 2.32$ the boundary becomes an "envelope of characteristics."

RESULTS

Once the characteristic field has been mapped, the stresses at any point of the field are easily determined by the use of Equations [6] and [4], and the stresses at any point of the boundary by Equations [6] and [12].

Fig. 10 shows the stress distribution along the line $y = 0$, and Fig. 11 the distribution plotted versus the distance along the boundary. Figs. 12, 13, and 14 show the stress distribution computed along vertical cross sections taken at different points in the plastic material. The graphs show good qualitative agreement with the results obtained for the frictionless case by Sokolovsky (6) and Shevchenko (4).

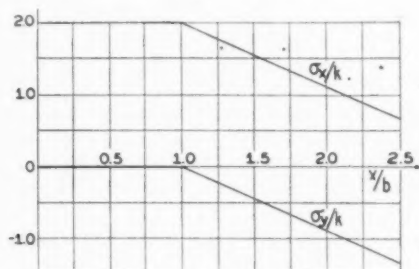


FIG. 10 STRESS DISTRIBUTION ALONG x -AXIS

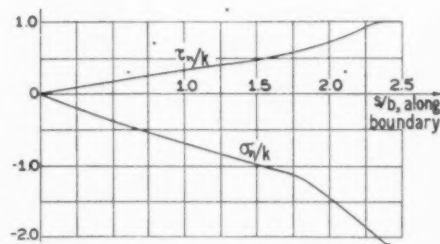


FIG. 11 STRESS DISTRIBUTION ALONG BOUNDARY

It was found that at the beginning of the region PEDM, the characteristics can be approximated closely by a single circular arc. This suggests that for small thickness-to-radius ratios the problem can be solved with sufficient accuracy by using a single circular arc to replace the entire segment of a characteristic extending from the center line to the boundary. In addition if the total angle of grip γ_{\max} does not exceed 10 deg, the transcendental friction law at the boundary given by Equation [14] can be linearized, thus simplifying case (c) of the preceding section.

With these simplifications the problem has been solved graphically using $b/R = 1/160$ and boundary values of the section, "Boundary Conditions." The resulting stress distribution is shown in Fig. 15. At $x/b = 12$, the horizontal stress along the y -axis is $\sigma_x/k = 0.20$, and the normal stress at the boundary is $\sigma_n/k = -1.8$. Sachs(1) gives $\sigma_x/k = 0$, and $\sigma_n/k = -2$ for $x/b = 12$.

DETERMINATION OF PLASTIC-ELASTIC BOUNDARIES

The process of forming a sheet between fixed guiding surfaces will be one of the following three cases:

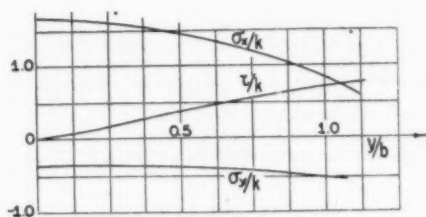
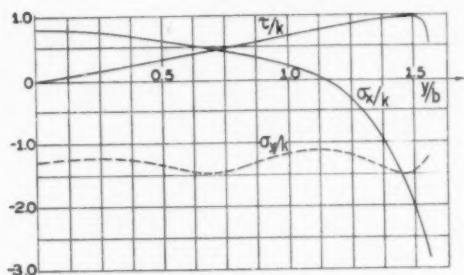
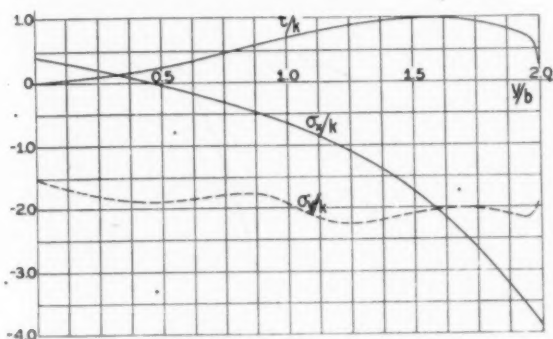
Fig. 12

Fig. 13

Fig. 14

(a) P to the
plied at
(b) L the exit
(c) E at the
termini
portion
requir
be app
another
gion at

A m
remain
section
Conse
the po
which

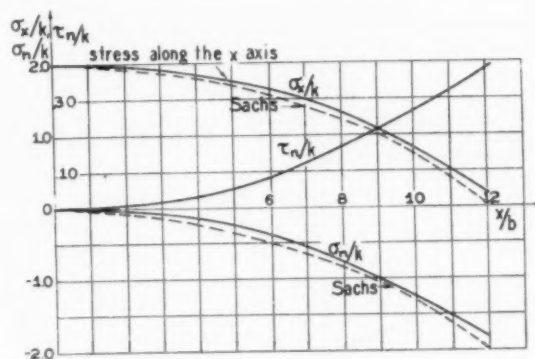
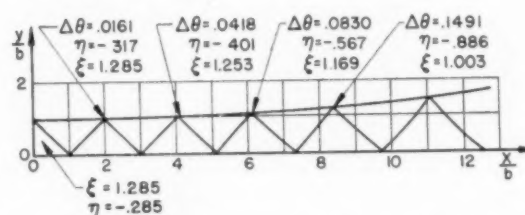

 FIG. 12 STRESS DISTRIBUTION ALONG VERTICAL SECTION AT $x/b = 1.38$

 FIG. 13 STRESS DISTRIBUTION ALONG VERTICAL SECTION $x/b = 2.32$

 FIG. 14 STRESS DISTRIBUTION ALONG VERTICAL SECTION $x/b = 3.0$

(a) *Pure Drawing.* In this case a drawing force is applied to the sheet at the exit from the guides, but no force is applied at the entrance.

(b) *Drawing Under Tension.* A drawing force is applied at the exit and a smaller tensile force at the entrance.

(c) *Extrusion.* In this case a compressive force is applied at the entrance and no force at the exit. For the purpose of determining the boundaries between the plastic and the elastic portions of the sheet the three cases may be summarized by requiring that a prescribed resultant horizontal force, say, F_{AB} , be applied to the plastic region at the exit from the guides and another horizontal force, say F_{PQ} , be applied to the plastic region at the entrance.

A material behaving according to the Saint Venant-Mises theory remains rigid up to the yield point. As a result of this, the entire section of the sheet between the guides must be in a plastic state. Consequently the plastic-elastic boundaries must pass through the points of the boundary (such as P , Q and A , B in Fig. 3), at which the sheet enters and leaves the guides.


 FIG. 15(a) STRESS DISTRIBUTION FOR $b/R = 1/160$, $f = 0.224$

 FIG. 15(b) GRAPHICAL SOLUTION FOR $b/R = 1/160$, $f = 0.224$

On the other hand, the resultant horizontal force transmitted across the boundary from the plastic to the elastic regions of the sheet¹⁰ must be equal to F_{AB} and F_{PQ} at the two respective boundaries. This condition is satisfied automatically at the exit by the method of solution used in this problem. It may be satisfied at the entrance to the guides by the following procedure:

Horizontal stress distributions, such as in Fig. 12, are plotted for a number of vertical sections in the plastic material. By interpolating between adjacent sections, a section is located along which

$$2 \int \sigma_x dy = F_{PQ}$$

integration being carried out from the center line to the boundary. If P and Q are used to denote the points at which this section intersects the boundary, then for any curve C joining P and Q through the plastic material

$$\int \sigma_s ds = F_{PQ}$$

the left side representing a line integral along C . This relation is easily seen by considering the horizontal equilibrium of a region such as $PMQN$ in Fig. 3. If the initial thickness of the sheet is now made equal to PQ , any such curve C will satisfy the conditions imposed on the plastic-elastic boundaries.¹¹ Thus the thickness of the sheet which may be formed under the con-

¹⁰ The transmitted shearing force will automatically be zero by the symmetry of the shearing stress distribution with respect to the x -axis.

¹¹ Determination of the actual shape of the plastic-elastic boundary curve depends on kinematic as well as dynamic considerations and is too involved to be attempted here.

ditions of this problem is uniquely determined for any prescribed system of loading.¹²

BIBLIOGRAPHY

- 1 "The Flow of Metals Through Tools of Circular Contour," by G. Sachs and L. J. Klinger, *Journal of Applied Mechanics*, Trans. ASME, vol. 69, 1947, p. A-488.
- 2 "Beitrag zur Theorie des Walavorganges," by Th. von Kármán, *Zeitschrift für angewandte Mathematik und Mechanik*, vol. 5, 1925, p. 139.
- 3 "The Forces Required for Rolling of a Steel Strip Under Tension," by A. Nadai, Trans. ASME, vol. 61, 1933, pp. 140-167.
- 12 It is important to keep in mind that this problem is solved under the assumption of negligible inertia forces. Thus the thickness determined in the foregoing represents the maximum thickness of the sheet which can be formed by the prescribed forces. If the thickness is smaller than the maximum, the sheet will accelerate, and the present solution is no longer applicable. If the thickness is greater, the sheet cannot be formed by the prescribed forces.
- 4 "The Plastic State of Stress and the Flow of Metals in Cold Rolling and Drawing,"¹³ by K. H. Shevchenko, *Izvestia Akademii Nauk USSR, Otdelenie Tekhnicheskikh Nauk*, 1946, no. 3, pp. 329-354.
- 5 "Rolling and Drawing at High Speeds,"¹⁴ by A. Iu. Ishlinsky, *Prikladnaia Matematika i Mekhanika*, vol. 7, 1943, pp. 226-230.
- 6 "Teoria Plastichnosti," by V. V. Sokolovsky, *Izdalelstvo Akad. Nauk, Moscow, USSR*, 1946.
- 7 "Discontinuous Solutions in the Theory of Plasticity," by W. Prager, *R. Courant Anniversary Volume*, New York, N. Y., 1948, pp. 289-300.
- 8 "Theory of Elasticity," by S. Timoshenko, McGraw-Hill Book Company, Inc., New York, N. Y., 1934.
- 9 "Differentialgleichungen Reeler Funktionen," by E. Kamke, *Akad. Verlagsgesellschaft, Leipzig, Germany*, 1930, pp. 296-301.
- 10 "Anwendungsbeispiele zum Henckyschen Satz ueber das plastische Gleichgewicht," by L. Prandtl, *Zeitschrift für angewandte Mathematik und Mechanik* vol. 3, 1923, p. 401.
- 13 A translation of the paper has been prepared for the D. W. Taylor Model Basin, U. S. Navy, by the Graduate Division of Applied Mathematics, Brown University.

Mo

The
applica
motor,
fication
nating-
the op
grades.
have go
The lat
ice on
Virgini
constru

I N h
ous
the
mend it
the ser
ducing,
without
which f
motive
effort o

The
motor s
to main
power
purpos

On t
armatu
motor
voltage
on the
transfo
motors
date th
cation
than 4
motor
commo
than 2
for col
for act
output

¹ Ele
W. Va.
² Su
Wenat
³ Pr
pany,
Com
Annua
AMERI
Not
under
of the

Motor-Generator Locomotives, Their Design and Operating Characteristics

By J. C. FOX,¹ J. F. N. GAYNOR,² AND F. D. GOWANS³

The motor-generator type of locomotive permits the application of the direct-current series-wound traction motor, with its highly desirable characteristics, to electrifications deriving their power from a single-phase alternating-current trolley. This is of particular benefit in the operation of heavy-drag freight trains on mountain grades. Nearly 30 years of design and operating experience have gone into the development of this type of locomotive. The latest examples are the units recently placed in service on the electrified sections of the Great Northern and Virginian Railways. Noteworthy features in the design, construction, and operation of these units are discussed.

GENERAL CHARACTERISTICS

IN heavy-drag freight-train service, encountered in mountainous territory, involving relatively long and heavy gradients, the direct-current series-wound motor has much to recommend its use. In addition to relative simplicity of construction, the series-wound motor has the characteristic ability of producing, without appreciable damage to itself, high initial torques without accompanying armature rotation—a characteristic which finds practical utilization when the motor is used in a locomotive that is required to “lay up” against a heavy train in the effort of getting the train under way.

The drop in speed and rapid increase in torque of the series motor as its loading is increased, with the accompanying tendency to maintain, to a certain extent, a relatively constant load on the power source, make this type of motor well suited for traction purposes.

On the other hand, the presence of a commutator on the motor armature restricts the voltage which can be used across the motor to a relatively low value, as transmission and distribution voltages are judged. Hence the desire to employ a high voltage on the contact system is accompanied by the necessity of using a transforming medium between the contact line and the traction motors if these be of the direct-current series-wound type. To date the highest practicable contact-line voltage for direct application to the direct-current series-wound motor is something less than 4000 volts, with the application made by connecting two motor armatures permanently in series and gearing them to a common gear on the driving axle. Thus with something less than 2000 volts per motor armature, valuable space is required for conductor insulation, and this space might better be used for active material, i.e., copper and iron, to secure the maximum output from the restricted spaces in which traction motors are

required to work. This is done by the use of relatively low-voltage motors, such as are used in the motor-generator and Diesel-electric types of locomotives.

There is no practically usable static transformer-rectifier combination commercially available to the locomotive builder that will transform high-voltage alternating-current single-phase energy to low-voltage direct-current energy suitable for use with the simple direct-current series-wound motor in traction service. The mercury-arc rectifier, in recent years, has been viewed as a possible candidate for this role. Corrective measures must be taken to minimize primary-power-supply wave distortion, characteristic of single-phase-rectifier operation. Interference must be reduced to values acceptable from the viewpoint of communications-lines interference, which would render this type of transformation unacceptable from the locomotive builder's and operator's point of view.

The alternating-current synchronous-motor direct-current generator set, in combination with a suitable static transformer of the conventional alternating-current type seems to be the most practicable means of energy conversion for locomotive use where direct-current series-wound traction motors are employed.

Hence the motor-generator type of locomotive and its justification in heavy traction service.

ADVANTAGES

There are several incidental but valuable advantages attendant upon the use of the synchronous-motor-generator locomotive. These may be cited as follows:

- 1 The maintenance of power factor in the railroad-owned transmission and distribution lines at values close to unity, and, in some cases, of leading power factors, is practicable by the control of the synchronous-motor excitation.

- 2 The motor-generator locomotive is essentially a constant-horsepower machine and, accordingly, the avoidance of large power demands under heavy grade or accelerating conditions is of direct benefit to the operating company's power bills, as influenced by peak-demand charges.

- 3 The motor generator set and its control lend themselves to flexibility of control functioning during regenerative-braking and motoring periods, with a consequent flexibility of locomotive and train control.

- 4 The performance characteristics of the locomotive are independent of contact-system voltage drop, down to a limit dictated by synchronous-motor pull-out torque.

- 5 The performance characteristics of this type of locomotive appear to be admirably suited to the operation of railroads traversing long stretches of terrain at river grade, interrupted with severe mountain gradients of appreciable length. Thus relatively fast schedules are secured for a limited given power demand.

- 6 Because the motor-generator locomotive is, to a large extent, similar to the Diesel-electric in that both employ driven direct-current generators and associated traction motors, the same design of traction motor can be used in both types of locomotives. Thus the benefits of standardized production of

¹ Electrical Engineer, The Virginian Railway Company, Princeton, W. Va. Mem. ASME.

² Superintendent, Electrical Operations, Great Northern Railway, Wenatchee, Wash.

³ Project Engineer, Locomotive Division, General Electric Company, Erie, Pa. Mem. ASME.

Contributed by the Railroad Division and presented at the Semi-Annual Meeting, San Francisco, Calif., June 27-30, 1949, of THE AMERICAN SOCIETY OF MECHANICAL ENGINEERS.

NOTE: Statements and opinions advanced in papers are to be understood as individual expressions of their authors and not those of the Society. Paper No. 49-SA-7

traction motors are available to the operator of motor-generator locomotives.

HISTORY

The motor-generator locomotive is not a recent development. The first one built in the United States was an induction-motor-generator unit operating under a 2300-volt 60-cycle single-phase overhead-contact system. This was in the nature of an experimental locomotive built by General Electric in 1910, for a small privately owned railroad desiring to use the commercial form of energy available to it without conversion apparatus. The line has long since been abandoned.

In the middle 1920's the New Haven Railroad purchased five 1120-hp, 1-B+B-1, 138-ton motor-generator freight locomotives, Fig. 1, and two B+B, 100-ton switching locomotives of the same rating (1).⁴ These were built for use in electrified territory where contact-system power-factor correction was an objective.

When the Great Northern Railway relocated its line through the Cascade Mountains in the late 1920's, a relocation which involved the abandonment of operation through the old 2.75-mile Cascade Tunnel and the driving of a new bore 7.79 miles in length, 15 years of operating experience with the then existing 6600-volt three-phase electrification indicated that a more flexible system was desirable for the new section of line. Accordingly, the 11,000-volt 25-cycle single-phase system, with motor-generator locomotives, was adopted (2, 3).

The first locomotives purchased for the new electrification

⁴ Numbers in parentheses refer to the Bibliography at the end of the paper.

were built by Baldwin-Westinghouse as 1-D-1, 179-ton, 1830-hp (cont.) 2165-hp (one-hour) units, operable in multiple in combinations of two to five cabs, see Fig. 2, under the control of one engineman (4). These were supplemented by a 1-C+C-1, 270-ton, 3000-hp (cont.) 3300-hp (one-hour) design built by American Locomotive and General Electric, shown in Fig. 3, also capable of being operated in multiple to provide large concentrations of motive power under the control of a single engineman (5).

NEW LOCOMOTIVES

Early in 1947 the Great Northern took delivery from the General Electric Company of two B-D+D-B, 360-ton, 5000-hp single-cab locomotives, Fig. 4, bringing the total number of units now operated by this railway to twenty (6).

Table 1 gives dimensional and other salient characteristics of the locomotives composing the Great Northern fleet.

With the delivery in the early part of 1948, of four 6800-hp double-cab 500-ton locomotives (7), the Virginian Railway became the fourth⁵ railway in the United States to operate this type of motive power. These locomotives, with somewhat more than a million pounds on drivers, classify as the heaviest (in so far as driver weight is concerned) and the most powerful continuously rated electric locomotives in service in the United States.

Principal characteristics of the Virginian locomotives are shown in Table 2, and one of the units is shown in Fig. 5, at the

⁵ The Detroit, Toledo and Ironton R.R. operated two motor-generator locomotives on a 16.6 route-mile electrification in 1926. This electrification has since been abandoned.

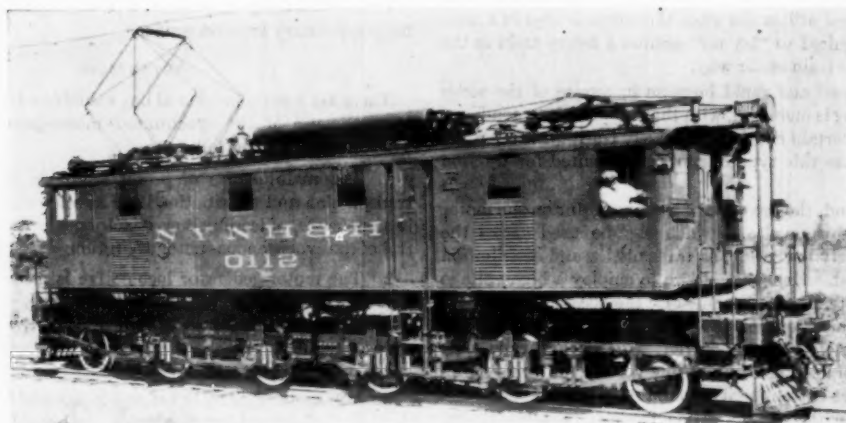


FIG. 1 FREIGHT LOCOMOTIVE ON THE NEW HAVEN RAILROAD



FIG. 2 TWO 1830-HP UNITS BUILT BY BALDWIN-WESTINGHOUSE FOR THE GREAT NORTHERN RAILWAY

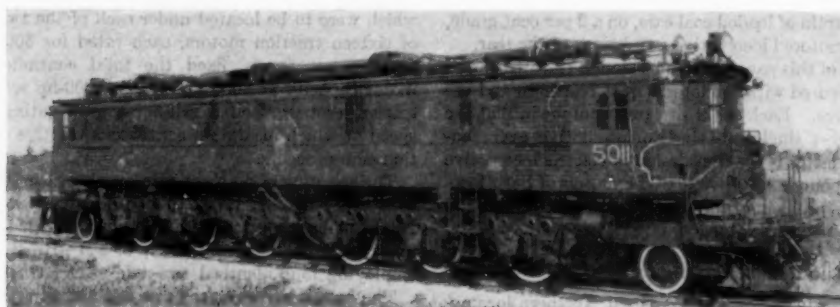


FIG. 3 GENERAL ELECTRIC 3000-Hp LOCOMOTIVE FOR THE GREAT NORTHERN RAILWAY

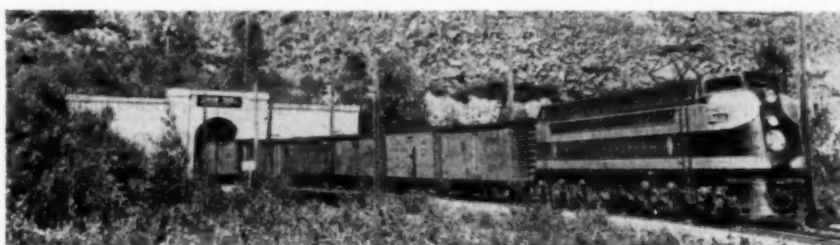


FIG. 4 5000-Hp FREIGHT-PASSENGER UNIT WITH TRAIN ON THE GREAT NORTHERN RAILWAY



FIG. 5 6800-Hp DOUBLE-CAB LOCOMOTIVE WITH TRAIN HELPED BY AN INDUCTION-MOTORED THREE-CAB UNIT ON THE VIRGINIAN RAILWAY

TABLE 1 GREAT NORTHERN 11,000-VOLT, MOTOR-GENERATOR LOCOMOTIVES

	Baldwin	American	General Elec.
Builder, mechanical	Westinghouse	General Elec.	General Elec.
Builder, electrical			
Wheel arrangement.....	1-D-1	1-C+C-1	B-D+D-B
Hp (cont.) at rail.....	1830	3000	5000
Total weight, lb.....	371100 ^a	539000 ^b	735000
Weight on drivers, lb.....	284800 ^a	426200 ^b	735000
No. driving axles.....	4	6	12
Cont. tract. effort, lb.....	44250	60500	119000
Cont. adhesion, per cent.....	15.5	14.2	16.2
Speed at cont. t.e., mph.....	15.5	18.6	15.75
Max safe speed, mph.....	45	50	65
Length over couplers, ft-in.....	47-2	73-9	101-0
Rigid wheel base, max, ft-in.....	16-9	15-4	16-9
Height over-all, ft-in.....	56	15-3	16-0
Driving-wheel diam, in.....	56	55	42
No. in operation.....	10	8	2
Year built.....	1926-28-29	1927-28-30	1947

^a The first four locomotives weighed 357,700 lb with 275,000 lb on drivers.^b The first two units weighed 518,200 lb with 410,600 lb on drivers.

TABLE 2 VIRGINIAN RAILWAY MOTOR-GENERATOR LOCOMOTIVE

	General Electric
Builder, mechanical.....	General Electric
Builder, electrical.....	General Electric
Wheel arrangement.....	2 (B-B+B-B)
Hp (cont.) at rail.....	6800
Total weight, lb.....	1033832
Weight on drivers, lb.....	1033832
No. of driving axles.....	16
Cont. tract. effort, lb.....	162,000
Cont. adhesion, per cent.....	15.8
Speed at cont. tract. effort, mph.....	15.75
Maximum safe speed, mph.....	50
Length over couplers ft-in.....	150-8
Rigid wheel base, maximum, ft-in.....	9-0
Height over-all, ft-in.....	16-3
Driving wheel diam, in.....	42
No. in operation.....	4
Year built.....	1948

head of a 6000-ton train of loaded coal cars on a 2 per cent grade, with an induction-motored locomotive as a helper at the rear.

It is the purpose of this paper to discuss design features of and operating results secured with the latest Great Northern and the Virginian locomotives. Each of the designs is unique in that the former is the longest single-cab electric locomotive ever constructed, while the latter is the first design of electric locomotive to carry a million pounds on drivers. The design of both locomotives involved problems not heretofore encountered in locomotive-development work.

BASIC DESIGN CONSIDERATIONS

Basic requirements in the case of the Great Northern locomotive were as follows:

- 1 A total of 5000 hp at the rail at a continuous rating, to be available continuously at a low speed of between 15 and 20 mph.
- 2 Locomotive to be built in a single-cab unit.
- 3 All weight to be on drivers.

The specification of 5000 hp at the rail indicated a synchronous-motor rating of 6000 hp, with an over-all electrical-transmission efficiency, between the synchronous motor and rail, of approximately 83.5 per cent. Synchronous-motor design factors, restricted by a permissible stator diameter of 83 in., which allowed a 17 in. width of aisle and 3 in. for each cab-wall thickness, and a synchronous speed of 750 rpm, made necessary the use of two separate set driving motors, each having a continuous rating of 3000 hp.

Similar restrictions, applying to traction-generator design, resulted in the use of two generators to be driven by each of the synchronous motors.

The traction motor which was selected is the GE-746, a standard series-wound motor originally designed for Diesel-electric locomotive applications with maximum axle loading of 60,000 to 62,500 lb on 42-in-diam wheels with 65 mph (top speed) single-reduction gearing. The motor is rated as being suitable for use with a traction generator involving 500-hp input from the prime mover (in this case, the synchronous motor) per traction motor. Thus for a synchronous-motor rating of 6000 hp, twelve traction motors, with a total locomotive weight of 720,000 to 750,000 lb, were indicated.

With these design elements fixed, the over-all problem resolved itself into one of designing a running gear with twelve motored axles that would negotiate 10 deg main-line curvature coupled to trains and 17 deg wye trackage alone, and that would match with a double-end cab of sufficient length to house the two 3000-hp three-unit motor generator sets and their associated auxiliary and control equipment.

Preliminary specifications for the Virginian motive power stipulated a continuous rating such as to permit the haulage of trains as large as those being handled by the three-cab 6000-hp induction-motored locomotives with which the railway has been operating since the electrification of the Mullens-Roanoke section of its line.

The impracticability of mounting so large a rating in a single cab was obvious at the outset and a two-cab locomotive was selected as the basis of design.

A study of the service requirements and the performance of the existing motive power indicated that a locomotive carrying approximately a million pounds on drivers would be required. Since the top speed involved (50 mph) was moderate, it was decided that all weight would be on drivers and no special guiding axles would be required.

The desire to utilize the GE-746 traction motor, with a permissible axle loading of 62,500 lb with maximum reduction gearing resulted in the selection of sixteen motored axles, eight of

which were to be located under each of the two cabs. The use of sixteen traction motors, each rated for 500-hp input to the traction generators, fixed the total continuous synchronous-motor capacity at 8000 hp, or two 4000-hp sets. Transmission efficiencies permitted a rail-horsepower rating of 6800 at the speed at which maximum continuous tractive effort of the traction motors occurs.

The selection of an eight-axle running gear for each of the two cabs was narrowed down to two designs, a B-D-B arrangement employing a main frame, integral with the cab structure, and two two-axle swivel trucks; or a B-B-B-B arrangement, employing four identical two-axle swivel trucks.

The second arrangement was selected in the interests of easy maintenance, interchangeability of trucks, and over-all superior flexibility of operation. The resulting locomotive nomenclature of this arrangement of running gear is 2 (B-B-B-B), and each of the two units composing the locomotive is, for all practical purposes, a duplicate of the other. One unit, however, carries two pantographs (one being a spare collector), while the second carries but one. A second collector may be added to the second unit if operating experience indicates this to be advisable.

CAB DESIGN

In conformity with current appearance styling practices, the cabs of both locomotives have been streamlined, combining appearance with practical utilization of space and good visibility. Nose compartments and operating cabs are practically identical in both designs. A full-size model of these portions of the cabs was made before construction to determine characteristics.

For optimum visibility with a long hood or "nose" section, a 16-ft radius over the cab roof from the track center line at a rail level was used, which results in positioning of the operator's eyes but a few inches below the maximum at the cab center line. The right-hand running rail can be seen from normal eye level at a distance 50 ft ahead of the coupler.

The top of the hood extending down to the level of the window sill is made up on a three-piece form, two outside sections—left and right—and a center section. By changing the width of the center section the form is made suitable for cabs of different widths, within certain limits of course. From the window sill to the bottom of the cab the hood sheets are perfectly straight, cut on a bias, and wrapped around the hood. Above the sills the windows and cab side sheets have been drawn in at an angle of 15 deg. This was done for appearance reasons only in this case, to set off the superstructure from the side sheets and relieve the otherwise boxy appearance. However, in a number of other instances this has been done to meet clearance restriction and is quite practical. On both locomotives the striping and lettering have been arranged to relieve the side-sheet expanse and embrace the air-inlet grilles.

PLATFORM DESIGN

Although the outward appearances of these locomotive cabs, as shown in Figs. 6 and 7, are very similar, the supporting structures are quite different. This is due chiefly to the horsepower requirements for a single-cab unit. A unit of the Virginian locomotive rating 4000 hp represents the practical maximum rating of a single motor generator which can be accommodated in the width and height available, even though both locomotives are unusually high and wide. The Great Northern locomotive, requiring 6000 hp in a single unit, would not accommodate a set this large, and the cab had to be stretched out to accommodate two 3000-hp sets end to end, as shown in Fig. 8. For this reason the cab is long, with a center-plate distance of 56 ft 6 in. This determined the nature of the structure, which is a truss designed to keep the deflection within design limits.

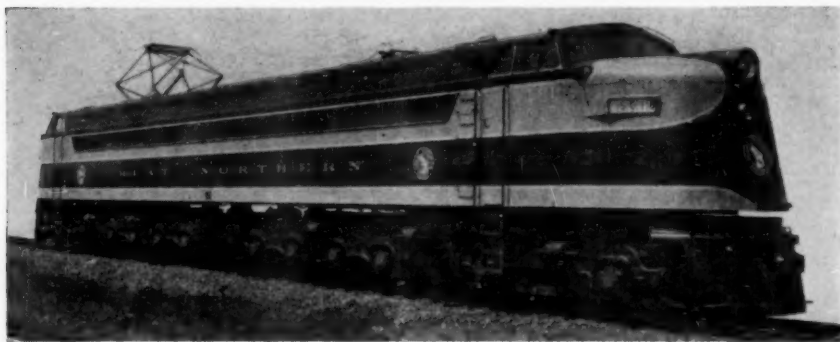


FIG. 6 GREAT NORTHERN 5000-HP MOTOR-GENERATOR LOCOMOTIVE



FIG. 7 VIRGINIAN 6800-HP MOTOR-GENERATOR-LOCOMOTIVE

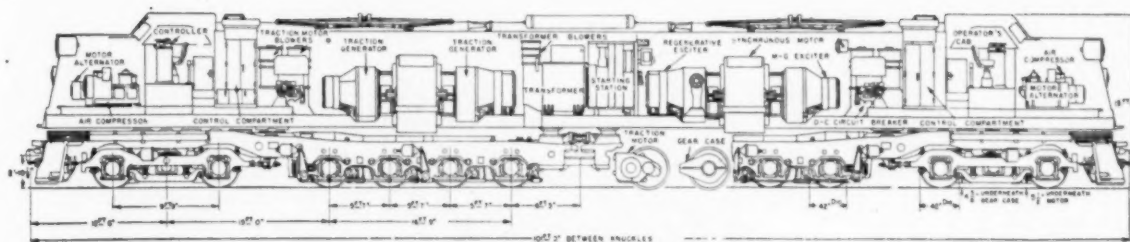


FIG. 8 CROSS-SECTIONAL ELEVATION OF 5000-HP GREAT NORTHERN LOCOMOTIVE

The truss supports a central equipment platform with end bulkheads, intermediate cross-ties, and lateral bracing. Fig. 9 shows center of gravity and weight distribution. The symmetry of cab and truss construction, together with equipment location from each end to the center, results in unusually good weight distribution.

On the Virginian locomotive, Fig. 10, the center-plate distance is shorter, namely, 34 ft 6 in., permitting the use of a suitably deep platform instead of a truss. The main sills are 24 in. deep between the bolsters and reduce to 18 in. for the end extensions.

Procurement of the desired weight distribution on the Virginian

locomotive was difficult because the large pieces of equipment (motor generator set and transformer) necessarily were forced to the rear by the single-end operating cab and hood. Since the railway desired to avoid the use of loading pads between the cab and truck, all the cab weight had to be carried on the two center plates. By very careful arrangement of equipment, proper weight distribution was secured. The preliminary loading diagram, Fig. 11, shows the center of gravity of the cab only 1 in. to the rear of the center line, and the rear center-plate load only 1730 lb heavier than the front one. The matter of span bolster weight distribution had to be considered since the front

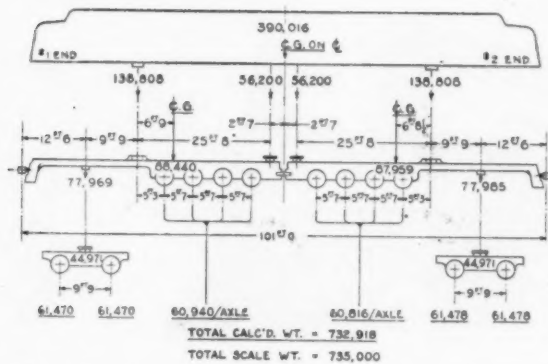


FIG. 9 WEIGHT-DISTRIBUTION DIAGRAM FOR GREAT NORTHERN UNIT.

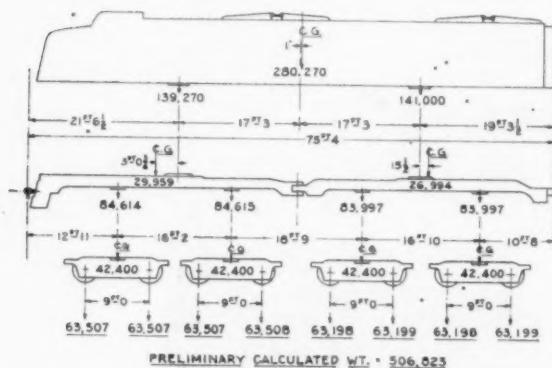


FIG. 11 PRELIMINARY WEIGHT-DISTRIBUTION DIAGRAM FOR THE VIRGINIAN LOCOMOTIVE

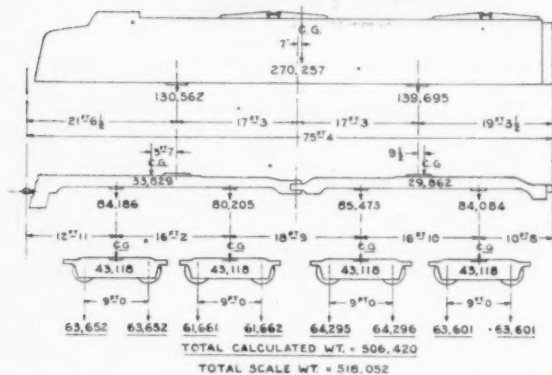


FIG. 12 FINAL WEIGHT-DISTRIBUTION DIAGRAM FOR THE VIRGINIAN LOCOMOTIVE

bolster was longer and carried the pilot and draft gear on the extreme end.

A study of the loading diagram indicates the truck arrangement employed to balance these loads. Since the actual expected weight was not known until some time after the design dimensions were fixed, the weight distribution actually secured was remarkably close to calculations, even though a difficult time was encountered with the first locomotive weighed. When it was weighed, there was 10,000 lb weight difference between the

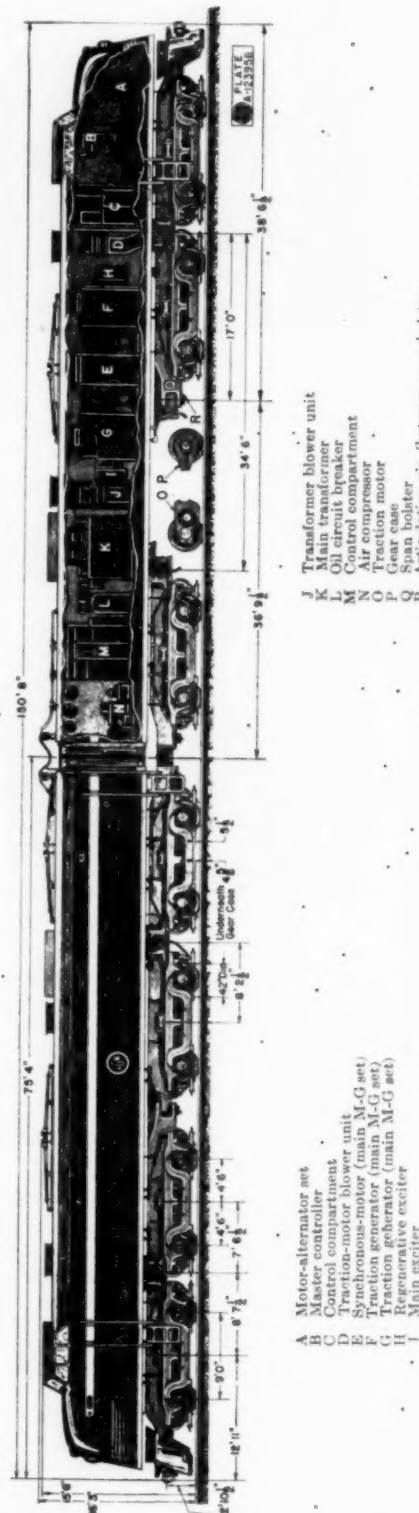


FIG. 10 CROSS-SECTIONAL ELEVATION OF 6800-HP VIRGINIAN LOCOMOTIVE

heavy covered drawing were of actual

Fig. locomotives passenger posts an ultimate bottom withstanding sufficient 18 in. These attached at the sills. sheets This structural limits within framing of each

Here previous the passenger traction GE-740 synchro North The sters and the co truck frames boxes, propor The w pressed with r require directio

Req the Gr esting

In 2-C+ very s tain th to this to acc to the B-D

With determ wheel accom way re thickn mainta layers of each mit th

heaviest and the lightest axles.' Upon investigation it was discovered that some equalizer springs which were not within the drawing tolerances had been used, and both cab center plates were out of alignment. The final calculated weights and the actual weights secured by weighing are shown in Fig. 12.

Fig. 13 shows the collision structure of the Great Northern locomotive. It is designed to meet AAR specifications for new passenger cars. The sum of the section moduli of both vertical posts and their reinforcement is 66.75 in.³ Each post has an ultimate shear value of 316,800 lb where it is attached at the bottom to the underframe. The top attachment is designed to withstand a force of 27,800 lb when the post is subjected to a force, sufficient to develop the yield point of the material, of 85,500 lb, 18 in. above the bottom attachment.

These posts are further strengthened by means of plates attached to the top and running diagonally to the side structure at the corners of the front bulkhead, at the level of the window sills. On the outside the contour of these plates follows the hood sheets and provides a connection for the top and side hood sheets. This structure is expected to withstand collision forces within the limits indicated, yielding as the forces increase but absorbing them within limits to protect personnel and equipment. Collision framing with this same stiffness is provided at the front and rear of each of the Virginian cabs.

TRUCKS

Here the two designs are widely divergent. As has been noted previously, the number of axles was determined in each case by the performance specifications and the selection of a particular traction motor to meet speed-tractive-effort requirements. The GE-746 motor rating 500 hp, on the basis of output from the synchronous motor, dictated twelve motored axles on the Great Northern and sixteen (eight per unit) on the Virginian machines.

The use of simple swivel two-axle trucks, supporting span bolsters and cab, was made possible on the Virginian locomotive by the comparatively low top speed specified. Span bolster and truck frames are of grade A unannealed cast steel. The truck frames are supported on double equalizers, which span the journal boxes, by means of helical and semielliptic springs. Loads are proportioned on the springs in the ratio of 65 to 35, respectively. The wheels are rolled steel, class C, 42 in. diam. They are pressed on axles which have $7\frac{1}{2}$ -in. \times 13-in. journals equipped with roller bearings. No restraining or guiding devices were required. All trucks are completely interchangeable in either direction.

Requiring twelve axles to carry the single cab, the design of the Great Northern unit presented a number of new and interesting problems.

In considering running gear and wheel arrangement, the 2-C+C-2 arrangement had been employed a number of times very successfully. It has ten axles but only six drivers. To obtain the required number of drivers with an arrangement similar to this it was necessary to increase the length of the main truck to accommodate four axles instead of three and apply motors to the guiding axles. Such an arrangement is classified as B-D+D-B.

With the wheel arrangement settled, the next problem was to determine the length of the four-axle main trucks. The rigid wheel base of this truck developed to be 16 ft 9 in. long. To accommodate the maximum lateral displacement ($1\frac{1}{2}$ in. each way required at the two inside axles on the 17-deg curve), the thickness of the pedestal was reduced at these points in order to maintain identical journal boxes, and a device made up of three layers of rubber vulcanized to intermediate layers of steel on top of each journal box was used. This device was designed to permit the required displacement at a force approximating 10 per

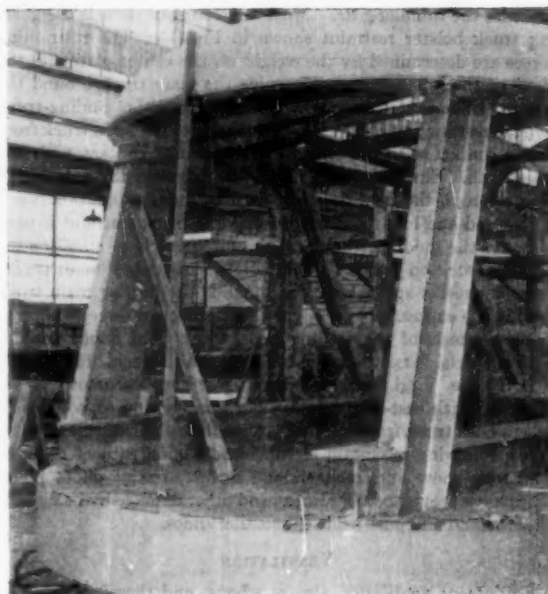


FIG. 13 COLLISION POST CONSTRUCTION EMPLOYED IN NOSE OF LOCOMOTIVE CAB

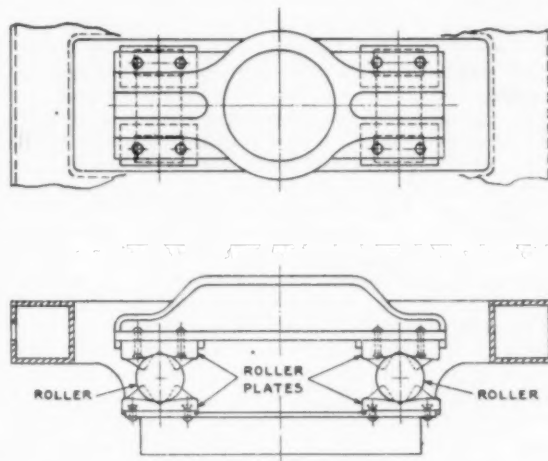


FIG. 14 GUIDING-TRUCK RESTRAINT AS USED ON THE GREAT NORTHERN UNIT

cent of the journal load. This force is sufficient to restore the axle to its normal position and maintain stability on a tangent track.

The over-all length of the running gear was approximately 3 ft shorter than the cab, making it necessary to use a drawbar between the main trucks instead of an articulation.

The loading pads required at the rear of each main truck to obtain proper load distribution required loading to 28,100 lb each on four pads.

Motored guiding-truck axles required the same-size wheels and the same load as the main-truck axles. Consequently the bolster and centering devices had to be designed for these loads.

A number of restraining devices were required to guide and

stabilize the running gear. Most interesting of these is the guiding truck bolster restraint shown in Fig. 14. The restraining forces are determined by the weight on the center plate and the slope of the roller plates. To guide the main truck around the curves, sufficient resistance is designed into the guiding-truck bolster restraint to slip the leading wheels of the main truck from flange contact with the outside rail to flange contact with the inside rail. Since centrifugal force enters into the calculation of the forces, the final design had to be a compromise between high-speed and low-speed conditions. A spring restraint is used between the guiding truck and the main truck to stabilize the guiding truck on tangent track. Between the two main trucks there is another spring restraint to guide the trailing main truck around the curves. It is designed with sufficient force to slip the leading wheels of the trailing main truck from flange contact with the outside rail to flange contact with the inside rail.

Both the Virginian and Great Northern locomotives are equipped with cast-steel pilots. Fortunately, it was possible to design both truck frames for the same pilot. The nature of these roads, following mountain streams and slopes, subject them to numerous snow and rock slides. Strong, heavy pilots many times have prevented derailment and other damage by being able to withstand and push aside the smaller slides.

VENTILATION

Equipment ventilation always affects, and therefore must be considered in, the mechanical design. The unusual air requirements (100,000 cfm for the Great Northern and 82,000 cfm for a single unit of the Virginian) made evident the seriousness of the problem at the beginning. A factor which led to a solution of this problem was a means for starting the single-phase synchronous motors. It is desirable, because of the power and additional equipment involved in single-phase alternating-current starting, to employ other means of bringing the motor up to approximately half-speed before applying alternating-current power. Means used previously were not considered altogether satisfactory. Further investigation led to the use of a small motor generator set for furnishing starting power. This set, driven by a single-phase 1500-rpm induction motor driving a direct-current generator, could be used to motor the main generators and thereby start the synchronous motor. It could have a very high short-time rating sufficient for main-set starting purposes, and a continuous rating sufficient for control and battery charging during normal operation. In order to take advantage of the simplicity and ruggedness of the induction motor for auxiliary drives, a three-phase synchronous generator was added to the starting set, making it a three-unit two-bearing set, and power was thus secured to operate induction-motor-driven blowers. Combinations of the synchronous-generator and induction-motor poles give the desired blower speeds. In general, a ten-pole generator and four-pole motors to give a motor speed of 3600 rpm have been used. This relatively high speed secures advantages in both space and weight. Another advantage in the use of this system is the simplicity of its control. The generators are designed so that all blowers can be started at once by simply closing the generator-field contactor.

Characteristics of the high-speed axial-flow blower are admirably suited for locomotive applications. Combining high flow and pressure in relatively small space, it has been used to great advantage on both of these locomotives. On the Virginian motive power, where fine coal dust, water, and dirt are a constant menace to electrical equipment; air cleaning blowers, forced ventilation for the main motor generator set, and air taken directly from the outside instead of from the apparatus cab, were specified. A mechanical cleaning device forming the blower inlet was developed and tested. The results indicated as much

as 75 per cent efficiency under standard test-code conditions.

Of special significance on the Great Northern electrification is the operation through the Cascade Tunnel. Temperature in the tunnel is practically constant at 55 F. To avoid condensation of moisture on the electrical equipment when entering the tunnel from a colder outside temperature, means are provided for recirculating the transformer and motor generator set cooling air. By recirculating this air, the machine temperatures can be kept above the dew point.

AIR BRAKES

Both designs of locomotives employ type 8EL air-brake equipment. Requiring overspeed control, the Great Northern unit uses the KS-8-PB brake valve, while the Virginian locomotive uses the plain K-8-PA valve. The Virginian machines, handling 9000-ton trains, require higher compressor and reservoir capacity than the Great Northern units. Each cab of the Virginian locomotive is equivalent in air-compressor capacity to the Great Northern, having two motor-driven compressors with a total displacement of 300 cfm and reservoir capacity of 75,000 cu in.

Foundation brakes on the Great Northern locomotive are designed to use a single shoe on each wheel. Each cylinder on either side of the truck serves two axles. The same braking ratio (70 per cent at 50 psi cylinder pressure) is used on both the guiding and main-truck axles. A conventional clasp brake is used on the Virginian design. The braking ratio is 75 per cent at 50 psi cylinder pressure.

OPERATION OF THE GREAT NORTHERN

Since the Great Northern has been operating motor-generator locomotives in its electrified territory since 1926, the new locomotives initiated in 1947, were not novel in so far as type is concerned. As a consequence the introduction of the new locomotives into service involved primarily an extension of well-established operating methods, taking into account the greater ratings and capabilities over the older motive power.

The electrified section of the Great Northern has been described in numerous articles appearing in the technical press (3, 4, 5), and a detailed description of the installation is outside the scope of this paper. It will be well to note here, however, that operation involves gradients of 2.2 per cent and a tunnel approximately 8 miles in length, with the line running through mountainous territory subjected to heavy snowfalls and a temperature range between -20 and +110 F. The profile of the line is shown in Fig. 15.

Preliminary tests on the locomotives indicated a freight-train tonnage rating of 2000 to 2100 tons as a continuous loading on the 2.2 per cent grades. Scaled-weight trains of these tonnages on the 2.2 per cent grades loaded the locomotive traction motors to continuous-rating values, indicating total tractive effort of 123,000 lb at a continuous speed of 15.75 mph. Thus the rail horsepower delivered at continuous rating developed to be 5160 hp. Starting tests on these grades developed adhesions of 26.5 per cent and accelerations were accomplished quite readily without the use of sand on clean dry rail.

With full-rated tonnages, the locomotives are worked at adhesion values approximating 17 per cent on tangent track with dry rail, and there appears to be little, if any, tendency for driving wheels to "creep" under these conditions. Some creep is experienced in entering and leaving curvature. With poor rail conditions some creep with no attendant loss in train speed is experienced on tangent track. In heavy curvature, however, the degree of creep encountered results in train-speed loss of 1 to 2 mph. Average all-weather running adhesions of 15 per cent to 16 per cent on track, involving curvature of 8 deg to 10 deg, have been found to be practicable.

No m
fected h
locomot
55 to 5
The e
regener
motives
be it st
electric
ing ton
head en
Pass
ing ten
boilers
track li
While
horsep
deman
short t
powers
the new
Pow
by mar
motor-
operat
the ma
tem is
The
miles
motive
per ho
grade
miles
older
weigh
locom
The n
The
axles i
as to
Obser
ing w
Howe
of tra
develo
ture.

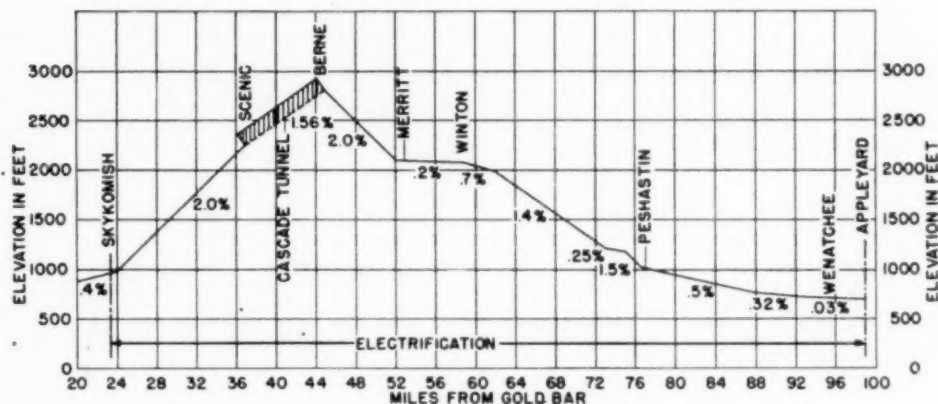


FIG. 15 CONDENSED PROFILE OF ELECTRIFIED SECTION OF THE GREAT NORTHERN RAILWAY

No noticeable differences in operable adhesion values as affected by driving-wheel diameter have been observed. The new locomotives have 42-in. drivers while the older machines have 55 to 56-in.-diam driving wheels.

The extreme fineness of control afforded in both motoring and regenerating operations permits the ready use of the new locomotives in freight trains with any type of motive power operated, be it steam, Diesel-electric, or the older types of motor-generator electric locomotives. Heavy freight operations involving trailing tonnages of 5000 tons are worked with locomotives at the head end, in the middle and at the end of the train.

Passenger trains with consists of 14 to 17 Pullmans and a heating tender (the locomotives are not equipped with train-heating boilers) are handled up to speeds of 50 and 60 mph consistent with track limitations and passenger comfort.

While the motor-generator locomotive is basically a constant-horsepower machine, lending itself nicely to the practice of peak-demand control by power dispatchers, it can be overloaded for short times as occasions and emergencies demand. Rail horsepower approximating 5800 have been secured on occasion from the new locomotives.

Power-factor control of the supply system is readily obtained by manipulation of the synchronous-motor excitation on all of the motor-generator motive power. Unlike the Virginian Railway operation, no induction-motored locomotives are operated, and the maintenance of unity to 0.95 leading power factor on the system is readily accomplished.

The efficiency of operation measured in terms of gross-ton-miles per hour seems to be somewhat better for the new locomotives than for the older units. A figure of 6.8 gross-ton-miles per hour per kilowatt at the substation on a 2.2 per cent grade holds for the new machines compared to 6.2 gross-ton-miles per hour per kilowatt for the average performance of the older machines. Undoubtedly, this is due in part to the lesser weight per horsepower of locomotive 147 lb applying to the new locomotives, compared to 180 and 203 lb for the older machines. The new locomotives have all the weight on the drivers.

The use of the B—D+D—B running gear with four motored axles in each of the main-truck frames gave rise to some question as to the effect the locomotives might have on the track structure. Observations during initial operations indicated that good tracking was being secured over the whole range of speeds operated. However, shortly after operation had commenced, some sections of track were rebalanced in routine maintenance, and complaints developed that the locomotives were moving track in sharp curvature.

Measurements were made which indicated no deflection at speeds above 30 mph. However, at speeds of 10 to 15 mph permanent deflections of the track toward center of curvature, as much as 1/2 in. were recorded, when drivers Nos. 3 and 10 moved by the recording point. These observations indicated that the initial resistance (24 per cent) of the variable-resistance centering device was too high. Pending installation of new roller plates, temporary relief was secured by removing the wear plates from the journal boxes and pedestals on drivers Nos. 3 and 10 which increased the lateral to approximately 1 1/2 in.

New roller plates were supplied which reduced the initial resistance to 18 per cent, building up to 20 per cent in the first inch. With these changes, the locomotives have been operating satisfactorily.

Some interesting observations of the added train resistance occasioned by the "piston action" of trains in long tunnels have been made. Comparing train-power demands, as indicated by the locomotive metering equipment, approximately 7 per cent more power in motoring is required to move a train against the tunnel grade than is required for operation at the same speeds on open grades of the same severity. The amount of regenerated energy is affected to the same degree, and less energy is required to hold a train at given speeds in the tunnel than is required for similar grade and speed conditions in the open.

Observations involving the added train resistance occasioned by 4 to 6 in. of snow on the tracks indicate an increase of resistance of approximately 15 per cent.

A minimum of rail sanding is employed since tests indicate that train resistance may be increased by as much as 10 per cent by the over-liberal use of sand in making train starts with heavy trains on heavy grades.

OPERATION ON THE VIRGINIAN

The electrified section (9) of the Virginian's lines extends eastward from Mullens, W. Va., to Roanoke, Va., a distance of 134 miles, traversing heavy mountainous territory crossing the Appalachians with a maximum ruling grade eastbound of 2.07 per cent. The profile of the electrified section and data pertinent thereto are shown in Fig. 16. The line is single-tracked with the exception of 22 miles of double track eastward from the Mullens terminus. The 11,000-volt 25-cycle single-phase system was installed in 1925, and, until the recent acquisition of motor-generator locomotives, has been operated with two-speed (constant speeds at 14 and 28 mph) 6000-hp induction-motored locomotives (10).

The two-speed induction-motored locomotives were entirely

alternating-current series commutator motor, and the other the direct-current series motor. For traction circuits the former uses a step-down transformer with a number of secondary taps to provide the range of voltages required for acceleration and running; the latter uses a step-down transformer with a minimum number of secondary taps for supplying proper voltage for the synchronous motor which drives the direct-current generator. From the standpoint of amount of major equipment and control required, the locomotive using the alternating-current series traction motor is the simpler. The offsetting feature, however, of the motor-generator type of locomotive is its use of the standard railway type direct-current series traction motor.

Granted that both types of locomotives can be built to produce the general operating characteristics required, the long-range factor of cost of maintenance and cost of operation in respect to power consumed must be considered.

While the modern motor-generator locomotives described in the paper are too new as yet to judge what their maintenance cost will be, nevertheless, it would be reasonable to suppose that over the life of the locomotive it would be higher for the motor-generator type than for the other type. Certainly it would be interesting and valuable to follow this feature in connection with these locomotives.

As to the power-consumption question, it would be expected that the motor-generator-type locomotive would entail more losses than its alternating-current traction motor counterpart, though admittedly this particular feature would be in some degree offset by power-factor correction.

Certainly the experience of the New Haven Railroad with motor-generator-type freight and switching locomotives, starting in 1926, points to the significance of both of these questions, of maintenance and power consumption.

The authors have done a fine job of describing the design and operating characteristics of the latest motor-generator-type locomotives built for the Great Northern and the Virginian Railways, and it is hoped that a companion paper of equal merit will be prepared covering the actual operating and maintenance experience of these locomotives over the period culminating in their first major overhaul.

CHARLES KERR, JR.⁷ In the heavy-grade territory served by the Great Northern and Virginian railroads, the type of power described in the paper should give a good account of itself.

The authors make a strong case for the advantages of low voltage direct-current traction motors. These advantages are not denied. However, it is thought that credit might be given to improvements being made in locomotives equipped with alternating-current traction motors. In this connection, the following comparison is given between the two motor-generator locomotives discussed in this paper and locomotives now under construction for the Pennsylvania, equipped with alternating-current traction motors:

	Great Northern	Virginian	Pennsylvania
Trolley voltage.....	11000	11000	11000
Frequency cycles.....	25	25	25
Maximum speed, mph....	65	50	65
Locomotive weight lb....	735000	1033832	540000
On drivers, lb.....	735000	1033832	540000
Continuous hp.....	5000	6800	5625
Maximum hp.....	5800	...	7500
Continuous tractive effort, lb.....	119000	162000	90000
Rated per 100 tons on drivers			
Continuous hp.....	1361	1361	2084
Maximum hp.....	1578	...	2777
Continuous tractive effort, lb.....	32370	31340	33330

For equal driver weights, the Pennsylvania locomotive with

alternating-current motors produces a maximum tractive effort equal to the MG type. At speeds, it produces greater horsepower for the same weight, making a more versatile locomotive for territories where both drag and high-speed service may be encountered.

Any railroad, using the alternating-current system, can be assured of excellent motive power with locomotives of the MG type, or with those using alternating-current traction motors.

T. M. C. MARTIN.⁸ Motor-generator locomotives are virtually without peer in western mountain-grade applications. Hence the writer is somewhat at a loss to understand the reasons why motor-generator locomotives are so greatly underrated by the motive-power fraternity. It would seem that they are deserving of much more attention and respect than they customarily receive. In spite of this paper, and its apparently enthusiastic support by equipment-manufacturing personnel, nevertheless, the impression exists that the motor-generator locomotive is not openly espoused with great joy by the builders. It is said to be the most expensive type to build. The writer is not in a position to say, but does believe there may be economic reasons to support a somewhat higher first cost.

The apparent recipient of the builders' most extravagant praise in recent years is the straight alternating-current series motor locomotive similar to the Pennsylvania's GG-1 class. Although it is freely admitted that, as originally conceived and built, the GG-1 could not fulfill the requirements of "laying-up" against the load in mountain-grade operations without benefit of armature rotation, as described in the paper, there seemingly is agreement that a locomotive of the series alternating-current type can be built that will equal the performance of the motor-generator type in this respect. There are rumors that such a locomotive is even now being erected.

Be all this as it may, and the writer does not wish to be recorded as a scoffer on the basis of the possible physical performance of a series alternating-current locomotive, it occurs to him that there would still be two or three characteristics peculiar to the motor-generator type that would clothe it with definite superiority over other electric locomotives.

Consider, for example, power factor. If it be assumed that a series alternating-current type locomotive would have an average operating power factor of about 0.8 lagging, it is evident that a unit of continuous output rating comparable to the Great Northern's 5018 class motor-generator type would have the approximate 5-4-3 right-triangle relationship of 5000 kva, 4000 kw, and 3000 rkva.

Even to approximate the Great Northern 5018 class, such a locomotive should be equipped with capacitors capable of supplying at least 3000 rkva. The placement of perhaps 1500 cu ft of capacitors, together with their control apparatus on the locomotive, might require some little ingenuity. It may be doubted that such a locomotive could be brought up to unity, much less leading power factor anywhere near as easily or economically as it is accomplished automatically in the motor-generator locomotive.

Next is the matter of regenerative braking. It is generally agreed that the motor-generator locomotive is the ideal type for regenerative braking. We may disregard the operating advantages of regenerative braking since the series alternating-current type could be provided with a dynamic brake that would be almost, if not quite, as good.

What cannot be brushed aside lightly is the economic waste involved in dissipating valuable electric energy unnecessarily in resistance grids when it might be returned to the line to serve

⁷ Consulting Transportation Engineer, Westinghouse Electric Corporation, East Pittsburgh, Pa. Mem. ASME.

⁸ Electrical Engineer, Bonneville Power Administration, United States Department of the Interior, Portland, Ore.

useful purposes elsewhere. Evidently most engineers do not appreciate fully the economic value of regeneration on western railroads, and the writer would like to develop this subject briefly with respect to Great Northern operations.

In terms of present utilization on the Great Northern, the 5018 class is able to approximate only 1.5 round trips or 225 miles per day. This is about 80,000 miles per year—not a particularly impressive figure. In freight service with about 2400 gross tons, including locomotive, this is equivalent to about 192,000 kgm⁹ per locomotive per year. On the present Great Northern electrified zone, the gross energy consumption (motoring) will be about 50 kwhr/kgm, the regeneration will be about 10 kwhr per kgm, making a net consumption of about 40 kwhr/kgm (all energy figures are as of 3-phase, 60 cycles supply points).

The value of regeneration then is about 1,920,000 kwhr per year, which, at the present rate schedules in effect on the Great Northern (fractionally in excess of 1.0 cent per kwhr) amounts to about \$20,000 per year per locomotive.

Lest this appear to be too special a case built around a relatively high proportion of heavy-grade operation, let us suppose that the Great Northern electrification is extended both ways from present termini until it includes the entire main line from Seattle to Spokane, some 330 route miles. In this event, individual locomotive mileage could quite easily be brought up to 500 per day or 180,000 miles per year. It is estimated that motoring and regenerative energy would approximate 32 kwhr and 4 kwhr per kgm, respectively. The locomotives would now be handling 2400×180 or 432,000 kgm per year. At 4 kwhr/kgm this would mean an annual total of 1,728,000 kwhr of regenerative energy, having a value of some \$18,000 per year at present Great Northern power rates.

The Great Northern examples cited are believed to be entirely typical. Most sections of western main line that are economically feasible of electrification have profiles embodying sufficient regeneration potentialities to warrant adoption of motor-generator-type locomotives for economic reasons alone. Even if present electric power rates are cut in half, it seems evident that not

⁹ kgm = thousands of gross-ton-miles.

less than \$10,000 can be saved per locomotive per year through utilization of regeneration. Couple this with the ability of the motor-generator locomotive to produce rather than use reactive power, and another 20 per cent saving can be claimed annually. The potential savings from these two factors would appear to run from \$12,000 to \$24,000 per locomotive per year, depending upon the basic rate schedules under which electric power is purchased. If money is assumed to be worth, for example, 6 per cent, this is equivalent to saying that a railroad can afford to expend from \$200,000 to \$400,000 more per locomotive for motor-generator locomotives even if it is believed there are no other reasons for preferring them. It wouldn't appear that they need to cost this much more per unit to build, and, as the authors have shown in this paper, there are many important reasons why motor-generator-type locomotives are superior.

It would appear to the writer that before a railroad purchases alternating-current series motor-type locomotives of clearly inferior characteristics as regards power factor and regeneration capabilities merely on the basis of lower initial cost, it should understand fully that it is probably going to be paying a very substantial premium in the form of higher operating costs. It can be demonstrated that in the case of most western railroads, the differential savings resulting from the operation of motor-generator locomotives will support a much higher initial cost for such locomotives should this be found to be really necessary.

J. STAIR, JR.¹⁰ For the profile and train movements encountered on the electrified sections of the Great Northern and Virginian Railways, the motor-generator type of locomotive appears to be well-adapted. The present paper covers the situation admirably.

It would add to the value of the paper, as a permanent record, if "speed-traction effort" and "speed-braking effort" curves were included for the latest class of electric locomotive on each of these railways.

¹⁰ Electrical Engineer, "The Pennsylvania Railroad," Philadelphia, Pa.

Two Slants on Postwar Wood Finishing

Part I—Current Practice

By P. S. KENNEDY,¹ NEWARK, N. J.

The postwar period has witnessed much activity and growing interest in the finishing of wood. This has been due to the following factors: (1) The ever-present objectives of greater speed and reduced cost. (2) The desire for better and more resistant finishes. (3) Increasing recognition that ultimate cost, rather than package cost, should be the yardstick of value for finishing products. (4) The vital need for a quick and consistent method for anticipating the check resistance of lacquer films, in particular. This trend has been accentuated by unusual circumstances. These aspects of current conditions in the wood industries are treated in this paper.

GREATER SPEED AND REDUCED COST

IN line with general experience, the postwar period has included a seller's market in the wood industries, together with radical increases in labor cost. Accordingly, aims have been to produce finished units rapidly, plus all possible economies.

Probably the sorest spot in wood-finishing materials is the filler which must be applied on open-grain woods such as mahogany, walnut, and the like, and intensive activity has been directed to a cure. In the prewar period, filler was generally regarded as a necessary evil, as well as a staple product to be purchased at a staple price, like flour or sugar. It was relatively slow drying—overnight being the usual minimum drying period—but in addition, subsequent performance was unpredictable—particularly with lacquer finishes. Various deviltries developed periodically, the most poignant of which were the so-called "graying of pores" and an unsightly "muddying"—usually in sections—of what should properly be a uniformly clear transparent-film effect.

One of the most constructive results of this postwar experience has been the growing appreciation by the consumer that the established practice of buying filler "at a price" could be short-sighted. When one of these epidemics of graying of pores, or muddying of films was encountered, the corrective labor expense invariably produced a staggering ultimate price tag. Sufficient consumers adopted this line of reasoning to encourage the finish manufacturer, for the first time, to spend time and money on the development of filler, with the assurance that a successful effort would receive a just return.

A receptive attitude was also created toward tolerance of change in long-standing shop practice for the handling and application of filler. For instance, a new filler development, because it had to be handled faster, might require two men to wipe off a large unit, rather than one man. Actual man-hours would be the same, however. Again, a new filler development might not suspend as well after reducing for use, and thus require an occasional stirring which would not have been necessary with the older type.

¹ Vice-President, Finishes Division, Interchemical Corporation. Mem. ASME.

Contributed by the Wood Industries Division and presented at the Wood Industries Division Meeting, Jamestown, N. Y., September 27, 1949, of THE AMERICAN SOCIETY OF MECHANICAL ENGINEERS.

NOTE: Statements and opinions advanced in papers are to be understood as individual expressions of their authors and not those of the Society. Paper No. 49—WDI-2.

Thus fillers have come into use, employing various synthetic vehicles, as contrasted with the long-accepted linseed-oil vehicle, and drying time, not only shortened to periods such as an hour, but also giving better clarity, which is another way of saying "proof against pore graying and muddled films." The ultimate in this direction has been achieved with the stain-filler combinations, employing fast-to-light dyes. The best of these products not only give "tops" in clarity; but they are absolute proof against pore graying. The explanation for this is that the translucent inert pigments, used in the filler, are themselves actually dyed. They therefore do not "dry out" or "wash out" to an unsightly pore condition.

Particularly in fast production, such as radio cabinets, operators, who have been open-minded in adjusting labor practice to conform with the product, have been able to effect important economies by the elimination of both material and labor costs. For example, a good-quality finish, employing stain and filler separately, first calls for the material and operation of applying a coat of stain. Next, a sealer wash coat of either lacquer or shellac of low solids content, followed by a scuff-sanding operation. The purpose of this is to seal the pores so that when the filler is subsequently applied some of its vehicle is not sucked away by stray capillaries in the wood, robbing the full strength of the filler, as well as giving "smeary" pore effects at such points.

With a stain-filler combination, all of this is combined into a single operation with a single product. But while, from this point on, the application of the top coats would be identical, the danger of graying still exists with the simple filler. Sometimes precaution is taken against this by formulating so that the filler is tinted with so-called oil-soluble anilines. When the top-coat material is applied, these anilines "bleed" and in so doing stain the inert pigment. The objection to this is that it is a temporary measure, as these colors are not fast to light and may subsequently provide embarrassment. Another method of obviating against graying is the application of a shading stain over all. While this tends to color over potential gray pores, it is at some sacrifice of finish clarity, plus being an additional operation.

In all frankness, it must be admitted that these so-called fast fillers and stain-filler combinations, are not as foolproof as the old-fashioned filler for wiping and cleaning up; nor for packing the pores quite as full. But the good ones do a most acceptable job, as the mechanic gets the hang of them. Supplemented by the continuing laboratory work of the maker, further improvements and refinements are being progressively achieved.

The best of these synthetic types of fillers do not "heave" like the old-fashioned filler. This is temporary "lifting" from the pores, which occurs when top-coat material is freshly applied, and gives the illusion of a most flushy filled job. Unfortunately, there is a subsequent collapsing which shows up as "shrinkage." The best of synthetic fillers frequently look "hungry" by comparison because they are not so affected by freshly applied top coat, with the pore filling remaining fixed. With the continued support and co-operation of the user, the future outlook for filler is most promising.

Another angle of reduced cost applies most specifically to lacquer jobs. From the standpoint of speed, saving of floor space,

and fast and easy touch-up and repair, lacquer is the ideal finish for wood. But it does have the shortcoming of what might be termed low solids or film thickness.

There is a definite limit to the amount of solids which can be incorporated in lacquer and still maintain a suitable spraying viscosity. Roughly speaking, varnish will have twice the solids or double the film thickness of a lacquer coat. Much work has recently been done to improve this deficiency in lacquer, and along two lines; one by increasing the solids content of the lacquer, and the other, by hot-spray application. While both of these measures have proved effective, from the standpoint of giving possibly a 50 per cent increase in film thickness over what is regarded as normal (a 21 per cent lacquer) sufficient resistance and objection have developed to prevent general adoption.

A resultant trend has been to secure the desired film thickness by means of synthetic coatings—of which alkyd-urea base compositions would be typical—and these are currently finding some usage. The cure of these coatings is activated by means of a catalyst, and while some are available in air dry form, most of them require stimulation by heat. The average temperature ranges employed are between 130 and 135 F, as there is a pronounced feeling that in exceeding that maximum temperature vagaries of wood and glue are apt to cause complications. However, on some current government furniture work, specifications call for 150 F.

Best and surest satisfaction is secured by adding the catalyst to the coating just prior to the time of use; although some of the products are supplied with catalyst added. In this connection, there is always a question of package stability, and potential difficulty exists if the user does not have a rigidly enforced system of first using up the oldest finishing material on hand.

Investigation by finishing manufacturers is currently under way with various kinds of synthetics, and further developments can be confidently expected with synthetic clear coatings.

BETTER AND MORE RESISTANT FINISHES

The advent of the synthetic finishes, besides affording savings because of heavier film thickness, introduces varying degrees of resistance, which are highly interesting from the sales and service angle. When cured, many of them have outstanding resistance to alcohol and many other materials which affect lacquer and ordinary varnish films.

The maximum properties in these finishes are secured when the work is top-coated entirely with these coatings. But for various shop reasons there is quite a general trend toward using an undercoat of lacquer-type sealer, followed by a top coat of the synthetic. Importantly involved in this is the economy in sanding and the avoidance of possible "shelving" of coats of the synthetic

itself when the cure of the undercoat has been carried too far to permit of proper knitting between the coats.

Here again, however, this is a matter amenable to ready control in a well-regulated finishing room, because it is possible to get satisfactory sanding on undercoats of synthetic, and to provide against too complete curing of undercoats.

ULTIMATE COST VERSUS PACKAGE COST

There has been a decided and significant increase in the application of accounting practice in wood-finishing departments to more careful and detailed segregation of costs. In these instances the package or container cost of finishing products is no longer the prime consideration, and many revealing instances have occurred as the result of teamwork between the purchasing agent and the finishing superintendent.

Actual mileage is not necessarily the most important factor. Hospitalization—or touch-up and repair—is frequently the most potent figure. Accessories, such as sandpaper, cost real money these days, but are too often taken for granted, rather than investigated from the angle of whether much less would be used with another finishing product. Savings in sanding, rubbing, and polishing time all add up to the careful scrutiny which is being given, more and more, and the net importance of which cannot be over-emphasized.

QUICK METHOD OF TESTING LACQUER FILMS

The rugged winter of 1947-1948 not only accentuated the need of a greater margin of safety for lacquer films, but for a quick method of evaluating them. To be factual, the blame for the widespread finish failures should not be laid entirely to the finishing materials—specifically lacquer. Because of rush and shortages, much lumber and veneer were used, which were not in normal condition, to say the least, and the stresses and strains which they created placed an undue load upon the lacquer coats.

However, it emphasized a fundamental deficiency in formulations to meet abnormal conditions—not only weather like 1947-1948, but changes in merchandising conditions. Typical of these would be warehousing of finished products, which will increase importantly. It is well known that ordinary lacquer films lose check resistance on standing; so there is the double problem of pronounced improvement in lacquer films, and a practical method of measuring their strength.

The present accepted methods for so-called "cold check" are not only time-consuming and expensive, but undesirably open for error. Hence a radical correction of this situation would be of such dynamic importance that the companion paper which follows as Part 2 warrants thorough consideration.

Two Slants on Postwar Wood Finishing

Part II—Suggested Method for Predicting Check Resistance of Lacquer Films

By W. T. SMITH,¹ NEWARK, N. J.

This paper presents details of equipment and technique for performing control tests on film-forming materials. Typical tests are interpreted and correlated, and illustrated examples are given of test results on various lacquers.

THE tendency of clear, lacquer-type furniture finishes to fail by severe checking or cracking, especially under exposure to wide and abrupt changes in temperature, has long resisted accurate and significant laboratory prediction and control. In an effort to perform control tests of the film-forming media, carefully controlled and presumably representative wood panels are prepared, aged for a period of up to 2 weeks and then subjected to a systematic cycle of temperature extremes in an effort to establish the limits of check resistance of the finishing system in question.

Distinct stresses are set up in a cellulosic film in the process of setting. This effect is influenced by the nature of the incorporated resin as pertains to solvent release and basic molecular arrangement, the viscosity of the cellulose, and the thickness of the film. The actual moisture content of the film itself, especially in the presence of alkyd resins and/or vegetable oils, is a directly pertinent influence on tendencies to check at low temperatures. It is indicated by Koenig² that mechanical failures such as checking and cracking are rupture phenomena, and the result of external and/or internal forces. These phenomena are influenced by non-uniformity of the film or the substratum which leads to local stresses.

Checking of lacquer films is due to three factors, as follows:

- 1 The deforming force.
- 2 Nonuniformity of the film.
- 3 Local stresses exceeding the film strength.

Deforming forces may be caused by changes in the substrate. Moreover, the film may undergo contraction on aging, and this may lead to stresses and strains in the film which are dependent upon the mechanical properties of the coating. The solvent will evaporate from the lower layers much more slowly than from the outer layers. Consequently, the stresses in the outer layer will grow more rapidly than in the lower layers, reach a maximum value in the surface layer, and decrease in the direction of the substrate. However, as the drying and aging proceed, the distribution of stresses will become more uniform. Shrinkage takes place at a measurable rate for a period of 30 days or more and, together with progressive development and relief of stresses, is not confined to a short time interval. When films dry and age,

shrinkage occurs, which results in deformation and causes stresses. The theoretical examination of the mechanical processes taking place during film formation indicates that stresses occur even while the film dries.

WOOD-PANEL TESTS

Variation has long been a persistent attending factor in the performance of wood-panel tests for cold-checking tendencies of lacquer systems. In an effort to identify the variables influencing the result of wood-panel tests, an evaluation of a representative furniture-finishing system was made by finishing large plywood specimens and cutting them later into smaller test pieces in an attempt to minimize wood source variations. The tests were performed on specification panel stock, especially constructed and furnished for test purposes. This panel stock consists of a $\frac{3}{16}$ -in. yellow-poplar core, $\frac{1}{32}$ or $\frac{1}{16}$ -in. yellow-poplar cross-banding, and face and back of mahogany and sap gum, respectively, of about $\frac{1}{32}$ in. to make up a $\frac{3}{16}$ -in. resin-bonded panel.

The lacquer system involved is of the conventional radio-cabinet type, consisting of the following:

- 1 Non-grain-raising stain.
- 2 A light cellulosic wash coat.
- 3 A paste filler.
- 4 A 20 per cent nonvolatile sanding sealer.
- 5 Two coats of a 21 per cent clear rubbing-type finishing lacquer.

This single representative system was used in all tests described herein.

The cold-check cycle referred to consists of the conventional 1 hr at 120 F, followed immediately by 1 hr at -5 F to complete each cycle. Inspection is made at an oblique angle in strong light after each cold period.

CONCLUSIONS

1 The major and basic conclusion evident here is that wood-panel tests for cold-check tendencies in any normal scope of handling and condition are rampantly inconsistent.

2 The moisture content of the wood at time of finishing, especially within the range of conventional precision woodworking practice, is not a significant factor to a consistent degree.

3 Moisture sealing of the wood member on all unfinished surfaces has the effect of causing a slight increase in resistance value in isolated sections, but causes a somewhat wider spread of results to the end of increasing the inconsistency of the test results.

4 Moisture conditioning of the finished member by storage in varying conditions of relative humidity is the most influential factor observed here. Variation of moisture content of the finished member—wood and finish—from 5 to 10 per cent moisture content, will effect a variation in check resistance of from 500 to 800 per cent.

5 While the combined precautions of moisture conditioning and moisture sealing will, in a majority of cases, prove slightly

¹ Supervisor, Physical Testing Laboratory, Finishes Division, Interchemical Corporation.

² "Shrinkage and Deterioration of Paint Coatings—Part I," by W. Koenig, *Paint, Oil and Chemical Review*, 111, No. 19:15, September 16, 1948.

Contributed by the Wood Industries Division and presented at the Wood Industries Division Meeting, Jamestown, N. Y., September 27, 1949, of THE AMERICAN SOCIETY OF MECHANICAL ENGINEERS.

NOTE: Statements and opinions advanced in papers are to be understood as individual expressions of their authors and not those of the Society. Paper No. 49-WDI-2.

better than moisture sealing alone, this result is not completely consistent.

6 Checking results cannot be assigned to any continuity or relationship of wood structure, even in adjacent sections of the same original stock.

7 It must be concluded that wide variation in results on wood test panels may be expected from unpredictable, natural variations in wood density, structure, and composition, over and above the demonstrated sensitivity to handling and ambient condition, to the extent that it is not practical or feasible to evaluate the checking tendencies of an organic-finish film conclusively by this method.

FILM TESTS ON A METAL SUBSTRATE

The most exhaustive study of cold-check evaluation on the media of wood surfaces will serve mainly to emphasize the number and complexity of variables present, or potential, in a wood substrate. Such are these variables and vagaries of behavior that they cannot all be measured, classified, or even recognized. In setting out to evaluate the unknown checking potential behavior of a finish film on a wood surface, we are employing an unknown element over a substrate of a similarly unknown and unpredictable nature. In order to permit equitable measurement of a potential value in a material of unknown behavior, an accompanying medium of known and controllable properties is indispensable. Constructive thinking in various fields has led experimenters toward the employment of such constants.

C. W. Smith³ states that stress lacquers have long been used as a surface indicator to show, by induced checking, the presence of stress lines in the body of the substrate under scrutiny. Stress lacquers are specially formulated brittle materials of a known and controlled behavior as pertains to tolerance of lateral stresses. Castings and similar metal parts are coated to a thickness of from 0.0003 to 0.0008 in. with these lacquers and subjected to heavy operational stress and strain in suitable testing apparatus. By the nature and direction of the resulting fracture lines in the brittle coating, the stress reaction of the substrate in question may be observed and evaluated.

Since checking failure of wood finishes is the result of an inability of the surface coating to cope with dimensional changes in the substrate, it would seem to follow that systematic controlled manipulation of an amenable substrate would permit the assignment of a specific resistance to the finish film under scrutiny.

Attempted manipulation of the substrate is the principle involved in conventional wood-panel checking tests, but the direction and extent of the induced dimensional change cannot be controlled or predicted in other than very general terms.

An applicable substrate may be found in the form of very thin sheet copper of known and specified temper and ductility. When such a surface is coated with the film under test, the sheet and the film together may be deformed systematically under hydraulic pressure to form a "dimple" or hemispherical section, the surface area of which represents a measurable increase or distention of its original dimensions.

If the film is cured to a constant state, the distention performed at controlled low temperature and the distention on the radius of the spherical section measured to 0.0001 in., the actual substrate expansion at the point of fracture failure of the film may be expressed to an accuracy of 0.1 per cent.

Small⁴ states that film flexibility, as evidenced by cold-check failure, may be correlated with elongation data, and that there is a

striking correlation between cold-check resistance and the degree of elongation. Comparison of values so obtained on standardized formulations, on which cold-check data from wood-panel tests, as well as from field applications, have been accumulated over a period of years, serves to correlate results of the distention method with those obtained on wood surfaces. Such comparisons also serve to indicate the limits of movement of conventional wood surfaces in terms of per cent of area increase and lead to the conclusion that finish failures on wood surfaces are avoided by maintaining a standard of distention potential, at low temperature, at a level offering a margin of safety over the range covered by the behavior of wood.

In so calibrating the "distention-potential test," a series of thirty materials was used, the relative cold-check resistances of which, in terms of hot and cold cycles, have been well established. The distention potentials of these materials fall, Table 1, into well-defined groups or fields which have been designated arbitrarily as Classes I to IV inclusive. The accuracy of the distention factor as a criterion of checking potential has been found to be such that a specific formulation will not fall out of class unless there has been error in compounding. Repetition of tests of the same lot of material show an operational aberration in result of between 5 and 10 per cent only.

TABLE 1 CLASSIFICATION OF 30 REPRESENTATIVE LACQUER FORMULAS BY DISTENTION-POTENTIAL TEST

	Class IV	Class III	Class II	Class I
Tolerated distention	Not over 0.0700	0.0700 to 0.0850	0.0850 to 0.1000	Over 0.1000
Per cent increase in area	Not over 1.4 per cent	1.4 to 2.3 per cent	2.3 to 2.8 per cent	Over 2.8 per cent
Considered	Poor	Fairly good	Good	Excellent
Approximate Wood cycles—	3 or less	8 to 10	15 to 18	Infinite number
<i>Sealers</i>				
Under 21 per cent.....				4
21 to 25 per cent.....	1	3		
Over 25 per cent.....	2			
<i>Lacquers</i>				
21 per cent solids.....	8	5, 6, 7, 17, 18	21, 22, 23	9, 10, 11, 12, 13, 28
25 per cent solids.....	16		24, 25, 26, 29	
28 to 30 per cent.....	14	19, 30, 20*	27	15

Routine control methods of this test are such that by use of a standardized substrate and controlled coating and curing methods it is possible to make an accurate cold-checking evaluation within an elapsed time of 24 hours after the sample is received in the laboratory.

PREPARATION OF SPECIMENS

Choice of coating methods of the copper specimens is limited by the flimsy and flexible nature of the thin sheet which is 0.0050 in. \pm 0.0004 in. The most convenient and practicable method of coating was found to be by controlled pour or flowdown. A 7-in. length of the 6-in. strip is affixed by masking tape, extending $\frac{1}{4}$ in. over the sides, to a stand or easel at 50 deg from the horizontal. Since two separate flowdowns are made on each such specimen plate, $\frac{1}{8}$ -in. tape may be applied vertically to the center of the panel as a separator. One fluid ounce of the lacquer under test is brought to 25 \pm 1 deg C and flowed down over the 2 \times 7-in. area, pouring as closely as possible to the top edge and completing the pour in four rapid passes across the 2-in. space. If the surplus is recovered as it flows from the lower edge, it will be found that about 24 ml will be recovered, requiring a consumption of about 6 ml or $\frac{1}{4}$ fluid oz (approximately) for the test film.

Consideration or control of viscosity or nonvolatile content of the materials under test is not made at the time of coating these specimens. Since most furniture-type lacquers are supplied ready for use, it is presumed that the material under test is of

³ "Brittle Lacquer Stress Analyzers," by C. W. Smith, *Paint Incorporating Paint Manufacture*, vol. 17, October, 1947, pp. 333-335.

⁴ "Improvements Derived From Using Resins Designed Specifically for Lacquers," by J. O. Small, *Official Digest*, Federation of Paint and Varnish Production Clubs, no. 288, January, 1949, pp. 23-35.

viscosity and solid content amenable to normal spray application. Experimentation therefore has been based upon lacquers ranging naturally from 21 per cent to 30 per cent nonvolatile, and in viscosity from 45 sec to 70 sec, ASTM No. 7 Cup, as a representative coverage for clear cellulosic materials at spraying consistency. Since distention is made of each pour at three stations for an average result, the thickness of film deposited at the respective stations has been observed and considered carefully. Station A is at 1½ in. from the top of the pour, Station B at 3½ in., and Station C at 5½ in., respectively.

Film thickness of the pour, for lacquers at spraying consistency, will be found to range from 0.0005 to 0.0007 in. at Station A, according to viscosity and nonvolatile content and to increase about 0.0002 in. at each subsequent station. Such is the secondary influence of the viscosity and nonvolatile factors that their influence on film thickness may be ignored in the process of achieving a distention-potential value of cellulosic materials at spraying consistency.

Application of the distorting pressure is made in a modification of the familiar Mullen tester used for paper testing, and which is modified to a distention apparatus by the addition of a 0.0001-in. dial gage, mounted with the plunger contacting the center of the operating area for the purpose of measuring the spherical radius of the distention.⁵

CURING THE FILM

The cure of films for the significant evaluation of distention potential must be constant for a dual purpose: to bring the films to a constant condition as pertains to solvent content, and to insure a consistent condition of moisture in the film. It has been found that films of this thickness on a copper substrate may be brought to a very satisfactory constant condition by curing for 16 hr at 120 F in a forced-draft convection oven. This forcing period may be applied at any time after 15 min following application of the films, up to 8 hr.

TEMPERATURE AT TIME OF TEST

Actual performance of the distention operation at room temperature was found to result in a certain instability and inaccuracy of result. While the actual degree of error prevailing is not significantly great, it is found that the numerical value of the distention factor obtained is approximately proportional in direct ratio

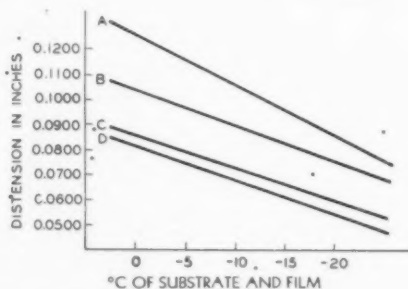


FIG. 1 EFFECT OF TEMPERATURE AT TIME OF DISTENSION ON FOUR REPRESENTATIVE LACQUER FILMS

to the temperature of the film and substrate at the moment of drawing, Fig. 1.

The process of arriving at the correct temperature for testing, where a machine based on the Model C Mullen tester is cooled by placing it within a refrigerator, is shown in Fig. 2. It will be

⁵ U. S. Patent no. 2,332,818.

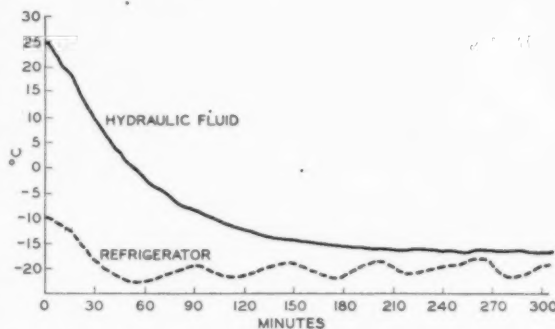


FIG. 2 PROGRESSIVE COOLING OF HYDRAULIC FLUID OF DISTENTION MACHINE WHEN PLACED IN A REFRIGERATOR AT -20 C

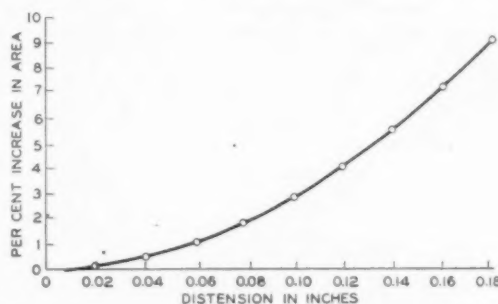


FIG. 3 RATIO OF DISTENSION OF FILM IN 0.0001 IN. ON RADIUS OF SPHERICAL DISTENSION TO ACTUAL INCREASE IN AREA IN PER CENT

noted that the hydraulic fluid of the machine will have reached a temperature of about -3 C (26.6 F) in 1 hour, a point generally satisfactory for making check evaluation distentions.

PERFORMANCE OF TEST

Specimens are removed directly from the oven for placement in the distention machine for testing. Reduced as the films are by the 16 hr of elevated temperature curing to a minimum constant as pertains to moisture content, the film will absorb atmospheric moisture rapidly after removal from the oven. Since the checking potential of many films is affected by moisture content, it is important that this factor be maintained constant.

Under a concentrated light, such as from a microscope illuminator, directed obliquely on the exposed circular area within the clamp of the machine, the incidence of failure of the film by abrupt fracture is positive and instantaneous and readily observed. The possible variation of rate of application of pressure is not great, though turning of the compressing screw at a constant speed is advisable. The motor-driven machine operates at 120 rpm. On observation of fracture failure, the pressure increment is stopped at once, and the vertical distention at the center of the spherical distortion is read to 0.0001 in. accuracy. Expression of the distention-potential factor in per cent of expansion of the area involved is plotted in Fig. 3. The per cent increase of the circular area distended into a spherical segment is calculated by the formula

$$P = \frac{100D^2}{R^2}$$

where

D = vertical distention as read from dial gage of distention machine

R = radius of distended area, or 0.59375 in.

Stations A, B, and C, representing progressive distances from the top of the flowdown as previously described, are run successively, and the results in 0.0001 in. are averaged for the expressed value for the material under test.

INFLUENCE OF FILM THICKNESS ON CHECKING TENDENCY

While it has been customary to assume in both tests and practice that, all else being equal, checking hazard increases more or less in proportion to film thickness, viz., that a heavy film is immediately more conducive to checking failure, experience in reading distention potentials and, ergo, the tendency of the film to exhibit failure by checking, serves to indicate that this ratio is not a true proportionate one. Koenig² indicates that the rate and extent of the development of stresses in a cellulosic film drying by evaporation of solvent, is influenced not only by the thickness of the film, but by the rate of evaporation, viz., the nature of the solvents and the ambient condition of the atmosphere, the solvent-retention properties of the nonvolatile constituents, and the aging factor of the stress development. While it cannot be denied that film thickness is a factor in checking propensity, the number of variables present is such that prognostications of proportionate influence cannot be made with impunity.

Examinations made of films ranging from 0.0005 in. to 0.0050 in. thickness by the distention-potential method show relatively little proportionate effect due to the fact that a standard procedure of curing the films for test will not develop in all thicknesses of film the same degree of stress. The greater mass of the heaviest films is prevented from early failure by the presence of unreleased solvent and the incomplete development of stresses. The very fact that the release of solvent is more gradual, in itself, affects the final extent, direction, and nature of the end stresses developed. The exact extent and behavior of the end stresses developed in any one application and of any one formulation of film-forming material defying comprehensive regimentation, it does not seem possible to formulate a rule for the exact effect of film thickness on checking tendency.

The normal effect of film thickness on the distention-potential test for one representative low-potential material is shown in Fig. 4. An increase here of slightly over 100 per cent in film thickness—from 0.0007 in. to 0.0015 in.—serves to reduce the distention potential about 200 points, causing its classification to descend from Class III into Class IV. The actual differential represented would probably amount to from 3 to 5 cycles of panel

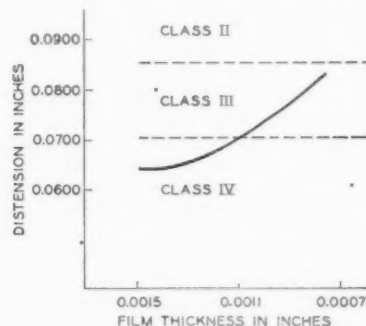


FIG. 4 EFFECT OF 100 PER CENT INCREASE OF THICKNESS OF TEST FILM OF CONVENTIONAL CLASS III LACQUER

checking value. This material is a sealer, and since the curve enters Class IV at a film thickness of slightly over 0.0010 in., it is considered a Class III material with a normal checking potential of 8 to 10 cycles.

Film thickness of ready-to-spray lacquers may be disregarded in this test since the film deposited by the temperature and angle of incident flowdown is in itself a characteristic of the individual material. The natural flow and "hang" of the material, as affected by viscosity, rate of solvent release, and nonvolatile content, will induce a similar corresponding effect in commercial application. Thus a material which, as offered at spraying consistency, deposits a film of certain thickness having a distention potential of a specific value for this normally deposited film of the material, may be assigned a significant evaluation of its potential behavior in commercial use.

Commercial application of course connotes a heavier film than is used in the laboratory distention evaluation. It is possible, however, by correlation of these results with field experience to assign a relative value to the behavior of uniformly cured films which is an equitably accurate criterion of their ultimate behavior in field use.

INTERPRETATION AND CORRELATION OF RESULTS

Values in checking potential which are assigned, therefore, through the Class I to Class IV evaluation just described, are so adjusted as to connote a prediction of the behavior of the material in question in conventional practice.

All coating materials are evaluated singly whether designed and used as an undercoat or as a finishing coat. Such materials are usually formulated for reciprocal association and, as such, will be found to fall into a similar bracket of distention potential. In this case the resulting distention value is considered the value for the complete system, consisting usually of an undercoating and two finishing coats.

Where a wide divergence of value between under and finishing elements is obtained, it is indicated that the finishing coat is the dominant factor in checking. Not only is a greater amount of this material applied in the double coat in conventional use, but by being superimposed in the system and exposed to the air, earlier development of complete stress is realized. If the undercoat exhibits a lower distention potential, its effect will be much delayed by the slower development of stresses due to its submergence in the system. Further, the undercoat, lying adjacent to the insulating substrate formed by wood, is never subjected to as abrupt thermal shock as is the surface coating.

Adequately accurate predictions of the potential checking resistance of furniture-type finishing systems may be made by assigning a value to the system, based upon the proportionate application of the respective materials in question. Thus if an undercoat and finishing coat fall into the same distention potential class, that value may be accepted as the value for the system. Unless the distention potential of the undercoat is two or more classes below that of the finishing coat, the value of the finishing coat may be accepted for the entire system in practically all cases. Where the differential between materials is several classes, the aggregate point for the system will fall a point between the extremes proportionate to the number of applications of each respective material. For example, in case of a wide divergence in undercoat and top coat to be used as a single and double coat, respectively, the potential checking-point value will be approximately one third of the differential between the individual values below the greater.

It may be that the underlying causes of cold checking, especially as pertain to basic formulation characteristics, have not been understood completely. Sanding sealers, for example, are generally considered to be "short" materials as a concession to their incorporated sanding property. The issue, however, is confused in a measure by the fact that not all the factors conducive to production of a "short film," are contributors to early cold-checking tendency. The use, for example, of metallic soaps as sanding

agents does not contribute largely to checking tendency, nor does the amount of added plasticizing agent or the rate of solvent release. The principal offender in cold-check failure is the hard resin. Softness or "cheesiness" of a sealer film, or even some degree of brittleness, as evinced by some such test as a mandrel bend, do not necessarily connote low cold-check resistance. Decrease or omission of plasticizer in a typical furniture-lacquer formulation will be reflected in the distention potential, and in a manner which reveals that the effect of plasticity so induced is not proportionate but takes the form of a logarithmic curve.

In Fig. 5, material (A), a high-grade piano lacquer, falls from its normal position as a Class I material at a distention factor of 0.1153 to Class III, distention factor 0.0833 with the omission of 25 per cent of the normal plasticizer. It remains thereafter in Class III even when plasticizer is omitted completely. Material

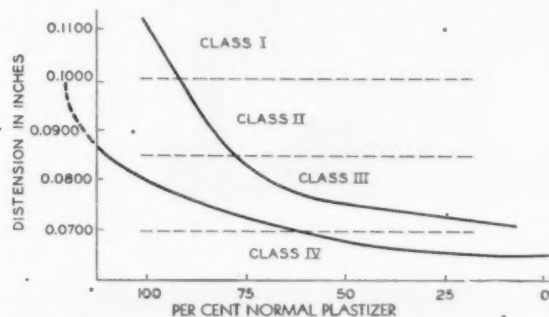


FIG. 5 EFFECT OF PLASTICIZER CONTENT ON DISTENTION OF A HIGH-POTENTIAL PIANO LACQUER (UPPER CURVE) AND A CLASS II RADIO-CABINET MATERIAL

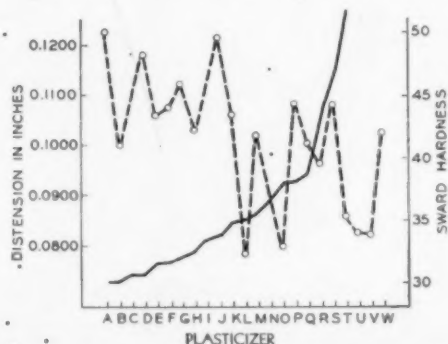


FIG. 6 LACK OF RELATIONSHIP BETWEEN DISTENTION POTENTIAL (SOLID LINE) AND SWARD HARDNESS (BROKEN LINE) OF CELLULOSIC SOLUTION WITH 23 DIFFERENT PLASTICIZERS

(B), a conventional furniture rubbing lacquer, has, as shown, a normal distention potential of approximately 0.0800. Elimination of 37.5 per cent of the plasticizer causes the rating to fall into Class IV, where it remains throughout the progressive elimination of the remainder of the plasticizer. The addition of extra plasticizer, to the extent of overplasticizing the material by 20 per cent, serves to raise the distention potential of the material into Class I at sacrifice of course of other such essential properties as resistance to printing and shrinkage.

Significant development of high distention potential does not occur until the maximum permissible plasticity (as gaged by other pertinent factors) is approached or exceeded. Varying amounts of plasticizer will not affect the distention potential of a film in the

same ratio as they will a mandrel bend or similar flexing or bend test.

That distensibility is a distinct property of the film is shown clearly in Fig. 6. Here a standard cellulose-resin solution was treated with 23 different plasticizers. Distentions were made, and the results plotted in ascending order. Sward hardnesses of the films drawn on plate glass by doctor blade are plotted in superimposed position over the distentions. The obvious absence of relationship in these properties needs no comment.

Fig. 7 shows equipment for distention of test sheets. Fig. 8 shows a typical test plate. Two pours, or flowdowns are shown, each with its respective three test stations. This is a lacquer of very high distention potential showing no failure here with all stations drawn to approximately 0.1840 in. in a vertical direction.

Fig. 9 shows a typical failure in a high-grade piano lacquer. The film thickness here is 0.0011 in., and the recorded distention potential, 0.1080, making this a Class I material which might be expected to resist efforts to check it on wood panels for an almost infinite number of cycles.

Fig. 10 shows the same piano lacquer having the distention test run on a heavy film of 0.0023 in. thickness. The "veined leaf" pattern is typical of the failure obtained from a thick film of high-potential material. The distention potential obtained here is 0.0963, showing that the excessive film causes a recession of value to the extent of one class only.

Figs. 11 and 12 are typical extreme fractures obtained from very brittle materials of low checking potential. The concentric fracture and glasslike shattering are typical. Fig. 11 is a clear furniture lacquer showing a distention potential of 0.0648. This is a Class IV material which would not be expected to exceed 3 cycles of panel testing. Fig. 12 of the same basic formula is a low-potential batch failing at 0.0567. Note the glasslike shattering combined with concentric fracture rings.

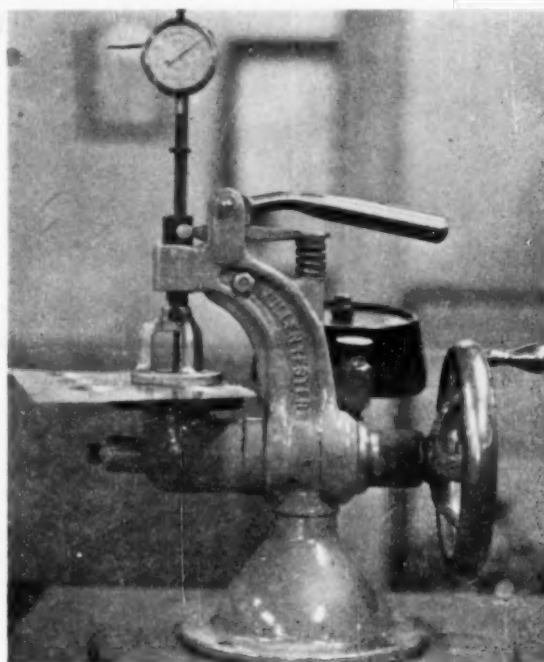


FIG. 7 EQUIPMENT FOR THE HYDRAULIC DISTENTION OF TEST SHEETS (U. S. Patent 2,332,818.)

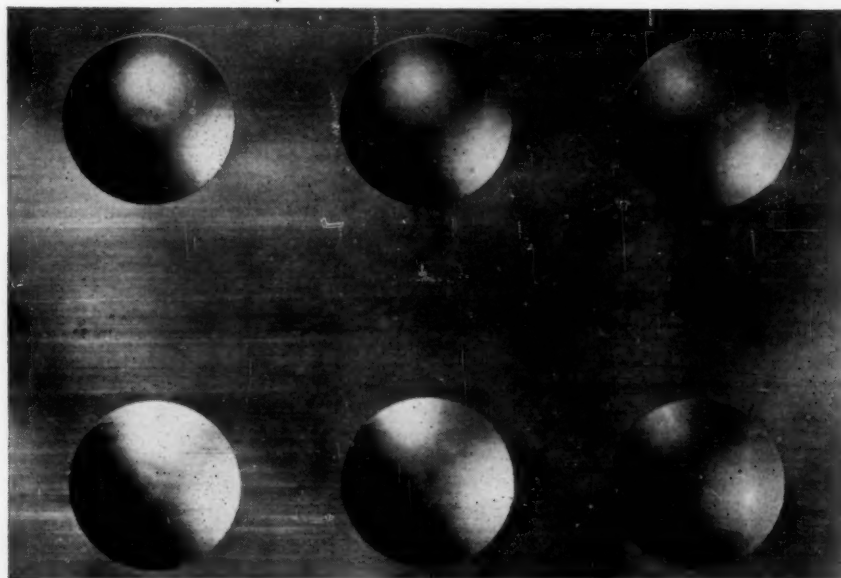


FIG. 8 TEST PLATE SHOWING TWO FLOWED SPECIMENS AND THREE TEST STATIONS ON EACH



FIG. 9 TYPICAL FAILURE OF A HIGH-POTENTIAL PIANO LACQUER



FIG. 10 "LEAF" PATTERN FAILURE OF A HEAVY (0.0023-IN.) FILM OF PIANO LACQUER SHOWN IN FIG. 9

Fig. 11

Fig.
check
tratio
sistan

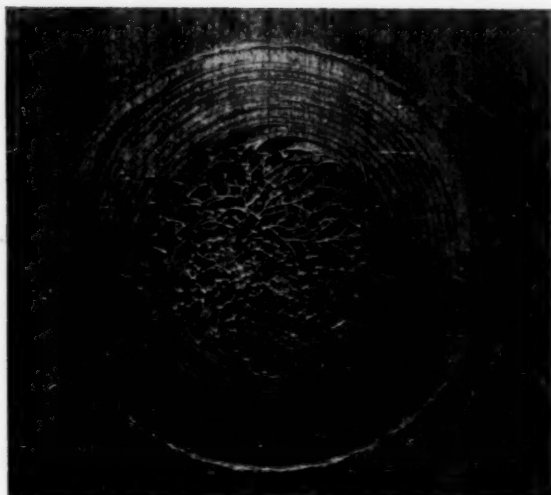


FIG. 11 FAILURE OF A LOW-POTENTIAL BRITTLE LACQUER SHOWING TYPICAL CONCENTRIC FRACTURE

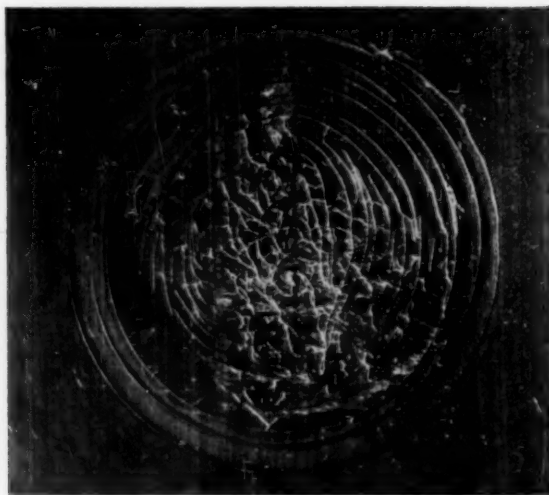


FIG. 12 FAILURE OF A VERY BRITTLE LOW-POTENTIAL LACQUER (Concentric fracture supplemented by glasslike shattering)

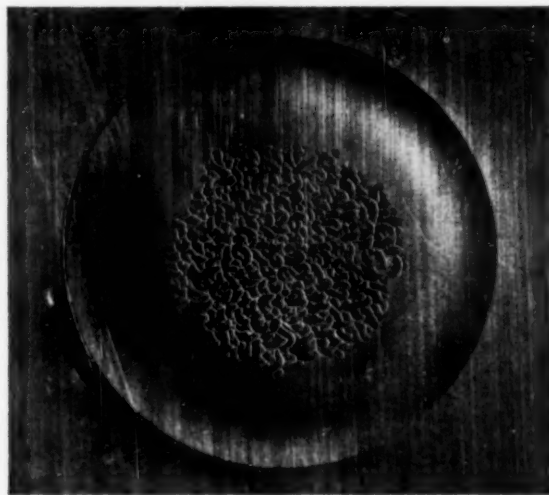


FIG. 13 TYPICAL "ALLIGATOR" PATTERN FAILURE OF A SOFT FLEXIBLE FILM OF HIGH DISTENTION POTENTIAL

Fig. 13 illustrates the characteristic uniform small-pattern check of a soft "cheesy" film material. Here, as in the other illustrations, the fracture pattern itself is not a criterion of check-resistance potential, but the failure, when reached, will take these

general forms in accordance with respective film types. The material shown in Fig. 13 is a sanding sealer. It is a high-check-resistant material having a distention of 0.0924 or Class II, and connoting a panel-test resistance of 15 to 18 cycles.

The
tane,
mensi
lamin
smalle
for all
The b
test w
lamin
modul
after
The us
thems
given p

INF
our
evi
specific
purpose
This
effects
weight,
tative l
involve
The cor
for diffe
of test v

In vie
herein e
to draw
more of
This
Standar
assistan

The m
grades s
experim
The exp
saturate
cotton f
strength
nate, tw
pressure
C cotton

¹ Physi
² Physi
Contrib
the Fall
CAN SOCI
NOTE:
understo
of the Soc

Effect of Fuel-Immersion on Laminated Plastics

By W. A. CROUSE,¹ MARGIE CARICKHOFF,² AND MARGARET A. FISHER²

The effects of cyclic and of continuous immersion in heptane, toluene, and SR-6, a test fuel, on the weight, dimensions, and flexural properties of nineteen samples of laminated plastics are reported. No one sample exhibited smaller changes than all other samples in all properties for all fuels, and for both cyclic and continuous immersion. The best weight and dimensional stability in the cyclic test was shown by a glass-fabric unsaturated-polyester laminate. The changes in flexural strength as well as in modulus of elasticity were losses in the majority of cases after the cyclic- and the continuous-immersion test. The unsaturated-polyester laminates varied widely among themselves in regard to the magnitude of the changes in a given property after an immersion test.

INTRODUCTION

INFORMATION regarding the effects of immersion in various fuels on the properties of laminated plastics is needed to evaluate these materials for use on aircraft, and to prepare specifications for such materials as are found suitable for this purpose.

This paper presents the results of tests made to determine the effects of cyclic and continuous immersion in three fuels on the weight, dimensions, and flexural properties of nineteen representative laminated plastic materials. The cyclic-immersion test involved alternate 24-hr periods of fuel-immersion and air-drying. The continuous-immersion test involved immersion in the fuels for different periods of time between 7 and 360 days. Both types of test were carried out at only one temperature, 77 F.

In view of the variability in properties to which the materials herein examined are usually subject, no attempt has been made to draw general inferences regarding the superiority of one or more of these materials relative to the others.

This investigation, conducted at the National Bureau of Standards, was sponsored by and conducted with the financial assistance of the National Advisory Committee for Aeronautics.

MATERIALS AND FUELS

The materials used in this investigation included commercial grades such as Grade C, L, and AA phenolic laminates, and several experimental materials of interest for aircraft application. The experimental samples were as follows: A number of unsaturated-polyester resin laminates reinforced with glass and cotton fabrics, a cotton-fabric melamine-resin laminate, a high-strength-paper phenolic laminate, a rayon-fabric phenolic laminate, two experimental phenolic laminates made with high pressure and low pressure, respectively, using the same Grade C cotton fabric as filler, and a paper-base lignin laminate.

The materials are described in detail in Table 1. They were obtained in the form of sheets approximately $\frac{1}{8}$ in. thick.

The fuels used were heptane (an aliphatic hydrocarbon), toluene (an aromatic hydrocarbon), and SR-6, a representative aircraft test fuel (a blend of aliphatic and aromatic hydrocarbons). The heptane used was a commercial *n*-heptane and the toluene, a technical toluene, both supplied by the Phillips Petroleum Company. The SR-6 used was a mixture of di-isobutylene (60 per cent), toluene (20 per cent), xylene (15 per cent), and benzene (5 per cent), and 0.2 lb of aviation-gasoline inhibitor per 1000 gal, supplied by the Standard Oil Company of New Jersey. The inhibitor consists of 50 per cent of *n*-butyl-*p*-aminophenol, 30 per cent of isopropyl alcohol, and 20 per cent of anhydrous methanol, and is added in order to hinder the oxidation of the di-isobutylene, a diolefin, with consequent gum formation.

TEST PROCEDURES

Specimens. The dimensions of the test specimens were 1 in. \times 3 in. \times the thickness of the sheet. The specimens were machined on a surface grinder with tap water as a coolant. The length and width were kept to within ± 0.005 in. of the given dimensions. One surface of each sheet was arbitrarily designated as the reference surface. The specimens of the cloth laminates were cut so that the direction with the greater number of threads per inch in the reference surface was lengthwise. As all the paper laminates were crossed-ply materials, the lengthwise direction of these specimens was arbitrarily taken parallel to one edge. The weight of the specimens varied from approximately 7 to 12 grams.

The specimens which were to be immersed were conditioned for 48 hr at 77 F and 50 per cent relative humidity (RH) prior to starting the tests.

Weight and Dimensions. The weight was determined to the nearest milligram. The length was measured to the nearest 0.001 in., and the width and thickness to the nearest 0.0001 in. The length was measured at two places, and the width and thickness at three places. The changes in weight and dimensions were determined with two specimens of each material. The changes in the length and width columns presented in the tables were determined by taking the mean of the average length changes and the average width changes.

Flexural Properties. The flexural tests were made in accordance with method No. 1031 of Federal Specification L-P-406a,³ using the 1200-lb scale of the 2400-lb-capacity hydraulic testing machine shown in Fig. 1. The flexural apparatus, Fig. 2, has been described.⁴ Load-deflection graphs were obtained in each test on a Southwark-Templin autographic recorder, which was operated by a Southwark-Peters plastics extensometer.

The 1 \times 3-in. specimens, which were immersed in the various test fuels, were cut into two 1 \times 1.5-in. specimens for the

¹ Physicist, National Bureau of Standards, Washington, D. C.

² Physical Science Aide, National Bureau of Standards.

Contributed by the Rubber and Plastics Division and presented at the Fall Meeting, Erie, Pa., September 28-30, 1949, of THE AMERICAN SOCIETY OF MECHANICAL ENGINEERS.

NOTE: Statements and opinions advanced in papers are to be understood as individual expressions of their authors and not those of the Society. Paper No. 49-F-32.

³ Federation Specification L-P-406a: Plastics, Organic; General Specifications, Test Methods; Government Printing Office, Washington, D. C., January 24, 1944.

⁴ "A Variable Span Flexure Test Jig for Plastic Specimens," by B. M. Axilrod, R. W. Thiebaud, and G. E. Brenner, ASTM Bulletin no. 148, October, 1947, p. 96.

TABLE 1 DESCRIPTION OF MATERIALS

Item No.	Material	Type of Laminate	Manufacturer	Thick- ness (in.)	Density (lb./cu. in.)	Resin Designation	Content, by Weight (%)	Reinforcement		Fiber Count Per Square Inch	No. of Pressure Plies (16/in.)	Welding Conditions		Time Cooling (min.)			
								Type	Material			Pressure (psi)	Temperature (°F)				
C	High-Strength-Paper Phenolic		Consolidated Water Power and Paper Co.	0.121	1.42	--	--	Fiber	--	--	Crossed	250					
D	Lignin Paper		Formica Insulation Co.	0.128	1.38	Lignin		Lignin Paper			Crossed						
E	Glass-Fabric Unsat- rated Polyester		Seedling Aeroplastics Corp.	0.134	1.69	Marco MB-1A	55-63	Glass Fabric, plain weave		29	17	Crossed	7				
F	Muslin-Cotton-Fabric Unsaturated Polyester		Seedling Aeroplastics Corp.	0.123	1.31	Marco MB-1A		Cotton Fabric (Muslin), twill weave		70	45	7					
H	Enamel-Duck Cotton- Fabric Unsaturated Polyester		Pittsburgh Plate Glass Co., Columbia Chemical Division	0.147	1.36	Allymer CR 39	62-65	Cotton Fabric (Enamel Duck), plain weave, 8 oz/yd ²		36	32	Crossed	6	1-5	158	239	2 hr at Gradual 1500F, 1 hr at 154-2500F
I	Grade C Phenolic		Synthane Corp.	0.124	1.35	Bakelite BV-1112	45	Cotton Fabric, plain weave, 10 oz/yd ²		50	40	Crossed	7	1600	340	50	20
J	Grade L Phenolic		Synthane Corp.	0.124	1.34	Bakelite BV-1112	44-52	Cotton Fabric, plain weave, 3.7 oz/yd ²		80	80	Parallel	19	1630	330	45	25
K	Grade AA Phenolic		Synthane Corp.	0.135	1.49	Bakelite BV-2427	47	Asbestos Fabric, plain weave, 18 oz/yd ²		18	16	Parallel	5	1800	340	50	20
L	Enamel-Duck Cotton- Fabric Phenolic		Bakelite Corp.	0.132	1.36	Bakelite BV-1687	59	Cotton Fabric (Enamel Duck), plain weave, 8 oz/yd ²		84	28	Crossed	9	250	335	30	
M	Canvas-Cotton-Fabric Melamine		Formica Insulation Co.	0.145	1.47		50-55	Cotton Fabric (Canvas), plain weave, 8 oz/yd ²		90	26	Parallel	11	1400	284-288		
N	Canvas-Cotton-Fabric Unsaturated Polyester		Formica Insulation Co.	0.150	1.13	Lantane	50-55	Cotton Fabric (Canvas), plain weave, 8 oz/yd ²		90	26	Parallel	7	15	23-246		
O	High-Strength-Paper Phenolic		Consolidated Water Power and Paper Co.	0.122	1.42	Bakelite BV-1056	30	High Strength Vitecherlon Paper		--	--	Crossed	54	250	310±10	12	Gradual
V	Low-Pressure Grade C Phenolic		Synthane Corp.	0.130	1.26	Bakelite BV-1687	51	Cotton Fabric (Army Duck), plain weave, 10 oz/yd ²		50	40	Crossed	7	180	320	50	
W	High-Pressure Grade C Phenolic		Synthane Corp.	0.138	1.36	Bakelite BV-1112	47	Cotton Fabric (Army Duck), plain weave, 10 oz/yd ²		50	40	Crossed	7	1600	330	50	
X	Glass-Fabric Unsat- rated Polyester		Pittsburgh Plate Glass Co., Columbia Chemical Division	0.125	1.64	Allymer CR 149	50-55	Glass Fabric (ECG-11-162), plain weave, 12 oz/yd ²		24	16	Crossed	6	1-5	176	207	18 hr at Gradual 1700F, 1 hr at 2070F
Y	Glass-Fabric Unsat- rated Polyester		Pittsburgh Plate Glass Co., Columbia Chemical Division	0.114	1.66	Allymer CR 39	44-50	Glass Fabric (ECG-11-162), plain weave, 12 oz/yd ²		28	16	Crossed	6	1-5	176	207	15 hr at Gradual 1700F, 1 hr at 2070F
Z	Rayon-Fabric Phenolic		Formica Insulation Co.	0.160	1.35	Iron- side 91-1	37-40	Rayon Fabric (Cellulose Corp., WG-3975), high tenacity Fortisan rayon warp thread, cotton filling thread, twill weave, 12.5 oz/yd ²		75	12	Crossed	6	1100	330	20	Temper- ature al- lowed to cool to over 3000F for 20 min.
AA	Glass-Fabric Unsat- rated Polyester		Marco Chemicals Inc.	0.118	1.69	Marco MB-17B	45-5	Glass Fabric (ECG-11-162), plain weave		29	17	Parallel	7	None	140	240	1 hr at 1400F, 1 hr at 2400F
AB	Glass-Fabric Unsat- rated Polyester		Army Air Forces, Air Technical Service Command	0.130	1.64	Plaston 940	43	Glass Fabric (ECG-117), Heat Treated, plain weave		40	40	Parallel	45	40	160	220	2 hr at 1600F, 2 hr at 2200F

A. Average for all specimens tested.

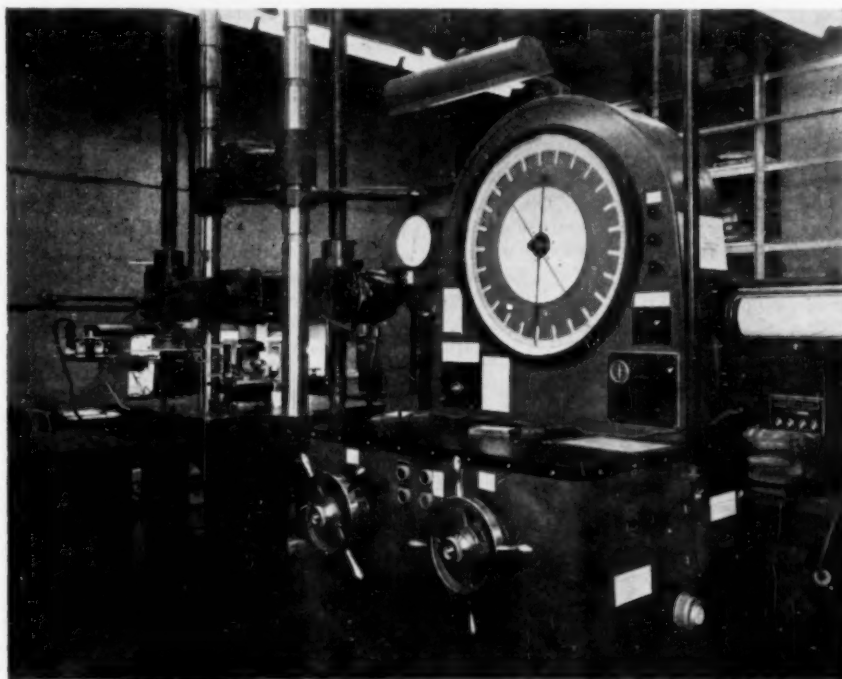


FIG. 1 HYDRAULIC TESTING MACHINE

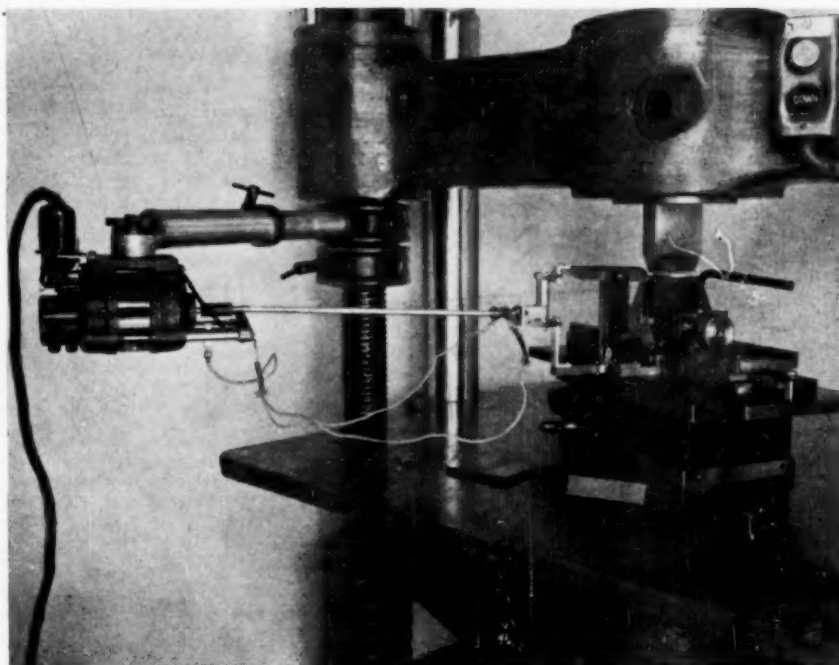


FIG. 2 FLEXURAL APPARATUS

flexural tests. Because the test specimens were too short, a span-depth ratio of 8:1 was used instead of 16:1, as prescribed by Federal Specification L-P-406a. The reference surface of the specimen was on the tension side during the test. The radius of the support and pressure pieces was $1/32$ in. The relative rate of head motion was 0.01 ipm.

The flexural strength and the flexural modulus of elasticity were calculated in accordance with the equations given in method No. J031 of Federal Specification L-P-406a. The flexural-strength values reported are considered to be accurate to 1 per cent, and the flexural modulus of elasticity values to 3 per cent. All the values for the flexural properties are the averages obtained with four specimens except the initial values, which are the averages for six specimens.

The initial values for the flexural properties were determined on specimens which were heated in a circulating-air oven at 122 F for 48 hr and then conditioned for 48 hr at 77 F and 50 per cent RH prior to test. The changes in the flexural strength and the flexural modulus of elasticity as a result of immersion in the various fuels were calculated from these initial values.

Cyclic and Continuous Fuel-Immersion Tests. Each cycle of the cyclic fuel-immersion test consists of a 24-hr immersion and a 24-hr drying period. The specimens were immersed individually in 200 ml of test fuel in closed glass containers. Weight and dimensional measurements and flexural tests were made after 10 cycles of test and reconditioning at 77 F and 50 per cent RH for 48 hr.

The continuous fuel-immersion test consists of 7, 30, 90, 180, and 360 days of immersion. The specimens were immersed individually in 200 ml of test fuel in closed glass containers. Weight and dimensional measurements and flexural tests were made immediately after removing the specimens from the fuel on one set of specimens, and after reconditioning for 7 days at 77 F and 50 per cent RH on a second set.

TABLE 2 CHANGES IN WEIGHT AND DIMENSIONS OF LAMINATED PLASTICS AFTER THE CYCLIC FUEL-IMMERSION TEST^a

NBS Material Designation	Change ^b in Weight in			Average ^b of Length and Width Changes in			Change ^b in Thickness in		
	Heptane (\$)	Toluene (\$)	SR-6 (\$)	Heptane (\$)	Toluene (\$)	SR-6 (\$)	Heptane (\$)	Toluene (\$)	SR-6 (\$)
Lignin paper									
D	0.08	0.52	0.06	0.02	0.05	0.00	0.3	0.2	-0.1
Phenolic; high-strength paper									
E	0.09	0.42	0.01	0.00	0.01	-0.01	0.1	0.0	-0.1
S	0.10	0.35	0.04	0.02	0.04	-0.04	0.2	0.2	0.1
Phenolic; cotton fabric									
J (Grade L)	0.07	0.42	0.01	0.02	0.05	-0.01	-0.1	0.1	-0.1
I (Grade C)	0.10	0.36	0.02	0.01	0.05	-0.02	0.2	0.0	-0.5
W (Grade C)	0.14	0.85	0.05	0.04	0.07	0.02	0.1	0.0	-0.3
L (Grade C; low pressure)	0.26	0.88	0.14	0.03	0.09	-0.03	0.5	0.1	1.6
Phenolic; rayon fabric									
Z	0.34	0.33	0.32	0.04	0.05	0.04	0.0	0.2	0.0
Phenolic; asbestos fabric									
K	0.16	0.83	0.20	0.02	0.05	0.03	0.0	0.2	0.5
Melamine; cotton fabric									
M	0.16	0.65	-0.03	0.03	0.08	-0.03	0.1	0.4	-0.2
Unsaturated polyester; cotton fabric									
P	0.09	0.54	0.00	0.02	0.08	-0.03	0.0	0.3	-0.4
II	0.19	0.60	0.04	0.04	0.09	0.01	0.1	0.2	-0.1
N	0.49	2.83	1.54	0.11	0.14	0.16	0.4	2.3	1.2
Unsaturated polyester; glass fabric									
E	0.09	0.30	0.14	0.00	-0.02	0.00	0.0	0.5	-0.4
X	0.08	0.08	0.08	0.01	0.01	0.01	0.0	-0.1	-0.1
Y	0.12	0.20	0.16	0.01	0.01	0.01	0.1	0.3	-0.4
AA	0.00	0.29	0.06	0.00	0.00	0.01	0.7	0.6	0.2
AB	0.17	0.21	0.19	0.03	0.01	0.03	0.2	0.0	0.1

^a Each cycle of the test consists of a 24-hour immersion and a 24-hour drying period. Weight and dimensional measurements were made after 10 cycles of testing and reconditioning at 77° F and 50 percent relative humidity for 48 hours.

^b Based on average value for two specimens.

RESULTS AND DISCUSSION

Weight and Dimensional Changes. The changes in weight, length, width, and thickness of the laminates immersed in heptane, toluene, and SR-6 are shown in Table 2 for cyclic fuel immersion, and in Tables 3 to 5, and Figs. 3 to 5, inclusive, for continuous fuel immersion. The samples having changes greater than ± 1 per cent for weight, ± 0.1 per cent for length and width, and ± 0.5 per cent for thickness in the cyclic fuel-immersion test and after 360 days of continuous fuel immersion are shown in Table 9. The data for the low-pressure Grade C phenolic laminate V were not included in the tables and in the discussion because of its great variability, but are shown in Figs. 3 to 5.

(a) **Cyclic Fuel-Immersion Test.** In the cyclic fuel-immersion test, practically all of the weight changes of the samples for all the fuels as well as the majority of the dimensional changes for heptane and toluene are positive. In SR-6 nearly one half of the changes in length and width, and over one half of the changes in thickness are negative. The positive changes indicate that there is some retention of liquid accompanied by a slight swelling. Considering the magnitude of the changes for each sample in the three fuels regardless of sign, in the majority of cases the greatest changes in weight, and length and width of the samples occurred in toluene, whereas in thickness, the greatest changes were fairly well distributed between toluene and SR-6. The greater positive changes obtained with toluene compared to heptane may be partly ascribed to the greater volatility of heptane.

None of the samples showed weight changes in heptane of over 0.5 per cent, and about one half of them exhibited changes of 0.1 per cent or less. In toluene, the cotton-fabric unsaturated-polyester laminate N showed a change of 2.83 per cent. The remainder of the laminates changed less than 1 per cent, and about one half of the samples showed changes of less than 0.5 per cent. In SR-6 the laminate N showed a change of 1.54 per cent. The remainder of the samples showed changes of less

than 0.35 per cent, and nearly one half of the samples exhibited changes of 0.05 per cent or less. The glass-fabric unsaturated-polyester laminate X had the smallest average change for the three fuels, with individual values of less than 0.1 per cent.

The laminate N showed length and width changes of 0.11, 0.14, and 0.16 per cent in heptane, toluene, and SR-6, respectively. The remainder of the samples exhibited changes of less than 0.1 per cent.

The cotton-fabric unsaturated-polyester laminate N in toluene and SR-6, and the low-pressure Grade C phenolic L in SR-6, showed thickness changes of 2.3, 1.2, and 1.6 per cent, respectively. The remainder of the samples changed less than 1 per cent.

The laminate X exhibited the greatest stability and the laminate N the least.

(b) **Continuous Fuel-Immersion Test.** In the continuous-immersion test the majority of the changes in weight and dimensions were positive. The

TABLE 3. CHANGES IN WEIGHT OF LAMINATED PLASTICS AFTER CONTINUOUS IMMERSION IN HEPTANE, TOLUENE, AND SR-6 FUEL BLEND

Material notation	Specimen	Change ^b After Immersion in Heptane For:			Change ^b After Immersion in Toluene For:			Change ^b After Immersion in SR-6 For:		
		7 Days	30 Days	90 Days	7 Days	30 Days	90 Days	7 Days	30 Days	90 Days
		(%)	(%)	(%)	(%)	(%)	(%)	(%)	(%)	(%)
Lignin paper										
D	I*	0.12	0.24	0.05	0.26	0.10	0.24	0.07	0.16	0.04
	I*	0.22	0.34	0.06	0.36	0.11	0.37	0.10	0.22	0.05
Phenolic:high-strength paper										
C	I	0.07	0.20	0.12	0.23	0.30	0.05	0.24	0.05	0.14
	I	0.14	0.20	0.16	0.32	0.32	0.15	0.33	0.07	0.52
S	I	0.05	0.16	0.26	0.47	0.18	0.08	0.20	0.09	0.56
	I	0.16	0.25	0.34	0.46	0.30	0.14	0.27	0.04	0.55
Phenolic:cotton fabric										
J (Grade L)	I	0.13	0.26	0.16	0.24	0.18	0.13	0.34	0.13	0.42
	I	0.16	0.31	0.07	0.45	0.12	0.15	0.30	0.06	0.66
I (Grade C)	I	0.76	0.53	0.14	0.46	0.28	0.27	0.65	0.14	1.18
	I	0.26	0.42	0.08	0.69	0.16	0.22	0.37	0.06	1.00
W (Grade C)	I	0.35	0.63	0.36	1.13	0.42	0.56	0.61	0.32	1.43
	I	0.37	0.86	0.38	0.80	0.11	0.36	0.53	0.10	1.92
L (Grade C; low pressure)										
	I	0.54	0.97	0.75	1.52	0.76	1.00	1.14	0.64	1.82
	I	0.28	0.35	0.25	0.68	-0.04	0.24	0.40	0.02	1.48
Phenolic:rayon fabric										
Z	I	0.14	0.33	0.26	0.72	0.43	0.24	0.40	0.25	1.02
	I	0.11	0.15	-0.04	0.44	0.15	0.09	0.18	-0.04	0.64
Phenolic:acetate fabric										
K	I	0.62	1.25	0.94	1.15	0.74	1.57	1.35	1.64	1.70
	I	0.18	0.24	0.06	0.45	0.17	0.24	0.52	0.31	1.28
Melamine:cotton fabric										
M	I	0.24	0.55	0.28	0.82	0.35	0.56	0.64	0.42	1.04
	I	0.05	0.20	-0.10	0.36	0.02	0.13	0.29	0.00	0.50
Unsaturated polyester:cotton fabric										
P	I	0.09	0.24	-0.04	0.48	-0.23	0.66	1.52	1.18	1.19
	I	0.16	0.21	-0.04	0.42	0.16	0.20	0.55	0.52	0.90
H	I	0.14	0.24	0.13	0.50	0.14	0.35	0.50	0.37	1.27
	I	0.20	0.26	0.04	0.60	0.04	0.30	0.44	0.38	1.38
W	I	1.45	4.06	4.28	5.24	6.60	7.01	9.44	10.42	13.46
	I	0.20	0.49	0.30	0.85	0.52	1.60	3.42	4.77	5.66
Unsaturated polyester:glass fabric										
E	I	0.11	0.22	0.28	1.16	0.34	0.46	8.39	3.73	6.80
	I	0.06	0.12	0.12	0.20	0.21	0.36	1.00	1.62	2.24
X	I	0.06	0.05	0.07	0.16	0.11	0.07	0.12	0.08	0.24
	I	0.04	0.06	0.04	0.14	0.11	0.03	0.08	0.04	0.19
Y	I	0.17	0.36	0.13	0.32	0.32	0.32	0.54	0.77	1.44
	I	0.02	0.03	-0.04	0.18	-0.01	0.08	0.24	0.52	0.65
AA	I	1.20	1.95	0.35	1.96	1.44	1.76	2.80	3.21	4.30
	I	-0.14	-0.15	-0.16	-0.04	-0.21	0.06	0.26	0.58	1.17
AB	I	0.13	0.22	0.26	0.52	0.60	0.18	0.84	0.34	0.59
	I	0.07	0.11	0.02	0.20	0.06	0.04	0.14	0.34	0.34

a. Data for this column: I = Tested immediately.

b. Based on average value for 7 days at 70° F and 50 percent relative humidity.

c. Based on average value for two specimens.

TABLE 4 AVERAGE OF CHANGES IN LENGTH AND WIDTH OF LAMINATED PLASTICS AFTER CONTINUOUS IMMERSION IN HEPTANE, TOLUENE, AND SR-6 FUEL BLEND

Material Designation	When Tested	Change ^b After Immersion in Heptane For:		Change ^b After Immersion in Toluene For:		Change ^b After Immersion in SR-6 For:								
		7 Days	30 Days	7 Days	30 Days	7 Days	30 Days							
Lignin paper														
D	1	-0.23	0.04	0.01	0.11	0.03	0.01	0.03	0.01	0.01	2.09	0.01		
	2	0.03	0.05	0.01	0.09	0.02	-0.02	0.10	0.02	0.01	-0.31	-0.01		
Phenolic-high-strength paper														
G	1	0.20	0.01	0.01	0.06	0.03	0.01	0.00	0.00	0.05	0.02	0.21	0.05	
	2	0.02	0.01	0.00	0.04	0.06	0.02	0.03	0.01	0.06	-0.03	0.07	0.03	
H	1	0.00	-0.01	0.02	0.02	0.05	0.02	0.01	0.02	0.06	0.04	0.00	0.05	
	2	0.00	0.01	0.01	0.06	0.03	0.02	0.01	0.02	0.05	0.00	0.02	0.04	
Phenolic-cotton fabric														
J (Grade L)	1	-0.01	0.01	0.00	0.10	0.02	0.01	0.04	0.01	0.11	0.06	-0.01	0.07	0.03
	2	0.02	0.04	0.02	0.12	0.04	0.02	0.05	-0.01	0.12	0.06	0.00	0.09	0.03
I (Grade C)	1	-0.01	0.04	0.02	0.12	0.05	0.02	0.03	-0.04	0.12	0.02	0.01	0.12	0.01
	2	0.03	0.03	0.00	0.09	0.03	0.04	0.04	-0.01	0.13	0.03	0.01	0.13	0.00
W (Grade C)	1	-0.01	0.02	0.01	0.11	0.04	0.00	0.03	0.01	0.13	0.04	0.02	0.12	0.01
	2	0.02	0.04	-0.03	0.11	0.04	0.03	0.05	0.01	0.11	0.02	-0.03	0.09	0.01
L (Grade C; low pressure)	1	0.00	0.03	0.00	0.11	0.01	0.01	0.02	-0.02	0.13	0.03	0.00	0.12	0.02
	2	0.04	0.03	-0.01	0.11	0.04	0.04	0.05	-0.04	0.10	0.02	0.01	-0.02	-0.01
Phenolic-rayon fabric														
Z	1	-0.02	0.01	-0.01	0.07	0.05	0.01	0.00	0.00	0.08	0.04	0.00	0.03	0.02
	2	0.02	0.02	-0.01	0.07	0.04	0.03	0.02	0.00	0.08	0.03	0.00	0.02	0.04
Phenolic-asbestos fabric														
K	1	-0.01	0.01	0.03	0.04	0.05	0.10	0.03	0.06	0.16	0.14	0.04	0.11	0.07
	2	0.02	0.00	-0.01	0.06	0.03	0.04	0.07	0.03	0.16	0.14	0.02	0.10	0.10
Melamine: cotton fabric														
M	1	0.02	0.01	-0.02	0.09	0.03	0.03	0.03	0.00	0.11	0.07	0.01	-0.02	0.01
	2	0.01	0.02	-0.03	0.06	0.02	0.02	0.05	-0.01	0.11	0.04	0.05	-0.01	0.01
Unsaturated polyester:cotton fabric														
P	1	0.00	0.06	-0.01	0.07	0.01	0.00	0.06	0.07	0.15	0.27	0.00	0.13	-0.02
	2	0.01	0.06	0.01	0.09	0.00	0.01	0.04	0.04	0.15	0.15	0.00	0.11	0.02
H	1	0.00	0.01	0.01	0.16	0.05	0.02	0.05	0.04	0.29	0.17	0.03	0.16	0.09
	2	0.04	0.04	-0.02	0.11	0.04	0.04	0.07	0.02	0.24	0.13	0.02	0.16	0.07
W	1	0.09	0.08	0.13	0.23	0.22	0.37	0.25	0.63	0.85	0.66	0.23	0.56	0.42
	2	0.04	0.08	0.07	0.15	0.26	0.02	0.26	0.41	0.62	0.53	0.10	0.44	0.42
Unsaturated polyester:glass fabric														
E	1	0.03	0.04	0.02	0.04	0.04	0.03	0.09	0.05	0.09	0.10	-0.01	0.03	0.05
	2	0.00	0.02	0.01	0.04	0.03	0.02	-0.02	-0.03	-0.02	-0.02	0.00	0.02	0.04
X	1	-0.01	0.03	-0.01	0.02	0.01	0.01	0.04	-0.01	0.06	0.05	-0.01	-0.02	0.04
	2	-0.01	0.01	0.01	0.04	0.04	-0.01	0.00	0.02	0.04	0.05	-0.02	0.01	0.05
Y	1	-0.01	-0.02	0.00	0.04	0.03	-0.01	0.00	0.02	0.05	0.06	0.01	0.00	0.05
	2	0.00	0.00	0.00	0.02	0.02	-0.02	0.00	0.02	0.05	0.05	0.01	0.04	0.03
AA	1	-0.02	-0.01	-0.01	0.03	0.01	0.05	-0.01	0.02	0.03	0.07	0.03	0.01	0.06
	2	-0.03	0.01	0.00	0.01	0.02	-0.02	-0.03	0.00	0.04	0.02	-0.03	0.03	-0.02
AB	1	0.01	0.01	0.00	0.05	0.04	0.00	0.04	0.01	-0.01	0.04	0.03	0.01	0.05
	2	0.02	0.01	-0.01	0.06	0.03	-0.03	0.00	-0.02	0.04	0.03	0.02	0.00	0.01

a. Code for this column:
1 = Tested immediately.
r = Tested after reconditioning for 7 days at 77° F and 50 percent relative humidity.

b. Based on average values for two specimens.

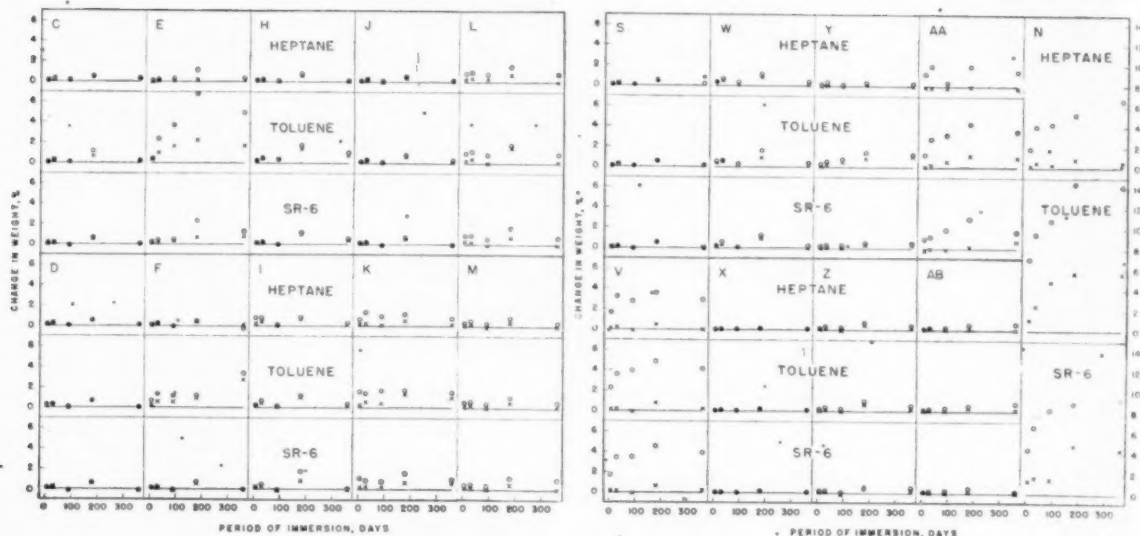


FIG. 3 CHANGES IN WEIGHT OF LAMINATES IN PROLONGED FUEL-IMMERSION TESTS
(O-tested immediately after removal from the fuel. X-tested after reconditioning for 7 days.)

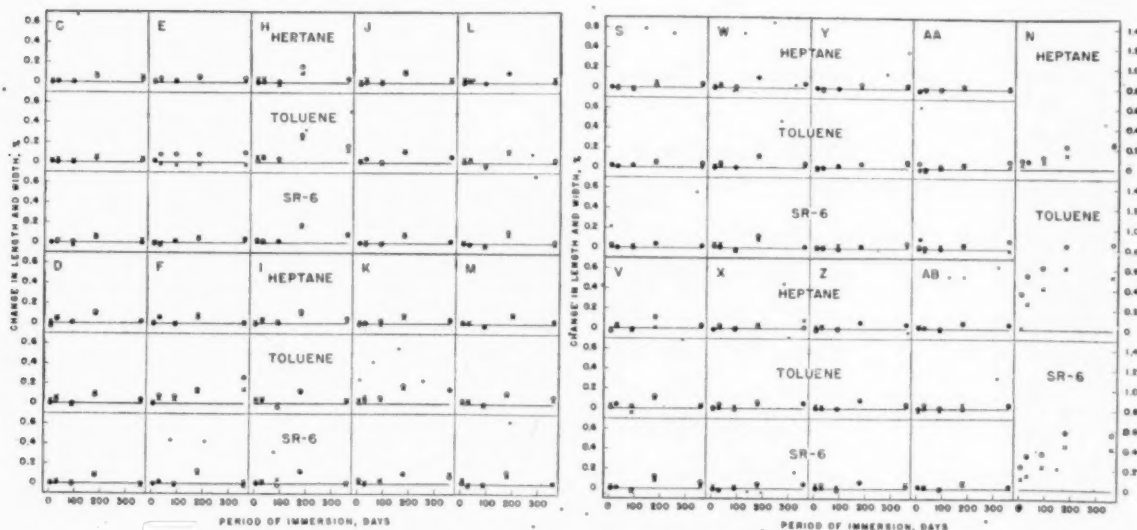


FIG. 4 CHANGES IN LENGTH AND WIDTH OF LAMINATES IN PROLONGED FUEL-IMMERSION TESTS
(O-tested immediately after removal from the fuel. X-tested after reconditioning for 7 days.)

changes, regardless of sign, were equal to or higher for the "tested immediately" condition, as compared with the "reconditioned 7 days" condition in the majority of cases. In the majority of cases toluene caused the greatest changes. In weight and dimensions, the changes in the majority of cases attained their maximum values at the 180-day period. The reduction in the changes during the succeeding 180-day period indicates that the fuels may have dissolved some of the resin.

It is noted that for a given type of laminate, the weight changes varied considerably among the samples. For example, samples J, I, and W are all Grade C laminates made with the same phenolic resin. In most cases the changes for sample W for all three fuels are about double the corresponding values for sample J.

Among the glass-fabric unsaturated-polyester laminates, samples E and AA exhibited changes higher than 1 per cent in each of the three fuels during the course of the 360-day immersion tests, compared with sample X which at no time changed as much as 0.3 per cent. The cotton-fabric unsaturated-polyester laminate H showed changes roughly one tenth of those of sample N, a material absorbing greater than 5 per cent of liquid in each of the fuels.

Similar behavior, namely, a wide spread in the changes for samples of a given type of laminate, is evident (Table 5) in the thickness changes of the unsaturated-polyester laminates.

A comparison of the changes in the various samples after 360 days of immersion in the fuels follows:

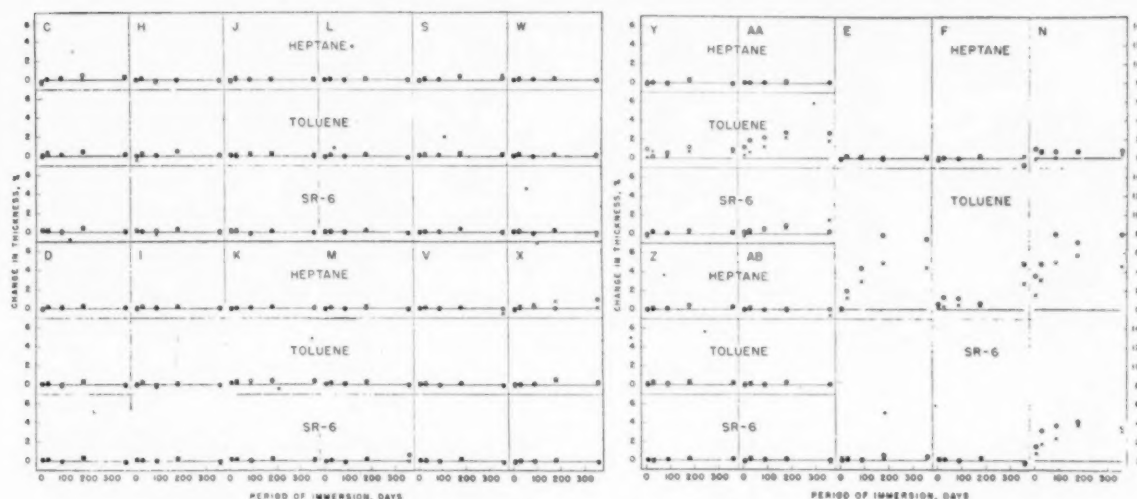


FIG. 5 CHANGES IN THICKNESS OF LAMINATES IN PROLONGED FUEL-IMMERSION TESTS (O—tested immediately after removal from the fuel. X—tested after reconditioning for 7 days.)

Weight Changes at 360 Days. In heptane the cotton-fabric unsaturated-polyester laminate N and the glass-fabric unsaturated-polyester laminate AA in the "tested immediately" condition showed changes of 6.60 and 1.44 per cent, respectively. The remainder of the samples exhibited changes of less than 1 per cent, both when tested immediately and after 7 days of reconditioning. In toluene more than one half of the samples when tested immediately and more than three fourths of the materials in tests after reconditioning 7 days showed changes of less than 1 per cent. In SR-6 the laminates N, E, and AA in the tested immediately condition, and the laminate N in the 7-day condition showed changes of 9.32, 1.30, 1.65, and 4.34 per cent, respectively. The remainder of the samples had changes of less than 1 per cent. The lignin paper laminate D, the Grade C phenolic laminate J, and the glass-fabric unsaturated-polyester laminate X have the least average changes for all fuels, and both test conditions with no individual changes greater than 0.3 per cent.

Length and Width Changes at 360 Days. The laminate N in heptane and SR-6, and the laminates F, H, K, and N in toluene showed changes greater than 0.1 per cent. The remainder of the samples exhibited changes of 0.1 per cent or less.

Thickness Changes After 360 Days. The unsaturated-polyester laminates F, N, and X in heptane, E, F, N, Y, and AA in toluene, and N and AA in SR-6 showed changes greater than 0.6 per cent in either test condition or both. The remainder of the samples had changes of 0.6 per cent or less.

Changes in Flexural Properties. The changes in flexural strength and flexural modulus of elasticity of the laminates after immersion in heptane, toluene, and SR-6 are shown in Table 6 for cyclic fuel immersion, and in Tables 7 and 8 and Figs. 6 and 7, for continuous fuel immersion. The laminates exhibiting losses greater than 10 per cent for flexural strength and 5 per cent for flexural modulus of elasticity in the cyclic fuel-immersion test, and after 360 days of continuous fuel immersion are listed in Table 9. The data for the low-pressure Grade C phenolic laminate V were not included in the tables and in the discussion because of its great variability but are shown in Figs. 6 and 7.

(a) Cyclic Fuel-Immersion Test. In the cyclic fuel-immersion test approximately two thirds of the changes in flexural strength and in flexural modulus of elasticity are negative in each fuel.

Considering the changes for each sample in the three fuels, it is noted that the losses are well distributed among the three fuels. The Grade AA phenolic laminate K exhibited the greatest positive changes in all three fuels in both flexural strength and flexural modulus of elasticity, although the initial values of these two properties for sample K are among the lowest.

Of the eighteen samples tested in each fuel, only four, none of which was a cotton-fabric phenolic, had losses in flexural strength greater than 5 per cent. Two samples, the glass-fabric unsaturated-polyester laminate E, and the cotton-fabric unsaturated-polyester laminate N had losses greater than 10 per cent in each of the three fuels.

Approximately one half of the materials exhibited losses in flexural modulus of elasticity less than 5 per cent in each fuel. Only the enameled-cotton-fabric unsaturated-polyester laminate H and the Grade L phenolic laminate J had losses greater than 10 per cent in each of the three fuels.

The samples which showed the greatest flexural stability in the three fuels were the cotton-fabric melamine laminate M, the cotton-fabric phenolic laminate L, the high-strength-paper phenolic laminate S, the cotton-fabric unsaturated-polyester laminate F, and the glass-fabric unsaturated-polyester laminate AB. The changes in both flexural strength and flexural modulus of elasticity did not exceed 5 per cent. Samples X and K, which showed increases but no decreases greater than the foregoing limits, were considered to have withstood the cyclic immersion test favorably. The cotton-fabric unsaturated-polyester laminate N exhibited the greatest changes.

(b) Continuous Fuel-Immersion Test. In the prolonged fuel-immersion test most of the changes in flexural strength and flexural modulus of elasticity are negative. Eighty per cent of the differences in the percentage values between the "tested immediately" and "reconditioned 7 days" conditions of test for the three fuels in flexural strength and flexural modulus of elasticity are 5 or less. It is considered that differences of this order are not significant. This indicates that in the majority of cases the deterioration occurred during the immersion, and that retained solvent in the tested immediately condition had little effect on the strength and modulus of elasticity. Most of the differences for flexural strength and flexural modulus of elasticity were approximately the same for the three fuels in the two test condi-

TABLE 6 CHANGES IN FLEXURAL PROPERTIES AFTER THE CYCLIC FUEL-IMMERSION TEST^a

VES Material Designation	Initial Flexural Strength ^b (10 ³ lb/in. ²)	Change ^c in Flexural Strength in Heptane Toluene SR-6		Initial Flexural Modulus of Elasticity ^b (10 ⁶ lb/in. ²)	Change ^c in Flexural Modulus of Elasticity in Heptane Toluene SR-6	
		(%)	(%)		(%)	(%)
Lignin paper						
D	23.5±0.4	-7	-8	1.92±0.05	-10	-5
Phenolic; high-strength paper						
C	35.1±0.4	-4	-7	2.57±0.03	-8	-4
S	33.7±0.3	-2	-2	2.47±0.01	-4	-5
Phenolic; cotton fabric						
J (Grade L)	17.4±0.2	3	3	1.12±0.04	-13	-11
I (Grade C)	20.9±0.3	-2	-2	1.24±0.02	-8	-3
W (Grade C)	20.7±0.2	8	3	1.20±0.04	0	-7
L (Grade C; low pressure)	20.7±0.1	5	2	1.02±0.03	-4	2
Phenolic; rayon fabric						
Z	46.4±0.5	-2	-3	2.22±0.04	-9	-7
Phenolic; asbestos fabric						
K	9.0±0.1	19	9	0.99±0.06	5	10
Melamine; cotton fabric						
M	25.4±0.6	-2	-3	1.62±0.02	-3	2
Unsaturated polyester; cotton fabric						
F	16.1±0.4	-4	-3	0.71±0.02	-2	-1
H	13.1±0.1	-4	-3	0.67±0.02	-14	-12
N	12.1±0.2	-12	-19	0.45±0.01	-8	-16
Unsaturated polyester; glass fabric						
E	34.1±0.1	-13	-16	1.81±0.04	-9	-17
X	41.2±0.3	2	5	1.68±0.01	4	6
Y	34.5±0.2	-6	-5	1.44±0.02	2	1
AA	20.3±0.9	11	0	1.32±0.05	-6	-8
AB	56.5±0.9	-3	3	2.85±0.02	0	-3

a. Each cycle of the test consists of a 24-hour immersion and a 24-hour drying period. Flexural tests were made after 10 cycles of test and reconditioning at 77°F. and 50 percent relative humidity for 48 hours.

b. Average value for six specimens. The accompanying plus and minus value is the standard error.

c. Based on average value for four specimens.

TABLE 7 CHANGES IN FLEXURAL STRENGTH OF LAMINATED PLASTICS AFTER CONTINUOUS IMMERSION IN HEPTANE, TOLUENE, AND SR-6 FUEL BLEND

NBS Material Designation	Initial Flexural Strength (psi)	Specimen Tested	Change ^c After Immersion in Heptane for:			Change ^c After Immersion in Toluene for:			Change ^c After Immersion in SR-6 for:		
			7 Days	30 Days	90 Days	7 Days	30 Days	90 Days	7 Days	30 Days	90 Days
Lignin paper			(%)	(%)	(%)	(%)	(%)	(%)	(%)	(%)	(%)
D	23,500.4	1	-3	-5	-4	-6	-3	-2	-11	-6	-5
		2	-8	-9	-7	-3	-3	-2	-6	-1	-5
Phenolic; high-strength paper											
G	35,100.4	1	-5	-6	-9	-17	-9	-7	-8	-6	-11
		2	-5	-1	-5	-7	-7	-9	-3	-7	-10
S	31,700.3	1	-4	-3	-3	-2	-2	-6	-3	0	-3
		2	-7	-6	-6	-1	-2	-3	-3	-3	-4
Phenolic; cotton fabric											
J (Grade I)	17,400.2	1	-1	1	-1	-3	-1	1	-2	1	-6
		2	0	-1	-1	-3	-1	1	-1	3	-3
I (Grade C)	22,900.3	1	-10	-3	-7	-4	-5	-6	-2	-3	-7
		2	-5	-3	-1	-7	-5	-5	-3	-5	-7
K (Grade C)	20,700.2	1	-4	-1	-7	-1	-4	-3	-1	1	-2
		2	-2	-3	-3	-1	-1	-3	-1	1	-3
Melamine; cotton fabric											
L (Grade C; low pressure)	20,700.1	1	-2	-2	-1	3	1	2	-1	1	-1
		2	-7	-1	-10	-3	-3	-2	-4	3	17
Phenolic; rayon fabric											
Z	46,400.1	1	-6	-4	-5	-3	-4	-5	-3	-3	-5
		2	-6	-2	-4	-3	-4	-5	-3	-3	-7
Phenolic; asbestos fabric											
K	9,000.1	1	11	11	17	13	10	21	18	19	12
		2	11	8	17	20	13	14	9	11	13
Melamine; cotton fabric											
M	25,400.6	1	-9	-5	-6	-2	-2	-4	-6	-7	-5
		2	-7	-5	-8	-2	-2	-5	-6	-5	-7
Unsaturated polyester; cotton fabric											
P	16,100.4	1	-2	-6	-4	-2	-2	-11	-1	-1	-7
		2	-7	-4	-4	-2	-5	-15	-9	-11	-2
N	13,100.1	1	-3	-6	-3	-2	-6	-7	-5	-3	-7
		2	-3	-5	-3	-2	-9	-8	-5	-5	-8
B	12,100.2	1	-19	-29	-19	-9	-12	-34	-37	-30	-31
		2	-17	-21	-17	-7	-16	-30	-27	-21	-23
Unsaturated polyester; glass fabric											
X	34,100.1	1	-17	-12	-11	-20	-14	-16	-16	-15	-20
		2	-17	-13	-14	-22	-14	-16	-13	-13	-25
Y	51,800.3	1	4	7	5	-2	-3	1	7	8	-2
		2	7	5	-5	-2	-3	-5	2	1	-5
AA	34,500.2	1	-11	-9	-14	-2	-13	-16	-11	-11	-15
		2	-11	-8	-11	-2	-17	-17	-7	-11	-16
AB	20,300.9	1	-2	-3	-5	-2	-3	-6	1	8	-3
		2	-5	-5	-5	-2	-3	-5	1	7	-1
	56,500.9	1	-5	1	-3	-2	-2	-1	-7	-7	-8
		2	-5	1	-3	-2	-2	-1	-7	-7	-9

a. Average value for specimens. The average value or minus value is the standard error.

b. One test at 100% humidity.

c. Tested after reconditioning for 7 days at 77°F and 50 percent relative humidity.

d. Based on average value for four specimens.

TABLE 8 CHANGES IN FLEXURAL MODULUS OF ELASTICITY OF LAMINATED PLASTICS AFTER CONTINUOUS IMMERSION IN HEPTANE, TOLUENE, AND SR-6 FUEL BLEND

Material Designation	Initial Flexural Modulus of Elasticity (10 ⁶ lb/in. ²)	Change ^a after immersion in heptane for 7 days			Change ^a after immersion in toluene for 7 days			Change ^a after immersion in SR-6 fuel for 7 days		
		(1)	(2)	(3)	(4)	(5)	(6)	(7)	(8)	(9)
Lignin paper										
D	1.92 ± 0.05	1	-8	-10	-11	0	-1	-10	-11	0
		7	-11	-9	-2	-6	-3	-12	-4	6
Phenolic; high-strength paper										
G	2.57 ± 0.03	1	-6	-11	-10	-14	2	-5	-11	-5
		7	-9	-10	-4	-1	2	-5	-8	-1
S	2.47 ± 0.01	1	-8	-3	0	6	6	-6	-2	-1
		7	-6	-10	-4	1	8	-6	-8	0
Phenolic; cotton fabric										
J (Grade I)	1.12 ± 0.04	1	-20	-14	-2	-5	-2	-16	-14	-4
		7	-15	-16	-6	1	1	-13	-14	-2
I (Grade O)	1.24 ± 0.02	1	-22	-17	2	-8	0	-13	-8	-1
		7	-14	-8	1	-6	0	-10	-2	-2
W (Grade O)	1.20 ± 0.04	1	-15	-6	-2	-11	-2	-17	-19	-3
		7	-15	-11	-9	-9	-2	-16	-1	-5
L (Grade O; low pressure)	1.02 ± 0.03	1	-7	-5	1	-7	4	-3	-4	2
		7	-7	-5	1	-7	4	-3	-4	2
Phenolic; rayon fabric										
Z	2.22 ± 0.04	1	-14	-13	-11	-8	-4	-13	-13	-3
		7	-17	-15	-12	-6	-3	-15	-9	-5
Phenolic; asbestos fabric										
K	0.99 ± 0.06	1	7	-2	12	15	22	-10	12	9
		7	7	-2	12	15	22	-10	12	9
Melamine; cotton fabric										
M	1.62 ± 0.02	1	-7	-4	1	-3	-3	-2	-4	3
		7	-7	-4	1	-3	-3	-2	-4	3
Unsaturated polyester; cotton fabric										
P	0.71 ± 0.02	1	-5	-3	16	19	12	-9	-9	-7
		7	-5	-3	16	19	12	-9	-9	-7
H	0.67 ± 0.02	1	-10	-12	-5	10	-5	-12	1	-10
		7	-12	-11	-7	5	6	-10	-10	-11
N	0.45 ± 0.01	1	-14	-21	-6	1	-1	-14	-16	-17
		7	-17	-16	-8	-1	-1	-14	-16	-17
Unsaturated polyester; glass fabric										
X	1.41 ± 0.04	1	-4	-5	-13	-22	3	-12	-22	-40
		7	-9	-5	-4	-18	-3	-8	-25	-32
Y	1.64 ± 0.01	1	4	4	0	4	24	5	5	0
		7	4	4	0	4	24	5	5	0
AA	1.44 ± 0.02	1	-5	-1	-2	0	5	-2	2	1
		7	-5	-1	-2	0	5	-2	2	1
AB	1.62 ± 0.05	1	-14	-20	1	-5	-5	-23	-26	-6
		7	-8	-9	-1	-5	-5	-23	-26	-6
		7	-7	-7	-9	-9	-1	-9	-8	-4
		7	-11	-12	-7	-3	-5	-11	-5	-9

a. Average values for six specimens. The accompanying plus or minus value is the standard error.

b. Code for this column: 1 = Tested immediately.

7 = Tested after reconditioning for 7 days at 77°F and 50 percent relative humidity.

8. Based on average values for four specimens.

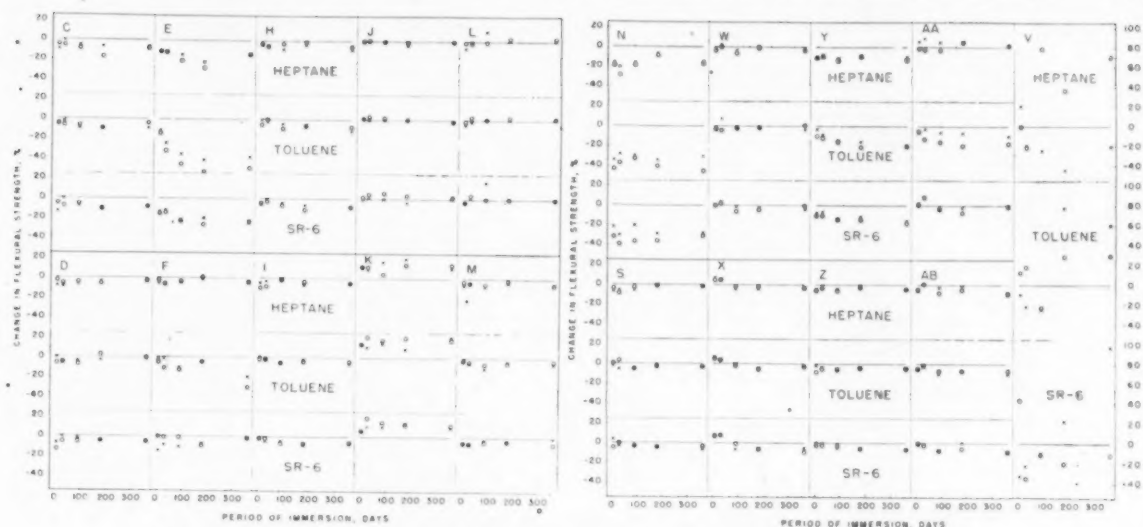


FIG. 6 CHANGES IN FLEXURAL STRENGTH OF LAMINATES IN PROLONGED FUEL-IMMERSION TESTS (O-tested immediately after removal from the fuel. X-tested after reconditioning for 7 days.)

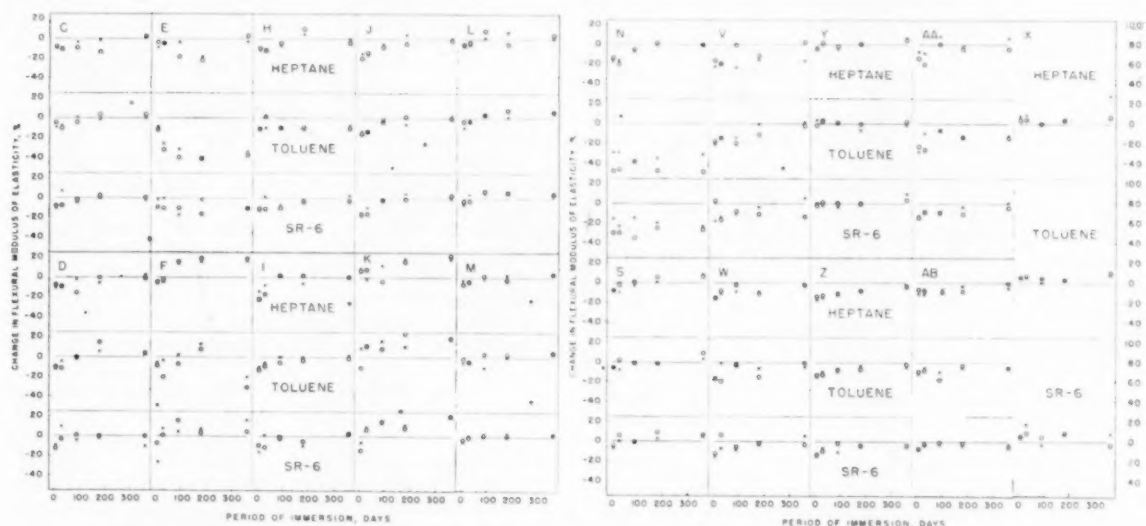


FIG. 7 CHANGES IN FLEXURAL MODULUS OF ELASTICITY OF LAMINATES IN PROLONGED FUEL-IMMERSION TESTS (O-tested immediately after removal from the fuel. X-tested after reconditioning for 7 days.)

tions; where there were exceptions, the differences were usually greatest in toluene. Most of these large differences took place in the unsaturated-polyester laminates.

At no time during the continuous-immersion test, did any cotton-fabric phenolic laminate show losses in flexural strength exceeding 10 per cent in the three fuels. This was also true of two glass-fabric unsaturated-polyester materials, X and AB, the paper-phenolic laminate S, and the rayon-phenolic laminate Z. The cellulose-filled phenolic laminates exhibited the following trend with regard to the flexural modulus of elasticity in the course of the immersion tests: After 7 days of immersion, the changes were losses, and as the test progressed the losses decreased with some samples showing gains at the end of the test. The changes for the cotton-fabric phenolic materials were about

—10 to —20 per cent at 7 days, and at 360 days the changes were about —5 to +5 per cent.

It is noted that, just as in the cyclic-immersion test, the various samples of polyester laminates varied considerably in their flexural-strength behavior on prolonged immersion.

A comparison of the changes in the flexural properties of the various samples after 360 days of immersion in the fuels follows:

Flexural Strength Changes at 360 Days. In heptane only the unsaturated-polyester laminates E, N, and Y showed losses greater than 10 per cent. In toluene the only samples that showed losses greater than 10 per cent in either test condition were all unsaturated-polyester laminates. Samples X and AB were the only materials of this type which did not exceed 10 per cent loss. In SR-6 only the unsaturated-polyester laminates E, N,

TABLE 9 SAMPLES WITH CHANGES IN PROPERTIES GREATER THAN SELECTED VALUES INDICATED IN THIS TABLE AFTER IMMERSION IN HEPTANE, TOLUENE, AND SR-6 FUEL BLEND^a

Property	Heptane	Toluene	SR-6
Weight (> ±1 per cent change):			
Cyclic immersion.....	...	N	N
Continuous immersion, 360 days:			
Tested immediately.....	N, AA	E, F, H, K, N, Y, AA	E, N, AA
Reconditioned.....	...	E, F, N, Y	N
Length and width			
(> ±0.1 per cent change):			
Cyclic immersion.....	N	N	N
Continuous immersion, 360 days:			
Tested immediately.....	N	F, H, K, N	N
Reconditioned.....	N	F, H, K, N	N
Thickness (> ±0.5 per cent change):			
Cyclic immersion.....	AA	N, AA	I, L, M
Continuous immersion, 360 days:			
Tested immediately.....	F, N, X	E, F, N, Y, AA	M, N
Reconditioned.....	AB	E, F, N, Y, AA	M, N, AA
Flexural strength			
(> -10 per cent change):			
Cyclic immersion.....	E, N	E, N	E, N
Continuous immersion, 360 days:			
Tested immediately.....	E, N, Y	E, F, N, Y, AA	E, N, Y
Reconditioned.....	E, N	E, F, H, N, Y	E, N, Y
Flexural modulus of elasticity			
(> -5 per cent change):			
Cyclic immersion.....	C, D, E, H, I, J, N, Z, AA	E, H, J, N, W, Z, AA	H, I, J, N, W, Z, AA
Continuous immersion, 360 days:			
Tested immediately.....	...	E, F, H, N, AA, AB	E, N, AB
Reconditioned.....	...	E, F, H, N, AA	D, E, N

^a The letters are the designations for the laminates tested as shown in Table 1. Due to the variability of the V material, it was not included in this summary.

and Y showed losses greater than 10 per cent. In each of the three fuels and for both test conditions, nearly one half of the samples had losses greater than 5 per cent. The Grade AA phenolic laminate K was the only material which exhibited increases for both test conditions in each of the three fuels:

Flexural Modulus of Elasticity Changes at 360 Days. In heptane none of the samples exhibited losses greater than 5 per cent for either test condition. In toluene the unsaturated-polyester laminates X and Y showed losses of 1 per cent or less in either test condition. The remaining unsaturated-polyester laminates showed losses of 5 per cent or more. In SR-6 the only samples which had losses greater than 5 per cent in either test condition were the unsaturated-polyester laminates E, N, and AB, and the lignin-paper laminate D. The phenolic laminates K, L, and S, and the melamine laminate M were the only samples which exhibited increases for both test conditions in all three fuels, and the phenolic laminate K had the largest increases.

The only sample which exhibited changes not exceeding 5 per cent^b in both flexural strength and modulus of elasticity after 360 days of immersion in each fuel was sample J. Other samples exhibiting satisfactory behavior were the asbestos-fabric phenolic laminate K, which exhibited positive changes, and the cotton-fabric phenolic laminates L and W, which showed no losses greater than 5 per cent but whose increases were more than 5 per cent in some instances. The cotton-fabric unsaturated-polyester resin laminate N showed the greatest losses in flexural properties.

CONCLUSIONS

The following conclusions refer to the actual numerical results obtained in this investigation. Since there may be appreciable differences in the properties of individual sheets taken from the same batch, in different batches made by the same manufacturer, and in similar laminates made by different manufacturers, any general inferences drawn from these data about a given type of laminate should be considered tentative.

^b Changes in the flexural properties less than 5 per cent are not considered significant due to the variability of the material.

1 No one sample exhibited smaller changes than all the other samples in all properties for all fuels and for both cyclic and continuous immersion.

2 In all three fuels, the weight changes of the majority of the laminates were less than 1 per cent in the cyclic test, and did not exceed 1.5 per cent after 360 days of continuous immersion. The largest weight changes were usually obtained with the unsaturated-polyester laminates in toluene.

3 With very few exceptions, mainly cotton-fabric unsaturated-polyester samples, the length and width changes after either the cyclic or the 360-day immersion in the fuels did not exceed 0.1 per cent. In both types of test the changes in thickness were, in the majority of cases, less than 1 per cent. The exceptions occurred mainly in the 360-day immersion test for several unsaturated-polyester laminates in toluene.

4 The best weight and dimensional stability in all three fuels in the cyclic test was observed with the glass-fabric unsaturated-polyester laminate X.

5 After the 360-day immersion test, the weight and dimensional changes were, in the majority of cases, higher for the samples when tested immediately as compared with measurements after reconditioning for 7 days.

6 The changes in flexural strength for the cyclic test and after the 360-day immersion test were, in the majority of cases, negative. However, the losses were less than 10 per cent for all samples, except some unsaturated-polyester laminates. For the latter samples in the 360-day test, greater losses usually occurred in toluene than in the other fuels.

7 The changes in flexural modulus of elasticity were, in the majority of cases, negative in the cyclic and the continuous-immersion tests. In the cyclic test no losses greater than 10 per cent were shown by the samples, except one phenolic laminate and several unsaturated-polyester samples. After 360 days of immersion, no losses greater than 10 per cent occurred except for some unsaturated-polyester laminate samples in toluene or in SR-6 or in both.

8 The unsaturated-polyester laminate samples varied widely among themselves in regard to the magnitude of the change in a given property after the immersion tests.

Current Design Practices for Gas-Turbine Power Elements

By H. D. EMMERT,¹ MILWAUKEE, WIS.

A brief description is presented of certain principles of design and analysis for power elements of commercial gas-turbine plants. These principles are based upon the experience of the gas-turbine engineering group of the author's company. The discussion comprises a review of procedures for analysis of turbine performance and design of blading and blade-carrying elements. Since the mechanical reliability and useful service life of a gas-turbine plant are governed almost entirely by the design of the power element, such a design must be a compromise between requirements for high efficiency, dependability, and low first cost. The fulfillment of these requirements is assisted by the organization of fundamental principles and experience into basic design practices.

INTRODUCTION

NUMEROUS technical discussions have been published concerning the general features and potentialities of gas-turbine plants for land, marine, and air service. This paper is restricted to the consideration of a single component of the gas-turbine plant, namely, the basic power element. The problems under discussion comprise (a) the design of the turbine blade path from the standpoint of fluid mechanics, and (b) the basic principles of stress analysis used for the blades and blade-carrying elements. The mechanical construction of such parts as casings, bearings, supports, and governors is not included.

GENERAL DESIGN PRINCIPLES

Importance of Optimum Design. The net output of a gas-turbine plant is represented by a surplus in power produced by an expansion element over the power demand of a compression element. On an average, the ratio of gross power to net power is of the order of 2 or 3 to 1. Assuming a constant compressor demand, an increase of 1 per cent in turbine efficiency results in a gain of from 2 to 3 per cent in net output and efficiency. This indicates the importance of improving power-element performance to the maximum practical level.

Mechanical reliability and useful service life of a gas-turbine plant are governed to a large degree by the design of the power element. In this element occurs the particularly critical combination of high temperature and high dynamic stress. Reliability and long life are of primary importance for commercial turbines. These requirements are reflected by a tendency toward conservatism in temperature and stresses in such machines when compared with aircraft-turbine practice. Since performance requirements for commercial applications do not permit any appreciable sacrifice in fuel economy, it is necessary to offset the effects of moderate cycle temperatures by increasing

power-element efficiencies at some expense in over-all weight and size.

Basic Turbine-Design Principles. The most important factors which control the type of construction adopted for any specific gas turbine are as follows:

- (a) Desired efficiency level.
- (b) Expected useful service life.
- (c) Required maximum-load capability.
- (d) Desirable variable-load characteristics.

The particular problems associated with commercial applications indicate that certain design principles have definite advantages:

1 The premium placed on performance almost invariably results in the employment of a multistage construction. Turbine efficiency is thereby considerably improved over the level which can be obtained with the lightweight single-stage turbines ordinarily used in aircraft units.

2 The large volumetric flows inherent in high-capacity designs necessitate correspondingly large annular flow areas. These are best provided by high ratios of active blade height to blade-rising mean diameter. Three-dimensional flow considerations therefore become of considerable importance, and the mechanical design of the blading and spindle becomes more difficult.

3 High speeds are desirable to reduce physical size as much as possible. Procurement of large ingots is difficult with many of the better gas-turbine alloys. In addition, handling and fabricating problems in the shops increase rapidly with size of part.

The foregoing principles lead to the conclusion that the most practical design for commercial application is one incorporating a plurality of stages, employing maximum blade-height ratios in the low-pressure elements, and rotating at a maximum speed. Fig. 1 shows a cross section through the blade path of such a turbine, this particular design being representative of units intended for commercial power applications.

BLADE-PATH DESIGN AND PERFORMANCE ANALYSIS

Turbine Efficiency. The internal efficiency of a turbine relates the actual power produced by the turbine stages to the theoretical power available in an isentropic expansion from the total pressure and temperature at the turbine inlet to the static pressure at the turbine exhaust. It is a function of the following basic variables

$$\eta_i = (\eta_s)(RF) - \% \Delta h_L \dots \dots \dots [1]$$

where

- η_i = internal efficiency, per cent
 η_s = average stage efficiency, per cent
 RF = reheat factor
 $\% \Delta h_L$ = leaving loss, per cent

The stage efficiency takes into account the losses incurred in each element due to gas friction and leakage. It is primarily dependent upon the operating conditions and configuration of the staging, and it can be controlled within fairly wide limits by the designer.

The reheat factor originates from the fact that as the gas

¹ Engineer in Charge, Engineering Design, Turbo-Power Development Department, Allis-Chalmers Manufacturing Company, Mem. ASME.

Contributed by the Gas Turbine Power Division and presented at the Annual Meeting, New York, N. Y., November 28-December 3, 1948, of THE AMERICAN SOCIETY OF MECHANICAL ENGINEERS.

NOTE: Statements and opinions advanced in papers are to be understood as individual expressions of their authors and not those of the Society. Paper No. 48-A-170.

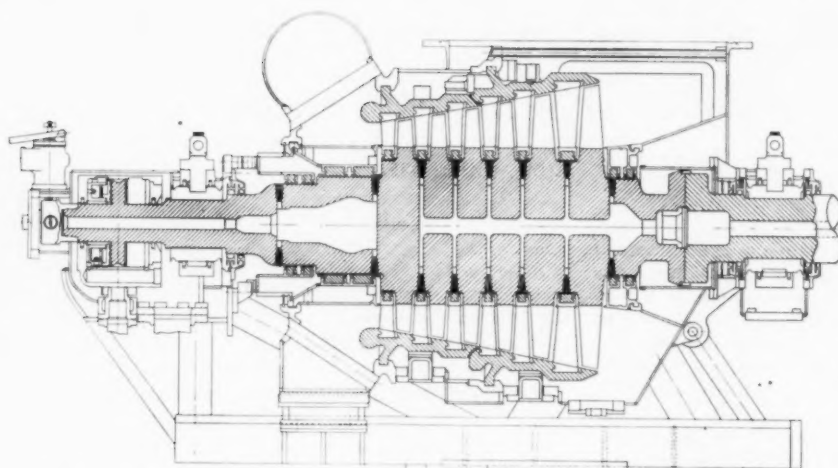


Fig. 1 Cross Section Through Typical Commercial Gas-Turbine Power Element

progresses through the blading, friction and leakage cause the actual temperatures to be slightly above those corresponding to an expansion without losses. This has an apparent effect of increasing the over-all efficiency slightly above the incre-

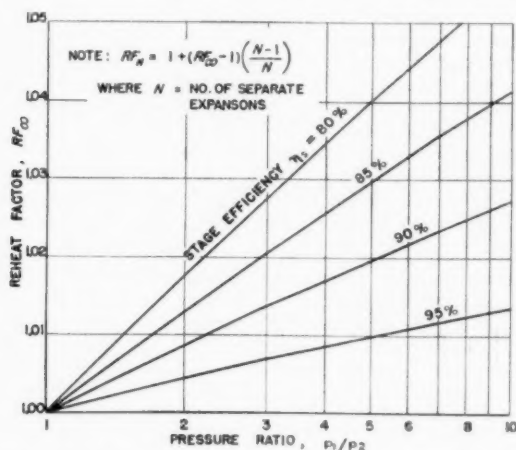


Fig. 2 Reheat Factors for Gas-Turbine Expansions
(Curves are based upon a mean-specific-heat ratio of 1.350.)

mental stage efficiency. Fig. 2 shows a reheat-factor plot computed from the following formula (1)²

$$RF_{\infty} = \frac{1}{\eta_s} \left[\frac{1 - \left(\frac{p_2}{p_1} \right)^{\eta_s \frac{k-1}{k}}}{1 - \left(\frac{p_2}{p_1} \right)^{\frac{k-1}{k}}} \right] \dots \dots \dots [2]$$

where

RF_{∞} = reheat factor for infinite stages
 p_1 = turbine inlet pressure
 p_2 = turbine exhaust pressure
 k = mean-specific-heat ratio

² Numbers in parentheses refer to the Bibliography at the end of the paper.

Leaving loss is proportional to the residual kinetic energy contained in the gas leaving the turbine. Shaft power is generally the only useful output from a commercial gas turbine, and residual kinetic energy is unavailable for further use. The magnitude of the leaving loss is primarily dependent upon the relation between the total volumetric flow of gas and the annular flow area at the last row of blades. The large volumetric flow in high-capacity units necessitates the use of a considerable amount of exhaust annulus area if the leaving loss is to be held to an acceptable value.

Stage Performance. Both theory and experience indicate that the following basic factors almost completely control the performance of an individual stage:

- 1 Primary factors: (a) Isentropic velocity ratio
 (b) Stage reaction
 (c) Leakage configuration
- 2 Secondary factors: (a) Pressure ratio
 (b) Parasitic losses
 (c) Viscosity effects

Numerous tests have shown that isentropic velocity ratio is the most important criterion establishing general performance level of a stage, regardless of the actual physical configuration. This parameter measures the energy loading for the stage and is defined by the following relation

$$\frac{u}{c_0} = \sqrt{\frac{\Delta h_u}{\Delta h_s}} \dots \dots \dots [3]$$

where

u = blade velocity at blade-ring mean diameter, fps
 c_0 = gas velocity corresponding to stage isentropic enthalpy drop, fps

$$\Delta h_u = \text{stage equivalent blading energy, Btu per lb} \\ = \frac{u^2}{2gJ}$$

$$\Delta h_s = \text{stage isentropic enthalpy drop, Btu per lb} \\ g = 32.17 \text{ ft/sec}^2 \\ J = 778.26 \text{ ft-lb/Btu}$$

For a given set of blading operating with a moderate pressure drop, changes in flow kinematics within the blading are adequately reflected by changes in the isentropic velocity ratio. Fig. 3 shows two examples of basic blading-efficiency curves as derived by test. Curves such as these represent blading performances only, and stage efficiencies ordinarily will be somewhat lower due to the effects of other factors.

As a general rule, the number of stages to be employed in a specific turbine design is determined from the selection of a

* Reaction-turbine designers customarily use the isentropic drop per row, rather than per stage, in Equation [3]. However, the use of the stage drop is more general in application.

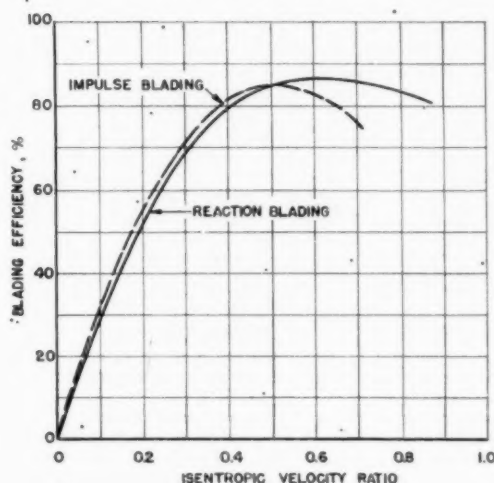
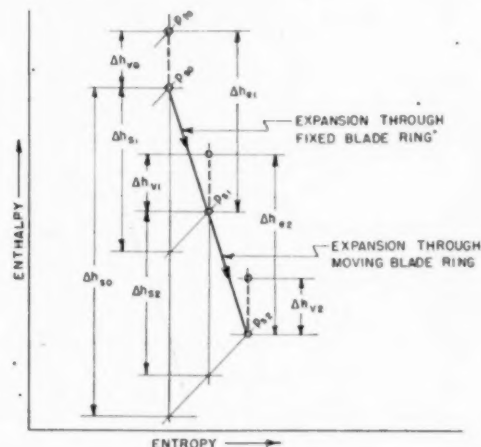


FIG. 3 TYPICAL BLADING-EFFICIENCY CURVES



- Δh_{v0} = KINETIC ENERGY ENTERING STAGE
 Δh_{s0} = STAGE ISENTROPIC ENTHALPY DROP
 Δh_{s1} = ISENTROPIC ENTHALPY DROP ACROSS FIXED BLADE RING
 Δh_{e1} = EFFECTIVE KINETIC ENERGY LEAVING FIXED BLADE RING
 Δh_{v1} = KINETIC ENERGY ENTERING MOVING BLADE RING (RELATIVE TO MOVING BLADE RING)
 Δh_{s2} = ISENTROPIC ENTHALPY DROP ACROSS MOVING BLADE RING
 Δh_{e2} = EFFECTIVE KINETIC ENERGY LEAVING MOVING BLADE RING (RELATIVE TO MOVING BLADE RING)
 Δh_{v2} = KINETIC ENERGY LEAVING STAGE

FIG. 4 ENTHALPY-ENTROPY DIAGRAM OF STAGE EXPANSION

desirable velocity ratio at the normal operating load. The curves in Fig. 3 show that high velocity ratios are required for good efficiency. However, the number of stages rises rapidly as the velocity ratio increases. A considerable amount of investigation of each design is necessary to obtain a satisfactory balance in this respect.

The second major factor affecting stage performance is the stage reaction. This parameter is best explained by reference to Fig. 4 which shows the energy quantities in a stage on an enthalpy-entropy diagram. The expansion through a stage is accomplished in two distinct steps, namely, a partial expansion

through the fixed blade ring, followed by an additional expansion through the moving blades. The distribution of energy assigned to these two successive expansions is at the control of the designer and is established by means of the stage reaction. Stage reaction is defined as the ratio of the isentropic enthalpy drop across the moving blades to the isentropic enthalpy drop across the stage.

Two opposing considerations influence the amount of reaction used in a specific turbine. Purely from the performance standpoint, it is preferred to use a stage reaction of approximately one half. This corresponds to the conditions in normal reaction blading, and maximum efficiency is obtained provided velocity ratio is high and leakage losses are low. If the turbine isentropic enthalpy drop is large, the number of stages may become excessive. When this occurs it is frequently desirable to decrease the number of stages by decreasing the average velocity ratio of the high-pressure elements. The reaction in these elements is also lowered, and they assume the form of a normal impulse-blading configuration. This is particularly desirable when high temperatures and stresses are involved, since a reduction in stage reaction lowers the effective impact temperature on the moving blades.

Leakage control plays a dominant part in establishing stage efficiency level. Gas leakage through operating clearances between rotating and stationary parts represents a loss of working fluid. It is therefore desirable that clearances be kept to the minimum value consistent with reliability, and that the leakage gas path be made as tortuous as possible.

Both shrouded and open-ended blades are used. For blades operating at high tip velocities, shroud weight adds considerably to the centrifugal stress at the blade base. If the blade is long, the leakage and end-loss effects can be kept small and at the same time safe operating clearances at the blade tip can be maintained. Open-ended construction is preferred in such a design (see Fig. 1). Leakage control for short blades is better if shrouding is installed.

Spindle glands are normally designed with step-type labyrinth seals similar to those shown in Fig. 1. This same construction is used for interstage seals in disk-and-diaphragm blade paths. Accurate tests have been made and correlated by simple theory (2) to determine the leakage characteristics of various types of seals. The performance with air of a typical standard labyrinth design is summarized in Fig. 5.

Pressure ratio is listed as a secondary factor influencing stage performance. For single-stage turbines, pressure ratio may become of major importance. Compression shock losses and poor control of fluid direction may seriously depreciate efficiency

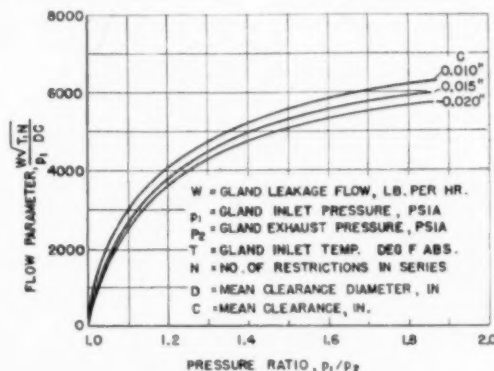


FIG. 5 LEAKAGE FLOW CHART—SUMMARY OF TESTS OF STEP-TYPE SPRING-BACK LABYRINTH SEAL

when high pressure drops are employed across individual elements. However, the pressure ratio across each stage of a multistage turbine is generally small, with a corresponding decrease in influence on the individual elements. The Mach number of the mean fluid stream relative to the blading seldom exceeds about 0.65. This magnitude causes little difficulty due to shock or choking as long as the flow is accelerated.

Parasitic losses resulting from disk or spindle gas friction are not high in gas turbines of the type under consideration. However, they are accounted for in performance estimation through empirical formulas derived from test analysis.

The influence of viscous forces within turbine staging is measured by the Reynolds number. Laboratory tests on small turbine elements are known to indicate a Reynolds-number effect, but the importance of this factor has not been apparent from tests on full-scale commercial turbines. The influence is sufficiently small in large units so as to be indeterminate in the presence of other more powerful factors.

Basic Stage Analysis. Requirements for optimum performance at high speed make it necessary in most cases to design the blading configuration for a new turbine to conform to a specific application. It is therefore essential that there be available detailed procedures for turbine-stage analysis. The designer is thereby able to predict the approximate actual conditions existing within each element and can proportion the blades accurately with respect to shape and setting.

Blading analyses by means of filament-flow theory and vector diagrams are as old as the steam-turbine art, but these conceptions still represent the most powerful tools available to the practical gas-turbine designer. Two basic requirements must be met in applying vector diagrams to blading performance and flow analysis:

- 1 The velocity magnitudes must represent integrated mean values rather than highly peaked or depressed local values.
- 2 The velocity directions must represent mean fluid directions, and not necessarily blade-profile geometric angles.

Cascade tests have contributed to a certain extent to the alignment of current design information, but the main source of data has always been analyses of over-all turbine tests. Actual working procedures are admittedly oversimplified from the viewpoint of the highly developed mathematics of modern aerodynamics. It cannot be assumed that the actual flow conditions within a stage are in exact agreement with predictions from simplified vector-diagram analyses. However, reasonable correspondence between prediction and performance has been thoroughly demonstrated, provided suitable control is exerted by continual comparison with test results.

The basic variables in blade-ring calculations are shown in Fig. 6. The data apply to either fixed or moving blades, provided the velocity magnitudes and directions are taken relative to the blade ring under consideration. The most important quantity required in blade-ring analysis is the effective kinetic energy at the ring outlet. This energy is computed from the following relation

$$\Delta h_{e2} = \phi^2_E (\Delta h_{e1} + C_i \phi^2_i \Delta h_{e1}) \dots \dots \dots [4]$$

where

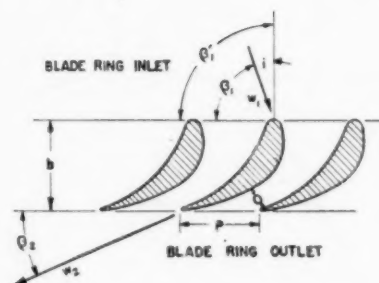
ϕ^2_E = expansion-energy coefficient

C_i = incidence coefficient

ϕ^2_i = kinetic-energy coefficient

See Fig. 6 for other symbols.

The primary loss resulting from turbulence and wall friction within the blade passage is reflected by the expansion-energy coefficient. This coefficient is determined from the profile



BLADE RING DATA:—

- b = AXIAL WIDTH, IN.
- β_1 = BLADE INLET ANGLE, DEG.
- O = THROAT OPENING, IN.
- P = CIRCUMFERENTIAL PITCH, IN.
- O/P = OPENING COEFFICIENT
- β_2 = ANGLE OF EFFLUX, DEG.
- $\gamma = \sin^{-1}(O/P)$ (SEE FIG. 12)
- θ = DESIGN DEFLECTION ANGLE, DEG. $\theta = 180^\circ - (\beta_1 + \beta_2)$

GAS FLOW DATA:—

- ϕ_1 = GAS INLET ANGLE, DEG.
- i = INCIDENCE ANGLE, DEG.
- $\phi_1 = \phi_1 - \phi_1$
- w_1 = INLET VELOCITY, FPS
- w_2 = EFFECTIVE OUTLET VELOCITY, FPS
- Δh_{e1} = KINETIC ENERGY AT INLET, BTU/LB.
- Δh_{e2} = ENTROPIC ENTHALPY DROP, BTU/LB.
- Δh_{e2} = EFFECTIVE KINETIC ENERGY AT OUTLET, BTU/LB.

FIG. 6 BLADE-RING ANALYSIS

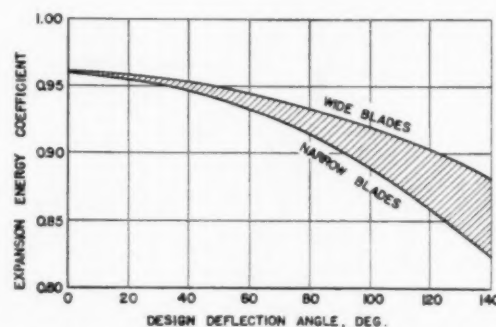


FIG. 7 VARIATION OF EXPANSION-ENERGY COEFFICIENT WITH DESIGN DEFLECTION ANGLE

width and deflection angle, as shown in Fig. 7. Tests indicate that the effective energy obtained from a given amount of inlet kinetic energy is less than that which is realized when the same quantity of available energy is supplied by pressure drop. In Equation [4] the inlet kinetic energy is reduced by a kinetic-energy coefficient. This coefficient is normally assumed to be equal to the expansion-energy coefficient. The rule is rough, but it is justified by an elementary theory of blade friction loss. (3). When the inlet velocity vector forms a definite incidence angle with reference to the blade leading edge, an additional loss occurs which is evaluated by means of the incidence coefficient. This coefficient is a function of the blade-nose design and the angle of incidence as shown in Fig. 8.

The angle of efflux from the ring is assumed to be approximately equal to arcsine (O/P) , where O is the blade throat opening and P is the blade circumferential pitch. The accuracy of this simple rule is adequate for small efflux angles. It is discussed in more detail in a later section.

Establishment of the average velocity magnitudes and directions within a stage permit the determination of tangential velocity components. Estimated blading output per pound of gas flow may then be found by entering these data into the basic turbine equation

$$\Delta h'_w = \frac{u_1 c_{t1} - u_2 c_{t2}}{gJ} \quad [5]$$

where

$\Delta h'_w$ = blading output, Btu per lb

u_1 = blade velocity adjacent to the fixed-ring outlet mean diameter, fps

u_2 = blade velocity at the outlet mean diameter of the moving ring, fps

c_{t1} = tangential component of effective velocity leaving fixed ring, fps

c_{t2} = tangential component of velocity leaving stage, fps

The gas flow is found from the continuity equation using the effective velocity, area, and gas density at the blade-ring throat. Net stage output may then be calculated by subtracting clearance and parasitic losses from the gross blading output.

Three-Dimensional Considerations. Radial variations in circumferential pitch between blades increase as the blading is lengthened. If the blades are installed with normal pitch at the blade-ring mean diameter, the pitch at the tip may become excessive and result in poor control of fluid direction. At the inner radii, the pitches may become so small as to restrict the gas considerably. Furthermore, unless the flow is controlled properly, the tangential velocity components along the outlet plane of the fixed blade ring tend to throw the fluid outward. This

centrifugal action results in a massing of the flow toward the tips and a starving of the blade passages at the roots.

The three-dimensional flow problem has been attacked quite thoroughly using approaches based on aerodynamic theory. For practical purposes, however, a simple and adequate solution is obtainable from rather elementary conceptions. The basic elements of the problem are presented in Fig. 9. The upper diagram shows the velocity components of a fluid stream leaving a fixed ring of blades at a given radius. In the lower diagram the same velocities are projected onto the outlet plane of the blades. Consideration of the forces acting on an incremental mass of gas indicates that the static pressure at the fixed-ring outlet must gradually increase with radius in accordance with the following equation

$$\frac{dp}{dr} = \rho \frac{c_t^2}{r} \quad [6]$$

where

p = static pressure at fixed-ring outlet, psfa

r = radius, ft

ρ = mass density of gas, lb-sec²/ft⁴

c_t = tangential component of velocity leaving fixed ring, fps

Three controlling premises are made in the practical design of blading where special provision is to be incorporated for maintenance of radial equilibrium:

- 1 The basic equation for radial stability of flow, as given in Equation [6], is to be satisfied over the entire outlet plane of the fixed blade ring.
- 2 The mass flow through the stage is to be distributed evenly over the entire stage annulus.
- 3 The isentropic enthalpy drop across the stage is to be constant at all radii in the stage annulus.

Stages designed in accordance with these conceptions exhibit the following characteristics:

- 1 The fixed blades have almost symmetric profiles at all radii.
- 2 The moving-blade profiles vary with radius. At the inner radius, the profile shape approaches that of a normal impulse blade. An approximately normal reaction-blade profile is used at the mean radius. At the tip, the profile assumes the form of a low-cambered airfoil of medium thickness.

Analyses of tests on both steam and gas turbines incorporating such blading have indicated that appreciable improvements in efficiency are attained in comparison with more conventional designs. In addition, improved accuracy has been obtained with respect to prediction of mass-flow characteristics.

Turbine Performance. The performance of a complete turbine depends primarily upon the characteristics of the individual stages composing the turbine. However, it is essential that the design be established and controlled from the standpoint of the complete unit, rather than as an assembly of completely independent elements. Poor design of any one stage affects elements both upstream and downstream from that point. The residual kinetic energy from each stage except the last is available to the succeeding stage. With adequate care in design, this energy is recoverable to a large extent.

Other factors than stage design may have appreciable effects on performance. Pressure drops in the inlet and exhaust passages are particularly important. Low velocities, gentle changes in flow direction, and freedom from obstructions are essential if harmful reductions in both performance and load capability are to be prevented (4). Radiation losses may reach significant values in high-temperature units, particularly at light load. Adequate insulation is mandatory, not only for the turbine proper

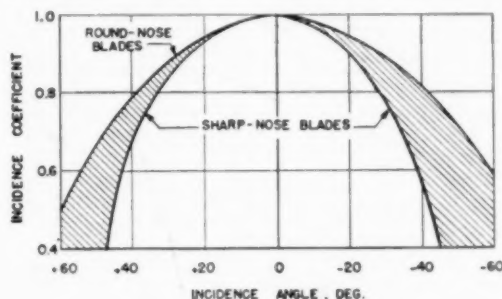


FIG. 8 VARIATION OF INCIDENCE COEFFICIENT WITH INCIDENCE ANGLE

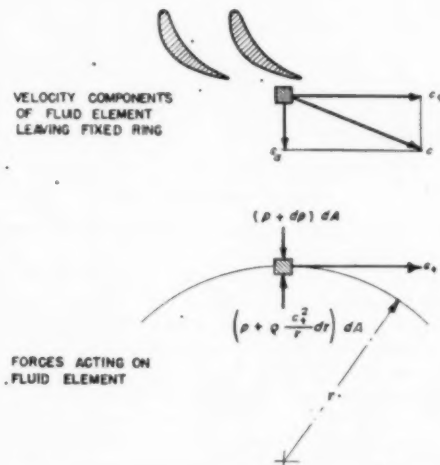


FIG. 9 VELOCITY COMPONENTS AND FLUID FORCES AT FIXED-BLADE-RING OUTLET

but also for all interconnecting piping handling hot gas. Mechanical losses, as imposed by bearings, reduction gears, and lubrication and governor oil pumps, are generally small for commercial gas turbines.

Over-all turbine performance is determined analytically by combining the results of stage calculations and then correcting for the external effects just discussed. Dimensional analysis assists in correlating the influences of the various factors. For practical purposes the performance of a given turbine can be represented adequately in terms of the following simplified parameters.

$$\left(\frac{W \sqrt{T_{01}}}{p_{02}} \right), (\eta_t) = f \left(\frac{p_{01}}{p_{02}} \right), \left(\frac{n}{\sqrt{T_{01}}} \right) \dots \dots \dots [7]$$

where

- W = gas flow, lb per hr
- T_{01} = total temperature at inlet, deg F abs
- p_{01} = total pressure at inlet, psia
- p_{02} = static pressure at exhaust, psia
- η_t = internal efficiency, per cent
- n = turbine speed, rpm

Fig. 10 is a general performance map in terms of these parameters for a turbine rated at 12,000 gross bhp. The calculation of

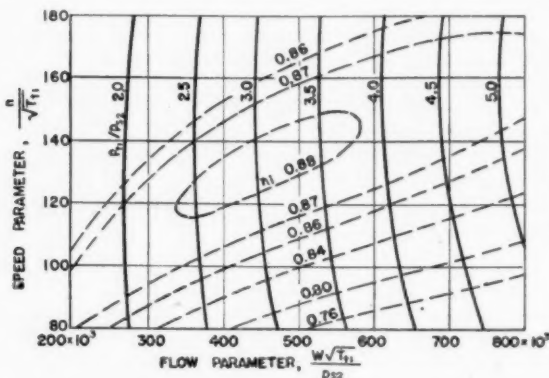


FIG. 10 TYPICAL GAS-TURBINE POWER-ELEMENT PERFORMANCE MAP

such a chart represents the final step in the thermodynamic analysis of each turbine design. The accuracy of the over-all design procedure is measured by the degree of correlation on such a chart between computed and test performance.

TURBINE-BLADE DESIGN

Standard Blade Profiles. Each steam-turbine manufacturer has conducted over a period of years extensive shop and field tests on the blading configurations used in his particular turbine designs. These programs have resulted in a standardization within each company of not only blade profiles but also blade pitches and settings for the best compromise between efficiency and cost (5).

A number of commercial gas turbines have been built utilizing standard blade profiles of various types. These machines have given excellent performance within their normal ranges of application. The general trend, however, has been toward higher rotative speeds with the accompanying advantages of reduced size and weight. Ratios of blade length to mean diameter are of necessity increased in such machines, and considerations of both

three-dimensional flow effects and blade stresses have led to the general adoption of blades with warped surfaces and high degrees of taper. Standard profiles are, therefore, not ordinarily applicable, and each new turbine design requires special profile development to some degree.

Basic Profile-Design Principles. The significant dimensions and angles used to control profile design are illustrated in Fig. 11. The most important parameter is the opening coefficient, which is defined as the ratio of the minimum passage width or throat opening between adjacent blades to the circumferential pitch of the blades. Control of both fluid efflux angle and mass flow is exerted primarily by means of the opening coefficient. As long ago as 1924, test data published by the Steam Nozzles Research Committee in England (6) showed that, for the particular nozzles and blades tested, the fluid angle was given quite closely by arcsine (O/P). Subsequent tests, both published and unpublished, have verified this approximate relationship within a reasonable range. General experience indicates that the curve in Fig. 12 provides a relatively accurate guide. The curve shows an increasing deviation of the fluid angle from arcsine (O/P) as the opening coefficient is increased.

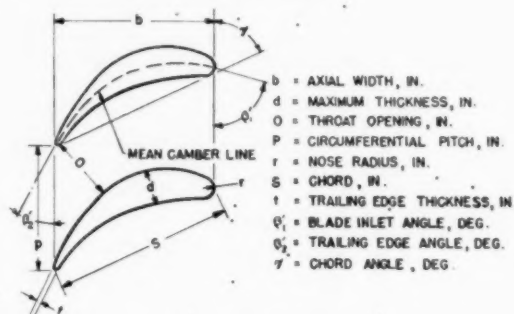


FIG. 11 PROFILE AND BLADE-RING NOMENCLATURE

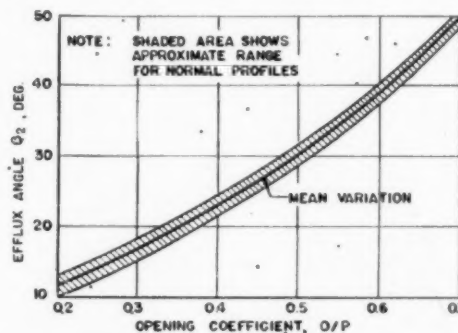


FIG. 12 VARIATION OF EFFLUX ANGLE WITH OPENING COEFFICIENT

Blading performance is affected to a large extent by the aerodynamic loading on the profiles. The resultant force acting on a profile corresponds to the integrated pressure differences between the convex and concave surfaces. In closely pitched blades, these pressure differences and their accompanying turbulence losses are reduced. However, losses due to surface friction are increased. Wide pitching decreases surface-friction loss, but aerodynamic loading is increased. This may induce stalling with an accompanying rapid drop in performance.

Aerodynamic loading is a function of the cascade solidity or chord/pitch ratio. The permissible ranges of blading solidity for

standard profiles have been fairly accurately established by test. Complete correlation of test results has not been attained for all types of profiles over the range from sharp-edged high-deflection impulse blades to low-camber small-deflection airfoils. However, sufficient data to permit interpolation between known optimum settings have been assembled and interpreted in terms of an aerodynamic loading coefficient (7).

For the practical design of a blade, vector diagrams at control points along the blade height are established from the data in the previous sections. The requirements for fixed blade rings are generally such that normal reaction profiles can be used. The contours, pitches, and settings at all radii are established from experience with such configurations. The vector diagrams for long moving blades require that the profiles be varied along the radius. The fluid deflection angle at the blade base is generally large, and highly cambered, closely pitched profiles must be used. Depending upon the stress conditions and the root design, a ratio of circumferential pitch to axial width of from 0.45 to 0.60 is ordinarily selected. The profile at the tip is normally designed as a low-camber airfoil of medium thickness. The aerodynamic loading coefficient is brought into use here, the solidity being established such that the loading coefficient does not exceed a permissible maximum value.

Blade Layout. Required blade pitches, throat openings, and axial widths or chords are established by application of the principles described in the previous paragraphs. Profiles are then laid out with the following considerations for guidance:

- 1 The stress in a blade due to centrifugal force is proportional to the blade volume above the point of stress. Profile thicknesses and cross-sectional areas must therefore be closely controlled within limits prescribed by preliminary stress analysis.

- 2 Geometric inlet and outlet angles are set at approximately the desired fluid angles. Exact correspondence is not necessary and is seldom obtained. The selection of inlet angle varies with the partial-load performance requirements for the stage and turbine.

- 3 Profile nose design depends upon stress conditions and fluid velocities. Moderately small nose radii are ordinarily prescribed. Trailing-edge thicknesses are consistent with the particular manufacturing process to be used and vary from approximately 1 per cent of the chord to not over 8 per cent of the throat opening.

It is considered essential that the passage area between adjacent blades converge at all points in the direction of flow. The walls of the passage as formed by the blade surfaces are kept

free of sharp changes in radius of curvature. The actual contours of the profiles are described by combinations of either circular arcs or parabolic arcs, depending upon the desired degree and rate of change of curvature. Fig. 13 shows a set of profiles designed in accordance with these principles.

For ease in manufacture, it is usually desirable that the blade surfaces between the base and tip profiles be in the form of warped conical surfaces generated by a series of straight lines. Such a design greatly simplifies the diemaking problem for forged and cast blades. It is essential when the blades are to be produced by standard machining processes.

The moving blading of a stage designed in accordance with these general procedures is shown in Fig. 14. The stage efficiency determined by test for the element incorporating this particular wheel is approximately 88 per cent at the design conditions. This indicates the general performance level obtainable from such blading.

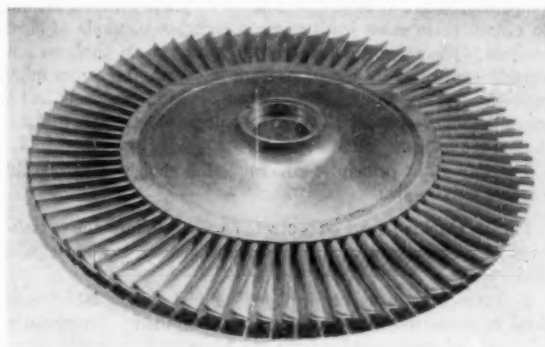


FIG. 14 BLADED GAS-TURBINE DISK

MATERIALS AND DESIGN STRESSES

High-Temperature Materials. There are many considerations which influence the selection of materials for gas-turbine construction. Of necessity, a limited number of criteria must be established to permit direct comparisons of available alloys, and certain properties must be adopted for quantitative use in design calculations.

Allowable working stresses in high-temperature portions of the blade path are based on rupture strength. Adequate 1000-hr stress-rupture data are available for nearly all materials considered applicable to commercial gas-turbine use (8). Consequently, little extrapolation of data is necessary for relatively short-service-life designs. Some uncertainty is generally involved for long-life turbines, but extrapolation is a relatively safe procedure as long as it is limited to approximately one logarithmic time cycle, and ductility can be predicted to remain sufficiently high. Materials which show a tendency toward brittle failure in long-time rupture tests are avoided.

For parts operating at moderate temperatures, the use of yield strength as a design stress criterion has been adopted from steam-turbine practice. Adequate yield strength is essential to prevent harmful deformations due to pure overstressing. Judgment must be exercised, however, since for most alloys yield strength and ductility vary somewhat inversely. Low ductility has been considered acceptable in certain cases, but it is believed that adequate test-bar elongation must be maintained in materials for large thick parts, particularly since uncertainty exists with many alloys regarding changes in ductility over extended periods of time at high temperature.

At the present time, creep-rate and total-deformation data

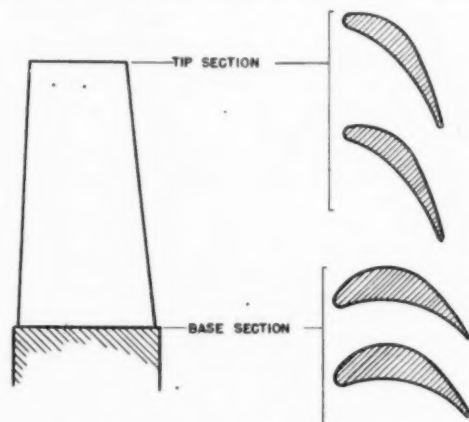


FIG. 13 TYPICAL MOVING-BLADE PROFILES

are seldom used for establishing actual working stresses for rotating parts. Stresses which are considered to be permissible from the standpoints of rupture strength and yield strength generally correspond to low values of total deformation. Such deformations are slow and steady in nature and are subject to determination by periodic inspection after a machine has been placed in operation.

Fatigue strength at operating temperature is of considerable importance in selecting blade materials. Accurate fatigue data are not available for many high-temperature alloys, and some materials exhibit no well-defined endurance limit, particularly where conditions conducive to stress corrosion are also present. Compensation for inadequate fatigue data is obtained by keeping bending stresses low and controlling blade vibrational characteristics.

Selection of Design Stresses. The present state of knowledge concerning the effects of temperature on metals and the actual temperatures and stresses encountered by parts within a turbine, do not in most cases justify overly complex methods of stress analysis. Discrepancies involved in using simple analyses adequately controlled by experience are less than the errors inherently present due to variations in properties of materials and to unpredictable stresses. These considerations make essential the use of moderate design stresses.

The important principles governing the choice of permissible working stresses are:

- 1 The machine must be protected against failure due to either fracture or excessive local deformations, under any anticipated load conditions.
- 2 Protection must be provided against unavoidable variations in properties of the materials as installed. Unwarranted rejections of materials for large machines lead to costly delays in manufacture and shipment.
- 3 Some margin is essential due to inaccuracies in stress analysis. These inaccuracies result primarily from a lack of complete knowledge of the true stresses existing in many parts. They also arise to some extent from the use of certain simplified stress-analysis procedures which are tolerated only for the purpose of shortening engineering time.

Of the many types of stresses which are encountered in gas-turbine design, average stresses in tension, compression, shear, and bending are most easily determined. Therefore they are used as the guiding criteria. Local high stresses due to stress raisers of various types are taken into account where necessary by stress-concentration factors. In many cases, such stresses are safely relieved by local yielding without failure, as a result of the plasticity of the material at operating temperature. Variable stresses are generally estimated from computed average bending stresses.

The selection of working stress is based on the operating temperature of the part and the specified service life for the turbine. For a given operating temperature, service-life considerations lead to a wide variation in permissible working stress. As a general rule, turbines are classified as short-life units if their expected-life cycle at maximum temperature is less than 10,000 hr, and as long-life units if the corresponding time is 10,000 hr or more.

The type of materials-data curve shown in Fig. 15 is used for general gas-turbine design calculations. The practical value of this type of presentation lies in the fact that all parts of a given turbine are normally designed for the same life, but large differences in operating temperature exist between the high and low-pressure ends of the unit. The appropriate working stress for a particular part is determined by applying the selected factors

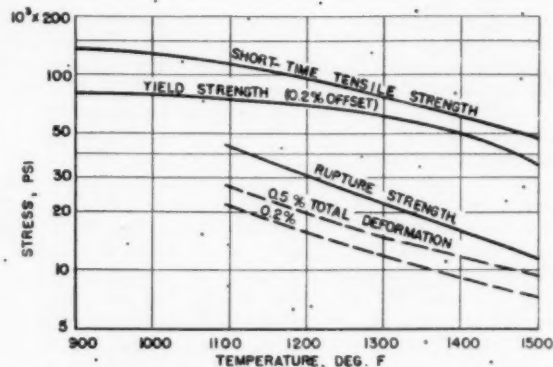


FIG. 15 MATERIALS-DATA CURVE—WROUGHT S-590 10,000 HOURS

of safety to the material properties at the proper temperature ordinate.

STRESS ANALYSIS

Blade Stresses. Blading stress analysis is concerned with a determination of the stresses set up by the centrifugal and bending forces generated by rotation and fluid pressure differences. The highest stresses encountered are almost invariably those resulting from centrifugal forces in the rotating parts. The tensile stress imposed on the base profile of a blade by centrifugal force can be calculated from the following formula

$$s_c = 4.52 \gamma f_1 A \left(\frac{n}{1000} \right)^2 \dots \dots \dots [8]$$

where

- s_c = average tensile stress, psi
- γ = specific weight of blading material, lb per cu in.
- f_1 = taper factor
- A = annular area of blade ring, sq in.
- n = rotative speed, rpm

The taper factor is unity for constant-cross-section blades and, assuming constant density of blading material, the stress becomes a function of only annular area and speed. Tapered blades are used where the installation of constant-section blades would result in excessive stresses. The amount of taper permitted in any particular blade is dependent upon the degree to which both flexural strength and efficient blade shape can be maintained. Fig. 16 shows the stress reduction which can be accomplished with various degrees and types of taper.

Basic bending stresses are generated by changes in gas velocity through the blades and by static pressure differences across the blades. Axial and tangential forces per unit length of blade are determined from the estimated flow conditions in the stage. Integration of these forces yields total component loads from which are determined the moments acting on any given profile of the blade.

The maximum stress in a blade is generally at the concave side of the leading edge of the base profile, since the stresses due to centrifugal force and gas bending force are additive in tension at this point. The total tensile stress resulting from centrifugal force and average bending force therefore constitutes the maximum steady stress in the blade. Variable stresses are expressed as percentages of the average bending stresses, and the effects of stress concentration are taken into account. As shown in Fig. 17, the maximum stresses in moving blades are

$$s_s = s_c + s_b \dots \dots \dots [9]$$

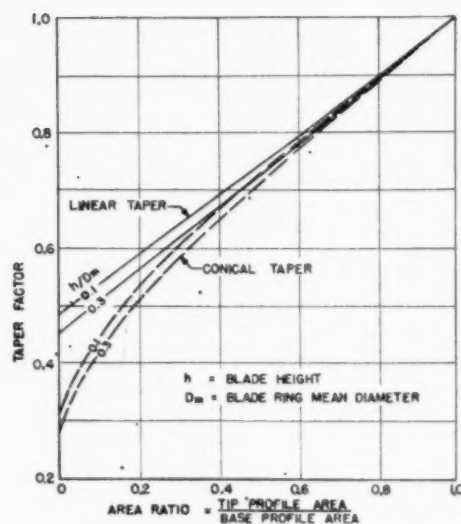


FIG. 16 VARIATION OF TAPER FACTOR WITH BLADE-PROFILE AREA RATIO

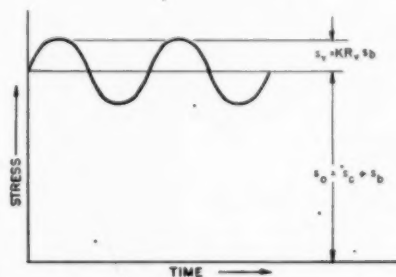


FIG. 17 ASSUMED BLADE-STRESS DIAGRAM

$$s_s = KR_s s_b \dots \dots \dots [10]$$

where

- s_s = maximum steady stress, psi
- s_v = maximum variable stress, psi
- s_c = centrifugal stress, psi
- s_b = average bending stress, psi
- K = stress concentration factor
- R_s = ripple factor

Fillet radii and thickness ratios are such that the stress-concentration factor seldom exceeds 1.5. The ripple factor is a function of the blade pitches, flow conditions, and blade frequency, and it may reach values as high as 0.5 under adverse circumstances. It is somewhat lower with blade frequencies remote from those of possible exciting forces.

Stresses as determined by the foregoing formulas are compared analytically with an assumed failure line on either an endurance limit-yield strength diagram (9) or an endurance limit-rupture strength diagram, as shown in Fig. 18. A minimum factor of safety of 2 is maintained for both comparisons. The actual stresses for use on the rupture-strength diagram are calculated at normal speed, and those for use on the yield-strength diagram are calculated at 120 per cent speed. This overspeed represents the maximum value for which commercial gas turbines

are normally designed to withstand harmful permanent deformations.

Blade-Frequency Analysis. Accurate control of blade frequency is essential to insure that vibratory stresses do not exceed the limits assumed in stress analysis. Normally, a new blade

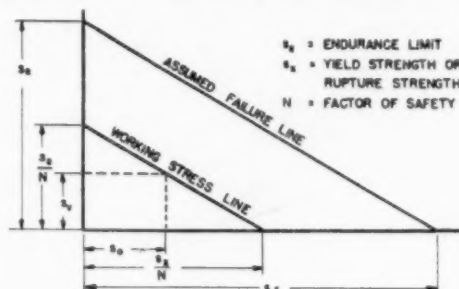


FIG. 18 ASSUMED FAILURE DIAGRAM

design is analyzed and suitably modified so that the frequency corresponding to the first mode of transverse vibration lies above the fourth multiple of the maximum rotational speed. This rule has been found to be safe for gas turbines operating from combustion chambers attached by relatively long ducting. If necessary, a safe condition is assured by tuning the actual blading after installation.

The frequency of the fundamental mode of vibration of blades in a given ring is expressed by the following formula

$$f_s = 11.0 C_f \frac{k}{h^2} \sqrt{\frac{E}{\gamma}} \dots \dots \dots [11]$$

where

- f_s = standing frequency, cps
- C_f = frequency correction factor
- k = radius of gyration of base profile, in.
- h = blade length, in.
- E = modulus of elasticity, psi.
- γ = specific weight of material, lb per cu in.

For a value of unity for the frequency correction factor, the formula is identical to that for the frequency of a uniform cantilever beam of equivalent properties. The tie between theory and actual conditions is by means of the frequency correction factor. This factor takes into account blade-taper effects and in addition is dependent upon the actual geometric configuration, the type of blade fixing, and the presence or absence of shrouding and lacing wire.

Moving blades are stiffened to some extent by centrifugal force. The running frequency is calculated from (10)

$$f_r = \sqrt{f_s^2 + B \left(\frac{n}{60} \right)^2} \dots \dots \dots [12]$$

where

- f_r = running frequency at n , cps
- B = rotation coefficient
- n = rotational speed, rpm

The rotation coefficient is dependent upon the degree of blade-root fixing, the geometric shape, and the blade-height ratio. The effect of rotation is generally small, and it can be predicted with practical accuracy for normal constructions from the data in Fig. 19.

Blade vibrational characteristics are best depicted on a frequency diagram similar to that shown in Fig. 20. Safe oper-

ating speeds for the turbine may be estimated from such a chart, with allowance for the effects of possible variations in blade frequency.

Disk Design. Fig. 21 shows the local elastic-stress distribution in a disk of uniform thickness, when carrying a prescribed rim load at a given rotational speed. The theory and formulation used to determine these stresses are of long standing (11). The stresses are essentially biaxial, consisting of both radial stresses

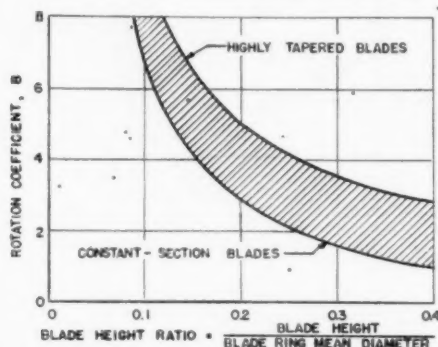


FIG. 19 VARIATION OF ROTATION COEFFICIENT WITH BLADE-HEIGHT RATIO

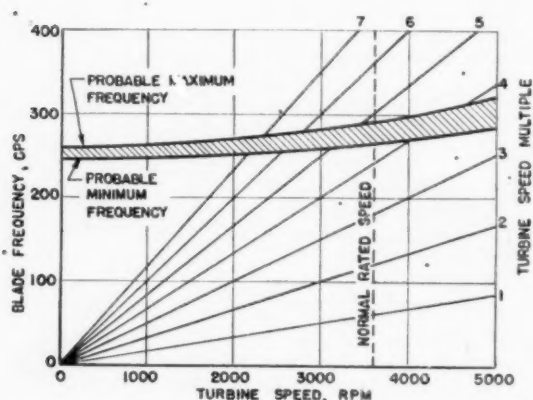


FIG. 20 TYPICAL BLADE-FREQUENCY DIAGRAM

and tangential stresses. The tangential stress at the inner radius of the center-bored disk is considerably above that at the center of the solid disk, which would apparently indicate a much lower safe speed for the former type.

Experimental evidence from a number of sources tends to refute this conclusion (12). The high stress at the inner radius of the center-bored disk is, in effect, a localized stress concentration, which is relieved to a large extent by plastic flow as soon as the elastic limit of the material is exceeded. There is little reduction in load-carrying ability of the disk as a whole.

In practical design, elastic stresses are calculated in detail for blade-carrying elements mainly for the purpose of insuring maximum utilization of the weight of material put into the elements. For comparative purposes, however, the primary criterion is the average tangential stress across the disk radial cross section. This approach assumes, in effect, that the total centrifugal load due to the blades, rim, and disk proper is carried uniformly across the cross-sectional area of the disk. The formula for the average stress is expressed as follows

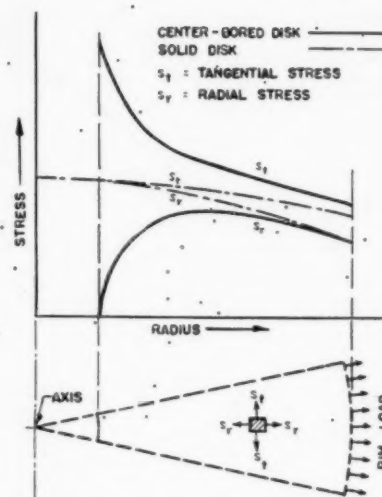


FIG. 21 LOCAL ELASTIC STRESS DISTRIBUTION IN DISK OF UNIFORM THICKNESS

$$s_{ta} = 28.42 \gamma \left(\frac{I}{A} \right) \left(\frac{n}{1000} \right)^2 + \frac{P}{2\pi A} \quad (13)$$

where

s_{ta} = average tangential stress, psi

γ = specific weight of disk material, lb per cu in.

I = moment of inertia of disk half section about axis of rotation, in.⁴

A = area of disk half section, sq in.

n = rotational speed, rpm

P = total centrifugal force due to rim load at speed n , lb

Overspeed tests analyzed in accordance with the conception of uniform stress distribution show much closer agreement between average tangential stress and test-bar tensile strength, than when the analysis is based on comparing local elastic stresses and test-bar strength. This is true for both solid and center-bored disks.

Normally, disk stresses as calculated by means of Equation (13) are limited to one half the rupture strength of the material for the specified service life and temperature for the part, when operating at rated speed. Rupture strength becomes of minor importance at moderate temperatures. In such cases, the average tangential stress is limited to one half the yield strength of the material at the specified service temperature, when rotating at 120 per cent of rated speed.

Disk stresses may be reduced considerably if the disk outline is profiled. Calculation of local elastic stresses is helpful in attaining the optimum degree of profiling, and disks are designed with a constant-stress form where possible. In general, thin rims and thick hubs are desirable from the standpoint of over-all stress reduction.

The effects of temperature variation may be of importance in the stressing of disks. These effects are secondary for industrial or utility turbines operating under almost constant load conditions with few start-ups and shutdowns. The temperature gradients during service are small and consistent, and the time intervals for placing the units in or out of service may be made sufficiently long to insure against any deleterious effects.

Stresses generated by thermal gradients may reach serious levels in units subjected to rapid load changes or where quick

starting is required. Since these stresses are transient in nature, they induce results similar to fatigue. This phenomenon, which is known as thermal shock, may rapidly lead to failure if not properly taken into account in the design. Without going into particulars, such conditions are best combated by preventing undesirable temperature gradients as much as possible. In this respect, experience up to the present time with artificial cooling of parts subjected to hot gas has been somewhat disappointing. Induced temperature gradients in some cases have led to deformations and failures which would not normally have occurred had the parts been permitted to assume more normal temperature distributions.

CONCLUSION

There are many problems in gas-turbine design which cannot be discussed adequately in a presentation such as this. An attempt has been made, however, to show the approaches to some of the more basic problems peculiar to the design of commercial gas-turbine equipment. These approaches are simple and systematic in all cases and they are based primarily upon fundamental theory, modified by experiment and experience.

The gas turbine is in a state of development. This development must be based upon a background of basic data which can be accumulated only through experience. Since the commercial gas turbine is in direct competition with other well-established types of prime movers, the requirements for efficiency, dependability, and low first cost must all be given special consideration. The fulfillment of these requirements is greatly assisted by the organization of fundamental principles and experience into basic design practices similar to those which have been outlined in this paper.

ACKNOWLEDGMENT

The author desires to express his appreciation to the Allis-Chalmers Manufacturing Company for permission to publish the data contained in this paper. He also wishes to acknowledge the invaluable guidance of Mr. R. C. Allen, during the preparation and review of the various drafts, and the able assistance of Mr. R. W. Rouse in preparing the final manuscript and drawings.

BIBLIOGRAPHY

- 1 "A New Theory of the Steam Turbine," by H. M. Martin, *Engineering*, vol. 106, July 19, 1918, pp. 53-54.
- 2 "Labyrinth Packings," by H. M. Martin, *Engineering*, vol. 85, Jan. 10, 1908, pp. 35-36.
- 3 "Investigation of Steam Turbine Nozzle and Blading Efficiency," by F. Dollin, *Proceedings of The Institution of Mechanical Engineers*, London, England, vol. 144, 1940, pp. 147-158; discussion by S. S. Cook, pp. 159-160.
- 4 "Some Effects of Pressure Loss on the Open-Cycle Gas-Turbine Plant," by J. I. Yellott and E. F. Lype, *Trans. ASME*, vol. 69, 1947, pp. 903-911.
- 5 "The Effect of Circumferential Pitch of Steam Turbine Blades on Torque," by R. Dowson, *The Institution of Mechanical Engineers*, London, England, vol. 1, April, 1938, pp. 267-284.
- 6 "Third Report of the Steam Nozzles Research Committee," *Proceedings of the Institution of Mechanical Engineers*, London, England, vol. 1, January-May, 1924, p. 469.
- 7 "The Spacing of Turbo-Machine Blading, Especially With Large Angular Deflection," by O. Zweifel, *The Brown Boveri Review*, vol. 12, December, 1945, pp. 436-444.
- 8 "A Summary of Heat Resistant Alloys From 1200 F to 1800 F," by N. J. Grant, A. F. Frederickson, and M. E. Taylor, *Iron Age*, vol. 161, March 18, 1948, pp. 73-78; April 8, 1948, pp. 75-81; April 15, 1948, pp. 84-93.
- 9 "Factor of Safety and Working Stress," by C. R. Soderberg, *Trans. ASME*, vol. 52, 1930, pp. 13-28.
- 10 "Vibration Problems in Engineering," by S. Timoshenko, D. Van Nostrand Company, Inc., New York, N. Y., 1928, pp. 270-273.

11 "Steam and Gas Turbines," by A. Stodola, McGraw-Hill Book Company, Inc., New York, N. Y., 1927, vol. 1, pp. 380-384.

12 "Bursting Tests of Steam-Turbine Disk Wheels," by E. L. Robinson, *Trans. ASME*, vol. 66, 1944, pp. 373-386.

Discussion

D. L. MORDELL.² The writer is disappointed to see that no mention is made of the possibility of using diffusion after the turbine. Rather than regarding the residual kinetic energy as a dead loss, by suitable design some of it may be recovered and used. The effect of any such recovery is simply to increase the effective expansion ratio over the turbine by maintaining subatmospheric pressure at the turbine exhaust annulus. At an exhaust velocity corresponding to Mach number 0.6, the kinetic energy represents 70 deg F or 14 per cent of the total turbine power in a typical simple case. Recovery of one half of this would increase the net or useful output by some 20 per cent. In point of fact, an exhaust Mach number of 0.4 is more probable, and if so, the net gain to be achieved by recovery of one half of the kinetic energy is 10 per cent. In the design shown in Fig. 1 of the paper, space limitations may be severe, but recent aerodynamic developments have indicated how diffusion can be allowed on a bend, if the boundary layer is suitably controlled.

D. G. TRAVER.⁴ A few specific questions have come to mind on which we should like the author to comment. In Fig. 3 of the paper, the impulse-blading efficiency peaks within a point to two of the reaction blading. What are the conditions of this comparison? Our information indicates a somewhat larger difference. However, there are details which influence this consideration. Thus our comparison would be at the same Reynolds number and aspect ratio (ratio of blade length to axial width), and our Mach number would be sufficiently below 1 not to influence this comparison. In general, the author's curve substantiates ours in that we believe an impulse stage can be made which performs almost as well as a reaction stage. Frequently the mechanical advantages of the impulse stage counterbalance this small sacrifice in efficiency.

The popular classification of turbines into pure impulse and pure reaction types has almost lost its meaning to the gas-turbine designer, for he often deals with large-diameter-ratio blading in which three-dimensional effects are large, and in which there may be a radial variation in degree of reaction. Gas-turbine designers often depart from impulse or reaction conditions at the mean diameter even for small diameter ratios, for they may find a partial reaction stage better suited to their design requirements. There is no real justification for designing to the arbitrary limits of reaction or impulse stages, and it must be assumed that some sort of continuous efficiency envelope between these two types exists. Would the author indicate what form this envelope might take, and what he considers a "typical" impulse stage?

Referring to Fig. 7 of the paper, we use aspect ratio as a design parameter, and we would be interested in knowing the aspect ratios of these two curves. Our data for aspect ratio of 3 and Reynolds number = 100,000 (based on the throat hydraulic diameter as characteristic length) are the average of the author's curves over the entire range. Does Fig. 7 apply equally to impulse and reaction blading?

In Fig. 12 our findings are identical to the author's in the range of opening coefficients which we normally use in turbine design.

² Associate Professor of Mechanical Engineering, McGill University, Montreal, Can.

⁴ Research Engineer, Analytical Section, Elliott Company, Jeanette, Pa.

In regard to the author's discussion of aerodynamic loading and optimum pitch as developed by Zweifel, we use a variable optimum load coefficient that varies linearly with the reciprocal of aspect ratio, because the theory is developed for two-dimensional (infinite aspect ratio) flow conditions only. Our test data verify this variable load coefficient for normal reaction blading. However, our data do not agree, even in the two-dimensional case, with the optimum spacing indicated for impulse blades, but indicate a larger optimum pitch than calculated by Zweifel. This can be rationalized by assuming a more realistic ideal pressure distribution for impulse blades than the rectangular one assumed by Zweifel.

AUTHOR'S CLOSURE

Mr. Mordell points out the possibility of using diffusion to recover a portion of the residual kinetic energy from turbine-exhaust blading. The practicability of reducing leaving loss by this method is dependent upon the amount of kinetic energy available for recovery and upon space requirements for efficient diffusion. In multistage turbines of the general type shown in Fig. 1, the axial velocity of the gas leaving the last row of blades seldom exceeds 400 fps at rated load. Recovery of 50 per cent of the energy corresponding to this velocity would improve power-element efficiency about one per cent. However, power-element length would have to be increased over 25 per cent to provide an efficient diffusing turn for the exhaust gas. An increase in length of this magnitude is not practical for many installations, particularly for locomotive and marine service, in view of the small resultant gain in over-all efficiency.

With reference to Mr. Traver's questions concerning Fig. 3, the title is misleading in that the word "typical" applies to the curves rather than to the blading. Instead of identifying the stages as "reaction" and "impulse," it would be more proper to refer to them as "symmetrical" and "unsymmetrical." In both cases Reynolds number and aspect ratio are sufficiently high that their influences are small. The impulse or unsymmetrical staging has warped moving blades with a stage reaction at design conditions of zero at the root diameter and about 25 per cent at the mean diameter. The blading efficiency is somewhat better than that of a more conventional stage. The reaction or symmetrical blading is designed for 50 per cent reaction at all radii.

We have insufficient experimental evidence to plot, as suggested by Mr. Traver, a continuous efficiency envelope for blading varying in stage reaction from zero to 0.50. The shape of such a curve can be deduced to a certain extent from the following experimental results:

- 1 The efficiency of normal reaction blading is not affected by small unbalances in stage reaction above or below 0.50. The slope of the efficiency envelope curve must therefore be essentially zero at a stage reaction of 0.50.

- 2 The efficiency of a nominal impulse stage is generally improved by the introduction of a small amount of reaction, pro-

vided reasonable control over blade clearances is maintained to prevent gas leakage. The slope of the efficiency envelope curve must therefore be slightly positive for a stage reaction of zero.

We can probably assume from the foregoing that the efficiency envelope curve is roughly parabolic in form with a peak at a stage reaction of 0.50. However, the curve would be of academic interest only, as the internal configuration of any specific stage as regards blade height, diameter ratio, profile form, and operating clearance always exerts a major influence on its general efficiency level.

Concerning Mr. Traver's questions on Fig. 7, which shows expansion energy coefficient curves used in performance analysis, these data are assumed to apply to two-dimensional flow when the Reynolds number based upon throat-opening hydraulic diameter is 100,000 and higher. A value of 100,000 represents the lower limit of normal design practice, and over-all turbine tests seem to indicate only minor changes in efficiency as operating conditions are varied a moderate amount from this level.

Since the data in Fig. 7 apply only to two-dimensional flow, a gross stage power output calculated using these coefficients must be corrected for three-dimensional effects. The correction is made in terms of an end loss which includes clearance leakage, interference effects, and other secondary flow losses. The magnitude of the end loss is estimated from the blade height, blade profile, operating clearance, and clearance configuration. An aspect ratio such as defined by Mr. Traver (ratio of blade length to axial width) is not used as a design parameter.

The energy coefficients shown in Fig. 7 were determined by analyses of over-all turbine tests, and the curves may be considered to represent statistical averages. Individual tests show moderate variations above and below the curve values. The fact that wide blades generally show improved efficiency (provided the blades are of reasonable length) is believed to be due to two influences:

- 1 In practice it is seldom possible to maintain exact geometric similarity between wide and narrow blades. Trailing edge-wake loss generally increases as blading is narrowed, with a consequent slow decrease in over-all blade-energy coefficient.

- 2 Reynolds number effects have not been isolated satisfactorily in over-all turbine tests, but undoubtedly they are responsible for some reduced efficiency in narrow blades at moderate Reynolds number levels.

The data in Fig. 7 apply in general to both impulse and reaction blades. The expansion-energy coefficient of reaction blades or nozzles with very small outlet angles may fall slightly below the level of the curves. The kinetic-energy coefficient of impulse blades with very low deflection angles is generally somewhat higher than the expansion-energy coefficient as determined from Fig. 7. However, these types of elements are not normally employed in gas-turbine blade paths, so that the general accuracy of Fig. 7 is not affected for practical application.

Bending of an Ideal Plastic Metal¹

By J. D. LUBAHN² AND G. SACHS³

The stresses and strains in plastically bent parts have been analyzed for the two limiting conditions of (a) a very wide plate (plane strain), and (b) a very narrow bar (plane stress). The complete solution is presented for a hypothetical metal with no strain-hardening, and the method is described for treating any actual metal. The solution was obtained by a method of successive approximations, each approximation employing various graphical processes. The gradual change in cross-sectional contour with progressive bending was obtained by considering small successive intervals of increasing curvature. The final solution shows the movement of the neutral axis toward the compression surface, the decrease in the radial dimension of the part, and the gradual divergence between the tangential strains at the inside and outside surfaces. The solutions for plane stress and plane strain were nearly identical as regards the tangential strains and the changes in the radial dimension. Experimental measurements of surface strains and cross-sectional contour of bends conformed well with the results of the calculations.

NOMENCLATURE

The following nomenclature is used in the paper:

- A = angle subtended by a portion of the bend
- a = radius to concave surface of bent part
- a as a subscript refers to concave surface of bent part
- b = radius to convex surface of bent part
- b as a subscript refers to convex surface of bent part
- e = conventional strain
- F = component of force acting on an element of volume
- f as a subscript denotes final (strained) condition
- h = height or dimension in radial direction
- k = flow stress, i.e., uniaxial stress necessary to cause plastic flow
- L = element of length (tangential unless otherwise specified)
- m as a subscript denotes center (with respect to curvature, i.e., h_0/a) of a finite interval of bending
- n as a subscript denotes neutral axis, i.e., point of zero tangential stress or zero tangential strain differential
- r = radius to an arbitrary point
- r as a subscript denotes radial direction
- s = stress

t as a subscript denotes tangential direction (will be omitted where no ambiguity arises)

V = volume

w = breadth $[= w_0(1 + e_w)]$

w as a subscript denotes lateral direction

x = distance from an element of volume to concave surface ($= r - a$)

0 as a subscript denotes initial (unstrained) condition

1 as a subscript denotes direction of largest principal strain or stress

2 as a subscript denotes direction of intermediate principal strain or stress

3 as a subscript denotes direction of smallest principal strain or stress

ϵ = natural strain $[= \ln(1 + e)]$

$\bar{\epsilon}$ = uniaxial tensile strain causing an equivalent strain-hardening (when flow stress is a function of three principal strains)

' = beginning of finite interval of bending

" = end of finite interval of bending

INTRODUCTION

The bending of metal bars and plates by amounts sufficient to cause plastic deformation of practically the entire volume of the metal causes a condition of stress and strain throughout the part which is exceedingly complex. Under certain conditions, however, it is possible to treat the problem quantitatively, as discussed later, although the solution is involved and tedious. The simplifying conditions which are necessary to allow mathematical treatment of the problem are as follows: (a) It must be considered that the part is externally loaded only by end moments, i.e., that there is no pressure against the concave or convex surface, except at the ends of the bent portion; (b) the region of elastically deformed metal must be negligibly small; (c) all elements of volume of the part must have either zero lateral⁴ stress (condition of plane stress) or zero lateral strain (condition of plane strain); and (d) the bend must be long enough in the circumferential direction so that the end effects do not disturb the behavior of the metal near the center of the bend. These circumstances will be approached rather closely in bars which are sufficiently wide (approaching plane strain) or sufficiently narrow (approaching plane stress) and which contain a bend that is neither too mild nor too sharp.

Previous treatments (1, 2, 3, 4)⁵ of plastic bending have dealt with an even simpler set of circumstances where only the stresses and strains in the circumferential direction have been considered, the changes in cross-sectional contour have been neglected, and the effects of curvature on the position of the neutral axis have been disregarded.

In the present paper an "ideal plastic metal," i.e., one exhibiting no strain-hardening, will be assumed. Even with this assumption, however, the solution of the plastic-bending problem requires graphical methods for determining both the stresses and strains in a narrow bar and for determining the strains in a wide plate; only the stresses in a wide plate are obtainable algebraically. Consequently, for an actual metal with a specific stress-strain curve, the solutions would be but little more complex,

⁴ See Fig. 1 for definition of directions.

⁵ Numbers in parentheses refer to the Bibliography at the end of the paper.

¹ This paper originated in an investigation conducted at Case Institute of Technology, Cleveland, Ohio, under contract with the National Defense Research Committee of the Office of Scientific Research and Development. The completion of the analytical work reported in this paper and further experimental work were made possible by the Frederick Cottrell grant made by the Research Corporation, New York, N. Y. A preliminary report on the experimental work is in preparation.

² Research Associate, Research Laboratory, General Electric Company, Schenectady, N. Y. Formerly of Case Institute of Technology, Cleveland, Ohio. Jun. ASME.

³ Metals Research Associates, Inc., Cleveland, Ohio. Formerly Professor of Physical Metallurgy, Case Institute of Technology, Cleveland, Ohio. Mem. ASME.

Contributed by the Metals Engineering Division and presented at the Annual Meeting, New York, N. Y., November 28-December 3, 1948, of THE AMERICAN SOCIETY OF MECHANICAL ENGINEERS.

NOTE: Statements and opinions advanced in papers are to be understood as individual expressions of their authors and not those of the Society. Paper No. 48-A-168.

as will be shown. On the other hand, the solutions for the ideal plastic metal conform closely to the deformation characteristics of real metals, so it appears that little is to be gained by repeating the procedure to be given for any real metals. This statement does not apply to the stresses, however, and consequently the bending loads, springback characteristics, and other aspects of bending require consideration of the strain-hardening and cannot be deduced accurately from the results of the present analysis.

PLASTIC-FLOW LAWS AND CONDITIONS OF THE PROBLEMS

In the following solutions of plastic-bending problems, the behavior of the metal will be considered to be governed by the following empirical relations,⁶ which are generally accepted as the "laws" of plastic flow:

(a) The condition that the volume remains constant during plastic flow can be expressed in terms of the principal natural strains by

$$\epsilon_1 + \epsilon_2 + \epsilon_3 = 0 \dots \dots \dots [1a]$$

$$d\epsilon_1 + d\epsilon_2 + d\epsilon_3 = 0 \dots \dots \dots [1b]$$

where the natural strain ϵ , is defined in terms of the conventional strain e , or change in length divided by initial length, by

$$\epsilon = \ln(1 + e)$$

(b) The condition of stress under which plastic flow proceeds is given by the energy-of-distortion condition

$$(s_1 - s_2)^2 + (s_2 - s_3)^2 + (s_1 - s_3)^2 = 2k^2 \dots \dots \dots [2]$$

In this equation, k is the uniaxial stress necessary to cause plastic flow.

(c) The relation between the strains and stresses in the plastic state is given by

$$\frac{s_1 - s_2}{d\epsilon_1 - d\epsilon_2} = \frac{s_2 - s_3}{d\epsilon_2 - d\epsilon_3} = \frac{s_1 - s_3}{d\epsilon_1 - d\epsilon_3} \dots \dots \dots [3]$$

In addition to the foregoing relations governing the behavior of the metal itself, certain general principles of mechanics also apply to the situation at hand.

(d) For a stationary body, the equilibrium-of-force condition requires that the sum of the force components in any given direction (in particular, the radial direction) must be zero

$$\Sigma F_r = 0 \dots \dots \dots [4]$$

(e) For loading by end moments only, i.e., no external radial forces in the region considered, the equilibrium-of-force condition applied at the concave and convex surfaces of the bent part requires that the radial stresses at these surfaces be zero

$$s_r = 0 \text{ when } r = a \dots \dots \dots [5a]$$

$$s_r = 0 \text{ when } r = b \dots \dots \dots [5b]$$

SOLUTION FOR PLANE STRAIN

General Considerations. In the case of plane strain, the distribution of the stresses between initially unknown positions of the boundary surfaces can be determined algebraically. Subsequently, the position of the neutral axis can be determined, from which it is possible to calculate the strains and the height (see Fig. 1), and thus the positions of the concave and convex surfaces of the bent part.

If a wide plate is bent, the circumferential stretching at the convex surface tends to cause lateral contraction of this surface,

⁶ For a detailed discussion of these relations, see Nadai (1).

and similarly there is a tendency for the concave surface to expand laterally. This would cause lateral curvature of the part; but the resistance of the circumferentially curved plate prevents such lateral bending almost completely, and the lateral strains are therefore the same throughout the volume of the bend. Furthermore, the lateral resistance of the flat portions adjacent to the bend prevents any average lateral extension or contraction of the bend, so that the lateral strain ϵ_3 , is practically zero at every point.

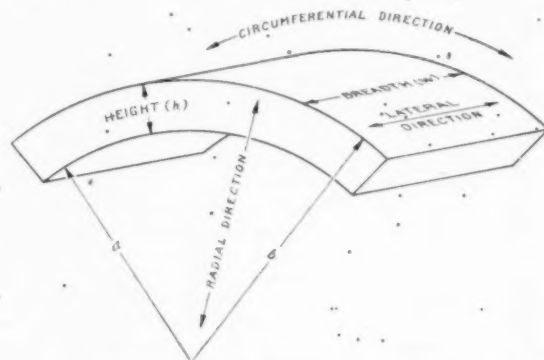


FIG. 1 DEFINITIONS OF DIRECTIONS AND DIMENSIONS IN BENT PART

From considerations of symmetry it can be seen that the shear stresses are zero on planes determined by the radial, lateral, and circumferential directions, and consequently these are the principal directions. Because of the constant volume condition, the value zero for the lateral strain will require this to be the intermediate principal strain ϵ_3 , and the intermediate principal stress will be the lateral stress. Applying $\epsilon_3 = 0$ to Equations [3] and [1b] yields

$$s_2 = \frac{s_1 + s_3}{2} \dots \dots \dots [6]$$

Then Equation [2] becomes

$$s_1 - s_3 = \frac{2k}{\sqrt{3}} \dots \dots \dots [7]$$

Stress Distribution for Plane Strain. For rotational symmetry, equilibrium of force in the radial direction Equation [4] yields the following differential equation relating the radial and tangential stresses (5)

$$\frac{ds_r}{dr} = \frac{s_t - s_r}{r} \dots \dots \dots [8]$$

At the convex surface, s_t is a tensile stress and s_r is zero, so that s_t is the largest and s_r is the smallest principal stress. Then Equation [7] becomes

$$s_t - s_r = \frac{2k}{\sqrt{3}} \dots \dots \dots [9]$$

Combining this with Equation [8] and rearranging yields

$$\frac{ds_r}{k} = \frac{2dr}{r\sqrt{3}}$$

Integrating between the boundary condition [5b] and an arbitrary point r , s_r

$$\frac{s_r}{k} = \frac{2}{\sqrt{3}} \ln \frac{r}{b} \quad [10]$$

Equation [10] shows that s_r becomes negative as r becomes smaller than b and consequently, as r deviates from b , Equation [10] is applicable as long as s_r and s_t are continuous.

At the concave surface, s_t is a compressive stress and s_r is zero, so that s_t is the largest and s_r the smallest principal stress. Then Equation [7] becomes

$$s_r - s_t = \frac{2k}{\sqrt{3}} \quad [11]$$

which, combined with Equation [8] and integrating between the boundary Condition [5a] and an arbitrary point, r , s_r becomes

$$\frac{s_r}{k} = -\frac{2}{\sqrt{3}} \ln \frac{r}{a} \quad [12]$$

According to Equation [12], s_r becomes negative, as r becomes greater than a , and consequently, as r deviates from a , Equation [12] is applicable as long as s_r and s_t are continuous.

The solutions Equations [10] and [12] for s_r will be identical at one and only one value of the radius, so that Equation [10] will apply at larger radii and Equation [12] at smaller radii. Consequently this is the point where the tangential stress changes from positive⁷ to negative, and it will be designated as the neutral axis, r_n . The position of the neutral axis is obtained by setting equal to each other the two expressions Equations [10] and [12] for s_r , yielding

$$r_n = \sqrt{ab} \quad [13]$$

The distributions of radial stress in bends of various curvatures are shown in Fig. 2, in terms of the as yet unknown height, h . These curves show clearly the increase in radial compression as the curvature increases. The distribution of tangential and lateral stresses, as well as the radial stress, are shown in Fig. 3 for one particular value of the curvature of the bar, namely, for $h/a = 1$.⁸

The Neutral Axis. When $r < r_n$, the tangential stress is the smallest principal stress, as discussed previously, and consequently the principal direction in which the algebraically smallest change, de_t , in strain occurs is the tangential direction, i.e., $de_t = de_3$. Since $de_3 = 0$ and considering Equation [1b], de_3 must be negative. Thus de_t is also negative for $r < r_n$. Likewise, de_t is positive when $r > r_n$ because the tangential stress is the largest principal stress in this region. Consequently, de_t is zero at the neutral axis; and the neutral axis may be defined not only as the point of zero tangential stress, but also as the point of zero tangential strain differential. The variation with curvature of the neutral axis with respect to the as yet unknown positions of the bounding surfaces ($r = a$ and $r = b$) is shown in Fig. 4. The fact that $de_t = 0$ when $r_n = \sqrt{ab}$, together with the value of the curvature and the condition that the distribution of (conventional) tangential strain is linear across the radius,⁹ constitute the necessary information for determining the radial distribution of tangential strains.

⁷ For very large curvatures (small radii (a/h_0) of curvature, s_r according to Equations [9] and [10] may be negative at $r = r_n$, but the magnitude of the discontinuity in s_t at r_n will still be $4k/\sqrt{3}$ (compare [9] and [11]).

⁸ It is interesting to note that the stress distribution in a plastically bent plate is identical with that which would be obtained if one thick-walled tube were shrunk onto another in such a manner that both were in a condition of complete plastic flow (6).

⁹ It can be shown experimentally that the radial distribution of tangential strains is linear near the (tangential) center of even a rather sharp bend.

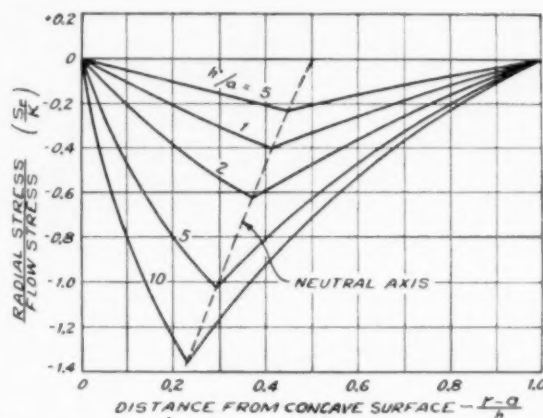


FIG. 2 DISTRIBUTION OF RADIAL STRESS IN BENDS OF VARIOUS CURVATURES FOR PLANE STRAIN

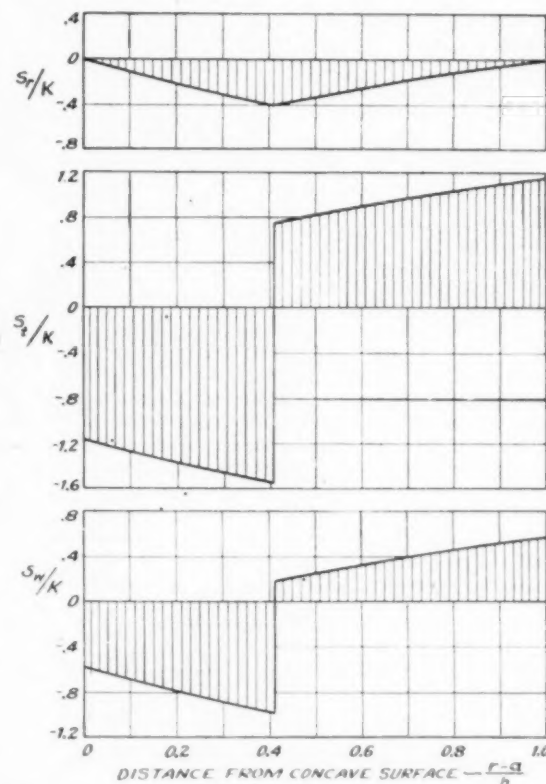


FIG. 3 RADIAL, TANGENTIAL, AND LATERAL STRESSES FOR PLANE STRAIN FOR $h/a = 1$

Strain Distribution. Because of the continuously changing position of the neutral axis with increasing curvature (see Fig. 4), the total tangential strain must be determined by integrating the differentials of strain occurring during small increments of bending in which the height remains constant and the neutral axis remains at a fixed distance ($r_n - a$) from the concave surface and the length L_n remains fixed, Fig. 5. Two cross sections bounding an initial length of the bar (before bending) of L_0 will subtend an

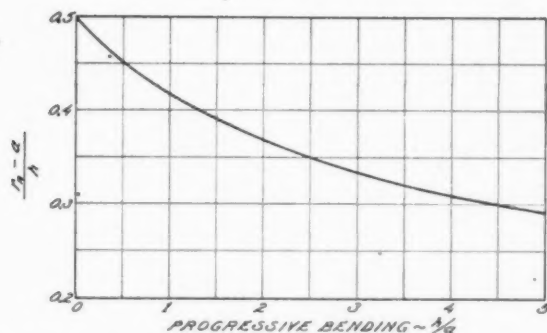


FIG. 4 CHANGE IN POSITION OF NEUTRAL AXIS DURING BENDING FOR PLANE STRAIN

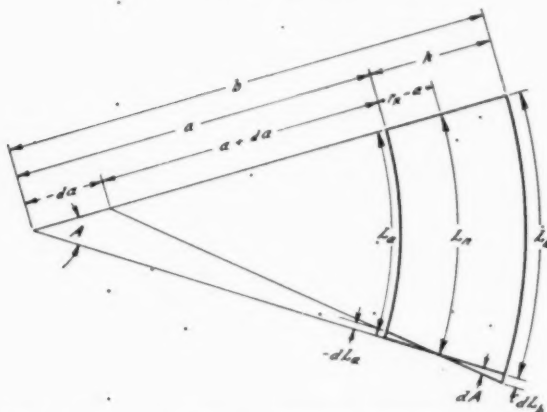


FIG. 5 GEOMETRICAL CHANGES DURING AN INFINITESIMAL INTERVAL OF BENDING

angle, A , during the interval, and may be considered as rotating about the ends of the neutral axis during the interval. If the radius a , to the concave surface changes by da during the interval, the cross section at one end of the neutral axis will rotate through an angle dA , with respect to the cross section at the other end of the neutral axis, Fig. 5. The lengths, L_a and L_b of the fibers at the concave and convex surfaces, respectively, will change by small amounts, dL_a and dL_b , respectively. Fig. 5 yields two equations each for the lengths L_b and L_a , of the surface fibers

$$L_a = Aa \quad L_b = Ab = A(a+h) \dots \dots \dots [14]$$

and

$$dL_a = (a - r_n)dA = [a - \sqrt{a(a+h)}] dA \dots \dots [15]$$

$$dL_b = (a + h - r_n)dA = [a + h - \sqrt{a(a+h)}] dA \dots [16]$$

The constant volume condition, Fig. 6, yields the relation

$$\frac{h(L_a + L_b)}{2} = h_0 L_0 \dots \dots \dots [17]$$

Since by definition

$$1 + e_a = \frac{L_a}{L_0} \quad 1 + e_b = \frac{L_b}{L_0} \dots \dots \dots [18]$$

Equation [17] reduces to

$$\frac{h_0}{h} = 1 + \frac{1}{2}(e_a + e_b) \dots \dots \dots [19]$$

In order to determine the surface strains (e_a and e_b) after a change in curvature from zero to h/a , a method of successive approximations has been used consisting of the following steps:

1a Obtain a first approximation to the strains by assuming that the height remains constant and integrating Equations [15] and [16] algebraically.

1b Obtain a first approximation to h by using Equation [19] and the results of step 1a.

2a Using the values of h found by step 1b, integrate Equations [15] and [16] graphically to obtain a second approximation to the surface strains.

2b Determine a second approximation to h using Equation [19] and the results of step 2a.

The foregoing procedure yields successive approximations to the correct solution, each of which is more nearly correct than the preceding one. Consequently the procedure described under steps 2a and 2b may be repeated until the desired accuracy is obtained.

Step 1a. Considering h constant and differentiating Equation [14]

$$dL_a = daA + Ada$$

$$dL_b = dA(a+h) + Ada$$

By means of these relations and Equation [14], A can be eliminated from Equations [15] and [16], yielding

$$\frac{dL_a}{L_a} = \frac{da}{a} - \frac{da}{\sqrt{a(a+h)}} \dots \dots \dots [20]$$

$$\frac{dL_b}{L_b} = \frac{da}{a+h} - \frac{da}{\sqrt{a(a+h)}} \dots \dots \dots [21]$$

These equations can be integrated between the limits $L_a = L_b = L_0$ when $a = \infty$, and the general condition of strain, yielding

$$\frac{L_a}{L_0} = 1 + e_a = \frac{4a}{2a + h + 2\sqrt{a(a+h)}} \dots \dots [22]$$

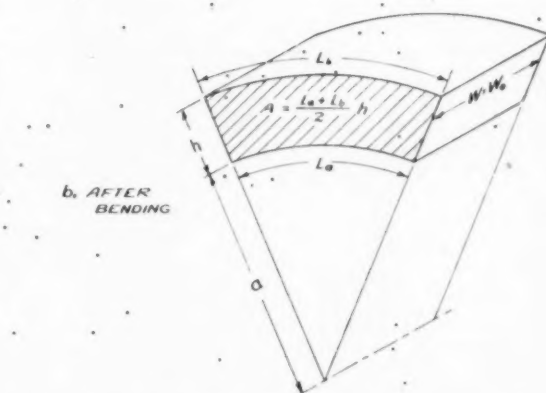


FIG. 6 CONSTANT VOLUME CONDITION FOR PORTION OF BENT SHEET

$$\frac{L_b}{L_0} = 1 + e_b = \frac{4(a+h)}{2a+h+2\sqrt{a(a+h)}} \dots [23]$$

These values of e_a and e_b are shown in Fig. 7, curve 1 (to designate the first approximation).

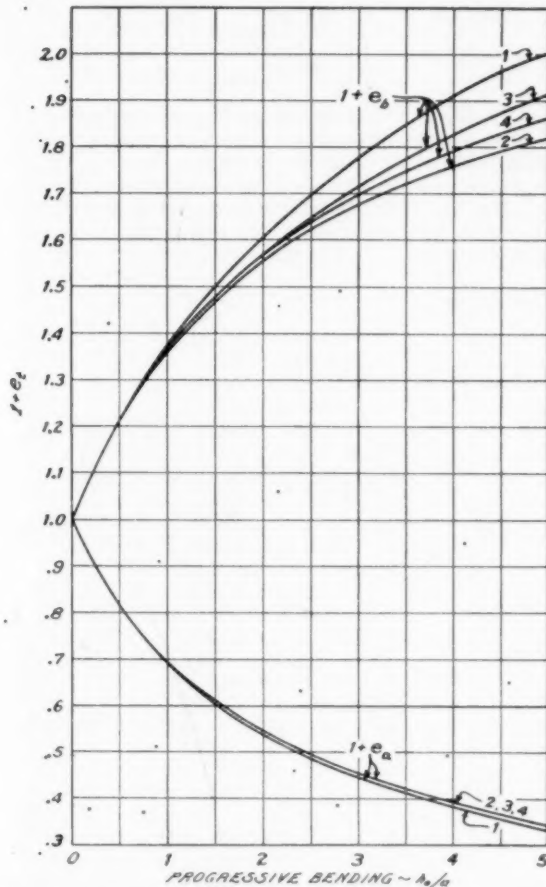


FIG. 7 SUCCESSIVE APPROXIMATIONS TO EXTREME TANGENTIAL STRAINS FOR PLANE STRAIN

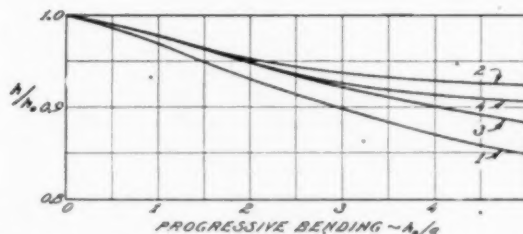


FIG. 8 SUCCESSIVE APPROXIMATIONS TO CHANGE IN HEIGHT ON BENDING FOR PLANE STRAIN

Step 1b. Using the surface strains given by Equations [22] and [23], the height (expressed as a fraction of the initial height) can be determined from Equation [19]. This is plotted in Fig. 8, curve 1 (to designate the first approximation).

Step 2a. For graphical integration of Equations [15] and [16], these equations may be applied to a small finite interval of

bending whose beginning is designated by prime, and whose end is designated by double prime. If the interval is sufficiently small, h and $(r_a - a)$ may be considered as constant during the interval and may be taken at a curvature midway (subscript m) between that at the beginning and that at the end of the interval. Then Equations [15] and [16] become

$$L''_a - L'_a = (A'' - A') (a_m - r_{nm}) \dots [24]$$

$$L''_b - L'_b = (A'' - A') (a_m + h_m - r_{nm}) \dots [25]$$

where

$$r_{nm} = \sqrt{a_m(a_m + h_m)}$$

Applying Equation [14] to the beginning and end of the interval yields values of A' and A'' which can be substituted into Equations [24] and [25] yielding

$$\frac{L''_a}{L'_a} = \left(\frac{a''}{a'} \right) \frac{a' - a_m + r_{nm}}{a'' - a_m + r_{nm}} \dots [26]$$

$$\frac{L''_b}{L'_b} = \left(\frac{a'' + h''}{a' + h'} \right) \left(\frac{a' - a_m + r_{nm}}{a'' - a_m + r_{nm}} \right) \dots [27]$$

Dividing numerator and denominator of the left member by L_0 and of the right member by h_0 yields the strains at the end of the interval in terms of the strains at the beginning of the interval and quantities available from the previous approximation

$$\left(\frac{L''_a/L_0}{L'_a/L_0} \right) = \frac{1 + e''_a}{1 + e'_a} = \left(\frac{a''/h_0}{a'/h_0} \right) \left(\frac{a'/h_0 - a_m/h_0 + r_{nm}/h_0}{a''/h_0 - a_m/h_0 + r_{nm}/h_0} \right) \dots [28]$$

$$\left(\frac{L''_b/L_0}{L'_b/L_0} \right) = \frac{1 + e''_b}{1 + e'_b} = \left(\frac{a''/h_0 + h''/h_0}{a'/h_0 + h'/h_0} \right) \times \left(\frac{a'/h_0 - a_m/h_0 + r_{nm}/h_0}{a''/h_0 - a_m/h_0 + r_{nm}/h_0} \right) \dots [29]$$

Values of h/h_0 at a'/h_0 , a_m/h_0 , and a''/h_0 , respectively, are given in Fig. 8, curve 1. The fact that intervals of h_0/a of one half are sufficiently small to give good accuracy can be shown by comparing the results of Equations [28] and [29] for this interval size and for a constant value of h , ($h = h_0$), with the results of Equations [22] and [23], respectively. The second approximation to the surface strains obtained by Equations [28] and [29] is shown in Fig. 7, curve 2.

Step 2b. Using the surface strains given in Fig. 7, curve 2, a second approximation to the height can be determined from Equation [19]. This is shown in Fig. 8, curve 2.

The third and fourth approximations (curves 3 and 4 in Figs. 7 and 8) show that consecutive solutions yield values approximately midway between those of the two preceding solutions. This information makes it possible to make an estimate directly of the final solution, which may be verified by applying steps 2a and 2b of the foregoing procedure to the estimate. The result, Fig. 9, shows that the estimate based upon four approximations is quite accurate.

The final solution for the surface strains is shown in Fig. 10 where the results are compared with the "conventional bending strains," i.e., those obtained by assuming constant height and that the neutral axis remains at the center of the height.

As will be shown, the tangential surface strains are the same for plane stress as for plane strain (within the limits of accuracy of the method); and in Fig. 10 are presented some data for various conditions between these limits, which show that the theoretical solutions agree closely with experimental measurements for bars or plates of any width. Of particular significance is the fact that

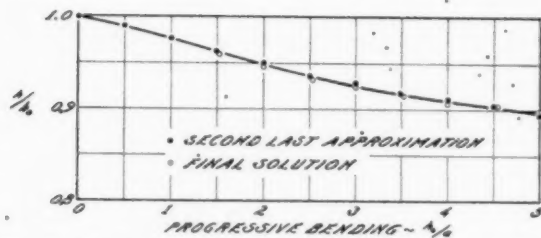


FIG. 9 HEIGHT CHANGE DURING BENDING FOR PLANE STRAIN ACCORDING TO LAST APPROXIMATION AND FINAL SOLUTION

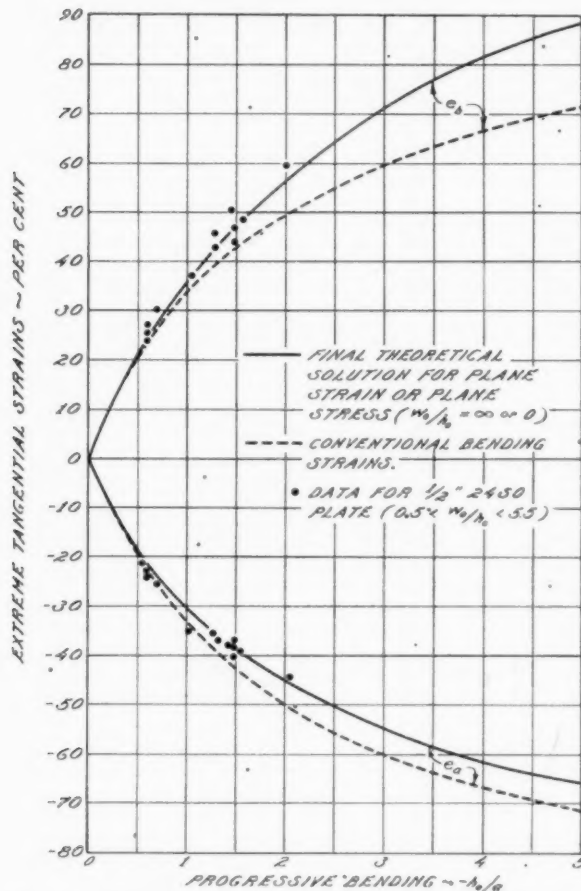


FIG. 10 COMPARISON OF MEASURED AND THEORETICAL CIRCUMFERENTIAL SURFACE STRAINS FOR WIDE RANGE OF W_0/h_0 VALUES BETWEEN PLANE STRAIN AND PLANE STRESS

the agreement is good between the theoretical solution for an ideal plastic metal and data for an actual metal. This means that the strain-hardening characteristics of the metal have but little influence on the strains in bending and consequently the foregoing solution should be applicable to a wide variety of metals, in so far as the strains are concerned. However, the stresses will vary considerably from metal to metal.

SOLUTION FOR PLANE STRESS

Development of Equations for the Stresses. A sufficiently thin

strip which is bent edgewise, Fig. 11, will have zero stress in the lateral direction (i.e., $s_w = 0$), and thus will be in a state of "plane stress." Since the radial stress is zero at the convex and concave surfaces, these surface fibers will be in a state of uniaxial tension and uniaxial compression, respectively, in the tangential direction, i.e.

$$\left. \begin{aligned} s_t &= s_l = k \text{ when } r = b \\ s_t &= s_l = -k \text{ when } r = a \end{aligned} \right\} \dots \dots \dots [30]$$

and

Under conditions of uniaxial tension and compression there are lateral contraction and expansion, respectively, causing the cross section to distort into a figure resembling a trapezoid, Fig. 11. Out of a bar with such a cross section, an element of volume having infinitesimal dimensions in the radial and tangential directions but the full breadth, w , of the bar in the lateral direction will have acting upon it the forces shown in Fig. 11. The sum

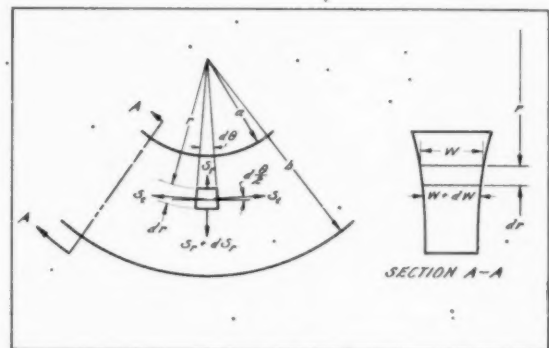


FIG. 11 FORCE ACTING ON AN ELEMENT OF VOLUME IN BENT BAR; PLANE STRESS

of the force components in the radial direction may be equated to zero, yielding

$$(s_r + ds_r)(w + dw)(r + dr)d\theta - s_r w d\theta - 2s_t dr (w + dw) \sin \frac{d\theta}{2} = 0 \dots \dots [31]$$

where $d\theta$ is an infinitesimal angle between the two radial planes which bound the element. Equation [31] reduces to

$$\frac{ds_r}{dr} = \frac{s_t - s_r}{r} - \frac{s_r dw}{w dr} = \frac{s_t - s_r}{r} - \frac{s_t de_w}{(1 + e_w) dr} \dots \dots [32]$$

To solve this equation, it is necessary to reduce the number of variables to two, namely, the independent variable r , and one dependent variable. This requires that e_w be known as a function of r and that there be a relation between s_t and s_r . The latter relation is furnished by combining Equation [2] with the condition of plane stress ($s_w = 0$), yielding

$$s_t = \frac{s_r \pm \sqrt{4k^2 - 3s_r^2}}{2} \dots \dots \dots [33]$$

Consideration of Equation [30] shows that the choice of sign in Equation [33] should be negative when $r = a$, and positive when $r = b$.

Procedure for Numerical Solution. The relation necessary for the solution of Equation [32], giving w as a function of r , i.e., the radial distribution of lateral strains in the bent part, is a complex function (see Equation [3]) of the stresses which in turn require for their determination the solution of Equation

[32]. Thus, at the best, an algebraic solution for Equation [32] would be very complex, and even then not adaptable to the solution for an actual (strain-hardenable) metal. Consequently a solution was obtained by a method of successive approximations, each approximation consisting of the steps shown in Table I, and resulting in a more accurate set of cross sections than the previous set. The final result of any one approximation must be expressed as a set of cross sections, rather than a single one, to represent the increasing "sharpness" of the bend, as expressed by the curvature, h_0/a , of the concave surface.

TABLE I OUTLINE OF STEPS FOR ONE APPROXIMATION

- For the first approximation, assume some arbitrary (but reasonable) set of cross sections which vary in shape with progressive bending. For all succeeding approximations, use the set of cross sections determined by the previous approximation.
- Using cross sections given by (a), solve Equation [32] for stresses.
- Determine position of neutral axis as point of zero tangential stress.
- Using this position of neutral axis and assumed condition of linearly distributed tangential strains, calculate extreme tangential strains.
- Determine lateral and radial strains.
- Integrate radial strains to obtain height. This, together with distribution of lateral strains, is necessary information for integrating Equation [32], which is first step of next approximation.

The results of the analysis¹⁰ show that the method of successive approximations as outlined is a converging process, i.e., each successive result is closer to a self-consistent final solution than the previous one. The method may be repeated as many times as necessary to obtain the desired accuracy, i.e., until the last and second last set of cross sections differ by less than the accuracy of experimental work.

Stress and Strain Distributions. The distributions of radial and tangential stress across the (initially unknown) height are shown in Figs. 12 and 13, respectively, for several curvatures, as

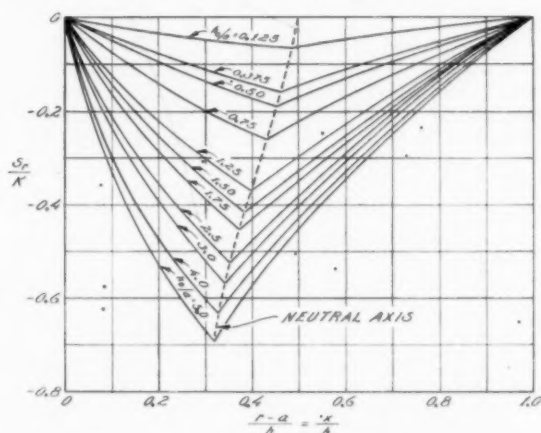


FIG. 12 VARIATION OF RADIAL STRESSES WITH PROGRESSIVE BENDING FOR PLANE STRESS; FIRST APPROXIMATION

calculated by the steps leading to the first approximation. Succeeding approximations yielded similar stress distributions.

The change in position of the neutral axis with changing curvature, Fig. 14, is nearly the same as for plane strain, Fig. 4. The neutral axis remains slightly closer to the center line in plane stress than in plane strain.

¹⁰ The detailed mathematical procedure of this analysis can be found in Report No. M-478 of the National Defense Research Committee of the Office of Scientific Research and Development entitled "Correlation of Information Available on the Fabrication of Aluminum Alloys (NA-126): Section V—Formability of Aluminum Alloys for Use in Military Aircraft, Part IV—Fundamentals of Pure Bending of an Ideal Plastic Metal Under Conditions of Plane Stress," by G. Sachs, J. D. Lubahn, and J. M. Taub, April 26, 1945.

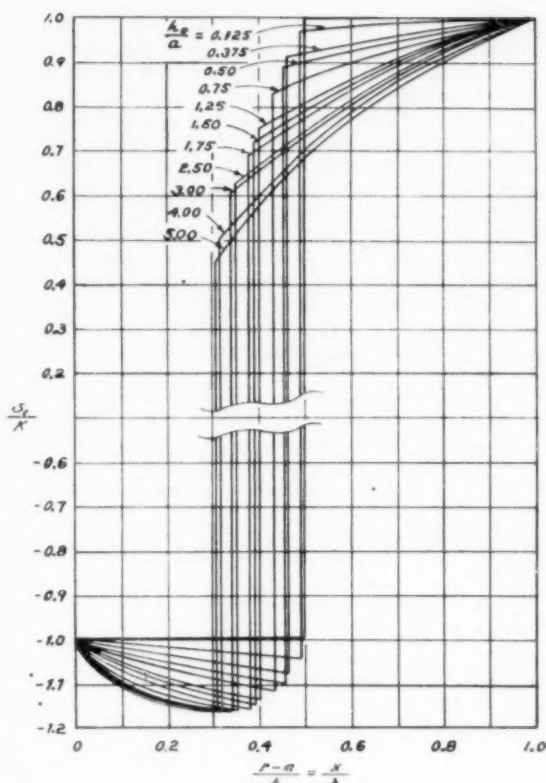


FIG. 13 VARIATION OF TANGENTIAL STRESSES WITH PROGRESSIVE BENDING FOR PLANE STRESS; FIRST APPROXIMATION

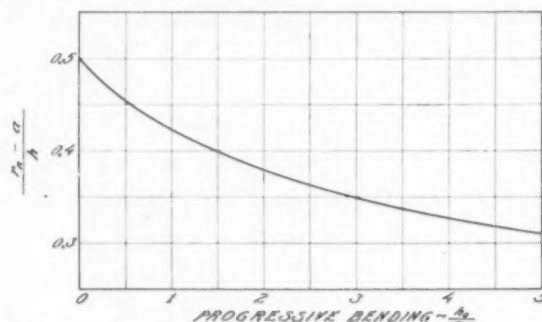


FIG. 14 SHIFT OF NEUTRAL AXIS FOR PLANE STRESS EXPRESSED AS FRACTION OF FINAL HEIGHT; FINAL SOLUTION

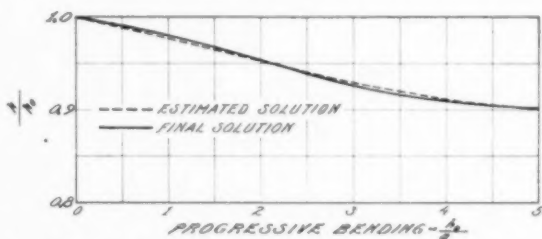


FIG. 15 VARIATION OF HEIGHT FOR PLANE STRESS FOR ESTIMATED AND FINAL SOLUTIONS

The height (the solid curve in Fig. 15) decreases with increasing curvature in almost the same manner as in plane strain (Fig. 9, solid curve). The change in height is slightly less for plane stress than for plane strain.

The tangential strains at the concave and convex surfaces are practically identical with those obtained for plane strain, and may be taken with sufficient accuracy directly from the solid curve in Fig. 10. The conditions of plane stress and plane strain represent the extremes of zero and infinity for the breadth-to-height ratio of curved parts. The identical results obtained for the tangential surface strains for these extremes suggest that these surface strains might apply to bars of all intermediate breadths. Fig. 10 shows data for bars having breadth to height ratios between 0.5 and 5.5. These results all agree within the experimental error with the theoretical strains for plane stress or plane strain.

The shape of the cross section can be expressed by the distribution of lateral strains across the height. The variation of these strains with increasing curvature is shown by the solid lines in Fig. 16. It is interesting to note that the breadth of the part increases slowly from the tension side to the center, and then more rapidly as the compression side is approached. Fig. 17 shows the radial distribution of lateral strain for a curvature (h_0/a) of 1.3, according to the theoretical solution for plane stress. A condi-

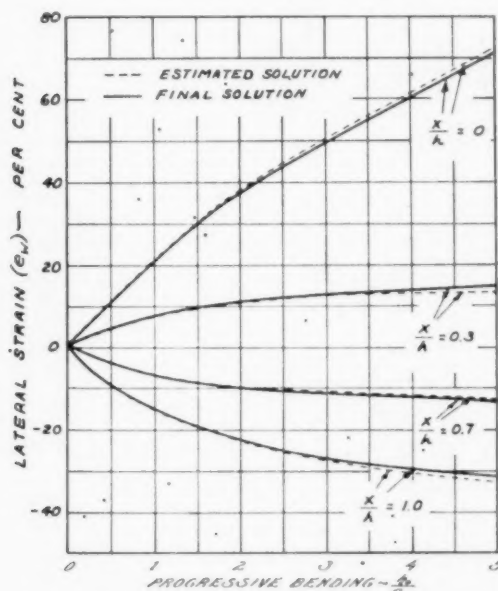


FIG. 16 VARIATION OF LATERAL STRAINS FOR PLANE STRESS FOR ESTIMATED AND FINAL SOLUTIONS

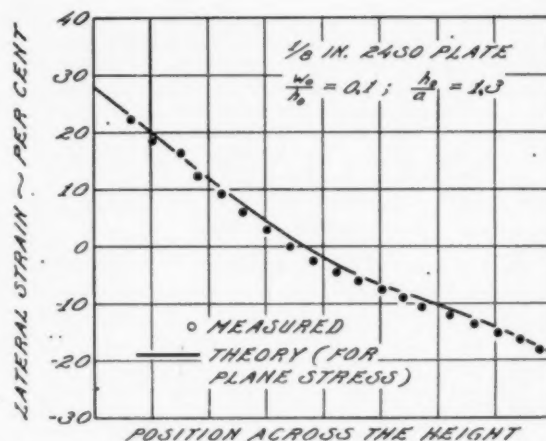


FIG. 17 MEASURED RADIAL DISTRIBUTION OF LATERAL STRAIN FOR $W_0/h_0 = 0.1$ AND THEORETICAL DISTRIBUTION FOR PLANE STRESS

tion of plane stress exists in a hypothetical bar whose breadth-to-height ratio is zero. An actual specimen with a very small breadth-to-height ratio (0.1) yielded a radial distribution of lateral strain very nearly that predicted by the theory for plane stress (for the same curvature), Fig. 17. This agreement not only bears out the theoretical analysis, but also indicates that a rather thin strip bent edgewise corresponds closely to a condition of plane stress.

ACKNOWLEDGMENTS

The authors are indebted to the War Metallurgy Committee of the National Research Council, which supervised the initial work, for permission to publish this paper. The authors also appreciate the assistance given by Messrs. L. J. Klingler, L. J. Ebert, and J. M. Taub.

BIBLIOGRAPHY

- 1 "Plasticity," by A. Nadai, McGraw-Hill Book Company, Inc., New York, N. Y., 1931.
- 2 "Mechanics of Sheet-Metal Bending," by W. Schroeder, *Trans. ASME*, vol. 65, 1943, pp. 817-827.
- 3 "Plastic Bending," by W. R. Osgood, *Journal of the Aeronautical Sciences*, vol. 11, 1944, pp. 213-226; vol. 12, 1945, pp. 253-262, 272, and 408-420.
- 4 "Effect of Bend Width Upon Minimum Bend Radii," by G. Gerard, *Journal of the Aeronautical Sciences*, vol. 13, 1946, pp. 161-170.
- 5 "Theory of Elasticity," by S. Timoshenko, McGraw-Hill Book Company, Inc., New York, N. Y., 1934, p. 55.
- 6 "The Strength of Inserted Dies," by G. Sachs, J. D. Lubahn, and L. J. Ebert (in publication).
- 7 "Plastic Flow in Metals," by J. J. Jelinek, A. J. Latter, E. G. Thomsen, and J. E. Dorn, Research Report No. W-200, War Production Board, Office of Production Research and Development, May, 1945.

History and Performance of the Oil-Refinery Steam-Electric Generating Stations of the Pacific Gas and Electric Company

By V. F. ESTCOURT,¹ SAN FRANCISCO, CALIF.

Design and operating characteristics are given for the three 1400-psi 940 F steam-electric generating stations built by the Pacific Gas and Electric Company for furnishing process steam and electricity to the three adjacent oil refineries, in addition to generating firm power for its own transmission system. An analysis is made of a number of special problems peculiar to this sort of undertaking, and both the advantages and limitations are discussed and evaluated, with emphasis upon the factors which must be considered in order to gain the maximum benefits from such a joint venture. It is pointed out that this type of plant can deliver the refinery's variable requirements for process steam without materially affecting the ability to generate firm power at high thermal efficiencies. However, high-sulphur fuels require higher exit-gas temperatures in order to avoid air-preheater corrosion, with resultant lower boiler efficiencies.

JOINT studies were conducted in 1937, in conjunction with the Tidewater-Associated, Shell, and Union Oil Companies for the purpose of working out the design details and contractual arrangements whereby the Pacific Gas and Electric Company would construct steam-electric generating stations respectively adjacent to the oil refineries of these three oil companies for the generation of electric power and process steam for the use of the refineries, plus electric power for the transmission system of the Pacific Gas and Electric Company. The three contracts as finally written were almost identical except for certain minor provisions relating to the fuels to be burned and the quantities of steam and power to be delivered to the refineries.

The first of these plants, located at Avon, Calif., adjacent to the Tidewater-Associated Company's oil refinery, was placed in operation on December 15, 1940; the second plant, located at Martinez adjacent to the Shell Oil Company's refinery, went into service on June 13, 1941; and the Oleum Plant, adjacent to the Union Oil Company's refinery, first went on the line on January 15, 1942. A second identical unit was installed at Oleum and placed in service on May 24, 1943. This unit was solely for the purpose of meeting the load growth on the Pacific Gas and Electric system.

A detailed description of the design of these stations already has been published in a paper by C. E. Steinbeck.² In that paper was included a plan of the station layout, a cross section of

the boilers and turbines, and a flow diagram showing both the conventional plant cycle and the superimposed process cycle for the generation of steam for the neighboring oil refineries. Mr. Steinbeck's paper was written before any of the plants had been placed in operation and therefore was confined to a description of the basic layout. This present paper may be considered as a continuation of the subject from the point where Mr. Steinbeck's discussion ended.

FUNDAMENTAL CONSIDERATIONS

There are certain fundamental considerations which must be taken into account before it is possible to write a contract which will be satisfactory to both parties on a long-term basis. The refinery, on the one hand, expects to get a cheaper and more reliable source of steam and electric power. On the other hand, if the undertaking is to be attractive to the utility, it must be possible to design the installation so that this sort of service can be given to the refinery at an over-all cost to the utility which is competitive with the cost of generating electric power in its conventional generating stations. This calls for a very careful and realistic analysis in order to avoid overlooking factors which might later prove to be detrimental to either party, or which might result in making commitments which cannot be met in practice, thereby disturbing the balance of the mutual advantages which rightfully can be anticipated in a carefully worked out agreement.

The plant must also be designed not only to meet the existing steam and electric requirements of the oil refinery but must be capable of reasonable expansion in anticipation of future growth not only of the oil refinery but also of the electric facilities of the utility. This may not be easy to do without sacrificing some of the original advantages unless the problem is given detailed consideration in the initial design.

The basic advantages which may be gained by the parties in entering into such an arrangement are as follows:

(a) The combined project, if properly conceived, will result in over-all economies which cannot be realized by either party separately. If the various technical and commercial factors are given realistic consideration, the resultant benefits can and should be shared equally by both parties.

(b) The oil refinery is provided with a reliable source of low-cost electrical energy and process steam.

(c) The oil refinery is provided with a commercial outlet for its waste fuels, and the burning of such fuels for the generation of electric energy is a contribution in the interests of conservation of our natural resources.

(d) In addition to the sale of electricity and steam to the oil refinery, an appreciable block of electrical energy with firm power value can be delivered to the transmission system of the utility.

(e) A stable source of fuel supply is made available to the utility not only to meet the refinery requirements, but also for the generation of the energy which is delivered into the utility's transmission system.

¹ Engineer of Steam Operation, Pacific Gas and Electric Company. Mem. ASME.

² "Power and Steam Plants for Oil-Refinery Service," by C. E. Steinbeck, Trans. ASME, vol. 61, 1939, pp. 733-740.

Contributed by the Power Division and presented at the Semi-Annual Meeting, San Francisco, Calif., June 27-30, 1949, of THE AMERICAN SOCIETY OF MECHANICAL ENGINEERS.

NOTE: Statements and opinions advanced in papers are to be understood as individual expressions of their authors and not those of the Society. Paper No. 49-SA-11.

PRINCIPAL FEATURES OF THE CONTRACT

The three contracts were signed during 1937 and 1938, and received the approval of what was then known as the California State Railroad Commission but which now functions under the name of California Public Utilities Commission. The maximum steam and electric quantities involved in each case are given in Table 1.

TABLE 1 STEAM AND ELECTRIC REQUIREMENTS OF REFINERIES

Name of company	Process steam, lb per hr	Electricity, kw
Tidewater-Associated Oil Company....	275000	15000
Shell Oil Company.....	325000	15000
Union Oil Company.....	275000	15000

The Pacific Gas and Electric Company agreed to furnish process steam and electric energy in quantities not to exceed the maximum demands given in Table 1, in exchange for certain quantities of "substitute fuels," plus cash payments based upon a demand charge plus a commodity charge. A formula was established wherein the barrels of substitute fuel to be delivered by the oil companies in part payment for the steam and electricity was obtained by multiplying by a certain factor the total pounds of steam or kilowatt-hours delivered to the refinery. There are different multiplying factors for steam and electricity, respectively.

The definition of substitute fuel, as applied in the contract is "any liquid or gaseous fuel, including refinery-waste fuel such as acid sludge, tars, waxes, and gases which will not leave an unburnable residue in excess of 2 per cent by weight, and will produce substantially the same output of steam from the boilers as when fired to capacity with fuel oil." In addition to the foregoing, a further provision was made at the Oleum Steam Plant to include pulverized petroleum coke having the following analysis:

Volatile constituents.....	not less than 10 per cent
Fixed carbon.....	not more than 90 per cent
Ash.....	not more than 1 per cent
Sulphur.....	not more than 2 per cent
Impregnated oil.....	not more than 2 per cent

Provision was also made for the purchase by the Pacific Gas & Electric Company of certain quantities of "excess fuel oil" over and above the amounts delivered to it in payment for steam and electricity. This feature provided a firm source of fuel supply for the generation of electric power for the company's own transmission system. In Fig. 1 is given a diagrammatic representation of the disposition of the various quantities of steam, electricity, fuel, and cash involved in the operation of the contract. Based upon a nominal maximum load of 46,000 kw, more than 30,000 kw is delivered to the company's transmission system, and a little under 12,000 kw is delivered to the oil refinery, plus

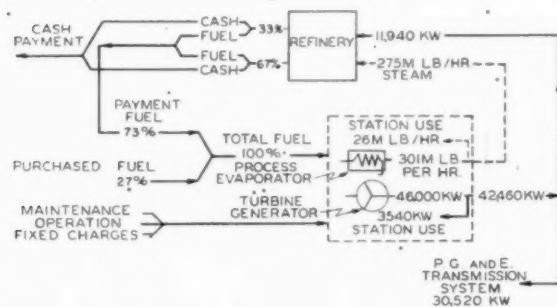


FIG. 1 DISTRIBUTION OF STEAM AND ELECTRIC LOADS, CASH AND FUEL PAYMENTS, ETC., AVON STEAM PLANT

275,000 lb per hr of process steam. Of the total payment in terms of fuel and cash for these quantities of steam and electricity, 67 per cent is for steam and 33 per cent is for electric energy. Under the operating conditions shown in the diagram, the total payment fuel represents 73 per cent of the total fuel requirements of the station, and the remaining 27 per cent must be purchased under the excess-fuel-oil clause in the contract.

DESIGN AND OPERATING CHARACTERISTICS

In order to meet the operating requirements of the Pacific Gas and Electric system, the turbine generators had to be capable of providing a firm electrical power source for its own system without being dependent upon the process-steam demands of the oil refinery. It was also necessary to make the installation self-sufficient as an electric generating station even though the contract with the oil refinery were discontinued at some future date. From this point of view, a straight back-pressure turbine presented distinct disadvantages, because in this case there must be an outlet for the exhaust steam before the turbine is able to generate power. Therefore, single 50,000-kw, 3600-rpm tandem-compound units with automatic extraction at the exhaust of the high-pressure turbine were selected for each of the three stations, and are designed for an initial steam pressure of 1400 psig and a total steam temperature of 940 F. Although these units are nominally rated at 50,000 kw, they have under favorable extraction conditions operated as high as 55,000 kw. Their average capability under the usual refinery steam loads is about 46,000 kw.

The turbine is designed so that it may be operated either as a straight condensing tandem-compound machine or as an automatic extraction unit. It is only on rare occasions that it is necessary to operate on a straight condensing basis; and, under these conditions, the capacity of the unit is reduced to approximately 41,000 kw. Thus, should the oil refinery temporarily curtail or discontinue taking process steam, as was the case during the recent Pacific Coast oil-refinery strike, the plant is able to continue generating more than 80 per cent of its nominal capacity. Should the refinery permanently discontinue taking process steam, it would be feasible to add a second low-pressure condensing element of approximately 25,000 kw capacity, thereby raising the nonextraction capacity of the unit from 41,000 to 66,000 kw with the same installed boiler capacity.

The low-pressure turbine exhausts into a condenser which is somewhat smaller than would be used for a conventional condensing machine for the reason that large quantities of steam normally are extracted at the exhaust of the high-pressure element, thus unloading the condenser. This feature is illustrated by the curve in Fig. 2 showing that at 40,000 kw and with a contract demand of 275,000 lb per hr of process steam, the flow to the condenser is only 172,000 lb per hr, as compared with 324,000 lb per hr for straight condensing operation; or stating it in another way, the condenser flow for these conditions, when operating on an automatic extraction basis, is approximately 53 per cent of what it would be for straight condensing operation. Obviously, any reduction in condenser losses with the same kilowatt output results in a substantial gain in economy in the over-all cycle, as well as a saving in initial investment for the smaller condenser. Due to the relatively few hours of operation on a straight condensing basis, it is economical to overrate the condenser for these conditions at some sacrifice in efficiency.

There is a somewhat complicated relationship between the electric generating capability of the turbine generator and the process-steam flow to the oil refinery. From the curves in Fig. 3 it can be seen that, as the refinery steam load increases, the electric load on the turbine generator can be held constant or increased until the control valves on the low-pressure turbine are wide open. When this optimum point is reached, any further in-

crease in the electric load can be made only by increasing the refinery steam load. In this connection it is interesting to note that the second unit installed at Oleum made it possible to divide the extraction load between the two units and thereby operate more nearly at this optimum extraction point, so that the capability of the first machine was slightly increased as a direct result of installing the second unit. At a refinery steam demand of 275,000 lb per hr and with all of the extraction steam coming from one machine, the capacity of the turbine is 46,000 kw, as compared with 48,000 kw on each of two units with the extraction divided equally between them.

The steam which is extracted from the high-pressure turbine is passed through the process evaporator coils, and the condensate is returned to the plant cycle. The heat exchange with the process feedwater results in the generation of steam at approximately

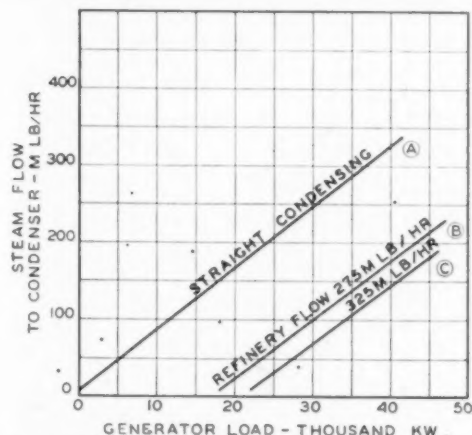


FIG. 2 STEAM FLOW TO CONDENSER FOR DIFFERENT GENERATOR LOADS UNDER BOTH STRAIGHT CONDENSING AND EXTRACTION OPERATION OF 50,000-KW TURBINE-GENERATOR AT AVON STEAM PLANT

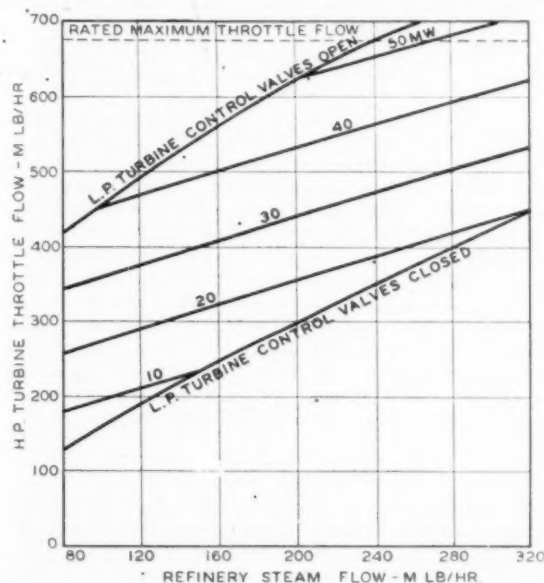


FIG. 3 OPERATING CHARACTERISTICS OF 50,000-KW TURBINE GENERATOR AT AVON STEAM PLANT FOR VARIOUS ELECTRIC AND EXTRACTION LOAD CONDITIONS

165 psig. The evaporators were selected for a moderate temperature head which varies both with the process steam load and the cleanliness of the evaporator coils. The extraction pressure is controlled by a feeler line connected to the 165-psig steam pipe to the oil refinery. Thus, although the nominal extraction pressure at the exhaust of the high-pressure turbine has been referred to as 240 psig, actually this pressure varies automatically with the evaporator load as indicated in Fig. 4. This serves to hold the temperature head at a minimum, thereby reducing the inherent loss in cycle efficiency where a heat exchanger is interposed, in order to recover as condensate the steam extracted from the high-pressure turbine.

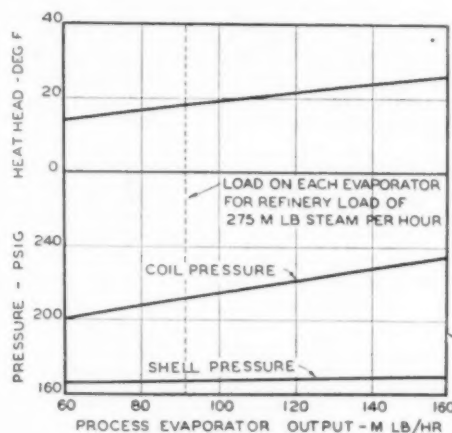


FIG. 4 PROCESS-EVAPORATOR OPERATING CHARACTERISTICS AT DIFFERENT OUTPUTS—AVON STEAM PLANT

In view of the foregoing, the losses resulting from the use of a closed cycle are not as great as sometimes have been indicated. The only other alternative is to deliver the extracted steam from the exhaust of the high-pressure turbine directly to the oil refinery. This immediately introduces a major problem in controlling the chemical content of large quantities of raw make-up water which must be fed to the high-pressure boilers. It is usually difficult to obtain condensate returns from the oil refinery which are free enough from oil contamination for satisfactory high-pressure boiler feedwater. Therefore the added investment cost in water-conditioning equipment plus increased operating and maintenance costs will in some instances offset the theoretical gain in cycle efficiency.

In electric systems such as ours, where an appreciable percentage of the power output is generated from hydroelectric sources, there sometimes occur seasonal conditions wherein all or at least a considerable number of the steam plants must be operated at minimum load in order to prevent loss of water over the dams during periods of high run-off. As indicated in Fig. 5, the amount of process steam required by the refinery determines the minimum electric load which can be carried by the turbine generator when operating on a strictly automatic extraction cycle. This minimum occurs when the low-pressure-turbine control valves are closed so that the high-pressure turbine is functioning as a straight back-pressure machine with its load fixed by the amount of extraction steam being delivered to the evaporator coils. In order to reduce the load below this minimum, it is necessary to by-pass a portion of the steam requirements for the process evaporators around the turbine and through the reducing valves which are provided primarily for occasions when the turbine is shut down for overhaul. Obviously, there is considerable loss in efficiency when

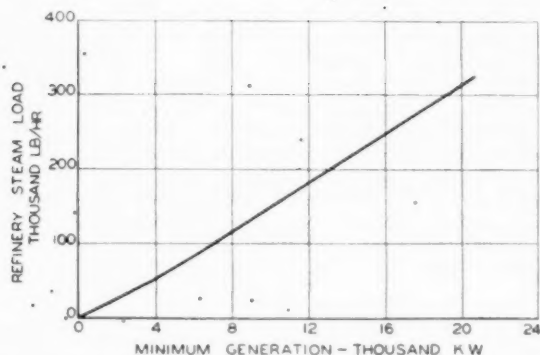


FIG. 5 MINIMUM POSSIBLE LOADS ON 50,000-KW TURBINE GENERATOR FOR VARIOUS REFINERY STEAM LOADS WHEN OPERATING ON AUTOMATIC EXTRACTION—AVON STEAM PLANT

all or part of the steam supply for the evaporators is passed through the reducing valves, and these factors must be evaluated in determining the average cost of steam and electric energy supplied to the oil refinery. On many power systems it may be feasible never to operate below the minimum load possible with full-automatic extraction, and therefore the only time when it will be necessary to use the reducing valves will be for the short periods during which the turbine is shut down for overhaul.

One of the problems requiring special consideration is the size and number of boilers. Due to the burning of waste fuels the boiler availability is somewhat less than is possible with good commercial fuels, and furthermore, the oil refinery cannot be expected to curtail or shut down its plant in order to permit the utility to carry on routine maintenance. Therefore special consideration must be given to this problem in the boiler layout. As indicated by the curve in Fig. 6, there are three boilers per turbine, each having a continuous rated capacity of 200,000 lb of steam per hr and an overload capacity of 230,000 lb per hr. It is of interest

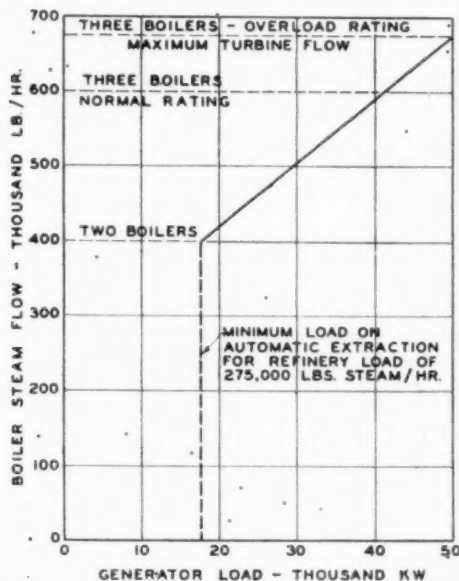


FIG. 6 BOILER STEAM-FLOW REQUIREMENTS FOR VARIOUS TURBINE-GENERATOR LOADS AND A REFINERY STEAM LOAD OF 275,000 LB PER HR

to note that, due to the base load which must be carried by the boilers in order to meet the demand for process steam, the loss of one boiler, representing one third of the total boiler capacity, results in an electric-load reduction of more than 50 per cent. Thus it is clear that it is desirable not only to carry some additional reserve boiler capacity in order to offset the slightly lower boiler availabilities with waste fuels, but it is also necessary to install several small boilers rather than a lesser number of large boilers, in order to avoid an excessive load reduction on the turbine generator when one boiler is out of service.

HEAT RATE FOR ELECTRIC GENERATION

In Fig. 7 the estimated heat rate per kilowatthour of electric generation has been plotted as a separate item by segregating the proportions of fuel chargeable, respectively, to the generation of process steam and electricity. There are various methods of com-

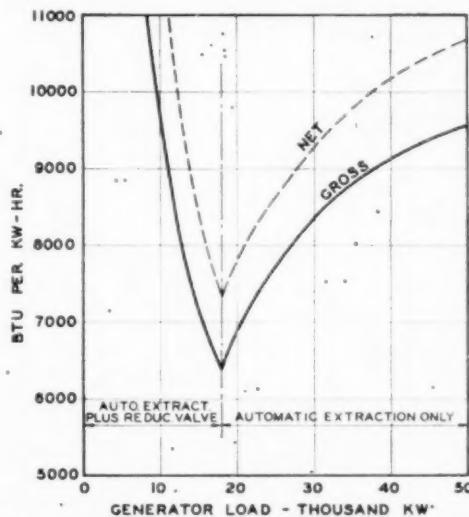


FIG. 7 HEAT RATE IN BTU PER KW-HR OF ELECTRIC GENERATION AFTER DEDUCTING FUEL REQUIRED FOR GENERATION OF 275,000 LB PER HR OF PROCESS STEAM—AVON STEAM PLANT

puting the proper allocation based upon the initial premises which are set up; but for the purpose of establishing the curve in Fig. 7 it was decided to credit the total fuel consumption for both process steam and electricity with the amount of fuel that would be required to generate the contract demand for 275,000 lb per hr of process steam in low-pressure boilers. Then the balance of the total fuel used is all that is chargeable against electric generation. It is fully realized that this method of allocating the fuel for process steam and power is debatable, but a study of other methods of arriving at a solution based upon a breakdown of the various components of the plant cycle led to the conclusion that these also left much to be desired and involved more complication than appeared to be justified for the present objective.

BURNING OF WASTE FUELS

The physical and chemical characteristics of refinery-waste fuels are subject to considerable change from time to time, and the fuel-burning equipment at the plant must be sufficiently flexible to anticipate such changes. The design of the boiler must also be such that fuels which are high in ash and sulphur may be burned with reasonable boiler availability. Some of these liquid-petroleum-base fuels present operating difficulties which are not

usually encountered with coal. Therefore the commercial aspects of the contract must be worked out properly so that the extra handling and maintenance costs plus lower boiler availability associated with certain of these waste fuels will not penalize the utility in the cost of electric generation.

The types of fuels burned differ somewhat in each of the three plants under consideration; and from time to time there have also been radical changes both in the type and quality of the fuels delivered to any particular plant due to the changes in the manufacturing programs at the respective refineries. To date the types of fuels which have been burned are given in Table 2. The analyses of these fuels are given in Table 3.

TABLE 2 TYPES OF FUELS BURNED

Avon	Martinez	Oleum
Acid sludge	Recovered oil	Pulverized petroleum coke
Pitch	Cracked asphalt	High-sulphur fuel oil
Heavy fuel oil	Heavy fuel oil	Commercial fuel oil
High-sulphur fuel oil	High-sulphur fuel oil	Natural gas
Commercial fuel oil	Commercial fuel oil	
Natural gas	Natural gas	

TABLE 3 TYPICAL ANALYSES OF CRITICAL FUELS

	Per cent by weight	
	Sulphur	Ash
Acid sludge	2.9-4.6	0.03-0.06
Recovered oil	6.0-9.0	0.01-0.09
Pitch	0.05	0.70
High-sulphur fuel oil	3.0-4.6	0.08-0.14
High-sulphur petroleum coke	4.0-4.2	0.51-0.84

The curves in Fig. 8 show historically the types and quantities of each kind of fuel which have been burned at the Avon plant since it was started up in December, 1940. It is interesting to note that during the war years, large quantities of natural gas were burned as a result of a co-operative effort between the Pacific Gas and Electric Company and the oil refineries on the one hand, and the United States Navy on the other hand, in order to make the maximum amount of fuel oil available for the Navy. Again, during the months of September, October, and November, 1948, it became necessary to burn natural gas in order to keep our plants in operation during the Pacific Coast oil-refinery strike.

Our early experience with the burning of acid sludge resulted in rather low boiler availability owing to external fouling of the boiler heating surfaces; and because of combustion instability, supporting gas or oil pilot fires must be used. However, as a result of research on the part of the oil company, changes were made in its equipment and processes so that the modified acid sludge could be burned with fairly high boiler availability. Due to the high water content, it must not be heated much above 190 F in order to avoid a boilover in the heated storage tanks, and this temperature is satisfactory at the burners.

The problem of burning pitch or cracked asphalt is confined merely to maintaining its temperature at the burners at approximately 400 F in order to obtain a satisfactory viscosity for burning it under the boilers. At ordinary temperatures it is in the solid state, and therefore considerable care must be exercised in seeing that the temperature of this material is never allowed to go too low. This is accomplished by means of steam tracer lines bound to the fuel lines and surrounded by insulation. Other than this, it has proved to be a fairly acceptable fuel which can be burned almost as satisfactorily as the commercial grade of fuel oil derived from the same crude, although it is somewhat higher in ash content and therefore will produce slightly more deposits on the boiler heating surfaces than will the fuel oil.

So-called "recovered oil" is the end product after extracting a large percentage of the sulphuric acid present in acid sludges resulting from the manufacture of lubricating oil. Both acid sludge and recovered oil are highly corrosive, and the products of combustion are very corrosive at temperatures which normally would

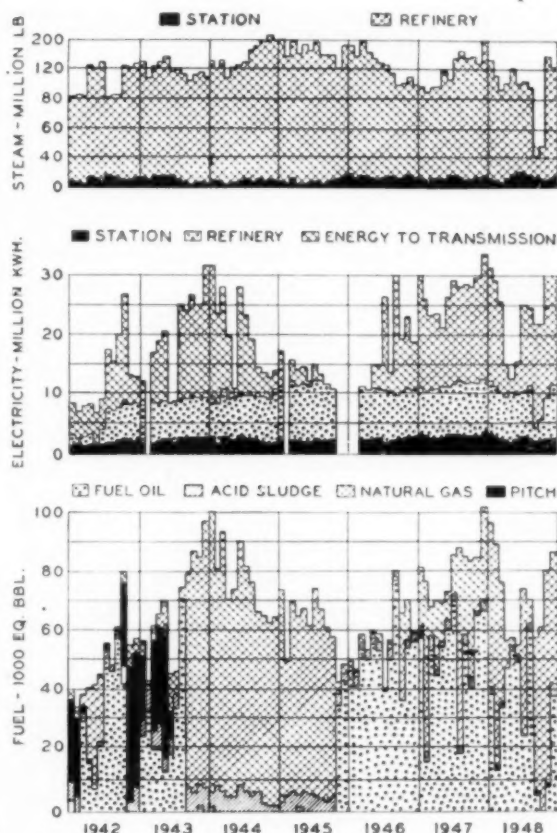


FIG. 8 HISTORICAL CHART SHOWING PROCESS STEAM AND ELECTRIC ENERGY DELIVERED TO OIL REFINERY, AND TYPES OF FUEL BURNED AT AVON STEAM PLANT

exist in the air preheater of the boiler. All fuels with high sulphur contents such as acid sludge, recovered oil, high-sulphur fuel oil or coke, and the like, make it necessary to provide for partly by-passing the air preheater so that the exit-gas temperature can be held above the dew point. The effect of the presence of sulphur, or rather of sulphur trioxide, upon the dew point of the exit gases is fairly well understood, and it is necessary, in order to avoid air preheater corrosion, to maintain these temperatures in general conformity with the curves shown in Fig. 9 as the sulphur content in the fuel increases. This results in an appreciable reduction in boiler efficiency which should be taken into account in working out the commercial details of the contract.

HIGH-SULPHUR FUEL OILS AND PETROLEUM COKE

Certain so-called high-sulphur fuel oils and petroleum cokes require special consideration in order to be able to burn them with reasonable boiler availability and maintenance costs. The particular fuel oil referred to here has the sulphur and ash contents shown in Table 3. The degree of external fouling of the boiler heating surfaces appears to be influenced by the combination of both the high sulphur and ash contents. It is not felt that the presence of high sulphur by itself would result in appreciable fouling, but it also has been fairly well demonstrated that, in the presence of a high ash content, the combination will produce a bad fouling problem. In certain temperature zones, a binding action exists which results in maximum deposits on the heating surfaces

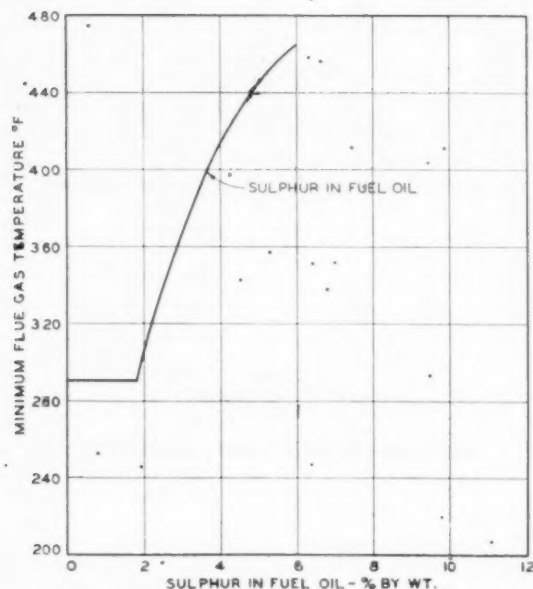


FIG. 9 MINIMUM SAFE FLUE-GAS TEMPERATURES FOR VARIOUS PERCENTAGES OF SULPHUR IN FUEL OIL IN ORDER TO AVOID AIR-PREHEATER CORROSION

in that area. The mechanism by which deposits are formed on a heating surface has to do primarily with the fusion and softening points of the ash. Deposits will occur largely in those parts of the boiler where the gas envelope surrounding the tube is within approximately 200 deg F of the softening point of the ash. The other critical zone is at temperatures near or below the dew point of the flue gases, where corrosion of the metal also takes place and further aggravates the fouling problem.

The characteristic of the ash content in high-sulphur fuel oil produces a fouling problem which is quite different from that usually experienced with coal, owing to the fact that the fusion point of the ash is in the neighborhood of 1600 F. As may be seen from the schematic cross section of the heating surfaces of the boiler shown in Fig. 11, this temperature zone lies in the first bank of superheater tubes. With coals, the fusion point of the ash is frequently well above 2200 F, which fixes the fouling zone in the boiler-generating tubes. In such instances, it is possible to control to a very large extent the whole problem of fouling by going to a low-heat-release furnace, so that the temperature of the gases leaving the furnace are for the most part below the softening point of the ash. The boiler and superheater tubes for coal-firing are widely spaced in order to provide low velocities for the gases of combustion, which appears to be helpful in preventing the fly ash from depositing on the tubes, and also because the mechanical strength of coal slags is usually greater than that from petroleum-base fuels, thereby increasing the tendency to bridge across between tubes.

In connection with the firing of high-sulphur fuel oil and petroleum coke, interesting proof of the sharply defined temperature conditions which control deposits on boiler heating surfaces was obtained by fanning out the first bank of superheater tubes so that the spacing at the bottom was increased from $3\frac{1}{2}$ to $4\frac{1}{2}$ in. centers for $2\frac{1}{2}$ -in.-OD tubes. This was accomplished simply by inserting 2-in. spacers between the lower ends of the tubes, thus increasing the clear space between tubes from 1 to 2 in. Actually, with only 1 in. of clear space, some of the tubes were much closer than this, or even touching one another due to warpage. The

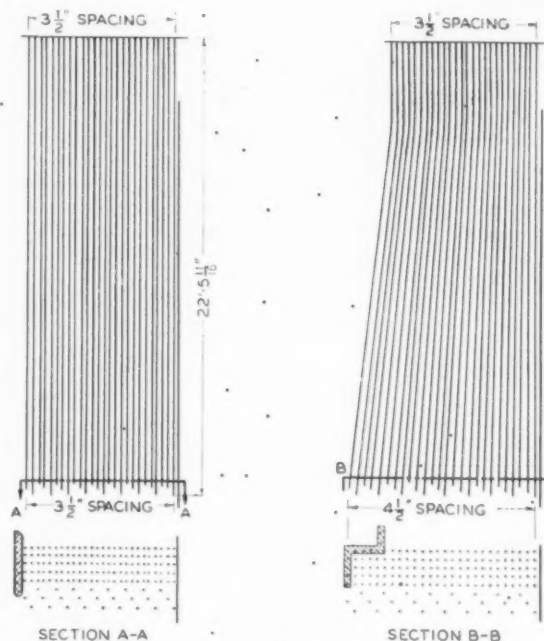


FIG. 10 METHOD OF FANNING-OUT BOILER SUPERHEATER TUBES TO INCREASE CLEAR SPACE BETWEEN TUBES—OLEUM STEAM PLANT

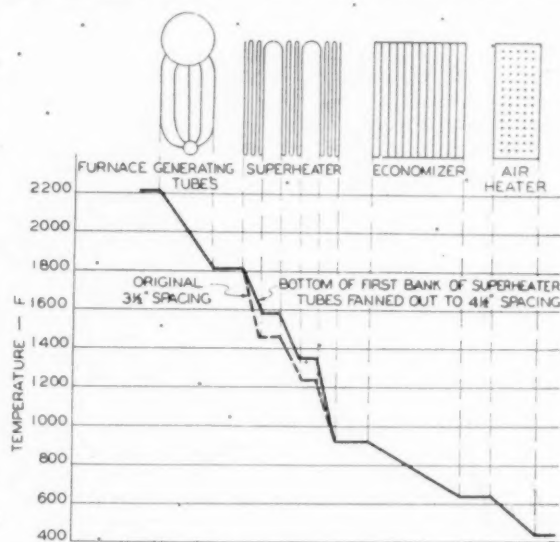


FIG. 11 TEMPERATURE GRADIENT OF FLUE GASES BEFORE AND AFTER FANNING OUT SUPERHEATER TUBES, AS SHOWN IN FIG. 10

method of accomplishing this is illustrated in Fig. 10, and the effect on the temperature gradient of the flue gases is shown in Fig. 11.

Before making the change just mentioned, in the superheater-tube spacing, the fouling zone was concentrated initially in the first bank of the superheater, and as the deposits continued to build up, the temperatures ultimately were raised in the second bank to the point where fouling would commence in that zone. The tubes were so closely spaced that effective soot-blowing was

impossible. However, after fanning them out, the amount of fouling in the first bank and the first three rows of the second bank was materially reduced, and it was possible to keep these tubes clean by means of soot-blowing. There was some increase in the amount of deposits in the last few rows of the second bank. It has been concluded that this is due to lack of penetration of the soot blowers. It is anticipated that installation of additional blowers between the second and third superheater banks will remove these deposits.

Increasing the spacing by the method described was considered as an experiment in order to determine the optimum spacing of the superheater tubes. However, such a noticeable improvement in the operating periods between cleanings was obtained at nominal expense that nine of the twelve boilers in the three plants are in the process of being changed in a similar manner. The other three boilers, which are designed for coke-firing as well as fuel oil, are to undergo a more radical change in superheater-tube spacing as a further experiment. The conclusion to be drawn from the foregoing experiment appears to be that soot-blowing can be made effective for these special fuels if the optimum spacing of the superheater tubes is predicted correctly. From this optimum point, the indications are that the effectiveness of the blowers will decrease either for narrower or wider spacing.

Additional problems were encountered in the furnace owing to the particular kind of ash found to be present in either the high-sulphur fuel oil or coke derived from the same crude stock. From the analysis of the ash given in Table 4, it can be seen that appreciable quantities of vanadium and nickel are present, and that the

TABLE 4 ANALYSIS OF ASH IN PETROLEUM COKE

Substance	Per cent by weight
(1) SiO_2	7.9
(2) Al_2O_3	2.6
(3) TiO_2	0.2
(4) CaO	1.3
(5) MgO	3.0
(6) FeO	0.3
(7) NiO	10.5
(8) SO_2	20.9
(9) V_2O_5	29.9
(10) Na_2O (calculated)	23.4
Total of items 7-8-9-10	84.7

total of NiO , SO_2 , V_2O_5 , and Na_2O represents nearly 85 per cent of the entire sample. The presence of these compounds introduced a phenomenon of furnace-wall growth which eventually progressed to a point where the expansion spaces at the corners of the furnace walls were completely taken up, thereby setting up very heavy stresses which in turn resulted in serious distortion of the steel members between the buck stays and the furnace walls. This condition was first observed after a period during which approximately 25,000 tons of petroleum coke had been burned.

The furnace walls consist of waterwall tubes which are studded and faced with plastic chrome ore. In the process of combustion, sulphates and vanadates of the alkalis are formed; and these appear to have a strong affinity for the chrome ore and penetrate the pores and cracks which occur during successive cooling and heating of the furnace. Under such temperature reversals these compounds pass back and forth from the solid to the liquid state, thereby penetrating the chrome ore with resultant growth in volume. The coefficient of expansion of the slag is greater than that of the chrome ore, and the combination produces a very dense mass which brings about a progressive growth of the entire wall. The resultant mechanical forces which are set up are sufficient to force the water-wall tubes to spread further apart until all the expansion space in the corners of the furnace walls has been taken up. This condition has been overcome by the addition of more tie bars for holding the waterwall tubes in place, and the substitution of a different type of refractory facing for the tubes.

In Table 5 is shown a rough correlation between the proportion

TABLE 5 PROPORTION OF CRITICAL FUELS BURNED, COMPARED WITH AVERAGE NUMBER OF BOILER SHUTDOWNS PER YEAR FOR EXTERNAL CLEANING OF HEATING SURFACES

Year	Station	Proportion of critical fuels burned, per cent of total	Average number of cleaning outages per year per boiler
1948	Avon	45	2.7
	Martinez	69	2.7
	Oleum	59	1.7
1947	Avon	66	4.0
	Martinez	73	3.0
	Oleum	78	1.7
1946	Avon	92	3.0
	Martinez	70	2.7
	Oleum	73	2.0
1945	Avon	18	1.7
	Martinez	17	1.7
	Oleum	14	1.2

NOTE: The number of cleaning outages in the last column includes the regular annual overhaul and inspection.

of critical fuels burned and the average number of boiler shut-downs per year for external washing of the heating surfaces. It can be noted that, during 1945, on account of the war, much smaller percentages of critical fuels were burned, and the average number of cleaning outages was the lowest during the 4 years shown in the tabulation. However, due to the improvements which are being made in overcoming the problem of deposits, boiler availabilities increased during 1948.

This problem of burning special types of fuels has been treated at some length because it has to do with one of the major points of difference between a conventional plant and the semi-industrial type which is the subject of this paper. On the other hand, the data which have been presented clearly show that, although the problem should not be underestimated in entering upon a joint undertaking of this nature, waste fuels can be burned with reasonable boiler availability, and that operating experience has brought to light the possibility of boiler-design modifications and improved soot-blowing techniques, which should bring these availabilities still closer to what can be obtained with commercial grades of fuel.

RAW-WATER SUPPLY

The large quantities of raw water required for the process evaporators are supplied from a slough in the San Joaquin River about 10 miles north of the Avon steam plant. However, due to a combination of tidal conditions and seasonal variations in river flow, the salt water from San Francisco Bay tends to back up in the river and the salinity of the water becomes prohibitive at certain seasons of the year. Shortly after the Avon station was started up, an alternate supply became available from the Contra Costa Canal which is an irrigation project of the United States Bureau of Reclamation. The source of this canal is located at a higher point up the San Joaquin River, but conditions are such that, at certain seasons of the year, the salinity from Mallard Slough is less than that which prevails in the Contra Costa Canal, and it has been found desirable to switch from one source to the other during the year, as indicated in Fig. 12. The chemical conditioning of this raw water for evaporation involves a formidable treating plant which is illustrated in Fig. 13. The average analyses of the raw water are given for both Mallard Slough and the Contra Costa Canal and the analyses at various points in the treating cycle are also given.

The problem of preparing the raw water for evaporation without carry-over and consequent contamination of the entire system is of major importance. However, it is felt that this is a subject which does not stand out as peculiar to this type of plant, except with respect to the very large quantities of water to be handled. Therefore the matter will not be elaborated here in such detail as has been the case with the special problems directly related to this type of station.

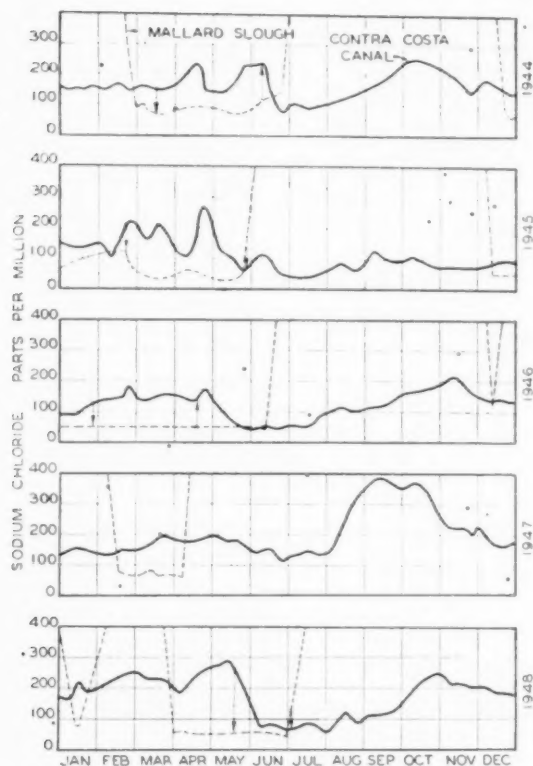


FIG. 12 HISTORICAL RECORD OF SALINITY OF RAW-WATER SOURCES FOR AVON AND MARTINEZ STEAM PLANTS
Vertical arrows indicate time of change-over from one source of supply to the other.)

CONCLUSION

An attempt has been made to point out and evaluate the special problems which enter into the design and operation of a plant of this type. The advantages that are inherent in such a joint undertaking should be obvious, but it is possible to wipe out a large proportion of these benefits by the failure to give proper weight to the various factors involved. It is therefore hoped that the somewhat detailed analysis of the more important problems which have been set forth in this paper will be helpful in developing a sound basis for making a realistic appraisal of any such similar undertaking which might come up for consideration in the future.

Discussion

F. S. CUMMINGS.³ This paper is of particular interest on two points:

1 It gives operating results of a modern high-pressure public-utility generating plant, operating in conjunction with a large industrial plant, requiring both electric energy and large quantities of moderately high-pressure steam for process work.

2 It covers what is believed to be the first published information on the problems of burning, under modern high-pressure boilers, practically all of the waste products from a modern oil refinery.

In the last 25 or 30 years there have been many industrial plants built to supply process steam and electric energy for plant uses. Sometimes these plants operate as independent units, and sometimes they operate in parallel with a public-utility system to better take care of any unbalance in electric and steam requirements of the industry. However, there have been relatively few public-utility plants built for the express purpose not only of supplying electric energy to the utility distribution system, but

³ Vice-President and Chief Engineer, C. C. Moore & Company, Engineers, San Francisco, Calif. Mem. ASME.

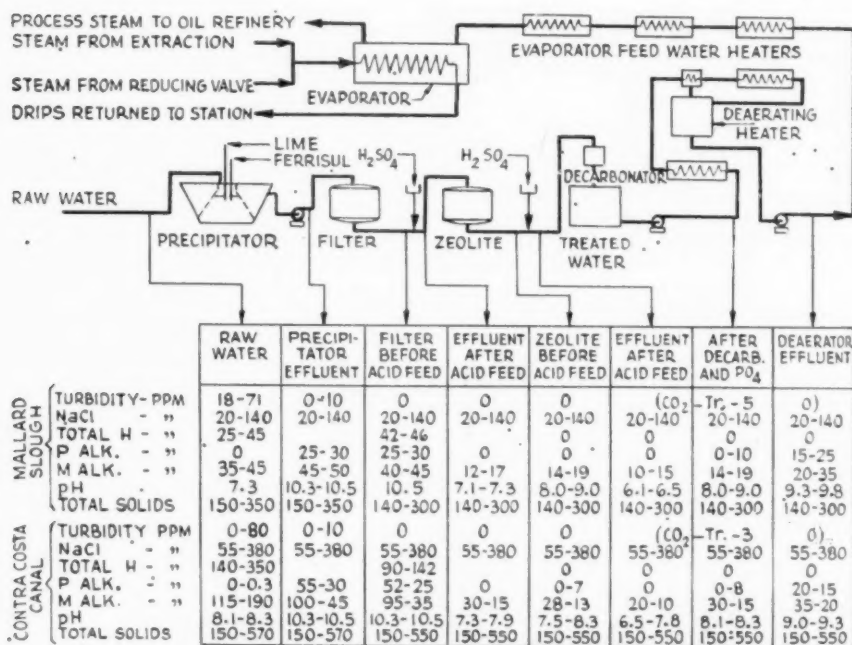


FIG. 13 FLOW CYCLE AND CHEMICAL-TREATING CYCLE FOR RAW-WATER SUPPLY TO PROCESS EVAPORATORS AT AVON AND MARTINEZ STEAM PLANTS

also to supply electric energy and steam for an adjoining industrial plant. Further, there have been still fewer such plants built to operate at high pressures and temperatures.

As pointed out in the paper, both the utility and the industry can gain much by such a tie. The advantages to be gained are so many that future planners should consider them seriously. Probably one of the more important reasons for a utility being reluctant to tie in with an industrial plant has been the fear on the part of the utility that it would lose some of its flexibility in the generation of electric power which of course is its basic reason for existence. The plants discussed in the paper have been in operation for a number of years, and the operation has given ample proof that there need be no serious difficulties.

Until perhaps the last 15 or 20 years, fuel oil was considered to be perhaps the most ideal of fuels. Compared to the use of coal and other fuels, boiler outage was relatively low, maintenance was also relatively low, the elimination of expensive storage,

handling, and burning equipment meant lower first cost, and operation was generally more flexible. All of this has changed in more recent years. The change in quality of fuel oil available during the war years, and changes in refining methods, have created many new problems for the boiler designer and operator—problems which are not always solved by referring to experience in burning coal. Years ago oil-fired boilers were relatively small, of comparatively low pressure, and ran at moderate ratings. Central-station boilers today are of large capacity, high pressure and temperature, and operate at high ratings. These factors have increased the problems confronting the designer and operator.

On the West Coast the quality of fuel oil also has deteriorated because of the decreasing supply of crude, which has necessitated an increased use of crudes which are relatively high in impurities. These impurities are sulphur and sometimes small quantities of rare metal oxides which have a peculiar action on the ash which is in the fuel. While fuel oils themselves many times have these

troublesome characteristics, the various types of waste fuels, burned in the three plants under discussion, produce aggravated difficulties because of the higher percentage of impurities.

It is most interesting to note that boiler and plant design has been such that even the worst of the waste fuels have been handled with some considerable success. The operating experience gained has been most valuable in the design and operation of new units; it is by studying the operating difficulties encountered that future plants can be built with increased reliability equal to the best of modern coal-burning plants.

F. X. GILG.⁴ It may be of interest to show a cross section through the steam-generating units which were installed as part of the Oleum, Avon, and Martinez projects, described by the author.

Fig. 14 herewith shows a cross section through the boilers which are radiant-type single-pass gas flow, designed to generate 200,000 lb. of steam per hr. continuously at 1450 psi and 950 F at the outlet of the superheater. Final steam temperature is controlled by means of a gas by-pass around the superheater at one side of the boiler, the quantity of gas

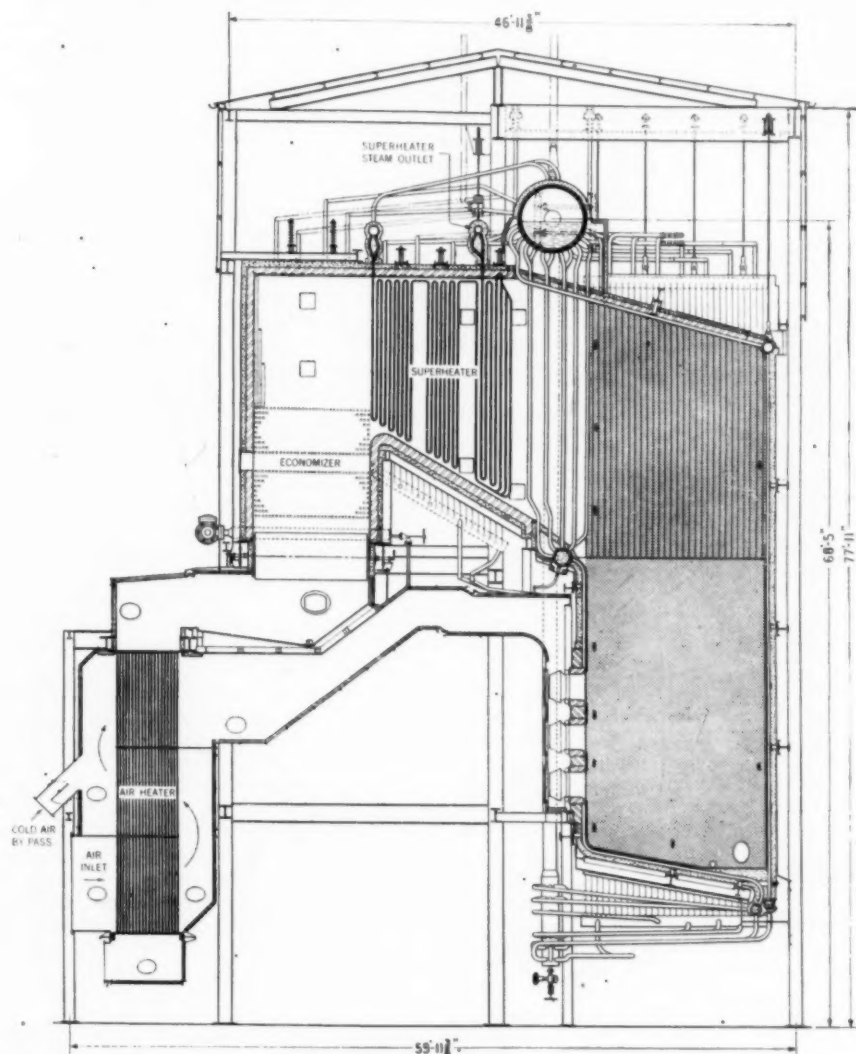


FIG. 14 CROSS SECTION THROUGH STEAM-GENERATING UNIT AS INSTALLED AT OLEUM, AVON, AND MARTINEZ STATIONS

⁴ Application Engineer, The Babcock & Wilcox Company, New York, N. Y. Mem. ASME.

by-passed being controlled by dampers located in the cooler zone under the economizer.

The furnaces are completely water-cooled and designed to accommodate oil, gas, or pulverized fuel.

The economizer is of the continuous-tube type and extends across the full width of the setting including the superheater by-pass area.

A cold-air by-pass is provided in the tubular air heater so that the tube-metal temperature can be raised to minimize corrosion when burning high-sulphur fuels.

The boilers are installed outdoors with just a protecting roof over them.

As pointed out by the author, experience gained on these units burning refinery-waste fuels has been helpful in designing later units so that the superheater surfaces do not foul up as quickly and can be cleaned by soot blowers in service. As can be seen from the temperatures in Fig. 11 of the paper, it is more complicated than simply providing more space between superheater tubes, because the absorption decreases with wider spacing, resulting in higher gas-temperature levels in the subsequent banks of superheater tubes and the possibility of transferring the troublesome area. It is to be noted that after fanning the lower ends of the first-bank superheater tubes so that the clear space was 2 in. instead of 1 in. between tubes, the temperature of the gases entering the second bank of superheater tubes increased from 1450 F to 1580 F. However, indications are that the wider spacing resulted in less plugging of the first bank of superheater tubes, which was so troublesome from the beginning.

F. G. PHILO.⁵ Experience obtained in burning natural gas and high-impurity fuel oils in large quantities at the Long Beach Steam Station, through evolution, has led to a number of boiler-design, operating, and maintenance betterments which are incorporated in the boiler installation of the Redondo Steam Station which was placed in service late in February, 1948. In connection with the present paper it may be helpful to mention several of these improvements. The more important changes are as follows:

- 1 Elimination of all gas baffles.
- 2 Graded spacing of furnace screen, superheater and economizer tubes.
- 3 Watertight acid-resistant sloping floor and hopper beneath superheaters, economizers, and air preheaters to facilitate water washing.
- 4 Downflow of gases through economizer and air preheater.
- 5 Permanent provision to collect and conduct wash water with dissolved and other solids to a point of convenient disposal.

In a general way, with high-impurity fuel oils, including rather high sulphur content, such as Pacific Coast 400 or Bunker C, the boiler, superheater, economizer, and air-preheater surfaces operate within a very wide range and number of gradations of skin temperatures (on the surfaces of deposits especially) and function quite effectively as fractionating condensers.

Most of the impurities enter the boiler passages in the vapor or gas phase and tend to deposit throughout the heat-transfer system wherever temperature and moisture conditions are favorable for deposit. The situation to a large degree may be likened to the changing nature of deposits often found in successive stages of a steam turbine due to carry-over of solids from the boiler.

Referring to the accompanying sectional outline of one of the Redondo boilers, Fig. 15, the changes previously itemized will be noted as follows:

⁵ Chief Mechanical Engineer, Southern California Edison Company, Los Angeles, Calif. Mem. ASME.

TABLE 6 TUBE SPACINGS

Location	No. rows deep	Tube OD, in.	Space between tubes, in.	
			Across	Deep
Furnace screen.....	3	4	14	8
Furnace screen.....	2	4	5	8
Secondary superheater.....	3	2 1/2	4 1/2	2 1/2
Secondary superheater.....	5	2 1/2	4 1/2	2 1/2
Primary 2nd section superheater.....	8	2 1/2	1	1 1/2
Primary 1st section superheater.....	10	2 1/2	1	1 1/2
Economizer 2nd section.....	21	2 1/2	2	1 1/2
Economizer 1st section.....	20	2 1/2	2	1 1/2

1 Elimination of all gas baffles facilitates water washing; certain areas may be washed both from front and back.

2 The lateral and "front to back" tube spacings are as given in Table 6 herewith.

Gradation of cross spacing between tubes has prevented appreciable increase of draft loss due to fouling.

Although, at the time of installation, the boilers were equipped with the latest design of retractable mass-action soot blowers, deposits do adhere to the various heating surfaces and cause a gradual but slow reduction in the range of superheater control.

The greatest deposits occur on the surfaces of the economizer tubes. This particular deposit is rather loose and soft and, fortunately, is highly soluble and easily removed with a generous stream of water slushed over the top row of tubes in each of the two tube banks of the economizer. This is done with a very low fire and can be completed in a period of about 2 hr "off-line" at full boiler pressure.

3-4-5-Watertight, acid-resisting floors and soot hoppers, downflow of the gases and wash water in the economizers and air preheaters, and washing toward the cold end of the economizers and the air preheaters, especially in the case of the air preheater, combine to wash deposits out of the preheater instead of through the air preheater.

To those unacquainted with the problem of deposits from relatively high-ash and sulphur fuel oils, it may be of interest to know of the quite effective cleaning job that may be accomplished by the occasional use of natural gas for several days, as a cleaning agent for surfaces fouled by noncombustible residues from fuel oil. Where limited amounts of natural gas are available in oil-burning plants, it has been found good practice to rotate or alternate the firing of gas and oil. The reasons for the cleaning effect of gas are still undetermined.

Operation with regenerative air preheaters to date has been encouraging as most of the troubles previously experienced with the older tubular air-preheater deposits have not been encountered. It is felt that a great deal of the corrosion and deposits difficulties previously experienced with the tubular air preheaters was chargeable to uneven distribution of air and gas flow around and through the individual tubes. Scott Jensen⁶ has surveyed the pattern of gas temperatures from the individual tubes of large preheaters at the Long Beach Steam Station which were installed in 1928-1930. Corrections of local flow rates in the preheaters have raised the lower local gas temperatures sufficiently to mitigate corrosion greatly and also plugging by deposits on the cold ends of the air preheater tubes.

The writer feels that the problem of oil-ash residues has not received its warranted study by the boiler and soot-blower manufacturers. Intensive study of this important problem is suggested as it is reasonable to expect increasing troubles with higher concentrations of oil-impurity residues anticipated from fuel oils produced by improved refinery processes of the future.

W. F. RYAN.⁷ The advantages of co-operation between process

⁶ Steam Plant Engineer, Southern California Edison Company, Los Angeles, Calif. Mem. ASME.

⁷ Engineering Manager, Stone & Webster Engineering Corporation, Boston, Mass. Fellow ASME.

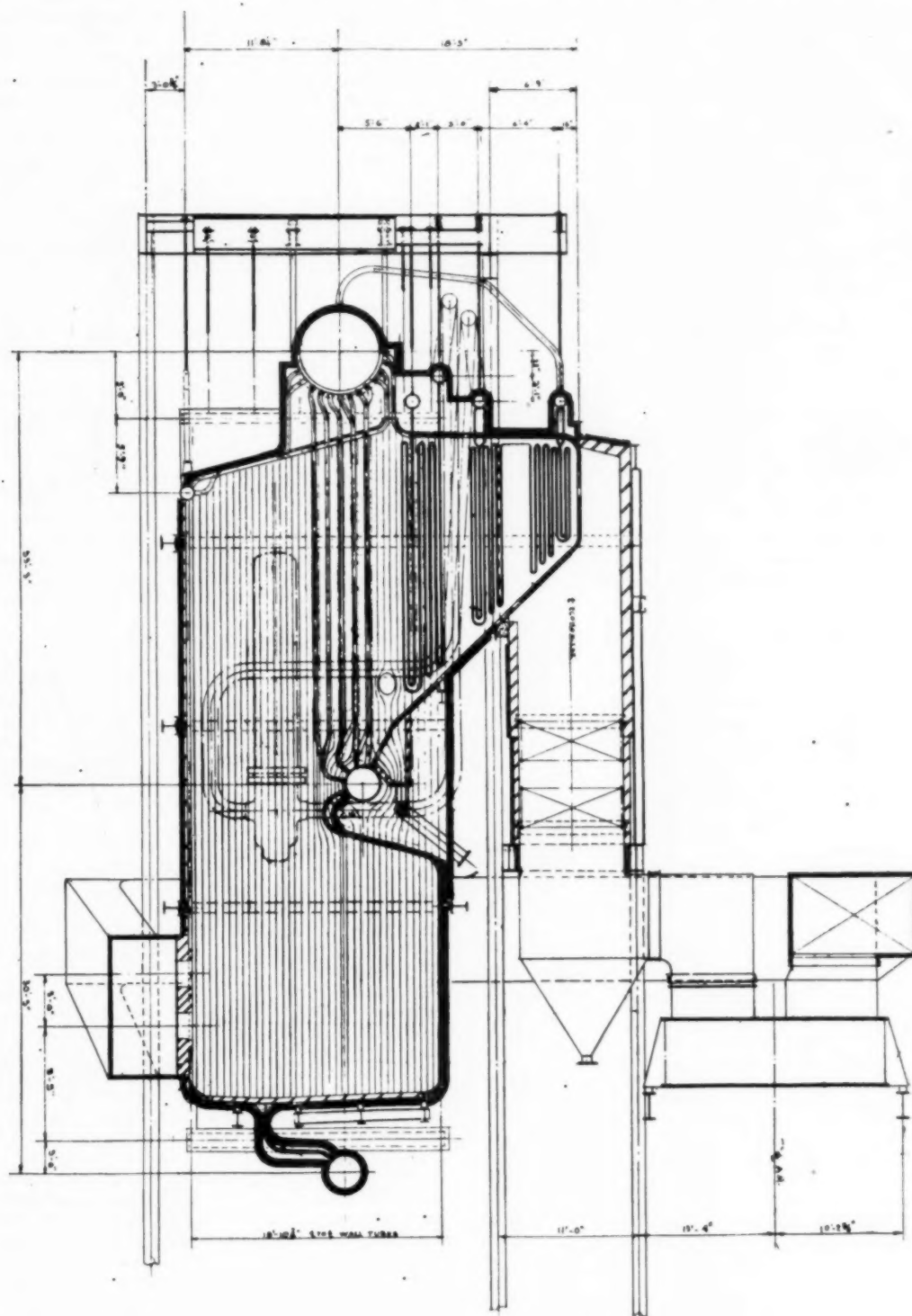


FIG. 15 CROSS SECTION THROUGH STEAM GENERATOR AT REDONDO STATION OF THE SOUTHERN CALIFORNIA EDISON COMPANY
(Maximum capacity 400,000 lb of steam per hr; design pressure 1000 psi; total steam temperature 900 F.)

industries and public utilities for wholesale generation of electric power have never been better stated than by the author in this paper. If these advantages were more widely comprehended, an appreciable portion of steam-generated power in this country might be derived from plants like those described in the paper, with benefit to the national economy from availability of lower-cost electric power, lower-cost process steam, and conservation of our fuel resources. As the author points out, the advantages of the setup should be equitably divided between the utility and the manufacturer. An equitable arrangement is not always easy to arrive at, and it is even less easy to convince both parties that the arrangement is equally advantageous to each. Nevertheless, meticulous and patient appraisal of each detail will be well-rewarded whenever the basic conditions are favorable for such an enterprise.

When these plants were built, the pressures and temperatures selected were probably regarded as the maxima commercially practicable. There should be no obstacle, in the design of future plants, to the use of higher pressures and temperatures. Certainly, if higher pressures and temperatures can be justified for the straight-condensing units in the normal utility plant, there is much greater justification in plants such as these when a substantial portion of the output is generated with a back pressure in excess of 200 psi. Raising the pressure from 1500 to 2500 psi, and the temperature from 940 F to 1050 F increases the energy potential about 8.5 per cent, with 1.5 in. Hg back pressure, but the corresponding increase, with a back pressure of 240 psi, is over 31 per cent. The yield of "by-product" power is correspondingly increased.

Further increase in the yield of by-product power could be effected by interposing a desuperheating heater in the extracted-steam connection between the turbine and the evaporators. The author does not indicate the temperature of the extracted steam, but with a throttle temperature of 940 F, the amount of superheat at 200–240 psi must be substantial. It has been shown by Cross and Wells⁸ that the use of the feedwater to desuperheat this steam before it enters the evaporator provides an increase in the yield of by-product out of all proportion to the cost of the simple equipment required. For the steam conditions at the Pacific Gas & Electric Company plants, the increase would be about 8.0 per cent.

With 2500 psi initial pressure, reheat would be desirable for the condensing part of the cycle. With this reheat taking place at about 470 psi, the combined effect of higher pressure, reheat, and the interposition of a desuperheating heater in the extraction line would increase the yield of by-product power by more than 48 per cent. This larger noncondensing operation probably would justify the use of turbine-generators of 60,000 to 80,000 kw, which might be more suitable for large power systems such as that of P.G. & E.

These thermodynamic considerations are well-known, and relatively unimportant in comparison with the business aspects of this kind of undertaking, and the practical operating results which are so ably reported in this paper. We are greatly indebted to the author and to the Pacific Gas and Electric Company for making these data public. It is hoped that this report may inspire other utilities and other process industries to develop like opportunities to the advantage of themselves, and to the benefit of the public which ultimately profits both from lower costs of power and lower costs of processed products.

H. G. THIELSCHER.⁹ A significant fact is the foresight shown

⁸ "An Improved System in the Application of Noncondensing or Extraction Turbines," by H. W. Cross and E. S. Wells, Jr., Trans. ASME, vol. 62, 1940, pp. 37–40.

⁹ Resident Engineer, Combustion Engineering-Superheater, Inc., New York, N. Y. Mem. ASME.

by the designers of the station described in selecting a steam pressure of 1500 psi and 940 F 12 years ago when that temperature was not at all common, even in central-station practice. This selection of steam conditions leaves the utility in an attractive position today should it ever become necessary to operate these plants as electric-generating stations only.

Fig. 3 of the paper indicates a throttle flow of 680,000 lb per hr for 50,000-kw turbine load and a refinery flow of 275,000 lb of steam per hr. For the steam conditions selected and with a straight regenerative cycle and 4 stages of extraction, we might expect a throttle flow of 450,000 lb for 50,000-kw turbine load. The difference between this figure and the 680,000 lb of steam provided, or 230,000 lb per hr, represents a considerable additional investment in the cost of the boiler plant.

Other major items which make the plant cost more than a conventional electric-generating station are the turbine-generator, process-steam evaporators, process-steam piping, and water-purification plant.

No doubt these factors were taken into consideration when figuring the charge for process steam and electric energy. As an offset to the additional fixed charges imposed by these items, it is to be noted that the heat rate per net kilowatt-hour generated averages much less than that of a conventional plant.

The oil industry generally practices the policy of writing off its investment in new equipment in a few years compared to utility practice of, say, 30 years. It would be interesting to know whether a quick write-off of the extra investment involved in this plant, compared to a conventional generating plant, was figured in arriving at the charges to be made for the products supplied to the refinery.

P. H. WOODS.¹⁰ It has been both a pleasure and a privilege to have participated from its inception in the development of the arrangement for supply of steam and electric power by the Pacific Gas and Electric Company to the oil companies as described in this paper. The author has outlined the principal features of the contract and of the technical problems encountered in the operation of the steam plants. Therefore the writer will limit his comments to the arrangement as seen from the oil-company point of view.

In the 8½ years that have elapsed since utilities were first supplied to us by the Avon Steam Plant, Tide Water Associated Oil Company has had little reason to regret entering into the contract. The oil company is in the business of making petroleum products, and we have been quite happy to leave generation of power in the hands of the utility—that is, the business they are in.

At the time the present arrangement was first suggested, Associated was in the midst of a major plant expansion which included enlargement of our steam-generating facilities. We had, in fact, entered into a contract for construction of a new 850-psi-pressure boiler plant and were seriously considering installation of electric-generating facilities as well. Fortunately, as we see it now, the suggestion came early enough in our program to permit cancellation of our boiler-construction contract and to switch to the present setup.

Before the Avon Steam Plant was built, Associated generated all of its own steam, partly at 150 psi pressure, and partly at 250 psi, and purchased electric energy from the utility through a single substation at 2400 volts. Now we take delivery of steam at 165 psi pressure with some superheat, and receive electric power through three substations. The old 150-psi boilers have been out of service for some years, as the contract maximum on steam gives us a comfortable margin over actual demand. The arrange-

¹⁰ Chief Engineer, Tide Water Associated Oil Company, Associated, Calif. Mem. ASME.

nient has encouraged us to electrify new construction for the sake of economy in operating costs, and in many cases has enabled us to replace old steam-driven units with electric drives at substantial savings.

Economies have accrued in another direction as well. Formerly we burned sludges and other wastes in a disposal furnace. These noncommercial products are now turned over to the utility in part payment for energy. Some conditioning of these fuels is necessary, but generally this can be accomplished by minor modifications in the manufacturing process. Refinery operating personnel works in close co-operation with steam-plant operators as to characteristics of this type of fuel.

Reliability of supply of electric energy to the refinery has been improved materially. Our second and third substations are fed directly from the steam plant 12-ky bus, and interruptions to this supply are rarities. This factor is important to us, as process units built since 1940 are much more complex than older units, therefore more difficult to get back on stream after a power interruption, and shutdown time is expensive.

In normal steam-plant operation, three evaporators are on-stream to supply the refinery steam load. Fouling requires that they be taken down, one at a time, for periodic cleaning. At such times, when availability is down one third, Associated supplies the difference from its 250-psi system. This second refinery steam system is necessary for process reasons and was in existence prior to the time the steam-plant studies were begun. For several reasons, both process wise and economic, no attempt was made to incorporate a 250-psi steam source into the steam-plant design.

AUTHOR'S CLOSURE

The author is very much indebted to all of those who have presented written discussions. It is felt that all of the remarks are timely and constructive, and have added materially to the value of this paper. It is interesting to note the great amount of interest displayed in the subject of external fouling of boiler heating surfaces.

The observation by Mr. Cummings, to the effect that the problems encountered in burning present-day fuel oil are not always solved by referring to experience in burning coal, has been well substantiated by the experiences of plants on the eastern seaboard which have recently changed from coal to fuel-oil firing. Such plants, originally designed for firing with coal, have changed to fuel oil because of the availability of the latter fuel at competitive prices. In some instances the resulting boiler availabilities have been reduced below that which is obtained on the Pacific Coast with the similar types of fuel oil. This is partly due to the fact that, when firing with fuel oil, deposits tend to build up in the first superheater bank which, in a boiler designed for coal firing, sometimes consists of as many as 12 or 14 rows of tubes, thus making it impossible to obtain effective soot-blower penetration. As has already been pointed out, slag deposits do not usually occur in this zone when firing coal due to the usually much higher fusion point of the ash. Effective results from soot blowing cannot be obtained on superheater banks deeper than about six or eight rows of tubes. Satisfactory penetration is obtained by blowing from both the front and back of such banks with mass type blowers.

With reference to the last paragraph of Mr. Gilg's discussion, it is important to emphasize that the one inch clear space between tubes in the first superheater bank cannot consistently be maintained due to a certain amount of warpage which takes place in this temperature zone, thereby producing a very serious obstruction to the path of the gases and making it almost impossible to obtain effective soot-blower penetration. A cross section of one of the boilers is included as Fig. 14 in Mr. Gilg's dis-

cussion, and by comparing this with Section AA or BB in Fig. 10 representing the lateral spacing of the tubes in the first superheater banks, it will be noted that there are three rows of relatively wide-spaced tubes at the front of this bank. This arrangement provides a clear space of 3 in. between these tubes, but tends to reduce the effective penetration of the soot blowers through the more closely spaced tubes because of the interference of these first three rows, which also have the effect of keeping the soot blowers further away from the close-spaced rows. Thus the wide-spaced rows, particularly in view of the fact that they are staggered, appear to do more harm than good from the standpoint of fouling of the heating surfaces.

As an experiment on one boiler, the first two staggered rows of wide-spaced tubes have been moved back into line with the third row, thus having the effect of adding one more close-spaced row in place of the three wide-spaced rows, and making it possible to move the soot blowers a distance of approximately 10 in. closer to the close-spaced rows in that bank. This is very important from the standpoint of effective soot-blower penetration, and there is every indication that this modified tube arrangement, plus 2 in. clear space between the tubes and the proper installation of mass blowers, will make it possible to keep this first superheater bank clean for considerably longer periods of time. It has also been demonstrated that the effectiveness of mass-type blowers can be greatly increased by the addition of specific quantities of water. This applies to either air or steam blowers, and results in far less temperature shock than occurs when 100 per cent water washing is resorted to under load. A few plants have actually adopted the latter practice at intervals of, say, 30 days to augment regular soot blowing.

Mr. Philo's discussion is very pertinent and brings out some of the design modifications which have been adopted almost universally on recent Pacific Coast installations. The provisions cited in Item 3 of Mr. Philo's discussion, to facilitate water washing of the boiler while it is off the line, tend to produce a better job of cleaning with less boiler outage time. In connection with Item 2, it has already been emphasized by the author that increased spacing between superheater tubes to some figure greater than 1 in., particularly in the first bank, is highly desirable. However, it does not follow that, by progressively increasing this spacing, we shall obtain correspondingly improved results from the standpoint of less deposits. Operating experience during the past year suggests that there is an optimum spacing which will obviate abnormal restriction of the gases due to slag deposits and at the same time provide for maximum effectiveness of the soot blowers. It is fairly certain that this optimum clear spacing is somewhere between 2 and 3 in. for the superheater banks, and approximately 2 in. for the economizer section. For oil fuel, it is doubtful whether spacing as little as one inch can be justified at any point in either the superheater or economizer sections.

The investigation conducted by Scott Jensen and referred to by Mr. Philo in connection with the survey of the pattern of gas temperatures leaving individual tubes of large tubular air preheaters, represents a valuable contribution to the problem. It provides a basis for the installation of baffles so that proper gas-flow distribution is obtained throughout the preheater, thereby eliminating localized low-temperature zones which have a major influence on both corrosion and plugging by deposits at the cold end of the preheater.

With reference to Mr. Ryan's comment on the gains which can be realized by desuperheating the extraction steam before it enters the evaporator, it should be stated that this has been accomplished, at least in part, by means of a steam-to-steam heat exchanger whereby the superheat in the high-pressure turbine exhaust is removed by adding superheat to the evaporator vapor. The refineries require 50 F superheat in the process steam at the

point of delivery. In the last paragraph of Mr. Ryan's discussion he has emphasized the importance of the business aspects of this kind of undertaking. This is indeed true because it is absolutely essential to make proper allowance in the financial setup for the various technical factors which enter into the operation of such an undertaking. However, it cannot be too strongly emphasized that an intimate knowledge of the practical operating problems and related technical factors are the essential prerequisites to the conclusion of a satisfactory business arrangement between the two parties.

In connection with Mr. Thielscher's remarks regarding the increased investment in boiler plant over what would be required for a conventional plant, it should be pointed out that additional boiler capacity is required to generate the process steam which is sold to the oil refineries. The working agreement, of course, provides that the revenue from such steam sales will be adequate to

pay for this incremental capacity, and it should also be pointed out that the additional high-pressure steam generates by-product power in the high-pressure turbine at extremely high efficiencies. In reply to Mr. Thielscher's question in the last paragraph of his remarks, it should be stated that all three of the contracts with the oil refineries were written for a period of 20 years with provisions for automatic extension beyond that period unless twelve months' written notice is given by either party stating its desire to terminate the agreement.

It is gratifying that Mr. Woods has contributed to the discussion by giving the point of view of the oil refinery, setting forth the advantages which have accrued to them as a result of this undertaking. We should like to add that the day-to-day working relations between the respective operating personnel of the utility and the refinery have been highly satisfactory and consistently take place in the spirit of fine co-operation.

Steam-Electric Power Expansion in Southern California

By W. L. CHADWICK,¹ LOS ANGELES, CALIF.

This paper presents the background of the postwar expansion of steam power in Southern California, the requirements of the area served, a brief discussion of some of the war and postwar influences bearing upon power needs, the disposition of the new generation, the design trends in the area, and the influences bearing thereon. A description is given of the major features of the Redondo Steam Station of the Southern California Edison Company.

INTRODUCTION

FOLLOWING the late war and the necessity of restricting to the maximum the manufacture and installation of electric power-generating equipment of every kind and also the purposeful loading of all existing reserve generation with war production, it has been a common experience throughout the country to have postwar power loads increase more rapidly than new generation capacity could be provided. Perhaps, however, the situation in California is sufficiently different to be noteworthy and of interest.

A companion paper² treats of the northern part of the state; this paper will treat of the southern part. California may be said to consist economically of three metropolitan and industrial areas, and a large agricultural hinterland in which there are also some industrial and residential centers. The metropolitan areas of course are those around San Francisco Bay in Northern California, and those around Los Angeles and San Diego in Southern California. Although geographically, Southern California includes only ten of the state's 58 counties and only 37 per cent of the area of the state, it contains more than one half of the state's population and utilizes about one half of the electric power. Another fact which has a large bearing on power resources, particularly hydraulic power, is that the Southern California area possesses only about 1 per cent of the state's water resources.

Because fuel was then scarce and steam power generation was inefficient, the first electric power developed in the state was hydraulic. However, during the first decade of power development, a severe drought so reduced the water supply that some systems found it necessary to move boilers and engines to hydro plants to meet the deficiencies in the hydro output. Since that time, steam power has been an intimate part of power supply, but being always more costly to operate than hydro, it has been used only as complementary or supplementary energy. This condition has begun to change, and in the future base-load steam generation will be required in increasing amounts.

SOUTHERN CALIFORNIA POWER SYSTEMS

Southern California is served by eight different power systems.

¹ Manager of Engineering Department, Southern California Edison Company. Mem. ASME.

² "Postwar Planning for Steam Capacity in Northern California," by C. C. Welchel and W. R. Johnson, published in this issue of the Transactions, pp. 237-246.

Contributed by the Power Division and presented at the Semi-Annual Meeting, San Francisco, Calif., June 27-30, 1949, of THE AMERICAN SOCIETY OF MECHANICAL ENGINEERS.

NOTE: Statements and opinions advanced in papers are to be understood as individual expressions of their authors and not those of the Society. Paper No. 49-SA-16.

The city of Los Angeles is supplied by its municipal Department of Water and Power, with energy generated (a) in its own hydro plants, (b) at Hoover Dam, and (c) in three steam stations. The cities of Pasadena, Glendale, and Burbank have municipally owned systems each supplied from its own steam station, in addition to purchasing hydro energy from Hoover Dam. The Imperial Irrigation District supplies energy generated by hydro along the All American Canal and by Diesel to the Imperial Valley area, and is now constructing a steam station. The metropolitan area surrounding San Diego is served by the San Diego Gas & Electric Company through a system which gets most of its energy from base-load steam, but obtains the remainder from wholesale purchases.

A portion of the eastern side of the coastal plain and some of the desert area is served by California Electric Power Company through a system supplied mainly by hydro plants in the Sierra Nevada Mountains, and by purchases from Hoover Dam and other agencies. The remainder of the Southern California area is served by Southern California Edison Company with energy supplied from Sierra Nevada and other hydro plants, from Hoover Dam, and from two large steam stations, a total system capacity of 1,583,000 kw. Further detail on these systems and their generating capacities are given in Table I, and the map, Fig. 1.

POWER RESOURCES

At the end of the war the power resources of Southern California systems consisted of a total of 2,535,000 kw in operating capacity, installed by the eight agencies; 65.5 per cent of this capacity was hydro, 33.2 per cent was steam, and 1.3 per cent Diesel. Of the hydro, 39.6 per cent of the installed capacity was in 30 plants in the Sierra Nevada Mountains, or in plants utilizing water brought from those mountains; 59.4 per cent was at Hoover Dam, and 1 per cent was in miscellaneous smaller plants. Hydro energy output is ordinarily considered on three bases, namely, (1) that for a year of average water supply, (2) that for a year of low water supply, i.e., a dry year, and (3) that for a year of exceptional water supply, i.e., a wet year. These outputs vary from 6,579,000 kwhr for a dry year to 9,036,000 kwhr for an average year to 10,470,000 kwhr for a wet year. In other words, there is about 27 per cent less in a dry year than during an average year, and about 16 per cent more in a wet year than in an average. Except for the effect of the large storage at Hoover Dam, there would be 50 per cent less in a dry than in an average year.

This situation presents the basic need for steam generation up to the time the war began. Ordinarily, sufficient reserves are maintained either in stored water or steam-generating capacity to meet not only emergency system needs, resulting from breakdowns and seasonal and other peaks, but also for the full deficiency which occurs in a dry year. It is usually considered that about 40 per cent of a system's total capacity is required in steam generation to meet these needs.

WAR-END AND MORE RECENT CONDITIONS

During the war the presence of reserve capacity in Southern California led the War Production Board to locate several defense plants, including one each for magnesium and aluminum reduction, in the area. The effect of these additions was to reduce

the reserves to the point where load curtailment would have been necessary in a year of subnormal water supply. As the war ended, it was generally thought that postwar adjustment would reduce considerably the need for industrial power and hence allow a period during which to regain reserves by building new

TABLE 1 CAPACITY OF ELECTRIC GENERATING SYSTEMS SERVING SOUTHERN CALIFORNIA AS OF AUGUST 1, 1948^a

	Total kva capacity of main units derived from name-plate rating			
	Hydro	Steam	Internal combustion	Total
California Electric Power Co.	55463	11250	293	67006
City of Burbank	..	25000	..	25000
City of Glendale	..	50000	..	50000
City of Los Angeles	157532	331430	..	488962
City of Pasadena	1500	62500	..	64000
Imperial Irrigation District	18000	..	15000	33000
San Diego Gas and Electric Co.	..	253500	..	253500
Southern Calif. Edison Co.	508650	604981	37500	1151131
Hoover Dam ^b
U. S. Department of Interior, Bureau of Reclamation	1030000	1030000
Total	1771145	1338661	52793	3162599

^a From figures compiled by California Public Utilities Commission.

^b Of this capacity approximately 495,000 kva is operated for the Department of Water and Power, City of Los Angeles, and the cities of Pasadena, Glendale, and Burbank; 330,000 kva for Southern California Edison Company and 40,000 kva for the California Electric Power Company. In addition, 165,000 kva of capacity, which is installed for the primary use of the Metropolitan Water District of Southern California, is operated for the Southern California Edison Company and the California Electric Power Company during times that the full capacity is not required by the Metropolitan Water District.

TABLE 2 ADDITIONS IN CAPACITY TO ELECTRIC GENERATING SYSTEMS SERVING SOUTHERN CALIFORNIA, ARRANGED CHRONOLOGICALLY—1946 TO 1951

					Approximate name-plate rating of main generators, kva	
					Hydro	Steam
Southern California Edison Co.	Long Beach	August, 1947	25000	..
City of Glendale	..	October, 1947	25000	..
City of Los Angeles	Harbor	November, 1947	81250	..
Southern California Edison Co.	Redondo	March, 1948	70588	..
San Diego Gas & Electric	Silvergate	April, 1948	75000	..
Southern California Edison Co.	Redondo	April, 1948	70588	..
Southern California Edison Co.	Big Creek #3	April, 1948	35000
City of Los Angeles	Harbor	December, 1948	93750	..
City of Los Angeles	Harbor	February, 1949	93750	..
City of Los Angeles	Harbor	Spring, 1949	93750	..
Imperial Irrigation District
City of Burbank	El Centro	April, 1949	25000	..
City of Pasadena	..	August, 1949	25000	..
Southern California Edison Co.	Redondo	September, 1949	43750	..
Southern California Edison Co.	Redondo	October, 1949	70588	..
Imperial Irrigation District	Drop 4	March, 1950	12500
San Diego Gas & Electric	Silvergate	October, 1950	75000	..
City of Los Angeles	Owens Gorge	December, 1950	75000
City of Los Angeles	Owens Gorge	Spring, 1951	37500
Southern California Edison Co.	Big Creek #4	Late 1951	84000
Total	244000	938602

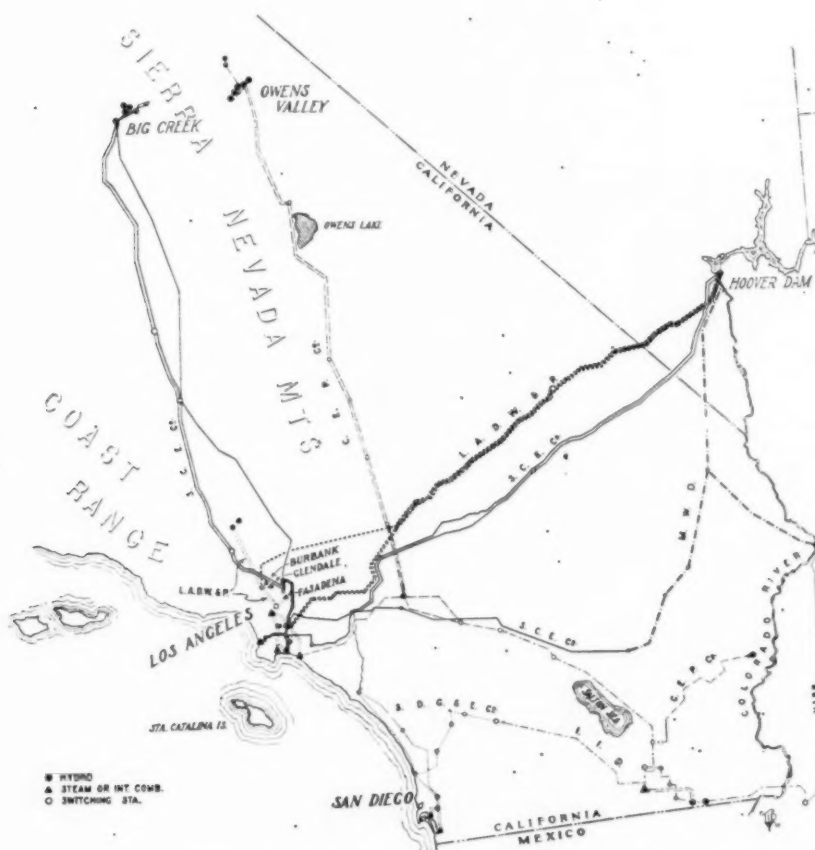


FIG. 1 GENERAL SCHEME OF POWER SYSTEMS SERVING SOUTHERN CALIFORNIA

capacity. Although industrial load did drop for a time, its effect was more than offset by expanding energy use in other classifications.

By the first of 1946 it was apparent that in California, as well as elsewhere in the country, there would be no respite, but that the load, at least for some time, would increase faster than new generation could be built. From over the nation, orders were placed much faster than turbines, generators, and transformers could be built. Delivery promises increased from 16 months to 39. Strikes of all kinds during 1946 added months to delivery expectations.

Population Trend. In the meantime, population and loads were growing. Population in Southern California increased 47 per cent between 1940 and 1948. On the Southern California Edison Company's system during the 4 years between January, 1944, when voluntary wartime power rationing in this area ceased, and January, 1948, residential power use increased 52 per cent, commercial use increased 58 per cent, agricultural 75 per cent, and industrial 18.6 per cent. The over-all increase was 41 per cent.

Conditions in 1948. Combined with these influences, rainfall in the early part of 1948 was the lowest for many years, not only causing hydro production to fall off all over the state but also greatly increasing the demand for power for off-season irrigation pumping. In some areas, curtailment became necessary. Southern California had been successful enough in building new steam generation so that when that new capacity was combined with daylight saving and good rains, curtailment there was unnecessary. Also, by co-operative pooling of generating resources, it was possible to transmit large blocks of energy to the curtailed areas with the combined fortunate result that curtailment anywhere in the state was short-lived.

SOUTHERN CALIFORNIA CONDITIONS AFFECTING STEAM-POWER EXPANSION

Southern California steam-power expansion has been noteworthy for the following characteristics and developments:

- 1 The rapid increase in the steam-hydro ratio during the past 5 years.
- 2 The use of moderate steam pressures and temperatures.
- 3 Exclusive use of natural gas and oil but with space allowance for future coal.
- 4 The earliest use of outdoor plant construction.
- 5 The use of special operating methods, controls, and construction to obtain minimum-time load pickup from minimum to maximum.
- 6 Extensive use of high-pressure mechanical oil atomization.
- 7 Successful use of thermal control of marine fouling organisms.
- 8 The recent field rebuilding of three large-sized turbine generators during conversion from 50 to 60-cycle operation.

Hydro-Steam Ratio. As noted previously, at the end of the war the capacity serving Southern California was 2,535,000 kw consisting of 1,659,000 kw of hydro, 844,000 kw of steam, and a small amount of Diesel. Percentage-wise for hydro and steam, this amounts to 65.5 and 33.2 per cent, respectively. Since that date (that is, to January 1, 1949) 34,000 kw of hydro and 388,000 kw of steam have been added, bringing the steam capacity currently to 41.7 per cent. Installations now in design and under construction will bring this ratio to 54.4 per cent hydro, 44.8 per cent steam by January, 1952 (Table 2).

Moderate Pressures Used. To the present time, two influences have tended to keep steam-power developments in Southern California in the moderate pressure and temperature range, namely, (1) relatively low cost of fuel because of the area being figuratively on top of large oil and gas fields, (2) availability of large

quantities of relatively cheap hydro power and the resulting low load factor available for steam operation. Under the latter conditions, 35 per cent is a fair estimate of steam-power load factor. Accordingly, economy has required that new installations be designed and built for the pressures around 850 psi and temperatures of 900 F. With the increase in fuel-oil cost from 18 cents per million Btu to 36.1 cents between the war's end and January, 1949, and waning additional projects for hydro development, interest in more economical cycles is keener. One turbine is on order for 1250 psi 950 F, but no plant so far has been built in the area to utilize the reheat cycle.

Gas and Fuel Oil Only. Prior to the war, fuel gas was in abundant supply at costs of from 9 to 11 cents per million Btu, and oil at about 13 cents. With the increase in demand during the war for gas for industrial and domestic heating, except where gas could be obtained by direct purchases from the oil fields for boiler use, it became available only on a "dump" basis. This means that during warm weather when domestic use is light, and on week ends and holidays when industrial use is light, gas for power generation may be had in quantity, but there is no firm supply except where obtained by direct field purchase. Pipe-line importations are now being made from Texas, and others are in prospect, but again they afford no firm supply. As a result, power generation is principally supported by oil fuel. Some petroleum coke has been available but not in sufficient supply to be important.

As previously stated, no Southern California plant so far has been equipped with coal-handling and burning equipment although several have been built with space provision for bunkers, ash hoppers, pulverizers, and burning equipment.

A rough comparison of the cost of the three fuels under present (February, 1949) conditions is gas about 30 cents per million Btu, oil 31.2 cents to 32 cents per million Btu, depending upon the viscosity supplied, coal from Southern Utah about 44.7 cents per million Btu. With a large increase in fuel-oil stocks during recent months, oil prices for firm delivery have broken somewhat, backing off any immediate necessity for considering coal fuel seriously.

Early Use of Outdoor Construction. Mild weather and economy led to outdoor design for the two plants built by the cities of Burbank and Glendale about 10 years ago, two of the first to make use of such construction. The new Redondo Station of Southern California Edison Company has outdoor boilers, air preheaters, fans, and oil heaters. Three stations have been built on the unit principle with one boiler per turbine unit. Further use of this principle in the near future seems certain.

Quick Pickup Important. Because of the position in the load curve which steam power must take with respect to hydro, and hence of the frequent necessity of steam standing by at minimum loads for immediate operation in the event of an emergency, such as transmission-line or equipment loss, close attention is given in Southern California stations to the minimum load pickup time. The Redondo Station of Southern California Edison Company, for instance, is designed to increase from 5 per cent to full load in 15 sec. Other stations on systems depending upon long transmission lines for an important part of their resources have similar features.

High-Pressure Mechanical Atomization. With the increase in the use of cracking and other newer refining techniques, the production of fuel oil has passed from one in which this fuel was crude oil with the lighter and more valuable fractions removed by distillation to one where it is now a refinery residuum carrying tars, free carbon, and other heavy ends, plus considerable amounts of combustible and noncombustible residual chemicals. The resulting product while containing around 6,250,000 Btu per bbl possesses viscosities as high as 190 sec SSF and averages around 175

see SSF for Bunker C fuel. This heavier fuel requires heating to between 80 F and 100 F to permit its conveyance from tanks to final heaters where temperature is increased to 200-210 F before supply to the burners. Further, this fuel produces deposits which adhere to closely spaced heat-transfer surfaces, particularly in superheaters, economizer and preheater sections which require washing down of external surfaces to permit maintaining anywhere near normal heat absorption.

Further, with the increased industrial use of fuel oil in the area, the need to minimize smoke emission, because of the special topographical and meteorological characteristics of the Southern California coastal area, has also made efficient combustion of first-order importance. To meet this need, a burner and supply system has been developed which utilizes a maximum burner supply pressure of 900 psi, obtained by screw pumps in the primary fuel-supply lines and booster pump connected to a recirculation line, which permits maintaining a burner pressure of not less than 300 psi at minimum load. The result is (1) wider range (1 to 20) between minimum and maximum boiler load, and (2) finer atomization, and hence better and more smoke-free combustion.

REDONDO STATION

Replaces Former Station. The Redondo Steam Station of the Southern California Edison Company is situated directly on the Pacific Ocean at Redondo Beach on an enlargement of the site of an earlier station which was considered uniquely efficient in its day. That original station was built a little more than 40 years ago and contained three 5000-kw General Electric generators, each driven at 100 rpm between two double angle-compound McIntosh & Seymour reciprocating engines supplied with steam at 175 psi and 475 F. The design and construction contract provided for a bonus payment for efficiency better than 170 kw-hr per bbl of fuel oil (about 36,760 Btu per kw-hr). Performance was 50 per cent above this requirement, earning a handsome bonus for its builders. Strangely enough, the advance in steam power generation was so rapid that within less than 4 years a turbine-driven generator was added, making the original units obsolete. Seventeen years later the station was sufficiently obsolete to put it only on the very peak of the load curve, and in another 9 years it was decommissioned and its boilers salvaged. The building was wrecked to permit construction of the new Redondo Steam Station.

Necessary to Utilize Previously Designed Equipment. Design of the new station was started early in 1946, at a time when (1) there was an unprecedented shortage of designers and draftsmen not only for station design but for equipment design and development, (2) strikes were tying up the entire production of the major electrical-equipment manufacturers and such basic industries as steel, coal, and transportation. Postwar adjustments were further delaying deliveries of power-plant equipment of all kinds.

In spite of these influences, it was necessary to have the new station in operation at the earliest practicable date. To offset these delays as much as possible, all major equipment was specified so that proposals could be offered for equipment which had been previously designed and preferably used, thus minimizing design and manufacturing time.

The joint AIEE-ASME Standards Committee had only recently issued its preferred standards for turbine generators, and some design work had been done on the largest or 60/66,000-kw size. Use of these standards and the estimated probable load factor for the station on the combined hydro system, fixed steam conditions at 850 psi and 900 F and turbine speed at 3600 rpm. One each General Electric and Westinghouse units were purchased at the outset, and one each additional late in 1946.

Boilers also were specified to fit radiant types which previously

had been built and used successfully. Multiple and single boilers per unit were considered, but, although more expensive, multiple boilers were selected because, under system conditions, they afforded the greatest reliability and flexibility. To serve the first two units, four 400,000 lb per hr Babcock & Wilcox boilers were provided affording one spare. The final installation will include seven such boilers for four turbines, also affording one spare.

Station Arrangement. The station is laid out with the turbine generators arranged longitudinally along the center of a turbine building 73 ft wide and 485 ft long. A 45-ft-wide auxiliary and control bay parallels this room and forms the firing aisle for the seven boilers. One 200-ft reinforced-concrete stack is provided for each pair of boilers. The boilers, preheaters, forced- and induced-draft fans, secondary fuel-oil heaters, and deaerating heaters are outdoors on the inshore side of the turbine building. Because of the salt-spray-laden fogs which occur along the California coast, no consideration was given to outdoor turbine settings.

Cooling-Water System Design. The coast along which the Redondo Station is situated is exposed and subjected to heavy waves during the late fall, winter, and early spring. The original station had used an exposed vacuum-primed syphon pipe line with 9-ft drop legs set in the surf line to supply circulating water. This system was frequently in trouble from sand, seaweed accumulations, and storm damage. In designing the new station, every effort was made to afford a trouble-free circulating-water system. To obtain this objective, it was considered necessary (1) to keep the pipe lines below the ocean floor; (2) to keep the lines under positive pressure; (3) to avoid any exposed structure; (4) to extend the lines far enough seaward to set the intakes in water deep enough to afford 20 ft of water below low tide, and in order to avoid sand entrapment, to set the intake chime or inflow lip not less than 10 ft above the ocean floor; (5) to afford means of controlling marine fouling organisms which would make shutdown of the pipe lines for cleaning unnecessary. To effectuate the first conditions, both the intake and discharge lines are built of 10-ft-diam precast lock-joint concrete-pipe sections 16 ft in length laid below the ocean floor. The intakes are vertical tee sections 14 ft diam at the end of the 10-ft lines and set in 32 ft of water.

Marine Fouling Control. To control fouling organisms, an extensive investigation of chlorine injection was carried out, but previously it had been observed at the company's Long Beach Station that although the intake tunnels accumulated 4 to 6 in. of marine growth during the growing season, almost no growth occurred in the discharge tunnels. The only reason assignable for the difference was the difference in circulating-water temperatures. Using this long-time laboratory observation, it was decided to provide for fouling control both by means of chlorination and by periodically raising the temperature of the lines by alternately using each as a discharge. To check the possibility of satisfactory control by such means, the assistance of marine biochemists was sought, particularly that of Dr. D. L. Fox, of Scripps Institute of Oceanography.

The eventual solution was two separate 10-ft-diam lines extending an average of 1900 ft offshore where each is provided with an intake structure. These structures were set 200 ft apart, diagonal to the beach, to minimize recirculation. To permit alternate use as discharge and intake and likewise to enable chlorination without the need for chlorination lines extending seaward, a reversing chamber was provided on shore where flows may be reversed in 5 min and recirculated to build up any desired discharge temperature. By chlorinating the discharge line only and reversing pipe lines within the lethal chlorination cycle, all chlorine injection could be accomplished on shore.

Originally, it was considered that it might be necessary both to chlorinate and to elevate temperature and to put each line through such a cycle as frequently as each 8 hr. So far, control by heat alone has been so satisfactory that no chlorine has yet been used in the offshore lines. Furthermore, reversals only once each 2 weeks with temperature elevation to 95 F for 6 to 7 hr, to 102 F for 1½ hr have killed off all organisms before they could mature to objectionable size. The arrangement of these features is shown diagrammatically in Fig. 2.

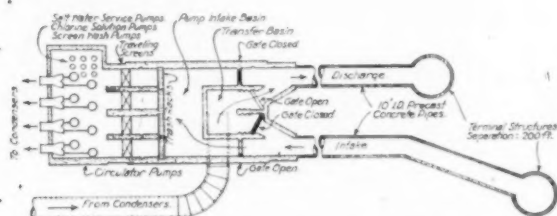


FIG. 2 SCHEMATIC DIAGRAM OF COOLING-WATER SYSTEMS AND PROVISIONS FOR REVERSING FLOW, REDONDO STEAM STATION

Cooling-Water Lines a Difficult Construction Problem. Construction of the cooling-water lines proved the most difficult part of the project but was successfully accomplished by Maceo Corporation, the contractors, without delaying the operation of the station. Pipe laying was done entirely under water by divers served from a temporary trestle supporting excavating equipment, and a gantry crane for pipe handling. The courage and skill shown in handling the 42-ton sections suspended by slings and cable hoists in depths up to 50 ft, while subjected to fairly high seas, is a fine tribute to the construction fraternity, particularly since the visibility of a diver was often less than 1 ft, making work by touch only necessary most of the time.

Cooling-Water and Condensate System. Flow into and out of the reversing chamber is controlled by motor-operated welded steel gates, 7 ft × 10 ft. Automatic controls pair the gates during the reversing process. Trash racks with traveling rakes and stainless-steel revolving screens prevent the passage of fish or mats of seaweed into the pump chamber. Pumping to each condenser is by means of two vertical 25,000-gpm centrifugal pumps driven by two-speed motors for ease of adjustment from stand-by service to full load. Circulating-water temperatures vary from 55 to 70 F. The condensers are of Ingersoll-Rand manufacture and have 42,500 sq ft of surface. Water boxes and hot wells are divided. Condensate and condensate booster pumps are provided in duplicate with each able to return the condensate from 70,000 kw of load with all heaters in service. Three boiler feed pumps of 785 gpm capacity at 1100 psi are provided for each unit with a steam-driven pump for emergency use on either of each pair of units.

Boilers. All boilers are interconnected on the steam, the feed-water, and fuel sides. Each boiler is equipped with an outside heat-exchanger type of attenuator. Each also is provided with an extra large main steam drum (72 in.) to protect against carry-over during water swell on quick load pickup. Each boiler is provided with automatic equipment which performs the following functions:

- Controls the flow of fuel to the burners.
- Controls the induced-draft-fan inlet louvers and outlet damper, except as modified by the fuel-air ratio controller to maintain a preset metered-fuel-air ratio.
- Controls the forced-draft-fan inlet vanes and outlet damper, except as modified by the furnace-draft controller to maintain a preset furnace draft.

Combustion Control. The combustion-control system was designed specifically for quick load pickup and also for wide load range. The following features were incorporated into the design:

- 1 Steam flow rather than steam pressure provides the impulse to increase the supply of fuel and air.
- 2 Air loading pressure is transmitted direct and simultaneously to the controls for fuel, air volume, and draft.
- 3 Control drives are of the "high-speed" type with extra large pilot valves and air-supply lines for rapid admission of operating air.
- 4 Combustion air is measured by a Venturi section in the air duct rather than being measured subsequent to combustion, thereby decreasing the lag in adjusting air flow to correspond to steam flow.

Fuel System. After primary heating, fuel oil is forced at about 725 psig by Sier-Bath screw pumps, to the main oil heaters adjacent to the boilers where it is raised to about 200 F, and forced to the "constant differential" pumps which raise the pressure to the burners to a full-load pressure of 900 psig and 200 F. The constant differential pumps afford a 20 to 1 load range. Automatic controls are provided in this system to start additional fuel-oil pumps in accordance with load demands, to control recirculation of oil to storage tanks, and to control flow of steam used for heating the oil. Furnace and burner protection is obtained through interlocking controls which shut off fuel to the burners if:

- (a) Oil-supply pressure is low.
- (b) Fan motors fail.
- (c) Furnace has not been purged prior to "lighting off."

Turbine Generators. As previously stated, the turbine generators are the largest AIEE-ASME Preferred Standard, namely, 60,000/66,000 kw tandem-compound 850 psi, 900 F, 3600 rpm units, 13.8 kv voltage, 0.85 short-circuit ratio, built for either 0.5 or 15 psi hydrogen pressure. The heat balance for these units and the station is shown in Fig. 3. Each of the first two units has been tested and operated at loads to prove a safe output of 66,000 kw net.

Auxiliary Power. Two 6000-kw, 15-sec response, noncondensing house sets provide auxiliary power in the event a system voltage or frequency drop threatens the auxiliary power supply ordinarily supplied by two transformer banks connected to the system. On a drop in system voltage, these sets start automatically from standstill and come to full speed and voltage ready to carry full auxiliary load in 15 sec, but must be connected manually to the load at the time the auxiliary banks are disconnected from the system.

GENERAL

Each generator is connected to a 70,000-kva transformer bank. The output of the plant is controlled by a double bus switchyard and is transmitted over six 69-kv transmission lines to a major transmission substation about 5 miles away.

The station structures include an administration and service wing where all offices, shops, and chemical laboratory are housed. Because the region is subject to earthquakes, all structures are designed for a seismic coefficient of 0.2 gravity. This factor is twice that required for public school buildings in the state but is selected in the public interest to assure service continuity should a serious earthquake affect the area.

The station is equipped to burn either gas or fuel oil and space has been provided for pulverized-coal equipment should such become necessary. Some gas is available direct from the fields, but the principal fuel is oil. Storage is provided on the site for 220,000 bbl.

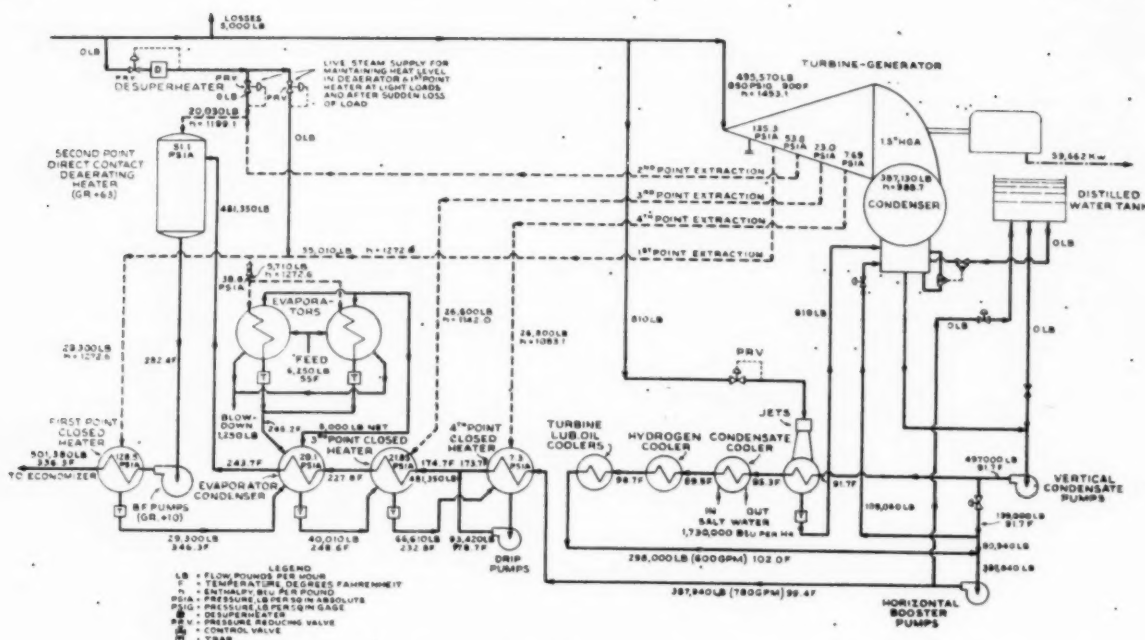


FIG. 3 HEAT-BALANCE DIAGRAM, REDONDO STEAM STATION OF THE SOUTHERN CALIFORNIA EDISON COMPANY

Because of the demand in California during late 1947, and early 1948, for every possible kilowatt of generating capacity, construction of the Redondo Station was under heavy pressure. The first turbine generator was erected from receipt of bedplate to first synchronization with the system in 70 elapsed days, and the second in 51 days. So urgent was the need for the station that it was put into operation as soon as the fundamentally essential manual controls could be completed, and several months ahead of the time when it would have been possible to provide a fully tested and automatically controlled plant. In spite of many threatened construction delays because of postponed equipment deliveries, the station was delivering energy to the system less than 18 months after excavation on the site was started. Operators, engineers, and construction men all co-operated to the latter end. Base-load operation has been the order of the day ever since the first unit was first put on the line.

The station was designed and constructed by the Stone and Webster Engineering Corporation in close collaboration with the Engineering and Operating Departments of the Southern California Edison Company.

FIELD REBUILDING OF LARGE UNITS FOR FREQUENCY CONVERSION

Incidental to conversion of most of the Southern California Edison Company power system for operation at 60 cycles instead of 50 cycles, it was necessary to rebuild two 100,000-kw 450-psi 750 F tandem-compound double-flow General Electric and one 60,000-kw 400-psi 700 F single-cylinder General Electric turbine generators in the field. In each instance it was necessary to replace the high-pressure casings, high and low-pressure spindle, front bearing pedestal, the governor, and the generator field. Further, to allow for the higher speed and greater steam space, it was necessary to reduce the stages in the larger machines from 21 to 17, and in the smaller machine from 20 to 17. This latter required machining new ledges for the new diaphragms.

All parts were manufactured in the factory and shipped to the field without benefit of check assembly of low-pressure parts.

The machining of the intermediate and low-pressure casings was accomplished by field forces of the manufacturer, using a large boring bar operating in the bearings of the turbine. The first job was on one of the 100,000-kw machines and was completed during a 4½ months' outage, the second was completed in 4 months, and the third in 3½ months. Each machine went into service immediately after it was dried out and without clearance, balance, or other adjustment being necessary. All three were delicate and difficult shop and field manufacturing jobs most competently completed.

In the process of rebuilding, 10,000 kw additional capacity was built into each of the larger machines and nearly as much into the smaller one.

With an expansion of 760,000 kw in steam-generating capacity either constructed or in progress since the end of the war, the power systems of Southern California are determined that power supply to that area shall be in time and enough.

Discussion

F. X. GILG.² The steam-generating equipment for Redondo as furnished by the writer's company consisted of four radiant boilers which were placed in service during the early part of 1948, and three additional radiant boilers of identical design which are about ready to be placed in operation. We would like to describe the principal features of the steam-generating equipment.

Fig. 4 of this discussion shows a cross section through these boilers, each of which is designed to generate 400,000 lb of steam per hr continuously at 875 psi and 900 F at the outlet of the superheater. The furnaces are of water-cooled construction, designed to burn either gas or oil. The contour of the water-cooled furnace makes it possible to adapt this furnace to pulverized-coal firing at some future date, if this becomes desirable.

² Application Engineer, The Babcock & Wilcox Company, New York, N. Y. Mem. ASME.

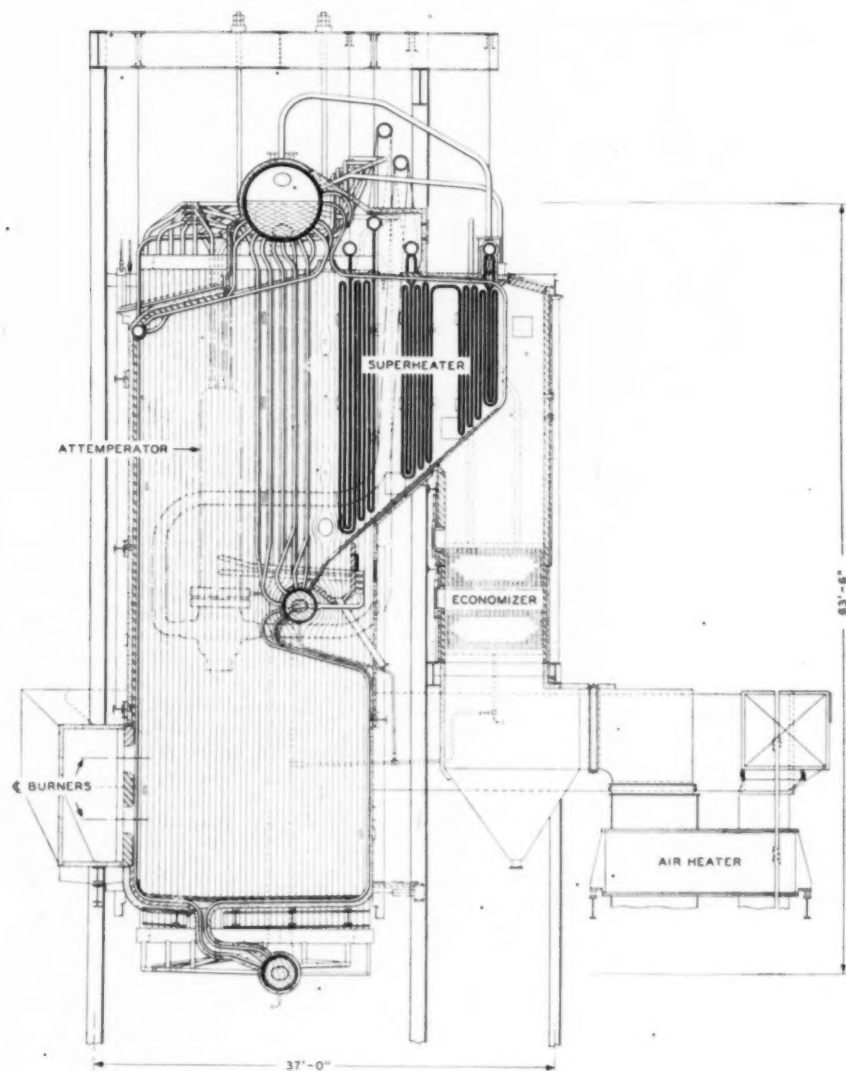


FIG. 4 CROSS SECTION THROUGH REDONDO STATION STEAM GENERATOR

The boiler and superheater tubes are arranged on wide centers to minimize tube fouling from oil-fuel slag. The first rows of boiler tubes are 4 in. OD on 18 in. centers, while the remaining three rows are 4 in. OD on 9-in. centers. The first bank of superheater tubes consists of $2\frac{1}{2}$ -in. tubes on 7-in. centers. The second and third banks of superheater tubes are $2\frac{1}{2}$ in. OD on $3\frac{1}{2}$ -in. centers.

The steam drum is 72 in. diam to provide water storage and space for water-level rise during quick load pickups. The steam drum contains cyclone separators and steam scrubbers so that the solids content of the steam leaving the boiler will not exceed 1 ppm even during sudden load pickup.

Steam temperature is maintained at 900 F from 250,000 to 400,000 lb of steam per hr by means of a shell-type attemperator connected between the first and second sections of the superheater through which a portion of the superheated steam will flow, giving up some of its heat to boiler water which circulates around the

outside of the tube bundle in the attemperator. The amount of steam that goes through the attemperator tube bundle is controlled automatically by a rotary valve. Quick response of temperature control is an important factor in steam-generating units designed for quick pickup of load.

The economizer is of the continuous-tube type, discharging into the steam drum through cyclone separators.

To facilitate the cleaning of troublesome deposits from superheater tubes, the floor under the superheater is arranged with a drain hopper so that the superheater surfaces can be washed with water during out-of-service periods. The economizer and air heater are also arranged so that they can be washed during out-of-service periods.

The expected efficiency of 81.41 per cent on gas fuel and 85.46 per cent on oil fuel have been exceeded on heat-balance tests which showed 82.24 per cent efficiency on gas, and 86.42 per cent efficiency on oil.

C. L. HATHAWAY.⁴ Mr. Chadwick has presented a very clear picture of the conditions in Southern California relative to the electrical demand in this area and to the facilities for meeting this demand. He has also brought to our attention many very interesting design details of the new Redondo Steam Plant. Of much interest is the method of controlling the growth of marine life in the circulating-water system, a very serious problem which the pioneering efforts of his company have solved successfully.

This discussion of Mr. Chadwick's paper will be limited to the following comments concerning the most southerly coastal portion of the area considered, that of San Diego. Several years before the war it became evident that the power facilities of the San Diego Gas & Electric Company would have to be expanded to meet the rising demand. This was due to the very great increase in the population of the area with its increase in domestic load requirements, to the rapid development and growth of the aircraft industry, and to the expansion of the needs of the United States Government. The company had at that time only one generating plant, Station B. This is a low-pressure steam station operating at 235 psi 700 F, located in downtown San Diego. Expansion of Station B was not advisable. The cost of increasing the circulating-water supply would have been prohibitive, and property values were comparatively high. A topping installation was considered, but the idea was abandoned because the load cycle did not lend itself well to this type of operation and because building alterations would have been excessive. In addition, any appreciable increase in the station's generation would have required extensive changes in the electric-transmission system in this area. For these and other reasons, it was deemed advisable to build a new station.

The site of the Silver Gate Station was chosen for several reasons; property values were reasonable, the station could be built near the San Diego Bay so that circulating-water problems would not be serious, and the location would be in a central part of the distribution system, with close proximity to the rapidly growing South Bay area.

Work was begun in 1941, and the station was placed in commercial operation in March, 1943. This plant consists of a 35,000-kw General Electric turbine, driving a 50,000-kva hydrogen-cooled General Electric generator at 3600 rpm. Steam is supplied at 850 psi and 900 F by two 200,000-lb per hr Babcock & Wilcox type F integral furnace boilers.

Before unit No. 1 was placed in service it was apparent that it would not be sufficient to meet the rapidly increasing load. Therefore, in December, 1941, the company placed an order for the second unit (50,000 kw). This was later canceled by government order so that all manufacturing facilities might be directed exclusively to further the war effort. It was not until late in 1945 that it was possible again to place orders. Work of installation was begun in 1946, and unit No. 2 was placed in service in April, 1948.

The delay in the installation of unit No. 2 due to the war, and the unexpected increase in load at the cessation of war activities, has made unit No. 3 an immediate necessity. Plant construction is now under way, and it is hoped that it may be placed in service early in the summer of 1950. This unit will operate at 1250 psi 950 F. This increase was deemed advisable in view of the increasing cost of fuel. Studies are now under way for unit No. 4, which will be the last at this site. Ultimate capacity of the station, based upon turbine ratings, will be 185,000 kw.

Fig. 5 herewith is an average of the actual week-day load conditions of the San Diego Gas & Electric Company for the month of January, 1949. This shows the peculiarities of loading in a comparatively small system in which the load is largely domestic.

⁴ Superintendent, Electrical Production, San Diego Gas and Electric Company, San Diego, Calif.

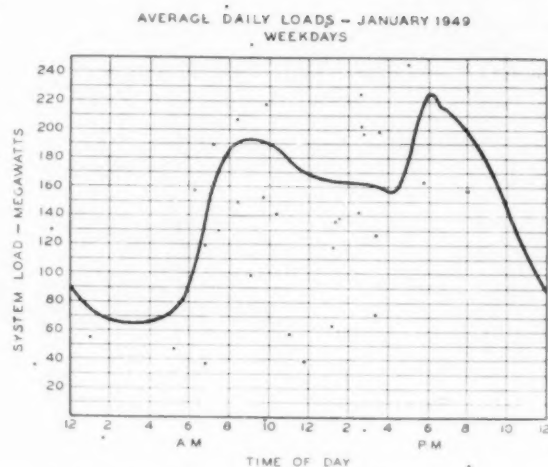


FIG. 5 AVERAGE DAILY LOADS ON WEEKDAYS, JANUARY, 1949

This load demand must be met by an all-steam system, as the company has no hydroelectric generating stations. Serious operating problems are introduced by the extremely high rate of load change, particularly when going from the minimum to the morning peak. This represents an increase of 150 per cent in $2\frac{1}{2}$ hr. This figure is not impressive if we consider the expected performance of a true stand-by plant; but it must be remembered that this is a daily occurrence and that a large part of this system pickup must be handled by the 99,000-kw low-pressure station, whose increase is in the nature of 500 per cent.

An explanation of the San Diego Gas & Electric Company's recent development in steam generation can best be made by describing Silver Gate unit No. 2. In listing the various items of equipment, comment will be made upon certain features which have been changed from the design of unit No. 1 and certain other points of interest.

The turbine is a General Electric 3600-rpm "Handbook" tandem-compound machine with double flow in the low-pressure section. It is rated at 50,000 kw with an overload rating of 25 per cent, or 62,500 kw. It was designed for and uses four points of extraction for feedwater heating. The hydrogen-cooled General Electric generator is rated at 60,000 kw at 80 per cent power factor (PF), or 75,000 kva. This rating is for $\frac{1}{2}$ psi hydrogen pressure. The main exciter is driven through a reduction gear coupled to the generator shaft and runs at 1775 rpm. It is a 220-kw 250-volt unit. The pilot exciter, a 4-kw 250-volt unit, is overhung from the end of the main exciter shaft.

Fig. 6 of this discussion is a heat balance for unit No. 2. The values shown are the turbine-generator manufacturer's estimates for a generator load of 62,095 kw (approximately $\frac{3}{4}$ turbine rating). This is a simple system with four-point regenerative feedwater heating. Generator hydrogen and exciter air are cooled by the full condensate flow from the hot-well pump. Condensate flow through these coolers and through the air-ejector condensers is increased during start-up, and at low loads by recirculation to the condenser. Make-up to the system is supplied by an evaporator receiving steam from the second turbine extraction point (10th stage) and discharging its vapor to the deaerating heater. The deaerator pressure is not held constant, but swings with that of the turbine third extraction point (14th stage) as load on the unit changes.

The turbine lubricating-oil system of unit No. 2 differs from earlier units in that there is no shaft-driven pump. Instead, there

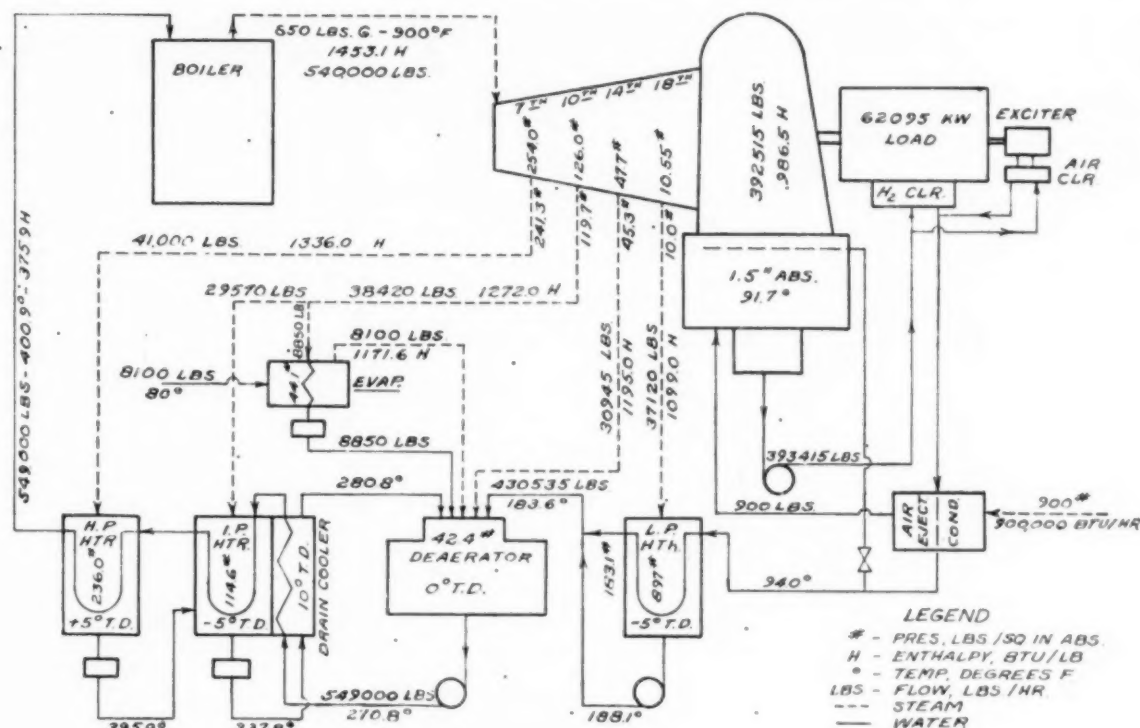


FIG. 6 HEAT-BALANCE DIAGRAM SILVER GATE UNIT No. 2
(60,000 kw, 3600 rpm, 0.8 pf, hydrogen-cooled generator, 850 psig, 900 F, 1 1/2 in. Hg abs.)

are two motor-driven pumps, so interlocked that the reserve pump will start on an outage of the preferred pump. There is also a steam-driven pump, which starts on low pressure, for emergency use. This pump rotates continuously at low speed, as a small amount of steam is fed through its turbine to keep it warm and available for immediate service.

The boilers of unit No. 2 are two Babcock & Wilcox integral furnace-type F which supply steam at 850 psi 900 F to the turbine. Each has a capacity of 300,000 lb per hr with an overload capacity of 10 per cent for 4 hr. As with unit No. 1, each boiler has two superheaters, with an externally mounted at-temperat in series between them. Considerable difficulty has been experienced with slag formation on the tubes of the unit No. 1 primary superheaters when oil fuel has been used. These deposits have been so heavy that actual bridging between tubes has resulted. This has caused excessive draft loss, requiring reduction in boiler load. The material on the tubes is hard and tough so that an extended outage is necessary to remove it mechanically. Use of natural gas as fuel tends to remove the deposit, but as gas is available only in certain seasons and then in limited supply, it cannot be depended upon to maintain cleanliness. Although the deposit is softened by water and is readily washed off, it has not been deemed advisable to water-wash these superheaters for fear of damage to the refractories and possible corrosion of the superheater headers and the boiler mud drum. For this reason the design has been changed for unit No. 2. The superheaters are of the pendant type with the headers above, and hoppers have been provided to drain off the wash water properly. It is felt that these superheaters can be quickly and effectively cleaned. In addition to this, the tube spacing in the primary superheater has been increased to 6 in. between centers, giving

much greater space for gas passage than in the older superheaters where tubes were spaced at 3 in. This has necessitated locating part of the primary superheater in the second gas pass of the boiler.

The waterwalls of the furnaces of the unit No. 2 boilers are the touching-tube type, instead of the stud-tube design of unit No. 1. This greatly reduces the amount of refractory required and increases materially the radiant-heat absorption. Boiler convection surface is reduced somewhat by the increased size of the superheater.

Boilers of both unit No. 1 and unit No. 2 are equipped with tubular air preheaters. The preheaters of unit No. 1 have horizontal tubes with the air on the inside and the gas on the outside. During the war period it was necessary to burn fuel oil with a comparatively high sulphur content. The resulting high-dew-point flue gas caused sufficient condensation on the cold-end tube sheet for chemical attack, so that a large number of the tubes were cut completely off at this point. In order to avoid this trouble in unit No. 2 preheater, the design was changed materially. The hot gases are on the inside of the tubes with the air outside. The preheater is divided into two sections, a main section and a short-tube cold-end section. It was thought that if high-dew-point conditions were again encountered it would be a simple matter to replace tubes in the cold-end section or, if necessary, alloy tubes might be used. As a further protection a cold-air by-pass was provided to control the cold-end temperatures at low load operation.

Both the forced-draft and induced-draft fans of unit No. 1 use vane control. Considerable trouble was experienced in the vane bearings of the induced-draft fans. Because of the high temperatures to which they were exposed the lubricant carbon-

ized and froze the balls in position, which resulted in operating difficulties and in high maintenance. Although this condition has been largely removed by the use of silicone lubricants, it was decided to use a different control for the induced-draft fans of unit No. 2. These fans are driven at variable speed through hydraulic couplings. Additional control is obtained by the use of dampers in the fan ducts.

Fuels used at Silver Gate are natural gas and industrial fuel oil Bunker D. In unit No. 1 this oil is delivered to the control valves at 280 psi. A centrifugal pump which maintains constant differential of 100 psi between the burner supply and return, raises this to about 350 psi at maximum demand. For unit No. 2, centrifugal booster pumps raise the pressure to 660 psi at the control valves, and a 250 psi differential is maintained at the burners, giving a full-load maximum of about 900 psi. This increase in fuel-oil pressure is to permit the use of smaller burner tips and thus to obtain better atomization and better combustion at low loads. It is planned to convert unit No. 4 to the same pressure levels, and a comparable change will be made at Station B.

Fuel-oil storage is by three steel-lined concrete tanks located beneath the 12.5-kv substation structure. Each tank has a capacity of approximately 5300 bbl, with a normal net of a little over 4000 bbl. Delivery to these tanks is by pipe line from the oil company's tanks or direct from tankers. The storage afforded by these tanks is not deemed adequate, so it is planned to provide an 80,000-bbl tank for additional reserve.

High-pressure steam piping in unit No. 2 uses welded joints throughout. All joints were checked by gamma ray. This is a change from unit No. 1 piping where octagonal ring-flanged joints are used.

Bearing and jacket cooling at Silver Gate is supplied by fresh water. This is a closed system, common to both units, in which

city water is circulated through salt-water heat exchangers. The fresh water is treated to maintain a noncorrosive condition. Make-up to this system is by condensate drains, so that the solids concentration is less than that of the city water. The only use of salt water is in these exchangers and in the main condensers.

Fig. 7 herewith is a diagram showing the station's hookup with the distribution system. Electric generation is at 12,500 volts. Each generator feeds a ring bus which is connected on one side to the two main buses of a 12.5-kv substation, and on the other to the transformer banks for the 69-kv system. Station auxiliaries for each unit are supplied at 2400 volts by two transformers, one from the generator bus and one from a feeder from the 12.5-kv substation. The larger units operate at 2400 volts, the smaller ones at 220 volts.

The Silver Gate Station is not of the outdoor or semioutdoor type, in that both the turbine and boiler rooms are enclosed. The partially open type of plant was considered, but the advantages of the closed building were believed to more than offset its increased cost. It might be well to mention a few of the points considered in making this decision. A slight increase in operating efficiency results from the partial recovery of radiation heat losses. This is effected by placing the forced-draft fans on the top floor of the boiler room. Next, it is possible to do maintenance work in any part of the plant on short notice, regardless of weather conditions. This is of considerable importance in a small all-steam system, such as that of the San Diego Gas & Electric Company. Further, morale of the operating personnel is definitely better with the closed plant. This is a point that is always considered but usually not credited with sufficient importance. There are other advantages to the enclosed station; such as, greater ease in maintaining plant cleanliness, less chance of neglect of routine operating duties, etc.

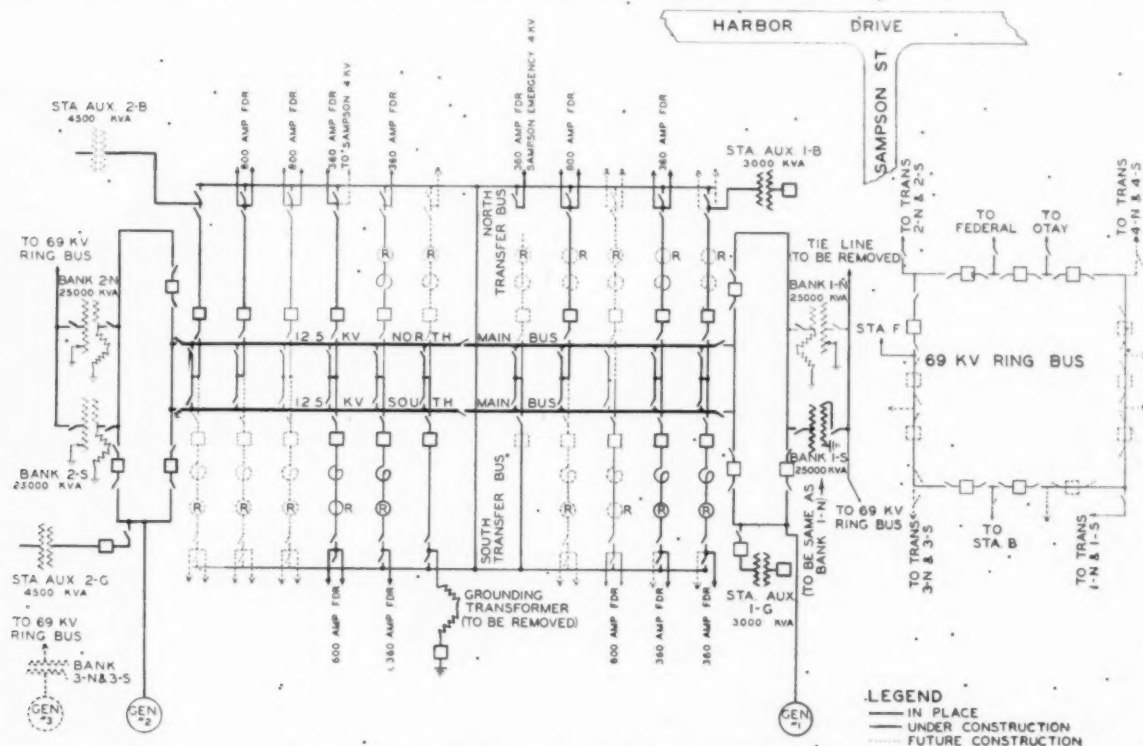


FIG. 7 SILVER GATE STATION HOOKUP WITH DISTRIBUTION SYSTEM

TABLE 3 PRINCIPAL POWER-PLANT EQUIPMENT AT SILVER GATE STATION UNIT NO. 2

TURBINE GENERATOR UNIT	
Turbine.....	General Electric Company
50,000 kw, 3600 rpm, tandem-compound, double-flow, condensing steam turbine 850 psi, 900 F, 1 1/2-in. exhaust; 4 bleed points.	
Generator.....	General Electric Company
60,000 kw, 0.8 pf, 12,500 volt, 3 phase 60 cycle, hydrogen cooled. Main exciter direct connected through reduction gear, 1775 rpm, 220 kw, 250 volt, pilot exciter 4 kw, 250 volts.	
Condenser.....	Worthington Pump & Machinery Corporation
Two-pass, divided water box, surface type with 40,700 sq ft effective surface. Tubes are of arsenical aluminum brass, tube sheets of rolled muntz metal.	
Circulating-water pump.....	Worthington Pump & Machinery Corporation
Two 36-in. vertical, 21,000-gpm, 390-rpm, motor drive, 150 hp, 2300 volts.	
STEAM-GENERATING EQUIPMENT	
Boilers.....	Babcock & Wilcox Company
Two integral-furnace type, 875 psi 900 F 300,000 lb per hr; overload capacity 330,000 for 4 hr. Heating surface, boiler and furnace: 21,500 sq ft superheater, pendant type, three steam passes. Temperature control by external attenuator.	
Air preheater.....	Babcock & Wilcox Company
Vertical tubular, 2 sections, 2 gas passes, gas in tubes, 3 air passes. Heating surface 44,674 sq ft.	
Forced-draft fans.....	Buffalo Forge Company
One per boiler, 101,000 cfm at 120 F, 1180 rpm, variable vane control.	
Induced-draft fans.....	Buffalo Forge Company
One per boiler, 181,000 cfm at 435 F. Control is by variable-speed drive through hydraulic coupling, and dampers.	
Fuel burners.....	Peabody Engineering Company
Four per boiler, type H-26, combination gas and oil. Oil burners are wide-range mechanical-atomizing with constant differential of 250 psi, and a maximum top pressure of 900 psi.	
Safety valves.....	Crosby Steam Gate & Valve Co.
Three per boiler, 4 in.	
Combustion control system.....	Bailey Meter Company
Fuel flow-air flow on both fuels; temperature control.	
CONDENSATE AND FEEDWATER SYSTEM	
Condensate pumps.....	Worthington Pump & Machinery Corporation
Two 3-stage 1183 rpm, 963 gpm	
Feedwater heater No. 1.....	Foster Wheeler Corporation
Low-pressure, vertical, 4-pass, 1915 sq ft surface. Steam from 18th stage extraction.	
Feedwater heater No. 2.....	Cochrane Corporation
Deaerator, 750,000 lb per hr, storage capacity 124,000 lb. Steam from 14th stage extraction, evaporator vapor, etc.	
Feedwater heater No. 3.....	Foster Wheeler Corporation
High-pressure, vertical, 4-pass, 2506 sq ft surface; has drain cooler section. Steam from 10th stage extraction.	
Feedwater heater No. 4.....	Foster Wheeler Corporation
High-pressure, vertical, 4-pass, 2206 sq ft surface. Steam from 7th stage extraction.	
Evaporator.....	Foster Wheeler Corporation
Type H.P., single effect, with preheating and degassing section. Capacity 12,000 lb per hr. Pressures: coils, 250 psi; shell 50 psi.	
Boiler feed pumps.....	Ingersoll-Rand Company
Three 850 gpm, 3568 rpm, 2880 ft total head, motor-driven, barrel-type casing.	
Feedwater regulators.....	Bailey Meter Company
Three-element control.	
PIPING, VALVES, AND FITTINGS	
Piping contractor.....	Midwest Piping & Supply Co.
Main steam line.....	Chrom-moly ASTM A-280-46T
Main steam valves.....	Crane Company
Stop-check valves.....	Edward Valve Company
Blow-off valves.....	Edward Valve Company
Boiler feed pump check valve.....	Chapman Valve & Mfg. Co.
Small high-pressure valves.....	Edward Valve Company
Steam traps.....	Henry Vogt Machine Company
	Armstrong Machine Works
	Yarnall-Waring Company
ELECTRICAL EQUIPMENT	
Main transformers.....	Westinghouse Electric Corp.
Two TCUL, 12.5/69 kv	
25,000 kva	
Station transformers.....	Westinghouse Electric Corp.
Two 12.5/2.3 kv, 4500 kva	
Station auxiliary transformers.....	Pennsylvania Transformer Co.
Two 2400/240 volt, 750 kva	
Station lighting transformers.....	Kuhlman Electric Company
Two 2400/240/120 volt, 200 kva	
Generator oil circuit breakers.....	Kelman Electric & Manufacturing Company
Two 15 kv, 3000 amp	
2400-volt switchgear.....	General Electric Company
Indoor type, metal clad	
220-volt power centers.....	ITE Circuit Breaker Company
Motors:	
Boiler feed pump.....	Westinghouse Electric Corp.
Fans.....	General Electric Company
Circulating-water pumps.....	Westinghouse Electric Corp.
Hot-well pumps.....	Westinghouse Electric Corp.
Compressors.....	General Electric Company
MISCELLANEOUS EQUIPMENT	
C.W. traveling screens.....	Chain Belt Company
Control air compressors.....	Ingersoll-Rand Company
Heater drain pumps.....	Ingersoll-Rand Company
Fuel-oil booster pumps.....	Byron Jackson Company
Sump pumps.....	Yeomans Brothers Company
Differential oil pumps.....	United Iron Works

The Silver Gate plant is a windowless building except for the office bay. Air is supplied by a ventilation system which takes in outside air at the top-floor level. This gives a supply of fresh air to the station more nearly free of dust than would be provided by windows or louvers at near street elevation.

As a one-unit plant, the Silver Gate Station was operated by a four-man crew, in addition to a part-time electrician. This consisted of one engineer, one fireman, and two auxiliary engineers. When unit No. 2 was placed in service an additional fireman was provided, bringing the total to five men.

The engineer, in addition to his duties as turbine operator, handles all the electrical operations frequently performed in a separate control room. Synchronizing and breaker operation are controlled at the turbine-generator panel. This of course does not include operation of the substation which is by supervisory control by the system load dispatchers.

Table 3 gives a list of the major equipment of Silver Gate Station unit No. 2.

B. G. HUME.⁵ The City of Los Angeles' Harbor Steam Plant is located adjacent to the Los Angeles Harbor. This plant was designed, built, and is operated by the Department of Water and Power, a municipally owned corporation serving the 450 square-mile area within the limits of the City of Los Angeles. This location was selected for a plant site as it afforded an ample supply of cooling water for a plant of large capacity, combined with proximity to the center of the city's industrial load.

Studies made in 1939, of the anticipated growth of load on the system, indicated that it would be necessary to add additional

⁵ City of Los Angeles, Department of Water and Power, Los Angeles, Calif.

steam-generating capacity to the system by about 1943. This study of system requirements indicated that more stand-by steam power would be needed in the form of spinning reserve, and that this type of operation probably would change to base-load operation as the number of steam units on the system increased. Therefore it was decided to build a new steam plant, the first two units of which would provide spinning reserve and, when required, carry system peaks or base load.

Accordingly, orders were placed for two 81,250-kva units, the first to go into operation in 1943, and the second about a year later. The war interfered with this program, however, and the second unit did not go into operation until late in 1947.

By 1946 it became evident that unless considerable additional generating capacity was added as soon as possible, there would be a power shortage in Los Angeles. Orders were then placed for three additional units having a capacity of 93,750 kva each.

The curves in Fig. 8 of this discussion show the growth of load in terms of kilowatthours generated and kilowatt peak, respectively. These curves are extended beyond the year 1948, showing the probable growth of the load on the Department's system to and including the year 1952. Unit No. 2 was completed in November, 1947, just in time to prevent a serious power shortage on the system. Likewise, units Nos. 4 and 3 were completed in December, 1948, and February, 1949, respectively, in time to enable the department to help alleviate the shortage of power in California.

There are five turbine-generator units now installed in this plant. The fifth unit will go into service in the near future. This will complete the plant to its ultimate rated capacity of 355,000 kw on the main units. Unit No. 1 and unit No. 2 each consists of a 65,000-kw, 0.8-power factor (pf), 3600-rpm tandem-compound

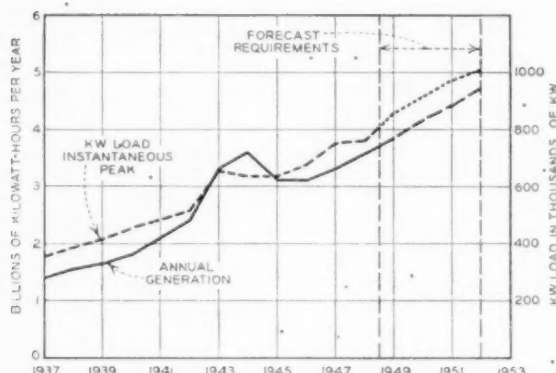


FIG. 8 POWER SYSTEM OF THE CITY OF LOS ANGELES DEPARTMENT OF WATER AND POWER

turbine connected to a 81,250-kva, 60-cycle, 3-phase, 13,800-volt hydrogen-cooled generator. Units Nos. 3, 4, and 5, each consists of a 75,000-kw, 0.8-pf, 1800-rpm, single-cylinder turbine connected to a 93,750-kva, 60-cycle, 3-phase, 13,800-volt hydrogen-cooled generator. The nominal steam pressure and temperature at rated capacity is 850 psig and 900 F. Each turbine exhausts into a twin condenser, consisting of an exhaust trunk connected to the turbine exhaust which divides the steam and discharges it into two one-half size condensers located on either side of the foundation. This design permits low center of gravity and low siphon leg on the cooling-water outlet.

Circulating water is supplied to each twin condenser unit by two vertical mixed-flow pumps driven by vertical splash-proof motors.

The plant requires approximately 300,000 gpm cooling water. This water is taken from slip No. 5 of the harbor by means of two 8-ft-diam precast concrete pipe tunnels 1200 ft long and discharged into the West Basin through two similar tunnels approximately 1400 ft long. The temperature of the water varies from 55 F in the winter to 70 F for a short period of time in the summer.

Each turbine is supplied with steam from one steam-generating unit. The first two boiler units installed have a rated capacity of 570,000 lb of steam per hr and a 2-hr overload capacity of 760,000 lb per hr. The remaining three steam-generating units have a continuous rating of 650,000 lb of steam per hr, with a 2-hr overload rating of 825,000 lb per hr. These units are equipped to burn oil and gas and can be converted to burn pulverized coal at reduced rating if it should be necessary to burn the latter fuel at some future time.

All auxiliaries are motor-driven except for the emergency boiler feed pumps which are driven by steam turbines. The cycle is a straight regenerative cycle with four extraction points.

Horizontal feedwater heaters are arranged vertically, one above the other in the auxiliary bay, to provide positive drainage at low loads and to take care of surges when the load is suddenly increased.

As the first two units were to be designed for either base-load, peaking, or stand-by service, they would have to be capable of carrying the least possible load when there was plenty of hydroelectric power available and to pick up full maximum load instantly at the time of an outage and carry it until such time as the system might be restored to normal, or to carry a base load for protracted periods of time during dry years or whenever the system load exceeded the capacity of the hydroelectric plants. For the latter reason, these two units were designed for good econ-

omy when operating on base load. The wisdom of building economy into this type of plant has been proved during the past power shortage, as it was necessary to operate most of the time on a base load. The performance of 10,900 Btu per net kw-hr at the most efficient load has been realized from these units.

When it became necessary to add the last three units, it was decided to eliminate the extreme requirements for stand-by operation, imposed on the first two units, by eliminating the excess fan and fuel-burning capacity built into the first two units. While the last three units afford considerable stand-by power, if required, they have not been designed for the very low load operation. This was considered unnecessary because of the greater proportion of steam to hydroelectric power existing at the later date.

Units Nos. 1 and 2 have been designed to operate on a minimum block load of 5000 kw indefinitely and, when the occasion demands, assume full rated load instantly. In order to accomplish this result, it was necessary to provide the following features in the design of the plant:

- 1 Absolute minimum carry-over in the steam under all conditions of operation.
- 2 Wide-range burners.
- 3 Positive, fast-acting fan control over a wide range.
- 4 Positive superheat control over a wide range.
- 5 Positive, fast-acting automatic combustion control
- 6 Positive heater drainage at all loads.
- 7 Automatic boiler feed pump control.

The boilers were designed for a minimum water-storage capacity of 3500 cu ft. The controls were designed to maintain a constant steam pressure in the steam drum. A dry drum was provided to prevent carrying over of any quantity of water to the turbine during periods of quick pickup and also to prevent carry-over of solids into the superheater and turbine during normal operation. This design provided maximum heat storage in the boiler and maximum steam pressure at the throttle when the unit was operating on stand-by load.

The fans and burners were designed to have about one and one-half times the required full-load capacity in order that the unit could be fired at a rate high enough to enable the boiler to supply steam for the highest possible quick-pickup load and at the same time recover full steam pressure in the least possible time.

These requirements made it necessary to install oil and gas burners having a maximum range of 15 to 1, and fan drives that could control the speed of the fans accurately enough for the automatic combustion control to function properly when the unit is carrying a 5000-kw load. At the same time, these fan drives had to be able to increase the rate of firing the boiler fast enough to enable the turbine to assume full rated load instantly without permitting the steam pressure at the throttle to drop lower than 750 psig. Motor-generator sets with a modified type of Ward-Leonard control were the only system of fan drives available that would meet these specifications. The turbines are designed to carry rated load on the minimum steam pressure and are provided with a minimum steam-pressure load-limiting device that will cut back on load should the steam pressure fall below this value.

Should an outage occur, the turbine is released automatically from the low block and instantly assumes approximately full rated load. This load is limited by the high-block limit device. The steam pressure in the boiler drum immediately begins to drop. The fans come up to the full speed and the fuel valve opens wide. Fuel is then fired to the boiler until steam pressure is restored to normal for the corresponding load. As soon as equilibrium is restored, the high load limit is moved out of the way and

the turbine generator can take load up to its maximum capability.

Results of tests on the system show that the fuel valve opened wide in about 8 sec, and the fans came up to speed in 10 sec. During this time the steam pressure dropped from 1040 psig to 770 psig. The steam pressure then began to rise until full operating pressure was restored in 8 min. It was not possible to duplicate exactly an actual system outage. Hence the load pickup to 48,000 kw instantly, and to 58,000 kw in 40 sec was somewhat slower than would be the case should a system outage occur.

Units 3, 4, and 5 depart from standard practice in one important respect, namely, the regulation of feedwater by controlling pump speed. Feedwater control in units Nos. 1 and 2 is accomplished by means of a conventional throttling feedwater regulator. At low loads this results in extremely high pressures in the feedwater system on the discharge side of the pumps. It also results in a considerable waste of power at all loads. Economic studies indicated that the power saved by installing variable-speed hydraulic drives would justify the additional cost, and expensive boiler-feed regulating valves could be eliminated. Furthermore, intangible savings in maintenance could be effected by eliminating the high excess pressure on piping valves and heaters.

The speed of the pumps is regulated by the boiler's demand for feedwater. This means of control is very stable and no trouble has been experienced in regulating the level of the water in the drums in this manner.

E. H. KRIEG.⁶ To have constructed such an unusual station as Redondo in less than 18 months would have been a good record under any conditions, but the author has good reason to tell of the achievement so that others may know what can be done.

The design and construction of a power plant on the seashore is indeed a challenge, and the response to that challenge has been unusual in the development of reversal of circulating water for control of mussels and marine organisms in the circulating water system. The average power-plant operator has a healthy respect for what happens when the flow of water in even small-diameter short-length feedwater lines is stopped even without being reversed, but when the designer and operator must think in terms of 10-ft-diam tunnels that are each 1900 ft long, it takes courage and keen imagination to anticipate the many conditions which can arise to avoid the large losses in investment and outage that anything else but complete success would entail.

No doubt an entire paper could be written on the ingenuity called for in arranging for such quick load pickup, from 5 per cent to full load in 15 sec, particularly when many operators ordinarily try to follow turbine-loading rates of perhaps 5 per cent of rating per min even when no steam-temperature change is involved. Further to plague the designer was the need of providing earthquake protection, not only in the structure but to insure that heavy masses would not start swinging out of phase with other lighter masses to which they are connected. This refers particularly to the intricate problems involved in supporting and damping the vibrations in various parts of a piping system where a relatively light steam line is connected to a heavy nonreturn valve or a heavy turbine emergency stop valve that may weigh 5 or 6 tons.

Now that there are no great hydroelectric developments like Hoover Dam on the horizon to augment system capacity, the author states that future capacity is to be steam-driven. Fuel costs of 30 cents per million Btu are high to one accustomed to thinking in terms of 15 or 20 cents. This naturally develops the thought, expressed by the author, that the reheat cycle has a

great deal to offer. This is particularly true of a system which has a great deal of steam-turbine-driven capacity, 20 years old and more, that is so economical for handling short-time peaks overlying a broad base of capacity to be supplied by very efficient units. In other words, where 35 per cent load factor had been commonly associated with steam units, a base is now beginning to develop where steam units in the future will have load factors of 60 per cent and over, even if the full-term life of the unit is taken into account.

High fuel costs point the way toward more efficient units, offering a temptation to go to higher pressures and temperatures. High temperature is the element much more likely to place a limit on quick load pickup which is so important to the system. Reheat is fundamentally more conservative than the higher temperatures for an equivalent heat rate. For example, the reheat cycle is equivalent to approximately 150 F higher temperature in a straight regenerative cycle, and there is little doubt that a 950 F—950 F reheat cycle is more conservative than an 1100 F regenerative cycle at the present time.

When oil is the major fuel, high steam temperatures must be looked at carefully, if not askance, to avoid the very serious wastage of exterior surfaces of tubes caused by vanadium pentoxide which has given so much trouble when used with tubes having external skin temperatures over 1100 F.

The judicious use of partial outdoor construction shows an appreciation of the advantages and also the limitations that such a layout affords. Where salt fogs are possible, protection against condensation in electrical equipment must be provided.

Because Hoover Dam played such a large part in supplying the electricity needs of Southern California during the last two decades, considerable foresight and ingenuity should characterize the decisions to be made on capacity additions during the next decade as they will be mostly of the steam type. Further, the new plants must anticipate burning coal as well as utilizing gas and oil while it is still available. That this challenge is clearly recognized is evidenced by the author's statement: "With an expansion of 760,000 kw in steam-generating capacity either constructed or in progress since the end of the war, the power systems of Southern California are determined that power supply to that area shall be in time and enough."

AUTHOR'S CLOSURE

Each of the discussions includes many interesting items which were not covered by the author and which add to the value of the paper. Mr. Gilg has described the features of the steam-generating equipment at Redondo most capably. Messrs. Hathaway and Hume have presented excellent discussions of Southern California generating stations whose basic characteristics were determined by the general conditions mentioned in the author's paper, but which have individual features of design which were influenced by local conditions and preferences. Mr. Hathaway has included an able presentation of the arguments favoring the all-indoor station. However, these arguments should be balanced against the savings in construction costs of several dollars per kilowatt which are possible with semioutdoor construction. Mr. Krieg's broad experience in the design of steam-electric generating stations makes his discussion particularly welcome. His comments on the advantages of the reheat cycle are especially pertinent.

The downward trend in Southern California fuel prices, which was mentioned in the paper, has continued. As of October 20, 1949, gas is 16.0 cents per million Btu and fuel oil is 20.6 cents per million Btu. There has been no significant change in the estimated cost of coal.

The increased importance of steam power throughout the Pacific Southwest (Arizona, California, and Nevada) is shown by

⁶ Consulting Engineer, Stone & Webster Engineering Corporation, Boston, Mass. Fellow ASME.

the change in margin between installed hydro capacity and the maximum demand. Prior to 1940, under favorable water conditions, it would have been possible to carry the maximum demand of the area on the available hydro generation. By 1948, in spite of the addition of nearly 1,000,000 kw of hydro capacity, the demand was 1,400,000 kw more than the total installed hydro capacity.

In the Southwest in 1940 only 11 per cent of the power was generated by steam, whereas in 1948 steam power produced 38 per cent of the kilowatthours for the area. The increases in demand since the war, and the further increases which are forecast in all estimates of future demands, indicate increased dependence on steam power for base-load generation throughout California and the Pacific Southwest.

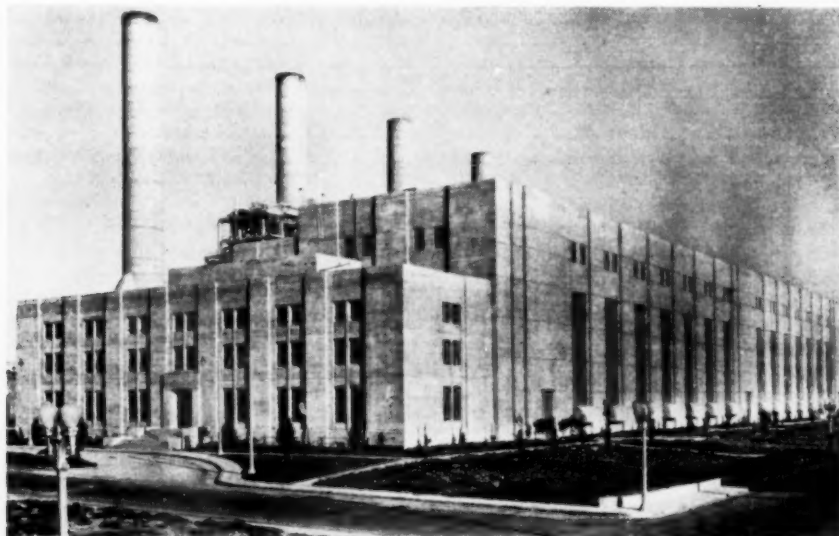


FIG. 9 COMPLETED REDONDO STEAM STATION, FRONT VIEW

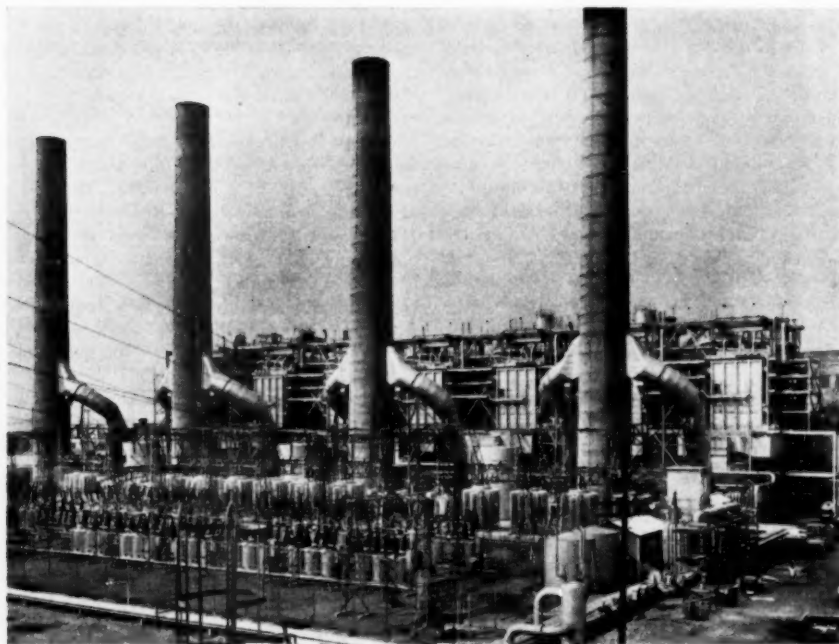


FIG. 10 COMPLETED REDONDO STEAM STATION, REAR VIEW

Postwar Planning for Steam Capacity in Northern California

By C. C. WHELCHER¹ AND W. R. JOHNSON,² SAN FRANCISCO, CALIF.

The estimated population for northern and central California on January 1, 1949, was 4,950,000. This represents an increase since 1940, of 1,667,000 or about 51 per cent. The Pacific Gas and Electric system peak in 1940 was 1,125,000 kw. In December, 1948, it was 2,050,000 kw under daylight-saving time. Standard time would have added 160,000 kw. If the current trends continue, it is estimated the peak in 1951 will be 2,633,000 kw. Planning the required steam-generating capacity to carry its proper share of this unprecedented load growth is discussed in this paper.

INTRODUCTION

THE northern and central part of California served by the Pacific Gas and Electric Company comprises an area of approximately 90,000 square miles with a population approaching 5,000,000. Along with other sections of the West Coast, this area is experiencing an unusual postwar growth in population, in industry, and in the general level of business and agricultural activity. This growth is reflected in the increasing electric power load, and by the current construction program of the authors' company, under which nearly 1,300,000 kw of new hydroelectric and steam-electric generating capacity will be added to the resources of the area before the end of 1951.

The purpose of this paper is to present the background leading up to this current expansion program, to discuss reasons for the location and amounts of steam capacity being added to the system, and to explain unusual technical features of these new plants.

LOAD GROWTH AND POWER SUPPLY

The territory served with electric power largely by the Pacific Gas and Electric Company is a naturally coherent geographical area nearly 500 miles in length, and between 150 and 200 miles in width. The heart of this region is the great valley of the Sacramento and San Joaquin Rivers, bounded by the Sierra Nevada on the east, by the coast ranges on the west, and by other mountain groups on north and south. The natural outlet for the valley, both geographic and economic, is through the San Francisco Bay region.

In Fig. 1 certain features of this territory are shown, including its main watercourses, and location of the company's hydro and steam-electric power plants. The hydro plants, with minor exceptions, are scattered along the western slopes of the Sierra Nevada. They are located on many different rivers, progressing from the Pit in the north, down along the Feather, Yuba, Bear, American, Mokelumne, Stanislaus, San Joaquin, Kings, and finally the Kern River in the extreme south. Hydro developments by others are not indicated; notable among these omissions are the

¹ Chief, Division of Steam Engineering, Pacific Gas and Electric Company. Mem. ASME.

² Division of Hydro-Electric and Transmission Engineering, Pacific Gas and Electric Company.

Contributed by the Power Division and presented at the Semi-Annual Meeting, San Francisco, Calif., June 27-30, 1949, of THE AMERICAN SOCIETY OF MECHANICAL ENGINEERS.

NOTE: Statements and opinions advanced in papers are to be understood as individual expressions of their authors and not those of the Society. Paper No. 49-SA-10.



FIG. 1 TERRITORY SERVED BY THE PACIFIC GAS AND ELECTRIC COMPANY

(The scale for this map is roughly 1 in. to 100 miles.)

Big Creek development on the San Joaquin by the Southern California Edison Company, Ltd., the Shasta and Keswick powerhouses of the United States Bureau of Reclamation, the City and County of San Francisco plants on the Tuolumne, and various irrigation district projects.

Steam-electric plants are indicated by solid triangles. They are located in the San Francisco Bay region, along the coast, and in the extreme southern part of the territory. Plants built, or under construction, in the postwar expansion program are indicated by a double triangle.

After a brief decline in the early 1930's, the consumption of electric energy has climbed steadily upward. This is shown by the curves of annual peak kilowatts and energy in Fig. 2. During the war years growth was accelerated. As the peak of war activity passed there appeared to be a slight decrease in the rate of growth, particularly in 1945 and 1946. It was commonly anticipated, by business and government alike, that a return to prewar

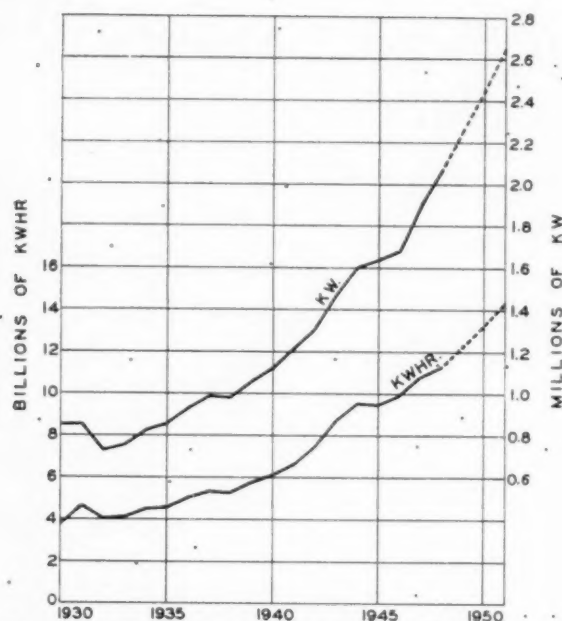


FIG. 2 ANNUAL PEAK KILOWATTS OF LOAD AND ENERGY OF PACIFIC GAS AND ELECTRIC COMPANY SYSTEM

trends would occur. The incorrectness of this reasoning is clearly indicated by the load growth experienced in 1947 and 1948. The system peak of 2,078,900 kw in 1948, represented an increase of 9 per cent over the 1947 peak; while 1947, showed an increase of 13 per cent over 1946.

From 1940, the last prewar year, to 1947 inclusive, peak demand increased from 1,125,700 kw to 1,906,200 kw. This increase of 780,500 kw in 7 years is a growth of 69 per cent, or an average yearly increase of approximately 8 per cent.

In this same period the Pacific Gas and Electric Company brought 206,000 kw of hydro capacity and 100,000 kw of steam capacity into operation, a total addition of 306,000 kw. Also the United States Bureau of Reclamation brought into operation two units at Shasta Dam with a name-plate rating of 150,000 kw. The additions by the power company were projects well started and equipment largely manufactured prior to the war. Exceptions were 32,000 kw of peaking capacity at Pit River No. 1, obtained by enlarging forebay capacity for existing units, and two small steam units in the Eureka area in 1946-1947. Orders for two large steam units placed prior to the war in 1941, were held in abeyance in the interest of the over-all national defense program. These orders were reinstated at the end of the war, and both units went into operation during 1948—seven years after the original orders were placed.

In addition to the two large steam turbogenerators and the smaller installations, just mentioned, planning for other new generation was pursued vigorously as the war period drew to a close. The program, however, faced serious delays beyond the company's control. Manufacturers found themselves swamped with orders for major equipment items; the wave of labor difficulties delayed production. Furthermore, the vagaries of nature brought subnormal rainfall during 1947, followed by the driest January and February, on record in 1948.

In spite of the most strenuous efforts by the company, the effects of drought in reducing hydrogeneration and greatly increasing the agricultural irrigation pumping load, made necessary a power-curtaillment program. This period was of short duration

owing to the combined effects of daylight-saving time, heavy spring rains, power delivered from southern California, and completion of new plants in northern California. The new plants brought into operation at this time were the first major units completed in a postwar program of considerable magnitude.

THE POSTWAR PROGRAM

A construction program of great magnitude is now well under way to restore adequate power margins and to serve the rapidly growing needs of the area. The estimated net generation capacity increases, constructed and planned for the 1946-1951 period, are given in Table 1.

TABLE 1 ESTIMATED NET GENERATION CAPACITY INCREASES—1946-1951

	Steam, kw	Hydro, kw	
1946-1947	Two additional units, boilers and improvements to existing plant in the Eureka area (approx).....	Pit River No. 1 forebay peaking increase on existing units.....	32000
1948	Kern No. 1.....	New Electra ^a	87000
1949	Hunters Point.....	West Point.....	13000
	Hunters Point.....	New Colgate ^a	23000
1950	Kern No. 2.....	Cresta.....	68000
	Moss Landing.....	Rock Creek.....	110000
		Potter Valley—peaking increase on existing units.....	4000
1951	Moss Landing.....		
	Moss Landing.....		
	Contra Costa.....	Total hydro.....	337000
	Contra Costa.....		
	Contra Costa.....		
	Total steam.....		987000

^a Replaces existing generation at the two plants totaling about 30,000 kw.

This program was decided upon after consideration of many factors relating to the amounts of steam and hydro capacity to be added. The basic reasons for the large proportion of steam generation include the following:

1 Steam-capacity additions postponed by the war. The first units at Kern and Hunters Point are in this category. These steam-capacity additions had been planned prior to the war as necessary to maintain the desirable steam-hydro ratio in the area.

2 Steam capacity required because of the changing economic steam-hydro ratio. The economic and other factors entering into the optimum proportions of steam and hydro capacity have been discussed fully in earlier papers. As the more favorable hydroelectric sites are developed,^{3,4} those remaining are more costly. At the same time technological improvements in steam-plant design, such as larger unit size and higher efficiency, have tended to reduce the relative cost of steam. Offsetting this has been a rising fuel cost. However, the over-all result has been a gradual shifting of the economic steam-hydro ratio from approximately 75 per cent hydro and 25 per cent steam to nearly equal amounts of each.

This trend is illustrated in Fig. 3, which shows the annual energy sources for the company's system from 1930 on, in per cent of the total for each year. The energy shown coming from "other sources" is almost entirely from hydroelectric plants owned by others. The proportion of energy from fuel plants is as low as 3 per cent in 1935, and is seen to be increasing gradually, reaching 36 per cent in 1947. However, the trend is partially obscured by the effect of variations in precipitation, both 1947 and 1948 being below average. In such years the amount of steam energy is much greater than normal.

3 Steam capacity for support of hydro developments planned by the company after 1951.

³ "Aspects of Steam Power in Relation to a Hydro Supply," by A. H. Markwart, *Mechanical Engineering*, vol. 48, 1926, pp. 557-561.

⁴ "Mingled Hydro and Steam Power Production in California—Past, Present, and Future," by A. H. Markwart, *Trans. AIEE*, vol. 59, 1940, pp. 775-781.

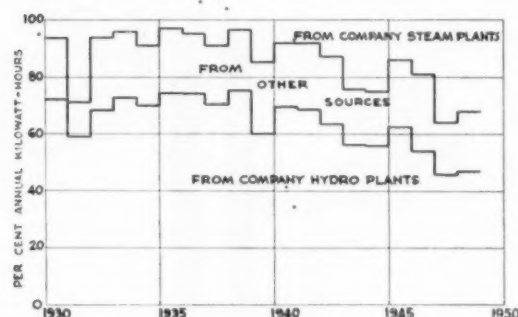


FIG. 3 ENERGY SOURCES FOR THE PACIFIC GAS AND ELECTRIC COMPANY SYSTEM

4 Factors in planning and construction. Nearly all new hydro developments require procurement of licenses and water rights involving Federal agencies and other interests. Until satisfactory agreements are reached on these matters, design and manufacture of the major equipment cannot be commenced, nor preliminary construction begun.

Steam turbogenerators, on the other hand, do not have their design dictated by the site where they are to be installed. Therefore, orders may be placed and design commenced far in advance of the procurement of a satisfactory site.

5 The company has always followed a policy of planning to facilitate the absorption of hydroelectric energy produced by irrigation districts, the United States Bureau of Reclamation, and other agencies as a by-product of water-conservation projects. The prime importance of development and best use of California's water resources have long been recognized. The company endeavors to co-operate to the utmost in the utilization of incidental power from these projects for the greatest possible benefit to the project.

SYSTEM INFLUENCES ON STEAM-PLANT LOCATIONS

With some artistic liberties, the problem of load and power supply on the company's system for an estimated average water year, as of 1951, is shown in Fig. 4. Energy from hydroelectric sources is represented by the unshaded arrows, that which must be supplied from steam plants by shaded arrows, and the quantity of energy involved is proportional to the arrow width. It is rather apparent that major steam plants should be located in the southern and west-central portions of the area if transmission losses are to be minimized.

Planning for steam plants of the capacities needed for this program required consideration of factors not involved in smaller installations located in metropolitan areas where power may be fed directly into the distribution network. It is not feasible on the company's system to take away the full output of a large plant entirely over distribution voltage circuits, nor can the large blocks of generated power be absorbed locally at periods of light load.

In view of the foregoing the new plants were designed for system, as well as local area use, and it was necessary in each case to provide full-capacity outlets directly to the transmission system. With such outlets the general plant locations were determined after considering such factors as area power supply and load, availability of fuel, make-up water, condenser circulating water, foundation conditions, transmission outlets, and the possibility of future expansion.

All four of the new large steam plants required construction of high-voltage transmission connections. This was accomplished for Hunters Point by means of 115-kv underground-cable connections to a transmission substation in combination with power sup-

ply to a new 115-kv distribution substation in downtown San Francisco. The Kern plant connects directly to the 115-kv transmission by overhead lines to substations in the vicinity, and is provided with transformer auto taps to feed into the 70-kv subtransmission. At Moss Landing two of the units will have auto tap connections tying into the 115-kv transmission lines, in the area, but all three units will have full-capacity outlet by 230-kv lines to the San Joaquin Valley and the lower San Francisco Bay regions. While the other plants have connections to the 115-kv or subtransmission, the entire output of the Contra Costa plant will be transmitted over the 230-kv high-voltage network.

KERN STEAM PLANT^{5,6}

Agriculture has long been recognized as the basic industry in California and the one which in a large measure is responsible for the prosperity of the state. The San Joaquin Power Division of Pacific Gas and Electric Company, with headquarters at Fresno, represents over 70 per cent of the system's agricultural load. In 1946, the peak for this division was 415,000 kw. In 1948, it was 578,000 kw. The estimate for 1951, based upon present trends is 800,000 kw, which represents a 93 per cent increase above 1946, a 5-year period.

⁵ "Control is Centralized at Kern station," *Electrical World*, vol. 130, Sept. 25, 1948, pp. 90-91.

⁶ "Centralized Control at Kern," *Electrical West*, vol. 101, 1948, pp. 79-80.

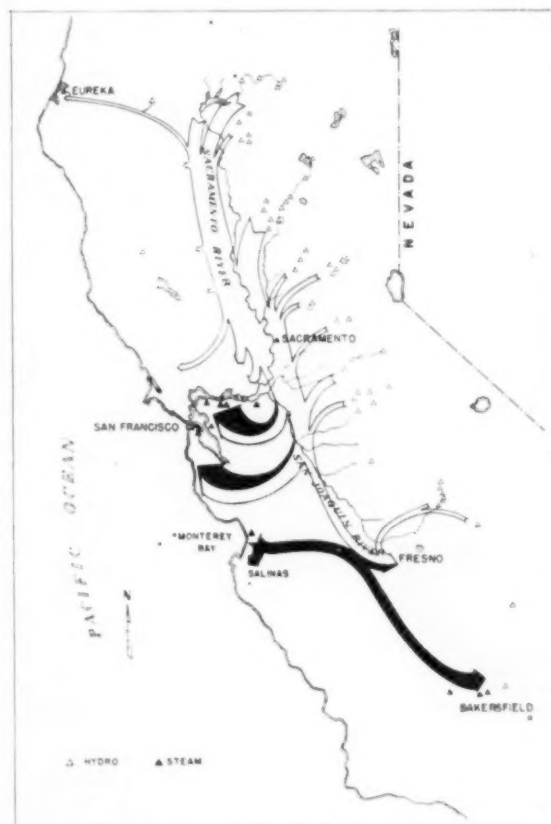


FIG. 4 ESTIMATED LOAD AND POWER SUPPLY FOR THE PACIFIC GAS AND ELECTRIC COMPANY SYSTEM IN 1951, WITH AN AVERAGE WATER SUPPLY

(The scale for this map is roughly 1 in. to 100 miles.)

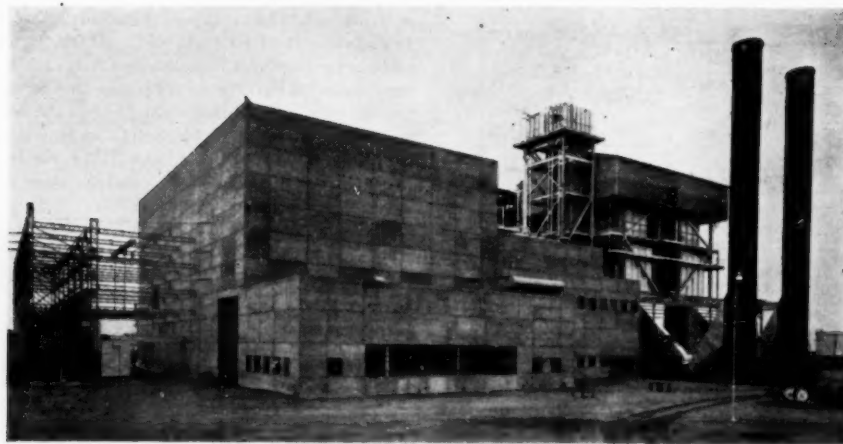


FIG. 5 KERN STEAM PLANT

In the lower end of this territory, power had been supplied from transmission sources, small hydro and steam plants, and from an interconnection with the Southern California Edison Company at Magunden. Upon termination of the Edison Company's interchange agreement in December, 1947, a replacement of this power source was required. Additional steam capacity in the Bakersfield area proved to be an economical means of replacing this supply, as well as providing for a portion of the load growth in the lower San Joaquin Valley. Since there are no rivers in the area capable of supplying condenser circulating water, cooling towers must be used, and their make-up is supplied by wells. The use of cooling towers permitted the plant to be located on a level 160-acre plot near oil refineries which supply fuel oil by pipe line. To those not accustomed to obtaining condensing water in this manner, it may at first seem strange to locate a large steam power station in an open field. That, however, proved to be most suitable for this station which is 5 miles west of Bakersfield on the Santa Fe Railroad.

The first main unit at Kern, which is rated at 75,000 kw, has been in commercial operation since May 10, 1948. A 100,000-kw second main unit is scheduled to be placed in operation during January, 1950. There will be two accompanying house units of 6000 and 7500 kw, respectively. Each of the four boilers has a normal full-load evaporation rate of 450,000 lb of steam per hr. These boilers are designed to burn either fuel oil or natural gas. A general view of this plant is shown in Fig. 5.

MOSS LANDING STEAM PLANT

Another important agricultural center, sometimes called the "Salad Bowl of America" because of its tremendous production of lettuce, celery, and artichokes, is located along the coast of Monterey Bay, with much of the business activity centering at Salinas. The agricultural lands here must also be irrigated by water pumped from wells. In this area at Moss Landing, a 270-acre site was selected as the location of a new plant in which three 100,000-kw main units and three 7500-kw house units will be installed initially. As in the other stations, two boilers per turbine have been provided. An appreciable amount of the power from this plant will be used locally with much of the remainder normally being transmitted east over the coast range mountains to the San Joaquin Valley in the general areas of Fresno and Bakersfield.

Condenser circulating water will be drawn from Moss Landing Harbor and discharged into Elkhorn Slough to the north. Since

Elkhorn Slough is connected to the harbor, a careful study of the possible effects of recirculation was undertaken. It was concluded that while certain conditions of unfavorable tidal flow may result in some temperature elevation, this will occur infrequently and should not affect the capacity of the first three turbines. Operating experience with the initial installation will determine what, if any, further precautions must be taken when additional units are installed. Fresh water for the station will be obtained from wells located on the property.

Fuel oil will be delivered by 120,000-bbl tankers through a submerged pipe line extending approximately 3500 ft out into Monterey Bay. A flexible hose at the sea end of this line will be taken aboard the tanker upon arrival and connected to the discharge of its unloading pumps. When not in use, the hose will rest on the bottom of the sea. If conversion to coal operation should become desirable at this station, a spur of the Southern Pacific Railroad will be available for coal deliveries. There is ample space at the plant for the simultaneous storage of fuel oil and coal. Grading at the site was started in September, 1948.

"STATION P," HUNTERS POINT¹

Load growth in San Francisco and on the Peninsula necessitated an increase in power supply for this area. Studies indicated that this could be obtained most economically by installing additional steam capacity at Station P where space was available and a good condenser circulating-water system had already been developed. The original unit at this station was placed in operation in 1929, and is rated 35,000 kw.

The two new 100,000-kw main units and two 7500-kw house units are supplied steam by four new boilers entirely independent of the old unit so far as operation is concerned. Circulating water is drawn from San Francisco Bay. Fuel oil is delivered by barge or tanker to a filling line carried on a pier extending into the bay.

Power generated by the new units is stepped up to 115 kv and transmitted by high-voltage underground cable to the new Mission substation in the heart of the city. Two 115-kv underground cables also connect Station P with Martin substation from where the power may be taken during light load periods over transmission lines to the system outside the city.

The first new unit at Station P was placed in commercial operation on December 12, 1948, and the second followed on January 25, 1949. Construction started in July, 1947, and about 18 months were required to bring the first unit into operation.

¹ "Station P," *Power*, vol. 92, 1948, pp. 586-588.

CONTRA COSTA STEAM STATION

The most concentrated industrial area of the company's system lies in the East Bay region and along the lower Sacramento and San Joaquin Rivers near where they empty into San Francisco Bay. The Contra Costa Station has been located in this area at a point $2\frac{1}{2}$ miles east of Antioch on the San Joaquin River.

The backbone of the electrical transmission system is the 230-kv network running the length of the great Central Valley and carrying power from the many hydroelectric plants in the Sierra Nevada to the principal load centers in the San Francisco Bay area and below. The Contra Costa steam plant was placed astride this network. Its power will be used wherever required in the system, and its location on the San Joaquin River was, among other considerations, decided on the basis of availability of circulating water and proximity to fuel-oil supplies along the upper bay. Circulating water will be drawn from the river which, although subject to tidal action is still essentially fresh. It is believed that stratification and the large volume of water available will reduce the effect of recirculation during unfavorable conditions of tidal and stream flow. Fuel oil will be delivered by barge, tanker, or pipe line. Coal when and if required in the future can be delivered to a spur of the Santa Fe Railroad entering the property.

The initial installation at this plant will include three 100,000-kw main units, three 7500-kw house units and six steam generators. All units are scheduled to be in operation during the first 6 months of 1951. Construction was started in February, 1949.

POWER-PLANT DESIGN AND STATION EQUIPMENT

The steam program outlined in this paper has been and is being planned and co-ordinated by the Pacific Gas and Electric Company's engineering department but, except for the units at Eureka, the plant design and the construction are being carried out by others. Stone and Webster Engineering Corporation has this responsibility for Kern, Station P, and Moss Landing. The Bechtel Corporation has similar responsibilities in connection with the Contra Costa plant.

Structure. In general, each of the four new steam stations is of semioutdoor design, with the turbine room and control bay entirely housed. The boilers are protected by an umbrella-type roof of corrugated transite. The firing aisle is completely enclosed. The buildings are of steel-frame construction with reinforced-concrete walls and roofs. A plan and section of the Contra Costa steam plant are shown in Figs. 6 and 7.

Turbine Generators. Except for the two 1800-rpm Kern units, where delivery was a prime consideration, the remaining eight main turbine generators involved in this postwar program, each with a nominal rating of 100,000 kw, 15 lb hydrogen, are 3600-rpm machines designed for 1300 psig and 950 F. The turbines are of the tandem-compound double-flow condensing type and have four extractions to supply steam to the feedwater evaporators and the closed feedwater heaters. The condensers are single pass with divided water boxes to permit part-load operation on one of the two circulating-water pumps.

The eight accompanying automatic-extraction house turbo-generators are rated 7500 kw and are designed for the same steam conditions as the main units. They operate condensing with a single extraction opening supplying steam for the deaerating feedwater heater. The house units are installed to provide an independent electric power supply for the vital station auxiliaries. They are simple rugged units expressly designed immediately to assume full load in the event of a system disturbance. Normally they will be in operation supplying extraction steam at a constant 5-psig pressure to the deaerating feedwater heaters. System frequency or voltage dips, severe enough adversely to affect station operation, automatically disconnect the main units from the

house bank. Thus, the main units will operate at whatever frequency and voltage the system can develop and will carry essentially full load. Meanwhile the house units furnish normal voltage and frequency to the auxiliaries.

A heat-balance diagram, which is typical of each of the eight main and house units at Station P, Moss Landing, and Contra Costa is given in Fig. 8, for the 100,000-kw load condition.

Steam Generators. All steam generators included in this program are of the radiant type with tangent waterwall tubes in the furnace. Two different methods of superheat control are employed. At Contra Costa and Moss Landing, a portion of the gases are by-passed around the primary superheater, and the position of the by-pass dampers determines the temperature of steam leaving the superheater. At Kern and Station P, the control is by means of a heat exchanger installed in an enlarged lower drum. Part of the steam leaving the primary superheater is passed through this attemperor and is cooled prior to mixing with the remainder. All steam then passes through the secondary superheater and thence to the turbines. Two different types of air heaters are also employed. The first eight boilers in the program are equipped with tubular air heaters, whereas the last twelve use the regenerative type, wherein the heat-exchange elements are exposed alternately to furnace exhaust gases and to incoming air.

The steam generators for Station P and Kern were designed for oil and gas fuels. Conversion to coal, should this become desirable, can be accomplished with some loss in capacity. At Moss Landing and Contra Costa, on the other hand, provision is being made for possible use of coal with full-capacity output. Not only is space being provided for installation of such auxiliary equipment as pulverizers, coal bunkers, and dust eliminators, but the steam generators themselves are provided with larger furnaces to permit burning coal efficiently and without reducing the steaming rate. The difference in furnace size is illustrated by the heat-release rate, which for Kern and Station P is about 30,000 Btu per cu ft-hr on oil at rated load. Heat release for the same conditions at Moss Landing and Contra Costa by contrast is approximately 18,000 Btu per cu ft-hr.

In addition to providing greater volume to permit the slower-burning coal to be consumed before the gases leave the furnace, greater space between tubes in the superheater is provided to minimize effects of slagging of these surfaces. The minimum clear space between tubes in the Kern and Station P superheaters is 1 in. The Moss Landing and Contra Costa superheaters have 2 in. clear. These more conservatively designed boilers are expected to be able to stay on the line longer when burning oil fuel and thereby improve boiler reliability.

Quick Pickup. All of the new steam stations at times will be operated at low loads on stand-by duty and may then be called upon to provide nearly full-load output in a matter of 20 to 30 sec. This quick-response requirement is reflected in the selection of equipment. Boiler feed pumps and draft fans are operated always at full speed immediately ready for full-capacity demand. This is achieved at some loss in cycle efficiency because of the need to resort to dampers, throttling valves and recirculation of boiler-feed-pump flow. The fuel burners and auxiliary equipment have a capacity range of 20 to 1 at Kern and Station P, and 10 to 1 for Moss Landing and Contra Costa. All burners are always in service.

Centralized Control. Centralized control is a basic feature of the general plant layout of each of the stations and the operator at the key point in the control room is in position to maintain visual contact with helpers operating the principal items of equipment. He is able to see the main turbines, house units, and boiler feed pumps on the one hand, and the boiler firing aisle on the other. In addition, he is aided in the operation of the plant by a very spe-

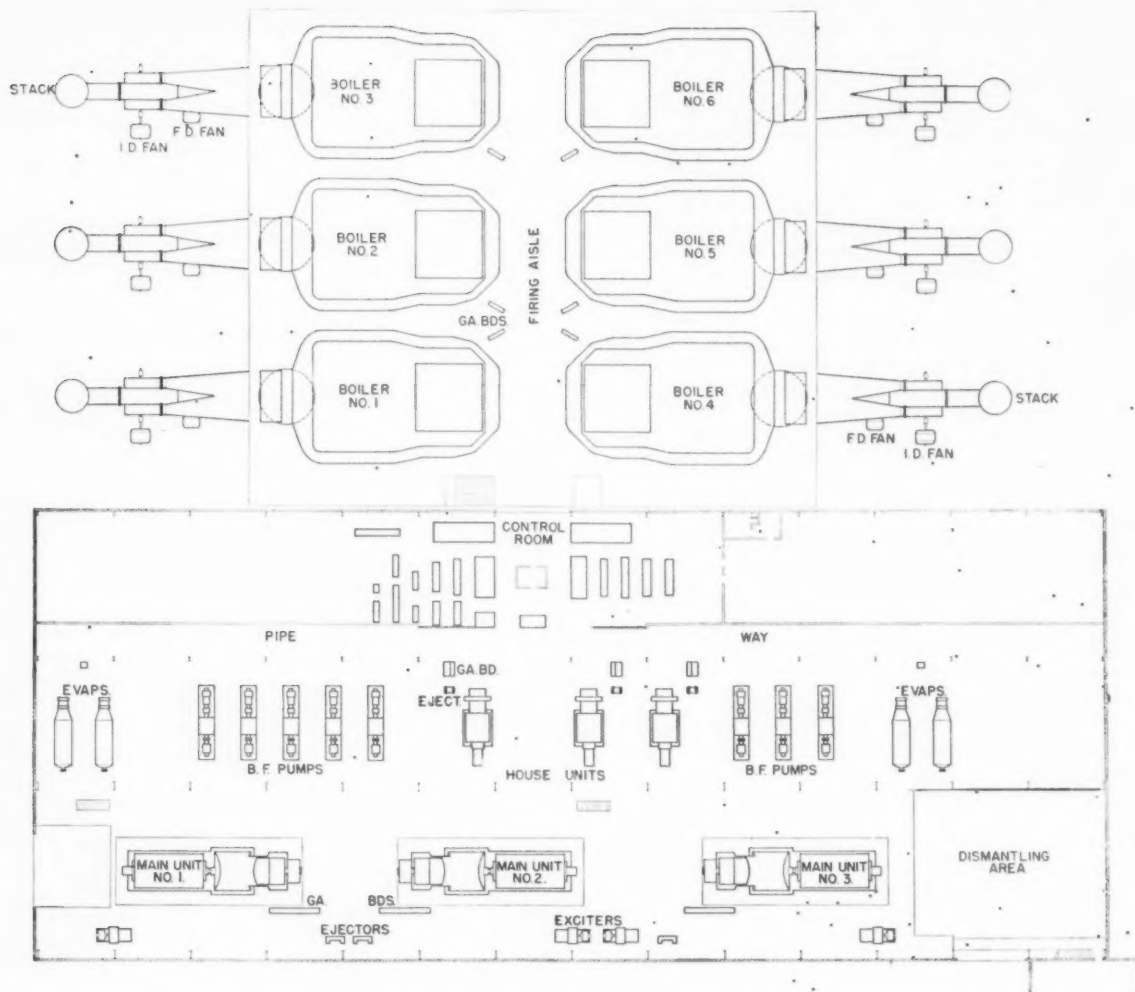


FIG. 6 PLAN OF CONTRA COSTA STEAM PLANT

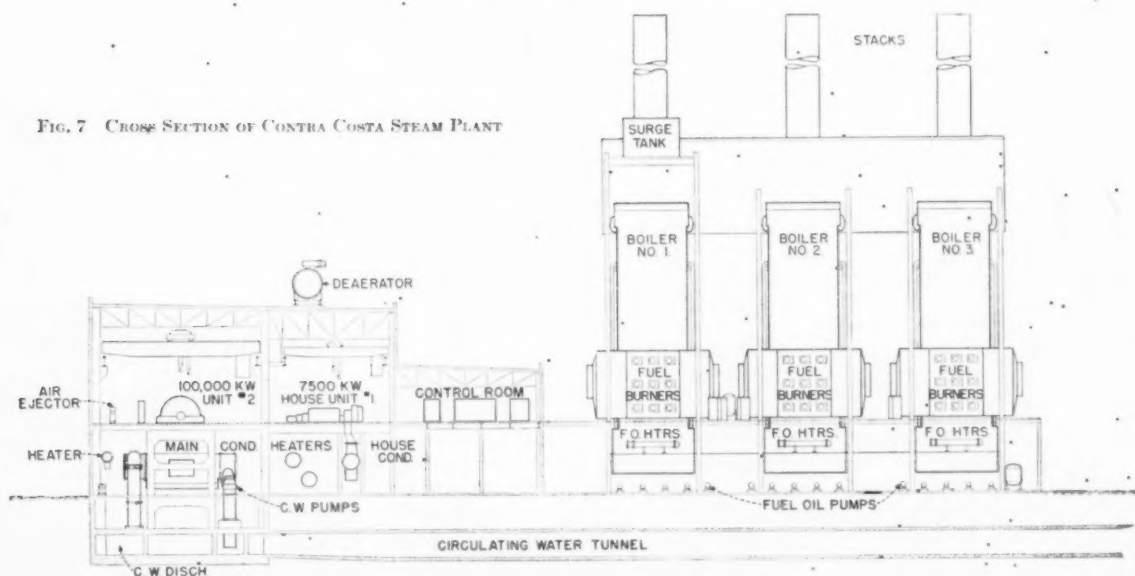


FIG. 7 CROSS SECTION OF CONTRA COSTA STEAM PLANT

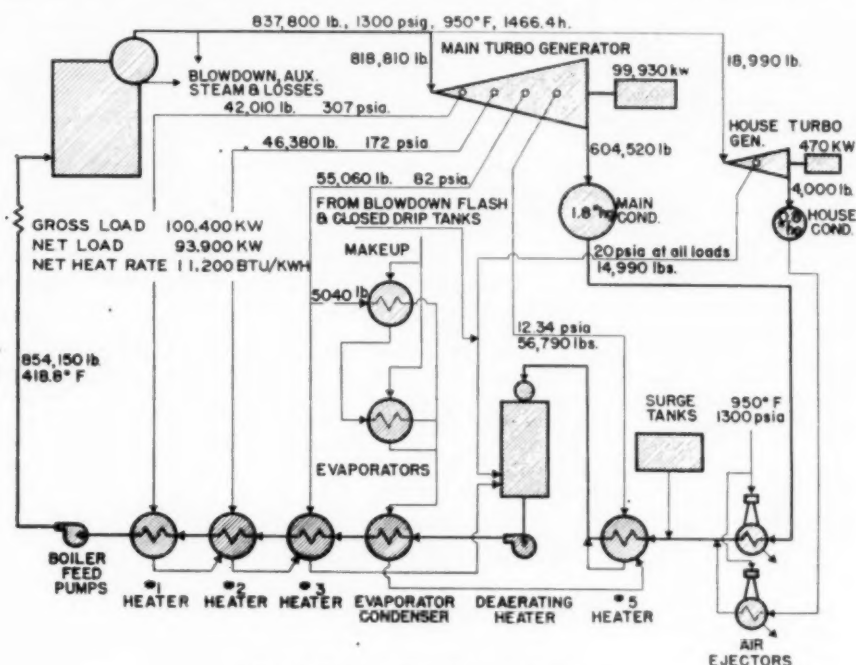


FIG. 8 TYPICAL HEAT-BALANCE DIAGRAM

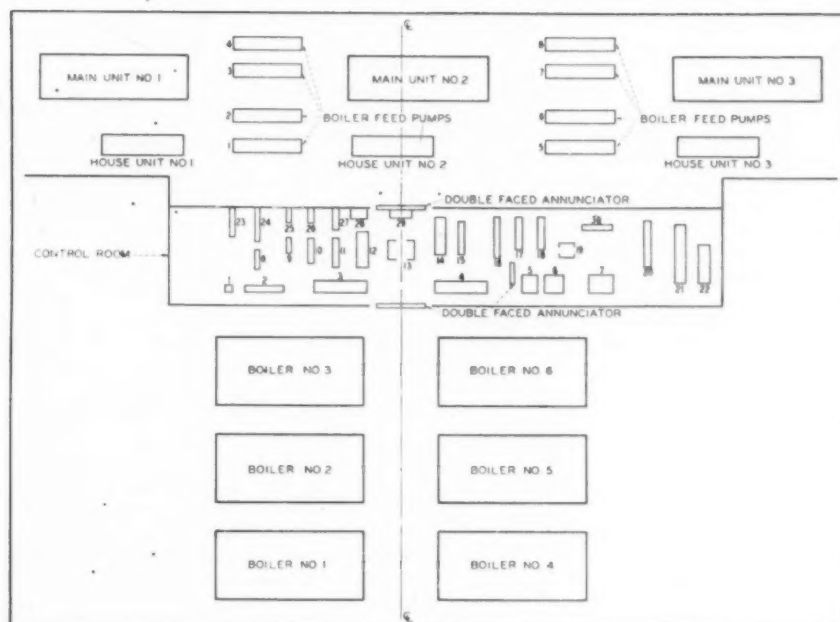


FIG. 9 CONTROL ROOM AT MOSS LANDING

- 1 Control air-compressor auxiliary board.
- 2 Fuel-oil control board.
- 3,4 Individual boiler control boards.
- 5 110-Kv control board.
- 6 Generator and transformer banks.
- 7 220-Kv control board.
- 8 Fuel-oil heaters control board.
- 9 Miscellaneous heaters control board.
- 10 Ratio control board.
- 11 Feedwater meter board.
- 12 Master control board.
- 13 Plant operator telephone booth.
- 14 House-generator control boards.
- 15 House-turbine auxiliary control boards.
- 16 Load-frequency control board.
- 17 4.16-Kv control board.
- 18 480-Volt control board.
- 19 System operator telephone booth.
- 20 Excitation boards.
- 21,22 125-Volt d-c station service switchboards.
- 23 Soot-blower reducing-valves control board.
- 24 Miscellaneous recording meter board.
- 25 Miscellaneous pumps gage board.
- 26 200-Lb reducing-valves gage board.
- 27 Feedwater-pump gage board.
- 28 Feedwater control board.
- 29 Main generator control boards.
- 30 Electrical recording meter board.

cial annunciator system consisting of banks of large light-type indicators mounted above the various control boards and on the control-room walls between the turbine and boiler rooms. By a combination of horns and signal lights, he is warned of abnormal operating conditions anywhere in the plant. By use of a color code, the relative urgency of corrective measures is emphasized.

At Kern and Station P two main units and their auxiliaries are controlled from one room. At Moss Landing and Contra Costa three main units will be controlled from one room. A block diagram of the Moss Landing Station with identification of the individual control boards is shown in Fig. 9.

Station Auxiliary Power System. The primary auxiliary power system in each of the stations is 4160-volt 3-phase. The switchgear used therewith is metal-enclosed with magnetic-type air breakers. The buses are connected in the form of a ring, one ring bus for each main generating unit. Each bus has connected to it, a house turbine and a house transformer bank. The bus sections are connected together through a bus tie switch, allowing parallel operation if necessary.

The secondary auxiliary-power-system voltage is 480 volt 3-phase, and is a selective radial type consisting of load centers located at strategic locations around the plants. Each load center is equipped with a number of 3-pole electrically operated air breakers of proper interrupting duty. The main load centers are supplied with power from 4160/480-volt stepdown transformers. These main load centers supply power to other load centers scattered around the plant. Each center is sectionalized so that only one half the equipment is lost in case of a bus failure.

Motors of 250 hp and above are connected to the 4160-volt system, while smaller motors are connected to the 480-volt system. In addition, the power for the lighting system is 3-phase, 4-wire, 216/125-volt, supplied by numerous small 3-phase lighting transformers stepping down from 480 volts to 216 volts.

CONCLUSION

The construction program outlined in this paper covers almost 1,000,000 kw of new steam-electric generating capacity which will be added to the area before the end of 1951. This amount of capacity clearly indicates the increased importance of fuel-burning plants to the Pacific Gas and Electric Company. From a system standpoint, the new steam stations not only add generating capacity, but the required interconnecting transmission lines and switching stations will further contribute to system reliability. As integration and growth continues, the need for "quick pickup" steam stations and multiple-boiler per turbine installation probably will tend to decline. The future trends of steam-station design here as well as elsewhere is expected to be in the direction of simplification of equipment and plant layout and still lower station heat rates.

Discussion

M. W. CARTY.⁵ The authors give a clear presentation of the salient factors considered in providing additional electric power supply for the requirements in the great central-valley area of California. The rapid rate of growth in peak demand in that area is probably unprecedented in the United States for any comparably sized territory. It is of interest to note that the economics of the situation for the extensive territory served will lead by 1951 to a 50-50 per cent ratio of steam and hydroelectric power-generating plants. In the power developments recently completed since the end of the war in this area, or now under construction, the added steam capacity will be three times as great as the added hydro power.

⁵ Senior Mechanical Engineer, Stone & Webster Engineering Corporation, Boston, Mass. Mem. ASME.

Fig. 4 of the paper shows clearly the preponderant dependence on hydroelectric power in the northern part of the system and makes evident the strategic value of added steam capacity in the San Francisco Bay area. It is a wise precaution to locate the large steam plants where fuel oil is readily available by tanker delivery as the quantities of fuel are large. The Moss Landing steam plant will produce a net output of 565 kw/hr per bbl of oil when operating under full-load conditions, and approximately 12,800 bbl of oil will be required per day under these conditions. If the plant is operated at the minimum capacity at which the turbines will be capable of quick pickup of load, approximately 1000 bbl of oil will be burned per day without any net output of energy.

The steam plants have multiple boilers per main turbine-generator and this was decided upon, having in mind the requirements of quick pickup of load, the need to remove from time to time metallic adhesions on the furnace tubes resulting from oil burning, and the need to wash off occasionally deposits on the superheater tubes. Satisfactorily large water storage in the boiler steam drums is helpful to give accumulator action at times of quick pickup of load, and multiple boilers are better in this respect than single equivalent large boilers. In a completely integrated and compact system, as distinct from the central-valley area with its long transmission lines, it would be desirable to come closer to the "unit principle" of one boiler per turbine generator without cross-connections, in the interest of lower investment cost and operating simplicity.

The advantages of centralized control are apparent, and this has been a major factor in the general arrangement of the steam plants. The operators have direct vision from the central operating point to the key centers at the turbine generators, boiler feed pumps, and house turbines.

Referring to Fig. 5 of the paper, which shows the Kern steam plant, it is not entirely apparent that the two principal operating levels, main operating floor and ground floor, are each arranged at one continuous uniform level which adds to the convenience of the operators and ease of maintenance activities. This plant is dependent upon cooling towers for cooling the condenser circulating water. For make-up and other requirements at full-load operation, the water requirement is at the rate of 4000 gpm, which is readily obtained from deep wells on the power-plant property.

Fig. 9, the Moss Landing steam plant, shows the boiler-feedwater pumps located on the main operating level, and consequently they are always under the observation of an operator. The house units also are located in readily observable positions and are easily accessible. Fuel oil for this station will come from tankers having a capacity of 120,000 bbl and will be discharged by the tanker pumps operating at 125 psig pressure and will be heated to 140 F, if necessary, in the tanker before delivery. It is expected that the tanker will be able to deliver up to a maximum rate of 8000 bbl of oil per hr through an 18-in. submarine pipe and a 24-in. on-shore pipe, extending to the storage tanks at the steam plant, a distance of approximately 1 3/4 miles.

Arrangements in the steam plants are made with a view to the safety and comfort of the operators, and primarily for reliability of service.

Prevention of trouble from mussel accumulation in the circulating-water lines has received special attention at the Moss Landing steam plant. There are two supply lines to each main condenser, and it is planned to circulate water warmed to 95 F back through one line at a time. The single-pass divided-water-box arrangement of the condenser is well-adapted for this operation. A routine backwash may be established for one condenser circuit per week end, resulting in a normal 3-week time cycle. Perhaps a longer cycle will suffice, and the usual chlorine concen-

tration for reduction of slime formation inside condenser tubes may be increased during the backwashing operation.

C. H. WOOLLEY.⁹ The Pacific Gas & Electric Company is very progressive and has consistently purchased efficient and modern designs of power-generating equipment in order to best serve the rapidly growing population. In 1938 the company with which the writer is affiliated installed the first oil-fired radiant-type boiler for P.G.&E. The single-pass principle of gas flow which results in low fan-power costs and improved operation was incorporated in this design. When these boilers were designed, the serious fouling of superheaters with oil slag had not yet been encountered in California; however, the front row of superheater tubes was staggered to form a 3-row slag screen.

When the next expansion of this company was contemplated

⁹ Proposition Division, Babcock and Wilcox Company, New York, N. Y. Mem. ASME.

in 1941, for Kern steam plant and Hunters Point, the same modern radiant-type boiler was selected, but at that time the oil-slag problem had been encountered, and special provisions were included in the design to reduce the possibility of an outage due to the effect of oil slag. The furnace was changed from the older stud-tube design to touching-tube design, in order to provide a cooler furnace and to eliminate the growth of furnace walls, caused by oil slag penetrating the refractory on the studded tubes, as reported by V. F. Estcourt.¹⁰ The tubes in the first two sections of the superheater were spaced far apart so that oil slag could not close the lanes. The superheater banks were made shallow in order to permit better cleaning by the soot blowers. Provision was made to water-wash the superheater, economizer, and air heater. Drain hoppers were installed under all three of these units of equipment.

Unfortunately, the war delayed the installation of the boilers, and they were not placed in operation until 1948.

When it was necessary to purchase the boilers for Moss Landing and Contra Costa, there was not sufficient operating experience to determine if the same improvements would render the units free from the increasing oil-slag troubles. As the degree of trouble due to this slag had increased throughout the country, it was believed that even greater precautions should be taken to insure continuous operation. The possibility of future coal-firing required that the furnace for the new stations should be larger, and this automatically gave a lower temperature entering the tube bank with oil-firing than would have been used normally for a straight oil-fired job. Fig. 10 of this discussion shows the boilers for the Moss Landing Steam Plant, with which the writer is familiar. The additional precautions against tube fouling were as follows:

The front bank of superheater tubes were placed on 12-in. centers primarily to guard against coal-slag troubles, but automatically, operation became safer for oil-firing. As the gas temperature was reduced and reached the second superheater section the spacing was changed to 6-in. centers which is adequate in this temperature zone to insure against tube-lane pluggage with

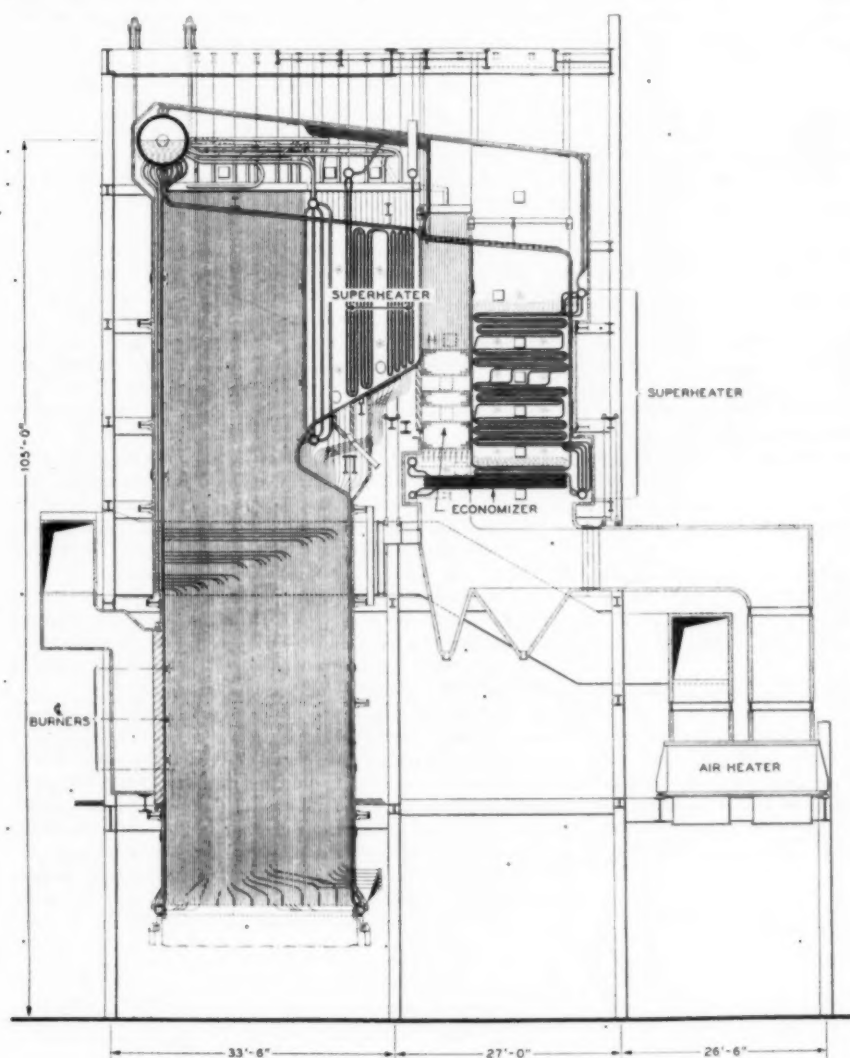


FIG. 10 BOILER FOR MOSS LANDING STEAM PLANT

¹⁰ "History and Performance of the Oil-Refinery Steam-Electric Generating Stations of the Pacific Gas and Electric Company," by V. F. Estcourt, published in this issue of the Transactions, pp. 209-222.

either coal or oil slag. Experience has indicated that oil-slag pluggage becomes much less troublesome in the lower-temperature zone existing after passing over two banks of superheater tubes, and it is probable that no pluggage would result if the tube spacing were reduced to 1 in. clear between tubes. However, since fuel-oil slag has become progressively more troublesome, it was decided to make the minimum clearance between tubes in the cooler section of the superheater not less than 2-in. The superheater banks were made extremely shallow so that the soot blowers could penetrate the bank properly. Provision for water-washing the superheater, economizer, and air heater was also incorporated.

The experience of the Pacific Gas and Electric Company in its own plants and the boiler manufacturer's experience in other plants in California, Florida, and elsewhere, were combined in an effort to design and build a boiler unit that would be as reliable as is humanly possible. If the hopes of the designers and operators are realized in these new units, perhaps the availability records will permit the next expansion program to be of the single-boiler single-turbine design, resulting in a further simplified plant design and operation.

ALF HANSEN.¹¹ This paper describes the power system of Northern California, and gives a clear, factual picture of the background and planning of the current expansion program.

Normal rainfall in California varies from $\frac{1}{2}$ in. per year in the desert area in Southern California to 114 in. per year in the northwest area. Water available for hydro-power generation in a dry year is about 40 per cent of a normal year. This can be increased to 60 per cent by the use of storage. Therefore there must be available enough steam-generating capacity to firm up 40 per cent of the hydro capacity.

As the power system grows, available hydro sites become less attractive from a firm power standpoint, a larger percentage of the capacity must be firmed up with steam, and initial cost of development increases. Only about 20-25 per cent of the consumers' dollar pays for the fuel used in a steam-generating plant. Therefore steam generation will assume an increasingly greater share of the power load.

Before the war the power company estimated the division of generating capacity as 60 per cent hydro, 25 per cent steam, and 15 per cent from other sources.

At present (including current expansion) the ratios are 40 per cent hydro, 50 per cent steam, and 10 per cent from other sources.

In the future, best estimates indicate the ratios should be 20-25 per cent hydro, 70 per cent steam, and 5-10 per cent from other sources.

The peak-load curve of the P.G. & E. system from 1914 to date shows the effects of two world wars, drought periods, depressions, and business booms; but if a smooth line is drawn through this curve it indicates an average annual increase of slightly more than 6 per cent. Inspection of the annual peak kilowatt curve in Fig. 2 of the paper shows no increase in 1938, and about 13 per cent in 1947. Therefore there must be enough spare capacity on the system to take care of such unpredictable increases in load as effected by war and business booms.

¹¹ Turbine Engineer and Specialist, Pacific District, General Electric Company, San Francisco, Calif. Mem. ASME.

At the present rate of normal growth, the Northern California power system needs 200,000 kw of additional firm generating capacity every year, a large portion of which will be steam.

Before the war P.G. & E. had about 100,000 kw capacity in old steam units which were shut down and served as "cold stand-by." It is clearly seen from figures given in the paper that these units had to be brought into service, and had to be operated at high load factor during the war. When they are again returned to serve as cold stand-by by the current expansion program, 28 per cent more electrical energy will be produced from the same quantity of fuel. Such improvement in efficiency tends to hold down the cost of electricity in spite of rising prices on equipment and labor. It also helps conserve our resources.

The authors mention that a power-curtailment program became necessary in the spring and early summer of 1948. During the 2-year period 1947-1948, the system-peak demand increased some 400,000 kw over the 1946 peak. Subnormal rainfall during this same period greatly reduced hydro generation and increased irrigation pumping load. During the actual curtailment, the load on the power system was 28 per cent greater than for the same period the preceding year, and in certain irrigation areas 400-1800 per cent greater than during the same period of a normal year.

By close co-operation of the power companies in the West, and pooling of their resources, plus effective use of daylight-saving time, the utility companies were able to pull through without interruption of service and with only a minor rationing program for a short period. This is an achievement of which they may be justly proud.

When the interchange agreement with Southern California Edison Company was terminated in December, 1947, some 70,000 kw of firm power obtained from this source had to be replaced with new steam-generating facilities. However, the first new 75,000-kva unit at Kern near Bakersfield did not go on the line until May 10, 1948, so it was fortunate that the Southern California Edison Company continued to supply power on a nonfirm basis after the expiration date of the firm power agreement.

The paper clearly brings out that irrigation pumping is an ever-increasing portion of the system load. This accounts for the August peak being equal to the December peak in a normal year, and will even exceed it in a dry year. The load factor for the July-August peak is 73-74 per cent, and for the December peak 62-63 per cent.

Centralized control of steam plants has considerable merit from an economic point of view. Reducing the operating force in a steam plant by one man per shift, effects a net annual saving of \$15,000. Such a saving will justify a capital expenditure of about \$120,000 for laborsaving features and devices.

We have stated that the peak-load curve shows an average annual increase of a little more than 6 per cent. Some time in the future the shape of this curve must change, or the power company would have to double its capacity every 12 years. Experts claim there is a definite relationship between the amount of rainfall in a certain area and the number of people that area can support. According to this theory, the saturation point for the State of California is between 23 and 32 million people. Therefore one might venture to guess or predict that the peak-load curve will continue at the present slope for another 12 years.

The Design of Sewaren Generating Station and No. 1 Unit at Essex Station, Public Service Electric and Gas Company

By F. P. FAIRCHILD,¹ NEWARK, N. J.

The author outlines the more important considerations leading to the design of the 100,000-kw unit at Essex and the four-unit Sewaren Generating Station. Outstanding features are semioutdoor boilers at latitude 41°; 1050 F steam temperature; a simplified plant layout, including the unit system; central control; shaft-end house generators; and all-electric auxiliary drive. The improvements in calculated plant heat rates are shown for the progressive steps of the program. Some of the more important electrical and architectural features are described.

THIS paper is concerned primarily with the new Sewaren Generating Station, but inasmuch as the Essex 100,000-kw unit was a definite step in the development of many Sewaren innovations and principles, the two may be considered almost as progressive steps in the same program.

PRELIMINARY STUDIES

The Sewaren site, located on an arm of the ocean between Staten Island and the New Jersey coast in Woodbridge Township, was acquired by the Public Service Electric and Gas Company in 1928. With outlet rights of way it consists of approximately 150 acres, of which 35 acres are used in the present development.

Various studies of the method to be used in developing this site, together with probable capital costs and operating economies, had been made from time to time over a period of years. The essentials of the present layout first were developed in a preliminary way the latter part of 1944, at which time consideration was also being given to the removal of an old 22,500-kw unit at Essex, and the substitution of a 100,000-kw, 3600-rpm, modern unit in its place.

Early in 1945, construction of a simple model of a unit station with semioutdoor boilers was begun. The purpose of this model was to provide better visualization of the unit principle of generating-station design, and looking toward Sewaren in particular, it also incorporated outdoor-boiler-plant design and two-level operation. This preliminary model proved to be of considerable use in discussions with the operating department, executives, and others.

GENERAL DESCRIPTION—ESSEX PROJECT

In March, 1945, the work at Essex Generating Station in Newark, N. J., was authorized. The capacity situation was uncertain at the time, but the installation was justified by economies to be obtained which amounted to an annual saving of about 16 per cent of the estimated cost of the installation. The final completed cost was roughly \$9,300,000.

¹ Chief Engineer, Electric Engineering Department, Public Service Electric and Gas Company. Mem. ASME.

Contributed by the Power Division and presented at the Semi-Annual Meeting, San Francisco, Calif., June 27-30, 1949, of THE AMERICAN SOCIETY OF MECHANICAL ENGINEERS.

NOTE: Statements and opinions advanced in papers are to be understood as individual expressions of their authors and not those of the Society. Paper No. 49-SA-15.

It was decided to go ahead with the Essex installation with one boiler and one turbine, and to adopt all features of a complete unit system, namely, one boiler and one turbine generator with a shaft-end generator to carry all essential auxiliaries, without any cross-connections tying into other units in the station. Central control was also adopted as far as was possible in this installation.

Essex embodied a considerable advance in the design of 3600-rpm turbines and generators. The turbine was the first 3600-rpm machine to use 23-in. buckets. These buckets were put through very thorough tests in a special test wheel before installation on the spindle.

Prior to the Essex installation, the largest 3600-rpm generator in existence was rated 65,000 kw. The Essex main generator was rated 95,000 kw and in addition to being the largest generator at that time, it was also the first to be designed for a hydrogen pressure of 25 psi.

Forced- and induced-draft fans, air preheaters, and flue-dust collectors were placed above the boiler, out of doors. For this outdoor service the manufacturers, in co-operation with Public Service engineers, developed fans with air-cooled bearings, large motors of the totally enclosed fan-cooled type, and air-to-oil coolers for hydraulic couplings, to eliminate water-cooling connections of any kind. In the interest of simplicity and the reduction of make-up, it was decided to omit the usual auxiliary steam header. This departure involved the development of a motor-driven condenser air removal pump, a satisfactory substitute for the usual steam-driven auxiliary oil pump of the turbine, the use of air soot blowing, and the elimination of the reserve steam-driven boiler feed pump. Commercial operation of the Essex unit started in December, 1947.

GENERAL DESCRIPTION—SEWAREN PROJECT

On January 21, 1946, authorization was given for the construction of a generating station at Sewaren, consisting of two 100,000-kw units to operate at 1500 psi and 1050 F. These units were required to meet the system load as forecast for 1948. Substantial operating savings were indicated. These two units started commercial operation at the end of November, 1948. A time-table of important dates concerning these two units appears in Table 1.

A third Sewaren unit was authorized January 9, 1947, because of the rapid growth of load on the system. This unit is scheduled to operate in the fall of 1949. It is a twin of the second unit.

On December 11, 1947, funds were appropriated for the purchase of the fourth turbine generator with step-up transformers at Sewaren, in order to obtain shipment early in 1951. No. 4 is similar to the first three units except that it will be rated at 125,000 kw, and will operate with reheat to 1000 F. Prior to this time a 100,000-kw nominal rated turbine generator was the largest 3600-rpm single-shaft machine available. Studies indicated that the larger equipment can be installed in the space provided for the fourth unit without crowding, and that substantial fuel savings will result from the improved efficiency of the reheat cycle.

TABLE 1 TIME-TABLE TO DESIGN, BUILD, AND ERECT FIRST TWO 100,000-KW UNITS AT SEWAREN GENERATING STATION

	Starting dates
Design.....	Jan. 1946
Purchases:	
Turbine generators.....	March 1946
Boilers.....	May 1946
Erection in field:	
Excavation.....	Jan. 1947
Pile driving.....	March 1947
Concrete.....	May 1947
Structural steel.....	July 1947
Boiler:	
No. 1.....	Oct. 1947
No. 2.....	Nov. 1947
Turbine generator:	
No. 1.....	May 1948
No. 2.....	June 1948
Commercial operation:	
Unit No. 1.....	Dec. 1, 1948
Unit No. 2.....	Nov. 30, 1948

The present estimated unit cost of the four-unit station is \$132 per kw for name-plate conditions. This includes all electrical equipment to the high-voltage side of the transformers.

The approach to the basic design of Sewaren was the same as Essex, namely, to develop the unit system to the greatest extent practicable. Here, however, as architectural and structural limitations did not exist, it was possible to accomplish much more in this direction. The Sewaren design makes use of all the features developed for Essex plus two-level operation, semioutdoor boilers, and central control of units in pairs.

SEWAREN PLANT ARRANGEMENT COMPARED TO ESSEX

The Essex unit was installed in the area occupied for 32 years by a 22,500-kw turbine generator and four boilers. Fig. 1 is a view of the Essex turbine room with the new unit in the foreground. No. 2 unit, next to it, is a twin of the original No. 1. The new equipment was arranged to suit the building; whereas at Sewaren, the building was designed to accommodate the equipment. The cross sections of the two plants show this difference. At Essex, Fig. 3, on account of limited floor area,

the fans, air preheaters, flue-dust collector, and stack are above the boiler; coal is brought from the existing bunker by conveyor to a hopper which feeds the pulverizers.

In contrast to this, the Sewaren auxiliary equipment is laid out as near ground level as possible, Fig. 2. The circulating-water pumps are at the screen well; the fans, air preheaters, and dust collectors are out of doors; the stacks are on separate foundations; the pulverizers are placed under the coal bunker. The plant is spread out horizontally.

SEMIOUTDOOR BOILERS

The Sewaren boilers are of the semioutdoor type in which the building encloses the front and one side of each boiler. The exterior of the boilerhouse is shown in Fig. 4. The form of the building in the vicinity of the boilers is shown more clearly in the simplified sketch, Fig. 5. This type of construction saved about \$1,000,000 in first cost of three units. Because of the smaller building volume and reduced heat radiation in the boilerhouse, the building is easier to ventilate and keep clean.

Boiler overhauls will be on an annual basis and will be scheduled for warm weather. By far the greater portion of the boiler-maintenance work is performed inside the boiler furnace, gas passes, and boiler drums. Arrangements have been made to keep the inside of the furnaces and gas passages warm during winter shutdowns, not only for maintenance work but also to prevent freezing of the superheaters.

BOILER DESIGN

The designs of the Essex and Sewaren steam-generating equipment are particularly adapted to each plant layout. At Essex, where the limitation was floor area, the steam generator and its auxiliaries occupy an area of about 70 ft × 60 ft. Coal hopper, pulverizers, coal piping, and burners are fitted compactly under the superheater, economizer, and uptake duct. Coal is brought from the station bunker to the hopper by conveyers.

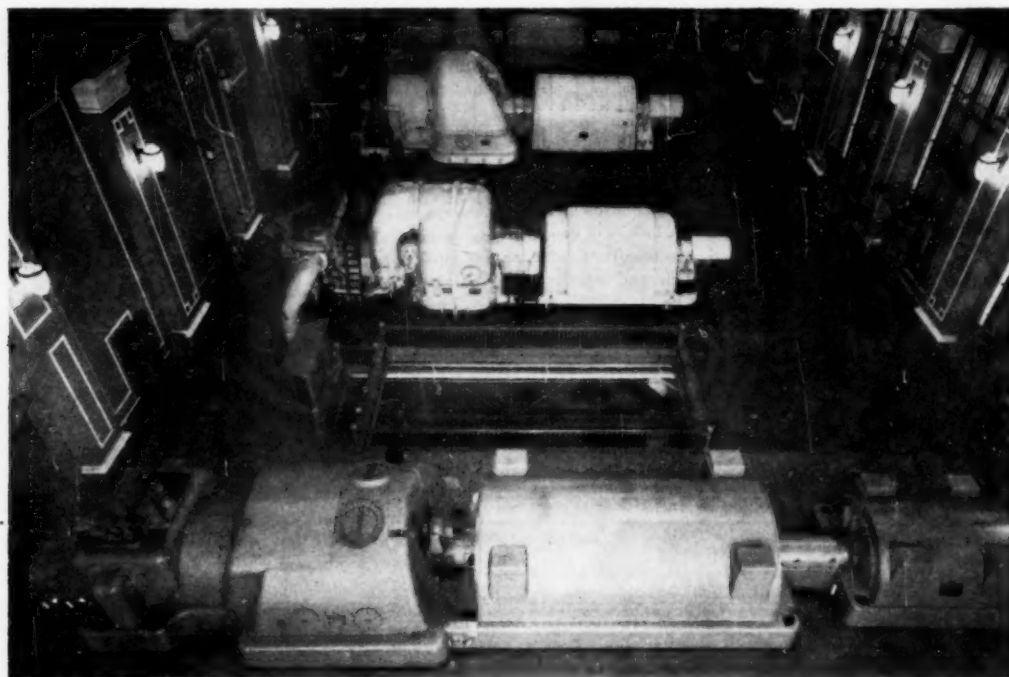


FIG. 1 TURBINE GENERATOR OF 100,000 KW INSTALLED AT ESSEX IN AREA FORMERLY OCCUPIED BY 22,500-KW TWIN OF ADJACENT UNIT

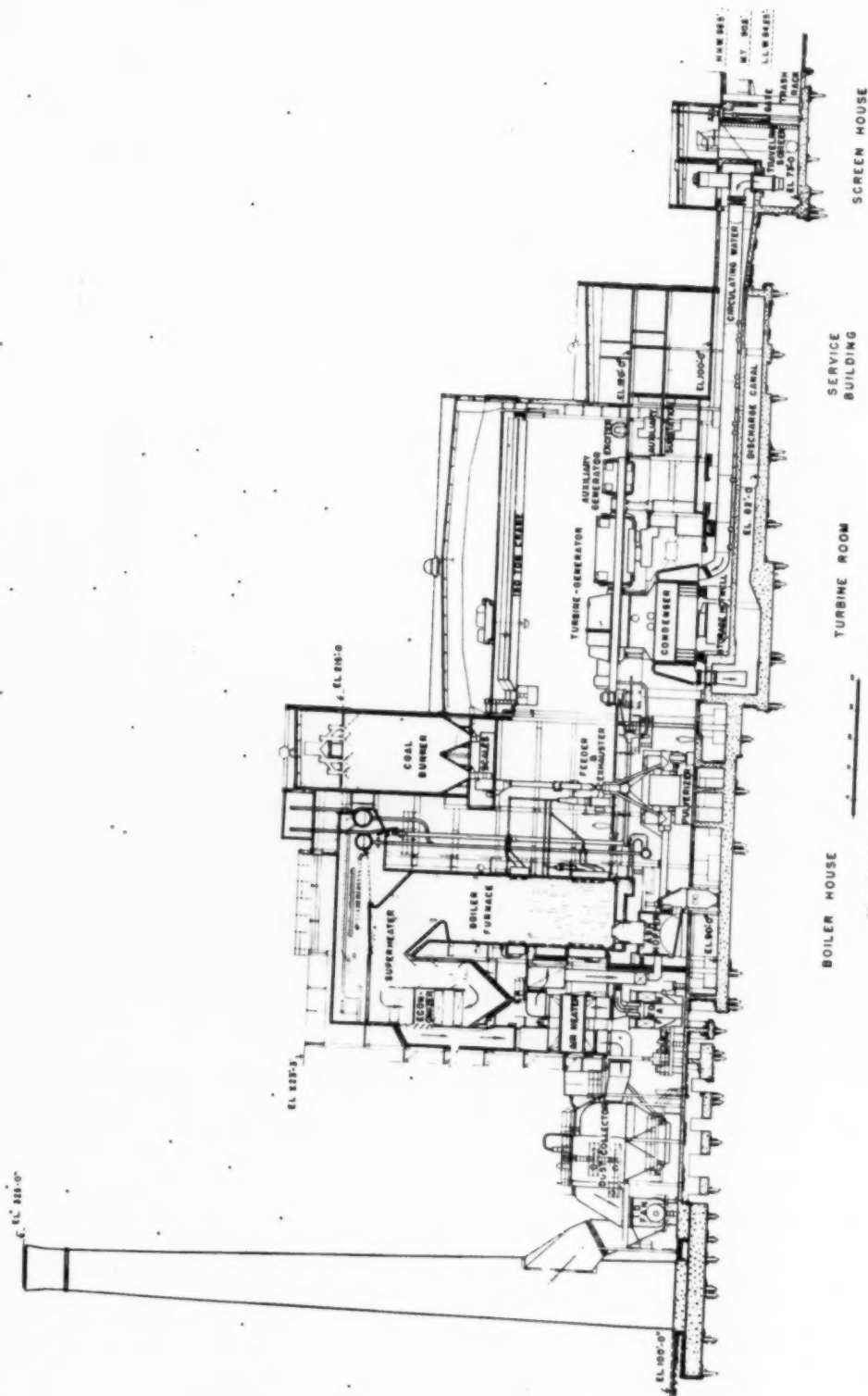
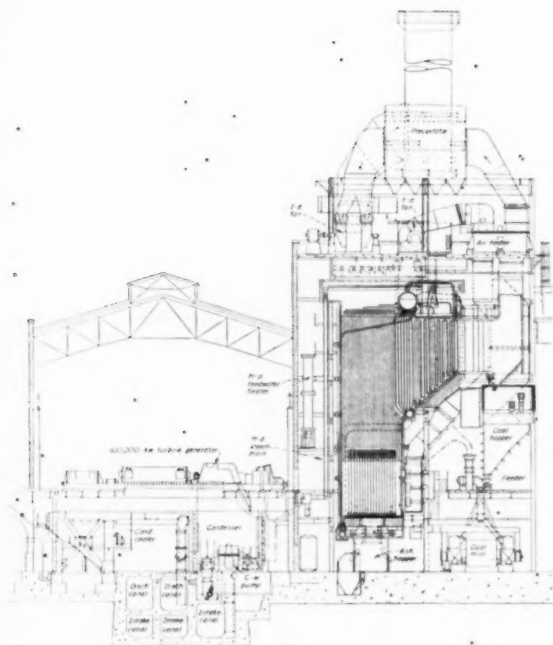


Fig. 2 Plant Cross Section, No. 2 Unit—Sewaren



The Essex boiler, Fig. 6, is a two-drum radiant type, having a continuous rating of 900,000 lb per hr and a maximum rating of 1,000,000 lb per hr for 4 hr with throttle conditions of 1250 psi and 1000 F. The slag-tap furnace, which has a volume of 47,800 cu ft, is divided into two equal volumes by a center waterwall having interconnecting ports in the flame area. Three horizontal ball-type pulverizing mills serve the twelve combination pulverized coal-mechanical atomizing oil burners. Outlet steam temperature is controlled by means of a spray-type attenuator placed between the two sections of the superheater. Auxiliaries include two forced- and two induced-draft fans, two Ljungström air heaters, an economizer, and an electrostatic dust collector.

At Sewaren, where the design objectives included the semi-outdoor feature, two-level operation, and the utmost simplicity, the area occupied by the steam generator and auxiliaries is roughly 160 ft \times 50 ft, about twice the area used at Essex. The drums and superheater outlet header are offset from the furnace so that they are housed in the building. This facilitated the semioutdoor design of the boilerhouse.

Each of the first three Sewaren boilers, Fig. 7, is of the three-drum, radiant type, having a continuous rating of 850,000 lb per hr, and a maximum of 950,000 lb per hr for 4 hr with throttle conditions of 1500 psi and 1050 F. The slag-tap furnace, which has a volume of 52,450 cu ft, is arranged for tangential corner firing at two levels, with combination pulverized-coal and oil burners vertically adjustable to permit positioning of the turbulent burning zone in order to obtain optimum slagging conditions on the walls and floor of the furnace and to effect a certain amount of superheat control. Final steam temperature is controlled by a damper which by-passes part of the furnace gases from the primary superheater to the economizer. As at Essex, there are three pulverizers, two Ljungström air heaters, an economizer, and two forced- and two induced-draft fans. The dust collector is a combination mechanical-electrostatic unit, with the mechanical section ahead of the electrostatic.

FIG. 3 (left) PLANT CROSS SECTION,
No. 1 Unit—Essex

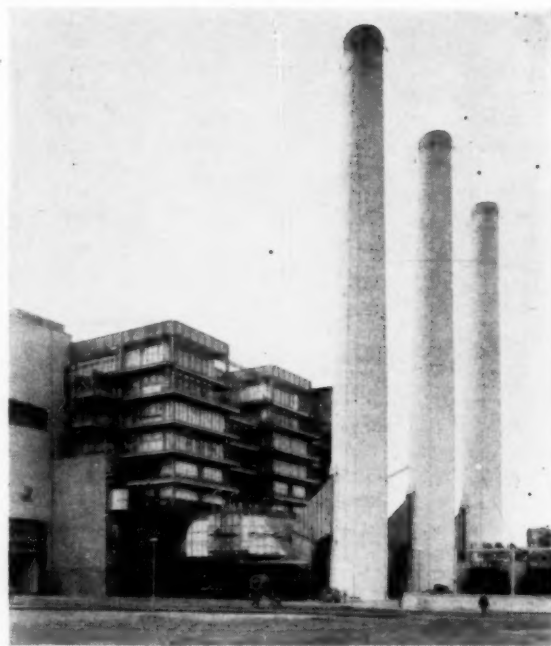


FIG. 4 SEMIOUTDOOR BOILERS—SEWAREN

TURBINE DESIGN AND HEAT RATES

At its best point, the Essex unit has a calculated plant heat rate (based upon turbine guarantees) of 10,400 Btu per net kw-hr. Steam conditions are 1250 psi, 1000 F, and the turbine has a double-flow low-pressure cylinder, Fig. 8. This unit operated 8149 hr of the 8784 hr in 1948 at an average turbine load of about 97,800 kw. The capacity factor was 90.7 per cent. The average heat rate for the year was 10,500 Btu per kw-hr, which is approximately the calculated rate for that load. The average circulating-water temperature was 60.6 F; average back pressure was 1.36 in. Hg. The unit operates regularly at a rating of 110,000 kw.

No. 1 unit at Sewaren is essentially similar to Essex No. 1, except that the steam conditions are increased to 1500 psi and 1050 F. The improvement in heat rate is 4.6 per cent at the best point. This increment includes a one-point improvement

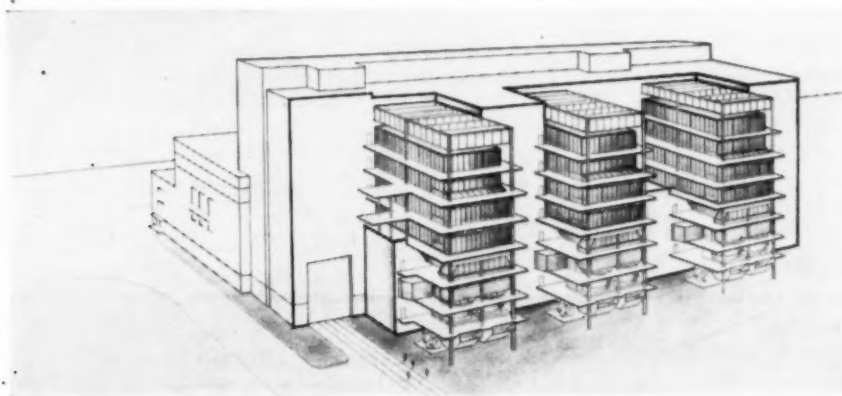


FIG. 5 SKETCH OF EXPOSED PARTS OF BOILERS—SEWAREN

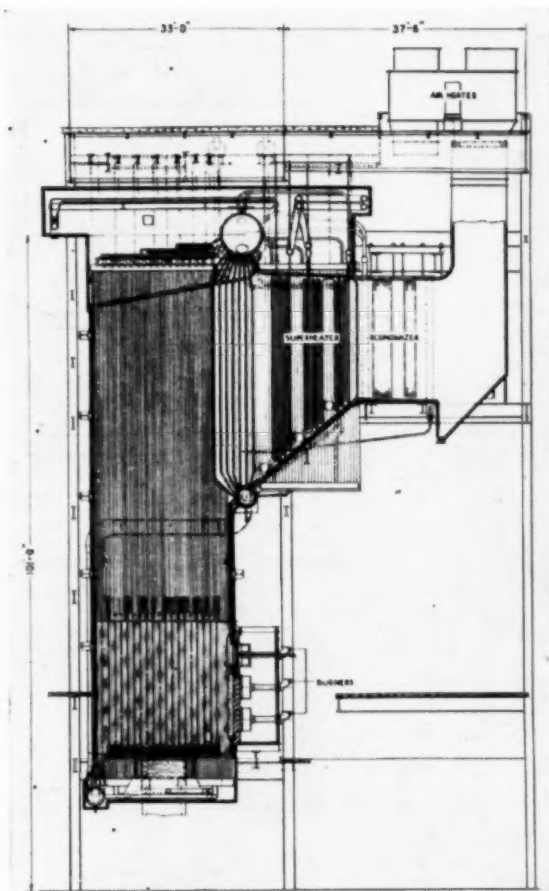


FIG. 6 BOILER CROSS SECTION—ESSEX

in boiler efficiency. The cross section of the turbine is shown in Fig. 9.

No. 2 and 3 units at Sewaren are similar to No. 1 unit except that they have triple-flow low-pressure cylinders. The improvement over No. 1 unit (Sewaren) is 1.4 per cent at the best point. The cross section of the turbine is shown in Fig. 10.

No. 4 unit is similar to No. 2 and 3 at Sewaren except that it is a larger machine, and the steam is reheated to 1000 F. The improvement over No. 2 and 3 units is 4 per cent at the best point, Fig. 11.

The calculated plant heat rates for the units are shown in Fig. 12. The heat-balance diagram for No. 2 and 3 units at Sewaren, Fig. 13, is typical. The system operates without a heater-drain pump. Although the diagram does not show it, the hot-well pump is of the re-entry type. The condensate re-entry is made after passing through the condensate cooler, generator, hydrogen and air coolers, and oil and miscellaneous coolers.

CENTRAL CONTROL

Unit design, with only one boiler per turbine, greatly facilitates central control in a modern electric generating station. For example, the control-panel areas of No. 1 unit at Sewaren compared with the corresponding areas of No. 6 unit at Burlington, a 125,000-kw cross-compound unit with two cross-connected boilers installed in 1943, show some interesting figures. At Sewaren there are 521 sq ft of panel in one location; at Burlington there are 695 sq ft in five separate locations. This concentration of control results in better co-ordinated operation and a reduction in operating attendance.

The arrangement of the control panel at Essex is shown in Fig. 14. Care was taken to make it short so that the operator can see the maximum number of instruments and can reach the greatest number of controls with the least movement. Instruments and controls of lesser importance were placed on the end of the panel wings to make room for the more essential items on the front and center of the panel. While there is no distinct separation between boiler, turbine, and auxiliary boards, the controls are placed on the panels in relative arrangement similar to that of the equipment controlled. The board is arranged so that, in the future, it can be enclosed in a separate room. The plan of the Essex operating floor, Fig. 15, shows the location of the control board. In this installation the generator and electrical auxiliary supply controls were located in an existing electrical control room.

The two Sewaren control rooms are tee-shaped, with the electrical benchboard, Fig. 16, forming the crossbar. The operator sees the two turbine generators through windows just above the benchboard. The other sides of the room, Fig. 17, are occupied by the panels controlling the turbines, boilers, and their auxiliaries. At the rear, there are two windows looking toward the boilers. There are three operators in the control room. Normally, one operates the electrical benchboard of two

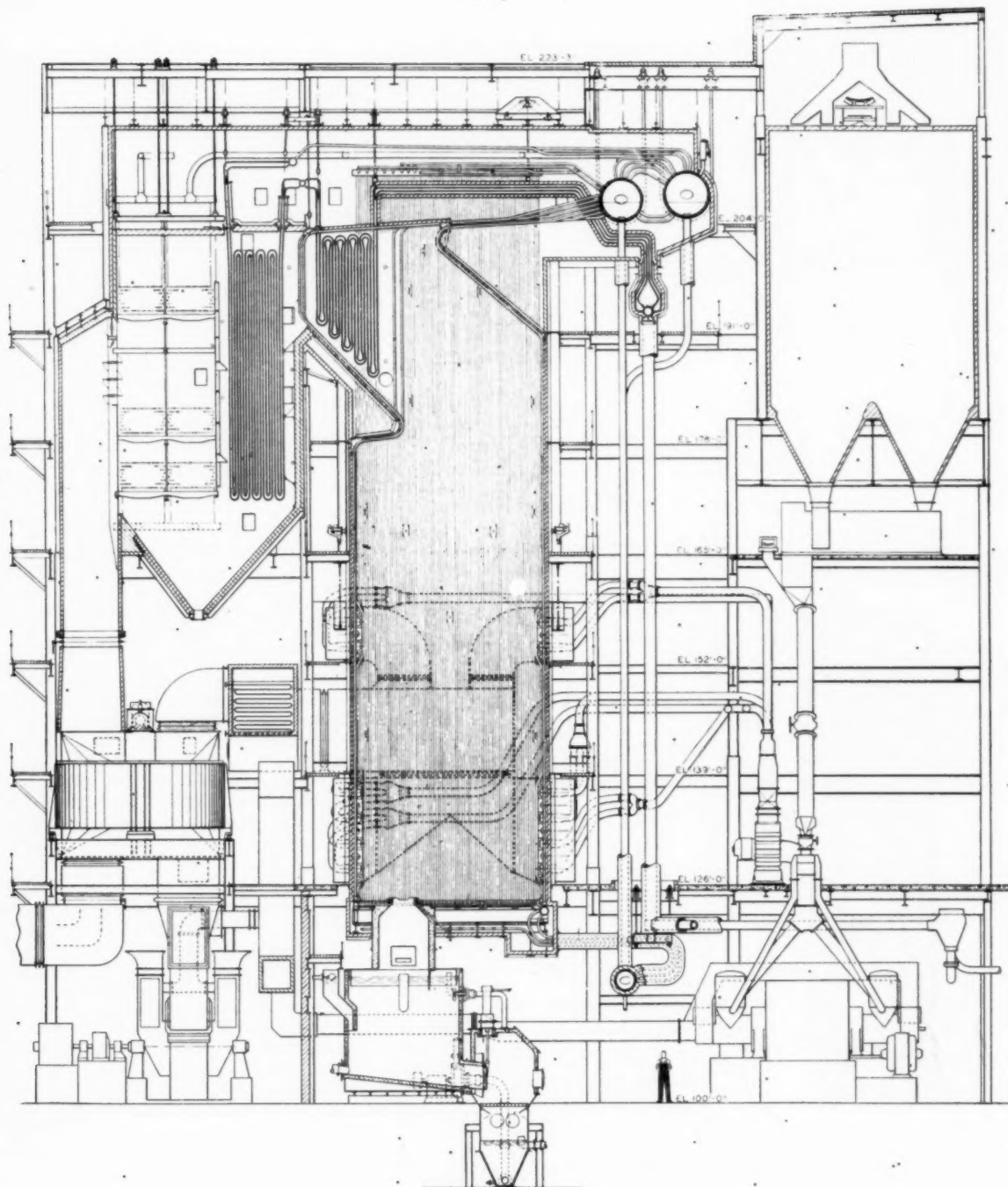


FIG. 7 CROSS SECTION, NO. 1, 2, AND 3 BOILER. —SEWAREN

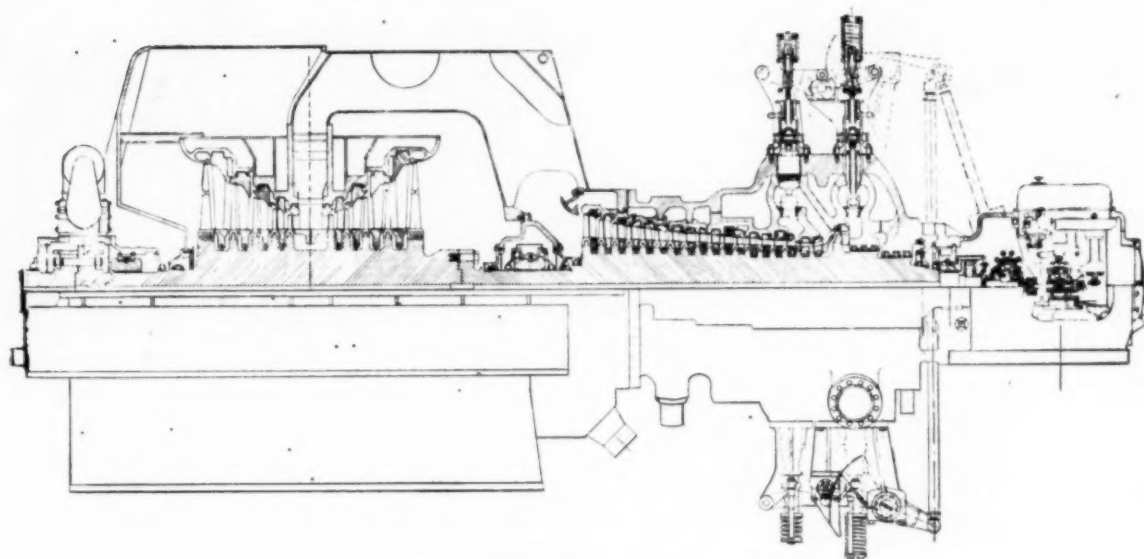


FIG. 8 TURBINE CROSS SECTION—ESSEX

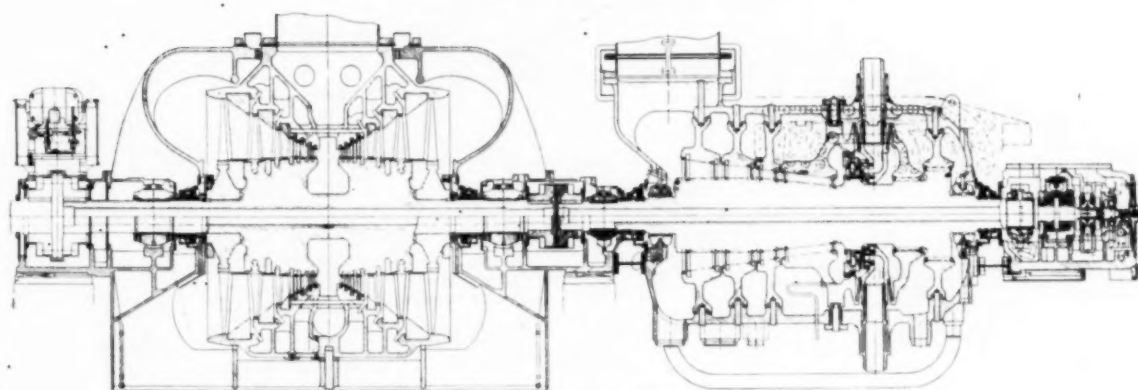


FIG. 9 CROSS SECTION, NO. 1 TURBINE—SEWAREN

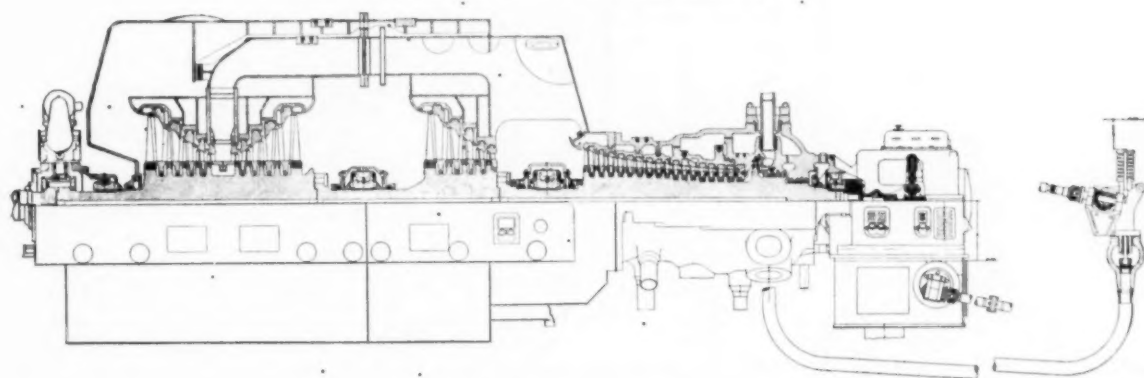


FIG. 10 CROSS SECTION, NO. 2 AND 3 TURBINES—SEWAREN

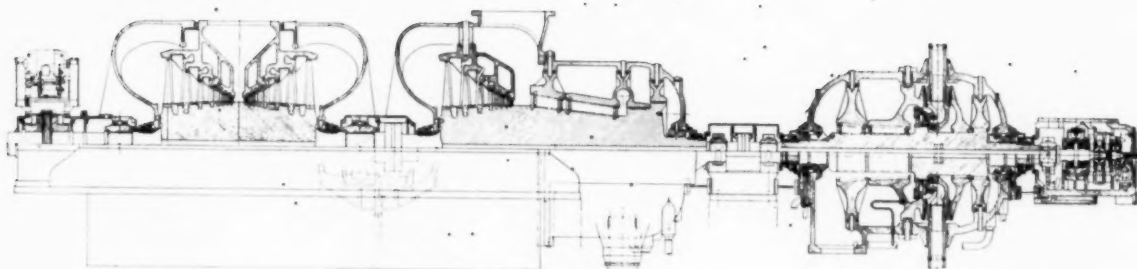


FIG. 11 Cross Section, No. 4 Turbine—Sewaren.

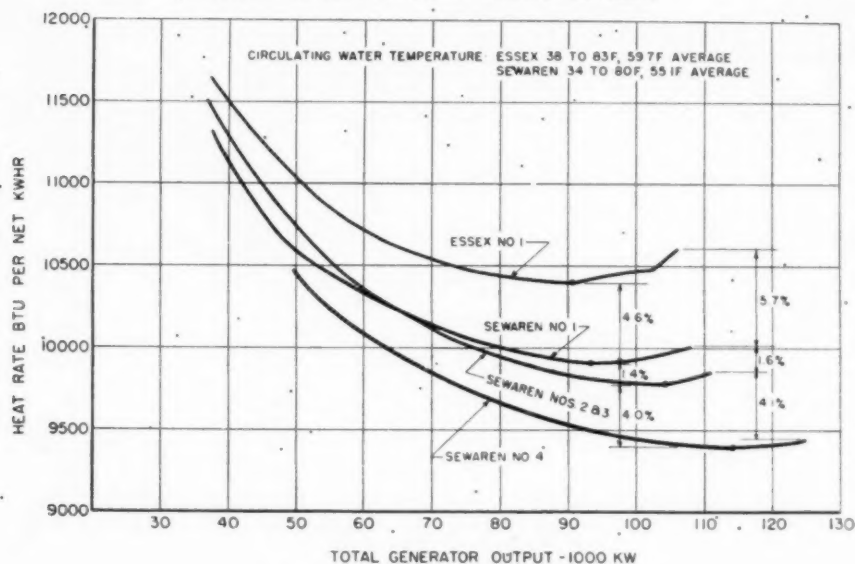


FIG. 12 Calculated Plant Heat Rates

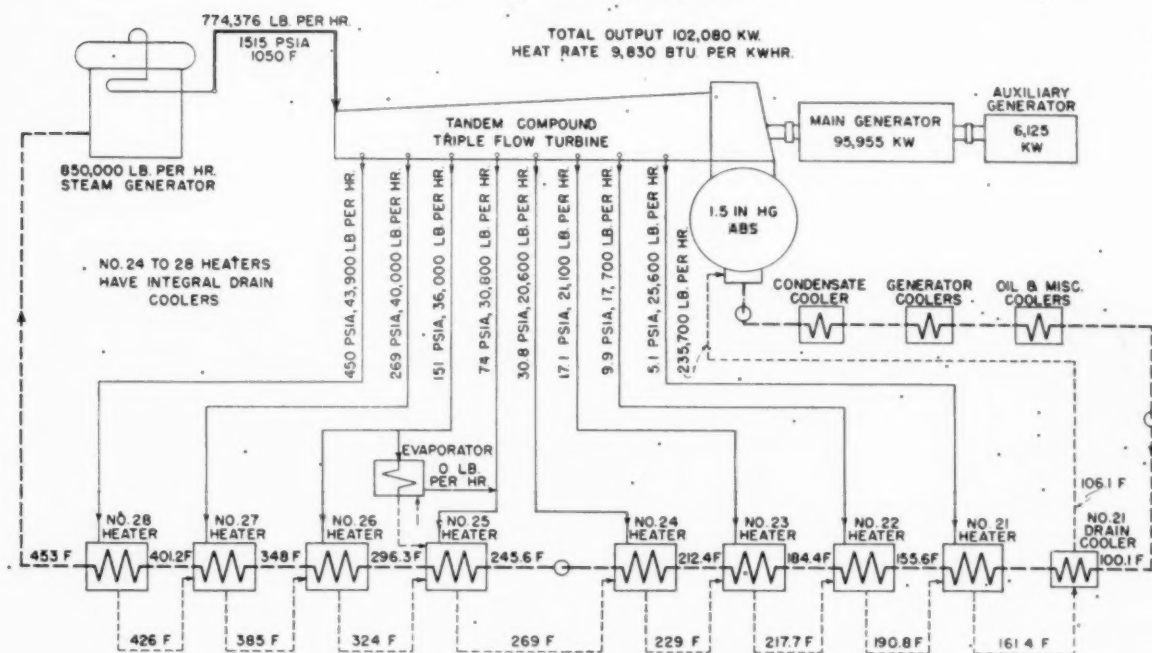


FIG. 13 Heat-Balance Diagram, No. 2 and 3 Units—Sewaren

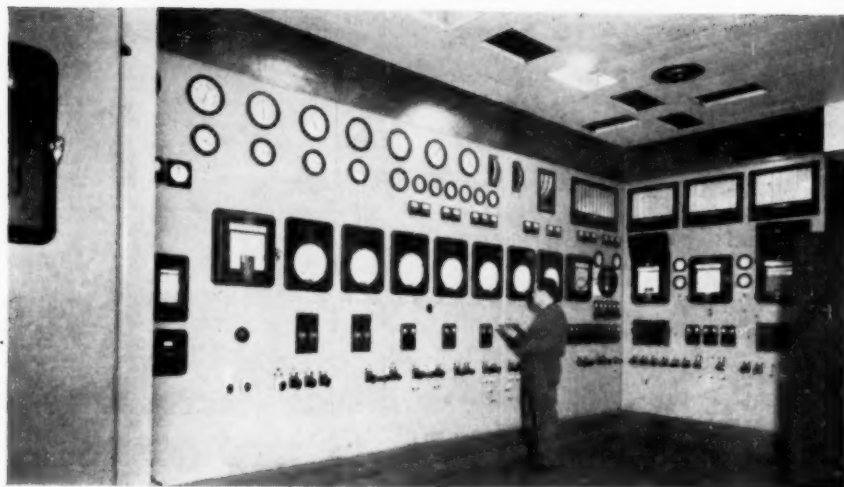


FIG. 14 ESSEX CONTROL PANEL

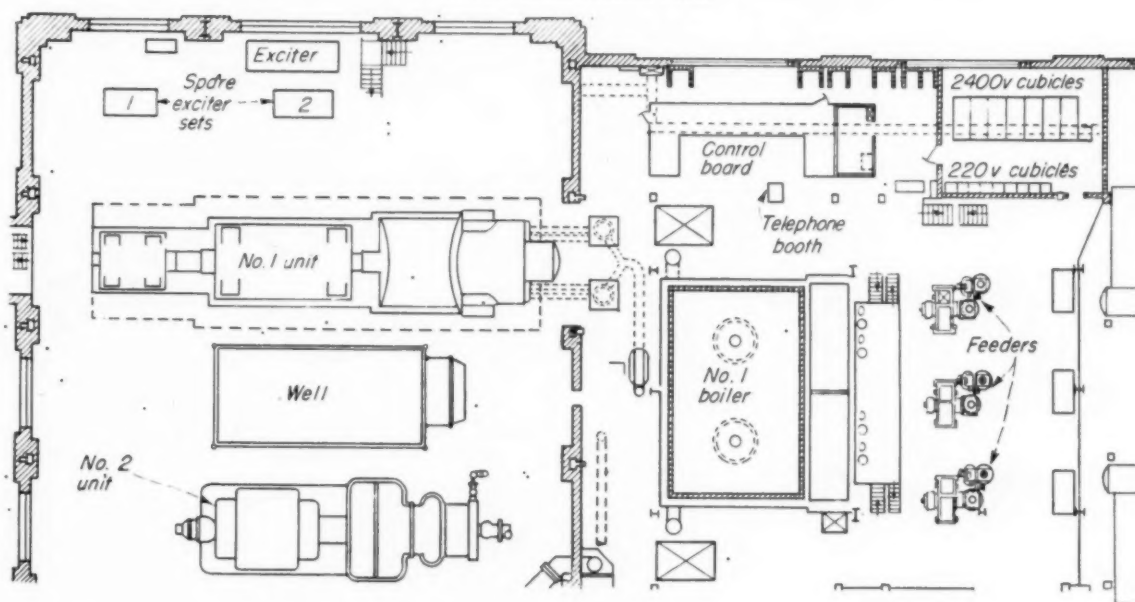


FIG. 15 PLAN OF MAIN OPERATING FLOOR—ESSEX

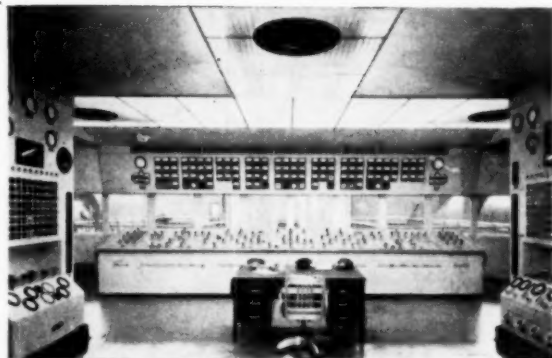


FIG. 16 ELECTRICAL SECTION OF SEWAREN CONTROL ROOM

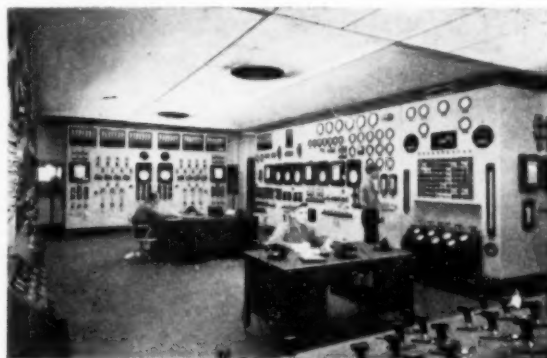


FIG. 17 MECHANICAL SECTION OF SEWAREN CONTROL ROOM

units, and each of the other two operates the mechanical equipment of one unit. However, the operators are trained to handle both mechanical and electrical controls, and, at present, each one rotates around the three operating jobs in the control room. The control rooms are air-conditioned and soundproofed. Special attention was given to the lighting, particularly of the vertical panels, for which totally indirect lighting is provided by means of a cove and arched-ceiling design. In the areas between sections of arched ceiling, vinylite eggerate plastic was used to provide a luminous ceiling, which avoids the contrast between lighted and unlighted areas which a solid ceiling would have given. The final design was the result of studies made of a mock-up, erected in the basement of the Public Service Terminal Building in Newark, N. J.

Each control room is situated at the center of the area occupied by the main equipment under its supervision, Figs. 18 and 19.

HIGH-TEMPERATURE PARTS

The steels used in the pressure parts exposed to the highest-temperature steam are listed in Table 2.

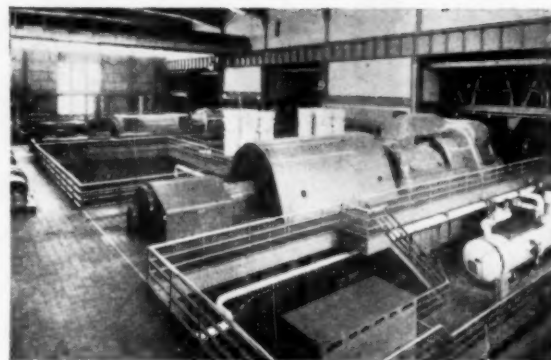


FIG. 19 NO. 1 AND 2 TURBINE GENERATORS AND CONTROL ROOM—SEWAREN

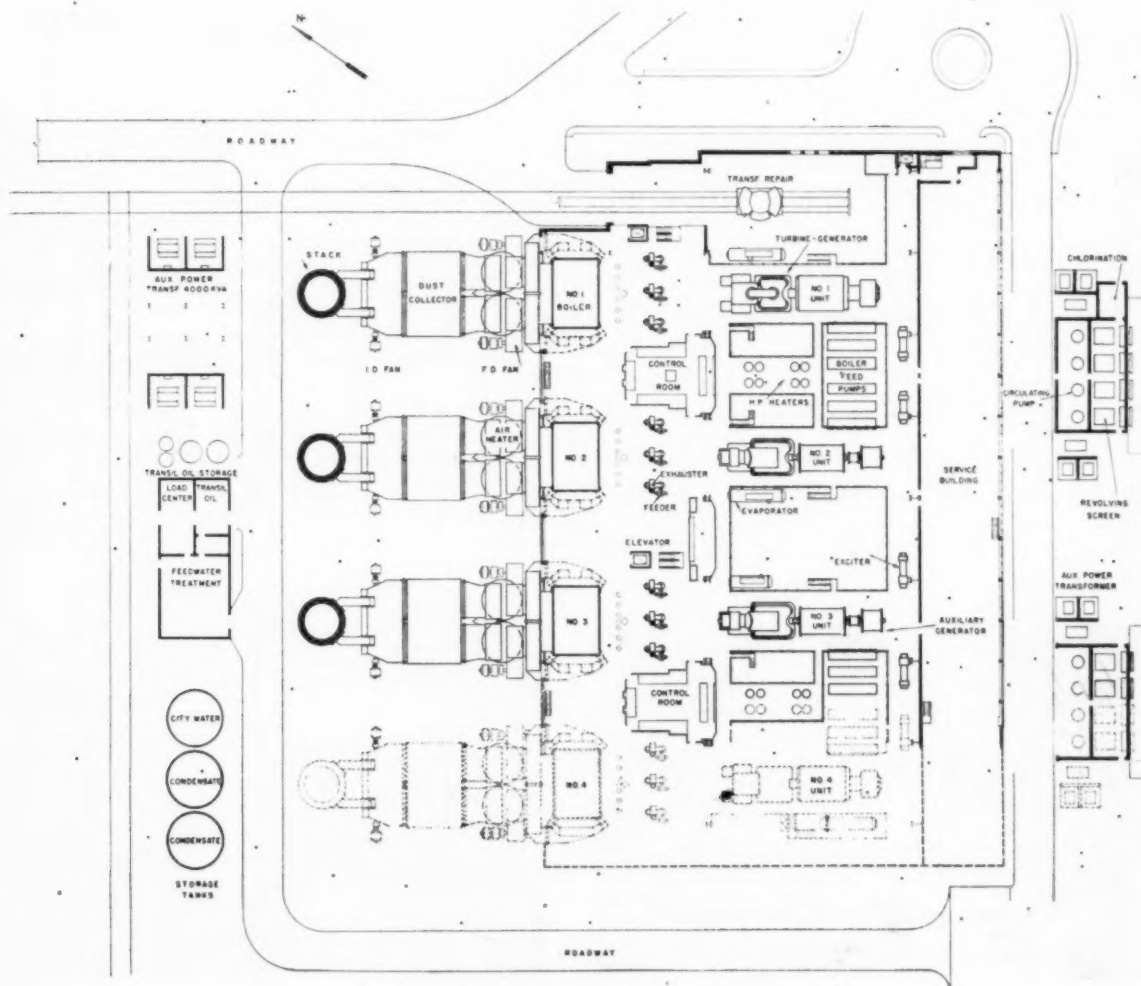


FIG. 18 PLAN OF UPPER OPERATING FLOOR—SEWAREN

TABLE 2 STEELS USED IN PRESSURE PARTS EXPOSED TO HIGHEST-TEMPERATURE STEAM

	Essex	Sewaren	
	No. 1 1000 F	No. 1 1050 F	No. 2 and 3 1050 F
Superheater tubes . . .	9 Chromium 1.3 Molybdenum	19 Chromium 11 Nickel Titanium stabilized	19 Chromium 11 Nickel Titanium stabilized
Steam piping	2 1/4 Chromium 1 Molybdenum	3 Chromium 1 Molybdenum	3 Chromium 1 Molybdenum
Turbine valves	0.14 Vanadium 1.1 Molybdenum	18 Chromium 8 Nickel Columbium* stabilized	17 Chromium 14 Nickel 2 Molybdenum Columbium stabilized
Turbine cylinder	0.14 Vanadium 1.1 Molybdenum	2 1/4 Chromium 1 Molybdenum	17 Chromium 14 Nickel 2 Molybdenum Columbium- stabilized
Turbine buckets	12 Chromium	13 Chromium	12 Chromium 5 Cobalt 3 Tungsten 0.15 Molybde- num

NOTE: All compositions given in per cent of alloying materials.

At Sewaren, each unit has two welded joints between the austenitic steel of the stop valves and the ferritic steel of the steam piping. As the stainless steel expands about 50 per cent more than the chrome-moly steel in the range from 70 to 1050 F, there was some concern about the adequacy of a welded joint between the two metals in heavy wall thickness. With the co-operation of the boiler, turbine, and pipe suppliers, a cyclic-heating test was made on several full-size, heavy-wall, welded pipe joints between austenitic and ferritic steels. This test has been des-

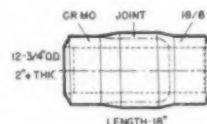


FIG. 20 KELCALOY TRANSITION PIECE

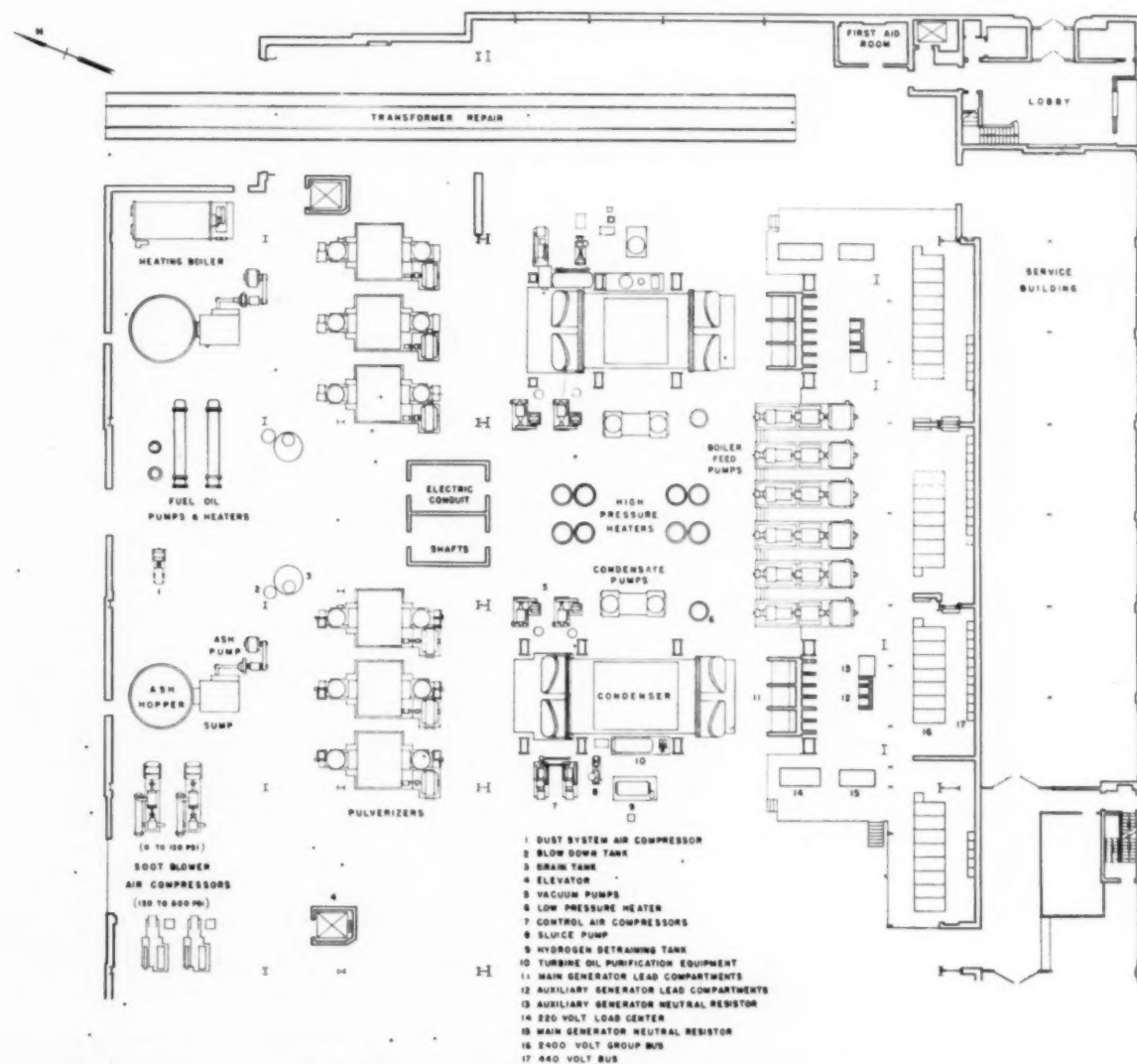


FIG. 21 PLAN OF LOWER OPERATING FLOOR—SEWAREN

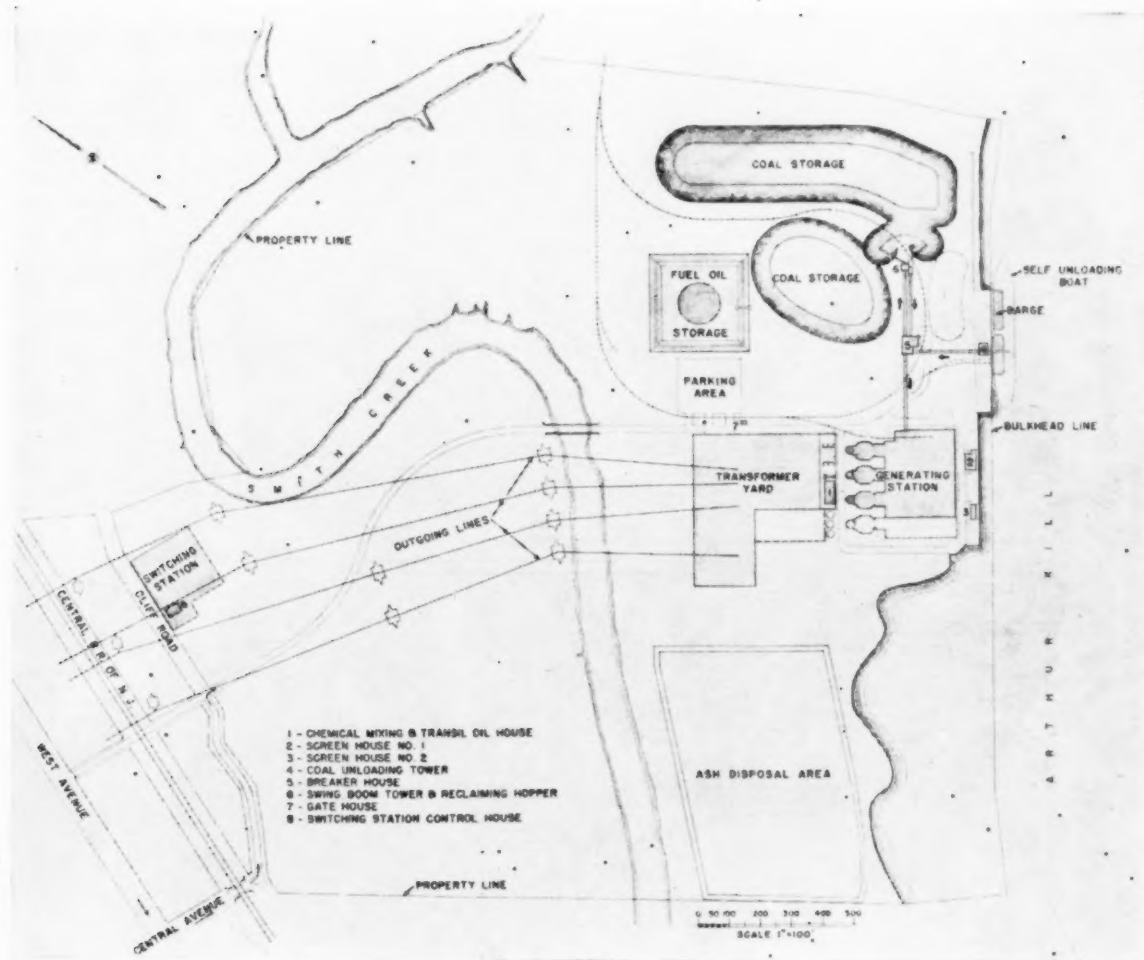


FIG. 22 SEWAREN PROPERTY MAP

cribed fully by H. Weisberg.² The Kelcaloy transition piece finally selected is shown in Fig. 20. The purpose of this arrangement is that the major portion of the interface between the dissimilar metals is longitudinal to the pipe rather than transverse, and therefore is subject principally to shear stress resulting from internal pressure or bending. If failure occurs at the joint between the two metals it should appear as a lap or lamination rather than as a separation straight across the pipe. The transition piece is welded to the stop valves in the shop, leaving a ferritic weld to be made in the field.

The spindles of the stop and control valves of No. 2 and 3 turbines at Seward are cooled with steam from the intermediate header of the superheater. No. 1 turbine valves are not provided with any cooling arrangement.

AUXILIARY POWER

Shaft-end auxiliary generators are used to provide the essential auxiliaries with a direct source of power free from outside dis-

turbances. Normally, each auxiliary generator carries the essential auxiliaries of its own unit. It is rated 7500 kw at 2400 volts, 80 per cent power factor, and is separately excited. The 2400-volt auxiliary buses of each unit can be fed either from the auxiliary generator or from auxiliary transformers connected to an outside source. The two are never paralleled. Relays are installed to throw over automatically from generator to transformer in case of loss of voltage on the generator. Manual throw-over in the other direction is provided for transferring auxiliaries from transformer to auxiliary generator when starting up.

AUXILIARIES

Steam from the high-pressure boilers is used only to run the main turbines. All auxiliaries are electric-motor-driven. At Seward, steam for heating fuel oil, mixing chemicals, and heating the building is supplied normally from the evaporators. There is a heating boiler for use in the event of a complete station shutdown. Every effort has been made to reduce make-up to a minimum.

With the shaft-end auxiliary generator as the source of auxiliary power, the elimination of steam-driven auxiliaries becomes a relatively easier step in station design. One of the problems in

² "Cyclic Heating Test of Main Steam Piping Joints Between Ferritic and Austenitic Steels, Seward Generating Station," by H. Weisberg, Trans. ASME, vol. 71, 1949, pp. 643-664.

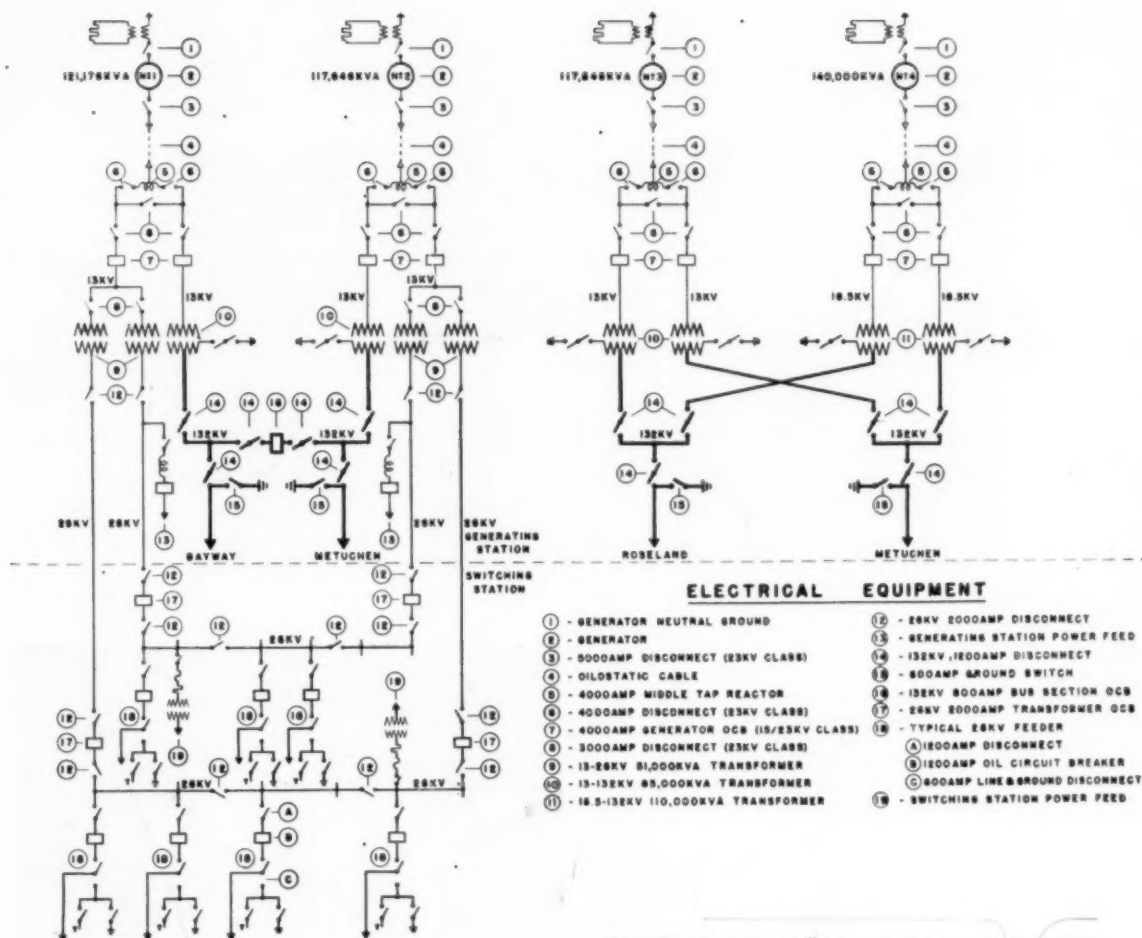


FIG. 23 ULTIMATE CONNECTION DIAGRAM OF THE FOUR SEWAREN GENERATORS

this connection was the substitution of motor-driven, positive-displacement, rotary vacuum pumps for the usual steam-jet ejectors for the removal of noncondensable gases from the condenser.

Before proceeding with this new departure, a Kinney pump of this type was tried out on No. 10 condenser at Marion Generating Station for about 1000 hr. This test revealed that most of the troubles were related to separating the lubricating oil from the water vapor associated with the gases coming from the condenser air coolers. As these difficulties appeared to be surmountable, it was decided to use Kinney pumps at Essex because they offered the following advantages over the steam-jet air pumps: (a) Sufficient capacity at low vacuum to eliminate the need of starting evactors; (b) adaptability to remote push-button starting and stopping; and (c) more complete removal of corrosive gases such as ammonia and carbon dioxide from the system, as there are no inter- and after-condensers (or, alternatively, no wastage of condensate to get rid of these gases).

It was evident after a few months' operation of the Essex pumps that they would do the job and, accordingly, orders were placed for the Sewaren pumps. Operating experience to date has confirmed the expectation of satisfactory operation.

The traditional steam-driven auxiliary oil pump of the turbine

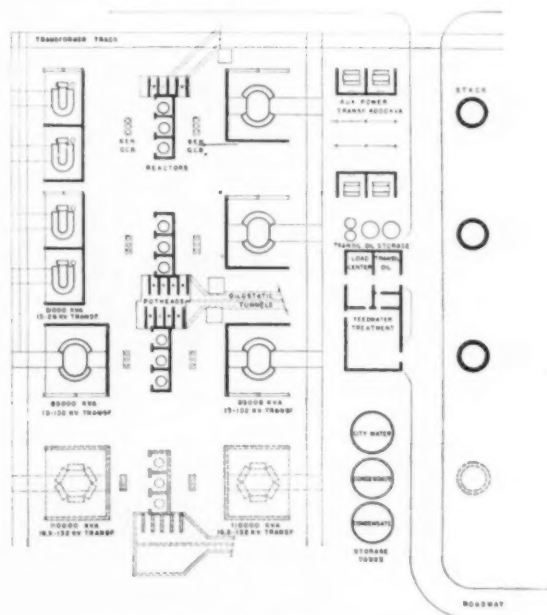


FIG. 24 PLAN OF TRANSFORMER YARD—SEWAREN

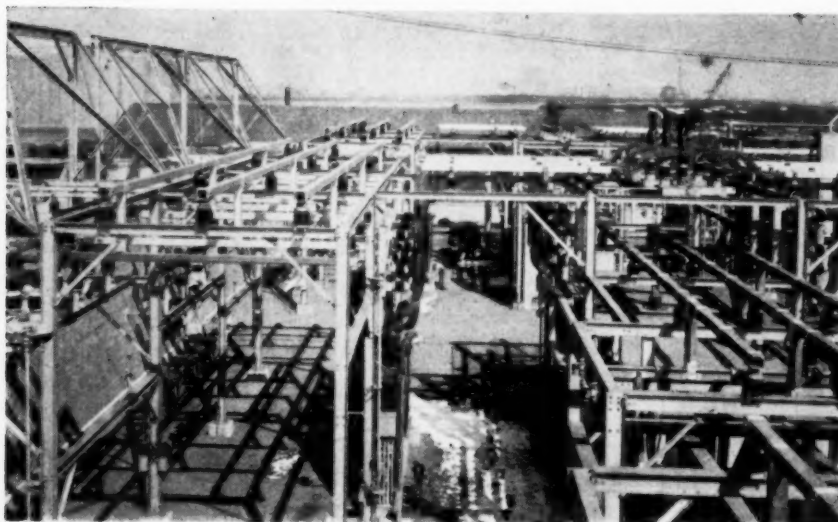


FIG. 25 13-KV ALUMINUM BUSES AT SEWAREN

generator was replaced by a full-capacity alternating-current motor-driven pump, backed up by a smaller direct-current motor-driven pump operating from the station battery. This latter pump has sufficient capacity to bring the turbine-generator to a stop if both main and auxiliary pumps should fail.

The arrangement of auxiliaries at the lower operating level of Sewaren is shown in Fig. 21. This plan, which includes only the first two units, is typical for the second pair.

FUEL HANDLING AND STORAGE

Sewaren is designed for normal operation with water-borne fuel. The plan of the property, Fig. 22, shows the coal-unloading tower and breaker house, where the coal is sent either to the bunker or to the swing-boom tower for storage by tractor and carry-all. Both the dock and the unloading tower are designed so that in the future the unloading tower could be mounted on wheels and moved along the dock. Coal arriving by rail or reclaimed from yard storage is dropped into track hoppers feeding a conveyor to the breaker house. A 125,000-bbl fuel-oil tank is located north of the main building.

PRINCIPAL ELECTRICAL FEATURES—SEWAREN

The ultimate connections of the four Sewaren generators to the system are shown in Fig. 23. Each generator feeds into the midpoint of a reactor which takes the outgoing current into two channels. All switching is done between the generator and transformer at 13 kv, except for one 132-kv oil circuit breaker which ties together two lines, closing a transmission loop when the station is shut down. The 26-kv circuits feed the area immediately adjacent to Sewaren, while the 132-kv lines connect to the transmission system for utilization in more remote areas. Fig. 24 shows the arrangement of equipment in the transformer yard.

The 13-kv generator leads extend about 500 ft to the transformer yard in 8-in. oilstatic pipes in tunnels on foundation slabs carrying station power and control cables in one case, and transformer track supports in another case.

Placing the oilstatic cables in tunnels enabled the use of forced cooling, by means of which the copper cross section of the conductors was reduced from 12 to 6 million circular mils per phase, thus effecting a saving in cost and permitting the use of small easily handled cables. Forced air is used to cool the pipes in No.

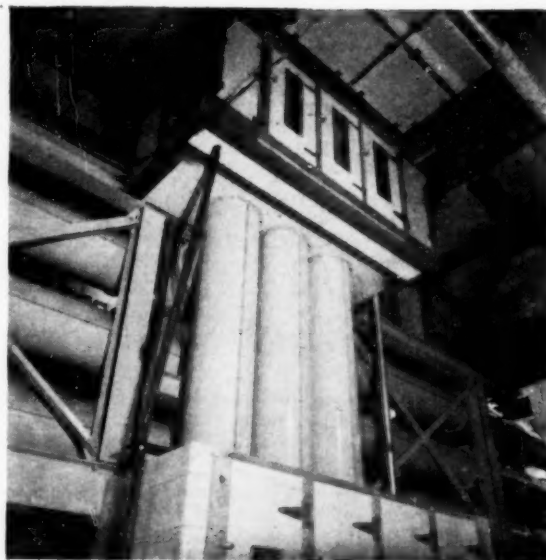


FIG. 26 ISOLATED PHASE BUS LEADS FROM AUXILIARY GENERATOR—SEWAREN

1 and 3 tunnels. For generator No. 2, the oil is circulated in the oilstatic pipe by a pump and gives up its heat in an oil-water heat exchanger. The forced cooling is required only in hot summer weather. Each generator has twenty-four 750,000-circular-mil oilstatic cables, six in each 8-in. pipe.

The aluminum bus¹ was adopted for the transformer yard after a study showed considerable savings in its installation. Fig. 25 shows portions of the square 13-kv aluminum buses. At the left they are tubular and at the lower right they are formed from two angle sections. A large portion of the savings lies in the use of the

¹ "Welded Aluminum Bus in Outdoor Transformer Yard of Sewaren Generating Station," by D. M. Quick, Edison Electric Institute Bulletin, December, 1948.

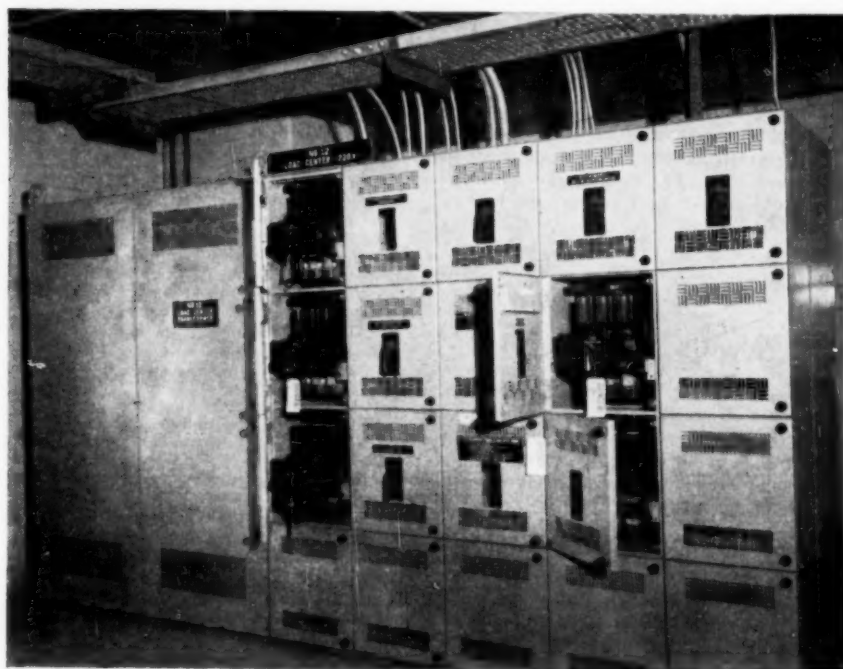


FIG. 27 220-VOLTS LOAD CENTER—SEWAREN

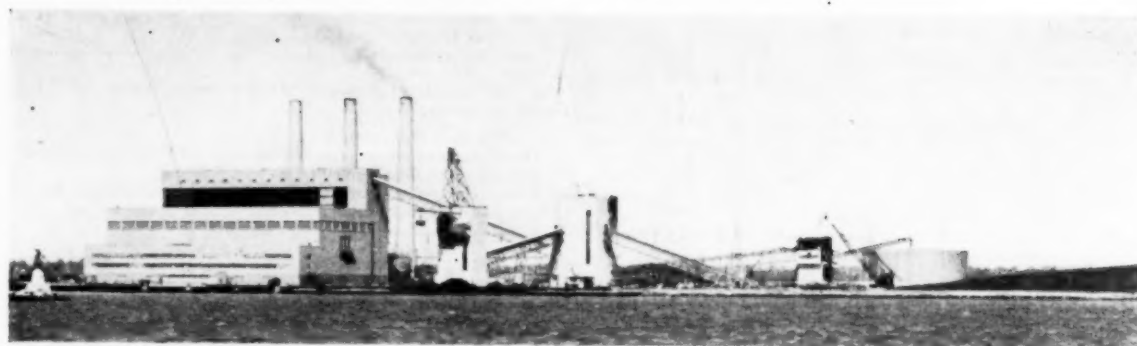


FIG. 28 SEWAREN GENERATING STATION

newly developed inert gas-shielded arc system of welding in lieu of the usual bolted connections. This is the first installation ever made using inert gas-shielded-arc welding on outdoor buses of such heavy cross section.

The isolated phase bus leads coming from the auxiliary generator to the 2400-volt service buses are shown in Fig. 26. A stovepipe bus comes from the main disconnecting switch to a potential transformer compartment and to the cross bus. Toward the right it terminates in a rectangular metal-clad enclosure feeding one of the 2400-volt auxiliary buses.

Motors rated at 200 to 2000 hp are supplied at 2400 volts; those between 25 and 200 hp at 440 volts; while those below 25 hp are fed at 220 volts. These latter motors and the station lighting are supplied by air-cooled transformer load center units located throughout the station, Fig. 27.

Totally enclosed motors have been used to the greatest extent practicable. In addition to the fan motors already mentioned,

all motors for the coal-handling system, boiler feed pumps, and the circulating-pump motors of No. 3 and 4 units, are totally enclosed.

BUILDINGS

The architectural treatment of the buildings is simple and functional, with strong horizontal lines resulting from continuous rows of sash and glass block, Fig. 28. At the permanent end of the turbine room there is a visitors' observation balcony which affords an outside view of the easterly end of the property and an inside view of the turbine room. The main entrance and lobby are at the permanent end of the service building. All the window sash are of aluminum, and the principal entrance doors are of stainless steel.

The turbine-room roof is supported by arched girders rather than by the conventional open-truss construction. The temporary end is covered with corrugated asbestos sheets secured to steel

girls. The coal-handling buildings are enclosed with flat transite sheets.

LIGHTING

A high level of illumination is provided throughout the station in the belief that it will yield dividends in better operation, safety, and general housekeeping. In this connection, special attention was given to the turbine room, Fig. 19. Combination incandescent-fluorescent units are mounted flush against the bottom flange of the roof beams to form a continuous fixture containing sixteen 500-watt incandescent lamps with control lenses, and sixty-four 40-watt fluorescent tubes, about 10 kw of lighting load per beam. Relamping and cleaning are accomplished readily from the top of the crane.

SUMMARY

The objectives in the Sewaren design were straightforward simple arrangement which with central control would simplify operation and make for minimum man power per kilowatt; a reasonably efficient cycle that would not be obsolescent at too early a date; and a simple building construction involving a minimum of maintenance throughout its life.

ACKNOWLEDGMENT

The author gratefully acknowledges the assistance of Messrs. E. H. Snyder, H. Weisberg, and P. A. Salmon, all of the Public Service Electric and Gas Company.

Appendix

PRINCIPAL EQUIPMENT FOR NO. 1, 2, AND 3 UNITS AT SEWAREN

Turbine-Generators and Auxiliaries:

1 Turbine-generator (Westinghouse), having nameplate data as follows:

Steam turbine, rated 100,000 kw, maximum 109,500 kw; initial pressure 1500 psi, initial temperature 1050 F, exhaust pressure 1.5 in. Hg, rpm 3600, 32 stages.

Alternating-current generator, rated 121,176 kva, power factor 0.85, hydrogen pressure 30 psi, frequency 60 cycles, phases 3, voltage 13,100 to 14,500, star connected, speed 3600 rpm.

Auxiliary alternating-current generator, rated 9375 kva, power factor 0.80, air cooled, speed 3600 rpm.

2 Turbine-generators (General Electric) each having nameplate data as follows:

Steam turbine, rated 100,000 kw, 23 stages, speed 3600 rpm, maximum capacity 108,500 kw, steam pressure 1500 psig, temperature 1050 F, exhaust pressure 1.5 in. Hg abs.

Alternating-current generator, hydrogen cooled, 2 poles, 60 cycles, 3 phase wye-connected for 13,800 volts; rating at 15 psig hydrogen pressure 111,765 kva at 0.85 power factor, armature 4670 amp, field 1040 amp, exciter 250 volts. Capacity at 25 psig hydrogen 117,647 kva at 0.85 power factor; armature 4920 amp, field 1070 amp.

Auxiliary alternating-current generator, rated 9375 kva, power factor 0.80, air cooled, speed 3600 rpm.

3 Single-pass, divided water box, spring supported, welded steel-shell Foster-Wheeler condensers with storage-type deaerating hot well; one 50,000 and two 60,000 sq ft surface, and 7/8-in.-OD X No. 18 BWG aluminum brass and aluminum bronze tubes.

9 Low-pressure, 2-pass, closed feedwater heaters (Westinghouse), located horizontally in condenser neck.

3 Low-pressure, 4-pass, closed vertical feedwater heaters; and 12 high pressure, 2-pass, closed vertical feedwater heaters (Foster Wheeler Corp.)

3 Condensate coolers, using salt water for cooling (Graham Manufacturing Co.).

Steam-Generating Units and Auxiliaries:

3 Boilers (Combustion Engineering-Superheater, Inc.), each rated 850,000 lb per hr continuous, 1500 psi, 1050 F throttle steam conditions, 52,450 cu ft furnace volume, 15,080 sq ft boiler heating surface; vertically adjustable, tangential firing burners, continuous

slag tap; 2-stage pendant, convection superheaters, 41,800 sq ft heating surface; continuous tube, counterflow, 39,600 sq ft economizer.

6 Ljungstrom regenerative air heaters (Air Preheater Corp.), 104,350 sq ft.

Superheater and economizer refractory walls, sectionally supported (M. W. Detrick Co., George Allen & Son).

3 Ash hoppers, 3 ash pumps and 1 dewatering bin, Allen-Sherman-Hoff Co.

Ductwork, Connery Construction Co.

Boiler and boiler gas-duct insulation, H. W. Porter Co.

Hot air duct insulation, Chas. S. Wood & Co.

Air soot blowers, automatic sequential operation, Diamond Power Specialty Corp.

9 Hardinge pulverizers, 19 tons per hr; 9 raw-coal feeders; and 9 mill exhausters, Foster Wheeler Corp.

6 Variable-speed forced-draft fans, driven through hydraulic couplings, American Blower Corp.

6 Air-cooled radiator for cooling oil of forced-draft-fan hydraulic couplings, Young Radiator Co.

6 Induced-draft fans, 2 driven through hydraulic couplings, 4 louvre controlled, American Blower Corp.

2 Fan-cooled radiators for cooling oil in the induced-draft-fan couplings, General Electric Co.

3 Stacks, double shell, radial brick, 225 ft high, 15 ft diam at top, M. W. Kellogg Co.

Zeolite water softening system, Worthington Pump & Machinery Corp.

3 Evaporators, 30,000 lb per hr each (2 Foster Wheeler Corp.; 1 Griscom-Russell Co.).

3 Evaporator deaerators, Worthington Pump & Machinery Corp.

Coal-Handling Equipment:

Unloading tower and barge puller, McKiernan-Terry Corp.

Bradford breaker, Pennsylvania Crusher Co.

Conveyors, traveling tripper, and swing boom, Robins Conveyors, Division of Hewitt-Robins Inc.

Conveyor belts, Thermoid Rubber Co.

Magnetic separator, Ding's Magnetic Separator Co.

Weightometer, Merrick Scale Manufacturing Co.

12 Automatic coal scales, Richardson Scale Co.

Raw-coal hoppers and stainless-steel chutes, Heilman Boiler Works; Allied Steel Products Corp.

Gates in raw-coal chutes and at bunker outlets, Stock Engineering Co.

2 Tractors, bulldozers and carryalls, Smith Tractor Co.; East-coast Equipment Co.

Dust-Handling Equipment:

Dust collectors, multiclone-Cottrell, Western Precipitation Corp.

Fuller-Kinyon dust-conveying system, Fuller Co.

Redder conveyers between precipitators and dust-pump hopper, Stephens-Adamson Manufacturing Co.

Variable-speed drives, Reeves Pulley Co.

Screw conveyers between economizers and dust-pump hopper, Link Belt Co.

Star feeder valves, precipitator, and economizer hoppers, United Conveyor Corp.

Dust-storage silo, Heilman Boiler Works

Pumps:

6 Vertical, mixed-flow, 47,000-gpm, 345-rpm circulating-water pumps, Foster Wheeler Corp.

6 Rotating-plunger-type, single-stage, vacuum pumps, 550 cfm at 1.5 in. Hg, Kinney Manufacturing Co.

6 Vertical, centrifugal 4-stage, re-entry type condensate and booster pumps; 2090 gpm at 517 ft head, 884 rpm; Worthington Pump & Machinery Corp.

9 Horizontal, centrifugal 8-stage, 1115-gpm at 4,680 ft head, 3465-rpm boiler feed pumps, Worthington Pump & Machinery Corp.

9 Variable-speed hydraulic couplings driving boiler feed pumps, rated 2000 hp at 3550 rpm, American Blower Corp.

4 Vertical, DeLaval, 2500-gpm at 250 ft head, 1760-rpm salt-water service pumps, Turbine Equipment Co.

3 Ash sluice pumps, 2000 gpm at 25 ft head, Worthington Pump & Machinery Corp.

1 Centrifugal fire pump, 1600 gpm, Gould Pumps, Inc.

1 City-water booster pump, 500 gpm, Gould Pumps, Inc.

3 Vertical, DeLaval, rotary-screw, fuel-oil pumps, 140 gpm at 325 psi, Turbine Equipment Co.

2 Pumps for acid-cleaning system, 1000 gpm at 70 ft head, Worthington Pump & Machinery Corp.

9 Sump pumps, Quimby Pump Division, H. K. Porter Co. Inc.

2 Condensate storage tank pumps, Ingersoll-Rand Co.

3 Evaporator feed pumps, Gould Pumps, Inc.

1 High-pressure chemical feed pump, Worthington Pump & Machinery Corp.

4 Continuous chemical feed pumps, Milton Roy, Inc.

2 Condensate return pumps, Worthington Pump & Machinery Corp., and Federal Pump Corp.

1 Circulating pump for oilstatic cable cooling, Sier-Bath Gear & Pump Co., Inc.

1 Laboratory vacuum pump, Schutte & Koerting Co.

2 Fuel-oil-reclaiming pumps, Sier-Bath Gear & Pump Co., Inc.

Air Compressors:

4 Horizontal, single-stage, 150-cfm at 100 psi carbon-ring-control air compressors, Ingersoll-Rand Co.

1 Horizontal, duplex, 2-stage, 660-cfm at 125 psi station-service air compressor, Ingersoll-Rand Co.

2 Rotary, 2-stage, 1035-cfm at 120 psi soot-blower air compressors, Fuller Co.

2 Horizontal, single-stage, 1000-cfm, 120 to 500 psi high-pressure soot-blower air compressors, Ingersoll-Rand Co.

6 Dual-tower silica-gel air dryers for control air, Dehydriair Corp.

1 Air receiver, 1000 cu ft, 500 psi, A. O. Smith Corp.

3 Air receivers, 60 cu ft, 250-320 psi, American Locomotive Co.

Instruments and Controls:

Three-element control of boiler feed pump speed, Bailey Meter Co. Automatic combustion-control equipment, Hagan Corp.

160-point bearing and superheater-tube temperature recorders; and 90-point miscellaneous temperature recorder, Leeds & Northrup Co.

Automatic control of superheater by-pass damper, Leeds & Northrup Co.

Condenser-hot well-level control equipment, Hagan Corp.

Automatic fuel-oil pressure control, Hagan Corp.

Yarway remote boiler-drum-level indicators, Yarnall-Waring Co. Boiler meters, Bailey Meter Co.

Clear and bi-color gage glasses for boiler drums, Diamond Power Specialty Corp.

Miscellaneous gage glasses, Ernst Water Column & Gage Co.

Boiler-draft and pressure gages, Republic Flow Meters Co.

Ashcroft Duragages, Hajoca Corp.

CO₂, pH, temperature, and conductivity recorders, Leeds & Northrup Co.

Industrial thermometers, Taylor Instrument Co.

Piping:

Main steam and high-pressure boiler feed piping, M. W. Kellogg Co.

Intermediate and low-pressure piping, Midwest Piping and Supply Co.; Cornell & Underhill

Circulating-water 48-in. reinforced concrete pipe, Lock Joint Pipe Co.

Strainers, Andale Co.; Leslie Co.

Insulation, Chas. S. Wood & Co.

Valves:

Steel gate and check valves, high pressure, The Lunkenheimer Co. Steel gate and check valves, Wm. Powell Co.; Walworth Co.

Safety valves, Foster Engineering Co.; Manning, Maxwell & Moore Inc.

Bleeder check valves, Schutte & Koerting Co.

Boiler blowdown valves, Yarnall-Waring Co.

Regulating valves, Bailey Meter Co.; Fisher Governor Co.; Swartwout Co.; Schutte & Koerting Co.

Pressure relief valves, Manning, Maxwell & Moore Inc.; Farris Engineering Co.; Foster Engineering Co.; Crosby Steam Gage & Valve Co.

Iron valves, Crane Co.; Chapman Valve Manufacturing Co.; Darling Valve and Manufacturing Co.; Walworth Co.

Butterfly valves for circulating water, Henry Pratt Co.

Electrical Equipment:

9 Reactors, single-phase, mid-tap, 5000 amp, General Electric Co.

4 Transformers, 85,000 kva, 13.2-132 kv, forced oil-forced air, Westinghouse Electric Corp.

4 Transformers, 51,000 kva, 13.2-26.4 kv, forced air, General Electric Co.

4 Station power transformers, 4000 kva, 26.4-2.4 kv, Moloney Electric Co.

2 Station power transformers, 1500 kva, 2400-440 volts, Allis-Chalmers Mfg. Co.

Lightning arresters, 15 kv (6 General Electric Co.; 3 Westinghouse Electric Corp.)

Oil circuit breakers, 15, 34.5, and 132 kv, Westinghouse Electric Corp.

Main generator leads of oilstatic cables, Okonite-Callender Cable Co. Inc.

Auxiliary generator-lead housings, Railway and Industrial Engineering Co.

Disconnecting switches 7.5, 23, 34.5, 132 kv, Railway and Industrial Engineering Co.; Delta Star Electric Co.; Pringle Manufacturing Co.

228 Transformer cooling fans, Diehl Manufacturing Co.

Metal-clad switchgear, 2400 and 440 volts, Westinghouse Electric Corp.

Load centers, 220 volts, Westinghouse Electric Corp.; I-T-E Circuit Breaker Co.

Storage batteries, 125 and 250 volts, Electric Storage Battery Co.

Electric motors, 220, 440, and 2400 volts, 3-phase, 60 cycles, Westinghouse Electric Corp.; Allis-Chalmers Manufacturing Co.; General Electric Co.

Mulsifyre fire-protection equipment, Grinnell Co.

Miscellaneous:

6 Sluice gates, operated by air motors, Coldwell-Wilcox Division, Krajewski Pesant Manufacturing Corp.

1 Traveling water screens, basket type, Link-Belt Co.

1 Traveling water screen with continuous screen cloth, Stephens-Adamson Mfg. Co.

Chlorination equipment, Wallace & Tiernan Products, Inc.

150-ton turbine-room crane, Whiting Corp.

2 Boiler-house elevators, Otis Elevator Co., Westinghouse Electric Corp.

1 Service-building elevator, Otis Elevator Co.

Ventilation and air conditioning, Buensod-Stacey Inc.

Heating boiler, Cleaver-Brooks Co.

Test Department furniture, Laboratory Equipment Co.

DeLaval turbine and transil oil-purifying equipment, Turbine Equipment Co.

Structural steel: Main building, Lehigh Structural Steel Co.; Turbine-generator supports, American Bridge Co.; Coal-handling structures, Morris, Wheeler & Co.

125,000-bbl fuel-oil tank, Bethlehem Steel Co.

Fuel-oil tank heaters, Griscom-Russell Co.

Fuel-oil pressure heaters, American Locomotive Co.

3 Water-storage tanks, 125,000 gal each, Bethlehem Steel Co.

Equipment insulation, Chas. S. Wood & Co.

NOTE: List of principal equipment for No. 1 unit, Essex Generating Station, was published in October, 1948, issue of *Power*.

Designers, Electric Engineering Department, Public Service Electric and Gas Company.

Builders, United Engineers & Constructors Inc.

Architectural consultants, Walker & Poor.

Discussion

C. B. CAMPBELL.⁴ The author has presented a most interesting report on the background experience of his company, culminating now in the modern Sewaren generating station. Certainly this is a plant whose continuing performance will be watched with great interest by all who are concerned with steam-power-generating problems.

The author refers to the installation of new equipment to modernize Essex Station as a definite step in the development of many Sewaren innovations and principles. Actually, it seems, at the expense of greater length and detail, that he could have included the progressive developments previously made by his company in its Burlington, Essex, and Marion generating plants as also having contributed to the latest accomplishment. Taken in their entirety, this whole program presents an excellent chronological picture of the progress in American steam-power-plant practice over the past 15 years.

Table 2 of the paper lists materials used in pressure parts exposed to the highest-temperature steam for the specific units

⁴ Manager of Engineering, Steam Division, Westinghouse Electric Corporation, Philadelphia, Pa. Mem. ASME.

indicated by column headings. It is believed there may be some misunderstanding of these data on the part of those not intimately acquainted with details of design of the equipment. We would like, therefore, to amplify this matter somewhat as regards Sewaren turbine, unit No. 1.

While the main steam-piping system leading to the turbine is of 3 per cent Cr 1 per cent Mo alloy as listed, the inlet steam piping connecting the separately supported turbine control-valve chests to the several first-stage nozzle groups is of 17-20 per cent Cr, 9-13 per cent, Ni, Cb-stabilized steel. Higher alloy was selected for these inlet pipes in order to reduce wall thickness and the length of loop necessary to care for expansion and relative displacement of the terminal connections.

In so far as the turbine is concerned, highest-temperature steam, that is, at 1050 F, is confined only to the throttle valves, control-valve chests, inlet piping, nozzle chambers, and nozzle blocks. Steam does not come into contact with the turbine cylinder proper until heat has been extracted by work performed in the first turbine stage, and its temperature even at maximum loading has decreased to approximately 970 F. It is this reduction from the maximum temperature of the steam supplied which permits the use of $2\frac{1}{4}$ per cent Cr, 1 per cent Mo alloy for the inner turbine cylinder.

The throttle and control-valve bodies and bonnets are of steel forgings of the composition shown in Table 2 under "Turbine Valves." Of the parts enumerated in the preceding paragraph as being subjected to 1050 F steam, castings were used only for the relatively small individual nozzle chambers. These castings are of 16-18 per cent Cr, 11-13 per cent Ni, 1.75-2.75 per cent Mo, with Cb stabilizer.

W. L. CHADWICK.⁵ The author has presented a valuable paper on an outstanding power station, a station which it was the writer's good fortune to inspect early in 1949. The Public Service Electric and Gas Company and its engineers are to be complimented on their courage and foresight in (1) pioneering the use of large units operating on steam at 1050 F, (2) the high efficiencies obtained, (3) building semioutdoor boilers in a comparatively severe climate; and further, for their ingenuity in simplifying plant layouts, centralizing controls, and in eliminating so many of the customary steam auxiliaries. Doubtless many of the new developments which are being field-tested and proved in Essex and Sewaren will soon be accepted standard practices.

The increases in efficiency which the author reports are impressive, the No. 4 unit at Sewaren being expected to gain nearly 10 per cent in efficiency when compared with the Essex unit, which latter unit is an efficient generator by any present standard. This efficiency represents about 665 kwhr per bbl of oil on the Pacific Coast base of 6,250,000 Btu per bbl. Some of the newer stations being built throughout the country are designed for as much as 100 kwhr per bbl less than this 665. The use of eight feedwater heaters in the cycle appears somewhat elaborate, but the efficiency and the station cost seem to justify that use. The use of triple-flow turbine exhausts to offset the higher exhaust losses usually attending 3600-rpm designs is commendable.

The clean simplicity of Sewaren's unit design described by the author not only reduced first cost, but should make for considerably greater operating reliability through elimination of headers and manifolds with their multitude of fittings and valves, each of which is a potential source of an outage. The use of semi-outdoor boilers on the East Coast at a latitude of 41° is an interesting and bold step, but one which seems well-justified by a saving of \$1,000,000 in construction costs of the first three units. The structure arrangement, which encloses the front and one

side of each boiler, is ingeniously planned to give protection to weather-vulnerable equipment at minimum building costs. It is also notable that this efficient station is being built for a total cost of \$132 per name-plate kilowatt.

The advances in simplifying auxiliaries are also significant. The development of air-cooled bearings and fluid couplings, and of totally enclosed motors to facilitate outdoor operation is interesting and creditable. The use of motor-driven vacuum pumps to replace the usual condenser jets puts to test the results of considerable recent discussion and development with several valuable advantages. The air soot blowers and the consequent elimination of many auxiliary steam lines also tests in a major station other recent developments and is a progressive step.

The Sewaren control system is efficient and convenient. The contrast which the author notes between the 521 sq ft of panel at one location at Sewaren and the 695 sq ft of control panel at five separate locations for a comparable unit at the Burlington Station is an interesting indication of the advantages of central control. The Sewaren design, which groups the control of each pair of units into a single control room is practical, convenient, and effective in reducing operating labor.

Electrically, Sewaren is ingeniously fitted to special system requirements.

The use of main turbine-driven house generators for auxiliary power appears to be contrary to the current trend. Most of the newer steam stations supply auxiliaries for each unit as a separate group, as at Sewaren, but use transformer banks, usually directly connected to the generator leads, as auxiliary power sources.

LOUIS ELLIOTT.⁶ To one who knows the author of this paper and holds him in high regard, the description of Sewaren and its basis of design exemplify his tireless application and his high competence. The writer is sure he will take pride, through the years to come, in the great plant to which he has given so much care and work, from the initiation of the project to the completion of construction.

While the design incorporates many modern refinements and new developments, the unit cost reported—\$132 per kw—is moderate.

The writer was interested in the reported reduction in total construction cost, by adoption of semioutdoor steam generators. The saving is given as \$1,000,000 for three units; this is at the rate of roughly \$3 per kw—which happens to be approximately the same unit saving as has been observed in other plants, achieved by similar reduction in structures. It is gratifying to see the adoption of this type of plant construction by a number of utilities operating properties in the East and Middle West, where severe winter conditions are experienced, as well as by companies in the West. The economy achieved is worth while, and the design should not entail serious difficulties in operation and maintenance.

The next step in reduction of structures in steam-plant construction involves use of an outdoor gantry crane, tramping over a low structure housing the turbine generator. This is figured to save around \$3 per kw, additional, in plant cost. The third step calls for the installation outdoors of the turbine and considerable other equipment, with housing limited to that for control room and for protection of certain delicate equipment. The saving as compared with a fully housed plant may be of the magnitude of \$10 or more per kw.

A recent example of the third step in economy is a gas-burning plant just now going into operation in the South, with two 66-mw turbine generators each served by one steam generator. The

⁵ Manager, Engineering Department, Southern California Edison Company, Los Angeles, Calif. Mem. ASME.

⁶ Consulting Mechanical Engineer, Ebasco Services Incorporated, New York, N. Y. Mem. ASME.

executives and engineers on this property are thoroughly in accord with the adoption of the design, and with its substantial savings.

Many of the outdoor plants have been in the South, but a number of stations involving the second step in reduction of structures have been installed and operated in locations experiencing winter conditions.

Plants designed during the past 10 years, incorporating various types of outdoor and semioutdoor construction, have aggregated between 3,000,000 and 4,000,000 kw in capacity. The 150 to 200 plant-years of successful operation of these stations have demonstrated the practicability as well as the economy of that character of design.

C. C. WHELCHER.² The author clearly explains the evolution of the Seward design over a brief but significant period starting with the Essex unit and ending with the reheated Seward unit No. 4. Through all, economic considerations have been a keynote as well as consideration of reliability, always aiming at the designers' goal—the lowest annual cost. This entails not only the most careful consideration of initial capital and operating cost, but also efficiency.

The semioutdoor boiler arrangement has proved to be a natural point of savings here in California and has been used for this reason for many years, but it would seem to present problems, although not insurmountable, where winters are more severe. Serious operating difficulties were encountered this last winter at one of our plants when unprecedented cold weather resulted in the freezing of exposed control and gage lines. This brief contact with the freezing problem has instilled in us considerable respect for the problems which must have been encountered in evolving the semioutdoor design for a colder section of the country. For example, a report has reached us of an experience of a boiler-water level gage freezing on an operating boiler due to a severe building air leakage. We would be interested in a brief résumé of methods used to avoid cold-weather difficulties at Seward.

As pointed out by the author, the centralization of control results in better co-ordination of operations and reduction in operating attendance. It is apparent that this may have been carried to a practical limit. The designer must be aware that as long as equipment is functioning properly few operators are required. The real test of adequacy is during and immediately after disturbances.

The effort expended to minimize required make-up is believed to be well-placed. It is probable that while this will show returns, as far as annual operating costs are concerned, little if any benefit can be derived in the sizing of make-up equipment.

While the omission of the deaerating heater from the Seward cycle may have simplified plant design and operation, and in addition, resulted in a lower initial cost, it would appear that the hazard of feed-pump seizure due to flash may be introduced upon sudden load changes or condensate-pump failures. This problem has been solved satisfactorily in the case of pumps fed from the deaerating heater.

² Chief, Division of Steam Engineering, Pacific Gas and Electric Company, San Francisco, Calif. Mem. ASME.

AUTHOR'S CLOSURE

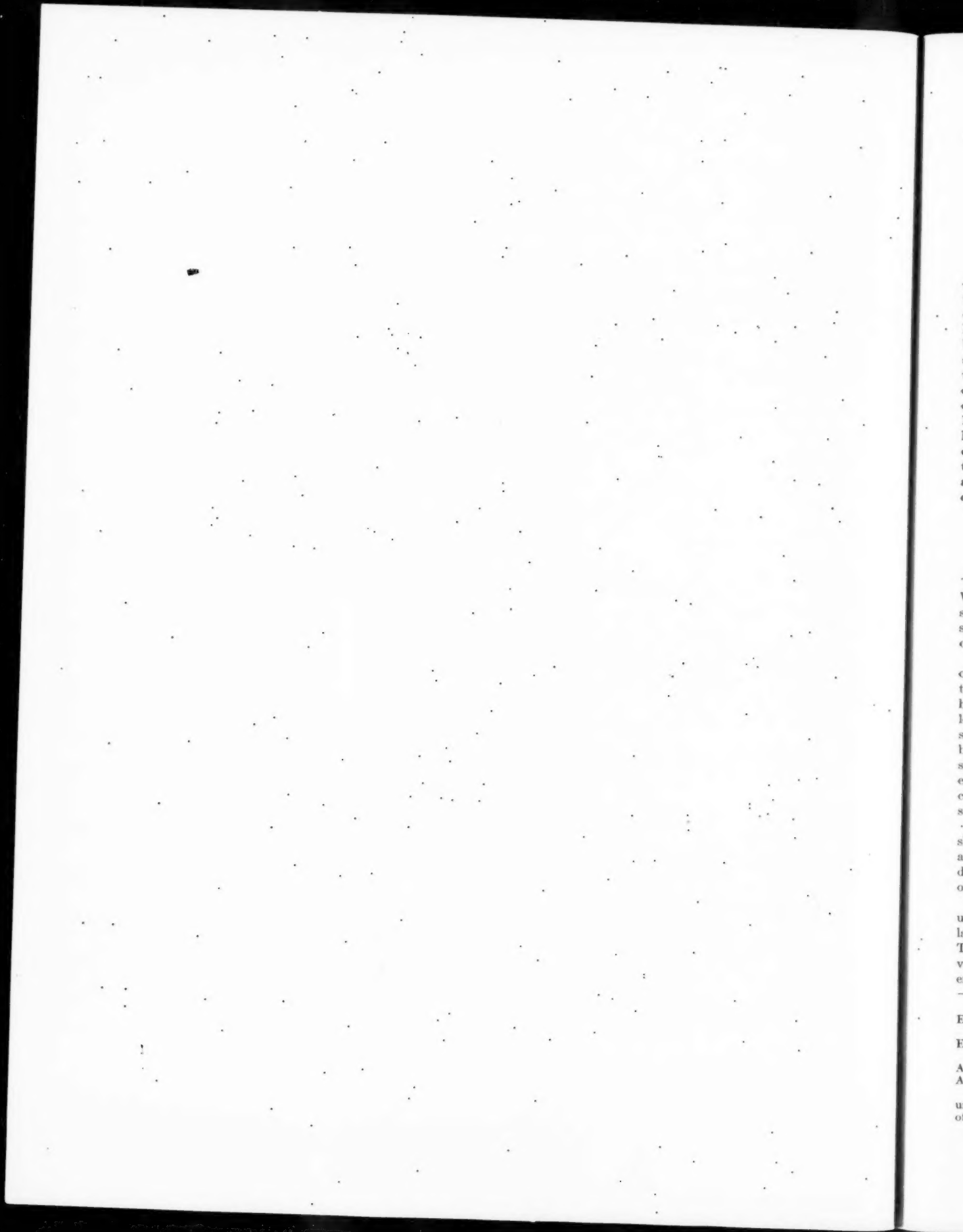
The author thanks Mr. Campbell for the information clarifying Table 2.

With regard to Mr. Chadwick's comment about main turbine-driven house generators for auxiliary power, the primary objective, as stated in the paper, was to provide the auxiliaries with a direct source of power free from outside disturbances. This is particularly important with pulverized-coal firing where there is danger of the fire being extinguished due to slowing down of the pulverizing equipment with a system voltage drop and relighting when the voltage is restored. We have had a number of trip-outs of high-tension transmission circuits due to dancing conductors caused by ice formation. In some instances these trip-outs have resulted in the separation of parts of the system and the loss of the main generators and their transformer-fed auxiliaries at our older stations. In using a shaft-end auxiliary generator supplying auxiliary buses not tied in with the main system nor the auxiliary system of any other unit, we expect our auxiliaries to operate undisturbed through the most severe disturbances. We realize, of course, that the ultimate in dependability is accomplished by a separate house turbine. The complication involved, however, is too great for the advantages gained. Also, our policy is to drop load rather than allow frequency to diminish.

An important consideration was the size of the turbine-generator unit. At the time that this station was designed, the upper limit of the rating of a single-shaft turbine-generator unit was determined by generator size. Thus the rating of the unit was increased by generating auxiliary power in a separate, shaft-end machine.

In accordance with Mr. Whelcher's suggestion, the following is a brief description of cold-weather precautions for outdoor equipment. The boiler drums, superheater outlet header, gage glasses, and safety valves are placed forward of the boiler and inside the boiler-operating aisle. All stairways serving the outdoor boiler platforms are indoors. Silica-gel driers are used to remove moisture from the compressed air which operates control devices and other similar equipment. Soot-blower mechanisms and other control devices which are vulnerable to icing, are provided with covers or are placed in individual enclosures. Draft fan bearings are cooled by air flow induced by suction from the induced-draft side of the air heaters. Low pour-point lubricating oil of a relatively narrow viscosity range is used in bearings and hydraulic couplings, the same grade being used in winter and summer. Heat generated by slip of the hydraulic couplings of the forced-draft fans is transferred to the air entering the fans by means of radiators mounted at the fan inlets. In the case of the hydraulic couplings of the induced draft fans of No. 1 Unit, radiators with motor-driven fans are used for the same purpose. Air heater bearings are cooled with air supplied by a motor-driven fan.

With reference to Mr. Whelcher's comment about the omission of the deaerating heater, the feed pumps are protected against the hazard of seizure upon sudden load changes by a large storage hot well under the condenser which operates as a surge tank. This hotwell receives water from the head tank via the condenser deaerator when the level falls below a certain point. The system is protected against condensate pump failure by the same head tank which holds a five-minute supply of condensate available to the feedpump suction through a check valve which is held closed by normal pressure from the condensate pump.



Operating Characteristics of the 100,000-Kw Essex Turbine Generator

BY STANFORD NEAL¹ AND VINAL S. RENTON²

On December 18, 1947, the largest 3600-rpm tandem-compound steam-turbine generator ever built up to that time was placed in service at the Essex Generating Station of the Public Service Electric and Gas Company, Newark, N. J. Since it was the first of a new class of turbine for both the manufacturer and the operating company, and since the throttle steam temperature was 1000 F, extensive tests were made to determine practical operation procedures for the new machine. These tests indicate that, even with the high steam conditions of 1250 psig this 1000 F turbine generator can safely withstand starting and loading rates higher than those normally used. The operating instructions for this machine can be revised to take advantage of these characteristics. Additional data are needed for wider application to other machines and designs.

INTRODUCTION

A TURBINE generator must be designed to operate safely and efficiently for many years under conditions of high pressures, high temperatures, and large centrifugal forces. Within 14 ft of the casing length of this particular turbine, the steam pressure changes from 1250 psig to 0.5 psia, and the corresponding temperatures change from 1000 to 80 F. The highest circumferential speed is 1393 fps.

With careful design, a turbine generator can be constructed to operate satisfactorily at a constant load under these severe conditions, but rapidly changing loads or temperatures impose stresses higher than occur at constant load. If all conditions of starting, load change, and steam-temperature change were imposed very slowly, the additional stresses due to changing conditions would be insignificant compared to those of constant load. Since very slow changes are not practical, it is necessary to determine the effects of rapid load and temperature changes, design the machine to withstand them, and then to specify, where possible, safe operating procedures during such changes.

Previous operating experience with turbine generators has shown that, without proper control, the length of starting time and rapid load and temperature changes may cause mechanical damage to the turbine or generator. To illustrate the importance of good operation, several of the extreme cases are mentioned here.

Both the turbine casing and shaft may bow because of non-uniform cooling, after unloading, and the shaft may rub the labyrinth packings during the subsequent start and bow still more. The resulting unbalance can increase to such an extent that vibration may cause damage if the machine is handled improperly. This trouble has been largely prevented in later machines

by rotating the shaft at very low speeds as the machine cools or is heated in preparation for starting.

Since the rate of heat transfer to the various parts is greatly different, crushing of internal fits and surfaces may occur, and the resulting stresses may permanently distort the parts.

When the rotor and stationary parts expand at different rates, mechanical contact may occur and wear the rubbing strips which minimize steam leakage. No serious mechanical damage will result from rubbing strip wear.

An infrequent but unusually severe condition exists during emergencies when water slugs are carried over from the boiler. Thrust-bearing failures and permanent distortions may result.

To reduce the possibility of such troubles, starting and loading rates have, in the past, been determined by experience. The tests described here, and recent tests of other investigators³ indicate that, in some cases, those procedures of starting and loading are unnecessarily conservative, and may even be harmful. An adequate theory of starting and loading effects, substantiated by test data, should permit the establishment of more realistic operating procedures. Such information is important both to designer and operator.

DESCRIPTION OF TURBINE GENERATOR

Since the mechanical description of the machine has been reported separately,⁴ only a few details will be mentioned here. The semisection of the turbine is shown in Fig. 1, and the outline of the turbine and generator in Fig. 2. Figs. 3 and 4 show the inner and outer high-pressure shells. The latter three figures also show the location of several of the instruments used in this investigation.

The tandem-compound machine has a nominal rating of 100,000 kw, and the steam conditions are 1250 psig and 1000 F. The high-pressure section has 19 stages with extraction connections from the 7th, 10th, 13th, 16th, and 19th stages. The double-flow low-pressure section is on the same shaft and has 5 stages with extraction connections from each of the two 20th, 21st, and 22nd stages.

The main generator is rated 111,765 kva at 0.85 power factor with 15 psig hydrogen pressure and 117,647 kva at 0.85 power factor with 25 psig hydrogen pressure. The house or auxiliary generator is air-cooled and rated 7500 kw at 0.80 power factor. Separate motor-driven exciters supply the field electrical requirements.

The turbine and two generators are coupled solidly to one shaft. The unit has an over-all length of 77 ft 7 1/4 in., and weighs 1,120,000 lb.

OBJECTS OF TEST

It was expected that there would result criteria for optimum operation with respect to safety, economy, and flexibility and, further, procedures for operation during emergency conditions.

¹ "Quick Starting of High-Pressure Steam-Turbine Units," by J. C. Falkner, R. S. Williams, and R. H. Hare, *Trans. ASME*, vol. 70, 1948, pp. 201-209.

² "The Design of Sewaren Generating Station and No. 1 Unit at Essex Station, Public Service Electric and Gas Company," by F. P. Fairchild, published in this issue of the *Transactions*, pp. 247-266.

¹ Section Engineer, Steam Turbine Engineering Division, General Electric Company, Schenectady, N. Y. Mem. ASME.

² Engineer, Electric Engineering Department, Public Service Electric and Gas Company, Newark, N. J. Mem. ASME.

Contributed by the Power Division and presented at the Semi-Annual Meeting, San Francisco, Calif., June 27-30, 1949, of THE AMERICAN SOCIETY OF MECHANICAL ENGINEERS.

NOTE: Statements and opinions advanced in papers are to be understood as individual expressions of their authors and not those of the Society. Paper No. 49-SA-28.

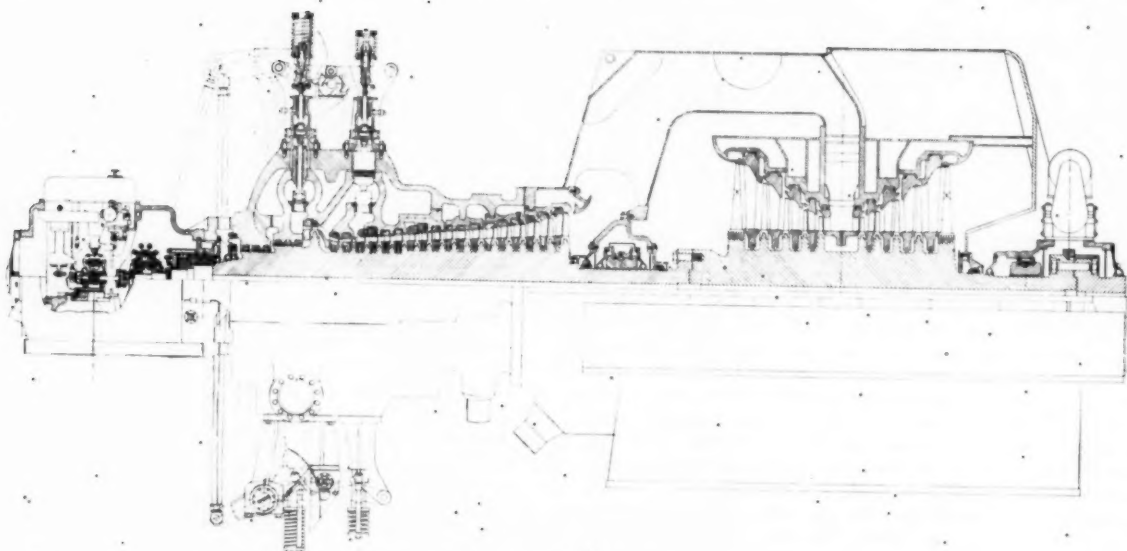


FIG. 1 SEMI-SECTION OF UNIT NO. 1 TURBINE AT ESSEX GENERATING STATION OF PUBLIC SERVICE ELECTRIC AND GAS COMPANY

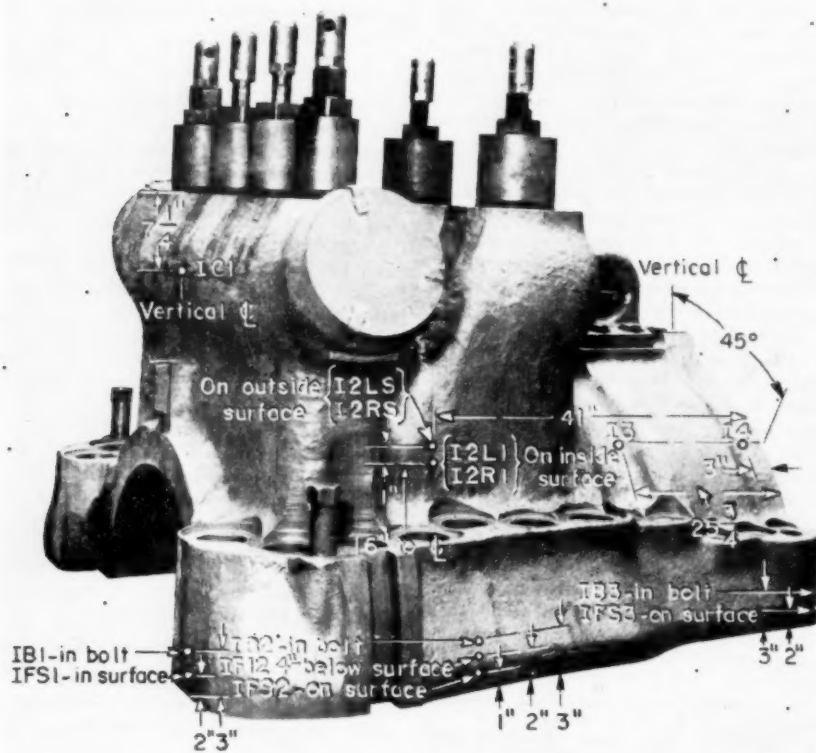
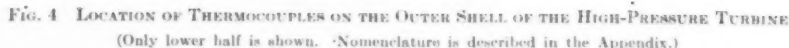
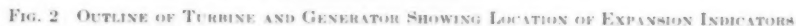


FIG. 3 LOCATION OF THERMOCOUPLES ON UPPER HALF OF INNER SHELL OF HIGH-PRESSURE TURBINE
(Nomenclature is described in the Appendix.)



5 Effect of preheating the generator field before or during

^b The generator preheating tests are expected to be the subject of an AIEE paper by F. W. Gay and H. D. Taylor.

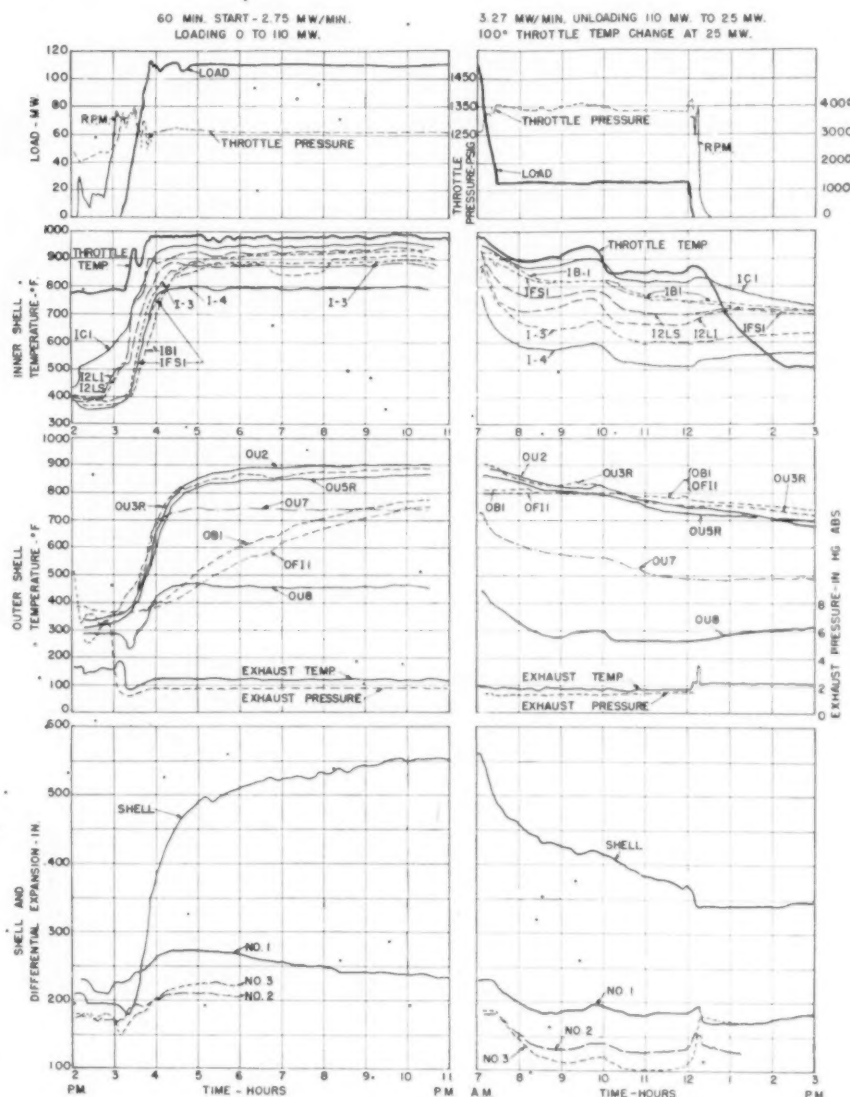


FIG. 6 TEMPERATURE AND EXPANSION DATA FOR (1) A 60-MIN START, FOLLOWED BY LOADING TO 110 MW AT 2.75 MW PER MIN, AND (2) UNLOADING FROM 110 MW TO 25 MW, FOLLOWED BY A THROTTLE-STEAM-TEMPERATURE DROP OF 110 F AT RATE OF 200 F PER HR AND THAT FOLLOWED BY A TURBINE SHUTDOWN

as soon as loading began it increased rapidly to about 975 F, then dropped rapidly to about 900 F, and then increased as the load increased, reaching 975 or 1000 F at about the same time the load reached 110 mw. The throttle-temperature change shown in Fig. 6 is quite typical, except that the initial peak is low. The exhaust-pressure change is quite typical.

Unloading and Stopping. Unloading rates were varied from 0.5 to 3.27 mw per min from loads of 40 or 110 mw. For some tests, the unloading was stopped at 25 mw, and held until steady-state conditions were established. Eight unloading tests were made.

From the typical unloading-test data in Figs. 6 and 7 it can be shown that the turbine cooling rates are low when the throttle steam temperature is held as high as practical.

With normal operating procedure, the stop valve is closed as soon as the load is off and the machine coasts to a stop in

about 20 min. It is immediately put on the turning gear which rotates the shaft at about 3 rpm to prevent bowing because of nonuniform cooling. The stopping cycle introduces no trouble and no tests were planned or made.

Throttle Steam Temperature Change. The throttle steam temperature was changed to 100 F at rates of 50 F and 300 F per hr at a load of 110 mw and at 200 F per hr at a load of 25 mw. Five tests of this type were made. Typical tests are shown in Figs. 6 and 7.

Load Dump and Fast Pickup of Load. The load was dumped by opening the main- and auxiliary-generator circuit breakers. After a no-load period of from 3 to 15 min, loads of over 110 mw were picked up in times of 13 to 19 min. For one test, the auxiliary-generator circuit breaker was not opened. Three tests were made and are shown in Fig. 7.

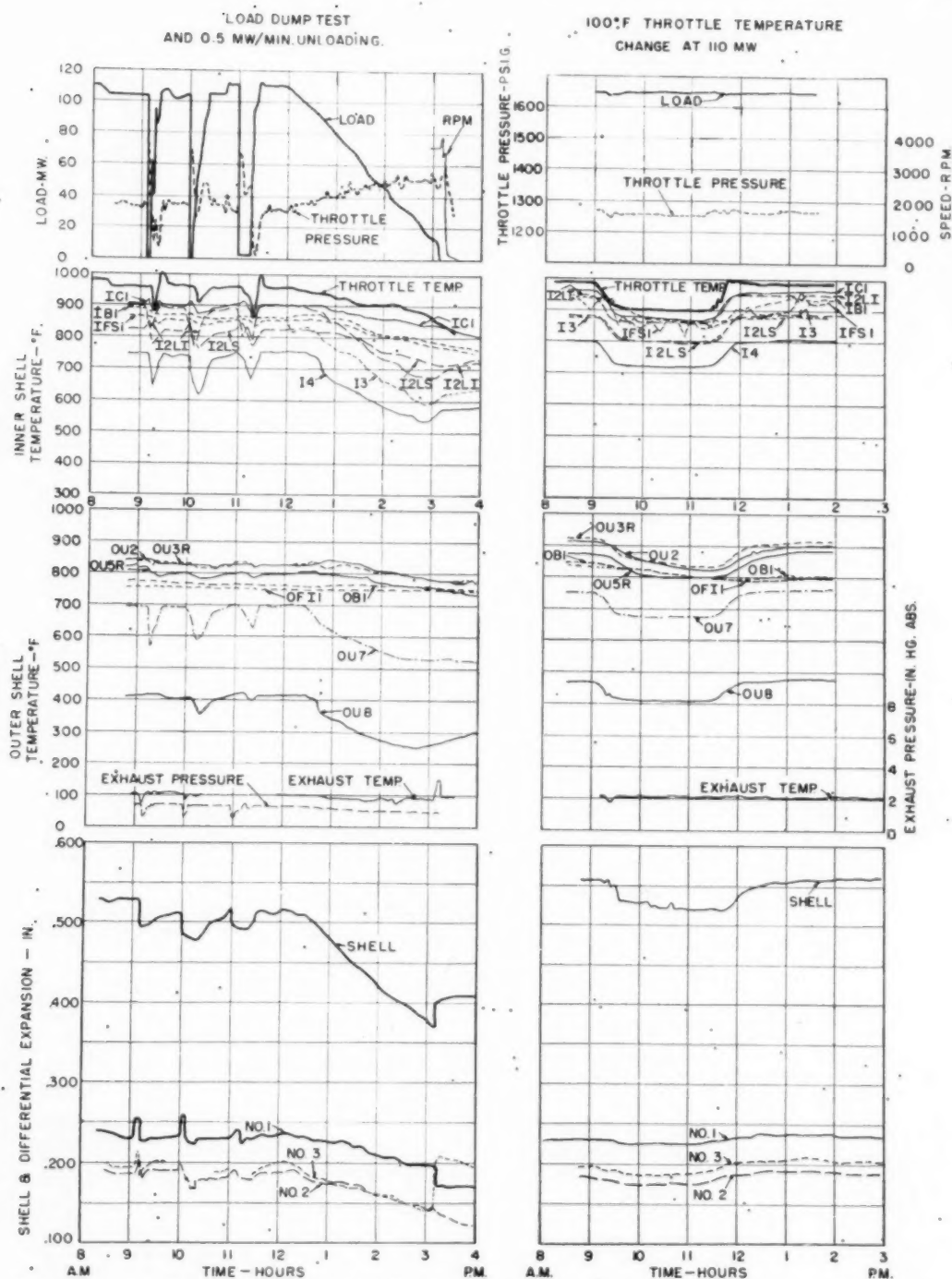


FIG. 7 TEMPERATURE AND EXPANSION DATA FOR (1) THREE LOAD DUMPS FROM ABOUT 110 MW, FOLLOWED BY RAPID PICK-UP OF LOAD, AND UNLOADING FROM 110 MW TO SHUTDOWN AT 0.45 MW PER MIN, AND (2) THROTTLE-STEAM-TEMPERATURE CHANGE OF 100 F AT RATE OF 300 F PER HR AT A LOAD OF 110 MW

As a matter of interest, the maximum speed reached by the turbine was 106.1 per cent of normal. A calculated time of only 0.85 sec is required for the turbine generator to reach 110 per cent speed after the circuit breakers are opened with full-load steam flow going through the turbine.

TEST RESULTS AND DISCUSSION

It would have been desirable to show more of the original data, but their volume made necessary the presentation of these few summarizing curve sheets. As an example of the amount of data obtained, a typical start and load cycle required about 7000 separate observations of temperatures, pressures, and loads, together with the continuous records of load, four expansions, and throttle, crossover, and exhaust temperatures and pressures.

Heating of Turbine. A description of the temperatures during a start is of great assistance in understanding the heating which occurs. Although the internal steam temperatures were not measured, these test data and previous experience indicate that the values quoted are of the right order of magnitude.

With the initial steam temperature at about 750 F during a start, and a calculated temperature drop of about 150 F in the first stage, steam will be supplied to the following turbine stages at a temperature of about 600 F. Steam of this temperature also leaks through the first section of the high-pressure packing and then divides to flow through the remaining sections of the high-pressure packing and between the inner and outer shells into the tenth stage or out to the tenth-stage feedwater heater.

Then, during a start, the valve chest and first-stage nozzle box should approach 750 F, and the remainder of the forward end of the outer and inner shells should approach a temperature of about 550 F. At the tenth stage the steam temperature will drop by perhaps 200 F, so that that section of the inner shell should approach an intermediate temperature between the inner steam of about 400 F and the outer steam of about 600 F. The last 9 stages of the high-pressure turbine will approach temperatures averaging about 350 F. Although the high-pressure turbine tends to equalize in temperature during cooling, the data show that the low-pressure end is usually about 100 F cooler than the high-pressure end. This distribution tends to match metal and steam temperatures. The first stages of the low-pressure turbine should approach a temperature of about 250 F, and the last stages should have temperatures ranging from 100 F to 250 F, depending upon the length of the start.

If the initial temperatures of the high-pressure turbine are approximately 450 F, there should be little change in turbine temperature during a start except in the valve chest and nozzle box. The initial temperature of the low-pressure turbine also should be little changed. Very short starts should then be possible, since the turbine and steam are near the same temperatures. The test data indicate that a starting time of 20 min is satisfactory for this condition.

If the initial temperatures of the high-pressure turbine are approximately 150 F, the start should be somewhat slower, since the turbine is cooler than the steam and heating will take place during the start. The longer start will permit the turbine to approach the 450 F equilibrium temperature for 750 F throttle steam. The test data indicate that a starting time of 50 min is satisfactory for this condition.

If the initial temperature of the high-pressure turbine is 750 F, the turbine should be started with 850 or 900 F steam to prevent cooling toward the 450 F equilibrium temperature which occurs with 750 F throttle steam. If the boiler cannot supply such high-temperature steam at the start, the starting time should be very short, followed by rapid loading to 30 or 40 mw. A starting time

of 10 min is suggested for this machine under these conditions.

With the turbine at initial temperatures of about 450 F, some starts show very rapid temperature drops of 50 or 100 F at the steam chest and in sections of the outer shell near the inlet steam pipes. It is believed that more careful heating of the steam pipes and stop valve might prevent this cooling and so keep the subsequent heating gradients at a lower value. Further testing is necessary to establish the proper techniques. A similar effect occurs when the turbine is started with steam colder than the machine and this, likewise, should be avoided.

Typical heating curves at several places in the turbine casing are shown in Figs. 6 and 7. An examination of the rate of heating will give a measure of the stresses caused by the transient. With initial temperatures of the high-pressure turbine of approximately 400 F and, during starts of 20 to 60 min, only the steam chest and two other temperatures on the inner shell show any appreciable change. All other temperatures rise only after loading starts. Fig. 8 shows the maximum rate of heating as a function of the rate of load increase. Not only does the maximum rate of heating vary at different places, but it occurs at different

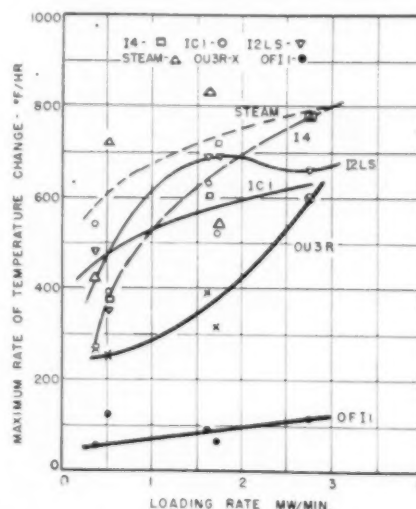


FIG. 8 MAXIMUM RATE OF TEMPERATURE CHANGE AT REPRESENTATIVE LOCATIONS DURING STARTING AND LOADING PERIOD

times during the heating cycle. The steam chest shows its highest rate when loading starts and as steam temperature rises very rapidly by about 200 F. The lowest value of the maximum gradient in the high-pressure turbine occurs in the outer-shell flange 10 to 30 min after a load of 110 mw is reached. As an example of heating rates at a particular time, Fig. 9 shows the rates at a load of 50 mw during loading to 110 mw.

With the initial temperatures of the high-pressure turbine at approximately 150 F, considerable heating takes place before loading. However, the maximum rates are not reached until after the loading starts. The preliminary heating is of such an amount that the subsequent maximum gradients are not greatly different from those that occur when a start is made from an initial turbine temperature of 450 F.

The heating data in Figs. 6 and 8 show that some of the temperature gradients in the turbine are very nearly the same as the temperature gradient of the steam. If the rate of increase of steam temperature were constant during the loading period, the maximum heating gradients in the shell could be reduced to about a quarter or third of the test values.

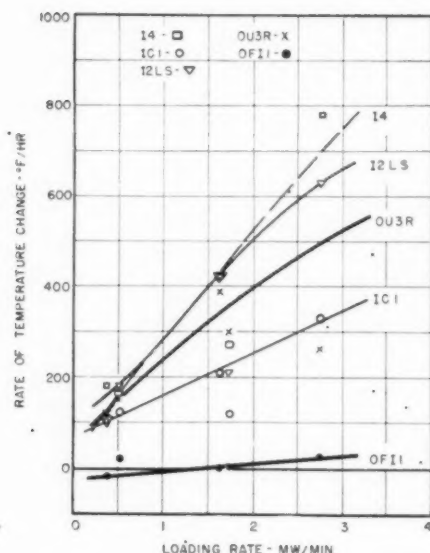


FIG. 9 RATE OF TEMPERATURE CHANGE AT REPRESENTATIVE LOCATIONS AT 50 MW DURING LOADING FROM ZERO TO 110 MW

A study of the calculated heat-transfer coefficients shows that the rate of turbine heating as the load is increased should not be greatly different from the rate of cooling as the load is decreased for the same change of load and the same rate of load change. The order of difference is probably about 30 per cent for the range of $1/2$ to full load. This occurs since, over that load-range, the range of temperatures caused by the load change is relatively small. However, when the turbine is started and loaded from room temperature, the temperature differences become relatively large. In stages which change from dry to wet as the load changes, the rate of cooling will be somewhat higher and the general relation given in the foregoing will not apply.

Longitudinal and Circumferential Temperature Distribution. The relation between steam and shell temperatures is shown in Figs. 10 and 11, for loads of 35 and 117 Mw. Of particular interest is the effect of discharging the steam from the first section of the high-pressure packing through the outer shell at the tenth stage. This tends to keep that portion of the outer shell much hotter than the tenth-stage steam. The flanges on both inner and outer shells remain appreciably colder than the corresponding cylindrical sections of the shells. A large section of the inner shell is colder than the outer shell at the light loads. These effects can be explained as a rather complicated combination of the radiation from the steam chest, heat transfer from the packing and valve steam leakage, and heat conduction through the inner shell.

The circumferential temperature distribution was measured at several sections of the outer shell. At constant load, the largest difference around the shell was about 50 F. Differences of about 125 F were observed during both loading and cooling cycles. Previous experience indicated that the differences during cooling would be much greater if the turning gear were not used.

At one shutdown, the exhaust-hood manholes were opened shortly after the machine was shut down and with the turbine still on the turning gear. The ventilation with room air cooled the machine very rapidly. Temperature differences of about 300 F were observed between top and bottom of the outer shell. Certain turbine parts cooled 500 F in 20 min with the major part of the temperature drop at the rate of 3000 F per hr. Such rates are considered to be undesirably high.

Shell and Differential Expansion. Shell expansion is a measure of the average temperature of the shell and, during temperature changes, shows the speed with which the average shell temperature approaches the steady-state value. Differential expansions are important since they indicate the relative movement of the rotor and shell and show when rubbing can occur.

The magnitude of the expansions for steady-state conditions is shown in Fig. 5. (For a more specific description of how these expansions were measured, see the Appendix.) For transient conditions, the greatest change from the initial, steady-state values during load and temperature variations, is shown in Fig. 12. With loading rates higher than 1.0 mw per min, the maximum change for the No. 1 differential expansion is practically constant for either loading or unloading and is well below the value, which would cause rubbing. No. 2 and No. 3 reach maximum values of the greatest change and then decrease as loading rate is further increased. Since the clearances in the low-pressure turbine are relatively large, the higher maximum differences cause no concern.

Such deviations of differential expansion are functions not only of loading rate but also of the size of the load change and of the initial temperature of the turbine (or the initial load). The maximum change of the No. 1 differential expansion is plotted in Fig. 13 as a function of loading rate. The dotted and solid lines show the effects of load ranges of 0 to 40 and 0 to 110 mw, respectively. The effect of initial turbine temperature is large and shows why loading rates must be adjusted for this factor.

With the longitudinal variations of shell and steam temperature such as are shown in Figs. 10 and 11, the shell and differential expansions can be calculated for the steady-state conditions and show reasonable checks with the measured values. For this purpose the turbine-rotor temperatures were estimated from the steam and bearing-oil temperatures.

An exact calculation of the differential expansion during transients is difficult because of the irregular shapes, the wide variation of steam velocities and heat-transfer coefficients, and the indeterminate heat-transfer characteristics of metal joints of various types. From the measured differential expansions, estimates of the over-all heating rates of both the rotor and shell can be made. With these rates and the calculated steady-state expansions, maximum values of the differentials during transients can be predicted for any turbine of this type. The rates and predicted expansions check well with previous experience.

Change of Throttle Steam Temperature. A change of throttle steam temperature causes a change of turbine temperatures and expansions. In some load ranges, these changes are much like the effect of a load change at constant throttle temperature.

Since this machine has stage valves which by-pass the second and third stages starting at loads of about 93 mw, the change in temperatures and expansions is small for the load range from 93 to 117 Mw. However, between loads of 37 and 93 Mw, a load change of 33 Mw at constant throttle temperature is somewhat the equivalent of a throttle temperature change of 100 F at constant load. It follows that a load change at the rate of 1.65 Mw per min is similarly the equivalent of a throttle-temperature change at the rate of 300 F per hr under the conditions just given.

The data show that the differential expansions for a load change from 0 to 40 Mw are about the same as those for a throttle-steam-temperature change of 100 F.

This concept of similarity is useful in analyzing and applying the test results, although it should be noted especially that local effects, such as heating of the steam chest and the first-stage nozzle, are very different for the two types of change.

Exhaust-Steam Temperature. During a start, the maximum temperature of the steam in the exhaust hood occurred just be-

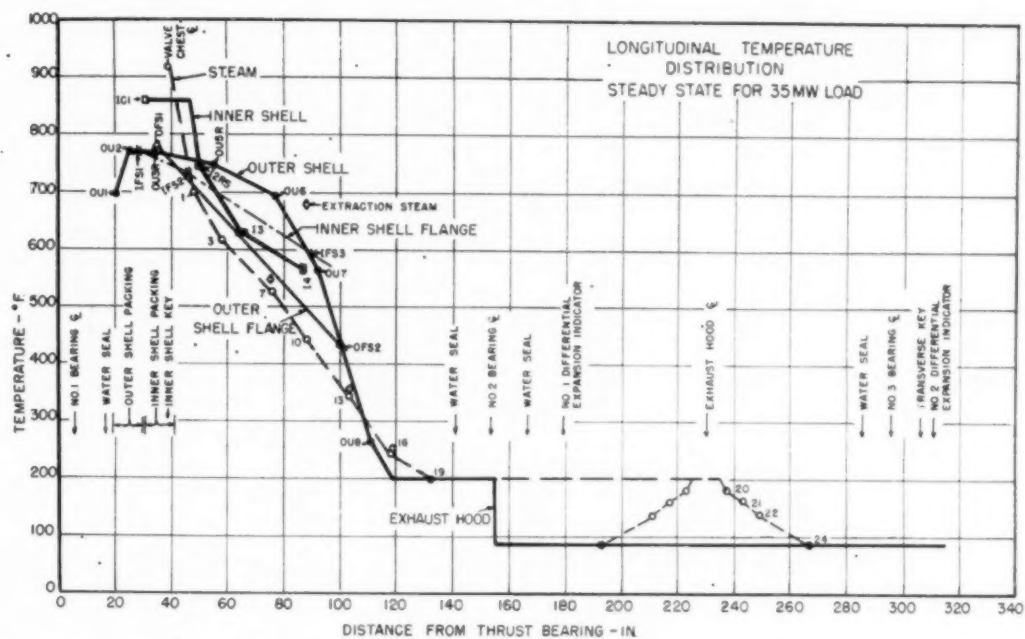


FIG. 10 LONGITUDINAL TEMPERATURE DISTRIBUTION AT CONSTANT LOAD OF 35 MW
(Steam temperatures from heat-rate test.⁷)

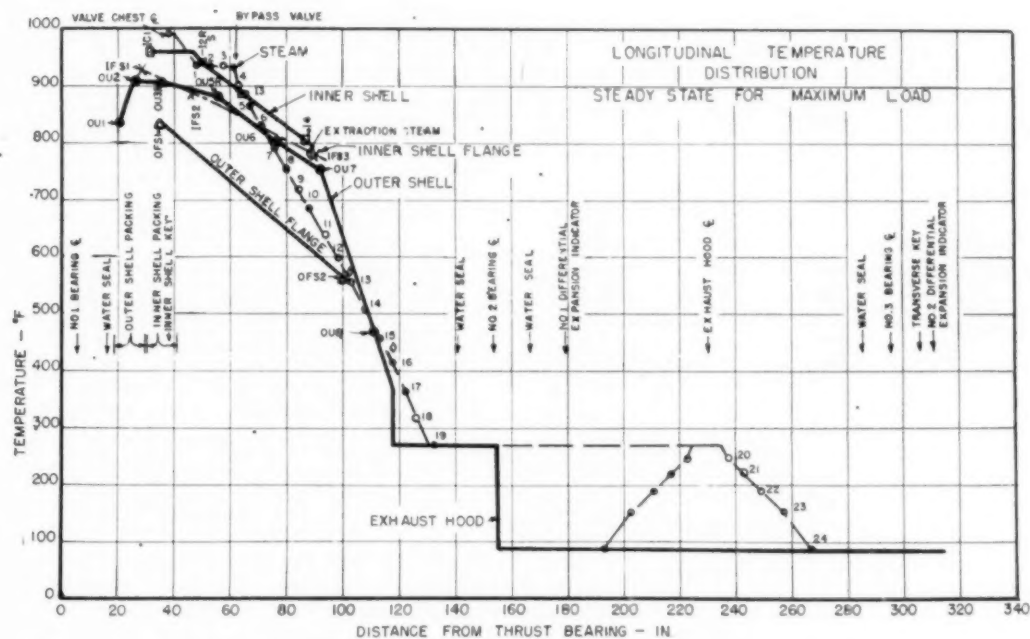


FIG. 11 LONGITUDINAL TEMPERATURE DISTRIBUTION AT CONSTANT LOAD OF 117 MW
(Steam temperatures from heat-rate test.⁷)

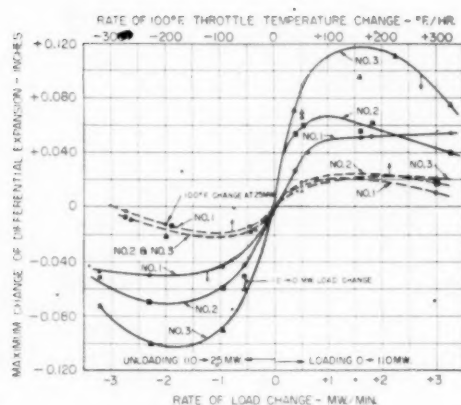


FIG. 12 MAXIMUM CHANGE OF DIFFERENTIAL EXPANSION (Solid lines show maximum change occurring during starting and loading, with initial turbine temperature approximately 450 F, and during unloading from full load to 25 mw. Dotted lines show maximum change during 100 F throttle temperature change at constant load.)

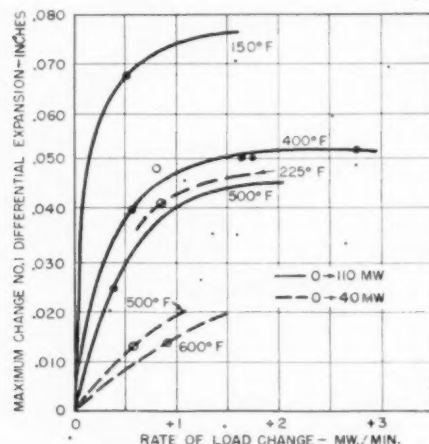


FIG. 13 MAXIMUM CHANGE OF DIFFERENTIAL EXPANSION FOR HIGH-PRESSURE TURBINE ONLY (Initial turbine temperature is shown as parameter. Solid lines show load changes from zero to 110 mw. Dotted lines show load changes from zero to 40 mw.)

fore the machine was loaded. The exhaust-steam temperature rises because of the large rotation losses in the last stages. Since those losses are proportional to exhaust pressure, and since that pressure was changing rapidly and was not the same for all tests, the data show some scatter. However, in general, the longer the starting time, the higher the maximum exhaust-steam temperature. The maximum temperature observed during a start was 230 F, which is well below the recommended maximum of 250 F.

At times it is necessary to operate a turbine generator at synchronous speed at no load. Although no tests of this nature were planned, operation for 30 min resulted in a temperature of 225 F. The exhaust pressure at that time was about 1.5 in. Hg. Steady-state conditions had not been reached, and the temperature would have risen further had the test been continued.

Steam-Chest Temperature. The largest observed difference between the throttle steam temperature and the outer surface of the steam chest was 300 F during a starting and loading period. Because of the high temperature drop from steam to

metal, the maximum temporary temperature gradient in the metal, calculated from the test data, was 270 F per in. which occurred when loading at 2.75 mw per min.

At steady loads, the gradient would be about 18 F per in., and the stress due to temperature would correspond to about 4500 psi in tension on the outer fibers and about the same amount in compression on the inner fibers. The calculated heat-transfer coefficient on the inside of the steam chest varied from about 3 to 350 Btu/(sq ft) (hr deg F) as the load changed from zero to maximum.

Inner-Shell Temperature. The temperatures of the inner and outer surfaces of the inner shell were measured at two places near the discharge of the first stage. At high loads, the temperature of the inner surface was hotter than the outer, although the steam flowing over each surface was supposed to be at the same temperature. The difference is largely due to the high heat gain on the inside, the high steam velocity, and the large heat loss by radiation from the outer surface. The magnitude of the difference varied from 75 F at constant load to 115 F during loading, and 70 F in the opposite direction during unloading, Fig. 14. The maximum temperature gradient in the inner fibers, as calculated from test data, was 54 F per in., and occurred during loading at the rate of 2.75 mw per min. This is only about twice the average gradient at constant load.

The 75 F temperature difference would cause a stress of about 7300 psi in the cylindrical part of the shell and should cause little concern. The maximum temperature gradient at the inner fibers of the inner shell will cause stresses of about 10,500 psi.

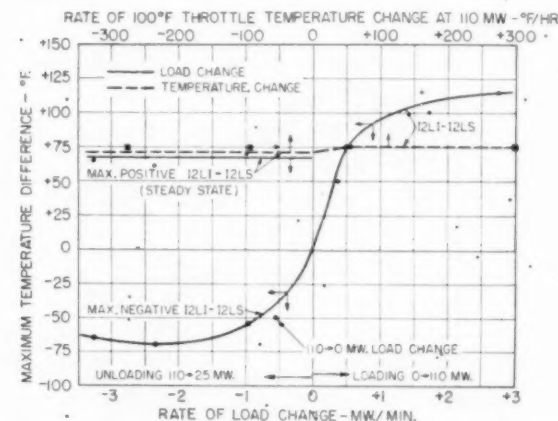


FIG. 14 MAXIMUM TEMPERATURE DIFFERENCE FROM INNER TO OUTER SURFACE OF INNER SHELL OF HIGH-PRESSURE TURBINE AT FIRST STAGE

(Solid lines show effect of starting and loading, and of unloading cycles. Dotted lines show effect of temperature changes at constant load. During unloading, direction of temperature difference reverses. Both positive, steady-state, and negative maxima are shown.)

Flange and Bolt Temperature. The greatest temperature difference between a bolt and its adjacent flange under steady-state conditions was about 30 F and was about the same for inner-shell studs and outer-shell bolts. During load and temperature changes, the maximum temperature difference between an outer-shell bolt and the adjacent flange was never more than 60 F, Fig. 15(D), for a loading cycle and was smaller for an unloading cycle. The bolt was hotter than the flange, and this indication, to a large degree, may be because the thermocouple inside the flange was not at the bolt center line, Fig. 18(E). Also the radiation from the hot side of the bolthole tends to heat

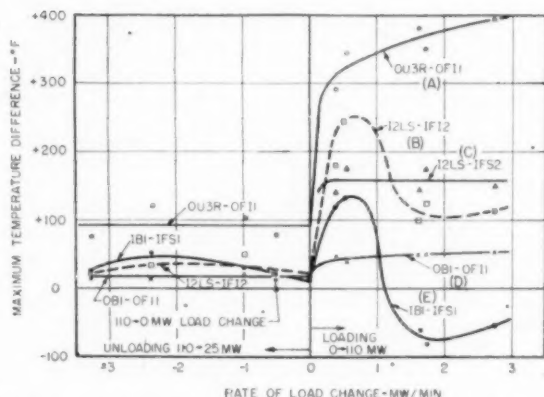


FIG. 15 MAXIMUM TEMPERATURE DIFFERENCES DURING LOAD CHANGES AT REPRESENTATIVE LOCATIONS IN TURBINE (Starting and loading data based on initial turbine temperature of about 450 F.)

the bolt faster than the flange, since the small space between bolts greatly restricts the flow of heat to the outside. It should be noted that the temperature of bolt and flange were measured only at one point.

The stress change with a bolt 60 F hotter than the flange would be about 12,000 psi with an incompressible flange and would relieve the initial tension on the bolt. Since the flange is compressed, the difference in stress may be reduced to about 9000 psi.

The temporary temperature differences between the hottest inner-shell bolt and adjacent flange were as large as +125 F and -75 F, Fig. 15E, during a loading period, and the direction of the difference changed with loading rate. The change is believed to be due to the relative amount of heat flow from the interior of the inner shell to the bolt.

Flange and Thin Section of Shell. The largest temperature differences observed in adjacent stressed parts were between the outside of the thin cylindrical section of the shell and the interior of the thick flange directly under the steam pipe (OU3R-OF11) and occurred during loading. These differences are shown in Fig. 15(A) as a function of loading and unloading rates.

As with the expansions, the important variables which affect this temperature difference are (1) rate of load or throttle-temperature change; (2) magnitude of the change; and (3) initial turbine temperature. Fig. 16 shows the test points with the curves extrapolated to 5 mw per min loading rate for several initial temperatures of the turbine. The extrapolation is believed to be accurate to about 75 F.

If this temperature difference is considered to be a measure of stresses, very interesting inferences can be made from the relation of that difference to loading and unloading rates. If repeated starts with loading at the rate of 1 mw per min can be made safely from an initial temperature of 150 F, with resulting temperature differences of 450 F (from Fig. 16), then loading at the rate of 5 mw per min will result in temperature differences of 530 F, or only 80 F more. Following the same argument, with initial turbine temperatures of 400 F or higher, loading

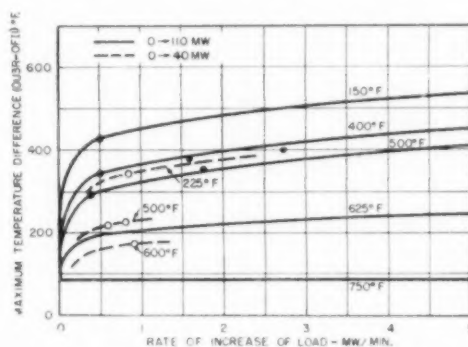


FIG. 16 MAXIMUM CHANGE OF TEMPERATURE FROM THIN CYLINDRICAL SECTION OF OUTER SHELL TO INTERIOR OF ADJACENT FLANGE (Initial turbine temperature is shown as parameter. Solid lines are for load change from zero to 110 Mw. Dotted lines are for load change from zero to 40 Mw.)

rates of greater than 5 mw per min can be made with no greater probability of trouble than for the start from 150 F and loading rate of 1 mw per min.

The temperature differences for load ranges of zero to 40 mw and of zero to 110 mw are shown by the dotted and solid curves in Fig. 16, with initial turbine temperature as the parameter. Initial turbine temperature appears to have a more important effect than the amount of loading when it is considered that the usual steady-state throttle-steam temperature is 80 F lower at a load of 40 mw than 110 mw. This is approximately the difference in temperature between the two sets of curves.

The highest calculated average heat-transfer coefficients on the interior of the outer shell are 3.2 and 11.9 Btu/(sq ft) (hr deg F) for convection and radiation, respectively. The low value of the convection coefficient is due to the low velocity of the steam flowing between the two shells.

The maximum temperature gradient on the inner surface, as calculated from the test data, was about 27 F per in., and was the same at the flange as at the thin section. This would correspond to the negligible stress of about 2000 psi. This stress affects only the inner fibers and is reduced progressively with distance from the inner surface. Other stresses, such as are caused by the difference between the temperature of the thin section of the shell and the adjacent flange, tend to distort the shell. The magnitude of these stresses and the amount of distortion depend upon the configuration and size of the shell and are difficult to analyze.

At steady state, the calculated average temperature gradient is about 5 F per in. in the thin section of the shell and about 3.5 F per in. through the flange. Fig. 17 shows the calculated and measured temperature change of a thin section of the shell and of the flange at the hot end of the outer shell as a function of time after start of loading. The agreement is good and represents a sample of the analysis now progressing.

Other Aspects of Test Results. The limitations of the tests must be realized. No temperatures were measured on the nozzle partitions, diaphragms, or rotor. The bucket and partition edges will heat rapidly because of the small mass and the high heat transfer and may cause permanent and undesirable distortions. The calculated heat-transfer coefficient of the first-stage nozzle partition is about 1000 Btu/(sq ft) (hr deg F).

It is known that the diaphragms will distort when heated or cooled rapidly. However, during the tests there was no evidence that the distortion was sufficient to cause the diaphragm packings to rub the shaft.

Temperature stresses in the shaft and wheels must be con-

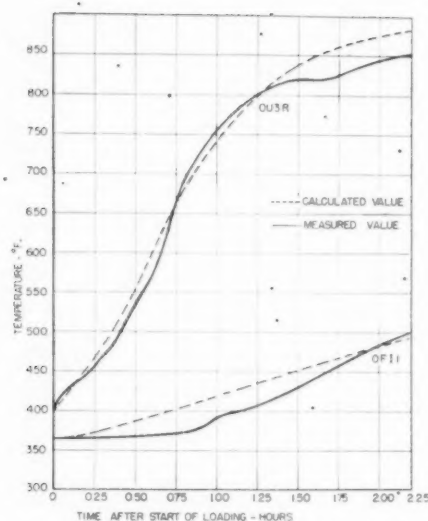


FIG. 17 MEASURED AND CALCULATED TEMPERATURE IN THIN SECTION OF OUTER SHELL AND INTERIOR OF ADJACENT FLANGE WITH LOAD CHANGE FROM ZERO TO 110 MW AT RATE OF 2.75 MW PER MIN (Initial temperature of turbine at start about 400 F.)

sidered, and it is hoped that techniques will be developed for measuring temperatures of the rotating parts. Such data will complement the theoretical work which is now proceeding.

Some effects of rapid changes of load or temperature may result in small permanent distortions which may be cumulative and which may be measurable only after many cycles.

FUTURE TEST PROGRAM

Analysis of these data is continuing and, after further study, it is expected that additional tests will be made at higher rates of load change and several initial turbine temperatures.

A similar 100,000-kw turbine generator but with steam conditions of 1500 psig and 1050 F, and a triple-flow low-pressure section has recently been installed in the Seward Generating Station of the Public Service Electric and Gas Company. The machine has been instrumented similarly since more severe steam conditions made temperature and expansion data even more desirable. Although the initial steam temperature is 50 F higher, preliminary data indicate that the outer shell is about 150 F cooler than that of the Essex turbine. This desirable end has been accomplished by an ingenious cooling scheme. It is expected that complete results will be reported later.

CONCLUSIONS

Although the analysis is not complete, the following procedures are justified by the test data and are consistent with previous experience. They are recommended specifically for the Unit No. 1 Essex turbine generator.

1 In an emergency, a load of any size can be dropped instantly and, after no-load synchronous-speed operation for as long as 45 min, with $1\frac{1}{2}$ in. Hg absolute exhaust pressure, the turbine generator can be loaded as fast as dry steam can be supplied.

2 Conservative starting and loading practice is determined by the rates at which temperatures throughout the machine will approach their steady-state values. Recommended starting times and loading rates are as follows:

Initial turbine temperature, deg F	Starting time, min	Loading rate, mw per min
150	50	1
450	20	3
750	10	5

The rate of throttle-steam-temperature increase should be made as constant as possible to reduce the temperature stress in the shells.

3 Loading or increase of throttle steam temperature can be done safely with respect to both expansion and temperature changes. With the turbine at any steady-state load, load can be increased to any other load at the rate of 5 mw per min at constant throttle temperature, or throttle temperature can be increased by 200 F at the rate of 500 F per hr at constant load.

4 Unloading or decrease of throttle-steam temperature must be considered carefully since the rotor contracts faster than the shell. The cooling gradients are usually low and uniform. As long as dry throttle steam is supplied, any amount of unloading can be done at the rate of 5 mw per min at constant throttle temperature, or throttle temperature can be dropped 200 F at the rate of 500 F per hr at constant load. The safest unloading procedure at any time consists of dropping all load instantly. During any unloading cycle, the throttle temperature should be held as high as possible.

5 The generator starting tests will be reported elsewhere.⁶ However, the test results show that there are no restrictions on starting time or loading rate of the generators, although it is recommended in the interests of longer life and lower maintenance that the main-generator field be preheated with a 850-amp current for 20 min immediately prior to operation at speeds above 1200 rpm.

These recommendations for this turbine generator are consistent with those previously published by the turbine manufacturer.^{6,7} However, initial turbine temperature is now taken into account and the recommendations are supported by specific test data.

After the remaining tests have been completed and analyzed, it is expected that these recommendations can be changed in the direction of higher rates of loading or temperature change. In interpreting these load rates for comparison to other machines, they should be compared on the basis of per cent of rated load.

The tests show that the Essex Unit No. 1 turbine generator is performing in accordance with design expectations both with respect to operation during transients and economy.⁸ Both the manufacturer and the operating company are well satisfied with the performance of the machine and its service record.

Appendix

THERMOCOUPLE NOMENCLATURE

The thermocouple locations are shown in Figs. 3 and 4. Designation of each couple has been made so that its approximate location can be deduced. The first letter indicates the inner or outer shell. The second and third letters indicate location on the shell. The number indicates longitudinal position starting at the high-pressure end. The meaning of each letter is given as follows:

⁶ Discussion by G. B. Warren, Supplement to Trans. AIEE, June, 1942, pp. 398-399.

⁷ "Steam Plant Performance on Fluctuating Loads—Part IV—Suitability of Modern Turbine Units," by E. E. Parker and C. W. Elston, Electric Light and Power, Chicago, Ill., April, 1949.

⁸ "Heat Rate Tests Results of the 100,000-Kw Essex Turbine Generator," by Vinal S. Renton and Stanford Neal, to be published in this issue of the Transactions, pp. 285-290.

- I Inner shell (or inside, if last letter)
- O Outer shell
- U Upper half
- L Lower half (or left side, if last letter)
- R Right side
- F Flange
- B Bolt
- C Steam chest

As an example, OU3R would indicate that the couple was in the outer shell, upper half, third position from the high-pressure end, and on the right side.

INSTRUMENTS AND THEIR APPLICATION

The special data required for this test were furnished by 4 expansion indicators and 40 thermocouples. All other data were taken from station instruments. These were the net load, steam pressure and temperature at the throttle, crossover, and exhaust hood, camshaft position, eccentricity of the shaft, vibration at each of the five main bearings, and turbine speed. The exhaust steam temperature was measured with three thermometers in the corners of the hood just above the horizontal joint. The exhaust pressures were measured in the plane of the exhaust-hood discharge.

The expansions were obtained by measuring the change in a magnetic circuit as the distance between the two pertinent parts changed. The instruments were the standard type usually supplied with General Electric Company turbines and were located at the positions shown in Fig. 2. One indicator was installed at the front bearing standard to measure the total expansion of the turbine shell from the exhaust hood to the front bearing standard. The No. 1 differential indicator was mounted at the coupling between the high- and low-pressure turbines and measured the difference in high-pressure-turbine rotor and shell expansion. That difference was measured from the thrust bearing which is located in the front bearing standard. The No. 2 differential indicator was mounted near the coupling between the turbine

and the generator and measured the difference in expansion of the entire turbine rotor and shell from thrust bearing to generator coupling. The No. 3 differential indicator was mounted at the coupling between the main and house generators and measured the movement of the turbine and generator shafts with respect to the foundation.

The difference between the indications of No. 1 and No. 2 is the difference in expansion of the low-pressure-turbine rotor and the exhaust hood. Since both the No. 2 and No. 3 indicators are essentially mounted on the foundation, the difference between their indications is the thermal expansion of the main-generator rotor less its elastic contraction in the longitudinal direction at speed relative to the foundation. When the expansion of the foundation is added to that difference, it is possible to deduce the average temperature of the rotor with a good degree of accuracy. The maximum thermal change in length of the generator foundation was small and was about 0.018 in. between room temperature and that corresponding to steady state, full load.

The No. 1 expansion indicator was in the exhaust hood in a steam atmosphere which occasionally reached 230 F, but no trouble was experienced for that reason. The other three indicators were in air at room temperature. The accuracy of the expansion measurement is believed to be from 0.002 to 0.004 in. No. 1 and the shell indicators were calibrated in place. No. 2 and No. 3 were calibrated before installation.

The shell temperatures were measured with 40 chromel-alumel thermocouples which were covered with silicone-varnish-impregnated glass insulation and were 80 ft long. The high-temperature ends of the couples were enclosed in stainless-steel tubing, and the junction of each couple was brazed to the tube, making a steamtight joint as shown in Fig. 18(A). The method of attachment of the couple to the shell is shown in Fig. 18(B). Fig. 18(C) shows the steamtight seal at the outer shell. The seal operated between steam conditions of 790 F, 400 psia and atmosphere. The steel sheath of each couple was brazed individually to the sealing diaphragm. The connecting pipe was made long enough

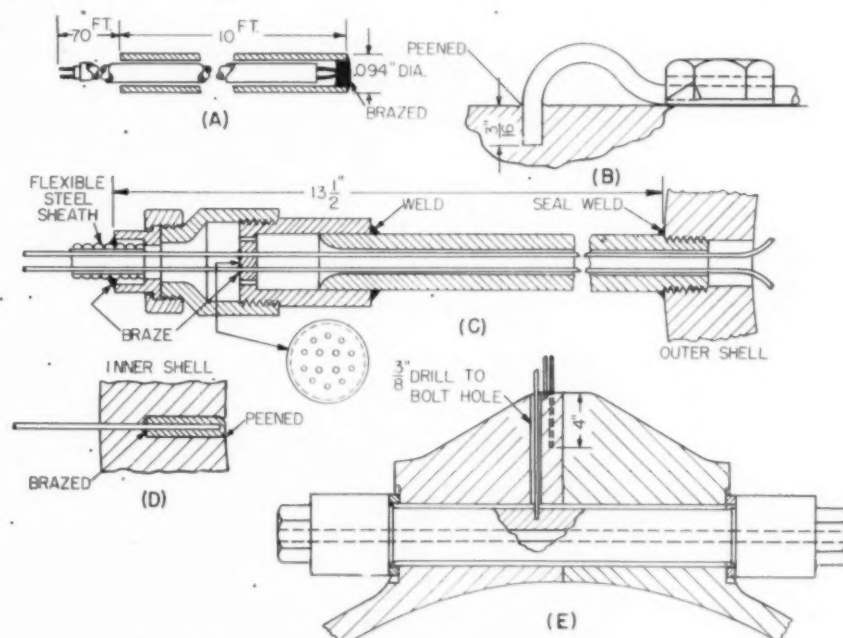


FIG. 18 DETAILS OF THERMOCOUPLE CONSTRUCTION AND INSTALLATION

to project through the turbine lagging so that the brazed assembly connections could be inspected or serviced. For protection of the fragile insulation, the couples were enclosed in a flexible steel sheath from the connection at the turbine to the potentiometer terminal board.

It was considered desirable to measure the temperature of the inner and outer surfaces of the inner shell at the first stage to determine the stresses due to unequal temperatures. The method of measuring the inner surface temperature is shown in Fig. 18(D). The couple was inserted through the hole in the shell and brazed to the cylindrical plug. The assembly was then pulled back into the shell, and the plug was peened in place. This construction was rugged and has given no trouble. The bolt and flange couples are shown in Fig. 18(E). All thermocouple potentials were measured by a self-balancing direct-reading potentiometer, which printed the temperatures at 4-sec intervals.

The couples were calibrated before installation, and the potentiometer was frequently checked during the progress of the test. It was expected that the thermocouples and potentiometer have a combined error of less than 4 F.

Some troubles were experienced during the 14 months of operation, and four of the couples are now open-circuited. Based upon this experience, it is believed that a couple can be made which will give accurate temperature readings for several years.

ACKNOWLEDGMENT

The authors express their appreciation to Messrs. E. M. Kratz and J. E. Phillips who were largely responsible for the instrumentation, testing, and evaluation of the data, and Messrs. H. G. Burk and J. Allhusen who supervised the operation of the unit during the tests.

Discussion

J. C. FALKNER.³ The tests on the Essex machine have confirmed the Consolidated Edison Company's tests on quick starting. That loading rates from 3.5 to 5 mw per min are safe is one of the most important conclusions of these tests, as many times we are faced with the necessity of loading machines rapidly to take care of sudden dark clouds, or thunderstorms. As the temperature of our high-pressure units after a 6- to 8-hr shutdown will be at 700 to 800 F, the rate of loading as shown by the paper should be as fast as desirable.

The Consolidated Edison Company of New York, like many other operating companies, had for years followed operating instructions given by the manufacturers as to how fast a turbine should be started, loaded, and what rate of steam-temperature change could be made safely during this starting and loading. In April, 1946, the company, pressed by steam conditions, departed from the manufacturers' instructions and began quick starting of high-pressure topping units. Since that time over 200 quick starts have been made, and there has not been a single instance where trouble developed during a start. There is every indication that the method is much better than that originally given by the manufacturers. However, after quick starting, a limitation of 100 F per hr rate of temperature change was maintained during loading. Loading rates have been held to values of $1/2$ to 1 mw per min after an initial loading of 4 mw. If the initial temperature of the turbine casing is 150 F or more lower than the steam temperature, the start is made at a slower rate. An hour is usually allowed for a start under these conditions.

The Consolidated Edison Company opened one of the topping

turbines at Waterside after operating 46,000 hr between November, 1942, and August, 1948. During this time there were 32 quick starts of approximately 15 min each, 74 water washes to wash off the phosphates, and four caustic washes to remove silica scale from the buckets. The machine was found in excellent condition, thus proving beyond any doubt that quick starting had not been injurious to the mechanical structure of the unit.

The quick starting of the turbines at Waterside led to trials at Sherman Creek Station, but conditions there were different as there is only one boiler per unit, while at Waterside there are two per unit with only one of the two boilers being used for starting. Therefore, temperatures as high as 700-750 F can easily be had on the starts at Waterside. On the 1,000,000 lb of steam per hr boiler at Sherman Creek, however, the steam temperature could not be brought over 500 F until a few minutes after starting. This meant that for a 6- to 8-hr shutdown the turbine metal temperature had to be reduced deliberately just before shutdown so that the initial steam temperature on the start would not cause a sudden drop and then a quick rise in cylinder temperature. In an effort to increase this initial steam temperature four oil burners were installed, high up in the furnace and pointed directly at the superheater. The results of typical quick starts with and without these oil burners are shown in Fig. 19 herewith.

In the start with oil burners the initial steam-chest temperature was allowed to be much higher than had been the usual practice, or 720 F, and the rolling time was cut down to 10 min. The turbine metal temperature drop was 50 F from 720 F to 670 F, and the rise was 100 F in 23 min, and only 150 F in the first hour. However, the steam temperature at the start was still only about 20 F above saturation, despite the use of the oil burners, and this temperature increased rapidly only after the throttle was opened, rising 105 F in the first 5 min. At the present time an additional by-pass around the topping turbine to the low-pressure machines is being designed so that the superheater will be cleared of water and the desired steam temperature will be obtained before opening the throttle. When this is installed the problem of steam-temperature control during starting will have been solved.

One of the latest and most important supervisory instruments used on turbine generators is the differential-expansion recorder which shows continuously the relative axial position of the cylinder and spindle and warns the operator of danger from an axial rub due to the spindle shrinking too fast in reference to the cylinder. In the paper the authors demonstrate that the differential-expansion recorder shows very little differential motion between spindle and cylinder when the turbine shell metal temperatures are between 400 and 450 F and the steam being admitted is at 700 to 750 F. This small relative motion is probably due to the fact that the heat in the steam is being dissipated and its temperature degraded while passing through the throttle and governor valve, and steam-chest structure.

Consolidated Edison Company, after the success of quick starting of topping turbines, tried the method on a 375-psi, 700 F, 160,000-kw tandem-compound condensing unit, and also on a 185-psi, 500 F, single-cylinder, 60,000-kw condensing unit. These trials were as successful as with the topping units, starting time being lowered on the large machines from $1 1/2$ hr to 20 min, and on the smaller machines from $1 1/2$ hr to 15 min. A decided improvement was obtained at the exhaust end of both units by lowering exhaust end temperatures immediately after the last-stage wheels by as much as 75 F to 100 F.

The Consolidated Edison Company expects to apply the quick-starting technique to all topping and condensing units on the system, and thereby realize an estimated annual saving of \$250,000.

In addition to the operating saving just mentioned, there are

³ Manager, Electric Production Department, Consolidated Edison Company, New York, N. Y.

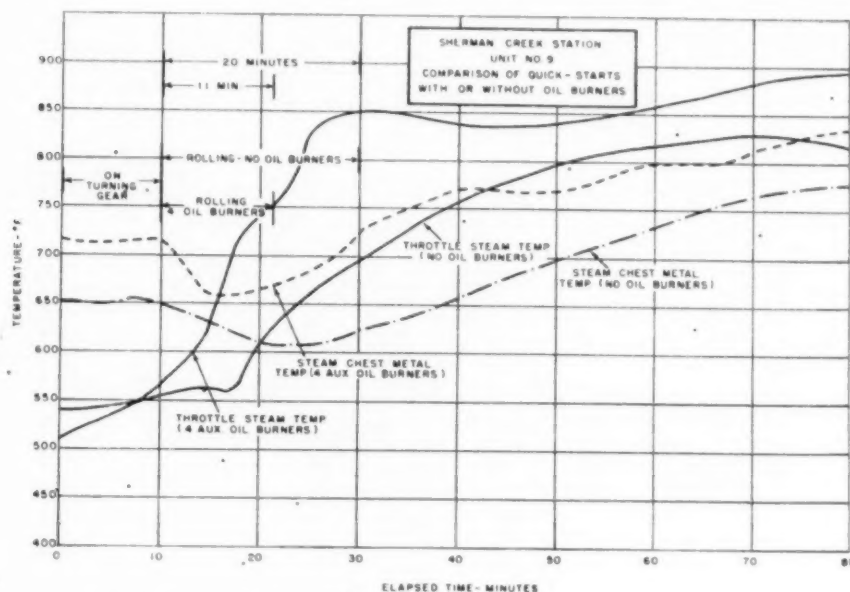


FIG. 19 RESULTS OF QUICK STARTS WITH AND WITHOUT AUXILIARY OIL BURNERS

many practical operating advantages which result from quick starting. A notable instance occurred on August 27, 1948, when the Manhattan Cooper Square network was de-energized because of failures of generator cables in Waterside No. 2, causing a simultaneous outage of three out of the four topping units in this station. As soon as the first generator cables were temporarily repaired on Unit No. 4, this machine was brought up to speed and was generating power in less than 15 min and the network was re-energized. If the old original 3-hr start had still been in vogue at the time, the network would have remained out of service at least $2\frac{1}{2}$ hr longer.

The short starting time relieves the man-power problem in the turbine room of each station during the start-up period. With the quick-starting technique perfected it is possible to put machines in service one after the other with fewer men, who can concentrate on one machine instead of on several.

With the potentialities of quick starting of large high-pressure turbine generators fully realized, the Consolidated Edison Company is now focusing its thoughts on quick starting of high-pressure boilers after week-end shutdowns. We think that it will be possible to start such boilers from cold and have them up to full pressure in 1 hr or less. Test work is being planned at present to develop the details of such high-pressure-boiler quick-start procedure and, if expectations are realized, it is felt that the economical advantages of the integrated quick starting of boilers and turbines will have been fully exploited. However, we believe that fast shutdown and quick starting of high-temperature high-pressure boilers will be best accomplished when an all-welded construction is used to join waterwall and generating tubes to their headers and drums.

H. H. POOR.¹⁰ To obtain information on boiler performance during rapid load swings, and to investigate the permissible rate of load pickup on a hot boiler, the writer's company participated in the last three load-dump and quick-pickup tests in the program at Essex Station described in the paper.

¹⁰ Staff Engineer, The Babcock & Wilcox Company, New York, N. Y. Mem. ASME.

Fig. 20 of this discussion shows a sectional side elevation of the steam-generating unit, which is a B&W radiant boiler designed to deliver 900,000 lb per hr of steam continuously at 1350 psi and 985 F from feedwater at 455 F, with a 4-hr peak load of 1,000,000 lb per hr. Twelve circular burners, arranged for either pulverized-coal or oil firing, deliver fuel to the slag-tap furnace. The burner region of the furnace is constructed of close-spaced tubes fully studded and covered with plastic chrome ore; the remaining upper portion of the furnace is of bare tube-to-tube construction. The furnace is divided by a central water-cooled division wall to provide more cooling surface in the furnace, without increasing furnace volume, than would be possible without such a wall. There is a boiler screen of three half-rows and four full rows of boiler tubes, two-stage pendant superheater with interstage spray attenuation, economizer, and air heater.

During the tests oil was fired because of greater operating flexibility, as compared with pulverized-coal firing. The boiler master controller, feedwater flow rate, fuel-oil flow rate, induced-draft fans, and forced-draft fans were on hand control; the spray attenuators were on full-automatic control. The feed pumps were on automatic control, but during load pickup were adjusted manually. Operators were stationed at the burners in order to remove the atomizers from service or put them back in service as rapidly as possible.

The last test was the most interesting because of the very rapid increase in load after 15 min at no load, following the full-load trip-out. As shown in Fig. 21 herewith, the trip-out took place at 11:00 a.m. when the boiler was delivering 970,000 lb per hr. The steam flow dropped immediately to the quantity necessary to roll the turbine at rated speed under no load (this was a reading of 70,000 lb per hr on the steam-flow chart). After $14\frac{1}{2}$ min, load pickup was started by an initial load increase of about 50,000 kw, and a steam flow of 920,000 lb per hr was regained in $3\frac{1}{2}$ min.

The drum pressure just before the trip-out was 1400 psi. When the steam flow was cut off, the superheater-outlet pressure rose at once, and the lowest set valve popped about 1 sec after the trip-out. All three superheater-outlet safety valves and some or

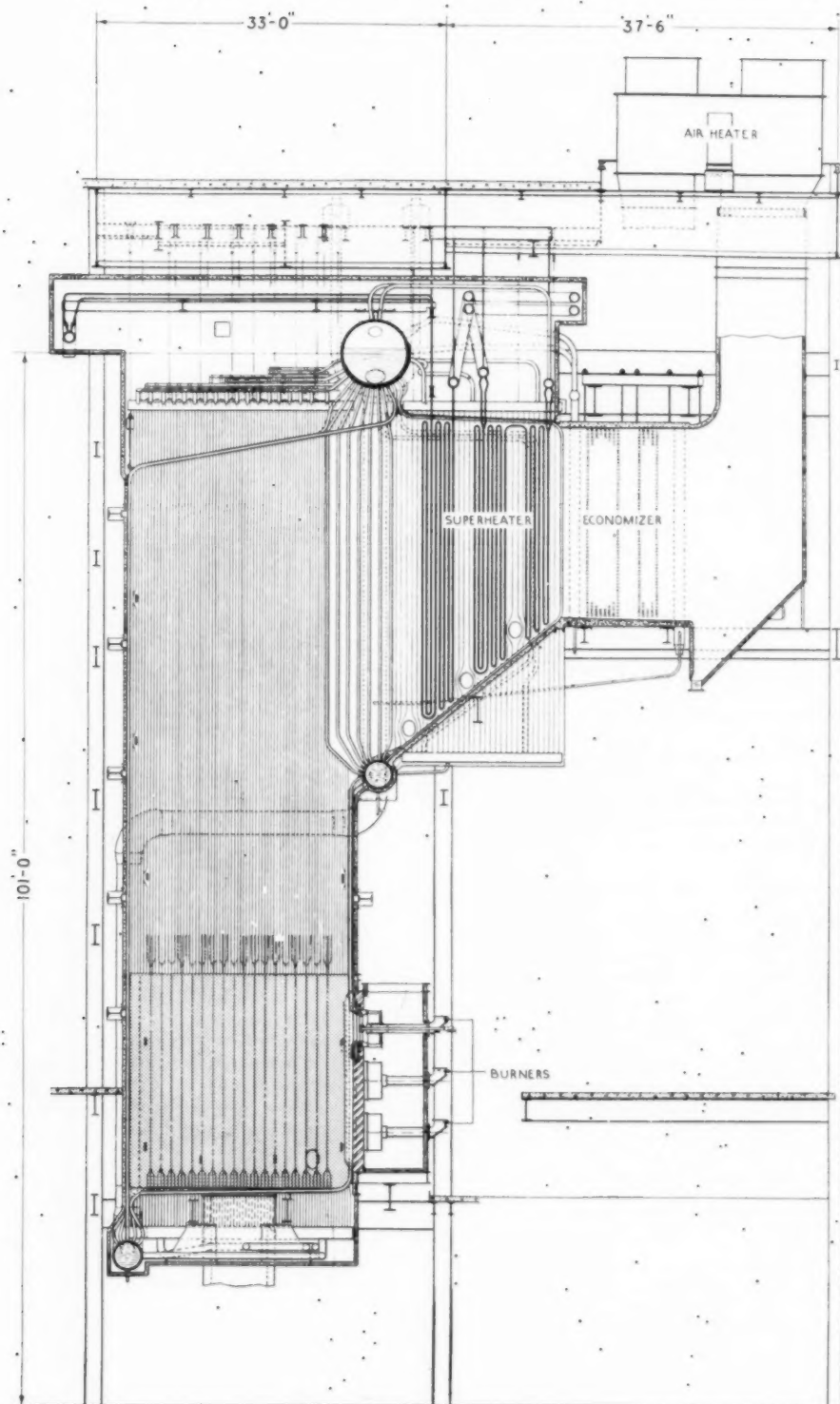


FIG. 20 BABCOCK & WILCOX RADIANT BOILER, ESSEX GENERATING STATION, PUBLIC SERVICE ELECTRIC & GAS COMPANY, NEWARK, N. J.

all of the drum safety valves opened, relieving the pressure as indicated in Fig. 21. The last valve closed a little more than 7 min after trip-out. The heat supplied by the two oil lighters remaining in service was sufficient to raise the steam pressure so that the low set valve reopened 10 min after trip-out at a pressure of 1370 psi, and reseated $2\frac{1}{2}$ min later at 1340 psi. When the load was applied, the drum pressure dropped to a minimum of 1230 psi, leveled out at 1250 psi for some time, and then climbed back to normal operating range.

Water level was measured by the panel-board recorder and was checked during the time that the water was visible in the gage glass by an observer stationed at the glass. At trip-out the water level dropped from $+1\frac{1}{2}$ in. to -13 in., but had returned to the

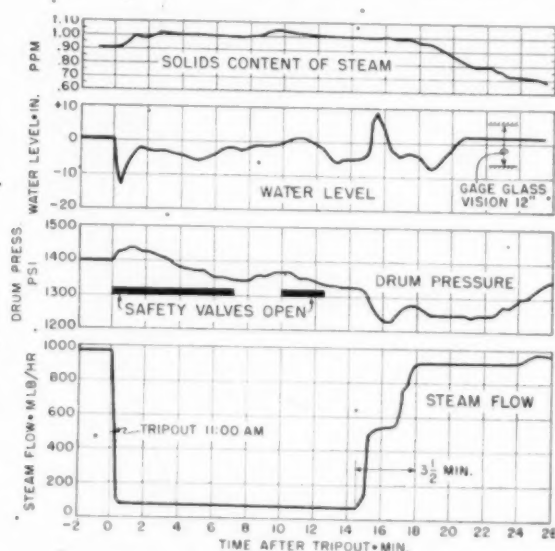


FIG. 21 RECORDS TAKEN DURING TRIP-OUT TEST

bottom of the gage glass 6 in. below the drum center line at the end of 1 min. The water level was held at 5 in. below the drum center line when the load pickup was approached. When the first block of load (approximately 50,000 kw) was applied to the turbine and the steam flow jumped from practically zero to 550,000 lb per hr, the water level rose 14 in. to a level 9 in. above the drum center line. The load was held at this value for about 2 min, during which time the drum level came back to -4 in., remaining in sight in the gage glass, except momentarily, during the remainder of the load pickup.

As a check for carry-over, saturated steam was taken through a sampling nozzle located in the center saturated-steam connection from the top of the drum, and passed through a cooling coil directly into a conductivity cell, with no attempt to remove dissolved gases. Before the trip-out the conductivity-cell indication corresponded to a solids content of 0.9 ppm. After the trip-out the indication increased to 1.0 ppm and finally to slightly above 1.0 ppm. There was no sign of carry-over increase when the load was picked up, despite the rise in water level, and, after full-load steam flow had been reached, the indicated solids content gradually decreased to less than 0.7 ppm.

Gas temperature entering the superheater was measured by a high-velocity thermocouple located in the gas stream halfway between the roof and floor at the superheater inlet, 10 ft from the right side wall. The gas temperature dropped from 2100 F be-

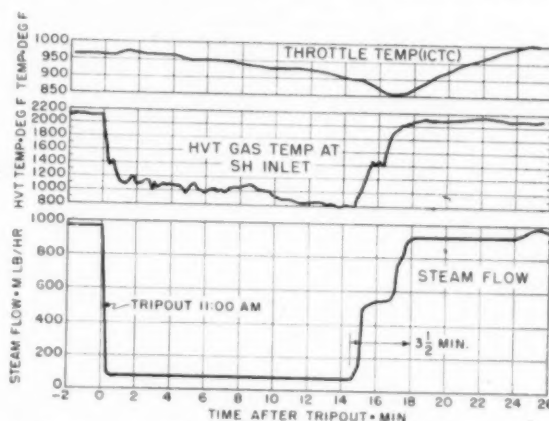


FIG. 22 RECORD OF CONDITIONS DURING AND AFTER TRIP-OUT

fore the trip-out to 1100 F in 1 min, and then drifted down in irregular fashion to 800 F during the low-load period. When load was resumed the gas temperature rose again to 2100 F.

Steam temperature at the turbine throttle was approximated by a bare 22-gage iron-constantan thermocouple inserted in an idle thermometer well at the turbine inlet. Due to the thermal inertia of the thermometer-well assembly, the temperature reading did not follow the steam temperature very closely. The steam temperature indication before the trip-out was 960 F, and during the no-load period slowly drifted down to 900 F. During the load pickup, a large quantity of saturated steam was passed through the superheater before the normal superheater absorption rate had been re-established, with the result that the steam temperature indication dropped to 850 F during load pickup. Then, as superheater absorption returned to normal the steam temperature climbed to 1000 F.

In so far as the boiler proper was concerned the limiting factor with respect to rate of load pickup was water level in the drum. Under the condition of test the rate of load increase was approximately 240,000 lb per hr per min; as a result of these tests we conclude that with optimum regulation and careful co-ordination of the feedwater with the rate of load increase, it would be possible to bring this boiler from no load to full load in somewhat less than 3 min, at a rate in excess of 300,000 lb per hr per min, without raising the water level more than 10 in. above the drum center line, and without increasing the solids content of the steam.

AUTHORS' CLOSURE

The authors wish to emphasize again that the rates of loading of 5 mw per min should be considered as applying only to this size machine and should be expressed as a percentage of rated machine capacity when these results are interpreted as applying to machines of different construction and capacity.

Mr. Falkner's use of burners located high in the boiler to give high steam temperatures at starting is a very interesting and apparently necessary development and should make safer and more practical the starting of a turbine after a relatively short shutdown.

One means of reducing the thermal stresses during fast loading is by holding the temperature of the steam high while the unit is operating in spinning reserve. Since most boilers have a drooping characteristic, the same high location of burners may be desirable when a turbine is held as spinning reserve. It is understood that some West Coast power companies are investigating this

procedure. It is to be understood that the higher throttle temperatures at low loads may require slightly higher minimum loads to maintain low exhaust-hood temperatures.

The annual saving of \$250,000, as quoted by Mr. Falkner, is impressive enough to justify the large amount of experiment necessary to establish the optimum starting and loading rates. The discussions of both Mr. Falkner and Mr. Poor illustrate the necessity of considering starting and loading the entire power plant, rather than the turbine, boiler, or auxiliaries alone. Mr. Poor's discussion also indicates a direction for boiler design if fast pickup of load is made a requirement.

A study of the temperature data taken by Mr. Falkner and others shows that quick starting of a hot turbine should not impose undesirable stresses on the machine when the quick starting is made under proper conditions and supervision. The inspection of the Consolidated Edison Company turbines, showing that a large number of quick starts had been made with no damage or increased maintenance, confirms this study. However, quick starting is by no means a universal panacea for all

starting or loading difficulties. There is no substitute for close mechanical supervision of any piece of machinery during such times. If anything, supervision during rapid starting and loading is even more important than at other times.

A primary requirement in starting and loading is that thermal stresses should be held to allowable limits. This involves the consideration of steam and metal temperatures and the heat-transfer coefficients. After the allowable limits for different material and different type of construction have been established by experience over a number of years, it will then be possible to establish starting times and loading rates for the allowable limits of thermal stress. It is probable that the loading rates will not be uniform over the complete load range of the machine and will be affected by the initial conditions of throttle steam and metal temperatures, as well as the conditions of starting. With further tests made possible by the co-operation of the operators and the manufacturers, further knowledge of this subject will be obtained and power-generating equipment may be operated nearer the point of its greatest usefulness.

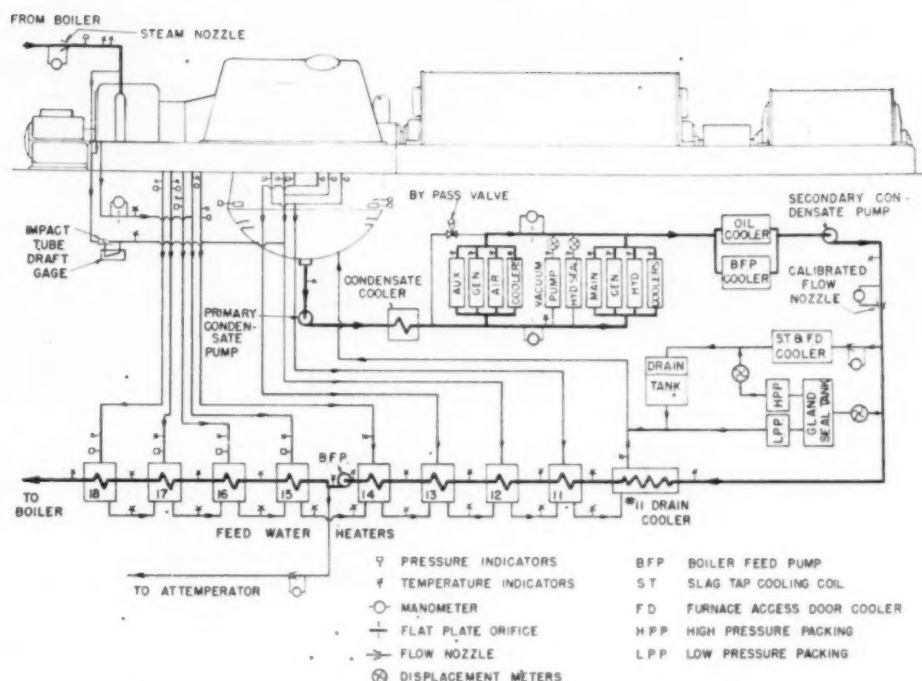


Fig. 1 DIAGRAM OF CYCLE AND LOCATION OF INSTRUMENTS

Heat-Rate Test Results of the 100,000-Kw Essex Turbine Generator

By VINAL S. RENTON¹ AND STANFORD NEAL²

A 3600-rpm, tandem compound, 100,000-kw turbine generator was recently installed at the Essex Generating Station of the Public Service Electric and Gas Company of New Jersey. Since it was, at that time, the largest machine of its type ever built, the first of a new class, and had initial steam conditions of 1250 psig and 1000 F, careful and extensive heat-rate tests were made jointly by the operating company and the manufacturer. The paper presents the results of the tests as an example of progress made in power-generating equipment.

INTRODUCTION

ON December 18, 1947, the largest 3600-rpm, tandem-compound steam turbine-generator ever built up to that time was placed in service as No. 1 unit at the Essex Generating Station of the Public Service Electric and Gas Com-

¹ Engineer, Electric Engineering Department, Public Service Electric and Gas Company, Newark, N. J. Mem. ASME.

² Section Engineer, Steam Research Section, Steam Turbine Engineering Division, General Electric Company, Schenectady, N. Y. Mem. ASME.

Contributed by the Power Division and presented at the Semi-Annual Meeting, San Francisco, Calif., June 27-30, 1949, of THE AMERICAN SOCIETY OF MECHANICAL ENGINEERS.

NOTE: Statements and opinions advanced in papers are to be understood as individual expressions of their authors and not those of the Society. Paper No. 49-SA-19.

pany, Newark, N. J. Since it was the first of a new class of units for the manufacturer and the operating company, extensive tests were made to determine its heat rate and operating characteristics. The operating characteristics are reported in a separate paper.³

The heat-rate tests, with which this paper deals, were made in the period from February 14 to February 24, 1948, jointly by the Testing Laboratory of the Public Service Electric and Gas Company and the Turbine Engineering Division of the General Electric Company.

Results of the test were consistent with and slightly better than the guarantees. They indicate that this machine, of advanced design performs in accordance with anticipations.

CYCLE AND TURBINE DESIGN

The turbine generator with its unit boiler, condenser, and auxiliaries, was designed to fit into the space occupied by the existing No. 1 unit, rated at 20 mw, which had been installed in 1915. The specifications for the new No. 1 unit called for a highly efficient cycle which was to have its best heat rate at loads between 70 and 90 mw.

The feedwater-heating arrangement is shown in Fig. 1. It is believed that this is the first time in this country that as many

³ "Operating Characteristics of the 100,000-Kw Essex Turbine Generator," by Stanford Neal and Vinal S. Renton, published in this issue of the Transactions, pages 267-284.

as eight stages of feedwater heating have been used for one turbine. The heater system is also unusual in that the drains are cascaded, then passed through a drain cooler and to the hot well, where deaeration is accomplished.

As shown in Fig. 1, most of the losses are used to heat condensate. For conditions of high turbine exhaust pressure with the resulting high temperature of the condensate, a cooler is provided to reduce the condensate temperature for cooling the auxiliaries.

DESCRIPTION OF THE TURBINE GENERATOR

The semisection of the turbine is shown in Fig. 2. A mechanical description is reported elsewhere,⁴ and the following discussion is limited to points pertinent to a study of the heat-rate results.

The tandem-compound turbine has a nominal rating of 100,000 kw, and the steam conditions are 1250 psig 1000 F. The high-pressure section has 19 stages with extraction connections from the 7th, 10th, 13th, 16th, and 19th stages. The double-flow low-pressure section is on the same shaft and has 5 stages with extraction connections from each of the two 20th, 21st, and 22nd stages.

The three feedwater heaters supplied, with steam from the three latter extractions, are placed horizontally in the condenser neck and directly under the low-pressure turbine to conserve space and reduce the length of the extraction piping. Model tests were made jointly by the manufacturers of the turbine and condenser to determine the best location of the heaters. The 23rd and 24th-stage moisture catchers are drained to the hot well.

Steam flow and load are controlled by eight primary valves which admit steam to the first stage, and four stage valves which by-pass steam from the discharge of the 1st stage to the inlet of the 4th stage. The valving sequence is arranged so that seven of the primary valves open consecutively for the first seven admissions. The four stage valves are next opened together for

the 8th admission, and the eighth primary valve is opened for the 9th admission.

The shaft of the high-pressure turbine is sealed by a labyrinth packing and an impeller-type water seal. The labyrinth packing at the high-pressure end has three sections with leakage steam from the 1st section going through the space between the inner and outer turbine shells and out to the 10th-stage heater. The leakage steam from the second section is piped to the 16th-stage heater, and that from the third section to the 21st-stage heater. The labyrinth packing at the low-pressure end has only one section, which is piped to the 21st-stage heater. The shaft of the low-pressure turbine has only impeller-type water seals.

The main generator is rated 111,765 kva at 0.85 power factor, with 15 psig hydrogen pressure, and 117,647 kva at 0.85 power factor with 25 psig hydrogen pressure. The house or auxiliary generator is air cooled and rated at 7500 kw at 0.80 power factor. Separate motor-driven exciters supply the field electrical requirements.

The turbine and the two generators are coupled solidly to one shaft, and the unit has an over-all length of 77 ft, 7 1/2 in. and weighs 1,120,000 lb.

MOISTURE REMOVAL

The quantity of drain flow was calculated by heat balances around each heater individually. Since all of the heater drains were cascaded through a drain cooler to the condenser, the quantity of total drain flow also was calculated by a heat balance at the drain cooler. The drain flow, so calculated, was found to be consistently and significantly higher than the sum of the calculated extraction steam flows to the eight heaters. That difference was considered to be the quantity of moisture discharged from the turbine into the extraction pipes and showed a high effectiveness of the moisture catchers. The amount of moisture thus indicated as removed in the wet extraction stages was about 10,000 to 12,000 lb of water per hr and was nearly constant irrespective of load. The amount of moisture removed from the 23rd-stage and the 24th-stage diaphragm was expected to be large but was not measured. An examination of the last-stage

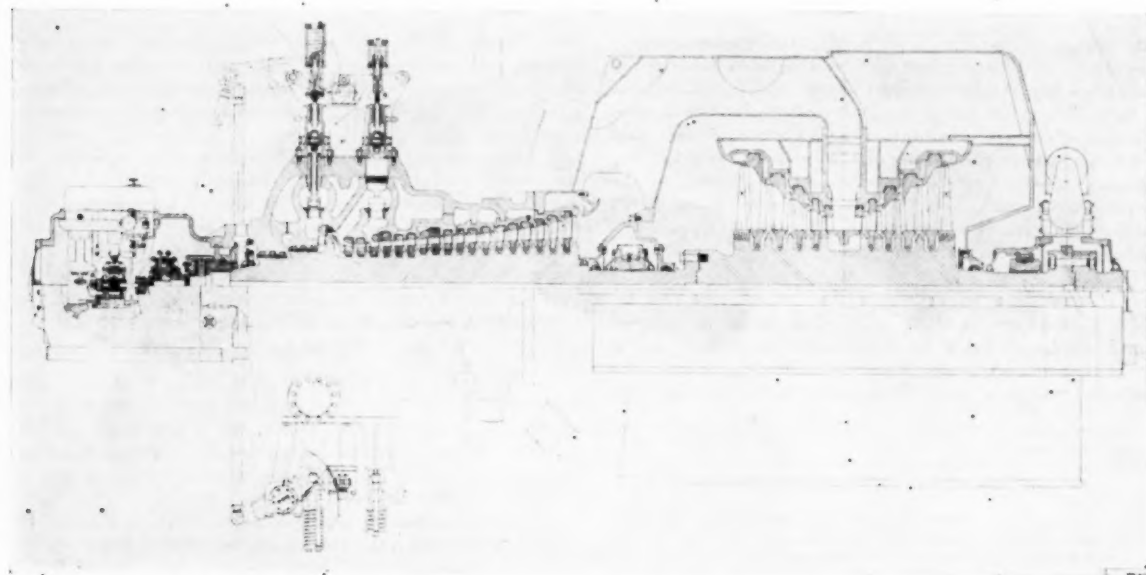


FIG. 2 SEMISECTION OF ESSEX NO. 1 UNIT TURBINE GENERATOR

⁴ "The Design of Seward Generating Station and No. 1 Unit at Essex Station, Public Service Electric and Gas Company," by F. P. Fairchild, published in this issue of the Transactions, pages 247-265.

buckets after 14 months of service confirmed this assumption since little erosion had occurred.

HEAT-RATE RESULTS

The heat rate of the turbine generator is defined as that quantity of heat supplied by the boiler (and the boiler feed and condensate pumps) necessary to produce 1 net kwhr of electricity. The net kilowatt-hour output is defined as the output at the terminals of the two generators minus the electrical inputs to the two generator fields.

Since the steam conditions and heater performance were not the same in every test, the test results have been corrected to a standard cycle to provide a uniform basis of comparison. The standard cycle differs from the test cycle principally in that:

- 1 The initial steam conditions were 1250 psig and 1000 F.
- 2 Exhaust pressures were 1.00 in., 1.50 in., 2.50 in., and 3.50 in. Hg abs.
- 3 Heater terminal differences and extraction-pipe pressure drops were assumed to be the same as in the turbine specification.
- 4 Attenuator flow was zero. (The attenuator was used only in 7 test points.)

The standard extraction cycle heat rates, based on test performance, are shown in Fig. 3 as a function of load for the four exhaust pressures. The points in Fig. 3 have been connected

by valve loops, the shapes of which have been determined by previous tests on other turbines. The rise in heat rate at loads above 93 mw is caused by the opening of the internal stage valves which provide a by-pass for the steam flow around the 2nd and 3rd stages. The heat-rate curve at 1.50 in. Hg exhaust pressure is well located with eleven points, but it should be noted that the curves at 1.00 in., 2.50 in., and 3.50 in. Hg are drawn from only three test points with the shape determined by the 1.50-in. curve.

The standard extraction cycle throttle and condenser steam rates based on test performance are shown in Fig. 4. It may seem surprising that the throttle steam rate is about 4 per cent better at 35 mw than at 117 mw while the heat rate is about 9 per cent poorer at the lower loads. This apparent inconsistency is explained readily since the amount of steam extracted for feed-water heating changes from about 22 per cent to 32 per cent over the same range of load. The larger percentage of condenser steam flow at 35 mw has the effect of reducing the amount of throttle steam per kilowatt-hour at the expense of a less efficient cycle with its higher heat rate. This example shows that a low throttle steam rate is not necessarily compatible with a low heat rate. Had this turbine been operated nonextracting, the steam rate would have been the same for both throttle and condenser flows and would have a value between the two sets of curves shown in the figure. As a matter of interest, the feed-

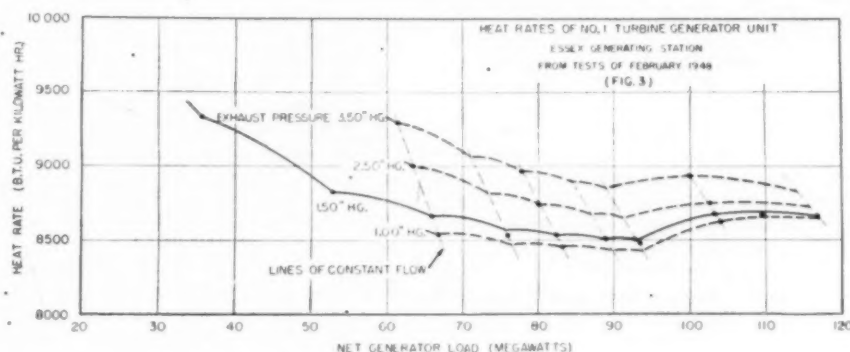


FIG. 3 HEAT RATE OF ESSEX NO. 1 UNIT TURBINE GENERATOR

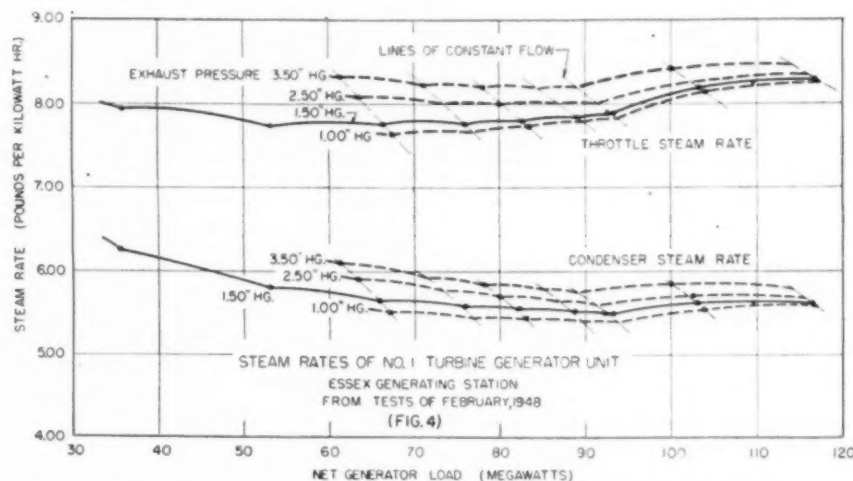


FIG. 4 THROTTLE AND CONDENSER STEAM RATES OF ESSEX UNIT NO. 1 TURBINE GENERATOR

water temperature leaving the last heater was 477 F at the highest load.

ACCURACY OF THE TESTS

Extreme care was taken in the isolation of the unit, selection, installation, and calibration of the instruments, and constancy of test conditions. It was expected that the absolute accuracy would be about $\frac{1}{2}$ per cent, and the reproducibility somewhat better. The one check point at 93 mw differs from the first point by about 0.15 per cent. Since one point was made at the beginning and the other near the end of the test, there was no appreciable change of performance of the unit during test. There was no evidence of deposits in the steam path either by inspection or from unit performance.

GENERATOR TEST

The results of the generator pre-heating test will be reported elsewhere,⁸ and will not be described here. The generator losses were of the magnitude predicted by the manufacturer and the maximum temperatures were well within the design limits.

CONCLUSIONS

At the best point, which was at 93 mw load, and at an exhaust pressure of $1\frac{1}{2}$ in. Hg abs, the heat rate of the turbine-generator and feedwater heaters was found to be 8498 Btu per kw-hr for the standard cycle used to compare the test points. The corresponding thermal efficiency is 40.16 per cent. The standard cycle differed from the operating cycle by only a few tenths of a per cent.

At the rated exhaust pressure of $1\frac{1}{2}$ in. Hg abs, the heat rate averages 0.76 per cent better, and the best point is 1.4 per cent better than the guarantee.

Test data on the complete unit including boiler, turbine, feedwater heaters, and auxiliaries indicate an approximate over-all heat rate of 10,100 Btu per kw-hr at the most economical point during winter conditions. The corresponding thermal efficiency is 33.79 per cent. With 13,500 Btu per lb coal, that heat rate corresponds to the consumption of 0.75 lb of coal to produce 1 net kw-hr of electrical energy at generator terminals.

During the entire year of 1948, the station records show that the over-all unit heat rate was 10,500 Btu per kw-hr at an average load of 97,800 kw for each hour of operation.

Tests of the operating characteristics have demonstrated that the unit operates satisfactorily with fast starts and high loading rates. Several load-dump tests followed by fast pickup of load have been made with excellent performance.⁹

The Essex No. 1 Unit has satisfied both the owner and the manufacturer with respect to efficiency, operating characteristics, and service record.

ACKNOWLEDGMENTS

The authors express their appreciation for the valuable assistance of Messrs. E. M. Kratz, P. C. Van Nørdstrand, and M. W. Leonard in making the test and calculations.

Appendix

DESCRIPTION OF TEST INSTRUMENTS

The location of each of the test instruments is shown in Fig. 1.

All important temperatures were measured with chromel P-copric thermocouples inserted in wells. A few temperatures were measured with copper-copric thermocouples peened into pipe walls. All thermocouple potentials were measured with precision

potentiometers. The condensate temperatures at the generator coolers were measured with precision-grade mercury-in-glass thermometers. All thermocouples and thermometers were calibrated before and after the test, except for the peened couples which necessarily were destroyed in disassembly. Temperatures were read at ten-minute intervals, with the exception of those at the throttle and at the discharge from the highest feedwater heater, which were read every 5 min.

Pressures above 25 psia were measured with dead-weight gages, those between 5 psia and 25 psia with mercury-filled manometers open to atmosphere, and the condenser pressures were measured with mercury-filled absolute gages. All gages, weights, and manometers were checked carefully before the test. For convenience and accuracy, all turbine pressures at levels below 25 psia were measured with air-filled connecting pipes. This was accomplished by bleeding a very small amount of air into each pipe.

The condensate flow was measured with either a 4.335-in. or a 2.794-in.-diam flow nozzle. Both were calibrated before the test by Prof. S. R. Beidler. The pressure difference was indicated on a mercury-filled manometer read at one-minute intervals.

As an independent check on the throttle flow, the pressure difference across the uncalibrated station steam-flow nozzle was read at one-minute intervals. However, the water legs could not be determined accurately, and the measurements were not entirely consistent or reliable. This trouble was corrected after the test.

The condensate flows to the gland-seal tank and from the high-pressure-turbine packings were measured with displacement-type integrating water meters. The flow quantity was recorded every 15 minutes.

The flow to the attemperator was measured with the station nozzle. Since the flows were small, a dibromoethane (specific gravity = 2.17) filled manometer was used to indicate the pressure difference. Readings were made at five-minute intervals. The maximum attemperator flow was $3\frac{1}{2}$ per cent of the throttle flow.

Slag-tap and boiler-access door cooling flow was measured with a flow nozzle and a mercury-filled manometer. Readings were made at five-minute intervals.

The flow of condensate through the generator coolers was measured by thin-plate orifices. The coefficients were taken from the ASME fluid meters report.¹⁰ The pressure differences were indicated on mercury-filled manometers and read at five-minute intervals. In order to obtain a larger temperature difference across the main generator coolers at several test points, the arrangement of the station piping made it necessary to by-pass some condensate around the auxiliary-generator coolers, which prevented measurement of the cooler flow. For that reason, only a few loss measurements could be made on the auxiliary generator.

The leakage flow from the second section of the high-pressure packing was measured with a thin-plate orifice and a mercury-filled manometer, read at five-minute intervals. The leakage flow from the third section of the high-pressure packing was measured with an impact tube placed at the axis of the pipe and a pipe-wall static pressure tap. The pressure difference was indicated on a draft gage and read at five-minute intervals. This method of measuring the flow was necessary, since there was not sufficient pressure available for an orifice measurement.

Storages in the hot well and heaters were measured by observing calibrated sight glasses at 15-minute intervals.

The electrical output of each generator was measured with three single-phase indicating wattmeters read at one-minute intervals. The voltage and current in each phase were observed at two-minute intervals. The power input to the two fields was measured with voltmeters across the slip rings and milliammeters across shunts.

⁸ The generator preheating test is expected to be the subject of an AIEE paper by F. W. Gay and H. D. Taylor.

¹⁰ "Fluid Meters, Their Theory and Application," THE AMERICAN SOCIETY OF MECHANICAL ENGINEERS, New York, N. Y., fourth edition, 1937.

All ammeters, voltmeters, and wattmeters were calibrated before and after the test, and the current and potential transformers and the shunts were calibrated before the test. Check readings were made on the station integrating watt-hour meter which was especially equipped for the test with a high-speed register.

The tests followed the procedures outlined in the ASME Power Test Code. The Keenan and Keyes Steam Tables⁷ were used to determine steam properties.

Before each test, the turbine and heater piping was carefully checked to make certain that the cycle used was the one shown in Fig. 1, and to check the isolation of the unit. Isolation was made positive in every connecting pipe not necessary to the cycle by inserting blind gaskets between flanges or by closing two valves in series and opening a "telltale" drain valve between them to prove that no flow passed through the pipe. A single valve was used for only one connecting line which went to the condensate head or surge tank. That valve was checked carefully for tight closing before, during, and after the test. It was not possible to double-valve this line from the standpoint of safety.

The losses of each generator were obtained by measuring the temperature rise and quantity of the condensate used to cool the hydrogen in the main generator, and the air in the auxiliary generator. Since the four coolers in each generator are connected in parallel and it was practical to make only one flow measurement for each generator, it was necessary to adjust the flow through each cooler to give the same temperature rise. The hydrogen pressure was maintained at 15 psig, except for the two highest load points where it was held at 25 psig.

All test points except one ($8\frac{1}{2}$ admission point) were made at a valve-intercept point. That point occurs just prior to the opening of the next higher valve. The intercept point could be set accurately by opening the governor until all lost motion is taken up in the cam-and-roller assembly of the next higher valve. Since a force of only a few hundred pounds was necessary to take up this lost motion and several thousand pounds to lift the valve away from the seat, a check of the force on the roller with a pinch bar permitted accurate setting of the valve within 2 or 3 thousandths of an inch. This method is considered to be the most accurate since a measurement of valve lift will vary slightly with different loads on the turbine as the temperatures of the valve mechanism and steam chest change. The valve-roller tightness and the position of governing mechanism were checked several times during each test to make certain the valves had not changed position. The governor was very stable and it was not necessary to reset the valve position during any test. During tests, the governor was set on the "load limit" which essentially kept the governor from increasing the load but still left control for reducing the load by normal governor action if an emergency should arise.

For different tests, the exhaust pressure at the condenser neck was held at $3\frac{1}{2}$ in., $2\frac{1}{2}$ in., $1\frac{1}{2}$ in. Hg abs, and the lowest that could be obtained. For the higher values, the pressure was held by bleeding air from the atmosphere into the condenser. This method is simple and permits rapid and close control of the exhaust pressure. It was usually held within 0.01 in. Hg.

Tests were made with an exhaust pressure of $1\frac{1}{2}$ in. Hg abs at each of the nine admission points, at the $8\frac{1}{2}$ admission point, and a check test was made at the 7th admission. Other tests were made at exhaust pressures of $3\frac{1}{2}$ in., $2\frac{1}{2}$ in., and best (about 1.1 in.) at the 3rd, 5th, and 8th admission points.

The initial steam conditions were held as closely as possible to the rating of 1250 psig and 1000 F. At the lighter loads, the

boiler characteristics resulted in lower throttle temperatures. The throttle temperature usually was held constant within ± 10 F, and the throttle pressure within ± 10 psi.

All test points at exhaust pressures of $1\frac{1}{2}$ in. Hg abs were of 2-hr duration. Those at other exhaust pressures were 1-hr tests. To insure constant conditions, the load was set and held for 1 hr before the test period.

Discussion

ADOLF EGLI.* The 100,000-kw turbogenerator tested is a brilliant example of progress in modern power-generating equipment. As regards steam-power-cycle development, this unit represents the highest perfection to date of the regenerative-feed-heating cycle. The writer is struck by the elegant simplicity of the layout of the turbine flow path as well as with the completeness of the regeneration system applied.

The thermodynamic perfection attained is astounding; 40.16 per cent thermodynamic efficiency of the turbogenerator unit and 33.79 per cent thermal efficiency of the complete power unit, including boiler and auxiliaries, are indeed excellent values for a plant without the complication of a reheat cycle.

Remarkable is the combination of a flat heat-rate curve with great overload capacity which has been attained by a clever arrangement of throttle valves and by-pass valves regulating the throttle steam flow. Between maximum load and half maximum load, the heat rate (at $1\frac{1}{2}$ in. Hg back pressure) varies only 1.7 per cent, the best value being obtained midway between these points at the most important output. Even at 30 per cent maximum capacity, the heat rate is only 9.5 per cent above the best value.

Of the test instrumentation, the dead-weight gages used to measure the high steam pressures, are most intriguing to the writer.

Would the authors be in a position to give a detailed description of the design and operation of these gages? Precise measurement of the high steam pressures on a turbine in operation is a difficult problem, and the proper application of the dead-weight system would appear to be a valuable step in improving test precision.

In particular, the writer is also interested in the accuracy attained with condensate-flow-nozzle measurement.

A detailed heat balance of the unit tested would also be most informative. By publishing this information the manufacturer and the Public Service Electric and Gas Company would indeed render valuable service in the general advancement of the art of power generation.

AUTHORS' CLOSURE

The authors thank Professor Egli for his comments on the design and application of the Essex turbine generator.

It has been the practice of the authors' company to use dead-weight gages in the tests of steam turbines since they provide the most practical fundamental and accurate type of pressure measurement. It is difficult to use this type of gage when the pressure fluctuates rapidly. However, modern methods of pressure control in generating stations are sufficiently good to permit the use of deadweight gages. Although more work is involved in its installation and use, the increase in accuracy is believed to justify the additional time and expense. The area of our dead-weight-gage cylinder is 0.1250 sq in. (a diameter of about 0.4 in.) and is larger than the usual dead-weight gage or dead-weight-gage tester. The sensitivity of about $\frac{1}{2}$ in. of water and the practical advan-

⁷ "Thermodynamic Properties of Steam," by J. H. Keenan and F. G. Keyes, first edition, twelfth printing, John Wiley & Sons, Inc., New York, N. Y., 1946.

* Professor of Mechanical Engineering, Towne Scientific School, University of Pennsylvania, Philadelphia, Pa. Mem. ASME.

tage of free plunger travel is believed to outweigh the inconvenience of the correspondingly large weights.

The gages are oil-filled and, in steam-turbine tests, are usually operated with water-filled lines, necessitating the usual water-leg correction. In operation, the pan is loaded with weights until the pressure is balanced, the weight pan being rotated by hand to remove any friction effect. Arrangements have been used with the pan loaded with a spring or balance arrangement of about 10 psi capacity to avoid the use of small weights. Such devices have also been used for the control of pressure with the rotation of the plunger accomplished by an air turbine. The radial clearance between the cylinder and plunger is held to about 0.0001 in. and the parts are usually made of nitraloy with lapped surfaces.

There is a question as to whether the area of the cylinder or of the plunger or some intermediate value should be used. With these close fits, the error involved when an average area is used

cannot be more than about 0.05 per cent. Calibrations by the Bureau of Standards and others confirm this opinion.

The two nozzles used in this test were made by the Bailey Meter Company and installed with straightening vanes in a pipe of suitable length. The two assemblies were calibrated by Prof. S. R. Beitler and are believed to represent the true coefficient within ± 0.2 per cent. Each nozzle was used only in the Reynolds number range of constant value of the flow coefficient. The smaller nozzle was used in the Reynolds number range of 1,200,000 to 1,600,000, and the larger from 1,200,000 to 2,200,000. While these ranges require extrapolation of the calibration to somewhat higher values than could be reached in the calibration, that extrapolation was in the region of the constant value of the flow coefficient and is well justified by experience.

The addition of heat balances at three loads was considered when this paper was prepared, but it was decided to omit these items because of lack of space.

Frictional Characteristics of O-Rings With a Typical Hydraulic Fluid

By L. E. CHEYNEY,¹ W. J. MUELLER,² AND R. E. DUVAL,³ COLUMBUS, OHIO

O-ring packings employed in aircraft hydraulic systems are subject to numerous operating variables, which affect the friction involved in their operation. A method for studying the friction is described, and the effects of several variables—pressure, time delay, squeeze, stroke speed, ring size, and surface finish of the moving metal part—have been determined.

INTRODUCTION

DURING the past several years there has been a strong trend in the aircraft industry toward the use of hydraulic systems, as a result of increases in the size of planes, where the required forces prohibit manual operation of many controls. The hydraulic system has an advantage over other possible systems because it assists in the movement of controls, but it still maintains the "feel" which is considered highly desirable.

Among the small but important parts of a hydraulic system are the packings. Earlier systems in use for aircraft employed one or more of the well-known V-ring, U-cup, or compression-type packings. The O-ring is a fairly recent development in the packing field, which has been shown to have many advantages over the older types.

To prevent sticking of moving parts and excessive wear on packings, the friction between the moving parts and the packing should be held to a minimum. It would be expected that the early compression-type packings would cause high friction because of their design. O-rings offer an opportunity to reduce this friction because of a much smaller area of contact with the moving part.

Previous published work on the subject of friction is meager. Several recent articles (1, 2, 3, 4, 5, 6, 7, 8)³ give limited data concerning the effect on packing friction of various characteristics of the hydraulic system, while the general frictional characteristics of rubber are treated in some previous publications (9, 10, 11). While these articles cover a part of the field, some of them freely admit that there is much work yet to be done.

EXPERIMENTAL PROCEDURE

An apparatus was designed so that friction caused by an O-ring could be measured under controlled conditions, with one factor varied at a time. In the apparatus employed, an actuating rod was drawn through a stationary O-ring. Frictional forces were transmitted from the ring, through a bellows arrangement, to a recording engine indicator.

The entire apparatus could be considered as composed of several individual units as follows:

¹ Formerly Assistant Supervisor, Resin and Rubber Research, Battelle Memorial Institute.

² Research Engineer, Battelle Memorial Institute.

³ Numbers in parentheses refer to the Bibliography at the end of the paper.

Contributed by the Rubber and Plastics Division and presented at the Annual Meeting, New York, N. Y., November 28–December 3, 1948, of THE AMERICAN SOCIETY OF MECHANICAL ENGINEERS.

NOTE: Statements and opinions advanced in papers are to be understood as individual expressions of their authors and not those of the Society. Paper No. 48—A-64.

1 The nucleus of the machine was a hydraulic press, to the ram of which was attached an actuating rod (SAE 4340 steel, Rockwell hardness 40 C). Ram speed of the machine could be varied from 85 to 300 ipm on the upstroke, and 60 to 215 ipm on the downstroke. A timing device was installed to allow an automatic variable time delay between strokes.

2 The hydraulic pressure unit consisted of a pump and reservoir with accessory equipment such as time switches, tubing, etc. The variable-flow pump employed was capable of producing 3000 psi fluid pressure. The oil reservoir, a large box made from steel plate, held about 50 gal of oil and was provided with cooling coils.

3 The assembly for holding the O-ring under fluid pressure consisted of a section of stainless-steel tubing with a cap screwed on each end. The end of each cap contained a hole, through which the actuating rod passed. One end of the tube was sealed by the O-ring, contained in a machined groove inside the cap. The other cap contained no packing but had a lap fit around the rod with a clearance of about 0.001 in. (The friction from this lap fit was found to be negligible.) The hydraulic pressure was applied to the inside of the sealed tube.

4 The friction-measuring unit consisted of a bellows connected to an engine indicator by means of copper tubing, the entire unit being filled with oil and sealed. The frictional force was transmitted from the ring to the bellows by a special cap, which in turn transmitted it through the oil to the recording engine indicator, which recorded the friction continuously.

In any work of this type the accuracy of test results should be considered. It is felt that the measuring unit is quite accurate because of its basic design. The spring on the engine indicator can be calibrated with dead weights and this is done at frequent intervals. A small error is involved in reading the engine indicator cards because a small distance between lines on the card corresponds to several pounds friction. This error is of the order of 3 or 4 lb maximum; it could probably be reduced if necessary by constructing a special micrometer-type scale for reading the cards. Assuming the measuring unit to be quite accurate, the accuracy of the work would then be limited only by the degree to which the friction would reproduce itself.

An effort was made to evaluate what were considered the more important variables, as indicated by previous work (1, 2, 3, 4). This study was concentrated upon one hydraulic fluid (Army-Navy Specification AN-VVO-366B). All of the work was performed using one typical ring size (-28 as described in Army-Navy Specification AN6227), except the study of ring-size effect. Testing was done at room temperature. All of the rings used in this study were aged in hydraulic fluid before testing, according to Army-Navy Specification AN-P-79.

EXPERIMENTAL RESULTS

Previously published data have recommended that the O-ring groove depth be 10 per cent less than the free diameter of the ring (6). The purpose of the shallow groove is to make certain that the ring is subjected to a positive squeeze at all times. This positive squeeze is necessary if the ring is to seal at low pressures where the pressure is not great enough to deform the ring and force it against the diametral clearance between the moving

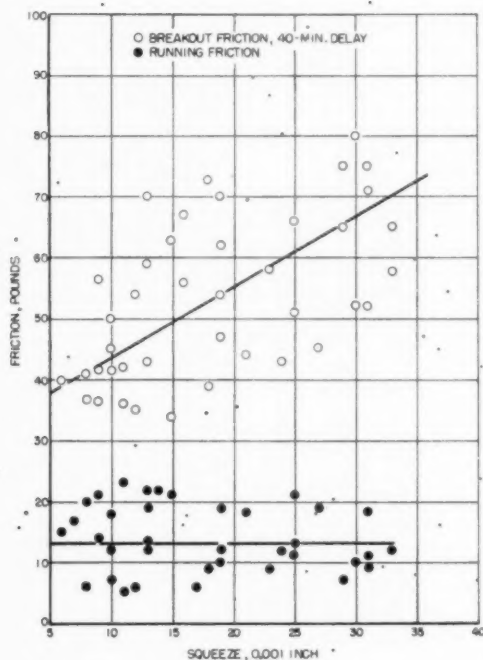


FIG. 1 EFFECT OF SQUEEZE ON FRICTION
(2.8-3.2 microinches surface finish, 300 ipm stroke speed, 500 psi pressure.)

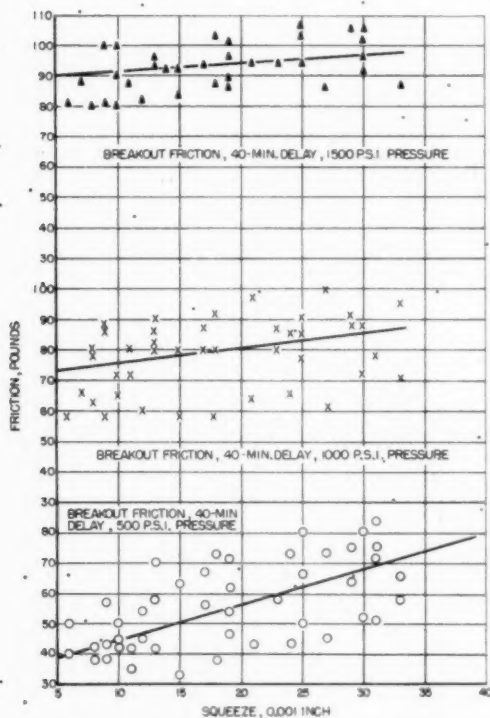


FIG. 2 EFFECT OF PRESSURE ON FRICTION
(2.8-3.2 microinches surface finish, 300 ipm stroke speed.)

and stationary parts. Army-Navy Specification AN-P-74 designates the minimum squeeze to be applied to an O-ring; this squeeze is approximately 10 per cent of the cross-section diameter of the ring.

Breakout- and running-friction determinations were made under various conditions of pressure and time delay, in addition to variation of squeeze. The result of a large number of tests shows that the running friction is largely independent of squeeze over the range covered. There is some tendency at higher pressures for the running friction to increase slightly with squeeze. A different situation exists in the case of breakout friction, where an increase in squeeze results in an increase in friction. Fig. 1 shows typical data of friction versus squeeze for running and breakout friction. The points shown are chosen as representative of about 2500 determinations. The range of results, as shown by the figure, is approximately ± 15 lb for the breakout friction and ± 8 lb for the running friction.

The effect of hydraulic pressure has been noted previously (1, 2). As there is a strong trend toward higher pressures in the newer aircraft systems, this is a very important factor. The effects of 500, 1000, and 1500 psi pressure were checked in this study. It was found that an increase in pressure resulted in a small increase in running friction and a large increase in breakout friction. Figs. 2 and 3 illustrate this point. The data shown here are typical of about 700 determinations. It can be seen that the accuracy is approximately ± 15 lb for the breakout friction and ± 10 lb for the running friction.

It has been generally felt that the breakout friction would be higher as time delay between strokes increased. Experimental results confirmed the original belief for time delays of less than 40 min. Time delays of more than 40 min, however, did not increase the friction appreciably.

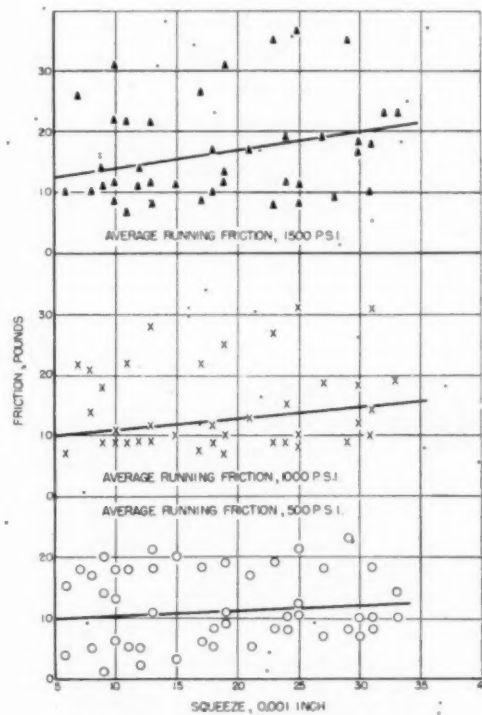


FIG. 3 EFFECT OF PRESSURE ON FRICTION
(2.8-3.2 microinches surface finish, 300 ipm stroke speed.)

Running friction was not expected to change with time delay between strokes. In this case also, the experimental data confirmed the original belief. Fig. 4 shows data, typical of about 1600 determinations, on the effect of time delay on the two types of friction. The accuracy of reproduction is about ± 10 lb.

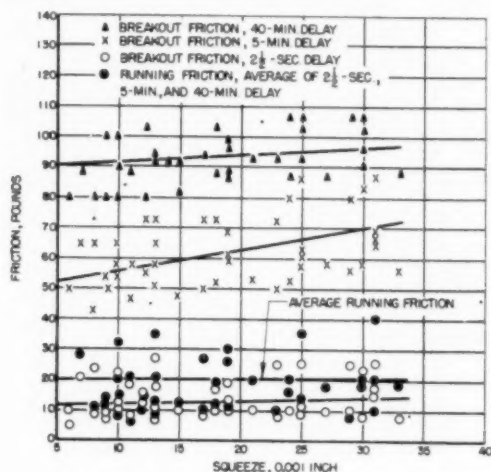


FIG. 4 EFFECT OF TIME DELAY ON FRICTION
(2.8-3.2 microinches surface finish, 300 ipm stroke speed, 1500 psi pressure.)

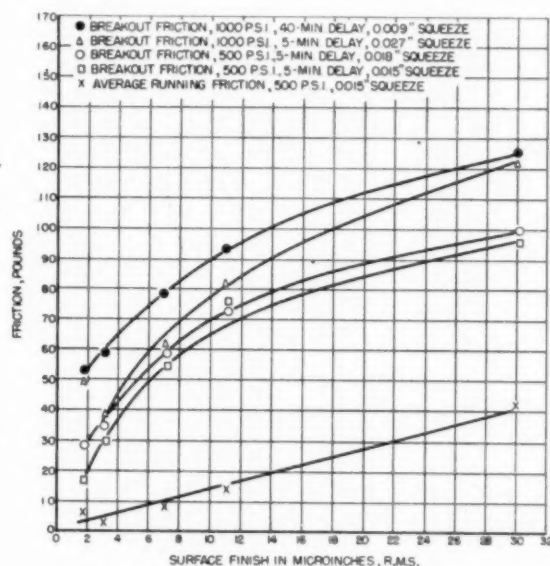


FIG. 5 EFFECT OF SURFACE FINISH ON FRICTION
(300 ipm stroke speed.)

The importance of roughness of the surface which rubs against the ring has been recognized by other investigators (1, 2). Army-Navy Specification AN-P-74 requires a surface finish (roughness) of 5-15 microinches root mean square (rms). (This is to be changed by eliminating the minimum requirement and retaining the 15-microinches rms maximum roughness.) In order to investigate this factor more thoroughly, a series of 4 rods was constructed. These rods were ground to finishes of 2.8-3.2, 6-8, 10-12, and 16-18 microinches rms. All four rods were evaluated with the same ring to eliminate any variability from that source.

These four rods represent a range of surface finishes not only covering, but also above and below the present specification limits. Fig. 5 shows typical curves for this series. It can be seen that there is a definite increase in friction with an increase in surface roughness.

An additional rod with a surface finish of 1.7-2.0 microinches rms was constructed and evaluated later in a manner similar to the four rods previously studied, although the same ring was not used. The data obtained for this rod are also included in Fig. 5 and show good agreement with the other values. The accuracy of these data is considered to be approximately ± 10 lb.

It has been reported that a chemical surface treatment was being used on some hydraulic parts. Several advantages were claimed for this treatment, particularly reduction of friction, because of better retention of an oil film on the surface. In order to investigate this point, a special rod was constructed and treated by the commercial process. This rod had a surface finish of 10 microinches rms before treatment and 30 microinches rms after treatment. This rod was included in the series showing the effect of surface finish on friction, Fig. 5. The frictional results obtained were apparently directly proportioned to the roughness of the finished rod.

A limited amount of work was done to determine the effect of stroke speed. Figs. 6 and 7 show these data. The running friction was almost independent of stroke speed over the range tested. An increase in breakout friction was noted with an increase in stroke speed at 1000 psi, but at other pressures the friction was independent of stroke speed. There are indications that factors other than stroke speed, for example, pressure, are more significant in determining the friction in a system.

The effect of ring size on friction has been reported by Pearl (2). This author showed the friction to be a function of pressure and projected area of ring exposed to pressure. The area of contact of a packing and moving surface would be expected to affect the amount of friction.

Four sizes of O-rings were given an evaluation to determine the effect of ring size. The ring sizes were —19, —23, —28, and —29 as described in Army-Navy Specification AN6227. The actual sizes are given in Table 1.

TABLE 1 SIZES OF O-RINGS

Ring	Cross-sectional diam., in.	ID, in.	OD, in.
—19	0.139	0.984	1.262
—23	0.139	1.234	1.512
—28	0.210	1.475	1.895
—29	0.210	1.600	2.020

The sizes were chosen to show the effect of diameter at constant cross section, using two different cross sections. Graphs of friction versus squeeze, at different conditions of pressure and time delay, where the data from all four rings were plotted on one graph, show that under some conditions one ring size gave the greatest friction while under other conditions another ring caused the greatest friction. Although the friction of all four rings followed the same general pattern, it could not be concluded that any one ring size consistently gave higher friction than another ring size, at least in the range of dimensions investigated.

Reproducibility of results has been checked in two different ways. One ring from each of several manufacturers was evaluated thoroughly and the comparative results recorded, then five rings from one manufacturer were evaluated in succession. Fig. 8 compares the reproducibility between rings from one manufacturer with that of rings from different manufacturers. It can be seen that the distribution of points in the two curves is very nearly the same, that is, reproducibility between rings of different manufacturers is approximately the same as reproducibility be-

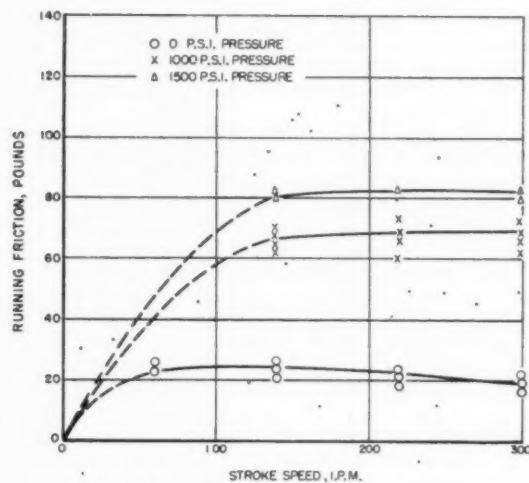


FIG. 6 EFFECT OF STROKE SPEED ON FRICTION
(2.8-3.2 microinches surface finish, 0.017 in. squeeze.)

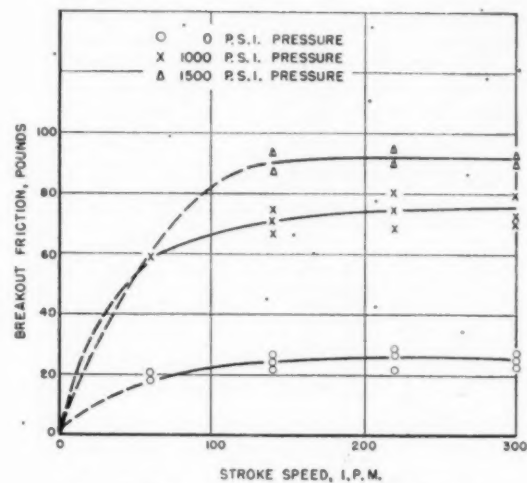


FIG. 7 EFFECT OF STROKE SPEED ON FRICTION
(2.8-3.2 microinches surface finish, 0.017 in. squeeze.)

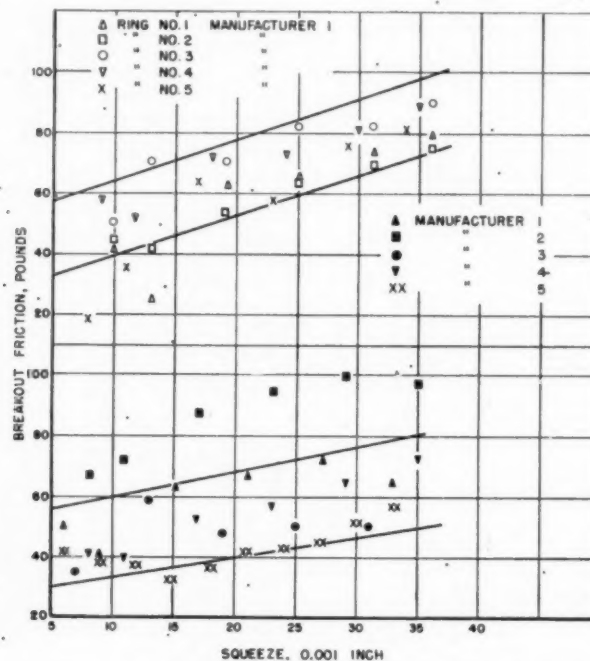


FIG. 8 REPRODUCIBILITY OF FRICTION OF O-RINGS
(2.8-3.2 microinches surface finish, 300 ipm stroke speed, 40-min delay, 500 psi pressure.)

tween several rings from one manufacturer. It can also be seen that the friction curves for the different manufacturers' rings are approximately the same within the accuracy of our testing. From this it can be concluded that all of the manufacturers whose aircraft hydraulic packings have been checked-produce rings of similar frictional characteristics, although there are insufficient data to justify a general conclusion that all are the same.

SUMMARY

Certain design and operating variables in aircraft hydraulic systems have been studied in relation to friction.

It is possible to summarize the resulting data in a fairly comprehensive form. Table 2 summarizes the effect of the variables studied on breakout and running friction.

ACKNOWLEDGMENT

The work described in this paper was carried out in connection with a research project sponsored by the Bureau of Aeronautics, Navy Department. Any opinions expressed here are those of the authors and do not necessarily represent those of the Navy Department. Acknowledgment is also made of the assistance rendered by other Battelle personnel.

TABLE 2 VARIATION OF BREAKOUT AND RUNNING FRICTION WITH CHANGES IN HYDRAULIC SYSTEM

Design or operating change	Breakout friction	Effect	
		Running friction	
Increase squeeze.....	Increase	No effect at low pressure (500 psi). Slight increase at high pressure (1000, 1500 psi).	
Increase time delay between strokes.....	Increase	No effect	
Increase hydraulic pressure.....	Increase	Increase (slight)	
Increase roughness of moving rod.....	Increase	Increase	

BIBLIOGRAPHY

- 1 "Hydraulic O-Ring Packing for Sealing Cylinders and Pistons," by R. E. Allen, *Product Engineering*, vol. 18, 1947, pp. 163-166.
- 2 "O-Ring Seals in the Design of Hydraulic Mechanisms," by D. R. Pearl, *SAE Quarterly Transactions*, vol. 1, 1947, pp. 602-611.
- 3 "Aircraft Hydraulic Systems—Factors Influencing Their Performance," by L. E. Cheyney and T. J. McCuiston, *Mechanical Engineering*, vol. 70, 1948, p. 675.
- 4 "Research on Aircraft Hydraulic Systems," by T. J. McCuiston, F. E. Clark, R. A. Clark, and L. E. Cheyney, *SAE Quarterly Transactions*, vol. 2, 1948, p. 227.
- 5 "Investigation of 10° Undercut Groove for O-Ring Packing," by B. R. Vennum, Douglas Aircraft Company Report SM-20063, Dec. 10, 1945.
- 6 "Performance of Linear LT2-70 Hydraulic O-Ring Packing Used With Chrome Retained Leather Back-Up Rings at 3000 Psi Pressure," by E. R. Broadbent, Douglas Aircraft Company Report SM-11809, April 4, 1946.
- 7 "Performance of Houghton No. 2216 Back-Up Rings With O-Rings on Large Struts at 3000 Psi Pressure," by E. R. Broadbent, Douglas Aircraft Company Report SM-11155, Jan. 1, 1946.
- 8 Letter from F. G. Newlon to L. E. Cheyney, Army Air Forces, Washington, D. C., Aug. 15, 1947.
- 9 "The Coefficient of Friction of Rubber," by J. B. Darieux, *Rubber Chemistry and Technology*, vol. 8, 1935, pp. 441-442.
- 10 "Frictional Properties of Rubber," by F. L. Roth, R. L. Driscoll, and W. L. Holt, National Bureau of Standards *Journal of Research*, vol. 28, 1942, pp. 439-462; *Rubber Chemistry and Technology*, vol. 16, 1943, p. 155-177.
- 11 "The Coefficients of Friction Between Rubber and Various Materials, Part II, Gripping Friction of Rubber Belting," by R. Ariano, *India Rubber Journal*, vol. 79, 1930, pp. 56-58; *Rubber Chemistry and Technology*, vol. 3, 1930, pp. 286-292.

Discussion

G. E. DAVISSON.⁴ The authors are to be congratulated on the excellent work that is summarized in the paper. A short history of this testing program will reveal its vital importance.

History of Testing Program. During the last war the Army Air Force and Navy Bureau of Aeronautics added the winterization requirements, calling for operation of aircraft hydraulic equipment at temperatures from -65 to +160 F, to the AN Specifications covering this equipment. This requirement made obsolete all of the old components of hydraulic equipment that were designed for operation to a minimum temperature of -40 F. It also made necessary an intensive program of development and testing by the services and the aircraft industry. The use of the original winterized O-rings with AN-VV-O-366b winterized hydraulic fluid resulted in an epidemic of so-called spiral failures and other miscellaneous types of O-ring failures.

In 1944 the Technical Advisory Committee on Hydraulic System Materials was formed. This committee is composed of representatives of the two services, and the manufacturers of aircraft, of hydraulic fluid, of packings, of hose, and of miscellaneous hydraulic equipment. The function of this committee is to assist the services in their program to improve performance of aircraft hydraulic systems. The committee makes recommendations for and co-ordinates the results of tests made on O-rings, hydraulic fluid, and all types of hydraulic equipment by industry.

⁴ Walker Manufacturing Company, Racine, Wis.

As the result of a great deal of test and development work by the services and by manufacturers of aircraft hydraulic fluid and packings, with help and advice of the Technical Advisory Committee on Hydraulic System Materials, there had been by 1946, a gradual improvement in the quality of hydraulic fluid and packings and in the compatibility of one with the other. However, there was urgent need for a comprehensive study of the fundamentals of packing and fluid behavior, which neither the services nor industry was in a position to undertake. Battelle Memorial Institute was found to be the organization that could undertake such a study. Battelle initiated test programs for both the Air Force and the Navy, and personnel of Battelle, active in this work, were made honorary members of the Technical Advisory Committee.

The present paper is based upon data obtained in this testing program. This information is valuable because it helps to build a foundation of scientific facts which will permit the services and industry eventually to eliminate the causes of packing failures in aircraft hydraulic systems. A great deal of progress has been made on this program, but a lot remains to be done. However, continued co-operation between the organizations involved eventually will insure that our pilots will fly better safer aircraft.

O-Ring Friction in Industrial Applications. The Battelle tests were for typical aircraft installations. For industrial applications, automotive type of cylinder oil is used more frequently than AN-O-366 hydraulic fluid. This is due to its ready availability, especially for refilling the systems. There will be less friction when cylinder oil is used. In most cases an O-ring made from a special industrial compound will be required for use with automotive cylinder oils. Use of brass or aluminum for piston rods or cylinders in place of the SAE 4340 steel will increase the friction, all other variables being the same.

O-Ring Friction in Pneumatic Systems. The friction in well-lubricated aircraft and industrial pneumatic installations normally will run higher than in comparable hydraulic systems. Friction is extremely high on poorly lubricated pneumatic installations where O-ring packings are used. Normally, O-rings are not recommended in unlubricated pneumatic installations, due to the excessive friction and the resultant high percentage of ring failures.

B. P. GRAVES.⁵ O-rings properly applied, are quite effective in preventing leakage between sliding surfaces, at least for a time. The important question to consider is—"How long will they last?" The writer has been seeking for some time to find a reliable answer to this question within our own personal applications and research, or in any of the papers on the subject of O-rings which have come to hand.

In discussing this subject with many hydraulic engineers and users of hydraulic equipment, the life of sliding O-rings has been questioned seriously, and the consensus of opinion seems to be that their life is too short. So instead of presenting a discussion on this paper, the writer finds it almost necessary to question the authors as follows:

Can the life of O-rings be extended to a practicable degree by practical methods, or ordinary shop methods? Of particular interest to us would be the effect on life of O-rings, of such matters as relative smoothness of the sliding surfaces, the condition of the grooves into which these O-rings fit, the composition of the O-ring and its hardness, amount of initial compression, working pressures, and speed of oscillation.

The several questions sum up to this one particular issue—is the life of an O-ring to be measured by the number of starts, the total

⁵ Director of Design, Brown & Sharpe Manufacturing Company, Providence, R. I. Fellow ASME.

distance traveled, or is it mainly a question of time under pressure?

We are particularly interested in the O-ring application because it offers a tantalizing picture of extreme compactness, high initial efficiency, and economy.

Answers to the foregoing questions would be of great value to the application engineer and to the user.

L. S. LINDEROTH, JR.⁶ It is most interesting to note the indications of uniform performance of rings made by different manufacturers. The data in the curves of running and breakout friction should be very helpful to the design engineer.

If future work is contemplated to carry on and amplify these data the writer would like to suggest a series of experiments to determine the possible variation in friction with different rod materials such as chrome plate, stainless steel, nonferrous alloys, and so on. From the designer's point of view it would be helpful to have the friction expressed in terms of rod or cylinder circumference. It would also be helpful to know whether the present AN specifications on the O-ring material are optimum for all types of service. Personally, the writer believes that for industrial use a better material can be compounded, since for one thing the extreme temperature requirements of the AN specifications are seldom encountered.

He has often wondered whether a rod or cylinder surface could be made too smooth, and perhaps the results indicated in Fig. 5 of the paper, on the running friction of the 1.7-2.0 rms rod bears this out. Notice that the point indicates a higher friction than the extended curve.

Personal experience has indicated that long time delays, several days to several months in duration, give extreme breakout friction values. This paper does not indicate whether any experiments considerably over 40 min duration were made. This is an important factor as relating to storage life of completed units and deserves considerable attention.

Were the points on the various curves measured with the rod going in one direction only or were directions measured and recorded? If both directions were recorded was there a difference between frictions with a dry and an oily rod?

On the measurement of the breakout friction with variation in rod speed, does not acceleration play a larger part than change in friction? With the bellows, fluid, and engine indicator parts all having appreciable mass, some question may arise as to the accuracy of the measurement of nonstatic loads. It may be desirable in future experiments to use a measuring means independent of mass in the measuring instrumentalities.

All tests in this paper were carried on at room temperature, presumably 70 F. It has been the writer's experience that most operating equilibrium temperatures are on the order of 150 F, unless special cooling is introduced. It would be helpful to know what effect temperature would have on the running and breakout friction with the time delay starting at the elevated temperature.

B. R. TEREZ.⁷ The study of all packings used in aircraft hydraulic systems regarding their frictional behavior due to change in squeeze, time delay between strokes, pressure and roughness of moving surfaces has always been of the utmost need. For years the aircraft hydraulic designers and engineers have been searching for such useful data to improve the operation of their equipment by reducing over-all friction. The discussion covered in this paper gives a clear-cut analysis of the frictional characteristics of

O-rings, most commonly used in the aircraft industry at this time, and the authors along with the Bureau of Aeronautics, should be complimented for this presentation.

In almost all aircraft hydraulic-equipment design work, there are two major points or locations where friction data on packing installation is badly needed. These two points are rod-gland-seal installation; and piston-head-seal installation. It is also pointed out that most of the serious problems in industry are with seals which are installed at rod ends of cylinders, where the leakage can be detected very easily.

The authors have discussed the investigation of this gland seal very thoroughly. In the test setup employed by the authors the O-ring does not change position at the start of the stroke. In an actual aircraft piston-ring seal the O-ring is at the side of the groove next to the pressure prior to starting the stroke. Therefore the O-ring must move to the opposite side of the groove as the pressure is applied, and as the stroke starts. This test information and data may not correlate with actual service experiences on piston-head seals. It is believed that in actual operating conditions the breakout friction will be less due to the rolling of the O-ring before the actual starting of the stroke.

It is surprising that in no place in this paper is there mention of friction tests at zero or very low pressures. Installations with such requirements are common in the aircraft industry.

There is also no mention of friction of O-rings with the use of leather back-up rings. This is understandable because there is an increased amount of work and testing involved for such an investigation.

It is stated in the paper that in the range of dimensions investigated, there was no appreciable difference in friction due to O-ring sizes. It is hoped that this will not be misinterpreted or confusing to designers because there must be a difference in friction due to change in size of O-ring as friction should be directly proportional to contact area.

The information covered in this paper is very valuable to the aircraft industry and also to all industrial hydraulic applications. It is important that it is leading to the discovery of causes of failure and other phenomena which occur in hydraulic systems. It is suggested that the authors, in their final analysis of friction characteristics of O-rings, prepare a technical chart wherefrom hydraulic designers can pick friction information for their particular designs at a glance.

AUTHORS' CLOSURE

The authors wish to thank the critics for their remarks about the work. Mr. Davison's discussion of the background of the project is a fitting addition to this summary of facts. Many of the questions raised in the discussion are beyond the narrow scope of this paper, but are welcomed because they propose a rather logical course for further investigation. They introduce problems of fundamental importance to the hydraulics industry.

For all data reported, rod travel was in a direction opposite to the direction of applied working pressure. This is almost always the performance condition for rod seals when an hydraulic cylinder is operated. However, limited tests were made for the reverse case in which travel was in the direction of the applied working pressure. A "toe-stubbing" or high-frequency "stick-slip" type of friction was observed which was considered unworthy of analysis. Recent endurance-cycling tests at Battelle indicate that this application shortens O-ring life.

This study was confined to room temperatures which averaged about 90 F, but actually ranged from 60 to 115 F. This was dependent somewhat upon operating conditions, but mostly upon the season of the year. This factor is considered to be only a minor cause for the rather wide deviations reported. Inspection of the data and temperatures at which single measurements were

⁶ Professor of Mechanical Engineering, Iowa State College of Agriculture and Mechanic Arts, Ames, Iowa. Mem. ASME.

⁷ Project Engineer, Aircraft Development, Weatherhead Company, Cleveland, Ohio. Mem. ASME.

made seems to indicate that running and breakout friction increase slightly with temperature. This was not demonstrated conclusively, however.

In so far as packing life at higher temperatures is concerned, it is well known that rubber ages much more rapidly at higher temperatures. Consequently, an appreciably shorter packing life would be expected for an application involving temperatures in excess of that for which the packing was designed. AN-P-79 packings are designed for a maximum temperature of 160 F. Many commercial-type packings have been designed for still higher temperatures. An upper limit for rubber-type packings is believed to be in the range of 250 F.

Zero-pressure breakout friction was not included in the work reported here. However, a study of certain unreported data has shown that zero-pressure breakout may be determined by extrapolation to zero pressure of the values determined at 500, 1000, and 1500 psi, when the other factors remain constant. This method generally determines values within the deviation limits cited, but they are occasionally high by as much as 50 per cent.

Time delays in excess of 40 min., and O-ring installations with leather back-up rings were not studied. Early work at Battelle showed that time delays of several days gave only slightly greater breakout friction than that obtained for 40 min. The maximum delays reported are, therefore, approximately representative of the maximum breakout developed by O-rings during pressurized stand-by periods. Over a long period of time, for example, several months in a service installation, other factors such as permanent set and fouling of the extended rod, due to heat and dust exposure, would be expected to increase breakout friction a significant amount.

Variable acceleration, if it existed, was dependent upon stroke speed, due to the nature of the test machine. Therefore, it is believed legitimate to express breakout friction as a function of stroke speed in Fig. 7 of the paper. Recent measurements have shown that rod acceleration was in the order of 100 fps per sec. Therefore, a full-stroke speed of 300 ipm was reached within about 0.004 sec after start. Recent oscillograph-type measurements of friction, which correlate very well with the engine indicator-type measurements of friction reported in this paper, show that breakaway occurs during this acceleration period.

The mass of the bellows and engine indicator are believed to have introduced some inertia factor into the breakout results reported. However, very little displacement of these components during breakout was observed, making this factor a negligible one, in light of the deviations reported. The authors realize the need for a method of measuring breakout friction which would be totally independent of any inertia interference.

The initial position of the O-ring recently has been observed to vary unpredictably during the stand-by period. An initial static-friction pull on the rod due to pressurization of the O-ring alone has been seen to vary from zero to 5 lb. Considering the high-order acceleration involved during breakaway, this is believed to account for the large deviations in the breakout-friction results. This irreproducibility would, however, be characteristic of actual O-ring installations in hydraulic systems.

It was seen that running and breakout friction decreased with increased rod smoothness for the range of surface finishes studied.

Although two points at 1.7–2.0 microin. rms in Fig. 5 of the paper, are out of line and indicate higher friction, a different O-ring was tested for this surface finish. The reproducibility of friction between different O-rings is illustrated in Fig. 8, and could account for the deviations from the smooth curves drawn in Fig. 5.

Since the presentation of this paper, considerable effort has been directed toward determining the effect of O-ring size on friction, and correlating the accumulated data into technical design charts. In general, it was found that the smaller sizes developed less friction, as expected. The resultant data, however, could not be fitted into a correlation which could be extrapolated to all sizes. This was due to the large variability in our data, and also to many dimensional factors which were difficult to control closely. Running-friction characteristics were much more consistent than breakout friction, and appear capable of being resolved into such charts. More sensitive test methods will be required to do this, however.

It cannot be said that the present AN specifications represent the optimum in O-ring material. Instead, they represent the minimum requirements, which would enable United States military aircraft to operate anywhere in the world with the same hydraulic fluid and packings. In the development of materials to meet this broad objective, many compromises in physical properties had to be made. Oil resistance, for example, was sacrificed for low-temperature flexibility. O-rings with physical properties superior to AN compounds have been formulated for individual industrial applications, where low-temperature flexibility is not a problem and wider latitude exists in the choice of a hydraulic fluid.

The frictional characteristics of O-rings are believed indicative of their expected life in service, within limits. High breakout friction is evidence of extrusion, where the packing is more susceptible to "nipping" when the rod is actuated. O-ring packings will tend to wear away faster by abrasion when running friction is high. Endurance cycling tests show, however, that the wearing rate of the packings does not correlate strictly with O-ring life, though wear is proportional to the number of completed strokes. Further investigation revealed that strict definition and control of pressure-time characteristics is of utmost necessity in conducting life tests, and being able to predict how long the O-rings will last in service. Accurate measurement and close control of the pressure-time relations in hydraulic systems is a serious problem in itself. This will have to be solved before the effect of the finite packing properties on O-ring life can be determined.

TABLE 3 SUMMARY OF GLAND-DESIGN FACTORS

Type of application	Low pressure (500 psi)		High pressure (1500 psi)	
	Squeeze	Surface finish	Squeeze	Surface finish
Intermittent cycling (breakout friction is important)	Maintain as low as possible	Maintain as smooth as possible	Unimportant 10 to 16%	Unimportant in 2- to 11-microin. range
Continuous cycling (running friction is important)	Maintain as low as possible	Maintain as smooth as possible	Unimportant 10 to 16%	Maintain as smooth as possible

It is believed that the friction studies point out certain gland-design considerations which can be applied to lengthen O-ring life. These are summarized in Table 3 of this closure.

Re
Co
AS

Strength-Variance Studies of Plastics

By W. J. GAILUS,¹ STEVEN YURENKA,² AND A. G. H. DIETZ³

Preliminary work of the plastics research program at the Massachusetts Institute of Technology, sponsored by the Plastic Materials Manufacturers Association is reported. A statistical study of the effect of pertinent variables likely to be encountered in gathering mechanical data from a representative system of plastics (polymethyl methacrylate) is described. Effect of manufacturer, rate of test, and nature of test specimen is reported.

INTRODUCTION

BASIC to the plastics research program reported in this paper was the need for a clear understanding of the variables likely to be important and for a rather complete knowledge, from a physical viewpoint, of the homogeneity and original "as-received" condition of the materials to be tested. To achieve this goal, it was decided to obtain randomized physical property data on the plastics concerned as part of a preliminary exploratory program. From such information it was hoped that it would be possible to reach a better-informed decision as to the number and distribution of test specimens to be used in the future major work; and consequently, the quantities and type of material required.

Polymethyl methacrylate was chosen as the first material to be studied in detail because it was a representative thermoplastic, was readily available in homogeneous form, and had a comparatively simple structure which could, however, be altered chemically under controlled conditions to give a variety of structural forms. The polymethyl methacrylate was supplied by two manufacturers (hereinafter referred to as A and B).

Since fairly large numbers of specimens of different shapes were to be used in the main program, uniformity as regards the material going into the various types of specimens was of prime importance, and so it was decided to machine them from cast-sheet stock. In order to obtain the requisite information just mentioned, a preliminary statistical program was designed to investigate the following variables:

1 Variation in the material supplied by manufacturers A and B to determine generally over-all differences in the material due to inherent variations, and differences in the manufacturing techniques used by A and B.

2 Variations of the material taken from different positions in a particular sheet—center, corner, center of edge, and intermediate—all with the view in mind of determining the degree of uniformity within any one sheet itself as regards positional variations.

¹ Research Associate, Plastics Research Laboratory, Department of Building Engineering and Construction, Massachusetts Institute of Technology, Cambridge, Mass. Jun. ASME.

² Research Associate, Plastics Research Laboratory, Department of Building Engineering and Construction, Massachusetts Institute of Technology.

³ Associate Professor of Structural Engineering; Director, Plastics Research Laboratory, Department of Building Engineering and Construction, Massachusetts Institute of Technology, Mem. ASME.

Contributed by the Rubber and Plastics Division and presented at the Fall Meeting, Erie, Pa., September 28-30, 1949, of THE AMERICAN SOCIETY OF MECHANICAL ENGINEERS.

NOTE: Statements and opinions advanced in papers are to be understood as individual expressions of their authors and not those of the Society. Paper No. 49-F-33.

3 Variation of the material taken from sheets of different thicknesses, $\frac{1}{4}$ in., $\frac{1}{2}$ in., and 1 in. to obtain an indication of the uniformity in the sheets as regards material cast in different sheet thicknesses.

4 Variation of material taken from the surface of the sheets, as compared with material from the center of the thicknesses, to indicate the uniformity of the material in so far as depth from the surface was concerned.

5 Variation in measured physical properties as influenced by two testing speeds, differing by ratios of approximately 10 to 1. The reason for including item (5) was twofold: (a) to get an indication of the importance of the rate of test; and (b), to have a basis of relative comparison for the importance of the first four variations. It is the results of this preliminary survey that are presented in this paper.

MATERIAL AND TEST PROCEDURE

The material investigated was supplied in duplicate by manufacturers A and B in the form of cast sheets in three thicknesses, $\frac{1}{4}$ in., $\frac{1}{2}$ in., and 1 in., and approximately 36 in. \times 36 in. in size. Manufacturer A supplied straight commercial-run stock while manufacturer B supplied material manufactured in a commercial run but under the supervision of laboratory personnel. In addition, the material supplied by B was given subsequent annealing treatments.

To facilitate that portion of the program concerned with specimen manufacture and of actual testing, it was decided to use simple bending tests throughout this preliminary work to obtain the physical data to be used in the calculations. The specimens employed were 0.2 in. thick, 0.5 in. wide, and of such length that the tests could be carried out with 3.2 in. between the supports (span-depth ratio of 16 to 1). Loads on the specimens were applied at the center of the span. The positions of the various specimens with respect to the sheets are as shown in Fig. 1.

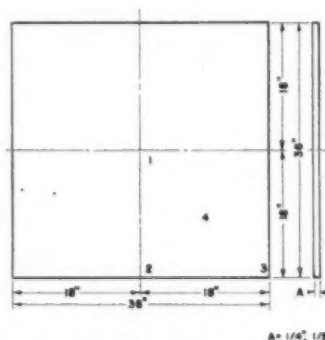


FIG. 1 SAMPLE POSITIONS CHOSEN FROM CAST SHEETS OF POLYMETHYL METHACRYLATE

The numbered positions are diagrammatic, i.e., the group of specimens from position 3, for example, might have been taken from any of the four corners, not necessarily the one shown. Surface specimens were machined from the same surface of the sheet; interior specimens were machined from the geometric center plane of the sheets. Since the major portion of the samples to be used in the main testing program would have machined surfaces,

it was felt desirable to minimize the complication of the "skin effect;" therefore the surface specimens were loaded with the molded skin on the upper, or compression, side. The tests were conducted in an air-conditioned atmosphere of 77 F and 50 per cent relative humidity (RH) at constant rates of crosshead motion (effectively constant rates of deflection) at speeds of 0.10 and 1.00 inches per minute.

ANALYSIS PROCEDURE

The value of an experiment is measured directly by the reliability of the measurements made. Reliable measurements in turn depend upon complete, or at least adequate, recognition of the variables involved and of their relative importance. The analysis of variance assigns to each of the five previously mentioned experimental variables (and combinations of them) its appropriate share of the total experimental variation and then tests whether each such share is significantly high or merely due to chance. With the aid of the results of such an analysis, any future program can be planned with confidence. If the analysis shows a large variation, for example, due to the position from which the specimen is taken in the sheet, or due to sheet thickness, then, in future work, an effort can be made to take specimens for a given series of tests from positions close to the same spot in a given sheet, or from sheets of the same thickness. In addition to evaluating the main sources of variation, these tests give a measure of the inherent and unavoidable variation in the results to be expected due to the host of uncontrolled variables which are acting, such as slight variations in temperature, humidity, speed of test, and dimensions. This uncontrollable variation or error is used as a base value in determining the number of tests, and so the amount of material, necessary for future testing work. Details on this point will be given in a later section.

In a complete formal analysis of the five variables being considered, there are 31 categories into which the total variation would be divided. These include the five main effects of testing rate, sheet thickness, manufacturer, position in the sheet, and "depth" in the sheet, i.e., surface as compared to internal specimens. These are the most likely sources of significant variation. In addition, there are ten first-order interaction effects such as the interaction of rate and sheet thickness, manufacturer and depth, position and depth, and so forth. The variation due to an interaction term would be a variation in one factor as caused by a variation in another factor. For example, consider the interaction term "testing rate and depth." It may very well be that the total average of maximum strengths would be the same for surface specimens as for internal specimens, yet the fast surface specimens may test significantly high compared to the fast internal specimens with the slow surface specimens significantly low compared to the slow internal specimens. The magnitude of the first-order interaction term, rate and depth, would indicate this condition. In addition to the fifteen variational terms already mentioned, there are ten second-order interaction terms such as "rate \times depth \times manufacturer," and "sheet thickness \times rate \times position." Further, there are also five third-order interaction terms, and one fourth-order term. These higher-order terms are of the same nature as the first-order interactions described, but much more difficult to comprehend and to associate with a physical meaning.

CALCULATION MECHANICS

The entire following discussion will be concerned with the maximum stress values obtained from the bending tests using the formula $s = Mc/I$. A completely separate and similar analysis must be made if the modulus of elasticity values are considered.

After the tests have been completed and the data tabulated

TABLE 1 MAXIMUM BENDING STRESS (Mc/I) PSI; TESTS AT CONSTANT RATE OF CROSS-HEAD MOTION

	Material A			Material B		
	Original Sheet Thickness			Original Sheet Thickness		
	$\frac{1}{8}$ "	$\frac{1}{4}$ "	1"	$\frac{1}{8}$ "	$\frac{1}{4}$ "	1"
<u>Surface Specimens</u>						
<u>Fast Rate Tests</u>						
Position 1	17,400	19,100	19,130	15,000	16,900	20,100
" 2	19,900	18,500	15,870	13,500	17,400	20,200
" 3	17,300	18,600	17,520	15,050	19,500	17,860
" 4	20,200	21,200	20,940	14,300	16,800	16,320
<u>Slow Rate Tests</u>						
Position 1	18,150	16,100	17,500	13,500	15,100	17,400
" 2	19,300	18,000	18,490	12,250	16,400	16,800
" 3	16,400	16,000	15,280	13,200	13,600	17,700
" 4	18,900	17,450	17,610	13,400	13,200	16,900
<u>Internal Specimens</u>						
<u>Fast Rate Tests</u>						
Position 1	18,600	22,300	9,990	15,800	18,800	20,200
" 2	19,900	22,400	13,760	14,850	16,500	11,960
" 3	14,200	16,500	16,320	15,450	16,100	16,320
" 4	20,450	22,600	13,400	14,100	15,400	16,820
<u>Slow Rate Tests</u>						
Position 1	16,800	18,500	9,640	14,100	14,850	16,700
" 2	18,000	20,600	15,190	13,800	15,100	16,800
" 3	17,500	18,950	12,820	11,850	16,200	17,800
" 4	18,050	19,400	13,790	13,400	15,800	16,600

TABLE 2 MODIFIED MAXIMUM BENDING-STRESS VALUES
(Actual stress less 10,000 and divided by 10)

Position	Material	Original Sheet Thickness			Total
		$\frac{1}{8}$ "	$\frac{1}{4}$ "	1"	
Slow Rate, Surface Specimens					
1	A	815	610	750	2,175
	B	350	510	740	1,600
2	A	930	800	849	2,579
	B	225	640	680	1,545
3	A	640	600	528	1,768
	B	320	360	770	1,450
4	A	890	745	761	2,396
	B	340	320	690	1,350
Sub Totals		A	3275	2755	8,918
		B	1235	1830	5,945
Total			4510	4585	14,863
Fast Rate, Surface Specimens					
1	A	740	910	913	2,563
	B	500	690	1010	2,200
2	A	990	850	587	2,427
	B	350	740	1020	2,110
3	A	730	860	752	2,342
	B	505	950	796	2,241
4	A	1020	1120	1094	3,234
	B	430	680	632	1,742
Sub Totals		A	3480	3346	10,566
		B	1785	3060	8,293
Total			5265	6794	18,859

TABLE 3 MODIFIED MAXIMUM BENDING-STRESS VALUES
(Actual stress less 10,000 and divided by 10)

Position	Material	Original Sheet Thickness			Total
		$\frac{1}{8}$ "	$\frac{1}{4}$ "	1"	
<u>Slow Rate, Internal Specimens</u>					
1	A	680	850	-36	1,494
	B	410	435	670	1,565
2	A	800	1060	519	2,379
	B	380	510	680	1,570
3	A	750	895	282	1,927
	B	185	620	780	1,585
4	A	805	940	379	2,124
	B	340	580	660	1,580
Sub Totals	A	3035	3745	1144	7,924
	B	1315	2195	2790	6,300
Total		4350	5940	3934	14,224
<u>Fast Rate, Internal Specimens</u>					
1	A	860	1230	-11	2,079
	B	580	880	1020	2,480
2	A	990	1240	376	2,606
	B	485	650	196	1,331
3	A	420	650	632	1,702
	B	545	610	632	1,787
4	A	1045	1260	340	2,645
	B	410	540	682	1,632
Sub Totals	A	3315	4380	1337	9,032
	B	2020	2880	2530	7,230
Total		5335	7060	3867	16,262

(Table 1), the information may be entered for analysis in the form shown in Tables 2 and 3. The original maximum stress values from Table 1 have been decreased by 10,000 and divided by 10 to reduce the size of the terms to be encountered in later arithmetical manipulations. (In general, all values in the initial data may be multiplied by a constant, or have a constant added to them without affecting the results in any way.)

The entire original data have been plotted in the frequency-distribution bar graph, Fig. 2. It can be seen that the maxi-

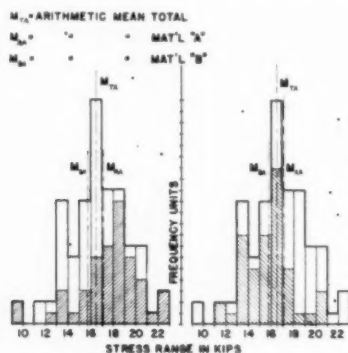


FIG. 2 VARIANCE SERIES FREQUENCY DISTRIBUTION: MAXIMUM STRESS IN BENDING

mum bending stresses range between 9000 and 22,000 psi, and that the arithmetic mean of the stresses for materials A and B and for their total lie between 15,000 and 17,000 psi. The ordinate of this graph is calibrated in frequency units or the number of specimens which broke within the range of stresses represented along the abscissa.

Below each table the sum of values for each thickness and manufacturer is formed, and horizontally, the sum of values for each position and manufacturer is similarly obtained. This is done to facilitate construction of further tables, as will presently be appreciated. The sum of all values for a given manufacturer

may be obtained by a summation of either the horizontal or vertical sums. This latter operation provides a check on the preceding computations.

Tabulations like the ones shown in Tables 4, 5, and 6 (there would be ten such tables if all were listed, one for each of the first-order interactions) are then filled in with the appropriate sums. The totals which were formed in Tables 2 and 3 are now found to be convenient aids for making all the entries into Tables 4, 5, 6, etc., except in the case of the position versus thickness table (Table 6). Here, for example, the first entry is obtained by using the individual values in Tables 2 and 3, or $815 + 350 + 740 + 500 + 680 + 410 + 860 + 580 = 4935$. Considering now for a moment Table 4, it may be seen that the first entry is the sum of all fast-rate, "A" specimens, or 10,566 (from Table 2) + 9032 (from Table 3) = 19,598. In a similar manner the remaining three entries are obtained. As a further example, consider Table 5. The first entry is the sum of all fast-rate, position 1 specimens or 2563 + 2200 (both from Table 2) + 2079 + 2480 (both from Table 3) = 9322. This procedure is followed in filling in the remaining values.

Finally, Table 7 may be made up, putting the "sum of squares of the deviation" in the first column.

The sum of squares of deviation is defined by the series

$$\sum_{i=1}^n (\bar{x} - \bar{x})^2$$

where \bar{x} is the mean value of maximum stress considering a particular variable and \bar{x} is the mean value of maximum stress considering all of the data; n is the total number of readings or values considered. To clarify this situation a bit, take, for example, the case of the interaction "position and thickness" (see Table 6). The discussion will be simplified considerably by introducing here a few symbolisms. Let

$\Sigma x =$ total sum of all maximum stress values = 64,208

$\Sigma x_P =$ total sum of maximum stress values for any one position

= 16,156 for position 1, etc. (four values in all)

$\Sigma x_T =$ total sum of maximum stress values for any one thickness

TABLE 4 VARIANCE COMPUTING TABLE: RATE OF TEST VERSUS MANUFACTURER

Manufacturer	Fast Rate	Slow Rate	Total
A	19,598	16,842	36,440
B	15,523	12,245	27,768
Total	35,121	29,087	64,208

$$(0) \text{ Sub-total sum of squares} = \frac{1}{n_{FM}} \sum_{i=1}^n (x_{FM})^2 = \frac{1}{24} [(19,598)^2 + \dots] = 44,109,921.7$$

$$(1) \text{ Sum of squares of Rate Deviations} = \sum_{i=1}^n (\bar{x}_R - \bar{x})^2 = \frac{1}{48} [(35,121)^2 + (29,087)^2] - \frac{1}{96} (64,208)^2 = 379,262.1$$

$$(2) \text{ Sum of squares of Manufacturers Deviations} = \sum_{i=1}^n (\bar{x}_M - \bar{x})^2 = \frac{1}{48} [(36,440)^2 + (27,768)^2] - \frac{1}{96} (64,208)^2 = 783,370.7$$

$$(3) \text{ Interaction of Rate vs. Manufacturer} = \sum_{i=1}^n (\bar{x}_{FM} - \bar{x}_R - \bar{x}_M + \bar{x})^2 = 2838.3$$

TABLE 5 VARIANCE COMPUTING TABLE; POSITION VERSUS RATE OF TEST

Position	Fast Rate	Slow Rate	Total
1	9,322	6,834	16,156
2	8,474	8,073	16,547
3	8,072	6,830	14,802
4	9,253	7,450	16,703
Total	35,121	29,087	64,208

$$(0) \text{ Sub-total sum of squares} = \frac{1}{n_{PR}} \sum_i (x_{PR})^2 = \frac{1}{12} [(9,322)^2 + \dots] = 45,121,653.2$$

$$(1) \text{ Sum of squares of Rate Deviation} = \sum_i (\bar{x}_R - \bar{\bar{x}})^2 = \frac{1}{48} [(35,121)^2 + (29,087)^2] - \frac{1}{96} (64,208)^2 = 379,262.1$$

$$(2) \text{ Sum of squares of Position Deviation} = \sum_i (\bar{x}_P - \bar{\bar{x}})^2 = \frac{1}{24} [(16,156)^2 + \dots] - \frac{1}{96} (64,208)^2 = 93,422.6$$

$$(3) \text{ Interaction of Position vs. Rate} = \sum_i (\bar{x}_{PR} - \bar{x}_P - \bar{x}_R + \bar{\bar{x}})^2 = 1,704,517.9$$

TABLE 6 VARIANCE COMPUTING TABLE; POSITION VERSUS THICKNESS

Position	Original Sheet Thickness			Total
	$\frac{1}{8}$ "	$\frac{1}{4}$ "	1"	
1	4,935	6,165	5,056	16,156
2	5,150	6,490	4,907	16,547
3	4,095	5,545	5,162	14,802
4	5,280	6,185	5,238	16,703
Total	19,460	24,385	20,363	64,208

$$(0) \text{ Sub-total sum of squares} = \frac{1}{n_{PT}} \sum_i (x_{PT})^2 = \frac{1}{8} [(4,935)^2 + (5,150)^2 + (4,095)^2 + \dots] = 43,547,174.7$$

$$(1) \text{ Sum of squares of Thickness Deviation} = \sum_i (\bar{x}_T - \bar{\bar{x}})^2 = \frac{1}{n_T} \sum_i (x_T)^2 - \frac{1}{96} (\sum_i x)^2 = \frac{1}{32} [(19,460)^2 + \dots] - \frac{1}{96} (64,208)^2 = 43,374,112.3 - 42,944,450.6 = 429,661.7$$

$$(2) \text{ Sum of squares of Position Deviation} = \sum_i (\bar{x}_P - \bar{\bar{x}})^2 = \frac{1}{24} [(16,156)^2 + \dots] - \frac{1}{96} (64,208)^2 = 43,037,937.2 - 42,944,450.6 = 93,422.6$$

$$(3) \text{ Interaction of Position vs. Thickness} = \sum_i (\bar{x}_{PT} - \bar{x}_P - \bar{x}_T + \bar{\bar{x}})^2 = 79,575.8$$

TABLE 7 OVER-ALL VARIANCE ANALYSIS

Cause	Sum of Squares of Deviation	Degrees of Freedom	Mean Square Deviation	M.S.D. 3490
1) Manufacturer	783,370.7	1	783,370.7	224.46
2) Rate of Test	379,262.1	1	379,262.1	108.67
3) Depth	109,080.2	1	109,080.2	31.26
4) Thickness	429,661.7	2	214,830.8	61.56
5) Position	93,422.6	3	31,140.9	8.92
6) Rate x Manufacturer	2,838.3	1	2,838.3	0.81
7) Depth x Manufacturer	34,504.1	1	34,504.1	0.99
8) Thickness x Manufacturer	1,645,879.8	2	822,939.9	235.80
9) Position x Manufacturer	435,061.9	3	145,020.6	41.53
10) Position x Depth	757.6	3	252.5	0.07
11) Rate x Depth	258,095.4	1	258,095.4	73.95
12) Thickness x Depth	927,902.5	2	463,951.3	132.94
13) Rate x Position	1,704,517.9	3	568,172.6	162.80
14) Thickness x Position	79,575.8	6	13,262.3	3.80
15) Thickness x Rate	91,670.0	2	45,835.0	13.13
16) 2nd 3rd 4th Order Interactions	219,868.9	63	3,490.0	1.00
17) TOTAL	7,195,535.4	95	-----	-----

= 19,460 for the $\frac{1}{4}$ in. thickness, etc. (three values in all)

Σx_{PT} = total sum of strength readings for any one combination of a specific thickness and a specific position
= 4935 for position 1, $\frac{1}{4}$ in. thickness, etc. (twelve values in all)

n_P = number of readings totaled to form each Σx_P
total number of values = 96
number of sums P = 4 = 24

n_T = number of readings totaled to form each Σx_T
total number of values = 96
number of sums T = 3 = 32

n_{PT} = number of readings totaled to form each Σx_{PT}
total number of values = 96
number of sums PT = 12 = 8

n = total number of values = 96

$i = \frac{n_T}{n_{PT}}$ = number of positions studied = 4

$j = \frac{n_P}{n_{PT}}$ = number of thicknesses studied = 3

The sum of squares of deviation between the mean maximum stress values for each thickness and the mean maximum stress for all values may now be written in the form

$$\sum_1^n (\bar{x}_T - \bar{x})^2 = \frac{1}{n_T} \sum_1^j (\Sigma x_T)^2 - \frac{1}{n} (\Sigma x)^2 \dots \dots [1]$$

The equation for computing the position deviation is analogous and of the form

$$\sum_1^n (\bar{x}_P - \bar{x})^2 = \frac{1}{n_P} \sum_1^i (\Sigma x_P)^2 - \frac{1}{n} (\Sigma x)^2 \dots \dots [2]$$

Finally, the equation for computing the deviation due to the interaction of position and thickness may be written in the form

$$\sum_1^n (\bar{x}_{PT} - \bar{x}_P - \bar{x}_T + \bar{x})^2 = \frac{1}{n_{PT}} \sum_1^i \sum_1^j (\Sigma x_{PT})^2 - \frac{1}{n_T} \sum_1^i (\Sigma x_T)^2 - \frac{1}{n_P} \sum_1^j (\Sigma x_P)^2 + \frac{1}{n} (\Sigma x)^2 \dots \dots [3]$$

Similar equations can be written for all other variables and interactions. The calculations involved in evaluating these equations numerically are shown for compactness, below each of the Tables 4, 5, 6, etc. as Equations [1], [2], and [3].

The procedure just described is followed for all entries in Table 7, including the total values, with the exception of the term consisting of the second-, third-, and fourth-order interactions. This term is equal to the total immediately below it minus all the terms above it.

The manner in which the foregoing procedure has been presented requires that the effects of the second-, third-, and fourth-order interactions be lumped together in one sum. To separate out the second-order interaction would require a duplication of about as much effort as has already been expended in making

up the present tables. A new sheet with ten additional three-way instead of two-way subtables would be required.

The degrees-of-freedom items of the second column of figures in Table 7 are obtained by subtracting one unit from the total number of items in each category. Thus, for example, because there are two manufacturers, and one of these may be "assumed," the degrees of freedom for the manufacturers is the remainder, or one. Also, since three different thicknesses of specimens were tested, and one of these may be assumed, the number of degrees of freedom is the remainder, or two, etc. Since the total number of specimens tested was 96, the total degrees of freedom is one less or 95.

The mean-square deviation, or variance, listed in the third column of Table 7, is obtained by dividing each sum of squares of deviation by its respective degrees-of-freedom value. Each of these mean-square deviations is an estimate of the variance of the 96 maximum stresses. If all 96 values were "alike," i.e., differed only at random, and had no significant trend between manufacturers, rates, thicknesses, etc., then all the estimates of variance would be alike. By alike is meant here that the values will differ from each other in magnitude, but not significantly.

Actually, from the values of the mean-square deviations shown in Table 7 we can conclude in the case of the first five causes that there was a significant difference in strength between materials A and B, since the estimate of variance due to manufacturers is significantly high. Furthermore, the estimate of variance due to position is significantly low compared to the values of the other four causes, which would indicate that there was not much difference in the maximum strength of specimens taken from various positions of the test plate or, in other words, the test plate is fairly homogeneous. It is important here to emphasize the fact that this conclusion is a relative one based upon consideration of the five primary causes, i.e., of these five causes, the position variation is the smallest. This is all that can be said at this point. The causes taken in order of importance of their influence on the maximum stress values obtained are as follows: (1) manufacturer, (2) rate of test, (3) thickness, (4) depth, (5) position.

In the case of the interaction terms, the analysis is not so simple, but here again it can be seen that the greatest influence on the maximum stress is that of cause (8), thickness versus manufacturer; and the least influence is that of cause (10) or position versus depth. The higher-order interaction terms (second, third, and fourth order in our case) do have physical meanings especially to engineers. Statisticians rarely include such in their analyses and indeed we have already obtained all the information we want so that the second and higher interactions are combined and taken as the variance or variability of the material due to such other variables not specifically considered here, such as fluctuations in temperature and humidity, and random errors in measuring dimensions, rates, deformations, etc. This variance is, so to speak, the basic, unavoidable, and unallocatable variation; and is used as the basis for comparison by which the other variances are judged significant.

The mean-square deviations which are smaller than the second-, third-, and fourth-order interactions combined obviously are not significant, but those which are considerably larger should be analyzed. To facilitate comparison, a convenient tabulation is obtained by dividing the mean-square deviation of the effect being tested by the mean-square deviation due to second-, third-, and fourth-order interactions (the lumped variation). The values obtained are shown in the last column of Table 7 and are further plotted in the form of a bar graph in Fig. 3. It is readily apparent that the general effect of manufacturer is greatly pronounced, overshadowing all else except thickness \times manufacturer, which

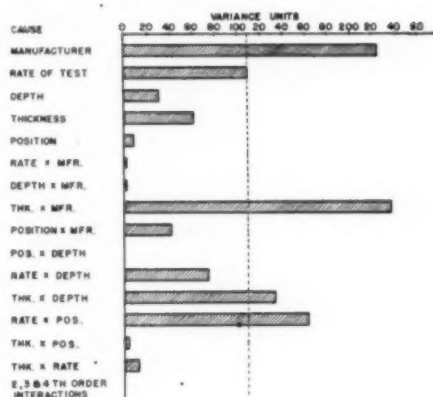


FIG. 3 VARIANCE SERIES COMPARATIVE VARIANCES

might conceivably also be due to the manufacturer participation. The rate of test is shown to be highly significant also, as might be expected. Thickness \times depth is certainly significant and would indicate the necessity of expecting different results from tests on specimens taken from different thicknesses at varying depths below the surface even when the tests are somewhat identical. The same is true for rate \times position.

SUBDIVIDED ANALYSIS

The over-all statistical studies here reported have grouped interaction terms which hinder specific allocation of effect to their proper factors. Thus to get a clearer idea of the relative magnitudes of the variations due to the various causes, a further, subdivided variance study has been made. Analyses of materials A and B separately to eliminate cross-terms attributable to variations between manufacturing techniques were thought most likely to clarify the situation. The computations made were carried out in the manner previously explained in detail, and have been summarized in Tables 8, 9, 10, and 11. The mean-square deviations in the last column of Tables 9 and 11 have also been plotted in the form of a bar graph in Fig. 4. Since the maximum order of magnitude was three, the analysis was carried out in detail to study the third-order effects, as shown in the tables and graphs.

Both of these subdivided analyses indicate that the largest deviation is caused by differences in physical properties of sheets of different thicknesses of apparently identical material. The remaining "mean-square-deviation" terms of the material B analysis seem to indicate that the effect of rate of loading is sizable, as normally would be expected, and, further, that positional variations and depth variations (surface versus internal

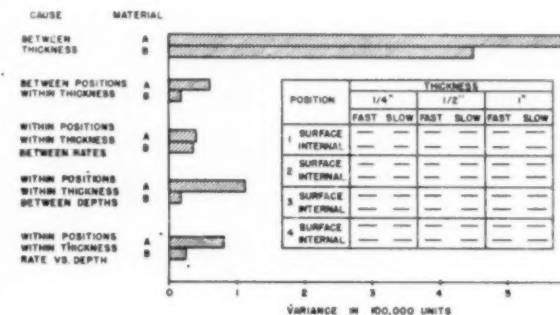


FIG. 4 VARIANCE SERIES COMPARATIVE VARIANCES

TABLE 8 VARIANCE STUDY; MATERIAL B COMPUTATIONS

Position		Thickness								
		1/4"			1/2"			1"		
		Fast	Slow	Total	Fast	Slow	Total	Fast	Slow	Total
1	Surface	500	350	850	690	510	1200	1010	740	1750
	Internal	580	410	990	880	485	1365	1020	670	1690
	TOTAL	1080	760	1840	1570	995	2565	2030	1410	3440
2	Surface	350	225	575	740	640	1380	1020	680	1700
	Internal	485	380	865	650	510	1160	196	680	876
	TOTAL	835	605	1440	1390	1150	2540	1216	1360	2576
3	Surface	505	320	825	950	360	1310	786	770	1556
	Internal	545	185	730	610	620	1230	632	780	1412
	TOTAL	1050	505	1555	1560	980	2540	1418	1550	2968
4	Surface	430	340	770	680	320	1000	632	690	1322
	Internal	410	340	750	540	580	1120	682	660	1342
	TOTAL	840	680	1520	1220	900	2120	1314	1350	2664

TABLE 9 VARIANCE STUDY; MATERIAL B ANALYSIS

Effect	Sum of Squares of Deviation	Degrees of Freedom	Mean Square Deviation
1) Between Thicknesses	899,784	2	449,892
2) Between Positions within Thicknesses	171,365	9	19,040.6
3) Within Positions within Thicknesses Between Rates	432,153	12	36,012.8
4) Within Positions within Thicknesses Between Depths	228,315	12	19,026.3
5) Within Positions within Thicknesses Rate vs. Depth	319,628	12	26,635.7
6) TOTAL	2,051,245	47	

specimens) are of the same order of importance, namely, about one half the magnitude of the deviation due to rate of loading, indicating fairly homogeneous material.

In the material A analysis, it is to be noted that the deviation "between thicknesses" is very high, indicating variability in the material taken from different sheets is significant. The analysis also indicates that deviation "between positions" is also high, indicating nonuniformity over a single sheet. Further, "depth" variation is also significant, indicating a nonhomogeneous structure in material near the surface of the sheet, as compared with material near the center plane.

CONCLUSION

This variance analysis of causes and interaction terms indi-

cates that studies correlating structural characteristics of a material, whether chemical, metallurgical, etc., with its physical properties had best be done by testing samples whose homogeneity and degree of representation (reproducibility) of a material are understood and can, therefore, be taken into consideration. Further, the importance of considering interaction effects has been indicated. The latter, if not considered, can easily lead to false conclusions or effectively mask effects that may occur.

In the case of the plastic materials analyzed in the paper, it has been found that in order to eliminate as many interactions as possible, future testing should be carried out using material (for particular phases of the work) from a single manufacturer, with samples taken from panels of the same thickness, using a predetermined random sampling procedure for obtaining specimens,

TABLE 10 VARIANCE STUDY; MATERIAL A COMPUTATIONS

Position		Thickness								
		1/4"			1/2"			1"		
		Fast	Slow	Total	Fast	Slow	Total	Fast	Slow	Total
1	Surface	740	815	1555	910	610	1520	913	750	1663
	Internal	860	680	1540	1230	850	2080	-11	-36	-47
	TOTAL	1600	1495	3095	2140	1460	3600	902	714	1616
2	Surface	990	930	1920	850	800	1650	587	849	1436
	Internal	990	800	1790	1240	1060	2300	376	519	895
	TOTAL	1980	1730	3710	2090	1860	3950	963	1368	2331
3	Surface	730	640	1370	850	600	1450	752	528	1280
	Internal	420	750	1170	650	895	1545	632	282	914
	TOTAL	1150	1390	2540	1510	1495	3005	1384	810	2194
4	Surface	1020	890	1910	1120	745	1865	1094	761	1855
	Internal	1045	805	1850	1260	940	2200	340	379	719
	TOTAL	2065	1695	3760	2380	1685	4065	1434	1140	2574

TABLE 11 VARIANCE STUDY; MATERIAL A ANALYSIS

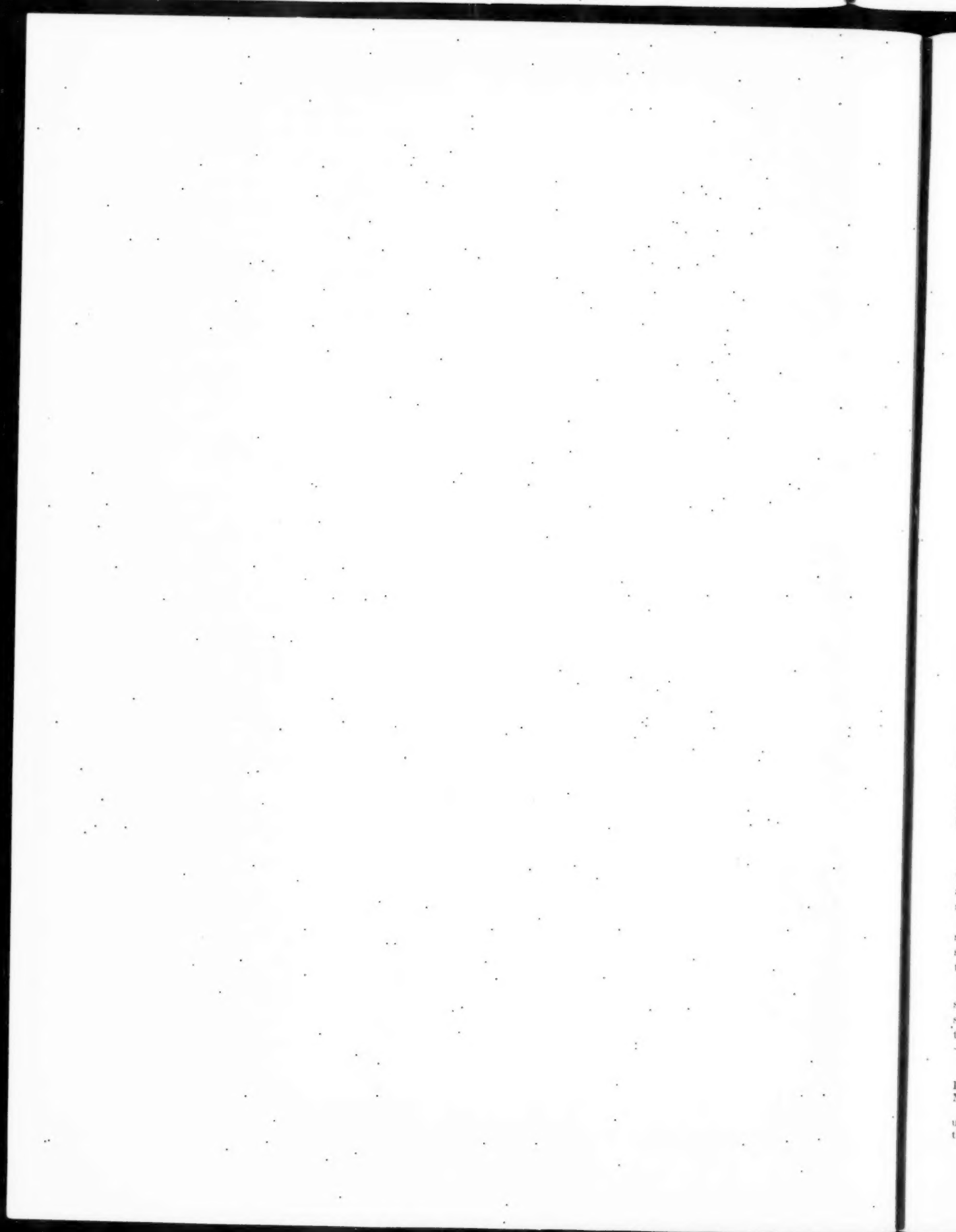
Effect	Sum of Squares of Deviation	Degrees of Freedom	Mean Square Deviation
1) Between Thicknesses	1,175,757	2	587,878.5
2) Between Positions within Thicknesses	543,511	9	60,390.1
3) Within Positions within Thicknesses Between Rates	470,464	12	39,206.2
4) Within Positions within Thicknesses Between Depths	1,389,377	12	115,781.4
5) Within Positions within Thicknesses Rate vs. Depth	929,810	12	77,484.2
6) TOTAL	4,508,919	47	

and using material which has been prepared by a carefully controlled technique.

ACKNOWLEDGMENT

The authors wish to express their appreciation especially to

Prof. L. C. Young for his invaluable assistance in applying and interpreting the techniques of the statistical approach, and to L. Lipschitz for his assistance in setting up the mechanics of the problem in the initial stages of the work. W. Campbell assisted in some of the tests.



0
0

t
s
s
s
t

s
s
t

I
M
u
th

Theoretical Considerations on the Optimum Adjustment of Regulators

By P. HAZEBROEK¹ AND B. L. VAN DER WAERDEN¹

In a companion paper, the authors propose some practical rules for the best possible adjustment of the parameters of automatic regulators with proportional-plus-integral action. The present paper will be concerned with the theoretical foundations of the method developed.

FUNDAMENTAL NOTIONS

IN this paper, we shall assume that a "single" variable is to be kept at a "constant" value by automatic regulation.

We begin by a short survey of the fundamental notions to be used.

Process and regulator are interconnected in such a way as to form a closed loop which we will call a "regulation circuit," Fig. 1. In a regulation circuit it is appropriate, for the purpose of our theory, to distinguish two interdependent variables as follows:

(a) The "regulated variable," which we will denote by x , which should be kept as constant as possible by suitable variations of our second variable.

(b) The "regulating flow," which we will denote by q .

We will assume that both x and q are measured from their normal value, which shall be taken as zero points and expressed in dimensionless units; for instance, as fractions of the maximum interval in which they may move.

The restriction shall be imposed that the relationship between x and q is such that the superposition principle is valid, in other words that the sum of two time-dependent disturbances of q (or x) causes a change of x (or q) which is the sum of the changes resulting from the two disturbances taken separately. This restriction has to be made in any general theory of regulation.

If the superposition principle holds good, we can confine ourselves, when studying the response of x (or q), to a "standard disturbance," i.e., a sudden deviation 1 from the normal value 0, remaining equal to 1 for all positive values of t .

We define two fundamental functions:

(a) The response function $X_R(t)$ of the "process" with respect to the considered variable x . This is the response of x to a standard disturbance of q , the circuit being open and assumed to be severed at A, between process and regulator, Fig. 1.

(b) The response function $Q_R(t)$ of the "regulator" is the response of q to a standard disturbance of x taken with a negative sign, the circuit being open and assumed to be severed at B between regulator and process.

Any time-dependent disturbance can be approximated by a succession of small "step functions" and hence can be represented by a linear combination (sum or integral) of standard disturbances. If the response corresponding to the standard dis-

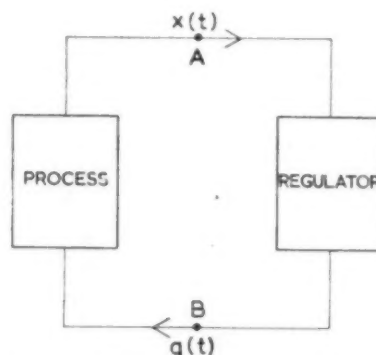


FIG. 1 DIAGRAM OF REGULATION CIRCUIT

turbance 1 of q is $X_R(t)$, the response corresponding to an arbitrary disturbance $q(t)$ will be

$$\frac{d}{dt} \int_0^t q(t-\tau) X_R(\tau) d\tau \dots \dots \dots [1]$$

which operation can be conveniently represented by the symbol $q(t) \circ X_R(t)$.

In the same way we have for an arbitrary disturbance $x(t)$

$$x(t) \circ Q_R(t) = \frac{d}{dt} \int_0^t x(t-\tau) Q_R(\tau) d\tau \dots \dots \dots [2]$$

Other quantities in the regulation circuit can be derived from $X_R(t)$ and $Q_R(t)$. Especially important is the following function:

Behavior of Regulated Variable $X_B(t)$. This is the response of x to an initial standard disturbance of x under the influence of the regulator. For the sake of brevity this will often be called the behavior function.

The behavior corresponding to an arbitrary time-dependent disturbance can be found by applying a formula of the same kind as Equation [1] or Equation [2] to $X_B(t)$.

TYPES OF RESPONSE CURVES

In order to study the behavior of the variables in a regulation circuit, it is convenient to assume hypothetical response curves representing mathematical functions distinguished by simple properties. By suitable adjustment to certain parameters occurring in these functions they are adaptable to a more or less close approximation of the majority of response functions met with in practice. The latter point has been treated more fully in the practical part.

For the present we shall confine ourselves to the discussion of the kind of regulation that is performed by a regulator with proportional plus integral action, and which may be represented by the idealized response function

$$Q_R(t) = \begin{cases} 0 & \text{for } t \leq 0 \\ a + bt & \text{for } t > 0 \end{cases}$$

¹ N. V. Bataafsche Petroleum Maatschappij, The Hague, Holland. Presented at the ASME Industrial Instruments and Regulators Division - Instrument Society of America Conference at St. Louis, Mo., September 12-16, 1949.

NOTE: Statements and opinions advanced in papers are to be understood as individual expressions of their authors and not those of the Society. Paper No. 49-IIRD-1.

As for the process, two classes of response functions will be considered as follows:

1 Processes with self-regulation of the following three types;

Type A. Curves having contact of the order $n - 1$ with the axis of t

$$X_R(t) = 1 - e^{-t} \left(1 + t + \frac{t^2}{2!} + \dots + \frac{t^{n-1}}{(n-1)!} \right) \dots [3]$$

Type B. Curves with dead time T_d

$$X_R(t) = \begin{cases} 0 & \text{for } t \leq T_d \\ 1 - \exp\left(-\frac{t - T_d}{T_e}\right) & \text{for } t > T_d \end{cases} \dots [4]$$

Type C. Abrupt response with dead time T_d

$$X_R(t) = \begin{cases} 0 & \text{for } t \leq T_d \\ 1 & \text{for } t > T_d \end{cases} \dots [5]$$

Type C is a limiting case of Type A ($n \rightarrow \infty$) and also of Type B ($T_e \rightarrow \infty$).

2 Processes without self-regulation of the following two types:

Type D.

$$X_R(t) = t - n + e^{-t} \left[n + (n-1)t + \frac{n-2}{2!} t^2 + \dots + \frac{1}{(n-1)!} t^{n-1} \right] \dots [6]$$

This function is obtained from Type A by integration from 0 to t .

$$X_R(t) = \begin{cases} 0 & \text{for } t \leq T_d \\ t - T_d & \text{for } t > T_d \end{cases} \dots [7]$$

Type E is a limiting case of Type B which may be obtained from the latter by multiplying Equation [4] by T_e and letting T_e become infinite.

As we have pointed out in the practical part,² the regulation has to satisfy different requirements according to the asymptotic behavior of the disturbance. In the case of processes with self-regulation, we have taken the standard disturbance as our fundamental disturbance. In the case of processes without self-regulation, we have considered as a fundamental disturbance the time integral of the unit disturbance

$$x(t) = t \quad (t > 0)$$

The behavior of the regulated variable resulting from this disturbance will be called the "second behavior function" and denoted by $X_B^*(t)$. It is the time integral of $X_B(t)$

$$X_B^*(t) = \int_0^t X_B(\tau) d\tau$$

In all these cases the main question is: What choice of the parameters a and b of the regulator gives the best possible regulation, and between what limits can a and b vary without making the regulation much worse?

CRITERION FOR BEST REGULATION

The new feature of our theory is the putting forward of a criterion for best regulation, which has been proposed by Prof. W. J. D. van Dijk. According to this criterion we shall have optimum performance when the parameters of the response function $Q_R(t)$ (in our case a and b) are given the values for which

(1) in the case of processes with self-regulation, the integral

$$S = \int_0^\infty X_B^*{}^2 dt \dots [8]$$

² "The Optimum Adjustment of Regulators," by P. Hazebroek and B. L. van der Waerden, companion paper presented at the IIR-ISA Conference at St. Louis, Mo., Sept. 12-16, 1949.

(2) in the case of processes without self-regulation, the integral

$$S = \int_0^\infty X_B^*{}^2 dt \dots [8a]$$

attains its minimum value. This is a reasonable condition as it meets both the requirements for good regulation:

(a) The regulated variable should be quickly reduced to its normal value.

(b) The fluctuations of this variable should remain small.³

These criteria seem to be especially adapted to the special types of fundamental disturbances we have assumed. We shall prove, however, that it is also satisfactory for more general disturbances.

We will first consider processes with self-regulation.

Let X_B be the behavior of x upon a standard disturbance of x , as previously calculated. The behavior due to an arbitrary disturbance X_D is

$$x = X_D \circ X_B = \frac{d}{dt} \int_0^t X_D(t - \tau) X_B(\tau) d\tau \dots [9]$$

Now suppose that X_B becomes practically zero after a certain time T , and that X_D is a continuous, differentiable bounded function of t , which means that no sudden, but only gradually increasing and decreasing disturbances occur. In this case Equation [9] may be written

$$x(t) = \int_0^T X_D'(t - \tau) X_B(\tau) d\tau$$

Now, by a well-known inequality of Schwarz

$$\left[\int_a^b f(x)g(x) dx \right]^2 \leq \int_a^b f^2(x) dx \cdot \int_a^b g^2(x) dx$$

we have

$$x^2(t) = \int_0^T X_D'^2(t - \tau) d\tau \cdot \int_0^T X_B^2(\tau) d\tau$$

In general, we may assume that the disturbances met with in practice do not occur so suddenly and so frequently and intensely that the first factor on the right becomes extremely large. As to the second factor, we can make it as small as possible by the application of our criterion. Now if the first factor is not too large and the second one is made small, the whole product will become small, that is, the deviation $x(t)$ will be small for all values of t , which is the object of regulation. Furthermore, if during some time T no disturbances occur, $x(t)$ will be zero after this lapse of time. This is all that reasonably may be expected.

Next we turn to processes without self-regulation. If we make use of the integral, Equation [8], also for these processes, it is found that b becomes zero. When b vanishes, however, the regulated variable would not revert to its normal value when the disturbance increases linearly. As we assume that in the present case the disturbance is of the latter type, the criterion has to be modified. If we replace in our first criterion the integral, Equation [8] by [8a], and if we assume further the disturbance X_D to

³ Some readers may be inclined to think that our criterion seems somewhat artificial. It might, for instance, be argued that it would be more plausible to choose a and b in such a way that the integral of the absolute value of $X_B(\tau)$

$$S_1 = \int_0^\infty |X_B(\tau)| d\tau$$

becomes a minimum. The main objection to this is, however, that this integral is very unsuitable for mathematical treatment. Moreover, the results would in most cases not differ very much from our own.

The same argument is, at least in part, at the bottom of the method of least squares, where the sum of the squares of the deviations is minimized rather than the sum of their absolute values. In fact our method also makes a quantity with the nature of a squared error a minimum.

increase linearly for large t , the foregoing argument is again valid with some slight modifications. The proof may be left to the reader.

Thus the principle of making the integrals, Equations [8] and [8a], respectively, as small as possible for standard disturbances is justified also on the assumption of nonstandard disturbances.

The parameters a and b sometimes must be subjected to certain restrictions, e.g., that the regulated flow should never exceed a prescribed value. In this paper, however, no such restrictions are imposed, and we shall only be concerned with the integral S .

QUALITY OF REGULATION

Let S_m be the minimum of S , corresponding to the best choice of a and b . We introduce an index for the quality of regulation. The quality number N is defined as the quotient

$$N = \frac{S_m}{S}$$

The maximum value $N = 1$ corresponds to the best regulation but regulation with quality number 0.9 is nearly as good.

CALCULATION OF BEHAVIOR OF REGULATED VARIABLE AND REGULATING FLOW

In order to find S and N , it is necessary to calculate the behavior $X_R(t)$ of the variable x .

If at time $t = 0$ a standard disturbance 1 is given to x , the response of q is given by $Q_R(t)$, and the response of x to this regulating flow is given, according to Equation [1], by

$$-F_1(t) = -Q_R(t) \circ X_R(t) = -(Q_R \circ X_R)$$

Hence the regulated variable x does not remain 1, but becomes

$$1 - F_1(t)$$

But this modified disturbance gives rise to a modified response of the regulating flow

$$-(1 - F_1) \circ Q_R$$

and this in turn causes a modified response of the variable x

$$\begin{aligned} -(1 - F_1) \circ Q_R \circ X_R &= -(1 - F_1) \circ F_1 \\ &= -F_1 + (F_1 \circ F_1) \end{aligned}$$

Hence the regulated variable becomes

$$1 - F_1 + F_2; (F_2 = F_1 \circ F_1)$$

By continuation of this process we finally find the behavior of x

$$X_R = 1 - F_1 + F_2 - F_3 + \dots \quad [10]$$

where

$$F_1 = Q_R \circ X_R = \frac{d}{dt} \int_0^t Q_R(t-\tau) X_R(\tau) d\tau \quad [11]$$

$$\left. \begin{aligned} F_2 &= F_1 \circ F_1 \\ F_3 &= F_2 \circ F_1 \end{aligned} \right\} \quad [12]$$

In simple cases, for instance, in the case of a step function X_R (Type C), the Equations [10], [11], [12] can be used directly to calculate the behavior X_R . In more complicated cases, other mathematical devices to be discussed later save a considerable amount of labor.

EFFECT OF A DEAD TIME

If one of the response functions Q_R or X_R has a dead time T_d , i.e., remains zero as long as $t \leq T_d$, the same dead time will appear in F_1 , double this time in F_2 , treble in F_3 , etc. Hence for any

finite value of t only a finite number of functions F_n will be different from zero, and the series, Equation [10], has for every finite value of t only a finite number of terms, each of which can be found by direct integration if the functions X_R and Q_R are not too complicated. For large values of t the number of terms may be large, but in that case the whole sum X_R is negligibly small if regulation is at all stable and efficient.

If both functions Q_R and X_R have dead times t_1 and t_2 , the sum of these $t_1 + t_2$ will be the dead time of F_1 according to Equation [11]. It is quite irrelevant which part of this sum is due to Q_R and which to X_R ; only the sum $t_1 + t_2$ matters. A dead time in Q_R has exactly the same effect as one in X_R ; hence we can always assume that Q_R has no dead time. For any satisfactory regulator the dead time has to be very small anyway.

The simplest case for an X_R with dead time is as follows:

Response Process Type C. We can take T_d as unit of time, hence Equation [5] becomes

$$X_R = \begin{cases} 0 & \text{for } t \leq 1 \\ 1 & \text{for } t > 1 \end{cases}$$

and

$$Q_R = a + bt \text{ for } t > 0$$

Equation [11] gives

$$F_1 = Q_R \circ X_R = \begin{cases} 0 & \text{for } t \leq 1 \\ a + b(t-1) & \text{for } t > 1 \end{cases}$$

By means of Equation [12], we get

$$F_n(t) = \begin{cases} 0 & \text{for } t \leq n \\ f_n(t-n) & \text{for } t > n \end{cases}$$

the polynomials f_1, f_2, \dots being defined by the recursion formulas

$$\begin{cases} f_1 = a + bt \\ f_n = af_{n-1} + b \int_0^t f_{n-1}(\tau) d\tau = \sum_{k=0}^n \frac{n!}{(n-k)!} \frac{a^{n-k} b^k}{k!} t^k \end{cases}$$

Finally, Equation [10] gives

$$X_R(t) = 1 - f_1(t-1) + f_2(t-2) - \dots$$

The result of the calculation is shown in Fig. 2, for $a = 0.5$, and $b = 0.8$.

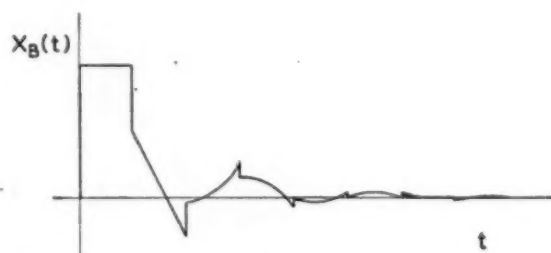


FIG. 2 BEHAVIOR OF REGULATED VARIABLE FOR TYPE C PROCESS

APPLICATION OF OPERATIONAL CALCULUS

In more complicated cases, when direct calculation of the series, Equation [10], is impracticable, the operational calculus is useful. The functions X_R and Q_R give rise to Laplace transforms

$$f(p) = \int_0^\infty p e^{-pt} X_R(t) dt$$

$$g(p) = \int_0^\infty p e^{-pt} Q_R(t) dt$$

The Laplace transform of the function $F_1(t) = Q_R \circ X_R$ is the product $f(p)g(p)$ and hence the transform of the series, Equation [10], is

$$\varphi(p) = \frac{1}{1 + f(p)g(p)} = \frac{F(p)}{G(p)} \dots [13]$$

In order to find the behavior function X_B , of which Equation [13] is the Laplace transform, use may be made of Heaviside's "expansion theorem," which is stated as follows:

If p_1, p_2, \dots, p_n are the roots of the equation $G(p) = 0$, each assumed to be different and none of them equal to zero, then Equation [13] is the Laplace transform of

$$X_B(t) = \frac{F(0)}{G(0)} + \sum \frac{F(p_i)}{p_i G'(p_i)} e^{p_i t}$$

The expansion theorem can be applied when $F(p)$ and $G(p)$ are polynomials, and also in the case of transcendental functions, where it becomes impracticable, however, for small values of t .

In the applications here considered, the Laplace transform of $Q_R = a + bt$ is

$$g(p) = a + \frac{b}{p} \dots [14]$$

As to $X_R(t)$, we will first consider the cases in which its Laplace transform $f(p)$ is a rational function (Types A and D). Next we shall deal with the cases in which $f(p)$ is a transcendental function (Types B, C, and E).

Formulas for S . When $f(p)$ is a rational function, the Laplace transform of $X_B(t)$ is a rational function

$$\varphi(p) = \frac{p(d_0 p^{n-1} + d_1 p^{n-2} + \dots + d_{n-1})}{p^n + c_1 p^{n-1} + \dots + c_n}$$

It is possible to find a general expression for the integral

$$S = \int_0^\infty X_B^2(t) dt$$

for any function $X_B(t)$ whose Laplace transform is a rational fraction

$$\varphi(p) = \frac{pE(p)}{(p - \alpha_1)(p - \alpha_2) \dots (p - \alpha_n)}$$

provided all the roots α_i of the denominator have negative real parts. The degree of $E(p)$ must not be higher than $n - 1$. The factor p in the numerator is necessary in order that $X_B(t)$ tends to zero for $t \rightarrow \infty$.

According to the expansion theorem, we have

$$X_B(t) = \sum_j \frac{E(\alpha_j) \exp(\alpha_j t)}{(\alpha_j - \alpha_1) \dots (\alpha_j - \alpha_{j-1})(\alpha_j - \alpha_{j+1}) \dots (\alpha_j - \alpha_n)}$$

and the value of the integral S is expressed by

$$S = - \sum_{k \neq j} \frac{E_k(\alpha_j)}{2\alpha_j \prod_{k \neq j} (\alpha_j - \alpha_k)^2} - 2 \sum_{(ij)} \frac{E(\alpha_i)E(\alpha_j)}{(\alpha_i + \alpha_j) \prod_{k \neq i} (\alpha_i - \alpha_k) \prod_{k \neq j} (\alpha_j - \alpha_k)}$$

It may be proved that S is a symmetrical function of the roots α_k , and thus can be expressed as a rational function of the coefficients c_k . Actually, S may be found more easily by means of a theorem to be stated later (Equation [15]). The general expression for S , which is rather long and complicated, is not given here but is only written down for those values of n which are of

practical interest. Also we have given the conditions of stability, according to the Hurwitz criterion

$n = 2$

$$S = \frac{d_1^2 + c_2 d_0^2}{2c_1 c_2}$$

$n = 3$

$$S = \frac{d_2^2 c_1 + (d_1^2 - 2d_0 d_2) c_3 + c_2 c_3 d_0^2}{2c_3(c_1 c_2 - c_3)}$$

Condition of stability

$$c_1 c_2 - c_3 > 0$$

$n = 4$

$$S = \frac{d_2^2(c_1 c_2 - c_3)}{2c_4(c_1 c_2 c_3 - c_3^2 - c_1^2 c_4)} + \frac{c_1(d_2^2 - 2d_1 d_3) + c_3(d_1^2 - 2d_0 d_2) + d_0^2(c_2 c_3 - c_1 c_4)}{2(c_1 c_2 c_3 - c_3^2 - c_1^2 c_4)}$$

Condition of stability

$$c_1 c_2 c_3 - c_3^2 - c_1^2 c_4 > 0$$

$n = 5$

$$S = \frac{d_4^2 \omega_0}{2c_5 G_5} + \frac{(d_3^2 - 2d_2 d_4) \omega_1 + (d_2^2 - 2d_1 d_3 + 2d_0 d_4) \omega_2 + (d_1^2 - 2d_0 d_2) \omega_3 + d_0^2 \omega_4}{2G_5}$$

$$\omega_0 = c_1 c_2 c_4 - c_3^2 - c_1^2 c_4 + c_1 c_5$$

$$\omega_1 = c_1 c_3 - c_3$$

$$\omega_2 = c_1 c_4 - c_5$$

$$\omega_3 = c_3 c_4 - c_2 c_5$$

$$\omega_4 = c_2 c_3 c_4 - c_2^2 c_5 - c_1 c_4^2 + c_4 c_5$$

$$G_5 = \omega_1 \omega_3 - \omega_2^2$$

Condition of stability

$$G_5 > 0$$

$n = 6$

$$S = \frac{d_5^2 \omega_0}{2c_6 G_6} + \frac{(d_4^2 - 2d_3 d_5) \omega_1 + (d_3^2 - 2d_2 d_4 + 2d_1 d_5) \omega_2}{2G_6} + \frac{(d_2^2 - 2d_1 d_3 + 2d_0 d_4) \omega_3 + (d_1^2 - 2d_0 d_2) \omega_4 + d_0^2 \omega_5}{2G_6}$$

$$\omega_0 = (c_2 c_4 - c_2 c_5 + c_1 c_6)(c_1 c_2 - c_3) - (c_1 c_4 - c_3)^2$$

$$\omega_1 = c_1 c_2 c_3 - c_3^2 - c_1^2 c_4 + c_1 c_5$$

$$\omega_2 = c_1 c_2 c_5 - c_2 c_5 - c_1^2 c_6$$

$$\omega_3 = c_1 c_4 c_5 - c_1 c_2 c_6 - c_3^2$$

$$\omega_4 = c_2 c_4 c_5 - c_2^2 c_6 - c_2 c_3^2 + c_1 c_4 c_6$$

$$\omega_5 = (c_2 c_3 - c_1 c_4 + c_5)(c_4 c_5 - c_3 c_6) - (c_1 c_6 - c_2 c_5)^2$$

$$G_6 = c_5 \omega_0 - c_3 c_6 \omega_1 + c_1 c_6 \omega_2$$

Conditions of stability

$$\omega_1 > 0$$

$$G_6 > 0$$

For higher values of n the expressions become too cumbersome for practical use. In some of these cases S may be found from the integral

$$S = \frac{1}{\pi} \int_0^\infty |\varphi(i\omega)|^2 \frac{d\omega}{\omega^2} \dots \dots \dots [15]$$

which follows from Parseval's theorem in the theory of the Fourier integral.

APPLICATION OF FORMULAS FOR S TO TYPES OF PROCESS A AND D.

Type A. The response of the process is given by Equation [3]. The Laplace transform is

$$f(p) = \frac{1}{(p+1)^n}$$

hence by Equations [13] and [14]

$$\varphi(p) = \frac{p(p+1)^n}{p(p+1)^n + ap + b} \dots \dots \dots [16]$$

Applying the formulas for S to the present case, Equation [16], we find, putting $a+1=k$ for $n=1$

$$S = \frac{b+1}{2bk}$$

$n=2$

$$S = \frac{bk + 2b + 2}{2b(2k-b)}$$

$n=3$

$$S = \frac{9 - k + 9b + 6bk - 3b^2}{2b(9k - k^2 - 9b)}$$

$n=4$

$$S = \frac{80 - 16k + 84b + 64bk - 66b^2 - 4bk^2 + b^2k}{2b[80k - 120b - (4k-b)^2]}$$

$n=5$

$$S = \frac{-(155b+1)x^2 + (23b^2+260b-70)x - b^3-8b^2+63b+55}{10b[-x^2-70x^3+(14b+55)x-b^2-22b]}$$

In the last case ($n=5$), we have put $k=5x$.

The values of a or k and b for which S becomes a minimum may be found by solving the equations

$$\frac{\partial S}{\partial k} = 0, \quad \frac{\partial S}{\partial b} = 0$$

It appears that there is only one set of roots of these equations which satisfies the conditions of stability.

For a table of values of a and b , we refer to the companion paper² (Table 1).

For larger values of n , the minimum of S can be found approximately by means of the integral, Equation [15].

For the case $n=4$ (third-order contact), the lines of constant N in the a, b -plane are shown in Fig. 3. It is seen that deviations of 40 per cent in a and b do not bring the quality number below 0.9. Thus a very rigorous adjustment of a and b is not necessary.

Type D (Without Self-Regulation). The method is exactly the same as in the preceding case. The Laplace transforms of the functions X_R and X_R^* are

$$f(p) = \frac{1}{p(p+1)^n}$$

$$\varphi(p) = \frac{p(p+1)^n}{p^2(p+1)^n + ap + b}$$

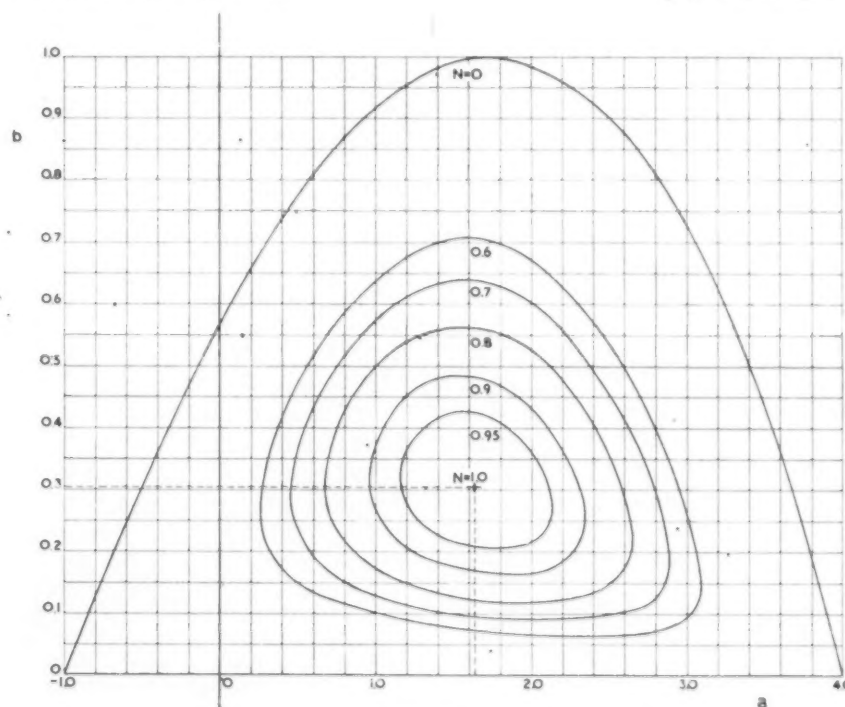


FIG. 3 LINES OF EQUAL QUALITY OF REGULATION FOR CASE $n=4$ OF TYPE A PROCESS

$$\left(N = \frac{S_m}{S}\right)$$

$n = 0$

$$S = \frac{1}{2ab}$$

$n = 1$

$$S = \frac{1+b}{2b(a-b)}$$

$n = 2$

$$S = \frac{2-a+4b+ab}{2b(2a-a^2-4b)}$$

$n = 3$

$$S = \frac{8-9a+27b+10ab-6b^2}{2b(8a-24b-9a^2+6ab-b^2)}$$

$n = 4$

$$S = \frac{64-112a+336b-a^3+156ab-176b^2-10a^2b+4ab^3}{2b(64a-256b-112a^2+144ab-64b^2-a^3)}$$

The values of a and b for which these expressions assume a minimum are given in Table 3 of the companion paper.²

PROCESSES OF TYPES B, C, AND E

In these cases the operational expression $\varphi(p)$ for $X_B(t)$ is transcendental and the determination of the most favorable values of a and b is far more troublesome, as the minimum value of S can only be found approximately by trial and error. For this purpose we have made use of the integral, Equation [15].

Type B. The response of the process is given by Equation [4]. Assuming $T_d = 1$, the Laplace transform of X_B is

$$f(p) = \frac{\exp(-pT_d)}{1+p}$$

hence

$$\varphi(p) = \frac{p(p+1)}{p(p+1) + (ap+b)\exp(-pT_d)}$$

In this case the integral, Equation [15], becomes

$$S = \frac{1}{\pi} \int_0^\infty \frac{(1+\omega^2)d\omega}{\omega^2(a + \cos \omega T_d - \omega \sin \omega T_d)^2 + (b - \omega \sin \omega T_d - \omega^2 \cos \omega T_d)^2}$$

In order to determine the minimum value of S , a and b have been systematically varied, and the integral has been evaluated numerically. It is only necessary to consider a finite interval from 0 to ω_0 where ω_0 must be assigned a suitable value depending upon the value of T_d . The contribution to S by the interval from ω_0 to ∞ remains nearly constant when a and b are varied, and thus does not materially affect the optimum values for a and b . It is again found that the quality of regulation remains good for a considerable latitude of variation of a and b .

The results of the calculation are recorded in Table 2 of the companion paper.²

After this somewhat more detailed exposition, we may be short about the remaining Types C and E. The best values of a and b are given in the companion paper.²

STABILITY

We conclude with a few remarks on stability of processes with dead time T_d .

When the process response has a dead time T_d the Laplace transform may be written

$$f(p) = e^{-pT_d}F(p)$$

and the Laplace transform of the behavior function $X_B(t)$ is

$$\begin{aligned} \varphi(p) &= \frac{1}{1 + e^{-pT_d}F(p) \left(a + \frac{b}{p} \right)} \\ &= \frac{p}{G(p)} \end{aligned}$$

The denominator of this function has an infinite number of roots, all of which should have negative real parts in order that regulation may be stable. Regulation becomes unstable for values of a and b for which a root crosses the imaginary axis. Moreover, b should be positive, as for negative values of b there would be a positive root.

In order to find the condition that $G(p)$ has purely imaginary roots, we substitute $p = i\omega$ and put $G(i\omega) = G_1(\omega) + iG_2(\omega) = 0$. Thus, a and b are expressed as functions of the parameter ω . These equations determine a spiral-shaped curve $\psi(a, b) = 0$ in the (a, b) -plane. The area enclosed by the smallest loop of this curve and the axis $b = 0$ is the region of stability.

As an example we consider a process of Type E with $T_d = 1$. The Laplace transform of $X_E(t)$ is in this case

$$\varphi(p) = \frac{p}{p^2 + e^{-p}(ap+b)}$$

and the limits of stability are given by the line $b = 0$, and the smallest loop of the curve

$$\begin{cases} a = \omega \sin \omega \\ b = \omega^2 \cos \omega \end{cases}$$

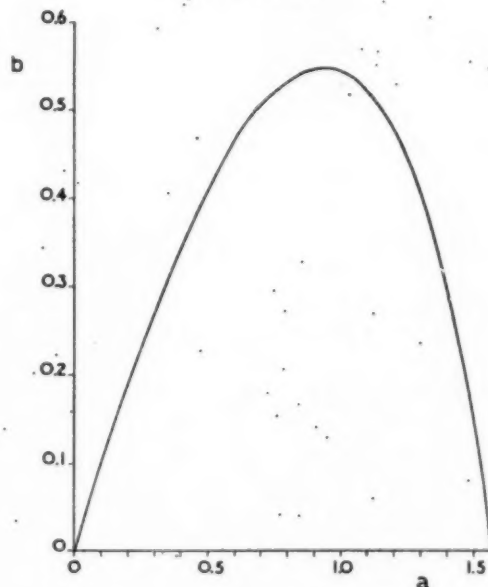


FIG. 4 REGION OF STABILITY FOR TYPE E PROCESS

ACKNOWLEDGMENT

Our acknowledgments are due to the N. V. de Bataafsche Petroleum Maatschappij for permission to publish this paper.

Discussion

M. D. CREECH.⁴ There are two requirements to be met in obtaining satisfactory control: One is that the amplitude of the controlled variable remain small; the other is that the amplitude approach zero at an early time. The integral of the absolute value of the amplitude gives about equal weight to the amplitude and the rapidity with which the amplitude approaches zero. As was pointed out by the authors, the integral of the square of the amplitude is more suitable to mathematical treatment. However, the integral of the square of the amplitude gives more weight to the magnitude of the amplitude and less weight to the time it takes for oscillations to die out. It now occurs to the writer that perhaps it might be better to use the integral of the fourth power or sixth power of the amplitude in certain cases.

An answer is requested to the following question: How can one tell when optimum control is obtained? Is it not possible that, in one case where the amplitude is large but quickly approaches zero and in another where the amplitude is small but takes a long time to become small, the minimum integral could be the same in both cases?

AUTHORS' CLOSURE

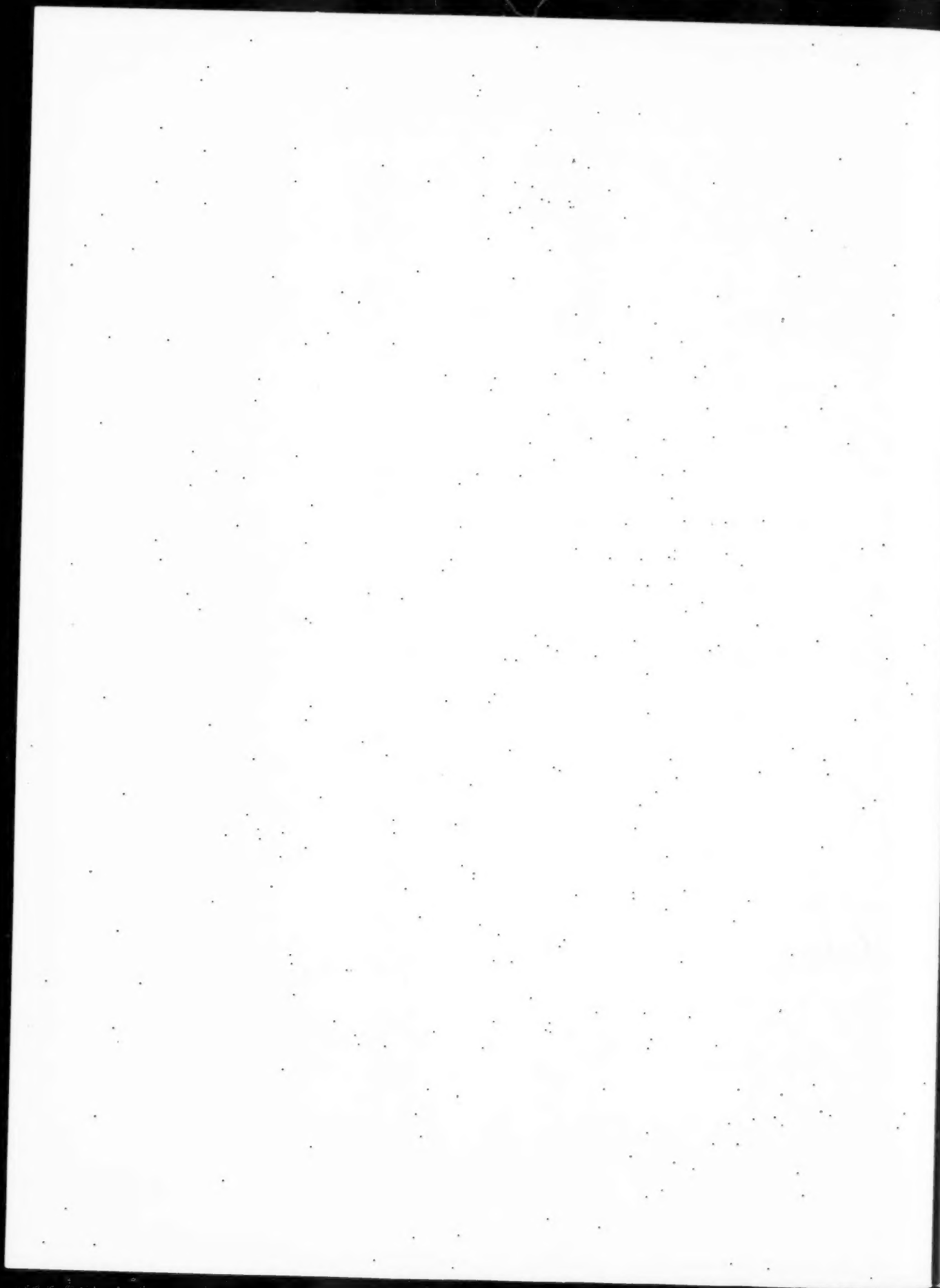
It may theoretically be admitted there might be some reason for the use of other than second powers in our minimum integral criterion, depending upon the relative weight of duration and amplitude of the regulated disturbance. It should however be recalled that: first, owing to several circumstances, our theory is only an approximation to any actual regulation; second, the optimum values of regulator parameters are not very critical, approximately forty per cent deviation from these values scarcely reducing the quality of regulation. For these reasons, apart

from mathematical difficulties, it seems an unnecessary refinement to consider other than second powers of amplitude, the more so as it would be difficult to decide which power should be chosen in any particular case.

The question whether our integral might have two approximately equal minimum values may be answered by the fact that in the cases we investigated, the function represented by our integral had only one single minimum, to which corresponds a definite set of values of regulation parameters. Hence in all these cases the behavior of the regulation circuit is uniquely determined. As our theory is only to be applied to regulation of processes whose response curves are sufficiently closely approximated by our hypothetical response curves, it may be expected also for these processes that optimum regulation according to our criterion is obtained for a unique set of values of regulation parameters. It may be granted that the case of two or even more minima of our integral is not a priori impossible, for example when there is more than one region of stability; it is, however, doubtful if such a case would ever be met with in practice. Anyway such a process would be beyond the scope of our theory.

At this place, reference may be made to "The Theory of Servo-Mechanisms," by James, Nichols, and Phillips, 1947, (McGraw-Hill Book Co., 1947), which came to the authors' attention after their papers had been submitted for publication. In a section of this book an approach to the control problems in many ways similar to that of the authors has been followed. The authors would like to avail themselves of this opportunity to express their thanks to Mr. N. B. Nichols of Taylor Instrument Co., firstly, for the stimulating influence of his repeatedly cited paper on "Optimum Settings for Automatic Controllers"; secondly, for discussions with members of our staff, which have resulted in considerable changes in our original design, especially of the companion paper; and thirdly, for his kindness in presenting these papers.

⁴ Professor, Mechanics and Metallurgy, The University of Oklahoma, Norman, Okla. Mem. ASME.



s
e
t
t
w
u
z
p
o
b
a
m
o
ca
va
be
re
ch
po
of
He
s
and
Re
par
E
Div
Sep
N
und
of t

The Optimum Adjustment of Regulators

By P. HAZEBROEK¹ AND B. L. VAN DER WAERDEN²

In this paper a practical method is proposed for the adjustment of regulators in order to obtain the most satisfactory regulation of a process variable which should be kept at a constant value. The regulator is assumed to perform proportional and integral action, derivative action not being taken into consideration for the present.

INTRODUCTION

SO far, little attention has been paid to the problem of assigning definite values to the parameters characterizing the action of a regulator in order to obtain optimum results. However, an important paper by J. H. Ziegler and N. B. Nichols,³ has been published, which gives some simple rules and which later on will be considered more closely.

The present authors, starting from other fundamentals, have developed new conditions for the adjustment of parameters. The novel feature of their theory is the proposal of a "general criterion for best regulation." This paper, which is intended to bring their theory within the scope of practical application, can be understood independently of the underlying theoretical foundation, which will be given in a separate paper.⁴

FUNDAMENTAL NOTIONS

Before considering the subject proper the authors will recall some well-known fundamental notions to be used later.

Let x be a "regulated variable," e.g., a temperature, pressure, etc., which should be kept as constant as possible. The value of this variable is obtained by measurement. The deviation from the regulation point, i.e., from the normal value, may be identified with the displacement of the recording pen from this point, measured in arbitrary units. The regulation point will be taken as zero point and thus x is the deviation from zero.

Let q be the "regulating flow." It can be measured by the position of the final regulating element, e.g., a regulating valve, or by the air pressure regulating it, assuming a linear relationship between them. Again, the normal value assumed by q in the absence of any disturbance is taken to be $q = 0$. The sign of q is made such that positive deviations of q cause positive deviations of x .

Process and regulator constitute a closed system which will be called a "regulation circuit," Fig. 1.

The "response of the process" is defined as follows: Let the valve be given at time $t = 0$ a sudden displacement q_0 and let it be kept in this position, the valve being disconnected from the regulator. The valve movement q_0 will cause in course of time a change in the regulated variable x , which is assumed to be proportional to the valve movement q_0 . The ratio x/q_0 as a function of time is called the "process response function" and is denoted

by $X_R(t)$. Thus, in other words, we may say that $X_R(t)$ is the deviation of x due to a sudden disturbance $q_0 = 1$. This latter disturbance will be called "unit" or "standard disturbance."

It follows from this definition that the process-response curve results from the properties both of the process and of the measuring part of the regulator.

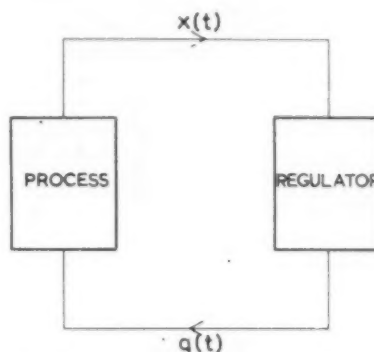


FIG. 1 DIAGRAM OF REGULATION CIRCUIT

The "response of the regulator" is defined as follows: Let the pen be given at time $t = 0$ a sudden displacement x_0 from its normal position and let the pen be kept in this position, the process being put out of circuit. The regulator will interpret the movement of the pen into a need for corrective action that is, the regulating flow $q(t)$ will become negative in order to compensate a positive x_0 . This change is assumed to be proportional to x_0 ; its opposite $-q(t)$ divided by x_0 is called the "response function of the regulator" $Q_R(t)$.

The response of a regulator with proportional plus integral action is represented by a function of the form

$$Q_R(t) = a + bt$$

From the response functions of process and regulator we may derive two functions describing the effect of regulation in the "closed" circuit. A sudden displacement x_0 of the recording pen will result in a response $x(t)$ of the regulated variable, and a response $q(t)$ of the regulating flow. The quotient $x(t)/x_0 = X_R(t)$ will be called the "behavior of the regulated variable," the quotient $-q(t)/x_0 = Q_B(t)$, the "behavior of the regulating flow."

It may happen that the theoretically best values of the regulation parameters would give rise to too violent fluctuations of the regulating flow. In this case Q_B must satisfy certain restricting conditions in consequence of which the said parameters are not allowed to exceed certain limiting values. These conditions depend upon the nature of the particular plant under consideration. As it is difficult to give satisfactory general rules, this point is merely mentioned here but henceforth will be left out of account.

CLASSIFICATION OF PROCESSES

By considering the process-response functions we can distinguish two classes of processes:

- 1 Those processes in which the regulated variable tends to a

¹ N. V. de Bataafsche Petroleum Maatschappij, The Hague, Holland.

² "Optimum Settings for Automatic Controllers," by J. H. Ziegler and N. B. Nichols, Trans. ASME, vol. 64, 1942, p. 759.

³ "Theoretical Considerations on the Optimum Adjustment of Regulators," by P. Hazebroek and B. L. van der Waerden, companion paper being presented at the present IIRD-ISA Meeting.

Presented at the ASME Industrial Instrument and Regulators Division-Instrument Society of America Conference, St. Louis, Mo., September 12-16, 1949.

NOTE: Statements and opinions advanced in papers are to be understood as individual expressions of their authors and not those of the Society. Paper No. 49-IIRD-2.

new fixed value, when a standard disturbance is applied to the regulating flow (processes "with" self-regulation).

2 Those processes in which the regulated variable increases or decreases indefinitely with time under the influence of a standard disturbance in the regulating flow (processes "without" self-regulation). We will consider especially the important case in which the increase is linear after a certain lapse of time.

TYPES OF DISTURBANCES

When defining the behavior functions as mentioned, a standard disturbance x_0 is assumed to be given to the regulated variable. In practice, however, the disturbances occurring in a process usually do not originate in the measuring part of the circuit, but may be introduced at any point in the process part. Hence the disturbance in the regulated variable in most cases is not a standard disturbance, but responds to some transformation of the initial disturbance somewhere else in the process.

We will distinguish the disturbances occurring in the regulated variable according to their asymptotic behavior for large values of t :

- 1 The disturbance tends to zero after a certain lapse of time.
- 2 The disturbance tends asymptotically to a fixed value. The simplest disturbance of this kind is the standard disturbance, introduced previously.
- 3 The disturbance increases indefinitely with time.

POSSIBLE COMBINATION OF PROCESSES AND DISTURBANCES

Each of the disturbances just classified may occur in each of the two classes of processes previously mentioned.

As the type of regulator to be chosen and its adjustment for optimum regulation depend on which of these cases we are considering, all these cases should be discussed from a theoretical point of view. In practice, however, two of the theoretically possible combinations are especially important: We will confine ourselves in this paper to these cases, which are as follows:

1 Processes with self-regulation, when a disturbance of the second kind is applied to the regulated variable. As will be shown later, it is sufficient for our purpose to consider the standard disturbance.

2 Processes without self-regulation whose response functions increase linearly with time, when a disturbance $x = t$ is applied to the regulated variable (special case of third kind of disturbance). An example is the regulation of a liquid level. The disturbance then usually results from a sudden change of the regulating flow, which is transformed into a linearly increasing disturbance of the regulated variable.

In this second case the behavior function $X_B(t)$, corresponding to a standard disturbance in the regulated variable, has mainly a theoretical significance. The response to a disturbance

$$x(t) = \begin{cases} 0 & \text{for } t < 0 \\ t & \text{for } t > 0 \end{cases}$$

(time integral of a standard disturbance) is far more important for judgment of the behavior of the regulated variable. This response function, which we shall call the "second behavior function" $X_B^*(t)$, is the time integral of $X_B(t)$

$$X_B^*(t) = \int_0^t X_B(\tau) d\tau$$

CONSTANTS OF REGULATOR

Two constants characterize the response function of the type

of regulator we are discussing: the sensitivity⁴ of proportional response and the "reset rate" b/a .

Sensitivity is concerned only with the first (vertical) part of the response curve; it is valve movement per pen movement. In practice it is customary to use in place of sensitivity the proportional band, defined as

$$PR = \frac{1}{a} \cdot \frac{q_m}{x_m} \cdot 100$$

where

q_m = maximum interval of the regulating flow

x_m = scale interval of the regulated variable

The reset rate is concerned with the second part of the curve; it is the number of times per unit of time that automatic reset repeats the proportional response a . Hence the reset rate b/a has the dimension of an inverse time; in fact, the reciprocal a/b , the reset time T , is the time in which proportional response is repeated, see Fig. 2.

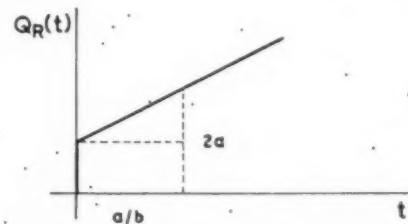


FIG. 2 RESPONSE CURVE OF REGULATOR OF PROPORTIONAL-PLUS-INTEGRATING TYPE

CRITERION FOR BEST REGULATION

Regulators with proportional plus integral action allow an adjustment of the parameters a and b/a within relatively wide limits. Hence the question arises: Which values of a and b/a will give the best regulation, reducing any disturbance of x to zero within a short time, without giving rise to violent fluctuations?

Before it is possible to answer this question, it should first be decided what we are to consider as the best possible regulation. The authors have adopted the following criterion, the justification of which they have given in their theoretical paper:³

1 For processes with self-regulation, optimum regulation will be obtained for those values of the parameters a and b for which the time integral of the square of the behavior of the regulated variable

$$S = \int_0^{\infty} X_B^2 dt$$

attains its minimum value.

2 For processes without self-regulation, the time integral of the square of the second behavior function

$$S = \int_0^{\infty} X_B^{*2} dt$$

should be minimized.

We have applied this criterion to a number of hypothetical process-response curves representing mathematical functions with particularly simple properties. For the details of the calculations we refer to our theoretical paper.³ These curves, to-

⁴ Sometimes sensitivity is identified with proportional band, which seems to us a confusing practice.

gether with the values of a and b , corresponding to optimum regulation, are given in Table 1.

TABLE 1

n	a	b
2	∞	∞
3	2.75	0.500
4	1.64	0.305
5	1.26	0.219
10	0.692	0.0913
25	0.555	0.0330
50	0.516	0.0162

Processes With Self-Regulation:

Type A

$$X_R(t) = 1 - e^{-t} \left(1 + t + \frac{t^2}{2!} + \dots + \frac{t^{n-1}}{(n-1)!} \right)$$

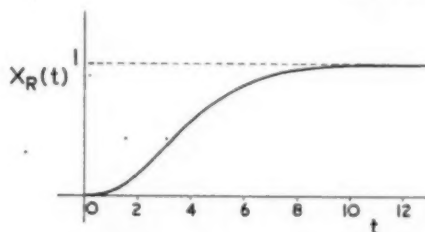
(Fig. 3 for $n = 4$)

FIG. 3 RESPONSE CURVE OF TYPE A PROCESS

Type B

$$X_R(t) = \begin{cases} 0 & \text{for } t < T_d \\ 1 - \exp\left(-\frac{t - T_d}{T_e}\right) & \text{for } t > T_d \end{cases} \quad (\text{Fig. 4})$$

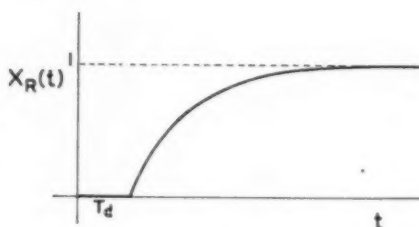


FIG. 4 RESPONSE CURVE OF TYPE B PROCESS

For time lag $T_d = 1$, we find approximately for different values of the time constant, data in Table 2.

TABLE 2

$\frac{1}{T_e}$	a	b
0.2	4.0	0.53
0.3	2.77	0.54
0.5	1.79	0.55
0.7	1.37	0.56
1	1.07	0.57
1.5	0.84	0.60
2	0.73	0.62
3	0.63	0.66
5	0.55	0.68
∞	0.50	0.80

Type C. Abrupt response with dead time T_d

$$X_R(t) = \begin{cases} 0 & \text{for } t < T_d \\ 1 & \text{for } t > T_d \end{cases} \quad (\text{Fig. 5})$$

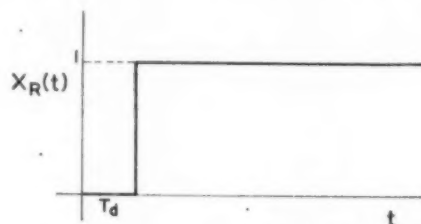


FIG. 5 RESPONSE CURVE OF TYPE C PROCESS

This is a limiting case of Type A when n becomes infinite and the time scale is transformed into $t' = T_d t/n$. It is also a limiting case of Type B when T_e becomes infinite. The most favorable values of a and b are

$$a = 0.50, \quad b = \frac{0.8}{T_d}$$

Processes Without Self-Regulation:

Type D

$$X_R(t) = t - n + e^{-t} \left(n + (n-1)t + \frac{n-2}{n!} t^2 + \dots + \frac{1}{(n-1)!} t^{n-1} \right)$$

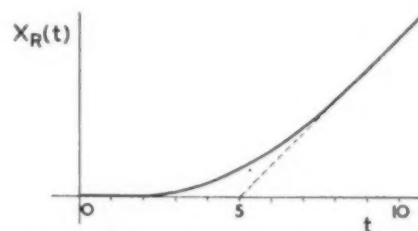
(Fig. 6 for $n = 5$)

FIG. 6 RESPONSE CURVE OF TYPE D PROCESS

Best values of a and b are given in Table 3.

TABLE 3

n	a	b
0 and 1	∞	∞
2	1.211	0.0917
3	0.571	0.0335
4	0.375	0.0174

Type E

$$X_R(t) = \begin{cases} 0 & \text{for } t < T_d \\ t - T_d & \text{for } t > T_d \end{cases} \quad (\text{Fig. 7})$$

Best values of a and b

$$a = \frac{1.11}{T_d}, \quad b = \frac{0.24}{T_d^2}$$

Type E may be obtained as a limiting case of Type D for $n \rightarrow \infty$ after having reduced both the time scale and the scale of the regulated variable by a factor T_d/n .

CHARACTERISTIC PARAMETERS OF PROCESS RESPONSE CURVES INTRODUCED BY ZIEGLER AND NICHOLS

In order to apply these theoretical results to the response curves produced by actual processes, it is necessary to define

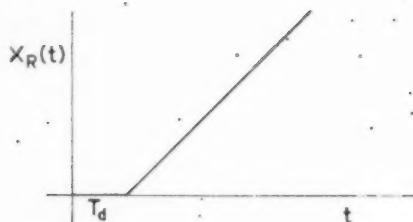


FIG. 7 RESPONSE CURVE OF TYPE E PROCESS

certain quantities which determine to a more or less close approximation the shape of the response curve. In this we follow the same lines as Ziegler and Nichols.

Ziegler and Nichols introduce two parameters occurring in a process-response curve (see Fig. 8)

R_1 = maximum slope of curve = time derivative in point of inflection⁵

L = time lag: distance along the axis from origin to point of intersection with inflection tangent.

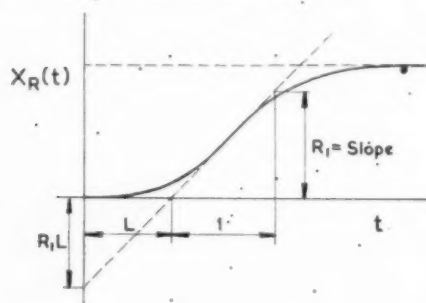


FIG. 8 CHARACTERISTIC PARAMETERS OF PROCESS-RESPONSE CURVE ACCORDING TO ZIEGLER AND NICHOLS

The parameters a and b/a of the regulator are now to be expressed in the introduced process parameters, in order to adapt the response curve of the regulator to the process-response curve.

Whereas L has the dimension of a time, the dimension of R_1L is "pen movement per valve movement." The inverse values $1/L$ and $1/(R_1L)$ have just the dimensions required for the reset rate and the sensitivity of a regulator. Hence Ziegler and Nichols define the optimum values of a and b/a by the formulas

$$\text{Sensitivity } a = \frac{0.9}{R_1L} \quad [1]$$

$$\text{Reset rate } \frac{b}{a} = \frac{0.3}{L} \quad [2]$$

The factors 0.9 and 0.3 are based on data obtained from practical experience.

COMPARISON OF ZIEGLER AND NICHOLS' RESULTS WITH PRESENT AUTHORS' RESULTS

We have applied Ziegler and Nichols' rules to a set of our response curves Type B. Each of the curves is characterized by its "time constant" T_e .

⁵ Ziegler and Nichols first introduce a quantity $R = \max \frac{dx}{dt}$ for arbitrary q_0 , but afterward they divide it by q_0 , and thus obtain the "unit reaction rate" R_1 .

Taking T_d as time unit, the values to be substituted in the formulas of Ziegler and Nichols are

$$\left. \begin{aligned} L &= T_d = 1 \\ LR_1 &= T_d \cdot \frac{1}{T_e} = \frac{1}{T_e} \end{aligned} \right\} \quad [3]$$

Hence the optimum sensitivity and reset rate would be, according to those authors

$$a = \frac{0.9}{LR_1} = 0.9 T_e \quad [4]$$

$$\frac{b}{a} = \frac{0.3}{L} = 0.3 \quad [5]$$

For comparison, the authors' results and those of Ziegler and Nichols are recorded side by side in Table 4.

TABLE 4 COMPARISON OF AUTHORS' RESULTS AND THOSE OF ZIEGLER AND NICHOLS

$\frac{1}{T_e}$	—Authors' results—		—Ziegler and Nichols' results—		
	a	$\frac{b}{a}$	a	$\frac{b}{a}$	
0.2	4.0	0.13	4.5	0.3	Reset rate high
0.3	2.77	0.195	3.00	0.3	
0.5	1.79	0.31	1.80	0.3	
0.7	1.37	0.41	1.28	0.3	
1.0	1.07	0.53	0.90	0.3	Good agreement
1.5	0.84	0.71	0.60	0.3	
2.0	0.73	0.85	0.45	0.3	Reset rate low
3.0	0.63	1.05	0.30	0.3	
5.0	0.55	1.24	0.18	0.3	Reset rate and sensitivity low
∞	0.50	1.38	0	0.3	

We have found that in all the cases we have computed, the minimum for S is very flat, so that for considerable deviations of a and b from their optimum values regulation still remains satisfactory. In our theoretical paper,³ we have given an instance where, even with deviations of 40 per cent, regulation remains good and, in other cases we have investigated, the conditions were found to be quite similar. Taking this into account, it may be stated that for $T_d < T_e$ (except when T_d/T_e is very small) the values of a and b found by both methods agree very well. For larger T_d/T_e , however, the reset rate given by Ziegler and Nichols' rule is far too low, and so is the sensitivity a for still larger T_d/T_e .

This conclusion is in accordance with a statement of Ziegler and Nichols in a later paper:⁴ "These settings appear to be very nearly correct on the processes tested for wide variations of R and L . On those infrequent processes in which L becomes greater than Z , Fig. 2,⁷ the settings given are too conservative."

Now L is our T_d and Z is our T_e , hence the "infrequent processes" to which Ziegler and Nichols' rules are admittedly not applicable are just the cases with $T_d/T_e > 1$. The cases with small lags ($T_d < T_e$) are those in which regulation is easy, whereas great lags make it difficult. As we shall see, it is possible to modify the rules of Ziegler and Nichols in such a way that they become generally applicable also in cases where the time lag is large.

MODIFICATION AND EXTENSION OF CONCEPTS INTRODUCED BY ZIEGLER AND NICHOLS

Ziegler and Nichols' formulas cannot be improved as long as only the constants L and R_1 , lag and slope of the process-response curve, are taken into account. Hence in order to give rules with

⁴ "Process Lags in Automatic-Control Circuits," by J. G. Ziegler and N. P. Nichols, Trans. ASME, vol. 65, 1943, p. 435.

⁷ Compare Fig. 9 of this paper where $L_2 = Z$.

a wider range of application, a third constant must be introduced. We can choose for this constant, in the case of processes with self-regulation in which x tends to a finite ultimate value, either the "height" H , of the horizontal asymptote or the "second lag" L_2 , described by Ziegler and Nichols as the time difference between the points of intersection of the inflection tangent with the t -axis and the asymptote (Fig. 9). H and L_2 are connected by the relation

$$H = R_1 L_2$$

For processes without self-regulation, H and L_2 are both ∞ .

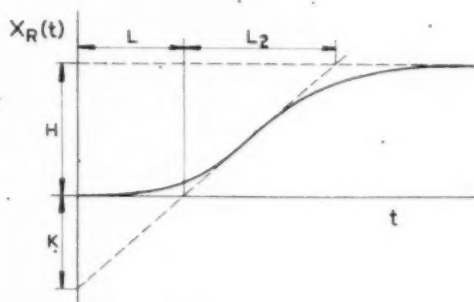


FIG. 9 EXTENDED DEFINITION OF CHARACTERISTIC PARAMETERS OF PROCESS-RESPONSE CURVE

Owing to the difference in definition of the criterion for best regulation, processes with and without self-regulation must be treated separately.

PROCESSES WITH SELF-REGULATION

The second lag L_2 has, like L , the dimension of a time. Hence the lag quotient

$$\lambda = \frac{L}{L_2} = \frac{R_1 L}{H} = \frac{K}{H} \quad [6]$$

is a dimensionless quantity. The product $R_1 L$ has a simple geometrical meaning; it is the "distance" K , measured from the origin down to the inflection tangent.

We now replace Equations [1] and [2] by the more general ones

$$\text{Sensitivity } a = \frac{\alpha}{R_1 L} = \frac{\alpha}{K} \quad [7]$$

$$\text{Reset rate } \frac{b}{a} = \frac{\beta}{L} \quad [8]$$

where the dimensionless quantities α and β are functions of λ , and are assigned such values that for curves Type B the Equations [7], [8] yield the exact optimum values of Table 2. For these curves the lag quotient is

$$\lambda = \frac{T_d}{T_c}$$

and since a , b , R_1 , and L are known in each of the ten cases, the coefficients α and β can be calculated from Equations [7] and [8], with the results given in Table 5.

For $\lambda < 0.2$

$$\alpha = 0.74 + 0.3\lambda, \quad \beta = 0.7\lambda$$

The case $\lambda = 0$ requires some comments. It will be seen from Equation [6] that λ may become zero in different ways, as follows:

TABLE 5 OPTIMUM VALUES OF a AND b FOR TYPE B RESPONSE

λ	α	β
0.2	0.80	0.14
0.3	0.83	0.20
0.5	0.89	0.31
0.7	0.96	0.41
1.0	1.07	0.54
1.5	1.26	0.71
2.0	1.46	0.85
3.0	1.89	1.05
5.0	2.75	1.23
∞	∞	1.60

1 When L becomes zero, which corresponds to a process with self-regulation and with dead time = 0.

2 When H becomes infinite, corresponding to a process without self-regulation and having a dead time different from zero.

Only the first possibility is of interest. We have seen that for processes without self-regulation our criterion for best regulation should be modified, so that the values for $\lambda = 0$, $\alpha = 0.74$, $\beta = 0$ are of no use for this second case.

TEST OF IMPROVED FORMULAS

In order to test whether Equations [7], [8] are also applicable to other process-response curves than those of Type B, for which they have been derived, we have applied them to Type A curves without dead time.

The optimum values of a and b have been given in Table 1 and the corresponding values of λ , α , and β , which can be found analytically, are recorded in Table 6.

TABLE 6 OPTIMUM VALUES FOR TYPE A RESPONSE

n	λ	α	β
3	0.218	0.600	0.146
4	0.319	0.523	0.265
5	0.410	0.526	0.366
10	0.773	0.535	0.774
25	1.500	0.832	1.10
50	2.326	1.200	1.28

For comparison, the values of α and β for both Type A and Type B response are represented graphically in Figs. 10 and 11. For small values of λ , comparison is impossible, because in the case of the A-curves for $n < 3$, a and b become infinite. For

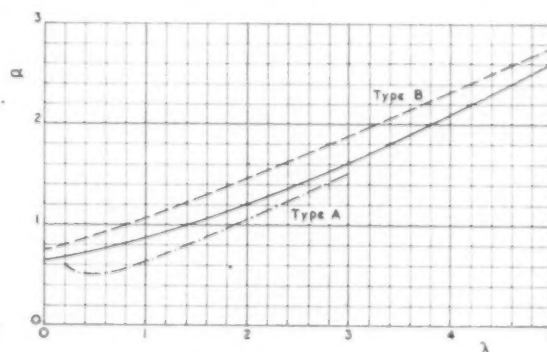


FIG. 10 CURVES REPRESENTING α AS A FUNCTION OF λ

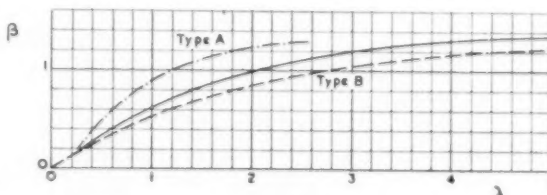


FIG. 11 CURVES REPRESENTING β AS A FUNCTION OF λ

small λ the best values of α and β depend very much upon the shape of the response curve near the origin. For these cases our theory would not be of interest anyway, as the values of our parameters become so high that on-and-off regulation would be the most favorable type of regulation that could be realized practically.

FINAL CHOICE OF α AND β

In view of the fact that a considerable deviation from the best values of the regulator parameters does not affect the quality of our regulation materially, the agreement of the α and β curves of both types may be considered fairly satisfactory. The response curves encountered in practice will have, roughly, the same shape as the curves of Types A and B. For any observed curve H , L , and L_2 or R_1 can be measured and thus λ is known. The corresponding optimum values of α and β will be somewhere near the values obtained for the Type A and B response curves. Owing to the relatively wide latitude of variation allowed for α and β we may assume universal values which we select somewhere intermediately between the two sets already found. These finally recommended values are recorded in Table 7 (for graphical representation see Figs. 10 and 11).

TABLE 7 SELECTED UNIVERSAL VALUES OF λ , α , AND β

λ	α	β	λ	α	β	λ	α	β
...	1.0	0.87	0.62	2.0	1.20	1.00
...	1.1	0.90	0.67	2.2	1.28	1.05
0.2	0.68	0.14	1.2	0.93	0.71	2.4	1.36	1.10
0.3	0.70	0.21	1.3	0.96	0.76	2.6	1.45	1.14
0.4	0.72	0.27	1.4	0.99	0.80	2.8	1.53	1.17
0.5	0.74	0.33	1.5	1.02	0.84	3.0	1.62	1.20
0.6	0.76	0.40	1.6	1.06	0.88	3.2	1.71	1.23
0.7	0.79	0.46	1.7	1.09	0.91	3.4	1.81	1.25
0.8	0.81	0.52	1.8	1.13	0.94	3.6	1.90	1.27
0.9	0.84	0.57	1.9	1.17	0.97	3.8	2.00	1.28
1.0	0.87	0.62	2.0	1.20	1.00	4.0	2.10	1.30

For $\lambda > 3.5$ the following formulas may be used

$$\left. \begin{aligned} \alpha &= 0.5\lambda + 0.1 \\ \beta &= 1.6 - \frac{1.2}{\lambda} \end{aligned} \right\} \dots \dots \dots [9]$$

It should be observed that these values of α and β should be used only for process-response curves of more or less "normal" shape. In exceptional cases one may meet with process-response curves which differ considerably from the hypothetical curves of Types A and B. For these cases the best values of the regulation parameters should be determined by separate investigation.

PRACTICAL RULES

Summarizing, we have the following practical rule: Find L , K , and H as indicated in Fig. 9, from the response curve of the process to a sudden increase q_0 of the regulating flow; calculate the lag quotient

$$\lambda = \frac{K}{H}$$

find α and β from Table 7, and take

$$\text{Sensitivity } a = \frac{\alpha}{K}$$

$$\text{Reset rate} = \frac{b}{a} = \beta/L$$

From the sensitivity, the proportional band (PB) may be computed easily.

$$\text{PB} = \frac{1}{a} \cdot \frac{q_m}{x_m} \cdot 100$$

where

$$\begin{aligned} q_m &= \text{maximum interval of regulating flow} \\ x_m &= \text{scale interval of regulated variable} \end{aligned}$$

The values of H , K , L , α , and β need be known only with an accuracy of, say, 10 per cent, because even a much greater variation in the adopted values of a and b does not make regulation materially worse.

It will be seen that the numerical values of the factors a , K , and H depend on the units of the variables q and x , whereas the b -values depend on the unit of time.

PROCESSES WITHOUT SELF-REGULATION

For processes without self-regulation the parameter λ becomes zero, and the parameters α and β may be defined in the same way as before by Equations [7] and [8]. The values of α and β calculated from the data for Types D (Table 3) and E are given in Table 8.

TABLE 8 VALUES OF α AND β CALCULATED FROM DATA FOR TYPES D AND E

λ	α	β
2	2.42	0.151
3	1.71	0.176
4	1.50	0.186
∞	1.11	0.22

Table 8 shows that there may be a considerable variation of the best values of a and b for different response curves possessing the same values of K and L . If we take as a reasonable compromise $\alpha = 1.5$, $\beta = 0.18$, we have the following practical rule for processes without self-regulation:

Find L and K from the response curve of the process and take

$$\left. \begin{aligned} \text{Sensitivity } a &= \frac{1.5}{K} \\ \text{Reset rate } \frac{b}{a} &= \frac{0.18}{L} \end{aligned} \right\} \dots \dots \dots [10]$$

Furthermore, the same observations which have been made with respect to processes with self-regulation apply here also.

Finally, we wish to stress the following points:

1 Our theory starts from idealized assumptions, viz., the validity of the superposition principle both for process and regulator, and ideal proportional and integral action of the regulator. Either of these assumptions is only realized to a rather rough approximation.

2 When testing our theory on actual processes this should be done with respect to our criterion of minimizing the integral S . It goes without saying that the adoption of any other criterion leads to other optimum values of a and b .

ACKNOWLEDGMENT

Our acknowledgments are due to the Management of the N. V. de Bataafsch Petroleum Maatschappij (Royal Dutch/Shell Group) for its kind permission to publish this paper. We would also mention Messrs J. van der Veen, F. C. L. van Vugt, and E. Wieringa of this company, whose comments and criticisms have had considerable influence on the final shaping of this paper, and Mr. H. J. Krajenbrink, who carried out most of the computations.

The Exhaust-Heated Gas-Turbine Cycle

By D. L. MORDELL,¹ MONTREAL, CANADA

The author describes and discusses a gas-turbine cycle in which the combustion chamber is placed behind the turbine, raising the exhaust temperature to a level at which all the heat required for the compressor air can be supplied by the heat exchanger. The possibilities of such a cycle for the utilization of low-grade solid or liquid fuels are explained and attention is drawn to the convenience with which steam can be generated from the otherwise wasted heat, and the over-all thermal efficiencies which may be obtained by a combination of gas and steam turbines.

INTRODUCTION

IN the past decade a great deal of experimental work has been done on the gas turbine, and much has been published on the subject. Surveying the present position, the advantages of the gas turbine, for fields other than aircraft propulsion, appear to be its compactness, low cost, and ease of control. With present metallurgical and aerodynamic limitations the simple "open cycle," with no allowances for auxiliaries, can achieve thermal efficiencies of the order 25 per cent, or, by the use of heat-exchange apparatus, 30 per cent. To improve compactness and specific weight, and to obtain a flat efficiency-load curve, resort may be had to compounding, intercooling, and reheating, which also will improve the thermal efficiency.

Criticisms which may be leveled at open-cycle gas turbines are that compared with a steam plant the efficiency is about the same, but the gas turbine demands more expensive fuels, as it is difficult to burn coal; and that, compared with the Diesel engine, although it can burn cheaper fuel, the gas turbine cannot yet approach the best efficiency of the Diesel.

By employing a closed cycle, the gas turbine can be made more compact and able to burn a wide range of fuels, including coal, but the engine becomes much more complex. There is no marked effect on thermal efficiency, which, as in the open cycle, depends on temperature, component efficiencies, and cycle layout.

It is the purpose of this paper to discuss a simple cycle in which solid and other low-grade fuels can be burned with a thermal efficiency of the order 20-25 per cent, excluding auxiliaries, and further to show how this may be brought up to nearly 40 per cent without departing from solid-fuel combustion, and without increasing the complexity of the plant unduly.

THE EXHAUST-HEATED CYCLE

The objection to burning solid fuels, and also certain low-grade liquid fuels, in an open-cycle gas turbine, lies in the difficulty of separating completely the ash from the combustion products. Ash passing through the turbine blades has a powerful erosive effect, while the accidental passage of any large pieces would be catastrophic. Furthermore, the deposition of solid matter on the blades has a deleterious aerodynamic effect that will demand frequent cleaning, necessitating opening the turbine. Residual fuel

oils also may contain metallic salts which, after oxidation, may condense on the turbine blades, with serious effects.

In the closed cycle, the compressed air is heated in a form of air heater, so that the working fluid is quite distinct from the combustion gases. The fluid passing through the turbine is pure air, while any deposition of solid matter from the combustion gases is confined to stationary heat-transfer surfaces, from which it may be removed easily, if necessary, even while the plant is running.

In what the author terms the exhaust-heated cycle, the air used for combustion is that rejected from the turbine, and heating of the air prior to entering the turbine is accomplished entirely by a heat exchanger. This is illustrated diagrammatically in Fig. 1. No detailed discussion of this type of cycle has been

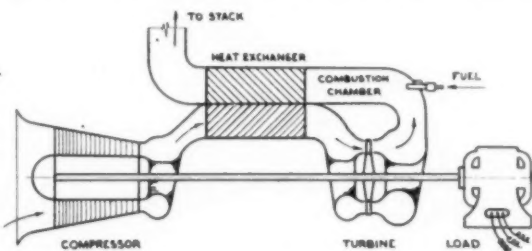


FIG. 1 DIAGRAM OF THE EXHAUST-HEATED GAS-TURBINE CYCLE

found by the author in the published literature, although the principle is disclosed in patents of Haverstick² and Lysholm.³

It is evident that in such a cycle, compared with a conventional open cycle operating at the same compression ratio, turbine temperature, component efficiencies, and so forth, the transposition of the combustion chamber will not affect the specific power output (power developed per pound of air circulating per second), and, if the exchanger had 100 per cent effectiveness or thermal ratio, would not alter the thermal efficiency. For any thermal ratio less than 100 per cent, however, the final discharge temperature obviously will be higher than in the open cycle, leading to a reduction in thermal efficiency.

CYCLE PERFORMANCE

In calculating cycle performance, the basic assumptions made are as follows: Compressor efficiency, 85 per cent; turbine efficiency, 87 per cent; system pressure losses, 10 per cent; combustion efficiency, 100 per cent.

It is appreciated that these figures may be considered optimistic or conservative, depending upon the particular circumstances, but it was felt that they represent a reasonable basis for a general survey, while any particular value for the combustion efficiency simply multiplies the thermal efficiency.

Fig. 2 shows values of thermal efficiency and specific power for various values of the heat-exchanger thermal ratio for an assumed turbine-entry temperature of 1300 F. It is at once evident that thermal ratios of the order 0.75 are necessary for reasonable efficiencies, and the accompanying curves are based on this value.

² U. S. Patent No. 2,438,635; J. S. Haverstick, March 30, 1948.

³ "A Contribution to the Solution of the Gas Turbine Problem," by A. J. R. Lysholm, Proceedings of The Institution of Mechanical Engineers, vol. 157, 1947, pp. 498-513.

¹ Associate Professor of Mechanical Engineering and Director of the Gas Dynamics Laboratory, McGill University. Mem. ASME.

Contributed by the Gas Turbine Power Division and presented at the Fall Meeting, Erie, Pa., September 28-30, 1949, of THE AMERICAN SOCIETY OF MECHANICAL ENGINEERS.

NOTE: Statements and opinions advanced in papers are to be understood as individual expressions of their authors and not those of the Society. Paper No. 49-F-6.

Fig. 3 shows the effect of turbine-entry temperature upon the performance. When using a heat exchanger, intercooling is usually beneficial, and Fig. 4 shows the effect of using an intercooler and a two-stage compressor. One stage of intercooling was assumed, placed so as to give equal temperature rises in each stage of the compressor. The improvement both in thermal efficiency and in specific power is quite considerable, and to complete the picture Fig. 5 shows the effect of reheating. This is accomplished as the air passes from the compressor turbine to the power turbine. Table 1 compares significant results. In each case we have assumed a heat exchanger of 0.75 thermal ratio and 1400 F turbine temperature.

The use of cooled blades in the turbine, permitting much higher gas temperatures, has not been presented at this stage. The benefits to specific output and efficiency are of course considerable, but their use is not considered practical in the immediate future because of the heat-exchanger tubes. For example, at 10 to 1 compression ratio, and turbine-entry temperature 2040 F, the specific output is 163 bhp per lb per sec, and the thermal efficiency 29.8 per cent, but the combustion temperature

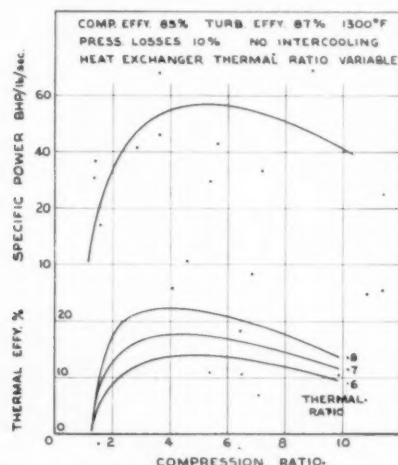


FIG. 2 THERMAL EFFICIENCY AND SPECIFIC POWER AS A FUNCTION OF THERMAL RATIO AND COMPRESSION RATIO

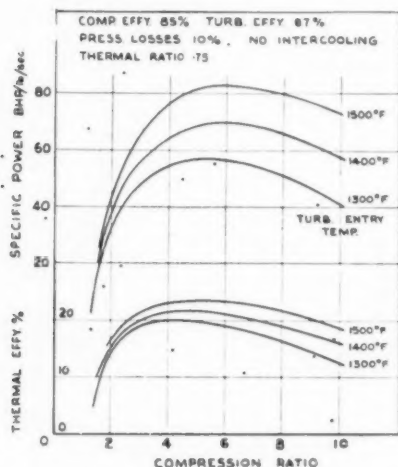


FIG. 3 THERMAL EFFICIENCY AND SPECIFIC POWER AS A FUNCTION OF MAXIMUM TEMPERATURE AND COMPRESSION RATIO

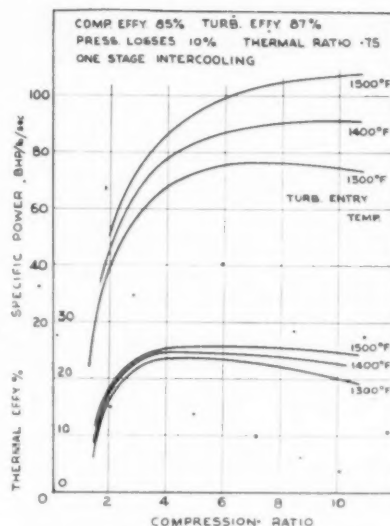


FIG. 4 EFFECT OF INTERCOOLING IN COMPRESSOR

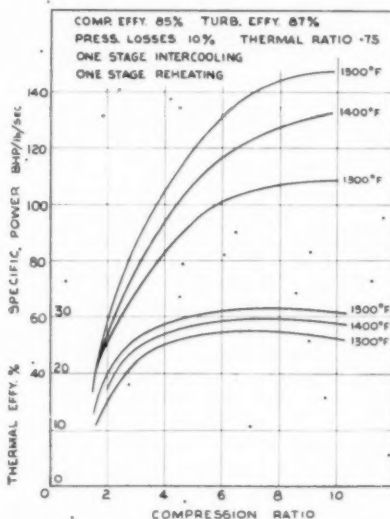


FIG. 5 EFFECT OF INTERCOOLING COMPRESSOR AND REHEATING IN TURBINE

TABLE 1 RESULTS OF PERFORMANCE ANALYSIS

	Compression ratio 5		Compression ratio 8	
	Specific output bhp/lb/sec	Eff. ciency, per cent	Specific output bhp/lb/sec	Eff. ciency, per cent
Simple open cycle	71.2	19.35	71.5	23.1
Open cycle with heat exchanger	69	28.5	65	26.6
Exhaust-heated cycle	69	22	65	19
Exhaust heat + intercooler	84	24.8	91	24
Exhaust heat + intercooler + reheat	108	28.5	127	30

required would be 2500 F, with metal temperatures at the hot end of the exchanger tubes of 2240 F.

CYCLE PERFORMANCE WITH EXHAUST STEAM GENERATION

The exhaust-heated cycle lends itself peculiarly well to the production of steam. The fact that exhaust temperatures are

higher, and that the heat exchanger is at the exhaust end of the cycle means that it is only necessary to include extra transfer surface past which the exhaust will flow after heating the compressed air. The steam may be used as process steam, for district heating, or in a turbine coupled to the gas-turbine shaft. Aspects and estimates of the waste-heat boiler were recently discussed by Fusner.⁴ The limitation on steam production is twofold. First we must not cool the exhaust below its dew point. This, however, owing to the large amount of excess air in the combustion chamber, will be in the region of 250 F, compared with the usual safe minimum temperature of 350–400 F used in boiler practice. The second factor is that in the production of the steam, a large fraction of the heat must be put in at, or above the saturation temperature, and this limits the amount of heat which can be extracted from the air by further cooling below the saturation temperature. Fusner based his estimates on the assumption that the air is cooled only down to the saturation temperature of the steam, so that his figures are somewhat conservative.

In Fig. 6 are shown the percentage heat transfer possible at various steam pressures and exhaust-gas temperatures, both for

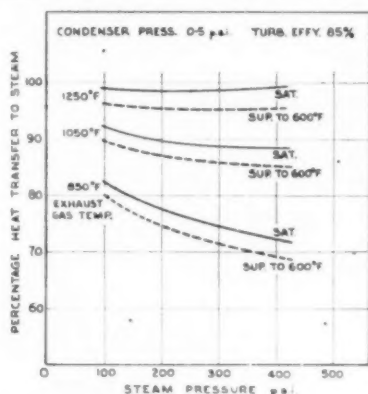


FIG. 6 FRACTIONAL HEAT RECOVERY IN A WASTE-HEAT BOILER

saturated and superheated steam. It should be emphasized that no account has been taken of dew-point considerations. The curves represent the thermodynamic limitations on heat transfer. The efficiency with which the steam is used also must be considered, and in Fig. 7 are shown the final results of using the steam produced by the waste-heat boiler in a steam turbine of 85 per cent efficiency and with a condenser pressure of 0.5 psi.

If we consider an exhaust-heated engine of compression ratio 4.5 to 1, with turbine-entry temperature of 1400 F, the thermal efficiency is 21.6 per cent. The exhaust temperature is just about 850 F. With this, using superheated steam, to avoid excessive moisture, we could recover 0.215×0.784 of the initial heat supply, or 16.8 per cent, giving an over-all efficiency of 38.4 per cent. The condenser and feedwater pump power demands probably would reduce this to about 36 per cent.

THE EXHAUST-HEATED CYCLE IN PRACTICE

So far we have considered only the thermodynamic aspects of exhaust heating. Summing up, exhaust heating gives a performance identical in specific output, and having about 75 per cent of the thermal efficiency of the conventional open cycle with heat exchanger. Let us now discuss the more practical aspects.

Combustion. The essential differences in the combustion chamber are that combustion is at an elevated temperature, prac-

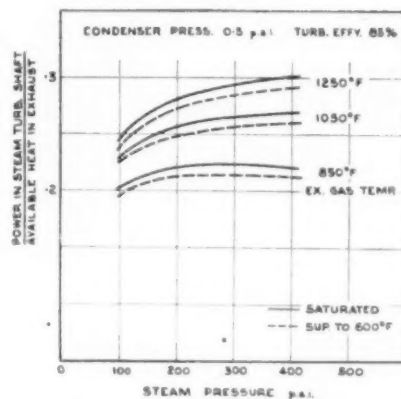


FIG. 7 EXHAUST-HEAT UTILIZATION IN A STEAM TURBINE

tically atmospheric pressure, and the combustion products have to pass only through the heat exchanger. Thus we may expect a larger combustion chamber due to the lower pressure, but at the same time it is no longer a pressure vessel, permitting simplification in its construction. It is essentially a firebox similar to those in boilers, and as such, should be capable of burning any fuel that is ordinarily burned as boiler fuel. The elevated air temperature will assist materially in handling low-grade and high-moisture fuels. Since it is at almost atmospheric pressure, and could be at subatmospheric pressure were an induced-draft fan used to overcome the pressure loss in the heat exchanger, firing arrangements can be simple. One can envisage a hand-fired gas turbine without much trouble!

If a conventional mechanical stoker is used to burn coal, the undergrate air could not conveniently be taken from the main air stream owing to its high temperature, but it is a simple matter to provide a fan, which need be of very small power ($1/2$ to 1 per cent of the net output) to supply cool air under the grates. By the use of a suitable stoker and firebox design it would be possible to burn coal or oil indiscriminately.

The Heat Exchanger. The exchanger obviously is going to require 3 or 4 times the heating surface of the conventional exchanger, in addition to running at a higher mean temperature. A high thermal ratio is essential. There is one factor, however, which enables a given thermal ratio to be obtained by less surface area relative to its duty than would be required for the exchanger of a conventional cycle. Since we are heating the air immediately prior to its entry to the heat exchanger by an amount which will necessitate air-fuel ratios considerably greater than stoichiometric, we would normally separate the air for combustion and subsequent dilution. However, in the exhaust-heated cycle there is no need to obtain a uniform stream of gas for a turbine, and we conveniently may retain the separation, using the hot gases resulting from nearly stoichiometric combustion, for a second pass of the heat exchanger, the first pass being heated by the "dilution" air, which of course is already at a fairly high temperature.

The optimum choice of design here to obtain the smallest heat exchanger is complex and requires further analysis, but offers a prospect of a small saving in weight and bulk.

Cleaning of the heat-exchanger surfaces can be accomplished by soot blowers, while the engine is running, while ash or slag removal can follow normal practice.

Control. If a liquid or pulverized solid fuel is being burned, the power output of the engine may be controlled easily by altering the fuel-supply rate. If solid fuel is being burned on a grate, the simplest control would be, in effect, to by-pass the air from

⁴ "The Gas Turbine With a Waste-Heat Boiler," by G. R. Fusner, *Mechanical Engineering*, vol. 70, 1948, pp. 515–518.

the firebox. This would lower the turbine-inlet temperature quite rapidly, depending upon the thermal capacity of the exchanger, while the hot fuel bed on the grate would remain, for quite a long time, at a temperature high enough to respond immediately as soon as air was readmitted under the grates.

For starting up, on solid fuel, a supply of air under the grates would be required to light the fire and, when this was going well, the main compressor could be rotated by a suitable starting motor in the usual fashion. Due to the heat capacity of the exchanger, the motor would be required for a longer period than with the conventional engine, but need not be any greater in capacity.

APPLICATIONS

The exhaust-heated engine can find application in any case where wide fuel utilization is important, and bulk and thermal efficiency are not prime considerations. It must be remembered that although the exchanger and combustion chamber are bulky, they must be compared with the equipment, such as gasifiers, or ash separators, or pulverizing systems that would be needed to burn solid fuel in the usual open-cycle unit. The thermal efficiency is only about 75 per cent of that of the conventional engines, but the price differential on the fuel consumable will be very much more than this, so that fuel costs will be considerably reduced. The first cost of the unit will be increased because of the larger exchanger, but in terms of cost per unit weight, the heat exchanger is about the cheapest component of the complete gas-turbine unit. The use of pure air in the turbines implies a reduction in maintenance costs, and this, together with the reduction in fuel costs, should more than make up for the extra initial cost, provided the utilization is high.

Electricity Generation. The combination of the exhaust-heated engine with steam generation, either for district heating, or extra shaft power, is most attractive. The thermal efficiency, at 36-38 per cent up, depending upon the auxiliaries, is obtained with few complications, and the plant consists essentially of a compressor, turbine, steam turbine, condenser, feed pump, vacuum pump, and combined combustor - heat exchanger - boiler.

The total transfer-surface area required will be about 2 sq ft per developed horsepower. The size of the combined heating unit for a 20,000-hp unit would be about $25 \times 25 \times 12$ ft.

If the utmost efficiency is desired, Fig. 5 shows that thermal efficiencies of very close to 30 per cent are possible, by the use of intercooling and reheat. Reheating leads to higher final exhaust temperatures, making possible higher recovery factors. With a gas-turbine efficiency of 30 per cent and 25 per cent recovery of the waste heat, an over-all efficiency of 47.5 per cent is possible. The complexity of such a plant would be less than a mercury-steam unit, and the air is much easier to handle than the mercury vapor.

It would be practical, with but very slight modifications, to burn solid or liquid fuels or low-pressure gas. In locations where low-grade fuel is very cheap, economy may be sacrificed by using a cheaper and smaller heat exchanger of lower thermal ratio. The resultant higher exhaust temperature will permit increased

utilization of the exhaust heat, so that even if the gas-turbine cycle efficiency drops to 10 per cent, the over-all efficiency of the dual-cycle plant can approach 32 per cent. Such a unit, in powers ranging up from, say, 4000 hp would be very attractive for some purposes.

Railroad Operation. Although the heat exchanger is large, it is not unreasonably so, and investigation has shown that there is enough room on a locomotive chassis to carry an exhaust-heated engine that is as powerful as a Diesel engine. A scheme for a 2000-hp unit is shown in Fig. 8. For railroad use, the ability of the same engine to run, with but minor modifications, on coal or oil may prove to be a considerable advantage, while its ability to produce steam is of advantage for car heating.

Marine Service. In very large sizes, the exhaust-heated engine probably will be too bulky to compete with the fully closed-cycle engine. Its indifference to fuel type and its convenient and economic steam production, however, render it especially suitable for ships requiring power, say, less than 20,000 shp.

CONCLUSIONS

The transposition of the combustion chamber of a conventional open-cycle gas-turbine unit to a position between the turbine exhaust and the heat exchanger results in an engine arrangement, which, although bulkier and less efficient than the usual arrangement, possesses advantages entitling it to very serious consideration for many applications. The main feature of this exhaust-heated cycle is the fact that the turbines operate on pure air, and the combustion products pass only through the heat exchanger, thus dispelling any serious fears of ash troubles or turbine-blade erosion. A further advantage is the ease with which steam can be generated from the otherwise wasted heat, permitting high efficiencies where the steam can be employed usefully.

Starting and control appear to present no serious difficulties, whether the unit is run on low-pressure gas, lump coal, or low-grade crude oil, any one of which conceivably could be burned in the same engine.

Under circumstances where the relatively large bulk of the heat exchanger and combustor present no installation difficulty, the possibility of burning really low-grade fuels—a feature assisted by the high-temperature level of combustion—makes the exhaust-heated cycle, with or without exhaust steam generation, worthy of close study. In this paper we have attempted a brief review of the more obvious aspects, and hope that it may lead to a much closer and more detailed study of some of the problems suggested.

ACKNOWLEDGMENTS

The author's thanks are due to Mr. W. A. Newman, manager of the research department, Canadian Pacific Railway, and Mr. J. I. Yellott, director of research, Locomotive Development Committee, for many valuable discussions and suggestions; and to Mr. A. G. Lane for assistance in the preparation of illustrations.

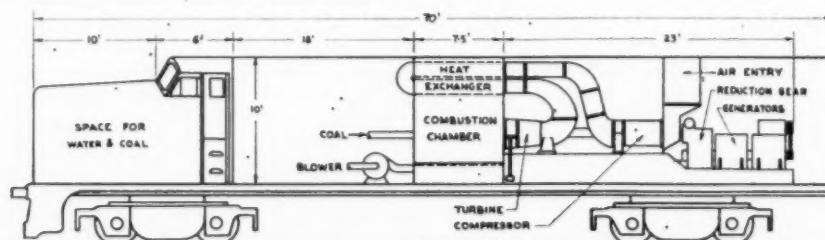


FIG. 8 DIAGRAM SHOWING A 2000-Hp EXHAUST-HEATED TURBINE IN A LOCOMOTIVE

Discussion

FREDERICK NETTEL.⁵ The basic arrangement which the author rightly recommends for many special applications is known from the time of the early air engines and was by no means overlooked when the gas turbine, or rather air turbine, created new possibilities in this field.

Since some relevant work was mentioned by reference to patents, it seems appropriate to draw attention to other work indicating new and substantial possibilities for improvement of the exhaust-heated gas turbine, by J. Kreitner and the writer.

As to Fig. 5 of the paper, it should be pointed out that the author evidently did not choose the optimum cycle which requires, after approximated isothermal compression, a temperature rise during compression

$$100 \times \frac{e(1-k)}{1-e(1-k)}$$

per cent of the absolute temperature at the start of the compression. This means that providing as the author does, for "equal temperature rise in each stage of the compressor" does not give best results. Nothing is said at what intermediate pressure reheat is applied. Optimal result requires a temperature drop during isentropic expansion, following approximated isothermal expansion, of

$$100 \times \frac{e(1-k)}{1-e^k}$$

per cent of the absolute temperature at the start of the expansion. In these formulas e is the thermal over-all efficiency of the practical cycle, and k the effectiveness of the heat exchanger.⁶

The application of the optimal hexagon cycle would have resulted in higher efficiencies than those shown in Fig. 5, or the same efficiencies with a smaller heat exchanger and smaller intercooler.

Exhaust-Heated Cycle in Practice. It seems always advantageous to divide the air leaving the air turbine into two separate streams and to use the smaller of these part streams for burning the fuel with an air surplus as used in steam boilers. The second, larger part stream is used for preheating the air coming from the compressor and leaves the plant clean. It is thus available for many uses; for example, in the chemical industries, food processing, water distillation, and the like. Only about one third of the total heating surface requires periodic servicing.⁷

The air supply proposed by the author for stoker firing is not only wasteful but unnecessary. In order to get air of suitable temperature for the coal drier in a pulverized-coal-firing plant, or air for the various compartments of a traveling stoker, it is more advantageous to tap it from the said larger second part stream at one or more points within the heat exchanger where the exhaust air has been cooled by "useful" heat exchange with the compressed air coming from the compressor to a suitable temperature or temperatures.⁸ This not only leads to considerable improvements in efficiency but also to better utilization of coal driers or of stokers, i.e., smaller stoker surfaces.

The exhaust-heated air turbine is by no means restricted to open cycles of comparatively small outputs, but can by modification to a semiclosed system be applied to plants of any size. In such high-pressure plants a turbopressure-charger set, han-

dling only about one third of the air circulating in the main high-pressure circuit, precompresses the ambient air for the main circuit. The same fraction of the hot air leaving the main turbine drives the turbine of the charger set, and after leaving the latter, is used as combustion air in the "air boiler" at near-atmospheric pressure.⁹

Another interesting application of the exhaust-heated air turbine can be envisaged in the production of large quantities of more or less heated compressed air, for example, for metallurgical furnaces. Here the air can be simultaneously sharply dried practically without additional cost, and the danger of surging of the compressor, generally associated with large fluctuations in the air demand, eliminated.¹⁰

The combination of the exhaust-heated air turbine with steam generation is surely advisable where steam is required for process purposes, district heating, etc., but from the point of view of efficiency of size of plant it does not appear necessary. It seems too early to speak of costs, but the advantage of low cooling-water requirements would surely be lost in an air-steam plant. Besides, working with two heat carriers must at best be considered an unavoidable evil in certain cases.

The cited references should, in the opinion of the writer, show that there exist no basic difficulties in burning lowest-grade oils or coals in plants of sizes which may interest the public utilities for locations where a severe shortage of cooling water exists. Improvement in plant efficiency and increase in power output during the winter months should prove another attraction.

Many of the improvements described are applicable to locomotives and can be expected to improve substantially the efficiency and performance beyond that of the arrangement proposed in Fig. 8 by the author. The decision as to the chances of the exhaust-heated air turbine for rail traction will depend on whether or not the long-awaited pulverized-coal-fired locomotive with mechanical ash removal from the compressed combustion gases will prove a success.

From the foregoing it seems possible that the present preferred position of the closed cycle for large marine plants may eventually be challenged.

We may thus conclude that the prospects for the exhaust-heated air-turbine plants are even brighter than pictured by the author.

D. G. SHEPHERD.¹¹ The author has offered a clear and concise discussion of the exhaust-heated gas-turbine cycle, a topic which as he says, has been mentioned from time to time, but has not received detailed attention.

From the practical point of view, the crucial problem is that of the heat exchanger or "air boiler" which has to handle hot gas at an entry temperature of about 1725 F, air entering at about 420 F and leaving at 1400 F. (Figures based upon the author's assumptions for a 75 per cent exchanger and 1400 F turbine-entry temperature.) The use of a counterflow arrangement involves a tube temperature intermediate between 1400 F and 1725 F and therefore it may be necessary to utilize parallel flow for the first part of the exchanger, whereby the metal temperature may be reduced to an intermediate value between 420 F and 1727 F. Under these conditions, the duty would seem comparable to that of known superheater practice, with the advantage of much lower stresses owing to the lower pressure. Some advantage in size over the conventional heat exchanger for turbine cycles can be gained from the fact that the heat exchanger is in reality an air

⁵ Consulting Engineer, Manhasset, Long Island, N. Y. Mem. ASME.

⁶ See also U. S. Patents 2,407,165, and 2,407,166.

⁷ See U. S. Patent no. 2,394,253.

⁸ See U. S. Patents nos. 2,434,950 and 2,420,335.

⁹ See U. S. Patent no. 2,472,846.

¹⁰ See U. S. Patent no. 2,457,594.

¹¹ Assistant Professor of Mechanical Engineering, Cornell University, Ithaca, N. Y. Jun. ASME.

boiler, and a considerable part of the necessary heat transfer may be effected by radiation.

The writer has found some difficulty in arriving at the figure of 22 per cent efficiency quoted in Table 1 of the paper for the exhaust-heated cycle of 5 to 1 pressure ratio, and it seems rather high. Possibly the difficulty lies in the evaluation of pressure losses, which are quoted as 10 per cent. Does this mean a loss of 10 per cent of the maximum absolute pressure, i.e., 7.35 psi, and if so, how is this loss apportioned before and after the turbine expansion? Perhaps the author will give us in more detail his basic assumptions in calculating the cycle performance.

For some applications, it will be more convenient to have a separate power turbine whose speed can be changed from that of the main shaft. This does not alter the conclusions of the author but does lend itself to some variants of the cycle. Thus the power turbine could have a separate combustion chamber with separate air supply bled off from the compressor. For the cycle mentioned, the work ratio is approximately $1/4$, so that with the same turbine temperature and pressure-loss ratios, the air would be split such that 2 parts go through the exhaust-heated side, which would act as a gas generator, and 1 part would provide the useful power. The power-turbine side would act on the conventional cycle, requiring fuel suitable for combustion before the turbine, with the gases from the turbine either passing through a separate exchanger or mixing with the main gas stream (as they have approximately the same exhaust temperature). This arrangement is illustrated in Fig. 9 of this discussion. Such a cycle gives an

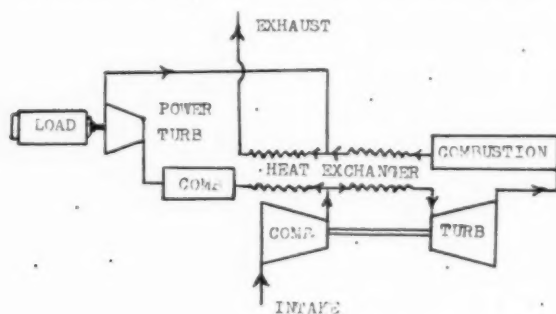


Fig. 9

efficiency intermediate between the plain exhaust-heated cycle and the plain open cycle, roughly in proportion to the amount of air by-passed to the power-output side. It does of course depart from the cycle as described, since it cannot be run entirely on solid fuel, but has the advantage of more flexibility of operation, as well as providing an intermediate fuel economy which may be useful, depending upon the ratio of fuel costs.

R. A. TYLER¹² AND D. C. MACPHEIL¹² Professor Mordel has presented an admirable introduction to an interesting gas-turbine cycle. This cycle has been the subject of a preliminary examination in these laboratories with the specific application in mind of a coal-burning power plant for locomotive use of about 5000 hp output. In a power plant of this size the air heater assumes proportions significant to the practicability of the system and various types of heater form have been investigated.

The locomotive application necessitates careful consideration of the choice of heater construction. Long service life, ease of cleaning, and maintenance are fundamental requirements. Gas-side pressure losses in particular must be kept to a minimum and volume and material requirements be of a reasonable order.

¹² National Research Council, Ottawa, Ontario, Canada.

It is believed that these requirements will best be met by a conventional shell-and-tube exchanger employing tubes of relatively large diameter for a reasonably small number of tubes under conditions of low-pressure loss. This type of exchanger can be constructed to incorporate the ruggedness necessary for locomotive operation and preliminary sketches indicate that a two-pass arrangement employing tubes as large as 1 in. in diameter can be accommodated in a locomotive layout of seventy feet over-all length. At this diameter an over-all tube run of about sixty feet would be required for a thermal ratio of 0.75 with a heat-transfer area per shp of about 3.5 sq ft. In view of the corrosive conditions and high temperatures prevailing in the shell it would appear impracticable to reduce the tube wall thickness below about 0.040 in. for a reasonable life expectation and the total weight of air heater would be about 10 lb per shp.

Stable operation and control of this form of power plant would appear to depend on a positive metering of a portion of the turbine exhaust to the firebox to effect a controlled rate of heat release, the metering being possibly effected by a simple valve of the constant-pressure type manually controlled from a "throttle" lever in the cab. This primary air in the form of hot furnace gas would be finally consumed in a separate mixing chamber with the remainder of the turbine exhaust, the mixed gases of uniform temperature proceeding to the shell of the air heater.

This physical separation of the primary and secondary air would appear desirable also from the point of view of grate-cooling requirements. The admission of fresh cooling air into the firebox must be kept to a minimum to avoid loss of over-all thermal efficiency through the rejection of this air at stack temperature. The throttle-controlled primary air entering the firebox would constitute about 25 per cent of the total turbine exhaust. The admission of cooling air into the primary air line could be effected by an automatic control of the cooling blower based on the limiting temperature (about 400°F) imposed by the grate. Under these conditions the reduction in over-all thermal efficiency due to cooling-air admission would be about 4 per cent, ignoring the negligible power requirements of the blower. The importance of controlling the cooling-air admission to a minimum level is illustrated by the extreme case in which the whole of the turbine exhaust is cooled to the limitation temperature. Under these conditions the over-all thermal efficiency would be of the order of 6 per cent.

The restriction of the firebox air to that required for the necessary heat release and the provision of a mixing chamber before the heater should result in a reduction of ash carry-over and a uniform temperature into the shell with consequent improved heater life. Further, with careful attention to the mixing-chamber design, a reduced pressure drop through the combustion system appears likely.

AUTHOR'S CLOSURE

Mr. Nettel has made many valuable suggestions for the proper application of the exhaust-heated cycle and it is obvious that he and his associates have been engaged on the close and more detailed study referred to in the conclusions.

In presenting performance calculations no attempt was made to find the optimum performance as such, we merely showed what could be done using reasonable compression ratios and maximum temperatures. For a given compression ratio equal division of the temperature rise between two stages gives the best compromise if the intercooler effectiveness be nearly unity, while in the use of reheat, practical convenience would make its application between the compressor and output turbine almost mandatory.

The suggestion to use some cooled "dilution" air to supply under the grates, rather than the separate supply envisaged by the author, is particularly valuable. The author shares with Mr.

Nettel a dislike of two heat carriers, but it seems that the rewards would make it attractive so long as water is available.

In answer to Professor Shepherd, the effect of pressure losses in the system was allowed for by assuming the expansion ratio to be 90 per cent of the compression ratio. There is thus no need to specify where the losses actually occur at this stage.

In presentation of the paper, the author eschewed discussion of all but the simplest possible engine in the interests of conciseness, but it is apparent that there are innumerable variations of more or less complexity, to suit special needs. Professor Shepherd's proposed compromise appears to the author to abandon the one selling point of the true exhaust-heated engine, namely, its ability to burn very low-grade fuels.

The possibilities of the exhaust-heated cycle obviously are going to depend on the size of a practical heat exchanger, and the comments of Mr. Tyler and Dr. MacPhail are particularly timely.

A recent report by Kays and London¹² also studies the design problems of a heat exchanger for this application, and it is of interest to compare the two solutions. Messrs. Tyler and MacPhail have considered a very rugged design whose weight comes out at 10 lb per shp, and surface area 3.5sq ft/ shp. Messrs. Kays and London have examined four cases using smaller tubes and in some cases extended surface area. The analysis suggests weight of the order 2.4–5.6 lb per shp with volumes between 67.5 and 86.3 cu ft per 1000 shp. The optimum choice of type awaits trials in service, although it would appear necessary for railroad application to use the heavier design in which, presumably, maintenance would be cheaper and simpler.

¹² "Gas Turbine Regenerator Design Studies," by W. M. Kays and A. L. London, Technical Report No. 8, Department of Mechanical Engineering, Stanford University, Calif., 1949.

Properties and Characteristics of Fuel Oils for Industrial Gas-Turbine Usage

By D. P. HEATH¹ AND E. ALBAT,² PAULSBORO, N. J.

Largely as a result of the rapid wartime development of gas turbines for aircraft usage, renewed emphasis has been placed upon the development of gas turbines for industrial applications. At the present time a number of domestic organizations are quite active in this field. One of the principal industrial applications of gas turbines in the United States is their use in the Houdry catalytic-cracking process in the oil-refining industry. Recent development work is centered around their use in the field of locomotive and marine propulsion using either coal or oil as fuel. The ultimate choice of a fuel is a complex problem involving such factors as fuel cost, engine performance and maintenance, and fuel availability. As far as fuel oils are concerned, the designer is further confronted with a wide variety of grades from which to choose. This paper presents information on the fuel properties and characteristics which are commonly employed for the identification and specification of such fuel oils, and also on those properties which are felt to be of significance with regard to fuel-system design and combustion-chamber and gas-turbine performance. Since fuel cost and availability are intimately related to supply and demand considerations, only limited regard is given to these factors in the present paper.

TYPICAL PROPERTIES OF FUEL OILS

THE classification of fuel oils into various grades has been tried several times with only limited success. A great many differences still exist among the systems employed by various oil companies; in addition, in many cases, there are considerable differences among the fuels produced by the different refineries of one oil company. A summary of several fuel-oil classifications is given in Table 1. Three different fuel-oil classification systems are presented in this table, ASTM Burner Oils, Pacific Coast Burner Oils, and ASTM Diesel Fuels. Of these three systems the ASTM Burner Oil Classification, which also has been adopted by the National Bureau of Standards, is the most widely used.

Average properties of the fuel oils produced in the United States are given in Tables 2, 3, and 4. In these tables the average properties and the normal variation in these properties are given for four types of distillate burner fuels, three types of residual burner fuels, and for three types of Diesel fuels.

The properties of the following four distillate-burning fuels are given in Table 2:

- (a) Kerosine.
- (b) Light distillate fuel oil.
- (c) Domestic fuel oil.
- (d) Heavy distillate fuel oil.

¹ Socony-Vacuum Laboratories, Division of Socony-Vacuum Oil Company, Inc., Research and Development Department.

² Contributed by the Gas Turbine Division and presented at the Fall Meeting, Erie, Pa., September 28-30, 1949, of THE AMERICAN SOCIETY OF MECHANICAL ENGINEERS.

NOTE: Statements and opinions advanced in papers are to be understood as individual expressions of their authors and not those of the Society. Paper No. 49-F-8.

The main usage of kerosine is in wick-feed lamps and stoves, and in pot-type domestic oil burners. The main requirement of a kerosine for these purposes is good burning quality, i.e., it should burn without causing objectionable odors, smoke, or deposits. To meet this requirement, kerosine must have a boiling range of about 300 to 500 F and be paraffinic in nature.

Light distillate fuel oil is a product that is very similar to kerosine in physical properties. However, it usually will not meet all of the rigid kerosine specifications. Light distillate fuel is used mainly in pot-type domestic oil burners. Both kerosine and light distillate fuel oil frequently are sold as light Diesel fuels.

Domestic fuel oil is the most widely used distillate fuel. It has a boiling range of about 400 to 700 F and is used in all types of domestic oil burners. To burn satisfactorily in most domestic oil burners, a fuel should have an ASTM 90 per cent point below 675 F, as fuels having appreciable amounts of material above 675 F tend to smoke and leave deposits in those burners of poorer design. In addition, domestic fuel oil should be noncorrosive and should not deposit gum or sediment in the burner, fuel lines, or fuel tank.

A few types of domestic oil burners can burn satisfactorily a fuel of slightly higher boiling range than domestic fuel oil. In some localities heavy distillate fuels are available for use in these burners. Heavy distillate fuels have boiling ranges of about 400 to 750 F and have somewhat higher heats of combustion on a volume basis.

The properties of light and heavy No. 5 fuel oils and No. 6 fuel oils are given in Table 3. These stocks all contain residual materials and are used as industrial and marine fuels. The chief physical requirement of these fuels is that they be sufficiently fluid to permit ready transfer by pumping. For this reason, the classification of fuels into light and heavy No. 5 and 6 types was made on the basis of viscosity. The No. 5 fuel oils can be pumped without heating, except during extremely cold weather. The No. 6 fuel oils usually require heating to considerably higher temperatures than No. 5 fuel oils.

Typical physical properties of light, medium, and heavy distillate Diesel fuels are given in Table 4. The two major requirements of Diesel fuels are ignition quality, as measured by cetane number, and volatility. In certain critical Diesel engines (high-speed) the more volatile fuels give less exhaust smoke and odor, and fuels of high cetane number promote easier starting and smoother operation. Inasmuch as Diesel engines of a wide variety of sizes and speeds are produced, the volatility and cetane-number requirements vary considerably.

Light Diesel fuel is of the same boiling range as kerosine. Frequently, to simplify supply and distribution problems, a product meeting the requirements of both water-white kerosine, and light Diesel fuel is produced and sold as a common fuel grade. Similarly, domestic fuel oil is sometimes sold as medium Diesel fuel.

Specifications for the three highest-quality fuels—kerosine, medium Diesel fuel, and domestic fuel oil—are quite rigid; hence the range of properties encountered among several samples of these fuels is much narrower than will be encountered with most other fuels. The properties of residual fuel oils, in particular, will vary over a wide range.

TABLE 1 COMPARISON OF FUEL-OIL CLASSIFICATIONS

Designation	Fuel Oils					Fuel Oils					Diesel Fuel Oils	
	U.S. Govt. (NBS) CS-12-40 ASTM D 396-40 T					Pacific Coast Standards					ASTM D 975-40 T	
	No. 1	No. 2	No. 4	No. 5	No. 6	No. 100	No. 200	No. 300	No. 400	No. 1-D	No. 4-D	
Date of specification	Aug. 16, 1940					May 20, 1947					Sept. 29, 1948	
Physical and chemical tests												
Gravity, °Api, min.	35	26	-	-	-	-	-	-	-	-	-	-
Distillation, ASTM method	420 max.	440 max. ^a	-	-	-	350 min. 420 max. 450 min.	425 min. 600 min.	-	-	-	-	-
10% evaporation deg F	625	675 max.	-	-	-	550 max.	-	-	-	625	675 max.	-
90% evaporation deg F	100 ^b	100 ^b	130 ^b	160	160	110 ^b	150	150	150	100 ^b	100 ^b	130 ^b
End point, deg F, max.	-	-	-	-	-	165	-	-	-	20 ^c	20 ^c	20 ^c
Flash point, deg F, min.	0	20	20	-	-	0.25	0.5	1.0	2.0	Trace	0.10	0.50
Flash point, deg F, max.	Trace	0	0.50	1.00	2.00 ^e	-	-	-	-	0.15	0.50	1.00
Pour point, deg F, max.	0	0.10	0.50	-	-	-	-	-	-	0.15	0.50	1.00
Water and sediment, % vol., max.	0.15	0.15	-	-	-	-	-	-	-	0.15	0.15	0.50
Carbon residue on 10% film, % wt., max.	0.15	0.15	-	-	-	-	-	-	-	0.15	0.15	0.50
Sulphur, % wt., max.	0.15	0.15	-	-	-	-	-	-	-	0.15	0.15	0.50
Sediment by extraction, % wt., max.	-	-	-	-	-	-	-	-	-	0.01	0.02	0.10
Ash, % wt., max.	-	0.10	0.10	-	-	-	-	-	-	0.01	0.02	0.10
Viscosity, temp., deg F	100	100	100	122	122	100	122	122	122	-	-	100
Max.	40 SSU	125 SSU	40 SSU	300 SSF	300 SSF	55 SSU	55 SSU	55 SSU	55 SSU	-	-	125 SSU
Min.	-	45 SSU	150 SSU	45 SSF	45 SSF	35 SSU	35 SSU	35 SSU	60 SSF	-	-	45 SSU
Kinematic viscosity, temp., deg F	100	100	100	122	122	-	-	-	-	100	100	-
Centistokes, max.	2.2	(4.3)	(26.4)	(81 @ 122 F)	(638)	-	-	-	-	5.8	5.8	-
Centistokes, min.	1.4	(5.6)	(32.1 @ 100 F)	(92)	(92)	-	-	-	-	1.4	1.4	-
Corrosion	No gray or black discoloration	-	-	-	-	-	-	-	-	Pass	Pass	-
Cetane number, min.	-	-	-	-	-	-	-	-	-	40 ^c	40 ^c	25

^a 440 F maximum for use in other than atomizing burners.

^b Or legal, see specification.

^c See specification for alternatives.

^d For use in diesel engines, cetane number is required.

^e See specification for method.

* Plus signs should appear before the number 20 across this line.

TABLE 2 PROPERTIES OF DISTILLATE-BURNER FUEL OILS

	Kerosine		Light distillate fuel		Domestic fuel		Heavy distillate fuel	
	Average	Variation	Average	Variation	Average	Variation	Average	Variation
Gravity, deg API	42.5	41-44	42.0	40-43	32.0	29-37	29.5	22-34
ASTM distillation, deg F	340	330-380	350	330-390	370	320-390	400	380-460
Initial boiling point	390	365-420	390	370-420	430	390-475	480	440-500
50% recovered	425	400-450	445	425-480	500	450-550	555	490-560
90% recovered	490	450-530	510	470-550	570	500-600	640	590-680
Final boiling point	530	500-550	540	510-625	620	560-650	680	600-730
Flash point, deg F (Tag)	135	125-155	135	130-160	160	135-190	180	160-210
Flash point, deg F (PM)	175	16-19	1.8	1.4-2.2	2.4	3.0	3.9	3.3-4.6
Viscosity, centistokes at 100 F	415	370-490	30	20-45	34	32-40	39	37-41
SSU at 100 F	130	115-145	30	20-45	20	0-40	10	25-35
Thermo viscosity at 60 F	130	115-145	30	20-45	20	0-40	10	25-35
Aniline cloud point, deg F	130	115-145	30	20-45	20	0-40	10	25-35
Sulphur, weight per cent	0.08	0.01-0.08	0.08	0.04-0.3	0.2	0.05-1.0	0.3	0.1-1.0
Copper strip corrosion, 1 hr at 212 F	Pass	+25	Pass	+10-25	Pass	0.05-1.0	Pass	0.1-1.0
Color, Saybolt	+25	+20-30	+15	+10-25	1 1/4	1-3	4	2-8
Color, ASTM	Nil	0.0-0.02	Nil	0.005-0.15	Nil	0-0.35	Nil	0-0.2
Water and sediment, vol per cent	0.01	0.0-0.02	0.01	0.005-0.15	0.05	0-0.35	0.2	0.1-1.4
Carbon residue on 10 per cent residuum, weight per cent	50	45-52	50	45-52	...	30-50	...	20-45
Cetane number	50	45-52	50	45-52	...	30-50	...	20-45

TABLE 3 PROPERTIES OF RESIDUAL BURNER FUEL OILS

	Light Average	No. 5 fuel Variation	Heavy Average	No. 5 fuel Variation	No. 6 fuel Average	Variation
Gravity, deg API	20	10-30	19	14-22	15	7-22
Flash point, deg F (PM)	200	170-320	220	180-240	270	160-410
Viscosity, SSU at 100 F	130	60-300	30	20-40	90	45-300
Centistokes at 100 F	27.5	10.5-65	130	65-200	480	260-750
Pour point, deg F	+20	-10-+80	5	-15-+50	45	+15-85
Sulphur, weight, per cent	1.0	0.2-3.0	1.0	0.5-2.0	1.2	0.7-3.0
Copper-strip corrosion, 1 hr at 212 F	Pass	...	Pass	...	Pass	...
Color	Black	...	Black	...	Black	...
Water and sediment, volume, per cent	0.2	Trace-1.0	0.3	0.05-1.0	0.4	0.05-2.0
Carbon residue, weight, per cent	3	1-10	6	3-8	7	5-13
Ash content, weight per cent	0.03	0-0.10	0.03	0-0.10	0.05	0.01-0.50

TABLE 4 PROPERTIES OF DIESEL FUEL OILS

	Light Diesel fuel— Average	Variation	Medium Diesel fuel— Average	Variation	Heavy Diesel fuel— Average	Variation
Gravity, deg API	42.0	42-43	36.0	33-41	28.0	22-31
ASTM distillation temperatures, deg F:						
Initial boiling point	345	330-390	370	350-460	390	360-430
10% recovered	395	380-420	450	420-510	470	460-480
50% recovered	445	430-460	510	465-550	540	520-560
90% recovered	500	490-515	550	530-675	600	590-680
Final boiling point	535	525-625	620	600-740	720	650-750
Flash point, deg F (PM)	135	130-160	160	140-220	185	160-200
Viscosity, SSU at 100 F	1.8	1.4-2.0	2.7	2.1-5.8	40	38-43
Centistokes at 100 F	30	+20-40	0	+20-15	0	3.6-5.2
Pour point, deg F	150	145-155	150	140-160	130	-30-+25
Aniline cloud point, deg F	0.05	0.005-0.5	0.2	0.04-1.0	0.4	0.2-2.0
Sulphur, weight, per cent	0.05	0.005-0.5	0.2	0.04-1.0	0.4	0.2-2.0
Copper-strip corrosion, 1 hr at 212 F	Pass	...	Pass	...	Pass	...
Color, Saybolt	+23	+16-+27	1-1/2	1-7	6	4-8
ASTM	Nil	...	Nil	Nil-0.10	0.01	0-0.50
Water and sediment, volume, per cent	Nil	...	Nil	Nil-0.10	0.01	0-0.50
Carbon residue on 10 per cent residuum, weight per cent	0.01	0-0.15	0.03	0.01-0.35	0.1	0.01-0.2
Cetane number	50	40-54	50	40-53	30	25-40

All of the ten classifications of oils listed in Tables 2, 3, and 4 are not available in any one locality. In most localities in the United States three to seven classifications of fuel oils will be available. The three fuels that are most widely distributed are kerosine, domestic fuel oil, and No. 6 residual fuel. Some changes in the availability of oil stocks can be expected from year to year, but residual fuels will continue to be the most plentiful, with domestic fuel oil being the most widely available distillate fuel.

SIGNIFICANCE OF PHYSICAL TESTS

In studying various physical tests of fuel oils, it should be kept in mind that no one test taken alone is of much value, but that a group of tests is necessary before the characteristics of the oil can be evaluated. With this in mind, the significance of the various tests listed in Tables 1 through 4 are discussed briefly.

API Gravity. API gravity is a direct measure of the density of an oil and is a good indication of its heating value. The density of an oil changes rather rapidly with temperature. Fig. 1 is useful in estimating the density at various temperatures when the API gravity is known. API gravity is also an indication of the composition of an oil. For example, of two oils having the same boiling range, the one having the higher API gravity is the more paraffinic.

ASTM Distillation. An ASTM distillation is one of the most common tests conducted on petroleum products. It is a measure of the boiling range of an oil and, as such, is of different significance with different products. In domestic fuel oils the amount of high-boiling material present gives an indication of the performance of the oil in certain types of burners. Specific burner types are commonly designed to operate on fuels of a given volatility. Use of a fuel higher in boiling range than that for which the burner was designed usually will lead to increased smoke and deposits. For example, most gun-type household burners can burn successfully a heavier fuel than pot-type burners, while an industrial-type burner can burn practically any liquid fuel.

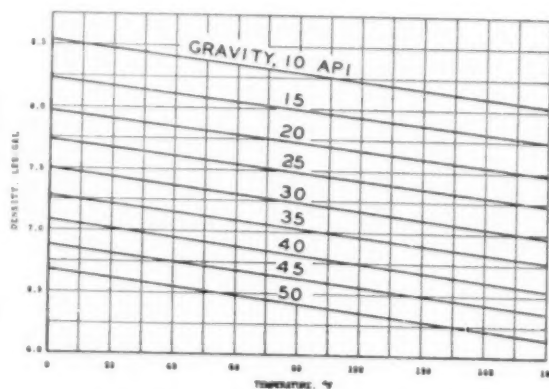


FIG. 1 DENSITY CHARACTERISTICS OF FUEL OILS

Flash Point. The flash point of an oil is the lowest temperature of the oil at which the vapor above the oil will burn if subjected to an open flame. Therefore the flash point of an oil is an indication of the temperatures at which an oil can be handled without undue fire hazard. Both the Pensky-Martens and Tag flash points, listed in Table 2, are determined in a closed container and agree quite well with each other; however, the Tag flash point procedure should not be used for oils having flash points above 175 F. The flash point determined in a closed container is always a few degrees lower than a flash point determined in an open container.

Viscosity. Several different methods of measuring viscosities are used for fuel oils, each grade of fuel oil having a particular viscosity method that is most widely used in its specification as shown in Table 5.

Kinematic viscosity at 100 F is gradually replacing the various Saybolt viscosity measurements as it is a more accurate and more

TABLE 5 METHODS OF MEASURING VISCOSITY

Product	Type viscosity measurement usually specified
Kerosine.....	Saybolt thermo viscosity at 60 F
Diesel fuels.....	Saybolt Universal or kinematic viscosity at 100 F
Distillate fuel oils.....	Saybolt Furol viscosity at 122 F
Residual fuels.....	Saybolt Furol viscosity at 122 F

flexible method of test. Kinematic viscosity at 100 F can be converted to the various Saybolt measurements by means of the scales given in Figs. 2 and 3. Typical viscosity-temperature curves for the various grades of fuel oil are also given in these figures. Since No. 6 fuel oils cover such a wide range of viscosities, two lines are given for this grade.

A lower limit of 30-sec Saybolt Universal at 100 F on Diesel fuels is generally recognized as being necessary to prevent leakage in worn fuel-injection equipment, and to furnish lubrication for the injection equipment of certain types of engines. For operation at atmospheric temperatures below 10 F, high-viscosity fuels are usually avoided to secure the required low pour point and increased volatility. If the viscosity of a Diesel fuel is unusually high, a solid stream may be obtained from the injector instead of a spray.

In the utilization of residual fuels in marine boilers, which usually do not have steam atomizers, an optimum viscosity of the

fuel at the nozzles can be found which results in the most efficient combustion. Preheating of viscous boiler fuels to give a viscosity of about 150 sec Saybolt Universal at the sprayer plates is standard U. S. Navy practice.

Detailed relationships of the effects of viscosity upon spray characteristics of gas-turbine fuel nozzles are not available, but it is expected that the design of the atomizing equipment will provide no difficult problem.

Viscosity is also related to ease of pumping. In general, if an oil has a viscosity of over 5000 to 10,000 sec Saybolt Universal, it is extremely difficult to pump. Inasmuch as the viscosity of an oil decreases rapidly as the oil is heated, very viscous oils require heating before they can be pumped. The temperatures to which an oil of a given viscosity must be raised to facilitate easy pumping can be estimated by the use of Figs. 2 and 3.

Pour Point. The pour point of an oil is the lowest temperature at which an oil will flow under specified test conditions. It is related directly to the wax content and viscosity of an oil. In general, the lowest practical pumping temperature is considered to be about 10 deg F above the pour point.

Aniline Cloud Point. The aniline cloud point is a measure of the paraffinicity of an oil, a low aniline point indicating an aromatic, naphthenic, or a highly cracked oil. Conversely, a high

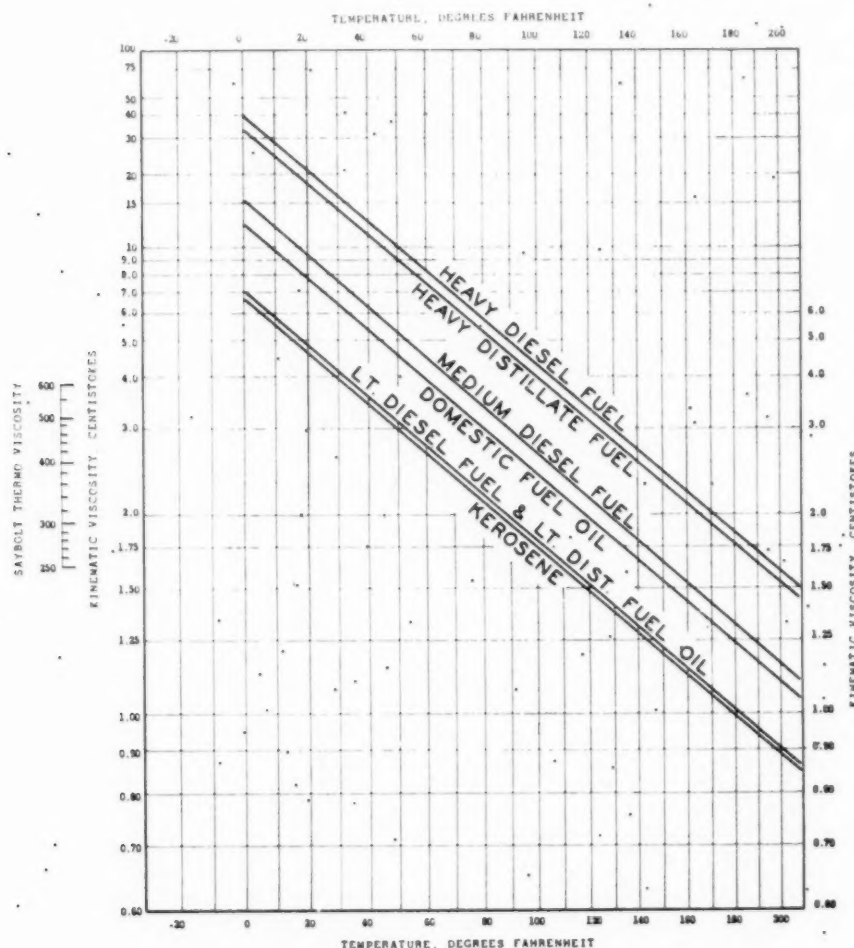


FIG. 2 VISCOSITY CHARACTERISTICS OF REPRESENTATIVE FUEL OILS

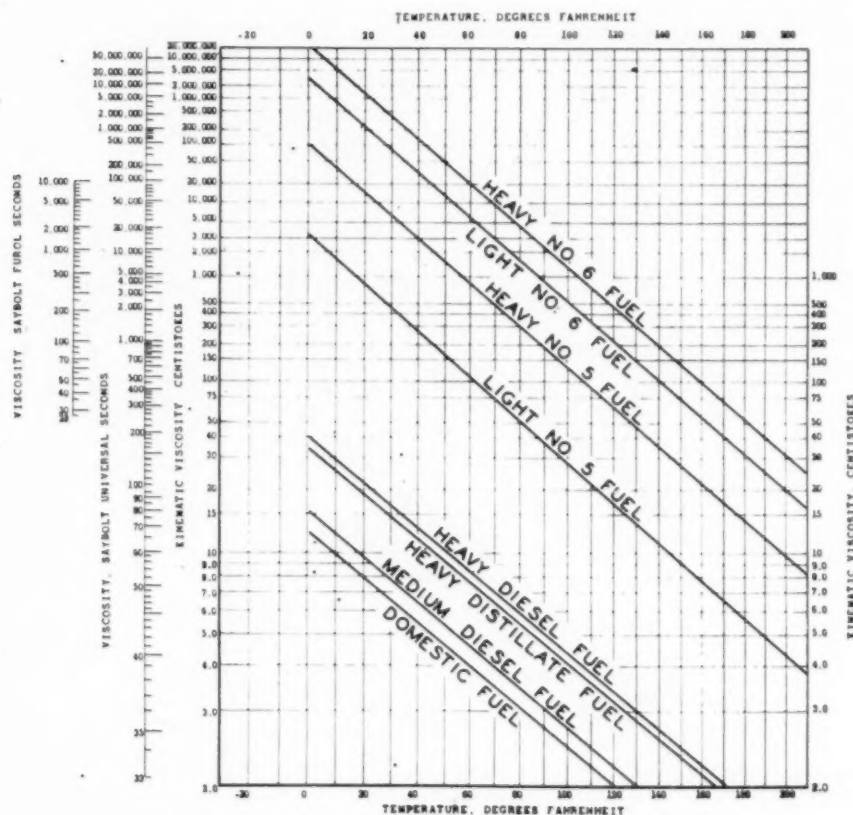


FIG. 3 VISCOSITY CHARACTERISTICS OF REPRESENTATIVE FUEL OILS

aniline point indicates a paraffinic straight-run oil. The major use of the aniline point is in the calculation of empirical constants related to some performance characteristics. These constants are discussed in a later section of this paper.

Sulphur Content. From a corrosion standpoint, sulphur content is important only when it is excessive. It must be remembered that sulphur occurs in many forms of which some are harmful and some are not.

The sulphur content of kerosines, which are to be burned in lamps or stoves indoors obviously should be quite low because of the resultant odor of the products of combustion. However, the sulphur content of other burner fuels is not of importance from the standpoint of corrosion in the exhaust or chimney unless the products of combustion are cooled sufficiently to condense the water in them. Sulphur dioxide is not a corrosive agent except in the presence of water.

With respect to corrosion at high temperatures, of the order normally encountered in gas-turbine applications, Avery (1)² presents quantitative data showing the effects of sulphur-bearing combustion gases on various metal alloys. It was shown that even high-sulphur gases do not cause a measurable increase in corrosion rate over that which would be obtained with air of the same temperature, when high-temperature-type alloy steels are used.

Copper-Strip Corrosion. Copper-strip corrosion tests attempt to measure the corrosive tendencies of an oil. Usually such tendencies are related to the presence of harmful sulphur com-

pounds. The results of corrosion tests are obvious for very bad fuels or very good fuels, but intermediate cases are not conclusive. The corrosion occurring in a system handling fuel oil is more frequently the result of the existing temperature-humidity conditions or the materials of construction rather than the result of operation on a corrosive fuel.

Color. The color of an oil is of little value as an indication of its performance characteristics except in extreme cases wherein contamination is indicated. The two common methods of measuring the color of petroleum oils are the Saybolt and ASTM methods. The Saybolt colorimeter is used on white products such as kerosine and gasoline. The Saybolt color scale runs from -16 (darkest) to +30 (lightest). The ASTM colorimeter is used to measure the color of fuel and lube oils. On the ASTM color scale, No. 1 is the lightest and No. 8 is the darkest color.

Water and Sediment. The presence of water and sediment is usually an indication of fuel-oil contamination. In the case of residual fuels, high values for this test may also be related to the instability of the fuel which is occasioned by the precipitation of heavy asphaltic or carbonaceous substances. The sediment-by-extraction test is another test frequently specified for heavy fuel oils and is supposed to give a similar indication of the insoluble material dispersed in the oil which ultimately will sludge out. Neither of these tests has been found to correlate with the pre-heater fouling characteristics of certain residual fuel oils. Presumably, polymerization and oxidation effects associated with the frequent recirculation of oil at relatively high temperatures over-balanced these factors. As a result, the Navy Department, in specifying stable residual fuel oil for its vessels, requires that it

² Numbers in parentheses refer to the Bibliography at the end of the paper.

pass a heater-fouling test which simulates preheater operation aboard ship.

Another well-known cause of sludge and sediment in fuel oils is that resulting from the incompatibility of mixtures. A gross example of this would be the mixing of a straight-run Diesel fuel with a deeply cracked bunker C fuel oil. Though neither fuel would have large amounts of sediment present, as indicated by the BS&W test, the mixture would have a very large amount which could plug lines, filters, and preheaters. Vessels are particularly susceptible to this type of fuel failure where bunker liftings from different countries are made. Where there is doubt concerning the compatibility of fuel oils, segregation of the stocks will of course minimize operating difficulties.

Ash Content. Residual fuel oils usually possess ash-forming constituents which indicate the presence of inorganic materials. A wide variety of metals may be found in the ash which originates in part from the metals inherent in the crude oil, the contamination by chemical compounds during the refining operation, and the entrainment of materials such as rust, seawater, etc. Sodium, iron, and vanadium are particularly deleterious to the brickwork in a furnace and cause rapid slagging of the refractory materials, necessitating frequent and costly replacement. In addition, these materials in the form of sulphates and oxides deposit on the closely packed superheater tubes and restrict the passage of the combustion gases through the furnace.

In so far as gas-turbine operation is concerned, a high ash content in the fuel oil may increase the rate of erosion of the burner chamber, turbine nozzles, and blading. In a recent test (2) with a high-ash-content fuel (1.5 per cent) no serious effects were noted. Efforts on the part of the refinery to reduce the ash in residual fuels have not been successful without a disproportionate increase in the cost of the fuel. Filtration and centrifuging were found to be partially effective, depending on the nature of the oil and the ash-forming constituents as well as the conditions of processing.

Carbon Residue. The carbon residue of distillate-type fuels is generally too small to be measured accurately. The carbon-residue test on the 10 per cent bottoms from the fuel is more reproducible and serves to indicate the presence of residual materials. Carbon residue has some relation to burner deposits caused by fuel oils and is felt to be related to combustion-chamber deposits in Diesel engines; however, no definite relationship has been found. In residual fuel oils, a high carbon residue indicates a deeply cracked fuel oil or, in some cases, residual materials from highly asphaltic crude. Paraffinic straight-run residual fuel oils are characterized by a relatively low carbon residue.

Heat of Combustion. The heat of combustion of an oil is usually estimated from the API gravity inasmuch as the actual determination is quite difficult. Fig. 4 shows the relationship between API gravity and the net or lower heating value. In general, the differences in heat of combustion between different batches of the same grade of fuel are too small to be reflected in engine or burner performance. However, in carefully controlled laboratory tests of Diesel engines, heat of combustion has been found to be a variable affecting power output and fuel consumption.

Cetane Number. Cetane number is of importance only in Diesel fuels. It is one of the factors affecting engine starting and roughness in operation, but appears to have little or no direct relation to exhaust smoke, power, or fuel consumption.

Heat Content and Related Thermal Properties. The thermal properties of fuels, such as heat content, heat capacity, and thermal conductivity, often must be estimated in the design of fuel-oil systems. Average values for these variables are given in Figs. 5 to 7, inclusive, which should prove useful to the design engineer.

Spontaneous-Ignition Temperature. A measure of the ease with which an oil will ignite in contact with a hot object in the presence of air is given by the spontaneous-ignition temperature.

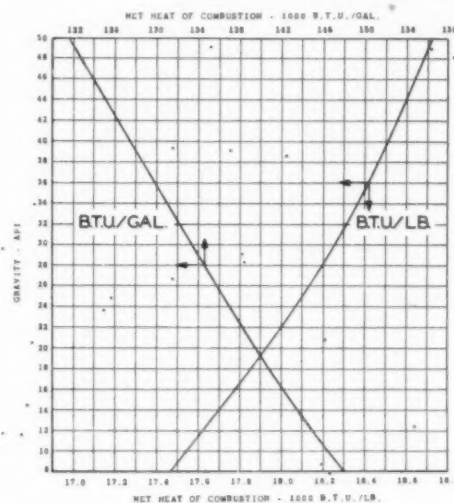


FIG. 4 HEAT OF COMBUSTION OF PETROLEUM FRACTIONS AT CONSTANT PRESSURE

It is not entirely a fuel property, however, as the values will vary considerably depending upon the apparatus used and the method of test employed. As an indication of the values obtained, some of the results of Edgar (4) are given in Table 6.

Surface Tension. Surface tension is the molecular force existing in the surface film of all liquids which tends to contract the volume into a form having the least surface area. Compared to water, petroleum products have relatively low surface tensions. Water has a surface tension of 76 dynes per cm at 20 C (68 F), while petroleum products have surface tensions varying from 15 to 40 dynes per cm at 20 C.

TABLE 6 SPONTANEOUS IGNITION TEMPERATURE OF PETROLEUM PRODUCTS (4)

Product	SIT, deg F
Aviation gasoline (100 octane leaded).....	960
W. W. kerosine (fly-spray).....	520
Diesel fuel (32 cetane).....	790
Diesel fuel (45 cetane).....	790
No. 1 fuel oil (Mid-Continent).....	530
SAE 60 aero lube oil (MC solv. ext.).....	750

This property in petroleum distillates appears to be a direct function of the density of the oil. In Fig. 8 the surface tensions of a number of pure hydrocarbons boiling in the gasoline range (5) are plotted against specific gravity. The line drawn in Fig. 8 is that given for petroleum distillates having end points up to 570 F (6).

The surface tension of petroleum products decreases with increasing temperature. From the limited amount of data available, it appears that all types of hydrocarbons have approximately the same rate of change of surface tension with temperature. In the range of 0 to 100 C (32 to 212 F), this rate of change is approximately 0.11 dynes per cm per deg C (0.061 dynes per cm per deg F).

In aqueous solutions, the addition of wetting agents or detergents causes an appreciable reduction in the surface tension of the liquid and gives a solution which will form a relatively stable froth with air. In petroleum products, however, the addition of antifoam agents or surface-active agents brings

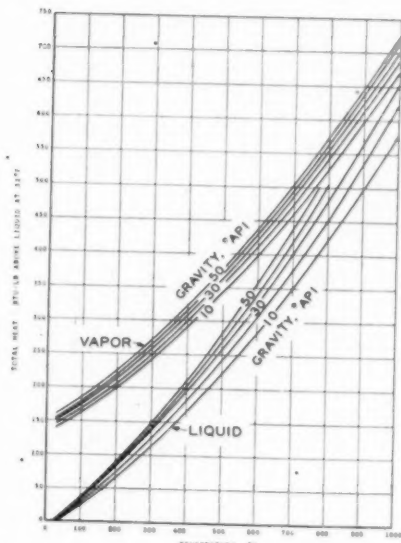


Fig. 5 TOTAL HEAT CONTENT OF PETROLEUM FRACTIONS (Average stock.)

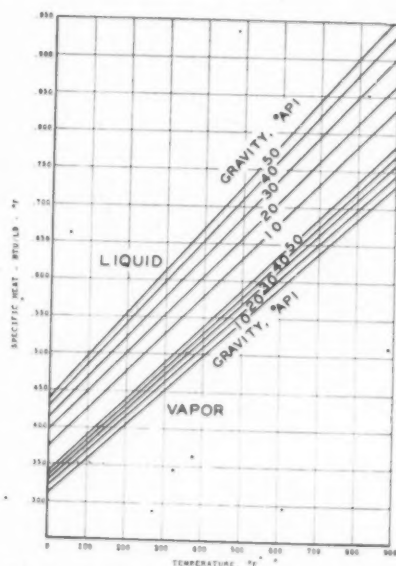


Fig. 6 HEAT CAPACITY OF PETROLEUM FRACTIONS (Average stock.)

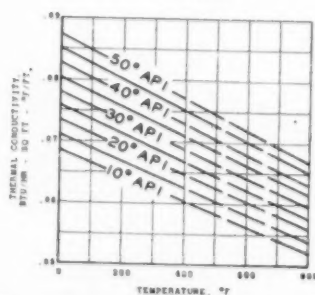


Fig. 7 THERMAL CONDUCTIVITY OF PETROLEUM LIQUIDS

about a reduction of less than 3 dynes per cm in the surface tension of the oil. Inasmuch as the surface tension of a petroleum distillate of a given boiling range will fall within a relatively narrow range, and this range can be changed only slightly by the use of addition agents, the surface tension of a fuel oil would ap-

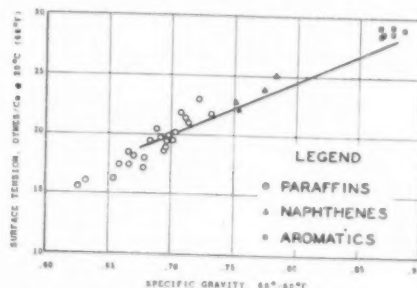


Fig. 8 SURFACE TENSION OF PETROLEUM OILS

pear to be a very minor variable affecting the characteristics of the fuel spray from a nozzle.

OTHER CHARACTERISTICS AND TESTS

Empirical Constants. It is apparent that the performance characteristics of an oil are quite difficult to estimate from the usual physical tests. Since performance tests are quite difficult and expensive to make, several empirical constants utilizing two or more physical tests have been developed for estimating product performance. These constants usually employ two or more of the following properties: API gravity, viscosity, aniline cloud point, and average boiling point. Since all of these properties are interrelated, the use of two of them is usually sufficient to obtain an indication of the composition of an oil and hence of its performance properties.

Diesel Index. Diesel index is a relatively reliable index to cetane number. It is usually several numbers higher than the corresponding cetane number, except in the case of fuels containing additives to improve the cetane number in which case the relationship may be reversed.

The relationship between Diesel index and cetane number is about as follows

Diesel index	Cetane number
43	40
50	45
59	50

Diesel index is applicable only to fuels having a boiling range similar to that of Diesel fuel. For example, aviation gasoline has a Diesel index of about 70, and a cetane number of below 10.

Diesel index is calculated from the API gravity and the aniline cloud point by the following equation

$$\text{Diesel index} = \frac{\text{API gravity} \times \text{aniline point, deg F}}{100}$$

UOP K-Value. The UOP K-value or characterization factor has been widely used as an index of composition in the correlation of thermal properties, such as heat content and specific heat of oils. It has also been used to indicate the burning qualities of fuel oils. The range of values obtained is quite limited. Most oils will be between 10.0 and 12.5 with the paraffinic stocks having the higher values. The K-value is calculated from the aver-

age boiling point and specific gravity by the following equation

$$K = \frac{\sqrt[3]{T_B}}{S}$$

where

$$T_B = \text{average boiling point, deg F} + 460$$

$$S = \text{specific gravity } 60/60 \text{ deg F}$$

Carbon-Hydrogen Ratio. The carbon-hydrogen ratio of distillate fuels has been found to correlate with the carbon deposits formed in domestic oil burners under certain operating conditions. Here again, the design of the burner is of primary importance and, in critical units, fuels having low carbon-hydrogen ratios, i.e., the more paraffinic fuels, will result in smaller deposits.

The carbon-hydrogen ratio of a fuel can be determined by burning a given amount of oil completely and analyzing the products of combustion. However, this procedure is extremely difficult to carry out accurately. A correlation for estimating carbon-hydrogen ratios of distillate fuels has been developed by Cauley and Delgass (7) and is presented in Fig. 8. This correlation is based upon aniline point, API gravity, and boiling point of a fuel (ASTM 50 per cent boiling point). The empirical formula expressing the relationship in Fig. 9 is as follows

$$C/H \text{ ratio} = \frac{28}{\sqrt{A + 47}}$$

Application of this correlation is limited to distillate fuel oils with mid-boiling points ranging from 350 F to 671 F.

PRODUCTION OF FUEL OILS

The production of fuel oils, in general, is controlled by refining

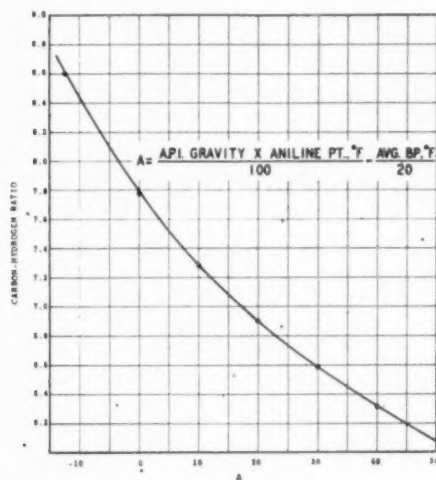


FIG. 9 CARBON-HYDROGEN RATIO OF DISTILLATE FUEL OILS

operations for the production of more valuable products. Fuel oils, ranging from light domestic fuel and high-speed Diesel fuel, to heavy marine and industrial fuel are obtained as distillates, or as residuum from primary crude-oil distillation, or from thermal and catalytic cracking. All types of fuel oils can be converted to gasoline by thermal or catalytic cracking, assuming the availability of suitable processing equipment.

Since refining operations are ordinarily carried out primarily to obtain the desired yield and quality of gasoline, it is not possible to exercise complete control over the characteristics of the fuel oils produced simultaneously. In the case of crude-oil distillation, the light-fuel boiling range can be controlled, but not much can be done about any of the other characteristics. In other words, the refiner simply isolates a fuel of desired boiling range and its characteristics depend only on the type of crude processed. In the case of heavy fuels, the chief property which can be regulated is viscosity. This characteristic is controlled by blending light fuel-oil (distillate) fractions in the residual (undistilled) fuel to the extent required. Similarly, the light fuel produced by thermal and catalytic cracking can be controlled as regards boiling range, but the other characteristics depend primarily on the type of stock being processed and on the severity of the cracking operation. The viscosity of the heavy fuel produced through thermal cracking is regulated, as in the case of crude-oil distillation, by blending-in light fractions. Thus the production of fuels of the desired characteristics is mainly a matter of selection and blending of available stocks.

The stability and performance specifications for kerosine, Diesel fuel, and domestic heating oils limit the types of refinery stocks suitable for these fuels. In general, burning kerosines contain only straight-run material, light Diesel fuel contains straight-run and catalytically cracked fuel, and domestic fuel oil can contain straight-run, catalytically cracked, and thermally cracked fuel.

AVAILABILITY OF FUEL OILS

It is difficult to predict reliably what the future relationship of supply and demand for fuel oils will be. With the completion of refinery-expansion programs, and the modernization of transportation systems, supply has more than kept up with demand. The result has been a cutback in crude-oil production today. The fact remains that, when needed, enough oil will be produced to satisfy all essential requirements in the near future, despite the predictions of some forecasters to the contrary.

An estimate of the future fuel-oil balance can be made from current consumption trends. For 1947, Table 7 (8) gives the consumption of fuels in the United States. It is noted that heating and industrial applications were the principal consumers of fuel oils. Residual fuels constituted the bulk of the oils and averaged about 56 per cent of the total; distillate fuels came next and comprised about 25 per cent. Kerosine and Diesel fuel made up the remainder of 11 and 8 per cent, respectively. At the moment, domestic oil-burning installations are proceeding at an accelerated rate which, together with the steam-to-Diesel con-

TABLE 7 U. S. CONSUMPTION OF FUEL OILS FOR 1947 (8) IN THOUSANDS OF BARRELS OF 42 GAL.

	Kerosine*	Diesel fuel	Other gas oil and distillates	Residual fuel oil	Total	Per cent of total* use
Heating.....	62482	9079	178359	56402	234761	25.5
Range oil.....	8209	20476	11632	...	24114	8.0
Tractor fuel.....	...	10389	4118	...	21406	2.3
Railroads.....	...	7100	3143	97500	121119	13.2
Industrial.....	...	17313	16291	177757	204437	22.2
Public utilities.....	...	5500	7116	60964	75180	8.1
Vessels.....	32012	17313	2338	121047	140698	15.3
Miscellaneous.....	102703	69857	5160	6859	49531	5.4
Total.....	102703	69857	228157	520529	921246	100.0
Per cent of total fuel oil.....	11.1	7.6	24.8	56.5	100.0	

TABLE 8 ESTIMATED U. S. CONSUMPTION OF FUEL OILS IN THOUSANDS OF BARRELS OF 42 GAL

Fuel	1947	1951	Per cent change over 1947
Kerosine.....	102703	113000	+10
Diesel fuel.....	69857	113000	+62
Distillate fuels.....	228157	329000	+44
Residual fuels.....	520529	474000	-9
Total.....	921246	1029000	+12

version program of the railroads, and the increased use of Diesel tractors, buses, and trucks, will impose increased demands on distillate-type stocks. The extent of these increases for 1951 is estimated in Table 8.

A reduction in the amount of residual fuel oils available is predicted. However, they will still be the main fuel-oil type for some years to come. Part of the increase in distillate fuels will be accomplished at the expense of residual stocks which will be cracked more extensively. In the immediate future, considerations of supply point to the use of these residual grades as the most attractive liquid fuel for gas-turbine usage.

BIBLIOGRAPHY

- 1 "Estimation of Scaling Resistance," by H. S. Avery, Alloy Casting Bulletin, No. 10, May, 1947, p. 9.
- 2 "Combustion System for Burning Bunker C Oil in a Gas Turbine," by B. O. Buckland and D. C. Berkey, Paper No. 48-A-109, presented at the Annual Meeting, New York, N. Y., November 28-December 3, 1948, of THE AMERICAN SOCIETY OF MECHANICAL ENGINEERS.
- 3 "Thermal Properties of Petroleum Products," Bureau of Standards, no. 97, 1929, p. 24.
- 4 "Prospects for Use of Safety Fuels in Spark-Ignition Aircraft Engines," by Frank C. Mock, discussion by Graham Edgar, SAE Transactions, vol. 34, 1939, p. 294.
- 5 "Annual Tables of Physical Constants," Section 700 (C), 1, Frick Chemical Laboratory, Princeton, N. J., 1941.
- 6 "International Critical Tables," National Research Council, McGraw-Hill Book Company, Inc., New York, N. Y., vol. 2, fig. 12, 1927, p. 157.
- 7 "Carbon Hydrogen Ratios of Distillate Fuel Oils," by S. P. Cauley and E. B. Deigass, *Oil and Gas Journal*, vol. 46, 1947, pp. 83-84.
- 8 "Mineral Market Report," No. MMS 1666, Bureau of Mines, Dec. 6, 1948.

Discussion

F. T. HAGUE.³ The total fuel cost for an industrial gas turbine must not exceed that of a Diesel engine if the gas turbine is to be a competitive engine. This means that it must burn residual oil. Residual oils as a group have two characteristics which must be controlled to insure satisfactory use. These are (1) the compatibility or freedom from sludge formations when batches of different origin and history are mixed together; and (2) the ash content of metallic salts which adheres to turbine blading and renders units inoperative.

In reference to the use of residual oil, it should be recognized that any gas-turbine manufacturer can develop a combustor for efficient combustion, and that the turbine-blade deposits, resulting from the use of an unsuitable batch of oil, are independent of the combustor design or the name of the turbine manufacturer. The problem of avoiding the use of unsuitable oil in a gas turbine has the characteristics of an industry problem, in that it is in the interest of the customer, the oil supplier, and the turbine manufacturer that the impossible not be attempted.

The industrial gas turbine gives promise of being a continuous outlet for a nominal percentage of residual oil. The oil industry's interest in developing this outlet for the otherwise surplus "what's left" of the refining process is commendable in all respects. Let's

consider the wealth of information at their disposal to do something constructive for the gas-turbine fuel-oil problem.

The oil suppliers know the field origin and the processing history of their residual oils. They recognize the typical ash content of the crudes from specific oil fields, such as the objectionable vanadium pentoxide from South America, and the sodium and calcium sulphates from domestic fields. We understand they recognize the impossibility of mixing refinery stocks from straight-run catalytically or thermally cracked processes without incurring incompatibility. This general type of information and experience is the present basis for preparing Navy Special residual oil.

The gas-turbine group must now become sufficiently articulate to tell the oil industry what it requires of a gas-turbine residual oil. Once the oil industry is convinced there is a gas-turbine residual-oil problem and takes the necessary steps to segregate and market a suitable "gas-turbine residual oil," it will be using its potential technical knowledge and experience most commendably. There is every indication that the various oil suppliers should get together and pool their experiences so that the availability of a gas-turbine residual oil fuel is a reality of tomorrow. Diesel oil fuel is closely controlled by specification because the Diesel and oil industries recognize the common-sense economics of using a suitable fuel. The gas-turbine industry is yet in the embryo stage, but the same common sense should rapidly mature the thinking on its fuel problem. Customers aren't going to like it otherwise.

ASHTON HOWARTH.^{4,5} More emphasis, it is believed, should be placed on ash content and its effects, as it constitutes one of the principal objections militating against the use of residual-type fuels in gas turbines. Serious as the corrosion problem may be, it is probable that susceptibility to attack by and deposition of vanadium compounds and other salts also are of great importance. Part of this problem is not much different from that encountered in steam-boiler practice where deposition of materials in the forms of sulphates, glasses, and oxides in superheater banks restricts the passage of combustion gases through the boiler and interferes with its operating efficiency.

The authors cite an example where a high-ash-content fuel produced no serious effect. Type of constituent is even more important than the amount; a low ash content of certain constituents can be much more offensive than higher amounts of other materials. Published analyses show one of the most bothersome constituents to be sodium sulphate.

Hughes and Voysey⁶ describe in great detail the ash and deposits found on gas-turbine blades and show that sodium is the most likely to form harmful deposits. They also discuss the various processes by which the ash adheres to the blades and possible means of dealing with this problem.

In connection with possible corrective measures, it is not to be overlooked that if the ash constituents are present in the vapor phase, their removal by mechanical means such as filtration is impractical.

E. W. JERGER.⁷ It is indeed true that the C/H ratio is difficult to obtain by a method of burning the fuel and analyzing the

⁴ Superintendent, Petroleum Division, Naval Boiler and Turbine Laboratory, Philadelphia Naval Shipyard, Philadelphia, Pa.

⁵ The opinions or assertions contained herein are the private ones of the writer and are not to be construed as official or reflecting the views of the Navy Department or the naval service at large.

⁶ "The Considerations Dealing With the Formation of Deposits in Gas-Turbine Plant," by Hughes and Voysey, *Journal of the Institute of Fuel*, April, 1949, p. 197.

⁷ Assistant Professor, Department of Mechanical Engineering, Iowa State College, Ames, Iowa, Jun. ASME.

³ Consulting Engineer, Steam Division, Westinghouse Electric Corporation, Lester Branch, Philadelphia, Pa.

combustion products. At present there is not available gas-analyzing equipment to enable one to make an extremely precise exhaust-gas analysis in oil burning. Then, in the calculation of the C/H ratio it would have to be assumed that the fuel is composed of only carbon and hydrogen. Ordinary heavy commercial distillates, even if low in sulphur content, rarely have greater than a 97 per cent combined carbon-hydrogen content. The aniline point and the (UOP) K factor, in fact, both are a measure of the paraffinicity of the oil. Hougen and Watson⁸ have shown that the K factor, average boiling point, and API gravity are related to the molecular weights of petroleum fractions. In general, paraffinic fractions have higher molecular weights than aromatic fractions with corresponding lower K factors, at approximately the same average boiling point. A correlation is also given between the hydrogen content and the K factor plus one other property. It seems that the C/H ratio with the molecular weight would indicate the general chemical structure of the compound.

The 50 per cent distillation temperature should only be used as the average boiling point for petroleum fractions of the same crude. A mixture of different-gravity distillates will exhibit a wide boiling range.

The writer takes exception to the correlation cited between Diesel index and cetane number. While the aniline point correlates well with the cetane number, the usual differences in API gravity for fuels taken from the same crude destroys a good correlation between the Diesel index and cetane number.

One property the author didn't mention that may have a bearing on the combustion-chamber design, from a combustion time standpoint, is the heat of vaporization. The heat of vaporization has also been empirically related to API gravity and boiling point, and can of course be calculated with the classical Clapeyron equation.

In regard to the mention of preheating fuel oil supplied to a burner; it has been the writer's experience that the preheat temperature should correspond to an optimum viscosity. The optimum viscosity seems to be a matter of droplet size, and is best found by experiment. Preheating a heavy residual No. 6 fuel oil to approximately 180 to 190 F seems to give the best results.

AUTHORS' CLOSURE

From the limited experimental and operational data available,

⁸ "Chemical Process Principles," Part 1, by Hougen and Watson, John Wiley and Sons, Inc. New York, N. Y., 1943.

the fuel problems associated with the use of residual fuels in gas turbines are by no means clear cut. Both railroads and merchant vessels, which are substantial consumers of residual fuels, have not suffered incompatibility difficulties though their fueling points cover a wide geographic area. The insistence of the Navy Department on a compatibility specification for its boiler fuels is probably based on the much greater area its vessels would be expected to cover as well as the necessity for minimizing operating difficulties however remote their possibility. Consequently, very few instances of incompatibility are anticipated in the utilization of residual fuel oils in gas turbines.

Hughes and Voysey in some commendable experiments did show that certain elements in fuel oils contribute more to turbine deposits than others. In their work with a 500-hp experimental gas turbine, deposit formation on the turbine blading was found to be progressive. Other turbine users, however, found that some deposits reached a maximum thickness and then remained constant indicating that operating conditions and turbine design were factors related to this phenomenon. The recent work of Buckland and Barkey on a 4800-hp commercial gas-turbine unit apparently did not lead into any deposit problems in the turbine even though residual fuels of varying ash contents were used. Corrosion, however, was encountered with a high-ash fuel containing vanadium. It is evident that more operating data on industrial gas turbines are needed to evaluate the effects of ash.

It is difficult to follow Jerger's contention that the 50 per cent distillation temperature should be used as the average boiling point only for petroleum fractions of the same crude. The C/H ratio correlations cited in the paper were developed from a series of 22 distillate fuels covering different crude oils and different refinery processing methods. The average deviation of estimated from actual C/H ratio was found to be 0.89 per cent and the maximum deviation was 3.27 per cent.

The aniline point of Diesel-fuels has not been found to correlate well with the cetane number. An estimation procedure utilizing only the 50 per cent boiling point and the API gravity⁹ of a fuel has been found to give acceptable estimates of cetane numbers for most fuels. The Diesel index correlation was presented because of its use as an alternate to the cetane-number requirement in a number of specifications.

⁹ "The Correlation of Cetane Number With Other Physical Properties of Diesel Fuels." Report by the Diesel Index Panel of Standardization Subcommittee No. 4, Gas Diesel & Fuel Oils, *Journal of the Institute of Petroleum*, vol. 30, 1944, p. 193.

Combination of Heat Sources and Sinks by the Method of Superposition¹

By F. H. BRIDGERS,² LOS ALAMOS, NEW MEXICO

A superposition method is proposed whereby the temperature pattern around a single buried heat source at a given temperature is used to arrive at the pattern obtained when several heat sources at the same temperature are placed at any distance apart. An equation is derived to give the "strength ratio," which is defined as the ratio of heat dissipated by one of a series of buried heat sources of equal temperature to the heat dissipated by a single heat source at the same temperature. This equation is plotted for a specific case to show the "strength ratio" as a function of heat-source spacing. Experimental temperature-distribution patterns around a heated tube buried in a box of sand are shown for the center tube of a group of three tubes. Although the proposed superposition method is subject to an inherent error, which may be severe at very close spacing of heat sources, the agreement between experimental and calculated results for the cases investigated in this work is good.

NOMENCLATURE

The following nomenclature is used in the paper:

A = distance from center of tube to "near" surface of equivalent slab

$$A = a + \frac{k_a}{f}$$

a = distance from center of tube to near surface in actual slab

B = distance from center of tube to "far" surface of equivalent slab; $B \gg A$

d = distance between tubes (center to center)

f = combined radiation-convection heat-transfer coefficient

$f(x, y)$ = mathematical function defined by Equation [1d]

$f(x, 2A-y)$ = mathematical function defined by Equation [1e]

k = thermal conductivity

k_a = thermal conductivity of equivalent slab

\ln = natural logarithm

q = heat flux per unit length of source

r = distance from line source or sink

r_0 = radius of cylindrical heat source

r_1, r_2, r_3, r_4 = distances from a particular line source or sink

$t_{x,y}$ = temperature of a point in a slab

t_w = temperature of tube surface

t_a = effective temperature of environment on heating side of slab; approximately equal to $\frac{t_a + t_s}{2}$

t_a = air temperature on heating side of slab

t_s = average surface temperature of surroundings on heating side of slab

t_e = effective temperature of environment on nonheating side of slab

α = constant defined by Equation [1a]

β = constant defined by Equation [1f]

γ = constant defined by Equation [1i]

Δ = constant defined by Equation [1b]

θ = temperature potential (point temperature minus sink temperature)

$\theta_0, \theta_1, \theta_2$ = temperature potentials due to a particular line source or sink

θ_p = temperature potential due to a combination of line sources or sinks

η = "strength ratio" defined as ratio of heat dissipated by one of a series of buried heat sources of equal temperature to heat dissipated by a single heat source at same temperature

π = mathematical constant, = 3.14159 . . .

$\psi(x, y)$ = mathematical function defined by Equation [1e]

$\psi(0, -B)$ = constant defined by Equation [1h]

$\psi(r, 0)$ = constant defined by Equation [1g]

INTRODUCTION

The solution of heat-transfer problems involving the two-dimensional steady flow of heat from a single heat source in a solid medium has been proposed by Carslaw (1)³ and others (2, 3). The various solutions are exact only when the boundaries of the solid mediums are isothermal sinks. For the case where the boundary of the solid medium is not isothermal, such as a pipe or cable buried in a wall, the solution is greatly complicated because of the complexity of establishing exact boundary conditions. Schofield (4) has shown that approximate solutions of such problems are possible by establishing simplified approximate boundary conditions. If there exists, instead of a single heat source, a series of heat sources at the same temperature buried in a slab, the mathematics of the problem becomes much more involved. This work will deal principally with the approximate solution of the type of problems where a series of cylindrical heat sources at the same temperature are buried in a solid medium. A practical example of such a case would be that of a floor-heating panel having hot water pipes buried in concrete. The boundary of the solid (panel surface) for the case considered will not be an isothermal sink, but will have a surface temperature distribution being governed by the balance at each point of the heat conducted to the surface from heat sources and that transferred from the surface by convection and radiation.

Vanderweil (5) has derived an equation to give the two-dimensional temperature distribution in a slab containing equally spaced heated tubes at the same temperature. His equation holds only when the tubes are located very near to one of the bounding surfaces of the slab, so that the percentage of heat flow

¹ Based on a Master's Thesis, 1948, School of Mechanical Engineering, Purdue University.

² Engineer, Charles S. Leopold, Consulting Engineering Firm, Philadelphia, Pa.

Contributed by the Heat Transfer Division and presented at the Fall Meeting, Erie, Pa., September 28-30, 1949, of THE AMERICAN SOCIETY OF MECHANICAL ENGINEERS.

NOTE: Statements and opinions advanced in papers are to be understood as individual expressions of their authors and not those of the Society. Paper No. 49-F-13.

³ Numbers in parentheses refer to the Bibliography at the end of the paper.

$$\theta_p = \theta_0 + \theta_1 = \frac{q}{2\pi k} \ln \frac{r_2}{r_0} + \frac{q}{2\pi k} \ln \frac{r_4}{r_3} \quad \dots\dots [4]$$

$$\theta_p = \frac{q}{2\pi k} \ln \frac{r_2 r_4}{r_0 r_3}$$

If the isothermal at r_0 represents the surface of a pipe with constant water temperature, the temperature potential at P will remain constant at θ_0 regardless of how close line source B ap-

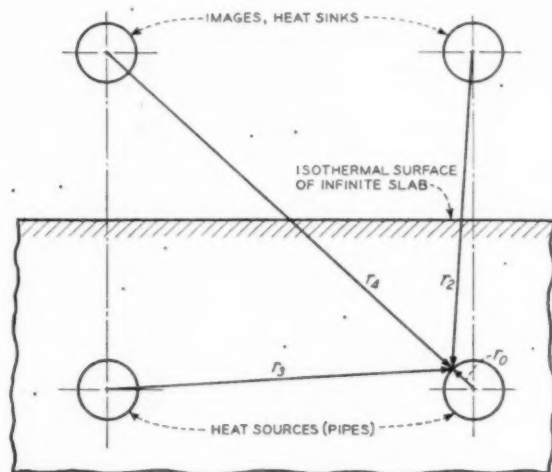


FIG. 2 COMBINATION OF TWO HEAT SOURCES IN AN INFINITE SLAB

proaches source A ; therefore Equation [4] does not hold. It is foreseeable that the strength, q (B hr⁻¹ ft⁻¹ of length), of each individual source, when combined with other sources in the solid at the same temperature will be less than the strength of the individual source alone in the solid. In other words, if two pipes at the same temperature were placed close together in a solid, each individual pipe would dissipate less heat than if one of the pipes were alone at the same temperature. Therefore, by fixing the temperature potential at r_0 , for the case of two sources close to one another, Equation [4] should be written in the form

$$\theta_p = \theta_0 = \eta \frac{q}{2\pi k} \ln \frac{r_2 r_4}{r_0 r_3} \quad \dots\dots [5]$$

where η is the "strength ratio," defined as the ratio of heat dissipated by one of the two tubes when together, to that dissipated by the same tube when by itself and at the same temperature.

Solving for η in Equation [5]

$$\eta = \frac{\theta_0 2\pi k}{q \ln \frac{r_2 r_4}{r_0 r_3}} \quad \dots\dots [6]$$

Solving for q in Equation [4] and substituting in Equation [6], we obtain

$$\eta = \frac{\theta_0}{\theta_0 + \theta_1} \quad \dots\dots [7]$$

In Equation [7], θ_0 is fixed as the difference between the temperature of the source and the temperature of the sink, while θ_1 is evaluated by means of Equation [3]. Equation [3] is given in terms of x, y -co-ordinates by Boelter and coworkers (6). Equation

[7] provides a good approximation for the change in strength q (B hr⁻¹ ft⁻¹ of length) of two pipes as a function of their distance apart in a slab. For the limiting case of two pipes when the distance apart approaches zero, η will approach 0.5, as would be expected for equal temperature pipes. As the distance apart increases, η will approach 1.0. The foregoing treatment is not limited to two pipes but could be applied to a series of pipes, and the decrease in strength of a single pipe could be similarly computed.

In applying the analytical treatment to an air-cooled slab with a series of embedded tubes, only an approximate solution can be obtained because of the complexity of establishing true boundary conditions. Equation [3], which was used to obtain Equation [7], holds only when the slab is bounded by an isothermal plane. Such is not the case for a finite slab with embedded tubes, but rather there is a definite surface-temperature gradient between the adjacent tubes. Vanderweil proposed approximate boundary condition in developing his theoretical equation which we may employ in the analytical approach of this treatment. He considered the actual slab, including the combined surface radiation-convection film, to be replaced by an equivalent slab of constant conductivity, which has the same resistance to heat flow as the actual slab. Such an equivalent slab is shown in Fig. 1 where the heat flow through the back side of the slab is neglected. If we assume the strength of three sources to remain unchanged upon combining, the temperature at point P , Fig. 1, would be

$$\theta_p = \frac{q}{2\pi k} \left[\ln \frac{r_2}{r_0} + \ln \frac{r_2}{r_1} + \ln \frac{r_4}{r_3} \right] \quad \dots\dots [8]$$

The strength ratio for the center tube can be obtained in the same manner as used to obtain Equation [7]

$$\eta_A = \frac{\theta_0}{\theta_p} \quad \dots\dots [9]$$

For an infinite number of equally spaced tubes the temperature potential at any point in the slab will be

$$\theta = \eta \frac{q}{2\pi k} \left[\ln \frac{r_1}{r_2} + \ln \frac{r_2}{r_4} + \ln \frac{r_4}{r_6} + \dots \right] \quad \dots\dots [10]$$

where r_2, r_4, r_6 are the distances from the sources to the point, and r_1, r_3, r_5 are the distances from the imaginary sinks to the point.

Fig. 3 shows a plot of the strength ratio versus tube spacing for the center pipe of a three-pipe combination at a 2-in. depth of burial in sand. The values for this plot were obtained by considering only three pipes and using Equations [8] and [9]. It is noteworthy that this curve will hold theoretically for any source temperature when employing Equations [8] and [9], provided bound-

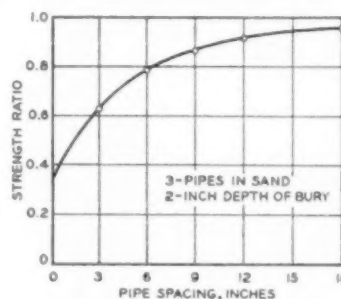


FIG. 3 STRENGTH RATIO AS FUNCTION OF PIPE SPACING FOR CENTER PIPE OF THREE-PIPE COMBINATION

any conditions are assumed to remain constant. Whether or not the curve will be valid for a wide temperature range in actual practice is a matter of experimental confirmation. In an actual slab where there is a series of tubes, it is obvious that when the pipes are spaced closely, there will be more than two pipes which will affect the temperature potential θ_p , and therefore the strength ratio. In any arrangement of a series of sources, one must take into account the effect of all those sources which influence the potential θ_p , Fig. 1.

It should also be mentioned that the smaller the depth of tube burial and the closer the tube spacing, the greater will be the error introduced by using this method based on line sources and sinks. In using the treatment based on line sources, the assumption was made that the isothermal at a distance r_0 (through point P , Fig. 1), from the source is circular and therefore represents the pipe surface. The isothermal through point P will not remain circular as two sources come close together, or as the distance to the surface becomes small, but will become distorted. The greater the distortion, the greater will be the error introduced.

An illustrated solution of the foregoing treatment is given in Fig. 4. This figure shows a method of using the temperature gradient along the horizontal center line from a single buried tube to obtain the gradient that would occur along the horizontal center line for a three-tube combination. For example, the resulting temperature potential at point P is given by

$$\theta_p = \eta_A \theta_{A_0} + \eta_B \theta_{B_0} + \eta_C \theta_{C_0} \quad [11]$$

where

$$\eta_A = \frac{\theta_0}{\theta_A}$$

and

$$\eta_B = \eta_C = \frac{\theta_0}{\theta_B} = \frac{\theta_0}{\theta_C}$$

Temperature potentials θ_0 , θ_p , θ_A , θ_B , θ_C , θ_{A_0} , θ_{B_0} , and θ_{C_0} are shown in Fig. 4. The resulting gradient along the horizontal center line connecting the three tubes is obtained by adding the potentials at a number of points as just shown. In this way, the temperature-distribution pattern of a single tube is used to obtain the temperature pattern of a combination of tubes for any particular tube spacing. If the experimental temperature gradients from the single tube are used in applying the illustrated superposition method, the results should be more accurate than the results obtained from an analytical solution where boundary conditions are approximated.

EXPERIMENTAL EQUIPMENT AND PROCEDURE

The experimental phase of this work consisted in obtaining data on the temperature-distribution patterns around single and multiple buried tubes, in order that the proposed superposition method could be checked. Temperature patterns were obtained for the following conditions:

- 1 Single tube as the only heat source in the solid.
- 2 The tube combined with either one or two other heat sources (tubes at the same temperature at a distance of 6 in. from centers).

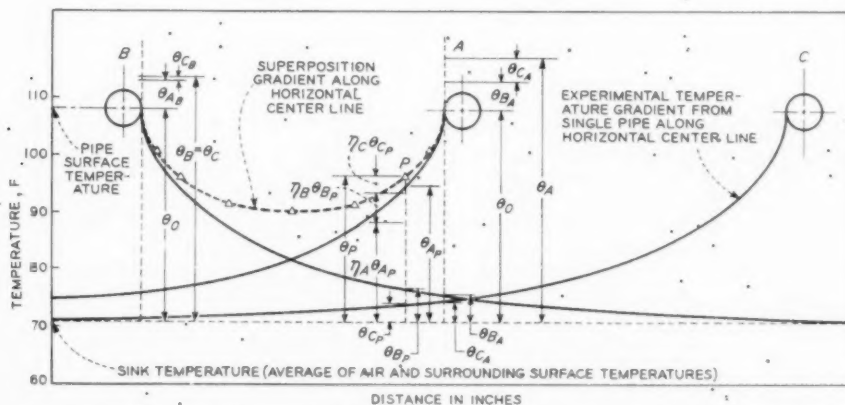


FIG. 4 ILLUSTRATED APPLICATION OF SUPERPOSITION METHOD FOR CASE OF THREE HEAT SOURCES

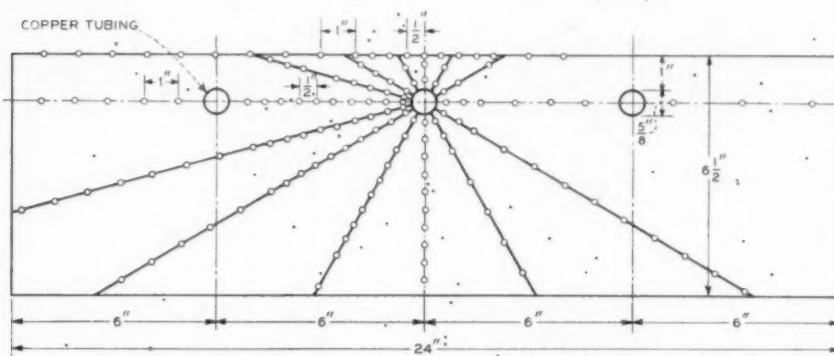


FIG. 5 THERMOCOUPLE ARRANGEMENT AT CENTER CROSS SECTION OF SLAB

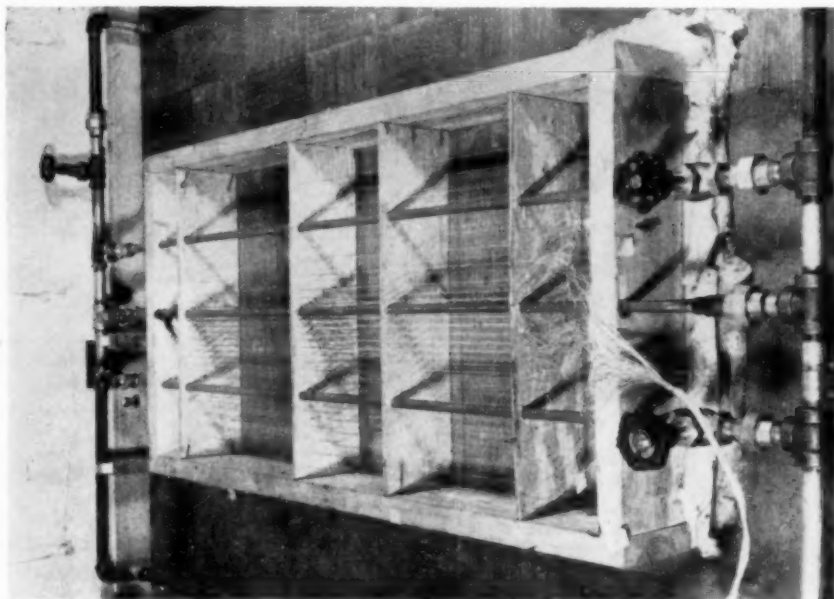


FIG. 6 EXPERIMENTAL EQUIPMENT SHOWING ARRANGEMENT OF THERMOCOUPLES

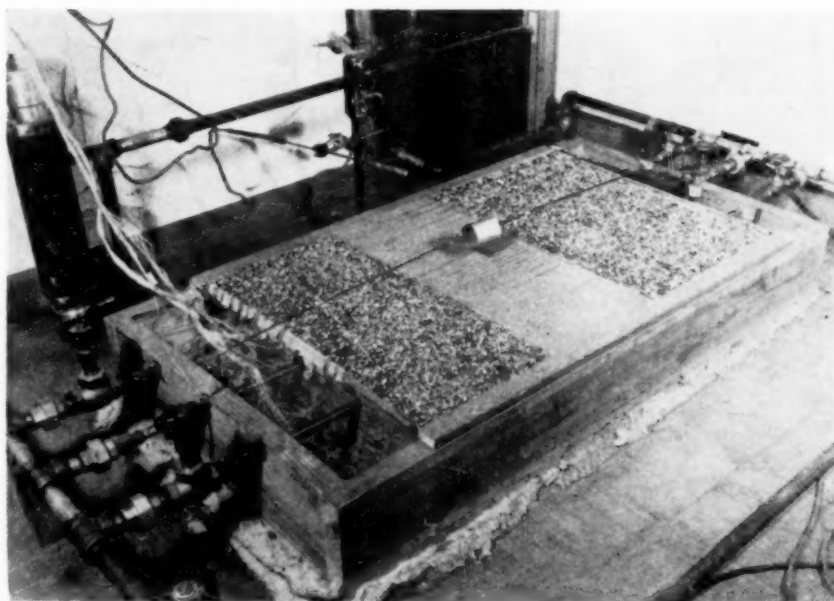


FIG. 7 EXPERIMENTAL EQUIPMENT SHOWING SLAB UNDER TEST

3 In both of these cases, three depths of burial were used, namely, $\frac{1}{2}$ in., 1 in., and 2 in.

The experimental equipment used to obtain the temperature pattern around the buried tubes consisted of a box containing three $\frac{3}{8}$ -in.-OD copper tubes buried in sand at various depths. Copper-constantan thermocouples were installed in a radial pattern around the middle tube at the center cross section of the slab. Fig. 5 shows the typical arrangement of the thermocouple

for the 1-in. depth of tube burial. The thermocouples indicating the tube temperature were soldered on top of each tube. All thermocouple leads were brought out parallel to the tubes. Fig. 6 shows the box containing the tubes and thermocouples before the sand was poured. The thermocouple leads were held in place by four $\frac{1}{8}$ -in. plywood boards which had small holes drilled to accommodate the leads, Fig. 6. Dry sand which had been sifted through a 16-mesh screen was poured into the center section,

care being taken to prevent movement of the thermocouples. The sand was not packed, but merely allowed to run freely into the box. Expanded vermiculite (loose particle size) was poured into the two end sections on each side of the sand to provide insulation to reduce the heat flow in the direction parallel to the pipes. Thus the heat flow in the sand slab was essentially two-dimensional. Fig. 7 shows the assembled slab with the copper tubes buried at a depth of 1 in. Additional thermocouples outside the box were placed as follows: One shielded thermocouple 2 in. above the sand over the center pipe to record the air temperature; two thermocouples between the box and the floor, one of which was above and the other below the blanket-type insulation which was placed between the box and the floor.

The thermocouple emf was measured by a semiprecision portable potentiometer which could be read accurately to within 0.2 deg. During all tests the water temperature in the tubes and the ambient room air temperature were maintained within approximately 1 deg.

Three tests were run for each depth of tube burial to determine the temperature-distribution pattern around the center tube. The first test was run with the water directed through the center tube only. Immediately after the temperatures were recorded for the first test, the valve on one of the outside tubes was opened and the water was passed through two tubes for the second test. Water was passed through all three tubes for the third test. During the equilibrium period, thermocouple readings were recorded along the horizontal center line. When the temperatures at points along this line ceased to change with time, it was assumed that steady-state conditions existed. The water temperature was maintained constant throughout the three tests for each depth of tube burial. The air temperature was also constant throughout the progress of the tests. After temperatures throughout the cross section of the box, and the air and floor temperatures were recorded, an exploring thermocouple was used to obtain the surface temperature of the surrounding walls and ceiling.

DISCUSSION OF RESULTS AND CONCLUSIONS

The results are summarized in Table 1, and Figs. 8, 9, and 10, which show a comparison between experimental temperatures, the temperatures obtained by using the superposition method and

temperatures computed by the Equation [1] proposed by Vanderweil.

In applying the superposition method, the temperature potential at any point in the slab was taken as the difference between the temperature at a given point and the "sink" (ambient) temperature. The true sink temperature would be difficult to obtain as it would depend on the following temperatures:

- 1 The true mean radiant temperature of the slab surface, which would be a function of the shape factor of the slab with respect to each of the surrounding room walls.
- 2 The room air temperature.
- 3 The temperature of the floor under the test box.

The true sink temperature would be a weighted average of the foregoing temperatures, proportioned according to the per cent of heat dissipated from the test box by radiation, convection, and conduction (through the bottom). A simplifying assumption was made in applying the superposition method by considering the sink temperature equal to either the air temperature or the average of the air temperature and surrounding surface temperatures, which in most cases would differ from the true sink temperature by less than 2 or 3 deg F, using the air temperature alone as the sink temperature might cause an appreciable error in some cases. Table 1 shows a comparison of point temperatures obtained by the superposition method in which both the air temperature and the average of the air and surrounding surfaces were used as the sink temperature.

The superposition-point temperatures are also compared with experimental values and point temperatures calculated using Vanderweil's theoretical equation (see Table 1). Vanderweil recommends that in applying his equation for calculating the minimum panel-surface temperature (midway between tubes) that the equivalent depth of the tube burial be multiplied by an experimentally determined correction factor; this correction factor would compensate for the increase in the equivalent boundary layer at that point due to a smaller temperature difference between the air and panel surface. In computing the temperatures shown in Table 1, this correction factor was not used, which might account partly for the deviation of surface temperatures calculated by this method compared with the experimental data.

TABLE 1 COMPARISON OF POINT TEMPERATURES OBTAINED BY EXPERIMENTAL, SUPERPOSITION, AND VANDERWEIL METHODS

One-Half Inch Depth of Tube Burial - Three Pipes - 107.2 F. Surface Temperature													
ALONG HORIZONTAL CENTER LINE							AT SURFACE OF SLAB						
Point	Experimental Values	Based on sink temp.	Based on sink temp.	Based on sink temp.	Based on sink temp.	Based on sink temp.	Point	Experimental Values	Based on sink temp.	Based on sink temp.	Based on sink temp.	Based on sink temp.	Based on sink temp.
1.312	0	90.0	90.1	90.1	90.8	90.8	1.0	0.812	92.2	93.1	93.1	94.9	94.9
2.312	0	83.8	84.6	84.6	86.2	86.2	1.5	0.812	82.8	83.6	83.6	87.4	87.4
3.0	0	83.0	83.6	83.6	85.2	85.2	3.0	0.812	79.0	80.5	80.5	84.3	84.3
One Inch Depth of Tube Burial - Three Pipes - 111.8 F. Surface Temperature													
1.312	0	96.0	94.3	95.0	95.9	95.9	1.0	1.312	90.0	88.8	89.6	89.5	89.5
2.312	0	91.0	88.9	89.7	91.6	91.6	1.5	1.312	85.3	85.6	85.3	86.4	86.4
3.0	0	90.0	87.8	88.3	90.8	90.8	3.0	1.312	82.0	81.7	81.7	84.0	84.0
Two Inch Depth of Tube Burial - Three Pipes - 108 F. Surface Temperature													
0.812	0	100.0	99.0	100.4	99.1	99.1	1.0	2.312	80.8	80.5	82.8	81.2	81.2
1.312	0	96.2	94.8	96.9	94.9	94.9	1.0	2.312	80.2	80.2	82.3	80.7	80.7
2.312	0	92.4	91.0	93.1	91.3	91.3	2.0	2.312	79.8	79.3	81.7	79.8	79.8
3.0	0	91.3	90.3	92.4	90.6	90.6	3.0	2.312	79.0	78.8	81.1	79.4	79.4

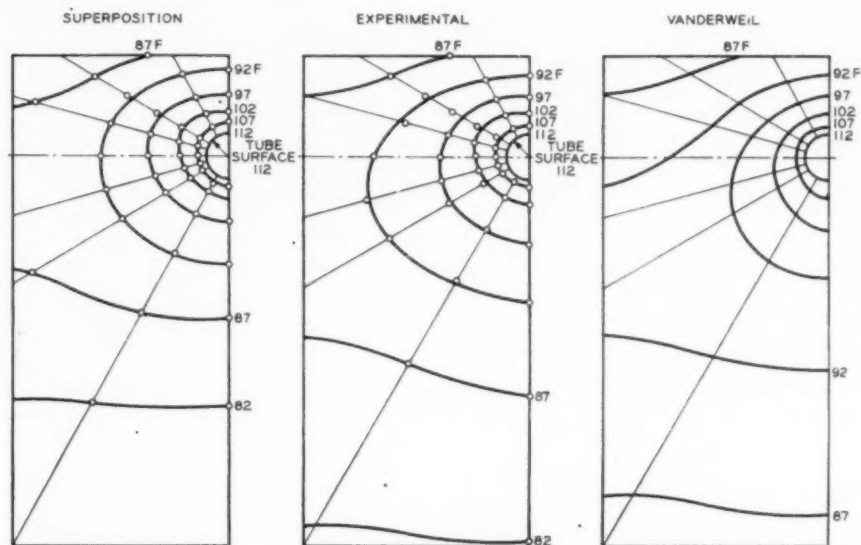


FIG. 9 COMPARISON OF ISOTHERMAL PATTERNS OBTAINED FROM EXPERIMENTAL, SUPERPOSITION, AND VANDERWEIL METHODS

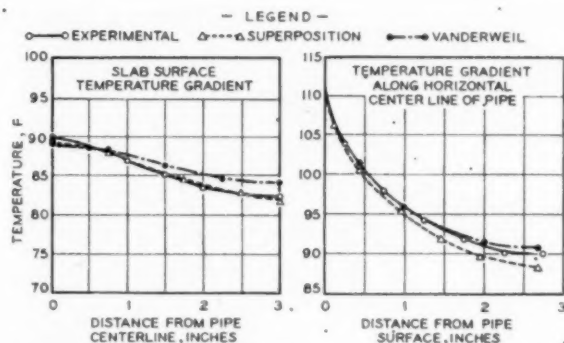


FIG. 8 COMPARISON OF EXPERIMENTAL GRADIENTS WITH GRADIENTS OBTAINED BY SUPERPOSITION METHOD AND VANDERWEIL EQUATION

Fig. 8 shows a comparison of the experimental temperature gradients along the surface and horizontal center line between tubes, compared with those obtained by the superposition and the Vanderweil method. The average of the air and surrounding surface temperatures was taken as the sink temperature.

Fig. 9 shows a comparison of the temperature-distribution patterns around the center tube of a three-tube arrangement obtained by the experimental, superposition, and Vanderweil methods. The average of the ambient air and surrounding surface temperatures was taken as the sink temperature for the superposition method.

Fig. 10 shows the same isothermal patterns that are shown in Fig. 9, superimposed on each other so as to give a more direct comparison. It is seen that the agreement is very good between the three methods above the horizontal center line of the tube. Below the horizontal center line, the experimental isotherms fall about half way between those determined by the superposition and Vanderweil methods. The deviation of the superposition method from the experimental might be partly explained by experimental difficulties. The floor temperature under the test box could not be controlled and varied as much as 4 or 5 deg F. Therefore the true sink temperature for the experimental case,

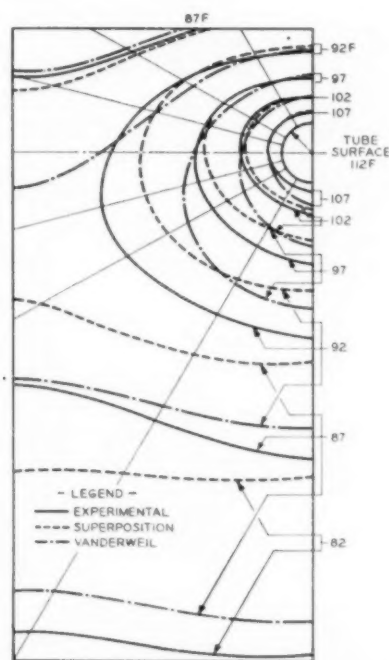


FIG. 10 SUPERIMPOSED COMPARISON OF ISOTHERMAL PATTERNS OBTAINED FROM EXPERIMENTAL, SUPERPOSITION, AND VANDERWEIL METHODS

and the sink temperature used in applying the method were different. This caused a change in temperature potentials for points below the tube, and thus resulted in a deviation between the experimental and superposition isothermal patterns.

Results presented here are for the 1-in. depth of tube burial only. For the $\frac{1}{2}$ -in. and 2-in. depths of burial the results of the superposition and Vanderweil methods deviated from the experi-

mental results by about the same amount as for the case of the 1-in. depth of burial.

The results obtained here by using the superposition method cannot be taken as conclusive validation of this method, even though there is reasonably good agreement with the experimental data. It should be remembered that only one tube spacing (6 in.), one type of material (sand), and one value of temperature difference between water in the tube and air (approximately 37 deg F) were investigated. On the basis of the results for the particular case considered, it can be concluded, however, that both the superposition and the Vanderweil methods may be used to give a good approximation of the temperature-distribution pattern around one of a series of embedded tubes.

Equation [7], which has been derived to give the strength ratio, may have application in many heat-transfer problems such as the spacing of tubes in a heating or cooling panel, the arrangement of tubes for ground coils used in conjunction with the "heat-pump" and many similar applications.

ACKNOWLEDGMENTS

The author wishes to express his sincere thanks to Dr. Y. S. Touloukian, Prof. F. W. Hutchinson, and Dr. Max Jakob for their encouragement and helpful suggestions throughout the course of this work.

The author is indebted to the Copper and Brass Research Association which made the funds available through the Purdue Research Foundation for carrying out this work.

BIBLIOGRAPHY

- 1 "Conduction of Heat in Solids," by H. S. Carslaw and J. C. Jaeger, Oxford Press, New York, N. Y., 1947, chapt. 15.
- 2 "The Heat Loss From a Cylinder Embedded in an Insulating Wall," by F. H. Schofield, *Philosophical Magazine*, vol. 12, 1931, pp. 329-349.

3 "Heat Flow When Boundary Condition Is Newton's Law," by J. H. Awbery, *Philosophical Magazine*, series 71, vol. 7, 1929, p. 1143.

4 "Steady Flow of Heat From Certain Objects Buried Under Flat Air-Cooled Surfaces," by F. H. Schofield, *Philosophical Magazine*, vol. 31, 1941, p. 471.

5 "Panel Heat Flow and Its Design Considerations," by R. G. Vanderweil, *Heating and Ventilating*, vol. 43, June, 1946, p. 63; also *Chase Radiant Heating Manual*, Chase Brass and Copper Company, 1945, p. 195.

6 "Heat Transfer Notes," by L. M. K. Boelter, H. V. Cherry, H. A. Johnson, University of California, July, 1942, pp. 4-10 and 8-8.

7 "Aerodynamic Theory," by W. F. Durand, editor, Julius Springer, Berlin, Germany, 1934, pp. 139-140.

Discussion

Y. S. TOULOUKIAN.¹ The author should be commended for his interesting and useful contribution. To the best of the writer's knowledge, this is the first time that the well-known theory of superposition has been adapted to the field of heat transfer, using a simple technique. It is thought that this semianalytical, semi-empirical method would be inherently better than a purely analytical approach on the equivalent convection radiation coefficient, because the author makes use of the experimental gradient for a single tube as the basis of his solution to obtain the surface temperature distribution for a series of tubes. This experimental gradient does take into account the exact influence of $(h_c + h_r)$.

Of course it should be kept in mind that this method does have limitations as set forth in the paper.

Further experimental work of broader scope would be a more conclusive check on the method presented in this paper.

¹ Assistant Professor of Mechanical Engineering, Mechanical Engineering School, Purdue University, Lafayette, Ind. Jun. ASME.

The Coal-Hydrogenation Demonstration Plant at Louisiana, Mo.

By J. A. MARKOVITS,¹ LOUISIANA, MO.

The 200 to 300-bbl per day capacity demonstration plant hydrogenates coal at 700 atm pressure in two stages. First, coal paste is liquefied with finely divided iron catalyst at 525 atm hydrogen partial pressure, then the middle oil distillate is further hydrogenated in the vapor phase on fixed catalyst beds. The hydrogen is made by catalytic reforming of natural gas with steam.

INTRODUCTION

BACKGROUND information on the national liquid-fuel situation and status of the American synthetic-fuel research has already been presented by Dr. Schroeder.² The report mentioned Bureau of Mines demonstration-plant activities at Louisiana, Mo. Two plants were erected adjacent to the government-owned synthetic-ammonia plant: A 200 to 300-bbl per day capacity coal-hydrogenation plant and an 80 to 100-bbl per day capacity gas-synthesis plant.

The gas-synthesis plant will not be discussed in this presentation. For general orientation it may be mentioned that, when completed, it will produce synthetic fuels by the Fischer-Tropsch synthesis method from hydrogen and carbon-monoxide mixtures derived from gasification of pulverized coal with oxygen and superheated steam. Major component parts of this installation are the 1-ton per hr capacity Linde-Frankl oxygen plant, the pulverized-coal gasification plant, the gas-purification plant, the Fischer-Tropsch synthesis plant, and the product-recovery unit or refinery. The total plant construction is nearing completion, but the component parts were started up as soon as progress of the construction made it possible. The oxygen plant started producing 98 per cent pure tonnage oxygen as early as January, 1949, and pulverized coal was gasified in the plant with oxygen and superheated steam in May. Operation of the integrated plant is anticipated in 1950.

The coal-hydrogenation-plant construction was completed in January, 1949, but partial test runs were under way by November, 1948. The plant produced the first synthetic liquid fuels from lignite derivatives in April, 1949. In this presentation the process will be described as it is practiced in the demonstration plant. Details of conventional procedures will have to be omitted for brevity.

The plant was designed and built by the Bechtel Corporation of San Francisco, Calif., under technical direction and supervision of the Bureau of Mines. In the plant, 10,000 psi operating pressures are combined with temperatures up to 1000 F, and the materials to be processed at these conditions range from gases to mixtures of viscous liquids containing high percentages of abrasive solid particles. These service conditions presented many un-

usual engineering problems. Coal has been hydrogenated in Germany on a rather extensive scale for the past 20 years, but the process was new in the United States. Few items were commercially available for the chosen process. Where there was a choice between importing equipment from Germany or building it here, the latter was done. It was the hard way, but it was considered desirable to acquire design "know-how" and to give American manufacturers an idea of the basic requirements for the design of future commercial-size plants. Within the limitations of the project the equipment was chosen and sized so that the results of operations would be representative of those expected in modern full-scale hydrogenation plants.

THE PROCESS

Coal and petroleum differ in appearance but are similar in chemical composition. The main constituents of both are carbon and hydrogen, although the carbon:hydrogen ratio, the arrangement of the atoms in the molecule, and the molecular weights are different. In addition, coal contains more oxygen, nitrogen, sulphur, and mineral impurities or ash. To convert coal into gasoline the carbon and hydrogen atoms have to be rearranged, the hydrogen:carbon ratio must be approximately doubled, and the ash has to be removed.

In the demonstration plant all this is done at the 700-atm pressure level and in two stages. In liquid-phase hydrogenation a pulverized coal-oil paste is liquefied with hydrogen at elevated temperatures in the presence of a finely divided catalyst, such as iron oxide. In the vapor phase the middle-oil cut of the liquefied coal, which boils below 625 F, is converted into gasoline and by-products with hydrogen over a solid bed of catalyst containing tungsten or molybdenum. Fig. 1 is a simplified flow diagram and shows the two main steps in proper relation to the necessary auxiliary operations.

The raw coal is first crushed to minus $\frac{3}{4}$ -in. size, then pulverized to minus 60 mesh in a ball mill and dried to 1 or 2 per cent moisture content by a gas-fired recirculating drier. The pulverized coal is mixed with a small quantity of catalyst, such as iron oxide or tin oxalate and with heavy oil, previously obtained from the liquid-phase process into a paste, containing approximately 47 per cent solids.

The viscous paste is injected into the paste preheater by steam-driven plunger pumps working at 10,000 psi. The preheater is of modified radiant type, in which the high-pressure tubing is protected by a superheated-steam jacket. Before the paste enters the preheater, a small volume of hydrogen is injected to reduce the viscosity. The mixture is then heated in the first section to about 570 F. At this stage, additional hot hydrogen and recycle heavy oil are added to jump the temperature to the 640 F level, circumventing coal-swelling difficulties that would occur around 600 F. After passing through the remainder of the preheater, the mixture leaves at about 815 F and passes into the first of two converters. For 95 per cent conversion of the coal to liquid and gaseous products, the residence time is approximately 1 hr. The reaction is highly exothermic, and to maintain the reaction temperature at 930 F, cooling hydrogen is added to the converters in controlled amounts at different points.

After the second converter, the reacted products enter the

¹ Assistant Chief, Coal-to-Oil Demonstration Branch, Office of Synthetic Liquid Fuels, Bureau of Mines.

² "Synthetic Liquid Fuels in the United States," by W. C. Schroeder, *Mechanical Engineering*, vol. 69, 1947, pp. 989-995.

Contributed by the Petroleum Division and presented at the Petroleum Mechanical Engineering Conference, Oklahoma City, Okla., October 2-5, 1949, of THE AMERICAN SOCIETY OF MECHANICAL ENGINEERS.

NOTE: Statements and opinions advanced in papers are to be understood as individual expressions of their authors and not those of the Society. Paper No. 49-PET-3.

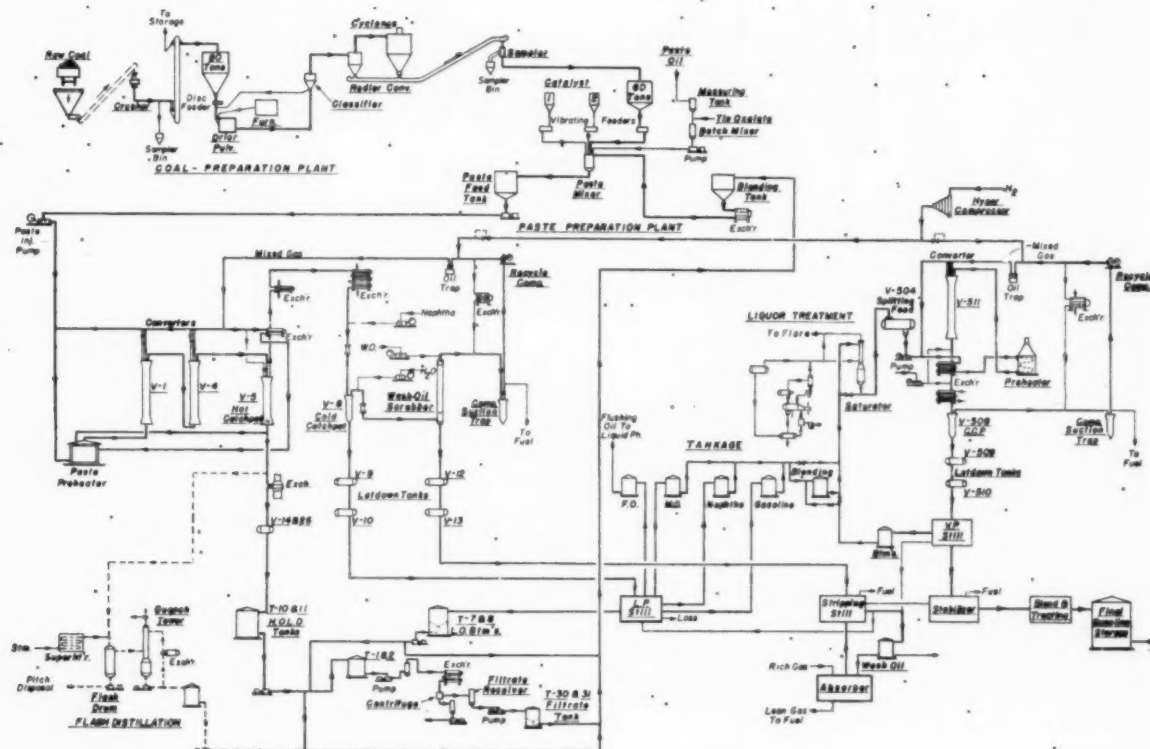


FIG. 1 PROCESS-FLOW DIAGRAM OF COAL-HYDROGENATION DEMONSTRATION PLANT

"hot catchpot," where the hydrogen and light ends separate from the solid-containing heavy-oil fraction. "Letting down" the heavy oil to near atmospheric pressure is the next step. This is extremely difficult, because the hot liquid contains large quantities of absorbed gases and up to 30 per cent of abrasive solids. The heavy-oil letdown valve, therefore, is considered one of the critical pieces of equipment and will be described in detail in a companion paper.

Two methods are provided for removing ash, catalyst, and unreacted coal from the heavy-oil letdown (HOLD). The first is a flash distillation unit (see Fig. 2), consisting mainly of a gas-fired heater for superheating steam to 1100 F, and a flash tower with high-velocity nozzles for instantaneous mixing of the hot steam and HOLD. The resulting mixture is quenched with saturated steam to prevent coking in the flash tower, which is 5 ft diam and 15 ft in height. Residue is withdrawn by steam-driven pumps and injected into a water-spray chamber for quenching. It is expected that the pitch will be hard and suitable for fuel; if not, other methods will be studied for the utilization of this waste product. The vapors from the flash tower pass to a quench tower and are cooled with oil of controlled temperature, to prevent congealing in the vessel. The recovered heavy-oil is used in the pasting-oil cycle.

The alternate method consists of a Bird and a Sharples centrifuge, with facilities for blending and diluting the feed as well as for temperature control on the inlet and jacketed drums and for collecting the filtrate and residue. The filtrate is used in the pasting-oil cycle and the residue burned or otherwise disposed of.

The gases and vapors leaving the top of the hot catchpot are cooled in a heat-exchanger and water-cooler system from about

850 F to 150 F, and the condensed liquid and vapor are separated in the "cold catchpot." The gas from the cold catchpot, containing about 70 per cent hydrogen, is washed with water at full operating pressure for the removal of NH_3 , H_2S , and water-soluble salts and is scrubbed with oil obtained in the liquid-phase distillation unit to separate the light hydrocarbons. After this purification, the hydrogen stream is recycled through the system with fresh make-up hydrogen. The liquid products from the cold catchpot and from the wash-oil scrubber go through let-down systems, where the pressure is reduced in two steps, first to 25 and then to 7 atm, and are then charged to the liquid-phase distillation unit. This two-step letdown facilitates economical separation of the C_1 and C_2 rich tail gases from the liquefied petroleum gases.

The bottoms from the liquid-phase distillation unit join the pasting-oil stream. Gasoline, naphtha, and middle-oil cuts are separated to establish weight relations and to prepare, by blending, after the separation of the washing oil, a feed stock of uniform composition for the vapor-phase hydrogenation. This stock is combined with a nearly equal amount of vapor-phase recycle middle oil and saturated with H_2S or with sulphur for the vapor-phase-hydrogenation step. The addition of some form of sulphur is necessary to preserve the activity of the vapor-phase catalyst.

The vapor-phase injection pumps, working at 10,000 psi, feed the charge, to which hydrogen is added, through a feed-product exchanger and a radiant-type vapor-phase preheater. The stream leaves the preheater at around 850 F completely vaporized. This vapor enters a single converter containing six fixed-catalyst beds. The catalyst is fuller's earth, treated with hydrofluoric acid and impregnated with compounds of zinc, molyb-

denu
at 70
tion,
quite
ing h
ture
react
of th
neglig
Th
where
hydro
liqui
phase
separ
sion
betw
to 60
hydro
RVP
storag
for fu
sulph
is uti
Ma
moist
Ordna
system
the re
 H_2 an
and c
per hi

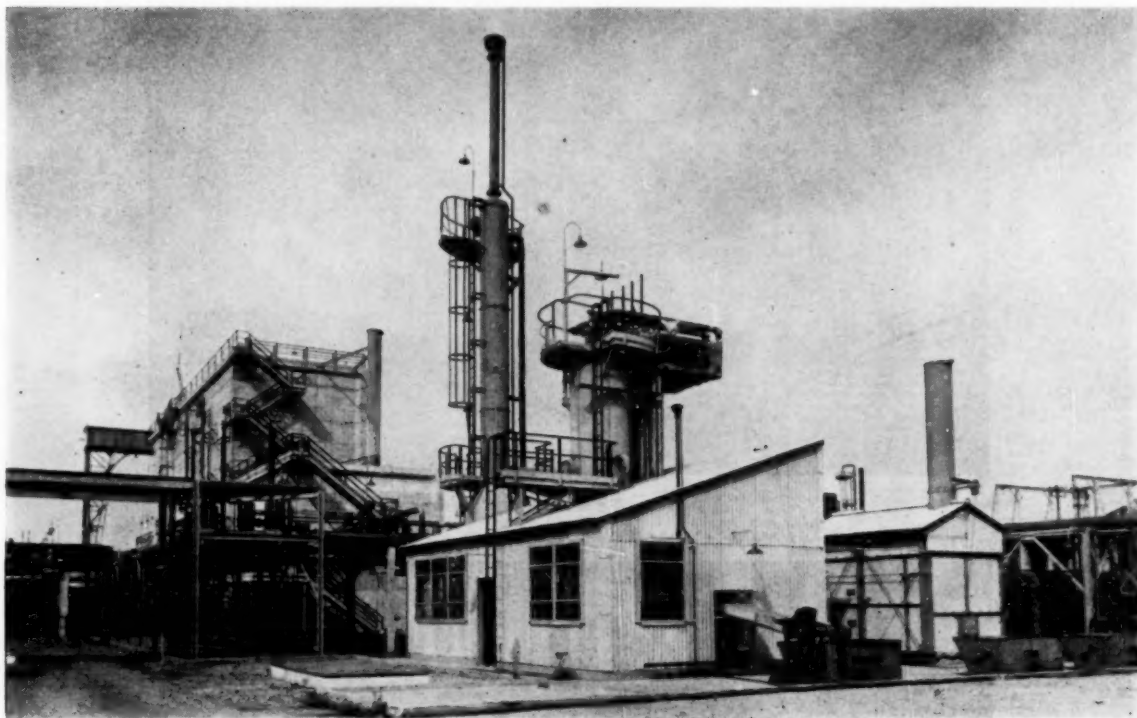


FIG. 2 HEAVY OIL LETDOWN FLASH DISTILLATION

denum, chromium, and sulphur. The catalyst is very rugged and at 700 atm performs the triple duty of the former German saturation, splitting, and dehydrogenation operations. The reaction is quite sensitive to temperature variations, and recirculated cooling hydrogen is added at every catalyst bed to keep the temperature between the 912 and 930 F operating limits. After the reaction is balanced, the feed-product exchanger provides most of the heat necessary, and the duty of the preheater becomes negligible.

The products then pass through a cooler and a cold catchpot, where the condensed oil and hydrogen are separated. The hydrogen is returned to the circulating compressors, and the liquid passes through a two-step letdown system to the vapor-phase distillation unit. The primary purpose of this unit is to separate the finished product from the recycle oil. Since conversion in the vapor-phase hydrogenation unit generally varies between 40 and 60 per cent, the distillation unit makes about 40 to 60 per cent bottoms, which are recirculated to the vapor-phase hydrogenation system; the overhead is stabilized to a 10-lb RVP gasoline, washed with caustic and water, and sent to final storage. Tail gases pass through an absorber before being used for fuel. Ammonia, CO_2 , and H_2S liquors are treated with sulphuric acid before going to the sewer, and the recovered H_2S is utilized to saturate the vapor-phase charge.

Make-up hydrogen of about 11 per cent by weight of the moisture- and ash-free coal is furnished from the former Missouri Ordnance Works' natural-gas reformer, scrubber, and compressor system. Here natural gas is cracked with steam at 1700 F, and the resulting H_2 and CO are shifted with more steam at 800 F to H_2 and CO_2 . The mixture is stored in a 300,000-cu-ft gas holder and compressed through three stages of a 7-stage 210,000-cu-ft per hr capacity compressor to 450 psi (see Fig. 3), at which pres-

sure the CO_2 is scrubbed out with water. After the 7th stage, around 11,000 psi, the remaining CO is changed by catalytic reaction into methane and water. The resulting 95 per cent pure hydrogen is ready for injection into the gas-circulating system.

The recirculating compressors shown in Fig. 4 provide the large excess of hydrogen necessary to keep the partial pressure of the system at 525 atm. Approximately 250 standard cu ft of recycle gas is circulated for each gallon of paste. The reaction is highly exothermic, and the circulating gas must be kept cold for temperature control. Failure of the gas-recycle system would result in coking up of the converters, runaway temperatures, and disaster. So important is this function, that the circulating gas is called the "bloodstream of the process." One steam-driven and one motor-driven recycle compressor are operated continuously for each hydrogenation phase at half load, so that in case of failure of any unit, the other would immediately pick up the whole load. The units are single-stage double-acting reciprocating compressors and are designed to maintain a pressure differential of 750 psi with a 450,000 standard cu ft per hr output.

PLANT EQUIPMENT

The facilities required to carry out the operations described can be subdivided into the following groups:

- | | |
|---|------------------------------|
| 1 Coal preparation. | 8 Vapor-phase hydrogenation. |
| 2 Paste preparation. | 9 Vapor-phase distillation |
| 3 Hydrogen manufacture. | 10 Ash removal. |
| 4 Hydrogen compression and purification | 11 Heavy-oil blending. |
| 5 Gas recycle and scrubbing. | 12 Gas recovery. |
| 6 Liquid-phase hydrogenation. | 13 Storage and transfer. |
| 7 Liquid-phase distillation. | 14 Instruments. |
| | 15 Auxiliaries |

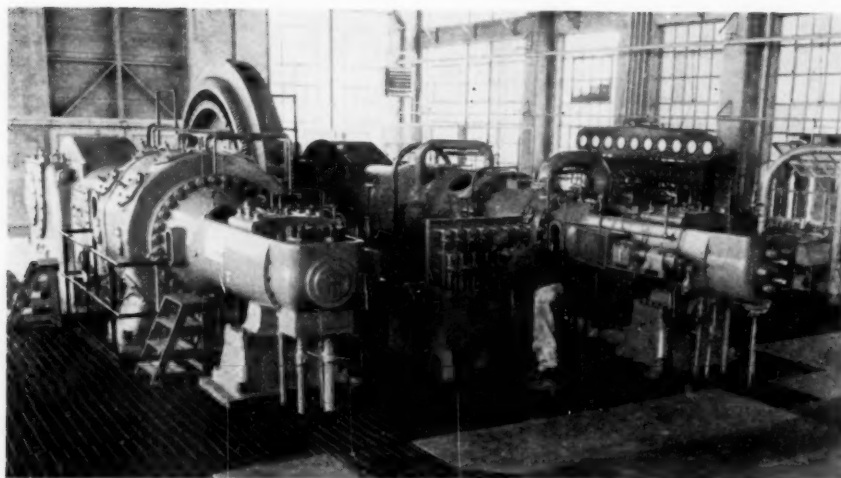


FIG. 3 MAKE-UP HYDROGEN COMPRESSOR

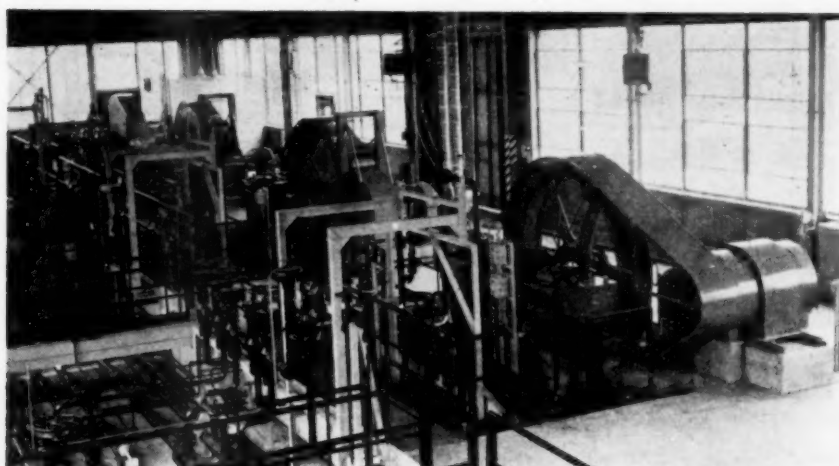


FIG. 4 CIRCULATING HYDROGEN COMPRESSORS

Detailed discussion of the foregoing groups will be omitted; and only a few comments will be offered, where necessary, to augment the process description. Thorough analyses of the more difficult coal-hydrogenation-equipment problems are given in companion papers elsewhere in this issue.

The coal-preparation plant was designed and furnished by Roberts & Schaefer Company, Chicago, Ill. It consists of track hopper, plate feeder, scraper conveyer, primary crusher, crushed-coal storage bin, feeder, gas-swept ball mill, gas-fired flue-gas heater, cyclones, fans, and water tumbler. It will pulverize and dry 10 tons per hr to 99 per cent minus 60 mesh, 85 per cent plus 200 mesh, 10 to 2 per cent moisture. Coal washing was eliminated from the original plans but may be added later if necessary.

The paste-preparation unit consists of a pulverized-coal storage bin, weighing feeder, paste mixer, paste storage tank, and facilities for mixing and adding measured quantities of dry or wet catalyst.

Paste is kept above 210 F and is circulated by Moyno pumps past the suction intake of the high-pressure injection pumps.

Although all lines and containers are steam-jacketed, viscosities as high as 1300 centipoises are encountered at this temperature. Coal and paste-preparation plants are shown in Fig. 5.

Hydrogen manufacturing, compression, purification, gas-recycle, and scrubbing facilities were described with the process. The technique employed and equipment used are adaptations of the Hercules Powder Company's 15,000-psi ammonia-synthesis practice. Make-up compressors and recycle-gas circulators were furnished by Ingersoll-Rand. The metallic packings used are quite satisfactory for these services.

The liquid and vapor-phase hydrogenation units are completely new in American industry. The high-pressure vessels, preheaters, exchangers and coolers, tubing, flanging, valves and instrumentation are subjects covered by companion papers.

The severe service conditions of the coal-paste injection pumps place them in the critical category. The paste has a viscosity of 4750 centipoises at the 200 F pumping temperature and 10,300 psig discharge pressure. The pumps are Union Steam Pump Co., 250-lb steam-driven, double-acting, duplex, forged-steel



FIG. 5 COAL-AND-PASTE PREPARATION PLANT

plunger pumps, working at 50 psi suction and 10,300 psi discharge pressure. With 24-in. \times 2 $\frac{1}{2}$ -in. bore and 18-in. stroke, capacity is 25 gpm at 14.6 rpm, and the developed hydraulic horsepower is 150. Application of this time-proved direct pumping method is a promising deviation from the oil-driven hydraulic pumps used previously. Oil, naphtha, and water-injection pumps are similar to the paste-charge pumps, except that the service conditions are not quite so severe. The heavy-oil recycle pump is a steam-driven plunger-type surge pump. It returns hot bottoms to the preheater at 750 F and 10,000 psi pressure. The pump is separated from the hot valve block, and cold, clean flushing oil is the surge medium. An Aldrich-Groff 40-hp motor-driven, vertical-triplex, variable-stroke injection pump is used in flushing-oil service, mainly to determine its adaptability for this type of work. This pump has Teflon packing. The Union Steam pump plunger packings were furnished by Garlock and have four Neoprene-impregnated chevron rings. The 8-in.-deep stuffing box, as well as the steam end, is oil-lubricated. It is felt that a lot will have to be learned by experience about high-pressure seals at the given operating conditions before the problem can be considered solved.

The most troublesome problem of the ash-removal and heavy-oil-blending steps is viscosity and settling of solids. Lines and pumps are steam-jacketed; tanks are equipped with heaters and mixing devices. An elaborate flushing-oil system is provided for these and other parts of the plant to eliminate plugging during shutdown periods.

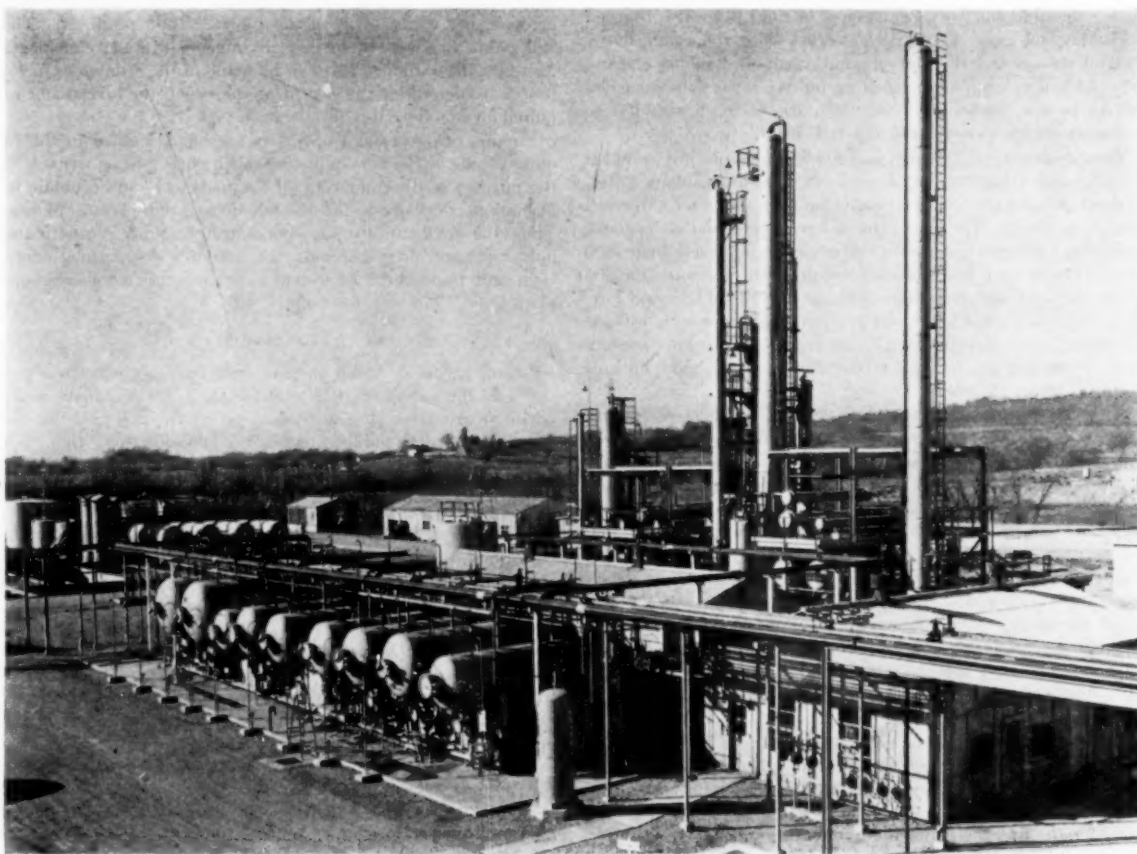


FIG. 6 COAL-HYDROGENATION DISTILLATION PLANT

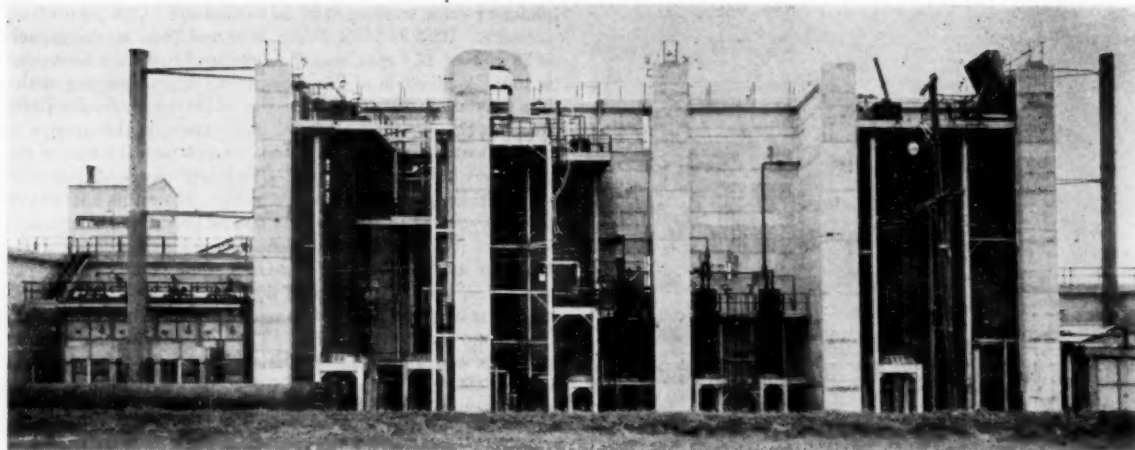


FIG. 7 LOOKING SOUTH AT OPEN END OF STALL

The liquid-phase distillation, vapor-phase distillation, gas-recovery, and liquor-treatment units are shown in Fig. 6. Gas recovery consists essentially of an oil absorber to recover enough butane to provide vapor-pressure control in the finished gasoline. No provisions are made for total C_3 , C_4 recovery, and after analyzing the different gas streams most of the LPG will be burned with the fuel gas. The stripper serves both the gas-recovery rich-oil stream and the high-pressure wash-oil scrubber stream. All distillation equipment, such as bubble towers, heating elements, pumps, exchangers, instrumentation, etc., are similar to conventional low-pressure refinery-type installations.

Complete storage, transfer, and loading facilities are provided to hold and handle 30 days' production. Steam, plant water, natural gas, and electricity are provided from the former Missouri Ordnance Works. The total connected power demand of the plant, including hydrogen generation and compression, is less than 4000 kw. Process and power steam requirement is about 100,000 lb per hr. Auxiliary facilities include elaborate high- and low-pressure flushing-oil and inert-gas purging systems, a tail-gas collecting system, and a vent and emergency letdown system with a burning pit. Fig. 7 shows the coal-hydrogenation unit from the converter side.

During plant construction it was found that neither the average American manufacturer nor the construction forces realized fully the severity of the service in a coal-hydrogenation plant. After the design was completed in painstaking detail and reasonably severe specifications were drawn, repeated difficulties were experienced with their enforcement. The importance of careful supervision, inspection, and testing during every step of the fabrication and installation became evident. Standards of excellence, applicable up to 2500-psi service conditions, were not necessarily good enough for 10,000-psi work. In numerous instances flaws in materials and unsatisfactory workmanship were not brought to light until after shop tests, or even after delivery to the job site. One of the companion presentations discusses these problems in detail.

It became evident at an early stage that the demonstration-plant program is really fulfilling its main functions. During the construction and break-in periods, many process and design improvements were developed. In addition, manufacturers gained considerable knowledge in high-pressure design and fabrication methods—a long step toward preparing them for building full-scale plant equipment.

OPERATION OF AN INTEGRATED PLANT

The second phase of the work is under way. It is the demonstration of the operation of an integrated plant, producing synthetic liquid fuels from coal. During this period, operating data are collected, analyzed, and interpreted to determine the effects of operating variables upon the processes and products. This will point the way to further improvements and refinements. More detailed studies will then be made of the economics of the process to determine the cost of products and the investment required for commercial-scale operations.

Finally, engineers and operators are being trained in the required skills of the new industry, and reports will be written for the purpose of disseminating all the technical and economic information developed in the demonstration-plant program. Thus the road toward an economically sound synthetic-fuel industry must lead through the actual construction, operation, and improvement of demonstration and commercial-size plants.

CONCLUSION

In conclusion, it should be mentioned that this paper was prepared in the spring of 1949. Subsequent developments in the coal-hydrogenation demonstration plant will probably be discussed in several publications. It seems advisable though to bring the six papers of this symposium up to date with a short reference to the two completed hydrogenation runs.

The first 10,000-psi vapor-phase hydrogenation run in America was conducted in April, first using a petroleum-crude charging stock, and, thereafter, hydrogenating low-temperature lignite tar oil, mainly into gasoline and Diesel fuel. The actual hydrogenation period lasted 9 days. At the May dedication of the demonstration plants, part of the Diesel oil produced was used on a 200-mile trial run in a Diesel-electric locomotive hauling a loaded 8-car passenger train from St. Louis to Louisiana and back. Since May all plant passenger autos, trucks and cranes, altogether 55 vehicles, have been operated on synthetic gasoline made in this operation.

During the summer all equipment was tested and prepared for the next operation.

The first liquid-phase hydrogenation break-in run was started on October 12, 1949, and terminated on December 2. High-temperature coal-tar oil was first circulated through the system at reduced temperatures, then hydrogenated. On November 25,

a paste was introduced containing 25 per cent of Rock Springs, Wyoming coal. Hydrogenated products from both charging stocks were nearly identical and consisted mainly of naphtha and middle oil suitable for vapor-phase hydrogenation stock.

Hydrogenation at 700 atm was never before attempted in this

country, and the work was conducted with inexperienced operators in a brand new plant containing untried equipment and experimental instruments; hence, the run was considered highly successful. All objectives of both the vapor- and liquid-phase hydrogenations were achieved.

T
sur
atta
pro
the
The
and

P

plas
try.
psi v
tack
fect
adec

T
vess
size
and
head
shell
proy
actio

M
type

A
12 p
B
moly
C

Ta
sign,
comp
Code
the i
Th
cludi
terial
inher
throu

¹ M
Office
² S
³ A
Synth
Cor
Petro
Okla.
Engin
No
under
the S

High-Pressure Vessels in Coal-Hydrogenation Service

By J. T. DONOVAN,¹ M. JOSEPHANS,² AND J. A. MARKOVITS³

The converters have to be built to resist 10,000 psi pressure and 1000 F temperature, complicated by hydrogen attack and H₂S corrosion. The three different designs proposed by American manufacturers are compared, and the vessels accepted for the plant are described in detail. The German spirally wound construction is discussed, and its expected advantages are enumerated.

INTRODUCTION

PRESSURES up to 15,000 psi have been used commercially in the synthesis of anhydrous ammonia and there is evidence of higher pressures applied for limited industrial production of plastics. These ranges, however, are unusual in American industry. Hydrogenation of coal combines working pressures of 10,300 psi with temperatures of 1000 F. The steels used must resist attack by high partial pressures of hydrogen and the corrosive effect of 1 per cent by weight of hydrogen sulphide, besides retaining adequate strength at elevated temperatures.

The 200-bbl per day demonstration plant required reaction vessels of 32 in. ID \times 39 ft 1 1/2 in. length. The vessels were sized to provide adequate residence time, proper space velocity, and complete accessibility upon removal of the top and bottom heads. To utilize a low-alloy steel it was desirable to keep the shell temperature as low as 500 F. This was accomplished by providing a 3-in.-thick asbestos-cement liner separating the reaction space from the shell.

COMPARISON OF PROPOSED DESIGNS

Manufacturers of high-pressure vessels proposed three different types of construction for this service, as follows:

- A A laminated wall of perforated carbon-steel plates with a 12 per cent chrome-alloy liner.
- B A two-layer compound cylinder with a perforated carbon-moly jacket over a 3 per cent chrome grooved inner shell.
- C A simple cylinder or solid wall forging of 3 per cent chrome.

Table 1 gives a comparison of the salient features of each design, and Figs. 1, 2, and 3 show the analysis of wall stresses as computed by the Lamé formula, stipulated by the API-ASME Code for vessels having wall thickness greater than 10 per cent of the inside diameter.

The laminated construction had many points in its favor, including the low-cost carbon steel, the close control of the wall material (insuring homogeneous construction), elimination of waste inherent in forging operations, and uniform stress distribution through the entire wall as shown in Fig. 1. On the other hand,

¹ Mechanical Engineer, Coal-to-Oil Demonstration Branch, Office of Synthetic Liquid Fuels, Bureau of Mines, Louisiana, Mo.

² Special Engineer, Koppers Company, Inc., Louisiana, Mo.

³ Assistant Chief, Coal-to-Oil Demonstration Branch, Office of Synthetic Liquid Fuels, Bureau of Mines, Louisiana, Mo.

Contributed by the Petroleum Division and presented at the Petroleum Mechanical Engineering Conference, Oklahoma City, Okla., October 2-5, 1949, of THE AMERICAN SOCIETY OF MECHANICAL ENGINEERS.

NOTE: Statements and opinions advanced in papers are to be understood as individual expressions of their authors and not those of the Society. Paper No. 49-PET-6

TABLE 1 VESSEL COMPARISONS

	A	B	C
Wall thickness, in.....	10 1/2	11	8 3/4
Shell construction.....	Laminated 1/4-in. plates	Forged compound cylinder	Solid forged
Type of steel.....	Carbon steel	5-in. inner shell-3% Cr 6-in. jacket-carbon moly	3% chrome
Maximum shell working stress, psi.....	17940	21460	25000
Ultimate tensile stress, psi.....	75000	90000	100000
Yield stress, psi.....	45000	50000	55000
Safety factor (based on ultimate tensile strength).....	4	4	4
Vessel weight, lb.....	312000	285000	180000
Vessel price, dollars.....	79876	88350	62600
Price per lb, cents.....	25.6	31	34.8

the built-up ends, where the solid flange is welded to the laminated wall section, gave certain fabrication difficulties that caused undesirable increase in both weight and cost.

The compound cylinder construction, similar to that used on large-caliber gun barrels, was considered an excellent and time-proven design for operation at high pressure. However, the close machining inherent in this method of fabrication, in addition to the 1/2 in. heavier wall, resulted in the most expensive unit. This design required perforation of the pervious jacket and machining of grooves on the outer surface of the inner cylinder to permit the

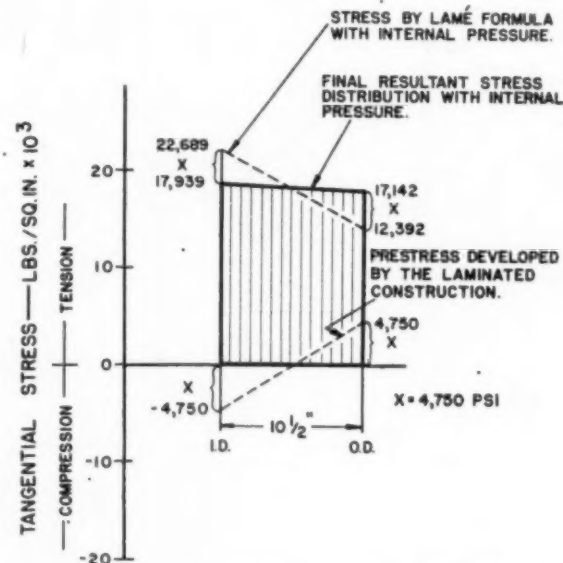


FIG. 1 WALL STRESSES OF MULTILAYER CONSTRUCTION

uniform release of the hydrogen, which diffuses through the alloy layer. These operations also contributed to the higher costs.

Referring again to Table 1, it is apparent that the solid-forged construction has the most points in its favor—it is lightest and lowest in cost; it combines the best physical and noncorrosive properties in one material.

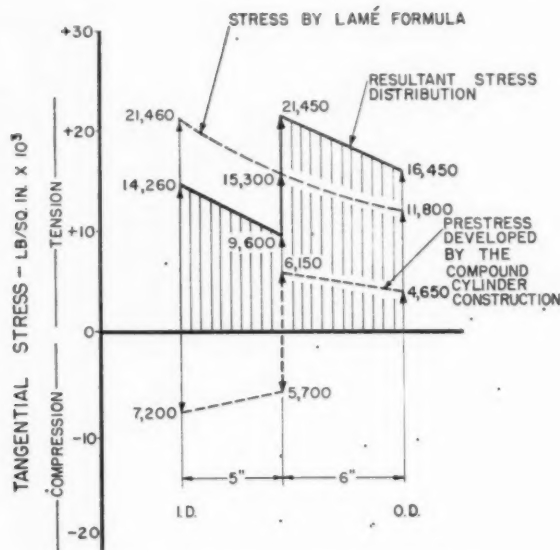


FIG. 2 WALL STRESSES OF COMPOUND CYLINDER

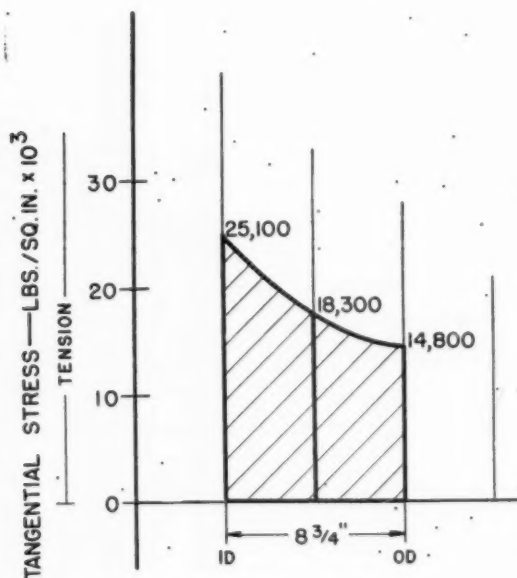


FIG. 3 WALL STRESSES OF SOLID FORGING

DEMONSTRATION-PLANT HIGH-PRESSURE VESSELS

The final design of these units furnished by the Midvale Company of Philadelphia, Pa., is as follows:

Liquid-Phase Converters. These vessels, shown in Fig. 4, are alloy-steel forgings, 32 in. ID \times 49 1/2 in. OD \times 39 ft 1 1/2 in. length, face to face of end flanges, with the ends flanged out to 61 in. OD. The heads are flat steel forgings, 21 1/2 in. thick \times 57 in. diam, provided with the necessary openings for the entry of the coal paste and hydrogen, and the exit of the products of reaction. There are no openings in the converter shell. The shell steel has 3 per cent chrome with 0.65 per cent nickel, 0.30 per cent molyb-

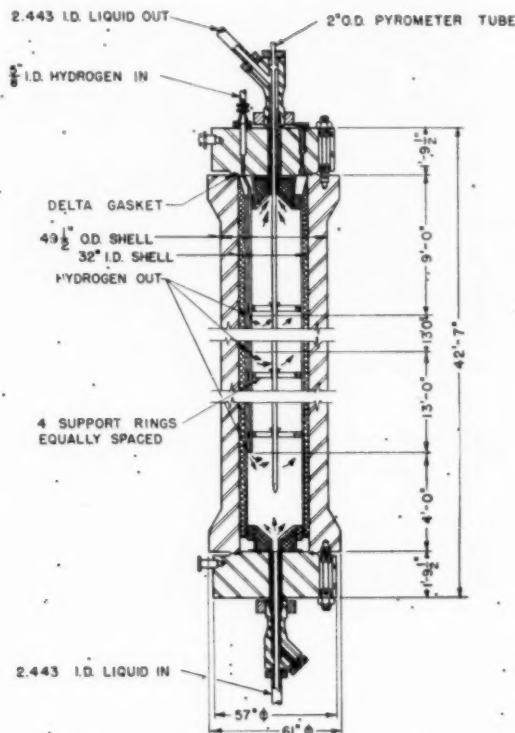


FIG. 4 LIQUID-PHASE CONVERTER ASSEMBLY

denum, and 0.25 per cent carbon, an ultimate tensile strength of 100,000 psi, and an elastic limit of 55,000 psi.

Past experience has shown that a minimum of 3 per cent chromium is desirable to resist penetration of hydrogen and the corrosive effect of H_2S at 500 F and 10,000 psi. The other constituents are necessary for adequate strength in an 8 3/4-in-thick converter wall, where the thickness is based on working unit stress of one fourth of the ultimate tensile strength at the shell temperature as required by the API-ASME Code. All vessels were tested hydrostatically to 1 1/2 times the operating pressure.

The converter heads are subjected to more severe temperature conditions; consequently, it was decided to use a slightly higher content of the same alloying elements, with heat-treatment to provide approximately the same physical properties. The head steel is 4 to 6 per cent chrome with 1 to 1.25 per cent nickel, and 0.40 to 0.80 per cent molybdenum. The head studs, of which there are 12 in each head on a 45 1/2-in-diam bolt circle, are 5 3/4 in. diam, of SAE-4340, with an ultimate tensile strength of 120,000 psi and an elastic limit of 90,000 psi. The stud nuts are of SAE-4140, with an ultimate tensile strength of 100,000 psi and an elastic limit of 70,000 psi. The shell proper weighs about 80 tons, each head about 7 1/2 tons, and the assembled converter, with internals, about 105 tons.

In determining the required head thickness the problem was approached by assuming a head thickness of 18 in. and substituting this value in Roarks' formulas⁴ for determining tension stresses in flat bolted cover plates

$$S_t = \frac{3w}{2\pi ml^3} \left[m + (m+1)L_s \frac{a}{r_0} - (m-1) \left(\frac{r_0}{2a} \right)^2 \right]$$

⁴ Roarks' Formulas for Stress and Strain, p. 18S.

where

$$a = 22.75 \text{ in.} = \frac{\text{bolt circle diameter}}{2}$$

$$r_0 = 16.625 \text{ in.} = \frac{\text{gasket contact diameter}}{2}$$

$w = 8,960,000 \text{ lb} = \text{total force on head from internal pressure}$

$t = 18 \text{ in.} = \text{head thickness}$

$m = 3, \text{ reciprocal of Poisson's ratio}$

Then

$$S_t = \frac{3 \times 8,960,000}{2\pi \times 3 \times 324} \left[3 + 4 \left(\frac{L_n}{16.625} \right) - (3 - \nu) \left(\frac{16.625^2}{4 \times 22.75^2} \right) \right]$$

$$S_t = 17,500 \text{ psi (without holes)}$$

This stress was then checked by using the API-ASME Code formula stipulated in paragraph W-316.

In an 18-in.-thick head this gives a value of 19,500 psi (without holes).

The thickness was then analyzed, taking into consideration the weakening effect of the large centrally located hole in the head.

Using formula⁵

$$S_t = \frac{Wk_1}{t^2}$$

where

$S_t = \text{allowable tensile stress at outer edge of hole} = 25,000 \text{ psi}$

$W = \text{total force from internal pressure} = 8,960,000 \text{ lb}$

$k_1 = 1.25 \text{ (derived from graph on ratio of bolt circle to gasket circle radii)}$

then t becomes 21.2 in.

It was decided to use a thickness of 21½ in. owing to possible higher temperatures which might occur on heads, and to reduce the elastic strain which might result in undesirable gasket action.

The bolts were sized in the conventional manner, based on a working load of 8,960,000 lb, which resulted in a working stress for the twelve 5½-in.-diam studs of 30,500 psi, or about one third of the elastic limit.

The asbestos-cement lining for the converter shell is mixed in the proportion of 1:1:1 by volume of granulated asbestos, quick-setting Portland cement and water. The mixture is poured and tamped in sections in the annular space between the shell and the basket. The basket is stainless-steel, ASTM-A240-347, and has a reaction space of about 110 cu ft. This steel was chosen for its good hydrogen and corrosive-gas resistance at temperatures up to 1000 F. The basket is 25½ in. ID with ¼-in.-thick wall, perforated with ⅜-in.-diam holes on 3-in. centers for pressure equalization.

The heads of the converter are insulated on the inside with 12 in. of asbestos cement and are sealed to the flanged ends by annealed SAE-1020 steel gaskets. The self-sealing gasket shown in Fig. 5 is of triangular cross section. The 33.250-in.-ID gasket fits into 0.35-in.-deep grooves in head and shell flange. About 0.002-in. copper plating was added to the polished gasket faces which improved the seal considerably by eliminating the galling of contact surfaces during fluctuation in pressure. The initial seal is created on opposite tips of the gasket by the bolting force. The

gasket becomes deformed after internal pressure is applied as shown by dotted lines in Fig. 5. Sealing actually takes place along faces marked a and b in the cross section. The soft-iron gasket is of small cross section and the internal pressure forces the entire gasket to expand in diameter when the pressure forces the bolted head away from the shell. At this writing it is still controversial how often a gasket can be re-used.

Temperature measurement within the converter is taken through a centrally located 40-ft-long, 2-in.-OD, ⅜-in.-ID seamless-steel pyrometer tube. This tube, held in place by several steel spiders, has a closed bottom and is designed to withstand an

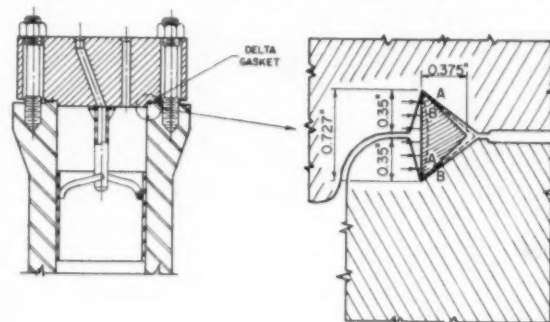


FIG. 5 DELTA GASKET ASSEMBLY

external pressure of 10,300 psi at 1000 F. Inside the tube is a ⅜-in. schedule-40 pipe of ASTM-A276-304 stainless steel, to which are attached six thermocouple elements on 6-ft centers. These elements transmit the temperatures at the various levels to a recording instrument located in the instrument house.

Vapor-Phase Converter. The vapor-phase converter, shown in Fig. 6, is identical with the liquid-phase converter in dimensions and composition of shell and heads. The inner insulation is also the same, except that the liner is ⅜-in. perforated stainless steel. The insulation is recessed for the ⅜-in. cooling hydrogen lines, so that the space inside of the insulation is unobstructed for the insertion and removal of the catalyst basket.

The removable catalyst basket, shown in detail in Fig. 6, is 24 in. ID, 36 ft 4¾ in. long, and made of ⅜-in. ASTM-A240-347 stainless-steel plate. Both top and bottom ends are bell-shaped and bolted to the body of the basket. Pressure equalization between basket and shell is obtained by holes in the top bell. The catalyst space of about 100 cu ft in the basket is subdivided into six compartments by perforated grids covered by a wire screen to support the 10-mm-diam × 10-mm-long pelleted catalyst. The grids are so constructed that they also serve as a gas-distribution chamber for uniform distribution of the hydrogen supplied to the bottom of each grid by separate ⅜-in. supply lines through the top head.

The pyrometer tube is similar to that in the liquid-phase converter, except that inside of the 2-in.-OD pyrometer tube there is a ⅜-in.-diam solid rod which carries 12 thermocouples for measuring the temperature at two points in each of the six catalyst chambers. The pyrometer tube is enclosed in a shielding pipe, permitting removal of the tube without disturbing the catalyst. The shield is closed at the bottom and made of ASTM-A240-347, schedule-160 pipe.

Hot Catchpot. This vessel receives the products of reaction from the liquid-phase converters. The heavy oil is drawn off at the bottom, while gases and vapors leave through the top of the hot catchpot. The general construction and dimensions shown in Fig. 7, as well as the materials of construction, are the same as for

⁵ "Stress and Deformation in Flat Circular Cylinder Heads," by Gilbert Dudley Fish, Trans. ASME, vol. 43, 1921, p. 615, No. 1805.

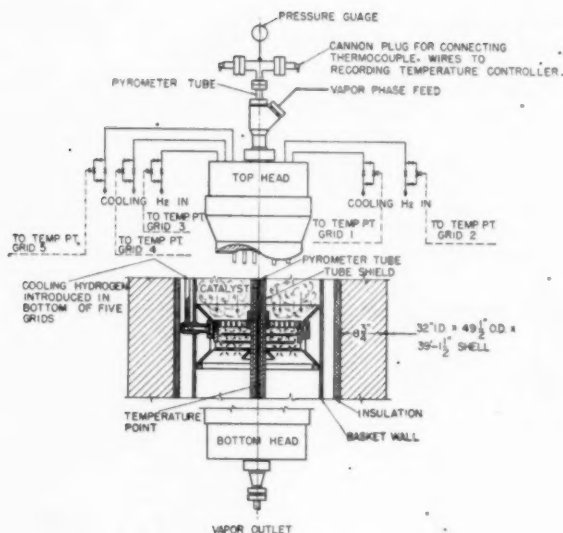


FIG. 6 VAPOR-PHASE CONVERTER INTERNALS

the liquid-phase converter, except that the shell is 25 ft 5 1/2 in. face to face of end flanges. The liquid inlet pipe extends downward through the top head a distance of 13 ft 6 in. The normal level of the liquid is about 5 ft above the bottom, while the liquid outlet pipe projects upward through the center of the bottom head to a height of 4 ft. To prevent settling of solids and coking at the bottom, a 1/2-in. size perforated, schedule-40 pipe bent to a 23 1/2-in.-diam ring is provided a few inches above the bottom for agitating and cooling the liquid with hydrogen.

Measuring and regulating the liquid level in the hot catchpot is a very important but troublesome operating function; and, in an attempt to make it foolproof, various methods were provided and are expected to work simultaneously. These methods are described in a companion paper on instrumentation.

The temperature of the hot-catchpot contents is observed by pyrometer readings. The pyrometer tube extends upward from the bottom about 2 ft above the normal liquid level. The thermoelements are spaced 12 in. on centers with at least two elements in the vapor space.

Cold Catchpots. Fig. 8 shows an assembly of these vessels. They are 24 in. ID, 37 3/4 in. OD, and 16 ft 11 5/8 in. inside length. They are flanged at the top to 47 in. OD and tapered at the bottom to a 2-in.-diam liquid outlet. The top head is 45 in. OD, and 18 7/8 in. thick, and is provided with product inlet and gas outlet openings. The 2 1/2-in.-diam product inlet pipe extends 2 ft below the head, where it is divided into two 1 1/2-in.-diam pipes, terminating in 3/8-in. x 1 7/8-in. rectangular outlets, discharging downward at 15 F, and tangentially along the inner surface of the shell. This arrangement will provide efficient separation of gases from liquids without foaming. At the elevation of the impinging stream, the vessel is lined with an interchangeable carbon-steel wear cylinder, 2 ft long x 3/8-in. wall thickness. The shell analysis is 2.50 to 3.25 per cent nickel, 0.75 per cent chromium, and 0.30 to 0.40 per cent molybdenum, and has an ultimate tensile strength of 100,000 psi and an elastic limit of 55,000 psi. The heads are carbon steel, and the head studs, nuts, and gaskets are the same as for the converters and the hot catchpot.

Since the normal operating temperatures are low, 150 F for the liquid phase, and 80 F for the vapor phase, the cold catchpots are neither insulated nor lined on the inside. For the same reason,

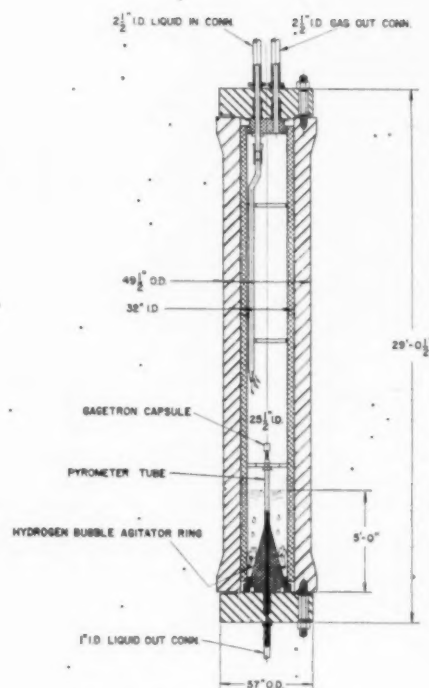


FIG. 7 HOT-CATCHPOT ASSEMBLY

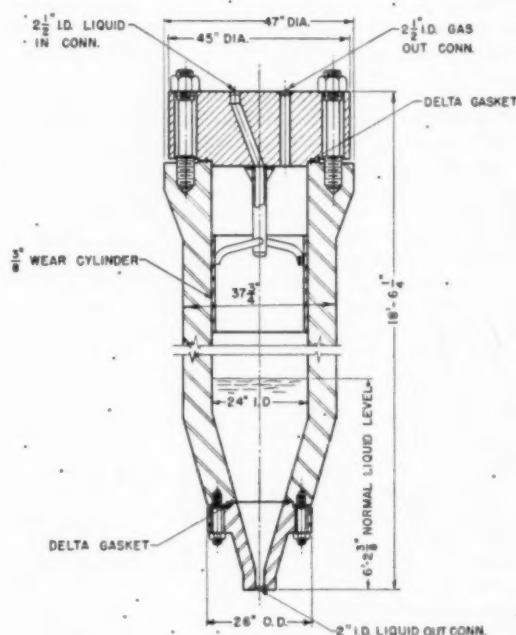


FIG. 8 COLD CATCHPOTS AND COMPRESSOR SECTION TRAPS

the shell steel contains only enough alloy metals to meet the required physical properties. The normal liquid level in the cold catchpot is 7 ft 8 $\frac{3}{4}$ in. above the bottom outlet flange.

Compressor Suction Traps. These vessels, also shown in Fig. 8, are installed in the recycle gas-compressor suction lines from the cold catchpots, to trap the moisture from the gas before it reaches the compressors. They are identical with the cold catchpots.

Wash-Oil Scrubber. The wash-oil scrubber is installed in the liquid-phase recycle gas-suction line between the cold catchpot and the compressor suction trap. The purpose of the scrubber is to wash out the hydrocarbons and impurities from the gaseous products of hydrogenation in order to maintain the partial pressure of hydrogen in the recycle gas at a minimum of 80 per cent. The scrubber is packed with 1 $\frac{1}{2}$ -in. \times 1 $\frac{1}{2}$ -in. steel Raschig rings.

The design conditions are similar to those for the cold catchpot, 10,300 psi at 120 F. In details of the shell, heads, and closures, materials of construction and general dimensions, the scrubber is identical with the cold catchpot, except that it is much longer, being 41 ft 7 $\frac{1}{4}$ in. over-all. Like the cold catchpot, it is tapered at the bottom from 24 in. ID in the body to a 2-in.-diam bottom outlet. The wash-oil inlet pipe through the top head extends down 6 ft to a perforated-steel distribution plate, below which is a packing space 28 ft 8 in. deep. The steel Raschig-ring packing is supported by a steel grate 3 ft 2 $\frac{3}{4}$ in. above the bottom head flange. The gas-inlet pipe extends up from the bottom to a point just below the packing grate and is surmounted by a serrated bubble cap. The normal liquid level in the scrubber is 4 ft above the packing grate. The liquid level is indicated and controlled in the same manner as in the cold catchpot.

STALL STRUCTURE AND REPAIR PIT

All high-pressure vessels are located within a heavy-walled reinforced-concrete structure 193 ft long, 28 ft wide, and 58 ft high, open on the top and rear. To minimize the danger of possible fires or explosions, the structure is divided into six stalls by 14-in. reinforced-concrete walls. A 130-ton gantry crane with a 70-ft lift and 60-ft span straddles the structure and facilitates handling of the heavy equipment. Fig. 9 shows the gantry crane carrying a converter to the stalls visible in the right background.

The two end compartments of the stalls house the preheaters. Next to the preheater are the hot stalls of each phase, containing the converters, high-temperature exchangers, and hot catchpot. In the center are the two cold stalls with the cold catchpots, coolers, and compressor suction traps. In a full-scale plant it is not considered necessary to enclose the cold vessels and preheaters. The experimental nature of the operation justified this extra precaution in the demonstration plant.

Adjacent to the stall area is a reinforced-concrete repair pit 35 ft deep. This pit facilitates the repair and cleaning of the large vessels by permitting vertical removal of internals.

NEW DEVELOPMENTS IN HIGH-PRESSURE-VESSEL DESIGN

The demonstration-plant high-pressure vessels described were built in accordance with the established practice of forged construction. However, during the initial stages of plant design, consideration was given to layer-vessel design and to the spirally wound vessels (Wickelofen) still in the industrial development stage in Germany. The carbon-steel-plate layer vessels proved to be too heavy and expensive, while the spirally wound vessels were not available from American manufacturers.

Latest investigations indicate that the spirally wound vessels have excellent possibilities in future American full-scale operations. Therefore a detailed description of this method seems to

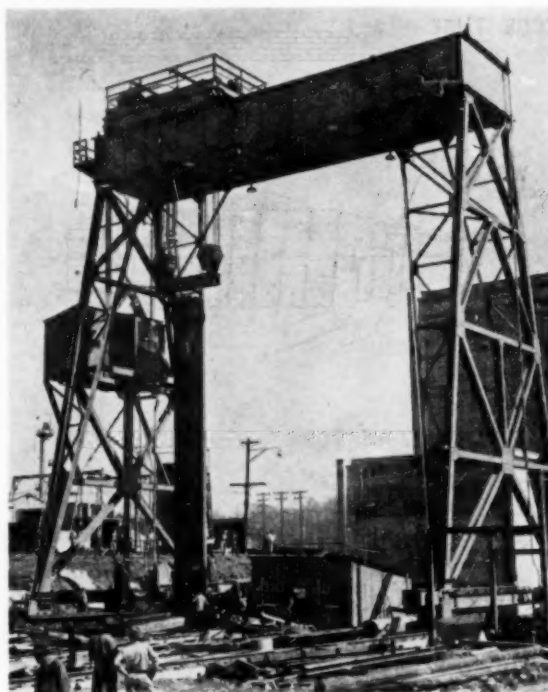


FIG. 9 PANORAMA OF STALL SHOWING GANTRY CRANE

be pertinent to this paper. The Germans developed this method of pressure-vessel construction shortly before the second world war as a modification to the layer vessel designed and constructed by the A. O. Smith Company of Milwaukee, Wis. Figs. 10, 11, and 12 help to visualize the spirally wound method of construction. The principle of design utilized by this method is the shrinkage of each successive layer of the wound strip upon the layer or core beneath. Shrinkage of the layers is achieved by continuously heating each strip electrically to between 1100 and 1550 F just before winding, followed by cooling to atmospheric temperature after it is pressed onto the underlying layer. The resultant predetermined contraction of the metal strip will set up circumferential prestressing necessary for minimum wall thickness. The intimate interlocking of the wound strips provides the necessary longitudinal strength.

The wound vessel is fabricated essentially as follows: The inner tube, which forms the core, may vary in thickness from $\frac{7}{8}$ in. for 30-in-ID to 1 $\frac{1}{4}$ in. for a 48-in-ID vessel. The inner tube must resist corrosion and hydrogen attack at high temperature and pressure. A 3 per cent chrome steel with 0.2 per cent C, 0.4 per cent Mn, 0.3 per cent Si, and 0.15 per cent V was normally used by the Germans for this purpose. A plate of commercial width is rolled to the desired diameter and butt-welded longitudinally. As many of these cylinders as are necessary for the desired length of the vessel are butt-welded together, and then stress-relieved. Dummy ends of plain carbon steel are welded to the ends of the inner tube. These dummy ends, to which the strip ends are welded, are later cut off when the vessel is finished.

The strip may vary in thickness from $\frac{1}{4}$ in. to $\frac{3}{8}$ in., and the width is usually about 10 times the thickness. It may be of plain carbon steel for the lower pressure and temperature ranges or low-alloy steel for higher temperatures and pressures, depending upon operating conditions or strength of material desired. As

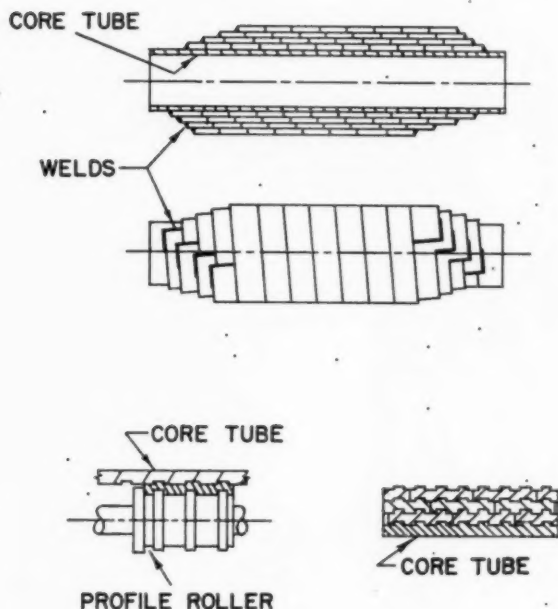


FIG. 10 DETAIL OF WICKELOFEN WRAPPING

shown in Fig. 10, the strip is rolled to a tongue-and-groove profile, preferably three or more grooves in width, so that the upper layer of strip can overlap by at least one third its width and still interlock amply for axial strength.

The wrapping lathe can be the same type used for machining solid wall vessels, Fig. 12. The tool carriage can be altered to run on a special track and accommodate a reel of strip, the strip heating and cooling equipment, and a profiled back-up roller. The strips, as received in mill lengths, are butt-welded end to end to a length required to wind a complete layer in one run.

The inner tube with its dummy ends is set on the lathe, and cooling water is turned on inside the tube. Spiral grooves are then cut into the outside face of the tube to match the tongues on the strip, at a pitch equal to the width of the strip, plus a slight clearance.

Before wrapping is started the end of the strip is welded to the dummy end of the inner tube at an angle corresponding to the pitch. The strip passes between guide rollers and is pressed against the vessel by two 6-in-diam profiled rollers diametrically opposite each other, to prevent distortion of the tube. The load on these rollers is about 1 ton. The guide rollers act as the connection for the electric current, which heats the strip as it unwinds from the reel onto the vessel. The power required to heat the strip to between 1100 and 1550 F is furnished at 30 to 40 volts and 4000 to 6000 amp.

After passing under the profiled roller, the strip is quenched by compressed-air jets and about five or six turns later by cold-water jets. The speed of wrapping is about 15 fpm.

After the first layer of strip is completely wrapped, the end is welded to the dummy end of the inner tube and the carriage returned to the other end of the lathe. The next strip is then welded to the first layer strip (see Fig. 10), so that it will overlap the joints of the underlying layer by one third of the width of the strip. The succeeding strips are then wrapped exactly like the first and second, until the required wall thickness is obtained.

To finish the ends of the vessel a flange is formed by the same wound method, a steel ring is shrunk over the strip ends, and the

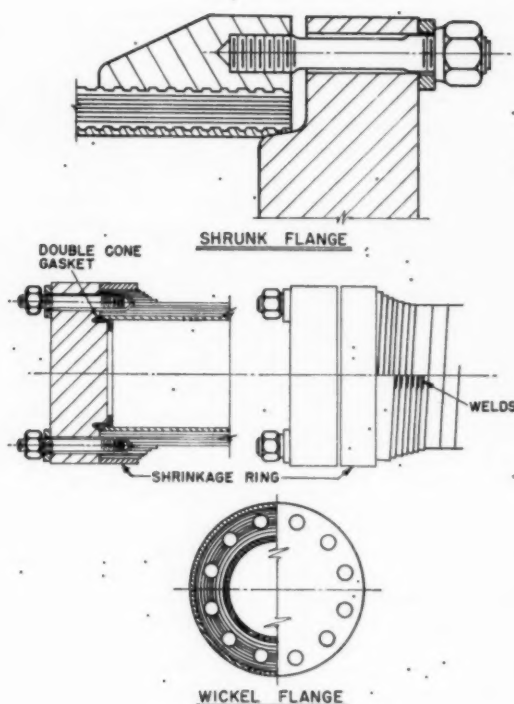


FIG. 11 WICKELOFEN FLANGES

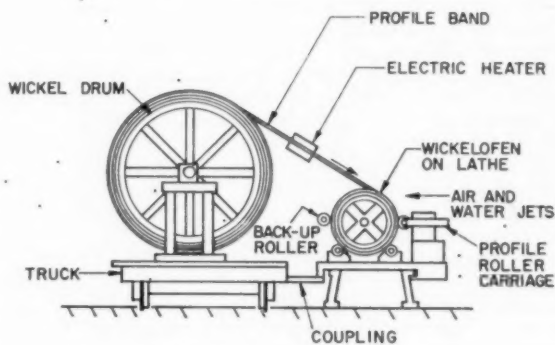


FIG. 12 WICKELOFEN WRAPPING LATHE

dummy inner-tube ends are cut off to the proper length Fig. 11. Instead of a wound flange of strips, a solid forged-steel flange may be screwed or shrunk on, if desired. Fig. 13 shows a German Wickelofen of the type described.*

Full-Scale Plant Converter. A layout has been made of a full-scale plant converter employing the spirally wound principle. A sectional sketch with the main dimensions and materials is shown in Fig. 14.

In order to take the best advantage of this type of construction, the wrapping strip steel should have a high yield strength. Also, the yield should not exceed 75 per cent, nor be less than 60

* For further particulars on the construction of the "Wickelofen" refer to "Engineering in Hydrogenation Plants in Germany," by J. F. Ellis, published by the British Intelligence Objectives Subcommittee, 32 Bryanston Square, London, W.1., or the office of Technical Services, U. S. Dept. of Commerce, Washington, D. C.



FIG. 13 FLANGED END OF WICKELOFEN

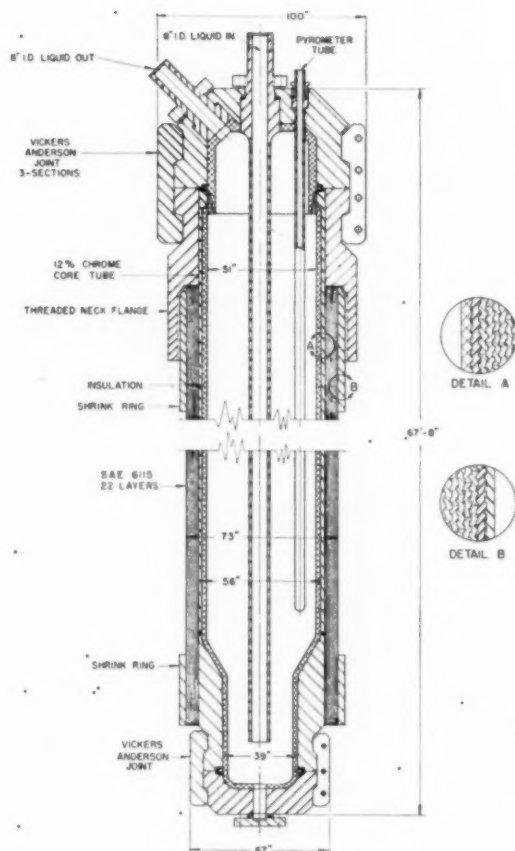


FIG. 14 FULL-SCALE PLANT CONVERTER

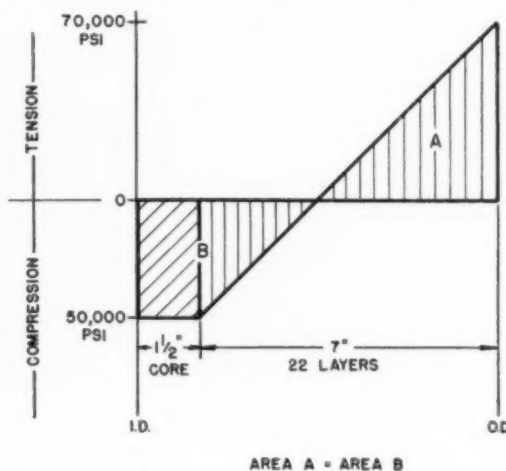


FIG. 15 WALL-STRESS DIAGRAM

per cent of the ultimate tensile strength. The elongation should not be lower than 17 per cent. It is believed that a low-chrome vanadium steel similar to SAE 6115 could be heat-treated in the wrapping procedure to secure the desired properties.

In designing the vessel shown in Fig. 15, a steel with 90,000 psi yield strength and about 130,000 psi ultimate tensile strength is used. In arriving at the wall thickness, the strip was stressed to 70,000 psi on the outside layer, resulting in compressive stress on the core tube of similar magnitude, Fig. 15. Twenty-two $\frac{3}{16}$ -in. layers were required over a $1\frac{1}{2}$ -in. inner tube. This resulted in an $8\frac{1}{2}$ -in. wall for the specified 56-in-ID vessel, weighing only 316 tons.

CONCLUSIONS

Many improvements are still possible in high-pressure vessel fabrication, particularly for large diameters required in commercial-scale hydrogenation plants.

The spirally wound construction is especially promising. A brief summary of the advantages claimed follows:

- 1 Economy in corrosion and hydrogen-resistant material, since only the core tube needs these properties.
- 2 The thin strips permit treating and forging operations to penetrate the innermost crystals. Thus the safety factor required for nonhomogeneous solid walls can be reduced.
- 3 The method of construction gives higher stress distribution on the outside layers, causing these to stretch uniformly, and thereby permitting visual inspection of amount of growth.
- 4 Reduction of wall thickness from increased physical properties secured by controlled heating and cooling of strip.
- 5 Material lost in machining is only one sixth of that lost in forging solid-wall vessels.
- 6 Fewer operators are required, and the manufacturing time is reduced to one fifth of that required in forging.
- 7 Wound vessels can be made at the plant-site shop, thus simplifying handling and transportation problems.
- 8 The size of vessels is limited only by the capacity of crane handling equipment in the field.

hy
to
di
inc

T
un
the
bri
A
cos
hig
are

I
pip
and
to
pra
tem
att
larg
to c
ity.

I
fail
gav
max
alon
mos
this

wh

1.
of Sy
2
Synt
3
Co
Petro
Okla
Eng
No
unde
of the

High-Pressure (10,300 Psi) Piping, Flanged Joints, Fittings, and Valves for Coal-Hydrogenation Service

By J. H. SANDAKER,¹ J. A. MARKOVITS,² AND K. B. BREDTSCHNEIDER³

The high-pressure piping components used in the coal-hydrogenation process are described briefly. Some factors considered in design are given. In addition, a short discourse on future design for commercial-scale plants is included.

INTRODUCTION

THE coal-hydrogenation demonstration plant required large quantities of 10,300-psi piping, flanged joints, fittings, and valves of various types. Service conditions introduce unique problems which have to be considered in the design of these elements. Some of these problems are touched upon briefly and resulting designs are described.

At this time it appears probable that most piping in future coal-hydrogenation plants would be made lighter by the use of higher-strength steels. However, the other piping components are unlikely to be changed radically in design.

PIPING

Design and standardization of the 10,300-psi-working-pressure piping presented numerous problems. In selecting materials and determining wall thicknesses, consideration had to be given to process-flow requirements, prevailing pipe-manufacturing practices, permissible stresses, including creep stresses at high temperature, and the effect of corrosion, erosion, and hydrogen attack. In addition, however, it early became apparent that large unit weights were involved; so that it became imperative to design for minimum weight consistent with safety and reliability.

It was realized that the many theories available to explain the failure of thick-walled cylinders from excessive internal pressure gave widely different results at the 10,000-psi design level. The maximum principal-stress theory, in which the tangential stress alone is considered to be the criterion for failure, proved to be the most suitable choice. The ASA code for pressure piping adopts this theory, and in paragraph 122b

$$tm = \frac{D}{2} \left(1 - \sqrt{\frac{S-P}{S+P}} \right) + C \dots \dots \dots [1]$$

where

¹Mechanical Engineer, Coal-to-Oil Demonstration Branch, Office of Synthetic Liquid Fuels, Bureau of Mines, Louisiana, Mo.

²Assistant Chief, Coal-to-Oil Demonstration Branch, Office of Synthetic Liquid Fuels, Bureau of Mines.

³Special Engineer, Koppers Company, Inc., Louisiana, Mo.

Contributed by the Petroleum Division and presented at the Petroleum Mechanical Engineering Conference, Oklahoma City, Okla., October 2-5, 1949, of THE AMERICAN SOCIETY OF MECHANICAL ENGINEERS.

NOTE: Statements and opinions advanced in papers are to be understood as individual expressions of their authors and not those of the Society. Paper No. 49-PET-2.

tm = minimum pipe-wall thickness in inches, excluding manufacturing tolerances,

P = maximum internal service pressure, psig

D = outside diameter, in.

S = allowable stress in material due to internal pressure, at the operating temperature, psi

C = allowance for threading and corrosion, in.

A study of Equation [1] reveals how wall thickness varies with allowable stress. By dropping the constant C and rearranging the equation, it becomes

$$\frac{D}{d} = \sqrt{\frac{S+P}{S-P}}$$

where D/d = theoretical ratio of outside diameter to inside diameter. Plotting D/d against allowable stress for the internal pressure of 10,300 psi, the graph shown in Fig. 1 is obtained. Several significant facts are evident from this curve. As the allowable stress approaches 10,300 psi, the D/d ratio approaches infinity. It is also apparent that at relatively low stress values, small increments cause large decreases in D/d ratio. The rate of decrease diminishes as the allowable stress increases.

Calculated data in Table 1 show an interesting comparison of

OUTSIDE DIA / INSIDE DIA, VS ALLOWABLE STRESS IN PSI FOR INTERNAL PRESSURE OF 10,300 P.S.I.

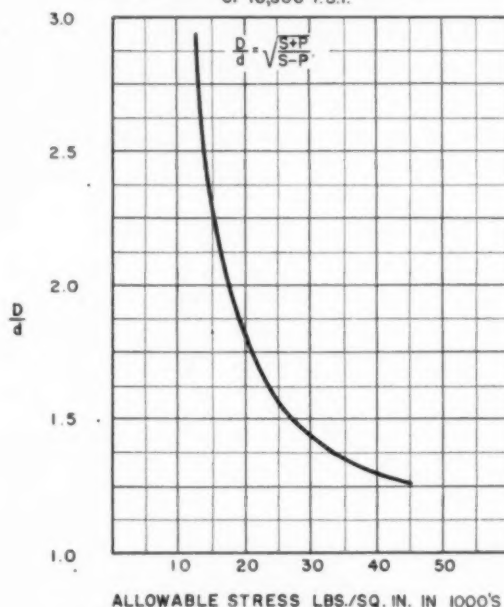


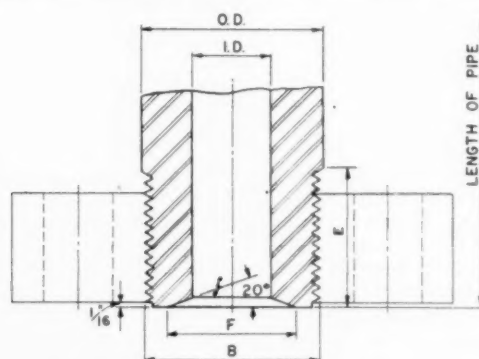
FIG. 1 GRAPH OF PIPE STRESS VERSUS OD/ID RATIO

wall thicknesses and unit weights for $2\frac{1}{2}$ -in-ID pipe, both with and without manufacturing tolerances, using ASTM-A-106, grade B carbon steel for which the ASA Code for Pressure Piping stipulates an allowable stress of 18,000 psi at 375 F, and alternately API 5L, grade C for which a stress of 22,900 psi is allowed at the same temperature.

TABLE 1 CALCULATED WALL THICKNESS FOR $2\frac{1}{2}$ -IN-ID 10,300-PSI PIPE

Material	Wall thickness excluding mfg. tolerances, in.	Weight lb per ft	Wall thickness including mfg. tolerances, in.	Weight lb per ft
ASTM A-106, grade B	1.25	57	1.875	88
API 5L, grade C	0.95	34	1.169	45

It is clear from the data that there was a distinct advantage in using API 5L for low-temperature service. Another notable fact is that manufacturing tolerances had a big influence in the final weight of the pipe. This was a factor which at the time had to be accepted as a necessary evil. Fig. 2 lists final pipe dimensions arrived at with manufacturing tolerances for seamless piping



DIMENSIONS						ALLOWABLE TOLERANCE	
NOM. SIZE	O.D.	I.D.	B	E	F	ON O.D.	ON WALL THICKNESS
$\frac{3}{8}$	$1\frac{1}{32}$	0.357	1"	$1\frac{1}{4}$	0.75"	$-\frac{1}{32}$ to $+\frac{1}{64}$	$\pm 15\%$
$\frac{1}{2}$	$1\frac{1}{16}$	0.637	$1\frac{1}{2}$	$1\frac{3}{4}$	1.125"	$-\frac{1}{32}$ to $+\frac{1}{64}$	$\pm 12\frac{1}{2}\%$
1"	$2\frac{9}{32}$	1.039	2"	$2\frac{1}{4}$	1.75"	$\pm \frac{1}{32}$	$\pm 12\frac{1}{2}\%$
$1\frac{1}{2}$	$3\frac{1}{32}$	1.461	3"	$3\frac{1}{4}$	2.35"	$\pm \frac{1}{32}$	$\pm 12\frac{1}{2}\%$
2"	$4\frac{1}{32}$	2.021	4"	$4\frac{1}{4}$	3.125"	$\pm \frac{1}{32}$	$\pm 12\frac{1}{2}\%$
$2\frac{1}{2}$	$4\frac{29}{32}$	2.443	$4\frac{3}{4}$	$5\frac{1}{4}$	3.75"	$+\frac{1}{32}$ to $-\frac{3}{64}$	$\pm 12\frac{1}{2}\%$

NOTES: THREADS AMERICAN NATIONAL 8 THREADS PER INCH, CLASS 2 FIT.
SMOOTH MACHINE SURFACE MARKED TO BE USED ON ALL H.P. PIPING SPECS.

FIG. 2 PIPE STANDARDS

which was to be finished by hot-rolling. After completion of some tubes, manufacturing difficulty necessitated a change to cold-drawing, so that there is some slight deviation from dimensions and tolerances listed.

Fig. 3 shows on the left a Croloy 9M tube obtained by hot-finishing. Note the squareness of the inside circumference. On the right is a well-shaped cold-drawn tube.

Following German precedent, materials for piping were divided into four different classes based upon service, as follows:

- Low temperature, up to 375 F.
- Medium temperature, 376 F to 850 F.
- High temperature, 851 F to 1000 F.
- Miscellaneous applications in which $\frac{3}{16}$ -in-ID \times $\frac{3}{16}$ -in-OD type 304 stainless steel or $\frac{1}{16}$ -in-ID \times $\frac{1}{4}$ -in-OD, chrome-molybdenum steel tubing was used.

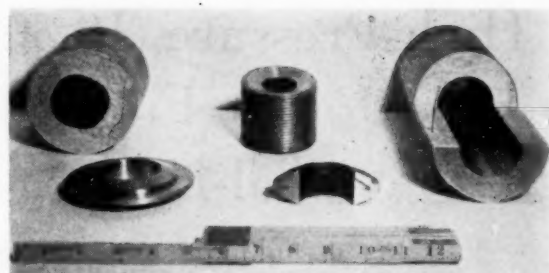


FIG. 3 PIPING AND GASKET SECTIONS

About the latter, used for instrument pressure leads, flushing, oil injection, nitrogen injection, hydrogen injection, and sampling lines, little need be said, since this type of tubing is regularly manufactured and can be obtained easily from suppliers.

The materials with their properties for the first three classes are listed in Table 2.

TABLE 2 HIGH-PRESSURE (10,300-PSI) PIPING MATERIALS

Maximum service temperature, deg F	Material	Yield point, psi	Ult. tens. strength, psi	Bhn
Low temperature: 0 to 375 (early design)	B & W MT-8040 equal to API-5L, grade C	45000 min	75000 min	159 min
0 to 375 (later design)	SAE 4130	45000 min	75000 min	180
Medium temperature: 376 to 850	Croloy 9M (Ref. B & W Tech. Bul. 6-D p. 49) HT-31,387 normalized and drawn at 1200 F	82000 min	103100 min	223
High temperature 851 to 1000	AISI Type 316	30000	75000 max attainable	

NOTE: Creep stress for 1 per cent elongation in 10,000 hr is about 22,800 psi.

The change in the low-temperature class to SAE 4130, a low-chromium-molybdenum steel, was made during construction of the plant, primarily for improved weldability.

The dimensions given in Fig. 2 are the same for all materials, for the sake of standardization of tubing, fittings, etc. The dimensions were based on the properties of API 5L, grade C, carbon-steel seamless tubing for which, as has been noted, the allowable stress is 22,900 psi at 375 F. It would appear that a higher design stress could have been used for Croloy 9M; however, at the time it was selected, not enough was known about its behavior at temperatures near 850 F to warrant taking full advantage of its strength. In addition, such procedure would have minimized standardization. It will be noted that the dimensions chosen bring the design stress up close to the creep stress for type 316 Babcock & Wilcox 16-13-3. It was considered more desirable to design on this basis than to exceed the OD/ID ratio of 2, which was about the maximum according to German experience. Thicker walls could be expected to give trouble due to greater likelihood of internal faults and to increased temperature stresses. Temperature changes especially would have a particularly detrimental effect on stainless steel with its high coefficient of expansion and low thermal conductivity. For this reason Croloy 9M, which has better thermal-shock properties, was used in emergency let-down lines where temperature could be momentarily over 1000 F and vary widely.

FLANGED JOINTS

In a good high-pressure flanged connection, the following features are desirable:

1 Tightness must be maintained in spite of pressure and temperature fluctuations and of usual piping stresses imposed by torsion, bending, and vibration.

2 Functioning should not be affected by minor pipe misalignments in construction or by slight surface imperfections either on gaskets or faces.

3 Since it is desirable to keep the weight of the joint low, tightness should be achieved with low bolt loads. The following contribute to this end:

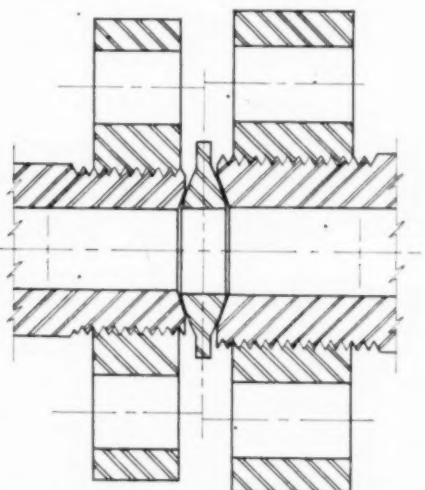
(a) A gasket pressure area as near the inside circumference of the pipe as possible.

(b) A design which provides high unit pressures on the gasket seat with relatively low bolt loads.

(c) At least a partial self-sealing at operating pressure.

4 A sufficient number of bolts should be provided so that failure of one during tightening will not cause the joint to fail completely.

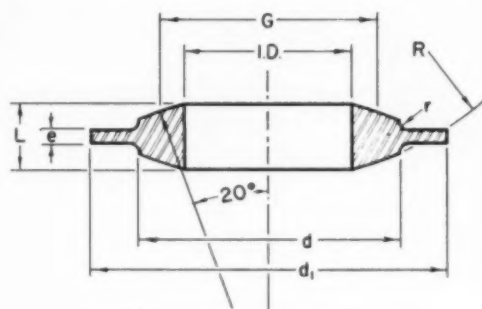
With these considerations in mind, a study was made of several types of flanged joints. Fortunately, data on the lens ring joint used in Germany were available for comparison with conventional types. This was finally chosen as the one having most of the desirable characteristics. Fig. 4 illustrates an assembled connection of this type for low-temperature lines. For comparison, a Bureau of Mines pipe, flange, and lens ring was shown mated with the closest-size German pipe and flange.



I. G. FARBEN END PIPE & FLANGE
BUREAU OF MINES SPECIFICATIONS END PIPE, FLANGE, & LENS GASKET.

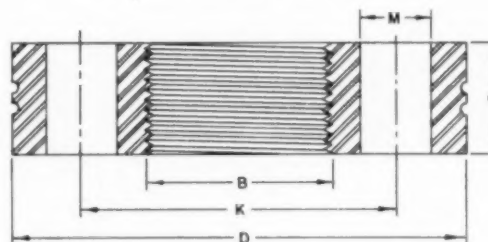
FIG. 4 FLANGED-JOINT ASSEMBLY.

Fig. 5 shows the shape and dimensions of low-temperature service lens-ring gaskets, and Fig. 6 shows the dimensions of flanges used. It should be noted that a spherical gasket surface is in contact with conical surfaces on the pipe ends. It is characteristic of a metal-to-metal ball-and-cone joint that, with small bolt load, the contact area is extremely small, though very high gasket unit seating pressures are achieved. The gasket is softer than the pipe and its action under load is both plastic and elastic. Plastic deformation takes place over an almost imperceptible area and seals off against minor imperfections in ma-



NOM SIZE	INSIDE DIA	d	d ₁	L	r	e	SPHER RAD	CONTACT CIRCLE
3/8"	357"	13/16"	—	11/32"	—	—	13/16"	556"
5/8"	637"	1-5/16"	—	3/8"	—	—	1-11/32"	921"
1"	1039"	175"	2-1/2"	17/32"	1/32"	5/32"	2-1/8"	1455"
1-1/2"	1461"	235"	3-1/4"	5/8"	1/32"	9/64"	2-15/16"	2009"
2"	2021"	3125"	4-1/4"	13/16"	1/16"	3/16"	4"	2735"
2-1/2"	2443"	375"	5"	31/32"	1/16"	1/4"	4-13/16"	3284"
3-1/2"	3500"	7-3/8"	10"	2"	1/16"	1-1/4"	9-5/8"	6531"

FIG. 5 SOLID-LENS GASKET STANDARDS



MACHINE ONE 1/16" RAD. IDENTIFICATION GROOVE ON MEDIUM TEMPERATURE FLANGES
MACHINE TWO 1/16" RAD. IDENTIFICATION GROOVES ON HIGH TEMPERATURE FLANGES

FLANGE DIMENSIONS				DRILLING		
NOM SIZE	B	C	D	K	M	NO HOLES
3/8"	1"	7/8"	3 15/16"	2 7/16"	11/16"	3
5/8"	1 1/2"	1"	4 7/16"	2 15/16"	11/16"	3
1"	2 1/4"	1 3/8"	5 9/16"	3 7/8"	7/8"	4
1 1/2"	3"	1 7/8"	6 3/4"	4 13/16"	1"	6
2"	4"	2 1/2"	8 5/8"	6 1/4"	1 1/4"	6
2 1/2"	4 3/4"	3 1/8"	10 3/16"	7 7/16"	1 1/2"	6

NOTE - TO BE USED ON ALL H.P. PIPING SPECS.

GENERAL NOTES

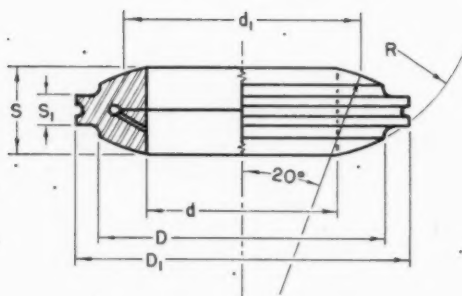
THREADS AMERICAN NATIONAL 8 THDS. PER INCH
CLASS 2 FIT HOLES TO BE EQUALLY SPACED AND
DRILLED ROUGH MACHINE ALL OVER

FIG. 6 FLANGE STANDARDS

chined surfaces. The greatest part of the deformation is elastic and occurs both radially and axially. Both the initial elastic deformation set up before pressure application and the internal pressure itself provide the self-sealing effect under operating conditions.

The ball-and-cone shapes allow the lens to find a seating position in spite of minor pipe misalignments. Though surface finish was specified to be very fine, it has been found that minor scratches and toolmarks do not cause leakage.

In spite of careful piping design, expansion stresses in high-temperature lines tend often to place added bending and torsion



NOM. SIZE	I.D. d	O.D. D1	CONTACT ϕ d1	D	WIDTH S	S1	SPHER. RAD. R	DIA. OF 20° C. SK. ON PIPE
1"	1.039"	2.04"	1.27"	1.69"	19/32	5/32	1.85"	1.75"
1-1/2	1.461"	2.75"	1.812"	2.35"	11/16"	3/16"	2.65"	2.35"
2"	2.021"	3-1/2	2.43"	3"	27/32	5/16"	3.54"	3.125"
2-1/2	2.443"	4-1/4	3"	3-5/8	1-1/8"	3/8"	4-7/16	3.75"
3-1/2	3.443"	5-1/2	4-1/4	4-1/2	2"	5/8"	5.55"	4.75"

FIG. 7 BELLWAS-GASKET STANDARDS

in the flanged connections. For this reason a bellows lens as illustrated in Fig. 7, is used in medium and high-temperature lines. This type of lens ring has still greater self-sealing effect because fluid under pressure enters the annular space in the lens and acts over a greater area. Should the bending moments tend to open mating flanges, the bellows lens tends to open and to follow the seating surfaces on the pipe.

Flanging materials and their physical properties are given in Table 3.

TABLE 3 MATERIALS—HIGH-PRESSURE (10,300-PSI) FLANGED JOINTS

	Material	Yield point, psi	Ult. tens. strength, psi	Bhn
LOW TEMPERATURE 0-375 F				
Flanges	Carbon steel ASTM-A-103, grade II	36000	70000	136 min
Lens-ring gaskets	Carbon steel ASTM-A-103, grade I	30000	60000	116 min 140 max
Bolts	ASTM-A-193-44, grade B-7 (SAE 4140) min draw temp. 1100 F	105000	125000	
Nuts	ASTM-A-194-40, class 2-h heavy series.			
MEDIUM TEMPERATURE 376-850 F				
Flanges (on tubing)	Carbon-moly ASTM-A-182-44 grade F-1	45000	70000	150 min
Flanges (on fittings and valves)	Alloy steel AISI type 304 ASTM-A-182, grade F-8	30000	75000	200 max
Lens-ring gaskets	AISI 405 chrome steel annealed	40900	64160	120 min 130 max
Bolts	Same as for low-temperature service			
Nuts	Same as for low-temperature service			
HIGH-TEMPERATURE 851-1000 F				
Flanges	Alloy steel AISI type 304 ASTM-A-182-44 type F-8	30000	75000	200 max
Lens-ring gaskets	AISI type 405 chrome steel annealed	40900	64160	120 min 130 max
Bolts	Same as for low-temperature service			
Nuts	Same as for low-temperature service			

The materials from which lens rings are made have in each application a Brinell number about 30-40 points below the piping materials. This follows German practice and is for the purpose of restricting plastic deformation to the lens rings, which are the

elements most easily replaced. Flanges are made of materials different from tubing to avoid galling of threads.

Some idea of the weight reduction achieved by use of the 10,300-psi lens-type joint can be obtained by comparing the weights of a flange for the 2 1/2-in. nominal-size pipe with the weight of an ASA-2500-lb screwed flange for the same pipe size. Each weighs about 50 lb.

Results of a test⁴ conducted in Germany on a 325-atm (4780-psi) working-pressure joint of this type for a pipe with an inside diameter of 4.73 in. are available. It was found that an initial total bolt load of 75,000 lb was increased to 99,000 lb by application of the design internal pressure corresponding to a total fluid force of 94,500 lb. The joint remained tight, and internal pressure had to be increased to 780 atm before signs of leakage appeared. Obviously, self-sealing took place. It is interesting to note that, at design pressure, the total bolt load exceeded the total fluid load by less than 10 per cent. Conclusions of the test report indicated that, for the joint under test, a bolt load between 1.8 and 2.5 times the total fluid load should be used in practice. The lower limit was set to avoid leakage when normal piping forces are applied, and the upper limit to avoid overstrain of bolts in service.

Lens-ring joints are used throughout except for instrument lines. These have conventional cinch joints.

FITTINGS

Fittings are limited to tees, 90-deg ells, and reducers, and all are forged and bored. Ells are made by bending straight forged and bored pieces. Table 4 gives materials and their physical properties.

TABLE 4 MATERIAL FOR FITTINGS

Service	Material	Ult. tensile strength, psi	Yield point, psi	Bhn
Low temperature 0 to 375 F	SAE 1030	75000	45000	163 min
Medium temperature 376 to 850 F	Type 304 18-8 stainless steel ASTM-A-182 grade F-8	75000	30000	max attainable
High temperature 851 to 1000 F	Type 316 stainless steel ASTM-A-182-44	75000	30000	max attainable

Details and dimensions of all flanged-type tees are given in Fig. 8. Fig. 9 illustrates welding-type ells. Fig. 10 shows a typical 2 1/2-in. high-pressure line with flanges and fittings.

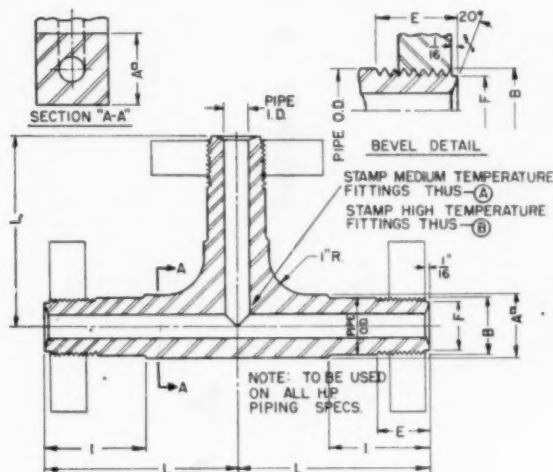
VALVES

In general, shutoff, throttling, check, and relief valves are used. All bodies are forged steel. Table 5 shows materials and physical properties.

TABLE 5 MATERIALS FOR HIGH-PRESSURE (10,300-PSI) VALVE BODIES

Service	Material	Ult. tensile strength, psi	Yield point, psi	Bhn
Low temperature 0 to 375 F	Carbon steel SAE-1030	75000	45000	163 min
Medium temperature 376 to 850 F and high temperature 851 to 1000 F	Alloy steel AISI type 316 ASTM-A-182-44 type F-8m	75000	30000	190 max

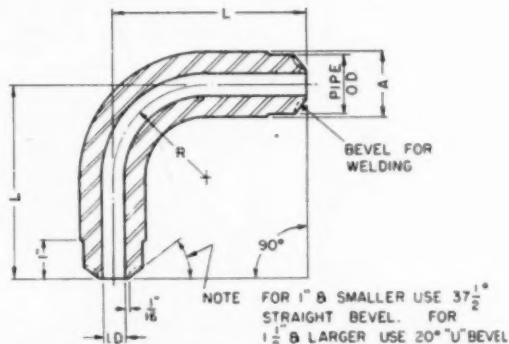
⁴ Report on the "Deformation of 120-Mm Sealing Rings of N5 Material Due to Internal Pressure and With Very Tightly Drawn Bolts," dated Ludwigshafen, July 12, 1936. Frames 6722-6728, inclusive of TOM Reel No. 181.



PIPE			TEE					
NOM SIZE	ID	OD	A	B	E	F	L	I
3/8	0.357	1 1/32	4 5/8	2 1/2	1 1/8	1 1/4	0.75	1 1/2
1/2	0.637	1 1/2	5	2 5/8	1 5/8	1 1/2	1.125	1 3/4
3/4	1.039	2 1/32	6 3/8	3 3/8	2 1/8	1 3/4	1.75	2
1	1.461	3 1/32	7 3/4	4 1/8	3 1/8	2 1/4	2.35	2 1/2
1 1/2	2.021	4 1/32	9 3/4	5 1/4	4 1/4	3	2.95	3 1/4
2	2.443	4 25/32	11 3/4	6 1/8	5	4 3/4	3.75	4

NOTES: THREADS AMERICAN NATIONAL 8 THDS PER INCH CLASS 2 FIT
SMOOTH MACHINE SURFACE MARKED
A⁰—THIS DIMENSION DESIGNATES SQUARE BODY

FIG. 8 FLANGED TEE



PIPE			ELBOW			
NOM SIZE	ID	OD	A	L	R	
3/8	0.357	1 1/32	1 1/8	4 5/8	2 1/4	
1/2	0.637	1 1/2	1 5/8	5	2 3/8	
3/4	1.039	2 1/32	2 1/8	6 3/8	3 1/4	
1	1.461	3 1/32	3 3/8	7 3/4	3 5/8	
1 1/2	2.021	4 1/32	4 1/4	9 3/4	4 3/4	
2	2.443	4 25/32	5	11 3/4	5 5/8	

NOTE TO BE USED ON H P PIPING SPEC
"AA" & "DD" ONLY

FIG. 9 WELDING ELL OF 90 DEG

All valves are angle type, except for a few vertical-lift check valves, which are straight-through type. The smaller sizes of shutoff and throttling valves are direct handwheel-operated and have screwed packing-gland nuts, while larger sizes, 1 1/2 in. and above, have bolted flanged packing glands, and are spur-gear- and handwheel-operated. Valves are so arranged that the pressure will be above the disk when closed.

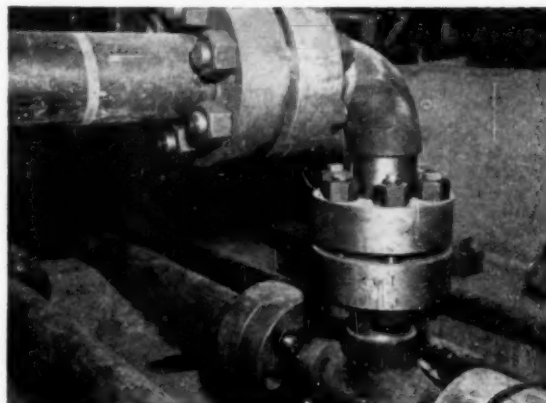


FIG. 10 FLANGED ELL AND TEE ASSEMBLY

High-pressure drops during opening and closing, even for mild service, are likely to cause severe erosion of disk and seat materials, unless proper precautions are taken in design. For this reason seat and disk are stellite for shutoff valves and kennametal for throttling valves. Because of the brittleness of kennametal, throttling valves cannot be used for shutoff. Provision must be made to avoid tight seating. This has been done either by providing a spring between spindle and removable disk, or by use of stop nuts on the valve spindle to limit the travel. In addition, throttling and shutoff valves must be paired and valve operations arranged so that all throttling is placed on throttling valves, while only shutoff valves are depended upon for tight shutoff.

Seat rings or bonnet closures for all valves are of the self-sealing type. This keeps down the weight of the valve and facilitates disassembly for replacement of valve internals. Valve packing, where used, is seven-ring type-220 durametalllic with nitrallloy base ring and gland.

Fig. 11 shows a section of a typical shutoff valve. In Fig. 12 a gear-operated 2-in. shutoff valve is compared with a 2-in. 150-psi screwed valve.

Throttling valves fall into two classes, depending upon whether service is severe or mild. Severe throttling valves are used where pressure drop would be from 10,300 psi down to about atmospheric pressure and the fluid is a mixture of liquids, gases, and solids consisting of unreacted coal, ash, and catalyst. Fig. 13 illustrates the valve used for such service. Velocities in the nozzle reach 700 to 800 fps. German experience with a similar valve indicated that a maximum service life with the best seat and disk materials available would be about 1 month. Design, therefore, had to be carried out with the object of attaining longest possible service life and of providing for the quickest and safest possible replacement of either valves or their worn elements. To minimize abrasion of the disk the valve was so designed that, with normal flow conditions, it would be fully open and all of the throttling would occur in the nozzle itself. Further, the nozzle was made with a divergent exit of 7 deg in order to prevent cavitation.

The stream leaving the nozzle enters an expansion chamber and impinges against a "target plate" made integral with the lens ring of the flanged joint on the outlet side of the valve. Flow through the plate is by means of a hole drilled eccentrically to the face which has a concave surface of stellite. The purpose of the expansion chamber and target plate is to provide for the dissipation of the energy of depressuring before entry of the fluid into the piping.

To permit rapid replacement of valve seat and disk, the con-

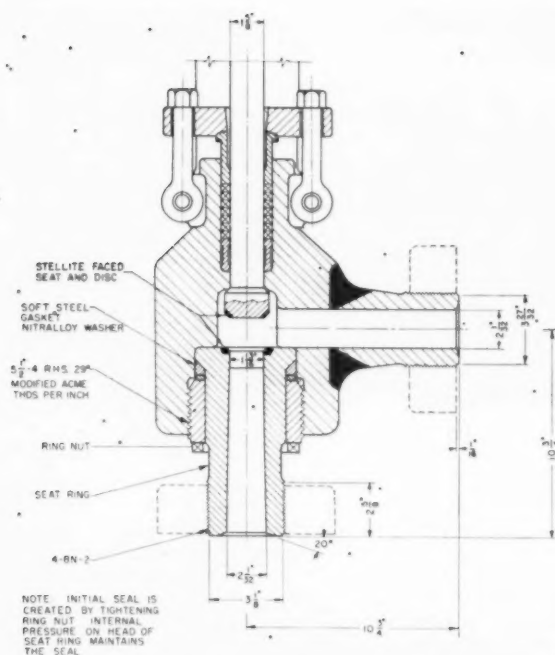


FIG. 11 SHUTOFF-VALVE ASSEMBLY

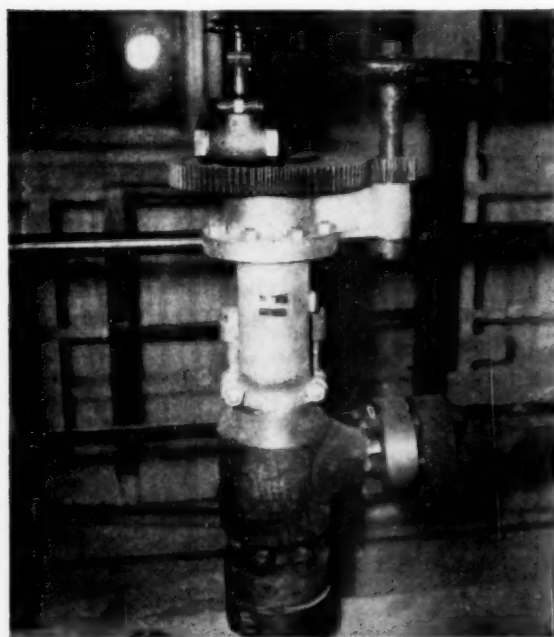


FIG. 12 2-IN. SHUTOFF-VALVE COMPARED WITH 2-IN. 150-PSI VALVE

struction is such that disassembly and removal of internals can be accomplished from the top without removal of the valve from the line. In the most severe service, three valves are used in parallel, two being controlled automatically and one hand-operated. One of the automatic valves and the hand-operated valve are spares.

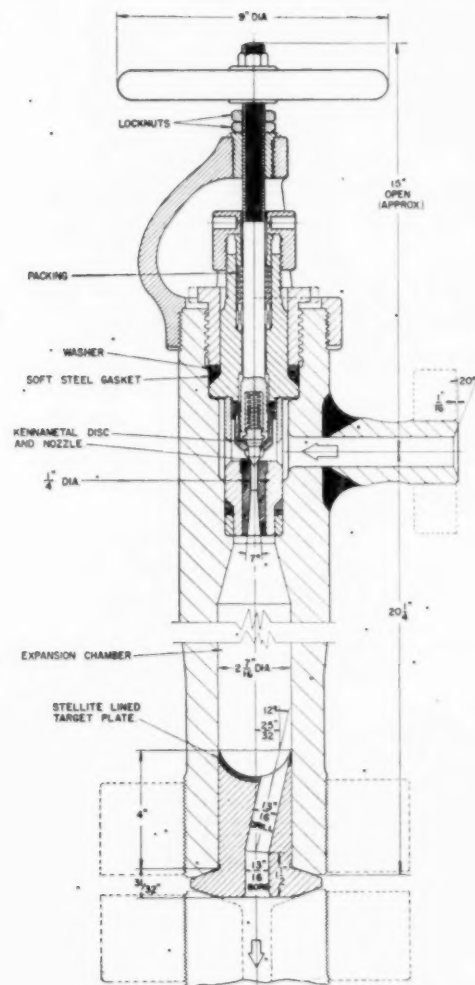


FIG. 13 SEVERE THROTTLING VALVE

Each of these valves is so arranged that three stop valves are on the upstream side and one on the downstream side, in order that it may be tightly isolated from the system for either removal or repair.

The mild throttling valve is much simpler in construction. Removable seat and disk cannot be taken out without removing the valve from the line, however. Fig. 14 shows the construction of one of the smaller sizes.

Check valves used are both angle and straight-through types. The angle type illustrated in Fig. 15 is used for gases and liquids free of solids. Both seat and disk are stellite-faced, and the seat is not removable. The disk is integral with the stem, which is spring-loaded sufficiently to keep the disk seated under conditions of no pressure differential. The spring space behind the stem is connected with the pressure space by a drilled hole for pressure equalization.

The straight-through vertical-lift check valve shown in Fig. 16 is used for slurries or liquids containing solids. It functions like a ball check, but the hollow disk is shaped like a small streamlined aerial bomb. Vertical movement is guided by three stellite-faced vanes 120 deg apart. Seat, disk, and vane guides are stellite-

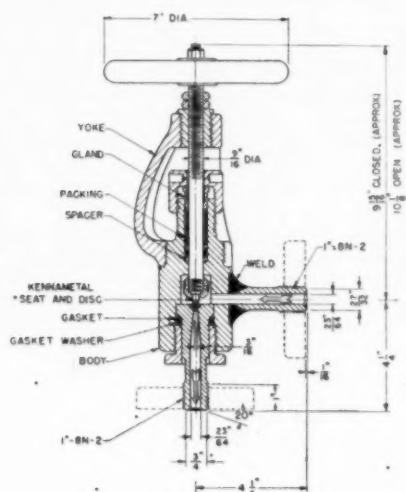


FIG. 14 MILD THROTTLING ANGLE VALVE

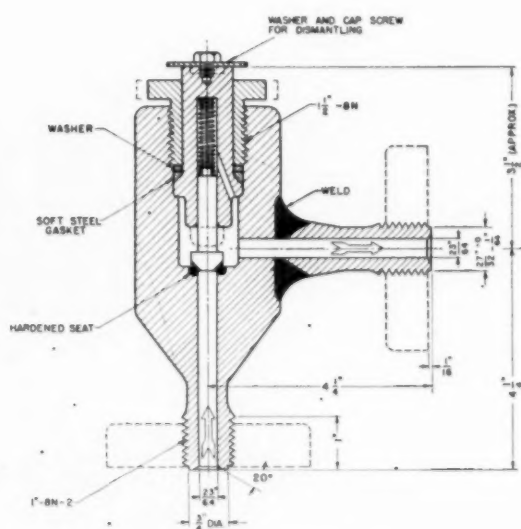


FIG. 15 ANGLE CHECK VALVE

faced also, and the seat is removable. This valve must always be installed with the disk and seat downward, and flow must always be upward.

Relief valves are spring-loaded, as shown in Fig. 17. Disk and seat are stellite and the seat is removable. The disk is integral with the stem, which extends through the coiled spring and is guided near the upper and lower ends.

Control valves are diaphragm type and have the same general features as hand operated valves.

Conventional 15,000-psi straight-through needle stop and angle check valves, and 25,000-psi microreregulating valves are used in high-pressure instrument lines.

FUTURE COMMERCIAL SCALE PLANT DESIGN

As it appears now, only minor changes would be made in design of fittings, flanged joints, and most valves for commercial scale

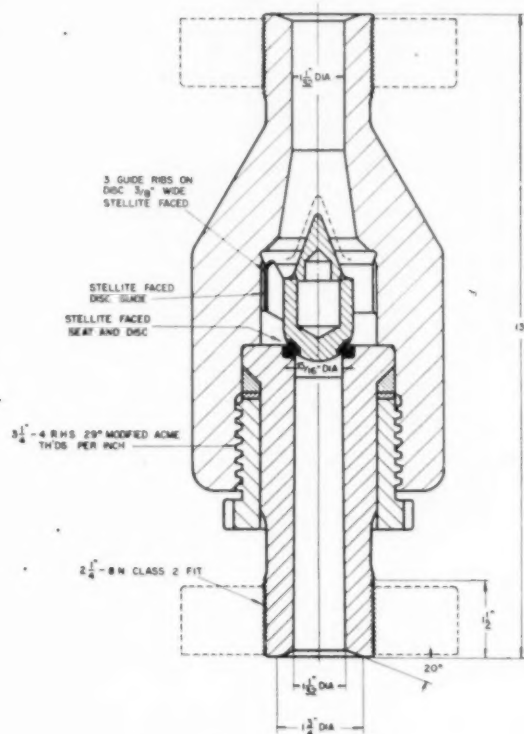


FIG. 16 VERTICAL CHECK VALVE

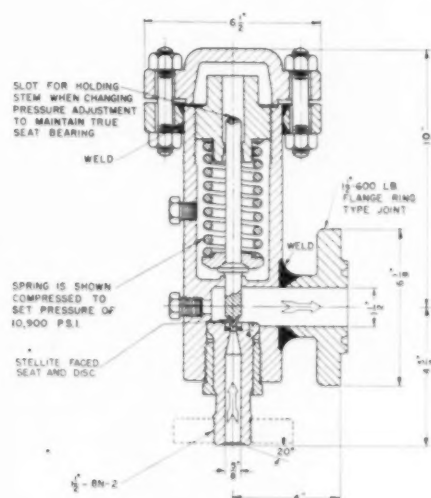


FIG. 17 RELIEF VALVE

plants. Possibly the severe throttling valve would be replaced by a pressure letdown engine.

The trend in piping, which is expected to reach a maximum size of 10 in. ID will probably be toward use of higher-strength materials in the low and medium temperature ranges, permitting higher design stresses. Possibly ends of pipe would be upset for threading so that the main body will not have excessively thick

walls. The thinner walls would allow manufacture of most of the required sizes by piercing and cold-drawing rather than by forging and boring. From about 6 in. ID to the maximum of 10 in. ID, manufacture undoubtedly would be by forging and boring.

It is expected that design stresses will be of the order of magnitude of 30,000 psi. A 4-in-ID pipe would then have an OD/ID ratio of about 1.53 and weigh about 60 lb per ft. Using the old design, a 4-in-ID pipe would have an OD/ID ratio of 1.88 and weigh about 108 lb per ft.

Further, it may be possible to substitute Croloy 7 or 5 for the Croloy 9M now in use. In addition, it may be desirable to break up the present medium-temperature service range into several

ranges, and to use a different material for each. Studies would have to determine whether such changes would be feasible metallurgically and if they would reduce costs appreciably.

At this time it is doubtful that a material for high-temperature service piping with a creep strength higher than AISI type 316 can be found. Heavier piping for this service will not affect the overall situation appreciably, since it represents only a small percentage of the total high-pressure piping in a coal-hydrogenation plant.

There are several super alloys in the development stage, but to date there is no evidence that any of them can be used successfully for high-temperature service tubing.

Instrumentation for Coal-Hydrogenation Service

By G. L. BRUNO,¹ F. W. GEYER,² AND J. A. MARKOVITS³

The process requirements of measurement and control are described as applied to high-pressure phases of the coal-hydrogenation process. Special emphasis is given to the details of development and application of special instruments.

INTRODUCTION

THE coal-hydrogenation demonstration plant includes nearly all types of instruments found in normal refinery practice. The instrumentation is not typical of that required in a commercial plant, as many measuring devices were installed for experimental purposes to gather operating data and to accommodate changes in operation with various types of coal. The text of this paper covers only high-pressure instrumentation with emphasis given to unusual items, new developments, and adaptations; it is discussed in the order of temperature, pressure, flow, differential pressure, level, and miscellaneous instruments.

Measurement and control in high-pressure services is not new. However, when applied to coal hydrogenation, other factors complicate the problem. In addition to pressures of 700 atm, there are temperatures of 1100 F, high-viscosity erosive liquids containing up to 50 per cent solids, hydrogen, and mixed hydrocarbon vapors, as well as severe pressure drops of as much as 675 atm, and freezing weather.

In German plants, automatic control was not an economic necessity; therefore instrumentation was not highly developed for this process. It was recognized that solution of the many complex instrumentation problems would offer great possibilities for improvement over the German plants and help adapt coal hydrogenation to the economics of the United States.

The necessity for protection against the hazards of the process established the basis of design for the control center. The control house is a reinforced-concrete building, 34 ft X 90 ft, with a solid 12-in. wall on the north or stall side as further protection. Directly outside the wall are located principal control valves and by-pass valves, the handles of which extend through the wall and panel board and are located directly under their respective instruments for manual operation. The instrument board, containing 121 instruments, consists of 30 control panels and 2 annunciator panels, with 18 panels on the north wall and 7 on each wing. The instruments are either pneumatic or electric receivers, eliminating explosive gases or high-pressure liquids from the control room. High-pressure controllers are on the north wall, with miscellaneous recorders and the annunciator system on the wings. High-pressure controls operate either automatically, remote pneumatically, or manually from the center.

¹ Project Engineer, Bechtel Corporation, San Francisco, Calif.

² Senior Engineer, Bechtel Corporation.

³ Assistant Chief, Coal-to-Oil Demonstration Branch, Office of Synthetic Liquid Fuels, Bureau of Mines, Louisiana, Mo.

Contributed by the Petroleum Division and presented at the Petroleum Mechanical Engineering Conference, Oklahoma City, Okla., October 2-5, 1949, of THE AMERICAN SOCIETY OF MECHANICAL ENGINEERS.

NOTE: Statements and opinions advanced in papers are to be understood as individual expressions of their authors and not those of the Society. Paper No. 49-PET-4.

TEMPERATURE INSTRUMENTS

The temperatures encountered in the process design range from atmospheric to 1800 F and makes the use of both iron-constantan and chromel-alumel thermocouples desirable. Twenty-gage thermal elements were used throughout the high-pressure system. This size was selected as the optimum possible, when considering thermal response in relation to thermowell ID and wall thickness, life of element, and resistance of the external instrument circuit. The thermowells used consisted of three types, skin, immersion, and vessel.

Skin-type thermocouple assemblies, as shown in Fig. 1, were required in furnaces, vessel shells, and lines containing abrasive solids. The assemblies were insulated to reduce radiation losses.

The immersion-type wells were used in all clean liquids and gas streams. The relationship of pressure to wall thickness presented the principal difficulties in the design of this type well. The design selected, illustrated in Fig. 2, afforded a minimum wall thickness at the junction of the element and incorporated the lens ring or sealing gasket which is the standard joint seal for high-pressure service.

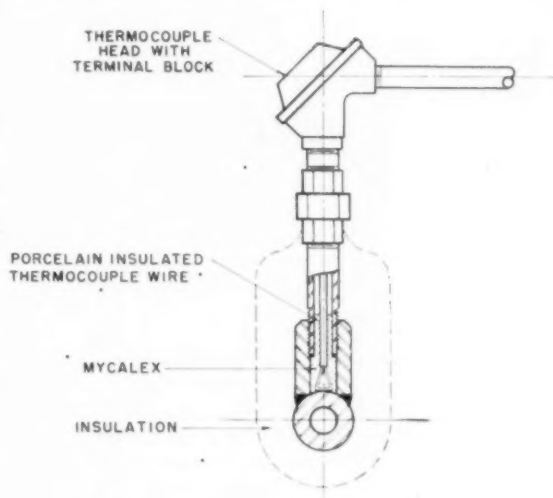


FIG. 1 SKIN-TYPE THERMOCOUPLE ASSEMBLIES

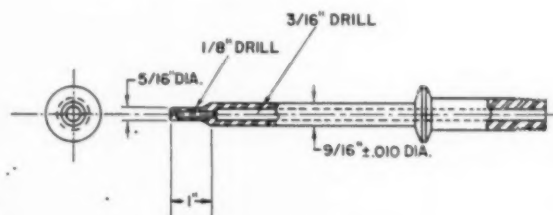


FIG. 2 IMMERSION-TYPE THERMOWELLS

Measurement of temperature in vessels such as converters and hot and cold catchpots was complicated by the requirement that all thermocouples enter either the top or bottom head of the vessel. The well design is identical for all vessels; however, the description of the method used is confined to the vapor-phase converter, which contained the maximum number of couples and presented the added difficulty of fixed beds of catalyst.

Due to the exothermic reaction of the process, it is necessary to introduce cooling hydrogen into the basket of the vapor-phase converter at each of the five removable grids. Hydrogen is mixed with the hot gases in the grid and flows downward through the next lower catalyst bed. A temperature point in the middle of each bed operates a diaphragm valve which controls the quantity of cooling hydrogen to the bed, maintaining the control temperature.

The pyrometer tube, as illustrated in Fig. 3, is encased in a shield which enables the tube to be removed for repairs without the catalyst falling through the grids. The shield, however, introduces a serious time lag owing to the low velocity of the gases in the converter and the devious path of heat transfer.

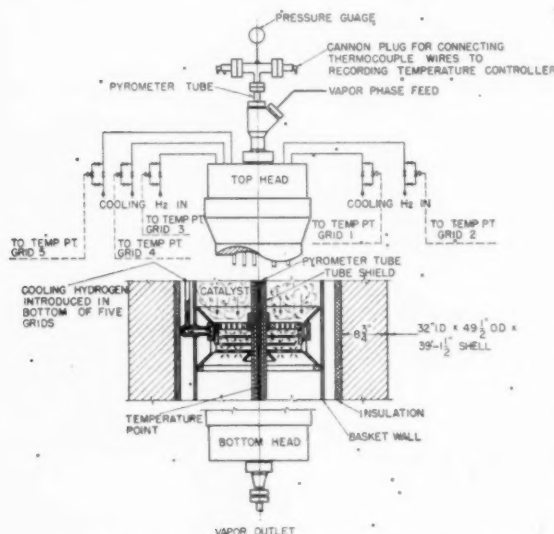


FIG. 3 VAPOR-PHASE CONVERTER AND PYROMETER TUBE

Due to hydrogen penetration of the pyrometer tube, it was necessary to seal the outlet where the 12 pairs of thermocouple wires leave the vessel. This was done by using a drilled soapstone bushing tapered at both ends. By tightening a follower nut the soapstone crushes around each wire and tightly seals the pressure in the pyrometer tube. To indicate hydrogen penetration by increased pressure, a special fitting was installed in the pyrometer tube above the vessel with a pressure gage and vent valve.

Temperature measurement and control were obtained by using standard electronic strip-chart multipoint recorders, circular-chart recorder controllers, and multipoint, self-balancing, precision indicators with switch cabinets of 48 and 96 points.

Temperature controllers were designed with manual by-pass panels, and it was felt necessary to incorporate full throttling and automatic-reset-type control. Multipoint recorders and controllers were equipped with high-temperature alarms which actuate the annunciator system. All ranges used on these instruments were standard, except one special circular-chart controller for controlling the vapor-phase feed temperature to the converters

by introducing cooling hydrogen to the stream. This instrument is unusual, in that its range is 850 to 900 F—a span and suppression not normally found in potentiometer-type instruments. This was necessary owing to the narrow span in which maximum hydrogenation efficiency is obtained.

PRESSURE INSTRUMENTS

Static pressure measurement was made with conventional alloy-steel Bourdon tubes in ranges to 20,000 psi. These instruments include indicating pressure gages, nonindicating pressure controllers, and indicating pneumatic transmitters.

The indicating gages are 8 in. diam, with safety features such as shatterproof glass and rupture-disk backs. Connections were made by using 1/2-in. straight pipe thread with annealed-copper gaskets as normally found in hydraulic work. Pressure elements installed in liquid services were equipped with a special high-pressure-design pulsation damper as normally required on services from reciprocating pumps. The measurement of static pressures in streams containing abrasive solids required special consideration, and for this purpose a diaphragm or "homogenizer" gage was used with flushing-oil connections to prevent plugging. This gage consists of a liquid-filled Bourdon tube actuated by the flexing of a flat-bulb-type diaphragm.

Nonindicating pressure controllers, ranging to 15,000 psi, were of conventional design, with special differential-cone-type high-pressure connections. As a protection against rupture of Bourdon tubes, excess-flow check valves were installed ahead of each tube. Transmission to recorders and recorder controllers was performed pneumatically by the conventional bellows system. Controllers were of the full-throttling type.

FLOW INSTRUMENTS

Flow measurement was made in streams consisting of hydrogen, vapors, clean liquids, and liquids containing abrasive solids by using a sharp-edged orifice in all cases except cooling hydrogen streams, where the small flow made orifice-plate measurement impractical. Orifice-plate design coefficients had to be established by extrapolation for the 3/4-in. to 2-in-ID special tubing. Additional problems were presented owing to pulsation from reciprocating pumps and compressors and the necessity of using nonstandard pipe taps of 8 diameters upstream and 8 diameters downstream to meet construction requirements of the lens ring joint, the lens gasket of which is incorporated as part of the orifice plate. It is anticipated that experimental data will be collected during operations to modify the preliminary design coefficients. The materials handled also required the use of accessories, such as seal pots, flushing oil and hydrogen purges, and steam tracing of meter legs.

For streams of small volume in the range of 100 cfh at operating conditions, a second type of primary element was used. The design consists of a helical rotor suspended on instrument pivots against jeweled bearings and contained within a high-pressure housing. A small alnico magnet is mounted on the rotor and as it turns, generates an alternating-current voltage in a pair of coils placed in the assembly. These coils are in series and connect to weatherproof terminals. The output from the transmitter is of a few millivolts magnitude, with frequency and amplitude proportional to the rate of turning of the rotor. This alternating-current voltage is fed to the receiving unit. A proposed alternate method for this service was an electric transmission-type rotameter; however, it was felt that a development such as the helical rotor, if proved practical, would be more suitable for the services and would be considerably cheaper.

The receiver for the rotor-type transmitter consists of 0-100 d-c panel-mounted microammeter. As the output of the transmitter is alternating current of a small magnitude, it must be rectified

and measured on a direct-current instrument. This rectification is done by a copper-oxide rectifier circuit and owing to the non-linear characteristics of the rectifier, it is necessary to bias the rectifier with a direct-current voltage to gain linear characteristics. Due to the biased voltage on the rectifier, it is further necessary to provide an opposing bias current on the indicating meter. This biasing current is supplied from a stabilized 6-volt d-c supply common to the 12 rotor installations in the plant.

Orifice-plate differential measurements were made by two types of transmitters. One consisted of a special 200-in. high-pressure mercury-filled manometer with an inductance-type transmitter. The transmitter consists of a soft-iron armature attached to the float and moves up and down in a nonmagnetic tube surrounded by a center-tapped inductance coil. Due to changing differential pressures, the position of the armature varies with respect to the center tap of the inductance coil. This movement changes the relative inductance of the two halves, the over-all inductance remaining constant.

The receivers for the mercury-manometer-type transmitters are a special adaptation of the electronic self-balancing recorder. They contain a transformer supplying 5.0 or 6.3 volt a-c for power to the system, and a self-balancing slide-wire which repositions itself to balance the voltage changes produced by the inductance-type transmitters. In other words, an alternating-current resistance-inductance Wheatstone bridge is formed between the transmitter and receiver. The simplified wiring diagram is shown in Fig. 8. It was necessary to use the more sensitive-type receiver rather than the standard electric-inductance flow receiver, as the changes in inductance produced by the transmitter-armature movement are much smaller than in the standard

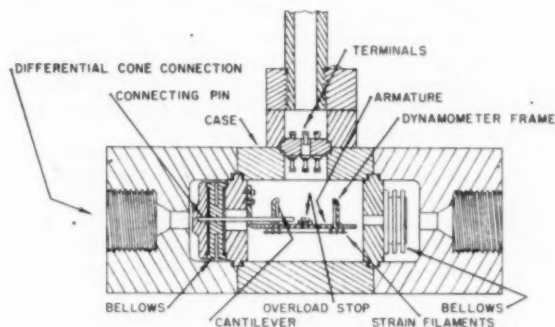


FIG. 4 SECTION OF DIFFERENTIAL STRAIN GAGE

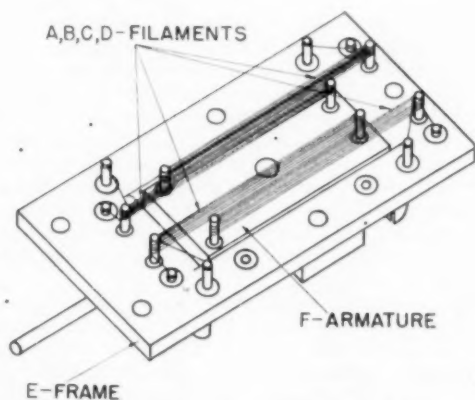


FIG. 5 DISPLACEMENT TRANSDUCER ELEMENT

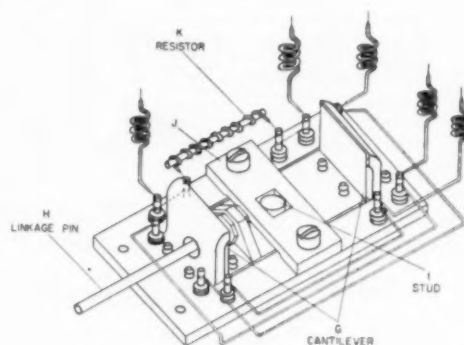


FIG. 6 REVERSE SIDE OF TRANSDUCER

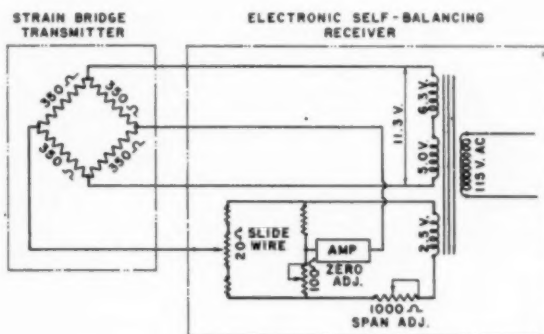


FIG. 7 SIMPLIFIED WIRING DIAGRAM OF STRAIN TRANSMITTER AND RECEIVER

transmitter. This reduction was a result of the heavy wall thickness of the nonmagnetic tube in the transmitter to withstand the higher operating pressures. These receivers are in all cases recording, full-throttling, automatic-reset, pneumatic controllers.

The second type consists of a high-pressure housing containing a measuring diaphragm and a sealing diaphragm between which is located an unbonded strain bridge or displacement transducer element immersed in a silicon liquid and connected to the measuring diaphragm, as shown in Fig. 4.

The displacement transducer element is shown in Fig. 5. It consists of a frame *E* supporting a movable armature *F* by two thin cantilever plates. Four sets of constant filaments, *A*, *B*, *C*, and *D*, are strung under initial tension between the frame and armature. When the armature is displaced longitudinally, two sets of filaments are elongated while two sets are shortened. The elongated filaments increase in resistance, and the shortened filaments decrease. The change in resistance of the filaments is proportional to their change in length. The transducer is so wired that the filaments are connected in a Wheatstone-bridge circuit. The resistance change of the filament alters the electrical balance of the bridge so that an electrical current flows in the output circuit. The reverse side of the transducer is shown in Fig. 6; *G* indicates the cantilever plates which support the armature; *H* is the linkage pin by which movement from the measuring diaphragm is transmitted to the armature; *I* is a stud attached to the armature which limits the movement of the armature to 0.0015 in. in either direction. This stop serves to protect the filaments against mechanical overload. The resistor *K* is a trimmer placed in series with one of the bridge elements. It is adjusted to equalize the resistance of the four elements of the bridge. If the bridge

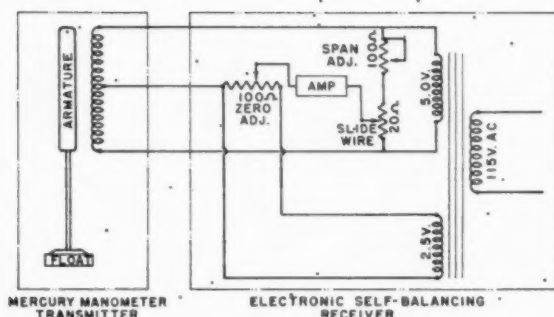


Fig. 8 SIMPLIFIED WIRING DIAGRAM FOR MERCURY-MANOMETER TRANSMITTER AND RECEIVER

is balanced at zero output before the displacement is applied, the unbalanced electrical output of the bridge bears a linear relationship to the displacement. The complete wiring diagram, including transmitter and receiver, is shown in Fig. 7.

The receivers for the differential strain transmitters are also special, although different adaptations of the electric self-balancing potentiometer. In this case it is an alternating-current potentiometer with both the strain bridge in the transmitter and the slide-wire in the receiver being supplied power from the same transformer located in the receiver. An alternating-current potentiometer-type circuit was chosen because by connecting the four strain elements in a bridge, the largest and most easily measured output could be obtained. The output is in the order of 25 millivolts for full scale deflection of the receiver whereas, had a resistance-measurement-type circuit been used, the total resistance change for full scale deflection would have been very small with the type of unbonded strain gage used. The span and zero adjustments are accomplished by means of a potentiometer rheostat network located in the receiver and shown on the simplified wiring diagram in Fig. 7. These receivers are in all cases circular-chart recorders.

It can be noted from the foregoing description that two different types of transmitters were used for differential flow measurements. Either type could have been used throughout. The mercury-manometer type was chosen for all control applications, as it seemed to offer the best possibility of maintaining its calibration over a long period of time while the strain-element type is known to have a zero calibration shift with time. The strain type was chosen for straight flow recording on the basis that it was cheaper, and that an instrument of this type should be developed.

DIFFERENTIAL-PRESSURE INSTRUMENTS

Most of the differential-pressure measurements in the demonstration plant were made for collecting experimental data on such items as plastic flow of viscous fluids and exchanger fouling factors. Very few data are available, particularly at high pressures, on the plastic flow of viscous fluids such as coal paste with a viscosity of 4750 centipoises at 200 F, and a Reynolds number considerably below the range of laminar flow; and it is therefore hoped that friction factors and empirical formulas may be developed by the differential-pressure data obtained. Differential-pressure measurements are also used as an indication of changes in fouling factors of exchanger equipment due to coke, salt, and hydrates; and for process control of water-injection rates necessary to reduce the scale and salt deposits in the exchanger tubes.

The primary measuring element and transmitter for these measurements is a differential strain gage as previously described in the flow section with modifications to the diaphragms for ranges of 100, 350, 500, and 1000-lb differentials.

The receivers for these measuring elements were an adaptation of a multipoint strip-chart potentiometer recorder. The basic electric circuit for each point was the same as previously described for single-point recorders under flow measurement; however, owing to the inherent difficulties in manufacture of the strain element, the calibration factors for each transmitter were different and required a separate span and zero adjustment for each point recorded. This span-and-zero adjustment for each transmitter was located behind the receiver case.

Automatic control of differential pressure was used in only two cases—the total differential pressure across the hydrogen-recycle compressors in the vapor-phase and the liquid-phase systems. Both systems are closed and operate independently. It was necessary to by-pass part of the recycle hydrogen at a high enough pressure, to be assured at all times of a sufficient pressure differential to force a controlled flow of cooling hydrogen into the converter, while still maintaining a constant flow of process hydrogen and feed to this same converter. To accomplish this, an excess of recycle compressor capacity is maintained at all times at a pressure differential of from 500 to 750 psi. This differential-pressure-recorder controller is the most important single controller in either phase, as enough cooling hydrogen must be available to prevent a runaway condition due to the exothermic reaction. These receivers are pneumatic, full-throttling, automatic-reset, circular-chart-recorder controllers, equipped with manual by-pass panels.

LIQUID-LEVEL INSTRUMENTS

Level measurement and transmission for all high-pressure vessels was accomplished by using 50-in. high-pressure mercury manometers of the type previously described in the section on flow instruments.

The receivers are circular-chart-recording, full-throttling, automatic-reset, pneumatic controllers with manual by-pass panels. The electric circuit for the receivers of the mercury manometers is the same as that used for the manometer-type flow receivers previously described.

The liquid-level measurement and control of the hot catchpot was the most difficult installation and is therefore described in detail. The hot catchpot is a vessel 24 in. ID \times 38 ft high and is used in the process as the hot liquid-vapor separator. The liquid flow to the hot catchpot is intermittent, and the sudden surges must be minimized by efficient control. The heavy-oil bottoms is a liquid containing approximately 35 per cent solids, consisting of unreacted coal, ash, and catalyst, and a high percentage of absorbed gases. From the foregoing description it can be seen that this service presented many problems as to measurement, control, and maintenance; therefore three separate and distinct level systems were employed. Two were of the pneumatic or bubbler-tube type in conjunction with 50-in. mercury manometers, and the third was of the gamma-ray type described later. The pneumatic liquid-level measuring device consists of a mercury manometer connected to tubes entering the top of the vessel. One tube is terminated near the top to measure the static pressure while the other extends into the vessel to a point near the bottom. The liquid head on the second tube produces the differential on the manometer. Hydrogen is introduced into the two manometer leads through two flow recorders in one case and through capillary throttling devices in the other. The arrangement is shown in Fig. 9.

Owing to the severe service conditions of the hot catchpot, it was felt that an additional type of level measurement and transmission should be employed. This is an electronic instrument utilizing gamma radiation which is capable of measuring changes of level through the heavy wall of the vessel without the use of an access opening. The gamma rays are produced as a result of

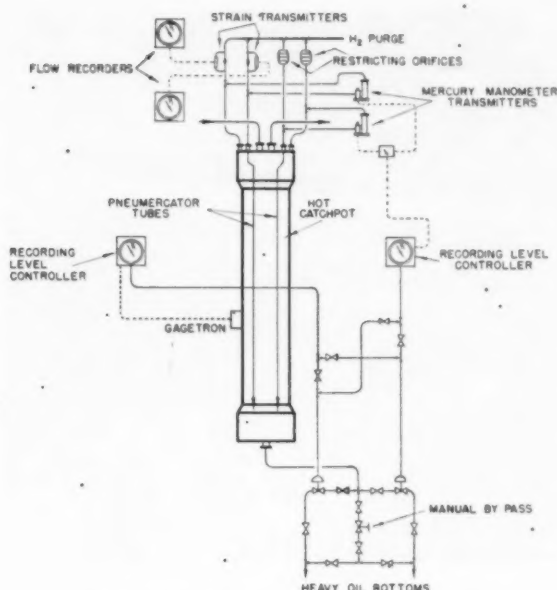


FIG. 9 HOT-CATCH-POT LEVEL-CONTROL SYSTEM

natural disintegration of radium in a capsule located within the vessel. The number of gamma rays that penetrate a section of the vessel wall are counted and averaged by a suitable Geiger counter amplifier-integrator circuit, which supplies an output of 0-50 millivolts d c. The intensity of the radiation from the radium source varies with the distance from the source to the counter and with the densities of various materials intervening. The counter is located about 2 ft higher on the outside of the vessel than the radium sources on the inside; therefore, as the liquid rises above the source, the radiation received at the counter is progressively reduced by this intervention of a material of a higher density. The reduction of intensity continues until the liquid level is directly opposite the counter producing a 2-ft operating range.⁴ The electric circuit of the receiver is a conventional self-balancing potentiometer with a range of 0-50 millivolts d c.

The manometer transmitters were wired through a switch on the control panel so that either of the two transmitters could be used on a common receiver controller. The output control air of this receiver was manifolded with that of the gamma-ray receiver controller so that either could be used to control the level in the hot catchpot. This controlled air operates either of the two diaphragm control valves of the severe throttling type, which remove the heavy-oil bottoms from the hot catchpot. A dual valve installation was required owing to the severe erosion caused by the 675-atm pressure drop of the material handled.

Special designed 15,000-psi test gage glasses also were installed on each of the vessels for manual operation and setting of control points.

MISCELLANEOUS EQUIPMENT

Two other types of instruments deserve mention: The thermal-conductivity hydrogen-analyzer recorders, and the Ranarex specific-gravity recorders, which are used as a check on the composition of the gas streams in both the liquid and vapor phase. The instruments are of conventional design. The continuous samples to these instruments were taken from the hydrogen re-

⁴ For further information on the type 79D1 Gagetron refer to the Engineering Laboratories, Inc., Tulsa, Okla.

cycle lines through 1-mm capillary tubing which was used to partly reduce the pressure and to reduce line volume to increase speed of response of the analyzers. The final high-pressure drop was taken across double manual throttling valves into a 10-in. WC bubbler, with part of the sample vented to atmosphere and the balance going to the hydrogen-analyzing cell and the gravimeter.

Instrument piping consisted of $\frac{3}{16}$ -in-ID \times $\frac{3}{16}$ -in-OD type 304 stainless-steel tubing, tees, connectors, and valves. Connections were made by use of a differential cone seal, as shown in Fig. 10. The connections were kept to a minimum by use of bends wherever possible.

The construction details of the diaphragm-control-valve bodies are covered in a companion paper on valves and fittings; however, some additional description covering the control operations is required. The valves are equipped with giant top works or diaphragm with 2-in. travel of the diaphragm through a linkage to give $\frac{3}{8}$ -in. travel of the inner valve. To insure ample power and accurate positioning of the inner valve, all control valves are equipped with valve positioners set for the $\frac{3}{8}$ -in. travel. The

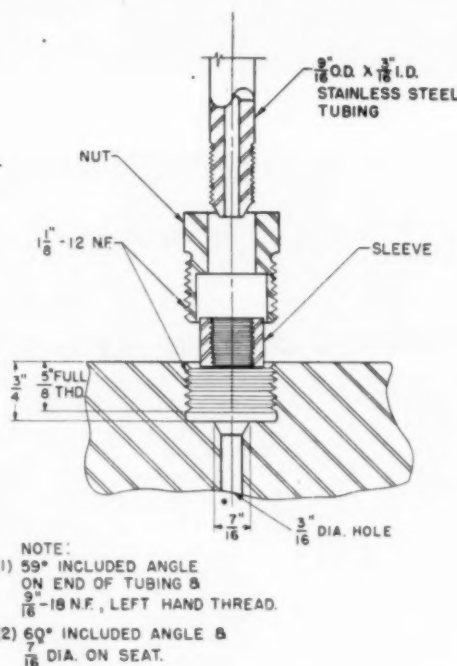


FIG. 10 INSTRUMENT-PIPING CONNECTIONS

port sizes range from $\frac{1}{8}$ in. to $\frac{1}{2}$ in. diam, and the plugs are characterized.

An elaborate annunciator system was installed with a normal amber light and an abnormal red light for each alarm circuit. A common howler with a reset button was used. The common-howler reset button will silence the howler for that circuit which has become abnormal, leaving the red light on and clearing the howler for operation from one of the other alarm circuits. The alarm circuits are used for high skin temperatures, thermocouple burnouts, high and low levels, low steam pressure, and low coal-paste pressure.

CONCLUSION

The special instruments described were developed primarily for

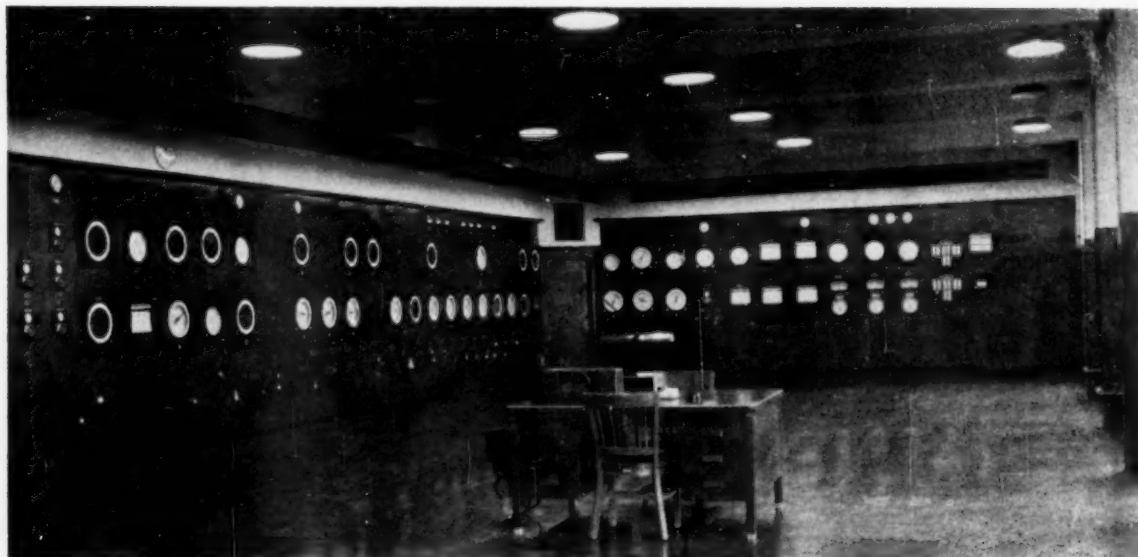


FIG. 11 INTERIOR OF HIGH-PRESSURE CONTROL HOUSE—LIQUID-PHASE INSTRUMENTS

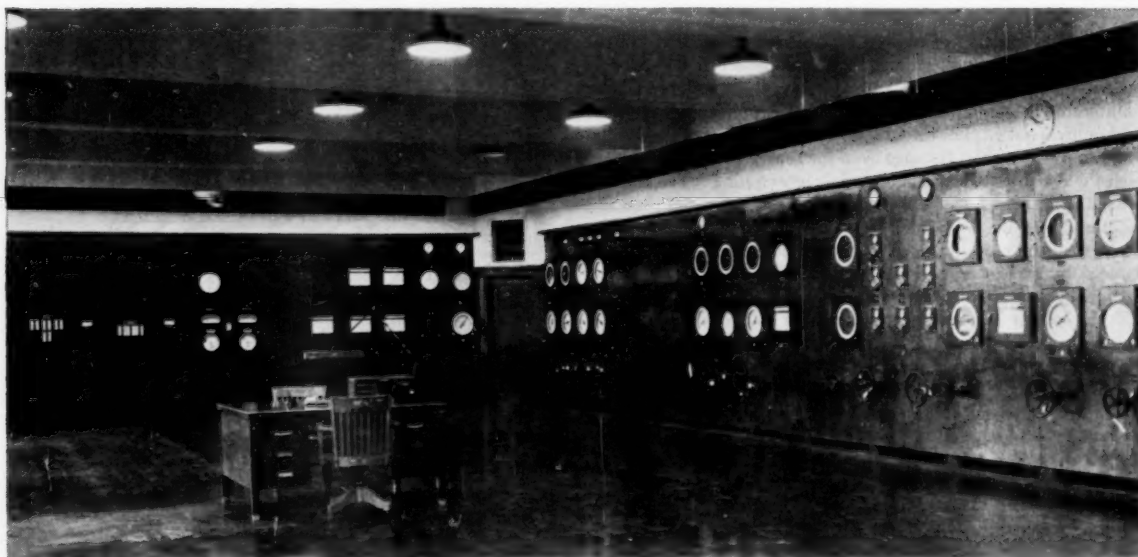


FIG. 12 INTERIOR OF HIGH-PRESSURE CONTROL HOUSE—VAPOR-PHASE INSTRUMENTS

the project through the splendid co-operation of interested manufacturers. The design of the project occurred during a period of peak demand for standard equipment; and it was therefore difficult to find suppliers to produce the equipment. Presentation of ideas to numerous manufacturers, even though they were not interested at the time, has now resulted in the development of some new equipment for high-pressure services. The instruments now in use represent the best that it was possible to develop and obtain but are by no means considered the only or final solution

to the problem. It is hoped that from operating experience and continued co-operation with manufacturers, improvements and new developments may be obtained that will be applicable not only to the coal-hydrogenation process but to any future processes of comparable services. The brief operating experience obtained to date indicates that some modifications and redesign will be required; and, after further and more conclusive information is obtained, it is hoped that additional papers will be written on the subject.

Metallurgical and Fabrication Considerations in the Coal-Hydrogenation Demonstration-Plant Construction

By B. H. LEONARD, JR.,¹ G. D. GARDNER,² AND J. A. MARKOVITS³

Special equipment, special steels, and heavy wall thicknesses were required to handle hydrogen and abrasive pastes at the high pressures and temperatures of coal hydrogenation. Some metallurgical and fabrication problems pertaining to this specialized process are discussed herein.

INTRODUCTION

COMPANION papers presented in this issue describe the coal-hydrogenation plant. An attempt will be made in this paper to show why certain materials were used and to point out some of the fabrication difficulties that were experienced. This discussion is necessarily limited to materials and equipment used for high pressures.

The primary consideration in the choice of materials for various services is the effect of hydrogen at different temperatures. From German and English experience in the hydrogenation field,⁴ it was learned that carbon steels resisted hydrogen attack at a pressure of 10,300 psig up to a temperature of 375 F. Chromium steels in excess of approximately 6 per cent Cr were found to be hydrogen-resistant at higher temperatures.⁵ At these higher temperatures, however, creep strength must also be considered. Above 800 F, straight chromium steels do not have high enough creep strength for the service conditions. These factors led to the establishment of three temperature classifications: 0 to 375 F for carbon steel, 376 to 850 F for intermediate chromium steel, and 851 to 1000 F for chromium-nickel stainless steel.

PIPING MATERIALS

To obtain materials suitable for high temperatures and high pressures, it was necessary to accept some undesirable features; one of these, common to all the metals, was hot-shortness. Seamless tubing was used throughout, with an approximate ID:OD ratio of 1:2. Because of the thick wall involved, difficulty was

experienced in maintaining uniform temperatures throughout the metal, and it was possible for part of the wall to be in the hot-short range at some time during the forming operation.

Low Temperature. The service conditions in the low-temperature range closely simulate those found in normal refinery practice, except for the higher pressures. Hydrogen attack on carbon steel in this temperature range is not evident. Therefore the piping specifications were established in compliance with the ASME Pressure-Piping Code, and specifically with the API 5L, grade C, classification.⁶ This specification requires a minimum yield value of 45,000 psi, and specifies a maximum allowable stress of 22,900 psi at 375 F. The most readily available material conforming to these specifications and adaptable to seamless piercing operations was MT-1040. Normal production of seamless tubing from this material employs a hot-roll finish. Due to the extremely heavy tube wall required, excessive ovality or squareness resulted from this procedure as shown in Fig. 1. Although minimum wall-thickness requirements were met, this

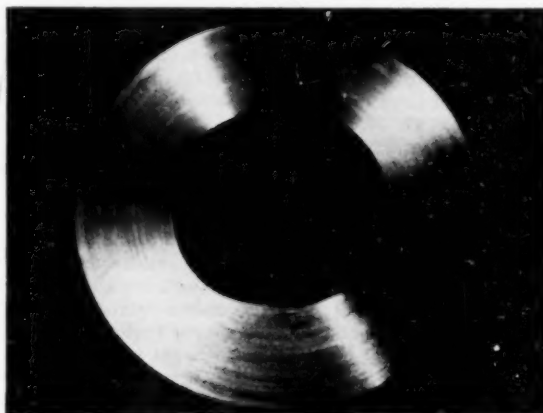


FIG. 1 SQUARED ID OF HOT-ROLLED MT-1040 STEEL TUBE

squareness was undesirable for the following reasons: (1) Tubes of nonsymmetrical cross section will develop undeterminable stress concentrations due to internal pressure; (2) indeterminate problems would result in the calculation of bending and shear stress caused by thermal expansion, pipe supports, and anchors; (3) starting points for corrosive and erosive action, sedimentation and coke formation would be established—especially at points where the squared ID of the tubing meets the round ID of the fittings; (4) proper fluid flow and heat transmission would be impaired; (5) systematic safety inspection of irregular tubes would be impossible.

To eliminate squareness and give a satisfactory finish to the

¹ Mechanical Engineer, Coal-to-Oil Demonstration Branch, Office of Synthetic Liquid Fuels, Bureau of Mines, Louisiana, Mo. Jun. ASME.

² Metallurgist, Coal-to-Oil Demonstration Branch, Office of Synthetic Liquid Fuels, Bureau of Mines.

³ Assistant Chief, Coal-to-Oil Demonstration Branch, Office of Synthetic Liquid Fuels, Bureau of Mines.

⁴ "The Effect of Highly Compressed Hydrogen Upon Unalloyed Steel," by F. K. Naumann, *Stahl und Eisen*, vol. 57, 1937, p. 889.

⁵ "The Effect on Various Steels of Hydrogen at High Pressure and Temperature," by N. P. Inglis and W. Andrews, *Journal of the Iron and Steel Institute*, vol. 128, 1933, pp. 383-397.

⁶ "The Effect of Alloying Additions on the Resistance of Steel to Hydrogen Under High Pressure," by F. K. Naumann, *Stahl und Eisen*, vol. 58, 1938, pp. 1239-1250.

Contributed by the Petroleum Division and presented at the Petroleum Mechanical Engineering Conference, Oklahoma City, Okla., October 2-5, 1949, of THE AMERICAN SOCIETY OF MECHANICAL ENGINEERS.

NOTE: Statements and opinions advanced in papers are to be understood as individual expressions of their authors and not those of the Society. Paper No. 49-PET-5.

⁶ ASME Code for Pressure Piping, 1942.

tubes required either boring or cold-drawing. The less expensive solution of cold-drawing was chosen. As a final step, the tubes were given a normalizing treatment for adjustment of mechanical properties.

One of the inherent properties of this steel is a hot-short range from 1400 to 1600 F. Forming should be done in a range of 1800 to 2000 F, and in no case should this material be cold-bent. Some of the tubing was found to have cracks, and it is believed that these cracks were caused by forming at too low a temperature, or in the hot-short range. A typical defect is shown in Fig. 2.

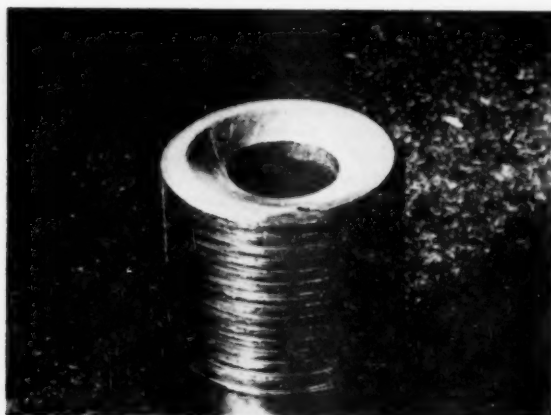


Fig. 2 HOT-SHORT CRACK IN MT-1040 STEEL TUBE

Intermediate Temperature. For the intermediate-temperature service, a steel with a chromium content exceeding 6 per cent was needed to resist hydrogen attack. Standardization of piping was based upon the maximum allowable stress of the low-temperature steel; 22,900 psi at 375 F. A study was made to find a material which at 850 F would have approximately this same allowable stress, and also have enough chromium to resist hydrogen attack. A stronger material would not have been economically sound; conversely, standardization would not have been possible without a material at least this strong. The most readily available material that could be heat-treated to give suitable mechanical properties and contained enough chromium to resist hydrogen was a 9 per cent chromium-molybdenum steel.

This material was found to have the same tendency to square during the customary hot-finishing operation as had been experienced on the low-temperature steel. It was necessary, therefore, to cold-draw this material also. For increased resistance to hydrogen penetration and to obtain required mechanical properties at working temperature, the chromium-molybdenum steel was normalized and drawn at 1200 F. The mechanical properties of this material could be expected to remain stable in operation because of the spread between the operating and draw temperatures. In tests on samples for 1000 hr at 800 and 900 F, only a minor loss could be found⁷ in mechanical strength at room temperature or 900 F.

For the extreme deformation required in the piercing operation, 9 per cent chromium-molybdenum steel should be heated to working range of 2000 to 2250 F. Within the range of 1500 to 1800 F this metal is hot-short, and deformation may lead to cracking at the points of maximum deformation. Because of the air-hardening characteristic of this material, rapid cooling

from above 1400 F could also produce cracks or checks. It is believed that the cracks found on some tubes of this material were caused by working in the hot-short range, Fig. 3.



Fig. 3 HOT-SHORT CRACKS IN 9 PER CENT CHROMIUM-MOLYBDENUM STEEL TUBE

High Temperature. The high-temperature requirements were the most difficult to meet. The material had to resist hydrogen attack and have high creep strength. Again, for standardization purposes, it was necessary to find a material with a creep strength at 1000 F, close to the maximum allowable stress of the low-temperature material, 22,900 psi. The stabilized materials in common use did not have enough strength. Careful control during operation eliminates corrosion and makes possible the use of unstabilized AISI type 316 stainless steel for the high-temperature service. This steel has the highest creep strength of the heat-resisting stainless steels for which data are available.⁸ Its strength for 1 per cent elongation in 10,000 hr is 23,000 psi.

AISI type 316 alloy is relatively refractory in piercing and rolling and has a tendency to surface-marking. It is therefore common practice to cold-draw this tubing to produce suitable surfaces, to eliminate notches and other stress raisers, and to save material. In addition, some cold work is applied to achieve some recrystallization on heat-treatment and to produce optimum grain size.

FITTINGS

The high-pressure fittings, consisting of tees, ells, and reducers, were forged from special steels required for the various temperature ranges. The tees were formed by forging solid blanks into the proper shape; these forgings were then bored to proper inside dimensions. Because of the thick walls required, it was very difficult to deform the entire mass sufficiently to modify completely the original cast structure. The ells were forged from straight bars, which were first bored eccentrically and then formed with the heavy side on the outside of the bend, in an attempt to secure uniform wall thickness.

Low Temperature. Zones of weakness in the high-pressure tees were found in the branch run. Here a minimum of work was required for the actual shaping of the forging. Fig. 4 shows a carbon-steel tee leaking at a pressure of 8000 psi during a hydrostatic test. Fig. 5 shows the cast (unworked) and the fibrous (partly worked) structures at the fractured surface of a defective tee, which had been broken to show the cause of leakage.

⁷ Test Report from Babcock & Wilcox Tube Company, Beaver Falls, Pa., July 14, 1948.

⁸ Metals and Alloys Data Book, S. L. Hoyt, Reinhold Publishing Company, New York, first edition, 1943, pp. 111 and 189-191.



FIG. 4 DEFECTIVE CARBON-STEEL TEE LEAKING UNDER HYDROSTATIC TEST PRESSURE OF 8000 PSI

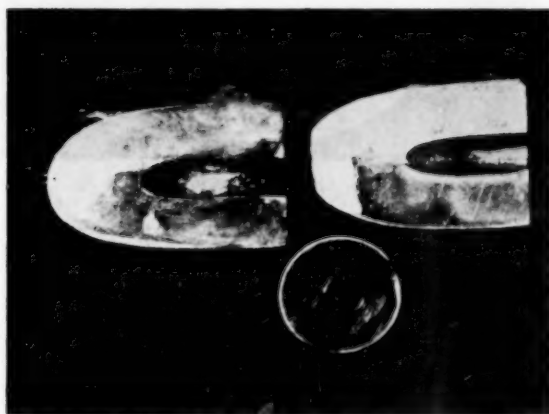


FIG. 6 DEFECTIVE AISI TYPE 304 STAINLESS-STEEL ELL CAUSED BY FORGING AT TOO LOW A TEMPERATURE

Other tees exhibited forging cracks, laps, and seams at the root of the branches; ells had some checks and laps, but few of these proved to be serious.

Intermediate and High Temperature. The intermediate-temperature forgings were of AISI type 304, and the high-temperature forgings were of AISI type 316 stainless steel. The forging range of these materials is very critical and narrow; 2200 to 1800 F. Forging at temperatures either slightly above or below these limits will result in cracks and checks. More blows are required to work these materials than are required for carbon steel, and the first few blows must be light, so as to harden and toughen the surface, after which heavier blows may be applied. Because of low thermal conductivity, very rapid cooling, and longer forging time, reheating must be done quite often. It is extremely important that the hot-work finish temperature be adhered to, since this material tends to work-harden while still very hot. Fig. 6 shows a forged ell which is believed to have been cracked, owing to forging at too low a temperature.

WELDING OF TUBING

In the fabrication of spool pieces by welding, the metallic-arc process was used exclusively, utilizing multipass procedure. Procedures and operators were qualified on the materials and thick-

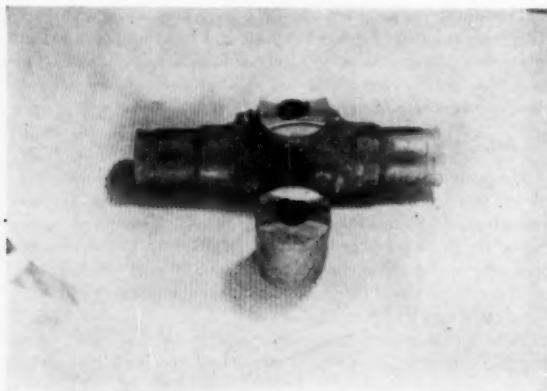


FIG. 5 TYPICAL STRUCTURE OF DEFECTIVE CARBON-STEEL TEE WHICH LEAKED UNDER HYDROSTATIC TEST

nesses involved. The joint design employed the conventional $37\frac{1}{2}$ -deg straight bevel for wall thicknesses up to $\frac{3}{4}$ in.; above this thickness a 20-deg U-type bevel was used. Backup rings were not used for the following reasons: (1) The small ID of the tubing made it impossible to remove the rings; (2) restriction to flow caused by a ring would be undesirable; rings would establish starting points for sedimentation and coke formation; (4) damage could result to valves or pumps, were a ring to come loose; (5) it was demonstrated that 100 per cent penetration could be obtained without the use of rings.

Tube tolerances often resulted in $\frac{1}{8}$ in. eccentricity. To prevent shoulders at the joints and to assure full penetration of the weld, the eccentric ID was taper-counterbored at the time of cutting the welding bevel. This also assured alignment of the inside diameters when the outside diameters were aligned, and facilitated setup of the spool pieces before welding.

Low-Temperature Material. Welding of the MT-1040 low-temperature material was difficult because of the high carbon content. To diminish the cooling rate and hardness of the heat-affected zone, a preheat of 400 F was used and maintained during welding. The length of time the preheat was applied was governed by the wall thickness involved. Contrary to common practice of using electrodes with minimum tensile strength at least equal to that of the parent metal, E-7010 electrode was used for the low-temperature-range steel. This choice sacrificed ultimate strength for a gain in ductility; however, yield values of the filler metal exceed yield values of the parent metal. The joint and the heat-affected areas were stress-relieved immediately upon completion of the weld. The heat-affected zone was heated to 1250 F, held at this temperature for 1 hr per in. of wall thickness, and slowly cooled in still air. In no case did the heat-treatment last less than $\frac{1}{2}$ hr. No attempt was made to restore the metal to the normalized condition as it was felt that the stress-relieved weld deposit would meet the necessary tensile requirements.

Intermediate-Temperature Material. Welding of the air-hardening chromium-molybdenum steel also required care. A preheat temperature of 600 to 800 F was used to insure a minimum of 500 F, and thus prevent cracking. Upon completion of the weld, and without any loss of temperature, the joint and heat-affected zone were soaked for 2 hr at 500 F to assist martensite transformation, so that, upon heating to 1200 F (subcritical temperature), holding for 4 hr, and cooling in still air, the weld would be tempered. A filler metal of composition similar to the parent metal was used.

High-Temperature Material. The austenitic AISI type 316 stainless steel required a preheat of 400 F, because of its low ther-

mal conductivity and because of the large mass of metal involved. To assure an austenitic weld deposit and to avoid possible sigma-phase formation, a 25 per cent chromium-20 per cent nickel electrode was used. Because of the high-temperature service condition, postheat was unnecessary.

MACHINING

Machining of the tube ends for the flanged lens joints also presented problems. To effect a seal, the tube ends had to have a smooth machine finish on a 20-deg bevel. This finish was obtained by means of a forming tool. Hard spots in the tube ends, however, would cause chatter of the tool bit and result in marks on the critical bevel face. Kerosene used as a cutting lubricant eliminated much of this trouble.

Tube and flange threads were gaged with "go" and "no-go" gages. If a tube thread were near the large limit and a flange thread near the small limit, binding would occur. This was especially troublesome with AISI type 316 material, which tended to gall. Cutting the tube thread deeper would not remedy a tight fit, but only change the thread profile. However, tube threads could be cut slightly oversize to accommodate oversize flanges. To eliminate this trouble, flanges and thread taps were supplied to the pipe-spool fabricator so that individual fitting could be achieved. These flanges were then used as thread protectors during shipping of the fabricated spool pieces. The critical bevel faces of the pipe spools had to be well protected also, for considerable time could elapse before a particular spool might be used. During this time the spool piece would lie in the pipe yard. Cosmolene was used to prevent corrosion, especially of the carbon steel, and various types of caps and plates were used to prevent damage. Even so, it was necessary to reface many tube ends before some pipe spools could be installed. This refacing was best accomplished by a tool similar to that shown in Fig. 7.⁹ The collar holds the tool square with the axis of the tube, and the

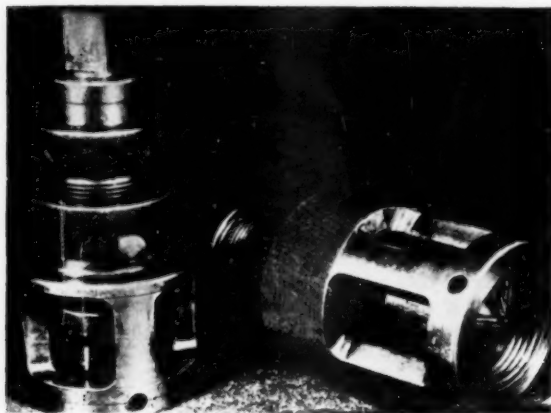


FIG. 7 TUBE-REFACING TOOL

straight cutting edges are mounted so as to sweep an imaginary, 140-deg, included, cone angle. This arrangement produces the required 20-deg bevel on the tube end. The tool is manually operated and care is exercised to maintain uniform rotation of the cutters when they are backed off. This precaution is necessary to prevent marking of the bevel face at the termination of the cut.

The other critical element of the flanged joint—the lens gasket—presented no serious fabrication difficulties. In all tempera-

ture ranges, the materials used for the lens gaskets were softer than the tube ends they were to seal. In the low-temperature range, the gaskets were made of AISI-1020 steel having a maximum Brinell hardness of 140. For the intermediate and high-temperature lens gaskets, AISI type 405 chromium stainless steel was used with a maximum Brinell hardness of 130. Impurities and lack of homogeneity caused voids in the middle of a forged bar of this material which did not show up until 26 pieces, approximately 1 1/2 in. long, had been cut, Fig. 8. The spherical surface of the lens gasket was a polished finish; however, since

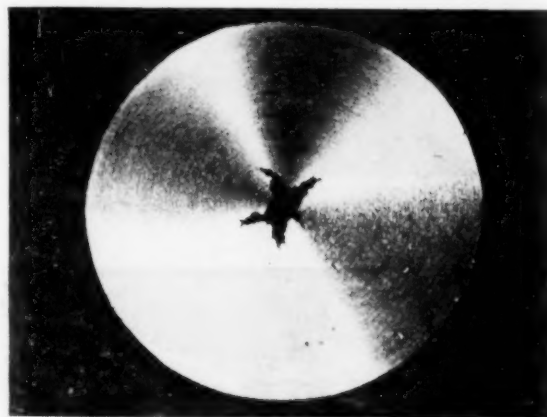


FIG. 8 PIPE IN AISI TYPE 405 STAINLESS STEEL

manufacture was done at the job site as needed, corrosive and handling damage was minimized and refacing could be accomplished easily.

OTHER PROBLEMS

The process equipment, including valves, pumps, heat exchangers, instruments, and vessels, is subjected to the same operating conditions as the tubing. Special steels and careful fabrication were required on these elements also. Hence special problems pertaining to each arose.

Materials. Cemented carbide is used for disks and seats of throttling valves and control valves. This material is very hard, but also very brittle, and slight pressure will cause fracture. It is therefore inadvisable to close these valves completely. Where both control and complete stoppage of flow are required, it is necessary to install throttling and stop valves in series. In some cases the cemented-carbide disks were replaced with stellite or hardened stainless steel, having less abrasive resistance but more toughness.

Two materials used for Bourdon tubes are straight 12 to 14 per cent chromium stainless steel and chromium-vanadium steel. Several chromium tubes failed after 5 days under hydrogen pressure. Tubes of similar material have been known to fail after short service in refinery operation because of corrosive attack of a deep cellular nature which causes excessive stress concentrations at tube corners. Fractures of the tubes in question also originated at corners of the cross section, and it is believed that similar attack occurred. Two of the chromium-vanadium tubes failed after 24 hr under hydrogen pressure. Fig. 9 illustrates a typical failure; in this case caused by corrosion fatigue. As a solution to this problem, tube-material specifications have been changed to a corrosion-resistant material, AISI type 316 stainless steel.

Welding. Welded pressure parts of equipment have to withstand the same service as welded tube joints. The proper preheat and postheat must be used regardless of how small the pressure

⁹ Tool designed by the Bureau of Mines, patent applied for.

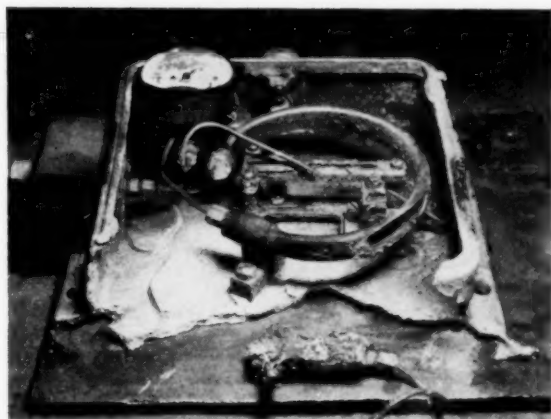


FIG. 9 BOURDON-TUBE ASSEMBLY AFTER RUPTURE FROM HYDROGEN PRESSURE OF 12,000 PSIG



FIG. 11 COLLAPSED THERMOCOUPLE WELL

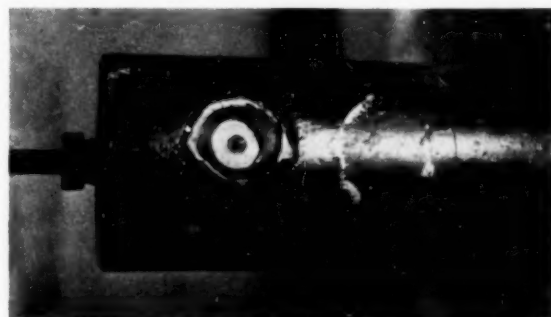


FIG. 10 FAILURE OF WELD ON AISI-1025 CARBON STEEL



FIG. 12 WELDED TEE

part might be; the electrode and welding bevel must be suitable for the materials and the thicknesses involved. One of the most important requirements is qualification of the welding operator.

Fig. 10 shows the weld failure of a plug connection of a sample bomb made of AISI-1025 steel which possesses good weldability. When joining light sections to heavy sections, the heavier section must be preheated to obtain good fusion and to avoid quenching the weld. The single-bead-weld fracture displayed a very brittle structure which would indicate insufficient preheat.

Seal welds were one of the most frequent weld failures. Several plugs in heat-exchanger header blocks leaked after a short time under pressure, and numerous pump-block plugs leaked during the pump break-in period. In both cases the weld was too small. Regardless of the tightness of a mechanical seal, the heat of the seal weld will in most cases destroy the fit. A good practice is to employ a seal-weld design capable of withstanding full pressure and to disregard any advantage that may be derived by mechanical means.

Machining. Thermocouple wells of stainless steel were difficult to machine. Two sizes are required: $11\frac{1}{4}$ in. long \times $\frac{9}{16}$ in. OD \times $\frac{3}{16}$ in. ID and $9\frac{3}{8}$ in. long \times $\frac{9}{16}$ in. OD \times $\frac{3}{16}$ in. ID. Both sizes reduce down near the tip to $\frac{9}{16}$ in. OD \times $\frac{1}{8}$ in. ID with a wall thickness of $\frac{2}{32}$ in. which is subjected to a collapsing pressure of 10,300 psig. The wells are turned from solid bars which are then drilled for the thermocouple leads. Drill drift resulted in eccentricity, thin walls, and subsequent failure as shown in Fig. 11. To eliminate the trouble, tips of all the wells were cut. Ec-

centric wells were rejected and concentric wells were reclaimed by welding repair. Replacements were made in two sections and welded together.

CONCLUSIONS

Experience gained in the construction of the hydrogenation demonstration plant evinces many possible improvements.

Some changes in materials and fabrication methods were made during the latter stages of construction. Most of these were effected because of a particular problem and have already been discussed. However, one change that was made to obtain better weldability and to lessen heat-treatment requirements was the use of AISI-4130, chromium-molybdenum steel for low-temperature tubing.

Investigation is being continued to find the most suitable materials to be used in contact with hydrogen at high pressures and temperatures.

One particular development in fabrication procedure is a welded-tee connection. This type of construction could be used to replace forged tees and thus eliminate two joints. An additional advantage is a close control of the material involved, Fig. 12.

Because of the seriousness of failures, one of the most stringent requirements in the construction of high-pressure and high-temperature plants is careful inspection. Materials must be thoroughly checked as to quality and suitability. Design must be commensurate with service conditions. Fabrication must be in accordance with the highest standards of workmanship.

The
the
son
Ge
the
hea
eli
cie

A
high
of n
pre
sibl
her

T
per
sur
mix
high
ver
pas
rea
me
con
ash
moi
the
The
ing
put

F
nee
as t
goo
terr

1
of S
2
3
Syn
C
Pet
Ok
Exc
N
und
of t

Design of Preheaters and Heat Exchangers for Coal-Hydrogenation Plants

By P. W. LAUGHREY,¹ W. I. GWILLIM,¹ H. SCHAPPERT,² AND J. A. MARKOVITS³

The preheater and the heat-exchanger possibilities of the coal-hydrogenation process are described. Comparison has been made between the demonstration and the German plant equipment. Emphasis has been placed on the importance of developing applicable high-pressure heat exchangers for commercial-size plants, in order to eliminate the preheaters and increase the thermal efficiency of the process.

INTRODUCTION

AN important step toward improving the economic aspect of the coal-hydrogenation process is to achieve high thermal efficiency. Various means have been suggested for a high thermal efficiency. Full utilization of the exothermic heat of reaction through an efficient heat-recovery system and proper preheater design become important in achieving this goal. Possible improvements in design and heat recovery are discussed herein.

PURPOSE OF PASTE PREHEATER

The function of the liquid-phase preheater is to raise the temperature of the coal paste-hydrogen mixture at 10,300 psi pressure from 250 F inlet temperature to about 815 F, before the mixture enters the converters. The reaction in the converters is highly exothermic. The amount of heat developed in the converters compares favorably with that necessary for preheating the paste to the reaction temperature. A summation of all of the reactions occurring in the converter during operations gives a mean heat of reaction of 800 Btu per lb of moisture and ash-free coal converted. This paste has about 40 per cent moisture and ash-free coal content (see Table 1), which means that 1 lb of moisture and ash-free coal makes 2.5 lb of paste. Gas is added to the paste in a ratio of about 16 standard cu ft per lb of paste. Therefore the preheating of this paste and gas requires the following heat quantities per pound of moisture and ash-free coal input:

$$\begin{aligned} 2.5 \times 0.54 \times (815-250) &= 770 \text{ Btu} \\ 40 \times 0.02 \times (815-100) &= 570 \text{ Btu} \\ \text{Total} &= 1340 \text{ Btu} \end{aligned}$$

From this computation it can be seen that the amount of heat needed for preheating the paste proper is approximately the same as the amount of the heat of reaction. It is obvious that with good heat exchange between feed and product, not only is no external heat needed, but a surplus of the major portion of the reac-

tion heat must be removed. Consequently, with a good product-feed heat exchange, there would be no need of a preheater. A small preheater would be needed only for start-up, and the size of this preheater would depend entirely on the length of time to reach full operating conditions. However, it is known that in the German plants, the preheater, especially for subbituminous-coal operation, was a very large and expensive piece of equipment which transmitted a large quantity of heat to the paste. The reason for this fact is to be found, for the most part, in the properties of the coal paste.

PROPERTIES OF THE PASTE

The main property of the coal paste which may determine the design and size of the coal-paste preheater is the viscosity. The change of viscosity of paste with temperature is shown in Fig. 1. An analysis of coal paste is presented in Table 1.

TABLE 1 ANALYSIS OF ROCK SPRINGS COAL PASTE

	Weight per cent
Moisture and ash-free coal.....	36.4
Pasting oil (solids free).....	55.4
Solids in pasting oil.....	6.5
Water.....	1.3
Ash and catalyst.....	1.4
Total.....	100.0

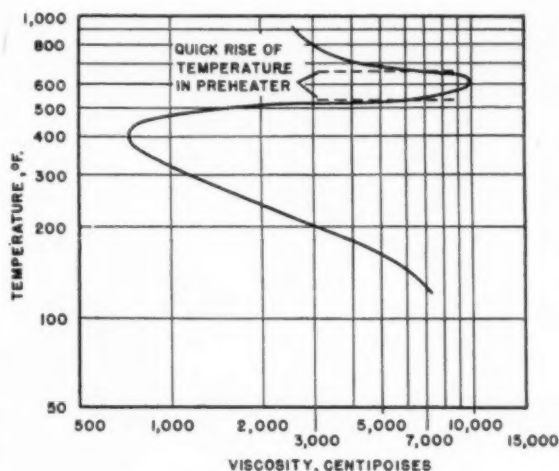


FIG. 1 VISCOSITY OF COAL-PASTE FEED

The products of hydrogenation, such as gasoline, Diesel oil, and the intermediate heavy-oil products, do not deviate from the ordinary behavior of natural hydrocarbons in regard to viscosity; but the coal paste has a singular behavior concerning viscosity, and this is caused by the swelling properties of the coal. The pulverized coal and the pasting oil are mixed, thereby surrounding each particle of coal with oil. The thickness of the oil film on the coal particles is determined by the ratio of pasting oil to coal and the sum of the entire surfaces of these coal particles. As long as

¹ Chemical Engineer, Coal-to-Oil Demonstration Branch, Office of Synthetic Liquid Fuels, Bureau of Mines, Louisiana, Mo.

² Special Engineer, Koppers Company, Inc., Louisiana, Mo.

³ Assistant Chief, Coal-to-Oil Demonstration Branch, Office of Synthetic Liquid Fuels, Bureau of Mines.

Contributed by the Petroleum Division and presented at the Petroleum Mechanical Engineering Conference, Oklahoma City, Okla., October 2-5, 1949, of THE AMERICAN SOCIETY OF MECHANICAL ENGINEERS.

NOTE: Statements and opinions advanced in papers are to be understood as individual expressions of their authors and not those of the Society. Paper No. 49-PET-1.

the oil film has a certain thickness, the viscosity of the paste is determined mainly by the viscosity of the pasting oil; but within a certain range, the coal swells, and consequently the viscosity increases markedly. This happens even in the presence of hydrogen, because at the beginning of the heating cycle the temperature is too low for hydrogenation of the coal. At higher temperatures hydrogenation and liquefaction take place, and the viscosity begins to decrease. The factors affecting this peculiar behavior of the paste are: Origin of the coal, solids content of the paste, fineness of the coal particles, and asphalt content of the pasting oil. In general, younger coals do not exhibit as marked a viscosity change in the swelling range. Increase of all the other factors mentioned tends to promote an increased viscosity of the paste in the swelling range.

Obviously, at a high viscosity of the paste, the heat transfer in the preheater is poor, and at a low viscosity it is good. Translating this viscosity effect into a more usable term, that of paste-film coefficient, the curve shown in Fig. 2 results. In the swelling-temperature range the paste-film coefficient reaches a minimum, and it improves with the beginning of the liquefaction. Since the tube-wall temperatures of the preheater are calculated by means of the paste-film coefficient, a knowledge of the values of this coefficient is very important. Characteristics of pastes derived from the various types of U. S. coals will be investigated in the preheater of the demonstration plant.

DESCRIPTION OF PASTE PREHEATER

An isometric drawing of the paste preheater is shown in Fig. 3. Because of the unusual viscosity and heat-transfer characteristics of the paste, which have been described, the paste preheater was designed with four separate cells, which are fired independently for optimum temperature control. It will be noted from the drawing that eight vertical hairpins are contained in each cell. The $2\frac{1}{2}$ -in-ID hairpins are surrounded with a 5-in-ID steam jacket, and the steam-jacket tube is exposed to radiant heat. The high-pressure tube is made of type-316 stainless steel, and the steam tube is made of 4 to 6 per cent chrome, and $\frac{1}{2}$ per cent molybdenum steel with dimensions as shown. The steam jacket

PREDICTED FILM COEFF OF COAL PASTE GAS MIXTURES
PASTE WITH 46% SOLIDS
BASED ON GERMAN DATA

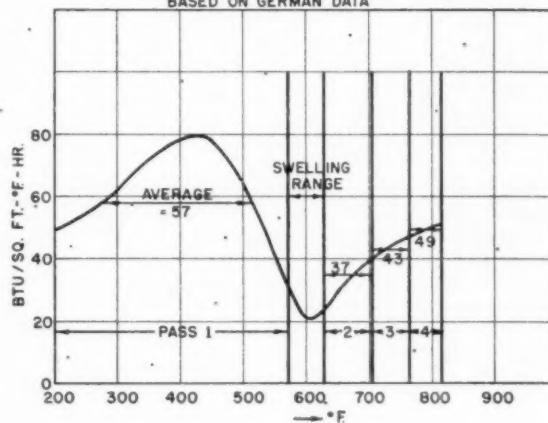


FIG. 2 PREDICTED FILM COEFFICIENTS OF COAL PASTE

promotes equal distribution of heat throughout the circumference of the high-pressure tube and aids in controlling the tube-metal temperatures.

Design data for the paste preheater applicable to operation on Rock Springs coal are given in Table 2.

OPERATION OF PASTE PREHEATER

The paste, with a small amount of gas, enters the first cell of the preheater. Addition of the gas improves the flow conditions, and therefore, the heat transmission. Between the first and second cells of the preheater, at about 570 F paste temperature, two outside streams are introduced into the paste. One is a hot stream of hydrogen at 710 F. The other stream is a heavy solids-containing oil, called "heavy-oil letdown" (HOLD). This latter stream flows hot (775 F) directly from the bottom of the hot

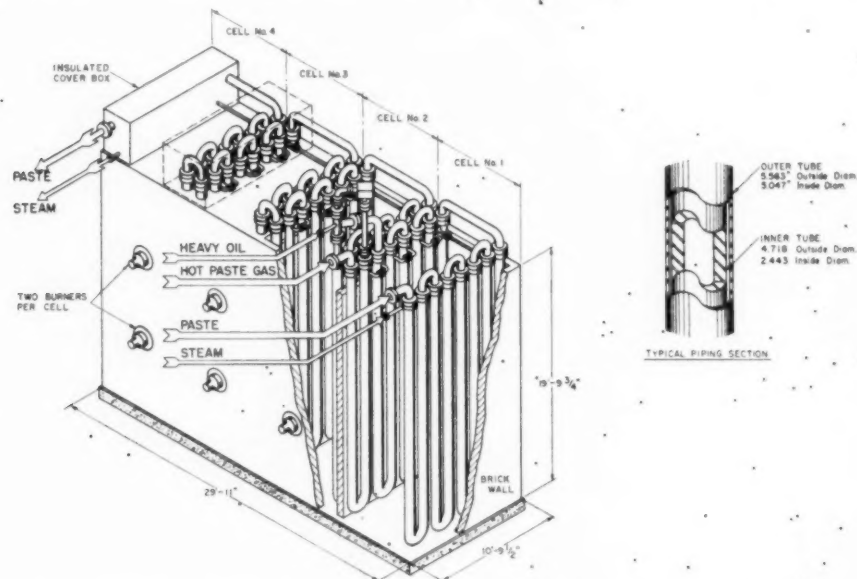


FIG. 3 ISOMETRIC DRAWING OF PASTE PREHEATER, COAL-HYDROGENATION DEMONSTRATION PLANT

TABLE 2 DESIGN DATA FOR PASTE PREHEATER (ROCK SPRINGS COAL)

	Maximum design conditions
Heat duty, Btu per hr:	
Paste.....	6560000
Gas.....	180000
Total.....	6740000
Quantity input, lb per hr:	
Coal paste at 250 F.....	20183
Heavy oil letdown at 775 F.....	2500
Hot paste gas at 710 F.....	3500
Total.....	26183
Steam into jacket (400 psig at 700 F), lb per hr.....	550
Inlet pressure, psig.....	10000
Maximum working pressure, psig.....	10300
Pressure drop, steam, psig.....	200-220
Firebox temperature, deg F.....	1400
Flue-gas temperature leaving furnace, deg F.....	1200
Heat fired, Btu per hr.....	10400000
Furnace efficiency, per cent.....	65

catchpot and is boosted with a surge-type pump. The injection of these two hot streams produces a sharp temperature rise in the paste to about 630 F, thereby causing the paste to pass over the swelling range of the coal quickly. Also, enough hydrogen is introduced into the paste to start the liquefaction of the coal.

The velocity in the coal-paste preheater is an important design factor. For the foregoing design conditions the velocities are cell No. 1, 3 fps; cell No. 2, 8.5 fps; cell No. 3, 9 fps; cell No. 4, 9.5 fps.

The velocity in the last three cells is increased owing to the addition of the hot gas and heavy-oil let-down. In the German plants, experience showed that a velocity of 15-20 fps was quite suitable for 4-in-ID preheater tubes. This velocity range assured a uniform flow of paste throughout the preheater, was under the erosion limit of approximately 25 fps, and did not cause an excessive pressure drop across the preheater.

Operating conditions for Rock Springs coal have been established, and various temperatures in the preheater under these conditions have been calculated as shown in Fig. 4. Fig. 5 shows that even if some coking of the tubes should occur, only a slight decrease in throughput is required to maintain tube-metal temperatures below the maximum allowable, 1000 F.

The throughput of various coals in the demonstration plant will vary according to the ease of hydrogenation, and therefore

the design velocities in the paste preheater are purposely rather low, in order to accommodate coals that hydrogenate easily. The demonstration-plant preheater is, therefore, suitably designed to solve all the problems involved in experimentation with all varieties of American coals.

LARGE-SCALE PASTE-PREHEATER INSTALLATIONS

All German preheaters were of the convection type. Tubes were arranged vertically in the form of hairpins in narrow cells in which flue gas was circulated at fairly high velocity. These hairpins were finned tubes with an outside:inside surface ratio of 20:1, to compensate for the low film heat-transfer coefficient on the flue-gas side. Tube-metal temperatures were controlled by regulating the quantity and temperature of the circulated flue gas.

A plan view of such a preheater is shown in Fig. 6. The inlet connections for heavy-oil and hot paste gas, shown in this drawing, indicate that the swelling range of the coal in this preheater was bridged in a similar manner to that in the preheater of the demonstration plant.

All things being equal, such as duty and maximum allowable tube-metal temperature, the total heating-surface requirement, based on inside area of the high-pressure tube is approximately the same for the finned-tube convection-type, the radiant-type, or the steam-jacketed radiant-type preheater of the demonstration plant. The reason for this fact is that the paste film represents 80 to 90 per cent of the total resistance to heat flow; therefore it is the determining factor in calculating the total surface requirement. The resistance to heat flow on the outside of the high-pressure tubes is lowered by the compensatory highly finned surface in the convection type, and the high-velocity steam flow in the steam-jacketed radiant type. A proper selection of a preheater for large-scale installations, therefore, must discard the convection type because of the added capital cost of fabricating the finned surfaces and the auxiliary equipment such as ducts and blowers. In comparing the conventional radiant type with the steam-jacketed radiant-type preheater, the operational features of the latter such as uniformity of heat distribution, prevention of coking, and optimum process control, must outweigh its slightly greater cost. It is conceivable that in the plant of the future a

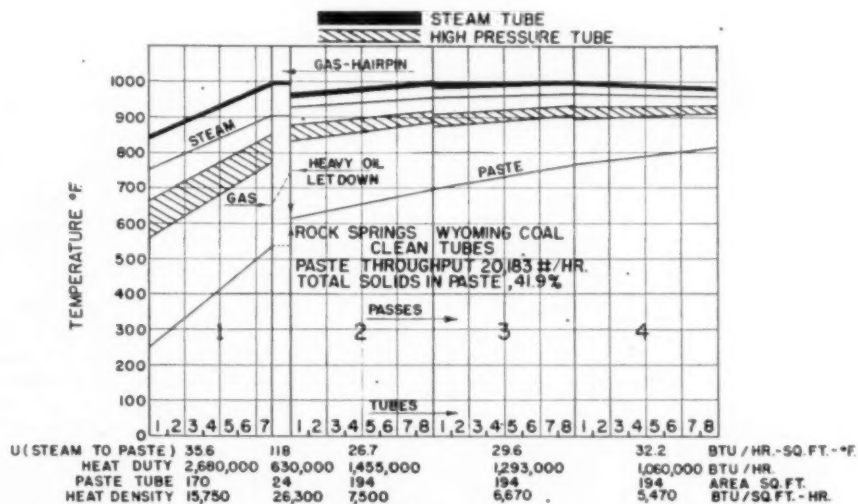


FIG. 4 CALCULATED TEMPERATURE GRADIENT WITH CLEAN TUBES, PASTE PREHEATER, COAL-HYDROGENATION DEMONSTRATION PLANT

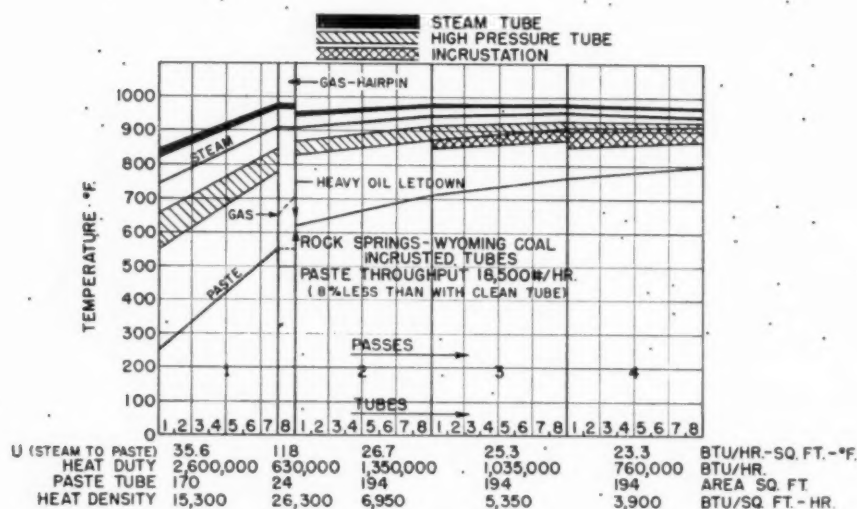


FIG. 5 CALCULATED TEMPERATURE GRADIENT WITH INCRUSTED TUBES, PASTE PREHEATER, COAL-HYDROGENATION DEMONSTRATION PLANT

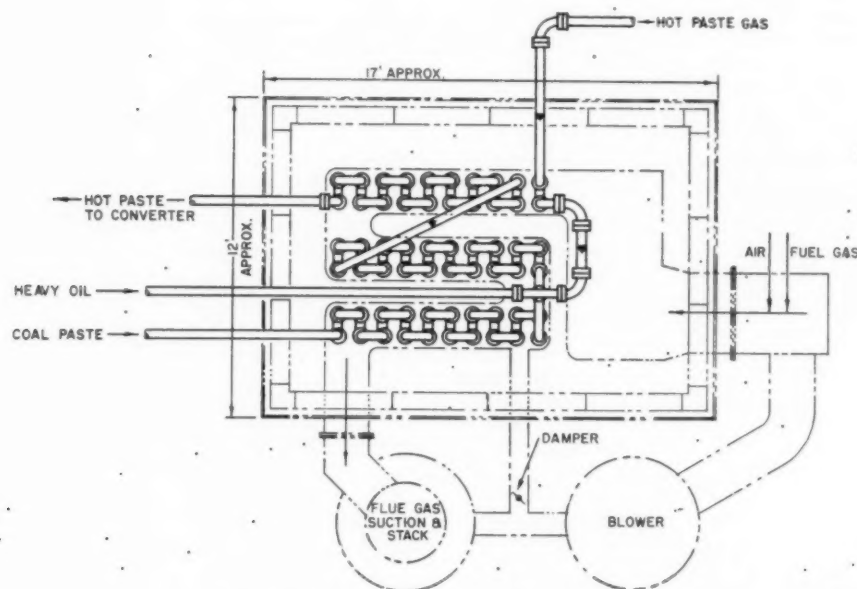


FIG. 6 PLAN VIEW OF CONVECTION-TYPE PREHEATER

conventional radiant-type preheater with low heat densities would be feasible. It can be designed along the following lines: The multicelled setting would take the form of a long, rectilinear box with hairpin tubes suspended from the roof in the center of the box. Firing would take place on each side of the box with short-flame burners and good burning characteristics, permitting wide variations in firing rate, with minimum percentages of excess air.

VAPOR-PHASE PREHEATER

For the first time in coal hydrogenation at 10,000 psig, a radiant-

type preheater is used in the vapor-phase hydrogenation demonstration plant. This preheater is gas-fired, contains thirty $1\frac{1}{4}$ -in-ID type 316, stainless-steel horizontal tubes arranged in two parallel streams, and has a design duty of 1,890,000 Btu per hr. Feed to the preheater consists of middle oil from the liquid-phase operation (620 F end point), and recycle oil from the vapor-phase distillation, which, together with hydrogen, comes from the product-feed exchanger with a temperature of about 780 F to the preheater. The preheater superheats the oil vapors to reaction temperature or to about 900 F.

Design data for the vapor-phase preheater are given in Table 3.

TABLE 3 DESIGN DATA FOR VAPOR-PHASE PREHEATER

	Maximum design conditions
Heat duty, Btu per hr.....	1890000
Quantity input, lb per hr—Vapor.....	15650
Inlet pressure, psig.....	10300
Maximum working pressure, psig.....	10300
Pressure drop (estimated), psig.....	430
Firebox temperature, deg F.....	1450
Flue-gas temperature leaving furnace, deg F.....	1200
Heat fired, Btu per hr (max).....	2910000
Furnace efficiency, per cent.....	65

Both the liquid- and vapor-phase preheaters were furnished by Alcorn Combustion Company, Philadelphia, Pa.

HEAT EXCHANGERS

The foregoing discussion shows how important it is to provide good heat exchange and how necessary it is to utilize fully the heat of reaction in the converters. The demonstration plant, however, was purposely not designed for maximum heat recovery, since the additional expense could not be justified in such a small plant. There are 40 heat exchangers in the plant. Thirty-one exchangers are designed for low-pressure service in the distillation and storage areas. Nine exchangers are designed for 700-atm operation in the liquid- and vapor-phase hydrogenation. All except the HOLD cooler are double-pipe exchangers, and only two of these high-pressure exchangers service process streams with the full 10,300 psi in both tubes. The wall thickness of the inside tube in these two exchangers is only 8 gage. It is designed for a differential pressure of 2000 psi so that testing and starting has to be done with both tubes under pressure. The other high-pressure exchangers are designed with full 10,300 psi operating pressure on the inside tube, the outside tube consisting of a low-pressure tube jacket in which either cooling water or low-pressure oil is flowing. The tube jackets are constructed of carbon steel, and the high-pressure tubes of 8-10 per cent chrome and $\frac{1}{2}$ per cent molybdenum alloy. The HOLD cooler is a forced-draft air cooler with eight hairpins, made with Croloy-9M tubes, 30 ft long and 1 in. ID, connected in series flow. The cooling air passes downward at 58 fps through a 64-in. \times 10-in. rectangular duct enclosing the

hairpins. All exchangers in high-pressure service were supplied by Industrial Engineers, Inc., Los Angeles, Calif.

The demonstration plant was designed in order that the following information may be obtained: (1) Heat balances to determine where the different heat quantities occur and in what relationship they occur; (2) the type of heat-exchange equipment most suitable for a particular heat-exchange job; and (3) determination of film heat-transfer coefficients and fouling factors. This information will be obtained on only the high-pressure equipment, since heat-exchange design in the low-pressure area follows conventional petroleum-refinery practice. All of the points mentioned must be investigated with the view of obtaining design data for commercial plants. As an example of the type of information to be obtained, a heat balance around the liquid-phase stall of the demonstration plant has been calculated as shown in Table 4 and summarized in Fig. 7.

Although this heat balance is applicable to the demonstration plant, the heat ratio of the top and bottom products will be maintained in commercial plants. This ratio is approximately 12,000,000 : 3,000,000 Btu per hr or 4 to 1. Heat exchange can best be carried out on the top product. The heat balance shows that the heat contained in the top product is sufficient to supply the following requirement:

Heat required:	
3793 lb per hr hydrogen.....	2,750,000
20,183 lb per hr paste (preheater).....	6,740,000
Total.....	9,490,000

Heat available from top product of the hot catchpot, Btu per hr.....	12,280,000
---	------------

It can be seen that the heat required is only about 75 per cent of the heat available. The problem is how to utilize fully this heat, and one answer to the problem may again be found in later German developments. These developments introduced a heat-exchange procedure in which two paste streams of different solids content were used. Thick paste with a total solids content of 53 per cent was heated in an exchanger train up to its swelling tem-

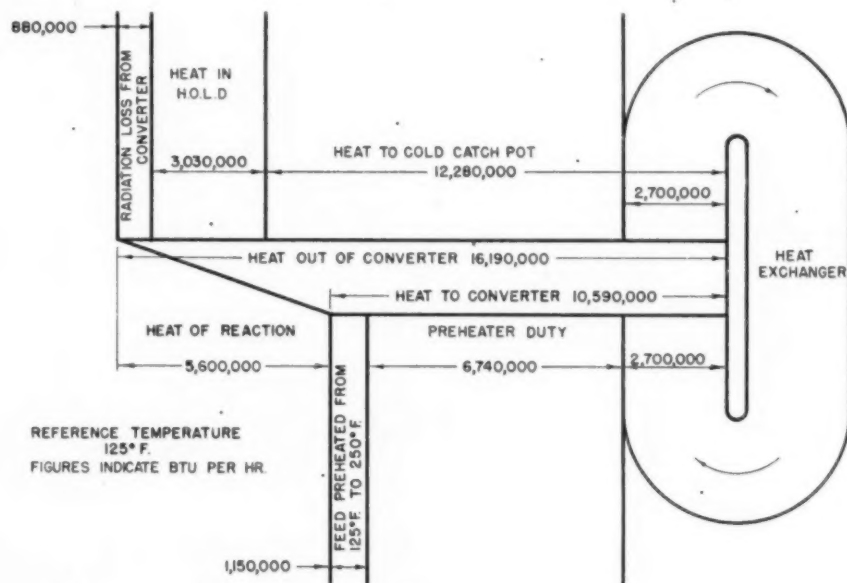


FIG. 7 HEAT BALANCE AROUND LIQUID-PHASE STALL

TABLE 4 HEAT BALANCE—LIQUID-PHASE STALL COAL-HYDROGENATION DEMONSTRATION PLANT, ROCK SPRINGS COAL
(Reference temperature, 125 F)

	Heat in					Heat out			
	lb per hr	spec. heat	Δt deg F	M Btu per hr		lb per hr	Spec. heat	Δt deg F	M Btu/hr
Feed preheat:					Heat to cold catchpot (hot catchpot overhead)				
Paste.....	20183	0.44	(250-125)	1100	Liquid-oil product.....	10775	0.62	(880-125)	5080
Paste gas (H ₂).....	293	1.31	(250-125)	50	Hydrogen-gas product.....	1297	0.76	(880-125)	750
Recirculated gas (H ₂ by heat exchange).....	3500	1.31	(710-125)	2700	Unreacted H ₂ gas.....	3375	1.31	(880-125)	3400
Preheater duty.....			(800-250)	6740	Water formed in reaction.....	660		1300 Btu per lb	860
Cooling gas (H ₂).....	2220	1.31	(125-125)	...	Cooling gas (H ₂).....	2220	1.31	(880-125)	2190
Total heat into converter.....				10590	Total.....	18327			12280
Heat of reaction.....				5600	Heat in HOLD (Hot catchpot bottoms).....	7869	0.57	(800-125)	3030
Total.....	26196			16190	Total.....	26196			15310
					Radiation loss.....				880
					Total.....	26196			16190

perature of 570 F. A thin paste with 42 per cent solids content made by diluting the thick paste with pasting oil, was heated in another exchanger train up to full reaction temperature with no difficulty. These two streams were then combined, and the remaining heat supplied in a small preheater. This procedure was not as advantageous as it should have been because of wide fluctuations in solids content of the various paste batches due to poor mixing technique.

It is anticipated in a projected 30,000-bbl per day coal-hydrogenation plant that a nearly perfect heat exchange can be achieved using a single paste with 47 per cent total-solids content. To do this, however, improved mixing controls must be introduced in order to insure a constant quality of paste. The preparation of the coal must also be such that all fines are eliminated from the process coal. These may be burned in the power plant. The heat-exchange system for the 30,000-bbl per day plant is shown in Fig. 8. The paste flow is divided into two streams, in such a manner that the larger stream (approximately 75 per cent), is heated up in exchangers to the reaction temperature without a preheater. The smaller stream is heated in exchangers to as high

a temperature as the remaining heat will allow, and further heat requirement is supplied with a small preheater. The extent of improvement by carrying out the foregoing procedure can be shown by comparison with conventional German design, that is, 3 times the German throughput can be obtained with the same number of preheaters of smaller duty.

Since the total heat requirement of the process can be supplied from the top products of the hot catchpot, the question arises as to how the heat from the bottom products can be used economically. There are several considerations as follows:

1 In the demonstration plant, the feasibility of a flash distillation of the heavy-oil let-down (HOLD) will be determined. Therefore it may be possible that in larger plants the bottom product of the hot catchpot may be flash-distilled without cooling.

2 If it becomes necessary to cool the HOLD for other treatment, such as centrifuging, steam can be produced by jacketing the HOLD lines.

3 If there is no need or demand for steam, the temperature can be lowered by a combination of air-and-water cooling.

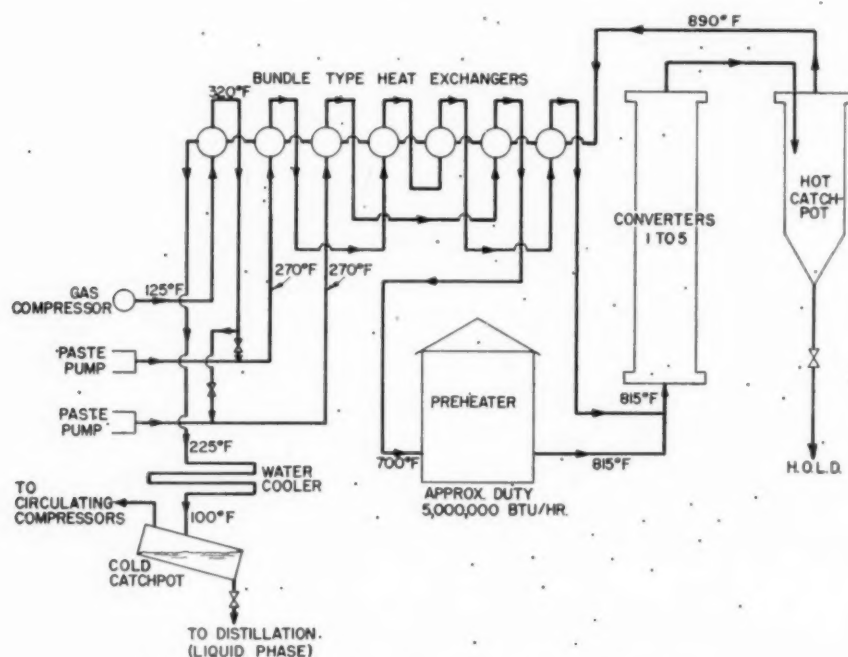


FIG. 8 PROPOSED HEAT-EXCHANGE SYSTEM FOR COMMERCIAL PLANT

There is no hot catchpot in the vapor-phase hydrogenation plant, and the heat of reaction is very high. Therefore a better heat exchange can be established in the vapor phase than in the liquid phase. The vapor-phase section can be operated without any external heat supply. Only a small preheater is necessary for starting-up operations.

The heat exchangers which were used in Germany were the shell-and-tube type designed for 10,000 psig operating pressure and placed in a vertical position. The bundle was inserted in a high-pressure internally insulated vessel and connected outside by means of a stuffing box on the top of the heat exchanger. The paste-feed stream flowed outside the tubes from bottom to top, and the product inside the tubes from top to bottom. The center-to-center distance of the tubes was determined by fabricating limitations and by the composition of the paste feed, that is to say, by the clogging tendency of the paste to form bridges between the tubes. A single design and size were used in both liquid-phase and vapor-phase operation. The tubes of this exchanger were designed for the full operating pressure of 10,000 psig. The bundle was designed with 199 tubes, (0.55 in. ID \times 0.91 in. OD), about 57 ft long, for use in a high-pressure vessel of 22 in. ID. The average heating surface was 2150 sq ft. Originally, forged shells were used, but later designs were based upon wrapped or spiral-wound construction.

In designing high-pressure heat exchangers for commercial plants, consideration has to be given to: (1) The thickness and material of the tube walls; (2) the minimum distance between center to center of the tubes; (3) pressure difference of the gas-recycle compressors, in order to determine the cross section of the heat-exchanger bundle; and (4) equal distribution of the product and the feed through the heat exchanger.

In special cases, for instance, with the heavy-oil letdown, double-pipe exchangers are quite effective. The HOLD stream flows through the tubes and the medium to be heated through the annular space. These double-pipe exchangers for 700-atm design pressure are cumbersome, owing to the extreme wall thickness.

FILM HEAT-TRANSFER COEFFICIENTS

Film heat-transfer coefficients of all gases increase greatly with pressure at constant linear velocity, as shown in the calculated example for pure hydrogen in Table 5. This, combined with the fact that the thermal conductivity of hydrogen is about 10 times that of other gases such as nitrogen, carbon monoxide, and carbon dioxide, makes for high film coefficients in coal-hydrogenation heat-exchange equipment.

The principal consideration in determination of the film co-

TABLE 5 EFFECT OF PRESSURE ON FILM HEAT-TRANSFER COEFFICIENT OF PURE HYDROGEN

	Pressure		
	1 atm	20 atm	700 atm
Standard cu ft per hr at 60 F.....	1000000	1000000	1000000
Cu ft per hr at flow.....	1000000	56000	2250
Pounds per hour.....	5320	5320	5320
Density, lb per cu ft.....	0.00532	0.095	2.56
Pipe ID, in.....	32.0	7.5	1.5
Linear velocity, fps.....	50	50	50
Mass velocity, lb per sec-ft ²	0.266	4.75	118
Calculated film heat-transfer coefficient, Btu per hr-ft ² -deg F.....	9	115	2100

efficient of the gas streams is the hydrogen purity, due to the effect of the high thermal conductivity of hydrogen on the film-transfer coefficient. Since the film coefficient for hydrogen-containing gases is high, especially at 700 atm, the use of the correct fouling factor also becomes very important. Fouling is quite rapid on new exchangers; therefore a film coefficient of about 110 Btu/hr-ft²-deg F for hydrogen of 80-90 per cent purity flowing at a velocity of about 15 fps, is a reasonable design figure.

Since coal paste is always heated up in the presence of hydrogen, its high thermal conductivity increases the film coefficient of the paste. The film coefficient is highly dependent on the solid concentration of the paste, and also on the fineness of the pulverized coal; but the fact was established in Germany that the film coefficient for the same paste was higher in the heat exchangers than in the preheater within the same temperature range. This effect was contributed to a better flow distribution through the heat-exchanger bundle. The film-coefficient values varied from 80-120 Btu/hr-ft²-deg F in the paste heat exchangers with a paste velocity of 8 fps.

Film coefficients range from 130-160 Btu/hr-ft²-deg F for middle oil and hydrogen in the relative portions used in vapor-phase hydrogenation where 15 to 30 cu ft of hydrogen is used per lb of oil at velocities from 6 to 15 fps. This range applies after a few months of operation.

The film coefficients for heavy-oil letdown (HOLD) have been determined from German data on air coolers. This coefficient varies with solids and asphalt content of the HOLD, but an average figure for this coefficient is 90 Btu/hr-ft²-deg F at velocities ranging from 9 to 15 fps and at temperatures above 400 F.

The German data quoted in this report were useful in designing the demonstration plant, and it is hoped that the operation of the plant will furnish the necessary information on all varieties of American coals. When these data are determined, perhaps an ideal heat-exchange system for future big-scale plants can be designed in both phases, and the use of both preheaters will become obsolete.

C
the
of l
shap
gave
negl
that
elem
the
acco
The
case
also

A

Ever
the s
coura
lems.

M
taken
the o
analy

It
simpl
a sha
with

In
slider
vario
very
face
probl
load
est lo

Fig. 1

Th
side l
speed
 h_1 , res

Wi
maxim

¹ Sc
² "N
iophic
Com
Petrol
York,
Societ
Not
stood
Society

A Simple Hydrodynamic Thrust Bearing

By F. R. ARCHIBALD,¹ PRINCETON, N. J.

Considerable mathematical difficulty has handicapped the designer in the application of the hydrodynamic theory of lubrication. This difficulty arises essentially from the shapes assumed by the oil films. In 1918 Lord Rayleigh gave a detailed analysis of the simple slider bearing, neglecting the side-leakage effect, in which he determined that the greatest load capacity occurs when the slider element gives a stepped convergence to the oil film. From the simple geometry of this oil film, a solution, taking account of side leakage, might be obtained fairly easily. The author proves this to be so, and gives solutions for the case of rectilinear motion with finite bearing width, and also the more practical sectorial case of a thrust bearing.

APPLICATIONS of the theory of lubrication have been handicapped by the considerable mathematical difficulties encountered in the solution of practical problems. Even in the elementary case of a flat inclined plate of finite width, the solution, given by A. G. M. Michell, is so difficult as to discourage much hope for the solution of many other practical problems.

Much of the mathematical difficulty arises from the shapes taken by oil films. Therefore, if a bearing can be devised in which the oil film has a simple shape there is a good prospect that an analytical solution can be given for its performance.

It might be thought impossible to obtain an oil-film shape simpler than that given by the inclined flat plate, but there is such a shape. At least there is a configuration much simpler to deal with in the lubrication problem.

In 1918 Lord Rayleigh² gave a detailed analysis of the simple slider bearing neglecting the side-leakage effect. He considered various shapes for the surface of the slider element. After showing very slight improvement in the load capacity when the slider surface was curved instead of being flat, he then set the variational problem to find the best possible shape from the point of view of load capacity. The result of this analysis was to show that greatest load capacity occurs if the slider element is made as shown in Fig. 1, giving a stepped convergence to the oil film.

The results of the flat inclined slider-bearing calculation, when side leakage is neglected, are well known. For a given viscosity, speed, length of slider, and minimum film thickness, μ , U , c , and h_1 , respectively, the maximum load per unit width is given by

$$W_{\max} = \frac{0.160\mu U c^2}{h_1^2}$$

With the shape given by Rayleigh it is possible to have a maximum load per unit width of

$$W_{\max} = \frac{0.206\mu U c^2}{h_1^2}$$

¹ School of Engineering, Princeton University.

² "Notes on the Theory of Lubrication," by Lord Rayleigh, *Philosophical Magazine*, vol. 35, 1918, pp. 1-12.

Contributed by the Research Committee on Lubrication and the Petroleum Division and presented at the Annual Meeting, New York, N. Y., November 27-December 2, 1949, of THE AMERICAN SOCIETY OF MECHANICAL ENGINEERS.

NOTE: Statements and opinions advanced in papers are to be understood as individual expressions of their authors and not those of the Society. Paper No. 49-A-29.

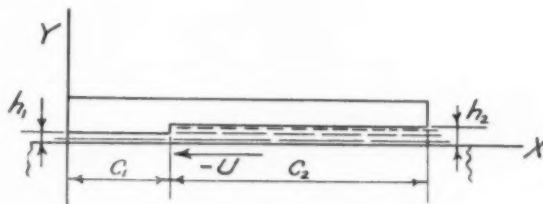


FIG. 1

This is about 29 per cent greater than for the inclined flat-plate bearing.

It would appear that with the simple geometry of this oil film, a solution, taking account of side leakage, might be fairly easy to obtain. This turns out to be so and solutions are given both for the case of rectilinear motion with finite bearing width and also the more practical sectorial case of a thrust bearing.

CASE WITH NO SIDE LEAKAGE

Before proceeding to the more complicated three-dimensional problem the case with no side leakage might be considered to advantage. The "calculus of variations" is perhaps not familiar to many who may be interested in the problem, and in any event this method of solution is available in Rayleigh's more elegant paper. Therefore the results will be obtained by the usual methods, but starting with the stepped-film shape. The notation will be the same as in Rayleigh's paper.²

From a consideration of the shear stress and velocity gradient in the film it is easily shown that

$$\frac{\partial^2 u}{\partial y^2} = \frac{1}{\mu} \frac{dp}{dx} \quad [1]$$

Upon integrating this equation twice with respect to y and substituting the boundary conditions; $u = -U$ when $y = 0$, and $u = 0$ when $y = h$, the following expression for u is obtained

$$u = \frac{y^2 - hy}{2\mu} - \left(1 - \frac{y}{h}\right) U \quad [2]$$

By integrating this expression over the film thickness the flow per unit width is obtained as

$$-Q = -\frac{1}{12} \frac{h^3}{\mu} \frac{dp}{dx} - \frac{1}{2} U h \quad [3]$$

This same expression for flow in the X -direction is obtained in the side-leakage problem, but in this case it is the rate of flow at a point rather than over a unit width. A partial derivative of p with respect to x is also necessary in this case. Because this relation is needed in the three-dimensional problem it will be given here

$$-q_x = -\frac{1}{12} \frac{h^3}{\mu} \frac{\partial p}{\partial x} - \frac{1}{2} U h \quad [3a]$$

From Equation [3]

$$\frac{dp}{dx} = \frac{6\mu U}{h^3} \left(\frac{2Q}{U} - h \right)$$

Call

$$\frac{2Q}{U} = H$$

Then

$$\frac{dp}{dx} = \frac{6\mu U}{h^3} (H - h) \quad [4]$$

If h is constant this equation can be integrated to give the pressure as follows

$$p = \frac{6\mu U}{h^3} (H - h)x + A \quad [5]$$

The evaluation of A depends on the boundary conditions. It is convenient here (and more so in the three-dimensional problem) to consider the problem for each stepped region separately. The co -ordinate axis being left as in Fig. 1 for region (1) and being moved forward by $(c_1 + c_2)$, i.e., to the leading edge, for region (2).

For region (1) when $x = 0$, $p = 0$ and $A = 0$

$$\therefore p = \frac{6\mu U}{h_1^3} (H - h_1)x \quad [6]$$

For region (2), when $x = 0$, $p = 0$, and $A = 0$

$$\therefore p = \frac{6\mu U}{h_2^3} (H - h_2)x \quad [7]$$

The pressure given by Equation [6] when $x = c_1$ is the same as that given by Equation [7], when $x = -c_2$

$$\frac{6\mu U}{h_1^3} (H - h_1)c_1 = -\frac{6\mu U}{h_2^3} (H - h_2)c_2$$

which upon solving for H gives

$$H = \frac{h_1 h_2 (c_1 h_2^3 + c_2 h_1^3)}{c_1 h_2^3 + c_2 h_1^3} \quad [8]$$

The load for each region is obtained by integrating the pressure over the areas as follows:

For region (1)

$$W_1 = \int_0^{c_1} p dx = \frac{6\mu U}{h_1^3} (H - h_1) \int_0^{c_1} x dx = \frac{3\mu U}{h_1^3} (H - h_1) c_1^2 \quad [9]$$

For region (2)

$$W_2 = \int_{-c_2}^0 p dx = \frac{6\mu U}{h_2^3} (H - h_2) \int_{-c_2}^0 x dx = \frac{3\mu U}{h_2^3} (h_2 - H) c_2^2 \quad [10]$$

The total load, $W = W_1 + W_2$

$$\begin{aligned} \therefore W &= 3\mu U \left[\left(\frac{H - h_1}{h_1^3} \right) c_1^2 + \left(\frac{h_2 - H}{h_2^3} \right) c_2^2 \right] \\ &= 3\mu U \left[H \left(\frac{c_1^2}{h_1^3} - \frac{c_2^2}{h_2^3} \right) + \frac{c_2^2}{h_2^3} - \frac{c_1^2}{h_1^3} \right] \quad [11] \end{aligned}$$

If H from Equation [8] is now placed in Equation [11] the load is obtained as a function of the parameters

$$W = 3\mu U \left[\frac{h_1 h_2 (c_1 h_2^3 + c_2 h_1^3)}{c_1 h_2^3 + c_2 h_1^3} \left(\frac{c_1^2 h_2^3 - c_2^2 h_1^3}{h_1^3 h_2^3} \right) + \frac{c_2^2 h_1^3 - c_1^2 h_2^3}{h_1^3 h_2^3} \right]$$

This expression for W will simplify to

$$W = 3\mu U c_1 c_2 (c_1 + c_2) \frac{h_2 - h_1}{c_1 h_2^3 + c_2 h_1^3} \quad [12]$$

If the total length of the bearing $c = (c_1 + c_2)$, and the minimum film thickness h_1 , are prescribed, the proportions for maximum load capacity can be found as follows

$$c_2 = c - c_1, \quad \text{and let } h_2 = kh_1$$

Then

$$W = \frac{3\mu U c c_1 (c - c_1) (k - 1)}{h_1^3 [c_1 (k^3 - 1) + c]}$$

$W = f(c_1, k)$ and will have a maximum when $\partial W / \partial c_1 = 0$ and $\partial W / \partial k = 0$

$$\frac{\partial W}{\partial c_1} = \frac{3\mu U c (k - 1)}{h_1^3} \times \left\{ \frac{[c_1 (k^3 - 1) + c] (c - 2c_1) - c_1 (c - c_1) (k^3 - 1)}{[c_1 (k^3 - 1) + c]^2} \right\} \quad [13]$$

For $\partial W / \partial c_1 = 0$ it is sufficient that

$$[c_1 (k^3 - 1) + c] (c - 2c_1) - c_1 (c - c_1) (k^3 - 1) = 0$$

which will reduce to

$$k^3 = \left(\frac{c - c_1}{c_1} \right)^2 \quad [14]$$

$$\frac{\partial W}{\partial k} = \frac{3\mu U c_1 c (c - c_1)}{h_1^3} \left\{ \frac{c_1 (k^3 - 1) + c - 3(k - 1) c_1 k^2}{[c_1 (k^3 - 1) + c]^2} \right\}$$

For $\partial W / \partial k = 0$ it is sufficient that

$$c_1 (k^3 - 1) + c - 3(k - 1) c_1 k^2 = 0$$

which will reduce to

$$c_1 = \frac{c}{1 - 3k^2 + 2k^3} \quad [15]$$

From Equation [14]

$$c = c_1 (k^{3/2} + 1)$$

Substituting in Equation [15]

$$c_1 = \frac{c_1 (k^{3/2} + 1)}{1 - 3k^2 + 2k^3}$$

which will reduce to

$$4k^3 - 12k^2 + 9k - 1 = 0$$

The three roots of this equation are

$$k = 1 \text{ and } k = 1 \pm \sqrt{3}/2$$

Obviously, the required value for maximum load is $k = 1 + \sqrt{3}/2 = 1.866$

Now $(c_1 + c_2) = c$, and from Equation [14]

$$c_1 (1 - 3k^2 + 2k^3) = c$$

With $k = 1.866$ these relations make $c_2 = 2.549c_1$

The maximum load from Equation [12] is now found as

$$W = 0.2062 \frac{\mu U c^2}{h_1^2} \quad [16]$$

These results are the same as given by Rayleigh.

STEPPED SHAPED SLIDER

The problem of the stepped shaped slider of finite width will next be considered. In this case a flow perpendicular to the direction of motion, i.e., a side-leakage effect, has to be included and recourse is had to Reynolds partial differential equation for pressure in a lubricating film

$$\frac{\partial}{\partial x} \left(h^3 \frac{\partial p}{\partial x} \right) + \frac{\partial}{\partial z} \left(h^3 \frac{\partial p}{\partial z} \right) = 6\mu U \frac{dh}{dx} \quad [17]$$

The scheme of the bearing is as shown in Fig. 2.

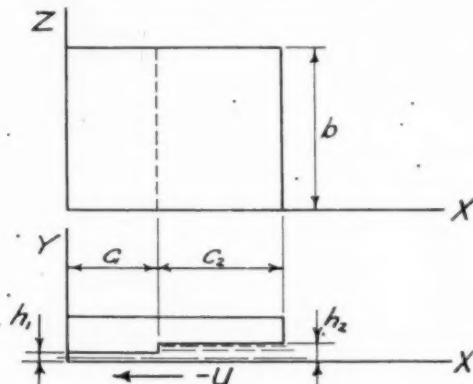


FIG. 2

The region in which h is constant at h_1 is called region (1), and the region in which h is constant at h_2 is called region (2). The X - Z plane is taken as the flat moving element having a velocity $-U$ as shown. It will again be found convenient to use two coordinate systems. For region (1) the co-ordinates are as shown, but for region (2) they will be moved forward so that the Z axis is on the leading edge of region (2).

If h is constant, the right-hand side of Reynolds equation is zero, and h^3 can be divided from the left-hand side leaving

$$\frac{\partial^2 p}{\partial x^2} + \frac{\partial^2 p}{\partial z^2} = 0 \quad [18]$$

This is the Laplace partial differential equation.

An interesting incidental result can be obtained at this stage. Consider a rectangular flat plate being moved parallel to another flat plate and separated from it by a fluid film of thickness h , Fig. 3.

In this case Equation [18] applies. However, if Laplace's

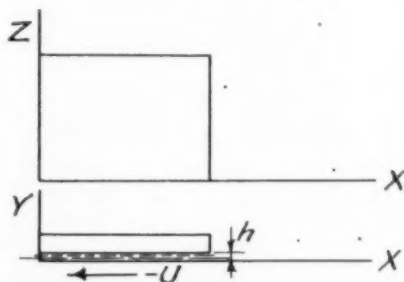


FIG. 3

equation applies to a region, on the boundaries of which the function is everywhere zero, the only solution is zero, i.e., $p = 0$ is the solution to the pressure equation in this case. This is a well-known result and is not of course restricted to a rectangular shape.

To return to the problem of the stepped slider. The pressure on the exterior boundaries of regions (1) and (2) is zero, but on the common boundary the pressure is not known. It is assumed that the pressure on this common boundary is given by the following Fourier sine series

$$p = \sum_{n=1,3,5,\dots}^{\infty} P_n \sin \frac{n\pi z}{b} \quad [19]$$

The summation is over the odd values because of the symmetry. P_n is the Fourier coefficient to be evaluated later.

The general solution for p can be put in the following form

$$p = \sum_{n=1,3,5,\dots}^{\infty} \left(A_n \cos \frac{n\pi x}{b} + B_n \sin \frac{n\pi x}{b} \right) \left(C_n \cosh \frac{n\pi x}{b} + D_n \sinh \frac{n\pi x}{b} \right) \quad [20]$$

The boundary conditions for region (1) are

$p = 0$ at $x = 0$ for all values of z I

$p = 0$ at $z = 0$ for all values of x II

$p = 0$ at $z = b$ for all values of x III

$$p = \sum_{n=1,3,5,\dots}^{\infty} P_n \sin \frac{n\pi z}{b} \text{ at } x = c_1 \text{ IV}$$

From conditions I and II, $A_n = C_n = 0$

From condition IV

$$\sum_{n=1,3,5,\dots}^{\infty} P_n \sin \frac{n\pi z}{b} = \sum_{n=1,3,5,\dots}^{\infty} B_n D_n \sin \frac{n\pi z}{b} \sinh \frac{n\pi c_1}{b}$$

$$\therefore B_n D_n = \frac{P_n}{\sinh \frac{n\pi c_1}{b}}$$

$$\therefore p = \sum_{n=1,3,5,\dots}^{\infty} \frac{P_n}{\sinh \frac{n\pi c_1}{b}} \sin \frac{n\pi z}{b} \sinh \frac{n\pi x}{b} \quad [21]$$

For region (2) a solution of the same form as Equation [20] is taken

$$p = \sum_{n=1,3,5,\dots}^{\infty} \left(E_n \cos \frac{n\pi x}{b} + F_n \sin \frac{n\pi x}{b} \right) \left(G_n \cosh \frac{n\pi x}{b} + H_n \sinh \frac{n\pi x}{b} \right) \quad [22]$$

The boundary conditions are

$p = 0$ at $x = 0$ for all values of z I

$p = 0$ at $z = 0$ for all values of x II

$p = 0$ at $z = b$ for all values of x III

$$p = \sum_{n=1,3,5,\dots}^{\infty} P_n \sin \frac{n\pi z}{b} \text{ at } x = -c_2 \text{ IV}$$

From conditions I and II, $E_n = G_n = 0$

From condition IV

$$\sum_{n=1,3,5,\dots}^{\infty} P_n \sin \frac{n\pi z}{b} = - \sum_{n=1,3,5,\dots}^{\infty} F_n H_n \sin \frac{n\pi z}{b} \sinh \frac{n\pi c_2}{b}$$

$$\therefore F_n H_n = - \frac{P_n}{\sinh \frac{n\pi c_2}{b}}$$

$$\therefore p = - \sum_{n=1,3,5,\dots}^{\infty} \frac{P_n}{\sinh \frac{n\pi c_2}{b}} \sin \frac{n\pi z}{b} \sinh \frac{n\pi x}{b} \dots [23]$$

In order that the pressure be calculable the Fourier coefficient, P_n , must now be evaluated. This is done by making use of the principle of continuity. At any point on the common boundary it will be seen that the rate of flow out of region (2) is the same as the rate of flow into region (1). The rate of flow in the X -direction is given by Equation [3a]

$$-q_x = - \frac{Uh}{2} - \frac{h^3}{12\mu} \frac{\partial p}{\partial x} \dots [3a]$$

The equality of the rate of flow for both regions at the common boundary is expressed as follows

$$\frac{Uh_1}{2} + \frac{h_1^3}{12\mu} \left(\frac{\partial p}{\partial x} \right)_{c_1} = \frac{Uh_2}{2} + \frac{h_2^3}{12\mu} \left(\frac{\partial p}{\partial x} \right)_{-c_2} \dots [24]$$

The partial derivative, $\partial p / \partial x$, for regions (1) and (2) must now be evaluated at $x = c_1$ for region (1), and at $x = -c_2$ for region (2).

For region (1)

$$\frac{\partial p}{\partial x} = \sum_{n=1,3,5,\dots}^{\infty} \frac{n\pi}{b} \frac{P_n}{\sinh \frac{n\pi c_1}{b}} \sin \frac{n\pi z}{b} \cosh \frac{n\pi x}{b}$$

$$\therefore \left(\frac{\partial p}{\partial x} \right)_{c_1} = \sum_{n=1,3,5,\dots}^{\infty} \frac{n\pi}{b} P_n \coth \frac{n\pi c_1}{b} \sin \frac{n\pi z}{b} \dots [25]$$

For region (2)

$$\frac{\partial p}{\partial x} = - \sum_{n=1,3,5,\dots}^{\infty} \frac{n\pi}{b} \frac{P_n}{\sinh \frac{n\pi c_2}{b}} \sin \frac{n\pi z}{b} \cosh \frac{n\pi x}{b}$$

$$\therefore \left(\frac{\partial p}{\partial x} \right)_{-c_2} = - \sum_{n=1,3,5,\dots}^{\infty} \frac{n\pi}{b} P_n \coth \frac{n\pi c_2}{b} \sin \frac{n\pi z}{b} \dots [26]$$

Equation [24] is rewritten using the values of $\partial p / \partial x$ from Equations [25] and [26]

$$\frac{Uh_1}{2} + \frac{h_1^3}{12\mu} \sum_{n=1,3,5,\dots}^{\infty} \frac{n\pi}{b} P_n \coth \frac{n\pi c_1}{b} \sin \frac{n\pi z}{b} = \frac{Uh_2}{2} - \frac{h_2^3}{12\mu} \sum_{n=1,3,5,\dots}^{\infty} \frac{n\pi}{b} P_n \coth \frac{n\pi c_2}{b} \sin \frac{n\pi z}{b} \dots [27]$$

which can be rearranged as follows

$$\sum_{n=1,3,5,\dots}^{\infty} \frac{n\pi}{b} P_n \left(h_1^3 \coth \frac{n\pi c_1}{b} + h_2^3 \coth \frac{n\pi c_2}{b} \right) \sin \frac{n\pi z}{b} = 6\mu U(h_2 - h_1) \dots [28]$$

The right-hand side of Equation [28] is expanded in a Fourier sine series by use of the standard sine series for $\pi/4$

$$\sum_{n=1,3,5,\dots}^{\infty} \frac{n\pi}{b} P_n \left(h_1^3 \coth \frac{n\pi c_1}{b} + h_2^3 \coth \frac{n\pi c_2}{b} \right) \sin \frac{n\pi z}{b} = \sum_{n=1,3,5,\dots}^{\infty} 6\mu U(h_2 - h_1) \frac{4}{n\pi} \sin \frac{n\pi z}{b}$$

The Fourier coefficient, P_n is thus

$$P_n = \frac{24\mu U b (h_2 - h_1)}{n^2 \pi^2 \left(h_1^3 \coth \frac{n\pi c_1}{b} + h_2^3 \coth \frac{n\pi c_2}{b} \right)} \dots [29]$$

The pressure can now be calculated at any point by placing this value of P_n in the pressure Equations [21] and [23]. However, the total load on the bearing is of more interest, and this is easily found. The load supported by region (1) is called W_1 and the load supported by region (2) is called W_2

$$W_1 = \int_0^b \int_0^{c_1} p \, dx \, dz$$

$$\therefore W_1 = \int_0^b \int_0^{c_1} \sum_{n=1,3,5,\dots}^{\infty} \frac{P_n}{\sinh \frac{n\pi c_2}{b}} \sin \frac{n\pi z}{b} \sinh \frac{n\pi x}{b} \, dx \, dz$$

$$= \int_0^b \sum_{n=1,3,5,\dots}^{\infty} \frac{b}{n\pi} \frac{P_n}{\sinh \frac{n\pi c_2}{b}} \left(\cosh \frac{n\pi c_1}{b} - 1 \right) \sin \frac{n\pi z}{b} \, dz$$

$$\therefore W_1 = \sum_{n=1,3,5,\dots}^{\infty} \frac{2b^2 P_n}{n^2 \pi^2 \sinh \frac{n\pi c_1}{b}} \left(\cosh \frac{n\pi c_1}{b} - 1 \right) \dots [30]$$

Again, for region (2)

$$W_2 = \int_0^b \int_{-c_2}^0 - \sum_{n=1,3,5,\dots}^{\infty} \frac{P_n}{\sinh \frac{n\pi c_2}{b}} \sin \frac{n\pi z}{b} \sinh \frac{n\pi x}{b} \, dx \, dz$$

$$= \int_0^b \sum_{n=1,3,5,\dots}^{\infty} \frac{b}{n\pi} \frac{P_n}{\sinh \frac{n\pi c_2}{b}} \left(\cosh \frac{n\pi c_2}{b} - 1 \right) \sin \frac{n\pi z}{b} \, dz$$

$$\therefore W_2 = \sum_{n=1,3,5,\dots}^{\infty} \frac{2b^2 P_n}{n^2 \pi^2 \sinh \frac{n\pi c_2}{b}} \left(\cosh \frac{n\pi c_2}{b} - 1 \right) \dots [31]$$

The total load, $W = W_1 + W_2$

Then

$$W = \sum_{n=1,3,5,\dots}^{\infty} \frac{2b^2 P_n}{n^2 \pi^2} \left(\frac{\cosh \frac{n\pi c_1}{b} - 1}{\sinh \frac{n\pi c_1}{b}} + \frac{\cosh \frac{n\pi c_2}{b} - 1}{\sinh \frac{n\pi c_2}{b}} \right)$$

By use of standard relations for the hyperbolic functions, W can be rewritten as

$$W = \sum_{n=1,3,5,\dots}^{\infty} \frac{2b^2 P_n}{n^2 \pi^2} \left(\tanh \frac{n\pi c_1}{2b} + \tanh \frac{n\pi c_2}{2b} \right)$$

If P_n from Equation [29] is substituted, the load is obtained as

$$W = \frac{48\mu U b^3 (h_2 - h_1)}{\pi^4} \sum_{n=1,3,5,\dots}^{\infty} \frac{1}{n^4} \frac{\tanh \frac{n\pi c_1}{2b} + \tanh \frac{n\pi c_2}{2b}}{h_1^3 \coth \frac{n\pi c_1}{b} + h_2^3 \coth \frac{n\pi c_2}{b}} \dots [32]$$

The foregoing solution applies to a rectangular slider having uniform rectilinear motion. This simplified problem is a logical first step because the mathematical work is more likely to be soluble. The result is also useful for comparison with the results of Michell's solution for the inclined flat-plate bearing. However, a more practical solution is possible, and this will be given before discussing the implications of Equation [32].

STEPPED SECTORIAL SLIDER

Instead of the stepped rectangular slider consider a stepped sectorial slider as shown in Fig. 4.

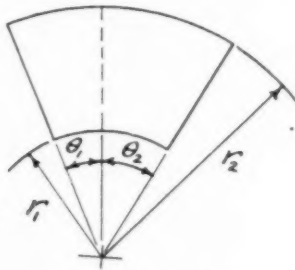


FIG. 4

With such a configuration, it is natural to adopt plane polar co-ordinates. Laplace's equation, that is Equation [18], in polar co-ordinates becomes

$$\frac{\partial^2 p}{\partial r^2} + \frac{1}{r^2} \frac{\partial^2 p}{\partial \theta^2} + \frac{1}{r} \frac{\partial p}{\partial r} = 0 \dots [33]$$

A new variable is introduced by letting $r = r_1 e^\rho$, where r_1 is the inner radius of the sector and ρ is the new variable. Clearly, when

$$r = r_1, \rho = 0, \text{ and when } r = r_2, \rho = \rho_2 = \log r_2/r_1$$

If the new variable ρ is substituted, Equation [33] becomes

$$\frac{\partial^2 p}{\partial \rho^2} + \frac{\partial^2 p}{\partial \theta^2} = 0 \dots [34]$$

The solution now proceeds on almost exactly similar lines to the rectangular case. It is assumed that the pressure on the common boundary is given by

$$p = \sum_n P_n \sin \frac{n\pi \rho}{\rho_2} \dots [35]$$

The question of what values of n are to be used in the summation is left open at this stage. It is fairly evident from the physical situation that the curve will not be symmetrical.

As in the previous cases, it is convenient to use two co-ordinate systems. For region (1) the zero of θ is taken through the trailing

edge of the slider. For region (2) the zero of θ is moved forward to the leading edge of region (2). The equations for pressure in regions (1) and (2) are obtained by the same methods as for the rectangular case and are identical in form. They are as follows:

For region (1)

$$p = \sum_n \frac{P_n}{\sinh \frac{n\pi \theta_1}{\rho_1}} \sin \frac{n\pi \rho}{\rho_1} \sinh \frac{n\pi \theta}{\rho_1} \dots [36]$$

For region (2)

$$p = - \sum_n \frac{P_n}{\sinh \frac{n\pi \theta_2}{\rho_2}} \sin \frac{n\pi \rho}{\rho_2} \sinh \frac{n\pi \theta}{\rho_2} \dots [37]$$

To calculate the Fourier coefficient P_n , it is necessary to use the rate-of-flow relation given by Equation [3a]. But now this must be expressed in polar co-ordinates. The rate of flow in the tangential direction is then

$$-q\theta = -\frac{r\omega h}{2} - \frac{h^3}{12\mu r} \frac{\partial p}{\partial \theta} \dots [38]$$

where ω is the rotational speed of the moving element.

On making the substitution $r = r_1 e^\rho$ this equation for flow becomes

$$-q\theta = -\frac{\omega r_1 e^\rho h}{2} - \frac{h^3}{12\mu r_1 e^\rho} \frac{\partial p}{\partial \theta} \dots [39]$$

The evaluation of $\partial p / \partial \theta$ at the common boundary is exactly the same as for the rectangular case and need not be repeated. The equality of the rate of flow out of region (2) into region (1) at any point on the common boundary, therefore, can be written down directly from Equation [39] and by analogy with Equation [27]

$$-\frac{\omega r_1 e^\rho h_1}{2} - \frac{h_1^3}{12\mu r_1 e^\rho} \sum_n \frac{n\pi}{\rho_2} P_n \coth \frac{n\pi \theta_1}{\rho_2} \sin \frac{n\pi \rho}{\rho_2} = -\frac{\omega r_1 e^\rho h_2}{2} + \frac{h_2^3}{12\mu r_1 e^\rho} \sum_n \frac{n\pi}{\rho_2} P_n \coth \frac{n\pi \theta_2}{\rho_2} \sin \frac{n\pi \rho}{\rho_2}$$

which can be rewritten as

$$\sum_n \frac{n\pi}{\rho_2} P_n \left(h_1^3 \coth \frac{n\pi \theta_1}{\rho_2} + h_2^3 \coth \frac{n\pi \theta_2}{\rho_2} \right) \sin \frac{n\pi \rho}{\rho_2} = 6\mu \omega r_1^2 e^{2\rho} (h_2 - h_1) \dots [40]$$

The factor $e^{2\rho}$ can be expanded in a Fourier series as follows

$$e^{2\rho} = \sum_n K_n \sin \frac{n\pi \rho}{\rho_2}$$

$$K_n = \frac{2}{\rho_2} \int_0^{\rho_2} e^{2\rho} \sin \frac{n\pi \rho}{\rho_2} d\rho$$

Upon evaluation of this integral, K_n is given for all integral values of n as

$$K_n = \frac{2n\pi[(-1)^{n+1}e^{2\rho_1} + 1]}{n^2\pi^2 + 4\rho_1^2} \dots \dots \dots [41]$$

Equation [40] can be written

$$\sum_n \frac{n\pi}{\rho_2} P_n \left(h_1^3 \coth \frac{n\pi\theta_1}{\rho_2} + h_2^3 \coth \frac{n\pi\theta_2}{\rho_2} \right) \sin \frac{n\pi\rho}{\rho_2} \\ = \sum_n 6\mu\omega r_1^2 (h_2 - h_1) K_n \sin \frac{n\pi\rho}{\rho_2} \dots \dots \dots [42]$$

This can be solved for P_n and gives, when K_n is substituted from Equation [41]

$$P_n = \frac{12\mu\omega r_1^2 \rho_2 [(-1)^{n+1}e^{2\rho_1} + 1] (h_2 - h_1)}{(n^2\pi^2 + 4\rho_2^2) \left[h_1^3 \coth \frac{n\pi\theta_1}{\rho_2} + h_2^3 \coth \frac{n\pi\theta_2}{\rho_2} \right]} \dots [43]$$

The pressure can now be found at any point of region (1) or (2) by use of Equations [36] and [37]. But, as in the rectangular case, the load is of more interest and is readily obtained by integrating over the areas. As before, W_1 will refer to the load supported by region (1), and W_2 will refer to the load supported by region (2). Then

$$W_1 = \int_{r_1}^{r_2} \int_0^{\theta_1} p r d\theta dr \\ = \int_0^{\rho_1} \int_0^{\theta_1} p r_1 e^{\rho} d\theta r_1 e^{\rho} d\rho \\ \therefore W_1 = \int_0^{\rho_1} \int_0^{\theta_1} \sum_n \frac{r_1^2 P_n}{\sinh \frac{n\pi\theta_1}{\rho_2}} e^{2\rho} \sin \frac{n\pi\rho}{\rho_2} \sinh \frac{n\pi\theta}{\rho_2} d\rho d\theta \\ = \int_0^{\rho_1} \sum_n \frac{r_1^2 P_n}{\sinh \frac{n\pi\theta_1}{\rho_2}} \frac{\rho_2}{n\pi} \left(\cosh \frac{n\pi\theta_1}{\rho_2} - 1 \right) e^{2\rho} \sin \frac{n\pi\rho}{\rho_2} d\rho \\ = \sum_n \frac{r_1^2 P_n}{\sinh \frac{n\pi\theta_1}{\rho_2}} \frac{\rho_2}{n\pi} \left[\frac{e^{2\rho} \left(-\frac{n\pi}{\rho_2} \cos n\pi \right) + \frac{n\pi}{\rho_2}}{\left(\frac{n^2\pi^2}{\rho_2^2} + 4 \right)} \right] \\ \left(\cosh \frac{n\pi\theta_1}{\rho_2} - 1 \right)$$

Since n may be even or odd, this can be written as

$$W_1 = \sum_n \frac{r_1^2 P_n [(-1)^{n+1}e^{2\rho_1} + 1]}{\left(\frac{n^2\pi^2}{\rho_2^2} + 4 \right) \sinh \frac{n\pi\theta_1}{\rho_2}} \left(\cosh \frac{n\pi\theta_1}{\rho_2} - 1 \right) \dots [44]$$

In the same way W_2 is given as follows

$$W_2 = \int_0^{\rho_2} \int_{-\theta_2}^0 \sum_n \frac{P_n}{\sinh \frac{n\pi\theta_2}{\rho_2}} e^{2\rho} \sin \frac{n\pi\rho}{\rho_2} \sinh \frac{n\pi\theta}{\rho_2} d\rho d\theta \\ \therefore W_2 = \sum_n \frac{r_1^2 P_n [(-1)^{n+1}e^{2\rho_1} + 1]}{\left(\frac{n^2\pi^2}{\rho_2^2} + 4 \right) \sinh \frac{n\pi\theta_2}{\rho_2}} \left(\cosh \frac{n\pi\theta_2}{\rho_2} - 1 \right) [45]$$

$$\therefore W = \sum_n \frac{r_1^2 P_n [(-1)^{n+1}e^{2\rho_1} + 1]}{\left(\frac{n^2\pi^2}{\rho_2^2} + 4 \right)} \left(\frac{\cosh \frac{n\pi\theta_1}{\rho_2} - 1}{\sinh \frac{n\pi\theta_1}{\rho_2}} + \frac{\cosh \frac{n\pi\theta_2}{\rho_2} - 1}{\sinh \frac{n\pi\theta_2}{\rho_2}} \right)$$

Placing in the value of P_n from Equation [43] and making use of the standard hyperbolic relations, W can be written as

$$W = 12\mu\omega r_1^2 \rho_2^3 (h_2 - h_1) \sum_n \left[\frac{(-1)^{n+1}e^{2\rho_1} + 1}{n^2\pi^2 + 4\rho_2^2} \right] \left[\frac{\tanh \frac{n\pi\theta_1}{2\rho_2} + \tanh \frac{n\pi\theta_2}{2\rho_2}}{h_1^3 \coth \frac{n\pi\theta_1}{\rho_2} + h_2^3 \coth \frac{n\pi\theta_2}{\rho_2}} \right] \\ \text{But } e^{2\rho_1} = (r_2/r_1)^2, \text{ and } \rho_2 = \log r_2/r_1 \\ \therefore W = 12\mu\omega \left(\log \frac{r_2}{r_1} \right)^3 (h_2 - h_1) \sum_n \left[\frac{(-1)^{n+1}r_2^2 + r_1^2}{n^2\pi^2 + 4 \left(\log \frac{r_2}{r_1} \right)^2} \right] \\ \times \left[\frac{\tanh \frac{n\pi\theta_1}{\log \left(\frac{r_2}{r_1} \right)^2} + \tanh \frac{n\pi\theta_2}{\log \left(\frac{r_2}{r_1} \right)^2}}{h_1^3 \coth \frac{n\pi\theta_1}{\log \frac{r_2}{r_1}} + h_2^3 \coth \frac{n\pi\theta_2}{\log \frac{r_2}{r_1}}} \right] \dots \dots \dots [46]$$

It is now a fairly easy matter to obtain the relations for the quantity of lubricant passing through the bearing and also to find the force and torque on the bearings. Since these are matters of secondary importance only the final formulas will be given.

FORCE REQUIRED TO MOVE FLAT ELEMENT IN RECTANGULAR BEARING

For the rectangular bearing, the force required to move the flat element is given by

$$F = \mu U b \left(\frac{c_1}{h_1} + \frac{c_2}{h_2} \right) + \frac{24 \mu U b^2 (h_2 - h_1)^2}{\pi^3} \sum_{n=1,3,5,\dots} \frac{1}{n^3 \left(h_1^3 \coth \frac{n\pi c_1}{b} + h_2^3 \coth \frac{n\pi c_2}{b} \right)} \dots \dots [47]$$

The quantity entering at the leading edge is

$$Q_2 = \frac{U h_2 b}{2} - \frac{4 U b h_2^2 (h_2 - h_1)}{\pi^2} \sum_{n=1,3,5,\dots} \frac{1}{n^2 \sinh \frac{n\pi c_2}{b}} \left(\frac{1}{h_1^3 \coth \frac{n\pi c_1}{b} + h_2^3 \coth \frac{n\pi c_2}{b}} \right) \dots \dots [48]$$

The quantity leaving at the trailing edge is

$$Q_1 = \frac{U h_1 b}{2} + \frac{4 U b h_1^2 (h_2 - h_1)}{\pi^2} \sum_{n=1,3,5,\dots}^{\infty} \frac{1}{n^2 \sinh \frac{n\pi c_1}{b}} \left(\frac{1}{h_1^3 \coth \frac{n\pi c_1}{b} + h_2^3 \coth \frac{n\pi c_2}{b}} \right) \dots [49]$$

The side leakage can be obtained by difference.

For the sector bearing the corresponding quantities are as follows:

The torque required to turn the bearing is given by

$$T = \frac{\mu \omega (r_2^4 - r_1^4)}{4} \left(\frac{\theta_1}{h_1} + \frac{\theta_2}{h_2} \right) + 6\pi (h_2 - h_1)^2 \mu \omega \left(\log \frac{r_2}{r_1} \right)^2 \sum_{n=1,3,5,\dots}^{\infty} \left[\frac{(-1)^{n+1} r_2^2 + r_1^2}{n^2 \pi^2 + 4 \left(\log \frac{r_2}{r_1} \right)^2} \right] \left(\frac{1}{h_1^3 \coth \frac{n\pi \theta_1}{\log \frac{r_2}{r_1}} + h_2^3 \coth \frac{n\pi \theta_2}{\log \frac{r_2}{r_1}}} \right) \dots [50]$$

The lubricant entering at the leading edge is given by

$$Q_2 = \frac{\omega h_2 (r_2^2 - r_1^2)}{4} - 2\omega \left(\log \frac{r_2}{r_1} \right) h_2^2 (h_2 - h_1) (r_2^2 - r_1^2) \sum_{n=1,3,5,\dots}^{\infty} \frac{1}{\left[n^2 \pi^2 + 4 \left(\log \frac{r_2}{r_1} \right)^2 \right] \sinh \frac{n\pi \theta_2}{\log \frac{r_2}{r_1}} \left(h_1^3 \coth \frac{n\pi \theta_1}{\log \frac{r_2}{r_1}} + h_2^3 \coth \frac{n\pi \theta_2}{\log \frac{r_2}{r_1}} \right)} \dots [51]$$

The lubricant leaving at the trailing edge is given by

$$Q_1 = \frac{\omega h_1 (r_2^2 - r_1^2)}{4} + 2\omega \left(\log \frac{r_2}{r_1} \right) h_1^2 (h_2 - h_1) (r_2^2 - r_1^2) \times \sum_{n=1,3,5,\dots}^{\infty} \frac{1}{\left[n^2 \pi^2 + 4 \left(\log \frac{r_2}{r_1} \right)^2 \right] \sinh \frac{n\pi \theta_1}{\log \frac{r_2}{r_1}} \left(h_1^3 \coth \frac{n\pi \theta_1}{\log \frac{r_2}{r_1}} + h_2^3 \coth \frac{n\pi \theta_2}{\log \frac{r_2}{r_1}} \right)} \dots [52]$$

The side leakage can be obtained by difference.

It will be observed that the series in Equations [32] and [46] converge very rapidly. For a square bearing a single term gives a result within 1 or 2 per cent of the actual value. The series for the sectorial bearing will converge somewhat less rapidly. For a "square" shape (i.e., the mean arc length equal to the radial depth), a satisfactory value can be obtained with 3 or 4 terms. In both cases the convergence becomes less rapid as the bearing becomes wider with respect to its length.

Equations [12], [32], and [46] give the load that can be supported on a bearing having the stepped-film shape. The conditions for a maximum of Equation [12] are fairly easily found, and this maximum is given in Equation [16]. The same device if applied to Equations [32] and [46] leads to great complication, and the method of trial is easier. It is found that the proportions for maximum load when side leakage is neglected are not the best proportions for a bearing of finite width. The values for the case of no side leakage were, $h_2 = 1.866 h_1$ and $c_2 = 2.549 c_1$. For a square bearing, it is found that the best values are, approximately, $h_2 = 1.7 h_1$ and $c_2 = 1.2 c_1$. However, the load capacity is not very sensitive to changes in the vicinity of these values.

COMPARISON OF LOADS WITH MICHELL FLAT-PLATE BEARING LOADS

It is interesting to compare the load given by Equation [32] for a square bearing to that given by Michell for an inclined flat plate. If the proportions given in the foregoing for the case of no side leakage are used, the bearing is about 6 per cent less effective than

the inclined-plane bearing. But if the best proportions are used it is about 3 per cent more effective. The 29 per cent improvement, obtained when side leakage is neglected, is reduced so that the bearing is only slightly better than the inclined-plane bearing in this respect. The side-leakage effect is no doubt aggravated because the large film thickness extends into the highest-pressure region, and thus offers an easier means of escape for the lubricant. If the bearing is made wider it gradually gains on the inclined-plane bearing and tends to approach the value given by Equation [16]. If it is made narrower it gradually gets less than the inclined-plane bearing.

A way in which the bearing could be improved to some extent

would be to make the stepped element as shown in Fig. 5. Such a shape would add to the mathematical difficulties and would be somewhat harder to produce unless it were etched. Probably the matter of increasing the capacity is not very important in practice as the loads that arise are already being taken by tilting-

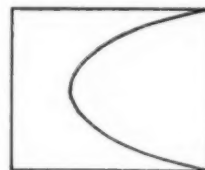


Fig. 5

block bearings of reasonable size, and it has been shown that these bearings are not quite as effective as the stepped arrangement.

An interesting conclusion can be drawn from Equations [32] and [46] by inspection. It will be recalled that the hyperbolic tangent approaches unity for quite small values of its argument. For example, $\tanh 3 = 0.99505$ and $\tanh 5 = 0.9991$. It is clear that if all other conditions are held constant, the load capacity is not increased appreciably by an increase in the length of the bearing beyond a certain point. This has particular significance in the case of a sector bearing because here there is a limit to the angle that can be subtended by a sector, viz., 360-deg. Thus if the ratio of outer to inner radii is 2, a pair of 180-deg sectors would

support almost exactly twice the load that could be carried by a single 360-deg bearing, other conditions being held constant. Also, three 120-deg sectors would be almost exactly 3 times as effective as a single 360-deg bearing (oil passages are neglected for simplicity in discussion; their influence would be small for large sectors). Obviously, there is a point at which this process of division would start to give a diminishing return. This could be fairly easily determined if the sector radii and oil-passage space were prescribed as well as the conditions of speed and viscosity. The matter is a little complicated by the fact that for each new angular condition the ratios of θ_2 to θ_1 and h_2 to h_1 will change for best conditions. However, a very good result would be obtained by holding these ratios constant at some reasonable value until the best number of sectors was found, and then making a more careful calculation in this vicinity to find best conditions.

CONCLUSION

The stepped-bearing arrangement has a good deal to recommend it in practice although there are two matters which are not especially in its favor. The bearing does not have any great advantage in load capacity over the inclined-plane bearing, and it is restricted to one direction of rotation. Offsetting these matters is its great constructional simplification over the tilting-block bearing, or even over those bearings in which the taper is machined into one of the elements. In addition, the fairly simple explicit equations for the load offer some advantage in design where the influence of each parameter is fairly easy to see and can be checked quite readily. It is true that viscosity has been taken as constant, and this can be quite misleading. However, there are ways of estimating the change in viscosity through the bearing, and a mean value seems to give fairly good results. In this respect the solution is no worse than others. It should be possible to apply this bearing to a great many thrust problems and in particular to those cases where space considerations are of importance.

Some experiments of a semiquantitative nature have been made with bearing models. It is well known that precise results by this means are rather difficult to obtain. However, reasonable agreement was found. An air-lubricated model in which the step height, i.e., $(h_2 - h_1)$, is about 0.00005 in. has been made and is entirely successful. Lord Rayleigh describes a simple test he made of the scheme in his paper.³

Discussion

J. R. MENKE.³ The author has presented a useful extension of Lord Rayleigh's calculations and has done a service in calling more general attention to this relatively unappreciated paper.⁴ The writer's attention was drawn to the paper in 1943-1944 by John E. Viscardi and Mayo D. Hersey with a practical result.

The author remarks in his discussion upon the behavior of the hyperbolic tangent terms in Equations [32] and [46]. This behavior is hardly surprising in the physical sense, indicating only that side leakage as usual reduces the advantage of increasing length in long, "thin" (i.e., not wide) bearings.

Fig. 5 of the paper indicates an interesting improvement, and one wonders about the estimated extent of this improvement. Is a large part of the potential 29 per cent gain over inclined-plate bearings feasible? Tests on this point should prove worth while.

The bearing examined is evidently simple in two respects; it can be readily understood and it can be manufactured cheaply. With such advantages and its indicated performance one might expect some industrial acceptance after these thirty-odd years since Lord Rayleigh's paper.

³ Nuclear Development Associates, Inc., New York, N. Y. Jun. ASME.

⁴ Author's reference (2).

Density-Pressure Relationships for Two Low-Viscosity Dimethyl Siloxanes

By S. R. GUNST,¹ PITTSBURGH, PA.

An instrument used to determine liquid compressibilities is described² as is its use in the determination of density versus pressure for hexamethyldisiloxane and octamethyltrisiloxane. Results at pressures to 10,000 psi, and at temperatures to 200 F for the hexamethyldisiloxane and to 300 F for the octamethyltrisiloxane are shown. The densities are precise within 0.3 per cent.

INTRODUCTION

THE dimethyl siloxanes are members of the group frequently called silicone liquids (1, 2, 3).³ They are heat-stable, chemically inert compounds (4). Their stability and small viscosity change with temperature suggest their potential excellence as viscometer-calibration standards, the objective which prompted this investigation.

In the rolling-ball viscometer (5), an instrument used for the determination of absolute viscosities of fluids at elevated pressures, the densities of the fluids under test conditions must be ascertained. This investigation was undertaken to determine the density-pressure relationships for two dimethyl siloxanes.

For mineral oils the density-pressure equation of Dow and Fink (6) has given satisfactory results; but for silicone liquids, in so far as is known, little experimental work from which such relations may be derived has been published (7, 8). Although the results of this investigation on only two silicone liquids are insufficient to yield a density-pressure equation for all silicones, they should be useful for the liquids tested, and subsequent work may lead to a density-pressure equation for silicones corresponding to that of Dow and Fink for mineral oils.

DESCRIPTION OF APPARATUS

For this investigation it was necessary to design and build an instrument for making measurements from which the compressibility of a liquid could be computed. A search of the literature (9, 10, 11) showed the many difficulties and attendant uncertainties experienced by the early investigators, and it is believed the instrument embraces the best principles of design known at this time. The pressure joints are self-sealing; the expansion of the pressure vessel is irrelevant; the test liquid is contained in a thin-walled, commercially available brass bellows, whose spring constant and bulk compression are negligibly small, and whose free end is unhampered by any sliding surfaces with their attendant friction; the instrument demands no calibration with a liquid whose compressibility is known; and it is continuously reading

so that a single charge of sample liquid within the bellows suffices for all pressures and temperatures encountered in this investigation.

A cross-sectional sketch of the instrument, hereafter referred to as the "compressibility meter," is shown in Fig. 1. The brass bellows 1, soldered to brass plugs 2 and 3, is filled with the test-liquid sample. The sample is trapped in the bellows by a steel taper pin 4, and a steel contact plate 5, which seals by compressing an aluminum gasket 6. The upper end of the bellows is held fixed by threading the upper plug 2 into the steel end plate 7, which is positioned in the steel pressure housing 8 by a steel end screw 9. A bakelite bushing 10, electrically insulates the brass bellows housing 11, with its brass micrometer spider 12, and steel micrometer screw 13, from the bellows. Adjustment of the micrometer screw is accomplished by turning the graduated brass knob 14. This turns a steel shaft 15, whose three steel fingers 16, engage the bakelite fluted coupling 17, attached to the micrometer screw. A steel spring 18, takes up the micrometer-screw backlash, and a thrust bearing 19, takes the load on the head of the shaft 15, resulting from internal pressure applied hydraulically inside the

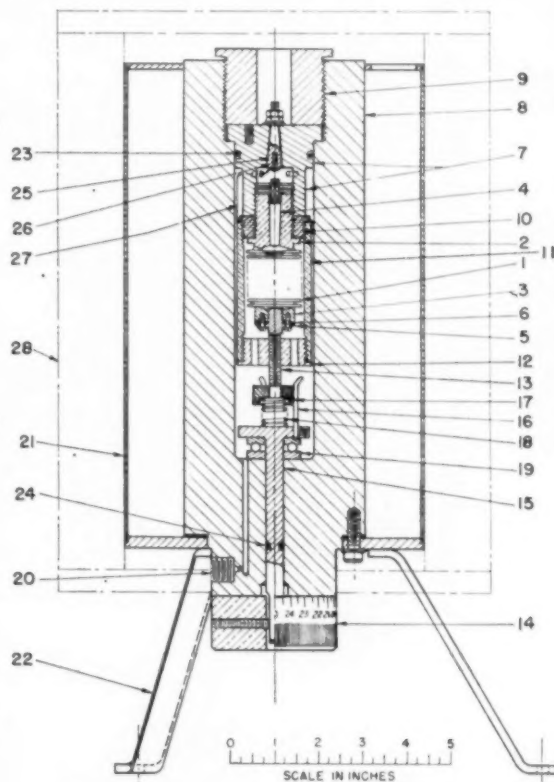


FIG. 1 SECTIONAL DIAGRAM OF COMPRESSIBILITY METER

¹ Gulf Research and Development Company, and University of Pittsburgh.

² Additional details can be found in a University of Pittsburgh thesis by the author.

³ Numbers in parentheses refer to the Bibliography at the end of the paper.

Contributed by the Research Committee on Lubrication and the Petroleum Division and presented at the Annual Meeting, New York, N.Y., November 27-December 2, 1949, of THE AMERICAN SOCIETY OF MECHANICAL ENGINEERS.

NOTE: Statements and opinions advanced in papers are to be understood as individual expressions of their authors, and not those of the Society. Paper No. 49-A-91.

pressure housing through the inlet 20. Three equally spaced annular slots in the top plate of the jacket 21, permit the admission of liquid into the jacket, and the immersion in this liquid of a strip heater, a stirrer, a thermoregulator, and a thermometer. Three steel legs 22, support the compressibility meter on a suitable workbench. Synthetic-rubber O-rings 23 and 24, serve as self-sealing gasket and packer, respectively, and a nylon bushing 25, serves both as a self-sealing gasket and an electrical insulator for the contact pin 26. A fiberglass-insulated wire 27, connects the contact pin to the bellows housing 11.

When the micrometer screw 13, is made to contact the contact plate 5, electrical connection is effected from the contact pin 26, to the bellows housing to the micrometer screw to the bellows to the pressure housing. Thus a suitable electrical indicator connected between the contact pin and the pressure housing will indicate contact between the contact plate and the micrometer screw. The micrometer screw has a major diameter of $1/4$ in. and 40 threads per inch. One turn advances the screw 0.025 in. Fifty graduations on the circumference of the knob 14, permit direct readings corresponding to a micrometer-screw advance of 0.0005 in. and estimations to 0.0001 in. With a suitably sensitive indicator, therefore, the variation in bellows length can be measured to 0.0001 in.

Hydraulic pressure, applied by means of a free-piston gage (12), commonly called a "dead-weight tester," is transmitted to all parts inside the pressure housing—to the bellows via six axial holes in the micrometer spider 12, and four axial slots (not shown in Fig. 1) in the bellows housing 11, and to the top of the taper pin 4, sealing the top of the bellows via four radial holes in the collar of the end plate 7. The application of pressure to the outside of the bellows compresses the test-liquid sample within the bellows and results in a decrease in bellows length, which can be measured as previously indicated.

In order to decrease heat loss, asbestos steam-pipe insulation 28, $1\frac{1}{2}$ in. thick, blankets the compressibility meter so that only the legs, the knob, the pressure inlet, and parts of the thermometer and temperature-control apparatus are exposed.

ANALYTICAL CONSIDERATIONS

Measurements of a variation in bellows length can be used to calculate the change in density of a test-liquid sample. For a mass m of liquid occupying a volume V the liquid density is given by

$$\rho = m/V \dots \dots \dots [1]$$

With atmospheric-pressure conditions denoted by a subscript 0, an isothermal change in density because of a change in pressure is given by

$$\Delta\rho = \rho - \rho_0 = (m/V) - (m/V_0) = \frac{m(V_0 - V)}{VV_0} \dots \dots [2]$$

Let $V = V_0 + \Delta V$ and Equation [2] becomes

$$\begin{aligned} \Delta\rho &= -\frac{m\Delta V}{V_0(V_0 + \Delta V)} = -\frac{\rho_0}{(V_0/\Delta V) + 1} \\ &= -\frac{\rho_0}{(m/\rho_0\Delta V) + 1} \dots \dots [3] \end{aligned}$$

Tests to determine the change in bellows volume with change in bellows length at constant temperature and pressure showed that $\Delta V = A\Delta L$, where ΔL is the change in bellows length and A is a constant, obviously the effective cross-sectional area of the inside of the bellows. Equation [3] can therefore be written

$$\Delta\rho = -\frac{\rho_0}{(m/\rho_0 A\Delta L) + 1} \dots \dots \dots [4]$$

from which the isothermal change in density resulting from a change in pressure can be calculated if all quantities on the right are known.

A graph of $\Delta\rho$ or ρ versus pressure p can be used to calculate the isothermal compressibility k of a liquid if desired. With isothermal conditions designated by a subscript T , k is given by

$$\begin{aligned} k &= -\frac{1}{V} \left(\frac{\partial V}{\partial p} \right)_T = -\frac{1}{V} \left(\frac{\partial \rho}{\partial p} \right)_T \left(\frac{\partial V}{\partial \rho} \right)_T = \frac{1}{\rho} \left(\frac{\partial \rho}{\partial p} \right)_T \\ &= \frac{1}{(\rho_0 + \Delta\rho)} \left(\frac{\partial \rho}{\partial p} \right)_T \dots \dots [5] \end{aligned}$$

Since the slope of the graph of $\Delta\rho$ or ρ versus pressure at any pressure is $(\partial\rho/\partial p)_T$, readily obtainable by graphical differentiation, k can be calculated.

TEST METHODS AND RESULTS

Preliminary investigations were made in order to establish methods for temperature measurement and control, to determine the effective cross-sectional area of the bellows, and to ascertain the effect of cubic compression of the various parts of the compressibility meter on bellows length measurements. The latter was found to be negligible.

The two liquids investigated were hexamethyldisiloxane and octamethyltrisiloxane, referred to by one manufacturer, the Dow-Corning Corporation, as DC-200 silicone fluid, viscosity 0.65 centistoke at 25 C, and DC-200 silicone fluid, viscosity 1.0 centistoke at 25 C, respectively. Equation [4] was used to calculate change in density $\Delta\rho$ for various temperatures and pressures.

1 The density ρ_0 :

The density ρ_0 at atmospheric pressure and test temperature was obtained from hydrometer tests by chemists at the author's laboratory and checked with the results of Hurd (3).

2 Effective bellows cross-sectional area A :

The cross-sectional area A of the bellows was found to be essentially independent of bellows length and pressure. The value of A of 0.764 sq in. determined by test at 75 F was used and corrected for thermal expansion, using a handbook value for the expansivity of brass.

3 The mass m of liquid filling the bellows:

Anticipated difficulties in filling the bellows with a test sample of liquid to the essential exclusion of air were easily overcome. The bellows assembly, with the taper pin removed, was immersed in an oil bath until only $1/8$ in. of the bellows taper-pin plug was exposed. The bath was maintained at a temperature above the maximum test temperature of a specific test liquid. A long-necked eyedropper inserted through the taper-pin hole was used to fill the bellows with test liquid. A glass stirring rod was used to agitate the bellows convolutions in order to rid them of air bubbles. The bellows was kept constantly filled by means of the eyedropper. After all evidence of bubbling through the taper-pin hole had ceased, the taper pin was driven into the taper-pin hole, thus sealing the test liquid within the bellows.

The mass m of test-sample liquid is the difference between the filled-bellows mass and empty-bellows mass obtained by the double massing method (13) with appropriate corrections for air buoyancy. The bellows assembly was carefully cleaned and dried prior to all mass determinations.

Only one filling of the bellows was necessary for all tests made

on each of the liquids and their corresponding masses were as follows:

Hexamethyldisiloxane mass $m = 13.630$ grams
Octamethyltrisiloxane mass $m = 13.575$ grams

4 Isothermal change in bellows length ΔL versus pressure:

Measurements of variation in bellows length at pressure intervals of 100 psi from 0 to 500 psi (gage), and at intervals of 500 psi from 500 to 10,000 psi (gage) were made for the two liquids at the following temperatures:

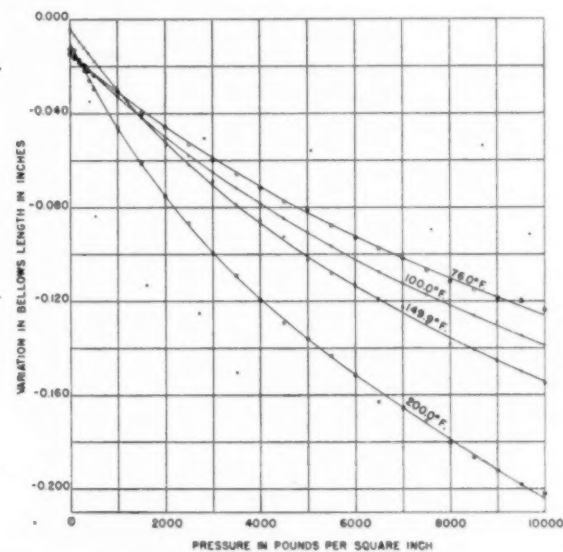


FIG. 2 MEASURED VARIATION IN BELLOWS LENGTH FROM ARBITRARY ZERO AT EACH TEMPERATURE VERSUS GAGE PRESSURE FOR HEXAMETHYLDISILOXANE

Hexamethyldisiloxane 76.0, 100.0, 149.9, 200.0 F
Octamethyltrisiloxane 77.5, 100.0, 150.0, 200.0, 250.0, 300.0 F

(At an absolute pressure of 760 mm Hg, the liquids have the following approximate boiling points: Hexamethyldisiloxane, 211 F; octamethyltrisiloxane, 306 F).

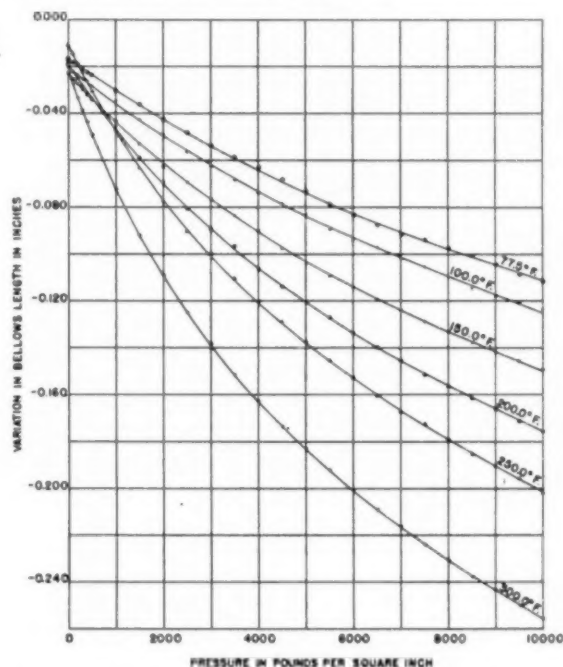


FIG. 3 MEASURED VARIATION IN BELLOWS LENGTH FROM ARBITRARY ZERO AT EACH TEMPERATURE VERSUS GAGE PRESSURE FOR OCTAMETHYLTRISILOXANE

TABLE 1 CHANGE IN DENSITY VERSUS PRESSURE FOR HEXAMETHYLDISILOXANE

Temp, F.	mass $m = 13.630$ grams				mass $m = 13.630$ grams				mass $m = 13.630$ grams			
	76.0	100.0	149.9	200.0	76.0	100.0	149.9	200.0	76.0	100.0	149.9	200.0
A , sq in.	0.764	0.764	0.765	0.766	0.764	0.764	0.765	0.766	0.764	0.764	0.765	0.766
ρ , gram per cu cm.	0.7634	0.7496	0.7194	0.6883	0.7634	0.7496	0.7194	0.6883	0.7634	0.7496	0.7194	0.6883
Gage pressure, psi	ΔL in.	$\Delta \rho$ gram per cu cm	ΔL in.	$\Delta \rho$ gram per cu cm	ΔL in.	$\Delta \rho$ gram per cu cm	ΔL in.	$\Delta \rho$ gram per cu cm	ΔL in.	$\Delta \rho$ gram per cu cm	ΔL in.	$\Delta \rho$ gram per cu cm
0	0.0000	0.0000	0.0000	0.0000	0.0000	0.0000	0.0000	0.0000	0.0000	0.0000	0.0000	0.0000
500	-0.0085	0.0046	-0.0105	0.0055	-0.0130	0.0062	-0.0195	0.0094	-0.0275	0.0123	-0.0365	0.0163
1000	-0.0160	0.0087	-0.0200	0.0105	-0.0255	0.0123	-0.0365	0.0163	-0.0480	0.0236	-0.0655	0.0298
2000	-0.0310	0.0169	-0.0370	0.0196	-0.0480	0.0236	-0.0655	0.0298	-0.0665	0.0331	-0.0895	0.0414
3000	-0.0440	0.0243	-0.0520	0.0279	-0.0665	0.0331	-0.0895	0.0414	-0.0825	0.0415	-0.1090	0.0511
4000	-0.0560	0.0312	-0.0650	0.0354	-0.0825	0.0415	-0.1090	0.0511	-0.0965	0.0491	-0.1260	0.0597
5000	-0.0675	0.0379	-0.0780	0.0426	-0.0965	0.0491	-0.1410	0.0676	-0.1090	0.0559	-0.1555	0.0753
6000	-0.0775	0.0438	-0.0895	0.0493	-0.1090	0.0559	-0.1690	0.0826	-0.1205	0.0623	-0.1820	0.0898
7000	-0.0865	0.0492	-0.0995	0.0552	-0.1205	0.0623	-0.1820	0.0898	-0.1310	0.0683	-0.1940	0.0965
8000	-0.0950	0.0544	-0.1090	0.0609	-0.1310	0.0683	-0.1940	0.0965	-0.1405	0.0738	-0.2095	0.1067
9000	-0.1035	0.0597	-0.1175	0.0660	-0.1405	0.0738	-0.2095	0.1067	-0.1495	0.0790	-0.2245	0.1141
10000	-0.1110	0.0643	-0.1255	0.0709	-0.1495	0.0790	-0.2245	0.1141				

TABLE 2 CHANGE IN DENSITY VERSUS PRESSURE FOR OCTAMETHYLTRISILOXANE

Temp, F.	mass $m = 13.575$ grams											
	77.5	100.0	150.0	200.0	250.0	300.0	77.5	100.0	150.0	200.0	250.0	300.0
A , sq in.	0.764	0.764	0.765	0.766	0.767	0.768	0.764	0.764	0.765	0.766	0.767	0.768
ρ , gram per cu cm.	0.8171	0.8046	0.7767	0.7479	0.7188	0.6900	0.8171	0.8046	0.7767	0.7479	0.7188	0.6900
Gage pressure, psi	ΔL in.	$\Delta \rho$ gram per cu cm	ΔL in.	$\Delta \rho$ gram per cu cm	ΔL in.	$\Delta \rho$ gram per cu cm	ΔL in.	$\Delta \rho$ gram per cu cm	ΔL in.	$\Delta \rho$ gram per cu cm	ΔL in.	$\Delta \rho$ gram per cu cm
0	0.0000	0.0000	0.0000	0.0000	0.0000	0.0000	0.0000	0.0000	0.0000	0.0000	0.0000	0.0000
500	-0.0065	0.0040	-0.0080	0.0048	-0.0110	0.0062	-0.0140	0.0073	-0.0195	0.0094	-0.0275	0.0123
1000	-0.0130	0.0081	-0.0155	0.0094	-0.0210	0.0119	-0.0275	0.0145	-0.0365	0.0179	-0.0510	0.0233
2000	-0.0255	0.0160	-0.0295	0.0180	-0.0385	0.0221	-0.0505	0.0271	-0.0660	0.0330	-0.0875	0.0409
3000	-0.0370	0.0234	-0.0415	0.0256	-0.0540	0.0313	-0.0700	0.0380	-0.0900	0.0458	-0.1175	0.0560
4000	-0.0475	0.0303	-0.0530	0.0330	-0.0675	0.0395	-0.0865	0.0476	-0.1100	0.0568	-0.1415	0.0680
5000	-0.0570	0.0367	-0.0635	0.0398	-0.0800	0.0473	-0.1010	0.0562	-0.1270	0.0663	-0.1615	0.0794
6000	-0.0660	0.0428	-0.0725	0.0458	-0.0910	0.0543	-0.1145	0.0643	-0.1420	0.0750	-0.1795	0.0894
7000	-0.0735	0.0479	-0.0810	0.0515	-0.1010	0.0607	-0.1260	0.0714	-0.1560	0.0833	-0.1950	0.0983
8000	-0.0810	0.0531	-0.0895	0.0573	-0.1100	0.0665	-0.1370	0.0783	-0.1680	0.0905	-0.2095	0.1067
9000	-0.0880	0.0580	-0.0970	0.0624	-0.1185	0.0722	-0.1465	0.0843	-0.1795	0.0975	-0.2220	0.1141
10000	-0.0940	0.0623	-0.1045	0.0677	-0.1270	0.0779	-0.1560	0.0904	-0.1905	0.1043	-0.2345	0.1217

The results of the tests for hexamethyldisiloxane, the dimer, are graphed in Fig. 2, and for octamethyltrisiloxane, the trimer, in Fig. 3.

COMPUTED RESULTS

Smoothed values of change in bellows length ΔL versus gage pressure, taken from the graphs in Figs. 2 and 3, are shown in Tables 1 and 2, as are the corresponding values of change in test-liquid density $\Delta \rho$ calculated from Equation [4]. The box headings of the tables bear appropriate values of the test-liquid temperature, the bellows cross-sectional area A , and the test-liquid density ρ_0 at atmospheric pressure. Graphs of test-liquid density ρ as a function of gage pressure are presented in Figs. 4 and 5, from which the density for any pressure can be read. Moreover, isobaric graphs of ρ versus temperature can readily be constructed from the graphs in Fig. 4 or 5, with which the density at any temperature from 75 to 200 F for the dimer, and from 75 to 300 F for the trimer and at any gage pressure from 0 to 10,000 psi for either can be determined.

Check tests confirmed results within experimental error.

The isothermal compressibilities, computed according to Equation [5], are shown in Figs. 6 and 7.

CONCLUSION

Calculations showed that the densities of the two dimethyl siloxanes were determined with a probable error no greater than 0.0018 gram per cu cm over a pressure range of 10,000 psi and at various temperatures.

ACKNOWLEDGMENT

The author is indebted to Mr. Paul G. Exline, formerly Section Engineer of Gulf Research and Development Company, for early suggestions concerning the problem and equipment design features; to Dr. David Halliday of the University of Pittsburgh, and to Mr. R. J. S. Pigott, Director of Engineering of Gulf Research and Development Company, for sponsoring this investigation; and to Dr. Paul D. Foote, Executive Vice-President and Director of Gulf Research and Development Company, for permission to disclose the results.

BIBLIOGRAPHY

- 1 "Nomenclature of Organosilicon Compounds," by E. O. Sauer, *Journal of Chemical Education*, vol. 21, 1944, pp. 303-305.
- 2 "Methylpolysiloxanes," by Winton Patnode and D. F. Wilcock, *Journal of the American Chemical Society*, vol. 68, 1946, pp. 358-363.
- 3 "Studies on Siloxanes: I. The Specific Volume and Viscosity in Relation to Temperature and Constitution," by C. B. Hurd, *Journal of the American Chemical Society*, vol. 68, 1946, p. 364.
- 4 "Dielectric Constants of Dimethyl Siloxane Polymers," by E. B. Baker, A. J. Barry, and M. J. Hunter, *Industrial and Engineering Chemistry*, vol. 38, 1946, pp. 1117-1120.
- 5 "Viscosity Determination of Subsurface Samples of Crude Oil," by P. G. Exline and H. J. EnDean, *Drilling and Production Practice*, 1939, pp. 659-665 (American Petroleum Institute), 1940.
- 6 "Computation of Some Physical Properties of Lubricating Oils at High Pressures," by R. B. Dow and C. E. Fink, *Journal of Applied Physics*, vol. 11, 1940, pp. 353-357.
- 7 "Further Rough Compressions to 40,000 Kg/cm², Especially Certain Liquids," by P. W. Bridgman, *Proceedings of the American Academy of Arts and Sciences*, vol. 77, 1949, pp. 129-145.
- 8 "Ultrasonic Investigation of Molecular Properties of Liquids. III. Linear Polymethylsiloxanes," by Alfred Weissler, *Journal of the American Chemical Society*, vol. 71, 1949, p. 93.
- 9 "The Physics of High Pressure," by P. W. Bridgman, The MacMillan Company, New York, N. Y., 1931; pertinent bibliographies on pp. 17-29, 147-148.
- 10 "The Design of High Pressure Plant and the Properties of Fluids at High Pressures," by D. M. Newitt, The Clarendon Press, Oxford, England, 1940; pertinent bibliography on p. 466.
- 11 "Recent Work in the Field of High Pressures," by P. W. Bridgman, *Review of Modern Physics*, vol. 18, 1946, pp. 1-93; pertinent

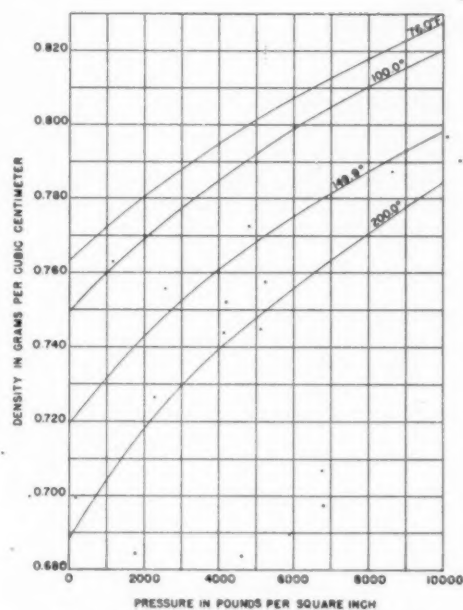


FIG. 4 DENSITY VERSUS GAGE PRESSURE FOR HEXAMETHYLDISILOXANE

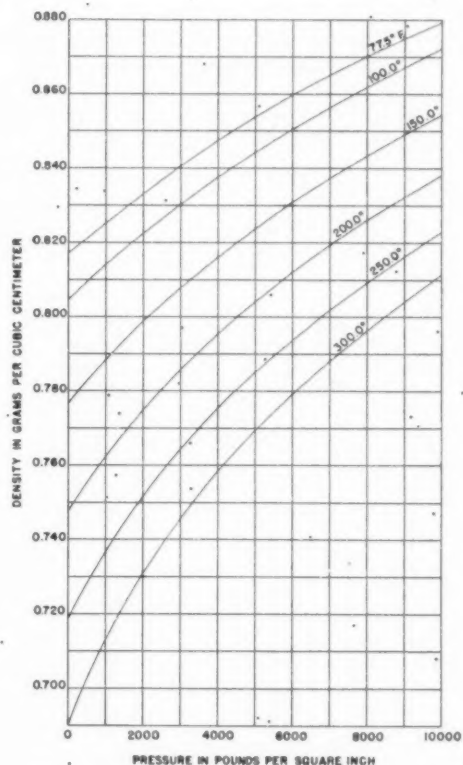


FIG. 5 DENSITY VERSUS GAGE PRESSURE FOR OCTAMETHYLTRISILOXANE

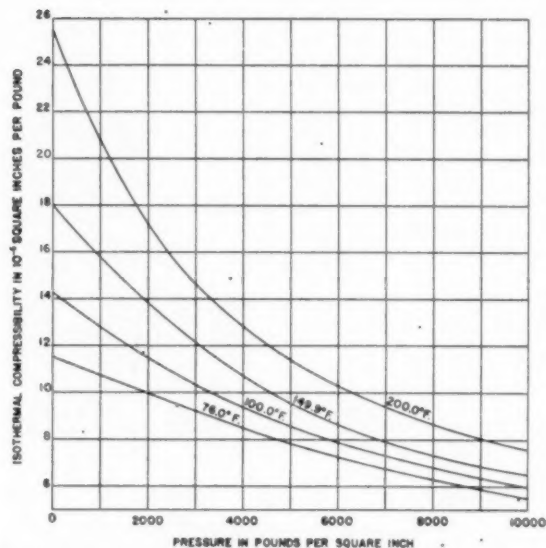


FIG. 6 Isothermal Compressibility Versus Gage Pressure for Hexamethyldisiloxane
(Precision is limited by graphical differentiation of Fig. 4.)

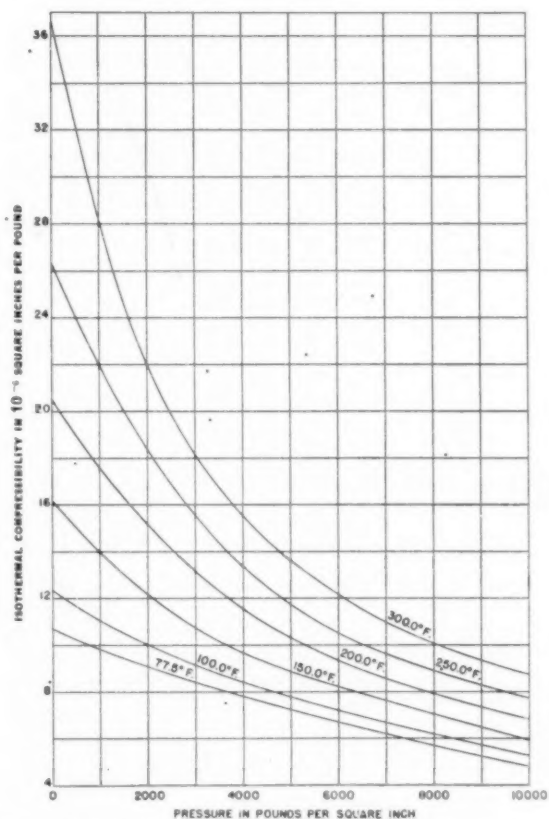


FIG. 7 Isothermal Compressibility Versus Gage Pressure for Octamethyltrisiloxane
(Precision limited by graphical differentiation of Fig. 5.)

bibliography on pp. 15-16; and *Journal of the Institute of Petroleum*, vol. 32, 1946, p. 254A.

12 "Pressure-Responsive Elements," by P. G. Edline, *Trans. ASME*, vol. 60, 1938, pp. 625-632.

13 "Heat," by A. G. Worthing and David Halliday, John Wiley & Sons, Inc., New York, N.Y., 1948, pp. 6-8.

Discussion

P. W. BRIDGMAN.⁴ This is an interesting and ingenious adaptation of the sylphon method of measuring compressibilities which the writer developed a number of years ago⁵ for use over a wider pressure range. For the purpose at present in view (determination of the density correction in rolling-ball viscometers used under pressure), and within the range of accuracy claimed (0.3 per cent on the densities), the apparatus seems entirely adequate. A check on this is afforded by comparing the author's results with those of the writer⁶ for the same two liquids at room temperature. After making corrections for slight differences of temperature, and expressing the results as fractional changes of initial volume instead of initial density, the writer finds for the author's value of $\Delta V/V_0$ at approximately 24°C at a pressure of 7110 psi (500 kg per sq cm) for hexamethyldisiloxane and octamethyltrisiloxane, respectively, 0.0552 and 0.0597. These values may be compared with the writer's of 0.0568 and 0.0586, respectively. The agreement is thus well within the claimed error, which would correspond to 0.003.

It would seem that the method should be capable of considerably greater accuracy than claimed, for 0.3 per cent on the absolute density is not high. It is to be regretted that the author did not take the opportunity to find the probable limits of accuracy. To do this, comparison with measurements by other methods is necessary, because there can be no question but there are intrinsic sources of error in the sylphon method owing to internal strains in the metal of the sylphon, which has been subject to very great deformations in the forming process. It may well be that the accuracy would prove great enough to justify use of the apparatus in making measurements of the compression of liquids for their own sake, as demanded in work on the equation of state of liquids. This apparatus has an especial advantage for such use in the wide temperature range that can be covered easily.

R. B. DOW.⁷ This paper represents a valuable contribution to the means available for calibrating high-pressure viscometers over the moderate pressure range of 10,000 psi. The writer and his collaborators have previously used a series of carefully chosen lubricating oils of such densities and viscosities as required to give suitable calibration curves for the rolling-ball type of viscometer. The present choice of silicone liquids is to be preferred chiefly because of the ready availability of a standard product, although the stability and small temperature coefficients of viscosity are valid reasons for considering them more suitable than oils. The author's results should be useful for all workers in this field who will welcome all advances toward standardization.

The compressibility meter is a well-designed and simple device which has been adapted from the sylphon piezometer of Prof. P. W. Bridgman. The techniques of measurement differ only in the method of measuring changes of length, Bridgman using changes of resistance of a fine manganin slide wire attached

⁴ Lyman Laboratory of Physics, Harvard University, Cambridge, Mass.

⁵ "The Volume of 18 Liquids as a Function of Pressure and Temperature," by P. W. Bridgman, *Proceedings of the American Academy of Arts and Sciences*, vol. 66, 1931, pp. 185-233.

⁶ See p. 143 of reference (7) in Bibliography of paper.

⁷ Bureau of Ordnance, Re9a, Navy Department, Washington, D. C.

directly to the top of the siphon instead of direct readings on a micrometer screw. The siphon piezometer has several obvious points of superiority over the old type of piston displacement in a pressure cylinder containing the test liquid. For the present pressure range the use of a micrometer is both direct and convenient since it can be used with a simple pressure seal which would not suffice at much higher pressures.

In respect to the corrections employed in the present work, it appears that the length of the screw was not corrected for possible changes due to changes of pressure and temperature. The correction for pressure would be negligible except at the highest pressure used, at which it would be of a magnitude about comparable with the accuracy of measurement. The correction for temperature, on the other hand, appears to be well within the accuracy of measurement between the limits of 76 and 200 F.

The value of the results are enhanced by the fact that several temperatures were used. It is suggested that, in addition to the value of 100 F, it would be desirable to have data at 130 and 210 F since the viscosities of oils are commonly measured at these temperatures.

P. G. EXLINE.⁸ This paper describes an instrument capable of determining liquid densities and compressibilities with a higher order of accuracy and with much greater convenience than has hitherto been obtainable. A single filling of the instrument suffices for all determinations over the allowable temperature and pressure range of the instrument. The pressure and temperature ranges covered by the author were rather arbitrarily limited by the materials tested and by the pressure-measuring instruments used. It would add to the value of the paper if a reasonable estimate could be given of the pressure and temperature limits to which the instrument could be used.

Although the author reports unusually high accuracy for determinations of this nature, the writer believes that an additional correction could well have been made. In determining liquid compressibilities in a vessel in which the internal pressure equals the external pressure, the direct observations yield the difference between the compressibility of the liquid and that of the material of the vessel.⁹ The fact that in the author's instrument the liquid is contained in a vessel capable of free axial elongation does not alter the situation, as the radius of the bellows is reduced by the pressure, and the brass bellows housing carrying the micrometer nut will be shortened. At the most, this correction would alter the reported values of $\Delta\rho$ by slightly under 1 per cent.

In calculating compressibilities from the density data the author has selected a definition of K which does not yield easily usable values, a mistake of which the writer has also been guilty.¹⁰

If the compressibility is defined as

$$K = \frac{1}{V_0} \frac{(V_0 - V)}{P}$$

where V is the volume at pressure P and V_0 is the volume at zero pressure, it is much more easily applied to numerical computations. In this case the compressibility can be expressed as a function of ρ as follows

$$K = \frac{\Delta\rho}{(\rho_0 + \Delta\rho)P}$$

⁸ President, Exline Engineering Company, Tulsa, Okla. Mem. ASME.

⁹ "A Text-Book of Physics—Properties of Matter," by V. H. Poynting and J. J. Thomson, 11th edition Charles Griffin & Company, Ltd., London, England, pp. 116–119.

¹⁰ "Leakage in Capillary Seals of Hydraulic Valves and Pumps," by P. G. Exline, *Product Engineering*, vol. 17, April, 1946, p. 292.

and the computations can be made directly from Tables 1 and 2 of the paper.

The initial values of K , computed this way, will be the same as in Figs. 6 and 7 of the paper, but the values at 10,000 psi will be 50 to 70 per cent higher.

The writer has had occasion to reduce the data reported in the paper to analytical expressions of the form $\rho = \rho_0(1 + \Delta P + bP^2 + cP^3)$. The values of the coefficients thus obtained are given in the following table:

Temp. deg F	ρ_0 gram per cu cm	a in. ² /lb	b in. ⁴ /lb ²	c in. ⁶ /lb ³
HEXAMETHYLDISILOXANE				
76	0.7634	1.196×10^{-8}	-4.65×10^{-13}	1.13×10^{-14}
100	0.7496	1.440	-7.13	2.28
149.9	0.7194	1.808	-12.3	4.63
200	0.6883	2.539	-20.5	9.13
OCTAMETHYLTRISILOXANE				
77.5	0.8171	1.038×10^{-8}	-2.95×10^{-13}	6.344×10^{-14}
100	0.8046	1.227	-5.80	1.94
150	0.7767	1.588	-8.85	3.00
200	0.7479	2.060	-13.35	4.84
250	0.7188	2.674	-20.60	8.38
300	0.6909	3.364	-26.0	10.0

ALFRED WEISSLER.¹¹ This interesting paper introduces a greatly improved instrument for the determination of isothermal compressibility. The measurement of sound velocity by means of the ultrasonic interferometer is an attractive, precise method for the determination of adiabatic compressibility, from which the isothermal compressibility may be computed if the heat capacity and thermal expansion coefficient are known.¹²

The latter method was utilized¹³ to measure the compressibilities (at atmospheric pressure and 86 F) of 16 methylsiloxane liquids, including the two studied in the present work. It is interesting to note that the values obtained from ultrasonic propagation are about 20 per cent higher than those found in the paper. This difference may be understood in terms of the rapid decrease in compressibility with increasing pressure, as shown in Figs. 6 and 7 of the paper. Inasmuch as the excess pressure attained in our ultrasonic interferometer is 0.1 psi or less, the compressibilities obtained thereby are valid for the range of 0 to 0.1 psi (gage). By contrast, the first measurement at each temperature in the present work gives the "average" compressibility over the range 0 to 100 psi (gage), from which it is not possible to extrapolate to zero pressure with any great accuracy. In the same connection, the isothermal compressibilities of these liquids determined at Dow Corning are considerably lower than those found in the present work, presumably because an even larger pressure interval was used.

It appears, therefore, that the ultrasonic interferometer is particularly valuable for the measurement of compressibility of fluids at zero gage pressure.

AUTHOR'S CLOSURE

The author gratefully acknowledges the stimulating discussion submitted by Professor Bridgman, Dr. Dow, and Messrs. Exline and Weissler, each of whom has made valuable contributions in the field of compressibility.

The corrections for changes in length of the micrometer screw because of temperature and pressure changes and for compression of the material of the vessel, suggested by Dr. Dow and Mr. Exline, respectively, are well within the reported probable error on the density ρ of 0.3 per cent. That the results could be im-

¹¹ Naval Research Laboratory, Washington, D. C.

¹² "Ultrasonics," by L. Bergmann, John Wiley & Sons, Inc., New York, N. Y., 1944, chapt. 3.

¹³ See reference (8) in Bibliography of paper.

proved by these and other corrections¹⁴ is true, although in many cases it is questionable if the increased accuracy obtained would justify the additional labor in computation.

The instrument described was designed as an engineering instrument with which results sufficiently accurate for most engineering uses could be obtained rapidly by a semiskilled technician with little supervision. The direct readings on the micrometer screw, the facility of testing at various temperatures, the single filling of the bellows for all temperatures and pressures investigated, and the omission of higher-order corrections to simplify the computations, are considered important features in the use of the instrument for engineering purposes.

The maximum possible precision obtainable with the instrument has not been investigated. Professor Bridgman's suggestion of comparison with measurements by other methods, and the application of corrections, such as those suggested by Dr. Dow and Mr. Exline, would be necessary in an investigation to determine the limits of accuracy obtainable with the instrument.

The maximum pressure and temperature to which the instrument could be used are limited primarily by the materials incorporated in the design. Synthetic-rubber O-ring seals in similar applications have been subjected to 40,000 psi at room temperature and to 12,000 psi at 400 F without failure in either case. The maximum temperature, however, is limited to approximately

350 F because a soft solder was used to join the bellows to the bellows plugs.

The isothermal compressibility K , defined by Mr. Exline, is approximately the integrated average between atmospheric and pressure p of the isothermal compressibility k shown in Figs. 6 and 7 of the paper. That Mr. Exline obtained results at 10,000 psi 50 to 70 per cent higher than those presented in Figs. 6 and 7, is therefore to be expected. In the opinion of the author, the isothermal compressibility defined by Equation [5] of the paper is more useful than that defined by Mr. Exline for theoretical analyses leading to calculations of such quantities as adiabatic compressibility and velocity of sound.

Mr. Exline's empirical equation for the density results should be useful, provided the user bears in mind that such expressions cannot safely be extrapolated nor differentiated. Since the labor involved in the evaluation of coefficients is considerable, Mr. Exline's contribution is especially appreciated.

Mr. Weissler's work¹⁵ on the adiabatic compressibility of methyl-siloxane liquids permitted him to calculate the isothermal compressibility at atmospheric pressure. His discussion unquestionably explains part of the difference between his results and those of this paper. Some of the difference, however, probably lies in the uncertainties in the quantities used in his calculations, notably the thermal expansivity and the specific heat at constant pressure.

¹⁴ See appendixes to the University of Pittsburgh thesis (MS) by the author (reference 2 of paper).

¹⁵ See reference (8) in Bibliography of paper.

A

O
num
lubr
the
from
form
(1),
resu
cate
diff
buti
pare
peri
con

T
a

A

F

H

M

1
vani
men
2
State
3
the p
Co
Petr
N. Y
OF M
No
unde
of th

A Mathematical Evaluation of Pressures in a Grease-Lubricated Bearing¹

By K. B. LAWRENCE,² STATE COLLEGE, PA.

Of the various methods proposed in the past for the numerical evaluation of pressures developed in a film of lubricant, perhaps the best method, in general, consists of the application of a finite-difference formula developed from the fundamental differential equation. Such a formula has been developed by Derman G. Christopherson (1),³ who also has shown that the formula gives accurate results when applied to calculations involving oil-lubricated bearings. The author herein applies the finite-difference formula to calculations of the pressure distribution existing in a grease-lubricated bearing and compares the results obtained with the results of a recent experimental investigation by Cohn and Oren (2), which was conducted under similar conditions of operation.

NOMENCLATURE

The following nomenclature is used in the paper:

- $a = r/L$ = dimensionless radius of a circle constructed about a central node o , which includes the surrounding nodes n upon its circumference
- A_o, A_{o-n} = influence coefficients
- C = eccentricity factor
- E = eccentricity of journal, in.
- F_o, F_{o-n} = residuals
- h = radial clearance or film thickness at point in film, in.
- h_o = radial clearance at point of closest approach
- $H = h/h_o$ = dimensionless ratio of radial clearance to radial clearance at point of closest approach
- L = length of bearing surface in direction of relative motion, in.
- $M = Z/Z_o$ = dimensionless ratio of absolute viscosity at points in film to viscosity at inlet to convergent section of channel
- n = subscript denoting points on circles of radius a or $2a$
- o = subscript denoting centers of circles
- p = pressure $\left[\frac{6Z_o UL}{(h_o)^2} \right] P$, psi
- P = dimensionless pressure
- U = rate of shear of viscous lubricant at point in film, ips
- x = distance measured in direction of relative motion, in.

y = distance measured in the plane of, and at right angles to relative motion, in.

Z = absolute viscosity at point in film, poise

Z_o = absolute viscosity at inlet to convergent section of channel, poise

η = radial clearance, in.

$\xi = x/L$ = dimensionless ratio of lengths measured along bearing arc from inlet position, to total length of bearing arc

INTRODUCTION

A method is to be shown herein for the solution of the pressure distribution in bearings lubricated with a copious supply of a non-Newtonian substance such as a grease or a polymer-laden oil. This subject is of considerable interest at the moment and has presented a problem of some difficulty because of the viscosity characteristics of the lubricants mentioned.

It has been shown by M. H. Arveson (3) and others that the apparent viscosity of greases varies as some function of the rate of shear, indicating an infinite value at zero rate of shear, with the viscosity approaching a constant value at extremely high rates of shear, such as indicated in Fig. 1. This effect is important in any analytical consideration of grease as well as of

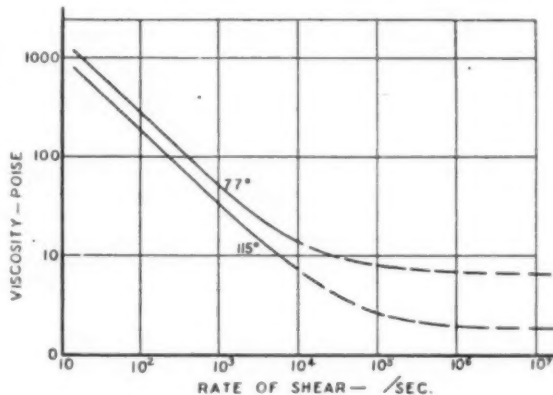


FIG. 1 VISCOSITY CURVES

other non-Newtonian substances used as a lubricant, inasmuch as the rate of shear is a variable under the conditions of thick-film lubrication of journal bearings.

It has been shown in hydrodynamic theory that the following equation formulated by Osborne Reynolds (4) applies in conditions of journal-bearing operation utilizing a copious supply of a viscous lubricant

$$\frac{\partial}{\partial x} \left(\frac{h^3}{Z} \frac{\partial p}{\partial x} \right) + \frac{\partial}{\partial y} \left(\frac{h^3}{Z} \frac{\partial p}{\partial y} \right) = 6U \frac{dh}{dx}$$

This equation, although admitting certain simplifications, remains general in so far as the viscosity characteristics of the lubricant are concerned, allowing viscosity changes in both

¹ This paper is an abstract of a thesis submitted to The Pennsylvania State College, June, 1948, in partial fulfillment of the requirements for a Master of Science degree in Mechanical Engineering.

² Instructor, Department of Mechanical Engineering, Pennsylvania State College.

³ Numbers in parentheses refer to the Bibliography at the end of the paper.

Contributed by the Research Committee on Lubrication and the Petroleum Division and presented at the Annual Meeting, New York, N. Y., November 27-December 2, 1949, of THE AMERICAN SOCIETY OF MECHANICAL ENGINEERS.

NOTE: Statements and opinions advanced in papers are to be understood as individual expressions of their authors and not those of the Society. Paper No. 49-A-69.

the X and Y -directions for any cause whatsoever. Considerable difficulty has been experienced, however, in the determination of a general, easily understood, and readily workable method for the solution of this equation. Much important work has been done in this respect by Reissner (5), Vogelpohl (6, 7, 8), Skinner (9), Kingsbury (10), and Christopherson (1). It is the last-named to whom we are indebted for the finite-difference formula which is to be used in this work.

In its very simplest elements, the solution of a differential equation in finite-difference form consists of the substitution of finite quantities in the place of the infinitely small differentials existing in the original. On this basis then, the equation containing the finite differences lends itself to numerical computations—however, at the sacrifice of accuracy. On the other hand, a satisfactory degree of accuracy can be obtained by limiting the finite differences to suitably small intervals simply as one approximates the slope of a graph by considering differences in the ordinates over suitably small intervals.

Christopherson (1) has determined the following finite-difference expressions as solutions of Reynolds equation:

$$\sum_{n=1}^4 a \left[\left(\frac{H^3}{M} \right)_n + \left(\frac{H^3}{M} \right)_a \right] P_n - P_o \sum_{n=1}^4 a \left[\left(\frac{H^3}{M} \right)_n + \left(\frac{H^3}{M} \right)_a \right] = 2a^2 \frac{\partial H}{\partial \xi}$$

which is accurate to the order of a^2 , or

$$16 \sum_{n=1}^4 a \left[\left(\frac{H^3}{M} \right)_n + \left(\frac{H^3}{M} \right)_a \right] P_n - \sum_{n=5}^8 2a \left[\left(\frac{H^3}{M} \right)_n + \left(\frac{H^3}{M} \right)_a \right] P_n - P_o \left\{ 16 \sum_{n=1}^4 a \left[\left(\frac{H^3}{M} \right)_n + \left(\frac{H^3}{M} \right)_a \right] - \sum_{n=5}^8 2a \left[\left(\frac{H^3}{M} \right)_n + \left(\frac{H^3}{M} \right)_a \right] \right\} = 24a^2 \frac{\partial H}{\partial \xi}$$

which is accurate to the order of a^4 .

The summations in the foregoing equation apply to points equally spaced on the circumference (n -points) and at the center (o -points) of circles of radius a or $2a$ such as shown in Fig. 2, situated in the hydrodynamic field in the plane of relative motion. These points are thought of as nodes formed by a grid of equally spaced lines covering the field which is transformed into the X, Y -plane as is shown in Figs. 2 and 3, where the latter shows the fine-grid node construction.

It is necessary also to apply the relaxation method of Southwell (11) to the results determined by the foregoing formulas, since these results will be in error due to the necessity of using a coarse grid, Fig. 2, at the starting points.

VISCOSITY ANALYSIS

Data are given in Table 1 for the reference grease which is to be used in the calculations. These data are for the same grease tested and reported by Cohn and Oren (2).

TABLE 1 CAPILLARY VISCOSITY DATA

U/h (rate of shear in reciprocal seconds)	Z (viscosity in poise)	
	77 deg F	115 deg F
15.6	1132.4	717.3
47.0	547.4	345.2
108.9	262.1	183.0
203.1	161.3	107.8
434.0	89.1	59.9
678.7	63.2	42.6
2737.0	26.4	16.4
8200.0	15.0	8.3

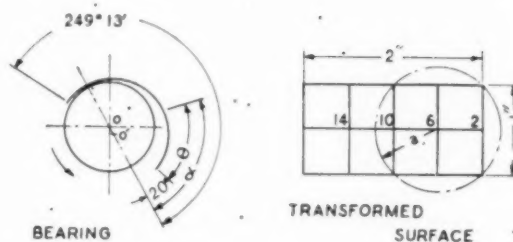


FIG. 2 INITIAL NODE ARRANGEMENT

n	13	12	11	10	9	8	7	6	5	4	3	2	1	0
$n+20$	33	32	31	30	29	28	27	26	25	24	23	22	21	20
$n+40$	53	52	51	50	49	48	47	46	45	44	43	42	41	40
$n+60$	73	72	71	70	69	68	67	66	65	64	63	62	61	60

FIG. 3 FINE-GRID NODE ARRANGEMENT

A mathematical formula is fitted to each of the viscosity sets of values by a standard textbook method (12) which results in the following

$$Z(\text{at } 77 \text{ deg F}) = 10,960 \left(\frac{U}{h} \right)^{-0.8018} + 6.8$$

$$Z(\text{at } 115 \text{ deg F}) = 6377 \left(\frac{U}{h} \right)^{-0.7800} + 1.82$$

This is done in order to extrapolate the existing data in the direction shown dotted in Fig. 1.

SOLUTION OF FINITE-DIFFERENCE FORMULA

A cylindrical 1-in. \times 1-in. bearing is selected for investigation. The bearing surface is transformed as in Fig. 2, and an area as indicated is selected for investigation in which positive hydrodynamic pressures are anticipated. Furthermore, the area, consisting of 2 in. of the bearing arc, is selected in particular to enable initial calculations to be made for pressures at nodes 6, 10, and 14, involving only pressures at nodes on the boundaries where the values for P_n are known to be zero.

The appropriate physical values are determined in the following calculations:

$$C = \text{eccentricity factor} = 0.46 \text{ (assumed)}$$

$$\eta = \text{radial clearance of bearing and journal} = 0.0082 \text{ in.}$$

$$E = \text{eccentricity of bearing and journal centers}$$

$$= 0.46 \times 0.0082 = 0.00377 \text{ in.}$$

$$\text{Mean film temperature } 115 \text{ F (assumed)}$$

$$\text{Journal speed } 250 \text{ rpm}$$

$$h_0 = \text{minimum film thickness} = 0.0082 - 0.00377 = 0.0044 \text{ in.}$$

$$h_s = \text{film thickness at entrance} = 0.0082 - 0.00377 \cos 20 \text{ deg} = 0.0117 \text{ in.}$$

$$\frac{U}{h_s} = \text{rate of shear at entrance} = \frac{\pi \times 1 \times 250}{60 \times 0.0177} = \frac{13.1}{0.0177}$$

$$= 1119 \text{ reciprocal sec}$$

$$Z_s = 6376 (1119)^{-0.789} + 1.82 = 30.6 \text{ poises}$$

$$\xi = \frac{x}{L} = \frac{r \theta}{L} = \frac{0.5 \theta}{2} = \frac{\theta}{4}$$

$$\begin{aligned}\alpha &= \theta + 20 \text{ deg} \\ H &= \frac{h}{h_s} = \frac{\eta + E \times \cos \alpha}{h_s} = \frac{\eta}{h_s} + \frac{E}{h_s} \cos (4\xi + 20) \\ \frac{\partial H}{\partial \xi} &= \frac{-4E}{h_s} \sin (4\xi + 20) = \frac{-4 \times 0.00377}{0.0044} \sin \alpha \\ &= -3.425 \sin \alpha\end{aligned}$$

TABLE 2

Node	α	%	H	U/h	Z	$M = Z/Z_s$	H^2/M	$\frac{\partial H}{\partial \xi}$
2	20	0.0177	2.66	1119	30.6	1.000	18.90	
6	77°18'	0.0090	2.042	1457	25.4	0.830	10.28	-1.932
10	134°36'	0.0056	1.272	2340	18.2	0.595	3.46	-2.442

It is to be noted in Table 2 that the viscosity of the grease calculated at each of the nodes is based upon the circumferential rate of shear which is assumed to be constant across the thickness of the film. This involves two cases in point. The one case involves the assumption just mentioned, and amounts to the neglect of the second-order effect of pressure on the velocity distribution across the film thickness. Further, it may be reasoned that the rate of shear as a function of x and y should be determined correctly in the direction of the flow at the points under consideration. However, since the flow in the X -(or circumferential) direction is of such a higher order of magnitude than the flow endwise at any point, it is reasoned that the circumferential rate of shear will be a satisfactory approximation and most especially so in this, the case of the highly viscous grease where the end flow is exceedingly low.

The dimensionless pressure at node 6 is now calculated as a sample

$$\begin{aligned}a &= \frac{0.5}{2 \times 0.707} = 0.3535 \\ P_6 &= \frac{2(0.3535)^2 \times 3.345}{2(18.9) + 2(3.46) + 4(10.28)} = 0.00974\end{aligned}$$

The pressures at nodes of progressively finer grids are calculated in a similar manner, using values at nodes previously determined.

Since the formula gives accurate results only for fine grids and the foregoing values were based upon values determined initially for an exceedingly coarse grid, it is necessary now to reduce the error by the relaxation technique.

APPLICATION OF RELAXATION METHOD

Numerical values called residuals are calculated by the reapplication of the finite-difference formula. The residuals defined by

$$\begin{aligned}F_0 &= \sum_{n=1}^4 a \left[\left(\frac{H^3}{M} \right)_n + \left(\frac{H^3}{M} \right)_s \right] P_n - \\ &\quad P_0 \sum_{n=1}^4 a \left[\left(\frac{H^3}{M} \right)_n + \left(\frac{H^3}{M} \right)_s \right] - 2a^2 \frac{\partial H}{\partial \xi}\end{aligned}$$

are in effect the numerical inequalities existing in the equation due to errors in the pressures. It is seen from the formula that a change in the residual may be made by effecting a change in the P_0 ; in addition, a change in P_0 results in an accompanying change in the residual at the neighboring nodes. To facilitate making these changes the quantities

$$\left[\left(\frac{H^3}{M} \right)_n + \left(\frac{H^3}{M} \right)_s \right]$$

and

$$\sum_{n=1}^4 a \left[\left(\frac{H^3}{M} \right)_n + \left(\frac{H^3}{M} \right)_s \right]$$

are given symbols A_{0-n} and A_0 , respectively, and are called influence coefficients. Then at the center

$$\Delta P_0 = - \frac{\Delta F_0}{A_0}$$

and at the n -nodes

$$\Delta F_n = \Delta P_0 \times A_{0-n} = - \Delta F_0 \frac{A_{0-n}}{A_0}$$

The ratios A_{0-n}/A_0 are calculated in advance and serve as multipliers.

In the manner then of reducing the residuals at each of the nodes successively according to the formulas given, values of corrected dimensionless pressures are obtained.

In this, the first case, an additional series of calculations are necessary to extend the area under consideration throughout the convergent section of the channel. The results obtained thereby are given in Table 3 and plotted in Figs. 4, 5, 6, and 7, as the No. 1 set of curves.

In a similar manner the values for the No. 2 set which were taken at the lower temperature, are determined, with the exception, however, that instead of determining initially approximate pressures by means of the formula, a rather arbitrary pressure distribution is assumed and corrections are made thereto by the relaxation method.

The No. 3 set of curves shows the results at the conditions of a higher temperature and increased eccentricity factor. These curves result from the application of the second and more accurate finite-difference formula in the determination of the residuals.

SUMMARY

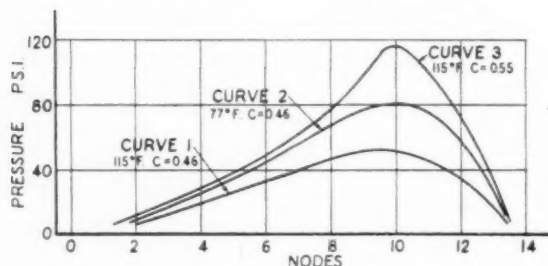
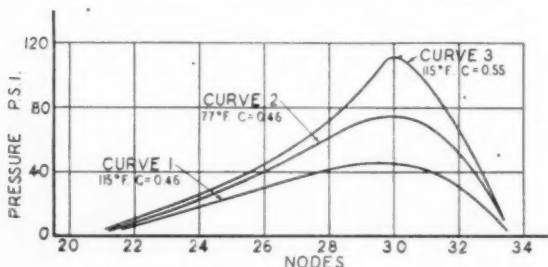
The reader's attention is invited first to the consideration of the viscosity curves in Fig. 1. It is here noted that the apparent viscosity levels off asymptotically at high values of rate of shear, which phenomenon has been reported by M. H. Arveson (3) and others, based upon experimental evidence. The term apparent viscosity is here used advisedly since the data given were determined by the capillary-tube method, and there is some question as to its applicability because of the possible coring effect in the capillary, which may be attributed to the non-Newtonian characteristic of the grease. However, these data are of sufficient accuracy to demonstrate the general behavior of the lubricant.

The curves in Figs. 4, 5, 6, and 7 are qualitatively similar to those of the oil family; however, no quantitative comparison is attempted here because of the basic differences in the two types of lubricants and the impracticability of establishing the conditions for a rational basis of comparison.

Finally, the curves in Fig. 8 are to be noted. Here the curves for the No. 2 set of conditions are compared with those determined by an experimental investigation by Cohn and Oren (2) on a bearing of similar dimensions. The latter are shown dotted. Rather good conformity is therein noted, although it should be emphasized that there is considerable uncertainty concerning the comparableness of some of the corresponding physical conditions existing in the two cases. Possibly the most notable deviation is the diversity in the unit radial clearance. In this work the value of 0.0164 in. per in. was used, while Cohn and Oren report for their bearing a value of 0.0071 in. per in. Of similar importance

TABLE 3 CORRECTED PRESSURES FOR CURVES NO. 1 PSI

n	$n + 0$	$n + 20$	$n + 40$	$n + 60$
1	0	0	0	0
2	7.74	6.95	5.50	4.20
3	13.88	12.77	9.42	6.10
4	20.99	19.85	16.12	9.77
5	26.39	24.88	20.52	13.43
6	32.62	30.66	24.97	15.08
7	39.6	37.0	29.9	17.5
8	46.1	42.6	34.6	20.7
9	50.8	47.0	39.6	23.8
10	51.1	45.0	35.4	23.8
11	47.2	43.1	35.6	21.4
12	35.1	32.0	26.0	16.0
13	17.7	14.1	13.2	7.4
14	0	0	0	0

FIG. 4 PRESSURE DISTRIBUTION AT n -NODES (CENTER)FIG. 5 PRESSURE DISTRIBUTION AT $n + 20$ NODES

is the matter of the running position of the shaft, since there is no reported value of eccentricity in the experimental investigation. The constant mean film temperature, as assumed herein for the lower (77 deg F) cases, roughly approximates the bearing shell temperatures observed by Cohn and Oren, and, although the finite-difference formula is adaptable to temperature variations in the film, no allowance was made for this occurrence in this work.

It is also to be noted that although the curves were plotted to the same scale on the abscissa, their relative location was chosen arbitrarily, since this mathematical treatment does not determine directly the angular position of the application of the load.

CONCLUSIONS

This work is presented as an illustration of the use of the finite-difference formula as applied to determining the pressure distribution in a journal bearing using grease as a lubricant. In a similar manner, this same method can be used equally as well where other non-Newtonian substances are used, as well as Newtonian substances. This method may be considered as valid in so far as the assumptions made herein apply, and presents the possibility of the establishment of a simpler method which can be applied to everyday lubrication problems involving non-Newtonian lubricants. This can be accomplished through the analytical survey of the whole field of application by this method. Then the evolution of a semianalytical method can be brought about, constructed on a rational basis.

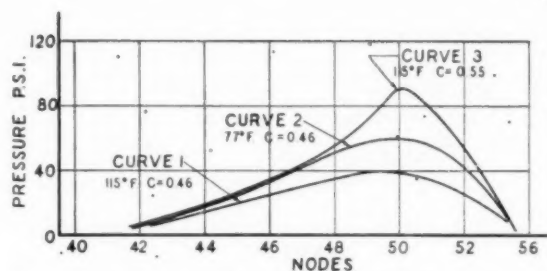
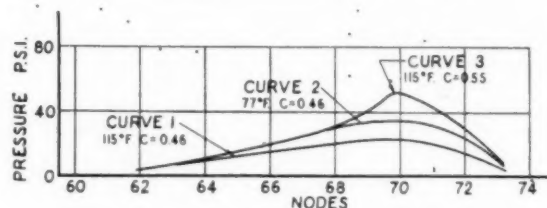
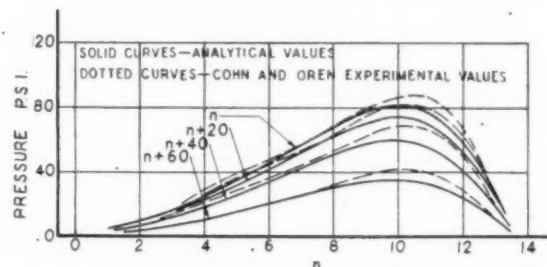
FIG. 6 PRESSURE DISTRIBUTION AT $n + 40$ NODESFIG. 7 PRESSURE DISTRIBUTION AT $n + 60$ NODES

FIG. 8 COMPARISON OF ANALYTICAL AND EXPERIMENTAL PRESSURES

ACKNOWLEDGMENTS

The author wishes to express his appreciation for the aid given in the preparation of the original thesis by Prof. L. J. Bradford, formerly of The Pennsylvania State College, and for the many helpful suggestions given in the preparation of this paper by E. M. Barber, F. J. Villforth, Jr., and J. R. Muenger of The Texas Company.

BIBLIOGRAPHY

- 1 "A New Mathematical Method for the Solution of Film Lubrication Problems," by D. G. Christopherson, The Institution of Mechanical Engineers, Journal and Proceedings, vol. 146, 1941, pp. 126-135.
- 2 "Film-Pressure Distribution in Grease-Lubricated Journal Bearings," by Gunther Cohn and Jess W. Oren, Trans. ASME, vol. 71, July, 1949, p. 555.
- 3 "Flow of Petroleum Lubricating Greases," by M. H. Arveson, Industrial and Engineering Chemistry, vol. 24, 1932, p. 71.
- 4 "On the Theory of Lubrication and Its Application to Mr. Beauchamp Tower's Experiments . . . (a), by O. Reynolds, Philosophical Transactions, Royal Society, vol. 177, part 1, 1886, pp. 157-234; (b) Papers on Mechanical and Physical Subjects, The Macmillan Company, New York, N. Y., vol. 2, 1901, pp. 228-310.
- 5 "Ebene und räumliche Strömung zäher inkompressibler trägheitsfreier Flüssigkeiten zwischen excentrischen, relative zu einander rotierenden Zylinderflächen. Beitrag zur Theorie der Schmierung," by H. Reissner, Zeitschrift für angewandte Mathematik und Mechanik, vol. 15, 1935, pp. 81-87; vol. 16, 1936, pp. 275-286, and 384.
- 6 "Zur hydrodynamischen Theorie der Lagerreibung," by G. Vogelpohl, Zeitschrift für angewandte Mathematik und Mechanik, vol. 15, 1935, pp. 278-285.
- 7 "Hydrodynamisch Lagertheorie und halbflüssige Reibung,"

by G. Vogelpohl, *Zeitschrift für angewandte Mathematik und Mechanik*, vol. 16, 1936, pp. 371-372.

8 "Beiträge zur Kenntniss der Gleitlagerreibung," by G. Vogelpohl, *Forschungsheft* 386, 1937, p. 28.

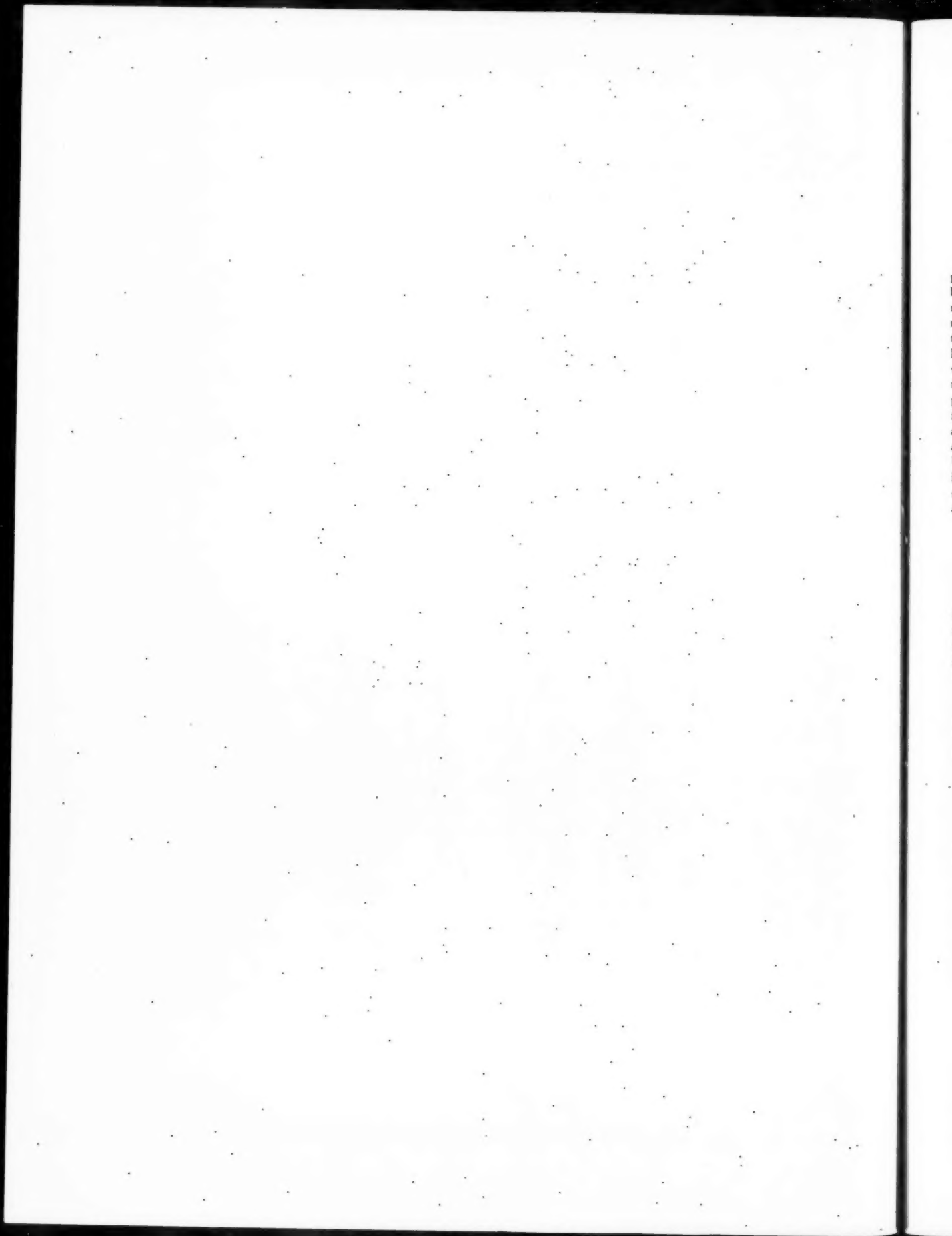
9 "Film Lubrication of Non-Planar Surfaces of Finite Width," by S. M. Skinner, *Bulletin, American Physical Society* vol. 12, 1937, p. 7.

10 "On Problems in the Theory of Fluid Film Lubrication, With

an Experimental Method of Solution," by A. Kingsbury, *Journal of Applied Mechanics*, Trans. ASME, vol. 53, paper no. APM-53-5, 1931, p. A-59.

11 "Relaxation Methods in Engineering Science," by R. V. Southwell, The Clarendon Press, Oxford, England, 1940.

12 "Empirical Equations and Nomography," by D. S. Davis, McGraw-Hill Book Company, Inc., New York, N. Y., 1943, pp. 11-14.



Investigation of Lubricants for Power Circuit Breakers

By R. R. BUSH,¹ PHILADELPHIA, PA.

This paper describes a technique for the selection of proper lubricants for power circuit breakers. The circuit breaker is described briefly, and its lubrication requirements for dependable operation are discussed. The laboratory methods set up to determine the performance of the grease best suited for this application are outlined. Results of the laboratory test data are shown and evaluated with reference to circuit-breaker requirements. Properties of some typical greases are compared with their performance for this particular application. Because performance depends not only upon grease properties, but also upon the process of manufacture, the greases tested are referred to only in code. Life tests on actual circuit breakers have checked laboratory results. Therefore it is concluded that tests may be set up to determine the suitability of a lubricant for any particular application and especially for power circuit breakers.

INTRODUCTION

PROPER lubrication of power circuit breakers is a problem of considerable importance because the operation of the entire power system depends so completely on the reliable operation of the breakers under any emergency. When a short circuit occurs on a power line, the portion in which the disturbance originated must be isolated quickly to prevent damage to associated apparatus and to restore service to the rest of the system. Its entire operation must be completed in less than $\frac{1}{10}$ sec. To obtain this high-speed operation, friction of all moving parts must be held to a minimum. The better the lubrication of all friction points, the lower the friction which will be encountered. This means higher speed of operation and longer life of all moving parts.

The lubrication problem in power-circuit-breaker bearings and other friction points is peculiar in that the motion is extremely intermittent, generally oscillatory, and generally heavily loaded. The contacts of the power circuit breaker are opened in response to the operation of a high-speed relay by means of a powerful driving force properly connected through cranks, cams, and rollers. The driving force is generally obtained from energy stored in compressed springs, or compressed air. Quick opening is accomplished by suddenly releasing this stored energy. Each passing year has seen the size and speed of circuit breakers increase. With each such increase, the duty on bearings has also increased, as indicated in Fig. 1. To keep friction and maintenance to a minimum, better and better lubricants have been required. Hand in hand with this development went the choice of the proper lubricant for the bearings depending on the duty they perform.

Fig. 2 is a magne-blast circuit breaker rated at 13,800 volts and

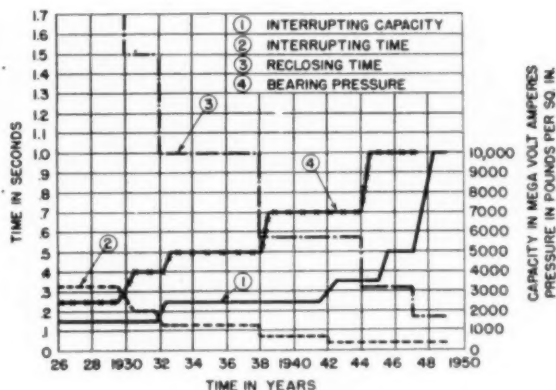


FIG. 1 GENERAL CHRONOLOGICAL DEVELOPMENT OF ALLOWABLE BEARING PRESSURES COMPARED TO OTHER POWER-CIRCUIT-BREAKER CHARACTERISTICS

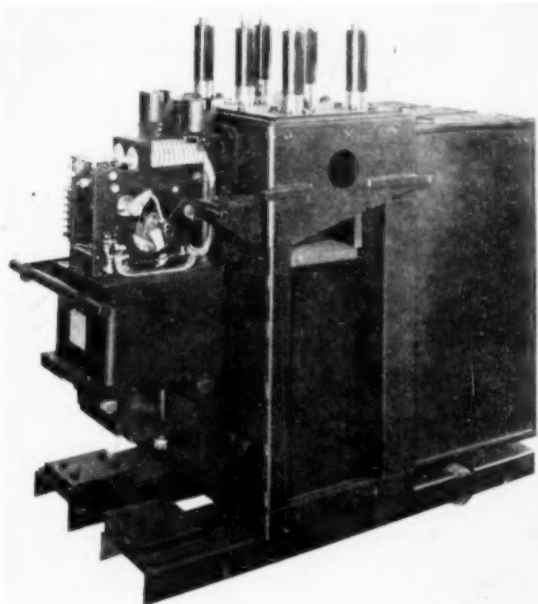


FIG. 2 MAGNE-BLAST POWER CIRCUIT BREAKER RATED 500,000 KVA AT 13,800 VOLTS
(Bearings must operate instantly but intermittently at medium speed and relatively heavy loading.)

500,000 kva interrupting capacity, which represents one of the smaller types of modern circuit breakers. Fig. 3 is a 360,000-volt circuit breaker with an interrupting capacity of 10,000,000 kva, which represents the highest-capacity circuit breaker yet developed

¹ Development Engineer, Switchgear Divisions, General Electric Company. Mem. ASME.

Contributed by the Research Committee on Lubrication and the Petroleum Division and presented at the Annual Meeting, New York, N. Y., November 27-December 2, 1949, of THE AMERICAN SOCIETY OF MECHANICAL ENGINEERS.

NOTE: Statements and opinions advanced in papers are to be understood as individual expressions of their authors and not those of the Society. Paper No. 49-A-17.

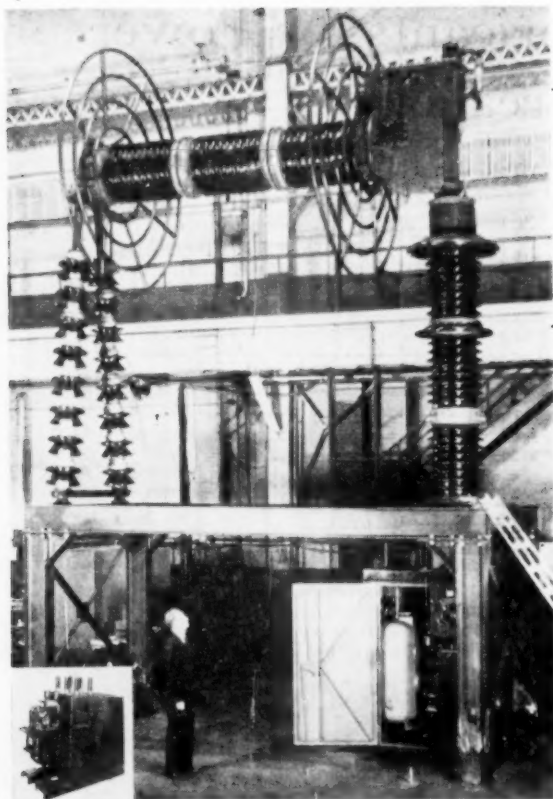


FIG. 3 LOW-OIL-CONTENT IMPULSE-TYPE OIL CIRCUIT BREAKER
RATED 10,000,000 KVA AT 360,000 VOLTS
(Interrupting time 0.05 sec.; reclosing time 0.167 sec.* Inset of breaker from
Fig. 2 compares sizes.)

Its 6 sets of contacts are designed to carry 1000 amp continuously, to open in 0.05 sec and reclose in 0.16 sec. For comparison of size, the inset at the lower left-hand corner shows the breaker from Fig. 2 to the same scale as this breaker. The development of most modern breakers would not have been possible without corresponding development in bearings and lubricants to keep friction to a minimum.

LUBRICATION REQUIREMENTS OF MODERN BREAKERS

It is well known that greases provide better lubrication than oils for power circuit breakers because they stay in the bearings better than oils under high pressures. They also exclude dirt to a greater degree than oils. This is especially true on textolite bearings,² and open antifriction or rolling-friction bearings. However, grease lubricants tend to stiffen up with time because of oxidation. In bearings in circuit-breaker mechanisms, where the available torque for initiating operation is low, this added friction may be serious because it may prevent the circuit breaker from opening. Some breaker bearings have been found in service in which the grease was practically solid around the rollers of trip latches. In cases when such breakers opened, it was found that the opening time had increased 3 to 5 times. This may be very serious under short-circuit conditions. Further investigation of

these cases showed the torque required to operate the trip latch had increased several times over the normal torque required for tripping, because of hardened grease. The only assurance users have had of proper operation of circuit breakers has been periodic checking with a time-travel recorder to see that they have the proper speed. On outdoor breakers, located in cold climates, the increase in consistency, or decrease in penetration, with temperature is also a problem with many greases.

Another duty that greases must perform in power circuit breakers is protection from corrosion and rusting of bearings and other sliding metal parts, both during storage before placing in service, and after being placed in service. Humidity or corrosive atmospheres are particularly severe on roller bearings unless they are properly protected with a film of lubricant.

In sleeve bearings, the coefficient of friction varies widely with the type and condition of the lubricant. This is critical because of the high bearing pressures used in circuit breakers. With older metallic-bushing bearings, the grease film must persist at pressures around 7000 psi and in the modern textolite-bushing bearings at around 10,000 psi. Many greases may be found to satisfy one or more of the requirements just outlined, but to find one which will satisfy all these requirements is much more difficult.

The dependable and trouble-free operation of power circuit breakers under all conditions, however, dictates that the lubricant used meet all these requirements. Preferably a single lubricant should be used in all locations of a given circuit breaker to avoid the necessity of selection on the part of the maintenance crew and to avoid the stocking of several types of greases. Hence this investigation was initiated to determine the best type of lubricant for use in modern power circuit breakers. It must be realized that the best grease from an over-all standpoint will not necessarily be the best grease from all standpoints. This review, therefore, is presented more to point out the method of investigation rather than as a grease recommendation; and, accordingly, all greases are referred to by number only.

METHOD OF ATTACKING THE PROBLEM

Engineers from a number of lubricating companies were asked to review the problem. All agreed it was worth while to look for one grease, although the possibilities of finding one suitable for all operating conditions were doubtful. Accordingly, the following specifications were set down for the grease:

- 1 High resistance to oxidation.
- 2 Operating temperature range from -30°F to $+150^{\circ}\text{F}$.
- 3 Good lubricating qualities.
- 4 Good corrosion protection.
- 5 Must not be forced out of bearing under high pressure.

With these points in mind, some thirty different greases were recommended for investigation.

The first check was on oxidation. The shelf life of the grease was considered the criterion for grease in antifriction bearings, because of the short working life and intermittent oscillatory motion imposed on them in circuit breakers. The Norma-Hoffman bomb test gave the best laboratory measure of this property, but the test was time-consuming.

For textolite sleeve bearings, it was considered that the oxidation of a thin film would be more indicative of the lasting qualities of the grease. In order to produce thin films for oxidation tests, a tool, shown in Fig. 4, was devised, the knife-edge of which spread an even thin film of grease on a chromium-plated steel plate measuring 1 in. \times 5 in. \times 12 in. This plate was lapped to a flatness of about 15 microinches before flash-plating with chromium about 0.0002 in. thick. The 0.001-in. thickness of

² "Heavy-Duty Bearings With Intermittent Oscillatory Motion," by R. R. Bush, presented at the Fall Meeting, Erie, Pa., September 28-30, 1949, of THE AMERICAN SOCIETY OF MECHANICAL ENGINEERS.

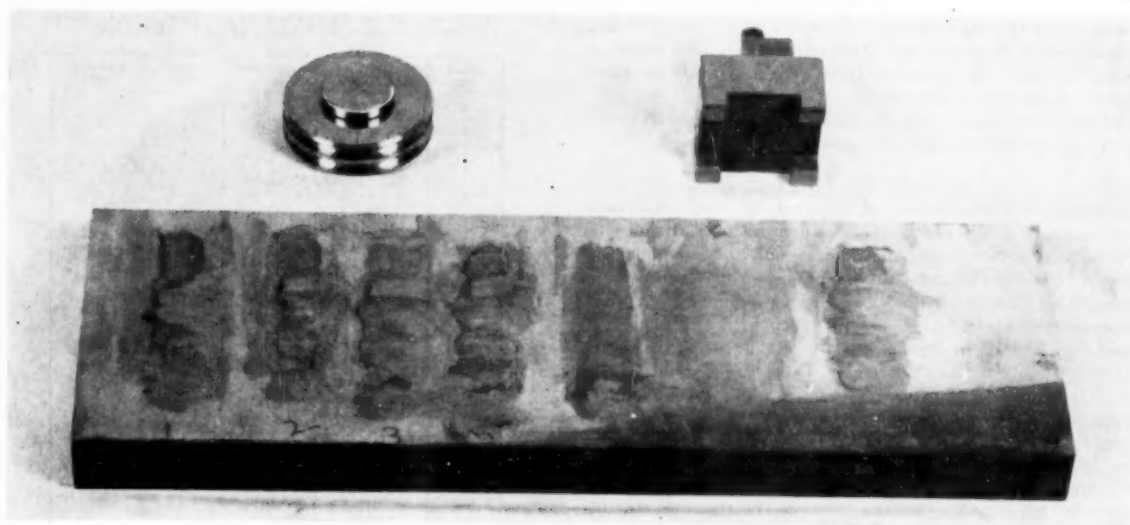


FIG. 4 APPARATUS FOR THIN-FILM OXIDATION TESTS

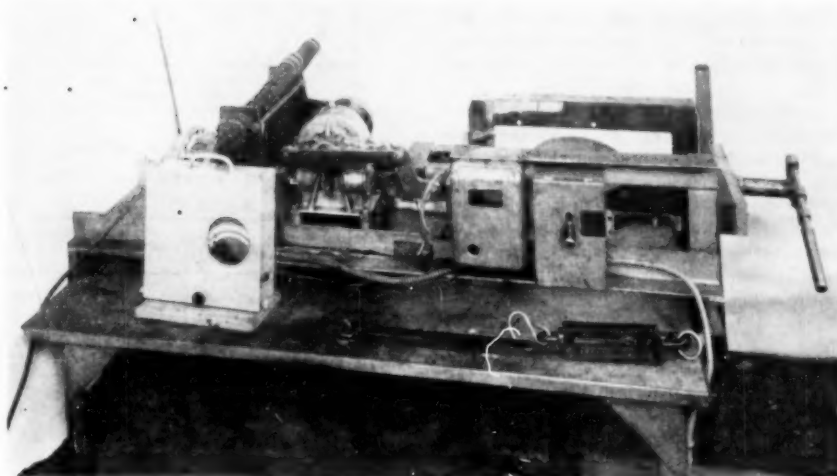


FIG. 5 BEARING TEST MACHINE FOR LIFE TEST AND FRICTION MEASUREMENTS

the film of grease as laid down was checked to within 0.0001 in. by a Gardner interchemical thickness gage.

Several greases were put on the plate at the same time and then placed in a circulating oven at 100 C. It was considered that any grease used for this purpose should remain relatively intact at this temperature and that the oxidation would be accelerated to give a comparative answer in a reasonable time. Greases which were not acceptable lost their lubricating properties in as short a time as 24 hr while many of the more acceptable ones lasted at least 120 hr. Some of the best greases retained their lubricating properties for even longer periods.

As soon as a grease indicated it might pass the thin-film oxidation test, it was checked in an ordinary refrigerator for 48 hr to see if it showed stiffening as lowered temperatures occurred. If it indicated satisfactory performance under these conditions, the grease was put on friction test in textolite bearings on the test machine shown in Fig. 5. Corrosion tests also were run at this time in both salt-spray and humidity chambers.

The friction test was run 100 operations at 8000 psi of projected area, 100 operations at 10,000 psi of projected area, and 100 at 12,000 psi. Starting and running friction were measured after each of the steps and if everything appeared satisfactory, a 14,000 operation life test was run at 12,000 psi. Starting and moving friction were determined at intervals during the run. Also, the machine was left standing overnight and over week ends and the starting friction measured just before resuming the run. The frictional values for both starting and running were compared because both are equally important in circuit breakers which must trip instantly and open at high speed. When a grease had passed the friction test, the thin-film test, the refrigerator cold test, and appeared to be satisfactory on the corrosion tests, then a Norma-Hoffman oxygen-bomb² test, and a torque-temperature

² "Some Applications of an Accelerated Test for Determining the Chemical Stability of Lubricating Greases," by F. L. Wright and H. A. Mills, Proceedings of the ASTM, vol. 38, part 2, 1938, pp. 525-538.

test in a ball bearing were run. To check with types of sliding bearings other than textolite, friction runs were also taken on bronze bearings. Evaporation tests were also made on those greases which showed promise.

With the laboratory tests all satisfactory, the grease was then put in actual circuit breakers as a final check.

RESULTS OF TESTS

Following will be a review of the results of tests made on a representative number of the greases investigated. It must be realized that any statement given applies only to the peculiar application investigated under the conditions outlined and is not a criterion for that grease under conditions different from those under consideration. Also, for the purpose of avoiding any possible undesirable reflection on any product, the greases are coded with only number reference. Table 1 is a tabulation of general performance as determined by test. Since readings were comparative, designations are listed as "acceptable" or "unacceptable." If any grease approaches acceptable in any given requirement, it is marked unacceptable and starred to indicate that further investigation is warranted. Table 2 lists general properties of several representative types of these greases together with general performance. Space does not permit listing all greases tested. Again, it is realized that the properties do not tell the whole story as to how a grease may perform. They are given merely to show any relation they might have to their performances under the conditions tested.⁴ For better understanding of these tables, the following curves show typical detailed test data.

Fig. 6 shows the performance of two greases acceptable for friction. Fig. 7 shows the performance of two greases unacceptable for bearing friction. No grease was considered acceptable which showed a marked tendency to exceed 0.10 coefficient of starting friction during a run. Starting friction after a long period of rest might exceed this figure but would not be desirable. The maximum reached when grease 21 was used was 0.128 in one case. With grease 14, the coefficient of friction never exceeded 0.11 when the grease was new. However, when quite old, it would permit scoring of the bearings and pin after a short run at the high pressures involved. Fig. 8 illustrates oxygen-pressure loss with time in the Norma-Hoffman bomb. These curves give relative resistance to oxidation of four different greases.

Fig. 9 shows torque-temperature properties of two greases of widely different composition. Both of the greases illustrated were acceptable on this test as it indicates low torque on ball bearings in cold weather. Fig. 10 illustrates the loss by evaporation of 5-g samples of different greases placed in an oven at 210 F.

Examination of the tables and charts will reveal that grease 21, when compared with others, performed most consistently acceptable in all tests to which it was submitted. It also will be noted that while its average performance is good all around for the purpose investigated, other greases exceeded it on some points; but fell down on others.

It appears that inhibitors against oxidation are mandatory. Rust inhibitors are a help against corrosion, but other ingredients may accomplish this protection. The sodium soap base appears to perform better on resistance to oxidation than calcium soap base, but either is good on friction when formulated with petroleum oil having in the neighborhood of 275 SUS viscosity at 100 F, and showing a consistency of around 275 penetration. The lithium soap base with a 300 SUS viscosity performed much better on the friction machine than those with lighter oils,

⁴ "Functional Tests for Lubricants and Their Interpretation," by T. G. Roehner and E. S. Carmichael, *Lubrication Engineering*, vol. 5 February, 1949, pp. 15-18 and 47.

TABLE 1 RESULTS OF PERFORMANCE TESTS AS CONDUCTED ON GREASES BY LABORATORY METHODS

GREASE NO.	Oxidation		Friction Mach.	Cold Reprig.	Corrosion Tests
	Film	Bomb			
1	U				
2	A	A	U	A	U
3	A		U	A	U
4	U				
5	U				
6	U				
7	U				
8	U				
9	U	U	U	U	
10	U*	U	U*	A	U
11	A		U		
12	U				
13	U				
14	U		A		A
15	U	U			
16	A	A	U	A	A
17	U				
18	A		U	U	
19	U			U	
20	U			U	
21	A	A	A	A	A
22	A		U	A	
23	A		U*		U
24	U				
25	U				

A = Acceptable
U = Unacceptable
* = Warrants further investigation

TABLE 2 CHARACTERISTIC PROPERTIES OF SEVERAL GREASES LISTED AGAINST RESULTS OF PERFORMANCE TESTS AS CONDUCTED BY LABORATORY METHODS

GREASE NO.	SOAP BASE	PROPERTIES				PERFORMANCE				
		TYPE	VELOC. 100°F	INHIBITORS	CONSIST. UNWORKED	THIN FILM	Friction Mach.	Cold Reprig.	Corrosion Tests	
21	Na	Pet.	200	Yes	Yes	300	A _b	A	A _c	A
11	Na	Pet.	125	Yes	No	300	A	U	U	-
14	Ca	Pet.	300	Yes	-	250	U	A	U	A
10	Ca	Pet.	285	No	No	350	U	U	U	-
23	Li	Pet.	300	Yes	Yes	275	A	U*	-	U
16	Li	Syn. & Pet.	72	Yes	-	265	A	U	A	A
2	Li	Syn.	70	Yes	Yes	290	A	U	A	U
3	Li	Syn.	70	Yes	Yes	250	A	U	A	U

A = Acceptable
U = Unacceptable
* = Warrants further investigation
b = Also bomb test—induction period exceeds 1000 hr
c = Also torque test—900 gm cm to start at -30 F

although the test results did not show up good enough. Generally, they gave the least protection in corrosion tests but showed very good resistance to oxidation.

It may be of interest here to mention that dry lubrication was tried on textolite bearings and stainless-steel shafts without success at any pressures in the ranges considered.

After the laboratory tests, grease 21 was put on life tests on large and small-sized breakers. Its performance met expectations in all cases except on high-speed open gearing. It lacked the ability to stick fast on these fast-rotating parts. Circuit breakers have few such applications in their design.

CONCLUSIONS

Review of the data reveals that much investigation is necessary to determine the suitability of a lubricant for any particular apparatus. It was possible to find a grease that fulfilled most of the

N • STOOD OVER NIGHT
W • STOOD OVER WEEKEND

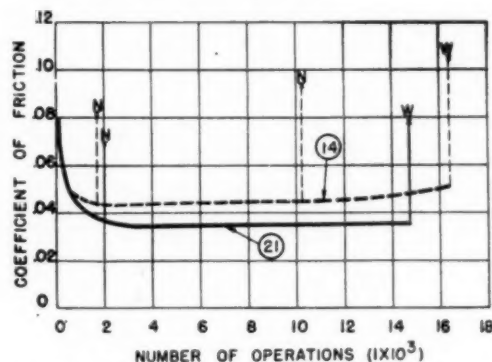


FIG. 6 CURVE SHEET SHOWING COEFFICIENT OF FRICTION OF BEARINGS WITH TWO ACCEPTABLE GREASES

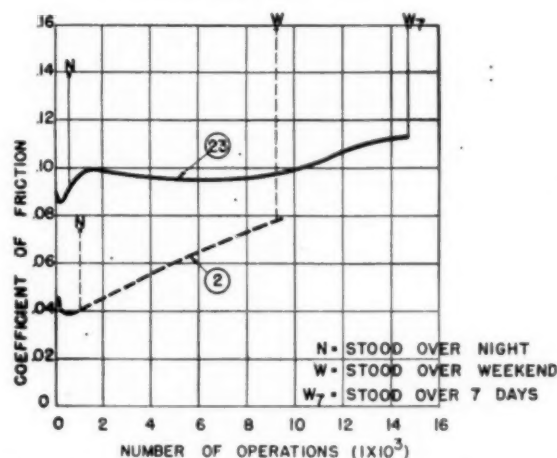


FIG. 7 CURVE SHEET SHOWING COEFFICIENT OF FRICTION OF BEARINGS WITH TWO UNACCEPTABLE GREASES

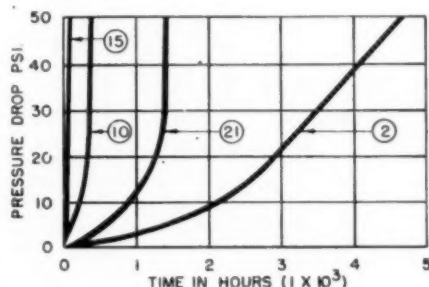


FIG. 8 CURVE SHEET SHOWING OXYGEN-BOMB TESTS AT 210 F OF SEVERAL GREASES

requirements set down for the particular application. For a few very special considerations a special lubricant is necessary. Investigation shows that laboratory tests are the quickest and the most reliable way to check a large number of possible greases for a specific application. Results obtained in an actual circuit breaker gave performance far superior to any of the standard greases previously used for this application. Each application,

however, will require its own peculiar tests of several lubricants, and different weights will be given to each characteristic to arrive at an acceptable solution for that application. Life tests then must be made on the apparatus itself to insure that performance on all points is satisfactory. In circuit breakers, such a lubrication investigation has yielded results far better than could have been obtained in any other way.

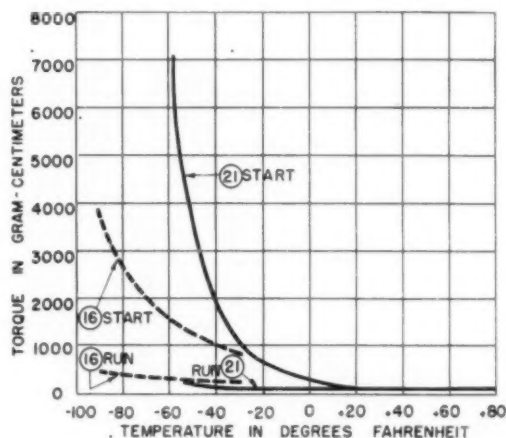


FIG. 9 CURVE SHEET SHOWING TEMPERATURE-TORQUE CHARACTERISTICS OF TWO GREASES

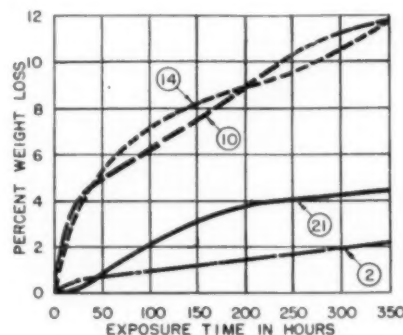


FIG. 10 CURVE SHEET SHOWING EVAPORATION LOSSES OF SEVERAL GREASES AT 210 F

Discussion

V. L. BARR.¹ One very important point which needs restressing is that this work was conducted to find a suitable lubricant for sleeve-type bearings, primarily textolite. The bearing pressures shown in Fig. 1 of the paper, for instance, are for this type bearing and not antifriction bearings. Successful applications of needle-type bearings under similar service conditions operate at much higher loading on a projected-area basis.

The data presented are applicable to antifriction bearings, but not in the same order of importance as shown in this paper. For ball and roller bearings, we would list the requirements in the following order:

¹ Director of Engineering, Roller Bearing Company of America, Trenton, N. J. Jun. ASME.

- 1 Resistance to oxidation.
- 2 Wide temperature range of operation.
- 3 Corrosion protection.
- 4 Good lubricating qualities.

The author's last requirement has no particular interest for antifriction bearings.

For the particular service required in circuit breakers, we are not too concerned with the lubrication properties of a grease. For continuous-rotating applications, however, this is not true.

With these points in mind and reviewing Table 1 of the paper, it is the writer's opinion that grease No. 16 would be very satisfactory for the antifriction bearings used in circuit breakers. Assuming corrosion conditions are not too severe, grease No. 2 would be highly satisfactory. Grease No. 11 we feel should be investigated further since it may be satisfactory for antifriction bearings.

Perhaps from Table 2 some of the greases may be recognized in terms of governmental specifications. In this respect, it is our opinion that service received from various manufacturers' products, meeting a particular specification, is quite varied. We believe any specifications for lubricants should include more performance-test requirements.

To stress further the difference in requirements between sleeve bearings and antifriction bearings, the variation between greases Nos. 21 and 16 from Fig. 9 will be noted. Grease No. 16 is much more desirable at the extreme low temperatures, yet, on the friction machine, grease No. 16 is unsatisfactory, while No. 21 was acceptable.

This last point suggests that for sensitive tripping mechanisms in extreme cold it may be absolutely necessary to use a grease such as No. 16 in the antifriction bearings.

AUTHOR'S CLOSURE

Mr. Barr has ably pointed out the difference between the requirements of an antifriction bearing used in a power circuit breaker and those of the same bearing working under what might be termed the usual running conditions. It must be remembered, however, that the grease selected for this application operates successfully in both the antifriction bearings and the textolite sleeve bearings working under the intermittent oscillatory motion encountered in circuit breakers.

Had the problem been restricted entirely to antifriction bearings, both greases No. 16 and No. 2 would have given better operation at lower temperatures than was required. Grease No. 11, however, was not as good in this respect as grease No. 21 which was chosen. The need for one all-purpose grease was imperative for this application and the selection was made on this basis.

The suggestion that specifications for lubricants should include more performance-test requirements is very timely. These requirements should be such that they can be checked in the laboratory with reasonable facility. The time required to work out a suitable set of tests as a procedure for screening the lubricants before final life tests will yield dividends. Each application will require its own peculiar tests of several lubricants, and different weights will be given to each characteristic to arrive at an acceptable solution for the application being considered.

Heat Transfer to Superheated Steam at High Pressures

By W. H. McADAMS,¹ W. E. KENNEL,² AND J. N. ADDOMS³

Local coefficients of heat transfer from a 12.3-in. length of 0.252-in. tubing to steam flowing upward in a vertical annulus were measured for pressures from 115 to 3500 psia, for temperatures from 430 to 1000 F, and for temperature differences from 100 to 620 F. All results are correlated in Fig. 8 in terms of the local Nusselt number, the Reynolds number, the Prandtl number, and the geometrical ratio L/D_s , with the physical properties evaluated at the film temperature. An improved correlation, employing new data on thermal conductivity, is presented in Fig. 10 of the Addendum.

NOMENCLATURE

The following nomenclature is used in the paper:

- A = area of heat-transfer surface, sq ft
- a = constant, dimensionless
- c = specific heat of fluid at constant pressure, Btu/(lb) (deg F)
- D = diameter, ft
- D_s = equivalent diameter, equal to 4 times the hydraulic radius based on total wetted perimeter, ft
- d = prefix, indicating first derivative, dimensionless
- f_m = mean value of friction factor, dimensionless
- G = mass velocity of fluid, lb/(hr) (sq ft of cross section)
- h = local coefficient of heat transfer, Btu/(hr) (sq ft) (deg F); h_m for mean value
- I^2R = rate of electrical generation of heat in wall of heater, Btu/hr
- K = function of L/D_s , defined by Equation [9]
- k = thermal conductivity of fluid, Btu/(hr) (ft) (deg F); k_A for wall of heater
- L = length of heat-transfer surface, ft
- m = exponent, dimensionless
- q = rate of heat transfer, Btu/hr
- q/A = density of heat flux, Btu/(hr) (sq ft)
- r = radius of wall of heater, ft
- S = cross section for fluid flow, sq ft; $\pi D^2/4$ inside tubes; $\pi(D_2^2 - D_1^2)/4$ in annuli
- t = bulk temperature of fluid, deg F
- V = average velocity of fluid, based on density at bulk-stream temperature, ft/hr
- X, X', X'' = abscissas of Figs. 4, 5, 6, dimensionless
- x_A = thickness of wall of heater
- Y, Y', Y'' = ordinates of Figs. 4, 5, 6, 8
- Δt = temperature potential, deg F

¹ Professor of Chemical Engineering, Massachusetts Institute of Technology, Cambridge, Mass. Mem. ASME.

² Research Department, Standard Oil Co. of Indiana, Whiting, Ind.

³ Assistant Professor of Chemical Engineering, Massachusetts Institute of Technology.

Contributed by the Special Research Committee on High Temperature Steam Generation, Joint Committee on Effect of Temperature on Properties of Metals, Heat Transfer, and Power Divisions, and presented at the Annual Meeting, New York, N. Y., November 27-December 2, 1949, of THE AMERICAN SOCIETY OF MECHANICAL ENGINEERS.

NOTE: Statements and opinions advanced in papers are to be understood as individual expressions of their authors and not those of the Society. Paper No. 49-A-32.

μ = viscosity of fluid, lb/(hr) (ft), equal to $2.42 \times$ viscosity in centipoises

π = 3.1416

ρ = density of fluid, lb/cu ft

Subscripts:

- 1, 2 = entering and leaving
- c = conduction and convection
- f = physical property evaluated at film temperature; t_f equals $(t + t_w)/2$
- i = inside wall of heater
- m = mean
- o = outside wall of heater
- r = by radiation
- t = total by conduction, convection, and radiation
- w = physical property evaluated at wall temperature t_w
- wi, wo = inside wall, outside wall, of heater

Dimensionless Moduli:

- $c\mu/k$ = Prandtl number
- DG/μ = Reynolds number based on inside diameter tube
- $D_s G/\mu$ = Reynolds number based on equivalent diameter D_s
- $DV\rho_w/\mu_w$ = modified Reynolds number
- hD_s/k = Nusselt number, local
- $h_m D/k, h_m D_s/k$ = Nusselt number, mean
- μ_w/μ = ratio of viscosities
- $L/D, L/D_s$ = geometrical ratios

INTRODUCTION

The object of this investigation was to determine local or point coefficients of heat transfer from metal to superheated steam at pressures up to 3500 psia, for a heater having an outside diameter of 0.25 in., concentrically located in an unheated vertical jacket having an inside diameter of 0.382 in. Mass velocities in the annulus were to be restricted to the range from 55,000 to 165,000 lb per hr per sq ft of cross section. Heater temperatures were to be as high as possible.

REVIEW OF THE LITERATURE ON HEATING AND COOLING

Turbulent Flow Inside Tubes. Various mathematical analogies between the transfer of heat and momentum lead to quantitative relations among four dimensionless moduli as follows:

$h_m D/k$, mean Nusselt number, based on heated length
 $c\mu/k$, Prandtl number, which is ratio of molecular diffusivity of momentum (μ/ρ) to molecular diffusivity of heat ($k/\rho c$)

$$\frac{DV}{\mu/\rho} = \frac{DG}{\mu}, \text{ "diameter" Reynolds}$$

number, which is a ratio of acceleration forces to viscous forces.

f_m , mean friction factor, equal to shear stress at wall, divided by $\rho V^2/2g_c$.

In deriving the analogies, various simplifying assumptions are made, such as, the flow is fully developed and incompressible, the physical properties are independent of temperature, and

the velocity distribution is known and is independent of Δt .

Owing to lack of fundamental information on temperature and velocity profiles, experimental data on mean heat-transfer coefficients are usually correlated empirically in terms of the first three of the dimensionless numbers just listed, or their equivalent. The empirical equations differ as to the temperatures at which the physical properties are evaluated. To allow for variation in properties with temperature, ratios such as μ/μ_w , ρ/ρ_w , and k/k_w are sometimes introduced.

In the last 16 years three types of equations have been accepted generally for predicting coefficients for heating fluids flowing inside tubes:

All physical properties are based on bulk-stream temperature t

$$\frac{h_m D/k}{(c\mu/k)^m} = a \left(\frac{DG}{\mu} \right)^{0.8} \quad [1]$$

Reference: ⁴	a	m	Equation
(6), (12)	0.024	0.4	[1a]
(10), (11)	0.023	0.4	[1b]
(7)	0.021	1/3	[1c]

All physical properties are based on bulk-stream temperature, except μ_f is taken at $t_f = (t + t_w)/2$

Reference:	a	m
(4)	0.023	1/3

All physical properties are based on bulk-stream temperature, except μ_w

$$\frac{(h_m D/k) \left(\frac{\mu_w}{\mu} \right)^{0.14}}{(c\mu/k)^m} = a \left(\frac{DG}{\mu} \right)^{0.8} \quad [3]$$

Reference:	a	m	Equation
(13)	0.027	1/3	[3a]
(2)	0.023	1/3	[3b]

The foregoing equations are based on experimental data for relatively small values of Δt ; at moderate Δt , they predict approximately the same values of h_m for water.

A recent paper (8) reports data on heating air at Δt up to 940 F and at DG/μ from 10,000 to 230,000. Regardless of whether the physical properties were evaluated at the bulk-stream temperature or at the wall temperature, the data fell on curves of changing slope, and the data were lower than predicted by Equations [1a] and [1b]. The data were brought into close agreement (8) by the equation

$$\frac{h_m D/h_w}{(c\mu/k)_w^{0.4}} = a \left(\frac{DV \rho_w}{\mu_w} \right)^{0.8} \quad [4]$$

wherein all physical properties are evaluated at the wall temperature, and a modified Reynolds number

$$\frac{DV \rho_w}{\mu_w} = \left(\frac{DV \rho}{\mu} \right) \left(\frac{\mu}{\rho} \right) \left(\frac{\rho_w}{\mu_w} \right) \quad [4a]$$

was employed. With a bellmouth entry (8), and for L/D of 60, the constant a was 0.022

$$\frac{h_m D/k_w}{(c\mu/k)_w^{0.4}} = 0.022 \left(\frac{DV \rho_w}{\mu_w} \right)^{0.8} \quad [4b]$$

Alternatively, $(c\mu/k)_w$ could be omitted (8) giving

$$\frac{h_m D}{k_w} = 0.018 \left(\frac{DV \rho_w}{\mu_w} \right)^{0.8} \quad [4c]$$

No other data at high Δt are available for heating gases. The

⁴ Numbers in parentheses refer to the Bibliography at the end of the paper.

literature contains no reliable data on heat transfer to steam under conditions of high pressure and high Δt .

Reference (1) shows curves of the local coefficient for air versus L/D for the entrance section of a tube at values of DG/μ from 17,000 to 56,000, for a number of entrance conditions. For flow in a tube following a sudden contraction, the initial value of h (for the first 0.56 diam) was roughly twice that at L/D of 10. Reference (3) reports results for DG/μ from 18,000 to 8000, which indicate that the local heat-transfer coefficient varies as the minus 0.15 power of L/D , for the first 31.5 diam.

Turbulent Flow in Annuli. While several equations have been proposed, the latest is that of reference (2)

$$\frac{h D_e/k}{(c\mu/k)^{1/3}} \left(\frac{\mu_w}{\mu} \right)^{0.14} = 0.023 \left(\frac{D_e G}{\mu} \right)^{0.8} \quad [5]$$

wherein all physical properties, except μ_w , are evaluated at the bulk-stream temperature; D_e is equal to 4 times the hydraulic radius based on total wetted perimeter, and is equal to $D_2 - D_1$.

Further support of the use of D_e is given by the results of reference (5) for rectangular passages; as shown in reference (11),⁴ these data ran 10 to 25 per cent below Equation [1b].

EXPERIMENTAL

Introduction. To accomplish the objectives, an apparatus capable of withstanding pressures of 3500 psia at 1000 F and per-

⁴ Reference (11), p. 198.

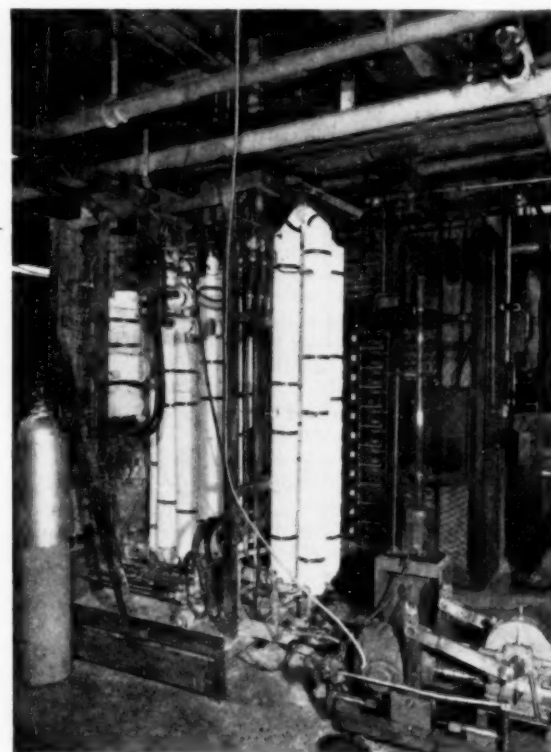


FIG. 1 HIGH-PRESSURE APPARATUS, WITH STEEL SAFETY BOOTH REMOVED

(Right foreground, adjustable-stroke 4-cylinder pump, feed reservoir, and condensate-measuring tube. Heavily insulated 13-pass electrically heated series boiler is located in front of the a-c switchboard, and condenser and cooler are visible. Heavily insulated test section, and the d-c busbars, are mounted just behind control panel near nitrogen cylinder.)

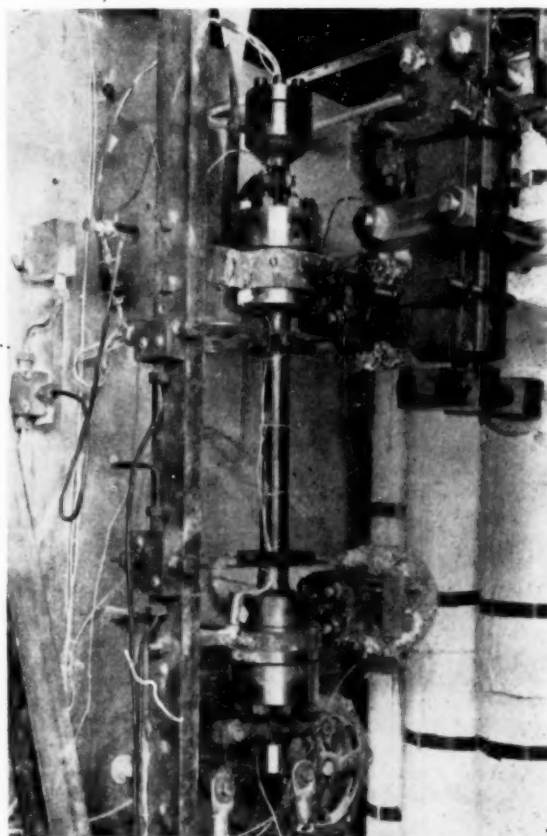


FIG. 2 TEST SECTION BEFORE INSULATING

(Leads to thermocouples installed inside heating tube are brought out through nitrogen-pressurized fitting at top. The d-c power connections and potential taps can be seen. Further details shown in Fig. 3.)

mitting accurate measurement of the local heat flow and local temperature driving force was required. Condensing mercury vapor, molten metals, and fused salts were considered as sources of heat but were discarded in favor of electric heat generated in the wall of a metal tube. Because the wall of the electrically heated tube had to be thin to avoid use of excessive current and to minimize longitudinal conduction of heat, it was impossible to use the tube itself as the pressure vessel. Consequently, the electrically heated tube was pressurized internally with nitrogen, and was located concentrically in a high-pressure jacket, thus forming an annular passage for flow of steam.

The procedure was to heat superheated steam as it flowed upward at a measured rate through the annular space. The heat dissipated by the heating element was calculated from electrical measurements; the corresponding temperature of the heating element was determined by measuring the inside temperature and correcting for the radial temperature gradient in the wall. The temperature of the steam was measured at the entrance and exit of the test section and was corrected for heat losses. The point coefficient of heat transfer could be calculated from the data for given flow conditions.

Apparatus. The apparatus was a flow system in which water was drawn from a reservoir and pumped through a preheater, a test section, throttle valves, a condenser and condensate cooler, and back to the reservoir. Views of the apparatus are shown in Figs. 1 and 2. Stainless steel, which has good corrosion resist-

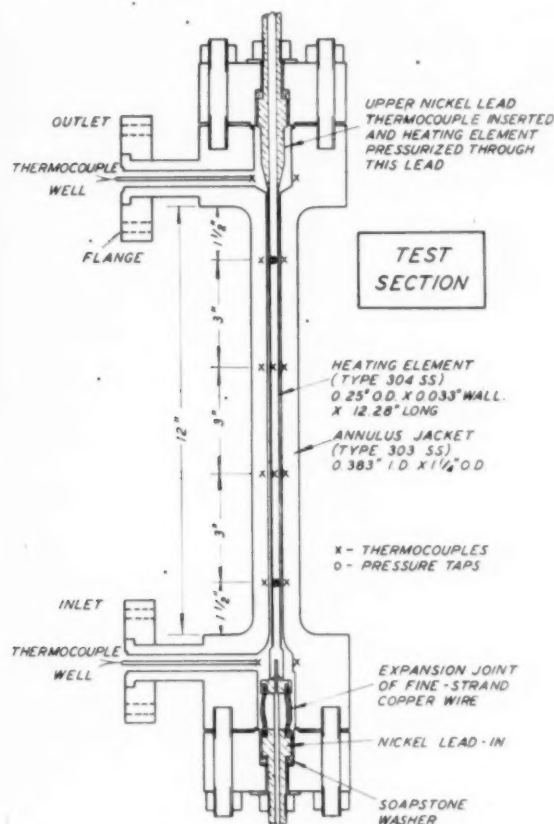


FIG. 3 DETAILED DRAWING OF TEST SECTION

ance and strength at high temperatures, was used as the material of construction. Safety devices included a movable steel booth enclosing the entire apparatus, two rupture disks calibrated to blow at 4400 psia, and an automatic device to shut off electrical power whenever the pressure decreased substantially.

A four-cylinder pump of the positive-displacement type drew water from the reservoir at atmospheric pressure and injected it into the high-pressure system. The flow rate was measured volumetrically at the inlet of the pump.

The preheater, seen in Fig. 1, took cold water from the pump and produced superheated steam at any desired temperature up to 900 F at flow rates up to 75 lb per hr. It consisted of 80 ft of $\frac{5}{8}$ -in. extra-heavy stainless-steel pipe covered with insulation and electrical windings capable of dissipating 35 kw at 110 alternating current. Power to the preheater was controlled by switches on each of 12 electrical windings and by a Variac on the last winding. Total preheater power was indicated by a wattmeter. A spiral strip of stainless steel was inserted in the last two 6-ft lengths of the preheater to impart a centrifugal motion to the fluid, so that any entrained liquid would contact the heated wall and thus be vaporized.

The test section (Figs. 2 and 3), consisted of a vertical annulus in which a stainless-steel heating element was mounted coaxially inside a pressure jacket which had an inside diameter of 0.382-in. Removable end closures on the pressure jacket were equipped with insulated nickel leads which supplied electrical power. The heating element was a stainless-steel tube having an outside diameter of 0.252 in., a length of 12.28 in., and a wall thickness of

0.0332 in. At the lower end it was silver-soldered to an adapter on a flexible connection which served as an expansion joint and electrical lead. At the upper end, the element was silver-soldered to a hollow nickel electrical lead through which were inserted four chromel-alumel thermocouples, spaced at 3-in. intervals. By means of a special fitting on the open end of the upper nickel lead, nitrogen pressure was applied to the inside of the heating element to prevent collapse under the external pressure of the steam.

Iron-constantan thermocouples were installed in wells at the entrance and exit of the test section to measure steam temperatures. Ten thermocouples were installed in small radial holes in the wall of the pressure jacket to permit estimates of temperature at the inner surface.

Power to the test section was supplied by a 15-volt 1000-amp direct-current generator. To measure voltage drop across the heating element a voltage-divider circuit, consisting of a 10-ohm resistor and a 1000-ohm resistor, was connected across the heating element. A calibrated 0.00005-ohm resistor was connected in series with the heating element to determine the current. The voltage drop across the 10-ohm resistor and the 0.00005-ohm resistor, and the potential generated by the thermocouples, were measured by means of a portable precision potentiometer.

Following the test section, $1/8$ -in. and $1/4$ -in. needle valves were installed in parallel to throttle the steam from operating pressure to that at the entrance to the condenser and cooler.

Operating Procedure. Before mounting a heating element in the test section, the resistances of its component parts were determined. The thermocouple assembly was then inserted in the heating element, which was mounted in the test section. The end closures were secured, and the system was pressure-tested.

The throttle valves were opened, the pump was started, and the desired flow rate was set by adjusting the stroke of the pump. The power to the preheater was then turned on and adjusted to approximately the desired value, and the temperature of the system was allowed to rise. The desired operating conditions were approached by adjusting the throttle valves and the power to the preheater. After a final adjustment of the pump to the desired flow rate, the system was allowed to come to a steady-state condition.

The approach to steady-state condition was determined by plotting the difference between the millivolt readings of the thermocouples measuring inlet and outlet steam temperature versus time. When this temperature rise became substantially constant, a run was begun. Each run was made with constant flow rate, pressure, and temperature of the inlet steam.

The first one or two data points in each run were taken with no power to the heating element, in order to determine the heat loss. Data points were then taken at various settings of power input to the test section. Most of the runs were concluded at power inputs such that the temperature inside the heating element did not exceed 1300 F, because early runs showed that operation at higher temperatures caused warping and discoloration.

Method of Calculation. For each setting of power to the test section, the total density of heat flux, the heat transferred by radiation (see Appendix), the temperature of the outside wall of the heating element, the bulk temperature of the steam, the Δt , and the local coefficient of heat transfer were calculated. Each of these factors was evaluated at four positions corresponding to the locations of the thermocouples inside the heating element.

The power dissipated by the heating element was calculated by using the product I^2R where I is the current through the heating element and R is the resistance at the average wall temperature. The density of heat flux was then calculated from the power dissipated and the dimensions of the heating element. The temperature of the outer wall of the heating element was

determined from the temperature of the inside wall by subtracting the temperature drop through the wall

$$t_{wi} - t_{wo} = \left(\frac{dq_i}{dA_o} \right) \frac{r_o}{k_h} \left(\frac{1}{2} - \frac{r_i^2}{r_o^2 - r_i^2} \ln \frac{r_o}{r_i} \right) \dots [6]$$

$$(\Delta t)_w = \left(\frac{dq_i}{dA_o} \right) \frac{x_h}{k_h} \left(\frac{1}{2} + \frac{x_h}{6 D_o} \right) \dots [6a]$$

Equation [6] was derived by assuming uniform generation of heat per unit volume of the wall and constant thermal conductivity at the average wall temperature; Equation [6a] follows upon expansion of the logarithmic term. For the densities of heat flux employed, the $(\Delta t)_w$ calculated from Equation [6a] was sufficiently close to that calculated by allowing for variation of thermal conductivity and electrical resistivity with temperature.

Since the temperature of the steam was measured only at the entrance and exit of the last section, it was necessary to calculate the temperature of the steam at the positions corresponding to the four thermocouples. The heat lost by the steam while it flowed from the entrance to any point in the test section was determined from data at zero heat input. The heat generated by the heating element up to the same position was calculated. The increase in the temperature of the steam from the entrance to the desired location was calculated by difference.

The local rate of heat transfer by the combined mechanisms of conduction and convection (dq_o/dA_o) was obtained by deducting an estimate for radiation (dq_r/dA_o) from the total local flux (dq_i/dA_o). Since the emissivity and absorptivity of water vapor for radiation have not been investigated at high pressure, it was necessary to extrapolate the values from atmospheric pressure (see Appendix). The radiation correction never exceeded 12 per cent and usually was less than 10 per cent.

The local Δt and the local density of heat flux dq_o/dA_o were used to calculate the local coefficient of heat transfer

$$h = \frac{\frac{dq_i}{dA_o} - \frac{dq_r}{dA_o}}{t_{wi} - t} = \frac{dq_o}{dA_o \Delta t} \dots [7]$$

RESULTS

Twenty-seven runs were made, of which twenty-five were successful. The ranges of pressure, temperature, and mass velocity are given in Table 1. Over-all heat balances were good, allowing for heat losses. Points of two kinds were eliminated; those for outer wall temperatures above 1300 F, and those with Δt less than 100 F. The points in the former category were discarded because there was the probability of distortion and oxidation of the heater. All data with Δt of less than 100 F were eliminated, since slight changes in line voltage to the preheater made precise control of the steam temperature difficult; a change of 1 per cent in the preheater power resulted in 10 to 12 F change in steam temperature.

The local Nusselt numbers, Prandtl numbers, Reynolds numbers, length-diameter ratios, and viscosity ratios were tabulated for all the data to be correlated. Local Nusselt numbers at L/D_o of 57 are plotted in Figs. 4, 5, and 6.

Plots similar to Figs. 4, 5, and 6 were made for local Nusselt numbers at L/D_o of 11.4; the trends were similar to those shown in Figs. 4, 5, and 6. In addition, plots similar to Figs. 4 and 6 were constructed for the local Nusselt numbers at L/D_o of 37 and 80.

The effect of L/D_o was determined from Fig. 6 and similar plots. The best straight line was drawn through each set of points, and the constant K in the equation

$$Y^* = K (X^*)^{0.89} \dots [8]$$

TABLE 1 RANGES OF VARIABLES

Pressure, psia	Run no.	G 1000	q_c/A_o 1000	t , deg F	Δt , deg F
115	27	55	30-53	477-735	267-540
	26	110	38-93	441-668	198-564
	24	165	44-110	429-591	178-513
	25	165	48-103	639-790	177-442
	1	56	11-61	569-821	107-624
500	2	110	26-48	541-643	130-291
	8	110	33-85	606-791	170-487
	9	110	33-56	617-729	168-357
	16	110	22-48	913-948	110-242
	3	165	47-108	544-673	167-507
1000	6	55	27-44	612-755	223-481
	4	110	27-74	590-705	120-444
	14	110	24-47	915-1000	116-250
	5	165	35-107	602-713	114-465
	7	55	24-40	711-812	166-425
2000	18	55	23-28	922-1011	171-258
	11	106	35-69	713-789	148-405
	15	110	25-48	934-1012	105-248
	12	164	57-98	730-808	193-402
	19	153	30-65	924-1012	104-238
3000	17	110	24-47	924-970	100-225
	22	97	29-51	886-967	130-284
	20	160	29-72	932-980	100-271
3500	23	96	27-52	891-964	112-293
	21	156	72-72	960-1000	226-238

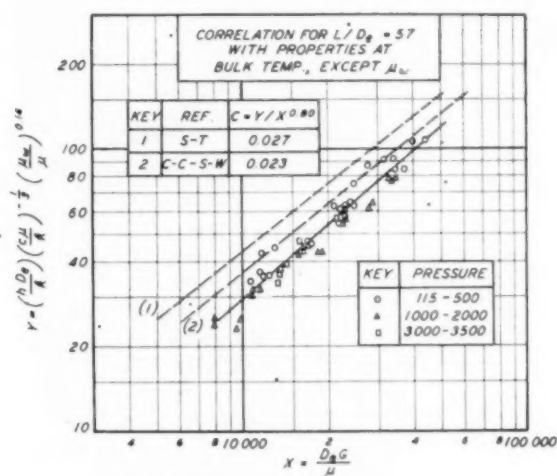
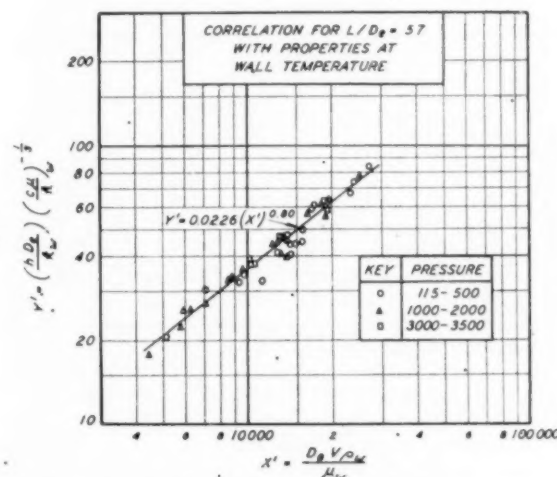
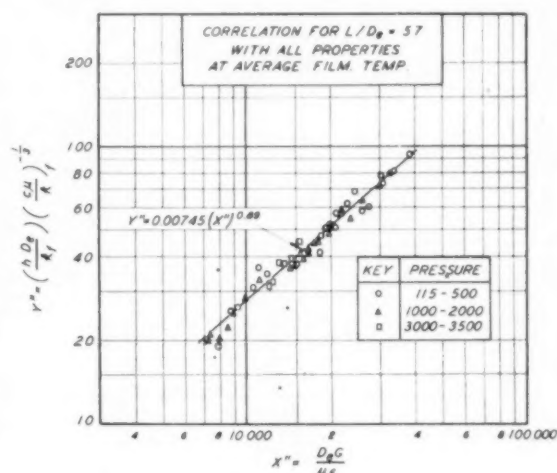
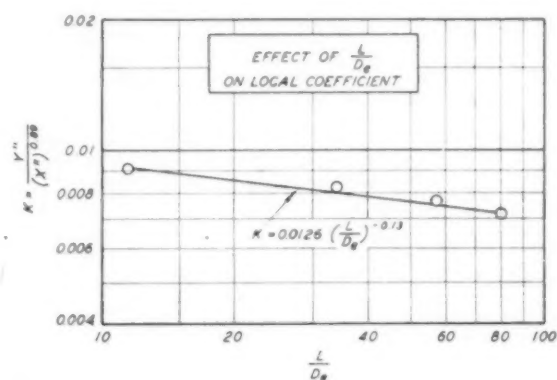
FIG. 4 CORRELATION OF DATA AT L/D_s OF 57 (Using co-ordinates of references 2 and 13.)

FIG. 5 DATA OF FIG. 4 REPLOTED WITH CO-ORDINATES OF REFERENCE (8)

FIG. 6 DATA OF FIG. 4 REPLOTED WITH ALL PROPERTIES EVALUATED AT FILM TEMPERATURE: $t_f = (t_w + t)/2$ FIG. 7 CROSS-PLOT OF RESULTS FROM FIG. 6, AND SIMILAR GRAPHS FOR VARIOUS VALUES OF L/D_s

was evaluated for each L/D_s . Fig. 7 shows these values of K plotted against L/D_s , yielding

$$K = 0.0126 (L/D_s)^{-0.13} \quad [9]$$

The final correlation, involving local coefficients at four different values of L/D_s , is given in Fig. 8

$$\frac{(h D_s / k_f) \left(\frac{L}{D_s} \right)^{0.13}}{(c \mu / k_f)^{1/4}} = 0.0126 \left(\frac{D G}{\mu_f} \right)^{0.89} \quad [10]$$

Since the simplified dimensional equation

$$\frac{h}{c G} = \frac{S}{A} \frac{(t_2 - t_1)}{(t_w - t)} = \frac{0.0144}{(D G)^{0.2}} \quad [11]$$

correlates data for certain common gases at moderate Δt , this type of correlation was tried for the present data on steam at one L/D_s . A plot of h/c versus G gave a slope of 0.87, but the maximum deviation from the main line was ± 40 per cent. The term $h/c G^{0.87}$ was plotted versus film temperature, but separate curves were obtained for the several pressures.

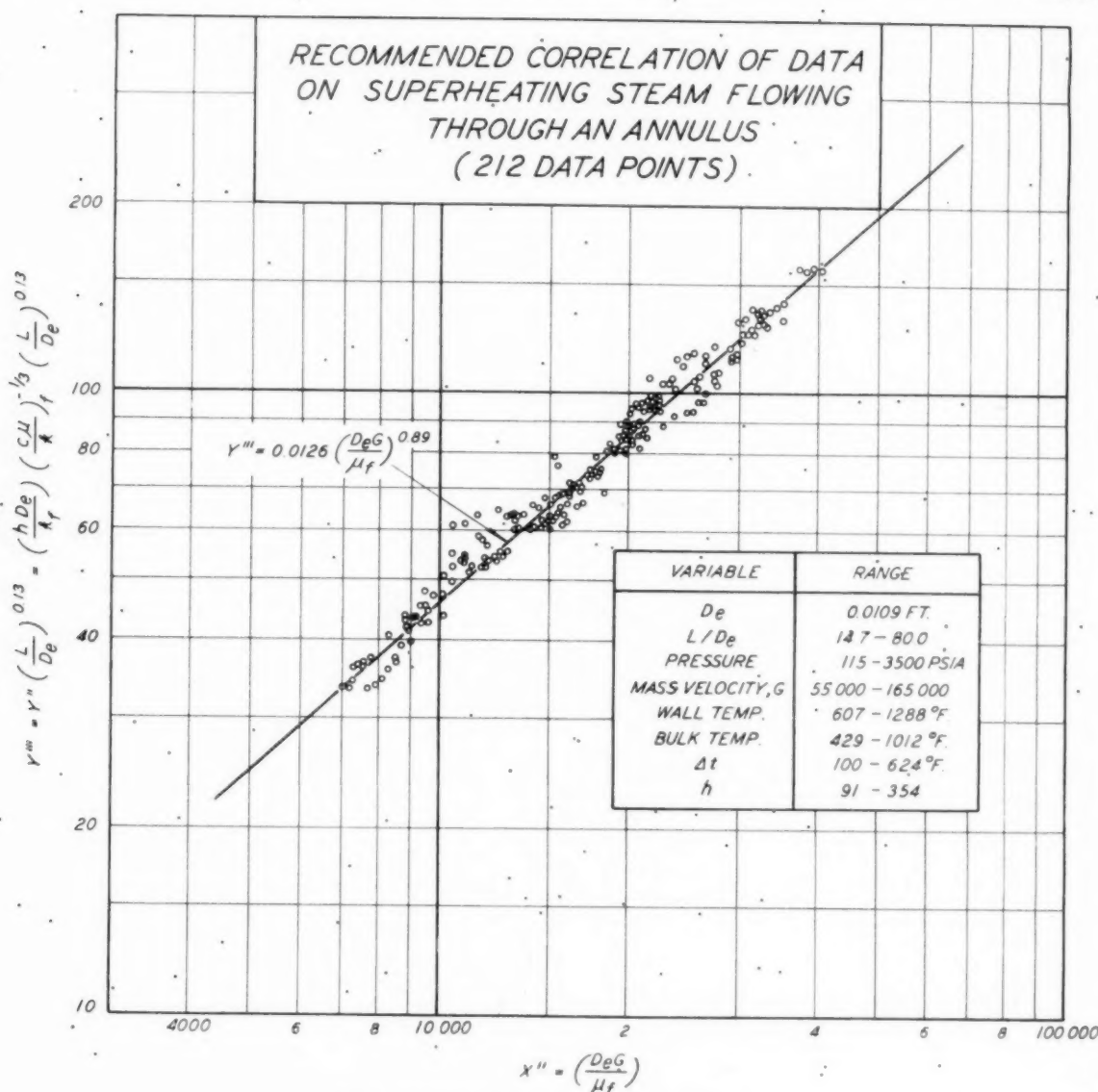


FIG. 8. RECOMMENDED CORRELATION OF ALL RESULTS

DISCUSSION OF RESULTS

In Fig. 4 all of the local Nusselt numbers lie below the dotted line of reference (13) for mean Nusselt numbers, and most of the data fall below the dotted line of reference (2). The solid line represents an average of the data. The points at pressures of 3000 to 3500 psia are close to the line, most of those for 115 to 500 psia are above, and most of those for 1000 to 2000 psia are below.

In Fig. 5 the correlation is better than in Fig. 4. The slope of the curve is the conventional value of 0.8, the same as that reported (8) for air flowing in a tube, with Δt up to 940 F. The ordinate contains an exponent of $1/3$ on the Prandtl number, in place of 0.4. For the pressures and temperatures involved, the ordinate would be changed but little by using $(c\mu/k)^{0.4}$ instead of $(c\mu/k)^{1/3}$. Consequently, it is interesting to note that Fig.

5 gives a constant of 0.0226 for the local Nusselt number at L/D_e of 57, as compared with 0.022 for the mean Nusselt number for L/D_e of 60, Equation [4b]. At a given pressure, the thermal conductivity of steam may either decrease or increase with increase in temperature, while for low-pressure air, k always increases with increase in temperature. Furthermore, as temperature increases, the Prandtl number decreases more rapidly for steam than for low-pressure air.

The plot (not shown) of Y' versus X' , at L/D_e of 11.4, gives a constant of 0.0267, which is higher than the constant of 0.0226 at L/D_e of 57.

In Fig. 6 the correlation is distinctly better than that in Fig. 4, and is somewhat better than that in Fig. 5; the same was true for L/D_e of 11.4. Consequently, the co-ordinates Y'' and X'' were employed for the final correlation. Fig. 7 shows that

L/D , entered to the minus 0.13 power. The recommended correlation of the local Nusselt numbers at the four values of L/D , is given in Fig. 8. The equation of the line is given by Equation [10], in which all physical properties are evaluated at the film temperature, t_f equals $(t_w + t)/2$. This equation correlates all the data, but should not be extrapolated outside the range of the data. At lower Reynolds numbers, modified streamline flow would prevail, and other dimensionless groups would be involved; at higher Reynolds numbers, the slope might decrease. At L/D , above 80, h may become asymptotic.

Values of viscosities were taken from reference (15), thermal conductivities were taken from reference (16), and the other properties were taken from steam tables (9). The range of values of μ_f , k_f and $c_{p\mu}/k_f$ for each pressure is shown in Table 2.

TABLE 2 RANGES OF PHYSICAL PROPERTIES

Pressure	t_f	μ_f	k_f	$(c_{p\mu}/k_f)$
115	518	0.0443	0.0240	0.95
	1011	0.0726	0.0525	0.79
500	606	0.0503	0.0294	1.01
	1132	0.0820	0.0646	0.77
1000	650	0.0535	0.0338	1.18
	1134	0.0830	0.0656	0.76
2000	787	0.0639	0.0441	1.21
	1140	0.0859	0.0673	0.82
3000	951	0.0765	0.0551	1.03
	1116	0.0874	0.0665	0.88
3500	947	0.0774	0.0580	1.13
	1120	0.0893	0.0675	0.92

CONCLUSIONS

1 The use of electric heat developed in a thin-walled tube minimizes longitudinal conduction and permits measurement of local coefficients of heat transfer to steam flowing upward through a vertical annulus.

2 For a given Reynolds number and Prandtl number, the local Nusselt number always decreases as L/D , increases, regardless of the temperature at which the physical properties are evaluated.

3 For a given L/D , the method of plotting used in Fig. 6, with all physical properties evaluated at the film temperature, is distinctly better than that in Fig. 4, and is somewhat better than that in Fig. 5; the quantitative effect of L/D , from 11.4 to 80 is shown in Fig. 7.

4 The recommended correlation of all the data is shown in Fig. 8 and is given by Equation [10], which should not be extrapolated outside the range of data shown in Fig. 8. For a given Reynolds number the maximum deviation in the ordinate is 28 per cent, and the average deviation is 7 per cent.

BIBLIOGRAPHY

- "An Investigation of Aircraft Heaters, XXVII, Distribution of Heat Transfer Rate in the Entrance Section of a Circular Tube," by L. M. K. Boelter, G. Young, and H. W. Iversen, Technical Note 1451, Washington, D. C., July, 1948.
- "Heat Transfer and Friction of Water in an Annular Space," by F. G. Carpenter, A. P. Colburn, E. M. Schoenborn, and A. Wurster, Trans. AICHE, vol. 42, 1946, pp. 165-187.
- "Heat Transfer: Local and Average Coefficients for Air Flowing Inside Tubes," by A. Cholette, Chemical Engineering Progress, vol. 44, 1948, pp. 81-88.
- "A Method of Correlating Forced Convection Heat Transfer Data and a Comparison With Fluid Friction," by A. P. Colburn, Trans. AICHE, vol. 29, 1933, pp. 174-210.
- "The Friction and Heat Transfer Coefficients of Rough Pipes," by W. F. Cope, Proceedings of The Institution of Mechanical Engineers, London, England, vol. 137, 1941, pp. 99-105.
- "Heat Transfer in Automobile Radiators," by F. W. Dittus and L. M. K. Boelter, University of California Publication in Engineering, vol. 2, 1930, pp. 443-461.
- "Heat Transfer Coefficients for Air Flowing in Round Tubes, Rectangular Ducts, and the Finned Passages of Blower-Cooled Cylinders," by R. E. Drexel and W. H. McAdams, Wartime Report W-108,

National Advisory Committee for Aeronautics, Washington, D. C. 1945.

8 "Heat Transfer From High Temperature Surfaces to Fluids I—Preliminary Investigation With Air in an Inconel Tube With a Rounded Entrance, Inside Diameter of 0.4 Inch and a Length of 24 Inches," by L. V. Humble, W. H. Lowdermilk, and M. Grele, Research Memorandum, No. E7L31, National Advisory Committee for Aeronautics, Washington, D. C., May, 1948.

9 "Thermodynamic Properties of Steam," by J. H. Keenan and F. G. Keyes, John Wiley & Sons, Inc., New York, N. Y., 1936.

10 "Heat Transmission," by W. H. McAdams, McGraw-Hill Book Company, Inc., New York, N. Y., first edition, 1933, p. 169.

11 "Heat Transmission," by W. H. McAdams, McGraw-Hill Book Company, Inc., New York, N. Y., second edition, 1942, pp. 168, 174.

12 "Heat Transmission to Liquids Flowing in Pipes," by T. K. Sherwood and J. M. Petrie, Industrial and Engineering Chemistry, vol. 24, 1932, pp. 736-745.

13 "Heat Transfer and Pressure Drop of Liquids in Tubes," by E. N. Sieder and G. E. Tate, Industrial and Engineering Chemistry, vol. 28, 1936, pp. 1429-1435.

14 "Thesis in Chemical Engineering," by H. S. Rice, Massachusetts Institute of Technology, Cambridge, Mass., 1931.

15 "The Determination of the Viscosity of Steam and Water at High Temperatures and Pressures," by D. L. Timroth, Journal Physics (USSR), vol. 2, 1940, p. 419.

16 "The Viscosity and Heat Conduction of Steam at High Temperatures and Pressures," by D. Timroth and N. Vargaftik, Journal of Technical Physics (USSR), vol. 9, 1939, pp. 461-469; 963-970; vol. 10, 1940, p. 1063.

Appendix

HEAT TRANSFERRED BY RADIATION

Since the present data were obtained for steam flowing in an annulus with an outer jacket that was colder than the flowing steam, an estimate was made of the net radiation from the heating element to the flowing steam and the outer jacket.

Professor H. C. Hottel of the Chemical Engineering Department at the Massachusetts Institute of Technology, derived an exact general solution of the problem by the method outlined by Hottel and Egbert (11). The result, a multiple-series equation, was too complex. A simplification, similar to the one used by Hottel and Egbert, gave the following equation

$$(q/A)_r = 0.173 \epsilon'_w \left\{ \left(\frac{T_w}{100} \right)^4 [\alpha_{L1} + (1 - \alpha_{L1}) \epsilon_j] \right. \\ \left. - \left(\frac{T_j}{100} \right)^4 \epsilon_j (1 - \alpha_{L2}) - \left(\frac{T_g}{100} \right)^4 \epsilon_{g L2} \right\} \dots \dots \dots [12]$$

where

- α = gas absorptivity for specified beam length and pressure
- ϵ_g = emissivity of steam for specified beam length and pressure
- ϵ_j = emissivity* of stainless jacket
- ϵ'_w = emissivity* of stainless heater at T_w
- ϵ'_w = effective emissivity of heating element equal to $(1 + \epsilon_w)/2$
- T_w, T_j, T_g = absolute temperatures of heating element, jacket, and steam, respectively, in deg Rankine
- $L1$ = effective beam length for gas radiation from heating element to gas
- $L2$ = effective beam length for gas radiation from gas to heating element

NOTE: Beam lengths $L1$ and $L2$ were assumed equal to 1.4 times clearance between heating element and jacket.

Since the present work was done at pressures far in excess of any for which gas-radiation data are available, the evaluation of the gas emissivities and absorptivities required an extrapolation of the existing data. Emissivities and absorptivities for gas

* The emissivity of stainless steel (14) was taken as a linear function of temperature, based upon 0.44 at 420 F and 0.36 at 914 F.

radiation (extrapolated to zero pressure were taken from Fig. 29 of reference (11), and were multiplied by the correction factor C_1 from Table 3, extrapolated from Fig. 30 of reference (11).

TABLE 3 - VALUES OF C_1

P , psia.....	115	500	1000	2000	3000	3500
P , atm.....	7.82	34.0	68.0	136	204	238
PL , atm-ft.....	0.119	0.515	1.03	2.06	3.09	3.60
C_1	1.85	1.75	1.65	1.50	1.45	1.42

As pressure increases C_1 decreases, but the emissivity at zero pressure increases faster than C_1 decreases; consequently the emissivity ($C_{1, \text{epw} = 0}$) increases. For example, at 1000 F, the emissivity increases from 0.156 at 115 psia to 0.568 at 3500 psia.

The simplified Equation [12] was shown to agree within 3 per cent of the exact equation for a typical case which was computed by both methods.

Addendum

Subsequent to the submission of this paper, new data on the thermal conductivity of steam became available through the courtesy of Prof. F. G. Keyes of the Department of Chemistry, M.I.T. The new data of Keyes and Sandell⁷ are shown in Fig. 9 of this addendum, for comparison with the earlier data of Timroth and Vargaftik (16) which were employed in the original correlation of Fig. 8. The new data have been extrapolated beyond a temperature of 660 F and pressure of 2200 psia by means of the correlating equation developed by Keyes and Sandell. The per cent deviation of the new data from the old becomes acute at high temperature, but is practically independent of pressure.

The new values of thermal conductivity were employed to recalculate all of the present data at L/D_e of 57. Plots of the recalculated data were made utilizing the parameters of Figs. 4, 5, and 6; the correlation of the type shown in Fig. 4 was very poor, that similar to Fig. 5 was fairly good, although the exponent on the Reynolds number was 0.71, and the best one was again the correlation employing film temperature similar to Fig. 6.

All the present data were then recomputed using the parameters of Fig. 6, and the effect of L/D_e was redetermined. The final revised equation, correlating all of the heat-transfer data and based upon the thermal conductivities extrapolated from the data of Keyes and Sandell is

$$\frac{h D_e}{k_f} = 0.0214 \left(1 + \frac{2.3}{L/D_e} \right) \left(\frac{D_e G}{\mu_f} \right)^{0.8} \left(\frac{c_p \mu_f}{k_f} \right)^{1/4} \quad [13]$$

As shown in Fig. 10 of the addendum, the maximum error is 17 per cent, as compared with 28 per cent for the correlation in Fig. 8.

⁷ "New Measurements of the Heat Conductivity of Steam and Nitrogen," by F. G. Keyes and D. J. Sandell, presented at the Annual Meeting, New York, N. Y., November 27-December 2, 1949, of THE AMERICAN SOCIETY OF MECHANICAL ENGINEERS.

Advantages of the revised correlation are (a) retention of conventional 0.8 power on the Reynolds modulus; (b) adoption of the fadeaway function for L/D_e , and (c) adoption of a value of 0.0214 for the constant in close agreement with established values at high L/D_e . It is worth noting that the fadeaway type of L/D_e correction could not have been obtained with the earlier value of thermal conductivity. The revised correlation is expected to be considerably better than the original one for purposes of extrapolation.

Further work remains to be done in extending the range of physical properties. Viscosities are still in question.

The authors desire to acknowledge the co-operation of Prof. F. G. Keyes in making his data available.

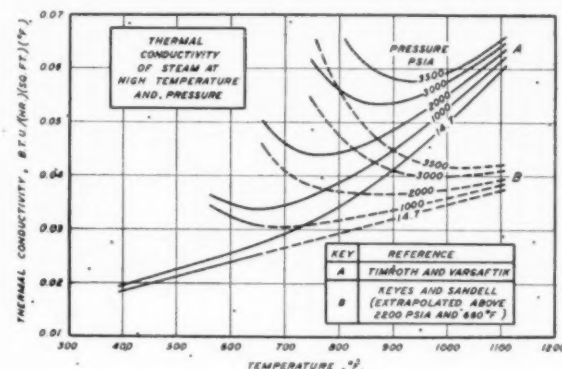


Fig. 9

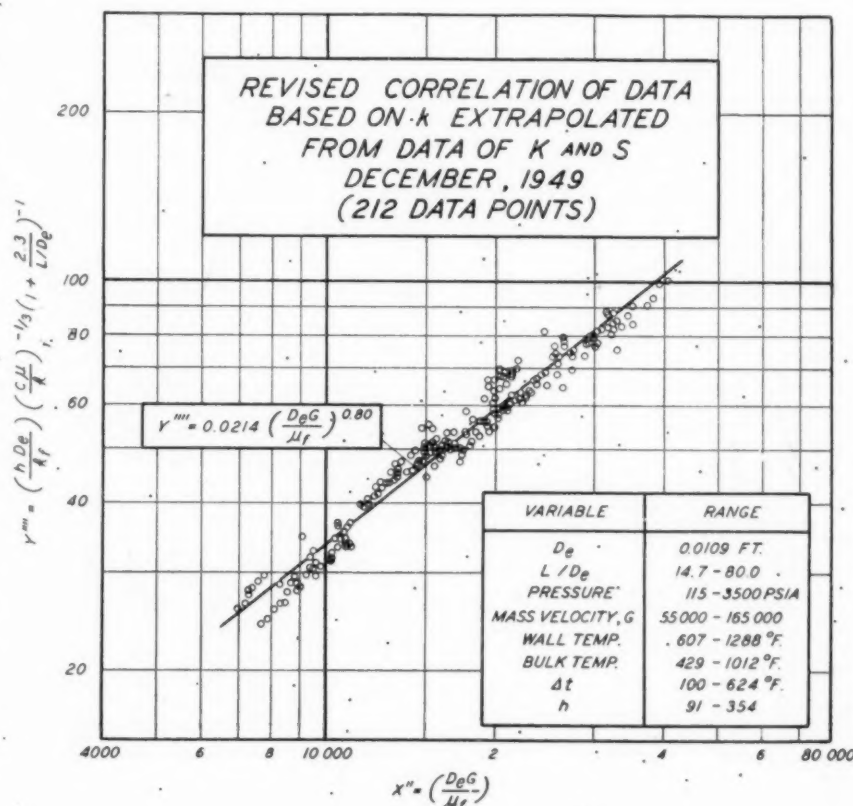


Fig. 10



FIG. 1 PETTY ISLAND STOCK PILES PRIOR TO 1946

Philadelphia Electric Company Adopts Mobile Coal-Handling Equipment

By E. C. RUSSELL,¹ PHILADELPHIA, PA.

The paper covers the change from storing and reclaiming coal by cranes and locomotives to the use of standard self-propelled earth-moving equipment. The size and type of equipment are described, as well as its use. The change in design of storage piles is also considered. Description of new storage systems designed for the use of mobile equipment is presented. An analysis of operating costs and capacities is made with a comparison of the two methods.

THE Philadelphia Electric Company in 1946 began to make a complete change in its method of handling coal into and out of coal-storage piles. Coal stock piles are maintained for emergency use only and are reclaimed only when there is an interruption of the regular supply.

Coal is delivered normally to all but one of the six generating stations by barge, where it is unloaded by coal-tower clamshell-bucket installations. At the sixth station, barge facilities are not available and rail coal is unloaded into track hoppers.

¹ Supervisor, Coal Bureau and Steam Heating Division, Philadelphia Electric Company.

Contributed by the Power, Fuels, and Materials Handling Divisions and presented at the Annual Meeting, New York, N. Y., November 27–December 2, 1949, of THE AMERICAN SOCIETY OF MECHANICAL ENGINEERS.

NOTE: Statements and opinions advanced in papers are to be understood as individual expressions of their authors and not those of the Society. Paper No. 49–A-63.

Prior to 1946 the company's method of coal storage was in piles between a system of parallel tracks. Fig. 1 shows the Petty Island coal-storage-plant stock piles prior to 1946. Fig. 2 is a recent view of the same location. These tracks were laid out on approximately 110-ft centers to give maximum height and width to the piles, using locomotive clam-shell cranes with 60-ft booms. This arrangement resulted in piles 100 ft wide and 30 to 35 ft high. On reclaiming, the cranes loaded into company-owned hopper cars. A locomotive switched these cars over track hoppers with a conveyer system which transported the coal to the normal bunker conveying system, or in the case of the Petty Island coal-storage plant, to a coal barge for transportation to a generating station. For storing coal, these same hopper cars were loaded at the coal tower by chutes fed by the coal-tower conveying system. A locomotive switched the cars to the storage yard, and the locomotive clamshell crane unloaded them.

CHANGE TO MOBILE EQUIPMENT

In March, 1946, we received the first piece of mobile coal-handling equipment on our initial order of three units. The other two units followed a short time later, and, by the end of the year we had acquired four more. Two more were put into operation early in 1949. These units are heavy earth-moving machines designed for construction work, self-propelled, bottom-loading, scraper type with four pneumatic tires. They have sufficient power to move their loads at relatively high speeds up



FIG. 2 PETTY ISLAND STOCK PILES FOR MOBILE EQUIPMENT

10 per cent grades and unload while moving, but need assistance in loading.

They are all Super "C" Tournapulls with Model LP Carryall scrapers, manufactured by R. G. LeTourneau, Inc., Peoria, Ill. The engines are 4-cycle 6-cylinder Diesel engines. Five of the nine are 150-hp Cummins engines, while the other four are 124-hp Hercules engines. The maximum speed of these units is 14.3 mph. The scraper capacity is 12.1 cu yd; heaped it has a 15-cu-yd capacity.

On the reclaiming cycle, we average $8\frac{1}{2}$ to 9 tons per load. On the storing cycle, since they are loaded by an overhead chute, a pant-leg-type hopper had to be designed to straddle the operating mechanism directly over the center line of the bowl of the scraper. This increases the tonnage per load on storing to 11 tons. Fig. 3 shows one of the units.

Self-propelled units have the advantage of the greater speed on the longer hauls and are usually more economical than the crawler-tractor-drawn scrapers on hauls over 600 or 800 ft on earth-moving work. However, the self-propelled units are favored even on the shorter hauls, for unlike most earth-moving work they are mechanically loaded when storing coal which theoretically is 50 per cent of their operation.

Self-propelled units being rubber-tired vehicles have the added advantage of being better-suited for use around paved station yards. They are also readily transferred over the road under their own power to another location. At times it is advantageous to be able to transfer a unit from one station to another to assist in the movement of coal.

TRACK-TYPE BULLDOZERS USED

Since the inception of mobile coal-handling equipment we have purchased four track-type bulldozer tractors. They are all Oliver Cle-Trac Model FDE with 130-hp Hercules Diesel engines. This is the largest tractor Oliver Cle-Trac make and is comparable in size to the International TD 18 or the Caterpillar D8. All four tractors are equipped with bulldozer blades as well as a power control unit on the rear. The power control unit is used to cable-operate a drawbar for towing the scrapers to assist loading on the reclaiming cycle.

The scrapers are equipped with a pusher pad on the rear for pusher-loading by a bulldozer. However, we have established a definite policy of not using this method of loading because our self-propelled scrapers are clutch-steered on the driving wheels. This presents the possible hazard of jackknifing if the bulldozer



FIG. 3 SCRAPER SHOWING PANT-LEG HOPPER



FIG. 4 TRACTOR DRAWBAR ENGAGING SCRAPER HOOK

is pushing faster than the scraper engine is driving it. Also there is some possibility of the bulldozer blade cutting a rear tire of the scraper if proper contact is not made. It is felt that our method of loading has the added advantage of leaving the scraper operator's hands free to operate the power control unit, and his attention therefore can be directed toward the loading of his machine, since the tractor is towing, and thus guiding its direction. Later models of Tournapulls have positive steering, and likely there are advantages in push-loading them.

One other point in connection with the clutch-steering model is that the ramps or inclines on the storage piles should be straight if possible, especially if the change is being made to this method of storage, and men are being trained in the operation of this equipment. This is mentioned because it is necessary to have power on the driving wheels for steering; if the practice is to coast down the incline with the engine idling, it is necessary to reverse clutch or "cross-steer." This of course is no problem for experienced operators.

The drawbars used for towing or snatch-loading are approximately 16 ft long with a 24-in. eye in a horizontal plane on the outboard end to engage a hook, mounted point down on the front end of the engine frame at the bottom. Fig. 4 shows a bulldozer preparing to snatch-load a scraper. The oil pan of the engine crankcase is protected with heavy plates so the eye can slide onto the hook. The drawbar is raised and lowered through a series of cables and sheaves by the power control unit on the rear of the tractor. Thus the scraper to be loaded drives up to the rear of the tractor in line with the drawbar. The drawbar is raised by the tractor operator, and upon engagement the tractor starts its tow. The operator of the scraper then concentrates upon the operation of the power control unit which raises the gate and lowers the bowl of the machine. When loaded, he lowers the gate, raises the bowl, speeds up, and turns to avoid the tractor, at the same time the tractor operator is lowering the drawbar.

METHOD OF STORING COAL WITH MOBILE EQUIPMENT

The method of storing coal with mobile equipment is entirely different from old methods with locomotive cranes. The Philadelphia Electric Company made the change-over to mobile equipment at an opportune time. Due to mine strikes, the coal stocks in 1946 were reduced to the lowest level at any time in the preceding 12 years. Thus we were able to remove the parallel tracks and relocate essential trackage where necessary, so that stock piles could be laid to the best advantage for this type of equipment.

It is readily apparent that one of the advantages of this method of storage is the increased quantity that can be stored on the same area. The parallel piles with the tracks between reduce the volume by approximately 50 per cent.

Figs. 1 and 2 show a very good comparison of the two methods of storing coal. The piles in Fig. 1 total approximately 150,000 tons of coal. The three piles shown in Fig. 2 total approximately 180,000 tons. It is quite apparent they have not even approached their maximum height. Close study of the two illustrations also will reveal that the piles in Fig. 2 extend possibly only one half the distance in the background compared with the piles in Fig. 1.

Furthermore, with mobile equipment, piles of much greater height are possible. Scraper-type equipment is ideal for storing coal, since this method of unloading allows the coal to be laid down in thin layers. Rolling or any other method of compaction as a fire preventive is not necessary as the mobile equipment with its large pneumatic tires has increased the density in our piles from 60 to 69 lb per cu ft. The old method of packing was to run a small crawler tractor, dragging a section of railroad rail on a bridle over the pile constantly while storing coal. We still follow this practice with the large tractors, but to a much lesser extent, and then only to maintain a fairly level surface, and to pack and spread the extreme edges of the pile where a self-propelled unit might encounter difficulties from its outside wheels sinking in the soft edges.

On the reclaiming cycle, the top of the pile is scraped off as evenly as possible, leaving the pile in shape for the time when coal is restocked again. One tractor will take care of the loading of two scrapers on the shorter hauls, while on the longer hauls three machines can be used.

Where possible, piles should be laid out with the ultimate tonnage desired in mind; so that the top of the completed pile will be as small as possible and still allow sufficient maneuverability for mobile equipment. This is essential because, in any case, there is a relatively large area of hard-packed coal, and the run-off of rain water resulting from a heavy downpour may be quite large. Provisions for handling this run-off should be made. If the top of the pile is made saucer-shaped, then the end result may be a small lake. At times of reclaiming, obviously, this is not desirable. The difficulties of handling wet coal in the usual chutes and conveyer systems, as well as the problems of burning extremely-wet coal are well known. We have had some success in grading the top toward one or more wooden chutes to lead the water down the side of the pile. These chutes require attention

occasionally, especially after a heavy rain. It is interesting to note that it has been found necessary to calk all cracks and keep the chute absolutely watertight or a serious washout beneath the chute may result.

In changing to mobile equipment the weight of the loaded unit must be considered if there are light paving slabs, manhole structure, or underground facilities too close to the surface. Also, in locations of limited area, minimum maneuvering space should be studied. The scrapers on our system will turn in a space 40 ft wide; however, we prefer a minimum width of 60 ft to improve maneuvering time.

The reclaiming of finer sizes of coal from the highly compacted piles made by mobile equipment has at times given some trouble with poor flow of coal in the pipes from bunkers to pulverizing mills and stokers. Former troubles in the stoker hoppers have been eliminated by the installation of agitators.

COAL-HANDLING FACILITIES

The Philadelphia Electric Company has stock piles at four generating stations, and a coal-storage plant on an island in the Delaware River. Petty Island—the coal-storage plant—serves the two stations without storage facilities by barge, and supplements the reclaiming at the other stations when necessary.

The change-over to mobile equipment required very little change in coal-handling facilities. The track hoppers in all locations had to be covered with some form of heavy steel grating designed to carry the load of a scraper. With the large-diameter wheels this grating can be made quite open.

On new installations, facilities are designed for the use of mobile equipment. At our Barbadoes Island Station where additional generating capacity was recently added, completely new coal-handling facilities were designed and installed for mobile-equipment use. This is the one station which must rely on rail coal delivery. The coal-unloading shed and track hoppers are laid out for the reclamation of coal by mobile equipment. The average haul distance is approximately 500 ft.

For storing coal, a scraper loading hopper was included in the design. This is a hopper of 20 tons capacity fed from the bunker conveying system so that a scraper can be loaded quickly without waiting for the normal flow of the 250 tons per hr of the conveying system, which would require approximately 3 min for loading. The haul distance for storing coal is approximately 400 ft.

A new coal-storage yard with an ultimate capacity of 1,000,000 tons is now in the planning stage. It is being designed to have a scraper loading hopper of 250 tons capacity and an ultimate rate of 500 tons per hr stocking by mobile equipment. For reclaiming, it is planned to have two unloading hoppers of 50 and 25 tons capacity, respectively, and a reclaiming rate by mobile equipment of 700 tons per hr.

ANALYSIS OF OPERATING EXPENSE

An analysis of the various accounts involving the storing and reclaiming of coal, and the operation and maintenance of cranes, locomotives, and mobile equipment reveals some interesting figures. However, these figures must be analyzed in the light of our operating conditions and accounting methods.

Three accounts were analyzed for the years 1944, 1945, 1947, and 1948. The year 1946 was excluded since that year involved the transition period from the old method of handling coal to the present method. The three accounts analyzed were (1) crane expense, (2) storing coal, (3) reclaiming coal.

It should be noted that the operating and maintenance expenses of a locomotive or locomotive crane is charged to the crane account regardless of its use. Some are regularly used by the Gas Department for handling coke, coal, and ashes, while others are digging ashes and slag as well as handling coal at the various

generating stations—or making occasional lifts of heavy equipment.

The crane account was analyzed in order to establish an average actual cost per hour of use for operating and maintenance expenses.

The storing and reclaiming coal accounts were studied to determine the hours of equipment operation and the tons of coal handled.

One year of the maintenance account on the cranes was analyzed completely to determine the ratio between material and maintenance labor so that the various years could be adjusted to 1948 costs by material and labor indexes. It was found that approximately 40 per cent of the account was material, and the remaining 60 per cent was maintenance labor. This agrees favorably with studies that have been made on generating-station maintenance accounts. Therefore it was assumed these figures would hold true for all years.

The maintenance labor costs of the various years were adjusted to 1948 costs by labor factors which have been established on actual conditions in the company. Materials in the maintenance account were also adjusted to 1948 costs by a materials index. A cost per hour of operation adjusted to 1948 costs was then derived for the cranes and locomotives for 1944 and 1945, and for the scrapers and tractors for 1947 and 1948.

These costs per hour of equipment use were then applied to the respective year's hours of equipment use on reclaiming and storing coal at two different locations. The two years for each method of operation were then combined to give weighted average costs.

Table 1 gives the comparison between the old method of using cranes and locomotives and the new, using scrapers and tractors, for both reclaiming and storing coal at the Petty Island coal storage plant. Table 2 is a similar tabulation for handling storage coal at Richmond Station.

TABLE 1 COMPARISON OF OLD AND NEW METHODS AT PETTY ISLAND PLANT

	Tons (1)	Tons per hr (2)	Equip- ment cost, dollars per hr (3)	Equip- ment cost, cents per ton (4)
RECLAIMING COAL				
Cranes and locomotives.....	87519	48.0	3.38	7.0
Mobile equipment.....	26066	60.2	3.50	5.8
STORING COAL				
Cranes and locomotives.....	63399	47.9	3.39	7.1
Mobile equipment.....	210009	74.2	3.43	4.6

TABLE 2 COMPARISON OF OLD AND NEW METHODS AT RICHMOND STATION

RECLAIMING COAL				
Cranes and locomotives.....	85856	43.6	3.33	7.6
Mobile equipment.....	140176	43.3	3.35	7.7
STORING COAL				
Cranes and locomotives.....	90839	35.1	3.36	9.6
Mobile equipment.....	186825	69.8	3.39	4.9

Referring to the tables, column (1) is the tons of coal handled. Column (2) is the tons per hour handled. Column (3) is the weighted average cost per hour of equipment use. Column (4) is equipment cost per ton of coal handled. All figures are a weighted average for the two-year period for the respective equipment.

To be explicit, the 87,519 tons in column (1), Table 1, are the total tons of coal reclaimed during 1944 and 1945, at Petty Island. Column (2) is the tons in column (1) divided by the hours of operation in the two years. The 3.38 dollars in column (3) are the result of dividing the total of 1944 and 1945 equipment expense by the total hours of operation for the two years. Column (4) is the total equipment expense divided by the tons of column

(1). Column (3) divided by column (2) will of course also produce column (4).

The same procedure was followed for the scrapers and tractors for the years 1947 and 1948.

It is apparent from column 3 of either table that the equipment cost per hour is practically the same for the two types of equipment. This was also found to be the case when the total 1944 and 1945 crane and locomotive account for the 28 pieces of equipment on the entire system was averaged and compared with a similar 1947 and 1948 figure for the 7 scrapers and 4 tractors. The two figures were 3.39 and 3.38 dollars, respectively, or so close that it would appear to have been intentional.

However, on comparing the results in either table for the two types of equipment, it is seen that the tons per hour handled are 25 per cent to 100 per cent greater than with the old method, with one exception, that is, reclaiming coal by mobile equipment at the Richmond Station.

It must be understood that the tons per hour in column (2) for either reclaiming or storing coal are per equipment-hour including tractors as well as the scrapers. For instance, on the reclaiming cycle we will have to assume that the normal method of operation was one tractor and two scrapers. To find the approximate scraper tons per hour the 60.2 tons on the second line of column 2 of Table 1 will be three pieces of equipment times 60.2 divided by two scrapers, or an average of 90.3 tons per hr reclaimed per scraper. However, on the storing cycle, the tractor is not usually used full time, hence the same ratio does not hold.

The foregoing partially explains the greater tonnage per hour moved on the storing cycle compared with the reclaiming cycle. Another factor is the 2 to 2½ tons or approximately 25 per cent greater capacity of the scrapers when storing coal. On the reclaiming cycle, too, a little more time is consumed on the pile loading the scrapers than in loading them to haul to the storage pile. Likewise, in discharging their load in the hoppers when reclaiming, the machine must come to a complete stop, but, when storing, the discharging is done on the move, and the machine continues on its route back to reload. The advantages of the self-propelled unit on storing are quite obvious regardless of the length of haul.

The low tons per hour reclaiming rate at Richmond Station as compared to the Petty Island operation is due to several factors, as follows:

- 1 The reclaiming hoppers at Richmond Station are not of sufficient capacity for mobile-equipment use. They are truck hoppers for unloading railroad hopper cars and are now in the process of being rebuilt with a greater capacity.

- 2 Operating conditions at the two locations are not the same. Petty Island is strictly a coal-storage plant and, when reclaiming, loads barges of as much as 2400 tons capacity. Richmond, being a generating station, reclaims the coal demands of the station. This station also burns two kinds of coal—stoker and pulverized—

and has two bunker belts in each bunker. Thus many times during a day of reclaiming there are short delays due to changing over bunker belts, changing from one bunker to the other, which also means changing from one storage pile to another. Furthermore, reclaiming stock coal, especially if wet, always causes some operating difficulties with conveyer systems. It cannot be expected under those conditions to deduct these short interruptions from the over-all equipment operating time. Hour meters installed on each machine would of course give the actual hours of operation.

It must also be pointed out that the total equipment-hours for either reclaiming or storing which were used to arrive at the hourly rate figure may include some nonproductive hours in so far as tons moved into or out of stock are concerned; since it is necessary at times to use the equipment to regrade a pile after considerable coal has been removed, or to clean up after a heavy rain may have damaged a pile. This time would be charged to one or the other accounts. Thus the data in the two tables are over-all figures for the two-year period and include all the equipment time relative to stock piles.

We know from several spot checks for periods ranging from 1 hr to a full day's work that a scraper is capable of reclaiming 70 to 90 tons per hr and will store better than 100 tons per hr.

A real saving in the use of mobile equipment is the resulting laborsaving. Formerly at Richmond Station it was necessary to use two cranes and a locomotive, and work longer hours at overtime rates to supply the demands of the station. This would require two engineers and two firemen for the cranes, an engineer for the locomotive and a brakeman, a total of six men. Stocking coal, one additional man would be required to pack and spread the coal with a tractor. Today, with mobile equipment more coal is reclaimed or stocked with but three men, namely, two scraper operators and one tractor operator. Furthermore, it takes far less time to train a scraper operator than a crane operator.

CONCLUSION

In conclusion, we feel that mobile coal-handling equipment is ideal for our conditions and methods of operation. For the first two full years of operation it has proved to be sound from an economy standpoint. We feel that the equipment is much more versatile than our former equipment for handling storage coal. If we find it necessary to store or reclaim coal on short notice it doesn't seem like the major operation that it appeared to be previously.

Finally, it must be remembered that mobile equipment is built primarily for earth moving and not for coal handling. Since coal is approximately one half the density of earth, it means that scrapers should be able to carry a considerably greater volume of coal than they are capable of handling. Therefore, from the standpoint of the buyer of equipment for coal-handling, improvements could be made.

of
in
ye
hi
pa
an

is
ste
It

Mo
sio
ve
cu
de
the
8.

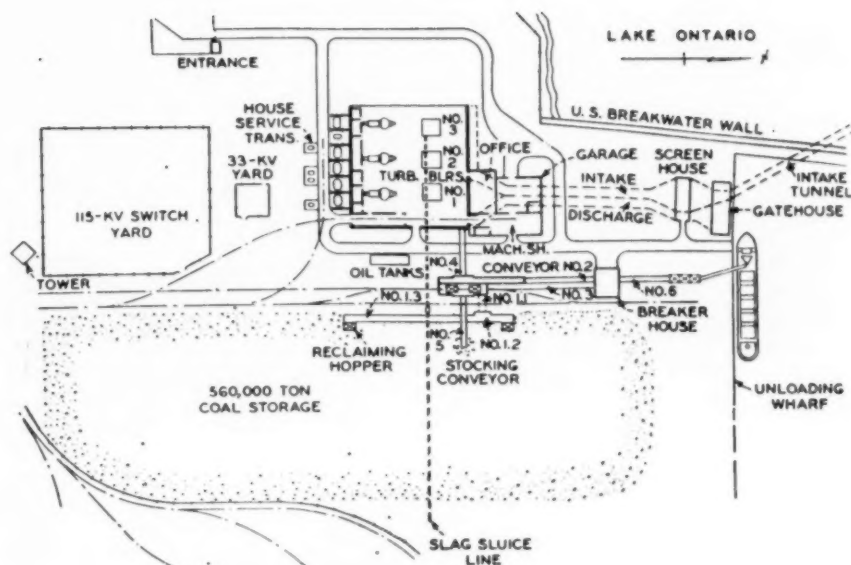


FIG. 1 PLAN OF COAL-HANDLING SYSTEM, OSWEGO STEAM STATION

Storing and Reclaiming Coal With Earth-Moving Equipment at the Oswego Steam Station

By J. N. EWART,¹ BUFFALO, N. Y.

Earth-moving equipment at the Oswego Steam Station of the Central New York Power Corporation has handled in excess of 3 billion ton-feet of coal during its first 9 years of operation. Coal is stored in a single pile 100 ft high with no danger of spontaneous combustion. The paper describes the operation of bulldozer-carryall units and presents operating and maintenance costs.

GENERAL DESCRIPTION

THE coal-handling system of the Oswego Steam Station of the Central New York Power Corporation is a simple one and lends itself readily to expansion of the station. Fig. 1 is a plan of the coal-handling system, showing the location of the storage pile and its relation to the receiving and reclaiming points. It also shows the arrangement of belt conveyers which permit

movement of coal to the house coal bunkers or to and from storage from either track hoppers or self-unloading lake boats.

Although provision is made for either rail or lake delivery of coal, all coal is received by self-unloading boats which discharge directly to either a receiving hopper or to one end of a 1400-ft-long \times 400-ft-wide stocking pile. This pile often reaches a height of 100 ft on the high end and has contained as much as 560,000 tons of coal, Fig. 2. From the receiving hopper the coal is carried through a Bradford breaker direct to the house coal bunkers or to a stocking conveyor, equipped with a telescopic chute which discharges to the stocking pile about 300 ft from the wharf end.

STOCKING AND RECLAIMING OPERATION

The coal is moved into storage from the discharge of the self-unloader or from the stocking pile entirely by means of bulldozer-carryall unit. During the stocking operation a bulldozer-carryall unit makes a round trip of approximately 2000 ft every 10 min. This trip starts at the stocking pile where the carryall picks up its load of 13 tons, carries it an average of 700 ft to the spreading area, and lays it down in a ribbon approximately 13 ft wide, 40 ft long and 10 in. thick, and then completes the circuit by returning for another load. Subsequent trips pack this ribbon of coal and integrate it with the rest of the pile to produce a section which is nearly impervious to air and water. Test pits have

¹ Chief Mechanical Engineer, Buffalo Niagara Electric Corporation. Mem. ASME.

Contributed by the Power, Fuels, and Materials Handling Divisions and presented at the Annual Meeting, New York, N. Y., November 27-December 2, 1949, of THE AMERICAN SOCIETY OF MECHANICAL ENGINEERS.

NOTE: Statements and opinions advanced in papers are to be understood as individual expressions of their authors and not those of the Society. Manuscript received at ASME Headquarters, October 8, 1949. Paper No. 49-A-98.

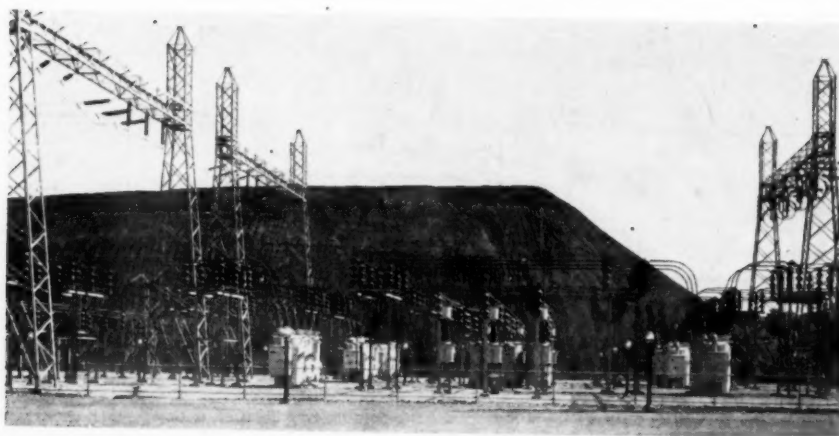


FIG. 2 COAL STORAGE PILE 100 Ft HIGH LOOKING EAST FROM GATE HOUSE

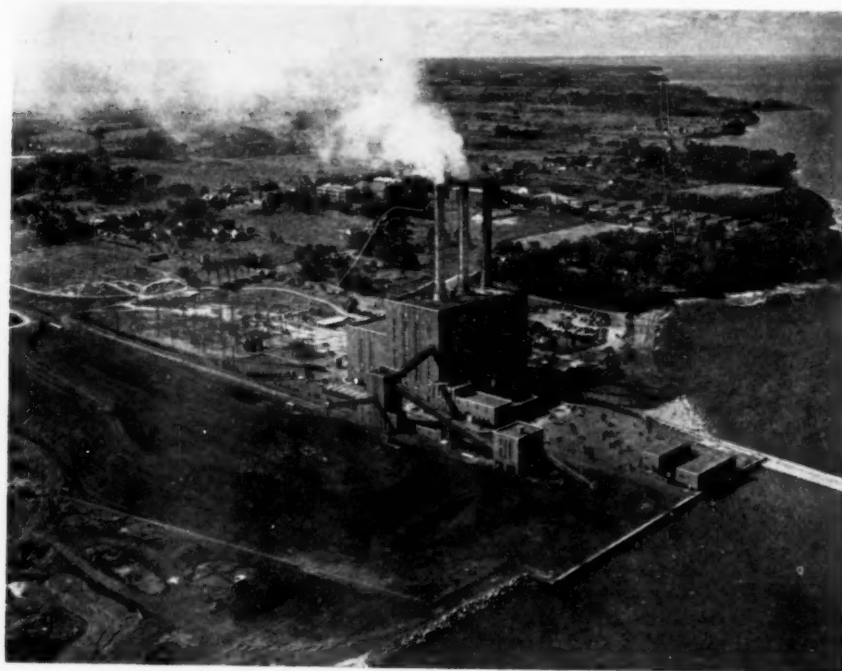


FIG. 3 AERIAL VIEW OF TOP OF STORAGE PILE DURING A STOCKING OPERATION

indicated that this coal is packed to densities of 80 lb per cu ft.

Fig. 3 shows the operation on the top of the pile during stocking. There have been no fires in this coal pile to date and sections of it have stood untouched for as long as 3 years.

Oswego's experience would indicate that many of the usual rules for successful storage of coal can be violated if coal is laid down in thin layers and adequately compacted. For example, no effort is made to avoid segregation though coal may be purchased from 60 mines varying in volatile matter from 17 to 37 per cent and sized from fine slack to double-screened and run of mine. Sulphur varies from 1 to 3 per cent. No particular effort has been made to provide a hard base or adequate drainage for the foundation, and there is no limit to the height of the pile.

Coal is reclaimed entirely by means of the bulldozer-carryall

units. Two reclaiming hoppers are located along the lengthwise toe of the storage pile, 300 ft apart. Additional hoppers can be provided if necessary to reduce the reclaim hauling distance. In reclaiming coal from the stock pile the coal is removed, in so far as possible, by working it off in vertical layers starting from one end of the pile. In this way the top surface of the pile is disturbed the least, and the nearly vertical surfaces which are exposed will absorb practically no water or snow. The coal is packed well enough that nearly vertical sides have been formed 40 ft high with no experience of a cave-in.

Since all of the coal is received by boat and, therefore, a year's supply must be obtained during the favorable navigation season of approximately 6 months, there is necessarily considerable movement of coal in and out of the storage pile over the period



FIG. 4 TRACK HOPPER BUILDING AND JUNCTION TOWER, OSWEGO STEAM STATION

of a year. For example, the total movement of coal in and out of storage for the 9-year period was 5,225,000 tons, compared with an amount burned during this period of 3,600,000 tons.

OPERATING DATA

Table 1 shows the operating and maintenance cost of the bulldozer-carryall equipment in dollars per 1000 ton-feet by years, covering the period 1945 to 1948, inclusive. Comparable information prior to these years is not available.

TABLE 1 BULLDOZER-CARRYALL OPERATING AND MAINTENANCE COST DATA AT OSWEGO STEAM STATION

Year	Total coal handled, tons	Dollars per 1000 ton-feet				
		Operation Labor	Fuel	Maintenance Labor	Material	Total
1945	614080	0.046	0.006	0.026	0.020	0.098
1946	444894	0.067	0.006	0.035	0.011	0.119
1947	700986	0.063	0.006	0.026	0.010	0.105
1948	828985	0.064	0.008	0.032	0.021	0.125
Average		0.060	0.006	0.030	0.016	0.112

Figures are shown in Table 1 on the basis of ton-feet in order to consider the length of the haul as well as the tonnage in arriving at the unit costs. It is recognized that there is not necessarily a straight-line relationship between cost and hauling distance. The incremental cost for distance, once the carryall is loaded and under way, may be relatively small. Using the average total value of 0.112 per 1000 ton-feet for the 4 years, it may be seen that Oswego's 700-ft out-haul cost was 7.8 cents per ton, and the 500-ft reclaiming cost, 5.6 cents per ton. It is believed that the maintenance cost of this equipment has reached its leveling-off value, except for possible increase in labor rates and material, since, at the end of 1948, the average life of the bulldozer-carryall units was 7 years, and a continuing program of replacing the older units has been developed.

It is interesting to note that one bulldozer handled approximately 500 million ton-feet before retirement.

INVESTMENT COST

The foregoing operating costs are exclusive of fixed charges on the capital investment. One of the advantages of mobile equipment, as compared with permanently installed machinery for handling storage coal, is that the initial investment can be small, and only that which is required for the initial installation. As and if the station expands, the storage area and coal-storage equipment can be expanded as required and always with modern equipment. Much in the way of improved and more efficient mobile equipment for handling coal has been developed in the last 5 years, and further improvements are inevitable.

Table 2 shows the capital investment in mobile equipment by years for the Oswego Station. Note that the initial investment was very small for the first few years of two-unit operation and increased as additional units were added. The original installation at Oswego consisted of two 80,000-kw rated, 100,000-kw maximum turbogenerator units with steam conditions of 1250 psi, 900 F. Each unit is supplied by a single boiler rated at 900,000 lb per hr. The third unit, essentially a duplicate of the first two, went into service in December, 1948. Installation of the fourth unit is now in progress and scheduled to be in service in 1951.

TABLE 2 CAPITAL INVESTMENT IN MOBILE EQUIPMENT AT OSWEGO STATION

Year	Station capacity, kw	Capital investment	Bulldozer units	Carryall units
1940	80000	\$54780	3	2
1941	160000	54780	3	2
1942-1947	160000	65544	4	2
1948	240000	73143	4	3

Fig. 4 is shown to emphasize that the coal-handling structures and even the coal pile itself can become not too unsightly if proper consideration is given to architectural lines and landscaping, followed by a desire on the part of the station operators to maintain a good appearance of the buildings and grounds.

of t
sign
of a
ing
and
com
sho
avoi
spee
dete
for
sim
the
whi
the
stre
blac
hav
com

I
with
some
dem
In
cour
been
pres
thro
hors
the
min
stres
obta
limi
the
vact
A
blad
The
whic
sum
typal
cert
fore
tion
vibr

1
& D
Co
Arch
Mee
AME
N
unde
of th

Vibration of Marine-Turbine Blading

By R. W. NOLAN,¹ NEWPORT NEWS, VA.

The purpose of this paper is to give a general explanation of the vibration phenomena encountered in turbine design. Detailed methods have been omitted. The behavior of a vibrating cantilever is expressed in terms of the exciting force and damping factor. The sources of damping and excitation are discussed. Impulse excitation is briefly considered and the reasons for its devastating effects are shown. The procedure of tuning low-pressure blading, to avoid resonance at the lower harmonics of the turbine speed, is explained in considerable detail. An apparatus for determining the natural frequency of blading, and another for applying both tensile and alternating bending stresses simultaneously, are described. The direct tensile stress in the test is plotted versus the alternating bending stress which causes failure, thus obtaining a curve which shows the resistance of the blade to any combination of these stresses. The designed stresses for certain turbine blades and the stresses involved in several blade failures have been plotted on this diagram for purposes of comparison.

GENERAL

IN recent years there has been a demand for decreased fuel consumption and a decrease in weight and space requirements for marine machinery. This of course had to be accomplished with no sacrifice in reliability because machinery failure can, on some occasions, endanger the life of the ship. The result of this demand has been a trend toward small high-speed turbines.

In the case of the high-pressure turbine, little difficulty was encountered in increasing speeds and a very rugged machine has been obtained. The low-pressure turbine, on the other hand, presents a complicated problem. The volume of steam passing through the last rows of blading is determined mainly by the horsepower and vacuum. This in turn approximately determines the diameter for the last blade row. With the diameter determined, the speed in revolutions per minute is then governed by stress considerations. The blade is made as long as possible to obtain maximum area for the steam passages, but its height is limited by considerations of stress and vibration. The blading in the last few stages is a compromise governed by steam flow, vacuum, efficiency, wheel stress, blade stress, and vibration.

At this point it should be mentioned that the last few rows of blading are not the only ones which can give vibration trouble. They are, however, the most susceptible to it and are the ones on which most vibration studies are concentrated. It is usually assumed that turbine blades are subjected to steady forces. Actually, this is not entirely true. All turbine blades are subject to certain variations in force. In the great majority of cases these force variations do no harm. Occasionally, however, the vibration characteristics of the blade might be such that a dangerous vibration could be set up by the exciting force variations which

are always present in the turbine. It is the duty of the designer to see that this does not happen.

BEHAVIOR OF BODIES SUBJECTED TO VIBRATORY FORCES

Before proceeding with specific turbine problems, it is desirable to review briefly the behavior of a simple vibrating structure, and to define the terms which will be used. For this purpose, consider a steel cantilever beam of constant rectangular cross section 2 in. \times 1/2 in. and 12 in. in length. These scantlings have been chosen because they give characteristics which are not too far from those of a low-pressure exhaust blade. Assume further, that this beam is subjected to a force which varies sinusoidally with a maximum value of 0.6 lb uniformly distributed over the broad side.

The behavior of the beam subjected to this force is shown in Fig. 1 in which the amplitude of vibration at the end of the blade is plotted as a function of the frequency of the applied force. At frequencies approaching zero, the amplitude of vibration is 0.000208 in. which is equal to the static deflection produced by a force of 0.6 lb. As the frequency of the exciting force is increased, the amplitude increases until it theoretically reaches infinity at 6800 cycles per minute (cpm) (following the solid curve). Above this frequency the amplitude drops sharply. If the frequency of the exciting force were increased sufficiently, the amplitude would be found to approach infinity again at 42,600 and 119,500 (cpm) and at still higher values.

The frequencies at which the amplitude reaches infinity are the natural frequencies of this blade. The natural frequency at 6800 cycles is the first critical or first mode and that at 42,600 cycles is the second critical or second mode. The turbine designer is usually interested only in the first mode. The term "resonance" is used to describe the action which takes place when the frequency of the applied force coincides with a natural frequency. The terms "resonant" frequency and "critical" frequency are frequently used for natural frequency.

The curve under consideration is based on the assumption that there are no losses of energy in the vibrating system. Such a condition would be the equivalent of perpetual motion. Actually, frictional forces are always present, and it is fortunate that they are. Otherwise all turbines would strip out their blades in a relatively short time.

In vibration problems the frictional resistance to vibration is expressed frequently as a damping coefficient.² The dotted curve in Fig. 1 shows the behavior of this same blade with a damping coefficient of 0.10. At resonance, the amplitude of the first

² "Vibration Problems in Engineering," by S. Timoshenko, D. Van Nostrand Company, Inc., New York, N. Y., second edition, 1937, chap. 1, sects. 8 and 9:

$$\text{Damping force} = c \frac{dy}{dx} \quad (\text{Damping is proportional to velocity}):$$

$$2n = c \frac{g}{w}$$

$$\gamma = \frac{2n}{p} = \frac{c g}{pw}$$

$$\gamma = \text{damping coefficient}$$

$$g = \text{acceleration of gravity}$$

$$p = 2\pi \times \text{natural frequency}$$

$$\frac{W}{g} = \text{mass}$$

¹ Engineering Technical Department, Newport News Shipbuilding & Dry Dock Company.

Contributed by the Power Division and the Society of Naval Architects and Marine Engineers and presented at the Annual Meeting, New York, N. Y., November 27-December 2, 1949, of THE AMERICAN SOCIETY OF MECHANICAL ENGINEERS.

NOTE: Statements and opinions advanced in papers are to be understood as individual expressions of their authors and not those of the Society. Paper No. 49-A-76.

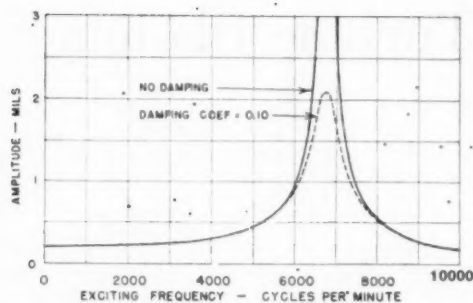


FIG. 1 VIBRATORY RESPONSE OF A CANTILEVER BEAM

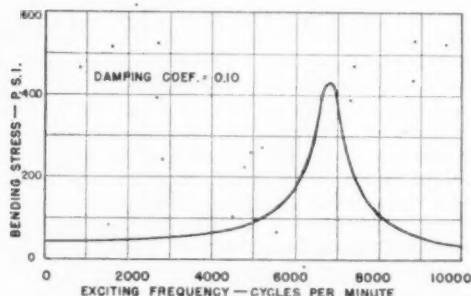


FIG. 2 VIBRATORY STRESS IN A CANTILEVER BEAM

critical (at 6800 cycles) is 0.00208 which is 10 times the amplitude at low frequencies.

For each deflection which is shown in Fig. 1, it would be possible to calculate the moment and stress in the material. This has been done in Fig. 2. At low frequencies the stress of 43.2 psi is equal to that produced by the exciting force of 0.6 lb acting statically. At other frequencies, the stress is proportional to deflection, and at resonance it amounts to 432 psi, or 10 times the stress at low frequency. The factor 10 is the magnification factor. It is equal to the reciprocal of the damping coefficient.

This method of applying the magnification factor to the static deflection applies strictly to a concentrated mass on a weightless spring. Its application to deflection and stress of a turbine blade is an approximation which is sufficiently accurate for first-mode vibrations. It is not necessarily suitable for higher modes or for other types of structure.

Those familiar with alternating-current theory, will recognize these curves to be the same as those obtained with resonant electric circuits. Magnification factor shown here is the same as the Q -factor which applies to series resonance in an electric circuit. The stress of 432 psi may appear low. It is low because a relatively high damping coefficient was used, in order to obtain a resonance curve which would plot well on a lantern slide. In actual turbine blades, the damping coefficient may be 0.005. This gives a magnification factor of 200 which would make the foregoing stress equal to 8640 psi.

CAUSES OF DAMPING IN A TURBINE

The factors which produce damping in turbine blades may be classified as elastic hysteresis, steam damping, and rubbing friction. Elastic hysteresis is internal friction in the blade material as it goes through the stress cycle. It varies widely with composition of the material and with temperature. It is difficult to determine experimentally; several investigators do not agree very well on the values. There is, however, enough information to permit a rough determination of the damping coefficient.

Another cause of damping is the resistance of the steam surrounding the blade. A rational method of determining the magnitude of steam damping would be to treat the velocity of vibratory motion as a change in blade speed, and to calculate the resultant change in tangential steam force. Application of this method shows the resultant damping forces to be rather small (less than hysteresis damping), and they usually are neglected.

The third cause of damping is rubbing friction between surfaces. There is always some minute sliding at the points of contact between the blade and the rotor, and between adjacent blades. The value of this damping is extremely variable, depending upon the design and on the fit which is obtained. Blades which are packed tightly together and are fitted accurately with considerable press fit, will have low frictional damping. Blades which are loose in the groove, or which are poorly fitted may have very high damping. In such cases the frictional damping will be many times that obtained by steam and hysteresis. This can be observed easily by striking the blades of a turbine rotor. Tight blades will ring clearly for a considerable time after striking. If the blades are loose, they have a dead sound because the vibratory energy is damped out almost immediately after striking. A natural reaction to this fact would be the suggestion that blades be installed loose to prevent vibration. This expedient might well be successful but one would hesitate to install loose blades, because of the possibility of wear caused by the movement. Furthermore, a blade which is poorly fitted may sometimes have its natural frequency lowered so that it falls into a resonant condition. It also may fail in the root, while tightly packed blades could not fail this way because they do not bend below the packing piece. Because of the uncertain nature of frictional damping, it is neglected in calculations.

A possible fourth source of damping is impact. It is closely related to frictional damping and may occur to some extent between adjacent faces of blade roots. There are patents on devices such as hollow blades containing loose rods or balls which are intended to cause impact damping if the blade vibrates. It is doubtful that these will ever find extensive application to marine turbines.

It thus appears that elastic hysteresis is the most dependable source of damping. Fig. 3 shows curves of the magnification

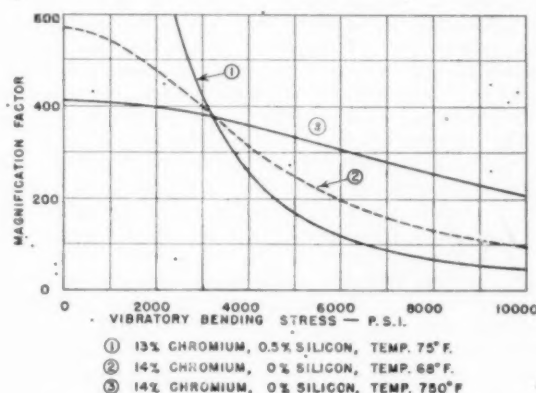


FIG. 3 MAGNIFICATION FACTOR FOR STAINLESS STEEL

factors of 13 and 14 per cent chromium stainless steel. These curves, based on data from an article by Andrew Gemant,³ are expressed as a function of the vibratory stress.

³ "Dependence on Stress of Damping Capacity of Alloys," by Andrew Gemant, *Mechanical Engineering*, vol. 67, 1945, p. 33.

EXCITING FORCES ACTING ON TURBINE BLADES

It was mentioned previously that there are always variations present in the tangential steam forces acting on blades. These may be due to many causes. Among them is the variation of pressure around the periphery of the wheel. Pressure variations cause variations in the steam velocity acting on the blade. These variations are difficult to measure experimentally because of the large number of pressure readings which must be obtained. Fig. 4, however, shows an approximate curve of pressure variation based on measurements at five points around the periphery of the last low-pressure stage of a turbine. One curve shows the discharge pressure and the other the inlet pressure for this stage. The last curve shows the variation in the Btu drop in the stage. In this case the maximum variation was about 12 per cent of the average heat drop. This is probably an extreme case since it is the last stage of a heavily loaded turbine.

Similar effects will be found at any point in the turbine where steam is being admitted or extracted. Designers frequently go to considerable pains to distribute steam uniformly in bleeder belts, chests, inlet belts, and in the space between the high-pressure first and second stages. In spite of their best efforts variations still exist.

Lack of uniformity in nozzles or blading also may be a source of uneven steam force. The discontinuity at the horizontal joint in the casing is a further possibility. It is difficult to keep the spacing of the nozzles, which span the joint, the same as that in the remainder of the ring. The conditions at the joint then may result in a different size of nozzle jet and, possibly, a different discharge angle. The blade rotating past these points will experience two impulses at each revolution.

The most severe form of excitation which occurs in turbines is known as impulse excitation. It usually occurs only in the high-pressure first stage and in astern turbines. In these stages steam is admitted to the wheel over a portion of the periphery, usually less than 180 deg. As the blade rotates, it enters the steam arc, receiving a sudden application of the full steam force. When it passes out of the steam arc, the sudden removal of the steam force is equally severe. The force variation is thus equal to 100 per cent.

Fortunately, the blades which receive this punishment are among the shortest and most rugged in the whole turbine. In spite of this, impulse excitation has been a serious problem to shore power plants, and it resulted in a number of failures before the cause was discovered. The shore turbines which suffered these breakdowns were high-pressure topping turbines which used large quantities of high-pressure high-temperature steam (1200 psi, 950 F). Conditions as severe as this have not yet been imposed on marine turbines and therefore failures of first-stage blading have been few. Present trends in marine steam conditions may bring on this trouble, and the designer must be alert to avoid it. A mild form of impulse excitation might be set up by damage which would partially close some of the nozzles in any turbine stage.

Blade vibration also may be excited by external forces. In one case, blade failure in a small geared turbogenerator was attributed to vibration set up by errors in the gear-tooth spacing. It is also possible that errors in the roundness of the journal may cause a motion which could set blading in vibration.

With the exception of impulse excitation, our knowledge of the magnitude of exciting forces is quite limited. We do know, however, that they are present in sufficient magnitude to cause failure of improperly designed blades. The uncertainty concerning the exciting forces and, to a considerable extent, the damping forces has led some of the large turbine manufacturers to adopt an empirical approach to the problem.

HARMONIC ANALYSIS OF EXCITING FORCES

Regardless of what may be the pattern of the exciting forces, it will be repeated periodically, usually once for each revolution of the turbine. Any periodically varying set of values, such as the exciting forces acting on a turbine blade, can be broken up into a series of sine and cosine curves. The frequencies of these harmonic components will be integral multiples of the frequency of the original curve.

For example, take the lower curve in Fig. 4, showing the distri-

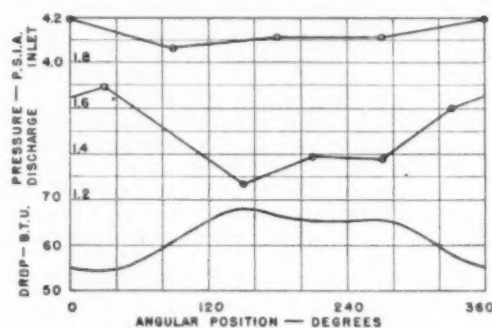


FIG. 4 PRESSURE AND HEAT DROP IN A TURBINE EXHAUST STAGE

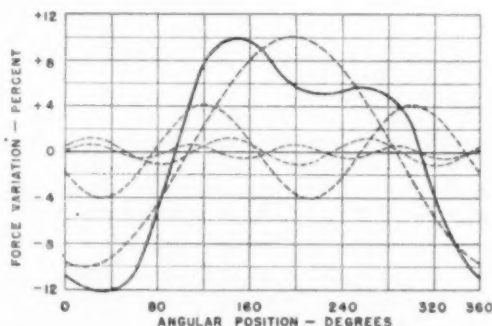


FIG. 5 HARMONIC ANALYSIS OF FORCE VARIATION IN A TURBINE EXHAUST STAGE

bution of heat drop around the circumference of the wheel. Assuming that the steam force, acting on a blade, is proportional to the heat drop, a curve of force variation has been plotted in Fig. 5 (solid curve). Each blade will be subjected to this force variation at each revolution.

By applying a Fourier analysis, the first four harmonics have been obtained. These also are shown in Fig. 5 (dotted curves.) Their amplitudes and phase angles are given in Table 1.

TABLE 1 AMPLITUDES AND PHASE ANGLES

Harmonic	Amplitude, per cent	Phase angle, deg
1	10.1	+253
2	4.1	+206
3	1.1	+24
4	0.6	+3

There was no justification in carrying this analysis beyond the fourth harmonic because there were so few points on the original curves from which the drop was calculated. It should be observed how the harmonics decrease in amplitude as their order increases. This is generally to be expected but it is not always so.

To illustrate the exciting forces generated by impulse excita-

tion, the diagram shown in Fig. 6 has been assumed. Here the nozzle arc is assumed to be 90 deg with instantaneous application and removal of the load taking place at the ends of the arc. The

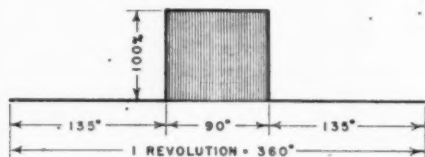


FIG. 6 STEAM-LOADING DIAGRAM FOR HIGH-PRESSURE FIRST-STAGE BLADING

instantaneous application and removal of the load is a rather severe assumption, but it is much less tedious to apply and therefore is more convenient for preliminary design purposes. Analysis of this diagram gives an infinite series of harmonics with every 4th one (4th, 8th, 12th, etc.) equal to zero. The values of the first ten harmonics in per cent of the steam loading F , are given in Table 2. Even the 30th harmonic has an amplitude of 2

TABLE 2 VALUES OF FIRST TEN HARMONICS

No. of harmonic	Intensity, per cent
1	45.0
2	31.8
3	15.0
4	0
5	9.0
6	10.6
7	6.4
8	0
9	5.0
10	6.4

per cent, which is sufficient to set up a vibration of considerable magnitude. This gives some indication of why impulse excitation can be so destructive. Further troublesome characteristics of impulse excitation will be brought out in the next section.

TUNING OF TURBINE BLADES

Whenever the frequency of one of the various harmonics of the exciting force coincides with a natural frequency of the blade, resonance will occur. As explained earlier, the vibration amplitude will be equal to the static deflection produced by the component, multiplied by the magnification factor. Assume, for instance, that a blade is subjected to a steady steam force of 6 lb plus a certain harmonic whose magnitude is 5 per cent. The harmonic force will then have an amplitude of 0.3 lb. The static deflection is then considered to be the deflection which would be produced by a force of 0.3 lb uniformly distributed over the blade. If the magnification factor is 200, the deflection at resonance would correspond to that produced by a force of 60 lb. The resultant vibratory stress also would be equal to that produced by a 60-lb load, and would thus be 10 times the stress produced by the total steam load which acts statically on the blade. Such bending stresses when superposed on the already high centrifugal stresses may cause fatigue failure if the turbine runs for long periods at a resonant condition.

As already mentioned, experience with turbines indicates that the lower harmonics usually have the largest amplitudes. There have been many failures which were caused by the 4th or lower harmonics. There also have been some failures at higher-order harmonics. It is therefore necessary to avoid resonance at the 4th and lower harmonics or, when it cannot be avoided, have it occur at a reduced speed where the centrifugal stress acting on the blade will be less than at full power.

A convenient means of visualizing this problem is the Campbell diagram, named for the late Wilfred Campbell of the General

Electric Company, who did much of the pioneer work on turbine vibration. The Campbell diagram is shown in Fig. 7. It consists of a series of curves of frequency (usually cycles per minute) plotted versus turbine revolutions per minute. On this diagram each harmonic is represented by a straight line passing through the origin. These lines give the frequencies of the exciting forces corresponding to the various harmonics, at all speeds of the turbine. The second harmonic will have twice the slope of the first, the third harmonic three times, etc. Usually, about eight harmonics are drawn.

After the frequencies of all of the important exciting forces have been plotted on the Campbell diagram, the natural frequencies of the blading are plotted. When the turbine is not rotating, the natural frequency of a blade (or group of blades joined by a shroud band), has a particular value which is called the static frequency. When the turbine is running, the centrifugal force has a stiffening effect on the blade, raising its natural frequency. This is the running frequency. These frequencies also can be plotted on the Campbell diagram. The curves for two stages, A and B, are shown in Fig. 7. The running frequency is fairly close to static frequency up to about half speed of the turbine. Above this speed the frequency increases appreciably. At maximum speed the increase in frequency is usually around 15 per cent for the longest blades.

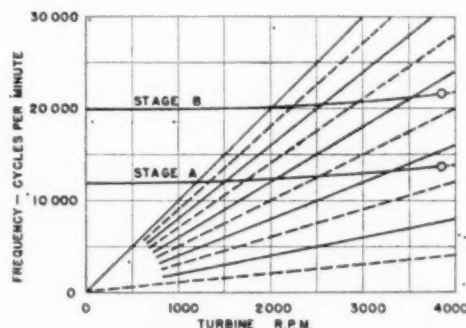


FIG. 7 CAMPBELL DIAGRAM

With the blade frequencies added, the Campbell diagram is complete. Each point at which the blade-frequency curve crosses one of the harmonics, represents a condition of resonance. There are thus numerous resonant conditions for each blade. Most of them are excited by high-order harmonics and are therefore not serious. The lowest order of resonance is the one of which to beware, because it occurs at the highest turbine speed and probably will have the largest exciting force.

Turning now to the curve for blade A, in Fig. 7, it can be seen that at maximum speed, resonance does not occur, and the blade frequency lies halfway between the 3rd and 4th harmonics. If the natural frequency of 13,500 is divided by the turbine rpm of 3850, the result is 3.5. This is usually called 3.5 vibrations per revolution. This value is not a coincidence. As originally laid out, this blade had 4.1 vibrations per revolution, which was very close to a dangerous resonant condition. It was not considered practical to stiffen the blade sufficiently to raise it to 4.5 vibrations per revolution, so, the blade section was reduced in order to lower the frequency to 3.5 vibrations per revolution. This process is called tuning. It is a fairly lengthy design process involving considerable work.

Referring back to the Campbell diagram, it will be seen that at 3300 rpm, stage A is in resonance with the 4th harmonic. At this condition, however, the steam load on the blade is less than at full power (probably down to 70 per cent of the full-power value) and

therefore the magnitude of the exciting force is reduced proportionately. In addition to this, the centrifugal stress in the blade is down to 12,200 psi, instead of the 16,600 psi which it had at full power. The total steam load on this blade at full power is 6.5 lb per blade, producing a steam bending stress of 550 psi. At 3300 rpm the bending stress may be assumed to be about 390 psi, (70 per cent of 550). If this steam force contained a 4th harmonic with a magnitude of 5 per cent of the steady steam force, and the vibration magnification factor were 200, the vibratory stress would be $390 \times 0.05 \times 200 = 3900$ psi.

A comparison of the blade stresses at full speed (3850 rpm) and at 3300 rpm, is given in Table 3.

TABLE 3 BLADE STRESSES AT 3850 AND AT 3300 RPM (STAGE A)

(a) Rpm.....	3300	3850
(b) Centrifugal stress, psi.....	12200	16600
(c) Static steam stress, psi.....	390	550
(d) Total steady stress (b + c), psi.....	12590	17150
(e) Vibratory stress, psi.....	3900	negligible
(f) Maximum stress (d + e), psi.....	16490	17150
(g) Minimum stress (d - e), psi.....	8690	17150

Thus it can be seen that although 4th-order resonance has not been avoided, it has been located at a speed where less severe stresses are encountered. Had 4th-order resonance occurred at full speed, the steady stresses would be 17,150 psi, and the vibratory stresses 5500 psi, leading to a maximum stress of 22,650 psi, and a minimum stress of 11,650 psi.

Stage B has been handled in a similar manner except that it is tuned to have the full-power condition fall between the 5th and 6th harmonics. Unless a blade is very highly stressed, it does not appear necessary to tune for harmonics above the 6th. Assuming the vibratory stress at resonance in stage B to be 10 times the steam bending stress, it will compare with stage A, as in Table 4.

TABLE 4 COMPARISON OF STRESSES IN STAGES A AND B

Stage	Resonant rpm	Harmonic	Centrifugal stress, psi	Steam bending stress, psi	Total steady stress, psi	Vibratory stress, psi
A	3300	4	12200	390	12590	3900
B	3550	6	12500	510	13010	5100

Although the stress in stage B is higher than that in stage A, when calculated by this arbitrary method, it should be remembered that the exciting force of the 6th harmonic will be much less than the 4th, and the factor of 10 is therefore rather severe.

It is in connection with tuning that one of the most objectionable features of impulse excitation becomes apparent. First-stage blades, which are subjected to impulse excitation, have high natural frequencies which ordinarily would put them well out of reach of vibration trouble. Their frequencies may be 25 or more vibrations per revolution. It was, however, mentioned in the preceding section, that even the 30th harmonic of impulse excitation may have an exciting force of 2 per cent. Thus these blades will be subjected to sizable exciting forces. Even assuming that it were possible to tune a blade accurately enough to obtain 24.5 vibrations per revolution, it would be in resonance at 25 vibrations per revolution when the speed dropped 2 per cent. This change is no more than that which would be encountered in going from light draft to load draft, or from clean bottom to foul bottom. It is thus impossible to avoid resonance at, or very close to, maximum speed. Therefore the blades must be designed to withstand such conditions. This can be done by keeping low bending stress and using materials which have good damping properties at the operating temperatures. Thirteen per cent chromium stainless steel has relatively good damping properties.

In the process of tuning, there are several ways of changing the frequency, and usually two or more of them are used together. In discussing the methods it would be well to consider the equa-

tion for the frequency of a cantilever beam of constant section, which shows the effect of several of the factors which determine blade frequency. This equation is

$$F_s = 660 \sqrt{\frac{EI}{Wl^4}} = \sqrt{\frac{EI}{\rho A l^4}}$$

where

F_s = static frequency, cycles per min (cpm)

E = modulus of elasticity, psi

I = moment of inertia of cross section, in.⁴

l = length of beam (length of blade), in.

ρ = density of material, lb per cu in.

A = area of cross section, sq in.

W = weight per in. of beam = ρA , lb per in.

In this equation, E and ρ may be considered fixed, since the material is usually settled in advance. That leaves the possibility of altering A , I , and l . Increasing the value of I , will increase the frequency. If a small increase is desired, it can be accomplished by thickening the blade slightly. If a large increase is needed, the necessary thickening would restrict the steam passage too much. In this case the entire blade section may be increased, maintaining the same geometric proportions. Either process increases the area A simultaneously. Moment of inertia, however, increases as the 4th power of the linear dimensions, while A increases as the 2nd. Thus frequency will increase about in proportion to the increase in lateral dimensions.

Another method of changing frequency is to change l . Since frequency varies as l^2 , this method is effective. It is usually an increase in frequency which is desired and, in this case, l would be decreased. This, however, may be a costly process because it will lower the efficiency of the stage. Therefore height decreases are used rather sparingly.

The third method of altering frequency is to taper the blade, or alter the taper on one which already has it. Tapering a blade not only increases the blade frequency, but it is most effective in reducing centrifugal stress. If the stage A in Fig. 7 were made with constant cross section (using the base section), its static frequency would be about 13 per cent lower, and the centrifugal stress 70 per cent higher. Tapered blades are also "twisted" frequently. This is done to suit the angle of the incoming steam.

Shroud bands and lacing wires affect the frequency. Shroud bands do not necessarily raise the frequency. They do stiffen the blades, but the added mass sometimes counteracts the added stiffness. In some cases, however, shroud-band alterations can be used as an aid in tuning. Lacing wires increase the frequency, particularly when there are two rows of them. Altering their size will alter the frequency.

Application of any of these methods of tuning usually is limited by the action of some other factor such as loss of thermodynamic efficiency, increase in stress, or difficulty of manufacture. It is for this reason that several methods may be applied simultaneously to obtain the desired result.

The subject of tuning cannot be dismissed without some mention of the calculating methods which must be applied with every change. Only the briefest discussion of them can be given in this paper because a detailed treatment would result in the writing of a textbook.

The calculation of a tapered twisted blade is a tedious process. It is necessary first to calculate maximum and minimum moments

of inertia and weight per inch of blade at several sections (usually at least three sections are taken and a curve is drawn through the three points thus obtained). For the actual frequency calculation, the Rayleigh method is frequently used. In this method, the potential and kinetic energy must be calculated for a given assumed deflection curve. Ordinarily, the static-deflection curve, obtained by loading the blade with its own weight, is taken as the assumed curve. In this case, the calculation is represented by the equation

$$F_s = 188 \sqrt{\frac{\int w y d l}{\int w y^2 d l}}$$

where

w = weight per unit length of blade
 y = ordinate of deflection curve
 $d l$ = differential length

If the assumed curve is reasonably close to the shape of the actual vibration curve, a good approximation is obtained. In using the static-deflection curve, the error seldom exceeds 2 per cent. If greater accuracy is required, it is necessary to make a second approximation, based upon the first calculation.

Twisted blades present a problem because the axes of the cross sections do not lie in one plane. This requires using two reference planes at right angles and working with co-ordinates. An expedient which has been used to avoid this, is to work two approximate calculations. In the first, the minimum moments of inertia for all sections are rotated into a single plane and the frequency calculated. This gives a frequency which is too low. The other calculation uses the moment of inertia, of each section, about an axis parallel to the minimum axis of the base section. This gives a frequency which is too high. By interpolating between these two frequencies and using factors obtained from tests, it is possible to obtain frequencies which are close enough for preliminary design work.

Final blade-frequency calculations involve the effect of the shroud band or lacing wires. In this case the structure is indeterminate and requires the application of strain-energy methods.

Finally, it is necessary to calculate the effect of centrifugal force. For blades of constant cross section, Campbell used the formula

$$F_r = \sqrt{F_s^2 + B N^2}$$

$$B = 1.56 \times \frac{R}{l} + 1.17$$

where

F_s = static frequency
 F_r = running frequency
 l = blade length
 R = radius to base of blade
 N = rpm of turbine

This formula may also be used for preliminary calculations on tapered blades. For final calculations, it is necessary to calculate the radial shortening caused by the lateral bending of the blade, and then calculate the potential energy which is stored up by producing this radial shortening against the action of centrifugal forces. The effect of centrifugal force on the vibration of a turbine blade is analogous in some ways, to the effect of gravity on the frequency of a pendulum.

BLADE TESTING

Consideration of the Campbell diagram shows that an error of a few per cent in the calculation of blade frequency could lead to

disaster. Therefore it is natural that testing should be an important phase of blade design. In this way the various factors affecting frequency can be determined, and empirical design coefficients chosen. For this purpose a vibrator can be used to determine the natural frequencies of blading. The vibrator, illustrated in Fig. 8, was built from a loud-speaker. The cone was sawed off and a small threaded nut cemented to the moving ele-



FIG. 8 VIBRATOR FOR DETERMINING NATURAL FREQUENCIES OF TURBINE BLADES

ment. One end of a small aluminum rod ($\frac{3}{32}$ in. diam) is screwed into this nut, and the other end is attached to the blade by means of a spring clip. The permanent-magnet field of the speaker has been replaced by an electromagnet of considerably greater field strength. By supplying an alternating current to the coil of the speaker, a corresponding alternating force of about 0.5 lb peak value can be obtained. A Hewlett-Packard 200-B, 1-watt oscillator is used for this purpose, and it supplies sufficient power to vibrate most turbine blades. The oscillator frequency is varied until resonance occurs, and the frequency can be read on the oscillator dial. By using a micrometer drive for the dial and calibrating with a cathode-ray oscillograph, very high precision can be obtained when needed.

Single blades to be tested are clamped to a heavy metal slab, usually using filler blocks which cover the root and packing piece. When testing an entire group of blades, complete with shroud band, the blades are mounted in a grooved block which simulates a section of the turbine rotor. Such a group can be seen in Fig. 8.

Another type of testing which is necessary in blade designing is the combined tensile and fatigue test. In this test a tensile load is applied to the blade to simulate centrifugal force. At the same time, vibratory stresses are simulated by the application of a lateral alternating force. A machine for making such tests is shown in Fig. 9. A beam, weight-loaded at the end, applies the tensile load (up to 21,000 lb). A connecting rod, attached to an adjustable eccentric, applies a bending deflection to the blade. The eccentric is driven by a motor with a speed range of 1000 to 2200 rpm. The bending stress in the blade is checked by means of bonded resistance-wire (SR-4) strain gages. This machine is used to determine the fatigue strength of blading, and also for comparative tests of modifications to blade roots. It was used in

FIG.

ALTERNATING BENDING STRESS-PSI.

arriv
 A an
 In
 load
 stres
 or w
 vers
 Fig.
 then
 Wit
 stan
 pap
 the
 cau
 stre
 this
 stre
 of s
 T
 cur
 plo
 plo
 all
 Th
 nat

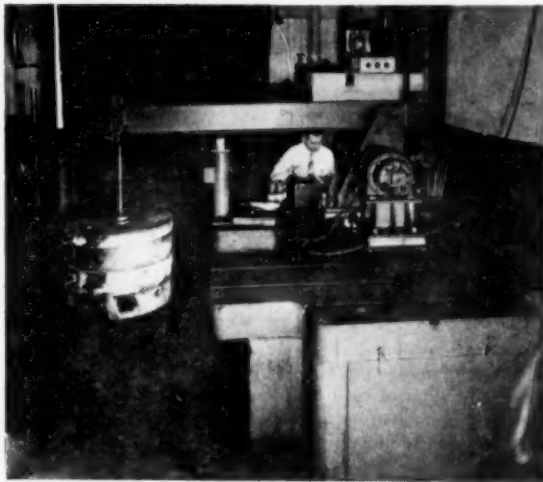


FIG. 9 MACHINE FOR MAKING COMBINED TENSILE AND FATIGUE TESTS

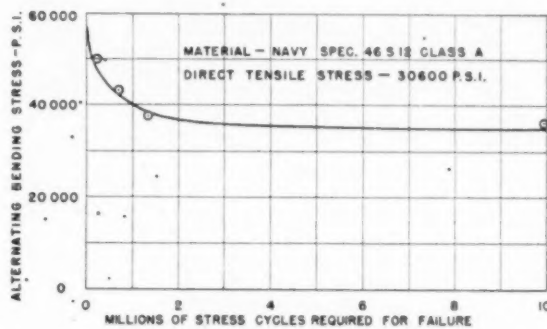


FIG. 10 FATIGUE TEST OF 2-IN. TURBINE BLADE

arriving at the size of fillet to be used in the roots of the stages, A and B, which were shown in Fig. 7.

In making combined tensile and fatigue tests, a certain tensile load is applied, and then a series of tests are run at different bending stresses. Each test is continued until the specimen either breaks or withstands 10,000,000 stress cycles. A curve of bending stress versus number of cycles is then plotted. Such a curve is shown in Fig. 10. It will be noticed that the curve falls rapidly at first and then levels off. At 10,000,000 cycles the curve is practically flat. With ferrous materials, it is assumed that a specimen which withstands 10,000,000 stress cycles will last indefinitely. In this paper the ordinate of the curve at 10,000,000 cycles will be called the endurance limit. This term must be used with caution because endurance limit is usually used to indicate the fatigue strength of the material subjected to alternating stress only. In this case there is a combination of steady stress and alternating stress. A separate endurance limit can be obtained for each value of steady stress.

The several values of endurance limit may be plotted on a curve such as that shown in Fig. 11. Here, endurance limit is plotted as the ordinate and steady stress as the abscissa. In the plot shown in Fig. 11 there are only two points. The tests were all run with 30,600 psi steady stress, which gave one of the points. The other point is the steady stress corresponding to zero alternating stress. This is simply the tensile strength of the material.

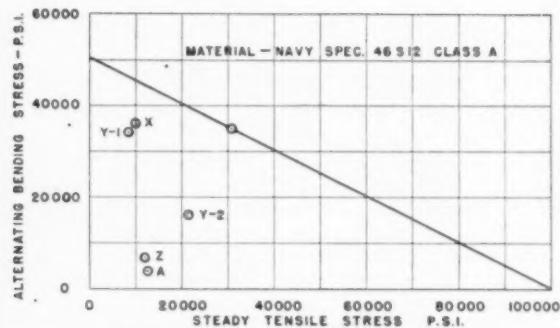


FIG. 11 FATIGUE-STRENGTH DIAGRAM FOR 2-IN. TURBINE BLADE

These have been joined by a straight line. Published literature on the subject indicates that this is a reasonable assumption to use when intermediate points are lacking. The resulting curve shows the strength of a particular blade for any combination of steady and vibratory stress. However, the curve should be representative of other blades of similar design.

FACTOR OF SAFETY

In most stress problems it is desirable to calculate a factor of safety. In turbine-blade vibration there is much that is not known and that is why designers prefer statistical methods aided by comparative stress and vibration calculations. The magnitudes of both exciting and damping forces are in considerable doubt. One manufacturer multiplies the steady steam bending stress by 10, adds it to the centrifugal stress at full power and considers that the working stress for the blade. This appears to be a reasonably rational approach when it is considered that it is equivalent to a harmonic exciting component of 5 per cent of the steady steam force, and an amplification factor of 180. The 5 per cent factor appears quite conservative in the light of the few measurements of variations in steam force which are available (except in the case of impulse excitation). In fact, it is difficult to see how this figure could be approached in a carefully designed turbine, unless there were some damage to blading or nozzles.

The amplification of 180 also appears reasonable for 13 per cent chromium stainless-iron blading in a low-pressure turbine. The 5 per cent exciting force and amplification of 200 which have been assumed several times in this paper are very nearly identical with it. What this method does appear to need is an additional factor whereby the decreasing intensity of higher harmonics could be considered.

Returning now to Fig. 11, we can plot the stresses for stage A from Table 3 of a previous section. The bending stress required for failure at the given static stress of 12,590 psi, is 44,000 psi, giving a factor of safety of $44,000 \div 3900 = 11.3$. At first glance this might seem to be an excessively high factor of safety. It is conservative, but turbine blades are subject to corrosion fatigue. Metals subjected to alternating stresses in an atmosphere of steam or water, have much lower endurance limits than in air. Because of this it would be reasonable to divide the foregoing factor of safety by 2, thus obtaining 5.6.

Four failures have been plotted in Fig. 11. The blades involved had the characteristics given in Table 5.

In each case the bending stresses have been multiplied by 10 before plotting in Fig. 11. Blades X and Y-1 both failed after several years of service. Both were in the last row of the high-pressure turbine, where they were subjected to relatively large variations in heat drop around the periphery. Since both had approximately 12 vibrations per revolution, they would not ordi-

TABLE 5 CHARACTERISTICS OF BLADES WHICH FAILED

Manufacturer	Turbine	Cent. stress, psi	Steam bending stress, psi	Total static stress, psi	Vibrations per rev	Failure
X	HP	6410	3610	10020*	11.9	Blade
Y (case 1)	HP	5000	3390	8390	12.5	Blade
Y (case 2)	LP	19800	1590	21390	4.0	Shroud
Z	LP	11200	700	11900	4.2	Root

narily be expected to give trouble. The bending stresses were, however, so high that even with the small excitation obtained from the 12th harmonic they succumbed to corrosion fatigue. In considering these stresses, it must be remembered that the factor of 10 is excessive for the high-order vibration. The remedy for such blade trouble is to lower the bending stress by using a heavier blade section.

With blade Y-2, 4th-order resonance was encountered at full power. The blade itself did not fail but the vibration was sufficiently severe to crack the shroud band. Broken shroud bands are liable to jam and tear up the blading. In the case of blade Z, failure was attributed to axial vibration of the wheel. However, exact diagnosis of blade failure is usually difficult, and the prox-

imity to 4th-order resonance appears suspicious.

In connection with design, it should be emphasized that great care must be exercised in proportioning all fillets on turbine blading. A sharp re-entrant corner at the base of the blade, or in the root can be the starting point for a fatigue crack which will cause the failure of an otherwise successful blade.

CONCLUSION

From the foregoing illustrations and discussion, it can be seen that the design of blading to resist vibration is far from an exact science. In spite of this, high efficiencies are being obtained, while blade failures from fatigue have been reduced to a point where they are considerably less than failures from other causes.

Theory of the Mechanical Properties of Hot Plastics

By S. J. LORING,¹ EASTON, CONN.

This paper describes a theory of large strain, rubber-like elasticity combined with stress relaxation, which is the character of the behavior of hot plastics indicated by a series of unpublished high extension rate tests on such materials as polystyrene, polyethylene, acetate, etc., in the molten or "soft" state.

NOMENCLATURE

a_{ij} = natural strain components
 A_{ij} = auxiliary strain quantities defined in terms of a_{ij}
 C = pressure gradient in channel or tube flow
 D = "diffusion coefficient" representing effect of thermal agitation of molecules on their phase-space co-ordinates
 f = representative molecular force
 $f(x_1)$ = designation for arbitrary function in channel- and tube-flow analysis
 f_{11}, f_{22} = functions representing stresses due only to elastic strain in channel and tube flows
 F_{22} = function representing stress due only to elastic strain in tube flows
 F_1, F_2, F_3 = forces on sides of parallelepiped of material
 G = modulus of rigidity entering specific strain-energy functions
 h = semiheight of channel or radius of tube
 H, H' = auxiliary parameters in analysis of channel and tube flows
 i, j, k = "dummy" indexes ranging over values 1, 2, 3
 K = constant of proportionality between representative molecular force f and length r
 l_{ij} = direction cosines relating directions of x_1, x_2, x_3 and y_1, y_2, y_3 axes
 L_1, L_2, L_3 = fixed reference lengths
 m_{ij} = direction cosines relating directions of x_1, x_2, x_3 and z_1, z_2, z_3 axes
 M_{ij} = auxiliary strain quantities defined in terms of a_{ij} and m_{ij}
 n = exponent in specific relaxation and strain-energy functions
 N = number of molecules per unit volume
 p = hydrostatic tension independent of elastic strain in incompressible materials
 p_0 = constant hydrostatic tension in channel or tube-flow analysis
 q = volume rate of flow per unit width in channel
 Q = volume rate of flow in tube
 r = representative length of chain molecule
 r_0 = reference value of r
 R_1, R_2, R_3 = functions describing relaxation process
 s = shearing rate in simple shear
 S = dimensionless measure of shearing rate s

t = time
 T = "relaxation time" entering specific relaxation functions
 v_0 = constant of integration in flow-velocity integrals for channel or tube
 v_1, v_2, v_3 = flow-velocity components in x_1, x_2, x_3 directions
 v_r = "drift" velocity of phase-space co-ordinates of a molecule due to molecular force
 W = work done on unit volume of material by external forces
 x_1, x_2, x_3 = fixed direction Cartesian co-ordinates; in dealing with strain a single prime (') denotes position of point in unstrained condition, and double prime (") in strained condition
 X, X' = auxiliary parameters in analysis of channel or tube flows
 x, y, z = Cartesian co-ordinates in phase space
 y_1, y_2, y_3 = Cartesian co-ordinates with same origin as x_1, x_2, x_3 but directed along lines in unstrained condition which become principal axes in strained condition. Single and double primes ('), (") have same significance as for x_1, x_2, x_3
 z_1, z_2, z_3 = Cartesian co-ordinates with same origin as x_1, x_2, x_3 but directed along lines of principal strain in strained condition. Single and double primes ('), (") have same significance as for x_1, x_2, x_3
 $\alpha_1, \alpha_2, \alpha_3$ = principal extension-strain ratios—referring to elastic strain in Sections 3, 4, and 5
 η = viscosity coefficient for Newtonian liquid
 η_c = apparent viscosity for flow in channel
 η_s = apparent viscosity for simple shear flow
 η_t = apparent viscosity for flow in tube
 θ = angle between principal strain axis z_1 and axis x_1 in two-dimensional strain
 θ_1 = angle between unrotated principal axis y_1 and axis x_1 in two-dimensional strain
 $\lambda_1, \lambda_2, \lambda_3$ = parameters in linear relations between M_{ij} and m_{ij}
 μ = assumed constant of proportionality between v_r and molecular force f
 ρ = distribution function in phase space
 ρ_0 = equilibrium distribution function
 $\sigma_1, \sigma_2, \sigma_3$ = principal stresses
 σ_{11}, σ_{22} = tension stresses on x_1, x_2 co-ordinate plane
 τ = shear stress on x_1, x_2 co-ordinate planes
 Φ, Φ' = auxiliary functions for channel flow
 ψ = strain-energy function

1 INTRODUCTION

The mechanical stress-flow properties of hot plastics are of considerable practical importance in the study of various plastic-manufacturing processes, such as extruding, molding, injection molding, etc. The results of a series of tension tests on several hot plastic materials, which are reported by the author,² indi-

² "Report on Tensile Tests on Hot Plastics at High Extension Rates"; report prepared for Plax Corporation by S. J. Loring, December, 1948.

¹ Consulting Engineer. Mem. ASME. Contributed by the Rubber and Plastics Division and presented at the Annual Meeting, New York, N. Y., November 27–December 2, 1949, of THE AMERICAN SOCIETY OF MECHANICAL ENGINEERS.

NOTE: Statements and opinions advanced in papers are to be understood as individual expressions of their authors and not those of the Society. Paper No. 49—A-60.

cate that the flow properties of these materials result from a rubberlike large deflection elasticity combined with a stress relaxation property.

The elastic and relaxation properties combine to produce flow characteristics which are in many ways similar to those of the classical Maxwell liquid. The classical Maxwell liquid theory, however, implies that the elastic strains are of infinitesimal, or at least very small magnitude as is also assumed in the classical theory of elasticity. In contrast, the subject materials exhibit very large elastic strains, with extension ratios of the order of 2 or even 10, and these large elastic strains have profound effects upon the behavior of the materials as compared to the classical Maxwell liquid.

The important novel effects introduced by large elastic strain as opposed to small strain originate from two principal sources. One source of novel effects lies in the geometrical properties of large strain itself, which are considerably more complex than those of small or infinitesimal strain. The other source of new complexities is the fact that both the elastic and relaxation rates are affected by the changes in internal structural arrangement of the materials which must accompany large strain; these rates no longer can be considered linear as in classical theories.

A theory of the mechanical behavior of materials exhibiting large-strain elasticity and stress relaxation is developed in the present paper, in which consideration is given both to the geometrical properties of large strain and to the nonlinearity of elasticity and relaxation which accompany large strain.

The theory is based upon the mathematical treatment of large strain presented in Section 2. This treatment differs from most other treatments of large strain in that it is developed from the specification of the state of strain at the individual points of a body rather than a general specification of the state of distortion of the body as a whole. The strain at the individual points is then related differentially to the distortion of the body as a whole by specifying its time rate of change in terms of flow velocities. This point of view appears simpler than the usual one because the current strain condition can be followed during the course of a deformation without the complexities and ambiguities that arise in relating the positions of points in the body directly to their original or unstrained positions. The viewpoint is, in addition, particularly well adapted to the treatment of the relaxation process in flows, which leads to real ambiguities with the older method.³

In Section 3 the mathematical specification of general elastic and relaxation properties is developed from a phenomenological and macroscopic point of view. It is pointed out at the end of that section that numerical implementation of this specification requires data relating to the internal structure of the materials.

A simple molecular representation of internal structure is set up in Section 4, and analyzed by the methods of statistical mechanics to illustrate the structural significance of the phenomenological concepts introduced to describe the macroscopic mechanical behavior. This analysis leads to definite mathematical functions which describe the elasticity and relaxation of the simplified representation, and which may be used as starting points for interpretation of test data on actual materials.

General solutions for the steady-state flows in channels and tubes are developed in Section 5, and their numerical application is illustrated by carrying out numerical computations with strain-energy and relaxation functions which are in accord with the tensile test data of the author.³ Comparison is made with some test data on flows through channels and tubes, and the agreement with the theory is encouraging.

Regarding extensions in the applications of this theory, it is interesting to note that the principal novel concepts in large elastic strain are very similar to those described by Bailey⁴ as orientation in cold plastics. It appears that the understanding of the mechanical properties of hot plastics may be extended and lead to understanding of the more complex properties of cold plastics.

In any event, it is hoped that the theory in its present form will serve as a basis for interpretation of observations on the mechanical behavior of hot plastics, and when fully implemented by such observations, will serve as a basis for rational and quantitative treatment of some of the flow problems involved in the manufacture of plastic articles.

2 GEOMETRY OF LARGE STRAINS

(a) *The Notion of Strain.* Since the properties of large strain differ in a number of ways from those of the small strain of classical theory, some of the commonly accepted attributes of small strain must be discarded in treating large strain. For this reason the developments of this section are introduced by an account of the general notion of strain of unrestricted magnitude. This account is directed to the viewpoint to be adopted in the following treatment of large strain.

A complete and detailed description of circumstances in which the relative positions of the points of a body change requires the notion of strain. Consideration of those circumstances will serve to bring out the basic concepts involved in the notion of strain.

Note first that change in the relative positions of the points of a body implies a comparison of two states of deformation of the body. Therefore two distinct configurations of the points of a body must be involved in the notion of strain; specifically, the comparison of the two configurations is involved.

Changes in relative position of distant points of the body result from vectorial addition of the changes of relative position of a number of closer intermediate points, and they are, therefore, implied by the latter changes. The closer the points of the body that are individually identified the more complete the description of the relative state of distortion in the two configurations.

In the limit, a complete description of a distortion of a body can consist of a catalog of the relative position changes of all its pairs of points which lie an infinitesimal distance apart. Such a catalog may be conceived as being composed of sections each of which is devoted to a particular point and contains the information for all pairs of points separated by an infinitesimal distance and of which the particular point is a member. Multiple listings required for this arrangement of the catalog will, of course, not affect its completeness, which is all that matters for the present purposes.

The information contained in that section of the catalog described in the preceding paragraph which is devoted to a particular point is just the information which is contained in a specification of the state of strain at the point. The mechanics of this specification, and its properties, form the subject matter of the present treatment.

Most classical treatments of strain are restricted to the case of "small" strains, in which case the changes in the distances between pairs of neighboring points are very small compared to these distances themselves. This restriction is inappropriate for the present purposes and is completely abandoned. In the treatment which follows no assumption is made as to the magnitude of the changes which take place in the distances between

³ See, for example, footnote, and discussion just prior to that reference.

⁴ "Stretch Orientation of Styrene and Its Interesting Results," by James Bailey, *India Rubber World*, vol. 118, May, 1948, pp. 225-231.

neighboring points, except that they are continuous from point to point and remain finite.

(b) *Specification of Strain at a Point.* In order to specify the strain at a point in a body, a set of Cartesian co-ordinates x_1, x_2, x_3 is set up with the origin at the point in question. The directions of these axes remain fixed, but the origin stays on the point of the body and moves with it during a deformation.

Let the x_1, x_2, x_3 -co-ordinates of any neighboring point be designated by x_1', x_2', x_3' "before the deformation," and let them be designated by x_1'', x_2'', x_3'' "after the deformation." Specification of the strain at the point consists of a general expression for x_1'', x_2'', x_3'' in terms of x_1', x_2', x_3' in which, however, these co-ordinates are limited to infinitesimal values.

Any relationship between x_1'', x_2'', x_3'' and x_1', x_2', x_3' can be expressed as power series in x_1', x_2', x_3' . The constant term in the series for each of x_1'', x_2'', x_3'' is zero since, by definition, the reference axes move with the reference point in the body, that is, $x_1' = x_1'' = x_3' = 0$ always implies that $x_1'' = x_2'' = x_3'' = 0$. Furthermore, since x_1', x_2', x_3' are limited to infinitesimal values, powers above the first may be neglected in the series. Accordingly, the most general expression for strain at a point is

$$\left. \begin{aligned} x_1'' &= a_{11}x_1' + a_{12}x_2' + a_{13}x_3' \\ x_2'' &= a_{21}x_1' + a_{22}x_2' + a_{23}x_3' \\ x_3'' &= a_{31}x_1' + a_{32}x_2' + a_{33}x_3' \end{aligned} \right\} \dots\dots\dots [1]$$

The strain is specified by the nine quantities $a_{11} \dots a_{33}$ which will be called the natural strain components. Though they are in a different form, the natural strain components are equivalent to the strain components usually employed in the classical theory of elasticity. However, as remarked before, in this work no assumption is made as to the magnitudes of the strain components except that they remain finite.

In the exposition which follows a number of equations will be encountered which, like Equations [1], have groups of similar terms in which only the indexes change. It will be convenient to shorten the writing out of these equations by use of the standard summation symbol Σ , and the letter indexes i, j, k , which range over the values 1, 2, and 3. The index to which the summation refers will be indicated by placing this index under the summation sign, and the ranges of other indexes will be indicated in parentheses after each expression. Thus Equations [1] can be written

$$x_i'' = \sum_j a_{ij}x_j', \text{ (for } i = 1, 2, 3) \dots\dots\dots [1a]$$

(c) *Resolution of Strain Into Three Principal Strains and a Rotation.* For treatment of the generalized types of elasticity and relaxation to be discussed in the sequel it is convenient to reduce the specification of a strain to a standard and uniquely simple form rather than to use the natural strain components of Equations [1].

It will be shown that any strain specified by Equations [1] is equivalent to, and can be resolved into three simple extensions along three suitably directed mutually perpendicular axes, plus a rigid-body rotation. The three simple extensions of this resolution are called the principal strains. Thus, according to this resolution, there are only three really independent components of strain proper; in addition to these three principal strains, the natural strain components a_{ij} also specify the orientation of the principal axes of strain and a rigid-body rotation. The resolution into principal strains will isolate these three aspects of a general strain given by Equations [1].

To effect this resolution introduce two additional sets of Cartesian co-ordinates with origins also staying on the point of the body which is the origin of the x_1, x_2, x_3 axes. These new co-ordinates are designated y_1, y_2, y_3 and z_1, z_2, z_3 ; their axes differ

from x_1, x_2, x_3 only in orientation, and expressions relating the co-ordinates themselves to x_1, x_2, x_3 are

$$y_i = \sum_j l_{ij}x_j, \text{ (for } i = 1, 2, 3) \dots\dots\dots [2]$$

and

$$z_i = \sum_j m_{ij}x_j, \text{ (for } i = 1, 2, 3) \dots\dots\dots [3]$$

In these relations l_{ij} and m_{ij} (for $i, j = 1, 2, 3$) are, respectively, sets of direction cosines relating two sets of orthogonal axes. They each satisfy the well-known identities for such direction cosines which express the orthogonality of the two sets of axes. These identities are used in subsequent derivations and will be written here for the m_{ij} for reference purposes

$$\sum_j m_{ij}^2 = 1, \text{ (for } i = 1, 2, 3) \dots\dots\dots [4]$$

$$\sum_j m_{ij}m_{kj} = 0, \text{ (for } i \neq k, \text{ and } i, k = 1, 2, 3) \dots\dots\dots [5]$$

It may be noted that Equations [5] comprise only three equations since for these equations i is specified to be not equal to k , and interchange of i and k does not change the terms of the summation. The terms that would result from $i = k$ in Equation [5] are the terms of Equations [4]. From the identities, Equations [4] and [5], the following similar identities can be derived

$$\sum_i m_{ij}^2 = 1, \text{ (for } j = 1, 2, 3) \dots\dots\dots [4a]$$

$$\sum_i m_{ij}m_{ik} = 0, \text{ (for } j \neq k, \text{ and } j, k = 1, 2, 3) \dots\dots\dots [5a]$$

Observations can be made concerning the identities, Equations [4a] and [5a], which are entirely similar to those already made concerning Equations [4] and [5].

Similar identities hold, of course, for the l_{ij} .

In a fashion similar to that already specified for x_1, x_2, x_3 , the single prime (') is used to designate the y - and z -co-ordinates of points in the body before deformation, and the double prime (") after deformation.

For each given strain, the orientation of the y - and z -axes, that is, l_{ij} and m_{ij} , are set as follows: The z_1, z_2, z_3 co-ordinate axes are directed along the three principal strain axes in the deformed body. The points of the body in the neighborhood of the reference point which lie on these principal strain axes after deformation will have lain along three mutually perpendicular straight lines before the deformation took place; these lines, however, generally have different directions than the principal strain axes in the deformed state, because of the rigid-body rotation component of the strain. The y_1, y_2, y_3 axes are directed along the three mutually perpendicular lines thus defined. It is seen then that the orientation of the z -axes, i.e., the m_{ij} , locates the principal axes of strain in the deformed body; and also that the difference in orientation between the z -axes and the y -axes, i.e., the m_{ij} and the l_{ij} , determine the rigid-body rotation part of the strain.

Let the three principal extension "strain ratios" be designated by α_1, α_2 , and α_3 . The strain expressed by Equations [1] is, then, asserted to be equivalent to a strain specified by

$$\left. \begin{aligned} z_1'' &= \alpha_1 y_1' \\ z_2'' &= \alpha_2 y_2' \\ z_3'' &= \alpha_3 y_3' \end{aligned} \right\} \dots\dots\dots [6]$$

or

$$z_i'' = \alpha_i y_i', \text{ (for } i = 1, 2, 3) \dots\dots\dots [6a]$$

The problem at hand is to show that a strain given by Equations [6] can be made to coincide with any given by Equations [1], by

suitable choices of the principal strain ratios α_i and of the direction cosines m_{ij} and l_{ij} ; and further to determine the α_i , m_{ij} , and l_{ij} in terms of the natural strain components a_{ij} of Equations [1]. The balance of this subsection is devoted to this problem.

Use the relations of Equations [2] and [3] to express Equations [6] in terms of the x_1, x_2, x_3 co-ordinates; thus

$$\sum_j m_{ij} x_j'' = \alpha_i \sum_j l_{ij} x_j', \quad (\text{for } i = 1, 2, 3) \dots \dots \dots [7]$$

Now, solve these three equations for x_1'', x_2'', x_3'' , respectively, by multiplying the respective equations first by m_{i1} and adding, then by m_{i2} and adding, and finally by m_{i3} and adding. This process solves the equations for x_1'', x_2'', x_3'' by virtue of the identities, Equation [4a] and [5a]. The coefficients of the x_j' in the resulting equations solved for the x_i'' , by comparison with Equations [1], are seen to be equal to the natural strain components a_{ij} . Thus

$$a_{ij} = \sum_k \alpha_k l_{kj} m_{ki}, \quad (\text{for } i, j = 1, 2, 3) \dots \dots \dots [8]$$

There is a total of nine separate equations in Equations [8], one for each of the nine a_{ij} .

In order to obtain explicit equations for the direction cosines m_{ij} , start by forming the following nine equations from Equations [8], with the help of the identities, Equations [4] and [5].

$$\sum_i a_{ij} m_{ki} = \alpha_k l_{kj}, \quad (\text{for } k, j = 1, 2, 3) \dots \dots \dots [9]$$

In these equations the m_{ij} occur only in the left-hand sides, while the l_{ij} occur only on the right. Now, with the help of the identities of the type of Equations [5] in the direction cosines l_{ij} , the three combinations:

$$\alpha_i \alpha_k \sum_j l_{ij} l_{kj} = 0, \quad (\text{for } i \neq k; i, k = 1, 2, 3) \dots \dots [10]$$

of the right-hand sides of Equations [9] may be formed which are identically zero. There are only three distinct relations, Equations [10] since $i \neq k$, and interchange of i and k does not change the relation. The corresponding left-hand sides of the combinations, Equations [10], of [9], which are equal to zero by Equations [10], comprise three equations in the m_{ij} . These three equations in combination with the identities, Equations [4] and [5], serve to determine the values of all the m_{ij} .

The three equations in the m_{ij} are most conveniently written with the help of the following auxiliary notation: Let

$$A_{ij} = A_{ji} = \sum_k \alpha_k a_{ik} a_{jk}, \quad (\text{for } i, j = 1, 2, 3) \dots \dots \dots [11]$$

and further, let

$$M_{ij} = \sum_k A_{kj} m_{ik}, \quad (\text{for } i, j = 1, 2, 3) \dots \dots \dots [12]$$

Note that, if a_{ij} are considered known, the A_{ij} are known constants, while the M_{ij} are "linear combinations" of the m_{ij} with these constants as coefficients. With this notation, the three equations in the m_{ij} may be written as follows

$$\sum_j m_{ij} M_{kj} = 0, \quad (\text{for } i \neq k; i, k = 1, 2, 3) \dots \dots \dots [13]$$

There are only three equations implied by Equations [13] since i is specified to be not equal to k , and the notation of Equations [11] and [12] implies that interchange of i and k does not alter the expanded or intrinsic form of Equations [13].

Comparison of Equations [13] with the identities, Equations [5], shows directly that the m_{ij} and their linear combinations M_{ij} must be connected by the relations

$$M_{ij} = \lambda_i m_{ij}, \quad (\text{for } i, j = 1, 2, 3) \dots \dots \dots [14]$$

where λ_i ($i = 1, 2, 3$) are constants which will be determined.

If the three of Equations [14] with any specific index i are substituted into the three of Equations [12] with the same index i , the following three linear homogeneous equations in m_{i1}, m_{i2}, m_{i3} are obtained

$$\left. \begin{aligned} (A_{11} - \lambda_1) m_{i1} + A_{21} m_{i2} + A_{31} m_{i3} &= 0 \\ A_{12} m_{i1} + (A_{22} - \lambda_1) m_{i2} + A_{32} m_{i3} &= 0 \\ A_{13} m_{i1} + A_{23} m_{i2} + (A_{33} - \lambda_1) m_{i3} &= 0 \end{aligned} \right\} \dots [15]$$

Furthermore, if these equations are to have solutions for the three unknowns m_{i1}, m_{i2}, m_{i3} which are not all zero—which must be the case because of Equations [4]—then the determinant of the coefficients must vanish. Thus

$$\begin{vmatrix} (A_{11} - \lambda_1) & A_{21} & A_{31} \\ A_{12} & (A_{22} - \lambda_1) & A_{32} \\ A_{13} & A_{23} & (A_{33} - \lambda_1) \end{vmatrix} = 0 \dots \dots [16]$$

The numerical values of m_{i1}, m_{i2}, m_{i3} can be obtained for any root λ_i satisfying Equations [16] by use of any two of Equations [15] and condition, Equation [4]. The expanded form of Equations [16] is a cubic equation which has three roots $\lambda_1, \lambda_2, \lambda_3$. These three roots give the values of m_{i1}, m_{i2}, m_{i3} for $i = 1, 2, 3$, respectively. Therefore all the m_{ij} are determined.

The determination of the l_{ij} can be carried out in an entirely similar manner starting with the relations

$$\sum_j a_{ij} l_{kj} = \alpha_k m_{ki}, \quad (\text{for } i, k = 1, 2, 3) \dots \dots \dots [17]$$

In a fashion entirely similar to that for Equations [9], these relations are obtained from Equations [8], with the help of the identities, Equations [4a], [5a]. The determination of the l_{ij} will not be carried out, since the formulas will not be required in the sequel.

Having shown how to determine the numerical values of the direction cosines m_{ij} and l_{ij} , these values may be considered as known. The values of the principal strain ratios α_i can be determined from Equations [9] by forming the three combinations

$$\alpha_i \sum_j l_{ij}^2 = \alpha_i, \quad (\text{for } k = 1, 2, 3) \dots \dots \dots [18]$$

of the right-hand sides. The resulting formulas for α_i are

$$\alpha_i = \sum_{j,k} m_{ij} l_{ik} a_{jk}, \quad (\text{for } i = 1, 2, 3) \dots \dots \dots [19]$$

Here the summation includes a term for each possible combination of j and k for $j, k = 1, 2, 3$. The summation has therefore nine terms, one for each of the a_{jk} .

The resolution of any strain given by Equations [1] into three principal strains in appropriate orthogonal directions and a rigid-body rotation has been effected. The local state of distortion of the material of a body near a point is completely specified by the α_i and the m_{ij} . The only role played by the direction cosines l_{ij} in specifying the strain is in defining the rigid-body rotation in conjunction with the m_{ij} . The rigid-body rotation does not contribute to the local distortion of the material at all, and it will be seen that for a number of purposes, the l_{ij} are extraneous, that is, they do not enter a problem at all. In fact, problems of this type would not have unique solutions in terms of the natural strain components a_{ij} , since the latter contain the extraneous rigid-body rotation.

Problems involving relaxation phenomena are often of this type, since the effect of relaxation on the rigid-body rotational component of the strains is in a sense indeterminate, that is, it depends upon the boundary conditions under which a partially relaxed body is allowed to become elastically restored to zero strain. These boundary conditions are unspecified and really ex-

traneous in problems in which the body is never allowed actually to restore itself to zero strain, for example, in a case of steady-state flow.

The general validity of this resolution is therefore of considerable theoretical significance in treating problems of flow in materials exhibiting relaxation properties. This is the main reason for treating the resolution in the completely general manner of the subsection, i.e., in terms of completely general three-dimensional strain. In the present work actual numerical use of the resolution is made in less general special cases.

(d) *Rate of Change of Strain Components Due to Flow.* The treatment of problems of flow is facilitated by relating the strains at the points of the body to the distortion of the body as a whole through differential relations for the rate of change of the strain components due to flow velocities. Some of these relations will be derived in their general three-dimensional form both in terms of the natural strain components and in terms of the principal strain components.

The unstrained co-ordinates x_1', x_2', x_3' of a point will not change as a direct result of a flow process;⁶ therefore in the present derivations these co-ordinates are considered independent of time. Differentiation of Equations [1] with respect to time gives the relations

$$\frac{\partial x_i''}{\partial t} = \sum_j \frac{da_{ij}}{dt} x_j', \quad (\text{for } i = 1, 2, 3) \dots [20]$$

The Eulerian velocity components along the x_1, x_2, x_3 co-ordinate directions are denoted by v_1, v_2, v_3 . The time rate of change of the displaced co-ordinates x_1'', x_2'', x_3'' of the particles of the body in the neighborhood on the reference point are therefore directly

$$\frac{\partial x_i''}{\partial t} = \sum_j x_j'' \frac{\partial v_i}{\partial x_j}, \quad (\text{for } i = 1, 2, 3) \dots [21]$$

In these Equations [21] the factors x_j'' in the terms of the right-hand side may be expressed in terms of x_j' by use of the relations, Equations [1]. The resulting right-hand sides of Equations [21] therefore become linear expressions in the x_j' and direct comparison of these coefficients with those in Equations [20] gives the expressions for the rates of change of the natural strain components due to flow. These expressions are

$$\frac{da_{ij}}{dt} = \sum_k a_{kj} \frac{\partial v_i}{\partial x_k}, \quad (\text{for } i, j = 1, 2, 3) \dots [22]$$

The principal strain ratios are given by Equations [19]. Their time derivatives are, accordingly, given by

$$\frac{d\alpha_i}{dt} = \sum_{j,k} \left(m_{ij} l_{ik} \frac{da_{jk}}{dt} + a_{jk} l_{ik} \frac{dm_{ij}}{dt} + a_{jk} m_{ij} \frac{dl_{ik}}{dt} \right), \quad (\text{for } i = 1, 2, 3) \dots [23]$$

The second and third terms in the summation of this equation vanish. This can be shown as follows: Sum the third terms with respect to j , and use Equations [9] to eliminate $a_{jk} m_{ij}$; the total contribution of this third term is thus seen to be

$$\sum_k \alpha_i l_{ik} \frac{dl_{ik}}{dt} = \frac{\alpha_i}{2} \frac{d}{dt} (\sum_k l_{ik}^2) = 0$$

⁶ The unstrained co-ordinates might be considered to change as an "indirect" result of a flow due to a relaxation phenomenon. For the present, however, only the direct results of flow are being considered. It will be seen later that this delicate question is sidestepped by use of the resolution into principal strains. In fact, this is the really fundamental reason for introducing this resolution.

Similarly, sum the second terms with respect to k and use Equations [17]; the contribution of this term is

$$\sum_j \alpha_i m_{ij} \frac{dm_{ij}}{dt} = \frac{\alpha_i}{2} \frac{d}{dt} (\sum_j m_{ij}^2) = 0$$

Thus only the first term in the summation on the right side of Equation [23] remains. Substitute Equations [22] into this first term and use Equations [17] to eliminate $a_{jk} l_{ik}$ factors; the resulting form of Equation [23] is

$$\frac{d\alpha_i}{dt} = \alpha_i \sum_{j,k} m_{ij} m_{ik} \frac{\partial v_j}{\partial x_k}, \quad (\text{for } i = 1, 2, 3) \dots [24]$$

It remains to determine the expressions for the rates of change of the direction cosines. These expressions will be derived only for the two-dimensional case in the next section.

(e) *Case of Two-Dimensional Flow and Strain.* The definition of two-dimensional strain in the x_1, x_2 -plane is that the deflection vector of all particles lies in the x_1, x_2 -plane, and all particles with the same x_1, x_2 -co-ordinates have the same deflection vector.

Referring to Equations [1], the condition on the natural strain components a_{ij} for two-dimensional strain in the x_1, x_2 -plane are

$$a_{13} = a_{31} = a_{23} = a_{32} = 0; \quad a_{33} = 1 \dots [25]$$

The corresponding two-dimensional flow is

$$\frac{\partial v_1}{\partial x_3} = \frac{\partial v_2}{\partial x_3} = v_3 = 0 \dots [26]$$

The relations for principal strains, principal strain directions, and rates of change of these due to flow are to be derived for this case of two-dimensional strain and flow.

The A_{ij} of Equations [11] for two-dimensional strain are

$$\left. \begin{aligned} A_{13} = A_{31} = A_{23} = A_{32} = 0; \quad A_{33} = 1 \\ A_{11} = a_{11}^2 + a_{12}^2 \\ A_{22} = a_{21}^2 + a_{22}^2 \\ A_{12} = A_{21} = a_{11}a_{21} + a_{12}a_{22} \end{aligned} \right\} \dots [27]$$

Thus Equations [15] for the direction cosines m_{ij} become

$$\left. \begin{aligned} (a_{11}^2 + a_{12}^2 - \lambda_i) m_{i1} + (a_{11}a_{21} + a_{12}a_{22}) m_{i2} &= 0 \\ (a_{11}a_{21} + a_{12}a_{22}) m_{i1} + (a_{21}^2 + a_{22}^2 - \lambda_i) m_{i2} &= 0 \\ (1 - \lambda_i) m_{i3} &= 0 \end{aligned} \right\} \dots [28]$$

The determinantal equation for λ_i is

$$(1 - \lambda_i)[\lambda_i^2 - (a_{11}^2 + a_{12}^2 + a_{21}^2 + a_{22}^2)\lambda_i + (a_{11}a_{22} - a_{12}a_{21})^2] = 0 \dots [29]$$

The root $\lambda_3 = 1$ is determined by the first factor in Equation [29]; substitution of this root into the first two of Equations [28] gives, with the help of Equations [4] and [4a]

$$m_{13} = m_{31} = m_{23} = m_{32} = 0; \quad m_{33} = 1 \dots [30]$$

With the values of Equations [30], the remaining direction cosines may be expressed as

$$m_{11} = m_{22} = \cos \theta; \quad m_{12} = -m_{21} = \sin \theta \dots [31]$$

where θ is the angle between the z_1 (principal) axis and the x_1 -axis. The meaning of Equations [30] is of course that the axes z_1 and z_2 lie in the x_1, x_2 -plane. The relative positions of these axes are shown in Fig. 1.

In order to determine the value of the angle θ , first determine the roots of the quadratic factor of Equation [29]. These roots are

$$\left. \begin{aligned} \lambda_1 &= \frac{1}{2} \left[(a_{11}^2 + a_{12}^2 + a_{21}^2 + a_{22}^2) \right. \\ &\quad \left. + \sqrt{(a_{11}^2 + a_{12}^2 - a_{21}^2 - a_{22}^2)^2 + 4(a_{11}a_{21} + a_{12}a_{22})^2} \right] \\ \lambda_2 &= \frac{1}{2} \left[(a_{11}^2 + a_{12}^2 + a_{21}^2 + a_{22}^2) \right. \\ &\quad \left. - \sqrt{(a_{11}^2 + a_{12}^2 - a_{21}^2 - a_{22}^2)^2 + 4(a_{11}a_{21} + a_{12}a_{22})^2} \right] \end{aligned} \right\} \quad [32]$$

Substitution of either of these values with Equations [31] into

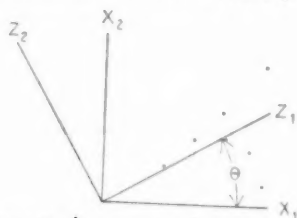


FIG. 1 POSITION OF PRINCIPAL STRAIN AXES z_1, z_2 FOR TWO-DIMENSIONAL STRAIN IN x_1, x_2 -PLANE

either of the first two of Equations [28] will determine the angle θ . The result is most easily expressed as

$$\tan 2\theta = \frac{2(a_{11}a_{21} + a_{12}a_{22})}{a_{11}^2 + a_{12}^2 - a_{21}^2 - a_{22}^2} \quad [33]$$

An expression for the rate of change of the angle θ is obtained by direct differentiation of Equation [33] with respect to time. This expression is

$$\begin{aligned} 2(\sec^2 2\theta) \times \frac{d\theta}{dt} &= \frac{2(a_{21} - a_{11} \tan 2\theta) da_{11}/(dt) + 2(a_{22} - a_{12} \tan 2\theta) da_{12}/(dt)}{a_{11}^2 + a_{12}^2 - a_{21}^2 - a_{22}^2} \\ &\quad + \frac{2(a_{11} + a_{21} \tan 2\theta) da_{21}/(dt) + 2(a_{12} + a_{22} \tan 2\theta) da_{22}/(dt)}{a_{11}^2 + a_{12}^2 - a_{21}^2 - a_{22}^2} \end{aligned} \quad [34]$$

Expressions [22] for the rate of change of the natural strain components due to flow become, for the two-dimensional case

$$\left. \begin{aligned} \frac{da_{11}}{dt} &= a_{11} \frac{\partial v_1}{\partial x_1} + a_{21} \frac{\partial v_1}{\partial x_2}, \quad \frac{da_{12}}{dt} = a_{12} \frac{\partial v_1}{\partial x_1} + a_{22} \frac{\partial v_1}{\partial x_2} \\ \frac{da_{21}}{dt} &= a_{11} \frac{\partial v_2}{\partial x_1} + a_{21} \frac{\partial v_2}{\partial x_2}, \quad \frac{da_{22}}{dt} = a_{12} \frac{\partial v_2}{\partial x_1} + a_{22} \frac{\partial v_2}{\partial x_2} \end{aligned} \right\} \quad [35]$$

Substitution of these relations into Equation [34] gives

$$\begin{aligned} 2(\sec^2 2\theta) \times \frac{d\theta}{dt} &= \left[\frac{-2(a_{11}^2 + a_{12}^2) \tan 2\theta}{a_{11}^2 + a_{12}^2 - a_{21}^2 - a_{22}^2} + \tan 2\theta \right] \frac{\partial v_1}{\partial x_1} \\ &\quad + \left[\frac{2(a_{21}^2 + a_{22}^2)}{a_{11}^2 + a_{12}^2 - a_{21}^2 - a_{22}^2} - \tan^2 2\theta \right] \frac{\partial v_1}{\partial x_2} \\ &\quad + \left[\frac{2(a_{11}^2 + a_{12}^2)}{a_{11}^2 + a_{12}^2 - a_{21}^2 - a_{22}^2} + \tan^2 2\theta \right] \frac{\partial v_2}{\partial x_1} \\ &\quad + \left[\frac{2(a_{21}^2 + a_{22}^2) \tan 2\theta}{a_{11}^2 + a_{12}^2 - a_{21}^2 - a_{22}^2} + \tan 2\theta \right] \frac{\partial v_2}{\partial x_2} \end{aligned} \quad [36]$$

The set of Equations [8] specialized for the two-dimensional case with the help of Equations [30] and [31] give

$$\left. \begin{aligned} a_{11} &= \alpha_1 l_{11} \cos \theta - \alpha_2 l_{21} \sin \theta \\ a_{12} &= \alpha_1 l_{12} \cos \theta - \alpha_2 l_{22} \sin \theta \\ a_{21} &= \alpha_1 l_{11} \sin \theta + \alpha_2 l_{21} \cos \theta \\ a_{22} &= \alpha_1 l_{12} \sin \theta + \alpha_2 l_{22} \cos \theta \end{aligned} \right\} \quad [37]$$

Further, reasoning similar to that used to derive Equations [31] shows that l_{11}, l_{12}, l_{21} , and l_{22} in the two-dimensional case may be expressed as

$$l_{11} = l_{22} = \cos \theta; \quad l_{12} = -l_{21} = \sin \theta \quad [38]$$

From Equations [37] and [38] the following relations may be obtained which are independent of the angle θ of Equations [38]

$$\left. \begin{aligned} a_{11}^2 + a_{12}^2 &= \alpha_1^2 \cos^2 \theta + \alpha_2^2 \sin^2 \theta \\ a_{21}^2 + a_{22}^2 &= \alpha_1^2 \sin^2 \theta + \alpha_2^2 \cos^2 \theta \end{aligned} \right\} \quad [39]$$

from which, finally

$$\left. \begin{aligned} \frac{2(a_{11}^2 + a_{12}^2)}{a_{11}^2 + a_{12}^2 - a_{21}^2 - a_{22}^2} &= \frac{\alpha_1^2 + \alpha_2^2}{\alpha_1^2 - \alpha_2^2} \times \sec 2\theta + 1 \\ \frac{2(a_{21}^2 + a_{22}^2)}{a_{11}^2 + a_{12}^2 - a_{21}^2 - a_{22}^2} &= \frac{\alpha_1^2 + \alpha_2^2}{\alpha_1^2 - \alpha_2^2} \times \sec 2\theta - 1 \end{aligned} \right\} \quad [40]$$

Substitution of the relations, Equations [40], into [36] yields the final expression for the rate of change of the principal strain directions with flow in the two-dimensional case. This final expression is

$$\begin{aligned} 2 \frac{d\theta}{dt} &= \left(\frac{\alpha_1^2 + \alpha_2^2}{\alpha_1^2 - \alpha_2^2} \times \sin 2\theta \right) \left(\frac{\partial v_2}{\partial x_1} - \frac{\partial v_1}{\partial x_2} \right) \\ &\quad + \left(\frac{\alpha_1^2 + \alpha_2^2}{\alpha_1^2 - \alpha_2^2} \times \cos 2\theta \right) \left(\frac{\partial v_2}{\partial x_1} + \frac{\partial v_1}{\partial x_2} \right) + \left(\frac{\partial v_2}{\partial x_1} - \frac{\partial v_1}{\partial x_2} \right) \end{aligned} \quad [41]$$

The important characteristic of this expression is that it involves only the quantities $\alpha_1, \alpha_2, \theta$ which describe the "strained" condition at a point; quantities relating back to the unstrained condition, that is, the l_{ij} or angle θ_i of Equation [38], do not enter the expression at all. Thus the question of whether the unstrained condition at a point of a body is changing due, for example, to a relaxation process, has been sidestepped. Previous reference has been made to this result.⁵ In this connection it should also be noted that Equations [24] for the rate of change of the principal strain ratios is also independent of the quantities l_{ij} .

(f) *Case of Steady-State Simple Shear Flow.* A particularly simple and important case of two-dimensional strain and flow is the case of a steady-state simple shear flow. Steady flows of materials through tubes and channels are often of this character. The relations of the preceding subsection can be further specialized for this case.

The flow considered is a flow in the x_1 -direction for which

$$\frac{\partial v_1}{\partial x_2} = s = \text{const}; \quad v_2 = v_3 = \frac{\partial v_1}{\partial x_1} = 0 \quad [42]$$

A flow of this character results in two-dimensional strain in the x_1, x_2 -plane, for which $\alpha_3 = 1$. With Equations [31] and [42] the relations, Equations [24] for rate of change of the principal strain ratios become

$$\left. \begin{aligned} \frac{d\alpha_1}{dt} &= \alpha_1 s \sin \theta \cos \theta = \frac{1}{2} \alpha_1 s \sin 2\theta \\ \frac{d\alpha_2}{dt} &= -\alpha_2 s \sin \theta \cos \theta = -\frac{1}{2} \alpha_2 s \sin 2\theta \\ \frac{d\alpha_3}{dt} &= 0 \end{aligned} \right\} \quad [43]$$

For the rate of change of the principal strain directions, Equation [41] gives

$$\frac{d\theta}{dt} = \frac{s}{2} \left(\frac{\alpha_1^2 + \alpha_2^2}{\alpha_1^2 - \alpha_2^2} \cos 2\theta - 1 \right) \dots \dots \dots [44]$$

3 PHENOMENOLOGICAL DESCRIPTION OF LARGE-STRAIN ELASTICITY WITH STRESS RELAXATION

(a) *Axiomatic Basis of Description.* The phenomenological description of the stress-strain properties of materials, exhibiting large-strain elasticity with stress relaxation, is developed from the following axiomatic statements:

1 The state of stress is dependent solely upon the state of "elastic" strain.

2 The time rate of change of elastic strain is equal to the time rate of "geometric" strain plus a spontaneous time rate of change which depends only upon the current elastic strain, and corresponds to the relaxation process.

The second statement defines the new concept of elastic strain which the first requires. This axiomatic foundation can be restated at greater length, and in a manner which emphasizes the meanings of the terms elastic and geometric strain.

Geometric strain has been treated in Section 2; it specifies the relative movements of the individual particles of a material. The time rates of change of the principal (geometric) strain ratios due to flow of a material are given by Equations [24], and of the principal (geometric) strain directions, for the two-dimensional case, by Equation [41]. Elastic strain is specified in the same terms as geometric strain, but differs in that its time rate of change is equal to the rate of change of geometric strain plus an additional term which describes a spontaneous relaxation of elastic strain. Because of this additional relaxation term, elastic strain does not specify relative movements of the individual particles of a material, though it is related to the history of these movements in a definite way. It is asserted axiomatically that the state of stress in the material is a function only of the elastic strain thus defined, and that the relaxation rate of elastic strain depends only upon the elastic strain itself.

The distinction between geometric strain and elastic strain may be illustrated further by stating how each might, in theory at least, be observed. The state of geometric strain would be observed by marking a number of particles of the material and noting how their relative positions change. The state of elastic strain might be observed by cutting a small cubical element out of a material under flow or stress, and, removing it from its environment, allowing it immediately to assume its natural zero-stress shape. The geometric strain which would have to be imposed to bring the element back to its cubical shape and size when cut would be the elastic strain in the material under the flow or stress condition, or would be closely related to it.⁸

The materials treated will further be assumed to be incompressible, and to have a property of isotropy generalized for the case of large elastic strain. This generalized property of isotropy is defined as follows:

1 When a material is in an elastically unstrained state, its mechanical behavior is identical in all directions in the material.

2 When a material is in an elastically strained state, its mechanical behavior in any direction depends only upon the relation of this direction to the principal strain directions, and upon the principal elastic strains themselves.

It may be noted that the difference between this generalized isotropy and the classical isotropy is that isotropic behavior is not

⁸ This reservation is made for a reason which will be referred to in the sequel.

postulated for the superposition of one elastic strain upon another. The analytical difference between large and small strains is of this character; superposition of large strains does not follow a simple addition law, while superposition of small strains does.

A numerical determination of the stress corresponding to any specified deformation process in a material requires mathematical expressions for the spontaneous time rate of change of elastic strain due to the relaxation process, and a mathematical relation between the state of elastic strain and the state of stress. The formulation of these mathematical expressions is the principal aim of the theory.

(b) *Elastic Strain and Relaxation Relations.* In accordance with the method of specification of large strain developed in Section 2, the state of elastic strain may be specified by the three principal strain ratios $\alpha_1, \alpha_2, \alpha_3$, and the principal strain direction cosines m_i , or, in the two-dimensional case, the angle θ . Henceforth this notation will be used without alteration to specify elastic strain. Special mention will be made if geometric strain is referred to, and it is different from elastic strain.

The time rate of change of the principal elastic-strain ratios is given by

$$\frac{d\alpha_1}{dt} = \left(\frac{d\alpha_1}{dt} \right)_{\text{geom}} + \left(\frac{d\alpha_1}{dt} \right)_{\text{relax}} \dots \dots \dots [45]$$

with two similar equations for α_2 and α_3 . The terms $(d\alpha_i/dt)_{\text{geom}}$ are the rates of change of the elastic strain corresponding to change of geometric strain; in a flow these terms are given by Equation [24], in which α_i on the right side is the elastic-strain ratio. The terms $(d\alpha_i/dt)_{\text{relax}}$ describe the relaxation property of the material, and, as properties of the material, these terms must be characteristic functions of the elastic-strain state only. As a result of the assumed property of isotropy these terms must be functions only of the principal strain ratios $\alpha_1, \alpha_2, \alpha_3$, and are designated by R_1, R_2, R_3 ; thus

$$\left. \begin{aligned} \left(\frac{d\alpha_1}{dt} \right)_{\text{relax}} &= R_1(\alpha_1, \alpha_2, \alpha_3) \\ \left(\frac{d\alpha_2}{dt} \right)_{\text{relax}} &= R_2(\alpha_1, \alpha_2, \alpha_3) \\ \left(\frac{d\alpha_3}{dt} \right)_{\text{relax}} &= R_3(\alpha_1, \alpha_2, \alpha_3) \end{aligned} \right\} \dots \dots \dots [46]$$

A further consequence of the property of isotropy is that R_1, R_2, R_3 must be obtainable from each other by interchanging the variables $\alpha_1, \alpha_2, \alpha_3$; thus there is actually only a single relaxation function to be determined.

It is also a consequence of the property of isotropy that the directions of principal elastic strain are not changed by relaxation. Equation [41] is therefore valid for the change of elastic-strain direction in two dimensions provided that α_1 and α_2 on the right-hand side are elastic strains.

A set of geometric-strain ratios which correspond to zero volume change in a material must satisfy the relation

$$\alpha_1 \times \alpha_2 \times \alpha_3 = 1 \dots \dots \dots [47]$$

The rates of change of geometric strain for incompressible materials must therefore satisfy the relation obtained by setting the time derivative of the left side of Equation [47] to zero

$$\frac{1}{\alpha_1} \left(\frac{d\alpha_1}{dt} \right)_{\text{geom}} + \frac{1}{\alpha_2} \left(\frac{d\alpha_2}{dt} \right)_{\text{geom}} + \frac{1}{\alpha_3} \left(\frac{d\alpha_3}{dt} \right)_{\text{geom}} = 0 \dots [48]$$

However, there appears to be no fundamental reason that the

rates of change of elastic strain, $R_i = (d\alpha_i/dt)_{\text{relax}}$, must also satisfy Relation [48]. If they do not for a particular material, then, even though the material be incompressible, the Relation [47] need not hold for the elastic strain. This is actually the case for the simple molecular representation analyzed in Section 4, and is the reason for the reservation referred to previously.⁶

(c) *Stresses and Strain-Energy Function.* For rapidly applied geometric strain it is evident from Equation [45] that, since the terms $(d\alpha_i/dt)_{\text{relax}} = R_i$ are functions of $\alpha_1, \alpha_2, \alpha_3$, the relative effect of relaxation upon the elastic strain becomes small, and the resulting elastic strain is nearly equal to the applied geometric strain. In the limit of very rapidly applied geometric strain the elastic and geometric strains become identical. This fact has important theoretical consequences.

Together with the axiomatic assumption that the stress depends only upon elastic strain the possibility of coincidence of elastic and geometric strain establishes the existence of a strain-energy function ψ . This function is equal to the recoverable strain energy per unit volume stored up as a result of the action of the elastic stresses. As a result of the assumed property of isotropy, ψ depends only upon the principal elastic-strain ratios in such a way that its values are unaltered by any interchange of $\alpha_1, \alpha_2, \alpha_3$.

A further result of the possibility of coincidence of elastic and geometric strain is that the principle of virtual work can be used to obtain expressions for the stresses in terms of elastic strain from the strain-energy function. In such application of the principle of virtual work, elastic-strain increments are treated as geometric-strain increments.

It may be recalled that any stress condition at a point is equivalent to three principal tension (or compression) stresses, to be denoted by $\sigma_1, \sigma_2, \sigma_3$, acting across planes normal to the three principal stress directions. It is a consequence of the property of isotropy that the principal elastic-strain directions and the principal stress directions coincide. The zero stress condition $\sigma_1 = \sigma_2 = \sigma_3 = 0$ will be associated with the elastically unstrained condition $\alpha_1 = \alpha_2 = \alpha_3 = 1$.

The relation between stresses and strains can be derived from the strain-energy function by considering the virtual work done on an elemental volume of material during a small virtual deformation specified by elastic strain changes $\delta\alpha_1, \delta\alpha_2, \delta\alpha_3$. As remarked before, elastic-strain changes can be identified with geometric-strain changes for the purpose of applying the principle of virtual work.

Consider an element of material in the shape of a rectangular parallelepiped with sides normal to the principal strain directions. The lengths of the sides of the parallelepiped must remain proportional to the elastic-strain ratios in any virtual deformation, and can therefore be represented by $\alpha_1 L_1, \alpha_2 L_2, \alpha_3 L_3$, where L_1, L_2, L_3 are constant lengths.

On the assumption of isotropy, as defined previously, the stress condition is one with principal stresses $\sigma_1, \sigma_2, \sigma_3$ acting on the faces of the parallelepiped, which have been placed normal to the principal strain directions. The force on each face of the parallelepiped, therefore, acts normal to the face. The magnitudes of these forces, designated by F_1, F_2, F_3 , are equal to the products of the stresses and areas of the respective sides, and are

$$\left. \begin{aligned} F_1 &= \sigma_1 \alpha_1 L_2 L_3 \\ F_2 &= \sigma_2 \alpha_2 L_1 L_3 \\ F_3 &= \sigma_3 \alpha_3 L_1 L_2 \end{aligned} \right\} \dots \dots \dots [49]$$

The parallelepiped and these forces are indicated in the diagram of Fig. 2. The work per unit volume δW done by the forces F_1, F_2, F_3 during a virtual displacement corresponding to elastic- (and geometric-) strain changes $\delta\alpha_1, \delta\alpha_2, \delta\alpha_3$ is

$$\delta W = \frac{F_1 L_1 \delta\alpha_1 + F_2 L_2 \delta\alpha_2 + F_3 L_3 \delta\alpha_3}{\alpha_1 \alpha_2 \alpha_3 L_1 L_2 L_3} = \frac{\sigma_1 \delta\alpha_1}{\alpha_1} + \frac{\sigma_2 \delta\alpha_2}{\alpha_2} + \frac{\sigma_3 \delta\alpha_3}{\alpha_3} \dots \dots [50]$$

The second form of this expression follows from the first by virtue of Equations [49]. This work is equal to the change $\delta\psi$ in the

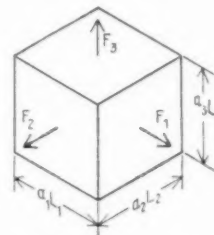


FIG. 2 FORCES ON AN ELEMENT OF VOLUME

value of the strain-energy function corresponding to the elastic-strain changes $\delta\alpha_1, \delta\alpha_2, \delta\alpha_3$. Thus

$$\delta W = \delta\psi = \frac{\partial\psi}{\partial\alpha_1} \delta\alpha_1 + \frac{\partial\psi}{\partial\alpha_2} \delta\alpha_2 + \frac{\partial\psi}{\partial\alpha_3} \delta\alpha_3 \dots \dots [51]$$

Both Equations [50] and [51] are valid for any arbitrary values of $\delta\alpha_1, \delta\alpha_2, \delta\alpha_3$; accordingly, the coefficients of each corresponding differential in the two expressions must be equal. Thus the required stress-strain relations are

$$\left. \begin{aligned} \sigma_1 &= \alpha_1 \frac{\partial\psi}{\partial\alpha_1} \\ \sigma_2 &= \alpha_2 \frac{\partial\psi}{\partial\alpha_2} \\ \sigma_3 &= \alpha_3 \frac{\partial\psi}{\partial\alpha_3} \end{aligned} \right\} \dots \dots \dots [52]$$

In the case of an incompressible material the virtual displacements must be restricted to those which correspond to no volume change, that is, to those for which

$$\frac{\delta\alpha_1}{\alpha_1} + \frac{\delta\alpha_2}{\alpha_2} + \frac{\delta\alpha_3}{\alpha_3} = 0 \dots \dots \dots [53]$$

It may be noted that in this case a hydrostatic pressure (tension) component

$$\sigma_1 = \sigma_2 = \sigma_3 = p$$

will not cause any virtual work by Equation [50] and correspondingly, may exist independent of the virtual-work expressions, Equation [53]. For incompressible materials the stress-strain relation which replaces Equations [52] is

$$\left. \begin{aligned} \sigma_1 &= \alpha_1 \frac{\partial\psi}{\partial\alpha_1} + p \\ \sigma_2 &= \alpha_2 \frac{\partial\psi}{\partial\alpha_2} + p \\ \sigma_3 &= \alpha_3 \frac{\partial\psi}{\partial\alpha_3} + p \end{aligned} \right\} \dots \dots \dots [54]$$

where p is an arbitrary hydrostatic tension which must be determined by external circumstances.

(d) *Recapitulation.* A quantitative and mathematical description of the stress-strain behavior of a material exhibiting large-strain elasticity and stress relaxation has been developed from a purely phenomenological viewpoint on the basis of two fundamental and axiomatic assumptions. The materials have further been assumed to be incompressible, and to possess a generalized property of isotropy.

The description is made in terms of a strain-energy function ψ , and relaxation functions R_1 , R_2 , and R_3 ; each of these functions is a characteristic function of the principal elastic strains α_1 , α_2 , α_3 . The description is quantitatively complete when the values of these functions are known. It may be remarked that, as a result of the assumed isotropy, when any one of R_1 , R_2 , or R_3 is given, the others follow by interchange of the arguments α_1 , α_2 , α_3 ; thus there are in reality only two independent functions to be determined, ψ and (say) R_1 .

If applications are limited to the case of infinitesimal strains, that is, α_1 , α_2 , α_3 , differing only by infinitesimals from unity, then the functions ψ and R might be replaced by the first terms of their Taylor series expansions about the point $\alpha_1 = \alpha_2 = \alpha_3 = 1$. This approximation leads to the classical Maxwell liquid theory.

However, when large deformations occur the behavior becomes more complex, and the abbreviated Taylor expansions are not adequate. It is necessary to use the complete functions or something closely resembling them. The functions ψ and R are properties of a material, and express the characteristics of internal structure which govern stress-strain behavior. They must be derived, therefore, either from a consideration of the internal structure of the materials or from rather extensive empirical observations or both.

4 A MOLECULAR REPRESENTATION OF MATERIALS EXHIBITING LARGE-STRAIN ELASTICITY AND RELAXATION

(a) *Purpose of Molecular Representation.* Plausible forms for the strain-energy and relaxation relations are to be obtained from an analysis of the behavior of a mechanical representation of the molecular structure of rubberlike materials. The large deformation elasticity, which is characteristic of rubberlike materials, is attributed to the bulk properties of highly elongated chainlike molecules of which these materials generally consist. The molecular representation proposed here is based upon the general descriptions given by several authors⁷ of these molecules.

This molecular representation is introduced primarily to illustrate the structural significance of the phenomenological concepts of elastic strain and relaxation which have been introduced in the preceding section. Detailed characteristics are not expected to be quantitatively realistic, but have been chosen to a large extent to lead to simple and exact mathematical solutions for mechanical behavior. However, the analysis of this model from an internal structural point of view does implement the phenomenological description already given, and the resulting forms for the strain-energy and relaxation functions serve as starting points for the interpretation of empirical observations, and can eventually be refined therefrom.

(b) *Description of Molecular Representation.* The molecular structure of the materials is represented by a matrix composed of a great number of structurally identical, highly elongated, chainlike molecules which behave in bulk as though they were embedded in an incompressible liquidlike medium. Each of the molecules assumes a more or less twisted and folded configuration, and is intertwined with numerous neighboring molecules. The whole assembly of molecules is in a state of continuous thermal agitation as a result of which the individual molecules have a certain

mobility or freedom of movement. This mobility is, however, also restrained in some degree by the interlaced configuration of the molecules.

Although, for purposes of visualization, the concept of a surrounding liquidlike medium in which the elongated molecules are embedded will be retained, the actual existence of a physical medium is not necessarily implied. The use of the concept may be considered merely as a graphic description of certain bulk properties of the matrix of intertwined molecules. The specific properties attributed to this surrounding "medium" are incompressibility and lack of resistance to change of shape.

It is assumed that at any particular instant the thermal motion of each individual molecule can be considered as a vibration about a defined position of equilibrium. The only effect of the thermal motions upon macroscopic mechanical properties is considered to be their statistical effect upon the mobility of the equilibrium positions of the molecules. All effects of the equilibrium configurations of the molecules are assumed to be represented by the lengths r between the two end points of each one, and by the directions of these lengths. The assumed form of this representation is as follows: The internal force within any molecule as well as its force interaction with its surroundings is equivalent to a simple tension force f tending to draw its end points together. The force f is proportional to the length r , thus

$$f = Kr \dots \dots \dots [55]$$

where K is a characteristic proportionality constant or stiffness with the dimensions (force) ÷ (length). The total effect of each molecular configuration upon the potential energy of the material is just the internal molecular potential energy of the force, Equation [55]. Thus the total potential energy of the material arising from molecular configurations is the sum of the contributions dW of each individual molecule

$$dW = \int f r dr = \frac{1}{2} Kr^2 \dots \dots \dots [56]$$

In any process involving only mechanical deformation the potential energy can be identified with the strain energy. Thus in such processes the sum of the contributions, Equation [56], for all molecules within a small volume of the material divided by the volume gives the value of the strain-energy function ψ for the material within the volume.

When the material is deformed, the equilibrium configurations of the molecules are assumed to change in accordance with the deformation as though their end points floated freely with the corresponding motion of the surrounding liquidlike medium. The molecular configuration may also change spontaneously with time under the sustained action of the forces, Equation [55], and also as a result of the random thermal agitation. The balance of these changes of molecular configuration, which give rise to the bulk properties of the material, are treated by the methods of statistical mechanics.

(c) *Statistical Mechanics of Molecular Representation.* The properties and macroscopic state of a material depend only upon certain statistical averages of the parameters which describe the detailed configurations of the individual molecules. In the case of the molecular representation now being considered these statistical averages involve only the magnitudes and directions of the effective molecular lengths, which have been designated by the symbol r .

For purposes of description it is convenient to think of these lengths and directions as being represented by vectors extending out from the origin of co-ordinates in a "phase space." The directions and lengths of the molecules are thus represented by the same vectors in the phase space as they would be represented

⁷ See, for example: J. Frenkel, *Kinetic Theory of Liquids*, Oxford, England, 1946, especially Chapter 8.

by in their actual physical positions; in the phase space, however, these vectors all issue out from the origin of co-ordinates. Cartesian co-ordinates in the phase space are designated by x, y, z . The molecular length vectors are, accordingly, represented by the points in the phase space at the outer ends of the vectors, or by the x, y, z -co-ordinates of these points. Thus in phase space

$$r^2 = x^2 + y^2 + z^2 \dots \dots \dots [57]$$

A statistical description is required of the configurations of the molecules within an element of volume of the material which is small enough that the macroscopic state, i.e., the stress, strain and temperature, may be considered constant throughout, but which is large enough to contain a very great number of molecules. In the phase space the end points of the vectors representing the individual molecular configurations will form a "cloud," the density of which describes the distribution of configurations over the various possibilities. Quantitative description of this cloud of points in the phase space is afforded by a "distribution function" ρ , which is a function of the phase-space co-ordinates x, y, z , with values such that the fraction of the molecules which have phase-space configuration vectors in the range

$$\left. \begin{aligned} x_0 < x < x_0 + \Delta x \\ y_0 < y < y_0 + \Delta y \\ z_0 < z < z_0 + \Delta z \end{aligned} \right\} \dots \dots \dots [58]$$

is given by

$$\rho(x_0, y_0, z_0) \Delta x \Delta y \Delta z \dots \dots \dots [59]$$

The magnitudes of the increments $\Delta x, \Delta y, \Delta z$ in Expressions [58] and [59] are understood to be large enough to include a representative number of vector end points, yet small enough that ρ is sensibly constant over the range of Expression [58]. Because of the immense number of molecules in even a very small macroscopic element of material, this requirement should not cause any theoretical difficulties.

An immediate consequence of the definition of the distribution function ρ is that it must at all times satisfy the relation

$$\int_{-\infty}^{\infty} \int_{-\infty}^{\infty} \int_{-\infty}^{\infty} \rho \, dx \, dy \, dz = 1 \dots \dots \dots [60]$$

It must also be remarked that, since the statistics of the molecular configurations may change with time, ρ must also be considered a function of time t as well as the phase-space co-ordinates x, y, z .

Let N denote the number of molecules per unit volume of the material; this number is a constant for any particular incompressible material. On the basis of the assumptions which have been made the value of the strain-energy function is, from Equations [56] and [57]

$$\psi = \frac{NK}{2} \int_{-\infty}^{\infty} \int_{-\infty}^{\infty} \int_{-\infty}^{\infty} (x^2 + y^2 + z^2) \rho \, dx \, dy \, dz \dots [61]$$

The conditions which govern the variation of the distribution function ρ are now to be set up. Thermal agitation itself causes a random change in the directions and magnitudes of the effective molecular lengths, that is, in their x, y, z -phase space components. The over-all thermal-agitation effect on the distribution function is, therefore, represented by the diffusion equation

$$\left(\frac{\partial \rho}{\partial t} \right)_{\text{thermal agitation}} = D \left(\frac{\partial^2 \rho}{\partial x^2} + \frac{\partial^2 \rho}{\partial y^2} + \frac{\partial^2 \rho}{\partial z^2} \right) \dots \dots [62]$$

in which the constant D is a "diffusion coefficient," and measures the balance between thermal-agitation forces and molecular-restraint forces due to intertwining of the molecules. The physi-

cal dimensions of D are (length)² ÷ (time). For purposes of this simplified theory D is considered a constant.

The effect of the internal molecular tension force, Equation [55], acting against the restraint of the molecules due to intertwining, may be represented in the phase space by a central attracting force acting upon the cloud of vector points against a viscous resistance to movement. The central force will cause an inward radial drift of the vector end points with a velocity v_r proportional to the force; thus

$$v_r = -\mu f = -\mu K r = -\mu K \sqrt{x^2 + y^2 + z^2} \dots [63]$$

The coefficient μ in this equation has the dimensions (length) ÷ (force × time), and is considered constant. The effect of this drift velocity in the phase space upon the distribution function is as follows

$$\begin{aligned} \left(\frac{\partial \rho}{\partial t} \right)_{\text{molecular force}} &= -\frac{1}{r^2} \frac{\partial}{\partial r} \{ \rho r^2 v_r \} = \frac{\mu K}{r^2} \frac{\partial}{\partial r} \{ \rho r^3 \} \\ &= \mu K \left(r \frac{\partial \rho}{\partial r} + 3\rho \right) = \mu K \left(x \frac{\partial \rho}{\partial x} + y \frac{\partial \rho}{\partial y} + z \frac{\partial \rho}{\partial z} + 3\rho \right) \dots [64] \end{aligned}$$

Combination of Equations [62] and [64] by the principle of direct superposition yields the following differential equation for the distribution function ρ , which holds in the absence of motion due to externally applied deformations

$$\begin{aligned} \frac{\partial \rho}{\partial t} = D \left(\frac{\partial^2 \rho}{\partial x^2} + \frac{\partial^2 \rho}{\partial y^2} + \frac{\partial^2 \rho}{\partial z^2} \right) + \mu K \left(x \frac{\partial \rho}{\partial x} + y \frac{\partial \rho}{\partial y} \right. \\ \left. + z \frac{\partial \rho}{\partial z} + 3\rho \right) \dots \dots [65] \end{aligned}$$

The constants D and μK of this equation are molecular constants in terms of which the bulk properties eventually will be expressed. For the present purposes they may be considered merely as constants of the material which might be evaluated from experimental observation.

The equilibrium distribution function ρ_0 , for which $\partial \rho_0 / \partial t = 0$, is the solution of the equation formed from Equation [65] by setting the time derivative $\partial \rho / \partial t$ equal to zero. Thus the equation for ρ_0 is

$$\begin{aligned} D \left(\frac{\partial^2 \rho_0}{\partial x^2} + \frac{\partial^2 \rho_0}{\partial y^2} + \frac{\partial^2 \rho_0}{\partial z^2} \right) + \mu K \left(x \frac{\partial \rho_0}{\partial x} + y \frac{\partial \rho_0}{\partial y} + z \frac{\partial \rho_0}{\partial z} \right. \\ \left. + 3\rho_0 \right) = 0 \dots \dots [66] \end{aligned}$$

The solution of Equation [66], which also satisfies condition [60], which may be verified by substitution into these relations, is

$$\rho_0 = \frac{e^{-(x^2 + y^2 + z^2)/r_0^2}}{(r_0 \sqrt{\pi})^3} \dots \dots [67]$$

where

$$r_0^2 = \frac{2D}{\mu K} \dots \dots [68]$$

is a fixed reference value of the effective molecular length r .

The distribution function ρ_0 of Equation [67] represents the material in a condition of statistical equilibrium. This function is directionally symmetrical so that the cumulative effect of the molecular forces, Equation [55], must be hydrostatic tension which can be balanced by the action of the surrounding liquid-like medium. Except for an arbitrary hydrostatic pressure p (see Equations [54]), which can have no effect on strain energy be-

cause of the assumed incompressibility of the material, the equilibrium distribution function corresponds to the zero stress condition, which is also the condition of no elastic strain

$$\alpha_1 = \alpha_2 = \alpha_3 = 1$$

A structural representation of elastic strain can be described by means of the distribution function ρ . Consider a body having initially the equilibrium distribution function ρ_0 to be deformed rapidly enough that relaxation effects during the deformation may be neglected. Without loss of generality this deformation can be considered to correspond with a strain having principal strain directions along the co-ordinate axes x, y, z of phase space. The strain imposed is arbitrary, except that it must conform to the condition of incompressibility

$$\alpha_1 \times \alpha_2 \times \alpha_3 = 1 \dots \dots \dots [69]$$

During deformation the end points of the molecules are assumed, as stated before, to follow freely the movement of the surrounding medium. Thus a molecule which had an effective length vector specified by the phase-space co-ordinates x_1, y_1, z_1 before the deformation, would have the co-ordinates x_1', y_1', z_1' after the deformation, where

$$\left. \begin{aligned} x_1' &= \alpha_1 x_1 \\ y_1' &= \alpha_2 y_1 \\ z_1' &= \alpha_3 z_1 \end{aligned} \right\} \dots \dots \dots [70]$$

The distribution function immediately after the deformation is obtained by substituting according to Equations [70] the values $(x'/\alpha_1), (y'/\alpha_2), (z'/\alpha_3)$ for x, y, z in Equation [67]. After this substitution is made, interest is restricted to the transformed phase-space co-ordinates x', y', z' ; therefore the primes may be dropped from the notation without confusion. The distribution function immediately after the deformation is, accordingly

$$\rho = \frac{1}{\alpha_1 \alpha_2 \alpha_3 r_0^3 \pi^{3/2}} \times e^{-[(x/\alpha_1)^2 + (y/\alpha_2)^2 + (z/\alpha_3)^2 + r_0^2]} \dots [71]$$

The factor $\alpha_1 \alpha_2 \alpha_3$ has been inserted into Equation [71] in order to satisfy formally the Condition [60]; this factor is, by Equation [69], equal to unity and so does not change the values of ρ in Equation [71].

(d) *Determination of Relaxation and Strain-Energy Functions.* Relaxation effects can now be examined by considering the material to be held by external forces in a deformed state, represented initially by the distribution function, Equation [71], and the principal strain ratios $\alpha_1, \alpha_2, \alpha_3$. The nonequilibrium Equation [65] for the distribution function is to be applied starting at $t = 0$ with the distribution function, Equation [71]

It may be verified by substitution of Equation [71] into Equation [65] that the solution for ρ under these conditions is a distribution function of the same form as Equation [71], but with $\alpha_1, \alpha_2, \alpha_3$ functions of time governed by the following differential relations

$$\left. \begin{aligned} \left(\frac{d\alpha_1}{dt} \right)_{\text{relax}} &= R_1 = -\frac{1}{2T} \left(\alpha_1 - \frac{1}{\alpha_1} \right) \\ \left(\frac{d\alpha_2}{dt} \right)_{\text{relax}} &= R_2 = -\frac{1}{2T} \left(\alpha_2 - \frac{1}{\alpha_2} \right) \\ \left(\frac{d\alpha_3}{dt} \right)_{\text{relax}} &= R_3 = -\frac{1}{2T} \left(\alpha_3 - \frac{1}{\alpha_3} \right) \end{aligned} \right\} \dots \dots \dots [72]$$

where $T = 1/(2\mu K)$ is the dimension time, and is of the nature of the "relaxation" time of the classical Maxwell liquid.

It can be seen, therefore, that the general solution for the distribution function ρ under any history of external deformation is

an expression of the form, Equation [71], where the variables $\alpha_1, \alpha_2, \alpha_3$ change with applied deformations in the same way that geometric strain does, and in addition have spontaneous time rates of change, or relaxation, given by Equations [72]. The variation of $\alpha_1, \alpha_2, \alpha_3$ is thus governed by conditions of the type specified by Equations [45].

Substitution of the general distribution function, Equation [71], into Equation [61] gives for the strain-energy function ψ , the expression^a

$$\psi = \frac{G}{2} (\alpha_1^2 + \alpha_2^2 + \alpha_3^2) \dots \dots \dots [73]$$

where $G = 1/2(NKr_0^2)$, and has the dimensions (force) + (length)² of a modulus of elasticity; it corresponds to the shear modulus of the classical Maxwell liquid. Thus since the strain-energy function has the arguments $\alpha_1, \alpha_2, \alpha_3$, and these variables are governed by relations of the form, Equation [45], it is clear that these variables are the structural representations of elastic strain.

5 APPLICATION OF THE THEORY TO FLOWS IN CHANNELS AND TUBES

(a) *Remarks on Applications.* Although the general stress-strain behavior of materials exhibiting large strain elasticity with relaxation is specified when the strain-energy and relaxation functions are known, the application of this specification to determine flows of materials under particular conditions is in itself a difficult task. The general problem is one of extreme complexity so that reliance must be placed on special techniques developed for specific problems.

As an illustration of the special techniques which may be employed, solutions are presented here for the important cases of steady-state flows in long uniform channels of infinite width, and in long straight circular tubes. These solutions are based on the observation that in steady-state flows in long tubes or channels, all particles of the material move in straight lines parallel with the tube or channel walls; the flow velocity does not vary in the direction of flow, but varies only in a direction normal to the flow. Consequently, the flow environment of each particle of the material is a steady-state simple shear parallel with the walls. The elastic strain of an element in a steady-state simple shear flow approaches a limiting steady value which is determined by equating to zero the net change of elastic strain, which is the sum of the changes due to change of geometric strain in the flow and that due to the relaxation process. This limiting steady elastic strain will prevail in the flows within long tubes and channels.

Thus, in these cases, the stresses can be determined directly in terms of the shearing rate. The flows themselves can be determined from the shearing-rate distributions which satisfy the stress-equilibrium conditions.

The course of these analyses is first indicated for general strain-energy and relaxation functions, and then illustrated by numerical examples using the following forms for strain-energy function ψ , and relaxation functions R_i

$$\left. \begin{aligned} \psi &= \frac{2G}{n^2} (\alpha_1^n + \alpha_2^n + \alpha_3^n) \\ R_i &= -\frac{\alpha_i}{nT} (1 - \alpha_i^{-n}) \end{aligned} \right\} \dots \dots \dots [74]$$

where n is a dimensionless constant. These are generalized

^a The indicated integrations of Equation [61] are carried out with the help of the known definite integrals

$$\int_{-\infty}^{\infty} e^{-(x/a)^2} dx = a\sqrt{\pi}; \quad \int_{-\infty}^{\infty} x^2 e^{-(x/a)^2} dx = a^3\sqrt{\pi}/2.$$

forms of the functions derived in the previous section which appear to fit data of the author² rather well with values of n in the range 1.1 to 1.5. For $n = 2$ these functions coincide with those of Equations [72] and [73]. The constants G and T have the same dimensions of an elastic modulus or stress and time, respectively, as those of Equations [72] and [73], and also have the same significance. For infinitesimal strain the Functions [74] for any value of n describe a classical Maxwell liquid; these functions were set up so that G and T will have their classical significance for each value of n . It may be noted that the behaviors specified by Equations [74] at infinitesimal strains are independent of the value of n .

The forms of Equations [74] were suggested in the course of a rather extensive study of the previous data.² Though these forms do fit the data of that reference within the experimental error, the data give relatively little information on the relaxation process because relaxation was a comparatively small factor in determining the stress at the rapid extension rates of those tests. The factor α_i in the relaxation functions R_i of Equations [74], which governs the relaxation rate at large extension ratios, was broadly verified by these tests; however, the tests give virtually no information on the factor $(1 - \alpha_i^{-n})$, which governs the relaxation rates for low stresses.

The strain-energy and relaxation functions, Equations [74], are presented, therefore, not as wholly realistic forms, but as the best information available at present upon which to base numerical examples.

Presentation of the analysis of the data which led to these forms will be postponed until the data from further tests, which will give information on the relaxation at low stresses, are available.

(b) *Elastic Strain and Stresses in Steady-State Simple Shear Flow.* Consider a two-dimensional flow referred to plane Cartesian co-ordinates x_1 and x_2 , in which the direction of flow at every point is parallel to the x_1 -axis, and the velocity of flow is independent of time and of the x_1 -co-ordinate. Each particle of the material travels along a straight line parallel to the x_1 -axis, and is subject to a continuous simple shear deformation at an unvarying rate specified by $s = (dv_1)/(dx_2)$. The geometrical strain relationships for this case have been analyzed in Section 2 to which reference is made.

Expressions for the rates of change of elastic strain and of the angle of the principal elastic strain directions due only to the geometric flow are given by Equations [43] and [44]. The net changes of these quantities when relaxation effects are included are, following relations, Equations [45] and [46]

$$\left. \begin{aligned} \frac{d\alpha_1}{dt} &= \frac{1}{2} s \alpha_1 \sin 2\theta + R_1 \\ \frac{d\alpha_2}{dt} &= -\frac{1}{2} s \alpha_2 \sin 2\theta + R_2 \\ \frac{d\alpha_3}{dt} &= R_3 \\ \frac{d\theta}{dt} &= \frac{s}{2} \left[\frac{\alpha_1^2 + \alpha_2^2}{\alpha_1^2 - \alpha_2^2} \times \cos 2\theta - 1 \right] \end{aligned} \right\} \dots \dots [75]$$

As just described, in the parallel flows being considered, each element of the material is subject to a steady-state shearing rate s . The values of α_1 , α_2 , α_3 , and θ will, therefore, adjust themselves in a period of time to the steady-state condition

$$\frac{d\alpha_1}{dt} = \frac{d\alpha_2}{dt} = \frac{d\alpha_3}{dt} = \frac{d\theta}{dt} = 0 \dots \dots \dots [76]$$

which, with Equations [75] yield four equations to determine the four quantities which specify the elastic strain as functions of shearing rate s .

The principal stresses σ_1 , σ_2 , and σ_3 are then given, for the incompressible case, by Equations [54]. The principal stress σ_2 acts in the direction normal to the plane of flow, while σ_1 and σ_3 act at an angle θ to the x_1 - and x_2 -axes, respectively, or along the x_1 - and x_2 -axes in Fig. 1. The in-plane direct stresses σ_{11} and σ_{22} acting normal, respectively, to the x_1 - and x_2 -axes, and the shear stress τ acting on each of these planes are given by

$$\left. \begin{aligned} \sigma_{11} &= \frac{1}{2} (\sigma_1 + \sigma_2) + \frac{1}{2} (\sigma_1 - \sigma_2) \cos 2\theta \\ \sigma_{22} &= \frac{1}{2} (\sigma_1 + \sigma_2) - \frac{1}{2} (\sigma_1 - \sigma_2) \cos 2\theta \\ \tau &= \frac{1}{2} (\sigma_1 - \sigma_2) \sin 2\theta \end{aligned} \right\} \dots \dots [77]$$

The positions and directions of these stresses are shown in Fig. 4.

A principal result of this analysis can be represented by an "apparent viscosity for simple shear" η_s , which is defined by

$$\eta_s = \tau/s \dots \dots \dots [78]$$

Since the shear stress τ is a function of s , this apparent viscosity is also a function of s . The apparent viscosity thus defined has the same dimensions, (force) \times (time) \div (length)², as the coefficient of viscosity of a Newtonian liquid, and has, for the particular flows being considered, a similar significance.

With the forms of Equations [74] for the relaxation functions, the conditions, Equations [76] for steady-state shear may be written

$$\left. \begin{aligned} \alpha_1 &= \left(1 - \frac{nS}{2} \sin 2\theta \right)^{-1/n} \\ \alpha_2 &= \left(1 + \frac{nS}{2} \sin 2\theta \right)^{-1/n} \\ \alpha_3 &= 1 \\ \cos 2\theta &= \frac{\alpha_1^2 - \alpha_2^2}{\alpha_1^2 + \alpha_2^2} \end{aligned} \right\} \dots \dots \dots [79]$$

into which the dimensionless measure of shearing rate $S = sT$ has been introduced.

The relations, Equations [79], can be solved explicitly for a series of values of the dimensionless shearing rate S by assigning a set of values to the quantity $(nS/2) \sin 2\theta$. Then α_1 and α_2 are determined explicitly for the first two of Equations [79], and θ by the last. The results of computations of this kind, and the subsequent determination of stresses and apparent viscosity are presented in Table 1, for $n = 5/4$ and $3/2$. The apparent viscosities are shown plotted as functions of the dimensionless shearing rate S in Fig. 3.

The case $n = 2$ allows a very simple analytical solution for the stresses. In this case the first two of Equations [79] may be written

$$\alpha_1^2 = \frac{1}{1 - S \sin 2\theta}; \quad \alpha_2^2 = \frac{1}{1 + S \sin 2\theta} \dots \dots [80]$$

When these expressions are substituted into the last of Equations [79], the results are

$$\cos 2\theta = S \sin 2\theta; \quad \text{or} \quad \cot 2\theta = S \dots \dots [81]$$

The principal stresses, from Equations [54], are

$$\left. \begin{aligned} \sigma_1 &= G\alpha_1^2 + p = \frac{G}{1 - \cos 2\theta} + p \\ \sigma_2 &= G\alpha_2^2 + p = \frac{G}{1 + \cos 2\theta} + p \\ \sigma_3 &= p \end{aligned} \right\} \dots \dots \dots [82]$$

The in-plane stresses on the co-ordinate planes, from Equations [74] are

$$\sigma_{11} - \sigma_{22} = 2GS^2; \quad \tau = GS \dots \dots \dots [83]$$

The apparent viscosity defined by Equation [78] is, in this special case, independent of shearing rate, and is equal to GT ; this result is in accord with the Maxwell liquid behavior.

(c) *Flow in Long Channels of Infinite Width.* In a typical steady-state flow at some distance from the entrance or exit of a long channel with parallel walls and of infinite width, all particles of the flowing material move in parallel straight lines which are also parallel with the walls. The flow is symmetrical with respect to a plane parallel to and lying midway between the channel walls. Since each element of the material is deformed in simple shear, acting parallel with the channel walls and in the direction of flow, the steady-state stress condition is given in terms of shearing rate by the analysis of the preceding subsection. The results of that analysis can be used in conjunction with the stress equilibrium conditions to determine the velocity and stress distributions in such channel flows.

Let Cartesian co-ordinates x_1, x_2, x_3 be set up in a channel with the x_1 -axis lying in the mid-plane in the direction of flow, the x_2 -axis in the mid-plane at right angles to the flow, and the x_3 -axis normal to the channel walls. Let the distance between the channel walls be designated by $2h$. The stresses in the plane of flow on a typical element of the material are those given by Equation [77], and are indicated in Fig. 4 which also shows the co-ordinate system and channel.

The equations of equilibrium for the stresses in the plane of flow indicated in Fig. 4 are

$$\left. \begin{aligned} \frac{\partial \sigma_{11}}{\partial x_1} + \frac{\partial \tau}{\partial x_2} &= 0 \\ \frac{\partial \sigma_{22}}{\partial x_2} + \frac{\partial \tau}{\partial x_1} &= 0 \end{aligned} \right\} \dots \dots \dots [84]$$

According to Equations [54], the principal stresses for an incompressible material may be considered to consist of two parts: the hydrostatic tension p which is independent of the elastic

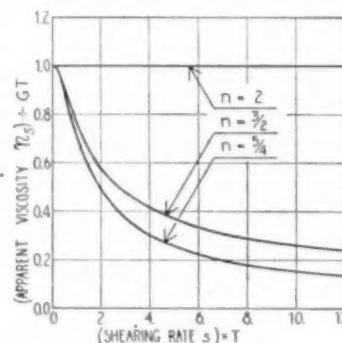


FIG. 3 APPARENT VISCOSITY FOR SIMPLE SHEAR VERSUS SHEARING RATE

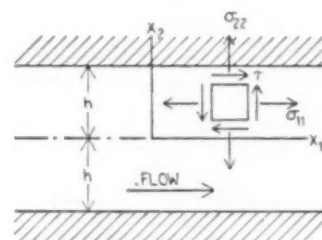


FIG. 4 CO-ORDINATES AND STRESSES ON TYPICAL ELEMENT FOR FLOW IN CHANNEL

TABLE 1 STRESSES AND ELASTIC STRAINS FOR STEADY-STATE SIMPLE SHEAR FLOW FOR THE STRAIN ENERGY AND RELAXATION FUNCTIONS OF EQUATION [74]

S	θ°	α_1	α_2	$\frac{\sigma_{11} - \sigma_{22}}{G}$	$\frac{\tau}{G}$	$\frac{\eta_a}{GT}$
0.0	45.0	1.00	1.00	0.0	0.0	1.000
0.337	35.9	1.20	0.804	0.21	0.317	0.949
0.793	26.9	1.51	0.764	0.90	0.615	0.776
1.613	18.5	2.08	0.687	2.41	0.893	0.553
2.383	14.0	2.62	0.654	3.88	1.032	0.433
2.972	11.9	3.03	0.639	5.02	1.107	0.373
3.822	9.7	3.62	0.625	6.70	1.191	0.312
5.165	7.6	4.56	0.612	9.46	1.291	0.250
7.660	5.4	6.31	0.598	14.89	1.452	0.186
9.413	4.5	7.54	0.593	18.93	1.499	0.159
12.164	3.6	9.48	0.589	25.64	1.598	0.131
17.313	2.5	13.13	0.584	39.03	1.738	0.100
30.982	1.5	22.87	0.579	79.09	2.004	0.065
∞	$45.8 + S^\circ$	0.718S	0.574	$1.057 \times S^{1/4}$	$0.845 \times S^{1/4}$	$0.846 \div S^{1/4}$
$n = 3/2$						
0.0	45.0	1.00	1.00	0.0	0.0	1.000
0.277	37.4	1.16	0.886	0.15	0.268	0.969
0.621	29.6	1.41	0.799	0.65	0.546	0.879
1.166	21.7	1.84	0.732	1.82	0.858	0.735
1.630	17.5	2.23	0.702	3.00	1.048	0.643
1.966	15.3	2.52	0.689	3.94	1.162	0.591
2.431	13.0	2.92	0.676	5.32	1.300	0.535
3.131	10.6	3.54	0.664	7.61	1.478	0.472
4.357	8.0	4.64	0.652	12.14	1.740	0.399
5.177	6.9	5.39	0.647	15.52	1.892	0.366
6.422	5.6	6.53	0.643	21.12	2.101	0.327
8.617	4.3	8.55	0.639	32.29	2.425	0.281
14.012	2.7	13.57	0.634	65.71	3.077	0.220
22.516	1.7	21.55	0.632	132.44	3.889	0.173
∞	$38.2 + S$	0.840S	0.631	$1.225 \times S^{1/2}$	$0.817 \times S^{1/2}$	$0.817 \div S^{1/2}$

strain; and the parts $(\alpha_i \partial \psi) / (\partial \alpha_i)$ which depend only upon the elastic strain. It will be convenient to consider the stresses entering Equations [84], which are given in terms of the principal stresses by Equations [77], to be composed of the corresponding two parts; thus

$$\left. \begin{aligned} \sigma_{11} &= (\sigma_{11} - p) + p = f_{11}(x_2) + p \\ \sigma_{22} &= (\sigma_{22} - p) + p = f_{22}(x_2) + p \\ \sigma_3 &= p \\ \tau &= \tau(x_2) \end{aligned} \right\} \dots \dots \dots [85]$$

The stresses $(\sigma_{11} - p)$, $(\sigma_{22} - p)$, and τ depend only upon elastic strain and therefore, in the present flows, must be functions only of the co-ordinate x_2 . This dependence is indicated in Equations [85] by introducing the functions f_{11} and f_{22} of x_2 only for $(\sigma_{11} - p)$ and $(\sigma_{22} - p)$, and by writing $\tau = \tau(x_2)$. Since the partial derivatives of f_{11} , f_{22} and τ with respect to x_1 are zero, use of the forms, Equations [85], in the equilibrium relations, Equations [84], reduces the latter to

$$\left. \begin{aligned} \frac{\partial p}{\partial x_1} + \frac{d\tau}{dx_2} &= 0 \\ \frac{\partial p}{\partial x_2} + \frac{df_{22}}{dx_2} &= 0 \end{aligned} \right\} \dots \dots \dots [86]$$

The second of Equations [86] contains only derivatives with respect to x_2 , and may be integrated at once to give

$$p = f(x_1) - f_{22}(x_2) \dots \dots \dots [87]$$

where $f(x_1)$ is an as yet undetermined function of x_1 only. Now, since τ and therefore also $(d\tau)/(dx_2)$ are functions of x_2 only, it follows from the first of Equations [86] that $(\partial p)/(\partial x_1)$ must be independent of x_1 . It then follows from the form of p in Equation [87] that $(\partial p)/(\partial x_1)$ must be a constant; therefore Equation [87] may be written

$$p = Cx_1 + p_0 - f_{22} \dots \dots \dots [88]$$

where p_0 is a constant of integration. Substitute this result into the first of Equations [86], thus

$$\frac{d\tau}{dx_2} = -C; \text{ or } \tau = -Cx_2 \dots \dots \dots [89]$$

Since by symmetry the shear stress on the midplane $x_2 = 0$ must be zero, there is no constant of integration in the expression for τ . Putting these results into the Equations [85], the general solution of the equilibrium equations for flow in a channel is

$$\left. \begin{aligned} \sigma_{11} &= Cx_1 + p_0 + f_{11} - f_{22} \\ \sigma_{22} &= Cx_1 + p_0 \\ \sigma_3 &= Cx_1 + p_0 - f_{22} \\ \tau &= -Cx_2 \end{aligned} \right\} \dots \dots \dots [90]$$

As remarked before, f_{11} and f_{22} depend only upon x_2 ; thus the constant C is the pressure gradient in the direction of flow.

The analysis of the steady-state shear conditions of the previous subsection has expressed the steady-state shearing rate $s = (dv_1)/(dx_2)$ as a function of the shearing stress τ ; therefore, with Equations [90] for the channel flows

$$\frac{dv_1}{dx_2} = s(\tau) = -s(-\tau) = -s(Cx_2) \dots \dots \dots [91]$$

Here $s(\tau) = -s(-\tau)$ follows from the necessary odd character of the shearing rate-shear stress relations. From the values of s the values of elastic strain and the stresses $(\sigma_{11} - p) = f_{11}$ and $(\sigma_{22} - p) = f_{22}$ follow from the steady-state shear analysis.

The velocity distribution over the channel is determined from Equations [91] by the integration

$$v_1 = v_0 + \int_0^{x_2} (dv_1/dx_2) dx_2 = v_0 - \int_0^{x_2} s(Cx_2) dx_2 \dots [92]$$

where the constant of integration v_0 is determined to make $v_1 = 0$ at the channel wall $x_2 = h$. Values of v_1 in the negative range of x_2 follow by symmetry. The volume rate of flow per unit width of the channel, denoted by q , is determined by a second integration

$$q = 2 \int_0^h v_1 dx_2 \dots \dots \dots [93]$$

The over-all resistance of a material to flow can be expressed conveniently by analogy to the flow of a Newtonian liquid. For Newtonian liquids the relationship between the volume flow rate q , the pressure gradient C , and the viscosity coefficient η is

$$q = \frac{2h^3 C}{3\eta} \dots \dots \dots [94]$$

An "apparent viscosity coefficient for flow in a channel" η_c may be defined in terms of the q given by Equation [93] and h and C by analogy to Equation [94]; thus

$$\eta_c = \frac{2h^3 C}{3q} \dots \dots \dots [95]$$

The solution, Equations [90], is perfectly general for all materials of the type considered, and holds in particular for materials of which the behavior is specified by the functions, Equations [74]. For these materials the dimensionless shearing rate $S = sT$ is a function of the dimensionless stress quantity τ/G . It is convenient to write Equations [91] in the following form for these materials

$$\frac{dv_1}{dx_2} = \frac{S(\tau/G)}{T} = -\frac{1}{T} \times S\left(\frac{Cx_2}{G}\right) \dots \dots \dots [96]$$

The integration specified in Equation [92] is written in terms of the dimensionless variables

$$X = \frac{Cx_2}{G}; \quad H = \frac{Ch}{G} \dots \dots \dots [97]$$

thus

$$v_1 = \frac{G}{CT} \phi(H, X) \dots \dots \dots [98]$$

where

$$\phi(H, X) = \int_0^H SdX' - \int_0^X SdX \dots \dots \dots [99]$$

The integral for the volume output rate q may be written

$$q = \frac{2G^2}{C^3 T} \Phi = \frac{2h^2}{T} \times \frac{\Phi}{H^2} \dots \dots \dots [100]$$

where

$$\Phi = \int_0^H \phi(H, X) dX \dots \dots \dots [101]$$

The apparent viscosity coefficient for flow in a channel is, from Equations [95] and [100]

$$\eta_c = GT \times \frac{H^3}{3\Phi} \dots \dots \dots [102]$$

The dimensionless measure of apparent viscosity $\eta_c/(GT)$ is a function of the single variable H , defined by Equations [97].

The dimensionless measure of the volume output rate qT/h^3 is also a function of H by Equation [100]. Therefore, $\eta_c/(GT)$ is a function of qT/h^3 , and their relationship characterizes the resistance to flow of these materials.

Numerical computations have been made for the case $n = 5/4$, using the relationship between S and τ/G given in Table 1. The results of these computations are summarized in Table 2, the $\eta_c/(GT)$ versus qT/h^3 plot in Fig. 6, and the velocity-distribution curves in Fig. 5.

Previous data of the author² indicate that the constants for polyethylene at 300.F are approximately as follows: $n = 5/4$, $G = 5$ psi, $T = 0.1$ sec, $GT = 0.5$ lb sec/in.² = 34,500 poises. As an example of an application of the numerical computations, the apparent viscosity for flow through a channel of height 0.01 in., and at a volume rate of 0.025 cu. in. per sec per in. width will be found. Thus

$$h = 0.005; qT/h^3 = 0.025 \times 0.1/0.000025 = 100$$

$$\eta_c/GT = 0.74(qT/h^3)^{-3/4} = 0.74/31.6 = 0.0234$$

$$\eta_c = 0.0234 \times 34,500 = 810 \text{ poises}$$

Values of this general order were found in measurements on the extrusion of polyethylene sheet at the Plax Corporation in June, 1947.

(d) *Flow in Long Circular Tubes.* The flow in any radial plane of a circular tube can be referred to x_1, x_2 -co-ordinates as in Fig. 4, if x_2 is interpreted as the radial co-ordinate, and h the tube radius. The stress notation of the previous subsection also can be used for the tube flow if σ_{22} is interpreted as radial stress, and σ_1 as circumferential stress. In the case of the circular tube the flow and stresses are symmetrical with respect to the tube axis x_1 , and the stress-equilibrium equations are

$$\left. \begin{aligned} \frac{\partial \sigma_{11}}{\partial x_1} + \frac{\partial \tau}{\alpha x_2} + \frac{\tau}{x_2} &= 0 \\ \frac{\partial \sigma_{22}}{\partial x_2} + \frac{\partial \tau}{\partial x_1} + \frac{\sigma_{22} - \sigma_1}{x_2} &= 0 \end{aligned} \right\} \dots \dots \dots [103]$$

As before, the stresses are represented in the form of Equations [85], and it is again noted that τ, f_{11} , and f_{22} , being functions only of elastic strain, must be dependent only upon the radial co-ordinate x_2 . The derivatives of these quantities with respect to x_1 vanish, and the equilibrium Equations [103] may accordingly be written

$$\left. \begin{aligned} \frac{\partial p}{\partial x_1} + \frac{1}{x_2} \frac{d}{dx_2} (x_2 \tau) &= 0 \\ \frac{\partial p}{\partial x_2} + \frac{1}{x_2} \frac{d}{dx_2} (x_2 f_{22}) &= 0 \end{aligned} \right\} \dots \dots \dots [104]$$

Integration of the second of these equations with respect to x_2 leads to the following form for p

$$p = f(x_1) - F_{22}(x_2) \dots \dots \dots [105]$$

where $f(x_1)$ is an as yet undetermined function of x_1 only, and F_{22} is given by

$$F_{22} = f_{22} + \int \frac{f_{22}}{x_2} dx_2 \dots \dots \dots [106]$$

and is, accordingly, like f_{22} a function of x_2 only.

It is noted as before that the first equation requires that $(\partial p)/(\partial x_1)$ be independent of x_1 , and must, from the form of Equation [105], be a constant C . Thus the general solution of the stress equilibrium equations for the tube can be written

TABLE 2 APPARENT VISCOSITY FOR FLOW IN CHANNELS

H	$\frac{qT}{h^3}$	$\frac{\eta_c}{(GT)}$
0.0	0.0	1.000
0.25	0.170	0.979
0.5	0.372	0.897
0.75	0.635	0.787
1.0	1.00	0.631
1.25	1.85	0.451
1.5	3.39	0.295
1.75	6.06	0.193
2.0	10.3	0.129
> 2	0.65×10^4	$1.03 \div H^3$

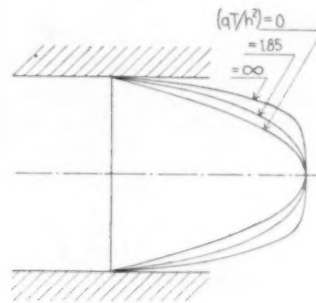
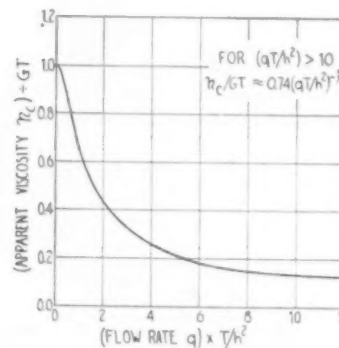


FIG. 5 VELOCITY DISTRIBUTIONS ACROSS CHANNELS

FIG. 6 η_c/GT VERSUS qT/h^3 FOR CHANNELS

$$\left. \begin{aligned} \sigma_{11} &= Cx_1 + p_0 + f_{11} - F_{22} \\ \sigma_{22} &= Cx_1 + p_0 + f_{22} - F_{22} \\ \sigma_1 &= Cx_1 + p_0 - F_{22} \\ \tau &= -Cx_2/2 \end{aligned} \right\} \dots \dots \dots [107]$$

Again p_0 is a constant of integration, and C represents the pressure gradient in the direction of flow.

The relation for the shearing rate s is

$$\frac{dv_1}{dx_2} = s(\tau) = -s(-\tau) = -s\left(\frac{Cx_2}{2}\right) \dots \dots \dots [108]$$

The functions f_{11} , f_{22} , and F_{22} of x_2 in the solution, Equations [107] are determined as before to fit the stress condition, which follows from the elastic strain corresponding to the shearing rate s given by Equation [108]. Equation [92] for the velocity distribution is valid in this case if the argument of s is made $Cx_2/2$. The volume rate of flow through the tube Q is given by

$$Q = 2\pi \int_0^h v_1 x_2 dx_2 \dots \dots \dots [109]$$

It is again convenient to use the analogy to the flow of a Newtonian liquid, this time in a tube, to determine an "apparent

viscosity, for flow in a tube" η_t as a measure of the over-all resistance to flow of a material. The formula in this case is

$$\eta_t = \frac{\pi h^4 C}{8Q} \quad [110]$$

For materials governed by the functions, Equations [74], the dimensionless shearing rate $S \approx sT$ is a function of τ/G ; thus in a fashion similar to that used in the channel-flow analysis

$$\frac{dw_1}{dx_2} = \frac{1}{T} S \left(\frac{\tau}{G} \right) = - \frac{1}{T} S \left(\frac{Cx_2}{2G} \right) \quad [111]$$

This equation differs from Equations [96] only by the factor 2 in the denominator of the argument of S , which comes from Equations [107] or [108]. In this case it is convenient to introduce the variables

$$X' = \frac{Cx_2}{2G}, \quad H' = \frac{Ch}{2G} \quad [112]$$

The velocity is, accordingly, given by

$$v_1 = \frac{2G}{CT} \phi'(H', X') \quad [113]$$

where

$$\phi'(H', X') = \int_0^{H'} S dX' - \int_0^{X'} S dX' \quad [114]$$

The volume-output integral Equation [109] gives

$$Q = \frac{16\pi G^3}{C^3 T} \Phi' = \frac{2\pi h^3}{T} \times \frac{\Phi'}{(H')^3} \quad [115]$$

with

$$\Phi' = \Phi'(H') = \int_0^{H'} \phi'(H', X') X' dX' \quad [116]$$

The expression for the apparent viscosity η_t is found by substituting the result, Equation [115], into Equation [110], and is

$$\eta_t = GT \times \frac{(H')^4}{8\Phi'} \quad [117]$$

The dimensionless measure of apparent viscosity $\eta_t/(GT)$ is a function of the parameter H' as is also the dimensionless measure of volume output rate GT/h^3 of Equation [115]; therefore, $\eta_t/(GT)$ is a function of QT/h^3 .

Numerical computations have been made for the case $n = 5/4$, and the results are presented in Table 3, and Fig. 7. The velocity distributions are qualitatively similar to those shown in Fig. 5 for the channels.

The viscosity-tube data in Fig. 8 of a report by James Bailey and R. W. Canfield⁹ are tabulated in Table 4, where they are also reduced to the form QT/h^3 and $\eta_t/(GT)$ by using values of the constants G and T , which are consistent with the tensile-test data of the author.² For values of QT/h^3 above about 0.35, there is good agreement of these measured apparent viscosities with the theoretical values in Fig. 7; the test points of Table 4 have been entered on the plot, Fig. 7. However, at very low rates of flow — QT/h^3 less than 0.3 — the measured viscosities are somewhat higher than the theoretical values. This discrepancy

⁹ "Report Covering Tests of Viscosity Tubes and Side Entrance Nozzle Made June 19, 20, and 21, 1944," report prepared for Plax Corporation by James Bailey and R. W. Canfield.

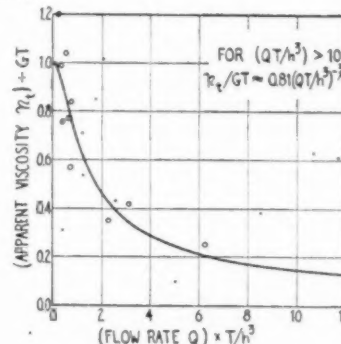
TABLE 3 APPARENT VISCOSITY FOR FLOW IN TUBES

H'	$\frac{QT}{h^3}$	$\frac{\eta_t}{GT}$
0.0	0.0	1.000
0.25	0.201	0.977
0.5	0.443	0.886
0.75	0.767	0.768
1.0	1.31	0.601
1.25	2.35	0.418
1.5	4.44	0.265
1.75	8.05	0.171
2.0	13.8	0.114
>2	$0.88 \times H^4$	$0.90 + H^4$

TABLE 4 VISCOSITY TUBE DATA OF FIG. 8^a

Exp. no.	h , in.	Q , in. ³ /sec	η_t , poises	$\frac{QT}{h^3}$	$\frac{\eta_t}{GT}$
Temp. = 437 — 440 F; $G = 4$ psi $T = 0.3$ sec; $GT = 83000$ poises					
1	5/8	0.082	350000	0.10	4.21
2	5/8	0.094	345000	0.12	4.15
3	5/8	0.250	258000	0.31	3.11
11	3/8	0.060	82000	0.34	0.99
4	5/8	0.448	86000	0.55	1.04
7	1/4	0.040	70000	0.77	0.84
12	3/8	0.394	29000	2.25	0.35
8	1/4	0.162	35000	3.11	0.42
9	1/4	0.325	20500	6.25	0.25
Temp. = 345 — 350 F; $G = 20$ psi $T = 0.3$ sec; $GT = 415000$ poises					
5	5/8	0.185	500000	0.23	1.20
13	3/8	0.042	655000	0.24	1.58
6	5/8	0.325	315000	0.40	0.76
10	1/4	0.034	325000	0.65	0.77
14	3/8	0.126	235000	0.72	0.57

^a See footnote 9.

FIG. 7 η_t/GT VERSUS QT/h^3 FOR TUBES

may be attributed to the factor $(1 - \alpha_1^{-n})$ of the relaxation functions in Equations [74], which, as remarked before, affect the apparent viscosity at low flow rates. This factor has not been substantiated by the previous tests³ for the reasons discussed at the beginning of Section 5.

ACKNOWLEDGMENT

The analyses presented in this paper were carried out by the author as a part of the research program of the Plax Corporation of Hartford, Conn., with whose permission they are published. The work was carried out under the general-direction of Mr. James Bailey, vice-president and research director of the Plax Corporation, and the author gratefully acknowledges the very valuable guidance of Mr. Bailey in planning and carrying out the work.

Discussion

JAMES BAILEY.¹⁰ On the subject matter of this paper the writer will confine his remarks to reasons why his company felt that a mathematical investigation of the flow of commercially used plastics was necessary.

¹⁰ Vice-President and Research Director, Plax Corporation, Hartford, Conn.

Preliminary experiments consisted of measuring the pressure drop through dies, tubes, screen packs, and various commercial apparatus, together with temperature and volume of material per unit of time. These data were analyzed mathematically, using the laws of pure viscous flow, and it was found that the computed viscosity varied over a very wide range.

These experiments were followed by experiments using especially large viscosity tubes having inside bores of $1/2$, $3/4$, and 1 in., and a length of 14 in. The tubes were equipped with a back-pressure valve at the outlet and four pressure gages arranged along their length. The computed viscosity was found to vary over a range of 17 to 1, when the output varied from a few pounds per hour to 60 lb per hr at the same temperature. Over-all back pressure had no practical effect.

In other experiments, frictional effects, heating effects due to the internal work necessary to maintain the flow, and a relaxation effect at the exit of dies were noted. Tests using a rapid stretching apparatus at controlled temperature showed similar behavior.

All of these effects presented so complicated a picture that it was felt correlation would be possible only by a mathematical procedure.

AUTHOR'S CLOSURE

To supplement Mr. Bailey's remarks on the origin of the studies reported in the paper the writer can add a few remarks on applications and future developments.

In the continuous blowing up of extruded thin-walled polyethylene tubing with internal pressure, a characteristic configuration of tube diameter often occurs wherein the tube diameter first decreases, and finally increases as it is drawn away from the die. This behavior is qualitatively inexplicable in terms of simple viscous flow theory, but is predicted according to the proposed flow theory.

Charts of pressure drop in channels and tubes of various sizes for varying flow rates and temperatures of several materials have been prepared on the basis of the results of section 5 of the paper, and are useful in design of equipment. Studies are also planned on the pressure-development characteristic in the melting section of extruder screws by use of the theory.

Further experimental and theoretical work is expected to improve the quantitative representation of the properties of specific materials, particularly with respect to variations with temperature and flow rate; work with molecular representations appears promising in this respect.

Extrapolation of Static Tests to Predict Operation of Jet Engines in Flight

By C. A. MEYER,¹ SOUTH PHILADELPHIA, PA.

The purpose of this paper is to present a method which enables a prediction of flight performance of a jet engine from data obtainable in the test cell. The range of flight performance obtained by the method is of course limited by the operating range covered in the static tests. The method is also useful in comparing static tests with flight or wind-tunnel data. A curve is also presented which is generally useful in the solution of many flow problems.

NOMENCLATURE

The following nomenclature is used in this paper:

A = exhaust-nozzle area
 a = acoustic velocity
 c = gas velocity
 c_p, c_v = specific heats, and constant pressure and volume
 D = diameter
 F, F_n = thrust, net thrust
 g = acceleration due to gravity
 J = mechanical equivalent of heat 778.26 ft-lb/Btu
 k = ratio of specific heats (c_p/c_v)
 n = rotational speed
 p, p_t = static and total pressures
 p_0 = standard sea-level pressure
 R = gas constant
 T, T_t = static and total absolute temperatures
 T_0 = standard sea-level temperature
 V = air speed
 W_a, W_f = weight rate of air, and fuel flow
 δ_{am}, δ_{t2} = relative absolute pressures, $P_{am}/P_0, P_{t2}/P_0$
 θ_{am}, θ_{t2} = relative absolute temperatures, $T_{am}/T_0, T_{t2}/T_0$
 1, 2 = subscripts referring to stations
 am = subscript for ambient

INTRODUCTION

Since the advent of jet propulsion, flight-performance figures of jet engines have been required by airframe builders in order that they could make suitable estimates of performance of proposed airplanes. This need for information was first met by the engine builders by supplying calculated estimates. These calculated estimates of engine performance were obtained by the following:

1 Testing or estimating the performance of the component parts of the engine, such as the compressor, burner, turbine, and exhaust nozzle;

2 Combining by means of calculations the performance of the components to obtain the over-all performance of the jet engine for various flight speeds, altitudes, rotational speeds, and

exhaust-nozzle sizes. Later, when jet engines actually were being tested, it became possible to obtain a better estimate of flight performance based on test-cell data rather than by combining the estimated or tested performance of the components.

This paper describes a method of carrying out such an estimate.

The curve, Fig. 1, which in this paper is used to carry out the calculations, will be found to be generally useful in the solution of various flow problems.

JET-MOTOR PERFORMANCE

The static performance of any given jet engine can be represented by the following relations:

$$A \text{ function of } \left(\frac{T_{t2}}{\theta_{t2}} \right), \left(\frac{n}{\sqrt{\theta_{t2}}} \right) \text{ and } A = 0 \dots \dots \dots [1]$$

$$A \text{ function of } \left(\frac{F}{\delta_{t2}} \right), \left(\frac{n}{\sqrt{\theta_{t2}}} \right) \text{ and } A = 0 \dots \dots \dots [2]$$

$$A \text{ function of } \left(\frac{W_a \sqrt{\theta_{t2}}}{\delta_{t2}} \right), \left(\frac{n}{\sqrt{\theta_{t2}}} \right) \text{ and } A = 0 \dots \dots \dots [3]$$

$$A \text{ function of } \left(\frac{W_f}{\delta_{t2} \sqrt{\theta_{t2}}} \right), \left(\frac{n}{\sqrt{\theta_{t2}}} \right) \text{ and } A = 0 \dots \dots \dots [4]$$

$$A \text{ function of } \left(\frac{P_{t2}}{P_{t2}'} \right), \left(\frac{n}{\sqrt{\theta_{t2}}} \right) \text{ and } A = 0 \dots \dots \dots [5]$$

The proof of the foregoing relations can be found by means of dimensional analysis of the jet engine.

As an example, the Relation [3] is developed in Appendix 1.

The Relations [1] through [5] give, respectively, the corrected top temperature, the thrust, the air flow, the fuel flow, and the exhaust-nozzle pressure ratio, in terms of the corrected rotational speed, and the exhaust-nozzle area taken as independent variables. It should be noticed that the various quantities given in the Relations [1] through [5] are corrected to the conditions (total pressure and total temperature) at inlet to the compressor. In this way the performance is given independent of the inlet-duct losses. Where the inlet-duct losses are negligible, this is the same as correcting the quantities to the ambient static pressure and temperature, since in this case the total pressure and temperature at the compressor inlet are respectively equal to the ambient static temperature and pressure.

Where it is desired to present the engine performance, including an inlet duct having finite losses, the quantities should be corrected to the ambient conditions.

Another very useful method of presenting jet-engine performance is to consider the engine to be a "hot-gas generator." This method simply presents the performance of the engine exclusive of inlet ducting and exhaust nozzle.

The combination of compressor, burner, and turbine is assumed to generate or supply a quantity of hot gases at a pressure above atmospheric. In the normal jet engine the hot gases are expanded in a nozzle to produce thrust.

¹ Thermodynamics Section Engineer, Aviation Gas Turbine Division, Westinghouse Electric Corporation. Jun. ASME.

Contributed by the Oil and Gas Power and Aviation Divisions and presented at the Annual Meeting, New York, N. Y., November 26-29, 1945, of THE AMERICAN SOCIETY OF MECHANICAL ENGINEERS.

NOTE: Statements and opinions advanced in papers are to be understood as individual expressions of their authors and not those of the Society.

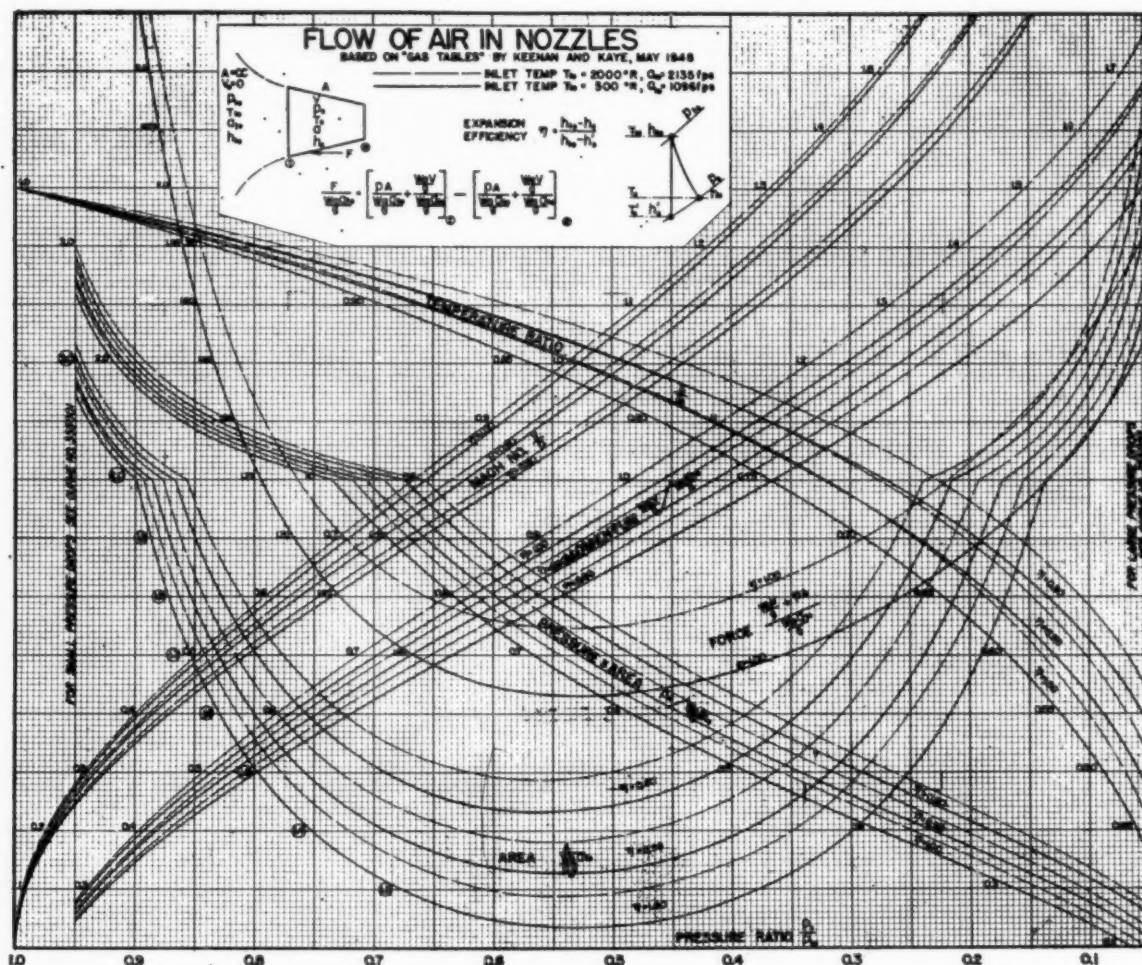


FIG. 1 FLOW OF AIR IN NOZZLES

If we analyze only the combination of compressor, burner, and turbine, we find we can present the performance as follows:

$$\text{A function of } \left(\frac{P_{t3}}{P_{t2}} \right), \left(\frac{T_{t4}}{T_{t2}} \right), \left(\frac{n}{\sqrt{\theta_{t2}}} \right) = 0 \quad [6]$$

$$\text{A function of } \left(\frac{T_{t3}}{\theta_{t2}} \right), \left(\frac{T_{t4}}{\theta_{t2}} \right), \left(\frac{n}{\sqrt{\theta_{t2}}} \right) = 0 \quad [7]$$

$$\text{A function of } \left(\frac{W_a \sqrt{\theta_{t2}}}{\delta_{t2}} \right), \left(\frac{T_{t4}}{\theta_{t2}} \right), \left(\frac{n}{\sqrt{\theta_{t2}}} \right) = 0 \quad [8]$$

$$\text{A function of } \left(\frac{W_f}{\sqrt{\theta_{t2} \delta_{t2}}} \right), \left(\frac{T_{t4}}{\theta_{t2}} \right), \left(\frac{n}{\sqrt{\theta_{t2}}} \right) = 0 \quad [9]$$

These relations give the generated pressure, the generated gas temperature, the air flow, and the fuel flow in terms of the top temperature and the rotational speed. All values are corrected to the compressor-inlet total pressure and temperature. The Relations [6] through [9] represent the "internal performance"

of a jet engine. Once this performance is determined, it can be combined with the characteristics of the inlet ducting and those of the exhaust nozzle to give the over-all performance of the engine.

THE EXTRAPOLATION METHOD

Let us assume we are testing a given jet engine, and during the test we arrange by means of an evacuating device to reduce the back pressure (P_{t2}) below atmosphere, and at the same time we reduce the exhaust-nozzle area so as to maintain the same conditions after the turbine (at point 5). The jet engine would now be operating under conditions which are similar to those in flight, because the total pressure at the compressor inlet will be greater than the static pressure at the outlet of the exhaust nozzle. Furthermore, since the conditions at the exit of the turbine were maintained constant, $(P_{t3}/P_{t2}) = \text{const}$, the internal performance of the jet engine would be unchanged by the reduction of back pressure and nozzle size.

We can now foresee that without performing the foregoing experiment, it is possible to predict a flight operating condition from the static-test data. The flight condition so calculated would correspond to a case with a reduced exhaust-nozzle size.

The method of carrying out such an extrapolation from a static test is summarized in the following:

Let us assume that we have corrected data taken from a single static test and represented by the quantities

$$\left(\frac{F}{\delta_{12}}\right)_T, \left(\frac{W_a \sqrt{\theta_{12}}}{\delta_{12}}\right)_T, \left(\frac{n}{\sqrt{\theta_{12}}}\right)_T, \left(\frac{T_{14}}{\theta_{12}}\right)_T, \left(\frac{W_f}{\delta_{12} \sqrt{\theta_{12}}}\right)_T, \left(\frac{P_{13}}{P_{12}}\right)_T, A_T$$

The subscript T represents the tested data while E represents extrapolated values.

(a) Calculate the corrected jet velocity from the thrust and air flow

$$\left(\frac{C_T}{\sqrt{\theta_{12}}}\right)_E = g \left(\frac{F}{\delta_{12}}\right)_T \left/ \left(\frac{W_a \sqrt{\theta_{12}}}{\delta_{12}}\right)_T \right.$$

(b) Assume a reduction in back pressure on the engine. The ratio of original to assumed back pressure becomes the flight (ram) pressure ratio $(P_{12}/P_{am})_E$ of the extrapolated point so that this pressure ratio can, if desired, be chosen to correspond to a given flight speed.

(c) Calculate the isentropic temperature ratio corresponding to the foregoing assumed flight (ram) pressure ratio

$$\left(\frac{P_{12}}{P_{am}}\right)_E^{\frac{k-1}{k}} = \left(\frac{T_{12}}{T_{am}}\right)_E = \left(\frac{\theta_{12}}{\theta_{am}}\right)_E$$

(d) To find the required reduction in nozzle area to maintain fixed conditions at point 5, we make use of curve 1, which is explained in Appendix 2. It should be noted that since curve 1 is a general working curve, its nomenclature differs from the remainder of the paper. Enter curve 1 with

$$\frac{P_s}{P_{10}} = \left(\frac{P_{12}}{P_{10}}\right)_T$$

and at an assumed exhaust-nozzle efficiency pick off the dimensionless area

$$\left[\frac{A}{(w_a a_{10}) / (P_{10} g)} \right]$$

Also pick off the dimensionless velocity

$$\frac{W_a V}{g} \left/ \frac{W_a a_{10}}{g} \right.$$

(e) Enter curve 1 again with

$$\frac{P_s}{P_{10}} = \left(\frac{P_{12}}{P_{10}}\right)_T \left/ \left(\frac{P_{12}}{P_{am}}\right)_E \right.$$

and again pick off the dimensionless area and velocity at the assumed nozzle efficiency.

(f) The ratios of the dimensionless areas and velocities obtained in (d) and (e) give the required reduction in exhaust-nozzle area and increase in jet velocity. By multiplication, we thus obtain A_E and $(C_T/\sqrt{\theta_{12}})_E$ which are, respectively, the exhaust-nozzle area, and the corrected jet velocity for the extrapolated point.

(g) Calculate the flight speed, corrected to atmospheric conditions, from the flight (ram) pressure ratio assumed under (b)

$$\left(\frac{V}{\sqrt{\theta_{am}}}\right)_E = \sqrt{2T_{am} g c_p f \left[\left(\frac{P_{12}}{P_{am}}\right)_E^{\frac{k-1}{k}} - 1 \right]}$$

(h) Calculate the rotational speed corrected to atmospheric conditions for the extrapolated point using the ram temperature ratio under (c)

$$\left(\frac{n}{\sqrt{\theta_{am}}}\right)_E = \left(\frac{n}{\sqrt{\theta_{12}}}\right)_T \sqrt{\left(\frac{\theta_{12}}{\theta_{am}}\right)_E}$$

(i) Calculate the extrapolated net thrust, corrected to atmospheric conditions from the ram pressure ratio, the air flow, and the jet and flight velocities

$$\left(\frac{F_s}{\delta_{am}}\right)_E = \frac{1}{g} \left(\frac{P_{12}}{P_{am}}\right)_E \left(\frac{w_a \sqrt{\theta_{12}}}{\delta_{12}}\right)_T \left[\left(\frac{C_T}{\sqrt{\theta_{12}}}\right)_E - \left(\frac{V}{\sqrt{\theta_{am}}}\right)_E \sqrt{\left(\frac{\theta_{am}}{\theta_{12}}\right)_E} \right]$$

(j) Calculate the corrected air flow

$$\left(\frac{w_a \sqrt{\theta_{am}}}{\delta_{am}}\right)_E = \left(\frac{w_a \sqrt{\theta_{12}}}{\delta_{12}}\right)_T \sqrt{\left(\frac{\theta_{am}}{\theta_{12}}\right)_E} \left(\frac{P_{12}}{P_{am}}\right)_E$$

(k) Calculate the corrected top temperature

$$\left(\frac{T_{14}}{\theta_{am}}\right)_E = \left(\frac{T_{14}}{\theta_{12}}\right)_T \left(\frac{\theta_{12}}{\theta_{am}}\right)_E$$

Other quantities, such as corrected specific fuel consumption, can be determined easily from the extrapolated quantities found in the foregoing equations.

In summary, the foregoing calculations have given us the net thrust, fuel flow, rotational speed, top temperature, jet velocity, and air flow, corresponding to a given corrected flight speed. All quantities are corrected to the atmospheric conditions before the engine.

DISCUSSION

As a practical application of the method, consider a case in which static tests have been run for various exhaust-nozzle openings. The results of these tests can be extended to flight conditions by extrapolating to smaller exhaust-nozzle areas.

If we are interested in performance data for only one value of exhaust-nozzle area, static tests can be run with various exhaust-nozzle passages which are larger (even diffusing) in size. The results can then be extended to flight conditions by extrapolating to the desired exhaust-nozzle size.

It is also possible to extrapolate in the reverse direction, in order to obtain performance with duct losses. Should it be necessary to extend the range to excessively high duct losses or to represent a case where the boundary layer is removed from the wings and fed into the inlet duct (greatly reducing the effective ram), an actual duct exhibiting such characteristic could be used, or even a simulated inlet duct in the form of a fine-mesh screen could be placed across the inlet.

Fig. 2 shows the flight range covered by the method. This

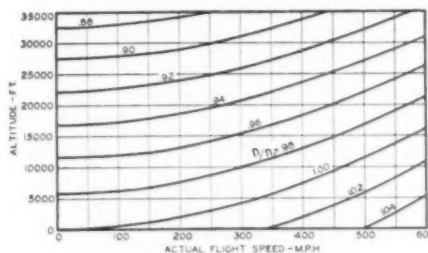


FIG. 2 EXTRAPOLATION RANGE FOR STANDARD SEA-LEVEL TEST CONDITIONS

curve assumes that the static tests are run under standard sea-level conditions. As illustrated by this curve, performance can

be obtained only up to 17,000 ft altitude for 600 mph with maximum allowable rotational speed and top temperature. Above this altitude the method will give performance only at reduced rotational speeds and top temperatures.

However, if the static tests are run on a day having a temperature less than the standard sea-level value, the limiting altitude will be increased accordingly. Likewise, it is possible to have the jet engine suck its air through a cooling turbine and in that way reduce the inlet-air temperature considerably below atmospheric. Naturally, this will extend accordingly the range of flight operation obtained; for here we are, in effect, extrapolating from a test condition corresponding to static altitude rather than static sea level.

It should be noted that the following liberties were taken in this extrapolation method:

- 1 Neglect of Reynolds-number effects.
- 2 Neglect of the effect caused by change in the properties of the fluid such as specific heat, gas constant, etc.
- 3 An exhaust-nozzle efficiency was assumed for the added expansion required by the method.

Appendix 1

DEVELOPMENT OF EQUATION [3]

The air mass flow W_a/g through any one of several geometrically similar jet engines depends upon the engine rotational speed n , the size of the engine represented by any convenient reference length D , the adjustable exhaust-nozzle area A , the compressor-inlet total pressure P_{t2} , the compressor-inlet total temperature T_{t2} , and the properties of the working fluid (in this case air) R and c_p .

A function of

$$\left(\frac{W_a}{g}\right) n D A P_{t2} T_{t2} R c_p = 0$$

We have in this analysis neglected to include the fluid viscosity or thermal conductivity. Thus, knowingly, we are neglecting Reynolds-number and Prandtl-number effects on the performance. These effects can be included later when sufficiently accurate test data are available.

By the methods of dimensional analysis, the foregoing relation can be reduced to a new relation between fewer dimensionless variables, for instance, a function of

$$\left(\frac{W_a a_{t2}}{P_{t2} A g}\right) \left(\frac{n D}{a_{t2}}\right) \frac{A}{D^2} k \frac{R}{C_p} = 0$$

We have in writing the foregoing relations assumed that the working fluid is a perfect gas with an acoustic velocity

$$a_{t2} = \sqrt{g k R T_{t2}}$$

Rather than use the dimensionless quantities in this relation in plotting engine performance, it has been found more convenient, although somewhat less general, to use the relation

$$\left(\frac{W_a \sqrt{\theta_{t2}}}{\delta_{t2}}\right) \left(\frac{n}{\sqrt{\theta_{t2}}}\right) A = 0 \dots \dots [3]$$

A function

This latter relation is restricted to use for a given-size engine, ($D = \text{const}$), and neglects variations of k and C_p of the working fluid. The inlet temperature and pressure are also given as ratios (θ_{t2} and δ_{t2}) to the standard sea-level total pressure and temperature, respectively.

The quantities appearing in the foregoing relation have dimensions and, therefore, are called "corrected values." They represent the tested values under standard sea-level conditions (for the case without inlet-duct losses), and give more reasonable numerical values for plotting test curves. Others have used, for instance, the quantity n/\sqrt{T} for corrected speed. The numerical values of this quantity for 16,000 rpm and 520 deg R would be 222 rpm/ $\sqrt{\text{deg}}$. The inconvenience is apparent.

Relation [3] simply states that the air flow for a given corrected speed and exhaust-nozzle area is proportional to the compressor-inlet total pressure ($\sim \delta_{t2}$) and inversely proportional to the square root of the compressor-inlet total temperature ($\sim \sqrt{\theta_{t2}}$).

The other relations appearing in the paper can easily be developed in a manner similar to the development of Equation [3].

Appendix 2

Fig. 1 is a working curve which is intended for use in the solution of many flow problems.

Often we are given a problem involving a flow through a channel or nozzle in which an area, a total temperature, and a velocity are given at one station, and we are required to find an area, temperature, or velocity at another station.

Fig. 1 has been constructed in such a way that areas, velocities, pressures, Mach numbers, and temperatures along the channel are given as dimensionless quantities in terms of inlet total pressure and temperature or inlet acoustic velocity. All curves are based upon the properties of air as given by Keenan and Kaye and are drawn for 2000 deg R and 500 deg R inlet temperature.

For other inlet temperatures, we interpolate between the curves.

The curve shows the variation of temperature, Mach number, momentum, area, and pressure \times area, with the static pressure, all given as dimensionless quantities.

Thus for fixed total conditions, the ratios of the dimensionless velocities at two stations along the nozzle are also the ratio of the velocities. Similarly, the ratios of the dimensionless areas are also the area ratio.

In the problem used in the extrapolation method of this paper we are assuming an extension of the exhaust nozzle with a corresponding reduction in back pressure so as to leave the conditions before the nozzle unaffected. We need only enter the curve with $(P_s/P_b) = (P_{t2}/P_{t3})_T$ and select a dimensionless velocity and area. For, say, a 10 per cent lower back pressure, we need only read the curve again with a value of P_s/P_b , which is 10 per cent lower than the original value. The ratios of dimensionless areas and velocities then give, respectively, the required area reduction, and velocity increase.

The thrust force on the channel is also easily calculated as shown on the curve.

It is no fatigue st-
ciable ext-
In order
of this sh-
ploying f-
two differ-
pared an-
factors th-
havior.
or altera-
the differ-
the rela-
localized
cross sec-
outward
the prim-
flexural f-

A GI reg-
str-
shape fac-
changes o-
strengths
fillet, hol-
been paid
tion may

In stud-
test resul-
Metals (3
seemed to
test speci-
specimens
lower tha-
of the sam-
specimen
higher th-

Based o-
tary elast-
son to su-
influence
terials su-

¹ Engin-
ASME.

² Cook

³ Engin-

⁴ Num-

the paper

⁵ Since

cles (11, 1

lar beams

machine.

Contrib

the Annu

1949, of 7

NOTE:

understo

of the Soc

The Influence of Shape of Cross Section on the Flexural Fatigue Strength of Steel

By T. J. DOLAN,¹ J. H. McCLOW,² AND W. J. CRAIG,³ URBANA, ILL.

It is not generally known or recognized that the flexural fatigue strength of a beam may be influenced to an appreciable extent by the shape of cross section of the member. In order to obtain further information on the magnitude of this shape effect, flexural fatigue tests were made employing four different shapes of cross section for each of two different steels. The results of these tests are compared and analyzed to clarify or explain some of the shape factors that may be of importance in affecting fatigue behavior. It is concluded that variations in residual stress or alterations of properties due to method of machining the different shapes play only a minor part in affecting the relative endurance limits. The susceptibility to localized inelastic action as governed by the shape of cross section and by the presence of "sore spots," such as outward projecting corners, are tentatively believed to be the primary elements leading to the differences noted in flexural fatigue strengths.

INTRODUCTION

A GREAT deal of data is available in the technical literature regarding the effects of the geometrical shape on the fatigue strength exhibited by a metal member. However, the shape factors usually considered by investigators are the abrupt changes of cross section which result in greatly reduced fatigue strengths due to the high localized stresses developed at a notch, fillet, hole, or other change of section. Very little attention has been paid to the possible manner in which the shape of cross section may influence the fatigue properties of a uniform beam.

In studying the effect of type of testing machine on fatigue test results, the ASTM Research Committee on Fatigue of Metals (1)⁴ found that a distinct change in fatigue strength seemed to be produced by altering the shape of cross section of a test specimen. In vibratory bending fatigue tests "rectangular" specimens exhibited fatigue strengths as much as 16 per cent lower than the fatigue strength obtained for "round" specimens of the same metal. Furthermore, it has been observed that round specimens tested in vibratory bending developed endurance limits higher than did similar specimens in rotating-beam tests (2, 3).⁴

Based on computations of nominal stress by means of elementary elastic theory (using the flexure formula), there is little reason to suspect that the shape of cross section should have any influence on the fatigue strength of a member. However, materials subjected to repeated stressing do not behave in accord-

ance with the basic assumptions of the theory of elasticity. One possible concept advanced to explain this phenomenon of a shape effect associates the relative amount of material at peak stresses with the propensity toward failure, that is, in a rectangular specimen a larger volume of material in the extreme fiber is subjected to peak stress than in a round specimen, and statistically, there is thus a greater chance for failure to occur. Little data is available to indicate whether factors such as residual stress, variations in machining procedure, or structural readjustments associated with the particular shape of cross section have a definite influence on the fatigue strength of machine parts in service.

OBJECT AND SCOPE OF INVESTIGATION

The purpose of this investigation was to obtain information regarding the relative magnitude of the effect of shape of cross section on flexural fatigue strength, and to analyze these data in an attempt to determine what factors influenced the fatigue behavior when the shape of the critical cross section was altered.

Flexural fatigue tests were made involving several shapes of specimen from each of two different steels. The size of the critical cross section in specimens of each metal was maintained as nearly constant as possible throughout each series of fatigue tests in order to eliminate as far as possible any size effect.

Four shapes of cross section were chosen for the test, namely, square, diamond, round, and a modified diamond. The techniques of manufacture of each specimen were studied rather critically in order to detect any possible changes in surface conditions and residual stresses which might arise to alter the fatigue properties exhibited by a member.

MATERIALS, TEST SPECIMENS, AND METHOD OF TESTING

The first series of test specimens were made of Mayari-R (a low-alloy structural steel) in a normalized condition and having the chemical and mechanical properties listed in Table 1. The second series of specimens were made of SAE 4340 steel, quenched and tempered to a static tensile strength of approximately 150,000 psi. The static mechanical properties and chemical analysis of this material are listed in Table 2, and a comparison of typical tensile stress-strain curves for the two steels is included in Fig. 1. These metals were selected for the investigation in order to compare the results for two steels having widely different mechanical strength. It was felt that the higher strength exhibited by the SAE 4340 steel would accentuate any shape effects which might be observed with the lower strength Mayari-R steel.

The dimensional details of the flexural-fatigue test specimens are shown in Figs. 2 and 3; these were all cut from 3/4-in.-diam bar stock; flats were milled on top and bottom to provide gripping surface for the testing machine.

The modified diamond section, Fig. 3(d), was prepared by removing from the extreme fiber of the diamond section the optimum amount to give the theoretically strongest beam. For example, the section modulus for the diamond shape was

$$I/c = 0.1178 d^3$$

in which d is the width of the side in the diamond section. By removing one eighteenth of the diagonal depth from both the top

¹ Engineering Experiment Station, University of Illinois. Mem. ASME.

² Cook Research Laboratories, Chicago, Ill.

³ Engineering Experiment Station, University of Illinois.

⁴ Numbers in parentheses refer to the Bibliography at the end of the paper.

⁵ Since this paper was written there have been published two articles (11, 12) in which the fatigue data also indicated that rectangular beams were weaker than round beams tested in the same fatigue machine.

Contributed by the Machine Design Division and presented at the Annual Meeting, New York, N. Y., November 27-December 2, 1949, of THE AMERICAN SOCIETY OF MECHANICAL ENGINEERS.

NOTE: Statements and opinions advanced in papers are to be understood as individual expressions of their authors and not those of the Society. Paper No. 49-A-55.

and the bottom, the section modulus for the diamond section became

$$I/c = 0.1243 d^3$$

which represents approximately $5\frac{1}{2}$ per cent increase in elastic flexural strength. For the square section (with the neutral axis of bending parallel to one face) the section modulus was

$$I/c = 0.1667 d^3$$

in which d represents the length of the side of the square.

Specimens of all four shapes, Figs. 2 and 3, were formed by machining the test section with longitudinal cuts, using a milling cutter having a 3-in. radius. A set of specimens of SAE 4340 steel with the round critical section, Fig. 2(c), was also prepared by turning with a single-point tool in a lathe (following the usual procedures for rotating-beam specimens), since the results of the first tests on round specimens seemed to indicate that a difference

TABLE 1 CHEMICAL COMPOSITION AND MECHANICAL PROPERTIES OF MAYARI-R STEEL

CHEMICAL COMPOSITION			
	Per cent		Per cent
Carbon.....	0.10	Nickel.....	0.35
Manganese.....	0.76	Chromium.....	0.67
Sulphur.....	0.028	Copper.....	0.58
Silicon.....	0.34	Phosphorus.....	0.096
MECHANICAL PROPERTIES ^a			
Upper yield point, psi.....			54800
Lower yield point, psi.....			52600
Tensile strength, psi.....			75200
Elongation in 2 in., per cent.....			33.2
Reduction of area, per cent.....			73.0
Brinell hardness number.....			147

HEAT-TREATMENT
Normalized at 1600 F

^a Each value represents the average of three tests.

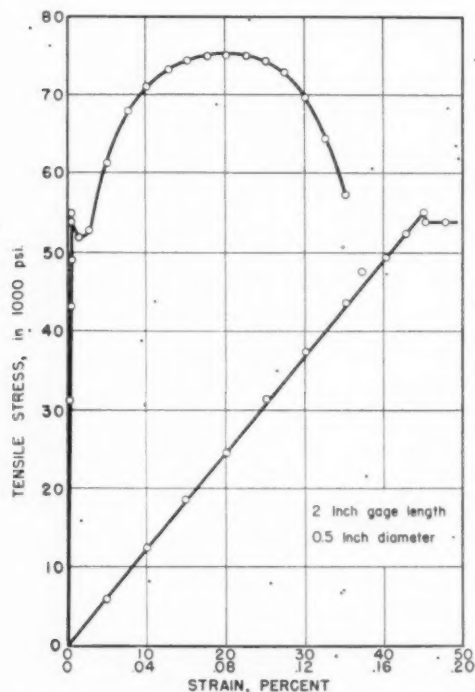


FIG. 1(a) STRESS-STRAIN DIAGRAM OF MAYARI-R STEEL

might exist between the results obtained from milled and from turned surfaces.

All round specimens were polished by means of emery paper wrapped around a rotating cylindrical bar which was moved slowly along the specimen by hand while the specimen was turning slowly in a lathe. For successive grades of polishing paper the direction of rotation of the specimen was reversed to change the direction of abrasive scratches; the final polishing scratches were parallel to the longitudinal axis of the specimen. All other specimens were polished by hand with scratches from successive papers being generated at right angles and finishing with a longitudinal motion with No. 2/0 paper slushed with machine oil.

All fatigue specimens were subjected to completely reversed cycles of flexural stress in Krouse plate-fatigue machines. In operation of these machines one end of the specimen is clamped rigidly in a vise B; and the other end is reciprocated vertically by means of a connecting rod and eccentric crank mechanism,

TABLE 2 CHEMICAL COMPOSITION AND MECHANICAL PROPERTIES OF SAE 4340 STEEL

CHEMICAL COMPOSITION			
	Per cent		Per cent
Carbon.....	0.39	Chromium.....	0.72
Manganese.....	0.66	Nickel.....	1.72
Phosphorus.....	0.012	Molybdenum.....	0.35
Sulphur.....	0.018		
MECHANICAL PROPERTIES ^a			
Upper yield point, psi.....			137500
Lower yield point, psi.....			133000
Tensile strength, psi.....			148800
Elongation in 2 in., per cent.....			20.9
Reduction of area, per cent.....			62.0
Brinell hardness number.....			322

HEAT-TREATMENT
Quenched in oil from 1525 F, tempered at 1150 F, cooled in air

^a Each value represents the average of five tests.

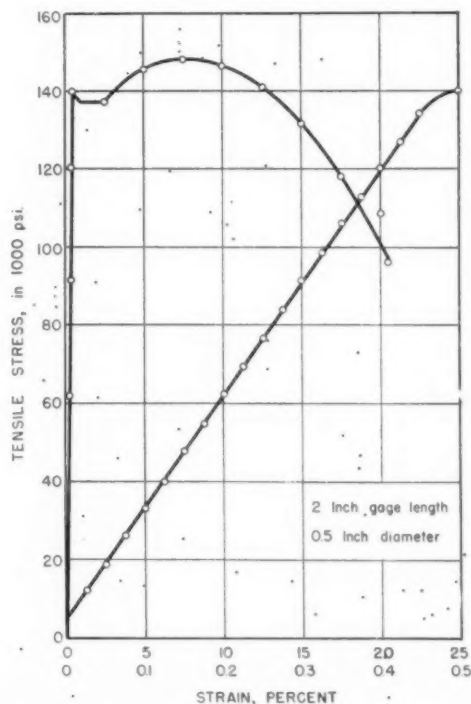


FIG. 1(b) STRESS-STRAIN DIAGRAM OF SAE 4340 STEEL

Fig. 4. A the critical with the position. both upw connecting eccentric dial indic reversed In orde mum stre the mach the deflec

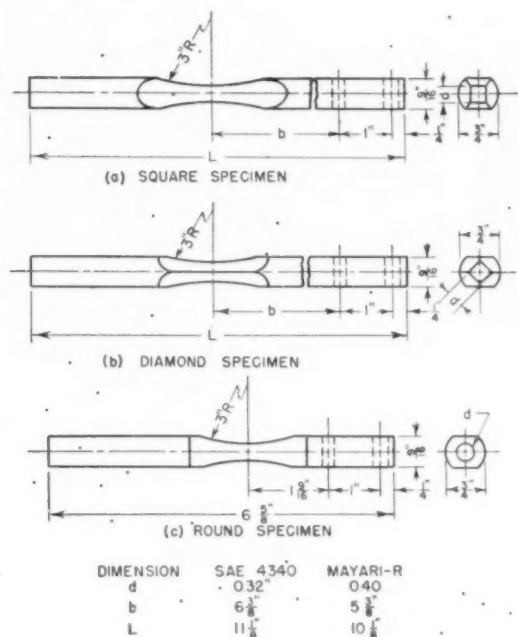


FIG. 2 SPECIMEN FOR CANTILEVER BENDING MACHINE

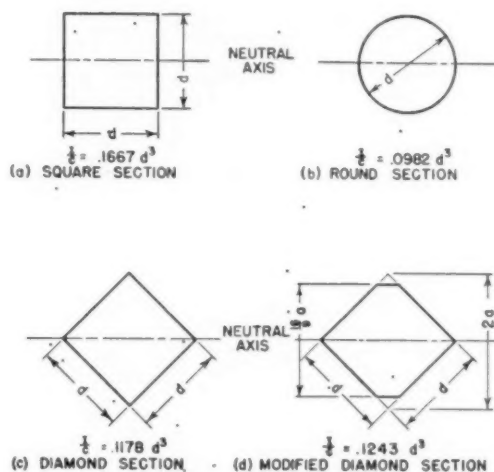


FIG. 3 VARIOUS CROSS SECTIONS USED IN TESTS

Fig. 4. A dead weight required to produce the desired stress in the critical-section S, is applied to the pin P, in the clamp C, with the connecting rod AP disconnected and swung out of position. The deflection is noted on the dial indicator D, for both upward and downward loads of the desired amount. The connecting rod AP is then coupled (as shown in Fig. 4), and the eccentric cam A adjusted to provide the same deflections of the dial indicator. For each revolution of the motor a completely reversed cycle of end deflection of the specimen is applied.

In order to check the stability and accuracy with which maximum stresses were reproduced throughout the duration of a test, the machines were stopped periodically and a recheck made of the deflection corresponding to the desired dead weight.

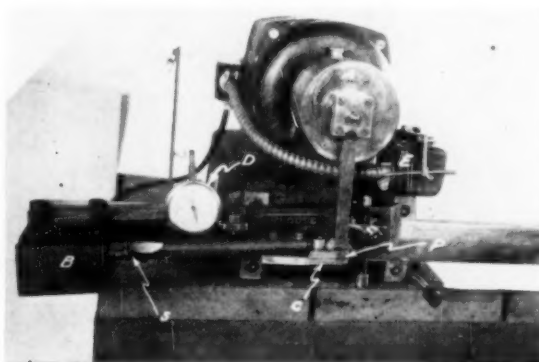


FIG. 4 KROUSE PLATE-FATIGUE TESTING MACHINE

RESULTS OF THE INVESTIGATION

The results of the fatigue tests on Mayari-R and SAE 4340 steels are plotted in the form of S-N diagrams in Figs. 5, 6, and 7. A summary of the fatigue limits obtained for these four shapes of cross section is given in Table 3, for the two steels. It will be noted that for each steel the round specimens exhibited fatigue limits appreciably greater than those obtained for the other three shapes tested. By utilizing the strength of the round specimens of each material as a "par" value, the relative fatigue limits for the various shapes of specimen are compared in the last two columns of Table 3. These ratios indicate that for either steel the general trend of decreasing endurance limits was in the following order: (a) round; (b) diamond; (c) modified diamond and square.

A comparison of the endurance limits for the square and the modified diamond cross sections reveals the fact that their strengths were almost the same, and that their relative order of strength was reversed when comparison is made between the tests on the two different steels. Thus it may be inferred that there was little, if any, difference between the strengths exhibited by the square and the modified diamond beams.

Possible Factors Contributing to a Shape Effect for Beams. In seeking an explanation for these apparently paradoxical differences in fatigue strength, the following concepts have been reviewed in a search for a possible explanation:

- 1 From a statistical viewpoint, the relative amount of material subjected to stresses greater than a certain percentage of the peak stress may influence the initiation of failure.
- 2 Possible regions of stress concentration or "sore spots," or the presence of highly stressed fibers that lack lateral support.
- 3 The presence of varying amounts of residual stresses in the various shapes which may be altered by the differences in manufacturing operations or processing.
- 4 Alterations in the mechanical properties of the surface fibers caused by differences in the amount of cold-working in the machining operations (and not entirely removed by polishing).
- 5 The effect of the shape of cross section in controlling the relative extent of "localized" inelastic action occurring on the extreme fibers of the beam.

The possible contributions of each of these items to the various differences in fatigue properties as noted in the tests will be discussed briefly.

By comparing the relative amount of material subjected to the peak stress in each of these cross sections and the sore spots (possible points of stress concentration), one finds that the round shape has a relatively small amount of material at peak stress,

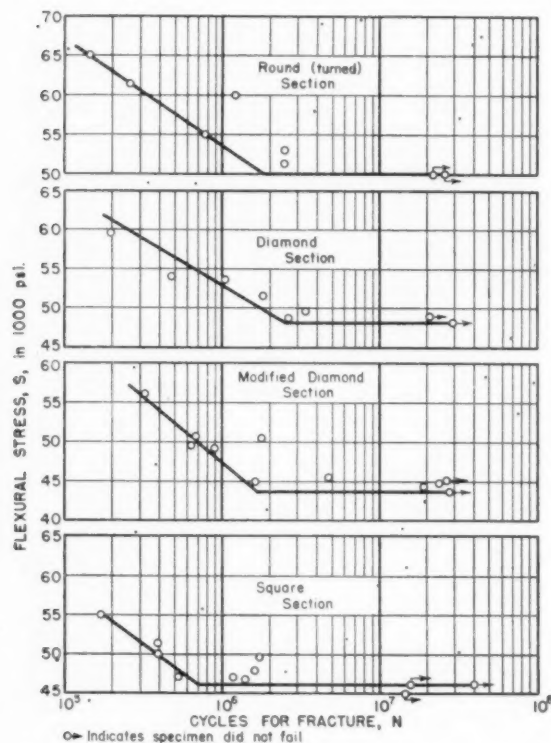


Fig. 5 VIBRATORY BENDING FATIGUE TESTS OF MAYARI-R STEEL OF VARIOUS CROSS SECTIONS

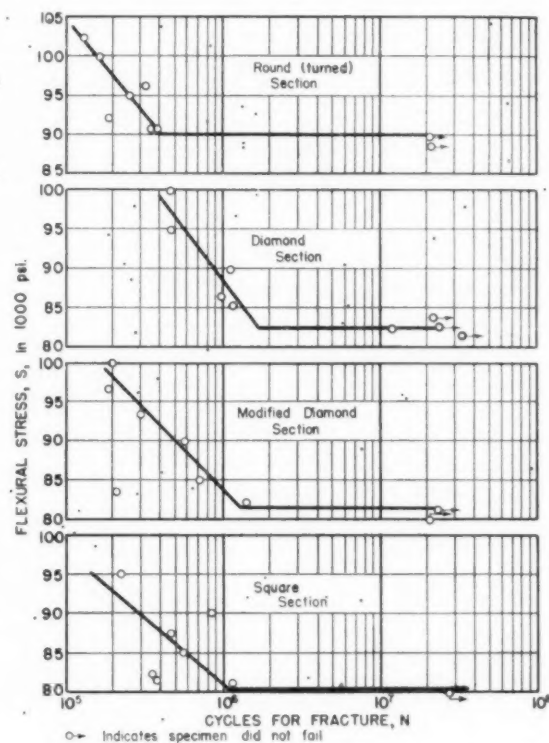


Fig. 6 VIBRATORY BENDING FATIGUE TESTS OF SAE 4340 STEEL OF VARIOUS CROSS SECTIONS

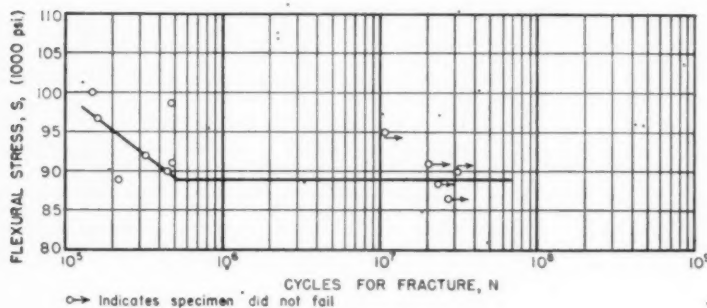


Fig. 7 (left) VIBRATORY BENDING FATIGUE TESTS OF SAE 4340 STEEL OF MILLED ROUND CROSS SECTION

TABLE 3 INFLUENCE OF SHAPE OF CROSS SECTION ON FLEXURAL FATIGUE STRENGTH

(Completely Reversed Cycles of Stress)

TEST RESULTS FOR MAYARI-R SPECIMENS

Specimen shape	Fatigue limit, psi	Ratio of fatigue limit to that of round	Per cent reduction in strength (based on round specimen)
Round (turned)*.....	50000	1.00	0
Square (milled).....	46000	0.92	8
Diamond (milled).....	48000	0.96	4
Modified diamond (milled)....	44000	0.88	12

TEST RESULTS FOR SAE 4340 STEEL SPECIMENS

Round (turned)*.....	90000	1.00	0
Round (milled).....	89000	0.99	1
Square (milled).....	80500	0.89	10.5
Diamond (milled).....	83000	0.92	7.7
Modified diamond (milled)....	82000	0.91	8.9

* Method of machining.

and does not contain sharp corners which may result in localized stresses due to outward projecting fins, or from nicks or scratches crossing the sharp corners. On the other hand, the diamond shape, with the minimum amount of material at peak stress, has one sharp corner which comprises the extreme fiber. This corner may lead to sore spots from which failure may initiate for two reasons, namely, (a) it is impossible to produce a sharp corner without some small intersecting scratches which may be effective as stress raisers, and (b) the outward projection is entirely unsupported except for the thin layer of metal below it, which in turn is rather highly stressed. Therefore this unsupported edge may be subjected to a localized buckling action during the compressive portion of a stress cycle. On this basis it seems reasonable that round specimens might develop a higher fatigue limit than those of diamond shape or other types with sharp corners.

In order to facilitate comparison of the relative amounts of

material
Fig. 8 an
depth in
and the
lying be
ble to pr
the spec
depths l
amount
tude (fo
has the
mond.
varies in
at peak
In opti
peak str
these tes

Fig. 8

material in the extreme fibers of these various shapes, the data in Fig. 8 are of interest. The ordinates in this figure indicate the depth in inches below the test surface for each type of specimen, and the abscissas represent the corresponding cross-sectional area lying between the extreme fiber and that depth. It is reasonable to presume that the failure is initiated in the outer fibers of the specimen at a depth not greater than about 0.004 in. For depths less than this amount the square shape has the greatest amount of material at peak stress; the order of decreasing magnitude (for amount of material at peak stress) for the other shapes has the following sequence: modified diamond, round, and diamond. Thus, by comparison with Table 3, the fatigue strength varies in a general manner inversely as the amount of material at peak stress.

In opposition to the thought that the amount of material at peak stress controls the fatigue limit, there are two instances in these tests for which the reverse tendency appeared, namely, (a)

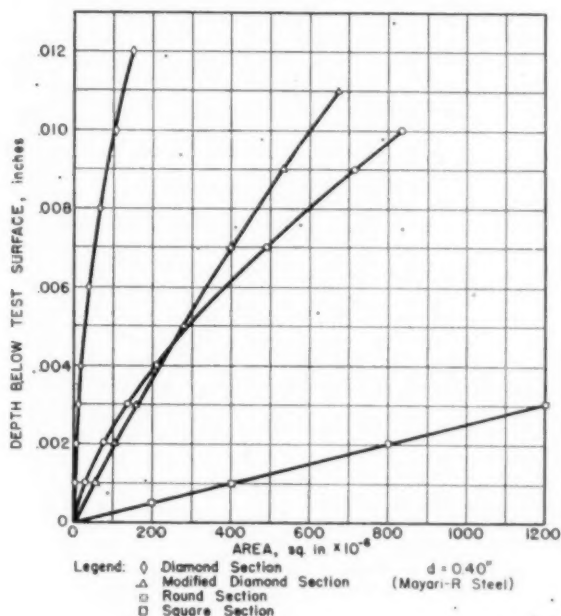


FIG. 8 RELATIVE AREAS OF EXTREME FIBERS IN CROSS SECTIONS OF SPECIMENS; MAYARI-R STEEL

the round specimens exhibited a higher endurance limit than the diamond shape, and (b) the fatigue limits for the square beams and for the modified diamond beams were practically the same, in spite of the fact that there was an appreciable difference in the volume of metal exposed to the peak stresses (in the extreme fibers) for these latter two shapes. It should also be kept in mind that both the modified diamond section and the square section have two sharp corners projecting outward from which failure may be initiated. The exact stress (including residual stresses) in the region of the corner of any of these shapes is unknown and difficult to evaluate, but it seems reasonable to assume that any abrupt change in shape may leave protruding fibers that may initiate fracture in these regions.

Metallographic examinations of the different specimens indicated that the diamond and modified diamond shapes did not have true sharp corners with flat plane faces. These projecting corners were found to have been rounded slightly in polishing, but this was desirable in order to remove any sharp fins of fragmented material. The cutting operations and cold-working involved in the machining of any specimen develop unknown amounts of residual stress in the surface layers which may be either of a macro (large-scale) or of a micro (small-scale) nature. In polishing a fatigue specimen, the removal of sufficient surface layers will reduce the surface residual stresses (4). However, no suitable methods exist today for measuring these residual stresses or of determining whether they have been removed.

A series of micro-indent (Knoop) hardness surveys were made on a number of test specimens to detect any hardness variations (strain-hardening) which might be a clue to the presence of (accompanying) residual stresses. Specimens with outward projecting corners might be particularly susceptible to the alteration of their physical properties by cold-working (and also to the development of residual stresses) owing to the fact that the pressures of cutting tools were applied in two different directions to the protruding corners. For the round specimens, conversely, this condition would not exist during the machining operations.

The microhardness surveys were made on transverse cross sections with particular attention being given to the material near the surface. However, the Knoop hardness values plotted in Figs. 9, 10, and 11 do not indicate any consistent increase in hardness near the surface. Only a small amount of material is examined at any one indent and hence random variations are to be expected.

The upper shaded area in Fig. 9 indicates the range of hardness found in pearlitic areas in the Mayari-R steel, and the lower shaded area shows the smaller spread of lower hardness found in ferrite grains or colonies of grains. This is in line with pre-

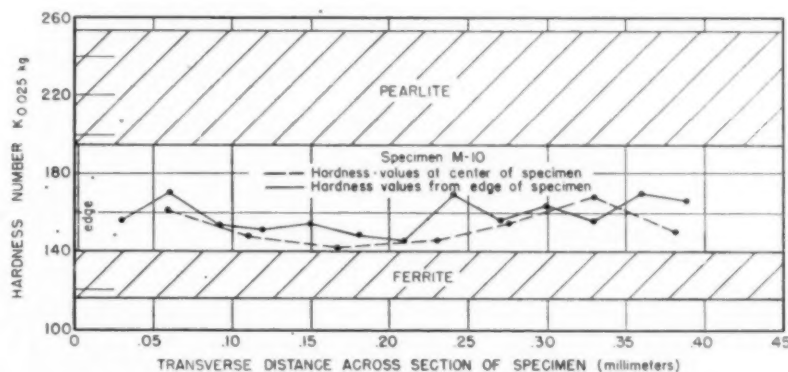


FIG. 9 HARDNESS SURVEY OF ROUND-TURNED-SPECIMEN OF MAYARI-R STEEL

vious observations that hardness will vary within a material, between different crystals, and also with different orientations and locations within the crystal itself (5). It will be noted that the variations in hardness from the center to the test surface fall entirely between these two bands and show no abnormal increase in the hardness of the surface crystals.

In Fig. 10 is shown a comparison of hardness surveys obtained on round SAE 4340 steel specimens produced by milling and produced by turning in a lathe. No correlation seemed to exist between the minor variations in hardness, and the differences in machining procedure used to form the specimen. In Fig. 11 three parallel surveys of hardness values from the outer surface to the center of a round milled specimen of SAE 4340 steel are plotted. Nevertheless, the random or erratic variations in hardness at each station fall within a fairly consistent band but exhibit no definite change in hardness of surface layers as compared with the material below the surface. Metallographic examination of the edges of transverse sections cut from the critical sections of several specimens did not show visual evidence of appreciable plastic deformation remaining from the machining operations. Thus it was felt that no plausible explanations for this shape effect in fatigue could be based on hardness variations or the presence of residual stresses resulting from cold-working in machining.

Tentative Explanation for Influence of Shape of Cross Section. Several investigators in recent years have supported the hypothesis that initial plastic yield under static loads occurs at a higher stress when a stress gradient exists (as in a beam) than the yield point for the same metal, when subjected to a uniformly distributed stress. Based on this assumption, it has been suggested (8) that a shape factor exists for the determination of yield strength in static flexural tests. However, further evidence indicates (9, 10) that the stress at which general yielding occurs in the extreme fibers of a beam is the same as that for the same metal under a uniform tensile stress, that is, the yield stress is not modified by the presence of a stress gradient.

The extent to which general plastic deformation progresses into a beam at loads above that which initiates yielding is, however, a function of the shape of the beam, Fig. 12. It is therefore probable that the microscopic, heterogeneously distributed inelastic actions that accompany the development of progressive fracture may likewise be influenced to some extent by the shape of cross section (or distribution of metal in the most highly stressed regions of a beam).

As evidence of variations in inelastic action at stresses above the yield point, Fig. 12 illustrates the theoretical curve of Morkovin and Sidebottom (10), in which the ordinates represent the ratio of the actual bending moment on the beam to the bending moment required to initiate yielding, and the abscissas represent the ratio of strain on the extreme fiber to the strain corresponding to the yield point. These curves are applicable to beams made of material with an abrupt yield point (horizontal tangent to the stress-strain curve at the yield point).

It will be observed that beams with the smallest amount of material on the extreme fiber (at peak stress) exhibit the smallest departure from linearity of load to strain for loading conditions above the yield point. However, the inelastic behavior of the metal is modified to some extent for materials which exhibit an upper yield point (as well as a lower yield point) in a static tensile test.

This modified behavior for a beam made of material having an upper yield point is illustrated by the curves in Fig. 13 in which the co-ordinates again represent ratios of the bending moment and strain, respectively, to the corresponding values at the lower yield point. The normal behavior for a beam "without stress raisers" would be to follow the linear relationship of moment to strain along the line *OAC* with no yielding until the load corresponding to the point *B* (upper yield point) is reached. Initial yielding corresponding to the conditions represented at point *B* creates a plastic wedge which acts as a stress raiser and leads to further propagation of yielding. Thus a condition of instability is created, and further yielding will progress at stresses equal to

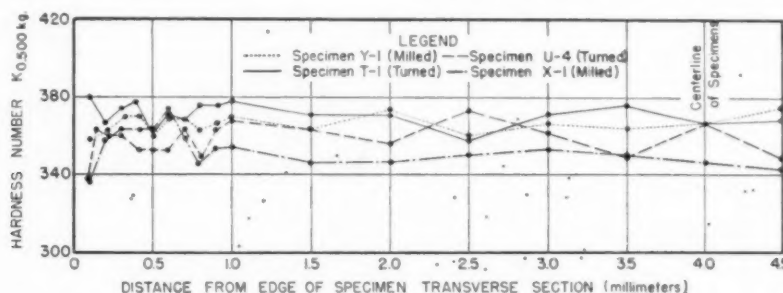


FIG. 10 HARDNESS SURVEY OF ROUND-MILLED AND TURNED-SPECIMENS OF SAE 4340 STEEL

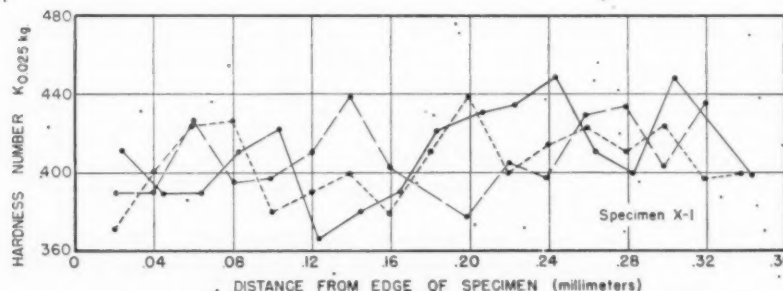


FIG. 11 HARDNESS OF ROUND-MILLED-SPECIMEN OF SAE 4340 STEEL
(Indents made in three parallel lines spaced 0.04 and 0.05 mm.)

Fig. 13

the lower
resented b
nitude of
trolled by
arise from
and meth
with stres
moment-s
lines *ACB*
correspon
stress conc
Morkov
ing corner
yielding b
outer surf
or branchi
At first l
discussion
which the
the yield
the nomina
ized stress
sisting the
nominal st

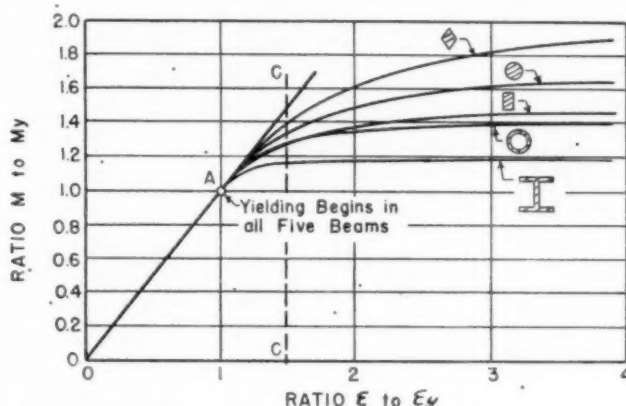


FIG. 12 THEORETICAL DIMENSIONLESS MOMENT-STRAIN DIAGRAM SHOWING EFFECT OF CROSS SECTION ON YIELDING IN MILD-STEEL BEAMS

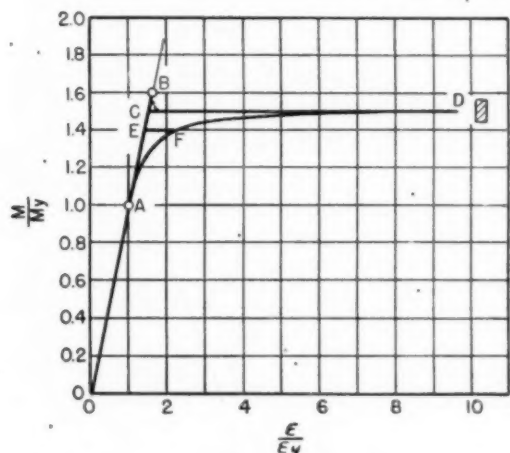


FIG. 13 MOMENT-STRAIN DIAGRAMS FOR RECTANGULAR BEAMS

the lower yield point of the material under constant loads as represented by the horizontal line CD , Fig. 13. However, the magnitude of the upper yield point exhibited by the material is controlled by the severity of the localized stresses present which arise from inherent stress raisers, inclusions, surface irregularities, and method of loading. It would be possible for the same beam with stress raisers (such as a roughened surface) to follow the moment-strain curve $OAFD$, or any intermediate curve between lines $ACBD$ and AFD . Initial yielding will start at the point A , corresponding to the lower yield point of the material, if the stress concentration is sufficiently acute.

Morkovin and Sidebottom also reported that outward projecting corners on a beam acted as nuclei from which localized plastic yielding branched out or was reflected along diagonal lines in the outer surfaces of the beam. No similar concentrations of strain or branching of plastic zones was observed for round specimens.

At first hand it may be difficult to visualize how the foregoing discussion applies to the actions progressing in fatigue tests in which the "nominal" computed stresses are considerably below the yield point of the material. However, it is obvious that the nominal stresses do not give a true index of the actual "localized stresses" developed by the individual crystals which are resisting the external loading. In a polycrystalline material, the nominal stress represents only the statistical average; the dis-

tribution of stresses on individual crystals will vary over a wide range above and below the nominal computed stress. It is highly probable that a number of the crystals in the surface fibers may either be favorably oriented for inelastic action or subjected to localized high levels of stress with corresponding strain conditions equivalent to the upper portions of the curves in Figs. 12 and 13. Thus localized inelastic actions progressing on a microscopic scale may in turn be influenced by the shape of cross section of the beam.

One might postulate, therefore, that a certain proportion of the crystals could be strained by an amount equivalent to that shown by the vertical line CC in Fig. 12. If it be assumed, as has been done by Orowan (6), that the mechanism leading to fatigue fracture is related to a critical amount of localized inelastic deformation, the line CC may be used as representative of a criterion for fatigue failure, and corresponds to the strain condition in localized crystals of the beam when repeatedly stressed at the endurance limit of the member.

By applying these observations to the present fatigue tests, it appears probable as a tentative hypothesis that the shape effects as noted in Fig. 12, were of influence in controlling the localized plastic actions, but since the materials employed in the fatigue tests had upper yield points, the modification in action portrayed in Fig. 13 must also be taken into consideration. Based upon these two concepts, the round beams which have little tendency to propagate appreciable inelastic action and which also have no stress raiser of geometric origin on the extreme fiber, should have exhibited the highest fatigue strength.

The diamond shape normally would resist somewhat greater static loads without a corresponding amount of inelastic action if the material did not display an upper yield point. However, for material exhibiting an upper yield point the fatigue limit probably was lowered by the stress-raising effect of the outward projecting corner (promoting inelastic action), and by the greater tendency for this sharp corner to act as a nucleus for the spread and reflection of slip. By following this comparison further, the modified diamond shape should be somewhat stronger than the rectangle, but somewhat weaker than the circle and diamond.

A load-strain diagram for the modified diamond shape (if added to Fig. 12), would fall somewhere between the diamond and the square shape, probably slightly below that curve representing the circular cross section. It also has two outward projecting corners which would make it behave in a manner structurally equivalent to that of the square shape.

On the basis of this reasoning, it appears logical to expect

that beams having different shapes of cross section should exhibit different fatigue strengths; the relative magnitudes of the endurance limit for each shape cannot be predicted accurately by any simple formula. In addition to the actual shape of cross section, several other strength factors influencing the fatigue limit might include: (a) the ratio of yield point to ultimate strength; (b) some parameter expressing the shape of the stress-strain curve in the region of the yield point, and (c) a consideration of whether the material exhibits an upper yield point.

In the foregoing explanation the tacit assumption has been made that localized inelastic action on a microscale induced by repeated stressing in the surface fibers contributes to fatigue damage, and that fracture results when these localized plastic actions exceed a certain level. While these assumptions are not susceptible to direct proof, there exists a great deal of experimental evidence that fatigue fracture is preceded or accompanied by plastic slip. This may be considered an indication that inelastic action due to repeated stressing is damaging in fatigue. The concepts of fatigue failure, outlined by Freudenthal and Dolan (7), also emphasize the fact that the first stage of failure in fatigue is that of crystal fragmentation (inelastic action) on a sub-microscopic scale.

CONCLUSIONS

Laboratory studies indicated that the flexural fatigue strength of a member was influenced to an appreciable extent by the shape of cross section; steel beams of circular cross section exhibited fatigue limits 8 to 10 per cent greater than the fatigue limits of beams of square cross section. Beams having a diamond cross section (square beams stressed with the neutral axis as a diagonal of the diamond) exhibited endurance limits from 4 to 8 per cent less than the round beams.

The susceptibility to localized inelastic action, as governed by the shape of cross section and by the presence of sore spots, such as outward projecting corners, is tentatively believed to be the primary element leading to the reduction of fatigue strength of the square and diamond shapes to values below that for the round. While the other factors (residual stresses, alterations of properties due to machining, and statistical aspects of the amount of material subjected to peak stress) may have been of some influence in these tests, it is felt that their effect on the fatigue strengths of beams of the shapes studied were of a minor nature.

ACKNOWLEDGMENTS

This investigation has been conducted by members of the staff of the Department of Theoretical and Applied Mechanics as a part of the work of the Engineering Experiment Station of the University of Illinois in co-operation with the Office of Naval Research, United States Navy, under Contract N6-ori-71, Task Order IV, Project NR-031-005. Appreciation is expressed to the Office of Naval Research for its financial assistance in this work.

BIBLIOGRAPHY

- 1 "The Effect of Type of Testing Machine on Fatigue Test Results," by Research Committee on Fatigue of Metals, Proceedings of the ASTM, vol. 41, 1941, pp. 133-151.
- 2 "Fatigue Characteristics of Rotating Beam Versus Rectangular Cantilever Specimen of Steel and Aluminum Alloys," by F. D. Fuller and T. T. Oberg, Proceedings of the ASTM, vol. 47, 1947, pp. 665-676.
- 3 "Certain Mechanical Strength Properties of Aluminum Alloys 255-T and X76S-T," by T. J. Dolan, NACA Technical Note No. 914, October, 1943.
- 4 "Work Hardened Surfaces of Fatigue Specimens," by F. C. Hull and H. R. Welton, *Metal Progress*, vol. 48, December, 1945, p. 1287.
- 5 "The Measured Knoop Hardness of Hard Substances and Factors Affecting Its Determination," by N. W. Thibault and H. L. Nyquist, *Trans. ASM*, vol. 38, 1947, pp. 271-323.
- 6 "Theory of the Fatigue of Metals," by E. Orowan, Proceedings of the Royal Society of London, series A, vol. 171, 1939, pp. 79-106.
- 7 "The Character of Fatigue," by A. M. Freudenthal and T. J. Dolan, Fourth Progress Report, ONR Contract, N6-ori-71, T. O. IV, University of Illinois, 1948.
- 8 "Effect of Stress Distribution on Yield Points," by F. G. E. Peterson, Proceedings of the ASCE, vol. 72, April, 1946, pp. 445-459.
- 9 "Raised Yield Strength in Bend Tests," by G. Brewer, *Metal Progress*, vol. 48, 1945, pp. 1306-1310.
- 9 "Raised Yield Point in Bend Tests," by T. J. Dolan and O. Sidebottom, *Metal Progress*, vol. 50, October, 1946, pp. 653-657; see also Proceedings of the ASCE, vol. 72, November, 1946, pp. 1275-1283.
- 10 "The Effect of Non Uniform Distribution of Stress on Yield Strength of Steel," by D. Morkovin and O. Sidebottom, Bulletin no. 372, Engineering Experiment Station, University of Illinois, December, 1947.
- 11 "Fatigue Characteristics of Aluminum Alloy 75S-T6 Plate in Reversed Bending as Affected by Type of Machine and Specimen," by T. T. Oberg and R. J. Rooney, Preprint No. 28, ASTM, June, 1949.
- 12 "Influence of Type of Machine, Range of Speed and Specimen Shape on Fatigue Test Data," by P. K. Roos, D. L. Lemmon, and J. T. Ransom, ASTM Bulletin, May, 1949, pp. 63-65.

Discussion

P. K. Roos.⁶ The authors point out that independent investigators have also reached the conclusion that rectangular beams are weaker than round beams when tested in the same fatigue machine. For the reader's convenience, the comparable data in reference (12), one such investigation, is summarized; the material tested was an SAE 4340 steel with a yield point of 107,000 psi and an ultimate strength of 127,000 psi; the machine was a Sonntag universal fatigue testing machine which tested specimens in pure reversed plane bending at 1800 reversals a minute; the comparable round and flat specimens tested had critical depth of beam dimensions of 0.30 in. compared to the 0.32 in. of the foregoing investigation.

Using the Dolan, McClow, Craig concept of the fatigue strength of the round specimen as a "par" of 1.00, the Roos, Lemmon, Ransom investigation⁷ gives a ratio of 0.92 for their flat specimens as compared to 0.89 for the present square specimen. Since the flat specimen had rounded sides, the corners were less severe "sore spots" than the corners in the square beam.

This thorough investigation certainly justifies the conclusion that the shape factor is the primary element leading to a reduction of fatigue strength, and, as immediate help to the designer, this is important. However, the concept of the statistical effect of the amount of material subjected to peak stresses as a fundamental part of the fatigue problem needing investigation, should not be forgotten.

AUTHORS' CLOSURE

The authors wish to thank Professor Roos for his contribution to the discussion of this rather intriguing "shape effect" in flexural fatigue tests.

In spite of the fact that the tests quoted by Professor Roos were conducted in a different laboratory, utilizing different types of fatigue machines and heat-treatment of material, it is reassuring to know that they obtained a similar reduction in fatigue strength of the flat or rectangular specimen as compared with the "par" value for a round cross section.

The seriousness of this shape effect is more dramatically emphasized by the pronounced variations in fatigue strength of 75S-T6 aluminum alloy, obtained recently by Oberg and Rooney

⁶ Associate Professor of Engineering Mechanics, The Pennsylvania State College, State College, Pa.

⁷ Influence of Type of Machine, Range of Speed, and Specimen Shape on Fatigue Test Data," by P. K. Roos, D. C. Lemmon, and J. T. Ransom; ASTM Bulletin, No. 158, May, 1949, pp. 63-65.

(11). These authors obtained values of 29,000 psi for the endurance limit of a round specimen as compared with 21,000 psi for a square specimen, and 17,500 psi for a rectangular specimen (whose width was three times the depth). Thus for this aluminum alloy the rectangular specimen exhibited a strength 40 per cent less than the par value obtained for a round specimen tested in the same machine. Much further work needs to be done to appraise the seriousness of (and to enable the designer to predict) these shape effects.

The authors agree that the statistical effect of the amount of material subjected to peak stresses is a fundamental part of all problems involving strength of materials, which should not be neglected in applications to shape effect in fatigue. In the present tests, however, the statistical effect evidently was not

the primary controlling factor, or the strengths of the various members tested would have been greatest for the diamond shape, next greatest for the round and modified diamond shapes, and the square cross section would have been by far the weakest of the group. Since the diamond cross section actually proved to be somewhat weaker than the round cross section, it was concluded that other factors of the test condition must have had a greater influence on the results than did the statistical effects of amount of material at peak stress.

The authors hope in the future to be able to conduct similar tests on somewhat the same shapes of cross section but with the critical section of greater size than in the present investigation, which should help to clarify some of our concepts of the factors contributing to this shape effect.

A study of sodium phosphate transfer properties in normal chemical systems that the indicator and, if this in

SOME

appears
This co
phosph
study o
out of p
was ad
keep a
11. W
would i
would l
phosph
loss of
sodium
or disod

After
the boil
with no
posits o
side of t

When
operatio
out did
sures inc
of low s
but whic
bility wa
to the v
sludge t
Conditio
deposit

¹ Rese
nois.

Contri
water St
Meeting
AMERICA

NOTE:
derstood
the Socie

Hide-Out of Sodium Phosphate in High-Pressure Boilers

By F. G. STRAUB,¹ URBANA, ILL.

A study has been made to explain a type of hide-out of sodium phosphate in steam boilers operating at about 1700 psi. This has shown that an insoluble form of a sodium phosphate is stable at temperatures above 620 F. This type of phosphate is scale-forming and is resistant to heat transfer. This sodium phosphate does not have the properties corresponding to those of the sodium phosphates normally encountered in steam-boiler water. Analyses by chemical means, x rays, and petrographic all indicate that this is a different form of sodium phosphate. Tests indicate that no insoluble potassium phosphate is formed and, if suitable potassium-to-sodium ratio is maintained, this insoluble salt will not form.

SOME difficulty has been experienced in boilers operating at a pressure of about 1600 to 1700 psi with loss of phosphate from solution while on steady load. This phosphate reappears in solution when the boiler rating or pressure is reduced. This condition was explained at first as so-called hide-out of phosphate due to conditions of circulation. However, a further study of the problem indicated that this was not the normal hide-out of phosphate. During operation of the boiler the phosphate was added continuously along with sodium hydroxide so as to keep a residual of about 20–40 ppm as Na_3PO_4 and a pH around 11. When the boiler rating was reduced, the soluble phosphate would increase to around 200–300 ppm, but the free hydroxide would be reduced from around 40 ppm to 0 ppm. This loss of phosphate with its subsequent reappearance accompanied by the loss of hydroxide indicated that it was not hiding-out as trisodium phosphate, but as a form more on the acid side, like mono or disodium phosphate.

After 2 or 3 months of operation, difficulty was experienced in the boiler because of failures in wall tubes. These tubes bulged with no indication of corrosion on the water side. Heavy deposits of calcium and sodium phosphate were found on the water side of the tube facing the furnace.

When the boiler pressure was reduced for a short period of operation to around 1300 psi, this peculiar type of phosphate hide-out did not take place. The absence of this action at lower pressures indicated that there might be a complex sodium phosphate of low solubility which was forming at the higher temperatures, but which was not stable at the lower temperatures. The possibility was considered that the calcium-phosphate sludge adhering to the wall surface might increase the temperature under the sludge to a point where the insoluble phosphate could form. Conditions were such that a complex sodium-calcium phosphate deposit also might be forming.

¹ Research Professor of Chemical Engineering, University of Illinois.

Contributed by the Joint Research Committee on Boiler Feed-water Studies and the Power Division and presented at the Annual Meeting, New York, N. Y., November 27–December 2, 1949, of THE AMERICAN SOCIETY OF MECHANICAL ENGINEERS.

NOTE: Statements and opinions advanced in papers are to be understood as individual expressions of their authors and not those of the Society. Paper No. 49-A-39.

LABORATORY INVESTIGATION

A laboratory investigation was undertaken to determine whether this reaction could be duplicated, and if so, to study the conditions causing the reaction. A small laboratory boiler, as shown in Fig. 1, was used. Heating was accomplished by means of electric resistance wire wound on the heating tube over a thin layer of alundum cement. The tubes were 1 in. ID \times 1 $\frac{3}{8}$ in. OD. The wire was wound on the tube for a length of 7 in. The heat input was approximately 50,000 Btu per sq ft per hr calculated on the inside area of the tube. In order to secure circulation in the tube, a smaller tube 0.75 in. OD \times 0.68 in. ID was inserted inside it. This inner tube was placed so that it had clearance at the bottom and extended well above the heated area.

The steam-water mixture traveled up the space between the tubes and water traveled down the inside of the inner tube. The presence of circulation in this area was indicated by the fact that the temperature gradient from the outside of the tube to the water in the main part of the boiler remained constant, at a value around 30 to 40 F. A thermocouple was peened into the outer surface of the heating tube at the center of the tube so as to measure the outside temperature of the heating tube. A thermocouple well was placed in the boiler directly above the outlet of the water coming from the heating tube into the main water-storage section. This is referred to as T_1 and that of the outside of the heating tube as T_2 .

The boiler held about 8 liters of water when cold. In order to operate at a constant heat input, a fan was directed so as to blow air on a bare steel tube on the top of the test boiler. When the temperature of the boiler water increased above the desired temperature, a temperature controller turned the fan on, and when the temperature was too low, it turned the fan off. This means of control allowed operation which would return the condensed steam without use of a pump. Since no steam was removed from the boiler during the test period, it was not necessary to have any make-up. The chemicals to be added during the test were pumped in solution into the main drum of the boiler.

BOILER TESTS

In order to test the boiler a solution of sodium hydroxide (1000 ppm) in distilled water was added to the boiler. The boiler was operated at temperatures from 400 F (250 psi) to 690 F (2900 psi) with constant heat input. The temperature drop ($T_2 - T_1$) was 30 F throughout the test and the concentration of sodium hydroxide also remained constant. This indicated that the hydroxide was evenly distributed throughout the test and that there were no localized spots in which concentration of the chemical might take place.

The inner tube was removed, and the boiler was run with a solution of sodium hydroxide, phosphate, and chloride in the boiler water. Table 1 gives the data collected during this test. After running 2 hr at 500 F, there was but slight temperature increase of the heating tube. When running at higher temperatures there was a slight increase of ($T_2 - T_1$), but a marked decrease in all the chemicals in solution. At the end of the test the heating was stopped and the contents of the boiler removed

TABLE 1 TEST RUN ON BOILER SHOWN IN FIG. 1, WITH CONSTANT HEAT INPUT AND NO FILLER IN TUBE
($T_2 - T_1$ = temperature differential from outside heating tube to water temperature in boiler)

Time Hours	Boiler Temp	Heat Input		NaOH	PO ₄	NaCl	pH
	° F	$T_2 - T_1$	Amps.				
2	500	35	26	85	870	498	11.4
4	525	42	26	43	820	430	11.4
22	550	50	26	55	440	359	11.5
24	610	45	26	18	172	153	11.5
26	610	45	26	3	38	76	11.2
28	610	45	26	12	10	88	10.8

Shut off heat and blow water from boiler while hot. Tube No. 4.

TABLE 2 TEST RUN ON BOILER SHOWN IN FIG. 1, WITH CONSTANT HEAT INPUT
($T_2 - T_1$ = temperature differential from outside heating tube to water temperature in boiler)

Time Hours	Boiler Temp ° F	$T_2 - T_1$	Heat Input Amps.	NaOH	PO ₄	NaCl
1	380	35	27	366	750	222
17	550	40	27	372	770	218
20	605	40	26	360	740	222
22	605	40	26	360	750	218
24	650	85	27	415	300	222
40	650	110	27	480	140	218

while the boiler and tube were hot. When the tube was removed and cut in half, a heavy hard deposit was found at the lower end of the heated area of the tube with no deposit at the middle of the tube or above. Since T_2 was measured at the middle of the tube, no appreciable indication of the deposit on the inside of the tube was detected. Analyses of this deposit gave the following results:

	Per cent
Fe =	0.11
PO ₄ =	60.32
Cl =	0.42
Na =	40.16
Total	101.01

The theoretical composition of Na₃PO₄ is 58 per cent PO₄ and 42 per cent Na. These results indicate that without the inner tube there is very little circulation in the tube, and that the steam leaving the tube causes the material dissolved in the boiler water to concentrate slowly until the solubility point of the salts is reached. At this point the insoluble excess salt crystallizes on the heating surface near the bottom where the concentration is highest. This test indicated that at 610 F, anhydrous trisodium phosphate was the stable phosphate. It also indicated that insertion of the inner tube aided in establishing circulation of boiler water through the heating tube.

The inner tube was replaced and the boiler was operated with a solution of sodium hydroxide, phosphate, and chloride in distilled water at temperatures from 380 to 650 F. Table 2 gives the results of this test. These results show that for water temperatures up to 605 F (1600 psi) there was no appreciable change in ($T_2 - T_1$), or the concentration of the various salts in solution. At 650 F (2200 psi) ($T_2 - T_1$) increased, accompanied by a loss of PO₄, an increase in NaOH, and no change in chloride. This indicated the hide-out of a sodium phosphate salt lower in sodium content than trisodium phosphate.

Table 3 gives the results of a similar test to determine the temperature at which the PO₄ starts to decrease. This test indicated that at 600 F there was no change in ($T_2 - T_1$), PO₄, or NaOH, but at 618 F, ($T_2 - T_1$) commenced to increase, with a loss in PO₄, and an increase in NaOH. At 670 F the phosphate had been reduced from 980 ppm to 40 ppm. The boiler was then cooled to room temperature and reheated to 528 F. The phosphate and the ($T_2 - T_1$) returned to normal. This indicated that the sodium-phosphate compound had formed on the heating surface at a temperature of 618 F (1750 psi) and above, but had redissolved when the boiler was operated at 528 F.

Another test was conducted in which sodium sulphate was added along with the phosphate, hydroxide, and chloride. Table 4 gives the results of this test. The phosphate again began to decrease at 620 F (1790 psi), with an increase in ($T_2 - T_1$). No reduction in the chloride occurred throughout the test, but the sulphate commenced to decrease at a temperature of 638 F with a loss of about 300 ppm at 675 F. When the run was finished, the heat was shut off and the contents of the boiler blown out while the water was still at the higher temperature. The heating tube was removed and cut in half (lengthwise). A deposit of a hard gray-white crystalline material was found evenly distributed throughout the area of the tube subjected to heat input. No deposit was found on the ends of the tubes which were not subjected to any heat input.

About 7.6 grams of this material was present on the heating surface.

A chemical analyses of this material gave the following results:

	Per cent
Sodium (Na)	31.78
Phosphate (PO ₄)	41.08
Sulphate (SO ₄)	17.99
Iron (Fe)	0.19
Total	91.04

TABLE 3 TEST RUN ON BOILER SHOWN IN FIG. 1, WITH CONSTANT HEAT INPUT
($T_2 - T_1$ = temperature differential from outside heating tube to water temperature in boiler)

Time Hours	Boiler Temp. ° F	$T_2 - T_1$	Heat Input Amps.	NaOH	PO ₄	NaCl	pH
1	500	40	27	177	960	435	11.4
3	550	50	26	171	960	427	11.3
5	600	50	26	177	960	438	11.3
19	618	67	26	232	780	438	11.3
23	628	82	26	256	680	427	11.3
26	625	85	26	262	670	427	11.3
27	635	95	26	274	575	427	11.4
43	635	115	26	394	350	427	11.5
46	650	115	26	342	240	427	11.4
50	650	120	26	348	270	427	11.5
71	650	130	26	344	140	427	11.4
76	670	120	25	338	45	427	11.4
78	670	125	26	336	35	427	11.4
95	670	125	26	351	40	450	11.4
2	510	45	26	287	1295	427	11.5
18	528	45	26	207	1250	427	—

TABLE 4 TEST RUN ON BOILER SHOWN IN FIG. 1, WITH CONSTANT HEAT INPUT
($T_2 - T_1$ = temperature differential from outside heating tube to water temperature in boiler)

Time Hours	Boiler Temp. ° F	$T_2 - T_1$	Heat Input Amps	NaOH	PO ₄	NaCl	Na ₂ SO ₄	pH
1	525	55	26	525	990	415	1670	11.5
21	560	60	26	575	970	405	1685	11.5
23	610	50	25	566	990	392	1730	11.5
24	620	60	26	555	880	398	1685	11.5
41	620	80	25	605	710	398	1670	11.6
46	630	80	25	598	630	392	1670	11.5
49	630	88	25	695	610	400	1650	11.5
66	638	130	25	640	300	405	1490	11.6
68	638	130	25	640	310	405	1470	11.6
70	648	152	25	646	180	410	1420	11.6
73	648	150	25	680	190	405	1450	11.6
90	655	185	25	654	80	400	1360	11.7
92	665	185	25	670	45	400	1345	11.7
94	665	185	25	665	40	408	1360	11.6
97	675	185	25	670	20	410	1330	11.6

Shut off heat and blow water from boiler while tube is hot. About 7.6 grams of scale on heating surface. Tube No. 3.

An x-ray diffraction analysis made by the Allis-Chalmers Manufacturing Company was reported as follows: "The deposit from Tube No. 3 from the laboratory test boiler gave quite a simple x-ray diffraction pattern, but we were not able to make an identification either from our library or from the ASTM card index. An incomplete chemical analysis indicated about 18 per cent sodium sulphate and 52 per cent disodium phosphate. The diffraction patterns, however, for both of these compounds are rather complex and none of the lines for either of these was found in the simple pattern. This would indicate that the two were present in the form of a double salt, crystallizing in rather simple form, perhaps the cubic system."

The sulphate was added in this test, since it is known that sodium sulphate has a decreasing solubility at higher temperatures. The phosphate decreased in concentration and deposited on the tube long before the sulphate began to decrease in concentration.

In order to study further the influence of circulation in the heating tube, the inner filler used in the tests reported in Tables 1, 2, and 3 was changed. The diameter was reduced from $\frac{3}{4}$ in. to $\frac{1}{8}$ in. OD. This changed the distance between the inner and outer tubes from $\frac{1}{8}$ to $\frac{3}{16}$ in. The phosphate started to decrease and $(T_2 - T_1)$ to increase again at 620 F (Table 5), while the sodium chloride remained constant. After 72 hr, when the heat input was reduced from 26 to 23 amp, the phosphate increased some, but did not return to the original value. When the tube was removed and examined the deposit did not cover the entire area of heat input. Deposit occurred on only about the middle two thirds of the heating area.

The deposit appeared to be in two layers. Analyses of these layers gave the following results:

	Top layer, per cent	Layer next to tube, per cent
Sodium (Na).....	28.36	31.30
Phosphate (PO ₄).....	56.90	58.62
Iron (Fe).....	14.96	10.24
Total.....	100.22	100.16

TABLE 5 TEST RUN ON BOILER SHOWN IN FIG. 1, WITH $\frac{1}{8}$ -IN-OD FILLER IN TUBE AND CONSTANT HEAT INPUT
($T_2 - T_1$ = temperature differential from outside heating tube to water temperature in boiler)

Time Hours	Boiler Temp ° F	$T_2 - T_1$	Heat Input Amps	NaOH	PO ₄	NaCl	pH
1	500	40	26	-24	820	488	11.4
18	610	50	26	+48	820	488	11.6
22	620	70	26	73	740	488	11.6
25	620	80	26	91	610	488	11.6
42	620	108	26	116	530	488	11.6
45	620	105	26	140	495	488	11.6
49	620	125	26	214	400	497	11.6
66	620	120	26	195	395	502	11.6
72	620	120	26	183	395	497	11.6
90	620	65	23	195	470	497	11.7
95	620	62	23	202	480	497	11.7
114	630	120	26	189	315	497	11.8
119	630	120	26	207	330	502	11.5
121	640	120	26	226	280	508	11.5
138	640	135	26	238	175	508	11.6
142	640	238	26	235	175	508	11.5
145	650	135	26	238	135	511	—
162	650	160	26	238	93	511	—
165	650	160	26	232	90	517	—
186	650	160	26	226	85	527	—
190	650	125	23	214	133	527	—
194	650	125	23	244	143	537	—
211	650	—	26	226	263	527	—
215	660	160	26	226	60	538	Intermittent heat input
218	660	150	26	210	60	538	Constant heat input
							11.5 Constant heat input

Shut off heat and blow water from boiler while hot. Tube No. 5.

The amount of sodium present is not sufficient to form trisodium phosphate.

BOILER MODIFIED FOR ADDITIONAL TESTS

The boiler shown in Fig. 1 was modified to give a different condition of circulation. Fig. 2 shows the modified boiler. The inner tube previously used was removed from the heating tube. The tests reported in Table 6 were made using this boiler. These results indicate that the reduction of the phosphate and the $(T_2 - T_1)$ changes were at a lower rate than on the boiler shown in Fig. 1. However, the reduction of the phosphate is evident at temperatures of 620 F and above. The deposit found on this tube at the end of the test was sent to the Victor Chemical Works for examination. The report was as follows:

"A microscopic examination of the scale from the pipe section submitted showed it to be made up of two materials. The greater part was a white amorphous material having a refractive index of 1.526. The balance was a very fine amorphous scale. This is believed to be due to decomposition of the amorphous material.

"The amorphous material, which was estimated to constitute 90 per cent of the scale, was obtained fairly pure by first scraping off the surface deposit. We did not find this to be readily soluble in water. It appears to decompose very slowly in water at room temperature, slightly faster when heated to 70 to 80 deg C. It is readily soluble in dilute acids and decomposes in hot dilute NaOH solutions. The exact composition was not determined, but qualitative tests show sodium, orthophosphate and ferrous iron to be present in appreciable quantities. From these tests the scale is believed to be a sodium ferrous phosphate. Optical properties did not identify the scale."

In order to study the effect of potassium, as compared to sodium, the boiler shown in Fig. 2 was used, and potassium hydroxide, phosphate, and chloride were added. The results of the tests are given in Table 7.

These results indicate that in the absence of sodium, the in-

soluble
presen
was n
sodium
equal
able c
crease

TABLE 6 TEST RUN ON BOILER IN FIG. 2, AT CONSTANT HEAT INPUT
($T_2 - T_1$ = temperature differential from outside heating tube to water temperature in boiler)

Time Hours	Boiler Temp ° F	$T_2 - T_1$	Heat Input Amps	NaOH	PO ₄	NaCl	pH
3	600	30	25	30	900	434	11.6
5	620	35	25	42	865	444	11.6
22	620	35	25	42	865	448	11.6
29	640	35	25	67	865	448	11.6
47	650	45	25	128	710	458	11.6
55	650	65	25	169	495	—	11.6
73	660	75	25	226	420	458	11.7
96	660	65	25	238	390	488	11.6
120	660	65	25	268	360	488	11.5
144	660	65	25	310	345	488	11.6
156	670	90	25	305	140	—	11.6
158	670	80	25	300	160	493	11.5
176	680	100	25	286	70	—	11.5
190	680	100	25	293	70	565	11.5

Steam leak in boiler

Shut off heat and blow water from boiler while hot. Tube No. 6.

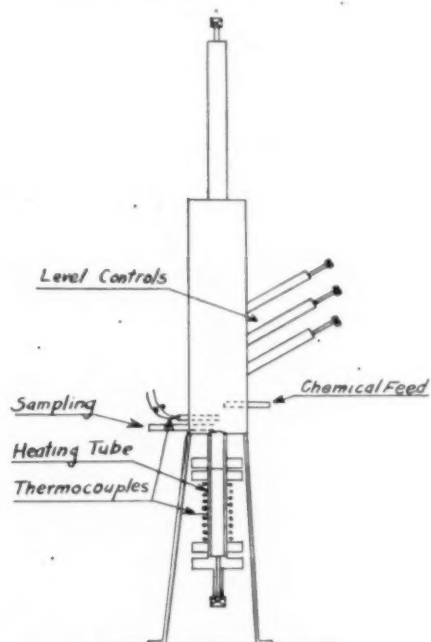


FIG. 1 TEST BOILER NO. 1

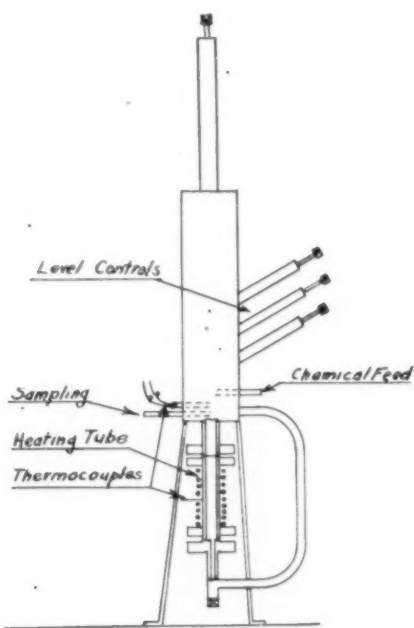


FIG. 2 TEST BOILER NO. 2

soluble phosphate will not form. Thus with potassium salts present, no appreciable change in PO₄, hydroxide, or ($T_2 - T_1$) was noticed even at a temperature of 680 F (2700 psi). When sodium is added as sodium chloride, so that the total sodium is equal to about 0.2 of the potassium present, hardly any appreciable change in PO₄ or $T_2 - T_1$ was noted. When this was increased to about 0.5 a loss of PO₄ and a change in ($T_2 - T_1$) was

observed. A further increase to around 1 made a further reduction in PO₄. This appears to indicate that in a closed-cycle plant, the use of potassium salts in place of sodium would prevent the deposition of the sodium phosphate at the higher temperatures. If there was leakage of sodium salts into the system, the sodium phosphate could form if the ratio of the sodium to the potassium became sufficiently high.

TABLE 7 TEST RUN ON BOILER SHOWN IN FIG. 2, USING POTASSIUM SALTS.
($T_2 - T_1$ = temperature differential from outside heating tube to water temperature in boiler)

Time Hours	Boiler Temp. ° F	$T_2 - T_1$	Heat Input Amps.	KOH	PO ₄	KCl	Total Cl as NaCl	pH
1	510	30	26	0	1000	457	—	11.7
3	630	43	26	0	1020	—	—	11.6
20	630	45	26	0	1000	453	—	11.6
22	660	45	26	0	1010	460	—	11.6
27	680	45	26	0	1030	—	—	—
45	680	40	26	0	1120	510	—	11.6
Add NaCl to boiler Water 2 grams -								
46	680	45	26	0	1050	—	1090	—
50	680	45	26	79	1000	—	1135	—
Add NaCl to boiler Water 4 grams -								
54	680	80	26	158	470	—	2600	—
66	680	80	26	202	470	—	2770	—
Add NaCl to boiler water 4 grams -								
75	680	85	26	183	270	—	4400	—

Shut off heat and blow water from boiler while hot. Tube No. 8.

When the tube was examined, a white deposit was found on the heating surface as expected.

Analysis of this material gave the following results:

	Per cent
Sodium (Na).....	10.46
Phosphate (PO ₄).....	51.91
Chloride (Cl).....	0.70
Potassium (K).....	1.08
Iron (Fe).....	2.87
Total.....	67.03

Two more tests were conducted with sodium phosphate hydroxide, and chloride in the boiler water in order to obtain more material for analyses. The results of the analyses of the deposit from these tests were as follows:

	Per cent	
	Tube no. 7.	Tube no. 9
Sodium (Na).....	31.72	30.70
Phosphate (PO ₄).....	60.32	60.32
Iron (Fe).....	8.80	9.36
Total.....	100.84	100.38

On tube No. 7 the deposit was 0.023 in. thick, and it caused an additional temperature gradient across the heating tube of 160 F. The x-ray diffraction pattern was the same as that obtained from tube No. 3 even though there was no sulphate present in this sample.

The results of examination of the deposit on tube No. 9 by another laboratory were reported as follows:

"Petrographic examination shows about 3/4 of the material to be a glassy isotropic substance with a refractive index of 1.52. The remainder is mostly anisotropic with refractive index values of about 1.595 and 1.68. These results do not correspond to any of the alkali phosphates in our available literature.

RESULTS OF ANALYSIS

Water-soluble material (76.2 per cent by weight):

	Per cent by weight
Sodium as Na ₂ O.....	40.1
Phosphate as P ₂ O ₅	36.0

Insoluble material (23.8 per cent by weight):

Silica as SiO ₂	0.5
Phosphate as P ₂ O ₅	6.4
Iron as Fe ₂ O ₃	12.7
Calcium as CaO.....	none
Magnesium as MgO.....	0.1
Sodium as Na ₂ O.....	trace

"The insoluble material is apparently composed of a small amount of magnesium silicate, a little silica, some iron phosphate, and some ferric oxide.

"The water-soluble material is evidently a mixture of various sodium phosphates, since the Na₂O ratio is too low for trisodium phosphate and too high for other alkaline phosphates known to exist. Microchemical tests furnish additional evidence in support of this view. A strong alkaline reaction to phenolphthalein indicates the absence of acid phosphates. Silver-nitrate reagent produces specks of both yellow and white precipitate, indicating the presence of orthophosphate (yellow precipitate) and other phosphates (white precipitate). The latter may be metaphosphates, pyrophosphates, or polyphosphates.

"With this possibility in mind, an attempt was made to analyze the sample in accordance with a method given by Loren T. Jones, *Industrial and Engineering Chemistry*, Analytical Edition, Vol. 14, p. 536, 1942. Very poor separations were obtained, as shown by the fact that the summation of the various phosphates determined by this method exceeds the total phosphate found by direct chemical analysis. No explanation is available for this discrepancy which was duplicated on a check run. Results follow:

	Per cent by weight
Orthophosphate as P ₂ O ₅	32.4
Hexametaphosphate as P ₂ O ₅	6.9
Trimetaphosphate as P ₂ O ₅	25.6
Pyrophosphate as P ₂ O ₅	4.9
Polyphosphates as P ₂ O ₅	None
Total.....	69.8
Total phosphate as P ₂ O ₅	41.2

TABLE 8 TEST RUN ON BOILER SHOWN IN FIG. 3, AT CONSTANT HEAT INPUT

Time Hours	Boiler Temp ° F	NaOH	PO ₄	NaCl	pH
16	600	256	900	306	11.5
18	620	305	865	301	11.5
20	620	323	850	306	11.6
23	620	317	800	306	11.6
40	620	390	750	306	11.6
43	620	440	750	306	11.6
45	650	482	660	315	11.6
48	650	530	590	315	11.6
64	650	585	500	301	11.7
68	670	598	240	306	11.7
72	670	585	260	315	11.8
93	600	420	680	301	11.7
113	600	438	660	295	11.8
117	660	560	500	340	11.8
120	660	550	480	335	11.8

A critical examination of the method used and the results obtained, suggest that the error lies in the determination of the ortho- and trimetaphosphate, since polyphosphates are absent, and the precipitation of hexametaphosphate and pyrophosphate seems quite straightforward. Assuming the latter determinations to be correct, and remembering that polyphosphates are absent, the per cent of ortho and trimetaphosphate may be calculated from the Na_2O to P_2O_5 ratio.

This calculation gives the following results, which are not capable of analytical proof, but which are considered to be a reasonable approximation of the composition of the sample:

	Per cent by weight
Sodium Hexametaphosphate . . .	9.9
Sodium Pyrophosphate	9.2
Sodium Orthophosphate	54.4
Sodium Trimetaphosphate	8.5

STUDY OF EFFECT OF RATE OF HEAT INPUT

To study further the effect of rate of heat input, a different design of boiler was used, Fig. 3. The heat is furnished by means of immersion heaters fitted inside of sealed tubes placed inside a drum. The rate of heat input was 10,000 Btu per sq ft per hr, which was lower than on boiler No. 1. The water passes around the tubes. Table 8 gives the results of the test using this boiler. These results again show that at about 620 F there is a reduction in the PO_4 content with an increase in the hydroxide, and no change in the chloride. The change in the phosphate was less than in the other boiler and there was a higher residual phosphate content at the higher temperatures than found when operating the boiler shown in Fig. 1.

RESULTS OF TESTS

With the small amount of data collected to date, it is rather difficult to draw very definite conclusions. The general trends may be summarized as follows:

1 At the boiler temperatures encountered in the pressure range of 1700 psi and above, there is present a stable insoluble sodium phosphate which will form as a deposit on the heating surface.

2 Anything which tends to raise the boiler-water temperature

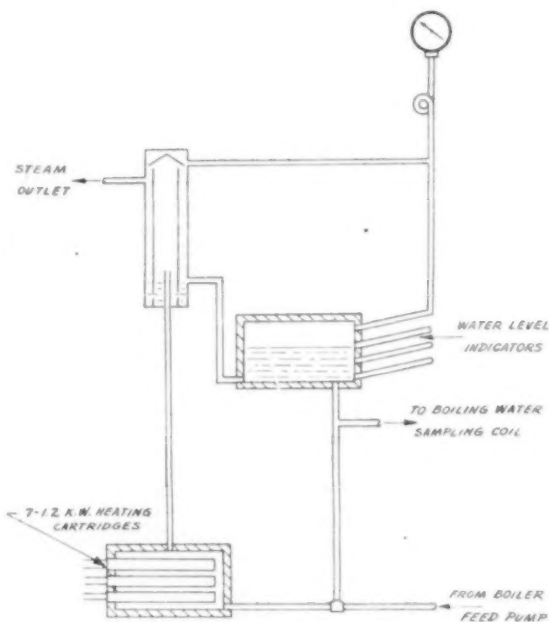


FIG. 3 HIGH-PRESSURE BOILER USED IN TESTS

will precipitate more of this slightly soluble phosphate from solution. Thus a heavy deposit of calcium phosphate at the heating surface will raise the water temperature at this location and cause precipitation of the insoluble sodium phosphate, which in turn will retard heat transfer and cause still higher temperatures and more deposit. A high rate of heat input may cause temperature increase and start the deposition of the phosphate.

3 The potassium phosphate does not form an insoluble salt at these temperatures. If the ratio of sodium to potassium can be kept low, it is possible to use potassium salts instead of sodium and thus stop the occurrence of this precipitation.

Discussion

ROBERT C. ADAMS.² The author has disclosed what may be a perplexing problem in operation of high-pressure boilers. Considerably more information may be obtainable from his test results to aid other investigators in the recognition and correction of the condition he describes.

He postulates the formation of an insoluble sodium phosphate having a $\text{Na}_2\text{O}:\text{P}_2\text{O}_5$ ratio less than 3. In both layers of the deposit corresponding to Table 5, and in the deposit on tubes 7 and 9, this ratio was reasonably uniform, ranging between 2.06 and 2.20. This suggests the deposition of a disodium phosphate. Some support for this idea can be deduced from the deposit in the run with added sulphate, corresponding to Table 4. If all the sulphate is assumed to be combined as Na_2SO_4 , the molecular ratio of the remaining sodium to phosphate is 2.34—only slightly higher than the above ratio.

This tentative confirmation is canceled, however, by the x-ray diffraction examination of the sodium-sulphate-phosphate deposit. The quoted report implies the formation of a single, crystalline compound, with neither sodium sulphate nor disodium phosphate present in recognizable form.

If the postulated compound exists, it should be possible to isolate and identify it in the deposits. The crystallographic approach should be more effective for this purpose than sole dependence on chemical analysis. The writer would urge the author to employ the petrographic microscope and x-ray diffraction for examination of all such deposits. The data from such examination, even though inconclusive in themselves, if presented systematically, would be most helpful to subsequent investigators. The joint study thus possible should lead to diagnosis and solution of the problem posed by the author.

I. B. DICK.³ The writer has some knowledge of one of the boilers referred to by Professor Straub in the first paragraph of his paper. It is substantially the same as that described in *Combustion*, August, 1943, pp. 28-34. Designed maximum steam generation is 1,000,000 lb per hr at 1742.5 psig drum pressure. Furnace volume is 54,400 cu ft, and calculated heat liberation at 1,000,000 lb per hr steam flow is 22,100 Btu per cu ft. Water-cooled furnace is formed of bifurcated tubes, 3 in. OD on 3 1/8 in. centers.

A hide-out condition was known to exist in this boiler, but no difficulty was experienced in keeping about 30 ppm of Na_3PO_4 in the boiler water. Phosphate, supplied directly to the boiler drum through a separate chemical distributor, was added as a solution of monosodium phosphate. Usage was very moderate, causing no especial concern about the known hide-out condition. The known hide-out amounted to about 100 ppm as Na_3PO_4 , which reappeared in the boiler water whenever pressure or rating were decreased about 20 per cent or more.

Following the loss of a wall tube in this unit, samples of boiler water taken while the boiler was dropping off line showed that the phosphate concentration reached a maximum of 800 ppm at about 600 psi and no load, at which point the free caustic soda in the boiler water had completely disappeared, and the water was slightly less alkaline than a solution of Na_3PO_4 . Customary limits for free NaOH are from 30 to 50 ppm. It appeared, therefore, that an acid phosphate was going back into solution.

This poses several questions:

1 In what manner can an acid phosphate be laid down from a boiler water containing at all times at least 30 ppm free NaOH?

² Superintendent, Chemical Engineering Laboratory, U. S. Naval Engineering Experiment Station, Annapolis, Maryland.

³ Division Engineer, Consolidated Edison Company of New York, Inc., New York, N. Y.

2 Under what conditions of operation can such a phosphate be laid down?

3 What would such an acid phosphate be?

4 Under what conditions would it reappear in solution?

5 How can this condition be corrected?

Professor Straub has contributed toward answering some of these questions. From all available information we construct a picture very much like this:

Acid phosphate cannot be laid down from a strongly alkaline water. Therefore in some manner the phosphate must be out of contact with the boiler water. Since the solubility of TSP is greater at operating temperature than the amount carried in the boiler water, it is evident the first precipitation must have occurred at temperatures in excess of saturation. Somehow this precipitated phosphate, which must at first be crystalline trisodium phosphate, is then converted into an acid phosphate.

There are two theories for the conversion to the acid phosphate, the one which has just been described by Dr. Partridge, and the other that has been alluded to in Professor Straub's paper, involving the formation of pyrophosphates or metaphosphates.

We hold no briefs for either of these two theories.

Since we now have two possible mechanisms for the acid phosphate to have been formed, it is apparent that such a phosphate will go back into solution whenever it is contacted with water at such temperatures that it has definite solubility. Here the observed pressure of about 1300 psi enters the picture, but the limited knowledge of the chemistry of the phosphates at temperatures in the range of 575 F impedes our applying this observation.

The remedy for the condition appears twofold:

1 So operate the unit as to permit frequent removal of precipitated soluble phosphates.

2 So treat the boiler water that the phosphates will not precipitate.

This, however, is another story.

In closing, the writer wishes to say that he believes Mr. Webb, in discussing this paper, is contributing substantially to our knowledge, and so to our food for thought, by reporting on the experiences of the American Gas and Electric Service Corporation in boilers of the 2000 psi class. It is hoped he will continue to do so.

E. P. PARTRIDGE AND R. K. SCOTT.⁴ It is naturally pleasing to us to have Professor Straub confirm in the laboratory the fact that potassium phosphate does not hide out under conditions simulating a "hot spot" in a high-pressure boiler. We accept his data with gratitude; at the same time we wish to present some interpretations differing in detail from those expressed or implied in his paper.

It might be mentioned that in designing his laboratory boiler, Professor Straub has duplicated faithfully, if unwittingly, a boiler in which gross hide-out of sodium phosphate was observed some fourteen years ago. This was the mercury condenser of the mercury-steam unit at Schenectady. Long nipples, closed at the bottom, projected downward from a horizontal tube sheet. An inner tube within each nipple was intended to act as a down-take. Mercury condensing outside of the nipples boiled the water within them, producing steam at a pressure of 425 psi. Deposits found in these nipples in 1935 were half insoluble sludge, half water-soluble salts, with sodium sulphate predominating over trisodium phosphate. Over week-end shutdowns, the sulphate and phosphate in the boiler water increased markedly.

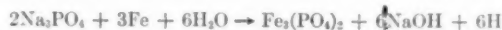
In an attempt to improve circulation, pairs of nipples were con-

⁴ Hall Laboratories, Inc., Pittsburgh, Pa.

needed together at the bottom to form U-tubes, but not until condensate was used for make-up was satisfactory operation attained. Later, in 1939, deposits found after a period of operation at increased load were essentially trisodium phosphate with less than 10 per cent of insoluble sludge constituents.

At the temperature of 450 F corresponding to 425 psi, it would have been necessary for the water in the nipples to concentrate until it contained 45 parts of Na_3PO_4 in 100 parts of water before the solid could be deposited (1).⁵

With respect to the changes in concentration of sodium hydroxide accompanying hide-out and redissolving of trisodium phosphate in the water of the experimental boiler, we believe there is an explanation both more simple and more sound than the one implied by the long quotation in the paper by Professor Straub. From the data given in his paper it is evident that concentrated trisodium phosphate actually did react with the steel of his boiler to produce ferrous phosphate, either as such, or combined as sodium ferrous phosphate, at the same time releasing sodium hydroxide. The reaction would be represented in simple over-all form as



The ferrous phosphate, stable in contact with the concentrated solution, would, however, hydrolyze as water of the normal low concentration washed over it at lower temperatures, with the resulting reversal of the reaction



in which sodium hydroxide is used up. The ferrous hydroxide would normally be converted further into black magnetic Fe_3O_4 .

The suggestion that molecularly dehydrated phosphates were formed from trisodium phosphate in the experimental boiler is based chiefly on the analytical results obtained by the Jones method. However, the report quoted in the paper shows that total P_2O_5 by adding up the various constituents "determined" by this method was 70 per cent greater than total P_2O_5 determined directly. From our fairly comprehensive knowledge of the phosphates as well as of the vagaries of the Jones method for the analysis of sodium phosphates, which would be aggravated in this case by the presence of considerable amounts of iron, we would conclude that metaphosphate and pyrophosphate need not have been present in the deposit.

At the ASME Annual Meeting six years ago, R. E. Hall presented his detailed paper (2) in which he pointed out the several ways in which the substitution of potassium for sodium ion in a boiler water should prove beneficial. With respect to hide-out, he mentioned the favorable experience in one plant where, under conditioning with sodium chemicals, "Both the sulphate and the phosphate skyrocketed when boiler load was reduced." After conditioning with potassium chemicals had been established, successive tests showed "complete absence of sulphate hide-out, and elimination of all but the barest trace of phosphate hide-out."

Subsequently, hide-out of sulphate and phosphate in the 2000-psi forced-circulation boiler at Somerset Station ceased when conditioning with potassium chemicals was commenced, as reported at the Annual Meeting four years ago (3). It was pointed out that the control limits for this boiler since the beginning of 1944 had included the maintenance of a minimum ratio of potassium to sodium in ppm of 3:1. This would mean a concentration of sodium (Na) in ppm not exceeding 0.2 times the concentration of potassium (K) in ppm.

Professor Straub may have been influenced by this and by similar reports from the field, not yet published, to undertake the experiments set forth in his paper. Like Kaufman and his associates (4) he has succeeded in confirming in the laboratory the fact that sodium phosphate hides out, while potassium phosphate does not. He has even reached the same conclusion as Hall (5), that 1 ppm of Na can be present in the boiler water for each 3 ppm of K without losing the improved behavior characteristic of full potassium conditioning.

When Professor Straub discussed the original paper by Hall six years ago, he urged caution and said, "The real importance of the suggested potassium substitution for sodium will depend upon the results obtained in actual operation," a dictum with which we thoroughly agree. With his knowledge of practical operating results in several plants during recent years, reinforced by the results of his laboratory tests, would Professor Straub now recommend potassium conditioning generally for high-pressure boilers afflicted with hide-out?

Hall and his associates continue to feel that potassium conditioning offers considerable promise as a treatment for the boiler disease of which hide-out is a symptom. In mild cases of this disease, an occasional good physic in the form of acid cleaning may suffice; where more severe conditions exist, the continuous mild laxative of potassium conditioning has paid for itself by keeping boilers on the line for longer periods than would otherwise have been possible. But when the disease is organic, surgery may be necessary for a boiler as for a human being. Let us consider some pertinent data.

According to the solubility studies of Schroeder and his associates (1), both trisodium phosphate and sodium sulphate become progressively less soluble as the temperature is increased beyond about 250 and 465 F, respectively. While each is substantially insoluble at the critical temperature of 705 F, nevertheless the amount which can be present in a normal boiler water is far greater than the solubility of most substances which form deposits in boilers. For example, the process of concentration in a boiler water at 1700 psi would have to proceed until 10,000 parts of Na_3PO_4 or more than 100,000 parts of Na_2SO_4 were present in a million parts of H_2O before the first crystal of solid could form. If the original dilute boiler water contained about the same amount of NaOH as of the salt, the limiting values would be even higher.

For trisodium phosphate or sodium sulphate to disappear from solution in boiler water by simple hide-out thus requires the development on some localized area of the boiler heat-transfer surface of a concentrated solution expressed more conveniently in per cent than in parts per million—a brine rather than a boiler water.

If the tube surface is hot enough to cause the concentrating film upon it to become saturated with trisodium phosphate, it is inevitably hot enough to cause continuing deposition of this substance as solid from the boiler water passing through the tube. The main body of boiler water is thus progressively robbed of phosphate as long as the local heat input remains sufficiently high.

The accumulation of solid may cause failure of the tube by simple overheating; wherever the deposit does not completely cover the steel, attack by the concentrated brine would also be likely, according to the experiments of Kaufman and his associates (4) as well as those of Professor Straub reported in the present paper.

What happens if, in a 1700-psi boiler which has consistently developed severe hide-out of sodium phosphate, we substitute potassium ion for sodium ion? The physical conditions which caused the boiler water to concentrate somewhere on strongly-heated tube surfaces remain the same, but instead of automatic

⁵ Numbers in parentheses refer to the Bibliography at the end of this discussion.

deposition of solid when the local concentration attains 10,000 ppm of Na_3PO_4 , the amount of K_2PO_4 in the concentrating film can increase without limit to whatever level is determined by the temperature produced in the film. The completely fluid condition maintained at the metal surface is advantageous in several respects. It does not interpose the increasing resistance to heat transfer and to fluid flow of a growing deposit of solid, and it does mingle rapidly with the normal dilute boiler water at every opportunity. The over-all effect in a number of boilers has been to prolong the life of the heat-transfer surfaces. If the local input of heat is high enough, however, the steel will be attacked by the water containing potassium salts just as it would by the water containing sodium salts, or, for that matter, by the purest water ever evaporated in a boiler.

Hall (2) has pointed out how the corrosivity of the concentrating film may be decreased by keeping the chloride high in relation to the hydroxide in the boiler water, or by eliminating free-hydroxide altogether and operating with only captive alkalinity. By such expedients much has been done to make the patient more comfortable.

Recently an impressive start has been made on investigations which could lead to prevention of the disease of which hide-out is a symptom. Studies of heat absorption in boiler furnaces, such as those at Tidd Station (6) and at Paddy's Run Station (7) can lead not only to greater efficiency in the utilization of heat, but also to decreased damage to the heat-transfer surfaces when we learn how to distribute the heat more uniformly to them.

BIBLIOGRAPHY

- 1 "Solubility Equilibria of Sodium Sulfate at Temperatures of 150 to 350° C. I. Effect of Sodium Hydroxide and Sodium-Chloride," by W. C. Schroeder, A. Gabriel, and E. P. Partridge, *Journal of the American Chemical Society*, vol. 57, pp. 1539-46 (1935); "III. Effect of Sodium Hydroxide and Sodium Phosphate," by W. C. Schroeder, A. A. Berk, and A. Gabriel, *ibid.*, vol. 59, pp. 1783-1790 (1937).
- 2 "A New Approach to the Problem of Conditioning Water for Steam Generation," by R. E. Hall, *Trans. ASME*, vol. 66, 1944, pp. 457-488.
- 3 "Water Conditioning for the 2000-Psi Boiler at the Somerset Station of Montaup Electric Company," by W. W. Cerna and R. K. Scott, *Trans. ASME*, vol. 68, 1946, pp. 443-451.
- 4 "The Behavior of Highly Concentrated Boiler Water," by C. E. Kaufman, V. M. Marcy, and W. H. Trautman, *Proceedings of the Sixth Annual Water Conference, Engineers Society of Western Pennsylvania*, 1945, pp. 23-49.
- 5 "Treatment of Steam Boiler Water," R. E. Hall, U. S. Patent 2,476,598, July 19, 1949.
- 6 "An Investigation of the Variation in Heat Absorption in a Pulverized-Coal-Fired Water-Cooled Steam-Boiler Furnace. I. Variations in Heat Absorption as Shown by Measurement of Surface Temperature of Exposed Side of Furnace Tubes," by L. B. Schueler, *Trans. ASME*, vol. 70, 1948, pp. 553-567.
- 7 "Furnace Heat Absorption in Pulverized-Coal-Fired Steam Generator, Using Turbulent Burners at Paddy's Run Station, Louisville, Ky. Part I. Variation in Heat Absorption as Shown by Measurement of Surface Temperature of Exposed Side of Furnace Tubes," by R. I. Wheeler and M. H. Howard. Presented at 1949 Annual Meeting, ASME, New York, N. Y., Nov. 27-Dec. 2, 1949. To be published in a later issue of the Transactions of the ASME.

W. L. WEBB.⁶ The author is to be commended for presenting data showing what may result from endeavoring to maintain high phosphate concentrations in boiler water when conditions are such to permit sodium phosphate hide-out. This paper indicates the inadvisability of feeding chemicals without establishing what becomes of them.

⁶ Mechanical Engineering Division, American Gas and Electric Service Corporation, New York, N. Y.

Based on the experience of the company with which the discussor is associated, it is more usual than unusual to find some degree of sodium phosphate hide-out in boilers of the 1200-1400 psi range. In such cases the phosphate feed is rigidly limited to restrict the quantity of hide-out. This results in substantially maintaining equilibrium PO_4 residuals which in the more serious cases may range from less than 1 ppm to perhaps 10 ppm.

Residual phosphate is customarily maintained in the boiler water not only to precipitate the small amount of hardness which normally enters the cycle with evaporator vapor and condenser leakage, but also to properly precipitate unusual surges of contamination, for example, from the priming of an evaporator or from the splitting of a condenser tube. The quantity of water in an operating boiler and the PO_4 residual in the boiler water establishes the number of pounds of phosphate available for precipitating incoming hardness. When this is limited by a low equilibrium PO_4 value by virtue of a hide-out condition, the objective of maintaining residual phosphate is partly defeated.

Disappearance of phosphate due to other than consumption by cycle contamination and losses by blowdown should be distinguished from actual hide-out. For example, following the acid-cleaning of a boiler there may be phosphate consumption in reforming a film on the freshly cleaned boiler metal. The extent of this consumption may be influenced by the type of so-called "conditioning boil" or boiler metal surface treatment which normally follows the rinsing operation after draining the acid solvent.

In case of extensive phosphate disappearance, particularly following acid-cleaning, it is considered good practice to make a careful check of the phosphate which returns to solution upon load reduction to definitely establish the existence of hide-out, and if it exists to limit the quantity hid out. Furthermore, the change in boiler-water alkalinity accompanying the return of phosphate to solution may give some clue to the form of phosphate hide-out. It may be of interest that in several cases boilers in which actual hide-out previously had not been observed have shown hide-out for periods of several months or longer after acid-cleaning. Why this condition should exist is not yet clear.

Following the acid-cleaning in April, 1949, of the Indiana and Michigan Electric Company's 2300-psi boiler at Twin Branch Plant, phosphate consumption was extensive and also hide-out existed to the extent that the equilibrium PO_4 value was less than 2 ppm. Previous to this acid-cleaning, hide-out had limited the PO_4 concentration to 8 to 10 ppm. As this new condition still existed in June, it was decided as an experiment, to see if hide-out could be prevented by the use of potassium chemicals. Phosphoric acid and potassium hydroxide were used because of the ease of control of both PO_4 and alkalinity in the boiler water. Potassium chloride was also employed both to assist in the control of the potassium-sodium ratio and to permit the use of the Cl concentration as a measure of the equivalent quantity of water in the boiler and for approximating blowdown.

Upon raising the K/Na epm ratio to about 1.5 (Na:K weight ratio of about 0.4:1) no phosphate returned to solution, presumably because the PO_4 residual of 1 to 2 ppm had been sufficient to prevent hide-out. However, SO_4 increased from 5 to 43 ppm. A further increase in the potassium concentration was accompanied by reappearance of no additional hid-out chemicals.

In a subsequent test just before the 2300-psi boiler was shut down for an extended period, the sodium concentration was progressively increased by the feeding of NaCl in an effort to show at what ratio phosphate and sulphate would start to hide out. At a K/Na epm ratio of about 1.0 (Na:K weight ratio of about 0.6:1), PO_4 decreased from about 24 to 17 ppm but SO_4 remained unchanged at about 29 ppm. A reduction of the ratio to about 0.5 (Na:K weight ratio of 1.2:1) made no appreciable change in

either PO_4 or SO_4 . By this time the boiler-water dissolved solids were sufficiently high to cause an increase in the conductivity of steam so the ratio was not further reduced.

The foregoing experience, as well as that with the 2000-psi boiler at Twin Branch Plant, leads the discussor to suspect that for pressures of this order, possibly 1700 psi and above as indi-

cated by Professor Straub, it may be advisable to employ potassium chemicals for internal treatment solely to prevent phosphate hide-out, particularly if hide-out seriously limits PO_4 residuals. Further data on the 2000-psi boilers shortly to be put into operation at the Philip Sporn Plant may permit conclusions to be more definitely drawn.

T
high
coil
is c
for
cycl
mer
soft
Peri
mal
at t

P
high
ture
tric
cond
plied
stati
Th
of 10
of th
chief
heat
mech
and

Th
avoi
comp
evap
pract
direc
loss
do no
into
degra
purp
prod

1 V
2 M
Servic
3 "
Sport
Trans
Col
water
Meet
THE
No
under
of the

Chemical Treatment, Demineralization, or Evaporation for Make-Up in High-Pressure By-Product Steam Plants

By J. D. YODER,¹ W. L. WEBB,² AND T. BAUMEISTER,³ NEW YORK, N. Y.

The increased power production obtained by exhausting high-pressure turbines directly to process rather than to coils of evaporators, which in turn produce process steam, is demonstrated. Typical heat balances are presented for systems employing evaporated make-up to the closed cycle and for 100 per cent make-up cycles using water treatments consisting of (a) silica removal and sodium-zeolite softening, and (b) demineralization and silica absorption. Performance data and costs are given for both evaporated make-up and 100 per cent treated make-up 1400-psi cycles at the Deepwater Operating Company's station.

INTRODUCTION

POWER manufactured as a by-product of process steam offers the lowest cost for fuel in mills per kilowatthour obtainable from any type of power plant. The most efficient high-pressure power plant which is devoid of the by-product feature and which delivers only one product—kilowatthours as electric energy—still wastes, as low-grade heat in cooling water of the condenser system, approximately 50 per cent of the heat supplied in fuel. The lowest heat rate as yet anticipated for a central station is 9300 Btu per net kw-hr for the Philip Sporn Station.³

The lowest heat rate of plants now in operation is of the order of 10,000 Btu per net kw-hr which represents a loss of 66 per cent of the heat supplied in the fuel. This waste or loss of heat is chiefly to the condensing water and the remainder is sensible heat of stack gases, combustion imperfections, hydrogen losses, mechanical and electrical losses, auxiliary power requirements, and other incidental and generally unaccounted-for items.

UTILIZING EXHAUST STEAM FOR PROCESS

The utilization of exhaust steam for process makes possible the avoidance of the heat loss to the cooling water. This is accomplished by using (1) high-pressure turbine exhausting to evaporator coils, which in turn deliver process steam at some practical lower pressure, or (2) high-pressure turbines exhausting directly to the process headers. Either method avoids the Btu loss to the condenser cooling water. The evaporators, however, do not permit the use of the full availability of heat for conversion into work, because the heat delivered to the evaporator coils is degraded by heat exchange to a lower steam pressure for process purposes. This greatly reduces the ratio of available low-cost by-product power to process steam.

¹ Vice-President, The Permutit Company. Mem. ASME.

² Mechanical Engineering Division, American Gas and Electric Service Corporation. Mem. ASME.

³ "The 2000-Psi, 1050 F, and 1000 F Reheat Cycle at the Philip Sporn and Twin Branch Steam-Electric Stations," by Philip Sporn, Trans. ASME, vol. 70, 1948, pp. 287-294.

Contributed by the Joint Research Committee on Boiler Feed-water Studies and Power Division and presented at the Annual Meeting, New York, N. Y., November 27-December 2, 1949, of THE AMERICAN SOCIETY OF MECHANICAL ENGINEERS.

NOTE: Statements and opinions advanced in papers are to be understood as individual expressions of their authors and not those of the Society. Paper No. 49-A-71.

When turbines exhaust directly to process, power is generated through the full steam expansion from boiler pressure to process steam pressure. The heat rate approaches the theoretical factor for the conversion of heat into mechanical energy, or 3413 Btu per kw-hr.

The major advantage of delivering exhaust steam to an evaporator instead of directly to process is that it permits the return of the condensed steam from the evaporator coils to the boiler feed system without further treatment. The requirements of the power cycle for make-up water are consequently comparable to those of a surface-condensing plant and are of the order of 1 or 2 per cent. This amount is readily supplied by a small-capacity evaporator.

When the turbine exhaust is delivered directly to process, it is necessary to prepare substantially 100 per cent treated make-up water for feed to the boilers. When high-pressure boilers were first installed to supply process steam under these conditions, designing engineers did not believe that the boilers could be operated successfully with 100 per cent treated make-up. With the accumulation of experience, however, it has been demonstrated that 100 per cent treated make-up can be fed even to high-pressure boilers (1400 psi) without operating hazard and with the advantage of the greatly increased by-product power rate.

When an industrial plant installs a high-pressure turbine to exhaust its steam to process, the boiler pressure is generally selected to balance the required power and process-steam demands, thus utilizing the maximum potential by-product power generation. This frequently results in installing 600-psi boilers where more low-cost power could be produced with a higher pressure such as 1400 psi.

When a public utility enters into an agreement to supply both process steam and power to an industrial plant, it is reasonable economy to install boilers to operate at maximum pressures, because any excess power produced by the turbine may be used advantageously by the utility to reduce its over-all cost of generation.

It is the purpose of this paper (1) to emphasize the greater amount of low-heat-rate by-product power which can be generated when turbines are exhausted directly to process rather than to evaporator coils; (2) to present operating data for a 1400-psi plant to substantiate these conclusions, and (3) to demonstrate the satisfactory chemical treatment of water for these conditions.

Fig. 1 illustrates the heat rate in Btu per kw-hr, for an efficient condensing plant as compared to the heat rate of by-product power plants when the turbine exhausts (1) to evaporator coils, and (2) directly to process. The plant heat rate with a process evaporator is less than one half of the heat rate for a surface-condensing installation. The heat rate for the case of turbines exhausting directly to process and using softened or demineralized feedwater is, in turn, somewhat less than with process evaporators.

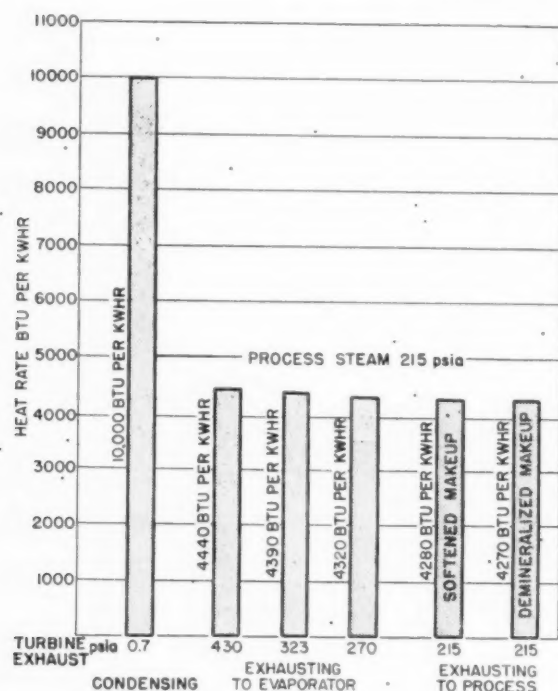


FIG. 1 PLANT HEAT RATES OF 1300 PSIA, 760 F TURBINE UNIT WHEN EXHAUSTING TO A CONDENSER, TO EVAPORATOR COILS, OR DIRECTLY TO PROCESS

ADVANTAGE OF EXHAUSTING DIRECTLY TO PROCESS

The great advantage of exhausting turbines directly to process instead of to evaporator coils is the greater amount of low-fuel-cost power that can be produced. This is illustrated in Fig. 2. Here the relative amounts of by-product power which can be produced with 1400-psi boiler steam for 100,000 lb per hr of 215-psia process steam are shown for (a) turbines exhausting to evaporator coils, (b) turbines exhausting directly to process and using (1) softened or (2) demineralized make-up.

The power, when using evaporators at a constant vapor pressure, increases as the differential in pressure between evaporator coils and process steam diminishes, or as the mean temperature difference across the evaporator surface is decreased. The amount of heating surface needed in the evaporator coils increases as the pressure or temperature differential becomes less, which correspondingly increases the cost of evaporators.

The chart indicates that when the turbine exhausts at 430 psia to the evaporator coils, the turbine produces 2920 kw of by-product power as compared with 4190 kw when exhausting the turbine at 270 psia. When the turbine exhausts to process and the feedwater is softened, as described later in this paper, the by-product power is 5340 kw, and, if the make-up water were demineralized, the available by-product power would be 5620 kw. The increased power generated, when using demineralized instead of softened make-up, results from less boiler blowoff and therefore less degradation of heat.

The heat-balance diagrams, Figs. 3 through 7, show the basic data for these graphs. The comparative study reflected in these data was greatly simplified by the requirement that process steam under all alternates be delivered at 215 psia and substantially saturated conditions. The heat rates and the amounts of by-

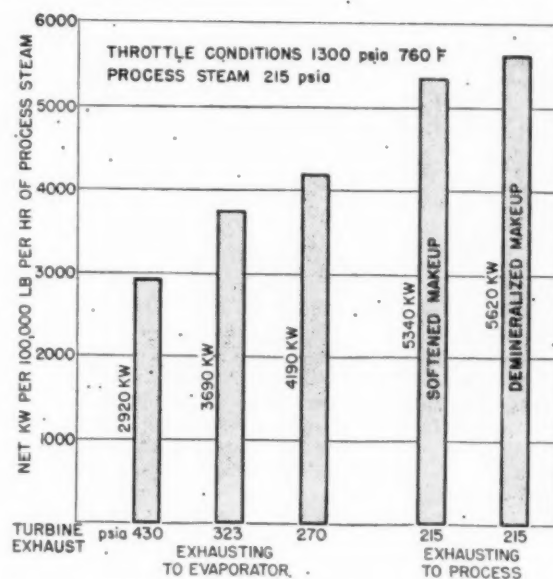


FIG. 2 COMPARATIVE POWER OUTPUTS FOR ALTERNATE TYPES OF BY-PRODUCT PLANTS

product power illustrated in Figs. 1 and 2 were thus determined by the feed cycles and heat balances of Figs. 3 through 7. In the preparation of these figures the following underlying performance estimates were used:

PERFORMANCE ESTIMATES

- 1 Process steam conditions, 215 psia dry and saturated.
- 2 Steam conditions at turbine throttle, 1300 psia, 760 F, and 1347 Btu per lb.
- 3 (a) Internal efficiency of main turbine, 80 per cent.
(b) Internal efficiency of heating turbine, 72 per cent.
- 4 (a) Exhaust pressure loss from main turbine shell to evaporator, to heating turbine, to heaters No. 1 and No. 3 or to station wall, 7 per cent.
(b) Extraction pressure loss from heating turbine to heater No. 2, 10 per cent.
- 5 Mechanical and electrical losses, 3 per cent of gross power generated.
- 6 Gland steam enthalpy, the throttle enthalpy minus 25 per cent of the enthalpy drop in the turbine.
- 7 Auxiliary power for the generating plant for all conditions, 6 per cent of the gross power generation obtainable with a condensing turbine operating at the given throttle conditions and flow, with a 10 lb per kw-hr water rate.
- 8 Boiler efficiency for power and process steam generation, 87 per cent.
- 9 Steam losses, 5000 lb per hr.
- 10 Blowdown losses:
 - (a) From boiler, fed with evaporated make-up, 1500 lb per hr, or approximately 1/4 per cent of boiler output (no heat recovery).
 - (b) From evaporator, 10 per cent of make-up (with heat recovery).
 - (c) From boiler fed with softened water, 21.6 per cent of make-up (with heat recovery).
 - (d) From boiler fed with demineralized water, 2.4 per cent of make-up (with heat recovery).

11 Terminal temperature differences on heat exchanger, closed heaters, and drain coolers taken the same for all conditions and as specified on the diagrams.

12 Cost of process steam computed as the heat in the process steam corrected for boiler efficiency, steam losses, auxiliary power allowance 2 per cent of the heat, and boiler blowoff 10 per cent of make-up (with heat recovery).

Fig. 3 shows a typical cycle diagram for the case of the turbine exhausting to evaporator coils. The heat balance of this figure is based upon operating the turbine at an exhaust pressure of 430 psia, under which condition the amount of by-product power pro-

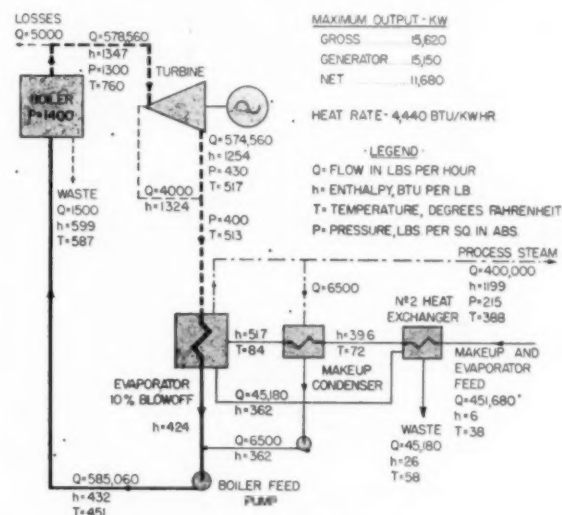


FIG. 3 HEAT BALANCE FOR HIGH-PRESSURE TURBINE UNIT EXHAUSTING AT 430 PSIA TO EVAPORATOR COILS

duced per 100,000 lb of process steam was 2920 kw and is so plotted in Fig. 2. Corresponding heat balances for evaporator operation with exhaust pressures of 323 and 270 psia are given in Figs. 4 and 5, respectively.

Fig. 6 is a typical cycle diagram for the delivery of exhaust steam directly from turbine to process and is applicable for the cases of feeding softened or demineralized make-up to the boiler. The heat balance of Fig. 6 is based upon softened make-up water of such analysis as to require a boiler blowdown of 21.6 per cent of make-up. The high-pressure turbine exhausts chiefly to process, but sufficient exhaust steam goes to the heating turbine to complete the heating of the feedwater from 38 F to 390 F. The steam flow through the high-pressure turbine is increased by an amount sufficient to compensate for the inadequacy of boiler blowoff for feed-heating purposes.

Fig. 7 differs from Fig. 6 in that only 2.4 per cent of make-up is blown down from the boiler because of the use of demineralized rather than softened make-up. Since there is less boiler blowoff with demineralized make-up, more steam must pass through the high-pressure turbine to provide the necessary heat in the feedwater. This additional flow increases the by-product power generation. Because less water goes to waste when demineralizing, the heat rate of by-product power is somewhat reduced as illustrated in Fig. 1.

Process-steam installations, similar to those shown in the heat balance, Figs. 3, 4, and 5, in which the high-pressure turbine exhausts to evaporator coils, and in Fig. 6 in which the 100 per cent softened make-up boiler supplies a high-pressure turbine exhaust-

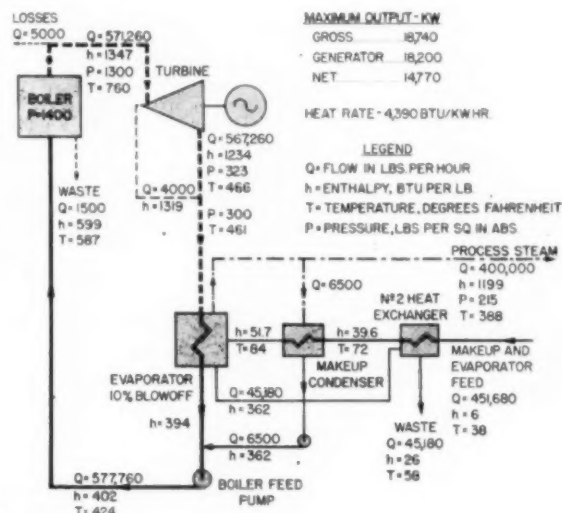


FIG. 4 HEAT BALANCE FOR HIGH-PRESSURE TURBINE UNIT EXHAUSTING AT 323 PSIA TO EVAPORATOR COILS

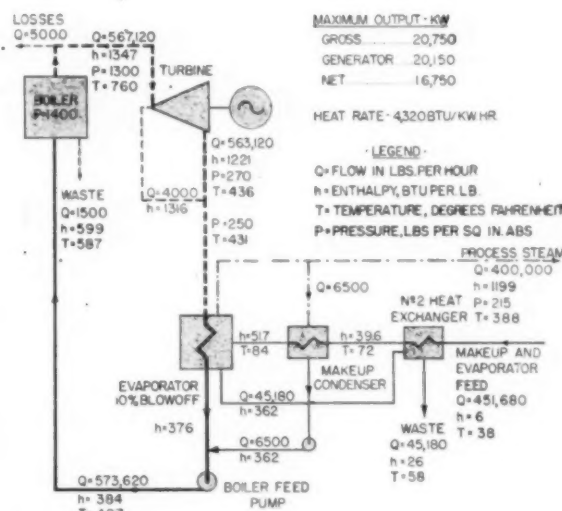


FIG. 5 HEAT BALANCE FOR HIGH-PRESSURE TURBINE UNIT EXHAUSTING AT 270 PSIA TO EVAPORATOR COILS

ing directly to process, were put into service at the Deepwater Operating Company's Station at Deepwater, N. J., in 1930 and 1942, respectively. Both employ nominally 1400-psi, 725-750 F initial steam conditions at the turbine throttle and supply 215-psia steam to process. No process condensate is returned to the powerhouse from the factory. Raw water separately treated for the two installations is taken from the nearby Salem Canal which is equipped with a valved dam, to prevent salines from the Delaware River from contaminating this surface supply.

DEEPWATER HIGH-PRESSURE TURBINE-EVAPORATOR UNIT

The 1930 Deepwater installation consists of two 331,000-lb-per-hr, 725 F cross-drum boilers which supply a 12,500-kw turbine, exhausting to the coils of 7 evaporators, having a combined rated

TABLE 1 DEEPWATER HIGH-PRESSURE TURBINE—EVAPORATOR UNIT
WATER CONDITIONS

	Process steam		400,000 lb per hr			
	Evaporator blowdown		21,000 lb per hr			
	Blowdown losses		21,000 lb per hr			
	Evaporator make-up		421,000 lb per hr			
	Raw water		Softener effluent		Evaporator shell water	
	(ppm)	(epm)	(ppm)	(epm)	(ppm)	(epm)
Calcium, Ca.....	19	0.94	1.2	0.06	2	0.10
Magnesium, Mg.....	7	0.54	0.4	0.04	1	0.08
Sodium, Na.....	13	0.56	55	2.41	1160	50.50
		2.04		2.51		50.68
Bicarbonate, HCO ₃	61	1.00	68	1.11	200	3.28
Carbonate, CO ₃	0	0	0	0	540	17.90
Hydroxide, OH.....	0	0	0	0	0	0
Sulphite, SO ₃	0	0	0	0	0	0
Sulphate, SO ₄	16	0.34	33	0.69	740	15.40
Chloride, Cl.....	25	0.70	25	0.71	500	14.10
		2.04		2.51		50.68
Silica, SiO ₂	8.6		8.6		124	
Carbon dioxide, CO ₂	7					
Color.....	25					
Iron, Fe.....	1.7		0.2			
Total hardness as CaCO ₃	74	1.48	5	0.10	9	0.18
pH.....		7.2		8.2		10.4
Dissolved solids.....	120		157		3267	
Suspended solids.....	30				113	
Total solids.....	150		157		3380	
Chemical requirements in terms of treating-plant effluent:						
			ppm	\$ per lb	\$ per million lb	
Ferrous sulphate, 98 per cent FeSO ₄ ·7H ₂ O.....			50	3.0	1.50	
Soda ash, 98% Na ₂ CO ₃			25	1.5	0.38	
Sodium chloride, 99% NaCl.....			240	0.6	1.44	
Sodium sulphate, 93% Na ₂ SO ₄			6	3.5	0.21	
Chemical cost per million lb treated water					\$3.53	

output of 400,000 lb per hr of 215-psia vapor. Turbine-exhaust pressure varies with load, and with the number of evaporators in service. At rated turbine capacity with 7 evaporators in service, exhaust pressure is approximately 300 psia. Make-up of 1.5 per cent to the 1400-psi cycle is supplied by house evaporators.

Raw water, coagulated and zeolite-softened, is fed to the process evaporators which are continuously blown down. The employment of softened water substantially has eliminated the need for scale-cracking operations. Representative water analyses for this unit are indicated in Table 1.

DEEPWATER 100 PER CENT SOFTENED MAKE-UP UNIT

Prior to undertaking the 1400-psi 100 per cent make-up installation at Deepwater, a pilot-plant test was conducted to establish that the raw water could be treated as contemplated, and that a high-pressure test boiler would operate satisfactorily with only treated-water make-up. This study was described by Carmichael.⁴

In the subsequent 1942 installation the raw water, after treatment for reduction of turbidity, color, silica, and hardness, is fed to a boiler which delivers 550,000 lb per hr of steam at 750 F total temperature. Substantially all the water-cooled surface of this boiler consists of vertical tubes, except the furnace roof and the hopper dry bottom. At full rating, the heat available is 62,000 Btu per hr per sq ft of projected water-cooled furnace area, as compared to 80,000-120,000 Btu per hr per sq ft for boilers of conventional design. Comparative values per cu ft of furnace volume are 13,800 and 18,000-24,000 Btu, respectively. The high-pressure steam is supplied to a 20,000-kw turbine exhausting directly to process.

A schematic diagram of the water-treating plant is shown in Fig. 8. As designed, precipitator No. 1 was for coagulation and color reduction, using ferric sulphate and sulphuric acid at a pH of about 4.5, followed by air agitation for carbon-dioxide removal, and precipitator No. 2 for silica reduction, using ferric sulphate and lime at a pH of 9 to 10. The precipitator effluent flows

through gravity filters and is discharged into the clearwell mixing chamber where pH was to have been reduced to 7.5 with sulphuric acid. Pumps transfer water from the clearwell through sodium Zeo-Karb softeners to elevated storage tanks and to the station for boiler make-up. Under this plan of operation, retention in the sedimentation sections of each Spaulding precipitator at rated raw-water flow of 625,000 lb per hr is 170 min.

Operating experience has indicated that sedimentation, and color and silica reduction can be accomplished in one step using ferric sulphate and lime at a pH of 9.2 to 9.6. This permits operating the two precipitators in parallel, thereby doubling the retention time. Because of deposition of slime on precipitator weirs and plugging of filters with organic matter and from carry-over of "wild floc," the raw water is chlorinated. Clay is fed with the lime to assist in weighting the floc.

Contrary to initial expectations that the zeolite material would be subject to attack from waters having pH values of 8 or higher, it has been established that a maximum pH of 10 is satisfactory. Supplementary chemicals consist of caustic soda and sodium sulphite fed at the deaerator discharge, and sodium phosphate and an organic dispersive fed directly to the boiler.

Table 2 indicates representative water conditions of the 100 per cent softened make-up cycle, and the cost of treating chemicals. For comparative purposes, Table 3 presents similar data on the basis of employing demineralization and silica absorption.

During the first 3 years of operation, semiannual outages were necessary for the removal of soft deposits of phosphate sludge and iron oxide from the water-cooled boiler surfaces. Initially this was done mechanically, and later by acid-cleaning. The employment of an organic dispersive in 1945, for maintenance of sludge in suspension, proved to be practically 100 per cent effective. Since 1945 the boiler has been acid-cleaned but once, and then as a precautionary measure. Since feeding the organic material, samples of deposit turblined from selected wall tubes indicated a deposition of some 2 grams per lineal foot of tube, which analyzed about 40 per cent carbon. This seemed to show that there had been some decomposition of the organic dispersive but subsequent examinations showed insufficient deposit to call for any change in treatment.

⁴ "Experimental Study, Feedwater Treatment for 1400-Lb Boiler Operating Pressure," by D. C. Carmichael, Trans. ASME, vol. 64, 1942, pp. 121-136.

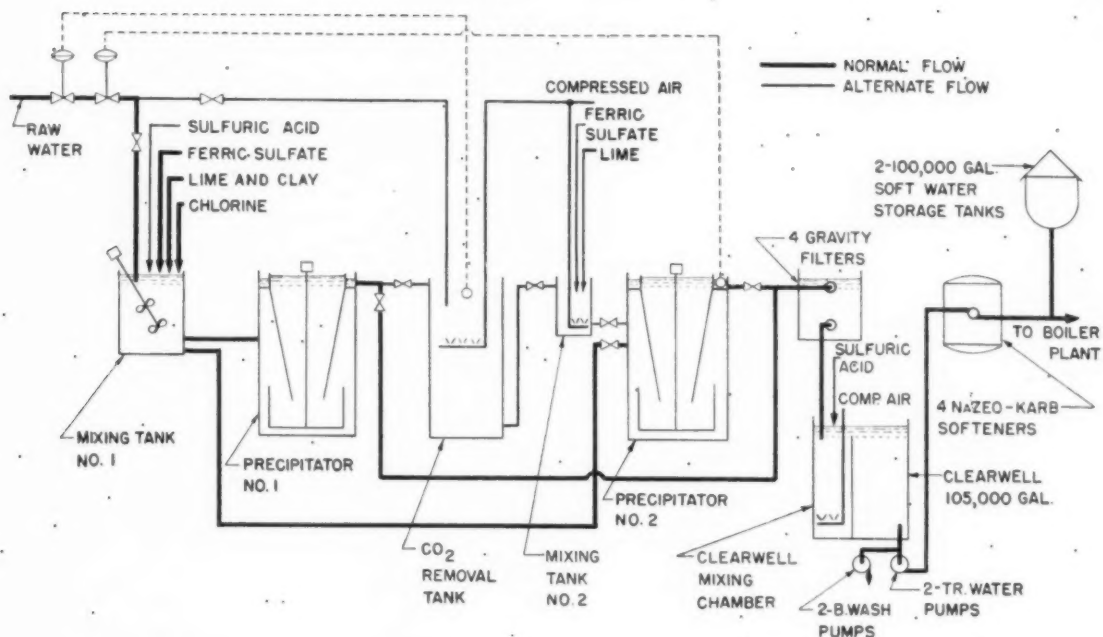


FIG. 8 SCHEMATIC DIAGRAM OF WATER-TREATING PLANT FOR THE DEEPWATER 100 PER CENT SOFTENED MAKE-UP UNIT

TABLE 2 DEEPWATER 100 PER CENT SOFTENED MAKE-UP UNIT WATER CONDITIONS

	Process steam		400,000 lb per hr					
	Steam losses		5,000 lb per hr					
	Boiler blowdown		75,000 lb per hr					
	Blowdown losses		45,000 lb per hr					
	Make-up		450,000 lb per hr					
	Raw water		Filtered precipitator effluent		Softener effluent		Boiler water	
	(ppm)	(epm)	(ppm)	(epm)	(ppm)	(epm)	(ppm)	(epm)
Calcium, Ca.....	19	0.94	60	3.00	0.6	0.03	0	0
Magnesium, Mg.....	7	0.54	6	0.52	0.1	0.01	0	0
Sodium, Na.....	13	0.56	12	0.52	94	4.09	600	26.12
		2.04		4.04		4.13		26.12
Bicarbonate, HCO ₃	61	1.00	17	0.28	17	0.28	0	0
Carbonate, CO ₃	0	0	2	0.08	2	0.08	8	0.27
Hydroxide, OH.....	0	0	0	0	0	0	40	2.35
Phosphate, PO ₄	0	0	0	0	0	0	15	0.47
Sulphate, SO ₄	0	0	0	0	0	0	10	0.25
Sulphate, SO ₄	16	0.34	140	2.92	140	2.92	850	17.71
Chloride, Cl.....	25	0.70	27	0.76	30	0.85	180	5.07
		2.04		4.04		4.13		26.12
Silica, SiO ₂	8.6		1.5		1.5		9	
Carbon dioxide, CO ₂	7		0		0			
Color.....	25		3		3			
Iron, Fe.....	1.7		0.1		0.1			
Total hardness, as CaCO ₃	74	1.48	176	3.52	2	0.04		
pH.....		7.2		9.2		9.2		11.2
Dissolved solids.....	120		257		277		1712	
Suspended solids.....	30						38	
Total solids.....	150		257		277		1750	
Chemical requirements in terms of treating-plant effluent:								
Treating plant			ppm		\$ per lb		\$ per million lb	
Ferric sulphate, 78% Fe ₂ (SO ₄)·2H ₂ O.....			220		1.5		\$3.30	
Lime, 90% Ca(OH) ₂			145		0.6		0.87	
Sulphuric acid, 93% H ₂ SO ₄			0		0.9		0	
Chlorine, 100% Cl ₂			6		9.0		0.54	
Sodium chloride, 99% NaCl.....			700		0.6		4.20	
Clay.....			50		1.0		0.50	
Chemical cost per million lb of treated water							\$9.41	
Supplementary treatment								
Disodium phosphate, 98 per cent Na ₂ HPO ₄			6.0		9.0		\$0.54	
Caustic soda, 98 per cent NaOH.....			2.5		2.5		0.06	
Sodium sulphite, 93 per cent Na ₂ SO ₃			6.5		3.5		0.23	
Organic dispersive.....			6.0		14.0		0.84	
Chemical cost per million lb of treated water							\$1.67	

TABLE 3 WATER CONDITIONS FOR A 100 PER CENT DEMINERALIZED MAKE-UP UNIT

	Process steam		400,000 lb per hr					
	Steam losses		5,000 lb per hr					
	Boiler blowdown		10,300 lb per hr					
	Blowdown losses		6,200 lb per hr					
	Make-up		411,200 lb per hr					
	Raw water		Filtered precipitator effluent		Demineralizer and silica absorber effluent		Boiler water	
	(ppm)	(epm)	(ppm)	(epm)	(ppm)	(epm)	(ppm)	(epm)
Calcium, Ca.....	19	0.94	34	1.68	0.2	0.01	0	0
Magnesium, Mg.....	7	0.54	7	0.54	0.1	0.01	0	0
Sodium, Na.....	13	0.56	13	0.56	1.8	0.08	107	4.66
		2.04		2.78		0.10		4.66
Bicarbonate, HCO ₃	61	1.00	65	1.07	4.3	0.07	0	0
Carbonate, CO ₃	0	0	6	0.20	0	0	0	0
Hydroxide, OH.....	0	0	0	0	0	0	40	2.35
Phosphate, PO ₄	0	0	0	0	0	0	15	0.47
Sulphite, SO ₃	0	0	0	0	0	0	10	0.25
Sulphate, SO ₄	16	0.34	39	0.81	0.5	0.01	38	0.79
Chloride, Cl.....	25	0.70	25	0.70	0.7	0.02	28	0.80
		2.04		2.78		0.10		4.66
Silica, SiO ₂	8.6		5.5		0.2		8	
Carbon dioxide, CO ₂	7		0		0.5		0	
Color.....	25		5		5		0	
Iron, Fe.....	1.7		0.1		0.1		0	
Total hardness, as CaCO ₃	74	1.48	111	2.22	1	0.02	0	11.3
pH.....		7.2		9.2		8.0		
Dissolved solids.....	120		162		6.5		246	
Suspended solids.....	30			40	
Total solids.....	150		162		6.5		286	

Chemical requirements in terms of treating-plant effluent:

Treating plant	ppm	¢ per lb	\$ per million lb
Ferric sulphate, 78% Fe(SO ₄) ₂ ·2H ₂ O.....	59	1.5	\$0.89
Lime, 90 per cent Ca(OH) ₂	39	0.6	0.23
Chlorine, 100 per cent Cl ₂	6	9.0	0.54
Caustic soda, 98% NaOH.....	458	2.5	11.45
Soda ash, 99 per cent Na ₂ CO ₃	94	1.5	1.41
Sulphuric acid, 93 per cent H ₂ SO ₄	337	0.9	3.03
Clay.....	50	1.0	0.50
Chemical cost per million lb of treated water			\$18.14
Supplementary treatment			
Disodium phosphate, 98 per cent Na ₂ HPO ₄	1.5	9.0	\$0.14
Caustic soda, 98 per cent NaOH.....	0	2.5	0
Sodium sulphite, 93 per cent Na ₂ SO ₃	0.9	3.5	0.03
Organic dispersive.....	2.5	14.0	0.35
Chemical cost per million lb of treated water			\$0.52

ECONOMICS

In any rational presentation of a subject such as this, it is necessary that some space be devoted to a consideration of the economic aspects of the design as well as to the technical features. It is of course true, here as elsewhere, that any "over-all," "average," "typical," or "representative" costs are bound to be associated intimately with the design details and local conditions. Broadly viewed, however, the alternative designs of by-product power plants using high-pressure turbines exhausting to process evaporators or exhausting directly to process, show an over-all investment requirement which justifies the selection of the latter. Experience has demonstrated that the investment for a high-pressure boiler make-up treating plant, alone, is substantially the same as an evaporator plant alone, for the same process-steam capacity. The complete power plant including boilers, turbines, buildings, and auxiliaries as well as the process-steam equipment is bound to require more investment for the installation exhausting directly to process. The turbine generator is nearly twice the size, and the boiler must be larger. Experience has shown that for a given process-steam output, say, 400,000 lb per hr at 215 psia:

(a) The increased by-product power capacity will be obtained at today's prices for an increment of investment in the neighborhood of \$100 per kw.

(b) The increment of production cost of the electrical energy as produced by the unit exhausting directly to process, as compared to the high-pressure turbine-evaporator unit will be less than the total production cost of a condensing plant using the same fuel.

These are favorable factors, and when it is recognized that the unit exhausting directly to process operates without undue labor or maintenance costs, and without sacrifice of reliability, the over-all economic picture is decidedly favorable to this solution of the problem of the multipurpose steam power plant.

ACKNOWLEDGMENT

Many of the details, figures, and calculations in this paper were prepared by Messrs. A. J. Fiehn and R. H. Marks.

Discussion

R. C. ADAMS.⁵ The authors have presented a convincing case for their major thesis, that chemical softening of make-up will produce more power per unit of process steam than evaporation of make-up. A further economic advantage from demineralization of the make-up is less certain.

A complete picture of relative costs cannot be obtained from the limited data of the authors. The only detailed costs they give are those for chemical costs of water treatment in Tables 2 and 3. From these and the comparison in Fig. 2 of the paper, a partial indication of relative expense can be derived.

Table 2, with total chemical costs of \$11.08 per million pounds and 450,000 lb per hr of make-up, indicates an hourly cost for chemicals of \$4.98. Referring this to the figures for power per unit of process steam in Fig. 2, shows a cost for treating chemicals of 0.023 cent per kw-hr. Similar calculations from Table 3 for de-

⁵ Superintendent, Chemical Engineering Laboratory, U.S.N. Engineering Experiment Station, Annapolis, Md.

mineralized make-up yield an hourly expenditure of \$7.67, and a chemical cost of 0.034 cent per kwh.

Chemical costs for water treatment are a minor, though not negligible, part of the expense of power generation. The hundredth of a cent per kilowatt-hour increase for demineralization instead of softening looks small. However, it should be recognized as a 50 per cent increase in chemical costs for all power generated.

If the increment in cost is divided by the increment of power, which is a more reasonable basis for appraisal of the process change, the result is even more striking. The 1120 additional kilowatts, attending the standard 400,000 lb per hr of process steam, cost \$2.69 per hr for treating chemicals alone. This means 0.24 cent per kwh. When it is considered that many favorably placed industries can purchase power for about twice this amount the probability of an over-all saving from demineralization shrinks.

This suggests that general application of demineralization for boiler make-up is far from assured. It is more likely that its application will be limited to special cases for some time to come.

S. B. APFLEBAUM.⁶ The authors mention two types of water-treating equipment for the make-up water to high-pressure boilers, as follows:

(a) Silica removal by contact of the water with precipitates of ferric hydroxide, followed by sodium zeolite to remove the hardness.

(b) Demineralization and silica adsorption by ion exchange.

The authors describe an actual installation at Deepwater, N. J., using the first method, and they present hypothetical tables showing what might be expected from a demineralizing plant for the same conditions. However, they do not describe demineralizing-silica removal plants in actual operation or being installed.

The purpose of this discussion is to supplement the paper by supplying information to show that there is a very definite trend toward the installation of plants which demineralize the water and remove the silica by ion exchange.

Case 1 Process Water. One of the earliest plants of this type was installed by the Liquid Conditioning Corporation, now a subsidiary of the writer's company, at a pharmaceutical plant in the Midwest. There had been a two-step demineralizing plant in operation which merely removed the cations and anions but did not remove the silica. However, the USP standards called for a total solids of 10 ppm including the silica and therefore the user purchased a third-step ion-exchange unit for the removal of the residual silica. At the same time, the original demineralizing plant was remodeled by using the most modern resins in the units and by improving the CO₂ removal of the decarbonator.

This plant has been in satisfactory operation for over two years now and Table 4 of this discussion gives the chemical results at various stages of treatment. The plant has a capacity of about 15,000 lb per hr, and it is now being remodeled to make it fully automatic in its operation.

A second plant is being installed by the same user, having a capacity of 20,000 lb per hr of the same general type except that the decarbonator will be of the vacuum type, in order to reduce oxygen as well as free CO₂ between the second and third stages. This plant also will be fully automatic and will contain the most modern resins.

The operation of this plant shows that the silica is reduced to under 0.2 ppm throughout the run and rises to 0.5 ppm at the

⁶ Manager of Cold Process Division, Cochrane Corporation, Philadelphia, Pa. Mem. ASME.

TABLE 4 CHEMICAL RESULTS FROM TREATMENT

Constituent	In ppm expressed as CaCO ₃				
	A	B	C	D	E
Cations					
Calcium (Ca ⁺⁺)	249	0-1	0-1	0-1	0-1
Magnesium (Mg ⁺⁺)	116	0-1	0-1	0-1	0-1
Sodium (Na ⁺)	27	0-1	0-1	0-1	0-1
Hydrogen F.M.A. (H ⁺)	0	113	0	0	0
Total cations	392	116	0-3	0-3	0-3
Anions					
Bicarbonate (HCO ₃ ⁻)	276	0	0-3	0-3	0
Carbonate (CO ₃ ⁻)	0	0	0	0	0-3
Hydroxide (OH ⁻)	0	0	0	0	0
Sulfate (SO ₄ ⁻)	100	100
Chloride (Cl ⁻)	16	16
Total anions	392	116	0-3	0-3	0-3*
Carbon dioxide, free	15	243	243	2-6	0
Silica	15	13	15	15	0-0.5*
pH	7.3	2.5-3.0	4.3-4.8	5.0-5.6	8.0-9.0
Total dissolved solids	18	8	2-6

* 2.5 average throughout run (total electrolytes).

† 0.1-0.2 average throughout run (SiO₂).

NOTES:

A. Raw.

B. From first step or cation units.

C. From second step or weakly basic anion units.

D. From decarbonator.

E. From third step or silica removal unit.

end of the run. The total electrolytes are reduced from nearly 400 ppm down to under 5 ppm. Therefore the effluent more than meets the USP standard of less than 10 ppm total solids, including the silica.

Although this water is not used for boiler-feed purposes, the continued satisfactory performance of this equipment has been reassuring to boiler-plant operators who were interested in the possibility of applying this system to boiler-feed make-up treatment.

Actually, during the last year there is evidence of a great increase in interest in this new system. A number of installations have been ordered.

Case 2 Central Power Plant. In the spring of 1949, a power plant in the Midwest, which had bought an evaporator for its make-up, decided to install a hydrogen-zeolite unit plus an alkali feed for neutralization plus a degasifier to pretreat the water to the evaporator. While receiving estimates of cost of this pretreating equipment the company also investigated the possibility of adding an anion exchanger for removal of the anions as well as the silica, and finally purchased a two-step demineralizer and silica-removal plant, using the evaporator as an emergency stand-by. The raw water comes from a well. The analysis is given in Table 5 of this discussion. The plant will have a capacity of 20,000#/hr, and is expected to be in operation early in 1950.

Case 3 Industrial Boiler Plant. Another order received was from an industrial plant on the West Coast. This plant previously used evaporators for producing distilled water for make-up purposes for the 420-psig boilers. Due to plant expansion it was necessary to provide for additional make-up. At that time it was decided to discontinue the evaporator and replace it by a demineralizer and ion-exchange silica-removal plant and to install a plant large enough to take care of the expansion.

One of the advantages of the demineralizer is that it permits the boiler to generate steam lower in free carbonic-acid content than the evaporator. This is due to the very low alkalinity of the demineralized effluent and its actual freedom from free CO₂. The pH value of the effluent is usually over 8.5 because the strongly basic anion exchanger absorbs free CO₂ as carbonic acid. The steam from the evaporator, on the other hand, would contain all the CO₂ that is formed by the decomposition of the feedwater alkalinity.

TABLE 5 ANALYSIS OF RAW WATER

	Ppm
Total hardness as CaCO ₃	240
MO alkalinity as CaCO ₃	217
Sulphates as CaCO ₃	13
Chlorides as CaCO ₃	3
Silica as SiO ₂	13
Free CO ₂ as CO ₂	36
Iron as Fe.....	0.3
Estimated pH value.....	7.2
Desired Quality of Effluent	
Total hardness as CaCO ₃	0 to 2
Total cations as CaCO ₃	2 to 5
Total anions as CaCO ₃	2 to 5
Silica as SiO ₂	under 0.5
pH.....	under 7.7

The raw water in this case has the following analysis:

		HCO ₃	40
Ca	50	CO ₂	8
Mg	17	Cl	19
Na	19	SO ₄	19
Total cations	86 ppm as CaCO ₃	Total anions	86 ppm as CaCO ₃
SiO ₂	11		
pH	8.5		

The demineralizing plant, which will have a capacity of 100,000 lb per hr, will consist of three steps, a cation exchanger in the first step, a weakly basic anion exchanger in the second step, then a decarbonator, and finally a strongly basic anion exchanger in the third step which will remove the residual anions and the silica. The quality of the effluent desired in this case is as follows:

	ppm		ppm
Ca	0-1	HCO ₃	0-3
Mg	0-1	SO ₄	0-1
Na	0-3	Cl	0-1
Total cations	0-5 as CaCO ₃	Total anions	0.5 as CaCO ₃
SiO ₂	under 0.2 ppm		
pH	over 8.0		

A number of similar installations are being made in the Midwest in central power plants and, judging from the inquiries and specifications that we are receiving calling for bids on this type of equipment, there can be no doubt that boiler users are becoming aware of the advantages of this system and that a definite trend has developed favoring that system instead of evaporators or ferric-hydroxide adsorption of silica.

Demineralizing by two-step ion exchange was in operation for some years, but the anion-exchange resin in the second step was of the weakly basic type which did not remove silica. Obviously, the removal of cations and anions without removing silica did not equal the performance of evaporators, because the boilers would have to be blown off heavily to keep the silica concentration low. It was discovered that by adding fluorides to the raw water, the ordinary demineralizer, using a weakly basic anion exchanger, would be able to remove the silica, and some plants were installed using this system. However, it had disadvantages of high operating cost, and there was a possibility of fluorides going over with the steam into the turbines.

With the advent of the highly basic anion-exchanger material, which removes silica, it is possible to remove silica without adding fluorides. The full advantage of the demineralizing process is, therefore, now available to produce a water of such low electrolyte and low silica content that it is the chemical equivalent of distilled water for boiler-feed purposes.

It is to be hoped that the actual experience with the plants which will be in operation during 1950, will be presented in papers before the Society so that additional evidence of the good results obtainable with this new process will be available.

D. C. CARMICHAEL.⁷ The paper presents a highly interesting subject and one upon which considerable study work was carried out before establishing that a 1400-psi boiler could be operated with 100 per cent make-up.

This work consisted of construction and operation of a 7-gpm water-treatment plant for color and silica removal. The results as to silica removal were much the same as later proved in the plant-size treatment system. The second step of this work was the operation of a 1400-psi boiler with a heating surface of approximately 4½ sq ft. The design of this boiler allowed for operation with a heat input up to and including 100,000 Btu per sq ft per hr. The feedwater for this experimental boiler was 100 per cent make-up from the mentioned water-treatment plant. The experimental boiler was operated for a total period of 120 days, and the prediction at that time was that the plant-size boiler would be operated for at least 6 months between internal cleanings.

The operating results in the Deepwater Operating Company's water-treatment plant may be of interest and are shown in Table 6 herewith. The constituents in the raw water do not vary widely from day to day, although the hardness has increased somewhat during 1948 and 1949. The hardness increase in the feedwater is due to the ferric sulphate and lime treatment. The silica content of the feedwater is fairly constant, irrespective of changes in the raw water. It may be said that the operation of the water-treatment plant is on a routine basis, although some interesting problems arose in the starting of the plant.

Fig. 9 of this discussion is a view of the precipitators, showing the lattice wave arrestors. When the plant was placed in operation, wind action stirred the water to the extent that water of a very unsatisfactory quality resulted. Covering of the tanks was considered but the wave action was overcome by a very low-cost idea—that of floating wood lath interlocked with nails as shown. This wave breaker was cheap and requires little maintenance.

⁷ Design Division, E. I. du Pont de Nemours and Company, Wilmington, Del. Mem. ASME.

TABLE 6 DEEPWATER OPERATING COMPANY—NO. 7 BOILER—WATER-TREATMENT DATA

	Raw Water		Filter Effluent		Chemical Feed	
	Total Hardness F.F.M.	SiO ₂ F.F.M.	Total Hardness F.F.M.	SiO ₂ F.F.M.	Ferric Sulphate F.F.M.	Lime F.F.M.
1944						
Min.	44	3.9	114	1.1	121	87
Max.	74	10.6	142	1.9	166	157
Avg.	56	8.5	129	1.8	139	111
1945						
Min.	41	4.0	111	1.2	122	90
Max.	55	10.5	146	1.9	207	156
Avg.	48	8.7	130	1.7	152	113
1946						
Min.	47	6.3	113	1.5	129	103
Max.	69	10.0	149	1.8	184	177
Avg.	58	8.3	126	1.7	155	127
1947						
Min.	46	2.3	115	1.0	105	105
Max.	80	10.6	176	1.8	224	182
Avg.	61	7.9	133	1.5	163	130
1948						
Min.	59	7.1	135	1.1	132	107
Max.	93	11.1	176	1.5	231	179
Avg.	71	9.2	158	1.3	195	141
1949 to date						
Min.	64	4.1	130	1.0	116	193
Max.	93	9.0	171	1.6	194	165
Avg.	75	7.0	152	1.2	168	126

Fig. 10 shows the operating valves of the gravity filters, the valves being located at floor level. They are readily accessible and make for lower investment than when a gallery floor is installed.

Fig. 11 shows the operating valves of the zeolite softeners. The softeners are located across the aisle from the filters, thus making for accessible operation to both the filters and softeners without the operator walking a long distance. In present-day design, only the operating valves and immediate piping would be housed with the shell proper outside, thus decreasing the building investment.

Table 7 of this discussion shows the boiler-water constituents.

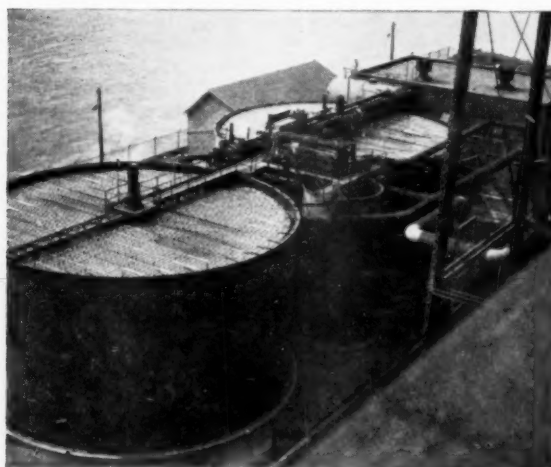


Fig. 9 VIEW OF PRECIPITATORS, SHOWING LATTICE WAVE ARRESTOR

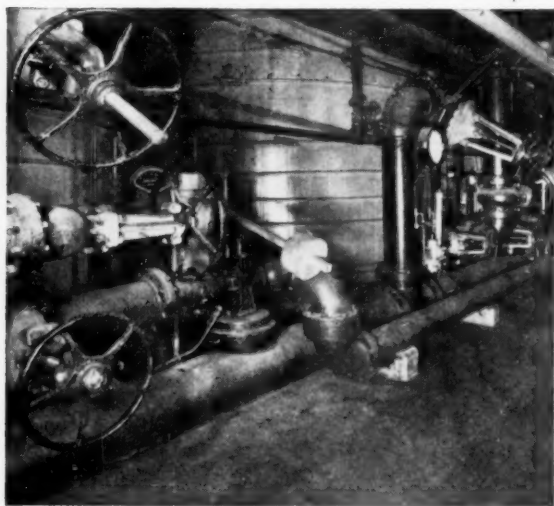


Fig. 10 PERMUTIT GRAVITY FILTERS—DEEPWATER OPERATING COMPANY

The blowdown varies from 15 to 20 per cent of the total feed-water, and no turbine-blade deposits have been encountered with the silica and total solid concentrations shown. The final criterion of the feedwater treatment is in the internal condition of the boiler.

TABLE 7 DEEPWATER OPERATING COMPANY—NO. 7 BOILER—BOILER-WATER CONCENTRATIONS

	Alkalinity PPM CaCO ₃	Hydroxide PPM CaCO ₃	SiO ₂ PPM	FeO ₂ PPM	MgSO ₄ PPM	SO ₄ PPM	Chloride PPM	Suspended Solids PPM	Total Solids PPM
1944									
Min.	98	87	6.9	11.9	9	624	74	22	1392
Max.	134	119	11.0	17.9	11	853	314	63	1655
Ave.	112	102	10.0	12.5	10	776	168	41	1560
1945									
Min.	112	94	7.0	12.2	9	718	97	60	1509
Max.	132	114	11.1	13.4	21	890	186	99	1686
Ave.	120	102	10.0	12.7	16	796	120	75	1567
1946									
Min.	122	104	9.4	12.8	18	704	90	62	1413
Max.	126	107	10.7	13.8	22	794	199	75	1679
Ave.	124	106	10.1	13.1	20	775	138	66	1606
1947									
Min.	124	105	6.4	13.2	18	662	105	55	1558
Max.	131	114	10.2	16.2	22	872	292	92	1711
Ave.	127	107	9.8	15.2	20	794	152	70	1630
1948									
Min.	125	106	9.5	15.8	18	596	102	50	1512
Max.	130	109	10.2	16.2	21	884	336	98	1694
Ave.	127	107	9.8	16.0	20	800	156	71	1650
1949 to date									
Min.	123	103	7.7	15.8	19	620	101	44	1566
Max.	145	126	10.0	16.4	20	867	354	73	1696
Ave.	131	111	9.2	16.0	20	793	178	60	1640

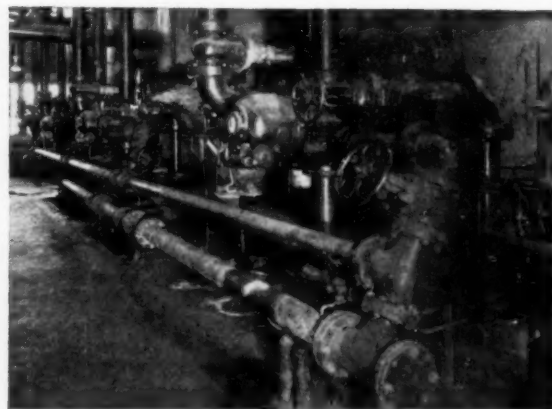


Fig. 11 PERMUTIT ZEOLITE SOFTENERS—DEEPWATER OPERATING COMPANY

Fig. 12 is a side-elevation view of the 1942 boiler installation operating with 100 per cent make-up as mentioned in the paper. The remaining views were taken during the annual inspection of the upper drum and lower drum to show the internal conditions.

Fig. 13 is of the upper drum, which indicates absence of scale or sludge in the drum itself as well as the cyclone separators. Fig. 14 is of the lower drum during the same inspection and likewise shows very little sludge present. These views were taken in June, 1948, after 3 years of operation since the previous cleaning.

The paper gives comparisons on 100 per cent softening versus 100 per cent demineralization. Equipment-cost comparisons between the two methods of treatment would be very enlightening. Likewise, would the boiler manufacturer agree to greater output in pounds per hour with the same unit on 100 per cent demineralized water, as compared to 100 per cent softened water, or would a lower-cost boiler unit be offered for the same output

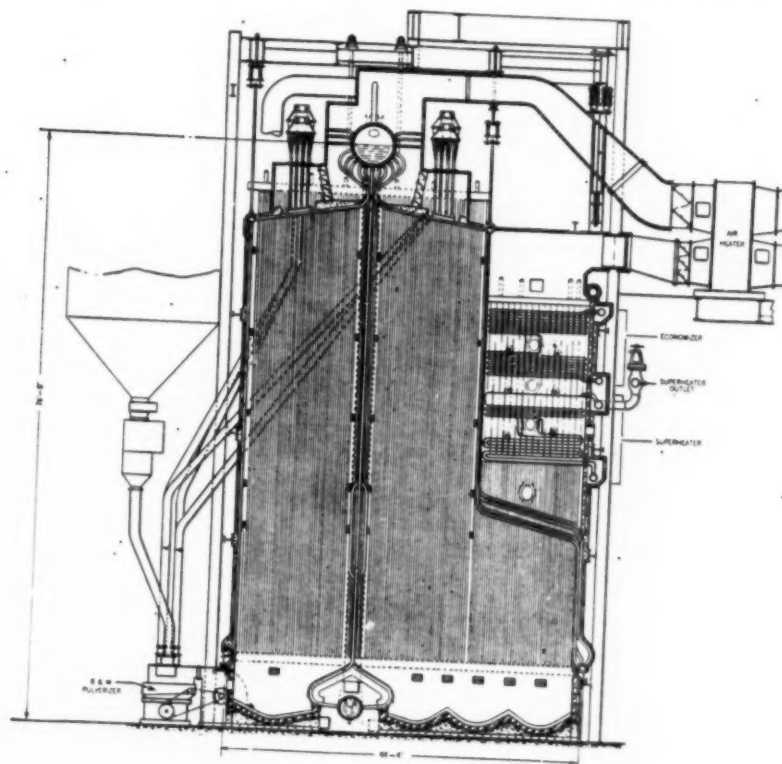


FIG. 12 SIDE ELEVATION OF NO. 7 BOILER

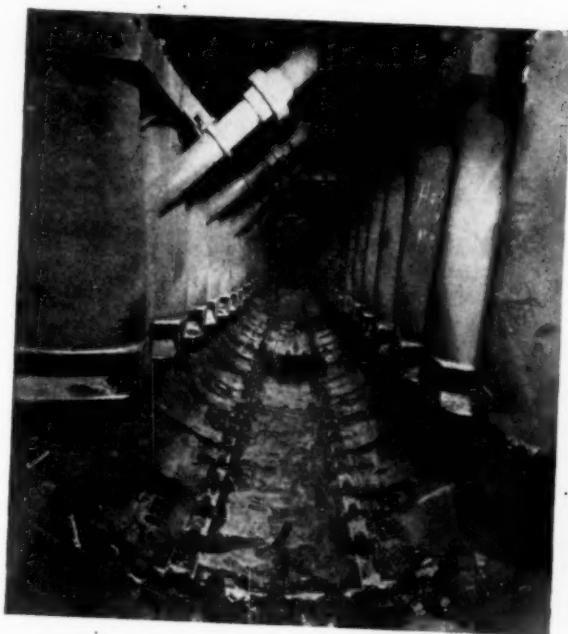


FIG. 13 UPPER DRUM OF NO. 7 BOILER

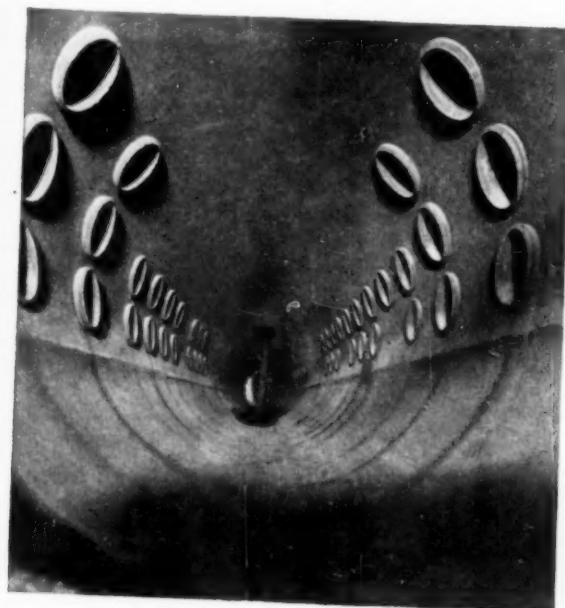


FIG. 14 BOTTOM DRUM OF NO. 7 BOILER

when 100 per cent demineralized water is the source of feedwater? After all, it is the economics of any installation which governs, to a large extent, the type of equipment and design.

In conclusion, it might be stated that the operating results on 100 per cent treated make-up show that the operating difficulties are no greater than have been experienced in many high-pressure boilers operating on low percentages of evaporated make-up.

P. H. KNOWLTON.⁸ The authors correctly emphasize the very high thermal efficiency of electric power production in plants where the power may be generated as a by-product of the generation of steam for other than power purposes. In the case of the Deepwater plant, elimination of the evaporator heat exchangers increases the amount of such high-efficiency power, which represents a gain in useful power output of the plant.

The improvements in feedwater treatment which make possible good operation without the evaporators constitute a valuable contribution to the development of more efficient power plants.

The authors point out that when a public utility and an industrial company co-operate in the design and use of a plant for producing steam and electric power, the tendency is to design a plant giving the largest amount of electric power, in proportion to steam, that can be shown to be economical. This tendency is to be commended, since it means that fuel resources are conserved, as the thermal efficiency at which this power is generated is much higher than by any other available means.

E. A. FIRSH.⁹ The authors have presented an interesting study of process steam plants generating by-product electric power. Heat balances are given for systems utilizing high-pressure turbines exhausting either directly to process or to the coils of evaporators, which in turn deliver the steam to process. The low heat rates in these types of plants show that the by-product power can be produced at a much lower fuel cost than is attainable in a central station which wastes heat to the condenser cooling water. The increasing number of plants which are operating successfully in this manner at or near 100 per cent make-up demonstrate the feasibility of such operation even under drastic water-treatment demands.

It is true that when high-pressure boilers were first installed the design engineers were reluctant to believe that they could be operated successfully with 100 per cent make-up. This attitude was in part based upon the knowledge that if excessive blow-down were to be avoided with the poorer quality of feedwater available to the high make-up boiler, it would be necessary to carry the boiler-water concentrations at much higher values. The capacity of the steam-separating equipment available at that time was influenced by increased boiler-water concentrations to a much greater degree than is the case with present-day steam-separating equipment. For this reason the maximum allowable steaming rate per foot length of drum was a more important consideration on over-all boiler design than it is at present.

The improved steam-separation and purification equipment now available permits a plant to carry boiler-water concentrations at higher values and to obtain better steam purity than was formerly possible. This results in a decreased blowdown requirement which is a very significant factor in the operation of high make-up boilers fed with water of relatively high dissolved-solid concentration.

There are now a considerable number of installations operating at or near 100 per cent make-up and at pressures ranging up to

2200 psi which deliver steam with a maximum total dissolved-solids content between 0.5 to 0.8 ppm, when carrying boiler-water concentrations up to 2500 ppm. The absence of tube failures and the long intervals between required cleanings on the waterside in these units is evidence that a properly designed boiler can be operated successfully under conditions of high make-up and high boiler-water concentrations, provided the boiler water is properly conditioned.

The pioneer design and operation of high-pressure boilers, which occurred during the 1920's, were beset with many new problems, and the design engineers, with justification, insisted that these boilers should operate with low make-up so as not to introduce unnecessary complexities through the use of a poorer-quality feedwater. It must be remembered that the science of water conditioning was in its infancy during this period, and the use of phosphates for water conditioning had just been introduced.

The accumulated knowledge obtained from experiences since that time has led to a clearer conception of the objectives to be achieved, a more thorough understanding of the principles involved, and the development of better and more economical means of feedwater- and boiler-water conditioning. Thus the quality of the feedwater for high make-up boilers has improved to the point where it is found economically practical in many instances to produce, by demineralization, a water whose purity approaches that of distilled water.

Proper conditioning of the sludge is of very great importance in a high make-up boiler because of the greater amounts which are present. The sludge must be in such condition that it is nonadherent to the surfaces in the boiler and must be kept in suspension so that it can be blown down from the unit. Sludge-dispersal agents have proved of tremendous value in performing these functions. The advances in the science of water conditioning must receive the major share of the credit for the demonstrated successful operation of high-pressure, high-make-up boilers.

The increasing demand for electric power in this country will stimulate the production of by-product power in process-steam installations, and the success of these plants must be credited in large part to the knowledge disseminated by those who have pioneered this type of operation.

W. C. WOODMAN.¹⁰ The authors have presented a paper which draws attention to the exceptional opportunities afforded in an industrial plant for obtaining power at fairly low cost where it is possible to generate this power as a by-product of process steam. The economics of the situation, as the authors point out, in the end often dictates the system or cycle to be employed, and present-day production costs require the adoption of pressures and temperatures, and the utilization of heat-saving devices not heretofore economically justifiable.

One such device which is particularly applicable to the type of plant chosen by the authors is the thoroughfare desuperheater. By employing this type of heat exchanger, a substantial increase in power may be developed without the generation of additional steam, or conversely, a considerable improvement in economy may be obtained with the same power development. When employing steam for process, that temperature which may be tolerated in the exhaust steam limits the turbine initial temperature to a value less than that which is often economically justifiable. With the use of a thoroughfare desuperheater, which is a wholly practicable heat exchanger, the initial temperature at the turbine inlet may be increased, while the temperature of the exhaust steam supplied to process is reduced on passing through this desuperheater to approximately the value which would be

⁸ Thermodynamic Engineer, Turbine Engineering Divisions, General Electric Company, Schenectady, N. Y. Mem. ASME.

⁹ Staff Engineer, The Babcock & Wilcox Company, New York, N. Y.

¹⁰ Mechanical Engineer, Stone & Webster Engineering Corporation, Boston, Mass. Mem. ASME.

obtained from a turbine having low initial steam temperature. Feedwater forms the cooling medium in the desuperheater. The heat balance, Fig. 15 of this discussion, illustrates the thoroughfare desuperheater applied to the cycle in the authors' Fig. 6. Over 5500 additional kilowatts, representing an increase of 26 per cent, have been obtained with substantially the same boiler output and cycle heat rate. To obtain this additional power, the boiler, turbine, and connecting piping must be designed for the higher temperature, and the thoroughfare desuperheater provided. It is estimated that these modifications can be installed for less than \$50 per kw of increased capacity, which is a relatively economical means of obtaining additional power.

For industrial plants where power and process-steam demand are not so nicely balanced as in the instances cited by the authors, an extraction-condensing turbine generator can be employed. The use of a thoroughfare desuperheater is equally adaptable for installation in the extraction steam line and permits realizing the added capacity or economy resulting from high initial temperature, without increasing the temperature of the extraction steam to process.

One economic fact in the authors' paper might be given more emphasis and that is the increased construction cost of demineralization over softening equipment. The extra power derived from the demineralization plant, Fig. 7 of the paper, over the softening plant, Fig. 6, is relatively costly. It is estimated that the extra cost of demineralization equipment over the cost of sodium zeolite would approximate the cost of equipping for the high-temperature operation described, and for the conditions assumed by the authors, the purchaser would get greater return on his investment by utilizing high-temperature equipment. The improvement in the cycle resulting from the use of a demineralizing plant develops a net increase of 1170 kw, which we estimate would have an incremental cost of approximately \$275 per kw, which seems to us to be more costly than the addition of a condensing end on the turbine.

This apparent advantage of one method of obtaining additional output over the method proposed by the authors serves also to emphasize the need for comprehensive analysis and engineering of each project.

AUTHORS' CLOSURE

The requests for supplementary and more detailed data on costs are natural and numerous. The problem, which confronts the authors, is to prepare such figures so that they will be of use and free of the possibilities of misinterpretation. When any attempt is made to give dollar values, which purport to be "averages" or "representative," they are always subject to misuse because of failure by all parties concerned to be on a common ground. This will occur despite the efforts to resolve differences. We are saddled with the inherent weaknesses of such approaches on the averages.

Mr. Adams correctly states that chemically softened make-up will produce more power per unit of process steam than evaporated make-up. Whether demineralization would be more economical than softening in a specific instance would depend upon many variables including not only water conditions, equipment and installation costs, and expenses for fuel and operating labor, but also upon the judgement of project designing engineers. Mr. Adams' figure of 0.24 cents per kwh obtained by dividing the increment of chemical cost by the increment of power is considerably less than the production cost of most condensing plants. Consequently it might be considered as an argument for demineralization.

As Mr. Applebaum indicates, demineralization is receiving much attention. Undoubtedly the ASME will welcome papers presenting conclusive operating results on this method of treatment.

Mr. Carmichael, because of his direct association with the design and initial operation of the Deepwater 100 per cent Make-up Unit, is well-qualified to discuss experiences with this

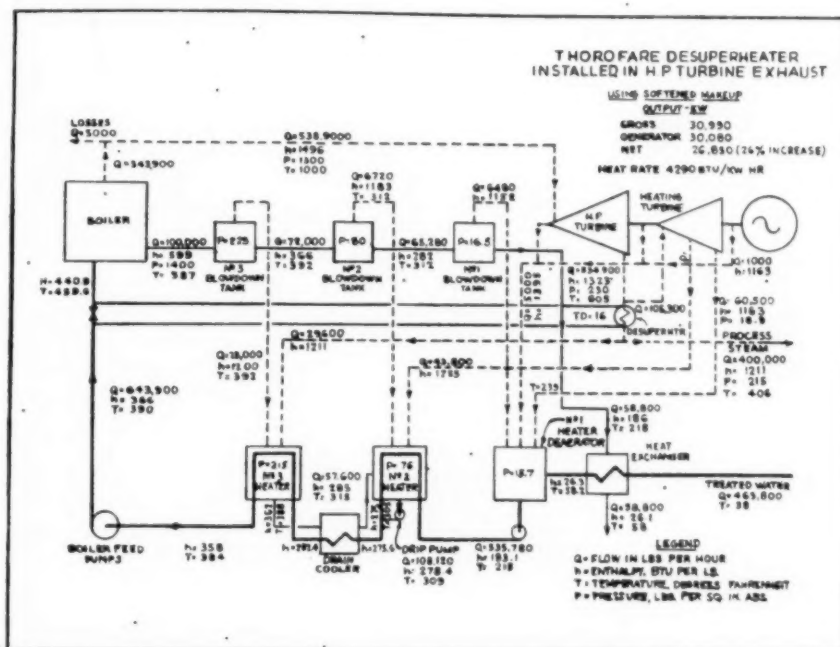


FIG. 15 THOROUGHFARE DESUPERHEATER INSTALLED IN HIGH-PRESSURE TURBINE EXHAUST

installation. The authors are most grateful for his contribution. However, as previously indicated, they are reluctant to give comparison of plant-equipment costs involved when employing softened and demineralized make-up. Mr. Carmichael's question concerning boiler design and cost for the two treatments represents only one of the variables which hinges largely on the judgment of the persons concerned. In a case where an existing condensing plant boiler is to be operated such to require high make-up, it probably would reflect good engineering judgment to demineralize rather than soften the make-up water.

It is gratifying to have Mr. Knowlton agree with the thesis of the paper and to emphasize the possibilities in reducing power costs by co-operation of public utilities and the industries requiring large quantities of process steam. Both he and Mr. Pirsh present pertinent observations.

It is most helpful of Mr. Woodman to have prepared a complete heat balance on the use of the thoroughfare heater. The data shown in his Fig. 15 are directly comparable with those contained in the body of the paper and the ASME should be grateful that Mr. Woodman has taken the time to work out such an exact analysis. He cites the gain in power for a given process-steam flow and ventures an estimate of the additional investment. In the case of the Deepwater 100 per cent softened make-up installation, the use of the thoroughfare heater was studied

but its installation was not considered to be justifiable on the basis of cost. Other specific cases, coupled with today's prices, could very reasonably lead to different conclusions.

In a similar fashion, any analysis made today should recognize the potentialities of mercury vapor for by-product power generation. Great strides have been made in this field and if a mercury boiler-turbine-condenser-steam unit were postulated instead of the combinations considered in this paper, the ratio of power to process steam would again run to much higher values.

If, for the conditions shown in the heat balances, the output of electric energy in Fig. 3, using a process-steam evaporator, could be considered for comparative purposes as 1.0, then the output with softened make-up, Fig. 6, would be 1.8, and with demineralized make-up, Fig. 7, 1.9. With the thoroughfare heater of Mr. Woodman's Fig. 15, this value for electric power output would climb to 2.4. If mercury vapor were used, then the by-product power would reach a value nearly double that of Fig. 15, actually about 4.4. This high ratio of power to process steam offers one of the real merits of mercury vapor. The disadvantage of the picture is the dollar cost of the increment investment. This, in many instances, is, at present, unfavorable to mercury vapor. But the continually changing prices for fuel and equipment are bound to alter any conclusions on the economic merit of the proposal and a continuing study is justified.

H
cha
7 un
abo
stor
uni
tion
mon
from
toge
appl

N
furni
study
The
believ
an in
The
the I
per h
press
opera
was p

The
that t
in con
of the
No.
line w
drum.
tically
the wa
would
At all
sentati
lecting
conditi
No. 2
in the f
the wat
the tub
chemic

¹ Supp
ASME.
² Chic
Contr
Studies
ing, Ne
AMERICA
NOTE
understo
of the S

Sulphite and Silica in Boiler Water at Springdale

By L. E. HANKISON¹ AND M. D. BAKER,² PITTSBURGH, PA.

Hydrogen sulphide was first detected in the gases discharged from the air ejector of the main condenser of No. 7 unit at Springdale Station of West Penn Power Company about 6 months after the unit was placed in service. The story of potassium sulphite and its connection with this unit will form the first part of this paper. Silica deposition on the turbine blades was quite rapid, and after 8 months operation it was necessary to sandblast the silica from the blades. The search for the source of this silica, together with the information found and the corrections applied, will also be discussed.

NO. 7 unit at the Springdale Station of the West Penn Power Company is a one boiler-one turbine installation, and is operated independently from the rest of the station. This furnishes an excellent opportunity to make a closely controlled study of the boiler and the turbine as regards water conditions. The unit is fully equipped with instruments as well as what was believed to be a fair complement of sampling facilities for making an investigation.

The boiler is a radiant-heat divided-furnace type furnished by the Babcock & Wilcox Company, and is rated at 800,000 lb per hr of steam at 930 F total temperature, and 1350 psi drum pressure. The turbogenerator is Westinghouse and is usually operated at 85,000 kw. This addition to the Springdale Station was put in regular operating service January 14, 1946.

SAMPLING BOILER WATER

The three original boiler-water sampling points were selected so that the samples obtained would show differences, if any existed, in concentration or chemical constituents at three different parts of the boiler. These are located as follows:

No. 1 This sample is collected from the continuous-blowdown line which extends from the left drumhead to the middle of the drum. It has small intake holes throughout its length. Theoretically, this blowoff pipe should give a representative sample of the water surrounding the length of the pipe, but at best this would be true only when a heavy blowdown was being made. At all other times the sample from this point would be representative of the water surrounding the first few holes in the collecting pipe. It is thought that the No. 1 sampling point gives conditions which exist only at the left end of the drum.

No. 2 This point is located 5 ft from the top end of No. 40 tube in the front wall. The sample obtained was supposed to represent the water in the left half of the boiler and was placed high up in the tube in order to determine if any difference existed in the chemical constituents of the boiler water because of hot spots or

faulty circulation. This wall contains 160 three-in-OD tubes 95 ft long.

No. 3 Similar to location of No. 2 sampling point, except this point is in tube No. 119 at the opposite or right half of the front wall.

The boiler water of the unit has always been conditioned with potassium salts. The chemicals used are potassium phosphate, potassium hydroxide, potassium chloride, and potassium sulphite. These chemicals were introduced into the boiler water at the drum in order that the least possible amount of solids would be in the water delivered to the attemperor. The use of potassium salts for boiler-water treatment has been described previously by the authors.³

Sulphite. West Penn Power Company considers sulphite an essential conditioning chemical in boiler water. Experience with lack of sulphite was quite expensive and was described by the authors of this paper in a previous presentation.⁴ It has been used in No. 77 boiler since it was first put in service, and its use is expected to continue.

It was noted quite early in the operation of the boiler that sulphite analyses of the boiler water were erratic and that the desired concentration was hard to maintain. Also, the water samples contained various quantities of finely divided black iron and copper oxides. The sulphite might vary from 10 ppm excess to none in two consecutive samples from the same sampling point. The day-by-day variations in all constituents in boiler-water analyses except sulphite were in proper proportion, and this gave confidence of correct methods of sampling. The varying results gave reason to question the equipment used to obtain the samples, and the water circulation in the boiler. These conditions, and particularly the unpredictable results of the sulphite analyses were the cause of much concern, and the reason for the boiler-water investigation.

Six months after the boiler was placed in service, intermittent shots of hydrogen sulphide were discharged at the air ejector of the main condenser. As time elapsed, the number and intensity of the shots became greater. The amount of hydrogen sulphide was sufficient to make the air in the turbine room offensive to the operators. The hydrogen sulphide in the 5 cfm of gases discharged from the air ejector was determined colorimetrically, using sodium plumbite. The amount usually found varied from 5 to 25 ppm. The maximum determined was 192 ppm by volume or 229 ppm by weight. This high figure does not represent a large amount of hydrogen sulphide, as 229 ppm by weight in 7200 cu ft of gases per day equals only 6.03 grams. This is equivalent to 1.12 ounces of potassium sulphite. At this time the sulphite fed was varying between 6 and 10 lb per day.

A probable reaction for the decomposition of potassium sulphite in high-pressure-boiler water is as follows



¹ Superintendent Efficiency, West Penn Power Company. Mem ASME.

² Chief Chemist, West Penn Power Company.

³ Contributed by the Research Committee on Boiler Feedwater Studies and the Power Division and presented at the Annual Meeting, New York, N. Y., November 27-December 2, 1949, of THE AMERICAN SOCIETY OF MECHANICAL ENGINEERS.

NOTE: Statements and opinions advanced in papers are to be understood as individual expressions of their authors and not those of the Society. Paper No. 49-A-75.

⁴ "History of Potassium Boiler-Water Treatment at Springdale," by L. E. Hankison and M. D. Baker, Trans. ASME, vol. 67, 1945, pp. 317-324.

⁵ "Corrosion and Embrittlement of Boiler Metal of 1350 Pounds Operating Pressure," by L. E. Hankison and M. D. Baker, Trans. ASME, vol. 69, 1947, pp. 479-486.

This reaction will occur with the dry salt-heated to a red heat. It has also been reported to occur in solution in the presence of copper or iron compounds at temperatures above 490 F.⁵ At this temperature, with the same catalysts, hydrogen sulphide can be produced from potassium sulphide as in the following



This reaction was confirmed by the high alkalinity of the boiler water at the time the hydrogen sulphide was most noticeable. During a period of several weeks the pH of the boiler water was in excess of 11.3 without feeding any caustic.

Boiler-water treatment was fed directly into the drum through a chemical feed bottle once each day. While not a constant occurrence, the heaviest discharge of hydrogen sulphide occurred 45 to 90 min after the chemicals were added. The minimum sulphite concentration was set at 3 ppm, and; to prevent going below this value, it was necessary to have 35 to 45 ppm of sulphite in the boiler water immediately after adding the chemical.

A theory that concentrations this high were the cause for the decomposition of sulphite with the resultant formation of sulphide was disproved. Tests were made on three other boilers of the same pressure with sulphite increased by shot treatment to concentrations of 60 to 90 ppm with no detected formation of hydrogen sulphide. The only difference in the chemical conditioning of the four boilers was in the rate of feed from the chemical bottles. The charge of chemicals in the bottle of No. 77 boiler would be emptied in a few minutes, while at least 1/2 hr was required to empty the bottle on each of the other boilers. In all four boilers, the high concentration of sulphite would be reduced to 10 ppm or less in 24 hr. No satisfactory explanation for this reduction or disappearance of sulphite in oxygen-free water is offered or has been found in the literature.

The set minimum concentration of 3 ppm of sulphite in No. 77 boiler was reduced to 1 ppm, but positive tests for hydrogen sulphide were obtained with 1 ppm of sulphite in the boiler water. This seemed to confirm the thought that the boiler had faulty circulation and was developing hot spots with the resultant decomposition of sulphite.

Two plans of action were started immediately, as follows:

- 1 Purchase and installation of a chemical feed pump that would permit continuous chemical treatment.
- 2 Installation of additional sampling coils which would permit sufficient samples to be obtained to determine if points of high concentration were occurring.

A Milton Roy pump of 3 gph capacity for continuous treatment was placed in service on April 5, 1947. The chemical treatment is pumped into the discharge line of the Hankison boiler-water recirculator which pumps water continuously from the boiler drum through the economizer for corrosion protection as described by Baker.⁶

Fig. 1 shows where the chemical feed pump discharges into the recirculator line before the water from the drum enters the main boiler feed line downstream from the attemperator connection. Since this pump was placed in service, continuous low sulphite concentrations have been easily maintained. Following this change in method of treatment there was a reduction in the intensity and frequency of the shots of hydrogen sulphide discharged by the air ejector, but 7 months elapsed before the production of this gas was entirely eliminated.

Fifteen additional sampling points were located on the boiler

⁵ "The Behavior of Sodium Sulphite in High-Pressure Steam Boilers," by R. M. Hitchens and J. W. Pursell, Trans. ASME, vol. 60, 1938, pp. 469-473.

⁶ "Economy in Boiler Water Recirculation," by M. D. Baker, Combustion, vol. 12, October, 1940, pp. 31-34.

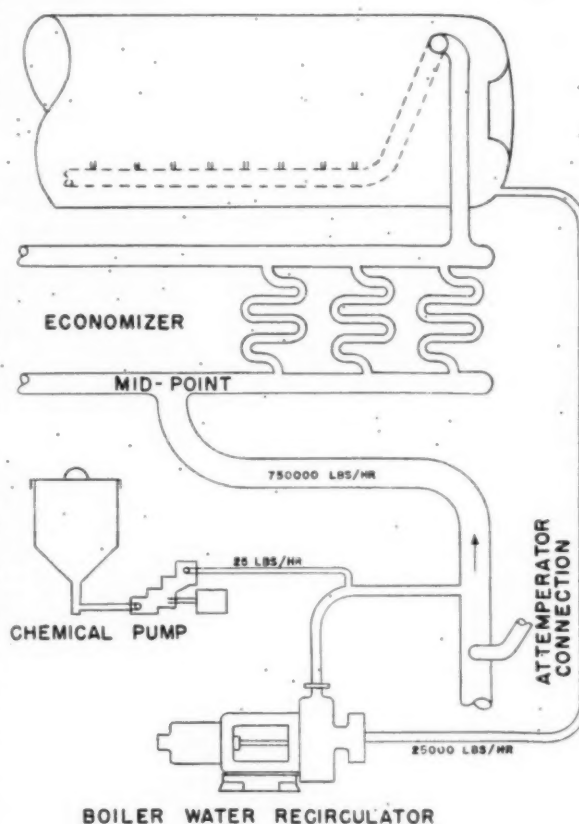


FIG. 1 BOILER WATER RECIRCULATOR

tubes and headers so that the complete study was made with 18 samples collected as nearly simultaneously as four men could collect them. The lower headers gave water conditions in each wall in accordance with the water supply from the drum. The additional tubes selected for sampling were thought to have the higher rates of evaporation, and consequently would be first to show faulty circulation.

Table 1 lists the points of sampling and gives a typical set of analyses obtained from the 18 sample points. The variation in ratio of sulphite to the other constituents was typical of the daily analyses made over a period of several months.

The boiler was acid-cleaned in April, 1947, to remove the heavy oxide deposit which was thought might be affecting circulation. It is estimated that the acid-cleaning and the subsequent washing of the drum and headers removed more than 500 lb of deposit. A partial analysis of the material which was removed is given in Table 2:

At the time the boiler was acid-cleaned the turbine was inspected. Severe active corrosion was found on the low-pressure-turbine casing at the discharge throat into the condenser. Also, the metals of the condenser were attacked where the condensed steam rained into the condenser. Subsequent inspections since the hydrogen sulphide disappeared show no active corrosion.

The hydrogen sulphide had attacked the tubes in the air-ejector condenser. The tubes in the inlet section could be broken easily by the hands. The tubes are made of admiralty metal and those replaced in April, 1947, are still giving satisfactory service.

TABLE 1 POINTS OF SAMPLING AND TYPICAL ANALYSES OBTAINED

Sample Date - 5/9/47

Sample Points	ppm SO ₃	Micromhos Cond.	ppm SiO ₂	ppm FeO	ppm Cl
Drum South End	11	720	5	28	100
South Wall Lower Header	11	708	4	26	96
South Division Wall Lower Header	11	695	3	24	89
South Convection Wall Lower Header	10	665	2	24	92
West Wall Lower Header	11	625	5	24	90
East Wall Lower Header	11	682	3	24	84
East Wall No. 40 Tube Bottom	11	714	4	22	98
East Wall No. 40 Tube Top	13	700	3	24	95
East Wall No. 66 Tube Bottom	7	678	3	24	100
East Wall No. 66 Tube Top	9	636	4	23	88
East Wall No. 119 Tube Bottom	5	650	3	22	85
East Wall No. 119 Tube Top	9	635	2	22	90
Drum Center	6	660	4	26	91
North Convection Wall Lower Header	6	626	3	22	86
North Division Wall Lower Header	10	660	4	24	92
North Division Wall No. I Tube Bottom	7	648	4	23	85
North Division Wall No. I Tube Top	6	645	2	24	92
North Wall Lower Header	11	660	2	24	85

TABLE 2 MATERIAL REMOVED FROM BOILER BEFORE ACID CLEANING

	Per cent
Silica as SiO ₂	0.1
Iron oxide as FeO	72.8
Copper as CuO	15.8
Phosphate as P ₂ O ₅	3.2

Theory of Hydrogen-Sulphide Formation. A probable theory for the formation of hydrogen sulphide is that while 45 ppm of sulphite was the maximum found in the boiler water after shot treatment, at the time of injection the concentration was much higher

and decomposition occurred. A large proportion of the gas was discharged from the air ejector, but some was absorbed by the condensate and recirculated in the boiler-water cycle. It is quite possible that a large number of cycles were required to discharge all the absorbed gas. The hydrogen sulphide when absorbed by the condensate produced an acid solution which attacked the metals of the system. These dissolved metals when finally concentrated in the boiler would settle out as oxides, but during the conversion from sulphide to oxide, they served as catalysts to break down more of the sulphite. With the removal of deposits by acid-cleaning, and the elimination of large excesses of sulphite, the desired boiler-water condition was slowly established, and the hydrogen sulphide gradually reduced.

The inconsistent sulphite analyses still persisted with the continuous feed of boiler-water chemicals. In the study to determine all inconsistencies it was noted that copper and steel were used in various combinations for sampling lines and inner coils of cooling coils. Table 3 shows the result of this phase of the study. It is to be noted that the samples collected through copper gave erratic sulphite results. Samples collected through steel gave consistent results.

The confirmation that copper reduced the sulphite in the sample was obtained from a series of tests made at the No. 40 tube top sample connection. The steel sample line from the valve was brought out to a tee. Each side of the tee was connected with the same length of steel tubing to sample coils; one with copper inner coil, the other with a stainless-steel inner coil. The flow was regulated at each coil so that the volume of sample was the same. Table 4 is typical of the results that were obtained on numerous tests with a copper coil and stainless-steel coil in parallel; and also with two stainless-steel coils in parallel. In all tests the sample from the copper coil gave a lower sulphite reading than was obtained in the sample from the stainless-steel coil.

Effect of Copper Tubing. Evidence of the effect of copper tubing on the disappearance of sulphite in the boiler water was found at the time of the failure of a section of tubing connecting the source of the sample with the cooling coil. The copper tubing could not be made tight at the fitting and was replaced. The section re-

TABLE 3 RESULTS OF TESTS WITH CONTINUOUS FEED OF BOILER-WATER CHEMICALS

	Sampling Tube Metal	Inner Coil Metal	5/23/47		5/29/47		6/3/47		6/23/47		7/7/47	
			SO ₃	Cond.	SO ₃	Cond.	SO ₃	Cond.	SO ₃	Cond.	SO ₃	Cond.
Drum South End	S	SS	14	792	2	696	3	762	11	922	9	730
South Wall Lower Header	S	Cu	14	774	2	654	3	750	7	898	5	716
South Division Wall Lower Header	S	Cu	14	762	2	610	3	725	9	875	9	697
South Convection Wall Lower Header	Cu	Cu	11	715	0	610	0	675	6	828	4	666
West Wall Lower Header	S	SS	12	697	2	603	2	658	10	820	8	656
East Wall Lower Header	S	SS	14	720	1	620	2	685	10	847	8	672
East Wall No. 40 Tube Bottom	Cu	Cu	15	773	2	665	2	728	8	900	0	725
East Wall No. 40 Tube Top	S	SS	14	750	2	635	3	715	10	865	8	710
East Wall No. 66 Tube Bottom	Cu	Cu	11	732	0	635	0	682	6	830	2	662
East Wall No. 66 Tube Top	Cu	Cu	9	700	0	592	0	610	6	808	0	658
East Wall No. 119 Tube Bottom	Cu	Cu	9	636	0	545	0	598	5	765	0	635
East Wall No. 119 Tube Top	S	Cu	12	630	2	538	2	585	3	750	3	634
North Convection Wall Lower Header	Cu	Cu	7	616	0	523	0	575	5	735	3	610
North Division Wall Lower Header	S	SS	13	648	4	546	2	610	9	786	7	665
North Division Wall No. I Tube Bottom	Cu	Cu	8	656	1	550	0	610	4	776	4	642
North Division Wall No. I Tube Top	Cu	Cu	8	650	1	545	0	655	4	750	0	642
North Wall Lower Header	S	SS	11	636	3	540	1	602	9	774	8	656

S - Steel
SS - Stainless Steel
Cu - Copper

TABLE 4 RESULTS WITH COPPER ON STAINLESS-STEEL COILS IN PARALLEL AND STAINLESS-STEEL COILS IN PARALLEL

Coil Metal	SO ₂	Conductivity	SiO ₂	PO ₄	CL
Sample date 7/16/47					
Copper.....	0	760	3	27	78
Stainless steel.....	5	808	3	28	83
Sample date 7/22/47					
Stainless steel.....	4	926	4	28	88
Stainless steel.....	4	929	4	27	88

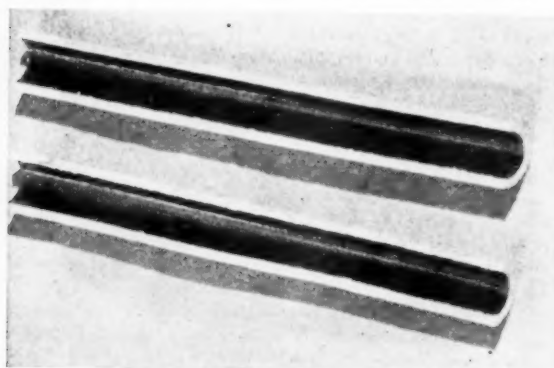


FIG. 2 SPLIT SAMPLING TUBE SHOWING COPPER OXIDE COATING

moved was split lengthwise and the inside was found to be coated with a black enamel-like coating that was badly cracked. In places, little chips of the coating had broken off exposing bare copper. Flakes of the coating removed for analyses were found to be copper oxide. Fig. 2 is a photograph of the split tube showing this oxide. A new section of bright copper tubing was installed. This section of tubing was inspected after a month of normal sampling service and showed definite discoloration. No further testing was done to determine the rate of attack as the copper tubing was replaced as soon as possible. No discoloration or metal attack has ever been found in steel tubing.

Analyses were not made to explain the disappearance of sulphite and the production of the copper-oxide coating. However, bright copper strips were exposed to cold boiler-water samples without discoloration. This would indicate that sulphide was not present in the boiler water. The least trace of sulphide added to these same samples would produce discoloration of the copper strip.

After it was determined that copper would reduce sulphite in boiler-water samples, all permanent boiler-water-sample connections and coils made of copper were replaced with steel. These changes corrected most of the erratic results, but it was found that variations in analyses still persisted and were more pronounced in warm weather than during cold weather. A study was made to determine the effect of temperature of the sample at the time of collection, and it was determined that:

1 Samples collected from an all-steel system at temperatures above 80 F may give low SO₂ results.

2 A sample collected through an all-steel sampling line, a stainless-steel inner cooling coil but with a short copper discharge tube from the coil will be affected if the sample has a temperature above 80 F.

3 A long copper cooling-coil discharge tube can, at any temperature, reduce materially the SO₂ content of the sample.

Some tests were made using monel sampling lines between the valve and cooling coils. Sufficient data were not obtained to arrive at definite conclusions but it was indicated that this metal would reduce the sulphite in the boiler-water sample, but not as much as copper.

Eliminating the erroneous results caused by the effect of copper on the sulphite content of the boiler water, the other data indicated that the boiler was free of circulation trouble.

SILICA DEPOSITION ON TURBINE BLADES

Silica. Silica deposition on turbine blades at Springdale has been mentioned in a previous paper.² The rate of deposition on No. 7 unit at Springdale confirms the findings of Straub and Grabowski³ that silica concentrations above 5 ppm in the boiler water will cause blade deposition. The rate of deposition on the unit at Springdale is measured by the increase in pressure at No. 3 bleed point. With clean blades and at a load of 85,000 kw on the turbine, the pressure at the third-stage bleed point is 128 psi. Any increase in this pressure usually indicates blade deposits.

A definite limit for maximum silica in the boiler water was not established during the period from starting the unit until September 14, 1946. Efforts were made to reduce the silica by blowdown, but no positive program was instituted. During the first 2 months of this period, silica in the boiler water varied between 18 and 25 ppm. During the remainder of the period the silica was gradually reduced to 8 ppm. At the time the unit was taken from service the third-stage pressure had increased to 155 psi. The cover was removed from the turbine and heavy blade deposits were found. The blades were cleaned by sandblasting which restored the turbine to a clean-blade condition. The unit was again placed in service October 1, 1946. During the first week after cleaning, the silica content of the boiler water varied between 13 and 21 ppm. After this the silica content of the boiler water was maintained between 4 and 8 ppm, except for a few short periods. High silica was found after each boiler outage. Blowdown was used to reduce this value to below 5 ppm.

All known sources of silica were investigated and eliminated. Silica due to evaporator carry-over was reduced to a minimum by maintaining the rate of evaporation at or below 50 per cent of rated capacity. Raw-water contamination could not be found. The possibility of silica in the water-conditioning chemicals was investigated and found to be negligible. Analytical procedure was investigated and, after a large amount of work, was found correct. With all these possibilities eliminated, unexplained sudden increases of the silica content of the boiler water were still experienced.

The increase in third-stage bleed pressure confirmed the presence of silica in the boiler water, with subsequent vaporization and deposition on the turbine blades. The pressure had increased to 152 psi so that on March 19, 1948, the turbine was caustic-washed to remove this silica. After caustic-washing, the condenser was tested using river water to fill the steam space. The river water was muddy and mud settled on the tube surface and was not drained out with the water. When the condenser was again placed in service a large amount of mud was carried into the boiler. After 20 hr. of operation, the silica in the boiler water was found to be 116 ppm. The third-stage pressure was 135 psi and increasing rapidly. Due to load conditions the unit could not be taken out of service.

Heavy blowdowns and vaporization of silica reduced the silica in the boiler water to 12 ppm by March 31, 1948, when the unit was again caustic-washed. By this time the turbine blades had enough deposit to cause the load on the unit to be reduced to 81,000 kw to prevent safety-valve operations on the heaters. With this reduced load the third-stage pressure was 150 psi, and it was estimated that at 85,000-kw load this pressure would be in excess of 165 psi. After the second washing, the third-stage pressure was down to 130 psi when operating at 85,000-kw load.

² "Silica Deposition in Steam Turbines," by F. G. Straub and H. A. Grabowski; Trans. ASME, vol. 67, 1945, pp. 309-316.

Fig. 3

Fly silica 5 ppm silica v showed the wir and i the sta feedwa operati tank to tive dra with th for rem the air drawn and the water h It is ho boiler w

Figs.

The b by the ppm sin of the stage pr 145 psi water ha of the fu

The co

1 Th 2 Co factory h num con 3 Co Steel sho tubes for 4 Sul collected

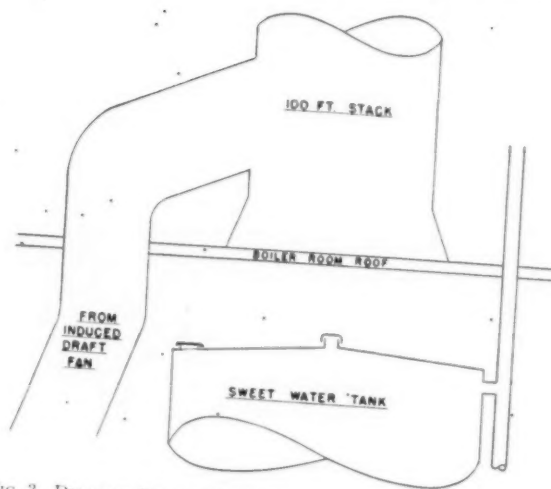


FIG. 3 DIAGRAM SHOWING RELATION OF SWEET WATER TANK AND VENTS WITH STACK

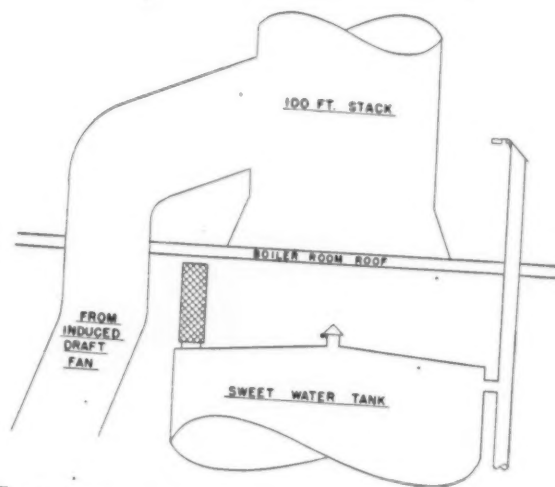


FIG. 4 SHOWING CHANGES MADE TO EXCLUDE FLY ASH FROM THE SWEET WATER SYSTEM AND PROVIDE BREATHING OF THE TANK

Fly Ash Cause of Deposits of Silica. With few exceptions the silica content of the boiler water has been maintained at or below 5 ppm since April 1, 1948. Occasional unexplained increases in silica were still experienced. A study of silica in the boiler water showed a relationship between silica increase and the direction of the wind. This apparently absurd observation was investigated and it was found that with a certain wind direction, fly ash from the stacks was blown into an open vent and entered the boiler feedwater system. Further investigation found that certain operations caused the manhole lid on a condensate-water storage tank to blow off. With this lid off, the roof vent caused a positive draft across the tank. This tank is located in the same room with the forced- and induced-draft fans, and the hydromix valves for removing the fly ash from the Cottrell precipitator. At times, the air in this room carries large quantities of fly ash which were drawn into the condensate tank. Correctives were applied, and the unexplained high peaks in the silica content of the boiler water have been reduced but have not disappeared entirely. It is hoped that when all desired changes are made, silica in the boiler water due to fly ash will be eliminated.

Figs. 3 and 4 show these changes in diagrammatic form.

The benefits of the elimination of the fly ash have been shown by the maintenance of the silica in the boiler water below 5 ppm since this source of contamination was discovered. Proof of the reduction in silica contamination is shown by the third-stage pressure on the turbine which has been constant at about 145 psi for the past 5 months. Reduction of silica in the boiler water has been made, but complete elimination is still a problem of the future.

CONCLUSIONS

The conclusions of the study are as follows:

- 1 The water circulation in the boiler is satisfactory.
- 2 Continuous chemical treatment is needed to obtain satisfactory boiler-water conditioning with the maintenance of minimum concentrations of conditioning chemicals.
- 3 Copper will remove sulphite from boiler-water samples. Steel should be used for sampling lines, cooling coils, and discharge tubes for collecting boiler-water samples.
- 4 Sulphite determinations may be in error if the sample is collected at or above 80 F.

- 5 Hydrogen sulphide in the water-steam circulation cycle of a power-station unit can produce severe corrosion.
- 6 Silica contamination of the feedwater system may occur because of failure of design engineers to recognize the possibility of contamination by fly ash.

Discussion

C. U. SAVOYE.* This paper is one of those rare exceptions in which anyone, other than the boiler manufacturers, is willing to make the statement that "the water circulation in the boiler is satisfactory."

Long live Mr. Hankison and Mr. Baker!

It takes less than half an hour to read this paper and to understand the results which seem so simple. It was quite a different matter for West Penn Power, looking into the problem from the front end. At that time they questioned everything, including boiler circulation; but instead of taking sides against it, they started out in their typical unbiased fashion to determine just what was the true cause and to cherish whatever they found. Obviously this attitude led them to the unexpected.

I do not know whether or not the West Penn people make a better quality of electricity than any other power company, but they should be high up among the electrical lum tums if there is any validity in that little inscription on my package of sodium bicarbonate, i.e., "The priceless ingredient in any product is the character and integrity of its maker."

AUTHORS' CLOSURE

It is indeed hard to present a suitable closure to such a discussion as Mr. Savoye has presented, and it now seems right and proper to simply thank the discussor for his very kind words.

It may be in order to state that the months between the time the paper was written and the present confirm the findings given in the paper in every particular. To those who are still fighting silica, it will be of interest to advise that a period of six weeks has just elapsed (April 20, 1950) during which time no blowdowns were made on the No. 77 boiler and the silica concentration in the boiler water has not exceeded 3.5 ppm.

* Executive Assistant, Babcock & Wilcox Company, New York, N. Y. Mem. ASME.

for
ge
th
be
ve
tw
co
ga
ele
th
su
du
m

P

alm
min
me
unc
am
sal
the
tivi
ana
pro
ste
effi
esse
pur

V
gase
dev
resu
to v
niqu
simp
conc
pres
Only
as g
or cl

1 S
2 P
3 J
ican
4 N
the p
Co
Stud
ing,
AME
No
derst
the S

An Automatic Degasser for Steam Sampling in Power Plants

By H. M. RIVERS,¹ W. H. TRAUTMAN,² AND G. W. GIBBLE³

Electrical conductivity procedures are widely preferred for measuring the purity of condensed steam. Because gases such as carbon dioxide and ammonia contribute to the conductivity as do dissolved salts carried over from the boiler, interpretation of conductivity measurements may be somewhat uncertain. A new degasser has been developed which automatically splits a steam sample into two approximately equal streams of condensate, one containing all solid impurities, the other containing all gaseous impurities in the original sample. Heat-exchange elements are combined in a unique way which guarantees that the weight ratio of one stream to the other will remain substantially constant. Both streams pass through conductivity flow cells so the degree of contamination can be measured continuously by conductometric means.

BECAUSE of the accuracy and ease with which the electrical conductivity of steam condensate can be measured (1),⁴ conductivity procedures are widely preferred—almost to the exclusion of all other methods—for precise determination of steam purity. Interpretation of the conductivity measured directly on a condensed sample of steam is frequently uncertain, however, because gases such as carbon dioxide and ammonia contribute to the conductivity just as do the dissolved salts which may have been carried over from the boiler. Either these gases must be removed from the sample before conductivity is measured, or they must be determined by chemical analysis so that a suitable correction can be applied. The latter procedure is cumbersome, time-consuming, and unsuitable when steam purity is to be determined continuously. Therefore an efficient steam-sample degasser, automatic in operation, is an essential requirement for continuous determination of steam purity by conductometric means.

Various devices have been developed in recent years to remove gaseous impurities from steam samples (2). In general, these devices operate by first condensing the sample completely. The resulting condensate is then either distilled, aerated, or subjected to vacuum in order to expel the dissolved gases. These techniques are reasonably effective for removing gases present in simple solution. However, all gases which can contribute to conductivity, such as the ammonia and carbon dioxide commonly present in steam, react with water, forming ionized compounds. Only the undissociated fractions of these dissolved gases behave as gases and are relatively easily removable. The dissociated or chemically combined fraction is very much harder to eliminate

by customary procedures. Ammonia especially and carbon dioxide to a lesser degree exhibit this behavior.

Ample experience in the past has shown how difficult it is to remove these dissolved gases from steam already condensed. The degasser to be described eliminates this problem altogether, simply by preventing the gases from becoming dissolved to any appreciable extent in the first place.

OPERATION OF DEGASSER

Fig. 1, a schematic diagram, shows the principal parts of the degasser. Operation is first described briefly and is then explained with additional details.

1 Steam, throttled to between 15 and 100 psig, enters the double reboil coil A immersed in a condensate pool in the separator. Heat exchange takes place between the fluids inside and outside of the coil. Steam in the coils is partially condensed before discharge through orifices, and condensate in the pool around the reboil coils is continuously boiled to eliminate traces of gases.

2 Uncondensed steam passing upward in the separator contacts the outside of the revaporizing chamber B. Partial condensation occurs, with water returning to the pool around the

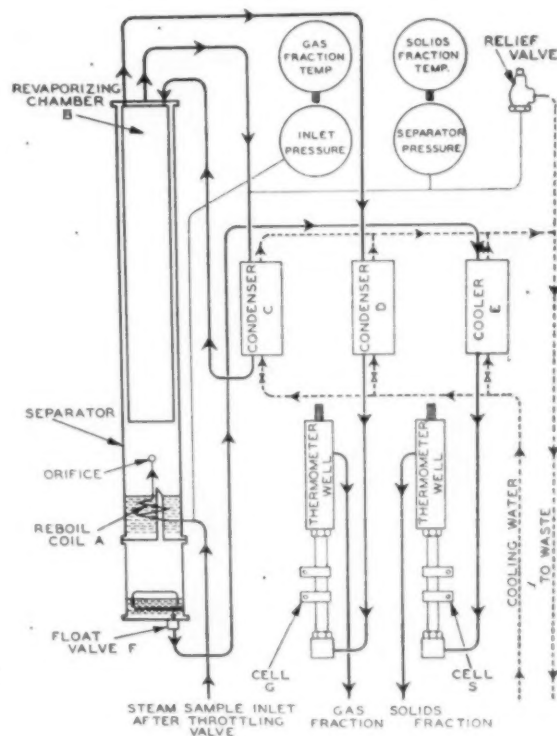


FIG. 1 SCHEMATIC DIAGRAM OF DEGASSER

¹ Service Department, Hall Laboratories, Inc., Pittsburgh, Pa.

² Research Department, Hall Laboratories, Inc.

³ Formerly with Hall Laboratories, Inc.; now with Arabian-American Oil Company, Ras Tanura, Saudi Arabia.

⁴ Numbers in parentheses refer to the Bibliography at the end of the paper.

Contributed by the Joint Research Committee on Boiler Feedwater Studies and the Power Division and presented at the Annual Meeting, New York, N. Y., November 27-December 2, 1949, of THE AMERICAN SOCIETY OF MECHANICAL ENGINEERS.

NOTE: Statements and opinions advanced in papers are to be understood as individual expressions of their authors and not those of the Society. Paper No. 49-A-74.

reboil coil A. The residual steam, containing gases, goes out the top of the separator.

3 The steam containing the gases ("gas fraction"), after leaving the separator, is completely condensed in condenser C.

4 The condensate leaving C is passed into revaporizing chamber B, where it absorbs heat from the steam on the outside and is completely vaporized, effecting the partial condensation in the separator, as mentioned in 2.

5 The gas fraction leaves the revaporizing chamber in the separator, is then condensed and cooled in condenser D, passes through conductivity flow cell G, and overflows to waste.

6 The water in the pool surrounding the reboil coil A contains the solids originally present in the steam but essentially no gases. This "solids fraction" overflows into a float chamber from which it issues continuously through float valve F.

7 The solids fraction is then cooled in cooler E, passes through conductivity cell S, and overflows to waste.

Reboil coil A does three important things: (a) Partial condensation of the steam sample provides water in bulk to collect all solid impurities in the original steam. (b) Condensation occurs only at boiling temperature; as a result of the low partial pressures of the gases and their lower solubility at higher temperature, they can contaminate the condensate only to a very slight extent. (c) Boiling outside coil A removes any traces of gas which may be picked up by condensate dripping down from the revaporizing chamber B. Thus all solid impurities—but practically no gases—remain in the condensate which overflows from the pool at A, and finally leaves through the float valve F. Cooled to room temperature at E, this stream of condensate is the solids fraction.

Heat given up by steam condensing in reboil coil A generates an equivalent amount of steam outside coil A. Condensate formed in coil A passes out of the orifices along with steam and then drops back into the pool, replacing the liquid lost by evaporation there. Thus the steam flow upward through the degasser is equivalent in weight to the total flow of steam sample.

Steam rising through the degasser passes revaporizing chamber B where some condensation occurs. This condensate (also substantially free from gas because it forms at high temperature and under low partial pressure of gases) falls into the pool where it is subjected to further reboiling.

All steam leaving the separator is completely condensed in C. This condensate is revaporized completely in B because of the pressure differential which is maintained between the outside and inside of this revaporizing chamber. In the process, an equivalent amount of steam is condensed outside of B. For each pound of steam leaving the outlet of B, essentially a pound of condensate drips back into the pool and eventually discharges through F. The steam sample is thus split automatically and continuously into two streams flowing at nearly equal rates, the solids fraction, substantially gas-free, and the gas fraction, substantially devoid of dissolved solids.

Since all the solids are concentrated in a fraction comprising about one half of the original weight of steam, and the gases are in a fraction of corresponding size, "magnification" of the two types of constituents is obtained. In each case the measured conductivity is multiplied by a factor which will approximate 0.5 to put the results on an original sample basis. The factor 0.5 can be approached closely if condensation in the steam-sample lines is minimized. This is accomplished by using small sample lines as short as possible, and by insulating thoroughly.

Since the concentration of solids in the solids fraction is about double that of the original sample, the accuracy of steam-purity measurements by conductometric or chemical means is materially improved, particularly when the amount of contamination is slight. For certain special studies such as investigations of

"volatile silica", or "selective carry-over," an even further concentration of solids in the solids fraction can be effected by bleeding off a portion of condensed gas fraction after condenser C. If a valve is inserted and used for this purpose, operation is no longer inherently automatic, but still will be reasonably stable.

Often it is desirable to have a continuous indication of total content of gases in the steam. A recording of the conductivity of the gas fraction serves admirably for this purpose. In some cases it may be necessary to determine how much carbon dioxide, ammonia, hydrogen sulphide, or other gas is individually present. While this cannot be done conductometrically, the gas fraction provides a convenient concentrated sample for such analysis by chemical means.

COMMERCIAL UNIT

The degasser¹ is shown completely assembled and ready for use in Fig. 2. Its total weight is about 90 lb with outside dimen-

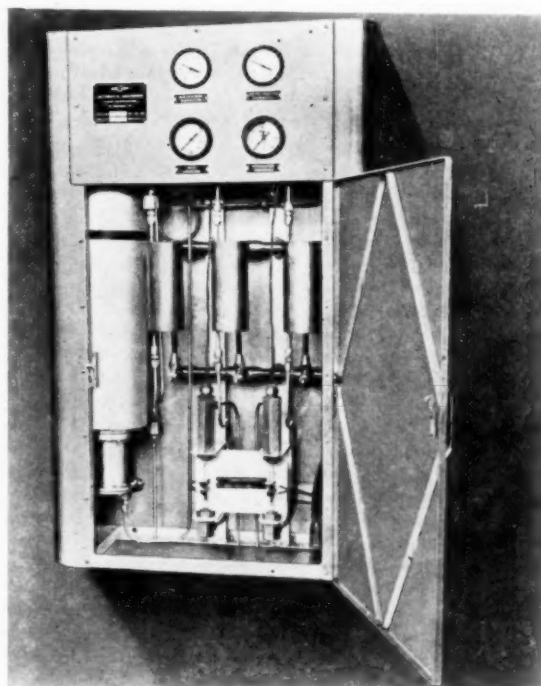


FIG. 2 THE COMMERCIAL UNIT

sions 40 in. \times 24 in. \times 9 in. The case is made of stainless steel to withstand corrosive atmospheres. All parts which contact steam or condensate flowing to the conductivity cells are fabricated of 18-8 stainless steel, thereby minimizing contamination of the sample. Regulation of cooling-water supply is easily accomplished by means of separate valves to the three coolers. Gages are provided to indicate the pressure of the throttled-steam sample and the operating pressure in the separator. Dial thermometers measure the temperatures of the condensed solids and gas fractions passing through the conductivity cells included with the equipment.

The conductivity cells which are an integral part of the degasser are small in volume, thus minimizing lag in response to any change in sample composition. Cells will ordinarily have a

¹ Manufactured by Hagan Corporation, Pittsburgh, Pa.

0.1 constant. However, for very pure steam, it is sometimes advisable to magnify readings, particularly when results are below 1 micromho. Thus if a 0.01 constant cell is substituted, a reading of 0.6 micromho, for example, which may be hard to follow at the edge of some charts, can be brought toward the middle of the charts.

The degasser is quite simple to install and can be moved from place to place with ease.

FACTORS PRODUCING DEPENDABLE AUTOMATIC OPERATION

In any degassing process, some water vapor must be vented away to remove the gaseous contaminants. If only a negligible fraction of the total sample is vented off, the high concentration of gas in the vented vapor tends to prevent complete gas removal from solution. On the other hand, if venting is copious, the volume of the remaining sample will be appreciably smaller, with the result that its solids content will be higher than in the steam undergoing test. These facts are almost universally ignored, with no attempt being made either to measure the vent loss or to control it within any but the widest of limits. Precise control over the rate of venting normally requires painstaking adjustment of cooling-water supply in proportion to rate of sample flow. This requirement for careful adjustment of sample and cooling-water flow rates—which generally must be done by hand—represents a serious shortcoming of most continuous degassers in use at the present time.

In the present degasser, this difficulty has been overcome effectively by the new combination of heat-exchange elements, the heat balance for which is presented in detail in the Appendix. The automatic method of splitting a continuously flowing steam sample into two nearly equivalent fractions depends on the thermal properties of steam and water—and nothing else. Since the total heat content of steam varies but little over the whole range of pressures encountered, the performance of the degasser is virtually independent of original steam pressure and operating pressure in the separator. Changes in rate of sample flow also have little effect. Fluctuations in temperature and pressure of the cooling water will affect the heat content of condensate leaving condenser C, but this variable is insignificant in comparison with the total heat value of steam, which governs the over-all heat balance.

Sample calculations in the Appendix assume certain values which represent extreme irregularities in such operational variables as original steam pressure, operating pressure in the degasser, sample flow rate and cooling-water temperature. It is to be taken for granted that these variables cannot always be held steady under practical plant operating conditions. Yet, in spite of the extreme conditions assumed, the ratio of solids fraction to total sample theoretically should not vary as much as 2 per cent.

This prediction has been consistently verified by field tests under actual plant operating conditions. In a given installation, the ratio of solids fraction to total sample remains substantially constant, varying no more than 1 to 2 per cent over long periods of time. The constancy of this ratio is altered only by virtually complete blockage of the cooling-water supply. On the other hand, to the extent that liquid water is carried over with the steam entering the degasser, the solids fraction will be increased in amount, as well as in conductivity. If gross carry-over occurs, the normal split will be restored when the carry-over ceases.

When the conductivity of a sample is to be measured continuously, it is important that the cell temperature be maintained at a nearly constant value so that the temperature compensator on the conductivity recorder will not have to be reset. The cooling coils D and E are generously designed in regard to heat-exchange surface, and they receive a copious supply of

cooling water. As a result, regardless of normal variations in the operation of the degasser, effluent temperatures of the two fractions remain practically constant. While it is desirable to inspect the apparatus daily, adjustments of any kind are seldom necessary. During operation, the degasser requires no more personal attention than any other instrument used continuously as a guide to boiler operation.

To be of greatest value, steam-purity data must correspond, as nearly simultaneously as possible, with records of other conditions of boiler operation, i.e., steam pressure, load, water level, etc. Every effort has been made to keep the liquid retention at a minimum so as to reduce time lag in the degasser. At normal sampling rates of approximately 30 lb per hr, only about 1 min elapses between an incident of steam contamination and the corresponding effect on the conductivity of the solids fraction. With this negligible time lag in the apparatus, momentary changes in steam purity are not blunted or obscured by dilution and the recorded conductivity can be compared readily with other boiler operating data.

FIELD EXPERIENCE WITH THE DEGASSER

The degasser has been field-tested in more than 25 plants to date. In practically all cases the effect of gases in the steam has been eliminated altogether. No measurable amount of carbon dioxide has ever been found in the solids fraction, even when a large quantity of this gas was purposely introduced into the inlet steam. Ammonia concentrations in the range of 2 or 3 ppm have been removed to such an extent that the insignificant residual amount could not be measured accurately by chemical means. In a few severe cases—deliberately chosen because of

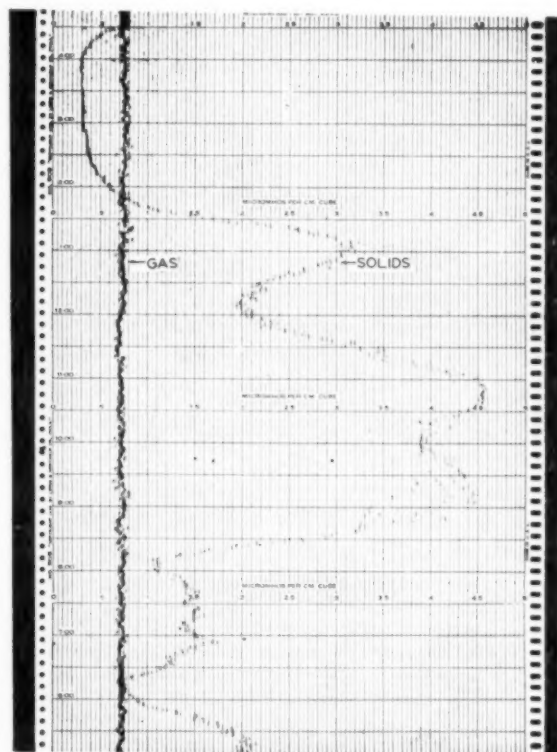


FIG. 3 CONDUCTIVITY RECORD FROM A CHEMICAL PLANT, INDICATING CONSTANT GAS FRACTION AND VARIABLE SOLIDS FRACTION (Multiply chart readings by 10.)

extreme ammonia contamination in the range of 10 to 25 ppm—the gas error was reduced to a very low and uniform value which permitted a simple correction to be made by conventional methods (3). Under all circumstances, at least 95 per cent of the ammonia entering has been removed.

The conductivity record shown in Fig. 3 was obtained during steam-purity tests on a 40,000-lb per hr boiler at a chemical plant. Saturated steam at 400 psig was sampled by means of a collecting header between the steam purifiers and inlets to the superheater tubes. The conductivity of the gas fraction remained relatively constant, showing only minor variations which were associated with irregularities in rate of feedwater admission to the boiler. Through most of the time covered by this chart, conductivity of the solids fraction fluctuated widely, revealing a severe carry-over condition. This particular case provided an unusually neat correlation between boiler load and conductivity

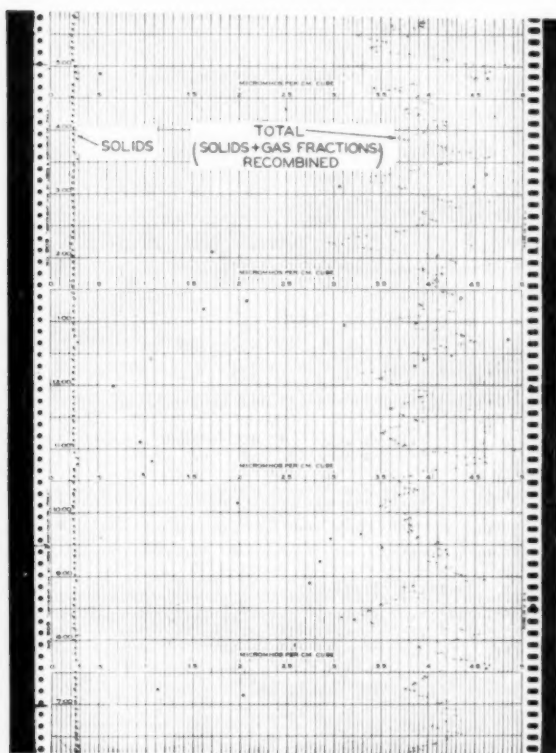


FIG. 4 CONDUCTIVITY RECORD FROM A STEEL MILL, SHOWING LOW CONSTANT SOLIDS FRACTION AND VARIABLE TOTAL STEAM SAMPLE (Multiply chart readings by 10.)

of the solids fraction, the respective values increasing and decreasing simultaneously and proportionally.

In contrast to Fig. 3, Fig. 4 presents the situation at a steel mill where gas content was extremely high and irregular while solid impurities remained very low and uniform. Conductivity due to solids represents only a small part of the total conductivity of solids and gases combined. Without the degasser, the difficulty in determining whether variations in conductivity were due to gas, to solids, or to both had previously prevented any certain conclusion concerning the extent to which carry-over might be occurring.

At the steel mill the solids fraction was practically constant at

about 53 per cent of the total sample flowing. This relationship was determined easily by measuring the volumes of solids-fraction and gas-fraction condensate collected simultaneously for a given interval of time. The ratio of solids-fraction to total sample was used as a multiplying factor to convert conductivity to the basis of the original sample. Of course corresponding data for the gas fraction can be converted to an original-sample basis in a similar way.

A single factor is used frequently to interpret the solids-fraction conductivity directly in terms of ppm total solids in the original steam. For example, at the chemical plant where Fig. 3 was developed, the solids fraction represented 56 per cent of the total steam sample. Assuming that 1 micromho of conductivity is equivalent to 0.65 ppm of dissolved and ionized solids, concentration of solid impurities in the original steam was found by multiplying the indicated conductivity by 0.56×0.65 , or 0.36.

It will be noted that a larger solids fraction flowed from the degasser at the chemical plant than at the steel mill. This came about because of a longer sampling line at the chemical plant. The greater the heat loss and attendant condensation in the sampling line, the larger will be the solids fraction, as shown mathematically in the Appendix.

An incident occurred at one plant which indicates the need for fully automatic conductivity-measuring equipment. Three boilers were operating at maximum capacity. Without warning, the gears driving the induced-draft fan on the boiler next to that attached to the degasser stripped. Although the whole plant was on automatic control, furnace gases, dirt, and the escape of steam from safety valves forced the men observing the test to leave hurriedly. With one boiler off the line, the two remaining were subjected to chaotic operation involving dropping of pressure and of water level in the drum. About 20 min elapsed before conditions were stabilized. On the return of the observers, the degasser was found to be operating normally. Both before and after the disturbance, conductivity of the solids fraction was low, indicating excellent operating conditions. Unfortunately, in this particular instance, only manual conductivity-measuring equipment had been available so that a complete record was not made.

At another plant, a coal fire in a bunker produced very erratic operation of a nearby 600-psig boiler. Personnel were required elsewhere and no attention could be given to the degasser, which, however, continued to function normally. Subsequent inspection of the continuous record showed the boiler had delivered quite pure steam through the whole period.

The degasser has proved very easy to start up. For example, a unit was installed to test the purity of steam generated by a 125-psig evaporator. The evaporator was shut down and drained without touching the degasser. When steaming of the evaporator was resumed, the degasser started to operate automatically. In this case there was no shutting off or opening of valves nor any adjustments.

Even relatively minor physical changes may be reflected in conductivity measurements made with the degasser. A small fire-tube boiler operating at 150 psig has been employed in testing degassers and for providing final design data for certain of the degasser components. The intermittent introduction of feedwater to this boiler showed up very clearly on the conductivity record of the gas fraction. Air introduced with the feedwater flowed through the gas-fraction conductivity cell and, by lessening electrode contact, produced a slight but quite noticeable drop in conductivity.

At one central heating plant, the correlation between load and conductivity was particularly close. In the morning, with increasing demand, conductivities of both solids and gas fractions tended to rise. More carry-over was produced and more gases were introduced into the system per unit time. At the end of

the business day, with dropping load, conductivities of both fractions dropped.

By using the degasser in acceptance tests on a new boiler, it was possible to prove rapidly as well as conclusively that negligible carry-over existed even at high loads, high water levels, and high boiler-water concentrations.

SUMMARY

A new degasser has been developed with the following features:

1 Under normal operating conditions substantially all ionizable gases are removed from the solids fraction. Even in extreme cases 95 per cent or more are removed.

2 Because of the inherently stable thermodynamic cycle employed, operation is automatic and cannot be affected materially by even abnormal changes in boiler operation.

3 Since steam and condensate flowing to the cells contact only stainless steel, minimum pickup of contaminants is assured.

4 The time interval from entrance of steam into the degasser to the passage of degassed condensate out of the conductivity flow cell for the solids fraction is of the order of 1 min. The averaging effect of holdup in blunting or spreading out over a period of time momentary conductivity changes is avoided.

5 Since the lag is small, conductivity-recorder charts made in conjunction with the degasser can be compared readily with steam flow, superheat temperature, or other operating charts to obtain a coherent over-all picture of the data.

6 The conductivity of the gas fraction is measured simultaneously by a second cell. The gas fraction can also be easily diverted for chemical analysis.

ACKNOWLEDGMENT

The authors acknowledge with thanks the helpful suggestions of R. E. Hall, E. P. Partridge, C. E. Kaufman, and other associates at Hall Laboratories, Inc.; A. A. Markson and R. R. Donaldson of the Hagan Corporation; and S. Andrews who did much of the detail design work on the commercial model.

The co-operation of the many plants in which the degasser was tested during development is particularly appreciated.

BIBLIOGRAPHY

- 1 "Electrical Conductance Measurements of Water and Steam, and Applications in Steam Power Plants," by Max Hecht and D. S. McKinney, *Journal of Applied Mechanics*, Trans. ASME, paper no. FSP-53-11, vol. 53, 1931, pp. 139-159.
- 2 "Design and Development of Apparatus for Measurement of Steam Quality by Electrical Conductivity Methods," by S. T. Powell, H. E. Bacon, Jr., I. G. McChesney, and F. Henry, Trans. AICHE, vol. 33, 1937, pp. 116-138.
- 3 "A New Degassing Steam Condenser for Use in Conductivity Determinations," by F. G. Straub and E. E. Nelson, Trans. ASME, vol. 63, 1941, pp. 645-648.
- 4 "Symposium on Problems and Practice in Determining Steam Purity by Conductivity Methods," Proceedings of the ASTM, vol. 41, 1941, pp. 1261-1340. Note especially "The Degassification of Steam Samples for Conductivity Tests," by P. B. Place, pp. 1302-1312; and "A New Type of Conductivity Apparatus for Use With Boiler Waters and Steam Samples," by A. R. Mumford, pp. 1314-1325.
- 5 "Calculation of Corrections to Conductivity Measurements for Dissolved Gases," by D. S. McKinney, part of Symposium listed in (2), Proceedings of the ASTM, vol. 41, 1941, pp. 1285-1301.
- 6 "Thermodynamic Properties of Steam," by J. H. Keenan and F. G. Keyes, John Wiley & Sons, Inc., New York, N. Y., 1936.

Appendix

HEAT BALANCE FOR THE DEGASSER

Heat balance is calculated for a system consisting of the steam-sampling line and of the separator shown in Fig. 1.

The following nomenclature is used in the Appendix:

H_1 = enthalpy of steam sample at sampling point, Btu per lb

H_2 = enthalpy of gas-fraction vapor leaving separator, Btu per lb

h_2 = enthalpy of solids-fraction liquid leaving separator, Btu per lb

h_3 = enthalpy of condensed gas-fraction liquid leaving condenser C, Btu per lb

H_4 = enthalpy of revaporized gas fraction leaving revaporizing chamber B, Btu per lb

L = total heat loss from separator and sampling-line surfaces, Btu per hr

W = flow rate of total steam sample, lb per hr

S = flow rate of solids fraction, lb per hr

G = flow rate of gas fraction, lb per hr

Development of Equations:

Total heat entering system, Btu per hr = $WH_1 + Gh_2$[1]

Total heat leaving system, Btu per hr = $Sh_2 + GH_2 + GH_4 + L$[2]

$G = W - S$[3]

Equating [1] and [2], and substituting [3]

$WH_1 + (W - S)h_2 = Sh_2 + (W - S)(H_2 + H_4) + L$[4]

$S(H_2 + H_4 - h_2 - h_3) = W(H_2 + H_4 - H_1 - h_3) + L$[5]

$(S/W)(H_2 + H_4 - h_2 - h_3) = H_2 + H_4 - H_1 - h_3 + L/W$[6]

Therefore

$\frac{S}{W} = \frac{H_2 + H_4 - H_1 - h_3 + L/W}{H_2 + H_4 - h_2 - h_3}$[7]

$G/W = 1 - S/W$[8]

Ranges in Variables. The solids fraction (S/W) and gas fraction (G/W) remain substantially constant in spite of wide fluctuations in the following variables: (a) Pressure of original steam at the sampling point; (b) steam pressure in the separator; (c) cooling-water temperature and rate of flow; (d) pressure of steam exhausting from revaporizing chamber B; (e) total heat loss from separator and sampling line; and (f) sample flow rate. The variations assumed are considerably greater than any likely to be encountered under normal operating conditions.

(a) In general, the pressure of saturated steam must vary from about 80 per cent to over 100 per cent to effect a change of 1 per cent in total heat content. Therefore most boilers deliver steam whose enthalpy is substantially constant despite normal fluctuations in pressure. Assume an extreme condition in which drum pressure fluctuates between 300 and 450 psig.

(b) Although steam pressure in the separator normally does not vary more than 2 or 3 psi, assume that it may range from a minimum of 5 psig to a maximum of 15 psig.

(c) Temperature and volume of cooling water generally can be controlled so as to hold the temperature of condensate leaving coil C within 5 deg F of any desired value. However, assume that this temperature varies from 60 to 80 F.

(d) Pressure of exhaust from revaporizing chamber B is not likely to fluctuate as much as 10 psi; but, as an extreme case, assume that it may range from 0 to 10 psig.

(e) Heat losses can be kept at a minimum through use of short well-insulated sampling lines and adequate insulation on the apparatus itself. Field tests indicate that the total heat loss can be reduced to about 1500 Btu per hr or less. It remains practically constant, for a given installation, being only feebly affected by reasonable changes in room temperature. Assume that this variable may range from 1425 to 1575 Btu per hr.

(f) Although it is difficult to maintain a precisely constant sample flow rate, simple devices (needle valve, orifice, capillary tubing, pressure-regulating valve) may be used to hold this flow reasonably steady. Assume that the sample flow rate may be anything from 25 to 30 lb per hr.

Constancy of Solids Fraction. The independent variables can be arranged according to their minimum and maximum values as in Table 1. The thermal values for steam and water were obtained from tables (4).

TABLE 1 RANGE OF VARIABLES

Variable	Minimum value	Maximum value
H_1 ...	(300 psig) 1203.3 Btu per lb	(450 psig) 1204.6 Btu per lb
H_2 ...	(5 psig) 1156.3 Btu per lb	(15 psig) 1164.1 Btu per lb
h_2 ...	(5 psig) 196.2 Btu per lb	(15 psig) 218.8 Btu per lb
h_3 ...	(60 F) 28.1 Btu per lb	(80° F) 48.0 Btu per lb
H_4 ...	(0 psig) 1150.4 Btu per lb	(40 psig) 1160.6 Btu per lb
L ...	1425 Btu per hr	1575 Btu per hr
W ...	25 lb per hr	30 lb per hr

By suitable substitution of the values given in Table 1 in Equation [7] minimum and maximum values for the S/W ratio can be readily calculated.

Minimum value for S/W ratio:

$$\frac{1156.3 + 1150.4 - 1204.6 - 48 + (1425/30)}{1156.3 + 1150.4 - 196.2 - 48} = \frac{1101.6}{2062.5}$$

$$= 0.534 \text{ or } 53.4 \text{ per cent}$$

with

$$G/W = 0.466 \text{ or } 46.6 \text{ per cent}$$

Maximum value for S/W ratio:

$$\frac{1164.1 + 1160.6 - 1203.3 - 28.1 + (1575/25)}{1164.1 + 1160.6 - 218.8 - 28.1} = \frac{1156.3}{2077.8}$$

$$= 0.557 \text{ or } 55.7 \text{ per cent}$$

with

$$G/W = 0.443 \text{ or } 44.3 \text{ per cent}$$

Thus the solids fraction varies only from 0.534 to 0.557, and the gas fraction from 0.466 to 0.443, although the controlling variables go through their entire ranges.

Discussion

O. M. ELLIOTT.⁶ The authors are to be congratulated for the development of a practical and usable improvement for steam-sampling degasification. It appears that this improvement will make the steam-degasifying and testing technique simple enough for any plant man to obtain reliable steam-contamination data. It is interesting to see how the authors have added to the previous work of Rummel, Gurney, Schwartz, Crosson, Straub, Nelson, Powell, Joos, and many others who have developed practical degasifying equipment for steam-conductivity measurements. Freeing the plant operators from the necessity of frequent adjustment of the degasser is a step in the right direction.

It is to be expected that degasification with this new equipment will be practically complete for most locations where the amount of ammonia in the steam is reasonably low. Where the amount of ammonia in the steam is high, difficulties can be expected with any degasifying equipment. It would be a welcome addition to the paper if in the written closure the authors would present detailed chemical data to show the degasification efficiency of the Hagan equipment for those more difficult conditions where ammonia is a problem. In particular, it would be useful

and easy to compare the NH_3 removing efficiency of the degasser to the simple expedient of boiling the totally condensed steam sample to the $1/2$ volume in an open flask to remove the gases. Many of us have used this simple $1/2$ -volume boiling solution to the degasifying problem for quick spot tests for a number of years. The Hagan organization has undoubtedly made this comparison in cases of extreme ammonia contamination, and the observed results would be a most useful addition to this paper.

Those who are less familiar with the Hecht and McKinney steam-conductivity method than the authors, should recall that this method only measures ionized contamination. Suspended solids in the condensate will not be ionized. Also, there are dissolved solids such as silica and iron with such a low order of conductivity that they will not be represented properly by conductivity tests, although they may be present in appreciable concentrations.

P. B. PLACE.⁷ The development of an effective degasser, and particularly one having stable and automatic operational control, is a most welcome addition to the art of steam-sampling and testing.

For many years, inconsistencies in steam-purity test results by conductivity have been evident in that the purity values have not reflected variations in steam output and/or boiler-water concentrations. In practically all cases, except where drum internal leakage has been involved, the measured steam conductivity has remained practically constant when steam flow and/or boiler-water concentration was increased or decreased several-fold. In some cases the conductivity values have been lower at the higher ratings and concentrations.

A possible interpretation of this inconsistency is that the variation in actual steam impurity is so small that it is completely submerged by sample-line contamination and residual gas effects on conductivity. It is gratifying to note that in the author's Fig. 4 the solids-fraction conductivity is in the order of $1/4$ micromho, a value that is roughly 4 times the impurity content, in ppm. Such low values have been conspicuously rare in steam-purity tests to date, and it seems possible that a new conception of the purity of commercial steam may be in the making.

It is hoped that further papers on this apparatus will be forthcoming in the near future, in which a comparison will be made with results obtained by some of the current methods such as evaporation and gravimetric determination of impurity, and correction for gases by chemical titrations. It would also be of interest to run gravimetric determinations on a silica-free gas fraction to see whether a solids-free result can be obtained by this method.

The steam-sampling rate of 30 lb per hr for this degasser seems rather low. Sampling rates should be sufficient to reduce any sampling contamination to a minor proportion of the measured conductivity. Low rates of flow are not generally adequate to insure good distribution of sampling with the usual perforated sampling nozzle. Very little reliable data are available along this line, however.

The variations in conductivity of the solids fraction in the authors' Fig. 3, which are assumed to be the result of changes in steam output, are typical of the characteristics of a small leakage carry-over rather than a normal variation due to rating alone. It would be expected that the conductivity of the gas fraction would show some variation, in view of the fact that gas liberation is a function of feedwater flow rather than steam output, and feed flow would change with changes in rating.

The significance and interpretation of steam-purity test re-

⁶ Water Conditioning Engineer, Sun Oil Company, Philadelphia, Pa. Mem. ASME.

⁷ Research and Development Engineer, Combustion Engineering-Superheater, Inc., New York, N. Y. Mem. ASME.

sults lie more in the manner in which conductivity values vary with changes in operating conditions than in their absolute value. It is therefore important that all such data be accompanied and correlated with such operating conditions as changes in feedwater and steam flow, changes in water level, and changes in boiler-water concentration.

S. T. POWELL.⁸ The fundamental principle upon which the degasser operates is sound and the method described by the authors for sampling steam is a definite improvement over earlier practice. Previous sampling technique was inadequate when ammonia and carbon dioxide were present in the steam in large quantities. The apparatus and its operation are more complex than some other equipment for this purpose but, where critical conditions are expected, such refinements may be justified.

The procedure of actually degassing samples thoroughly rather than trying to analyze chemically and then correct for ammonia and carbon dioxide is less time-consuming and has much merit, since it makes available a continuous record under all conditions and avoids subsequent recalculations to compensate for entrained gases.

The equipment illustrated in Fig. 2 of the paper appears to be well arranged and can be co-ordinated with other control instruments without complicated adjustments. The present trends in power-station design, and especially the trends to higher boiler pressure and temperature make the need for such appliances of growing importance.

W. L. WEBB.⁹ Because of the problem of scale formation from the use of surface and well waters for cooling steam and water samples, some plants, including the major stations of the American Gas and Electric System, are employing condensate from the cycles for cooling purposes. This plan commonly results in locating all of the sampling equipment for a unit at one common point both for the operators' convenience and to reduce the cost of cooling water and drain piping. This practice often results in sampling lines 100 ft or more in length.

In employing the Hagan degasser on samples conveyed through long lines, an insulation problem will result if the total heat losses, including those of the sampling line and of the degasser, are to be limited to the order of 1500 Btu per hr. Prospective users of the degasser would be interested in knowing to what extent heat losses in excess of this value affect performance.

In order to permit locating the degasser a considerable distance from the steam-sampling point, might it not be feasible to increase the sample flow rate and by-pass a portion of the sample to waste, provided there can be certainty that the portion entering the degasser is representative of the sample taken. An alternative plan might be to insert the sample tubing inside a line through which steam can be passed, in order to reduce loss of heat from the sample. The authors may wish to express their views on these proposals.

It is understood that the degasser can be used on steam from any source, provided it enters the reboil coil A at 15 to 100 psig, and that its heat content is such as to give an acceptable proportion of solids fraction to gas fraction. Can the authors state the permissible limits of this ratio as influenced by the gas concentrations in the sample?

AUTHORS' CLOSURE

The several discussers have made a valuable contribution to the paper as a whole, and their efforts are sincerely appreciated.

⁸ Consulting Chemical Engineer, Baltimore, Md. Fellow ASME.

⁹ Mechanical Engineering Division, American Gas & Electric Service Corporation, New York, N. Y.

Subsequent discussion is confined only to the specific questions which have been raised.

A tremendous amount of analytical data were collected in developing and proving the present degasser. In every instance where degassers of this type have been used in the field, the so-called "gas error" has been eliminated so completely that it no longer affected the reliability of the test data. A tabulation of gas residuals found in the solids fraction—mainly zero or bare-trace values for ammonia, and always zero for carbon dioxide—hardly seemed justified. However, in answer to Mr. Elliott's question regarding efficiency of gas removal under difficult conditions, steam at a certain steel mill contained 26 ppm of ammonia (the highest concentration encountered to date); despite this unusually severe contamination, 98.5 per cent of the total ammonia was carried off in the gas fraction, leaving a concentration of only 0.7 ppm in the concentrated solids fraction. As Mr. Elliott and Mr. Place suggest, many valuable studies can be made, not only to compare the present degasser with other methods of disposing of the gas error, but also to develop and expand our knowledge of steam contamination in general. It is hoped that the results of some of these studies can be presented in subsequent papers by engineers who have been using the degasser for some time in their own plants.

Mr. Place suspects that a sampling rate of 30 lb per hr may be inadequate either to minimize the effects of contamination picked up from the sample line or to insure good sampling. Condensed-steam samples frequently contain appreciable amounts of iron, but it is not safe to assume that all of this iron comes from the sample line. A goodly portion of it may exist as a contaminant in the original steam sample. Of course, when the steam sample flows through a considerable length of bare or lightly insulated pipe, as it does in many cases, hot condensate formed in the line may tend to pick up some iron. The possibility of such contamination is minimized with the present degasser, which uses short, well-insulated sample lines of small diameter. Where warranted, stainless-steel piping could be used to obviate contamination. As Mr. Place states, few reliable data are available concerning optimum steam-sampling rates. The first requirement of any steam sampling and testing procedure is that it provide purity data which can be accurately correlated with all conditions of boiler operation. This requirement has been well satisfied in tests with the degasser in many plants at sampling rates of about 30 lb per hr. While the present apparatus will accommodate flows higher than 30 lb per hr, little is gained by higher sampling rates, so far as actual interpretation of the purity data is concerned. A degasser could be built to any capacity whatever, but one important point should be remembered in this connection. Loss of heat in the steam sample, and the cost of water for cooling set a limit to the sampling rate which can be justified economically. This is especially true of permanent degasser installations.

A moderate amount of scale in the heat exchangers will not disturb the degasser's performance. Where scale-forming tendencies are severe, deposition of scale in the cooling system can be effectively prevented by simple and inexpensive chemical treatment which requires only a few minutes of attention once a month. Nevertheless, condensate is the ideal cooling medium, not only for reasons given by Mr. Webb, but also because the condensate is usually available at fairly constant temperature.

Mr. Webb raises an important question concerning the possible effects of condensation in long steam-sample lines. Condensate thus added to the solids fraction is not subject to automatic control since it does not enter into the basic heat-balance relationships. If the sample flow rate could be held steady, term LW in Equation [7] of the Appendix would remain constant, and a

comparatively high heat loss could be tolerated. It is desirable to keep the heat losses as low as possible so that sample flow rates can vary over a wide range without affecting the solids-fraction percentage. Calculations in the Appendix assume a total heat loss of about 1500 Btu per hr; but that is a typical, not a limiting, figure. In the plants to which Mr. Webb specifically refers, a conventionally insulated sample line 250 ft long should lose heat at the rate of about 6100 Btu per hr. Even under these admittedly extreme conditions, 10 per cent variations in either the total heat loss or the sample flow rate would have no significant effect on the accuracy of the test data. Where practicable, the expedients which Mr. Webb suggests would eliminate or greatly reduce the effects of condensation in long sample lines; obviously,

every precaution must be taken to insure that a truly representative sample enters the degasser.

Assuming that heat losses are kept at the usual minimum, the solids fraction will be approximately 50 per cent of the total sample. That is assured by the thermodynamic principle upon which the degasser is based. In a few cases, where it has been impossible to lag the sample lines properly, the solids fraction has run as high as 60 or 65 per cent without loss in efficiency of gas removal. No studies have been made to determine the limiting ratio of solids fraction to gas fraction, as this would entail deliberately throwing the degasser out of balance, resorting to manual instead of automatic operation, and setting up conditions not likely to be encountered in actual practice.

The Quality of Steam Condensate as Related to Sodium Sulphite in the Boiler Water

By R. C. ALEXANDER¹ AND J. K. RUMMEL²

Test data and conclusions are given in this paper which relate to the effect of various concentrations of sodium sulphite on the quality of condensed steam from high-pressure central-station boilers. Increase in sodium sulphite beyond certain limits was found to lower appreciably the pH and to raise the conductivity of the condensed steam. The acid material found in the steam resembles sulphurous acid. Test data, procedures, and equipment are described.

DURING the course of a research program, which had for its object the reduction of corrosion in the feedwater systems and high-pressure boilers at the Harbor Steam Plant of the City of Los Angeles, Department of Water and Power, efforts were made to increase the pH value of the condensed steam and feedwater, without addition of more than minimum amounts of alkaline materials.

A systematic search for the sources of materials which would promote acid conditions revealed that an appreciable increase in the sodium-sulphite concentration of the boiler water caused a definite decrease in the pH value of the steam condensate and feedwater. Conversely, a decrease in sodium-sulphite concentration caused an increase in pH. It was observed that simultaneously with the lowering of the pH value below 8, the conductivity of the steam condensate was increased. Likewise the amount of reducing material in the condensate increased with increase in sodium sulphite in the boiler water. These data made it evident that if the pH of the steam condensate and the feedwater were to be controlled in a satisfactory manner, it would be necessary first to control the concentrations of sodium sulphite in the boiler water.

With this in mind the authors conducted a joint investigation regarding the desirable limitations of sodium-sulphite concentration and the other effects which have been mentioned. Most of the work was carried out on the Harbor Steam Plant boilers³ which operate at 1050 psi, but Rummel⁴ has investigated separately the effects of sodium sulphite in boilers at other stations which operate at 950 psi and 375 psi, respectively. The operating conditions which relate to the data which are presented for the Harbor Steam Plant are shown in Table I. Garman and Rowse⁵ have given a complete description of the plant.

In many power stations it is customary to feed sodium sulphite

TABLE I OPERATING CONDITIONS HARBOR STEAM PLANT

Boiler pressure.....	1050 psi
Boiler-water temperature.....	552 F
Superheated-steam temperature.....	915 F
Feedwater treatment:	
Make-up water. Sodium-hydrogen zeolite softened followed by deaeration and evaporation.	
Feedwater—primary. Proportional feeding of sodium sulphite and pH control with caustic soda. Deaeration and venting of gases.	
Feedwater—secondary. Sodium phosphate direct to boiler plus caustic soda and sodium sulphite as required. Continuous blowdown to remove suspended matter and control the dissolved solids in boiler water.	

continuously to the feedwater and to maintain certain concentrations of sodium sulphite in the boiler water, in order to remove any residual dissolved oxygen which may be present in the water. The sodium sulphite will react with dissolved oxygen to form sodium sulphate, and the use of sodium sulphite to reduce corrosion, due to dissolved oxygen, is an accepted procedure.

The stability of sodium sulphite in water solution at various temperatures and pressures has been investigated by Taff, Johnstone, and Straub.⁶ Their investigation of the decomposition of sodium sulphite in steel bombs at temperatures above 528 F showed that as the temperature was increased up to 600 F, the rate of decomposition increased. At 530 F to 535 F the rate of decomposition, if any, appeared to be very slow. The data which are presented herein are confirming evidence that the sodium-sulphite solutions will decompose at measurable rates, but the principal decomposition product, which was found, differs from that reported by Taff, Johnstone, and Straub.⁶ This may be explained by the fact that in the boiler tests, emphasis was placed upon the analysis of the steam condensate whereas in the bomb tests the composition of the liquid in the bomb only was observed.

Hitchens and Purcell⁶ have reported on observations dealing with the behavior of sodium sulphite in boilers operating at 625 psi, 1400 psi, and 1775 psi. Tests were made for sulphite and sulphide as equivalent sulphur, in the saturated and superheated steam, and for sulphide in the boiler water. No mention was made of a change in pH or conductivity of the steam with a change in sodium-sulphite concentration of the boiler water, and it is assumed that such tests were not made or were not correlated with the other test data. The lead-acetate indicator-paper method used for the determination of total sulphite and sulphide consumed considerable time and required careful manipulation in order to obtain reproducible results. This procedure was not attempted in securing the data which are reported in this paper.

ANALYTICAL PROCEDURES

The analytical tests for the quality of the steam condensate included, pH, conductivity, reducing material as equivalent sulphurous acid, and hydrogen sulphide. The last two tests were not made for all test runs.

The pH value and conductivity were determined on flowing samples taken through stainless-steel sample lines and cooling

¹ Mechanical Engineer, City of Los Angeles, Department of Water and Power, Los Angeles, Calif.

² Chemical Engineer, Sheppard T. Powell. Consulting Chemical Engineer, Baltimore, Md. Mem. ASME.

³ "Harbor Steam Plant Goes on the Line," by C. P. Garman and W. C. Rowse, *Power Plant Engineering*, vol. 47, June, 1943, pp. 64-69.

⁴ Data Taken by J. K. Rummel at the Redondo Steam Station of the Southern California Edison Company and the Seal Beach Steam Plant of the City of Los Angeles.

Contributed by the Joint Research Committee on Boiler Feedwater Studies and Power Division and presented at the Semi-Annual Meeting, San Francisco, Calif., June 27-30, 1949, of THE AMERICAN SOCIETY OF MECHANICAL ENGINEERS.

NOTE: Statements and opinions advanced in papers are to be understood as individual expressions of their authors and not those of the Society. Manuscript received at ASME Headquarters, January 6, 1950. Paper No. 49-SA-37.

⁵ "Decomposition of Sodium-Sulphite Solutions at Elevated Temperatures," by W. O. Taff, H. F. Johnstone, and F. G. Straub, *Trans. ASME*, vol. 60, 1938, pp. 261-265.

⁶ "The Behavior of Sodium Sulphite in High-Pressure Steam Boilers," by R. M. Hitchens and J. W. Purcell, Jr., *Trans. ASME*, vol. 60, 1938, pp. 469-473.

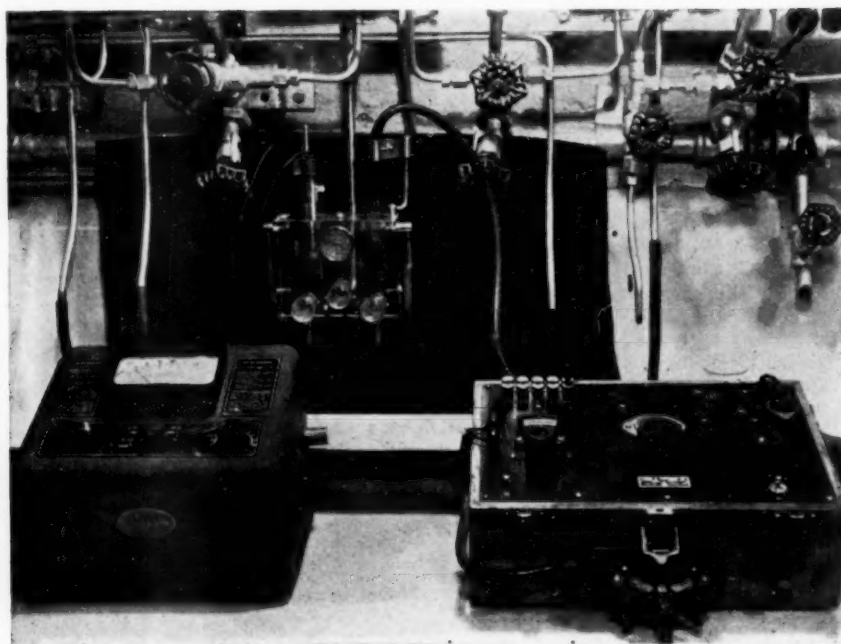


FIG. 1 FLOW CELL AND INSTRUMENTS FOR pH AND CONDUCTIVITY DETERMINATIONS

coils. A flow cavity, which was made by the authors, for holding the samples and the pH and conductivity cells, and the standard pH and conductivity meters, which were used for the measurements, are shown in Fig. 1.

The reducing material in the steam condensate was determined by direct titration with 0.002 N potassium-iodate solution, after first adding 2 ml of concentrated hydrochloric acid and 1 ml of 2.5 per cent potassium-iodide solution, to each 500 ml of sample. It was not practical to use starch as an indicator for this titration, and the end point was determined by use of an electronic indicator, which consisted of an electronic amplifier coupled to an indicator-ray tube (6E5 type) and a pair of plain platinum electrodes. The apparatus, together with the stirrer and micro-burette, is in all practical respects the same as that recommended by Ulmer, Reynar, and Decker⁷ for "dead stop" end point titrations, as for dissolved oxygen by the modified Winkler method. The indicator tube and platinum cell assembly is sensitive to not more than one drop or 0.05 ml of 0.002 N potassium-iodate solution, which is equivalent to 0.0125 ppm of sodium sulphite, in a 500-ml sample. The test assembly is shown in Fig. 2.

Due to lack of a suitable method, no direct test for sulphurous acid could be made, and its positive identification remains to be completed.

Tests for hydrogen sulphide were made by the sodium-plumbite method recommended by Hitchens and Pursell.⁸ Briefly, the method consists of adding 2 ml of 20 per cent sodium hydroxide to each of two 50-ml samples and 1 ml of 1 per cent lead acetate to one of the samples. Comparison is made in matched tall-form Nessler tubes. If a darker color is found in the tube to which the lead acetate has been added, sulphides are present. The amount of sulphide is determined by making up standards from a 0.0005

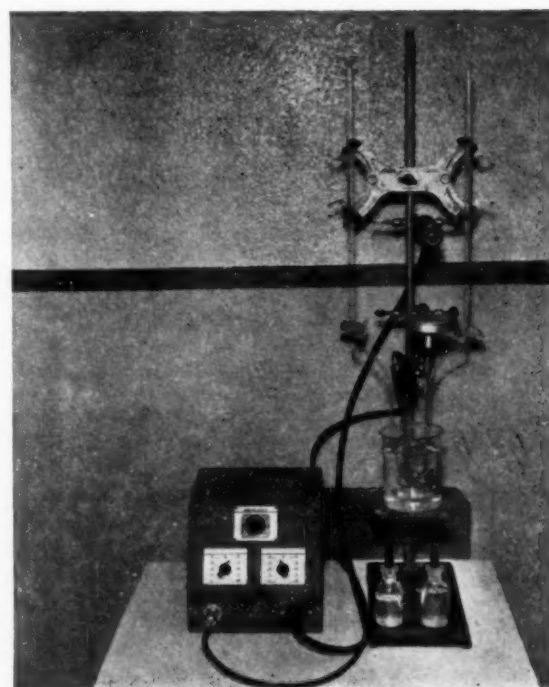


FIG. 2 TITRATING EQUIPMENT FOR MEASURING REDUCING MATERIAL

N sodium-sulphide solution and adding the reagents as already indicated. The method is said to be sensitive to 0.01 ppm of sulphide as equivalent sulphur.

⁷ "Applicability of the Schwartz-Gurney Method for Determining Dissolved Oxygen in Boiler Feedwater," by R. C. Ulmer, J. M. Reynar, and J. M. Decker, Proceedings of the ASTM, vol. 43, 1943, pp. 1258-1267.

EXPERIMENTAL PROCEDURE

Aside from the data obtained during normal operation of the boilers, a number of tests were made during which the sodium-sulphite concentration was increased rapidly by direct additions to the boiler water, and the quality of the saturated and superheated steam was measured, while gradually reducing the sodium sulphite concentration. The sodium sulphite concentration was raised to 60 ppm or over, in order to note the maximum effect on pH and conductivity of the steam condensate. Both commercial and pure sodium sulphites were used during the tests.

During most of the tests the pH of the boiler water was maintained near 11, and the total alkalinity at about 100 ppm. Several tests were made at a boiler-water pH of near 11.5 and a total alkalinity of 150 ppm or over, in order to determine the neutralizing effect of high boiler-water pH and alkalinity on the acid materials in the steam. One test was made at a boiler-water pH of 10.8 and a total alkalinity of about 60 ppm, in order to show the effect of low alkalinity.

For a good part of each test the boiler load was held to nearly maximum but, due to variable demand for power on the unit, the load was decreased at times to one third normal output. At these times equilibrium conditions were disturbed and there was a temporary change in the relationship between sodium sulphite in the boiler water and the quality of the condensed steam. However, the lowering of boiler load did not have any marked effect on the results.

Since one of the principal materials affecting the pH and conductivity of the steam condensate appeared to be sulphurous acid, several titrations were made in which known amounts of sulphurous acid were added to 2.5 liters of deaerated steam condensate, and the changes in pH and conductivity were recorded. Due to the calomel used in one of the glass electrodes for pH measurements, it was necessary to make separate titrations for conductivity. The apparatus used is shown in Fig. 3.

The sulphurous acid was made by adding strong sulphuric acid to sodium sulphite in a flask, and bubbling the sulphur dioxide gas, which was generated, into steam condensate in a gas-washing bottle. This solution was analyzed and diluted to the

required strength for the titrations. In order to avoid errors resulting from oxidation of the sulphurous acid to sulphuric acid it was necessary to make the tests in the minimum time possible. An atmosphere of nitrogen gas was maintained over the water in order to inhibit oxidation of the acid due to contact with air. These data were compared with the results of tests made on the steam condensate which included, as part of the data, the measurement of reducing material, as equivalent sulphurous acid.

RESULTS AND DISCUSSION OF BOILER TESTS

Before the sodium sulphite concentration in the boiler water had been reduced to less than the maximum range of 15 ppm to 45 ppm, the daily routine tests made on samples of steam condensate showed variations in pH of 6.2 to 7.2. The corresponding conductivity readings varied from 0.9 to 0.5 micromhos.

The results of the special tests, during which the sodium sulphite concentrations were purposely raised and lowered, and the effects of boiler water pH, are shown in Figs. 4, 5, 6, and 7.

Typical test results, with a boiler-water pH of 11 and a total alkalinity of 100 ppm, are shown in Fig. 4. The sodium sulphite concentration was varied between 3 ppm and 57 ppm. At maximum sodium sulphite concentration, the pH of steam condensate was 5.9, and at the minimum sodium sulphite concentration the pH was 8.3. At nearly the same time the conductivity of the steam condensate varied between 1.1 micromhos and 0.45 micromhos. However, after the conductivity had reached the lowest value, which corresponded to pH 7.8, it rose again to 0.7 micromho for a corresponding pH of 8.3. This is explained by the greater conductivity of the more alkaline materials which were present. These data show that if the boiler water has an alkalinity of about 100 ppm, a pH of 11, and a sulphite concentration of over 7 ppm, the probabilities are that the pH of the steam condensate will be lower than if the sodium sulphite concentration is less than 7 ppm. If the sodium sulphite concentration is as high as 20 ppm, which is a normal value for many boiler waters, the pH of the steam condensate may be less than 7. At sodium-sulphite concentrations in excess of 20 ppm, the pH was definitely on the acid side of 7.

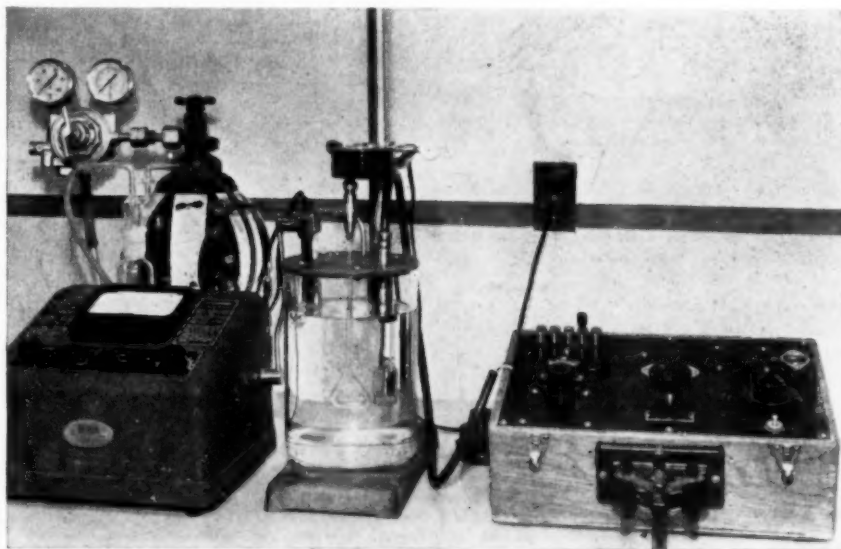


FIG. 3 EQUIPMENT FOR MEASURING CHANGE IN pH AND CONDUCTIVITY OF STEAM CONDENSATE WITH ADDITION OF SULPHUROUS ACID

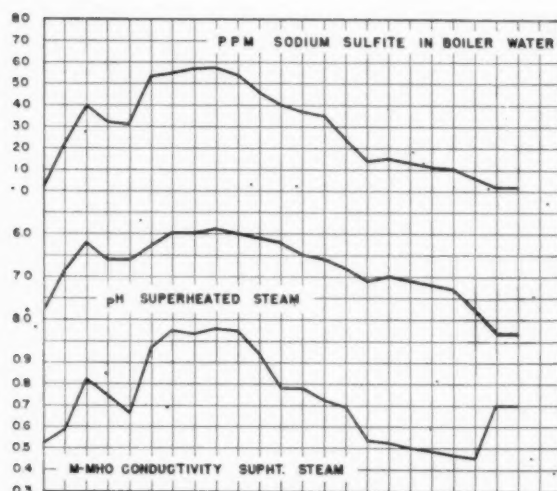


FIG. 4 TEST RUN TO SHOW EFFECT OF SODIUM SULPHITE ON STEAM QUALITY BOILER WATER pH 11 TO 11.1

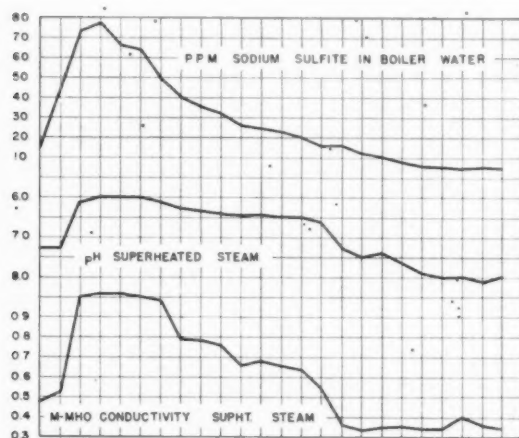


FIG. 5 TEST RUN TO SHOW EFFECT OF SODIUM SULPHITE ON STEAM QUALITY BOILER WATER pH 11

It is to be noted that the conductivity data will not show exactly how the quality of the steam is being affected by sodium sulphite. The conductivity, together with the pH of the steam condensate, are required in order to observe the variations in steam quality.

The foregoing pH and conductivity data, for various sodium sulphite concentrations, and a pH of 11 in the boiler water, were confirmed within close limits by the test data obtained for the boilers at the Redondo Steam Station, of the Southern California Edison Company. The data for one test, made during a period of full load, are shown in Fig. 5. At this time the boiler was operated at 950 psi, and the superheated-steam temperature was 900 F. The total alkalinity of the boiler water was approximately 100 ppm, and the pH was near 11.

Of special interest are the data which show that a concentration of sodium sulphite in excess of approximately 60 ppm appears to have little further effect on lowering of the pH and raising the conductivity of the steam condensate. It seems that the pH and alkalinity of the boiler water may at this point re-

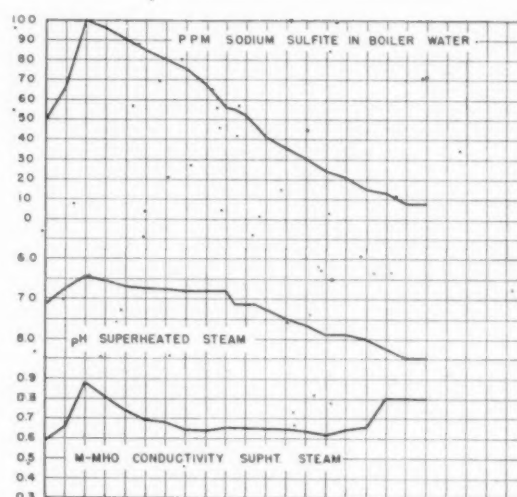


FIG. 6 TEST RUN TO SHOW EFFECT OF SODIUM SULPHITE ON STEAM QUALITY BOILER WATER pH 11.5

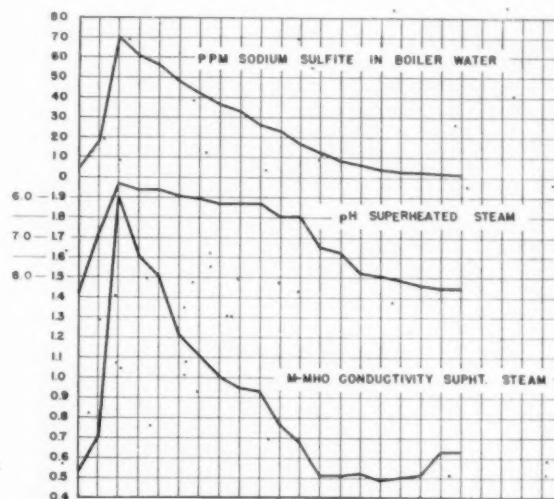


FIG. 7 TEST RUN TO SHOW EFFECT OF SODIUM SULPHITE ON STEAM QUALITY BOILER WATER pH 10.8

tard any further increase in the amount of acid ions which are present in the steam.

As in the case of Fig. 4, the data in Fig. 5 show that if the pH of the steam is to be held at near maximum values, while carrying a boiler water pH of 11 and an alkalinity of 100 ppm, it will be necessary to limit the sodium sulphite in the boiler water to a maximum of 7 ppm.

The test data for the steam condensate show that the pH varied between 6 and 8.1, and the conductivity between 1.0 micromho and 0.3 micromho when the sodium sulphite in the boiler water was varied between 78 ppm and 5 ppm. The slightly lower pH and conductivity values obtained for the steam condensate at Redondo Steam Station are believed to be due principally to the presence of less ammonia. A concentration of not over 0.01 ppm was indicated. At the Harbor Steam Plant the

ammonia in the steam condensate was found to vary between 0.02 ppm and 0.03 ppm.

In order to study the effect of boiler water pH and alkalinity on the action of sodium sulphite concentration, a number of test runs were made during which the boiler water pH was increased to 11.5 and 11.6 instead of the normal pH of 11 to 11.1. The results of a typical test are shown in Fig. 6. The pH of the boiler water was held at 11.5, and the total alkalinity was 150 ppm. These data are similar to those obtained at a boiler-water pH of 11.6 and 200 ppm of alkalinity. The boiler was operated at 17 per cent of normal full load.

The data show less change in pH and conductivity with high sodium sulphite concentrations than when the pH of the boiler water was lower. For example, the minimum pH of the condensate was 6.5, instead of 6.0 for a lower boiler water pH. Also, a pH of 7.9 is reached at a sodium sulphite concentration of 24 ppm. However, it will be seen that the pH of the steam condensate continues to increase with decrease in sodium sulphite concentration until, at the maximum of pH 8.5 the sodium sulphite is 8 ppm. Thus a pH of 11.5 in the boiler water was found to have a limited beneficial effect in attaining the maximum pH of the steam condensate.

In order to show the effect of low pH and alkalinity in the boiler water on the action of sodium sulphite, a test was made during which the pH was held at 10.8, and the total alkalinity at about 60 ppm. The results, as given in Fig. 7, show that except for concentrations below about 10 ppm, the sodium sulphite had a definitely greater effect on the pH and conductivity of the steam condensate than when the pH of the boiler water was higher. The amount of reducing material found in the steam was also definitely greater than for higher boiler-water pH.

Each of the foregoing test runs required from 3 to 5 days for completion, during which the condition of the boiler feedwater was maintained as nearly constant as was possible. No large variations in the composition of the feedwater were observed.

The test results for the saturated-steam condensate are not shown, but it is of interest that the saturated steam showed a slightly higher pH than has been reported for the superheated steam. Generally, the difference did not exceed about 0.2 pH.

The tests made at the Seal Beach Steam Plant, on a boiler operating at 375 psi, failed to show any significant changes in pH or conductivity of the steam condensate which could be attributed to the sodium sulphite concentration in the boiler water. Confirming tests should be made under more favorable feedwater conditions, as when a minimum of carbonate is present.

DATA RELATING TO REDUCING MATERIAL IN STEAM

Identification of the reducing materials in the steam condensate, which were related to changes in sodium sulphite concentration in the boiler water, the amounts of reducing material in the steam, and the pH and conductivity of the steam condensate, was of interest. This information was not considered to be an essential part of the practical test results obtained, or the main conclusions which were reached in regard to control of the quality of the steam. However, as a matter of interest the data now available are presented. These data and observations may be of use in any further investigation of the decomposition of sodium sulphite in the boiler.

The actual composition of the acid material and the reducing materials in the steam condensate were identified by process of elimination, and by correlation of the reducing material found in the steam condensate with pH and conductivity changes in steam condensate to which reducing material in the form of sulphurous acid was added. The conductivity readings were useful in showing that there were limited amounts of total solids and dissolved gases in the steam condensate.

On numerous occasions, during normal operation, and during several of the experimental runs, tests were made from the presence of sulphides in the steam condensate. In some instances it was believed that a trace of sulphide was present, especially when the condensate had a slight odor resembling sulphide. However, the amount was not sufficient to determine by quantitative analysis, and it was concluded that sulphides represented only minor amounts of the total reducing material found in the steam condensate.

It was assumed that at least part of the reducing material found in the steam was sodium sulphite or other neutral reducing material. During most of the test runs, the increases in reducing materials in the steam condensate corresponded with increases in acidity, decreases in pH, and increases in conductivity. These data have indicated that the amounts of neutral reducing material will vary with the pH of the boiler water and with the alkaline materials present in the steam condensate.

During some of the tests, there was present considerable excess of reducing material over that which can be accounted for by changes in pH of the steam condensate. At high boiler-water pH, the conductivity change was relatively small. These variations have not been explained fully.

The amounts of reducing material found during several of the boiler tests and the corresponding sodium sulphite in the boiler water are shown in Fig. 8. It was observed that within limits, the

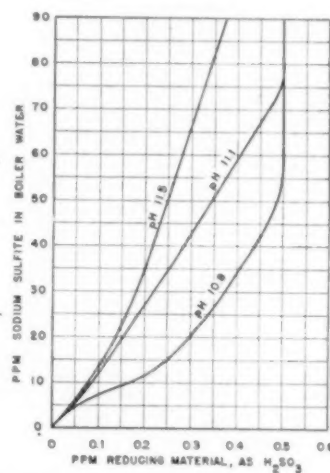


FIG. 8 VARIATION IN REDUCING MATERIAL IN STEAM CONDENSATE WITH CHANGE IN SODIUM SULPHITE CONCENTRATION AND pH OF BOILER WATER

amount of reducing material in the steam tends to increase with increase in the sodium sulphite in the boiler water, but since each change in boiler water pH, or other condition, gives a different ratio of reducing material to sodium sulphite, it is not possible to show one curve which will apply to all of the boiler tests. Therefore the data shown in Fig. 8 should be checked for each test run that is made. As a matter of convenience, the reducing material is shown as equivalent sulphurous acid.

The effect of measured additions of sulphurous acid on the pH and conductivity of steam condensate is shown in Figs. 9 and 10. Due to the presence of ammonia and other materials in the condensate, these data are not assumed to be applicable to all boilers. The effect of the alkalinity of the condensate is seen at the start of the pH and conductivity curves. The relationship between pH and sulphurous acid was used in reaching the conclusion that a

considerable amount of the reducing material in the steam was sulphurous acid.

In order to compare these data with the test results, it will be necessary to refer first to Fig. 8 which shows the equivalent sulphurous acid found in the steam condensate for different concentrations of sodium sulphite in the boiler water. The sulphurous acid and sodium sulphite values shown may then be used to note whether or not the pH and conductivity results actually obtained for a given sodium sulphite concentration and pH value in the boiler water will parallel the changes in the pH and conductivity values found by additions of sulphurous acid to steam condensate.

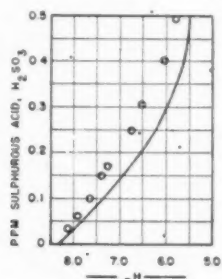


FIG. 9 CHANGE IN pH OF STEAM CONDENSATE WITH CHANGE IN SULPHUROUS ACID CONCENTRATION
(0 Equals pH equivalents for test run shown in Fig. 7.)

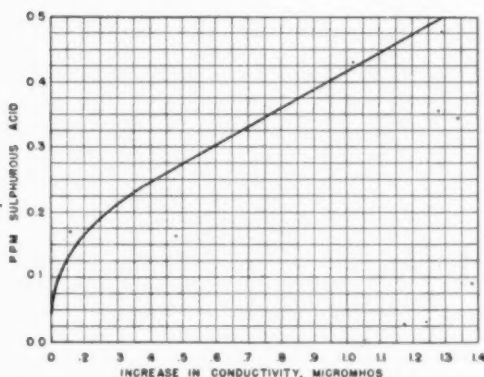


FIG. 10 CHANGE IN CONDUCTIVITY OF STEAM CONDENSATE WITH CHANGE IN SULPHUROUS ACID CONCENTRATION

By way of illustration, identifying marks have been made in Fig. 9 to show how closely the boiler-test data shown in Fig. 7 parallels the change in pH, when equivalent amounts of reducing material, in the form of sulphurous acid, are present.

Attention is called to the fact that small increases in the amount of acid or alkaline material will cause a considerable change in the pH and conductivity of the steam condensate, and that care is required in obtaining the measurements.

CONCLUSIONS

Based on the data obtained from boilers operating at 900 psi and over, the following conclusions have been reached:

It is probable that when more than 5 ppm to 8 ppm of sodium sulphite is present in the boiler water, the quality of the steam will be affected.

The extent to which the composition of the steam is changed will depend largely on the concentration of sodium sulphite, and

to some degree on the alkalinity and pH of the boiler water.

The change in steam quality is seen in the lowering of pH, increase in the conductivity and increase in the reducing material of the steam condensate.

A large part of the reducing material found in the steam condensate resembles sulphurous acid.

When the steam contains sufficient ammonia or other alkaline material to overbalance the acid effects of carbon dioxide, it is probable that with small amounts of sodium sulphite in the boiler water, the point of lowest conductivity of the steam condensate will be near a pH of 8. Near this point, increasing the sodium sulphite concentration will lower the pH and raise the conductivity of the condensate, but lowering of the sodium sulphite will increase both the pH and conductivity.

The test data which are presented are of special interest when using conductivity readings to estimate the solid-matter content of the steam condensate and in regulating the amount of solid matter in the form of acid-reducing material.

The quality of the steam from boilers operating at pressures below 900 psi, should be studied further, in order to show the effects of sodium sulphite in the boiler water.

ACKNOWLEDGMENTS

To the executive staffs of the City of Los Angeles, Department of Water and Power, the Southern California Edison Company, and to Sheppard T. Powell, appreciation is expressed for the support given to the investigation and for permission to publish the data. Special acknowledgment is given to H. T. Duplice, Harbor Steam Plant Superintendent, and his laboratory staff for the assistance received in arranging and carrying out the tests.

Appendix

After the completion of the foregoing tests, which show the effect of sodium sulphite in the boiler water on the quality of the steam condensate, it was decided to investigate the extent to which the reducing material, expressed as equivalent sulphurous acid, in the steam would carry on through the feedwater system. Accordingly, a test-run was made during which the sodium sulphite in the boiler water was raised to 65 ppm by direct injection into the boiler drum, no sodium sulphite was added to the feedwater, and the sodium sulphite in the boiler water was allowed to diminish while testing the steam condensate for pH-value conductivity and reducing material in the condenser hot-well condensate and the feedwater leaving the deaerator for reducing material. The data are shown in Fig. 11. The results of this test confirm some of the previous data and, at the same time, show the rate at which the acid sulphite in the water is oxidized as it passes through the condenser and the various heaters and the deaerator. Furthermore, the test data show the possibility of maintaining a sufficient concentration of sodium sulphite in the boiler water, in order to maintain some reducing material in the feedwater and thus remove dissolved oxygen.

It appears that if the sodium sulphite in the boiler is as great as 10 ppm to 15 ppm, the feedwater before the deaerator will contain a significant amount of reducing material. However, the results found at Harbor Steam Plant are not likely to be duplicated at other plants, and similar tests would need to be made in order to determine the actual condition. It should be noted especially that the rate of reaction of sulphite with oxygen will increase with increase in temperature and, no doubt, to some extent on the concentrations of dissolved oxygen and reducing material. The presence of catalysts also will have a decided effect on reaction rates.

The actual pH value of the steam condensate and feedwater

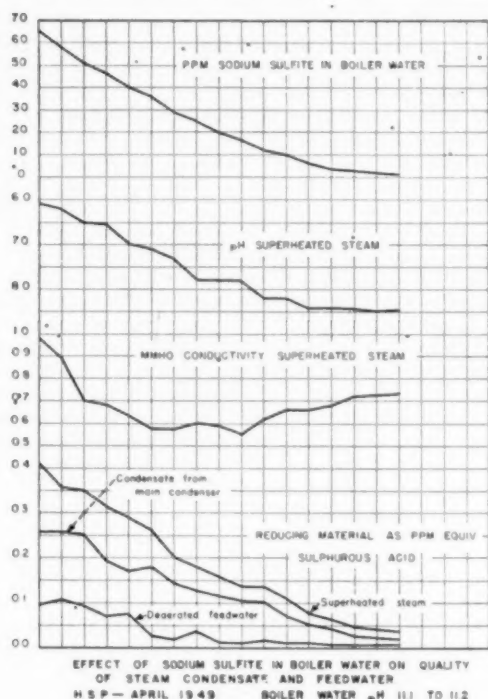


FIG. 11

at Harbor Steam Plant was influenced to some extent by the ammonia naturally present in the water. The ammonia had the effect of neutralizing the acid sulphite and other acid materials in the steam.

These data suggest certain possible advantages in selection of the concentration of sodium sulphite in the boiler water, provided this concentration does not depress unduly the pH value of the steam condensate and the feedwater.

Discussion

M. D. BAKER.⁸ Mr. Alexander and Mr. Rummel have presented an interesting paper and the data given is a worth-while contribution to the study regarding the behavior of sodium sulphite when used as an oxygen scavenger in boiler water.

The fact that all conclusions are based on superheated-steam condensate and not sufficient data were presented on saturated-steam condensate to make a comparison between saturated and superheated-steam condensate eliminates any conclusions regarding mechanical carry-over with subsequent decomposition of sodium sulphite in the superheater. Some of the results obtained indicate that mechanical carry-over occurred and it would be valuable information if the authors could make any definite comparisons.

The conclusion that sodium sulphite concentrations of 7 ppm or less will not affect the pH of the steam condensate and the data used to obtain the curves in Fig. 5 indicate that the authors have information that should be a worthy contribution in the study of sulphite behavior in boiler water. This leads to several questions. First, do the authors feel that they have sufficient data to make a statement regarding the point of stability of sodium sulphite in boiler water? What is meant; can they state from numerous

test data that 7 ppm of sodium sulphite is the minimum concentration at which decomposition due to excess sulphite will occur? When above 7 ppm of sodium sulphite what causes it to decompose and what are the mechanics of the decomposition?

In Fig. 5 does their interpretation of the curves mean that above 50–60 ppm of sodium sulphite the rate of automatic decomposition is constant and continues so until the concentration is lowered to 10–20 ppm of sodium sulphite?

C. E. KAUFMAN.⁹ In the authors' careful investigation of the decomposition of sodium sulphite in boiler water, the emphasis has been on the production of small amounts of sulphurous acid through hydrolysis. Quantitatively, there may easily be some question as to the exact amount of material produced in the steam since the over-all effect is so small. However, the actual fact of SO_2 or H_2SO_3 production would not be unexpected from a physical-chemical standpoint. In fact, substances subject to this sort of behavior might well be listed in a series. For example, in decreasing order of tendency to contribute material to the steam, we might list sodium carbonate, sodium sulphite, and sodium silicate.

In general, with all of these materials, greater amounts of the corresponding acid would be expected to be released as pH of the boiler water is dropped.

In the case of sodium sulphite, the fact of hydrogen sulphide development should not be neglected. The authors found rather negative evidence in this regard but there have been a number of occasions in the experience of the discussor's organization where hydrogen sulphide was a major product.

The difficulty of analyzing for small quantities of sulphur compounds brings up a question. Was it not possible to secure a sampling point where concentration of gases could occur? The aftercondenser on a steam-jet ejector for a turbine condenser will frequently provide rather remarkable and convincing samples. For example, in a number of cases at such a location, "odorific" analysis (rotten-egg smell) alone proved that hydrogen sulphide was an important breakdown product. In like manner, appreciable concentrations of ammonia, far higher than in the over-all steam, have been found.

Ten years ago we investigated the behavior of a 1400-psig boiler which produced steam of increasing conductivity after feed of sodium sulphite. Fig. 12 shows the similarity of this action to that reported by the authors. Only traces of sulphur com-

⁹ Hall Laboratories, Inc., Pittsburgh, Pa.

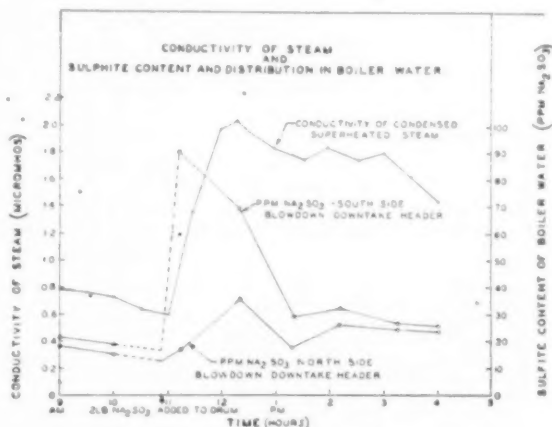


FIG. 12

⁸ Chief Chemist, West Penn Power Company, Pittsburgh, Pa.

pounds were found by field tests in the steam from regular sampling connections. Slower feed of chemical reduced the effect.

What is the significance of sulphur compounds in the steam? The presence of hydrogen sulphide may indicate that hot spots exist in the boiler with attendant auto-oxidation of sodium sulphite to produce sulphate and sulphide. In other words, sulphide production may be a symptom of somewhat critical conditions. Sulphur dioxide or sulphurous acid in the steam may contribute to somewhat lower pH in the condensate but its total effect will be little more conducive to acid corrosion than a small amount of carbon dioxide. In fact, the use of alkaline materials such as ammonia and amines in the steam should undoubtedly be as effective for SO_2 as for CO_2 .

The presence of SO_2 (or CO_2) in the steam going to a turbine will be of no concern. Before condensation it is obvious that the dry steam containing gases can have no effect on the metal. Even at a condensing end, solubility relationships dependent on temperature and partial pressures can permit only a trace of gas in solution. In other words, internal corrosion of turbines during operation due to dissolved gases is most improbable.

Thus, although the breakdown of sulphite is of considerable theoretical interest, the small effect which may occur lacks much practical significance. Years of trouble-free experience with boilers at many pressures provide assurance that there is no cause for alarm.

F. G. STRAUB¹⁰ AND H. D. ORGMAN.¹¹ Sodium sulphite has been used as an oxygen scavenger in steam boilers for almost twenty years. Taff, Johnstone, and Straub called attention¹² to the possibility of the decomposition of this material in concentrated solutions (4000 ppm) at temperatures above 540 F to form sodium sulphide and sodium sulphate. Hitchens and Purcell¹³ reported the results of their study of steam from boilers operating at pressures up to 1400 psi. Their conclusions were that the decomposition to sodium sulphide and sulphate did not take place at concentrations normally carried in the boiler water.

In the intervening years the prevailing opinion appears to have been that in concentrations below 20-30 ppm of sodium sulphite very little, if any, sulphide appears to form. However, if areas in the boiler exist where the sulphite can concentrate, sodium sulphide forms and hydrogen sulphide is found in the steam at steam pressures around 1200 psi.

Some plants have used an excessive amount of sulphite when feeding it intermittently to boilers. This was reduced to a much smaller amount when fed continuously even in cases of practically no blowdown from the boiler. This indicated the possibility of some loss of sulphite at the higher concentrations occurring during intermittent feeding of the chemical.

In order to explain some of the peculiar behavior of the sulphite and to study the limitations of its use, the authors started a study in which a small laboratory steaming test boiler was used. This work is not completed. However, since they have observed the same action that the authors of this paper have, it was deemed advisable to discuss this paper at this time.

The laboratory tests have covered the behavior of sodium sulphite at various concentrations in the boiler water from 250 to

1550 psi. The steam in all cases shows a reduction in pH and an increase in conductance which is almost proportional to the sulphite concentration in the boiler water. The effect is almost proportional to the steam pressure.

The authors' conclusion that sulphurous acid is being distilled from the boiler water appears to be a logical one. In many power plants there has been sufficient ammonia or caustic carry-over from the boiler to mask the pH reducing effect of the small amount of sulphurous acid in the steam. The authors of this paper have been fortunate in having steams with low ammonia content with which they could run their determinations.

The results of these tests should be correlated with the experience in other plants before the power-plant operators become panicky about the effect of sulphite treatment on their preboiler equipment. In many plants sufficient ammonia is present to neutralize the small amount of sulphurous acid in the steam. It indicates the need of control of sodium sulphite in the boiler water to within reasonable limits and at the same time an adequate means of continuously adding the sodium sulphite to the system as to reduce the high peaks of concentrations to a minimum.

W. D. BISSELL,¹⁴ W. W. CERNA,¹⁵ E. L. KNOEDLER,¹⁶ L. G. VON LOSSBERG,¹⁷ AND E. B. POWELL.¹⁸ The authors have made a very important contribution to boiler-water chemistry, adding valuable information on the reaction products from sodium sulphite and also contributing constructively to water chemistry, in general, by bringing to attention clearly how sparse and sketchy is the actual knowledge of reactions at moderately high temperatures in this field.

Taff, Johnstone, and Straub in their 1937 paper,¹² as the present authors comment, make no mention of analyses of steam sampled from their bombs but find from analyses of the reacting solutions increasing rates in conversion of sodium sulphite to sodium sulphide and sodium sulphate with temperature increase in the range of about 530 F to 600 F. As reported by Parks¹⁹ it was found in operation of the 2000-psi boiler at Somerset Station that sodium sulphite, when maintained at more than a few parts per million in the boiler water, resulted in considerable contamination of the steam with hydrogen sulphide. As reported by Parks in the paper just mentioned, and by Cerna and Scott,²⁰ use of potassium-base chemicals in place of sodium-base chemicals was begun at Somerset Station in 1943. As affecting the sulphite radical the change in nature of chemical base apparently brought no very significant change in reactive tendency or essential nature of reaction products. Observations on the 2000-psi boiler at Somerset Station with water temperatures in the range of about 600 F to 625 F have indicated that, for the associated operating conditions, concentrations of sulphite chemical in excess of 4 or 5 ppm SO_2 are accompanied by evolution of hydrogen sulphide and formation of sodium sulphate and some alkali, as evidenced by methyl orange, but scarcely more than a trace of sodium sulphide. Considered together, the observations of the three independent investigating groups suggest that at temperatures of about 530 F and above, sulphites when

¹⁴ Superintendent of Engineering, Montaup Electric Co., Fall River, Mass. Mem. ASME.

¹⁵ Engineer, Hagan Corporation, Pittsburgh, Pa. Mem. ASME.

¹⁶ Chemical Engineer, Sheppard T. Powell, Baltimore, Md. Mem. ASME.

¹⁷ Chemical Engineer, Sheppard T. Powell, Baltimore, Md.

¹⁸ Consulting Engineer, Stone & Webster Engineering Corporation, Boston, Mass. Mem. ASME.

¹⁹ "Experience With Sodium and Potassium Chemicals for Boiler-Water Conditioning at Montaup Electric," by G. U. Parks, Trans. ASME, vol. 67, 1945, pp. 335-338.

²⁰ Water Conditioning for the 2000-Psi Boiler at the Somerset Station of the Montaup Electric Company, by W. W. Cerna and R. K. Scott, Trans. ASME, vol. 68, 1946, pp. 443-451.

¹⁰ Research Professor in Chemical Engineering, University of Illinois, Urbana, Ill. Mem. ASME.

¹¹ Research Assistant in Chemical Engineering, University of Illinois, Urbana, Ill.

¹² "Decomposition of Sodium-Sulphite Solutions at Elevated Temperatures," by W. O. Taff, H. F. Johnstone, and F. G. Straub, Trans. ASME, vol. 60, 1938, pp. 261-265.

¹³ "Behavior of Sodium Sulphite in High-Pressure Steam Boilers," by R. M. Hitchens and J. W. Purcell, Jr., Trans. ASME, vol. 60, 1938, pp. 469-473.

presen
tions
other
perat
625
tinea
tance

Su
sodium
quant
occurs
high-t
tinea
need
i urg
salts
phite
have
sembl
sound
vestig
ferent
conclu
and p
treatm
establi

Hyd
sources
cases
produc
densat
feedwa
the fil
crushe
9.0, an
phide
secure
free of
replace
presenc
nated.

The
discuss
been p
ference
steam
into th
little d
example
steam
Since th
sulphite
the char
sodium
With re
position
boiler w
not show
the boiler

²¹ Con

present in boiler water in excess of some rather small concentrations may be expected to decompose or react with constituents other than dissolved oxygen, and that there exists critical temperature or critical temperatures within the range of 530 F and 625 F above and below which such sulphite reactions are of distinctly different nature, and doubtless other factors are of importance which may even shift the critical reaction temperatures.

SHEPPARD T. POWELL.²¹ In spite of the extensive use of sodium sulphite as a deoxygenating chemical, there is a dearth of quantitative information on the mechanism of the reaction which occurs and the rate and extent of dissociation of sulphites under high-temperature conditions. These phenomena are not particularly significant for low-pressure boiler operation, but the need for such data for high pressure and temperature conditions is urgent. Many operators have concluded that the sulphite salts break down, and have noted the presence of hydrogen sulphite qualitatively in condensate. The authors of these papers have contributed much reliable information, and the data assembled and their extensive investigation have established a sound basis for control of this essential treatment. Other investigators have approached the problem from a somewhat different angle, but their findings generally confirm the authors' conclusions. This paper is a major contribution to the subject and presents definite and reliable data for control of sulphite treatment which, up to the present time, have not been definitely established.

Hydrogen sulphide in steam and condensate has come from sources other than sulphites. The writer has encountered two cases where extensive breakdown of sulphides occurred, which produced heavy concentrations of hydrogen sulphide in the condensate. At both the stations where the difficulty occurred, the feedwater was treated by hot-process softening systems, and the filter material in pressure filters used to filter the effluent was crushed magnetite. The pH value of the water was between 9.0 and 10.5. The sulphides were dissolved from the iron sulphide present in the magnetite ore. An attempt was made to secure magnetite free from sulphide, but no material completely free of iron sulphide could be obtained. It was found necessary to replace the filter material with anthracite coal, after which the presence of sulphide in the condensate was completely eliminated.

AUTHORS' CLOSURE

The authors wish to thank the various commentators for their discussion dealing with the usefulness of the data which have been presented. In answer to Mr. Baker's question on the difference between the quality of the saturated and superheated steam condensates and the effect of carry-over of sodium sulphite into the superheater, it has been stated that we found only a little difference in the quality of the two steam samples. For example, during most of the tests the pH value of the saturated steam was about 0.2 higher than for the superheated steam. Since this difference can be observed with only a trace of sodium sulphite in the boiler water, we have not been able to attribute the changes in pH value of the superheated steam to carry-over of sodium sulphite, followed by decomposition in the superheater. With regard to Mr. Baker's questions on the stability or decomposition levels of various sodium-sulphite concentrations in the boiler water, the conditions of testing were such that the data do not show exact equilibrium conditions. It was indicated that for the boilers under test and the analyses of the boiler water, the

pH value and conductivity of the steam condensate would not be changed appreciably when the concentration of sodium sulphite was held at not over 5 ppm to 8 ppm.

In answer to Mr. Kaufman, the authors have on various occasions tested the gas and water leaving the after condenser of the steam jet ejector for the main condenser and have used this data for the control of ammonia in the system. At times we found traces of hydrogen sulphide. However, there are obvious difficulties to be overcome in making quantitative tests of steam quality at this point, and direct tests on the steam samples are recommended.

It was observed that very small amounts of hydrogen sulphide could be detected by smell, but that on a quantitative basis the hydrogen sulphide was of very minor significance during any of the tests which have been described. With regard to the significance of corrosive sulphur compounds in the steam, the authors have been concerned with the amounts of iron oxide and copper found in the water at the condenser hot well and the iron oxide produced in the feedwater systems and the boilers. Concerning the suggested use of amines; an amine which has been used in power plants to raise the pH value of steam condensates decomposed and disappeared rapidly in one of the boiler systems under study and in the absence of a stable material, it is not recommended that amines be used in high-pressure boilers.

In order not to increase the solubility of copper alloys it was not desired to increase the ammonia content of the feedwater and the steam. However, when the acid gases in the system were reduced to a minimum, ammonia in concentrations of as low as 0.02 ppm was found to be effective in maintaining a pH value of 8 or better in the steam condensate.

The authors are very appreciative of information submitted by Drs. Straub and Orgman. Their conclusions, in regard to recent laboratory boiler tests made at various pressures and concentrations of sodium sulphite and pH value, are in confirmation of the conclusions reached by the authors. Due to the broader scope of their studies the completed data and conclusions will be of considerable interest. As has been indicated, the authors are in full agreement with the recommendation that tests be made at individual power plants in order to note the effect of sodium sulphite in the boiler water on the quality of the steam condensate.

The information submitted by Messrs. Bissell, Cerna, Knoedler, von Lossberg, and E. B. Powell have been of interest and we are especially appreciative of the favorable comment which has been offered. Due to limitations in operating pressure for the tests made by the authors, we are unable to verify the indication that hydrogen sulphide is an important product of sodium sulphite decomposition in boilers operated at 2000 psig, but it is suggested that the test methods mentioned in this paper be considered.

In answer to Mr. S. T. Powell's favorable comment, the authors have not been able to confirm the work of others on the production of appreciable amounts of hydrogen sulphide. On the contrary, hydrogen sulphide appeared only as traces and during periods of highest sodium sulphite concentrations in the boiler water. Mr. Powell has mentioned the very interesting possibility that sulphides may be introduced from sources other than sodium sulphite and in this connection the composition of the cooling water to the main condensers should be taken into account.

In closing it is again suggested that the analytical methods which have been presented be considered and that similar quantitative tests on operating boilers be carried out. At this time the decomposition products of sodium sulphite may be measured quantitatively and it should be possible to distinguish between smell and amount of any sulphides which are present.

²¹ Consulting Chemical Engineer, Baltimore, Md. Fellow ASME.

ger
the
the
ope
suc
tio
tes

I

at
last
betw
pers
and

D
in p
only

In
rang
whic
the
has
wat
prod

T
whic
tran

D
the r
tube
has
the s
units
main
to av
tuna
treat
satis
oped

As
feedw

¹ M
and P
² C
Engin
Cor
water
Meeti
Societ
Nor
unders
of the
Janua

Feedwater Treatment During Early Operation of Steam-Electric Stations

By R. C. ALEXANDER¹ AND J. K. RUMMEL²

Based upon the experience with five high-pressure steam-generating units installed at the Harbor Steam Plant of the City of Los Angeles during the last six years, the authors devise some basic practices to follow during early operation of such installations. Their study includes such items as cleaning the feed system, corrosion prevention, chemical control of corrosion, sampling and control tests of the feedwater system, and inspection of equipment.

DURING the last six years a total of five high-pressure steam-generating units have been installed at the Harbor Steam Plant. The boilers of the first two units operate at 1050 psig drum pressure. The boiler-drum pressure for the last three units varies with load demand. Normally, it varies between 900 psig and 1000 psig. The superheated-steam temperature is 915 F for all units. The first unit was started in 1943, and the last unit began operating on load in July, 1949.

During this time it was found that the items to be considered in preparing the units for service and early operation were not only numerous, but deserved considerable detailed attention.

In general, it has been necessary to study the design, the arrangement of equipment, and the particular local conditions which affected the satisfactory control of the make-up water and the feedwater. Usually the most important single consideration has been the maintenance of minimum corrosion of the feedwater-system equipment, and the disposal of corrosion by-products which lodge in the heaters and the boilers.

These by-products are for the most part iron oxide and copper, which are likely to encourage further corrosion, reduce heat-transfer rates, and cause overheating of boiler tubes.

Due to the highly corrosive harbor water used for cooling in the main condensers, there have been a large number of condenser-tube failures, and contamination of the feedwater with sea water has been a frequent occurrence. This has added considerably to the suspended matter and insoluble solids found in the boilers of units Nos. 1 and 2. At the same time, it has been necessary to maintain a close watch on the condition of the feedwater in order to avoid serious consequences from sea-water leakage. It is fortunate that there have been available the facilities for testing and treatment control, which were installed with each unit, and that satisfactory methods of procedure have been provided or developed as they were required.

CLEANING THE FEED SYSTEM

As shown by past experience, it is highly important that the feedwater system and interconnected equipment be cleaned

thoroughly of dirt, grease, rust, and other foreign material which would cause difficulties in operation of the pumps, heat exchangers, and the like, or be carried on to the boilers. When this important step is neglected, the resulting maintenance costs are found to be disproportionate to the probable cost of the preliminary cleaning.

Present practice at Harbor Steam Plant is first to clean by hand all surfaces which can be reached, such as the condenser shell and hot well, the heat exchangers, and the deaerator with its storage tank. Heat-exchanger tubes are cleaned with air and water, and any grease on the tube ends is removed with brushes and a detergent solution. Preliminary cleaning of the unit was followed by circulation of a hot detergent solution through the feed system. This operation simulated the "boiling out" of the boiler. It was effective in removing soluble oil coatings on parts of the equipment and in loosening the dirt for removal by the water flushing which followed. Finally, all traps where dirt collected, such as the bottoms of tanks and the condenser hot wells, were cleaned by hand.

The results of the foregoing cleaning operations have been highly satisfactory, as was reflected in a minimum amount of material carried into the boilers from the feed system, general freedom from clogging of screens used in preliminary operations, and no known damage to pumps or other equipment. After preliminary operation, an examination of one of the boiler units showed that only 2 to 4 grams of deposit could be removed from the tubes, and very little dirt was seen in the feedwater-system equipment. The amount of deposit in the boiler tubes was determined by placing a cloth filter bag over the end of the tube, followed by cleaning with an air-driven rotary wire brush. The bag was then shaken out over a clean paper and the material weighed.

The boiler tubes and drums were washed with water from a hose in order to remove the loose materials, and recently a high-pressure water-washing nozzle has been made for lowering down the tubes in order to clean them more thoroughly.

All of the superheater tubes are washed individually with condensate, flowing at high velocity, in order to remove both insoluble and soluble deposits such as would cause overheating or be carried through the steam turbine and into the feedwater system. A specially designed washing connection is used, which is held in the tube ends with air pressure while the water is flowing through. The washing time is regulated by use of an electronic conductivity indicator and a dip cell. This shows the completion of removal of the soluble material. Visual examination of the wash water shows the removal of insoluble material.

CORROSION PREVENTION

Returning to the main problem of corrosion prevention, it has been found that both iron and copper are present in the feedwater, and that the deposits found in the feedwater-system equipment and the boilers are composed mostly of iron oxides and copper.

During early operation a large part of the iron oxide comes from the mill scale on the surfaces of the equipment, but after the loose scale has been removed the corrosion process continues to add iron to the feedwater. In the older units the iron in the feed-

¹ Mechanical Engineer, City of Los Angeles, Department of Water and Power, Los Angeles, Calif.

² Chemical Engineer, Sheppard T. Powell. Consulting Chemical Engineer, Baltimore, Md. Mem. ASME.

Contributed by the Joint Research Committee on Boiler Feedwater Studies and Power Division and presented at the Semi-Annual Meeting, San Francisco, Calif., June 27-30, 1949, of THE AMERICAN SOCIETY OF MECHANICAL ENGINEERS.

NOTE: Statements and opinions advanced in papers are to be understood as individual expressions of their authors and not those of the Society. Manuscript received at ASME Headquarters, January 6, 1950. Paper No. 49-SA-48.

water was about 0.1 ppm and the copper about 0.03 ppm. These data show that appreciable corrosion of the copper alloys in the feedwater system is to be expected, and in this connection it has been realized that there is present a considerably larger area of copper alloy than iron.

Visual inspections of the equipment have shown that corrosive attack has been most rapid where the pH of the water has been lowered by acids and where dissolved oxygen is present. In the deaerator vent condensers, ammonia no doubt has played a part in hastening the failure of brass condenser tubes, but in zones of lower ammonia, acid, and dissolved-oxygen concentrations, no appreciable attack has been seen, and no failures due to corrosion have been experienced.

In some instances erosion has hastened the tendency for corrosion to take place. This was especially noticeable on the turbine-casing surfaces which are in the path of the steam entering the main condenser. However, the attack on the main condenser shell has taken place more rapidly in the air off-take section where the steam condensate contained relatively large amounts of dissolved oxygen and acids.

Another point of local corrosive attack, due to adverse water conditions, has been in the condensate drip-system equipment, which carries the condensate from the evaporator condenser and the stage heaters. This has been noticed in the first unit installed which, during its early operation, carried the vented vapor from the evaporator condenser. This vapor is now vented to atmosphere, and the pH of the water is more favorable. Previously the pH of the water was as low as 5.5 and is now seldom less than pH 7.

Considering the action of carbonic acid alone, it is of interest to note that for an equivalent reduction in pH, much more of this acid is required than if a mineral acid is present. Also, when the acidity of the water has been increased to give a pH of a little less than 5, the carbonic-acid solution is found to be more corrosive than a solution of the same pH to which only hydrochloric acid is

added. Whitman, Russell, and Altieri² have examined this action experimentally and their results are shown graphically in Fig. 1. It is explained that since at pH 5.4 the carbonic acid is only 6 per cent dissociated and hydrochloric acid is nearly 100 per cent dissociated, the carbonic acid would be about 16 times more concentrated than the hydrochloric acid. It is seen from these data that the corrosion rates may at times depend more largely

² "Effect of Hydrogen Ion Concentration of the Submerged Corrosion of Steel," by W. G. Whitman, R. P. Russell, and V. J. Altieri, *Industrial and Engineering Chemistry*, vol. 16, 1924, pp. 665-670.

"The Acid Corrosion of Metals," by W. G. Whitman and R. P. Russell, *Industrial and Engineering Chemistry*, vol. 17, 1925, pp. 348-354.

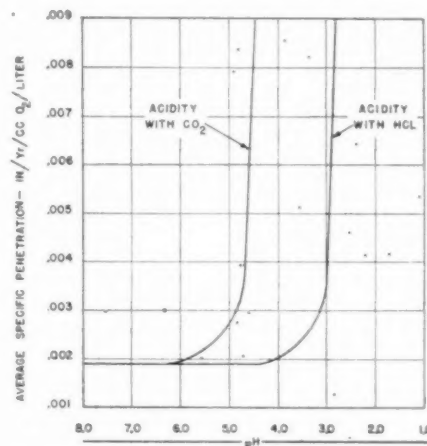


FIG. 1 COMPARISON OF RATES OF CORROSION FOR CARBONIC ACID AND HYDROCHLORIC ACID

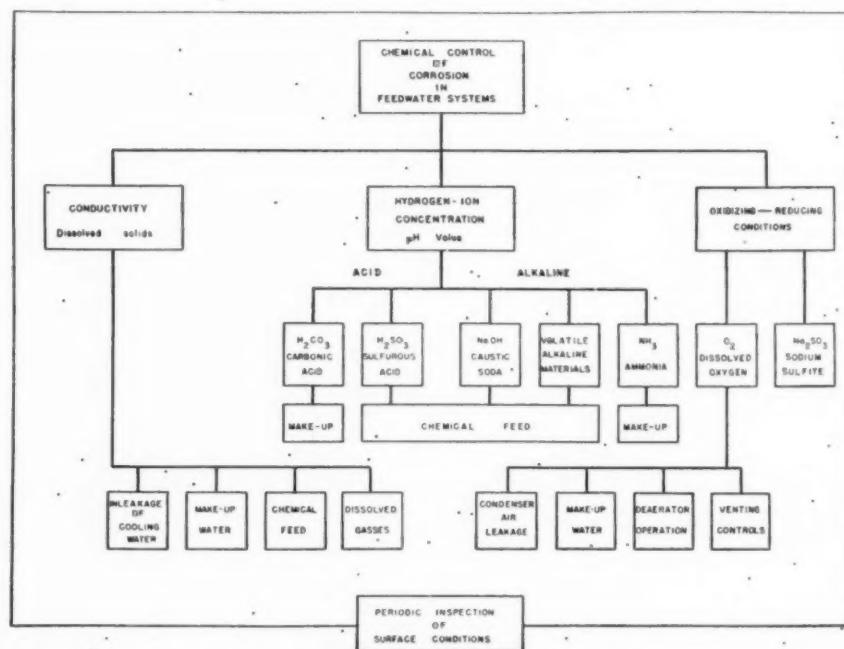


FIG. 2 ITEMS ENTERING INTO CHEMICAL CONTROL OF CORROSION

upon the acid concentration than the pH value, and a low pH due to carbonic acid may cause a serious amount of corrosion.

CHEMICAL CONTROL OF CORROSION

For purposes of discussion, the principal items which have entered into chemical control of corrosion in the feedwater systems are shown in Fig. 2. It is indicated here that the principal controls are conductivity, pH, and oxidizing or reducing conditions. Under these are subheadings showing the materials which are present or are added to the feedwater, to counteract any adverse conditions. Other subheadings show sources of feedwater impurities. This type of chart is useful in visualizing the chemical conditions which may exist and the corrective measures which should be taken.

As is indicated, emphasis has been placed upon avoiding high conductivity due to condenser leakage, adjustment of the pH to the highest practical value, and the maintenance of reducing conditions in all parts of the system where such control is feasible.

Dealing with the details of chemical control, it has been realized that all of the factors listed in Fig. 2 are somewhat interrelated and that the corrosion rates may be dependent upon a combination of conditions. This interrelationship is not always clear, but it has required consideration when making adjustments to the treatment control or in evaluating the corrosion found.

The effect of conductivity on corrosion rate has not been shown definitely but it is obvious that the higher the conductivity of the water the better the opportunity for electrochemical corrosion to proceed. Therefore any unnecessary increase in feedwater conductivity has been avoided. This matter has not been considered when adding the chemicals for treatment, since their beneficial effects are assumed to be much greater than any adverse effect due to conductivity. The avoidance of condenser leakage or addition of other high-conductivity water has been given first consideration.

The control of pH in the steam condensate, the feedwater, and the drip returns is considered to be of primary importance and has been given the greatest amount of attention.

As is known, the steam condensate, which is practically the whole of feedwater, is unbuffered, and any small amounts of acid or alkali will make a considerable change in the pH value. Therefore the elimination of dissolved carbon dioxide which forms carbonic acid, and the minimum generation of acids from sodium sulphite in the boiler water, are given close attention. As a first step, the pH value of the steam condensate is maintained in excess of pH 8.2 by careful regulation of the boiler-water alkalinity and sulphite concentrations, and the exclusion of carbonates from the feedwater. The retention of 0.02 ppm to 0.04 ppm of ammonia in the feedwater assists in neutralization of any small amounts of acid elements in the steam and raises the steam condensate above its neutral point of pH 7.

A detailed account of the effects of sulphite in the boiler water on the quality of the steam condensate is given in a separate paper by Alexander and Rummel.⁴

In order to exclude carbonates from the feedwater, close attention is paid to maintaining a low alkalinity in the make-up water to evaporators and in reducing condenser leakage. The elimination of carbonic acid from the system has been given considerable study. It has been found that most of the dissolved gases can be removed by use of the deaerating equipment which was installed, but that adequate venting of the deaerators and evaporator condensers is of great importance to the control. This venting is a necessary part of the pH control and the removal of dissolved oxygen.

⁴ "The Quality of Steam Condensate as Related to Sodium Sulphite in the Boiler Water," by R. C. Alexander and J. K. Rummel, published in this issue of the Transactions, pp. 519-527.

The final adjustment of the pH of the feedwater is accomplished by continuous addition of caustic soda, and most of the residual dissolved oxygen is removed by addition of sodium sulphite. The pH value of the feedwater, which was formerly held to pH 8 to pH 8.2, has been raised to pH 8.5 to pH 9. The higher pH is believed to be beneficial in reducing corrosive effects due to dissolved oxygen which is present in measurable amounts in the water leaving the main condenser and probably persists as traces in the water leaving the deaerators.

In units Nos. 1 and 2, the caustic soda and sodium sulphite are added after the condenser hot-well pumps in order to afford further protection of equipment between the hot well and the deaerator. Formerly, these chemicals were added to the deaerator storage tank. The change in the point of feeding has presented some problems in keeping the feed rate constant, but this method of feeding has caused no apparent interference in the removal of carbon dioxide at the deaerator, as was originally feared. Irregular feeding of the chemicals, due to intermittent pump operation, was overcome in part by use of an equalizing tank, but there is some hope of replacing this later with a variable-speed direct-current-motor drive for the pumps.

There has not been sufficient time to determine the effect on corrosion due to the increase in the pH of the water and the further removal of dissolved oxygen, but the amounts of iron and copper in the feedwater are believed to be reasonable for the operating conditions which are experienced. This investigation is being continued and recorders for hydrogen and pH are being used in collecting the data.

TABLE 1 TYPICAL WATER ANALYSIS, UNITS NOS. 1 AND 2 HARBOR STEAM PLANT

BOILER WATER											
	pH	P-ALK	M-ALK	NaCl	Na ₂ SO ₃	Na ₂ SO ₄	PO ₄	S.O ₂	Fe	SiO ₂	LOAD
Normal	11.1	60	85	125	7	135	25	2	600		10-60
Max	11.2	85	110	175	9	175	40	3	1050		10-60
Min	11.0	45	70	75	3	75	20	1	600		10-60
FEEDWATER											
	pH	CO ₂	NH ₃	Na ₂ SO ₃	Na ₂ SO ₄	PO ₄	S.O ₂	Fe	SiO ₂	LOAD	
Normal	8.7	0	.02	3							10-60
Max	9.0	0	.04	5							10-60
Min	8.5	0	.01	2							10-60
MAIN CONDENSER CONDENSATE											
	pH	CO ₂	NH ₃	Na ₂ SO ₃	Na ₂ SO ₄	PO ₄	S.O ₂	Fe	SiO ₂	LOAD	
Normal	7.9	.2	.02	1.0							10-60
Max	8.1	.03	1.2								10-60
Min	7.6	.3	.01	0.8							10-60
JET CONDENSER CONDENSATE											
	pH	CO ₂	NH ₃	Na ₂ SO ₃	Na ₂ SO ₄	PO ₄	S.O ₂	Fe	SiO ₂	LOAD	
Normal	7.0	0.8	0.4	5.0							10-60
Max	6.8	0	5.0	3.0							10-60
SATURATED STEAM											
	pH	CO ₂	NH ₃	Na ₂ SO ₃	Na ₂ SO ₄	PO ₄	S.O ₂	Fe	SiO ₂	LOAD	
Normal	8.4	0	.02	.7							10-60
Max	8.6	0	.04	.9							10-60
Min	8.0	2	.01	.5							10-60
EVAPORATOR CONDENSATE											
	pH	CO ₂	NH ₃	Na ₂ SO ₃	Na ₂ SO ₄	PO ₄	S.O ₂	Fe	SiO ₂	LOAD	
Normal	7.0	.4	.03	.65							10-60
Max	7.4	.3	.04	1.7							10-60
Min	6.3	.4	.02	.60							10-60
SUPERHEATED STEAM											
	pH	CO ₂	NH ₃	Na ₂ SO ₃	Na ₂ SO ₄	PO ₄	S.O ₂	Fe	SiO ₂	LOAD	
Normal	8.3	0	.02	.65							10-60
Max	8.5	0	.04	.80							10-60
Min	7.9	.2	.01	.50							10-60
EVAPORATOR LIQUID											
	pH	CO ₂	NH ₃	Na ₂ SO ₃	Na ₂ SO ₄	PO ₄	S.O ₂	Fe	SiO ₂	LOAD	
Max	4.00	550	30	40	4000						10-60
Min	3.25	400	10	10	3000						10-60
AUX CONDENSER CONDENSATE											
	TIME	pH	CO ₂	NH ₃	Na ₂ SO ₃	Na ₂ SO ₄	PO ₄	S.O ₂	Fe	SiO ₂	LOAD
											10-60

Results as PPM except as noted

The analytical results, which are typical of present operating conditions for units Nos. 1 and 2, are shown in Table 1.

FREQUENCY OF SAMPLING AND USE OF CONTROL TESTS

A schematic flow diagram of the feedwater system and the location of various sample points which are available are shown in Fig. 3. The sample points which are used for routine tests are circled by a solid line and the samples which are taken less frequently are shown by dotted lines.

Generally, sufficient chemical-treatment control has been

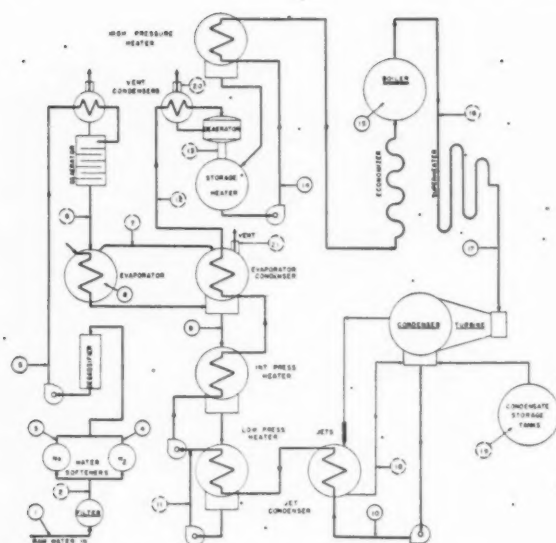


FIG. 3 FLOW DIAGRAM SHOWING SAMPLE POINTS

maintained by daily tests made on the steam, the feedwater from the deaerator, the condensate from the evaporator condenser, the boiler water, and the effluents from the zeolite softeners.

To determine the minimum vent settings, at times it is necessary to examine the condensed vented vapor for pH and gas content, and to compare the pH of the evaporator condensate or the feedwater with the vent opening.

In order to determine the effectiveness of oxygen removal in the deaerators and the prevention of in-leakage of oxygen in the vicinity of the condenser hot well and condensate pumps, it is necessary to make weekly tests for dissolved oxygen. Indirect tests for dissolved oxygen can be made at any time by determination of the sodium sulphite remaining in the feedwater. This test is much more rapid than the direct method, but, for the present, the direct modified Winkler method is being retained. As a matter of normal routine, the increase and decrease in sodium sulphite demand for maintenance of minimum sulphite concentration in the boiler water can be interpreted as showing the presence of more or less oxygen in the feedwater.

Occasional to frequent tests are made of the water leaving the aftercondenser in the vacuum system of the main condenser. These and related data are used to show when it is advisable to

throw the condensate to waste instead of returning it to the system. For example, if the ammonia content of the feedwater is higher than is necessary to maintain the desired pH in the steam condensate, the aftercondenser condensate will run high in ammonia, and a part or all of this condensate may be thrown to waste. In some other system or at another time the free carbon dioxide in the water may be the main consideration.

As has been indicated, the tests most frequently made on the samples of steam condensate are pH value and conductivity expressed as micromhos. Tests for free carbon dioxide and ammonia are made less frequently, but sufficient tests are made to control adequately the venting of deaerators, the evaporator condensate, and to show any need for other adjustments which may be possible.

The determination of iron and copper in the feedwater are being made frequently during investigations of corrosion, and it is likely that these tests will be made occasionally in the future.

Tests for soap hardness, alkalinity, and free chlorine are made on the raw city-water supply, and hardness alkalinity, and free mineral-acid tests are made of the effluents from the zeolite softeners and the blended soft water from the degasifying tower. The alkalinity of this water is maintained at approximately 25 ppm.

At the Harbor Steam Plant it has been found necessary to schedule the minimum amount of test work which should be done, but the laboratory personnel are expected to make such additional tests as may be indicated by the control tests which are made on schedule.

INSPECTION OF EQUIPMENT

At times of overhaul, or during other shutdown periods, the opportunity has been taken to inspect the equipment for signs of corrosion and the presence of deposits on the metal surfaces. Inspections now being made by competent personnel are being used as a guide to the effectiveness of corrosion control by feedwater treatment at Harbor Steam Plant. It has been noted that those parts of the system in which the dissolved oxygen has been present and the pH values low, are most likely to show corrosive effects. No severe general corrosion has been found in any of the units, and this is attributed to the care which has been taken in applying the chemical controls which have been recommended. At this time it is believed that satisfactory progress has been made in improving the feedwater conditions so that local corrosive attack may be reduced to a practical minimum.

Finally, it has been shown by tests and inspections that effective deaeration throughout the system for removal of corrosive gases is of prime importance to the success of corrosion control.

Th
the
roun
calcu
stan
Calc
for st

T

A =
A₀ =
E =
E' =
R =
S =
S₁ =
S₂ =
S_e =
S_u =
S =
W =
W_e =
W =

The
spheric
the cor
round
concept
second
tributo
The
design
nesses
hoped
Unfired
The
mán an

¹ Prof.
ASME.
² Star
³ Gra
Jun. AS
⁴ Num
of the p
Contr
Vessels
mittee o
tion and
vember
CHANICA
NOTE
understo
of the So

Allowable Eccentricity of Spherical Heads Convex to Pressure

By R. G. STURM,¹ L. W. SMITH,² AND H. L. O'BRIEN³

This paper discusses the variables and considerations in the design of spherical heads or shells, initially out-of-round, when subjected to external pressure. A method of calculating charts for design purposes based upon the instantaneous modulus of elasticity is presented herein. Calculations and charts for aluminum 3SO, and charts for stainless steel, 17-7 and "A" nickel are shown.

NOMENCLATURE

THE following nomenclature is used in this paper and is the same as that previously used for similar papers (1, 2, 3):⁴

- A = maximum value of deflection, in.
- A_0 = maximum initial departure from a perfect sphere, in.
- E = modulus of elasticity (Young's Modulus), psi
- E' = tangent modulus of elasticity, psi
- R = radius of spherical shell, inches.
- S = total stress in the shell (direct stress and bending), psi
- S_1 = average stress in shell due to pressure only, psi
- S_2 = stress in deflected shell due to bending, psi
- S_c = stress in shell at collapse, psi
- S_u = ultimate strength of material, psi
- S = modulus of failure, psi
- W = actual applied pressure, psi
- W_c = collapsing pressure for perfect shell, psi
- \bar{W} = collapsing pressure for an out-of-round shell, psi

INTRODUCTION

The design of spherical shells or pressure vessels with heads of spherical contour subjected to external pressure or pressure on the convex side is complicated by the unavoidable initial out-of-roundness of the manufactured shell or head. Beside the basic concepts of the strength of materials, other factors, such as secondary stresses due to bending, must be recognized as contributors to buckling action.

The analysis presented herein leads to curves which may aid designers in the proper selection of spherical shell or head thicknesses when manufacturing tolerances are considered. It is hoped that such curves will be of value to the ASME Code for Unfired Pressure Vessels.

The type of eccentricity is an important factor. Th. von Kármán and H. Tsien (4) point out that a full cup deflection is a stable

condition, but a flat deflection is very unstable. The size of the deformed area is also a critical factor.

Investigators have attacked the problem in two general ways. Von Kármán and Tsien (4) have used the theoretical approach as applied to thin shells, whereas Zick and Carlson (5), and Mariner and Keith (6) have approached the problem from the experimental viewpoint.

This paper treats each shell as a departure from a perfect shape in which the bending stress contributes to yielding and collapse. The methods used are primarily analytical and follow similar analytical studies for cylindrical vessels. The analysis for cylindrical vessels has been substantiated by tests and serves as the basis for computing allowable out-of-roundness charts for the present ASME Code for Unfired Pressure Vessels.

ANALYSIS

The basic equation for the buckling of a perfect sphere which is thin enough to buckle elastically is

$$S_c = 0.6 E \left(\frac{t}{R} \right) \quad [1]$$

If, however, the head is perfectly spherical but buckling does not occur until the compressive stress in the wall is above the proportional limit, a close approximation of the buckling stress is obtained by using a reduced value for the modulus of elasticity (1). For this case, the tangent modulus of elasticity E' is used. The effective, or tangent, modulus of elasticity is the slope of the tangent to the stress-strain curve at the stress considered. Von Kármán and Tsien corroborate the use of this modulus in preference to the secant modulus (4). The resulting equation is

$$S_c = 0.6 E' \left(\frac{t}{R} \right) \quad [2]$$

which is more useful when written as

$$S_c/E' = 0.6 \left(\frac{t}{R} \right) \quad [2a]$$

In Equation [2a], the physical properties of the metal (S_c/E') are separated from the geometrical dimensions inherent to the head or shell.

The general expression for the maximum value of deflection for an elastic structure initially out-of-round is given by the equation

$$A = A_0 \left(\frac{W}{W_c - W} \right) \quad [3]$$

At collapse W becomes \bar{W} , and this expression gives the value of the moment arm which together with the force in the shell or head wall makes possible the computation of the secondary stresses due to bending.

From the basic laws of statics, the average compressive stress in the wall of a spherical shell under external pressure is given by the equation

$$S_1 = \frac{WR}{2t} \quad [4]$$

¹ Professor, Purdue University, West Lafayette, Ind. Mem. ASME.

² Standard Oil (Indiana) Fellow, Purdue University.

³ Graver Tank and Manufacturing Company, East Chicago, Ind. Jun. ASME.

⁴ Numbers in parentheses refer to the Bibliography at the end of the paper.

Contributed by the Special Research Committee on Strength of Vessels Under External Pressure, and Pressure Vessel Research Committee of the Welding Research Council of The Engineering Foundation and presented at the Annual Meeting, New York, N. Y., November 27-December 2, 1949, of THE AMERICAN SOCIETY OF MECHANICAL ENGINEERS.

NOTE: Statements and opinions advanced in papers are to be understood as individual expressions of their authors and not those of the Society. Paper No. 49-A-70.

At the collapsing pressure for a perfect spherical shell, this stress is great enough to cause collapse. In out-of-round shells, the additional stress due to bending must be included in the computation for collapse. From Fig. 1, the moment due to the com-

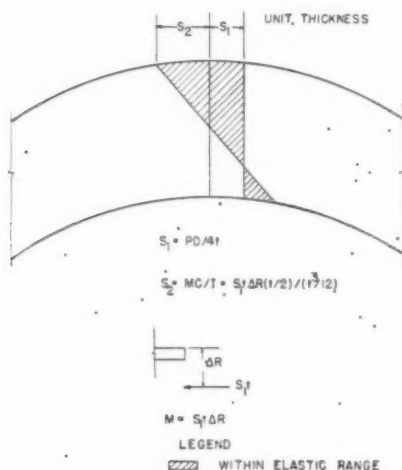


FIG. 1 DERIVATION OF STRESSES IN WALL OF SHELL

pressive force in the shell and the total radial deflection of the shell from its true spherical form causes a bending stress of

$$S_2 = \frac{M_0}{I} = \frac{S_1 t \Delta R \left(\frac{t}{2} \right)}{1 \left(\frac{t^3}{12} \right)}$$

which reduces to

$$S_2 = 6 S_1 \frac{\Delta R}{t} \quad [5]$$

Therefore the combined effects of Equations [4] and [5] give the total localized stress in the out-of-round shell or head. Thus the general expression for the maximum total stress in the shell at any pressure is

$$S = S_1 + S_2 = S_1 \left(1 + 6 \frac{\Delta R}{t} \right) \quad [6]$$

At collapse, the maximum deflection ΔR in Equation [6] is the value of A given by Equation [3]. The stress at collapse is, then

$$S = S_1 \left(1 + \frac{6A}{t} \right) \quad [7]$$

The ratio between the collapsing pressure of an out-of-round shell and the collapsing pressure of a sphere can be defined as a reduction ratio C_R , which may be expressed mathematically as

$$C_R = \frac{\bar{W}}{W_0} \quad [8]$$

This value of C_R introduced into Equation [3] gives

$$A = A_0 \left(\frac{C_R}{1 - C_R} \right) \quad [9]$$

which gives a measure of the value A at the pressure causing collapse of the out-of-round vessel.

A term often used to predict the maximum load-carrying capacity of beams is the modulus of failure, \bar{S} , which is the hypothetical value of stress obtained from the ordinary flexure stress formula $S = \frac{Mc}{I}$, using the value of M corresponding to the maximum load on a test beam. The value thus obtained is used to predict the maximum value of M for other beams.

From a consideration of a simple rectangular beam, such as a narrow strip of a shell wall (see Fig. 2), a value for this modulus of failure can be arrived at analytically for the case of pure bending. At maximum load, the actual stress distribution will be that indicated by the curved line in Fig. 2, which shows a maximum stress equal to the nominal tensile strength S_u of the material. The hypothetical stress distribution is the straight line which terminates at the modulus of failure \bar{S} .

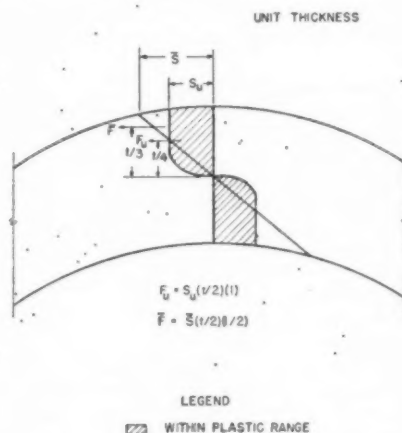


FIG. 2 DERIVATION OF MODULUS OF FAILURE

By equating the moment from the hypothetical stress distribution to that from the actual stress distribution, approximated as constant stress across half of the beam, the following relation is obtained

$$2 S_u (1) \left(\frac{t}{2} \right) \left(\frac{t}{4} \right) = 2 \bar{S} (1) \left(\frac{t}{2} \right) \left(\frac{t}{3} \right)$$

from which we get

$$\bar{S} = 1.5 S_u \quad [10]$$

Numerous tests have indicated that for narrow beams \bar{S} is usually less than $1.5 S_u$, and for wide beams or plates \bar{S} is often appreciably greater than $1.5 S_u$. For a usable approximation in this paper, however, the relation given by Equation [10] has been used.

At collapse of an out-of-round shell, the maximum localized stress would then be expected to be practically equal to the value of \bar{S} . When this value is substituted for the value of S in Equation [7] and the value of A from Equation [9] substituted in Equation [7] the relation becomes

$$\bar{S} = S_1 \left(1 + \frac{6A_0}{t} \cdot \frac{C_R}{1 - C_R} \right) \quad [11]$$

This equation then may be solved for the ratio of A_0/t in terms of the allowable reduction in strength represented by C_R , the ratio

of the thickness to the radius (t/R) represented by S_1 and the material in the vessel represented by S . The resulting equation is

$$\frac{A_0}{t} = \frac{\bar{S} - S_1}{6S_1 \frac{C_R}{1 - C_R}} \quad [12]$$

At collapse of an out-of-round vessel, the value of S_1 is $(WR)/(2t)$. For a perfect shell at collapse, the average stress is $S_e = (W_e R)/(2t)$. Therefore

$$\frac{S_1}{S_e} = \frac{W}{W_e} = C_R$$

Now, the right side of Equation [12] may be divided by S_e , the average stress in a perfect shell at collapse, to give

$$\frac{A_0}{t} = \frac{\bar{S}}{S_e} - C_R \quad [13]$$

PROCEDURE

As the first step toward evaluation of the A_0/t values, a range of design characteristics, thickness to diameter ratio, was selected (see Table 1, column 1). This choice made the geometric design conditions the independent variables in the calculations of A_0/t ,

and all physical properties of the material were later determined from appropriate charts.

The values of C_R for computations are listed in column 2, Table 1, and values of S_e/E' , calculated from Equation [2a], are listed in column 3; thus columns 1 through 3 are independent of any physical and metallurgical properties and can be used when constructing tables for all metals.

The figures listed in Table 1 are for 380 aluminum. The values of S_e for column 4 were obtained (2) from the ordinate of Fig. 3 at the intersection of the S_e/E' , (abscissa) value, and the appropriate curve. With proper regard to existing data, the modulus of failure for 380 aluminum was taken as 21,000 psi (7).

The component parts of Equation [13] were calculated, and listed in Table 1. The resultant values of A_0/t , listed in column 11 do not consider a safety factor. However, any suitable factor may be applied to the resulting curves by dividing the pressures at collapse by that factor.

The results of the foregoing calculations are presented in Fig. 4. This chart was composed by designating the abscissa as the maximum initial departure from a true sphere divided by the head thickness (A_0/t) and the ordinate as the ratio of the collapsing pressure for the out-of-round head to the collapsing pressure for a perfectly spherical head (C_R). The curves were plotted for various ratios of diameter to thickness and for vessels operating under standard temperature conditions.

Charts for ordinary temperatures were also calculated and

TABLE 1 DESIGN CHARACTERISTICS OF 380 ALUMINUM

(1)	(2)	(3)	(4)	(5)	(6)	(7)	(8)	(9)	(10)	(11)
t/D	C_R	$1.2(\frac{t}{D})$	S_e	C_R^2	$1 - C_R$	$\frac{6C_R^2}{1 - C_R}$	$1.5 S_u$	$1.5 \frac{S_u}{S_e}$	$1.5 \frac{S_u}{S_e} - C_R$	A_0/t
.0002	.3	.00024	2400	.09	.7	.772	21000	8.85	8.55	11.1
	.4			.16	.6	1.6			8.45	5.21
	.5			.25	.5	3.0			8.35	2.78
	.6			.36	.4	5.4			8.25	1.53
	.7			.49	.3	9.8			8.15	.831
	.8			.64	.2	19.2			8.05	.42
	.9			.81	.1	48.6			7.95	.164
	1.0			1.0	0	0			7.85	0
.001	.3	.0012	3720	.09	.7	.772	21000	5.64	5.34	6.9
	.4			.16	.6	1.6			5.24	3.27
	.5			.25	.5	3.0			5.14	1.71
	.6			.36	.4	5.4			5.04	.933
	.7			.49	.3	9.8			4.94	.504
	.8			.64	.2	19.2			4.84	.257
	.9			.81	.1	48.6			4.74	.098
	1.0			1.0	0	0			4.64	0
.002	.3	.0024	4430	.09	.7	.772	21000	4.73	4.43	5.74
	.4			.16	.6	1.6			4.33	2.71
	.5			.25	.5	3.0			4.23	1.41
	.6			.36	.4	5.4			4.13	.765
	.7			.49	.3	9.8			4.03	.411
	.8			.64	.2	19.2			3.93	.205
	.9			.81	.1	48.6			3.83	.079
	1.0			1.0	0	0			3.73	0
.005	.3	.0060	5570	.09	.7	.772	21000	3.77	3.47	4.48
	.4			.16	.6	1.6			3.37	2.11
	.5			.25	.5	3.0			3.27	1.09
	.6			.36	.4	5.4			3.17	.586
	.7			.49	.3	9.8			3.07	.313
	.8			.64	.2	19.2			2.97	.155
	.9			.81	.1	48.6			2.87	.059
	1.0			1.0	0	0			2.77	0
.010	.3	.012	6540	.09	.7	.772	21000	3.21	2.91	3.77
	.4			.16	.6	1.6			2.81	1.755
	.5			.25	.5	3.0			2.71	.903
	.6			.36	.4	5.4			2.61	.483
	.7			.49	.3	9.8			2.51	.256
	.8			.64	.2	19.2			2.41	.1255
	.9			.81	.1	48.6			2.31	.0476
	1.0			1.0	0	0			2.21	0
.020	.3	.060	7410	.09	.7	.772	21000	2.83	2.53	3.28
	.4			.16	.6	1.6			2.43	1.52
	.5			.25	.5	3.0			2.33	.777
	.6			.36	.4	5.4			2.23	.413
	.7			.49	.3	9.8			2.13	.217
	.8			.64	.2	19.2			2.03	.1065
	.9			.81	.1	48.6			1.93	.0317
	1.0			1.0	0	0			1.83	0

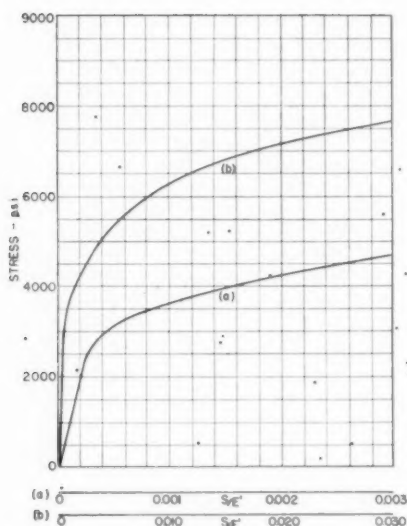


FIG. 3 CURVES USED FOR DETERMINING MODULUS OF ELASTICITY OF ALUMINUM, 380

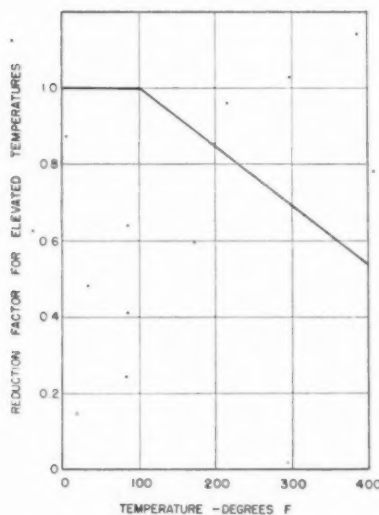


FIG. 5 CHART FOR DETERMINING STRENGTH REDUCTION FACTOR FOR 380 ALUMINUM AT ELEVATED TEMPERATURE

drawn for 17-7 stainless steel and "A" nickel, and are represented in Figs. 8 and 9, respectively. The S/E' curves for these materials may be found (2) in Figs. 6 and 7, respectively.

Both the modulus of elasticity and the yield strength of metals operating under elevated-temperature conditions are lower than the same properties at standard conditions. Thus charts similar to those of Figs. 4, 8, and 9, should be drawn for various temperature conditions. However, a strength-reduction factor for aluminum, 380, can be obtained from Fig. 5. This chart gives a reduction factor which corrects for both the reduction in modulus of elasticity and yield strength of 380 aluminum. The factor is applied by multiplying the value of W obtained from Fig. 4 by the correction for the desired temperature to get the reduced value of collapsing pressure at an elevated temperature.

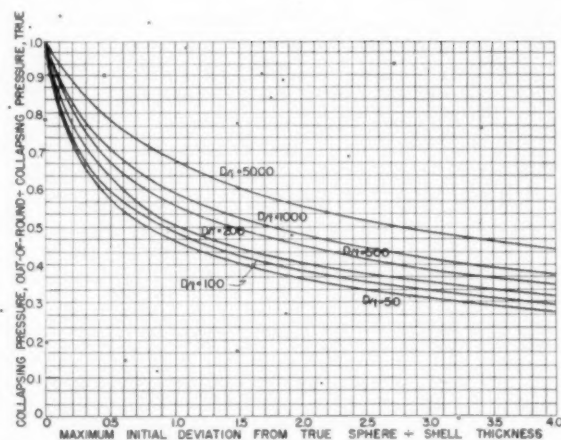


FIG. 4 CHART FOR DETERMINING WORKING PRESSURE FOR AN INITIALLY OUT-OF-ROUND SHELL CONSTRUCTED OF ALUMINUM, 380

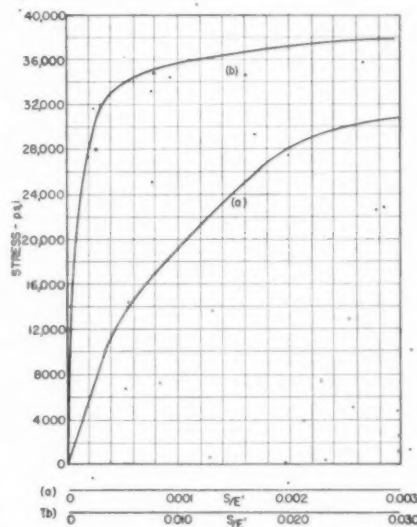


FIG. 6 CURVES USED FOR DETERMINING MODULUS OF ELASTICITY OF STAINLESS STEEL, 17-7

SUMMARY

1. Unavoidable out-of-roundness incurred in the manufacture of spherical heads or shells necessitates a consideration of the decrease in strength of such vessels due to additional stress caused by the initial deviation from a true sphere.

2. The type and size of deviation from a true sphere is important. A small cup deflection actually stabilizes the shell, but a flat deflection contributes to instability and will give rise to buckling failure.

3. A relation between the collapsing pressure of an out-of-round shell or head, and the value of the initial deviation from a true sphere has been analytically derived, and charts prepared for three representative metals.

4. A method by which similar charts may be constructed is presented herein. This method separates the physical properties of the metal from the geometrical dimensions of the shell.

5. Suitable reduction factors may be applied to determine the

FIG. 7

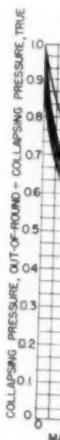


FIG. 9
TALL

collapsi
ture. T
pressure
the redu
factor is
tions.

6 Fa
here for
recalcul
stress, b
collapsin
7 Ex
desirable

1 "A
by R. G.
vember, 1

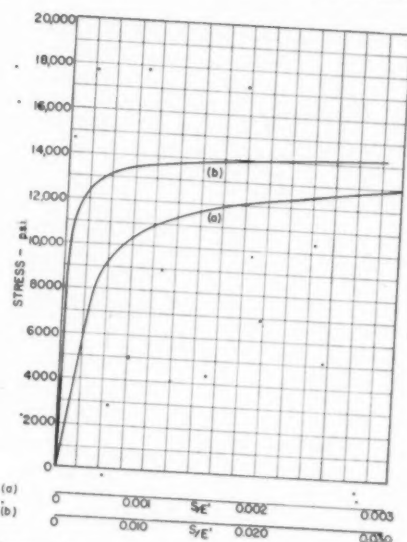


FIG. 7 CURVES USED FOR DETERMINING MODULUS OF ELASTICITY OF "A" NICKEL

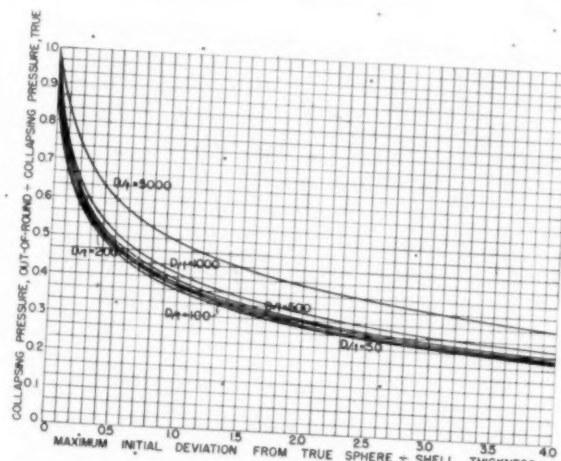


FIG. 9 CHART FOR DETERMINING WORKING PRESSURE OF AN INITIALLY OUT-OF-ROUND SHELL CONSTRUCTED OF "A" NICKEL

collapsing pressure for 350 aluminum at an elevated temperature. This may be accomplished by multiplying the collapsing pressure for the out-of-round vessel at standard temperature by the reduction factor for the desired temperature. The reduction factor is less than unity for temperature above standard conditions.

6 Factors of safety may be applied to the results presented here for industrial use. This consideration would not necessitate recalculations of the fundamental relations utilizing the allowable stress, because a suitable factor could be applied directly to the collapsing pressure.

7 Experimental verification of the charts presented herein is desirable.

BIBLIOGRAPHY

- 1 "A Study of the Collapsing Pressure of Thin Walled Cylinders," by R. G. Sturm, University of Illinois Bulletin, vol. 39, no. 12, November, 1941.

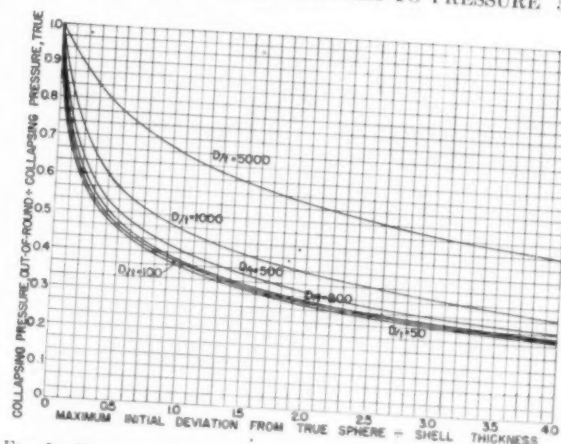


FIG. 8 CHART FOR DETERMINING WORKING PRESSURE OF AN INITIALLY OUT-OF-ROUND SHELL CONSTRUCTED OF STAINLESS STEEL, 17-7

- 2 "Computing Strength of Vessels Subjected to External Pressure," by R. G. Sturm and H. L. O'Brien, Trans. ASME, vol. 69, 1947, pp. 353-358.
- 3 "Collapsing Strength of Out-of-Round Vessels," by R. G. Sturm and H. L. O'Brien. Paper presented at the Annual Meeting, New York, N. Y., November 29-December 3, 1948, of The American Society of Mechanical Engineers.
- 4 "Buckling of Spherical Shells by External Pressure," by Th. von Kármán and H. Tsien, *Journal of the Aeronautical Sciences*, vol. 7, December, 1939, pp. 43-50.
- 5 "Vacuum Tests of Sphere to Failure," by L. P. Zick and C. E. Carlson, *Water tower*, vol. 34, November, 1947, pp. 6-7.
- 6 "Buckling Tests on Models of the Hemispherical Heads for the 16-Inch by 16-Inch Supersonic Wind Tunnel Vacuum Chamber," by J. Mariner and J. Keith, North American Aviation, Inc., Report.
- 7 "Spherical Shells Under External Pressure," by M. Holt, Aluminum Research Laboratories Report.
- 8 "Unfired Cylindrical Vessels Subjected to External Pressure," by F. Hartman, Trans. ASME, vol. 69, 1947, pp. 337-344.

Addendum

In determining the moment arm for the derivation of Equation [5], the initial deflection, A_0 , was omitted. Consideration of this value alters Equation [3], since

$$\Delta R = A \equiv A_0 \left(\frac{W}{W_c - W} \right) + A_0 = A_0 \left(\frac{W_c}{W_c - W} \right)$$

and

$$A = A_0 \left(\frac{1}{1 - C_R} \right) \quad [9]$$

The value of A thus obtained satisfies the definition of A in the nomenclature, and changes Equation [13] to

$$\frac{A_0}{t} = \frac{\frac{S}{S_c} - C_R}{6 C_R (1 - C_R)}$$

This materially changes column (11) of Table 1, Design Characteristics, with the result that the abscissas for the curves are changed. This is accomplished by multiplying the values of A_0/t by C_R at each value of C_R and t/D . By means of this modification the curves in Figs. 4, 8, and 9 as published can be used for design.

Discussion

MARSHALL HOLT.¹ Coincidentally Equation [1] of the paper also applies to the buckling of thin-wall circular cylindrical shells under axial load. Inasmuch as test data and theories of large deflections indicate that the coefficient 0.6 is too large, the question naturally arises as to the validity of this value of the coefficient in the problem of spheres. Von Kármán and Tsien arrive at a value of 0.18² for shells which are extremely thin and whose deviation from circularity gives the minimum elastic buckling strength. Although this coefficient does not enter the mathematics of this paper, it will be of great importance to the experimenter who tries to deduce from test results the out-of-roundness that must have existed in his specimens.

In establishing the equation for maximum stress, no consideration is given to the fact that the shell plate is bent in two directions. It would seem that Poisson's ratio should enter this equation. On the other hand, the modulus of failure is deduced from the results of a test under uniaxial stress without consideration of the effects of biaxial loading on the ultimate strength of materials. The authors, no doubt, expect these two effects to compensate for each other.

¹ Aluminum Research Laboratory, New Kensington, Pa.

² "The Buckling of Spherical Shells by External Pressure," by Th. von Kármán, and Hsue-Shen Tsien, *Journal of Aeronautical Sciences*, vol. 7, 1939, pp. 43-50.

AUTHORS' CLOSURE

Dr. Holt has raised a very interesting question which should have been covered in the original paper. The work by von Kármán and Tsien deals with extremely thin shells in which the material has an indefinitely high elastic limit. The coefficient 0.18 determined by von Kármán and Tsien represents the reduced value of the classical coefficient, 0.60 for perfectly spherical shells.

This reduced value results from a consideration of an eccentricity sufficient to produce a flat spot over an area which will make the value of the coefficient a minimum. Therefore the coefficient 0.18 cannot be used as a basis for determining the initial out of roundness because it intrinsically includes the effects of out of roundness.

Dr. Holt is correct in expecting the effects of Poisson's ratio and biaxial loading to compensate for each other. A consideration of the maximum distortion energy theory for biaxial bending reveals that when the two bending stresses are nearly equal and the stress normal to the shell is negligibly small the critical stress for inception of plastic action is the same as for unidirectional stress.

For elastic action Poisson's ratio is included in the derivation of the coefficient, 0.60. For plastic action the analysis and derivations may not be as precise as for elastic action but have been found to give reliable results for engineering usage.

This
Lehigh
welding
cusses
effects
tion pr

TH
ve
de
Research
desired
mechanic
this info
codes of
responses
the Press
at Lehigh

In ear
lated fal
changes
material.
plastic st
treatment
This re
was desir
respond
of plastic
welding,

For the
from sever
deoxidatio
of the ste
A (A-201)
and F (A
pecially fo
stock. Sh
according
these anal

¹ Progre
Steels Used
Pressure V
of The Eng

² Former
University

³ Resear
versity, Be

⁴ Associat

⁵ Directo
gineering, I

⁶ Number

paper.

Contribu
Vessels Un

Committee

Annual Me

of The AM

NOTE: S

derstood as

Society. F

Effect of Welding on Pressure-Vessel Steels¹

By A. F. SCOTCHBROOK,² L. ERIV,³ R. D. STOUT,⁴ AND B. G. JOHNSTON⁵

This paper presents the results of a study using the Lehigh slow notched-bend test to determine the effects of welding on as-received and prestrained plate. It also discusses the effects of different heat inputs in welding, the effects of plate thickness, of carbon content and deoxidation practice, and of heat-treatment after welding.

INTRODUCTION

THE effect of fabrication processes on steels used in pressure vessels is a subject to which considerable attention has been devoted by the Fabrication Division of the Pressure Vessel Research Committee of the Welding Research Council. It is desired to know which fabrication operations are harmful to the mechanical properties of steels, and to what extent. Eventually this information should lead to materials specifications and to codes of recommended fabrication practice, based upon measured responses of steel to various treatments. With these objectives, the Pressure Vessel Research Committee is sponsoring a project at Lehigh University.

In earlier investigations (1, 2, 3)⁶ the effects of various simulated fabrication operations were determined by measuring the changes in transition temperature, strength, and ductility of the material. These fabrication processes included various degrees of plastic strain produced by uniaxial stress, followed by various heat-treatments (3).

This report considers another fabrication process—welding. It was desired to know how different grades of pressure-vessel steels respond to welding, and to observe the effects of plate thickness, of plastic strains before welding, of high and low heat input during welding, and of heat-treatments after welding.

MATERIALS

For the tests reported here, six plain-carbon steels were selected from several mills to cover a range of grades, carbon contents, and deoxidation practices. A complete history is available (2) for two of the steels used, A-201 and A-70, each in two thicknesses, steels A (A-201) and E (A-70) of $\frac{3}{8}$ -in. thickness, and steels B (A-201) and F (A-70) of $1\frac{1}{4}$ in. thickness. These steels were made especially for research purposes. The others came from regular mill stock. Samples for chemical analysis were taken from the steels according to recommended ASTM procedure, and the results of these analyses are given in Table 1. Also included in Table 1 are

strength and ductility data for the as-rolled plate, as determined by standard 0.505-in. tensile tests at Lehigh University.

SPECIMEN PREPARATION AND TESTING

The transition temperature of each steel was determined for each of the following conditions:

- Welded.
- Welded and heat-treated at 500 F.
- Welded and heat-treated at 1150 F.
- Elongated 5 per cent and welded.
- Elongated 5 per cent, welded, and heat-treated at 500 F.
- Elongated 5 per cent, welded and heat-treated at 1150 F.

This schedule was followed for two heat inputs: 175 amp at 10 ipm with an E6010 $\frac{3}{16}$ -in. electrode (called W1), and 275 amp at 8 ipm with an E6010 $\frac{1}{4}$ -in. electrode (called W2). To cut down on expensive machining operations, conditions (b) and (e) were not used for the $1\frac{1}{4}$ -in. plate (steels B and F).

The longitudinal bead notch-bend test, Fig. 1, was used as de-

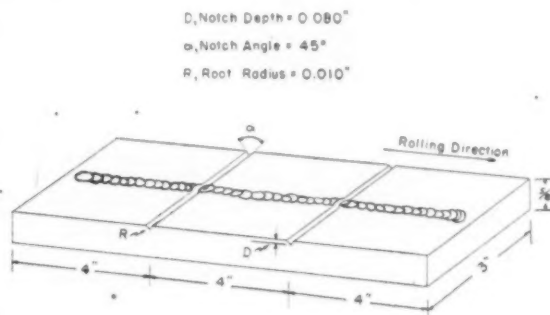


FIG. 1 LEHIGH SLOW NOTCHED-BEND SPECIMEN WITH WELD

veloped by a Welding Research Council project at Lehigh University (4). With an automatic welding machine, a weld bead 10 in. long was deposited on a plate surface of the 3-in. \times 12-in. specimen. Heat-treating was done one day after welding. The $\frac{3}{8}$ -in. plate was then notched and tested at plate thickness, while the $1\frac{1}{4}$ -in. plate was shaped down on the unwelded surface to a thickness of $\frac{3}{8}$ in. before notching. Specimens were tested 1 week after welding.

The 5 per cent prestrain for the foregoing conditions (d), (e), (f) was produced by stretching strips $9\frac{1}{2}$ -in. \times 16-ft in an 800,000-lb testing machine. Gage marks were scribed at 2-ft intervals along the strips, and the distances between marks were measured regularly during the pulling. A 2-ft section from each end of each strip was discarded to avoid using material which had been nonuniformly deformed because of the restraints at and near the testing-machine grips.

The specimens were tested in bending, as in Fig. 2. Three measurements were made on each specimen—per cent lateral contraction, per cent of the fracture area which was cleavage, and energy absorbed by the specimen from the start of the test until the load had passed its maximum and dropped to a value equal to half the maximum. The per cent contraction values were obtained by measuring with a pointed micrometer the width of the

¹ Progress Report No. 4 on the Effect of Fabrication Processes on Steels Used in Pressure Vessels, submitted to the Fabrication Division, Pressure Vessel Research Committee of the Welding Research Council of The Engineering Foundation.

² Former Research Assistant, Fritz Engineering Laboratory, Lehigh University, Bethlehem, Pa.

³ Research Assistant, Fritz Engineering Laboratory, Lehigh University, Bethlehem, Pa.

⁴ Associate Professor of Metallurgy, Lehigh University.

⁵ Director, Fritz Engineering Laboratory, and Professor of Civil Engineering, Lehigh University.

⁶ Numbers in parentheses refer to the Bibliography at the end of the paper.

Contributed by the Special Research Committee on Strength of Vessels Under External Pressure, and the Pressure Vessel Research Committee of the Welding Research Council and presented at the Annual Meeting, New York, N. Y., November 27–December 2, 1949, of THE AMERICAN SOCIETY OF MECHANICAL ENGINEERS.

NOTE: Statements and opinions advanced in papers are to be understood as individual expressions of their authors and not those of the Society. Paper No. 49–A-49.

TABLE 1 RESULTS OF ANALYSES

Project Letter	A.S.T.M. No.	Deoxidation	Plate Thickness	C	Mn	P	S	Si	Al	Al ₂ O ₃	N ₂	Lower Yield Strength p.s.i.	Maximum Strength p.s.i.	% Red. of Area	% Elongation
I	A-285 Grade A	Rimmed	5/8"	.15	.38	.012	.030	.01	.010	.007	.004	34,650	59,150	63.8	38.0
K	A-285 Grade A	Semi-killed	5/8"	.09	.43	.014	.027	.02	.011	.006	.004	29,600	51,450	73.5	42.3
L	A-285 Grade C	Rimmed	5/8"	.20	.40	.011	.030	.01	.008	.006	.003	32,050	61,400	56.3	37.5
E	A-70 Grade C	Rimmed	5/8"	.22	.37	.019	.028	.02	.010	.002	.004	33,850	64,300	63.2	38.5
F	A-70 Grade C	Rimmed	1 1/4"	.20	.36	.018	.028	.02	.021	.003	.003	26,250	56,300	63.1	39.5
A	A-201 Grade A	Killed	5/8"	.17	.55	.020	.022	.21	.041	.003	.005	35,450	63,150	68.6	38.0
B	A-201 Grade A	Killed	1 1/4"	.15	.56	.020	.019	.20	.041	.006	.004	31,600	63,300	64.6	36.8
F	A-201 Grade A	Killed	5/8"	.12	.41	.015	.027	.19	.018	.007	.003	32,850	57,350	66.7	38.9

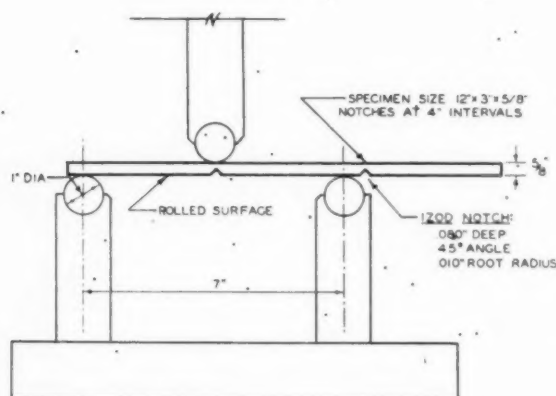


FIG. 2 THE LEHIGH SLOW NOTCHED-BEND TEST

specimen $1/32$ in. below the notch before and after the test. Per cent cleavage measurements were made on a fractured section with a steel scale. Energy values were determined by measuring with a planimeter the area under a load-deflection curve obtained autographically during the test.

Twelve specimens, or twenty-four notch tests, were used for each condition, four tests at each of six temperatures. The average values at each temperature were connected by straight lines, and the transition temperature was the point at which the per cent contraction, per cent cleavage or energy was equal to half its maximum. When occasionally the transition curve formed a plateau near the transition temperature, a transition range was reported as well as a transition temperature. This range extended from the temperature of -10 per cent to that of $+10$ per cent of the half-maximum value of contraction, cleavage, or energy which had defined the transition temperature. T_N and

T_E , the transition temperatures obtained from per cent contraction and energy curves, respectively, were considered the transition temperatures of the material with the original notch. T_E , obtained from per cent cleavage curves, was considered the transition temperature of the plate when notched by a crack. All three temperatures are listed in Tables 2, 3, and 4.

T_E , as described here, is a transition temperature not previously determined or reported in the earlier papers. T_E was found to agree very closely with T_N for unstrained material, and to be consistently lower than T_N for strained material. Fig. 3 shows typical energy and contraction curves for strained and unstrained material.

To determine the effects of welding, the transition temperatures of welded specimens were compared with those of unwelded specimens from the same material. Although transition curves for the as-received condition have been made earlier for steels B and F (1, 3), they were repeated for use in the present work. It was found that there were some differences between the two sets of curves, which are shown in Figs. 4 to 7. The discrepancies between the curves must be accounted for by variation from plate to plate (2), and by inaccuracy caused by the method of plotting. From these curves it appears that variations in transition temperature as high as 30 F could be intrinsic to plate variations and to the testing and plotting methods, and could not be attributed with surety to the variable being studied.

DISCUSSION OF RESULTS

Effect of Welding As-Rolled Plate. Welding increased notch-sensitivity of as-received plate when measured by per cent contraction or energy. The difference between unwelded and welded plate was shown by a significant rise in the transition temperatures T_N and T_E , both of which are affected by the material directly below the machined notch. The rise in T_N caused by welding as-received plate is shown graphically in Fig. 8. The order of transition temperatures after welding was quite different from that before welding.

TABLE 2 EFFECT OF WELDING ON TRANSITION TEMPERATURE—CRITERION— T_N

Steel	As Rolled	Weld w ₁ Unstrained	Weld w ₂ Unstrained	Weld w ₁ Post Heat 500°F	Weld w ₂ Post Heat 500°F	Weld w ₁ Post Heat 1150°F	Weld w ₂ Post Heat 1150°F	Strain 5% un- welded	Strain 5% welded w ₁	Strain 5% welded w ₂	Strain welded w ₁ Post Heat 500°F	Strain welded w ₂ Post Heat 500°F	Strain welded w ₁ Post Heat 1150°F	Strain welded w ₂ Post Heat 1150°F
A	-35	33	-18	15	-8	-30	3	-45	35	20	3	20	-18	6
B	-85	43	47	-	-	7	19	-35	89	93	-	-	-15	0
P	-73	18	30	27 ^a	-11	-55	-24	-75	77 ^b	11	0	31 ^c	-20 ^d	-24
I	-28	28	66	41	28	-18	35	-53	45	26	40 ^e	15	-5	-11
K	-53	12	-17	8	-30	-40	-25	10	71	40	53	27	-16	-23
L	-51	63	58	79	59	35	56	-7	92	88	45	83	-10	48
E	-13	75	68	68	63	30	50	8	80	58	58	40	-13	38
F	-71	81	66	-	-	17	21	48	150	62	-	-	88	18

o w₁ - Welded using 175 amperes at 10 inches per minute with an E6010 3/16" electrode.oo w₂ - Welded using 275 amperes at 8 inches per minute with an E6010 1/4" electrode.

a - Temperature Range - 5 to 32

b - Temperature Range - 45 to 82

c - Temperature Range - 0 to 43

d - Temperature Range - 26 to 32

e - Temperature Range - 0 to 50

TABLE 3 EFFECT OF WELDING ON TRANSITION TEMPERATURE—CRITERION— T_E

Steel	As Rolled	Weld w ₁ Unstrained	Weld w ₂ Unstrained	Weld w ₁ Post Heat 500°F	Weld w ₂ Post Heat 500°F	Weld w ₁ Post Heat 1150°F	Weld w ₂ Post Heat 1150°F	Strain 5% un- welded	Strain 5% welded w ₁	Strain 5% welded w ₂	Strain welded w ₁ Post Heat 500°F	Strain welded w ₂ Post Heat 500°F	Strain welded w ₁ Post Heat 1150°F	Strain welded w ₂ Post Heat 1150°F
A	-36	29	-34	-11	-16	-80	-3	-59	7	-5	-18	-18	-59	-8
B	-96	45	55	-	-	-18	5	-58	90	88	-	-	-24	-25
P	-74	17	22	20	-35	-41	-23	-67	49	-18	-26	-36	-41	-46
I	-33	29	61	27	5	-68	-15	-84	0	-2	-18	-13	-13	-33
K	-54	11	-27	2	-31	-50	-21	-39	46	18	33	15	-28	-29
L	-58	52	51	75	40	13	53	-20	26	38	-26	16 ^a	-25	25
E	-13	65	50	33	2	-62 ^b	30	-13	14	13	3	8	-31	12
F	-75	100	69	-	-	7	33	-11	136	3	-	-	30	22

o w₁ - Welded using 175 amperes at 10 inches per minute with an E6010 3/16" electrode.oo w₂ - Welded using 275 amperes at 8 inches per minute with an E6010 1/4" electrode.

a - Temperature Range - 3 to 60

b - Temperature Range - 58 to 15

TABLE 4 EFFECT OF WELDING ON TRANSITION TEMPERATURE—CRITERION— T_B

Steel	As Rolled	Weld w ₁ Unstrained	Weld w ₂ Unstrained	Weld w ₁ Post Heat 500°F	Weld w ₂ Post Heat 500°F	Weld w ₁ Post Heat 1150°F	Weld w ₂ Post Heat 1150°F	Strain 5% un- welded	Strain 5% welded w ₁	Strain 5% welded w ₂	Strain welded w ₁ Post Heat 500°F	Strain welded w ₂ Post Heat 500°F	Strain welded w ₁ Post Heat 1150°F	Strain welded w ₂ Post Heat 1150°F
A	65	68	53	35	53	45	25	50	90	108	115	111	84	68
B	81	78	70	-	-	67	64	83	95	118	-	-	91	94
P	-50	13	30	13	-11	28	-16	-10	57	65	56	44	48	38
I	45	80	75	83	74	84	61	79	114	85	113	86	88	57
K	55	66	47	55	38	60	75	79	117	97	103	86	80	61
L	87	97	93	92	108	110	100	108	156	148	153	142	131	107
E	110	95	98	109	119	133	113	118	153	150	175	127	125	115
F	180	157	158	-	-	156	164	163	163	212	-	-	156	166

c w₁ - Welded using 175 amperes at 10 inches per minute with an E6010 3/16" electrode.

oo w₂ - Welded using 275 amperes at 8 inches per minute with an E6010 1/4" electrode.

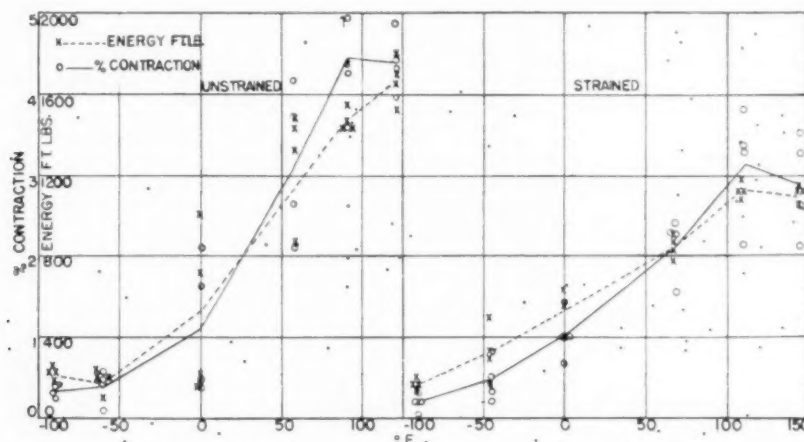


FIG. 3 COMPARISON OF PER CENT CONTRACTION AND ENERGY CURVES FOR WELDED A-201, 5/8-IN. MATERIAL

The notch sensitivity measured by fracture appearance was little affected by welding. This is shown in Fig. 9 by a small rise, or even a drop, in T_B values from unwelded to welded plate.

Effect of Welding Prestrained Plate. As seen in Fig. 10, prestraining often but not always raised somewhat the transition temperatures of as-received plate. The effect of welding this plastically prestrained plate is shown in Figs. 11 and 12. As in the case of as-rolled plate, the T_N for strained plate was significantly raised by welding, Fig. 11. The T_N level after welding strained metal was a little higher than that after welding unstrained metal, Fig. 13.

When the effect of welding prestrained steel is considered in the light of the transition temperature T_B in Fig. 12, it can be seen that T_B for strained steel was raised up to 75 F by welding. T_B for strained and welded plate was, in most cases, appreciably higher than that for unstrained and welded plate, Fig. 14.

Effect of Heat Input. In comparing the differences in level be-

tween W1 and W2 in Figs. 8, 9, 11, and 12, it may be noted that, except in two cases, the two heat inputs resulted in about the same transition temperature for these plain-carbon steels.

Effect of Plate Thickness. It can be seen from Figs. 8 to 11 that welding usually caused greater increases in T_N for steels B and F, which were welded at 1 1/4-in. thickness, than it did for the other steels, welded at 5/8 in. thickness. Since all the steels were tested in 5/8 in. thickness, this indicates that the increased cooling rate after welding, imposed by the thicker plate, resulted in a higher T_N transition temperature. The T_B transition temperature, Figs. 9 and 12, was changed by welding to about the same degree for 1 1/4-in. and 5/8-in. plate.

Effect of Carbon Content and Deoxidation Practice. There appeared to be some correlation between carbon content and transition temperatures, both before and after welding, as shown in Fig. 15. This figure contains only the values for the steels of 5/8 in. thickness.

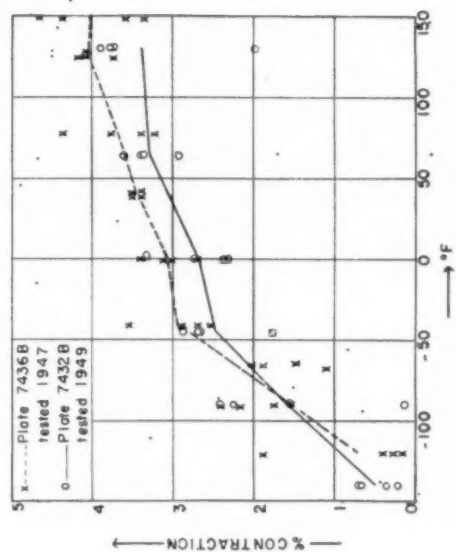


FIG. 4 TRANSITION CURVES FOR SAME A-201, $1\frac{1}{4}$ -IN. MATERIAL DETERMINED IN 1947 AND 1949
(Lehigh slow notched-bend test. Criterion: Per cent cleavage.)

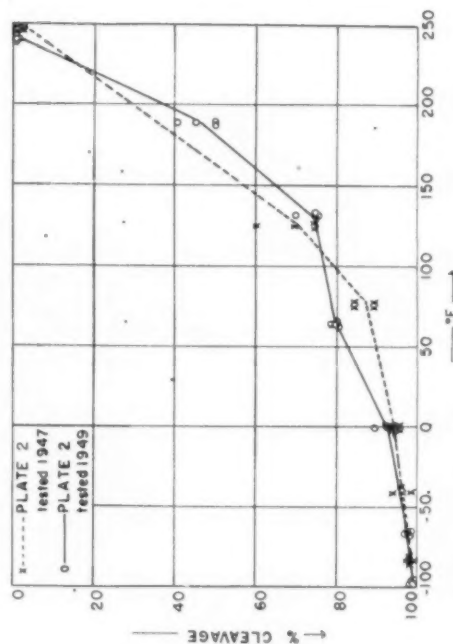


FIG. 6 TRANSITION CURVES FOR SAME A-70, $1\frac{1}{4}$ -IN. MATERIAL DETERMINED IN 1947 AND 1949
(Lehigh slow notched-bend test. Criterion: Per cent cleavage.)

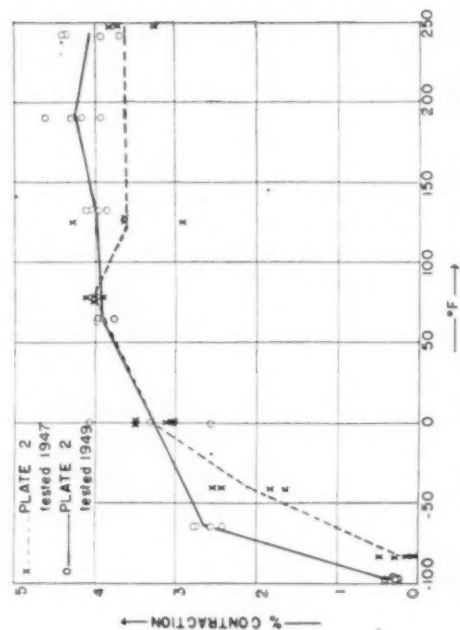
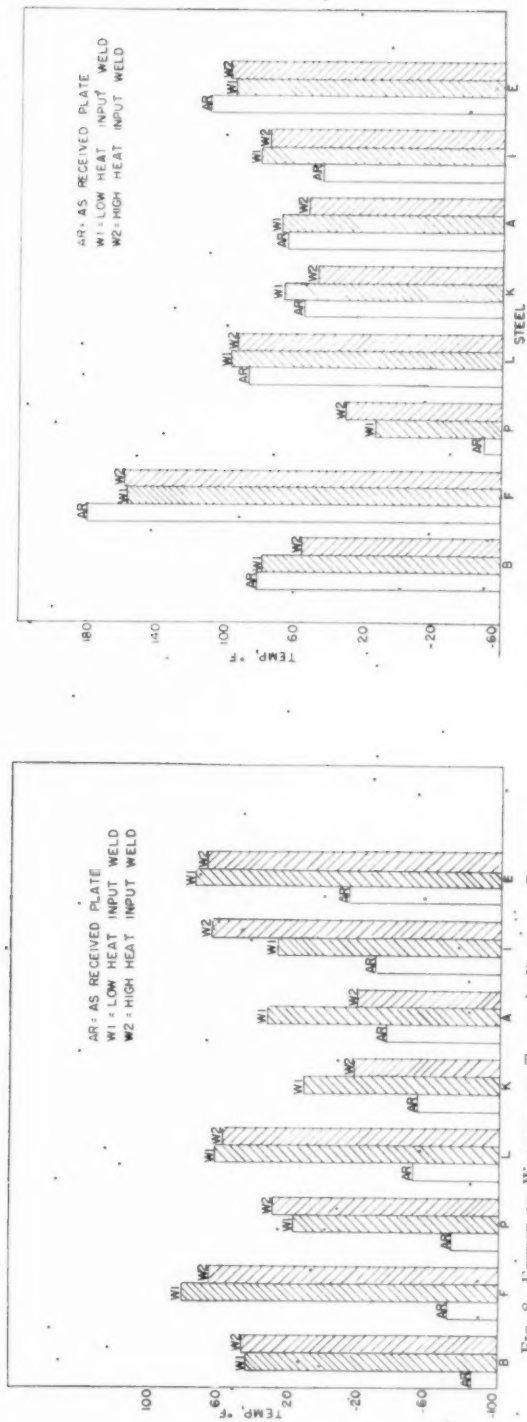
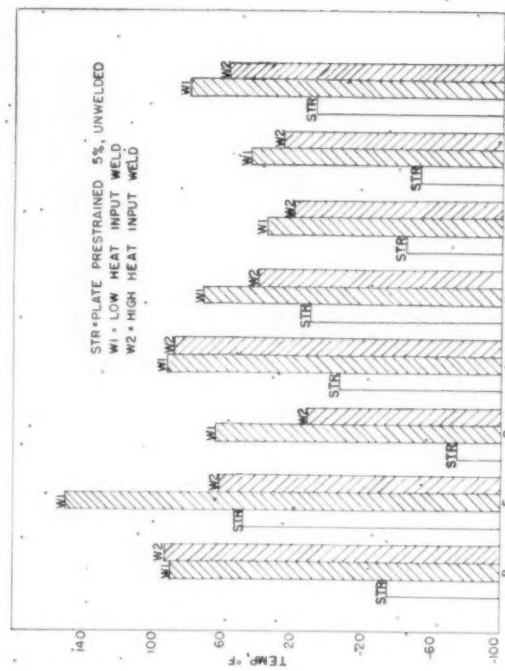
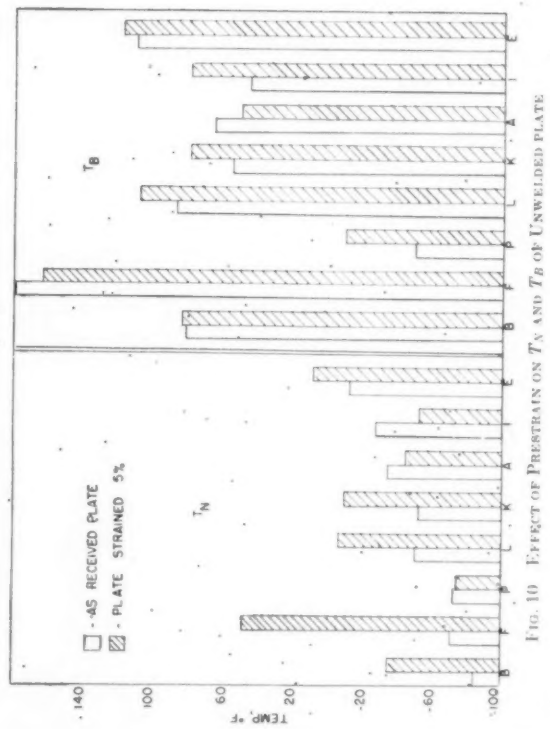


FIG. 7 TRANSITION CURVES FOR SAME A-70, $1\frac{1}{4}$ -IN. MATERIAL DETERMINED IN 1947 AND 1949
(Lehigh slow notched-bend test. Criterion: Per cent contraction.)

FIG. 5 TRANSITION CURVES FOR SAME A-201, $1\frac{1}{4}$ -IN. MATERIAL DETERMINED IN 1947 AND 1949
(Lehigh slow notched-bend test. Criterion: Per cent contraction.)

Fig. 9 EFFECT OF WELDING ON T_B OF AS-RECEIVED PLATEFig. 11 EFFECT OF WELDING ON T_N OF STRAINED PLATEFig. 10 EFFECT OF PRESTRAIN ON T_N AND T_B OF UNWELDED PLATE

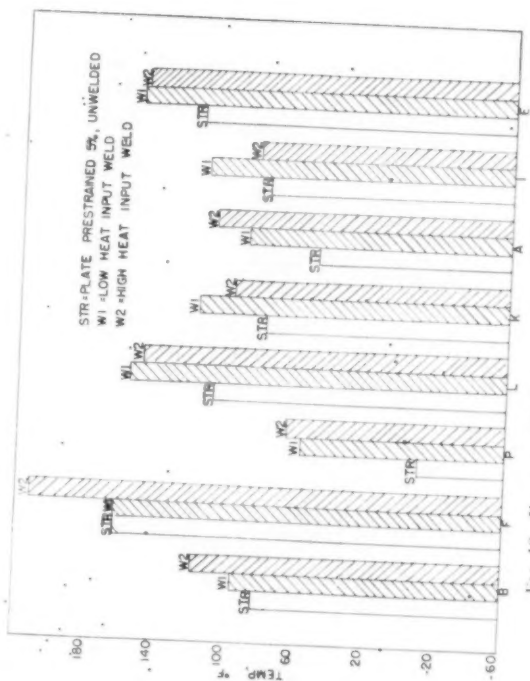


FIG. 12 EFFECT OF WELDING ON T_B OF STRAINED PLATE

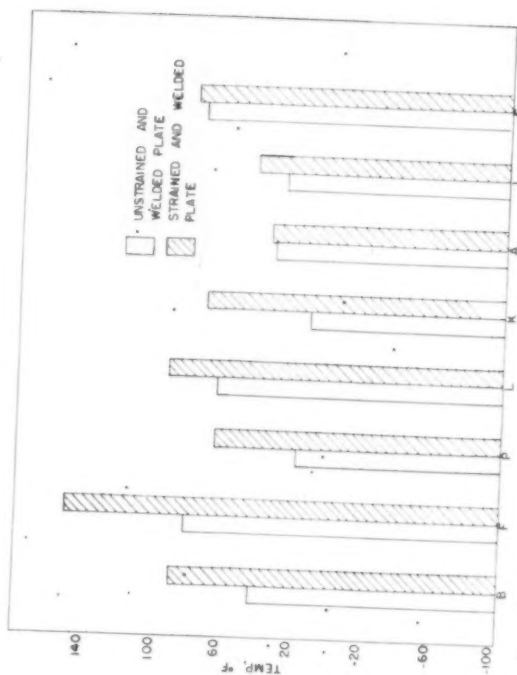


FIG. 13 COMPARISON OF T_N FOR UNSTRAINED AND WELDED PLATE WITH STRAINED AND WELDED PLATE

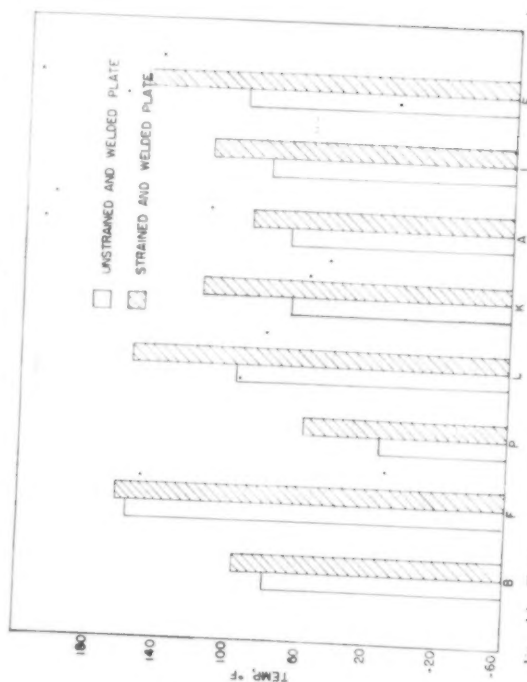


FIG. 14 COMPARISON OF T_B FOR UNSTRAINED AND WELDED PLATE WITH STRAINED AND WELDED PLATE

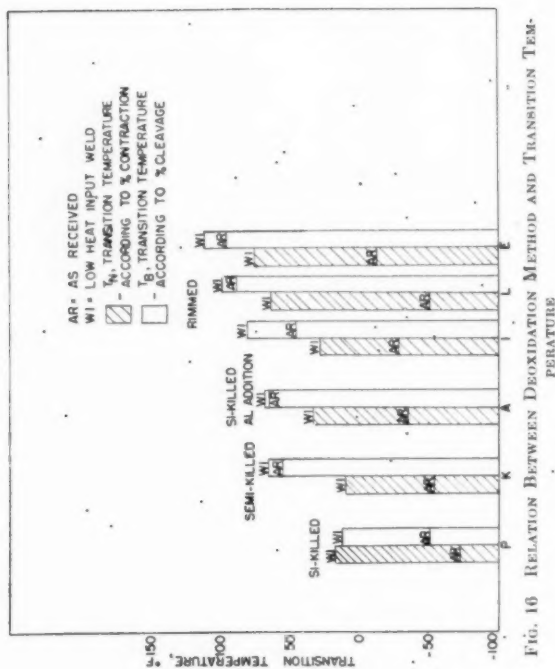


FIG. 16 RELATION BETWEEN DECARIDATION METHOD AND TRANSITION TEMPERATURE

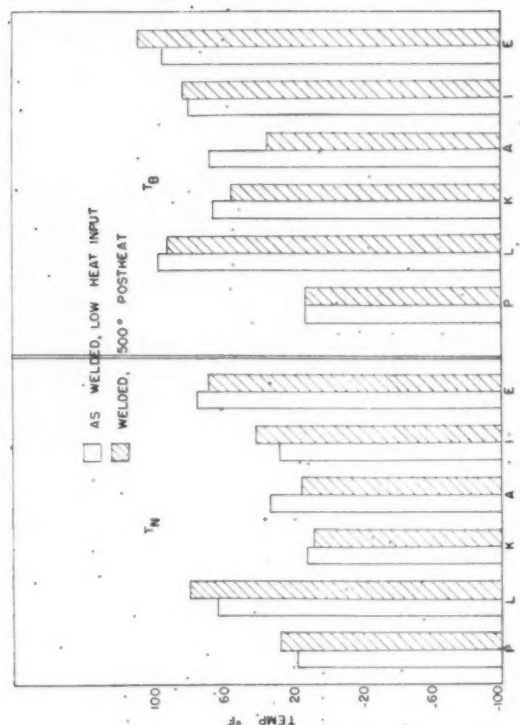


FIG. 17 EFFECT OF 500 DEG POSTHEAT ON UNTRAINED AND WELDED PLATE

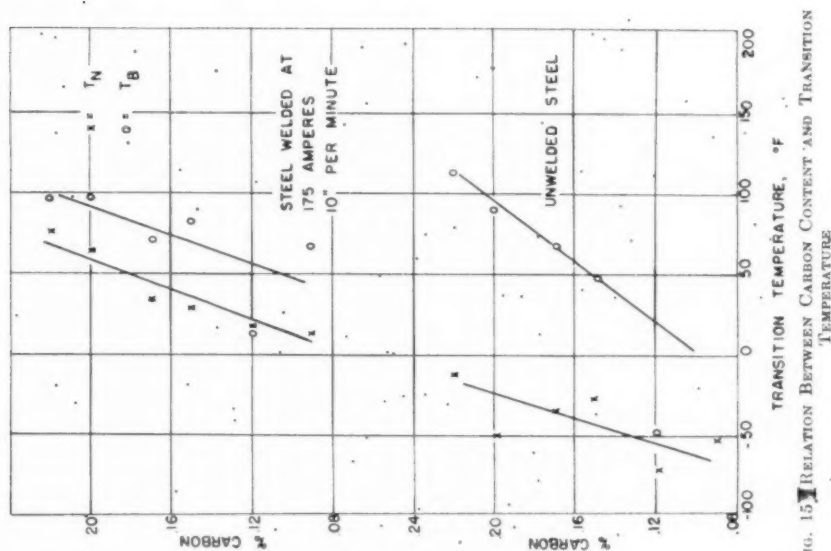


FIG. 15 RELATION BETWEEN CARBON CONTENT AND TRANSITION TEMPERATURE

In
pract
the h
with
straig
steels
with
purpo
Eff
F heat
input
effect
raised
 T_N by
Str
to he
deg p
The 1
of T_N
The
weld.
Eff
ness o
It rev
ness i
soften

1
mater
tempe
2
slight
3
more
4
of car
5
proved
impro
mater

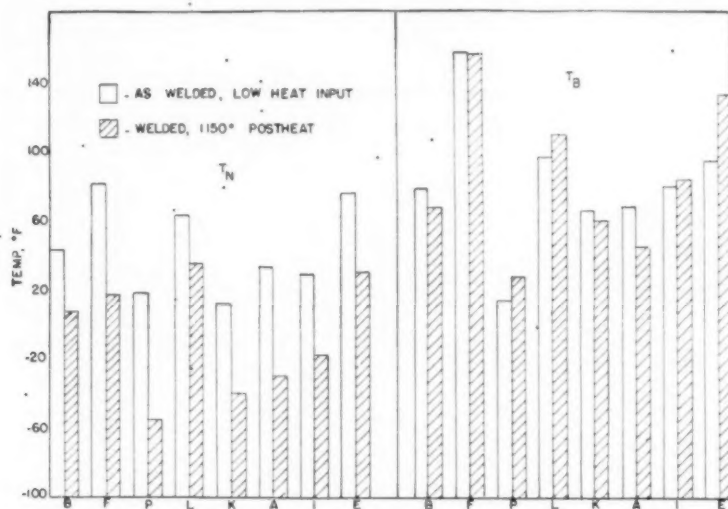


FIG. 18 EFFECT OF 1150 DEG POSTHEAT ON UNSTRAINED AND WELDED PLATE

In Fig. 16 the steels are grouped according to deoxidation practice. According to either T_N or T_B , the rimmed steels had the highest transition temperatures after welding, the killed steel with aluminum addition next, followed by the semikilled, and straight silicon-killed steels. It is interesting to note that the four steels selected at random from mill stock compared favorably with the two pedigreed steels prepared especially for research purposes.

Effect of Heat-Treatment After Welding. The effect of a 500 F heat-treatment after welding unstrained metal at the lower heat input is illustrated in Fig. 17. The heat-treatment has little effect—it sometimes lowered T_N and T_B slightly and sometimes raised them. The 1150 F postheat, however, Fig. 18, lowered T_N by as much as 70 deg, while T_B was unaffected.

Strained and welded metal, however, responded more readily to heat-treatment. In Fig. 19 it can be seen that even the 500 deg postheat lowered T_N somewhat, and it left T_B unchanged. The 1150 deg postheat, as shown in Fig. 20, resulted in a lowering of T_N by as much as 100 deg, and also a consistent lowering of T_B .

The same responses were found after the higher-heat-input weld.

Effect of Welding on Hardness. A study was made of the hardness of the material immediately below the weld in all conditions. It revealed little beyond the fact that welding increased the hardness in this area, and that the 1150-deg postheat had a very slight softening effect.

SUMMARY

- 1 Welding appreciably increased the notch sensitivity of the material. The increase could not be predicted from the transition temperature of the unwelded plate.
- 2 Welding prestrained material resulted in a T_N and T_B of slightly higher level than welding unstrained plate.
- 3 Welding raised the T_N transition temperature of thick plate more than thin plate.
- 4 The level of transition temperature was apparently a function of carbon content and deoxidation practice.
- 5 An 1150 F heat-treatment after welding greatly improved the material affected by the weld. A 500 F postheat improved strained and welded material, but not unstrained welded material.

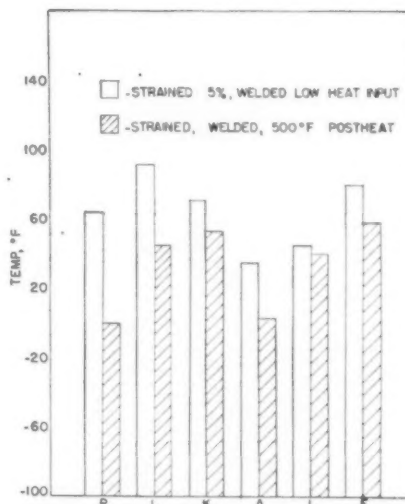


FIG. 19 EFFECT OF 500 DEG POSTHEAT ON STRAINED AND WELDED PLATE

ACKNOWLEDGMENTS

This work was sponsored by the Pressure Vessel Research Committee of the Welding Research Council, which is directed by William Spraragen. Walter Samans is chairman of the Pressure Vessel Research Committee and Boniface E. Rossi is executive secretary. Harry Boardman is chairman of the Fabrication Division of the Pressure Vessel Research Committee, which guided the project staff in this work.

The project was carried on jointly by the Fritz Engineering Laboratory of the Civil Engineering Department, and the Metallurgy Department of Lehigh University.

The execution of work was made possible by the co-operation of Kenneth R. Harpel, laboratory foreman, and the entire laboratory staff.

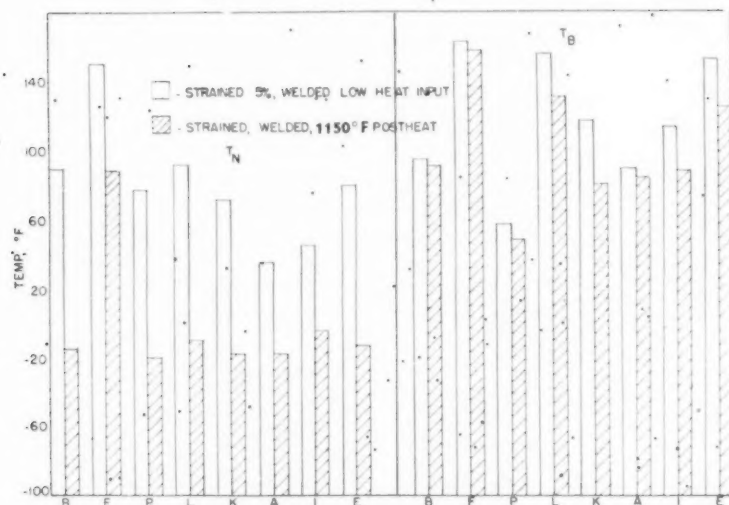


FIG. 20 EFFECT OF 1150 DEG POSTHEAT ON STRAINED AND WELDED PLATE

BIBLIOGRAPHY

- 1 "Comparison of Notch Tests and Brittleness Criteria," by C. J. Osborn, A. F. Scotchbrook, R. D. Stout, and B. G. Johnston, *The Welding Journal*, vol. 28, 1949, Research Supplement, pp. 24s-33s.
- 2 "Composition and Property Variation of Two Steels," by C. J. Osborn, A. F. Scotchbrook, R. D. Stout, and B. G. Johnston, *The Welding Journal*, vol. 28, 1949, Research Supplement, pp. 227s-235s.

- 3 "Effect of Plastic Strain and Heat Treatment," by C. J. Osborn, A. F. Scotchbrook, R. D. Stout, and B. G. Johnston, *The Welding Journal*, vol. 28, 1949, Research Supplement, pp. 337s-353s.
- 4 "Effect of Welding on Ductility and Notch Sensitivity of Some Ship Steels," by R. D. Stout, L. J. McGeady, C. P. Sun, J. F. Libsch, and G. E. Doan, *The Welding Journal*, vol. 26, 1947, Research Supplement, pp. 335s-357s.

TH
tors
syste
a rel
are c
basie
feren
plan
and
ence

I
of the
one p

Th
to be
and a
instal

Spe

(a)
(b)
bility.

(c)
in ave

It i
four p
this p
Select
startin
tions,
design
tion, h
that a
be of i

Fou
for inv
turbine
(2) res
tion.
100-m
ators.
connec
direct
turbine

¹ Eng
ASME
Cont
Meeting
AMERIC
NOTI
derstood
the Soc

Some Factors Influencing the Economics of Reheat Installations

By R. W. HARTWELL¹ AND H. A. WAGNER,¹ DETROIT, MICH.

This paper presents a discussion of some economic factors concerned with choosing between a battery boiler system as compared to a unit boiler-turbine system, and a reheat as compared to a nonreheat plant. Annual costs are compared for four power plants containing the several basic design features. Emphasis is placed upon the difference in average availability of capacity of the four plants, effect on availability of two maintenance schedules, and result of assigning capital charges based upon difference in average available capacity.

IN any study concerned with economics of a new power plant, there are numerous factors which require consideration. Basic assumptions in each case must suit the characteristics of the particular power system involved, hence a study made for one plant will not necessarily fit the requirements for another.

This paper covers only certain of the economic factors believed to be pertinent in choosing between (1) a battery boiler system and a unit boiler-turbine system; (2) a reheat and a nonreheat installation.

Special consideration was given to the effect on over-all cost of:

- (a) Availability of capacity in each of the schemes.
- (b) The result of different maintenance schedules on availability.
- (c) Assignment of capital charges resulting from the difference in average capacity available.

It is not the intent of the paper to prove that any one of the four plant schemes studied is the preferred arrangement since this paper represents only a part of a study now being made. Selection of one or two schemes from this analysis should be the starting point for further investigation as to other throttle conditions, different sizes and types of turbine-generators, and other design characteristics such as outdoor or semioutdoor construction, heat-cycle arrangement, and so on. It is believed, however, that an analysis of the effect of some of the foregoing factors will be of interest to those concerned with power-plant economics.

BASIC DESIGN FEATURES OF PLANTS STUDIED

Four plant designs were selected for study to provide a means for investigating the economic desirability of (1) the unit boiler-turbine systems as compared to a battery boiler system; and (2) resuperheating or reheat as compared to a nonreheat installation. Each plant has an installed capacity of 400 mw in four 100-mw tandem-compound double-flow 1800-rpm turbine-generators. Plant A, the battery boiler system, consists of five interconnected boilers; plant B has four boilers, each connected directly to its own turbine; plant C has four boilers, one for each turbine, which are connected by a crossover; plant D is the unit

system as for plant B, but provided with reheat. These plants have totally enclosed boiler rooms and pulverized-fuel-burning boilers equipped with unit coal-pulverizing mills.

The estimated total cost for each of the four types of plants considered, and the cost per kilowatt which was based upon name-plate turbine-generator capacity, are given in Table I. The better thermal economy of the reheat installation is reflected in smaller boilers, condensers, boiler feed pumps, piping, etc., all of which have been evaluated in arriving at the total cost of the reheat plant.

Throttle Conditions. Plants A, B, and C were assigned the 1300-psi 950 F throttle condition in comparing the battery boiler system with the unit system, since use of higher steam conditions would have increased piping costs to a disproportionate extent, and unduly penalized the battery boiler system. Detroit Edison installed two 100-mw 1300-psi 950 F turbine-generators and four boilers at Trenton Channel power plant during 1949, for which accurate cost data are available. Also, two similar machines with the same steam conditions, together with four boilers, will be installed for service at the Connors Creek plant in 1951.

In setting up the reheat installation, plant D, an effort was made to choose conditions which were high enough to favor a reheat cycle and yet which were somewhat comparable with the nonreheat condition. The 1450-psi operating steam pressure seems to be popular because the cost of turbine-generators for 1450 psi apparently is no more than for 850 psi, assuming the same temperature for both pressures. Subsequent studies may investigate the economic advantages of reheat and nonreheat installations with equivalent throttle conditions.

Boiler Capacity and Arrangement. Of the 970,000-lb per hr boilers in plants A and B, each has approximately 10 per cent excess steam-generating capacity over the maximum steam requirements of one 100-mw turbine-generator. In the battery boiler system of plant A one spare boiler was provided, and all boilers supply steam to a common main steam header. Provision of more boilers of a smaller size in the battery boiler scheme was not included since it was determined that more boilers would involve a higher cost with no compensating economic return. Plant B has four entirely separate unit boiler-turbine combinations, while plant C is laid out as a unit system with sufficient crossover piping so that any of the four boilers can supply steam to any of the four turbines. The 1,100,000-lb per hr boilers were sized so that any three boilers can supply sufficient steam to carry rated load, 100 mw, on each of the four turbine-generators. The larger boilers are desirable to secure a higher average plant availability made possible by the crossover.

The reheat boilers in plant D are comparable with those in plant B in that about 10 per cent excess steam-generating capacity over maximum turbine requirements is provided and the four boiler-turbine units are entirely separate.

Pump and Heater Arrangement. The arrangement of the pumps and heaters for all plants is essentially the same. Each turbine has two full-size condenser pumps and three half-size combination boiler feed and heater feed pumps. Five feedwater

¹ Engineering Department, The Detroit Edison Company. Mem. ASME.

Contributed by the Power Division and presented at the Annual Meeting, New York, N. Y., November 27-December 2, 1949, of THE AMERICAN SOCIETY OF MECHANICAL ENGINEERS.

NOTE: Statements and opinions advanced in papers are to be understood as individual expressions of their authors and not those of the Society. Paper No. 49-A-100.

TABLE 1 COMPARISON OF NEW PLANT BOILER-TURBINE ARRANGEMENTS; NAME-PLATE CAPACITY 400 MW
(Four 100-mw turbine generators)

Plant Designation	A	B	C	D
	Battery Boiler System 5-970,000 lb per hr boilers	Unit System - No Crossover 4-970,000 lb per hr boilers	Unit System - With Crossover 4-1,100,000 lb. per hr boilers	Unit System - Reheat No Crossover 4-800,000 lb per hr boilers
Throttle Conditions	1300 psi - 950 F	1300 psi - 950 F	1300 psi - 950 F	1450 psi - 1000 F - 1000 F
Total Plant Cost	\$ 72,000,000	\$ 65,751,000	\$ 67,805,000	\$ 67,612,000
Cost per kw	\$ 180.00	\$ 164.40	\$ 169.50	\$ 169.05
Annual fixed charge per kw based on a 10 per cent fixed charge rate	18.00	16.44	16.95	16.91
Availability, per cent				
Maintenance Schedule A - Single Shift	95.2	90.4	93.8	90.4
5 week tri-annual turbine overhaul				
2 week annual boiler overhaul				
1 1/2 week annual boiler inspection				
Maintenance Schedule B - Double Shift on Overhauls	96.9	94.2	96.0	94.2
2 1/2 week tri-annual turbine overhaul				
1 week annual boiler overhaul				
1 week annual boiler inspection				
Average annual available capacity based on a maximum net turbine capability of 113,000 kw	430,300	408,600	424,000	408,600
Maintenance Schedule A, kw	430,000	425,800	434,000	425,800
Maintenance Schedule B, kw				

HAB

heate
six he

The
has be
cause
trend
loads.

The
peak l
ble to
summe
circula
a redu
mainin
availa
system
are 75
the an

Man
nance
tenanc
period
report
tenanc
schedu
nance,
Each s
hours

TABLE

Sch
Un

The
person
the bo
period
ticipat
day fo
mainte
acid-ch
stalled

The
outage
of such
require

The
one co
utilitie
indicat

Ava
A four
operat
schedu
assum
in Tab

Tu
August

heaters are provided for the turbines in plants A, B, and C whereas six heaters are provided for the reheat turbines in plant D.

PLANT AVAILABILITY

The scheduling of Detroit Edison turbine-generator overhauls has become increasingly difficult during the postwar years because summer peak loads have shown a pronounced upward trend and are now about 88 per cent of the previous winter peak loads.

The 12 per cent difference between the summer and winter peak loads represents the theoretical amount of capacity available to accommodate equipment maintenance and overhaul in the summer. All of this margin is not available, however, as higher circulating-water temperatures during the summer months cause a reduction in machine capacity of about 4 per cent. The remaining 8 per cent of the winter peak, which is about 120 mw, is available for summer maintenance. Overhaul scheduling for a system which includes 28 turbine generators, many of which are 75 and 100 mw capacity, is seriously affected, therefore, by the anticipated availability of the various machines.

Maintenance Schedules. In establishing a new plant-maintenance schedule, it is necessary to forecast the average maintenance time for the boilers and turbines for a minimum 35-year period. Operating records for equipment in the system and reports of other companies provide a basis for assuming maintenance schedules. For the purposes of this analysis, two schedules have been used: one based upon single-shift maintenance, and the other on double-shift maintenance (Table 2). Each schedule provides approximately the same number of man-hours for the equipment overhauls and inspections.

TABLE 2 MAINTENANCE SCHEDULES, BASED UPON 35 YEARS OF OPERATION

	Schedule A single shift	Schedule B double shift
Scheduled outages:		
Turbine overhaul, triannual.....	5 weeks	2½ weeks
Boiler overhaul, annual.....	2 weeks	1 week
Boiler inspection, annual.....	1½ weeks	1 week
Unscheduled outages:		
Turbine forced outage, annual.....	2 days	2 days
Turbine maintenance, annual.....	2 days	2 days
Boiler forced outage, annual.....	½ day	½ day

The annual boiler-inspection period gives the maintenance personnel an opportunity to check thoroughly the condition of the boiler and to make necessary repairs. With an inspection period scheduled about 6 months after a boiler overhaul, it is anticipated that no other boiler outages will occur, except the ½-day forced outage per year. In setting up the lifetime boiler-maintenance schedules, it was assumed that all boilers would be acid-cleaned, and that a spare coal-pulverizing mill would be installed so that no boiler outage will result from mill maintenance.

The allowance thus made for unscheduled turbine-maintenance outage is to cover minor repairs, or adjustments, or other troubles of such a nature that immediate outage is not caused but which require correction within a reasonable length of time.

These two schedules represent possible practice on the part of one company. Other maintenance practices in force in other utilities² will have an important bearing upon availability as is indicated by the difference between schedules A and B.

Availability Calculation for a Four Turbine-Four Boiler Plant. A four turbine-four boiler plant arranged on a unit-system basis, operating with a single-shift maintenance schedule, such as schedule A, would have availability over a typical 3-year period, assuming best coincidence of boiler and turbine repairs as given in Table 3.

TABLE 3 AVAILABILITY OF FOUR TURBINE-FOUR BOILER PLANT

Scheduled outages:	
1st year	
One turbine and one boiler overhaul.....	5 weeks
Three boiler overhauls.....	6 weeks
Four boiler inspections.....	6 weeks
Total for 1st year.....	17 weeks
2nd year	
Same as 1st year.....	17 weeks
Total for 2nd year.....	17 weeks
3rd year	
Two turbine and two boiler overhauls.....	10 weeks
Two boiler overhauls.....	4 weeks
Four boiler inspections.....	6 weeks
Total for 3rd year.....	20 weeks
Average scheduled outages per year.....	18 weeks
Unscheduled outages, per year:	
Boiler forced outage.....	2 days
Turbine forced outage.....	8 days
Turbine maintenance outage.....	0 days
Average unscheduled outage per year.....	2 weeks
Total outage per year.....	20 weeks

$$\text{Availability} = 100 \left[1 - \frac{20}{52 \times 4} \right] = 90.4 \text{ per cent}$$

In these calculations, the effect of increase in frequency of forced outage due to addition of forced boiler outage to the forced turbine outage in the unit system is minimized, since average capacity of the several plants is based only upon availability. If the total reserve against forced outage were computed by probability methods, the increase in reserve required by the greater frequency of outage of the unit system would be a significant amount.³ The extra reserve capacity so determined would be added to the increase in reserve needed for summer maintenance for the unit system as indicated herein, to make all plants equivalent in average available capacity.

The availability figures for all plans under consideration and for both maintenance schedules are shown in Table 1.

CAPACITY CHARGES

In studying the merits of the four plant designs shown in Table 1, it is desirable to make each design comparable with the other from a capacity standpoint. As is shown in Table 1, plant A with its battery boiler system, has the best availability and hence the highest average available capacity. Conversely, plants B and D, designed as unit systems without crossover piping, have the poorest availability and the lowest average available capacity. The difference in the average available capacity should be considered if, as pointed out heretofore, maintenance schedules require that summer peak loads must be met with reserves no better than under winter peak-load conditions. With the latter, it is assumed in all schemes that full capacity is available. The capacity charge is determined by applying fixed charges on the investment required to provide the difference in average available capacity, as indicated by the following example:

Method of Calculation. With maintenance schedule A in effect, plant A has a 430,300-kw average available capacity, which is 21,700 kw more than the 408,600-kw average capacity of plant B. One means of making these two plants equivalent would be to install 21,700 kw of additional capacity in plant B. The cost of this capacity at \$164.40 per kilowatt for plant B would be about \$3,570,000. Annual fixed charges on this investment, which include taxes, insurance, depreciation, and interest, would be \$357,000. As is demonstrated in this simple calculation, the amount of the capacity charge is influenced by equipment availability, the cost of the new capacity involved, and the fixed-charge rate.

Partial Capacity Charges. The annual capacity charge of \$357,000 computed in the foregoing represents a 100 per cent capacity charge. This assumes that each year plant B is in

² Turbine and Boiler Overhaul Practice, EEI Publication No. R-13, August, 1949.

³ "Outage Expectancy as a Basis for Generator Reserve" by H. P. Seelye, Trans. AIEE, vol. 66, 1947, pp 1483-1488.

service will be one during which a close maintenance schedule is in effect wherein careful consideration must be given to peak loads during the summer months as well as during the winter months. Furthermore, it is assumed that added system capability correctly matches load growth, and only a minimum amount of reserve capacity is available at all times.

The likelihood that all of the years in the life of a power plant will be prosperous ones, during which power loads remain high, is remote. Past experience indicates that there will be depression years, during which peak loads tend to fall off, and with these lower loads machine availability becomes less important. In depression years, capacity reserves are high, and therefore capacity charges do not seem justified. Because of this condition, it is postulated that a partial charge should be made against the plant designs which have poorer machine availability.

In many cases reserve capacity might be bought from interconnected systems during the close maintenance years, thereby saving the charges during depression years. Then too, a company interconnected to a system which generates hydropower might arrange the purchase of excess power during the summer months. It is recognized, however, that reserve capacity or power purchase agreements are often on a short-term basis, and may not cover the life of a plant.

The contention that capacity charges should be made only when the amount of capacity involved is influential in deciding when to install an additional machine, should be considered. Actually, many factors are involved in establishing the amount of capacity which has sufficient effect on the system to warrant installation of a new machine, and hence to require a special capacity charge. Some of these factors are matters of policy, such as reserve allowance and equipment maintenance, while others pertain to conditions under which a company is operating, i.e., system size, interconnections, machine sizes, load characteristics, etc. In one case the deficiency of 21,700 kw of capacity, which is the difference between that provided by plants A and B, could require the installation of new capacity, while in some other case the deficiency of this amount of capacity might not affect the expansion policies of the company.

Thus it is evident that conditions may require a full 100 per cent capacity charge, whereas others require none at all. This study therefore includes capacity-charge rates of 0, 50, and 100 per cent.

ANNUAL OVER-ALL COSTS

In developing the annual costs for the plants, four basic cost items were considered. These were (1) the fixed charges on the investment, (2) coal costs, (3) labor costs, and (4) capacity charges.

Fixed Charges. Annual fixed charges which include property taxes, insurance, depreciation, and interest were computed at 10 per cent on the investments.

Income taxes were not included as a fixed-charge item since they are associated with revenue rather than with investment. The economies of one plant design over another is not necessarily subject to income taxes as these savings might be considered applied to rate reductions, for averaging out with less profitable phases of the business, or to offset increasing costs without rate increases. It would appear that income taxes should be considered on completion of the analysis, so that the effect of such items as coal and labor costs can be included. No deductions for income taxes have been applied in this study.

Coal Costs. The basic coal cost assumed in this study was 25.8 cents per million Btu, representing a coal having 11,800 Btu per lb heating value and a long-range cost of \$6.10 per ton delivered.

Since it is extremely difficult to forecast long-term coal costs, one of the annual operating-cost comparisons was made holding the annual plant factor constant while varying coal costs from 16 to 32 cents per million Btu.

In computing the coal costs for the various plants, it was assumed that for a specific annual plant factor the same number of kilowatthours would be required by the system. The base generation therefore would be equal to the net plant capability times per cent availability of the battery boiler system times annual plant factor. It is assumed that the net plant capability is 113 mw per machine, or 452 mw for the plant. A plant with a poorer availability would be unable to produce all of the required generation and therefore some kilowatthours would be supplied by less efficient machines on the system. The foregoing does not include a capacity charge. With a 50 per cent capacity charge, only one half of the generation deficiency need be transferred to the less efficient capacity. If a 100 per cent capacity charge is made, it may be assumed that all of the required kilowatthours will be generated on high economy capacity. The charge against plants with poorer availability will depend upon the heat rates of the machines to which the generation is transferred.

Labor Costs. In a new plant with centralized control features, modern coal-handling equipment, and large turbines and boilers, the number of men per megawatt of capacity is considerably less than found in many existing plants. It was estimated that the labor complement, including operating and maintenance personnel, for plant A would be about 210 men. Plant C, with its unit system and crossover, has one less boiler to overhaul each year and therefore requires fewer maintenance personnel. It was assumed that more boiler-maintenance overtime or additional maintenance personnel would be required in plants B and D, as compared to plant C, as boiler outage means turbine outage in plants B and D.

Based upon the foregoing, the assumed labor costs, including wages and such items as social security, pensions, insurance, etc., for each plant are given in Table 4.

TABLE 4 ASSUMED LABOR COSTS

Designation	Plant Description	Annual labor cost—	
		Maintenance schedule A	Maintenance schedule B
A	Battery boiler system	\$830000	\$830000
B	Unit system—no crossover	813000	843000
C	Unit system—crossover	802000	802000
D	Unit system—reheat	813000	843000

Capacity Charges. Operating cost data are presented for three different capacity charge rates, 0, 50, and 100 per cent. The method of computing these charges and a brief discussion of the reasons for including them in an economic analysis which involves equipment with different availabilities was presented earlier in the paper.

Annual Operating-Cost Comparisons. Table 5 presents the annual operating-cost comparisons for the four plants under consideration, assuming a 70 per cent annual-plant factor and a coal cost of 25.8 cents per million Btu. The annual plant factor is the ratio of the kilowatthours generated on the machine in a year to the product of the kilowatt name-plate rating \times 8760 hr. Total operating costs are shown for both maintenance schedules and the three selected capacity charge rates, 0, 50, and 100 per cent. In all cases the cost of operating the battery boiler system that is, plant A, was found to be the highest and therefore this arrangement was used as a basis for comparison. The savings over the cost of operating plant A are shown for the other three plants.

COMPARISON OF PLANT OPERATING COSTS

The curves drawn in Figs. 1, 2, and 3 offer a means of comparing the plants from the standpoint of total operating costs. These

TABLE 3 COMPARISON OF NEW PLANT BOILER-TURBINE ARRANGEMENT: NAME-PLATE CAPACITY 400 MW
(Four 100-mw turbine generators)

Plant Designation	A Battery Boiler System 8-970,000 lb per hr boilers				B Unit System - No Crossover 4-1,100,000 lb per hr boilers				C Unit System - With Crossover 4-1,100,000 lb per hr boilers				D Unit System - Reheat No Crossover 4-800,000 lb per hr boilers			
Annual Cost of Operation - Maintenance Schedule A 70% APF - No Capacity Charges	Fixed Charges	\$ 7,200,000			\$ 6,575,000				\$ 6,780,000				\$ 6,762,000			
	Coal Cost	6,518,000			6,518,000				6,562,000				6,359,000			
	Labor Cost	830,000			830,000				802,000				813,000			
	Capacity Charge	0			0				0				0			
	Total Annual Cost	\$ 14,548,000			\$ 14,060,000				\$ 14,164,000				\$ 13,934,000			
Maintenance Schedule A 70% APF - 50% Capacity Charges	Fixed Charges				\$ 489,000				\$ 404,000				\$ 614,000			
	Coal Cost				\$ 6,575,000				\$ 6,780,000				\$ 6,762,000			
	Labor Cost				6,518,000				6,539,000				6,274,000			
	Capacity Charge				830,000				813,000				813,000			
	Total Annual Cost				\$ 14,548,000				\$ 14,175,000				\$ 14,032,000			
Maintenance Schedule A 70% APF - 100% Capacity Charges	Fixed Charges				\$ 397,000				\$ 373,000				\$ 516,000			
	Coal Cost				\$ 6,575,000				\$ 6,780,000				\$ 6,762,000			
	Labor Cost				6,518,000				6,518,000				6,189,000			
	Capacity Charge				830,000				813,000				813,000			
	Total Annual Cost				\$ 14,548,000				\$ 14,227,000				\$ 14,131,000			
Maintenance Schedule B 70% APF - No Capacity Charges	Fixed Charges				\$ 285,000				\$ 341,000				\$ 417,000			
	Coal Cost				\$ 6,575,000				\$ 6,780,000				\$ 6,762,000			
	Labor Cost				6,518,000				6,546,000				6,284,000			
	Capacity Charge				830,000				802,000				843,000			
	Total Annual Cost				\$ 14,548,000				\$ 14,148,000				\$ 13,869,000			
Maintenance Schedule B 70% APF - 50% Capacity Charges	Fixed Charges				\$ 525,000				\$ 420,000				\$ 659,000			
	Coal Cost				\$ 6,575,000				\$ 6,780,000				\$ 6,762,000			
	Labor Cost				6,518,000				6,531,000				6,237,000			
	Capacity Charge				830,000				802,000				843,000			
	Total Annual Cost				\$ 14,548,000				\$ 14,168,000				\$ 13,945,000			
Maintenance Schedule B 70% APF - 100% Capacity Charges	Fixed Charges				\$ 469,000				\$ 400,000				\$ 603,000			
	Coal Cost				\$ 6,575,000				\$ 6,780,000				\$ 6,762,000			
	Labor Cost				6,518,000				6,518,000				6,189,000			
	Capacity Charge				830,000				802,000				843,000			
	Total Annual Cost				\$ 14,548,000				\$ 14,137,000				\$ 14,000,000			
Saving over Battery Boiler System					\$ 411,000				\$ 360,000				\$ 448,000			

Coal cost assumed at 25.8 cents per million Btu.

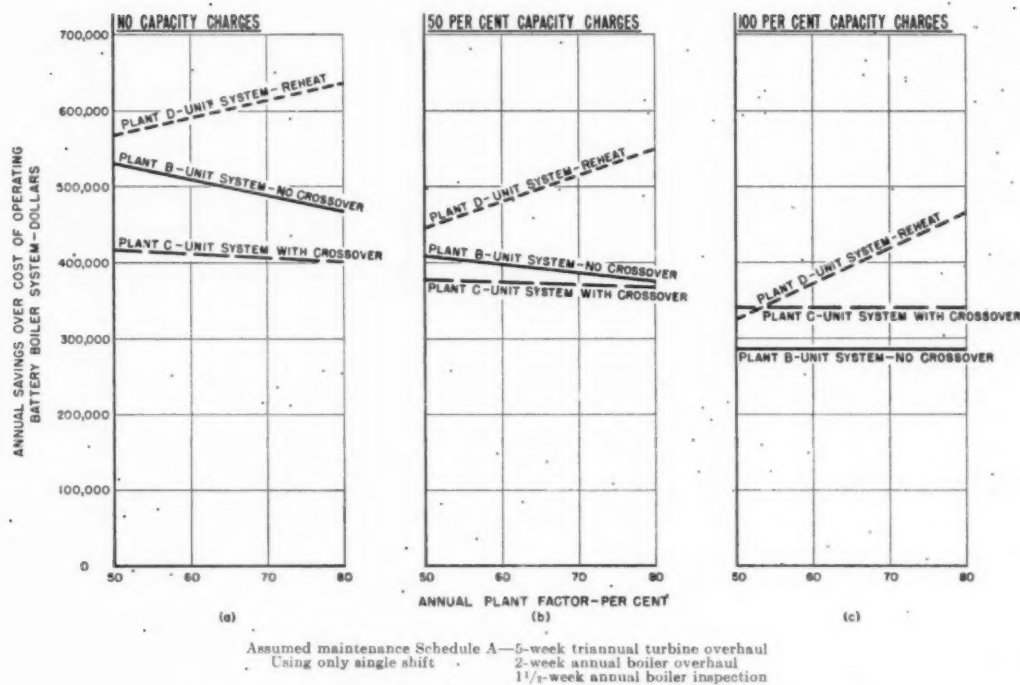


FIG. 1 BOILER-TURBINE ARRANGEMENT COMPARISON—MAINTENANCE SCHEDULE A
(Each arrangement has four 100-mw turbines and boiler capacity as shown in Table 1. Assumed coal cost 25.8 cents per million Btu.)

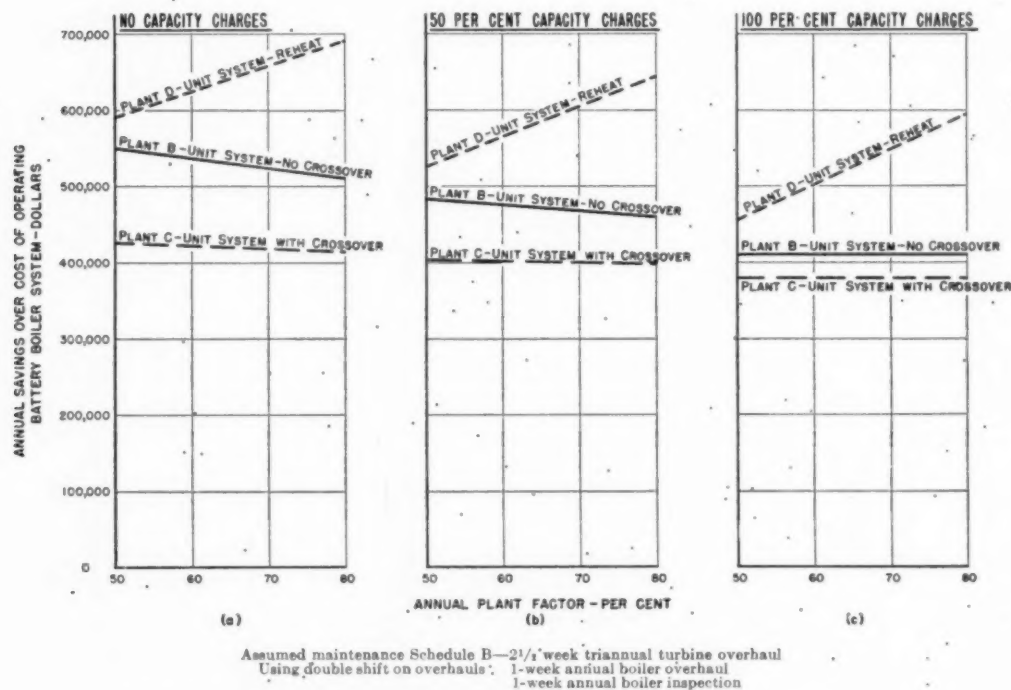


FIG. 2 BOILER-TURBINE ARRANGEMENT COMPARISON—MAINTENANCE SCHEDULE B
(Each arrangement has four 100-mw turbines and boiler capacity as shown in Table 1. Assumed coal cost 25.8 cents per million Btu.)

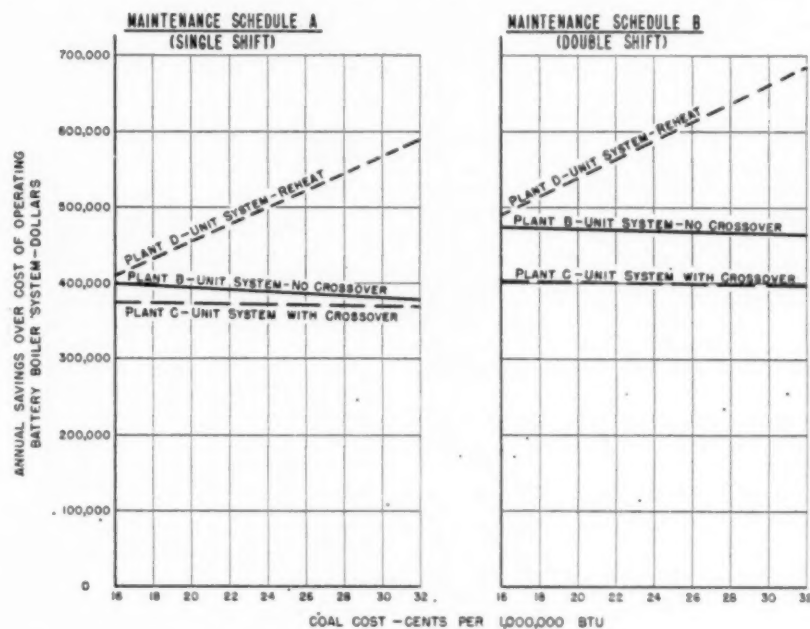


FIG. 3 BOILER-TURBINE-ARRANGEMENT COMPARISON; EFFECT OF COAL COSTS ON RELATIVE POSITIONS OF ARRANGEMENTS UNDER CONSIDERATION
(Assumptions: 50 per cent capacity charges; 70 per cent annual plant factor.)

curves show the effect of including capacity charges, of varying the annual plant factor, of shortening the maintenance time on boilers and turbine generators, and of varying the coal costs. In drawing these curves, the unit-system plants, with and without the crossover, and with reheat, are compared with the cost of operating a battery boiler plant.

For example, it might be concluded that the new plant would operate under the following conditions over its useful life:

- 1 Maintenance schedule A.
- 2 Capacity charge, 50 per cent.
- 3 Annual plant factor, 70 per cent.
- 4 Coal cost, 25.8 cents per million Btu.

Fig. 1(b), which presents curves based upon these assumptions, shows that the operating costs for a reheat installation would be \$135,000 less per year than the annual costs for a 1300-psi 950 F unit system with no reheat. Over a 35-year period, which might represent the minimum life of the equipment from an obsolescence standpoint, this saving would amount to \$4,725,000. In comparing the costs of plants B and C, which should reflect the added cost of the crossover and larger boilers, it appears that the installation of a unit system could not necessarily be justified on the basis of economics alone, as the saving is only about \$13,000 per year. The choice between these two designs might be decided on the basis of operating flexibility, or possibly the difference in the total investment.

Effect of Capacity-Charge Variation. Including capacity charges in the comparison of two plant designs favors the plant with the highest availability. This relationship is clearly shown in Fig. 1 wherein plants B and C are compared for 0, 50, and 100 per cent capacity-charge rates. When no capacity charges are assessed, plant B, unit system without crossover, has a significant advantage over the unit system with a crossover installation, plant C. The relative position of the curves for these two plants is reversed, however, when 100 per cent capacity charges are in-

cluded. In Fig. 2, where maintenance schedule B is in effect, the savings curves for plants B and C tend to come together as capacity charges are included, but do not reverse positions. The variation in the effect of including the capacity charges results from the difference in availability under the two maintenance schedules.

The curves for plant B, for instance, tend to become horizontal as the capacity-charge rate is increased, because the amount of generation transferred to low-economy equipment varies inversely with capacity charges.

Effect of Annual Plant-Factor Variation. As the annual plant factor for a comparatively low-availability installation, such as has been assumed in plants B and D, is increased, the amount of generation transferred to low-economy machines must be increased. This means that increasing the annual plant factor reduces the savings for unit-system plants. In the case of the high-economy reheat plant, the loss of savings due to generation transfer is more than offset by fuel savings at high load factors. This accounts for the divergence of the curves for plants B and D in Figs. 1 and 2.

The reheat machines would probably have higher annual plant factors than the 1300-psi 950 F machines in the other plants, since the lower heat-rate capacity would carry more of the off-peak loads. A credit which would reflect the added coal savings made possible by a higher-use-factor reheat plant could be computed and included in the coal-cost calculations. This factor is not included, however, since the amount involved is relatively small and is dependent upon the questionable accuracy of long-term load growth and daily load-curve assumptions. On the other hand, if reheat machines are operated over any considerable part of their life at loads below 75 per cent of their name-plate rating, consideration should be given to possible reduction in thermal economy at such loads.

Effect of Changing the Maintenance Schedule. Reducing the number of days the boilers and turbines are out of service for gen-

eral maintenance, improves the savings rate of all unit-system plants. This improvement is more pronounced in the case of plants B and D where equipment availability is low. The amount of time required for boiler overhauls and inspections has more effect on the operating expenses of the unit-system plants than the time required for turbine maintenance. This conclusion is based upon an analysis of a third maintenance schedule which required double-shift boiler maintenance and single-shift turbine maintenance. Detailed calculations on this schedule have been omitted from this analysis to avoid complicating the presentation.

The schedules for general maintenance of boilers and associated auxiliaries are matters of individual preference resulting from operation of a variety of equipment. This is another of the factors on which a single value acceptable to the industry cannot be specified.

Effect of Coal-Cost Variation. A change in cost of coal has a pronounced effect on the savings made possible in a reheat plant. Fig. 3, drawn for a 70 per cent annual plant factor and a 50 per cent capacity-charge rate, shows that the savings from a reheat plant increase sharply as the cost of coal increases. This increase occurs under both maintenance-schedule assumptions. The heat-rate savings in the reheat plant offset the loss of savings which is common to each of the unit-system plants. These small reductions in savings which result in a slight negative slope of the

curves for plants B and C are caused by the increased cost of generating the kilowatthours transferred to low-economy machines.

CONCLUSIONS

In so far as conclusions can be reached on a partial study, it is evident that assignment of fixed charges where justified by minimum reserve capacity, may have a pronounced effect on the cost of operation of the four types of plants considered. Likewise, variation in annual plant factor, single or double-shift maintenance, and increase in coal cost all have a significant influence on the annual operating cost.

Figs. 1, 2, and 3 are based upon the substantial savings to be realized by the unit system, the unit system with crossover, or the reheat installation as compared with the battery boiler system. It is believed that the trend toward the unit system can be explained in part at least by this comparison.

The reheat installation appears favorable economically in all cases, although if 100 per cent capacity charges are assigned, and annual plant factors of 60 per cent or lower are used, the savings in favor of reheat are considerably reduced. In this case, any extra complexity in operation, possible reduction in coal cost, or long-time partial-load operation at less than 75 per cent name-plate rating, would militate against a reheat installation.

S

I
Lig
kw
stal
Thi
for
upo
econ
life

I
as N
that
Desi
lecte
and

In
used
60,00
1939
coal
first
tion
were
for in
million
increa
most
As
modat
stand
900 F
bodyin
bility
cles.

The
timate

¹ Ser
Compa
² Ass
and Po
Cont
Meetin
AMERIC
NOT
derstoo
the Soc

Selection of Steam Conditions for No. 4 Unit— Riverside Generating Station

By R. C. DANNETTEL,¹ AND G. S. HARRIS,² BALTIMORE, MD.

In the summer of 1948, the Consolidated Gas Electric Light and Power Company of Baltimore ordered a 75,000-kw-capability, 3600-rpm, straight-condensing unit for installation as No. 4 Unit in its Riverside Generating Station. This selection was made after consideration of units both for straight-condensing and reheat cycles and was based upon judgment that the nonreheat unit should be more economical in total dollar costs to the company during the life of the unit.

IN THE summer of 1948, the Consolidated Gas Electric Light and Power Company of Baltimore ordered a 75,000-kw-capability, 3600-rpm, straight-condensing unit for installation as No. 4 Unit in its Riverside Generating Station. It is expected that this machine will be placed in operation in the fall of 1951. Design throttle steam conditions of 1450 psig, 1050 F were selected after consideration was given to the following sizes of units and operating conditions:

- 66,000-kw capability, 850 psig, 900 F
- 75,000-kw capability, 1250 psig, 950 F,
with reheat to 950 F
- 75,000-kw capability, 1450 psig, 1000 F,
with reheat to 1000 F
- 75,000-kw capability, 1450 psig, 1050 F

In the study leading to the final selection, the 850-psi unit was used as a measuring stick. The company has in operation four 60,000-kw, 850 psi units which were ordered in the period from 1939 to 1946, and which represented the economic selection for the coal market and equipment market of that period. When the first of this series of units was placed in service at Westport Station in 1941, the fuel cost per million Btu and construction costs were such that it was not economical to spend additional money for improvement in heat rate. By 1948, however, the cost per million Btu had practically doubled, and construction costs had increased sufficiently to warrant a careful reconsideration of the most economical steam conditions.

As a unit with 75,000-kw maximum capability could be accommodated by the system, the study centered around a "preferred standard" 60,000-kw unit with 66,000-kw capability for 850-psig 900 F steam conditions, and three alternative arrangements embodying 60,000-kw, nominally rated, 75,000-kw, maximum-capability units both for straight-through condensing and reheat cycles.

CONSTRUCTION-COST ESTIMATES

The first step involved the preparation of construction-cost estimates. These were carefully made by bringing up to date the

¹ Senior Engineer, Consolidated Gas Electric Light and Power Company of Baltimore. Mem. ASME.

² Assistant Electrical Engineer, Consolidated Gas Electric Light and Power Company of Baltimore. Mem. ASME.

Contributed by the Power Division and presented at the Annual Meeting, New York, N. Y., November 27–December 2, 1949, of THE AMERICAN SOCIETY OF MECHANICAL ENGINEERS.

NOTE: Statements and opinions advanced in papers are to be understood as individual expressions of their authors and not those of the Society. Paper No. 49-A-62.

actual costs of preceding units in the station and substituting current bids for those items affected by change in size and heat balance. The result was somewhat surprising since it indicated a spread of less than 2 per cent in the cost per kilowatt of capability. The 1250-psig 950/950 F unit showed the lowest installation cost per kilowatt of capability with the 1450-psig, 1050 F, straight-condensing unit a very close second. The 1450-psig 1000/1000 F design showed the highest installation cost. Fixed charges were of course in the same order. Computation of fixed charges included consideration of return on the investment, depreciation, property taxes, and income taxes based upon three methods of financing the project, that is, by bonds, by stock, and from surplus.

OPERATING COSTS

The next step was an investigation of operating costs. The heat rates showed a wide range with the 1450-psig 1000/1000 F design about 12½ per cent better than the 850-psi unit. There were, however, a number of corollary problems to be disposed of before operating costs could be set down in terms of dollars per year.

The question of operating labor proved to be easy to solve since it is not planned to augment the operating force at the station to take care of this unit, regardless of its size or steam conditions.

Perhaps the most difficult problem in the determination of operating costs was the selection of annual generation on which to base fuel costs. It was realized that load-duration curves would be of little value since, with units differing somewhat in capability, the load-duration curves would have corresponding differences. The matter was settled by arbitrarily using 6000 hr operation at 66,000 kw for all units.

The cost per ton of fuel is of course a variable and was handled by computing the annual fuel cost for each unit over a wide range of fuel prices.

In order to combine all of these factors and find a parameter for comparison of the units, a curve sheet, Fig. 1, was prepared with

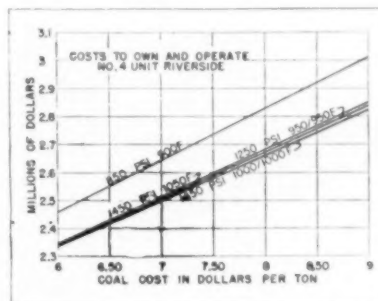


FIG. 1 COSTS TO OWN AND OPERATE NO. 4 UNIT RIVERSIDE

the cost to "own and operate" plotted as ordinates and with the cost of coal in dollars per ton as abscissas. The cost to own and operate was, for the purpose of this study, considered to be the sum of fixed charges and fuel costs. Because of the annual generation selected, the fixed charges for the 75,000-kw units were re-

duced proportionately to 66,000 kw for comparison purposes. The coal cost in dollars per ton can be interpreted as the cost of coal delivered to the bunker. The cost of coal at the time the study was made amounted to about \$8.50 per ton. It was found that with the cost to own and operate approximately \$3,000,000 per year, there was a spread of about \$180,000 or about 6 per cent, Fig. 2. The highest cost was for the 850-psig 900 F unit; the

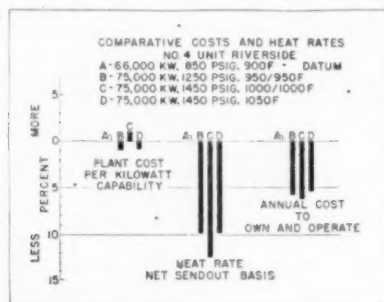


FIG. 2 COMPARATIVE COSTS AND HEAT RATES NO. 4 UNIT RIVERSIDE

lowest cost was for the 75,000-kw, 1450-psig 1000/1000 F unit. The annual cost to own and operate the 75,000-kw, 1450-psig, 1050 F straight-condensing unit was computed to be about \$24,000 above that of the 1000 F reheat unit.

The difference in cost to own and operate was considered to be within the limits of accuracy of estimating and led to the opinion that the 1450-psig 1050 F, straight-condensing unit, and the 1450-psig 1000/1000 F unit could be considered on the same basis

in so far as total expense for fuel and fixed charges was concerned. The final selection then rested on judgment as to availability, reliability, and maintenance.

AVAILABILITY, RELIABILITY, AND MAINTENANCE

The control gear for a reheat unit is sufficiently complicated to lessen reliability somewhat; the unit could not so readily adapt itself to the sudden changes in load which may be expected with system disturbances; and the unit could not be used to regulate frequency on the system. The multiplicity of piping and controls to and from the reheat turbine might well add to station maintenance. Two superheaters and superheat controls would be needed. For the Riverside unit, where the selection of the boiler was influenced by the obvious savings in engineering costs made possible by duplicating the furnace and mill arrangement of other units in the station, one of these controls would be a spray desuperheater which has undesirable features. The gains from reheat are doubtful during the light-load operation which can be expected as the unit ages. Steam and fuel would be wasted at times to protect the reheater from overheating.

The nonreheat unit has a single superheater and control and a minimum of high-temperature piping and valves. The use of 1050 F presents no serious metallurgical problems. This plant should require less maintenance than a reheat unit and should therefore be less expensive to operate.

In comparison with reheat units, the 1450-psig, 1050 F-straight-condensing unit should be simpler to install and operate; with less controls should be more reliable and available; should be more adaptable during system disturbances and for frequency regulation; and, considering maintenance and probable light-load operation, should be more economical in total dollar costs to the company during the life of the unit.

A Comparison of Costs of Reheat Versus Nonreheat for 100-Mw Units

By R. P. MOORE,¹ BUFFALO, N. Y.

This paper analyzes the differences in cost of the various elements of a steam-electric power plant, as affected by choice of the reheat or nonreheat cycle applied to units of about 100,000-kw capability.

ANY economic study, the object of which is to ascertain whether or not the use of the reheat cycle in a proposed steam-power-plant development is justified, necessarily must start with differences in capital investment. These then can be compared to the improvement in plant efficiency to be expected from the use of reheat.

The author does not attempt, in this study, to cover all possible combinations of size of unit, plant arrangement, pressures, temperatures, and the like. The data contained herein, while presented in as general a form as possible, are based upon units of 100-mw capability in a single boiler-single turbine arrangement with throttle steam at 1450 psig, superheated and reheated to 1000 F. The reheat turbines are reverse-flow, double-flow, single-shaft, tandem-compound units for 3600 rpm, with bleeding for regenerative heating. They are compared to nonreheat units of similar arrangement, except that the steam passes straight through from throttle to condenser. The fuel is pulverized bituminous coal. Mechanical dust collectors are used.

COST ELEMENTS OF REHEAT CYCLE

The use of reheat affects the original cost of various parts of a steam-electric power plant in different ways. If it is assumed that the capability of the plant is to be the same whether the cycle is reheat or nonreheat, then the boiler plant and parts pertaining to it, excepting the boiler itself, would cost less. This is a direct result of the improved fuel economy. Certain other parts would cost even less than is indicated by the improvement in cycle efficiency. These are the parts carrying the cycle fluid, such as the feedwater system and the condensing system. The generator and the main bus and switch structure are unaffected by the choice of cycle. Finally, there are parts that cost more. Table 1 divides the main items of a plant into these four categories.

Opinions will differ as to the category in which some of the items should be placed. Certainly all of the items in any one of the groups will not follow exactly the same formula in figuring differences in the cost of equipment for the two cycles. A few examples will serve to illustrate.

1 Most pieces of equipment are built in standard sizes. Reducing the fuel requirements by adopting reheat may or may not permit the use of a smaller-size pulverizer, for instance. If it does, the step in cost may be greater than the step in required capacity. It is believed that plus and minus errors of this nature will essentially balance each other.

2 If the plant or unit under consideration is an extension of

existing facilities, there may be a number of items which, though they otherwise might be reduced in cost, must be extended as previously installed, without having advantage of savings possible in a new project.

3 Table 1 shows the condenser in the category, the size of which varies approximately with the heat rejection. However, the flow of steam through the last wheels of a reheat turbine is so much less than that through the corresponding nonreheat machine (if the same-size wheels are used) that the reheat turbine possibly can make better use of improved vacua and thereby justify a larger condenser than indicated by the flow. This, however, would seem to be a subject for a separate study involving, in addition, triple versus double flow.

TABLE 1 PLANT COMPONENTS FOR COST ESTIMATING

I Parts of a plant which vary in size generally inversely with cycle efficiency	
Coal storage	Dust collectors
Coal handling	Ash disposal
Fuel-burning equipment	Boilerhouse structure
Fans and ducts	Auxiliary electrical equipment
II Parts of a plant which vary more in size than efficiency would indicate:	
(A) Generally directly with the flow of cycle fluid:	
High-pressure steam pipe	
Condensate and boiler feed pumps	
Condensate and feedwater piping	
Bleeder heaters and piping	
(B) Generally directly with heat rejection to condenser:	
Condenser	
Circulating water pumps	
Intake and discharge flumes	
Screening equipment	
III Parts of a plant which are affected little, if any, by cycle efficiency:	
Land and improvements	Electrical structures
Generator and main transformer and connections	Evaporators
Metering and controls	Feedwater treatment
Turbine hall	Offices, locker rooms, shops, and administration space
IV Parts of a plant which cost more for reheat than for nonreheat, capability of unit remaining the same:	
Turbine	
Boiler	
Reheat piping	

GAIN IN ECONOMY OF REHEAT

Messrs. E. E. Harris and A. O. White² have shown that, for reheat pressures below 500 psia, the per cent gain in economy of reheat over nonreheat is 5 or better. Their figure² can be used for the purposes of this paper. The reduction of cycle fluid flow at full capacity is 16.4 per cent and of the heat rejection to the condenser 8.7 per cent, all other conditions, except for reheat remaining the same.

An examination of cost data on plants of the size described, both under construction and recently completed, reveals that at the present time the cost of those items listed in category I, Table 1, totals about \$22.50 per kw of capability. For category II(A), Table 1, the total cost is \$8, and for II(B) \$7.50 per kw of capability. These figures apply to nonreheat units. The cost of items in category III have no effect upon this discussion. For category

¹ Mechanical Engineer, Buffalo Niagara Electric Corporation. Mem. ASME.

Contributed by the Power Division and presented at the Annual Meeting, New York, N. Y., November 27-December 2, 1949, of THE AMERICAN SOCIETY OF MECHANICAL ENGINEERS.

NOTE: Statements and opinions advanced in papers are to be understood as individual expressions of their authors and not those of the Society. Paper No. 49-A-99.

² "Development in Resuperheating in Steam Power Plants," by E. E. Harris and A. O. White, Trans. ASME, vol. 71, 1949, pp. 685-691, Fig. 11.

IV, the difference in cost between reheat and nonreheat units is approximately \$3.88 per kw of capability.

The cost of power-plant equipment does not vary directly as its size, generally speaking. A machine having 10 per cent greater capacity than another does not cost 10 per cent more. Experience shows that a factor of about 0.7 applied to the difference in capacity will express the difference in cost. In other words, the machine having the 10 per cent greater capacity should cost approximately 1.07 times as much. This factor varies from 0.65 to 0.75, but experience indicates that 0.7 is a good figure for estimating purposes. Authority for it is not readily found outside of price books and quotations, but an article by Alfred Iddles² substantiates the figure.

Applying these data to the difference in cost between reheat and nonreheat the ledger stands as follows:

Credits:

For items in category I (Table 1)

$$22.50 \times 0.05 \times 0.7 = \$0.79 \text{ per kw}$$

² "Planning New Capacity," by Alfred Iddles, *Electrical World*, vol: 105, 1935, pp. 983-986.

For items in category II(A)

$$8.00 \times 0.164 \times 0.7 = 0.92$$

For items in category II(B)

$$7.40 \times 0.087 \times 0.7 = -0.45$$

Total credits for reheat..... \$2.16 per kw

Debits:

For items in category IV \$3.88

Total charges for reheat..... \$3.88

Net charge for reheat..... \$1.72 per kw

These figures apply only to new locations where presumably all possible savings can be made.

With coal costing \$7.50 per ton of 2000 lb, and a coal rate of 0.8 lb per kw-hr and 5000 hr per year use (57 per cent capacity factor), the saving per year using reheat instead of nonreheat would be \$0.75 per kw per year. After allowing 10 per cent for interest, insurance, and taxes, there remains \$0.58 which would write off the additional cost in 3 years. Even if coal cost only one half as much, the writeoff can be accomplished in 8 years if the capacity factor averages 57 per cent. No allowance is made for additional operation or maintenance as the author feels that none will be required.

General Discussion of Reheat Papers

LOUIS ELLIOTT.¹ Noting the decisions reached as to reheat versus regenerative cycle, in designing steam plants, and without knowing detailed conditions and special methods of reasoning, it sometimes appears that one engineer wants reheat and recommends it, for a relatively small turbine and moderate fuel costs, and another does not like reheat and rejects it, although the turbine in question is a large unit and fuel costs are relatively high. However, in most or all cases, a careful study is given to the economics of the cycle to be selected, as is evidenced by the three papers on this subject.^{2,3,4}

Considering that the use of reheat is one of the most important methods of improving steam-plant efficiency, aside from utilization of higher steam temperatures, the decision as to cycle is an important one, and warrants the closest attention. It is necessary, in arriving at a rational conclusion, to determine with some completeness the character of major equipment that would be used for the regenerative- or reheat-cycle plant, and obtain close estimates of cost. These estimates should of course include all elements in which there is a significant difference in investment. Similarly, careful study must be given to relative efficiencies, again taking into consideration all elements showing significant differences, and making sure that for each cycle the plant design and operation are quite thoroughly worked out.

It happens that no recommendation to a client, in which this discussor has been involved, has specified a reheat installation. It may be that this results from the fact that most of the turbine units have been in the moderate or smaller sizes, and that fuel costs on clients' properties have frequently been much lower than those prevailing in the North and East. Recommendations as to plant cycle have been made for a large number of turbines of the magnitude of 60 mw nominal rating—which have indeed been bought for clients in larger numbers than any other one size.

Ordinarily, the estimated saving in production costs, effected by the use of reheat, is expressed as a percentage of incremental investment for the reheat design. To justify reheat, percentage return on increase in investment should be somewhat higher than the normal assigned for charges on cost of station as a whole. In the first place, depreciation of a boiler plant is higher than the average on the entire station. In addition, a reheat plant involves greater complication, perhaps slightly greater expense for operation and maintenance, and possibly some little penalty in reliability.

With respect to magnitude of fixed charges, the papers under discussion show a wide range in allowances made—from 10 to 15 per cent—for all elements of fixed charges and taxes applying to power-station investment. It is now general practice to include, as an element of fixed charges and taxes, an allowance for federal income tax, and state income tax, if any, which must be earned before net return. Federal income tax may frequently be figured, conveniently, as a percentage of investment. It is usually necessary to obtain from management estimates or information on the following: Cost of money, or desired return; average proportion

of total capital that will be borrowed; average interest rate to be paid on borrowed capital; method of accounting for depreciation or amortization; life of plant or period of amortization to be assumed; ad valorem or other local taxes. Some of these data can be obtained from annual financial reports, but as the percentages required are those that may obtain through life of property or period of amortization, a new approach is desirable. With such basic values established, an equivalent constant percentage may be taken from annuity tables, covering cost of money plus allowance for depreciation or amortization.

The general subject of station design as affecting magnitude of reserve or system reliability, together with the economics of reheat, were discussed in the Wagner-Hartwell paper.⁵ Engineers should appreciate the careful analysis of the influence of plant design on system reserves and reliability. The mathematical process, based upon a mass of outage data and the long and consistent history of operation in large cities, certainly give interesting results, developing the effect of such elements as cross-connection of steam generators and provision of reserve boiler capacity in a large installation.

However, the writer is inclined to feel that, for the usual power system, the long-time influence of differences in design on magnitude of reserves required may be exaggerated. Indeed, it appears that in a good many cases undue stress is laid upon the highest reliability of utility plants, and that continuity of service is "over-sold." While New York and other great cities doubtless do call for special treatment, for the smaller cities and for interconnected systems covering large territories, it appears that adherence to a mathematical standard for reliability may be unwarranted.

Almost all the recommendations for plant design in which the writer has been involved have called for one steam generator per turbine generator, with no interconnection between boilers; this has applied to units up to 100 mw in size. There are tangible and intangible values in simplicity, and, aside from saving in investment cost, there is an element of ruggedness and reliability in the avoidance of steam and water interconnections.

G. A. TAYLOR.⁶ We have given a great deal of study to the Hartwell-Wagner paper² and have found that study very well worth while. The writer, with others, has set up a method of evaluating power-plant equipment that is very complete and has many unique features. We believe that this method can be used advantageously by all of us, but we must keep in mind that there are many conditions peculiar to each system. Care must be taken to evaluate these conditions properly.

The authors state that better thermal economy of the reheat installation is reflected in smaller boilers, etc. The boilers are smaller when rated in pounds of steam per hour. The boilers are about 5 per cent smaller when rated by heat input. We have found that the size of the reheat boiler is almost the same as the size of a nonreheat boiler for the same pressure and temperature, other conditions being equal. Since the heat input to the reheat boiler is about 5 per cent less than the heat input to the nonreheat boiler, the firing equipment can be slightly smaller, the furnace can be 5 per cent smaller, but the superheater and reheater require much more space than the superheater on a nonreheat boiler. With all other design factors being equal, our experience shows that the cost of a reheat boiler is about 5 per cent more than the cost of a nonreheat boiler. This was brought out

¹ Consulting Mechanical Engineer, Ebasco Services Incorporated, New York, N.Y. Mem. ASME.

² "Some Factors Influencing the Economics of Reheat Installations," by R. W. Hartwell, and H. A. Wagner, published in this issue of the Transactions, pp. 549-556.

³ "Selection of Steam Conditions for No. 4 Unit, Riverside Generating Station," by R. C. Dannett, and G. S. Harris, published in this issue of the Transactions, pp. 557-558.

⁴ "A Comparison of Costs of Reheat Versus Nonreheat for 100-Mw Units," by R. P. Moore, published in this issue of the Transactions, pp. 559-560.

⁵ Project Manager, The Babcock & Wilcox Company, New York, N. Y.

previously by Messrs. Rowand, Raynor, and Gilg.⁶ We believe it is very important when comparing reheat to nonreheat boilers to keep all other design factors the same.

Boilers are being bought today for comfortable operation with a minimum of man power. It appears that for schemes "A" and "C" of the paper consideration should be given to the possibility of using the short-time overload capacity of the boilers when one boiler is out of service. The use of this overload capacity might mean that more man power would be required to keep the heating surfaces clean but it might be worth while.

The 12 per cent difference between the summer and winter peak loads is an interesting bit of data and certainly makes it evident that more spare capacity on the system will be required now than in the past. This condition of course would be most troublesome to those systems that use old and inefficient generating equipment as stand-by for the modern equipment. We believe it will be necessary for the engineers making a study similar to this on any specific system to estimate the cost of power generated by the old equipment. On many systems the "capacity-charge" method of calculation would result in error because of the very high cost of stand-by power. It also can be true when power is purchased. We have observed that depending upon purchased power can be very dangerous because when one power system is operating at high load the power systems from which power can be purchased are also operating at high load and may not have any surplus available.

One feature of the battery boiler system is disturbing to us, that is, the thermal stresses set up in the main steam header whenever a boiler is cut into service. We can visualize 650 F steam being turned into a header, the temperature of which is between 950 F and 1050 F. We would like to suggest that the designers provide some protection against such thermal shocks.

This paper² brings out very forcibly the fact that rating boilers in thousands of pounds of steam per hour is no longer satisfactory. Not many years ago the practice of rating a boiler in "horsepower" was satisfactory until increased pressures and steam temperatures made this method inadequate and caused us to go to rating boilers in thousands of pounds of steam per hour. The popularity of reheat cycles with high pressures and temperatures has now made it necessary for us to start using another yardstick. We should begin to think of "heat input," "heat output," or "megawatts" when thinking of the capacities of modern boilers.

E. E. HARRIS.⁷ R. P. Moore's paper⁴ states, "This paper analyzes the differences in cost of the various elements of a steam-electric power plant, as affected by choice of the reheat or nonreheat cycle applied to units of about 100,000-kw capability."

It appears that the author's approach is a more logical method for determining the costs between a reheat and a nonreheat station. He attempts to evaluate only the differences between two such plants.

In his Table 1 various parts of a power station have been placed in different classifications, depending upon how the cost of these parts varies. Some equipment changes cost due to a change in heat consumption, while other equipment changes cost due to a change in liquid flow. Other parts do not change cost by changing heat consumption or cycle flow. There is an increase in cost for the turbine and boiler, with an additional charge for reheat piping.

In Table 1, Section II-A, Bleeder Heaters and Piping, it would be inferred that the cost of these would be reduced directly with the flow of the cycle fluid. The heater and the extraction piping

next below the reheat point may increase in cost due to higher-temperature steam to this heater than would be obtained for a nonreheat unit. This additional cost may be of small magnitude.

Table I, Item III—Metering and Controls—probably would cost more for the reheat installation. The turbine hall, depending upon the arrangement, may cost more due to the increase in length of a reheat machine over a nonreheat unit. Evaporators may cost less, as well as the feedwater-treatment apparatus. If these items in Section III balance out to zero differential in cost, then they do not enter into a cost difference between reheat and nonreheat.

The paper states, "Net charge for reheat \$1.72 per kilowatt." This addition is based upon costs assigned to the various items in Table 1. If they represent average costs, then \$1.72 per kilowatt corresponds to between 1 and 2 per cent additional cost for a reheat station over a nonreheat station. Such an increase in cost for the reheat station compared with the gain in economy obtained by reheating makes reheating appear very favorable.

E. H. KRIEG.⁸ At the 1948 Annual Meeting of the Society, an outstanding group of papers was presented which discussed the engineering aspects of the reheat cycle quite completely, with the exception of its economic aspects. Desiring to present a few thoughts on the economics of reheat from the stockholders' or management's viewpoint while interest was still warm, and to supplement the data given in "Comparative Costs of Resuperheating Installations,"⁹ Mr. Stanley Stokes and the writer prepared a paper, "Union Electric Finds Attractive Return in Reheat."¹⁰ Some of the points therein bear reiteration when discussing the present papers.^{3,4} Engineers will welcome these good papers on economics, for no engineering study can be complete without justification of the proposed investment.

We agree with the conclusion reached in R. P. Moore's paper,⁴ that, although a plant designed for the reheat cycle costs more, its adoption is justified in many cases. This discussion is intended to amplify that conclusion.

The Hartwell-Wagner paper³ mentions the often forgotten concept that to justify interconnected boilers, extra capacity is required either in the form of an extra boiler or larger boilers. The hours per year when the interconnection would be used may prove to be too small to justify the interconnection otherwise. The paper³ does not mention that availability of battery boilers is sometimes adversely affected by the sectionalizing valve (or its by-pass) in the interconnecting steam and water lines. When a boiler or turbine is down and steam or water leaks into it from the adjacent active unit, a total of two units must come off. The writer wonders if Mr. Steinberg assumed¹¹ that valves always remain tight and never need maintenance, with consequent outage of two boilers instead of one, or possibly two turbines instead of one. The question is: Won't the valves in the several interconnections cause almost as many lost kilowatt-hours over 30 years as they will save? We have many data on turbine availability, but little on the effect of valve tightness on availability other than the recollection of operators of specific cases. There is a need for some factual data on such cases.

Messrs. Dannett and Harris⁵ state: "When the first of these series of units was placed in service at Westport Station in 1941, the fuel cost per million Btu and construction costs were such that it was not economical to spend additional money for improve-

⁸ Consulting Engineer, Stone & Webster Engineering Corporation, Boston, Mass. Fellow ASME.

⁹ *Electrical World*, vol. 132, Sept. 10, 1949, pp. 87-91.

¹⁰ *Electrical World*, vol. 132, Dec. 17, 1949, pp. 93-96.

¹¹ "Relation of Thermal Plant Design to Reserve Capacity," by M. J. Steinberg, *Electrical Engineering*, vol. 69, January, 1950, pp. 64-67.

⁶ "High-Pressure Boilers With Reheaters," by W. H. Rowand, A. E. Raynor, and F. X. Gilg, *Trans. ASME*, vol. 71, 1949, pp. 719-727.

⁷ General Electric Company, Schenectady, N. Y.

ment in heat rate. By 1948, however, the cost per million Btu had practically doubled, and construction costs had increased sufficiently to warrant a careful reconsideration of the most economical steam conditions." It is admittedly difficult to do so, but power-station design should not be concerned with present fuel costs but with the cost of fuel 16 years from now, that is, the average of the 3 to 33-year period hence.

Metallurgically, there are such meager long-term data on the characteristics of certain steels at 1050 F and over that some speculation attends their use at the present time. The incremental dollar savings do not always appear to balance the incremental headaches.

In the paper by Messrs. Dannett and Harris,⁶ could not a more direct comparison between reheat and nonreheat costs be made for approximately the same thermal performance, e.g., 1450 psi, 1050 F compared with 1250 psi, 950 F/950 F reheat? The paper admirably presents the small cost difference between reheat and nonreheat: "The result was somewhat surprising indicating a spread of less than 2 per cent in the cost per kilowatt of capability."

Availability might be better served with 950 F reheat cycle than for a 1050 F straight-through cycle, because in one study it was noted that the former enjoyed a lower furnace-gas exit temperature which should give less slagging. This is especially important with strip coal.

It is regretted that the effect of system interconnections seems to be omitted from many studies. Load factor of a unit is a function of how that unit serves an integrated group of systems on which there are usually some low-efficiency units for taking low load factors, giving new units better load factors. When engineers expect the load factor of a new unit to decrease in the future, that decrease will not take place unless more efficient units are installed.

Reviewing the issues developed thus far, the enigma of reheat is not the mere estimation of investment costs nor return on the investment. Rather, much of the problem or the enigma appears to be one of "futures" in coal and labor. The present price of coal has no bearing on the problem because the proposed plant does not begin to burn coal until some 3 years after the decision has been made to build the plant. Then, if the amortization period is 30 years, the coal price between 3 and 33 years from now is all that is significant—similarly for labor costs. What fuel will cost in the future has a greater effect on the choice of cycle than whether one cycle is 5 per cent more efficient than another. It seems too bad that, relatively, so little attention is focused on actual past and probable future fuel costs in journals devoted to power plants. Perhaps some enterprising power-industry publication will favor us with regular fuel-cost forecasts needed by power-plant engineers. A great deal of attention, perhaps too much, is given to calculating the difference a few Btu may make, using existing costs without proportionate attention being given to what future fuel costs may be.

Even this is not the whole story, for the effect of a higher coal price during the early years is of far greater significance than during its later years. During the first 5 years the load factor of the plant will certainly be high, and a high fuel cost then will produce a large return. But during the 25 to 30-year-old period when a low load factor may well be the case, a low fuel cost means little, for the earnings made during "boyhood" will support its "old age." If an inefficient plant is built today, its future fate inevitably will be low load factor; interconnection contracts will take care of that. The better the performance that is designed into today's plant, the less will it be backed off by future plants.

No two people can agree on what coal prices will be during the next 33 years, and it is anybody's right to estimate or speculate on what they will be. At the risk, or rather with the certain

knowledge that others will disagree, this slant on future coal prices may have some guidepost value.

W. F. RYAN.¹² No matter which set of assumptions is used, the Messrs. Hartwell and Wagner² find an annual saving of about \$130,000 for a unit system with reheat (Plan D) compared with a nonreheat unit system (Plan B). The maximum differential is \$137,000 and the minimum \$126,000 per year. This is the net return, before income taxes, on an increment investment of \$1,861,000.

A factor which should not be overlooked is that, assuming regulated and limited net profits for the utility, the \$130,000 more or less reduction in annual production expense represents an ultimate saving to the customer on his energy charge, while the \$1,861,000 added investment represents an increase in his demand charge.

Some of us can remember the "great depression" when power customers whose markets had evaporated, and whose gross income had shrunk in proportion to sales, refused to understand why the power company demanded so much money for such small amounts of energy. Those of us who remember those days might hesitate to accept this return on what is ultimately an increase in demand charge. We remember that when a customer is using a lot of energy, he is prosperous and can pay for it. When he is not using much energy, he is hard up, and complains bitterly about paying for his previously established demand.

The savings which accrue from the use of a unit system are assignable to the demand factor, exclusively. Therefore it is not only a substantial saving, but it is a saving in the right place. We are indebted to the authors for so clear a demonstration of the advantage of unit installation.

Under other conditions the case for reheat may be more convincing. For example, in dealing with larger units, the lowest cost undoubtedly will be obtained by installing the greatest capacity economically feasible on a single-shaft 3600-rpm machine. In this case capacity may be increased several thousand kilowatts by the use of reheat, effecting a substantial saving comparable to that shown in this paper² in production expense, and also in the unit capital cost of the plant.

SABIN CROCKER.¹³ The authors are to be congratulated on contributing an excellent paper on a timely subject that warrants careful analysis. They have done well in offering an objective presentation of data concerning the relative availability of boiler-turbine units installed with and without crossovers. The paper affords a variety of factual data from which the reader can select the set that best suits his own conception of availability and what share of capital charges should be assessed against any loss thereof.

One of the important facts brought out by the paper is the reduction in outage time obtained by using two-shift maintenance instead of one shift. For the straight unit system without crossovers, this represents a gain in availability of 3.8 per cent as shown in Table 1. This gain in availability can be obtained at little expense for premium pay since only the controlling jobs of longest duration need to go on double shift; other jobs can be finished in time on one shift with a normal crew or by putting extra men on the one shift where more can work to advantage simultaneously.

With two-shift maintenance the authors show the difference in availability of the unit system with and without crossovers to be something less than 2 per cent which agrees with the experience of operating companies that have had unit systems in

¹² Engineering Manager, Stone & Webster Engineering Corporation, Boston, Mass. Fellow ASME.

¹³ Mechanical Engineer, Ebasco Services Incorporated, New York, N. Y. Mem. ASME.

use for some time. In fact, the engineers of some operating companies contend that there is less outage without crossovers than with because the extra valves and other items associated with the crossovers and with operating the boilers in battery constitute an added source of outage. In any event the operation of a boiler and turbine on the straight unit system without crossovers permits omitting the nonreturn valve as well as two or more gate valves per unit. This results in a considerable reduction in pressure-drop losses and perhaps an ensuing saving in boiler cost together with the saving in cost of the valves and piping omitted. Furthermore the straight unit system permits a simplification of steam and feedwater controls and metering which both facilitates operation and reduces cost. Inasmuch as the authors have shown a difference in investment of \$5.10 per kw changeable to the crossovers plus some extra boiler capacity, the writer concludes that they have made due allowance for differences in piping, controls, and metering. Nevertheless, more details concerning estimated differences in investment would be helpful.

Granting for the purposes of discussion that the authors were right in assigning about 2 per cent in round figures less availability without the crossovers (see Table 1 for 96.0-94.2 = 1.8 per cent), the writer would like to apply this figure in trying to analyze what it means as applied to an actual system. Assuming an existing name-plate rating of 1,700,000 kw for units installed on the electrical system, the addition of 400,000 kw would bring the installed capacity up to 2,100,000 kw. The last 400,000 kw, by assumption, would have an availability 2 per cent less without crossovers than if such had been provided. Thus for an addition of 400,000 kw, the loss of availability would be diluted to the following extent:

$$\frac{400,000 \times 2 \text{ per cent}}{2,100,000} = 0.38 \text{ per cent}$$

A loss in availability of less than 0.4 per cent when spread over the system as a whole seems within the capability of existing reserves to carry without installing more capacity on this account. Continuing the reasoning on this basis, it would be perhaps 15 to 20 years before the further dilution of availability due to adding successive units without crossovers could approach 1 per cent loss in availability for the electrical system as a whole. This still remains a small figure with respect to other uncertainties to be considered in determining what constitutes reasonable reserve.

Theoretically, on an electrical system having aggregate name-plate ratings of 2,100,000 kw, a difference, 0.4 per cent represents only 8400 kw which is a relatively small amount to obtain by way of assistance over an interconnection or, in a pinch, by temporarily reducing voltage or dropping nonessential load. From a practical operating standpoint, a loss in availability of this order is apt to mean that one of the new large boiler-turbine units without crossovers would be off the system at some remote time when full reserve for backing it up is not available. On a system having units of various sizes it is to be expected that a smaller unit would be in reserve for this contingency which, plus about 8000 kw aid from a tie line, or as otherwise noted above, would tide things over.

CLOSURE BY R. W. HARTWELL AND H. A. WAGNER

The authors believe that Mr. Elliott is quite right in his statement that the reliability standards indicated in the paper may not be applicable to small power systems where continuity of service and other factors may differ materially from those considered suitable for large systems. Such variables make it impractical to apply the results of our analysis directly to another power system.

Mr. Taylor has raised an interesting point with reference to rating of boilers in terms of heat input or output rather than steam output. He is, of course, correct. To many engineers, however, the capacity of a boiler in terms of steam output conveys a better appreciation of size, even though not strictly accurate, than heat input or output in million Btu. The authors agree, however, that we should begin to think in terms of heat rather than pounds of steam.

Mr. Krieg's discussion concerning the cost of coal over the life of the equipment is certainly pertinent. In stating, however, that the fuel cost over the first five years of a plant is the more important, some of the uncertainty of speculating on long-time coal costs is removed. Whereas the fuel purchaser will be extremely hesitant about predicting the cost of coal for a 30 to 40-year period, he probably would not be too hesitant in giving a figure for the next five years. The authors feel sure that Mr. Krieg would agree that the inability to predict the long-time coal cost should not be considered a reason to stop the quest for more efficient power plants.

Mr. Ryan makes a very good point that the amounts of money involved in the several schemes differ greatly. It is entirely possible that a somewhat less efficient plant might prove a much better choice depending on future business and load conditions.

Mr. Crocker correctly points out that small differences in availability are difficult to evaluate in terms of capacity. Whereas an increment of capacity considered individually might be considered too small to warrant a capacity charge, several of such increments, however, could add up to a capacity which could not be overlooked. Again, numerous factors require consideration as to whether a charge for small capacity differences is warranted on a particular system.

The authors appreciate the comments made by the discussers of this paper. These comments represent an important addition to the information presented in the symposium on the economics of reheat power plants.

CLOSURE BY R. C. DANNETTEL AND G. S. HARRIS

The authors appreciate the helpful suggestions of the discussers and, in general, agree with them. The importance of some of these points justifies further discussion for clarification.

Mr. Elliott emphasizes that estimates should include "all elements in which there is a significant difference in investment." The surprising result in the authors' investment studies was the small difference when all elements were considered as contrasted with the much larger spread of costs indicated by consideration of a few major elements. With respect to magnitude of fixed charges, the constant percentage used by the authors was determined by a staff member of the Company's Economic Planning Committee who was familiar with the taxes, interest rates, and amortization rates mentioned by Mr. Elliott and who also was in a position to weigh the effects of stock-bond-surplus financing of the project. There is full agreement with Mr. Elliott's comment "To justify reheat, percentage return on increase in investment should be somewhat higher than the normal assigned for charges on cost of station as whole."

Mr. Krieg is correct in saying, "It is admittedly difficult to do so, but power-station design should not be concerned with present fuel costs but with the cost of fuel 16 years from now, that is, the average of the 3 to 33-year period hence." The authors based their computations on a study of the estimated average cost of coal for a 30-year period prepared by the Company's purchasing agent. Mindful of the severe changes in fuel costs between 1941 and 1948, and acknowledging the difficulty of predicting future prices, the authors graphed their results with coal costs as abscissas (Fig. 1 in paper) to permit evaluation with wide latitude in estimates of future coal cost.

The authors agree with Mr. Krieg's statements that the "problem of reheat" appears to be one of "futures" in coal and labor with the further complication of future load factor. The graphs plotted against coal cost offer a partial solution to the first part of this problem by predicting in advance the effect of a wrong guess in estimating fuel cost. The second part is best answered by a composite load-duration curve including estimated effects of system interconnection and the progress of the manufacturers and the central-station industry in producing more efficient units in the future. A curve of thermal rates plotted against years shows clearly the achievements to date and promises better efficiency for future units; sound engineering dictates that each improvement be weighed as it becomes available and incorporated in the system whenever a study of all elements of cost shows that its selection would result in greater over-all return to the

stockholders over the life of the unit. It may be of interest that a study conducted along these lines one year later than the one reported confirms the assumptions made for No. 4 Unit at Riverside and indicates similar general conclusions.

Mr. Krieg is correct in stating that the 1450 psi, 1050 F, and the 1250 psi, 950 F/950 F cycles would have approximately the same thermal performance and should offer a more direct comparison than 1450 psi, 1050 F compared with 1450 psi, 1000 F/1000 F. The results of this comparison are shown in the graphs and indicate that the cycles with approximately the same thermal performance differ very slightly from each other in costs.

The authors frankly admit that their computations show a small saving by use of the reheat cycle but are in full agreement with Mr. Krieg that "the incremental dollar savings do not always appear to balance the incremental headaches."

C

The strain and the reference to other applied locally the d opera is dis given ing-st of ap The e surin hydro

IN su gi shells pierced at a ra spheric opening up ben from po

In th whose Blaser, the inn of thes outer w by one bending and ben idea of better loads an multiply moment ness squ

A plo the vess

Man Babcock

Engi

"Exp

Kooistra tions, pp

Contri presented

of THE A

NOTE: understood of the Soc

Analysis of Experimental Data Regarding Certain Design Features of Pressure Vessels

By G. J. SCHOESSOW¹ AND E. A. BROOKS,² BARBERTON, OHIO

This paper presents an analysis of data obtained by strain-gage experimental stress analysis on drum heads and nozzle openings in drum shells. This analysis, while referred particularly to power boilers, is also applicable to other types of pressure vessels. The data obtained are reduced to dimensionless form so that they may be applied to drums of other size and thickness but geometrically similar, and to illustrate more clearly the action of the drum in resisting pressure. The relationship between operating-stress level and the life of the vessel in service is discussed with particular reference to a drum that has given over 40 years of satisfactory service with an operating-stress range over a considerable area of the vessel of approximately the ultimate strength of the material. The effect of prestress created in the vessel by overpressuring, such as applying the $1\frac{1}{2}$ -times working-pressure hydrostatic test, is discussed.

IN A vessel of complicated shape subjected to internal pressure, the simple membrane-stress concepts do not suffice to give an adequate idea of the stress situation. Cylindrical shells are somewhat out of round, vary in thickness, and are pierced by openings. Their end closures tend to dilate radially at a rate different from that of the shell, they deviate from a true spherical shape, often markedly, and are themselves pierced with openings. These deviations from a true membrane shape set up bending in the vessel wall and cause the direct loading to vary from point to point.

In the series of experimental stress analyses on pressure vessels whose technique has been reported by L. F. Kooistra and R. U. Blaser,³ resistance strain gages were bonded in opposite pairs to the inner and outer walls of the test drums. From the readings of these gages may be computed the stresses at the inner and outer walls. The direct stress on the wall at that point is given by one half the sum of the stresses inside and outside, while the bending stress is given by one half their difference. These direct and bending stresses, plotted over the vessel wall, give an excellent idea of how the vessel behaves under pressure. A somewhat better conception is obtained if, instead of stress, the actual loads and moments be plotted. The direct load is obtained by multiplying the direct stress by the vessel thickness; the bending moment, by multiplying the bending stress by one sixth the thickness squared.

A plot of the distribution of direct loading and moment over the vessel surface would show how the vessel takes the loading

due to its internal pressure. The direct loading is diverted from the more flexible to the more rigid portions of the vessel, the deviations setting up bending in the shell. The information so obtained is instructive, but applies only to the specific vessel tested. It is necessary further to interpret the data to apply the test results to prototype vessels.

The direct load at any point of a vessel is proportional to the internal pressure and to the inside radius, so that if we divide the load per inch of shell (T) by the pressure and by the inside radius, we obtain a dimensionless value showing the relative loading at each point, the value of unity corresponding to the simple membrane stress in a cylinder, the value 0.5 to the simple membrane stress in a sphere. The bending moment at any point is proportional to the direct load and to a geometric eccentricity, which latter is proportional to the inside radius. If then we divide the moment per inch of shell (M) by the pressure and by the inside radius squared, we obtain a dimensionless value showing the relative bending at each point, the value zero corresponding to a direct loading without bending. The values so obtained are independent of the size of the vessel, depending only on its shape.

To use these charts in finding the actual stresses in a prototype vessel, the foregoing procedure is reversed. The dimensionless value for direct load is multiplied by the pressure and by the inside radius to give the load (T) per inch of shell, which is divided by the shell thickness to give direct stress. The value for bending is multiplied by the pressure and by the inside radius squared to give moment (M) per inch of shell, which is divided by one sixth the thickness squared to give bending stress. The direct and bending stresses are added algebraically to give the stresses at the inside and outside surfaces of the prototype vessel.

HEADS

The results obtained for dished heads of different shapes are shown in Figs. 1 to 8, inclusive. In each case the radius shown is the inside radius of the cylindrical skirt of the head. The circumferential direction is parallel to the circumference of the skirt. The meridional direction is perpendicular thereto, lying in a plane containing the axis of the drum. A positive load value corresponds to tensile load, a positive moment value corresponds to tension on the inside surface of the vessel, both with internal pressure applied.

Figs. 1 to 8 show the loading distribution in dished heads. In general, the dished heads tend to move toward the spherical shape giving circumferential compression and rapid changes of bending moment, indicative of large shears, at the knuckle. This circumferential compression carries well into the cylindrical portion of the shell. At the crown of a blankhead, the curvature increases under pressure, producing compression inside. At the opening in a manhead there is found a high circumferential tension with local bending in the flued-in manway.

Figs. 6 and 7 show an ellipsoidal blankhead and a similar head with an opening so reinforced as to dilate at the same rate as the portion of the blankhead crown replaced. During fabrication the reinforcement was displaced axially, causing the bending shown near the reinforcement. Otherwise the reinforcement is seen to perform satisfactorily. The unreinforced hemispherical manhead, Fig. 8, is seen to perform about as would be predicted

¹ Manager and Chief Engineer, Engineering Department, The Babcock & Wilcox Company. Mem. ASME.

² Engineer, The Babcock & Wilcox Company.

³ "Experimental Technique in Pressure-Vessel Testing," by L. F. Kooistra and R. U. Blaser, published in this issue of the Transactions, pp. 579-589.

Contributed by the Power and Applied Mechanics Divisions and presented at the Fall Meeting, Erie, Pa., September 28-30, 1949, of THE AMERICAN SOCIETY OF MECHANICAL ENGINEERS.

NOTE: Statements and opinions advanced in papers are to be understood as individual expressions of their authors and not those of the Society. Paper No. 49-F-19.

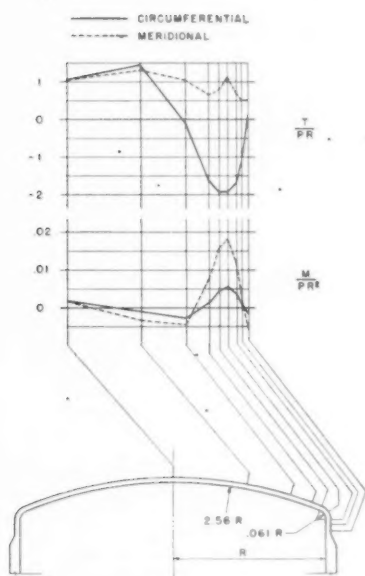


FIG. 1 LOADING DISTRIBUTION IN SHALLOW BLANKHEAD OF TYPE USED PRIOR TO 1915

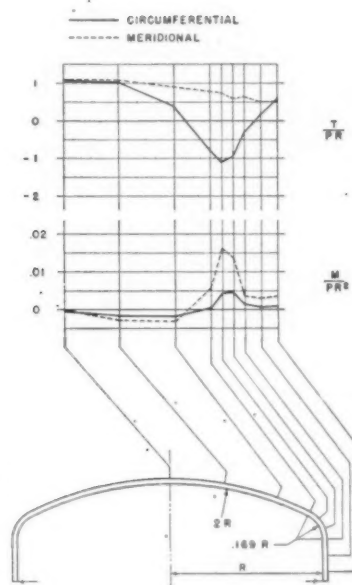


FIG. 3 LOADING DISTRIBUTION IN SHALLOW BLANKHEAD OF TYPE IN CURRENT USE

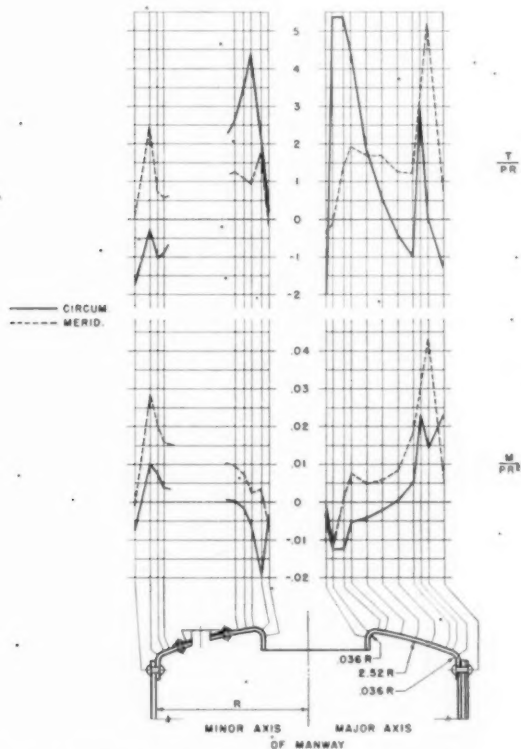


FIG. 2 LOADING DISTRIBUTION IN SHALLOW MANHEAD FABRICATED IN 1906

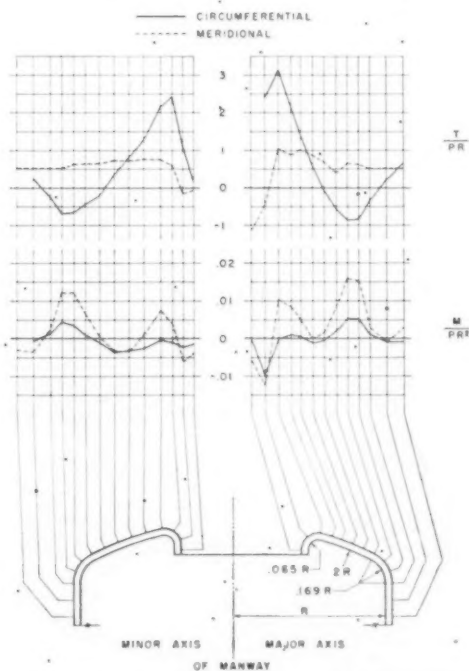


FIG. 4 LOADING DISTRIBUTION IN SHALLOW MANHEAD OF TYPE IN CURRENT USE

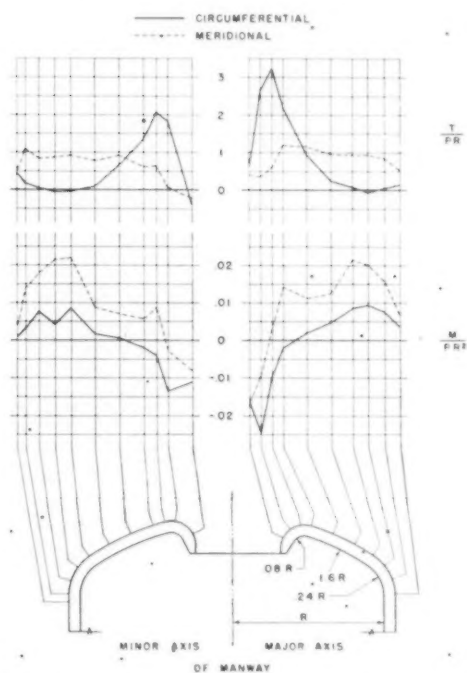


FIG. 5 LOADING DISTRIBUTION IN MARINE-TYPE MANHEAD

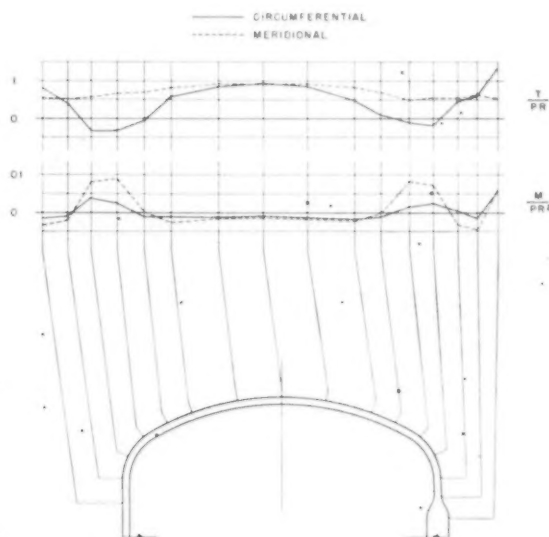


FIG. 6 LOADING DISTRIBUTION IN 2:1 ELLIPSOIDAL BLANKHEAD

from theoretical considerations. The circumferential stress at the edge of the opening is twice that in the head elsewhere. The increased deflection near the opening causes a reduction in the curvature of the head, with positive bending throughout.

OPENINGS

Round Openings. Openings in a cylindrical shell are focal points for the initiation of failure, particularly when operating at

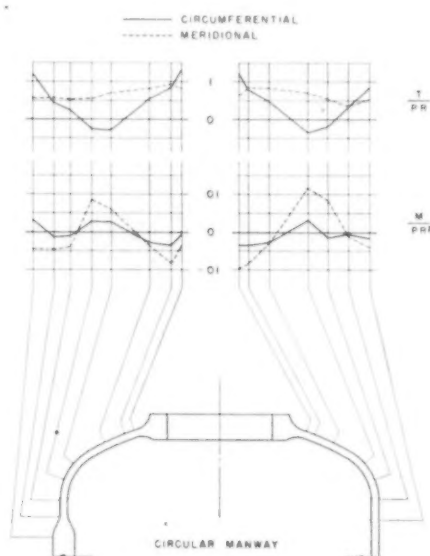


FIG. 7 LOADING DISTRIBUTION IN 2:1 ELLIPSOIDAL REINFORCED MANHEAD

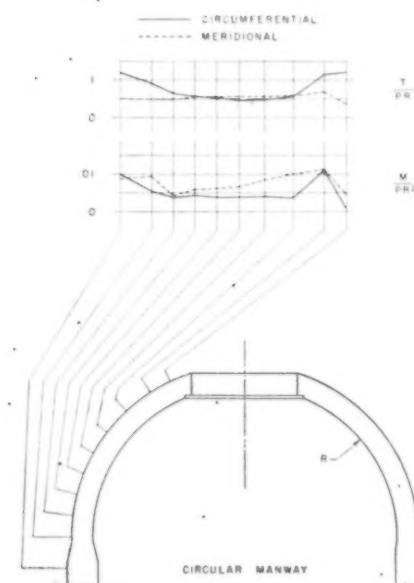


FIG. 8 LOADING DISTRIBUTION IN HEMISPHERICAL MANHEAD

high stress levels in services involving frequent pressure changes. The designer will seek to reinforce such openings by adding metal locally around the hole. Each such addition of metal reduces the stress at the opening but as more metal is added the reinforced area becomes more rigid. If this be carried on sufficiently, the stresses at the outside edge of the reinforcement will rise to values higher than at the opening, and the opening becomes over-reinforced.

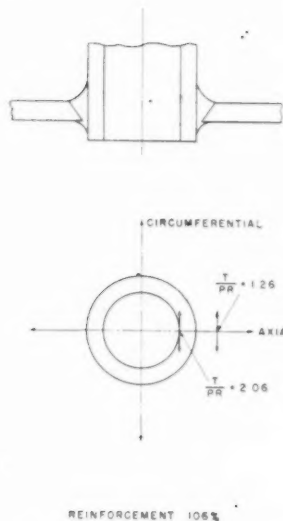


FIG. 9 MAXIMUM LOADINGS AT INSERTED CIRCULAR NOZZLE

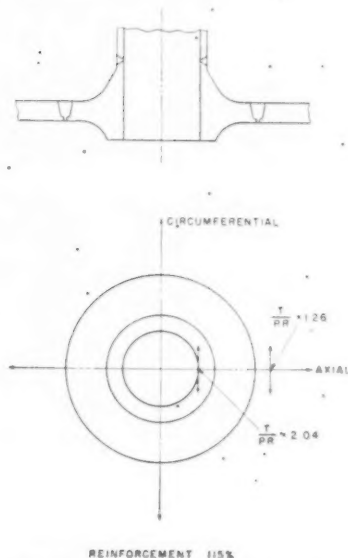


FIG. 10 MAXIMUM LOADINGS AT CIRCULAR NOZZLE OPENING WITH INTEGRAL REINFORCEMENT

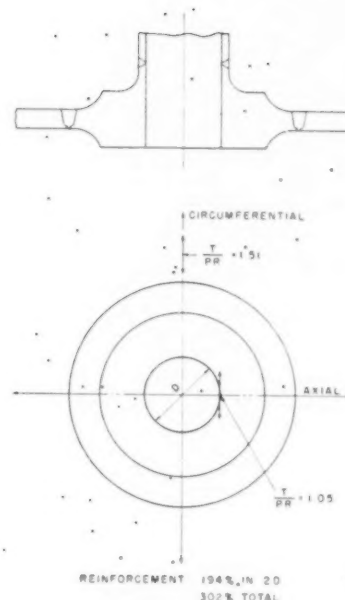


FIG. 11 MAXIMUM LOADINGS AT CIRCULAR NOZZLE OPENING WITH THICK INTEGRAL REINFORCEMENT

Figs. 9 to 12, inclusive, show the effect of adding reinforcement in various degrees at the opening.

Fig. 9 shows a heavy inserted nozzle. Counting only that part of the nozzle and weld that is symmetrical about the center of the vessel shell, the added reinforcing area is 106 per cent the area cut out in the opening. This is considerably more than required by present design rules, and a little more than would be required if the provision allowing 2-in. free opening without reinforcement were removed from the present rules. It is seen that the maximum stress at the bore has been dropped to 2.06 from the 2.50 times the average shell stress that is found at an unreinforced round opening. This is a relatively minor improvement.

Fig. 10 shows an inserted nozzle with welds that are readily radiographed. The changes in thickness are less abrupt, while the total reinforcing area is only slightly increased to 115 per cent. The maximum stress at the bore is only slightly reduced to 2.04 times the average shell stress, corresponding to the slight increase in area of reinforcement over the nozzle of Fig. 9.

Fig. 11 shows the effect of increasing considerably the reinforcement by adding metal close to the opening. The added reinforcement within one opening diameter as specified by present rules is 194 per cent, and the total added area is 302 per cent. The maximum stress at the bore is 1.05 times the average shell stress but the stress in the shell just outside the reinforcing area is now 1.51 times the average shell stress, showing the rigidity of the thick reinforcement.

Fig. 12 shows the effect of increasing the diameter of the reinforcement and reducing the thickness so as to maintain reinforcing area while reducing rigidity. Here the added reinforcement is 147 per cent within one opening diameter either side of the opening, 380 per cent total. The maximum bore stress is now 1.16 times the average shell stress and the maximum shell stress is 1.26 times the average.

Further experimentation with reinforcement shape can yield forms of still better performance. All the reinforcements tested were essentially the same shape in both circumferential and meridional sections. Tapering to a different shape in the circumferential direction will be most effective in reducing the rigidity of

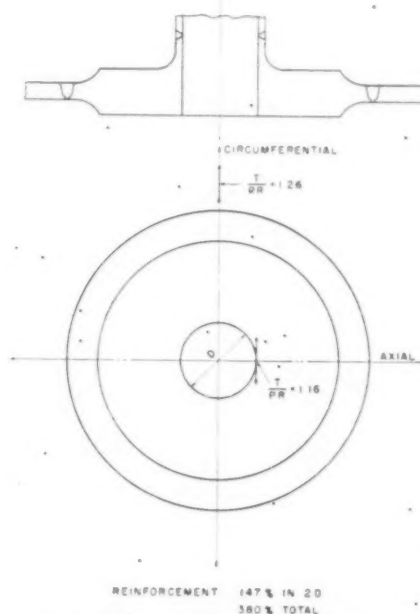


FIG. 12 MAXIMUM LOADINGS AT CIRCULAR NOZZLE OPENING WITH LARGE-DIAMETER INTEGRAL REINFORCEMENT

the reinforcement, while keeping down the stress at the bore. All such designs are expensive to fabricate and are bulky, occupying shell surface needed for functional drum attachments. As openings are usually for the flow of fluids, there is no necessity that the opening be round. The virtue of the round opening lies in its simplicity. If this virtue is to be lost in reinforcement to

give u
perm
advan
Ell
in tw
minor
The n
load
length
direct
the pe
plate
means

Fig. 13

Fig. 14

give uniform stress levels throughout the vessel, then it becomes permissible to examine the performance of openings having more advantageous shapes.

Elliptical Openings. The wall of a cylindrical vessel is loaded in two principal directions, the major load circumferential, the minor axial and of a little less than one half the magnitude. The minimum stress concentration at an opening in a plate so loaded is obtained by making the opening elliptical with the lengths of the axes proportional to the plate loadings in the same directions. So designed, the tangential stress is uniform around the periphery of the hole and is equal to the sum of the unpierced plate stresses in the major and minor directions. In drums this means that the opening is an ellipse with axis ratio 2:1, and with

peripheral stress 1.5-times the average circumferential stress in the drum shell. Several such elliptical nozzles were built and tested with results shown in Figs. 13 to 16, inclusive.

Fig. 13 shows a thin-walled nozzle designed to give minimum reinforcement. In the longitudinal section, the area added that is symmetrical about the vessel wall is 16 per cent of the area lost in the opening. The maximum stress is found in the inside of the nozzle, equal to 1.40 times the average circumferential stress in the vessel. Here even a small amount of reinforcement has produced an appreciable reduction in maximum stress from the 1.50 factor expected without reinforcement.

Fig. 14 shows a nozzle with a thick wall, the reinforcing area symmetrical about the vessel wall being 113 per cent the area cut out. This is seen to be too heavily reinforced, for the stress inside the opening is 0.77 the stress in the vessel wall, while the stress factor in the plate outside the nozzle has risen to 1.19.

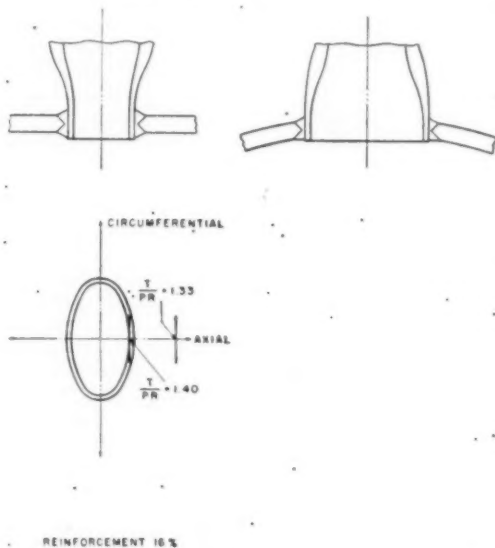


FIG. 13 MAXIMUM LOADINGS AT ELLIPTICAL NOZZLE OPENING WITH MINIMUM REINFORCEMENT

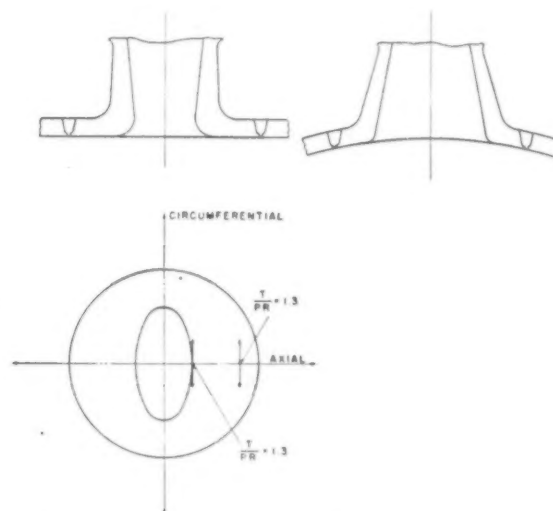


FIG. 15 MAXIMUM LOADINGS AT CAST ELLIPTICAL NOZZLE INSERTED INTO CIRCULAR OPENING IN DRUM

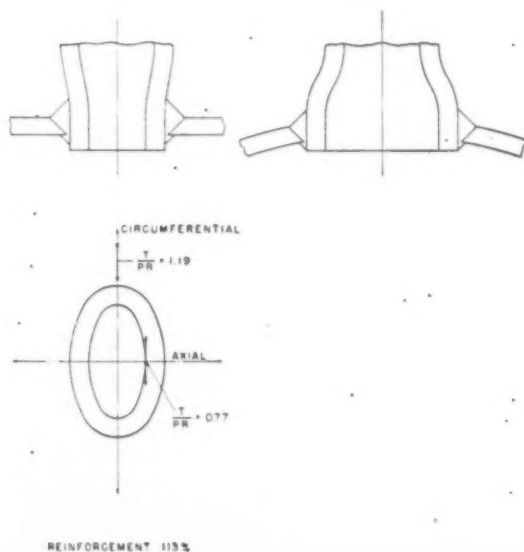


FIG. 14 MAXIMUM LOADINGS AT HEAVY INSERTED ELLIPTICAL NOZZLE

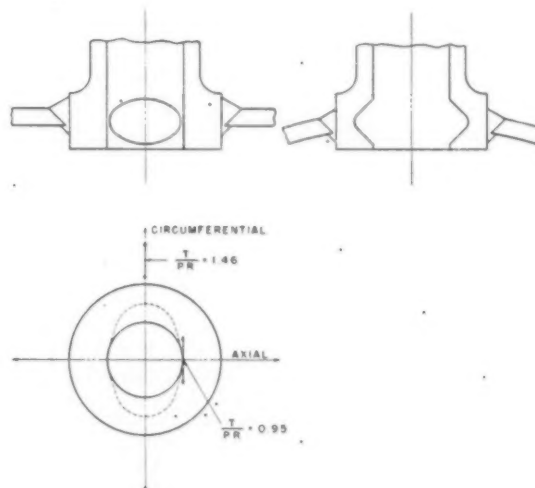


FIG. 16 MAXIMUM LOADING IN CIRCULAR INSERTED NOZZLE WITH SECTION OF OVAL SHAPE IN PLANE OF SHELL

With an optimum design of intermediate thickness, a stress level but slightly above that in the unpierced plate can be achieved.

The designs in Figs. 13 and 14 occupy an absolute minimum of area of drum shell, often a very valuable consideration. They do, however, require the cutting of an elliptical hole in the shell which may be objectionable, and do not permit of ready x-ray examination of the welds.

Fig. 15 shows a cast nozzle with elliptical opening which inserts into a round hole in the shell. This proved to be a little light in design with a stress factor of 1.3. A somewhat heavier version of this nozzle should prove to be a near perfect nozzle.

Fig. 16 shows a heavy nozzle with a round hole machined to an oval shape at the vessel wall. It performed about as might have been expected for the same amount of reinforcement on a round opening, so that the oval shaping made little difference.

DESIGN METHODS

In the past the design of many boiler parts has been on an arbitrary rule-of-thumb basis. In the case of dished heads and reinforced holes, for example, there has been available no adequate theory nor any method of determining experimentally the behavior of these parts. The experimental techniques of Kooistra and Blaser² have now filled the latter deficiency, so that a re-examination of the methods of design of heads and openings is in order.

The general method of design of boiler parts has been to set up a reasonable appearing formula involving the pressure, the dimensions of the part, and one or more arbitrary constants relating to the material used, and to experience with the part obtained from service or from proof-pressure test. It is unfortunate that one of these constants has had the dimensions of stress, for this practice has given the impression that such a stress level actually existed in the vessel, with the corollary that these stress levels were the maximum desirable. It is significant that in the case of complicated pressure-vessel elements, such as stay bolts, stress factors are not used. If we are to apply our new knowledge of the behavior of boiler parts to design, we must be prepared to alter our ideas concerning permissible stresses, or our new knowledge will do us a disservice.

ALLOWABLE STRESS

With the means available to determine stress levels throughout a vessel, we must find a reliable method of determining allowable stresses in a vessel for a given service. The service test is the most reliable test of a design, but it takes a long time to complete. Safety considerations make it impractical to determine limiting stresses in this manner.

The test to destruction by overpressure is quickly accomplished, but has the serious difficulty that often the shape just before failure is much different from that of the vessel in operating condition, and the properties of the material have changed markedly, so that the vessel at failure is quite different from the vessel it was desired to test. The overpressure test will not usually show the effect of high local stresses, as at notches, which may cause failure in service.

The fatigue test, produced by the cyclic application of pressure, does not distort the vessel and may be relied upon to show the existence of any important stress raisers. It simulates in a short time the variations of pressure which the prototype will experience in service, and can be run to failure without hazard so that limiting stress values can be obtained. It is, however, open to the objection that the fast cycling of the fatigue test may not produce the same effect in the vessel as the slow cycling in service, with long periods at nearly constant pressure. The validity of this objection can be established only by service tests.

The fatigue test, generally performed with cold water as a

pressure medium for safety and convenience, does not reproduce the effect of temperature on the vessel. Temperature does affect the physical properties of the vessel material, so must affect the life of the vessel. Up to the saturation temperatures of high-pressure boilers, the change in short-time physical properties of steel is small.

The work of Kooistra and Blaser³ on fatigue of pressure vessels at elevated temperatures shows no significant effect of temperature on the fatigue life of steel in the saturation-temperature range. It appears unnecessary to perform fatigue tests at temperatures in the saturation range. The fatigue test is also open to the objection that it does not reproduce the effect of corrosive media on the vessel material. The validity of this objection must also be determined by service tests.

In the past, due to insufficient knowledge, vessels containing parts operating at high stress levels were fabricated and operated. A study of the history of such vessels may prove a valuable aid in determining allowable stress levels. There are a large number of such vessels available. If we determine the stress levels actually obtaining in such vessels by experimental stress analysis when the vessel is retired, we will be better able to assess the validity of the fatigue test.

Prior to 1915 boiler-drum heads were of the shallow dished-and-flanged type shown in Figs. 1 and 2. Recently, in the course of a modernization program at a district steam-heating plant, a drum with a satisfactorily long life at full design pressure became available. The boiler was first installed in 1906 and was removed from service in 1948. Design pressure was 200 psi, with 175 psi being maintained on the main steam headers, so that the actual drum pressure was between those values. A 300-psi test pressure was applied on starting up each fall, and at other times after opening up the boiler. No accurate log of boiler operation was kept; however, all boilers of the plant were required during the colder periods of winter, some boilers were banked or shut down during milder weather, and all were laid up dry each summer.

Such service is in many ways more severe than steady operation, for it involves many more stress cycles, and exposes the drum to corrosion while cold and in contact with moist air. No close estimate can be given of the number of stress cycles applied during the 42 years of operation, but it would appear that the cycles of 300-psi test pressure would number about 75, while the cycles of operating pressure would number several thousand.

The high stress level is clearly portrayed in Fig. 17, showing the pattern of Lüders' lines formed on a head of this drum. This pattern was so fully developed that it showed up clearly even after sandblasting the scale from the surface. This drum was made from 55,000 UTS open-hearth steel plate. Extensive sectioning and testing of the highly stressed regions of the head showed no significant change in physical properties over those given in the original mill tests of the plate. The interior surface in contact with boiler water was covered with a smooth coating of scale, but showed no signs of corrosive attack. The exterior surface showed a few deep pits, apparently at points where the boiler brickwork was in contact with the drum shell. From any visible evidence this drum was in good shape and ready for another extended period of service.

Fig. 18 shows the stresses actually measured in this drum at 200 psi pressure. These of course represent stress range at this pressure after a preceding 300-psi test pressure. It appears that the stress range at any point did not much exceed twice the yield point of the material at design pressure. At test pressure the stress range exceeded twice the yield point over limited areas.

From the foregoing data on this drum we are in a position to draw some tentative conclusions concerning the relative importance of the various factors in drum life.

We do not have any data as to the fatigue strength of the ma-

Fig. 17

terial of number of considerable Neither the failure It would service life

There is of cycles The destr which will the desired safe margin factors show pressure sufficient i

The app test, will s pressure in ficial effect Considered raised from portions of zero stress If the vess



FIG. 17 LÜDERS' LINES ON OUTER SURFACE OF KNUCKLE OF SHALLOW DISHED MANHEAD FABRICATED IN 1906

terial of this drum, but, considering the severity and probable number of the stress cycles, we may assume safely that a considerable portion of the fatigue life of this drum has been spent. Neither time nor exposure to boiler water has greatly accelerated the failure, for the drum was to all appearances in good condition. It would then appear that the fatigue test is a reliable test of service life for boiler drums.

There is a general relationship between stress range and number of cycles to failure, expressed in the conventional S-N curve. The desirable maximum stress range in a vessel is that range which will produce a service life of the vessel which shall exceed the desired service life, expressed in number of service cycles, by a safe margin. In the determination of stress range all contributing factors should be considered, such as thermal stresses, not merely pressure stresses alone. We now have available or obtainable sufficient information to design vessels on such a basis.

PRESTRESS

The application of an initial overpressure, as by a pressure test, will so prestress a vessel as to reduce the stress at working pressure in various portions of the vessel. This may have a beneficial effect on the life of the vessel.

Consider a vessel so constructed that when the pressure is raised from zero to design pressure, the growth of various localized portions of the vessel corresponds to a stress range varying from zero stress to over twice the yield point of the vessel material. If the vessel pressure is simply raised to design pressure without

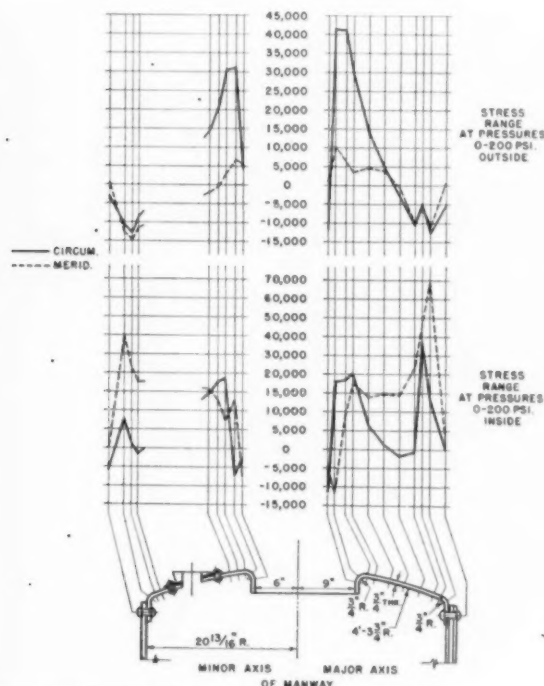


FIG. 18 STRESS RANGE AT 200 PSI IN MANHEAD FABRICATED IN 1906

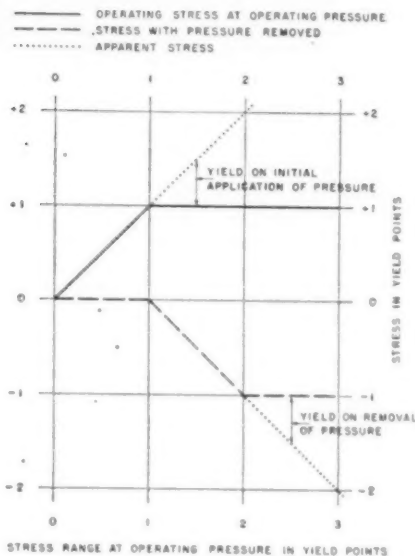


FIG. 19 BEHAVIOR OF VESSEL AT LOCALLY HIGH STRESSED POINTS WITH NO INITIAL OVERPRESSURE

any initial overpressure, then the stress picture is that indicated in Fig. 19. Those portions with stress ranges between once and twice yield point operate at yield point with no yielding on subsequent pressure applications. With pressure off, these same portions have prestresses varying down to negative yield point. Those portions of the vessel with a stress range of over twice the

yield point must yield with each application and release of pressure.

If an initial overpressure is applied, Figs. 20 and 21 show that the operating stress is lowered for portions with an operating stress range of less than twice the yield point. If an overpressure of $3/2$ working pressure is applied, then the operating stress for those portions of the vessel with an operating stress range less than $5/3$ yield point does not exceed $2/3$ yield point. If an overpressure of 2 times working pressure is applied, then the operating

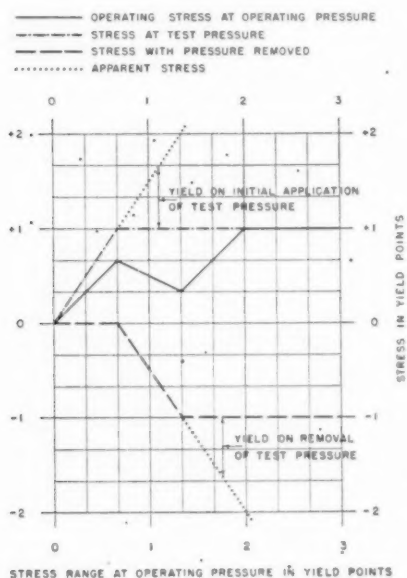


FIG. 20 BEHAVIOR OF VESSEL AT LOCALLY HIGH STRESSED POINTS WITH INITIAL OVERPRESSURE 1.5 TIMES WORKING PRESSURE

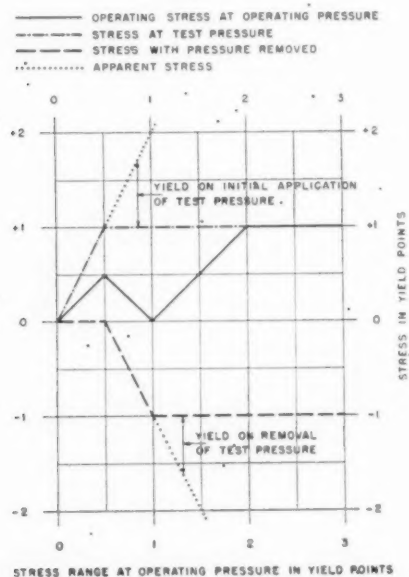


FIG. 21 BEHAVIOR OF VESSEL AT LOCALLY HIGH STRESSED POINTS WITH INITIAL OVERPRESSURE 2.0 TIMES WORKING PRESSURE

stress for those portions of the vessel with an operating stress range less than $3/2$ yield point does not exceed $1/2$ yield point. Similar relationships apply for other values of initial overpressure. No initial prestress can benefit those portions of the vessel which have an operating stress range of over twice the yield point, for these portions must yield with each application and release of operating pressure.

The foregoing discussion assumes that only limited portions of the vessel have these high stress ranges so that their yielding will not affect appreciably the general stress level of the vessel. To the extent that this assumption is not justified, that yielding of the higher stressed portions does increase the general stress level, then to that extent is the amount of prestress obtainable restricted. A vessel with a uniform stress range throughout cannot be prestressed.

It has also been assumed that yield point is a simple, definite stress. Actually, the yield point is not a clearly defined value in any case, and is considerably influenced by previous cold-working of the material, and by the stress conditions in the perpendicular directions. The effect of these considerations is to round off the sharp corners of the curves in Figs. 19, 20, and 21, and to alter the value of yield point selected, but does not change the general relationship.

It has been shown that the effect of prestress is limited to portions of the vessel having stress ranges within certain limits as set forth. Whether this prestressing will increase vessel life depends upon whether corrosion resistance or fatigue life is improved. Experience with older drums, such as the case already cited, would indicate that corrosion due to contact with properly treated boiler water is negligible for boiler plate at any stress level. There may, however, be benefits in services using other media. Fatigue-test data indicate that there may be some improvement in fatigue life of mild steel by prestressing at ranges below twice yield point, but that this improvement is in a life already many hundred times the number of pressure cycles possible in boiler service.

We may conclude that prestressing is not significantly beneficial to the life of boiler drums. The pressure test is of course of value in boilers to show up safely incipient failures in parts weakened by erosion or other cause. The value of prestress in other services should be determined by the effect on corrosion and fatigue life in that service.

CONCLUSION

The results of many experimental stress analyses of boiler drums have been given in a form permitting their ready application to other vessels of the same general shape.

The significance of these results is discussed with particular reference to allowable stress levels in design. It is shown that in power-boiler service there is no selective corrosive attack of boiler plate at stress ranges of twice the yield point. It is also shown that present design rules are not correct as regards dished heads and reinforced openings.

Discussion

H. C. BOARDMAN,⁴ This paper is timely because it treats of problems now of great interest to the ASME Boiler Code Committee and to the Design and Fabrication Divisions of the Pressure Vessel Research Committee of the Welding Research Council. It brings out into the open stress factors which present codes for pressure vessels either conceal or only mention in cautionary phrases. Surely it will stir code writers to a keener awareness of the deficiencies of their work, and of their obligation

⁴ Director of Research, Chicago Bridge & Iron Company, Chicago, Ill. Mem. ASME.

to keep
consider

The
veys a
has cor
ing. S
should
already
tanks.
Tanks,

"It is
tanks c
necessi
recogni
informa

A sim
sure-ves

Prestu
of shell
per inch

Appl
stress sy
from the
deviation

to the m
nozzles
to keep

ments es
perpendi
the cited
and other

In calc
and bend
shell, the
and the s

the produ
which is
that the

just as th
on the co
another e

conical-he
the three
cylinder r

used in de
The aut

load and
of 1 in., u
eccentricit

cylinder d
probable?
dependent

Is not a g
cisely appl
ness, are p

Neverthele
when appli
doubtless t

Dished h
believed to
analysis and

gratifying t
spheres cha

Openings
how shape

to keep rules of design as close to the forefront of knowledge as considerations of safety will permit.

The technique and interpretation of electric-strain-gage surveys are well established and understood; the authors' company has contributed much both to this technique and this understanding. Such surveys, complemented by mathematical analyses, should be accepted as a basis for the design of pressure vessels, as already they are officially accepted for the design of storage tanks. The Standard Specifications for Elevated Steel Water Tanks, Standpipes and Reservoirs states:

"It is recognized that no specifications for the design of elevated tanks can be sufficiently specific and complete to eliminate the necessity of judgment on the part of the designer. It is also recognized that strain gage surveys are a proper source of design information."

A similar statement could well be made with reference to pressure-vessel design.

Presumably "direct load," "direct loading," and "load per inch of shell" are synonymous; also "bending moment" and "moment per inch of shell."

Aptly descriptive of how connections upset the membrane stress system is the statement: "The direct loading is diverted from the more flexible to the more rigid portions of the vessel, the deviations setting up bending in the shell." These words convey to the mind a picture of "direct-load" contours bunching up near nozzles and supports and correspondingly thinning out elsewhere to keep their sum total equal to the bursting pressure. The moments established in this way are of two kinds—those in planes perpendicular to and tangent to the shell. The latter are due to the cited shifting of direct loadings because of vessel attachments and other geometric irregularities.

In calculating their dimensionless values for "relative loading and bending" the authors have assumed that, at any point in the shell, the "load per inch of shell" is proportional to the pressure and the shell radius, and that the "moment per inch of shell" is the product of the "direct load" times a "geometric eccentricity" which is proportional to the shell radius only. How is it known that the geometric eccentricity is not a function of pressure too, just as the eccentricity of a column is a function both of the load on the column and the geometry of the unloaded column? As another example, the moment per inch of shell at a cylinder to a conical-head connection varies approximately as the product of the three-halves power of the pressure and the square of the cylinder radius, and inversely as the square root of the unit stress used in designing.

The authors' dimensionless values for a cylinder are the direct load and moment per inch of shell for a cylinder having a radius of 1 in., under a pressure of 1 psi, assuming that the geometric eccentricity for this small cylinder is the eccentricity for the actual cylinder divided by the radius of the actual cylinder. Is this probable? What is meant by: "The values so obtained are independent of the size of the vessel depending only on its shape"? Is not a given set of the authors' dimensionless numbers precisely applicable only to vessels which, including the shell thickness, are photographic enlargements or reductions of each other? Nevertheless, such dimensionless numbers should be quite useful when applied to vessels departing from photographic similarity; doubtless the authors intend that they be so used.

Dished Heads. The reported results for the heads tested are believed to be in line with the results of crude mathematical analysis and with intuitive knowledge of how heads behave. It is gratifying to observe that properly reinforced circular openings in spheres change little the normal stresses in adjacent shell plates.

Openings. This section is a real contribution because it shows how shape refinements, commonly known as streamlining, can

reduce stress concentrations. Although elliptical openings have been used for some time, it is probable that this paper for the first time demonstrates their advantages quantitatively. Are not such openings amenable to fairly accurate mathematical analysis?

Incidentally, there is now being conducted at the Chicago plant of the writer's company, a strain-gage survey of a large rectangular clean-out door, installed in the bottom ring of a section of an oil storage tank 100 ft diam, with the bottom of the opening flush with the upper surface of the horizontal tank bottom plate. To carry the normal ring-tension stresses in the shell around the opening, without causing bending in the tank shell and tank bottom, there is provided a continuous bar with its width perpendicular to the shell, which bar forms the top and bottom of the opening, and is shaped to a parabola around each end of the opening. Of course this bar is welded to the shell. In this case the parabola is the equilibrium curve for the shell loads on the bar. However, in the case of a cylindrical pressure vessel, the 2:1 ellipse is not the equilibrium curve for the shell loads upon it and therefore is subject to bending as well as direct stresses. The 1.414:1 ellipse in a cylindrical shell is free of bending moments but is subject to a variable direct stress.

Design Methods and Stresses. This portion of the paper is very stimulating and helpful. The authors truly state: "If we are to apply our new knowledge... to design we must be prepared to alter our ideas concerning permissible stresses, or our new knowledge will do us a disservice." The same thought has been expressed many times in meetings of the ASME Boiler Code Committee, and really is an indirect way of saying that the inevitable changeover, from the crude idea that the nominal stresses of simple design formulas are the actual stresses in the vessel, to the idea that the working stress at points of stress concentration may safely be practically at the yield point, must involve a period of education and conditioning to make acceptance possible. Such education and conditioning result in one of the greatest products of the Pressure Vessel Research Committee and in papers such as the one under discussion.

The service history of the boiler-drum heads built in 1915 is most encouraging and gives assurance that the heads of the 1950 ASME Unfired Pressure Vessel Code are quite safe for the services intended.

It is startling to read "It appears that the stress range at any point did not much exceed twice the yield point of the material at design pressure," and "The desirable maximum stress range in a vessel is that range which will produce a service life of the vessel which shall exceed the desired service life, expressed in number of service cycles, by a safe margin." The first statement arouses a bit of doubt as to whether the stress range did really exceed twice the yield point; perhaps the tensile and compressive yield points were sufficiently raised by the straining to keep the stress range between them. The second statement, extended to the limit, appears to mean that, if a vessel were so streamlined as to be free of stress concentrations, it could for most services be operated safely at general stress levels practically up to the yield point in tension. This is plenty of food for thought.

The writer questions the reasoning by which the authors reached the conclusion that "the fatigue test is an accurate test of service life for boiler drums." How the fact that a boiler drum, poorly designed by present standards, withstood service conditions for over 40 years, and then appeared to be in good condition, leads to the conclusion that the fatigue test is an accurate test of service life for modern boilers, is rather obscure.

Prestress. The questions of prestress and the hydrostatic test are inseparable, especially for vessels not thermally stress-relieved. In such vessels cold-forming and welding lock up very complex stress systems which, in a sense, are prestress systems.

These the hydrostatic test modifies by plastic-straining, particularly in the welds and in regions where there are fabricating misalignments and design discontinuities such, for example, as the direct connection of a conical head to a cylindrical shell.

The real question is whether the residual-stress system after the hydrostatic test is more favorable to vessel service than the locked-up stress system which would develop in service if the hydrostatic test were omitted.

Since the major stresses induced by pressure are tensile, it seems that the highest tensile prestrain short of general yielding is the most beneficial because it most reduces misalignments and, in regions of design discontinuities, results in the lowest subsequent "pressure-on" tensile stress in service. Furthermore, should the latter effect be overdone, to the extent that plastic compressive yielding occurred upon release of pressure, such secondary yielding would again modify the residual-stress system so that thereafter the pressure-on tensile stress in service would be the lowest possible, and the "pressure-off" stress would be the compression yield point. Of course the extreme tolerable stress cycle is between the highest possible compressive and tensile yield points short of failure.

On the other hand, if no overpressure were applied prior to service, the pressure-off compressive stresses at regions of stress concentrations would be the lowest possible, and the pressure-on stress would be the tensile yield point if plastic yielding occurred when the working pressure was first applied.

Does the Bauschinger effect in any way change this reasoning? Does embrittlement due to cold-working?

The concluding statement: "It is shown that present design rules are not correct as regards dished heads and reinforced openings" cannot be denied in an absolute sense. However, the burden of proof is on him who claims that the dished heads of the 1950 ASME Unfired Pressure Vessel Code are inadequate for boiler and other pressure-vessel services. Although in theory these heads could be improved by providing a transition spiral (like a railroad transition spiral), between the cylinder proper and the head proper, such refinement and complication seem inadvisable in view of the practically perfect performance of modern dished heads, both torispherical and ellipsoidal.

Commendation is due the authors for this most stimulating, instructive, and forward-looking paper.

D. S. JACOBUS.⁶ The authors should be commended for showing the way in which advances may be made in designs and constructions.

The advantage of diminishing stress concentrations is well known but, as shown by the tests and data given in the paper, such concentrations exist in some of the usual constructions.

If models of new designs were tested in the way described in the paper, progress could be made in formulating rules to provide the necessary safety with a minimum amount of material.

Let us hope that the work of the authors will cause such a movement to be started and perpetuate their efforts.

AUTHORS' CLOSURE

It is indeed gratifying to the authors of a paper to find their work has been to some avail, that their paper has been read thoroughly and with discernment, and that it has evoked searching discussion. The original paper, being necessarily limited in length, passed lightly over much experience and analysis that influenced the conclusions drawn. Mr. H. C. Boardman has pointed out several significant gaps in the paper which we will endeavor to fill in this closure.

In connection with the dimensionless constants set up to as-

say the behavior of a shell or dished head, it has been pointed out that the geometric eccentricity implicit in the moment constant is a function of pressure as well as vessel size for a given vessel shape. We have found this to be only a minor factor. The doubly curved surface of a drum head is so rigid that its shape changes only slightly with pressure unless the pressure is carried so high that a large portion of the head material has yielded. In such a case a new head shape is formed which behaves somewhat differently. We have had only a few opportunities of checking heads of similar shape but varying ratios of thickness to diameter. In each case the load and moment coefficients have checked to within the geometric accuracy of the vessels.

The testing so far has been confined to vessels of the proportions in general use. As our company uses progressively deeper heads with increasing pressure, there has been no opportunity to test any shape over a wide range of thicknesses. We would expect, however, that in very thick heads there would be a non-linear stress distribution through the wall at places where the curvature is high in relation to the thickness, much as in a curved beam. Properly evaluated, the same loading and bending constants might well still hold for thick heads.

The elliptical openings were designed from the analysis of C. E. Inglis as given by Timoshenko.⁸ In high-pressure drums, the addition of material to form a reinforcement for an opening is sometimes undesirable, both for fabrication and for service life. Reinforcement is then best provided by increasing the shell thickness. The optimum opening shape without local reinforcement is an ellipse whose axes are parallel and proportional to the principal stresses. The local tangential stress around the opening is the sum of the principal stresses. This is predicted from the analysis and closely verified experimentally. If local reinforcement is added to further reduce local stresses, then the optimum opening shape becomes less elongated, until, in the limit, for no disturbance in the shell plate, the optimum opening shape becomes an ellipse whose axis ratio is the square root of the ratio of the principal stresses. This result is important in the design of efficient low-pressure vessels, and we are much indebted to Mr. Boardman for his analysis of the latter condition.

In the case of the old-type drum which was strain-gage tested, the metallurgical examination showed only normal 55,000-psi UTS plate. There was no elevation of the yield point or abnormal corrosive attack even in the zone showing extensive Lüders' lines. The physical properties checked the original mill-test reports to the usual accuracy of such tests. The strain gages definitely showed a stress range at working pressure of at least twice yield point, and proportionally more at test pressure. A measured yield point is a function of the shape as well as the material of the specimen, and actual yielding in the direction of load is also affected by the stresses in the perpendicular directions, so that we cannot say that an operating stress range of twice the yield point of a standard 0.505 specimen means actual yielding in the vessel. Nor can it be determined from the behavior of any gage that yielding has taken place at that gage, for yielding at an adjacent location at another stress level will increase the load on the metal under the gage to show an apparent yielding.

In applying strain gages to a vessel, it is unlikely that the gage will be applied exactly to the highest stressed location. The gage indicates average strain over its gage length so that the peak stress is always larger than indicated. All these factors add so that it may be stated confidently that the peak-stress range in the head of the old drum tested was well over twice the nominal yield point of the material as given by a standard 0.505 specimen.

⁸ "Theory of Elasticity," by S. Timoshenko, McGraw-Hill Book Company, Inc., New York, N. Y., 1934, p. 175.

⁶ Past-President, ASME.

The extensive and well-formed system of Lüders' lines shows that there was much plastic action during the drum life.

Service tests have shown no definite upper limit for allowable stress in boiler drums. Given the usual good water conditions, local stress ranges at working pressure of twice the nominal yield point seem to operate with complete satisfaction. As it is manifestly impractical to operate a vessel with the general stress level at yield point, it is seen that isolated stress raisers may have a concentration factor of at least 2.

This of course applies to boiler drums and present boiler plate. Contact with other fluids and the use of high-strength steels may alter these conclusions markedly and will require a separate evaluation.

Certain features of design are not susceptible to stress analysis, either mathematical or experimental. Examples are the fillet at a gasket seat and the built-in crack at the root of a fillet weld. For such cases, an accelerated service test is desirable. The simplest such test is the room-temperature fatigue test. This fatigue test can be invalid on three counts: (1) Its results may be unrelated to service life; (2) they may be overly optimistic, or, (3) pessimistic in predicting service life.

1 A room-temperature fatigue test, using water as the pressure fluid, will certainly not predict performance under corrosive conditions or at high temperatures in the creep range. However, our tests have revealed no invalidating evidence in the range of saturation temperatures in boiler work up to 650 F.

2 The speed of cycling is necessarily much higher in a fatigue test than in boiler service, and there is an observed small increase in fatigue strength with increase of cycling frequency. It is possible that very slow cycling might show some lowering of fatigue strength. However, we may note that fatigue strength is unaffected by testing frequency from the slowest normally run up to about 5000 cycles per min. An increase to 1,000,000 cycles per min will raise the endurance limit by a factor of the order of 30 per cent. We would not expect to find any serious lessening of fatigue strength at very slow cycling rates. Our service experience shows no corrosive attack from boiler water during these slow cycles.

3 Several factors apply which may make service life greater than that predicted from fatigue-testing. If the fatigue life is determined by the number of cycles at peak or test pressure, then the cycling at lower operating pressures may raise the endurance limit appreciably. If the service life is predicted from number of cycles at working pressure, properly weighted for the damage caused by occasional overpressuring, then the effect of the mild heat-treatment at saturation temperature may be underestimated.

The amount of information available from service experience, concerning operation at stress ranges higher than twice yield point, is very small. Feed nozzles have developed cracks when quenched with cold water. Fired mud drums have cracked when in-

sulated from the water inside by scale or oil. Boiler sectional headers have cracked when intermittently quenched by improper use of the water lance. All of these cases have involved estimated thermal stress ranges of 100,000 psi or more and at least several hundred cycles. The service life obtained under such conditions is about what could be predicted from fatigue-test data. Certainly, if the service life were very much less than might be predicted from fatigue data, the old drums built prior to 1915 would not have the long service life actually afforded. If we require that a design when submitted to fatigue test, shall exhibit a life, measured in number of cycles that shall exceed the desired service life by a wide margin, say by a factor of 10, then the safety of the design is certainly assured. There are several commonly used details of current boilers that may not meet such a test.

The stress ranges in blankheads designed in accordance with the ASME Power Code are shown in Fig. 22 of this closure. It

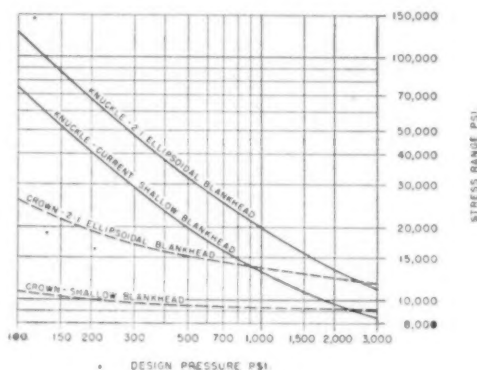


FIG. 22 ACTUAL OPERATING STRESS RANGE IN 2:1 ELLIPSOIDAL AND SHALLOW DISHED BLANKHEADS SIMILAR TO FIGS. 6 AND 3. DESIGNED IN ACCORDANCE WITH ASME POWER CODE: $S = 14,000$ PSI

is seen that the stress range is high in the thinner low-pressure heads and very low in high-pressure heads. This is inherent in any head-design formula which specifies a thickness proportional to pressure. The company with which the authors are connected has no service experience with the thin low-pressure heads.

For many years, long before these tests were conducted, it has been our practice to use shallow dished heads at pressures below 300 psi, 2:1 ellipsoidal heads from 300 psi to about 1000 psi, and hemispherical heads at higher pressures. Heads designed for 160 psi are used at lower pressures. This practice, it is now seen, has kept operating stress ranges under 50,000 psi. Dished heads might well be used at much higher pressures than is now the practice, if the Code were modified to permit a reasonable stress range at such pressures.

T
boi
me
ods
as v
pre
duc
vess
in a
The
tus

E

pape
take
It ha
neces
a fac
sider
reduc

In
by m
Fore
Bald
more
much
sis cr
there
nique
use o

Be
levels
terna
tions
tempe
were
fatigu
tempe
tions
high-t
in an
larily
in this
pose v

¹ As
Compe
² He
pany,
Con
presen
of TH
Nor
unders
the Soc

Experimental Technique in Pressure-Vessel Testing

By L. F. KOOISTRA¹ AND R. U. BLASER,² ALLIANCE, OHIO

The latest designs of pressure vessels for high-pressure boiler service have been investigated by means of experimental stress analysis and hydraulic fatigue tests. Methods have been developed to measure strain on the inside as well as on the outside of pressure vessels under internal pressure. Pulsating hydraulic fatigue tests were conducted on full-scale high-pressure drums. Scale-model vessels of about one tenth actual size were similarly tested in a saturated-steam and water atmosphere of 2000 psi. The technique used in these tests, and the special apparatus built for the purpose are described.

INTRODUCTION

EXPERIMENTAL development of pressure vessels has been carried on for many years during which various testing techniques and procedures have been used. This paper will discuss certain phases of this development that have taken place in the authors' company during the past 10 years. It has long been felt that the use of a design factor of 5 was unnecessarily large, and that more appropriately it could be called a factor of ignorance rather than a factor of safety. The very considerable amount of work herein described was undertaken to reduce the number of unknown factors in pressure-vessel design.

In the earlier stages, experimental stress analysis was conducted by means of Berry strain gages and somewhat later by using DeForest scratch gages. These tools were later replaced by the Baldwin-Southwark SR-4 gages. The SR-4 gages were so much more accurate and sensitive and could be used with so much greater facility that the art of experimental stress analysis came into its own with the use of this tool. This paper, therefore, will deal largely with the development and the technique employed for experimental stress analysis starting with the use of the SR-4 gage.

Besides the use of SR-4 gages, which tell the designer what stress levels are reached in the various parts of the structure under internal pressure, other methods for determining stress concentrations were employed, such as room-temperature and high-temperature fatigue tests. The room-temperature fatigue tests were conducted on full-size drums, and the high-temperature fatigue test on scale-model cylindrical specimens. The room-temperature full-size drums were subjected to hydraulic pulsations by means of apparatus specially built for this purpose. The high-temperature specimens were placed inside of a steam drum in an atmosphere of saturated steam and water and were similarly tested by means of hydraulic pulsations. The methods used in this kind of testing and the special apparatus built for this purpose will be described.

¹ Assistant Director, Materials Laboratory, Babcock & Wilcox Company, Research and Development Department. Mem. ASME.

² Head, Engineering Physics Section, Babcock & Wilcox Company, Research and Development Department.

Contributed by the Power and Applied Mechanics Divisions and presented at the Fall Meeting, Erie, Pa., September 28-30, 1949, of THE AMERICAN SOCIETY OF MECHANICAL ENGINEERS.

NOTE: Statements and opinions advanced in papers are to be understood as individual expressions of their authors and not those of the Society. Paper No. 49-F-20.

The results of the experimental stress analysis, and the merit of various design features are discussed in a companion paper by Schoessow and Brooks.³

Problems in fabrication of fusion-welded pressure vessels, and the inspection and control of the materials entering into this type of product, are described in another companion paper by O. R. Carpenter.⁴

EARLY CONSIDERATIONS

For a great many years it has been accepted practice to subject pressure vessels to a hydrostatic proof test. Sometimes a procedure of hammer testing was also included. Test measurements in the early days were limited to visual observations, linear measurements by rule, or tape measure, and mechanical gages. Such mechanical gages became more refined as dial indicators, Berry gages, and Huggenberger tensometers became available for measuring strain due to pressure loading. All these were restricted to readings on the outside of pressure vessels. Strain determinations on the inside of vessels under pressure first became practical through the advent of the DeForest scratch gage.

Requirements of such extensometers and strain-measuring devices are small size, sensitivity, ease of multiple application, reliability, low cost, little or no damage to specimens, and stability. Slightly more than 10 years ago the resistance-wire strain gage, combining all these requirements, was introduced. This measuring tool has done much to further the art of experimental analysis. It has made possible a clearer understanding of the distribution of stress, both on inside and outside surfaces of pressure vessels. Because of the advantages mentioned, the SR-4 electric-resistance strain gage has been used in most of the work herein described.

At various times brittle coatings, such as whitewash, and later "Stresscoat" have been used to determine the locations of maximum stress. Stresscoat is particularly useful in many cases where the location and direction of maximum stresses is obscure. In this application it serves as an excellent detective measure to determine critical or maximum stress points.

EXPERIMENTAL STRESS ANALYSIS

In testing pressure vessels under internal pressure, a problem immediately arises as to the choice of pressure medium to be used. For the regular hydrostatic tests, water is generally used for this purpose. When stress measurements were made on the outside of the vessel, water was entirely satisfactory. Even later, when DeForest type scratch gages were used for internal-stress measurements, water was not objectionable. The SR-4 gage, being an electrical device, is naturally sensitive to moisture. Consequently, a great deal of development work has been done by several experimenters toward waterproofing SR-4 gage setups.

For atmospheric work, a Petrosene wax coating proved very satisfactory. Waterproofing for internal hydraulic pressure, however, was not available at the time of the earlier SR-4 tests

³ "Analysis of Experimental Data Regarding Certain Design Features of Pressure Vessels," by G. J. Schoessow and E. A. Brooks, published in this issue of Transactions, pp. 567-577.

⁴ "Fabrication of Pressure Vessels," by O. R. Carpenter (not printed).

(1942) and for that matter is still not reliable for high-pressure work.

For the first test in which internal stresses were determined, compressed air was chosen as a pressurizing medium. For this purpose the drum was set up on end, which was permissible in this case since only the stresses in the manhead on one end were to be measured.

Fig. 1 shows the upper end of the drum with the SR-4 gage arrangement. After filling the drum with air at 200 psi, water from the hydraulic line was admitted at the bottom. The rising water column then compressed the air further until the desired test pressure was reached. Maximum pressures of 1268 psi were

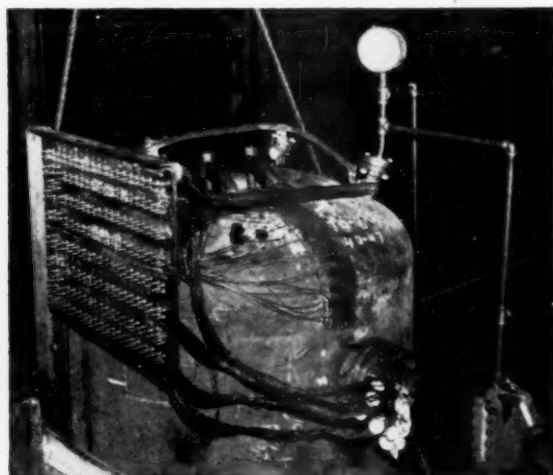


FIG. 1 VIEW OF TEST SETUP OF STEAM DRUM IN VERTICAL POSITION USING COMPRESSED AIR AS PRESSURE MEDIUM

obtained without the water level touching the lowermost gage wires. No particular difficulties were experienced in obtaining consistent data.

Using a compressible gas in high-pressure vessels, sometimes at double the working pressure, was considered dangerous, particularly for experimental vessels. Therefore a method having less energy storage was highly desirable.

In searching for a dry, high-resistance pressurizing liquid, the choice naturally falls on transformer oil. After testing several oils for this purpose, an inexpensive light lubricating oil proved equally satisfactory. The next problem was to bring the necessary gage wires through the pressure shell, electrically insulated and pressure-tight. A special plug was designed for this purpose.

This multiwire plug is shown in Fig. 2 as it looks in the process of assembly. Once put together, several feet of wire are left on either side of the plug so that rewiring the plug is not necessary since soldered connections are made at the end of the leads. Construction details of this plug are shown in Fig. 3. This plug has been used with pressures up to 3750 psi and has been completely satisfactory both with respect to the absence of leaks as well as electrical insulation.

To check the reliability of strain gages under pressure, a separate test was conducted with a weighted cantilever beam inside a small pressure chamber. This pressure chamber could be taken to whatever pressure was desired up to a maximum of 5000 psi, Fig. 4. It could be rotated about a central point so that the cantilever beam would be horizontal, vertical, or at any intermediate angle. Near the fixed end the cantilever beam was pro-

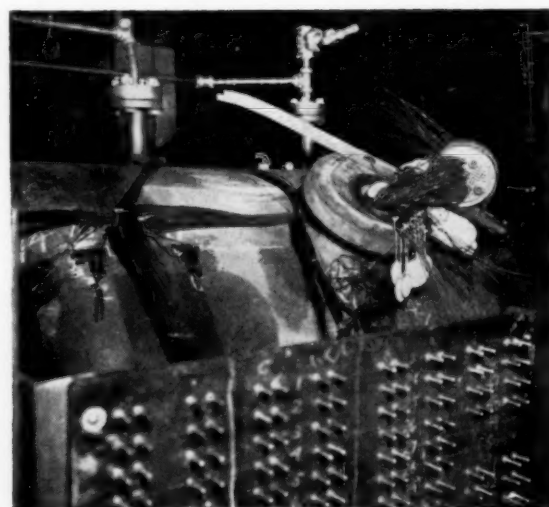


FIG. 2 VIEW OF SR-4 GAGE SETUP SHOWING MULTI-WIRE PRESSURE SEAL IN PROCESS OF ASSEMBLY

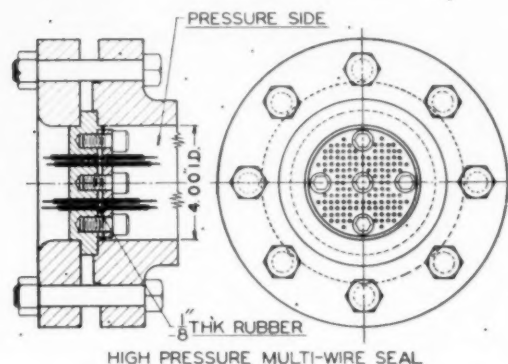


FIG. 3 HIGH-PRESSURE MULTI-WIRE SEAL

vided with machined flats, top and bottom, on which the SR-4 strain gages were applied. Since the cantilever was surrounded on all sides by the high-pressure atmosphere in which it was placed, the gages registered a compression strain as expected. By rotating the assembly, bending stresses independent of internal pressure could be induced in the cantilever beam so that strains due to bending could be isolated from those due to internal pressure. Some variations between gages resulted. Further investigation revealed that these variations were due to differences in technique of application, such as, variation in thickness of the cement layer between metal and gage, air bubbles, etc.

Fig. 5 shows results obtained using an inside reference gage. Briefly, the conclusion is that SR-4 strain gages are reliable at least up to the maximum test pressure of 5000 psi if applied correctly.

For the large vessel tests it is customary to use a dummy gage to correct for temperature changes. When measuring stress under hydraulic pressure, this dummy gage is placed inside the vessel for the inside gages. The dummy-gage specimen is of course in compression on all sides and will show a compression strain. Gages on the inside surface of the vessel have pressures radial to the surface, and a Poisson's ratio effect is present for both dummy



FIG. 4 APPARATUS FOR CALIBRATING SR GAGES UNDER HYDRAULIC PRESSURE

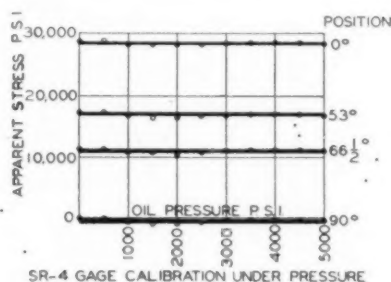


FIG. 5 EFFECT OF HYDRAULIC PRESSURE ON SR-4 GAGE READINGS

and test gages. The theoretical correction for pressure on a dummy block will be as follows

$$\text{Apparent strain } \epsilon_x = \frac{P(1 - 2\mu)}{E}$$

$$\text{Stress correction} = E \epsilon_x = P(1 - 2\mu) \text{ psi}$$

in which:

P = internal pressure, psi

E = modulus of elasticity

μ = Poisson's ratio

ϵ_x = apparent strain

These corrections are negligible in the testing of drums and pressure vessels at comparatively low pressure, and in most cases have been neglected.

INSTRUMENTATION

SR-4 strain gages from $1/8$ in. to 6 in. gage length, and rosettes of various types have been used. The original tests were made

with the Baldwin-Southwark galvanometer-type control box. Later, the electronic SR-4 strain indicator greatly increased the facility of taking strain data. The latest-type K strain indicator is now used. A six-channel Brush Development Company pen-and-ink recorder and amplifier setup is now in use on some dynamic measurements. These are also applicable to measuring stresses during fatigue tests which will be described later.

Although from an electronic point of view stranded lead wire for the multiwire plug may be desirable, solid wire is essential to prevent leakage. Consequently, solid wire of sizes from No. 22 to No. 18 gage have been used in all high-pressure work.

For switching from one gage to another in a multiple setup, plugs similar to those used on household appliances, such as toasters, irons, etc., have proved quite satisfactory. These double-terminal plugs were very simple and enabled rapid manual changing from gage to gage. With two men, several hundred gage locations can be read in one hour. The hydraulic pressure is of course held constant during this interval.

Figs. 6, 7, and 8 show arrangements of representative jobs. The outside views show the terminal board in place. It has been found that the material from which this terminal board is made is critical. It should be of a moistureproof material. This requirement also applies to more modern switching arrangements including multipoint tap switches and automatic switching units.

FATIGUE TESTING

There are many cases on record and in the literature where pressure vessels have been tested to destruction under hydraulic pressure. These vessels usually fail at pressures from 3 to 5 times the allowable working pressure. In those instances where the pressure vessel was made of one of the regular boiler-plate materials, the failure generally occurred after very considerable distortion of the original shape. The relatively large amount of plastic deformation, which of necessity occurs in the weakest section of the design, goes so far beyond the operating strain range in these locations that the final values have very little bearing on the behavior of such a vessel in regular operation. It has been argued successfully that in the final stages of a static-pressure destruction test, one will not be testing the same shape nor the same material as that of the original vessel. Therefore it would be more to the point to test the design in a shape and condition similar to actual service.

It is for this reason that considerable work has been done on testing pressure vessels under conditions of pulsating fatigue from zero to a maximum internal pressure. Although this type of test does not simulate the service conditions of many types of pressure vessels either, it does bring out points of severe stress concentration, or is a means of demonstrating that such stress concentrations do not exceed those that are unavoidable in pressure-vessel design. Where a boiler drum, for example, may be subjected to but a few hundred major cycles during its service life, a pulsating fatigue test of 100,000 cycles at or above working pressure will establish confidence that the design does not contain regions of severe strain which could result in premature failure. Although a more pertinent test is desirable, none has so far been devised except for the high-temperature fatigue test described later, where operating temperature is taken into consideration.

As long as the test pressure did not exceed the hydraulic line pressure available, the pulsation fatigue tests were conducted by means of a motorized valve. This device admits water from the hydraulic system to the test drum and discharges the volume expansion after a certain predetermined maximum pressure has been reached.

When drums with a design pressure of over 1000 psi had to be tested, the 1500-psi hydraulic pressure was insufficient to produce pulsation for $1\frac{1}{2}$ times working pressure. Hence it was decided



FIG. 6 EXTERNAL VIEW OF DRUM SPECIMEN WITH REINFORCED MANHOLE AND VARIOUS NOZZLE DESIGNS

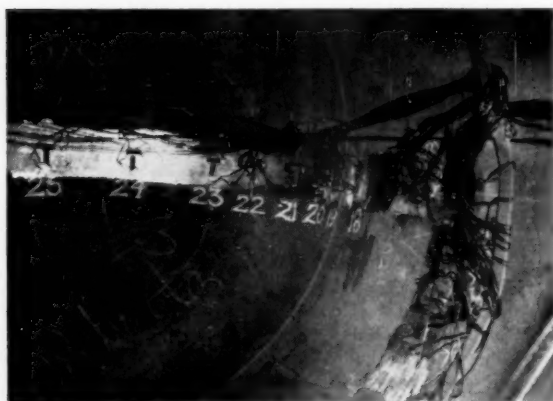


FIG. 7 INSIDE VIEW SR-4 TEST SETUP SHOWING GAGE-WIRING ARRANGEMENT AND NOZZLE OPENING



FIG. 8 INSIDE VIEW SHOWING SR-4 GAGE TEST SETUP IN STIRLING BOILER MUD DRUM
(This drum had been subjected to severe overpressure.)

to build an apparatus that would extend the pressure range up to 6000 psi.

The energy required to pump water at the rate necessary for testing full-size specimens up to a pressure of 6000 psi and then release it, amounts to about 450 hp. This not only would be a sizable piece of apparatus but would become quite expensive for continuous testing in so far as power is concerned. It was therefore thought economical to build a balanced apparatus in which only the frictional forces would have to be overcome. This apparatus consists of two opposed plungers actuated by a central cam, as shown diagrammatically in Fig. 9. Each plunger is connected to a closed hydraulic system completely filled with water. In many tests two drums will be tested simultaneously, one on each plunger. When only one specimen is to be tested the opposing piston is connected to a balance or "dummy" drum to form the elastic counterpart.

When a plunger is pushed into the cylinder, the water in the system is compressed up to the end of the stroke, and on the re-

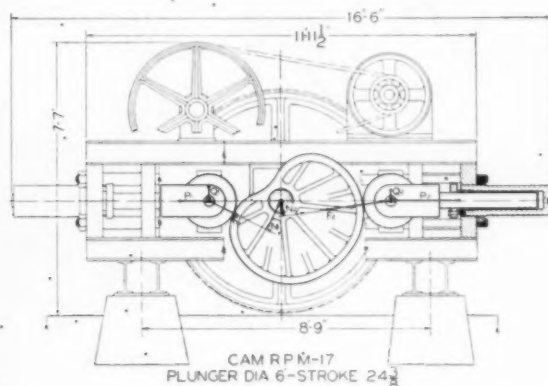


FIG. 9 DIAGRAM SHOWING CAM AND ROLLER MECHANISM OF PULSATOR

turn stroke the plunger is forced outward by the elastic action of the compressed water. Disregarding friction, the work done by forcing the piston in is equal to the work delivered when it is pushed out. By opposing two plungers and actuating them with a suitable cam, the actual energy input can be reduced to frictional losses only. The shape of the cam, however, has to be designed so that the torque required by the ingoing plunger is equal to the torque delivered by the outgoing plunger.

Referring to Fig. 9, the shape of the cam must satisfy the following relationship

$$F_1 \times N_1 = F_2 \times N_2$$

where

- F = resultant of P and Q
- N = radius on which F operates
- P = proportional to plunger travel
- Q = vertical reaction on crossheads

Although there is a theoretical solution for the shape of the cam when the stroke and the diameter of the roller are known, the shape had to be approximated with four sections of circles to avoid making the machining of the cam too costly. A torque analysis of the final shape shows that the simultaneous torque curves very nearly overlap one another, see Fig. 10.

The apparatus was equipped with a 75-hp motor. Only a fraction of this power has been necessary to drive it. The cyclic speed is about 17 pulsations per min for each plunger. Plungers are 6 in. diam and have $24\frac{3}{8}$ in. stroke, providing a displacement of 687 cu in.

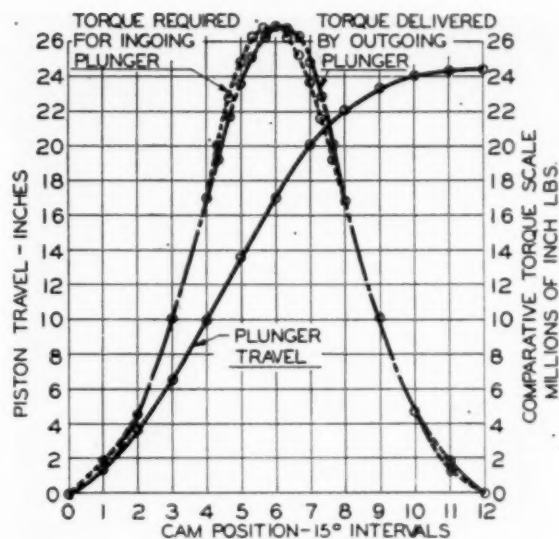


FIG. 10 TORQUE-AND-PLUNGER TRAVEL DIAGRAM FOR PULSATOR-CAM MECHANISM

In order to avoid injury to operating personnel, test drums have been protected by heavy blasting mats made of $\frac{3}{8}$ -in.-diam steel cables.

The heaviest vessel tested on this apparatus is that shown in Fig. 11, having an inside diameter of 46 in. and shell thicknesses of $3\frac{3}{16}$ and $4\frac{1}{4}$ in. The maximum testing pressure used to date is $1\frac{1}{2}$ times the working pressure of the specimens, or 3750 psi. The compressibility of water for room-temperature operation (100 F) is shown in Fig. 12. For large-size high-pressure specimens, the volume expansion still is several times the total displacement of the pulsator plunger. It is therefore necessary to displace the major part of the water volume in the specimen drum by a much less compressible solid. In the beginning pig iron was used for this purpose but when even this became a critical material during the war, it was found that dense paving brick made an excellent substitute.

The elastic displacement during a pressure cycle is due, for the major part, to the compressibility of the water and to a lesser degree is a result of the dilation of the vessel under the action of internal pressure. These values can be calculated from known equations as long as the physical constants of the material are known.

In most tests the pulsator was operated only during working hours, with rest periods at night and over week ends. One run would consist of 100,000 cycles, after which the specimen drum was carefully inspected, visually and with magnetic-particle technique. The first run is usually conducted at working pressure, others at higher pressure up to 1.5 times working pressure.

In so far as boiler service is concerned, the first run would demonstrate that, from the point of view of cyclic loading, the drum is good for many times its natural service life. The second and third run are superimposed to obtain additional information as to its margin of strength and its ability to withstand considerable overpressure on infrequent occasions.

It is realized that the stepwise increase in cycle pressure will result in somewhat better fatigue life than would be obtained on a straight run. This procedure was followed only as a matter of economy in testing time. If the cycle pressure is chosen too low, a test to failure would last indefinitely at the slow speed of 17 rpm,

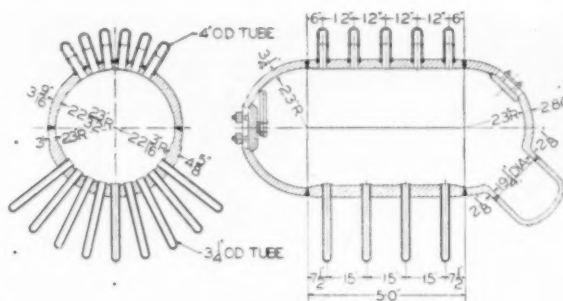


FIG. 11 FULL-SIZE-DRUM FATIGUE SPECIMENS

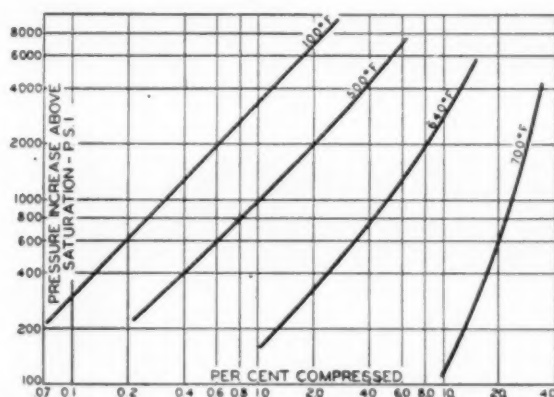


FIG. 12 COMPRESSIBILITY OF WATER AT VARIOUS TEMPERATURES

and if chosen too high the number of cycles to failure might be so few that the test could be considered insignificant and not justify the high cost of the specimen. The extra number of cycles that may have been obtained from the "coaxing" effect can easily be discounted in the large margin of fatigue life obtained on a properly designed vessel. Failures like those shown in Fig. 13 bring out stress-concentration points at which design improvements are required.

The pulsation test on all important specimens is preceded by an experimental stress analysis, as shown in Fig. 14. Lately the experimental stress analysis in turn has been preceded by a brittle-lacquer test cycle to determine points of maximum stress, and to indicate the best location for the SR-4 gages for measuring maximum stresses.

SLOW CYCLE TEST

When observing a vessel that is being subjected to fairly rapid cycles of pulsating pressure, there appears to be a difference in response to this type of cycle compared to bringing the pressure up to the maximum and then holding it there. In heavy vessels, a time factor or a brief period of readjustment seems to enter. This is particularly noticeable when the drum contains a multiplicity of closely spaced expanded tubes.

In testing the specimen drum shown in Fig. 15, this observation led to a change in the pressure cycle. For this specimen, which contained six $4\frac{1}{2}$ -in.-diam, four $3\frac{1}{8}$ -in.-diam, twenty 2-in.-diam, and ninety-four 1-in.-diam tube holes, the pressure cycle was as follows:

After opening the hydraulic valve, the pressure was allowed to rise to the maximum test pressure, was kept there for $2\frac{1}{2}$ minutes, and then released by opening the discharge. After $2\frac{1}{2}$ minutes at



FIG. 13 VIEW SHOWING FATIGUE FAILURE IN HIGH-PRESSURE-DRUM SPECIMEN



FIG. 14 OUTSIDE VIEW OF HIGH-PRESSURE-DRUM SPECIMEN SHOWING PUSHOUT DOWNCOMER CONNECTION ON NEAR HEAD

zero pressure, the cycle was repeated. This cycle seemed to be more severe than the continuous cycle without rest periods. At $1\frac{1}{2}$ times working pressure, several leaks were developed on the expanded tube seats. This was particularly true on the small-diameter tubes and provided an opportunity to improve the method of expanding this size tube. Fig. 16 is an inside view of the tube ligaments.

HIGH-TEMPERATURE FATIGUE TEST

All the tests described were conducted at room temperature. Under actual service conditions, however, the metal of the drum is exposed to saturated steam and water. It was therefore desirable to investigate the effect of temperature as well as the contact with steam and boiler water. An apparatus to perform a pulsating fatigue test under simulated service conditions was designed to investigate this phase.

Although this apparatus went through a few evolutionary stages, only the final arrangement will be considered here. The test was performed on scale models, since compressibility of high-temperature water is such that plunger displacement for full-size specimens is beyond the scope of practical possibilities. Compressibility values for water at elevated temperatures are given in Fig. 12.

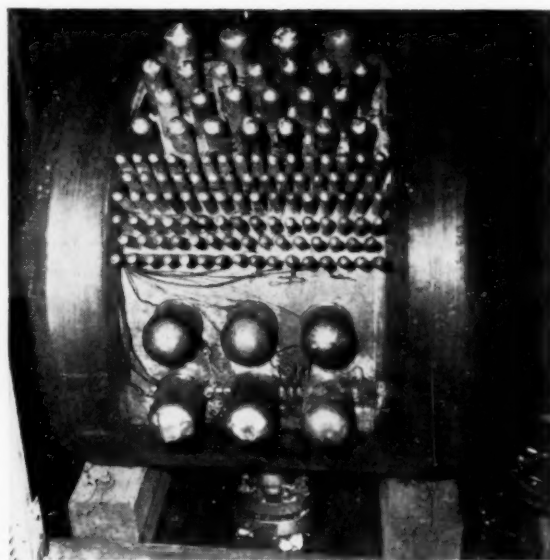


FIG. 15 EXTERNAL VIEW OF FULL-SIZE DRUM SPECIMENS SHOWING TEST SETUP ON TUBE LIGAMENTS



FIG. 16 INSIDE VIEW OF TEST SETUP ON TUBE LIGAMENTS

A diagrammatic arrangement of the test apparatus is shown in Fig. 17. Since the hydraulic pulsations were provided by a high-pressure triplex pump, only three specimens or pairs of specimens could be tested at any one time. The inlet and discharge valves were removed from the pump so that the plungers only pulsated the water without actual pumping action.

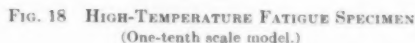
The specimens were placed in a 24-in. ID \times 5-ft-long steam drum which was operated at a pressure of 2000 to 2500 psi. The location of the specimens was such that approximately one half was above the water line and the other below it. The water in the drum was representative of average boiler-water conditions, namely, a pH of 10.5-11, a NaSO_4 to NaCl ratio of 3 to 1, and a total solids concentration of 1500-2000 ppm.

The inside of each specimen is connected to one of the three plunger bodies of the triplex pump. The maximum pressure of the fatigue cycle was 7500 psi so that the pressure difference between inside and outside of the specimens was 5000 psi. In parallel with the specimens in the steam drum, three similar



Specimens were 6 in. ID and $\frac{3}{8}$ in. thick with heavy hemispherical ends and about 24 in. long on the straight cylindrical part, as shown in Fig. 18. The cylindrical sections were made of regular $1\frac{1}{8}$ -in.-thick boiler plate bent to a semicylindrical shape, welded together, and then machined inside and out.

The maximum pressure reached in the pulsing circuit depends upon the total water content of the circuit, the temperature of



This core was made of such size that the maximum cycle pressure would rise above that necessary for this test. Some additional water volume was then provided on the outside of the steam drum by connecting to each circuit a high-pressure buffer vessel somewhat smaller than the specimen itself. By regulating the temperature in the buffer vessels, the compressibility of the water contained in them could be varied at will, and thus the over-all compressibility of the circuit controlled.

Considerable trouble was experienced due to leakage of high-pressure valves, particularly check valves and high-pressure relief valves. These troubles were gradually overcome by proper design, and operation settled down to a watchful routine.

RESULTS OF FATIGUE TESTS

Full-Size Specimens. Quite a large number of pressure vessels have been tested by the authors' company using techniques similar to those described. Some of the early tests were reported by Prof. H. F. Moore.⁵ The work reported was continued to include various drum designs with and without tube holes. Later tests included banded vessels as well as many pressure vessels covering the range of thicknesses from $1\frac{1}{2}$ in. to $4\frac{3}{4}$ in. Details of several of these test vessels and the results will be included here.

Test Drum, Fig. 15. The test drum, shown in Figs. 15 and 16, was also made of SA-212 plate and included a total number of 124 expanded tube nipples ranging from 1 in. diam up to 4 $\frac{1}{2}$ -in. diam. This drum was designed for a pressure of 980 psi at a stress of 22,500 psi in the shell proper. The drum was given 100,000

^a "Tests of the Resistance to Repeated Pressure of Forged Riveted and Welded Boiler Shells," by H. F. Moore, Trans. ASME, vol. 53, 1931, pp. 55-60.

cycles at 1078 psi pressure and 1400 slow cycles at 1470 psi pressure as described previously. Strain-gage tests have indicated stresses at various locations, as given in Table 1.

TABLE 1 STRESSES IN TEST DRUM, FIG. 15

Cycles	Pressure, psi	Stresses, psi		
		Tube ligaments	Manhead	Blank head
4	980 WP	23600	39400	35600
100000	1078	26000	43300	39200
1400	1470	34500	57500	51700

The results of this fatigue test were leaks at some of the tube seats. This development resulted in changes in tube-expanding methods which will not be discussed here. There were no indications of incipient failure in any of the other locations, such as the shell proper or in the head knuckles.

Drum With Intentionally Faulty Welds. For another vessel a piece of rimmed steel, SA-70 plate, having laminations and non-metallic inclusions, was used for the shell and the blank head. The manhead was SA-212 plate. The thicknesses of shell, blank head, and manhead were $1/2$ in., $5/8$ in. and $11/16$ in., respectively. This test was conducted to determine the effect of welding defects on the fatigue life of a vessel and both submerged-arc welding and automatic multipass welding were used. The final failure was in a highly stressed section of the manhead knuckle, although incipient cracks also appeared in the defective longitudinal weld seam. The conditions of failure are described in greater detail in the companion paper by Carpenter.⁴ The physical properties and chemistry of some of the parts of this drum are given in Table 2.

TABLE 2 PROPERTIES OF PARTS OF TEST DRUM

	Blank head	Shell	Manhead	Manhead
MILL REPORTS 0.505 IN. (AFTER TEST)				
Tensile, psi.....	56700	56600	79900	82900
Yield point, psi...	36900	37200	42400	43300
Elongation, per cent	32.5	32.0	30.7	28.8
CHEMISTRY, PER CENT				
C.....	0.21	0.21	0.28	
Mn.....	0.41	0.41	0.69	
P.....	0.015	0.015	0.012	
S.....	0.040	0.040	0.027	
Cu.....	0.32	0.32	0.22	
Si.....			0.20	

The stresses and cycles in the shell proper are given in the following tabulation, but due to stress concentration, the inside of the knuckle of the head has probable stresses as high as 35,000 psi. The series of cycles follows:

100000 cycles at 560 psi pressure	13750 hoop stress
100000 cycles at 615 psi pressure	15000 hoop stress
161000 cycles at 840 psi pressure	20600 hoop stress

Even under these adverse conditions the vessel withstood a number of pressure cycles far beyond actual service requirements both in number and magnitude.

High-Pressure Drum. This drum, shown in Fig. 11, was designed for a working pressure of 2500 psi, and tested at pressures up to 3750 psi. The average ligament stress in the upper shell was 23,585 psi calculated in accordance with the 1943 ASME Codes. This drum was made of SA-212 steel with the physical properties given in Table 3.

TABLE 3 PHYSICAL PROPERTIES OF TEST DRUM

	Upper shell	Lower shell
Plate thickness, in.....	$3 \frac{1}{2}$	$4 \frac{1}{2}$
Tensile strength, psi.....	70820	68250
Yield point, psi.....	36750	37500
Elongation in 2 in., per cent.....	35	33
Reduction of area in 2 in., per cent.....	56	55.7

The first point of stress concentration located was a failure in the sharp corner of the manhole-cover seat shown in Fig. 13. This occurred after 100,000 cycles at 2500 psi pressure and 57,240 additional cycles at 3000 psi pressure. This point in the original construction was improved by a change in design. During the pulsating fatigue test this drum was subjected to the series of pulsations given in Table 4.

TABLE 4 PULSATIONS ON TEST DRUM

Cycles	Pressure psi	Calculated average ligament stress, psi	Maximum stress range in tube hole, psi
100000 at working pressure (WP).....	2500	23585	41600 test
100000 at 1.2 WP.....	3000	28300	51200*
100000 at 1.4 WP.....	3500	33000	59730*
12000 at 1.5 WP.....	3750	35380	65500 test

* Values calculated from the average measured stress-concentration factor for this location of 1.81.

The test was terminated after the cycles indicated, owing to a fatigue failure which resulted in a leak at a welded-tube stub in the upper shell. This was a radial crack starting at the inside of the tube hole on the longitudinal center line. Further inspection revealed 13 such failures in the upper shell tube sheet. The test was dismantled and metallurgical inspection of these failures will be made.

Model Tests. In the high-temperature fatigue tests, 15 specimens were tested, 9 of which were of the type shown in Fig. 18, and will be reported here. Of the latter, 4 were tested at room temperature and 5 in direct comparison in the steam drum at 2000-psi saturated-steam and water atmosphere. All failures occurred in the weld or weld-affected zone, and all of them were in a longitudinal direction, i.e., transverse to the maximum stress. The test data are given in Table 5, and are plotted on logarithmic co-ordinates in Fig. 19. As a means of comparison an S-N curve for full-size welded specimens is also shown.⁶ The stress range of the cycle is not exactly alike, however, since the latter specimens were tested from zero to a maximum tension, and the model specimens were tested from a hydraulic compressive stress of the steam-drum atmosphere of 2000 psi to a maximum biaxial cylinder stress resulting from internal pressure.

This comparison brings out the following:

- 1 The test results of the cylindrical specimens are lower than those of the flat-plate specimens.
- 2 In the scatter band there is no particular preference between the points of the hot specimens and the cold specimens. There is apparently no significant change in the endurance limit resulting from the high-temperature steam-drum environment.

CONCLUSION

The foregoing testing techniques are the outgrowth of many years of pressure-vessel development work. They do not in every case result in data leading to absolute conclusions but are, rather, several approaches to the problem of reducing the wide margin for unknown factors in this field of engineering. By measuring stresses, by subjecting both model and full-size specimens to static as well as cyclic loading, and at room temperature as well as under simulated service conditions, the background of knowledge has been extended. The results attained are as follows:

- 1 A reliable method of measuring stress on the inside surface of heavy vessels under high internal pressure has been developed.

⁶ Bulletin no. 27, University of Illinois, Engineering Experiment Station.

TABLE 5 DATA ON CYLINDRICAL MODELS IN HIGH-PRESSURE STEAM-AND-WATER ATMOSPHERE

Specimen description	No.	Tensile strength, psi	Yield point, psi	Weld metal ^a	Stress relief	Average hoop stress, psi	Number of cycles	Location of failure ^b
Series A X made of bent 1/8-in. plate, not polished, welds ground flush (hot)	1	77090	43390	A	No	38000	49267	1 in. from longitudinal weld seam and parallel
	2	77090	43390	A	No	43000	34289	Junction of long and girth weld
	3	77090	43390	B	No	41700	31360	Longitudinal weld seam
Series D • specimens made of bent 1/8-in. thick plate, medium polish inside and outside (hot)	1	70000 to 74600	40600 to 48700	A	No	31700	269000	Edge of longitudinal weld seam
	2			A	Yes	32800	340000	Girth weld seams
	3			B	No	34500	76000	Longitudinal weld seam
Series F ○; hot specimen made of SA-212 plate, machine inside and outside (see Fig. 18)	1			A	Yes	35000	105212	Longitudinal weld steam space
	2			A	Yes	35000	192085	Longitudinal weld steam space
	3	74700	52160 ^c	A	Yes	33600	306018	Longitudinal weld steam space
	4			A	Yes	34000	186221	Longitudinal weld steam space
	5			A	Yes	33200	242123	Longitudinal weld water space
Series G □; room temperature, specimens same as Series F	1	72180	46090 ^c	A	Yes	33700	54942	Longitudinal weld
	2			A	Yes	35200	219611	Longitudinal weld
	3			A	Yes	34400	247958	Longitudinal weld
	4			A	Yes	33600	268550	Longitudinal weld
Weld metal.....		71500	79990	on test plate longitudinal and transverse are approximately equal				

^a Electrode designation: A, Carbon-moly coated electrode (0.33 C, 0.5 Mo); B, 25 Cr 20 Ni coated electrode.

^b All failures were longitudinal cracks; i.e., transverse to the maximum stress, starting at small mechanical weld defects.

^c These physical properties were determined on one hot and one cold specimen after test.

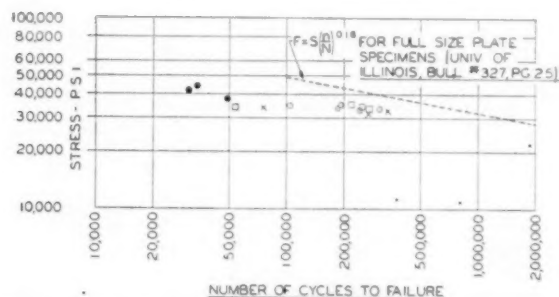


FIG. 19 SOME RESULTS ON CYLINDRICAL SPECIMENS SUBJECT TO CYCLIC PULSATION

- × = Specimens in series A of Table 1
- = Specimens in series D of Table 1
- = Specimens in series F of Table 1
- = Specimens in series G of Table 1

This work resulted in the use of oil as a pressurizing medium.

2 A simple and reliable device for bringing a multiplicity of gage wires through the wall of a pressure vessel in a manner suitable for accurate strain-gage measurements was designed and successfully used.

3 A method has been developed to isolate the effect of hydraulic pressure on SR-4 gages and to calibrate them in a setup employing an inside "dummy."

4 An apparatus has been designed and built for pulsating full-scale pressure vessels economically up to a maximum pressure of 6000 psi at room temperature.

5 A method of pulsating model vessels in an atmosphere of saturated steam and water at elevated pressure and temperature has been built and operated, and a limited check made to determine the effect of such an environment compared to that of room-temperature water.

As the problem of pressure-vessel design at the present time is under intensive investigation, it is hoped that this work will contribute in some small measure to developing the optimum design from an economic, engineering, and service point of view.

Discussion

HENRY LIESSENBERG.⁷ The authors stated that in applying the slow cycle test, which had proved more severe than the first pulsation test, leaks developed on the expanded tube ends, particularly on the small-size tubes. It would be helpful if the authors would state whether tube expansion was controlled by the elongation method, or what other method for control in expanding was applied; also the amount of expanding before test and additional amount of rerolling required to eliminate leakage.

The authors are to be congratulated on the brilliant conception of their high-temperature fatigue test, even if small models had to be used. It is interesting that the test indicated practically no difference in number of cycles between hot and cold specimens. It is the writer's belief that if the shell is exposed to furnace gas, which is of much higher temperature than the inside water temperature as used in model test, different results would be encountered. To conduct such a test would require considerable expenditure. It would be helpful if the authors would state to what percentage failures occurred between longitudinal and circumferential welds, or if all failures occurred in longitudinal welds only, as well as type of failures. Did any failures occur in the attachment weld of the tube nipples?

The statement that endurance-limit tests on cylindrical specimens are considerably lower than on flat-plate specimens is in agreement with previous conclusions, i.e., that in a curved plate, as used in drums, initial residual stresses due to rolling, pressing, or forming are never fully eliminated by annealing.

Were microphotographs taken of weld and adjacent plate before test and after failure to indicate possible change in grain structure under fatigue test? If so, will the authors supply such photographs for study?

H. L. O'BRIEN⁸ AND E. WETTERSTROM.⁹ The discussion

⁷ Combustion Engineering-Superheater, Inc., New York, N. Y.

⁸ Research Engineer, Graver Tank and Manufacturing Company, East Chicago, Ind. Jun. ASME.

⁹ Graver Research Fellow, Purdue University, Lafayette, Ind. Mem. ASME.

which follows has a twofold purpose: Primarily, the mathematical development of experimental techniques for analyzing biaxial-stress conditions is directed toward the end of illustrating that the authors' assumptions are accurate within the limits of their test. Nevertheless, it is to be pointed out that appropriate corrections must be made when the SR-4 electrical resistance strain gage is utilized under certain conditions of loading.

The nomenclature resorted to in this development is as follows:

- $\bar{\epsilon}_0, \bar{\epsilon}_1, \bar{\epsilon}_2$ = strain as read, in./in.
 $\epsilon_0, \epsilon_1, \epsilon_2$ = actual strain, in./in.
 P = hydrostatic pressure, psi
 E = modulus of elasticity, psi
 μ = Poisson's ratio
 S = stress, psi

The basic equation of biaxial stress is¹⁰

$$S_1 = \frac{E}{(1-\mu^2)} (\epsilon_1 + \mu\epsilon_2) \quad [1]$$

From this relationship it is apparent that the stress in any direction can be determined if the strain in that direction and the strain at 90 deg are known. When these strains are being evaluated by an SR-4 strain-gage circuit, there is no assurance that the strains are correct "as read," owing to the difference in loading the active gage and the dummy gage. The former is subjected to pressure in one direction only; whereas the dummy gage is under pressure from all sides. These conditions are illustrated in Figs. 20 and 21, herewith, along with the co-ordinate system.

Writing the equation for strain in the stressed body, we obtain

$$\epsilon_1 = \frac{P}{E} \mu - \frac{S_2}{E} \mu + \frac{S_1}{E} \quad [2]$$

$$\epsilon_2 = \frac{P}{E} \mu + \frac{S_2}{E} - \frac{S_1}{E} \mu \quad [3]$$

A solution to simultaneous Equations [1] and [2] is obtained by multiplying Equation [3] through by μ and adding

$$\begin{aligned} \epsilon_1 &= \frac{P}{E} \mu - \frac{S_2}{E} \mu + \frac{S_1}{E} \\ \mu\epsilon_2 &= \frac{P}{E} \mu^2 + \frac{S_2}{E} \mu - \frac{S_1}{E} \mu^2 \\ (\epsilon_1 + \mu\epsilon_2) &= \frac{P}{E} (\mu + \mu^2) + \frac{S_1}{E} (1 - \mu^2) \end{aligned}$$

$$\text{Then } \frac{S_1}{E} (1 - \mu^2) = (\epsilon_1 + \mu\epsilon_2) - \frac{P}{E} (\mu + \mu^2) \quad [4]$$

Introducing the argument $\epsilon_1 = \bar{\epsilon}_1 - \epsilon_0$ Equation [4] may be rewritten as

$$\begin{aligned} \frac{S_1}{E} (1 - \mu^2) &= [\bar{\epsilon}_1 - \epsilon_0 + \mu(\bar{\epsilon}_2 - \epsilon_0)] - \frac{P}{E} (\mu + \mu^2) \\ \frac{S_1}{E} (1 - \mu^2) &= [\bar{\epsilon}_1 + \mu\bar{\epsilon}_2 - \epsilon_0(1 + \mu)] - \frac{P}{E} (\mu + \mu^2) \end{aligned}$$

Substituting $\epsilon_0 = (P/E)(1-2\mu)$ we obtain

$$\frac{S_1}{E} (1 - \mu^2) = \bar{\epsilon}_1 + \mu\bar{\epsilon}_2 - \frac{P}{E} (1 - 2\mu)(1 + \mu) - \frac{P}{E} (\mu + \mu^2) \quad [5]$$

¹⁰ "Theory of Elasticity," by S. Timoshenko, McGraw-Hill Book Company, Inc., New York, N. Y., 1934, p. 162.

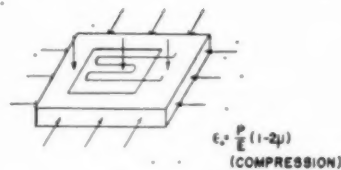


FIG. 20 DUMMY GAGE BLOCK SUBJECT TO PRESSURE FROM ALL DIRECTIONS

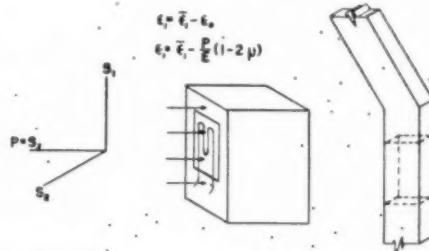


FIG. 21 ACTIVE GAGE SUBJECT TO PRESSURE FROM ONE DIRECTION ONLY

Clearing Equation [5] results in a stress relation

$$S_1 = \frac{E}{(1-\mu^2)} \left[(\bar{\epsilon}_1 + \mu\bar{\epsilon}_2) - \frac{P}{E} (1 - \mu^2) \right] \quad [6]$$

A more useful form of Equation [6] may be expressed when each side of the equation is divided by P

$$\frac{S_1}{P} = \frac{E}{P(1-\mu^2)} (\bar{\epsilon}_1 + \mu\bar{\epsilon}_2) - 1 \quad [7]$$

and

$$\frac{S_2}{P} = \frac{E}{P(1-\mu^2)} (\bar{\epsilon}_2 + \mu\bar{\epsilon}_1) - 1 \quad [8]$$

The ratio $S/P: D/t$ illustrates that thick-wall cylinders have a low S/P value. For this reason the constant "1" becomes increasingly significant as the shell thickness increases.

Example: A cylinder of 46 in. ID is 4 in. thick. The theoretical Lamé stress at 2000 psi internal pressure is 24,100 psi. The corresponding S/P ratio is approximately 12 units. If this same stress is determined experimentally by using the SR-4 strain-gage readings in Equation [1] of this discussion, the ratio of S/P will be 13 units; the discrepancy is accounted for only when Equation [8] is utilized. An error of $1/13 = 7.7$ per cent is encountered in the use of Equation [1].

L. P. ZICK.¹¹ If the G-E magnetic gage were substituted for the DeForest scratch gage, the history described could very easily pass as a description of our own early activities in this field. The SR-4 strain gages and equipment now dominate our work. However, our techniques and methods and those of the authors' company have taken quite different paths, the chief difference being that we have used water (with all its troubles), as the pressure medium because of the size and the corresponding lower pressures of the vessels tested.¹²

Experimental Stress Analysis. The method of keeping the

¹¹ Research Engineer, Chicago Bridge & Iron Company, Chicago, Ill.

¹² "Strain Gage Survey Around the Supports of a 48-Foot Diameter Hortonsphere," by L. P. Zick and C. E. Carlson, Proceedings of the Society for Experimental Stress Analysis, vol. VI, no. II, pp. 41-60.

liquid level below the gage locations should surely save some difficulties. However, one word of caution—if separate leads of any length are used they, too, should remain above the liquid.

The cantilever bar tests showing the reliability of the strain gages under very high pressures is certainly encouraging.

Fatigue Testing. The method and test ranges for the fatigue tests gain additional merit in that the authors realize that the values of the various ranges vary. On the other hand, the statement, "After the initial proof test of $1\frac{1}{2}$ or 2 times working pressure there will be no further plastic deformation in the vessel during its entire service life," rightly or wrongly, seems to ignore the Bauschinger effect and strain-aging. The observations during the slow-cycle testing also seem contrary to this statement.

The use of double balanced plungers with the activating cam combined with the use of noncompressible ballast is an ideal example of a method revelation which will probably save someone else time, trouble, and expense.

High-Temperature Fatigue Test. The high-temperature fatigue tests are very interesting and have required considerable planning. The statement that all the specimens to date have failed in or near the weld does not agree with the results found by Professor Wilson. Has the possibility of a difference in welding technique been studied as a source of reduced fatigue strength?

AUTHORS' CLOSURE

We greatly appreciate the favorable comments of many engineers and acknowledge that our techniques may not apply in many applications which we did not cover. We will attempt to answer some of the detailed questions which have been submitted.

Mr. Liessenberg has asked for details on the tube-expansion method. Most of these tubes, especially the small size, were ball drift-expanded and, since the ball has a specific size, the amount of expansion does not need control by additional means. As to the amount of expansion before test and any additional rerolling, it is true that some repetition of expanding was necessary. In fact, the complete set of smaller tubes was replaced during tests of various tube seat designs.

Exposure of the high-temperature specimens to hot gases undoubtedly would have an effect on the results, but this effect becomes of real importance only on the heavier walled vessels. Our particular interests were in applications where this contact with hot gases is not present, since most of our high-pressure boiler drums are either outside the furnace proper or have adequate protection against the hot gases. In order to give a more complete record on the high-temperature tests, Table 5 was added to the final paper. The last column in this table and note (b) show that all of the failures were longitudinal cracks resulting from circumferential stresses. Out of fifteen failures, only one was at a girth seam, and one at the junction of a girth and longitudinal seam, but even these were in a longitudinal direction.

A metallurgical investigation of some of the failures indicated that they were initiated at minute, mechanical, weld defects, such as entrapped slag or small gas pockets. There were no failures in the tube-nipple connection welds. We regret that no microphotographs of the weld and plate were taken before the test for the comparison of grain structure. Such photographs of this location after failure are available, however, and we will be pleased to supply them for study.

Messrs. O'Brien and Wetterstrom have contributed a satisfactory algebraic combination of the strain-gage correction and the effect of pressure radial to the inside surface.

This combined formula is not applicable in at least two cases. Of first importance in this is the study of the actual unit strains which are present with relation to yield points, plastic flow, and

residual stresses. Another case is where an external dummy gage must be used with inside gages. In the latter case the radial pressure inside must still be evaluated without the "dummy" block correction. In studying true-strain values, the dummy strain correction alone must be made since the effect of radial pressure at the test location is part of the study.

For the tests in which they are applicable, the formulas of Mr. O'Brien and Mr. Wetterstrom give the same stress result as our procedure. However, we believe it is highly desirable to consider stresses in a three-dimensional system and not to confuse corrections with actual stresses. Our interpretation is then as follows:

1 The compression of the inside dummy gage block due to pressure results in a false strain reading for the test gage. This is, therefore, a true correction which must be made, and the value for this "apparent strain ϵ_1 " was given in the original paper.

2 The effect of pressure on the test location is not a correction but a true stress which must be included in the triaxial stress system. This evaluation must then be made by use of the basic strain equation as follows:

$$\epsilon_1 = \frac{1}{E} (S_1 - \mu S_2 - \mu S_3)$$

in which S_3 becomes the pressure. This should not be interpreted as a correction, but is a true existing stress radial to the surface.

3 Our usual approach then is to make the strain correction, caused by the dummy compression, on all the strain readings in inside gages. This is a true correction, similar to those made for gage factor resistances outside the instrument range, temperature differences, etc. The pressure is then evaluated as an existing stress in a three-dimensional system.

We agree that for the particular purpose of plotting the S/P ratio for inside gages, as is done in some of the PVRC projects, for example, the formula proposed by Messrs. O'Brien and Wetterstrom is a useful short cut. It must be used with considerable caution, however, in the applications described above.

Mr. Zick cautioned about keeping the leads out of the water, which we agree is necessary. In the case of the vertical vessel, the leads were definitely kept above the water. The drum in Fig. 1 of the paper was provided with a gage glass at a location that made it possible to observe the water level if it should rise above a maximum allowable level.

Concerning the Bauschinger effect, we believe that a properly designed pressure vessel would not have stress ranges equal to the range between tension and compression yield points. We believe any strain-aging effect will be insignificant because of insufficient deformation occurring in the pressure vessel.

The particular application of the slow cycles and the time element required involved expanded tubes where there was relative motion between surfaces held together primarily by friction. We believe it is more important in this study than in the major part of the pressure vessel. The statement regarding the behavior of a vessel after the initial proof test only appeared in the first draft and after due consideration was deleted, but not in time to correct the preprints.

Mr. Zick also mentions that the fatigue data do not agree with those obtained by Professor Wilson and asks whether differences in technique can be the answer.

This is quite likely since the weld deposit and basic weld rod may be considerably different from the tensile plate investigations of Professor Wilson. An additional effect of a difference in environment is also a possibility. Other differences of course include the biaxial stress condition in the cylindrical specimens as well as size effect and speed of testing.

A
in
high
whi
stud
sus
of a
cou
effe
bus
of i
incr
proc
igni
com
ant

V
with
press
term
also
least
more
migh
sion
add
is giv
A
of pu
the to
effect
furna
to ma
depen
suffic
possib
hot s
tures

¹ A
the re
Engin
² Fo
Instit
fornia
³ M
of Tec
⁴ N
the pa
Com
Meeti
THE A
Not
unders
of the
ary 9,

Effect of Pressure on the Combustion of Pulverized Coal¹

By T. T. OMORI² AND A. A. ORNING³

A theoretical study of heat transfer to a sphere suspended in cold air and suddenly exposed to radiation from a high-temperature source indicated an effect of air pressure which had not been disclosed by previous theoretical studies relating to the ignition of pulverized coal in air suspension. Experimental investigation, in the absence of an extended flame so that the source of radiant heat could be independently controlled, showed an adverse effect of elevated pressures upon completeness of combustion which was much larger than a beneficial effect of increased partial pressures of oxygen. It appeared that increased pressure, through a lower initial heating rate, produced less reactive combustion residues which lost ignition before combustion was complete. Complete combustion could be obtained only by increasing the radiant intensity responsible for ignition.

INTRODUCTION

WITH the appearance of the gas turbine as an economical prime mover, considerable interest has been aroused in the combustion of fuels under pressure. Experience with gas turbines has shown that liquid fuels can be burned under pressure with good efficiency at extremely high burning rates in terms of heat release per unit volume. While pulverized coal can also be burned in such units at very high combustion rates, at least as compared to steam boiler practice (1),⁴ it has appeared more difficult to avoid high combustible losses in the fly ash. It might seem that such losses could be reduced by the simple provision of more combustion space. However, it will appear that added space will not improve combustion unless proper attention is given to flame conditions.

A study of the ignition and combustion of individual particles of pulverized coal under atmospheric pressure (2) showed that the temperature responsible for ignition, presumably through its effect upon the initial heating rate of the fuel as it entered the furnace, had a marked effect upon the ability of residual particles to maintain ignition. Maintenance of ignition was found to be dependent upon the ability of the burning particles to maintain sufficiently high temperatures, certainly higher than 1000 and possibly on the order of 2000 C. Accordingly, except possibly in hot slagging furnaces, burning residues must maintain temperatures considerably above those of their surroundings if good

combustion of such particles is to be maintained as they move out of the flame into cooler parts of the furnace.

Since subsequent loss of ignition appears somehow related to the conditions under which ignition occurs, the various theoretical studies of the ignition of pulverized coal are of particular interest. These studies involve the calculation of the temperature history, prior to ignition, of a particle suspended in air and suddenly exposed to a high-temperature source of radiant heat.

Nusselt (3) calculated theoretical ignition times of various fuels on the assumption that a spherical particle received heat by radiation from the furnace walls and lost heat by conduction into the particle and into surrounding gases. However, some of the basic assumptions made were of doubtful validity. An infinite thermal conductivity of the particle, a simplifying assumption facilitating solution, was implied though not explicitly stated. Further, the heating of a particle to its ignition temperature is a transient phenomenon; the assumption of a steady-state heat-transfer coefficient between particle and surrounding gas is subject to question. Nusselt gave his heat flow equation in the form

$$(4/3)\pi a^3 \rho c \frac{dt_p}{dt} = \phi \sigma \left[\left(\frac{T_w}{100} \right)^4 - \left(\frac{T_p}{100} \right)^4 \right] 4\pi a^2 - 4\pi a k(t_p - t_a) \quad [1]$$

where

- a = particle radius
- c = specific heat per unit weight of particle
- σ = radiation constant
- ϕ = radiation-angle factor
- t_p = particle temperature, deg C (T_p , deg K)
- t_w = radiation temperature of furnace walls, deg C (T_w , deg K)
- t_a = temperature of air and of particle at θ equal zero; also, temperature of air at infinite radius
- k = thermal conductivity of air
- ρ = particle density
- θ = time

The term to the left of the equality is the rate of heat absorption, assuming infinite thermal conductivity for the particle. The first term on the right is the rate at which heat is received by the particle due to radiation from the furnace walls, while the second represents loss by conduction from the particle to surrounding air. The second term can be derived by assuming that heat flow to the surrounding air is given by the steady-state equation

$$-4\pi r^2 k \frac{dt}{dr} = 4\pi a k(t_p - t_a) \dots \dots \dots [2]$$

which integrates to the form

$$t = \frac{a}{r} (t_p - t_a) + t_a \dots \dots \dots [3]$$

where

- r = distance from center of sphere
- t = air temperature at distance r

This indicates that the temperature distribution in the surrounding air was assumed to be proportional to $1/r$.

¹ Abstract from a thesis by T. T. Omori in partial fulfillment of the requirements for the degree of Doctor of Science in Chemical Engineering at Carnegie Institute of Technology.

² Formerly Member of Staff, Coal Research Laboratory, Carnegie Institute of Technology, Pittsburgh, Pa.; present address: California Institute of Technology, Pasadena, Calif.

³ Member of Staff, Coal Research Laboratory, Carnegie Institute of Technology, Pittsburgh, Pa. Mem. ASME.

⁴ Numbers in parentheses refer to the Bibliography at the end of the paper.

Contributed by the Fuels Division and presented at the Annual Meeting, New York, N. Y., November 27-December 2, 1949, of THE AMERICAN SOCIETY OF MECHANICAL ENGINEERS.

NOTE: Statements and opinions advanced in papers are to be understood as individual expressions of their authors and not those of the Society. Manuscript received at ASME Headquarters January 9, 1950. Paper No. 49-A-72.

Neglecting heat loss due to back radiation, Nusselt simplified his original equation to

$$\frac{c\rho a^2}{3} \frac{dt_s}{dt} + k(t_s - t_0) - \phi\sigma a \left(\frac{T_w}{100}\right)^4 = 0 \dots\dots [4]$$

which integrates to

$$t_s = t_0 + \frac{\phi\sigma a}{k} \left(\frac{T_w}{100}\right)^4 (1 - e^{-3k\theta/c\rho a^2}) \dots\dots [5]$$

For sufficiently small times this equation may be approximated as

$$t_s = t_0 + \phi\sigma \left(\frac{T_w}{100}\right)^4 \frac{3\theta}{c\rho a} \dots\dots [6]$$

This indicates an initial rate of temperature rise inversely proportional to the particle radius and to the heat capacity per unit volume of solid but independent of the thermal properties of the gas.

For sufficiently large times the equation may be approximated as

$$t_s = t_0 + \frac{\phi\sigma a}{k} \left(\frac{T_w}{100}\right)^4 \dots\dots [7]$$

indicating final temperatures directly proportional to the particle radius and to the intensity of radiation, but inversely proportional to the thermal conductivity of the gas, a quantity which is essentially independent of pressure.

Starting with a heat-balance equation which was essentially the same as Nusselt's, Traustel (4) introduced a correction for the effect of a finite amount of excess air. This was accomplished by assuming that the average air temperature to which the particle was losing heat could be expressed as a function of time and a dimensionless quantity N , the ratio of heat capacities of the associated quantities of air and coal. The constant term t_w was replaced by a function of θ and t_s . Integration led to the form

$$\frac{1}{D} = \frac{1 - e^{-n}}{2 \left(1 + \frac{1}{N}\right)^2} + \frac{2Z}{(N+1)D^2} \dots\dots [8]$$

where

$$D = \frac{2a\phi\sigma}{k(t_s - t_0)} \left(\frac{T_w}{100}\right)^4 \dots\dots [9]$$

$$Z = \frac{3\phi^2\sigma^2\theta}{c\rho k(t_s - t_0)^2} \left(\frac{T_w}{100}\right)^8 \dots\dots [10]$$

$$n = \left(1 + \frac{1}{N}\right) \frac{3k\theta}{c\rho a^2} \dots\dots [11]$$

The limiting forms of Equation [8] are of particular interest. For sufficiently small times, such that the exponential may be replaced by the first two terms of its binomial expansion, the result is identical with that obtained for Nusselt's equation, indicating an initial heating rate independent of the excess amount as well as of the thermal properties of the air. For sufficiently large times, such that the exponential may be neglected, the equation becomes

$$t_s = \phi\sigma \left(\frac{T_w}{100}\right)^4 \left[\frac{N^2 a}{(N+1)^2 k} + \frac{3\theta}{(N+1)c\rho a} \right] + t_0 \dots [12]$$

With infinite excess air, this is identical with the final limiting form of Nusselt's equation, while with finite excess air it indicates

a final rate of temperature rise proportional to the ratio of the heat capacity of the coal to the heat capacity of the coal plus the air.

Traustel's analysis involves all of Nusselt's assumptions, both failing to find any dependence upon pressure if proper account is taken of the ratios of heat capacities. Accordingly, it would appear desirable to examine the heat-transfer system more rigorously. The coal particles, suspended in relatively cold gas initially at the same temperature as the coal, are suddenly introduced into a hot furnace. Heat transfer to the particle surface from the furnace can be assumed to be by radiation through transparent gas. Over the interesting range of surface temperatures, the fourth power of the absolute surface temperature can be neglected as compared to that of the source of radiant heat. The rate of heat transfer by radiation to the surface depends only upon the radiation temperature and the extent and character of the particle surface. Under these conditions, the surface can be considered as a heat source of constant strength. Heat loss from the surface is by conduction into the particle and into the surrounding gas.

Though general solutions of the problem as posed have not been found, the solution for a spherical heat source of constant strength with heat diffusing both inward and outward, the two regions having the same thermal properties, has been given by Carslaw (6)

$$t = \frac{Q}{8\pi k r^{3/2}} \int_{(1/2)\sqrt{\rho c/k\theta}}^{\infty} [e^{-(r-a)^2 r^2} - e^{-(r+a)^2 r^2}] \frac{dr}{r} \dots [13]$$

where Q is the strength of the spherical source (Carslaw's $q\rho c$).

Integration by parts followed by expansion in a power series, and omission of all but the leading terms leads to an approximation valid within 1 per cent when

$$\frac{(r+a)}{2} \sqrt{\frac{\rho c}{k\theta}}$$

is less than 0.2

$$t = \frac{Q}{4\pi k r} - \frac{Q}{4\pi k} \sqrt{\frac{\rho c}{k\theta}} + t_0 \text{ for } r > a \dots\dots [14]$$

and

$$t = \frac{Q}{4\pi k a} - \frac{Q}{4\pi k} \sqrt{\frac{\rho c}{k\theta}} + t_0 \text{ for } r < a \dots\dots [15]$$

where t_0 is arbitrarily added as the air temperature at $r = \infty$. For large times the temperature outside the sphere varies as $1/r$ as assumed by Nusselt. With air at 100 C and r slightly greater than a , the minimum time at which the expressions are valid is

$$\theta_m = (79.1)a^2 P \dots\dots [16]$$

where P is expressed in atmospheres, and a in centimeters. For a 100- and 200-mesh particle, each in air at 1 atm pressure, these times are 0.0043 and 0.0011 second, respectively.

Accordingly, after a few milliseconds, the inward heat flow becomes comparatively negligible and the outward flow becomes

$$Q_0 = \frac{4\pi k a(t_s - t_0)}{1 - a \sqrt{\frac{\rho c}{k\theta}}} \dots\dots [17]$$

Comparison with the assumption made by Nusselt

$$Q_N = 4\pi k a(t_s - t_0) \dots\dots [18]$$

shows that Nusselt underestimated the outward heat flow by failing to include the factor

$$1 - a \sqrt{\frac{\rho c}{\pi k \theta}} \dots \dots \dots [19]$$

This factor applies to a system having the same thermal properties within and without the sphere. With dissimilar materials, coal and air, the system may be assumed to have reached a quasi-steady state after a few milliseconds, and the estimate of outward heat flow as a function of the density and thermal properties of, and the temperature drop through, the air is probably fair. Estimated corrections to be applied to Nusselt's assumption are shown in Fig. 1. The corrections are strongly dependent upon pressure and indicate considerably larger values for the smaller times where estimates are not available.

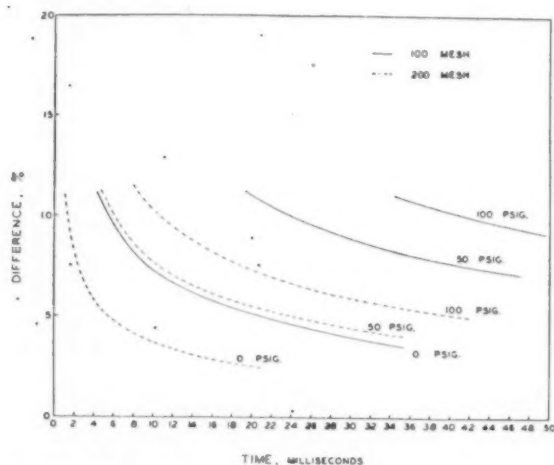


FIG. 1 CORRECTIONS TO BE APPLIED TO NUSSLETT'S ESTIMATES OF OUTWARD HEAT-FLOW RATE

These estimates have taken no account of relative velocities between coal and air. Rigorous solutions for the simultaneous conduction and convection problem are not available. An approximate solution by Johnstone, Pigford, and Chapin (7) leads to an estimate of outward heat flow

$$q = 0.714 D_p^{2/3} (t_g - t_0) \sqrt{k V \rho c} \dots \dots \dots [20]$$

where D_p is the particle diameter and V the relative velocity. The rate of convective heat loss appears proportional to the square root of the gas density and hence proportional to the square root of the total pressure.

If there is any appreciable relative velocity between the particle and surrounding gas, an increase in pressure will tend to increase the rate of heat loss from the surface. Owing to the dependence upon temperature drop, this effect starts at zero and increases with time. A pressure effect arising out of the transient character of the heat-flow system should be superimposed. Since the latter, as shown in Fig. 1, is greatest at the start, the combined effect would be a continued influence of pressure upon the rate of heat loss from the particle into the surrounding atmosphere. This loss concerns only part of the heat-transfer system responsible for the initial temperature history of the coal particle. However, it is only this part which should depend upon pressure. Any other dependence must arise out of mechanical action such as restraint of particle swelling or cenosphere (2) formation.

Since the solution for the heat-transfer problem, though not rigorous, indicated a decreased initial heating rate with increased pressure and, since there was a possibility of direct mechanical

action, an experimental investigation of the effect of pressure upon ignition seemed highly desirable. The investigation required such "thin" streams of coal particles that ignition resulted from heat transfer from controlled wall temperatures rather than from a flame. Use of various partial pressures of oxygen was indicated to determine any pressure effects resulting from increased availability of oxygen. Provision had to be made for collection of combustion residues in order to determine the effect of ignition conditions upon ensuing combustion.

APPARATUS AND PROCEDURE

The furnace used for the study of the ignition and combustion of pulverized coal under pressure is shown in Figs. 2 and 3. The furnace was built in a 24-in. length of Shelby tubing, 6 in. ID and 1/4 in. wall thickness. A water-cooling jacket covered the central 13 in. of the tube. The tube was mounted horizontally and provided with a window along the center of the bottom side. A sheet of single-strength window glass was inserted about 1 in. above the pyrex-glass pressure window. A stream of secondary air, introduced between the two glasses and passed through nozzles around the upper glass, further protected the window

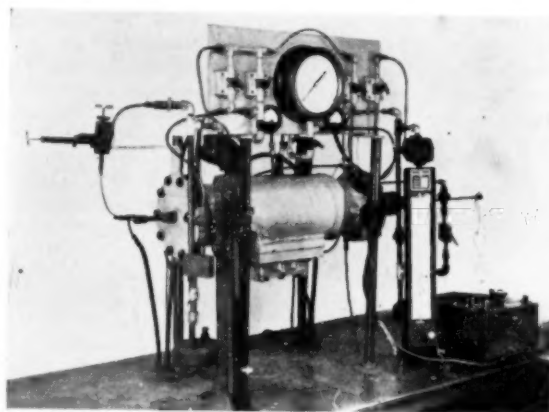


FIG. 2 VIEW OF APPARATUS

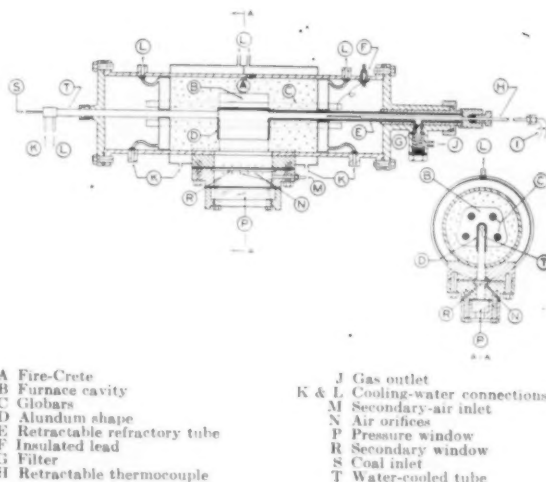


FIG. 3 SECTIONS OF PRESSURIZED FURNACE

from the furnace heat and provided some upward air flow through the combustion space.

The furnace insulation was cast from "Hi-Temperature Fire-Crete" to provide support for the "Globar" heating elements, the water-cooled feed tube, the ceramic outlet tube, and the alundum tunnel which limited the combustion space. Water-cooled end plates held the furnace elements in place and protected the electrical connections in the end compartments. A power input of 4 kw brought the furnace to 1300 C, as indicated by an optical pyrometer sighted upon the inside of the alundum tunnel, but this temperature could not be maintained with full air flow.

The coal was fed from a removable brass cartridge into the primary-air stream by a screw-feed plunger assisted by a vibrator. Suitable isolation valves permitted reloading without depressuring the furnace. Any gas leakage through the plunger packing gland had to be by-passed around the cartridge to keep the coal from packing against the plunger. Orifice meters were used to measure the air-flow rates. The volume flow rates at furnace pressure and room temperature were held constant, 0.0053 cfm for the primary, and 0.177 cfm for the secondary air admitted past the window. These flow rates appeared to be optimum values for carrying the coal through the 5-in. distance across the top of the tunnel and into the outlet tube. The transit time for the coal particles was somewhat uncertain. Based upon jet conditions it was 0.015 sec, while exit conditions would indicate 0.065 sec, varying somewhat with exit-gas temperature. The removable outlet tube, 1/2 in. ID and 18 in. long, had a side opening placed just over a filter plate ahead of the throttling valve used for pressure control. While some combustion residues fell to the observation window, the greater portion was always found in the outlet tube or on the filter plate.

The percentage combustion was determined on the basis of ash analyses. Residues from the filter plate, from the outlet tube, and from the window, if any, were collected and analyzed individually. Any residues falling upon the hot surface of the outlet tube near the furnace cavity had to be discarded and ignored. While such residues had ample time for complete combustion in a temperature-controlled reaction on the hot surface, no appreciable further combustion would have occurred had they been promptly carried out of the hot zone.

A retractable thermocouple was placed in the outlet tube. The thermocouple indication agreed with the optical pyrometer sighted through the window onto the inside of the alundum tunnel when no gas was flowing, but showed substantially lower temperatures with gas flowing. The optical pyrometer indication was taken as the temperature for correlation with percentage combustion.

EXPERIMENTAL RESULTS

The proximate analyses of the coals studied are given in Table 1. The degree of combustion of these coals in various atmospheres as a function of furnace temperature is shown in Figs. 4 through 10. Fig. 4 gives data for 100-140 mesh Pittsburgh seam coal in air at zero, 50, and 100 psig. Figs. 5 and 6 show similar data for Illinois No. 6 and Pocahontas No. 3 seam coals, respectively. The curves, relating the degree of combustion to furnace radiation temperature at constant pressure, show a progressive change in form as the pressure is increased and, to a lesser extent, as the

rank of the coal increases. The curve for the Illinois coal at atmospheric pressure is displaced furthest to the left and is everywhere concave downward. The Illinois coal at intermediate pressure and the Pittsburgh and Pocahontas coals at atmospheric pressure show curves with points of inflection within the temperature range explored. The steepest points of the curves for the Pittsburgh and Pocahontas coals occur at temperatures which had previously been shown to be the minimum for uniform ignition of these coals (2). The remaining curves must become concave downward as combustion reaches completion with furnace temperatures above 1100 C. Whatever the significance of this change in the form of the curves, it appears that higher furnace temperatures were necessary to obtain the same percentage combustion with higher furnace pressures or higher rank coals.

Fig. 7 shows curves for 170-200 mesh as compared to 100-140 mesh Pittsburgh seam coal. While the curve for atmospheric pressure is shifted upward and its point of maximum slope shifted somewhat to higher temperatures, the curves at the higher pressures are not appreciably different from those found for the coarser-sized coal. Similar studies at 50 psig showed insignificant changes for the Pocahontas coal and an upward shift of 5 to 10 percentage points for the Illinois coal. Minus 200-mesh Pittsburgh seam coal was also studied, Fig. 8. It was difficult to obtain reproducible results with this size coal. Based upon a number of duplicate points for the atmospheric-pressure curve, large circles were drawn representing probable error limits. These show that a more involved curve than that shown is not justified. These curves all show points of inflection but the maximum slopes occur at higher temperatures than those found for coarser sizes of this coal.

Figs. 9 and 10 show the effect of higher partial pressures of oxygen with the Pittsburgh seam coal. Proceeding to 50 per cent and 90 per cent oxygen in nitrogen mixtures, the curves, at each total pressure, move somewhat upward and to the left with increasing partial pressure of oxygen. However, the effect is not so marked as the depressive effect of increasing total pressure. The difference would be even greater if the pressure effect was taken at constant partial pressure of oxygen rather than at constant composition. Only at 90 per cent oxygen and 50 psi pressure was the effect great enough to make a substantial change in the form of the curve.

INTERPRETATION OF DATA

In order to interpret the experimental data, it is necessary to

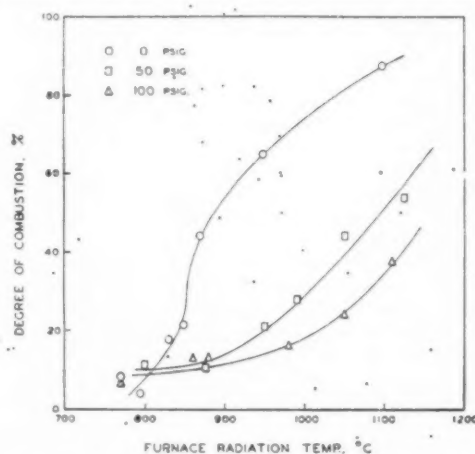


FIG. 4 DEGREE OF COMBUSTION OF PITTSBURGH SEAM COAL (100-140 mesh. Gas composition: 20 per cent oxygen, 80 per cent nitrogen.)

TABLE 1 PROXIMATE ANALYSES OF COALS STUDIED

Seam	County	Moisture per cent	Volatile matter per cent	Fixed carbon per cent	Ash per cent	Btu
Pittsburgh	Fayette, Pa.	1.9	33.6	57.0	7.5	13,910
Pocahontas No. 3	McDowell, W. Va.	0.8	15.3	78.3	5.6	14,760
Illinois No. 6	Franklin, Ill.	6.7	33.9	50.3	9.1	12,270

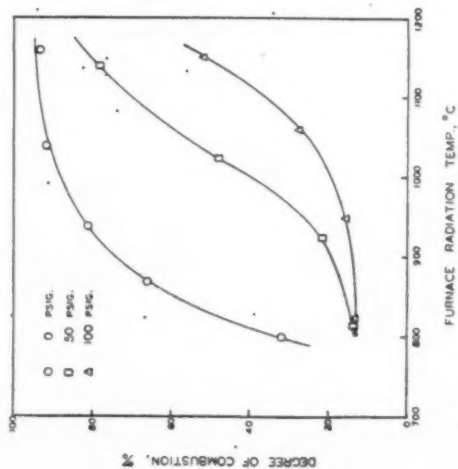


FIG. 5 DEGREE OF COMBUSTION OF ILLINOIS No. 6 SEAM COAL. Gas composition: 20 per cent oxygen, 80 per cent nitrogen.

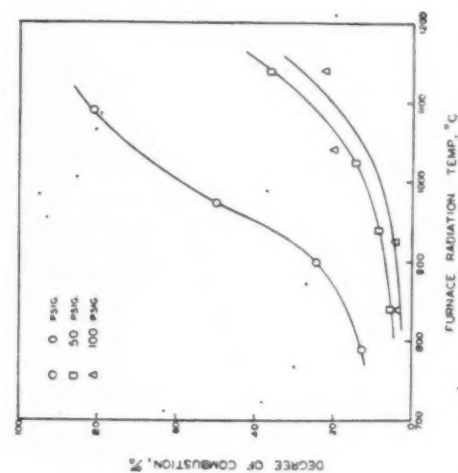


FIG. 6 DEGREE OF COMBUSTION OF POCAHONTAS No. 3 SEAM COAL. Gas composition: 20 per cent oxygen, 80 per cent nitrogen.

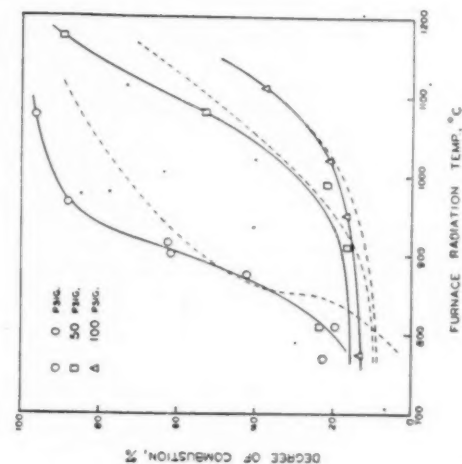


FIG. 7 DEGREE OF COMBUSTION OF PITTSBURGH SEAM COAL. (Solid lines, 170-200 mesh; dashed lines, 100-140 mesh. Gas composition: 20 per cent oxygen, 80 per cent nitrogen.)

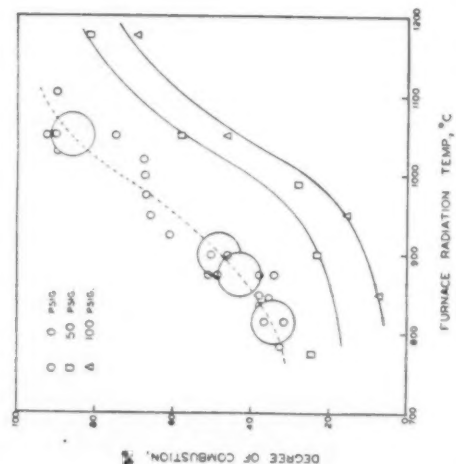


FIG. 8 DEGREE OF COMBUSTION OF PITTSBURGH SEAM COAL. (Minus 200 mesh. Gas composition: 20 per cent oxygen, 80 per cent nitrogen.)

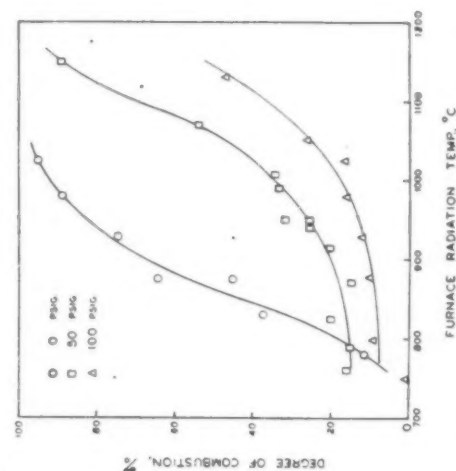


FIG. 9 DEGREE OF COMBUSTION OF PITTSBURGH SEAM COAL. (100-140 mesh. Gas composition: 50 per cent oxygen, 50 per cent nitrogen.)

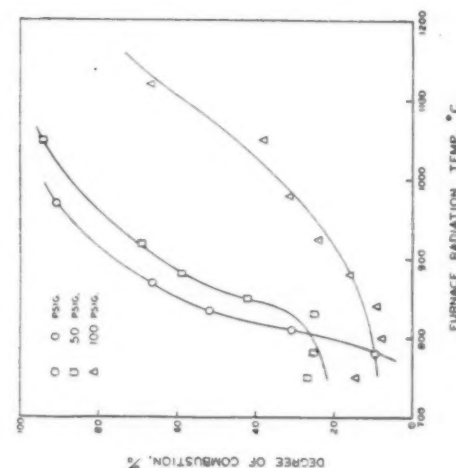


FIG. 10 DEGREE OF COMBUSTION OF PITTSBURGH SEAM COAL. (100-140 mesh. Gas composition: 90 per cent oxygen, 10 per cent nitrogen.)

recognize the conditions under which the coal was ignited. The coal and the primary-gas stream entered together at the water-cooling temperature. The primary air entered as a jet moving through the secondary air which had some opportunity to approach furnace temperature. The coal probably remained within the jet long enough so that the hotter secondary gas had little chance to influence the ignition process. The two gas streams ultimately mixed but never reached the radiation temperature of the furnace walls. Thermocouple indications were always lower than the furnace radiation temperature and, with the furnace at 1200 C, fell to 600 C in the outlet tube where the thermocouple probably came nearest to measuring the gas temperature.

In all instances the active burning times were less than the transit times across the furnace. The burning particles generally were incandescent for only a small portion of the total distance of travel across the combustion chamber. Nevertheless, the degree of completeness of combustion, even at temperature levels giving uniform ignition, increased strongly with increasing temperature, increased moderately with partial pressure of oxygen, but was strongly depressed by increasing total pressure.

It would seem evident that these variables influenced the degree of combustion through an effect upon loss of ignition. The burning particles, failing to consume the oxidizing gas as rapidly as it can be transported by convection and diffusion to the burning surface, fall to a temperature somewhere between that of the immediately surrounding gases and the radiation temperature of the furnace. At the lower temperature, the rate of burning is so low as to contribute practically nothing during the limited time of transit through the furnace.

The ability to consume the oxidizing gas as rapidly as it can reach the burning surface depends upon the particle temperature. Since the heat capacity of the particle is relatively small, as compared to its heat of combustion, this temperature is such as to obtain a balance between the rates of heat release and heat dissipation to the surroundings. Heat loss to the immediately surrounding gas should depend upon pressure, but these gases have been heated to a high temperature by the combustion process reducing any heat loss to such a level that it would seem that increasing the partial pressure of the oxygen, making it more readily available to combustion, should easily offset any such effect. This is contrary to the relative effects found. Changing pressure and gas composition should have little effect upon heat loss by radiation. Further, the burning-particle temperatures probably were so high that back radiation from the furnace was not an important factor. The previous studies at atmospheric pressure showed a marked effect of furnace temperature with little difference whether the active burning period ended within the furnace or in an environment at room temperature (2).

However, the temperature required to maintain ignition does depend upon the reactivity of the burning residue; the more reactive the surface the lower the temperature at which the oxidizing gas will be consumed as rapidly as it can reach the surface and the more completely the particle will be expected to burn out before it loses ignition. While the arguments relating the different variables to the balance between heat release and heat dissipation are not rigorous, it appears that these variables could exert their influence through an effect of the initial heating rate of the coal as it enters the furnace upon the reactivity of the combustion residues.

The alternate suggestion that the effect might have been due to an influence upon cenosphere size (8) seems not to be correct, since it was observed qualitatively that the cenosphere size decreases with increasing pressure, while previous work showed that, within the temperature ranges giving uniform ignition, the cenosphere size also decreases with increasing furnace temperature.

Failure to find a marked effect of coal size is of particular inter-

est. Traustel's (4) analysis indicated an optimum size, giving most rapid initial rates of temperature rise; the finer sizes heat less rapidly owing to more intimate contact with the heat capacity of the surrounding air. This is not in contradiction to large furnace practice. Increasing coal fineness produces a shorter and more intense flame, favoring increased rates of heat transfer to the incoming fuel. Any effect of higher resistance to heat flow with finer coal would be overpowered by the increased flame intensity.

Such interplay between the influence of various factors upon ignition with a controlled igniting source and the influence of these factors upon the ability of a flame to supply heat transfer for ignition should be the basis for further experimental investigation. The controlled source with low-density suspensions leads to particulate ignition, each particle igniting independently. Increasing the density of suspension beyond some critical value, collective ignition occurs with the appearance of a definite flame front (2). The influence of fuel character, size distribution, coal-to-air ratio, and aerodynamic factors upon this limit should be investigated. The influence of such factors upon the intensity of radiation from flames should be studied, in order, for instance, to determine to what extent the more intense radiation from a short flame of fine coal can offset the more difficult ignition of a finer coal particle.

Such information will be particularly useful in the development of combustion systems for gas-turbine cycles where good combustion is much more difficult to obtain than in large furnaces. High gas velocities and early introduction of high excess air tend to reduce the rate of heat transfer into incoming fuel. The adverse effect of pressure upon the rate of temperature rise further decreases the reactivity of combustion residues. Corrective measures must involve increased flame intensity held close to the point of entry of fuel into the combustion chamber. Increasing volumes available for combustion will be of no avail unless the wall temperatures are high enough, probably in the slagging range, to avoid loss of ignition.

SUMMARY AND CONCLUSIONS

- 1 A theoretical study of heat transfer indicated an adverse effect of pressure upon the ignition of pulverized coal, the rate of heating falling with increased pressure.
- 2 Apparatus and procedures were devised for studying the effect of total as well as oxygen partial pressure with controlled igniting conditions upon the resulting combustion process. The resulting data confirmed the indication from earlier work at atmospheric pressure that decreased initial heating rates under pressure would lead to less complete combustion.
- 3 Particularly in application to gas-turbine cycles, good combustion demands high rates of heat transfer to incoming fuel. Increased volume for combustion cannot replace inadequate ignition intensity.

BIBLIOGRAPHY

- 1 "Experimental Combustion of Pulverized Coal at Atmospheric and Elevated Pressures," by H. R. Hazard and F. D. Buckley, *Trans. ASME*, vol. 70, 1948, pp. 729-737.
- 2 "Combustion of Pulverized Coal," by A. A. Orning, *Trans. ASME*, vol. 64, 1942, pp. 497-508.
- 3 "Der Verbrennungsvorgang in der Kohlenstaubfeuerung," by W. Nusselt, *Zeitschrift Verein deutscher Ingenieure*, vol. 68, 1924, pp. 124-128.
- 4 "Verbrennung in der Schwebe," by Sergei Traustel, *Feuerungstechnik*, vol. 29, 1941, pp. 1-6, 25-31, 49-60.
- 5 "Chemistry of Coal Utilization," H. H. Lowry, editor, chapt. 34—"The Combustion of Pulverized Coal," by A. A. Orning, John Wiley & Sons, Inc., New York, N. Y., 1945, pp. 1522-1567.
- 6 "Mathematical Theory of Conduction of Heat in Solids," by H. S. Carslaw, Macmillan and Company, London, England, 1921, pp. 149-152.

7
John
Bulle
8
A. A.
izec
ence

H.
exper
of inc
of pre
ness
tests
tical
prete
One
result
ary ai
throu
psia,
increa
conve
cussed
combu
below
used a
they r
Thus
the eff
increa
The
oxygen
bustion
oxygen
directl
portion
sure.
increas
The
plified
noticed
In the
was pr
indicate
onstrat
barely
particle
combus
particle

The f
to the in
did exist
that eq
was exp
history.
ignition
would d
combus
that ign
In one,
tremely
of the pe

* Assis
Ohio. J

7 "Heat Transfer to Clouds of Falling Particles," by H. F. Johnstone, R. L. Pigford, and J. H. Chapin, University of Illinois Bulletin, vol. 38, No. 43, June 17, 1941.

8 "The Mechanism of the Combustion of Pulverized Fuel," by A. A. Orning—"Papers to Be Discussed at a Conference on Pulverized Fuel," Harrogate, England, June, 1947, Pulverized Fuel Conference Committee, The Institute of Fuel, London, England, pp. 45-64.

Discussion

H. R. HAZARD.⁵ The authors have done an excellent piece of experimental work in which they have controlled the environment of individual particles of burning coal to determine the influence of pressure, temperature, and oxygen concentration on completeness of combustion. However, the conditions under which the tests were run were far removed from conditions existing in practical combustion chambers, and therefore data must be interpreted carefully if they are to be of practical value.

One factor which may have had an important bearing on the results was the use of constant volumes of primary air and secondary air at all pressures. Thus at 115 psia, the mass flow of air through the test combustion chamber was 7.8 times that at 15 psia, though the coal-firing rate was probably unchanged. This increased the Reynolds number by a factor of 7.8, thus increasing convection heat transfer from the particle to some degree not discussed in the paper. This probably would reduce completeness of combustion, because air temperatures were always considerably below wall temperatures. If the extremely high air/fuel ratios used at 115 psia also resulted in very low exit-gas temperatures, they might account in part for poor combustion at 115 psia. Thus the poor combustion found at 115 psia was not necessarily the effect of pressure alone, but probably reflects the very large increase of air flow with pressure.

The manner in which the authors discuss partial pressure of oxygen suggests that oxygen is more readily available for combustion at higher static pressures because partial pressure of oxygen is higher. Actually, while the mass rate of diffusion is directly proportional to the partial pressure, it is inversely proportional to density, and is, therefore, independent of static pressure. The availability of oxygen can thus be increased only by increasing the proportion of oxygen in the mixture.

The value of the method used was that it isolated and amplified small combustion effects which might have passed unnoticed in combustion chambers designed for practical operation. In the test furnace, a definite effect of pressure was shown which was probably much greater than mathematical analysis would indicate. The effect shown can be regarded as a qualitative demonstration that, under temperature conditions where ignition is barely maintained, and where gas temperatures are below both particle temperatures and wall temperatures, pressure will affect combustion adversely because of heat loss by convection from the particle.

The final completeness of combustion is not necessarily related to the initial heating rate in all equipment, though such a relation did exist in the authors' test equipment for obvious reasons. In that equipment, the radiation temperature to which a particle was exposed was essentially constant throughout its combustion history. Low furnace temperatures thus resulted in early loss of ignition as well as slow ignition, while high furnace temperatures would delay loss of ignition as well as accelerate ignition. Two combustion chambers operated at Battelle have demonstrated that ignition intensity and loss of ignition need not be related. In one, a gas-turbine combustor 30 in. in diam, ignition was extremely rapid, with flame temperatures above 2600 F within 6 in. of the point of coal admission. However, the flame passed close

to very cold walls, and was quickly diluted by large quantities of excess air, and combustion efficiency was only 60 per cent. In another investigation, low-volatile coal was burned in a tubular refractory furnace 18 in. diam and 8.5 ft long. Ignition was so slow that at distances of 1 ft, 2 ft, and 3.3 ft from the burner, flame temperatures were only 1935, 2060, and 2240 F, respectively; however, at 6 ft from the burner, both gas temperature and refractory temperature were 2570 F, and at 8.5 ft from the burner 97 per cent of the coal had been burned. In this test, rate of heating was much lower than in the gas-turbine combustor, but combustion took place under nearly adiabatic conditions so that loss of ignition did not occur until burning had practically run its course.

In gas-turbine practice the combustor-inlet and combustor-outlet temperatures, and the volume rate of air flow would be nearly constant over a wide range of pressures. Mass rate of air flow and fuel flow would vary in almost direct proportion to pressure. Because of higher flame density and higher firing rates at higher pressures, it would be expected that flame temperatures would be considerably higher than at low pressures. This would result in higher radiating temperatures for ignition, which might be expected to compensate to a great degree any adverse convection effect. At the end of combustion, gas temperatures in an air-cooled combustor would be higher than wall temperatures by perhaps 1000 F, so that increased convection at high pressures actually should benefit combustion rather than cause early loss of ignition noted under the authors' test conditions.

At Battelle, as referred to by the authors,⁶ tests have been run to determine the effect of pressure on combustion in a pulverized-coal flame. Conditions differed from gas-turbine practice in that firing rate was not proportional to pressure, but was nominally constant for all tests, at 120 lb of coal per hr. Flame temperatures of about 2800 F were obtained near the burner. Under these conditions no large effect of pressure was found. If ignition was retarded by pressure, the effect on practical operation was negligible.

Inspection of the authors' curves, Figs. 7 through 10, suggests that if the tests had been run at temperatures of 2500 to 3000 F (1370 to 1650 C), complete combustion might have been obtained at all pressures.

The data presented are of interest principally because they point out that not all the combustion effects resulting from use of high pressures are favorable, and care must be exercised to minimize the unfavorable effects which might be expected.

AUTHORS' CLOSURE

The questions raised by Mr. Hazard involve interpretation of the data presented as an alternative to that presented in the paper. His analysis requires extension of empirical correlations from large-scale experiments to the microscopic scale involved in these studies of combustion of pulverized coal. This requires caution in the absence of rigorous mathematical solutions for either mass or heat-transfer rates in processes involving both convection and diffusion.

Some confusion appears between these attempts to explain loss of ignition and the demonstration of effects of pressure, acting through the initial heating rate, upon the ease of maintaining ignition. Ignition is easily maintained in a hot furnace in the slugging range, but is increasingly difficult with high excess air and rapid cooling of the burning particle by radiation to cold walls. Under the latter conditions the data show that ignition must be effected by a more intense source of radiant heat with increased pressure than at atmospheric pressure in order to maintain ignition. Otherwise, combustion will be less complete and increased combustion space alone will not be adequate.

⁶ Reference is to authors' bibliography (1).

⁵ Assistant Supervisor, Battelle Memorial Institute, Columbus, Ohio. Jun. ASME.

This
the ga
tures i
design
are giv
the ga
checke
limits
to the
metho
the qu
tributo

TH
T
pe
sef of h
barrel o
natural
plement
the futu
Estab
the synt
ful oper
graphica
operate
sources
Many
for the p
reviews
only sun
tages and

¹ Chem
Synthetic

² Super
Branch, I

³ Assist
Synthetic

⁴ "Oxy
L. L. New
559.

⁵ "Futu
Powell, G

⁶ "Rece
British C
12, 1948,

⁷ "Gasi
tion Rese

Contrib
Meeting,

AMERICAN

NOTÉ:
derstood a

the Societ

Continuous Gasification of Pulverized Coal With Oxygen and Steam by the Vortex Principle

By H. PERRY,¹ R. C. COREY,² AND M. A. ELLIOTT³

This progress report presents the preliminary results of the gasification of pulverized coal by steam-oxygen mixtures in a vortex reactor. The basic principles of reactor design, and an illustrative example of their application are given. A method of calculating the composition of the gas produced in this reactor is presented and has been checked experimentally. The carbon conversion and the limits of operation have been found to be closely related to the type and uniformity of the coal distribution. A method of improving the operation of the equipment and the quality of the gas by a change in the type of coal distributor appears to be promising.

INTRODUCTION

THE manufacture of synthetic liquid fuels by the Fischer Tropsch process, which appears to be a future commercial possibility in this country, requires approximately 30,000 scf of hydrogen and carbon monoxide (synthesis gas) for each barrel of product. Although synthesis gas can be made from oil, natural gas, or coal, it is obvious that if synthetic fuels are to supplement a substantial percentage of the liquid fuels consumed in the future, coal must be looked to as the primary source.

Established gasification processes in this country could supply the synthesis-gas requirements, but since they depend for successful operation on coke, or classes of coal found only in certain geographical areas, there is an urgent need for a process that will operate with any class of coal, thereby removing fuel costs and sources as restrictions.

Many methods have been proposed for the gasification of coal for the production of synthesis gas, and since several excellent reviews of these methods have been published^{4,5,6,7} they will be only summarized here for the purpose of showing the advantages and disadvantages of each, and the basis for the present in-

vestigation. The methods have been classified by Newman⁴ into the four following groups:

- 1 Fine fuel gasified in a fluidized bed.
- 2 Fine fuel gasified in a fixed bed.
- 3 Lump fuel gasified in a fixed bed.
- 4 Fine fuel gasified in suspension.

The fluidized-bed processes, of which the Winkler is typical, require a highly reactive and noncoking coal or char, a large reactor volume, and a relatively large consumption of oxygen per pound of fuel gasified. The dust loading and the carbon dioxide in the gas produced are high. Where cheap fines of a highly reactive fuel are available, this process might be suitable for use in the United States.

The processes in which fine fuel is gasified in a fixed bed at atmospheric pressure are an extension of the use of air-blown gas producers. The necessity of using either sized coke or anthracite severely limits these processes both economically and from the viewpoint of available raw materials. The Lurgi process, which involves a fixed-bed operation at 20 to 30 atm with small-sized fuel, suffers the same limitations from the standpoint of coal requirements, and, in addition, produces substantial quantities of methane, which is a diluent in the Fischer Tropsch process and would require an expensive reforming process if the product were to be used for synthesis gas.

The fixed-bed processes using lump fuel have the advantage of requiring only a modification in design and operation of existing water-gas generators, and thus the years of accumulated experience with such equipment could be used. However, from a commercial standpoint, high-temperature coke is the only suitable fuel, and this imposes a serious limitation on the use of the conventional water-gas process.

One of the most promising methods appears to be the gasification of pulverized coal in suspension in a stream of oxygen and steam. Favorable characteristics inherent in such a process appear to be: (1) Relatively high specific rates of gasification due to the high specific surface of the fuel; (2) the advantages of a continuous process in ease of control and the need of a small plant size for large throughputs; and (3) the use of any class of coal.

Suspension gasification of pulverized coal may be classified, in general, in two ways, depending upon the path of the coal particle with respect to the gas: (a) The coal may flow with one or both of the reacting gases; (b) the coal may have relative motion with respect to the reacting gases, thereby making use of the fact that the speed of the diffusion-controlled phases of the gasification reactions is increased.

Early in 1947, when this investigation was under consideration, the latter classification appeared to merit further experimental work. The Fuel Research Board in England,⁸ and the Loco-

¹ Chemical Engineer, Research and Development Branch, Office of Synthetic Liquid Fuels, Bureau of Mines, Pittsburgh, Pa.

² Supervising Engineer, Combustion Research Section, Coal Branch, Bureau of Mines, Pittsburgh, Pa. Mem. ASME.

³ Assistant Chief, Research and Development Branch, Office of Synthetic Liquid Fuels, Bruceton, Pa. Mem. ASME.

⁴ "Oxygen in the Production of Hydrogen or Synthesis Gas," by L. L. Newman, *Industrial and Engineering Chemistry*, vol. 40, 1948, p. 559.

⁵ "Future Possibilities in Methods of Gas Manufacture," by A. R. Powell, *Gas Times*, vol. 52, 1947, pp. 164, 167-168, 233-234 and 237.

⁶ "Recent Trends in Gas Producer Practice," by T. J. Brozowski, British Coal Utilization Research Association, Monthly Bulletin, vol. 12, 1948, p. 237.

⁷ "Gasification Methods," by M. W. Thring, British Coal Utilization Research Association, Monthly Bulletin, vol. 8, 1948, p. 69.

Contributed by the Fuels Division and presented at the Annual Meeting, New York, N.Y., November 27-December 2, 1949, of THE AMERICAN SOCIETY OF MECHANICAL ENGINEERS.

NOTE: Statements and opinions advanced in papers are to be understood as individual expressions of their authors and not those of the Society. Paper No. 49-A-73.

⁸ "Complete Gasification of Pulverized Coal in a Vortex Chamber," Report of the Fuel Research Board for Year ending March 31, 1938, p. 141.

motive Development Committee⁹ had investigated the use of a vortex reaction chamber as a combustor. This reactor appeared to have special advantages for use as a gasifier. One other method of suspension gasification had been tried in the Ruhr, Germany. A pilot plant was operated during the war using a process developed by the Heinrich Koppers Company, which used pulverized coal with oxygen and steam under turbulent conditions. It was claimed to be superior to the Winkler process, but sufficient design details and operating data were not available to the Bureau of Mines to evaluate completely its applicability to commercial operation in this country. In April, 1949, the Bureau placed into operation a synthetic-liquid-fuels demonstration plant in Louisiana, Mo., using a modified Heinrich Koppers unit, designed to gasify 25 tons of coal a day for the Fischer Tropsch plant.

The original work on the vortex reactor was done by the Fuel Research Board in England⁸ and was used for the production of producer gas with encouraging results. A few tests were also made using steam-air mixtures, and a typical gas composition was as follows: Analysis, per cent by volume, nitrogen free; CO₂ 45.1 per cent, O₂ 0.8 per cent, CO 20.5 per cent, H₂ 30.3 per cent, CH₄ 3.3 per cent, carbon conversion approximately 50 per cent.

It was thought that the high carbon dioxide in the gas resulted from high heat losses because of the small size of the unit. The same principle was studied in 1946 at Battelle Memorial Institute for the Locomotive Development Committee⁹ with the objective of developing a combustor for pulverized coal. In these tests heat releases up to 4,000,000 Btu per cu ft were observed.

Careful study of the theory and the results of each of these applications of the vortex principle led to the conclusion that it might be adapted to the gasification of pulverized coal with oxygen and steam. Accordingly, the Research and Development Branch of the Office of Synthetic Liquid Fuels, in co-operation with the Combustion Research Section of the Coal Branch, each of the Bureau of Mines, designed and built a pilot plant at the Pittsburgh Station to gasify 100 lb of coal per hr. This size was selected because it was thought to be large enough to have low heat losses and to be small enough to be operated with reasonable quantities of materials.

THEORY OF THE VORTEX

The design of the vortex required a mathematical analysis of the aerodynamics of the unit and of the forces on the particles. The approximate feed conditions are established by the requirements for making a gas of desired composition. To avoid slagging of ash on the walls, the vortex should be designed so that the largest particles do not reach the wall. The outlet radius must be selected such that the ash and unburned carbon will leave at the exit pipe before reaching the floor of the vortex.

The basic law of the free vortex is the conservation of angular momentum. The fluid is introduced tangentially at the wall and its angular momentum is $M_1 V_1 R_1$, where V_1 is the tangential velocity at radius R_1 (wall radius), and M_1 is mass of the gas. At any other radius R_2 within the vortex the angular momentum must be the same as at the wall, so that $M_1 V_1 R_1 = M_2 V_2 R_2$, or $V_2 = V_1 R_1 / R_2$. Thus since $R_2 < R_1$, as the gas moves toward the outlet in the center of the chamber the tangential velocity increases. Since the fluid also moves radially toward the outlet, its resulting path is a spiral. If a solid particle is introduced into this moving stream, it is accelerated rapidly to the velocity of the stream, and the forces acting on the particle are (1) centrifugal

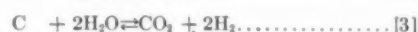
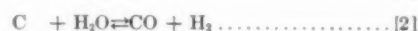
force due to the circular path of the particle, (2) viscous drag of the gas stream, (3) and gravity. If the particle size is such that the centrifugal force and the viscous drag on the particle are equal at some radius within the vortex, and if the particle does not react and change size, it will move downward in a helical path.

If the coal particles are gasified they continually change size. For each size of the coal particle there is a new equilibrium radius—the smaller the particle the nearer the equilibrium radius to the center of the chamber. Thus a reacting particle not only moves in a circular path with the gas stream but also moves across the gas stream seeking new equilibrium radii. This movement of the particle across the gas stream sweeps the products of the reaction from the coal surface, leaving a fresh surface for the reaction to take place.

The method of application of these principles to the design of a vortex for a particular set of feed conditions is shown in the Appendix.

GAS COMPOSITION FROM EQUILIBRIUM CONSIDERATIONS

In the absence of methane in the make gas, the chemical reactions in a mixture of carbon, oxygen, and steam at elevated temperatures are



At atmospheric pressure and at the temperatures involved in these calculations, Reaction [1] is assumed to go to completion and the dissociation of steam and carbon dioxide is assumed to be negligible. In the vortex reactor, Reaction [4] was found to take place so slowly as not to influence the final make-gas composition. Equation [5] (water-gas shift reaction) is the only remaining independent equation since Equation [5] = Equation [3] — Equation [2].

The equilibrium composition of the gas produced has been calculated for a variety of conditions from a knowledge of the following:

- 1 Coal feed rate and ultimate analysis.
- 2 Gross heating value of coal.
- 3 Oxygen feed rate and analysis.
- 4 Steam feed rate and preheat temperature.
- 5 Heat loss from the unit.
- 6 Per cent of carbon gasified.

In addition, the following assumptions have been made:

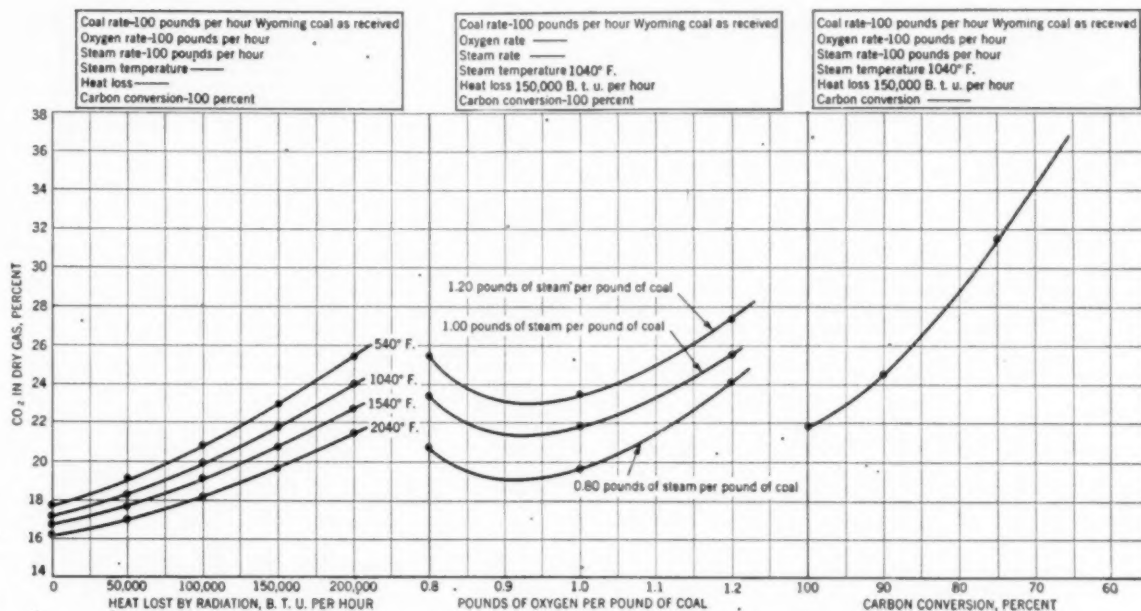
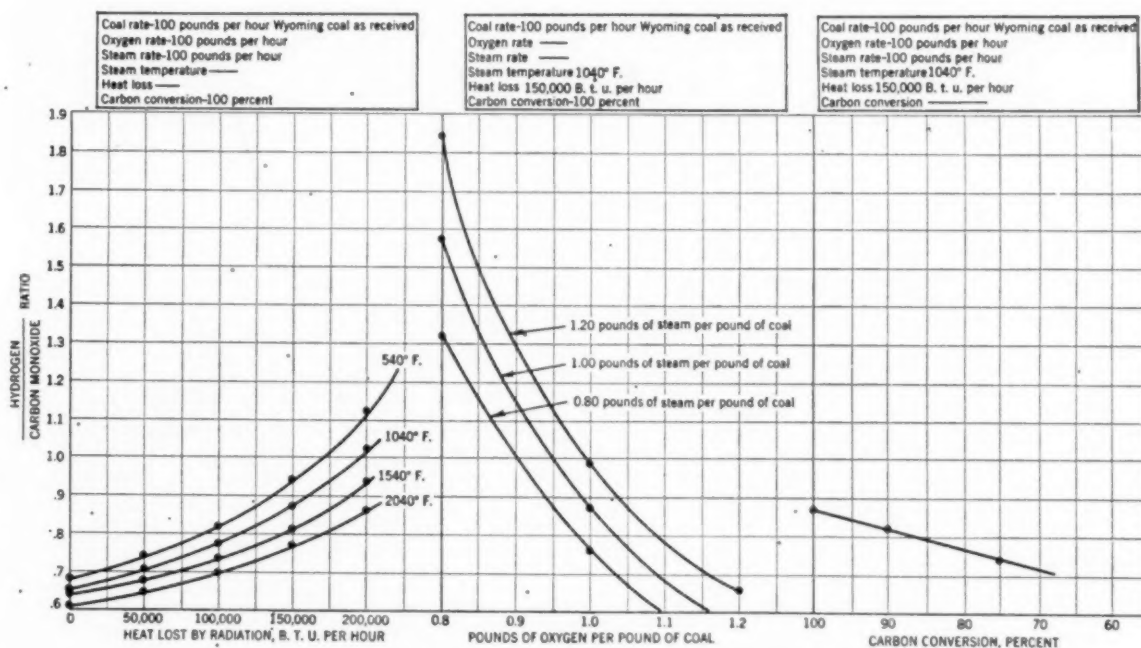
- 1 Water-gas shift equilibrium is reached (Equation [5]).
- 2 Boudouard reaction Equation [4], does not influence the final gas composition.
- 3 The oxidation of C to CO₂ goes to completion.
- 4 No dissociation of CO₂ and H₂O.
- 5 No methane is formed.
- 6 All sulphur in the coal appears as H₂S in the make gas.

The first four assumptions have been found to be essentially correct for the vortex reactor. Small amounts of methane (2-3 per cent) appear in the make gas, but affect the equilibrium calculations only slightly. The form in which the sulphur appears in the make gas has not been determined, but for the low-sulphur coals used in these tests it could appear in any form without changing the equilibrium calculations appreciably.

The per cent of CO₂ in the dry make gas, the per cent steam

⁹ "Progress Report on Pressurized Combustion of Pulverized Coal," by J. I. Yellott and C. F. Kottcamp, presented by the Fuels Division, Annual Meeting, New York, N. Y., 1946, of THE AMERICAN SOCIETY OF MECHANICAL ENGINEERS.



FIG. 1 CALCULATED VALUES OF PER CENT CO₂ IN DRY MAKE GAS AS FUNCTION OF PROCESS VARIABLESFIG. 2 CALCULATED VALUES OF H₂-TO-CO RATIO IN DRY MAKE GAS AS FUNCTION OF PROCESS VARIABLES

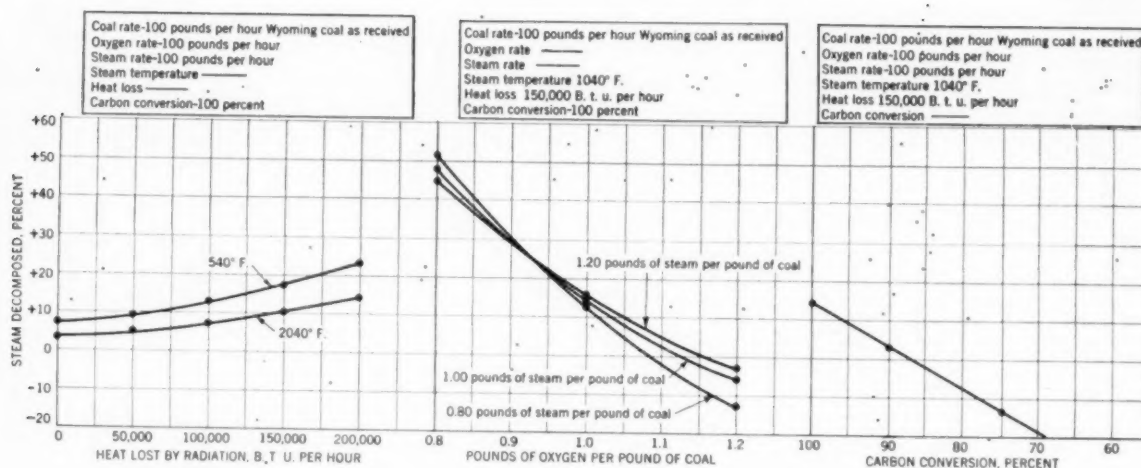


FIG. 3. CALCULATED VALUES OF PER CENT STEAM DECOMPOSED AS FUNCTION OF PROCESS VARIABLES

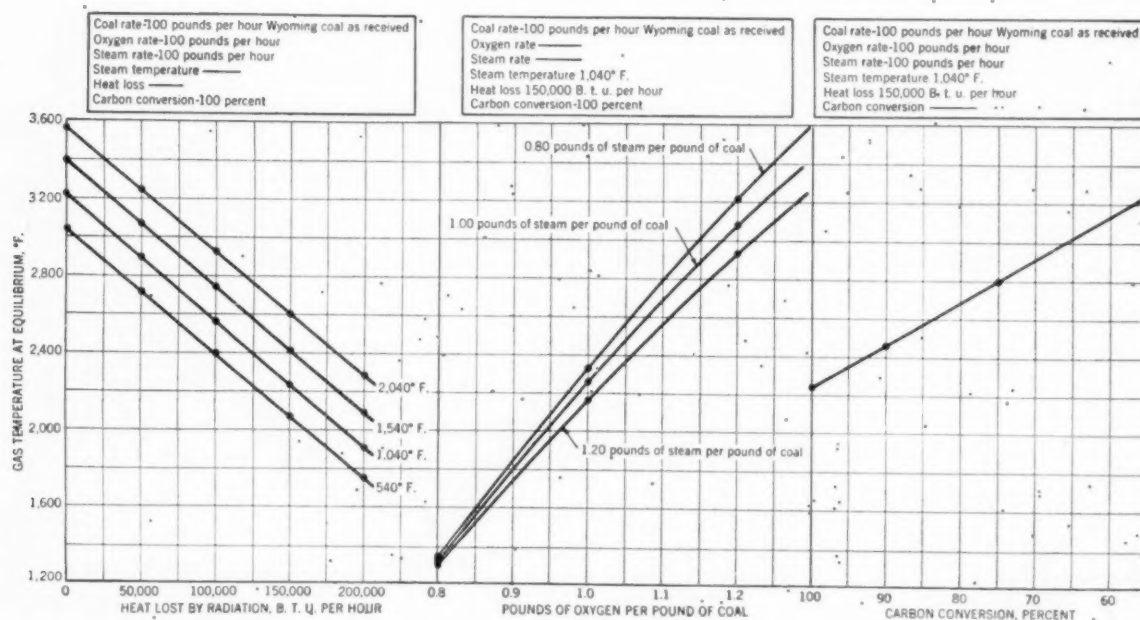


FIG. 4. CALCULATED VALUES OF EQUILIBRIUM TEMPERATURE OF GAS AS FUNCTION OF PROCESS VARIABLES

decomposition, and the ratio of hydrogen to carbon monoxide have been calculated as a function of the following:

- 1 Heat lost by radiation.
- 2 Steam preheat.
- 3 Oxygen to coal ratio.
- 4 Steam to coal ratio.
- 5 Per cent carbon gasified.

The coal used for these calculations was a Rock Springs No. 9, Wyoming coal, the composition of which is given in Table I.

In the calculations in which the carbon gasified was assumed to be less than 100 per cent, the residue was assumed to be entirely carbon and ash. This agrees with the experimental results.

TABLE I. ULTIMATE ANALYSIS (3.5 PER CENT MOISTURE), PER CENT

H ₂	5.3	O ₂	15.4
C	71.6	S	0.9
N ₂	1.5	Ash	5.3

Gross heating value = 12,620 Btu per lb

The results of these calculations are shown on Figs. 1, 2, 3, 4. Fig. 1 indicates that the production of CO₂ is a minimum for a weight ratio of oxygen to coal of approximately 0.9. For this feed, therefore, the CO + H₂ is at a maximum. The position of the minimum CO₂ is affected slightly by the steam-to-coal ratio. As the percentage carbon gasified decreases, the CO₂ in the dry make gas increases rapidly.

Fig. 2 shows that as the O_2 -to-coal ratio decreases, the H_2 -to-CO ratio increases rapidly.

Fig. 3 shows that the percentage of steam decomposed is almost independent of the steam-to-coal ratio, at an oxygen to coal ratio of 0.9.

Fig. 4 shows the effect of the process variables on the exit gas temperature. Increasing heat losses decrease the exit gas temperature, while increasing the oxygen-to-coal ratio in the feed and decreasing the carbon conversion cause the exit gas temperature to increase.

APPARATUS

A flow diagram of the apparatus is shown in Fig. 5. The steam superheater was gas-fired and the heat-transfer surface consisted of two stainless-steel coils. The oxygen, obtained from

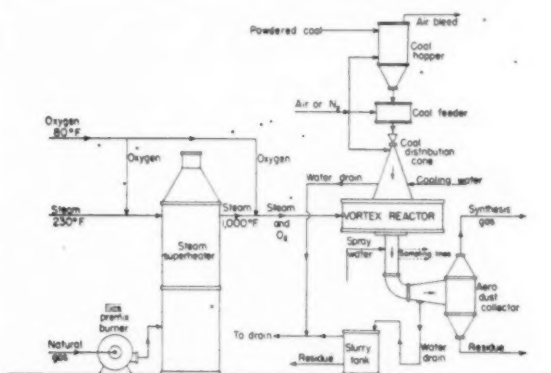


FIG. 5 FLOW SHEET FOR VORTEX GASIFIER

a Linde Cascade unit, was mixed with the superheated steam and split into four feed lines to the reactor. Pulverized coal was fed from an aerated hopper by a star-wheel feeder to a distributor, and then to the vortex reactor. The gases produced, ash, and unburned carbon, left the reactor at the bottom and passed through a 4-in. refractory-lined pipe. Gas-sampling and temperature measurement were made in this section. The gases and solids were then cooled by a water spray to about 500 F, and part of the solids was recovered with the excess spray water. In the first tests, multiple cyclone separators were used in an attempt to remove the remaining solids, but these proved unsatisfactory and their use was discontinued.

The construction of the vortex reactor is shown in Fig. 6. Babcock & Wilcox Bafflemix refractory was used to line the outer steel shell, while the slots, top, and bottom of the reaction chamber were cast from B & W Kaocast. Provision for two sight holes and a gas burner was made in the top of the reaction chamber. Movable Pt-PtRh thermocouples were placed in the top and side of the reactor.

The steam and oxygen were measured by means of calibrated sharp-edged orifices. Steam from the service line was throttled to the desired pressure and preheated before measurement at the orifice. The steam temperature leaving the superheater was measured with a Pt-PtRh thermocouple.

The coal hopper held approximately 150 lb of coal and was aerated by an air distributor at the base of the hopper. Mechanical agitation of the coal was tried and resulted in packing of the coal in the hopper. The hopper was connected to the feed mechanism by a standpipe 31 in. high and 4½ in. diam. The fluidized coal fell from this standpipe through two openings in the bottom of the pipe (180 deg apart), was picked up by a rotating impeller wheel, carried through 90 deg around the plate

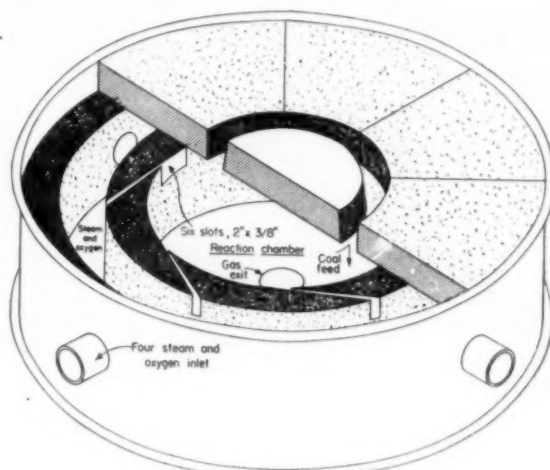


FIG. 6 SCHEMATIC DRAWING OF VORTEX GASIFIER

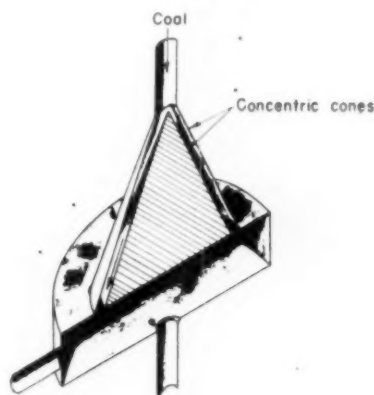


FIG. 7 CONE DISTRIBUTOR

and dropped through two outlets to the two feed pipes. A small stream of air was injected into the impeller teeth at both outlet pipes to dislodge the coal. Calibration of the feeder indicated that the coal rate was proportional to the speed of the impeller wheel and varied, at constant speed, by approximately ± 3 per cent over 5-min intervals. The feeder and hopper were mounted on scales and connected to the distributor with rubber tubing so that coal-feed rates could be checked regularly.

The metered coal fell by gravity to the coal distributor, shown diagrammatically in Fig. 7. The streams of coal were split by the inner cone and passed down the annulus between the two cones into the reaction chamber. The bases of both the inner and outer cones, which were level with the top of the reaction chamber, were water-cooled. A Syntrol vibrator was fastened to the distributor to insure steady flow of the coal down the cone. The coal entered the reaction chamber around the entire circumference at a distance 3 in. from the wall of the reactor.

A second type of distributor has been used. In this distributor, the coal, metered as described, falls on a water-cooled spinning plate at the top center of the reactor and is thrown toward the walls in an umbrellalike pattern by the rapidly rotating plate.

EXPERIMENTAL PROCEDURE

Before admitting coal, the reactor was preheated to about 2000 F with a natural gas - air mixture. Primary air was mixed

with the gas, and secondary air, preheated in the superheater, was introduced through the slots in the reactor. When the temperature in the reactor reached 1000 F, the secondary air was replaced gradually with the steam-oxygen mixture required for gasification, and heating was continued to 2000 F.

The coal hopper was charged through a $1/2$ -in. \times $1/2$ -in. screen, with the fluidizing air turned on to prevent packing of the coal while charging. After filling, the charged hopper and standpipe were fluidized for about 30 sec with an air stream introduced at the star wheel.

When the chamber was preheated to the desired temperature, the coal was started into the vortex, and as the temperature of the exit gases rose sharply, the gas-fired burner was removed from the chamber, and the gas and primary air shut off.

A continuous record of the exit-gas temperature was made, and readings of steam flow, oxygen flow, speed of coal feeder, and the weight of the coal hopper were taken periodically. At regular intervals gas samples were taken at the exit pipe with a water-cooled probe.

RESULTS

Limits of Operation. Approximately 45 tests have been made on the unit with the conical coal distributor. In the first eleven tests Bruceton (coking) coal was used and the coal distributor became coked in every test. When Wyoming (noncoking, 70 per cent through 200 mesh) coal was used and when the optimum slot sizes were determined the unit was operated continuously at coal rates between 45 and 85 lb per hr. At both higher and lower rates, unburned coal accumulated on the vortex floor. At the lower rates the small quantities of steam and oxygen required for gasification produced such low tangential velocities in the reactor that the incoming coal stream was not picked up by the gas. At the higher coal rates the density of the incoming coal stream was such that even at the high tangential velocities part of the coal reached the vortex floor before being picked up by the gas.

An attempt to use the same Wyoming coal at rates of 50 lb per hr but with a larger size consist (only 30 per cent through 200 mesh) resulted in an accumulation of unburned carbon in the vortex. One further attempt to use coking coal, under the optimum conditions of slot size and coal-feed rate, also failed.

The limits of operation are a function of the type of coal distributor. In all of the tests in which unburned carbon accumulated on the vortex floor, it was found in irregular piles. At times one side of the vortex was completely clean while the other side was partially filled with coal, indicating uneven feed. With a coking coal, in the cone type of distributor, bridging of coke occurs across the outlet of the distributor, and all of the coal must then be fed through the remaining open area. With a noncoking coal this irregular accumulation of unburned carbon indicates improper design of the distributor. It appears probable that if a noncoking coal were fed uniformly around the circumference by the distributor, the vortex could be operated at both lower and higher coal rates than are now possible.

There is some evidence that this nonuniformity of coal distribution not only affects the operational limits of the unit, but also the composition of the make gas and the gasification efficiency. One test was run for a period of $1\frac{1}{2}$ hr without accumulation of unburned coal, but with a known poor distribution of the coal feed. The resulting gas was extremely high in carbon dioxide, and the gasification efficiency was low, when compared to tests with the same feed conditions but with better coal distribution. This nonuniformity of feed also may be the cause of the variation in results for similar feed conditions.

Size Consist of Coal. The vortex was designed so that particles of approximately 325 mesh have an equilibrium radius equal

to that of the outlet pipe. The coal actually used in these tests contained 55 per cent by weight of particles smaller than this. For commercial use it is impractical to grind coal with 1 or 2 per cent on 100 mesh and have much less than 45-55 per cent through 325 mesh. To approach practical operating conditions, the usual commercial grind of pulverized coal was used, even though it was realized that the unburned carbon might be high. To reduce the carbon loss caused by the high percentage of fines the outlet diameter of the vortex would have had to be reduced below 4 in., causing a pressure rise in the vortex and excessive velocities in the exit pipe (see Appendix).

Calculation of Results. All of the data have been calculated from an elemental balance on the unit using the feed rates of steam, coal, and oxygen, and the composition of the dry make gas. The residue from all tests consisted essentially of carbon and ash, and if the small amounts of hydrogen and oxygen in the residue are neglected, the calculations are affected by less than 0.5 per cent. From the elemental balance, the moles of dry gas per hour, moles of steam per hour, and the amount of unburned carbon per hour can be calculated. To check the calculated values, it would have been desirable to determine one of these streams experimentally, and some attempts were made to measure the humidity of the make gas and to collect and weigh all of the residue. Both determinations proved to be rather difficult, and, because of the multitude of other problems, were deferred until a gas approaching the desired composition is produced. However, even without a check on the absolute values of these calculated quantities, certain trends appear and are reported.

Data. In the equilibrium calculations, made to determine the composition of the make gas that could be expected with this reactor, the assumption was made that the water-gas equilibrium shift would be satisfied. In Fig. 8 the values of the equilibrium constant, calculated from the make-gas composition, are

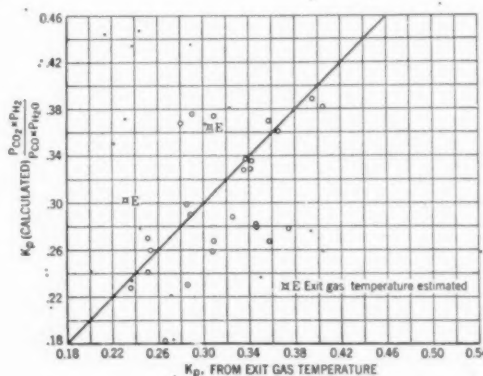


FIG. 8 COMPARISONS OF CALCULATED AND THEORETICAL WATER-GAS EQUILIBRIUM CONSTANTS

plotted against the values of the constant corresponding to the measured exit-gas temperature. About one half of the points agree almost exactly, and the remainder are scattered almost equally above and below the line. Considering the errors in temperature measurement and the errors possible in calculations, based on an experimentally unchecked elemental balance, this agreement is excellent.

The other assumption made concerning equilibrium in calculating the theoretical gas composition was that the rate of the $\text{CO}_2 + \text{C} \rightleftharpoons 2\text{CO}$ reaction would be slow enough not to influence the final gas composition. The equilibrium constant for this reaction was calculated as described and is plotted in Fig. 9.

There is considerable scatter of the experimental values but they are roughly $1/10,000$ of the equilibrium values corresponding to the exit-gas temperature, indicating that the rate of this reaction is such as to influence only slightly the final gas composition.

Thus the major assumptions made in calculating gas compositions, i.e., the water-gas-shift equilibrium is reached, and the effect of the Boudouard reaction is negligible, have been justified for this reactor. It was shown, in the calculation of

the equilibrium gas composition, that if the foregoing assumptions are correct, and if the amount of carbon gasified and the heat losses are known for a given set of feed conditions, the make-gas composition can be calculated. Estimate of the heat losses can be made for any size of unit. The per cent of carbon gasified is a characteristic of the type of reactor and is the variable which will determine the practicability of the reactor for gasification purposes.

The data for the test with the cone-type distributor are presented in Table 2. For this table the percentage heat loss is defined as

Heat lost by radiation, convection, etc.

Enthalpy in feed — heat of combustion of unburned carbon

The high percentage of carbon dioxide in the synthesis gas appears to be a result of the excessive heat losses occurring in this small unit. Figs. 10 and 11 show the effect of percentage heat loss on the production of carbon monoxide plus hydrogen, and carbon dioxide per pound of coal gasified. At higher throughputs, the percentage heat loss was reduced and the carbon monoxide and hydrogen produced per pound of coal increased, while the carbon dioxide produced per pound of coal decreased. The dotted curves in these figures are for those tests in which the steam-to-coal ratio was low, and in which the gas produced had a carbon monoxide-to-hydrogen ratio of 2:1 instead of the 1:1 ratio observed in other tests. The relatively high yield of carbon

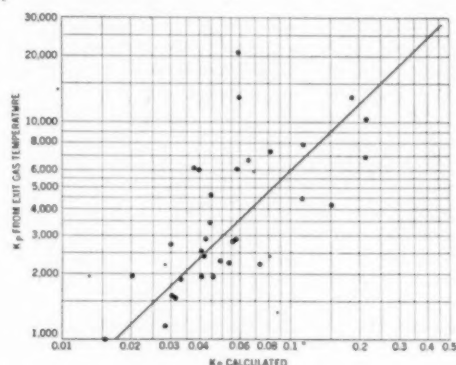


FIG. 9 COMPARISON OF CALCULATED AND THEORETICAL EQUILIBRIUM CONSTANTS FOR THE $\text{CO}_2 + \text{C} \rightleftharpoons 2\text{CO}$ REACTION

TABLE 2 DATA FROM TESTS ON CONE-TYPE DISTRIBUTOR

Test No.	S No.	Coal Rate pds/hr	pds O_2 per pd coal	pds H_2O pd coal	% C gasified	Exit gas temp.	Gas made cuft/hr	GAS ANALYSIS			% heat loss
								CO_2	CO	H_2	
43	4	44.8	.905	.800	49	2240	724	50.3	19.5	20.6	36.1
43	3	49.2	.931	.742	52	2320	818	48.0	23.6	18.8	35.9
28	3	53.8	.995	1.222	63	2270	1050	49.6	20.8	24.4	31.1
28	5	52.0	1.023	1.277	66	2340	1070	48.0	22.6	24.4	29.4
28	4	50.3	1.059	1.280	70	2330	1089	47.8	22.4	23.4	30.0
43	2	49.2	1.063	.408	57	2495	888	49.6	23.4	14.8	41.3
43	7	48.0	1.075	.785	62	2375	931	49.2	25.0	19.5	37.3
43	6	48.0	1.077	1.152	65	2370	1027	46.9	22.7	21.2	27.2
30	2	48.0	1.096	1.375	67	2285	996	48.8	24.6	22.6	29.4
30	1	46.8	1.128	1.390	67	2235	942	53.0	21.6	20.2	32.4
30	3	46.0	1.137	1.440	74	2315	1065	46.6	25.2	23.0	29.8
18	AV	46.3	1.157	1.378	70	2360	962	53.7	20.9	22.3	31.3
16	4	46.0	1.197	1.165	74	2180	1030	53.2	19.0	19.6	37.8
43	1	42.0	1.245	.881	73	2410	966	50.2	21.6	15.2	38.0
16	2	50.0	1.292	1.580	76	2150	1130	58.4	15.8	18.2	39.4
16	3	46.0	1.405	1.717	86	2285	1202	55.2	17.2	18.4	35.9
16	5	46.0	1.452	1.165	90	2540	1207	54.4	21.8	17.6	36.7
30	4	48.0	1.452	1.373	85	2860	1173	55.8	23.6	16.6	30.8
<hr/>											
38	2	67.0	1.157	.963	69	2570	1442	47.2	26.6	20.4	30.9
38	4	60.0	1.280	.453	83	2680	1345	44.0	40.4	14.0	35.5
35	3	65.0	1.304	1.232	80	2880	1553	50.6	26.4	20.8	27.2
<hr/>											
42	5	84.0	.804	.787	47	2360	1326	43.4	24.2	26.2	27.5
42	6	82.0	.823	.326	50	2465	1328	38.8	32.6	25.6	31.7
42	7	82.0	.912	.843	56	2400	1533	40.6	28.8	25.6	28.9
42	4	84.0	.910	.325	55	2570	1387	38.0	38.8	19.8	31.8
42	1	82.0	.916	.864	50	2555	1220	53.4	23.6	22.2	31.6
33	1	80.0	.989	.970	61	2315	1537	44.2	27.8	24.0	28.5
42	2	84.0	1.000	.772	59	2750	1442	49.6	26.6	20.2	29.6
42	3	84.0	1.012	.518	60	2750	1433	43.2	38.4	17.6	34.1
35	2	76.0	1.015	1.047	63	2480	1480	48.8	23.0	24.6	31.0
37	4	76.0	1.035	.905	67	2595	1660	42.5	27.0	24.7	25.8
33	2	78.0	1.100	.994	73	2470	1730	41.8	32.2	23.2	26.2
33	3	76.0	1.142	1.055	75	2620	1791	40.9	31.7	23.3	25.1

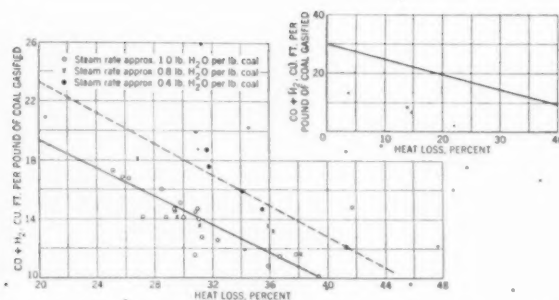
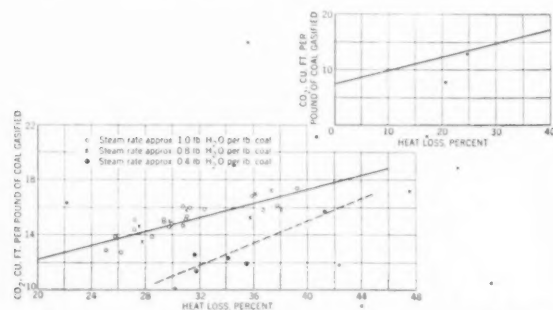
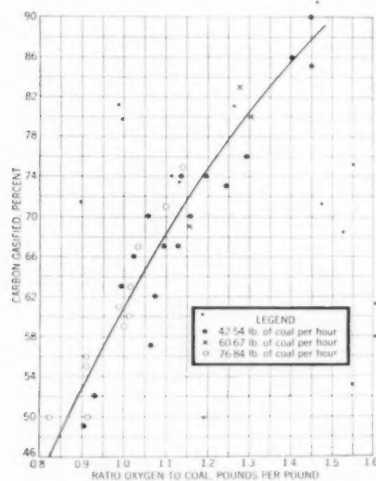
FIG. 10 EFFECT OF HEAT LOSS ON PRODUCTION OF $\text{CO} + \text{H}_2$ FIG. 11 EFFECT OF HEAT LOSS ON PRODUCTION OF CO_2 

FIG. 12 PER CENT CARBON GASIFIED AS FUNCTION OF COAL RATE AND OXYGEN-TO-COAL RATIO

monoxide and hydrogen per pound of coal at these conditions probably resulted from the higher temperatures in the reaction zone in the presence of low steam concentrations, and the formation of a higher carbon monoxide-to-carbon dioxide ratio in the initial oxidation step.

In the inserts in Figs. 10 and 11 the data are replotted and extrapolated to zero heat loss. Under adiabatic conditions, it appears that a yield of 30 to 40 cu ft of hydrogen and carbon monoxide per lb of coal gasified would be obtained, which compares favorably with other gasification processes, and the synthesis gas would contain 15 to 20 per cent carbon dioxide. Thus

in large units, where the heat losses are small, the vortex may be expected to produce a satisfactory yield and quality of synthesis gas.

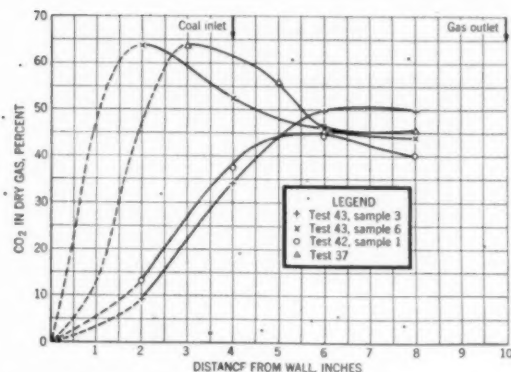
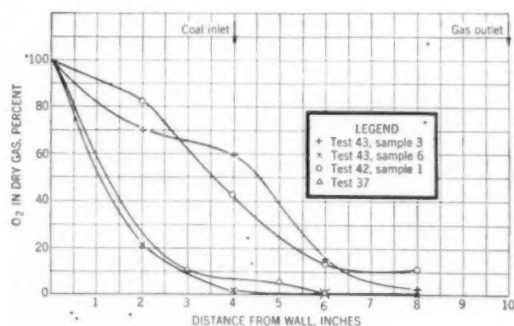
Fig. 12 indicates that for the conditions tested and with the cone distributor, the per cent carbon gasified is independent of the coal rate and almost directly proportional to the pounds of oxygen per pound of coal in the feed. The proportionality between the oxygen in the feed and the carbon converted is evident, since the oxygen concentrations in the make gas were always less than 1 per cent regardless of the quantity of oxygen fed to the reactor. The nearly constant percentage of carbon gasified for different throughputs is probably a function of the hydrodynamics of the unit. As the coal rate was increased the steam and oxygen were increased proportionately and, since the same slot sizes were used in all tests, the tangential wall velocity increased with the increasing throughputs. Increased values of the tangential wall velocity result in smaller carbon particles having an equilibrium radius within the vortex. However, the radial velocity of the fluid in the vortex also increases with increasing throughputs and causes a larger-sized particle to leave the vortex. Calculations indicate that by keeping constant the steam-coal-oxygen ratio, increasing the throughput from 40 to 80 lb of coal per hr should decrease the carbon conversion between 2 and 4 per cent, for the inlet slot conditions used in these tests. This is within the experimental error of measurement.

The carbon conversions range from 50 to 75 per cent for the oxygen-to-coal ratios that are feasible for gasification, and this value is low when compared to the 95 per cent reported for the German Koppers dust process. However, as was noted previously, the vortex was tested with a size consist of coal such that low carbon conversions would be expected. With the cone-type distributor, it was found impossible to operate with a coarser coal.

In some tests, gas samples were taken at different radii within the vortex in an attempt to study the order in which the chemical reactions take place. These data are plotted in Figs. 13, 14, 15, and 16. Although the data were taken for varying feed conditions, the differences in results cannot be explained by this alone, and probably were caused by irregular distribution of the coal in the vortex by the cone distributor. Despite these differences, however, it appears that:

- 1 The oxygen reacts with volatiles in the coal and with the carbon to form CO_2 and H_2O , thereby minimizing tar formation.
- 2 Only when the oxygen has been consumed does the steam-carbon reaction begin.

There are several possible methods of increasing the carbon conversion in the vortex. A constant coal-feed rate and a uniform distribution of the coal appear to be effective, and increasing the tangential velocity for the same throughput also should increase the carbon conversion. Since the reaction of carbon with oxygen is extremely rapid and apparently goes to completion, any method of increasing the rate of the steam-carbon reaction will increase the carbon conversion, and this can be accomplished by having a higher density of carbon in the zone of the steam-carbon reaction. To accomplish this the coal must be fed near the center of the vortex and be thrown out toward the walls. One other possible method of increasing the carbon conversion appears to be increasing the depth of the vortex chamber. From Equation (29) (Appendix), which considers only the aerodynamics of the reactor, as the depth of the reaction chamber, h , is increased the size of the particle, a , which will remain in the vortex becomes smaller, and the carbon conversion should be increased. In addition, increasing h increases the time available for gasification and should aid in increasing the carbon conversion.

FIG. 13 PER CENT CO₂ IN DRY GAS AT VARIOUS POSITIONS IN VORTEXFIG. 14 PER CENT O₂ IN DRY GAS AT VARIOUS POSITIONS IN VORTEX

Several preliminary tests were made with the spinning-plate coal distributor in which the coal is introduced near the center of the reaction chamber. This distributor was designed to increase the carbon density near the center of the reactor, to increase the total path of the carbon particle, and to give more uniform coal distribution. Mechanical difficulties with the driving mechanism caused early shutdowns in every test, but the composition of the gas was much improved over that obtained with the conical coal distributor. Further tests are planned when the mechanical problems are overcome.

CONCLUSIONS

These tests confirm the assumption that from the knowledge of the feed conditions, heat losses, and the per cent carbon gasified, the approximate composition of the gas produced can be predicted for this reactor. In these tests the carbon conversions were low, and the resulting make gas was high in carbon dioxide. For a given set of feed conditions any means of increasing the carbon conversions will improve the quality of the gas. In order for this reactor to be commercially feasible the carbon conversions must be increased.

The results of these initial tests show that the uniformity and the method of coal distribution strongly influence the amount of carbon conversion, the quality of the gas produced, and the maximum and minimum throughputs. The conical coal distributor was unsatisfactory in that the coal was fed nonuniformly near the outer perimeter of the vortex. The few preliminary tests with the spinning-plate distributor suggest that these difficulties have been overcome.

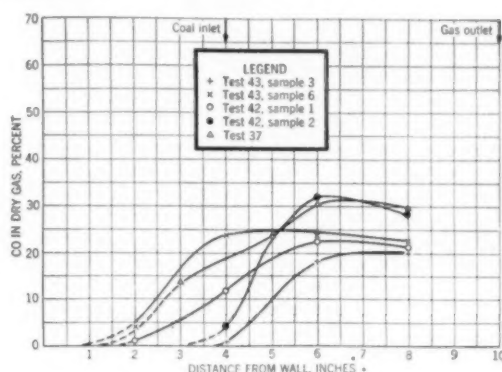
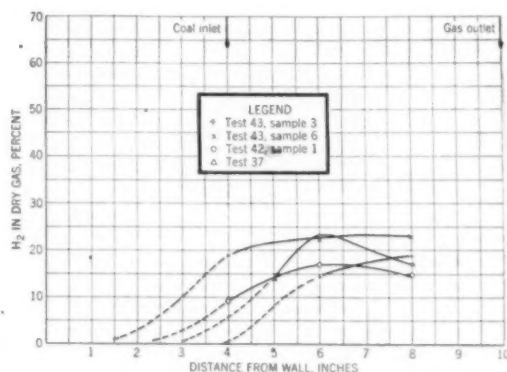


FIG. 15 PER CENT CO IN DRY GAS AT VARIOUS POSITIONS IN VORTEX

FIG. 16 PER CENT H₂ IN DRY GAS AT VARIOUS POSITIONS IN VORTEX

Other possible methods of increasing the carbon conversion are available, i.e., (1) using a coarser size consist of coal with the spinning-plate distributor, (2) increasing the height of the reaction chamber, and (3) increasing the tangential velocities at constant coal rates. Further tests are planned with the new distributor when the mechanical difficulties have been overcome, and the effect of the foregoing variables on the carbon conversion will also be investigated.

Appendix

NOMENCLATURE

- a = particle radius, ft
- b = settling velocities of particles, fps
- h = depth of vortex chamber, ft
- M_1 = mass of inlet gas, lb per hr
- M_2 = mass of inlet gas plus coal, lb per hr
- r = radius at any point in vortex, ft
- R_1 = radius of vortex at inlet, ft
- R_2 = radius of vortex at outlet, ft
- t = gasification time, sec
- u = radial velocity of gas at any radius r , fps
- U_1 = radial velocity at R_1 , fps
- U_2 = radial velocity at R_2 , fps
- v = tangential velocity of gas at any radius r , fps
- V_1 = tangential velocity at R_1 , fps
- V_2 = tangential velocity at R_2 , fps

Z_1 = volume of gas at R_1 , cfs

Z_2 = volume of gas at R_2 , cfs

η = viscosity of gas in vortex, $\frac{\text{lb}}{\text{sec-ft}}$

ρ = density of coal, lb per cu ft

PROBLEM CONSIDERED

The following treatment is an extension of the analysis by Hurley¹⁰ of the forces on a particle in a vortex. To illustrate the application of the theory to the design of a vortex, a particular set of feed conditions will be considered as follows:

100 lb per hr of oxygen) 600 F

100 lb per hour of steam)

100 lb Wyoming coal per hr—as received

Size consist of coal, 70 per cent through 200 mesh, 1-2 per cent on

100 mesh

Inlet Conditions. The basic law of the ideal free vortex is the conservation of angular momentum

$$M_1 V_1 R_1 = M_2 V_2 R_2 \quad [6]$$

The horizontal forces on a particle at any radius, r , in the vortex are

$$\text{Centrifugal force} = \frac{(4/3\pi a^2 r) v^2}{r} \quad [7]$$

$$\text{Viscous drag} = 6\pi a \eta u \quad [8]$$

When the forces are balanced

$$v^2 = \frac{9\eta u r}{2a^2 \rho} \quad [9]$$

From Equation [6] and for $\rho = 130$ lb per cu ft

$$V_1^2 = 3.46 \times 10^{-2} \frac{\eta u r^2}{R_1^2 a^2} \left(\frac{M_2}{M_1} \right)^2 \quad [10]$$

Using a viscosity which is the average for the inlet and outlet conditions: $\eta = 0.043$ centipoises = 2.89×10^{-5} lb/sec-ft. For the selected feed $M_1 = 200$, and $M_2 = 200 + 100 = 300$ lb and Equation [10] becomes

$$V_1^2 = 2.25 \times 10^{-8} \frac{u r^2}{a^2 R_1^2} \quad [11]$$

If no change in temperature or total number of moles of gas occurred in the reactor, by a material balance across cylinders with radii r and R_1

$$u r = U_1 R_1 \quad [12]$$

For this feed there are 8.7 moles of gas per hr at the inlet and 14.1 moles of gas per hr at the outlet. The average is 11.4 moles per hr. The temperature change is from 1060 R to 2960 R, therefore

$$u r = \frac{2960}{1060} \times \frac{11.4}{8.7} U_1 R_1 = 3.66 U_1 R_1 \quad [13]$$

This correction for the change in the number of moles will be approximately the same for any set of feed conditions suitable for gasification, and the correction for temperature change will depend largely upon the amount of steam preheat.

From Equations [11] and [13]

¹⁰ "Some Factors Affecting the Design of a Small Combustion Chamber for Pulverized Fuel," T. F. Hurley, *Institute of Fuel*, vol. 4, 1931, p. 243.

$$V_1^2 = 8.24 \times 10^{-6} \frac{U_1^2 r^2}{a^2 R_1^2} \quad [14]$$

If the maximum-size particle permitted in the feed is 100 mesh then $a = 0.000246$ ft, and Equation [14] becomes

$$V_1^2 = 1.362 \times 10^3 \frac{U_1^2 r^2}{R_1^2} \quad [15]$$

But U_1 is equal to the inlet feed volume divided by the wall area

$$U_1 = \frac{Z_1}{2\pi R_1 h} \quad [16]$$

Substituting in Equation [15]

$$V_1^2 = 21.7 \frac{r^2 Z_1}{R_1^2 h} \quad [17]$$

or

$$V_1 = 4.66 \frac{r}{R_1} \sqrt{\frac{Z_1}{h}} \quad [17]$$

To keep a 100-mesh particle off the wall $r < R_1$, and this is true for any value of R_1 . For the limiting case of $r = R_1$, Equation [17] becomes

$$V_1 = 4.66 \sqrt{\frac{Z_1}{h}} \quad [18]$$

This equation is approximately true for any throughput if the ratio of steam to coal to oxygen is 1:1:1, and the steam-oxygen mixture is at 600 F. The values of V_1 required at different throughputs and for different chamber depths are shown in Fig. 17.

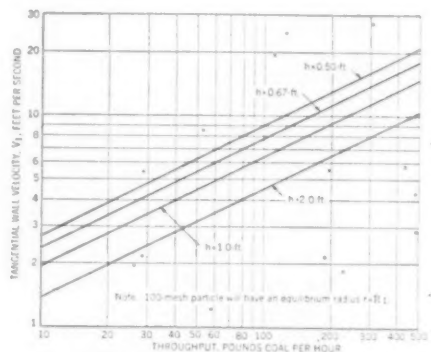


FIG. 17 REQUIRED TANGENTIAL WALL VELOCITY AS A FUNCTION OF THROUGHPUT AT DIFFERENT CHAMBER DEPTHS

For the feed conditions selected, i.e., 100 lb per hr each of coal, oxygen, and steam, and with the steam and oxygen at 600 F, $Z_1 = 1.865$ cfs, and from Equation [18]

$$V_1 = \frac{6.36}{\sqrt{h}} \quad [19]$$

The value of R_1 cannot be determined from this relation, but a value can be established if the outlet conditions are considered (to be mentioned).

Any value of h may be chosen for the selected feed conditions if the tangential velocity, at the wall, V_1 , required to satisfy Equation [19] can be obtained with the reactor. However, other

physical factors determine h . The depth of the chamber must be such that the particle will leave the chamber before it reaches the vortex floor. The settling velocities of the particle and the gasification time must be known since then

$$h = bt \dots \dots \dots [20]$$

The settling velocities, b , of coal particles of various sizes can be calculated from Stokes' law if the particles are assumed to be spheres and the viscosity of the fluid is known. These values are plotted in Fig. 18 for a viscosity of 0.043 centipoise.

The estimation of gasification time is more difficult. From the little available data a value of 0.5 to 1.0 sec appeared to be adequate. The design figure actually used was 0.70 sec. From Fig. 18 the settling velocity of a 100-mesh particle is approxi-

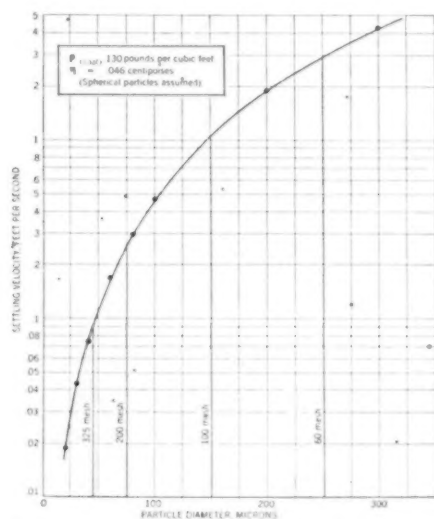


FIG. 18 SETTLING VELOCITY OF COAL PARTICLES

mately 1 fps, and, using a gasification time of 0.70 sec, the height of the chamber becomes

$$h = (1) (0.70) = 0.70 \text{ ft} \approx 8 \text{ in.} \dots \dots \dots [21]$$

The required value of V_1 can now be calculated from Equation [19].

$$V_1 = \frac{6.36}{\sqrt{0.67}} = 7.8 \text{ fps.} \dots \dots \dots [22]$$

A series of tests were made to determine the values of V_1 for different throughputs and for various arrangements of the inlet slots. These data were required since it was found that different slot arrangements resulted in markedly different tangential wall velocities even at the same throughput.

A vortex with $R_1 = 1 \text{ ft}$, $h = 1/2 \text{ ft}$, and $R_2 = 1/4 \text{ ft}$ was used in these tests. The values obtained for different slot sizes and shapes and at different throughputs are plotted in Fig. 19. If the loss in energy in the fluid expanding from the slot into the vortex chamber were a pure expansion loss then it would be directly proportional to the throughput. In this case other variables must be involved since the tangential wall velocity is proportional to $Z_1^{0.75}$ for all $3/8$ -in-wide slots, $Z_1^{0.57}$ for $1/2$ -in-wide slots, and $Z_1^{0.38}$ for the $1/8$ -in-wide slot. Sufficient data were not obtained to develop an empirical equation to fit all of the experimental data, but enough information was obtained to design the slots for the V_1 values used in these tests.

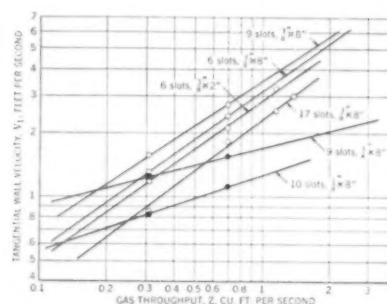


FIG. 19 TANGENTIAL WALL VELOCITY AS FUNCTION OF GAS THROUGHPUT

Outlet Conditions. For the feed conditions selected there are approximately 14 moles of gas leaving the reactor at 2500 F. To calculate the particle size that will just leave the reactor, i.e., $r = R_2$ from Equation [6]

$$V_2 = \frac{200}{300} \frac{V_1 R_1}{R_2} \dots \dots \dots [23]$$

and since

$$Z_2 = 8.4 \text{ cfs.} \dots \dots \dots [24]$$

therefore

$$U_2 = \frac{8.4}{2\pi R_2 h} = \frac{1.337}{R_2 h} \dots \dots \dots [25]$$

At the outlet $\eta = 0.06$ centipoise $= 4.03 \times 10^{-6} \text{ lb/sec-ft}$. A particle at the outlet is subject to the same forces as a particle at the inlet so that from Equation [9]

$$V_2^2 = \frac{9}{2} \frac{\eta U_2 R_2}{a^2 \rho} \dots \dots \dots [26]$$

or

$$a^2 = \frac{9}{2} \frac{(4.03 \times 10^{-6}) 1.337}{130 h V_2^2} = \frac{1.863 \times 10^{-6}}{h V_2^2} \dots \dots \dots [27]$$

and from Equation [23]

$$a^2 = \left[\frac{1.86 \times 10^{-6}}{(h) (0.667)^2 V_1^2} \right] \frac{R_2^2}{R_1^2} \dots \dots \dots [28]$$

or

$$a = \left[\frac{2.05 \times 10^{-3}}{\sqrt{h} V_1} \right] \frac{R_2}{R_1} \dots \dots \dots [29]$$

From Equation [19], $\sqrt{h} V_1 = 6.36$ so that

$$a = 3.22 \times 10^{-4} \frac{R_2}{R_1} \dots \dots \dots [30]$$

Thus the smaller the ratio R_2/R_1 the smaller will be the particle that will just leave the vortex, and the higher will be the carbon conversion. To operate the vortex at atmospheric pressure, a value of R_2 greater than 1 in. is required, and a value of 2 in. was found to be more satisfactory. Thus when $R_2 = 1/4 \text{ ft}$ then when

$$\begin{array}{ccc} R_1 = & 0.5 \text{ ft} & 1.0 \text{ ft} & 1.5 \text{ ft} \\ a = & 1.072 \times 10^{-4} \text{ ft} & 0.537 \times 10^{-4} \text{ ft} & 0.358 \times 10^{-4} \text{ ft} \end{array}$$

Since the weight of carbon leaving the reactor is proportional to a^3 , increasing the value of R_1 to greater than 1 ft decreases the

weight per cent of carbon leaving only slowly. Thus a value of $R_1 = 1$ ft was selected.

From the use of both inlet and outlet conditions, the vortex designed for feed conditions of 100 lb per hr each of coal, oxygen, and steam had

$$R_1 = 1 \text{ ft}$$

$$R_2 = \frac{1}{6} \text{ ft}$$

$$h = \frac{2}{3} \text{ ft}$$

and required $V_1 = 7.8$ fps. The final slot arrangement, 9 slots each $\frac{3}{8}$ in. \times 8 in., was selected to give the maximum values of V_1 . For the feed conditions selected and at the temperatures at which the steam-oxygen mixture pass through the slots, V_1 should be approximately 6.5 fps. Although this value is slightly lower than that required by the calculations, it was the maximum value obtainable using any of the slot arrangements tested, and it appeared to be satisfactory in view of the factors of safety in design used in calculating the values of V_1 required.

co
de
are
on

T
A
A
a
a
b
b
C
c
c
D
D
f
G
g
h
K
K
k
L
n
P
R
r
T
t
U
V
V
v

1 Pro
Mem.
2 Ac
sity.
Cont
and pr
27-July
NEERS.
NOT
underst
of the S

The Gas-Turbine Regenerator—the Use of Compact Heat-Transfer Surfaces

By A. L. LONDON¹ AND W. M. KAYS,² STANFORD, CALIF.

This paper illustrates the application of high-rating compact surfaces of the plate-fin-type to the regenerator-design problem for typical gas-turbine cycles. Comparisons are made with designs employing circular tube surfaces one inch and one-quarter inch in diameter.

NOMENCLATURE

The following nomenclature is used in this paper:

A = heat-transfer area, sq ft
 A_c = free-flow area, sq ft
 a = nonflow dimension of heat exchanger, ft
 a = plate-metal thickness or tube wall thickness, ft
 b = gas-flow dimension of heat exchanger, ft
 b = plate spacing, ft
 C = air or gas capacity rate, $C = Wc_p$, Btu/(hr)(deg F)
 c = air-flow dimension of heat exchanger, ft
 c_p = specific heat at constant pressure, Btu/(lb deg F)
 D_i = inside diameter of tubes, ft
 D_o = outside diameter of tubes, ft
 f = Fanning friction factor, dimensionless
 G = mass velocity, $G = \frac{W}{A_c} = V\rho$ lb/(hr)(sq ft) of A_c
 g = proportionality factor in Newton's second law, $g = 32.2$ lb ft/#-sec²
 h = unit conductance for thermal convection heat transfer, Btu/(hr ft² deg F)
 K_c = contraction loss coefficient for flow at heat-exchanger entrance, dimensionless
 K_e = expansion loss coefficient for flow at heat-exchanger exit, dimensionless
 k = thermal conductivity, Btu/(hr sq ft deg F/ft)
 L = flow length used in the definition of hydraulic radius, ft
 n = number of passes in multipass cross flow heat exchanger, dimensionless
 P = pressure, psi, psf
 R = Reynolds number, dimensionless
 r_h = hydraulic radius, $r_h = \frac{A_c L}{A}$, ft
 T = temperature, deg R
 t = temperature, deg F
 U = unit over-all thermal conductance, Btu/(hr ft² deg F)(sq ft) of A_g
 V = heat exchanger total volume, cu ft
 V = velocity, fps
 v = specific volume, cu ft/lb

W = specific flow rate, lb/(1000 shp-hr)
 x_l = longitudinal tube-bank pitch, dimensionless
 x_t = transverse tube-bank pitch, dimensionless
 α = ratio of total transfer area of one side of exchanger to total volume of exchanger, ft²/ft³
 β = ratio of total transfer area of one side of exchanger to volume between the plates of that side, ft²/ft³
 δ = fin metal thickness, ft
 Δ = with P denotes inlet minus outlet pressure difference
 ϵ = heat-exchanger effectiveness, a function of (NTU , C_a/C_g , flow arrangement), dimensionless
 η = over-all temperature effectiveness of plate-fin heat-exchanger surface, dimensionless
 ρ = density, lb/ft³
 σ = ratio of free flow to frontal area, dimensionless
 μ = viscosity, lb/(hr ft)

Dimensionless Groupings

N_{St} = Stanton's number, (h/Gc_p) , a heat-transfer modulus

N_{Pr} = Prandtl's number, $(\mu c_p/k)$, a fluid-properties modulus

$N_{St} N_{Pr}^{1/3}$ = generalized heat-transfer grouping. This factor versus R defines the heat-transfer characteristics of the surface

R = Reynold's number, $(Gr_h G/\mu)$, $(D_o G/\mu)$

f = Fanning friction factor. This factor versus R defines the friction characteristics of the surface

NTU = Number of heat-transfer units, $(A_g U/C_a)$

ϵ = heat-exchanger effectiveness, a function of (NTU , C_a/C_g , flow arrangement)

Subscripts

a = air-side condition
 g = gas-side condition
 f = film average condition
 l = fluid entrance condition to heat exchanger
 avg = average fluid condition

Miscellaneous

lb = pounds mass in distinction to
 $\#$ = pounds force
 \cong = approximate equivalence

INTRODUCTION

The high-efficiency gas-turbine plant, unlike other prime-mover systems, requires a design philosophy of close attention to details in all respects. This insistence on optimum design is mandatory because operation at temperatures approaching metallurgical limits, large specific flow rates (lb/shp-hr) of the working substance, the high "back-work" input to the compressors multiplying the cost of flow-friction power, are all coupled with the requirement of a compact machinery arrangement. The requirement of compactness is a major consideration in the transportation application of the gas-turbine plant if its basically light weight aspect is to be capitalized upon.

During the present pioneering development of the gas-turbine system, relatively little attention has been devoted to the heat-

¹ Professor of Mechanical Engineering, Stanford University, Mem. ASME.

² Acting-Instructor of Mechanical Engineering, Stanford University. Jun. ASME.

Contributed by the Gas Turbine Power and Aviation Divisions and presented at the Semi-Annual Meeting, San Francisco, June 27-July 1, 1949, of THE AMERICAN SOCIETY OF MECHANICAL ENGINEERS.

NOTE: Statements and opinions advanced in papers are to be understood as individual expressions of their authors and not those of the Society. Paper No. 49-SA-9.

exchanger components—primarily the regenerator. However, for a gas-turbine plant having a specific fuel consumption over a fairly wide load range comparable to that of a steam plant, a regenerator of considerable specific transfer area is required. For instance, in an open-cycle plant such as described by Soderberg, Smith, and Scott (7),³ a transfer area of the magnitude of 3 to 4 sq ft/shp rating is needed. This requirement is several times that of the boiler plus condenser of a steam power plant. It is evident, therefore, that if compactness and lightweight are to be realized, boiler or condenser-type surfaces cannot be used. As an illustration of a practical result of the application of such surfaces, reference (8) describes a 5000-kw gas-turbine plant for central-station application. The regenerator of 75 per cent effectiveness, consisting of 1-in.-diam tubes providing about 3.9 sq ft/shp, has a weight of the order of 21 lb/shp plant rating. While this massiveness and its concomitant cost and bulk may be admissible in a conservatively designed central-station-type plant, it cannot be extended to the transportation-type prime mover.

This discussion emphasizes the ultimate necessity of the development of types of heat-transfer surfaces for the regenerator having substantially higher area-to-volume ratio characteristics than conventionally used boiler and condenser-tube banks. Thus attention is directed to the use of either small, circular, or flat tube surfaces of the order of $1/4$ -in. hydraulic diameter, or else extended surfaces. In the latter case it will be necessary to have a type of construction allowing extended area on both the hot and cold gas sides since each heat-transfer film resistance is of the same order of magnitude, and the coefficients are sufficiently low to permit satisfactorily high "temperature effectiveness" for the fin surfaces.

To illustrate the wide variance in inherent compactness of different surfaces, Table 1 compares the area-to-volume ratio of the several types of surfaces described in Fig. 1. The 10:1 difference for plate-fin surfaces as compared to the 1-in.-diam tubes and the 2:3:1 comparison even with $1/4$ -in. tubes is striking and demonstrates the basic advantages of the extended surface.

The aircraft intercooler application is somewhat akin to that of the regenerator, as gas-to-gas heat transfer exists and the requirements of compactness and lightweight are paramount. Here, both the extended plate-fin and tubular direct surfaces are competitive, but it has been necessary to resort to $1/4$ -in.-diam tubes and smaller to match the over-all performance of extended surfaces. This experience is probably indicative of the competition that will exist in the regenerator application for the open-cycle gas-turbine plant.

While manufacturing methods are available for constructing tubular surfaces into high-temperature heat exchangers, such is not the case for extended surfaces. Heretofore, these have been used primarily in the aircraft intercooler and/or air-conditioning fields, and the production methods for low-temperature service cannot be directly extrapolated to the high-temperature regenerator application. Therefore there is a question as to whether or not the development of methods of high-temperature fabrication is worth the major effort it will undoubtedly require. A response to this question requires the prior technical answer to the following:

- 1 What are the advantages in shape, size, and weight of the extended as compared to the direct-surface regenerator?
- 2 Can extended surfaces be cleaned, and will the fouling rates be excessive?
- 3 Will the extended surface be less expensive assuming that manufacturing methods can be developed?

It is the objective of this paper to answer the first question by comparison of extended and direct-surface exchanger cores de-

³ Numbers in parentheses refer to the Bibliography at the end of the paper.

TABLE 1 COMPARISON OF AREA-VOLUME RELATIONS FOR SOME HEAT-EXCHANGER SURFACES

	Area/volume (ft ² /ft ³)	
	Outside	Inside
1-in.-OD circular tubes..... ($x_1 = 2, x_2 = 1, D_i/D_o = 0.9$)	18.85	16.96
$1/4$ -in.-OD circular tubes..... ($x_1 = 2, x_2 = 1, D_i/D_o = 0.9$)	74.3	67.9
Plate-fin surface (see Fig. 1)..... (12 fins/in., $1/4$ -in. plate spacing)	175.8	

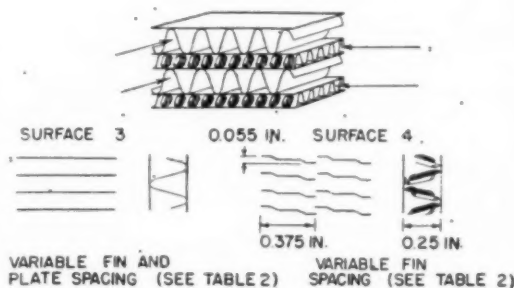
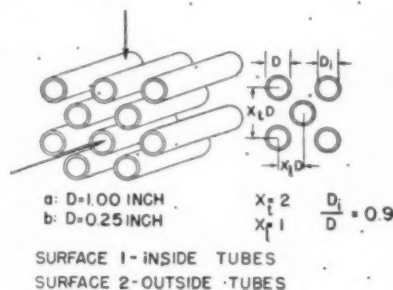


FIG. 1 DESCRIPTION OF FOUR HEAT-EXCHANGER SURFACES (Refer to Table 2 for further details of geometry and Fig. 4 for basic heat-transfer and flow-friction data.)

signed for the same performance. The other two questions cannot be answered categorically at this stage, but several points of interest will be considered.

Heretofore, comparative studies of this character were impossible because of the lack of basic heat-transfer and flow-friction data for surfaces other than circular tubes. Under the sponsorship of the U. S. N. Bureaus of Ships and Aeronautics, and the Office of Naval Research, however, basic data have recently been made available for a number of variations of the plate-fin type of surface of Fig. 1 (1, 2, 3, 4, 5, 6).

REGENERATOR DESIGN CONSIDERATIONS

The primary considerations influencing regenerator design may be summarized as follows: (1) manufacturing and cost limitations, (2) maintenance and cleaning requirements, (3) mechanical-design problems including a thorough consideration of thermal stresses, (4) weight, space, and shape limitations, (5) allowable flow-friction limitations, and (6) desired exchanger heat-transfer effectiveness.

As indicated in the introduction, only items 4, 5, and 6 will be considered in any detail in this paper. This will be accomplished in the following manner:

- 1 Several gas-turbine cycles will be selected for consideration.
- 2 Several different types of the extended and direct surfaces will be specified along with their basic heat transfer-flow friction characteristics.

3
flow f
4
cycle.
On
of reg
pariso

The
rates,
transf
fer an
for a p
ing th

where
The
fer rat
by the
tio of a
let-hot
tiveness
heating
The
times
For th

EFFECTIVENESS %

Fig. 2

3 A nominal per cent pressure drop for hot-side plus cold-side flow friction will be specified for each cycle under consideration.

4 A heat-transfer effectiveness also will be specified for each cycle.

On this basis estimates will be made of the size, shape, and weight of regenerators utilizing the different surfaces. A critical comparison will then follow.

HEAT-TRANSFER AND FLOW-FRICTION EQUATIONS

The exchanger-flow arrangement, the heat-transfer area, flow rates, exchanger effectiveness, and over-all conductance for heat transfer from the hot to cold gas sides are related by heat transfer and thermodynamic considerations. The resulting relations for a particular flow arrangement may be expressed in a form using the following dimensionless groupings

$$\epsilon = \phi \left(NTU, \frac{C_a}{C_g} \right) \dots \dots \dots [1]$$

where ϕ denotes a functional relation.

The exchanger effectiveness ϵ compares the actual heat-transfer rate in the exchanger to the maximum possible rate as limited by thermodynamic considerations. This is equivalent to the ratio of actual cold-air temperature rise to the difference between inlet-hot-gas and inlet-cold-air temperatures, that is, the effectiveness compares the actual to the maximum possibility for air heating.

The capacity-rate ratio, C_a/C_g , compares the mass-flow rate times specific-heat capacity product of the cold and hot streams. For the regenerator application, because of the small contribution

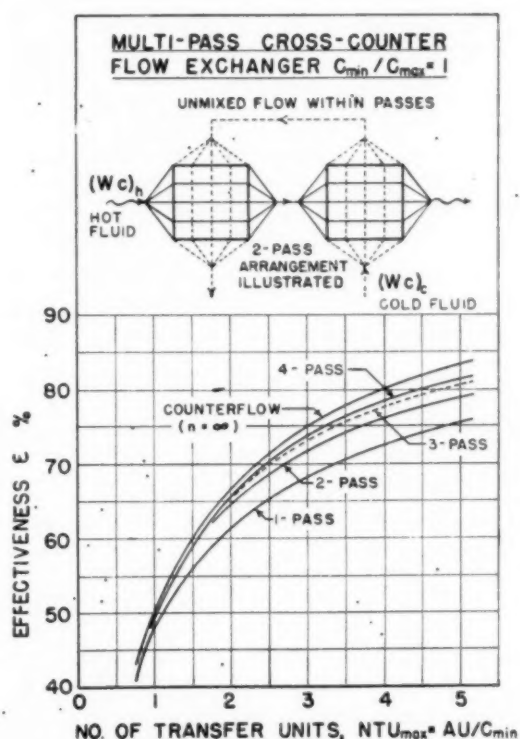


FIG. 2 REGENERATOR EFFECTIVENESS—NUMBER OF HEAT-TRANSFER UNITS RELATION

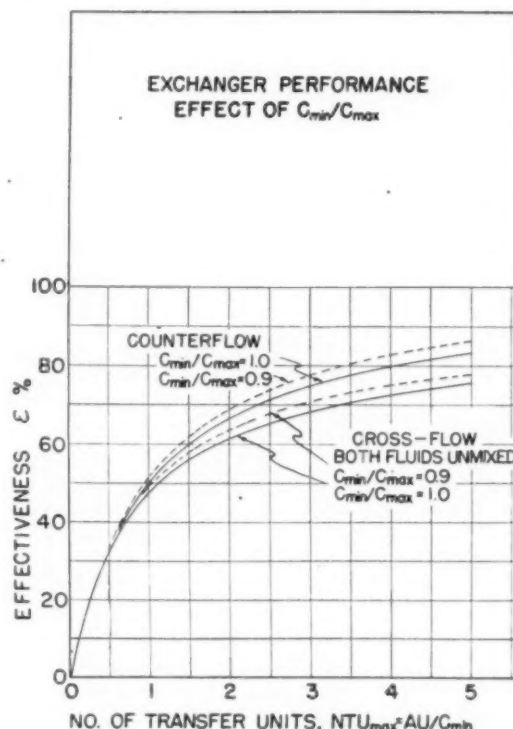


FIG. 3 INFLUENCE OF CAPACITY-RATE RATIO ON REGENERATOR EFFECTIVENESS

(For the gas-turbine system $C_{air}/C_{gas} = C_{min}/C_{max} = 0.95$ to 0.98 .)

of fuel to the hot-gas rate and the slightly higher specific heat with temperature, C_a/C_g is of the order of 0.96 to 0.98.

The number of heat-transfer units, $NTU = AU/C_a$, is a dimensionless expression of the "heat-transfer size" of the exchanger. Note that the NTU is defined in terms of the minimum capacity rate ($C_a < C_g$).

Fig. 2 gives Equation [1] in graphical form for a number of flow arrangements, and the condition that $C_a/C_g =$ unity, a condition approximately satisfied in the regenerator. The influence of capacity-rate ratio is shown in Fig. 3 for C_a/C_g both unity and 0.90. Any intermediate condition can be established by interpolation.

Flow pressure drop through the exchanger can be determined from the following relation

$$\frac{\Delta P}{P_1} = \frac{G^2 v_1}{2g P_1} \left[(K_e + 1 - \sigma^2) + 2 \left(\frac{v_2}{v_1} - 1 \right) + \right. \\ \left. f \frac{A}{A_c} \frac{v_{avg}}{v_1} - (1 - \sigma^2 - K_e) \frac{v_2}{v_1} \right] \dots [2]$$

entrance effect flow acceleration

core "skin" friction exit effect

The terms associated with the flow contraction on entrance to the core, the flow acceleration or deceleration due to the heat-transfer influence on density, the friction within the core, and the pressure recovery on flow expansion at exit are all indicated in Equation [2]. For multipass arrangements, losses in return headers must be accounted for separately.

The correct average specific volume to be used in the indicated skin-friction component is

$$v_{avg} = \frac{1}{A} \int_0^A v dA \quad [3]$$

For the sensibly unity magnitude of C_a/C_g in the regenerator, flow temperatures vary linearly with transfer area, A . Thus to a good approximation

$$\frac{v_{avg}}{v_1} \cong \frac{P_1}{P_{avg}} \frac{T_{avg}}{T_1} \quad [4]$$

where T_{avg} , P_{avg} are the arithmetic average of the terminal magnitudes.

For the heat-exchanger comparisons of this paper, a simplification of Equation [2] is employed by using nominal magnitudes for K_e , K_g , σ , and v_2/v_1 terms in the brackets. The result is for the hot-gas side

$$\left(\frac{\Delta P}{P_1}\right)_g \cong \frac{G^2 v_1}{2g P_1} \left[f \frac{A}{A_c} \frac{P_1}{P_{avg}} \frac{T_{avg}}{T_1} \right] \quad [5]$$

and for the cold-gas side

$$\left(\frac{\Delta P}{P_1}\right)_a \cong \frac{G^2 v_1}{2g P_1} \left[2 + f \frac{A}{A_c} \frac{P_1}{P_{avg}} \frac{T_{avg}}{T_1} \right] \quad [6]$$

For the hot side, the entrance effect tends to cancel the influence of both the flow exit and flow deceleration pressure rises, but for the cold-gas side, flow acceleration on heating adds to the entrance pressure drop. This consideration accounts for the difference between Equations [5] and [6]. In any event, as the core friction term $\left(f \frac{A}{A_c} \frac{P_1}{P_{avg}} \frac{T_{avg}}{T_1}\right)$ is of the order of 15 to 50, the over-all pressure drop is not markedly influenced by the other flow effects.

The total regenerator flow-friction work expenditure is proportional to

$$\left(\frac{\Delta P}{P_1}\right)_{total} = \left(\frac{\Delta P}{P_1}\right)_a + \left(\frac{\Delta P}{P_1}\right)_g$$

for a given cycle and a given operating pressure ratio. This fraction pressure drop is simply related to either the additional compressor work requirement or the diminution of turbine work arising from flow friction. A one per cent pressure drop on the air side causes just as much "loss" as one per cent on the gas side.

With respect to the distribution of friction losses on the air and gas sides, the following general comments can be made:

If the plant is to be operated primarily at full load, an approximately equal distribution of flow-friction work is desirable, i.e.

$$(\Delta P/P_1)_a / (\Delta P/P_1)_g = 0.7 - 1.5$$

as it tends to result in minimum regenerator volume. Should high part-load efficiencies for the plant be desirable, however, the regenerator designs should tend toward

$$(\Delta P/P_1)_a / (\Delta P/P_1)_g < 0.25$$

at full load. This conclusion stems from the fact that while the hot-side density is relatively constant with load for the open-cycle plant, the air-side density decreases markedly as pressure ratio is decreased. The consequence is, while the gas-side loss in terms of plant specific fuel consumption tends to remain fairly constant, the air-side loss increases strongly as load is decreased. Thus if $(\Delta P/P_1)_g$ controls at full load the total loss will remain fairly constant rather than have an undesirable rising characteristic with decreasing load (7).

HEAT-TRANSFER SURFACES

Only four types of surfaces will be considered in this paper: (1) flow inside circular tubes, (2) flow normal to circular-tube bundles, and (3), (4) two plate-fin surfaces, Fig. 1. However, each surface is susceptible to considerable variation as by changing fin and plate spacing and tube diameter. The specific variations in this respect are summarized in Table 2 as 1a, 2b, etc.

For the circular tube surfaces, in all cases specifically considered here, the hot gas flows normal to the tubes and the cold air within the tubes, as this arrangement results in a minimum weight and volume regenerator. The effect of interchanging the flows, on the shape of the core, will be considered later.

The basic heat-transfer and flow-friction data for each of the four surfaces are presented using the usual dimensionless plots of $N_{St} N_{Pr}^{1/3}$ and f versus Reynolds number, R , in Fig. 4. Only for circular tube surfaces, Nos. 1 and 2, Fig. 1, is exact geometrical

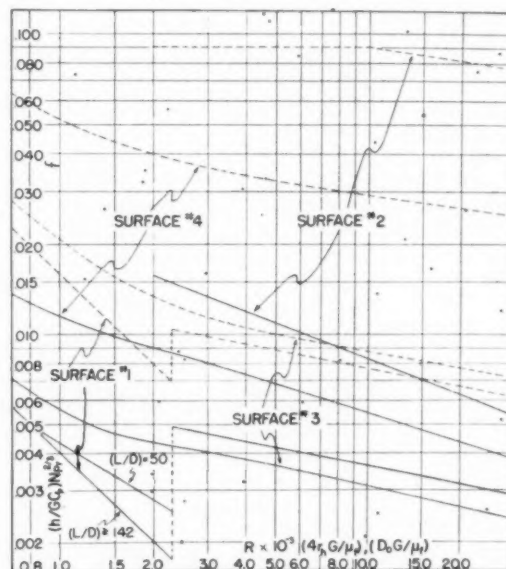


FIG. 4 BASIC HEAT-TRANSFER AND FLOW-FRICTION DATA FOR THE SURFACES OF FIG. 1

--- denotes f characteristic; — denotes $N_{St} N_{Pr}^{1/3}$ characteristic.
[Data for surfaces Nos. 3 and 4 from references (2, 3), and for surfaces 1 and 2 from reference (10).]

similarity maintained for all the variations. Nevertheless, for surfaces 3 and 4, even though complete geometrical similarity is not maintained, the use of a single $N_{St} N_{Pr}^{1/3}$ versus R and a single f versus R characteristic for each surface does not introduce serious error. This has been demonstrated in references (3, 4, 5) which show an excellent heat-transfer correlation for the different fin spacing with Reynolds number based on the flow hydraulic radius, r_h . The f correlation is not as good but the departure from the average characteristics shown in Fig. 4 is less than 15 per cent.

GAS-TURBINE CYCLES

Four distinct gas-turbine cycles are included in this regenerator design survey:

1 Cycle (A) is an open cycle with a 9:1 pressure ratio, 90 per cent intercooling and 75 per cent regeneration with $(\Delta P/P_1)_{total} < 3$ per cent. Such a system, designed for central-station power generation, is described in reference (8).

2 Cycle (B) is a closed cycle identical with cycle (A) except that the pressure levels are increased by a factor of four.

3 Cycle (C) is an open-cycle system designed for a locomotive application with a 4.8:1 pressure ratio, no intercooling, and about 60 per cent regeneration with $(\Delta P/P_1)_{\text{total}} < 5$ per cent. A similar system is described in reference (9).

4 Cycle (D) is an open "exhaust-combustion" cycle of 3:1 pressure ratio with 75 to 80 per cent regeneration and $(\Delta P/P_1)_{\text{total}} < 7$ per cent. This system (11) is of possible interest in the coal-burning-locomotive application. All the thermal energy provided to the turbine working substance after leaving the compressor comes from heat transfer in the regenerator. The turbine exhaust air is combusted with the requisite amount of fuel and is then fed into the regenerator before exhausting to the atmosphere. The basic advantage of this cycle for the coal-fueled plant is that the turbine working substance is clean air and not the products of combustion with attendant fly-ash erosion and fouling problems.

The operating conditions for the regenerator for these cycles are summarized in Table 3, giving the inlet state for hot and cold gases—pressure, temperature, and specific volume; the nominal average gas properties used in the heat-transfer friction calculations—viscosity, unit heat capacity, and Prandtl's number, N_{Pr} ; and the capacity rate ratio, C_a/C_g , together with the specific air-flow rate, W_a lb/(1000 shp-hr).

GEOMETRICAL RELATIONS

As a preliminary to the consideration of the results of the analysis for core shapes for the different regenerator applications, certain readily derivable geometrical relations first will be established. These equations relate core dimensions and volume, the free flow:frontal area ratios for the two sides, the flow mass velocities, and the specific flow rate, W lb of air or gas/1000 shp-hr. The air and gas-flow dimensions are independent of the plant rating but the nonflow dimension (or dimensions for true counterflow) is, of course, directly dependent on plant rating. The more obvious relations for single-pass crossflow, 2-pass cross-counterflow, and true counterflow are summarized in Fig. 5. This illustration also defines the nomenclature specifying over-all core geometry. From these relations follow directly

For any number of air-passes, n , in a cross-counterflow arrangement (single-pass on gas side)

$$\begin{aligned} a &= \left(\frac{n W^2}{V} \right) \frac{1}{\sigma_a \sigma_g G_a G_g} \\ b &= \left(\frac{V}{W} \right) \sigma_g G_g \\ c &= \left(\frac{V}{n W} \right) \sigma_a G_a \end{aligned} \quad [7]$$

For a true counterflow arrangement

$$\begin{aligned} a \cdot b &= \frac{W}{\sigma_a G_a \sigma_g G_g} \\ c &= \left(\frac{V}{W} \right) \sigma_a G_a = \left(\frac{V}{W} \right) \sigma_g G_g \end{aligned} \quad [8]$$

The conclusions to be drawn from these relations are as follows:

- 1 Counter and single-pass crossflow cores will have about the same air-flow dimension, c .
- 2 Counterflow cores can be designed for any nonflow dimensions, a or b , only satisfying the (ab) product requirement given by the first of Equations [8].
- 3 For any number of passes in cross-counterflow, as long as all

the passes are on the air side, the gas-flow-dimension is invariant with n , but the air-flow dimension varies inversely and the non-flow dimension directly with the number of passes, n .

4 If the nonflow dimension tends to be too-large for a particular regenerator application, counterflow will give the best shape with single-pass crossflow next.

5 For the crossflow arrangements, the nonflow dimension may be reduced by (a), reducing the number of passes, $a \propto n$; (b), reducing the specific flow rate, $a \propto W^2$; (c), increasing the volume, $a \propto 1/V$; (d), maximizing the mass velocities G_a, G_g ; (e), maximizing the $\sigma_a \sigma_g$ product.

In this last respect, 5(e), not too much can be accomplished directly inasmuch as $\sigma_g + \sigma_a \leq 0.9$. Consequently, σ_a can vary from 0.3 to 0.6 with no marked change in the $\sigma_a \sigma_g$ product. However, for the extended surfaces in particular, the σ magnitudes can have an important influence on transfer area per unit volume, hence on total volume, V , and as a result, indirectly on the nonflow dimension a .

As crossflow cores tend to be better adapted to machinery arrangements as compared to counterflow, and since the plate-fin surfaces to be considered are more readily formed into crossflow cores, no further consideration of counterflow will be attempted in this paper. Additionally, since the air-flow length tends to be considerably greater than the gas-flow length because of the great differences in density, in the specified n -pass arrangements all the passes are on the air side. It is possible to arrange for multipasses on the gas side as well, without a fundamental change in the relative flow geometry, as pictured in Fig. 5, for a

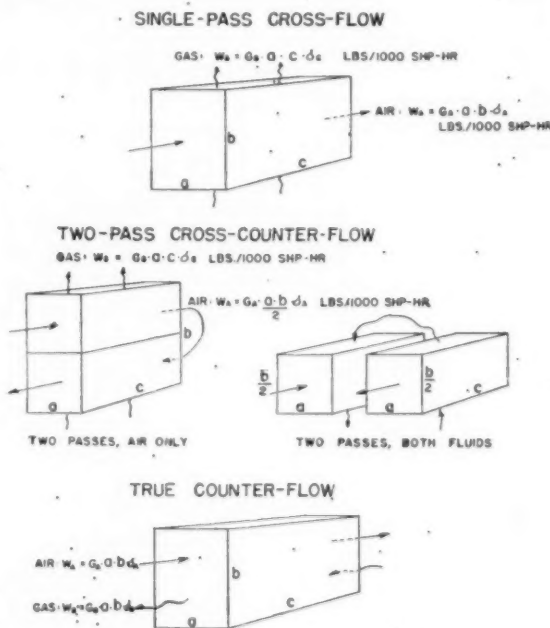


FIG. 5 DESCRIPTION OF CORE GEOMETRY
(See Equations [7] and [8].)

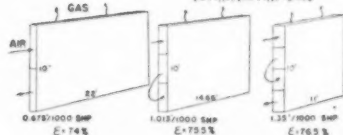
core with two passes on both gas and air sides. However, this expedient just results in a further increase in the nonflow dimension with the somewhat doubtful advantage of a decrease in an already small gas-flow dimension.

REGENERATOR CORE SHAPES

The foregoing considerations together with the data for the

CYCLE A - ARRANGEMENT "1"

1" TUBES, GAS OUTSIDE, AIR INSIDE
VOLUME = 1485 ft³/1000 shp
WEIGHT = 5385 lbs/1000 shp
NTU = 3.41 $(\Delta P/P)_{\text{total}} = 2.88\%$
 $(\Delta P/P)_h / (\Delta P/P)_c = 0.140$



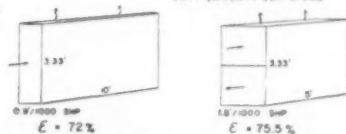
CYCLE A - ARRANGEMENT "2"

1/4" TUBES, GAS OUTSIDE, AIR INSIDE
VOLUME = 3675 ft³/1000 shp
WEIGHT = 1334 lbs/1000 shp
NTU = 4.78 $(\Delta P/P)_{\text{total}} = 2.69\%$
 $(\Delta P/P)_h / (\Delta P/P)_c = 0.109$



CYCLE A - ARRANGEMENT "3"

AIR SIDE - SURFACE 3a, 1/2 INCH PLATE SPACING
6 FINS PER INCH
GAS SIDE - SURFACE 3f, 1/2 INCH PLATE SPACING
12 FINS PER INCH
VOLUME = 30 ft³/1000 shp, WEIGHT = 1941 lbs/1000 shp
NTU = 3.80 $(\Delta P/P)_{\text{total}} = 2.86\%$
 $(\Delta P/P)_h / (\Delta P/P)_c = 0.362$



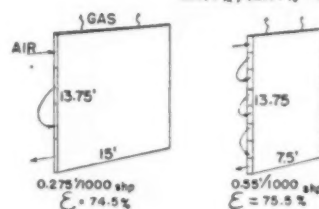
CYCLE A - ARRANGEMENT "4"

AIR SIDE - SURFACE 4a, 1/2 INCH PLATE SPACING
6 FINS PER INCH, 1/2 INCH LOUVERS
GAS SIDE - SURFACE 3f, 1/2 INCH PLATE SPACING
12 FINS PER INCH
VOLUME = 27 ft³/1000 shp, WEIGHT = 1750 lbs/1000 shp
NTU = 3.79 $(\Delta P/P)_{\text{total}} = 2.97\%$
 $(\Delta P/P)_h / (\Delta P/P)_c = 0.359$



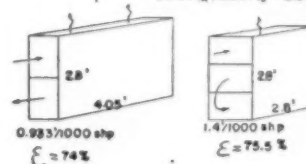
CYCLE B - ARRANGEMENT "1"

1" TUBES, GAS OUTSIDE, AIR INSIDE
VOLUME = 56.7 ft³/1000 shp
WEIGHT = 2060 lbs/1000 shp
NTU = 3.09 $(\Delta P/P)_{\text{total}} = 2.67\%$
 $(\Delta P/P)_h / (\Delta P/P)_c = 0.1125$



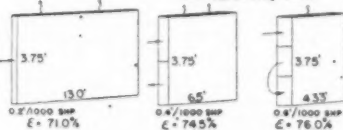
CYCLE B - ARRANGEMENT "2"

1/4" TUBES, GAS OUTSIDE, AIR INSIDE
VOLUME = 10.96 ft³/1000 shp
WEIGHT = 398 lbs/1000 shp
NTU = 3.35 $(\Delta P/P)_{\text{total}} = 2.59\%$
 $(\Delta P/P)_h / (\Delta P/P)_c = 0.0508$



CYCLE B - ARRANGEMENT "3"

AIR SIDE - SURFACE 3a, 1/2 INCH PLATE SPACING
6 FINS PER INCH
GAS SIDE - SURFACE 3c, 1/2 INCH PLATE SPACING
12 FINS PER INCH
VOLUME = 9.75 ft³/1000 shp, WEIGHT = 656 lbs/1000 shp
NTU = 3.52 $(\Delta P/P)_{\text{total}} = 2.33\%$
 $(\Delta P/P)_h / (\Delta P/P)_c = 0.195$



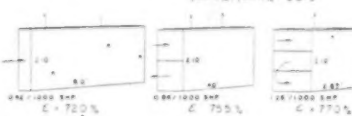
CYCLE B - ARRANGEMENT "4"

AIR SIDE - SURFACE 4a, 1/2 INCH PLATE SPACING
6 FINS PER INCH, 1/2 INCH LOUVERS
GAS SIDE - SURFACE 3c, 1/2 INCH PLATE SPACING
12 FINS PER INCH
VOLUME = 8.83 ft³/1000 shp, WEIGHT = 594 lbs/1000 shp
NTU = 3.47 $(\Delta P/P)_{\text{total}} = 2.13\%$
 $(\Delta P/P)_h / (\Delta P/P)_c = 0.190$



CYCLE B - ARRANGEMENT "5"

AIR SIDE - SURFACE 4a, 1/2 INCH PLATE SPACING
6 FINS PER INCH, 1/2 INCH LOUVERS
GAS SIDE - SURFACE 4c, 1/2 INCH PLATE SPACING
12 FINS PER INCH, 1/2 INCH LOUVERS
VOLUME = 705 ft³/1000 shp, WEIGHT = 475 lbs/1000 shp
NTU = 3.67 $(\Delta P/P)_{\text{total}} = 2.8\%$
 $(\Delta P/P)_h / (\Delta P/P)_c = 0.243$



CYCLE C - ARRANGEMENT "1"

1" TUBES, GAS OUTSIDE, AIR INSIDE
VOLUME = 1450 ft³/1000 shp
WEIGHT = 526 lbs/1000 shp
NTU = 191 $(\Delta P/P)_{\text{total}} = 4.82\%$
 $(\Delta P/P)_h / (\Delta P/P)_c = 0.357$



CYCLE C - ARRANGEMENT "2"

AIR SIDE - SURFACE 3a, 1/2 INCH PLATE SPACING
6 FINS PER INCH
GAS SIDE - SURFACE 3f, 1/2 INCH PLATE SPACING
12 FINS PER INCH
VOLUME = 20.6 ft³/1000 shp, WEIGHT = 1333 lbs/1000 shp
NTU = 1.985 $(\Delta P/P)_{\text{total}} = 4.81\%$
 $(\Delta P/P)_h / (\Delta P/P)_c = 0.583$



CYCLE D - ARRANGEMENT "1"

AIR SIDE - SURFACE 3a, 1/2 INCH PLATE SPACING
6 FINS PER INCH
GAS SIDE - SURFACE 3f, 1/2 INCH PLATE SPACING
12 FINS PER INCH
VOLUME = 86.3 ft³/1000 shp, WEIGHT = 5596 lbs/1000 shp
NTU = 5.14 $(\Delta P/P)_{\text{total}} = 6.71\%$
 $(\Delta P/P)_h / (\Delta P/P)_c = 0.864$



CYCLE D - ARRANGEMENT "2"

1/4 INCH TUBES, GAS OUTSIDE, AIR INSIDE
VOLUME = 67.5 ft³/1000 shp, WT = 2450 lbs/1000 shp
NTU = 5.13 $(\Delta P/P)_{\text{total}} = 6.34\%$
 $(\Delta P/P)_h / (\Delta P/P)_c = 0.893$



FIG. 6 REGENERATOR CORE DESIGNS

(Refer to Tables 2, 3, and 4 for further details of surfaces and operating conditions.)

TABLE 4 SUMMARY OF DESIGN DATA

	CYCLE A				CYCLE B				CYCLE C				CYCLE D			
	1	2	3	4	1	2	3	4	5	1	2	3	4	5	1	2
Surfaces:																
Gas.....	2a	2b	3f	3f	3f	2a	2b	3c	3c	4c	2b	3f	3f		3f	2b
Air.....	1a	1b	3a	3a	3a	1a	2a	3a	4a		1b	3a	3a		3a	1b
Weight/1000 shp, lb.....	5285	1334	1941	1750	2060	56.7	398	656	594	475	526	1333	5596		2450	2450
Volume/1000 shp, ft ³	148.5	36.8	30.0	27.0	10.96	8.83	7.05	9.75	8.83	7.05	14.5	20.6	86.3		67.5	67.5
Flow Lengths, ft:																
Air.....	44.0	9.00	10.0	6.00	55.0	8.40	13.0	7.80	8.00	8.00	4.53	6.18	9.34		9.00	9.00
Gas.....	10.0	2.48	3.33	3.00	15.0	2.80	3.75	3.40	2.10	2.10	1.08	1.79	4.52		2.50	2.50
Non-flow, l-pass.....	0.3375	1.650	0.90	1.50	0.06875	0.4670	0.200	0.333	0.420	0.420	2.960	1.860	2.140		3.00	3.00
($\Delta P/P_1$)/g, %.....	2.53	2.42	2.10	1.89	2.40	2.46	1.98	1.79	2.26	2.26	3.07	1.77	3.60		3.35	3.35
($\Delta P/P_1$)/a, %.....	0.35	0.27	0.76	0.68	0.27	0.13	0.38	0.34	0.55	0.55	1.75	3.04	3.11		2.99	2.99
($\Delta P/P_1$)/total, %.....	2.88	2.69	2.86	2.57	2.67	2.59	2.36	2.13	2.81	2.81	4.82	4.81	6.71		6.34	6.34
h_g , Btu/(hr ft ² of h_g).....	19.4	34.2	13.1	13.1	42.2	75.5	43.2	43.2	68.7	68.7	47.1	14.6	13.9		39.3	39.3
h_a , Btu/(hr ft ² of h_a).....	32.5	36.6	42.9	56.6	89.8	91.5	92.7	113.5	134.5	134.5	61.9	54.3	31.3		39.6	39.6
η_g	---	---	0.775	0.778	---	---	0.827	0.827	0.765	0.765	---	0.758	0.767		---	---
η_a	---	---	0.864	0.848	---	---	0.777	0.750	0.729	0.729	---	0.839	0.893		---	---
U, Btu/(hr ft ² of A_g).....	11.7	16.8	5.72	6.36	27.7	39.4	19.8	21.4	28.4	28.4	25.5	6.55	5.13		12.7	12.7
A_g , ft ²	2800	2732	6360	5720	1069	815	1713	1552	1240	1240	1077	4365	18310		5030	5030
A_g/A_a	0.900	0.900	0.353	0.353	0.900	0.900	0.628	0.628	0.628	0.628	0.900	0.354	0.353		0.900	0.900
NTU.....	3.41	4.78	3.80	3.79	3.09	3.35	3.52	3.47	3.67	3.67	1.91	1.985	5.14		5.13	5.13
G_g , lbs/(hr ft ²).....	6270	6275	7610	7610	28620	23730	39800	39800	27600	27600	10440	8950	6290		6390	6390
V_g , ft/sec.....	46.0	48.0	58.2	58.2	43.3	45.4	68.5	68.5	52.8	52.8	84.8	72.8	65.7		66.3	66.3
G_a , lbs/(hr ft ²).....	35950	29700	42790	28500	128500	92800	115900	76700	98700	98700	57000	57800	25530		29750	29750
V_a , ft/sec.....	27.8	33.0	33.0	22.0	24.9	18.0	22.4	14.9	19.1	19.1	83.1	84.3	75.3		87.8	87.8
R_g	7150	1787	1110	1110	25920	6760	4630	4630	3570	3570	2900	1270	768		1519	1519
R_a	38500	7940	9800	6540	137700	24830	26400	17630	22650	22650	15250	13280	5000		6790	6790

specified surfaces were employed to design thirteen regenerator cores. Four heat-transfer surface variations were used for Cycle (A), the 9:1 pressure ratio central-station-type plant. Five surfaces were considered for the closed-cycle plant (B). Two surface variations were selected for each of the locomotive-plant cycles, (C) and (D). All designs for a particular cycle were made for approximately equal heat-transfer effectiveness and total per cent pressure drops as specified in Table 3. Deviations from uniformity in this respect arise from the necessary trial-and-error successive approximation method of calculation characteristic of heat-exchanger design. The tedium of attaining exact equivalence was considered not to be worth the effort.

These thirteen designs are shown in Fig. 6. More detailed information with respect to film coefficients, mass velocities, Reynolds numbers, temperature effectiveness of extended surfaces, etc., are summarized in Table 4.

From these comparisons the following factors are most strikingly evident:

1 One-inch tube regenerators weigh 3 to 5 times as much as $1/4$ -in. tube or extended plate-fin surface regenerators.

2 One-inch tube designs have the smallest nonflow dimension for a given number of cross-counterflow passes. However, the other dimensions are so large that the volumes are 4 to 8 times as great as the other designs.

3 For small flow frictions, i.e. $(\Delta P/P_1)_{\text{total}} < 3$ per cent, the plate-fin surfaces have the following advantages relative to the $1/4$ -in. tube surface: (a) smaller volume, by 10 to 15 per cent, (b) smaller nonflow dimension, by 10 to 60 per cent. However, the weight is greater by 20 to 60 per cent.

4 For large flow frictions, i.e. $(\Delta P/P_1)_{\text{total}} \geq 5$ per cent, the $1/4$ -in. tube surface has the advantage of (a) smaller volume by 30 per cent, (b) smaller weight by 20 to 50 per cent. However, even here the nonflow dimension is substantially poorer by 20 to 30 per cent as compared to the plate-fin surface.

5 Low-effectiveness regenerators, i.e., cycle (C), although of considerably smaller volumes, tend to have large nonflow dimensions. Reference to Equation [7] will demonstrate the reasons. The combination of smaller volume and the characteristically higher specific flow rate, W , combine to give a larger nonflow dimension in spite of larger mass velocities permitted by the higher friction allowance.

6 In the exhaust combustion cycle (D), as the effectiveness ϵ must be high and since the specific flow rate is large, the volume of the exchanger is inherently quite large, e.g., 70 to 90 cu ft/1000 shp as compared to 30 to 40 cu ft/1000 shp for cycle (A). To fit the requisite exchanger into a locomotive cab for ratings greater than 2000 shp will necessitate the use of small tubes ($1/4$ in.) or extended surfaces.

7 The regenerator volume in the closed-cycle plant (B) is only 25 to 30 per cent of that for the comparable open cycle (A). Most of this reduction of volume is realized by a much smaller nonflow dimension. In turn this means much better regenerator shapes for the large-capacity closed cycle as compared to the open-cycle system.

8 Contrary to general opinion, the extended surfaces of the plate-fin type, even when made of thin sheet (0.010 in.) and low thermal conductivity material ($k = 12$ Btu/(hr sq ft deg F) characteristic of high-temperature alloys), will have a fairly high temperature effectiveness on the order of 70 to 80 per cent, that is, the plate-fin surface per unit area will transfer 70 to 80 per cent as much heat as a prime or direct surface operating with the same temperature and film coefficient conditions. This conclusion also holds for the closed-cycle plant even with the much higher film coefficients, h_g, h_a .

These designs, Fig. 6, are not necessarily of "optimum" shape

for the particular surface selected, because optimum conditions depend on the machinery arrangement and rating of the plant in question. However, it is believed that the geometries shown will yield a qualitative idea of what can be accomplished with the different surfaces considered.

For the circular tube surfaces with interchanged flow, i.e., gas inside and air flow normal to the tubes, calculations for several examples yielded the following comparisons with the comparable gas-inside-of-tube systems: (1) volume is increased by 20 per cent, (2) the nonflow dimension is essentially unchanged, (3) the gas-flow dimension is almost exactly doubled, (4) the air-flow dimension is almost exactly halved, and (5) the gas-side velocities are increased two and a half fold and the air-side velocities are reduced three and a half fold.

FOULING CHARACTERISTICS

The foregoing designs incorporated no allowance for fouling. Until more is known about this behavior for the different surfaces, to include such a factor might be conservative but would be very much guesswork. Cognizance was taken of the problem, however, to the extent that for all the gas-side plate-fin surfaces of the open-cycle plants (A), (C), and (D), plain fins were used in preference to louvered fins, the opinion being that louvered surfaces would provide edges for the accumulation of soot deposits.

The plate-fin surfaces on the gas side operate with somewhat higher average and maximum velocities than the tube surfaces with air flow inside the tubes. Also, there are no low-velocity regions except of course for the boundary layer. Consequently, it is believed that the plate-fin surfaces will have a reduced fouling tendency. In fact, the high velocities (50 to 70 fps) and the smooth passage walls may provide a continuous soot-blowing action. In any event, mechanical cleaning of the gas side will not be feasible for either $1/4$ -in. tube surfaces or for the plate-fin surfaces. In all probability water or chemical washing methods must be employed.

One advantage of interchanging the flow for the circular tube surfaces, which may outweigh the cost of increased volume, is that for gas flow inside the tube the gas velocities are on the order of 120 fps as compared to 50 fps for gas flow normal to the tubes. These high velocities in smooth tube passages, as in the case of the plate-plain-fin surface, should provide for a very effective self-cleaning action.

MANUFACTURING COSTS

The plate-fin surfaces have several advantages in principle from the point of view of labor and material costs, provided that suitable high-temperature furnace brazing and/or automatic production-welding techniques can be developed.

1 High-temperature alloys in sheet form have a substantially lower cost because of the high cost of the die-drawing procedure used for tubing.

2 The $1/4$ -in. tube surface regenerator of Cycle (A) requires 4650 9-ft tubes/1000 shp for the single-pass crossflow arrangement. For the n -pass arrangement a proportionately greater number of tubes of shorter length are required. On this basis it would appear that the hand labor involved in providing for more than 9000 tube-sheet joints per 1000 shp rating would be prohibitive. In the case of the plate-fin surface, the tube-sheet periphery requiring sealing is greatly reduced, and possibly furnace-brazing techniques could completely obviate the necessity of hand labor in this respect.

CONCLUSIONS

The conclusions and opinions that may be formed from the foregoing discussion are as follows:

1 In order that circular tube surfaces can become competitive with extended surfaces of the plate-fin type with respect to volume, weight, and shape, it is necessary to resort to small diameters of the order of $1/4$ in. Even then the plate-fin surface will have the advantage of a smaller nonflow dimension.

2 Units fabricated from small-diameter tubular surfaces in high-alloy material will probably have a higher material and labor cost than the plate-fin surface, provided that methods of furnace-brazing fabrication can be developed for the latter.

3 If compact regenerators have to be realized, mechanical cleaning methods cannot be employed. In this respect the plate-fin type of surface appears to be more cleanable and will probably show less tendency to foul as compared to $1/4$ -in. tube or similar surfaces.

4 It is believed that these conclusions justify a considerable developmental effort devoted to plate-fin surface fabrication for high-temperature service.

5 The geometric advantages of true counterflow as compared to n -pass cross-counterflow arrangements in many cases may warrant the difficulties of header design.

6 Conceivably, other superior types of compact surfaces are available or can be developed. Firm conclusions regarding each surface can be made only after their basic heat-transfer and flow-friction characteristics are determined. The lack of such data has tended to restrict current regenerator thinking to the shell-and-tube-type surface.

7 In all probability experience will demonstrate that there is no one best surface for the regenerator application and that the designer will need information on a number of surfaces so that the best solution may be made for the particular cycle and machinery arrangement.

ACKNOWLEDGMENT

The Office of Naval Research, the U. S. N. Bureau of Ships, and the U. S. N. Bureau of Aeronautics are currently sponsoring a heat-transfer research program for compact surfaces at Stanford University. The authors prepared this paper on this program and express their appreciation to the sponsoring organizations.

BIBLIOGRAPHY

- 1 "Test Results of High-Performance Heat-Exchanger Surfaces Used in Aircraft Intercoolers and Their Significance in Gas-Turbine Regenerator Design," by A. L. London and C. K. Ferguson, Trans. ASME, vol. 71, 1949, p. 17.
- 2 "Gas-Turbine Plant Regenerator Surfaces," by A. L. London and C. K. Ferguson, Bureau of Ships Research Memorandum 2-46, NavShips (250-338-3), July, 1946.
- 3 "An Investigation of the Effect of Fin Spacing on the Performance of Louvered Plate-Fin Heat Exchanger Surfaces," by W. M. Kays, Tech. Rpt. No. 3, Navy Contract N6-ONR-251, Task Order VI (NR-035-104) Stanford University, December 15, 1948.
- 4 "Basic Heat-Transfer and Flow-Friction Data for Gas-Turbine Plant Regenerator Surfaces," by John J. Dinan, U. S. N. Engineering Experiment Station Report No. C-2171-D, August, 1947.
- 5 "Basic Heat-Transfer and Flow-Friction Data for Gas-Turbine Plant Regenerator Surfaces," by John J. Dinan, U. S. N. Engineering Experiment Station Report No. C-2171-E, 1948.
- 6 "Basic Heat-Transfer and Flow-Friction Data for Gas-Turbine Plant Regenerator Surfaces," by John J. Dinan, U. S. N. Engineering Experiment Station Report No. C-2171-F, 1948.
- 7 "A Marine Gas-Turbine Plant," by C. R. Soderberg, R. B. Smith, and A. T. Scott, Transactions of the American Society of Naval Architects and Marine Engineers, vol. 53, 1945, pp. 249-289.
- 8 "A 5000-Kw Gas Turbine for Power Generation," by A. Howard and C. J. Walker, 1948 ASME Annual Meeting paper No. 48-A-83. See digest in *Mechanical Engineering*, vol. 71, 1949, p. 38.
- 9 "Construction of a Gas Turbine for Locomotive Power Plant," by William B. Tucker, *Mechanical Engineering*, vol. 70, 1948, p. 877.
- 10 "Heat Transmission," by W. H. McAdams, McGraw-Hill Book Company Inc., New York, N. Y., second edition, 1942.

11 Personal Communication, J. I. Yellott; and "The Exhaust-Heated Gas-Turbine Cycle," by Donald L. Mordell, Trans. ASME, vol. 72, 1950, p. 17.

12 "Gas-Turbine Regenerator-Design Studies," by W. M. Kays and A. L. London, Tech. Rpt. No. 8, Navy Contract N6-ONR-251, Task Order VI (NR-035-104) Stanford University, December 15, 1949.

Discussion

D. ARONSON.⁴ A realistic comparison between tubular heat exchangers and extended-surface plate-fin types is extremely difficult to make. The characteristics of tube-and-shell design have been established as a result of years of experience, and manufacturing costs are readily estimated. In so far as this writer knows, only three models of a large-size plate-fin extended-surface exchanger for high-temperature service have been built. The cost of manufacturing these three pioneer models is several times higher than a tubular design for the same service due partly to high cost of development. However, there are no cost data on operations comparable to those involved in the fabrication of extended-surface regenerators to encourage the view that they will be cheaper than tubular units. Engineers have a tendency to look more favorably upon new designs whose full assortment of hobgoblins have not yet made an appearance.

There is a special field of application for each type. For small installations it is possible to obtain better performance with small-diameter tubing or with closely spaced fins than with larger-size tubing. As the size of the gas turbine increases, the need for small diameters diminishes. This arises from the fact that the effectiveness of a regenerator is a function of the length-to-diameter ratio of passages. In small units either length must be obtained by a multipass arrangement or small diameter must be employed. A comparison such as made by the authors on the basis of dimensions per shp is not strictly valid.

The need for further development of plate-fin surface fabrication is very real as regards brazing techniques, end connections, thermal stresses, fin effectiveness, and resistance to oxidation.

The superiority of plate-fin-type surface for minimum weight and volume mentioned in the text of the article is not borne out by the authors' own calculations as shown in Table 4. In every instance the weight and surface are least for $1/4$ -in. tubes and in most instances the volume is just a little less for the tubular design. The comparison is as follows:

	Weight, lb	
	$1/4$ -in. tubes	Best design plate-fin extended surface
Cycle A	1050 ^a	1750
Cycle B	436 ^a	475
Cycle C	526	1333
Cycle D	2450	5996

	Volume, cu ft	
	$1/4$ -in. tubes	Best design plate-fin extended surface
Cycle A	29.3 ^a	27.0
Cycle B	12.0 ^a	7.05
Cycle C	14.5	20.6
Cycle D	67.5 ^a	86.3

	Surface, sq ft (total of both passages)	
	$1/4$ -in. tubes	Best design plate-fin extended surface
Cycle A	4170 ^a	8050
Cycle B	1705 ^a	2150
Cycle C	2060	6250
Cycle D	9600	25,700

^a The figures for the tubular design have been modified proportional to the ratio of the NTU of the tubular design to that of the extended surface so that the comparison will be somewhat closer to a fair picture.

The advantage of the plate-fin surface in having a smaller nonflow dimension is not quite clear from the authors' remarks. The virtue of the plate-fin surface can perhaps be better expressed in a different way. It possesses a greater degree of design flexibility in that the proportion of surface on the hot side to that on

⁴ Elliott Company, Jeannette, Pa. Mem. ASME.

the cold side can be varied over a wide range. This flexibility makes it possible to fit the regenerator into any particular geometry with maximum effectiveness for a given pressure drop. Where volume of regenerator is the sole criterion the non-flow dimension should be made as large as possible.

The dimensions of a tubular unit often result in an inefficient ratio of heat-transfer coefficients on the cold side to that on the hot side, and since the surface areas on the two sides are related directly as the diameter ratios, there is no opportunity for improving the utilization of surface. As a result, it will often be found that for a particular geometry of available space for the regenerator the plate-fin design can give a higher effectiveness for the same pressure drop. The price to be paid for this better performance will be a greater surface area, possibly a greater weight, and a greater cost.

The writer of this discussion presented at the ASME Annual Meeting, December, 1949, a method of designing for optimum performance, which includes consideration of some of the foregoing factors.

AUTHORS' CLOSURE

The authors agree with Mr. Aronson that a realistic comparison of general validity between tubular and extended surface gas-turbine regenerators is next to impossible to make. Even for a particular application, a comparison made now would not be valid at some later time because of rapidly changing conditions with respect to costs, methods of fabrication, and the development of new surfaces. Nevertheless, if limited comparisons can be made they should be made with as complete a realization as possible of the limitations. These are the "hobgoblins" referred to by Mr. Aronson. If engineers fail to look ahead, that is, "look favora-

bly on new designs," the gas-turbine development will not overcome the advantage of the entrenched position now occupied by the conventional prime mover systems.

The comparison of regenerator geometry on the basis of non-flow dimension per 1000 shp will allow ready visualization of the size of heat exchanger required for any plant capacity, large or small. Mr. Aronson's objection to this basis is not clear to the authors.

There is no disagreement between the authors' text and the comparisons presented by the discussor regarding the "superiority of plate-fin-type surfaces." However, it was perhaps not emphasized that $1/4$ in. tubes probably represents the most compact circular tube surface that is practical while it is quite probable that more compact and more effective plate-fin surfaces exist or can be developed. As a matter of fact, current studies (12) confirm this view.

It is obvious from the first of Equations [7] that an increase of volume brought about by a change of surface will tend to decrease the nonflow dimension. It should be pointed out, however, that for a *given surface* the minimum volume design will also be very close to the minimum nonflow-dimension design. The increase of volume which produces a smaller nonflow dimension comes about from the use of a less compact surface. Thus the use of compact heat-transfer surfaces tends to yield small-volume heat exchangers but with large nonflow dimensions, as can be seen by an examination of the various designs for Cycle (A). If small volume is the only criterion then a large nonflow dimension will have to be accepted, as Mr. Aronson points out. It seems to the authors, however, that both "good" shape and "small" volume and "high" effectiveness are criteria which have to be in some measure mutually compromised in the usual design.

Perforated
present
perimeter
heat exchanger
built up
num pl
perpend
by caus
passage
and gas
Results
drop ef
tions of

The fo

a

A_1

A_2

A_3

A_w

b_e

b_f

b_L

b_w

c

D

f_L

g_e

G_{max}

h_1

h_2

h_3

i

k, k_w

L

L_g

L_s

n

N_L

¹ Arth

Contri

sions and

ber 27-1

ENGINEER

NOTE:

understo

of the So

A Perforated-Plate Heat Exchanger

By H. O. McMAHON,¹ R. J. BOWEN,¹ AND G. A. BLEYLE, JR.¹

Performance data of heat transfer and flow resistance are presented for the continuous heating of air in several experimental variations of a new type of perforated-plate heat exchanger. These exchangers consisted of sections built up by stacking multiple units of a perforated aluminum plate and a neoprene gasket, to form parallel channels perpendicular to the plate faces. Tests were conducted by causing air to flow countercurrently through these passages. The effects of hole diameter, plate thickness, and gasket thickness (or plate separation) are indicated. Results are presented jointly in the form of a pressure-drop efficiency factor versus Reynolds number for portions of the range between 800 and 4300.

NOMENCLATURE

The following nomenclature is used in this paper:

- a = numerical coefficient, dimensionless
- A_1 = surface area inside holes of one set of channels, sq ft
- A_2 = total heat-transfer surface on both faces of plates of one set of channels, sq ft
- A_3 = effective heat-transfer surface on both faces of plates of one set of channels, sq ft
- A_c = mean area of cross section of fins in one set of channels, sq ft
- b_a = distance between centers of adjacent holes, in.
- b_f = length of fin (i.e., channel width), ft
- b_L = channel height, ft
- b_m = gasket ligament width (i.e., metal path between channels), ft
- c = specific heat of air, Btu/(lb)(deg F)
- D = diameter of holes in plates, in.
- f_L = friction factor based on plate thickness, defined by Equation [5], dimensionless
- g_c = gravitational conversion factor, (lb)(ft)/(sec²)(lb force)
- G_{max} = mass velocity, based on hole diameter, lb/(hr)(sq ft)
- h_1 = average heat-transfer coefficient of fin, arbitrarily based on A_1 , Btu/(hr)(sq ft)(deg F)
- h_2 = actual local heat-transfer coefficient, based on A_2 , Btu/(hr)(sq ft)(deg F)
- h_3 = actual local heat-transfer coefficient, based on A_1 , Btu/(hr)(sq ft)(deg F)
- j = heat-transfer factor for fluid flow, dimensionless
- $j = \left(\frac{h_1}{cG_{max}} \right) \left(\frac{c\mu}{k} \right)^{1/4}$
- k, k_w = thermal conductivity of air and fin material, respectively, (Btu)(ft)/(hr)(sq ft)(deg F)
- L = plate thickness, in.
- L_g = gasket thickness, compressed, in.
- L_e = length of exchanger section, ft
- n = numerical exponent, dimensionless
- N_L = number of plates per exchanger section

N_{Re} = Reynolds number, based on hole diameter, dimensionless $\left(N_{Re} = \frac{DG_{max}}{12\mu} \right)$

ΔP_{avg} = averaged pressure difference across warm and cool channels of exchanger, lb force/sq in.

q_{avg} = rate of heat transfer, averaged for the warm and cool channels, Btu/hr

$scfm$ = volumetric flow rate, std cu ft/min

T_1 = cool-side inlet-gas temperature, deg F

T_2 = cool-side outlet-gas temperature, deg F

T_3 = warm-side inlet-gas temperature, deg F

T_4 = warm-side outlet-gas temperature, deg F

T_5 = gas temperature after rotameter, deg F

ΔT_0 = temperature difference between root of fin and gas stream, deg F

ΔT_m = length-mean temperature difference between fin and gas stream, deg F

ΔT_w = temperature difference in metal between channels (i.e., between roots of adjacent fins), deg F

ΔT_{lm} = log-mean temperature difference for exchanger, deg F

U = over-all heat-transfer coefficient, based on A_1 , Btu/(hr)(sq ft)(deg F)

V = gas velocity in holes, ft/min

$\eta = \frac{\Delta T_m}{\Delta T_0}$ = fin effectiveness, dimensionless

ρ = gas density at average exchanger conditions, lb/cu ft

μ = gas viscosity at average exchanger gas stream temperature, lb/(hr)(ft)

INTRODUCTION

During the past decade, and particularly since the end of the war, several industrial processes have been developed which entail the handling of large volumes of gases and depend for commercial feasibility on a high degree of heat economy with a small to moderate capital investment. For example, there are the proposed techniques for tonnage production of oxygen (1)² as well as various specialized applications of the gas turbine. However, in none of these cases can the prime requisites of large effective surface area per unit volume of equipment and high efficiency of heat transfer with low flow resistance be satisfactorily met by the use of conventional designs of gas-to-gas heat exchangers. Consequently, process planners have been paying close attention to each promising new design of extended-surface exchanger.

Since the appearance of the definitive paper by Norris and Spofford (2), there have appeared in the technical and patent literature descriptions of many apparently practical design variations of extended-surface heat exchangers. Generally they consist of enclosures of separate, adjacent, fluid-flow channels formed from concentric piping or parallel sheets of highly conductive metal, the free spaces of which are partially occupied by some form of extended surface bonded to the channel-defining walls. Some fin-forming materials which have aroused considerable interest are the edge-wound helixes of copper ribbon devised by Collins (3, 4), louvered or smooth crimped metal plates (5), pin-fins formed from square helixes of wire (6) and stacked, louvered sheet-metal stampings (7), fin-base continuity being obtained in

¹ Arthur D. Little, Inc., Cambridge, Mass.

Contributed by the Heat Transfer and Gas Turbine Power Divisions and presented at the Annual Meeting, New York, N. Y., November 27-December 2, 1949, of the AMERICAN SOCIETY OF MECHANICAL ENGINEERS.

NOTE: Statements and opinions advanced in papers are to be understood as individual expressions of their authors and not those of the Society. Paper No. 49-A-92.

² Numbers in parentheses refer to the Bibliography at the end of the paper.

each case by means of brazed or soldered contacts at the channel walls.

The ideal heat exchanger would appear to have the following characteristics: Simplicity of manufacture from low-cost materials; adaptability of the basic design for varying conditions of use; the possibility of effecting repairs to the interior of the unit without total replacement; a relatively simple manifolding problem, particularly for switch or reversing service; the ability to carry fairly large differential pressures in adjacent channels; a minimum effect of longitudinal heat conduction; interchannel heat conduction through "parent" metal without the use of thermal bonding, together with the basic considerations of large heat-transfer capacity and low resistance to flow.

It is the purpose of this paper to present a range of performance data of heat transfer and flow resistance for the heating of air in several variations of three basically similar experimental models of a unique perforated-plate type of extended-surface heat exchanger designed particularly for air separation. Exchangers of this type possess a great many of the characteristics of an ideal heat exchanger, particularly those of large heat-transfer capacity with moderate frictional losses. In recognition of this a patent application has been filed. The data presented are not comprehensive in the sense that they cover only a limited range of variation of the numerous parameters at the control of the designer. It is felt, however, that the range covered is sufficiently broad to include most of the probable engineering applications.

DESCRIPTION OF EXCHANGER

It will become evident that the dimensions and materials of construction of perforated-plate exchangers can vary widely and that the optimum specifications cannot yet be considered as definitely determined for any specific application. For this reason, the present description will be confined to a presentation of the essential details and properties of the particular experimental units

studied in this investigation, some sample components of which are shown in Fig. 1. However, it should be noted that commercial-size units are being fabricated, the basic design of which is similar to that of the Groups I-II runs. (See Table 1.)

The experimental exchanger section was $3\frac{1}{2}$ in. square and from 1.5 to 3.5 ft in length, completely insulated externally, the only outside connections being the inlet and outlet pipes and two pressure taps at each end. Such a section was built up in the form of a stack of units, each consisting of a thin square plate of precision-punched 2-S aluminum sheet placed on a thin die-cut neoprene gasket to form four individually gastight, parallel, narrow, longitudinal flow channels of matched metal openings, each approximately $\frac{1}{2}$ in. wide \times 3 in. high. The complete stack, together with a cast aluminum header at each end, was held together by means of steel tie rods bolted to the periphery of $\frac{1}{4}$ -in.-thick steel end plates. Piping connections were provided in the end plates.

The circular punched holes in the plates were spaced evenly along rows parallel to a side and offset from each other in the perpendicular direction at the vertexes of equilateral triangles to form a series of horizontal unit fins, as indicated in Fig. 2.

Gases could thus pass in countercurrent turbulent motion along two sets of adjacent flow passages, transferring heat by conduction through the perforated metal. Actually, the cool and warm gas streams were each divided by the headers, allowing the cooler incoming gas to flow in the two outer channels, while the warmer gas passed in the opposite direction through the inner channels. The center passage was blocked off and served as a dead space.

This design of heat exchanger has certain obvious advantages. The turbulence of flow induced by the presence of the gasket spacers, together with the high proportion of exposed fin surface, provide for a favorable rate of heat transfer. The perforated-plate construction enables the attainment of very high fin efficiencies, by proper choice of fin length and flow conditions. The

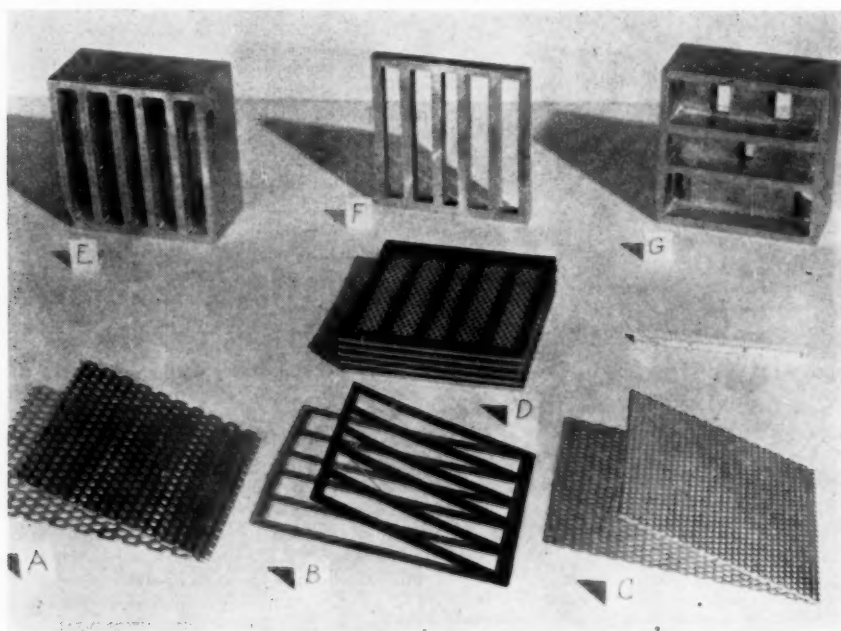


FIG. 1 SOME HEAT-EXCHANGER COMPONENTS

[(A) Plate with $\frac{1}{8}$ -in. holes on $\frac{1}{4}$ -in. staggered centers; (B) typical neoprene gasket; (C) plate with $\frac{1}{16}$ -in. holes on $\frac{1}{4}$ -in. staggered centers; (D) portion of stacked exchanger; (E) inner face of header, note pressure taps; (F) center spacer; (G) outer face of header.]

TABLE 1 PHYSICAL DETAILS OF EXCHANGERS

RUN	L _g (in.)	L _g (in.)	L _g (in.)	L _g (in.)	b _g (ft.)	b _g (ft.)	b _g (ft.)	L _g (ft.)	H _L	A _g (sq.ft.)	A _g (sq.ft.)
A.											
Group 1											
1	.013	.0833	.0625	.125	.0417	.250	.0130	1.59	246	6.32	0.237
2	.022	"	"	"	"	"	"	1.77	240	6.17	0.231
3	.045	"	"	"	"	"	"	2.20	"	"	"
4	.069	"	"	"	"	"	"	2.66	"	"	"
5	.081	"	"	"	"	"	"	2.13	"	"	"
6	.102	"	"	"	"	"	"	3.36	"	"	"
B.											
Group 11											
1	.042	.0833	.125	.125	.0417	.250	.0130	2.98	240	12.35	0.463
2	.047	"	"	"	"	"	"	1.77	120	6.17	0.231
3	.070	"	"	"	"	"	"	2.00	120	6.17	0.231
4	.078	"	"	"	"	"	"	1.75	100	5.15	0.193
5	.093	"	"	"	"	"	"	1.88	100	5.15	0.193
C.											
Group 111											
1	.027	.125	.0625	.1875	.0384	.244	.0156	1.58	208	2.91	.199
2	.060	"	"	"	"	"	"	2.13	160	2.24	.153
3	.078	"	"	"	"	"	"	2.23	186	2.60	.178
4	.143	"	"	"	"	"	"	1.67	104	1.63	.099

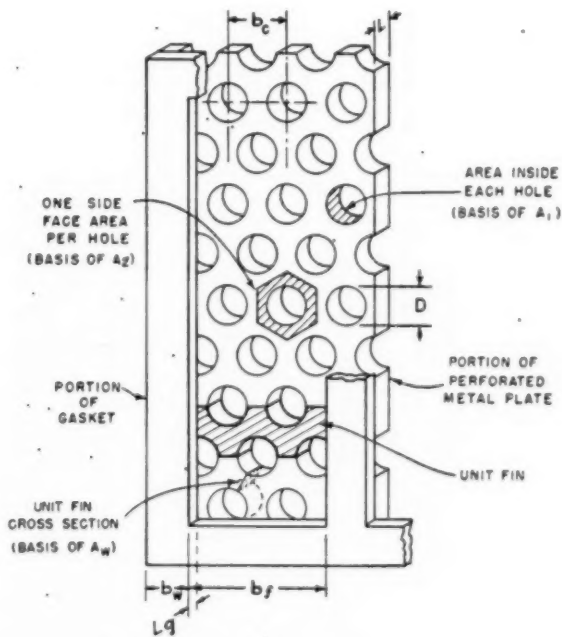


FIG. 2 SCHEMATIC REPRESENTATION OF FIN

employment of aluminum makes use of the usually higher ratio of thermal conductivity to cost per unit mass of that material compared to the value for other more conventional heat-transfer media, an important consideration for oxygen plants. The simplicity of construction is evident, as is the fact that an exchanger of this type can be disassembled plate by plate and reconstructed to meet new situations. Also, where necessary, several materials of construction or techniques of assembly can be used in a single section. Through the use of neoprene gaskets, heat conduction along the length of an exchanger is effectively eliminated. The use of neoprene also affords a very tight locked-in-place seal between plates, which can be maintained almost indefinitely, even at the temperatures of liquid air. Finally, it is possible by regulation of the hole diameters, spacing of centers, channel width, and

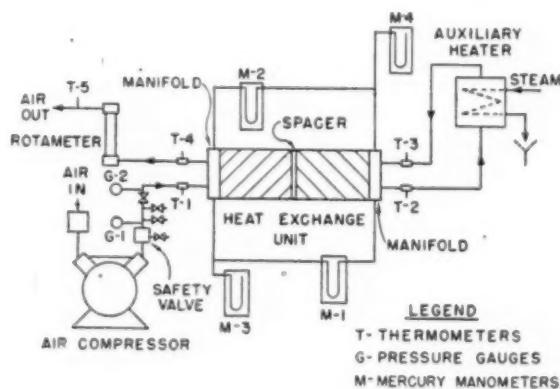


FIG. 3 EXPERIMENTAL INSTALLATION

gasket and plate thicknesses to vary the amount and type of induced turbulence as well as the fin efficiency, thereby to obtain the optimum values of heat transfer and friction losses for specified conditions of operation. As will be shown later in this paper, save for certain technical difficulties involved in the preparation of adequate low-cost gaskets, this design seems to offer possibilities of great utility to the field of gas-to-gas heat transfer. Indeed, the results of preliminary tests of furnace-brazed construction employing aluminum gasket spacers have indicated already that the economic position of this exchanger design can be improved greatly with little sacrifice of intrinsic performance characteristics.

TEST INSTALLATIONS

A schematic representation of the arrangement of the equipment used in this investigation is shown in Fig. 3.

Filtered test air was drawn into the system through a compressor of 30 cfm capacity. The air was then moved through the outer cool channels of the exchanger, through a small steam coil heater, and out through the inner warm channels of the exchanger, before being exhausted to the atmosphere.

Gages G-1 and G-2 were used to indicate the approximate inlet air pressure. Temperatures were measured by means of mercury thermometers. Static pressures and pressure drops were meas-

ured by means of mercury manometers. Flow rates were measured by means of a rotameter.

The complete exchanger, including manometer taps and thermometer wells, was thermally insulated with 6 in. of closely packed mineral wool.

Because of the simplicity of construction, few difficulties were encountered in the operation of these installations.

PROCEDURE

Experimental: The greatest installation problems were encountered during the assembly of the first exchanger section. Finally, a technique was developed to insure uniformity of procedure and freedom from interchannel leaks. For this purpose a U-shaped metal frame was constructed, in which were stacked, in order, a face plate with two $1/2$ -in. pipe connectors, a heavy neoprene gasket, and a rough-cast-aluminum header, Fig. 1 (G), and then, alternately, gaskets and perforated plates to form half of a unit. A $3/8$ -in.-thick cast-aluminum spacer, Fig. 1 (F), was then added and the second half of the exchanger completed, with the exception that the aluminum plates in this half were reversed as to the direction from which they had been punched. This latter expediency was considered necessary after preliminary tests of frictional effects had demonstrated a certain variation of pressure drop with direction of fluid flow through these plates caused by the difference in roughness of the hole ends. To assure uniformity of alignment still further, the precaution was taken to index the plates as to the direction from which they had been punched. Compared with examples of mill-run punched sheets which have been observed, these plates were quite accurately punched. The exchanger sections were held together by means of tie rods passing along the sides and bolted to the face plates. By taking up on the tie-rod nuts, the thickness of the gaskets could be varied over a range of about 30 per cent. The assemblies were then tested for leaks with air at 200 psig. In the only case of failure, the gasket between a manifold and a face plate gave way under a hydrostatic pressure of 1000 psig. It was observed that the gaskets between plates were actually locked into place by the expansion of the neoprene into the perforations. This same assembly technique was used with good success for the three groups of runs. The auxiliary test equipment was assembled with pipe fittings in a conventional manner. The rotameter was calibrated with a standard orifice.

Three separate groups of runs were carried out, using a different design of perforated plate for each group. The gasket thicknesses were varied as noted in Table 1. It should be pointed out that in the runs of Group II, the $1/8$ -in. plate thickness was achieved by the use of units consisting of two $1/16$ -in. plates cemented together. In this case an effort was made to assure that the direction of perforation was the same for each $1/16$ -in. plate, but it is not certain that this was always achieved. In any case, the juxtaposition of two slightly conically tapered holes, $1/16$ in. in length, varying in diameter from end to end by as much as 5 per cent, certainly introduced a complication of the friction situation in comparison to the single-plate installations of Groups I and III.

The capacity of the compressor limited the range of flow rates to between 5 and 29 scfm. The use of mercury manometers necessitated approximations of uncertain precision in the case of pressure drops at the lowest flow rate. The static pressure of the air was kept at about 5 psig.

In the conduct of a run, inlet air was heated from approximately 70 to 220 F in the outer cool channels of an exchanger. This air was then passed through an auxiliary heater, after which it passed back through the warm channels in which it cooled from about 250 to 100 F. Actually, the log mean temperature difference in the exchanger varied from run to run between 11 and 35 F. A typical run to obtain a single series of flow data points

required 6 hours for completion. Two extra hours were consumed in obtaining steady temperatures and smooth operation. At least three check values were obtained for each piece of data at 6 points in the range of flow rates for each plate design and gasket thickness.

Treatment of Data: The various temperatures, pressures, pressure differentials, and flow rates measured experimentally were combined with the data on the physical characteristics of the exchangers given in Table 1, to provide values of the heat-transfer coefficients, heat-transfer factors, friction factors, and heat-transfer efficiency factors, some of which are presented in Table 2, together with some of the important lesser variables.

As a matter of convenience, all reported values of heat-transfer coefficients have been based arbitrarily on A_1 , the area inside the holes of the aluminum plates. It is recognized that the actual effective area for heat transfer must also include a portion of the face surfaces of each plate, the amount being strongly influenced by the value of the gasket thickness employed, especially when that value approaches the thickness of the plate.

The Reynolds numbers have been based on the hole diameters. In other words, the effect of gasket thickness on heat transfer has been treated as in the nature of a controlled nonconducting artificial roughness or interruption on the surface of otherwise smooth small metal tubing.

Over-all heat-transfer coefficients have been calculated from averaged values of warm- and cool-side heat-transfer rates by means of mass flow rates and air temperatures, as follows

$$U = \frac{q_{avg}}{(A_1)(\Delta T_{lm})} \quad [1]$$

Utilizing the fact that the temperature difference between the fin roots of the warm and cool channels was small, it was possible to calculate the values of the effective heat-transfer coefficient (ηh_1) by means of the following expression

$$\eta h_1 = \frac{2}{\frac{1}{U} - \frac{b_w A_1}{k_w A_w}} \quad [2]$$

and check them against the equivalent equation

$$\eta h_1 = \frac{2q_{avg}}{A_1(\Delta T_{lm} - \Delta T_w)} \quad [3]$$

The average of the foregoing values of (ηh_1) was solved simultaneously with the definition of fin-effectiveness (2) by trial and error, to give values of η and h_1 , as follows

$$\eta = \frac{\Delta T_m}{\Delta T_0} = \frac{\tanh \sqrt{\frac{h_1 A_1 b_f}{k_w A_w}}}{\sqrt{\frac{h_1 A_1 b_f}{k_w A_w}}} \quad [4]$$

Values of h_1 are presented versus N_{Re} for the Group III runs in Fig. 4, from which can be seen their advantage in comparison to the smooth tube coefficients.

Utilizing the foregoing values of h_1 , heat-transfer factors were calculated from the following

$$j = \frac{3.30 h_1}{G_{max}} \quad [5]$$

thereby providing a function of h_1 which is only slightly influenced by the mass velocity. Values of j are presented versus N_{Re} in Fig. 5a, b, and c.

McMAHON, BOWEN, BLEYLE—A PERFORATED-PLATE HEAT EXCHANGER

627

TABLE 2 (A) SUMMARIZED DATA AND CALCULATIONS

GROUP I RUNS

$U = 1/12$ in., $L = 1/16$ in., $b_c = 1/8$ in.

DATA	$L_g = .013$ in.					$L_g = .022$ in.					$L_g = .046$ in.				
SCFM	6.05	10.16	14.65	19.16	23.95	28.34	6.23	10.23	15.21	19.82	24.92	29.03	34.24	40.27	45.25
ΔP_{ave} lb./sq.in.	.084	.185	.270	.445	.688	.840	.080	.209	.430	.706	1.01	1.28	.070	.220	.427
T-1 °F.	79.3	79.3	79.3	79.9	79.0	78.7	65.2	67.2	64.2	65.5	66.5	63.8	64.0	63.3	64.1
T-2 °F.	234.0	238.7	241.3	243.3	243.3	242.0	191.3	192.3	194.2	193.8	193.2	191.8	201.0	201.7	202.0
T-3 °F.	263.7	273.0	276.0	277.7	278.3	277.7	211.0	214.0	215.0	215.0	214.5	214.7	217.7	219.7	220.0
T-4 °F.	101.3	107.3	108.0	108.3	108.7	109.3	78.8	81.8	81.2	83.5	84.8	83.2	76.5	78.8	79.5
G lb./hr.(sq.ft.)	3353	5640	8124	10608	13284	15708	3483	5663	8410	10985	13825	16078	3414	5688	8436
N_{Re}	489	788	1136	1483	1857	2196	509	833	1234	1606	2030	2258	509	839	1240
ρ lb./cu.ft.	.065	.068	.072	.078	.085	.093	.068	.071	.075	.081	.088	.094	.068	.071	.076
$f_{L/2}$.042	.033	.025	.026	.025	.026	.040	.028	.039	.039	.039	.039	.034	.040	.038
q B.t.u./hr.	1102	1897	2779	3874	4598	5401	928	1509	2306	2958	3678	4332	998	1648	2443
Δt_{lm} °F.	25.52	31.08	31.61	31.77	31.77	31.11	16.83	18.52	18.68	18.61	19.84	21.06	14.47	16.73	16.71
U B.t.u./(hr. sq.ft.)(°F.)	6.81	9.66	13.91	18.30	22.93	25.82	8.94	13.14	20.01	24.46	30.05	33.32	11.18	15.97	23.70
$\frac{\Delta T_g}{b_w}$ °F./ft.	.472	.825	1.21	1.60	2.00	2.35	.413	.672	1.03	1.32	1.64	1.93	.444	.734	1.09
n_1 B.t.u./(hr.)(sq.ft.)(°F.)	21.10	31.44	43.47	56.88	66.09	79.34	19.34	29.61	48.04	61.60	79.72	91.62	24.80	37.10	59.17
J	.0142	.0124	.0128	.0135	.0141	.0139	.0184	.0172	.0188	.0185	.0190	.0188	.0236	.0215	.0231
V ft./min.	692	1162	1676	2192	2740	3242	713	1171	1742	2270	2855	3321	714	1175	1744
$3/f_1$.350	.378	.502	.523	.556	.528	.518	.459	.488	.480	.488	.482	.700	.542	.607
η	.96	.94	.92	.89	.86	.84	.95	.92	.88	.85	.82	.80	.93	.90	.86

TABLE 2(A) (Continued)

GROUP I RUNS (cont.)

$U = 1/12$ in., $L = 1/16$ in., $b_c = 1/8$ in.

DATA	$L_g = .069$ in.					$L_g = .082$ in.					$L_g = .108$ in.				
SCFM	6.29	10.38	15.46	20.07	25.22	29.77	6.23	10.26	15.24	19.76	24.83	29.04	6.30	10.43	15.54
ΔP_{ave} lb./sq.in.	.095	.305	.560	1.06	1.66	2.17	.108	.368	.792	1.18	1.70	2.20	.112	.469	1.03
T-1 °F.	61.5	61.0	60.8	60.8	61.8	60.1	61.0	65.5	65.3	65.7	67.0	66.0	61.8	60.5	60.2
T-2 °F.	201.7	203.3	203.0	202.7	201.3	200.0	205.3	208.0	207.3	205.3	203.3	198.7	207.5	209.0	207.9
T-3 °F.	211.3	218.3	218.7	218.7	218.7	217.7	227.7	227.7	227.3	227.0	227.3	226.3	224.0	226.0	226.0
T-4 °F.	71.5	72.3	73.5	75.2	76.2	75.7	76.2	76.5	79.8	83.2	85.2	81.8	68.8	70.0	70.8
G lb./hr.(hr.)(sq.ft.)	3484	5936	8980	11136	13968	16512	3490	5688	8448	10944	13764	16104	3494	5760	8624
N_{Re}	513	847	1261	1638	2057	2430	506	835	1243	1608	2023	2348	514	851	1267
ρ lb./cu.ft.	.069	.071	.076	.082	.091	.098	.068	.072	.076	.083	.090	.099	.068	.072	.078
$f_{L/2}$.046	.036	.038	.059	.064	.065	.052	.069	.071	.069	.068	.070	.054	.065	.072
q B.t.u./hr.	1026	1701	2559	3483	4089	4843	2030	3720	5336	6820	8974	1090	1867	2720	3472
Δt_{lm} °F.	11.73	13.67	14.50	15.12	15.79	16.58	15.73	16.09	17.11	17.59	18.96	22.35	11.08	12.88	13.26
U B.t.u./(hr.)(sq.ft.)(°F.)	14.18	21.10	28.60	35.70	41.97	47.46	14.76	24.04	33.36	39.76	48.61	58.19	15.95	22.98	31.25
$\frac{\Delta T_g}{b_w}$ °F./ft.	.458	.758	1.14	1.48	1.82	2.15	.635	1.06	1.56	1.99	2.45	2.83	.486	.814	1.22
n_1 B.t.u./(hr.)(sq.ft.)(°F.)	34.30	51.29	75.01	101.36	128.10	152.28	33.68	60.01	94.14	105.60	130.15	147.86	36.82	56.95	82.00
J	.0306	.0275	.0288	.0300	.0302	.0304	.0322	.0324	.0360	.0318	.0312	.0302	.0248	.0126	.0352
V ft./min.	719	1188	1709	2296	2885	3405	712	1173	1743	2260	2840	3322	721	1193	1778
$3/f_1$.681	.526	.497	.508	.472	.470	.631	.506	.508	.465	.460	.434	.619	.388	.384
η	.91	.87	.83	.78	.74	.71	.91	.86	.80	.77	.74	.71	.90	.86	.80

TABLE 2(B) (Continued)
GROUP II RUNS
D = 1/12 in., L = 1/8 in., b_c = 1/8 in.

DATA	Lg = .022 in.						Lg = .047 in.						Lg = .070 in.					
SCFM	6.26	10.33	15.42	20.11	25.40	29.36	6.26	10.31	15.36	19.93	25.02	29.09	6.22	10.25	15.06	19.72	24.89	28.73
ΔP_{ave} lb./sq. in.	.140	.387	.795	1.34	1.93	2.38	.120	.412	.872	1.38	1.98	2.49	.162	.524	1.08	1.74	2.44	3.01
T-1 °F.	62.3	61.7	62.7	62.8	64.0	63.5	62.5	62.2	62.0	62.5	63.0	62.2	67.2	67.0	69.0	68.0	70.0	70.7
T-2 °F.	206.7	208.0	207.7	208.7	207.7	207.0	207.5	208.5	208.5	207.0	206.0	203.0	214.3	216.0	216.0	214.3	212.7	211.7
T-3 °F.	223.0	224.3	225.0	225.0	224.7	224.5	227.0	229.5	230.0	230.0	230.0	229.5	235.0	236.3	238.0	237.3	237.0	236.3
T-4 °F.	70.5	71.7	72.7	73.3	74.5	74.8	74.2	76.0	77.0	79.0	80.5	79.5	77.3	77.5	82.2	82.8	85.7	87.7
G_{avg} b./.(hr.)(sq.ft.)	3472	5708	8556	11160	14064	16272	3468	5724	8514	11052	13878	16110	3445	5688	8352	10932	13836	15912
N_{Re}	511	841	1259	1640	2071	2395	511	841	1253	1625	2042	2373	508	836	1229	1608	2037	2343
ρ lb./cu.ft.	.068	.072	.077	.083	.092	.098	.068	.072	.077	.084	.092	.100	.068	.071	.077	.084	.093	.100
$f_{L/2}$.034	.036	.036	.038	.038	.037	.038	.077	.079	.081	.079	.080	.078	.099	.102	.105	.100	.100
q B.t.u./hr.	1068	1775	2635	3439	4289	4948	1072	1777	2644	3484	4297	4861	1039	1800	2621	3410	4219	4793
ΔT_{lm} °F.	11.78	12.91	13.33	13.20	13.49	14.13	15.30	17.11	18.06	19.56	20.60	21.54	14.77	16.13	17.04	18.62	19.67	20.79
U B.t.u./.(hr.)(sq.ft.)(°F.)	7.36	11.13	16.05	21.10	25.74	28.35	11.36	16.84	23.74	28.05	33.10	36.59	11.93	18.10	24.95	29.70	34.78	37.31
$\frac{\Delta T_w}{b_w}$ °F./ft.	.237	.390	.580	.757	.944	1.09	.478	.791	1.18	1.53	1.87	2.17	.486	.804	1.17	1.52	1.88	2.14
h_1 B.t.u./.(hr.)(sq.ft.)(°F.)	15.75	24.68	37.15	54.8	85.82	74.03	25.20	39.20	59.02	73.14	90.91	104.77	26.60	42.76	62.97	78.80	97.57	107.38
j	.0150	.0143	.0143	.0152	.0154	.0150	.0240	.0226	.0228	.0218	.0216	.0214	.0255	.0248	.0248	.0238	.0233	.0223
V ft./min.	716	1181	1764	2300	2905	3358	716	1180	1757	2279	2862	3327	711	1172	1723	2256	2947	3286
$J/\frac{f_L}{2}$.447	.401	.405	.409	.413	.412	.417	.296	.292	.272	.277	.271	.326	.256	.249	.231	.239	.227
η	.95	.93	.90	.87	.84	.83	.93	.90	.86	.83	.80	.78	.93	.89	.85	.82	.79	.77

TABLE 2(B) (Continued)
GROUP II RUNS (cont.)
D = 1/12 in., L = 1/8 in., b_c = 1/8 in.

DATA	Lg = .078 in.						Lg = .093 in.					
SCFM	6.14	10.10	15.10	19.47	24.41	28.95	6.16	10.14	15.02	19.40	24.34	28.68
ΔP_{ave} lb./sq. in.	.150	.440	.847	1.32	1.90	2.42	.128	.418	.838	1.32	1.85	2.44
T-1 °F.	71.3	70.5	71.2	71.3	72.5	73.7	66.0	66.0	67.0	68.5	68.2	69.5
T-2 °F.	229.0	230.7	229.0	226.7	224.3	220.7	267.0	267.5	269.0	267.0	263.0	260.5
T-3 °F.	250.7	253.3	252.7	252.3	250.7	249.7	295.5	298.0	299.0	299.0	297.5	295.5
T-4 °F.	85.8	88.3	90.8	93.0	95.2	97.2	84.5	87.2	90.0	95.8	97.5	101.0
G_{avg} b./.(hr.)(sq.ft.)	3405	5592	8376	10800	13524	16056	3414	5634	8334	10746	13500	16344
N_{Re}	501	825	1232	1584	1992	2362	502	826	1225	1583	1986	2340
ρ lb./cu.ft.	.066	.070	.074	.080	.088	.096	.064	.067	.073	.078	.085	.094
$f_{L/2}$.088	.100	.092	.092	.092	.092	.072	.090	.089	.090	.088	.090
q B.t.u./hr.	1138	1889	2774	3514	4312	4982	1459	2414	3538	4480	5523	6356
ΔT_{lm} °F.	17.84	20.16	21.43	23.32	24.49	26.15	23.21	24.68	27.06	29.54	32.04	33.24
U B.t.u./.(hr.)(sq.ft.)(°F.)	12.39	18.19	25.14	29.27	34.19	37.03	12.21	18.99	25.39	29.44	33.48	37.12
$\frac{\Delta T_w}{b_w}$ °F./ft.	.605	1.01	1.44	1.88	2.30	2.66	.778	1.28	1.89	2.39	2.95	3.39
h_1 B.t.u./.(hr.)(sq.ft.)(°F.)	27.68	42.97	63.43	77.54	95.43	116.55	27.16	45.22	64.52	78.06	92.69	107.33
j	.0268	.0253	.0250	.0237	.0233	.0219	.0262	.0264	.0255	.0240	.0226	.0222
V ft./min.	703	1156	1727	2226	2793	3312	705	1160	1717	2219	2784	3281
$J/\frac{f_L}{2}$.307	.254	.273	.261	.256	.244	.372	.294	.289	.268	.263	.248
η	.93	.89	.85	.82	.79	.77	.93	.88	.84	.82	.80	.77

TABLE 2(C) (Continued)

GROUP III RUNS																									
$D = 1/8$ in., $L = 1/16$ in., $b_c = 3/16$ in.																									
$(L_g = .080$ in.)																									
$(L_g = .123$ in.)																									
SCFM	6.14	10.07	14.79	19.40	24.39	29.06	6.12	10.07	14.95	19.25	24.25	28.75	6.13	10.09	14.98	19.42	24.35	28.73	5.98	9.79	14.53	18.80	23.56	28.01	
ΔT_{ave} lb./sq.in.	.074	.362	.760	1.21	1.76	2.31	.110	.307	.622	1.02	1.44	1.96	.119	.483	.913	1.46	2.02	2.64	.113	.355	.707	1.13	1.60	2.10	
T-1 °F.	68.5	69.0	70.3	70.3	70.7	70.3	68.8	68.7	69.7	70.0	70.8	71.3	71.3	71.3	71.0	71.7	72.8	73.8	77.7	77.7	77.0	76.8	76.8	76.8	
T-2 °F.	230.5	229.3	228.3	226.0	223.3	219.7	220.0	220.0	220.7	218.0	216.0	213.0	210.0	207.3	207.3	204.7	201.0	207.7	224.7	236.7	237.0	234.0	230.3	221.0	
T-3 °F.	237.5	237.0	237.0	235.3	233.7	232.3	228.3	225.0	220.7	218.0	216.0	213.0	210.0	207.3	207.3	204.7	201.0	207.7	224.7	236.7	237.0	234.0	230.3	221.0	
T-4 °F.	85.0	91.3	93.7	95.2	97.0	98.3	88.3	91.5	94.7	97.5	100.0	100.7	86.0	88.7	91.8	94.5	96.8	99.2	104.3	108.7	111.7	115.0	117.7	120.3	
Q_{max} lb./hr.	424.8	6972	10024	13428	16824	20112	4236	6948	10344	13320	16776	19824	4236	6972	10356	13440	16860	19872	4328	6744	10044	12984	16276	19356	
h_{20}	880	1444	2120	2781	3498	4167	888	1443	2173	2761	3476	4177	879	1447	2148	2785	3492	4119	858	1400	2083	2695	3379	4013	
ρ lb./cu.ft.	.066	.070	.075	.081	.089	.097	.075	.075	.075	.075	.080	.087	.066	.069	.075	.081	.088	.097	.065	.068	.073	.079	.086	.095	
$f_{L/2}$.037	.071	.075	.074	.074	.075	.075	.082	.080	.085	.082	.085	.067	.105	.098	.100	.096	.098	.125	.154	.148	.152	.146	.150	
q B.t.u./hr.	1179	1887	2714	3521	4337	5099	1094	1810	2811	3730	4758	5758	1200	1947	2859	3636	4432	5118	1123	1826	2667	3362	4101	4708	
ΔT_{lm} °F.	23.05	24.91	25.93	27.01	28.35	29.17	23.43	25.64	27.12	29.72	31.27	33.45	18.87	21.45	23.92	26.44	27.35	28.99	30.82	33.92	37.21	40.34	42.75	45.42	
U B.t.u./hr. (sq.ft.)	17.28	26.03	35.97	45.02	52.59	60.11	20.68	31.52	42.98	50.02	58.55	62.86	24.46	34.93	45.96	52.54	62.31	67.91	25.13	37.12	49.43	57.48	66.16	71.18	
ΔT_{lm} °F./ft.	.930	1.49	2.14	2.78	3.42	4.02	1.12	1.86	2.60	3.42	4.21	4.88	1.06	1.72	2.52	3.20	3.91	4.51	1.78	2.89	4.22	5.33	6.50	7.47	
h_1 B.t.u./hr. (sq.ft.)	39.20	61.56	90.50	121.05	151.02	181.76	47.03	77.13	114.08	139.50	174.76	194.39	56.93	87.21	124.82	149.33	191.66	219.48	59.61	94.44	137.71	170.27	211.16	236.75	
J	.0304	.0291	.0292	.0297	.0295	.0298	.0366	.0315	.0314	.0345	.0344	.0322	.0443	.0413	.0397	.0367	.0375	.0364	.0468	.0452	.0452	.0432	.0427	.0403	
V ft./min.	880	1444	2121	2782	3499	4168	877	1444	2145	2761	3477	4123	879	1447	2149	2785	3493	4121	858	1403	2084	2697	3379	4017	
$J/\frac{V}{L}$.823	.411	.392	.402	.396	.398	.491	.446	.458	.405	.421	.374	.670	.394	.408	.366	.392	.374	.380	.301	.326	.285	.292	.269	
η	.94	.90	.87	.83	.79	.77	.92	.88	.84	.81	.77	.76	.91	.87	.82	.80	.76	.73	.86	.81	.78	.74	.72	.72	

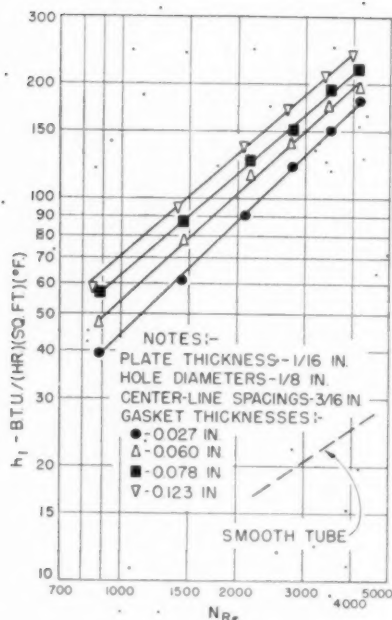


FIG. 4 HEAT-TRANSFER COEFFICIENT, h_1 , BASED ON HOLE AREA VERSUS REYNOLDS NUMBER FOR GROUP III RUNS

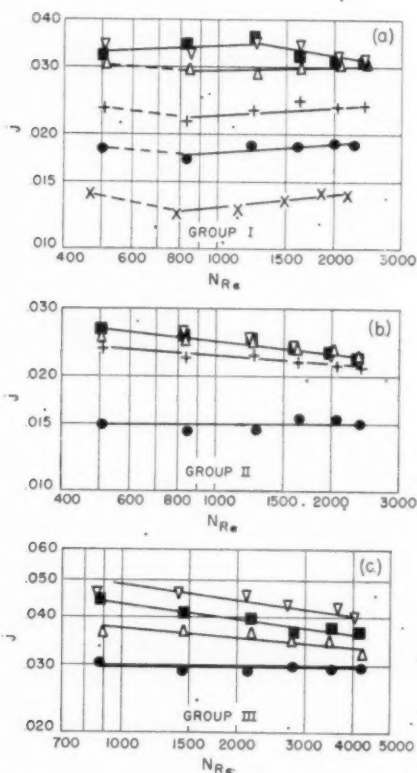


FIG. 5 (a, b, c) HEAT-TRANSFER FACTOR VERSUS REYNOLDS NUMBER
[(a) Group I runs, (b) Group II runs, (c) Group III runs.]

The effects of friction losses were calculated from net pressure drops averaged across the warm and cool channels, by means of the Fanning equation for turbulent flow, as follows

$$f_L = \frac{(72) (\Delta P_{ave}) (\rho) (g_s) (D)}{(N_L) (L) (G_{max})^2} \quad [6]$$

Values of $f_L/2$ are presented versus L_g in Fig. 6.

The final results of the heat-transmission and frictional-resistance calculations are presented in terms of the pressure drop efficiency factor $j/(f_L/2)$ versus N_{Re} in Fig. 7.

DISCUSSION OF RESULTS

Heat Transfer: From theoretical considerations it can be postulated that the transfer of heat from a stream of gas to the metal of a perforated plate through which it is flowing, should be viewed as the resultant of two simultaneous actions. If, for a given mass flow rate, attention is focused on the events transpiring along the length of a single series of matched holes in a channel of an exchanger section, one plate and gasket of which are shown schematically in Fig. 2, certain predictions can be made concerning the probable variation in the heat-transfer process as the gasket thickness is changed. For a zero gasket thickness and a stipulated 100 per cent fin efficiency, the amount of heat transferred will be small and essentially identical to that for a smooth tube of the same diameter. As the gasket thickness is increased and assumes small finite values, the heat-transfer coefficient, h_1 , based on the area A_1 inside of the holes, will rise rapidly because of the interruption and periodic destruction of the laminar-flow boundary layer near the tube walls and the resultant turbulence. As gasket thickness is increased somewhat beyond a moderate fraction of plate thickness, no further improvement in h_1 occurs, presumably because turbulence already is fully developed. This primary effect is shown clearly in the lower portions of the two curves of h_1 versus L_g in Fig. 8, where the cases of $N_{Re} = 1000$ and 2000 for the Group I runs are presented. But as the spacing is further increased, portions of the total surface, A_2 , on the faces of the plates become available for heat transfer, approaching a maximum of availability when the gasket thickness approximates a small multiple of the width of face area per hole, $(b_s/2) - D$, as indicated by the upper portions of the curves of Fig. 8. Thus the actual conditions of heat transfer might perhaps be more realistically represented in the following manner

$$h_1 = h_2 \left(\frac{A_2}{A_1} \right) + h_s \quad [7]$$

Unfortunately, sufficient data were not available from this investigation to do more intergroup correlation than to indicate the general agreement between the results of the Groups I and III runs and the predicted curve shapes. It was not felt advisable to attempt a comparison of the Group II results with those of the other runs, because of the uncertain nature of the surfaces of the hole interiors and the probability that they were not reproducible.

It should be emphasized that the average values of h_1 , some of which are presented in Fig. 4, are based on only the surface area inside the holes, and are somewhat higher than the true local fin coefficients. However, even if one allowed for a liberal correction factor of 50 per cent, the point values would still be considerably higher than those estimated for smooth tubes at the same fluid-flow rates. Probably it would have been more realistic to base the heat-transfer coefficients on an average value of surface, such as $A_1 + (A_2/2)$. However, the present values will serve for design calculation purposes. When more data become available, it should be possible to determine with accuracy the point values of

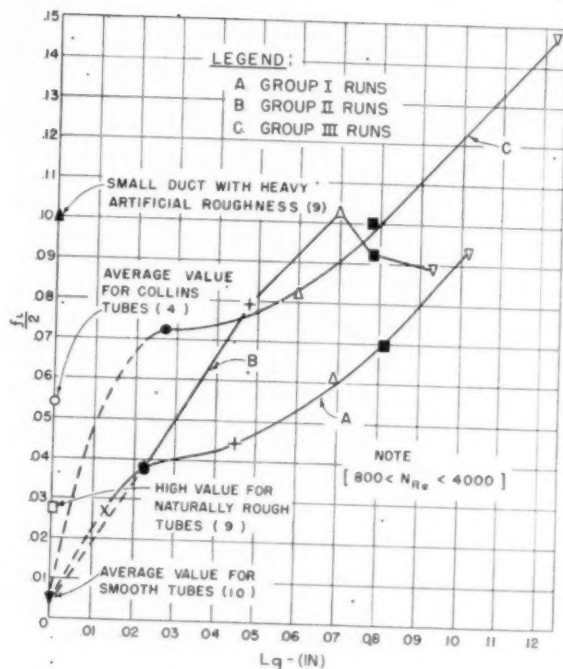


FIG. 6 HALF FRICTION FACTOR VERSUS GASKET THICKNESS

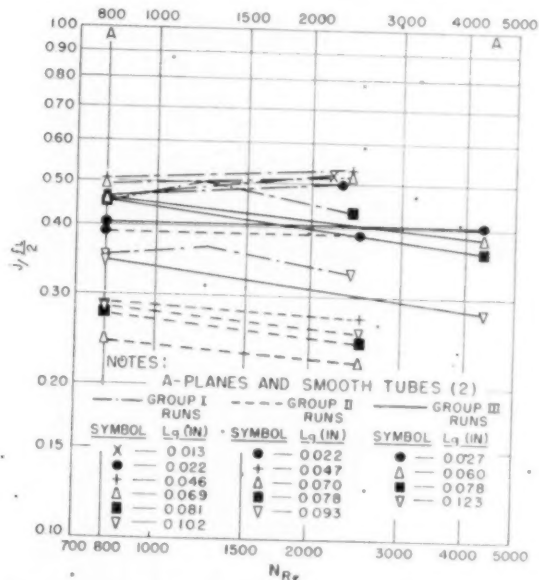
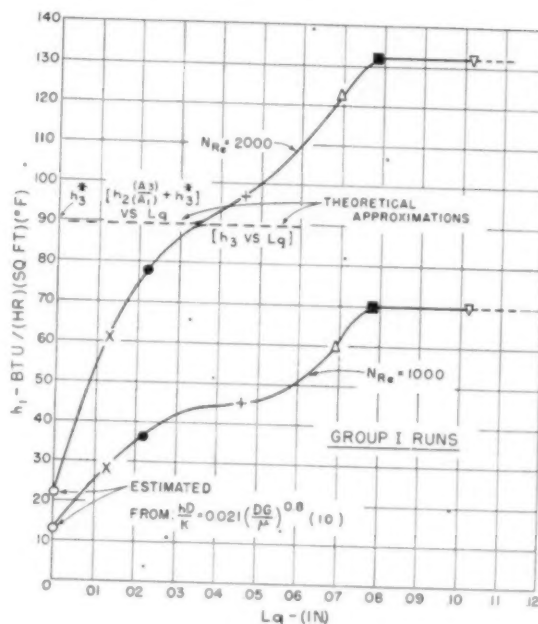


FIG. 7 PRESSURE-DROP EFFICIENCY FACTOR VERSUS REYNOLDS NUMBER FOR ALL RUNS

h or, better still, to effect an exact correlation of average h_i 's with exchanger dimensions.

Save for the case of the lowest values of Reynolds number in the Group I runs, which may indicate a transition region, the variation of h_i with N_{Re} , was found to be a simple power function, as follows

$$h_i = a (N_{Re})^n \quad [8]$$

FIG. 8 HEAT-TRANSFER COEFFICIENT h_i AT CONSTANT MASS FLOW RATE VERSUS GASKET THICKNESS

In the range of N_{Re} covered here, the value of n varied with increasing gasket thickness from approximately 1.14 to 0.88. Since normal turbulent-flow heat exchange inside tubes varies as the 0.8 power of N_{Re} , it seems apparent that even at the lowest values of N_{Re} encountered here, normally considered to be in the region of streamline flow or transition, turbulent conditions prevailed. This was also borne out by the friction results. The fact that h_i varied to lower powers of N_{Re} as gasket thickness increased may be attributable to a change in the nature of the turbulence. At low values of L_g , but greater than a certain minimum, the constant boundary-layer interruption would not permit normal smooth-tube turbulence. However, conceivably, normal turbulence can exist if gasket thickness is great enough.

The dependence of the heat-transfer factor j , on N_{Re} is shown to be slight in Fig. 5(a, b, and c). The fact that the slopes of these curves vary from positive to negative as gasket thickness is varied is unusual, but depends on the variation of the exponent n just noted.

The values of fin effectiveness, η , presented in Table 2, are generally high, varying between 0.70 and 0.96. From Equation [4] it is seen that any variable which can influence the value of $(h_i A_i)$, such as mass flow rate or plate and gasket dimensions, will change η . The greatest control was exerted by the mass flow rate in these experiments.

Flow Resistance: Plate thickness was chosen as the unit of length for friction factors. It is interesting to note that in comparing values of $f_L/2$ versus N_{Re} , in Table 2, save for the runs at lowest flow rates where pressure-drop data were of uncertain precision, the friction factors are essentially independent of the mass flow rate, but a strong function of the gasket thickness. This relationship is shown in Fig. 6. The curve for the Group I runs can be seen to possess a shape similar to that for the h_i -versus- L_g curves in Fig. 8. The somewhat erratic nature of the results obtained by use of doubled $1/8$ -in. plates in the Group II runs is evident from the shape of the $f_L/2$ versus L_g plot. For this reason, straight lines were used between points.

9 "A Study of the Data on the Flow of Fluids in Pipes," by E. Kemler, Trans. ASME, vol. 55, paper no. HYD-55-2, 1933.

10 "Heat Transmission," by W. H. McAdams, McGraw-Hill Book Co., Inc., New York, N. Y., second edition, 1942, pp. 170-171.

That the friction factor should be greatly influenced by the gasket thickness is obvious if one thinks in terms of tubes with controlled roughness, as mentioned earlier. Indeed, in smooth tubing several inches in diameter, the resistance to a moderately turbulent air-flow rate is raised severalfold by the presence on the pipe wall of a band of paper tape a few thousandths of an inch in thickness (8). This phenomenon bears out the laminar-boundary-layer interruption theory and forms the basis of our proposed explanation for the h_1 versus N_{Re} results of this investigation. There is some evidence from previous work with artificially roughened pipes (9) to indicate the independence of friction factor from Reynolds number in the range covered by this work. At least one author presents values of $f_L/2$ in excess of 0.10. While these previous artificial roughnesses did not begin to approach that of the plate exchangers, the agreement in principle is satisfactory.

In general, then, the results of this series of experiments have indicated that for plate exchangers, friction losses rise with mass flow rate, hole diameter, plate thickness, and gasket thickness.

The plate-exchanger friction when compared to the average Collins tube value (4), shown in Fig. 6, or to the correlations for the various fin constructions of Norris and Spofford (2), is seen to be more satisfactory than the former and to compare somewhat less favorably, even for the optimum plate design of this work, with the most efficient fin systems presented by the latter.

Efficiency Factor: Following the device used by Norris and Spofford, a "pressure-drop efficiency factor," $j/(f_L/2)$, is plotted versus Reynolds number. According to Reynolds analogy this factor is unity for forced convection over a single infinite plane and is less than unity for all other surface types. It is to be noted that the values for the perforated-plate exchangers compare favorably with those for most other forms of extended surface.

It is to be observed that the pressure-drop efficiency factor varies somewhat with Reynolds number, as would be expected from the similar variation of the heat-transfer factors.

These pressure-drop efficiency factors, regardless of the basis of N_{Re} , can be compared approximately with those for the Collins tube and for the single-plane and the finned surfaces presented by Norris and Spofford. In the case of the best values for the plate exchanger, i.e., Group I runs, the efficiencies are somewhat higher than for the Collins tube and more than 80 per cent those of most of the extended-surface designs. They are better than pin fins by about 20 per cent, averaging about 50 per cent of the value for smooth single planes and tubes.

Thus the highest efficiency factors for these plate exchangers were obtained with the smaller hole diameter, the thinner plate, and the smallest gasket thickness.

CONCLUSIONS

From this investigation of three basically similar designs of aluminum perforated-plate exchangers, the following specific conclusions are indicated:

1 In the range of flow rates, $800 < N_{Re} < 4800$, the average heat-transfer coefficient, based on the area inside of the holes, is a simple power function of N_{Re} , exponent variations with increasing gasket thickness of from 1.14 to 0.88 having been observed. The highest value of these film coefficients was 237 Btu/(hr) (sq ft) (deg F), obtained in the Group III runs.

2 Heat-transfer and flow-resistance phenomena can be ex-

plained on the basis of a two-function theory. The gasket thickness is considered to cause turbulence by the interruption of the laminar-flow layers at the walls of the tube portions, as well as by making available heat-transfer area on the faces of the plates.

3 The influence on fluid friction and heat transfer of increasing hole diameter is to increase them. The influence of increasing plate thickness is to increase fluid friction and to decrease heat transfer somewhat. (This comment is subject to the limitation mentioned previously concerning reproducibility of the Group II plate design.)

4 In the range of flow rates studied, for a given gasket thickness, the fluid friction factor is independent of the mass velocity.

5 Pressure-drop efficiency factors for these exchangers are substantially independent of mass flow rate, the absolute values varying from a low of 0.22 in the case of the Group II runs to a high of 0.53 in the Group I runs. In general, the influence of an increasing gasket thickness was, first, to increase and then to decrease this efficiency factor. Increase of hole diameter or plate thickness lowered the value of the factor. It is apparent that the type of turbulence produced by the frequently interrupted flow passages is quite efficient as a promoter of high heat transfer with only a moderate amount of fluid friction.

6 While much remains to be learned concerning the properties of perforated-plate exchangers, and the problem of gasket economics also requires additional attention, it can be stated that this type of unit possesses very attractive operational characteristics for large-scale gas-to-gas heat exchange. At the present time full-scale commercial units are being constructed in connection with a special assignment in the field of liquid-oxygen production. It is planned to publish information regarding cost analysis and plant performance in the near future.

ACKNOWLEDGMENTS

It is a pleasure to acknowledge the valuable assistance and advice of many of the staff members of Arthur D. Little, Inc., particularly that of Messrs. R. B. Hinckley and A. Latham, Jr. The kind interest and co-operation of Profs. S. C. Collins and A. H. Shapiro of the Mechanical Engineering Department of the Massachusetts Institute of Technology are also gratefully acknowledged.

[AUTHORS' NOTE: Following presentation of this paper, a question was raised concerning the observed small differences between the temperature changes of the fluid in adjacent channels. The temperature drops in the warm channels were consistently greater than the rises in the cool channels. Calculation showed this to be attributable to heat leak to the surroundings. Thus, for practical purposes, it was possible to eliminate the effect by using temperature changes averaged, between channels.]

BIBLIOGRAPHY

- 1 "Air Separation Principles and Technology," by the editors, *Chemical Engineering*, vol. 54, 1947, pp. 126-134.
- 2 "High-Performance Fins for Heat Transfer," by R. H. Norris and W. A. Spofford, Trans. ASME, vol. 64, 1942, pp. 489-496.
- 3 "Reversing Exchangers Purify Air for Oxygen Manufacture," by S. C. Collins, *Chemical Engineering*, vol. 53, 1946, p. 106.
- 4 "The Design of Ribbon-Packed Exchangers for Low-Temperature Air Separation Plants," by P. R. Trumpler and B. F. Dodge, *Chemical Engineering Progress*, vol. 43, 1947, pp. 75-84.
- 5 "Basic Heat Transfer and Flow Friction Data for Gas Turbine Plant Regenerator Surfaces," Report No. EES-C-2171-E, U. S. Naval Engineering Experiment Station, June 11, 1948.
- 6 Same title, Report No. EES-C-2171-F.
- 7 "New Commercial Tonnage Oxygen System," by B. H. VanDyke, *Steel*, vol. 123, 1948, p. 103.
- 8 Personal Communication, A. H. Shapiro.

E

The effects were tical st tempe The ef quiren

A

planning should to use smaller to this whole e

In a apply to engineer since it this poin internal ever, if ally as t such as

Similar unit size difference following engines ing the c which n addition from the can be de

where R length of describe complete in the va Similar engine an as separa cylinders

Profes Contrib Annual M of The A NOTE: s stood as in Society.

Effect of Size on the Design and Performance of Internal-Combustion Engines

By C. F. TAYLOR,¹ CAMBRIDGE, MASS.

The importance of the problem is outlined and size effects isolated from other effects. Three similar engines were tested at the Sloan Laboratories at M.I.T. Mechanical stresses, volumetric efficiency, heat losses, and wall temperatures are explained as a function of cylinder size. The effects of cylinder size on combustion and fuel requirements are pointed out.

INTRODUCTION

A BASIC problem in the production of power, and indeed in many other fields of machine technology, is involved in the question of unit size. At an early stage in the planning of any engineering enterprise the following question should be asked: "To accomplish the required work, is it better to use few units of relatively large size, or a larger number of smaller units?" On the success in arriving at the correct answer to this question may well depend the success or failure of the whole enterprise.

In a broad sense, the discussion which follows can be taken to apply to most types of machinery dealt with by the mechanical engineer. However, since it is the author's chosen field, and since it is an excellent example of the problems involved, from this point on the discussion will be confined to the reciprocating internal-combustion engine. It would be disappointing, however, if the broader implications were entirely forgotten, especially as they apply to other types of power-producing machinery such as turbines, generators, etc.

RECIPROCATING INTERNAL-COMBUSTION ENGINES

Similar Engines. In order to study properly the question of unit size, it is necessary to eliminate differences in shape and differences in structural material. This process leads to the following definition of "similar engines." Similar engines are engines of different size in which each linear dimension describing the design has the same ratio to a basic linear dimension, l , which may be conveniently taken as the cylinder bore. In addition, corresponding parts in such engines must be constructed from the same material. The geometry of a series of such engines can be described by the following notation

$$(R_1, R_2, R_3, \dots, R_n)$$

where R stands for the ratio of the length of a certain part to the length of the basic dimension, and enough R 's are included to describe the design completely. Any engine in the series is then completely specified by the R series, by a list of materials used in the various parts, and by the magnitude of the dimension l .

Similar Cylinders. In so far as the cylinders of a reciprocating engine are independent of each other, they can be considered as separate similar machines. Excluding the influence of other cylinders through the crankshaft, crankcase, and manifold,

this discussion can be applied with equal force to the question of whether or not an engine should have few large or many small cylinders to furnish the required power.

Weight of Similar Engines. There are certain characteristics of a series of similar engines which can be predicted from mathematical considerations alone. For example, it is obvious that weights will be proportional to l^3 and areas to l^2 . Less obvious, perhaps, are certain important stress relations in such a series.

Stresses in Similar Engines. If it be assumed that the output end of each crankshaft turns with a constant angular velocity, Ω , and that deflections are negligible, it is easy to show that all "inertia" stresses, that is, stresses due to the mass and motion of the parts, will be the same at corresponding points in all engines when the values of (Ω) and the crank angle, θ , are the same.

In most practical cases, however, there are cyclic variations in angular velocity, and deflections under load, which cannot be ignored from a stress point of view. The deflections set up vibratory stresses which may be exceedingly important. In order to deal with vibratory stresses it is necessary to assume equal damping due to friction at the rubbing surfaces and to assume that the apparatus driven by the output shaft is similar in the same sense as the engines, or else that the engines are dynamically isolated from the driven apparatus. Under these circumstances, if the pressure cycles in all the engines are the same, the variation of angular velocity with crank angle will again be the same when the values of (Ω) at a given point in the cycle are equal. Appendix 1 indicates how this relation may be proved.

If the cycles of cylinder pressure versus crank angle are all the same, it is obvious that the stresses directly attributable to gas pressure will be the same at the same crank angle. The question of the circumstances under which pressure cycles will be the same is discussed in a later section.

Since the product (Ω) , together with the necessary design ratios and the angle θ , describe the linear velocity of a given point in any one of the engines, it can be said that, under the limitations just stated, the stress-versus-crank-angle cycle caused by gas pressure and by inertia forces will be the same in each engine of the series if the linear velocities of corresponding parts are the same. The implications of this statement for turbines, electrical machinery, etc., are obvious. In reciprocating engines, a convenient measure of linear velocity is the "mean piston speed."

It should be noted that the similitude in stress pattern at a given value of (Ω) includes stresses due to vibration in any mode of the system. This conclusion follows not only from considerations of dimensional analysis, but because in similar structures natural frequencies of vibration are inversely proportional to the characteristic linear dimension. Thus, at a given value of (Ω) the ratio of forcing frequencies to natural frequencies will be the same in each engine of the series, provided the gas-pressure cycles and the damping are the same and the connected equipment is isolated or is dynamically similar.

Such conditions would be fulfilled by a series of engines connected to a series of similar generators or propellers. These conditions will also be present in the case of motor vehicles, where the driven system is virtually isolated from the engine, dynamically, on account of the great torsional flexibility of the shafting between engine and wheels.

¹ Professor, Massachusetts Institute of Technology.

Contributed by the Oil and Gas Power Division and presented at the Annual Meeting, New York, N. Y., November 27-December 2, 1949, of THE AMERICAN SOCIETY OF MECHANICAL ENGINEERS.

NOTE: Statements and opinions advanced in papers are to be understood as individual expressions of their authors and not those of the Society. Paper No. 49-A-116.

Although stresses due to the force of gravity are seldom of much importance in reciprocating engines, it is interesting to note that in a series of similar engines these stresses increase in proportion to the linear dimension. A proof of this statement is given in Appendix 1. The practical conclusion to be drawn from this relation is that gravitational stresses will become important if unit size is made sufficiently large. Evidence of this trend is indicated by the fact that in studying the balance and vibration of very large engines, gravitational forces are usually considered.

The remaining type of stress to be considered is that due to temperature differences. In structures of similar geometry made of the same materials, it can be shown that such stresses will not be the same unless temperatures at corresponding points are the same. This question is more fully discussed in a subsequent section.

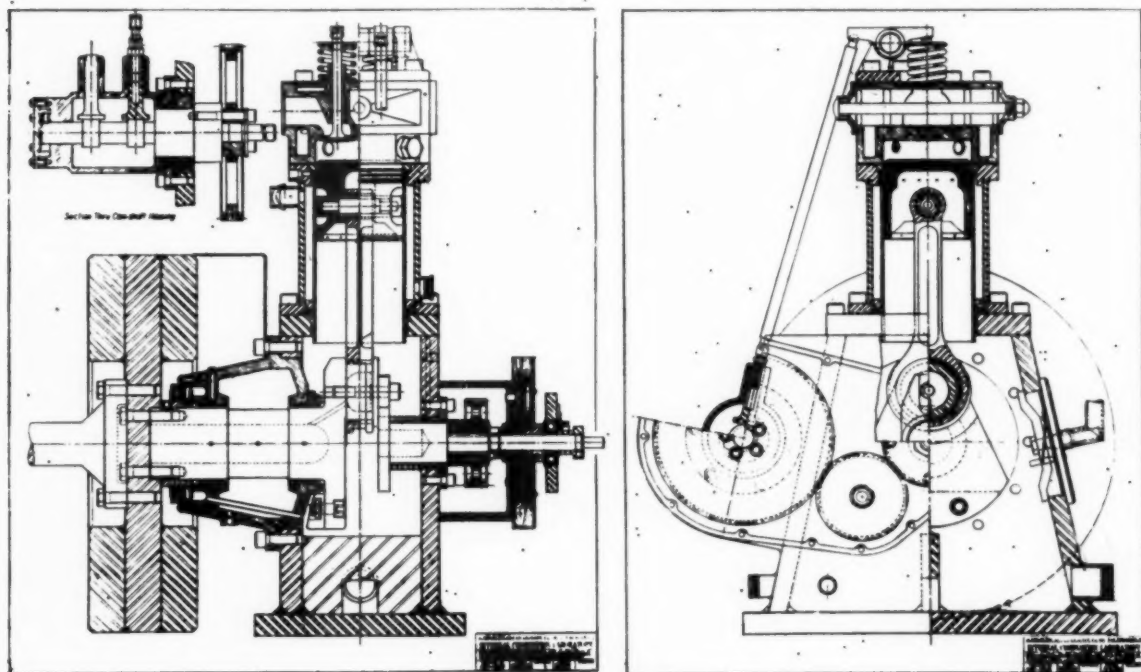
A point to be noted in connection with stress considerations is that, in the absence of resonance effects, stresses due to inertia increase with the square of the linear velocity. It may be predicted, therefore, that inertia stresses are likely to constitute a most important limitation on linear velocities. A corresponding limitation is even more obvious in the case of turbines.

M.I.T. Similar Engines. The foregoing relations are capable of mathematical proof which leaves little doubt of their general validity. When it comes to the more complicated questions of fluid flow, heat flow, combustion, etc., theory does not give the complete answer.

In order to afford opportunity for experiment in this highly important field, there have been constructed at the Sloan Laboratories of the Massachusetts Institute of Technology, three single-cylinder engines which fulfill with considerable exactness the definition of similitude on which the foregoing discussion is based. Fig. 1 is a cross section of these engines. One drawing serves for all three, with only a change in scale. The bores are 2 1/2, 4, and 6 in., respectively, and the strokes are 3, 4.8, and 7.2 in. All details are in proportion, including bearing clearances, wall thicknesses, and screw threads. As installed for test, inlet and exhaust systems are similar.

At present these engines are arranged for four-stroke spark-ignition operation using a premixed gaseous charge. Later they can be converted to Diesel operation, or, with new cylinders, to operate on the two-stroke cycle.

Similar Operating Conditions. For internal-combustion engines the important independent operating variables include inlet-air pressure and temperature, exhaust pressure, fuel-air ratio and coolant-supply temperature. These variables are controlled primarily by factors other than size, and they will be considered to be held the same for all engines in a similar series, unless otherwise noted. Also, the ignition or injection timing will be taken as optimum in each case. Test results presented for the M.I.T. similar engines have been made under these circumstances. The remaining important independent variable, rotational speed, is limited by size considerations as already indicated.



	Bore in.	Stroke in.	Piston Area in. ²	Displ. Vol. in. ³
Small	2.500	3.000	4.91	14.71
Medium	4.000	4.800	12.57	60.35
Large	6.000	7.200	28.27	203.54

FIG. 1 CROSS SECTIONS OF THE THREE M.I.T. GEOMETRICALLY SIMILAR ENGINES
(Single-cylinder, water-cooled, compression ratio, $r = 5.74$.)

Although stresses due to the force of gravity are seldom of much importance in reciprocating engines, it is interesting to note that in a series of similar engines these stresses increase in proportion to the linear dimension. A proof of this statement is given in Appendix 1. The practical conclusion to be drawn from this relation is that gravitational stresses will become important if unit size is made sufficiently large. Evidence of this trend is indicated by the fact that in studying the balance and vibration of very large engines, gravitational forces are usually considered.

Although stresses due to the force of gravity are seldom of much importance in reciprocating engines, it is interesting to note that in a series of similar engines these stresses increase in proportion to the linear dimension. A proof of this statement is given in Appendix 1. The practical conclusion to be drawn from this relation is that gravitational stresses will become important if unit size is made sufficiently large. Evidence of this trend is indicated by the fact that in studying the balance and vibration of very large engines, gravitational forces are usually considered.

Although stresses due to the force of gravity are seldom of much importance in reciprocating engines, it is interesting to note that in a series of similar engines these stresses increase in proportion to the linear dimension. A proof of this statement is given in Appendix 1. The practical conclusion to be drawn from this relation is that gravitational stresses will become important if unit size is made sufficiently large. Evidence of this trend is indicated by the fact that in studying the balance and vibration of very large engines, gravitational forces are usually considered.

Air Flow in Similar Engines. One interesting relation here is quite obvious. Since the speed of sound is the limiting gas velocity at the smallest cross section of a flow system, when pressures and temperatures on the upstream side of this section are the same (and shapes are the same), maximum mass flow will be proportional to the square of the typical dimension. We are used to this relation in turbines, where critical flow through the nozzles is customarily considered. In the case of reciprocating engines the inlet-valve opening is usually the smallest cross section. It is thus easy to see that, under similar operating conditions, the maximum mass rate of air flow, and hence the maximum possible power output, is proportional to an area rather than a volume. For flows less than critical, the foregoing considerations suggest that a Mach index, that is, an index defining the relation of flow velocity to sound velocity, will be of great importance.

In dealing with questions of mass flow of air in reciprocating engines, it is convenient to use the parameter called "volumetric efficiency," which will be defined here as the ratio of the actual mass flow to a mass flow equal to the displaced volume multiplied by the air density in the inlet manifold of the engine.

Appendix 2 shows that, for a series of similar engines operating under similar conditions, volumetric efficiency is a function of the two nondimensional parameters

$$s/c \text{ and } sl\rho/g_{0u}$$

where s is mean piston speed, c is speed of sound in air at inlet conditions, ρ is inlet-air density, μ is viscosity of air at inlet conditions, l is the typical dimension, and g_0 is the coefficient relating force and mass.

It will be noted that the first fraction in the series is in the nature of a Mach index and the second has the characteristics of a Reynolds index. The same system of parameters applies to a gas turbine by substituting rotor tip velocity for mean piston speed.

Volumetric Efficiency Versus Mach Index. It might be inferred that, in reciprocating engines, variations in viscous forces and in heat-transfer coefficients, which depend on the Reynolds number, will be of considerably less importance in this particular case than the forces due to inertia of the gas, which are dependent upon the Mach number. If this be the case, the curve of volumetric efficiency versus Mach index should be the same for similar engines under similar operating conditions. Fig. 2, constructed from tests on the M.I.T. similar engines, shows this assumption to be valid within the size range employed and within the accuracy of the measurements.²

There is evidently no discernible trend on the basis of cylinder size, which would not be the case if the Reynolds index had an important influence on volumetric efficiency.³

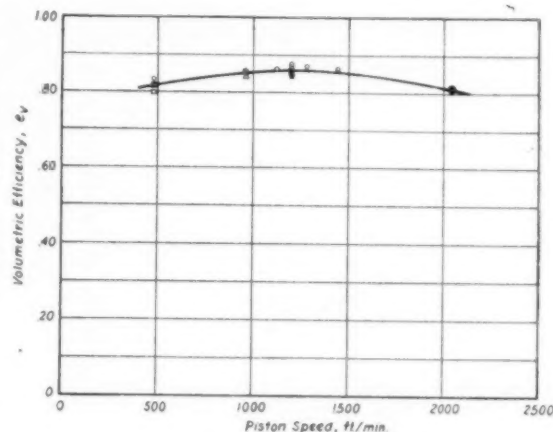
The foregoing statement is not intended to imply that heat transfer is an unimportant factor in connection with volumetric efficiency, or in other aspects of engine performance. As a matter of fact, heat transfer to the inlet gases accounts for a considerable portion of the difference between the actual and ideal volumetric efficiencies of most engines.⁴ What appears to be unimportant, from the M.I.T. tests, is the effect of size on the part which heat transfer plays in determining volumetric efficiency.

Another important item to be noted is that the volumetric

² Since inlet temperature was the same, the value of the speed of sound c was the same for all engines, and volumetric efficiency has been plotted against s rather than against s/c .

³ Only a limited amount of testing has been completed as yet with the M.I.T. engines. The accuracy of measurement and reproducibility of results are, therefore, not yet as good as is hoped for later.

⁴ "Rise in Temperature of the Charge as It Passes Through the Inlet Valve. . .," by J. E. Forbes and E. S. Taylor, Technical Note No. 839, National Advisory Committee for Aeronautics, January, 1942.



Range of rpm				
Piston Speed ft/min.	450	900	1200	2040
□ Small	960	1920	2400	4080
○ Medium	600	1200	1500	2550
△ Large	400	800	1000	1700

FIG. 2 VOLUMETRIC EFFICIENCY VERSUS PISTON SPEED OF M.I.T. GEOMETRICALLY SIMILAR ENGINES

($r = 3.74$; $F = 0.073$; optimum spark advance: $p_i = 28$ in. Hg, $p_e = 32$ in. Hg absolute; $T_i = 150$ F.)

efficiency versus piston-speed relation will not be the same for similar engines unless the connected inlet and exhaust systems are similar. Without such similitude, pressure-wave patterns in the inlet and exhaust piping will not be the same at the same piston speed.

A third point to be noted is that the foregoing discussion applies to supercharged engines, provided the superchargers and their connections are similar. This conclusion follows, because the theory has placed no limitations on design detail.

Since it has been common practice to regard "rpm" as an important parameter of engine performance, the curve in Fig. 2 has been plotted versus rpm in Fig. 3. Obviously, rpm is a poor index where cylinder size is not the same.

Heat Losses. The coefficient of heat transfer between a fluid and a solid surface depends on geometry, and on the local Reynolds number and Prandtl number.⁵ Assuming the same fluids and gases in our system of similar engines, the Prandtl numbers will be the same. Assuming internal Reynolds numbers to be a function of the Reynolds index, $sl\rho/g_{0u}$, with the same inlet conditions and at the same piston speed, heat-transfer coefficients will evidently vary with size. Dimensional analysis, together with existing knowledge of less complicated heat-transfer systems indicates that, under the conditions specified:

1 Heat-transfer coefficients grow less as cylinder size increases, because of the increasing local Reynolds numbers both inside the cylinder and in the cooling system.

2 In spite of the decreasing coefficients, mentioned in (1), temperature differences across the cylinder walls, piston, valves, etc., increase with increasing size, due to the longer heat-flow paths.

3 Heat loss per unit wall area decreases with increasing size.

Fig. 4, taken from the M.I.T. similar engines under similar operating conditions, confirms the second statement. These temperatures were taken by means of thermocouples embedded at corresponding points in the cylinder heads, close to the inner surface of the wall.

⁵ "Heat Transmission," by W. H. McAdams, McGraw-Hill Book Company, Inc., New York, N. Y., 1942.

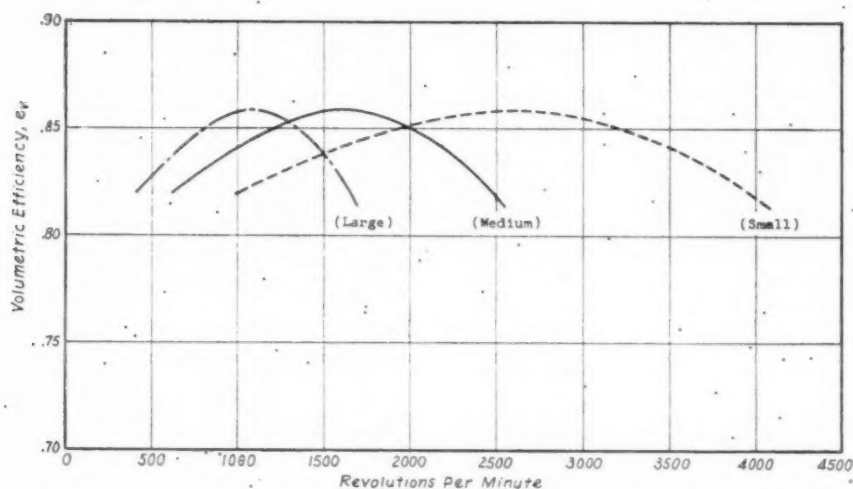


Fig. 3 VOLUMETRIC EFFICIENCY VERSUS RPM OF THE M.I.T. GEOMETRICALLY SIMILAR ENGINES
(Same operating conditions as in Fig. 2.)

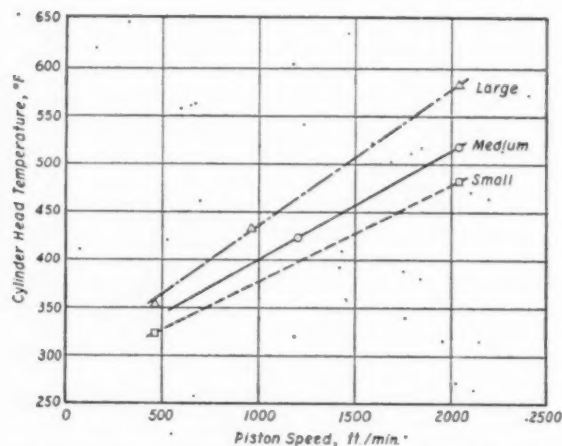


Fig. 4 CYLINDER-HEAD TEMPERATURE VERSUS PISTON SPEED OF M.I.T. GEOMETRICALLY SIMILAR ENGINES
(Same operating conditions as in Fig. 2. Temperatures were taken at corresponding points near inside surface of cylinder heads.)

The implications of the second conclusion are highly important. It follows that, for similar engines run under similar operating conditions and at the same piston speed, stresses due to temperature differences will increase with cylinder size. In practice, this results in departures from similitude in the direction of more effective cooling as cylinder size increases. Oil or water circulation within the pistons and exhaust valves of large cylinders is an example.

Indicated Mean Pressure. At the same volumetric efficiency and fuel-air ratio, indicated mean effective pressure will be the same, provided thermal efficiency is the same. This statement is simply a matter of accepted definitions.

At the same piston speed and fuel-air ratio, therefore, indicated mean pressure will be proportional to thermal efficiency. Due to the smaller heat losses of the larger cylinder one would expect its thermal efficiency to be higher. Fig. 5 shows, however, that within the range of size of the M.I.T. engines, the differences in efficiency are smaller than the uncertainties of measurement, and the imep versus piston-speed curves are the same.

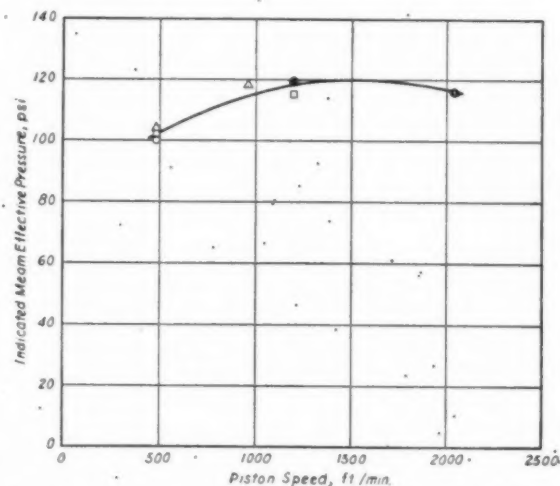


Fig. 5 INDICATED MEAN EFFECTIVE PRESSURE VERSUS PISTON SPEED OF M.I.T. GEOMETRICALLY SIMILAR ENGINES
(Symbols and operating conditions same as in Fig. 2)

Figs. 6 and 7 show indicator diagrams made from the three engines at the same piston speed and under similar operating conditions. The diagrams are the same within the accuracy of measurement. At the same rpm the diagrams are quite different. Figs. 6 and 7 lend further confirmation to the foregoing theory, including the predominant influence of the Mach index on volumetric efficiency.

Following up this subject further, the author has plotted, Fig. 8, indicated thermal efficiency versus bore for a number of commercial Diesel engines, based on manufacturers' data. If the data for large bores are representative, a trend in the expected direction is indicated.

Fuel and Combustion. In spark-ignition engines, flame speed tends to be proportional to piston speed, regardless of cylinder size. This being the case, the time required for the flame to cross the combustion chamber of similar engines running at the same piston speed increases in proportion to the bore. The time required for autoignition of the end gas, however, remains constant

Fig. 6

(Pist

with a
tenden
as cylin
that th
creases
rapid,
used.
sirable
ing may
out sup
raised a
effective
sion rat
be requ
tion wh
limit th
for mos

In Di

* For c
plete dis
Engine,"
Company

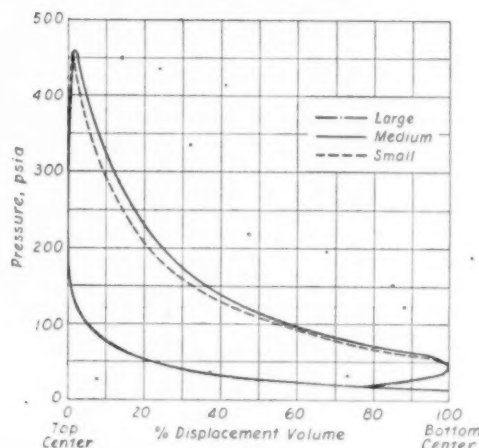


FIG. 6 INDICATOR DIAGRAMS OF M.I.T. GEOMETRICALLY SIMILAR ENGINES

(Piston speed = 2040 fpm; other operating conditions same as in Fig. 2.)

with a given fuel and fuel-air ratio. Thus there is an increasing tendency toward autoignition of the end gas, causing detonation,⁶ as cylinder bore increases. Another way of stating this relation is that the detonation-limited indicated mean effective pressure increases with decreasing bore. Fig. 9 shows this increase to be very rapid, although the slope of the curve may vary with the fuel used. This relation would tend to make small cylinders very desirable for aircraft engines, or in other services where supercharging may be used and very high specific output is desirable. Without supercharging and with a given fuel, compression ratio may be raised as cylinder size decreases, thus increasing indicated mean effective pressure and decreasing fuel consumption. If compression ratio is not changed, a fuel more resistant to detonation will be required as the bore increases. It is considerations of detonation which, perhaps more than any other factor, have tended to limit the bore of spark-ignition engines to a maximum of 6 or 7 in. for most purposes.

In Diesel engines, on the other hand, most of the difficulty in

⁶ For definitions of "detonation," "end gas," and for a more complete discussion of this whole subject see "The Internal Combustion Engine," by C. F. Taylor and E. S. Taylor, International Textbook Company, ed. 1948, chapt. 6.

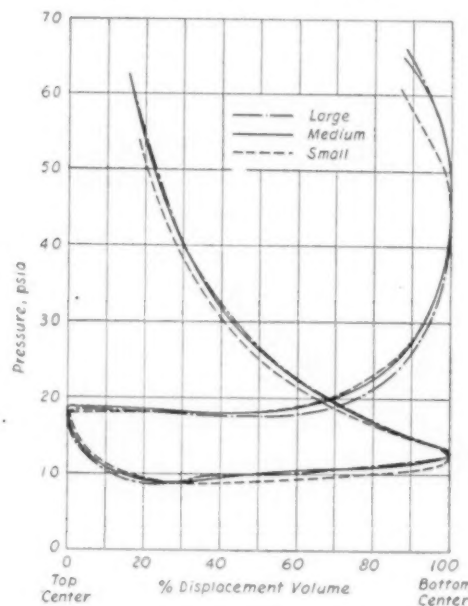


FIG. 7 LIGHT-SPRING INDICATOR DIAGRAMS OF M.I.T. GEOMETRICALLY SIMILAR ENGINES

(Piston speed = 2040 fpm; other operating conditions same as in Fig. 2.)

securing satisfactory combustion rates centers around the "delay angle," that is, the crank angle between the start of injection and the beginning of rapid combustion. The larger this angle, the more difficult it is to avoid excessively high rates of pressure rise. At the same piston speed, as cylinders get larger the time to traverse a given crank angle grows correspondingly longer. Thus fuels with longer ignition delays can be tolerated as the bore increases, which is of great practical advantage. In the other direction, as bore gets smaller and rpm increase, either fuels with better ignition quality are required, or the design must be changed to incorporate prechambers designed to limit the rate of pressure rise over the piston.

From these considerations it is easy to see why engines with very large cylinders are invariably Diesels.

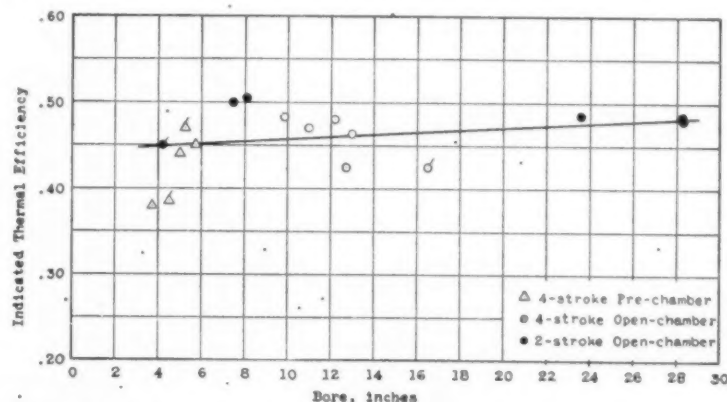


FIG. 8 INDICATED THERMAL EFFICIENCY OF DIESEL ENGINES AT $0.60 \times$ CHEMICALLY CORRECT FUEL-AIR RATIO
(From manufacturers' performance data, 1949.)

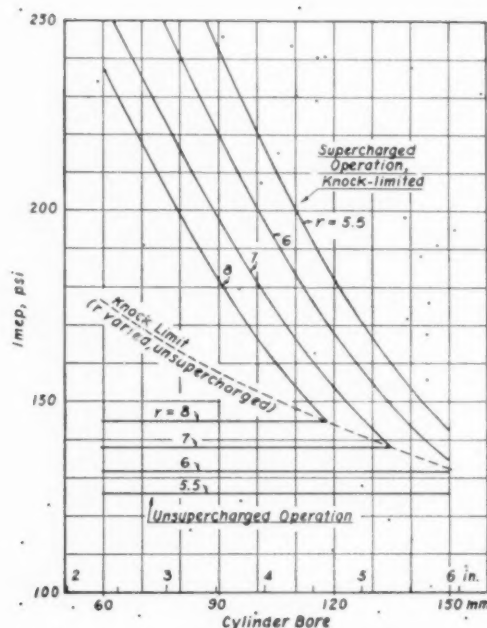


FIG. 9 EFFECT OF SIZE ON KNOCK-LIMITED IMEP IN SIMILAR CYLINDERS

(Piston speed = 2170 fpm, adapted from Kamm, *Schriften der Deutschen Akademie der Luftfahrtforschung*, March 3, 1939, r is compression ratio.)

Friction. It is well known that the coefficient of friction of well-lubricated bearings of similar design is a function of the parameter ($\mu N/p$), in which μ is the oil viscosity, N is the angular velocity, and p is the unit load. We have shown that in similar engines running at the same piston speed and under similar operating conditions, p will be the same; N , obviously, will be inversely proportional to the dimension, l , so that for the friction parameter to be the same for all engines of the series, μ/l must be the same. In other words, oil viscosity must be proportional to the characteristic dimension. Similar considerations lead to the same conclusion for sliding bearings under conditions of fluid-film lubrication.

There remains the question of bearings operating under conditions of partial lubrication. Less is known about this type of friction, but since it constitutes only a very small fraction of the total friction, the assumption that all the coefficients of mechanical friction will be the same if oil viscosity is proportional to bore, seems justified.

Since unit bearing pressures in our similar engines under similar operating conditions will be the same at the same piston speed, unit friction forces should be the same, which means that the mean effective pressure to overcome friction should be the same.

Experiments on the M.I.T. similar engines have not borne out this theory, the mechanical friction mep being smaller as engine size increases, Fig. 10. The differences are larger than expected, especially in view of Fig. 11 which shows nearly equal values of friction mep versus piston speed for two engines of enormously different size. Further investigation of the causes for the wide differences in friction mep of the M.I.T. similar engines is indicated.

Brake Mean Effective Pressure. With equal indicated mep and equal friction mep, brake mean effective pressure will be the same. Even if friction mep is not the same, it is generally small enough compared to indicated mep so that the resulting differences due to

engine size should be small. Thus it is not surprising that engines for similar service tend to be rated at the same brake mep and piston speed, as indicated by Fig. 12.

Power Output and Weight. Since power output is proportional to the product of piston area, brake mean effective pressure, and piston speed, the output of similar engines running at the same piston speed will be nearly proportional to l^2 , that is, nearly proportional to the "piston area" rather than the piston displacement. Since weight is obviously proportional to l^3 , or to displacement, the weight per unit output increases with the linear dimension. In spite of wide differences in design, this trend is indicated by Fig. 13. This relation constitutes one of the strongest arguments for the use of small units or small cylinders, where feasible.

Wear and Life. While the mechanism of wear and how to control it is not yet clearly understood, there seems good basis for the following assumptions:

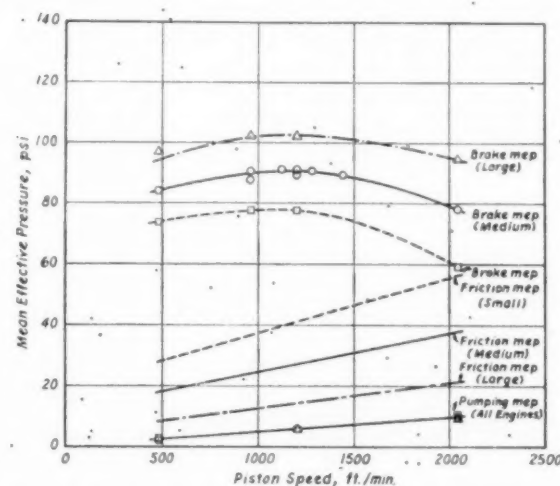


FIG. 10 BRAKE, FRICTION, AND PUMPING MEAN EFFECTIVE PRESSURE VERSUS PISTON SPEED OF M.I.T. GEOMETRICALLY SIMILAR ENGINES

(Same operating conditions as in Fig. 2. Friction mep includes pumping cycle. For mechanical friction only, subtract pumping mep.)

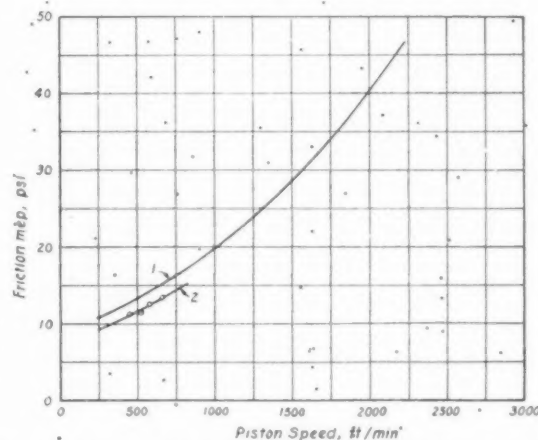


FIG. 11 FRICTION MEAN EFFECTIVE PRESSURE OF TWO ENGINES (Curve 1 from motoring test of G-M 6-cylinder two-stroke Diesel engine, 4.25 in. \times 5 in., single-acting, with scavenging pump. Curve 2 from indicator cards of Sulzer 8-cylinder two-stroke Diesel engine, 19.6 in. \times 35.3 in., single-acting, with scavenging pump.)

(a) Depth of corrosive wear per unit time should be independent of size.

(b) With the same materials, same unit pressures, depth of contact wear should be proportional to distance traveled. Therefore depth of contact wear per unit time should be the same for similar engines running at the same piston speed.

Wear "damage" should be measured by depth of wear divided by the dimension of the worn part. Therefore, if (a) and (b) be true, wear damage per unit time varies in proportion to the reciprocal of the bore. In other words, the "life" of similar engines, as limited by wear, increases as the cylinder bore increases. This conclusion is in line with common experience.

Costs of Manufacture. These depend on weight of materials, size of parts, and on the number and character of machine operations. The small unit would appear to have the advantage in respect to weight and size, but of course requires more parts for the same power output. However, small parts lend themselves to mass-production methods better than do large ones. The following figures apply to two engines with cylinders of nearly similar design:

Engine	No. cyls.	Bore, in.	Stroke, in.	Rpm	Hp	Weight, lb/hp	Retail price, \$/hp
GM 6-71	6	4 1/4	5	1800	180	12.1	28
GM 16-278	16	8 1/2	10 1/2	750	1600	17.5	31

NOTE: Prices include d-c generator, were quoted in Boston, Mass., 1949. Other figures from *Diesel Power*, April, 1949.

It is known that the cost per horsepower of Diesel engines with very large cylinders is much higher than the figures given.

American Diesel Engines. Maximum rated brake mean effective pressure and the piston speed at maximum rating are shown for U. S. Diesel Engines in Figs. 14 and 15, respectively.

Mean effective pressures and piston speeds, on the average, decrease slightly with bore, partly due to considerations of increasing temperature stresses, and partly to the fact that as engines get larger there is less opportunity for development work and ratings must, therefore, be conservative.

A Contrast. Fig. 16 shows a composite view of a Nordberg 29-in. \times 40-in. two-stroke Diesel engine and an Arden 0.495-in. \times 0.516-in. model airplane engine, also a two-stroke compression-ignition type. In spite of the considerable difference in size and field of these two engines, the last three figures in Table 1 show their basic similarity.

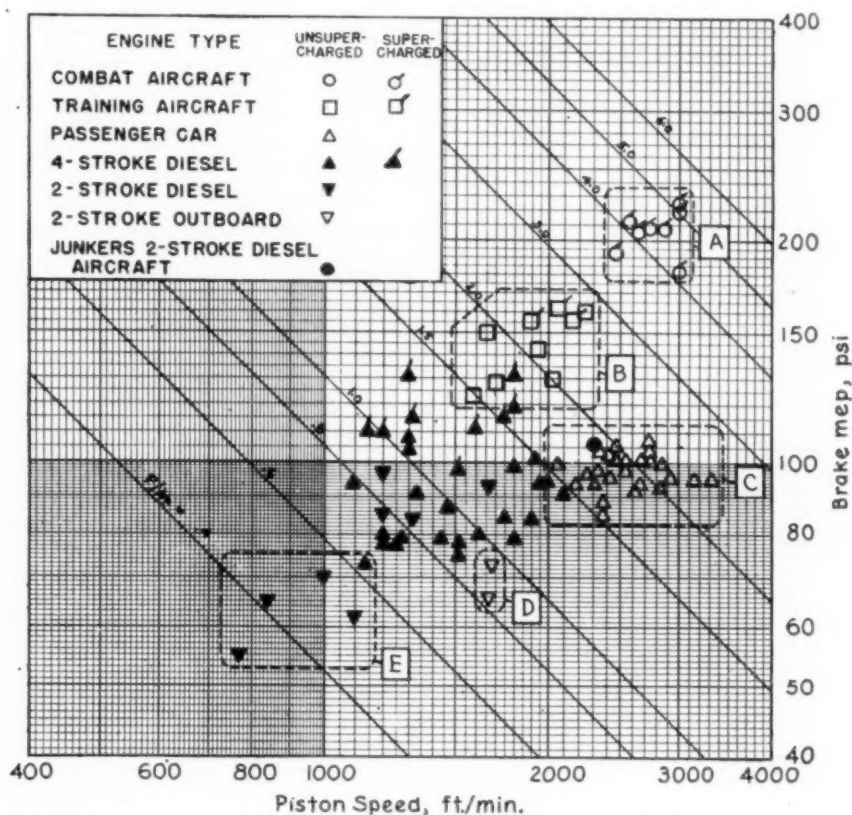


FIG. 12 RATED BRAKE MEAN EFFECTIVE PRESSURE, PISTON SPEED AND POWER PER SQUARE-INCH PISTON AREA OF VARIOUS TYPES OF ENGINES

(Published ratings, 1945: Combat aircraft-engine ratings are at sea-level take-off with 100-octane gasoline, without water injection; P/A_p lines are constant ratios of horsepower to piston area in sq. in. for 4-stroke engines; multiply by 2 for 2-stroke engines.)

Group A, Combat aircraft engines
Group B, Training aircraft engines
Group C, Passenger-car engines
Group D, Outboard marine engines
Group E, Heavy-duty Diesel engines

Remaining points are for miscellaneous Diesel engines including automotive and locomotive types.)

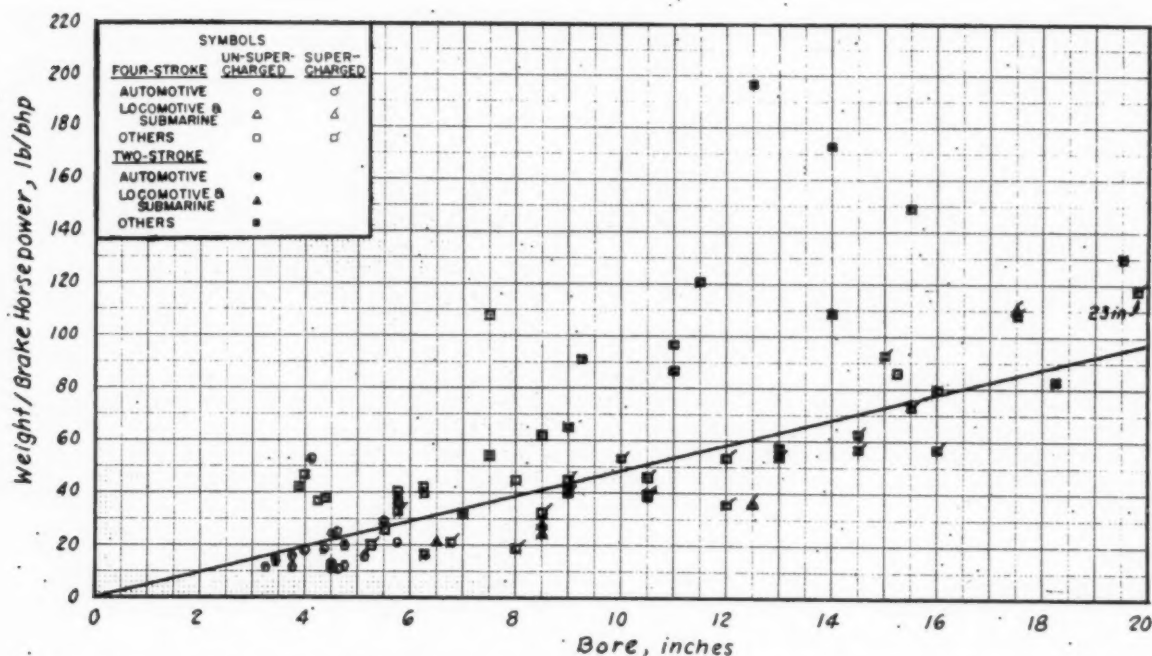


FIG. 13 WEIGHT PER RATED BRAKE HORSEPOWER VERSUS BORE OF REPRESENTATIVE U. S. COMPRESSION-IGNITION ENGINES
(Data from *Diesel Power* and *Diesel Transportation*, April, 1947.)

TABLE 1 ENGINE DETAILS

	Arden	Nordberg
Bhp per cylinder.....	0.136	710
Rpm.....	11400	164
Cylinder displacement, in. ³	0.10	26500
Piston speed, fpm.....	980	1100
Bmep, psi.....	47	66
Weight ÷ bore ³ , lb/in. ³	3.1	3.2

The performance figures for the Arden were obtained by test at M.I.T. at maximum output. Those for the Nordberg are the manufacturer's ratings. The weight of the Arden has been corrected on the assumption that the aluminum parts are changed to cast iron, to correspond with the materials used in the larger engine.

CONCLUSION

Table 2 has been prepared to summarize the practical aspects of the foregoing discussion.

TABLE 2 SUMMARY OF ENGINE DATA DISCUSSED

For a given output and for:	Unit size should be	Cylinder size should be
1 Smallest weight.....	small	small
2 Smallest volume.....	small	small
3 Lowest first cost.....	small	small
4 Lowest fuel consumption, Diesel.....	...	large
5 Cheapest fuel, Diesel.....	...	large
6 Lowest fuel consumption, spark ignition.....	...	small
7 Cheapest fuel, spark ignition.....	...	small
8 Longest life (wear).....	large	large

Appendix 1

Similar Engines. These will be taken as engines in which all corresponding length ratios are the same and in which the same materials are used in corresponding parts. Such engines can be completely described by the following notation:

Typical dimension..... l
Design (length) ratios..... $(R_1, R_2, R_3, \dots, R_n)$
A bill of materials

Basic properties of the materials can be specified by the value for a given material. For example:

All moduli of elasticity will be proportional to a characteristic modulus, E .

All densities of material will be proportional to a characteristic density ρ .

The same can be said for heat conductivities, etc.

Fundamental Dimensions

For purposes of this discussion, the fundamental dimensions are taken as follows:

Length.....	L
Force.....	F
Time.....	t
Mass.....	M
Absolute temperature.....	T

Inertia and Gravitational Stresses. In so far as stresses due to inertia and gravity are concerned, only the following properties will be important:

Name	Symbol	Dimension
Characteristic length.....	l	L
Design ratios.....	(R_1, \dots, R_n)	0
Characteristic density.....	ρ	ML^{-3}
Characteristic modulus of elasticity.....	E	FL^{-2}
Angular velocity.....	Ω	t^{-1}
Crank angle.....	θ	0
Damping coefficient ^a	C	$FL^{-1}t^{-1}$
Acceleration of gravity.....	g	Lt^{-2}
Dimensional constant connecting force, mass, and acceleration.....	g_0	$MLT^{-2}F^{-1}$

^a The damping coefficient here referred to is the damping force per unit area and per unit velocity between rubbing surfaces. The internal damping coefficients of the materials will of course be the same in similar engines.

Introducing the typical stress σ , which has the dimensions FL^{-2} we can write the dimensionless equation

$$\psi_1 \left(\frac{\rho l^2 \Omega^2}{\sigma g_0}, \frac{\rho l^2 \Omega^2}{E g_0}, \frac{g_0 l}{\sigma g_0}, \frac{C g_0}{\rho \Omega}, \theta, R_1, \dots, R_n \right) = 0.$$

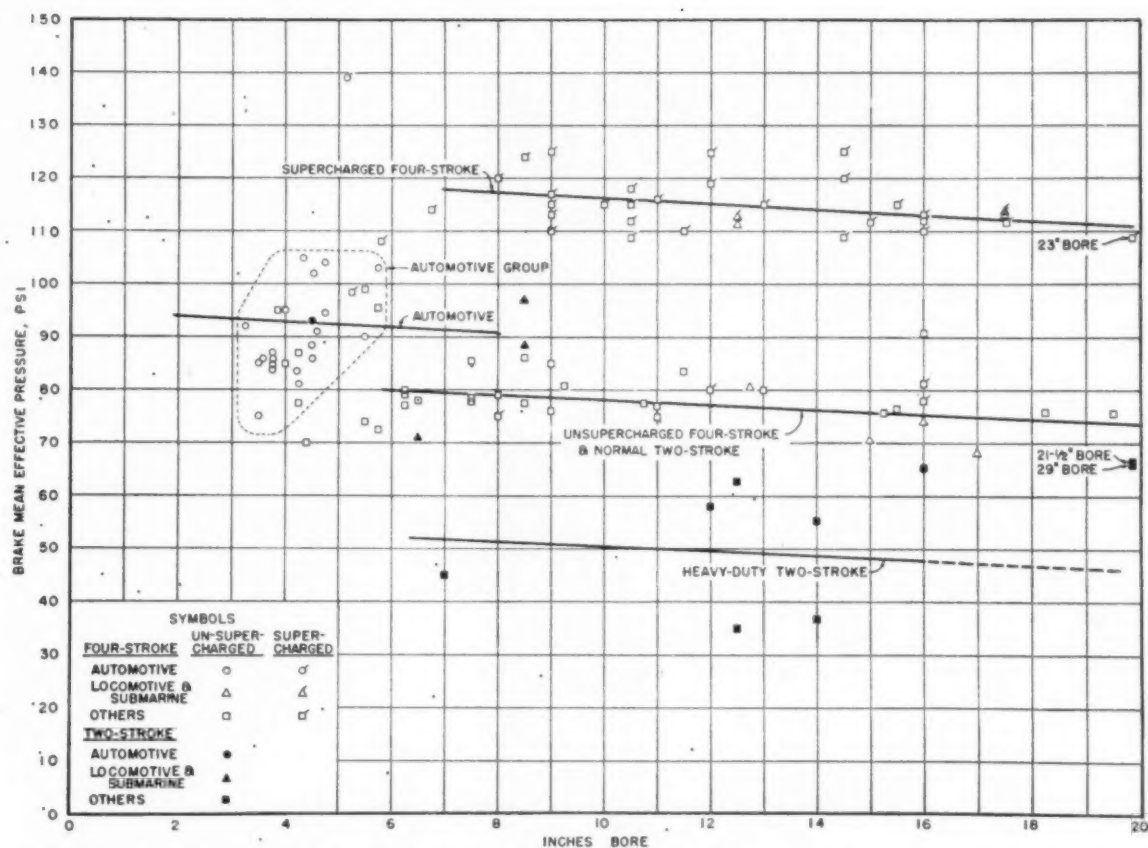


FIG. 14 Rated Brake Mean Effective Pressure Versus Bore of Representative U. S. Compression-Ignition Engines
(Data from *Diesel Power* and *Diesel Transportation*, April, 1947.)

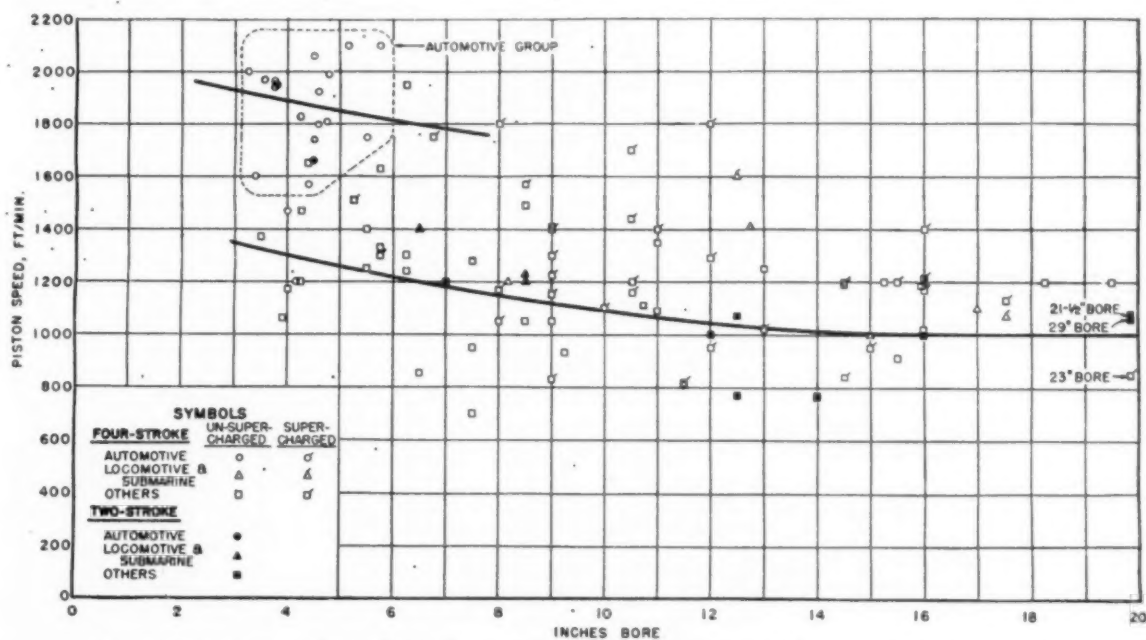


FIG. 15 Piston Speed at Rated Power Versus Bore of Representative U. S. Compression-Ignition Engines
(Data from *Diesel Power* and *Diesel Transportation*, April, 1947.)

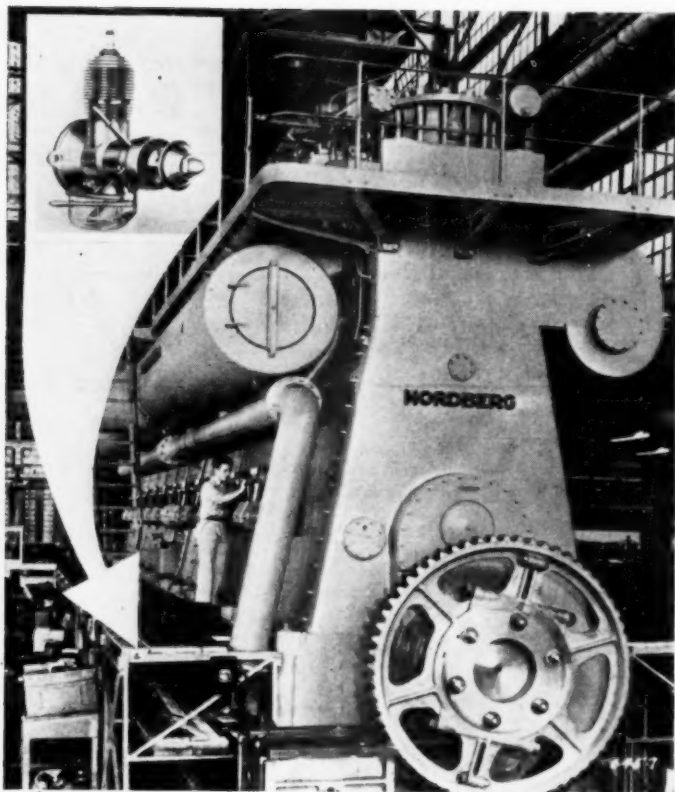


FIG. 16 COMPARISON OF A NORDBERG DIESEL ENGINE AND AN ARDEN MODEL AIRPLANE ENGINE

	Arden	Nordberg
Bore, in.	0.495	29
Stroke, in.	0.516	40
Cylinder displacement, in. ³	0.19	26500
No. of cylinders	1	10
Bhp per cylinder	0.136	710
Rpm.	11400	164
Piston speed, fpm	980	1100
Bmeep, psi	47	66
Weight ÷ bore ³ , lb/in. ³	3.1	3.2

where ϕ_1 indicates a function of what follows. This notation means that if values are assigned to all but one of the terms in the parentheses, the value of the remaining term is determined. The third term in parentheses describes a parameter controlling stresses due to gravity. It is evident that these stresses vary with the typical length, l . Assuming such stresses to be negligible, and omitting all constant terms gives

$$\phi_2 \left[\frac{\rho(l\Omega)^2}{\sigma g_0}, \frac{\rho(l\Omega)^2}{E g_0}, \frac{C g_0}{\rho l \Omega}, \theta \right] = 0$$

C will be the same in similar engines provided the oil viscosity is proportional to the bore. Assuming this to be the case, and eliminating all constant quantities, we can write the following equation, no longer dimensionless

$$\sigma = \phi_3(l\Omega, \theta)$$

This equation indicates that corresponding stresses will be the same at the same values of mean piston speed and crank angle.

Appendix 2

Volumetric Efficiency of Similar Engines. Assuming similar design, the independent engine variables which affect volumetric efficiency can be taken as follows:

Variable	Symbol	Dimensions
Typical length	l	L
Angular velocity	Ω	t^{-1}
Inlet pressure	p_i	FL^{-2}
Exhaust pressure	p_e	FL^{-2}
Inlet temperature	T_i	T

Variable	Symbol	Dimension
Coolant temperature	T_j	T
Fuel-air ratio	F	0
Inlet-gas characteristics:		
Density	ρ	ML^{-3}
Viscosity	μ	$FL^{-1}T$
Speed of sound	c	Lt^{-1}
Ratio of specific heats	k	0
Prandtl number	π_p	0

Since the Prandtl number is the same for real gases, it can be omitted from further consideration. Adding volumetric efficiency, ϵ_v , which is the dependent variable under consideration, we can write

$$\phi_1 \left(\epsilon_v, \frac{l\Omega}{c}, \frac{\rho l^2 \Omega}{g_{0\mu}}, \frac{p_e}{p_i}, F, \frac{T_j}{T_i}, k \right) = 0$$

Let it be assumed that similar engines all use the same inlet gas (air), and that the fuel-air ratio, pressures, and temperatures are held constant. Omitting the constant arguments yields

$$\phi_2 \left(\epsilon_v, \frac{l\Omega}{c}, \frac{\rho l^2 \Omega}{g_{0\mu}} \right) = 0$$

omitting all constant quantities

$$\epsilon_v = \phi_3(l\Omega, l)$$

The function indicated by ϕ_3 now contains constants which are not dimensionless. It indicates that, under similar running conditions, the volumetric efficiency of similar engines is a function of piston speed ($l\Omega$) and of the bore (l). The presence of the term (l) comes from the Reynolds index. If viscous forces and variations

in heat
fluence
alone.

L. I.
has be
problem
science
of prog

In a
efficient
effectiv
overlo
cylind
the pap
per cul
The h
efficient
we kno
for the
conclu
out by
manifo
points
sion dr
essenti
these t

In g
effect o
perien
at anal
smaller
consum
trying
strippe
most o
make a
compre
show th

Perh
rate of
walls d
bore.
does al
horsep
indicat
walls w
a comp
differen
levels o
and tim
a pump
the ind
is a los
which
In this
pared i
stroke
a strok
whereas
edly is

Staff
Peoria,

in heat-transfer coefficient are considered to have a negligible influence, volumetric efficiency becomes a function of piston speed alone.

Discussion

L. E. JOHNSON.⁷ The thesis Professor Taylor has presented has been carefully developed in two ways: analytically as a problem involving mechanics, hydraulics, and empirically other sciences; and by testing and studying the actual performance of products that are essentially similar.

In any discussion of the effect of engine size on volumetric efficiency, the effect of the residual or unscavenged gases on the effectiveness of the succeeding induction stroke should not be overlooked. Because of lower heat transfer from gases to the cylinder wall with increase in cylinder bore, as pointed out in the paper, these residual gases are measurably higher in enthalpy per cubic inch of displacement than in the smaller-size cylinders. The hotter gases, undoubtedly, tend to reduce the volumetric efficiency of larger engines. However, as a matter of experience, we know that the volumetric efficiency is essentially identical for the same piston speed in cylinders of varying size. We may conclude that the heating effect of residual gases is balanced out by the reduced heat transfer to the incoming air in the manifolds of the larger bore engines, a factor which the author points out but adjudges insignificant. Thus, while the conclusion drawn by the author regarding volumetric efficiency is still essentially correct, for a full understanding of the phenomena these two balancing factors should not be overlooked.

In general, the experience of engine manufacturers with the effect of engine size on friction horsepower is in line with the experience cited in the paper and contrary to the conclusion arrived at analytically, that f_{mep} should remain constant. In general, smaller engines have higher f_{mep} and, as a result, higher fuel consumption at a given b_{mep} than do larger bore engines. In trying to determine where the extra losses occur, we have stripped our smaller engines part by part and have found that most of the difference results from greater heat losses which make available for recovery a smaller percentage of the work of compression. The indicator card may not be accurate enough to show this but motoring tests certainly do.

Perhaps the difference may be explained by the difference in rate of heat transfer per cubic inch of displacement to the cylinder walls during the compression and expansion strokes with varying bore. Presuming that greater heat transfer in the smaller engines does alter cylinder pressures, then the determination of friction horsepower by computing the difference between b_{hp} and card indicated horsepower would not reveal the loss to the cylinder walls whereas friction determined by motoring would. However, a comparison of very accurate indicator diagrams obtained on different sizes of similar engines should reveal lower pressure levels on the smaller bore engines, providing compression ratios and timing events are identical. This difference in friction is not a pumping loss in the normal sense, to be measured by analyzing the indicator diagram during the intake and exhaust stroke, but is a loss of a portion of the energy stored during compression, which cannot be returned to the crankshaft during expansion. In this regard it should be pointed out that the two engines compared in the paper, namely, the GM 671 and the large Sulzer two-stroke cycle Diesel are quite dissimilar in design. The former has a stroke to bore ratio of 1.18 and operates on fast-burning fuels, whereas the latter has a stroke to bore ratio of 1.8 and undoubtedly is operated on bunker C or other heavy fuel.

In general, bearing friction is a very small proportion of engine friction at normal operating temperatures. While the conclusion drawn is that bearing friction will be an identical fraction of output in similar engines, the inference that the large engine should be supplied with a heavier oil than the small engine may be in question. Certainly for equal unit friction, oil viscosity must be greater in the bearings of the larger engine. However, due to the longer leakage path across the bearing of the larger engine with the same average hydrodynamic pressure as in smaller engines, the larger bearing must run with greater clearance. This in itself results in a lower rate of shearing per unit volume of lubricant which in turn produces less bearing temperature rise within the engine. This results in less reduction in viscosity, requiring still more flow clearance and still less heating, sufficient to establish the required balance of pressure and viscosity. Thus automatically the oil is more viscous due to less heating in the bearing of the large engine to a degree which may eliminate completely any difference in viscosity grade of oil required.

Any manufacturer concerned with engine design for wide customer acceptance, is concerned with production and maintenance costs. Some analysis of the relation between the costs of similar engines of different sizes would be intensely interesting. This analysis would be complicated by the wide spread in unit costs for parts made in different quantities per year. This is particularly significant in analyzing the cost of wear. While the smaller part may have to be discarded in a shorter period of time due to less capacity for wear, the replacement cost is often so much less due to the combined factors of size of part and use of mass-production tooling, that replacement cost per horsepower-hour is competitive. The labor involved in installing the smaller part is also less as is also the cost of invested capital that is tied up during the life of the engine and during nonproductive time.

Perhaps the tendency of manufacturers to operate large-bore engines at lower b_{mep} is not because of the inherently poor capabilities of the larger cylinders, but rather because of the different nature of the applications to which the different engine sizes are applied. It is our experience with similar engines in similar service that the opposite is true, that the larger cylinder can operate at higher b_{mep} , providing that piston temperatures which tend to be higher are controlled.

On the other hand, the trend to lower piston speeds for large-bore engines has several practical explanations: Piston temperature drops at a greater rate through reduction in piston speed than it does from reduction in b_{mep} so that lowering speed is a more desirable method of controlling piston temperatures than is lowering of b_{mep} . In fact, it is possible, by lowering piston speed and increasing b_{mep} , to reduce piston temperatures without reducing horsepower output of a given-size cylinder. Another consideration is that the slower-burning heavy fuels have their widest use in the larger engines and are more completely burned at lower piston speeds.

An analysis of the effects of b_{mep} and piston speed on piston temperatures indicates that piston speed should not be held as a constant factor for similitude in rating similar engines. However, the product of piston speed and b_{mep} will be constant for equal service life of similar engines provided piston speed is adjusted downward with increase in cylinder bore sufficiently to maintain piston temperature constant.

The effect of Diesel-engine speed on ignition delay varies from one type of Diesel combustion system to another. In some engines the conclusion drawn in the paper that ignition delay in crank-angle degrees increases with speed may be true. However, ignition-delay time in precombustion-chamber engines tends to vary inversely with engine speed in similar engines, undoubtedly because of increased turbulence at increased speed. It is interesting in this regard to point out that supercharging reduces ignition

⁷ Staff Engineer, Research Department, Caterpillar Tractor Co., Peoria, Ill.

lag in Diesel engines to an insignificant interval, from a practical standpoint.

T. C. Tse.⁸ The author has attacked a basic problem with clarity, both by theoretical analysis and by experimental investigation. The paper contributes greatly toward making engine design more of a science than an art.

In connection with the curves of friction mep versus piston speed, Fig. 10 of the paper, the writer would like to ask whether or not the three similar engines were made with the same degree of surface finish, particularly on the pistons, piston rings, and cylinder walls.

To be exactly geometrically similar, of course, the engines should have different degrees of surface finish. If they were made with the same degree of finish, then, relatively speaking, the small engine would be rougher than the medium engine, and the medium engine rougher than the large engine. In this event the friction mep naturally would increase with decreasing size, in view of the fact that lubrication between the pistons and cylinder walls is relatively poor.

E. T. VINCENT.⁹ The paper under discussion is of some theoretical interest but seems to the writer to be of minor practical importance since no design criteria for any particular type of application is involved in the analysis. True, it is shown that, given the correct parameters, a number of similar engines have similar characteristics, but this does not mean that any one of such a series is of special application to any particular job. It is the engine least suited to its own particular application that has the least chance of success.

Again by employing data from a large number of engines the author draws a series of straight lines from which he infers that an average engine fulfills his theoretical approach. It is true that the average line, in some cases, does so indicate. However, as an example, if one has not formed an opinion as to how the line should be drawn, the automotive engines in Fig. 14 of the paper lie along a line with a slope of about 45 deg up toward the right much better than the approximately horizontal line drawn by the author.

Again comparison is made between engines of small bore and high speed, and large-bore slow-speed engines. Is not the rating of the latter deliberately held down in order to achieve long life?

The question of rating is peculiar to the application. The writer knows of a comparison, somewhat similar to the author's, made many years ago, of engines for a particular duty in which the assumed conditions were somewhat different. Not only was a specific requirement laid down, but a given space was prescribed at the same time. This was a submarine application where space is of vital importance. The result of these differing assumptions was a totally different answer to that of the author. In this case, for a given output and space limitation the largest cylinder that could be employed, coupled with the fewest number of cylinders was proved, in an equally satisfactory manner as that of the author's, to result in the smallest weight for the required maximum power output. It will be observed that these results are in direct opposition to those in the paper under discussion, illustrating the great effect the initial assumptions can have on the final results.

The writer would differ from the author's conclusion that the lowest fuel consumption for a spark-ignition engine is attained in the small cylinder. This is contrary to practice where it is well

known that a fairly large cylinder is required for good fuel consumption, e.g., the work at Studebaker during the last war to develop the most economical engine. This was not done in small bores.

In practice it is well known that high speeds are conducive to high frictional losses which is confirmed by the results observed from the M.I.T. similar engines. The mean-piston-speed comparison in Fig. 11 is not considered to cover a wide enough range to bring out any effective result, since comparison over about 400 to 700 fpm is out of range for the high-speed engine of, say, 300 to 2500 fpm.

While on the subject of frictional losses, the author states that the friction mep is, in general, such a small quantity compared with the imep. The writer would hardly consider 30 per cent of the imep a small quantity that could be neglected in the comparison; and that is the value to be expected in many high-speed small-bore engines which are unsupercharged.

Some figures of interest regarding the comparison in Table I of the paper are given as follows:

	Four-cycle locomotive engine	Two-cycle locomotive engine
Bhp per cylinder	50	65
Rpm	800	1400
Bmep	80	82
Weight bore ³	0.965	1.35

Both of the Diesel engines listed have considerable life, the first having operated on railroads for many millions of miles. Comparing these figures with the author's seems to indicate that the comparison in the paper was somewhat accidental.

The writer would like to suggest another reason for the similarity of the various engines in some of the different groups, viz., competition. The manufacturer cannot afford to produce an outstanding engine and sell it in a certain field against competition with a cheaper unit that will perform with a reasonable degree of satisfaction, the result being that each type of application has very similar engines built by different manufacturers. If the trade would stand for a better engine, there are many cases where great improvements can be made at some increase in cost, etc., and the result would be that most of this data would not plot near the author's lines and would tend to make curves in place of straight lines.

AUTHOR'S CLOSURE

In replying to Mr. Johnson, let us assume that the residual gases fill the clearance space at exhaust pressure when the inlet valve opens. Then the temperature of the residual gases has little direct effect on volumetric efficiency because the volume of residuals plus fresh mixture is not altered appreciably by the mixing process. The chief thermal effect on volumetric efficiency is due to heat transferred to the fresh mixture from the engine parts, and this would tend to be less with the larger cylinder, as stated in the paper. The author sees no effect which would tend to balance this one out as bore increases.

With regard to engine friction, indicator diagrams taken both before and since writing the paper show both light-spring and heavy-spring diagrams to be identical at the same piston speed. The differences in "friction" are, therefore, truly frictional and are not connected with heat losses from the gases. Further testing since the paper was written shows that the motoring friction mep is substantially the same at the same piston speed for all three engines, but that the difference between indicated and brake mep is substantially the "friction mep" shown in Fig. 10 of the paper. At present we are inclined to agree with Mr. Johnson that these differences in friction are characteristic of the differences in cylinder size, but the explanation is not yet ob-

⁸ Research Associate, The Pennsylvania State College, State College, Pa. Mem. ASME.

⁹ Professor, Mechanical Engineering, University of Michigan, Ann Arbor, Mich. Mem. ASME.

vious. One reason might be the higher wall temperature of the larger cylinder, which reduces oil viscosity below proportionality with bore.

With regard to bearing friction, the author does not agree that the larger bearing with proportionately larger clearance will have less temperature rise in the oil at the same value of $(\mu N/p)$. Bearing wall temperatures will be higher in the large bearing, due to the longer path for heat conduction from the bearing, so that at the same nominal value of $(\mu N/p)$ the actual value may be lower.

The author is in agreement with Mr. Johnson regarding the importance of production and maintenance costs, and hopes that more study will be given to the effect of cylinder size on such costs. With regard to the effect of cylinder size on engine ratings, Figs. 14 and 15 of the paper show that, on the average, both bmep and piston speed fall off with increasing bore at about the same rate. Apparently manufacturers, in general, have not appreciated the possibility of holding temperatures down by raising bmep and lowering piston speed as the bore increases.

In reply to Mr. Tsu, the surface finish in the three engines is approximately the same, and therefore is not geometrically similar. However, within the usual limits, surface finish has negligible effect on engine friction. The effect of surface finish on wear, however, may be quite important.

Referring to Professor Vincent's comments, the author's experience is that the relations expressed in this paper are of the greatest practical importance, especially in design, and that they have been unconsciously recognized and used for a long time. Of course each design must be made to meet its particular needs, but in recognizing the limitations common to all machines of a given type, an excellent basis is laid for the necessary modifications for a particular case.

With regard to the drawing of the curves in Figs. 14 and 15, it is obvious that the lines for the automotive group were drawn parallel to those indicated by groups which cover a much wider range of cylinder size.

In answer to Professor Vincent's third question, it is agreed that ratings for large cylinders tend to be held down for long life as well as for the other reasons stated in the paper. The author's only surprise is that the average bmep and piston speed of large engines are so little smaller than those of small engines of the same class. It might be expected that the average curves in Figs. 14 and 15 would fall off more rapidly with increasing bore than they actually do.

In the case of the submarine engine quoted as an example by Professor Vincent, the author would be interested to learn what the assumptions were and whether or not this installation is still current. Perhaps the assumption of direct propeller drive was used, in which case the rpm was set by the propeller, and the largest cylinder, which would give a reasonable piston speed, would be the logical choice.

With regard to the effect of cylinder size on fuel consumption of spark-ignition engines, the small cylinder has a lower fuel consumption only if the compression ratio is allowed to rise to hold the knock limit the same. The conclusion reached from the Studebaker tests was, if the author remembers correctly, that the large cylinder had no poorer fuel consumption than the small one. Since both cylinders had the same compression ratio, the larger one could be expected to have a slightly better fuel consumption

at the same piston speed, owing to smaller heat losses and friction losses.

With regard to Fig. 11 of the paper, it is to be regretted that the points for curve No. 2 cover such a small speed range. Professor Vincent can be assured, however, that the curve of friction mep versus piston speed of this engine would not flatten out, but would follow essentially the path of the other curve. He states: "High speeds are conducive to high friction losses." The author agrees with this statement entirely, but when cylinders of different sizes are being compared, the speed must be piston speed in order to make the statement accord with reality.

The author fails to see the relevance of the table of figures given by Professor Vincent. Table 1 of the paper refers to a pair of two-stroke loop-scavenged engines whereas his table compares a four-stroke and a two-stroke engine. No claim is made that similitude can be stretched to cover both types. However, although the Arden and Nordberg engines were chosen for comparison before their performance data were available, we could hardly expect such close agreement on weight/bore,² except by chance.

With regard to the last statement of Professor Vincent's comment, the author is in total disagreement. As engines are improved toward optimum design for a given service, they correlate better and better on the basis of rated mep and piston speed. This trend can easily be verified by plotting a graph, similar to that of Fig. 12, for the year 1910, or by leaving obsolescent engines out of Fig. 12 of the paper.

In conclusion, the theory of similitude is offered not as a panacea, but as a tool which can be of great assistance toward rationalization of the design process, which is all too empirical at best. Its validity, at least in many respects, is shown by the performance of the M.I.T. similar engines. Since commercial engines are not similar, they can be expected to follow the laws of similitude only in a general way with wide departures in individual cases. Such wide departures usually indicate either a mistake in rating or some unusual feature. If the departure is below the average there should be an immediate investigation by the producer, and if above the average, by his competitors. Used in this way, the theory, intelligently applied and with a full appreciation of its limitations, can result in significant improvements in the art of engine design.

Previous Work on Similitude. It should have been stated in the paper that the general theory of similitude in engines, and particularly the importance of piston speed as a limiting factor, is not new. A list of references on the subject follows; the paper is simply an attempt to explain and extend the theory and to compare its predictions with the behavior of actual engines.

"Design Limitations of Aircraft Engines," by E. S. Taylor, *Aero Digest*, vol. 26, January, 1935, pp. 22-27 and 45.

"Diesel Engine Design," by H. F. P. Purday, D. Van Nostrand Company, Inc., New York, N. Y. (Constable and Company, Ltd., London, England), 1937; revised, 1948. See especially chapt. 5.

"Ergebnisse von Versuchen mit geometrischen Gebauten Zylinder verschiedenen Grösse und Folgerungen für die Flugmotorenentwicklung," by W. Kamm, *Schriften der Deutschen Akademie der Luftfahrtforschung*, vol. 12, March 3, 1939, 33 pp.

"Dynamic Similitude in Internal Combustion Engines," by O. Lutz, NACA Technical Memorandum No. 978, May, 1941.

"Heat Transfer in Geometrically-Similar Cylinders," by P. Riekert and A. Held, NACA Technical Memorandum No. 977, May, 1941.

"Die Dynamik der Verbrennungskraft-Maschine," by H. Schrön, Julius Springer-Verlag, Vienna, Austria, 1942.

In

In the angle with diameter, compressible a wind tunnel on the surface numbers pressure small in range the drical P elements of particula that for the cylinder creases.

THE por app "direction ing veloci be used f and it is c fans, and Consider whose axi the cylind the press the illustrat

FIG. 1

with angl ference is A and C, pressure p

¹ Engine Francisco, ² Profess Lafayette, Contrib presented 27-December ENGINEER

NOTE: understood the Society

Influence of Compressibility on Cylindrical Pitot-Tube Measurements

By L. W. THRASHER¹ AND R. C. BINDER²

In the cylindrical Pitot tube, an opening at the critical angle with the flow gives the static pressure. For small-diameter tubes this critical angle is $39\frac{1}{4}$ deg for incompressible fluids in a certain range of turbulent flow. Using a wind tunnel, the distribution of pressure was measured on the surface of $\frac{1}{8}$ -in. and $\frac{3}{16}$ -in.-diam. cylinders at Mach numbers ranging from 0.13 to 0.87. The change in the pressure distribution on the surface of the cylinders was small in the range of Mach numbers up to 0.25. In this range the critical angle was constant, and a simple cylindrical Pitot tube would be convenient for direct measurements of static pressure. At the higher Mach numbers, particularly above 0.4, the critical angle increases above that for incompressible flow. The directional accuracy of the cylindrical Pitot increases as the Mach number increases.

THE measurement of velocity in a gas stream is of basic importance in fluid mechanics, both in research and industrial applications. The cylindrical Pitot tube, or the so-called "direction-finding" Pitot tube, is one device of several for measuring velocity. This tube has advantages in certain cases. It can be used for the measurement of both magnitude and direction, and it is convenient for various mountings, as in surveys in pumps, fans, and compressors.

Consider the two-dimensional flow around a circular cylinder whose axis is perpendicular to the stream some distance ahead of the cylinder. Let p_i represent the upstream static pressure, and p the pressure at some point on the surface of the cylinder. As illustrated in Fig. 1, the pressure difference ($p - p_i$) decreases

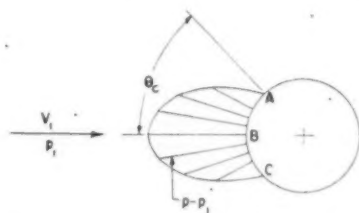


FIG. 1 PRESSURE DISTRIBUTION ON SURFACE OF CYLINDER

with angle on each side of the stagnation point B until the difference is zero at points A and C. If pressure taps were placed at A and C, the pressure transmitted to a gage would be the static pressure p_i . The critical angle θ_c is defined as the angle between

the stagnation point on the cylinder and the point on the cylinder at which the surface pressure is equal to the static pressure.

If the critical angle for a flow range is known, then for that range a Pitot tube can be constructed for measuring velocity in both magnitude and direction. Various constructions are possible. In one type, a hollow cylinder can be arranged with two holes; each hole leads to a separate compartment connected to a suitable gage. The angle between the holes is twice the critical angle, as the angle between A and C in Fig. 1. The tube in a stream of unknown direction can be rotated about its axis until the pressure at each hole is p_i . In this position the bisector of the angle between the holes gives the flow direction. If the tube is rotated about its axis so that an opening is in line with V_i , this opening will give the stagnation pressure.

The foregoing discussion indicates the use and importance of experimental data on the critical angle. Information is useful particularly for small-diameter tubes, because it is desirable to minimize disturbances of the flow.

PREVIOUS WORK

Various data for incompressible flow have been reported. For example, Dryden (1)³ was one of the first to present measurements of critical angle. A critical angle of $39\frac{1}{4}$ deg for $\frac{3}{16}$ -in. and $\frac{1}{8}$ -in.-diam tubes at a tube Reynolds number of 1.2×10^4 was the result of a large number of tests with air reported by Fechheimer (2). Binder and Knapp (3) used a critical angle of $39\frac{1}{4}$ deg on $\frac{3}{16}$ -in. and $\frac{1}{8}$ -in.-diam tubes. These tests were made in water at a Reynolds number approximately that of Fechheimer's tests.

There is a definite need for further experimental information on the cylindrical Pitot tube, particularly for compressible flow around small tubes. The following presentation gives the results of measurements designed to help fill the gap in present literature.

EXPERIMENTAL INVESTIGATION

Using a wind tunnel, the distribution of pressure was measured on the surface of $\frac{1}{8}$ -in. and $\frac{3}{16}$ -in.-diam cylinders at Mach num-

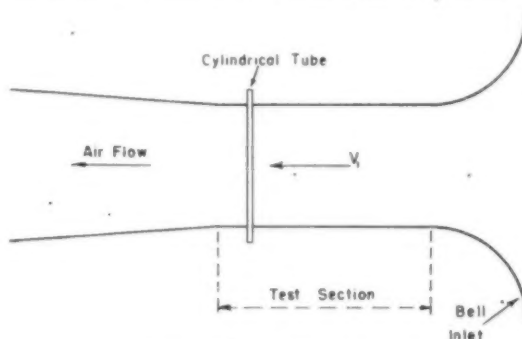


FIG. 2 DIAGRAMMATIC SKETCH OF WIND TUNNEL

bers ranging from 0.13 to 0.87. Fig. 2 shows a diagrammatic sketch of the tunnel. Atmospheric air entered the bell inlet and

³ Numbers in parentheses refer to the Bibliography at the end of the paper.

¹ Engineering Department, Arabian-American Oil Company, San Francisco, Calif. Jun. ASME.

² Professor of Mechanical Engineering, Purdue University, West Lafayette, Ind. Mem. ASME.

Contributed by the Research Committee on Fluid Meters and presented at the Annual Meeting, New York, N.Y., November 27-December 2, 1949, of THE AMERICAN SOCIETY OF MECHANICAL ENGINEERS.

NOTE: Statements and opinions advanced in papers are to be understood as individual expressions of their authors and not those of the Society. Paper No. 49-A-31.

passed through the test section. In the test section the area normal to the flow was a square 5 in. on each side. The diffuser at the end of the test section was connected to the inlet of a compressor. A screen and an egg-crate type of straightener were mounted at the bell inlet. The flow through the test section was parallel and uniform.

Each cylinder was placed in the test section as indicated in Fig. 2. Each cylinder was a seamless brass tube with a No. 80 (0.0135-in.) hole. Care was taken to have a radial hole, a hole free from burrs, and a smooth tube surface free from scratches. The pressure p at the tube hole was measured by water and mercury manometers. The reference static pressure p_1 was measured at tunnel-wall pressure taps, in a test plane normal to the flow and passing through the cylinder.

For the type of tunnel used, assume that there is no heat transfer through the tunnel walls. As the air expands from the atmosphere to the test plane, a tube placed at the test plane will then measure a stagnation pressure p_2 equal to the atmospheric pressure. Tests showed this assumption to be accurate.

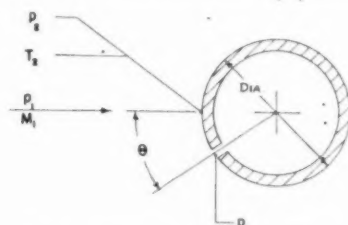


FIG. 3 NOTATION FOR MEASUREMENTS

Let M_1 represent the Mach number of the flow just upstream from the Pitot; $M_1 = V_1/c_1$, where c_1 is the acoustic velocity. Fig. 3 illustrates the notation. Let $k = c_p/c_v$, where c_p is the specific heat at constant pressure, and c_v is the specific heat at constant volume. In the test section, the energy equation for an isentropic process applied between the undisturbed flow and the stagnation point on the Pitot can be arranged in the form

$$\frac{p_2}{p_1} = \left[1 + \frac{(k-1)}{2} M_1^2 \right]^{\frac{k}{k-1}} \quad [1]$$

In Equation [1], p_2 and p_1 are absolute pressures. From the adiabatic relation between pressure and temperature, we can write

$$\frac{T_2}{T_1} = 1 + \left(\frac{k-1}{2} \right) M_1^2 \quad [2]$$

where T_2 is the absolute stagnation temperature, and T_1 is the absolute static temperature. The stagnation temperature was taken as the temperature of the atmospheric air. For an ideal gas, $c_1 = \sqrt{kgRT_1}$, where g is gravitational acceleration, and R is the gas constant. Thus from measurements of pressures and temperature, it was possible to determine M_1 , c_1 , and V_1 .

Fig. 4 shows typical pressure-distribution curves at low Mach numbers. The pressure difference ($p - p_1$) is plotted as a function of angle. The critical angle θ_c for the $1/8$ -in.-diam tube at both Mach numbers of 0.13 and 0.25 was $39\frac{1}{4}$ deg. Fig. 5 shows a plot of a dimensionless pressure ratio versus angle for a range of Mach numbers. At the low Mach numbers the curves are close together. As the Mach number is increased, the critical angle increases.

The solid line in Fig. 6 shows a plot of Mach number versus critical angle for a $1/8$ -in.-diam tube. For Mach numbers up to about 0.25, the critical angle is constant. For higher Mach numbers, the critical angle increases. For the Mach number range from 0.1 to 0.9, the corresponding tube Reynolds number varies from about 0.7×10^4 to 5.9×10^4 .

For incompressible frictionless flow, the critical angle is 30 deg. This result can be shown by a purely theoretical study. For real fluids the critical angle is always higher than 30 deg. In Fig. 6 the dashed curve marked "theory" was calculated from a theoretical analysis by Kaplan (4) for frictionless, subsonic flow. The experimental curve follows a trend similar to that of the theoretical up to a Mach number of about 0.6 (a constant difference of roughly 19 deg between the two curves).

Fig. 7 shows a plot of Mach number versus critical angle for a $3/16$ -in.-diam tube. The trend for the $3/16$ -in.-diam tube was

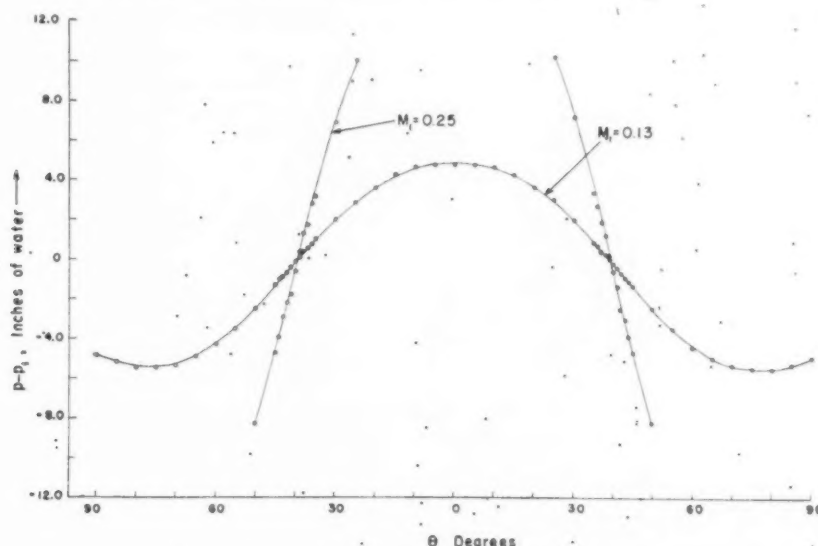


FIG. 4 PRESSURE DISTRIBUTION ON $1/8$ -IN.-DIAM CYLINDER

(The stagnation-point pressure p_2 was 29.62 in. of mercury abs. and the stagnation-point temperature 74 F.)

Fig. 6

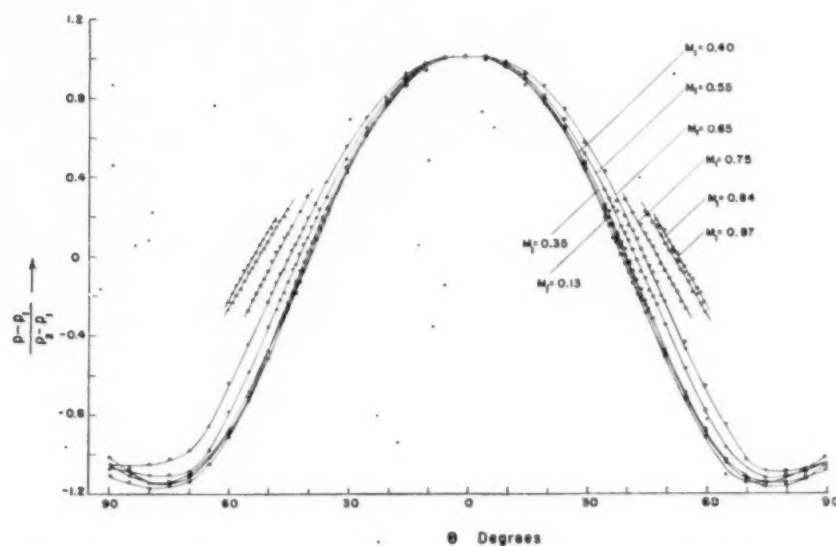


FIG. 5 PRESSURE DISTRIBUTION ON $1/8$ -IN-DIAM CYLINDER FOR DIFFERENT MACH NUMBERS

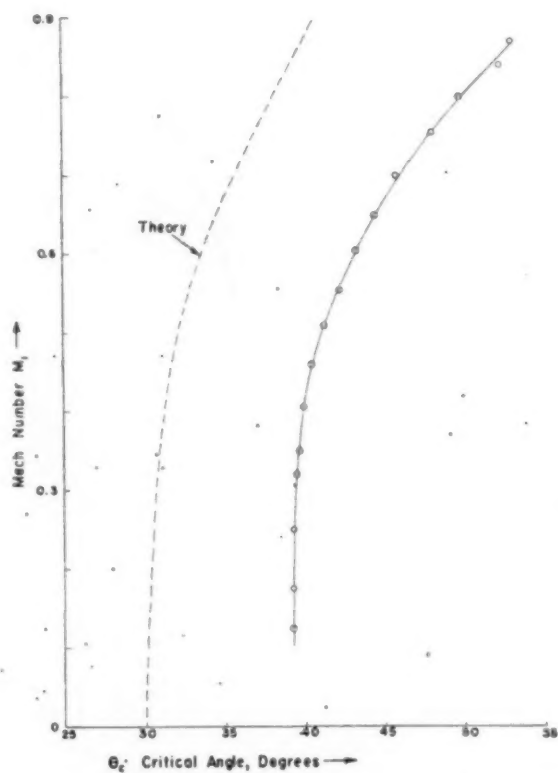


FIG. 6 PLOT OF MACH NUMBER VERSUS CRITICAL ANGLE FOR $1/8$ -IN-DIAM CYLINDER

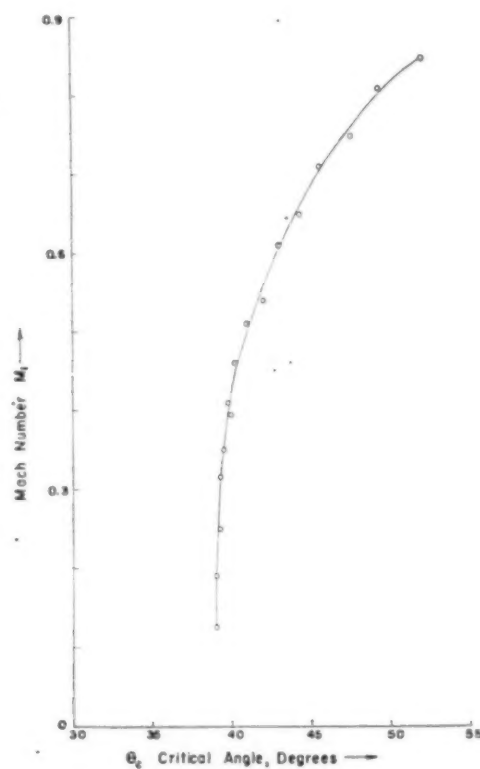


FIG. 7 PLOT OF MACH NUMBER VERSUS CRITICAL ANGLE FOR $3/16$ -IN-DIAM CYLINDER

the same as that for the $1/8$ -in.-diam tube. The critical angles for the $3/16$ -in. tube were slightly lower ($1/4$ deg lower in the Mach number range up to 0.25), than the critical angle for the $1/8$ -in. tube. This small difference may be due to a wall effect. For the Mach-number range from 0.1 to 0.9 for the $3/16$ -in.-diam tube, the corresponding tube Reynolds number varied from about 1.0×10^4 to 8.8×10^4 .

CONCLUSIONS

The change in the pressure distribution on the surface of the circular cylinders was small in the range of Mach numbers up to 0.25. In this range the critical angle was constant. A simple cylindrical Pitot tube in this range would be convenient for accurate, direct measurements of static pressure. At the higher Mach numbers, particularly above about 0.4, the critical angle increases above that for incompressible flow. At the higher Mach numbers, the static-pressure measurement is more indirect, and requires a calibration over a range of Mach number.

Typical plots, as in Fig. 4, show that the pressure gradient (pressure difference per degree) increases as the Mach number increases. Thus the directional accuracy of the cylindrical Pitot tube increases as the Mach number increases.

ACKNOWLEDGMENT

The authors are grateful to Dean A. A. Potter, Dean of Engineering, and Prof. H. L. Solberg, Head of the School of Mechanical Engineering, both of Purdue University. These gentlemen made possible the facilities for these tests. This paper includes material adapted from a master's thesis (5).

BIBLIOGRAPHY

- 1 "Air Forces on Circular Cylinders," by H. L. Dryden, Scientific Paper No. 394, U. S. Bureau of Standards, vol. 16, Sept. 4, 1920.
- 2 "Measurement of Static Pressure," by C. J. Fehheimer, Trans. ASME, vol. 48, 1926, p. 965.
- 3 "Experimental Determinations of the Flow Characteristics in the Vortices of Centrifugal Pumps," by R. C. Binder and R. T. Knapp, Trans. ASME, vol. 58, 1936, p. 649.
- 4 "Two-Dimensional Subsonic Compressible Flow Past Elliptic Cylinders," by C. Kaplan, NACA Technical Report No. 624, 1938.
- 5 "Influence of Compressibility on Cylindrical Pitot Tube Measurements," by L. W. Thrasher, MS thesis, Purdue University, February, 1949.

Discussion

L. J. HOOPER.⁴ Some work along the lines of that reported in this paper was done at the Alden Hydraulic Laboratory, in 1932. This test work was conducted just below the throat of a 36-in. \times 16-in. Venturi meter operating with water. Several factors were studied which had an influence on the registration of a cylindrical Pitot tube.

Fig. 8 of this discussion shows the results of tests to determine the effect of piezometer size on the angle of zero impact pressure. These tests were made at a constant Reynolds number of 69,000. On the curve sheet the piezometer size is presented as a ratio to the size of the rod in which it was installed. The actual rod diameter was $1/16$ in., and the piezometer diameters were varied successively from $1/16$ to $7/8$ in. It is seen that the angle for zero impact pressure varied from 37 to 56 deg for the range of piezometer sizes tested.

In Fig. 9 herewith the angle required to secure zero impact pressure was determined as a function of Reynolds number. It is seen that for the limited range of the tests (5 to 30 fps), the

⁴ Professor, Hydraulic Engineering, Worcester Polytechnic Institute, Worcester, Mass. Mem. ASME.

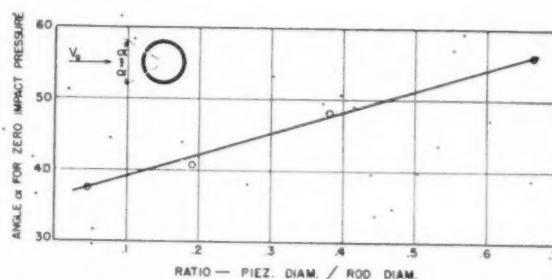


FIG. 8 EFFECT OF PIEZOMETER SIZE ON POSITION OF ZERO IMPACT PRESSURE ON A CYLINDRICAL TIP

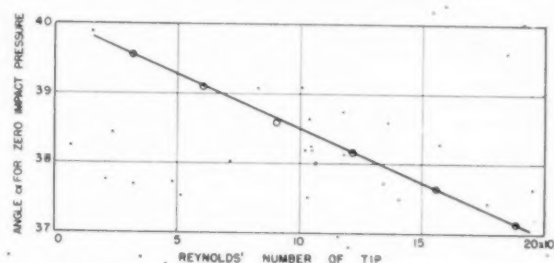


FIG. 9 EFFECT OF REYNOLDS' NUMBER ON POSITION OF ZERO IMPACT PRESSURE ON A CYLINDRICAL TIP

variation in the angle for zero impact pressure plotted as a straight line between 39.6 and 37.1 deg.

These tests indicate that other factors besides Mach number might have been affecting the results quoted in the paper. It would seem that tests in a water tunnel as well as in a wind tunnel would offer a very convenient way of separating the Reynolds and Mach number effects.

AUTHORS' CLOSURE

It is of interest and value to have available the data presented by Professor Hooper. Care should be exercised, however, in comparing the authors' data with those presented by Professor Hooper.

Note that in the authors' tests the tube diameters were $1/8$ in. and $3/16$ in., and the channel was 5×5 in. In Professor Hooper's tests the tube, $1/16$ in. diam, was a larger portion of the channel size than the tube in the authors' tests. Thus Professor Hooper's data may show a large variation due to a wall effect; this large effect was not present in the authors' tests.

Note also in the authors' tests that the diameter of the pressure hole was 0.0135 in., whereas in Professor Hooper's tests the hole size varied from $1/16$ to $7/8$ in. The variation of pressure over the surface of the cylinder is not linear. An opening of $1/2$ in. diam or $7/8$ in. diam subtends a relatively large angle. The data in Fig. 8 are open to question. There is a question as to interpretation. What is the meaning of the "angle for zero impact pressure?" The angle indicated in Fig. 8 may not be the actual angle at which the pressure is the static pressure of the stream.

In the authors' tests the wall effect was small. The small pressure opening covered a relatively small angle. The experimental trend, as indicated by Fig. 6, followed the general trend indicated by an analysis of the compressibility effects. We feel, therefore, that the authors' test data indicates clearly the influence of compressibility.

Determination of ASME Nozzle Coefficients for Variable Nozzle External Dimensions

By R. G. FOLSOM,¹ BERKELEY, CALIF.

Specifications for ASME long-radius nozzles do not include external dimensions. A series of tests have been made in an 8-in. pipe to determine the influence of the external nozzle diameter on pressures measured at several points downstream from the nozzle flange. The results are expressed in terms of per cent of the differential head measured at the standard corner tap locations.

INTRODUCTION

THE internal geometrical configuration and pressure-tap locations for long radius (ASME) flow nozzles are specified in reports of the ASME Special Research Committee on Fluid Meters.² Nozzle discharge coefficients are available for several standard pressure-tap locations. Since the nozzle external dimensions have not been specified, the change in discharge coefficient with different widths of the annulus or clearance between the outside contour of a nozzle and the pipe wall are unknown. The experimental investigations reported here are part of a study to determine the preferable location for the outlet pressure tap to be used with the standard long-radius flow nozzles.

EXPERIMENTAL EQUIPMENT

Four 8-in. pipe nozzles with approximate throat diameters of $7\frac{1}{8}$ in., $6\frac{1}{8}$ in., $5\frac{1}{8}$ in., and $5\frac{1}{16}$ in. were tested. The external surface of the nozzle was formed by a wire-mesh-reinforced "Hydrostone" sleeve cast around the nozzle and turned on a lathe to the desired constant external diameter. A clear synthetic resin was applied to the machined surface of the Hydrostone to prevent deterioration by water during the test period. Successive cuts to smaller external diameters and treatment with the resin were used to provide a series of finite widths of annulus between the nozzle outer surface and the pipe inner wall. Fig. 1 shows a test nozzle with the Hydrostone sleeve and ready for insertion into the test pipe.

The test station consisted of 60 diam of straight upstream pipe from a header to the test flange, followed by 30 diam of straight pipe to a 90-deg elbow. Centrifugal pumps driven by induction motors discharged into the header. A downstream control valve and about 20 diam of pipe discharging 1 ft above the elevation of the test section completed the circuit. The pipe was 8-in. nominal diam standard new galvanized iron pipe with standard extra-heavy flanges to hold the test nozzle. The upstream pipe was smooth to the edge of the thin circumferential slit between the end of the pipe and the upstream nozzle face. The flanges were machined to provide a special slit both upstream and downstream of the nozzle for corner-tap pressures. Measure-

ments of the pipe on eight diameters at three sections upstream from the nozzle showed the following:



FIG. 1 NOZZLE NO. 8.506.1 WITH CAST HYDROSTONE SLEEVE FINISHED TO MAXIMUM DIAMETER

Pipe end	$3\frac{1}{2}$ in. upstream	$10\frac{1}{2}$ in. upstream
8.066 in. $\left\{ \begin{array}{l} +0.026 \\ -0.049 \end{array} \right.$	8.069 in. $\left\{ \begin{array}{l} +0.074 \\ -0.056 \end{array} \right.$	8.077 in. $\left\{ \begin{array}{l} +0.123 \\ -0.085 \end{array} \right.$

Centering pins were provided in the flanges to place the nozzle concentric with the pipe.

Pressure taps were made at several points downstream and near the nozzle on the underside of the pipe. The longitudinal position of the taps is shown in Table 1. The circumferential spacing of the downstream holes was such that no one hole was directly in line downstream from another. The pressure connection was made by drilling a $\frac{3}{16}$ -in.-diam hole radially into the pipe and brazing a $\frac{1}{8}$ -in. standard coupling to the outside of the pipe.

TABLE 1 PRESSURE TAP LOCATIONS

Tap no.	Longitudinal location, in.	Type of pressure tap
2'	8.1 ^a	Hole ($\frac{3}{16}$ in. diam)
1'	0.0 ^a	Slit (width less than 0.15 in.)
1	0.0	Slit (width less than 0.15 in.)
2	2.2	Hole ($\frac{3}{16}$ in. diam)
3	3.2	Hole ($\frac{3}{16}$ in. diam)
4	4.2	Hole ($\frac{3}{16}$ in. diam)
5	5.2	Hole ($\frac{3}{16}$ in. diam)
6	6.2	Hole ($\frac{3}{16}$ in. diam)
7	7.2	Hole ($\frac{3}{16}$ in. diam)
8	8.2	Hole ($\frac{3}{16}$ in. diam)
9	9.2	Hole ($\frac{3}{16}$ in. diam)

^a Measured upstream from the upstream face of the nozzle; all other measurements downstream from the downstream face of the nozzle flange. Thickness of nozzle flange was $\frac{3}{8}$ in. and a metal-to-metal fit was obtained between the nozzle face and the holding flanges.

Plastic or rubber tubes were used as connecting lines from the couplings to the manometers. Since petcocks can be closed without displacement of fluid, all petcocks in the connecting lines were operated by a single lever linkage to function simultaneously and allow corresponding instantaneous observations to be made. Other petcocks were installed to bleed air from the high points in the upstream and downstream piping.

Air-water differential manometers (length of 8 ft) were used to measure pressure differences between taps 2' and 4 (approximate

¹ Professor and Chairman, Division of Mechanical Engineering, University of California. Mem. ASME.

² "Fluid Meters, Their Theory and Applications, Part 1," Reports of the ASME Special Research Committee, ASME, 1937.

Contributed by the Research Committee on Fluid Meters and presented at the Annual Meeting, New York, N. Y., November 27-December 2, 1949, of THE AMERICAN SOCIETY OF MECHANICAL ENGINEERS.

NOTE: Statements and opinions advanced in papers are to be understood as individual expressions of their authors and not those of the Society. Paper No. 49-A-110.

standard radius tap locations) and taps 1' and 1 (standard corner-tap locations). The remainder of the pressure taps were connected to vertical open-end 2-in.-diam plastic tubes with point gages mounted to determine the water elevation at the center of the tube. The point gages had a least count of 0.001 ft. Water and air temperatures were recorded, and the manometers were shielded from the sun.

TESTING PROCEDURES

Flow was established in the circuit, all air bled, and equilibrium conditions checked. The petcock linkage was closed and all manometer readings recorded. After opening the petcock linkage and checking equilibrium, the linkage was closed and the manometer readings recorded again. This procedure was repeated to obtain from four to six sets of readings. The manometer zero positions were checked before and after a series of runs.

Clearances of the annulus at the pressure taps were measured with the aid of a machinist micrometer before or after the series of tests on a specific nozzle external diameter. Since the pipe is out of round, the clearances varied. Typical values are shown in Table 2. Curves and data are reported in terms of the average clearances.

TABLE 2 CLEARANCE (ANNULUS) FOR NOZZLE NO. 8.506.1

Pressure tap no.	2	3	4	5	6	Average
Nominal clearance						
$1/16$ in.	0.084	0.075	0.060	0.033	0.056	0.062
$1/8$ in.	0.120	0.103	0.092	0.067	0.085	0.093
$3/16$ in.	0.145	0.132	0.121	0.098	0.126	0.124
$1/4$ in.	0.174	0.163	0.150	0.126	0.148	0.152
$5/16$ in.	0.295	0.291	0.275	0.245	0.272	0.276
$3/4$ in.	0.424	0.413	0.396	0.370	0.396	0.400

^a Clearance magnitudes in inches.

RESULTS

Following the general methods applied by Bean and Beitler,³ test results are expressed in terms of dimensionless ratios. The pressure loss coefficient is defined as

$$k_n = \frac{100\delta_n}{\Delta_c}$$

where δ_n is the pressure difference between a downstream pressure tap at position n and the downstream corner tap. Δ_c is the differential pressure across the corner taps. The positive value

³ "Some Results From Research on Flow Nozzles," by H. W. Bean and S. R. Beitler, Trans. ASME, vol. 60, 1938, pp. 235-244.

TABLE 3 SUMMARY OF EXPERIMENTAL RESULTS

Nozzle No. 8.506.1; Clearance = 0.062 in.

Δc	$Re \times 10^{-3}$	Δc	k_1	k_2	k_3	k_4	k_5	k_6	k_7	k_8	k_9
1.04	3.2	1.10	0.09	0	0.09	0.46	0.64	1.36	2.09	2.54	
2.50	4.9	2.67	0.04	0	0.08	0.45	0.71	1.31	2.21	2.66	
3.27	5.6	3.48	0.06	0.03	0.12	0.55	0.92	1.47	2.41	3.04	
4.04	6.2	4.30	0.05	0.04	0.14	0.58	1.05	1.53	2.63	3.14	
4.96	7.5	5.30	0.06	0.04	0.15	0.59	1.11	1.57	2.68	3.15	
6.87	8.1	7.33	0.06	0.07	0.19	0.61	1.25	1.62	2.93	3.18	
Average			0.06	0.03	0.13	0.54	0.95	1.48	2.49	2.95	

NOTE: Space did not permit publication of the complete table which consists of 26 sections similar to the one presented. The complete table is on file at ASME Headquarters, 29 West 39th Street, New York, N. Y., for reference.

TABLE 4 k_n FOR NORMAL NOZZLES (AS SUPPLIED)

Pressure tap no.	1	2	3	4	5	6	7	8	9
X/D (a)	0	0.27	0.40	0.52	0.64	0.77	0.89	1.02	1.14
X/D (b)	0.09	0.35	0.47	0.60	0.72	0.85	0.97	1.09	1.22
Nozzle									
8.506.1		0.09	0.17	0.25	0.36	0.60	0.74	1.25	1.59
8.562.1		0.06	0.15	0.20	0.35	0.59	0.72	1.38	1.81
8.615.1		0.06	0.08	0.15	0.24	0.54	0.63	1.44	2.11
8.715.1		0.03	0.03	0.10	0.42	0.63	1.16	2.44	0.74

(a) X/D expressed in terms of X measured from downstream face of flange.

(b) X/D expressed in terms of X measured from upstream face of flange.

of δ_n indicates a reduction in pressure at the downstream tap with respect to the corner tap. At Reynolds numbers greater than some minimum value, the pressure-loss coefficient should be independent of the flow rate. The experimentally determined values of k_n are given in Table 3. This table includes values of Δ_c and Δ_R (the differential pressure across the approximate radius taps), as well as the Reynolds number based on the throat-diameter conditions. Table 4 presents the average k_n -values for the normal nozzles (as supplied without sleeves). The pressure-tap locations are expressed in terms of pipe diameters X/D , where the distance X is measured from the upstream or the downstream face of the nozzle flange as indicated.

Fig. 2 presents the data of Table 4 in graphical form. The values of k_n have been plotted as positive in the downward direction of the ordinate due to the definition of k_n . The shape of the curve represents the relationship of static pressures measured at the wall with respect to the distance along the pipe axis. The curves in Fig. 2 show a decrease in static pressure as one passes downstream for the range of the experiments, except for the last point on the $\beta = 0.79$ curve ($\beta =$ ratio of nozzle throat diameter to pipe diameter). When the X/D -values are less than about 0.8, all nozzles show similar characteristics for k_n . Beyond the end of the nozzle and at the larger area ratios, appreciable differences in k_n exist over the region of the tests.

The range of values measured for k_n for nozzle No. 8.506.1 is indicated in Fig. 3. The area designated as "range of all normal nozzle tests" is bounded by the minimum and maximum magnitudes given in Table 3 under clearance of 1.080 in. (as supplied). Thus this area includes all test results over the limits of flow rates investigated for the normal nozzle. The other area in Fig. 3 is bounded by the minimum and maximum average values at a given tap for all other clearances and flow rates as tabulated

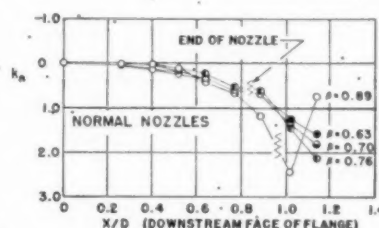


FIG. 2 COEFFICIENTS (k_n) FOR THE ALL NORMAL ASME NOZZLES "AS SUPPLIED"

in Table 3. Within the accuracy of the test results, it is impossible to discover a trend of k_n with clearance at taps before the end of the nozzle.

The average values of k_n given in Table 3 are plotted in Figs. 4, 5, and 6 for three nozzles, the results for a specific nozzle being plotted in a single figure. The general shape of the curves is similar to those in Fig. 2, with separate curves applicable to each

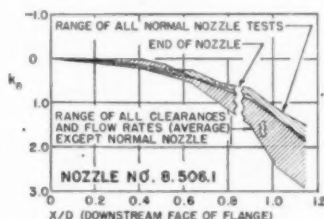


FIG. 3 VARIATION IN COEFFICIENTS (k_n) AS DETERMINED FOR THE TEST RANGE IN REYNOLDS NUMBERS

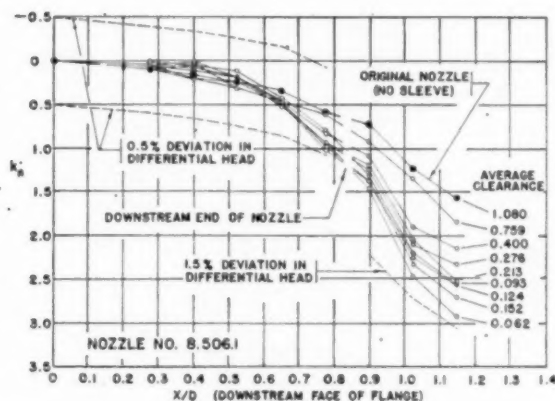


FIG. 4 SUMMARY OF TEST RESULTS ON NOZZLE NO. 8.506.1

sleeve clearance investigated. In general, consistent and definable changes with sleeve clearance appear only at points downstream from the end of the nozzle. The region of $\pm 1/2$ per cent deviation from the normal nozzle magnitudes is indicated for the tap locations before the end of the nozzle. Although this deviation is small (less than $1/2$ per cent for all points in Figs. 4 and 5), it increases as the diameter ratio increases. Fig. 6, for the largest nozzle, shows four points outside the $1/2$ per cent deviation limits; these points being at the smaller sleeve clearances. For points beyond the end of the nozzle, the deviation of points for smaller sleeve clearances reduces as the diameter ratio increases. In Figs. 4 and 5 all clearances show k_n magnitudes greater than those for the normal nozzles, a $1 1/2$ per cent range for Fig. 4, and a 1 per cent range for Fig. 5. In Fig. 6 all results except one point are within $1/2$ per cent of the normal nozzle characteristics.

The magnitudes of k_n indicate the per cent difference in heads due to measurements at different pressure taps. The corresponding difference in calculated rate of flow (if no change in nozzle coefficient is considered) is one half the per cent difference in head. The test results show that for any pressure-tap location upstream from the downstream end of the nozzle, an error of less than $\pm 1/4$ per cent in calculated flow rate results from changes in nozzle external diameters, as compared to results with the normal external contours of the standard test nozzles.

No experimental investigation was made of the change in nozzle coefficient for the corner taps when the nozzle external dimensions were changed.

Fig. 7 has been included to demonstrate the change in k -values of pressure for No. 4 as the clearance increases. Data from three nozzles are included. Since this tap is near the location of the standard downstream radius tap, the magnitudes of variables in Fig. 7 correspond approximately to conditions for radius taps.

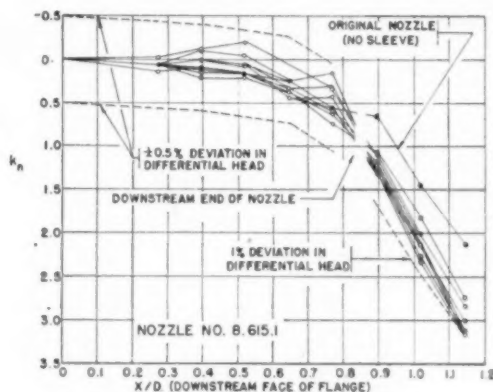


FIG. 5 SUMMARY OF TEST RESULTS ON NOZZLE NO. 8.615.1

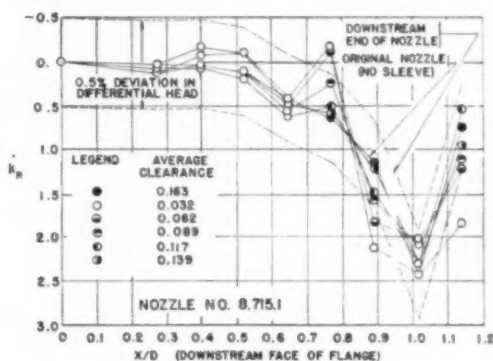


FIG. 6 SUMMARY OF TEST RESULTS ON NOZZLE NO. 8.715.1

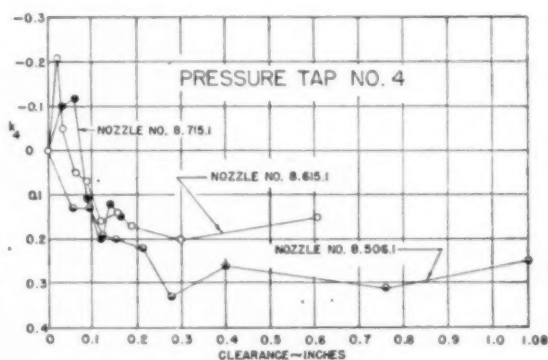


FIG. 7 CHANGE IN COEFFICIENT (k_n) AT NO. 4 PRESSURE TAP WITH CHANGE OF CLEARANCE IN ANNULUS

CONCLUSIONS

The discharge coefficients for standard ASME long-radius nozzles are almost independent of the clearance in the annulus between the pipe wall and the nozzle external diameter at all pressure-tap locations between the holding flange and the end of the nozzle. At pressure-tap points downstream from the end, appreciable changes in the coefficient with clearance exist with larger differences corresponding to smaller diameter ratios.

The tabular and graphical results are expressed in terms of per cent of the differential pressure across the corner taps. The maximum difference in heads (pressure at downstream corner

tap minus pressure at given downstream tap) at a given downstream tap between the nozzle with reduced clearance in the annulus and the normal nozzle (as supplied) was $1\frac{1}{2}$ per cent for the range of the conditions tested in this investigation.

ACKNOWLEDGMENTS

The author gratefully acknowledges the co-operation of the ASME Special Research Committee on Fluid Meters in making the standard nozzles available for testing, and the assistance of L. Gray, W. C. Shepherd, and K. J. Bermel in making the tests and reducing the data.

This
the m
respon
Experi
of ther
in. are
a rang
locitie
were c
therm
sented
fabrica
tempe
radiat

A

given
Due to
peratu
fields
of the
data o
wires.

One
respon
subjec
gram
tus, d
collect
compo
wire s
experi
atmos
F.

Bef
surve
Many
invest
corpo
the in

¹ B.
autho

² E.
Richl

³ In
versit

⁴ W.
versit

Unive

Co

Annu

of Th

No

unde

the S

The Response of Thermocouples to Rapid Gas-Temperature Changes¹

By M. W. CARBON,² H. J. KUTSCH,³ AND G. A. HAWKINS⁴

This paper presents practical data which were taken from the main results of a research program dealing with the response of thermocouples to changing gas temperatures. Experimental and theoretical data for the response time of thermocouples ranging in wire size from 0.01 to 0.0005 in. are presented. The experiments were performed over a range of temperatures from 70 F to 950 F, and for air velocities ranging from 0 to 125 fps. All of the experiments were carried out in such a way that the hot junction of the thermocouple was always cooled. An equation is presented for computing the response time for thermocouples fabricated from fine wires and subjected to sudden air-temperature changes. Heat transfer by conduction and radiation were negligible in the experiments performed.

INTRODUCTION

A THERMOCOUPLE placed in a gas stream, the temperature of which suddenly changes, will usually indicate a temperature different from that of the true value at any given time before the equilibrium condition has been attained. Due to the fact that the measurement of instantaneous gas-temperature changes is becoming increasingly important in the fields of heat transfer and thermodynamics, this particular part of the main investigation was undertaken to obtain and correlate data on the response time of thermocouples fabricated from fine wires.

One of the purposes of this investigation was to study the response of a thermocouple made from fine wires, by suddenly subjecting it to a low-temperature air stream. The research program consisted of the design and construction of suitable apparatus, development of a satisfactory welding technique, and the collection and analysis of experimental data. Thermocouples composed of platinum and platinum 10 per cent rhodium with wire sizes of 0.01, 0.002, 0.001, and 0.0005 in. were used in the experiments. All of the work was carried out at approximately atmospheric pressure. The temperature range was 70 F to 950 F.

Before undertaking the experimental part of the program, a survey of the literature available to the authors was undertaken. Many of the contributions and suggestions made by previous investigators, as reported in the technical literature, were incorporated in the program. Space limitation does not permit the inclusion of the many references studied, hence only a short

Bibliography⁵ is included. However, the authors are cognizant of the value of the work of previous investigators.

DESCRIPTION OF THE APPARATUS

Welding Apparatus. Before the actual experimental investigation could be undertaken, it was first necessary to develop suitable apparatus and a technique for welding the fine wires. Many different methods were tried before a satisfactory technique was developed. Finally a satisfactory method was obtained whereby the wires were electrically welded between graphite electrodes. The wires were joined by first crossing the ends and placing the intersection of the wires on the surface of a horizontal graphite rod. A second graphite rod was placed at right angles to the first and then rolled over the intersection of the two wires. A satisfactory weld was obtained when the rods were connected to a 3-volt d-c source. After welding, the excess material was removed carefully from the junction of the thermocouple.

Recently Hammel (1)⁵ described a butt-welding technique based on the use of a special jig. By means of this apparatus successfully butt-welded thermocouples have been constructed from wires as small as 0.003 in. diam. If the same apparatus may be used for fabricating thermocouples of even smaller diameter, this procedure may prove to be more effective than the method used by the authors.

Recording Apparatus. Since the object of this phase of the work was to study the response of thermocouples during very rapid temperature changes, it was not possible to use standard laboratory equipment. As a result a large amount of time was spent in constructing suitable recording apparatus.

The thermocouple voltage change was finally recorded by means of an apparatus consisting of an interrupter, alternating-voltage amplifier, oscilloscope, and a rotating-drum camera equipped with a modulator tube for placing timing marks on the photographic paper. Due to unstable operation of the direct-current amplifiers, it was finally decided to use a voltage interrupter in the circuit and a stable alternating-voltage amplifier. The rotating-drum camera was found to be very satisfactory for recording the trace on the oscilloscope. The apparatus was designed on the basis of the idea previously advanced by Champion and Brokaw (2).

Test Apparatus. Two devices were used to subject the thermocouples to a sudden decrease in temperature. The first apparatus consisted of a T-shaped section of aluminum mounted in such a way that it could be moved instantly a short distance in a horizontal direction. In the normal operating position a jet of high-temperature air passed through a slot in the aluminum section and flowed over the test thermocouple. Horizontal displacement of the section shut off the high-temperature air stream, and a second slot allowed a cold-air stream to pass over the thermocouple. Whenever the T-section was moved, the hot-air stream was suddenly replaced by a cold-air jet which subjected the thermocouple to an instantaneous air-temperature change.

The second method consisted of placing a thermocouple in a low-temperature air stream and raising the temperature of the

¹ Based on a PhD thesis, Purdue University, 1949, by one of the authors.²

² Engineer, Pile Technology Division, General Electric Company, Richland, Wash. Jun. ASME.

³ Instructor, School of Mechanical Engineering, Purdue University, Lafayette, Ind.

⁴ Westinghouse Research Professor of Heat Transfer, Purdue University; Visiting Professor, 1949-1950, Division of Engineering, University of California, Los Angeles, Calif. Mem. ASME.

Contributed by the Heat Transfer Division and presented at the Annual Meeting, New York, N. Y., November 27-December 2, 1949, of THE AMERICAN SOCIETY OF MECHANICAL ENGINEERS.

NOTE: Statements and opinions advanced in papers are to be understood as individual expressions of their authors and not those of the Society. Paper No. 49-A-148.

⁵ Numbers in parentheses refer to the Bibliography at the end of the paper.

wire by passing a current through it. After a desired temperature had been reached, the current was cut off, and the couple allowed to cool rapidly in the air stream.

In all tests the thermocouples were placed in a horizontal position, the wires extending in opposite directions from the junction. The horizontal thermocouple was mounted at right angles to the air stream. In this way the thermocouple resembled a very thin cylinder placed at right angles to the air flow.

EXPERIMENTAL PROCEDURES

Before undertaking the main part of the experimental program, calibration tests and preliminary calculations and experiments were conducted.

Experiments were conducted to ascertain as to whether or not conduction of heat along the lead wires of the thermocouples was of large enough magnitude to merit consideration. The results obtained indicated that the heat loss by conduction was negligible.

Calculations indicated that for the experimental range of the apparatus, the transfer of heat by radiation from the junction of the thermocouple to the surroundings was very small in comparison with the convective heat transfer; hence it could also be neglected.

Several experiments were carried out in an effort to determine the maximum air velocity which the couples could withstand without breaking. The results obtained indicated that the couples could be used for velocities up to 400 fps.

Considering only convective heat transfer to or from the couple, a heat balance was written and the final result written in a form similar to that used by Rhodes (3), Harper (4), Fiock (5), and Bailey (6), which follows

$$(t_i - t) = (t_i - t_a)(1 - e^{-\tau/\beta}) \quad [1]$$

$$\beta = \frac{\rho D c}{4h} \quad [2]$$

where

t_i = initial temperature as indicated by thermocouple before temperature change occurs

t = temperature indicated by thermocouple τ millisecond after change occurs

t_a = temperature of air stream after temperature change occurs

ρ = density of thermocouple material

c = specific heat of thermocouple material

h = coefficient of heat transfer

D = diameter of thermocouple wire

τ = time elapsed after temperature change occurs

If the time elapsed τ is selected equal to β , then Equation [1] reduces to the following

$$(t_i - t) = 0.632(t_i - t_a) \quad [3]$$

when $\tau = \beta$. This means that if τ is equal to β , then the temperature change $(t_i - t)$ is 63.2 per cent of the total change $(t_i - t_a)$.

Therefore it was decided to measure on the records obtained the time elapsed τ , when the temperature change had reached a value of 63.2 per cent of the total. The average experimental values obtained for τ are recorded in Table 1. The averages are based on 103 individual experiments.

In order to check the experimental values, a mean coefficient of heat transfer was considered during 63.2 per cent of the change and was computed by means of the following correlation given by McAdams (7)

$$\frac{hD}{k_f} = 0.32 + 0.43 \left(\frac{DV\rho}{\mu_f} \right)^{0.53} \quad [4]$$

In order to determine the values for the thermal conductivity, viscosity, and density of the air for use in Equation [4], a mean temperature was used as found by use of the following equation

TABLE 1 EXPERIMENTAL AND COMPUTED DATA

Thermocouple number	Diam of wire, in.	Initial temp of thermocouple t_i , deg F	Air temp, t_a , deg F	Average air velocity, fps	Average for 63.2 per cent response time obtained from photographic records, millisecond	Calculated Reynolds number NRe	Calculated time for 63.2 per cent response, millisecond
701	0.0005	776	84	24.5	3.6	3.18	3.4
701		794	83	47.1	2.8	6.05	2.6
711		665	87	22.5	4.5	3.17	3.5
711		677	86	49.4	3.5	6.92	2.6
711		667	83	106.8	2.4	15.15	1.9
700	0.001	834	99	49.4	8.0	12.04	7.7
700		840	103	28.8	11.0	6.93	9.7
701		867	104	28.9	12.7	6.83	9.6
701		852	102	48.4	10.8	11.72	7.7
703		814	91	29.2	11.5	7.29	9.6
703		821	90	50.7	9.7	12.62	7.6
703		795	88	118.0	6.5	30.19	5.2
704		580	74	27.3	9.2	8.43	9.9
704		580	70	48.9	7.9	15.22	7.7
500	0.002	908	104	18.2	34.3	8.32	34.8
500		916	100	27.9	31.1	12.77	29.1
500		915	96	50.4	24.9	23.24	22.4
500		910	93	73.8	22.3	34.32	18.7
500		913	91	98.3	20.1	45.70	16.3
500		902	90	124.8	15.2	58.90	14.6
501		853	99	11.1	34.9	5.32	42.5
501		860	93	23.6	31.5	11.40	31.4
501		870	90	49.0	24.8	23.55	22.5
501		886	89	98.8	18.9	47.00	16.3
502		803	104	11.9	35.0	5.93	41.4
502		807	98	26.2	27.2	13.02	29.9
502		818	97	48.9	21.5	24.23	22.6
502		843	92	102.0	16.0	49.95	16.1
542		429	64	25.4	26.4	18.20	30.2
542		372	64	48.9	21.1	37.00	22.3
501		531	80	25.5	28.8	16.07	30.8
501		520	80	48.9	22.3	31.50	22.5
543		417	62	23.7	27.5	17.24	30.9
543		574	84	24.1	26.1	14.73	30.8
542		815	81	21.6	31.4	10.97	32.4
542		830	80	48.9	24.0	24.53	22.6
705	0.01	570	66	54.5	237.0	171.8	246.0
705		574	63	107.4	180.0	340.1	178.0

$$t_f = \frac{\frac{t_i + t}{2} + t_a}{2} \dots \dots \dots [5]$$

The symbols have the same significance as previously mentioned.

In the development of Equation [4], the Prandtl number was considered constant, which is a satisfactory assumption for the temperature range used in this investigation.

Using the value for h , together with the density, specific heat, and diameter, the theoretical values for τ were determined for 63.2 per cent of the total time by means of Expression [2] since τ is equal to β under the condition specified.

RESULTS AND CONCLUSIONS

The values for the theoretical response for various sizes of couples for the range of temperatures and velocities covered in the experiments are shown by the solid lines in Figs. 1 and 2. The points represent the experimental values obtained. From the results it may be concluded that the relations developed may be used to predict the time required for a thermocouple to cool to a value of 63.2 per cent of the total impressed temperature difference for the temperature and air-velocity ranges covered during the investigation. The air velocity was varied from approximately 0 fps to 125 fps. The temperature range was 70 F to 950 F.

Although the experimental data have not been evaluated for other response times, it is felt that other values for the response interval may be calculated by using different relationships for τ and β , such as the following:

Relation between τ and β	Value for ratio $\frac{t_i - t}{t_i - t_a}$
$\tau = \beta$	0.632
$\tau = 2\beta$	0.865
$\tau = 3\beta$	0.95

or by evaluating β by use of Equations [2] and [4] and solving for τ in Equation [1].

ACKNOWLEDGMENT

The authors wish to express thanks to E. I. duPont de Nemours and Company for financial assistance and encouragement during the course of the main project. One of the authors² held the duPont Company Postgraduate Fellowship in Mechanical Engineering at Purdue University for the 1948-1949 academic year. The authors wish to thank Dr. Max Jakob for valuable suggestions and advice given during the course of the investigation.

BIBLIOGRAPHY

- 1 "Method for the Preparation of Butt-Welded Thermocouples Using 3-Mil Diameter Wire," by E. F. Hammel, Documents Distribution Subsection, Publication Section, Technical Information Branch, AEC, P. O. Box E, Oak Ridge, Tenn., Reference MDDC 776, LADC 393.
- 2 "A High-Speed Multiple-Temperature Recorder," by A. R. Champion and G. K. Brokaw, Temperature—Its Measurement and Control in Science and Industry, American Institute of Physics, Reinhold Publishing Corporation, New York, N. Y., 1941.
- 3 "Industrial Instruments for Measurement and Control," by T. J. Rhodes, McGraw-Hill Book Co., Inc., New York, N. Y., 1941.
- 4 "Thermometric Lag," by D. H. Harper, 3rd, *Bulletin of the Bureau of Standards*, vol. 8, 1912, p. 664.
- 5 "Development of Thermocouple Pyrometers for Gas Turbines," by E. F. Fiock and associates, National Bureau of Standards, Reference III-2/ITPU (3225), Washington, D. C.
- 6 "The Response of Thermocouples," by N. P. Bailey, *Mechanical Engineering*, vol. 53, 1931, pp. 797-804.
- 7 "Heat Transmission," by W. H. McAdams, McGraw-Hill Book Co., Inc., New York, N. Y., second edition, 1942, p. 220, Equation 4.
- 8 "The Platinum Metals and Their Alloys," edited by E. M. Wise, The International Nickel Company, Inc., New York, N. Y.

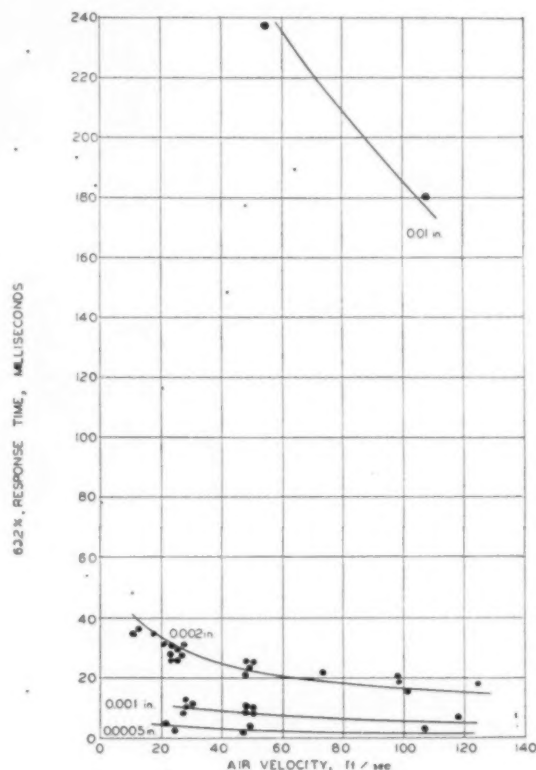


FIG. 1 RESPONSE TIME VERSUS AIR VELOCITY

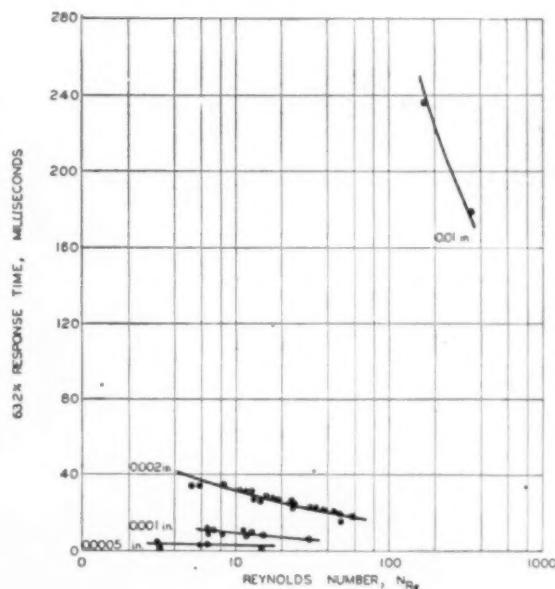


FIG. 2 RESPONSE TIME VERSUS REYNOLDS NUMBER

C

Ch
have
norm
tests
cusse
equa
press
turb
tests
on vi
press
sume
impo

W

"large
cussio
larger
line g
nomin
larger
steel,
impro
increa
rather
rates
accura
portan
of new
presen

In h
that th
applic
familia

In this
expres
feet.
in the
termin
This
be exp

¹ Sta
Cont
Petrole
Okla., C
ENGINE
Not
underst
the Soc

Crude-Oil Flow Characteristics Experienced in Large-Diameter Lines

By L. E. ANDERSON,¹ TULSA, OKLA.

Characteristics of crude-oil flow in large-diameter lines have been investigated by gathering data on lines under normal operating conditions. A description of these tests, and a summary of the results obtained are discussed in this paper. From these tests, an exponential equation has been derived to determine capacity or pressure drop for all trunk lines pumping crude oil in the turbulent-flow region. In connection with these flow tests, an investigation was made into the effect of pressure on viscosity in the range of normal pipe-line operating pressures. This effect, which in the past has been assumed to be a negligible one, is shown to be of definite importance.

WITH the advent of larger-size lines for crude-oil transportation, the question has arisen as to the flow characteristics encountered in these larger lines. The term "large diameter" is of course a comparative one, but in this discussion will refer to lines with outside diameter of 16 in. and larger, as prior to the last few years there were few crude-oil pipe-line systems of any appreciable length composed of lines with a nominal diameter greater than 12 in. The increased laying of larger lines has paralleled the development of higher-strength steel, permitting higher station operating pressures, together with improved methods of laying line. A further parallel has been the increased use of technical data for the design of new systems rather than rules of thumb formerly used. Since the pumping rates through these larger lines are much greater, the need for an accurate knowledge of available throughput is gaining in importance so that the optimum-size line will be used in the design of new facilities, and the length of loops required to enlarge on present facilities can be determined accurately.

BASIC HYDRAULIC FORMULAS

In hydraulic calculations involving crude oil, it has been found that the basic formula as introduced by Darcy in 1857, is the most applicable of the various flow formulas. This equation is a familiar one to all engineers and in its basic form is

$$h_f = \frac{f l v^2}{2gd}$$

In this form the equation is solvable if the various quantities are expressed in foot-pound-second units, giving the value of h_f in feet. This form is rather cumbersome, however, as units required in the foregoing equation are not commonly used in pipe-line terminology.

This equation, after conversion to a more practical form, can be expressed as

¹ Stanolind Pipe Line Company. Jun. ASME.

Contributed by the Petroleum Division and presented at the Petroleum Mechanical Engineering Conference, Oklahoma City, Okla., October 2-5, 1949, of THE AMERICAN SOCIETY OF MECHANICAL ENGINEERS.

NOTE: Statements and opinions advanced in papers are to be understood as individual expressions of their authors and not those of the Society. Paper No. 49-PET-13.

$$P = \frac{34.87 f B^2 s}{D^5} \dots \dots \dots [1]$$

where each of the terms has the following significance:

- P = pressure drop, psi per mile.
- B = line throughput, bbl per hr
- s = specific gravity of oil pumped
- D = internal diameter, in.
- f = friction factor

In Equation [1] it is possible to measure physically all quantities, with the exception of the dimensionless friction factor which must be determined experimentally.

The customary means of expressing f is to plot its value against the corresponding value of Reynolds number R , which is in existence in the line at that particular time. It is not necessary to dwell at length on this number as it also is familiar to all engineers. In its basic form it is expressed as

$$R = \frac{dv\rho}{\mu} \dots \dots \dots [2]$$

where

- d = diameter of pipe
- v = velocity of fluid
- ρ = density of fluid
- μ = absolute viscosity

Any consistent set of units can be used such that the value of R will be dimensionless. This equation also can be expressed in a form more readily used and remembered by engineers. This converted form is

$$R = \frac{2214 \times B}{D \times \nu} \dots \dots \dots [3]$$

where B and D have the same significance as previously given, and ν is the kinematic viscosity of the oil moving through the line, expressed in centistokes. To clarify the formula further, the relationship between centistokes and Saybolt Universal seconds (SUS), a more common way of expressing viscosity, can be set forth by a simple equation

$$\text{Centistokes} = 0.22t - \frac{180}{t} \dots \dots \dots [4]$$

where t represents Saybolt Universal seconds.

A basic relationship between f and R has been established for streamline flow and verified by many experimenters so will be valid for the lines here investigated. This relationship can be expressed by the equation $f = 64/R$ which when substituted in Equation [1] gives

$$P = \frac{1.008 B \mu}{D^4} \dots \dots \dots [5]$$

where μ is the absolute viscosity in centipoises.

RESEARCH ON FLUID FLOW

Experimental work done by Stanton and Pannell on fluid flow through pipes embraced a wide set of flow conditions and has been recognized as one of the most authoritative pieces of work on this subject. Their experiments were carried out using air and water moving at different rates through smooth drawn brass pipe varying in diameter from 0.361 cm to 2.855 cm. The curve propounded by these authors is shown in Fig. 1, plotted in double logarithmic form. This shows the two distinct regions of flow, streamline and turbulent.

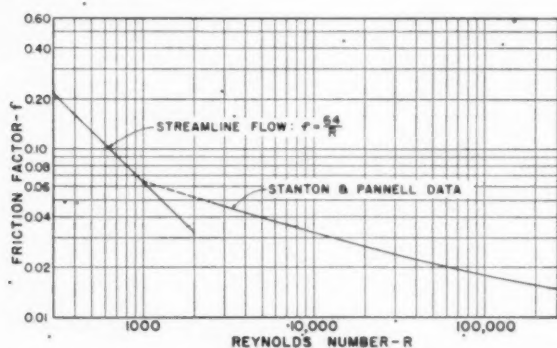


FIG. 1 PLOT OF FRICTION FACTOR VERSUS REYNOLDS NUMBER SHOWING BASIC EQUATION FOR STREAMLINE FLOW AND STANTON AND PANNELL DATA FOR TURBULENT FLOW

It is the purpose here to describe tests run recently for the evaluation of the friction factor f in large-diameter lines in the turbulent-flow region and to express the results obtained from these tests. The intent in carrying out this investigation was to secure data that would be of direct use in hydraulic calculations on commercial pipe lines rather than procuring data that would be of academic interest only. Numerous papers such as that of Stanton and Pannell have been written on the value of f , as determined by laboratory experimentation, using various fluids such as water and air in small-diameter lines. Our purpose was to determine which data, if any, obtained from these laboratory experiments would be confirmed by results secured from large-diameter lines moving crude oil. Various authors concur with the reasoning that their results obtained from smaller lines may not hold true for larger lines.

To get information such as was desired, sections of line in our system were utilized as test sections, thus providing the best large-scale laboratory possible. The friction factor was determined in each of a series of test runs on each section of line. This was done by using Equation [1], measuring the four quantities, P , s , B , and D , and solving for the unknown friction factor.

To measure the pressure drop P , recording pressure gages were normally used. One was installed at each end of the test section of line and calibrated in place by means of a dead-weight tester. For the measurement of specific gravity, periodic samples were taken from the line, and the gravity determined by means of a hydrometer. The gravities of the crude in the lines tested varied from 32 deg API to 44 deg API. For any one test, the gravity remained essentially constant. An accurate measurement of the volume of oil pumped through the line was necessary in order to obtain the pumping rate, B . This was done by pumping decrease out of one tank so that the actual volume was determined from hourly tank gages. The internal diameter used was the nominal internal diameter of the line with no allowance being made for manufacturing tolerances. Just prior to the running of a test, a pig-type scraper was run through the line to remove any wall

deposits which would have the effect of reducing the internal diameter, which in turn would give a higher value for the calculated friction factor.

To compute the value of R to correlate with the value of f , it is necessary to determine the viscosity of the oil being pumped, this value then being used in Equation [3]. The ordinary method of measuring viscosity is by use of a commercial viscosimeter, such as the Saybolt type of instrument, which measures the time of efflux of a prescribed amount of liquid through a calibrated orifice.

These tests run at atmospheric pressure, however, do not give the true viscosity of the oil while moving through the line under pressure. It was known that viscosity increased with pressure, but a perusal of available literature on the subject yielded nothing that was specific enough to be applicable for our use. The effect of pressure on viscosity is gaining in importance due to the trend toward higher operating pressures.

To obtain information on conditions existent in our system, tests were run to determine how viscosity varied with pressures normally encountered in pipe-line operation. Fig. 2 shows the results obtained from two crudes analyzed in this manner by means of a falling-ball type of viscosimeter. The East Central Texas crude is one of the lightest common stream crudes handled in our system, and the Wyoming crude is the heaviest common stream crude moved through our lines. An examination of Fig. 2 shows that the relationship between pressure and viscosity is apparently a straight-line function. At higher temperatures, the

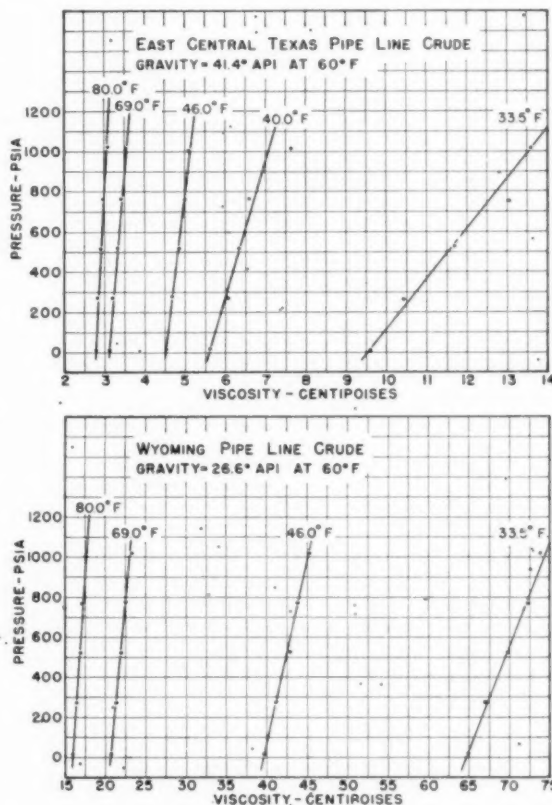


FIG. 2 EFFECT OF PRESSURE ON VISCOSITY OF TWO CRUDE OILS IN RANGES OF PRESSURE AND TEMPERATURE NORMALLY ENCOUNTERED IN ACTUAL OPERATION

per cent increase in pressure is the same for the Wyoming crude. The increase in viscosity at higher pressures, it is shown, is not as great as there may be at lower pressures.

It is obvious that the apparent viscosity of the oil is a function of pressure and temperature. The apparent viscosity of the oil is a function of pressure and temperature. The apparent viscosity of the oil is a function of pressure and temperature.

Although the apparent viscosity of the oil is a function of pressure and temperature, the apparent viscosity of the oil is a function of pressure and temperature. The apparent viscosity of the oil is a function of pressure and temperature.

As a crude oil is pumped through a pipe line, the apparent viscosity of the oil is a function of pressure and temperature. The apparent viscosity of the oil is a function of pressure and temperature.

Most crude oils are characterized by a high apparent viscosity at low temperatures and a low apparent viscosity at high temperatures. The apparent viscosity of the oil is a function of pressure and temperature.

per cent increase in absolute viscosity per 1000 psi is about the same for the two crudes, but at lower temperatures the effect of pressure is much greater on the lighter crude than on the heavier Wyoming crude. Also, for either of the particular crudes, the increase in viscosity due to increased pressure is a greater percentage at lower temperatures. From the trend indicated on the curves, it appears that if the temperature is increased sufficiently, there may be a point at which pressure will have no effect on viscosity. However, this supposition would have to be proved or disproved by actual tests.

VISCOSITY IN FLOW CALCULATIONS

It is obvious now that using viscosity determined at atmospheric pressure by means of commercial viscosimeters will give erroneous values. With this added information, our problem now is to seek to utilize this information in a simple manner. As realized from past experimentation and evidenced by this investigation, the science of turbulent flow is not an exact one such as is experienced under streamline-flow conditions. Instead, the basic equation includes the empirical term f which is dependent on many variables and which will itself vary over a certain range for the same type of pipe. Because of the inability of measuring f quantitatively, it is proposed to make its value dependent on one more variable—the change in viscosity due to pressure. Since the operating pressures of most trunk-line stations do not vary widely, this effect will be a fairly consistent one, so it is proposed not to use a viscosity correction factor, but instead to plot the values of f determined against the apparent value of R . The apparent value of R will be the value of this term based on the viscosity determined at atmospheric pressure.

Although the effect of viscosity change in turbulent flow is an indirect one, by reference to Equation [5] it is seen that in streamline flow, the pressure drop is directly proportional to the absolute viscosity. Therefore, using the correct viscosity is of major importance. Normally, crude-oil flow is in the turbulent region, but there are cases where streamline flow is encountered such as in winter months in lines moving the heavy Wyoming oil shown in Fig. 2. Since pressure versus viscosity gives a straight line, the viscosity determined at atmospheric pressure can be corrected by using a correction factor based on the average line pressure. It is difficult to determine the average line pressure exactly because of ground profiles being very irregular, but, for most cases, the average line pressure in a section of line can be assumed to be one-half the station discharge pressure. No investigation has been made into streamline flow in actual operations to determine how closely theoretical conditions will be approximated.

As a counteraction to the effect of pressure on viscosity, some crudes are of a thixotropic nature, i.e., their apparent viscosity decreases as the shear rate increases. The shear rate in any one size line would increase as the pumping rate increases. This characteristic is noticed especially in high-paraffin-base crudes, such as those produced in southwestern Wyoming. On one pipeline system operating in this area, normal operating pressures as high as 2000 psi are encountered, thus resulting in a large throughput and a corresponding high shear rate. In expressing the viscosities of these crudes, viscosities determined by an efflux-type viscosimeter will give a false indication of the viscosity of the oil moving through the line. Instead, a viscosity-temperature curve should be used showing apparent viscosities determined from a study of actual operations.

Most crude oils are of the Newtonian type, however, as their apparent viscosity at any certain temperature is constant regardless of shear rate. For this type of crude, a normal temperature-viscosity curve, as determined by means of an efflux viscosimeter, can be used for determining uncorrected line viscosities.

RESULTS OF TESTS

The section of the Stanton and Pannell f versus R curve between Reynolds numbers of 30,000 and 240,000 has been reproduced in Fig. 3, and the author's experimentally determined values for f have been plotted against the apparent R . As shown on the graph, these points were obtained from tests run on lines of 16 in., 20 in., and 30 in. diam. An examination of the graph shows that the author's points determined from the 16-in. lines approximate the Stanton and Pannell curve very closely. The average of the points from the 20-in. line fall slightly above the curve, and the three points representing the 30-in. line are still higher above the curve.

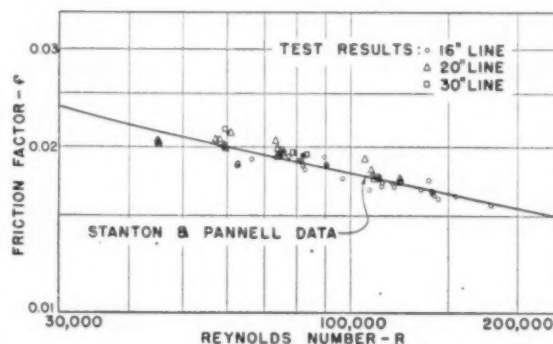


FIG. 3 PLOT OF EXPERIMENTAL POINTS DETERMINED FROM CRUDE-OIL LINES IN ACTUAL OPERATION, AS COMPARED TO DATA OF STANTON AND PANNELL

The values of f from the 16-in. and 20-in.-diam lines were determined in all cases from sections of trunk line many miles in length, which in most cases included very few valves and no junctions, making the values representative of straight pipe. Much of the 16-in. line has been in West Texas sour-crude service for a period of over 5 years. The 20-in. sections tested have been used for both sour and sweet crude, and have been in service for from 1 to 2 years.

The values shown for the 30-in.-diam line were obtained from a section of tank line approximately one-half mile in length. This line was just recently laid and is used for sour West Texas crude. Because of its short length and corresponding small pressure drop, it was necessary to measure the pressure differential by means of a manometer installed at each end of the line. Due to insufficient data on the 30-in. line, no definite conclusions can be reached, but it is felt that in trunk-line service, the friction factor for this size line will be somewhat lower than shown here. The 30-in. tank line tested was $1/8$ -in. wall pipe and was laid above ground so was probably not perfectly round, as the pressure in the line did not exceed 15 psi. In addition, the test section included an expansion joint which would have the effect of increasing the pressure drop slightly, resulting in a higher apparent friction factor.

Moody² has drawn a family of friction-factor curves based upon different relative roughnesses. The lowest curve in this family is for smooth pipe and approximates the Stanton and Pannell curve. The relative roughness, ϵ/D , as given by Moody for commercial steel pipe in the range of sizes here discussed, is low enough that it can be considered as smooth pipe in the range of Reynolds numbers normally encountered.

² "Friction Factors for Pipe Flow," by L. F. Moody, Trans. ASME, vol. 66, 1944, pp. 671-684.

Drew, Koo, and McAdams¹ made a survey of work done on determination of the friction factor to ascertain if Lees' equation, which was based upon the data of Stanton and Pannell, gave values for f that were representative of smooth pipe. Their investigation showed that the majority of experimental work, up to a Reynolds number of 500,000, validated Lees' equation. These authors also studied work done on commercial iron and steel pipe and, as a result of this study, presented a curve for f somewhat higher than that for smooth pipes. The work they reviewed was all carried out on small-diameter pipe, and they state that smaller-size pipes generally give higher values for f .

Other experimental work has been done by Heltzel⁴ at lower Reynolds numbers on lines of 6 to 12 in. diam in crude-oil service, and the validity of the Stanton and Pannell curve for this use has been verified by him. It is believed the test data accumulated here are sufficient confirmation of this curve to warrant using it for large-diameter lines. Although these tests did not cover the entire range of R encountered in these lines, the range covered includes the majority of normal flow conditions.

DETERMINING TRUNK-LINE CAPACITY

Because the Stanton and Pannell curve has thus been substantiated for a wide range of pipe sizes, an expedient equation based on this curve will be developed for determining directly trunk-line capacity. The use of Equation [1] for determining line capacity is rather laborious, as it is necessary to use a cut-and-try method for determining the value of f to use in the equation. The range of R normally encountered in our crude-oil lines does not exceed 200,000 with the majority of flow conditions giving a value of R less than 100,000.

Our problem now is to develop a relationship between f and R which will give fairly consistent results over the entire range of turbulent-flow conditions encountered in our work. To do this, a straight line is drawn between points on the Stanton and Pannell curve corresponding to R of 6000 and 130,000, as shown in Fig. 4. It can be seen that this straight line does not vary widely from the curve at any point. By simple mathematics, the equation of this line is calculated to be

$$f = \frac{0.3305}{R^{0.382}} \quad [6]$$

but

$$R = \frac{2214 \times B}{D \times v}$$

which substituted in Equation [6] gives

$$f = \frac{0.0474 D^{0.252} v^{0.252}}{B^{0.382}} \quad [7]$$

This in turn is substituted in Equation [1] and the resultant form is

$$P = \frac{1.653 B^{1.748} v^{0.352g}}{D^{4.748}} \quad [8]$$

Solving this equation for B gives the following

$$B = \frac{0.750 P^{0.572} D^{2.718}}{v^{0.144} g^{0.572}} \quad [9]$$

While this is unwieldy to use, it does give a direct means of solving

¹"The Friction Factor for Clean Round Pipe," by T. B. Drew, E. C. Koo, and W. H. McAdams, Trans. AIChE, vol. 28, 1932, pp. 56-72.

⁴"Fluid Flow and Friction in Pipe Lines," by W. G. Heltzel, *The Oil and Gas Journal*, vol. 29, June 5, 1930, pp. T203-T224.

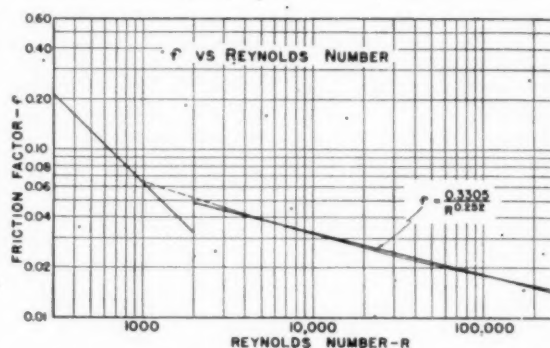


FIG. 4 STRAIGHT-LINE RELATIONSHIP BETWEEN FRICTION FACTOR AND REYNOLDS NUMBER FOR TURBULENT FLOW, BASED UPON STANTON AND PANNELL CURVE

ing for the capacity of a line. The greatest value of this type of equation lies in its adaptability to logarithmic charts or a logarithmic slide rule, providing a convenient means of solution.

PRACTICAL VERIFICATION

It is felt that the choice of the straight line for f versus R above the Stanton and Pannell curve will approximate actual conditions very closely as the use of a higher friction factor will give a greater pressure drop than encountered in a straight pipe line. This higher pressure will compensate for certain factors not now considered which have the effect of increasing the operating pressure. Under our present method of calculating, no provision is made for the additional pressure loss through valves, fittings at junctions, and station manifolds. The basis of our calculations is the actual distance of line between stations with the correction for elevation head being taken as the difference in elevation between the station floors. Though most of our stations operate with a tank floating on the line, there are times when they pump their entire stream into a tank at the next station. This would have the effect of increasing the discharge pressure at the pumping station due to the additional pressure drop through the tank line. No correction is made for these operating conditions although the tank lines are one-half mile in length at some stations.

An additional factor that will be corrected for, by using a higher line for f , is the decrease in effective internal diameter between the running of scrapers. As the lines grow older, the value of f experienced may increase due to internal corrosion in some lines, although past performance has shown this factor to be a negligible one in trunk lines where velocity is sufficient to prevent the settling out of water, the primary cause of internal corrosion.

Considering the effect on capacity, the maximum difference encountered is 2.7 per cent less capacity when using the straight line for f instead of the Stanton and Pannell curve for f .

CONCLUSION

While it is realized that the data presented here are not all-inclusive, it is felt that it is a realistic addition to the field of pipeline hydraulics. The accumulation of data such as included here is time-consuming as well as costly, but it is hoped that further study can be made of flow conditions in commercial pipe-line systems, for information gathered in this manner will be of definite aid to the pipe-line engineer.

ACKNOWLEDGMENTS

The author wishes to acknowledge the help of members of the Engineering Department of the Stanolind Pipe Line Company, and particularly the aid of Messrs. L. E. Tomlinson and W. E.

Roads, who suggestions

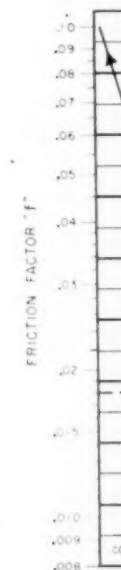
F. M. Van actual operat friction factor confirms the mal operatin used. From This discussi consistent w factors, delin factor relatio calculators, th exponentials

The writor olds number has been deli by the writor chart, inasm drawn mater chart or tabl being entered

The writor for materials

A series of 60,000 and 13 by the autho on fines repr

⁵ Assistant N. Y. Mem. ⁶ Author's



Roads, who assisted in some of the test work and offered helpful suggestions in compiling the data here presented.

Discussion

F. M. VAN DEVENTER.⁵ The author has demonstrated that actual operating data on 16-in., 20-in., and 30-in. lines indicate a friction factor versus Reynolds number relationship which closely confirms the Stanton and Pannell data, and that within the normal operating range for oil lines, a straight line may safely be used. From that straight line, he establishes his Equation [9]. This discussion will show that the author's formula is entirely consistent with the D'Arcy general flow formula and friction factors, delineated by the most recent revisions of the friction-factor relationship. Reference will also be made to mechanical calculators, the use of which eliminates the necessity of calculating exponentials of the author's formula.

The writer's Fig. 5 is a graph of the friction factor versus Reynolds number relationship based upon the Colebrook function and has been delineated by Prof. L. F. Moody.⁶ This form, prepared by the writer, is considered to be an improvement over Moody's chart, inasmuch as scales are appended for steel, cast iron, and drawn materials. Hence it is unnecessary to refer to a separate chart or table from which the value ϵ/D is obtained; that value being entered on the friction-factor chart.

The writer includes a scale ϵ/D so that solution may be made for materials other than the three referred to.

A series of five circles in the Reynolds-number range between 60,000 and 150,000 are shown in Fig. 5. This is the range covered by the author's tests. It will be noted that if the chart is entered on lines representing 16-in., 20-in., and 30-in. steel pipes, these

lines converge so as to become almost indistinguishable in the range under discussion. That line in turn conforms closely with the Stanton and Pannell line, and hence with the author's test data. It is also interesting to observe that this line corresponds to a hydraulic efficiency of about 98 per cent.

A word of caution is in order concerning the limitation of the author's formula if used for Reynolds numbers too far outside the limits covered by the Stanolind tests. This may be demonstrated by observing the spread of friction factors for pipes of 16 in. to 30 in. diam, operating with Reynolds numbers of the order used in natural-gas transportation. (It is recognized that the author's formula is not intended for such use, but this comparison will serve to illustrate the point.)

Modern natural-gas transport lines operate at Reynolds numbers in the range of 8 million to 16 million. The spread of friction factors in this range is represented by the group of small circles plotted on the friction-factor chart. It will be noted that for 16-in. pipes the expected friction factor is 0.012, and for 30-in. pipes, 0.011. In this range there is a particular friction factor corresponding to each pipe size. In comparing this group of points with the oil group, it is interesting to observe that the hydraulic efficiency of the 16-in. and 30-in. pipes would be about 80 per cent and 90 per cent, respectively.

In the interest of labor and timesaving, the writer recommends the use of "mechanical brains" for the solution of most problems concerning the flow of fluids. Some such devices are based upon crude approximations or empirical data, hence satisfactory accuracy may not be obtained. On the other hand, some of them are based upon a formula of the D'Arcy type, means being provided whereby the friction factor may be compensated so as to represent the pipe size and material actually used.

The writer's Fig. 6 is a graphic comparison of the results obtained from (1) the author's formula; (2) the D'Arcy formula; (3) the Polyflo computer. The following assumptions were

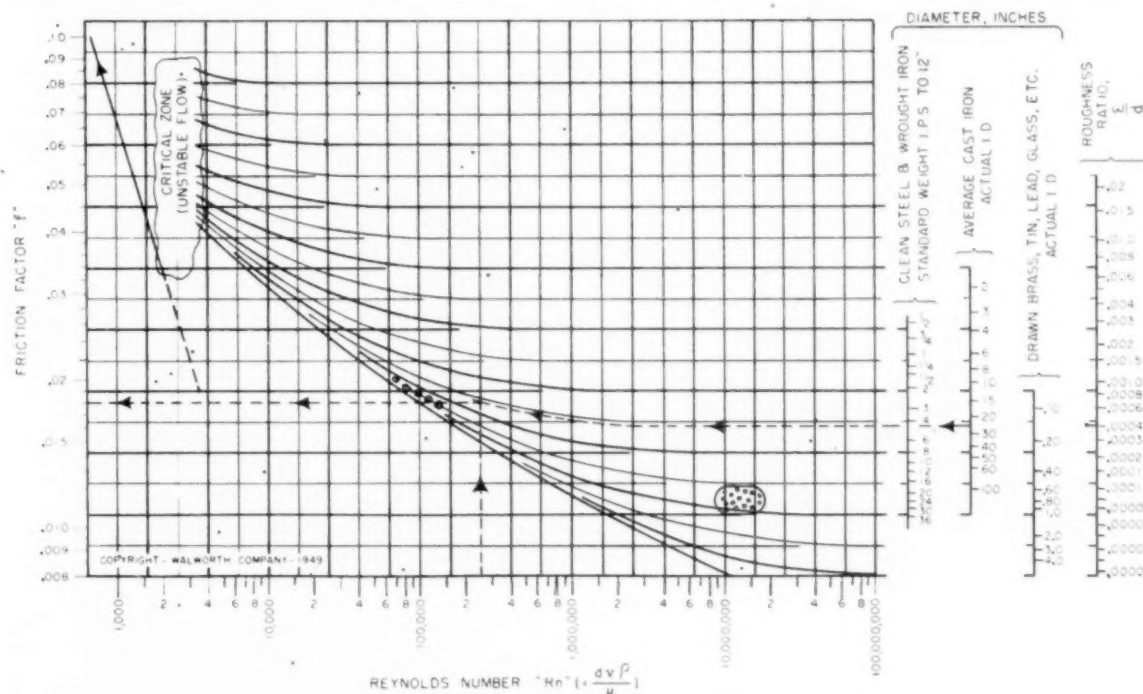


FIG. 5

⁵ Assistant Chief Engineer, Walworth Company, Inc., New York, N. Y. Mem. ASME.

⁶ Author's reference 2.

made: ID of pipe, 20 in.; specific gravity, 0.90; viscosity, 10 centistokes.

Values of 4, 8, 13, and 22 psi per mile were assumed. Barrels per hour was calculated by the author's formula and plotted as shown.

A second set of values for pounds per square inch per mile was computed by the D'Arcy formula, using friction-factor values from the writer's Fig. 5, and the results plotted.

A third set of calculations was solved by the Polyflo computer and plotted. It will be noted that a single line fairly represents the results from all three methods.

It is true that the exponent representing the relation between

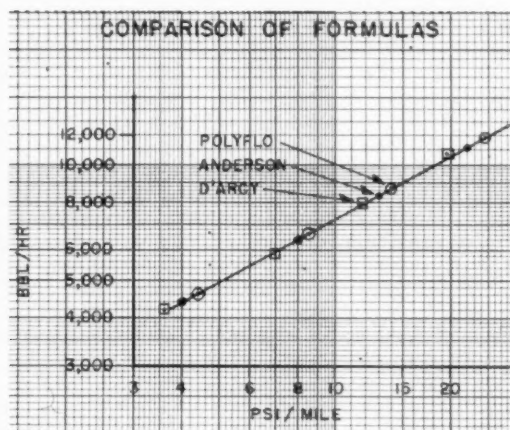


FIG. 6

rate of flow and pressure loss is slightly different for each of the three methods. Hence it is analytically deduced that there should be three separate lines in Fig. 6. However, it may also be shown that within the range of this chart, the difference between any two of these three methods would be in the order of 2 to 3 per cent. Inasmuch as the spread of plotted points in the author's Fig. 4 is plus or minus 5 per cent, it seems reasonable to conclude that a mechanical calculator such as the Polyflo has a degree of accuracy consistent with the solution of most flow problems.

W. G. HELTZEL.⁷ The writer suggested in a paper:⁸ "In view of the trend to higher operating pipe-line pressures it would be worth while having some information on the viscosity of crude oils under pressures used in pipe-line operation." In so far as is known, the data in the present paper are the first to be presented on this subject. It is noteworthy that there is a 50 per cent increase in the viscosity of the East Central Texas crude oil at 33.5 F, corresponding to an increase in pressure from atmospheric to 1000 psi. Likewise, an increase of only 10 per cent for the viscous low-gravity Wyoming crude oil under similar conditions is interesting.

Because pressures up to 1400 psi are used for pumping operations, and since temperatures as low as 32 F are experienced, this subject should be studied further. It is of sufficient importance that the industry should undertake an extensive investigation through the API or one of the engineering societies for the purpose of confirming the author's data and to determine what the relationship is between pressure and viscosity of crude oils. At the same time, a study of the crude oils of a "thixotropic" nature should be made so that a pipe-line engineer will have some way of

identifying such a crude oil—and for the purpose of developing suitable means of obtaining a true viscosity. The pipe-line engineer needs more reliable means than those at his disposal now for determining accurately the viscosity of very viscous crude oils.

It would be interesting if the author would report any observations on the pipe line system, referred to in his paper, that is, transporting a thixotropic crude oil at 2000 psi. It is presumed that this is the La Barge Wyoming crude oil. How do the operating results compare with the theoretical calculations for the line, using the viscosities obtained from both the Saybolt and Brookfield types of viscosimeters at atmospheric pressure? In this case can the author give any information as to what extent the increased shear rate offsets the viscosity?

Are there any operating results to compare with theoretical calculations in the case of the 50 per cent increase in the viscosity of the East Central Texas crude oil at 33.5 F, as shown in Fig. 2?

The pipe-line engineer will be interested in knowing more about the manner of conducting the viscosity tests under pressure.

That the author's data for the coefficient of friction fall along the Stanton-Pannell curve is what might be expected. The results for the 16-in. line fall very close to the Stanton-Pannell curve; perhaps these data are the most reliable because, as the writer understands, they were obtained from a long 16-in. pipe line. One would expect the results for the 20-in. and 30-in. lines to be as low or lower than those for the 16-in. line. However, the results are rather consistent for data obtained from operating pipe lines; the shortness of the 30-in. line probably accounts for the higher values obtained in that case. It would be helpful if the author would define in some detail the pipe lines for which the data were obtained, particularly the length of the sections and the period of observations. The author makes reference to some data reported by the writer in 1926, showing that the coefficients of friction for lines in sizes as small as 8 in. and 12 in. lie near the Stanton-Pannell curve. These tests were made on a 12-in. screw-joint line in Wyoming in 1923. The data were obtained by recording the pressure and temperature at 1/2-mile intervals for about 8 miles, and at some longer intervals outside of this stretch. The tests covered about 180 successive days, using 24-hr recording instruments.

The Moody curves show coefficients of friction higher than the Stanton and Pannell curve. There is no reason for doubting the dimensionless analysis expressed by the Colebrook function; however, we should recognize that the absolute coefficient of roughness cannot be determined too accurately. The author's data and other information on the operation of large-diameter crude-oil lines that is gradually coming to light, indicate that the relative roughness of these large-diameter lines approximates that for the small smooth brass tubes used in Stanton and Pannell's experiments. This factor is of such importance in the design of large-diameter lines that the industry should endeavor, through a joint effort, to determine these coefficients for the practical design of crude-oil pipe lines.

It is the writer's opinion now that the empirical formula, as developed in the paper, can be used safely for the design of crude-oil pipe lines. The results probably will be as accurate as those obtained by trying to be precise. It is doubtful if the factors entering into the calculations can be determined accurately enough to warrant striving for precision beyond the results that would be obtained by this formula. In a paper written in 1930, the writer offered two formulas developed in a manner similar to the present method. One covered a range from 3000 to 57,000 for Reynolds number, and another for the region beyond 57,000. Now one formula for the whole range is adequate for practical purposes. The design of many miles of crude-oil pipe lines over the past 26 years, using the Stanton and Pannell curve, has, in general, and for all practical purposes proved satisfactory.

⁷ Consulting Engineer, Tulsa, Okla. Mem. ASME.

⁸ Author's reference (4).

AUTHOR'S CLOSURE

The author wishes to express his appreciation to Messrs. Van Deventer and Heltzel for the foregoing discussions submitted by them.

As Mr. Van Deventer states, and as brought out in the text of this paper, the turbulent-flow formula is not applicable for all values of Reynolds numbers. The formula was derived with the intent of using it for crude-oil flow problems only; it is sufficiently accurate for values of R from the lower turbulent-flow region to a maximum R of approximately 150,000. This range includes the majority of crude-oil flow conditions encountered in the turbulent-flow region.

With reference to transporting the thixotropic La Barge crude, only a limited amount of data have been obtained from a study of daily reports on operations. Apparent viscosities were determined from these data by using the author's derived equation. These apparent viscosities at low temperatures are lower than the viscosities obtained from the temperature-viscosity curve for this crude oil. The values for the temperature-viscosity curve were determined from viscosity tests run at atmospheric pressure by means of the Saybolt viscosimeter at high temperatures and

by the Brookfield viscosimeter in the lower-temperature range.

No data are available from actual operations on the transporting of the East Central Texas crude oil at 33.5 F since our lines transporting this crude in its pure form reach a minimum line temperature in the winter months of only 50 F.

The viscosities under pressure were determined by use of the Humble viscosimeter which is a falling-ball type of viscosimeter designed to measure the viscosity of a small subsurface oil sample under actual reservoir conditions. It is equipped with a water bath to permit viscosity determinations at different temperatures.

Mr. Heltzel suggested that additional information on the lines tested would be helpful. Two different sections of 16-in. line were utilized, a 40-mile section in West Texas and a 15-mile section in Oklahoma. Tests on each of the lines were run over a period of about three weeks with data secured from as wide a range of flow rates as was conveniently possible. The tests conducted on the 20-in. lines were carried out for about the same length of time. Two sections of 20-in. line were also used: one section in Missouri was 74 miles in length, and the other section, which was in Oklahoma, consisted of 57 miles of pipe.

**This p
Commit
volved.
water-ha
petroleu**

IN OUR
flow
mach
vision is li
varying c
It is to th

In the
that there
on water
American
approxim
handbook
serious re

A preli
activity b
1931 the
the surve
on the sta
committe
had contr
years.

The m
members
the Amer
did not b
mittee be
Engineers
to The En
the desira
surges an
ship also
represent
versity pr
power co
United St

As the
pared, it
where a c
covering
available

¹ Consul
Inc.; Cha
² Norma
S. Quick, I
Contrib
Petroleum
Okla., Oct
ENGINEER

NOTE:
understood
of the Soci

Surge Problems in Pipe Lines—Oil and Water

By S. LOGAN KERR,¹ PHILADELPHIA, PA.

This paper outlines the work done by the Water Hammer Committee of the Society, outlining the publications involved. A general review and summary are given of water-hammer studies as they can be applied to the petroleum pipe-line surge problem.

IN OUR Society, The Hydraulic Division is concerned with the flow of water and other fluids and their use in hydraulic machinery, turbines, pumps, valves, and conduits. The Division is likewise interested in the behavior of flowing fluids under varying conditions where cavitation or water hammer is present. It is to this latter phenomenon that attention is now directed.

In the years from 1920 to 1930 it was increasingly apparent that there was a great dearth of reliable and accurate information on water hammer. Only a few articles had been published in American engineering literature prior to 1930, but many different approximate formulas had found their way into textbooks and handbooks and were widely used by designers, sometimes with serious results.

A preliminary survey indicated the need of some continuing activity by the Hydraulic Division, to remedy this situation. In 1931 the Committee on Water Hammer was set up to continue the survey, to sponsor programs, solicit articles, prepare reports on the state of the art, and to stimulate interest in this subject. A committee of six was appointed, consisting primarily of those who had contributed articles on water hammer in the preceding 10 years.

The membership of the Committee² was not restricted to members of the Society, but included some who were members of the American Society of Civil Engineers, and one member who did not belong to any society. At least two members of the committee belonged to both The American Society of Mechanical Engineers and the American Society of Civil Engineers, as well as to The Engineering Institute of Canada. Great stress was laid on the desirability of co-operation between all groups interested in surges and water-hammer problems. The committee membership also was independent of company affiliations and included representatives of the hydraulic-turbine manufacturers, a university professor, and two representatives of one of the largest power companies operating hydroelectric equipment in the United States and Canada.

As the survey continued, and committee reports were prepared, it was felt desirable to hold a series of technical sessions where a carefully selected group of papers could be presented, covering the various aspects of water hammer and thus make available in English a comprehensive treatise on water hammer.

¹ Consulting Engineer, and President, S. Logan Kerr & Company, Inc.; Chairman, Committee on Water Hammer. Mem. ASME.

² Norman R. Gibson, Eugene E. Halmos, Lewis F. Moody, Ray S. Quick, Earl B. Strouger, and S. Logan Kerr.

Contributed by the Petroleum Division and presented at the Petroleum Mechanical Engineering Conference, Oklahoma City, Okla., October 2-5, 1949, of THE AMERICAN SOCIETY OF MECHANICAL ENGINEERS.

NOTE: Statements and opinions advanced in papers are to be understood as individual expressions of their authors and not those of the Society. Paper No. 49-PET-9.

Field test data to substantiate the theory were to be made available wherever possible.

Two years of preparation resulted in the first Symposium on Water Hammer, held at the time of the Century of Progress Exposition in Chicago, June, 1933, when several national engineering societies were having conventions, and a maximum attendance could be expected. It was sponsored jointly by The American Society of Mechanical Engineers, Hydraulic Division, and the American Society of Civil Engineers, Power Division, with other societies co-operating.

A comprehensive committee report and seven papers were privately published as a 90-page booklet, in advance of the meeting, and were widely distributed to promote active discussion. These discussions were included in a 60-page supplement which later was combined in a single publication and two editions were rapidly exhausted.

In February, 1949, the Symposium on Water Hammer, 1933, was republished by this Society, and once more is available to engineers and students for study and reference.

1 STATE OF THE ART—1933

The committee report (1)³ outlined the historical development of surge wave theory, beginning with the experiments by Joukovsky in Moscow in 1897, described in an article (2), published in 1904 by the American Water Works Association. Subsequent treatises were analyzed and evaluated as this fundamental research was extended and amplified by many engineers in Europe and America, the best known being the work by Allievi (3) in Italy and translated into many languages. The English version by E. E. Halmos was published in 1925, under the sponsorship of this Society and the American Society of Civil Engineers, with funds supplied by the late John R. Freeman.

An annotated bibliography was prepared as a part of the committee report, together with a tabulation of symbols used by different authors in their treatises on water hammer. The committee also recommended a uniform nomenclature and symbol system in an attempt to avoid confusion in terminology.

An appendix to the report evaluated the various theories and the approximate formulas in general use prior to 1933. Some of these formulas were derived analytically, some from piecemeal translations of European authors, notably Allievi, and were frequently tagged with his name as the source. These partial abstracts reached American engineering literature by devious routes. The original Allievi treatises were published in Italian, translated into German or French by Swiss engineers, and subsequently, translated from German into English by others. There were many opportunities for substantial departures from the original concept during this process, since the use of formulas alone without full understanding of their limits of accuracy or the assumptions upon which they are based may give results that are frequently in error.

Fig. 1 gives a comparison of the computations of a specific surge problem by several approximate formulas in current use at

³ Numbers in parentheses refer to the Bibliography at the end of the paper.

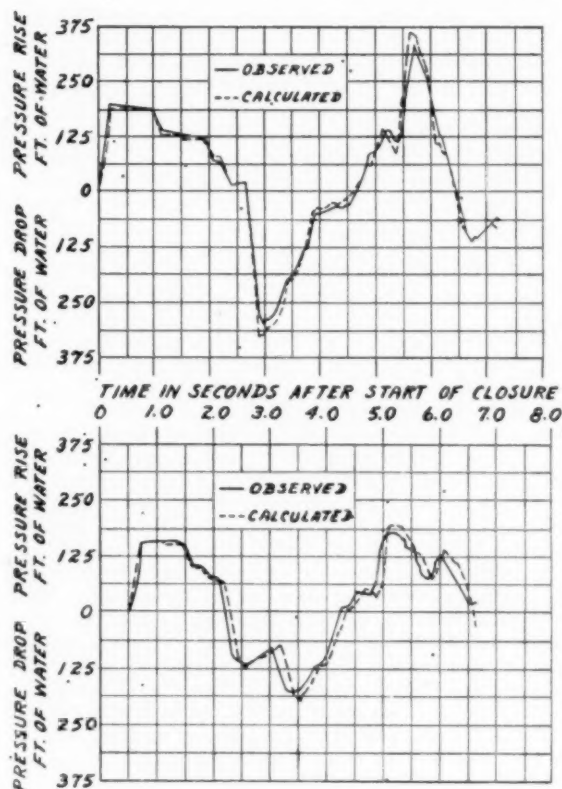


FIG. 2 COMPARISON OF THEORETICAL AND FIELD TEST PRESSURES
(Seira penstock No. 1, 4550 ft long, of which 663 is 61 in. diam; 527 ft of 55 in. diam; 1872 ft of 49.2 in. diam, and 2071 ft of 43.3 in. diam. Thickness varied 0.375 in. at top to 1.688 in. at bottom. 15.5 cfs stopped in 0.22 sec.)
(a) Pressure-time curves at control valve
(b) Pressure-time curves at lower end 49.2-in. section, 0.455 L from valve

5 Approximate formulas, short cuts and general assumptions, were a source of great potential error and should be eliminated from use, unless the formula itself was accompanied by a statement of its limitations, and the range of application within it agreed reasonably well with the elastic-wave theory.

6 Field-test programs had confirmed the accuracy of the theoretical approach.

EXPANDED ACTIVITIES

So successful was this first endeavor that two additional steps were authorized as follows:

1 To invite representatives from other societies in the United States and Canada to serve as associate members of The American Society of Mechanical Engineers' Water Hammer Committee.

2 To broaden its activities to include representatives of engineering societies in other countries, or to designate individuals to serve as associate members of the committee in other countries.

Within a year representatives were designated by the American Society of Civil Engineers, the American Water Works Association, The Engineering Institute of Canada, and The Institution of Mechanical Engineers of Great Britain.

Engineers in other countries were invited to become associate members to represent their own countries, and such delegates were designated in France, Switzerland, Germany, Austria, Brazil, and Australia.

With this broadened scope of activities, The American Society of Mechanical Engineers' Committee on Water Hammer became, to a large extent, the clearing house for accumulating publications on water hammer throughout the world. Many interesting contributions were being received from abroad and much investigation and development work was being carried out in the United States and Canada.

The second Symposium was planned for December of 1937, and the papers presented at that time were published in the November, 1937, issue of Transactions, ASME, and were available for study in advance of the meeting.

The international flavor which this committee had acquired was apparent in the author representation at this second Symposium. While the first Symposium was confined to engineers in the United States and Brazil, the second program in 1937 included contributions from engineers in Canada, Great Britain, Switzerland, Italy, and Brazil, in addition to those from the United States.

The onset of the European war, with its extension to World War II, naturally curtailed the activities of the committee and, while representation of other engineering societies in the United States and in Canada was maintained, the associate memberships from other foreign countries were discontinued until some future time when this very valuable world-wide program of technical co-operation could be resumed.

One major factor in the success of the committee in carrying out its objectives of placing in American and Canadian engineering literature, accurate and authoritative treatises on water hammer, has been the spirit of cordial relationship among engineers who are interested in this subject.

The free interchange of technical information in the form of articles submitted to the committee for possible presentation and publication, the interchange of information by correspondence or by personal visits, have brought about a friendly co-operative situation that could not help but bring success to the program.

Discussion of papers was carried out in an unbiased manner, and there is not on record a single case where personal animosity, personal ambition, or company policies or attitudes were allowed to interfere with constructive progress in this highly technical field. The publication of articles was not confined to the journals of any one society. Outstanding contributions can be found in Transactions, ASME; Proceedings, American Society of Civil Engineers; the Journal of the American Water Works Association; the Journal of The Engineering Institute of Canada, and the Proceedings of The Institution of Mechanical Engineers of Great Britain. Discussions were received from all over the world, and abstracts or republications of many of the symposium articles appeared in technical publications of France, England, Switzerland, Germany, and Italy.

2 STATE OF THE ART IN 1949

In the year 1949, some 18 years after the formation of the Committee on Water Hammer, many of the original objectives have been attained. There are now available, in English, a number of reliable articles dealing with practically every phase of water hammer and surges, as applied to water flowing in closed conduits. A selected list of such papers is included in the Bibliography, that, with few exceptions, are all available in engineering reference libraries.

Graphical methods of solution of the complex surge-wave equations have been developed and are proving most useful in analyzing complex problems (12, 13, 14).

Nonlinear valve characteristics can be accounted for simply. The effect of motor-driven centrifugal pumps on surge pressures during sudden shutdown can be predetermined. The performance

of relief valves and their behavior in reducing surges can be related to control-valve operation.

Much progress has been made in applying surge-wave theory to analyses during the design of installations and in advance of construction. It is now possible to predict with a great degree of accuracy the magnitude of surge pressures in any given installation, and thus to design remedial devices with assurance that they will function as desired.

There is a growing interest in water-hammer and surge-wave theory. In several engineering schools, graduate research projects include theses on water hammer.

Some typical examples are included to demonstrate such methods of solving surge problems.

GRAPHICAL SOLUTION OF EXAMPLE IN FIG. 1

The example used for the comparison of the various approximate formulas, Fig. 1, can also be solved by the graphical method. If the hydraulic characteristics of a given system are plotted on rectangular co-ordinates, Fig. 3(a), it is possible to show along the vertical axis the head or pressure, and along the horizontal axis the velocity of flow in the conduit.

Under any steady-state condition with fixed valve opening, the relationship between velocity and head will be given by a curve (B_0) which follows the square-root relationship between head and discharge. If friction is neglected in this particular example, the static head can be represented as a horizontal line through the vertical axis at a point corresponding to 165 ft.

The static-head line and the steady-state head-velocity relationship intersect at point 1, which represents the normal operating

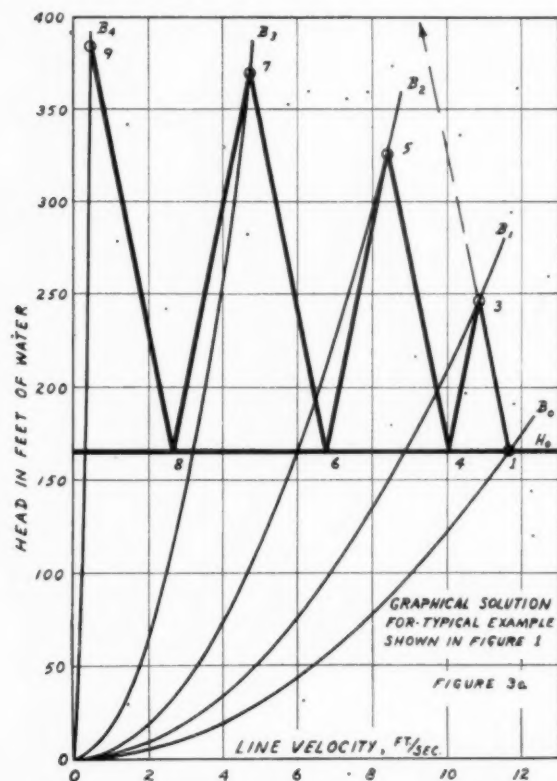


FIG. 3(a) GRAPHICAL SOLUTION FOR TYPICAL EXAMPLE SHOWN IN FIG. 1

ing point. Assume that the rate of cutting off flow is uniform with respect to time, and the closure takes place in 2.1 sec. The length, diameter, and material of construction of the pipe give a velocity of the pressure wave of 3220 fps. The critical time ($2L/a$ sec) for a surge wave to travel from the valve to the intake and return is approximately 0.51 sec, and hence the closure will be in slightly over 4 such intervals.

Additional curves which represent the intermediate steady-state condition of the control valve at each unit of critical time can be drawn (B_1, B_2, B_3 , and B_4).

A further relationship exists between head and velocity, namely, that the surge pressure is equal to aV/g , whenever the closure rate is in a time equal to or less than the critical time of the conduit.

This becomes a straight line when represented graphically and has a slope of a/g , either plus or minus, depending on whether it is a wave of positive pressure or negative pressure.

If the closure is made instantaneously, then this straight line, having its origin at the initial steady-state condition, point 1, will intersect the zero-velocity line at some point 2 (not shown on diagram), and will result in a surge of 1175 ft above normal.

If the closure is made in a time greater than $2L/a$ sec, then the valve stroke can be assumed to be made in a series of increments each equal to $2L/a$ sec. In this case, the line would start at point 1 and would intersect the next steady-state condition at point 3. It would then be reflected to point 4 along the line drawn with a downward slope, until it intersected the normal head line. Here again, it would be reflected until it reached the point corresponding to two intervals opening under a steady-state condition, shown as point 5. This is continued until the valve is closed.

It will be noted that points 1, 3, 5, 7, and 9 represent the pressures at time increments of $2L/a$ sec. If they are drawn as shown in Fig. 3(b), a curve of pressure rise above normal with respect to

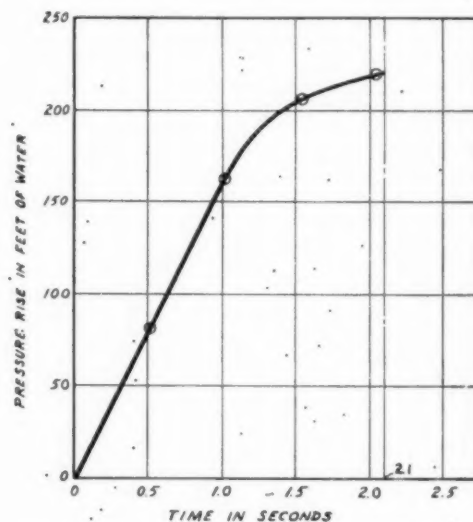


FIG. 3(b) PRESSURE-TIME DIAGRAM FOR EXAMPLE, FIG. 3(a)

time will result, and the shape of the surge wave can be determined. After the valve is closed, the oscillations of pressure, unless damped, will continue above and below the normal head line and can be represented on the diagram accordingly. The maximum pressure as indicated from the graphical solution, is identical with that obtained by the use of the elastic-wave-theory equations, and no new element of theory has been introduced.

In making on the hydro behavior of the flow.

The usual on the folio

(a) The form rate.

(b) The area and h

In a given rate of 5 in reduction of of change graphical s Fig. 4(d), s

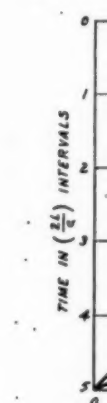


FIG. 4(a)



FIG. 4(b) VELO

NONLINEAR VALVE MOVEMENT

In making surge analyses, it is essential to have all of the data on the hydraulic characteristics of the system, including the behavior of the valves or of other devices which may be controlling flow.

The usual assumption of uniform rate of flow reduction is based on the following fallacies:

- (a) That the stroke of the valve stem cuts off area at a uniform rate.
- (b) That the flow through a valve is in direct proportion to area and hence to stem travel.

In a given system, with an initial flow of 5 fps, and a shutoff rate of 5 intervals of time ($2L/a$ sec), the uniform rate of flow reduction could be represented as curve A in Fig. 4(a). The rate of change of velocity (dv/dt) would be 0.50 fps per sec. The graphical solution is given in Fig. 4(b), and pressure-time curve A, Fig. 4(d), shows a rise of 60 ft above normal.

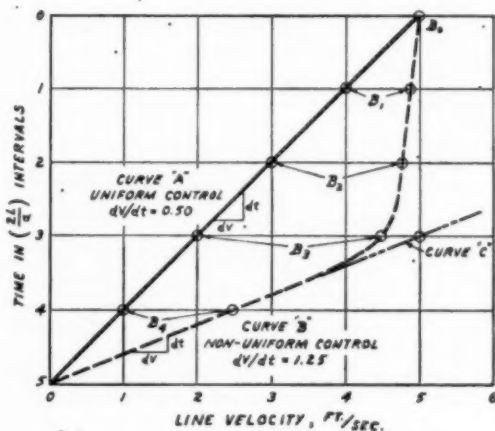


FIG. 4(a) COMPARISON OF UNIFORM AND NONUNIFORM RATES OF VELOCITY CONTROL WITH RESPECT TO TIME

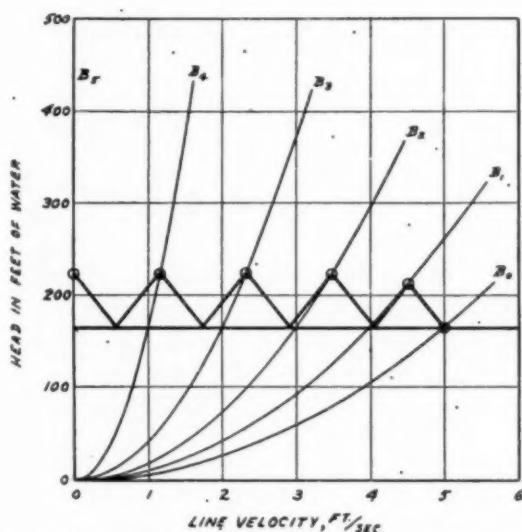


FIG. 4(b) GRAPHICAL SOLUTION FOR UNIFORM VARIATION OF VELOCITY WITH RESPECT TO TIME, CURVE A, FIG. 4(a)

By contrast, in actual practice, when an ordinary gate valve is closed, there is little or no effect upon the discharge until a point is reached about one half to one third of the full valve opening. The flow then begins to be reduced far more rapidly as the valve continues on toward the seat. Fig. 4(a) shows such a typical relationship for an ordinary gate valve, curve B. It will be seen that the maximum rate of change of flow (dv/dt) is $2\frac{1}{2}$ times that for uniform closure assumptions, reaching a value of 1.25 fps per sec.

The graphical method can account for variable rates of change of flow by taking the steady-state velocity relationship from curve B, Fig. 4(a), at each interval of time. The B_1, B_2 , etc., points, as shown in Fig. 4(c), give the corresponding relationships, and the solution follows the same procedure as with uniform flow cutoff. The pressure rises very slowly until the valve begins to

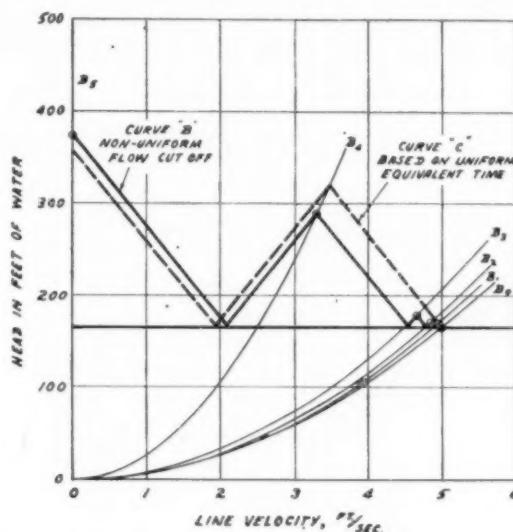


FIG. 4(c) GRAPHICAL SOLUTION FOR NONUNIFORM VARIATION OF VELOCITY WITH RESPECT TO TIME, CURVE B, FIG. 4(a) AND CURVE C (EQUIVALENT TIME)

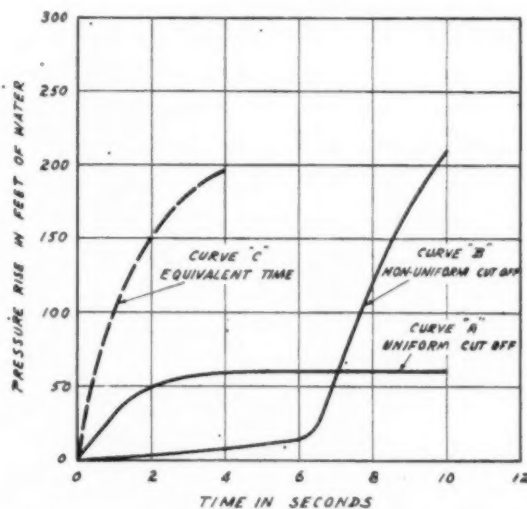


FIG. 4(d) PRESSURE-TIME CURVES FOR FIGS. 4(a), 4(b), AND 4(c)

cut off flow, then after three intervals of time the pressure rise is very much greater than it would have been if the flow rate had been cut off uniformly throughout the whole stroke.

Fig. 4(d) shows the difference in pressure-time curves for these two cases. The rise above normal for nonuniform cutoff, curve B, is about 210 ft, as compared with 60 ft for uniform closure, or $3\frac{1}{2}$ times as great. Such differences can explain many pipe-line failures.

In the water-works and hydroelectric fields, a reasonably valid short cut is used to approximate the effect of nonuniform flow-rate cutoff. Since it is the maximum rate of change of flow that determines the maximum rise in pressure, a line tangent to this maximum cutoff rate can be drawn, curve C, Fig. 4(a), and a so-called "equivalent time" is secured.

In the present case the equivalent uniform rate would be two intervals of time rather than five. The dash line in Figs. 4(c), and (d) give the graphical solution of this case. A rise above normal of 195 ft results, as compared with 210 by the more precise method, in an error of only 7 per cent, as compared with 250 per cent by the assumption of curve A.

Using this so-called short cut, the required total time of travel to limit surge pressures to permissible maximum values can be obtained.

EFFECT OF INITIAL VALVE OPENING

It is also interesting at this time to analyze the effect of the initial starting point of valve closure upon the magnitude of surge pressures obtained.

Closure from some intermediate point down to zero may give a much higher surge value than closing at the same uniform rate from the wide-open valve position down to zero. Fig. 5(a) shows, for the same example (Fig. 4, curve A), the graphical solution which indicates this relationship. It will be seen that higher surge pressures result when closure is initiated from 60 per cent or from 20 per cent flow rates than when full flow is interrupted. Fig. 5(b) gives the pressure-time curves and shows the change in wave shape as well.

When the closing rate is greater than $2L/a$ sec, there will be some intermediate point from which the valve can be closed to

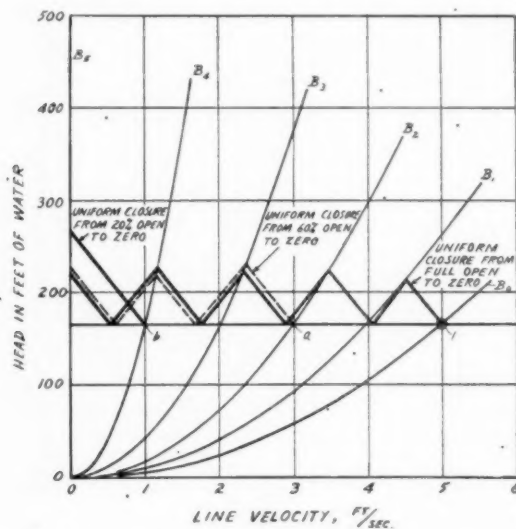


FIG. 5(a) GRAPHICAL SOLUTION FOR UNIFORM VARIATION OF VELOCITY WITH RESPECT TO TIME, CURVE A, FIG. 4(a), WITH DIFFERENT INITIAL VALVE POSITIONS

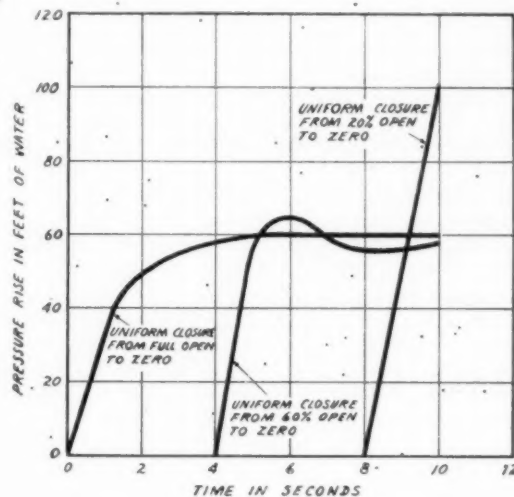


FIG. 5(b) PRESSURE-TIME CURVES FOR FIG. 5(a)

zero in exactly $2L/a$ sec, and this will result in instantaneous water hammer for that smaller flow. Nonuniform valve operation can aggravate this effect.

VARIATION IN SURGE PRESSURE ALONG CONDUIT

It is interesting to note the variation in wave form at the control gate and at intermediate points along the pipe line for different rates of closure. If closure is made instantaneously, then aside from any natural damping of the wave due to internal friction, compressibility of the fluid, or expansion of the pipe walls, this wave will travel undiminished from control valve to the point of origin of flow and the distribution of pressure along the line will be ABFC.

If the closure is in $2L/a$ sec or over, the surge pressure will diminish uniformly between the control valve and the point of origin of flow and will appear as shown in Fig. 6, as line (ABD).

If the closure is made at some intermediate time, between zero and one interval of $2L/a$, the wave will travel undiminished up the line a distance BF corresponding to the proportion of time that the closure is less than time $2L/a$ sec, and from that point (F),

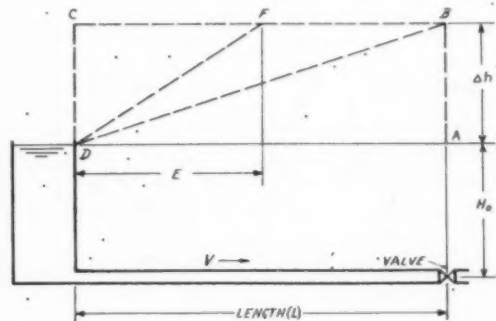


FIG. 6 DISTRIBUTION OF SURGE WAVE ALONG PIPE LINE WHEN

Time (T) = 0, Line ABC

Time (T) = $\frac{2L}{a}$, Line ABD

Time (T) > 0 < $\frac{2L}{a}$, Line ABFD, with $E = \frac{Ta}{2}$

will gradually
ABFD.

Comparative and
from closure
proportion
origin of flow

These same
the graphic
taking into
through the
number of
distance from
is desired to

It is also
control centre

If the
posed on the
station point

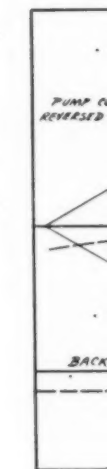


FIG. 7 GRAPHICAL SOLUTION FOR UNIFORM VARIATION OF VELOCITY WITH RESPECT TO TIME, CURVE A, FIG. 4(a), WITH DIFFERENT INITIAL VALVE POSITIONS

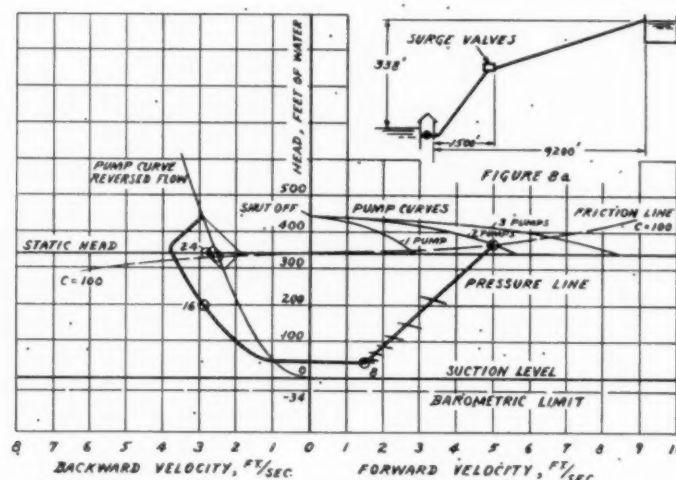
throttling-
sired.

If an
power fail
sloped line
drawn, and
terminated.

If the fl
motor is k
time incre
tion for ea
time interv
of the pun

The suc
of the pun
such cond
water-wo
pared to t
no check
its rotation

At a point of about 1500 ft beyond the pump house, the sub-normal pressure fell below the barometric limit, and the water column parted at this point, the upper portion gradually slowed down, coming to rest and reversing, while the lower portion of the



FIGS. 8 (a) (b) GRAPHICAL ANALYSIS, LONG LAC PIPE LINE
(9200 ft long, 36-in.-diam pipe, two pumps tripped out, no check valve in operation.)

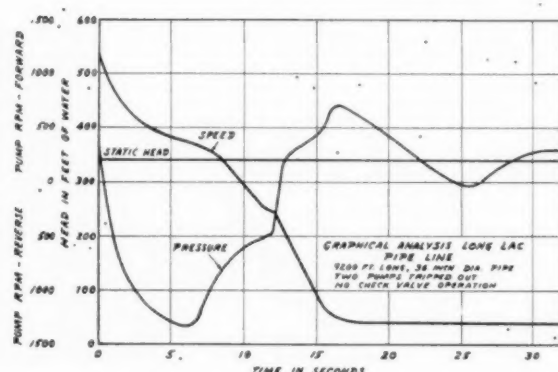


FIG. 8(c) PRESSURE-TIME DIAGRAM FOR LONG LAC PIPE LINE.

column continued to flow back through the pump after having reversed at a much more rapid rate. The upper column gradually picked up momentum and rejoined the lower column, resulting in an instantaneous surge pressure which was much greater than that due to check-valve closure. A resultant surge pressure, upon rejoining the water column, of about 250 lb above normal would be experienced if no remedial devices were installed.

On this installation, some quick-opening, slow-closing air valves were utilized at the crest of the hill, to admit air to act as a cushion to slow up the rate at which the two columns were rejoining.

An analysis in advance of design indicated that a surge pressure of about 70 psi would be experienced and would be within a safe limit of design based on the stress in the thin-wall pipe. The actual tests made in the field, when one pump was tripped-off, showed a surge pressure of 65 psi. While only the operating gages were available for this check test, such readings as were secured indicated an extremely close agreement between the theoretical design values obtained nearly a year previously, and the actual test values recorded under service conditions.

BASIC RELATIONS

It may be well at this point to restate a few of the fundamental relationships in surge-wave theory which determine the magni-

tude of the pressure rise and its distribution along a conduit. These comments relate to gravity flow or discharge lines from centrifugal pumps only.

1 The pressure rise for instantaneous closure is directly proportional to the fluid-velocity (V) cutoff, to the magnitude of the surge-wave velocity (a), and is independent of the length of the conduit. Its value is

$$h = aV/g \text{ ft of water}$$

or

$$p = aWV/144g = (a/g) (\text{sp gr}/2.3) V \text{ psi}$$

where

$$a = 12 \sqrt{\frac{W}{g} \left(\frac{1}{k} + \frac{d}{Ee} \right)} \text{ fps}$$

and

$2L/a$ = critical time of conduit, sec

T = closing time, sec.

N = number of intervals of $2L/a$ for closing time T .

L = length of conduit, ft

h = pressure rise above normal, ft of water

p = pressure rise above normal, psi

V = velocity of flow, fps

W = weight per cu ft of fluid, lb

sp gr = specific gravity of fluid (water = 1.0)

k = bulk modulus of compressibility of liquid, psi

E = Young's modulus of pipe-wall material, psi

d = inside diam of conduit, in.

e = thickness of conduit wall, in.

g = acceleration due to gravity (32.2 fps per sec)

2 When the flow rate is changed in a time greater than zero but less than or equal to $2L/a$ sec, the magnitude of the pressure rise is the same as with instantaneous closure, but the duration of the maximum value decreases as the time of closure approaches $2L/a$ sec.

3 Under the conditions in paragraph 2, the pressure distribution along the pipe line varies as the time of closure varies. The

pressure
sec. Th
length o
travels u
uniform
4 Th
pendent
total pre
5 For
pressure
flow with
6 No
timing d
sired lim
7 Th
valves o
method
8 Th
station
The min
mum wh
line.

9 Pa
tremely
10 T
any sur
of the no
11 T
of a sur
hydrauli
12 T
field-test
theory i

3
With
applied
with co
rise will
emergen
ing devi
How,
petroleu

1 In
mechan
2 Th
same m
the phy
3 T
fluids a
ture fro
limitati

By ex
possible
our atte
The
structu
passes,
unchan

Cent
but dri
introdu
valves,
iary de

pressure decreases uniformly along the line if closure is in $2L/a$ sec. The maximum pressure at the control valve exists the full length of the line with instantaneous closure, and for slower rates travels up the pipe a distance equal to $(L-Ta/2)$ ft, then decreases uniformly.

4 The surge-pressure distribution along the conduit is independent of the profile or ground contour of the line so long as the total pressure remains above the vapor pressure of the fluid.

5 For closing times greater than $2L/a$ sec, the maximum pressure rise will be a function of the maximum rate of change in flow with respect to time (dv/dt).

6 Nonlinear closures can be investigated, and the proper valve timing determined to hold the maximum pressure rise to any desired limiting value.

7 The effect of centrifugal pumps and quick-closing check valves or control valves can be investigated using the graphical method of analysis.

8 The profile of the conduit leading away from a pumping station may have a major influence upon the surge conditions. The minimum effect will be found when the line is level, the maximum when the line is steep, or when high points occur along the line.

9 Parting and rejoining of the liquid column can produce extremely high pressures and may cause failure of the conduit.

10 The effect of friction can be accounted for graphically in any surge problem, and, when such losses are less than 5 per cent of the normal static or working pressure usually can be neglected.

11 The greater the degree of accuracy desired for the results of a surge analysis, the more must be known about the various hydraulic and physical characteristics of the system.

12 The agreement between theoretical analyses and actual field-test results has confirmed the accuracy of the elastic-wave theory in water conduits.

3 APPLICATION TO PETROLEUM SYSTEMS

With this broad knowledge and practice of surge-wave theory applied to water conduits, it has been possible to design projects with complete assurance that the limit set for maximum pressure rise will not be exceeded in actual operation. Behavior under emergency conditions can be predicted, and remedial or alleviating devices utilized to protect the installation.

How, then, can this broad base of knowledge be applied to petroleum pipe lines and their associated apparatus?

1 In either case, there exists a basic physical-hydraulic-mechanical system subject to analysis by the elastic-wave theory.

2 The differences in behavior between dissimilar fluids in the same mechanical system can be accounted for by the differences in the physical properties of the fluids themselves.

3 There may be differing requirements in handling certain fluids as compared with others. This does not represent a departure from established fundamental theory, but merely places limitations on the design of the installations.

By examining the things that are the same in both systems it is possible to select the few factors that are different and concentrate our attention upon them.

The pipe itself, the thickness, diameter, and material of construction, its length, the profile of the country through which it passes, the branches, dead ends, parallel conduits, all these are unchanged by the fluid within a given system.

Centrifugal pumps, differing slightly in details of construction, but driven by electric motors as they are in water systems do not introduce new factors as between oil and water, nor do they control valves, check valves, shutoff valves, relief valves, or other auxiliary devices for regulating flow.

The only basic difference between water systems and petroleum systems is the fluid itself, and possibly the trend today toward lowered factors of safety in crude-oil pipe-line designs, as compared with water-supply systems.

The velocity of the pressure wave a , is a fundamental factor in any surge study, as the surge pressures are directly proportional to its value. The velocity of surge wave is dependent upon the diameter, thickness, material of the pipe walls, and the density and compressibility of the fluid in the pipe.

Our knowledge concerning the physical characteristics of the pipe material is fairly complete. Young's modulus for steel lines can be taken at 30,000,000 psi as an average between 29,000,000 to 31,000,000 psi. If the ratio of diameter to thickness is known, it is necessary to know only the density and the compressibility of the liquid within the pipe to determine the value of a .

Within the range of ordinary operating temperature for water, 32 to 100 F, and for pressures from 0 to 1000 psi, the specific gravity can be taken at 1.00.

In the same range the modulus of compressibility or "bulk modulus" has been measured and checked by field tests to be approximately 300,000 psi with a variation of plus or minus 3 per cent.

For other pipe-wall materials, cast iron, asbestos cement, or concrete, the physical factors are sufficiently well known that a chart, Fig. 9, can be used to determine the value of a when the inside diameter and wall thickness are known.

For crude oil the variations in density and compressibility are greater than with water. Composition of the crude varies from field to field, and the presence of more or less of the highly volatile components may change these two factors at standard conditions.

It is important to know just how these factors vary with pressure and temperature in the ranges encountered in pipe-line pumping, so that such variations can be accounted for in surge investigations. A variation in the bulk modulus will vary the velocity of the pressure wave and thus change the surge intensity by an appreciable amount.

Fig. 10 has been prepared to show the change in surge-wave velocity for different values of specific gravity and compressibility. The range of values has been taken to cover as fully as possible all commonly known crudes.

In a proposed installation it was found that there could be as much as 10 per cent variation in surge-wave velocity due only to variations in compressibility between the terminal pressure at the suction of one pumping unit, as compared with the initial pressure in the discharge of the station.

Where fluid temperatures also vary between pumping stations or between seasons, an additional correction may be necessary, if the value of the surge-wave intensities is to be determined within limits of 2 per cent.

If the limits are not closer than 10 per cent of the actual surge magnitude, then this refinement may be eliminated, and an average surge-wave velocity may be utilized for a given installation.

Where accuracy is needed in determining surge pressures, it is highly desirable to obtain a sample of crude and make a compressibility determination at several different temperatures throughout the range of pressures which may be experienced. Published literature references now available are not dependable for bulk modulus values as applied to surge studies.

It is obvious that the greater the compressibility of a given fluid the more damping effect there will be present and hence the more rapid dying away of the after waves and the lowering of the maximum surge pressures.

When pumping refined products, similar data are needed and the problem is rendered more complex when several different

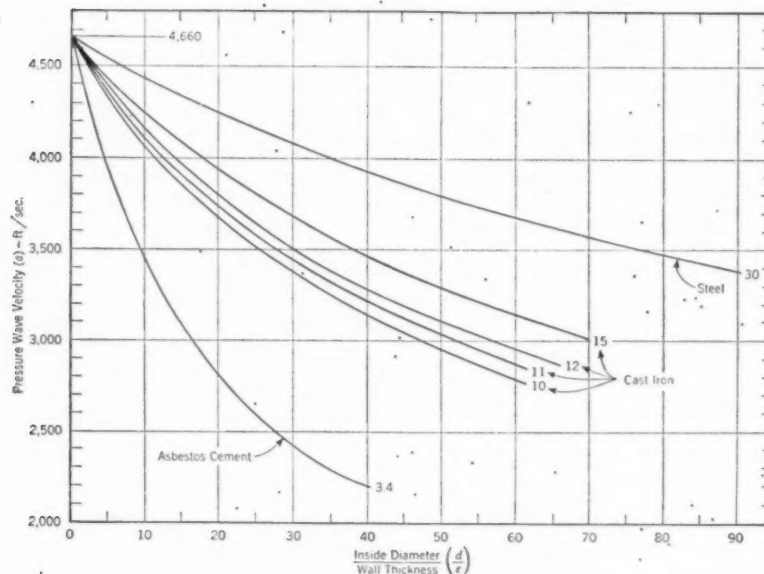


FIG. 9 SURGE-WAVE VELOCITY CHART FOR WATER

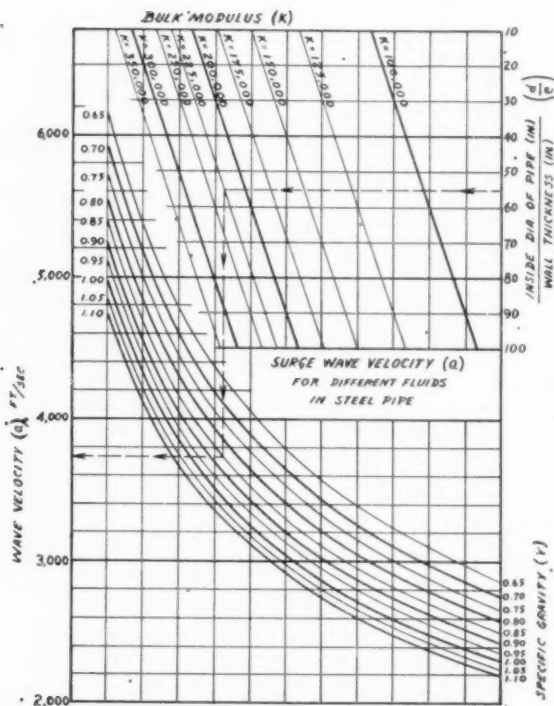


FIG. 10 SURGE-WAVE VELOCITY FOR DIFFERENT FLUIDS IN STEEL PIPE

products are in a given line at one time. The interfaces probably will act as points of partial reflection, in a manner similar to a change in diameter or thickness of the pipe wall.

Once these physical characteristics of the fluid have been determined, the solution of any surge problem (exclusive of positive-

displacement pumping), can be obtained by the proper application of the elastic-surge-wave theory developed for water problems.

POSITIVE-DISPLACEMENT PUMPING

The analysis of surges occurring in positive-displacement pumping of fluids has been described in great detail in the classic work of Diederichs and Pomeroy (15), presented before the Petroleum Division in 1929. In 1936 DeJuhasz published two excellent papers (16, 17), extending such analyses to the injection systems of Diesel engines using graphical methods.

In the Diesel-engine field it is well known that the degree of compressibility of Diesel fuel oils will have an effect on the performance of the engine. As the fuel pumps force the liquid into the engine, they store up energy within the system and the pressure wave is slightly delayed in reaching the spray nozzle. When the fuel pump stops delivering oil, this locked-up energy is dissipated, causing the spray nozzle to continue to discharge for a relatively short period of time after the fuel flow is supposed to be cut off.

Analyses have been made using the elastic-wave theory to establish adjustments in the crank-angle setting for fuel injection in the cylinders which are remote from the fuel pumps. Improved performance has resulted from this timing adjustment as it compensates for the surge effect within the fuel lines and makes the torque applied to the crankshaft more uniform.

With positive-displacement pumps on petroleum pipe-line service, harmonic surges can be set up if the impulses from the individual cylinders of two or more pumps get into step with each other. Still another factor enters, namely, the design of station piping and the arrangement of headers, manifolds, branch pipes, and dead ends which may have natural periods of surge-wave oscillations and could aggravate further any "in-step" harmonics between pumping units.

The magnitude of such harmonic surges can be many times the value calculated from the mere starting and stopping of a liquid column by a control valve.

General solutions for the problem have not been too successful,

and more
of corre

In co
the M
felt nee
sure sur
Since
the des
October
prepare
comple
at other
Some
mentio
as follo

(a)
tween s
of crud
was less
(b)
some 20
of the p
(c)
normal
units w

It w
closely
taking
gravity
time of
Then
applie

As h
over a
formul
culated
proper
metho
The
of mal
water-
studies
starts.

As t
comes
field, t
assura
knowle
better

1
Water
2
Ameri
3
by Eu
4
Dodki
mer, p
5
L. F. L
1933, 1

and more detailed studies are usually required to arrive at a means of correcting harmonic surges.

JOINT SURGE CONFERENCE

In connection with the design of large crude-oil pipe lines for the Middle East, and in the United States and elsewhere, it was felt necessary to acquire a more thorough knowledge of the pressure surges that might be experienced.

Since several large lines are now under construction, or are in the design stage, a Joint Surge Conference was organized in October, 1948, to make investigations, conduct field tests, and prepare reports on the subject. The major program has been completed and will doubtless be reported upon in greater detail at other technical meetings in the near future.

Some very interesting results were obtained which can be mentioned briefly. Three sets of field tests were carried on as follows:

- (a) Gravity series to check the fundamental correlation between so-called "water-hammer" theories and the actual behavior of crude oil in a pipe line, under field conditions where friction was less than 15 per cent of the static pressure.
- (b) Gravity and pumping series in an actual operating line, some 20 miles long, where friction amounted to 80 to 90 per cent of the pressure available.
- (c) Operating tests of 50 odd miles of products line, under normal and emergency starting and stopping of the pumping units when operating as a closed system.

It was found that, in every case, the field-test results checked closely with theoretical studies, using the elastic-wave theory and taking into account the differences in bulk modulus and specific gravity of the particular oil or refined product in the line at the time of the test.

There was complete confirmation of the elastic-wave theory as applied to petroleum lines.

CONCLUSIONS

As has been found in the water-supply and hydroelectric field over a period of many years, there is no simple quick and easy formula to solve surge problems. Surge conditions can be calculated and predicted during the design stage of a project by proper application of the elastic-wave theory using the graphical method.

The results obtained have been well worth the time and expense of making such analyses, and the practice is increasing in the water-supply and hydroelectric fields of carrying out detailed studies on surges for any proposed installation before construction starts.

As the knowledge of surge-wave theory of "liquid" hammer becomes more widely disseminated in the petroleum-pipe-line field, then, as in the water field, it will be used more and more with assurance. Designs can be based on more accurate advance knowledge of surge conditions, and better designs always lead to better performance of the finished project.

BIBLIOGRAPHY

- 1 "Report of Committee on Water Hammer," Symposium on Water Hammer, ASME, vol. 55, 1933 (republished 1949), pp. 3-24.
- 2 "Water Hammer," by Olga Simin, Proceedings of the American Water Works Association, 1904, pp. 336-424.
- 3 "Theory of Water Hammer," by Lorenzo Allievi, translated by Eugene E. Halmos, 1925, distributed by the ASME.
- 4 "High Head Penstock Design," by A. W. K. Billings, O. H. Dodkin, A. Santos, Jr., and F. Knapp, Symposium on Water Hammer, published by ASME, 1933 (republished 1949), pp. 29-61.
- 5 "Simplified Derivation of Water-Hammer Formula," by L. F. Moody, Symposium on Water Hammer, published by ASME, 1933, pp. 25-28 and reprinted, 1949, pp. 1-152.

- 6 "Computation of Water-Hammer Pressures in Compound Pipes," by R. E. Glover, Symposium on Water Hammer, published by ASME, 1933, pp. 64-71.
- 7 Ibid., discussion F. Knapp, pp. 128-133.
- 8 Ibid., discussion E. B. Strowger, pp. 133-139.
- 9 "Surge Control in Centrifugal Pump Discharge Lines," by R. S. Quick, Symposium on Water Hammer, published by ASME, 1933, pp. 81-83.
- 10 "Water-Hammer Tests in Croton Lake Pumping Plant," by S. L. Kerr, Symposium on Water Hammer, published by ASME, 1933, pp. 84-87.
- 11 "Complete Characteristics of Centrifugal Pumps and Their Use in the Prediction of Transient Behavior," by R. T. Knapp, Trans. ASME, vol. 59, 1937, pp. 683-689.
- 12 "Water Hammer in Pipes, Including Those Supplied by Centrifugal Pumps; Graphical Treatment," by R. W. Angus, Proceedings of The Institution of Mechanical Engineers, London, England, vol. 136, 1937, pp. 245-291.
- 13 "Methods of Calculating Water-Hammer Pressures," by F. M. Dawson and A. A. Kalinske, *Journal, AWWA*, vol. 31, November, 1939, pp. 1835-1864.
- 14 "Elements of Graphical Solution of Water-Hammer Problems in Centrifugal-Pump Systems," by A. J. Stepanoff, Trans. ASME, vol. 71, 1949, pp. 515-534.
- 15 "The Occurrence and Elimination of Surge or Oscillating Pressures in Discharge Lines From Reciprocating Pumps," by H. Diederichs and W. D. Pomeroy, Trans. ASME, vol. 51, 1929, PET-51-2, pp. 9-49.
- 16 "Graphical Analysis of Transient Phenomena in Linear Flow," by K. J. DeJuhasz, *Journal of The Franklin Institute*, vol. 223, 1937, pp. 463-493, 643-654 and 751-778.
- 17 "Hydraulic Phenomena in Fuel-Injection Systems for Diesel Engines," by K. J. DeJuhasz, Trans. ASME, vol. 59, 1937, pp. 669-677.

Discussion

F. M. VAN DEVENTER.⁴ The author has described one hydraulic line which was periodically shut off by the manual operation of a valve. During this operation an expansion joint failed on several occasions, and this despite his instructions to spread the closing operation over a 5-min interval. His investigation disclosed the fact that, although the full time was used, the operator had divided the time into ten $\frac{1}{2}$ -min periods. He then rotated the valve handwheel one tenth of full travel every 30 sec. It

⁴ Assistant Chief Engineer, Walworth Company, Inc., New York, N. Y. Mem. ASME.

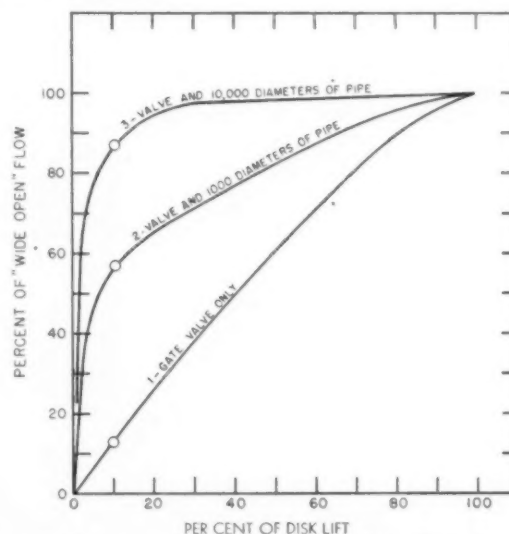


FIG. 11 CURVES OF PER CENT OF WIDE-OPEN FLOW PLOTTED AGAINST PER CENT OF DISK LIFT

was observed that the joint failed during the final increment of stem travel. Gradual and continuous closing eliminated the trouble.

It seems appropriate to present here an interpretation of valve-closing characteristics, often overlooked, and which may explain the experience reported by the author.

Fig. 11, herewith, presents three curves of per cent of wide-open flow plotted against per cent of disk lift.

Curve 1 represents a typical gate valve with a round disk sliding over a round port. The valve is attached directly to the reservoir, has free discharge, and hence functions as a variable orifice. The characteristic approximates a straight line; hence uniform disk travel during the closing operation would be accompanied by a nearly uniform velocity decrease.

Now, if a length of pipe equal to 1000 or 10,000 pipe diam be connected to the discharge side of the valve, then the flow characteristic will be determined by the resistance of the valve and pipe as a system, rather than by the restraining influence of the valve alone.

Curves 2 and 3 represent those conditions.

Referring to curve 3, it will be noted that if the valve disk be moved 90 per cent of its closing travel, the flow will still be at about 86 per cent of wide-open capacity. (Compares to 14 per cent for valve without pipe.) In this case, most of the flow control takes place during the last small increment of stem travel.

The obvious conclusion is that either manual or mechanical control of valves should be scheduled so as to reduce the rate of

stem travel gradually as the closed position is approached. The extent to which this adjustment should be applied will depend upon the characteristic of the pipe and conduit considered as a whole.

AUTHOR'S CLOSURE

Mr. Van Deventer has raised a most interesting question concerning the relative effect of valve operation when controlling flow in long conduits. These factors can be related with reasonable accuracy by using a calibration of the valve where the pressure drop and discharge capacity at various positions of the valve, from wide open to closed position, has been established. It is possible to co-ordinate this data with the friction factor of the lines being controlled and thus secure the net effect of the valve. This will then give the rates at which flow is cut off as the valve travels through its stroke.

It would appear from Fig. 11 that the gate valve acting alone showed almost a uniform rate of change of flow, which is rarely found in any control valve. The normal characteristics of a gate valve operating at free discharge or in a pipe line usually looks more like curve *B* in Fig. 4a in the author's paper. The same comment would apply to some degree to the curve in Fig. 11 with the valve in combination with various lengths of pipe. It would be interesting to know whether the curves in this illustration were developed from actual tests or whether it was assumed that flow varied uniformly with the area through the valve, neglecting changes in the discharge coefficient.

P

The
prob
flow
situa
main

It
bend
old
length
of los
and
than
two
are
given
metr
than
latic
some
the p
from
or ve
tests
smoo
roug
invol
tion
lelin
that
relia
diffe

tion
latic
it is
over
test
tion

S

flow
is no
Emo
test
lish
work
same
Si

1 C
Fello
2 N
page
Co
Petro
Okla
Engi
No
stood
Soci

Pressure Losses in Tubing, Pipe, and Fittings

By R. J. S. PIGOTT,¹ PITTSBURGH, PA.

This paper is a continuation of the second half of the problem involved in the writer's 1933 paper on pipe flow and Prof. Lewis F. Moody's 1944 paper. The pipe-flow situation is shown to be in satisfactory condition; the main attention is on bends and fittings.

It has been customary in the past to rate the losses in bends and fittings as a function of velocity head. Another old method, less used, was to rate the loss in equivalent length of pipe. In the case of bends and fittings two types of loss are superposed, i.e., skin friction or pipe-loss type, and bend loss. The methods of test are less accurate than for pipe as they involve getting the difference between two much larger readings. Consequently the test data are much poorer than for pipe, for several reasons: one given above; another that the pipe fittings are not geometrically similar; and the test data are very much less than those on pipe. It seems clear that a rational formulation, however, could be attempted if we can establish some picture of the factors involved in the losses. Up to the present time bend and fitting losses have been taken from a range of factors unconnected with size, roughness, or velocity of flow. This formulation, on the basis of the tests, endeavors to show that there is a true bend loss for smooth fittings underlying the superposed losses due to roughness and Reynolds number. The final formulation involves an evaluation of the true bend loss and an evaluation of the roughness and Reynolds number effects paralleling the friction factor in pipe. The final conclusion is that the equivalent pipe length is by all means the most reliable and convenient method of tabulating losses in different kinds of fittings and bends. The final formulation is $\xi = \xi_1 + \xi_2 = 0.106 \left(\frac{r}{d}\right)^{-2.5} + 2000f^{0.5}$. This formulation has been checked against the test results and while it is obvious that the factors will be both plus and minus over a considerable range, the general correlation of the test data appear to be as good as our present test information will permit.

SINCE Osborne Reynolds' development of the Reynolds criterion dp/μ , a great variety of empirical and limited-range formulations for the variation of pressure drop with flow rate continued in use because the effect of surface roughness is not covered in Rn . In 1931 and 1932, the author and Dr. Emory Kemler undertook analysis of all published data on flow test of water, oil, air, and steam, the results of which were published by Dr. Kemler (1)² in 1933. This study was the groundwork on which the author's hypothesis that roughness had the same effect as reduction of diameter was based (2).

Since 1933 this formulation of friction factor has received

rather general adoption, and there is now ample proof of its advantages and much more general application over the earlier formulations. For example, extensive tests on commercial crude-oil pipe lines by W. B. Heltzel (Stanolind) and by Standard Oil of New Jersey, 6-in. to 12-in. sizes, and tests on gasoline in drawn aluminum tubing by CRC (Dr. O. C. Bridgeman, Bureau of Standards) both corroborate the corresponding curves in the formulation.

In 1944 Prof. Lewis F. Moody made a further valuable improvement (3). By the use of the Colebrook equations (4), he established smooth curves for f versus Rn for each relative roughness, and also confirmed the important fact that at some Reynolds number for each relative roughness, the friction factor ceased to vary with Rn and became a constant. This condition had been uncovered 30 or more years ago by Prof. W. S. Pardoe to be the case for Venturi-meter coefficients. Since the reduction of coefficient from a value of 1.00 in a properly designed Venturi is due to skin friction, it acts like a pipe, and the evidence of hundreds of highly accurate Venturi tests is that for each size and roughness, at some Reynolds number and above, the coefficient becomes constant. A similar behavior is also found for long-radius nozzles (ASME Special Research Committee on Fluid Meters).

The formulas for pipe flow are given again in the following:

Viscous or laminar flow

$$\text{Round pipes, } \Delta p = \frac{0.00691 \mu l v}{d^2} \dots \dots \dots [1]$$

For pipes or conduits not circular, the following formula for shapes where the maximum diameter is not more than 25 per cent greater than minimum diameter, is

$$\text{Approximately circular or rectangular } \Delta p = \frac{0.000432 \mu l v}{M^2} \dots [2]$$

For shapes greatly different from circles or squares, such as capillary slits or bearing clearances, it has been demonstrated by J. M. Cunningham that Equation [2] is not exact; in fact, for the capillary slit, such as a bearing clearance, the value of Δp correctly calculated, is just 1.5 Δp calculated by Equation [2].

Viscous flow, that is, flow below the critical velocity where $Rn = 1200$ to 2500, is likely to be found in heavy crude-oil pipe lines, most oil lines between oil tank and engine, internal lubrication passages such as drilled crankshafts, oil galleries, drilled connecting rods, and all bearing clearances. It will also be found in drill pipe and hole when handling mud in oil-well drilling, in cement slurries, and heavy sewage.

Turbulent flow will be found in practically all cases involving water, air, natural and manufactured gas, and steam.

Turbulent flow, $Rn > 2500$

$$\text{Round pipes } \Delta p = \frac{0.000108 f l v^2}{d} \dots \dots \dots [3]$$

$$\text{Other shapes } \Delta p = \frac{0.000027 f l v^2}{M} \dots \dots \dots [4]$$

In the case of turbulent flow, there is no limitation on Equation [4] as to shape, and the mean hydraulic radius is a fully satisfactory criterion which was not the case in viscous flow.

¹ Chief Engineer, Gulf Research and Development Company, Fellow ASME.

² Numbers in parentheses refer to the Bibliography at the end of the paper.

Contributed by the Petroleum Division and presented at the Petroleum Mechanical Engineering Conference, Oklahoma City, Okla., October 2-5, 1949, of THE AMERICAN SOCIETY OF MECHANICAL ENGINEERS.

NOTE: Statements and opinions advanced in papers are to be understood as individual expressions of their authors and not those of the Society. Paper No. 49-PET-22.

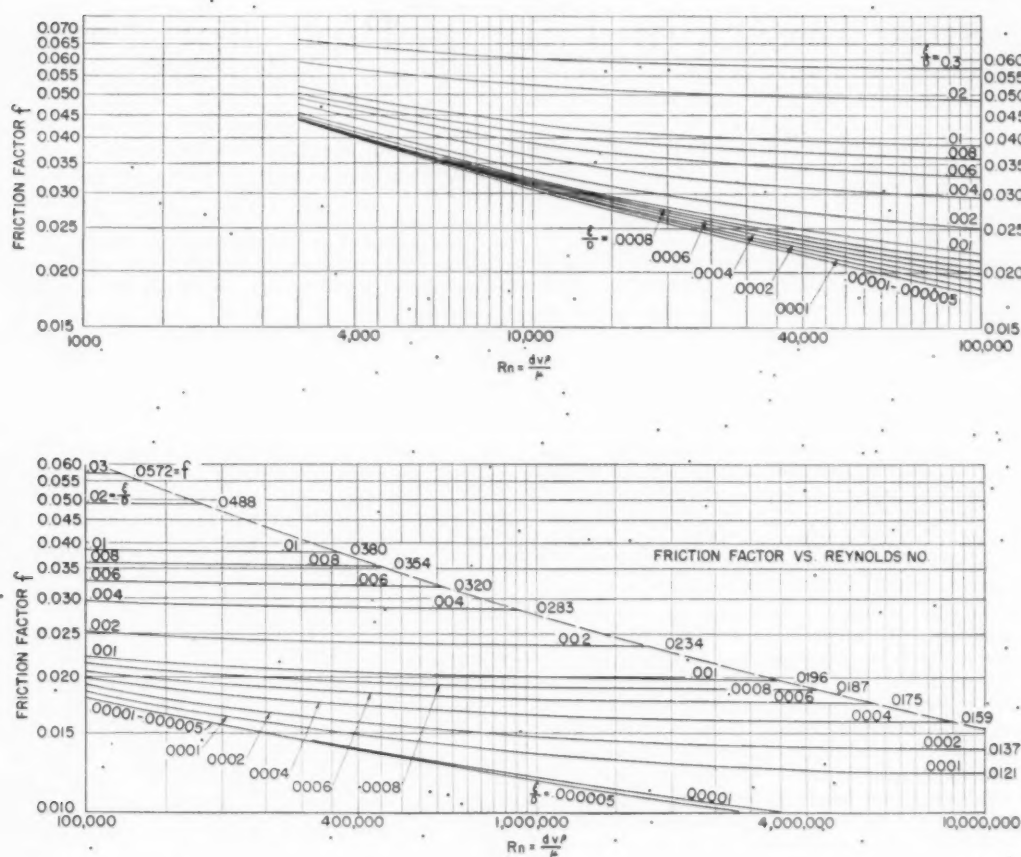


FIG. 1

Professor Moody's plot of f versus Rn was arranged with different log scales for f and Rn ; this gives a convenient sized plot for compactness; but the f lines at each value of ϵ/r are quite sharply curved. The original-type plot, Fig. 1, with equal coordinates gives no higher accuracy, but the f lines are so nearly straight over large ranges that generally the whole range of flow likely to be of interest in any particular case can be conveniently predicted by the relation

$$\Delta p \propto v^{2-n} \quad [5]$$

where n is the slope of the f line for the particular roughness. This procedure offers the convenience that only one flow rate need be calculated by Equation [2]; all other values may be obtained from this value by using Relation [5]. Table 1 gives the roughness for the commonly used materials.

It is of interest to note that, within the ordinary design range, the values in the author's 1933 plot and Professor Moody's 1944 improved plot do not differ over ± 2.5 per cent, and this is well within the limits of accuracy even for smooth pipe (± 5 per cent). Our selection of ϵ/d for the rougher pipes such as old cast-iron, concrete, or riveted pipe is open to still wider errors.

We have for the past decade been in a satisfactory position in so far as calculating pipe friction with sufficient accuracy is concerned; but the other half of the task, the losses in bends and pipe fittings, has hitherto not been covered in any consistent manner.

TABLE 1 RELATIVE ROUGHNESS ϵ/d

	Brass and Tubing	Galv. Air Duct	Steel Pipe	Asphalted Cast Iron	Galv. Steel	Cast Iron	Concrete Smooth	Concrete Average
1/2	.000107		.0032		.0120	.0206		
3/4	.000076		.0022		.0080	.0136		
1	.000057		.0017		.0060	.0102		
1-1/4			.0014		.0050	.0081		
1-1/2	.000046		.0012		.0040	.0069		
2	.000029	.00015	.00090		.0030	.0051		
2-1/2	.000021	.00012	.00070		.0026	.0041		
3	.000020	.00010	.00060	.00150	.0020	.0034	.0065	.016
4	.000015	.000075	.00045	.00120	.0015	.0026	.0030	.012
6	.000010	.000050	.00030	.00090	.0010	.0017	.0020	.0080
8		.000038	.00021	.00080	.00075	.0013	.0015	.0060
12		.000018	.00010	.00040	.00040	.00070	.0012	.0050
16	.000005	.000025	.00015	.00030	.00030	.00050	.0010	.0040
20			.00010	.00020	.00020	.00040	.00080	.0030
24		.000013	.000075	.00010		.00030	.00050	.0020
36			.000050	.00010		.00020	.00030	.0010
	Riveted Light	Riveted Heavy						
3	.0120							
6	.0090							
8	.0065							
10	.0045	.005						
12	.0030	.003						
16	.0021	.002						
20	.0016	.0015						
24	.0015	.0015						
36	.0010	.0010						
72		.0005						
144		.00025						

NOTE: The 12-in.-diam values are also the absolute roughness; ft.

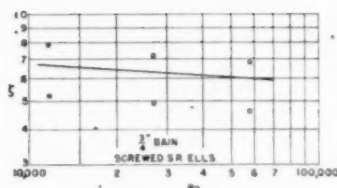


FIG. 2

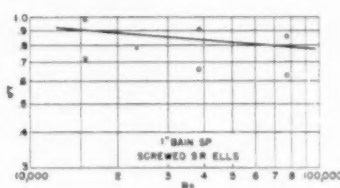


FIG. 3

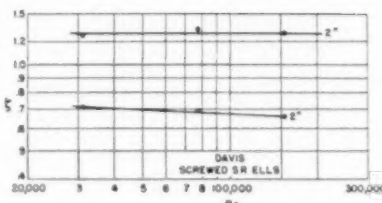


FIG. 4

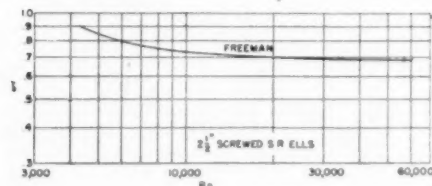


FIG. 5

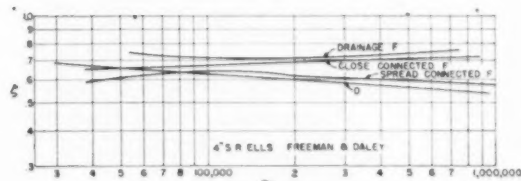


FIG. 7

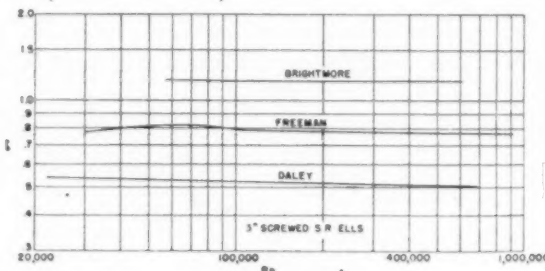


FIG. 6

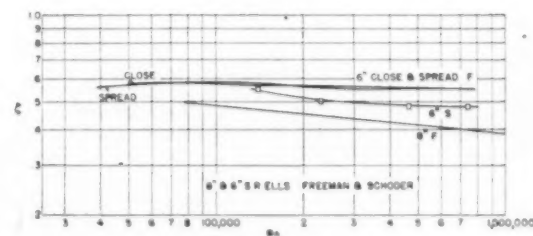


FIG. 8

PREDICTING LOSSES IN BENDS AND FITTINGS

The problem of predicting losses in bends and fittings is much more uncertain than for pipe for the following reasons:

1 The mechanism of flow is not clearly defined; at least two types of loss are superposed—skin friction (pipe loss), and bend loss.

2 The dimensions of fittings, particularly screwed fittings, vary both in the actual body diameter and the ratio of diameter to radius of bend r/d , as commercially produced.

3 The method of test involves taking differences between relatively much larger readings, and the disturbances in flow occasioned by the fitting are not usually completely eliminated at the outlet thereof. In pipe flow, consistency between tests on brass tubing varies ± 5 per cent, clean steel ± 10 per cent, and for the rougher materials, up to ± 30 per cent. Furthermore, for fittings, the variations between tests by different experimenters, and different fittings by the same experimenter, may vary more than 300 per cent.

4 There are very much less test data for fittings and bends than for pipe.

Probably the most extensive and accurate test data on fittings are those by J. R. Freeman (5), covering a range from $2\frac{1}{2}$ in. to 8 in. diam, several r/d values, and both screwed and flanged types. With this range of sizes, Freeman's work could be supplemented by the work of others, down to $\frac{3}{4}$ in., with some assurance that the correlation would be good enough to furnish a base for rationalization.

The test data have first been plotted ζ versus Rn .

NOMENCLATURE

The nomenclature used is given as follows:

d = pipe diameter, ft

v = average velocity, fps $\left(\frac{Q}{(\pi/4d^2)} \right)$

Q = volume flow, cfs

ρ = density of fluid, lb per cu ft

μ = absolute viscosity, ft-lb-sec units, ($= 0.000672 \times$ centipoises)

f = friction factor, a number

l = length of pipe, ft

l_e = equivalent length of pipe for ζp

l_f = length of fitting flow path, ft

M = mean hydraulic radius $\left(\frac{\text{area}}{\text{wetted perimeter}} \right) = (d/4 \text{ for round pipe})$

ϵ = absolute roughness, ft

$\frac{\epsilon}{d}$ = relative roughness, a number

ζ = bend loss factor, a number; does not include pipe friction; fraction of velocity head

ζ_1 = true bend loss factor, a number

ζ_2 = Rn and roughness factor, a number

p = pressure, psi

Δp = pressure loss, psi, for length l

Rn = Reynolds number $\frac{dv\rho}{\mu}$ or $\frac{4Mv\rho}{\mu}$

r = radius of bend, ft

In all cases the values of ζ are for bend loss only. The pipe friction for the length l_f of the fitting path is eliminated; this has been the customary method of handling.

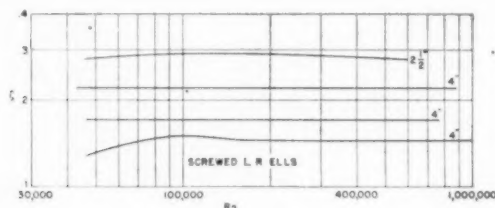


Fig. 9

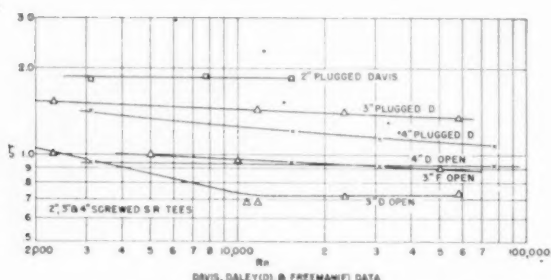


Fig. 11

TEST DATA

Figs. 2 to 8, inclusive, show test data for short-radius (SR) screwed elbows. Test points have been omitted for all Freeman data as there are from 15 to 20 or more points for each, and the curves are simply replotted from the Freeman report (5).

For all other investigators except Hopmann, the experiments were much less extensive, usually 2 or 4 points for each fitting. The scatter is so great as to render any combination of the curves on a single sheet too confusing to read.

Figs. 9 and 10 show long-radius elbow tests (Freeman). Fig. 11 shows SR tees, flow entering run, with the leaving end of the run both plugged and open. Plugging the run end of these tees shows a higher loss than when opening free into the pipe. Plugging in this case is equivalent to converting the tee into a very rough miter bend, and is not a normal use of the tee.

Fig. 12 shows three other sizes of SR tees and two sizes of long radius. Plugging in the case of the long-radius tees does not affect the turn loss, as there is a sufficient length of water between the turning point and the plug, and it behaves the same as if open to the line.

Fig. 13 shows five sizes of short-radius tees, flow entering the branch, and one size of long-radius tee.

An examination of these curves, Figs. 2 to 13, inclusive, discloses some facts likely to be of use in spite of bad scatter.

1 Generally the curves show a decrease of f with increase of R_n at the lower values of R_n , and are flat at higher values of R_n . One or two which show apparent increase of f with R_n are for few test points and probably due, therefore, to experimental error.

2 There is a definite reduction of f with size at the same value of R_n . Since cast iron has the same absolute roughness for all sizes, this means that f varies with relative roughness independently of R_n .

3 There appears to be no difference in f for screwed and flanged fittings.

From Figs. 1 and 2 we may infer that the variation of f is rather similar to f for pipe flow; at low R_n values f decreases with

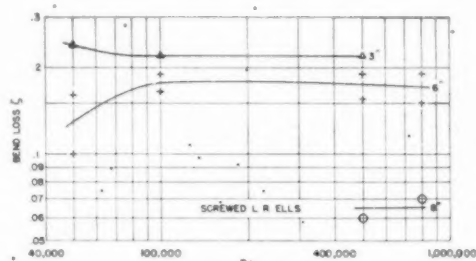


Fig. 10

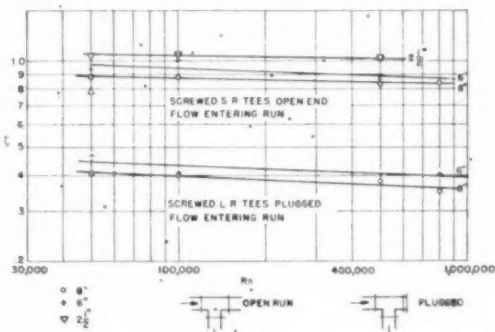


Fig. 12

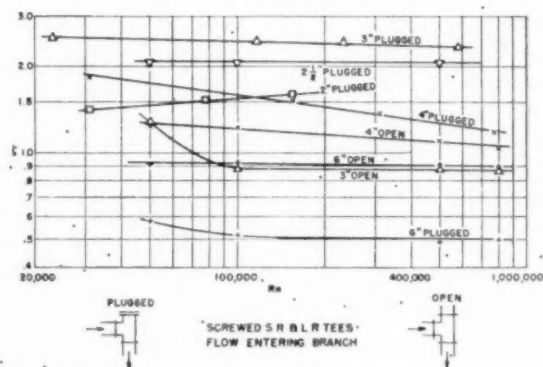


Fig. 13

increase of R_n and then becomes constant for further increase.

In so far as can be determined from the relatively small amount of data and bad scatter, for the rougher surfaces (cast iron in small sizes), the value of f becomes constant at about the same R_n as f in the Moody chart for pipe. In the smoother materials, f becomes constant at lower values of R_n , than f .

Fig. 14 shows the test results on bends, mostly steel pipe (7, 8, 9; 11, 12). In this figure are plotted some screwed and flanged (S and F) cast-iron ells; likewise some small aluminum tubing and Hofmann's (6, 10) two sets of tests on machined brass bends, both smooth and artificially roughened with sand and varnish coating. The scatter is again bad, but again there is a general decrease of f with roughness.

Fig. 15 shows test results on 3-in., 12-in., and 33-in. air duct. Even for 12-in. square, on which most of the data were taken, the

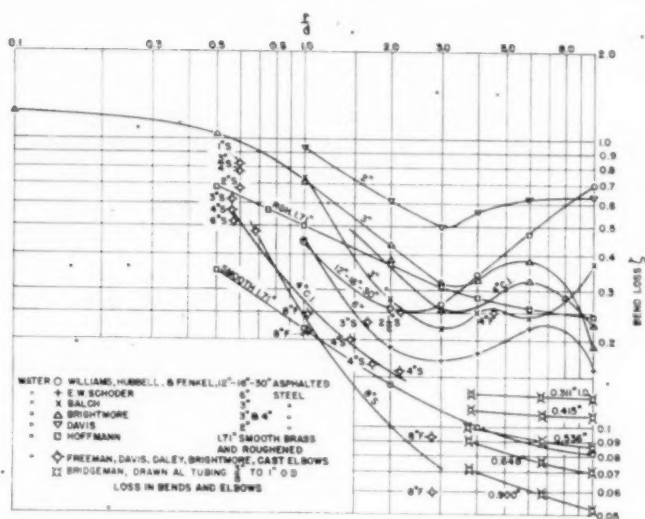


Fig. 14

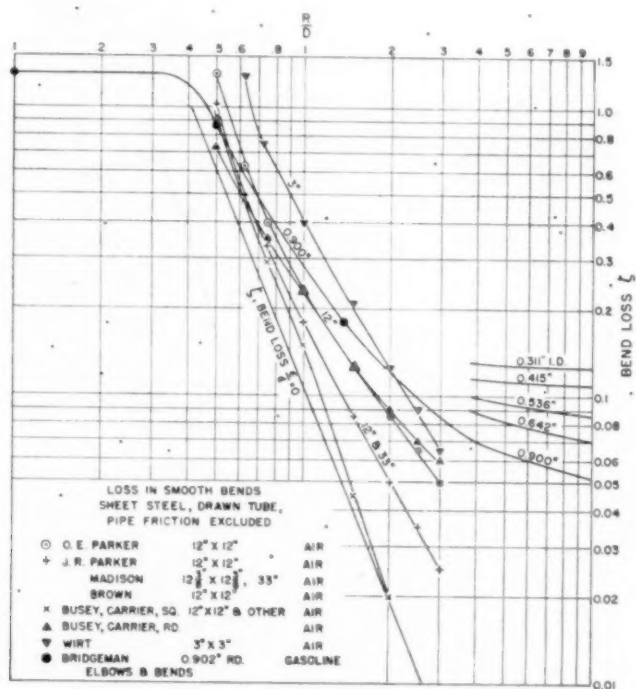


Fig. 15

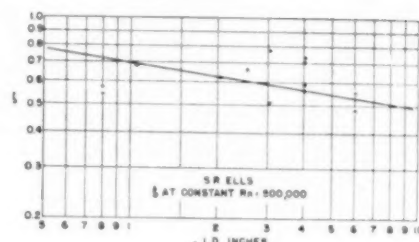


Fig. 16

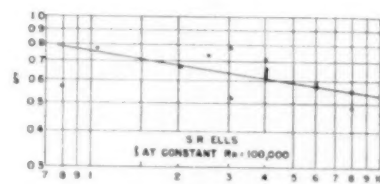


Fig. 17

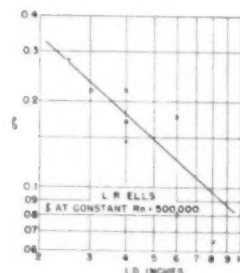


Fig. 18

CORRELATION OF DATA

Fig. 16 shows the values of ζ with size, for cast-iron, short-radius elbows, at $Re = 100,000$; and Fig. 17 the same, at $Re = 500,000$. Fig. 18 shows the same for long-radius, cast-iron elbows at $Re = 500,000$.

These three curves show the nature of the ζ variation with size in a single material, and, consequently, with relative roughness. The rest of the curves for tees, steel bends, and air ducts are not given, as the sample curves are enough to establish the nature of the variation. Using the same plots for tests of SR tees, it was found that the average ζ for flow entering the run, leaving the branch (same size) averaged 1.48 times that for the corresponding elbow. For flow entering the branch, leaving the run, 1.95 times that for the ell. Factors of 1.50 and 2.00 seem satisfactory. The plugged short-radius-tee runs are disregarded as they uniformly show high values, and in any case, are not the normal use of the tee, practically converting it into a rough miter elbow. The value for long-radius tees is correspondingly 2.50 times that for short-radius elbows for both cases of flow entry through run and through branch.

We may now, with the foregoing data, attempt to find some formal relationship.

Inspection of Figs. 14 and 15 shows quite plainly that there is the expected reduction of ζ with increase of r/d ; an obvious variation of ζ with ϵ/d ; and since the values of ζ are all high at low values of r/d , roughness alone cannot account for all the variation in ζ and there is likely to be an underlying true bend

scatter is considerable as r/d increases; this could be expected, as the value of ζ is a very small difference between two relatively large values (total loss — pipe friction).

Both Fig. 14 and Fig. 15 were plotted on data at the higher values of Re , where ζ had become substantially constant. In these curves, therefore, variation of Re is eliminated, leaving only r/d and ϵ/d variation.

The foregoing figures comprise substantially all of the reliable data and we can attempt correlation.

loss for dead smooth materials (which of course do not exist) that is dependent only on r/d .

TEST PLOTS OF VARIOUS MATERIALS

The first move was to plot tests of each kind of material (same absolute roughness) on several kinds of co-ordinate paper to indicate trends. The plot chosen was relative roughness (ϵ/d) versus ξ . The semilog plot proved the most useful as the intercept at $\epsilon/d = 0$ should be the approximate value of the dead smooth pipe-bend loss. These plots are not given since they are merely the working means of approximately the quantities we want. At this point it appeared that the total loss in an elbow or bend is likely made up of three elements:

- 1 The ordinary pipe friction.
- 2 A minimum true bend loss for dead smooth conduit, depending only on r/d .
- 3 A turbulence loss due to the relative roughness of the pipe and affected by Reynolds number and roughness.

Since we are dealing with ξ in the more usual way, pipe friction for the fitting or bend is eliminated (calculated separately with the rest of the pipe friction), and we need only deal with the items 2 and 3.

From the ξ versus ϵ/d plots, it was found that the value of ξ_1 , the zero roughness loss, was between 0.40 and 0.50 at $r/d = 0.58$; and 0.02 to 0.09 for $r/d = 1.78$, except for some of the steel pipe bends which are higher.

Using the range just given, the line for ξ_1 was drawn in Fig. 15, corresponding to the equation

$$\xi_1 = 0.106(r/d)^{-2.5} \quad [6]$$

This line shows a satisfactory slope referred to the test curves, and leads us to the next step. Subtracting the values of ξ_1 from the test value of ξ , yields ξ_2 , the roughness and Reynolds-number factor.

Since in pipe friction f covers both Reynolds number and roughness, and since the value of ξ seems to vary in much the same way as f , with Rn , it appeared that a good plot would be ξ_2 versus f . The value of f is taken for the fitting or bend roughness. The correlation was closest for

$$\xi_2 = 2 \times 10^3 f^{2.5} \quad [7]$$

Of course it must be admitted that other power correlations fit nearly as well, since the scatter of test points for ξ_2 is several hundred per cent. The correlation was tried for both ξ_1 and ξ_2 at powers of 2, 2.5, and 3.

Comparing with other methods of estimating ξ , most of these have been based upon a straight velocity-head relationship, no variation with Rn or ϵ/d . Examination of all the test data compels one to recognize that ξ does vary with both Rn and ϵ/d , the same as f , and not alone with $(v^2)/(2g)$.

The Tentative Standards of the Hydraulic Institute, which are probably the latest collection of data from many sources, have been checked against this present formulation

$$\xi = \xi_1 + \xi_2 = 0.106 \left(\frac{r}{d} \right)^{-2.5} + 2000 f^{2.5} \quad [8]$$

For example, the range of values given in the Hydraulic Institute standards for short-radius screwed elbows corresponds to $1\frac{1}{4}$ in. to 6 in. by Equation [8]. For flanged short-radius elbows, the Hydraulic Institute range of values covers the 3-in. to 12-in. range by Equation [8].

The formulation also agrees well with the air-duct tests, but is considerably lower than the test data for steel bends, except for one case. There appears to be a reason: With the exception of

Freeman, Bridgeman, and Hofmann, most investigators took fitting or bend loss close to the fitting or bend. This procedure can give erratic results, which are quite evident in Fig. 14. It is clear that the up and down variation with r/d is completely inconsistent for various sizes. It does not seem possible for the resistance of a bend, less the pipe friction, to increase to a higher value at $r/d = 10$ than at $r/d = 1$. The air-duct and smooth-tube experiments do not show any such inconsistent behavior. One other point—the tests on steel bends are generally relatively old, made at a time when steel pipe was rolled considerably rougher than now; much of present production is from smooth rolled plate, or seamless. The greater roughness undoubtedly raised the ξ -values. Moreover, in some cases, cast-iron bends were included with steel, of course raising the averaged results.

The Hofmann tests on a surface as rough as cast iron bear out this view. It seems quite unreasonable to suppose that cast-iron fittings, both short and long radius, should be considerably below steel, a smoother material. The author has given the most weight to Freeman's work, after that to Hofmann's, and the investigators of air-duct bends. These are much more consistent between different experimenters than the steel-pipe tests. The formulation also yields results agreeing quite well with the drawn aluminum-tube tests by CRC (Bridgeman) and fairly well with Hofmann's smooth-tube data. However, the latter gives values for ξ below the true bend loss at values of r/d from 0.5 to 1.0; and higher than Bridgeman at values of r/d greater than 1.0.

PRESENT-DAY STEEL-PIPE VALUES

Therefore it would seem reasonable to assume, since Equation [8] gives results in good agreement with tests on the roughest material, cast iron, and with the smoothest materials, drawn tube and air duct, that the values calculated from Equation [8] for present-day steel pipe are probably nearer the truth than the older steel-pipe tests on a material definitely rougher than now and including some cast iron. This formulation attempts a consistent, rationalized expression for ξ to overcome the rather haphazard and wholly unrelated values hitherto used. This formulation is thought to be justified by the following:

1 ξ has hitherto been treated as corresponding to velocity head and r/d only. Tests show (particularly the more recent work) a definite variation of ξ with Rn and ϵ/d .

2 The use of a formulation covering Rn , ϵ/d and r/d renders results consistent and eliminates the use of range of values, to be selected on judgment alone.

3 The older simple method of equivalent pipe-loss computation may be developed safely.

Referring to item 3, it becomes clear that since ξ_2 , involving f , is always a substantial fraction of ξ , the old method of representing fitting and bend loss by length of equivalent pipe is not only likely to give good accuracy, but eliminates all the work of calculating the power formula, Equation [8], if tables are set up. The friction loss for equivalent length of pipe is

$$\Delta p_e = (0.000108 \rho v^2) \frac{f l_e}{d} \quad [9]$$

The bend loss, not including pipe friction, is

$$\Delta p_b = \xi (0.000108 \rho v^2) \quad [10]$$

Therefore the value of ξ in terms of feet of pipe of the same roughness is

$$l_e = \frac{\xi d}{f} \quad [11]$$

The calculated values of ξ for cast-iron elbows are given in

Fig. 1
sheet 1

3/4
1-1/2
2
3
4
5
6
7
8
9
10
11
12
13
14
15
16
17
18
19
20
21
22
23
24

3/4
1-1/2
2
2-1/2
3
4
5
6
7
8
9
10
11
12
13
14
15
16
17
18
19
20
21
22
23
24

3
4
5
6
7
8
9
10
11
12
13
14
15
16
17
18
19
20
21
22
23
24

.511
.415
.336
.268
.200
.141
.100
.071
.051
.036
.026
.018
.013
.009
.006
.004
.003
.002
.001

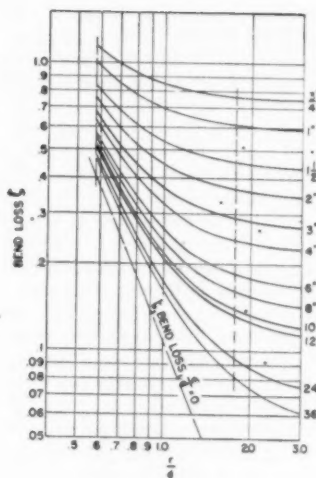


FIG. 19

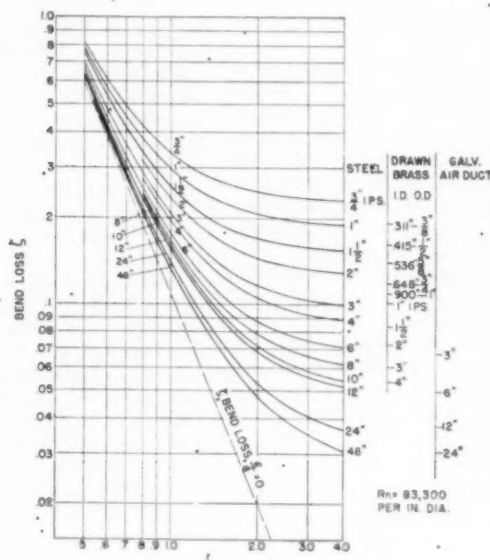


FIG. 20

Fig. 19. Those for drawn tubing, steel pipe, and galvanized-sheet air duct are given in Fig. 20. Table 2 gives the calculated

 TABLE 2 CALCULATED f

$$f = 0.106 \frac{r^{-0.85}}{d} + 2000r^{0.85}$$

C.I. Pipe

	$f = 0.5$	$f = 0.58$	$f = 1$	$f = 1.78$	$f = 2$	$f = 3$	$f = 4$
3/4	1.158	.850	.769	.763	.753	.749	
1	1.002	.694	.613	.607	.596	.591	
1-1/2	.844	.556	.455	.449	.437	.433	
2	.754	.445	.355	.359	.347	.343	
3	.679	.370	.289	.293	.271	.267	
4	.633	.325	.244	.238	.226	.222	
6	.575	.267	.196	.190	.168	.164	
8	.550	.242	.162	.155	.143	.139	
10	.528	.220	.139	.132	.114	.110	
12	.521	.213	.132	.124	.114	.110	
24	.483	.176	.094	.088	.076	.072	
36	.459	.161	.080	.074	.062	.058	

Steel

	$f = 0.5$	$f = 0.58$	$f = 1$	$f = 1.78$	$f = 2$	$f = 3$	$f = 4$
3/4	.829	.644	.535	.525	.515	.511	
1	.760	.603	.495	.485	.475	.471	
1-1/2	.752	.567	.459	.449	.439	.435	
2	.726	.541	.433	.423	.413	.409	
2-1/2	.706	.521	.413	.403	.393	.389	
3	.697	.512	.404	.394	.384	.380	
4	.686	.501	.393	.383	.373	.369	
6	.660	.483	.375	.365	.355	.351	
8	.650	.474	.366	.356	.346	.342	
10	.652	.467	.359	.349	.339	.335	
12	.646	.460	.352	.342	.332	.328	
18	.642	.457	.349	.339	.329	.325	
20	.638	.453	.345	.335	.325	.321	
24	.634	.449	.341	.331	.321	.317	

Air Duct

	$f = 0.5$	$f = 0.58$	$f = 1$	$f = 1.78$	$f = 2$	$f = 3$	$f = 4$
3	.644	.479	.371	.361	.351	.347	
6	.646	.481	.373	.363	.353	.349	
12	.634	.469	.361	.351	.341	.337	
24	.627	.462	.354	.344	.334	.330	

Drawn Tubing, Brass or Other

	$f = 0.5$	$f = 0.58$	$f = 1$	$f = 1.78$	$f = 2$	$f = 3$	$f = 4$
.311	.769	.603	.495	.485	.475	.471	
.415	.760	.594	.486	.476	.466	.462	
.536	.737	.571	.463	.453	.443	.439	
.648	.718	.552	.444	.434	.424	.420	
.900	.706	.540	.432	.422	.412	.408	
1 I.P.S.	.698	.532	.424	.414	.404	.400	
1-1/2	.690	.524	.416	.406	.396	.392	
2	.682	.516	.408	.398	.388	.384	
3	.657	.491	.383	.373	.363	.359	
4	.650	.485	.377	.367	.357	.353	

become constant, and this is near enough to the usual design maximum flow to be satisfactory. To make sure of the values of f at lower flows, in which we are occasionally interested, the calculated values were checked for lower R_n values. Since they are affected by f , they follow the test curves, Figs. 2 to 15, quite reasonably.

values by Equation [8], from which these curves were plotted.

Applying Equation [11] to this table gives the equivalent feet of pipe; but we use both cast-iron and steel pipe with cast-iron and steel fittings, and brass pipe with cast-brass fittings. Therefore we need three sections, for the three line materials, using the f for maximum design flow for cast-iron, steel, and drawn tube for the three cases. The values are given in Table 3. For bends, the bend and the line material will be the same. Table 4 gives the equivalent pipe length; since galvanized air duct is near to drawn tube in roughness, the equivalent lengths come out so nearly alike that they could be combined in one set of figures. All of these tables have been based on the values of f after R_n was great enough to

TABLE 3 EQUIVALENT FEET OF STRAIGHT PIPE

Cast 90-deg Elbows

CAST 90 DEG. ELBOWS

	C.I. Pipe		Steel Pipe		Brass Pipe	
	$f = 0.58$	$f = 1.78$	$f = 0.58$	$f = 1.78$	$f = 0.58$	$f = 1.78$
3/4	1.0	1.2	2.9	1.9	3.9	2.5
1	2.2	1.6	3.5	2.1	4.7	3.1
1-1/2	2.7	1.5	3.6	2.3	4.3	3.1
2	3.2	1.7	4.9	2.6	6.2	3.3
2-1/2	5.1	2.2	6.2	2.9	7.8	3.7
3	6.1	2.5	7.6	3.3	9.4	4.1
4	6.1	2.5	8.8	3.5	11.0	4.4
6	12.4	2.9	11.5	4.2	14	5.1
8	17	3.8	17	5.3	20	6.3
10	22	5.6	30	7.7		
12	27	6.4	37	8.9		
24	59	11.1				
36	93	16				

TABLE 4 EQUIVALENT FEET OF STRAIGHT PIPE

90-deg Bends

		Brass Tub. & Pipe, Sheet Steel Ducts				Steel Pipe			
OD	ID	$f = .5$	$f = 1$	$f = 2$	$f = 3$	$f = .5$	$f = 1$	$f = 2$	$f = 3$
	3/8	.311	.32	.31	.22	.20			
	1/2	.415	1.1	.39	.27	.26			
	5/8	.536	1.5	.49	.32	.29			
	3/4	.648	1.9	.59	.36	.32			
1	1	.769	2.7	.72	.41	.37			
	3/4 I.P.S.	2.3	.72	.41	.38				
		2.2	.93	.53	.45	2.3	.81	.59	.55
1-1/2	1	4.1	1.2	.62	.52	1.2	1.2	.71	.65
	1-1/2	5.1	1.4	.71	.59	1.2	1.2	.78	.71
2	2	6.9	1.8	.88	.71	1.4	1.4	.94	.88
	2-1/2	9.1	2.2	1.1	.84	1.4	1.4	1.2	1.2
3	3	12.9	2.7	1.2	1.0	1.3	2.3	1.5	1.3
	4	15	3.6	1.6	1.2	20	5.2	2.6	2.1
6	6	24	5.4	2.2	1.9	29	7.1	3.3	2.6
10	10					37	8.9	3.9	3.0
12	12	11.6	11	4.2	2.9	46	11	4.6	3.4
18	18					64	15	5.7	4.2
24	24					82	19	6.9	5.0
30	30	11.7	26	8.0	4.8	102	22	8.2	5.0

CONCLUSIONS

It has been believed generally that screwed fittings of given r/d offered higher resistance than the corresponding flanged fittings. The test evidence, mostly Freeman, does not support this view. The reason is that all the screwed fittings average approximately 12 to 15 per cent larger diameter of body than the inside pipe diameter; this circumstance lowers the turbulence effects sufficiently to offset the loss due to enlargement of section leaving the pipe at entry of the fitting, and the subsequent contraction at exit from the fitting to the line again.

This formulation (Equation [8]), cannot of course be considered final, and it must be admitted it takes an optimist to take the necessary risks with such scattering data.

With regard to gate and globe valves, check valves, unions and couplings, it is thought that skin friction has little part, and that the sharp turns, changes of section, contractions and expansions are the principal cause of loss. Therefore in these cases ξ can be treated as largely varying with velocity head only.

BIBLIOGRAPHY

- 1 "A Study of the Data on the Flow of Fluids in Pipes," by Emory Komler, Trans. ASME, Hydraulics Institute, HYD-55.2, vol. 55, 1933, pp. 2-22.
- 2 "The Flow of Fluids in Closed Conduits," by R. J. S. Pigott, *Mechanical Engineering*, vol. 55, 1933, pp. 497-501 and 505.
- 3 "Friction Factors for Pipe Flow," by L. F. Moody, Trans. ASME, vol. 66, 1944, pp. 671-678.
- 4 "Turbulent Flow in Pipes, With Particular Reference to the Transition Region Between the Smooth and Rough Pipe Laws," by C. F. Colebrook, *Journal of the Institution of Civil Engineers*, London, England, vol. 11, 1938-1939, pp. 133-156.
- 5 "Flow of Water in Pipe and Pipe Fittings," by J. R. Freeman, ASME, New York, N. Y., 1941.
- 6 "Loss in 90-Degree Pipe Bends of Constant Circular Cross-Section," by Albert Hofmann, Transactions of Munich Hydraulic Institute, Bulletin No. 3; authorized translation published by ASME, vol. 57, 1935, pp. 29-41.
- 7 "New Data for the Design of Elbows in Duct Systems," by Loring Wirt, *General Electric Review*, vol. 30, 1927, pp. 286-296.
- 8 "Loss of Pressure Due to Elbows in the Transmission of Air Through Pipes or Ducts," by F. L. Busey, Trans. ASH&VE, vol. 19, 1913, pp. 366-376.
- 9 "Pressure Loss in Rectangular Elbows," by R. D. Madison and J. R. Parker, Trans. ASME, vol. 58, 1936, pp. 167-176.
- 10 "CRC Reports on Loss in Aluminum Tubing, Elbows and Fittings, 1939-1940," by O. C. Bridgeman (not published).
- 11 "Pressure Losses for Fluid Flow in 90° Pipe Bends," by K. Hilding Beij, R. P. 1110, Bureau of Standards, vol. 21, July, 1938.
- 12 "Tube Turns, by J. E. Busher, Bulletin 3002, 1937.

Discussion

S. LOGAN KERR.² The author has demonstrated in a very interesting manner the application of the friction-flow theory for pipe lines to the determination of losses in fittings, tubes, and pipes. The comparisons between the various theories are most interesting and confirm the contributions which Prof. Lewis F. Moody made in 1944.

The validity of experimental work in the field of pressure losses in pipes, valves, and fittings is dependent entirely on the methods that are used for measuring pressures and flow. It is well known that pressure taps immediately downstream from obstructions to flow do not give an accurate indication of the head loss. It is necessary to have a series of piezometers above and below the valve or fitting to be investigated, establish from them the normal slope of the pressure loss versus length in straight pipe, then project these lines to the upstream and downstream limits of the fitting or valve, and measure the difference between

them in this manner. These multiple piezometers should be located over a distance of not less than 5 diam upstream and downstream from the valve under test. In some cases, 10 to 15 diam will be necessary in order to develop a uniform straight line of pipe loss with respect to length of pipe.

The use of multiple piezometers also aids in detecting errors due to the improper design of piezometers and of their position with respect to the pipe wall which may affect the readings.

There is some question as to the practice of reporting losses through valves and fittings, and it is important that an accurate definition of gross loss and net loss be included in any test reports or studies of friction loss through valves and fittings.

It is the practice of certain manufacturers of valves and fittings to deduct from the gross pressure drop the amount of friction that would occur in a straight piece of pipe of the same length as the face-to-face dimensions of the valve or fitting. This gives a net pressure loss over and above that in straight pipe. On large valves with high velocities through them, it is essential that a careful designation be made as to whether or not the equivalent straight-pipe loss has been deducted, or whether the loss as reported is for the valve itself without adjustment.

The condition of flow entering the test section is also of great importance, as whirling or eddying of the fluid will affect the piezometer readings. It has been found frequently in larger conduits that the presence of a bend or transition section ahead of the test section will distort the results and make them meaningless. It has also been found that repeat runs at the same velocities will not check each other, due to a so-called "rolling-flow" condition which is not identical in the two series of observations.

Mr. Floyd Nagler reported a number of tests made at the University of Iowa on large rectangular conduits with 90 and 180-deg bends. The variation of test results from one run to another indicated a rolling flow, and visual observations made of the flow pattern showed this very clearly. The roughness factor also must be considered in proportion to the size of the conduit. In analyzing the results of pressure-loss investigations, it is essential to have full data on this factor.

F. M. VAN DEVENTER.⁴ In the author's 1933 paper⁵ he presented the friction-factor relationship using straight lines. The writer is one of the multitude who accepted and used that paper for precise calculations.

The use of that chart involved a supplementary table of pipe sizes and roughness values. That combination of chart and table did not permit smooth interpolation since any reading was taken from one or another of the 18 lines. Thus a comparison of two successive pipe sizes could be quite misleading.

The writer prepared a chart using Pigott's basic data, but with scales appended for steel, cast iron, and drawn tubes. Thus, for most problems, reference to a supplementary table was avoided and smooth interpolation obtained. That chart was published in the general catalog 1937, 1942, and 1947 editions of the writer's company.

As the author has reported, Professor Moody, in his 1944 paper,⁶ faired the curves in accordance with the Colebrook equation. He also spaced the plotted lines to correspond to preferred values of relative roughness ϵ/D , and appended a chart from which values of ϵ/D are obtained for known diameter and roughness.

Smith and Shebeko, in designing the "Polyflo" computer, also used the Colebrook data.

The author's present contribution likewise embraces the Colebrook principle and, therefore, yields results commensurate with

⁴ Assistant Chief Engineer, Walworth Company, Inc., New York, N. Y. Mem. ASME.

⁵ Refer to author's bibliography (2).

⁶ Refer to author's bibliography (3).

² Consulting Engineer, Philadelphia, Pa. Mem. ASME.

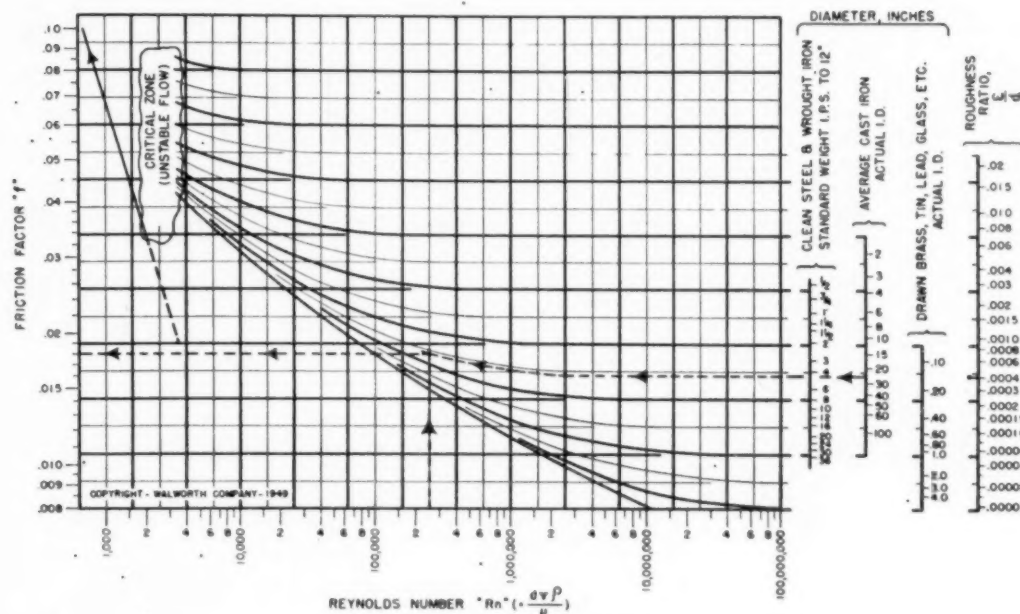


FIG. 21 FRICTION-FACTOR CHART

Moody's. He has adopted ϵ/D in plotting, but again uses a supplementary table from which values of ϵ/D are obtained.

The writer's Fig. 21 is a revision of his 1937 edition, using the Moody and Pigott faired curves. Again, scales are provided directly on the chart for steel, cast iron, and drawn tubes. A fourth scale of ϵ/d values permits solutions involving other materials, provided the absolute roughness is known. Thus reference to supplementary tables or charts is avoided. The use of a uniformly spaced grid also facilitates following the guide lines with a minimum of confusion.

The following statement from the paper requires clarification: "...within the ordinary design range, the values of the author's 1933 plot and Professor Moody's 1944 improved plot do not differ over ± 2.5 per cent..." At Reynolds numbers in the range 100,000 to 1,000,000, the old and new plots cross. At lower Rn , the old values were high, and at higher Rn , the old values become increasingly deficient, e.g., at $Rn = 40,000,000$, the old values were 50 and 40 per cent low for $1/2$ -in. and 2-in. steel, respectively. The author implies that this is not in the "ordinary design range." Albeit, the writer is presently concerned with design problems running the gamut of Reynolds numbers from 500 to 50,000,000. Oil transport lines operate in the 40,000 to 200,000 range, natural-gas transport lines 1,000,000 to 20,000,000, and flow channels feeding supersonic wind tunnels and jet-propulsion devices may exceed 50,000,000. The sooner the author's 1933, and the writer's 1937 friction-factor charts are definitely replaced by the more accurate Moody 1944,—Pigott and Van Deventer 1949 versions—the better.

The author has presented in Figs. 2 to 12, graphs for pipe fittings plotting lambda versus Rn . This nomenclature (lambda) has been used by foreign writers, while most American authors have used K . Either lambda or K is the number of velocity heads lost, or the coefficient K in the formula

$$h = K \times \frac{v^2}{2g}$$

This is not made clear in the paper, though loosely implied in the explanation of symbols.

In the several graphs, only upper and lower limits are plotted. One must still use judgment in selecting a datum between these limits. Such being the case, the same end is attained by tabulating the high and low values as has been done by other authors.

To facilitate the use of lambda or K values the writer offers the following formulas for the evaluation of velocity pressure

$$\text{Fitting turbulence loss, psi} = K \times VP \quad [12]$$

$$VP \text{ for any liquid} = \frac{0.00116 \times \text{gpm}^2 \times G_w}{d^5} \quad [13]$$

$$VP \text{ for any gas} = \frac{0.00113 \times \text{cfm}^2 \times G_a \times Z}{P \times d^5} \times \frac{T}{520} \quad [14]$$

$$VP \text{ for steam} = \frac{0.28 \times 10^{-6} \times \text{lb/hr}^2 \times V}{d^5} \quad [15]$$

where

- psi = loss, psi
- K = fitting factor, or number of velocity heads lost
- VP = velocity pressure, psi
- gpm = gallons per minute
- cfm = cubic feet per minute measured under standard condition, 14.7 psia and 60 F
- lb/hr = pounds per hour, for steam
- d = inside diameter, in.
- G_w = specific gravity relative to water
- G_a = specific gravity relative to air
- P = absolute pressure of flowing gas, psia
- Z = compressibility factor, if gas deviates from Boyles law
- V = specific volume of steam, cu ft per lb

The only objection to the use of the D'Arcy formula is that it is slower and more cumbersome than most of the less precise empirical formulas for specific fluids. It is necessary to obtain from tables, viscosity and density data for the fluid in question. Then two separate solutions must be accomplished: First for Reynolds number, then the basic flow formula. In the interest of time-sav-

ing and facility, several forms of special slide rules or "mechanical brains" have been devised. Some of these are eminently satisfactory. The Polyflo type, for example, is based upon a modification of the D'Arcy formula and yields compatible results. Friction factor is easily compensated for correct e/d . Gage points are provided covering almost any fluid met in general engineering practice; hence reference to viscosity tables is unnecessary. The writer, after extended use of this device, recommends it as a general purpose, time-saving tool.

AUTHOR'S CLOSURE

The author is glad to get Mr. Kerr's support of the idea that for testing of hydraulic elements such as fittings, bends, and valves, great care must be used in placing and instrumenting the readings. It must be admitted that much of the early test data lacks a perception of some of these conditions and therefore has added to the difficulties by giving greater scatter to the results.

In preparing this paper the author was preoccupied chiefly with the task of the ordinary designer of a power or industrial plant where the relatively smaller sizes of materials are much in use. In the line in which Mr. Kerr is most interested, the subject covers, as a general rule, by far the largest sizes of piping with which we are concerned and it is readily agreed both that irregularities of flow, such as rolling flow, and other velocity distortions may take a more prominent part than they are likely to do in smaller sizes. The reason is that we are generally dealing with water (low viscosity) and, in these large sizes, cast iron and concrete have very low relative roughness, and therefore the irregularity of the flow plays a considerably greater part. Almost the only man who widely investigated the difference between close-coupled and spread-fitting configurations was John Freeman and there was no consistency even in his results.

The author feels sure that there are some deviations from average results even in the smaller size of piping which can be produced by piping configuration, such as, for example, two short-radius elbows in planes at right angles to each other. We have not enough data to decide upon what increase of loss would occur from such an arrangement, nor indeed do we know how it might vary with Reynolds number or roughness. It is quite agreed that since the pipe loss per foot of length is small, fitting and bend losses will vary more in the large-sized equipment used in hydraulic plants. The present information we have on valves is relatively unsafe for the large valves used in such plants, particularly where the valves are of special design to reduce loss, for example, the Johnson valve.

Referring to Mr. Van Deventer's discussion, in the author's original 1933 paper¹ the roughness table was prepared from a chart of exactly the same nature as Professor Moody's in his 1944 paper (see Fig. 2 of 1933 paper), but both in his own plots as well as Professor Moody's it was found that many kinds of pipe have a range of values which overlap each other and it gets quite confusing to read the chart without error. It should be borne in mind also that the author spent little time in making convenient charts, but only in getting one idea across, i.e., that the loss in bends and fittings is, in general, not proportional to $V^2/2g$ only, but is affected by Reynolds number, roughness, and a true bend loss; therefore equivalent length of pipe turns out to be both convenient and more accurate. It is felt that it was wiser in a paper such as this to keep the matter purely on the basis of the original argument and to take up the question of plotting for greater convenience separately. The author feels that Mr. Van Deventer's form of plot is going to be very useful.

With regard to his comment on the "ordinary design range," it should be borne in mind again that this paper is in terms of designing so far commonly done in power plants and industrial plants in which the design habits that have been used are something around 80,000–85,000 R_n per in. diam and this applies pretty well both for air and gas, or liquids. In the example which Mr. Van Deventer gave at the meeting, using, if recollection is right, 2 in. pipe on gas, he was dealing with velocity rather close to the acoustic and this is certainly not yet ordinary design. Of course it is true that in the near future, with our ideas opened up during the war period, we may be changing design ranges very considerably.

The author is thankful for the comments by Mr. Kerr and Mr. Van Deventer and wants to reiterate his statement that this was a first crack at the subject. He feels that the values given are not the final ones because there is certainly need of a great deal more testing of elbows and bends than we have had hitherto. It is felt, however, that the use of this method of approach tends to reduce the amount of judgment required of the designer in selecting the values of ξ for any given circumstance. There is not much to be gained by carefully selecting a value by judgment when the variation between tests is in some cases greater than the whole range over which judgment is to be exercised. The writer believes he would rather use a curve which automatically gives better probability in accuracy from a single value.

¹ "Flow of Fluids in Closed Conduits," by R. J. S. Pigott, *Mechanical Engineering*, vol. 55, 1933, p. 497.

A th
ation a
one en
pressu
upon i
elemen
compr
fluid a
Accou
compl
are su
for us
soidal

The

A =
C =
D =
E =
L =
M =
Q =
T =
V =
b =
c =
k =
m =
n =
p =
s =
t =
x =
z =
γ =
δ =
η =
λ =
μ =
ν =
ξ =
ρ =

1 T
proj
2 P
Stand
"Th
in th
Wash
Col
of Tr
at th
St. L
No
under
the S

Attenuation of Oscillatory Pressures in Instrument Lines¹

By A. S. IBERALL,² WASHINGTON, D. C.

A theoretical investigation has been made of the attenuation and lag of an oscillatory pressure variation applied to one end of a tube, when the other end is connected to a pressure-sensitive element. An elementary theory based upon incompressible viscous fluid is first developed. The elementary solution is then modified to take into account compressibility; finite-pressure amplitudes; appreciable fluid acceleration; and finite length of tubing (end effects). Account is taken of heat transfer into the tube. The complete theory is derived in an appendix.³ The results are summarized in eight graphs in a form convenient for use in computing the lag and attenuation of a sinusoidal oscillation in a transmission tube.

NOMENCLATURE

The following nomenclature is used in the paper:

- A = tube area
- C = velocity of sound
- D = inside diameter of tube
- E = elastic modulus
- L = tube length
- M = mass flow
- Q = volumetric flow
- T = absolute temperature
- V = instrument volume
- b = compressibility factor for liquid
- c = any arbitrary constant
- k = compressibility of a liquid
- m = exponent of "polytropic" expansion in instrument volume
- n = exponent of polytropic expansion in tube
- p = pressure
- s = tube-wall thickness
- t = time
- x = axial distance along tube
- z = dimensionless parameter of fluid regime
- γ = ratio of specific heats
- δ = phase angle
- η = density ratio
- λ = time constant
- μ = fluid viscosity
- ν = kinematic viscosity
- ξ = fractional pressure excess
- ρ = fluid density

¹ This work was supported by the Office of Naval Research under a project on "Basic Instrumentation for Scientific Research."

² Physicist, Mechanical Instruments Section, National Bureau of Standards.

³ This paper with a mathematical appendix is also to be published in the *Journal of Research* of the National Bureau of Standards, Washington, D. C.

Contributed by the Industrial Instruments and Regulators Division of THE AMERICAN SOCIETY OF MECHANICAL ENGINEERS and presented at the National Instruments Conference, September 12-16, 1949, at St. Louis, Mo.

NOTE: Statements and opinions advanced in papers are to be understood as individual expressions of their authors and not those of the Society. Paper No. 49-IIRD-5.

χ = attenuation factor

ω = angular frequency

INTRODUCTION

In many industrial processes it is necessary to know or to utilize the pressure at one or more points in a fluid conduit. It is not always possible to connect an instrument directly into the conduit at those points. Instead, recourse must be had to remote indication or control. In the case that a fluid is used for transmitting the pressure, it is often of interest to the designer or user of such systems to know their response to variations in pressure. At the present time, the only solution easily available to the engineer is generally based on an elementary theory which considers the system as equivalent to an R-C electrical network.⁴ The main defect of the theory is that it does not provide criteria for the limits of its applicability.

In the present paper a relatively complete treatment is given for the transmission of oscillatory pressures in tubing. Primary consideration is given to simplifying the design of high-quality transmission systems for relatively low frequencies.

The elementary solution is derived, and then extended to apply for oscillatory pressures that are an appreciable fraction of the absolute mean pressure, for appreciable frequencies of oscillation, and for tubing short enough to require end corrections. The effect of heat transfer in modifying the oscillatory response of the tube is also discussed.

The chief utility of knowing these corrections is that it permits the designer to choose the size of tubing for specific applications with greater confidence than can otherwise be generally done.

In this paper the elementary theory of transmission lags is developed, and the corrections are discussed. The complete theory is presented in graphical form for the convenience of the designer. A number of examples of the use of the design charts are also given. All mathematical symbols used in this paper are defined in the nomenclature, and also when they are first used.

The theory is developed and more exact results are given in a mathematical appendix,³ here omitted but included in the complete paper.

ELEMENTARY THEORY

Fig. 1 is a schematic drawing of the system that will be dis-

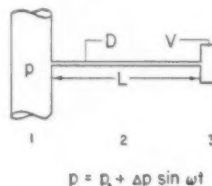


FIG. 1 SCHEMATIC DIAGRAM OF A FLUID TRANSMISSION SYSTEM (1, conduit, 2, transmission tube, 3, pressure instrument.)

cussed throughout the paper. A tube transmits fluid pressure from a conduit to a pressure-sensitive instrument. The conduit

⁴ "Pressure Drop in Tubing in Aircraft Instrument Installations," by W. A. Wildhack, NACA Technical Note 593, 1937.

applies an oscillatory (sinusoidal) pressure to the entrance of the transmission tube. The tube, which transmits the pressure, is characterized by a constant cross-sectional area, and its length. The pressure-sensitive instrument, which receives the pressure, is characterized by its enclosed volume. It is assumed that if the walls enclosing the instrument volume are flexible (either elastic or pistonlike), the enclosed volume can be replaced by a larger equivalent rigid volume that will store the same mass of fluid per unit pressure change. It is further assumed that the pressure-sensitive instrument will be so chosen that its indication is independent of the frequency of expected pressure oscillations.

In deriving the elementary theory, it is assumed that Poiseuille's law of viscous resistance holds at each point in the tube; that the fluid is incompressible in the tube; that the sinusoidal pressure oscillations at the beginning of the tube are of small amplitude compared to the mean absolute pressure; and that, if the fluid is a gas, it expands and contracts isothermally in the instrument volume.

The same assumptions applied to an incompressible fluid (e.g., a liquid) lead to the conclusion that there is no loss in amplitude or lag in a liquid-filled system, since a liquid would not expand or contract in the instrument volume.

We may write

$$\frac{\partial p}{\partial x} = -\frac{128}{\pi} \frac{\mu_0}{D^4} Q \quad [1]$$

for Poiseuille's law, and

$$\frac{\partial M}{\partial x} = -A \frac{\partial p}{\partial t} \quad [2]$$

for the equation of continuity. Here

- p = instantaneous pressure at any point in tube
- x = distance along tube measured from its entrance
- μ_0 = mean fluid viscosity
- D = tube diameter
- Q = volumetric flow at any point in tube
- ρ = instantaneous density at any point in tube
- M = the mass flow at any point in tube
- A = cross-sectional area of tube
- t = time

We infer from the equation of continuity and the assumption that the fluid is incompressible in the tube, (i.e., $\partial \rho / \partial t = 0$) that the mass flow, and, therefore, the volumetric flow does not vary along the tube, but at most varies only with time (the fluid motion is pistonlike).

By differentiating Equation [1], we then obtain

$$\frac{\partial^2 p}{\partial x^2} = 0 \quad [3]$$

along the tube.

Our boundary conditions are that at $x = 0$

$$p = p_0 + \Delta p e^{j\omega t} \quad [4]$$

a sinusoidal pressure variation about the mean pressure, and that at $x = L$

$$\left. \begin{aligned} Q &= \frac{V}{p_0} \frac{\partial p}{\partial t} \\ \frac{\partial p}{\partial x} &= -\frac{128}{\pi} \frac{\mu_0}{D^4} Q \end{aligned} \right\} \quad [5]$$

The first line of Equation [5] expresses the rate at which a compressible fluid entering a rigid volume builds up pressure, while

the second line of Equation [5] states that the flow into the volume is limited by the pressure gradient at the end of the tube. Here

- p_0 = mean pressure at entrance
- Δp = amplitude of pressure oscillation applied at conduit
- V = instrument volume
- ω = angular frequency of pressure oscillation
- L = length of tube

It is convenient to introduce a new variable ξ , the fractional pressure excess, defined as

$$\xi = \frac{p - p_0}{p_0} \quad [6]$$

so that Equations [3], [4], and [5] become, respectively

$$\frac{\partial^2 \xi}{\partial x^2} = 0 \quad [7]$$

at $x = 0$

$$\xi = \xi_0 e^{j\omega t} \quad [8]$$

and at $x = L$

$$\left. \begin{aligned} \frac{\partial \xi}{\partial x} &= -\frac{128}{\pi} \frac{\mu_0}{p_0} \frac{V}{D^4} \frac{\partial \xi}{\partial t} \\ &= -\frac{\lambda_0}{L} \frac{\partial \xi}{\partial t} \end{aligned} \right\} \quad [9]$$

where

$$\left. \begin{aligned} \lambda_0 &= \frac{128}{\pi} \frac{\mu_0}{p_0} \frac{L}{D^4} \frac{V}{D^4} \\ &= 32 \frac{\mu_0}{p_0} \left(\frac{L}{D} \right)^2 \frac{V}{AL} \end{aligned} \right\} \quad [10]$$

Here

- ξ = fractional pressure excess
- ξ_0 = amplitude of fractional pressure excess at origin (= $\Delta p / p_0$)
- λ_0 = time constant of system

It is of further convenience to separate the pressure excess into a part that varies with x and one that varies with t .

Let

$$\xi = \tilde{\xi} e^{j\omega t} \quad [11]$$

where $\tilde{\xi}$ is the maximum amplitude of the pressure excess at any point of the tube.

Our equations then become

$$\frac{d^2 \tilde{\xi}}{dx^2} = 0 \quad [12]$$

at $x = 0$

$$\tilde{\xi} = \xi_0 \quad [13]$$

and at $x = L$

$$\frac{d\tilde{\xi}}{dx} = -\frac{\lambda_0 \omega}{L} j \tilde{\xi} \quad [14]$$

The solution of Equation [12] which satisfies Equations [13] and [14] is

$$\tilde{\xi} = \xi_0 \frac{1 + \lambda_0 \omega \left(1 - \frac{x}{L} \right) j}{1 + \lambda_0 \omega j} \quad [15]$$

The ratio of the amplitude of the pressure excess at the end of

the tube to that at the beginning of the tube is then given by

$$\left. \begin{aligned} \frac{\tilde{\xi}_L}{\xi_0} &= \frac{1}{1 + \lambda_0 \omega j} \\ &= \frac{1}{1 + \chi_0 j} \end{aligned} \right\} \dots \dots \dots [16]$$

where

$$\chi_0 = \lambda_0 \omega \dots \dots \dots [17]$$

Here

$\tilde{\xi}_L$ = maximum amplitude of pressure excess at instrument volume

χ_0 = attenuation factor

The real part of Equation [16] is the attenuation in amplitude of the pressure excess, while the imaginary part is the phase lag, or

$$\left. \begin{aligned} \left| \frac{\tilde{\xi}_L}{\xi_0} \right| &= \frac{1}{[1 + \chi_0^2]^{1/2}} \\ \tan \delta_0 &= \chi_0 \end{aligned} \right\} \dots \dots \dots [18]$$

where δ_0 is the lagging phase angle.

We will regard Equation [18] as the elementary solution of our problem.

It indicates that a transmission system is characterized by a time constant λ_0 , which can be computed from a knowledge of the dimensions of the tube, the effective internal volume of the end device, and the average conditions of the gas in the tube; and an attenuation factor χ_0 , for each angular frequency, from which one can compute the attenuation and phase lag in a tube. The tube dimensions and the instrument volume furnish the analog to the resistance and capacitance of an electrical network.

In principle, although difficult in practice, from a knowledge of the response to a sine wave, one can obtain the response to square waves, step functions, etc., by Fourier analysis.

DISCUSSION OF CORRECTIONS

The assumptions made in the elementary theory are restrictive, and in the appendix³ these are modified, one at a time, until finally we arrive at a complete solution that accurately takes into account all first-order phenomena, and partially takes into account second-order phenomena. Complete results are presented in convenient graphical form in Figs. 2 to 9, inclusive.

The factors that must be taken into account are as follows:

Compressible Flow in Tube. The effect of fluid compressibility is to introduce a time constant and corresponding attenuation factor (λ_T , χ_T) depending on the tube volume in addition to the ones depending on the instrument volume. (The time constant and attenuation factor depending upon the instrument volume will be referred to as λ_I and χ_I henceforth instead of λ_0 and χ_0 .) In terms of the electrical analog, the tube volume represents a distributed capacitance in addition to the equivalent capacitance of the instrument volume.

Finite Pressure Excess. The effect of the application of a finite pressure excess to a compressible fluid in a transmission tube is to introduce harmonic distortion and to modify the mean pressure. However, the attenuation of the fundamental is essentially independent of the magnitude of the pressure excess. The percentage of distortion is approximately proportional to the applied pressure excess.

Fluid Acceleration. The effect of fluid inertia is to modify the time constants of the system. Both the attenuation of the fundamental and the magnitude of harmonic distortion are affected. A dimensionless parameter z , analogous to the Q of an electrical system, characterizes the fluid regime and determines whether fluid inertia may or may not be neglected.

When fluid inertia is negligible, a transmission tube acts like a highly damped system; when fluid inertia is large, a transmission tube acts like an undamped system, and elementary acoustic theory is applicable.

Finite Length of Tubing. The effect of fluid acceleration at the ends of the tube results in further distortion of wave form, which must be taken into account in short tubes.

Heat Conduction. If there were no heat transfer from outside the tube to inside, the oscillatory processes would take place adiabatically; if there were perfect heat transfer into and through the tube, the processes would take place isothermally. The effect of finite heat conduction is to make the real process occur in between these extremes, although in a rather complicated fashion. At low frequencies the process may be regarded as isothermal.

Although an exact result is given in the appendix,³ it is advantageous to utilize the thermodynamic equation of condition, discussed in the following section, for elucidating the problem of attenuation in tubing.

THERMODYNAMIC EQUATION OF CONDITION

In the case of an oscillatory variation of fluid flow, the equation relating the thermodynamic parameters of the fluid lies between the adiabatic and the isothermal equations of condition. For high frequencies, as in sound waves, it is well known that the adiabatic equation holds. However, for viscously damped motion, the adiabatic relation is not, in general, attained.

For a gas, we assume, and justify in the appendix³ that the processes can be described as "polytropic," that is, characterized by a constant exponent n , in the expression

$$p = c \rho^n \dots \dots \dots [19]$$

with

$$1 \leq |n| \leq \gamma$$

where

- n = exponent of polytropic expansion in tube
- γ = ratio of specific heats
- η = density ratio (ρ/ρ_0)
- ρ_0 = average density in tube
- c indicates any constant

The viscosity of gases is independent of the pressure, and, as an approximation, proportional to the absolute temperature. (The more rigorous approximation is that the viscosity is proportional to $(T)^{1/2}/(1 + c/T)$, but over a small range this can be approximated by the temperature to a power close to 1. For example, for air at room temperature, a power of 0.8 fits experimental data quite well. The difference from unity is unimportant for our purpose.)

Therefore

$$\left. \begin{aligned} \mu &= cT \\ \frac{\mu}{\mu_0} &= (1 + \xi)^{\frac{n-1}{n}} \\ \frac{\mu}{\mu_0} &= \eta^{n-1} \end{aligned} \right\} \dots \dots \dots [20]$$

follows from the gas laws and Equation [19]. Here

- μ = instantaneous fluid viscosity
- T = absolute temperature

Equations [19] and [20] thus express the variation of viscosity, density, and pressure, respectively, in a polytropic process in a gas. At low frequencies, the polytropic exponent may be regarded as equal to unity.

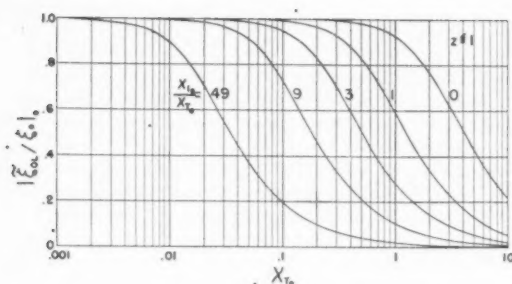


FIG. 2 AMPLITUDE RATIO OF FUNDAMENTAL $|\xi_0 L / \xi_0|_0$ IN A VOLUME-TERMINATED TUBE AS A FUNCTION OF A PARAMETER PROPORTIONAL TO FREQUENCY (X_{T0}) FOR VARIOUS RATIOS OF INSTRUMENT VOLUME TO TUBE VOLUME (X_{I0}/X_{T0}) WITH LARGE DAMPING ($z \leq 1$)

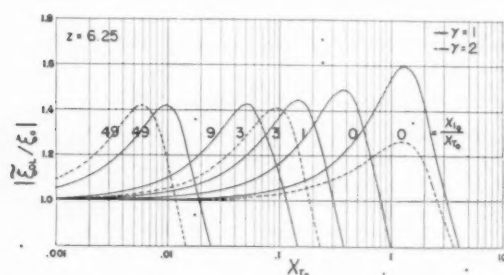


FIG. 4 AMPLITUDE RATIO OF FUNDAMENTAL $|\xi_0 L / \xi_0|$ IN A VOLUME-TERMINATED TUBE AS A FUNCTION OF A PARAMETER PROPORTIONAL TO FREQUENCY (X_{T0}) FOR VARIOUS RATIOS OF INSTRUMENT VOLUME TO TUBE VOLUME (X_{I0}/X_{T0}) AND FOR TWO VALUES OF SPECIFIC HEAT RATIO (γ) WITH INTERMEDIATE DAMPING ($z = 6.25$)

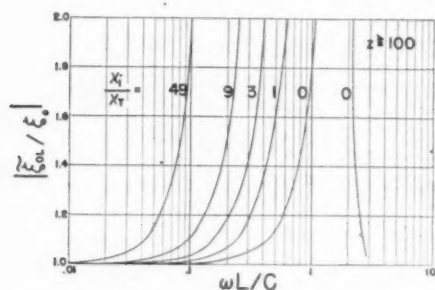


FIG. 6 AMPLITUDE RATIO OF FUNDAMENTAL $|\xi_0 L / \xi_0|$ IN A VOLUME-TERMINATED TUBE AS A FUNCTION OF A PARAMETER PROPORTIONAL TO FREQUENCY ($\omega L / C$) FOR VARIOUS RATIOS OF INSTRUMENT VOLUME TO TUBE VOLUME (X_I / X_T) WITH LITTLE DAMPING ($z \geq 100$)

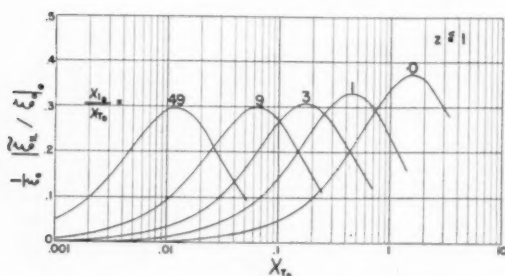


FIG. 8 RELATIVE AMPLITUDE OF DOUBLE HARMONIC DISTORTION ($|\xi_1 L / \xi_0|_0 / |\xi_0 L / \xi_0|_0$) IN A VOLUME-TERMINATED TUBE AS A FUNCTION OF A PARAMETER PROPORTIONAL TO FREQUENCY (X_{T0}) FOR VARIOUS RATIOS OF INSTRUMENT VOLUME TO TUBE VOLUME (X_{I0}/X_{T0}) WITH LARGE DAMPING ($z \leq 1$)

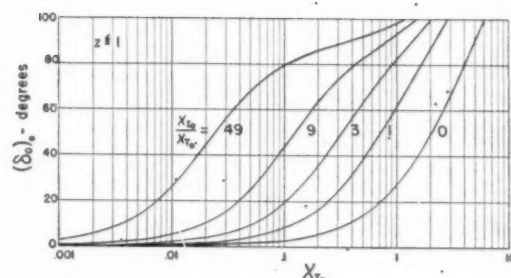


FIG. 3 PHASE LAG OF FUNDAMENTAL $(\delta_0)_0$ IN A VOLUME-TERMINATED TUBE AS A FUNCTION OF A PARAMETER PROPORTIONAL TO FREQUENCY (X_{T0}) FOR VARIOUS RATIOS OF INSTRUMENT VOLUME TO TUBE VOLUME (X_{I0}/X_{T0}) WITH LARGE DAMPING ($z \leq 1$)

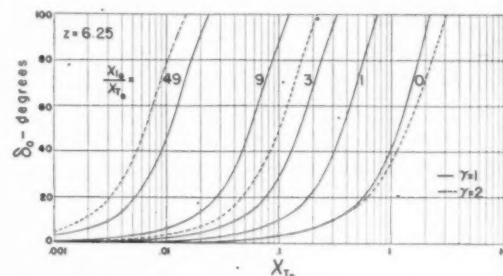


FIG. 5 PHASE LAG OF FUNDAMENTAL (δ_0) IN A VOLUME-TERMINATED TUBE AS A FUNCTION OF A PARAMETER PROPORTIONAL TO FREQUENCY (X_{T0}) FOR VARIOUS RATIOS OF INSTRUMENT VOLUME TO TUBE VOLUME (X_{I0}/X_{T0}) AND FOR TWO VALUES OF SPECIFIC HEAT RATIO (γ) WITH INTERMEDIATE DAMPING ($z = 6.25$)

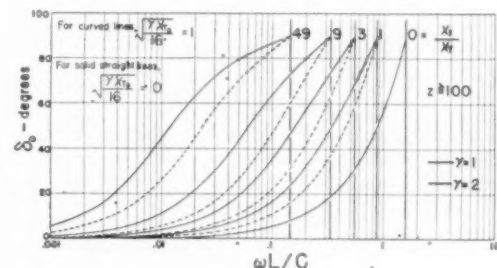


FIG. 7 PHASE LAG OF FUNDAMENTAL (δ_0) IN A VOLUME-TERMINATED TUBE AS A FUNCTION OF A PARAMETER PROPORTIONAL TO FREQUENCY ($\omega L / C$) FOR VARIOUS RATIOS OF INSTRUMENT VOLUME TO TUBE VOLUME (X_I / X_T) INDICATING THE DIFFERENCE BETWEEN NO DAMPING $[\gamma X_{T0} / 16]^{1/2} = 0$, AND SMALL DAMPING $[\gamma X_{T0} / 16]^{1/2} = 1$, FOR TWO VALUES OF SPECIFIC HEAT RATIO (γ) WITH SMALL DAMPING ($z \geq 100$)

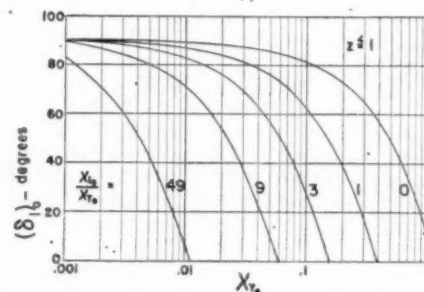


FIG. 9 PHASE LEAD, AS MEASURED ON FUNDAMENTAL TIME SCALE, OF DOUBLE HARMONIC DISTORTION $(\delta_1)_0$ IN A VOLUME-TERMINATED TUBE AS A FUNCTION OF A PARAMETER PROPORTIONAL TO FREQUENCY (X_{T0}) FOR VARIOUS RATIOS OF INSTRUMENT VOLUME TO TUBE VOLUME (X_{I0}/X_{T0}) WITH LARGE DAMPING ($z \leq 1$)

For liquids, we assume that the equation of condition in a polytropic process is given by

$$\rho = \rho_0 + c p^n \quad [21]$$

where

$$1 \leq |n| \leq \gamma$$

For liquids, however, γ lies so close to unity that we may satisfactorily assume $n = 1$.

Equation [21] can then be written in the form

$$\eta = 1 + b\xi \quad [22]$$

where

b = compressibility factor ($= k_0 p_0$)

k_0 = liquid compressibility at average conditions in tube

The variation in viscosity of a liquid over a small range of temperature can be neglected, so that in a polytropic process

$$\mu = \mu_0 \quad [23]$$

Actually, the implication in Equations [22] and [23] is that in a liquid-filled transmission line, the effect of conditions appreciably different from isothermal is negligible.

It is also necessary to take into account heat exchange at the instrument.

For an isothermal process with a gas in the instrument volume, we previously assumed that

$$Q = \frac{V}{p_0} \frac{\partial p}{\partial t} \quad [5]$$

represents the influx of fluid. If, instead, we assume a polytropic process in the instrument, characterized by an exponent m (the heat exchange may differ in the tube and instrument volume so that m is not necessarily equal to n), then Equation [5] should be modified to

$$\left. \begin{aligned} Q &= \frac{V}{mp} \frac{\partial p}{\partial t} \\ Q &= \frac{n}{m} \frac{V}{p} \frac{\partial p}{\partial t} \end{aligned} \right\} \quad [24]$$

in the case of gases; or to

$$Q = \frac{Vb}{p_0} \frac{\partial p}{\partial t} \quad [25]$$

in the case of liquids.

If the fluid is regarded as a spring, the exponent of the polytropic process for a gas, or the small compressibility of a liquid may be viewed as quantities which make the fluid spring stiffer in the case of gases, or almost infinitely stiff in the case of liquids. It is shown in the appendix³ that these polytropic exponents modify the time constants of the tube and volume.

GENERAL PROCEDURE, WITH EXAMPLES, FOR COMPUTING TRANSMITTED PRESSURE

The computation of the attenuation and phase lag at one end of a transmission tube of a sinusoidal pressure variation imposed at the other end can be carried out with the aid of Figs. 2 to 9. These figures are based upon the theory largely developed in the appendix. The computations are made primarily for the attenuation at the fundamental frequency. An estimate of the distortion arising from finite input amplitudes with high damping is made in the appendix.³ The computation for the first harmonic in the distorted output can be made with the aid of Figs. 8 and 9. An

outline of procedure for making computations follows:

1 Compute

$$z = \frac{D^2}{4} \frac{\omega}{v_0} \quad [26]$$

a dimensionless parameter of the fluid regime which characterizes the amount of damping present. When this parameter is less than one (large damping), use Figs. 2 and 3; when greater than 100 (small damping), use Figs. 6 and 7. For intermediate values of this parameter, use Figs. 4 and 5 as an aid to interpolation.

2 Compute the attenuation factors

$$x_{T0} = \frac{32\mu_0\omega}{p_0} \left(\frac{L}{D}\right)^3 \quad [27]$$

$$\frac{x_{I0}}{x_{T0}} = \frac{1}{m} \left(\frac{V}{AL}\right) \quad [28]$$

for a gas, or

$$x_{T0} = 32\mu_0 k_0 \omega \left(\frac{L}{D}\right)^3 \left(1 + \frac{p_0 - p_a}{p_0} \frac{1}{k_0 E} \frac{D}{s}\right) \quad [29]$$

$$\frac{x_{I0}}{x_{T0}} = \frac{V}{AL} \frac{1}{\left(1 + \frac{p_0 - p_a}{p_0} \frac{1}{k_0 E} \frac{D}{s}\right)} \quad [30]$$

for a liquid. These quantities x_{T0} and x_{I0} are factors based on the tube volume and instrument volume, respectively. The zero subscript means that they are values for the case of large damping.

3 Compute the input pressure excess

$$\xi_0 = \frac{\Delta p}{p_0} \quad [31]$$

4(a) For values of z less than 1, enter Fig. 2 with x_{T0} and x_{I0}/x_{T0} to find the amplitude ratio $|\tilde{\xi}_{OL}/\xi_0|_0$, and enter Fig. 3 to find the lagging phase angle $(\delta_0)_0$.

4(b) The output pressure excess is then computed from

$$|\tilde{\xi}_{OL}|_0 = \xi_0 \left| \frac{\tilde{\xi}_{OL}}{\xi_0} \right|_0 \quad [32]$$

5(a) For values of z greater than 100, compute

$$\frac{\omega L}{c} = \left[\frac{zx_{T0}}{8\gamma} \right]^{1/3} \quad [33]$$

$$\frac{x_I}{x_T} = \gamma \frac{x_{I0}}{x_{T0}} \quad [34]$$

For liquids, assume $\gamma = 1$.

The quantities x_I and x_T are the attenuation factors for the case of low damping. With low damping, it is convenient to use the dimensionless parameter $\omega L/C$ which is proportional to frequency, as the independent variable. The quantity C represents the velocity of sound.

5(b) Enter Fig. 6 with $\omega L/C$ and x_I/x_T to find the amplitude ratio $|\tilde{\xi}_{OL}/\xi_0|$ and enter Fig. 7 to find the lagging phase angle δ_0 . It is necessary to estimate the phase angle by interpolation. For very small values of x_{T0} compared to 1, the lagging phase angle is zero up to the first resonance. In Fig. 7 curves have been presented to indicate the phase angle for $(\gamma x_{T0}/16)^{1/3} = 0$ and $(\gamma x_{T0}/16)^{1/3} = 1$. One may linearly interpolate for values lying between 0 and 1.

6(a) For values of z lying between 1 and 100, one may interpolate between the values of amplitude ratio and lagging phase angle obtained in step 4(a) and those obtained in step 5(b) by the use of Figs. 4 and 5. Enter Figs. 4 and 5, with x_{T0} and x_{I0}/x_{T0} to find the amplitude ratio $|\tilde{\xi}_{OL}/\xi_0|$ and lagging phase angle δ_0 . These are the values for $z = 6.25$. In order to interpolate, plot a logarithmic graph with z as abscissa and the amplitude ratio or phase angle as ordinate. Plot the values from step 4(a) at $z = 1$, from step 6(a) at $z = 6.25$, and from step 5(b) at $z = 100$, draw a curve through these three points, and interpolate on this curve for the intermediate value of z .

COMPUTATION OF DOUBLE-FREQUENCY DISTORTION

This computation represents only an estimate of the double-frequency distortion, and is strictly only valid for values of z less than 1.

Compute x_{T0} and x_{I0}/x_{T0} . Enter Figs. 8 and 9 to obtain the relative amplitude ratio $|\tilde{\xi}_{IL}/\xi_0|_0/\xi_0$ and leading phase angle $(\delta_1)_0$ for the double-frequency wave. The leading phase angle is measured on the time scale of the fundamental where the input is a cosine term.

Compute the pressure excess of the double frequency $|\tilde{\xi}_{IL}|_0$ from

$$|\tilde{\xi}_{IL}|_0 = \left(\frac{1}{\xi_0} \left| \frac{\tilde{\xi}_{IL}}{\xi_0} \right|_0 \right) \xi_0^2 \quad [35]$$

Compute the mean pressure at the instrument volume which is larger than the mean pressure at the tube entrance by $\xi_0 \Delta p (1 - |\tilde{\xi}_{OL}/\xi_0|_0^2)/4$.

The various quantities in this section are defined as follows:

- μ_0 = mean fluid viscosity
- ν_0 = mean kinematic viscosity
- p_0 = mean fluid pressure
- p_a = ambient pressure external to tube
- Δp = amplitude of applied sinusoidal pressure
- ξ_0 = applied fractional pressure excess
- ξ_{OL} = pressure excess of fundamental at instrument volume
- ξ_{IL} = pressure excess of double frequency at instrument volume
- δ_0 = lagging phase angle of fundamental at instrument volume
- δ_1 = leading phase angle of double frequency at instrument volume
- k_0 = mean fluid compressibility
- V = equivalent rigid internal volume of instrument
- A = internal cross section of tube
- D = internal diameter of tube
- s = wall thickness of tube (assumed small compared to diameter)
- E = elastic modulus of tube material
- L = length of tube
- C = velocity of sound in fluid
- γ = ratio of specific heats of fluid (assumed to be 1 for liquids)
- m = coefficient of polytropic process in instrument volume.
(In lieu of other information, it may be assumed to be 1.)
- z = dimensionless parameter characterizing fluid regime
- ω = angular frequency applied
- x_T = attenuation factor based on tube volume
- x_I = attenuation factor based on instrument volume

Subscript T refers to parameters based on tube volume.

Subscript I refers to parameters based on end volume.

Subscripts O or 1 adjacent to a letter denote fundamental or first harmonic.

An end subscript of 0 denotes a value for case of large damping.

The attenuation of the fundamental may be computed validly from the formulas developed in this paper when

$$\left. \begin{aligned} \frac{p_0}{CD} < 1 \\ \frac{p_0 \omega}{C^2} < 1 \end{aligned} \right\} \quad [36]$$

The second harmonic distortion, which was only estimated approximately, may be validly computed from the formulas developed when

$$z = \frac{\omega D^2}{4\nu_0} < 1 \quad [37]$$

and for applied pressure amplitudes small enough to guarantee laminar flow.

EXAMPLES OF COMPUTATIONS

The calculation of attenuation by the General Procedure outlined will be illustrated by a number of examples.

(a) What is the longest length of $3/16$ -in-ID tubing that can be used to transmit air pressure to a Bourdon-type pressure gage (equivalent internal volume assumed negligible) up to a frequency of $1/2$ cycle per sec (cps) with a loss in amplitude not greater than 25 per cent? What will be the double-frequency distortion? For air, assume $\mu_0 = 2 \times 10^{-4}$ poise, $\nu_0 = 1/6$ stokes, $m = 1$, $\gamma = 1.4$, $p_0 = 10^6$ dynes/cm² (atmospheric pressure), angular frequency $\omega = \pi$.

Using Equation [26], $z = 1.1$ (computed in consistent units). This value is sufficiently close to unity to permit the use of Figs. 2 and 3.

Enter Fig. 2 with $|\tilde{\xi}_{OL}/\xi_0|_0 = 0.75$ and $x_{O1}/x_{T0} = 0$, since the instrument volume is negligible, to find $x_{T0} = 2.1$. Compute L in Equation [27] to be 160 ft.

Enter Fig. 3 with $x_{T0} = 2.1$, to find that the maximum phase lag will be 53 deg.

Enter Fig. 8 to find that the relative amplitude of the double frequency $|\tilde{\xi}_{IL}/\xi_0|_0/\xi_0 = 0.35$. For initial pressure excesses of 0.1, 0.3, and 1, respectively, the double-frequency amplitude, relative to the input amplitude, will be $3^{1/2}$, $10^{1/2}$, and 35 per cent, respectively.

(b) What lengths of 0.1-in-ID tubing (nominally $3/16$ -in-OD tubing) can be used for quality transmission of air pressure for frequencies up to 1, 10, 100, 1000 cps into pressure instruments with equivalent rigid volumes of 0.1 cu in. and 1 cu in.?

We will define quality transmission as that in which there is no more than ± 5 -per cent change in fundamental amplitude or more than ± 30 -deg phase shift (whichever is more stringent).

Assume that $\mu_0 = 2 \times 10^{-4}$ poise, $\nu_0 = 1/6$ stokes, $m = 1$, $\gamma = 1.4$, $D = 0.1$ in., $A = 0.0079$ sq in., $p_0 = 10^6$ dynes/cm², $\rho_0 = 0.0012$ g/cm³.

We will calculate for each frequency separately.

Let $f = 1$ cps:

Using Equation [26], $z = 0.61$, therefore use Figs. 2 and 3.

Assume $AL = \infty$, therefore, by Equation [28], $x_{I0}/x_{T0} = 0$.

Enter Fig. 2 for $|\tilde{\xi}_{OL}/\xi_0|_0 = 0.95$ to find $x_{T0} = 0.80$.

Enter Fig. 3 for $(\delta_0)_0 = 30$ deg to find $x_{T0} = 1.1$; use 0.80 since more stringent.

Calculate L from Equation [27] to be 450 in.

Calculate AL to be 3.5 cu. in.

Compute x_{I0}/x_{T0} from Equation [28] to be 0.029 for $V = 0.1$ cu in.; to be 0.29 for $V = 1$ cu in.

In Fig. 2, x_{T0} is modified negligibly for $V = 0.1$ cu in.

Therefore $L = 450$ in. = 37 ft for $V = 0.1$ cu in.

Re-enter Fig. 2 for $|\tilde{\xi}_{OL}/\xi_0|_0 = 0.95$, $x_{I0}/x_{T0} = 0.29$ to find $x_{T0} = 0.5$.

Calculate L to be 350 in. = 29 ft for $V = 1$ cu in.

Let $f = 1000$ cps:

Using Equation [26], $z = 610$, therefore use Figs. 6 and 7.

Assume $x_I/x_T = 49$ (the line volume will probably be small).

Enter Fig. 6 for $|\tilde{\xi}_{OL}/\xi_0|_0 = 1.05$ to find $\omega L/C = 0.031$.

Calculate L from Equations [33], [26], and [27] to be 0.066 in.

Calculate AL to be 0.00052 cu in.

Using Equation [34], it is seen that x_I/x_T is greater than assumed so that $\omega L/C$, and therefore L is less than the previous estimate. One may note that the estimated length will be so small that the theory essentially predicts that no transmission tubing at all may be used. In fact, the acoustic impedance of the entrance orifice into the pressure instrument, or the mechanical impedance of the pressure instrument itself will probably govern the response at this high frequency.

Let $f = 10$ cps:

Using Equation [26], $z = 6.1$, therefore use Figs. 4 and 5.

Assume $AL = \infty$, therefore $x_{I0}/x_{T0} = 0$.

Enter Fig. 4 with $|\tilde{\xi}_{OL}/\xi_0| = 1.05$, and $\gamma = 1.4$ to find $x_{T0} = 0.12$.

Compute L from Equation [27] to be 58 in.

Compute AL to be 0.45 cu in.

Compute x_{I0}/x_{T0} from Equation [28] to be 0.22 for $V = 0.1$ cu in.; = 2.2 for $V = 1$ cu in.

In Fig. 4, x_{T0} is modified to about 0.07 for $V = 0.1$ cu in.

Therefore L is reduced to about 4 ft for $V = 0.1$ cu in.

Enter Fig. 4 for $|\tilde{\xi}_{OL}/\xi_0| = 1.05$, and $x_{I0}/x_{T0} = 2$ to find $x_{T0} = 0.018$.

Compute L to be 22 in. for $V = 1$ cu in.

Compute AL to be 0.17 cu in.

Compute $x_{I0}/x_{T0} = 6$.

Enter Fig. 4 to find $x_{T0} = 0.007$.

Compute L to be 14 in.

Compute AL to be 0.11 cu in.

Compute $x_{I0}/x_{T0} = 9$.

Enter Fig. 4 to find $x_{T0} = 0.004$.

Compute L to be 11 in.

Compute AL to be 0.09 cu in.

Compute $x_{I0}/x_{T0} = 11$.

In Fig. 4, x_{T0} is modified negligibly. Therefore $L =$ about 1 ft for $V = 1$ cu in.

To check the phase angle, enter Fig. 5 with $x_{I0}/x_{T0} = 11$, and $x_{T0} = 0.005$, to find 4 deg.

Let $f = 100$ cps:

$z = 61$ (interpolation is necessary).

First estimate from Figs. 6 and 7.

Assume $x_I/x_T = 9$.

Enter Fig. 6 to find $\omega L/C = 0.068$.

Compute L to be 1.5 in.

Compute AL to be 0.011 in.

Compute $x_I/x_T = 9.1$ for $V = 0.1$ cu in.; = 91 for $V = 1$ cu in.

By Fig. 6, $\omega L/C$ is negligibly modified for $V = 0.1$ cu in.

Therefore $L = 1.5$ in. for $V = 0.1$ cu in. is our first estimate.

For $V = 1$ cu in., we find again that an extremely small tube is predicted, so that the impedance of the entrance orifice will probably govern.

For $V = 0.1$ cu in., and $L = 1.5$ in., estimate $(\gamma x_{T0}/16)^{1/2}$ to be 0.01.

From Fig. 7 we find that the phase lag is negligible.

Compute $x_{T0} = 0.0009$, from Equation [27] for $\omega = 200 \pi$.

Enter Fig. 4 for $x_{I0}/x_{T0} = 9$, to find $|\tilde{\xi}_{OL}/\xi_0| = 1.00$.

Interpolating between $|\tilde{\xi}_{OL}/\xi_0| = 1$ at $z = 6.25$ and $|\tilde{\xi}_{OL}/\xi_0| = 1.05$ at $z = 100$ for $z = 61$, we find that $|\tilde{\xi}_{OL}/\xi_0|$ is negligibly affected.

Therefore $L = 1.5$ in. for $V = 0.1$ cu in.

Then
mainta
period
ured v
estima
be sus
Both o
the th
year.
precisi
creep.
use in
greater

O

fairly v
exceed
moplas
have b
vide m
plastic

Creep
for two
with fu
aspect
cluded
the thr
will alv
sued in
present

It is
creep,
fect so
sisting
stresse
under
direct
moldin
ture.
ances
or defo
undue
was us

Creep
one lab

¹ Re
² Re
³ Nu
Con
the An
1949, c
Nor
unders
of the

Long-Time Tension and Creep Tests of Plastics

By C. E. STAFF,¹ H. M. QUACKENBOS, JR.,² AND J. M. HILL,¹ BLOOMFIELD, N. J.

Thermosetting and thermoplastic materials have been maintained under constant load at 25 C and 75 C for periods ranging from 1000 to 14,500 hr. Creep was measured with electric strain gages and, from its course, an estimate has been made of the maximum stresses that can be sustained for 5 years by the thermosetting materials. Both creep and crazing govern the maximum stresses for the thermoplastics, and these have been estimated for 1 year. An examination has been made of the accuracy and precision of the electric strain gage in measurements of creep. It is believed that the results are not confined to use in potential structural applications but have their greatest value in many current problems.

INTRODUCTION

OVER the past 8 years more than a dozen papers have appeared on the creep of rigid plastics and yet our knowledge is far from complete. The common laminates have been fairly well covered, but tests on thermosetting products have not exceeded 1000 hr (1, 2, 3)² with one exception (4), and of the thermoplastics only cellulose acetate and polymethylmethacrylate have been investigated (5, 6). It is the aim of this paper to provide more information about the thermoplastic and thermosetting plastics.

Creep tests for plastics have usually been justified in the past for two reasons: (a) The results were thought to be connected with fundamental physical properties. In the present paper this aspect will be neglected, although the physical chemist is not excluded from making his own interpretation. (b) Plastics were on the threshold of light structural uses. Good creep data, of course, will always find use in structural design, but this study was pursued mainly with the conviction that the results relate to many present applications.

It is not generally recognized that two practical aspects of creep, namely, sustained stress and continuing deformation, affect so many common molded parts. Examples are fan blades resisting centrifugal stresses, material around metal inserts under stresses that have arisen from differential contraction, parts under stress from differential water absorption, objects bearing direct load (e.g., coat hangers and bottle caps screwed tight), and moldings shrinking under the influence of high ambient temperature. Under such circumstances creep may either change tolerances or cause weakening and even fracture. The period of stress or deformation may easily be several years, and in order to avoid undue extrapolation from laboratory to field, the creep test here was usually continued 5000 hr while a few tests lasted 14,500 hr.

Creep usually has been measured with optical devices except in one laboratory (1, 2, 3), where the value of electric strain gages

has been demonstrated. Such a gage was preferred here because of its economy and simplicity. The reliability of an electric gage over a long period of time has been questioned, and a secondary objective of this study was to resolve this doubt.

PROCEDURE

The thermosetting materials examined were all commercial combinations of a filler and a two-step resin polymerized from phenol and formaldehyde. The percentage and type of resin varied from one material to another. These materials were compression-molded. The thermoplastics were injection-molded with the exception of vinyl copolymer which was cut from sheet. Fifty bars of each material were prepared at the same time and kept at 25 C and 50 per cent RH until used; for periods ranging from 1 month minimum to 2 years maximum.

The procedure for most creep tests was as follows: The specimen bearing two SR-4 gages connected in series was put into the grips and hung in the rack. (These SR-4 gages, supplied by Baldwin-Southwark, have been described before, reference 1). The gages were balanced electrically, as shown by an SR-4 meter, against two other ("dummy") gages on a similar specimen, or on a steel bar, hanging nearby under no load. Specimens and clamps are shown in Fig. 1. Ten-point switches designed for use with

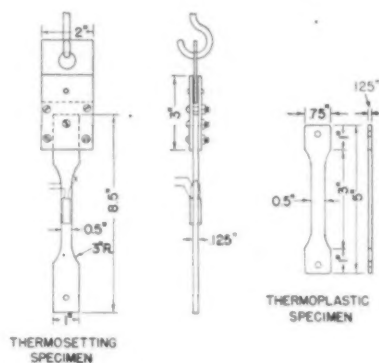


FIG. 1 SPECIMENS, ONE GRIP AND HOOK FOR LOADING IN CREEP TESTS

thermocouples were found satisfactory in allowing several specimens and their dummies to be connected to the SR-4 meter in turn. Load was applied directly with iron or lead weights to a pan hooked to the lower grip. Ten 20-lb weights gave a stress of about 3200 psi in the specimen. Strain was observed for each increment of load during loading, in order to determine modulus of elasticity. After loading, strain was observed every one, two, or three days, depending on the duration of the test. Elastic and delayed recovery on unloading were also observed when desired.

Two ambient conditions were maintained; 25 C and 50 per cent RH in a conditioned room, and 75 C and uncontrolled low relative humidity in an ordinary air-circulating oven. Holes were drilled in this oven, and it was supported so as to surround only the specimen and grips. The weights and frame were outside.

¹ Research and Development Department, Bakelite Corporation.

² Research Engineer, Bakelite Corporation. Jun. ASME.

³ Numbers in parentheses refer to Bibliography at end of paper.

Contributed by the Rubber and Plastics Division and presented at the Annual Meeting, New York, N. Y., November 27-December 2, 1949, of THE AMERICAN SOCIETY OF MECHANICAL ENGINEERS.

NOTE: Statements and opinions advanced in papers are to be understood as individual expressions of their authors and not those of the Society. Paper No. 49-A-61.

At 25 C and at 75 C the dummy gages were cemented to a specimen resembling that under test. Such a practice is supposed to eliminate fluctuations arising from minor variations in temperature. At 75 C, in addition, the dummies were carried on steel bars.

Tensile tests were made at 25 C and 75 C in a testing machine, and strain to failure was measured usually with a mechanical extensometer at 75 C and SR-4 gages at 25 C. The specimens for tensile tests at 75 C were first exposed for 100 days at that temperature. Details of procedure appear in the Appendix.

DISCUSSION

Creep of Thermosetting Materials. Creep curves are of most value when they are linear and so can be extrapolated if wished. Four of the six materials tested at 25 C followed a course that was linear on logarithmic co-ordinates. These four had fillers, respectively, of woodflour, floc, kraft paper, and fabric. Two of them are illustrated in Figs. 2 and 3. Note that the ordinate is total deformation, the sum of the initial elastic deformation, which occurs immediately on loading, and creep which accumulates with time.

With a filler of asbestos, the creep curve eventually becomes a straight line on rectangular rather than logarithmic co-ordinates, Fig. 4. When the filler is mica, the creep is so small, Fig. 5, that it might be interpreted as linear on almost any kind of plot.

The original points usually have been omitted, in order to make the diagrams more effective. The points were first plotted on rectangular co-ordinates and the best smooth curve was drawn

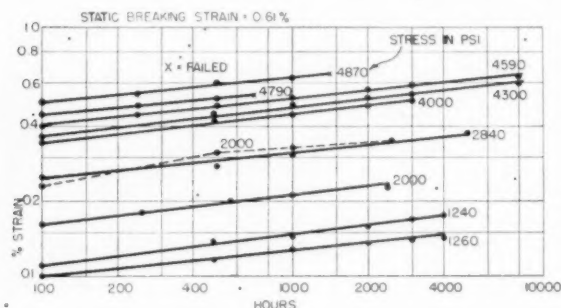


FIG. 2 CREEP AT 25 C FOR COMBINATION OF WOODFLOUR AND PHENOL-FORMALDEHYDE RESIN
(Strain shown includes initial elastic deformation which was 0.078 per cent per 1000 psi. Lines not straight in this and in Fig. 3 are dotted.)

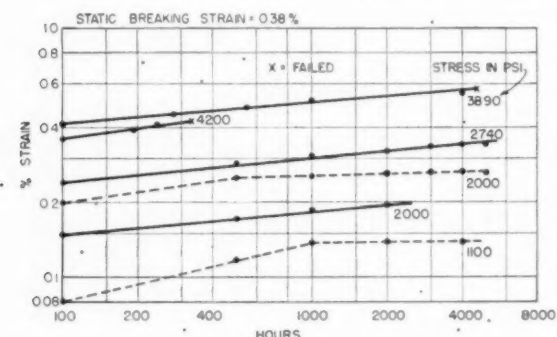


FIG. 3 CREEP AT 25 C FOR COMBINATION OF MACERATED FABRIC AND PHENOL-FORMALDEHYDE RESIN
(Not shown are two tests at 4450 and 4830 psi which ended in failure in 1-3 days with total deformations of 0.42 per cent and 0.44 per cent, respectively. Strain shown includes initial elastic deformation which was 0.067 per cent per 1000 psi.)

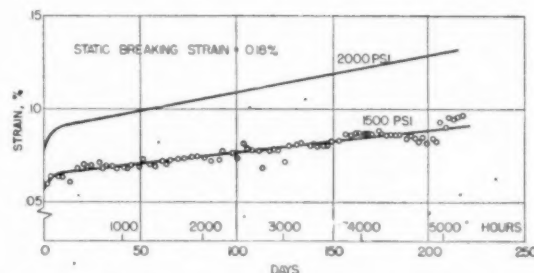


FIG. 4 CREEP AT 25 C FOR COMBINATION OF ASBESTOS AND PHENOL-FORMALDEHYDE RESIN
(Strain at zero time represents initial elastic deformation.)

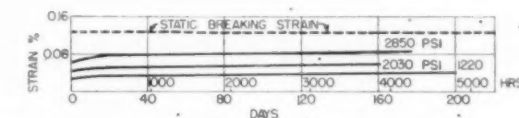


FIG. 5 CREEP AT 25 C FOR COMBINATION OF MICA AND PHENOL-FORMALDEHYDE RESIN
(Strain at zero time represents initial elastic deformation.)

through them, as illustrated for one curve in Fig. 4. Where the co-ordinates are rectangular, the diagrams in this paper show this curve alone, and where logarithmic, the few points shown have been taken from this original curve.

At 75 C creep and shrinkage go on together. Creep itself is measured by comparing the stressed specimen with an unstressed one at the same temperature. Figs. 6 and 7 show the same tendency to linearity as at 25 C. The net strain was given by reference to a steel bar at 75 C, and shrinkage was taken as creep minus net strain. Shrinkage itself follows a linear course on a semilogarithmic plot, Fig. 8, and was found independent of stress.

In introducing the subject of creep, it was mentioned that continuing deformation is of practical importance. Figs. 2 to 7, inclusive, inform us of deformation under stress, and Fig. 8 is of interest in connection with operation at an elevated temperature under no stress. All the lines may be extrapolated to longer times if wished.

Sustained stress is also of importance, and one often wishes to know the maximum stress that can be borne without failure for, say, 5 years. In this connection consider Fig. 3. Four tests ended in failure in a period of 180 days, and in each the total deformation (elastic plus creep) was somewhat in excess of that measured in failure in the short-time tensile test. A similar tendency at 25 C was noted in Fig. 2. At 75 C one failure for each of three materials occurred at the corresponding level of deformation.

Thus the 5-year strength is established by finding a stress such that the creep line extrapolated to 5 years does not quite reach the level of tensile breaking strain. Strengths predicted in this way are presented in Table 1. The estimates are conservative, especially at 75 C where the creep data are rather incomplete.

In order to fortify these predictions, one specimen of each material was kept loaded for 19 months (14,500 hr) at 25 C, Fig. 9. The woodflour and asbestos materials, under higher stresses than those predicted, almost reach the dangerous levels, and the lower stresses of Table 1 are more appropriate. The others withstand comfortably the predicted stresses.

There are two points of practical importance about these long-time strengths; (a) they are quite low in relation to the tensile strengths, (b) they hold only for unnotched specimens. If a sharp notch (or equivalent) is present in the specimen or in a

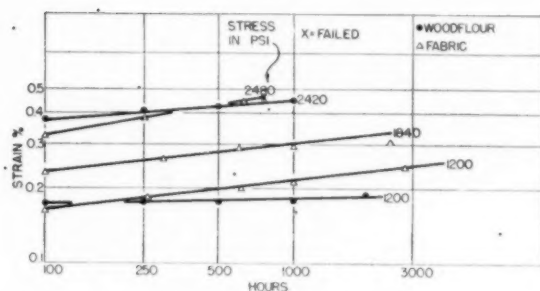


FIG. 6 CREEP AT 75 C FOR PHENOLFORMALDEHYDE RESIN COMBINED WITH FILLERS INDICATED

(Strain shown includes initial elastic deformation, which was about 0.098 per cent for each 1000 psi woodfloc and 0.084 per cent fabric, but excludes shrinkage.)

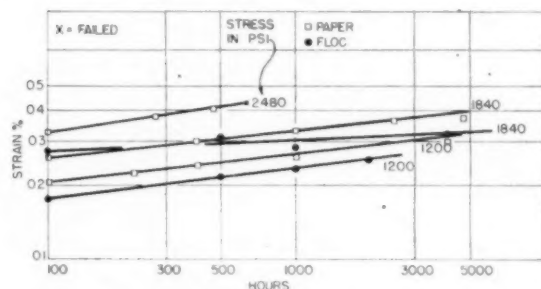


FIG. 7 CREEP AT 75 C FOR PHENOLFORMALDEHYDE RESIN COMBINED WITH FILLERS INDICATED

(Strain shown includes initial elastic deformation, which was about 0.090 per cent for each 1000 psi with both materials, but excludes shrinkage.)

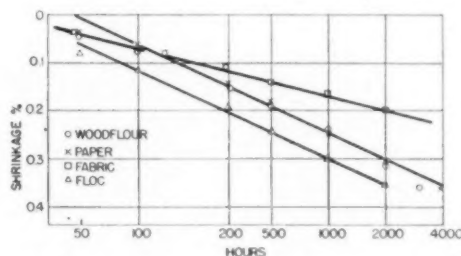


FIG. 8 SHRINKAGE AT 75 C FOR PHENOLFORMALDEHYDE RESIN COMBINED WITH FILLERS INDICATED

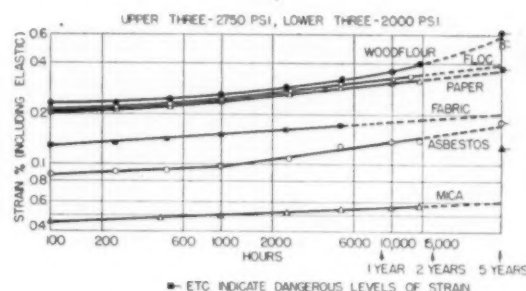


FIG. 9 CREEP TESTS LASTING 14,500 HR AT 25 C FOR SEVERAL THERMOSETTING MATERIALS

(Elastic deformations as in Figs. 2, 5.)

molded object, the figure should be divided by the "notch sensitivity" of Table 1.

A quantitative relation between creep and stress is usually of interest. It is remarkable that one equation covers the four materials having fillers of woodfloc, fabric, paper, and floc, namely

$$\log_{10} \left(\frac{\epsilon}{\sigma} \right) = 0.103 \log_{10} t + 0.713 \quad [1]$$

where

t = time, hr

ϵ = per cent strain (elastic plus creep) $\times 10^3$

σ = stress, psi

Within ± 20 per cent, this line describes the results for Figs. 2, 3, and 9, and for the data not illustrated for the floc and paper fillers—at four stresses for each, ranging from 1180 to 2750 psi maintained for 2500 to 5000 hr. The exceptions are the three curves in Figs. 2 and 3 that are not linear, and the curve which begins to curve upward at longer times. The equation is not valid for times less than 50 hr.

At 75 C a similar equation correlates the results except that creep is about 1.5 times greater at any given time. The results are more scattered, reflecting some instability of the electric circuit at that temperature.

In several papers, one of Findley's, for example (5), appear graphs relating stress versus time to fracture. For four materials here, Equation [1] can be manipulated, in conjunction with the constant level of critical breaking strain, to demonstrate that such a graph would be linear on logarithmic co-ordinates.

Relaxation, or the decline of load necessary to maintain constant strain, is sometimes of interest. Usually the greater the creep the greater the relaxation. A closer connection has not been evolved except for thermoplastics under high temperature. One relaxation curve is shown in Fig. 10.

No extensive measurements were taken of creep recovery after unloading. Instantaneous elastic recovery at 25 C is equal to the

TABLE 1 PREDICTED LONG-TIME (5-YEAR) TENSILE STRENGTHS OF PHENOL-FORMALDEHYDE MATERIALS

Filler	25 C				75 C			
	Tensile strength, psi	Tensile modulus, psi $\times 10^{-4}$	5-year strength, psi	Notch sensitivity	Tensile strength, psi	Tensile modulus, psi $\times 10^{-4}$	5-year strength, psi	
Woodfloc	7800	1.28	2000	2.0	8000	1.30	1200	
Asbestos	4400	2.47	1500	1.7	4800	2.3		
Chopped kraft paper	7700	1.42	2700	1.3	6500	1.39	1200	
Macerated fabric	5600	1.49	2000	1.0	5600	1.45	1200	
Cotton floc	7500	1.40	2700	1.4	6100	1.48	1200	
Mica	5700	4.5	2000	1.3	6000	

NOTE: Products are commercial. Type and content of resin varied. They were all virtually linear to failure in tension and strain to failure can be found by dividing strength by modulus of elasticity. Notch sensitivity is the ratio of the breaking load in flexure for an unnotched bar 0.4 in. deep to the breaking load for a bar 0.5 in. deep containing the standard ASTM notch (0.1 in. deep, 0.01 in. radius) in the lower face.

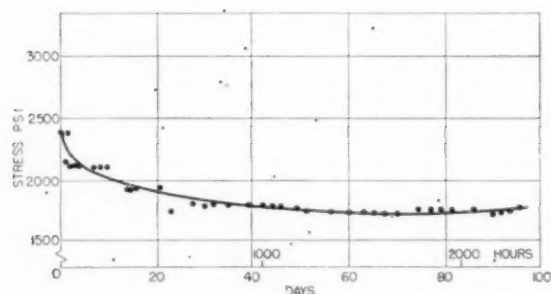


FIG. 10 RELAXATION—CONSTANT STRAIN—AT 25 C OF A THERMOSETTING MATERIAL WITH A FILLER OF KRAFT PAPER (Initial stress was 2400 psi.)

original elastic deformation. In thirteen instances the difference between these two elastic deformations averaged 0.004 per cent only. After the usual exposure to 75 C for 1 hr before a creep test was started, the modulus of elasticity was about 20 per cent lower than at 25 C. The instantaneous recovery on unloading after several hundred hours at 75 C was always lower than the initial elastic deformation, because the modulus had risen about 20 per cent in that time.

Few other results exist for comparison. The several materials exposed for 1000 hr by Telfair, Carswell, and Nason (1), and the one material for several thousand hours by Findley (4) resemble the ones in this paper. The curves are not linear on rectangular or semilogarithmic co-ordinates but might become linear on logarithmic co-ordinates. The creep deformation is of the same order. The several authors of the one paper predict, by a procedure not described, a "stress below which no practical danger of failure exists." The predictions agree with those of Table 1. In spite of this apparent success of forecasts based on 1000 hr, it is suggested that a new material be run at least 5000 hr. Lower times might be sufficient for a product resembling quite closely one already tested.

It has been suggested (2) that elevated temperatures promote further curing and hence shrinkage in molded thermosetting specimens. Another possibility is that such shrinkage is connected with the loss of water by diffusion. Under conditions when further curing is probably absent (vacuum desiccation at 25 C), a woodflour-filled material shrinks about 0.20 per cent for each per cent of weight lost.

Measurements of the weight for a woodflour material at 75 C showed a loss of 2.4 per cent at 250 hr. At 1000 hr the loss reached 3 per cent and remained constant for longer times. If these losses are assumed to be all water, they are far too large to account for the shrinkage observed, assuming a shrinkage of 0.2 per cent for each per cent lost. It is not permissible to assume that other volatiles were lost and that the water alone would account for the shrinkage, because shrinkage continues after 1000 hr, although weight loss ceases. It is probable that shrinkage at 75 C is caused both by loss of water and by further curing.

Creep of Thermoplastics. The curves relating deformation and time generally become linear when plotted in the same way as the thermosetting materials, Fig. 11, 12, and 13. The cellulose plastics are exceptions, and their curves are shown on rectangular co-ordinates, Fig. 14. A comparison of creep alone for several thermoplastics is given in Fig. 15.

The data are not comprehensive enough to allow stress to be correlated with creep as in Equation [1]. Judging from results at two stresses, deformation increases out of proportion to stress. Temperature has a tremendous effect on creep. For example, between 24 hr and 2400 hr, polystyrene creeps 0.6 per cent under 3600 psi at 25 C, and at 75 C creeps the same amount under 400

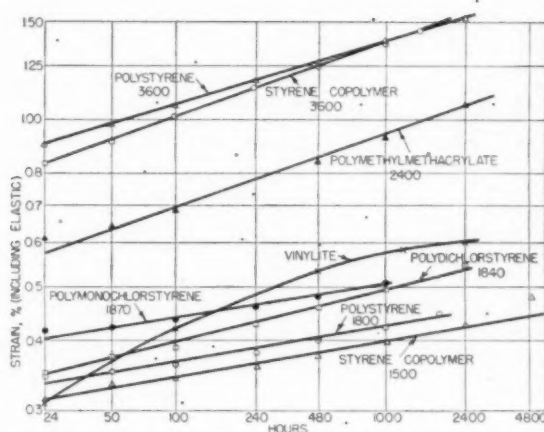


FIG. 11 CREEP AT 25 C FOR VARIOUS THERMOPLASTICS (Figure against each line represents stress in pounds per square inch. Initial elastic deformation included in strain shown may be calculated from moduli of Table 2.)

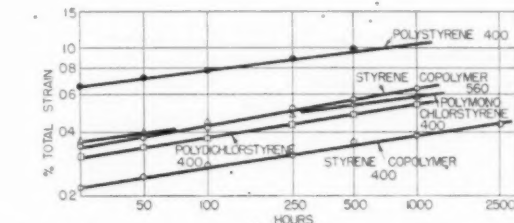


FIG. 12 CREEP AT 75 C FOR VARIOUS THERMOPLASTICS AT STRESSES SHOWN IN POUNDS PER SQUARE INCH (Strain shown includes initial elastic deformation but excludes shrinkage.)

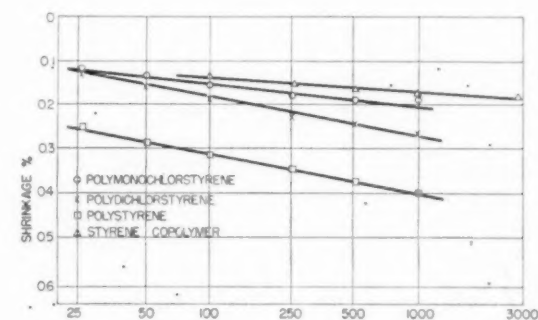


FIG. 13 SHRINKAGE OF THERMOPLASTICS AT 75 C

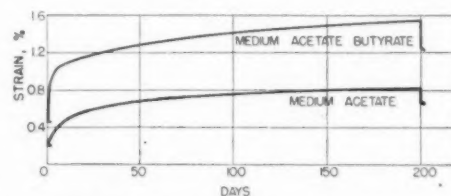


FIG. 14 CREEP OF CELLULOSIC PLASTICS AT 25 C UNDER 640 PSI (Strain at zero time represents initial elastic deformation.)

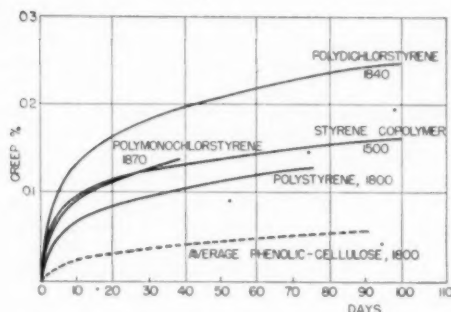


FIG. 15 CREEP ALONE OF THERMOPLASTICS AT 25 C
(Figures represent stresses in pounds per square inch.)

psi. The ratio of nine (3600/400) for polystyrene is lower for the other styrene polymers.

Several thermoplastics differ from other thermoplastics, and from thermosetting and laminated products, in that they can soon exhibit crazing or internal cracking under sustained load. Such crazing promotes premature failure. For example, polystyrene under 1800 psi at 25 C exhibits quite low creep, Fig. 11, and yet separation into two parts occurred in one test after 5700 hr. At a lower stress, 1200 psi, there is no danger of failure under 10,000 hr but definite craze marks were observed in 5 to 10 days. The user of polystyrene probably would feel uneasy or dissatisfied if craze marks did appear, and their appearance can be considered as defining failure.

This phenomenon of crazing under stress was observed with polystyrene from several sources, with annealed polystyrene, with a copolymer of styrene and acrylonitrile, and with polychlorostyrenes. Crazing occurred when SR-4 gages were not applied and therefore it cannot have arisen because of chemical attack by the cement. There was no crazing under the low stresses used at 75 C, and a limiting deformation provides the criterion of failure, as described in the following.

Crazing was not observed at 25 C with the cellulose plastics, with "Vinylite" (a copolymer of vinyl chloride and vinyl acetate), or with polymethylmethacrylate. (Under 3600–5400 psi the last was found to craze by Chasman, reference 6. The stresses exceed those suitable for enduring use.) With these plastics that do not craze, the deformation to failure, whether in a short or a long time, is much in excess of 1 per cent. However, a deformation of 1 per cent is usually the acceptable limit. A bar 8 in. long and 0.5 in. \times 0.5 in. in section when clamped at one end would deflect 0.8 in. at the other if the load there caused a strain of 1 per cent at the clamped end. Accordingly, the long-time strength will be such that the total deformation does not exceed 1 per cent. At 75 C the proper curves to which this criterion should be applied are those representing net deformation (total deformation minus shrinkage). However, there is so little knowledge of behavior at

75 C that a factor of safety will be applied by considering total deformation.

With the criteria of failure discussed in the foregoing, one can estimate long-time strengths. The data are less thorough than those for the thermosetting materials, and the predictions of Table 2 are for 1 year. The estimates are conservative. With polymethylmethacrylate at 25 C and polystyrene at 75 C, there are no creep data at the estimated stresses, and the very rough approximation was used that total creep is proportional to stress.

The results of Table 2 may be discussed in several ways. Thermoplastics often have a higher tensile strength but are less satisfactory for service under enduring stress than thermosetting materials. The heat distortion temperatures (ASTM D648-45T) for the four polymers of styrene are polystyrene, 83 C, copolymer of styrene and acrylonitrile, 92 C, polymonochlorostyrene, 100 C, polydichlorostyrene, 106 C. Evidently these values are a poor reflection of the serviceability at 75 C indicated by creep tests.

The problem of cracking around inserts may be analyzed. When a piece containing an insert cools after molding, stresses arise because the plastic shrinks more than the metal. At room temperature a stress will be present of a magnitude depending on the temperature at which the plastic becomes rigid and on the coefficient of expansion. With the four styrene polymers of Table 2, the coefficient of expansion falls as softening point rises in such a way that the expected stress is about the same for all. Their tendency to crack around inserts will be governed, therefore, by their long-time strengths at 25 C. Accordingly, polystyrene would crack most readily around inserts. There has been some practical confirmation of this.

The reason for the shrinkage of thermoplastics at 75 C is not known. The loss in weight of the styrene polymers is quite small. It reaches 0.1–0.5 per cent at 100 hr and remains constant for longer times. Coiling of the polymer chains probably accounts for shrinkage at 75 C.

Reliability of SR-4 Gage. Popular suspicion still attaches to the measurement of creep by electric strain gages. There are questions as to the reliability of the bond between the specimen and the gage, and as to the constancy of the electrical circuit over a period of time. The following experiments were designed to resolve the doubts.

The creep of a vinyl copolymer under 1560 psi at 25 C was measured simultaneously by dial gages, reading to 0.0001 in., and by SR-4 gages cemented with "Duco" cement. The specimen cut from a sheet 0.1 in. thick was made long to increase the accuracy of the dial gages. These gages were supported by the testing frame and were held against the edge of the specimen by the spring of the gage, contact being confined to a small area by means of clips, Fig. 16. The use of two dial gages eliminates any effect arising when the specimen shifts slightly in the upper grip or jaw. The SR-4 gages were applied on both sides in two locations to give a mean result. The creep shown by the SR-4 gages is lower than that given by the dial gages, Fig. 17.

Part of the discrepancy in Fig. 17 may arise because the elec-

TABLE 2 PREDICTED LONG-TIME (ONE YEAR) TENSILE STRENGTHS OF THERMOPLASTICS

Material	25 C			75 C	
	Tensile strength, psi	Tensile modulus, $\text{psi} \times 10^{-4}$	Strain to failure, %	One-year strength, psi	One-year strength, psi
Polystyrene	7500	0.48	2.1	800	250
Polymonochlorostyrene	9500	0.52	2.5	1200	400
Polydichlorostyrene	5900	0.60	1.0	1500	400
Styrene-acrylonitrile copolymer	9100	0.43	2.2	1500	560
"Vinylite"				1600	...
Cellulose acetate	6700	0.35	5.5	600	...
Cellulose acetate-butyrate	3900	0.16	9.5	less than 600	...
Polymethylmethacrylate	10100	0.43	4.2	2000	...

^a Properties can vary with the mode of preparation. This is especially true with the cellulose plastics.
^b "Medium" cellulose acetate and cellulose acetate-butyrate were used here.

tric gages actually stiffen the material in their neighborhood. After the creep experiment the central portion of the specimen in Fig. 16 was cut out and pulled in tension. The electric gages and mechanical extensometers applied to span them showed 15 per cent less elongation at a given load than mechanical extensometers outside the region covered by the electric gages. This means that of the 103 lb applied in the creep test, 15 per cent or 15.5 lb are carried by the SR-4 gages and only 87.5 pounds are taken by the adjacent vinyl copolymer. Outside the sections covered by

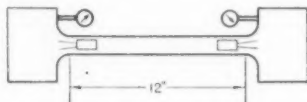


FIG. 16 MEASUREMENT OF CREEP BY ELECTRIC AND DIAL GAGES ON A PIECE OF VINYLITE, 0.1 IN. THICK

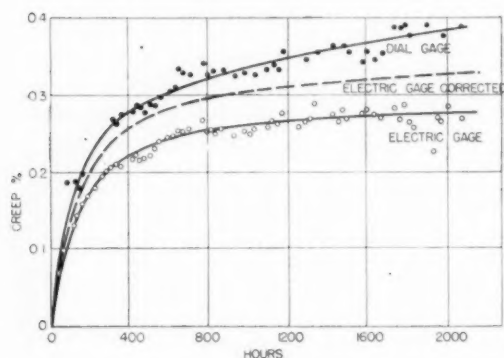


FIG. 17 CREEP OF VINYLITE AT 25°C UNDER 1569 PSI ACCORDING TO TWO KINDS OF GAGE

(Initial elastic deformation was 0.248 per cent according to the electric gages.)

the electric gages, the total load is of course borne by the plastic. In partial confirmation, one SR-4 gage (coated with Duco cement) when loaded by itself needed about 4 lb to register the initial elastic deformation of 0.248 per cent.

When creep starts, the load carried by the plastic may continue to be 87.5 lb or may change according to the way in which the SR-4 gage and the bond creep under their portion of load. Under the 4 lb just noted, the gage was found to creep (determined by readings on the SR-4 meter) more rapidly at first than the vinyl copolymer in Fig. 16, but after 72 hr settled down to approximately the same rate. When loaded with 7.75 lb (15.5 for two gages) the creep was much more rapid. It is uncertain whether we should prefer the load of 4 lb and the proper initial deformation of the gage, or the 7.75 lb which corresponds with the proper stiffening. It will be assumed that not only during initial loading but also during creep the plastic carries only 87.5 lb, and the adjacent gages 15.5 lb.

Therefore the creep curve using electric gages may be corrected for stiffening by multiplying all ordinates by 103/87.5, where creep is assumed proportional to stress. The corrected curve in Fig. 17 is still low, but it is fair to say that the electric gage gives a good indication of the actual creep in its area.

With several thermosetting specimens 1/8 in. thick, tensile loading was applied with and without electrical gages in the section spanned by a mechanical extensometer. For duplicability it was found necessary to apply the extensometer to each edge in turn rather than to the face of the specimen. The stiffening effect was 11 per cent with fillers of woodflour, floc, and asbestos. The

creep of these materials is comparatively low so that the 89 per cent of load borne initially by the specimen tends to increase during creep. If this is neglected the creep curves are about 11 per cent low.

It is easy to show theoretically that the percentage stiffening effect of the gages should be inversely proportional to the stiffness of the specimen (cross-sectional area \times modulus of elasticity). On this basis the stiffening effect for the thermosetting products, predicted from the 15 per cent for the vinyl copolymer, should be 4-6 per cent instead of the 11 per cent observed. This theoretical relation brings out that the thinner the specimen the greater the stiffening effect. It is not proper to measure creep on plastic specimens much under 0.10 in. thick. (Further, high sustained strains much exceeding 1 per cent probably cannot be measured reliably.)

The constancy of the electrical circuit over a period of time may be estimated by a method suggested by Tschebotarioff (7). Two pairs of electric gages are affixed to opposite ends of a steel bar, Fig. 18. A first reading is taken with the pairs connected in one way to the SR-4 meter ($A \rightarrow 1, B \rightarrow 2$) and a second with the pairs interchanged ($A \rightarrow 2, B \rightarrow 1$), by means of switches. The

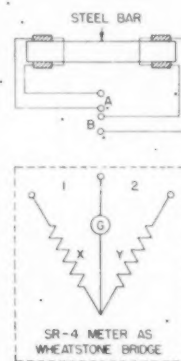


FIG. 18 MEASURING VARIABILITY OF ELECTRIC CIRCUIT

meter has been simplified to make the whole circuit a Wheatstone bridge. The same process is repeated daily. Typical readings are as follows:

	First reading	Δ_1	Second reading	Δ_2	$\frac{\Delta_1 - \Delta_2}{2}$	$\frac{\Delta_1 + \Delta_2}{2}$
Feb. 1	7-1120		0-940			
Feb. 2	7-1080	-40	0-980	+40	-40	0
Feb. 3	7-1070	-50	0-950	+10	-30	-20

Now two kinds of changes occur from day to day in the circuit in Fig. 18. The first is in the circuits of A and B, whether in the leads or switches (gages assumed to remain constant). Let it be a . It appears always as the difference between the changes that have occurred in A and B. The second change takes place in other parts of the circuit, for example, in the fixed resistance X. Let it be x . Therefore

$$\Delta_1 = a + x \quad [2]$$

$$\Delta_2 = x - a \quad [3]$$

where the deltas have the meanings in the foregoing tabulation. Hence

$$x = \frac{1}{2} (\Delta_1 + \Delta_2), \text{ and } a = \frac{1}{2} (\Delta_1 - \Delta_2) \quad [4]$$

The changes x , in the "permanent" part of the circuit for a period exceeding 2 years are shown in Fig. 19. Generally these fluctuations, expressed as strain in microinches/in., are not large, although

no special precautions were taken. In the foregoing argument no account was taken of changes that may occur in the switches when A and B are interchanged in the bridge circuit. Such variations in switching are part of the changes in the permanent portion of the circuit. Usually, they are quite small (≈ 10 microinches/in., as shown by repeated switching).

The changes α , may vary according to whether the changes in the individual circuits A and B happen to add or subtract. Over a period of 2 years they were usually ≈ 50 microinches/in.

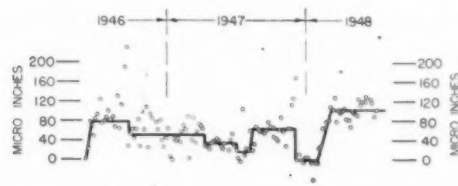


FIG. 19 VARIABILITY OF PERMANENT PART OF ELECTRIC CIRCUIT, EXPRESSED IN MICROINCHES

No check was made of reliability at 75 C. In another paper (1) a steel bar, carrying the AB gage recommended for measurements at 75 C (see Appendix) was bent beyond the elastic limit and held that way for one month at 75 C. The reading on the SR-4 meter, did not change in that time, and the bond and circuit were concluded to be good.

BIBLIOGRAPHY

- 1 "Creep Properties of Molded Phenolic Plastics," by D. Telfair, T. S. Carswell, and H. K. Nason, *Modern Plastics*, vol. 21, February, 1944, pp. 137-144 and 174.
- 2 "Creep Properties of Molded Phenolic Plastics at Elevated Temperatures," by W. J. Gailus and D. Telfair, *Modern Plastics*, vol. 22, May, 1945, pp. 149-154 and 192.
- 3 "Creep, Long-Time Tensile and Flexural Fatigue Properties of Melamine and Phenolic-Plastics Materials," by D. Telfair, C. H. Adams, and H. W. Mohrman, *Trans. ASME*, vol. 69, 1947, pp. 789-793.
- 4 "Mechanical Tests of Macerated Phenolic Molding Material," by W. N. Findley, *Modern Plastics*, vol. 25, December 1947, pp. 145-150, 218 and 238.
- 5 "Mechanical Tests of Cellulose Acetate," by W. N. Findley, *Modern Plastics*, vol. 19, September, 1941, pp. 57-62 and 78; vol. 19, August, 1942, pp. 71-73 and 114.
- 6 "Creep and Time-Fracture Strength of Plastics Under Tensile Stresses," by B. Chasman, *Modern Plastics*, vol. 21, February, 1944, pp. 145-148 and 176.
- 7 "Use of Electric Resistivity Strain Gages Over Long Periods of Time," by G. Tschebotarioff, *Experimental Stress Analysis*, vol. 3, 1946, pp. 47-52.

Appendix

As an adhesive for electric strain gages, "Duco" cement has been found satisfactory at 25 C for most common plastics except the polymers of styrene. The Duco cement produces a multitude of tiny superficial cracks in these. Such crazing is slight and the bond with the gage is good for the polymers of styrene other than polystyrene. With polystyrene the crazing is bad and the bond is firm only for a few days. Three cements that are effective with polystyrene are a solution of polyvinyl acetate in acetone, a solution of polystyrene in benzene and cold-setting glue (resorcinol-formaldehyde) normally used for wood. The latter is good only for small strains up to 1 per cent. When the adhesive is dry, the adhesion should be good enough to allow the gage to withstand prying with the fingernail and flexing of the test specimen by hand. If the gage is firmly attached it will usually give a proper measurement of creep. If the result is unexpectedly low it is advisable to check it with a gage bonded with another adhesive or

with dial gages. Finding that initial elastic deformation and instantaneous recovery after creep are equal is no assurance of the bond; it happened with a gage cemented to polystyrene with an aqueous emulsion of polyvinyl acetate whereas the creep under 1800 psi at 25 C appeared to be slightly negative.

For measuring strain at 75 C the special AB gages were applied to the thermosetting specimens. These gages have a special backing and are cemented with a thermosetting glue that must be baked at 100 C. Such a baking cycle rules them out with thermoplastics and so cold-setting glue or Duco cement was used with the ordinary paper gage. The results so obtained were judged reliable because the strains with gages affixed in this way to a thermosetting specimen agreed with those shown by AB gages on the same specimen up to 1000 hr. At that time the paper gage is somewhat charred. Between 1000 and 3000 hr the two curves diverge slightly and the charring becomes serious.

Apart from having the SR-4 gage well cemented, only the following precautions need be observed:

- 1 At elevated temperatures the dummy must be renewed for each test because it shrinks.
- 2 Switches should be cleaned every one or two weeks with a solvent and sandpaper to maintain fresh contacts of negligible resistance.
- 3 In the portable SR-4 meter, the enclosed batteries are small and they may be replaced advantageously with larger, more enduring batteries outside the meter. The sensitivity of the meter falls rapidly as the batteries become exhausted.

Discussion

JAMES BAILEY.⁴ The fact that the authors' specimens broke at unusually low stresses and that the cracks started in the interior of the injection-molded test specimens, indicates that the specimens had an inside portion which was under an initial tension due to thermal strains. Test specimens which had been annealed might show substantially higher long-time strength. Were the test specimens annealed?

HARRY MAJORS, JR.⁵ The authors have included as a third part of their paper the reliability of a bonded-wire resistance strain gage over long periods of time. It is to be noted that they do not mention what method was used for waterproofing the active gage and the dummy compensating gage. For precision work some system of waterproofing is desirable even though the laboratory conditions are fixed. Zero drift usually accompanies absorption of moisture which is due to the effect between that of the dummy-compensating gage and the active gage.

A method of determining the constancy of the SR-4 strain indicator as used by Mr. Ruge and Mr. Tschebotarioff is explained in the paper. It would have been interesting if the method had been extended to determine the constancy of the wire resistance gages mounted on a similar test specimen as the specimen under the creep test, but maintained at "zero stress" near the active specimen throughout the total time of testing. If this had been carried out using wire gages from the same lot and adequately waterproofed, one would have a measure of the constancy of the active measuring gages as well as that of the SR-4 strain indicator.

Fig. 16 of the paper is in conflict with the results in Fig. 17. The dial gages measure not only the uniform strain in the specimen, but also the increase in strain due to the stress concentration at the fillet. One would have been more satisfied if the dial gages

⁴ Vice-President and Research Director, Plax Corporation, Hartford, Conn.

⁵ Director, Engineering Experiment Station, University of Alabama, University, Ala.

were arranged so as to measure the strain in the straight section only, and if the wire gages had been moved just a bit more toward the center.

This paper is a further contribution to the correct technique in applying wire gages to the study of plastics.

AUTHORS' CLOSURE

The answer to Mr. Bailey is that the results are for thermoplastics that were not annealed. However, when polystyrene was found to craze at such low stresses, several fresh specimens were annealed and submitted to a sustained stress of 1500 psi. Crazeing was observed to appear to the same extent as for specimens that were not annealed. The annealed specimens were free of residual stress according to Mr. Bailey's test (no cracking of the specimen when drilled with holes of $1/16$ in. diam and immersed in kerosene).

Although Mr. Majors commends waterproofing we did not use it at all. In the first place it seemed unnecessary, in a laboratory maintained at constant temperature and humidity, for the degree of precision needed, and second we wished to avoid complications that would deter routine groups from considering this method.

The changes a discussed in the paper include any effects of humidity on the gages and leads. In regard to these changes a and the changes z we seem to have induced a misunderstanding. The changes a (≈ 50 microinches/in.) include changes in the sensitive wires of the gage and in the leads and in the switches outside the SR-4 meter. While these changes were measured for gages on a steel bar they should apply equally well to the active or dummy plastic specimens. Perhaps Mr. Majors is considering changes that we neglected; for example, two ends of a molded bar may gain or lose very slightly different amounts of water in attaining equilibrium with the ambient air, and in consequence may undergo a very slight differential change. This would show up in his proposed extension of the method to a plastic dummy but would not appear in our estimates of a . Fig. 16 is a pictorial representation prepared by a draftsman. The electric gages were actually close to the center of the specimen. The dial gages unavoidably measured the extension of a uniform 12-in. length and the extensions of two flared areas of small effective length.

Even a large error in an estimate of these effective lengths would hardly affect to ± 5 per cent the over-all length to be used in reducing the extension to a strain.

T
ma
tory
phe
vibr
spe
and
ter
velo
ma
test
cav
dev
ma
occ

A
Sep
sinc
to c
bee
tion
T
dur
Log
at t
The
app
high
cav
of t
cav

T
whi
ma
C
for
bo
to
is i
par
a b
C
var
cre

fac
the
C
Me
Am
der
So
194

Accelerated-Cavitation Research

By W. J. RHEINGANS,¹ MILWAUKEE, WIS.

The cavitation-pitting tests described in this paper were made with an accelerated-cavitation machine of the vibratory type. An attempt was made to solve some of the phenomena of cavitation by varying the amplitude of vibration, by varying the depth of submergence of the test specimen in the test liquid, and by using alkalis, acids, and oils for the test liquid. Other tests were made to determine the relative resistance to pitting of recently developed materials and techniques for applying these materials. Results showed that accelerated-cavitation tests can be used to determine some of the mechanics of cavitation, as well as to indicate that some of the newly developed materials might be suitable for use on hydraulic machinery under operating conditions where cavitation occurs.

AN accelerated-cavitation machine of the vibratory type was constructed by the Research Laboratory of the author's company in 1948, and was placed in operation in September of that year. It has been in continuous use ever since for making hundreds of tests on a large variety of materials to determine their relative resistance to cavitation and has also been used for investigations of some of the phenomena of cavitation and pitting.

These tests supplement the accelerated-cavitation tests made during the years 1934 to 1937, by J. M. Mousson (1),² and S. Logan Kerr (2), who tested almost all of the materials available at that time which were suited for use on hydraulic machinery. The development of new materials and new techniques for the application of materials since 1937, some of which have unusually high resistance to pitting or other advantages when used where cavitation occurs, indicated the necessity for continuous research of this type and resulted in the construction of the accelerated-cavitation machine described in this paper.

HISTORY OF CAVITATION

The following is a brief history of cavitation and the problems which brought about the development of accelerated-cavitation machines.

Cavitation as used throughout this paper is defined as the formation of voids within a body of moving liquid (or around a body moving in liquid) when the particles of liquid fail to adhere to the boundaries of the passageway. This occurs when there is insufficient internal pressure to overcome the inertia of the particles and force them to take sufficiently curved paths along a boundary which has a change or a variation in shape.

Cavitation affects the operation of hydraulic machinery in various ways. It can cause a loss of power and efficiency by increasing resistance to flow. It can produce noise and vibration

and it can produce pitting which is defined as the actual erosion of material subjected to cavitation.

The phenomenon of cavitation was anticipated as early as 1754 by Leonhard Euler (3) in his theory on hydraulic turbines, when he noted that an insufficient pressure in a perfect liquid can cause a divergence between theory and experiment and can result in zero resistance.

Some of the practical aspects of cavitation were first noted in connection with ship propellers operating at high speeds. Sidney W. Barnaby and Mr. Thorncroft, in a paper presented to The Institution of Civil Engineers in London in 1895, mentioned the occurrence of a new phenomenon during propeller trials of HMS *Daring* (4). They noted the formation of cavities in water which tended to become filled with water vapor. This condition was held responsible for waste of power and other difficulties. About the same time Charles A. Parsons (5) verified this by tests on the steamship *Turbinia* where loss of power on the first steam-turbine-driven propellers was traced to cavitation.

The first recorded indication that cavitation produced erosion or pitting of materials was in an article published in 1907, by W. Wagenbach (6), in which he described how the Francis turbine runners of the Jaice hydroelectric works in Bosnia failed after a few weeks of operation in 1890. The runners were so badly eroded by cavitation that they had to be replaced. After this there were numerous reports of pitting, both on hydraulic turbine runners and on ship propellers.

However, the wide variation in the resistance of different materials to pitting is a phenomenon that was first discovered during the 1920's. It is probable that prior to this period some engineers may have suspected such variations but there is no record of any published information on actual comparative tests.

J. Ackert, in his handbook published in 1926 (7), reported the relative resistance of cast iron, cast steel, and bronze to erosion or pitting.

In 1924 a cast-iron Francis runner with 15 patch plates of various types of materials fastened to the back sides of the runner blades near the discharge edge was installed at the Isle Malign Plant in Quebec. An inspection of this runner after 3½ years of operation showed that patch plates of stainless steel resisted pitting to a remarkable degree as compared to the cast iron in the runner, and as compared to other materials used in the remainder of the patch plates. About this time similar experiments with various materials, including stainless steel, were being made on hydraulic-turbine runners in a number of other power plants. However, it was soon realized that placing different types of material in a hydraulic turbine and then waiting a number of years for an answer was not a very satisfactory method of determining the degree of resistance to pitting of these materials. The time interval was entirely too long, and there was no satisfactory method for comparing materials tried in one turbine with those tried in another.

Therefore, starting about 1932, several types of machines were developed which were capable of producing accelerated cavitation whereby the resistance of various metals to pitting could be determined accurately under laboratory control within a reasonable period of time (8).

The earlier machines used the principle of passing water at a high velocity through a restricted area, followed by a sudden enlargement. This was known as the Venturi-tube type of machine.

¹ Assistant Manager, Hydraulic Department, Allis-Chalmers Manufacturing Company, Milwaukee, Wis. Mem. ASME.

² Numbers in parentheses refer to the Bibliography at the end of the paper.

Contributed by the Hydraulic Division and presented at the Annual Meeting, New York, N. Y., November 27-December 2, 1949, of THE AMERICAN SOCIETY OF MECHANICAL ENGINEERS.

NOTE: Statements and opinions advanced in papers are to be understood as individual expressions of their authors and not those of the Society. Manuscript received at ASME Headquarters, December 8, 1949. Paper No. 49-A-140.

In 1935 Dr. J. C. Hunsaker and Dr. H. Peters of the Massachusetts Institute of Technology, developed the vibratory method of accelerated cavitation (9, 10). This is the method used for the tests described in this article.

CAVITATION MACHINE

Fig. 1 shows a schematic layout of the vibratory type of accelerated-cavitation machine. Figs. 2 and 3 are views of the machine as originally built for temporary use, when only a few tests were being planned. However, the results of the tests were so revealing, so many new materials were being developed, and so many new ideas on the phenomena of cavitation were being advanced, that the machine has been in constant operation from the day it was completed. Since many additional tests are scheduled for this machine which may require several years to complete, it is being rebuilt in more permanent form, with cabinets for housing all of the electrical equipment, and with a neater arrangement of supports, connecting wires, and auxiliaries.

The apparatus follows the general description by S. Logan Kerr (2). It consists of a vacuum-tube oscillator which produces an alternating magnetic field through the nickel tube. When the frequency of the magnetic field is the same as the natural longitudinal frequency of vibration of the nickel tube, the tube will vibrate at maximum amplitude in the longitudinal direction.

The test specimen, Fig. 4, is attached to the end of the tube and immersed in the test fluid to a depth of $1/4$ in. Since the test fluid heats rapidly during a test run, the beaker containing the test fluid is set in a running-water bath to maintain a constant temperature of 76 plus or minus 1 F.

Since the frequency and amplitude of vibration of the test specimen have considerable effect on the rate of pitting, provisions are made to control these quantities at all times. The frequency of course is determined by the length of the nickel tube. The vacuum-tube oscillator circuit is tuned to the natural frequency of the nickel tube. All tests are made at a frequency of 6500 cycles per second (cps), this being the natural frequency

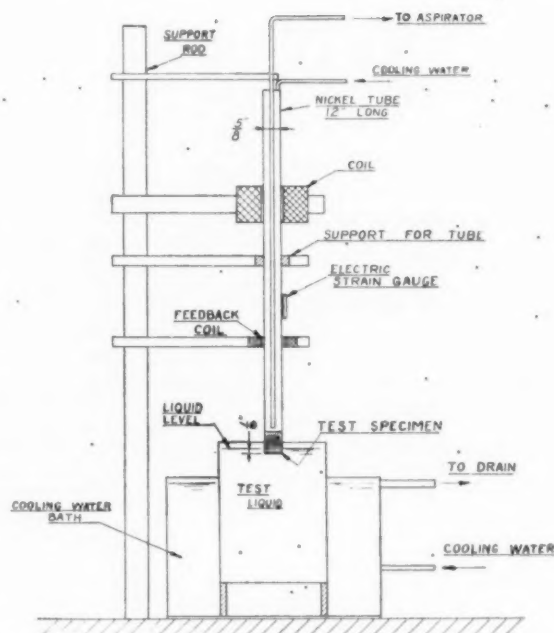


FIG. 1 SCHEMATIC LAYOUT OF VIBRATORY-TYPE ACCELERATED-CAVITATION MACHINE

of vibration of the nickel tube 12 in. long, with test button attached.

An electric strain gage is attached to the nickel tube to measure the amplitude of longitudinal vibration. It is calibrated at frequent intervals by measuring the actual movement of the test specimen by means of a stroboscopic light and a microscope with

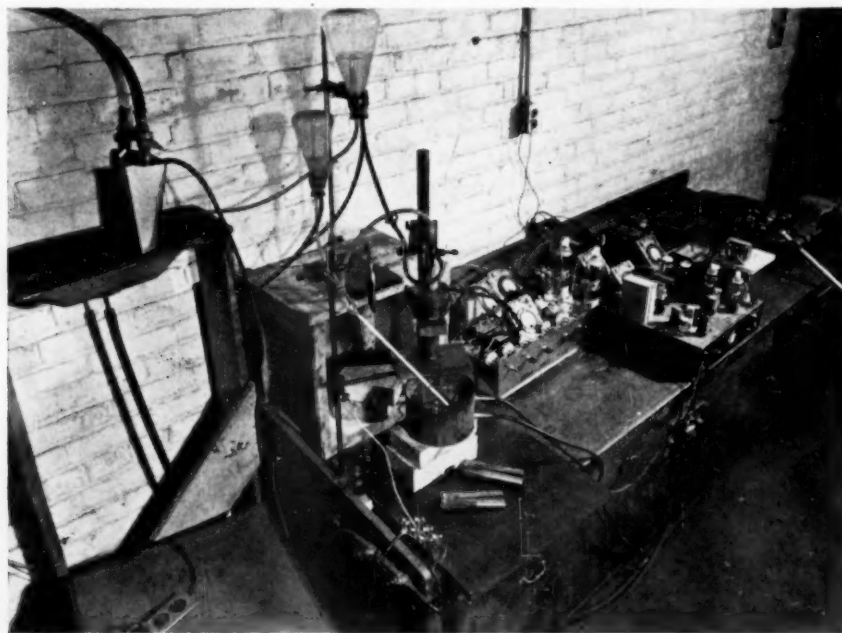


FIG. 2 HIGH-FREQUENCY OSCILLATOR AND ELECTRONIC CONTROL

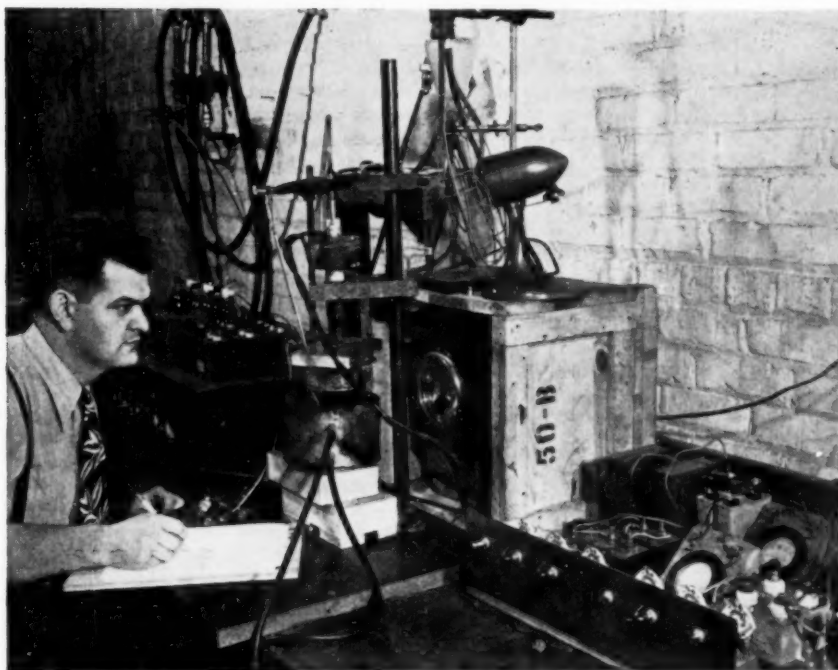


FIG. 3 HIGH-FREQUENCY OSCILLATOR

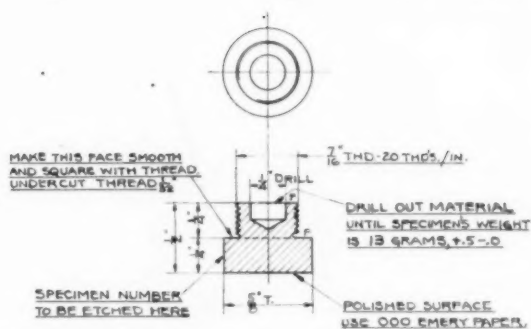


FIG. 4 BUTTONS USED FOR TEST SPECIMENS IN CAVITATION MACHINE

micrometer scale. All tests are made with an amplitude of vibration of 0.0034 in. In this paper the amplitude of vibration refers to the total travel of the test specimen. The criterion for rate of pitting is the loss of weight of the test specimen.

METHOD OF TESTING

As a check on the relative performance of the vibratory machine, it was decided to use a brass test specimen as a standard to be tested at frequent intervals. By comparing the rate of pitting of the various standard specimens, any serious deviation in the relative performance of the apparatus becomes apparent immediately.

At first, cast bronze was used for this purpose. However, it was found that this material would pick up water and actually increase in weight during the first 30 min of testing. The standard test specimen was then changed to rolled brass, ASTM Specifications B-16-44, which gave satisfactory results.

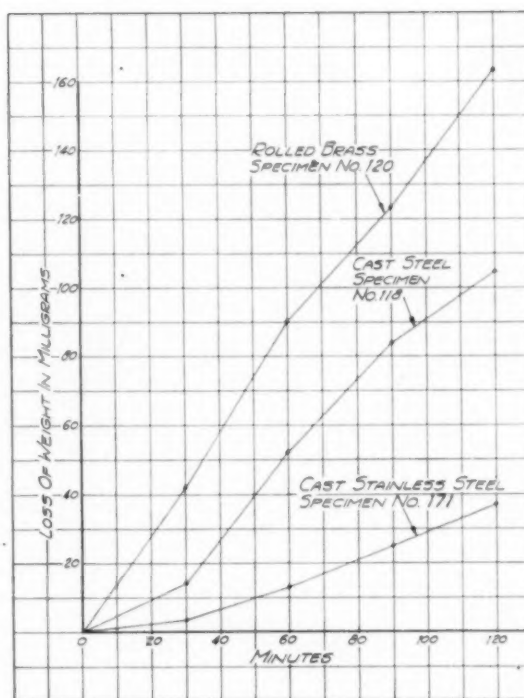


FIG. 5 LOSS OF WEIGHT OF TEST SPECIMENS

However, since most materials, particularly cast materials, have a tendency to pick up some moisture during the course of a 2-hr cavitation test, all of the test specimens are placed in boiling water for 30 min, before being tested and before being weighed.

All of the test specimens are carefully adjusted to the same weight within $\frac{1}{10}$ gram. They are all weighed accurately to the nearest $\frac{1}{10}$ mg in a chemical-balance scale. All specimens are weighed every 30 min during the test. It was found that the rate of loss of some of the metals increases for the first 60 to 90 min, but after that period the loss approaches a fairly constant rate. Therefore the length of each test was limited to 120 min. Fig. 5 shows how the rate of loss of metal varied with time. It was observed in several instances that a highly polished specimen had a slower rate of pitting during the first 60 min of testing than the same material with a dull finish. However, by the end of a 120-min test, the highly polished specimen would be pitting at the same rate as the duller specimen. Therefore, in comparing the relative rate of pitting of various materials, the rate of loss during the last 30 min, as well as the total loss of weight in 120 min, is used as a criterion.

EFFECT OF AMPLITUDE OF VIBRATION

An interesting series of tests were made on several materials to determine the effect on the rate of pitting by changing the amplitude of vibration of the test specimen. The construction of the accelerated-cavitation machine made it possible to control the amplitude of vibration by controlling the power output of the vacuum-tube oscillator. The amplitude was measured by means of an electric strain gage fastened to the nickel tube. This strain gage was calibrated at frequent intervals by means of a microscope micrometer. During these tests the frequency of vibration was the same as for all the tests described in this paper, namely, 6500 cps.

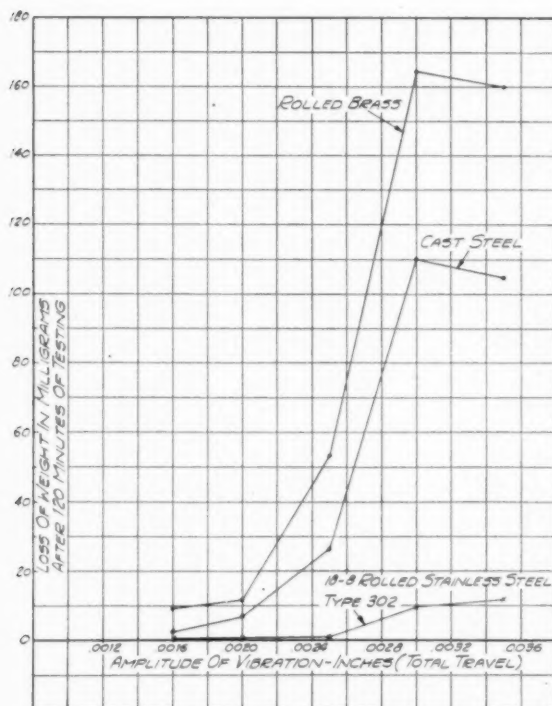


FIG. 6 EFFECT OF AMPLITUDE OF VIBRATION

Fig. 6 shows how the amount of pitting decreased as the amplitude was decreased. There was very little difference in the rate of pitting between 0.0030 in. and 0.0035 in. amplitude. For this reason, an amplitude of 0.0034 in. was selected for all the standard tests made on different materials to determine their relative resistance to pitting. Thus a slight variation in amplitude for different tests had very little effect on the relative rate of pitting of the test specimens.

The results of these tests indicate that a certain amplitude of vibration of the test specimen is needed to produce actual pitting, and that the magnitude of the amplitude required varies for different metals. The 18-8 rolled stainless-steel type 302 required an amplitude of 0.0025 in. before pitting became appreciable. The cast-steel specimen showed very little pitting below 0.0016 in. amplitude, and the brass specimen probably would have stopped pitting below 0.001 in., if the tests had been carried to such low values.

Apparently there is a difference in the minimum force required to produce pitting on different materials, and changing the amplitude of vibration seems to change the forces which produce pitting. This experimental data correspond to some of the field results, where cast iron or cast steel, which pitted rapidly, was replaced with stainless steel, which did not pit at all under the same operating and cavitation conditions.

Just what the forces are that are created by the vibrating specimen and which produce pitting is still open to speculation. The maximum velocity of the test specimen when vibrating at 6500 cps, with an amplitude of 0.0034 in. is only 5.8 fps, as computed from the sine-wave formula

$$V = \pi F A$$

where

V = maximum velocity

F = frequency

A = amplitude (full travel)

This velocity is much too low to produce any impact forces sufficient to cause pitting. However, the acceleration of the test specimen is quite high, as is shown in Fig. 7. At 0.0034 in. amplitude of vibration, the maximum acceleration is 7300 G's or about 235,000 ft per sec per sec. It is possible that this high rate of acceleration is responsible for the forces that produce pitting.

The most logical explanation is the theory by R. T. Knapp and A. Hollander (11) that bubbles form in the cavitation region where the absolute pressure drops below the vapor pressure of the surrounding liquid. They actually demonstrated by high-speed moving pictures that cavitation bubbles form in the liquid and then collapse at velocities up to 800 fps, depending upon the size of the bubble. These extremely high velocities of collapse produce pressures of approximately 50,000 psi, but only over a microscopically small area.

Observation of the test specimens, after having been tested at various amplitudes of vibration, showed that the pitted area on the bottom of the button, and the depth of pitting decreased with a decrease in amplitude. One of the reasons why the depth of pitting decreases with a decrease in amplitude is apparent when observing the test fluid in stroboscopic light. As the amplitude is decreased, the size of the vapor bubbles that form beneath the button also decreases. According to the theory of collapse of a vapor bubble, the smaller the bubble, the smaller the velocity of collapse and, therefore, the smaller the pressure produced.

The reason for the decrease in pitted area with a decrease in amplitude is also apparent from observation of the test fluid under stroboscopic light. As the amplitude decreases, the area covered by vapor bubbles also decreases. This is probably due to the lower vacuums produced under the test button at lower ampli-

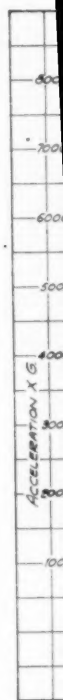


FIG. 7

tudes, and large areas. Further forces are what is

Another rate of men in stainless

The rolled-b with an cast sta per cen

On b surface

gence. the sam steel th creased $\frac{1}{8}$ in.

The eroded strobos form n ward t

Fig. Air bul drawn the liq

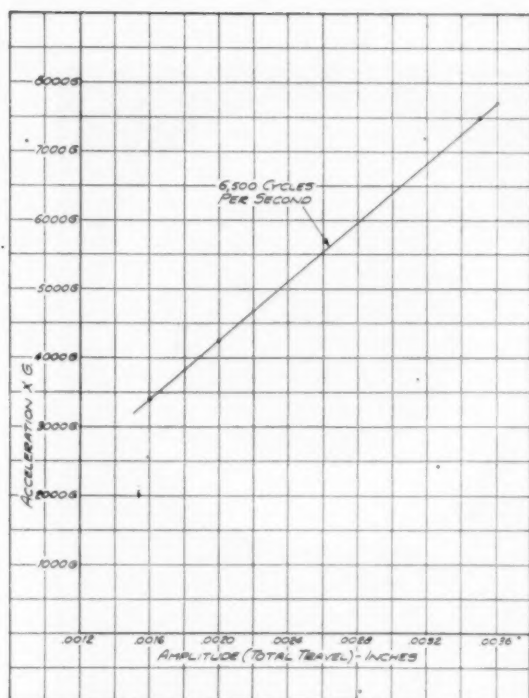


FIG. 7 ACCELERATION-DISPLACEMENT RELATIONSHIP AT 6500 Cps

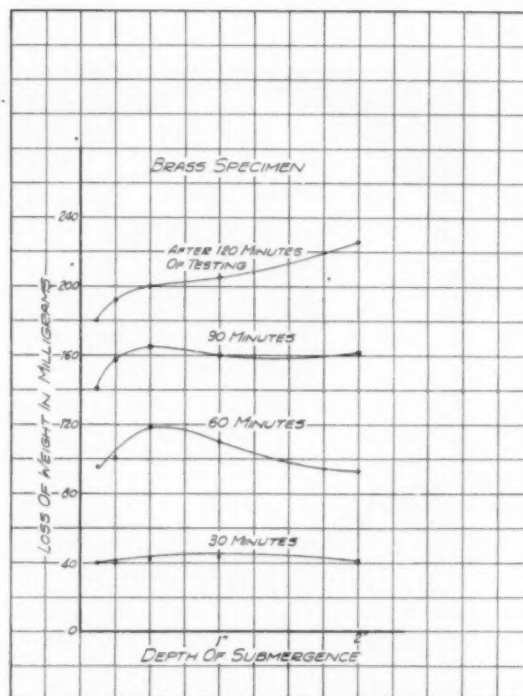


FIG. 8 CAVITATION TESTS TO DETERMINE EFFECT OF SUBMERGENCE ON BRASS SPECIMEN

tudes, and therefore the formation of vapor bubbles over a large area is prevented by the surrounding pressure.

Further tests are being made in an attempt to determine what forces are being produced under the vibrating test specimen, or what is actually taking place that produces the pitting.

EFFECT OF SUBMERGENCE IN TEST LIQUID

Another series of tests were made to determine the effect on the rate of pitting of various depths of submergence of the test specimen in the fluid. Tests were made on brass and on 18-8 cast stainless steel at various depths of submergence from $\frac{1}{8}$ to 2 in.

The results of these tests are shown in Figs. 8 and 9. With the rolled-brass specimen, the material removed increased 25 per cent with an increase of submergence from $\frac{1}{8}$ to 2 in. With the 18-8 cast stainless-steel specimen, the material removed decreased 60 per cent with an increase of submergence from $\frac{1}{8}$ to 2 in.

On both the brass and the stainless steel, the area of the pitted surface on the specimens increased with an increase in submergence. However, on the brass the depth of pitting remained about the same for all depths of submergence, while on the stainless steel the depth of pitting decreased as the submergence was increased. Fig. 10 shows the pitting of brass and stainless steel at $\frac{1}{8}$ in. submergence and at 2 in. submergence.

The reason why only the central portion of the specimen is eroded or pitted is apparent when observing the test liquid with stroboscopic light. As the test specimen vibrates, vapor bubbles form near the center of the bottom of the button and flow downward to the bottom of the container in a continuous stream.

Fig. 11 shows this action with a test specimen vibrating in oil. Air bubbles are also visible in the liquid. Apparently air is being drawn down along the side of the test button from the surface of the liquid. This air flows underneath the button to prevent

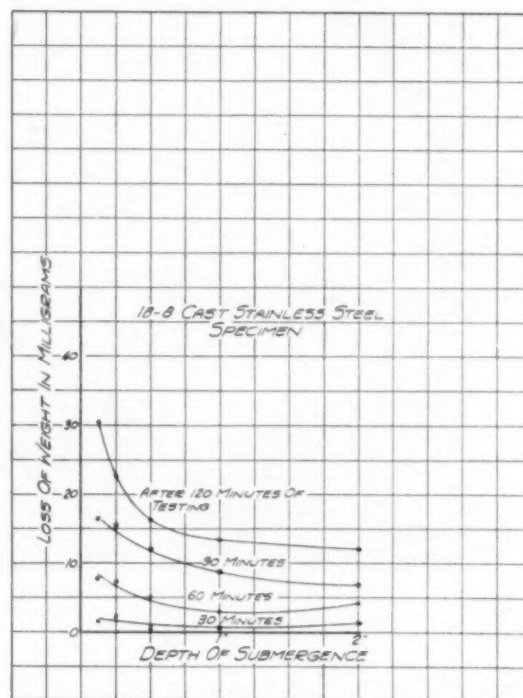


FIG. 9 CAVITATION TESTS TO DETERMINE EFFECTS OF SUBMERGENCE ON STAINLESS-STEEL SPECIMENS

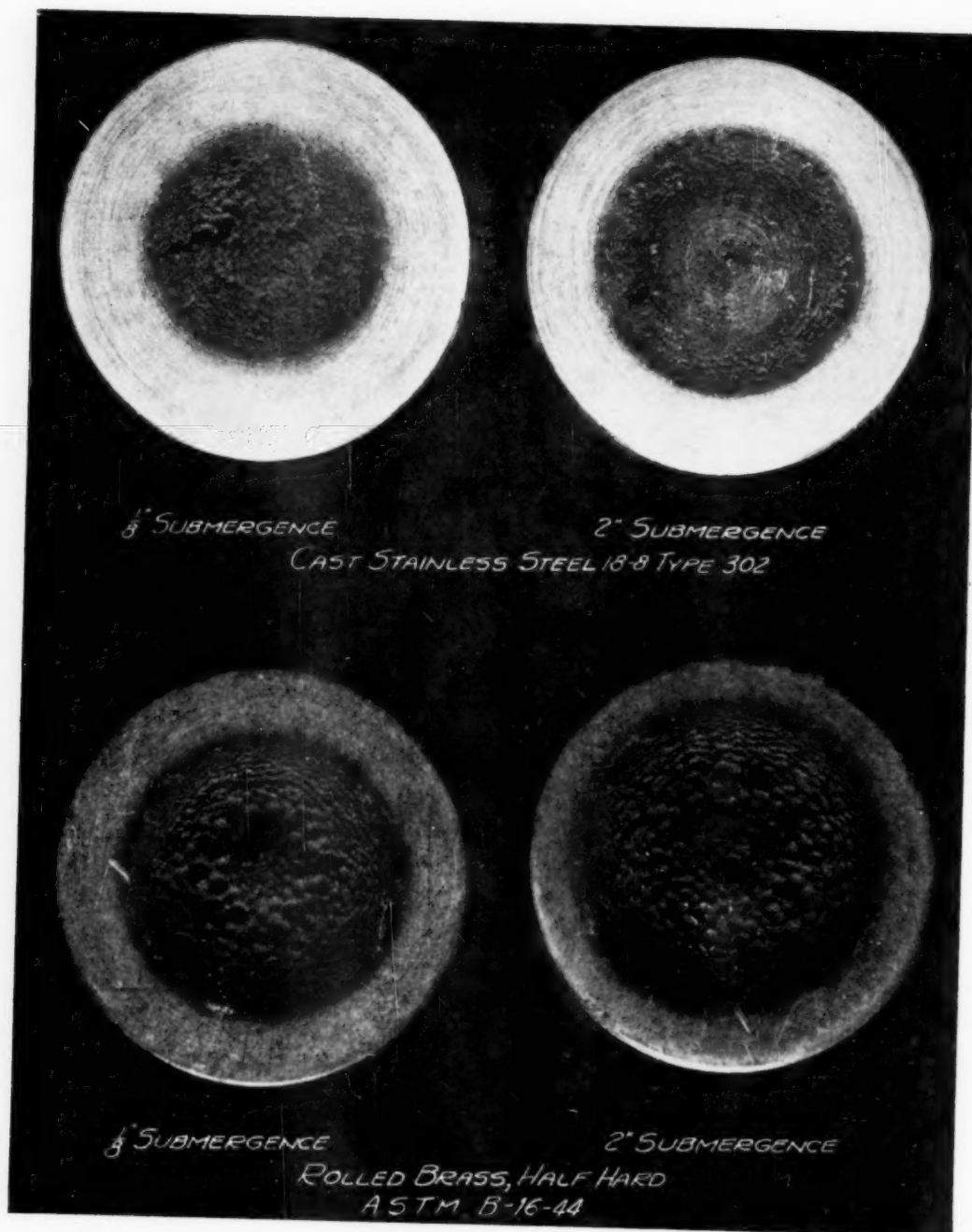


FIG. 10 BRASS AND STAINLESS STEEL AT $\frac{1}{8}$ IN. AND 2 IN. SUBMERGENCE

form
of su
air c
form
air is
with
from
speci
Th
at al



FIG. 11 SPECIMEN VIBRATING IN OIL

formation of the vapor bubbles at the outer edges. As the depth of submergence of the test specimen is increased, the quantity of air drawn from the surface decreases, thereby permitting the formation of larger pitted areas on the test specimen. This flow of air is not visible on any of the photographs, but close observation with stroboscopic light indicates that air is being drawn from the surface of the liquid to the bottom of the vibrating test specimen.

The reason why the brass specimens pitted to the same depth at all depths of submergence, and why the pitting on the stainless

steel decreased with an increase of depth, cannot be explained quite as easily. It might be expected that pitting would decrease with increased submergence, because, with increased pressure, the formation of vapor bubbles decreases. It is possible that the severity of cavitation actually did decrease with an increase in submergence, but that the brass specimen was so susceptible to cavitation that it was not very sensitive to a change in the cavitation forces. On the other hand, the stainless steel was probably close to the borderline between pitting and not pitting and therefore was sensitive to any slight differences in the cavitation forces such as would occur due to an increase in the depth of submergence. This is similar to what occurred when the amplitude of vibration was decreased as shown in Fig. 6.

Further tests are being made to determine the effect of submergence on the rate of pitting of other materials. All of the other tests described in this paper were made at $1/8$ in. depth of submergence in the test liquid.

EFFECT OF DIFFERENT TEST LIQUIDS

One of the most interesting series of tests was made using different test liquids. Most of the standard tests to determine the relative resistance of different materials to pitting have been made in distilled water. S. Logan Kerr made some tests using salt water (2) which showed very little difference in the rate of pitting as compared to fresh water.

The present series of tests used liquids such as sulphuric acid, hydrochloric acid, oils and water, treated with a chromate inhibitor. The materials tested were brass, stainless steel, cast steel, and special cast irons.

Table 1 lists the results of tests on various cast irons when tested in distilled water and in water treated with chromate (Na_2CrO_4). The chromate solutions were alkaline, having a pH number of 8.6. The chemical compositions of the five different cast irons tested are shown in Table 2.

The purpose of these tests was to determine whether addition of an inhibitor such as chromate to water would reduce pitting. With the exception of the heat-treated low-alloy cast iron, none of the test results indicated that addition of chromate increased the resistance to pitting any appreciable amount.

However, since the Brinell hardness was determined for all of the test specimens, it was noted that the loss of metal of the various materials after 120 min of testing varied with hardness. This is shown in Fig. 12, and, despite the fact that this curve

TABLE 1- EFFECT OF INHIBITOR IN TEST LIQUID ON RESISTANCE TO PITTING

Material	Test liquid	Rate of loss mg per min during last 30 min of test	Total loss in mg in 120 min
Low-alloy gray iron, as cast, Rockwell A55.....	Water (distilled)	0.60	68
Low-alloy gray iron, as cast, Rockwell A55.....	0.2% chromate (Na_2CrO_4) 99.8% water, pH = 8.6	0.57	67
Low-alloy gray iron, as cast, Rockwell A55.....	0.4% chromate, Na_2CrO_4 99.6% water, pH = 8.6	0.55	67
Low-alloy gray iron, heat-treated, Rockwell A71..	Water (distilled)	0.67	59
Low-alloy gray iron, heat-treated, Rockwell A71..	0.2% chromate (Na_2CrO_4) 99.8% water, pH = 8.6	0.36	36
Low-alloy gray iron, heat-treated, Rockwell A71..	0.5% chromate (Na_2CrO_4) 99.6% water, pH = 8.6	0.32	31
Type no. 1 Ni-Resist, Rockwell A43.....	Water (distilled)	0.58	136
Type no. 1 Ni-Resist, Rockwell A43.....	0.2% chromate (Na_2CrO_4) 99.8% water, pH = 8.6	0.53	115
Type no. 1 Ni-Resist, Rockwell A43.....	0.4% chromate (Na_2CrO_4) 99.6% water, pH = 8.6	0.79	122
Type no. 2 Ni-Resist, Rockwell A35.....	Water (distilled)	1.03	166
Type no. 2 Ni-Resist, Rockwell A35.....	0.2% chromate (Na_2CrO_4) 99.8% water, pH = 8.6	0.99	166
Type no. 2 Ni-Resist, Rockwell A35.....	0.4% chromate (Na_2CrO_4) 99.6% water, pH = 8.6	1.02	181
Type no. 3 Ni-Resist, Rockwell A42.....	Water (distilled)	1.00	133
Type no. 3 Ni-Resist, Rockwell A42.....	0.2% chromate (Na_2CrO_4) 99.8% water, pH = 8.6	0.89	130
Type no. 3 Ni-Resist, Rockwell A42.....	0.4% chromate (Na_2CrO_4) 99.6% water, pH = 8.6	0.79	115

TABLE 2 CHEMICAL COMPOSITION OF MATERIALS TESTED IN CHROMATE SOLUTION

Material ^a	Chemical composition, per cent							
	Fe	Si	Mn	Ni	Cr	Cu	P	S
Low-alloy gray iron as cast.....	3.15	2.14	0.64	2.17	0.08	0.08
Low-alloy gray iron heat-treated.....	3.15	2.14	0.64	2.17	0.08	0.08
Type 1 Ni-Resist....	2.97	1.82	1.21	13.82	2.24	6.14	0.08	0.08
Type 2 Ni-Resist....	2.74	2.32	1.20	19.98	2.00	..	0.08	0.08
Type 3 Ni-Resist....	2.47	1.81	0.71	29.75	3.00	..	0.08	0.08

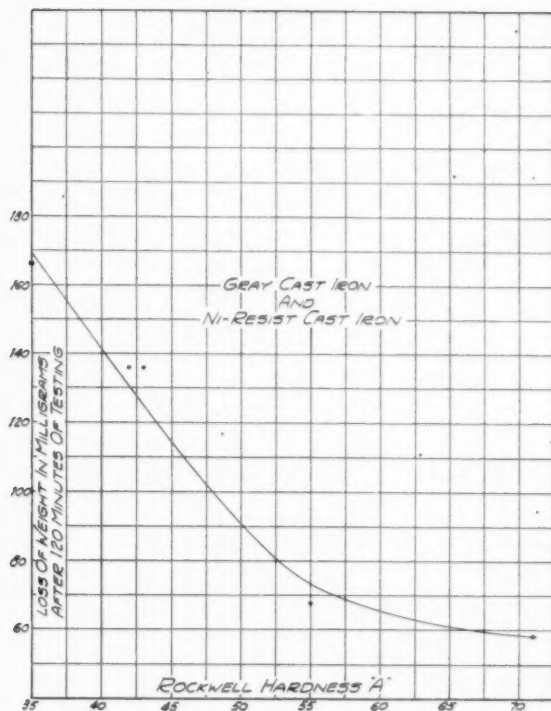
^a Furnished by International Nickel Company.

FIG. 12 EFFECT OF HARDNESS OF CAST IRON ON RESISTANCE TO PITTING

represents cast iron with various chemical compositions, there is a definite relation between hardness and resistance to pitting.

Table 3 lists the results of tests on half-hard rolled-brass bar stock using various solutions of sulphuric and hydrochloric acid, and also oils. The first group of tests seemed to indicate that the greater the concentration of sulphuric acid, the greater the resistance to cavitation. In the second series, however, where both the water and the acid solutions were wetted to give approximately the surface tensions of the oils used, there seemed to be very little difference in the resistance to pitting between distilled water and various concentrations of acids. The biggest variation was found when oil was used as the test liquid. The results showed that there was a marked drop in loss of weight of the test specimen when vibrated in either mineral seal oil or transformer oil. A test was also made mixing the mineral seal oil with chloroform to increase the specific gravity and decrease the viscosity, bringing these values closer to that for water. This mixture showed an increase in the loss of weight of the test specimen.

Table 4 lists the results of tests on cast stainless steel, type 302. Again the acid solutions showed no marked increase or decrease, but the test in the seal oil showed a big decrease in pitting.

TABLE 3 ROLLED-BRASS BAR STOCK, ASTM, B-16-44, HALF-HARD

(Cu 60 per cent, Zn 27 per cent, PB 3 per cent, 90 Bhn)

Test liquid	Properties of liquid			Rate of loss mg per min during last 30 min of test	Total loss in mg in 120 min
	Specific gravity	Viscosity 100 F. centistokes	Surface tension, dynes per cm		
Water (distilled)...	1.00	0.77	76.5	1.37	190
5% H ₂ SO ₄ , 95% H ₂ O.....	1.058	0.83	76.1	1.13	174
25% H ₂ SO ₄ , 75% H ₂ O.....	1.226	1.20	71.2	1.44	154
50% H ₂ SO ₄ , 50% H ₂ O.....	1.424	2.99	65.5	0.73	77
Water (wetted to reduce surface tension).....	1.00	0.77	34.6	1.26	145
25% H ₂ SO ₄ , 75% H ₂ O (wetted).....	1.226	1.20	32.0	1.27	166
5% HCl, 95% H ₂ O (wetted).....	1.100	0.76	49.1	1.10	156
25% HCl, 75% H ₂ O (wetted).....	1.057	0.86	41.0	2.36	164
Mineral seal oil.....	0.838	4.98	32.3	0.010	1.2
Mineral seal oil and chloroform.....	0.993	1.86	31.5	0.42	39
Transformer oil.....	0.897	10.95	34.7	0.047	4.7
(Spec. N-2698, Sun Oil Company T-92304-6199 Sun X 2587)					

TABLE 4 CAST STAINLESS STEEL, TYPE 302 (18 per cent CR, 8 per cent Ni, 0.11 per cent C)

Test liquid	Properties of liquid			Rate of loss mg per min during last 30 min of test	Total loss in mg in 120 min
	Specific gravity	Viscosity 100 F. centistokes	Surface tension, dynes per cm		
Water (distilled)...	1.00	0.77	76.5	0.47	35
25% H ₂ SO ₄ , 75% H ₂ O (wetted).....	1.226	1.20	32.0	0.24	25
25% HCl, 75% H ₂ O (wetted).....	1.057	0.86	41.0	0.48	48
Mineral seal oil and chloroform.....	0.993	1.86	31.5	0.028	2.1

TABLE 5 CAST STEEL, FEDERAL SPECIFICATION QQ-S-681 b CLASS 2 MEDIUM

Test liquid	Properties of liquid			Rate of loss mg per min during last 30 min of test	Total loss in mg in 120 min
	Specific gravity	Viscosity 100 F. centistokes	Surface tension, dynes per cm		
Water.....	1.00	0.77	76.5	0.75	104.4
25% H ₂ SO ₄ , 75% H ₂ O (wetted).....	1.226	1.20	32.0	1.91	155.5
25% HCl, 75% H ₂ O (wetted).....	1.057	0.86	41.0	0.99	146.0
Mineral seal oil and chloroform.....	0.993	1.86	31.5	0.073	6.9

TABLE 6 LOSS OF WEIGHT OF TEST SPECIMENS DUE TO CORROSION WHEN IMMERSED STATICALLY IN TEST LIQUID FOR 120 MIN

Material	Test liquid	Loss of weight in mg in 120 min
Rolled brass, ASTM, B-16-44, half-hard..	25% H ₂ SO ₄ , 75% H ₂ O	0.3
Rolled brass, ASTM, B-16-44, half-hard..	50% H ₂ SO ₄ , 50% H ₂ O	2.2
Cast stainless steel, type 302.....	25% H ₂ SO ₄ , 75% H ₂ O	6.5
Cast stainless steel, type 302.....	25% HCl, 75% H ₂ O	5.2
Cast steel, QQ-S-681 b, Class 2 med.....	25% H ₂ SO ₄ , 75% H ₂ O	51.8
Cast steel, QQ-S-681 b, Class 2 med.....	25% HCl, 75% H ₂ O	67.3

Table 5 lists the results of tests on cast steel. These tests indicate a definite increase in loss of weight with the acid solutions. However, the acid solutions have a definite corrosive effect on cast steel and can cause an appreciable loss of weight due to corrosion alone during the 2-hr test period. This static loss of weight of the test specimens in the acid solutions is shown in Table 6. The brass and stainless-steel losses due to corrosion are negligible. However, when the static loss due to corrosion for cast steel is subtracted from the loss of weight of the test specimens, as determined during the cavitation tests, there again is an indication that the acid solutions do not affect the resistance to pitting.

The general conclusion from all of these tests is that acid solu-

tions do not change the cavitation forces, and there is some evidence that the greater the acid concentration, the smaller the amount of pitting. On the other hand, when the test specimens are vibrated in oil, the weight loss is greatly reduced. The explanation for this phenomenon is not quite clear. However, Dr. W. A. Weyl and F. C. Marbae (12) have suggested that water molecules can be fractured under high negative pressures such as are present where cavitation occurs, and produce a solution of H^+ and OH^- ions. This is comparable to a combination of a strong acid and a strong base, which produces strong corrosion. If this theory is correct it will explain why the pitting of metals decrease as the acid concentration is increased, since the water molecules available to be fractured decrease. It will also explain the exceedingly large decrease in pitting when the metals were vibrated in oil. However, it will not explain the pitting of such materials as glass and rubber. Therefore further investigations along these lines are required before any definite conclusions can be reached.

Tables 7 to 19, inclusive, list practically all of the materials tested in the accelerated-cavitation machine. These materials were tested at a depth of immersion of $1/8$ in. in distilled water at 6500 cps with a total travel amplitude of 0.0034 in.

Each specimen was tested for a total period of 120 min, but the loss in weight was determined every 30 min.

CAST AND ROLLED STAINLESS STEELS

Table 7 lists tests on a number of cast stainless steels, which indicate quite a variation in resistance to pitting. Even cast stainless steels of the same type but cast in different foundries show considerable variation in their resistance to pitting. For example, cast stainless-steel type 302, which contains 18 per cent chrome and 8 per cent nickel, showed losses of 12, 22, and 35 mg, respectively, as furnished by three different foundries. This is a maximum variation of 300 per cent in the resistance to pitting. Some of these variations may be due to the materials being cast for different purposes. Other causes for variations are the carbon content of the steel, where the specifications for a particular type permit a wide variation in carbon. The heat-treatment of the casting and the hardness of the material also affect its resistance to pitting.

Table 8 lists the results of tests on a 12 per cent and a 13 per cent chrome cast steel with varying Brinell hardness. Fig. 13

TABLE 7 MATERIALS TESTED IN ACCELERATED-CAVITATION MACHINE

Specimen no.	Material	Rate of loss, mg per min during last 30 min of test	Total loss in mg in 120 min
CAST STAINLESS STEELS			
159...	18% Cr, 8% Ni, 0.12% C, Type 302 ^a	0.19	12
103...	18% Cr, 8% Ni, 0.12% C, Type 302 ^a	0.18	13
137...	27% Cr, 10% Ni, 0.26% C, Type 312	0.18	13
108...	12% Cr, 0.10% C, Type 410	0.21	22
106...	18% Cr, 8% Ni, 0.10% C, Type 302 ^b	0.27	22
107...	17% Cr, 12% Ni, 0.10% C, Type 316	0.25	24
139...	21% Cr, 10% Ni, 0.11% C, Type 307	0.38	31
168...	18% Cr, 8% Ni, 0.11% C, Type 304 ^c	0.45	33
167...	18% Cr, 8% Ni, 0.11% C, Type 302 ^c	0.47	35
171...	13% Cr, 0.12% C, Type 420 ^c	0.40	38
169...	13% Cr, 0.12% C, Type 327 ^c	0.50	53
170...	13% Cr, 0.12% C, Type 410 ^c	0.55	59

^a Cast by Midvale. ^b Cast by Bonney Floyd Co. ^c Cast by Allegheny Ludlum.

TABLE 8 MATERIALS TESTED IN ACCELERATED-CAVITATION MACHINE; CAST STAINLESS STEELS—EFFECT OF HARDNESS

Specimen no.	Material	Rate of loss, mg per min during last 30 min of test	Total loss in mg in 120 min
	Cr, per cent		
182 ^a	12	0.20	20
196 ^b	13	0.26	25
194 ^b	13	0.43	49
195 ^b	13	0.39	51
181 ^a	12	0.55	54
193 ^b	13	0.46	57
192 ^b	13	0.51	70
180 ^a	12	0.73	141

^a Cast by Ohio Steel. ^b Cast by Allegheny Ludlum.

shows the loss in milligrams during a 2-hr test in the accelerated-cavitation machine plotted against Brinell hardness. For both the 12 per cent and the 13 per cent chrome steels, the test specimens were taken from the same castings, and the variation in Brinell hardness was obtained entirely by changing the heat-treatment of the two materials. These tests show the large effect that hardness of a material has on its resistance to pitting.

The large variations in resistance to pitting of the different cast stainless steels indicate the necessity for constant checks on such material when used in hydraulic machinery to assure that the desired resistance to pitting is being obtained.

Table 9 lists the results of tests on rolled annealed stainless steel. The wide variation in resistance to pitting of the two

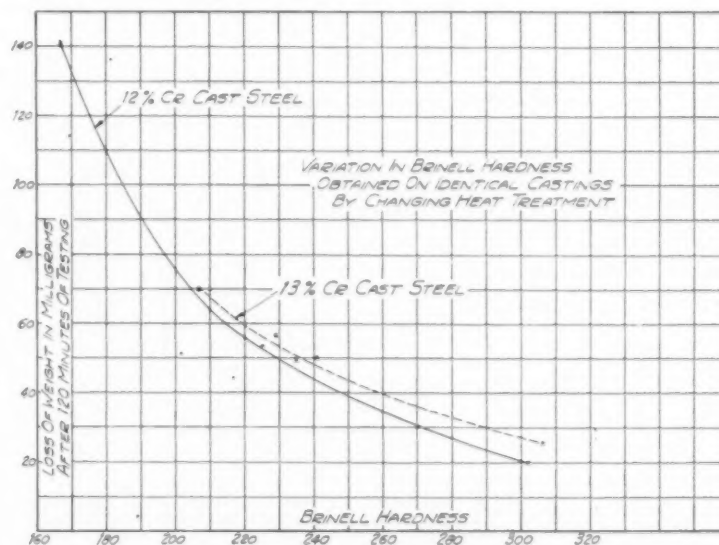


FIG. 13 (right) EFFECT OF BRINELL HARDNESS OF CAST-CHROME STAINLESS STEEL ON RESISTANCE TO PITTING

TABLE 9 MATERIALS TESTED IN ACCELERATED-CAVITATION MACHINE; ROLLED ANNEALED STAINLESS STEELS

Specimen no.	Material	Rate of loss, mg per min during last 30 min of test	Total loss in mg in 120 min
105.....	18% Cr, 8% Ni, 0.12% C, Type 302	0.107	8.0
137.....	18% Cr, 8% Ni, 0.12% C, Type 302	0.33	32

rolled stainless steels of the same type is another reason for the necessity of making careful accelerated cavitation tests on all materials of this type before using them for the purpose of resisting pitting.

WELDED STAINLESS STEELS

Table 10 lists the results of tests on welded stainless steels. These tests also show a wide variation in resistance to pitting, depending upon the type of material used.

TABLE 10 MATERIALS TESTED IN ACCELERATED-CAVITATION MACHINE; WELDED STAINLESS STEELS

Specimen no.	Material	Rate of loss, mg per min during last 30 min of test	Total loss in mg in 120 min
136.....	16% Cr, 7% Ni, 2 layers	0.057	9.4
135.....	19% Cr, 9% Ni-Cb, 1 layer	0.18	13
15.....	Lincoln A5	0.23	27
16.....	Steele 604	0.23	27
134.....	19% Cr, 9% Ni-Cb, 2 layers	0.83	36
132.....	25% Cr, 12% Ni-Cb	0.43	36
14.....	130x Inco Monel	0.36	37
133.....	25% Cr, 12% Ni-Cb, 1st layer	0.50	41
17.....	19% Cr, 9% Ni-Cb, 2nd layer	0.55	55
	Lincoln Aerisweld AE-124K		

TABLE 11 MATERIALS TESTED IN ACCELERATED-CAVITATION MACHINE; WELDED STAINLESS STEELS—EFFECT OF PREHEAT ON BASE METAL

Specimen no.	Material	Rate of loss, mg per min during last 30 min of test	Total loss in mg in 120 min
188....	18% Cr, 8% Ni on 12% Cr. Cast steel, preheated to 600 F	0.095	7.6
186....	18% Cr, 8% Ni, on 12% Cr. Cast steel, no preheat	0.099	7.8
187....	18% Cr, 8% Ni, on 12% Cr. Cast steel, preheated to 400 F	0.082	8.0
184....	12% Cr, on 12% Cr. Cast steel, preheated to 400 F	0.15	13
185....	12% Cr, on 12% Cr. Cast steel, preheated to 600 F	0.16	14
183....	12% Cr, on 12% Cr. Cast steel, no preheat	0.18	16.8

Table 11 shows the results of tests on welded stainless steels when welded to 12 per cent chrome, either preheated or not preheated. These tests show that preheating of the base metal has very little effect on the resistance to pitting of the welded deposit.

Table 12 lists the results of tests on various welded stainless steels and on various combinations of welded layers. The chromium and nickel contents refer to the commercial weld-rod designation and do not refer to the chemical analysis of the weld deposit. One object of this series of tests was to determine the resistance to pitting of different types of stainless-steel welds.

TABLE 12 MATERIALS TESTED IN ACCELERATED-CAVITATION MACHINE; WELDED STAINLESS STEELS—VARIATION IN LAYERS

Specimen no.	Material	Bhn	Rate of loss, mg per min during last 30 min of test	Total loss, in mg in 120 min.
	First layer of weld			
203....	17% Cr, 7% Ni, Type 301	308	0.098	10
201....	18% Cr, 8% Ni, Type 308	160	0.28	23
198....	25% Cr, 12% Ni, Type 309	145	0.36	26
204....	17% Cr, 7% Ni, Type 301	255	0.075	6
199....	25% Cr, 12% Ni, Type 309	145	0.36	31
202....	18% Cr, 8% Ni, Type 308	151	0.35	33
200....	25% Cr, 12% Ni, Type 309	175	0.40	35
	Second or final layer of weld			

Another object was to determine the effect of one and two layers of weld and of various combination of materials on the resistance of pitting. In each case the base metal consisted of cast steel, conforming to Federal specification QQ-S-681b, Class 2, medium.

The results indicate that of the three types of chromium-nickel steels tested, type 301, with 17 per cent chromium, and 7 per cent nickel, gave the highest resistance to pitting. There again appears to be a definite relationship between hardness of the material and its resistance to pitting, since type 301 had the highest Brinell.

The tests also show that two layers of type 301 weld are better than one layer, although the single layer had a higher Brinell hardness than two layers. This may be due to other characteristics of the welded material, since it is certain that the first layer is contaminated by the base metal and therefore its characteristics probably change materially while cooling.

An additional indication of such contamination is shown where a first layer of type 309 with a second layer of type 301 had less hardness and considerably less resistance to pitting than two layers of type 301.

The 18 per cent chromium, 8 per cent nickel stainless steel, type 308, did not seem to become contaminated very much by either the base metal or a first layer of type 309, but it had considerably less resistance to pitting than type 301.

One definite conclusion that can be made from this series of tests is that a first layer of type 309 has no beneficial effects on the resistance to pitting and, in the case of type 301, definitely lowers this resistance.

Since a lot of welded stainless-steel repairs and overlays are being made, using type 309 as a first layer, it was decided to determine whether this material had any other beneficial effects. One of the dangers of stainless-steel welds is that they may produce brittleness in either the weld deposit or in the base metal. A measure of brittleness is the bend test. Therefore, in preparing the test specimens for this series of tests, the weld was deposited on cast-steel bars 1 in. wide \times 8 in. long \times 1 in. thick. The cast steel conformed to Federal specification QQ-S-681b, Class 2, medium, which is a steel commonly used for hydraulic-turbine runners. In making the welds, only standard commercial weld rods were used.

The bend tests showed that in each case two weld layers gave a greater bend angle and therefore greater ductility than a single layer. Use of type 309 as a first layer did not increase the bend angle compared to any of the other two materials. However, two layers of type 308 had a higher bend angle than two layers of type 301.

The conclusion from these tests is that type 309 stainless steel as a first layer does not improve the characteristics of the weld. Although two layers of type 308 had greater ductility than two layers of type 301, this was more than offset by the greater resistance to pitting of type 301.

All of these tests indicate that for all welding repairs and all pre-welding of hydraulic-turbine machinery, two layers of stainless steel should be used and, if it is desired to obtain the maximum

resistance to pitting, type 301 stainless-steel weld rods should be used.

SPRAYED STAINLESS STEELS

Table 13 lists the tests on various sprayed stainless steels. These tests indicate that although some of the sprayed stainless materials had a resistance about equal to cast steel, others pitted very rapidly. These differences are probably due largely to the

TABLE 13 MATERIALS TESTED IN ACCELERATED-CAVITATION MACHINE: SPRAYED STAINLESS STEELS

Specimen no.	Material	Rate of loss, mg per min during last 30 min of test	Total loss in mg in 120 min
12.....	Metco Metcaloy No. 2	0.57	72
11.....	Metco Metcaloy No. 1	0.50	98
112.....	18% Cr, 8% Ni, Type 302	0.61	187
116.....	13% Cr, Type 420	0.70	192
179.....	Metcaloy No. 2	1.33	216

method of application of the sprayed metal, which accounts for the variance in field reports as to their effectiveness. Quite a number of the test specimens had to be scrapped before the 2-hr test period was completed, because the sprayed metal would separate from the base. The high acceleration (about 7300 G's) of the vibratory test is a severe test on the adhesion of the metal.

If the sprayed material is applied carefully it seems to have about the same resistance to pitting as cast steel, but considerably less resistance than a properly welded stainless steel. In general, the application of sprayed metal is cheaper than welding with mild or stainless steel, and it sometimes proves to be a satisfactory means of repair where pitting is not very severe, and where speed of application and low initial costs are a factor.

CAST STEELS

Table 14 lists the results of tests on the cast steel most commonly used for hydraulic-turbine runners. The tests on three castings from 3 different foundries do not show any appreciable variation.

TABLE 14 MATERIALS TESTED IN ACCELERATED-CAVITATION MACHINE: CAST STEELS

Specimen no.	Material	Rate of loss, mg per min during last 30 min of test	Total loss in mg in 120 min
178.....	Fed. Spec. QQ-S-681 b Class 2 medium	1.09	88
158.....	Fed. Spec. QQ-S-681 b Class 2 medium	0.75	104
118.....	Fed. Spec. QQ-S-681 b Class 2 medium	0.70	105

AMPECO BRONZES

Table 15 lists an interesting series of tests on Ampeco bronzes. Ampeco is the trade name for a bronze with an aluminum content varying from 10 to approximately 14 per cent. The Brinell hardness increases as the aluminum content increases. The results of the tests on the cast bronzes show that some of them have twice the resistance to pitting compared to the best stainless-steel castings. The welded bronzes also show a remarkable resistance to pitting. Fig. 14 shows cast and welded Ampeco bronze test specimens. Fig. 15 shows how the resistance to pitting of these materials varies with hardness. This curve indicates that while the resistance to pitting increases with hardness, there is a maximum point beyond which resistance to pitting decreases with increased hardness.

Unfortunately, there is very little information with reference to how these bronzes, either cast or welded, stand up under field conditions, which is really the final criterion. The author knows of only one instance where Ampeco bronze was used on a hy-

TABLE 15 MATERIALS TESTED IN ACCELERATED-CAVITATION MACHINE: BRONZES

Specimen no.	Material	Bin	Rate of loss, mg per min during last 30 min of test	Total loss in mg in 120 min
AMPECO ROLLED BRONZES				
111....	Ampeco no. 18 (Extruded)	190	0.15	12
AMPECO CAST BRONZES				
160....	Ampeco no. 20	235	0.095	5.8
161....	Ampeco no. 21	285	0.080	6.2
162....	Ampeco no. 22	340	0.115	9.5
123....	Ampeco 46	190	0.113	9.9
124....	Ampeco no. 18	170	0.12	12
121....	Ampeco A3	130	0.27	22
WELDED AMPECO BRONZES				
163....	Ampeco 200 on SAE 1010 steel	220	0.062	3.2
164....	Ampeco 250 on SAE 1010 steel	260	0.075	5.3
126....	Ampeco 160 on SAE 1010 steel	185	0.107	5.2
127....	Ampeco 160 on Ampeco 18	185	0.093	5.9
165....	Ampeco 300 on SAE 1010 steel	320	0.100	9.5
128....	Ampeco 160 on Ampeco 46	180	0.23	20
123....	Ampeco 10 on SAE 1010 steel	140	0.28	24
122....	Ampeco 10 on Ampeco A3	140	0.39	31

NOTE: Materials furnished by Ampeco Co.

draulic-turbine runner. In this case Ampeco bronze patch plates were alternated with ordinary bronze on the back sides of the blades of a hydraulic-turbine runner. After a period of operation the ordinary bronze patch plates had pitted to a considerable extent, while the Ampeco bronze showed very little sign of pitting.

Certainly the tests of the Ampeco bronzes in the accelerated-cavitation machine warrant experimenting with this material in field installations.

COLMONOY

Table 16 lists tests made on welded Colmonoy. The tests show that some types of welded Colmonoy have a high resistance to pitting.

Table 17 lists Colmonoy sprayed onto a base and then fused on at a temperature of 1850 F. These tests show that some of these materials also have a high resistance to pitting.

Colmonoy is a trade name for a material consisting primarily of iron, nickel, chromium, boron, silicon, and carbon. Before applying Colmonoy as a spray, the base metal is thoroughly grit-blasted. The Colmonoy is then sprayed uniformly over the grit-blasted area to a thickness of approximately 0.060 in. The sprayed area is then heated with an oxyacetylene flame or in a heat-treating furnace to a temperature of 1850 F. Colmonoy has the property of becoming very plastic at this temperature, thereby fusing itself to a grit-blasted area.

The author knows of no field tests on this material, but based on the results in the accelerated-cavitation machine, it merits consideration. One advantage is the ease of application, whereby the material is sprayed on and then fused with a torch or in an oven. However, the fusing process presents the problem of possible distortion of the base metal. The cost of the Colmonoy material also may be a deterrent to its general use in the prevention of pitting.

Several test buttons were prepared by spraying Colmonoy to a base, but eliminating the fusing process. It was impossible to obtain any pitting data on these specimens because the sprayed material separated from the base during the vibration tests.

THIOL RUBBER

Table 18 lists tests made on Thiokol rubber sprayed on various materials used for a base. The test specimens were prepared by the U. S. Navy. The loss of weight of the test specimens is not a very satisfactory means for determining the relative resistance of rubber because of its low specific gravity compared to metal. However, visual inspection of the test specimens indicated that the rubber overlay gave considerable resistance to pitting. Fig.

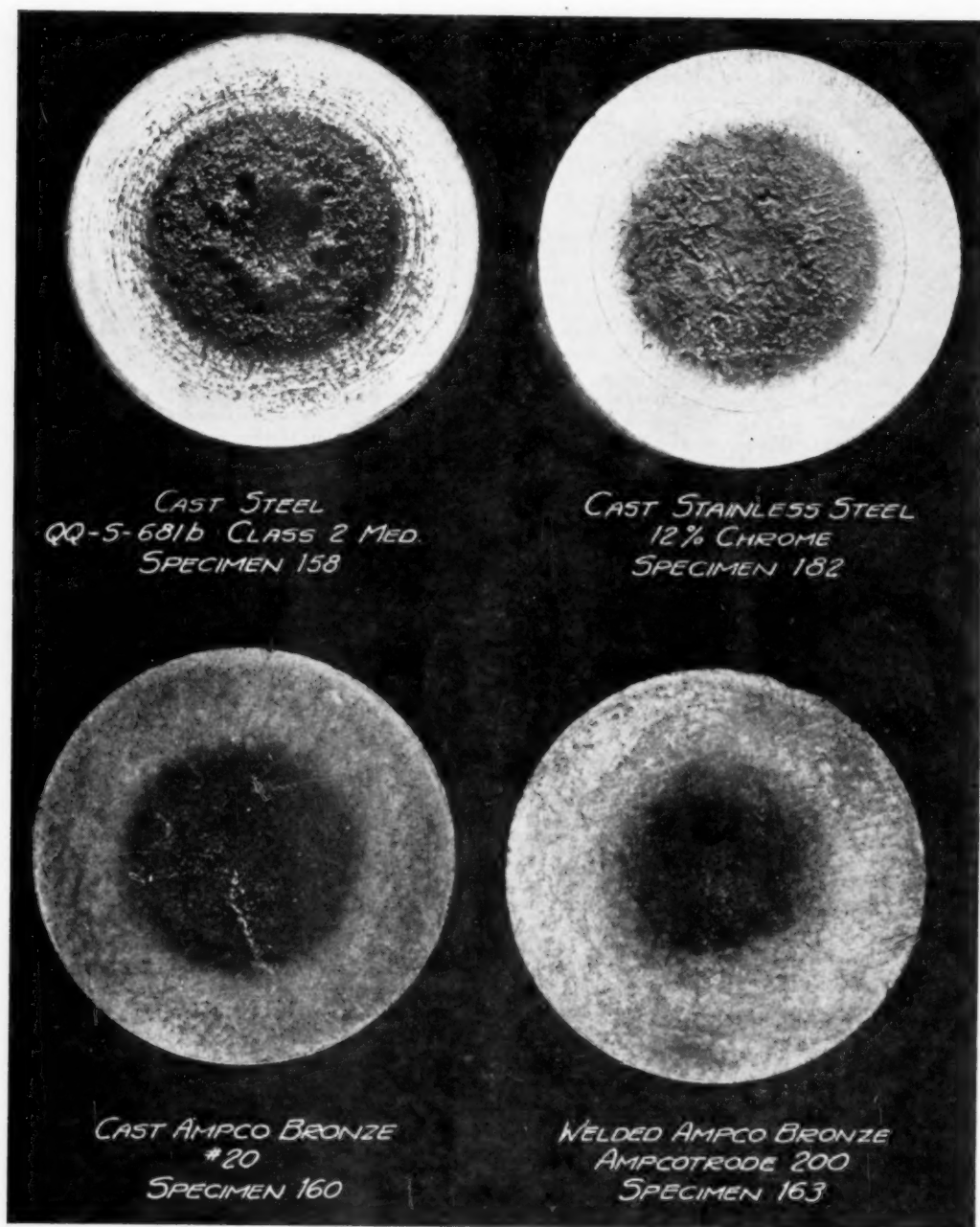


FIG. 14 CAST AND WELDED AMPCO BRONZE, COMPARED TO CAST STEEL AND CAST STAINLESS STEEL

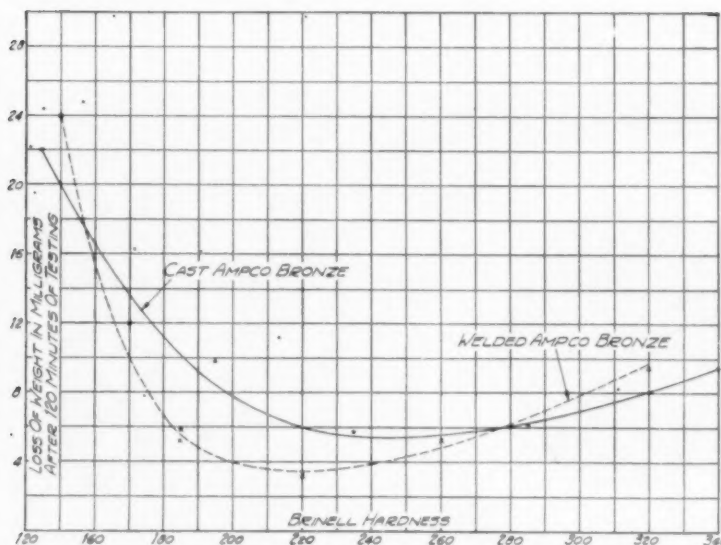


FIG. 15 EFFECT OF HARDNESS OF AMPCO BRONZES ON RESISTANCE TO PITTING

TABLE 16 MATERIALS TESTED IN ACCELERATED-CAVITATION MACHINE; WELDED OVERLAY^a

Specimen no.	Material	Rate of loss, mg per min during last 30 min of test	Total loss in mg in 120 min
148.....	Colmonoy WER-100, arc-welded	0.043	6.0
145.....	Colmonoy no. 6, arc-welded	0.070	8.4
129.....	Colmonoy—2 layers, gas-welded	0.20	19
130.....	Colmonoy—1 layer, gas-welded	0.24	23
147.....	Colmonoy no. 5, arc-welded	0.18	23
146.....	Colmonoy no. 4, arc-welded	0.21	29

^a "Colmonoy" furnished by Wall Colmonoy Company.

TABLE 17 MATERIALS TESTED IN ACCELERATED-CAVITATION MACHINE; COLMONOY SPRAYED AND FUSED TO BASE

Specimen no.	Material	Rate of loss, mg per min during last 30 min of test	Total loss in mg in 120 min
144.....	Colmonoy no. 6	0.064	8.0
156.....	Colmonoy no. 6	0.092	9.5
143.....	Colmonoy no. 5	0.19	16
141.....	Colmonoy no. 4	0.31	30
151.....	Colmonoy, sweat-on-paste arc application	0.32	30
150.....	Colmonoy, sweat-on-paste QXI-acetylene application	0.38	34

TABLE 18 MATERIALS TESTED IN ACCELERATED-CAVITATION MACHINE; THIOKOL RUBBER^a

Specimen no.	Materials	Rate of loss mg per min during last 30 min of test	Total loss in mg in 120 min
Navy no. 2..	Flame-sprayed on stainless steel	0.17	26
Navy no. 4..	Flame-sprayed on stainless steel, weld inlay	0.16	28
Navy no. 10.	Flame-sprayed on manganese bronze	0.18	30
Navy no. 8..	Flame-sprayed on mild welded steel	0.14	31
Navy no. 6..	Flame-sprayed on mild steel	0.16	33

^a Furnished by U. S. Navy.

16 shows several of the rubber overlays after 2 hr of testing in the accelerated-cavitation testing machine. These illustrations show how the center of the rubber overlay is eroded down to the base metal. The composition of the base metal apparently has very little influence on the resistance of the rubber to pitting, as is indicated in Table 18.

The U. S. Navy has used this rubber overlay with considerable

success on propeller shafts, rudders, and struts of naval vessels where pitting was being encountered. One of the important features of the successful use of rubber overlays is proper application. The U. S. Navy sandblasts the base metal to obtain a clean surface. The metal is heated to a temperature somewhat above the surrounding air temperature. The rubber is then sprayed on with a gun, using the powder and gun developed by the Schori Process Corporation.

The results of the tests in the accelerated-cavitation machine, and the results obtained by the Navy under actual operating conditions, indicate that it might be desirable to investigate the performance of this rubber when used for hydraulic-machinery parts subject to pitting.

MISCELLANEOUS MATERIALS

Table 19 lists some miscellaneous materials tested in the accelerated-cavitation machine. These include the base metals used by the Navy in connection with Thiokol rubber overlays. This table shows that stellite has by far the greatest resistance to pitting of all of the materials tested, which agrees with the results obtained in other accelerated-cavitation machines.

The stellite used in the present test was a rolled material consisting of 55 per cent cobalt, 33 per cent chrome, and 6 per cent tungsten, with a Brinell hardness of about 410. The stellite was brazed to the base metal with silver solder. Stellite can be obtained as a casting and also can be applied by welding. Its disadvantage for ordinary hydraulic machinery is its high cost, and

TABLE 19 MATERIALS TESTED IN ACCELERATED-CAVITATION MACHINE; MISCELLANEOUS MATERIALS

Specimen no.	Material	Rate of loss, mg per min during last 30 min of test	Total loss in mg in 120 min
Special.....	Stellite, Haynes no. 6, Rolled, Bhn 410	0.017	0.60
166.....	Nitraloy—Holcomb no. 218	0.07	14
Navy no. 3..	Welded stainless steel	0.35	28
Navy no. 1..	Stainless steel	0.46	47
Navy no. 9..	Manganese bronze	0.70	80
Navy no. 7..	Welded mild steel	0.79	97
Navy no. 5..	Mild steel	0.78	107
119.....	Brass, 70% Cu, 30% Zn	1.17	136
120.....	Roller brass B-16-44 half-hard bar stock used for standard to check cavitation machine, Cu 60%, Zn 27% Pb 3%, Bhn 90	1.01	162

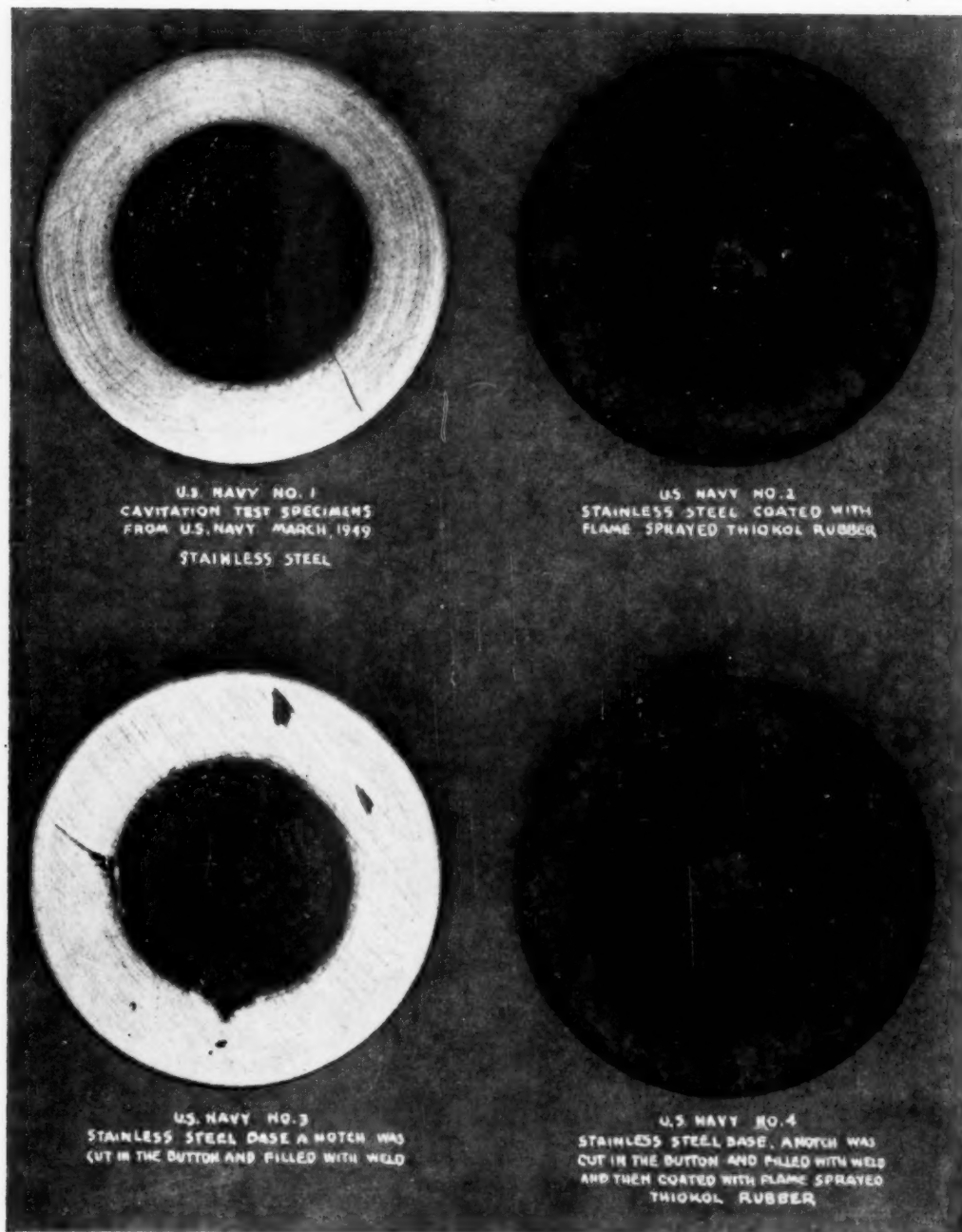


FIG. 16 THICKOL RUBBER SPECIMENS

the difficulty of machining and grinding it because of its extreme hardness. However, it has been used successfully for steam-turbine blading where the erosion problems are somewhat similar to pitting in hydraulic turbines.

CONCLUSIONS

The tests on variation in amplitude of vibration, on variation in depth of submergence and with various liquids, answered some of the questions regarding the phenomena of cavitation. Although these tests were not always conclusive, they indicated the type of additional investigations that should be made.

The standard accelerated-cavitation tests were made mostly on standard trade materials to determine the qualities of materials readily available to the industry. These tests showed the following:

- 1 That new materials such as the Ampco bronzes, Colmonoy, Thiokol rubber, and others, which are constantly being developed, might be suitable for hydraulic machinery and might have a distinct advantage over the materials now in use.
- 2 That the practical application of the materials, such as number of layers to be used when making repairs by welding or when prewelding, influences the resistance to pitting whereas preheating the base metal has very little effect on the resistance.
- 3 That hardness has a definite effect on resistance to pitting regardless of the material being used.
- 4 That it is desirable to make accelerated-cavitation tests on the special materials, particularly stainless steels, to insure obtaining the requisite resistance to pitting.

The results of all of the tests showed that the accelerated-cavitation machine can be used to:

- 1 Make further investigations on the phenomena of cavitation.
- 2 Test new materials and new techniques of application of materials for their relative resistance to pitting.
- 3 Test samples of all special materials to determine their resistance to pitting to avoid the wide variation of these qualities when the materials are obtained from different sources.

Although items 2 and 3 constitute practically a full-time test program for an accelerated-cavitation machine, any suggestions as to how it can be used for advancing the knowledge of the mechanics and phenomena of cavitation and pitting are welcomed.

ACKNOWLEDGMENTS

All of these accelerated-cavitation tests were made possible through funds provided by the Allis-Chalmers Manufacturing Company. The Research Laboratory of this company built the cavitation machine and kept it in operation. The tests were made under the direction of the Hydraulic Department.

The Ampco bronze test specimens were provided by the Ampco Metal Company, Milwaukee, Wis.

The Colmonoy specimens were furnished by the Wall Colmonoy Corporation, Detroit, Mich.

Cast stainless-steel specimens were provided by Allegheny Ludlum Steel Corporation, Brackenridge, Pa., Ohio Steel Foundry Company, Lima, Ohio, and Midvale Company, Midvale, Pa.

The Thiokol rubber specimens were supplied by the Material Laboratory, New York Naval Shipyard, Naval Base Station, Brooklyn, N. Y.

The cast-iron specimens for the tests with the chromate inhibitor were supplied by the International Nickel Company, New York, N. Y.

The author is indebted to these companies for making the facilities available for the tests, for furnishing test specimens, and for permission to publish the test results.

BIBLIOGRAPHY

- 1 "Pitting Resistance of Metals Under Cavitation Conditions," by J. M. Mousson, Trans. ASME, vol. 59, 1937, pp. 399-408.
- 2 "Determination of the Relative Resistance to Cavitation Erosion by the Vibratory Method," by S. Logan Kerr, Trans. ASME, vol. 59, 1937, pp. 373-397.
- 3 "Théorie plus complète des machines qui sont mises en mouvement par la réaction de l'eau" (More complete theory of machines driven by Hydraulic Reaction), by Leonard Euler, *Historie de l'Académie Royale*, Berlin, Germany, 1754.
- 4 "On the Formation of Cavities in Water by Screw Propellers at High Speeds," by Sydney W. Barnaby, Trans. Institution of Naval Architects, London, England, vol. 39, 1897, pp. 139-143.
- 5 "The Application of the Compound Steam Turbine to the Purpose of Marine Propulsion," by Charles A. Parsons, Trans. Institution of Naval Architects, London, England, vol. 38, 1897, pp. 232-237.
- 6 "Beiträge zur Berechnung und Konstruktion der Wasserturbinen" (Contribution to the Calculation and Construction of Hydraulic Turbines), by W. Wagenbach, *Zeitschrift für das Gesamte Turbinenwesen*, vol. 4, 1907, pp. 273-277.
- 7 "Kavitation" (Cavitation), by J. Ackert, *Handbuch der Experimentalphysik, Akademische Verlagsgesellschaft*, Leipzig, Germany, vol. 4, part 1, 1926.
- 8 "Korrosion durch Kavitation in einem Diffusor" (Erosion by Cavitation in a Diffusor), by Hellmut Schröter, *Zeitschrift Verein deutscher Ingenieure*, vol. 76, 1932, pp. 511-512.
- 9 "A Magnetostriction Oscillator Producing Intense Audible Sound and Some Effects Obtained" by Newton Gaines, *Physics*, vol. 3, 1932, pp. 2-9 and 229.
- 10 "Progress Report on Cavitation Research at Massachusetts Institute of Technology," by J. C. Hunsaker, Trans. ASME, vol. 57, 1935, pp. 423-424.
- 11 "Laboratory Investigations of the Mechanism of Cavitation," by R. T. Knapp and A. Hollander, Trans. ASME, vol. 70, 1948, pp. 419-431.
- 12 "Some Mechano-Chemical Properties of Water," by W. A. Weyl and E. C. Marbae, publication NAVEXOSP-571, Office of Naval Research, Navy Department, Washington, D. C.

Discussion

T. BAUMEISTER.³ This is the kind of document which adds greatly to our store of knowledge on a problem which is by no means limited to the field of hydraulics, or more particularly, the hydraulic turbine. The hydroelectric engineer probably has recognized the problem of cavitation for a longer period than have most other engineers. Likewise, he has tried to do something about it. He has not stood by waiting for someone to develop a solution.

This whole problem, however, of the aging and wasting of metals is one to which we must address ourselves more aggressively. The design of boilers has been changed radically in the last few years because of fly-ash-erosion problems which were formerly nonexistent or not recognized. Cavitation on water-wheels is one thing, but so is cavitation on (a) centrifugal and axial-flow pumps; (b) at the entrance to tubes in closed feedwater heaters or surface condensers; or (c) on rayon spinnerets. The examples are myriad. The pitting which results from cavitation must be met in a rational, practical way.

The contribution in the author's work is appreciated. His meticulous studies show the many variables which can influence this phenomenon. The accelerated technique should be of value to designers and users of equipment.

Criticism might be directed to the method, because it does not give absolute or theoretical values. It is in somewhat the same category as grindability testing devices; hardness testers; viscosimeters, and numerous other instruments. They all give useful data. The data obtained by the author's method should prove equally valuable, and it is to be hoped that he will con-

³ Professor of Mechanical Engineering, Columbia University; Consulting Engineer, American Gas and Electric Service Corporation, New York, N. Y. Mem. ASME.

tinue and extend his researches so that those of us who are concerned with attempting to correct the ill effects of cavitation will have better assurances of success.

R. C. GLAZEBROOK.⁴ The writer fears that as written the author's definition of cavitation may cause some confusion in the minds of some readers as to the difference between separation and cavitation. To the writer, cavitation, as defined, sounds more like separation. A more foolproof definition would be to state that it is a phenomenon occurring when the absolute pressure has been reduced to or below the vapor pressure of the liquid being handled so that the liquid flashes into the gaseous form, followed by a subsequent increase in pressure, resulting in a collapse of these cavities, which may be termed an implosion (the opposite of an explosion), a destructive shock phenomenon resulting in reduced performance, noise, and pitting.

The author's results show clearly that resistance to cavitation is definitely affected by the hardness of the materials, the harder materials being appreciably more resistant to cavitation. While not entirely confirmed by test, we have a somewhat conclusive suspicion that this is brought about by the finer grain size of the harder materials. It might be well to offer this as a possible explanation for this increased resistance with the harder materials, and draw forth some opinion on the subject which would be mutually helpful to the hydraulic profession in general.

W. R. MACNAMEE.⁵ Another source of damage to hydraulic equipment which frequently combines with cavitation is erosion. This is usually not serious as long as clear water is used, but when water at high velocities also carries in suspension hard material, such as sand, damage can be very rapid and severe.

Such conditions are not uncommon in South America, where the

⁴ Chief Engineer, Hydraulic Division, Fairbanks, Morse & Company, Beloit, Wis. Mem. ASME.

⁵ Assistant Supervising Engineer, Baldwin Locomotive Works, Philadelphia, Pa. Mem. ASME.

volcanic nature of much of the country, plus a rainy season of heavy and prolonged rainfall, combine to carry off large quantities of very finely divided solids of an abrasive nature.

The writer's company and the Braden Copper Company have been engaged in a program of materials testing to evaluate both standard and new materials under cavitation and erosive conditions.

The test program was carried out at the Pangal Plant of the Braden Copper Company, in Chile, where the nature of the water flow varies from clear water in the dry season to water heavily laden with silt in the rainy season.

By subjecting samples of various materials to a high-velocity jet of clear water, the resulting damage could be considered due to cavitation. During the rainy season, when turbid water was used, the rate of removal of test material was 5 to 10 times as great, and was no doubt due to erosion by the sand particles.

Fig. 17, herewith, shows the arrangement of test equipment, with and without the jet in operation.

A jet of water $\frac{1}{2}$ in. diam under 650 psi pressure was directed against the test specimen. The angle between the jet and the test specimen was 15 deg. A hole $\frac{1}{4}$ in. diam was purposely placed in each specimen at the point of impingement to produce severe cavitation. The two spots on the specimen downstream from the hole are typical of the patterns produced by cavitation in the clear-water tests. When tests were made with turbid water, the damaged area usually showed a smooth, though irregular surface, quite different from the characteristic pockmarks of cavitation.

For metals, the time of exposure to the jet varied from a few hours for the soft steels to 20 days for the hardest alloys.

As might be expected, the hard, strong materials were most resistant to erosion as well as to cavitation. The Colmonoy alloys, mentioned by the author, were outstanding in their excellent resistance to erosion. In general, materials showing good resistance to cavitation in the clear-water tests also performed well under erosive conditions with turbid water.

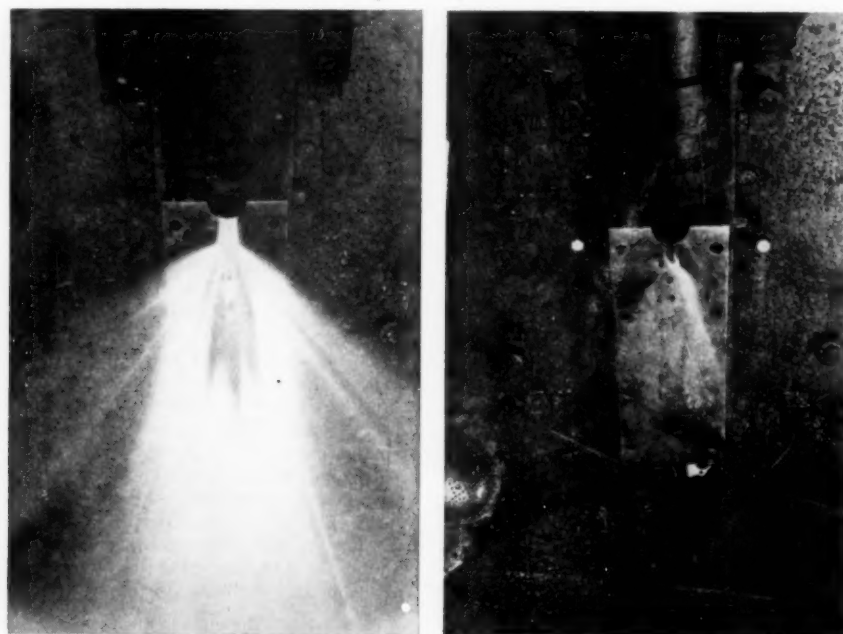


FIG. 17 ARRANGEMENT OF EQUIPMENT FOR TESTING EFFECT OF HIGH-PRESSURE JET IMPINGEMENT USING CLEAR WATER AND TURBID WATER FOR EROSION EFFECT

It was noted, however, that 18-8 stainless steel, which resisted cavitation far better than mild steel, performed but little better when erosion was combined with cavitation. It may be that the ability of 18-8 to work-harden was an important factor in this result. The repeated blows sustained under cavitation conditions may produce local work-hardening to a much greater degree than the cutting action of sand particles in the water.

The straight chromium steels of about 14 per cent chromium, heat-treated, were especially good in resisting erosion.

As tested here, rubber proved completely disappointing. Two samples, consisting of $1/8$ -in. rubber, vulcanized to steel plate under factory conditions, were tested with clear water only. Each failed in less than 1 min. Each time a strong odor of burned rubber was noticeable, and bits of rubber in the pit had the appearance of being charred. It appears that impingement of the jet produced sufficient working of the rubber to cause destructive internal heating.

One unexpected variable developed in these tests when it was discovered that the rate of pitting and erosion varied with barometric pressure, low pressure definitely accelerating removal of material.

It would be interesting to know if the author has detected any such correlation in his tests. Variation in barometric pressure would exceed considerably the variation in depth of submergence shown on the author's Fig. 8, although whether the variations shown there are due to the static-pressure change or variations in entrained air is not clear.

It is noted that the author makes no mention of tests of hard steels other than the stainless varieties. Such tests would round out the study in so far as materials commonly available are concerned.

At the present time there exists quite a gap between the existence of highly resistant alloys and their practical use, due not only to cost, but to the difficulty of applying them to the surfaces to be protected. In some cases, the necessity of obtaining a reasonably smooth surface after application is a difficult requirement.

These problems no doubt will decrease as improved techniques in the handling of these materials are developed, leading to longer and more reliable performance of hydraulic machinery.

H. S. VAN PATER.⁶ It is most interesting to compare the cavitation damage rates reported by the author with those reported in 1937 by S. L. Kerr and J. M. Mousson. The author shows much greater variations than found by Kerr with similar apparatus in the performance of particular materials from different sources. The loss rate for stellite is only 10 per cent of the lowest and about 1 per cent of the highest loss rates for the various stainless steels, whereas Mousson, using Venturi-type equipment, reported losses with stellite to be of the same order as with stainless steel. The author's results for aluminum bronze are somewhat better than reported by Kerr, but the check is quite good, and the excellent performance of type 301 stainless steel checks well with Mousson's findings.

The writer would appreciate some further comments from the author regarding his observation of the vapor bubbles at the specimen surface under stroboscopic lighting. Does one large bubble or a collection of small bubbles form over the area of damage with each upward movement of the specimen? What is the maximum size of these bubbles under the normal test conditions? Can the complete or partial collapse of the bubbles be observed by changing the phase of the light flashes gradually in relation to the movement of the specimen?

The effects of increasing the submergence in the test liquid are

rather surprising in degree if not in character. The writer suggests that the increase in damage area with increasing depth is due not to varying air content but to the greater inertia of the greater depth of water surrounding the specimen and supporting tube, which would reduce the rates of vertical and horizontal flow at the periphery of the test surface and allow the pressure over a larger area to drop below the vapor pressure.

With reference to the author's remarks concerning the effect of variation of the amplitude of vibration, it is indicated that tests were made under conditions which showed no pitting on some materials and measurable pitting on others. Has the author been able to determine the amplitude at which pitting begins for the various materials tested? This might give another measure of relative resistance to pitting, possibly bearing a closer relation to the performance under field conditions than the maximum rate of loss.

The author states, "all of these tests indicate that for all welding repairs and all prewelding of hydraulic turbine machinery, two layers of stainless steel should be used and if it is desired to obtain the maximum resistance to pitting, type 301 stainless-steel weld rods should be used." This is a surprising statement considering the excellent results with single-layer 301 stainless, the Ampeco bronzes, and stellite.

B. G. RIGHTMIRE.⁷ The experiments on the effect of amplitude, depth of immersion, and kind of liquid raise a number of interesting questions that the author has discussed qualitatively. In particular, he has suggested that air drawn in from the free surface reduces the damaged area more and more as the depth of immersion decreases. This explanation appears unlikely to the writer, for two reasons: (a) The air bubbles, which appear initially under the vibrating specimen, do not continue to form after dissolved gas has been partially removed, as by an extended period of vibration. (b) At small depths of immersion the free surface of the liquid near the vibrator is elevated slightly, indicating a mean pressure at the rim of the specimen greater than that at the same depth in the distant liquid.

In the writer's opinion, the flow set up by the vibrator suffices to explain the observed effects of depth of immersion. This flow can be visualized by imagining the vibrating member to be replaced by a pipe which alternately injects and removes liquid. When removing liquid, the pipe acts approximately like a point sink, that is, the flow tends to be radially inward toward the open end of the pipe. On the other hand, when the pipe discharges liquid, a jet is formed, separated by a surface of discontinuity of velocity from the surrounding liquid. The rapid alternation of these two tendencies results in a general circulatory flow exhibiting a high outward velocity along the normal to the vibrating surface, and a low return velocity along the walls of the container, in accordance with the requirements of continuity.

If the depth of immersion is small compared with the diameter of the vibrating member ($1/8$ -in. immersion), the velocity field of this circulation will be as shown in Fig. 18(a) of this discussion. Fig. 18(b) shows the velocity field if the depth is large compared with the diameter (2-in. immersion). The chief difference between these two fields is at the rim of the specimen, where the tendency for separation when the specimen moves upward is obviously greater in Fig. 18(b). One would thus expect the damaged area to be greater, the larger the depth of immersion.

Further tests along these fundamental lines can be planned and analyzed more effectively if the independent variables that are suspected to be of greatest importance are listed, and a dimensional analysis made. Thus one may assume here that for a

⁶ Chief Engineer, Hydraulic Division, Dominion Engineering Works, Ltd., Montreal, Can. Mem. ASME.

⁷ Assistant Professor of Mechanical Engineering, Massachusetts Institute of Technology, Cambridge, Mass. Mem. ASME.

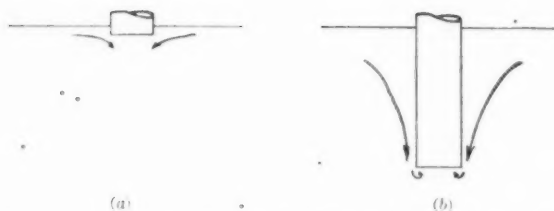


FIG. 18 ILLUSTRATING EFFECT OF DEPTH OF IMMERSION ON FLOW PATTERN AT SPECIMEN

given air content and a given material, the independent variables are as follows:

- α = amplitude of vibration, in.
- f = frequency of vibration, cps
- ρ = density of liquid, lb sec²/in.⁴
- $p - p_v$ = difference between pressure at specimen and vapor pressure of liquid, psi
- ν = kinematic viscosity of liquid, in.²/sec
- d = diameter of specimen, in.
- h = depth of immersion, in.

The dependent variable may be conveniently taken as the volume loss of the material at the end of a given period of vibration, V . A dimensional analysis shows that one possible arrangement of the variables is

$$\frac{V}{\alpha^3} = \text{function of} \left(\frac{p - p_v}{\rho f^2 \alpha^2}, \frac{f \alpha^2}{\nu}, \frac{d}{\alpha}, \frac{h}{\alpha} \right)$$

Two series of tests probing the effect of the first two dimensionless variables (cavitation number and Reynolds number) were made several years ago at M.I.T. It is hoped that the results will soon be released for publication.

C. G. SOUTHWAYD.⁸ The test data presented by the author is a welcome supplement to the investigations undertaken by J. M. Mousson and S. Logan Kerr some 12 years ago, in the determination of the resistance of various then available materials to the action of pitting. The advisability of, and necessity for, continual research of this type, particularly in the appraisal of new materials and techniques, cannot be questioned. The fact that it is possible to produce the phenomena of the cavitation in the laboratory, and so closely to parallel field experience is of special interest to the writer. This is particularly so when the apparatus does not in any way attempt to duplicate conditions under which cavitation is encountered in practice and yet affords a means whereby the effect of cavitation can be intensified and the relative resistance of different materials thereto appraised accurately.

For many years it has been suggested that the destructive action of pitting is at least partially due to chemical activity of the gases within the cavities, but the present investigations appear to confirm more recent theories which attribute the destructive action to mechanical forces alone.

In the discussion relative to the effect of the depth of submergence of the specimen in the test liquid, attention is drawn to the tendency for air to be carried down along the side of the test button and prevent the formation of cavities adjacent to the periphery of the specimen. Possibly tests undertaken in a pressurized chamber with constant depths of submergence but variable air pressure above the liquid would maintain a constant pattern of the pitting and so allow the loss of weight determination to give a true index of the benefit attained by increase of pressure at the location of the disturbance.

⁸ Manager, Hydraulic Division, Canadian Allis-Chalmers Ltd., Lachine, Inc., Canada. Mem. ASME.

When tests have been undertaken in the field to appraise the relative resistance of different materials to the destructive forces of cavitation on a single hydraulic turbine runner, it often has appeared that the application of stainless steel to the portions that are most seriously affected has a tendency to shift the position of "the affected area." The apparatus discussed would provide a means whereby it should be possible to apply stainless steel to half of the specimen (a semicircle), and to determine whether or not there is a tendency for a distortion of the pattern of the pitted surface on the parent metal. Probably such is not the case—although the premise is widely held.

In general, the relative resistance of the materials discussed in this paper to the action of cavitation closely corresponds to conditions found during field investigations. The suggestion that "there is a difference in the minimum force required to produce pitting in different materials," is most interesting, and the data supplied in Fig. 6 of the paper explains the apparent inconsistencies of field tests, when in some cases the substitution of rolled stainless steel for cast mild steel entirely eliminates destruction by cavitation in locations where this condition has been quite pronounced and yet in other cases the same stainless steel may be destroyed by this action (although at a considerably lower rate). The relatively small advantage attained by a high surface finish is also worthy of note.

Perhaps one of the greatest contributions is the disclosure of the very pronounced relationship between the resistance of any material to pitting and the hardness of that material. This may account for the wide divergence of much data obtained in the field during tests undertaken on materials of exactly the same chemical composition under comparable operating conditions. The data presented in Fig. 13 are most pertinent.

WILHELM SPANNHAKE.⁹ The consistent tests and their most interesting and practically important results remind the writer of a series of experiments which he initiated at the Technical University of Karlsruhe, Baden, Germany, in 1939. They have been carried through by Dr. Hans Nowotny and were published in 1942.¹⁰ These tests gave similar results for the curves showing the relationship between the loss of weight and the time of exposure of the material to the cavitation attack. However, Nowotny found that the loss of weight distinctly began after a certain "time of incubation," during which no loss of weight could be measured. For instance, with some sort of steel he found that during this incubation time, the material suffered about 6-10% hits of collapsing bubbles. He believes that during this time the material changes its properties, especially under the influence of heat created by the numerous blows concentrated on very small areas. He came to the conclusion that it is difficult to establish a general connection between the resistance against cavitation damage and the purely mechanical properties of materials as they are found at room temperature. By the same reason he finds that those high static pressures, which many authors believe to be necessary for an explanation of the cavitation damage, and which they failed to measure by experiments, are actually not necessary.

Nowotny went still further in analyzing the details of the destruction. He applied a very sensitive x-ray method, taking pictures not only of the various samples of material before and after cavitation, but also of the particles broken out of the sample and fished out of the liquid. In this way he found that not only the grain structure was destroyed, but that even the single

⁹ Senior Research Scientist, Armour Research Foundation, and Adjunct Professor, Illinois Institute of Technology, Chicago, Ill.

¹⁰ "Destruction of Materials by Cavitation," by Dr. Hans Nowotny (booklet in German), 1942; reprinted by Edwards Brothers, Ann Arbor, Mich., 1946.

grains were broken. The grains fished out of the liquid showed a distinct reduction in size.

These few details out of Nowotny's book have been given in order to demonstrate that the vibratory method is fit not only for practical purposes, but also for a very thorough basic investigation in order to establish a consistent theory of the particular form of wear and tear inherent in the cavitation phenomenon. It might be possible that by means of such a theory we may sometime succeed in "constructing" that material which has the strongest resistance against the cavitation damage.

On the other hand, the writer would recommend not to abandon the other methods of creating cavitation such as that in Venturi tubes or around specially shaped bodies. It is still important to compare the effects of different kinds of cavitation.

At the same time Nowotny made his experiments, the writer succeeded in creating in a high-power Venturi tube with a velocity of 250 fps in the throat, the same primary effects such as discoloring, and the like, after an exposure of the best steel for only 30 sec.

The scientists of both hydrodynamics and metallurgy should combine their efforts to clear this phenomenon of cavitation which has obtained so great an importance since high speeds are being applied more and more in so many fields of modern technique.

Any contribution out of the laboratories of the industry such as the author's should be highly appreciated.

AUTHOR'S CLOSURE

Mr. Baumeister's statement that the accelerated-cavitation method does not give absolute or theoretical values is correct. Up to the present time the test results have all been relative. However, there is a possibility that as our knowledge of the mechanics of cavitation increases, absolute or theoretical results can be obtained. For the time being we have to use the cut-and-try method of selecting materials for highest resistance to pitting.

The author does not agree with the limited definition of cavitation suggested by Mr. Glazebrook. It has been demonstrated experimentally¹¹ that actual voids or separations can be created in a liquid, and that the threshold of force required to create these voids varies with the gas content of the liquid and other factors. While the author's definition of cavitation could no doubt be improved, it should not be related to the vapor pressure of the liquid nor should it describe the details of some of the resulting phenomena as recommended by Mr. Glazebrook.

Although tests on materials with varying grain size¹² indicate that the finer the grain, the greater the resistance to pitting, there is no definite relationship between the hardness of a material and its grain size. However, fatigue strength is a determining factor in the ability of a material to resist pitting, and since those with a high hardness usually have a high fatigue strength, it may account for the increase in resistance to pitting with increased hardness.

Mr. MacNamee's description of the tests to determine the resistance to the erosion of various materials is very interesting. He should have sufficient data to warrant a separate treatise on this subject.

No tests have ever been made to determine the effect of barometric pressure on the rate of pitting. However, there is definite proof that the rate of pitting varies with the temperature of the liquid (1),¹³ and it is generally accepted that this variation is due

to the change of the vapor pressure with temperature. Therefore it can be assumed that barometric pressure has a similar effect on the rate of pitting.

The results of the tests which were made with different liquids are a further indication of the correlation between the rate of pitting and vapor pressure. These tests are described by the author as having been made with various concentrates of acids, and oils to determine whether the rate of pitting was affected by corrosive liquids. At the time the paper was written there was no good explanation for the results obtained. Recently a calculation was made on the vapor pressure of the liquids used in the tests. Plotting the rate of pitting against the vapor pressure of the liquid showed a definite straight-line relationship. This relationship is similar to the relationship Mousson (1)¹³ and Nowotny¹⁰ found in their tests by changing the temperature of the water, Fig. 19, herewith.

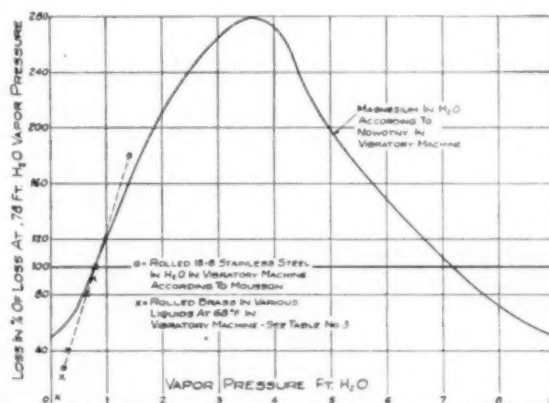


FIG. 19 Relation Between Vapor Pressure and Rate of Pitting as Measured by Loss of Metal of Test Specimen

The experiments by Mousson and the author were confined to the lower temperatures and vapor pressures, whereas Nowotny covered the entire range of temperature of water from freezing to boiling. The author is now conducting experiments with liquids with vapor pressures between 0.2 and 8.0 ft of water for comparison with Nowotny's curve.

The relationship between the rate of pitting and the vapor pressure of various liquids is very significant. It adds to our knowledge as to the nature of cavitation, and also indicates that there is a similarity between the cavitation produced by Mousson with a Venturi-tube type of machine and the cavitation produced with the vibratory machines.

Mr. MacNamee calls attention to the fact that the only hard steels tested were stainless steels. Accelerated-cavitation tests on various alloyed steels were made by both Mousson (1)¹³ and Kerr (2)¹³ and time did not permit the duplication of all of their tests.

In comparing the relative rate of pitting of stellite to other materials, Mr. Van Patter should take into consideration that there are various types and grades of stellite. The author tested rolled stellite which had shown high resistance to erosion in a special erosion testing machine. Mousson (1)¹³ tested both welded stellites and rolled stellites. The welded stellites showed losses from 3.4 to 10.8 cu mm, as compared to 0.9 to 2.8 cu mm for rolled stellites. This showed the large possible variation in the resistance to pitting of this material.

With reference to the formation of vapor bubbles on the test specimen, the stroboscopic light used did not have the high

¹¹ "Apparatus and Techniques for a Study of Cavitation," by F. G. Blake, Jr., Technical Memorandum no. 12, NR-014-903, Office of Naval Research, Department of the Navy, Washington, D.C.

¹² "Failure of Metal Due to Cavitation Under Experimental Conditions," by H. N. Boetcher, Trans. ASME, vol. 57, 1935, pp. 355-360.

¹³ Reference is to author's Bibliography.

frequency necessary to stop the movement of the specimen, and, therefore, the exact bubble formation could not be observed in detail. The author refers Mr. Van Patter to an article by M. Kornfeld and L. Suvorov,¹⁴ which gives a detailed description of the bubble formation, as observed in connection with a vibratory machine.

No tests have been made to determine at what amplitude pitting begins on various materials. However, this is an interesting subject and is scheduled for future investigation.

The author's statement that two layers of type 301 stainless-steel weld should be used for repairing and prewelding hydraulic turbine machinery, was based largely upon the practical application of weldments. The stellite tested by the author was a rolled plate and not a weldment, and therefore is not particularly suitable for repairs. Welded stellite is not practical because of its cost, and because it is difficult to grind and machine. There is very little information available at the present time on the performance of Ampco bronzes in field installations. Furthermore, the application of Ampco bronze weldments is more difficult and requires greater care than stainless steel and cannot be applied overhead.

Two layers of weld give a higher resistance to pitting and result in a better coverage of the welded surface than one layer. Also the first layer of stainless-steel weld on a mild-steel base has a tendency to become contaminated. Table 20 of this closure shows the chemical analysis of the weldments shown in

TABLE 20 CHROME AND NICKEL CONTENT OF STAINLESS-STEEL WELDMENTS*

Specimen no.	Type of weld-rod material		Content per cent	
	1st layer of weld	2nd layer of weld	Cr	Ni
203	301	...	12.5	4.9
201	308	...	16.5	7.8
198	309	...	16.9	11.2
204	301	301	15.8	6.5
199	309	308	19.9	10.3
202	308	308	19.6	9.7
200	309	301	19.9	10.3

* As shown in Table 12 of paper.

Table 12 of the paper. This indicates how the use of one layer of weld decreases the chromium content of the weldment. With two layers, the surface of the weldment approaches more closely the chemical composition of the weld rod used.

Mr. Rightmire gives a good explanation of the cavitation action at various depths of submergence. It is hoped that the results of the tests to which he refers will be published at an early date.

Mr. Southmayd refers to the tendency for pitting to shift on hydraulic-turbine runners when repairs are made with stainless

steel. This can probably be explained by the fact that the material erodes due to fatigue. Repairs are usually made only on the areas that have actually pitted and where the most severe cavitation occurs. However, in the surrounding areas where

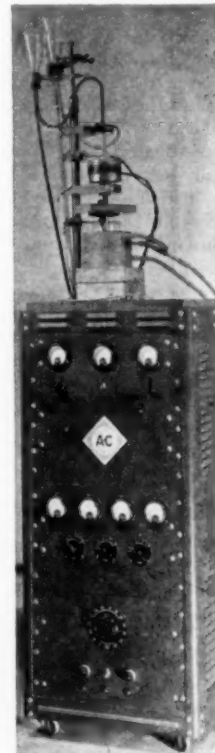


FIG. 20 ACCELERATED-CAVITATION MACHINE, VIBRATORY TYPE, AS ARRANGED FOR PERMANENT USE

cavitation is not quite so severe the material has already been weakened due to fatigue and therefore sometimes starts to erode soon after repairs have been made to the other areas.

Mr. Spannhake's reference to Nowotny's experiments is a valuable contribution.

The accelerated-cavitation tests described by the author in the original paper were made with the temporary machine shown in Figs. 2 and 3. Since then this machine has been rebuilt in more permanent form as shown in Fig. 20, herewith.

¹⁴ "On the Destructive Action of Cavitation," by M. Kornfeld and L. Suvorov, *Journal of Applied Physics*, vol. 15, 1944, pp. 495-506.

Zero-Pressure Thermodynamic Properties of Some Monatomic Gases

By J. A. GOFF,¹ SERGE GRATCH,² AND S. W. VAN VOORHIS,³ PHILADELPHIA, PA.

This paper presents definitive values of the zero-pressure thermodynamic properties of the stable naturally occurring isotopes and the normal isotopic mixtures of the following monatomic gases: Hydrogen (H), helium (He), carbon (C), nitrogen (N), oxygen (O), fluorine (F), sulphur (S), chlorine (Cl), argon (A), bromine (Br), iodine (I), mercury (Hg). These values cover the range 100 to 5000 deg R at the intervals indicated by the numbers in parentheses: 100(5)130(10)240(20)500(50)1000(100)2000(200)5000. They have been computed by the methods of quantum statistical mechanics from present best values of the relevant (a) general physical constants, (b) isotopic weights and fractional abundances, (c) spectroscopic data. Computational accuracy well beyond present physical accuracy has been maintained for practical reasons, final results being given to seven significant figures. Present physical accuracy is indicated by charts of estimated uncertainties. For some of the monatomic gases here considered, accurate values of their zero-pressure thermodynamic properties hitherto have been unavailable; for others the data presented are the first based upon recent spectroscopic and other input data to be made available at temperatures sufficiently close for convenient practical application.

INTRODUCTION

THE engineer will readily recognize the need of accurate information regarding the thermodynamic properties of some of the monatomic gases considered in this paper. Monatomic hydrogen is formed in appreciable concentrations in the atomic-hydrogen welding flame; helium seems destined to play an important role in nuclear-engineering developments; welding techniques have been advanced significantly through the use of argon and helium which therefore must be produced in increasing quantities; mercury is one of the working substances of the modern mercury power plant.

The need for accurate information regarding the thermodynamic properties of other monatomic gases will be more and more strongly felt by the engineer as it becomes more and more necessary for him to take account of the limitations imposed by chemical equilibrium in combustion processes. In attempting to predict the composition of a gas mixture at chemical equilibrium, it is usual to assume no transmutation of atomic species. Under

this assumption there are as many equations to be solved simultaneously, at a given pressure and temperature, as there are distinct atomic species. If the concentrations of the monatomic gases are used as unknowns, the equations for equilibrium take the same form regardless of the particular problem to which they are applied—only the terms to be included as making significant contributions to the pressure, volume, enthalpy, and entropy of the equilibrium mixture are different (1).⁴ This suggests the importance of having suitable tables giving the thermodynamic properties of the monatomic gases for use in making chemical equilibrium calculations.

THEORY

The formulations on which modern tables giving the thermodynamic properties of gases are based rest firmly on the zero-pressure values of the product pv , of the enthalpy h , and of the reduced entropy $s + R \log p$ as calculated from spectroscopic data by the method of statistical mechanics; direct experimental measurements are used only to extend these values to higher pressures. The general principles of the method have been summarized by Herzberg (2, 3) who also has reviewed the present state of our knowledge of the spectroscopic data for various common gases. When this knowledge can be expressed by equations giving wave number E (cm^{-1}) as a function of certain quantum numbers which independently can take on all non-negative integral values within prescribed limits, the constants appearing in these equations are called "spectroscopic constants."

To each wave number E_i there is assigned a definite energy hcE_i , where h denotes Planck's constant, and c the velocity of light in vacuo. Both E_i and hcE_i are referred to alternatively as "energy levels." To each set of values of the various quantum numbers corresponds a distinct quantum state; but there may be more than one, say, p_i , distinct quantum states having the same energy hcE_i in the absence of an external electric or magnetic field. The first step in the calculations is to form the state sum or partition function Q , defined by

$$Q = \sum p_i e^{-hcE_i/kT} = \sum p_i e^{-c_2 E_i} \dots \dots \dots [1]$$

where k is Boltzmann's constant, $c_2 = hc/k$ is the so-called second radiation constant, and τ denotes reciprocal absolute temperature T^{-1} . The summation is to extend over all accessible energy levels E_i . Values of the product pv , of the enthalpy h , and of the reduced entropy $s + R \log p$ are readily derivable from a knowledge of Q as a function of pressure p and temperature T .

In what follows it will be understood that the energy levels E_i are those that are strictly applicable only in the limiting case of "zero pressure" where the effects of intermolecular forces vanish. In some of the gases here considered, translation is the only mode of motion that contributes appreciably to the partition function Q up to 5000 deg R. As is well known, its contribution Q_{trans} is given by

$$Q_{\text{trans}}/nN_0 = [k(2\pi k/h^2 N_0)^{3/2}] \frac{M^{3/2} T^{3/2}}{p} \dots \dots \dots [2]$$

¹ Dean, Towne Scientific School and Director, University of Pennsylvania Thermodynamics Research Laboratory. Mem. ASME.

² Assistant Professor of Mechanical Engineering, Towne Scientific School, and Project Leader, University of Pennsylvania Thermodynamics Research Laboratory. Jun. ASME.

³ Formerly Research Assistant, University of Pennsylvania Thermodynamics Research Laboratory; now with The Lummus Company, New York, N. Y.

Contributed by the Research Committee on Properties of Gases and Gas Mixtures, and the Heat Transfer and Applied Mechanics Divisions, and presented at the Annual Meeting, New York, N. Y., November 27-December 2, 1949, of THE AMERICAN SOCIETY OF MECHANICAL ENGINEERS.

NOTE: Statements and opinions advanced in papers are to be understood as individual expressions of their authors and not those of the Society. Paper No. 49-A-145.

⁴ Numbers in parentheses refer to Bibliography at the end of the paper.

where n is the number of moles (on the chemical scale) of gas considered at absolute temperature T and absolute pressure p , and where M is the isotopic weight (also on the chemical scale) of the gas in question. The expression contains an additional general physical constant, namely, Avogadro's constant N_0 . The quantity Q_{trans}/nN_0 must necessarily be dimensionless, which means that the right-hand member of Equation [2] may also contain one or more conversion factors, depending upon the units chosen for temperature T and pressure p .

At all accessible temperatures for any gas, the partition function Q splits into two independent factors, namely

$$Q = Q_{\text{trans}} \cdot Q_{\text{int}} \quad [3]$$

where Q_{int} takes account of all internal energy levels. Possible contributions to Q_{int} from nuclear spin and other intranuclear levels will be excluded in accordance with usual practice because they are completely unaffected by ordinary chemical reactions not involving transmutation of atomic species. In the case of a monatomic gas the E_i contain only its electronic energy levels which, besides the second radiation constant $c_2 = hc/k$, are the only sources of uncertainty in the determination of its internal partition function Q_{int} .

The simplest procedure to follow in deriving the various thermodynamic properties of a gas from a knowledge of its partition function Q , as a function of pressure p and temperature T , is first to form its specific free enthalpy g , namely

$$g = -RT \log_e (Q/nN_0) \quad [4]$$

where $R = kN_0$, except possibly for a conversion factor which may be regarded as exact by definition. Free enthalpy g is a characteristic function for the choice of pressure p and temperature T as independent variables; from it the volume v , the enthalpy h , and the entropy s can be derived by application of the following identical relations of thermodynamics: $v = \partial g / \partial p$, $h = \partial (rg) / \partial r$, and $s = -\partial g / \partial T$, respectively. It is clear therefore that no new constants subject to experimental error are introduced in the derivation.

1 CRITICAL EVALUATION OF INPUT DATA

GENERAL PHYSICAL CONSTANTS

In conformity with the practice of the authors' laboratory, the 1941 Birge (4) best values of the general physical constants have been used in all calculations of thermodynamic properties. While the present calculations were in progress, DuMond and Cohen (5) published a revision of some of the Birge values which they later (6) corrected for a slight error of their origin value of Planck's constant h . Fortunately, the DuMond-Cohen revisions as corrected leave all of the general physical constants here considered well within the Birge uncertainty limits. For this reason, and especially since DuMond and Cohen feel that experimental determinations currently under way in various laboratories will soon warrant a systematic re-evaluation of the data, we have decided to retain the Birge values for the time being. Table 1 shows a comparison of the 1941 Birge and the 1949 DuMond-Cohen values of the general physical constants involved in the present analysis.

As illustrated by the data in Table 1, DuMond and Cohen have been able substantially to diminish the estimated uncertainties of the best values of the general physical constants. It seems unlikely that these will be increased by the systematic re-evaluation of the data to be undertaken when experimental determinations currently under way in various laboratories will have been completed. Therefore we have decided to recalculate the uncertainties of our tabulated results in order to bring them more

TABLE 1 GENERAL PHYSICAL CONSTANTS

Constant	1941 Birge	1949 DuMond-Cohen
N_0 (1/gmol)	(6.0228 \pm 0.0011) 10^{23}	(6.0235 \pm 0.0004) 10^{23}
k (erg/°K)	(1.38047 \pm 0.00026) 10^{-16}	(1.38062 \pm 0.00011) 10^{-16}
c (cm/sec)	(2.99776 \pm 0.00004) 10^{10}	(2.99776 \pm 0.00004) 10^{10}
h (erg sec)	(6.626 \pm 0.0024) 10^{-27}	(6.6237 \pm 0.0011) 10^{-27}
c_2 (cm °K)	1.4384 \pm 0.0003 $_4$	1.43853 \pm 0.00019
R (erg/°K gmol)	(8.31436 \pm 0.00038) 10^7	(8.31436 \pm 0.00038) 10^7

NOTE: gmol denotes a unit of weight of M grams, where M is molecular weight on the "chemical" scale.

nearly into line with the DuMond-Cohen uncertainties of the general physical constants, at the same time retaining, however, the 1941 Birge best values.

ISOTOPIC WEIGHTS

As can be seen from Equations [3], [4], the correct expression for specific free enthalpy g contains the additive term $-(3/2)RT \log_e M$ where M denotes the isotopic weight of the gas in question. In engineering it is customary to express these weights as numbers on the so-called chemical scale on which the apparent molecular weight of the normal isotopic mixture of diatomic oxygen is arbitrarily assigned the value 32. In general, the most accurate determinations of isotopic weight are those based upon measurements of close doublet separations by means of modern linear-scale mass spectrographs of high resolution. The direct determinations are always expressed as numbers on the so-called "physical" scale on which the isotopic weight of monatomic oxygen O^{16} is arbitrarily assigned the value 16. A numeric on the physical scale bears a definite ratio to the corresponding numeric on the chemical scale, this ratio being a constant which has to be determined experimentally. DuMond and Cohen accept Birge's best value, namely

$$r = 1.000272 \pm 0.000005$$

as, of course, do we.

As mentioned previously, the most accurate determinations of isotopic weight are usually those made with the mass spectrograph. For the technically important monatomic gases here considered, except in the case of one or two of the less abundant isotopes, nuclear-reaction determinations serve only as checks. In the mass spectrograph a beam of molecular (or atomic) ions is focused on a photographic plate, the location of the point of focus depending on the ratio of the mass to the electric charge of the ion. Two different ions, having neighboring values of this ratio, form on the photographic plate a close doublet, the separation of which yields a determination of the mass difference between the two ions when proper account is taken of the fact that their electric charges can differ only by integral multiples of the unit electric charge. The very slight effects of ionization and compound formation per se are negligible and well beyond the ability of the mass spectrograph to detect.

In mass-spectrographic work, all masses are compared directly or indirectly with that of monatomic oxygen O^{16} which is taken to be exactly 16 by definition. The first step is a direct determination of the masses of monatomic hydrogen H^1 , deuterium H^2 , and carbon C^{12} to be used as standards with which to compare the masses of other isotopes. Recent precision determinations of the masses of the isotopes of interest here have been carried out principally by Aston in 1936-1937, by Bainbridge and Jordan in 1936-1938, by Mattauch in 1936-1938, by Okuda, et al, in 1939-1941, and by Ewald in 1945-1946. In 1940-1941 Jordan reported preliminary results from a new mass spectrograph of greater resolving power and dispersion than were accessible to previous workers (7, 8).

The most recently published critical evaluations of existing data on isotopic masses are those of Livingston and Bethe (9) in 1937, of Birge (4) in 1941, of Flüge and Mattauch (10, 11)

in 1942 and 1943, of Aston (12) in 1942, of Cohen and Hornyak (13) in 1947, and of Bainbridge (14) in 1948. These evaluations seem to justify retention of the 1941 Birge (4) best values of the isotopic masses, at any rate for H^1 , H^2 , He^4 , C^{12} , C^{13} , N^{14} , N^{15} , O^{17} , O^{18} , I^{127} ; at the same time they seem to allow substantial diminution of Birge's probable errors or uncertainties.

Another critical evaluation of existing data on isotopic masses not referred to in the foregoing, was published in Japanese by Okuda (15) in 1942. We have reason, however, to question the mass determinations of the Japanese workers (15, 16, 17, 18, 19, 20, 21, 22). For one thing, they claim less accuracy for some of their important determinations than do other workers, even though they used a mass spectrograph of higher resolving power. They made no check on the internal consistency of their ground-doublet separation determinations. Their values ($679.3 \pm 0.7 \cdot 10^{-4}$ and $693.0 \pm 2.3 \cdot 10^{-4}$ for the mass-difference separations of the doublets $\text{C}_2^{12}\text{H}_2^1 - \text{A}^{40}$ and $\text{C}_2^{12}\text{H}_2^1 - \text{H}^1\text{A}^{40}$, respectively, are inconsistent. Their determinations of the masses of the two strongest nickel isotopes would assign to each an appreciably different packing fraction, which Aston (12) states "... is an unexpected result of great interest, if it is confirmed." Their values ($191.1 \pm 0.7 \cdot 10^{-4}$, $246.7 \pm 1.7 \cdot 10^{-4}$, and $421.7 \pm 0.9 \cdot 10^{-4}$ for the mass-difference separations of the doublets $\text{O}_2^{16} - \text{S}^{32}$, $\text{C}_2^{12}\text{H}_2^1 - \text{Cl}^{35}$, and $\text{C}_2^{12}\text{H}_2^1 - \text{Cl}^{37}$, respectively, differ appreciably from those of Aston (12), namely, ($177 \pm 3.2 \cdot 10^{-4}$, $225 \pm 7 \cdot 10^{-4}$, and $412 \pm 7 \cdot 10^{-4}$). Since we do have some question regarding the Japanese workers' determinations we feel obliged to disregard them and to disregard also the Flügge and Mattauch (10) values of the isotopic weights of S^{32} , S^{33} , S^{34} , S^{36} , Cl^{35} , Cl^{37} which have been based on these determinations. We will discuss in some detail the isotopic weight values that we have decided to accept for our present purposes.

Hydrogen. We accept the 1941 Birge values, namely

$$\begin{aligned}\text{H}^1 &= 1.00813 \pm 0.000017 \\ \text{H}^2 &= 2.01473 \pm 0.000019\end{aligned}$$

Helium. For He^3 , Livingston and Bethe (9) have obtained the value 3.01707 ± 0.00012 from an analysis of the nuclear reaction $\text{H}^2(d,n)\text{He}^3$; Flügge and Mattauch (11) have obtained 3.016988 ± 0.000020 from an analysis of the nuclear reactions $\text{H}^2(d,n)\text{He}^3$ and $\text{Li}^6(p,\alpha)\text{He}^3$; Bainbridge (14) has obtained the value 3.017016 ± 0.000032 from an analysis of various nuclear-reaction and mass-spectrographic data. The last of these seems to us to be the best value available and we therefore accept it along with the 1941 Birge value of the He^4 mass; thus we accept

$$\begin{aligned}\text{He}^3 &= 3.017016 \pm 0.000032 \\ \text{He}^4 &= 4.00389 \pm 0.00007\end{aligned}$$

Carbon. We accept the 1941 Birge values, namely

$$\begin{aligned}\text{C}^{12} &= 12.00386 \pm 0.00004 \\ \text{C}^{13} &= 13.00761 \pm 0.00015\end{aligned}$$

Nitrogen. We accept the 1941 Birge values, namely

$$\begin{aligned}\text{N}^{14} &= 14.00753 \pm 0.00005 \\ \text{N}^{15} &= 15.0049 \pm 0.0002\end{aligned}$$

Oxygen. We accept the 1941 Birge values, namely

$$\begin{aligned}\text{O}^{17} &= 17.0045 \\ &\quad \text{(no uncertainties given)} \\ \text{O}^{18} &= 18.0049\end{aligned}$$

Fluorine. Aston (24) has obtained the value $(183.3 \pm 2.6) \cdot 10^{-4}$ for the mass-difference separation of the doublet $\text{O}^{16}\text{H}^2\text{H}^1 - \text{F}^{19}$. Combined with mass values already accepted this gives

$$\text{F}^{19} = 19.00453 \pm 0.0003$$

which we regard as the best value presently available.

Sulphur. We accept Aston's value for S^{32} . Flügge and Mattauch (11) have determined the mass of S^{32} from an analysis of the nuclear reactions $\text{S}^{32}(d,p)\text{S}^{33}$ and $\text{Cl}^{35}(d,\alpha)\text{S}^{33}$ using the values of Okuda, et al (18), for S^{32} and Cl^{35} ; we accept their value as the only one available at present, not bothering to correct it to strict consistency with our accepted values for S^{32} and Cl^{35} because the concentrations of S^{33} with which we have to deal are so very small. For S^{34} we accept the Livingston and Bethe (9) value, which happens to agree closely with that of Okuda and Ogata (16, 22), as corrected by Flügge and Mattauch (11). For S^{36} the best we can do is infer a value from Flügge and Mattauch's estimate of its packing fraction, namely, -6.5 , since there are no mass-spectrographic or nuclear-reaction data to go on. Our accepted values are

$$\begin{aligned}\text{S}^{32} &= 31.9823 \pm 0.0003 \\ \text{S}^{33} &= 32.98014 \pm 0.00040 \\ \text{S}^{34} &= 33.978 \pm 0.0020 \\ \text{S}^{36} &= 35.977 \pm 0.002\end{aligned}$$

Chlorine. We accept Aston's (25, 33, 12) value for Cl^{35} which happens to be in good agreement with that of Okuda, et al (18), as corrected by Flügge and Mattauch (11), namely, 34.97884 ± 0.00019 , with that of Livingston and Bethe (9) obtained from an analysis of the nuclear reaction $\text{S}^{32}(\alpha,p)\text{Cl}^{35}$, using Aston's value for S^{32} , namely, 34.9803 ± 0.00060 , and especially with that of Gibert, Roggen, and Rossel (23), namely, 34.98054 (no uncertainty given). We also accept Aston's (25, 12) value for Cl^{37} , although it disagrees somewhat with that of Livingston and Bethe (9), namely, 36.9779 ± 0.0012 , based upon his value for S^{32} ; also with that of Okuda, et al (18), as corrected by Flügge and Mattauch (11), namely, 36.97769 ± 0.00010 . Our accepted values for chlorine are

$$\begin{aligned}\text{Cl}^{35} &= 34.9808 \pm 0.0007 \\ \text{Cl}^{37} &= 36.9785 \pm 0.0008\end{aligned}$$

Argon. We accept Aston's (26, 12) value for A^{36} as determined from the mass-difference separations of the doublets $\frac{1}{2}\text{A}^{36} - \text{O}^{16}\text{H}_2^1$ and $\text{A}^{36} - \text{C}_2^{12}$ which happens to agree with that of Flügge and Mattauch (11) obtained in roundabout manner from nuclear-reaction data, namely, 35.97790 ± 0.00040 . We accept Flügge and Mattauch's value for A^{38} which agrees well with that of Livingston and Bethe (9), namely, 37.974 ± 0.0025 , but is based on more recent data. Following Aston (12), we accept Mattauch's 1938 value for A^{40} (27), even though the latter subsequently has revised his substandards somewhat (28) so that, strictly speaking, the 1938 value should be revised correspondingly, except that the original substandards were in closer agreement with the Birge values already accepted. Our accepted values for argon are

$$\begin{aligned}\text{A}^{36} &= 35.9780 \pm 0.0010 \\ \text{A}^{38} &= 37.97461 \pm 0.00030 \\ \text{A}^{40} &= 39.97564 \pm 0.00015\end{aligned}$$

Bromine. We accept Aston's (29, 30) values for Br^{79} and Br^{81} as the only ones presently available. His determinations were based upon the observed mass-difference separation of the doublet $\frac{1}{2}\text{Br}^{79} - \frac{1}{2}\text{Xe}^{132}$ and on the assumption of equal packing fractions for Br^{81} and Br^{79} . He had previously determined provisionally the mass value of Xe^{132} (31) from an unsatisfactory overlapping doublet and from comparison with the mass value of Xe^{130} . In 1942 he (12) brought his value up to date by correcting it for changes in his substandards. Our accepted values for bromine are

$$\begin{aligned}\text{Br}^{79} &= 78.9415 \pm 0.0020 \\ \text{Br}^{81} &= 80.9401 \pm 0.0020\end{aligned}$$

Iodine. Aston (32) reported in 1927 that he had found I^{127} to have the same packing fraction as Ne^{120} , namely, -4.1 . This is the only mass-spectrographic evidence regarding the mass of I^{127} . Accepting his provisional value for Ne^{120} (31), a value of 126.948 would be computed for I^{127} . Birge (4) derives the value 126.915 ± 0.004 (on the chemical scale) from available chemical-reaction data; it is directly applicable to I^{127} , the only stable isotope of iodine. Mainly for the sake of consistency but also because Aston's value seems somewhat doubtful, we accept the Birge value, namely

$$I^{127} = 126.915 \pm 0.004 \text{ (chemical scale)}$$

Mercury. Published data on the masses of the mercury isotopes are meager and lacking in precision. In 1937 Aston (33) gave a provisional value of $+1.4$ for the packing fraction of Hg^{200} , based upon a somewhat doubtful comparison with the fundamental substandards through Ne^{120} and Ne^{122} ; subsequently, he revised this value to $+1.7$ to accord with revisions in the substandards themselves (12). In his 1927 report, Aston (32) states that the mass intervals of the mercury isotopes can hardly be distinguished from unity. If we accept this statement and assume the same packing fraction $+1.7$ for all the isotopes, and if we accept the data on fractional abundances given in the "Fifth Report of the Committee on Atoms of the International Union of Chemistry," 1940 (34), we obtain the value 200.59 (on the chemical scale) for ordinary mercury which compares well with the value 200.61 given in the "Thirteenth Report on Atomic Weights of the International Union of Chemistry" (35), based on chemical-reaction data. While this favorable comparison is not convincing evidence of the accuracy of the mass-spectrographic determinations, still the Aston mass (12) values suffice for our purposes because larger errors can be tolerated in the case of mercury. We have used the following values:

$$\begin{aligned} Hg^{180} &= 196.033 \pm 0.02 \\ Hg^{182} &= 198.034 \pm 0.02 \\ Hg^{190} &= 199.034 \pm 0.02 \\ Hg^{200} &= 200.034 \pm 0.006 \\ Hg^{201} &= 201.034 \pm 0.02 \\ Hg^{202} &= 202.034 \pm 0.02 \\ Hg^{204} &= 204.035 \pm 0.02 \end{aligned}$$

We conclude our discussion of isotopic weights by listing in Table 2 some recent values by Cohen and Hornyak (13), Bainbridge (14), and Ewald (36, 37) for some of the lighter elements. Undoubtedly, these are more precise than the ones we have accepted as just noted, but we have not attempted to use them because it would hardly be feasible for us to do so in a thoroughly consistent way.

ISOTOPE ABUNDANCES

Ordinary oxygen, for example, is a mixture of the six different isotopic molecules that can be formed from the isotopes O^{16} , O^{17} , O^{18} . The atom fractions, or fractional abundances, of these isotopes in the mixture have been determined to be 0.99763, 0.00040, 0.00197, respectively. Using the isotopic weights previously adopted, namely, 16, 17.0045, 18.0049, respectively, we readily compute the value 32.00970 for the apparent molecular

weight of ordinary oxygen on the physical scale. Its apparent molecular weight on the chemical scale is exactly 32 by definition, whence the value 1.000272 for the ratio between corresponding values on the two scales.

We require information regarding the isotope abundances of other normal isotopic mixtures. Existing data have been reviewed critically and evaluated by Livingston and Bethe (9) in 1937, by the Committee on Atoms of the International Union of Chemistry (34) in 1940, by Birge (4) in 1941, by Aston (12) in 1942, by Flüge and Matthauch (11) in 1943, and by Seaborg and Perlman (38) in 1948. We accept the 1941 Birge values for hydrogen, carbon, nitrogen, and oxygen. In this connection it may be well to mention that the isotope abundances of ordinary oxygen have been investigated recently by Thode and Smith (39) and by Urey (40), who have detected significant variations among samples obtained from various sources. For helium we accept the values of Aldrich and Nier (41, 42) applicable to well (natural-gas) helium. For fluorine, sulphur, chlorine, argon, iodine, and mercury, we accept the "Fifth Report of the Committee on Atoms of the International Union of Chemistry" (34) values with uncertainties estimated from the Seaborg and Perlman (38) data, and with Nier's (43) value of the fractional abundance of S^{32} in ordinary sulphur. The isotope abundances of argon have been investigated recently by Dibel, Mohler, and Reese (44), whose results agree fairly well with those of Nier (45), which in turn do not dispute the values accepted here within the accuracy given. The isotope abundances of bromine have been investigated recently by Williams and Yuster (46) and by White and Cameron (47) with almost identical results; we accept those of the latter investigators because of their somewhat smaller uncertainties.

We conclude this brief discussion of isotope abundances by listing in Table 3 the values we have decided to accept for our present purposes.

TABLE 2 FRACTIONAL ABUNDANCES ACCEPTED FOR USE HERE

H^1	0.9998551 \pm 0.0000022	Cl^{35}	0.754 \pm 0.0018
H^2	0.0001449 \pm 0.0000022	Cl^{37}	0.246 \pm 0.0018
He^3	0.00000016 \pm 0.00000004	A^{32}	0.0031 \pm 0.000038
He^4	0.99999984 \pm 0.00000004	A^{33}	0.0006 \pm 0.000016
C^{12}	0.98925 \pm 0.00024	A^{34}	0.9963 \pm 0.000054
C^{13}	0.01075 \pm 0.00024	Br^{79}	0.5051 \pm 0.0005
N^{14}	0.99631 \pm 0.00008	Br^{81}	0.4949 \pm 0.0006
N^{15}	0.00369 \pm 0.00008	I^{127}	1.0000
O^{16}	0.99762 \pm 0.00007	Hg^{180}	0.0015 \pm 0.000055
O^{17}	0.00040 \pm 0.00005	Hg^{182}	0.1011 \pm 0.0016
O^{18}	0.00197 \pm 0.00004	Hg^{190}	0.1703 \pm 0.0024
F^{19}	1.00000	Hg^{200}	0.2326 \pm 0.0029
S^{32}	0.951 \pm 0.0010	Hg^{201}	0.1217 \pm 0.0019
S^{33}	0.0074 \pm 0.00016	Hg^{202}	0.2945 \pm 0.0021
S^{34}	0.042 \pm 0.0008	Hg^{204}	0.0672 \pm 0.0011
S^{36}	0.00016 \pm 0.000016		

SPECTROSCOPIC DATA

If in the expression $Q = \sum p_i e^{-E_i/RT}$, we replace the E_i with the differences $E_i - E_0$, where E_0 is a constant for the gas in question, we merely augment Q by the factor $e^{E_0/RT}$, diminish the free enthalpy g and the enthalpy h by a constant amount $N_0 E_0$, but leave the entropy s unaltered. Furthermore, if for the mon-

TABLE 2 SOME NEWER VALUES OF ISOTOPIC WEIGHT

Isotope	Cohen-Hornyak	Bainbridge	Ewald
H^1	1.008128 \pm 0.000003	1.0081283 \pm 0.0000028	
H^2	2.014718 \pm 0.000005	2.0147186 \pm 0.0000055	
He^3		3.017016 \pm 0.000032	
He^4		4.003880 \pm 0.000032	
C^{12}	12.003847 \pm 0.000016	12.003858 \pm 0.000019	
C^{13}			13.007581 \pm 0.000025
N^{14}	14.007589 \pm 0.000015	14.007586 \pm 0.000022	15.004649 \pm 0.000030
N^{15}			

atomic gases here considered E_0 is understood to denote the energy of the ground electronic state so that $E_i > E_0$ for all other electronic levels, then $NhcE_0$ may be identified as the amount contributed by the electronic levels to the null-point ($T = 0$, $p = 0$) energy \bar{u} of the gas in question. We have ascertained by preliminary calculations that for all gases considered here, separations $E_i - E_0$ exceeding 50,000 reciprocal centimeters (cm^{-1}) cannot affect our final results and therefore may be disregarded. In the case of hydrogen, for example, the next to the lowest electronic energy level lies some 82,000 cm^{-1} above the ground level so that we may, within the accuracy of our final results, take $Q_{\text{lat}} = p_0 e^{-C_0/T_0}$, where p_0 is the statistical weight of the ground level. It is well known that $p_0 = 2$ (exactly) for hydrogen, and we absorb the constant E_0 in the null-point energy \bar{u} ; hence no detailed discussion of the spectroscopic data for hydrogen is necessary for our purposes.

Regarding the spectroscopic data for the other gases considered here, no general statement can be made at present. Among several excellent reviews of existing data are those of Bacher and Goudsmit (48) in 1932, of Robinson and Shortley (49) in 1937, of Shenstone (50) in 1938, of Moore (51) in 1945, of Meggers (52) in 1946, and of Moore (53) in 1948. These reviews serve as excellent guides to the literature, the first and last of them providing extremely useful tables of energy levels also. We proceed on the basis of this and other information separately to discuss each atom considered here.

Hydrogen. The ground state is a $1s: ^1S_{1/2}$ state (48) with $p_0 = 2$, the next higher level lying some 82,000 cm^{-1} above it.

Helium. The ground state is a $1s^2: ^1S_0$ state (48) with $p_0 = 1$, the next higher level lying some 160,000 cm^{-1} above it.

Carbon. The ground state is a $1s^2 2s^2 2p^2: ^3P_0$ state (48) with $p_0 = 1$. The only low-lying levels are the $2s^2 2p^3: ^4P, ^4D, ^4S$ and the $2s 2p^3: ^4S$ states, the next higher level having been rather definitely established as lying some 60,000 cm^{-1} above the ground level (54). Until recently the location of the 4S state was in doubt, but Shenstone (55) has now obtained direct experimental evidence placing it at 33,735.2 \pm 0.1 cm^{-1} above the ground state; he has also confirmed the findings of Chulanovskii and Mokhaatkin (56) regarding the locations of the 4P_1 and the 4P_2 states. Edlén (54) has confirmed the values of Bacher and Goudsmit (48) for the locations of the 4D_2 and the 4S_0 states. We have based our calculations for carbon on the following data: 1(0.0); 3(16.56 \pm 0.1); 5(43.47 \pm 0.1); 5(10192 \pm 1); 1(21647 \pm 1); 5(33735.2 \pm 0.1); 1(60331.3). The number before the parentheses is the statistical weight p_i of the level whose separation $E_i - E_0$ from the ground level is given within the parentheses in reciprocal centimeters (cm^{-1}).

Nitrogen. The ground state is a $1s^2 2s^2 2p^3: ^4S_{3/2}$ state (48) with $p_0 = 4$. The only low-lying levels are the $2s^2 2p^3: ^4D, ^4P$ states, the next higher level lying some 83,000 cm^{-1} above the ground level. The most reliable data on the arc spectrum of nitrogen appear to be those of Ekefors (57), who was the first to detect the predicted splitting of the $^4D^0$ levels. Others (58, 59, 60) have confirmed his results (on the splitting of the $^4D^0$ levels) and, in addition, have confirmed the prediction that the splitting of the $^4P^0$ levels is quite small; it is of no interest to us here because it does not improve the accuracy of Ekefors' data. A brief analysis of the recent work of Kamiyama and others (61, 62, 63) suggests that their apparatus was incapable of resolving the $^4D^0$ levels and that, therefore, a detailed analysis would be unlikely to locate the low-lying levels more accurately than do the data of Ekefors. We have based our calculations for nitrogen upon the following data: 4(0.0); 6(19223 \pm 2); 4(19231 \pm 2); 6(28840 \pm 2); 2(83285.5).

Oxygen. The ground state is a $1s^2 2s^2 2p^4: ^3P_2$ state (48) with $p_0 = 5$. The only low-lying levels are the $2s^2 2p^4: ^4P_1, ^4P_0, ^4D_3, ^4D_1$

states, the next higher level lying some 74,000 cm^{-1} above the ground level. The latest and most reliable data on the arc spectrum of oxygen have been given by Edlén (64) in an excellent review article. We accept his values for the low-lying levels, assigning approximate uncertainties which we feel sure are of the right order of magnitude. Thus we have based our calculations for oxygen upon the following data: 5(0.0); 3(158.5 \pm 0.1); 1(226.5 \pm 0.1); 5(15867.7 \pm 0.1); 1(33792.4 \pm 0.2); 5(73767.8).

Fluorine. The ground state is a $1s^2 2s^2 2p^5: ^2P_{3/2}$ state (48), with $p_0 = 4$. The only low-lying level is the $2s^2 2p^5: ^2P_{1/2}$ state, the next higher lying some 102,000 cm^{-1} above the ground level. The most recent and probably the best data on the ultraviolet-arc spectrum of fluorine are those of Edlén (65) which we accept. It may be well to mention, however, that Edlén has redetermined the separation of the $2p^5: ^2P_{3/2, 1/2}$ levels to be 404.0 cm^{-1} , which differs slightly from Bacher and Goudsmit's (48) value of 407.0 cm^{-1} , obtained from Dingle's (66) evaluation of Bowen's (67) data. The very recent data of Lidén (68) are not concerned with the low-lying levels. We have based our calculations for fluorine on the following data: 4(0.0); 2(404.0 \pm 0.5); 6(102406.50).

Sulphur. The ground level is a $1s^2 2s^2 2p^3 3s^3 p^4: ^3P_2$ state (48) with $p_0 = 5$. The only low-lying levels are the $3s^3 3p^4: ^3P, ^1D, ^1S$ and the $3s^2 3p^3 4s: ^4S_0$ levels, the next higher lying some 72,000 cm^{-1} above the ground level. Bacher and Goudsmit (48) give values for the $3p^4: ^3P_{0,1,2}$ and the $3p^3(^4S)4s: ^4S_0$ levels based on the data of Hopfield (69), of Bungartz (70), and of Hopfield and Dieke (71). More recent investigations are those of Frerichs (72), of Meissner, Bartelt, and Eckstein (73), and of Ruedy (74, 75). In 1936, Bowen (76) revised Ruedy's (75) value of the 4S_0 level in order to align the p^4 configurations better with those of other similar atoms. Robinson and Shortley (49) disagree with this revision, but Edlén (77) has adduced rather convincing evidence in favor of it. We have decided to accept Ruedy's values as revised by Bowen, because they appear to be the most accurate direct determinations of the low-lying levels, and especially because they have been carefully checked by Edlén. We have based our calculations for sulphur upon the following data, the uncertainties given being only approximate: 5(0.0); 3(397.2 \pm 1); 1(574.7 \pm 0.5); 5(9239.8 \pm 0.5); 1(22182.2 \pm 1); 5(52623.8).

Chlorine. The ground state is a $1s^2 2s^2 2p^3 3s^3 3p^5: ^2P_{3/2}$ state (48) with $p_0 = 4$. The only low-lying level is the $3s^3 3p^5: ^2P_{1/2}$ level, the next higher lying some 72,000 cm^{-1} above the ground level. The latest reported work on chlorine is that of Kiess (78) which, however, does not evaluate the $^2P_{1/2}$ term; for this we must rely on Turner (79) even though his data are not as accurate as might be wished. We have based our calculations for chlorine upon the following data, the uncertainty given being only approximate: 4(0.0); 2(881 \pm 3); 6(71954.00).

Argon. The ground state is a $1s^2 2s^2 2p^6 3s^3 3p^6: ^1S_0$ state (48) with $p_0 = 1$. The next higher level almost certainly lies some 93,000 cm^{-1} above the ground level, such large separations being characteristic of the inert gases as remarked by Herzberg (80).

Bromine. The ground state is a $1s^2 2s^2 2p^6 3s^3 3p^3 3d^{10} 4s^2 4p^5: ^2P_{3/2}$ state (48) with $p_0 = 4$. The only low-lying level is the $4s^2 4p^5: ^2P_{1/2}$ level, the next higher lying some 63,000 cm^{-1} above the ground level. The latest reported work on bromine is that of Kiess and de Bruin (81) which, however, does not evaluate the $^2P_{1/2}$ term; for this we must rely upon Turner (79). We have based our calculations for bromine upon the following data, the uncertainty given being only approximate: 4(0.0); 2(3685 \pm 3); 6(63000).

Iodine. The ground state is a $1s^2 2s^2 2p^6 3s^3 3p^3 3d^{10} 4s^2 4p^4 4d^{10} 5s^2 5p^5: ^2P_{3/2}$ state (82) with $p_0 = 4$. The only low-lying level is the $5s^2 5p^5: ^2P_{1/2}$ level, the next higher lying some 54,000 cm^{-1} above the ground level according to what evidence is available.

The most recent and probably the best data on the arc spectrum of iodine are those of Murakawa (82) which are supported by the earlier work of Turner (79), of Evans (83), of McLeod (84), and of Hellerman (85). We have based our calculations for iodine on the following data, the uncertainty given being only approximate: 4(0.0); 2(7602.7 \pm 1); 6(54630.0).

Mercury. The ground state is a $1s^2 2s^2 2p^6 3s^2 3p^4 3d^{10} 4s^2 4p^4 4d^{10} 4f^{14} 5s^2 5p^5 5d^{10} 6s^2$ 1S_0 state (48) with $p_0 = 1$. The only low-lying levels are the $6s 6p$ $^3P_{0,1,2}$ levels, the next higher lying some 54,000 cm^{-1} above the ground level. These low-lying levels have been very accurately located by Fukuda (86), by Stiles (87), and by Foote, et al (88), respectively, whose data we accept. Thus, we have based our calculations for mercury on the following data: 1(0.0); 1(37641.97 \pm 0.7); 3(39412.25 \pm 0.3); 5(44039.21 \pm 2); 3(54065.7).

2 WORKING TABLES WITH ESTIMATED UNCERTAINTIES

CALCULATION OF THERMODYNAMIC PROPERTIES

From previous statements in this paper, it is clear that specific free enthalpy g is given by the expression

$$e^{-g/RT} = [k(2\pi k/h^2 N_0)^{3/2}] e^{-c_{27} E_0} \sum p_i e^{-c_{27}(E_i - E_0)} \frac{M^{3/2} T^{5/2}}{p} \quad [5]$$

We replace the factor $e^{-c_{27} E_0}$ with unity, knowing that we thereby merely diminish the free enthalpy g and the enthalpy h by the constant amount $N_0 h c E_0$, which we absorb in the null-point ($T = 0$, $p = 0$) energy \bar{u} , without affecting the entropy s . We introduce the so-called characteristic temperatures

$$\theta_i = c_{27}(E_i - E_0) \quad [6]$$

and define the dimensionless temperature functions

$$\begin{aligned} \alpha &= \sum p_i e^{-\theta_i \tau} \\ \beta &= \sum p_i (\theta_i \tau) e^{-\theta_i \tau} \\ \gamma &= \sum p_i (\theta_i \tau)^2 e^{-\theta_i \tau} \end{aligned} \quad [7]$$

Finally, using the 1941 Birge (4) values of the general physical constants, together with the conversion factors 1.8 $^\circ\text{R}/^\circ\text{K}$ and 1,013,246 dyne/cm² atm, we derive

$$\begin{aligned} \log_e p - (g - \bar{u})/RT &= -5.13397_5 + \frac{3}{2} \log_e M \\ &+ \frac{5}{2} \log_e T + \log_e \alpha \quad [8] \end{aligned}$$

in which pressure p is to be expressed in international atmospheres (atm) and temperature T in degrees Rankine ($^\circ\text{R}$). In Equation [8] it is understood that M denotes isotopic weight on the chemical scale.

As mentioned previously, free enthalpy g is one of the characteristic functions of thermodynamics when expressed in terms of temperature T and pressure p as independent variables. Applying to Equation [8] the identical relations $v = \partial g / \partial p$, $s = -\partial g / \partial T$, $h = \partial(g\tau) / \partial \tau$, and the definition $c_p = \partial h / \partial T$, we easily derive

$$\left. \begin{aligned} (pv)_{p=0} &= RT \\ [s/R + \log_e p]_{p=0} &= -2.63397_5 + \frac{3}{2} \log_e M + \frac{5}{2} \log_e T \\ &+ \log_e \alpha + \beta/\alpha \\ [(h - \bar{u})/RT]_{p=0} &= 5/2 + \beta/\alpha \\ [c_p/R]_{p=0} &= 5/2 + \gamma/\alpha - (\beta/\alpha)^2 \end{aligned} \right\} \quad [9]$$

In each of Equations [9] the subscript $p = 0$ has been affixed to the left-hand member in order to emphasize that the expression is valid only in the absence of intermolecular forces, that is to say, it is valid only in the limiting case of zero pressure. The first contains the theory of the practical realization of absolute temperature, T . The quantity in brackets on the left of the second expression is what we call "reduced entropy," $s + R \log_e p$ divided by the gas constant R . The third is an expression for "mean isobaric specific heat" $(h - \bar{u})/T$ except that, strictly speaking, the null-point energy \bar{u} should be replaced by the null-point enthalpy \bar{h} which exceeds \bar{u} by a finite, though for our purposes, negligibly small amount. The fourth is an expression for the "instantaneous isobaric specific heat," c_p . The fact that none of Equations [9] is valid at extremely low temperatures, say, below 0.01 $^\circ\text{R}$ does not concern us here.

To illustrate the use of Equations [9], we shall apply them to the case of monatomic hydrogen H^1 at 1000 $^\circ\text{R}$. For H^1 : $M = 1.00813/1.000272$; $p_0 = 2$; $\theta_0 = 0$; all other θ_i being negligibly high at the temperature in question, $\alpha = 2$ and $\beta = \gamma = 0$. We readily compute: $3/2 \log_e M = 0.01173_4$; $5/2 \log_e T = 17.26938_4$; $\log_e \alpha = 0.693147$. Accordingly, for the limiting case of zero pressure

$$\begin{aligned} s/R + \log_e p &= 15.34029_4 \\ (h - \bar{u})/RT &= 2.5 \\ c_p/R &= 2.5 \end{aligned}$$

UNIT OF ENERGY

There has been much discussion of late on the bothersome question of the calorie, which discussion Keenan (89) has summarized in a memorandum to members of the ASME Special Research Committee on Properties of Gases and Gas Mixtures. Prior to 1929, a large number of different kinds of calorie were in use, the circumstances surrounding the development of thermodynamics being intolerably confused thereby. At the First International Steam Tables Conference held in London, England in 1929, the question of removing this confusion was discussed at length, and it was unanimously decided to adopt and promote the use of a single calorie, to be called the International Table calorie (IT cal), defined as 1/860 (mean) international watt-hour. This was the first unit of its kind to have international sanction. The conference which defined it included among its members: Prof. H. L. Callendar, the acknowledged British expert on the properties of steam; several representatives of the German Physikalisch-Technische Reichsanstalt; delegates from Czechoslovakia; and an American delegation including Dr. N. S. Osborne and Dr. H. C. Dickinson, both of the U. S. Bureau of Standards. In all subsequent publications dealing with the thermodynamic properties of steam, from virtually all sources throughout the world, including the U. S. Bureau of Standards, either the International Table calorie or the international electrical unit in terms of which it was defined, was used.

Unfortunately, the efforts of the First International Steam Tables Conference to promote the use of a single calorie have not been entirely successful. In 1930 Dr. E. W. Washburn of the U. S. Bureau of Standards proposed to the Commission on Thermochemistry of the International Union of Chemistry that the Commission agree to use a different calorie defined as 4.1833 international joules in order to preserve as many as possible of the numerical values given in International Critical Tables (90) in terms of a calorie defined as 4.185 absolute joules. This so-called artificial or thermochemical calorie (4.1833 international joules) was officially adopted by the Commission in 1934, and since has become firmly established. Thus, and mainly through lack of foresight, there has been erected an artificial barrier between the engineer on the one side and the thermochemist on the

other. The two calories differ by as much as 1 part in approximately 1500.

Recently steps have been taken to abandon by international agreement the so-called international electrical units and to use instead the absolute or mechanical units. The 1941 Birge (4) value for the ratio between the two units is 1.00020 ± 0.00004 , abs kwhr/(mean) int kwhr. DuMond and Cohen (91, 92) adopt the conversion factor 1.000165 abs kwhr/(NBS) int kwhr as exact by definition. Mueller and Rossini have proposed to redefine the thermochemical calorie as 4.1840 absolute joules, having previously (93) expressed the hope that "in the course of time physical scientists will become more and more familiar with the joule as the unit of energy, thermal and otherwise, and that the arbitrary conversion of joules to artificial (thermochemical) calories will become a chore that will gradually cease to be necessary."

We know of no completely satisfactory way out of the above dilemma but, being engineers, we have decided to adopt for the purpose of this paper a unit of energy called the International Tables Btu (IT Btu), defined by the conversion factors: 1 IT Btu g °K/IT cal lb °R; 860 IT cal/(mean) int whr; 1.00020 ± 0.00004 , abs whr/(mean) int whr. Accordingly, we derive from the 1941 Birge (4) values of the general physical constants

$$R = 1.98581_{11} \pm 0.00018 \text{ IT Btu/}^\circ\text{R mol} \dots \dots [10]$$

where the symbol "mol" denotes the pound-mol on the chemical scale. Thus our calculated values of the reduced entropy $s + R \log p$ (with pressure expressed in international atmospheres), mean isobaric specific heat $(h - \bar{u})/T$, and instantaneous isobaric specific heat c_p for monatomic hydrogen H^1 at 1000°R and, strictly speaking, zero pressure are: 30.46293 , IT Btu/°R mol, 4.964528 IT Btu/°R mol, and 4.964528 IT Btu/°R mol, respectively.

ESTIMATED UNCERTAINTIES

In our calculations and subsequent interpolations we have tried to avoid any approximations that would affect our final results by more than ± 2 in the eighth significant figure; before tabulating these results, however, we have rounded them off to seven significant figures. In this manner we have sought to achieve computational accuracy well beyond present physical accuracy for practical reasons. We wish now to give some indication of the limits of present physical accuracy and, for this purpose, shall compute what we call the estimated uncertainties of our final results.

In our calculations we have used the 1941 Birge (4) best values of the general physical constants consistently throughout. In estimating the uncertainties of our final results, however, we shall use the DuMond-Cohen (92) probable errors augmented by the differences, in absolute value, between the Birge and DuMond-Cohen best values. This procedure will tend to make our estimated uncertainties somewhat too conservative, but we believe it is the best one to use pending the systematic re-evaluation of all the data, which will surely be undertaken when experimental determinations currently under way in various laboratories have been completed.

From Equation [5] we see that the probable error of the quantity g/RT is to be derived in part from the probable errors of the constant $\log_e [k(2\pi k/h^2 N_0)^{3/2}]$, the ratio 1.000272 , the conversion factor $1,013,246$ erg/cm²atm, and the isotopic weight M on the physical scale. We have calculated this constant or "translational" part of the uncertainty of g/RT for each of the isotopic monatomic gases here considered and have found it to lie between ± 0.00066 and ± 0.00069 in all cases.

The temperature function α is the only remaining source of uncertainty in our calculated values of g/RT . It makes what

we may call the "electronic" contribution which arises jointly from the probable error of the second radiation constant c_2 and from those of the observed electronic-energy levels $E_i - E_0$. The corresponding electronic contributions to the uncertainties of the quantities $s/R + \log p$, $(h - \bar{u})/RT$, and c_p/R come from the functions $\log_e \alpha + \beta/\alpha$, β/α , and $\gamma/\alpha - (\beta/\alpha)^2$, respectively, in accordance with Equations [9]. We show these latter electronic uncertainties graphically in Figs. 1, 2, 3. To the electronic uncertainty of the quantity $s/R + \log p$ shown in Fig. 1, there must, of course, be added the constant amount 0.0007 (approximately) representing the translational uncertainty; the translational uncertainties of the quantities $(h - \bar{u})/RT$ and c_p/R are both nil in accordance with Equations [9].

Now we do not tabulate the dimensionless quantities just referred to, but rather the reduced entropy $s + R \log p$, the mean isobaric specific heat $(h - \bar{u})/T$, and the instantaneous isobaric specific heat c_p . To each of these tabulated quantities the relative probable error of the gas constant R contributes an additional uncertainty which we estimate to be 0.0091 per cent of the quantity tabulated. When the International Tables calorie was adopted in 1929, it was anticipated that the time would come when this calorie would have to be redefined in terms of the absolute or mechanical units. A move in this direction has been taken recently. When and if such a redefinition is adopted officially, it will be possible to state a relative probable error in the gas constant R only about one half as large as that just stated, that is, approximately 0.0046 per cent.

Returning to Figs. 1, 2, 3, it will be noticed that these cover only oxygen, carbon, sulphur, bromine, chlorine, fluorine, and iodine. In the cases of hydrogen, deuterium, helium, and argon, the electronic uncertainties are entirely negligible in the temperature range here considered. In the cases of nitrogen and mercury these uncertainties are not entirely negligible but are, nevertheless, too small to warrant complicating the figures to include them.

ISOTOPE EFFECTS

In general, each isotope of a particular atom possesses a slightly different set of electronic energy levels, $E_i - E_0$. It was through an investigation of these slight differences in the case of hydrogen that the existence of deuterium (heavy hydrogen) was first shown. Herzberg (94) states that the differences are only of the order of 2 cm^{-1} and in many cases considerably smaller. Accordingly, we use the same spectroscopic data for each isotope (of a particular atom) and thereby assign to each the same mean isobaric specific heat $(h - \bar{u})/T$, the same instantaneous isobaric specific heat c_p , and, to within an additive constant amount $3/2 R \log_e (M/M_0)$, the same reduced entropy $s + R \log p$. In this expression M_0 denotes the isotopic weight of a particular reference isotope. Thus it suffices to tabulate the thermodynamic properties of only one reference isotope of each monatomic gas if an auxiliary table is provided in which values of the quantity $(3/2) R \log_e (M/M_0)$ are listed. Table 4 is such an auxiliary table.

The reduced entropy $s + R \log p$ of the normal isotopic mixture of a given monatomic gas exceeds that of the reference isotope of isotopic weight M_0 by the constant amount $(3/2) R \sum x_i \log_e (M_i/M_0) - R \sum x_i \log_e x_i$, where the x_i are the fractional abundances (mol fractions) and the M_i are the isotopic weights of the various constituents of the mixture. Slight inaccuracies in the x_i do not appreciably affect the first sum if none of the M_i/M_0 differs much from unity, since in any event the x_i must add up to unity. The "mixing entropy," $-R \sum x_i \log_e x_i$, is, however, quite sensitive to inaccuracies in the x_i , and for this reason is listed separately in Table 4.

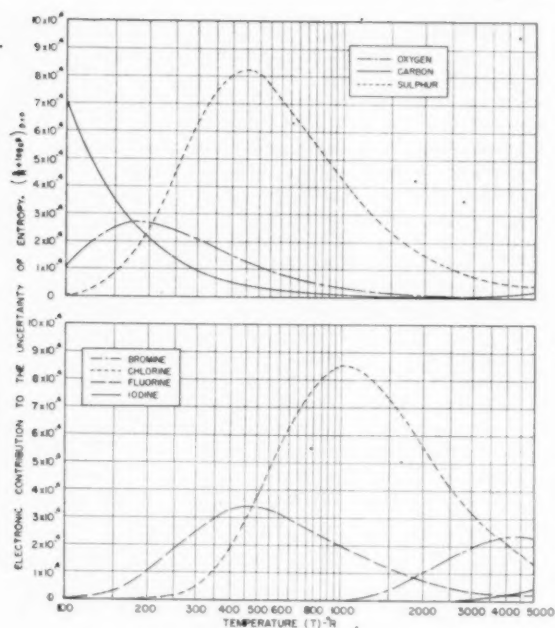


FIG. 1 ELECTRONIC UNCERTAINTY CONTRIBUTION

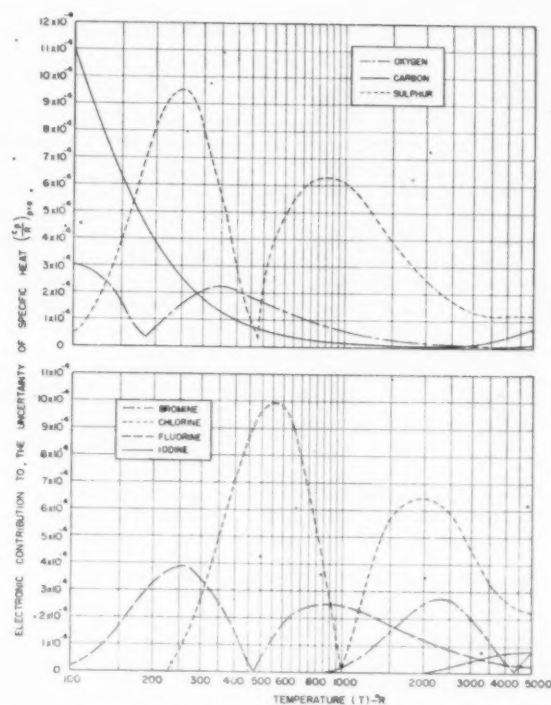


FIG. 3 ELECTRONIC UNCERTAINTY CONTRIBUTION

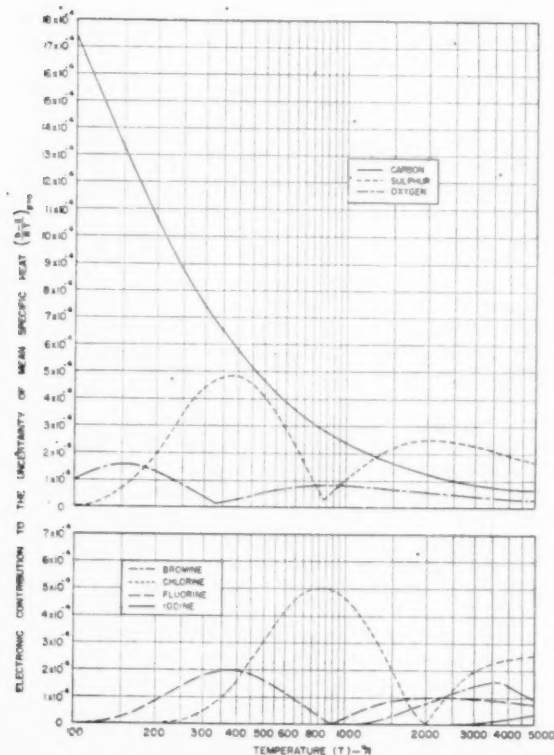


FIG. 2 ELECTRONIC UNCERTAINTY CONTRIBUTION

WORKING TABLES

The working tables here presented require little explanation beyond that already given. The original calculations were carried out with a precision of ± 2 in the eighth significant figure; at 16°R intervals from 100 to 5220°R for hydrogen, helium, and argon; at the intervals shown in parentheses, namely, 76(8)-212(16)388(32)740(64)1580(128)5348°R for the other gases. The calculated values were then interpolated to the intervals, 100(5)130(10)240(20)500(50)1000(100)2000(200)5000°R for tab-

TABLE 4 REDUCED ENTROPY CORRECTIONS
(IT Btu/°R mol)

To get $s + R$ $\log p$ for	Add	Add add mixing entropy	To $s + R$ $\log p$ for
H ¹	+2.06243		H ¹
Mixture	+0.00030	+0.00283	H ¹
He ³	-0.84297		He ⁴
Mixture	0.00000	0.00000	He ⁴
C ¹²	+0.23919		C ¹²
Mixture	+0.02571	+0.11800	C ¹²
N ¹⁴	+0.20488		N ¹⁴
Mixture	+0.00076	+0.04817	N ¹⁴
O ¹⁷	+0.18137		O ¹⁶
O ¹⁸	+0.35165		O ¹⁶
Mixture	+0.00077	+0.03529	O ¹⁶
F ¹⁹	0.0		F ¹⁹
S ³²	+0.09152		S ³²
S ³⁴	+0.18030		S ³²
S ³⁶	+0.35088		S ³²
Mixture	+0.00831	+0.43416	S ³²
Cl ³⁷	+0.16543		Cl ³⁶
Mixture	+0.04070	+1.10791	Cl ³⁶
A ³⁶	-0.31385		A ⁴⁰
A ³⁸	-0.17094		A ⁴⁰
Mixture	-0.00983	+0.05173	A ⁴⁰
Br ⁸¹	+0.07448		Br ⁷⁹
Mixture	+0.03686	+1.38525	Br ⁷⁹
I ¹²⁷	0.0		I ¹²⁷
Hg ¹⁹⁶	-0.06018		Hg ²⁰⁰
Hg ¹⁹⁸	-0.02993		Hg ²⁰⁰
Hg ¹⁹⁹	-0.01493		Hg ²⁰⁰
Hg ²⁰¹	+0.01485		Hg ²⁰⁰
Hg ²⁰²	+0.02963		Hg ²⁰⁰
Hg ²⁰⁴	+0.05911		Hg ²⁰⁰
Mixture	+0.00903	+3.35767	Hg ²⁰⁰

TABLE 5. ISOBARIC SPECIFIC HEAT $c_{p,0}$, FOR SOME SELECTED MONATOMIC GASES (IT Btu/mol °R)

1987

1988

1989

1990

1991

1992

1993

1994

1995

1996

1997

1998

1999

2000

2001

2002

2003

2004

2005

2006

2007

2008

2009

2010

2011

2012

2013

2014

2015

2016

2017

2018

2019

2020

2021

2022

2023

2024

2025

2026

2027

2028

2029

2030

2031

2032

2033

2034

2035

2036

2037

2038

2039

2040

2041

2042

2043

2044

2045

2046

2047

2048

2049

2050

2051

2052

2053

2054

2055

2056

2057

2058

2059

2060

2061

2062

2063

2064

2065

2066

2067

2068

2069

2070

2071

2072

2073

2074

2075

2076

2077

2078

2079

2080

2081

2082

2083

2084

2085

2086

2087

2088

2089

2090

2091

2092

2093

2094

2095

2096

2097

2098

2099

2100

2101

2102

2103

2104

2105

2106

2107

2108

2109

2110

2111

2112

2113

2114

2115

2116

2117

2118

2119

2120

2121

2122

2123

2124

2125

2126

2127

2128

2129

2130

2131

2132

2133

2134

2135

2136

2137

2138

2139

2140

2141

2142

2143

2144

2145

2146

2147

2148

2149

2150

2151

2152

2153

2154

2155

2156

2157

2158

2159

2160

2161

2162

2163

2164

2165

2166

2167

2168

2169

2170

2171

2172

2173

2174

2175

2176

2177

2178

2179

2180

2181

2182

2183

2184

2185

2186

2187

2188

2189

2190

2191

2192

2193

2194

2195

2196

2197

2198

2199

2200

2201

2202

2203

2204

2205

2206

2207

2208

2209

2210

2211

2212

2213

2214

2215

2216

2217

2218

2219

2220

2221

2222

2223

2224

2225

2226

2227

2228

2229

2230

2231

2232

2233

2234

2235

2236

2237

2238

2239

2240

2241

2242

2243

2244

2245

2246

2247

2248

2249

2250

2251

2252

2253

2254

2255

2256

2257

2258

2259

2260

2261

2262

2263

2264

2265

2266

2267

2268

2269

2270

2271

2272

2273

2274

2275

2276

2277

2278

2279

2280

2281

2282

2283

2284

2285

2286

2287

2288

2289

2290

2291

2292

2293

2294

2295

2296

2297

2298

2299

2300

2301

2302

2303

2304

2305

2306

2307

2308

2309

2310

2311

2312

2313

2314

2315

2316

2317

2318

2319

2320

2321

2322

2323

2324

2325

2326

2327

2328

2329

2330

2331

2332

2333

2334

2335

2336

2337

2338

2339

2340

2341

2342

2343

2344

2345

2346

2347

2348

2349

2350

2351

2352

2353

2354

2355

2356

2357

2358

2359

2360

2361

2362

2363

2364

2365

2366

2367

2368

2369

2370

2371

2372

2373

2374

2375

2376

2377

2378

2379

2380

2381

2382

2383

2384

2385

2386

2387

2388

2389

2390

2391

2392

2393

2394

2395

2396

2397

2398

2399

2400

2401

2402

2403

2404

2405

2406

2407

2408

2409

2410

2411

2412

2413

2414

2415

2416

2417

2418

2419

2420

2421

2422

2423

2424

2425

2426

2427

2428

2429

2430

2431

2432

2433

2434

2435

2436

2437

2438

TABLE 7 REDUCED ENTROPY $(s^* + R \log p)_{\text{calc}}$ FOR SOME SELECTED MONATOMIC GASES (IT Btu/mol °R)

1999
 1997
 1995
 1993
 1991
 1989
 1987
 1985
 1983
 1981
 1979
 1977
 1975
 1973
 1971
 1969
 1967
 1965
 1963
 1961
 1959
 1957
 1955
 1953
 1951
 1949
 1947
 1945
 1943
 1941
 1939
 1937
 1935
 1933
 1931
 1929
 1927
 1925
 1923
 1921
 1919
 1917
 1915
 1913
 1911
 1909
 1907
 1905
 1903
 1901
 1899
 1897
 1895
 1893
 1891
 1889
 1887
 1885
 1883
 1881
 1879
 1877
 1875
 1873
 1871
 1869
 1867
 1865
 1863
 1861
 1859
 1857
 1855
 1853
 1851
 1849
 1847
 1845
 1843
 1841
 1839
 1837
 1835
 1833
 1831
 1829
 1827
 1825
 1823
 1821
 1819
 1817
 1815
 1813
 1811
 1809
 1807
 1805
 1803
 1801
 1799
 1797
 1795
 1793
 1791
 1789
 1787
 1785
 1783
 1781
 1779
 1777
 1775
 1773
 1771
 1769
 1767
 1765
 1763
 1761
 1759
 1757
 1755
 1753
 1751
 1749
 1747
 1745
 1743
 1741
 1739
 1737
 1735
 1733
 1731
 1729
 1727
 1725
 1723
 1721
 1719
 1717
 1715
 1713
 1711
 1709
 1707
 1705
 1703
 1701
 1699
 1697
 1695
 1693
 1691
 1689
 1687
 1685
 1683
 1681
 1679
 1677
 1675
 1673
 1671
 1669
 1667
 1665
 1663
 1661
 1659
 1657
 1655
 1653
 1651
 1649
 1647
 1645
 1643
 1641
 1639
 1637
 1635
 1633
 1631
 1629
 1627
 1625
 1623
 1621
 1619
 1617
 1615
 1613
 1611
 1609
 1607
 1605
 1603
 1601
 1599
 1597
 1595
 1593
 1591
 1589
 1587
 1585
 1583
 1581
 1579
 1577
 1575
 1573
 1571
 1569
 1567
 1565
 1563
 1561
 1559
 1557
 1555
 1553
 1551
 1549
 1547
 1545
 1543
 1541
 1539
 1537
 1535
 1533
 1531
 1529
 1527
 1525
 1523
 1521
 1519
 1517
 1515
 1513
 1511
 1509
 1507
 1505
 1503
 1501
 1499
 1497
 1495
 1493
 1491
 1489
 1487
 1485
 1483
 1481
 1479
 1477
 1475
 1473
 1471
 1469
 1467
 1465
 1463
 1461
 1459
 1457
 1455
 1453
 1451
 1449
 1447
 1445
 1443
 1441
 1439
 1437
 1435
 1433
 1431
 1429
 1427
 1425
 1423
 1421
 1419
 1417
 1415
 1413
 1411
 1409
 1407
 1405
 1403
 1401
 1399
 1397
 1395
 1393
 1391
 1389
 1387
 1385
 1383
 1381
 1379
 1377
 1375
 1373
 1371
 1369
 1367
 1365
 1363
 1361
 1359
 1357
 1355
 1353
 1351
 1349
 1347
 1345
 1343
 1341
 1339
 1337
 1335
 1333
 1331
 1329
 1327
 1325
 1323
 1321
 1319
 1317
 1315
 1313
 1311
 1309
 1307
 1305
 1303
 1301
 1299
 1297
 1295
 1293
 1291
 1289
 1287
 1285
 1283
 1281
 1279
 1277
 1275
 1273
 1271
 1269
 1267
 1265
 1263
 1261
 1259
 1257
 1255
 1253
 1251
 1249
 1247
 1245
 1243
 1241
 1239
 1237
 1235
 1233
 1231
 1229
 1227
 1225
 1223
 1221
 1219
 1217
 1215
 1213
 1211
 1209
 1207
 1205
 1203
 1201
 1199
 1197
 1195
 1193
 1191
 1189
 1187
 1185
 1183
 1181
 1179
 1177
 1175
 1173
 1171
 1169
 1167
 1165
 1163
 1161
 1159
 1157
 1155
 1153
 1151
 1149
 1147
 1145
 1143
 1141
 1139
 1137
 1135
 1133
 1131
 1129
 1127
 1125
 1123
 1121
 1119
 1117
 1115
 1113
 1111
 1109
 1107
 1105
 1103
 1101
 1099
 1097
 1095
 1093
 1091

TABLE 8. ENTHALPY ($h - u$) _{$P=0$} FOR SOME SELECTED MONATOMIC GASES (IT° BRU/mol)[illegible]

ulation. Before final tabulation, however, they were rounded off to seven significant figures.

Table 5 lists values of isobaric specific heat c_p for all isotopic gases considered; Table 6 lists values of mean isobaric specific heat $(h - \bar{u})/T$; Table 7 lists values of reduced entropy $s + R \log_e p$ (with pressure expressed in international atmospheres); Table 8 lists values of enthalpy $h - \bar{u}$ for all isotopic gases considered. Strictly speaking, the data listed in these tables are valid only in the limiting case of zero pressure where the effects of intermolecular forces vanish. The unit of energy is the International Tables Btu (IT Btu) in terms of which the universal gas constant takes the value $R = 1.98581$, IT Btu/°R mol, the symbol "mol" being understood to denote the "pound-mol" on the chemical scale.

COMPARISON WITH OTHER DATA

The principles and procedures for calculating zero-pressure thermodynamic properties from spectroscopic and other data by the methods of quantum statistical mechanics have been well understood for some time. It appears, nevertheless, that only six papers of any consequence dealing with the zero-pressure thermodynamic properties of the monatomic gases here considered have hitherto been published. The only tables previously available are (a) various skeleton tables giving values of free enthalpy—actually the quantity $(g - \bar{u})/T - R \log_e p$ —for the monatomic gases, hydrogen, nitrogen, oxygen, sulphur, chlorine, and iodine; (b) the familiar skeleton tables of the U. S. Bureau of Standards (95) for hydrogen, carbon, nitrogen, and oxygen; (c) a skeleton table of reduced free enthalpy for carbon (96) at intervals of 1000° K from 2000 to 6000° K. Except in the Bureau of Standards table (95), the published data have been based on the now obsolete values of the general physical constants and atomic weights given in International Critical Tables (90) and, in some cases, on obsolete spectroscopic data.

In Table 9 we compare our results with those of previous authors. The data in this table are values of the quantity $(g - \bar{u})/T - R \log_e p$ or $(h - \bar{u})/T - (s + R \log_e p)$ for some normal isotopic mixtures, mixing entropy excluded in accordance with the practice followed by previous authors. Before listing the data of previous authors in Table 9, we have corrected them to the value of the gas constant R used in this paper, in order to make them comparable with our data. The comparison shows that most of the discrepancies between our values and those of previous authors can be ascribed to the use of different values of the general physical constants. Only in a few cases have recent changes in spectroscopic data produced significant changes in the thermodynamic properties. It is especially interesting to note that the agreement between our values and those of the Bureau of Standards (95) is quite good except in the case of carbon.

ACKNOWLEDGMENT

It is a pleasure to acknowledge the generous support and active co-operation of the Navy Department, Bureau of Ships, and Office of Naval Research, in sponsoring our work through our University of Pennsylvania Thermodynamics Research Laboratory. We wish especially to thank Dr. G. Herzberg of the National Research Council of Canada, a member of our Laboratory's Advisory Committee, for his very valuable suggestions and criticisms, not only on the subject of atomic spectra but on the work of this project as a whole. We wish also to thank Miss Helen Tulloch, Miss Eleanor Smith, and Mrs. Jean Okada of the Laboratory's computing staff, for their painstaking efforts to achieve computational accuracy in the results presented in this paper.

BIBLIOGRAPHY

- 1 "Thermodynamics of Gas Mixtures," by J. A. Goff—a lecture delivered at the Brown University Course of Advanced Instruction in Research in Mechanics during the summer of 1945, Brown University, Providence, R. I., 1945.
- 2 "Infrared and Raman Spectra of Polyatomic Molecules," by G. Herzberg, D. Van Nostrand Company, Inc., New York, N. Y., 1945, pp. 501-530.
- 3 "Molecular Constants From Spectroscopic Data," by G. Herzberg, *Trans. ASME*, vol. 70, 1948, pp. 623-624.
- 4 "A New Table of Values of the General Physical Constants," by R. T. Birge, *Reviews of Modern Physics*, vol. 13, 1941, pp. 233-239.
- 5 "Our Knowledge of the Atomic Constants F , N , m , h in 1947 and of Other Constants Derivable Therefrom," by J. W. M. DuMond and E. R. Cohen, *Reviews of Modern Physics*, vol. 20, 1948, pp. 82-108.
- 6 "Erratum: Our Knowledge of the Atomic Constants F , N , m , h in 1947 and of Other Constants Derivable Therefrom," by J. W. M. DuMond and E. R. Cohen, received April 23, 1949.
- 7 "The $C^{12}H_2-N^{14}$ Mass Difference," by E. B. Jordan, *Physical Review*, vol. 58, 1940, pp. 1009-1010.
- 8 "The Mass Differences of the Fundamental Doublets Used in the Determination of the Isotopic Weights of C^{12} and N^{14} ," by E. B. Jordan, *Physical Review*, vol. 60, 1941, pp. 710-713.
- 9 "Nuclear Physics. C. Nuclear Dynamics, Experimental," by M. S. Livingston and H. A. Bethe, *Reviews of Modern Physics*, vol. 9, 1937, pp. 245-390.
- 10 "Nuclear Physics Tables and an Introduction to Nuclear Physics," by J. Mattauch and S. Flügge, 1942; translated by E. P. Gross and S. Bargman, Interscience Publishers, Inc., New York, N. Y., 1946.
- 11 "Isotopenbericht 1942," by S. Flügge and J. Mattauch, *Physikalische Zeitschrift*, vol. 44, 1943, pp. 181-201; *ibid.*, p. 391.
- 12 "Mass Spectra and Isotopes," by F. W. Aston, second edition, Longmans, Green and Co., New York, N. Y., 1942.
- 13 "Least Squares Fit of the Fundamental Mass Doublets," by E. R. Cohen and W. F. Hornyak, *Physical Review*, vol. 72, 1947, p. 1127.
- 14 "Isotopic Weights of the Fundamental Isotopes," by K. T. Bainbridge, National Research Council, Division of Mathematical and Physical Sciences, Nuclear Science Series, Preliminary Report No. 1, June, 1948.

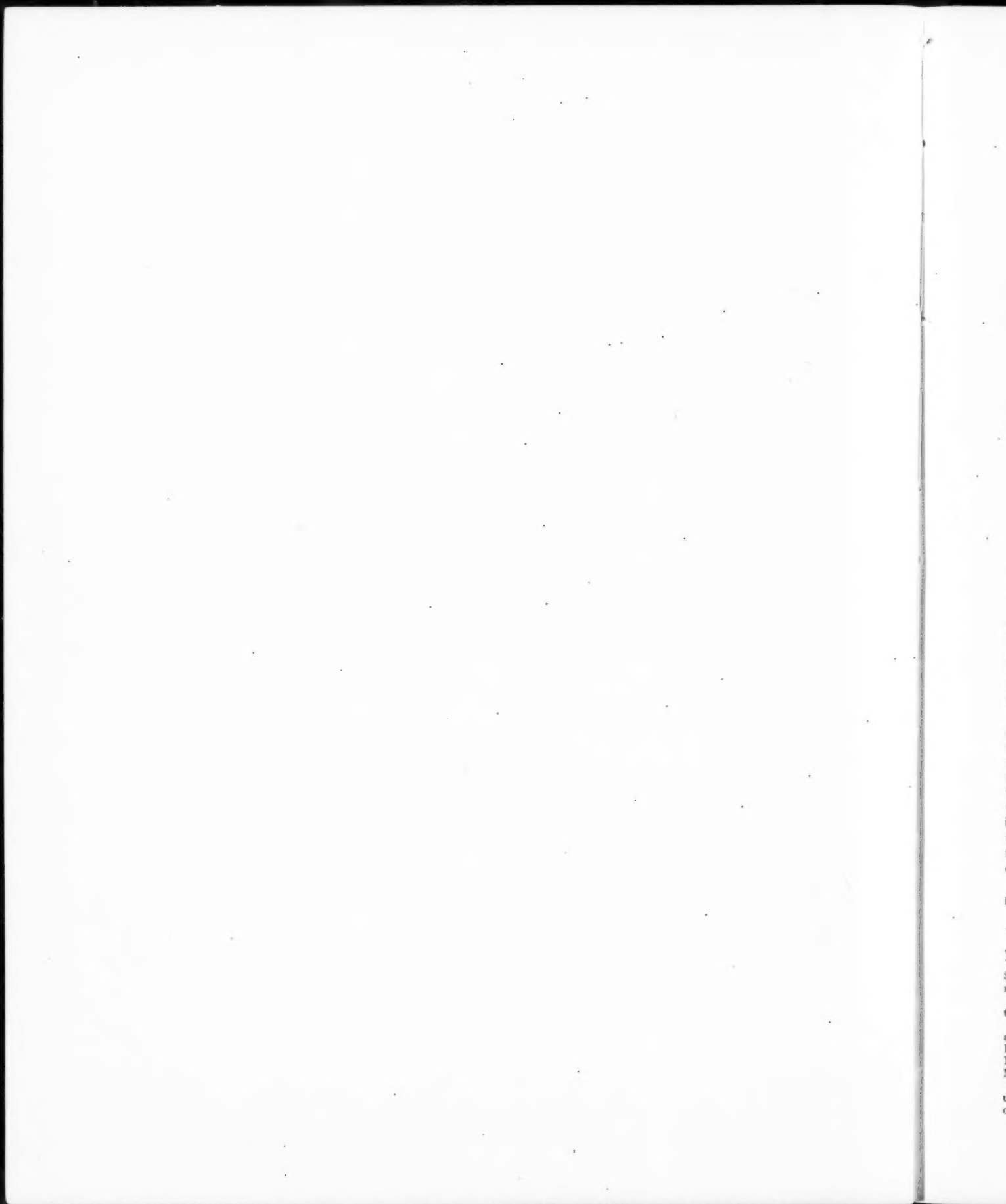
TABLE 9 COMPARISON WITH OTHER DATA

		The function $(g - \bar{u})/T - R \log_e p$ for some normal isotopic mixtures (IT Btu/°R mol; mixing entropy excluded)				
Gas	Reference	900°R	1800°R	2700°R	3600°R	4500°R
Hydrogen...	(97)	-24.995	-28.436	-30.449	-31.878	-32.985
	(95)	-24.976	-28.416	-30.430	-31.858	-32.966
	GGV*	-24.97564	-28.41079	-30.42973	-31.85794	-32.96574
Carbon.....	(95)	-35.183	-38.703	-40.744	-42.186	-43.304
	GGV	-35.19919	-38.72347	-40.76443	-42.20733	-43.32600
	(98)	-34.205	-37.646	-39.659	-41.087	-42.196
Nitrogen....	(95)	-34.191	-37.632	-39.646	-41.074	-42.181
	GGV	-34.19104	-37.63219	-39.64514	-41.07341	-42.18208
	(99)	-35.832	-39.448	-41.526	-42.988	-44.117
Oxygen.....	(95)	-35.815	-39.433	-41.510	-42.972	-44.102
	GGV	-35.81491	-39.43201	-41.51032	-42.97253	-44.10127
	(100)	-37.526	-41.261	-43.407	-44.909	-46.064
Sulphur....	GGV	-37.51143	-41.24726	-43.39345	-44.89719	-46.05637
	(101)	-37.050	-40.663	-42.813	-44.322	-45.485
	GGV	-37.04437	-40.65989	-42.79753	-44.30648	-45.46968
Iodine.....	(102)	-40.772	-44.213	-46.225
	GGV	-40.75596	-44.19712	-46.21073

* The initials GGV (Goff, Gratch, Van Voorhis) refer to this paper.

- 15 "Determination of Masses of Atoms by Mass Spectra," by T. Okuda, *Bulletin of the Institute of Physical and Chemical Research* (Tokyo), vol. 21, 1942, pp. 1-17. (see *Chemical Abstracts*, vol. 41, 1947, p. 5389f)
- 16 "Isotopic Weights of Sulfur and Titanium," by T. Okuda and K. Ogata, *Proceedings of the Physico-Mathematical Society of Japan*, vol. 25, 1943, pp. 374-375. (see *Chemical Abstracts*, vol. 41, 1947, p. 6142g)
- 17 "Preliminary Report on the Mass of ^{12}C and ^{14}N ," by T. Asada, T. Okuda, K. Ogata, and S. Yoshimoto, *Nature*, vol. 143, 1939, p. 797.
- 18 "On the Isotopic Weights of Chlorine, Argon, and Iron by the Doublet Method," by T. Okuda, K. Ogata, K. Aoki, and Y. Sugawara, *Physical Review*, vol. 58, 1940, pp. 578-579.
- 19 "On the Isotopic Weight of C^{12} ," by K. Ogata, *Proceedings of the Physico-Mathematical Society of Japan*, series 3, vol. 22, 1940, pp. 486-491.
- 20 "On the Isotopic Weights of Carbon and Nitrogen by the Doublet Method," by T. Asada, T. Okuda, K. Ogata, and S. Yoshimoto, *Proceedings of the Physico-Mathematical Society of Japan*, (3) vol. 22, 1940, pp. 41-45.
- 21 "Isotopic Weights of Ni Isotopes by the Doublet Method," by T. Okuda, K. Ogata, H. Kuroda, S. Shima, and S. Shindo, *Physical Review*, vol. 59, 1941, p. 104.
- 22 "Isotopic Weights of Sulfur and Titanium," by T. Okuda and K. Ogata, *Physical Review*, vol. 60, 1941, p. 690.
- 23 "Sur les Masses de C^{12} et C^{13} ," by A. Gibert, F. Roggen, and J. Rossel, *Portugaliae Physica*, vol. 1, 1944, pp. 43-46.
- 24 "New Data on Isotopes. Isotopic Weights by the Doublet Method," by F. W. Aston, *Nature*, vol. 137, 1936, p. 613.
- 25 "Isotopic Weights by the Doublet Method," by F. W. Aston, *Nature*, vol. 138, 1936, p. 1094.
- 26 "Isotopic Weight of ^{12}C ," by F. W. Aston, *Nature*, vol. 139, 1937, p. 922.
- 27 "Die Substandards in der Massenspektrographie," by J. Mattauch, *Zeitschrift für technische Physik*, vol. 19, 1938, pp. 578-582.
- 28 "Discussion on the Isotopic Weight of C^{12} ," by J. Mattauch, *Physical Review*, vol. 57, 1940, pp. 1155-1159.
- 29 "Packing Fractions of Bromine, Chromium, Nickel, and Titanium," by F. W. Aston, *Nature*, vol. 141, 1938, p. 1096.
- 30 "Masses of Some Light Atoms Measured by Means of New Mass Spectrograph," by F. W. Aston, *Nature*, vol. 137, 1936, pp. 357-358.
- 31 "Packing Fractions of Krypton and Xenon," by F. W. Aston, *Nature*, vol. 140, 1937, p. 149.
- 32 "A New Mass Spectrograph and the Whole Number Rule," by F. W. Aston, *Proceedings of the Royal Society of London*, series A, vol. 115, 1927, pp. 487-514.
- 33 "A Second-Order Focusing Mass Spectrograph and Isotopic Weights by the Doublet Method," by F. W. Aston, *Proceedings of the Royal Society of London*, series A, vol. 163, 1937, pp. 391-404.
- 34 "Fifth Report of the Committee on Atoms of the International Union of Chemistry," by F. W. Aston, N. Boer, O. Hahn, W. D. Harkins, F. Jolot, R. S. Mulliken, and M. L. Oliphant, *Journal of the Chemical Society*, London, 1940, pp. 1416-1417.
- 35 "Thirteenth Report of the Committee on Atomic Weights of the International Union of Chemistry," by G. P. Baxter, M. Guichard, and R. Whytlaw-Gray, *Journal of the American Chemical Society*, vol. 69, 1947, pp. 731-736.
- 36 "Eine Neukonstruktion des Mattauch-Herzog'schen doppel-fokussierenden Massenspektrographen. Die Massen von ^{12}C und ^{14}N ," by H. Ewald, *Zeitschrift für Naturforschung*, vol. 1, 1946, pp. 131-136.
- 37 "Massenspektroskopische Atomgewichtbestimmungen," by H. Ewald, *FIAT Rev. German Sci.*, 1939-1946, Inorg. Chem. Part I, 1948, pp. 12-25.
- 38 "Table of Isotopes," by G. T. Seaborg and I. Perlman, *Reviews of Modern Physics*, vol. 20, 1948, pp. 585-667.
- 39 "The Natural Abundances of the Oxygen Isotopes," by H. G. Thode and H. R. Smith, National Research Council of Canada, Atomic Energy Project Report MX-129, April, 1945.
- 40 "Oxygen Isotopes in Nature and in the Laboratory," by H. C. Urey, *Science*, vol. 108, 1948, pp. 489-496.
- 41 "The Abundance of He^3 in Atmosphere and Well Helium," by L. T. Aldrich and A. O. Nier, *Physical Review*, vol. 70, 1946, pp. 983-984.
- 42 "The Concentration of He^3 in the Liquid and Vapor Phases of He^4 ," by H. A. Fairbank, C. T. Lane, L. T. Aldrich, and A. O. Nier, *Physical Review*, vol. 71, 1947, pp. 911-913.
- 43 "The Isotopic Constitution of Calcium, Titanium, Sulfur, and Argon," by A. O. Nier, *Physical Review*, vol. 53, 1938, pp. 282-286.
- 44 "Mass-Spectrometer Study of the Rare Gases," by V. H. Dibeler, F. L. Mohler, and R. M. Reese, *Journal of Research of the National Bureau of Standards*, vol. 38, 1947, pp. 617-620, Research Paper RP1799.
- 45 "A Mass-Spectrographic Study of the Isotopes of Argon, Potassium, Rubidium, Zinc, and Cadmium," by A. O. Nier, *Physical Review*, vol. 50, 1936, pp. 1041-1045.
- 46 "Isotopic Constitution of Tellurium, Silicon, Tungsten, Molybdenum, and Bromine," by D. Williams and P. Yuster, *Physical Review*, vol. 69, 1946, pp. 556-567.
- 47 "Natural Abundance of Isotopes of Stable Elements," by J. R. White and A. E. Cameron, *Physical Review*, vol. 74, 1948, pp. 991-1000.
- 48 "Atomic Energy States," by R. F. Bacher and S. Goudsmit, McGraw-Hill Book Co., New York, N. Y., 1932.
- 49 "The Coupling of p -Electron Configurations," by H. A. Robinson and G. H. Shortley, *Physical Review*, vol. 52, 1937, pp. 713-723.
- 50 "Atomic Spectra," by A. G. Shenstone, *Reports on Progress in Physics*, Physical Society of London, England, vol. 5, 1938, pp. 210-227.
- 51 "A Multiplet Table of Astrophysical Interest," by C. E. Moore, Princeton University Observatory, Princeton, N. J., 1945.
- 52 "Spectroscopy, Past, Present, and Future," by W. F. Meggers, *Journal of the Optical Society of America*, vol. 36, 1946, pp. 431-448.
- 53 "Atomic Energy Levels as Derived From the Analyses of Optical Spectra," by C. E. Moore, Circular of the National Bureau of Standards 467, vol. 1, sec. 1, 1948.
- 54 "Wellenlängen und Termsysteme zu den Atomspektren der Elemente Lithium, Beryllium, Bor, Kohlenstoff, Stickstoff, und Sauerstoff," by B. Edlén, *Nova Acta Regiae Societatis Scientiarum Upsalienis*, series IV, vol. 9, No. 6, 1934, pp. 1-153.
- 55 "The s State of Carbon," by A. G. Shenstone, *Physical Review*, vol. 72, 1947, pp. 411-414.
- 56 "The Fine Structure of the Triplet $(2s^2)(2p)(3s)^2P \rightarrow (2s^2)(2p)^2P$ of the Carbon Atom," by V. M. Chulanovskii and M. P. Mokhnatkin, *Comptes rendus de l'Académie des sciences de l'URSS (N.S.)*, vol. 2, 1934, pp. 18-19.
- 57 "Das Bogenspektrum von Stickstoff," by E. Ekefors, *Zeitschrift für Physik*, vol. 63, 1930, pp. 437-443.
- 58 "Die Feinstruktur des metastabilen $\text{D}_{3/2,3/2}$ -Terms des Stickstoffatoms," by W. Tschulanovsky, *Zeitschrift für Physik*, vol. 82, 1933, pp. 134-145.
- 59 "The Metastable D -Level of the Nitrogen Atom," by H. Stücklen and E. P. Carr, *Physical Review*, vol. 43, 1933, pp. 944-945.
- 60 "The Fine Structure of the Metastable Levels of Nitrogen," by B. Stepanov, *Physikalische Zeitschrift der Sowjetunion*, vol. 8, 1935, pp. 352-353.
- 61 "The Arc Spectrum of Nitrogen (N I). Part II-A. Extreme Ultraviolet Region," by M. Kamiyama, *Scientific Papers of the Institute of Physical and Chemical Research*, Tokyo, Japan, vol. 36, 1939, pp. 375-384.
- 62 "The Arc Spectrum of Nitrogen (N I). Part I. Historical, and Part IIB. Near-Infra-Red Region," by M. Kamiyama and T. Sugiura, *Scientific Papers of the Institute of Physical and Chemical Research*, Tokyo, Japan, vol. 37, 1940, pp. 479-487.
- 63 "The Arc Spectrum of Nitrogen (N I). Part III. The Intermediate Region," by M. Kamiyama and H. Noguchi, *Scientific Papers of the Institute of Physical and Chemical Research*, Tokyo, Japan, vol. 39, 1942, pp. 475-483.
- 64 "The Arc Spectrum of Oxygen, O I," by Bengt Edlén, *Kungliga Svenska Vetenskapsakademiens Handlingar*, series III, vol. 20, No. 10, 1943, 31 pp.
- 65 "Beitrag zu den Spektren F III, F II, und F I," by B. Edlén, *Zeitschrift für Physik*, vol. 93, 1934, pp. 433-449.
- 66 "The Spectrum of Fluorine (F I) Part II," by H. Dingle, *Proceedings of the Royal Society of London*, series A, vol. 117, 1927, pp. 407-416.
- 67 "Series Spectra of Boron, Carbon, Nitrogen, Oxygen, and Fluorine," by I. S. Bowen, *Physical Review*, vol. 29, 1927, pp. 231-247.
- 68 "Wave-Length Measurements and New Energy Levels in the Arc Spectrum of Fluorine, F I," by K. Lidén, *Arkiv för Matematik, Astronomi och Fysik*, vol. 35A, No. 24, 1948, 13 pp.
- 69 "Series Spectra in Oxygen and Sulfur," by J. J. Popfield, *Nature*, vol. 112, 1923, pp. 437-438.
- 70 "Beitrag zur Kenntnis des Sauerstoff- und Schwefelspektrums," by E. Bungartz, *Annalen der Physik*, series 4, vol. 76, 1925, pp. 709-728.
- 71 "PP' Groups in the Elements S(I) to K(IV)," by J. J. Hopfield and G. H. Dieke, *Physical Review*, vol. 27, 1926, p. 638.

- 72 "Zum Bogenspektrum des Schwefels," by R. Frerichs, *Zeitschrift für Physik*, vol. 80, 1933, pp. 150-160.
- 73 "Zur Kenntnis des Schwefel-Bogenspektrums," by K. W. Meissner, O. Bartelt, and L. Eckstein, *Zeitschrift für Physik*, vol. 86, 1933, pp. 54-81.
- 74 "The Arc Spectrum of Sulfur in the Ultraviolet," by J. E. Ruedy, *Physical Review*, vol. 43, 1933, p. 1045.
- 75 "The Arc Spectrum of Sulfur in the Ultraviolet," by J. E. Ruedy, *Physical Review*, vol. 44, 1933, pp. 757-760.
- 76 "Forbidden Lines," by I. S. Bowen, *Reviews of Modern Physics*, vol. 8, 1936, pp. 55-81.
- 77 "On s^2p^4 S and sp^5 P in the S I Isoelectronic Sequence," by B. Edlén, *Physical Review*, vol. 62, 1942, pp. 434-437.
- 78 "A New Description and Analysis of the Arc Spectrum of Chlorine," by C. C. Kiess, *Journal of Research of the National Bureau of Standards*, vol. 10, 1933, pp. 827-839, Research Paper RP570.
- 79 "The Arc Spectra of Iodine, Bromine, and Chlorine in the Schumann Region," by L. A. Turner, *Physical Review*, vol. 27, 1926, pp. 397-406.
- 80 "Atomic Spectra and Atomic Structure," by G. Herzberg, Dover Publications, New York, N. Y., 1944, pp. 146-147.
- 81 "The Arc Spectrum of Bromine and Its Structure," by C. C. Kiess and T. L. de Bruin, *Journal of Research of the National Bureau of Standards*, vol. 4, 1930, pp. 667-692.
- 82 "Ueber die Spektren J II, J I, und Cl II," by K. Murakawa, *Zeitschrift für Physik*, vol. 109, 1938, pp. 162-174.
- 83 "The Arc Spectrum of Iodine," by S. F. Evans, *Proceedings of the Royal Society of London, England, series A*, vol. 133, 1931, pp. 417-430.
- 84 "New Lines in the Ultraviolet Spectrum of Atomic Iodine," by J. H. McLeod, *Physical Review*, vol. 49, 1936, pp. 804-807.
- 85 "Ueber die Hochfrequenz- (Kurzwellen-) Anregung einiger Spektren in fernen Ultraviolet," by M. Hellerman, *Zeitschrift für Physik*, vol. 104, 1937, pp. 417-429.
- 86 "The New Lines ($1s-2p_{1,2}$) of Zinc, Cadmium, and Mercury," by M. Fukuda, *Scientific Papers of the Institute of Physical and Chemical Research*, Tokyo, Japan, vol. 4, 1926, pp. 171-175.
- 87 "A Determination of the Wave Lengths (International System) for the Arc and Spark Spectrum of Mercury," by H. Stiles, *Astrophysical Journal*, vol. 30, 1909, pp. 48-61.
- 88 "The Excitation of Forbidden Spectral Lines," by P. D. Foote, T. Takamine, and R. L. Chenault, *Physical Review*, vol. 26, 1925, pp. 165-175.
- 89 "Memorandum on the Definition of the Calorie," by J. H. Keenan, an unpublished memorandum sent in April, 1949, to members of the ASME Special Research Committee on properties of Gases and Gas Mixtures.
- 90 "International Critical Tables," National Research Council, McGraw-Hill Book Company, Inc., New York, N. Y., vol. 1, 1926, p. 16 ff.
- 91 "Our Knowledge of the Atomic Constants F,N,m,h in 1947 and of Other Constants Derivable Therefrom," by J. W. M. DuMond and E. R. Cohen, *Reviews of Modern Physics*, vol. 20, 1948, pp. 82-108.
- 92 "Erratum: Our Knowledge of the Atomic Constants F,N,m,h in 1947 and of Other Constants Derivable Therefrom," by J. W. M. DuMond and E. R. Cohen, received April 23, 1949.
- 93 "The Calory and the Joule in Thermodynamics and Thermochemistry," by E. F. Mueller and F. D. Rossini, *American Journal of Physics*, vol. 12, 1944, pp. 1-7.
- 94 "Atomic Spectra and Atomic Structure," by G. Herzberg, Dover Publications, New York, N. Y., 1944, pp. 182-185.
- 95 "Selected Values of Properties of Hydrocarbons," by F. D. Rossini, K. S. Pitzer, W. J. Taylor, J. P. Ebert, J. E. Kilpatrick, C. W. Beckett, M. G. Williams, and H. G. Werner, Circular of the National Bureau of Standards C461, November, 1947, pp. 173, 191, 209, 227, and 280.
- 96 "The Free Energy of Diatomic Carbon Vapor," by A. R. Gordon, *Journal of Chemical Physics*, vol. 5, 1937, pp. 350-352.
- 97 "The Entropy of Hydrogen and the Third Law of Thermodynamics. The Free Energy and Dissociation of Hydrogen," by W. F. Giauque, *Journal of the American Chemical Society*, vol. 52, 1930, pp. 4816-4831.
- 98 "The Heat Capacity and Entropy of Nitrogen. Heat of Vaporization. Vapor Pressures of Solid and Liquid. The Reaction $\frac{1}{2}N_2 + \frac{1}{2}O_2 = NO$ From Spectroscopic Data," by W. F. Giauque and J. O. Clayton, *Journal of the American Chemical Society*, vol. 55, 1933, pp. 4875-4889.
- 99 "The Dissociation of Oxygen to 5000°K. The Free Energy of Atomic Oxygen," by H. L. Johnston and M. K. Walker, *Journal of the American Chemical Society*, vol. 55, 1933, pp. 187-193.
- 100 "The Free Energy of Sulfur Monoxide and the Dissociation Constants of S_2 ," by G. W. Montgomery and L. S. Kassel, *Journal of Chemical Physics*, vol. 2, 1934, pp. 417-418.
- 101 "The Hydrogen, Chlorine, Hydrogen Chloride Equilibrium at High Temperatures," by W. F. Giauque and R. Overstreet, *Journal of the American Chemical Society*, vol. 54, 1932, pp. 1731-1744.
- 102 "The Free Energy of Iodine and Hydrogen Iodide From Spectroscopic Data," by G. M. Murphy, *Journal of Chemical Physics*, vol. 4, 1936, pp. 344-350.



Zero-Pressure Thermodynamic Properties of Carbon Monoxide and Nitrogen

By J. A. GOFF¹ AND SERGE GRATCH,² PHILADELPHIA, PA.

In this report are presented tables of the principal thermodynamic properties of carbon monoxide and of nitrogen along the zero-pressure isobar in the range 100 to 5000 deg R at the intervals indicated by the numbers in parentheses as follows: 100[5]130[10]240[20]500[50]1000-[100]2000[200]5000. The data have been computed by the method of quantum statistical mechanics in the University of Pennsylvania Thermodynamics Research Laboratory under Project G-3. Computational accuracy well beyond present physical accuracy has been maintained for practical reasons. It is believed that the tables given herein should supersede all previous ones. The calculated values are in satisfactory agreement with those obtained from calorimetric and acoustic velocity measurements.

INTRODUCTION AND THEORY

THIS is the third of a series of reports on the calculation of thermodynamic properties of gases along the zero-pressure isobar by the methods of quantum statistical mechanics. These calculations were carried out at the University of Pennsylvania Thermodynamics Research Laboratory under the sponsorship of the United States Navy, Bureau of Ships, as an essential part of an extensive program for the determination of the thermodynamic properties of some technically important gases. The general aims of this program and the theoretical basis for the calculations have been outlined in the first two reports (1, 2).³ Only as much of the theory will be reviewed in the present report as is necessary for an understanding of the special results obtained in the case of carbon monoxide and nitrogen.

The spectroscopic data are usually expressed by an equation giving wave number E (cm^{-1}) as a function of certain quantum numbers which independently can take on all non-negative integral values within prescribed limits; the constants appearing in this equation are called spectroscopic constants. To each wave number E_i there is assigned a definite energy $\epsilon_i = hcE_i$, where h denotes Planck's constant, and c the velocity of light in vacuo. To each set of values of the various quantum numbers there corresponds a distinct quantum state; but there may be more than one, say, p_i distinct quantum states having the same energy ϵ_i in the absence of an external electric or magnetic field.

The first step in the calculation is to form the state sum or partition function Q defined by

$$Q = \sum p_i e^{-\epsilon_i/kT} = \sum p_i e^{-\epsilon_i/\tau} \dots [1]$$

¹ Dean, Towne Scientific School; Director, University of Pennsylvania Thermodynamics Research Laboratory. Mem. ASME.

² Assistant Professor of Mechanical Engineering, Towne Scientific School; Project Leader, University of Pennsylvania Thermodynamics Research Laboratory. Jun. ASME.

³ Numbers in parentheses refer to the Bibliography at the end of the paper.

Contributed by the Research Committee on Properties of Gases and Gas Mixtures, and the Heat Transfer and Applied Mechanics Divisions, and presented at the Annual Meeting, New York, N. Y., November 27-December 2, 1949, of THE AMERICAN SOCIETY OF MECHANICAL ENGINEERS.

NOTE: Statements and opinions advanced in papers are to be understood as individual expressions of their authors and not those of the Society. Paper No. 49-A-50.

where k is Boltzmann's constant, c_2 is the so-called second radiation constant hc/k , and τ denotes reciprocal absolute temperature T^{-1} . The summation is to be extended over all accessible energy levels ϵ_i . Now the specific free enthalpy g of the gas in question is given by

$$g = -RT \log_e (Q/nN_0) \dots [2]$$

where n is the number of mols of gas with state sum Q and N_0 is Avogadro's number. This is subject to augmentation by an arbitrary constant \bar{u} , which can be identified as the null-point ($p = 0$, $T = 0$) energy of the gas in question, since the numerical value to be assigned to the energy ϵ_0 of the lowest level is arbitrary.⁴ Since free enthalpy g is a characteristic function of pressure p and temperature T , the enthalpy h , reduced entropy $s + R \log_e p$, and product pv can be derived from it in a simple manner by application of well-known identical relations of thermodynamics, namely, $h = \partial(\tau g)/\partial \tau$, $s = -\partial g/\partial T$, and $v = \partial g/\partial p$, if the state sum Q in Equation [2] is expressed as function of p and T . From the first of these relations it is to be noticed that enthalpy h , like free enthalpy g , is subject to augmentation by a constant amount \bar{u} ; the second shows that such augmentation does not affect the entropy s .

In a previous report (1) it was explained that the contributions to the state sum from translation can be evaluated separately from those for internal motions (rotation, vibration, etc.). If the effect of intermolecular forces is neglected, the following result is obtained

$$\begin{aligned} [\log_e p - g/RT]_{p=0} = \frac{5}{2} \log_e T + \log_e \{ (2\pi Mk/h^2 N_0)^{3/2} k \} \\ + \log_e Q_{\text{int}} \dots [3] \end{aligned}$$

where M denotes the molecular weight, and Q_{int} is the contribution to the state sum from internal motions only. Consistent units must be used in the arguments of the logarithms. The subscript $p = 0$ is affixed to the quantity on the left to emphasize that Equation [3] is strictly valid only in the absence of intermolecular forces, that is, it is valid only in the limiting case of zero pressure. At not too low temperatures the effects of intermolecular forces remain small until fairly high pressures are reached; therefore the zero-pressure properties can be used without correction in ordinary engineering calculations not involving too-high pressures.

INTERNAL STATE SUM

The energy levels ϵ_i entering the internal state sum Q_{int} represent the rotational, vibrational, electronic, and nuclear contributions. It has been shown that the contribution from nuclear spin may be disregarded if the resulting properties are to be used only in the analysis of processes which involve no transmutation of atomic species, provided, of course, that the practice is followed consistently for all molecules. In the case of carbon monoxide and nitrogen the electronic contributions are negligible in the temperature range here considered. In this

⁴ Not completely arbitrary, because the null-point energy of a molecular gas is definitely related to the null-point energies of the associated monatomic gases.

range, therefore, it is only necessary to take account of the rotational-vibrational energy levels for the ground electronic state, which is the $X^1\Sigma_g^+$ state in the case of nitrogen (N_2) and the $X^1\Sigma^+$ state in the case of carbon monoxide (CO) (3). For these states the rotational-vibrational energy levels can be expressed by the following equation for the corresponding wave numbers E_i measured from the lowest level

$$E_i = \omega_0 v - \omega_0 x_0 v^2 + \omega_0 y_0 v^3 - \dots + B_e J(J+1) - D_e J^2(J+1)^2 + F_e J^3(J+1)^3 - \dots \quad [4]$$

with

$$B_e = B_0 - \alpha_0 v + \dots; B_0 = B_e - \frac{1}{2} \alpha_0 + \dots \quad [4a]$$

$$D_e = D_0 - \beta_0 v + \dots; D_0 = D_e - \frac{1}{2} \beta_0 + \dots \quad [4b]$$

$$F_e = F_0 - \gamma_0 v + \dots; F_0 = F_e - \frac{1}{2} \gamma_0 + \dots \quad [4c]$$

$$\omega_0 = \omega_e - \omega_e x_e + \frac{3}{4} \omega_e y_e - \dots \quad [4d]$$

$$\omega_0 x_0 = \omega_e x_e - \frac{3}{2} \omega_e y_e + \dots \quad [4e]$$

$$\omega_0 y_0 = \omega_e y_e - \dots \quad [4f]$$

where

- ω_e = zero-order vibrational frequencies
- x_e, y_e, \dots = anharmonicity constants
- B_e = rotational constant⁵
- D_e, F_e, \dots = rotational stretching constants
- $\alpha_e, \beta_e, \gamma_e, \dots$ = rotation-vibration coupling constants
- v, J = quantum numbers

In the case of $^1\Sigma$ states, such as the ones here considered, the statistical weights p_i (neglecting the contribution from nuclear spin) are given for heteronuclear molecules, such as CO, by

$$p_i = 2J + 1$$

In the case of homonuclear molecules, such as N_2^{14} , these statistical weights must be multiplied by additional factors which are different according to whether J is even or odd. At not too-low temperatures it may be shown (4) that the internal state sum over the even values of J differs from that over the odd values of J by only a negligible amount and that, as a result, the effect of the additional factor in the statistical weights is equivalent to dividing all the statistical weights $(2J + 1)$ by a symmetry number σ , which has the value 2 for homonuclear molecules, and of course has the value unity for heteronuclear molecules. At very low temperatures this is not the case and as a result a homonuclear gas like N_2^{14} must be considered as a mixture of two different species, the so-called ortho and para modifications. In the case of nitrogen at 100 deg R and higher temperatures, the difference between the two modifications is entirely negligible; the method of calculating the properties of the ortho and para modifications, of the equilibrium mixture, and of the normal mixture at lower temperatures is discussed in general terms in many references, e.g. (4), and its application to the case of nitrogen is treated in a previous report from this laboratory (5). Of course, if the two atoms of the nitrogen molecule are different

isotopes, as in the case of $N^{14}N^{15}$, the molecule is heteronuclear, and therefore its symmetry number is unity.

MATHEMATICAL REARRANGEMENT⁶

The first step in the evaluation of the internal state sum Q_{int} for the set of energy levels given by Equation [4] is to evaluate the sum over J for arbitrarily fixed values of the vibrational quantum number v . This can easily be done by application of the Euler-Maclaurin formula. The result is

$$\Sigma(2J + 1)e^{[-b_1(1-s_1v)J(J+1) + b_2(1-s_2v)J^2(J+1)^2 - \dots]} = (\Sigma y_i v^i)/b_1, \dots \quad [5]$$

where the y_i are simple functions of $b_1 = c_{27}B_0$, $b_2 = c_{27}D_0$, $b_3 = c_{27}F_0, \dots, s_1 = \alpha_0/B_0$, $s_2 = \beta_0/D_0, \dots$ which have been listed elsewhere (5) and need not be reproduced here. The summation on the left extends over all nonnegative, integral values of the rotational quantum number J . Strictly speaking, that on the right extends over all nonnegative, integral values of the index i . However, in the case of nitrogen and carbon monoxide the sum over i is very rapidly convergent, and in the temperature range here considered it is sufficient to include in the sum only the first seven terms.

Substitution of Equations [4] and [5] into Equation [1] yields

$$\sigma b_1 Q_{int} = \Sigma y_i v^i e^{[-c_{27}(\omega_0 v - \omega_0 x_0 v^2 + \omega_0 y_0 v^3 - \dots)]} \quad [6]$$

The summation extends over i and v . The latter should cover all non-negative, integral values up to the dissociation limit. For nitrogen and carbon monoxide up to at most 5000 deg R, as long as only the first seven values of i are considered, no significant error is introduced by extending the summation over v to infinity.

The contribution to the exponential in Equation [6] from the quadratic and cubic terms in v can be reduced to a power series in v by expansion in a Taylor series. This reduction facilitates evaluation of the quantities Y_i defined by

$$Y_i = (1 - x) \sum_{v=0}^{\infty} v^i x^v e^{c_{27}(\omega_e x_e - \omega_e x_0 x^2 - \omega_e y_0 x^3 + \dots)}$$

where $x = e^{-c_{27}\omega_0}$. Each Y_i is a combination of sums of the form

$$A_n = (1 - x) \sum_{v=0}^{\infty} v^n x^v$$

These sums can be expressed as simple functions of $y = x/(1 - x)$, which have been listed elsewhere (1, 5).

After having evaluated the y_i and Y_i , it is a straightforward matter to calculate Q_{int} from

$$\sigma b_1 (1 - x) Q_{int} = \Sigma y_i Y_i = \alpha \quad [7]$$

Algebraic expressions for the first and second derivatives of α are obtained easily (5) from the results just given and need not be reproduced here.

ZERO-PRESSURE PROPERTIES

Having evaluated the sum α in Equation [7] it is possible to write down convenient expressions for the various zero-pressure thermodynamic properties of particular interest. This part of the mathematical rearrangement is completely analogous to the corresponding part previously published for carbon dioxide.

⁵ B_e is inversely proportional to the largest principal moment of inertia I_e at the equilibrium internuclear separation, that is, $B_e = h/8\pi^2 c I_e$.

⁶ A more detailed derivation of the working equations has been given elsewhere (5). It must be noted that the notation used in previous reports was slightly different from that used in this paper.

(1), and therefore only the final results will be given here. These are

$$[\log_e p - (g - \bar{u})/RT]_{p=0} = \frac{7}{2} \log_e T - \log_e(1 - e^{-\theta r}) + \log_e \alpha + \log_e [(2\pi Mk/h^2 N_0)^{3/2} (k/\sigma c_2 B_0)] \dots [8]$$

$$[(h - \bar{u})/RT]_{p=0} = \frac{7}{2} + \frac{\theta r}{e^{\theta r} - 1} + T \frac{d \log_e \alpha}{dT} \dots [8a]$$

$$[s/R + \log_e p]_{p=0} = [\log_e p - (g - \bar{u})/RT]_{p=0} + [(h - \bar{u})/RT]_{p=0} \dots [8b]$$

$$[c_p/R]_{p=0} = \frac{7}{2} + \frac{(\theta r)^2 e^{\theta r}}{(e^{\theta r} - 1)^2} + T \frac{d^2(T \log_e \alpha)}{dT^2} \dots [8c]$$

where again it is noted (a) that the free enthalpy g and the enthalpy h are subject to augmentation by a constant amount \bar{u} representing the null-point energy, and (b) that the arguments of the logarithms in Equation [8] must be expressed in consistent units. The quantity $\theta = c_{200}$ is the so-called characteristic temperature of the gas considered.

The terms containing $\log_e \alpha$ essentially represent the combined corrections for anharmonicity, rotational stretching, and rotation-vibration coupling. Approximate expressions for $\log_e \alpha$ have been obtained (5) and may be useful for rapid calculations of the properties of other similar gases. Formulas for correcting $\log_e \alpha$ and its derivatives for small changes in the spectroscopic constants have also been obtained (5). These formulas may be useful for future revisions of the tables, as well as for the calculation of the properties of other than the most abundant isotopes, in which case the tabulated values have to be corrected for small isotopic effects on the spectroscopic constants.

PHYSICAL CONSTANTS AND CONVERSION FACTORS

In conformity with the practice of this laboratory the 1941 Birge (6) values of the general physical constants have been used consistently. As explained in another report (2), the probable errors given by Birge have been revised on the basis of the analysis of DuMond and Cohen (7). The adopted constants are

$$R = (8.31436 \pm 0.00038) \times 10^7 \text{ erg deg K}^{-1} \text{ g-mol}^{-1}$$

$$c_2 = 1.43848 \pm 0.00024 \text{ cm deg K}$$

$$\log_e [(2\pi k/h^2 N_0)^{3/2}] = -5.13397_5 \pm 0.00065 \text{ (with argument in g-mol}^{3/2} \text{ atm deg R}^{-3/2} \text{ g}^{-3/2})$$

$$\text{ratio of physical to chemical atomic weights} = 1.000272 \pm 0.000005$$

Following usual steam-table practice, the Btu has been used as unit of energy in preparing the tables presented in this report. The particular Btu used is defined by the following conversion factors: 1.8 Btu g/ITcal lb and 860/1.00020 ITcal/abs kwhr.² Temperature on the Rankine scale (deg R) is used as independent argument and the pound-mol (mol) is used as unit of weight, in order to simplify the analysis of problems involving gas mixtures. In the case of reduced entropy $s + R \log_e p$, it is to be understood that pressure is expressed in international atmospheres (atm).

ATOMIC WEIGHTS

The available data on the weights of the various isotopes of

² In the previous report on the properties of carbon dioxide (1) the conversion factor 860/1.00019 ITcal/abs kwhr was given by mistake. Actually the value 860/1.00020 had been used in the calculations, with the corresponding value $R = 1.98581$ Btu/mol deg R.

carbon, oxygen, and nitrogen have been reviewed in a previous report (2). The values used in the present calculations are those recommended by Birge (6), for consistency with previous calculations from this laboratory. The changes indicated by more recent data are altogether negligible. The adopted values of the isotopic weights and of the relevant abundance ratios are listed in Table 1.

TABLE 1 ISOTOPIC WEIGHTS OF CARBON, OXYGEN, AND NITROGEN (PHYSICAL SCALE)

Isotope	Weight	Abundance
C ¹²	12.00386	92
C ¹³	13.00761	1
N ¹⁴	14.00753	270
N ¹⁵	15.0049	1
O ¹⁶	16.0000	506
O ¹⁷	17.0045	0.204
O ¹⁸	18.0049	1

The molecular weights of the various possible carbon monoxide and nitrogen molecules can be computed directly from the data in Table 1, converting them to the chemical scale by division by 1.000272. The following are of particular interest:

$$\text{C}^{12}\text{O}^{16} : M = 27.99625 \text{ (chemical scale)}$$

$$\text{CO} : M = 28.01139 \text{ (normal isotopic mixture, chemical scale)}$$

$$\text{N}_2^{14} : M = 28.00744 \text{ (chemical scale)}$$

$$\text{N}_2 : M = 28.01480 \text{ (normal isotopic mixture, chemical scale)}$$

The values for the normal isotopic mixtures are in excellent agreement with those adopted by the Committee on Atomic Weights of the International Union of Chemistry (8).

SPECTROSCOPIC CONSTANTS FOR NITROGEN

The best complete analysis of the vibrational structure of the ground electronic level ($X^1\Sigma_g^+$) of diatomic nitrogen is that given by Birge and Hopfield (9) in 1928; they give for the vibrational contribution to the wave numbers

$$2345.16 v - 14.445 v^2 \text{ (cm}^{-1}\text{)}$$

The constants in this expression are subject to a relatively large uncertainty since they were obtained from the band heads rather than the band origins. Several new bands have been analyzed since 1928 (10, 11, 12, etc.). All these newer results indicate that there should be no revision of the first two vibrational constants, even though R. Herman (12), on the basis of her own measurements as well as those of Wulf and Melvin and of Janin, proposes the addition of cubic and quartic terms, obtaining the following expression for the vibrational contribution

$$2345.16 v - 14.445 v^2 + 0.0064958 v^3 - 0.000509 v^4 \text{ (cm}^{-1}\text{)}$$

The contribution from the last two constants to the thermodynamic properties up to 5000 deg R is not significant. Therefore, since these two constants appear to have a rather large probable error, it was decided not to include them in the present calculations. Available data do not permit a reliable estimate of the uncertainties of the vibrational constants just quoted. More or less arbitrarily we have assumed a probable error of ± 0.1 cm⁻¹ for the first constant 2345.16, and a probable error of ± 0.01 cm⁻¹ for the second constant 14.445.

The earlier rotational analyses have been revised by Watson and Koontz (13), whose results have been confirmed by Spinks (14). According to their analysis, the rotational constants for the ground electronic state of nitrogen are

$$B_0 = 1.998 \pm 0.002 \text{ cm}^{-1}; \alpha_0 = 0.018 \text{ cm}^{-1}$$

It appears safe to assume that the probable error of α_0 is at most ± 0.001 cm⁻¹. These values are in excellent agreement with the somewhat less accurate values obtained by Rasetti (15)

from the Raman spectrum, and by Janin (10) from the Vegard-Kaplan bands. Other rotational constants have not been determined from direct measurements but may be calculated from approximate theoretical equations which are reviewed by Jevons (16) and Birge (17). Spinks (14) lists values of D_0 and β_0 calculated from these formulas; however, his values are only preliminary and are not correct. From the constants adopted for these calculations and the quoted formulas, we obtain

$$D_0 = 5.808 \times 10^{-6} \text{ cm}^{-1}; F_0 = 4 \times 10^{-12} \text{ cm}^{-1}$$

The calculated values of β_0 and of other rotational constants are negligible. While it is not possible to state the probable error of the constants thus obtained, it seems safe to assume that the probable error of the value of D_0 given in the foregoing does not exceed $0.1 \times 10^{-6} \text{ cm}^{-1}$, and that the probable error of F_0 has no significant effect on the accuracy of the thermodynamic properties herein presented.

In conclusion the constants adopted for the ground electronic state of diatomic nitrogen (N_2^{14}) are those listed in Table 2. Constants not listed there are assumed to be negligibly small. The first excited electronic state is the $A^2\Sigma^+$ state, which is about $50,000 \text{ cm}^{-1}$ above the ground state (3), and therefore does not make a significant contribution to the thermodynamic properties in the temperature range here considered.

TABLE 2 SPECTROSCOPIC CONSTANTS FOR NITROGEN (N_2^{14}) IN THE GROUND ELECTRONIC STATE

$\omega_0 = 2345.16 \pm 0.1 \text{ cm}^{-1}$	$B_0 = 1.998 \pm 0.002 \text{ cm}^{-1}$
$\omega_{00} = 14.445 \pm 0.01 \text{ cm}^{-1}$	$\alpha_0 = 0.018 \pm 0.001 \text{ cm}^{-1}$
	$D_0 = (5.808 \pm 0.1) \times 10^{-6} \text{ cm}^{-1}$
	$F_0 = 4 \times 10^{-12} \text{ cm}^{-1}$

The data given in Table 2 suffice also for the calculation of the constants for N_2^{15} and $N^{14}N^{15}$. Indeed, the vibrational and rotational constants of isotopes are related through the following theoretical equations (18):

$$\left. \begin{aligned} \omega_i^i &= \rho \omega_e \\ B_i^i &= \rho^2 B_e \\ D_i^i &= \rho^4 D_e \end{aligned} \right\} \dots \dots \dots [9]$$

$$\left. \begin{aligned} \omega_i^i x_e^i &= \rho^2 \omega_e x_e \\ \alpha_i^i &= \rho^2 \alpha_e \\ \rho &= \sqrt{\mu/\mu^i} \end{aligned} \right\}$$

where superscript i indicates the heavier isotope and μ is reduced mass. It must be noted again that $N^{14}N^{15}$ is heteronuclear and therefore has a symmetry number $\sigma = 1$.

SPECTROSCOPIC CONSTANTS FOR CARBON MONOXIDE

Until recently the best available analysis of the vibrational structure of the ground electronic level ($X^1\Sigma^+$) of carbon monoxide was that given by Read (19), and the most reliable set of rotational constants was that of Gerö, Herzberg, and Schmid (20). A tabulation of the thermodynamic properties of carbon monoxide based upon those constants has been issued by this laboratory (21). Recently, new data have been obtained and a more accurate analysis has been completed by associates of G. Herzberg. Dr. Herzberg has very kindly communicated to us the new spectroscopic constants in advance of publication. These constants, which have been adopted for the calculation of the tables of properties herein presented, are listed in Table 3. The probable error in each constant will be assumed to be five units in the last tabulated figure, except in the case of B_e and α_e , in which case the probable error will be assumed to be five units in the penultimate figure. This assignment of probable

TABLE 3 SPECTROSCOPIC CONSTANTS FOR CARBON MONOXIDE ($C^{12}O^{16}$) IN THE GROUND ELECTRONIC STATE

$\omega_e = 2170.21 \text{ cm}^{-1}$	$B_e = 1.9313_5 \text{ cm}^{-1}$
$\omega_{00} = 13.461 \text{ cm}^{-1}$	$\alpha_e = 0.0174_5 \text{ cm}^{-1}$
$\omega_{000} = 0.0308 \text{ cm}^{-1}$	$D_e = 6.43 \times 10^{-6} \text{ cm}^{-1}$
	$S_e = -0.04 \times 10^{-4} \text{ cm}^{-1}$

errors is quite arbitrary, but sufficient data are not available to the authors for a more rational assignment. The additional constant $F_0 = 6.5 \times 10^{-12}$ has been calculated from previously mentioned, theoretical formulas (16, 17). Other constants are considered to be negligible. The first excited electronic state of carbon monoxide is the $a^3\Pi$ state, which is about $48,000 \text{ cm}^{-1}$ above the ground state (3, 22), and therefore makes no significant contribution to the tabulated properties in the temperature range here considered. The properties of other isotopes may be obtained easily by means of Equation [9].

FINAL RESULTS

The final results of the present calculations are given in Table 4. It might be well to repeat that the data listed in this table are characterized by computational accuracy well beyond present physical accuracy. The unit of energy used is the (International Steam Tables) Btu in terms of which the universal gas constant R has the value $1.98581 \text{ Btu/mol deg R}$. The usual practice of excluding the contribution to the reduced entropy from nuclear spin has been followed.

The probable errors of the tabulated data arise from several separate factors. All the properties contain as a factor the universal gas constant R , and therefore have at least a relative error equal to the relative error of R . The latter depends on the choice of units. If the units chosen can be defined directly in terms of the absolute units of energy, then the relative error contributed by R is ± 0.000046 or ± 0.0046 per cent. If the units chosen are defined in terms of the international electrical units, then the relative error contributed by R is about twice as much, namely, ± 0.000091 or ± 0.0091 per cent.

In order to discuss the other sources of error independently of R , we shall consider next the errors in the dimensionless quantities obtained by dividing by R the following tabulated properties: reduced entropy, mean isobaric specific heat, and specific heat. In the case of the last two named quantities, the probable error originates only from errors in the rotational-vibrational contributions. This probable error is shown in Fig. 1. In the case of the entropy, an additional probable error of about ± 0.0007 (dimensionless) arises from the translational contribution. In this case most of the error in the rotational contribution arises from the classical term $\log(c_2 B_0 \sigma)$. The probable error of this term has the value ± 0.0012 in the case of nitrogen, and ± 0.00043 in the case of carbon monoxide. Since these errors are constant, they cancel in calculations for processes not involving chemical changes. Therefore, only the probable errors in the rotational-vibrational contributions exclusive of the classical term $\log(c_2 B_0 \sigma)$ are of general interest. These are shown graphically in Fig. 1.

The zero-pressure properties presented in this paper apply to the most abundant isotopes, namely, carbon monoxide $C^{12}O^{16}$ and nitrogen N_2^{14} . All the data necessary to obtain the properties of molecules containing other isotopes have been given in this report, and these properties may be obtained easily by applying small corrections to the values listed in Table 4. Detailed tables for each isotope are not given here because of space limitations.

Regarding the thermodynamic properties of the normal isotopic mixture of nitrogen (N_2), the following statements may be made: Its enthalpy and isobaric specific heat are almost identical with those of the most abundant isotope N_2^{14} ; its reduced entropy exceeds that of N_2^{14} by about $0.00078 \text{ Btu/mol deg R}$ because it contains some isotopes of higher molecular weight M than that of N_2^{14} , by about $0.0102 \text{ Btu/mol deg R}$ because the statistical weights p_i of $N^{14}N^{15}$ differ from those of N_2^{14} , and by a mixing entropy of about $0.086 \text{ Btu/mol deg R}$.

TABLE 4 ZERO-PRESSURE PROPERTIES OF DIATOMIC NITROGEN (N_2) AND OF CARBON MONOXIDE (CO)

T degR	Reduced Entropy ($s + R \log p$) _{p=0} Btu/mol degR		Mean Isobaric Specific Heat [(h-U)/T] _{p=0} Btu/mol degR		Enthalpy (h-U) _{p=0} Btu/mol		Isobaric Specific Heat $c_{p=0}$ Btu/mol degR	
	N_2	CO	N_2	CO	N_2	CO	N_2	CO
100	34.04942	35.50111	6.91620	6.91754	691.620	691.754	6.95091	6.95099
105	34.39855	35.84025	6.91785	6.91913	726.374	726.509	6.95092	6.95100
110	34.71191	36.16361	6.91935	6.92059	761.189	761.264	6.95093	6.95102
115	35.02099	36.47260	6.92073	6.92191	795.994	796.019	6.95095	6.95104
120	35.31672	36.76343	6.92199	6.92312	830.838	830.774	6.95096	6.95106
125	35.60047	37.05219	6.92315	6.92424	865.393	865.530	6.95097	6.95108
130	35.97309	37.32432	6.92422	6.92527	900.149	900.285	6.95099	6.95110
140	36.39822	37.83995	6.92613	6.92712	969.659	969.796	6.95103	6.95114
150	36.96779	38.31953	6.92779	6.92872	1039.17	1039.31	6.95106	6.95119
160	37.31640	38.76915	6.92925	6.93013	1108.69	1108.82	6.95110	6.95123
170	37.73791	39.19957	6.93053	6.93137	1178.19	1178.33	6.95114	6.95129
180	39.13513	39.59900	6.93169	6.93249	1247.70	1247.85	6.95118	6.95133
190	39.51096	39.96274	6.93271	6.93347	1317.21	1317.36	6.95122	6.95139
200	39.96751	40.31930	6.93363	6.93437	1386.73	1386.87	6.95126	6.95143
210	39.20667	40.65846	6.93447	6.93519	1456.24	1456.39	6.95131	6.95149
220	39.53004	40.99194	6.93524	6.93592	1525.75	1525.90	6.95135	6.95153
230	39.93905	41.29025	6.93594	6.93660	1595.27	1595.42	6.95139	6.95159
240	40.13489	41.56671	6.93659	6.93723	1664.78	1664.94	6.95143	6.95164
260	40.69131	42.14314	6.93773	6.93834	1803.91	1803.97	6.95152	6.95174
280	41.20648	42.65833	6.93978	6.93930	1942.94	1943.00	6.95161	6.95185
300	41.68609	43.13796	6.93959	6.94014	2081.87	2082.04	6.95170	6.95196
320	42.13474	43.58663	6.94034	6.94088	2220.91	2221.08	6.95179	6.95207
340	42.55620	44.00910	6.94102	6.94155	2359.95	2360.13	6.95188	6.95220
360	42.95356	44.40549	6.94162	6.94214	2498.99	2499.17	6.95199	6.95236
380	43.32944	44.78138	6.94217	6.94268	2638.03	2638.22	6.95211	6.95257
400	43.69604	45.13901	6.94267	6.94319	2777.07	2777.27	6.95227	6.95294
420	44.05254	45.47725	6.94313	6.94365	2916.12	2916.34	6.95247	6.95322
440	44.34969	45.90072	6.94356	6.94410	3055.17	3055.40	6.95273	6.95375
460	44.65775	45.10994	6.94397	6.94453	3194.23	3194.49	6.95310	6.95449
480	44.95368	45.40594	6.94436	6.94497	3333.29	3333.59	6.95359	6.95545
500	45.23755	45.69980	6.94474	6.94541	3472.37	3472.71	6.95405	6.95674
550	45.90049	47.35306	6.94572	6.94665	3920.14	3920.66	6.95695	6.96174
600	45.50599	47.95914	6.94693	6.94823	4169.10	4169.94	6.96171	6.97005
650	47.05351	49.51750	6.94925	6.95035	4515.36	4517.73	6.96930	6.98244
700	47.58037	49.03555	6.95012	6.95322	4865.09	4867.26	6.99034	6.99952
750	48.06245	49.51919	6.95262	6.95702	5214.46	5217.76	6.99529	7.00153
800	48.51420	49.97319	6.95596	6.96157	5564.69	5569.49	7.01440	7.04847
850	48.94043	50.40142	6.95997	6.96797	5915.97	5922.59	7.03769	7.08005
900	49.34344	50.80710	6.96502	6.97507	6268.52	6277.57	7.06500	7.11584
950	49.72624	51.19298	6.97109	6.98351	6622.53	6634.33	7.09607	7.15530
1000	50.09109	51.56096	6.97819	6.99315	6979.18	6993.15	7.13050	7.19790
1100	50.77423	52.25123	6.99545	7.01587	7695.01	7717.45	7.20755	7.29949
1200	51.40495	52.98963	7.01563	7.04269	8419.95	8451.22	7.29235	7.39631
1300	51.99216	53.49472	7.04124	7.07299	9153.62	9194.76	7.39135	7.48447
1400	52.54848	54.04294	7.06976	7.10576	9896.28	9948.06	7.47161	7.58119
1500	53.06102	54.56919	7.09860	7.14059	10647.9	10710.9	7.55097	7.67453
1600	53.55179	55.06736	7.13022	7.17876	11409.4	11482.8	7.64757	7.76390
1700	54.01792	55.54054	7.16312	7.21757	12177.3	12263.4	7.75063	7.84685
1800	54.45204	55.99129	7.19695	7.25111	12954.3	13052.0	7.86942	7.92490
1900	54.86629	56.42173	7.23107	7.28851	13739.0	13849.2	7.93363	7.99745
2000	55.26245	56.83368	7.26546	7.32565	14530.9	14651.3	7.95317	8.06464
2200	56.05649	57.60907	7.33391	7.39941	16134.4	16276.5	8.07854	8.18409
2400	56.76419	58.32466	7.40050	7.46624	17761.2	17923.8	8.16697	8.29544
2600	57.48232	58.99140	7.46468	7.53455	19409.2	19589.8	8.28053	8.37260
2800	58.03995	59.51467	7.52591	7.59713	21072.5	21272.0	8.36132	8.44597
3000	58.61927	60.19227	7.58399	7.65597	22752.0	22967.9	8.43130	8.51079
3200	59.16540	60.75078	7.63990	7.71118	24444.5	24675.7	8.49219	8.56614
3400	59.69187	61.27156	7.69059	7.76291	26149.3	26393.9	8.54543	8.61439
3600	60.17167	61.76516	7.73950	7.81141	27862.2	28121.1	8.59225	8.65871
3800	60.63736	62.23423	7.78580	7.85690	29594.9	29856.2	8.63366	8.69912
4000	61.09115	62.68104	7.82994	7.89951	31351.4	31598.4	8.67049	8.73758
4200	61.50501	63.10759	7.86972	7.93975	33052.8	33347.0	8.70345	8.77171
4400	61.91059	63.51560	7.90630	7.97753	34795.5	35101.1	8.73309	8.79405
4600	62.29939	63.90561	7.94475	8.01313	36545.9	36840.4	8.75990	8.80632
4800	62.65396	64.28195	7.97924	8.04673	38300.3	38644.3	8.78429	8.83050
5000	63.03178	64.64285	8.01189	8.07849	40059.4	40392.5	8.80659	8.85083

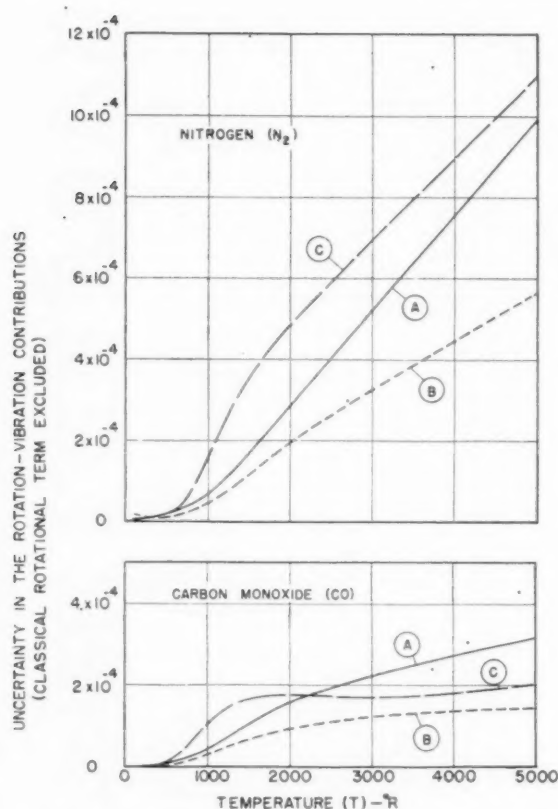


FIG. 1 UNCERTAINTY IN THERMODYNAMIC PROPERTIES (A. Reduced entropy; B. mean isobaric specific heat; C. isobaric specific heat.)

The mixing entropy has been estimated on the assumption that the mixture contains in significant concentration only N₂¹⁴ and N₂¹⁵.

Regarding the thermodynamic properties of the normal isotopic mixture of carbon monoxide (CO), the following statements may be made: Its enthalpy and isobaric specific heat are almost identical with those of the most abundant isotopes C¹²O¹⁶; its reduced entropy exceeds that of C¹²O¹⁶ by about 0.00161 Btu/mol deg R because it contains some isotopes of higher molecular weight *M* than that of C¹²O¹⁶, and by a mixing entropy of about 0.153 Btu/mol deg R. The mixing entropy has been estimated on the assumption that the mixture contains in significant concentration only C¹²O¹⁶, C¹²O¹⁷, C¹²O¹⁸, C¹³O¹⁶.

In addition to the foregoing corrections there are, strictly speaking, some temperature-dependent corrections to account for the isotopic effect on the rotational and vibrational constants. These, however, can reasonably be expected not to exceed the uncertainties in the calculated properties, and therefore may be ignored.

COMPARISON WITH OTHER DATA

The first extensive tabulation of the zero-pressure thermodynamic properties of nitrogen is that of Giauque and Clayton (23), who published tables of the free enthalpy of this gas. Trautz and Adler (24) published tables of the specific heat of nitrogen and other gases, but their tables were rather inaccurate. Johnston and Davis (25) reviewed the available data on the spectroscopic constants and calculated tables of the entropy and of

the specific heat of nitrogen. Wagman, et al (26) corrected the Johnston and Davis tables for recent changes in the accepted values of the general physical constants and atomic weights, but not for some significant changes in the rotational constants. Woolley (27) in 1944, prepared an unpublished tabulation of the principal thermodynamic properties of nitrogen by correcting the Johnston and Davis tables for changes in the rotational constants as well as in the general physical constants and atomic weights. In 1944, Woolley used essentially the same constants as those herein adopted, except that he apparently used the incorrect values of *D_e* and *β₀* given by Spinks (14). In 1947 Woolley revised and extended his earlier tables, presumably using the spectroscopic constants adopted for the calculations of tables previously issued from this laboratory (5).

The results of the present calculations for nitrogen are compared with those of previous authors in Table 5, the comparison being based on the isobaric specific heat *c_p*=0. In the second

TABLE 5 ZERO-PRESSURE ISOBARIC SPECIFIC HEAT OF NITROGEN

<i>T</i> , deg R	(Values in Btu/mol deg R)		Goff and Gratch
	Johnston and Davis	Wagman	
180	6.951	...	6.951
900	7.067	7.065	7.065
1800	7.817	7.811	7.809
2700	8.329	8.324	8.322
3600	8.599	8.596	8.592
4500	8.756	8.753	8.747

column are listed the original Johnston and Davis (25) values converted to Btu/mol deg R by multiplication by 1.98581/1.9869 = 0.99945. In the third column are listed the Wagman, et al, (26) revisions of the Johnston and Davis values converted to Btu/mol deg R by multiplication by 1.98581/1.98718 = 0.99931. In the fourth column are listed values interpolated from our final tables rounded off to the number of figures used by the other authors for greater ease of comparison. No comparison with the 1947 Woolley (27) unpublished tables is shown, since his tables are essentially equivalent to ours, except for the fact that we maintained greater computational accuracy.

While the differences between the three sets of values listed in Table 5 are small, they are significant, since they definitely exceed the probable error of our values. The conclusions to be drawn from comparisons of the other properties are similar; these comparisons are not shown here because of space limitations. It should be noted that most of the previous tabulations are for the normal isotopic mixture, but they do not include the mixing entropy and the effect of the heteronuclearity of N¹⁴N¹⁵. Therefore the values of reduced entropy given by the other authors should exceed our values for N₂¹⁴ by about 0.0015 Btu/mol deg R because of differences in molecular weights.

The first extensive tabulation of the zero-pressure thermodynamic properties of carbon monoxide is that of Clayton and Giauque (28), who published tables of the free enthalpy of this gas. Kassel (29) tabulated the specific heat of carbon monoxide. Gordon and Barnes (30) calculated a single set of values of the thermodynamic properties of carbon monoxide at 3000 deg K. Johnston and Davis (25) reviewed the available data on the spectroscopic constants and calculated tables of the entropy and of the specific heat of carbon monoxide. Wagman, et al (26) corrected the Johnston and Davis tables for recent changes in the accepted values of the general physical constants and atomic weights, but not for some significant changes in the spectroscopic constants.

The results of the present calculations for carbon monoxide are compared with those of previous authors in Table 6, the comparison being based on the isobaric specific heat *c_p*=0. In the second column are listed the Kassel (29) values converted to

TABLE 6 ZERO-PRESSURE ISOBARIC SPECIFIC HEAT OF CARBON MONOXIDE

T, deg R	(Values in Btu/mol deg R)			
	Kassel	Johnston and Davis	Wagman	Goff and Gratch
180	6.949	6.950	6.951	6.951
900	7.111	7.118	7.115	7.116
1800	7.914	7.932	7.927	7.925
2700	8.390	8.417	8.413	8.411
3600	8.626	8.662	8.659	8.657
4500	8.758	8.802	8.800	8.796

Btu/mol deg R by multiplication by 0.99945. In the third column are listed the Johnston and Davis (25) values similarly converted to Btu/mol deg R. In the fourth column are listed the Wagman, et al (26) revisions of the Johnston and Davis values converted to Btu/mol deg R by multiplication by 0.99931. In the fifth column are listed values interpolated from our final tables rounded off to the number of figures used by the other authors for greater ease of comparison.

The differences between the four sets of values listed in Table 6 are small but significant, since they definitely exceed the probable error of our values. The differences of our tables from the previous tabulations are due primarily to the recent revision of the vibrational and rotational constants. As in the case of nitrogen, no comparison of the other properties is given here because of space limitations. In the case of the entropy, since the tables by other authors are for the normal isotopic mixture (mixing entropy excluded), the values given by the other authors should exceed our values for $C^{18}O^{16}$ by about 0.0032 Btu/mol deg R because of differences in molecular weights.

As has been previously pointed out by Johnston and Davis (25), the available results from calorimetric adiabatic expansion, velocity of sound, and explosion measurements are much less accurate than those from spectroscopic data, at least in the case of carbon monoxide and nitrogen. Anyway a partial comparison with those data (based on isobaric specific heat) is shown in Fig. 2. The older data, in particular those from acoustic velocity measurements, have been omitted since they are too inaccurate. Also several recent results near room temperature have been

omitted to avoid overcrowding the graph. The two points credited to Fenning and Whiffin (35) were calculated from their formulation, which supposedly is valid from 2370 to 3060 deg K. The points credited to Henry (31) are Henry's smoothed values, and not the original experimental values. The most accurate values used for this comparison are probably those obtained by Eucken and Lude (32) and by Eucken and Mücke (33) by means of an adiabatic expansion experiment; these values are reported to be accurate to about 0.1 per cent. The Eucken and Lude (32) results for nitrogen, which are in excellent agreement with the spectroscopic values, could not be shown in Fig. 2 because of overcrowding.

Taking account of the relative lack of accuracy of the experimental values, their agreement with the spectroscopic values is quite satisfactory.

ACKNOWLEDGMENT

It is a pleasure for the authors to acknowledge the extremely valuable advice and suggestions of Dr. Gerhard Herzberg, Director, Division of Physics, National Research Council of Canada. It is also a pleasure to acknowledge the substantial co-operation of the Navy Department, Bureau of Ships, which sponsored the project leading to the preparation of the tables presented in this report. The co-operation of the computational staff of the Thermodynamics Research Laboratory is also gratefully acknowledged.

BIBLIOGRAPHY

- 1 "Zero-Pressure Thermodynamic Properties of Carbon Dioxide," by Serge Gratch, *Trans. ASME*, vol. 71, 1949, pp. 897-902.
- 2 "Zero-Pressure Thermodynamic Properties of Some Monatomic Gases," by J. A. Goff, Serge Gratch, and S. W. Van Voorhis, *Trans. ASME*, vol. 72, 1950, pp. 725-739.
- 3 "Molekülspektren," by H. Sponer, Julius Springer, Berlin, vol. 1, 1935 (Tabellen), pp. 14, 32.
- 4 "Statistical Thermodynamics," by R. H. Fowler and E. A. Guggenheim, Cambridge University Press, London, 1939, p. 187.
- 5 "Zero-Pressure Properties of Diatomic Gases. I. Nitrogen," by Serge Gratch, Annual Report From the Thermodynamics Research Laboratory, University of Pennsylvania, July, 1946, Project G-3.
- 6 "A New Table of Values of the General Physical Constants," by R. T. Birge, *Reviews of Modern Physics*, vol. 13, 1941, pp. 233-239.
- 7 "Our Knowledge of the Atomic Constants F , N , m , and h in 1947, and of Other Constants Derivable Therefrom," by J. W. M. DuMond and E. R. Cohen, *Reviews of Modern Physics*, vol. 20, 1948, pp. 82-108; see also "Erratum," privately communicated, received April 23, 1949.
- 8 "Thirteenth Report of the Committee on Atomic Weights of the International Union of Chemistry," by G. P. Baxter, M. Guichard, and R. Whytlaw-Gray, *Journal of the American Chemical Society*, vol. 69, 1947, pp. 731-736.
- 9 "The Ultra-Violet Band Spectrum of Nitrogen," by R. T. Birge and J. J. Hopfield, *Astrophysical Journal*, vol. 68, 1928, pp. 257-278.
- 10 "Le spectre d'émission de l'azote sous la pression atmosphérique. Analyse des bandes du système de Vegard-Kaplan," by J. Janin, *Cahiers de physique*, vol. 18, Dec., 1943, pp. 48-54.
- 11 "Extension of the A-X System of Nitrogen," by R. Herman, *Nature*, vol. 157, 1946, p. 843; see also Comptes rendus des séances de l'Académie des sciences, vol. 222, 1946, pp. 1226-1227.
- 12 "Contribution à l'étude des spectres de la molécule d'azote," by R. Herman, *Annales de physique*, vol. 20, 1945, pp. 241-291.
- 13 "Nitrogen Molecular Spectra in the Vacuum Ultraviolet," by W. W. Watson and P. G. Koontz, *Physical Review*, vol. 45, 1934, p. 561; *ibid.*, vol. 46, 1934, pp. 32-37.
- 14 "Rotational Structure of the Birge-Hopfield Bands of N_2 ," by J. W. T. Spinks, *Canadian Journal of Research*, vol. 20, sect. A, 1942, pp. 1-5.
- 15 "Incoherent Scattered Radiation in Diatomic Molecules," by F. Rasetti, *Physical Review*, vol. 34, 1929, pp. 367-371.
- 16 "Band-Spectra of Diatomic Molecules," by W. Jevons, The Physical Society, London, Cambridge University Press, 1932, p. 27.
- 17 "Molecular Spectra in Gases," by E. C. Kemble, R. T. Birge, W. F. Colby, F. W. Loomis, and L. Page, *Bulletin of the National Research Council*, vol. 11, part 3, December, 1926, p. 237.

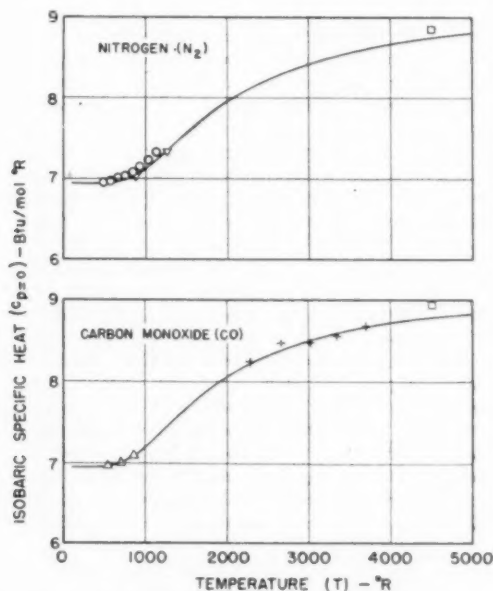


FIG. 2 COMPARISON WITH OTHER DATA
(—Goff-Gratch; ○ Henry (31); △ Eucken-Lude (32); ▽ Eucken-Mücke (33); + Sherratt-Griffiths (34); □ Fenning-Whiffin (35).)

- 18 "Molecular Spectra and Molecular Structure. I. Diatomic Molecules," by G. Herzberg, Prentice-Hall, Inc., New York, N. Y., 1939, pp. 151-155.
- 19 "Rotational and Vibrational Structure of the Fourth Positive Bands of Carbon Monoxide," by D. N. Read, *Physical Review*, vol. 46, 1934, pp. 571-575.
- 20 "On the Cameron Bands ($\Pi - \Sigma$) of Carbon Monoxide," by L. Gerö, G. Herzberg, and R. Schmid, *Physical Review*, vol. 52, 1937, pp. 467-471.
- 21 "Zero-Pressure Properties of Diatomic Gases. II. Carbon Monoxide," by Serge Gratch, Annual Report From the Thermodynamics Research Laboratory, University of Pennsylvania, July, 1947, Project G-3.
- 22 "Zur Vervollständigung des Termschemas von Kohlenoxyd. II," by R. Schmid and L. Gerö, *Zeit. für Physik*, vol. 106, 1937, pp. 205-211.
- 23 "The Heat Capacity and Entropy of Nitrogen. Heat of Vaporization. Vapor Pressure of Solid and Liquid. The reaction $\frac{1}{2} N_2 + \frac{1}{2} O_2 = NO$ from Spectroscopic Data," by W. F. Giauque and J. O. Clayton, *Journal of the American Chemical Society*, vol. 55, 1933, pp. 4875-4889.
- 24 "Spektroskopische Berechnung der Molwärmen von Luft, O_2 , N_2 ," by M. Trautz and H. Adler, *Zeit. für Physik*, vol. 89, 1934, pp. 1-11.
- 25 "Heat Capacity Curves of the Simpler Gases. IV. Extension of the 'Free Energy' Formula of Giauque and Overstreet to Yield Reliable Approximation Formulas for the Calculation of Entropy and of Heat Capacity From Spectroscopic Data. Entropy and Heat Capacity of Carbon Monoxide and of Nitrogen From Near Zero Absolute to 5000°K," by H. L. Johnston and C. O. Davis, *Journal of the American Chemical Society*, vol. 56, 1934, pp. 271-276.
- 26 "Heats, Free Energies, and Equilibrium Constants of Some Reactions Involving O_2 , H_2 , H_2O , C , CO , CO_2 ," by D. D. Wagman, J. E. Kilpatrick, W. J. Taylor, K. S. Pitzer, and F. D. Rossini, *Journal of Research of the National Bureau of Standards*, vol. 34, 1945, pp. 143-161, Research Paper RP1634.
- 27 "Thermodynamic Functions for Molecular Nitrogen in the Ideal Gas State," by H. W. Woolley, National Bureau of Standards, private communication, unpublished, 1944; revised, 1947.
- 28 "The Heat Capacity and Entropy of Carbon Monoxide. Heat of Vaporization. Vapor Pressures of Solid and Liquid. Free Energy to 5000°K From Spectroscopic Data," by J. O. Clayton and W. F. Giauque, *Journal of the American Chemical Society*, vol. 54, 1932, pp. 2610-2626; *ibid.*, vol. 55, 1933, pp. 5071-5073.
- 29 "Mathematical Methods for Computing Thermodynamic Functions from Spectroscopic Data," by L. S. Kassel, *Journal of Chemical Physics*, vol. 1, 1933, pp. 576-585.
- 30 "Evaluation of the Series Which Arise in the Calculation of Thermodynamic Quantities from Spectroscopic Data," by A. R. Gordon and C. Barnes, *Journal of Chemical Physics*, vol. 1, 1933, pp. 297-307.
- 31 "Specific Heats of Air, Oxygen, Nitrogen From 20°C to 370°C," by P. S. H. Henry, Proceedings of the Royal Society of London, part A, vol. 133, 1931, pp. 492-500.
- 32 "Die spezifische Wärme der Gase bei mittleren und hohen Temperaturen. I. Die spezifische Wärme der Gase: Luft, Stickstoff, Sauerstoff, Kohlenoxyd, Kohlensäure, Stickoxydul und Methan zwischen 0° und 220°C," by A. Eucken and K. v. Lüde, *Zeit. für Physikalische Chemie*, part B, vol. 5, 1929, pp. 413-441.
- 33 "Die Bestimmung der wahren spezifischen Wärme einiger Gase bei hohen Temperaturen nach der Lummer-Pringsheim'schen Methode," by A. Eucken, and O. Mücke, *Zeit. für Physikalische Chemie*, part B, vol. 18, 1932, pp. 167-188.
- 34 "The Determination of the Specific Heat of Gases at High Temperatures by the Sound Velocity Method. I. Carbon Monoxide," by G. G. Sherratt and E. Griffiths, Proceedings of the Royal Society of London, series A, vol. 147, 1934, pp. 292-308.
- 35 "The Specific Heat of Gases at High Temperatures," by R. W. Fenning and A. C. Whiffin, Philosophical Transactions of the Royal Society of London, series A, vol. 238, 1939, pp. 149-212.

Discussion

H. W. Woolley: The computations described in this paper seem to have been made carefully and

ambiguity in his private communication of 1944 (27),⁹ which must have led to the statement that for one of his tables incorrect spectroscopic constants D_e and β_e , given by Spinks (14), apparently were used. Spinks' constants were not used, but instead computed constants which were essentially identical with those used in the present paper. Before accepting the statement that the constants by Spinks are incorrect, one might consider a deviation plot of divided differences of vibrational term values, according to actual observational data (9, 15),¹⁰ as shown in Fig. 3 of this discussion. The sloping straight line represents the equation given by Birge and Hopfield, drawn with a half-width equal to 0.1 cm^{-1} the uncertainty assigned to ω by the authors of the present paper. The scattering of the data of Birge and Hopfield are regarded by the writer as consistent with careful measurement, since they had to measure their photographic film to $1/1000$ mm to determine a line to one wave number. The uncertainty of 2 cm^{-1} given by Rasetti for his 1929 Raman value, is shown on the

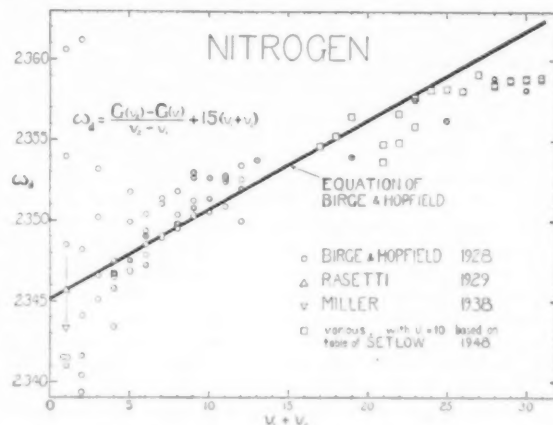


FIG. 3 VIBRATIONAL DATA FOR NITROGEN

diagram. The 1938 Raman value of Miller is 2.4 cm^{-1} below the value of Rasetti. If one takes the uncertainty in ω from that for the Raman data, and the uncertainty in α as assigned by the authors, then the values of Spinks for D and β are covered by their uncertainties.

In spite of the possibility of further improvement in the spectroscopic constants, the writer has considered the new table for nitrogen to be a satisfactory basis for a table in the NBS-NACA series of "Thermal Properties of Gases." This table, Table 11.10 of that series, extends on upward in temperature to 5000 K, using the writer's 1947 results, which were obtained quite simply by using the tables of Gordon and Barnes with a small corrective addition appropriate for higher temperature. His results were in excellent agreement with the results presented in this paper, but were based on four-decimal-place tables so there was no thought of five-decimal-place accuracy.

A year ago Professor Gratch presented values of zero-pressure thermodynamic properties of carbon dioxide at a meeting of the Society (1).⁸ His results for the specific heat are shown in a deviation plot in Fig. 4 of this discussion. The writer has been quite puzzled about their lack of fit to the temperature range above 2000 K. Comparison with an admitted uncertainty of 0.1 cal/deg

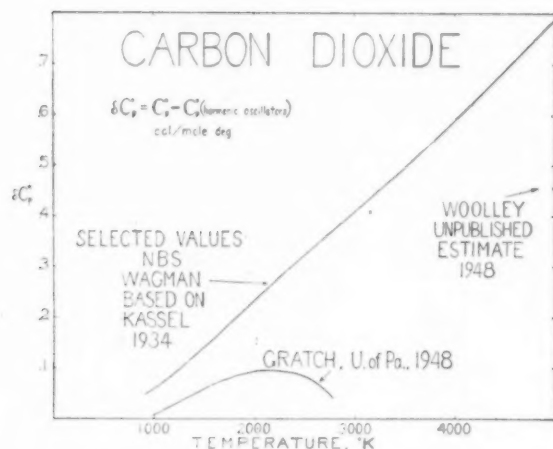


FIG. 4. COMPARISON OF ESTIMATES FOR SPECIFIC HEAT FOR CARBON DIOXIDE

based on Kassel's results, and with an estimate which was made for 5000 K have led the writer to think that there might be something in the results which should be investigated further. In spite of this, the results presented by Professor Gratch for carbon dioxide have been included in the NBS-NACA tables as the only recently computed table available. It is the writer's private impression, however, that if any rocket researchers or others are interested in very accurate values for calculations at elevated temperatures, they should take Fig. 4 of this discussion into account and be aware that values obtained by a wrong extrapolation might possibly be in error by several units in the first decimal place in such a function as the specific heat, with corresponding errors in the other thermodynamic functions.

AUTHORS' CLOSURE

We regret that we must disagree with most of Mr. Woolley's criticisms of our paper. Consider first his criticism of the standard error ($\pm 0.1 \text{ cm}^{-1}$) we have assigned to the Birge-Hopfield best value (2345.16 cm^{-1}) of the vibrational constant ω_0 . His plot of the observed vibrational data, Fig. 3, is entirely misleading because it gives undue weight to the low-quantum-number data. After all, it is the quantity $G(v) = \omega_0(v + \frac{1}{2}) + \dots$ that is important for the determination of zero-pressure thermodynamic properties; hence the problem is to determine these values of ω_0 , $\omega_0 x_0$, etc. which, when inserted in the Birge-Hopfield-Herman equation, give the best values of $G(v)$ from the least squares point of view. If he had plotted observed values of $G(v) - G(v_0)$ as deviations from the corresponding values calculated from the

Birge-Hopfield-Herman equation and then analyzed these deviations by the method of least squares after weighting them properly, he would have found that $\pm 0.1 \text{ cm}^{-1}$ is indeed a reasonable estimate of the standard error of ω_0 despite the fact that individual wave-length measurements may be uncertain by as much as several reciprocal centimeters, especially at low quantum numbers.

Next, consider Mr. Woolley's comments on the rotational constants D_e and β_0 . Theoretically, D_e should be approximately equal to the quantity $4B_e^2/\omega_0^2$. From this it is clear that the disagreement between us regarding the uncertainty of ω_0 is entirely irrelevant to the discussion of D_e ; Fig. 3 has no bearing on the matter whatsoever. The largest observed rotational quantum number J is about 20; D_e is of order of magnitude 6×10^{-4} ; the corresponding value of $D_e J^2(J+1)^2$ is about 1 cm^{-1} ; this is probably well within the uncertainty of the rotational wave-length measurements which cannot, therefore, yield reliable values of D_e and β_0 . But, in order to calculate reliable values of the zero-pressure thermodynamic properties of nitrogen even up to temperatures as high as 5000 deg R we must take account of rotational levels up to $J = 100$; therefore we are practically forced to rely on the theoretical values of D_e and β_0 . When we found that our calculated values of these rotational constants differed appreciably from those of Spinks we consulted Professor Herzberg who assured us that ours were correct and that those of Spinks were definitely in error. We can admit no ambiguity in Mr. Woolley's statement to one of us (SG) that his original (1944) calculations of the zero-pressure thermodynamic properties of nitrogen were based on Spinks' incorrect values of D_e and β_0 ; furthermore, we note that the results of Mr. Woolley's subsequent (1947) calculations differ from those of his original calculations by amounts that are accurately accounted for by an assumed change from the Spinks to the theoretical values of D_e and β_0 .

Mr. Woolley has been good enough to comment upon a previous paper by one of us (SG) entitled, "Zero-Pressure Thermodynamic Properties of Carbon Dioxide." We heartily agree with him that the results presented therein may not stand extrapolation to temperatures as high as 5000 deg K and we second his warning to rocket researchers and others against placing reliance on any rule-of-thumb extrapolation. In our opinion Mr. Woolley's Fig. 4 is an excellent example of the kind of extrapolation to be avoided especially since it starts away down at 1000 deg K, the highest temperature for which Kassel made accurate calculations. It is our impression that Mr. Woolley made a number of rather drastic approximations in arriving at his unpublished estimate of the value of zero-pressure isobaric specific heat at 5000 deg K and that, therefore, accurate calculations may or may not confirm it. We see no reason to conclude that the downward concavity of the Gratch curve below 2700 deg K (Fig. 4) must persist above that temperature. In short, we are inclined to think that the comparison of Fig. 4 is entirely meaningless.

18 "Molecular Spectra and Molecular Structure. I. Diatomic Molecules," by G. Herzberg, Prentice-Hall, Inc., New York, N. Y., 1939, pp. 151-155.

19 "Rotational and Vibrational Structure of the Fourth Positive Bands of Carbon Monoxide," by D. N. Read, *Physical Review*, vol. 46, 1934, pp. 571-575.

20 "On the Cameron Bands (Σ — Σ) of Carbon Monoxide," by L. Gerö, G. Herzberg, and R. Schmid, *Physical Review*, vol. 52, 1937, pp. 467-471.

21 "Zero-Pressure Properties of Diatomic Gases. II. Carbon Monoxide," by Serge Gratch, Annual Report From the Thermodynamics Research Laboratory, University of Pennsylvania, July, 1947, Project G-3.

22 "Zur Vervollständigung des Termschemas von Kohlenoxyd. II," by R. Schmid and L. Gerö, *Zeit. für Physik*, vol. 106, 1937, pp. 205-211.

23 "The Heat Capacity and Entropy of Nitrogen. Heat of Vaporization. Vapor Pressure of Solid and Liquid. The reaction $\frac{1}{2} N_2 + \frac{1}{2} O_2 = NO$ from Spectroscopic Data," by W. F. Giauque and J. O. Clayton, *Journal of the American Chemical Society*, vol. 55, 1933, pp. 4875-4889.

24 "Spektroskopische Berechnung der Molwärmen von Luft, O_2 , N_2 ," by M. Trautz and H. Adler, *Zeit. für Physik*, vol. 89, 1934, pp. 1-11.

25 "Heat Capacity Curves of the Simpler Gases. IV. Extension of the 'Free Energy' Formula of Giauque and Overstreet to Yield Reliable Approximation Formulas for the Calculation of Entropy and of Heat Capacity From Spectroscopic Data. Entropy and Heat Capacity of Carbon Monoxide and of Nitrogen From Near Zero Absolute to 5000°K," by H. L. Johnston and C. O. Davis, *Journal of the American Chemical Society*, vol. 56, 1934, pp. 271-276.

26 "Heats, Free Energies, and Equilibrium Constants of Some Reactions Involving O_2 , H_2 , H_2O , C , CO , CO_2 ," by D. D. Wagman, J. E. Kilpatrick, W. J. Taylor, K. S. Pitzer, and F. D. Rossini, *Journal of Research of the National Bureau of Standards*, vol. 34, 1945, pp. 143-161, Research Paper RP1634.

27 "Thermodynamic Functions for Molecular Nitrogen in the Ideal Gas State," by H. W. Woolley, National Bureau of Standards, private communication, unpublished, 1944; revised, 1947.

28 "The Heat Capacity and Entropy of Carbon Monoxide. Heat of Vaporization. Vapor Pressures of Solid and Liquid. Free Energy to 5000°K From Spectroscopic Data," by J. O. Clayton and W. F. Giauque, *Journal of the American Chemical Society*, vol. 54, 1932, pp. 2610-2626; *ibid.*, vol. 55, 1933, pp. 5071-5073.

29 "Mathematical Methods for Computing Thermodynamic Functions from Spectroscopic Data," by L. S. Kassel, *Journal of Chemical Physics*, vol. 1, 1933, pp. 576-585.

30 "Evaluation of the Series Which Arise in the Calculation of Thermodynamic Quantities from Spectroscopic Data," by A. R. Gordon and C. Barnes, *Journal of Chemical Physics*, vol. 1, 1933, pp. 297-307.

31 "Specific Heats of Air, Oxygen, Nitrogen From 20°C to 370°C," by P. S. H. Henry, Proceedings of the Royal Society of London, part A, vol. 133, 1931, pp. 492-506.

32 "Die spezifische Wärme der Gase bei mittleren und hohen Temperaturen. I. Die spezifische Wärme der Gase: Luft, Stickstoff, Sauerstoff, Kohlenoxyd, Kohlensäure, Stickoxydul und Methan zwischen 0° und 220°C," by A. Eucken and K. v. Lude, *Zeit. für Physikalische Chemie*, part B, vol. 5, 1929, pp. 413-441.

33 "Die Bestimmung der wahren spezifischen Wärme einiger Gase bei hohen Temperaturen nach der Lummer-Pringsheim'schen Methode," by A. Eucken, and O. Mücke, *Zeit. für Physikalische Chemie*, part B, vol. 18, 1932, pp. 167-188.

34 "The Determination of the Specific Heat of Gases at High Temperatures by the Sound Velocity Method. I. Carbon Monoxide," by G. G. Sherratt and E. Griffiths, Proceedings of the Royal Society of London, series A, vol. 147, 1934, pp. 292-308.

35 "The Specific Heat of Gases at High Temperatures," by R. W. Fenning and A. C. Whiffin, Philosophical Transactions of the Royal Society of London, series A, vol. 238, 1939, pp. 149-212.

Discussion

H. W. WOOLLEY.⁸ The computations described in this paper seem to have been made carefully and to show considerable ingenuity in the arrangement of the method of calculation.

In regard to nitrogen, the writer wishes to apologize for some

⁸ Thermodynamics Section, National Bureau of Standards, U. S. Department of Commerce, Washington, D. C.

ambiguity in his private communication of 1944 (27),⁹ which must have led to the statement that for one of his tables incorrect spectroscopic constants D_e and β_0 , given by Spinks (14), apparently were used. Spinks' constants were not used, but instead computed constants which were essentially identical with those used in the present paper. Before accepting the statement that the constants by Spinks are incorrect, one might consider a deviation plot of divided differences of vibrational term values, according to actual observational data (9, 15),¹⁰ as shown in Fig. 3 of this discussion. The sloping straight line represents the equation given by Birge and Hopfield, drawn with a half-width equal to 0.1 cm^{-1} the uncertainty assigned to ω by the authors of the present paper. The scattering of the data of Birge and Hopfield are regarded by the writer as consistent with careful measurement, since they had to measure their photographic film to $1/1000$ mm to determine a line to one wave number. The uncertainty of 2 cm^{-1} given by Rasetti for his 1929 Raman value, is shown on the

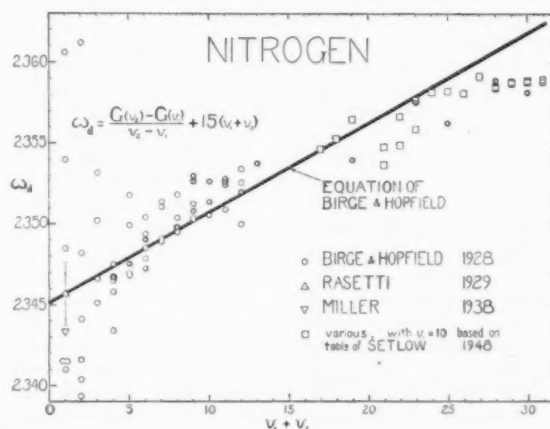


FIG. 3 VIBRATIONAL DATA FOR NITROGEN

diagram. The 1938 Raman value of Miller is 2.4 cm^{-1} below the value of Rasetti. If one takes the uncertainty in ω from that for the Raman data, and the uncertainty in α as assigned by the authors, then the values of Spinks for D and β are covered by their uncertainties.

In spite of the possibility of further improvement in the spectroscopic constants, the writer has considered the new table for nitrogen to be a satisfactory basis for a table in the NBS-NACA series of "Thermal Properties of Gases." This table, Table 11.10 of that series, extends on upward in temperature to 5000 K, using the writer's 1947 results, which were obtained quite simply by using the tables of Gordon and Barnes with a small corrective addition appropriate for higher temperature. His results were in excellent agreement with the results presented in this paper, but were based on four-decimal-place tables so there was no thought of five-decimal-place accuracy.

A year ago Professor Gratch presented values of zero-pressure thermodynamic properties of carbon dioxide at a meeting of the Society (1).⁹ His results for the specific heat are shown in a deviation plot in Fig. 4 of this discussion. The writer has been quite puzzled about their behavior in the temperature range above 2000 K. Comparison with an admittedly uncertain extrapolation

⁹ Reference is to authors' bibliography.

¹⁰ Authors' bibliography (9, 15) and the following:

"A Note on the Raman Spectra of Nitrogen," by C. E. Miller, *Journal of Chemical Physics*, vol. 6, 1938, pp. 902-904.

"High Energy States of N_2^+ and N_2 ," by R. B. Setlow, *Physical Review*, vol. 74, 1948, pp. 153-162.

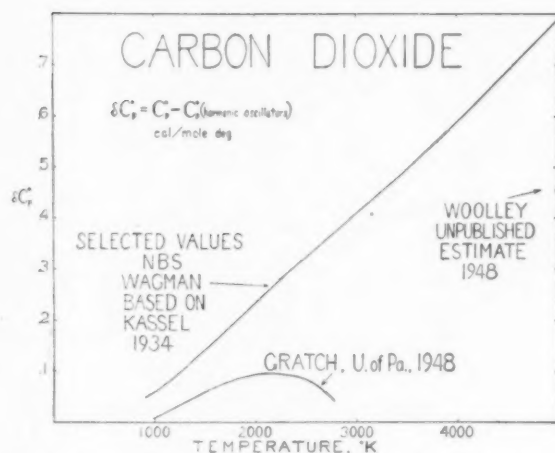


FIG. 4. COMPARISON OF ESTIMATES FOR SPECIFIC HEAT FOR CARBON DIOXIDE

based on Kassel's results, and with an estimate which was made for 5000 K have led the writer to think that there might be something in the results which should be investigated further. In spite of this, the results presented by Professor Gratch for carbon dioxide have been included in the NBS-NACA tables as the only recently computed table available. It is the writer's private impression, however, that if any rocket researchers or others are interested in very accurate values for calculations at elevated temperatures, they should take Fig. 4 of this discussion into account and be aware that values obtained by a wrong extrapolation might possibly be in error by several units in the first decimal place in such a function as the specific heat, with corresponding errors in the other thermodynamic functions.

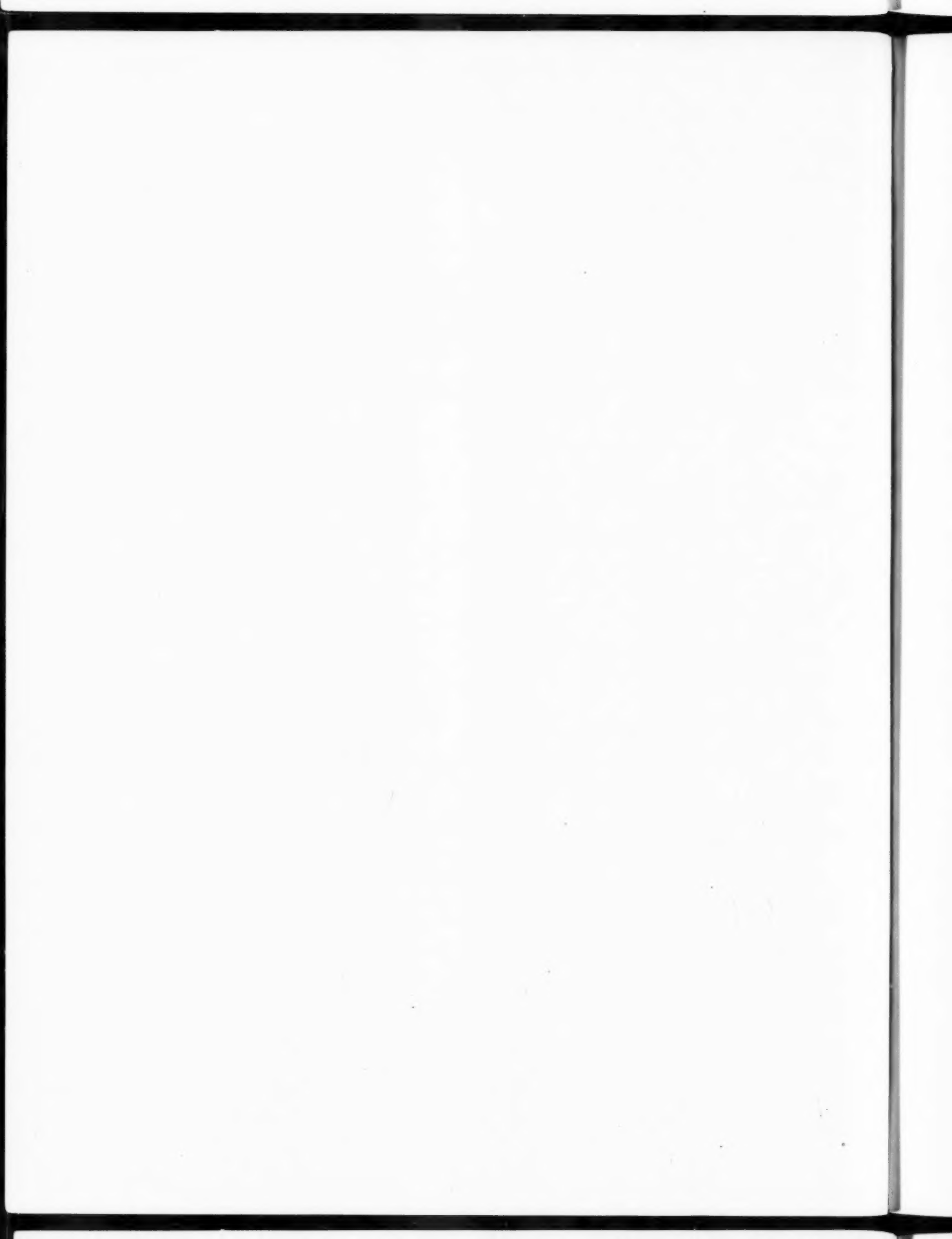
AUTHORS' CLOSURE

We regret that we must disagree with most of Mr. Woolley's criticisms of our paper. Consider first his criticism of the standard error ($\pm 0.1 \text{ cm}^{-1}$) we have assigned to the Birge-Hopfield best value (2345.16 cm^{-1}) of the vibrational constant ω_0 . His plot of the observed vibrational data, Fig. 3, is entirely misleading because it gives undue weight to the low-quantum-number data. After all, it is the quantity $G(v) = \omega_e(v + 1/2) + \dots$ that is important for the determination of zero-pressure thermodynamic properties; hence the problem is to determine those values of ω_e , $\omega_e x_e$, etc. which, when inserted in the Birge-Hopfield-Herman equation, give the best values of $G(v)$ from the least squares point of view. If he had plotted observed values of $G(v_2) - G(v_1)$ as deviations from the corresponding values calculated from the

Birge-Hopfield-Herman equation and then analyzed these deviations by the method of least squares after weighting them properly, he would have found that $\pm 0.1 \text{ cm}^{-1}$ is indeed a reasonable estimate of the standard error of ω_0 despite the fact that individual wave-length measurements may be uncertain by as much as several reciprocal centimeters, especially at low quantum numbers.

Next, consider Mr. Woolley's comments on the rotational constants D_e and β_0 . Theoretically, D_e should be approximately equal to the quantity $4B_e^2/\omega_e^2$. From this it is clear that the disagreement between us regarding the uncertainty of ω_0 is entirely irrelevant to the discussion of D_e ; Fig. 3 has no bearing on the matter whatsoever. The largest observed rotational quantum number J is about 20; D_e is of order of magnitude 6×10^{-6} ; the corresponding value of $D_e J^2(J+1)^2$ is about 1 cm^{-1} ; this is probably well within the uncertainty of the rotational wave-length measurements which cannot, therefore, yield reliable values of D_e and β_0 . But, in order to calculate reliable values of the zero-pressure thermodynamic properties of nitrogen even up to temperatures as high as 5000 deg R we must take account of rotational levels up to $J = 100$; therefore we are practically forced to rely on the theoretical values of D_e and β_0 . When we found that our calculated values of these rotational constants differed appreciably from those of Spinks we consulted Professor Herzberg who assured us that ours were correct and that those of Spinks were definitely in error. We can admit no ambiguity in Mr. Woolley's statement to one of us (SG) that his original (1944) calculations of the zero-pressure thermodynamic properties of nitrogen were based on Spinks' incorrect values of D_e and β_0 ; furthermore, we note that the results of Mr. Woolley's subsequent (1947) calculations differ from those of his original calculations by amounts that are accurately accounted for by an assumed change from the Spinks to the theoretical values of D_e and β_0 .

Mr. Woolley has been good enough to comment upon a previous paper by one of us (SG) entitled, "Zero-Pressure Thermodynamic Properties of Carbon Dioxide." We heartily agree with him that the results presented therein may not stand extrapolation to temperatures as high as 5000 deg K and we second his warning to rocket researchers and others against placing reliance on any rule-of-thumb extrapolation. In our opinion Mr. Woolley's Fig. 4 is an excellent example of the kind of extrapolation to be avoided especially since it starts away down at 1000 deg K, the highest temperature for which Kassel made accurate calculations. It is our impression that Mr. Woolley made a number of rather drastic approximations in arriving at his unpublished estimate of the value of zero-pressure isobaric specific heat at 5000 deg K and that, therefore, accurate calculations may or may not confirm it. We see no reason to conclude that the downward concavity of the Gratch curve below 2700 deg K (Fig. 4) must persist above that temperature. In short, we are inclined to think that the comparison of Fig. 4 is entirely meaningless.



The Thermodynamic Properties of Helium

By S. W. AKIN,¹ SCHENECTADY, N. Y.

Evaluation has been made of the density, enthalpy, entropy, viscosity, and thermal conductivity of helium in the range of pressures from atmospheric to 6000 psia and at temperatures from -440 F to 600 F. These data are composed of observed values published prior to 1945, and of extrapolations based upon the Beattie-Bridgeman equation of state and kinetic theory. The results evaluated to four significant figures are tabulated for particular values of pressure and temperature. Graphic plots of the same information are also presented, with an accuracy sufficient for investigations of flow and heat-transfer processes involving high-pressure helium.

INTRODUCTION

THE properties of helium for engineering use presented in this paper are based upon the most acceptable values of experimental data as reviewed and evaluated by Keesom (1).² The range of these observed data was extended where necessary by extrapolation procedures which are described under headings for each of the properties. In summary, the respective range of pressures and temperatures included by experimental data and extrapolation is shown in Table 1. For the density data, this information is shown in Fig. 1.

TABLE 1 RANGE OF PRESSURES AND TEMPERATURES STUDIED

	Observed range		Extrapolated range	
	Pressure, psia	Temperature, deg F	Pressure, psia	Temperature, deg F
Viscosity.....	Independent	-435 to 1525	None	None
Thermal conductivity.....	Independent	-424 to 212	None	212 to 1100
Enthalpy.....	14.7 to 900	-440	900 to 6000	-440 to 600
Entropy.....	14.7 to 900	-440	900 to 6000	-440 to 600

To maintain consistency in the thermodynamic properties, two independent equations were used in the evaluations. The numerical results were in agreement within 0.5 per cent. Where graphical solutions were necessary, plotting was arranged to permit the reading of values to a corresponding degree of accuracy.

DENSITY

To determine the densities at the temperatures and pressures selected in this report, the reciprocal of density (specific volume) was evaluated from the Beattie-Bridgeman equation of state (2). For convenience, the values of the constant terms given in refer-

¹ General Engineering and Consulting Laboratory, General Electric Company. Jun. ASME.

² Numbers in parentheses refer to the Bibliography at the end of the paper.

Contributed by the Special Research Committee on Properties of Gases and Gas Mixtures and the Heat Transfer and Applied Mechanics Divisions and presented at the Annual Meeting, New York, N. Y., November 27-December 2, 1949, of THE AMERICAN SOCIETY OF MECHANICAL ENGINEERS.

NOTE: Statements and opinions advanced in papers are to be understood as individual expressions of their authors and not those of the Society. Manuscript received at ASME Headquarters, October 10, 1949. Paper No. 49-A-96.

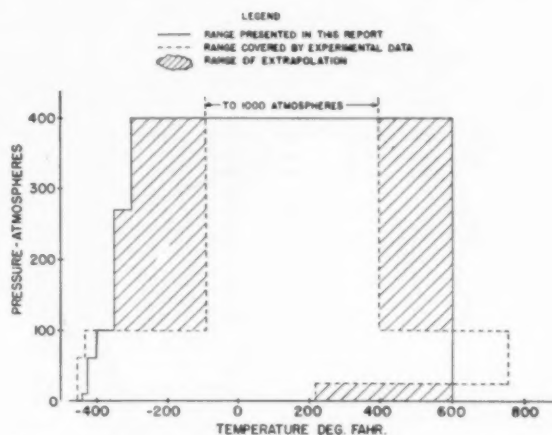


FIG. 1 PLOT COMPARING RANGE OF TEMPERATURES AND PRESSURES COVERED BY OBSERVED VALUES OF DENSITY FROM REFERENCE (1) AND DENSITIES PRESENTED IN PAPER (Shaded portion indicates the range of extrapolation.)

ence (2) were converted to the engineering units indicated.

$$p = \frac{RT(1-\alpha)(v+B)}{v^2} - \frac{A}{v^2} \quad [1]$$

where

p = absolute pressure, psia

T = absolute temperature, deg R

$T^\circ R = t^\circ F + 459.69$

v = specific volume, ft³/lb

$R = 2.6829, \frac{\text{ft}^3 \cdot \text{lb}}{^\circ R \cdot \text{lb} \cdot \text{in.}^2}$

$\alpha = \frac{C}{vT^2}$, dimensionless

$A = A_1 \left(1 - \frac{a}{v}\right)$

$A_1 = 5.0906, (\text{ft}^3/\text{lb})^2 \times (\text{lb}/\text{in.}^2)$

$a = 0.23963, \text{ft}^3/\text{lb}$

$B = B_1 \left(1 - \frac{b}{v}\right)$

$B_1 = 0.056063, \text{ft}^3/\text{lb}$

$b = 0$

$C = 934.17, \frac{\text{ft}^3 T^2}{\text{lb}}$

The specific volumes are given in Table 2.

At several pressures and temperatures throughout the range of calculations, the specific volumes computed from Equation [1] were compared with values determined from the equation of state in the virial form, as follows

$$p = \frac{RT}{(v-B_0)} \quad [2]$$

The second virial coefficient B_0 was evaluated using the relation

TABLE 2 PROPERTIES OF HELIUM

Absolute Pressure, Lbs. per sq. in., 14.696	v , Specific volume, cu ft per lb															s , Entropy, Btu per lb, deg F		h , Enthalpy, Btu per lb		T , Total temperature, deg F	
	-144	-125	-100	-75	-50	-25	0	25	50	75	100	125	150	175	200	25	50	25	50	25	50
v	3.431	6.315	10.92	20.08	29.20	38.33	47.46	56.59	65.72	74.85	83.97	93.10	102.2	111.3	120.5	130.7	140.8	150.9	161.0	171.1	181.2
h	26.5	46.2	76.9	138.8	200.9	263.0	325.1	387.1	449.2	511.3	573.3	635.4	697.4	759.5	821.5	883.6	945.6	1007.7	1069.7	1131.8	1193.8
s	2.002	3.394	4.045	4.807	5.276	5.616	5.893	6.133	6.390	6.697	6.942	7.147	7.322	7.478	7.615	7.738	7.851	7.955	8.050	8.136	8.214
v	0.8947	1.847	3.225	5.925	8.613	11.30	13.98	16.67	19.35	22.02	24.70	27.37	30.04	32.71	35.38	38.05	40.72	43.39	46.06	48.73	51.40
h	24.9	43.4	76.7	139.0	201.1	263.2	325.3	387.4	449.5	511.6	573.7	635.8	697.9	759.9	822.0	884.1	946.2	1008.3	1070.4	1132.5	1194.6
s	1.997	2.749	3.435	4.197	4.667	5.008	5.275	5.495	5.682	5.869	6.054	6.234	6.409	6.578	6.742	6.901	7.056	7.207	7.355	7.500	7.642
v	0.209	0.6166	1.094	2.001	2.901	3.797	4.693	5.589	6.484	7.380	8.276	9.172	10.06	10.96	11.85	12.74	13.63	14.52	15.41	16.30	17.19
h	21.3	43.5	75.9	139.3	201.8	264.0	326.2	388.3	450.4	512.5	574.6	636.7	698.8	760.9	823.0	885.1	947.2	1009.3	1071.4	1133.5	1195.6
s	1.269	2.196	2.664	3.040	3.331	3.582	3.799	4.000	4.195	4.384	4.568	4.747	4.921	5.090	5.254	5.413	5.568	5.719	5.866	6.010	6.151
v	0.2566	0.4344	0.7768	1.116	1.453	1.790	2.127	2.463	2.800	3.137	3.474	3.811	4.148	4.485	4.822	5.159	5.496	5.833	6.170	6.507	6.844
h	41.5	75.7	140.3	203.4	266.0	328.3	390.5	452.7	514.9	577.1	639.3	701.5	763.7	825.9	888.1	950.3	1012.5	1074.7	1136.9	1199.1	1261.3
s	1.618	2.380	3.156	3.631	3.973	4.241	4.481	4.699	4.906	5.101	5.294	5.486	5.677	5.867	6.056	6.243	6.428	6.611	6.792	6.972	7.150
v	0.199	0.3094	0.5327	0.7990	1.0944	1.209	1.434	1.658	1.882	2.107	2.331	2.555	2.779	3.003	3.227	3.451	3.675	3.899	4.123	4.347	4.571
h	41.3	75.4	141.0	204.7	267.5	330.0	392.3	454.6	516.9	579.2	641.5	703.8	766.1	828.4	890.7	953.0	1015.3	1077.6	1139.9	1202.2	1264.5
s	1.396	2.176	2.955	3.428	3.770	4.039	4.259	4.446	4.611	4.765	4.909	5.053	5.197	5.340	5.483	5.626	5.769	5.912	6.055	6.198	6.341
v	0.146	0.221	0.3704	0.5212	0.6717	0.8080	0.9720	1.122	1.421	1.720	2.019	2.317	2.616	2.914	3.212	3.510	3.808	4.106	4.404	4.702	5.000
h	43.0	75.0	142.1	206.6	269.6	332.5	395.0	457.3	519.7	582.0	644.3	706.6	768.9	831.2	893.5	955.8	1018.1	1080.4	1142.7	1205.0	1267.3
s	1.176	1.984	2.750	3.224	3.567	3.836	4.057	4.245	4.432	4.619	4.806	4.993	5.180	5.367	5.554	5.741	5.928	6.115	6.302	6.489	6.676
v	0.11	0.154	0.2410	0.3310	0.4214	0.5118	0.6021	0.6922	0.7822	0.8722	0.9622	1.0522	1.1422	1.2322	1.3222	1.4122	1.5022	1.5922	1.6822	1.7722	1.8622
h	75.2	144.3	210.5	274.5	337.6	400.4	463.2	526.0	588.8	651.6	714.4	777.2	840.0	902.8	965.6	1028.4	1091.2	1154.0	1216.8	1279.6	1342.4
s	1.752	2.498	2.968	3.311	3.560	3.801	4.000	4.195	4.384	4.568	4.747	4.921	5.090	5.254	5.413	5.568	5.719	5.866	6.010	6.151	6.292
v	0.09	0.11	0.163	0.2166	0.2707	0.3251	0.3795	0.4338	0.4882	0.5422	0.5966	0.6510	0.7054	0.7598	0.8142	0.8686	0.9230	0.9774	1.0318	1.0862	1.1406
h	148	217	282.2	346.1	409.0	472.0	535.0	598.0	661.0	724.0	787.0	850.0	913.0	976.0	1039.0	1102.0	1165.0	1228.0	1291.0	1354.0	1417.0
s	2.255	2.712	3.054	3.324	3.545	3.734	3.902	4.060	4.218	4.376	4.534	4.692	4.850	5.008	5.166	5.324	5.482	5.640	5.798	5.956	6.114
v	0.07	0.09	0.119	0.151	0.185	0.219	0.253	0.286	0.320	0.354	0.388	0.422	0.456	0.490	0.524	0.558	0.592	0.626	0.660	0.694	0.728
h	164	227	293.9	358.9	422.7	486.5	550.3	614.1	677.9	741.7	805.5	869.3	933.1	996.9	1060.7	1124.5	1188.3	1252.1	1315.9	1379.7	1443.5
s	2.036	2.479	2.816	3.067	3.286	3.481	3.660	3.834	4.003	4.167	4.331	4.495	4.659	4.823	4.987	5.151	5.315	5.479	5.643	5.807	5.971
v	0.06	0.07	0.09	0.114	0.137	0.160	0.183	0.205	0.227	0.249	0.271	0.293	0.315	0.337	0.359	0.381	0.403	0.425	0.447	0.469	0.491
h	240	309.4	375.9	440.6	504.4	568.2	632.0	695.8	759.6	823.4	887.2	951.0	1014.8	1078.6	1142.4	1206.2	1270.0	1333.8	1397.6	1461.4	1525.2
s	2.279	2.614	2.881	3.102	3.292	3.460	3.618	3.766	3.904	4.042	4.180	4.318	4.456	4.594	4.732	4.870	5.008	5.146	5.284	5.422	5.560

from reference (3) with the constants converted to engineering units

$$B_0 = 0.305937 \tau^{3/4} - 1.845 \tau^{2/4} - 0.822 \tau^{1/4} \dots [3]$$

where

B_0 is expressed in ft³/lb

τ = reciprocal temperature (1/T°R)

T°R = (t°F + 459.69)

Calculations showed that the coefficients given by this equation were in substantial agreement with the values adopted by Keesom (1).

The comparison indicates that for pressure less than 2500 psia and for densities less than 4.32 lb per cu ft (critical density), good agreement exists between the two equations. At higher pressures, the values determined from Equation [1] were from 3 to 10 per cent larger. However, Keesom (1) points out that no equation had been proposed which agrees exactly with observed facts. On the strength of his remarks, densities determined which were larger than 10 lb per cu ft have been reported to only one significant figure in order to show possible trends.

Another comparison was made at 30°C with the equation for the isotherm observed by C. A. Johnson (4). The greatest difference was about 1 per cent at 6000 psia. The equation is

$$pv = 1462.391 + 0.047232 p - 2.98 \times 10^{-7} p^2 \dots [4]$$

where

p = absolute pressure, psi

v = specific volume, ft³/lb

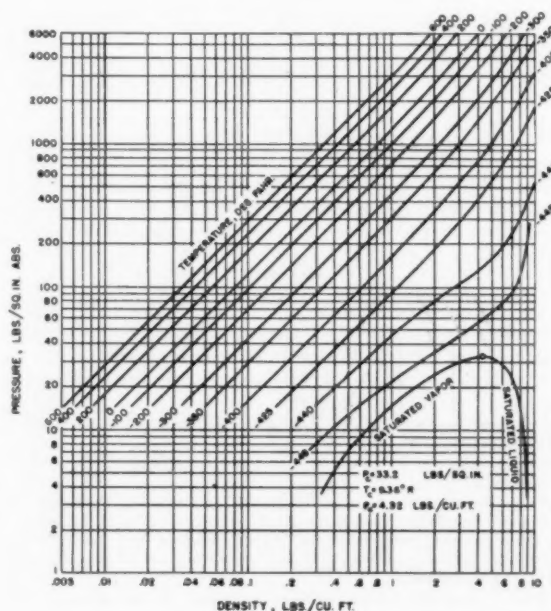


Fig. 2 DENSITY OF HELIUM PLOTTED AS FUNCTION OF ABSOLUTE PRESSURE FOR SELECTED RANGE OF TEMPERATURES

Fig. 2 shows a plot of the pressure, density, and temperature relations calculated from Equation [1]. Values for the saturated liquid and saturated vapor were taken directly from Zelmanov's data (5).

VISCOSITY

The following equation (1) was used to determine the viscosity of helium as plotted in Fig. 3

$$\eta = 8.315 (T)^{0.657} \times 10^{-4} \dots \dots \dots [5]$$

where

η = viscosity, lb (mass)/hr ft

T = absolute temperature, deg R

$T^{\circ}R = (t^{\circ}F + 459.69)$

The values found by this equation represent the true viscosity

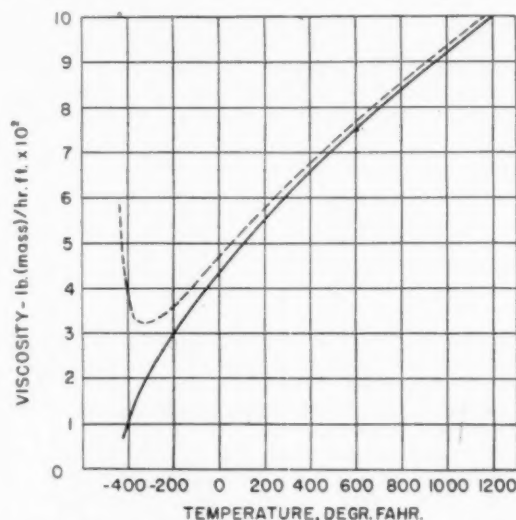


FIG. 3 VISCOSITY OF HELIUM PLOTTED AS FUNCTION OF TEMPERATURE
(Dashed line indicates estimated values for 6000 psia.)

with an accuracy of 1 per cent in the range of $-450^{\circ}F$ to $2000^{\circ}F$ and independent of pressure.³

Values determined in Equation [5] were compared with two

³ From consideration of kinetic theory, it is expected that viscosity should be independent of pressure (4). But at 6000 psia, the volume of the molecules is an appreciable part of the volume occupied by the gas, and therefore we might suppose helium would display the properties of a "dense" gas. To check this possibility, the variation of viscosity at high density was determined from the equation (6)

$$\frac{\eta'}{\eta} = b\rho \left(\frac{1}{b\rho x} + \frac{4}{5} + 0.7614 b\rho x \right)$$

where at a given temperature using any consistent set of units

η' is viscosity at high pressure

η is viscosity at atmospheric pressure

$$b = \frac{2}{3} \pi \frac{\sigma^2}{m}$$

σ = molecular radius

m = mass of helium atom

ρ = mass density

$$x = 1 + \frac{5}{8} b\rho + 0.2869 (b\rho)^2$$

The results of this computation are shown as the dashed line in Fig. 3, and indicate that at normal temperatures, the effect of increased pressure is not great. However, until data on the viscosity of helium at high pressures are available, these calculations should be considered only as an estimate of the possible variation.

separate equations covering the full temperature range. The first equation valid from $-258^{\circ}C$ to $-22^{\circ}C$ is (7)

$$\log_{10} (\eta) = 6.90595 - 10 + 0.650 \log_{10} T^{\circ}R \dots \dots \dots [6]$$

The second equation is a form of Sutherland's formula with constants suggested by Keyes (4), and is valid above $-100^{\circ}C$

$$\eta = \frac{249.67 \times 10^{-7} \sqrt{T}}{1 + \frac{100.4}{T}} \dots \dots \dots [7]$$

where for both equations

η = viscosity, lb (mass)/hr ft

T = temperature, deg R

$T^{\circ}R = (t^{\circ}F + 459.69)$

Agreement was within plus and minus 2 per cent from $-432^{\circ}F$ to $700^{\circ}F$, and within $3\frac{1}{2}$ per cent up to $1200^{\circ}F$.

THERMAL CONDUCTIVITY

The thermal-conductivity values given in Fig. 4 and listed in Table 3 combine three sources of information. In the range 3 R to 161 R, recent data published by Ubbink and de Haas (8) were used. In the range 161 R to 672 R, values were taken from a smoothed curve based upon an evaluation of the observed data

TABLE 3 INTERCEPT VALUES OF THERMAL CONDUCTIVITY AS A FUNCTION OF TEMPERATURE TAKEN FROM FIG. 4

k expressed as Btu/hr-ft ² (°F/ft)			
$T^{\circ}F$	$k \times 10^4$	$T^{\circ}F$	$k \times 10^4$
-456	22	-100	673
-450	63	0	792
-440	106	200	1000
-430	133	400	1191
-420	160	600	1365
-410	186	800	1524
-400	210	1000	1675
-300	400	1100	1750
-200	530		

by several experimenters (1). In the range 672 R to 1572 R, extrapolation was made by use of the following kinetic-theory (9) relation

$$k = \eta c_p \dots \dots \dots [8]$$

in which

k = thermal conductivity, Btu/hr-ft² (°F/ft)

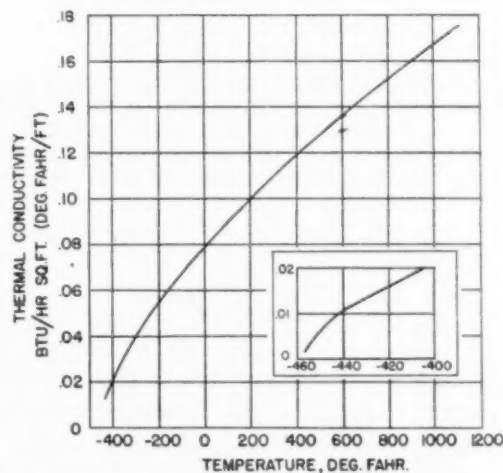


FIG. 4 THERMAL CONDUCTIVITY OF HELIUM PLOTTED AS FUNCTION OF TEMPERATURE

- η = viscosity, lb/hr-ft
 c_v = specific heat at constant volume, 0.7445 Btu/lb-°F
 ϵ = proportionality constant

A value for the proportionality constant, which could be used with reasonable certainty above 672 R, was obtained as follows: Equation [8] was solved for ϵ in the range 60 R to 672 R, using observed values of thermal conductivity, viscosity, and constant-volume specific heat. Above 540 R, ϵ had a constant value of 2.44. This value was then used in Equation [8] with the observed values of viscosity to determine the conductivity up to 1572 R. Table 3 gives the intercept values taken graphically from the smoothed curve in Fig. 4, with temperatures converted to the Fahrenheit scale.

ENTHALPY-ENTROPY

In order that the extrapolated enthalpy and entropy values presented in this paper would be consistent with recently published data, the following values (5 and 10) were taken as the datum⁴ for computation

- T_0 = absolute temperature, 19.69 R (−440 F)
 P_0 = absolute pressure, 14.7 psia
 h_0 = enthalpy, 26.56 Btu per lb
 S_0 = entropy, 2.602 Btu per lb-deg F

Evaluation of the enthalpies given in Table 2 proceeded as follows: Changes in enthalpy with increasing temperature at constant pressure were found from Equation [4]

$$h_T = h_0 + \int_{T_0}^T c_{p_0} dt + \int_{T_0}^T \left(\frac{\partial B_0}{\partial \tau} \right)_p dp \dots [9]$$

in which

- h_T = enthalpy at temperature T , Btu per lb
 h_0 = enthalpy at −440° F, 26.56 Btu per lb
 c_{p_0} = specific heat at constant pressure as $p \rightarrow 0$, 1.241 Btu per lb-°F
 p = absolute pressure, atm

The expression

$$\left(\frac{\partial B_0}{\partial \tau} \right)_p$$

obtained by operating on Equation [3], using the same notation is

$$\left(\frac{\partial B_0}{\partial \tau} \right)_p = 0.38242 \tau^{1/4} - 3.229 \tau^{3/4} - 1.850 \tau^{5/4} \dots [10]$$

The enthalpies at atmospheric pressure for the selected temperatures were calculated by substituting Equation [10] in Equation [9]. Letting these enthalpies at atmospheric pressure be the datum, the Joule-Kelvin coefficients were used to find the changes in temperature with increasing pressure. At the chosen enthalpies

$$\Delta T = \mu \Delta P \dots [11]$$

where, by definition

$$\mu = \left(\frac{\partial T}{\partial P} \right)_h = \text{deg R/psia}$$

T = absolute temperature, deg R

The Joule-Kelvin coefficients have been determined experimentally from 15 psia to 2930 psia in the range 572 F to −310 F

⁴ The datum for these values was chosen by the original investigator so that the enthalpy and entropy of liquid helium at 14.7 psia were equal to zero. The values given were obtained by graphical interpolation after suitable unit conversion.

(11). Down to −248 F, the coefficient is independent of pressure, but at lower temperatures it increases with increasing pressure.

To establish a reasonable basis for extrapolation to higher pressures, values of μ were calculated from 15 psia to 6000 psia in the range of 600 F to −300 F, using the well-known equation

$$\mu = -\frac{1}{c_p} \left[V - T \left(\frac{\partial V}{\partial T} \right)_p \right] \dots [12]$$

where $[(\partial V)/(\partial T)]_p$ was obtained by operation on the Beattie-Bridgeman equation of state.

The calculated coefficients showed a dependence on pressure at all temperatures which amounted to a variation of plus or minus 8 per cent from the average of the calculated values. Further, these average values were from 2 to 5 per cent less than the experimental values. The observation can be made that overall discrepancies of this magnitude in μ can cause errors in the enthalpies at 6000 psia of only about 1 per cent at −300 F, and even less at higher temperatures. On this basis, use of the experimental values listed in Table 4 for the entire range of pressures was concluded to be sufficiently accurate for this work.⁵

TABLE 4 JOULE-KELVIN COEFFICIENTS USED IN THE DETERMINATION OF ISENTHALPS FROM 15 PSIA TO 600 PSIA

Temp, deg F	°R/psia
600	0.00759
400	0.00759
200	0.00759
0	0.00735
−100	0.00710
−200	0.00655
−300	0.00480

It was possible to show a consistency in the variation of μ with temperature by checking the enthalpies for a given pressure found through Equation [11] by use of Equation [9]. At selected temperatures down to −300 F, the enthalpies were in disagreement by no more than 0.5 per cent.

Below −300 F, a temperature-enthalpy chart was constructed using Zelmanov's data below −425 F, and the previously calculated data above −300 F. Graphical interpolation with a readable accuracy of 0.1 Btu was used to determine the enthalpies listed in Table 2.

Additional auxiliary temperature-enthalpy curves were made to large scale from which the values for the isenthalps in Figs. 5, 6, and 7 were found. The accuracy of this graphical plot was within plus or minus 1 deg and one Btu.⁶

Using the values at atmospheric pressure given by Zelmanov, changes in the entropy with increasing temperature were made using the following equation

$$s_T = S_0 + c_p \ln \left(\frac{T}{T_0} \right) \dots [13]$$

When entropies had been calculated for the selected temperature, the entropies at higher pressures at these same temperatures were then determined, using the values at atmospheric pressure as the datum, and the following equation

$$s_p = S_0 + \int_{V_0}^V \left[\left(\frac{\partial p}{\partial T} \right)_V dv \right]_T \dots [14]$$

⁵ It is well to point out that the coefficients adopted by this procedure may not truly represent the actual phenomenon, and that experimental data at higher pressures would be desirable for checking the data given here.

⁶ Subsequent to the preparation of Figs. 5, 6, and 7, a slight error was found in checking the calculations. This error amounts to no more than 0.5 per cent at any temperature or pressure; this did not justify replotting the data. This accounts for the obvious discrepancies between Table 2 and Figs. 5, 6, and 7.

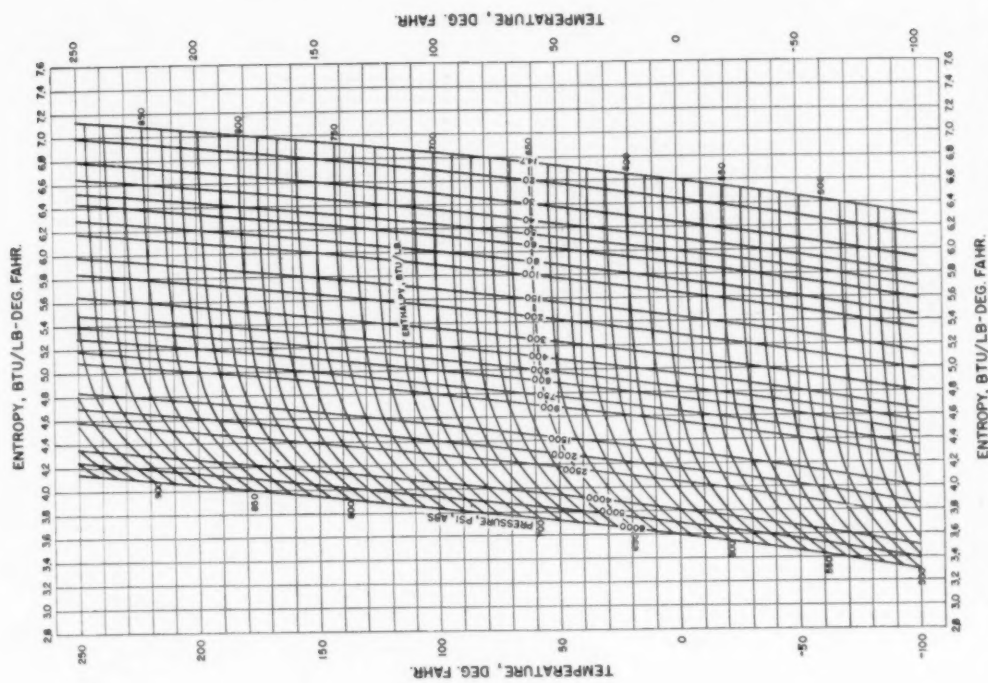


FIG. 5 TEMPERATURE-ENTROPY DIAGRAM FOR HELIUM IN RANGE -450 F TO -100 F FOR SELECTED SERIES OF PRESSURES AND SHOWING LINES OF CONSTANT ENTHALPY

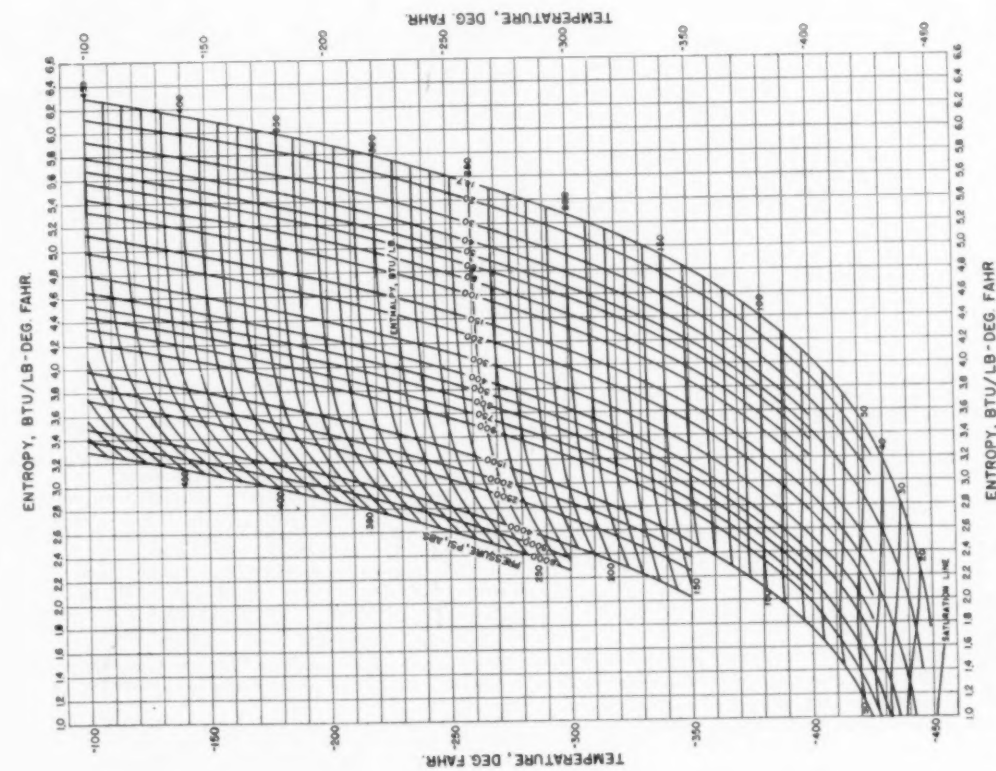


FIG. 6 TEMPERATURE-ENTROPY DIAGRAM FOR HELIUM IN RANGE -100 F TO 250 F FOR SELECTED SERIES OF PRESSURES AND SHOWING LINES OF CONSTANT ENTHALPY

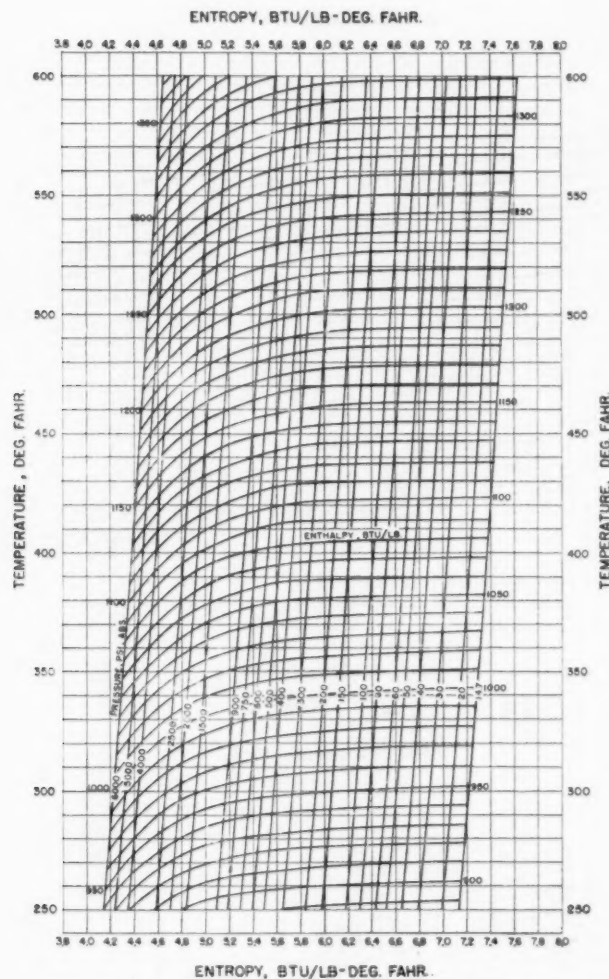


FIG. 7 TEMPERATURE-ENTROPY DIAGRAM FOR HELIUM IN RANGE 250 F TO 600 F FOR SELECTED SERIES OF PRESSURES AND SHOWING LINES OF CONSTANT ENTHALPY

The function $[(\partial p)/(\partial T)]_v$ was calculated by operating on the Beattie-Bridgeman equation. Again at the higher pressure, the entropy differences corresponding to selected temperatures were checked by use of Equation [13]. In no case were the entropies in disagreement by more than $1/2$ per cent.

The values of entropy have been entered in Table 2 and plotted in Figs. 5, 6, and 7. Entropies for the intermediate pressures were obtained by graphical interpolation with an accuracy of 0.5 per cent.

ACKNOWLEDGMENTS

Appreciation is expressed for the valuable information supplied by Prof. Frederick G. Keyes of the Massachusetts Institute of Technology, and for the instructive assistance by Mr. R. H. Norris of the General Electric Company. The author is indebted to Mr. R. M. Woody and Miss V. Demeo who performed the calculations, and to Mr. F. T. Rohrs who prepared the curve plots.

BIBLIOGRAPHY

- 1 "Helium," by W. H. Keesom, Elsevier, Amsterdam, Holland, 1942, pp. 27-142.
- 2 "Equations of State," by J. A. Beattie and W. H. Stockmayer, Reports on Progress in Physics, vol. 7, 1940, p. 207.
- 3 "Temperature," published by American Institute of Physics, Reinhold Publishing Corporation, New York, N. Y., 1941, p. 55.
- 4 "Personal Letter to Author," from Frederick G. Keyes, Massachusetts Institute of Technology, October, 1946.
- 5 "The Entropy Diagram for Helium at Low Temperatures," by J. Zelmanov, *Journal of Physics, USSR*, vol. 8, 1944, pp. 135-141.
- 6 "The Mathematical Theory of Non-Uniform Gases," by S. Chapman and T. G. Cowling, Cambridge University Press, London, England, 1939, pp. 274-286.
- 7 "Chemical Engineers Handbook," by John H. Perry, McGraw-Hill Book Company, Inc., New York, N. Y., second edition, 1941, p. 792.
- 8 "Thermal Conductivity of Gases," by J. B. Ubbink and W. J. de Haas, *Physics*, vol. 10, 1943, pp. 465-470.
- 9 "Kinetic Theory of Gases," by E. H. Kennard, McGraw-Hill Book Company, Inc., New York, N. Y., first edition, 1938, pp. 178-180.

10 "Specific Heat and Enthalpy of Helium at Low Temperatures," by J. Zelmanov, *Journal of Physics*, USSR, vol. 8, 1944, pp. 129-134.

11 "Joule-Thomson Effect in Helium," by J. R. Roebuck and H. Osterberg, *Physical Review* (2), vol. 43, 1933, p. 60.

Discussion

F. G. KEYES.⁷ The author gives a comprehensive survey of the factual data upon which his tables are based, and Fig. 1 of the paper, leads quickly to a grasp of the extrapolation required because of the limitations in range of measurements of the p - v - T properties.

The present tables are believed to be the most exact that can be compiled at this time, and cover the entire superheat from a

⁷ Department of Chemistry, Massachusetts Institute of Technology, Cambridge, Mass.

few degrees above the critical temperature to a temperature (600 F or 315.5 C) reached by a restricted amount of the experimental data. However, the analytic functions used to represent the basic observational data are of a form known to be reliable for extrapolation.

The basic data for viscosity are fairly complete, that for heat conductivity less so, and no pressure effects, which are small, have been measured.

AUTHOR'S CLOSURE

The author wishes to thank Prof. F. G. Keyes for his instructive remarks. It is gratifying to learn that the data presented here should be useful in commercial design work. Realizing many of the inevitable shortcomings inherent in the preparation of extrapolated information, the author hopes that additional experimental work will be undertaken on the properties of this gas.



Some New Values of the Second Enthalpy Coefficient for Dry Air

By J. R. ANDERSEN,¹ PHILADELPHIA, PA.

Measurements of the second enthalpy coefficient for dry CO₂-free air are reported for three temperatures: 0 C, 10 C, and 30 C. These values, which are in excellent agreement with the best data on air in the literature, were formulated, together with the data of Eucken, Clusius, and Berger by the equation

$$\beta = -0.05442G(0.01244 T), \text{ ft}^3/\text{lb}$$

The second virial coefficient was then calculated by means of the equation

$$B = 0.05442 F(0.01244 T) - 2.33 \times 10^{-3}T, \text{ ft}^3/\text{lb}$$

where the value of the constant of integration was adjusted to give the best fit with the Holborn and Schultze compressibility data. These equations represent adequately all reliable data on air in the temperature range -80 C to 200 C. The functions F and G are the well-known Lennard-Jones functions, abridged tables of which are given in the Appendix.

INTRODUCTION

THIS report presents the results so far obtained in an experimental program for the determination of the thermodynamic properties of gases and gas mixtures at low pressures. The preference for low pressures is of course due to the interesting inferences which may be drawn as to the intermolecular force potential through the application of statistical mechanics. The method used, which is called by us the "Isothermal Joule-Thomson Experiment," consists of the measurement of the change in enthalpy with pressure at various constant temperatures. The method is generally similar to the Joule-Thomson experiment in that a steady flow of gas at constant inlet and exit pressures flows through a calorimeter in which there is an orifice or other constriction to induce a drop in pressure, but differs from it by the introduction of a heater to restore the outlet temperature to its inlet value. Our choice of this type of experiment was dictated mainly by the following considerations: (a) the low-pressure data are determined directly, that is, without the necessity for extrapolation or differentiation of high-pressure data; and (b) certain design problems inherent in Joule-Thomson or specific-heat calorimeters are less onerous in this experiment, because it is not necessary to maintain temperature differences at the two ends of the calorimeter.

In order not to complicate the development of the calorimeter by the necessity for solving other difficult problems concurrently, it was decided at the outset to use air as the experimental fluid and

to limit the range of physical conditions accessible to the apparatus. The upper limit of pressure was set at 4 atm, and the temperature range selected was 0 C to 30 C.

Measurements of the second enthalpy coefficient for dry CO₂-free air are reported for three temperatures: 0 C, 10 C, and 30 C. These values are in excellent agreement with the best data on air available in the literature and serve to indicate that the apparatus in its present form is capable of producing reliable data on the low-pressure properties of gases and gas mixtures in the range of physical conditions accessible to it.

THEORY AND PRACTICAL REALIZATION OF EXPERIMENT

The equation of state of a gas is conveniently expressed as a power series in pressure

$$pv = (pv)^0 + Bp + Cp^2 + \dots \dots \dots [1]$$

where $(pv)^0$ is the zero pressure value of pv , and B, C, \dots are called virial coefficients. $(pv)^0$ and B, C, \dots are temperature functions. The enthalpy of a gas can also be expressed as a power series in pressure

$$h = h^0 + \beta p + \gamma p^2 + \dots \dots \dots [2]$$

where h^0 is the zero pressure enthalpy and β, γ, \dots are herein called enthalpy coefficients. h^0 and β, γ, \dots are temperature functions. If $(pv)^0$ and h^0 are finite the second law of thermodynamics asserts that $(pv)^0$ is proportional to a universal temperature function called absolute temperature, i.e., $(pv)^0 = RT$.

The virial coefficients B, C, \dots and the enthalpy coefficients β, γ, \dots are related. Consider the identical relation of thermodynamics

$$(\partial h / \partial p)_T = v - T(\partial v / \partial T)_p \dots \dots \dots [3]$$

It follows that

$$\beta = d(B\tau)/d\tau; \gamma = \frac{1}{2}d(C\tau)/d\tau \dots \dots \dots [4]$$

where the reciprocal temperature $\tau = 1/T$ is used. Numerical values of the virial coefficients can be obtained from the enthalpy coefficients by integration of these equations

$$\left. \begin{aligned} B &= (1/\tau) \left[\int_{\tau_0}^{\tau} \beta d\xi + C_1 \right] \\ C &= (2/\tau) \left[\int_{\tau_0}^{\tau} \gamma d\xi + C_2 \right] \end{aligned} \right\} \dots \dots \dots [5]$$

provided that some means of evaluating the constants of integration are available.

A steady-flow calorimeter suitable for the determination of the enthalpy coefficients consists of the following elements: (a) An entrance section for measurement of the inlet pressure and temperature; (b) an orifice or other constriction to induce a drop in pressure; (c) an electric heater; and (d) an exit section for measurement of the exit pressure and temperature. Furthermore, in order to eliminate the need for making difficult and uncertain corrections to the data, it is desirable to have the kinetic energy of flow of the experimental fluid negligibly small in the entrance and exit sections, and to establish adiabatic conditions along the walls of the calorimeter between the entrance and exit sections so that the rate of heat absorption between these sections is just that

¹ Assistant Professor of Mechanical Engineering, Towne Scientific School, University of Pennsylvania; Project Leader, University of Pennsylvania Thermodynamics Research Laboratory. Jun. ASME.

Contributed by the Research Committee on Properties of Gases and Gas Mixtures and the Heat Transfer and Applied Mechanics Divisions and presented at the Annual Meeting, New York, N. Y., November 27-December 2, 1949, of THE AMERICAN SOCIETY OF MECHANICAL ENGINEERS.

NOTE: Statements and opinions advanced in papers are to be understood as individual expressions of their authors and not those of the Society. Paper No. 49-A-40.

deliberately introduced by the electric heater. In addition, it is necessary to provide (a) accurate control of the inlet and exit pressures; (b) a thermostat to establish the temperature level of the apparatus; and (c) means for measurement of the rate of flow of the experimental fluid.

Under steady-flow conditions, with negligible kinetic energy of flow in the inlet and exit sections, conservation of energy requires that

$$h_2 - h_1 = {}_1Q_2/G \dots \dots \dots [6]$$

where h_2 and h_1 are the enthalpies of the experimental fluid at the exit and entrance sections, respectively, ${}_1Q_2$ is the rate of heat absorption between these sections, and G is the rate of flow of the experimental fluid. If the rate of heat input is adjusted to restore the exit temperature to its inlet value, there is obtained

$$(h_2 - h_1)_T = ({}_1Q_2)_T/G \dots \dots \dots [7]$$

The pressure drop $p_2 - p_1$ is also determined. These measurements yield numerical values of the ratio

$$[(h_2 - h_1)/(p_2 - p_1)]_T = ({}_1Q_2)_T/(p_2 - p_1)G \dots \dots \dots [8]$$

that is, values of the change in enthalpy with pressure at constant temperature are determined.

The enthalpy coefficients are obtained readily from these data since

$$[(h_2 - h_1)/(p_2 - p_1)]_T = \beta + \gamma(p_1 + p_2) + \dots \dots \dots [9]$$

If the measurements are carried out at a sufficiently low pressure (strictly zero pressure), the second enthalpy coefficient β is determined directly.

Statistical mechanics predicts that for molecules whose intermolecular force potential $E(r)$ is independent of orientation, the second virial coefficient B is related to it by the expression

$$B = 2\pi N_0 \int_0^\infty (1 - e^{-E(r)/k}) r^2 dr \dots \dots \dots [10]$$

in which r is the separation of any pair of molecules, N_0 is Avogadro's number, and k is the Boltzmann constant. This relation results from two basic assumptions, both of which are very nearly fulfilled at sufficiently high temperatures. It is assumed that a Maxwellian velocity distribution prevails and, further, that the kinetic and potential energies of the molecules are completely independent of each other and continuously variable. It follows that the second enthalpy coefficient β is related to the intermolecular force potential by the expression

$$\beta = 2\pi N_0 \int_0^\infty \{1 + [E(r)/k - 1]e^{-E(r)/k}\} r^2 dr \dots [11]$$

Thus accurate values of the second enthalpy coefficient can give important information on the intermolecular force potential. Furthermore, Equations [10] and [11] with a plausible empirical form for the intermolecular force potential $E(r)$ can be used effectively in the formulation of experimental data.

One widely used empirical form for the intermolecular force potential is that of Lennard-Jones

$$E(r) = 4\epsilon [(r_0/r)^{12} - (r_0/r)^6] \dots \dots \dots [12]$$

In this expression ϵ and r_0 can be regarded as parameters for empirical adjustment. The Lennard-Jones potential is shown graphically in Fig. 1. Using the Lennard-Jones form for the intermolecular force potential in Equations [10] and [11], the necessary integrations can be carried out. The results are

$$B = (2\pi N_0 r_0^3/3) F(kT/\epsilon) \dots \dots \dots [13]$$

$$\beta = -(2\pi N_0 r_0^3/3) G(kT/\epsilon) \dots \dots \dots [14]$$

The functions F and G have been tabulated by J. O. Hirschfelder, R. B. Bird, and E. L. Spotz (1)² and others. An abridged table of these functions is given in the Appendix.

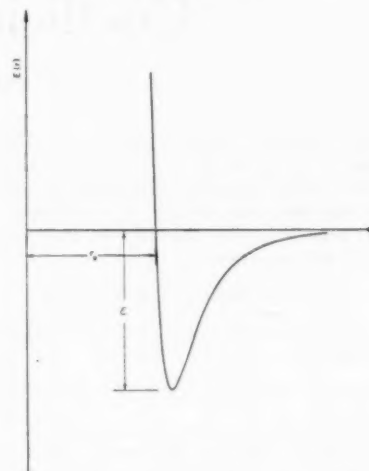


FIG. 1 LENNARD-JONES INTERMOLECULAR FORCE POTENTIAL

DESCRIPTION OF APPARATUS

The arrangement of the apparatus used is shown schematically in Fig. 2.

The thermostat temperature-regulation system was of conventional construction and operation. The temperature range selected for experimentation permitted the use of water as thermostat fluid. The temperature of the thermostat was controlled by the circulation of an auxiliary fluid through coils immersed in the thermostat. The circulation of the auxiliary fluid was controlled by a conventional mercury-alcohol thermoregulator operating a circulating pump through a thyatron circuit. The temperature of the auxiliary fluid was maintained at the proper value by either an electric heater or a refrigeration machine as required. The auxiliary fluid was a mixture of water and ethylene glycol. The temperature regulation obtained with this system was of the order of ± 0.005 deg C as ordinarily operated. The regulation could have been improved by the utilization of a more careful operating technique, but this was not thought to be necessary, since the temperature fluctuations were effectively damped by the heavy vacuum jacket surrounding the calorimeter. The inlet air to the calorimeter passed through a thermal ballast chamber to reduce its temperature fluctuation to negligible proportions.

The air was supplied during a test by a small compressed-air cylinder suspended from one arm of a sensitive balance. The rate of flow was determined by recording the time required for a certain weight of air to flow from this cylinder. The weight of air withdrawn was determined by the replacement method, the weights being placed directly over the center of gravity of the cylinder. Since weighing under flow conditions was necessary, a flexible take-off tube was provided. Balance was indicated by a balance signal and timing device, operated by a needle and mercury thimble mounted on the balance. The rate-of-flow determination as made with this system was the least reliable of the measurements. The reproducibility of the flow-rate measurement under identical flow conditions was seldom better than 1 part in 1000 and often not better than 1 part in 500. The difficulty

² Numbers in parentheses refer to Bibliography at the end of the paper.

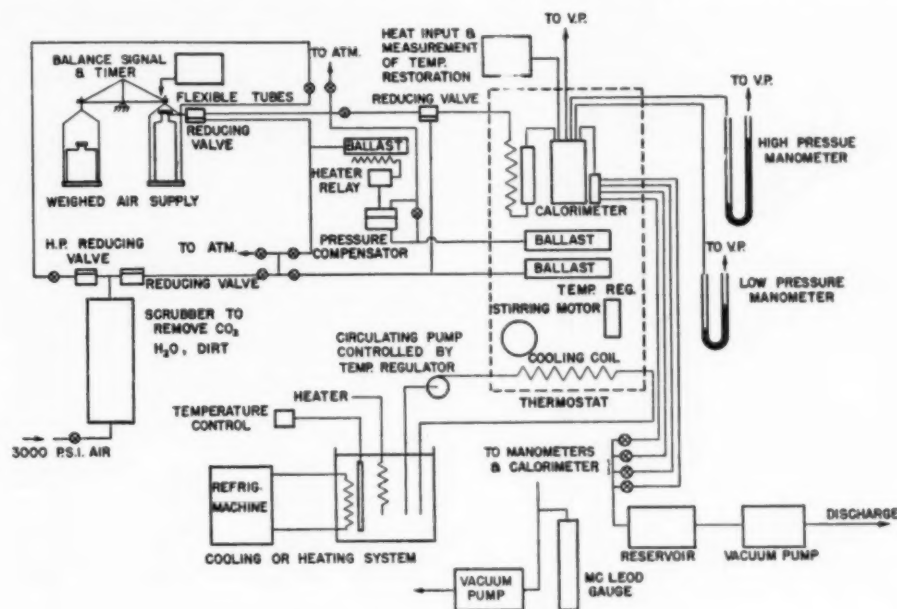


FIG. 2 SCHEMATIC DIAGRAM OF APPARATUS

seemed to be due to vibrations transmitted to the balance from other machinery in the laboratory.

The rate of flow and inlet pressure were controlled by the calorimeter orifice in conjunction with two reducing valves in series.

For convenience of operation and to make the reducing-valve settings independent of room temperature and barometric pressure, both of these reducing valves were arranged for pneumatic operation. The first reducing valve was compensated for drift in its discharge pressure by an electric heater wound around the ballast cylinder in its pneumatic system. This heater was actuated by a diaphragm pressure-compensating device which compared the discharge pressure of the reducing valve with a reference pressure maintained by a ballast cylinder submerged in the thermostat. The second reducing valve had its pneumatic system pressure maintained by another ballast cylinder submerged in the thermostat. The pressure regulation obtained with this system was of the order of ± 0.002 in. Hg.

The back pressure in the calorimeter was controlled by a bank of four orifices in parallel so arranged that any one or a combination of them could be opened to give the desired back pressure. This bank of orifices was thermostated to eliminate the effect of room-temperature changes. All orifices were operated with their back pressures less than the corresponding critical back pressure to make the flow through them depend only on the upstream temperature and pressure so that the settings of the pressures and the rate of flow were separated from any influence arising from adjustment of the heat input.

The pressures were measured by mercury manometers. The manometers had one leg evacuated to eliminate the effect of barometric pressure variation and also in order to give the absolute pressure directly. The absolute pressure in the vacuum system was measured with a McLeod gage. The manometers were of one-piece glass construction, the tubes having a bore of about $\frac{1}{2}$ in. to minimize the effect of capillary depression. The menisci were located by means of small telescopes mounted on micrometer screws whose settings were established by comparison with a steel scale mounted on the manometer frame.

The essential features of the calorimeter in its final form are shown in Fig. 3. In use this device was mounted inside a heavy evacuated submarine which was in turn submerged in the thermostat. The experimental fluid entered the calorimeter through tube 1 after being brought to the thermostat temperature by passing through a cooling coil submerged in the thermostat and the thermal ballast. The inlet conditions were measured at section 2.

The high-pressure manometer was connected to tube 3. A five-junction copper-constantan differential thermocouple 4 was used to indicate temperature restoration between the inlet and outlet sections. The remainder of the calorimeter consisted of an inlet labyrinth 5, orifice 6, heater 7, outlet labyrinth 8, mixing screens 9, and radiation shields 10 and 11. The heater wires were brought out through the capillary tubes 12 and the packing glands 13. The low-pressure manometer was connected to tube 14.

The design of the inlet labyrinth may seem to be unnecessarily elaborate but this design was evolved after extensive experimentation with simpler arrangements clearly demonstrated their inadequacy in respect to heat leakage to the orifice by conduction along its inlet pipe. The orifice consisted of a thin brass disk cemented to the end of a long, thin-walled, lucite tube. The outlet labyrinth served to provide additional radiation shielding for the heater and helped to promote uniform flow conditions at the outlet section. The mixing screens served also to promote uniform flow conditions.

The entire calorimeter was constructed of brass with the exception of the orifice mounting tube and the form on which the heater element was wound which were of lucite. Demountable connections had neoprene gaskets coated with shellac on assembly. The electrical energy to the heater was supplied by Willard DD-5-1 storage batteries which had excellent voltage stability for the low discharge rates used in this application. The heat-input circuit consisted of the batteries, voltage dividers for adjustment, the heater element, and a standard resistance. The potentials across the heater and the standard resistance were measured with a Leeds and Northrup type K-2 potentiometer making use of a volt box

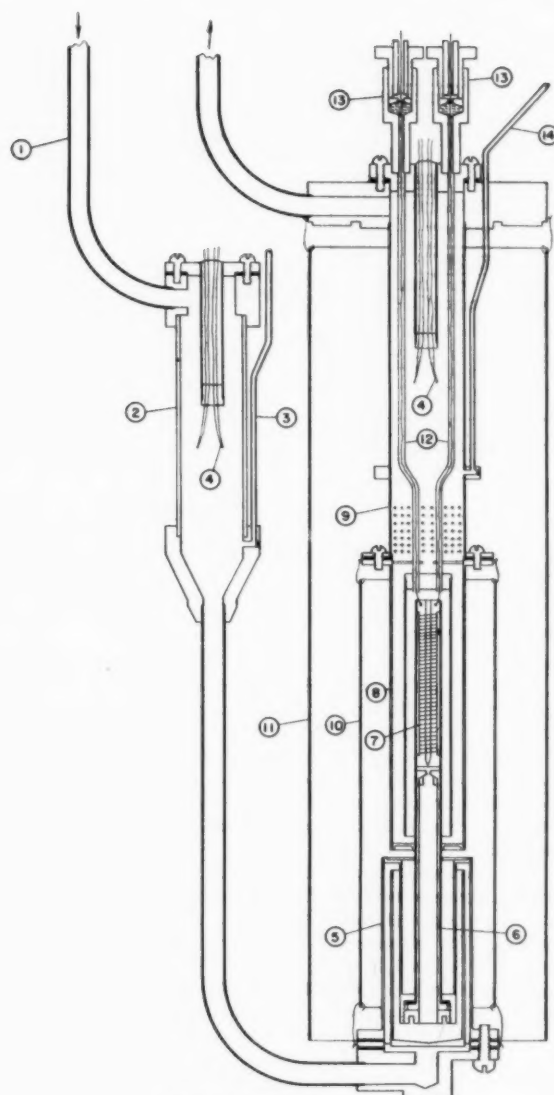


FIG. 3 THE CALORIMETER

when necessary. Temperature restoration was indicated by a high-sensitivity galvanometer connected directly to the differential thermocouple. The sensitivity of the indication of temperature restoration was about ± 0.0005 deg C.

EXPERIMENTAL MEASUREMENTS

The measurements made on dry CO_2 -free air with the apparatus in its final form are given in Table 1. It will be noted that at each temperature, measurements were made at two different pressure drops. Since the same orifice was used, this resulted in two different rates of flow. These two series of measurements served to show (a) that the results were not sensitive to the rate of flow, and (b) that $[(h_2 - h_1)/(p_2 - p_1)]_T$ was not a function of pressure within the sensitivity of the apparatus. Dependence of the results on the rate of flow was taken as evidence of heat leakage to the orifice in the calorimeter. In the earlier arrangements used, the results had a pronounced sensitivity to the rate of

TABLE 1 MEASUREMENTS ON AIR

Run	t (°C)	$p_1 - p_2$ (lb/ft ²)	$G \times 10^5$ (lb/sec)	$h_2 - h_1$ (ft-lb/lb)	$-\beta$ (ft ³ /lb)
34	10	2857.20	2.9069	158.120	0.04099
35	10	2845.27	2.9150	157.854	0.04105
36	10	2849.35	2.9074	156.728	0.04072
37	10	2855.34	2.9168	157.888	0.04095
39	10	6651.79	4.7405	274.970	0.04070*
40	10	6621.50	4.7561	273.470	0.04066*
41	10	6632.05	4.6882	275.511	0.04090*
42	10	6629.76	4.6926	271.214	0.04091
43	10	6632.40	4.6837	272.875	0.04114
44	10	2784.17	3.0071	150.945	0.04010
45	10	2784.44	3.0313	154.059	0.04070
Av.	10				0.04080
58	0	4716.04	3.7982	212.654	0.04509
59	0	4716.81	3.8061	212.118	0.04497
60	0	6701.83	4.7700	300.968	0.04491
61	0	6710.00	4.7968	299.782	0.04468
62	0	6714.34	4.7861	300.660	0.04478
63	0	6709.24	4.7913	299.925	0.04470
64	0	4754.15	3.8190	210.379	0.04444
65	0	4756.36	3.7782	214.186	0.04520
Av.	0				0.04465
66	30	4694.57	3.6955	164.978	0.05514
67	30	4696.15	3.6928	165.427	0.05523
68	30	4700.05	3.6867	164.556	0.05501
69	30	4695.59	3.7002	165.715	0.05487
70	30	6674.81	4.6418	232.611	0.05485
71	30	6676.53	4.6501	232.117	0.05477
72	30	6669.68	4.6574	233.423	0.05500
73	30	6672.00	4.6528	234.644	0.05517
Av.	30				0.05500

* These values were corrected for the presence of water.

flow, but successive improvements made in the thermal isolation of the orifice to reduce its heat leak reduced this sensitivity. Since the final measurements had a negligible dependence on the rate of flow, it was concluded that heat leakage to the orifice in the final design was negligible. The range of pressures used was not sufficient to reveal any dependence of $[(h_2 - h_1)/(p_2 - p_1)]_T$ on pressure, so these values were taken as a direct measure of the second enthalpy coefficient, β .

There was evidence that in runs 39, 40, and 41, water was present in the calorimeter. This was attributed to adsorption of water on the walls of the calorimeter as a result of exposure to the atmosphere when the calorimeter was disassembled for repair just prior to run 39. These runs were corrected for the presence of water on the assumption that the inlet air to the calorimeter was saturated with water at 10 C. This correction was calculated from the data by J. A. Goff (2) and had the magnitude 0.00064 ft³/lb.

FORMULATION OF DATA

The data were formulated, using Equation [14], with the constants $2\pi N_0 r_0^3/3$ and k/ϵ , adjusted by the method of least squares to fit the three average values of β at 0 C, 10 C, and 30 C. The results were

$$2\pi N_0 r_0^3/3 = 0.05254 \pm 0.0062, \text{ ft}^3/\text{lb}$$

$$k/\epsilon = 0.01226 \pm 0.00056, \text{ deg K}^{-1}$$

The standard error of each of the three experimental values based on this formulation is ± 0.00039 ft³/lb. Of course, the use of statistical methods with so few experimental values does not lead to reliable conclusions, but may be used as an indication of the goodness of fit. Values calculated from this formulation are compared with the experimental values in Table 2.

TABLE 2 COMPARISON WITH FIRST FORMULATION

T (deg K)	Observed	Calculated	Deviation
273.16	0.04485	0.04466	-0.00019
283.16	0.04080	0.04112	0.00032
303.16	0.03500	0.03487	-0.00013

It was felt that the only other reliable values of β for air in the literature were those of A. Eucken, K. Clusius, and W. Berger (3). Therefore the least-squares adjustment of the constants in Equation [14] was repeated using their values as well. Their values were given a weight of one third as compared with the values from the present investigation. The results of this formulation were

$$2\pi N_0 r_0^3/3 = 0.05442 \pm 0.00187, \text{ ft}^3/\text{lb}$$

$$k/\epsilon = 0.01244 \pm 0.00019, \text{ deg K}^{-1}$$

The standard error of each of our experimental values based on this formulation is $\pm 0.00027 \text{ ft}^3/\text{lb}$. Thus the results of this investigation can be formulated together with the Eucken, Clusius, and Berger data by means of Equation [14] with no significant change in the constants. A comparison of values calculated from this formulation and the experimental values is given in Table 3 and shown graphically in Fig. 4.

TABLE 3 COMPARISON WITH SECOND FORMULATION

T (deg K)	Observers	β (ft ³ /lb)		
		Observed	Calculated	Deviation
273.16	Andersen	0.04485	0.04473	-0.00012
283.16		0.04080	0.04115	0.00035
303.16		0.03500	0.03483	-0.00017
193.0		0.08994	0.08947	-0.00047
249.5	Eucken	0.05335	0.05452	0.00117
273.2	Clusius	0.04509	0.04474	-0.00035
289.8	Berger	0.03919	0.03892	-0.00027

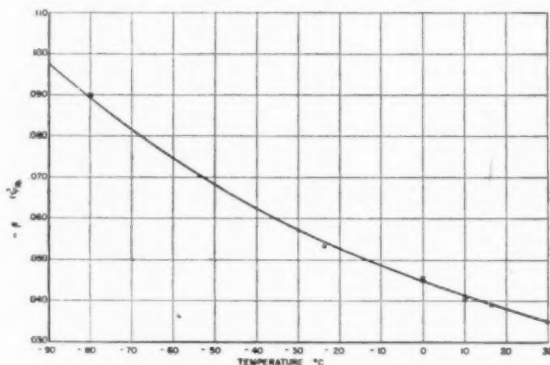


FIG. 4 THE SECOND ENTHALPY COEFFICIENT FOR AIR
(O, Andersen; X, Eucken, Clusius, Berger; — $\beta = -0.05442 G(0.01244 T)$.)

The agreement shown in Table 3 is excellent; therefore it is felt that Equation [14] with the second set of constants represents adequately the best available data on the second enthalpy coefficient for air in the temperature range -80°C to 30°C . This formulation, however, must be considered an empirical one since (a) air is a mixture of gases so that β should be represented by a linear combination of integrals of the type given in Equation [11] rather than by a single such integral; and (b) the Lennard-Jones form for the intermolecular force potential only approximates the correct potential. Therefore to deduce values of the second virial coefficient B , one would expect to modify Equation [13] to

$$B = (2\pi N_0 r_0^3/3) F(kT/\epsilon) + C_1 T \dots \dots \dots [15]$$

in accordance with Equations [5] since there would be no good reason to expect the constant of integration to be zero.

A comparison of Equation [15], using the constants of the second formulation with the values of B obtained from the Holborn and Schultz compressibility data, quoted by Curtiss and Hirschfelder (4), and with a single unpublished value obtained in this laboratory by W. Pfeifferle, is given in Table 4.

TABLE 4 COMPARISON OF B WITH OBSERVED DATA

t (deg C)	B (ft ³ /lb)		
	Observed	Calculated	Deviation
0	-0.00653	-0.00665	-0.00012
30*	-0.00300*	-0.00301	-0.00001
50	-0.00126	-0.00112	0.00014
100	0.00209	0.00243	0.00034
150	0.00475	0.00474	-0.00001
200	0.00669	0.00713	0.00044

* This value is due to W. Pfeifferle.

TABLE 5 COMPARISON OF FORMULATIONS OF β

t (°C)	$-\beta$ (ft ³ /lb)					
	(a)	(b)	(c)	(d)	(e)	(f)
100	0.01821	0.02147	0.02335	0.02258	0.02202	0.02199
75	0.02344	0.02544	0.02715	0.02655	0.02604	0.02614
50	0.02951	0.03025	0.03161	0.03075	0.03017	0.03116
25	0.03671	0.03614	0.03694	0.03601	0.03648	0.03739
0	0.04475	0.04360	0.04341	0.04245	0.04346	0.04379
-25	0.05514	0.05529	0.05145	0.05051	0.05215	0.05183
-50	0.06828	0.06854	0.06175	0.06093	0.0630	0.06146
-75	0.08530	0.08475	0.07554	0.07501	0.0770	0.07549
-100	0.10850	0.11251	0.09427	0.09525	0.0966	0.09377

(a) Present formulation (Equation [15])
 (b) Bridgeman (1929) (7)
 (c) Beattie-Bridgeman (1928) (9)
 (d) Claitor-Crawford (1948) (8)
 (e) Curtiss-Hirschfelder (1949) (4)
 (f) Roebuck-Murrell (1941) (5)

The agreement is excellent, showing that Equations [14] and [15] with the constants $2\pi N_0 r_0^3/3 = 0.05442 \text{ ft}^3/\text{lb}$, $k/\epsilon = 0.01244 \text{ deg K}^{-1}$, $C_1 = -2.33 \times 10^{-5} \text{ ft}^3/\text{lb-deg K}$ represent all existing extensive information on air [except the Roebuck Joule-Thomson data, reference (5)] adequately over the temperature interval -80°C to 200°C . This seems to show that the Roebuck data are systematically in error. This conclusion is in agreement with the observations of de Groot and Michels (6) on the Roebuck Joule-Thomson data for CO_2 .

A comparison of the present formulation of the second enthalpy coefficient for air with several other current ones is given in Table 5. All of the quoted formulations except the present one and that of Bridgeman (7) have apparently given too much weight to the Roebuck data in the temperature range considered.

It may be remarked that the agreement of the present formulation and that of Claitor and Crawford (8) improves at lower temperatures and is quite good at -150°C to -180°C . This is encouraging, since the Claitor and Crawford formulation gives much weight to the accurate velocity-of-sound data available at these low temperatures.

CONCLUSIONS

Some new experimental values of the second enthalpy coefficient for dry, CO_2 -free air are reported. These values were formulated together with the data of Eucken, Clusius, and Berger (3) by the equation

$$\beta = -0.05442 G(0.01244 T), \text{ ft}^3/\text{lb} \dots \dots \dots [16]$$

The second virial coefficient was then calculated by means of the equation

$$B = 0.05442 F(0.01244 T) - 2.33 \times 10^{-5} T, \text{ ft}^3/\text{lb} \dots [17]$$

in which the value of the constant of integration was adjusted to give the best fit with the Holborn and Schultz compressibility data for air. The conclusion is that Equations [16] and [17] represent adequately all reliable data on air in the temperature range -80°C to 200°C .

ACKNOWLEDGMENT

It is a pleasure for the author to acknowledge the aid of Dean John A. Goff, under whose direction this investigation was carried out. It is also a pleasure to acknowledge the aid of the Bureau of Ships and the Office of Naval Research, both of the United States Navy, who sponsored the project through the University of Pennsylvania Thermodynamics Research Laboratory. The aid of the members of the laboratory staff, particularly in the matter of construction of parts of the apparatus, is greatly appreciated. The helpful suggestions of Mr. Serge Gratch, particularly in regard to methods of formulating the data, were invaluable.

BIBLIOGRAPHY

- 1 "Viscosity and Other Physical Properties of Gases and Gas Mixtures," by J. O. Hirschfelder, R. B. Bird, and E. L. Spots, paper presented at the Annual Meeting, New York, N. Y., November 28-December 3, 1948, of THE AMERICAN SOCIETY OF MECHANICAL ENGINEERS. (Preprints available from the Towne Scientific School, University of Pennsylvania.)
- 2 "Final Report of the Working Subcommittee of the International Joint Committee on Psychrometric Data," by J. A. Goff, paper presented at the Annual Meeting, New York, N. Y., November 28-December 3, 1948, of THE AMERICAN SOCIETY OF MECHANICAL ENGINEERS. (Preprints available from the Towne Scientific School, University of Pennsylvania.)
- 3 "Eine Apparaten zur exakten Messung des isothermen Drossel-effektes bei verschiedenen Temperaturen und Drucken," by A. Eucken, K. Clusius, and W. Berger, *Zeitschrift für Technische Physik*, vol. 13, 1932, pp. 267-270.
- 4 "Thermodynamic Properties of Air," by C. F. Curtiss and J. O. Hirschfelder, Navy Bureau of Ordnance Report, University of Wisconsin, CM-472, June 1, 1948.
- 5 "The Kelvin Scale From the Gas Scales by Use of Joule-Thomson Data," by J. R. Roebuck and T. A. Murrell, *Temperature*, Reinhold Publishing Corporation, New York, N. Y., 1941, pp. 60-73.
- 6 "The Joule-Thomson Effect and the Specific Heat at Constant

Pressure of Carbon Dioxide," by S. R. de Groot and A. Michels, *Physica*, vol. 14, 1948, pp. 218-227.

7 "The Joule-Thomson Effect and Heat Capacity at Constant Pressure for Air," by O. C. Bridgeman, *Physical Review*, vol. 34, 1929, pp. 527-533.

8 "Thermodynamic Properties of Oxygen, Nitrogen, and Air at Low Temperatures," by L. C. Claitor and D. B. Crawford, paper presented at the Annual Meeting, New York, N. Y., November 28-December 3, 1948, of THE AMERICAN SOCIETY OF MECHANICAL ENGINEERS. (Preprints available from the Towne Scientific School, University of Pennsylvania.)

9 "A New Equation of State for Fluids," by J. A. Beattie and O. C. Bridgeman, *Proceedings of the American Academy of Arts and Sciences*, vol. 63, 1928, pp. 229-308.

Appendix

LENNARD-JONES FUNCTIONS F AND G

KT/ϵ	F	G	KT/ϵ	F	G
0.30	-27.878	104.47	2.60	-0.2664	1.4211
0.40	-15.797	44.046	2.70	-0.2256	1.3235
0.50	-8.7204	25.637	2.80	-0.1845	1.2359
			2.90	-0.1485	1.1513
0.60	-6.1978	17.450	3.00	-0.1150	1.0750
0.70	-4.7102	12.965			
0.80	-3.7539	10.189	3.10	-0.0843	1.0043
0.90	-3.0474	8.3300	3.20	-0.0559	0.9387
1.00	-2.5580	6.9663	3.30	-0.0292	0.8776
			3.40	-0.0048	0.8207
1.10	-2.1450	5.9555	3.50	0.0185	0.7674
1.20	-1.8552	5.1728			
1.30	-1.5842	4.5476	3.60	0.0403	0.7176
1.40	-1.3755	4.0420	3.70	0.0608	0.6707
1.50	-1.2008	3.6146	3.80	0.0800	0.6267
			3.90	0.0953	0.5852
1.60	-1.0515	3.2577	4.00	0.1134	0.5461
1.70	-0.9232	2.9525			
1.80	-0.8119	2.6887	4.10	0.1315	0.5089
1.90	-0.7141	2.4591	4.20	0.1465	0.4738
2.00	-0.6277	2.2572	4.30	0.1606	0.4405
			4.40	0.1743	0.4089
2.10	-0.5505	2.0781	4.50	0.1871	0.3788
2.20	-0.4820	1.9180			
2.30	-0.4200	1.7744	4.60	0.1995	0.3503
2.40	-0.3638	1.6450	4.70	0.2112	0.3232
2.50	-0.3129	1.5278	4.80	0.2228	0.2972
			4.90	0.2332	0.2725
			5.00	0.2435	0.2489

Discussion

F. G. KEYES.³ The measurement of an isothermal property is always to be preferred to a nonisothermal one because of the great difficulty of controlling heat flow. Thus in the case of the Joule-Thomson effect, for example, a sharp fall or rise of temperature is produced in a length of tube through which a fluid passes a constriction in the tube, and the quantity desired is the ratio of temperature change to the pressure difference across the constriction or expansion plug. The long history of the efforts to secure accuracy in the measurements of the Joule-Thomson effect is largely an account of successive improvements to control heat flow caused by the temperature difference being measured, and also kinetic effects induced in the gas by expansion at the "plug."

Professor Andersen's measurements of the enthalpy pressure coefficient of air

$$(\partial h / \partial p)_T = v - T(\partial v / \partial T)_T = (\partial v / \partial \tau)_p, \tau = T^{-1}$$

are most encouraging, not only because they are made by a method which is, in principle, of the isothermal type, but also because the results lead directly to a quantity representative of the departure of a gas from the ideal state. The Joule-Thomson effect

(μ) is, however, an involved function of "gas imperfection" as the equation

$$\mu = [T(\partial v / \partial T) - v] / [C_p^* - \int T(\partial^2 v / \partial T^2) dp]$$

indicates. Indeed it is possible to design the apparatus for the measurement of both $(\partial h / \partial p)_T$ and $(\partial h / \partial T)_p$, $[C_p^* + \int T(\partial^2 v / \partial T^2) dp]$, thus obtaining complete factual information on the equation of state and thermal properties in the equilibrium state. Moreover, by the use of this method the adverse effects of adsorption are avoided since a "flow" method is employed and measurements may be extended to temperatures practically inaccessible to apparatus employed for measuring p-v-T properties directly.⁴

The first exposition of the importance of measuring the quantity $(\partial h / \partial p)_T$ is due to Edgar Buckingham⁵ and a full discussion

⁴ Measurements of the p-v-T properties of helium have recently been reported by W. G. Schneider to 600°C ; a remarkable achievement. "Compressibility of Gases at High Temperatures. II. The Second Virial Coefficient of Helium in the Temperature Range 0 to 600°C ," by W. G. Schneider and J. A. H. Duffie, *Journal of Chemical Physics*, vol. 17, 1949, p. 751.

⁵ "On a Modification of the Plug Experiment," by Edgar Buckingham, *Philosophical Magazine*, vol. 6, 1903, p. 519.

³ Department of Chemistry, Massachusetts Institute of Technology, Cambridge, Mass.

of the significance and uses of both the enthalpy coefficient and the Joule-Thomson coefficient was published twelve years later by Harvey N. Davis.⁶ The development of the required experimental procedures took place independently (1932) in Germany⁷ and in the United States.⁸ The methods used differed, however, in an important particular. In Germany the investigator allowed the gas to expand as in a Joule-Thomson measurement with subsequent warming to the initial temperature, thereby foregoing entirely any attempt to conduct an isothermal measurement. The United States workers expanded the gas in a uniform-bore platinum-iridium capillary tube in the walls of which an electric current was flowing sufficient to produce the heat needed to compensate for the Joule-Thomson cooling of the gas; a condition indicated by the equality of the temperature of the gas entering and leaving the capillary.^{9,10}

It will be observed that the flowing gas experiences a sharp change of velocity within the restriction and the attendant increase in kinetic energy of the gas will be compensated at the expense of the sensible heat of the fluid. There will also be energy amounts due to the friction of the fluid in the constriction besides entrance and exit effects. Accordingly $(\partial h / \partial p)_T$ cannot be made a rigorously isothermal experiment throughout the path of flow except in the limit of zero mass movement. However, the temperature changes due to the kinetic effects in the constriction are small relative to the Joule-Thomson effect, excluding the special region of inversion where $(\partial h / \partial p)_T$ tends to zero. Above the inversion temperature heat must be abstracted from the expanding gas and this cooling could be applied with precision by making use of the Peltier effect that occurs in proportion to electric-current flow at one of a pair of junctions formed by two metallic wires of differing substance.

The author employs for the correlation of his measurements

⁶ "Note on the Value of Joule-Thomson Observations for Computing Steam Tables," by Harvey N. Davis, *Physical Review*, vol. 5, 1915, p. 359.

⁷ "An Apparatus for Exact Measurement of the Isothermal Porous Plug Effects at Various Temperatures and Pressures," by A. Eucken, K. Clusius, and W. Berger, *Zeitschrift für Technische Physik*, vol. 13, 1932, p. 267.

⁸ "The Pressure Variation of the Heat Function as a Direct Measure of the van der Waals Forces," by F. G. Keyes and S. C. Collins, *Proceedings of the National Academy of Science*, vol. 18, 1932, p. 328.

⁹ The further development of the method is reported in a paper, "The Heat Capacity and Pressure Variation of the Enthalpy for Steam From 38 to 125 C, Part V, Steam Research Program," by S. C. Collins and F. G. Keyes, *Proceedings of the American Academy of Arts and Sciences*, vol. 72, 1938, p. 72. This method can also be used to determine the heat of a chemical reaction for gaseous dissociations of the type $A_2 \rightarrow 2 A_1$.

¹⁰ "Note on the Year's Progress on the Precise Measurement of the Effects of Intermolecular Potential in Gases," by S. C. Collins and F. G. Keyes, *Journal of Physical Chemistry*, vol. 43, 1939, p. 5.

the intermolecular potential, Equation [12] which is a convenient special form of the so-called Lennard-Jones formula for the potential energy of intermolecular interaction, namely, $E = \gamma r^{-n} - \mu r^{-m}$, where n/m is taken to be 2, and m is 6 in accord with the first approximation for the negative part of the potential based on the quantum theory. Equation [12] has been widely used, as the author states. The writer's colleague, Prof. I. Amdur,¹¹ has succeeded in measuring the repulsive or positive part of the potential in the case of He-He and He-H₂, and finds for the first and second pair of particles the following potential forms

$$\begin{aligned} \text{He-He, } V_+(r) &= 11.3 \exp(-4.63 r^{1/2}) \times \\ &\quad 10^{-10} \text{ ergs } (r \text{ range } 0.55 - 1.05 \text{ \AA}) \\ \text{He-H}_2, V_+(r) &= 0.846 \exp(-24.9 r^2) + \\ &\quad 0.211 \exp(-2.40 r^2) \times 10^{-10} \text{ erg } (r \text{ range } 0.28 - 0.70 \text{ \AA}) \end{aligned}$$

The foregoing equations are illustrative of the complexity of the analytical forms required to represent within experimental accuracy the positive potential. For the negative part of the potential it has long been known that where accuracy of knowledge of the potential is required, the following type of expression is to be used

$$V_-(r) = -\mu r^{-6}(1 + \mu_1 r^{-2} + \dots + \mu_n r^{-2n})$$

It is therefore clear that Equation [12] must be regarded as a rough expedient sufficient for exploratory purposes or as a first approximation, provided the ranges of representation are restricted. In the present case the range from -90 to 30 C is accurately represented and it is hoped measurements may be extended to temperatures of perhaps 500 C, or higher if possible.

AUTHOR'S CLOSURE

The remarks by Professor Keyes are greatly appreciated. To have Professor Keyes give a short history of the "Isothermal Joule-Thomson Experiment" is a welcome supplement to the paper since the author had not been willing to take the space for it and further since Professor Keyes has personally contributed such a great deal to it.

Professor Keyes' further remarks on the proper representation of the intermolecular force potential are very interesting and point up the difficulty in obtaining accurate analytical expressions for any thermodynamic property over an extended range of physical conditions. The interesting feature of the formulation presented in the paper is not that any particular virtue is associated with the use of the Lennard-Jones form for the intermolecular force potential but rather, that this crude approximation to the correct form for the intermolecular force potential represents the data so well.

¹¹ "Repulsive Interaction Potentials at Small Interaction Distances: He-He and H₂-H₂ Systems," by I. Amdur, *Journal of Chemical Physics*, vol. 17, 1949, p. 844.

New Measurements of the Heat Conductivity of Steam and Nitrogen¹

By F. G. KEYES² AND D. J. SANDELL, JR.,³ CAMBRIDGE, MASS.

The heat conductivity of steam has been measured by Timroth and Vargaftig (1940) from approximately 100 to 550 C and to pressures of 250 atm, using the hot-wire type of conductivity cell, wherein the wire of pure platinum serves as thermal emitter, and its electrical-resistance change provides the temperature indication. The new measurements in the present paper were obtained using a concentric cylinder type of conductivity cell in which the heater and thermometric parts were isolated from contact with the material whose conductivity was being measured. Vargaftig had published (1937) measurements of the heat conductivity of nitrogen in substantially the same cell used for steam. The new measurements on nitrogen are in tolerable agreement with the Vargaftig measurements, but in the case of steam the new measurements are considerably lower in magnitude. A comparison of the two sets of steam data indicates some peculiarities of temperature trend in the Timroth and Vargaftig data which find no correspondence in the data of any other substance, and also differs from the trend relative to the new data. A formulation of the steam and nitrogen data is given in terms of pressure and temperature as independent variables.

MEASUREMENTS of the heat conductivity of steam for pressures of about 1 kg per cm² were published in 1937 by Vargaftig (1)⁴ for the temperature range 69 to 550 C. A few years later, however (1940), data appeared by Timroth and Vargaftig (2) for the temperature range 250 to 550 C and to pressures of 250 kg per cm². These later data were correlated by one of the authors and a table of the values given in the Keenan and Keyes Steam Tables (3) beginning with the 1943 printing.

The only earlier measurements for steam are those of Moser (4) who gave values relative to air at 100 C and somewhat less. The most comprehensive earlier data, however, were published by Milverton (5) who carried out a painstaking investigation in the temperature region just below 100 C. Milverton detected a pressure effect; roughly, one tenth of that deducible by extrapolation from the data of Timroth and Vargaftig. Milverton's formulated data give a value for the heat conductivity of steam at 100 C at

zero pressure,⁵ in fair agreement with Vargaftig's 1937 value: $5.77 \cdot 10^{-8}$ and $5.63 \cdot 10^{-8}$, respectively, in cgs units. Moser's values are now mainly of historic interest.

The present measurements of the heat conductivity of nitrogen are associated with those of steam for several reasons, as follows:

1 All the measurements on steam have been obtained using the "hot-wire" method originally due to Schleiermacher (6); a method which makes use of a wire of pure platinum stretched axially within a tube containing the fluid of interest. The wire serves as an electrical heater for measured heat losses and also as a resistance thermometer. The method during the past 25 years has been brought to a high state of perfection for the measurement of heat conductivities of gases at low pressures. The Timroth and Vargaftig (2) measurements on steam represent an attempt to adapt the hot-wire method to measurements with steam and nitrogen [Vargaftig (1)] under pressure. It is desirable, however, to confirm the accuracy of the existing results through the use of a different method, and the alternate measurements of nitrogen and steam in the steam cell constitute a control which has proved highly desirable.

2 The case of steam presents difficulties of a fundamental nature in interpreting the apparent heat conductivities due to its highly polar character,⁶ namely, its property of absorbing and emitting radiation. All metals emit radiation when heated and in varying degrees depending upon the state of the emitting surface. Thus silver under the most favorable conditions will reflect close to 99 per cent of radiant energy, while platinum wire in practice may, as shown by Milverton, reflect only 90 per cent or less. The use of nitrogen, which is transparent to radiation, served as a means of controlling the behavior of the steam cell.

The effect of radiation absorption on the heat conductivity (the latter defined as proportional to the temperature gradient) may be described by noting that the gradient, when determined by measuring the surface temperatures of the metal, or other material, walls of the conductivity cell between which the steam is confined, does not correspond to the actual gradient since a part of the radiant energy emitted by the hotter surface is absorbed depending on the

¹ The meaning to be attached to the phrase, "heat conductivity at zero pressure, λ_0 ," in the case of gases, is similar to "specific heat at zero pressure, C_p^0 ." The concept relates to the fact of experience that on extrapolation of the quantities measured at finite pressures to lower pressures, the "pressure effect" becomes linear to an increasing degree as the limit zero is approached, and λ_0 is the limiting value in the sense of this ultimate extrapolation. Experience shows, however, that at very low pressures, beginning at about 0.1 mm (about 0.002 psia), gases begin to exhibit properties in containers of finite size in contrast to the properties manifest when the distance interval between molecular collisions is microscopic relative to the dimensions of the container. Thus in the heat-conductivity cell used in the present investigation at a pressure of 0.0000002 psia, the number of molecules between the walls has become so small that the amount of heat transferred by them is not measurable in comparison to the heat transferred by radiation. It follows also that the quantities λ_0 and C_p^0 are functions of temperature only as $(p)^0$ is solely temperature-dependent.

² The term "polar" refers to the fact that the water molecule, due to its structure and in complete contrast to nitrogen, possesses a permanent electric dipole of large magnitude. The presence of the dipole is responsible for the strong energy radiation absorption and emission characteristics of steam.

¹ Results recorded in this article are from a thesis submitted as partial fulfillment of the requirements for the degree of Doctor of Philosophy in Chemistry at the Massachusetts Institute of Technology.

This paper is a summary of part of the results obtained in the course of a program of research supported by the Office of Naval Research.

² Professor of Physical Chemistry, Massachusetts Institute of Technology. Mem. ASME.

³ Graduate Student, Massachusetts Institute of Technology.

⁴ Numbers in parentheses refer to the Bibliography at the end of the paper.

Contributed by the Research Committee on Properties of Gases and Gas Mixtures, Heat Transfer, and Applied Mechanics Divisions and presented at the Annual Meeting, New York, N. Y., November 27-December 2, 1949, of THE AMERICAN SOCIETY OF MECHANICAL ENGINEERS.

NOTE: Statements and opinions advanced in papers are to be understood as individual expressions of their authors and not those of the Society. Paper No. 49-A-43.

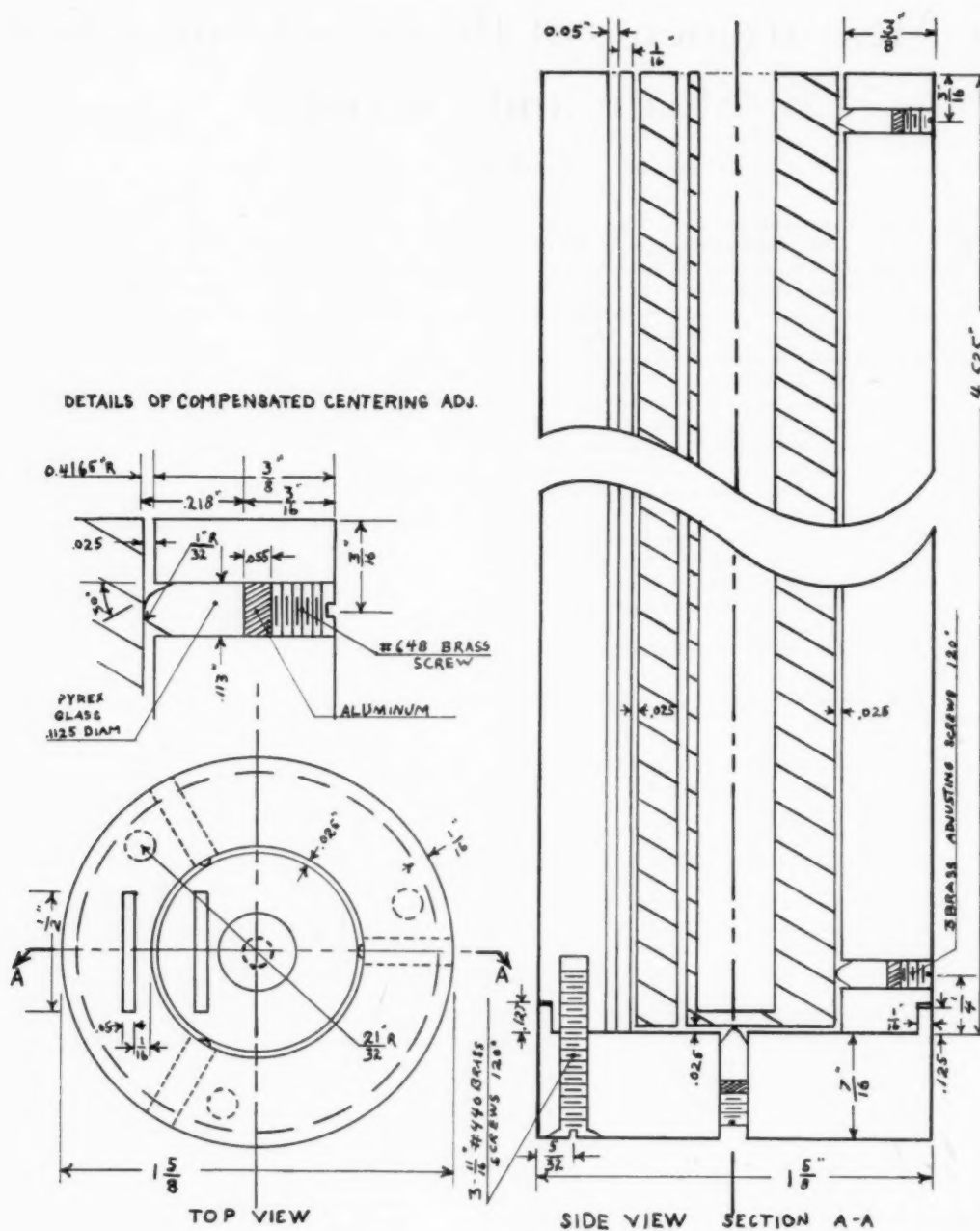


FIG. 1 CONDUCTIVITY CELL AND HEATING CYLINDER
(Material—silver.)

geometry and distance of separation of the surfaces and the detailed structure of the emission spectrum of the steam. The usual procedure of subtracting the total amount of the radiation due to the hotter surface from the total energy input to the cell is permissible in the case of a radiation-transparent gas like nitrogen, but evidently not in the case of the polar substance water vapor, unless the radiation effect is of the same order of magnitude as the experimental error of the conductivity measurement or less. In so far as is known, the rational adjustment of measurements of heat conductivity of polar substances to allow for radiation-absorption characteristics has never been made or discussed.

Finally, the choice of cell design in the case of steam must be governed by the finite electrical conductivity which is a property of water and adsorbed water vapor on surfaces. The disturbing effects of moisture, for example, on the behavior of platinum-resistance thermometers has long been known.

The leads from the cell used by Timroth and Vargaftig were in contact at room temperature with liquid water at the point of exit from the cell case. This circumstance along with possible disturbance to the functioning of the platinum wire as a resistance thermometer because of adsorbed water vapor and the Thomson effect⁷ was not discussed in their paper and the question of radiation "corrections" was referred to without sufficient detail for critical judgment. Since Vargaftig in the 1937 paper gives tests of a steam cell using nitrogen as well as steam, a comparison of the results using nitrogen and steam in our steam cell proves interesting.

THE STRAIN-FREE AND THE STEAM CELL

There has been in use during the past year a silver "strain-free" cell and also the steam cell whose heaters and thermocouples and all leads were encased to prevent contact with steam or water. The encasement predisposed the cell to thermal strains which were absent in the strain-free type where the heater and thermocouples were in direct contact with the substance under measurement. The leads from the strain-free cell parts were, however, so delicate (0.003-in. \times 0.0155-in. ribbon) that no strain or distortion of recognizable amount could occur through temperature or pressure change.

The general form of cell employed, Fig. 1, was the concentric cylinder type of fine silver with an axial heater throughout the length of the inner cylinder, and thermocouples in the cylinder walls of the inner or emitter cylinder and the outer or receiver cylinder. A bottom portion of silver was attached, adjusted in distance of its inner surface from the lower face of the emitter by an amount (0.025 in. \pm 0.0001 in.) equal to the annulus formed by the emitter and receiver. Thermal contact of the bottom piece to the receiver was secured by means of three screws holding the surfaces at the receiver piece in contact.

Above the cell there is a "heat station" or heat guard to intercept the flow of heat to or from the emitter along the electrical leads.⁸ The heat station contains a heater and a thermocouple along with means for bringing about good thermal contact of the leads with the body of the heat station. The temperature of the heat station, as indicated by its thermocouple, was maintained the same as that of the emitter as recorded by its thermocouples.

⁷ The Thomson effect is a measure of the amount of distortion of a temperature gradient due to an electric-current flow. If σ denotes the Thomson coefficient, q the heat absorbed or evolved depending upon the direction of current flow, then $q = \sigma i(dt/dx)dx$. The effect has never been given consideration in interpreting the data from "hot-wire" conductivity cells.

⁸ The intercepting of heat flow along the leads is necessarily imperfect in the case of the heater leads because of the higher temperature which the heater wire must have to effect heat transfer to the body of the emitter. This heater-wire temperature will be greater as the energy imparted to the heater is increased.

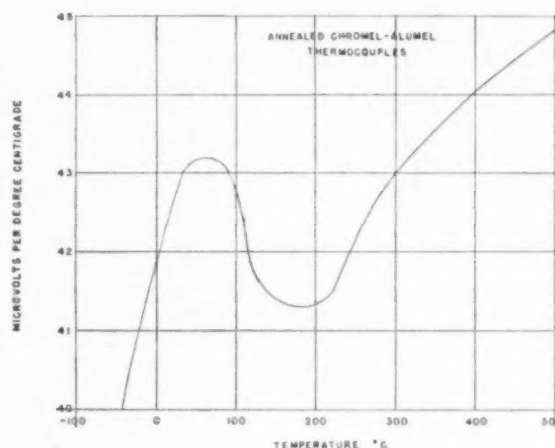


FIG. 2 ANNEALED CHROMEL-ALUMEL THERMOCOUPLES

The thermocouple wire employed was chromel-P and alumel, chosen because of its adaptability to high temperatures, its large and moderately constant value of dE/dt over the temperature range of the measurements.

It was necessary to develop means for measuring $\Delta E/\Delta t$, where E is the electromotive force (emf) of the couple, and Δt , the temperature difference between hot and cold junction, was 2 to 5 deg C. The course of the $\Delta E/\Delta t$ values is represented in Fig. 2 and a confirmation of the accuracy of the values was obtained by comparing the graphically obtained integral values from the $\Delta E/\Delta t$, t -plot from zero to various temperatures with measured integral values between the ice point and corresponding temperatures. For example, the 0-deg to 100-deg-C measured value of the emf is 4289 μ v, while the integrated value 4290 was found by graphical integration under the dE/dt , t -curve. All thermocouple wire used was in ribbon form 0.003 in. thick and 0.0155 in. wide, annealed to 500 deg C for 205 hr in the presence of carbon dioxide. The potentiometer was sensitive enough for readings to 0.1 μ v, equivalent to 0.0025 deg C for a single junction. For the 25-ohm platinum-resistance thermometers a Mueller bridge of Wolff manufacture was employed.

THE CELL CONSTANT

The dimensions of the silver emitter and receiver were obtained through the use of the length-measuring facilities and standard gages of the mechanical engineering department (M.I.T.). However, to obtain the mean diameter of the inside cylindrical surface of the receiver, it was first measured for length and outer diameter prior to drilling the thermocouple and centering holes. From the weight of the receiver in air and water, using Archimedes' principle, it accordingly became possible to deduce the mean inner diameter. The dimensions, Fig. 1, of the steam cell were approximately as follows: Length of annulus, 4.5 in.; smaller diameter of annulus, 0.8512 in.; larger 0.9012 in.; annular width 0.025 deg. The strain-free cell was very closely of the same dimensions.

The Fourier theory of heat conduction leads to the following equation for a steady state of heat flow in the case of an infinite cylindrical annulus where λ is the heat conductivity of the material in the annulus; r_2 its larger and r_1 its smaller radius; L the length; t_2 and t_1 the temperatures corresponding to the surfaces of radii r_2 , r_1 ; and q , the heat flow per sec in the steady state

$$q/(t_2 - t_1) = \lambda \frac{2\pi L}{\ln r_2/r_1} \dots \dots \dots [1]$$

The heat-temperature difference ratio for the circular bottom of the emitter is $q_b/(t_2 - t_1) = \lambda(\pi r_1^2)/(\Delta r)$ where Δr is $r_2 - r_1$. There will also be a small additional flow of heat at the corners of this bottom disk, an item, $q_c/(t_2 - t_1) = (c\lambda)/(\Delta r)$, approximately $1/200$ of the whole. We have then

$$\lambda = \Sigma q / \Delta t \left(\frac{1}{\frac{2\pi L}{\ln r_2/r_1} + \frac{\pi r_1^2}{\Delta r} + \frac{c}{\Delta r}} \right) = \Sigma q / \Delta t \times \dot{C} \dots [2]$$

where C is the cell constant equal to the quantity in parentheses, a function only of the cell dimensions.

A question arises regarding the degree of approximation to infinite length for the actual cell described. The ratio of length to annular width is 180. However, the material silver has a conductivity 17,000 times that of air at 0 deg C and 1 atm, and while toward the bottom heat is actually flowing axially as well as radially, the proportion is only 1 in 22 of the whole for the entire emitter surface, while at the top heat is largely prevented from flowing axially owing to the presence of the heat station at the same temperature as the emitter. However, the main reliance justifying the use of the infinite cylinder formula rests on the fact of the enormously greater heat conductivity of the silver tending to prevent to a good approximation any variation of temperature at points on the radius of the emitter near the bottom. Tests with a brass cell at the outset of the investigation indicated no "measurable" differences in temperature at the ends of the emitter relative to temperatures at the middle.

Using the computed cell constant in the case of the strain-free cell, the following values were obtained for the heat conductivity of air at 0 deg C.

Strain-free brass cell $\lambda \cdot 10^5 = 5.83$ (steam calories per cm per sec per deg C)
Strain-free silver cell $\lambda \cdot 10^5 = 5.80$
Correlation value $\lambda \cdot 10^5 = 5.77$

The "correlation" value quoted is obtained from a consideration of all the published data to 1947, for the heat conductivity of air. The smoothing equation found to be satisfactory follows

$$(\text{Air}) \lambda_0 \cdot 10^5 = \frac{0.6302 \sqrt{T}}{1 + 245.1\tau/10^{12}\tau^2}, \text{ IT cal per cm per sec per deg C} \dots [3]$$

where λ_0 signifies the conductivity for the limiting pressure zero, T denotes Kelvin scale temperature, and τ its reciprocal T^{-1} . The large amount of data for air extending over the temperature range about 100 deg to 600 deg K lies for the greater part in a deviation band of width ≈ 3 per cent.

MODE OF TAKING AND TREATING OBSERVATIONAL DATA

It is a well-known fact that the amount of energy which is radiated from the surface of a solid surface is very sensitive to the state of the surface. The presence of a film of oil, oxide, or even in some instances vapors, is known to increase markedly the radiation absorbed or emitted. The experimental arrangement in the present measurements permitted the cell case to be highly exhausted to the point where residual gas made no measurable contribution to the loss of heat from the emitter. The measured losses in vacuo were then due to conduction at the points of support of the emitter at the pyrex cone contact, Fig. 1, along the copper leads of the heater and to radiation from the emitter surface.⁹ At each

⁹ The radiation loss from the silver surface may be assumed related to temperature according to the fourth power of the Kelvin temperature. It has been found that the emissivity of silver formulated by this relationship is a function of temperature. Evidently the radiation loss of heat becomes very great at high temperatures and for this

temperature of observation in the strain-free cell used for the nitrogen measurements, a determination of the in-vacuo heat loss was made. In the case of the steam cell, in-vacuo heat-loss determinations were made at 100 C and the cell constant determined using the control gas nitrogen. At higher temperatures the in-vacuo heat loss was determined through the use of nitrogen.

The quantities measured are the heat input to the emitter in joules of electrical energy, the temperature of the emitter at a point about 1 mm from the emitter surface, and similarly the temperature of the receiver. The temperature of the surface of the emitter and the receiver is not the same as the temperature of these elements at a finite distance from the surface, except for infinitely small energy rates to the emitter. Also, only in the limit of small energy input will the lead loss along the heater leads, due to the unavoidable higher heater-wire temperature, become negligible. Turbulence or natural heat convection, while allowed for in the design, can be regarded as rigorously absent only when the temperature difference approaches zero.¹⁰ Therefore at least three complete sets of observations of the steady-state values for increasing energy input with corresponding readings of the temperatures of the cell elements were made for each constant temperature of the surrounding environment of the cell case and constant pressure of the substance under measurement. By graphical treatment the value of $q/\Delta t$, the energy input divided by the corresponding temperature difference, was obtained for $q^2/\Delta t$ approaching zero. The following considerations indicate the reason for using the latter variable:

The total heat input q is assumed given by the following equation

$$q = \lambda C \Delta t + C_r(\bar{T})^3 \Delta t + G \Delta t + C_e q^2 \dots [4]$$

where λ is the heat conductivity of the gas within the cell in a fixed state, C is the cell constant, and Δt the temperature difference corresponding to the energy input q . C_r is the radiation constant for the cylindrical silver emitter, \bar{T} the mean temperature of emitter and receiver, G the constant appropriate to the conduction of heat along the centering supports maintaining the emitter in an axial position within the receiver, while C_e is a constant of proportionality relating to the elevation of temperature at the heater-copper lead junction above the mean temperature of the heat station.¹¹ Dividing the left-hand member of Equation [4] by Δt leads to the justification for the choice of variables.

An equation similar to Equation [4] results for the in vacuo situation with the term containing λ absent. Therefore, by determining the limiting value of $q/\Delta t$ for the in-vacuo condition, it becomes possible to compute λ . All the heat conductivities listed were obtained by this procedure of multiple observations, and their graphical extrapolation to obtain $(q/\Delta t) q \rightarrow 0$.

reason the accuracy of measurements of heat conductivity becomes progressively impaired with advancing temperature. It will also be observed as mentioned earlier that the difficulty of interpreting the observational data becomes greatly enhanced in the case of polar substances among which steam is an outstanding example.

¹⁰ H. Kraussold (7) has shown that the criterion for negligible convection requires that the annulus width δ in the concentric cylinders be given by the following relationship

$$\delta \geq 10 \left(\frac{\mu k}{\rho^2 g \beta \Delta t c} \right)^{1/2}$$

where c is the specific heat, μ the viscosity, ρ the density, g the gravitational acceleration, β the volume exhaustivity with temperature, and Δt the temperature difference.

¹¹ The temperature elevation of the heater wire above the mean temperature of the emitter necessarily required to effect heat transfer may be assumed to vary with energy transferred as the energy input for small inputs, or $\Delta t/\Delta q \sim q$, which leads to the relation ϵ , the elevation of junction temperature, proportional to q^2 . The latter relationship follows from the empirical finding of a linear relation between $q/\Delta t$ and $q^2/\Delta t$.

TABLE 1 HEAT CONDUCTIVITY OF STEAM
(IT cal per sec per cm per deg C)

t , °C	p , atm	$10^8 \lambda_{\text{obs}}$	$10^8 \lambda_{\text{calc}}$ *	Dev.**
102.86	0.03	5.666 a	5.665	0.0
102.82	0.47	5.734 a	5.719	+ 0.3
199.84	4.67	8.064 c	7.773	+ 3.6
199.80	12.52	8.650 c	8.310	+ 3.9
202.30	0.03	7.391 a	7.580	- 2.6
202.34	4.70	7.580 a	7.819	- 3.2
202.40	9.26	7.973 a	8.102	- 1.6
202.30	12.52	8.264 a	8.340	- 0.9
297.85	4.71	9.668 c	9.584	+ 0.9
297.77	12.52	9.887 c	9.792	+ 1.0
297.91	21.97	10.144 c	10.090	+ 0.5
297.21	43.49	10.712 c	11.024	- 2.9
300.40	73.87	12.517 c	13.187	- 5.3
306.64	39.98	10.752 b	10.894	- 1.3
306.40	63.92	11.333 b	12.249	- 8.1
306.82	21.54	10.325 b	10.199	+ 1.2
307.52	4.57	9.938 b	9.759	+ 1.8
307.39	4.57	9.915 b	9.759	+ 1.6
307.76	12.70	10.205 b	9.958	+ 2.4
307.33	12.70	10.171 b	9.958	+ 2.1
351.18	12.52	10.560 c	10.741	- 1.7
350.53	43.71	11.470 c	11.473	0.0
350.76	72.86	13.032 c	12.522	- 3.9
349.01	103.77	13.925 c	14.229	- 2.2
350.40	149.93	18.681 c	18.686	0.0

* Computed from the following equation

$$10^8 \lambda_p = 10^8 \lambda_0 + 1.096 (10^{0.934} \times 10^8 e^{-ap} - 1)$$

where $a = T^{-1}$ and p is in atm.

$$\text{and } 10^8 \lambda_0 = \frac{1.5456 \sqrt{T}}{1 + 1737.3 \tau / 10^{13.7}}$$

** The deviation is given by the expression:

$$\frac{\lambda_{\text{obs}} - \lambda_{\text{calc}}}{\lambda_{\text{obs}}} \times 100$$

a represents values of heat conductivity in steam cell No. 1

b represents values of heat conductivity in revision No. 1 of steam cell No. 1

c represents values of heat conductivity in revision No. 2 of steam cell No. 1

THE STEAM DATA

The value of λ , the heat conductivity for steam, deduced from the observations taken to August, 1949, are assembled in Table 1.

The basis for correlating the data requires λ_0 , the heat conductivity corresponding to zero pressure, since the quantity is a function of temperature only, and it is convenient in the absence of any adequate theory of the effect of pressure on heat conductivity to assume that λ generally may be represented by the following form of relationship

$$\lambda = \lambda_0 + f(\tau)p \dots \dots \dots [5]$$

It is likely that when more complete data for a variety of substances become available the pressure dependence can be more simply expressed in terms of density and temperature as independent variables, but convenience at present is served by a pressure-temperature function.

It may be supposed that the pressure effect will diminish as T increases ($T^{-1} = \tau$ small), and this indeed proved to be the case when, some years ago, the Timroth and Vargaftig data were correlated. The form of function $f(\tau, p)$ found to represent the Russian data most satisfactorily was as follows

$$f(\tau, p) = C [e^{a\tau p} - 1] \dots \dots \dots [6]$$

a relationship which vanishes as p approaches zero and also as T becomes very large for any finite pressure. Also, for small pressures at all finite temperatures the pressure effect of $f(\tau, p)$ becomes $(Ca)\tau p$, on expanding the exponential in Equation [6], a linear dependence.

At constant pressure λ_0 , as has long been known, increases indefinitely and regularly with temperature while $f(\tau, p)$ of Equation [6] decreases. Therefore, for a particular value of the temperature along the isopiestic heat conductivity-temperature curve, there will be a minimum in λ , the minima for increasing isopiestic occurring at progressively higher temperatures. This is exactly what the Timroth and Vargaftig data show with λ falling from the saturation-pressure value, reaching the minimum and again increasing. Therefore, for the isopiestic above the minimum there are two temperatures with numerically equal λ -values.

The value of C in Equation [6] was taken to be 1.096 for the new steam data with $0.934 \cdot 10^9$ (2.151 $\cdot 10^9$ nat logs) for a . The λ_0 values employed in computing the values in Table 1 were obtained from the following equation based on the 1-atm measurements

$$10^8 \lambda_0 = \frac{1.5456 \sqrt{T}}{1 + 1737.3 \tau / 10^{13.7}}, \text{ IT cal per sec per cm per deg C} \dots [7]$$

The fifth column of Table 1 lists the deviations of the observed conductivities from those computed and there appears to be no pronounced trend in sign except the tendency to negative values around 200 deg and positive at about 307 deg C. It will be observed that the $f(\tau, p)$ chosen is a two-constant form and, when additional data are available, it may be found that a less simple correlative equation is required.

The Timroth and Vargaftig data were represented some years ago (3) by the form of Equation [6], with, however, the constants $c = 2.486$ and $a = 1.832 \cdot 10^9$ (nat logs) for pressure in atmospheres, τ in reciprocal Kelvin degrees, and $10^8 \lambda$ in IT cal per sec per cm per deg C. Accordingly, the pressure effect is considerably larger for the Timroth and Vargaftig observations. It was also found that the λ_0 , or more accurately, the λ_1 values for 1 kg per cm² exhibited an exponential rise with temperature beginning at about 250 C, and extending to 550 C. The equation obtained for the Timroth and Vargaftig λ_1 data (1 kg per cm) follows

$$10^8 \lambda_1 = 0.3191 \sqrt{T} e^{1.5234 \cdot 10^{-3} T^2}, \text{ cal per sec per cm per deg C} \dots \dots \dots [8]$$

However, taking the ensemble of low-pressure data published in the 1937 paper of Vargaftig (1), and the 1940 paper of Timroth and Vargaftig (2), it is possible to correlate the data from below 100 to 550 C with the following form

$$10^8 \lambda_1 = \frac{1.0446 \sqrt{T}}{(2.191 \cdot 10^3 \tau / 10^{1.59 \cdot 10^4 \tau^2} - 1)} \dots \dots \dots [9]$$

TABLE 2 HEAT CONDUCTIVITY OF STEAM
($10^3 \lambda$ in IT cal per sec per cm per deg C)

t	$10^3 \lambda$ (IT) calc (a)	$10^3 \lambda$ (IT) obs (b)	$10^3 \lambda$ (ES) (c)
	20 kg per cm ²		
250	10.58	10.97 (+3.9)	9.33 (+11.4)
300	11.14	11.33 (+1.7)	10.04 (+11.0)
350	12.18	12.21 (+0.3)	10.87 (+12.0)
400	13.05	13.61 (+6.6)	11.78 (+15.9)
500	18.20	18.55 (+2.0)	13.70 (+35.8)
	50 kg per cm ²		
300	12.49	12.22 (-2.2)	10.80 (+15.7)
350	13.01	12.67 (-2.6)	11.33 (+14.9)
400	14.03	14.11 (+0.8)	12.08 (+17.6)
500	18.09	19.05 (+2.3)	13.84 (+33.6)
	60 kg per cm ²		
300	14.35	13.69 (-4.2)	11.91 (+20.5)
350	14.06	13.39 (-4.8)	11.93 (+17.6)
400	14.86	14.96 (+0.5)	12.45 (+19.4)
500	18.80	19.50 (+3.7)	14.02 (+34.0)
	100 kg per cm ²		
350	17.09	15.83 (-7.3)	13.78 (+24.0)
400	16.59	16.26 (-1.9)	11.46 (+25.3)
500	19.94	20.22 (+1.5)	14.35 (+35.4)
	150 kg per cm ²		
350	23.53	23.67 (+1.9)	18.11 (+30.0)
400	19.77	18.61 (-5.9)	15.39 (+25.3)
500	20.69	20.83 (+0.7)	15.09 (+28.1)

(a) Correlation values computed from the following equations based on Timmer and Vargaftik's values reported in 1940:
 $10^3 \lambda = 0.103 \sqrt{t} \cdot 10^{-0.616 \times 10^{-3} t} + 10^3 \lambda_0 + 2.46(10^{-0.77 \times 10^{-3} t} - 1)$

Pressure in kg per cm²

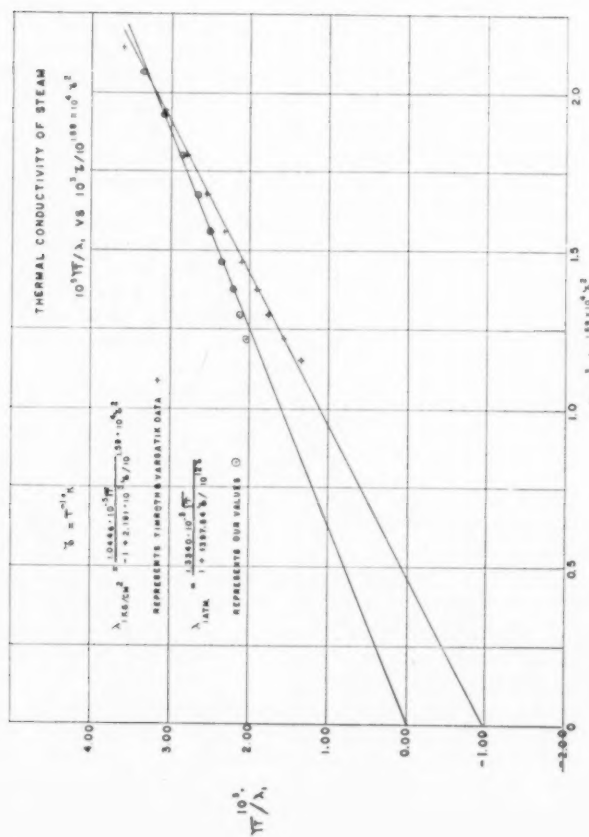
(b) Timmer and Vargaftik's reported values. The bracketed number is the quantity $\frac{\lambda_{obs} - \lambda_{calc}}{\lambda_{calc}} \times 100$.

(c) Values computed from the following equations based on the new data and the new correlation values reported in Table 1. The bracketed adjacent numbers are the deviation in percent relative to the IT computed value.

$$10^3 \lambda = \frac{1.016 \sqrt{t}}{1 + 1737.3 \sqrt{t} / 10^{0.2} t} + 10^3 \lambda_0 + 1.09(10^{-0.94 \times 10^{-3} t} - 1)$$

Pressure in atm.

Note: The equation designated $10^3 \lambda_0$ in the Steam Tables and based upon the Timmer and Vargaftik's values is actually based upon their case kilogram per cm² values. Accordingly the $10^3 \lambda$ equation labeled $10^3 \lambda_0$ and (p-1) substituted for p in the (p-2) part of the $10^3 \lambda$ equation. However the error introduced by assuming $10^3 \lambda_0$ equal to $10^3 \lambda$ is inconsequential in the temperature range 250 to 500°C.

FIG. 3 THERMAL CONDUCTIVITY OF STEAM $10^3 \sqrt{t} / \lambda_0$ VERSUS $10^3 \sqrt{t} / 10^{0.2} t \times 10^{0.2}$

The implications contained in the form Equation [9] are made evident by considering Fig. 3 where $10^8 \sqrt{T}/\lambda_1$ is plotted versus $\tau/10^{1.59-10\tau}$. In the figure the observed Vargaftig, and Timroth and Vargaftig data are represented and also the authors' data for 1 atm. The Russian $\lambda_1 \sqrt{T}$ data in the variable \sqrt{T}/λ_1 decrease so rapidly with increasing temperature (declining τ) that the extrapolation to higher temperatures than 550 C is moving to negative values in contrast to the trend of the new data. Extrapolation of λ_1 by means of either Equation [8] or Equation [9] to 2000 K would cause λ_1 to assume very large values; literally infinite values for temperatures which would cause the denominator of Equation [9] to vanish. Actually, however, the new data (λ_0 instead of λ_1) are best represented by Equation [7]; an equation of the form which correlates satisfactorily the λ_0 values for a

TABLE 3 HEAT CONDUCTIVITIES OF STEAM FOR PRESSURES APPROACHING ZERO

t °C	$10^8 \lambda_1 (T.V.)^a$	$10^8 \lambda_0 (T.V.)^b$	$10^8 \lambda_0 (K.S.)^c$	Dev. d
250	9.078	9.046	8.518	6.1
300	10.178	10.156	9.522	6.7
350	11.517	11.502	10.522	9.3
400	13.177	13.166	11.533	14.2
500	17.941	17.934	13.566	32.2

a Computed from the equation $10^8 \lambda_1 = 0.3194/T \cdot 10^{0.6616-10\tau}$ see "Notes" at foot of Table 2.

b The values in column three are the λ_1 values (1 kg per cm²) of Timroth and Vargaftig corrected by using the Keyes and Sandell $f(\infty, p)$ relation. See "c" at foot of Table 2.

c These values are computed from the $10^8 \lambda_0$ equation based on the new observations.

$$d \quad \frac{\lambda_0 T.V. - \lambda_0 K.S.}{\lambda_0 K.S.} \times 100$$

number of other gases from low (—200 C) temperatures to about 300 C (air, nitrogen, oxygen, hydrogen, helium, carbon monoxide, and carbon dioxide).

The data of Timroth and Vargaftig are compared with the new data on heat conductivity in Table 2 for temperatures from 250 to 500 C at pressures from 20 kg per cm². The comparison is made of the computed Timroth and Vargaftig values with computed values using the correlative equations based upon the new data and given at the bottom of the table. The corresponding observed values of Timroth and Vargaftig are also listed in the table to supply an impression of their accord with the computed values. In every case the new values as represented by the correlative equations are less than the Timroth and Vargaftig values. However, the temperatures of the new observations do not extend above 350 C.

It is of interest to compare the low pressure λ_0 , or λ_1 , values from the Timroth and Vargaftig measurements with the similar new values. For this purpose Table 3 is given for the range 250 to 500 C. Below 250 C the agreement between the two groups of low-pressure data is more satisfactory, although the Timroth and Vargaftig data are the larger. From Table 3 it appears that a considerable part of the difference between the Timroth and Vargaftig data and the new data is caused by the larger λ_0 -value.

TABLE 4 NEW DATA FOR HEAT CONDUCTIVITY OF NITROGEN

t °C	p atm	$10^8 \lambda$ obs	$10^8 \lambda$ calc	Dev.
0.57	1	5.857 a	5.824	+ 0.6
0.70	1	5.790 b	5.824	- 0.6
0.69	45.5	6.370 b	6.388	- 0.3
0.48	93.7	7.106 b	7.105	+ 0.0
0.64	140.7	7.958 b	7.963	- 0.1
27.21	1	6.257 a	6.234	+ 0.4
29.40	25.0	6.609 a	6.527	+ 1.2
25.54	60.9	7.065 a	6.891	+ 2.5
24.38	91.2	7.340 a	7.291	+ 0.7
24.05	122.6	7.787 a	7.829	- 0.5
25.14	151.7	8.286 a	8.290	- 0.1
104.46	1	7.293 d	7.264	+ 0.4
104.15	1	7.292 a	7.264	+ 0.4
101.58	1	7.241 c	7.229	+ 0.2
104.12	44.7	7.781 a	7.637	+ 1.9
101.24	49.6	7.759 c	7.646	+ 1.5
101.63	100.7	8.328 c	8.170	+ 1.8
104.11	101.0	8.294 a	8.197	+ 1.2
200.55	1	8.394 d	8.410	- 0.2
202.29	1	8.402 a	8.430	- 0.3
199.80	1	8.374 c	8.402	- 0.3
202.49	24.9	8.813 a	8.588	+ 2.6
200.25	49.6	8.796 c	8.729	+ 0.8
202.61	91.0	9.344 a	9.070	+ 2.7
202.25	100.7	9.219 c	9.116	+ 1.1
202.69	146.9	9.772 a	9.547	+ 2.4
308.56	1	9.210 b	9.560	- 3.8
301.20	1	9.183 d	9.485	- 3.3
307.18	1	9.419 b	9.545	- 1.3
297.85	1	9.199 c	9.428	- 2.5
310.08	45.5	9.641 b	9.815	- 1.9
297.73	49.6	9.611 c	9.697	- 0.9
310.12	93.7	9.932 b	10.100	- 1.7
307.17	93.7	9.906 b	10.073	- 1.7
297.85	100.7	9.938 c	10.011	- 0.7
309.80	142.6	10.598 b	10.423	+ 1.7
348.88	1	9.753 c	9.960	- 2.1
351.76	1	9.801 d	9.985	- 1.9
349.13	49.6	10.010 c	10.208	- 2.0
347.11	100.7	10.268 c	10.475	- 2.0
401.13	1	10.455 d	10.459	0.0

Brass Cell

0	1	5.74	5.84	- 1.7
0	25.3	6.13	6.11	+ 0.1
0	50.1	6.52	6.44	+ 1.4
0	76.7	6.95	6.83	+ 1.8
0	101.4	7.14	7.33	- 2.7
0	126.3	7.82	7.68	+ 1.8

a signifies measurements in Steam Cell No. 1.

b " " " " " No. 1, Revision 1.

c " " " " " No. 1, Revision 2.

d " " " " " Strain-Free Cell.

* Computed from Equation [10].

NITROGEN HEAT-CONDUCTIVITY DATA

The data for 1 atm pressure in the case of gaseous nitrogen were taken in the silver strain-free cell, as were those for air, and used to determine the cell constant of the steam cell. Heat-conductivity values for nitrogen under pressure have not been completed but it is expected that a complete series of measurements will be made to at least 450 C. The data available are collected in Table 4 in which the computed values appear using the following equations

$$10^8 \lambda = 10^8 \lambda_0 + 2.5 (10^{0.52\tau p} - 1) \dots \dots \dots [10]$$

$$10^8 \lambda_0 = \frac{0.4508 \sqrt{T}}{1 + 84.07\tau/10^{12\tau}}$$

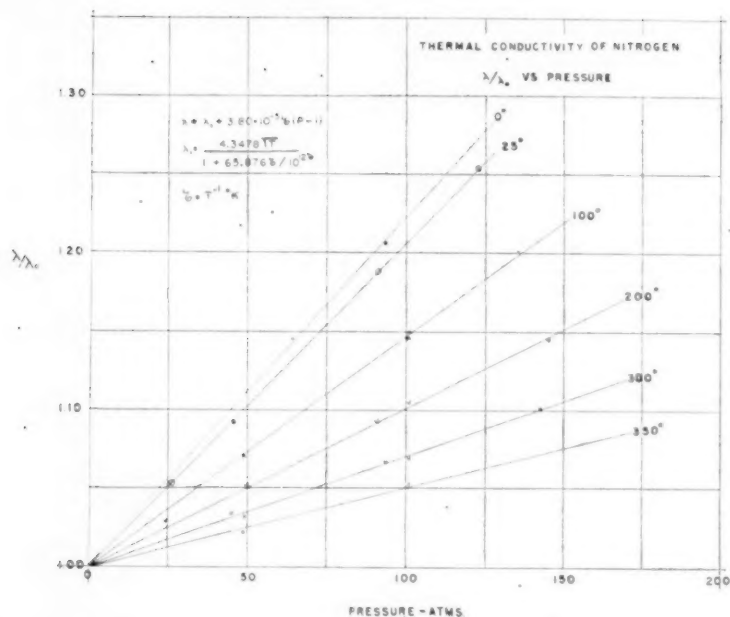
FIG. 4 THERMAL CONDUCTIVITY OF NITROGEN λ/λ_0 VERSUS PRESSURE

TABLE 5 COMPARISON OF HEAT-CONDUCTIVITY VALUES GIVEN BY VARGAFTIG FOR NITROGEN WITH NEW VALUES

t, °C	P, (atm)	$10^6 \lambda$ (V)	$10^6 \lambda$ (K.S.)	Deviation
40.3	0.968	6.444	6.455	+ 0.155
62.1	0.968	6.806	6.741	- 0.964
41.8	2.904	6.472	6.498	+ 0.400
63.0	2.904	6.833	6.775	- 0.856
41.7	6.775	6.500	6.544	+ 0.672
61.3	6.775	6.861	6.797	- 0.972
41.1	14.518	6.611	6.629	+ 0.272
60.9	14.518	6.944	6.880	- 0.930
40.9	19.357	6.667	6.686	+ 0.284
59.4	19.357	6.944	6.916	- 0.405
40.4	30.972	6.813	6.820	- 0.190
58.1	30.972	6.944	7.034	+ 1.279
40.0	46.458	6.972	7.004	+ 0.457
56.7	46.458	7.278	7.195	- 1.154
39.5	62.911	7.139	7.197	+ 0.806
55.2	62.911	7.417	7.368	- 0.665
38.9	87.108	7.556	7.486	- 0.935
53.4	87.108	7.778	7.630	- 1.940

(V) Refers to Vargaftig (1)

(K.S.) $\lambda_p = \lambda_1 + 3.8 \times 10^{-5} \phi(p-1)$

$$\lambda_1 = \frac{4.3478 \times 10^{-6} \sqrt{T}}{1 + 65.8761/10^{12} T^2}$$

representing nitrogen thermal conductivity values of the present investigation.

$$\text{Deviation} = \frac{\lambda(V) - \lambda(\text{calc}) (K.S.)}{\lambda(\text{calc}) (K.S.)} \times 100$$

The $f(\tau, p)$ of Equation [6] can also be assumed to be linear or of the following form which represents the data with tolerable accuracy to 100 atm

TABLE 6 NEW NITROGEN λ_0 -VALUES COMPARED WITH OLDER DATA

t, deg C	λ_0 (obs)	λ_0 (calc eq [10])	λ (eq [12])
-200	...	2.160 ^a	2.198
0	5.816	5.829	5.825
25	6.219	6.192	6.170
100	7.224	7.201	7.168
200	8.382	8.398	8.338
300	9.178	9.468	9.384
350	9.786	9.966	9.870
400	10.457	10.443	10.310

^a Extrapolated from 0 deg C by means of Equation [10]. Equation [12] is based upon all the older published observational data in the -200 C region and those extending to 400 C.

$$10^6 \lambda = 10^6 \lambda_1 + 3.8(p-1) \quad [11]$$

$$10^6 \lambda_1 = \frac{0.4348 \sqrt{T}}{1 + 65.887/10^{12} T^2}$$

Fig. 4 represents the new nitrogen data using the variable λ/λ_0 in relation to the linear isotherm for λ/λ_0 taken from Equation [11].

A comparison of the nitrogen heat-conductivity data of Vargaftig (1) in the range 40 to 63 C and to pressure of 87 atm with the new data (Equation [11]) is given in Table 5.

Table 6 gives a comparison of the $10^6 \lambda_0$ values for N_2 with the new observations for 1 atm reduced to zero pressure and round temperatures from the data of Table 4. In the fourth column the values obtained from a correlation of all the published data for nitrogen to 1947, are listed as computed from the following equation

$$10^6 \lambda_0 = \frac{0.442 \sqrt{T}}{1 + 76.927/10^{12} T^2} \quad [12]$$

No theoretical explanation of the pronounced difference between $f(\tau, p)$ for steam, $c(e^{\alpha \tau p} - 1)$, as compared with nitrogen, $c(e^{\alpha \tau p} - 1)$, is offered. The status of the theory of the pressure effect has been greatly affected by the absence of factual information on substances until recently. However, Enskog (8) has deduced a first-order form on the basis of a van der Waal's molecular

model; a relationship which has been tested recently by E. W. Comings and M. F. Nathan (9).

ACKNOWLEDGMENT

We take pleasure in acknowledging the continued general assistance of Miss Mildred Levin who took charge of the thermocouple and platinum-resistance thermometry.

BIBLIOGRAPHY

- 1 "The Dependence of the Coefficients of Thermoconductivity of Gases and Vapours on the Pressure," by N. Vargaftig, *Technical Physics* (USSR), vol. 4, 1937, p. 343.
- 2 "Thermal Thermoconductivity and Viscosity of Steam at High Temperatures and Pressures," by D. L. Timroth and N. Vargaftig, *Journal of Physics*, (USSR), vol. 2, 1940, pp. 101-111.
- 3 "Thermodynamic Properties of Steam," by J. H. Keenan and F. G. Keyes, John Wiley & Sons, Inc., New York, N. Y., table 7, 1943, and subsequent printings.
- 4 "Über die Wärmeleitfähigkeit der Gasen und Dampfen bei hohen Temperaturen," by E. Moser, Dissertation, Berlin, Germany, 1913.
- 5 "An Experimental Investigation of Thermal Conduction Through Vapors," by S. W. Milverton, Proceedings of the Royal Society of London, series A, vol. 150, 1935, pp. 287-308.
- 6 "Über die Wärmeleitungen des Quecksilberdampfes," by A. Schleiermacher, *Annalen der Physik*, vol. 36, 1889, pp. 346-357.
- 7 Mitteilung über Forschungsarbeiten auf dem Gebiete des Ingenieurwesens, Julius Springer, Berlin, Germany, Heft 21, 1905.
- 8 "Mathematical Theory of Non-Uniform Gases," by S. Chapman and T. G. Cowling, The Macmillan Company, New York, N. Y.; Cambridge, University Press, London, England, 1939, chap. 16.
- 9 "Thermal Conduction of Gases at High Pressures," by E. W. Comings and M. F. Nathan, *Industrial and Engineering Chemistry*, vol. 39, 1947, pp. 964-970.

Discussion

IRVING GRANET¹² AND R. M. GOULD¹³ The authors are to be congratulated for having completed successfully an accurate and extremely difficult experimental determination of the heat conductivity of steam. The need for an accurate determination of this property recently has been emphasized by the practical realization of units generating steam at 1000 F and 1350 psia.¹⁴ The data presented in the paper will aid the designer in better predicting the performance of such units and the researcher in correlating his data on a sounder basis.

Some time ago the writers had occasion to use the data of Timroth and Vargaftig as correlated and reported by Professor Keyes in the later printings of the "Steam Tables." At that time it was noted that the values of λ_0 (actually λ_1 for a pressure of 1 kg per cm²) listed in the Steam Tables exhibited a peculiar reverse curvature. These values were recomputed using the original correlation equation of Professor Keyes (Equation [8] of the present paper), and it was found that all of the 800 deg F values were incorrect as well as the values for saturated vapor at 32 F, 500 psia, and 1750 psia. The writers then differentiated this function twice and determined that a point of inflection does exist in the original Keyes equation. In Fig. 5 of this discussion is shown the original data of the Russian investigators and also a plot of the Keyes values as given in the "Steam Tables" for a pressure of 1 kg per cm². It will be noted that the error gives rise to a deviation from the original data of 11 per cent. The inflection

¹² Engineer, Research Department, Foster Wheeler Corporation, New York, N. Y. Jun. ASME.

¹³ Engineer, Research Department, Foster Wheeler Corporation, New York, N. Y.

¹⁴ "One Thousand Degrees F. . . . A New High in Steam Temperature," by Philip Sporn, *Electrical World*, vol. 126, Aug. 17, 1946, pp. 60-67. Reprinted as Bulletin B-46-20, Foster Wheeler Corporation, New York, N. Y.

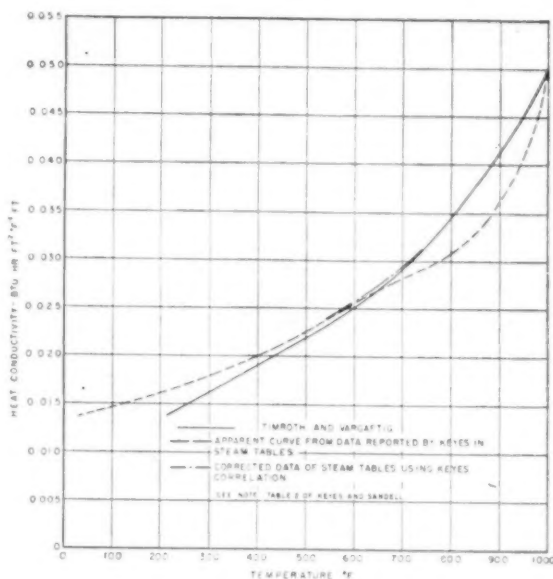


FIG. 5 COMPARISON OF KEYES CORRELATION, DATA REPORTED IN STEAM TABLES, AND ORIGINAL TIMROTH AND VARGAFTIG VALUES AT A PRESSURE OF 1 KG PER CM²

gives rise to no substantial deviation from the original Russian data.

In the present paper, Equation [7] is used to correlate the values of heat conductivity of steam at zero pressure. The writers felt that in view of certain similarities in Equations [7] and [8], and the discrepancies just noted, similar points might be exhibited by the present correlation. In order to test for such a condition, two devices were used. The values of λ_0 were calculated over a wide range of temperature using Equation [7], and a large-scale plot of these values was then made. This showed, in the range for which the plot was made, that while the reverse curvature was of such an order as to cause a negligible deflection in the correlation, two points of inflection seemed to exist—at about 200 F and at 1100 F. Since, to the writers' knowledge, the only other gas which exhibits such a reversal of curvature to any marked extent is hydrogen,¹⁵ it was felt that a further investigation of this point was justified. By a similar mathematical analysis it was determined tentatively that a point of inflection exists in this function between 1000 F and 1200 F. While it is puzzling to the writers to find such a phenomenon in an equation used to represent λ_0 which "... increases indefinitely and regularly with temperature. . .," it is noted that this phenomenon is of a negligible order.

In order to substantiate the present correlation some particular values of pressure and temperature were chosen, and the heat-conductivity values were calculated on the basis of the authors' correlation. For the values of temperature and pressure chosen, exact agreement was found with the corresponding values of heat conductivity listed in Table 2 of the paper.

It is understood that in the near future the values of heat conductivity of steam, as determined and correlated in this paper, will be incorporated in a new printing of the Steam Tables. To facilitate the use of this information in the interim, the writers have prepared Table 7 and Fig. 6 of this discussion. All values in Table 7 were determined by utilizing Equation [7] of the paper,

¹⁵ "An Investigation of Aircraft Heaters: II Properties of Gases," by M. Tribus and L. M. K. Boelter, NACA, October, 1942.

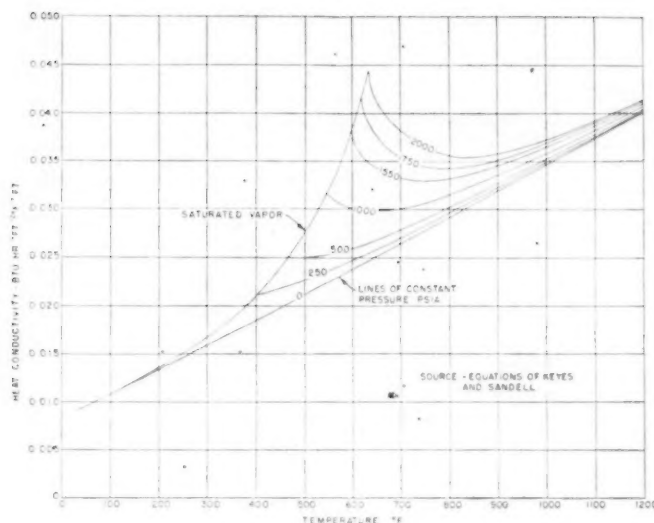


FIG. 6 HEAT CONDUCTIVITY OF STEAM

TABLE 7 HEAT CONDUCTIVITY $\times 10^2$ (Btu hr $^{-1}$ ft $^{-2}$ deg F $^{-1}$ ft)

	Temperature, deg F						
Sat. vapor	32	200	400	600	800	1000	1200
psia							
0	9.16	13.5	21.1	38.5			
250	9.16	13.3	18.4	23.8	29.2	34.7	40.1
500				24.7	29.7	34.9	40.3
1000				26.0	30.2	35.2	40.4
1500				30.1	31.4	35.7	40.7
1750				37.6	33.2	36.4	41.1
2000					34.3	36.8	41.3
					35.5	37.2	41.5

and the $f(p, \tau)$ as given by the authors. These values were determined to four significant places, but only three significant places are given in Table 7, since the writers feel that with the present data more than three places would not be warranted.

A word of caution must be noted at this time. When new accurate determinations of thermodynamic properties are made available, there is a tendency to use them in conjunction with the general heat-transfer relationships and equations made prior to the existence of the new data. For example, in the design of superheaters, the maximum tube temperature is a limiting factor. Using the present data for the heat conductivity of steam in the Poensgen¹⁶ correlation will indicate a temperature differential between the tube and the steam 30 per cent higher than that obtained using the data of Timroth and Vargaftig with the same heat-flux density. This would indicate erroneously a maximum heat-flux density, lower than that which could be used. Therefore the user of such equations should, where possible, determine the sources of the physical properties used by the correlator or investigator, as the case may be, and use the same sources in order to obtain reasonably accurate and correct predictions. If it is warranted, the user should recalculate previous data using the new physical properties.

SERGE GRATCH.¹⁷ These new data are certainly very accurate and reliable, and should supersede the older, apparently incorrect data by Timroth and Vargaftig.

The main value of the paper lies in the presentation of a greatly improved technique for the measurement of heat conductivity of

gases. In this connection engineers and scientists owe a great debt of gratitude to the senior author, Dr. F. G. Keyes, who for nearly half a century has been the leader in the development of new techniques for the accurate determination of properties of fluids. For resourcefulness and ingenuity in solving experimental problems Dr. Keyes is unequalled in his field, and stands high as guide and inspiration to the younger scientists.

R. L. SCORAH.¹⁸ The authors state clearly that the interpretation of the apparent heat conductivity measured for steam is complicated by the effect of radiation emitted and absorbed by the steam itself; and further, in so far as is known, the adjustment of heat-conductivity measurements to allow for radiation emission and absorption within the test material has never been made or discussed. This is a point of fundamental importance.

From the authors' description of their mode of taking and treating observational data, it appears that no allowance was made for the effect of radiation emitted and absorbed by the steam. When $(q/\Delta t)$ for $q = 0$ is obtained by graphical extrapolation, Equation [4] of the paper becomes

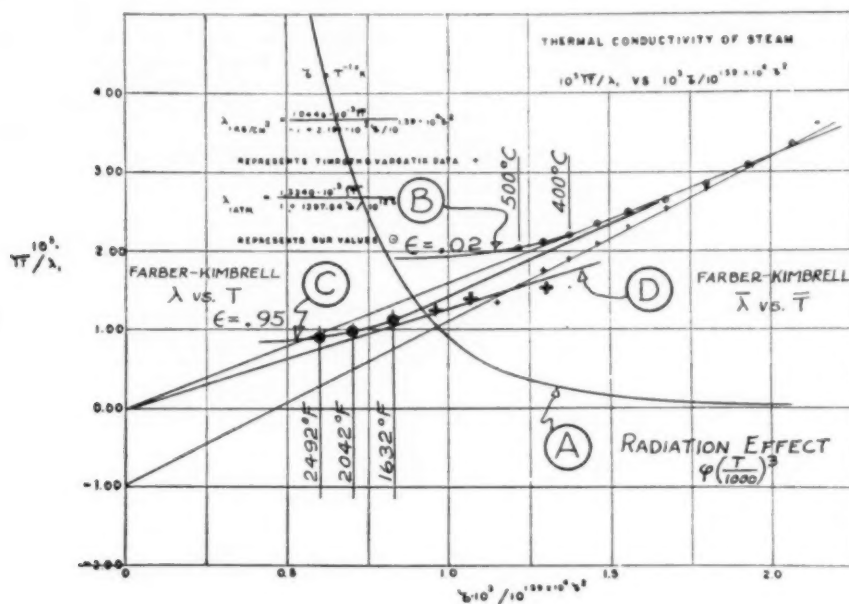
$$\left(\frac{q}{\Delta t}\right)_{q=0} = \lambda C + C_r(\bar{T})^4 + G + H$$

which is solved for λ . In general, the "radiation constant" C_r is a function of the surface temperature, emissivity, and shape, and the steam-film thickness and density. The new term H on the right-hand side of the foregoing equation has been added here to account for the effect of radiation emitted and absorbed within the film. The term C is fixed by the dimensions of the test cell, and the term G compensates for conduction within the emitter supports. The terms C_r and H , however, depend in part upon the emissivity of the test-cell surface material. The authors used silver and obtained lower values of conductivity than did the Russian experimenters who used platinum. This difference in results may be due in part to the difference in the emissivity of silver and platinum. Since engineering materials ordinarily show a much higher emissivity than polished silver, an emissivity correction would appear to be in order for applying heat-conductivity data measured by silver surfaces. This question must be clarified be-

¹⁶ "Heat Transmission," by W. H. McAdams, second edition, McGraw-Hill Book Company, Inc., New York, N. Y., 1942, p. 172.

¹⁷ University of Pennsylvania, Philadelphia, Pa. Jun. ASME.

¹⁸ University of Missouri, Columbia, Mo. Mem. ASME.

FIG. 7 THERMAL CONDUCTIVITY OF STEAM $10^5 \sqrt{T}/\lambda_1$ VERSUS $10^3 T^2 / (10^3 \lambda_1 \times 10^4)$

fore much confidence can be attached to any interpretation of heat-conductivity measurements for materials which absorb and emit radiation. It appears that with multiple observations at different emissivities, the heat conductivity with zero surface emission or absorption could be obtained by graphical extrapolation. The required emissivity correction could then be established.

Radiation becomes increasingly important at temperatures above 500 C, which is the limiting value of the authors' present paper. Our students have obtained rough values of the heat conductivity of steam at somewhat higher temperatures and at a pressure of 1 atm. For example, in the data of Farber¹⁹ for his April 25 tests, the last three runs were made with fully developed stable film boiling. From the optical measurements of J. T. Kimbrell,²⁰ the film was found to be 0.015 in. thick, as compared with the value of 0.025 in. in the authors' apparatus. Convection within this thin film was neglected. The radiation flux was estimated by the Stefan-Boltzmann equation, the temperatures being that of the wire surface and the saturation temperature of water; the emissivities, 0.95 for the wire and 0.963 for water. The remaining heat flux was considered as steady conduction, and the mean heat conductivity of the steam film was computed with the Fourier equation. No radiation correction of the type *H* was applied. The results are given in Table 8 of this discussion. Since the available data on the heat conductivity of

vapor line at 1 atm was considered to represent the Farber-Kimbrell experiments

$$k = 0.014 + 0.000043 (t-212) \dots \dots \dots [13]$$

At 500 C (932 F), this expression gives a value for the heat conductivity about 37 per cent greater than the zero-pressure value reported by the authors. Farber's experiments were never intended to measure the heat conductivity of steam, and while no high order of precision can be assigned to the numerical values, these data were obtained from steam films subjected to an intense radiation flux from a high-emissivity emitter. These data suggest an emissivity correction of considerable magnitude.

The correlation and extrapolation of steam-conductivity data is complicated when radiation phenomena are considered. As the temperature increases, the magnitude of the radiation flux increases very rapidly. Curve A in Fig. 7 herewith, is similar to the authors' *C*, term and is shown here only as a first approximation of the whole radiation effect. At high temperatures, the authors' data for an emissivity of about 0.02 departs from their straight line, as shown by Curve B. The departure begins at about 400 C. Since the radiation flux is increased approximately 50 per cent in the next 100 deg, the upward trend of Curve B may be due in part to this radiation increase. The fact that the trend of the authors' data is upward may be of special interest.

Curve C represents our student data. The instantaneous heat conductivity was computed for the test temperatures of the emitter by means of Equation [13] of this discussion. Considering the emissivity of about 0.95, these results do not appear to be completely inconsistent with those of the paper. The comparison of Curve B with Curve C suggests the possible range of the emissivity effect. Curve D represents the student data when using the mean heat conductivity calculated from Equation [13], and the arithmetic-mean film temperature. This plot enters the high-temperature region of the Russian data. Since at this writing we do not have the Russian papers, it is not clear what significance if any should be attached to this coincidence.

TABLE 8

<i>t</i> , deg F	<i>k</i> , Btu hr ⁻¹ ft ⁻² F ⁻¹ ft
1632	0.0465
2042	0.0492
2492	0.0640

steam is nearly linear at low pressures (the present paper included), the following linear relation passing through the saturated-

¹⁹ "Heat Transfer to Water Boiling Under Pressure," by F. A. Farber and R. L. Scoriah, Trans. ASME, vol. 70, 1948, pp. 369-384.

²⁰ Graduate Student, University of Missouri, Columbia, Mo.

AUTHORS' CLOSURE

The authors appreciate the careful discussion of the paper by Mr. Granet and Mr. Gould, who are correct in stating that the 800 F values in the Steam Tables are not in accord with the equations given in the text, section 7, page 23. The lambda-zero pressure value should be 34.42 instead of 30.55, and the pressure increments are correct. The new value is 29.2 as given in Table 7.

The authors had not been aware of the inflection feature of the correlating equation until it was brought to their attention by the commentators at the time of the meeting. The effect is small, however, as stated, and it does not invalidate the use of the correlative form which is in substantial accord with the kinetic-gas theory based on a van der Waals' molecular field. There is a qualification to this statement, however, due to the presence of the exponential term in Equation [7], a term which was found to be necessary if a long range of temperature is to be represented. Actually the Sutherland type formula is given in the classical kinetic-gas theory for the viscosity, and not for the heat conductivity,²¹ the latter coming out of the theory in the form: lambda proportional to the viscosity times the specific heat at constant volume.

The classical kinetic-gas theory gives no accounting of the temperature dependence of the specific heat, and since the specific heat for all except monatomic gases is a function of the temperature, it would be expected that the heat conductivity would involve a stronger temperature dependence as compared with the viscosity alone. The authors regard Equation [7] as a semi-empirical equation which appears to be of value in representing the observations on heat conductivity over considerable ranges of temperature. Reference should be made in this connection to the paper by J. O. Hirschfelder, R. B. Bird, and E. L. Spotz, a

report on the transport properties of gases and gas mixtures.²²

Substitute tables 6 and 7, of the Steam Tables have already been sent to the printers, and the commentators' Table 7 is in exact agreement with the authors' table.

Professor Scoriah's values given in Table 8 can be represented by a linear equation. It is important to observe, relative to Professor Scoriah's representation of the Table 8 values, that a linear equation is not suitable for long ranges of temperature. The Equation [7] is of the Sutherland type modified on the basis of a critical consideration of all the available heat conductivity data for the gases: air, helium, hydrogen, oxygen, nitrogen, CO, CO₂, as well as H₂O.²³

The difference in the emissivity of the wire used by Professor Scoriah's collaborators and that of silver used in the steam-heat conductivity work is very large, and there is insufficient data on the absorption spectrum and emissivity of steam to make the required correction of the apparent conductivity when the emissivity from the wire is as large as 0.95. Indeed under present circumstances the best that can be done is to use materials in the measurements that have as low an emissivity as possible, and silver appears to be better than any other metal.

As remarked in the text, the trend of the Russian data as given in Fig. 7 leads to an extrapolation impasse, namely, it tends progressively to very large values with increasing temperatures. This could be due in part to the high emissivity of the platinum wire which under operating conditions has been shown by Timroth and Vargaftig to be the order of 0.11; a figure in substantial agreement with Milverton's results for the platinum wire of his apparatus.

The authors thank the commentators for their encouraging and helpful comments.

²² "Viscosity and Other Physical Properties of Gases and Gas Mixtures," by J. O. Hirschfelder, R. B. Bird, and E. L. Spotz, Trans. ASME, vol. 71, 1949, p. 921.

²³ Final Report, Office of Naval Research, Task Order XI, M.I.T. Contract N5ori-78, Project Designation No. NR-059-037, October 1, 1949.

²¹ "Mathematical Theory of Non-Uniform Gases," by S. Chapman and T. G. Cowling, The Macmillan Company, Cambridge, Mass., 1939, p. 184.

Compilation of Thermal Properties of Wind-Tunnel and Jet-Engine Gases at the National Bureau of Standards

By HAROLD J. HOGE,¹ WASHINGTON, D. C.

A project for the preparation of a series of tables of thermal properties of gases is described. This project was undertaken by the National Bureau of Standards at the suggestion and with the co-operation of the National Advisory Committee for Aeronautics. The scope of the project, tables now available, work in progress, and plans for the future are described. The lack of adequate data at high temperatures and also at high pressures is pointed out.

INTRODUCTION

RESEARCH involving wind tunnels, jet engines, and missiles requires good thermal data on the gases which flow through the tunnels or jets, or which the missile encounters in its flight. The following are typical examples of the problems encountered:

1 Compressed gas in a tank at a known temperature and pressure expands to a low pressure as it passes through a wind tunnel. How do the temperature and velocity change along the tunnel? If water is present, at what temperature will it be precipitated, and will ice or liquid water be formed? Will the major constituents of the gas condense? Will condensation shock interfere with the measurements?

2 A missile flies through the earth's atmosphere, compressing and heating a layer of air in front of it. How much heat will be conducted to the missile and how hot will it get? How much deceleration will it experience?

3 Fuel is burned in a jet engine. What is the composition of the products of combustion? How does the efficiency of the engine depend on the operating temperature? Will the walls of the engine get too hot?

These questions and many others cannot be answered unless reasonably accurate thermal data are available.

Thermal data for the region near room temperature are available, although they are not always easy to locate or in convenient form for use. But as the interval from room temperature increases the data become more scarce, to the extent that above 900 or 1000 deg K data are practically nonexistent. A similar situation exists with regard to pressure. Near a pressure of 1 atm the data are fairly plentiful, but at high and low pressures they are scarce. This is especially true of the nonequilibrium properties such as viscosity and thermal conductivity.

A project for the compilation of tables of thermal data on

wind-tunnel and jet-engine gases has been established at the National Bureau of Standards with the co-operation of the National Advisory Committee for Aeronautics. This project was initiated by Dr. F. G. Brickwedde, chief, Heat and Power Division, who prepared a plan for the tables. This plan was sent to a large number of laboratories and individuals for comments and suggestions. After these had been received and considered, the program described in this paper was evolved. Several individuals have contributed to this program during the past year, and 16 tables have been published.

THE PROJECT

The program as it exists at present calls for the critical evaluation of available data, and the preparation of conveniently usable tables of thermal properties of the following gases:

Dry air	Carbon dioxide
Moist air	Carbon monoxide
Steam	Nitrogen dioxide (NO ₂)
Hydrogen	Nitric oxide (NO)
Oxygen	Helium
Nitrogen	Freon 12 (CF ₂ Cl ₂)
	Argon

The following properties are to be tabulated, in general, as functions of both temperature and pressure:

Heat capacity (C_p)	Velocity of sound
Enthalpy (total heat)	Relaxation parameters
Entropy	Viscosity
Gibbs free energy	Thermal conductivity
Compressibility factor	Prandtl number
Density	Vapor pressure
Ratio of specific heats	

Additions both to the list of gases and to the list of properties are anticipated as the project continues. For example, it is already evident that atoms and molecules formed by dissociation of certain gases in the list will have to be considered. The temperature and pressure ranges to be covered are almost always limited by the available data. At pressures below 1 or 2 atm, data are needed from the condensation temperature (vapor-pressure curve) to 3000 deg K. Throughout part of this temperature range, from room temperature to about 700 deg K, low-pressure data are not enough, and the aim is, where practical, to extend the tables to a pressure of 100 atm.

A few of the properties in the tabulation call for explanations or comment. Gibbs free energies are needed when equilibria are to be computed between products of combustion. Compressibility factor is the dimensionless quantity $Z = pV/nRT$, which equals unity for an ideal gas. The ratio of specific heats is of course C_p/C_v , the specific heat at constant pressure divided by the specific heat at constant volume. Relaxation is the process of distribution of energy among the various degrees of freedom of the molecule. When a gas is suddenly heated or cooled, the vibrational degrees of freedom do not gain or lose energy as fast as the translational or rotational degrees of freedom. This effect has often been neglected, but it can become quite important in

¹ Member, Thermodynamics Section, National Bureau of Standards.

Contributed by the Research Committee on Properties of Gases and Gas Mixtures and the Heat Transfer and Applied Mechanics Divisions, and presented at the Annual Meeting, New York, N. Y., November 27-December 2, 1949, of THE AMERICAN SOCIETY OF MECHANICAL ENGINEERS.

NOTE: Statements and opinions advanced in papers are to be understood as individual expressions of their authors and not those of the Society. Paper No. 49-A-56.

aerodynamic processes. The relaxation parameters to be tabulated are the relaxation time, the relaxation distance, and the specific heat (vibrational) associated with the relaxation. The Prandtl number $\eta C_p/k$ is the product of the viscosity and the specific heat at constant pressure divided by the thermal conductivity. It is particularly useful in heat-transfer problems at the surfaces of missiles.

In the preparation of the tables, emphasis is placed on convenience in use, and upon the inclusion of a brief summary of the more important questions involved in the critical evaluation. Suitably qualified estimates of the accuracy of the tables are given, even though these are sometimes very rough and approximate. In the present stages of the program we have thought it wise not to place extreme emphasis on accuracy, but simply to select the best data available and tell how good we think they are. When this has been done, so that the tables give a fairly good coverage of the selected field, we hope to begin to issue replacements for the less reliable tables. In most cases this will require new experimental work, or computations of an original nature. Some of this original work we expect to undertake ourselves, but for much of it we will have to depend on others. One of the minor functions of the project will be to show where there is greatest need for new experimental work.

In order to make the tables equally convenient regardless of the units to be employed, they are, wherever practical, expressed in dimensionless form. Then, on the same page with a given table, clearly labeled conversion factors are given which permit a quantity obtained from the table to be expressed in any units likely to be desired. This applies to the entries in the tables rather than to the argument or arguments (independent variables) of the tables. For example, a table giving the thermal conductivity of a gas at specified values of temperature and pressure will have as entries values of k/k_0 where k_0 is the thermal conductivity at some standard condition, such as 0 deg C and 1 atm. The arguments T and p , however, will normally be dimensional (T both in deg K and deg R, and p in atm, psia, or mm Hg). These have been left in dimensional form because it was felt that the use of too many dimensionless quantities might cause confusion.

The ease with which interpolations may be made is one of the most important factors in the practical use of a table. Seldom is it possible to avoid interpolation altogether. But linear interpolation is relatively simple and rapid as compared with higher-order interpolation, even when tables of interpolation coefficients² are at hand. Our goal has been to subtabulate to the point where linear interpolation can be used everywhere. Unfortunately, this has not always been practical, because in some cases it would have led to very large tables. In these cases care has been taken to indicate clearly where linear interpolation is not adequate.

One of the published tables is shown in Fig. 1. This table, No. 2.10, gives specific heat, enthalpy, and entropy of dry air as calculated from spectroscopic data (ideal gas state). The full-sized table consists of four $8 \times 10^{1/2}$ -in. pages printed by a photo-offset process. The original tables of the data proper were printed by International Business Machine typewriters actuated directly by punch cards, with rules and headings put in by hand. This procedure has been used whenever the data were already available on punch cards as a result of subtabulation or other operations performed on IBM equipment. It may be mentioned in passing that where IBM equipment has been used the tables can be furnished on punch cards.

The brief text accompanying a table contains a description of the table and how to use it, and an evaluation of the data upon which the table is based. In some cases a graph can be included

which shows the agreement between the table and the principal experimental data. Such a graph can quickly give the user of a table an idea of its accuracy that he could otherwise get only from hours of study of the original papers.

WORK ACCOMPLISHED AND IN PROGRESS

The tables now available for distribution are listed as follows (as of September, 1949):

- 2.10 Dry Air (Ideal Gas State), Specific Heat, Enthalpy, Entropy
- 2.42 Dry Air, Thermal Conductivity
- 5.42 Steam, Thermal Conductivity
- 7.10 Molecular Hydrogen (Ideal Gas State) Specific Heat, Enthalpy, Entropy
- 7.42 Molecular Hydrogen, Thermal Conductivity
- 9.10 Molecular Oxygen (Ideal Gas State), Specific Heat, Enthalpy, Entropy
- 9.42 Molecular Oxygen, Thermal Conductivity
- 9.50 Vapor Pressure of Oxygen
- 11.10 Molecular Nitrogen (Ideal Gas State), Specific Heat, Enthalpy, Entropy
- 11.42 Molecular Nitrogen, Thermal Conductivity
- 13.42 Carbon Dioxide, Thermal Conductivity
- 14.42 Carbon Monoxide, Thermal Conductivity
- 15.42 Nitrogen Dioxide, Thermal Conductivity
- 16.42 Nitric Oxide, Thermal Conductivity
- 18.42 Freon 12, Thermal Conductivity
- 19.42 Argon, Thermal Conductivity

So far it has been possible to keep each publication to a length of 4 pages or less. Undoubtedly, some will have to be longer, but it is planned to keep them as compact as is consistent with good legibility. A numbering scheme for the tables has been adopted which identifies both the substance and the properties treated in a table. For example, in table 9.50, the 9 shows that the substance is oxygen and the 50 shows that the property tabulated is vapor pressure.

Of the tables now issued, a large fraction gives ideal gas properties. These are computed from spectroscopic data. They furnish limiting values which should be approached by the real gas at low pressures, and they are virtually the only type of data available in the higher temperature ranges.

A large number of calculations of ideal gas properties have been published in the last 10 or 15 years. Many of these have become obsolete because of the subsequent publication of better molecular data. The process of selection of an ideal gas table is begun by checking the more recent tables at various temperatures. The table which appears to be most accurate is more carefully checked, sometimes by spot calculations starting from the molecular constants themselves. When the most adequate basic calculation of ideal gas properties has been accepted, it is generally necessary to subtabulate it. It is also converted to dimensionless units in such a way that the final table will be consistent with the latest values of the fundamental constants. Most of the tables of ideal gas properties published by the project to date have been prepared under the supervision of Harold W. Woolley.

In the field of real gas properties a considerable amount of effort has been put on the properties of dry and moist air. Curtiss and Hirschfelder^{3,4} have published two sets of tables that have served as the basis of this work. These have been retabulated with pressure rather than density as an independent variable, and some new intermediate values have been computed. Subtabulation has been performed; the tables have been made dimensionless and modified in some other respects. This work has been

² "Thermodynamic Properties of Air," by C. F. Curtiss and J. O. Hirschfelder, University of Wisconsin Naval Research Laboratory Report CM-472, June 1, 1948.

³ "Tables of Lagrangian Interpolation Coefficients," prepared by Mathematical Tables Project, WPA, Columbia University Press, New York, N. Y., 1944.

⁴ "Thermodynamic Properties of Air—II," by J. O. Hirschfelder and C. F. Curtiss, University of Wisconsin Naval Research Laboratory Report CM-518, December 21, 1948.

U. S. DEPARTMENT OF COMMERCE
Charles Sawyer, SecretaryNATIONAL BUREAU OF STANDARDS
E. U. Condon, DirectorTHE NBS-NACA TABLES OF
THERMAL PROPERTIES OF GASES

Table 2.10 Dry Air (Ideal Gas State)

Preliminary Issue

July 1958

Specific Heat, Enthalpy, Entropy

$$C_p^0/R, (H^0 - E_0^0)/RT_0, S^0/R$$

compiled by Harold W. Woolley

FOREWORD

This is one of a series of tables of Thermal Properties of Gases being compiled at the National Bureau of Standards at the suggestion and with the cooperation of the National Advisory Committee for Aeronautics. Recent advances in methods of propulsion and the high speeds attained thereby have emphasized the importance of accurate data on thermal properties of wind-tunnel and jet-engine gases. It is the purpose of the project on Thermal Properties of Gases to make a critical compilation of existing published and unpublished data, and to present such data in convenient form for application. The loose-leaf form has been chosen as being most convenient, and revisions are anticipated as new data become available.

The dimensionless character of the tables and their general format should facilitate calculations in aerodynamics, heat-transfer, and jet-engine problems. Suggestions for the extension or improvement of these tables are desired as well as information regarding unpublished data. Information and other correspondence regarding these tables should be addressed to Joseph Hilsenrath, Heat and Power Division, National Bureau of Standards. This table is also available on IBM punched cards.

$T^{\circ}K$	$\frac{C_p^0}{R}$	$\frac{(H^0 - E_0^0)}{RT_0}$	$\frac{S^0}{R}$	$T^{\circ}R$	$T^{\circ}K$	$\frac{C_p^0}{R}$	$\frac{(H^0 - E_0^0)}{RT_0}$	$\frac{S^0}{R}$
10	3.5009	0.1278	12.0382	18	400	3.5305	5.1182	24.9101
20	3.4941	0.2510	12.0462	36	410	3.5349	5.2476	25.0173
30	3.4926	0.3796	12.0578	54	420	3.5397	5.3771	25.1026
40	3.4918	0.5075	12.0683	72	430	3.5447	5.5061	25.1859
50	3.4915	0.6353	12.0783	90	440	3.5499	5.6356	25.2675
60	3.4914	0.7631	12.0890	108	450	3.5555	5.7667	25.3473
70	3.4914	0.8909	12.0998	126	460	3.5613	5.8979	25.4255
80	3.4913	1.0188	12.1094	144	470	3.5673	6.0274	25.5022
90	3.4913	1.1466	12.1195	162	480	3.5735	6.1561	25.5773
100	3.4913	1.2744	12.1298	180	490	3.5799	6.2851	25.6511
110	3.4914	1.4022	12.1402	198	500	3.5865	6.4202	25.7235
120	3.4914	1.5300	12.1506	216	510	3.5933	6.5513	25.7946
130	3.4914	1.6578	12.1608	234	520	3.6003	6.6831	25.8644
140	3.4914	1.7856	12.1712	252	530	3.6075	6.8152	25.9330
150	3.4915	1.9134	12.1816	270	540	3.6149	6.9475	26.0005
160	3.4916	2.0413	12.1920	288	550	3.6224	7.0799	26.0669
170	3.4916	2.1691	12.2024	306	560	3.6300	7.2127	26.1323
180	3.4917	2.2969	12.2128	324	570	3.6377	7.3457	26.1966
190	3.4919	2.4247	12.2232	342	580	3.6456	7.4789	26.2599
200	3.4922	2.5526	12.2336	360	590	3.6535	7.6126	26.3223
210	3.4924	2.6804	12.2440	378	600	3.6615	7.7466	26.3838
220	3.4927	2.8083	12.2544	396	610	3.6696	7.8807	26.4444
230	3.4932	2.9362	12.2648	414	620	3.6777	8.0152	26.5041
240	3.4937	3.0641	12.2752	432	630	3.6860	8.1500	26.5630
250	3.4945	3.1920	12.2856	450	640	3.6943	8.2851	26.6211
260	3.4953	3.3199	12.2960	468	650	3.7027	8.4205	26.6785
270	3.4963	3.4478	12.3064	486	660	3.7113	8.5561	26.7351
280	3.4975	3.5757	12.3168	504	670	3.7200	8.6922	26.7910
290	3.4989	3.7036	12.3272	522	680	3.7289	8.8289	26.8461
300	3.5005	3.8315	12.3376	540	690	3.7380	8.9659	26.9006
310	3.5024	3.9594	12.3480	558	700	3.7471	9.1027	26.9544
320	3.5044	4.0873	12.3584	576	710	3.7563	9.2393	27.0076
330	3.5068	4.2152	12.3688	594	720	3.7654	9.3766	27.0601
340	3.5095	4.3431	12.3792	612	730	3.7746	9.5147	27.1121
350	3.5127	4.4710	12.3896	630	740	3.7838	9.6529	27.1634
360	3.5163	4.5989	12.3999	648	750	3.7931	9.7913	27.2142
370	3.5203	4.7268	12.4103	666	760	3.8024	9.9297	27.2644
380	3.5248	4.8547	12.4207	684	770	3.8117	10.0682	27.3141
390	3.5298	4.9826	12.4311	702	780	3.8210	10.2068	27.3632
400	3.5355	5.1105	12.4415	720	790	3.8303	10.3452	27.4118
					800	3.8397	10.4837	27.4599

CONVERSION FACTORS

To Convert Tabulated Value of	To	Having the Dimensions Indicated Below	Multiply by
$C_p^0/R, S^0/R$	C_p^0, S^0	cal mole ⁻¹ °K ⁻¹ (or °C ⁻¹)	1.98719
		cal g ⁻¹ °K ⁻¹ (or °C ⁻¹)	0.008314
		joules g ⁻¹ °K ⁻¹ (or °C ⁻¹)	0.238946
		Btu lb mole ⁻¹ °K ⁻¹ (or °F ⁻¹)	1.98688
		Btu lb ⁻¹ °K ⁻¹ (or °F ⁻¹)	0.000930

FIG. 1 REPRODUCTION OF ONE OF THE TABLES IN THE NBS SERIES ON "THERMAL PROPERTIES OF GASES"

(Actual size of each of the 4 pages is 8 x 10 1/2 in.)

$T^{\circ}K$	$\frac{C_p^0}{R}$	$\frac{(H^0 - E_0^0)}{RT_0}$	$\frac{S^0}{R}$	$T^{\circ}R$	$T^{\circ}K$	$\frac{C_p^0}{R}$	$\frac{(H^0 - E_0^0)}{RT_0}$	$\frac{S^0}{R}$
800	3.8275	10.4882	27.4599	1440	1900	4.3337	27.1375	31.0047
850	3.8670	11.1924	27.6931	1530	1950	4.3452	27.9318	31.1175
900	3.9049	11.9037	27.9152	1620	2000	4.3561	28.7261	31.2276
950	3.9409	12.6218	28.1273	1710	2050	4.3666	29.5204	31.3353
1000	3.9750	13.3463	28.3303	1800	2100	4.3767	30.3267	31.4407
1050	4.0079	14.0769	28.5250	1890	2150	4.3864	31.1387	31.5438
1100	4.0391	14.8131	28.7121	1980	2200	4.3958	31.9524	31.6447
1150	4.0693	15.5547	28.8922	2070	2250	4.4048	32.7679	31.7436
1200	4.0987	16.3013	29.0658	2160	2300	4.4135	33.5849	31.8405
1250	4.1274	17.0535	29.2333	2250	2350	4.4219	34.4036	31.9355
1300	4.1548	17.8082	29.3953	2340	2400	4.4301	35.2237	32.0287
1350	4.1815	18.5679	29.5519	2430	2450	4.4380	36.0456	32.1201
1400	4.2075	19.3315	29.7036	2520	2500	4.4456	36.8684	32.2099
1450	4.2321	20.0988	29.8507	2610	2550	4.4530	37.6928	32.2980
1500	4.2553	20.8695	29.9935	2700	2600	4.4602	38.5186	32.3845
1550	4.2784	21.6434	30.1321	2790	2650	4.4672	39.3457	32.4695
1600	4.3003	22.4203	30.2669	2880	2700	4.4740	40.1740	32.5531
1650	4.3218	23.2001	30.3979	2970	2750	4.4807	41.0035	32.6353
1700	4.3429	23.9826	30.5255	3060	2800	4.4871	41.8343	32.7160
1750	4.3628	24.7678	30.6499	3150	2850	4.4933	42.6662	32.7955
1800	4.3815	25.5553	30.7711	3240	2900	4.4994	43.4992	32.8737
1850	4.3991	26.3453	30.8893	3330	2950	4.5053	44.3333	32.9507
1900	4.4157	27.1375	31.0047	3420	3000	4.5109	45.1684	33.0264

CONVERSION FACTORS

To Convert Tabulated Value of	To	Having the Dimensions Indicated Below	Multiply by
$H^0 - E_0^0/RT_0$	$H^0 - E_0^0$	cal mole ⁻¹	592.821
		cal g ⁻¹	18.7399
		joules g ⁻¹	78.4078
		Btu lb mole ⁻¹	976.437
		Btu lb ⁻¹	33.7088

DRY AIR

THE PROPERTIES TABULATED

The thermodynamic properties of dry air in the ideal gas state (without dissociation) are given in dimensionless form in this table. The properties listed are C_p^0/R , $(H^0 - E_0^0)/RT_0$, and S^0/R , tabulated as functions of temperature in degrees K, and degrees R. The values were obtained from the thermodynamic properties of the constituents of dry air, which was considered to be 78.088% N₂ [1], 20.9495% O₂ [2], 0.9324% A [3] and 0.0300% CO₂ [4]. This composition for dry air has been used in previous computations of properties of air [5], and corresponds to an average molecular weight of 28.966.

RELIABILITY OF THE TABLE

The uncertainties in the properties of dry air in the undissociated ideal gas state are considered to be roughly as great as for the ideal gas properties of molecular nitrogen, its principal constituent [1]. This implies that C_p^0/R and S^0/R are probably accurate to the next to the last place tabulated up to about 2000°K and might be uncertain by a little more than a unit in the next to the last place at 3000°K. $(H^0 - E_0^0)/RT_0$ may be uncertain by 0.004 at 2000°K and 0.006 at 3000°K.

INTERPOLATION

The validity of linear interpolation varies throughout this table depending upon the number of figures desired. The error produced by linear interpolation does not exceed one-eighth of the second difference. Where more precise values are desired, a four-point Lagrangian interpolation may be used [6].

CONVERSION FACTORS

The functions in this table have been expressed in dimensionless form in order that they may be converted readily to any system of units. Conversion factors are listed for the most often used units. For values of R and RT_0 not listed here see Table 1.30 of this series. The symbol R denotes the gas constant and T_0 is 273.15° Kelvin. The calorie used in the conversion factors is the thermochemical calorie and unless otherwise specified the mole is the gram-mole.

REFERENCES

- [1] Thermal Properties of Gases, Table 11.10, National Bureau of Standards.
- [2] Thermal Properties of Gases, Table 9.10, National Bureau of Standards.
- [3] S. Gretch and S. W. Van Vleet, Report of the University of Pennsylvania Thermodynamics Research Laboratory to the Navy Department, Bureau of Ships, for the period July 1, 1945 to April 30, 1946.
- [4] Tables of Selected Values of Chemical Thermodynamic Properties, National Bureau of Standards.
- [5] C. F. Curtiss and J. O. Hirschfelder, Thermodynamic Properties of Air (University of Wisconsin, June 1948) CM-472.
- [6] Tables of Lagrangian Interpolation Coefficients (Columbia University Press, New York, N. Y., 1944).

under the supervision of William S. Benedict. The available data on thermal conductivities of gases have been evaluated and tabulated by Ralph L. Nuttall, and some viscosity data have been furnished by Francis C. Morey.

Several experimental investigations for the determination of thermal data are in progress in the Heat and Power Division of the NBS. Among these are measurements of the heat capacities C_p , of carbon dioxide, water vapor, and freon 12 by Joseph F. Masi; measurements of thermal conductivities at high pressures and temperatures, by Ralph L. Nuttall; and measurements of vapor pressures by the author. Some of these investigations were undertaken simultaneously with the project for the compilation of data, to fill in gaps where data were urgently needed.

As a preliminary step in the compilation of the tables a card file of over 1000 references was prepared, primarily by a search of Chemical Abstracts back to 1926, but also by consulting survey articles and reports such as the group of papers on gas properties published by this Society.⁵ This file of references is gradually being processed as the tables are prepared, and in proportion as the references are read and evaluated, the file becomes more and more valuable. It is planned to maintain this file not only to promote the preparation of the tables, but also to aid in answering inquiries for thermodynamic data. The NBS receives a large number of such inquiries each year. These are welcomed, for it is one of the functions of this Bureau to supply or indicate sources of scientific information when these are known to members of its staff. Letters of inquiry are very useful to us as an aid in planning our future program.

PLANS FOR THE FUTURE

In the immediate future we expect to devote a large part of our effort to the tabulation of real gas properties. Ideal gas tables have been more readily available and our progress with them has been more rapid, but the properties of the real gases are necessary for accurate calculations. In addition to the tables, we plan to prepare charts and diagrams such as Mollier charts and entropy-temperature diagrams that will be more convenient than tables for problems where graphic accuracy is adequate. When most of the data in the field of the project have been tabulated, emphasis will be placed on filling in the gaps with new experimental work, and on revising tables that are out of date. We know already that there will be more gaps than filled places in our outline, and we hope that much new experimental work will be undertaken.

The most urgent needs for new data appear to be in the fields of high temperature and high pressure. Measurements are especially needed of heat capacities and thermal conductivities. A few of these are under way at NBS but much more work is needed.

In several instances unpublished work or work in process, of publication has been brought to our attention, and this has been extremely helpful to us. Communications of work in progress will be welcomed by any member of our group. If sufficient information becomes available the project will, if requested, act as a clearing house for information on work in progress in various laboratories. Those who have suggestions or comments concerning the tables, or who wish to obtain copies, should write to Joseph Hilsenrath, Thermodynamics Section, NBS, who is in charge of the project. At present the tables are being issued without charge.

Discussion

J. A. GOFF.* It is gratifying to note from the paper that

* Symposium on Gas Properties, Trans. ASME, vol. 70, 1948, pp. 621 ff.

* Dean, Towne Scientific School, University of Pennsylvania, Philadelphia, Pa. Mem. ASME.

excellent progress is being made at the National Bureau of Standards with the preparation of working tables and diagrams of the properties of technically important gases. This is an essential part of any really comprehensive program of gas-properties research and as such is of particular interest to the ASME Gas Properties Committee. Of no less interest to the committee are the Bureau's offer to act as a clearing house for information on work in progress in various laboratories and its plan to maintain a relatively complete file of gas-properties references. These are tasks that the committee hardly can hope to do itself in view of the difficulty it has encountered in obtaining financial support. The NBS-NACA Tables of Thermal Properties of Gases project, which the author describes, is sure to reveal serious gaps in existing knowledge regarding gas properties, and in so doing will render a valuable service.

Although the Bureau claims not to have placed extreme emphasis on accuracy in the present stage of its program, it is obvious that it has exercised great care in the selection and appraisal of the data it has so far tabulated. At the same time, its selection of units in terms of which to express the data seems ill-advised. Its claim that convenience in use is gained by selecting R as the unit of entropy and RT_0 as that of energy is difficult to allow. It is true of course that the probable error of the ratio c_p°/R , for example, is slightly less than that of c_p° itself, but this has nothing to do with convenience. In the opinion of the discussor, tables of c_p° itself with suitable conversion factors would have been a good deal more convenient and only very slightly less accurate than tables of c_p°/R with suitable conversion factors.

The writer also wonders why the Bureau proposes to tabulate the specific-heat ratio c_p/c_v since this cannot be substituted for k in the familiar expressions $pv^k = \text{const}$, and $a^2 = k g p v$, for the isentropes and the acoustic velocity, respectively, of a perfect gas with constant specific heats, to determine the isentropes and acoustic velocity of an actual gas with variable specific heats. There is considerable confusion on this point which tables of c_p/c_v would only serve to perpetuate.

In the auxiliary tables of conversion factors the symbol "cal" is understood to designate the thermochemical calorie which has recently been redefined as equal to 4.184 absolute joules exactly. The Btu referred to in these auxiliary tables is defined in terms of this calorie by the conversion factor 0.99934 Btu·g·°C/cal·lb·deg F. It is unfortunate that the simple numeric unity, has been lost in the struggle for individuality; perhaps something can yet be done to restore it.

C. N. WARFIELD.⁷ The compilation of thermal properties of wind-tunnel and jet-engine gases as described in the paper is a valuable contribution in that it presents the results of an extensive search for existing data and makes available to the engineer and scientist in convenient form what appears at the present time to be the best available values. The NBS staff is to be commended especially for the convenient form in which these data are made available, and for the expeditious manner in which the results have been released.

An examination of the 16 tables that are listed in the paper gives rise to comments on a number of specific topics as follows:

Nomenclature. Neither symbols, subscripts, nor superscripts are defined in the tables. A convenient reference, or list of such definitions, would be useful.

Ideal Gas State. A comparison of Table 2.10 with the tables of reference 5 thereto (Curtiss and Hirschfelder, U. Wis. Report, APL No. CM-472) reveals that the values listed for specific heat and for enthalpy correspond to the ideal zero-pressure state,

⁷ Applied Physics Laboratory, The Johns Hopkins University, Silver Spring, Md.

whereas the values listed for entropy correspond to a pressure of 1 atm. A statement of this fact would avoid confusion in regard to the use of the entropy values tabulated.

Although Report No. CM-472 is not listed as a reference for Table 11.10, a similar comparison indicates that the values of entropy for molecular nitrogen have been treated as in the case of dry air.

However, in Table 7.10 (for molecular hydrogen), it is conveniently stated that all values are for the "ideal gas state for a pressure of 1 atmosphere."

Thermal Conductivities. Table 2.42 lists values of thermal conductivity of dry air at various temperatures, but fails to give any indication concerning variation with pressure. Presumably the values listed are for a pressure of 1 atm, and a statement to this effect would be helpful. This comment is also applicable to the other tables for thermal conductivity, excepting only Table 5.42 (for steam) in which thermal conductivities are listed for 11 pressures (from 1 atm to 300 atm), as well as for various temperatures.

It is important to call attention at this time to the fact that some of the values listed may not be valid for direct use in those applications involving very rapid changes in pressure, temperature, etc., such as occur in shock waves and possibly in other applications in supersonic aerodynamics. In this connection the NBS tables on relaxation phenomena are awaited with considerable interest.

AUTHOR'S CLOSURE

Dean Goff raised a question as to the advisability of the choice of dimensionless units. We wish it were possible to find a set of units with dimensions acceptable in all fields where our tables will

find use. We are sympathetic with Dean Goff's point of view, but his selection of units would not have universal acceptance. Dimensionless variables were chosen because aerodynamic physicists and engineers, for whom these tables were undertaken, showed a greater preference for them than for any set of dimensional units. This may be so because dimensionless variables and properties are in general use in aerodynamics. From the NBS-NACA tables that are now in dimensionless units, tables in any other units may be prepared with little trouble.

Our conversion factors are so chosen that those who wish to work with calories will obtain values in terms of the thermochemical calorie, while those who prefer Btu's will obtain the kind of Btu that they are accustomed to. We believe that this is the way each group wants it. The thermochemical calorie = 4.1840 abs joules, and the Btu = 1055.040 abs joules. These are independent definitions. In these units, specific heats in calories per gram degree C are nearly, but not exactly, equal to specific heats in Btu per pound degree F. If the I.T. calorie is used, the equality becomes exact. Such a relationship has some advantage, but will probably not induce the users of either the thermochemical calorie or the present Btu to change their accustomed units.

With regard to Dr. Warfield's suggestion that symbols, subscripts, and superscripts be defined, it may be of interest that an introductory table for the series is being prepared. This table is to contain the definitions referred to and also lists of basic constants and conversion factors. Dr. Warfield's other comments are also well taken and we expect to adopt his suggestions in the preparation of future tables.

The careful consideration that the discussers have given to the NBS-NACA tables is much appreciated.

is
bl
vo
th
po

to
su
is
cis
wi
pro

1
The
2
par
3
ous
Sco

Eng
C
and
and
27-1
Eng
N
unde
the S

Pressure-Volume-Temperature Relationships of Gaseous Normal Hydrogen From Its Boiling Point to Room Temperature and From 0-200 Atmospheres

By H. L. JOHNSTON¹ AND DAVID WHITE,² COLUMBUS, OHIO

This paper presents a summary of accurate measurements on data of state for normal hydrogen gathered over a period of years by a group of investigators in The Ohio State University Cryogenic Laboratories. Results cover a wide range of temperature and pressure.

INTRODUCTION

ACCURATE measurements of data of state for normal hydrogen have been carried out by a group of investigators, in The Ohio State University Cryogenic Laboratories over a period of years. The purpose of the present paper is to present a summary derived from the results obtained over a wide range of temperature and pressure. A detailed description of the work will be published in a series of papers which will appear shortly. A survey of the P-V-T properties of hydrogen made by the Bureau of Standards³ summarizes existing data which cover this range of temperature and pressure. However, this is the first work to cover the entire range with a high degree of precision and accuracy throughout.

APPARATUS

A drawing of the apparatus in which the gas was compressed is shown in Fig. 1. The pipette *H* is surrounded by a series of blocks *E*, *F*, and *G* and enclosed in an evacuated can *J* to prevent heat leak. The pipette can be maintained to within a few thousandths of a degree of a specified temperature, at all temperatures, for at least 1/2 hr.

Briefly, the operation of the apparatus is as follows:

Gas is introduced into a pipette which has already been cooled to the desired temperature and compressed to the desired pressure. After thermal equilibrium has been established, the pressure is measured on an M.I.T. type dead-weight gage.⁴ The precision of this gage varies from 1 part in 10,000 to 1 part in 100,000 with increasing pressure. In some of the earlier work at high pressures, an American instrument-type gage was used with a

¹ Director, Cryogenic Laboratory, Department of Chemistry, The Ohio State University.

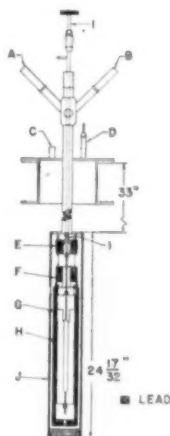
² Post-Doctorate Research Fellow, Cryogenic Laboratory, Department of Chemistry, The Ohio State University.

³ "Compilation of Thermal Properties of Hydrogen and Its Various Isotopic Ortho-Para Modifications," by H. W. Woolley, R. B. Scott, and F. G. Brickwedde.

⁴ "High-Pressure Technique," by F. G. Keyes, *Industrial and Engineering Chemistry*, vol. 23, 1931, p. 1375.

Contributed by the Research Committee on Properties of Gases and Gas Mixtures, Heat Transfer and Applied Mechanics Divisions, and presented at the Annual Meeting, New York, N. Y., November 27-December 2, 1949, of THE AMERICAN SOCIETY OF MECHANICAL ENGINEERS.

NOTE: Statements and opinions advanced in papers are to be understood as individual expressions of their authors and not those of the Society. Paper No. 49-A-149.



- A High-pressure gas inlet
- B Thermocouple tubes
- C Transfer-tube inlet for coolant
- D Safety T-tube and evacuation line for dewar in which apparatus is immersed
- E } Auxiliary upper and lower blocks
- F }
- G Calibrated pipette connected to auxiliary block by means of small capillary
- H
- I Pipette valve and stem which shuts pipette off from dead space
- J Evacuated outer can

FIG. 1 (left) THE P-V-T APPARATUS

precision of 1 part in 3000 or 4000. Both types of gages were calibrated using the vapor pressure of carbon dioxide at the ice point as a primary standard.⁵ The temperature of the gas is measured simultaneously with the pressure by means of thermocouples standardized with a helium thermometer. Temperatures can be read with a precision of 0.0005 deg C at room temperatures and of 0.003 deg at 20 deg K. The accuracy of the temperature scale is probably not better than 0.02 deg C at the lower temperatures, but is slightly better at the higher temperatures.

After first closing the valve above the pipette *I* (see Fig. 1), and pumping out the gas held in the dead space above this valve, the number of moles of gas is obtained by expanding the gas in the pipette into calibrated cylinders maintained at constant temperature. The expansions are generally carried out in two or three steps so that the pressures in the calibrated cylinders never significantly exceed 1 atm. Pressures are read on a constant-volume mercury manometer to within 0.03 mm Hg with the aid of a cathetometer.

The hydrogen used in this work was extremely pure. Impurities never exceeded 0.001 to 0.002 mole per cent. The gas was prepared by triple distillation of electrolytic hydrogen.

P-V-T DATA

A few sample isotherms, with experimental points, are shown in Figs. 2, 3, 4, and 5, to indicate the precision of the data. Figs. 2 and 3 show the low-pressure data, while Figs. 4 and 5 show the isotherms over the complete pressure range from 0 to 200 atm.

⁵ "A Fixed Point for Calibration of Pressure Gauges. The Vapor Pressure of Liquid Carbon Dioxide at 0°," by O. C. Bridgeman, *Journal of the American Chemical Society*, vol. 49, 1927, p. 1174.

TABLE 1 SMOOTHED PV/RT VALUES FROM BOILING POINT OF HYDROGEN TO ROOM TEMPERATURE AND FROM 0-200 ATM

Temp. °K.	1 atm	2 atm	5 atm	10 atm	15 atm	20 atm	25 atm	30 atm	35 atm	40 atm	45 atm
300	1.000528	1.001137	1.003047	1.005134	1.009221	1.012258	1.015355	1.018433	1.021570	1.024653	1.027785
250	1.000574	1.001308	1.003258	1.005572	1.009837	1.013202	1.016517	1.019832	1.023145	1.026412	1.029775
200	1.001386	1.002355	1.004550	1.008034	1.011679	1.015274	1.018859	1.022454	1.026120	1.029959	1.033737
175	1.000777	1.001473	1.003551	1.007181	1.010801	1.014491	1.018041	1.021522	1.025142	1.028831	1.032560
150	1.000453	1.001103	1.002970	1.005219	1.009437	1.012715	1.016045	1.019375	1.022949	1.026584	1.030583
125	1.000240	1.000529	1.002092	1.004431	1.006770	1.009109	1.011351	1.013590	1.016030	1.018954	1.022170
100	0.999719	0.999597	0.999109	0.998522	0.998500	0.998522	0.998556	0.998475	1.000450	1.002034	1.004227
90	1.000123	0.999311	0.997280	0.994166	0.991457	0.989425	0.988072	0.987230	0.987260	0.987537	0.989426
80	0.993357	0.997026	0.993055	0.985820	0.981335	0.973309	0.972043	0.968540	0.965102	0.964884	0.964579
75	0.998007	0.996058	0.990208	0.981271	0.973147	0.965997	0.960148	0.955273	0.951373	0.948773	0.946823
60	0.995452	0.991390	0.978391	0.957673	0.936346	0.916035	0.898161	0.882928	0.869929	0.859773	0.852461
50	0.991337	0.982627	0.958049	0.917410	0.875042	0.835890	0.796225	0.754345	0.725893	0.717137	0.717137
40	0.983327	0.967516	0.918258	0.830993	0.732174	0.619976	0.523590	0.449059	0.498049	0.523590	0.556732
35	0.974104	0.949439	0.873706	0.725367	0.472461	0.316480	0.350872	0.395686	0.443975	0.491568	0.538120
Temp. °K.	50 atm	60 atm	70 atm	80 atm	90 atm	100 atm	125 atm	150 atm	175 atm	200 atm	
300	1.030873	1.037048	1.043303	1.049437	1.055612	1.061827	1.077304	1.092903	1.108746	1.124589	
250	1.033139	1.039818	1.046691	1.053711	1.060925	1.068335	1.085907	1.105528	1.124150	1.142527	
200	1.037576	1.045436	1.053296	1.061401	1.069505	1.077609	1.098326	1.119531	1.141467	-----	
175	1.033489	1.044494	1.052918	1.061620	1.070500	1.079550	1.103040	1.127475	1.152954	1.179615	
150	1.034543	1.042683	1.051210	1.059819	1.069077	1.078579	1.104729	1.132585	1.162055	1.192753	
125	1.025579	1.033769	1.042542	1.052191	1.062133	1.072952	1.102778	1.135723	1.170910	1.209411	
100	1.006785	1.013355	1.021285	1.030788	1.041267	1.053086	1.089760	1.133014	1.179302	1.227930	
90	0.991322	0.996738	1.004592	1.014206	1.025445	1.038850	1.081358	1.131459	1.185758	1.243045	
80	0.964884	0.968033	0.975090	0.985449	0.998549	1.015611	1.057351	1.127576	1.192471	1.252087	
75	0.945848	0.945173	0.952673	0.965347	0.982408	1.001582	1.059591	1.129524	1.201231	1.275701	
60	0.848399	0.849517	0.853429	0.859755	0.914513	0.947517	1.042980	1.145349	1.250967	1.350850	
50	0.718354	0.740499	0.777730	0.825183	0.874095	0.925414	1.062931	1.158230	1.332557	1.455333	
40	0.591395	0.655535	0.741904	0.818527	0.893021	0.955995	1.149039	1.325597	1.495555	1.564115	
35	0.583976	0.674647	0.755318	0.854252	0.940059	1.025171	1.235347	1.435143	1.537287	-----	

TABLE 2 SMOOTHED PV/RT BELOW SATURATION CURVE OF HYDROGEN

Temp. deg K	0.2 atm	0.4 atm	0.6 atm	0.8 atm	1 atm	2 atm	3 atm	4 atm	5 atm	6 atm
30	0.993975	0.986571	0.978970	0.971567	0.964163	0.926037	0.886088	0.842840	0.794831	0.737993
25	0.989520	0.977901	0.966283	0.954418	0.942305	0.877046				
20	0.984540	0.965573	0.946901	0.928230						

TABLE 3 SMOOTHED PV/RT AT MINIMUM IN PV/RT VERSUS PLOT

Temp	Pressure at minimum	PV/RT at minimum
100	17	0.998500
90	32	0.987260
80	45	0.964579
75	54	0.945686
60	54	0.847383
50	46.8	0.716407
40	30.6	0.490295
35	19	0.315090

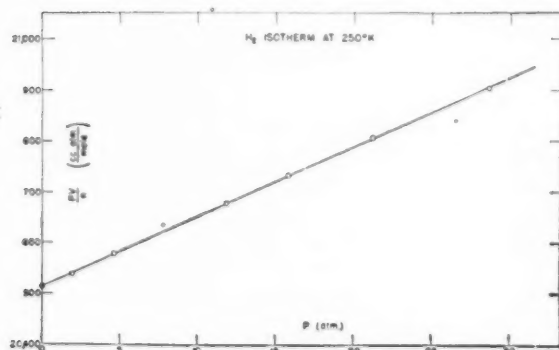


Fig. 2

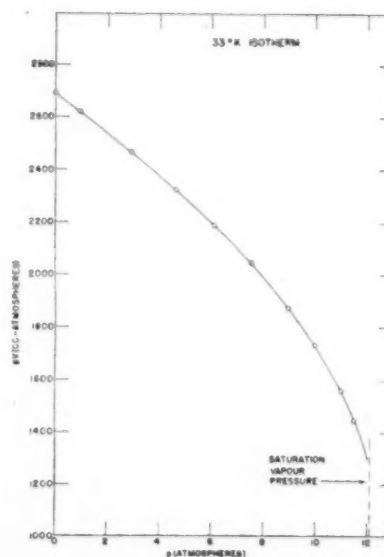


Fig. 3

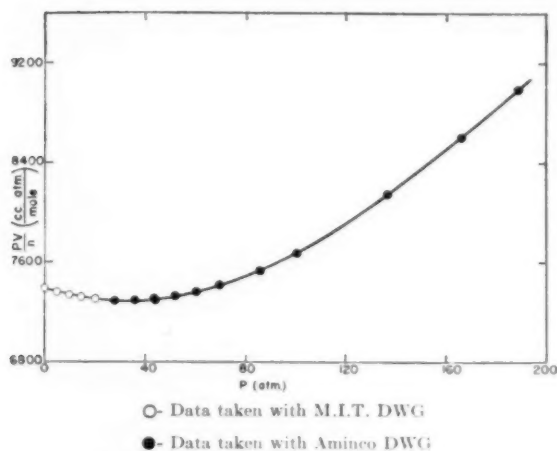


FIG. 4 HYDROGEN ISOTHERM AT 90 Deg K

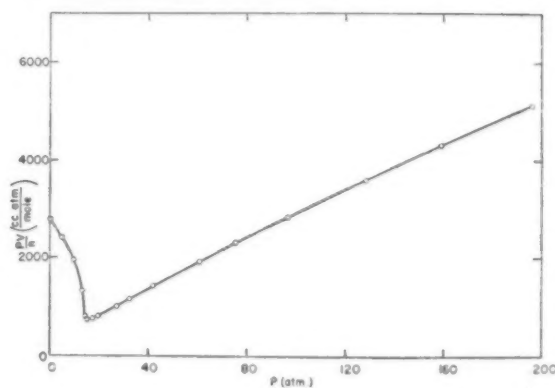


FIG. 5 HYDROGEN ISOTHERM AT 34 Deg K

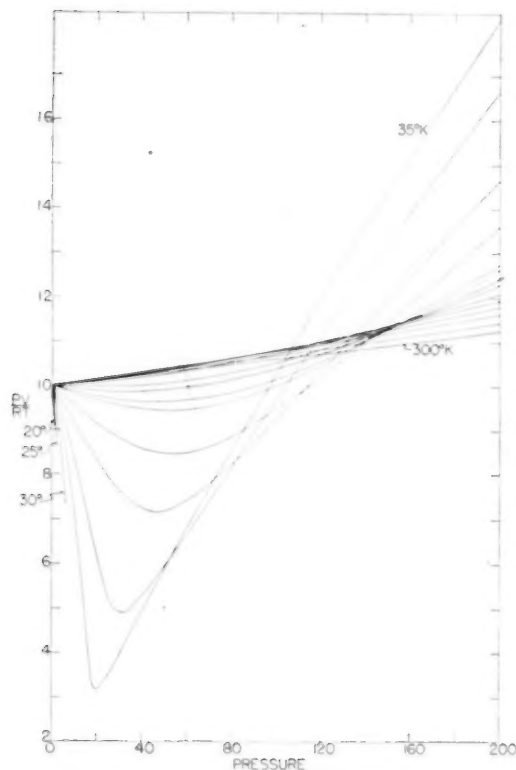


FIG. 6 RELATIVE ISOTHERMS FOR HYDROGEN
(Temperature of isotherms reading from top left-hand side down are 35, 40, 50, 60, 75, 80, 90, 100, 125, 150, 175, 200, 250, 300 deg Kelvin. Short isotherms at left represent data below critical temperature, 20, 25, 30 deg Kelvin, and extend only to vapor-pressure curve.)

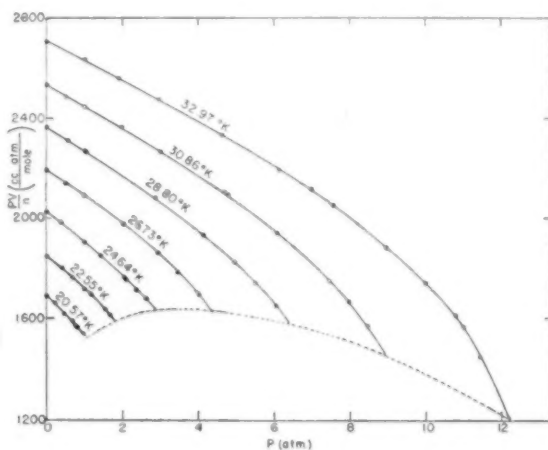


FIG. 7 P-V-T DATA OF HYDROGEN BETWEEN BOILING POINT AND CRITICAL TEMPERATURE
(Dotted line represents vapor-pressure curve of hydrogen between normal boiling point and critical temperature.)

Tables 1, 2, and 3 present a summary of the smoothed PV/RT values at integral values of the pressure and temperature. Isotherms below the "critical point" extend only to the saturation curve.

Analytical expressions are now being obtained for the individual isotherms by means of IBM machines using a virial form of equation. The constants of these equations will be correlated with temperature to give analytical expressions for all isotherms. These analytical expressions will be used to construct a Mollier diagram, which will be submitted for publication in the future.

Fig. 6 shows a plot of the data given in Tables 1, 2, and 3. Fig. 7 shows the experimental data taken below the critical temperature up to the saturation curve.

Jun
C
Am
194
N
und
of t

Heat Transfer to a Fluid Flowing Turbulently Between Parallel Walls With Asymmetric Wall Temperatures

By R. A. SEBAN,¹ BERKELEY, CALIF.

The case of heat transfer to a fluid of constant properties flowing turbulently between parallel walls having arbitrary but uniform temperatures is considered on an analytical basis, which is an extension of the work of Martinelli and of Harrison and Menke. Therefore, only conditions for a flow fully developed from the hydrodynamic and thermal standpoint are considered. It is shown that the existence of solutions for the case of one adiabatic wall enables the specification of the temperature distribution and heat-transfer coefficients for cases in which the walls have any uniform temperature values. The effect of inequality in the wall temperatures is shown to be small for Prandtl numbers greater than unity but significant for fluids of low Prandtl number, such as molten metals. To facilitate its use in the present applications, the existing solution for one adiabatic wall is extended.

NOMENCLATURE

CERTAIN temperatures are defined in Fig. 1 and these are not repeated in the following nomenclature which is used throughout the paper:

- a = thermal diffusivity, sq ft per sec
- c = heat capacity, Btu/(lb mass) (deg F)
- D = distance between the plates, ft
- h = heat-transfer coefficient Btu/(hr) (ft²) (deg F)
- k = thermal conductivity, Btu/(hr) (ft²) (deg F/ft)
- p = pressure, (lb force)/ft²
- q_0 = heat-transfer rate per unit area at wall, Btu/(hr) (ft²)
- T = temperature, deg F
- U = velocity, fps
- U_τ = friction velocity, $U_\tau = \sqrt{\frac{c_f}{2}}$ fps
- x = direction of flow, ft
- X = temperature-difference ratio, defined in Equation [8]
- y = direction normal to flow, ft
- ϵ = eddy diffusivity, sq ft per sec
- ν = kinematic viscosity, sq ft per sec
- ρ = fluid density, lb mass/ft³
- τ_0 = shear stress at wall, lb force/ft²

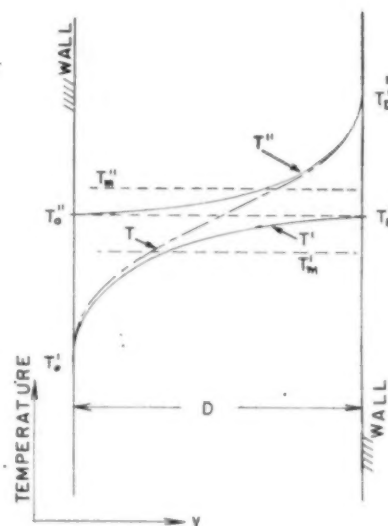


FIG. 1 SCHEMATIC REPRESENTATION OF COMPOSITION OF ADIABATIC-WALL SOLUTIONS

DIMENSIONLESS NUMBERS

- c_f = skin friction coefficient $\frac{2g\tau_0}{\rho U_m^2}$
- $\frac{2hD}{k}$ = Nusselt number ν/a = Prandtl number
- $\frac{2U_m D}{\nu}$ = Reynolds number $\frac{h}{\rho U_m c}$ = Stanton number
- D^+ = dimensionless channel width $\frac{DU_\tau}{\nu}$

SUBSCRIPTS

- m = mean value O, D = wall value
- 30 = value at point where $\frac{yU_\tau}{\nu} = 30$

INTRODUCTION

In a recent paper Harrison and Menke (1)² have extended the method of Martinelli (2) to the specification of the temperature distribution in the turbulent flow of a molten metal between parallel walls, one wall being adiabatic. It is the purpose of this paper to demonstrate that the existence of a solution for the case of one adiabatic wall enables the specification of the temperature distribution and, consequently, of the heat-transfer co-

¹ Lecturer in Mechanical Engineering, University of California, San Diego.

Contributed by the Heat Transfer Division and presented at the Annual Meeting, New York, N. Y., November 27-December 2, 1949, of THE AMERICAN SOCIETY OF MECHANICAL ENGINEERS.

NOTE: Statements and opinions advanced in papers are to be understood as individual expressions of their authors and not those of the Society. Paper No. 49-A-18.

² Numbers in parentheses refer to the Bibliography at end of paper.

efficients for the more general case in which the heat transfer takes place through both walls, the walls having any uniform temperatures. The solution for the case of one adiabatic wall has been extended so as to yield the quantities necessary for such a specification.

SPECIFICATION OF TEMPERATURE DISTRIBUTION

The problem considered herein involves the turbulent flow of a fluid of constant properties between two parallel walls, the temperatures of the walls having any uniform value. The flow is fully developed from a hydrodynamic and thermal standpoint, that is, the generalized velocity and temperature distributions in the flow cross section are assumed to be independent of the distance in the direction of flow.

The energy and momentum equations can be written as follows (neglecting any thermal effects of flow energy dissipation)

$$U \frac{\partial T}{\partial x} = \frac{\partial}{\partial y} \left[(\epsilon + a) \frac{\partial T}{\partial y} \right] \quad [1]$$

$$\frac{1}{\rho} \frac{\partial p}{\partial x} = \frac{\partial}{\partial y} \left[(\epsilon + \nu) \frac{\partial U}{\partial y} \right] \quad [2]$$

For the problem considered, the boundary conditions applying to the energy equation are at

$$\begin{aligned} y = 0 & \quad T = T_o \\ y = D & \quad T = T_D \end{aligned}$$

The usual method of solution of Equation [1] involves assumptions of the following type:

- (a) Separation of molar and molecular transfer effects into separate regions, after von Kármán.
- (b) The neglect of changes in stream thermal-energy content in those regions in which molecular transfer effects are appreciable.
- (c) The assumption that

$$U \frac{\partial T}{\partial x} = U_m \frac{\partial T_m}{\partial x}$$

Except for the assumption of constant velocity, this is correct for the case of constant wall heat-transfer rate and has yielded satisfactory results for cases of constant wall temperatures in previous applications of this type of analysis.

- (d) Integration of Equation [1] in terms of the diffusivity as calculated from Equation [2] and a specified velocity distribution.

The problem can be solved in this way, but a simpler development is realized by use of the available solution for one adiabatic wall. This solution satisfies Equation [1] under the restrictions just specified, for boundary conditions which are at

$$\begin{aligned} y = 0 & \quad T = T_o' \\ y = D & \quad \frac{dT'}{dy} = 0 \end{aligned}$$

and the solution may be specified as²

$$f'(y) = \frac{T' - T_o'}{T_D' - T_o'} \quad \text{so that} \quad \left. \begin{aligned} f'(0) &= 0 \\ f'(D) &= 1 \end{aligned} \right\} \quad [3]$$

Evidently the same solution is applicable if the heated and adiabatic walls are interchanged, so that the boundary conditions become at

$$\begin{aligned} y = D & \quad T = T_D'' \\ y = 0 & \quad \frac{dT''}{dy} = 0 \end{aligned}$$

² The prime superscripts as used herein are merely discriminating symbols, and do not indicate differentiation.

and this solution may be specified as

$$f''(D - y) = \frac{T'' - T_D''}{T_o'' - T_D''} \quad \text{that} \quad \left. \begin{aligned} f''(0) &= 0 \\ f''(D) &= 1 \end{aligned} \right\} \quad [4]$$

Because of the linearity of Equation [1], any sum of solutions is also a solution, and a proper addition of the solutions represented by Equations [3] and [4] will yield a temperature distribution satisfying the boundary conditions of the present problem. Fig. 1 reveals such a combination of solutions, which can be stated in the following way

$$T = T' + T'' - T_o'' \quad [5]$$

Then, in terms of the two adiabatic wall solutions given by Equations [3] and [4]

$$T = T_o' + (T_D' - T_o')f'(y) + T_D'' - T_o'' + (T_o'' - T_D'')f''(D - y) \quad [6]$$

The temperature distribution given by Equation [6] satisfies the energy equation in virtue of the fact that the solutions $f'(y)$ and $f''(y)$ satisfy that equation. Agreement with the boundary conditions of the present problem is demonstrated as follows:

$$\begin{aligned} \text{At } y = 0 & \\ T &= T_o' + (T_D' - T_o')(0) + T_D'' - T_o'' + (T_o'' - T_D'')(1) \\ T &= T_o' \end{aligned}$$

$$\begin{aligned} \text{At } y = D & \\ T &= T_o' + (T_D' - T_o')(1) + T_D'' - T_o'' + (T_o'' - T_D'')(0) \\ T &= T_D' + T_D'' - T_o'' \end{aligned}$$

and since the solutions are so combined that $T_D' = T_o''$, therefore $T = T_D'$ and the boundary condition at this point is fulfilled.

The determination of the temperature distribution specified by Equation [6] requires knowledge of the differences $T_D' - T_o'$ and $T_D'' - T_o''$, which are in turn related to the mean temperature of the fluid. This relation is determined by the use of Equation [6] in the specification of the mixed mean fluid temperature. This mean fluid temperature is defined as

$$T_m = \int_0^D \frac{1}{D} \frac{U}{U_m} T dy$$

and in consequence, from Equation [6]

$$\begin{aligned} T_m &= T_o' + T_D'' - T_o'' + (T_D' - T_o') \frac{1}{D} \int_0^D \frac{U}{U_m} f'(y) dy \\ &\quad + (T_o'' - T_D'') \frac{1}{D} \int_0^D \frac{U}{U_m} f''(D - y) dy \quad [7] \end{aligned}$$

Because of the assumed symmetry of the velocity distribution, U/U_m , about the flow center line, $y = D/2$, the two integrals occurring in the right side of the Equation [7] have the same value. Further, these integrals also express the ratio of the difference between wall and mean temperatures to the difference between the two wall temperatures for the solutions applying to the adiabatic wall cases as given by Equations [3] and [4]. Thus for the case of wall D being adiabatic

$$\frac{1}{D} \int_0^D \frac{U}{U_m} f'(y) dy = \frac{T_m' - T_o'}{T_D' - T_o'} \quad [8]$$

For convenience in what follows this temperature ratio is designated by the symbol X .

For the case of wall O being adiabatic

$$\frac{1}{D} \int_0^D \frac{U}{U_m} f''(D-y) dy = \frac{T_m'' - T_D''}{T_o'' - T_D''} = X \quad [9]$$

Introduction of these relations into Equation [7] yields the final expression

$$T_m = T_m' + T_m'' - T_o'' \quad [10]$$

or the alternative form

$$T_m = T_D'' + X(T_o'' - T_D'') + T_o' + X(T_D' - T_o') - T_o'' \quad [11]$$

It has been noted that the temperature distribution obtaining for wall temperatures T_o and T_D can be obtained from Equation [6] once the temperature T_o'' ($T_o'' = T_D'$) is known. This temperature is obtained from Equation [11] in terms of the mean fluid temperature, T_m , and the temperature-difference ratio X . The ratio X is obtained from the solution for one adiabatic wall and some magnitudes are indicated in the Appendix of this paper.

HEAT-TRANSFER COEFFICIENTS

Knowledge of the temperature distribution enables the specification of the heat-transfer coefficient in terms of the temperature gradient at the wall, under consideration. Thus at the wall $y = 0$

$$h = \frac{-k \frac{\partial T}{\partial y} \big|_{y=0}}{T_o - T_m} \quad [12a]$$

and at the wall $y = D$

$$h = \frac{+k \frac{\partial T}{\partial y} \big|_{y=D}}{T_D - T_m} \quad [12b]$$

Differentiation of Equation [5] so as to form $\partial T / \partial y$ and evaluation of this quantity at $y = 0$ and at $y = D$ reveals that the magnitude of the temperature gradient at the walls remains the same as for the adiabatic-wall solution for the wall considered. The heat-transfer coefficient given by Equation [12] is consequently different from that obtaining for one adiabatic wall only in so far as the prevailing wall temperatures affect the difference between the temperature of the wall considered and the mixed mean fluid temperature.

Thus at $y = 0$, the ratio of the heat-transfer coefficient obtaining for one adiabatic wall to that for the more general case here considered can be stated as

$$\frac{h'}{h} = \frac{T_o - T_m}{T_o' - T_m'} = 1 + \frac{T_o'' - T_m''}{T_o' - T_m'} \quad [13a]$$

and at $y = D$

$$\frac{h''}{h} = 1 + \frac{T_o'' - T_m'}{T_o'' - T_m''} \quad [13b]$$

As given by Equations [13a] and [13b], the heat-transfer coefficients are, in general, different for each wall, and they are the same for both walls only when the wall temperatures are the same or are equally above and below the mean fluid temperature.

Consideration of the definitions of the Nusselt and Stanton numbers indicates that Equations [13a] and [13b] can also be considered as ratios of these numbers, as well as ratios of the heat-transfer coefficients.

DISCUSSION

An immediate application of the foregoing theory is the specification of the maximum variation of the heat-transfer coefficient

due to changes in the wall-temperature values. Already it has been noted that the heat-transfer coefficient differs from that obtaining for the system with one adiabatic wall only in so far as the difference between the wall and mean fluid temperatures differs from that in the adiabatic-wall solution. Thus the extremes of variation occur for the case of equal wall temperatures ($T_o - T_m = T_D - T_m$), on one hand, and for wall temperatures equally above and below the mean fluid temperature ($T_o - T_m = T_m - T_D$) on the other. If Equations [13a] and [13b] are evaluated for these conditions, it is found that the ratio of heat-transfer coefficients specified by these equations depends only upon the temperature-difference ratio X . This ratio can be evaluated from the known adiabatic-wall solution and the ratio of the heat-transfer coefficient h , obtaining for one of the cases just considered, to the coefficient h' , obtaining for the adiabatic-wall solution, can then be determined. This ratio of heat-transfer coefficients is shown in Fig. 2 as a function of the Prandtl and Reynolds numbers.

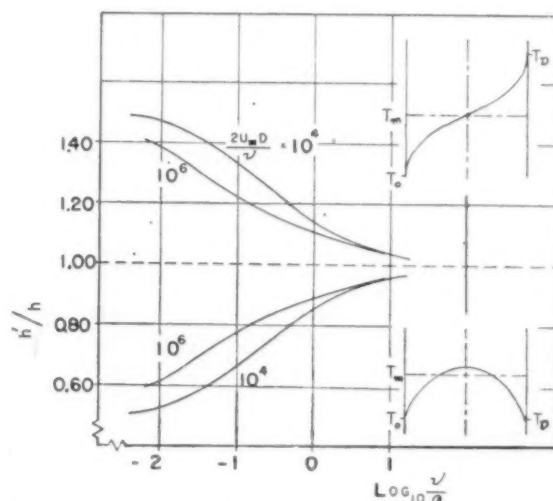
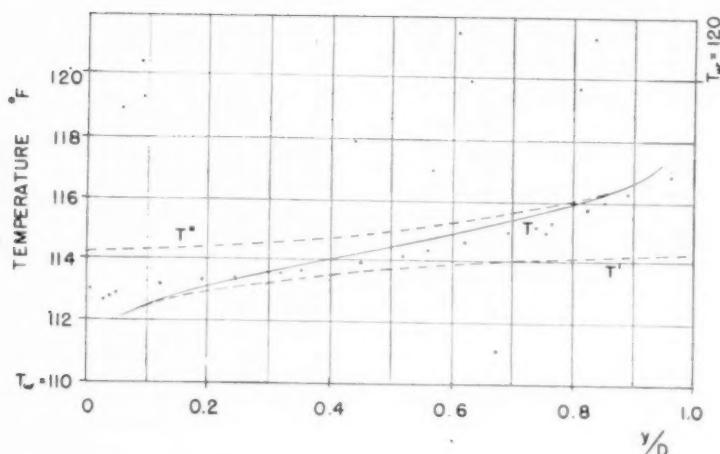


FIG. 2 VARIATION IN HEAT-TRANSFER COEFFICIENT DUE TO CHANGES IN MAGNITUDES OF WALL TEMPERATURES

(The two extreme cases are shown in reference to the case of one adiabatic wall. Temperature distributions are shown schematically adjacent to the curves depicting variation. The heat-transfer coefficient for one adiabatic wall is h' .)

The effect of variation in the wall-temperature values on the heat-transfer coefficient is seen to be significant only for fluids of relatively small Prandtl numbers. For fluids of high Prandtl number, the preponderant portion of the difference between wall and mean fluid temperatures occurs in the flow sublayers, and in consequence, the magnitude of the difference is not affected substantially by the relative wall-temperature magnitudes. Fig. 2 reveals that the variation in the heat-transfer coefficient is quite small for fluids having a Prandtl number greater than 10.

A specific example of the combination of two adiabatic wall solutions to obtain the temperature distribution for a case in which the wall temperatures are not equal consists in the comparison of this theory with the data of Corcoran (3), et al. These experimenters determined temperature distributions across the stream, and heat-transfer coefficients for air flowing turbulently in a rectangular duct having an aspect ratio of 16, the wall temperatures being uniform with respect to length. The data and the prediction according to the present theory are presented in Fig. 3, the prediction being obtained as follows:



Wall temperatures	110 and 120 F
Mean air temperature	114.5 F
Reynolds number	30,500
Measured Nusselt number: 120 F side	70
Predicted Nusselt number: 120 F side	53
110 F side	48

FIG. 3 (left) PREDICTED AND EXPERIMENTAL TEMPERATURE DISTRIBUTION FOR AIR FLOW IN A RECTANGULAR CHANNEL

Given: Mean air temperature 114.5 F; wall temperature $T_o = 110$ F; $T_D = 120$ F; Reynolds number = 30,500.

Solution: It is first necessary to determine the temperature-difference ratio X , obtaining for the Prandtl and Reynolds numbers of the flow. The use of Equation [18] (see Appendix) for the determination of $(T_o' - T_m')$ and of Equation [14] through [17] for the determination of $(T_o' - T_D')$ yields $X = 0.85$ for a Prandtl number of 0.72, and the given Reynolds number. (Linear interpolation of Fig. 4 yields $X = 0.84$.) The values associated with the two adiabatic-wall solutions from which the desired result is obtained are now determined as follows:

$$\begin{array}{ll} \text{From Equation [8]} & \text{From Equation [9]} \\ 0.85 = \frac{T_m' - 110.0}{T_D' - 110.0} & 0.85 = \frac{T_m'' - 120.0}{T_o'' - 120.0} \end{array}$$

and from Equation [10]

$$114.5 = T_m' + T_m'' - T_D''$$

Solution of these equations yields

$$T_D' = T_o'' = 114.2; T_m' = 113.6; T_m'' = 115.1$$

The temperature distribution is specified by Equation [6], the necessary "adiabatic-wall" temperature distributions being obtained from Equations [14] through [17] (see Appendix). This

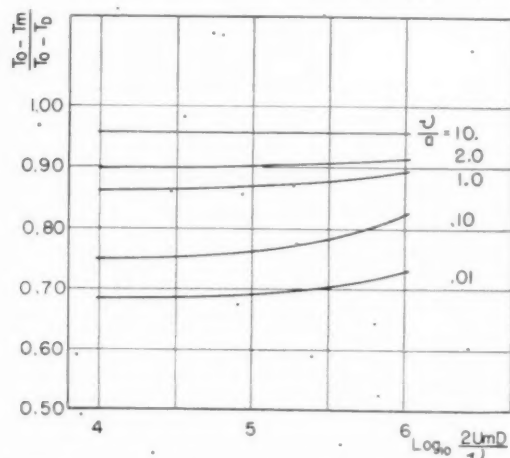


FIG. 4 TEMPERATURE-DIFFERENCE RATIO AS A FUNCTION OF REYNOLDS AND PRANDTL NUMBERS

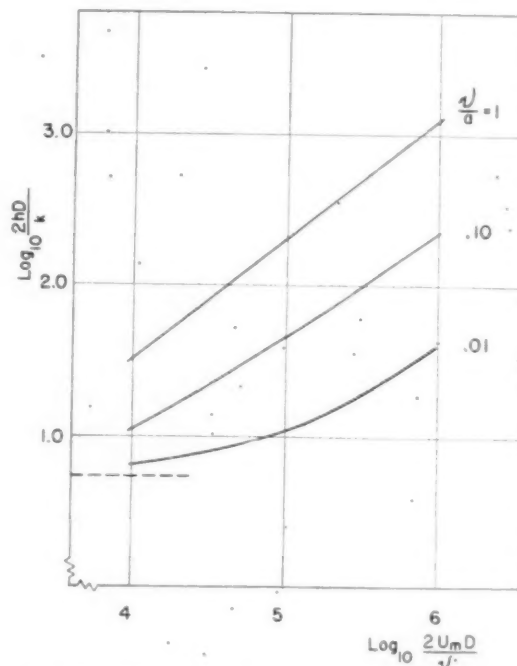


FIG. 5 NUSSLETT NUMBER AS A FUNCTION OF REYNOLDS AND PRANDTL NUMBERS

distribution already has been calculated in the process of evaluating the ratio X .

The determination of the heat-transfer coefficients does not require the determination of the temperature distribution, but knowledge only of the temperature quantities just noted. Thus the process is somewhat shortened if an approximate value of X is obtained from Fig. 4.

The Nusselt number for the adiabatic-wall case has been calculated as 60.2. (A magnitude can be approximated from Fig. 5.) Application of Equations [13a] and [13b] yields the Nusselt numbers for the case under consideration:

For the 110 deg F wall

$$\frac{h'}{h} = 1 + \frac{114.2 - 115.1}{110.0 - 113.6} \cdot \frac{2hD}{k} = \frac{60.2}{1.25} = 48$$

For the 120 deg F wall

$$\frac{h^*}{h} = 1 + \frac{114.2 - 113.6}{120.0 - 115.1}, \quad \frac{2hD}{k} = \frac{60.2}{1.12} = 53$$

The predicted Nusselt number is seen to be substantially less than the experimental value at the 120 deg F wall. A similar discrepancy can be noted between the measured and predicted temperature distribution. This might be ascribable to an inadequate starting length, except that the experimental apparatus had a 75-width length upstream from the measuring section.

CONCLUSIONS

The case of heat transfer to an incompressible fluid flowing turbulently between parallel walls has been considered for the case of arbitrary uniform wall-temperature values. A technique of calculating the heat-transfer coefficients and the temperature distribution has been indicated.

Variations in the magnitude of the heat-transfer coefficient due to the relative values of the wall temperatures have been shown to reside in variation of the difference between wall and mean fluid temperatures. Such variations are shown to be substantial only for fluids of low Prandtl number.

Presently available data are not sufficiently extensive to establish the accuracy of the solution for the general case. For the case of equal wall temperatures, the solution can be shown to coincide with existing solutions (2) for the case of equal wall temperatures, and these solutions are in accord with experimental data for the flow of air in ducts of large aspect ratio.

The extension of these concepts to the case of a fluid flowing turbulently in an annulus depends upon the radius of curvature involved. It is complicated by the dissimilarity of the two adiabatic-wall solutions necessary to a general solution, and the adiabatic-wall solutions are in turn complicated by the inequality of the skin-friction coefficients on the inner and outer cylindrical surfaces.

BIBLIOGRAPHY

- 1 "Heat Transfer to Liquid Metals Flowing in Asymmetrically Heated Channels," by W. B. Harrison and J. R. Menke, Trans. ASME, vol. 71, October, 1949, pp. 797-803.
- 2 "Heat Transfer to Molten Metals," by R. C. Martinelli, Trans. ASME, vol. 69, 1947, pp. 947-960.
- 3 "Temperature Gradients in Turbulent Gas Streams," by W. A. Corcoran, B. Roudebush, and B. H. Sage, *Chemical Engineering Progress*, vol. 43, March, 1947, pp. 135-142.
- 4 "Measurements of the True Temperature and Heat Exchange in a Catalytic Reaction," by M. Jakob, Trans. AIChE, vol. 35, 1939, pp. 563-586.

Appendix

TEMPERATURE DISTRIBUTION AND HEAT-TRANSFER COEFFICIENTS FOR THE CASE OF ONE ADIABATIC WALL

The basis of the method proposed for the calculation of the heat-transfer coefficient for the more general wall-temperature conditions is the availability of results for the heat-transfer coefficient and for the temperature ratio X for the case of heat transfer to a fluid flowing between parallel plates, one plate being adiabatic. Harrison and Menke (1) have outlined the method of solution for this case and have presented Nusselt numbers for fluids of low Prandtl number. In these results the temperature ratio X is not given. The solution is here extended by giving expressions for the temperature distribution and by a general result for the Nusselt number for cases of fluids of large Prandtl number. Values of the temperature ratio X are presented for some Prandtl numbers.

The assumptions necessary for a solution have been indicated

in the body of the paper. On such bases and upon the assumption of an eddy diffusivity, the temperature distribution across the channel can be obtained. In accord with the assumptions of Harrison and Menke, the diffusivity for heat has been presumed the same as for momentum transfer, and that diffusivity is obtained from the presumed linear shear distribution and the Prandtl-Nikuradse velocity distribution, except in the central region of the channel. In this region, from $y/D = 1/4$ to $y/D = 3/4$ the diffusivity has been assumed constant at its maximum value, which obtains at $y/D = 1/4$ in the basic calculation. The calculations of Harrison and Menke reveal this to be a plausible assumption.

The temperature distribution obtained from the integration of Equation [1] can be specified in terms of the following equations

$$\text{Region } 0 < \frac{y}{D} < \frac{y}{D}_{30} \\ \frac{T_0 - T_{30}}{2.5 \frac{q_0}{\rho c U_\tau}} = 2 \frac{y}{a} + 2 \log \left(5 \frac{y}{a} + 1 \right) \dots \dots [14]$$

$$\text{Region } \frac{y}{D}_{30} < \frac{y}{D} < \frac{1}{4} \\ \frac{T_{30} - T_{y/D}}{2.5 \frac{q_0}{\rho c U_\tau}} = \left[\frac{1}{4} - \frac{3}{8} \frac{1}{(m-n)} \right] \log \frac{\frac{y}{D} - m}{\frac{y}{D_{30}} - m} \\ + \left[\frac{1}{4} + \frac{3}{8} \frac{1}{(n-m)} \right] \log \frac{\frac{y}{D} - n}{\frac{y}{D_{30}} - n} \dots \dots [15]$$

where in this particular equation

$$m = \frac{-1 + \sqrt{1 + \frac{20}{D^{+v/a}}}}{-4} \quad n = \frac{-1 - \sqrt{1 + \frac{20}{D^{+v/a}}}}{-4} \\ \text{Region } \frac{1}{4} < \frac{y}{D} < \frac{3}{4}$$

$$\frac{T_{1/4} - T}{2.5 \frac{q_0}{\rho c U_\tau}} = \frac{1}{2.5} \left(\frac{1}{0.05 + \frac{1}{D^{+v/a}}} \right) \left[\frac{y}{D} - \frac{y^2}{2D^2} - \frac{7}{32} \right] [16]$$

$$\text{Region } \frac{3}{4} < \frac{y}{D} < \frac{y}{D} \text{ at } (D-y) \frac{U_\tau}{\nu} = 30 \\ \frac{T_{3/4} - T}{2.5 \frac{q_0}{\rho c U_\tau}} = \left[\frac{1}{4} - \frac{1}{8} \frac{1}{(m-n)} \right] \log \frac{y/D - m}{3/4 - m} \\ + \left[\frac{1}{4} + \frac{1}{8} \frac{1}{(m-n)} \right] \log \frac{y/D - n}{3/4 - n} \dots \dots [17]$$

where in this particular equation

$$m = \frac{-3 + \sqrt{1 + \frac{20}{D^{+v/a}}}}{-4} \quad n = \frac{-3 - \sqrt{1 + \frac{20}{D^{+v/a}}}}{-4}$$

For fluids with Prandtl numbers greater than unity, the effect of molecular conduction in the turbulent region of the flow becomes small. In such cases those terms in the foregoing expressions which involve the Prandtl number can be eliminated and substantially simpler expressions obtained.

The specification of the temperature distribution, together with the assumed velocity distribution, enables the evaluation of the mixed mean temperature of the fluid. This is expressed conveniently in the form of the difference between wall and mean fluid temperatures as

$$\frac{T_o - T_m}{2.5 \frac{q_o}{\rho c U_\tau}} = \frac{1}{U_m} \int_0^D U \frac{T_o - T}{2.5 \frac{q_o}{\rho c U_\tau}} dy \dots \dots [18]$$

The integral in Equation [18] is evaluated graphically or numerically by means of the temperature distribution as given in the previous equations. It is apparent that the evaluation of Equation [18] immediately yields an expression for the heat-transfer coefficient

$$h = \frac{q_o}{T_o - T_m}$$

Combination of Equation [18] with the expression for the difference between the wall temperatures yields an expression for the ratio

$$X = \frac{T_o - T_m}{T_o - T_D}$$

Fig. 4 reveals the general variation of this ratio with the Reynolds and Prandtl numbers. Consideration of the problems on the basis of the neglect of all turbulent diffusion effects on the heat transfer reveals a lower limit of about 0.66 on the value of X and reference to the figure indicates that conditions at $\nu/a = 0.01$ begin to approach this extreme.

The heat-transfer coefficient, expressed as a Nusselt number, is shown in Fig. 5. There the minimum value of the Nusselt number as derived by Jakob (4) for laminar flow is shown as a dashed line. A similar consideration, assuming heat transfer by conduction only and a uniform velocity for the entire flow, yields a Nusselt number only slightly higher, so that the dashed line indicates an approximate limit for all Reynolds-number values. The entrance effect under such conditions would be expected to be considerable.

For Prandtl numbers greater than unity, the negligible effect of molecular conduction in the turbulent core enables a specification of the mixed mean temperature which is independent of the Prandtl number if it is assumed that the mixed mean temperature of the fluid in the turbulent region of the flow is equal to the mixed mean temperature of the entire flow. This is a reasonable approximation even at low Reynolds numbers. It is found that for these cases the quantity

$$\frac{T_o - T_m}{2.5 q_o / \rho c u_\tau}$$

is a substantially linear function of the friction Reynolds number, $2U_\tau D/\nu$. This enables a convenient specification of the heat-transfer coefficient in the form

$$\frac{h}{U_m \rho c} = \frac{\sqrt{\frac{c_f}{2}}}{5 \frac{\nu}{a} + 5 \log \left(5 \frac{\nu}{a} + 1 \right) + 2.38 \log \frac{U_\tau D}{2\nu}} \dots [19]$$

It has been noted by R. Lyon (1) that the increased effect of the Prandtl number, when the Prandtl number becomes small, can be accounted for in an empirical expression of the Nusselt number of the type

$$\frac{2hD}{k} = A + B \left(\frac{2U_m D}{a} \right)^n$$

where A , B , and n are constants. Constant A serves to rationalize conditions at small Peclet numbers where the "limiting" value of the Nusselt number is approached. The Nusselt numbers presented in Fig. 5 can be expressed by the equation

$$\frac{2hD}{k} = 5.8 + 0.020 \left(\frac{2U_m D}{a} \right)^{0.8}$$

in the range

$$10^2 < \frac{2U_m D}{a} < 10^5$$

$$0.01 < \nu/a < 1.0$$

with an accuracy of ± 5 per cent.

Discussion

J. R. MENKE.⁴ The author has provided a worth-while extension to our understanding of heat transfer at low Prandtl number. He has noted the utility of superposition of the earlier solutions (1, 2),⁵ and he has extended and refined the calculations. The former result, the summation of solutions, is not altogether surprising, possible, as he of course points out, because of the linearity of the fundamental differential equations. The latter results, the calculations, are more complete (extending over the full range of 10^1 to 10^6 for Reynolds number, and 0.01 to 1.0 for Prandtl number) and probably more accurate than those given in (1).⁵ The results given in (1) and (2)⁵ have been subjected to a first experimental test with rather reasonable agreement and are reported in a paper by Dr. R. N. Lyon⁶ needing citation here.

We have, however, no new experimental information⁷ on the behavior of the eddy diffusivity near the center line of flow. The author, therefore, has used the earlier (and imperfect) assumptions of (1)⁵ with consequent limitations to accurate results. Powerful tools have been given to the experimenter to test these assumptions; measured traverses of temperature, t , and temperature derivative, $(\partial t)/(\partial y)$, will yield much information in fluids with low Prandtl numbers. One might, perhaps, suggest these measurements in a liquid metal flowing between plane parallel walls with almost all the heat flowing into one wall and out the other, i.e., heat flow "straight" across the channel. This approach is perhaps the most sensitive method for obtaining the differential description of the processes at work in the stream. A simplified method for measuring the integral result (the heat-transfer coefficient itself) is suggested in (1).⁵ Techniques for handling the liquid metals are rather well developed today; further studies with gases are also worth while.

Moreover, the question of the ratios of the eddy transports of heat, mass, and momentum is subject to more powerful attack with the availability of radioactive isotopes to compare measured mass transports with the foregoing measured heat transports.

RICHARD N. LYON.⁸ Dr. Seban has presented a powerful concept in his method for superimposing the heat flow from two

⁴ Nuclear Development Associates, Inc., New York, N. Y. Jun. ASME.

⁵ Author's Bibliography.

⁶ "Heat Transfer at High Fluxes in Confined Spaces," by R. N. Lyon, Dissertation, Doctor of Philosophy, University of Michigan, Ann Arbor, Mich., 1949.

⁷ Dr. B. H. Sage, California Institute of Technology, Pasadena, Calif., has indicated several forthcoming papers.

⁸ Oak Ridge National Laboratory, Oak Ridge, Tenn.

walls of a flat channel to enable calculation of the over-all heat-transfer effects. It will undoubtedly find wide application in the design of heat exchangers, as well as in future investigation of forced-convection heat transfer. The use of three relationships implied or stated by Dr. Seban in his paper, but not stressed by him, enable the usefulness of his concept to be shown clearly.

These are

$$h' = h'' \quad \dots \dots \dots [20]$$

$$T_{D'} = T_{O''} \quad \dots \dots \dots [21]$$

$$T_m = T_{m'} + T_{m''} - T_{O''} \quad \dots \dots \dots [10]$$

In most heat-transfer problems, the calculation of the actual heat-transfer coefficient at the two walls is not the ultimate objective. Usually one is interested in determining T_O , T_m , T_D , q_O , and q_D . Any three of these variables plus the values of the Reynolds number and of D for the system, together with the thermal conductivity of the fluid and its Prandtl number, will completely define the isothermal forced-convection system with smooth walls, as postulated by Dr. Seban. The value of h' or h'' can be calculated by the usual relationships for ordinary fluids, or by the last equation in the appendix of Dr. Seban's paper for the case of liquid metals. The value of X can be obtained from Fig. 4 with a knowledge of the Reynolds and Prandtl numbers. Any two of the five temperature and heat-flow variables listed herein can be calculated easily using a simple extension of Dr. Seban's paper as follows

$$T_m = T_{m'} + T_{m''} - T_{O''} \quad \dots \dots \dots [10]$$

or

$$T_m = \frac{q_O}{h'} - \frac{q_D}{h''} + T_O + T_D - T_{O''}$$

Since $h' = h''$ and $T_{O''} = T_{D'}$, this may be written

$$h'(T_m - T_O) = \frac{q_D}{X} + q_O - q_D \quad \dots \dots \dots [22]$$

or alternately as

$$h'(T_D - T_m) = \frac{q_O}{X} - q_O + q_D \quad \dots \dots \dots [23]$$

Adding Equation [22] to Equation [23] gives

$$h'X(T_D - T_O) = q_O + q_D \quad \dots \dots \dots [24]$$

Solving for q_O in Equation [22] and in Equation [24], and equating the solutions

$$h'(T_m - T_O) - q_D \left(\frac{1}{X} - 1 \right) = h'X(T_D - T_O) - q_D \quad [25]$$

Solving for q_D in Equation [23] and in Equation [24] and equating the solutions

$$h'(T_D - T_m) - q_O \left(\frac{1}{X} - 1 \right) = h'X(T_D - T_O) - q_O \quad [26]$$

Calculation of any of the five variables in terms of any three of the remaining variables plus h' and X may be accomplished by means of the appropriate equation from the following rearrangement of Equations [23], [24], [22], [25], and [26]

The symbol q_O represents the heat flux entering one wall from

$$h'T_m - h'T_D + \left(\frac{1}{X} - 1 \right) q_O + q_D = 0 \quad \dots \dots \dots [27]$$

$$h'XT_O - h'XT_D + q_O + q_D = 0 \quad \dots \dots \dots [28]$$

$$h'T_O - h'T_m + q_O + \left(\frac{1}{X} \right) q_D = 0 \quad \dots \dots \dots [29]$$

$$(1 - X)h'T_O - h'T_m + h'XT_D - \left(2 - \frac{1}{X} \right) q_D = 0 \quad \dots \dots \dots [30]$$

$$h'XT_O - h'T_m + (1 - X)h'T_D + \left(2 - \frac{1}{X} \right) q_O = 0 \quad \dots \dots \dots [31]$$

the fluid, while q_D represents the heat entering the fluid from the opposite wall. Negative values of q_O and q_D merely indicate heat flow in the opposite directions.

Values of h_O and h_D can be obtained if desired from the definitive equations

$$h_O = \frac{q_O}{T_m - T_O}; \quad h_D = \frac{q_D}{T_D - T_m}$$

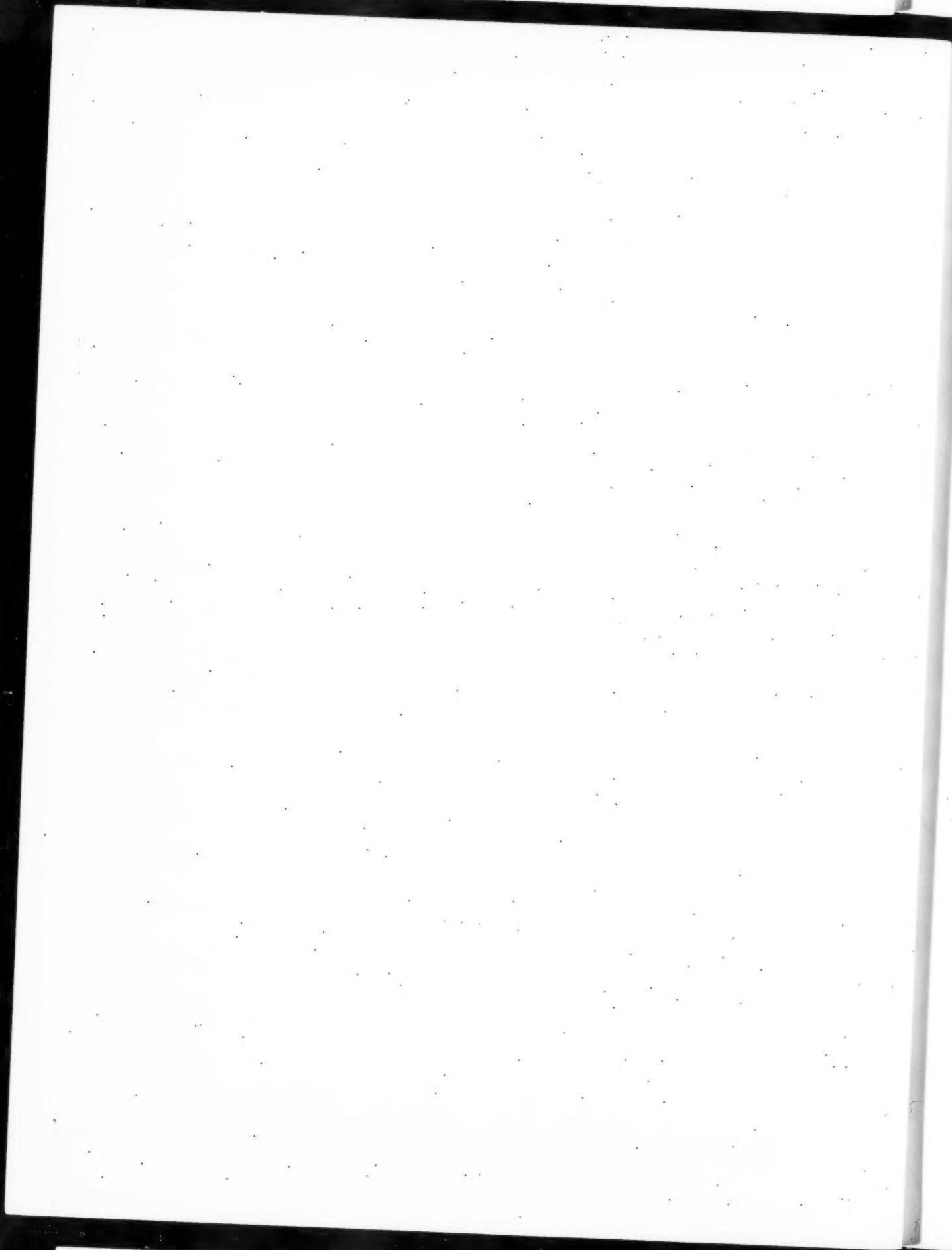
The writer hopes the foregoing comments will stimulate more rapid utilization of Dr. Seban's important contribution to the field of forced-convection heat transfer.

AUTHOR'S CLOSURE

Mr. Menke has appropriately emphasized the uncertainty concerning the magnitude of the eddy diffusivities for heat and momentum near the center line of the flow. In the present analysis, as in that of Harrison and Menke, a uniform diffusivity corresponding to the maximum value indicated by use of the Prandtl-Nikuradse expression for the velocity distribution in the turbulent region of the flow has been employed for the entire central half of the flow. Actual diffusivities are expected to be somewhat lower, and thus the heat-transfer rates predicted by the present analysis are somewhat too high. This discrepancy depends both upon the amount of heat flowing across the center line and upon the Prandtl number of the fluid. At the low Prandtl numbers typical of molten metals, particularly at low Reynolds numbers, the relative effect of molecular conduction is so great that the contribution of turbulent diffusion to the heat transfer is quite small.

There is a further question regarding the relation between the diffusion coefficients for heat and momentum transfer, which might be determined from measurements of the velocity and temperature and gradients thereof. Fig. 3 of the paper indicates experimental measurements on a system designed to realize such an objective and similar experimentation with fluids of low Prandtl number would be useful in indicating if there is any dependence of the eddy diffusivity for heat upon the Prandtl number.

Dr. Lyon's examination has produced a valuable generalization of the problem, expressed finally in the last five equations of his discussion. The flexibility of that expression of the results has there been noted, and one important point can be emphasized therefrom because these equations enable the specification of the wall temperatures in terms of the heat rates q_O and q_D . It can be shown that if the heat rates q_O and q_D are constant with respect to x , then the assumption "c" which follows Equation [2] is most precisely fulfilled. For such a case Equations [27] to [31] enable the relation of T_O and T_D to the mean fluid temperature T_m , the variation of which is linear with x because of the constant heat input to the fluid. Thus the linear variation of the wall temperatures corresponding to the constant-heat-rate case can be determined.



B

B

no
M
An
of
unc
of t

Heat-Transfer Rates in Centrifugal Compressors and the Effect of Internal Liquid Cooling on Performance

By W. E. TRUMPLER,¹ R. W. FREDERICK,² AND P. R. TRUMPLER³

This paper makes a preliminary exploration of the cooling rates which may be obtained in the internal passages of a centrifugal compressor. A mechanism for such calculations is proposed, data are given and correlated, and the results are used for prediction of performance of a compressor pumping 7500 cfm air to 100 psi, assuming various cooling arrangements.

NOMENCLATURE

The following nomenclature is used in the paper:

- A = area, sq ft; A_0 refers to diffuser wall, A_1 to diffuser side of plate, A_2 to return channel side of plate, A_3 to diaphragm wall in return channel
- c_p = specific heat of gas at constant pressure Btu/(lb_m) (deg F)
- D = hydraulic diameter, ft, equal to $\frac{4 \times \text{flow area}}{\text{wetted perimeter}}$
- g = acceleration of gravity, ft/sec²
- G = mass velocity, lb_m/(hr) (sq ft)
- h = heat-transfer film coefficient, Btu/(hr) (sq ft) (deg F)
- k = thermal conductivity of gas, Btu/(hr)(sq ft) (deg F/ft)
- K = thermal conductivity of diaphragm metal, Btu/(hr) (sq ft) (deg F/ft)
- n = exponent in polytropic change of state
- N = rotative speed, rpm
- p = absolute pressure, lb_f per sq ft; subscripts 1 and 2 refer to beginning and end of a succession of states.
- q = heat flow rate, Btu per hr; subscripts 0 to 3 have same meaning as for areas A
- Q = volume rate of fluid flow, cfm
- R = gas constant in $pv = RT$
- T = absolute temperature, deg F abs
- u = peripheral velocity of impeller, fps
- U = over-all conductance, Btu/(hr) (sq ft) (deg F)
- $(UA)_\infty$ = value of UA , assuming water film coefficient infinite
- v = specific volume, cu ft per lb_m
- V = fluid velocity, fps
- w = flow rate of gas, lb_m per hr
- Z = absolute viscosity lb_m/(hr) (ft)

$$\beta \text{ is defined as } \frac{1}{n-1} \left[\left(\frac{p_2}{p_1} \right)^{\frac{n-1}{n}} - 1 \right]$$

- γ = ratio of specific heats, c_p/c_v
- η = efficiency; subscript H refers to hydraulic efficiency
- μ = pressure coefficient
- ρ = density, lb_m per cu ft

Subscripts:

- d refers to diffuser
- r refers to return channel
- w refers to water

INTRODUCTION

For many applications the advantages resulting from cooling a gas during compression have been clearly established. Usually this cooling is obtained by withdrawing the gas from the machine at one or more intermediate points in the compression and passing it through heat exchangers. The construction of a centrifugal compressor is such that, without much added expense, the gas may be cooled as it flows through the fixed passages. Because of the high velocities in these passages the heat-transfer film coefficients are high. The questions may well be asked, what is the magnitude of these coefficients? how can one calculate the cooling effect which may be obtained in present commercial designs? and what is the effect of such cooling on over-all performance and other economic factors affecting users of centrifugal compressors?

It is the purpose of this paper to provide limited answers to these three questions. The answers are limited first in scope, concerning themselves only with one commercial centrifugal design, that manufactured by the authors' company, and applying the results to a study of only one process condition, namely, compression of 7500 cfm air at 68 F and 14.7 psia to 114.7 psia.

A second limitation is inherent in our method. As with most industrial research, the need for results was urgent and the man power limited. Therefore it was not possible to examine critically many of the assumptions upon which the theory is based.

FILM COEFFICIENTS IN COMPRESSOR PASSAGES

In Fig. 1 is shown an assembly of a commercial four-stage centrifugal compressor of the type used in the investigation. Outer diameter of all impellers is 18 in., and operating speeds vary from 7300 to 9800 rpm, depending on the application.

A detailed view of an intermediate stage is shown in Fig. 2. The gas first enters guide vanes, which direct the flow at the desired angle into the impeller. At the impeller periphery the gas leaves the wheel at a velocity near the acoustic. Conversion of velocity to pressure is accomplished in the diffuser, which, except for inlet and outlet, consists of two smooth parallel surfaces. At the return bend, the gas velocity is of the order of 300 fps. The gas approaches the next stage through the return channel which has integrally cast ribs, or return vanes, to direct the flow into the next stage. The casting, which encloses the return channel and the cooling-water passage, is known as the "diaphragm." Both diaphragms and inlet guide vanes are split on a horizontal diameter.

¹ Chief Engineer, Centrifugal Engineering Department, Clark Brothers Company, Inc., Olean, N. Y. Mem. ASME.

² Turtle Creek, Pa. Jun. ASME.

³ Professor of Mechanical Engineering, Illinois Institute of Technology, Chicago, Ill.; Consultant, Clark Brothers Company, Inc. Mem. ASME.

Contributed by the Heat Transfer Division and presented at the Annual Meeting, New York, N. Y., November 27-December 2, 1949, of THE SOCIETY OF MECHANICAL ENGINEERS.

NOTE: Statements and opinions advanced in papers are to be understood as individual expressions of their authors and not those of the Society. Paper No. 49-A-93.

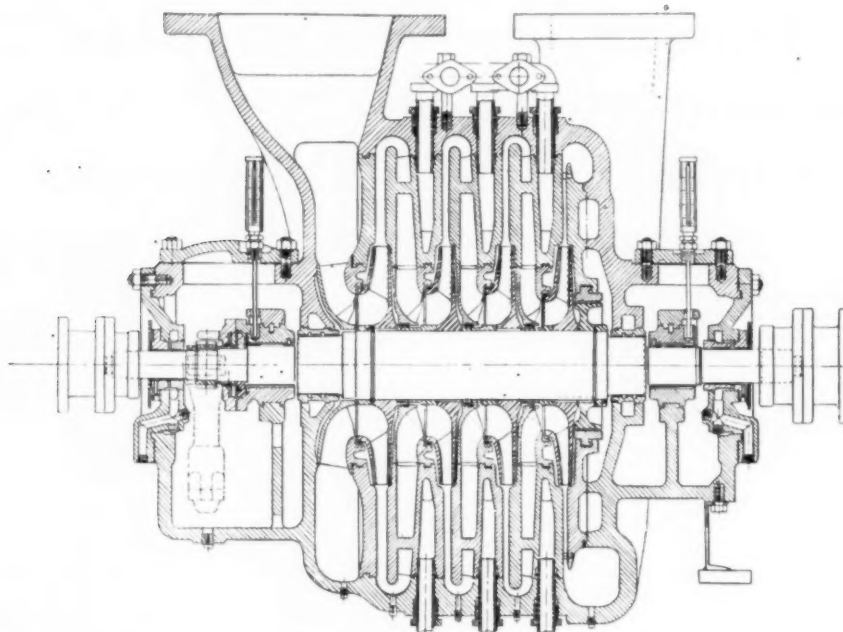


FIG. 1 SECTION THROUGH TYPICAL FOUR-STAGE CENTRIFUGAL COMPRESSORS

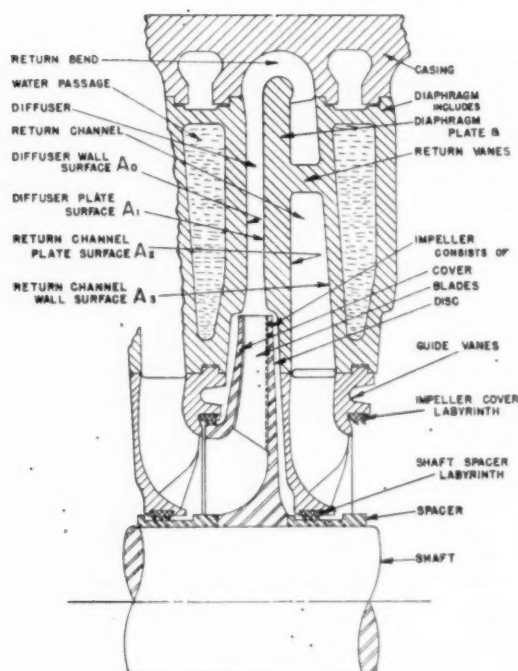


FIG. 2 REPRESENTATIVE INTERMEDIATE-STAGE CONSTRUCTION

Guide-vane sections may be either cast or fabricated by welding, with the latter method preferred. Three types of guide vanes are used in the standard design and provide for a gas flow approaching the impeller with an angular velocity in the direc-

tion of rotation (With), against rotation (Ag), or straight radial (Rad), with zero rotation. By changing the guide-vane selection the capacity of a given stage may be changed as much as ± 15 per cent without loss of efficiency, and without change in any other physical element or change in speed. By capacity is meant the actual volume per unit time flowing through the stage inlet.

Fig. 3 shows the design of an AB-diaphragm inserted between stages A and B. Two other designs are used for smaller-capacity stages, namely, B-diaphragm for insertion between B-stages and between B and C-stages, and C-diaphragms for all lower-capacity stages. Diffuser widths, which are specified to maintain the same velocity in each stage, may be controlled by different finishing dimensions on otherwise identical castings.

Each half-diaphragm has its own external water connections, thus eliminating internal connections at the split. The coring of the water passages is designed to obtain maximum water film coefficients with passages of reasonable size, and to minimize entrainment of air. Plugs around the diaphragm periphery permit some degree of mechanical cleaning of water passages, although chemical cleaning is recommended. The water-flow directions are indicated in Fig. 3. Normal flow rate for this size (No. 2) case is 100 gpm, divided equally between top and bottom halves, and 50 gpm flows through the half-diaphragms in series from one end of the machine to the other.

The diaphragms are cast iron or a high-conductivity bronze.

It will be clear that analysis of the heat transfer from the compressed gas through the irregular diaphragm wall to the water is a complex matter. Assuming that the water film resistance is small compared with the total thermal resistance, the heat-transfer problem may be divided into three parts, namely, gas film coefficient in diffuser, gas film coefficient in return channel, and resistance of metal wall. The effect of heat flow between casing and gas at the return bend, along the shaft, through the guide vanes and at the impeller walls was assumed sufficiently small that it could be taken into account adequately by the ex-

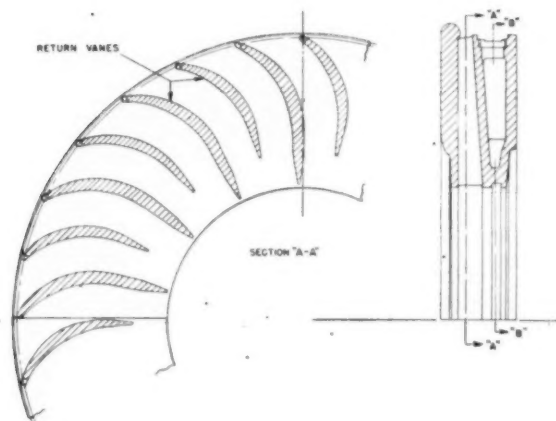


FIG. 3(a) SECTION THROUGH RETURN-CHANNEL VANES

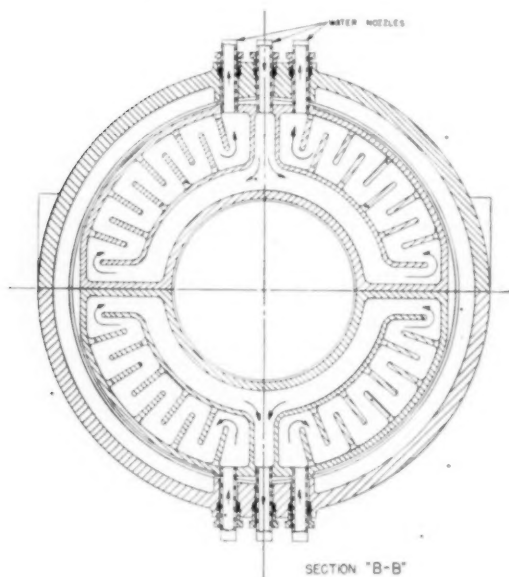


FIG. 3(b) SECTION THROUGH DIAPHRAGM COOLING-WATER PASSAGES

perimentally determined constant in the diffuser film-coefficient equation.

Three important assumptions are made in calculating the gas film coefficient in the diffuser, as follows:

1 Although there is a large variation in gas velocity, an average value of the coefficient is applied to the entire surface.

2 The value of h_d varies in accordance with an equation of the same form as that generally used for turbulent-flow film coefficients inside pipes or ducts⁴

$$\frac{h_d D}{k} = \text{const} \left(\frac{V D \rho}{Z} \right)^{0.8} \left(\frac{c_p Z}{k} \right)^{0.4} \quad [1]$$

with D taken as the diffuser width, and V directly proportional to the gas velocity entering the diffuser. Diffuser dimensions other than D are identical for a given size of machine.

⁴ "Heat Transmission," by W. H. McAdams, second edition, McGraw-Hill Book Company, Inc., New York, N. Y., 1942.

3 The velocity V is independent of the capacity and directly proportional to the peripheral velocity of the impeller. Since impeller diameter is uniform for each compressor size, this implies that V is proportional to rpm. The justification for this simplification is indicated in Fig. 4 which shows velocity diagrams at various loads at a given peripheral velocity, for the particular type of impeller being investigated.

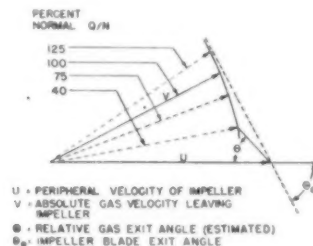


FIG. 4 VELOCITIES AT IMPELLER EXIT

As a consequence of these assumptions, and neglecting variation of the Prandtl modulus with gases, the equation for diffuser film coefficient becomes

$$h_d = 2.0 c_p (N \rho)^{0.8} \left(\frac{Z}{D} \right)^{0.2} \quad [2]$$

where the constant was determined by trial and error to fit a wide range of performance data on two size No. 2 (18-in.-diameter impeller) machines.

Gas properties were evaluated at total (stagnation) temperature and total pressure at the return bend. The stagnation temperature was used as the effective gas temperature for determining heat-flow potential between gas and surface.

The effective wall area A_0 in the diffuser was taken from the outer impeller diameter to the outer edge of the diaphragm, and the diffuser-plate area A_1 was taken from the outer impeller diameter to the maximum plate diameter.

It was assumed that the coefficient in the return channel could also be calculated by Equation [1] which, with a constant of 0.023 as recommended by McAdams and a Prandtl modulus of 0.78, becomes

$$h_r = 0.027 c_p G^{0.8} \left(\frac{Z}{D_r} \right)^{0.2} \quad [3]$$

In determining the gas-flow area through the return channels, the arithmetic average of the areas at the outer and inner edges of the diaphragm was used. The gas flow per unit time was taken as its value at the compressor discharge, thus neglecting leakage effects. The hydraulic diameter D_r was found for entrance and exit of the return channels, and the arithmetic average of their two-tenths power taken to evaluate $(D_r)^{0.2}$. Thermal properties were evaluated from stagnation temperature and total pressure at the adjacent return bend.

In the return channels, the plate area A_2 was equal to the diffuser side plate area A_1 minus the cross-sectional area of the vanes plus one half the surface area of the vanes. The area of the diaphragm wall A_3 was taken to be the area from the outer edge of the diaphragm to the point of contact with the inserted vanes minus the cross-sectional area of the integral return vanes plus one half the surface area of the integral vanes. The reason for the separation of the return-channel surface into plate area and diaphragm wall area will become clear with discussion of the wall resistance calculation.

Heat flow through the walls is calculated on the basis of the following assumptions:

1 The gas contacts four isothermal surfaces: namely, diffuser wall, diffuser plate, return-channel plate, and diaphragm wall, the effective surface areas of which have been previously defined.

2 The temperature difference between the two plate surfaces is the temperature drop calculated to conduct the heat flowing into the diffuser plate surface through the thickness of the plate.

3 Heat flow into the water takes place by three independent parallel paths: namely, (1) from the two plate surfaces through the return vanes, which have an effective length equal to the average width of the return channel, plus the thickness of the wall between the return channel and water passage, an effective heat-flow area equal to the total cross-sectional area of the vanes, and a temperature drop from the return-channel plate surface to the water surface, (2) from the diaphragm wall surface to surface on the water side of the wall from which return-vane cross-sectional area has been subtracted, and (3) from diffuser wall surface to water surface on the other side of the wall.

The water surfaces used for the three parallel heat-flow paths were the total return-vane cross-sectional area, the diaphragm wall surface A_d , and the diffuser wall surface A_o . A water conductance of 2000 based on these surfaces was assumed unless otherwise noted.

It should be understood clearly that the method here used for calculating heat flow through the complex diaphragm walls may limit seriously the generality of the conclusions. Solution by successive numerical approximation was attempted, but convergence was too slow.

Based on the heat-transfer mechanism just described, and with a knowledge of fundamental stage characteristics used to calculate the performance of uncooled machines, the performance of a cooled compressor may be established. The stage characteristics are the pressure coefficient μ and the hydraulic efficiency η_H , both as functions of the independent variable Q/N at the entrance to the stage. The definition of μ for one stage is

$$\mu = \frac{\int_{p_1}^{p_2} v dp}{u^2} \quad [4]$$

which for air as a perfect gas following the compression process pv^n constant, may be written

$$\mu = \frac{1725 T_1 \beta}{u^2} \quad [5]$$

where

$$\beta = \frac{1}{n-1} \left[\left(\frac{p_2}{p_1} \right)^{\frac{n-1}{n}} - 1 \right] \quad [6]$$

The definition of hydraulic efficiency is

$$\eta_H = \frac{\int_{p_1}^{p_2} v dp}{Wk_f} \quad [7]$$

where Wk_f represents the total mechanical work into the fluid being compressed. For a perfect gas following the process pv^n constant, with no heat transferred to the fluid, it may be verified that

$$\eta_H = \frac{\gamma}{n-1} \quad [8]$$

For air, a commonly used value for $(\gamma - 1)/\gamma$ is 0.283, which will be used in all calculations given in the paper. Temperatures and pressures at stage entrance and exit are related by the equation

$$\frac{T_2}{T_1} = \left(\frac{p_2}{p_1} \right)^{\frac{n-1}{n}} \quad [9]$$

Knowing the temperature T_1 , pressure p_1 , and volumetric gas flow Q at stage entrance, plus the impeller rpm, the values of μ and η_H are first determined at the given Q/N from characteristic curves determined from previous experiments on uncooled machines. Pressure p_2 at entrance to the next stage, and T_2 , the total temperature at impeller exit (same as temperature entering next stage in an uncooled machine) are then calculated. The gas temperature entering the next stage is determined on the basis of film coefficients and metal conductances as previously outlined. The calculation is a trial-and-error procedure. The temperature of the diffuser-plate surface must be such that the heat transferred to both sides of the plate is equal to the heat flowing through the return vanes.

The constant in Equation [2] was set to obtain agreement between calculated and observed performance of two different commercial machines.

TESTS OF WATER-COOLED COMPRESSORS

Important physical data on the two machines tested are given in Tables 1 and 2. Both were four-stage size No. 2 compressors, similar in design to the machine in Fig. 1. Both had 18-in.-diam impellers and were designed for operation at 9600 rpm. The first machine was designed for full-load volumetric suction flow of 7500 cfm air at 68 F and 14.7 psia, the second for 2700 cfm air at 85 F and 42 psia. Each machine was operated over the entire volumetric capacity range both with and without cooling water. Since the available power for these tests was limited, suction pressures at or below atmospheric were used. Speeds ranged from 9060 to 10,070 rpm.

TABLE 1 DIAPHRAGM DIMENSIONS

	Diaphragm type		
	AB	B	C
A_1 , sq ft.....	3.53	3.53	3.53
A_2 , sq ft.....	3.98	3.98	3.98
A_3 , sq ft.....	4.69	4.83	4.96
A_4 , sq ft.....	4.89	5.03	5.16
Return-channel D , in.....	0.637	0.633	0.625
Return-channel flow area, sq ft.....	0.346	0.319	0.291
Return-channel wall thickness, ft.....	0.0365	0.0365	0.0365
Return-vane cross-sectional area, sq ft.....	0.844	0.945	1.06
Return-vane axial length, ft.....	0.083	0.083	0.083
Plate thickness, ft.....	0.0704	0.0650	0.0704
Diffuser-wall thickness, ft.....	0.0442	0.0495	0.0650

TABLE 2 DIFFUSER WIDTHS

Impeller	Guide vane	Diffuser width, D , ft
A.....	Ag	0.0573
B.....	Ag	0.0469
C.....	Rad	0.0443
D.....	Ag	0.0312
E.....	Rad	0.0312
F.....	Ag	0.0312
G.....	Rad	0.0312

Standard ASME long-radius low-ratio nozzles of 5 and 6 in. throat diam, installed in accordance with the ASME Code, measured air flow out of the compressors. Speed was measured with a stop watch and a revolution counter geared to the shaft. All pressures were measured with impact tubes adjusted at each run to point directly into the air stream. Gas temperatures were measured with bare mercury-in-glass thermometers, except within compressor passages, where calibrated bare copper-constantan thermocouples were used. Since gas velocities were not

over approximately 300 fps, all recovery factors were taken as unity, that is, temperatures were considered as stagnation values. Each gas temperature was the average reading of at least two probes, and all pressures, except those inside the compressor case, were the average of at least two independent impact-tube readings.

Pressure and temperature readings were taken at the following locations: Upstream from the inlet flange, downstream from the discharge flange, and at the three return bends. One pressure point and two temperature points were located around the machine at each return bend.

It should be noted that instrumentation at the return bends was not adequate for the desired accuracy. Pressures, and particularly temperatures, varied around the circumference. Two temperature readings at a return bend usually were within 2 deg F, but differences up to 13 deg F were noted. Since each thermocouple was made of specially selected wire and checked with the assembled probe in a special hot-air calibration apparatus to read within 0.5 deg F of the standard Leeds and Northrup calibration curve, it was concluded that the readings reflected non-uniform conditions within the compressor. Differences would vary with change in load. It was not considered desirable to insert more probes into the machine in order to obtain a better average.

For many runs the suction flow to the compressor was throttled by means of two flat contiguous perforated plates which could

be moved with respect to each other. Thus the flow was throttled without setting up irregular velocity distribution at the compressor inlet. To insure an even better velocity distribution, three 12-in.-diam plates with 1/8-in.-diam holes on 5/16-in. pitch were inserted about six inches apart in the duct section between throttle plate and inlet flange. A gate valve in the compressor discharge line was used for control purposes.

In the cooling runs, water flow through the diaphragms (separate for the upper and lower casing halves) was measured with weighing tanks and platform scales. Temperature rise of the cooling water did not exceed 10 deg, and therefore thermometers with 0.1-deg divisions were used.

In all runs except a few in the surge region, data were taken at approximately 15-min intervals until two successive readings showed no appreciable difference. The average of these two readings was taken for calculation. Data on the various runs are presented in Tables 3 and 4.

In Figs. 5 and 6 are given the stage characteristic curves calculated from data on the test compressors operated without cooling. Since it was not convenient to obtain data at entrance to the guide vanes, the return-bend measurements were used instead. The first stage, therefore, extends from inlet flange to first return bend, the second stage from first to second return bend, the third stage from second to third return bend, and the fourth stage from third return bend to discharge flange. It will be seen that corrections were made for heat gain or loss in first and fourth stages

TABLE 3(a) TEST DATA, HIGH-CAPACITY COMPRESSOR, UNCOOLED

Calculations	Run 123-1	Run 123-2	Run 123-3	Run 123-4	Run 123-5	Run 123-6	Run 123-7	Run 123-8	Run 123-9	Run 123-10	Run 123-11
Nozzle diameter, in.	6.00	6.00	6.00	6.00	6.00	6.00	6.00	6.00	6.00	6.00	6.00
Nozzle coefficient	0.995	0.995	0.995	0.995	0.995	0.995	0.995	0.995	0.995	0.995	0.995
Nozzle-inlet temp, deg F	325.0	323.5	313.1	325.9	335.9	337.0	339.5	334.5	330.5	331.8	332.5
ΔP nozzle, in. water	31.58	32.02	35.26	30.84	28.25	24.34	16.94	14.19	10.50	8.20	3.74
Barometer, in. Hg	28.51	28.50	28.50	28.50	28.52	28.52	28.52	28.52	28.52	28.52	28.52
Air temp, suction, deg F	77.0	79.2	71.7	72.2	72.8	74.6	75.1	74.3	76.0	78.3	78.0
Air temp, 2nd stage (in), deg F	147.2	148.1	138.5	146.3	154.2	155.1	158.0	160.6	162.4	165.2	188.4
Air temp, 3rd stage (in), deg F	221.1	218.5	206.1	218.7	227.6	230.2	237.6	235.5	234.6	240.3	270.3
Air temp, 4th stage (in), deg F	289.9	289.5	278.0	289.5	303.6	305.4	314.8	312.5	311.6	317.3	342.8
Air temp, discharge, deg F	351.6	350.5	335.7	353.8	367.4	370.3	380.0	375.7	377.0	384.0	409.3
Pressure, suction, in. Hg	11.15	13.07	14.66	9.07	6.02	2.94	4.88	4.96	4.67	4.84	4.75
Pressure, 2nd stage (in), in. Hg	6.10	7.29	10.97	3.50	2.90	7.42	4.72	4.31	3.87	3.42	2.75
Pressure, 3rd stage (in), in. Hg	1.57	9.2	6.40	6.37	12.92	19.06	15.41	14.46	13.51	12.80	11.12
Pressure, 4th stage (in), in. Hg	10.20	6.49	1.16	16.38	24.99	32.53	27.75	26.29	24.30	23.30	20.54
Pressure, discharge, in. Hg	19.67	14.72	6.87	27.50	38.39	47.46	41.11	39.19	36.45	34.95	30.79
Time 14,400 blower rev, min	1.527	1.525	1.515	1.532	1.533	1.545	1.522	1.520	1.528	1.520	1.520
Rpm, N	9440	9450	9500	9400	9390	9320	9150	9470	9430	9470	9470
Inlet-air flow, cfm, Q	6190	6875	8180	5400	4450	3635	3280	3020	2575	2305	1555
Q/N inlet	0.656	0.728	0.861	0.575	0.475	0.390	0.347	0.319	0.273	0.243	0.164

TABLE 3(b) TEST DATA, HIGH-CAPACITY COMPRESSOR, COOLED

Calculations	Run 122-1	Run 122-2	Run 122-3	Run 122-4	Run 122-5	Run 122-6	Run 122-7	Run 122-8	Run 122-9	Run 122-10	Run 122-11	Run 122-12
Nozzle diameter, in.	6.00	6.00	6.00	6.00	6.00	6.00	6.00	6.00	6.00	6.00	6.00	6.00
Nozzle coefficient	0.995	0.995	0.995	0.995	0.995	0.995	0.995	0.995	0.995	0.995	0.995	0.995
Nozzle-inlet temp, deg F	260.0	257.6	255.6	263.8	260.0	258.5	257.0	257.8	245.0	244.0	244.0	227.0
ΔP nozzle, in. water	27.51	31.38	26.98	26.44	21.16	33.29	32.10	32.21	15.32	12.06	9.51	5
Barometer, in. Hg	28.45	28.46	28.48	28.49	28.62	28.55	28.55	28.58	28.58	28.58	28.59	28.59
Air temp, suction, deg F	76.4	76.1	76.5	76.7	72.9	72.5	69.8	67.5	71.3	73.3	73.5	73.5
Air temp, 2nd stage (in), deg F	140.4	140.3	145.5	146.6	149.9	131.6	134.2	133.8	143.3	148.4	151.1	152.3
Air temp, 3rd stage (in), deg F	192.2	192.0	194.2	198.6	202.3	182.8	187.0	187.7	195.3	194.1	196.8	195.5
Air temp, 4th stage (in), deg F	232.9	230.7	234.0	240.3	241.0	227.0	227.6	228.1	227.1	228.6	231.7	223.2
Air temp, discharge, deg F	279.2	274.2	274.3	285.2	282.7	274.8	274.3	268.6	268.6	270.8	278.5	258.5
Pressure, suction, in. Hg	-11.69	-8.70	-4.24	8.10	-4.21	-14.22	-12.18	-12.15	-5.30	-5.18	-4.98	-5.32
Pressure, 2nd stage (in), in. Hg	-6.72	-3.63	4.54	-0.78	5.57	-9.62	-6.43	-6.21	3.98	3.47	3.66	2.29
Pressure, 3rd stage (in), in. Hg	0.22	5.32	14.86	8.32	16.94	-3.67	0.52	0.64	14.63	13.64	13.86	11.20
Pressure, 4th stage (in), in. Hg	8.73	15.03	27.60	19.43	30.97	3.12	8.84	9.13	27.50	25.91	26.28	22.01
Pressure, discharge, in. Hg	18.76	26.35	42.28	32.67	47.43	10.96	18.80	19.25	43.26	40.90	41.29	35.10
Time 14,400 blower rev, min	1.538	1.568	1.590	1.535	1.536	1.531	1.552	1.549	1.539	1.517	1.500	1.532
Water flow, top, min/200 lb	0.629	0.642	0.675	0.571	0.573	0.572	0.568	0.577	0.467	0.475	0.489	0.440
Water flow, bot, min/200 lb	0.679	0.653	0.728	0.608	0.617	0.612	0.653	0.632	0.506	0.510	0.530	0.474
Water temp (in), deg F	71.4	71.6	71.6	71.8	71.6	71.2	70.95	70.75	68.5	68.45	68.3	68.2
Water temp (out) top, deg F	78.6	78.8	80.3	78.95	79.4	77.1	77.1	77.2	74.4	74.2	74.4	72.95
Water temp (out) bot, deg F	79.1	79.4	81.0	79.5	80.0	77.65	77.65	77.7	74.9	74.6	74.8	73.5
Rpm, N	9370	9190	9060	9380	9380	9400	9270	9300	9360	9500	9600	9400
Inlet-air flow, cfm, Q	6250	5660	4260	5020	3730	7960	6835	6815	3330	2970	2620	1982
Q/N inlet	0.667	0.616	0.4705	0.535	0.398	0.847	0.736	0.733	0.356	0.3125	0.273	0.211

TABLE 4(a) TEST DATA, LOW-CAPACITY COMPRESSOR, UNCOOLED

Calculations	Run 120-1	Run 120-2	Run 120-3	Run 120-4	Run 120-5	Run 120-6	Run 121-1	Run 121-2	Run 421-3	Run 121-4	Run 121-5	Run 121-6
Nozzle diameter, in.	5.00	5.00	5.00	5.00	5.00	5.00	5.00	5.00	5.00	5.00	5.00	5.00
Nozzle coefficient	0.990	0.990	0.990	0.990	0.990	0.990	0.990	0.990	0.990	0.990	0.990	0.990
Nozzle-inlet temp., deg F	261.7	310.1	339.4	292.4	348.3	273.5	335.9	337.2	336.2	333.5	332.8	348.6
ΔP nozzle, in. water	35.69	21.43	12.58	27.17	3.69	31.68	1.00	5.96	8.22	10.70	1.77	2.04
Barometer, in. Hg	28.63	28.62	28.60	28.60	28.61	28.62	28.59	28.59	28.59	28.59	28.59	28.59
Air temp suction, deg F	76.9	80.0	80.2	80.2	78.5	74.2	76.8	78.5	76.2	75.0	76.6	86.8
Air temp, 2nd stage (in), deg F	131.2	145.8	158.7	140.5	171.9	133.8	164.0	159.2	154.7	151.1	177.2	189
Air temp, 3rd stage (in), deg F	176.7	204.4	229.1	192.3	252.7	183.2	240.9	231.5	228	223.8	259.8	276.4
Air temp, 4th stage (in), deg F	225.8	270.5	303.7	252.8	334.8	238.3	318.3	308.8	304.8	298.1	338.9	359.4
Air temp, discharge, deg F	269.8	326.5	362.6	304.1	394.2	283.0	376.7	368.3	363.2	357.0	394.6	407
Pressure, suction, in. Hg	-4.94	-4.94	-4.72	-5.11	-4.79	-5.01	-6.86	-6.98	-7.18	-6.93	-6.20	-0.89
Pressure, 2nd stage (in), in. Hg	0.92	3.27	4.90	2.08	3.83	1.59	1.06	0.99	1.20	1.62	1.58	8.45
Pressure, 3rd stage (in), in. Hg	7.44	13.13	16.27	10.50	13.93	9.14	10.24	10.32	11.10	11.88	10.85	19.62
Pressure, 4th stage (in), in. Hg	14.82	25.12	30.25	20.49	25.81	18.01	21.37	21.42	23.16	24.31	21.60	31.82
Pressure, discharge, in. Hg	22.21	38.42	45.39	31.73	38.78	27.81	33.67	33.97	36.50	38.13	33.20	45.45
Time 17,500 blower rev, min	1.847	1.832	1.799	1.841	1.751	1.855	1.764	1.782	1.784	1.811	1.747	1.749
Rpm, N	9480	9550	9740	9500	10000	9440	9910	9820	9800	9660	10020	10000
Inlet-air flow, cfm, Q	3480	2622	1955	3010	1054	3245	1207	1488	1760	1980	784	685
Q/N , inlet	0.367	0.275	0.203	0.317	0.105	0.344	0.1218	0.1515	0.1795	0.205	0.0784	0.0685

TABLE 4(b) TEST DATA, LOW-CAPACITY COMPRESSOR, COOLED

Calculations	Run 118-1	Run 118-2	Run 118-3	Run 118-4	Run 118-5	Run 118-6	Run 119-1	Run 119-2	Run 119-3	Run 119-4	Run 119-5
Nozzle diameter, in.	5.00	5.00	5.00	5.00	5.00	5.00	5.00	5.00	5.00	5.00	5.00
Nozzle coefficient	0.990	0.990	0.990	0.990	0.990	0.990	0.990	0.990	0.990	0.990	0.990
Nozzle-inlet temp, deg F	209.5	219.5	220.0	216.5	203	210.1	201.9	208.4	216.5	195.4	194.6
ΔP nozzle, in. water	31.44	18.45	11.32	25.11	4.32	28.62	3.73	6.30	8.59	1.51	1.82
Barometer, in. Hg	28.63	28.62	28.63	28.63	28.63	28.63	28.63	28.63	28.63	28.64	28.64
Air temp suction, deg F	71.4	69.8	68.8	68.1	70.4	67.7	72.3	75.4	74.7	76.8	76.6
Air temp, 2nd stage (in), deg F	121.2	128.5	133.7	123.6	137.0	119.8	139.6	139.8	141.3	145.4	148.1
Air temp, 3rd stage (in), deg F	151.9	165.2	171.7	157.6	169.0	151.5	169.7	169.3	174.8	170.6	174.3
Air temp, 4th stage (in), deg F	182.4	196.8	202.2	190.3	190.0	183.3	190.2	193.9	202.6	184.6	187.6
Air temp, discharge, deg F	215.0	229.5	230.5	224.4	218.6	216.7	217.4	222.1	229.2	211.7	214.2
Pressure, suction, in. Hg	-4.98	-4.92	-5.93	-4.90	-4.30	-4.76	-6.99	-6.82	-6.83	-6.88	-4.09
Pressure, 2nd stage (in), in. Hg	1.26	3.39	3.39	-2.50	4.73	1.96	0.99	1.34	1.80	0.89	4.63
Pressure, 3rd stage (in), in. Hg	8.73	13.97	15.00	11.68	16.29	10.17	11.33	11.56	12.72	11.27	16.13
Pressure, 4th stage (in), in. Hg	17.99	27.81	30.41	23.44	31.11	20.42	24.60	24.80	27.15	24.66	30.94
Pressure, discharge, in. Hg	29.23	44.38	48.27	37.80	48.96	32.87	40.80	41.34	44.17	40.66	48.78
Time 17,500 blower rev, min	1.856	1.8405	1.812	1.851	1.764	1.872	1.753	1.772	1.790	1.739	1.756
Water flow, top, min/200 lb	0.602	0.620	0.610	0.614	0.641	0.671	0.920	0.875	0.873	0.924	1.00
Water flow, bot, min/200 lb	0.607	0.600	0.610	0.622	0.695	0.685	0.940	0.895	0.890	0.954	1.026
Water temp (in), deg F	71.4	71.4	71.35	71.3	70.95	70.55	67.8	68.0	68.1	68.1	68.2
Water temp (out) (top), deg F	76.05	76.9	77.1	76.45	76.75	75.75	75.6	75.75	76.55	75.35	76.9
Water temp (out) (bot), deg F	76.05	76.9	77.1	76.45	76.75	75.75	75.7	75.75	76.65	75.45	77.0
Rpm, N	9430	9510	9660	9450	9910	9340	9980	9860	9770	10070	9960
Inlet-air flow, cfm, Q	3360	2540	2073	2956	1214	3155	1344	1647	1906	819	794
Q/N , inlet	0.356	0.267	0.2147	0.3125	0.1224	0.338	0.135	0.167	0.195	0.0814	0.0796

for the low-capacity compressor. These corrected curves were used in subsequent analysis.

In Figs. 7 and 8 are shown the measured temperatures in each machine and those calculated on the basis of the method described in the previous section. The specific heat of air at constant pressure and the thermal conductivity of cast iron were treated as constants with values of 0.24 Btu/(lb) (deg F) and 27.0 Btu/(hr) (sq ft) (deg F/ft), respectively. The water temperature of any one diaphragm was considered constant and, for purposes of determining wall temperature, all diaphragms in one compressor were assumed to cause equal temperature rise of cooling water.

The agreement between observed and calculated temperature was considered satisfactory for general engineering use. At the lowest Q/N -values shown in Figs. 7 and 8, the machines were either in or close to surge. Under these conditions the assumption implicit in Equation [2] could hardly be expected to hold.

The results indicate that average gas-film coefficients in centrifugal compressors are quite high, varying in our tests from 54 to 180 Btu/(hr) (sq ft) (deg F) for the diffuser and 24 to 36 for the return channel. These values apply of course to the low absolute pressures of the tests.

For a machine of the same type, compressing from atmosphere to 100 psia, diffuser average film coefficients as high as 300 will be obtained. A test was actually made on a water-cooled two-casing machine compressing to 100 psia. Only one load condition was

run, however, but the calculated terminal temperatures checked the observed within the limits of experimental error.

PREDICTED PERFORMANCE OF COOLED MACHINES

The calculation procedure previously outlined was used to study five cooling arrangements for a centrifugal compressor designed to compress 7500 cfm air at 68 F and 14.7 psia to 114.7 psia with cooling water at 75 F. The compressor size and operating conditions were so selected because of general interest in utility air for large process or manufacturing plants. The five cooling arrangements considered were: (1) two four-stage cases with an intercooler, no diaphragm cooling, (2) two four-stage cases with an intercooler and cooled iron diaphragms, (3) one eight-stage compressor with cooled iron diaphragms, (4) one eight-stage compressor with cooled high conductivity ($K = 154$) bronze diaphragms,⁵ and (5) one eight-stage compressor with cooled diaphragms of infinite conductivity. The intercooler pressure drop, including that for interconnecting piping, was taken as 2 psi at full load, and air cooling to 100 F was assumed.

The characteristic curves in Fig. 9 were used, taking Q/N for each stage as 100 per cent for compressor operation at rated load, 7500 inlet cfm. Each arrangement was calculated on this basis for performance at 3750, 5000, 6250, and 7500 cfm inlet flow.

⁵ Material specifications supplied by P. R. Mallory and Company, Inc., Indianapolis, Ind.

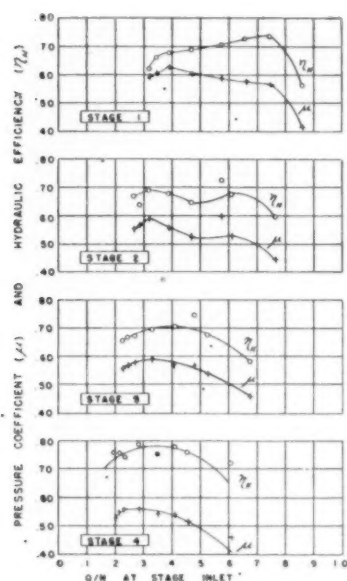


FIG. 5 HIGH-CAPACITY COMPRESSOR UNCOOLED-STAGE CHARACTERISTICS

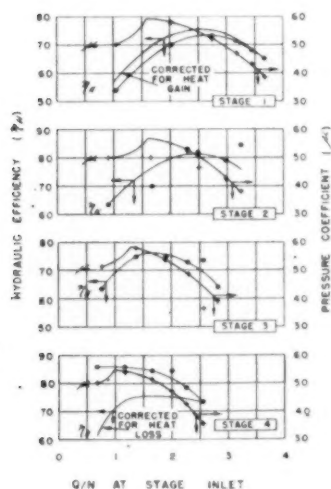


FIG. 6 LOW-CAPACITY COMPRESSOR UNCOOLED-STAGE CHARACTERISTICS

At part loads the Q/N -value for any stage differs from its value at rated load, and the ratio of the two multiplied by 100 is the "per cent Q/N " used as abscissa in Fig. 9.

It should be noted that Fig. 9 does not give maximum values for the type of compressor here described, and probably not average values. They are reasonable values, not uncommon in industrial practice, and were considered satisfactory for the purpose of this study.

The cooling-water flow was held constant for all loads. For the two cooled four-stage cases, a flow of 80 gpm parallel to the air flow was used for each case. For the eight-stage cases 80 gpm flowed through the first four diaphragms parallel to the air flow;

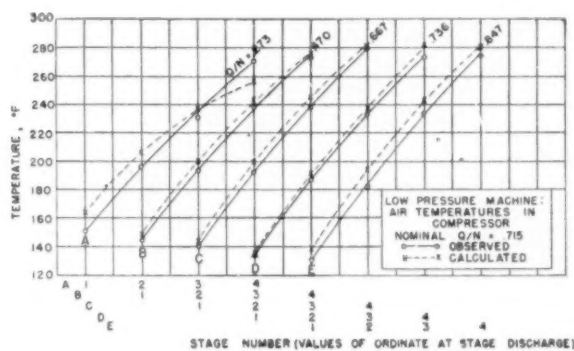


FIG. 7 HIGH-CAPACITY COMPRESSOR AIR-TEMPERATURE CORRELATIONS

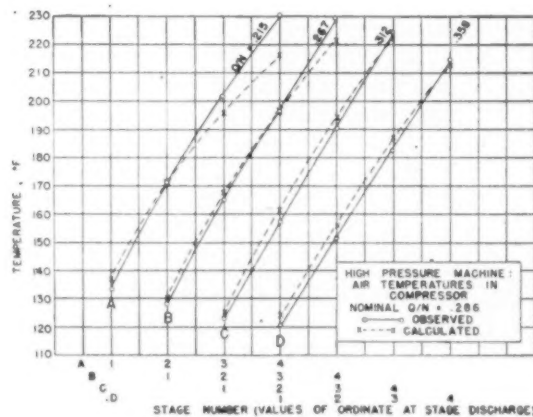


FIG. 8 LOW-CAPACITY COMPRESSOR AIR-TEMPERATURE CORRELATIONS

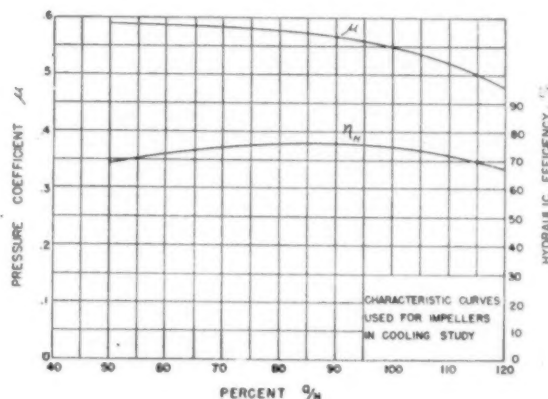


FIG. 9 CHARACTERISTIC CURVES OF COMPRESSOR STAGES IN COOLING STUDY

and another 80 gpm flowed through the last three diaphragms counter to the air flow.

The interstage operating temperatures calculated for the maximum and minimum inlet volumes are plotted in Fig. 10, and the over-all adiabatic and isothermal efficiencies and speeds for the complete range of inlet volumes in Fig. 11.

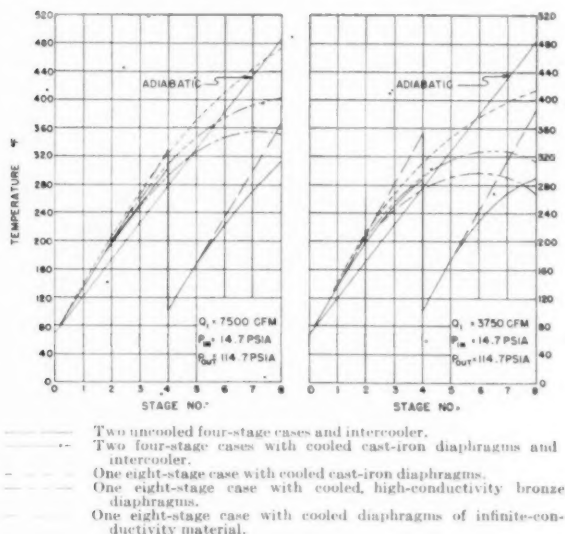


FIG. 10 OPERATING TEMPERATURE WITH VARIOUS COOLING ARRANGEMENTS

Three important conclusions may be noted from Fig. 10, as follows:

1 The air discharge temperature of the water-cooled machine with high-conductivity bronze diaphragms is approximately that of the uncooled machine with two casings and intercooling.

2 The air temperature in a diaphragm-cooled machine appears to reach a maximum and then decrease in further compression stages. A study of the heat-transfer mechanism will confirm the existence of this maximum. Furthermore, the maximum temperature with high-conductivity bronze is in the neighborhood of 400 F, which is well within the range of existing gas operating temperatures in centrifugal compressors. It also insures reasonable adiabatic efficiencies, even at high compression ratios.

3 At half capacity, the air temperature in the diaphragm-cooled machines is actually lower than at full load, while the temperature in intercooled machines has risen. Relatively better part-load performance of diaphragm-cooled machines, therefore, may be anticipated. This is a consequence of the high velocity maintained in the diffuser at light loads, which maintains high heat-transfer rates, and thus tends to counteract the effect of lower hydraulic efficiency.

Fig. 11 will verify the relatively better part-load performance of diaphragm-cooled machines. Other conclusions which may be drawn from Fig. 11 are as follows:

1 The diaphragm-cooled machine (using high-conductivity bronze) has an adiabatic efficiency about 3 percentage points lower than the standard arrangement of two uncooled cases with intercooler.

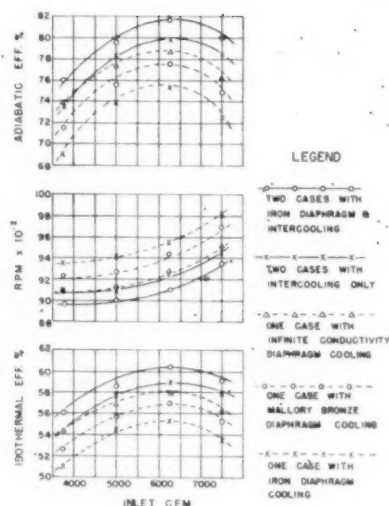


FIG. 11 EFFICIENCIES AND SPEEDS WITH VARIOUS COOLING ARRANGEMENTS

2 The use of high-conductivity bronze is probably justified, although not much can be gained by using a still higher-conductivity material. This conclusion is of course limited to the specific process application and to the geometry of the diaphragm.

3 If high efficiency is desired, diaphragm cooling will be a considerable aid to the intercooler in raising efficiency.

The relative desirability of each type of cooling is clearly a complex problem, involving such factors as space requirements, initial cost, maintenance, cost of power, availability and quality of cooling water, properties of the gas, and the gas process. From a study of a number of industrial applications it appears that diaphragm cooling should be considered seriously.

CONCLUSION

To many manufacturers and users, perhaps the most important conclusion to be reached from the findings of this investigation is that internal cooling makes possible low-cost, compact, multistage centrifugals for compression to relatively high pressures. In the past it has been general practice to supply air-compressor cases of only four or five stages, since more stages in a case would involve gas temperatures too high for economical compression. Thus the average 100-psig air compressor consists of two cases plus intercooler. Based on the study here presented, this arrangement can, with only a small loss in operating efficiency, be reduced to a compact single case containing all the stages without any external cooling.

ACKNOWLEDGMENT

The authors express their appreciation to Clark Brothers Company for permission to publish this paper.

The Hydrodynamic Lubrication of Cyclically Loaded Bearings

By E. M. SIMONS,¹ COLUMBUS, OHIO

The results of an experimental investigation of lubricating-film thicknesses in a journal bearing subjected to various loading conditions are presented and compared with theoretical predictions. General agreement with the theory has been found, except in the important cases of rotating and sinusoidally alternating loads applied at one half the frequency of shaft rotation. Here, instead of the theoretical eccentricity ratio of unity, finite film thicknesses have been observed. Free whirling in an unloaded bearing has been found to occur at slightly less than one half the shaft speed. High steady loads, high shaft speeds, and low lubricant viscosities have been found to inhibit journal whirl. The dependence of eccentricity ratio upon the extent of film rupture has been demonstrated for steady loads.

NOMENCLATURE

The following nomenclature is used in the paper:

- r = radius of journal or bearing
- w = axial width of bearing
- c = radial clearance, or difference between radii of bearing and journal
- e = distance between center of journal and center of bearing, called eccentricity
- $\eta = e/c$, called eccentricity ratio
- μ = absolute viscosity of lubricant
- N_j = average rotational frequency of journal in revolutions per unit time
- N = average frequency of rotation or oscillation of load, in revolutions or cycles per unit time
- N_e = mean frequency of rotation of journal center in its orbit, revolutions per unit time
- F = external load applied to bearing
- $P = \frac{F}{2rw}$ = load per unit projected area of bearing
- $S = \left(\frac{r}{c}\right)^2 \frac{\mu N_j}{P}$ = dimensionless parameter, often called Sommerfeld variable or Sommerfeld number
- Line of centers = line determined by center of journal and center of bearing
- Clearance circle = locus of journal center for $\eta = 1$; this is a circle whose radius is c

INTRODUCTION

Sleeve bearings subjected to rotating or fluctuating loads are commonly encountered in practice. Although a number of theoretical studies (1, 2, 3, 4, 5, 6, 7)² of the behavior of such

¹ Battelle Memorial Institute. Mem. ASME.

² Numbers in parentheses refer to the Bibliography at the end of the paper.

Contributed by the Special Research Committee on Lubrication and the Petroleum Division and presented at the Annual Meeting, New York, N. Y., November 27–December 2, 1949, of THE AMERICAN SOCIETY OF MECHANICAL ENGINEERS.

NOTE: Statements and opinions advanced in papers are to be understood as individual expressions of their authors and not those of the Society. Paper No. 49-A-41.

bearings have been published, little experimental work has been reported to prove or disprove the conclusions of these studies. Analytical treatments of even the simplest cases of cyclic loading require a number of questionable assumptions in order to reduce the mathematical complexity. Such studies indicate that there are certain speed and load conditions under which it is impossible for hydrodynamic lubrication to exist.

To check the validity of the mathematical investigations and to extend the knowledge of the effect of loading conditions on hydrodynamic lubrication, the National Advisory Committee for Aeronautics authorized an experimental study of the subject at Battelle Memorial Institute.

The plan of this investigation was to construct a testing machine in which constant or varying unidirectional, or constant rotating loads could be applied, singly or together, to a precision test bearing. The effect of the load diagram on hydrodynamic lubrication could be determined from the motions of the journal in the bearing.

Initially, simple loading conditions were studied, and then successively more complicated ones as the simpler conditions were understood. The loading conditions which are of interest are as follows:

- 1 Unloaded.
- 2 Constant unidirectional loads.
- 3 Constant rotating loads.
- 4 Unidirectional loads, varying in magnitude.
- 5 Combinations of the foregoing.

This study is by no means completed. Current work is aimed toward determining the sources of the discrepancies between theory and experiment and finding what modifications are required in the theory to bring the two into agreement.

APPARATUS

Spindle and Bearings. The testing machine designed and constructed for this study is presented in Fig. 1. The machine employs a ring-lapped 4-in.-diam spindle mounted in a support bearing (left), and a test bearing (right), both of which are precision-bored by a technique developed at Battelle (8).

The support bearing is a nonwhirling pivoted-pad type (9), consisting of four steel-backed babbit shoes, bored to provide 0.002-in. diametral clearance. The relatively large spindle length (28 in.), and the high stability of the support bearing make it possible to measure journal motions in the test bearing with a minimum contribution by motions excited in the support bearing.

The test bearing consists of a silver-plated steel shell pressed into the cast-iron housing and finish-bored in position. The diametral clearance is 0.004 in. The bearing has a 2-in. test length between two circumferential oil grooves and a 1/2-in. sealing section beyond each groove. Since the stiff pivoted-pad support bearing holds the shaft center line essentially fixed at one end of the shaft, the test bearing was bored tapered in order to keep the shaft surface approximately parallel to the test bearing along the line of nearest approach. The taper was made linear, the end farthest from the support bearing being 0.0003 in. larger in diameter.

Loading Systems. Loads are applied, by means of calibrated

compression springs, through two pressure-lubricated babbitt loading bearings, one for unidirectional loads and the other for rotating loads. The loading mechanisms are visible at the right of the test-bearing housing in Fig. 1. The small spring seen at the

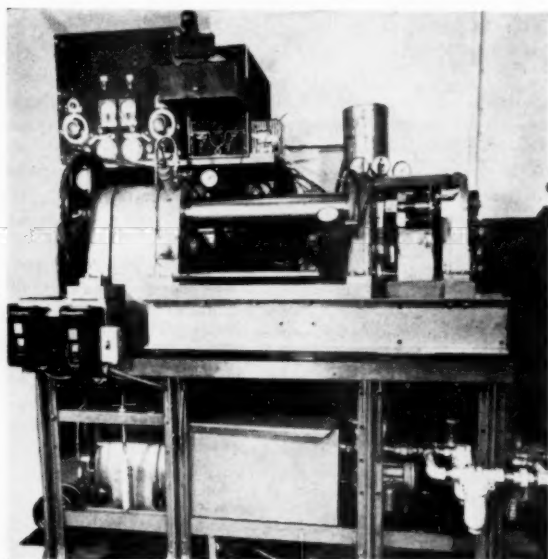


FIG. 1 MACHINE FOR TESTING HYDRODYNAMICALLY LUBRICATED SLEEVE BEARINGS UNDER VARIOUS LOADING CONDITIONS

top removes the weight of the shaft from the test bearing, enabling true no-load tests to be run. Sinusoidally alternating loads are applied by an adjustable cam which cyclically compresses the loading spring. Rotating loads are applied through a bell crank, one arm of which is attached to the loading bearing and the other to the loading spring. The bell crank pivots on a pin through the rotating-load jackshaft. The ranges of loads attainable are as follows:

Steady vertical load	0 to 500 lb ($62\frac{1}{2}$ psi)
Sinusoidally varying vertical load	± 0 to ± 250 lb ($\pm 31\frac{1}{4}$ psi)
Constant rotating load	0 to 500 lb ($62\frac{1}{2}$ psi)

Drive Arrangement. A 3-hp, 1740-rpm motor drives a jackshaft, through a Toledo Timer speed changer, with V-belts. The jackshaft is coupled to the independently mounted test spindle by a Lord bonded-rubber coupling to minimize the transmission of vibration. Spindle speeds of 25 to 2500 rpm can be obtained.

The camshaft is driven through change gears from the spindle, with the following ratios of spindle speed to camshaft speed available: 10:1, 6:1, 4:1, 2.80:1, 2.43:1, 2.11:1, 2.06:1, 2:1, 1.95:1, 1.89:1, 1.65:1, 1.43:1, 1:1, 0.67:1, 0.40:1. The flywheel on the camshaft tends to maintain uniform spindle speed during alternating-load tests.

The rotating-load jackshaft is driven through a gear-and-chain arrangement from the camshaft, and may be driven in either direction with respect to the spindle rotation.

Lubrication. All journal bearings are pressure-fed by a 12-gpm, 100-psi pump with by-pass pressure control. The two circumferential oil grooves in the test bearing have separate feed lines with independent control valves and gages. This arrangement provides good control of lubricant flow through the test bearing, while maintaining positive pressures at the ends. The lubricant is continuously filtered by micron filters, and is maintained near room temperature by cooling coils in the sump. An

oil reservoir is provided above the test bearing to permit operation with flood lubrication, if desired.

Radio-Frequency Micrometer. The instrument used to reveal the effectiveness of hydrodynamic lubrication is a specially built radio-frequency micrometer, the components of which are visible in Fig. 1. These consist of the receiver and power supply on the shelf at the upper left, the cathode-ray oscillograph to the right of the receiver, and the two probes, one of which is hidden from view, fastened to the left face of the test-bearing housing at an angle of 45 deg with the horizontal.

A description of the electrical circuits and the operation of the micrometer has been published (10). Briefly, minute displacements of the spindle are measured as a function of changes in electrical capacitance between the spindle and the micrometer probes. This capacitance is made part of the resonant circuit of a high-frequency radio oscillator, and variations cause sufficient changes in oscillator frequency to be readily measured by techniques developed for frequency-modulation broadcasting.

JOURNAL WHIRL

Types of Whirl. In general, the motion of a journal in a sleeve bearing is composed of two parts, i.e., a pure rotation about its own axis, and a combined rotation and translation of this axis with respect to the axis of the bearing. This latter motion is known as "whirling." Whirling may be self-excited, as in the case of oil whip, discussed by Newkirk, Taylor, and Grobel (11, 12), or it may be induced by external dynamic loads. It can be stable, with the journal center moving in a closed orbit with regular periodicity, or it may be transient.

In certain machines, such as high-speed turbine compressors, and steam turbines, serious vibration difficulties have been traced to journal whirl in sleeve-type bearings. This is particularly true where centrifugal forces resulting from journal eccentricity are large. Whirling could be troublesome in many other applications. For example, in machine-tool spindles, shaft whirl causes inaccuracies in machining and undesirable surface roughness. Whirling in sleeve-type propeller-shaft bearings, such as aircraft and marine shaft bearings, could easily contribute to fatigue-induced failures.

Frequency of No-Load Whirling. Robertson (2) has demonstrated mathematically that, neglecting oil-drag forces, the resultant oil-pressure force caused by journal rotation in an ideal bearing is at right angles to the line of centers and produces stable whirling at one half the rotational frequency of the journal. Swift (3) has shown analytically that an unloaded ideal bearing whirls in a circular orbit at any eccentricity whatsoever, with an angular velocity of exactly half of the journal speed.

To check these conclusions, precise measurements were made of the frequency of no-load transient whirling just after the journal had come up to speed from a standstill. It was necessary to use starting transients for these tests because sustained no-load whirling could not be obtained in the test bearing, regardless of the combination of speed, lubricant viscosity, and feed pressure employed. It was found that the natural whirl during no-load starting occurred at slightly less than one half the shaft speed, as seen in Table 1.

TABLE 1 FREQUENCY OF NO-LOAD SHAFT WHIRL, WITH SAE 10 OIL

Spindle speed, N_j , rpm	N_w/N_j , flood lubrication	N_w/N_j , 50 psig feed pressure
154	0.4980	0.4971
380	0.4968	...

These observations agree with the conclusions of Hagg (9), who states that one half the rotational frequency is the upper limit of whirling frequency for an unloaded ideal bearing, but that, in reality, this upper limit is reduced because of fluid friction and

bearing leakage." However, Taylor (13), in discussing Hagg's paper, points out that this was usually, but not always, the case in his own experiments, where frequency ratios as high as 0.6 were observed. In any case, it is difficult to see how fluid friction and side leakage alter the simple theory which demonstrates that an unloaded journal should whirl at one half the shaft speed.

Factors Influencing Shaft Whirl. Swift's work (3) would indicate that, in general, the journal center would not be stationary under no load, nor even under a constant load. On the contrary, the experiments have shown that in the absence of external periodic excitation, the ultimate equilibrium position of the journal center was always a stationary spot. For example, Fig. 2 shows that when the shaft was started from rest under no load, it moved in a spiral path which invariably ended in a steady position at the center of the bearing. However, the conditions of the particular test determined how quickly this equilibrium position was reached. Similarly, when the shaft was started from rest under a steady unidirectional load, the transient motion of the journal center never failed to die out at some fixed eccentricity ratio.

Obviously, the physical characteristics of the test setup were such that sufficient damping forces were present, over a wide range of operating variables, to prevent the journal center from moving continually in an orbit. Such damping forces are generally not considered in the theory. Experimentally, it was found that the most rapid damping of journal whirl was obtained with high steady loads, high shaft speeds, high lubricant feed pressures, or low-viscosity lubricants. The damping effect of higher lubri-

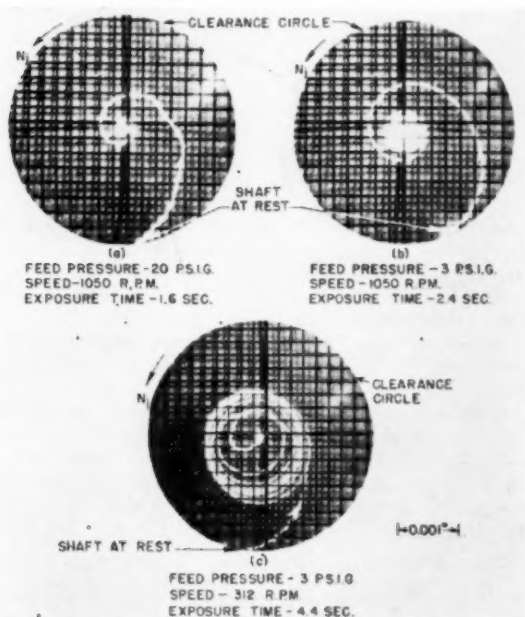


FIG. 2 TRANSIENT MOTIONS OF JOURNAL CENTER DURING NO-LOAD STARTING, USING KEROSENE AT 80 F AS LUBRICANT ($\mu = 1.52$ centipoises.)

cant pressure on whirling can be seen by comparing (a) and (b) in Fig. 2; the damping effect of high speed is strikingly shown by comparison of (b) with (c); while the steady influence of low viscosity is evident from the fact that it always took much longer to reach equilibrium when higher-viscosity lubricants were used at the same speed and lubricant feed pressure.

UNIDIRECTIONAL STEADY LOADS

Starting and Stopping Under Steady Load. Fig. 3 shows the motion of the spindle center when started from rest under an upward load of 50 psi. It is commonly thought that, upon starting from rest, the shaft crawls along the bearing wall in a direction opposite to that shown, until solid friction is reduced sufficiently by the formation of an oil film for hydrodynamic forces to take over. This effect was not observable in Fig. 3, indicating that a load-carrying oil film was generated much more rapidly than is usually assumed and that the rolling motion, if present at all, was too small to be detected in the photograph.

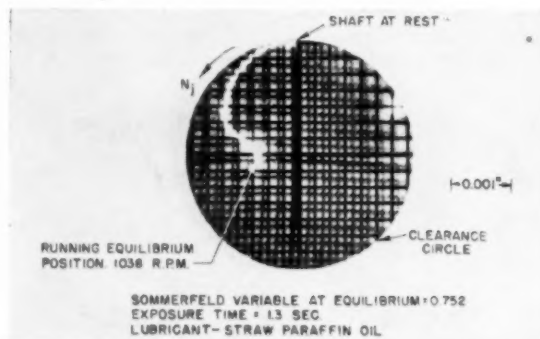


FIG. 3 TRANSIENT MOTION OF JOURNAL CENTER WHEN STARTED FROM REST UNDER 50-PSI UPWARD LOAD

Starting at the top of the clearance space, the shaft movement appeared to be first to the left and then downward as it came up to speed and the load-carrying capacity of the bearing increased. It then moved toward the center of the clearance circle, finally stabilizing at an eccentricity ratio of 0.27, which agrees with the theoretical predictions of Muskat and Morgan (14).

The absence of full spiraling motions like those obtained with no-load starting is apparent. Indeed, it has been found that free whirling of the journal is strongly damped by the application of an external load.

When the shaft was stopped under 50-psi upward load, its center retraced exactly the path in Fig. 3, moving to the left and then upward as the rotational motion slowed down and the load-carrying capacity of the oil film decreased.

Oil-Film Tension. In a flooded full journal bearing, the theoretical pressure distribution over the semicylinder on one side of the line of centers is the exact negative reflection of that on the semicylinder on the other side of the line of centers. This condition implies that the integrated pressure-area product in the film can have no component along the line of centers, so that the displacement of the journal in the bearing must be normal to the direction of load application. It also indicates that when a flooded full journal bearing is operated with an unbroken oil film, one half the external load is supported by hydrodynamic pressures above atmospheric on the loaded side, and the other half by equal pressures below atmospheric on the unloaded side. For example, if the external load is 10 psi, the average negative pressure on the unloaded side will be 5 psi, and the peak negative pressure may be in the vicinity of 3 times the average, say, 15 psi.

If this peak negative pressure exceeded 1 atm, the oil film would rupture in the region of theoretical pressures below absolute zero, unless the film were capable of carrying a tensile load. In the latter case, the rupture would occur when the negative pressures exceeded the tensile strength of the oil film. Any such break in the film will require that the journal move in the direction of load-

ing and generally result in higher eccentricities than those predicted by hydrodynamic theory for ideal bearings. This implies that a flooded bearing would operate with a continuous film only when the external loads were very low. However, the application of feed pressures in the circumferential oil grooves of the test bearing makes it possible to support higher loads without film rupture, because the feed pressure helps to prevent a tensile stress in the oil film.

Studies of the behavior of a unidirectionally loaded bearing were conducted by running the bearing at no load, and photographing the spindle motions as an upward load was applied gradually enough to maintain equilibrium at all times. Some views taken in this way are presented in Fig. 4. In (a), the shaft moved horizontally (normal to the direction of loading), in accordance with the theory, until the external load reached about 20 psi. At this

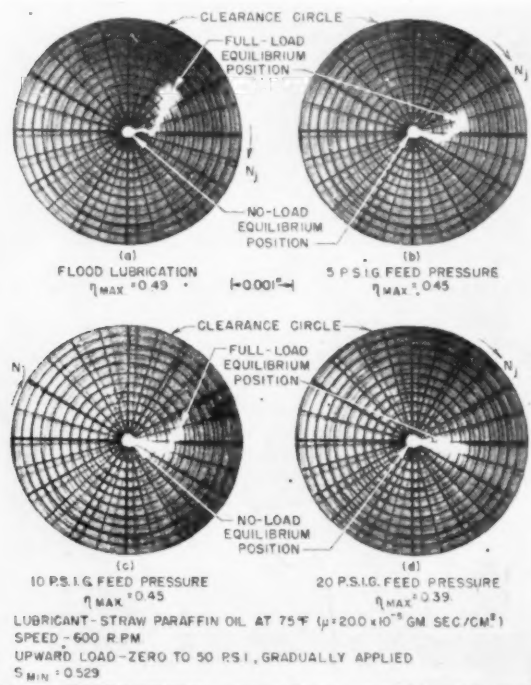


FIG. 4 EFFECT OF LUBRICANT FEED PRESSURE ON SHAFT POSITION DURING GRADUAL LOAD APPLICATION

point the negative pressures became too great, the oil film ruptured, and the shaft moved upward, in the direction of the load. As the feed pressures were increased [(b) and (c)], the rupture occurred at higher and higher loads, until, at a feed pressure of about 15 psig, the film remained apparently intact under the total load of 50 psi [cf. Fig. 4(d)], and no upward motion of the shaft took place. The rupture occurs suddenly in some cases, as evidenced by a sharp break from horizontal to upward motion, such as in Fig. 4(a) and (c).

Rough calculations of the magnitude of the negative film pressures indicate that the oil film is withstanding a small tensile stress, from a few to 50 psi. It is known that liquids can withstand tension under some circumstances and conditions in a bearing appear to be favorable.

Effect of Film Rupture on Eccentricity. Since the circumferential pressure distribution in a full journal bearing has rather sharp positive and negative peaks, it would be expected that, with

a gradual increase in load, incipient film rupture would occur in a highly localized region of peak negative pressure, spreading over a larger and larger fraction of the bearing area as the load was further increased. The dependence of eccentricity ratio upon the extent of such film rupture is demonstrated by the experimental results shown in Fig. 5 which is a plot of eccentricity ratio as a function of Sommerfeld number for steady, unidirectional loading.

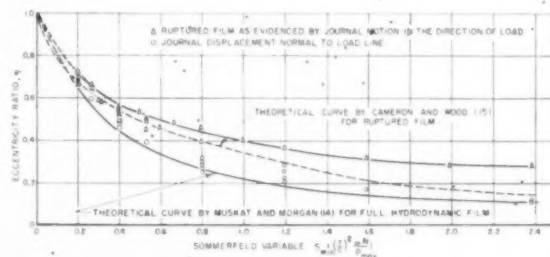


FIG. 5 OBSERVED AND THEORETICAL ECCENTRICITIES OF TEST BEARING UNDER STEADY UNIDIRECTIONAL LOADING

The lowest circled points agree, within experimental accuracy, with the theoretical curve from Muskat and Morgan (14), based upon a continuous oil film. The upper curve, drawn through the points showing the greatest departure from the curve of Muskat and Morgan, represents the cases where the oil feed pressure was low (flood lubrication), and film rupture had occurred to the greatest extent. Between these two curves are eccentricities which result from various degrees of film rupture, the points lying closest to the lower curve representing very small localized areas of rupture, and those lying near the upper curve representing rupture over more extensive areas. This range of eccentricity ratios was produced, at a given Sommerfeld number, by varying the oil feed pressure in the circumferential grooves, as illustrated in Fig. 4.

The curve of Cameron and Wood (15) in Fig. 5 is based upon numerically calculated results for what is essentially a ruptured film. The film is assumed to start at the large film-thickness end of the line of centers and extend to a point beyond the minimum film-thickness end where both the pressure and pressure gradient drop simultaneously to zero. The discrepancy between the curve of Cameron and Wood and the experimental curve for the ruptured film is very likely the result of this stringent restriction upon the extent of rupture.

Most theoretical treatments of journal bearings assume continuity of the oil film around the bearing arc. Fig. 5 demonstrates that these theories cannot be used to predict the behavior of bearings in practice unless the application involves high enough lubricant feed pressures or low enough external loads to preclude rupture at any point in the oil film.

CONSTANT LOAD ROTATING AT CONSTANT SPEED

Fig. 6 shows the eccentricities resulting from the application of a 7.8-psi load rotating at various frequencies. For all ratios of N_p/N_f greater than about 0.25, the orbits were circular, and the eccentricity ratio was taken as the ratio of the radius of the orbit to the radius of the clearance circle. However, when N_p/N_f was 0.25 or less, the orbits were stable and closed in one cycle of load application, but they were not circular. In such cases, the maximum value of eccentricity ratio was plotted in Fig. 6. This explains why the points at $N_p/N_f = 0.25$ and 0.167 fall above the curve drawn.

$N_p/N_f = 0$ represents a constant unidirectional load, and the measured value of η here agrees with Muskat's prediction (14) for a flooded full journal bearing under these conditions. As N_p/N_f is

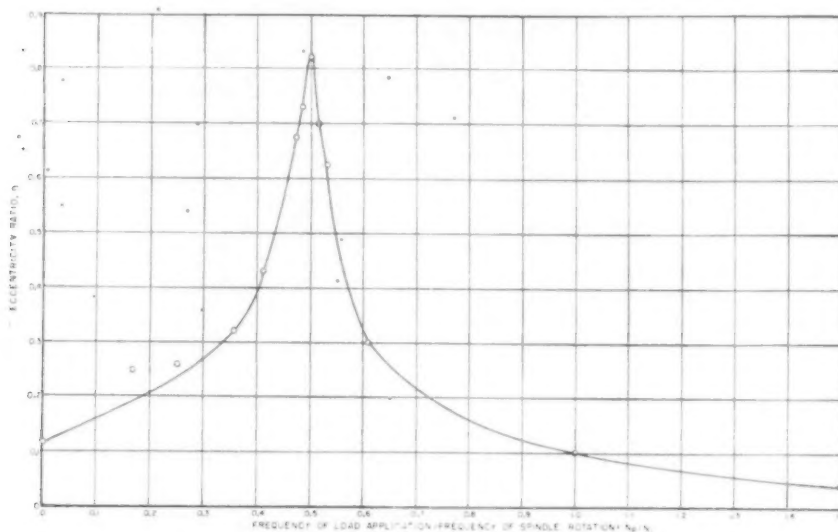


Fig. 6 Effect of Relative Frequency of Load Application on Eccentricity Ratio for Constant Load of 7.8 Psi Rotating at Constant Speed
($S = 2.38$; lubricant, kerosene.)

increased, η increases also, peaking sharply at $N_p/N_s = 0.5$. Further increase in N_p/N_s is accompanied by a drop in η , which has about the same value at $N_p/N_s = 1.0$ as at $N_p/N_s = 0$. This agrees with the findings of Burwell (17) and Underwood and Stone (16), viz., that a bearing subjected to a constant rotating load applied at the frequency of shaft rotation has a load capacity (as defined by eccentricity) numerically the same as if the load were stationary. Frequency ratios greater than 1.0 yield eccentricities lower than those obtained by constant unidirectional loading.

Robertson (2), Swift (3), Burwell (7), and others have demonstrated mathematically that when the load is rotating at one half the shaft speed, the bearing is unable to carry any load with an eccentricity ratio other than unity. Before this conclusion could be drawn, however, the following assumptions had to be made:

1. No end leakage.
2. Continuous oil film around the bearing.
3. No local changes in viscosity.
4. The oil has no inertia.
5. Oil pressure is constant along a radius.
6. The orbit is circular and concentric with the clearance circle ($d\eta/dt = 0$).
7. The angle between the line of centers and the load direction is constant. If so, its value is 90 deg.

In all the experiments run with $N_p/N_s = 0.5$, it was found that the eccentricity ratio was less than unity, decreasing slowly with decreasing load and decreasing rapidly with increasing speed. These effects are apparent in Fig. 7. Nevertheless, it is true that the eccentricity rises to a sharp peak when $N_p/N_s = 0.5$, Fig. 6, and that it is best to avoid such conditions in practice whenever possible. A knowledge of the factors which are favorable to the existence of an oil film under these conditions could provide valuable aid in the design of sleeve bearings for applications where cyclic load components at or near one half the frequency of shaft rotation are unavoidable.

One possible explanation for the presence of a load-carrying oil film, in violation of theoretical predictions when $N_p/N_s = 0.5$, lies in the discarding of higher-order terms in the development of the

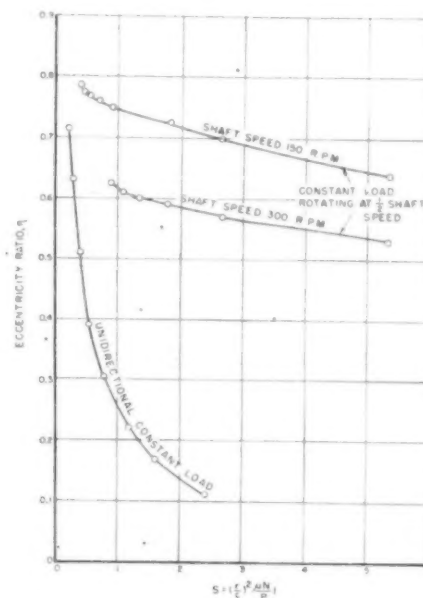


Fig. 7 Eccentricity Measurements for Load Rotating at $1/2$ Shaft Speed
(Flood lubrication with straw paraffin oil.)

theory (2). However, when this was investigated by substituting test conditions into the discarded terms, it was found that these terms were truly negligible, causing theoretical changes in eccentricity which were considerably smaller than the error in experimental measurements.

Another likely source of the discrepancy was the possibility of a dynamic stiffening effect in the pivoted-pad support bearing, which might prevent the journal from attaining the maximum eccentricity in the test bearing. The stiffening effect would have

to stem from dynamic forces, since it was possible to maintain contact between journal and bearing while rotating the load a full revolution slowly by hand. To ascertain the role of support-bearing hydrodynamic forces in stiffening, test-bearing motions were studied first with SAE 10 oil in the support bearing, and then with kerosene in the support bearing, while maintaining constant conditions at the test bearing. The tests showed that the viscosity of the lubricant in the support bearing had no effect on the eccentricity in the test bearing. This and other considerations proved that support-bearing stiffness did not limit journal motions in the test bearing.

A third explanation proposed for the nonunit eccentricity ratios obtained with $N_p/N_j = 0.5$ was that gyroscopic forces might oppose the hydrodynamic effects. However, simple computations showed that, because of the low journal speeds used in the tests, gyroscopic forces were much too small to have any noticeable effect on eccentricity.

Burwell has suggested (17) that thermal expansion of the oil in the minimum-film-thickness region might give rise to pressure development. He points out that the local rate of heat production, and hence of local temperature rise, will vary along the film inversely as the film thickness, being greatest at the point of minimum film thickness. Hence cooler oil will be dragged into the region of minimum film thickness, and the subsequently heated oil will be carried away. This plausible explanation has not been investigated as yet.

In an effort to obtain some clue from the appearance of the test bearing, the shaft was removed and the bearing studied. Burnish marks near both ends of the bearing gave strong indication that the shaft and bearing axes had somehow become misaligned. Very careful measurements revealed the fact that the axes diverged by 0.0006 in. in the 3-in. housing length. This misalignment was reduced to 0.00015 in. by straining the machine bed with short lengths of arc weld, which contracted the parent metal, causing the housings to move in the proper directions.

Table 2 shows that this improvement in alignment resulted in a closer approach to the theoretical eccentricity ratio of unity when $N_p/N_j = 0.5$, indicating that misalignment is probably a contributing factor in the discrepancy between theory and experiments.

TABLE 2 EFFECT OF BEARING MISALIGNMENT ON ECCENTRICITY, WITH ROTATING LOAD AT ONE-HALF SHAFT SPEED

Shaft speed, rpm	Eccentricity ratios—	
	0.0006 in. misalignment	0.00015 in. misalignment
150	0.72	0.83
300	0.61	0.66

NOTE: Rotating load, 12.5 psi at one-half shaft speed; SAE 10 oil, flood lubrication.

That misalignment might prevent a zero oil-film thickness when $N_p/N_j = 0.5$ can be seen from the qualitative discussion which follows. Assuming that center A, Fig. 8, whirls in a circular orbit, B and C are forced to rotate in circular orbits also (since one end of the shaft is essentially fixed), but the centers of the latter orbits will be displaced, respectively, below and above the center line of the bearing. This nonconcentric whirling of the shaft at every section except A will produce varying hydrodynamic forces F_1 and F_2 , equivalent to external loads superimposed on the applied rotating load. As will be discussed in a later section of this paper, such combined loads may reduce the eccentricity below that which would result from the rotating load alone, applied at one half the shaft speed. Furthermore, an increase in shaft speed would increase the hydrodynamic forces F_1 and F_2 and further reduce the eccentricity. This agrees with the results in Fig. 7 and in Table 2. Additional experimental effort along these lines is in progress.

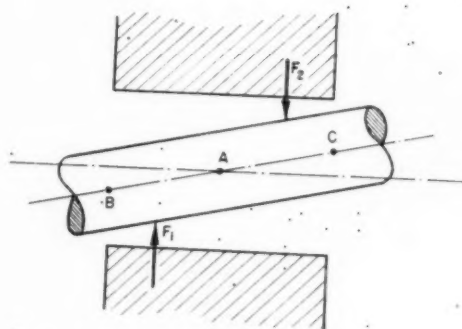


FIG. 8 EFFECT OF MISALIGNMENT ON SHAFT WHIRL

SINUSOIDAL ALTERNATING LOAD IN VERTICAL DIRECTION

Burwell (7) has extended the hydrodynamic theory of lubrication to the general case of a periodic load and has applied his findings to the solution of the problem of a sinusoidal reciprocating load with a journal rotating at constant speed. Since no analytical solution to his differential equations could be found, he carried out the solution by a step-by-step numerical integration, using trial-and-error methods to obtain closed-path solutions in one cycle of load application. Dick (4) studied the case of simple sinusoidal loading by assuming that the journal-center path was an ellipse and that the hydrodynamic load along one axis of the ellipse was zero. He then compared the hydrodynamic load along the other axis with a sinusoidal load.

Burwell's calculations produced orbits which resemble ellipses for sinusoidal alternating loads. He and Dick both found that the long axis was in the direction of loading when N_p/N_j was greater than 0.5, and that the long axis was perpendicular to the load line when N_p/N_j was less than 0.5. At $N_p/N_j = 0.5$, the orbit was the clearance circle. These shapes agree rather well, in general, with experimental findings, as may be seen from the examples in Fig. 9.

Furthermore, as Burwell pointed out, the paths become more complicated for values of N_p/N_j less than about 0.25. His orbit for $N_p/N_j = 0.25$ did not exhibit the extra loop shown in Fig. 10 (a), but this discrepancy can perhaps be attributed to the wide divergence between his value of S_{min} (0.0) and that used in the experiment (2.38). Fig. 10 (b) shows an interesting symmetric double-loop pattern, obtained with $N_p/N_j = 2/3$. The complicated gyrations of the shaft center before finally settling down to an equilibrium orbit are illustrated in Fig. 10 (c), which was photographed $1\frac{1}{2}$ min after the shaft had been started from rest. It took an additional $1\frac{1}{2}$ min to reach an equilibrium orbit similar in shape to Fig. 9 (a).

Most of the frequency ratios tested produced equilibrium orbits which closed in 1 cycle of load application. The exception to this was $N_p/N_j = 0.7$, in which case the path was an oscillating spiral between a larger and a smaller orbit. The time required to reach equilibrium, the complex transient patterns traced by the shaft center before equilibrium was reached, and the character of the ultimate equilibrium orbit indicate that certain N_p/N_j ratios produce equilibrium orbits which close in 1 cycle of loading only as a result of external damping conditions, or the fact that particular initial conditions existed. The behavior is analogous to the forced vibrations of a resonant system, in which the equations of motion contain terms dependent upon the initial conditions, and upon the resonant frequency. These terms can be neglected only after damping has eliminated the effect of initial conditions. There is a great deal of room for further work in correlating the theory with experiments.

Since the orbits were not circular, except when $N_p/N_j = 0.5$, it

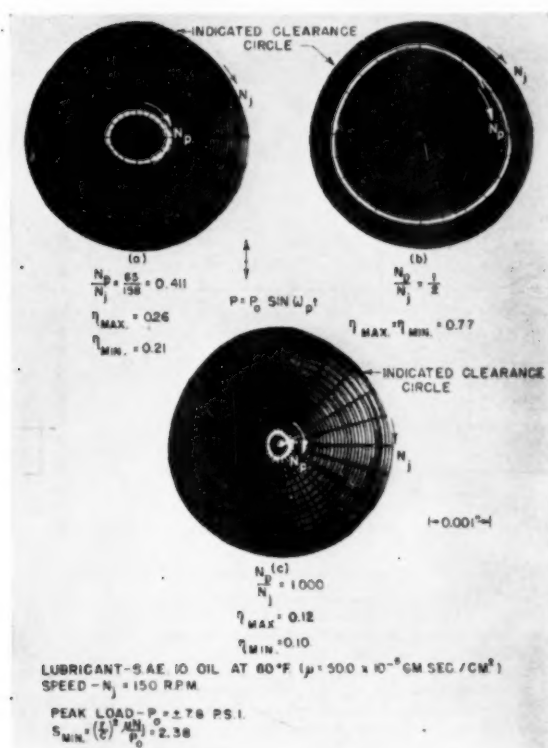


FIG. 9 JOURNAL CENTER ORBITS UNDER SINUSOIDAL ALTERNATING LOAD

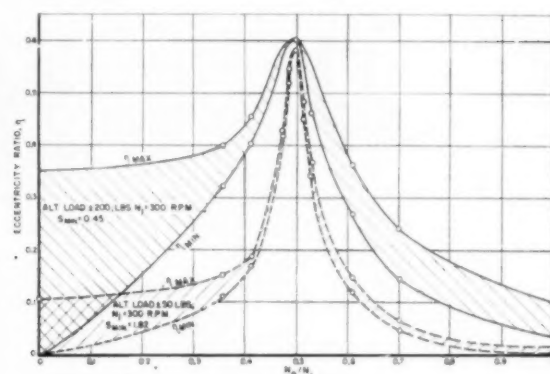
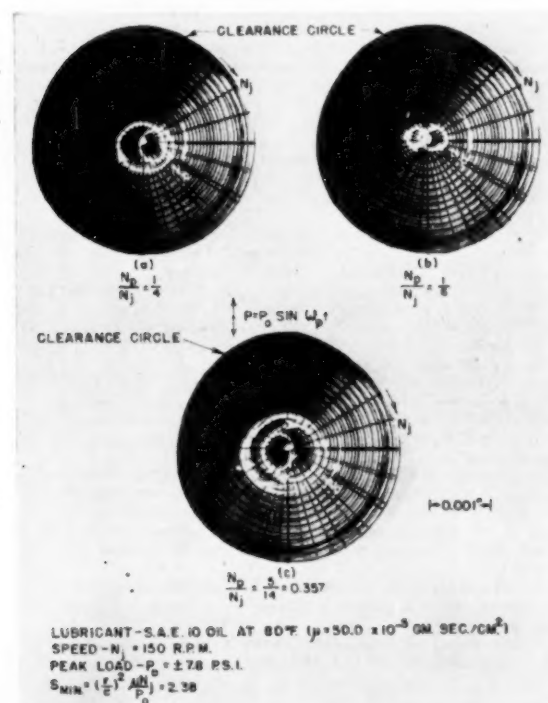


FIG. 11 SHAFT MOTIONS IN JOURNAL BEARING WITH SINUSOIDAL LOADS AT VARIOUS FREQUENCIES

was possible to measure a maximum and a minimum eccentricity. Plots of these values for two different values of S_{min} are shown in Fig. 11. When the load was applied at very low frequency ($N_p/N_j = 0$), the eccentricity varied from zero, when the load was zero, to a maximum which corresponded to the peak load applied continuously. As N_p/N_j was increased, both η_{max} and η_{min} increased, η_{min} increasing faster than η_{max} until N_p/N_j reached 0.5, at which point $\eta_{min} = \eta_{max}$, and the orbit was circular. Further increase in N_p/N_j resulted in a rapid drop in eccentricity, with η_{max} falling considerably below that for the constant unidirectional load, at values of N_p/N_j above about 0.65. These observations correspond generally to the relative load-capacity curves presented by Burwell (7) and Underwood and Stone (16).

The outstanding discrepancy between the results of the experiments and the theoretical work was the fact that, just as with a rotating load, the observed eccentricity ratios were not unity for sinusoidal loading at $N_p/N_j = 0.5$. A careful study was made of the effects of the various operating variables on eccentricity under this condition of loading. It was soon discovered that, above a certain very light load, the magnitude of the load had little influence on eccentricity. For example, as may be seen from Fig. 11, increasing the load by a factor of 4 raised the eccentricity ratio from 0.58 to only 0.60. The effects of speed and viscosity are apparent in Fig. 12 which shows that varying the viscosity in a given test seemed to have a small effect on the eccentricity when $N_p/N_j = 0.5$, while changing the speed had a pronounced effect. Under these conditions of loading, the Sommerfeld variable, which is a parameter of true hydrodynamic lubrication, provided no correlation between eccentricity and the operating variables.

The origin of load-supporting pressures in the lubricant film, with $N_p/N_j = 0.5$, is not known. It seems not unlikely that the explanation is the same for the case of the sinusoidal load as for a rotating load. Efforts to solve this problem are continuing.

COMBINED ROTATING AND ALTERNATING LOADS

Tests were run with a combination of rotating and alternating loads. The rotating load was applied at the frequency of shaft rotation to simulate centrifugal loading. The sinusoidal alternating load was applied at one half the spindle speed to represent, for example, gas-pressure loading in a four-stroke-cycle engine crankshaft bearing.

Fig. 13 shows the effect of increasing the rotating load while holding the alternating load constant. It is highly significant

FIG. 10 (left) JOURNAL CENTER PATHS UNDER SINUSOIDAL ALTERNATING LOAD

Discussion

J. T. BURWELL.³ The author is to be congratulated on having developed a most ingenious method for observing the instantaneous position of a journal inside a bearing and of using the method to study the performance of the journal bearing under various loading conditions. This information has been badly needed in order to provide a check on the theory of hydrodynamic lubrication upon which we are beginning to base design calculations for dynamically loaded bearings. It is interesting that a good many of the results of the simple theory such as the position of the journal under loads, its path under alternating loads, and oil-film rupture are now confirmed experimentally by this work. This gives us confidence that the theory can be used safely for the design of bearings subjected to varying loads. In this connection it is even more fortunate that the deviations from the simple theory that are found in the present work appear to be on the conservative side.

There appear to be five main discrepancies between the present experimental results and the predictions of the simple theory, as follows:

- 1 The shaft does not whirl in this apparatus under no-load conditions.
- 2 The transient whirl upon starting has a frequency slightly less than one half the shaft speed.
- 3 The shaft does not move in a periodic orbit under a constant unidirectional load.
- 4 The eccentricity ratio does not become unity under a constant load rotating at one half the shaft speed.
- 5 The eccentricity ratio does not become unity under a sinusoidal alternating load having a frequency of one half the shaft speed.

It is possible that all these discrepancies can be ascribed to a single cause. For instance, regardless of the exact nature of the cause, all five discrepancies are consistent with the single conclusion that a journal center rotation N_c equal to one half the shaft speed N_j is not for this bearing a natural or critical frequency. However, the explanation of this conclusion is not at all obvious.

It has been suggested that the absence of the periodic motions under no-load and under constant-load conditions must be due to damping forces not taken into account in the theory. For this reason the oil-drag forces on the whirling shaft have been re-examined to see whether they could be the source of the damping. It is found that their resultants parallel to and perpendicular to the line of centers are of the order of c/r times the corresponding resultants of the film pressures. This makes them equal to about 0.1 per cent of the film-pressure forces in the present experiments. More importantly it is difficult to understand how any forces of this nature can damp out these motions, since energy is being continually fed in by the rotating shaft. Rather, it would appear that positive forces directed radially inward are required to drive the journal center to the center of the clearance circle under no-load conditions as shown in Fig. 2 of the paper. The source of such radial forces, in the absence of oil-film rupture, is difficult to see unless it is a stiffness caused by the support bearing.

The oil-drag forces were found to give rise to a whirling speed very slightly less than one half the shaft speed, but unfortunately not in good agreement with the speed actually found. The expression for the ratio of the two speeds is

$$\frac{N_c}{N_j} = \frac{1}{2} - \frac{1}{12} \cdot \frac{c}{r} \cdot \frac{2 + \eta^2}{\eta^2} (1 - (1 - \eta^2)^{1/2}) \dots [1]$$

³ Massachusetts Institute of Technology, Cambridge, Mass.

where the symbols are as defined in the original paper. For a value of η near unity this becomes approximately

$$\frac{N_c}{N_j} \approx \frac{1}{2} - \frac{1}{4} \cdot \frac{c}{r} \dots [2]$$

With the dimensions of the present apparatus, this would lead to a value of N_c/N_j of approximately 0.4998 instead of 0.4980, as actually observed. The difference from $1/2$ becomes even less as η decreases. Furthermore, Equation [1], herewith, predicts no dependence of this ratio on shaft speed as shown by the data in Table 1 of the paper.

Since many lightly loaded shafts do show oil whip in practice, the conclusion of its absence in the present case cannot be entirely general. Possibly it is due to the absence of dynamic unbalance forces owing to the simple structure and the great accuracy with which the present shaft was made.

Turning to the last two disagreements with the theory, it seems most likely, as the author suggests, that the explanation of the two is the same. This is because the sinusoidal loading was found to induce a circular orbit having half the shaft speed, which is just the same orbit as that induced by the constant load rotating at this speed. The orbit, rather than the applied load, directly determines the pressure distribution in the oil film.

The writer has suggested that the explanation for these two discrepancies is probably to be found in the thermal expansion of the oil which was first suggested by Fogg⁴ to explain the load capacity observed in certain high-speed thrust bearings. This seems to be borne out by the strong dependence of the discrepancy on speed, since one would expect the amount of expansion which determines the load capacity to be dependent on the power consumption which is proportional to μN^2 rather than to μN for a purely hydrodynamic effect.

Furthermore, the resultant oil-film pressure due to thermal expansion will probably have a component parallel to the line of centers which can drive the journal toward the center of the clearance space. As discussed previously, this seems to be necessary to suppress its periodic motions under constant and no-load conditions.

It might be interesting to see whether there is some interrelation between the five discrepancies. For instance, the results in Table I of the paper indicate that while the journal will not whirl indefinitely, yet it does prefer a frequency slightly less than one half the shaft speed. This suggests that under a constant load rotating at one of the speed ratios given in Table 1, the eccentricity ratio might approach unity more closely than it does for the load rotating at exactly one half the shaft speed. Has the author tried this?

Nevertheless, in spite of the absence of any very satisfactory explanation the absence of the whirling and periodic motions under constant or no load is reassuring when using the theory to calculate the journal center path under sinusoidal and more complicated forms of loading such as occur on actual connecting-rod bearings. The solutions were obtained on the assumption⁵ that all transients arising from such motions would be absent and that only a steady-state motion, having the frequency of the applied load, would exist. The general agreement of the shape of the orbits shown in Figs. 9 and 10 of the paper, for a sinusoidal alternating load with those calculated under this assumption,⁶ give us confidence that calculations of more complicated types of loading on this assumption will be correct. In the absence of this assump-

⁴ "Film Lubrication of Parallel Thrust Surfaces," by A. Fogg, *Engineering*, vol. 159, 1945, p. 138.

⁵ Reference (7), author's bibliography.

⁶ *Ibid.*, Fig. 6.

tion the calculating problem becomes so complicated as to be well nigh impossible of solution.

E. F. MACKS.⁷ In 1946 the paper by Underwood and Stone⁸ verified experimentally the theory that a sleeve bearing would fail if subjected to a rotating load at one-half shaft speed, and to quote from the paper:

"It should be especially noted that the critical speed for zero load capacity is reached when the journal is twice the load speed. This proportion was proved for all journal speeds."

Now, however, another apparently very carefully prepared experimental paper appears which presents results some of which differ significantly from those of Underwood and Stone.

There are many very valuable experimental contributions given in this paper, but we feel the main thing in this report is the fact that an attitude of one was not obtained either with constant rotating load or sinusoidally alternating load at the theoretically critical speed; and the dependence of the attitude particularly upon speed but also upon viscosity and load. Since there is such a wide difference from theory, this work indicates either (a) that the theory must be revised to include terms which have been previously considered negligible or which have been entirely omitted, or (b) to find out what unique feature of the test machine contributes to the development of a hydrodynamic film in the test bearing.

Regarding possible changes in theory, the author's suggestion of thermal expansion may be a partial answer, but it should be recalled that in the equivalent system, that is, with respect to a fixed point on the load vector, there is no net flow circumferentially in the region of minimum film thickness, and therefore for any hot oil to be continually replaced, it must depend upon adherence to the moving members and upon side leakage. Also, inasmuch as the flow varies as the cube of the clearance, there will be little end flow in the region of the minimum film thickness.

Regarding the test machine, misalignment has been shown to be important, but we do not feel that it is the whole story. There may be something either in the test bearing or inherent in the test machine which prevents an attitude of one from being obtained under the critical conditions. We would like to ask the author if there is any possibility that the loading system—say, the loading springs involved or the manner in which the load is applied, or anything else—might contribute to a vibration conducive to the generation of a squeeze film or an unknown superimposed load on the test bearing. Also, any movement of the test-bearing housing is extremely critical, since the micrometer probes are attached to the housing. Is this a possibility? May we also ask if the author has found during operation that changes of speed or load affect the alignment and to what extent; and if he feels that such alignment changes may invalidate any of the results obtained or reported before it was discovered how sensitive the machine was to misalignment?

We feel that it would be well for the author to explain the care which was required to obtain a true clearance circle and the effect of a film on either the bearing or journal during this calibration, and also to mention how the oil-film temperature was determined to obtain the value of viscosity used in the calculation of the Sommerfeld number.

S. M. MARCO.⁹ Bearing theory has advanced through many stages from the time of Petroff and Osborne Reynolds to the

present. Although many papers have been written concerning both theoretical and experimental investigations of bearings, nevertheless the agreement between theory and experiment remains qualitative rather than quantitative. The true purpose of both theoretical and experimental investigations of bearings is to supply information to the designer so that he may arrive at bearing designs which are better. In general the situation at present is that the designer of bearings cannot rely too heavily on theory or experiment. He is forced to design bearings largely by trial and error, relying on his own experience and that of other designers to guide him in his selection of the various factors which affect the operation of a real bearing. The plain fact is that real bearings do not act in the way which theory predicts except in a qualitative sense. It is for this reason that those of us who are interested in the design field welcome all investigations which will lead eventually to a better understanding of the factors which affect the operation of a real bearing.

It seems to the writer that the investigation reported in this paper could well be the beginning of a long-time investigation which would lead eventually to an understanding of the relative importance of deviations of actual-bearing conditions from those which we are forced to assume in theoretical bearings. Such things as the effect of shaft deflection, the effect of restraints caused by adjacent bearings, the effect of complex periodic loading, and numerous other similar factors must be investigated if the designer is to be supplied with reliable quantitative information.

That the investigation reported by the author shows some of the discrepancies between bearing theory and experimental bearings is brought out in a number of instances. For example, this work shows that for the conditions of this test bearing, whirl in the absence of a periodic disturbing force is always damped out, whereas theory predicts that a steady-state whirl should be produced. Undoubtedly, this is due to the neglect in the theory of such damping forces as oil drag, shaft stiffness, constraints imposed by adjacent bearings, and the like. In this connection, would the author explain some of the factors which might be inferred from the paper but which are not explicitly stated? For example, in Fig. 2 does the exposure time indicate accurately the total length of time for damping to reduce the amplitude of whirl to zero? It would be of interest to know if the frequency of whirl is constant for a given set of conditions, i.e., does the frequency of whirl remain constant while the amplitude is decreasing? If it is, it would indicate a common type of damped vibration—a conclusion that might give a clue as to the type of damping involved. Apparently higher speed reduces the time required for damping but does it reduce the number of cycles required to bring the amplitude to zero? This is not quite clear from Fig. 2(b) and (c). The effects of load, lubricant viscosity, and feed pressure on damping are somewhat obscure. Also, it would be of interest to have the author explain the method of measuring the speed of whirl with the precision indicated in his Table 1.

In describing the unidirectional steady-load tests, the author states that upon starting from rest, this journal did not start to roll along the bearing wall as is commonly assumed. This is the action which is usually assumed when the journal has squeezed out sufficient oil so that dry friction exists. This paper does not indicate how fully this matter was explored. Fig. 3 of the paper indicates a bearing pressure of 50 psi which is a fairly low pressure. It is possible that because of the low pressures involved, the oil was never squeezed out completely, and therefore no dry friction resulted. Would heavier loads have resulted in the journal rolling along the bearing wall until a film had been built up? Since this is an important factor in bearing wear, this matter should be investigated thoroughly.

The work on oil-film rupture, as affected by feed pressure, is of

⁷ Flight Propulsion Research Laboratory, NACA, Cleveland Airport, Cleveland, Ohio. Jun. ASME.

⁸ Reference (16), Author's bibliography.

⁹ Professor of Mechanical Engineering, The Ohio State University, Columbus, Ohio. Jun. ASME.

great interest. The results of this work would indicate that most practical bearings, with the exception of a very few using extremely high lubricant feed pressures, operate with a partial film only. Since the theory of film lubrication predicts friction coefficient and load-carrying capacity on an assumed continuous film, it would appear again that the theoretical bearing is so different from the practical bearing that predictions based upon theory may well be completely unsafe for design purposes.

The investigation of rotating and sinusoidally varying loads brings out some interesting facts. Figs. 6 and 11 of the paper show that while a ratio of load frequency to shaft frequency of one half is serious, it does not result in a complete breakdown of the supporting film. Fig. 13 shows that a rotating load at shaft frequency, superimposed on a sinusoidal load at one-half shaft frequency, results in a lower eccentricity than for the case of the alternating load alone. The author states that this may be the reason that four-stroke-cycle engine crankshaft bearings can operate with complete film lubrication. It would take considerably more investigation with higher specific loads to prove this.

However, the writer feels that the fact that a thin film exists with sinusoidal load, i.e., the eccentricity ratio is not unity, is the reason that such bearings operate. The work of Needs¹⁰ would indicate that for a given bearing geometry, a larger eccentricity will support greater loads than will smaller eccentricities for the same oil viscosity and peripheral speed.

In the writer's opinion, Figs. 7 and 12 of the paper are of extreme importance since they show definitely that the Sommerfeld number is not an adequate parameter for describing the eccentricity of a bearing subjected to nonstatic loading.

It is to be hoped that the author of this paper can be encouraged and supported in a continuation and extension of this important piece of research.

B. L. NEWKIRK.¹¹ One item of especial interest in the paper is the indication of tensile stress in the liquid in the top of a full bearing. Under laboratory conditions, liquids have shown very considerable tensile strength. There has been doubt about the development of such strength in the lubricating film in apparatus under operating conditions. The presence of minute bubbles in the oil, or impurities which might promote the formation of bubbles, might inhibit the development of tensile stress in the liquid. In these experiments such tensile stresses amounting to perhaps 45 psi seem to have developed when a load of 50 psi was carried with a feed pressure of 15 psig. This is on the assumption that the peak negative pressure in the upper half is 3 times the average negative pressure of 25 psi. It would be interesting to know whether bearings in service could be counted on to behave reliably in this manner, what the effect of impurities in the oil would be, and whether higher feed pressures would produce higher tensile stress in the film. Theoretical values of tensile strength of liquids are very high. Possibly they may be realized in bearings.

The whirling shown in Fig. 2 of the paper is not the "oil-film whirl" which sometimes appears as a disturbing factor in the operation of machines. Such whirling develops when a machine runs at some speed that is approximately twice the shaft critical speed, or at some higher speed. There is an interaction between the elastic behavior of the shaft, and the oil film, and the shaft whirls at a frequency determined by its stiffness and the load it carries, while rotating at a much higher frequency. This model

has a very stiff shaft carrying no load except its own weight. The critical speed would be far above the speeds of these tests.

The possibility that a journal might whirl with a whirl speed equal to one-half running speed was pointed out in 1925.¹² The studies made at that time indicate that such a tendency did exist in an unloaded bearing during continuous operation, at all speeds up to as high as 2250 rpm, but that it is feeble and easily suppressed.

H. PORITSKY.¹³ This writer was particularly impressed by the verification loads of the predictions of the complete journal theory at low loads, where the displacement is perpendicular to the load, and the discrepancy between theory and tests at higher loads where the displacement has a component perpendicular to and one in the direction of the load. The explanation, as pointed out by the author, surely lies in the fact that the generally available theory requires the existence of negative pressures in the oil. While negative pressures up to a certain point might be sustained by oil, beyond that point the oil will foam, and the theory has to be modified correspondingly. When that is done, no doubt some of the discrepancies between existing "theory" and experiment will be eliminated.

In regard to the amplitudes of vibration or whirl in case of rotating and sinusoidally alternating loads, the writer's unpublished studies of some 10 years ago have shown that here, too, the discrepancy may be ascribed to negative pressures. Most of the published analytical studies of oil whirl show that a rotor should be unstable at all speeds, whereas, as has been discovered by Dr. B. L. Newkirk,¹² instability exists only at speeds above double the critical speed. When one takes into account the component of displacement in the direction of the load (due to the failure of the negative oil pressures required by theory), it is possible to show that this discrepancy may be largely explained. No doubt the displacement under sinusoidal loads can similarly be explained.

A. F. UNDERWOOD.¹⁴ This paper is helpful in bringing further attention to dynamically loaded bearings by contributing experimental results. It has become clear that no longer can we treat such bearings as statically loaded bearings.

The author points out that the study is not complete, and that further work is being done to investigate the existence of an oil film at the critical speed. The machine used to conduct the tests is extremely rigid in relation to the very light loads imposed on it, compared to most commercial machines. The highest eccentricity reported is 0.8 whereas many dynamically loaded bearings operate above 0.95. Although no failures caused by zero oil-film thickness were found by the author, we have had failure of bearings under 25 psi when operating at the critical speed. Other cases have come to our attention, in which bearing failure occurred when running at critical speeds, and we feel it is highly desirable to design bearings well outside of such conditions until the reasons for the results reported in this paper are understood thoroughly.

It is interesting to note the damping effect of higher lubricant pressure demonstrated in Fig. 2 of the paper. In tests reported previously,¹⁵ it was necessary to reduce the supply pressure to a very low value to stop the damping. Probably the effect would be less important if the bearing pressures were raised.

We are wondering how accurately the gas pressure on the bear-

¹⁰ "Effect of Side Leakage in 120-Degree Centrally Supported Journal Bearings," by S. J. Needs, *Trans. ASME*, vol. 56, 1934, p. 721.

¹¹ Professor of Vibration, Practice and Theory, Rensselaer Polytechnic Institute, Troy, N. Y. *Mem. ASME*.

¹² "Shaft Whipping Due to Oil Action in Journal Bearings," by B. L. Newkirk and H. D. Taylor, *General Electric Review*, vol. 28, August, 1925, p. 559.

¹³ Consulting Engineer, General Electric Company, Schenectady, N. Y. *Mem. ASME*.

¹⁴ General Motors Research Laboratory, Detroit, Mich.

¹⁵ Reference (16), author's bibliography.

ings of a four-cycle engine can be considered a true critically applied load. It is applied every other revolution, but each alternate revolution has practically no "half-speed" load during which time the oil film can be re-established.

The author suggests the use of an unbalance to reduce whirl when alternating loads are imposed at one half the shaft speed, and then damp the resulting vibrations. Another solution, when three or more bearings are in a machine, is to unbalance each one individually to apply a stabilizing load. However, by applying these loads so as to give an over-all balance to the machine, there will be very little resulting vibration transmitted to the mountings.

AUTHOR'S CLOSURE

Dr. Burwell raises the interesting point that, since the natural whirl frequency of this journal is slightly less than one half the shaft speed, a constant load rotating at this natural frequency might produce an eccentricity ratio closer to unity than does a load rotating at exactly one half the shaft speed. Unfortunately, no experiments of this nature have been tried, since the camshaft change gears do not permit the required frequency ratio of 0.498 or 0.497. However, the author feels that this idea has sufficient merit to warrant the installation of a separate variable-speed camshaft drive to check this point. This will be done at an early date.

With regard to Mr. Mack's question concerning the possibility that some phenomenon associated with the loading system might be responsible for eccentricity ratios less than unity when $N_p/N_j = 0.5$, recent efforts have been directed toward resolving this question. The natural frequencies of the loading springs are well outside the operating-speed range. However, preliminary measurements indicate that there is a small amount of relative motion between the test-bearing housing and the support-bearing housing, when the machine is running with a rotating load. This motion appears to occur at the loading frequency and amounts to several ten-thousandths of an inch in the axial direction at the shaft center line. No transverse motions were observed. The significance and exact mechanism of this movement are not yet known.

The only precaution which was necessary to obtain a good clearance circle was to be sure that the manual rotation of the load was accomplished slowly. Approximately 1 min for a complete revolution was found to give a maximum clearance circle. It is felt that any surface films remaining on the bearing or journal would be too thin to affect the pattern at the micrometer magnifications used. The oil temperature was measured by thermocouples in the feed lines just before the oil entered the bearing.

In response to Professor Marco's questions concerning Fig. 2 of the paper, the exposure times represent the actual periods during which the camera shutter was open. They are thus somewhat

longer than the exact duration of the whirling motion. Unfortunately, little quantitative information concerning damping can be derived from Fig. 2 because of this and because the periods of acceleration from rest to the whirl frequency are not known. Considerably more work is needed to ascertain precisely why high load, low viscosity, and high feed pressure produce the whirl-damping effects observed.

In the method used for determining the very exact ratios of N_p/N_j listed in Table 1 of the paper, only the departures from a precise 1:2 ratio were measured. The technique consisted of attaching a narrow piece of adhesive tape axially on the shaft at a point where it passed under the area of measurement of the probes. Because of the different dielectric constant of the tape compared to air, there was a distinct kick on the oscilloscope screen each time the tape passed under a probe. Since the spindle rotated approximately twice for each orbital revolution, and a kick was registered by each of the two probes, the pattern on the oscilloscope screen consisted of a circle with four distinct kicks. If the speed of orbital rotation were precisely one half the speed of shaft rotation, this pattern would remain stationary. Any departure from this precise 1:2 ratio was indicated by a slow rotation of the pattern, which could be timed easily. From the frequency and direction of this rotation, a very accurate value of N_p/N_j could be calculated.

Another point raised by Professor Marco concerns the fact that Fig. 3 shows no evidence that this journal started to roll along the bearing wall, when started from rest. It is possible that, in the tests, the loads were too light to squeeze out the oil film and permit dry friction. This matter was not explored fully.

The author agrees with Professor Newkirk that the matter of tensile stresses in journal-bearing oil films merits further consideration. Some qualitative studies were made with a lucite bearing on a steel shaft, observing the film conditions with ultraviolet light. The lubricant was introduced at a point source in the unloaded region of the bearing. It was found that film rupture started in localized areas on both sides of the oil hole, the evacuated areas extending, at times, for some distance circumferentially, but seldom reaching axially to the outside edges of the bearing. These observations led to the belief that film rupture, originating in a highly localized region of peak negative pressure and extending over only a small fraction of the bearing length, results in a redistribution of pressures on the unloaded side of the journal. Only when the load becomes high enough to rupture the film over a sizable fraction of the bearing area does the shaft move in the direction of the load, the amount of motion, and, hence the eccentricity, depending upon the extent of the rupture. The observations were only qualitative, since the lucite distorted under the influence of load and temperature. A glass bearing has been made to permit more exact tests, but no experiments have been run with it as yet.

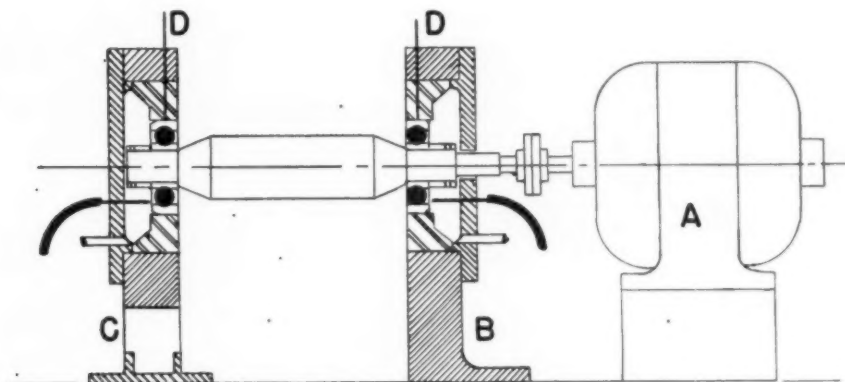


FIG. 1 DIAGRAM OF TEST EQUIPMENT
(A, motor; B, fixed pedestal; C, flexible pedestal; D, thermocouples.)

The Mechanism of Lubrication Failure in High-Speed Ball Bearings

By F. C. JONES¹ AND D. F. WILCOCK,² WEST LYNN, MASS.

When lubrication fails, the first point of distress in a high-speed ball bearing occurs at the rolling contact between a ball and a race. Because of the curvature of the race, sliding as well as rolling must occur in the contact area. Hence the absence of an oil film results in friction and heat. The localized heating and resultant differential expansion of the parts cause preloading of the bearing owing to loss of internal clearance. This process progresses rapidly to cause spalling or pitting of the races and balls, skidding balls, broken ball separators, and a jammed bearing.

INTRODUCTION

OPERATING conditions for antifriction bearings are becoming severe in certain applications; and today large bearings are being operated at high temperatures, high loads, and relatively high speeds. To meet these conditions, forced oil lubrication of the bearings has been necessary, particularly in order to help keep the bearings cool and to provide positive assurance of lubrication.

In machines with direct-connected oil pumps, there may be a short period during starting in which no oil will flow to the bearing, and therefore it becomes important to determine whether this situation might prove dangerous to the bearing. In a recent study,³ an improvement in roller bearings was described which

permits operation for extended periods without fluid lubrication. Three factors in addition to the material improvement make this type of operation possible, namely, (1) the pure rolling nature of the contact between rollers and races, (2) the light loading on the sliding surfaces between rollers and roll separator, and (3) the relatively large internal clearance. It was felt that the ball bearing, because of the nature of the rolling contact, would be much more marginal in its lubrication requirements.

Tests on high-speed ball bearings were arranged, under various conditions of lubrication. Examination of bearings after partial failure has provided interesting information as to the route by which failure occurs. Despite the opinion which is sometimes expressed,⁴ that the oil film is unimportant between balls and races because of the high pressures generated beneath the ball, these experiments have shown that it is precisely in the area between ball and race that the initial distress appears when the lubricant is depleted.

TEST APPARATUS

The ball bearings used in these tests are 50-mm-bore medium-series precision ball bearings, No. 310. Each bearing contains a complement of eight $\frac{3}{4}$ -in. balls, separated by a two-piece riveted retainer of laminated cloth-base phenolic material. The retainer is guided by the inner-race shoulders. The total radial internal clearance of the test bearings varies from 0.0013 to 0.0018 in.

The test equipment is shown in Fig. 1. It consists of a shaft carried by two of the No. 310 bearings and direct-coupled to a two-pole high-frequency motor. Motor power is furnished by a frequency changer. Motor speed is 13,200 rpm. A radial load of 19 lb is applied to each bearing due to the weight of the shaft. A thrust load of 300 lb is applied by adjusting the position of the bearing carrier in the flexibly mounted housing, in order to obtain the necessary deflection of the supporting reeds, as measured by a dial indicator.

⁴ "Methods of Lubricating High-Speed Ball Bearings," by A. F. Brewer, *Machinery Magazine*, vol. 55, 1948, pp. 172-178.

¹ Thomson Laboratory, General Electric Company.

² Thomson Laboratory, General Electric Company. Mem. ASME.

³ "Improved High-Speed Roller Bearings," by D. F. Wilcock and F. C. Jones, *Lubrication Engineering*, vol. 5, June, 1949, p. 129.

Contributed by the Research Committee on Lubrication and the Petroleum Division and presented at the Annual Meeting, New York, N.Y., November 27-December 2, 1949, of THE AMERICAN SOCIETY OF MECHANICAL ENGINEERS.

NOTE: Statements and opinions advanced in papers are to be understood as individual expressions of their authors and not those of the Society. Paper No. 49-A-36.

The bearing in the fixed coupling end housing is lubricated with 0.5 gpm of AN-O-8 grade 1065 oil, and functions as a guide bearing. The test bearing is located in the flexibly mounted housing and is lubricated as desired for each test. The test-bearing outer-race temperature is measured with an iron-Copnic thermocouple which is spring-loaded against the outer race.⁵ A high-speed G-E potentiometer-type photoelectric recorder is used to record the temperature-time curve during testing. A very rapid rise in temperature signals the depletion of the lubricant supply after which the test shaft usually is stopped as quickly as possible. After removal from the test shaft, the failed bearing is cut open for examination.

EXPERIMENTAL RESULTS

As part of the study of the amount of lubrication necessary in the ball bearing, a series of bearings were prepared with varying amounts of oil on the surfaces; and the length of time before a lubrication failure occurred was noted. Minute amounts of oil were added by immersing each bearing in oil solutions of varying concentrations. Because of slight oil absorption in the separator material, accurate determinations of the weight of oil added were not possible. The following schedule was followed in oil-coating the bearings:

- 1 Cleaned and soaked in solvent.
- 2 Air and furnace dried.
- 3 Cooled in a desiccator.
- 4 Soaked in a dilute oil-solvent solution.
- 5 Air and furnace dried.
- 6 Cooled in a desiccator.
- 7 Installed in the testing machine.

The running time to failure was found to be roughly proportional to the concentration of oil in which the bearing had been dipped, as shown in Fig. 2. By dipping an outer and inner race separately in a 5 per cent solution, the weight of oil added to the steel parts is estimated to be 13.5×10^{-6} gm per sq. cm, which corresponds to a layer 12 Ångströms thick, or about one molecular layer. Additional oil undoubtedly is absorbed at the separator surface and transferred to the balls in the actual bearing tests. No separator failures occurred during this testing.

The tests were stopped as soon as temperature rise of the outer race was noted. Fig. 3 shows a typical temperature record for the final portion of the test. The appearance of a bearing outer race

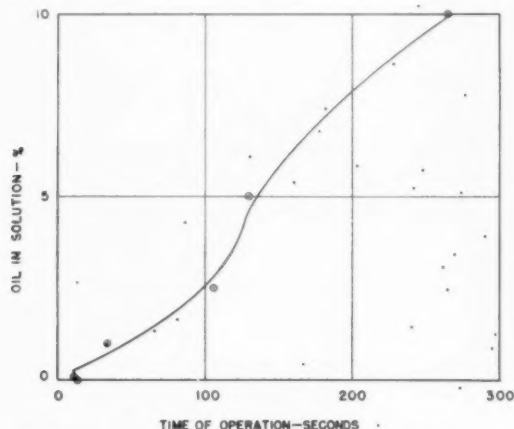


FIG. 2 VARIATION IN RUNNING TIME WITH CONCENTRATION OF OIL SOLUTION IN WHICH BEARING WAS DIPPED

after a partial failure is shown in Fig. 4. Three pitted areas in which sliding has occurred separated by two narrow shiny bands where only rolling took place are clearly visible. All the bearing

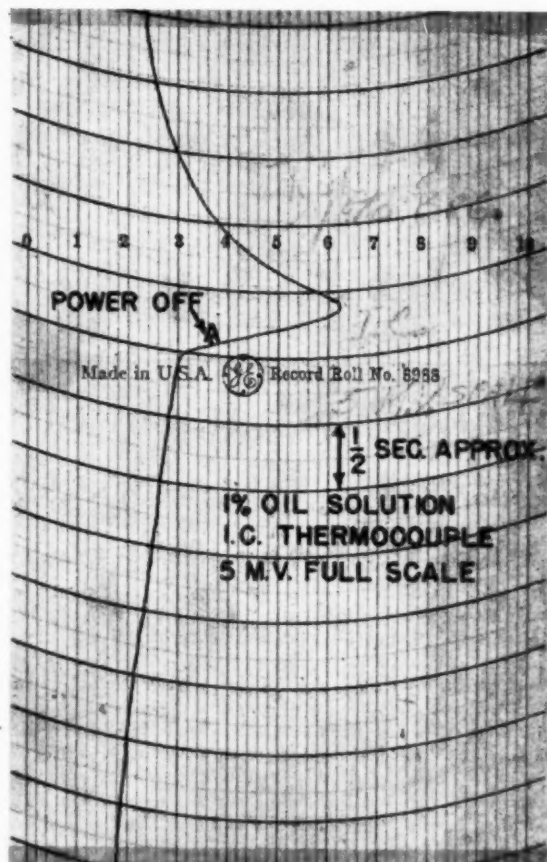


FIG. 3 TYPICAL CHART SHOWING RAPID TEMPERATURE RISE AT BEGINNING OF UNLUBRICATED PERIOD

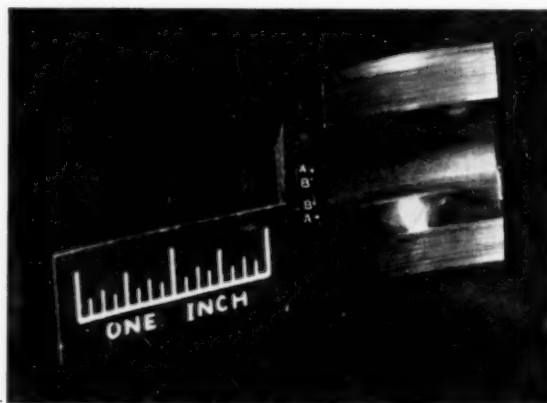


FIG. 4. CLOSE-UP OF PORTION OF BEARING OUTER RACE AFTER PARTIAL FAILURE, SHOWING ALTERNATING BANDS OF SLIDING AND ROLLING CONTACT (A-A edges of track; B-B lines of rolling contact.)

⁵ "Grease—An Oil Storehouse for Bearings," by D. F. Wilcock and M. Anderson, Special Technical Publication No. 84, ASTM, 1948, see p. 36.

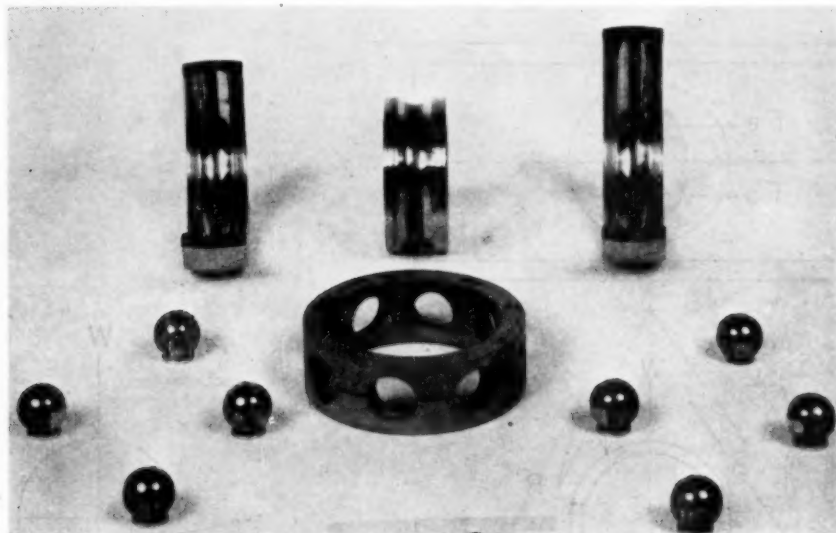


FIG. 5 BEARING PARTS AFTER PARTIAL FAILURE

parts are shown in Fig. 5 which illustrates the tracking which occurs on the balls and inner race, as well as on the outer race. Three other tests were made which are of interest. These are as follows:

1 A run using a large mass on the shaft to increase the radial load to 100 lb. A dry bearing was used, and no time could be recorded, since the bearing had not come up to speed before failure. The races and balls were darkened and covered with steel flakes. The separator broke during this failure, probably because of the greatly increased inertia of the weighted shaft which prevented the usual rapid stop.

2 A run was made in which the bearing was partially failed and then run with jet-oil lubrication. No complete failure occurred; and, although noisy, the operation was satisfactory during a 2-hr run.

3 A run was made carrying the failure beyond the point of rapid temperature rise. In this case the bearing seized without separator failure. There were steel flakes rolled onto the races and balls.

To investigate the possibility that the initial lubrication failure occurred between ball and race and not at the separator because of the better bearing characteristics of the phenolic separator, some tests have been made on standard No. 306 bearings with pressed-steel separators at speeds of 900 to 3600 rpm. These bearings also were lubricated with very small quantities of oil, of the order of 1 mg, applied from a 2 per cent solution in benzene. They were stopped at the first sign of distress, either noise or temperature rise. When the bearings were cut open, tracks were observed on the races similar to those in Fig. 4, but they were too faint to photograph readily. No marking or evidence of wear could be found on the steel surfaces of the separator, indicating again that the area of initial lubrication failure is between the ball and the race. When the bearings were not stopped immediately at the first sign of distress, very pronounced tracks were produced on the races together with brown iron-oxide powder. At this stage, some marking of the separator had taken place also.

DISCUSSION OF FAILURE CONDITIONS

The tracking observed on the races and balls after a partial

failure is an interesting verification of the conditions beneath a loaded ball which are predicted mathematically. The two shiny bands separating the three pitted strips in each track correspond to the lines where pure rolling motion occurs, sliding occurring over the balance of the area of contact.

A section of a ball bearing is shown in Fig. 6, indicating the loaded area between a ball and the outer race. Because of the differences in radii between the axis of rotation of the ball and the contact point with the outer race, the surface travel for a given angular rotation will vary from point to point, and, in general, will not agree with the corresponding portion of the outer-race circumference traversed by the ball. Thus if

r = the maximum distance from the axis of rotation of the ball to a point in the contact area

$r_1 = r - \Delta$ is distance to some other point in contact area

R = maximum radius of outer race

$R_1 = R - \Delta$ is outer-race radius corresponding to r_1

then the number of revolutions of the ball per revolution around the outer race is

$$n = \frac{2\pi R}{2\pi r} - 1 = \frac{R}{r} - 1 \dots \dots \dots [1]$$

and

$$n_1 = \frac{2\pi R_1}{2\pi r_1} - 1 = \frac{R - \Delta}{r - \Delta} - 1 \dots \dots \dots [2]$$

if no slip is assumed. It is apparent at once that since $R \neq r$, n is not equal to n_1 , and hence slip must occur. The ball must then roll in such a way that the forces due to sliding will balance as shown in Fig. 6. Sliding will occur in opposite directions in the areas marked A and B, and the boundaries between these areas represent the lines of rolling contact.

It is interesting to note that the ratio of the separation of the lines of rolling contact to the major diameter of the ellipse of contact is independent of the shape of the ellipse if it is assumed that the frictional force per unit area is constant and hence, that the areas A and B are equal. The calculated ratio of spread to major

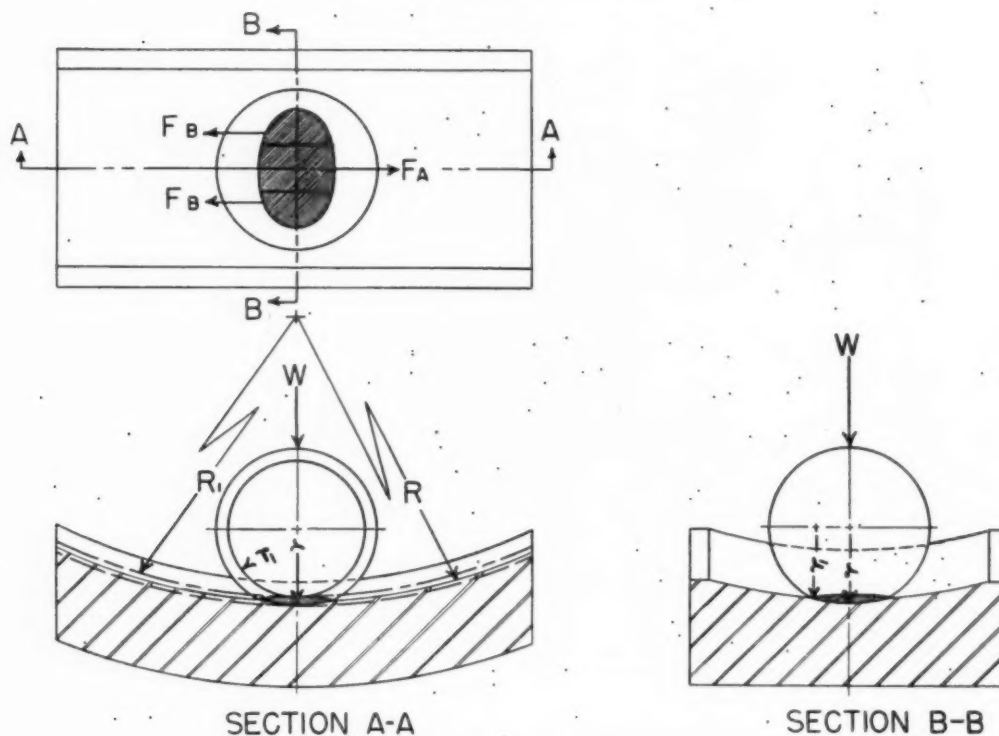


FIG. 6 SKETCH OF BALL BEARING UNDER RADIAL LOAD

diameter compares with the ratio measured on the outer race shown in Fig. 4 as follows:

$$\begin{aligned} \text{Calculated} & \dots\dots 0.405 \\ \text{Measured } \frac{0.0985}{0.246} & = 0.400 \end{aligned}$$

The bearing shown in Figs. 4 and 5 had a total internal radial clearance of 0.0015 in., and a maximum load per ball of 140 lb. Other pertinent bearing dimensions are as follows:

Radii of outer race	-1.950 in.,	-0.397 in.
Radii of inner race	+1.199 in.,	-0.387 in.

Application of the Hertz equations^{6,7} gives an outer race track width of 0.11 in. for the normal load of 140 lb plus the centrifugal load of 68 lb.

The observed track width of 0.246 in. corresponds to a ball load of about 2100 lb, or 15 times the normal load. The only logical source of a load of this magnitude is from preloading of the bearing caused by expansion of the balls due to the frictional heat. Thus this load was acting only after depletion of the lubricant supply and until the shaft was stopped. Maximum stress beneath the ball in the preloaded condition approaches 400,000 psi which, taken together with the frictional forces, appears ample to cause the spalling or pitting observed. The calculated interference required to create a ball load of 2100 lb is 0.003 in. on each side of the bearing or 0.006 in. total. If it is assumed that it is the balls which heat most rapidly from the friction, a temperature difference of about 800 F between balls and races is estimated. If

it is assumed that the balls and inner race both expand, a temperature difference of about 250 F is estimated. The hardness of the balls in the tracked area after test is 61-62 Rockwell C, so that it is doubtful whether more than a thin surface layer was heated severely. The peak outer-race temperatures were about 200 F.

Similar analysis of the No. 306 bearing showed it to have a track width of 0.102 in. corresponding to a ball load of 240 lb. The normal maximum ball load from the applied radial load of 160 lb is 113 lb.

THE COURSE OF A FAILURE

From the experimental observations and the analysis of their meaning, a fairly complete picture may be drawn of the course of a lubrication failure in a ball bearing. The following stages during failure are indicated, although many of the test bearings were not driven to complete failure.

Loss of Lubricant Film. It seems apparent from the minute quantities of oil which lubricate the ball bearings successfully that depletion of this oil supply beyond a certain critical value results in a lubrication failure. There doubtless is some lubricant remaining on the metal surfaces at this stage, but it is not sufficient to separate the high spots on the rubbing surfaces. Experiments with the No. 306 bearing appear to indicate that load and speed influence the quantity of lubricant remaining at failure, since the time of operation on a given small quantity of oil is strongly influenced by load and speed.

Local Heating Due to Friction. This localized heating occurs in the contact areas between the balls and the races as the result of sliding and friction in the absence of oil.

Loss of Radial Play. As a result of the local heating of the surfaces thermal expansion results in removal of the radial play or

⁶ "Analysis of Stresses and Deflections," by A. B. Jones, New Departure Division, General Motors Corporation, Bristol, Conn., vols. 1 and 2, 1946.

⁷ "Ball and Roller Bearing Engineering," by Arvid Palmgren, SKF Industries, Inc., Philadelphia, Pa., 1945.

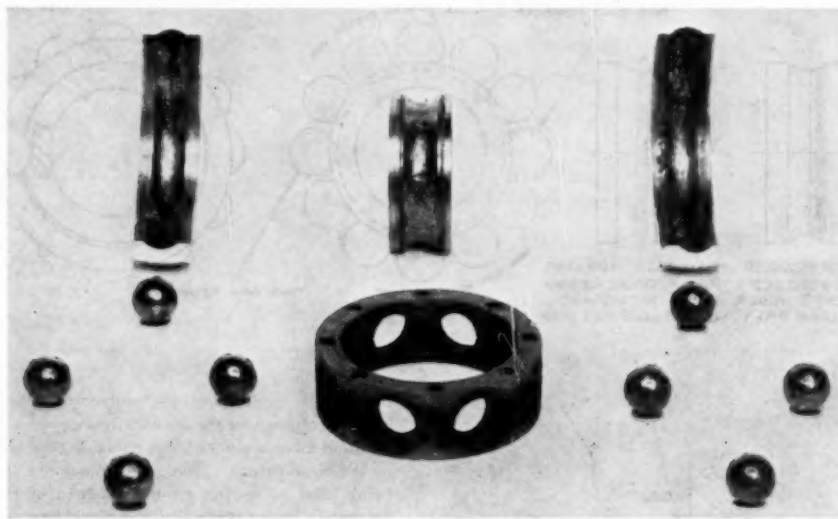


FIG. 7 BEARING PARTS AFTER FAILURE TO BALL-SKIDDING STAGE, SHOWING INDENTATION OF INNER RACE DUE TO PRELOADING

internal clearance of the bearing. A temperature difference of about 150 F between the balls and the races is sufficient to remove the radial play of 0.0015 in.

Preloading of Bearing. Continued heating beyond the point of zero clearance results in preloading because of "negative clearance." This results in high ball loads and high stresses beneath the contact areas.

Spalling or Pitting of the Contact Surfaces. Pitting appears to start as soon as the lubricant fails and it becomes severe when the preloaded condition is reached. Metal removed from the pits becomes rolled onto the races and balls.

Ball Skidding. Metal rolled beneath the balls causes skidding of one or more balls.

Separator Failure. The high tangential forces on the separator caused by the skidding balls break the separator.

Bearing Jammed. The bearing may jam before or after separator breakage depending upon the amount of inertia and power available in the shaft.

Indentation of Races. When the bearing is examined after a severe failure, i.e., after progression to the three preceding stages, the inner race is found to contain a number of indentations equal to the number of balls (see Fig. 7). This is an indication of the severe preloading at the time of failure.

Discussion

THOMAS BARISH.^{*} The authors' work to determine the actual mechanism of high-speed ball-bearing failures should be of great value in indicating to the ball-bearing manufacturers, some steps that can delay such failures.

The conclusion that the separator does not account for ball-bearing failures at high speeds is true only for certain special conditions; either pure radial load or pure thrust load combined with perfect alignment. The test conditions selected fill these special requirements, but are rarely met in actual practice. Separators account for a large proportion of the field failures, because the

contact angle changes around the circumference of the bearing, causing the ball speed to change and jam the separator.

To illustrate how serious and large this effect can be, we take the specific case quoted by the authors as a special test, 300 lb thrust, plus 100 lb radial load (when the cage did fail). The radial load is carried only on the bottom half of the bearing, and the contact angle changes from the top ball to the bottom ball, approximately as shown in Fig. 8. The change in contact angle on the inner race varies the ball speed from 3308 ft per min at the top, to 3172 at the bottom ball—a total change of 134 feet per min or 4.2 per cent.

Furthermore, this effect accumulates over half of the bearing causing an appreciable and dangerous displacement of the ball from its mean position—in this case, about 0.027 in. (Fig. 9^b). Part of this motion is absorbed by a displacement of the cage, as shown, but this effect cannot be large in high-speed bearings since cages cannot be very loose. The rest of the ball displacement produces cage distortion with resulting severe loads and heating. It is this effect which produces most high-speed failures in the field.

The authors had some difficulty in interpreting the very wide contact area. They deduced a load of 2100 lb per ball^b (a nomographic chart for making this calculation is given in reference^b), and attributed it to radial expansion caused by differential heating, the inner ring being hotter than the outer. Such a large load does not seem reasonable. The misapprehension is easily explained: the contact area appeared so wide because it moved.

On the test bearings, the following three conditions existed:

- 1 The initial bearing with 0.00155 in. looseness (average) contact angle 12.2 deg.
- 2 Add 300 lb thrust load, contact angle 16.2 deg.
- 3 Add radial expansion, say, 0.00155 in (85 deg temperature differential) contact angle 7.0 deg.

A radial preload as large as the authors' interpretation would have made the contact practically radial, but it is quite clear

^{*} Consulting Engineer, Washington, D. C.

^b "Ball Bearing Troubles," by Thomas Barish, *Product Engineering*, March, 1939.

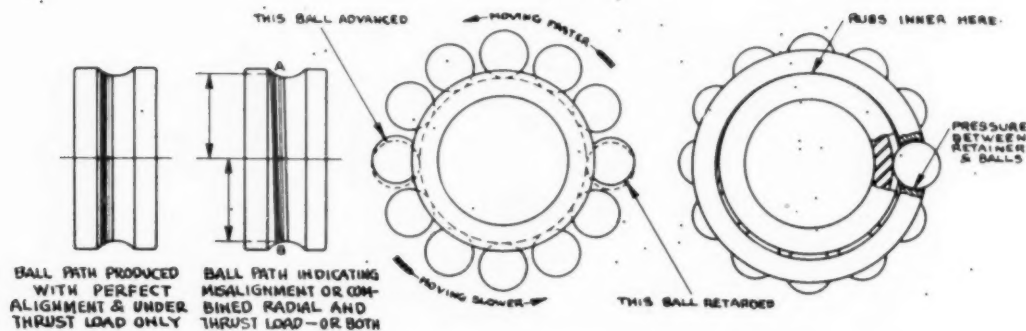


FIG. 9 INDICATING ACCUMULATIVE EFFECT OF VARIATION IN CONTACT ANGLE ON BALL POSITION AND IN CAGE

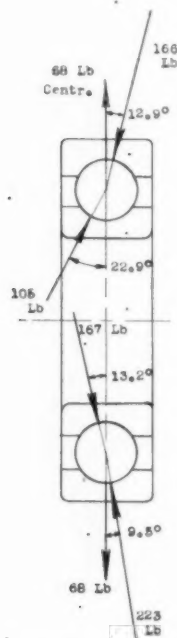


FIG. 8 VARIATION IN CONTACT ANGLE FROM TOP BALL TO BOTTOM UNDER 300 LB THRUST AND 100 LB RADIAL LOAD

from Fig. 4 in the paper that the area being measured was not radial, but at a considerable angle.

Hence most of the race marking in these tests occurred before the final excessive heating of the bearings. However, some heating and resultant contact movement took place during the initial run when the races were marked, or else the contact would not be so wide.

Incidentally, the authors' tests further confirm Poritsky's¹⁰ contention that the balls do not spin in angular contact bearings.

It is still to be proved that an oil film only one molecule thick can be an effective and necessary lubrication between the ball and the race. Lubricating unit pressures of over 200,000 psi do not appear feasible. Perhaps the oil film functioned to improve the heat transfer, rather than as a lubricant. It is suggested that very high pressures and slight movements are better lu-

bricated by such things as "molybde," which should then show better results under the authors' tests.

Much more testing of this valuable type should be undertaken in the near future. Too many machines like gas turbines are being used as testing grounds instead of running the bearings separately under controlled test conditions.

H. T. MORTON.¹¹ The authors amply described a test procedure which creates a lubrication failure of high-speed ball bearings. By stopping the test after various intervals of operation, the progressive figures of failure were observed.

During the writer's years of experience in the examination of bearings which have failed in service due to lack of lubrication, he has also observed similar steps leading to the complete failure of the bearing. Under normal operations the lubricant keeps a film between the ball surface and retainer surface to prevent friction and localized heating at these areas of contact. Likewise, experience requires changes in retainer materials for bearings operated at high speeds.

Under heavy loads or after the balls have expanded due to increase in temperature, the condition shown in Fig. 6 occurs. Here the ellipse of contact is divided into three areas separated by two lines. These lines were especially visible on the sample raceway Mr. Jones had with him at the meeting. These lines represented the position of rolling contact of balls. At all other positions of the ellipse, sliding friction occurred due to the difference in length between r and r_1 of Fig. 6 representing the distance from the point of contact to the axis of rotation of the ball. Thus the lubricant must have sufficient film strength to separate these surfaces or sliding friction will occur, which will increase the ball temperature and the raceway temperature. This increase in temperature will create expansion by heat and decrease of internal radial clearance, as explained by the authors.

It is interesting to note that the authors have computed the width of contact of the balls with the raceways, the stresses and temperatures to create this preload.

The authors also discovered the effect of stopping the bearing while the preload was in effect and plastic flow occurred both on the balls and raceways, leaving indentation in the bearing raceway surface.

Under preload conditions the retainer works all of the time under higher stresses. As a result, early fatigue failure occurs to break the retainers.

The important consideration in bearing service is that when the lubricant fails and the temperature of the bearing lubricant rises, the machine should be stopped immediately.

¹⁰ "Sliding Friction of Ball Bearings of the Pivot Type," by H. Poritsky, C. W. Hewlett, Jr., and R. E. Coleman, Jr., *Journal of Applied Mechanics*, Trans. ASME, vol. 69, 1947, pp. A-261-268.

¹¹ Standards Engineer, The Fafnir Bearing Company, New Britain, Conn.

E. F. MACKS AND E. E. BISSON.¹² The authors should be complimented upon presenting a paper on bearings which is fundamental in nature.

Inasmuch as this type of failure occurs in low-speed as well as high-speed ball bearings, we feel that the title may be too specific. In this regard, another type of failure which may occur in very high-speed ball bearings, and which has not been mentioned in the paper, is a lubrication failure at the cage locating surface. This type of failure may occur even with adequate lubrication at the points of contact between the balls and races.

The starting speed and rate of acceleration are important variables which have not been given. Flat spots on the balls are likely to occur during quick starts, particularly with faulty lubrication; such flat spots may affect the results. Have the authors checked for flat spots on a bearing before it had failed?

Inasmuch as the contact angle and therefore the track width vary with diametral clearance, the observed track width at the time of failure may be somewhat misleading regarding preloads as the balls have not retraced their paths but have gradually worked downward into the groove. Inasmuch as the three sliding and two rolling areas were evident in the failed bearings, the foregoing effect of reduced clearance on contact angle may be overshadowed by the high preloads at the time of failure. What is the author's opinion?

Is it not possible to tell from the tempering colors and hardness of an incipient failure what the ball and inner race maximum temperatures may have been? What have the authors found in this regard?

AUTHORS' CLOSURE

The authors appreciate the comments of the discussers concerning the interpretation of the data in the paper. Mr. Barish has raised some questions which deserve further discussion.

The paper neither states nor implies that the separator does not account for ball-bearing failures at high speeds, but rather that in the event of a "lubrication failure" or failure to supply adequate lubricant to the bearing, separator failure is not the primary cause but rather an end result of localized heating due to friction in the contact areas between balls and races. It was indeed surprising how much punishment this bearing could absorb from misalignment, combined load, and other sources, provided adequate lubrication was supplied. The paper clearly states in the description of special test No. 1, under 300 lb thrust and 100 lb radial load, that a "dry" bearing was used; and, because of the high ball-race friction, failure occurred before full speed was at-

tained by the same process observed in the high-speed failures of very lightly oiled bearings.

There is no difficulty in interpreting the wide contact area, since its width simply serves as a measure of the preload due to localized heating of the balls. For reasons of heat transfer it seems likely that the balls become hotter than either race. Whether the calculated load seems reasonable is a question of judgment in view of the permanent indentations left in the races, as illustrated in Fig. 7. That the contact area is wide because it moved appears highly unlikely for two reasons: (1) because the pitted contact surfaces were not found in the raceways of even scantily lubricated bearings after high-speed runs, and (2) because measurement of the position of the contact area illustrated in Fig. 4 of the paper shows that the contact was nearly radial as Mr. Barish has predicted it should be at the calculated high load.

We believe the evidence is clear that even under the high Hertz stresses, calculated for the contact area between a loaded ball and the raceway, the oil provided as lubricant serves the important function of reducing friction within the contact area. Since the relative motion is small and of short duration, it is possible that oil trapped in surface irregularities, aided by the increase in viscosity due to pressure, explains the beneficial effect.

Lubrication failure at the cage locating surface, as mentioned by Macks and Bisson, has been encountered by the authors in the case of roller bearings having land riding retainer. Undoubtedly similar failures would be encountered in the case of ball bearings constructed to have land riding metal retainers. The rate of acceleration used in these tests was not large—the rotor being brought to full speed in about ten seconds; and at no time were flat spots observed on the balls except after the most severe type of failure when they were obviously caused during failure. The authors have observed so many cases of colors similar to tempering colors arising from the effect of more moderate temperatures on thin oil films on bearing parts that they did not feel that this was a reliable method of judging temperatures. Measurement of hardness in the ball track after an incipient failure using the Rockwell C scale showed no change in hardness. Superficial hardness checks were made.

Bearing testing under controlled laboratory conditions can indeed be more informative than testing in complicated machines, where all too often a failed bearing has progressed so far toward complete destruction that the course of the failure cannot be ascertained. Doubtless it is for this reason that faulty separator lubrication, resulting in separator breakage, has been thought in the past to be the primary result of failure to supply lubricant to a ball bearing, when, in fact, it is the end result of a rapid progression of events originating in friction in the ball-race contact area.

¹² Technical Staff, NACA Lewis Flight Propulsion Laboratory, Cleveland, Ohio.

b
n
in
o
ol
at
be
al
du
in
ta
be

tica
len
obs
high
unc
pre
cor
bul
beh
S
bet
(1,
tion
spee
the
cyl
stat
high
was
met

1
2
the p
Co
Petr
York
Socr
No
unde
of th

Turbulence in High-Speed Journal Bearings

By D. F. WILCOCK,¹ WEST LYNN, MASS.

Measurements of the operating characteristics of journal bearings up to high surface speeds have revealed abnormalities beyond a certain critical value. A rapid increase in bearing torque, power loss, and oil-film temperature occurs as speed is increased beyond the critical value, while oil flow decreases below normal. These phenomena are attributed to the onset of instability or turbulence in the bearing oil film with an accompanying increase in energy absorption within the film. The experiments were conducted in a newly designed test apparatus capable of driving large bearings at high speeds. Maximum speed attained was 14,700 rpm, or 30,800 fpm, for an 8-in.-diam bearing, and 20,000 rpm, or 21,000 fpm, for a 4-in. bearing.

NOMENCLATURE

The following nomenclature is used in the paper:

- C = diametral clearance, in.
- D = shaft diameter, in.
- L = bearing length, in.
- N = shaft speed, rpm
- P = bearing load, psi
- T = torque on bearing, in-lb
- Z = absolute viscosity, lb min/in.²
- e = shaft eccentricity, in.
- g = gravitational constant, in./min²
- ν = kinematic viscosity, in.²/min
- ρ = liquid density, lb per cu in.

INTRODUCTION

In the course of an investigation of the operating characteristics of sleeve bearings over a broad range of diameter, clearance, length-to-diameter ratio, and design, anomalous behavior was observed in certain larger clearance bearings when operating at high rotative speeds. It was noted that the friction coefficient under these conditions was considerably higher than would be predicted from the f versus ZN/P curve for the bearing, and that correspondingly high oil-film temperatures were obtained. Turbulence in the oil film was suspected as being responsible for this behavior, since Reynolds numbers over 1000 were estimated.

Some years ago the problem of the stability of a fluid contained between concentric rotating cylinders was treated by G. I. Taylor (1, 2).² For the special case, in which the outer cylinder is stationary and the inner cylinder rotates, he was able to calculate the speed at which instability begins in terms of the fluid viscosity, the diameter of the inner cylinder, and the clearance between the cylinders. For the opposite case of a rotating outer cylinder and stationary inner cylinder, the fluid flow was found to be stable to higher speeds. The initial instability for inner-cylinder rotation was predicted mathematically to be in the form of uniform symmetrical vortexes or eddies, and this prediction was borne out by

careful, precise experiments. The symmetrical disturbances in the fluid changed to random turbulence as speed was increased above the transition speed.

It is interesting, therefore, to investigate whether the anomalous bearing performance observed at high rotative speeds obeys the relations derived by Taylor and may be ascribed properly to the effects of turbulence. Considerable differences in configuration and conditions exist between a loaded high-speed journal bearing and the annular space between smooth concentric cylinders. Consequently, deviations may be expected in applying the theory for cylinders to journal bearings. Some of the important differences are as follows:

- 1 Oil grooving in the bearings.
- 2 Eccentricity of the shaft in the bearing, as a result of the load applied.
- 3 Variations in oil viscosity throughout the bearing oil film.
- 4 Small clearance-to-diameter ratios.

The bearings used in this study are made with two longitudinal oil-distribution grooves at either side of the bearing located 90 deg from the load line. Thus, the external cylindrical surface is interrupted twice by oil grooves carefully blended with it. The smallest clearance-to-diameter ratio for the cylinders used by Taylor in his experiments was 0.0271, or 27 mils per in. The bearing tests have been made with much smaller clearance-to-diameter ratios ranging from 1.7 to 4.4 mils per in.

MATHEMATICAL RELATIONS

The essential mathematical relations are presented here without proof or derivation, for which the reader is referred to the original (1, 2). For the case of laminar flow of a fluid between concentric cylinders, the torque may be obtained directly from the definition of viscosity

$$T = \frac{(\text{surface area}) \times (\text{surface velocity}) \times (\text{viscosity}) \times (\text{radius})}{(\text{distance between surfaces})}$$

Neglecting the difference in diameter between bearing and shaft because of the relatively small clearance, and assuming a constant viscosity, this becomes

$$T = \frac{\pi^2 D^3 L N \rho \nu}{g C} \quad [1]$$

This may be rewritten in the following form in terms of two dimensionless variables

$$\left(\frac{Tg}{\rho N^2 D^4 L} \right) = \frac{\pi^2}{2} \left(\frac{\pi NDC}{2\nu} \right)^{-1} \quad [2]$$

A log-log plot of

$$\left(\frac{Tg}{\rho N^2 D^4 L} \right) \text{ versus } \left(\frac{\pi NDC}{2\nu} \right)$$

which is defined by Taylor as the Reynolds number, is a straight line with a slope of -45 deg. (It has been plotted in Figs. 6 and 7 as the "theoretical curve" for laminar flow.)

Taylor's criterion for the critical point beyond which instability should occur may be rewritten as

¹ Thomson Laboratory, General Electric Company. Mem. ASME.
² Numbers in parentheses refer to the Bibliography at the end of the paper.

Contributed by the Research Committee on Lubrication and the Petroleum Division and presented at the Annual Meeting, New York, N. Y., November 27-December 2, 1949, of THE AMERICAN SOCIETY OF MECHANICAL ENGINEERS.

NOTE: Statements and opinions advanced in papers are to be understood as individual expressions of their authors and not those of the Society. Paper No. 49-A-37.

$$\frac{\pi NDC}{2\nu} = \pi^2 \sqrt{\frac{D}{0.0577 C}} = 41.1 \sqrt{\frac{D}{C}} \dots [3]$$

for the case where C is small³ compared to D . At Reynolds numbers higher than those given by Equation [3], values of $(Tg)/(\rho N^2 D^4 L)$ higher than those calculated from Equation [2] are expected because of turbulence.

TEST EQUIPMENT

The experiments were conducted in test equipment designed and constructed in 1946-1947, and shown schematically in Fig. 1. The test bearing is located at the center of the test shaft. This shaft is supported by two pedestal bearings, which are usually smaller in diameter than the test bearing. It is driven through two step-up gears with an over-all ratio of 20:1 by a 200-hp d-c motor. An amplidyne control system is used to adjust the motor speed and to maintain it constant. With this drive, tests may be run at shaft speeds of 250 rpm to 30,000 rpm with full power available from 5000 to 30,000 rpm. Special control circuits permit full power to be used to stop the shaft in the event of a bearing seizure or other emergency.

Load is applied to the test bearing by means of a hydraulic cylinder located beneath it which can apply a maximum load of 133,000 lb. The load is transmitted to the test-bearing housing through a stationary pivot bearing supplied with high-pressure oil from the hydraulic cylinder. The pivot bearing is cylindrical, embracing 85 deg of arc, and contains four oil pockets symmetrically disposed. Oil is fed to each pocket individually through a small tube which restricts the flow and keeps the bearing balanced (3).

The pivot bearing is essentially frictionless and permits free rotation of the test-bearing housing which is restrained only by a torque arm and scale for measuring the torque reaction on the bearing during operation. The torque is measured with a precision of 0.05 ft-lb.

A general view of the installation without the scale is shown in Fig. 2. The control console and some of the oil piping are visible. The test bearing is supplied with filtered oil at controlled temperature and pressure. Each of the longitudinal oil grooves in the test bearing is fed through its own oil line containing a volumetric-type totalizing oil meter for the measurement of oil-flow rates. The pedestal bearings and the gears are supplied with oil from a second system completely independent of the test bearing.

³ Reference (2), Equations [3] and [5], p. 558.

Shaft speed is measured with a precision tachometer generator and meter. Shaft position in the bearing is measured with magnetic strain gages mounted radially to the shaft on the test-bearing housing. Changes in the gap between the gage armature and the shaft change the reactance of the gage coil which is measured in a bridge circuit.

Different size bearings may be mounted in the test-bearing housing and in the pedestals by means of adapters. Fig. 3 shows the installation of a 4-in.-diameter bearing in the test-bearing housing. The torque arm and part of the scale may be seen in the background.

The test bearing is usually fitted with a number of thermocouples for measurement of the oil-film temperatures and, at times, is also fitted with pressure taps for the measurement of oil-film pressures. The bearing thermocouples are copper-Copnic and are mounted so that the tips are open to the oil film and flush with the bearing surface. The wires are brought through a short section of two-hole ceramic insulator which is cemented in a close-fitting drilled radial hole. Softening of the cement by the oil is prevented by coating the exposed cemented surfaces with several coats of clear Glyptal cement. Temperatures read with thermocouples installed in the foregoing manner have been from 1 to 2 deg C above those read from adjacent thermocouples embedded in the babbit metal. The true oil-film temperature is not known, but it is thought that the disturbance of the bearing surface where the thermocouple is inserted causes a local disturbance in the oil film sufficient to circulate oil over the thermocouple bead.

EXPERIMENTAL RESULTS

Four bearings have been run at speeds high enough to exhibit the effects of oil-film instability. Three are 8-in.-diam bearings, 4 in. long. The fourth is a 4-in.-diam bearing, 4 in. long. Bearing and shaft dimensions are summarized in Table 1. The bearings are of the split cylindrical type shown in Fig. 4, with longitudinal oil-distribution grooves reaching to within 1/4 in. of each end.

Bearing D has 14 thermocouples at the oil-film surface, 10 of them in the lower half. Bearings E , L , and N each had four thermocouples disposed on a circumferential line 3/4 in. from one end of the bearing at 0, 45, 180, and 315 deg from the bottom of the bearing, respectively.

The tests were conducted at a bearing load of 150 psi of projected bearing area and with an oil-inlet temperature of 40 C (104 F) in most cases. Bearings D , E , and L were tested with an oil having a viscosity of 70 centistokes at 100 F. Bearing N was tested with an oil having a 100 F viscosity of 54 centistokes.

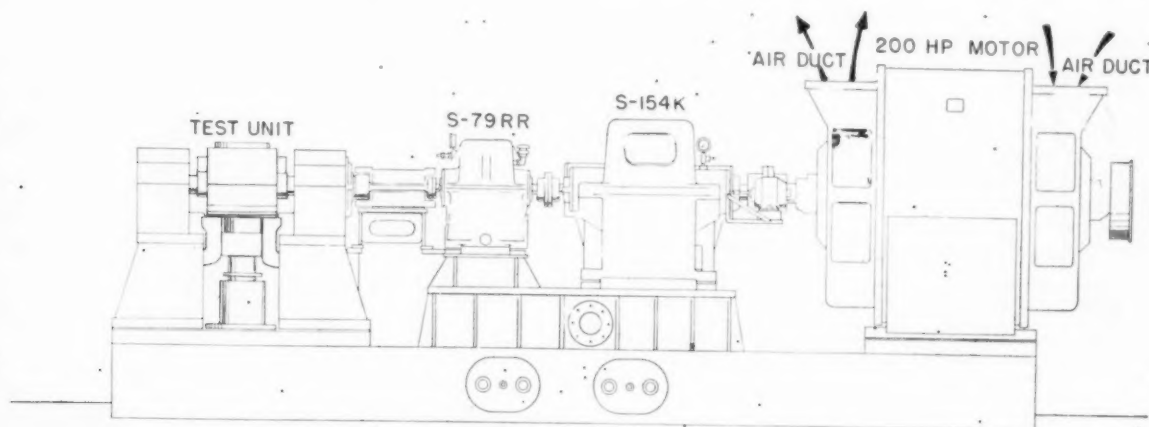


FIG. 1 SCHEMATIC DIAGRAM OF HIGH-SPEED JOURNAL-BEARING TEST STAND

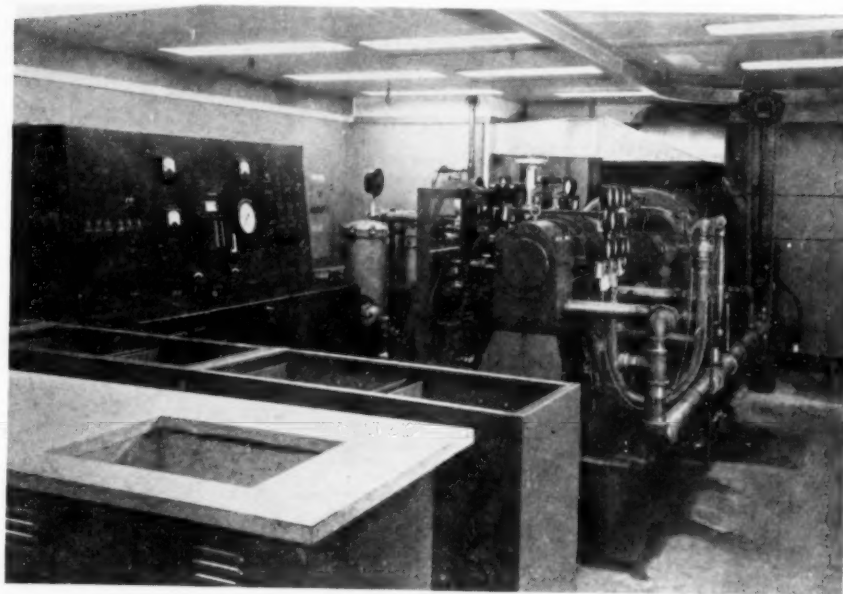


FIG. 2 VIEW OF JOURNAL-BEARING TEST STAND

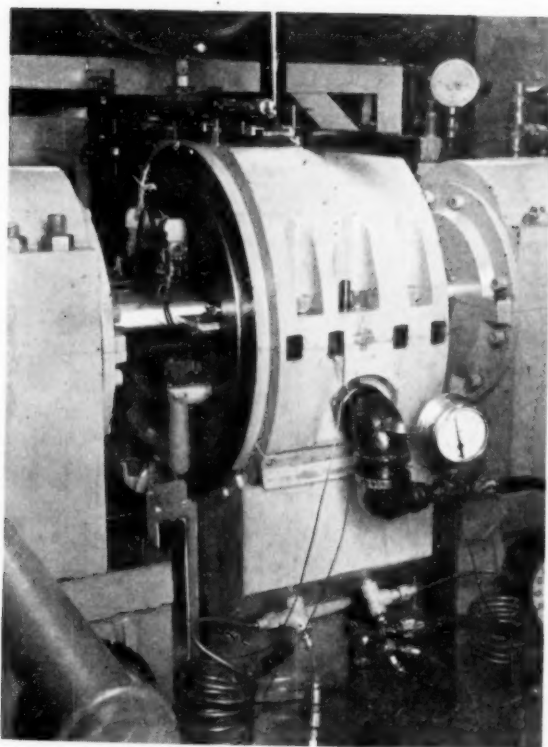
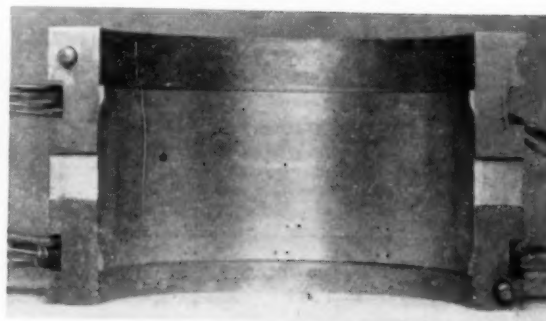

FIG. 3 VIEW OF TEST-BEARING HOUSING, SHOWING INSTALLATION OF 4-IN. \times 4-IN. BEARING, MAGNETIC FILM THICKNESS GAGES, AND TORQUE ARM


FIG. 4 TYPICAL TEST BEARING—LOWER HALF ONLY—SHOWING SHAPE OF OIL-FEED GROOVES, PRESSURE TAPS, AND THERMOCOUPLES

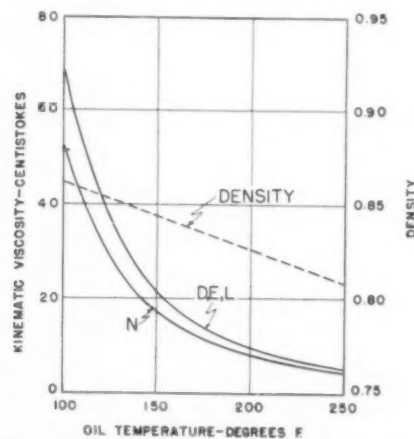


FIG. 5 VISCOSITIES AND DENSITIES OF TEST OILS AS A FUNCTION OF TEMPERATURE

TABLE 1 SUMMARY OF BEARING DIMENSIONS

Bearing	Shaft Diameter, Inches	Bearing Bore, Inches*			Bearing Clearance, Inches	Bearing Length, Inches
		Maximum	Minimum	Average		
D	8.0010	8.0118	8.0131	8.0139	0.0129	4
E	8.0000	8.0223	8.0190	8.0200	0.0200	4
L	8.0000	8.0358	8.0335	8.0349	0.0349	4
N	3.9998	4.0166	4.0137	4.0151	0.0153	4

*Measured with bearing clamped in test housing.

TABLE 2 TEST DATA ON 8-IN. \times 4-IN. \times 0.0129-IN. BEARING D

Run No.	Speed RPM	Shaft Torque ft-lbs	Horsepower	Inlet Oil Temp., °C	Outlet Oil Temp., °C	Max. Obsd. Brg. Temp., °C	Oil Flow GPM
D-12	250	8.4	0.40	39.0	40.7	48.2	0.7
D-11	500	8.95	0.85	39.3	43.3	48.7	1.0
D-15	1,000	10.9	2.1	40.2	46.0	59.8	1.5
D-5	2,720	17.4	8.9	40.2	57.3	78.0	3.1
D-18	5,000	24.2	23.0	40.5	68.9	84.5	5.3
D-24	7,510	33.3	47.5	42.9	85.1	98.6	7.4
D-54	9,500	42.6	76.9	51.8	109.8	130.2	8.6

TABLE 3 TEST DATA ON 8-IN. \times 4-IN. \times 0.0200-IN. BEARING E

Run No.	Speed RPM	Shaft Torque ft-lbs	Horsepower	Inlet Oil Temp., °C	Outlet Oil Temp., °C	Max. Obsd. Brg. Temp., °C	Oil Flow GPM
E-5	500	9.4	0.9	39.4	39.5	42.4	1.7
E-6	500	8.4	0.8	40.0	41.0	43.4	1.8
E-4	1,000	11.7	2.2	40.1	44.3	51.2	2.5
E-12	1,000	11.1	2.1	40.1	43.4	50.8	2.5
E-9	3,000	19.3	11.0	39.8	53.2	75.2	5.4
E-7	6,000	28.7	32.7	39.8	62.7	88.2	9.6
E-33	6,000	27.5	31.3	39.6	62.9	88.2	9.5
E-8	9,000	42.6	73.0	43.1	77.7	103.5	13.9
E-51	11,000	61.0	127.0	47.8	99.5	122.4	15.2

The viscosity-temperature curves for the two oils are shown in Fig. 5, together with the density-temperature curve.

The results obtained with the four bearings are given in Tables 2, 3, 4, and 5. Runs D, E, and N using bearings D, E, and N, were made with a constant inlet-oil pressure of 10 psi on both oil-feed grooves. In run L using bearing L, oil was fed only to the groove on the leading or downcoming side of the bearing above 4000 rpm, and modified inlet-oil conditions were permitted as shown in Table 4 because of limitations in the oil-supply system.

The oil line to the trailing-edge oil groove was closed above 4000 rpm. The shaft torques are obtained from the measured bearing-torque reactions by correcting for the torque due to the displacement of the shaft in the bearing at right angles to the load.

When the results are plotted in the dimensionless form used by Taylor, the curves, shown in Fig. 6 are obtained for $(Tg)/(\rho N^3 D^4 L)$ versus $(\pi NDC)/(2\nu)$, where the oil viscosity is calculated on the basis of the measured outlet-oil temperature. The vertical arrows indicate the critical values of $(\pi NDC)/(2\nu)$, calculated from

WILCOCK—TURBULENCE IN HIGH-SPEED JOURNAL BEARINGS

829

TABLE 4 TEST DATA ON 8-IN. \times 4-IN. \times 0.0349-IN. BEARING L

Run No.	Speed RPM	Shaft Torque ft-lbs	Horsepower	Inlet Oil Press. PSI	Inlet Oil Temp., °C	Outlet Oil Temp., °C	Max. Obsd. Brg. Temp.	Oil Flow GPM
L-2	1,000	20.4	2.0	10.0	40.0	41.9	49.9	7.6
L-35	1,000	9.5	1.8	10.0	39.8	41.6	49.7	7.6
L-8	2,000	13.1	5.0	10.0	39.7	43.4	55.0	10.0
L-6	3,000	15.8	9.0	3.0	40.5	47.1	51.9	9.7
L-11	4,000	15.3	11.6	3.0	40.2	47.6	72.0	10.8*
L-12	6,000	18.9	21.6	3.0	40.1	51.8	76.7	12.6*
L-13	8,000	23.7	36.0	3.0	39.7	57.2	78.0	13.8*
L-14	10,000	29.9	56.8	3.0	39.6	63.5	84.5	15.3*
L-16	12,000	41.6	94.9	3.0	45.8	80.9	99.2	18.2*
L-17	13,000	47.6	118.0	2.0	51.7	92.6	115.5	19.3*
L-19	14,000	53.8	143.0	1.5	52.4	99.6	121.0	19.8*
L-27	14,700	55.7	156.0	0.8	48.3	98.6	124.0	19.2*

* Oil feed to leading edge oil groove only.

TABLE 5 TEST DATA ON 4-IN. \times 4-IN. \times 0.0153-IN. BEARING N

Run No.	Speed RPM	Shaft Torque ft-lbs	Horsepower	Inlet Oil Temp., °C	Outlet Oil Temp., °C	Max. Obsd. Brg. Temp., °C	Oil Flow GPM
N-10	1,000	1.7	0.3	39.8	43.7	46.4	0.8
N-2	3,000	3.0	1.7	39.9	48.6	55.5	1.4
N-4	7,000	4.6	6.1	39.9	55.8	66.0	2.5
N-7	14,000	7.6	20.1	40.4	74.5	85.4	3.8
N-22	20,000	12.8	43.5	41.9	114.5	115.7	4.0

Taylor's criterion, Equation [3]. It is apparent that runs D, E, and N deviate markedly from the theoretical straight-line relation at values of Reynolds number above the critical. Run L shows a similar effect, but at a critical value considerably higher than calculated. Fig. 7 is a similar plot based on viscosities at the maximum observed bearing temperature. It shows the same marked deviation from the theoretical curve above the critical values of Reynolds number; and, in addition, the straight-line portions are more nearly parallel to the theoretical curve, Equation [2].

Surveys of bearing oil-film temperatures made with bearing D, among others, have shown that the outlet-oil temperature is approximately the same as the average oil-film temperature. Barber and Davenport (4) have made a similar survey on a 2-in.-diameter bearing. Consequently, the curves in Fig. 6 represent the bearing behavior based on average oil-film viscosities, while the curves in Fig. 7 refer to bearing behavior in terms of the maximum Reynolds number in the oil film. Further refinements in the calculation of Reynolds number, such as correcting for the effect of shaft eccentricity, do not appear to be warranted, since the measured bearing torque is the summation of the shear resistance over the entire bearing area.

Whether comparison is made on the basis of average or of minimum oil-film viscosity (Fig. 6 or Fig. 7), deviation from the

curve representing normal viscous behavior occurs at approximately the point predicted by the Taylor equation. Beyond the critical point, the frictional resistance of the bearing increases rapidly. The critical point for run L occurs at from 2 to 4 times the predicted value, depending upon the method of plot chosen. It is thought that this extension of the normal range may be related to the method of feeding oil only to the leading-edge oil groove rather than to both grooves as in the other runs.

EFFECTS OF TURBULENCE ON BEARING PERFORMANCE

In addition to the "Taylor plot," the presence of oil-film instability, or turbulence, reveals itself in a number of extremely practical effects. It affects power loss, oil-film temperatures, oil-flow rate, shaft eccentricity, and the Sommerfeld plot.

Power loss increases much more rapidly with speed after the critical Reynolds number is exceeded. Fig. 8 shows the relation of horsepower loss to speed. Below the critical point, horsepower varies as the 1.4 power of the speed; above the critical point, horsepower varies as the 2.7 power of the speed.

Oil-film temperatures tend to rise rapidly beyond the critical Reynolds number. Fig. 9 shows the maximum oil-film temperature, in terms of the rise above the inlet-oil temperature, as a function of shaft speed, and illustrates the rapid rise at high speeds.

The oil-flow rate is depressed at speeds above the critical point,

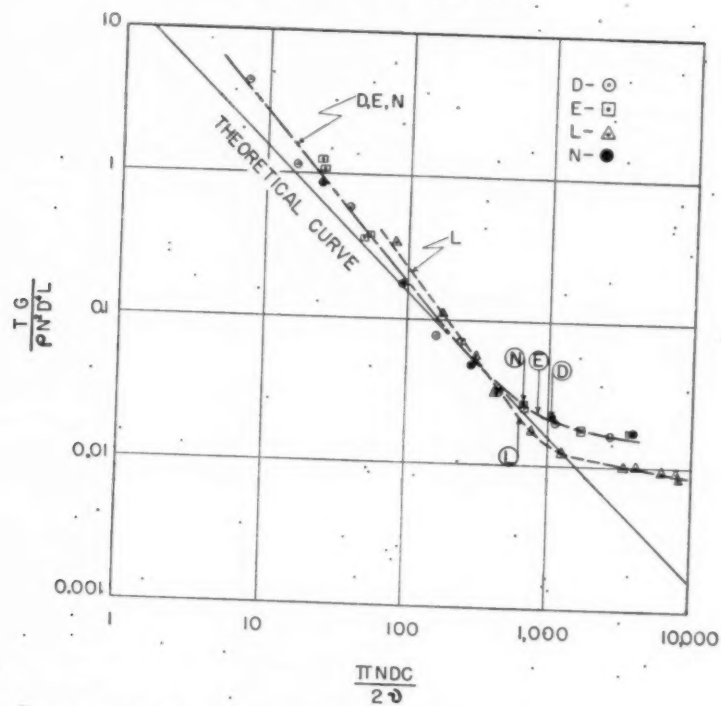


FIG. 6 TAYLOR PLOT BASED UPON VISCOSITIES AT OUTLET-OIL TEMPERATURES
(Vertical arrows indicate calculated transition points between laminar and turbulent flow.)

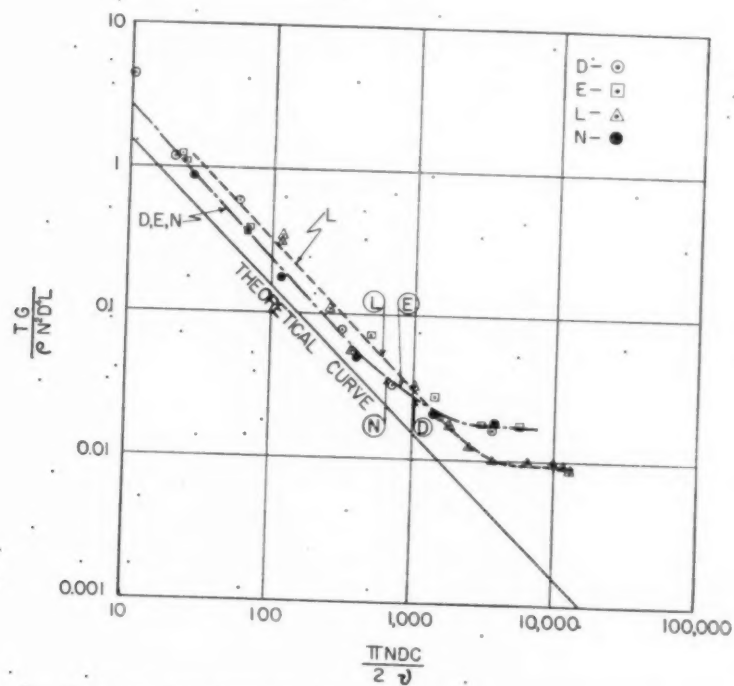


FIG. 7 TAYLOR PLOT BASED UPON VISCOSITIES AT MAXIMUM OBSERVED BEARING TEMPERATURES
(Vertical arrows indicate calculated transition points between laminar and turbulent flow.)

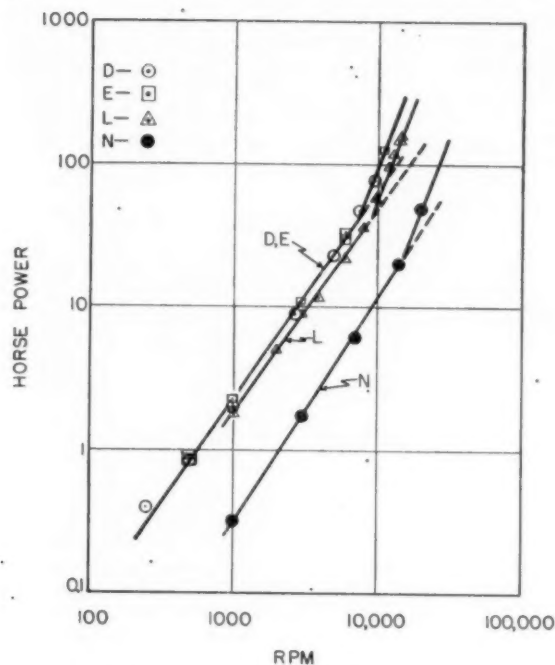


FIG. 8 BEARING POWER LOSS AS FUNCTION OF SPEED

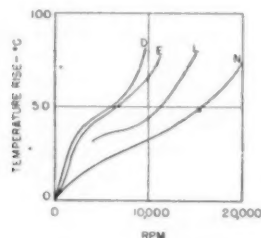


FIG. 9 MAXIMUM BEARING-TEMPERATURE RISE ABOVE INLET-OIL TEMPERATURE AS FUNCTION OF SPEED

as shown in Fig. 10. This occurs in spite of the fact that the higher inlet-oil temperatures occurring in the highest-speed runs should result in increased flow rates. Thus turbulence tends to obstruct oil flow, much as it does in a pipe line. The oil flow in run L is further depressed by the drop in inlet-oil pressure.

The effect of turbulence on shaft eccentricity is unusual and is shown in dimensionless form for runs E and L in Fig. 11 in which eccentricity ratio, $2e/C$, is plotted as a function of the Sommerfeld variable (5), based on the oil viscosity at the outlet-oil temperature. Above the critical Reynolds number, a sharp break in the eccentricity curve is observed. The Sommerfeld number decreases and the eccentricity simultaneously decreases toward the value predicted by the hydrodynamic theory for a complete cylindrical bearing without end leakage. It is presumed that the high eccentricities found in the normal range of operation are due to the effects of end leakage (oil flow) and of the oil-distribution grooves. The onset of turbulence then tends to reduce the effect of these factors.

Turbulence effects are sharply revealed in the Sommerfeld plot for friction factor (5), Fig. 12. The result of oil-film instability is a coefficient of friction greatly increased over the normal value at the same Sommerfeld number.

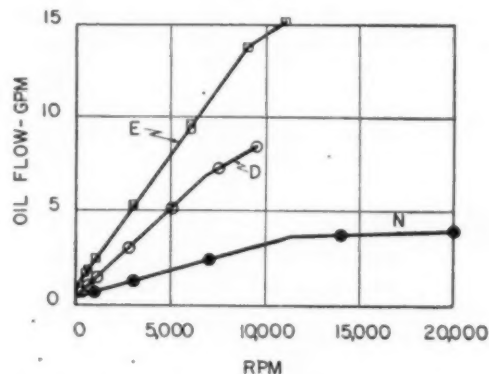
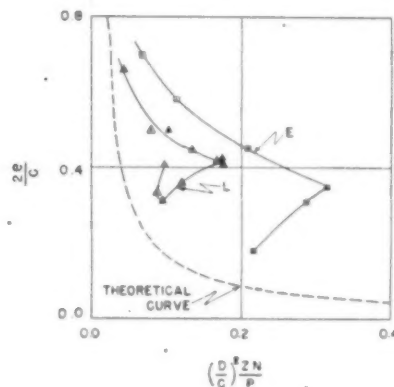
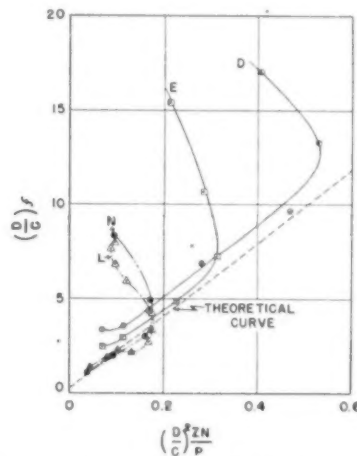


FIG. 10 OIL FLOW THROUGH TEST BEARINGS AS FUNCTION OF SPEED

FIG. 11 SHAFT ECCENTRICITY RATIO, $2e/C$, AS FUNCTION OF SOMMERFELD VARIABLE FOR BEARINGS E AND LFIG. 12 REDUCED FRICTION COEFFICIENT, $(D/C)F$, AS FUNCTION OF SOMMERFELD VARIABLE

HIGH-SPEED BEARINGS

There is a marked trend today toward higher rotative speeds in new turbine and gear designs. In many cases requirements for shaft stiffness dictate that these speeds be attained with large

shaft diameters, i.e., at high surface speeds. Do the experimental and theoretical effects outlined herein indicate a practical upper speed limit for cylindrical bearings?

The interplay of the several factors is complicated. The critical Reynolds number is inversely proportional to \sqrt{C} . Consequently, the requirement that a bearing of a given size operate in the normal range may be stated as,

$$N < \frac{K\sqrt{C}}{C^{3/2}}$$

in which K is a numerical constant. Thus the transition speed depends not only on the clearance but also upon the increase in oil flow as clearance is increased, and upon the corresponding increase in oil viscosity as outlet-oil temperature drops. Operation in the turbulent region is more feasible with the lower temperatures accompanying larger clearances, but opposed to this is the problem of machine alignment introduced by large-clearance bearings; for example, the larger clearances required between rotors and stators, and the possible improper meshing of gears. What do the experiments have to say about transition speeds at the critical Reynolds number and about practical top speeds?

The data on the three 8-in. \times 4-in. bearings indicate the following relation between clearance and the transition speed at which instability sets in:

Clearance	—Approximate transition speed, rpm—	
	Found	Predicted
D: 0.0129	7000	7500
E: 0.0200	6000	6700
L: 0.0349	8000	5500

The experimental transition speed is obtained from the Sommerfeld plot, but similar values may be obtained from the Taylor plot based on outlet-oil temperature. The predicted values are obtained from the Taylor plot using the calculated critical Reynolds numbers. Bearing in mind that the experimental transition speed for bearing L is high because of the method of oil feed, we see that lower transition speeds may be anticipated as clearances are increased.

The temperatures at the transition speed decrease as the clearance is increased as follows:

Clearance	—Approximate temperature, deg C—	
	Outlet oil	Max bearing
D: 0.0129	82	96
E: 0.0200	63	88
L: 0.0349	57	78

As a result, operation in the turbulent region will be safer at the larger clearances, and the safe top operating speed will increase somewhat as the clearance is increased. Referring to Fig. 9, the speed at which a bearing temperature 70 C (126 F) above inlet-oil temperature is reached is approximately as follows:

Clearance	Speed for 70 C	Excess over
	bearing temp rise,	transition speed,
	rpm	rpm
D: 0.0129	9000	2000
E: 0.0200	10500	4500
L: 0.0349	14000	6000

showing that the invasion of the turbulent speed region may be deeper at larger clearances. Decreasing the oil viscosity would be expected to have similar results, that is, it would decrease the speed at which the turbulent region begins but make possible operation at higher speeds for the same temperature rise.

The results on run L indicate that the region of normal operation may be extended considerably by feeding oil to the leading edge or downcoming side only. Confirmation of this effect of oil-feed method is furnished by the additional data for bearing E

at 9000 rpm shown in Table 6. Feeding oil only to the leading edge removed the bearing operation from the turbulent region, reducing the power loss from 73 hp to exactly the value calculated for laminar flow, 50 hp. Feeding oil to the leading edge also reduced the outlet-oil temperature, the maximum observed bearing temperature, and the oil flow. The effect of a similar change in oil feed at speeds below the transition speed is slight.

TABLE 6 EFFECT OF OIL FEED UPON BEARING OPERATION ABOVE CRITICAL REYNOLDS NUMBER

(Bearing E, 9000 rpm, 150 psi load Critical Reynolds number = 825)			
Oil-feed method	Both sides	Leading edge	Trailing edge
Inlet-oil temp, deg C	43.1	39.5	42.9
Outlet-oil temp, deg C	77.7	70.0	89.4
Maximum observed bearing temp, deg C	103.5	98.5	106.2
Oil flow, gpm	13.9	10.4	8.6
πNDC			
$\frac{2\pi}{NDC}$	3110	1290	2270
Power loss, hp	73	50	63
Power loss for laminar flow at indicated value of πNDC			
$\frac{2\pi}{NDC}$	21	50	28
Type of operation	Turbulent	Laminar	Turbulent

Feeding oil to the trailing edge (Table 6), results in much less reduction in the power loss which remains much greater than that calculated for laminar flow in the oil film. This method of feed also results in a decreased oil flow. However, outlet-oil temperature and bearing temperature are higher than when feeding to both grooves.

The beneficial effect of feeding oil only to the leading edge appears to be related to a decreased amount of oil in the upper half when feeding in this manner. Pressure measurements in the upper half of other bearings have indicated negative gage pressures with this type feed at locations which show positive pressures when feeding to both grooves or to the trailing edge. Because of the depressed position of the shaft in the bearing under load, the maximum Reynolds number normally occurs in the upper half where the clearance is largest, and consequently a reduced amount of oil in the upper half will result in less tendency toward turbulence in the bearing.

The depth of the oil-feed grooves doubtless results in the presence of turbulent eddies within them at even moderate speeds. These eddies will cause some slight increase in bearing friction. A. Rumpf (6), in comparing the performance of a cylindrical bearing with one with a circumferential groove in the upper half, has ascribed the increased friction of the latter bearing to turbulence in the circumferential groove. If such a bearing were operated with a restricted oil feed so that this groove did not run full of oil, considerably reduced friction would be expected because of the absence of turbulence.

CONCLUSION

The relation derived by G. I. Taylor for the Reynolds number at which fluid instability will begin between concentric cylinders with the inner cylinder rotating has been applied to the nonconcentric case of a journal bearing under load. With diameter-to-clearance ratios less than one tenth of those used experimentally by Taylor, the existence and location of the predicted critical point have been verified. The transition to turbulent oil-film conditions is evidenced by (a) increased power consumption, (b) increased bearing temperature, (c) reduced oil flow, (d) a sharp break in the dimensionless shaft-eccentricity plot, and (e) a break in the Sommerfeld friction-factor plot toward higher bearing friction. Feeding oil to the bearing through only the downcoming-side oil groove extends at least twofold the region of laminar oil-film behavior.

ACKNOWLEDGMENT

The assistance of W. Rogers, P. Lyons, and H. Stone in obtaining the experimental data is gratefully acknowledged.

BIBLIOGRAPHY

- 1 "Stability of a Viscous Liquid Contained Between Two Rotating Cylinders," by G. I. Taylor, *Trans. of the Royal Society of London, England, series A*, vol. 223, 1923, p. 289.
- 2 "Fluid Friction Between Rotating Cylinders," by G. I. Taylor, *Proceedings of the Royal Society, London, England, series A*, vol. 157, 1936, p. 546.
- 3 "Hydrostatic Lubrication," by D. D. Fuller, *Machine Design*, vol. 19, June, 1947, pp. 110-116; July, pp. 117-122; August, pp. 115-120; and September, pp. 127-131 and 188-190.
- 4 "Investigation of Journal Bearing Performance," by E. M. Barber and C. C. Davenport, *Pennsylvania State College Bull. No. 42*.
- 5 "Lubrication," by A. E. Norton, McGraw-Hill Book Company, Inc., New York, N. Y., 1942, pp. 119-120.
- 6 "Friction and Temperature Paths in Plain Bearings," by Adolf Rumpf, *VDI Forschungsheft, Ausgabe B*, vol. 9, November-December, 1938, 24 pp.

Discussion

M. D. HERSEY.⁴ The results of primary interest in this investigation are the confirmation of G. S. Taylor's criterion for turbulence under practical bearing conditions, and the exploration of performance characteristics for an appreciable distance into the turbulent region. There are also many important secondary results extending over the normal speed range which will establish this paper as one of reference value for some years to come.

Another form in which Taylor's criterion may be expressed is

$$N = \frac{\nu}{n^{1/2}} \left(\frac{77}{D^2} \right)$$

where N denotes the critical speed in thousands of revolutions per minute, D the journal diameter in inches, n the clearance in parts per thousand, and ν the kinematic viscosity in centistokes.

A formula for the occurrence of turbulent motion due to longitudinal flow in the clearance space was derived empirically by Edgar Buckingham (7) which may be written

$$\frac{CS}{\nu} = 2000$$

where S denotes the mean speed of flow through the clearance space toward each end of the bearing, the other quantities being expressed in the same system of units.

In referring to friction coefficients higher than expected from the ZN/P curve, it must be remembered that the correct use of the ZN/P diagram, under conditions where the density of the lubricant can effect its performance, requires a family of curves for constant values of the parameter $\rho N^2 D^2 / P$, or its equivalent, see page 84 of reference (8). It might be of interest to plot some of the author's data at the higher speeds in this manner.

Since it is difficult to evaluate the effective film viscosity Z , it may be more convenient to work with the inlet viscosity Z_1 . Approximate allowance can then be made for the variation in viscosity at different points in the film by introducing an additional parameter representing the more essential thermal properties of the lubricant, see discussion of the Linn and Irons paper,

⁴Mechanical Engineer, U. S. Naval Engineering Experiment Station, Annapolis, Maryland. Fellow ASME.

The opinions expressed in this discussion are those of the writer and do not necessarily reflect the views of the Navy Department or of the Naval Service at large.

page 623 of reference (9). This parameter may be written aP/q where a is the temperature coefficient of viscosity at the inlet temperature and q the mean heat capacity of the lubricant per unit volume. A separate family of curves will be required when any great change is made in the parameter p_1/P representing the ratio of inlet pressure to the load per unit area. Once laid out, such curves would be expected to apply to all geometrically similar bearings of whatever size, and to other lubricants besides those actually used in the tests. Two additional parameters are needed when loads are reached involving elastic deformation and the change of viscosity under pressure.

The beneficial effect of feeding oil only to the leading edge suggests that the conditions then prevailing are in some degree those of an externally pressurized bearing (3), and that the tendency for thermal expansion of the cooler entering oil also contributes to the lifting force of the film.

It is recommended that the factor g be omitted from Equation [1] in future publications. As it stands, this equation apparently states that the same operating conditions will create a greater friction torque on Pike's Peak than at West Lynn, Mass., which is plainly false in a physical sense, however accurate it may be made by virtue of specially chosen units. Lord Rayleigh (10) called attention to the practice of many engineers of putting g in their descriptions of phenomena that are in no way influenced by gravity, and leaving it out when it should be in. The aim of his criticism was to set up equations that will not merely serve for slide-rule work, but will convey a true physical picture of what happens.

BIBLIOGRAPHY

- 7 "Leakage Through Thin Clearance Spaces," by Edgar Buckingham, *Engineering*, vol. 15, 1923, pp. 225-226.
- 8 "Theory of Lubrication," by M. D. Hersey, John Wiley & Sons, Inc., New York, N. Y., 1936.
- 9 "Power Losses in High-Speed Journal Bearings," by F. C. Linn and D. E. Irons, *Trans. ASME*, vol. 63, 1941, pp. 617-629.
- 10 "The Principle of Similitude," by Lord Rayleigh, *Nature*, vol. 95, 1915, pp. 66-68.

H. PORITSKY.⁵ Offhand, one would not associate oil flow in bearings with the turbulence, and most of the theory of lubrication phenomena is based on the assumption of laminar flow of oil. The author is therefore to be congratulated on his precise delineation of one field of lubrication phenomena in which turbulent motion prevails.

It is of interest to point out that the turbulence occurring in the space between two cylinders of which the inner one is rotating and the outer one is stationary, first studied by Lord Taylor, is one of the few known cases of fluid motion in which it is actually possible to predict from theory the onset of turbulence. Turbulent fluid flow in a pipe, first studied by O. Reynolds some 90 years ago, has not as yet been fully explained.

The physical reason for the onset of turbulence in the case of an inner rotating cylinder may be visualized as follows. In laminar motion, the fluid particles move in circular paths with velocities varying from zero at the outer stationary cylinder to the speed of rotation at the inner cylinder. Thus the centrifugal force which tends to throw the particles out radially is largest on the inside and decreases to zero on the outside. The situation is completely analogous to a stationary layer of air which is warmed by contact with a heated surface at the bottom (for instance, atmospheric air, heated from the surface of the earth through the energy absorbed from solar radiation), and acquires buoyancy proportional to its temperature rise. When the temperature gradient becomes

⁵Consulting Engineer, General Electric Company, Schenectady, N. Y. Mem. ASME.

sufficiently large to overcome viscous resistance, convection currents will tend to get set up. Since the warm, lighter air cannot rise simultaneously everywhere, it is to be expected that circulation will be set up, with the warm air rising at some places and cooler air descending elsewhere. Thus vortices will be set up. A similar situation occurs in the fluid between a rotating and a stationary cylinder. Taylor's theory actually predicts size of these vortices, and Taylor verified it by injecting ink in the fluid between glass cylinders. Since he was concerned only with onset of turbulence, and used a linear theory retaining only the first powers of the circulation amplitude, he did not predict the amplitude of the vortices, nor the increased losses which occur as a result of onset of turbulence.

M. C. SHAW.⁶ When one cylinder rotates concentrically relative to another cylinder the motion of the fluid between the cylinders is observed to change its character with the speed of rotation. At relatively low speeds the fluid particles have circular paths, as in ordinary journal bearings which operate at normal speeds. As the speed is increased inertia forces become significant and pairs of ring vortices are found to appear in the film. As the speed is further increased the orderly vortex motion gives way to turbulence. Interesting photographs of the vortices formed during the second type of motion have recently been presented by W. W. Hagerty.⁷ This type of motion as well as turbulent motion in which there is a random intermingling of stream tubes will give rise to greater friction, temperature rise, etc., than will be obtained with the more usual laminar type of flow.

The experiments described by the author show a significant deviation from the friction characteristics based upon laminar flow with circular streamlines. However, from the data presented, it cannot be determined whether this increase in friction is due to the appearance of vortex pairs or truly turbulent motion. The critical value of Reynolds number given by Equation [3] is for the transition to turbulent motion. Therefore the statement in the conclusions that "...the existence and location of the predicted critical point have been verified" might possibly be too inclusive, since the increase in friction might be due to the onset of vortex motion rather than turbulent motion. In fact, one should expect the initial deviation from the laminar friction curve to be due to vortex motion; and a second rather abrupt increase in friction to accompany the beginning of turbulence.

A series of tests with concentric spheres have been reported^{8,9,10,11} by French workers which are of interest in connection with this problem. The friction torque was carefully measured when the inner sphere was rotated and the outer sphere was held stationary. At the same time the nature of the motion of the fluid was

observed as in Taylor's experiments. It was found that at low rotative speeds the fluid moved in circular paths parallel to the equator, but as the speed was increased vortex pairs appeared due to inertia effects. The fluid in the upper hemisphere was observed to move downward along the moving member, being deflected upward upon reaching the equator and thence flowing along the stationary member. At the same time a circulatory flow was established in the lower hemisphere in the opposite direction. The friction torque was observed to rise abruptly from the value corresponding to the usual flow with circular streamlines with the onset of the vortex motion. The observed increase in torque above that expected for circular stream lines was as high as 46 per cent, all of these tests being performed well below speeds required to give turbulence. Deviation from the usual curves was observed at very much lower speeds with spheres than the values Taylor found for cylinders for comparable values of clearance, diameter, and viscosity. Incidentally, these studies upon concentric spheres now verify the inertia induced circulatory flow postulated by Shaw and Strang¹² to explain the mode of operation of the Hydrosphere.

The tests presented in this paper are for a bearing in which the journal is in motion while the bearing is at rest. In discussing the question of turbulence in the oil film of a high-speed bearing in connection with a paper presented by A. E. Roach at the 1948 Annual Meeting, it was pointed out¹³ that even though Taylor observed different critical speeds for turbulence when either the outer or inner cylinders are rotated, this difference in the two critical speeds converges as the clearance-diameter ratio is decreased. By extrapolation the two critical speeds are found to converge to the same value for values of the clearance-diameter ratio usually employed in lubrication. Thus the material given in this paper should also be applicable to high-speed bearings in which the journal is stationary and the bearing surface is in motion.

AUTHOR'S CLOSURE

The author appreciates the helpful comments which the discussers have given. It is important to be able to delineate the region in which normal bearing operation with laminar oil flow in the bearing film can be expected; and the additional evidence cited will help in this regard.

It is not felt that the effect of feeding oil only to the leading edge in extending the region of laminar flow is due to the conditions mentioned by Mr. Hersey. In fact our measurements indicate that the shaft is riding somewhat lower in the bearing under these conditions, in agreement with Fig. 11. In other words, nonlaminar flow tends to restore the shaft toward the bearing center.

Mr. Hersey's recommendation on the use of the factor g is accepted with thanks. The confusion results from the failure to use a consistent system of units in the discussion.

The term turbulence has been used somewhat loosely, as Dr. Shaw points out, to mean "nonlaminar flow." The experiments indicate a gradual transition from the laminar region, which may be the region of vortex flow. Mr. Taylor's experiments at large clearances show the same type of transition, and in addition, his visual observations showed that beyond the transition region turbulence was experienced.

⁶ Associate Professor of Mechanical Engineering, Massachusetts Institute of Technology, Cambridge, Mass.

⁷ "Use of an Optical Property of Glycerine—Water Solutions to Study Viscous-Fluid-Flow Problems," by W. W. Hagerty, ASME Preprint 49—APM-21.

⁸ "Mesure du moment d'un couple par emploi du moteur chronométrique. Application à l'étude de la viscosité," by A. Guillet, *Comptes Rendus*, vol. 200, 1935, p. 442. "Sur le viscosimètre constitué par une sphère en rotation au sein d'un fluide," by A. Guillet, *Comptes Rendus*, vol. 200, 1935, p. 1522.

⁹ "Contribution à l'étude expérimentale de phénomènes anormaux en mécanique des fluides visqueux," by M. Jacques Huetz, *Comptes Rendus*, vol. 223, 1946, p. 534.

¹⁰ "Sur l'existence de plusieurs régimes, où les forces de viscosité sont linéaires en fonction de la vitesse," by M. Jacques Huetz, *Comptes Rendus*, vol. 223, 1947, p. 1205.

¹¹ "Sur le couple de viscosité entre deux sphères concentriques," by M. Aubert and Jean Villey, *Comptes Rendus*, vol. 224, p. 1271.

¹² "Movement of a Viscous Fluid Between Two Concentric Spheres," by F. Charron, *Publications Scientifiques et Techniques du Ministère de L'air*, No. 208, 1947, p. 1.

¹³ "The Hydrosphere—A New Hydrodynamic Bearing," by M. G. Shaw and C. D. Strang, Jr., *Journal of Applied Mechanics*, Trans. ASME, vol. 70, 1948, pp. 137-145. Discussion, *Journal of Applied Mechanics*, Trans. ASME, vol. 71, 1949, pp. 93-98.

¹⁴ "The Load-Carrying Ability of Hydrodynamic Oil Films," by A. E. Roach, *Mechanical Engineering*, vol. 71, 1949, pp. 293-296 and 326. Discussion by Milton C. Shaw, *Mechanical Engineering*, vol. 71, 1949, pp. 763-764.

Closed-Cycle Gas Turbine

Escher Wyss—AK Development, 1945-1950

By CURT KELLER,¹ ZURICH, SWITZERLAND

In 1945 Ackeret and the author made the first presentation in the United States of the basic theory and results of tests on the closed-cycle gas-turbine process, which had been pioneered by the author's company. Since then the development has progressed rapidly and larger industrial installations have been made. Compressed high-temperature air and other gases, used in closed-cycle turbines, have led to new designs of components and plant layouts. This paper describes new stationary units which will be in operation in the near future and discusses future work and possibilities.

THE gas turbine with a closed externally heated working cycle and variable pressure level is still a young proposal. The first plant of this kind, a test unit at the Escher Wyss works, produced 1000 kw for 7 hr in January, 1940. Early experience with this plant, theory of the cycle, and constructional proposals were covered in a paper (1)² presented in 1945.

Since 1945, when necessary materials again became available to Swiss industry, development has been rapid. Further experience has been gained with the test plant, research has gone ahead on individual components, and two large installations are under way. This report supplements the 1945 paper by covering the work of the past 4 years and outlining expected future trends.

In relation to its size, Swiss industry has made a great effort to bring the industrial gas turbine into being. Each firm, relying on its own resources, has taken the risk involved in exploring and developing one of several gas-turbine cycles—open, semiclosed, or closed.

Our work has been mainly with the closed cycle. The advantages we believe to be inherent have been discussed in previous papers (1, 4). They can be summarized as follows: (a) suitability for plants of large size; (b) possibility of using solid fuels; (c) use of clean air under pressure in working cycle gives advantages in design of rotating machinery and heat exchangers; and (d) regulation by variation of pressure level yields good part-load characteristics.

At present, one other firm which has been licensed under the basic patents Escher Wyss holds in most countries: Messrs. John Brown & Co., Ltd., Clydebank, Scotland, as our licensee in Great Britain, is also manufacturing plants of this kind. These will be referred to in this paper.

To avoid splitting our resources (man power as well as funds) we have concentrated first on the most promising projects—plants for central stations, industrial use, and ships (2). We have made only preliminary studies of closed-cycle possibilities for vehicles, locomotives, aircraft, and atomic-energy conversion, which would seem to be a most promising application in the future (1).

¹ Escher Wyss, Ltd. Mem. ASME.

² Numbers in parentheses refer to the Bibliography at the end of the paper.

Contributed by the Gas Turbine Power, Power, and Aviation Divisions and presented at the Annual Meeting, New York, N. Y., November 27-December 2, 1949, of THE AMERICAN SOCIETY OF MECHANICAL ENGINEERS.

NOTE: Statements and opinions advanced in papers are to be understood as individual expressions of their authors and not those of the Society. Paper No. 49-A-35.

Actual designs for the two 12,500-kw plants now under construction are based to a considerable extent upon experience with the 2000-kw shop plant and laboratory tests of components. We have been deliberately cautious in introducing new features and extrapolating from known information. Thus the essentially conservative design of these plants should not be regarded as more than an essential stage of development. Further progress, especially concerning size and simplification of heat-exchange apparatus, air heaters, and the like, as well as further improvements in machine efficiencies, are definitely in sight. Nevertheless, the plants under construction are expected to show a heat rate of 10,000 Btu per kw-hr. Every future rise of temperature will yield about three times as much efficiency gain as it would with steam, Fig. 1. Herein lies a major cause for optimism regarding the future application of gas turbines.

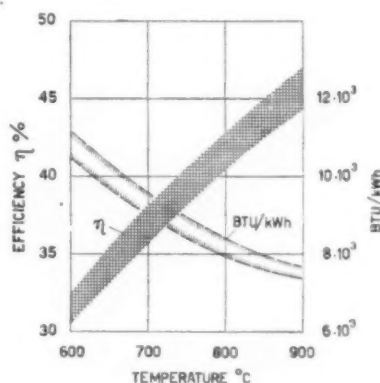


FIG. 1 APPROXIMATE OVER-ALL PLANT EFFICIENCIES—BASED UPON LOWER CALORIFIC VALUES—AND HEAT CONSUMPTION FOR CLOSED-CYCLE TURBINE INSTALLATIONS DEPENDING UPON WORKING TEMPERATURE

(Figures valid for today's constructional possibilities.)

LONG-TIME OPERATING EXPERIENCE WITH TEST PLANT

As the 2000-kw test plant is in many respects the basis of our present designs, a review of its 10-year record forms a good starting point. Despite many severe trials, it is still in good condition and ready for further work, Fig. 2.

Total running time (till spring, 1949) is close to 5000 hr. Apart from trial runs, more than 2.5 million kw-hr have been delivered to the grid. Official tests (5) were run after about 1000 hr total service, including a first 50-hr nonstop run at 650 C and 1000 kw output in December, 1943. After successful official tests in December, 1944, attention was focused on tests of component parts and especially on regulation, to check theoretical calculations.

In the test plant, the high-pressure turbine drives the compressor at 8000 rpm and the low-pressure turbine drives the generator at 3000 rpm. A gear set couples these two groups and maintains the speed relation. Tests on the pilot plant, without this intermediate gear, proved that with suitable simple regu-

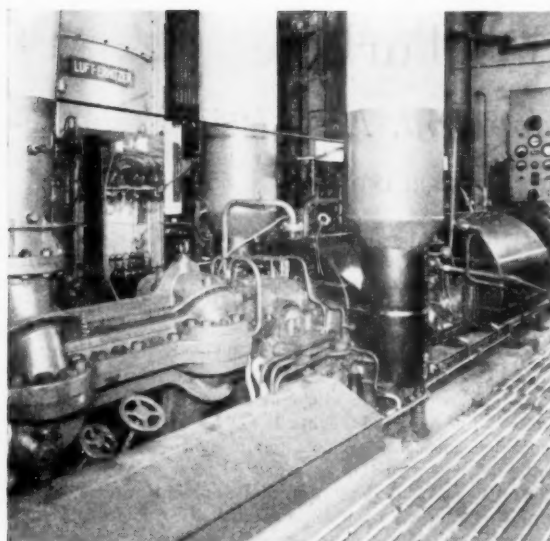


FIG. 2 VIEW OF MACHINE SET OF ESCHER WYSS 2000-KW TEST PLANT

(From left to right are shown compressor, high-pressure turbine, low-pressure turbine, generator. Note absence of inlet valve to high-pressure turbine. Vertical air accumulator in background.)

lating devices, the two groups are stable. Thus in most of the coming plant designs, the two turbine groups will run entirely separately.

Scarcity of hydroelectric energy in Switzerland during the past three winters offered the possibility of long nonstop runs, furnishing electricity to the town grid. The energy produced corresponded to the daily need of the Escher Wyss works. The main continuous operating periods were as follows:

First run, ended March, 1947.....	888 hr
Second run, ended November, 1947.....	1243 hr
Third run, ended March, 1949.....	1338 hr

All these were continuous, day and night, without any important interruptions caused by basic failures of the plant. A few short stops of several hours were caused by minor troubles with auxiliaries, electrical equipment, and instruments. We believe this represents a high order of reliability for a plant built for laboratory work, with much temporary auxiliary equipment. During the last long runs, two untrained men operated the plant each shift.

Neither air heater nor machines have experienced detrimental fouling. Air-heater tubes have never been cleaned since the beginning in 1940. Their surfaces are still almost unsoiled. Furnace oil as employed in Switzerland for industrial purposes, and synthetic oil were used. These are not the crudest grades.

Despite direct exposure to flame radiation, tube bundles are still in good order, Fig. 3. Since the beginning, about 250 starts and stops have been made, with corresponding heating and cooling. Nevertheless, over-all efficiency today is not lower than during official tests 4000 hr earlier. Average efficiency of the last 1338-hr run (loads between 650 and 800 kw, temperatures between 620 and 650 C) was 24.2 per cent, based on lower heating value. This corresponds well with the Quiby figure, taking account of temperature corrections. Between the second and third long-time runs, there was no revision or overhaul of machinery. The set was started at the beginning of 1949 in the same condition as at shutdown a year before.

The worst accident occurred after 1200 hr of running, in

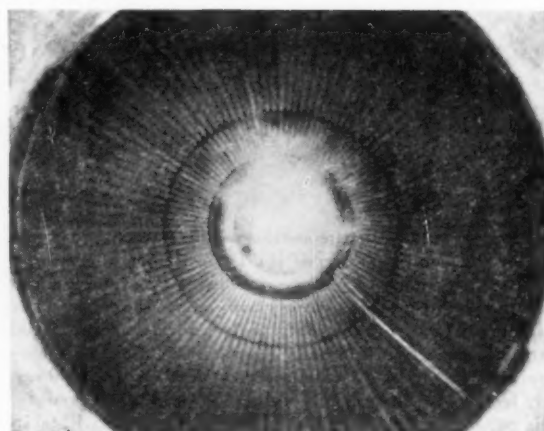


FIG. 3 VIEW INSIDE COMBUSTION CHAMBER OF TEST-PLANT AIR HEATER, SEEN FROM TOP UNDER OPERATION AT ONE THIRD FULL-LOAD



FIG. 4 BROKEN RIM OF FIRST STAGE OF EXPERIMENTAL TURBINE

December, 1943. The rim of the high-pressure turbine's first stage broke off; rotor and blading were badly damaged, Fig. 4. Close investigation furnished valuable information on the behavior of high-alloy heat-resisting steels. Following older steam-turbine practice, blades were attached to the first disk in a T-groove, not with the "fir-tree" fastening common today. Calculated stress in the outer rim from blade centrifugal forces amounted to about 17,000 psi. Due attention had not been given to rounding-off the T-root, and a sharp notch produced stress concentrations. Actually, a maximum stress of 28,000 to 35,000 psi must have been produced. This corresponds to the value which will cause rupture of this kind of material (Poldi AKRV steel—11.2 per cent Cr, 12.4 per cent Ni, 2.5 per cent Wo) in about 1000 hr. Tests established these values long after our rotor was ordered in 1935. In our new machines stresses are much lower.

The blades, of ATS steel (17.6 per cent Cr, 9.3 per cent Ni, 1 per cent Wo), behaved well. They were bent and twisted but none was broken. Ductility of the material had not suffered during its high-temperature service and there was no embrittlement.

Over the years, compressor design has changed to take advantage of later knowledge. Before putting new rotors into service in the test plant, efficiencies were carefully measured on a

special test bed. During the tests an amazingly quick and pronounced drop in rotor efficiency of 3 percentage points was measured after 12 hr, with ambient air taken from a relatively clean workshop.

Such compressor-efficiency drops would influence performance of the whole plant to a considerable extent. In two-stage plants of the kind we build, a 1 per cent compressor-efficiency drop results in 0.5 point loss of efficiency for the entire plant. This is equivalent to about 1.5 per cent rise in fuel consumption. Such detrimental effects of fouling are not encountered when the cycle is fully closed, as the long-time runs of the test plant demonstrate.

Regulation of closed-cycle plants has been explained in earlier publications (6). Practical operation of the test plant has proved that pressure-level variations combined with by-pass connections between high-pressure and low-pressure sections of the circuit can meet the demands usually imposed on steam-turbine plants. This principle was adopted for the 12,500-kw sets. Absence of moving parts, such as regulating valves, spindles, or throttling devices in the high-temperature region, and constant temperatures at each part of the plant for all loads, prove practical assets.

Because of accumulated heat in tubes and walls of the air heater and heat exchanger, combustion regulation need not follow load fluctuations quickly. If combustion rate is not properly adjusted, air temperature changes only relatively slowly. A load change as a consequence of altered temperature conditions will be compensated temporarily by a corresponding modification of pressure level. Fig. 5 shows the small change in pressure level (P/P_0) which is needed to hold plant output constant

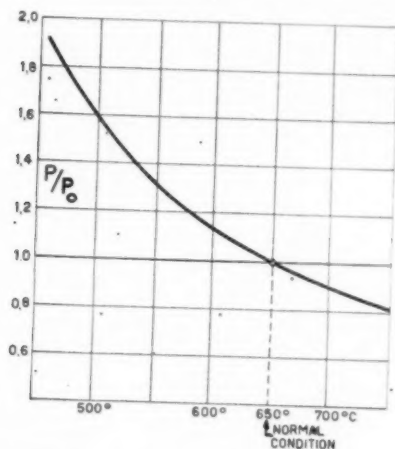


FIG. 5 COMPENSATION OF TEMPERATURE VARIATION BY CHANGING PRESSURE LEVEL

as turbine-inlet temperature varies. If, for instance, burner interruption causes a sudden drop from 650 to 600 C, a rise of only 12 per cent in pressure level, by releasing cold-storage air from the accumulators to the circuit, restores normal load. Such effects were quite clearly demonstrated in the test plant.

It is impressive, for example, to see that one can change fuel injection for several minutes without appreciable effect on output. Fig. 6 shows results of such demonstrations. Before point A, conditions were constant with normal output N_0 , maximum pressure P_0 , inlet temperature of 1050 F, and fuel consumption G_0 . At point A, load dropped suddenly to about 40 per cent of N_0 , and continued for about 10 min, to point B. Pressure level fell, too.

With no change in fuel-pump delivery, inlet temperature rose steadily, but at only 10 to 15 F per min. Increase in output from temperature rise was compensated automatically by gradual lowering of circuit pressure brought about automatically by the governing gear.

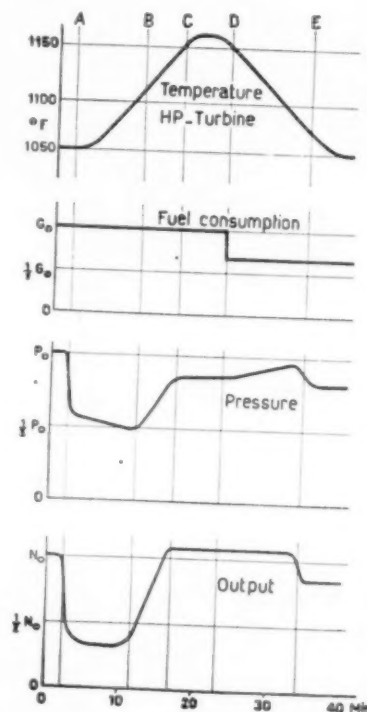


FIG. 6 TEST RESULTS AS TO ACCUMULATING EFFECT AT VARYING FUEL SUPPLY AND LOAD IN EXPERIMENTAL TURBINE

Between points B and C, load increased without an extra supply of fuel. Temperature still rises first as there are inertia effects. At point C load has reached its original value. Fuel supply remains constant to point D. This brings temperature to a maximum value of 1160 F. It then drops again. At point D fuel supply to air heater was suddenly reduced to 65 per cent. Normal output could be secured, in spite of falling turbine temperature, by the automatic pressure compensation (P_0 rose between D and E for another 10 min).

Shutting off fuel supply completely makes an impressive demonstration. With the test plant running at 1000-kw load, shutting oil supply off for a minute or two proves only slightly noticeable at the kilowatt meter. While these characteristics will be less pronounced in bigger plants because they depend on volumes and heat capacity of the installation, they will, in principle, help to make the set insensitive to unforeseen changes.

FIRST CLOSED-CYCLE PLANTS FOR CENTRAL STATIONS

At present, three closed-cycle plants are under erection, two for power plants and one for waste-heat use in a gas works. The central-station designs will be considered first, the industrial plant later.

Electricité de France has ordered a 12,500-kw oil-fired set for the St. Denis power station in Paris, Figs. 7 and 8. This plant will start operation late in 1950. Its regulation system enables it to follow load fluctuations independently of the network. This

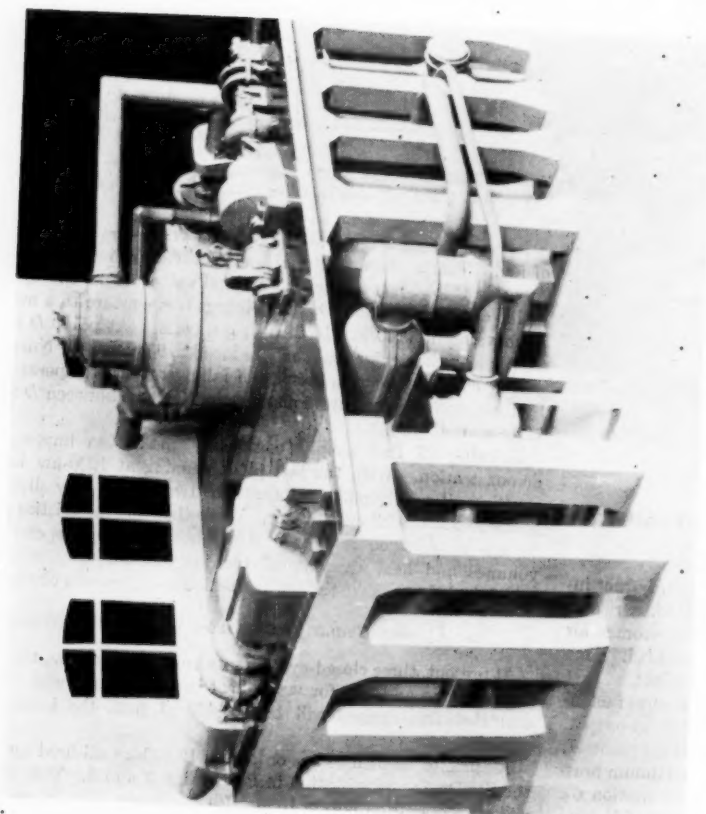


Fig. 7 MODEL OF 12,500-KW PARIS INSTALLATION
(At left, generator low-pressure turbine group; at right in foreground, high-pressure turbine-compressor group; center, upper part of air heater.)

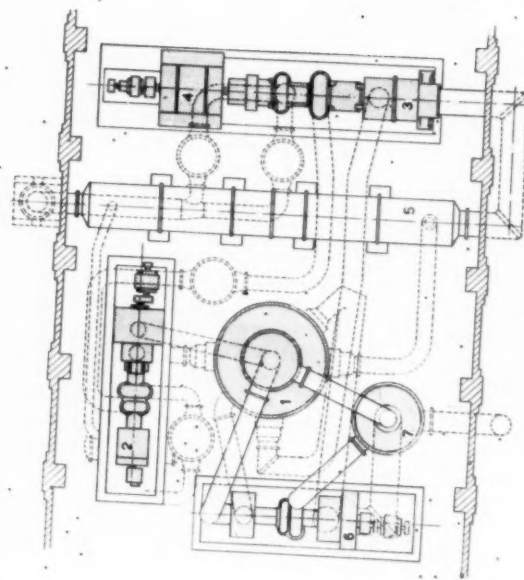
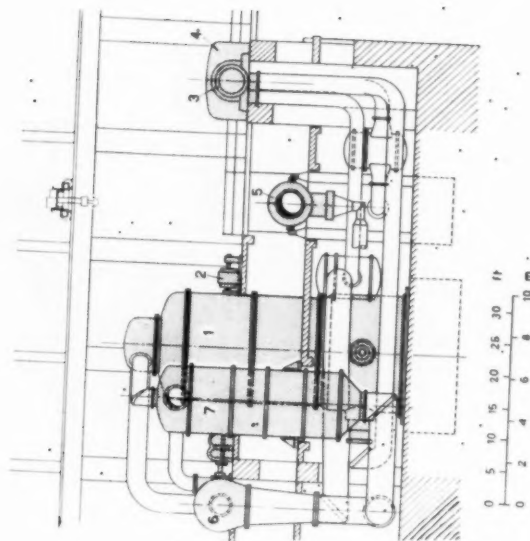


Fig. 8 (right) GENERAL LAYOUT OF PARIS INSTALLATION

- 1 Air heater
- 2 High-pressure turbine-compressor group
- 3 Low-pressure turbine with low-pressure compressor
- 4 Generator
- 5 Heat recuperator
- 6 Clamping set with return gas fan
- 7 Combustion-air preheater

FIG. 9* MODEL OF DUNDEE
INSTALLATION
(Seen from right lower corner of
Fig. 10.)

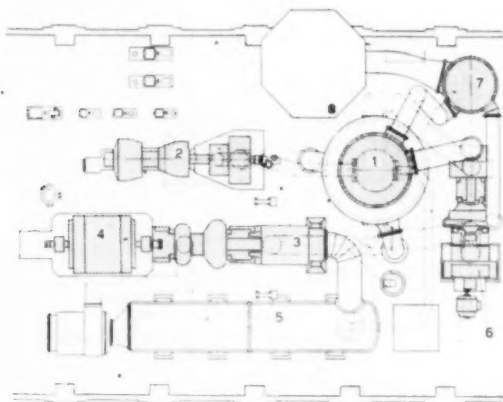
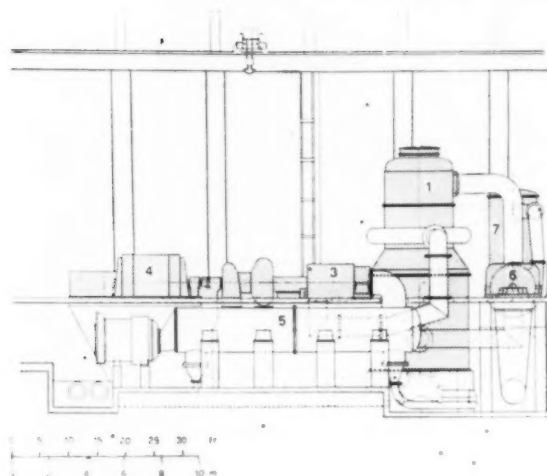
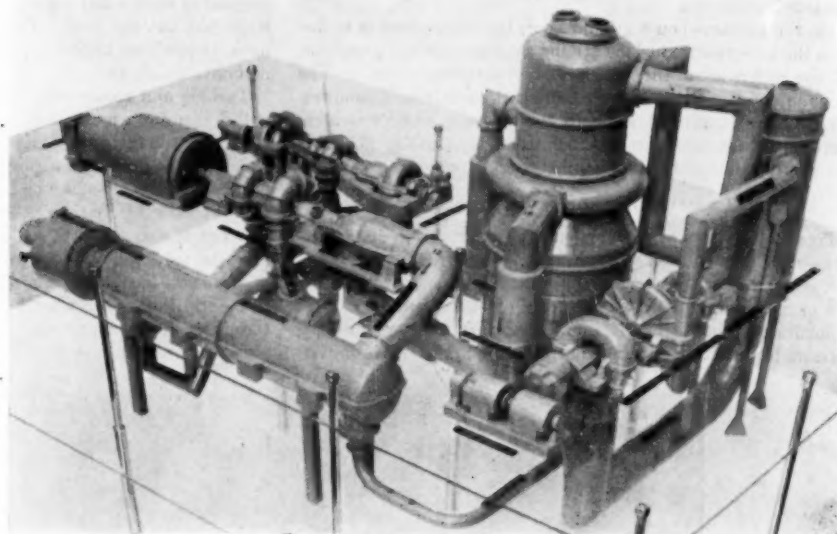


FIG. 10 GENERAL LAYOUT OF DUNDEE INSTALLATION
(Courtesy of Messrs. John Brown & Co., Ltd., Clydebank, and North of
Scotland Hydro-Electric Board; 8, chimney, other numbers same as Fig. 8.)

system works on the principle tried out in the test plant, using cold-storage air for changing pressure level in the circuit. Allowable generator speed variations for different load fluctuations are about the same as in corresponding steam plants. A heat rate of about 10,000 Btu per kw-hr is expected. At full load, working data are: Inlet of high-pressure turbine, 750 psia, 665 C; inlet of low-pressure turbine (reheat), 255 psia, 675 C; back pressure, 65 psia.

Layout of equipment was conditioned by a need to utilize given space in the old powerhouse. To provide good accessibility to all parts of this first industrial set, components are separated. This leads to unnecessarily long piping. The air heater stands in the center of the machine group. It extends into the cellar, which is unnecessarily high because the machine floor already existed.

Another 12,500-kw unit is being built by John Brown & Co., for the Carolina Port power station (Dundee) of the North of Scotland Hydro-Electric Board, Figs. 9 and 10. This forms part of the hydro scheme under development in Scotland, and it will operate as a base-load or stand-by plant depending on future needs. Regulation will be effected by pressure-level variation, but, as unforeseen load fluctuations will not occur in the same degree as at Paris, the system is somewhat simpler. No compressed-air accumulators are necessary; auxiliary reciprocating compressors introduce or withdraw air from the circuit. These take care of any eventual leakage also. Main circuit data for Paris and Dundee sets are the same.

This second set had to be fitted into an existing powerhouse also. As Fig. 10 shows, main machines and apparatus could be arranged in parallel, leading to shorter pipe connections. Good accessibility to major units is assured. Foundation height of this installation is less than that of the Paris plant. The two layouts show that a wide variety of machine arrangements is possible. In both cases, no special "boiler" room is foreseen. Machines can be easily dismantled as all inlets are below the machine floors.

If necessary in future plants, the space required can be reduced by combining the different elements. Fig. 11 shows a model of an ideal arrangement for a pulverized-coal-fired plant. The layout differs little from steam practice. Air heater and associated firing equipment would be separated from the machine set and heat ex-

changer. Since the heater uses no water, it is highly suited to outdoor installation.

On the machine-house ground floor, the regenerator is in line with the low-pressure turbine driving a compressor and generator. All the coolers are at the same level, beside the regenerator. The second floor carries the high-pressure turbine driving a compressor. This arrangement leads to short piping while providing ample space for operation and maintenance. (In Fig. 11, floors are partly omitted to show equipment.)

DESCRIPTION OF MAIN COMPONENTS

Figs. 12 to 19, inclusive, show some main parts of the 12,500-kw sets during manufacture at the Escher Wyss works. At the time this paper was written, some parts were still unfinished and erection of the power group in Paris was only just beginning.

Small size of the machines is impressive. Fig. 12 shows the high-pressure rotor having an actual output of 14,000 kw—it is only 20

in. diam. Small dimensions lead to comparatively low maximum stresses in blades and rotors. These do not exceed 7500 psi at 8500 rpm and full load. The useful-output turbine of Fig. 14, actually produces 18,500 kw, running at 3000 rpm. Tip diameter amounts to only 42 in.

Turbine and compressor shafts are sealed by compressed air withdrawn from a suitable point of the cycle, and oil sealing toward the ambient air. Fig. 14 shows this sealing arrangement, which proved quite satisfactory in the test plant, at the inlet side of a compressor. Sealing air for turbine shafts arrives at somewhat higher pressure than in the turbine and therefore flows into it, where it also serves to cool the first disk.

Model tests and calculations have been used in a careful study of cooling. Too-cold incoming air gives rise to temperature stresses in the rotor. Therefore, air of suitable higher temperature is used. Cooling effect is high because we work with high-pressure air from the circuit. Approximate temperature dis-

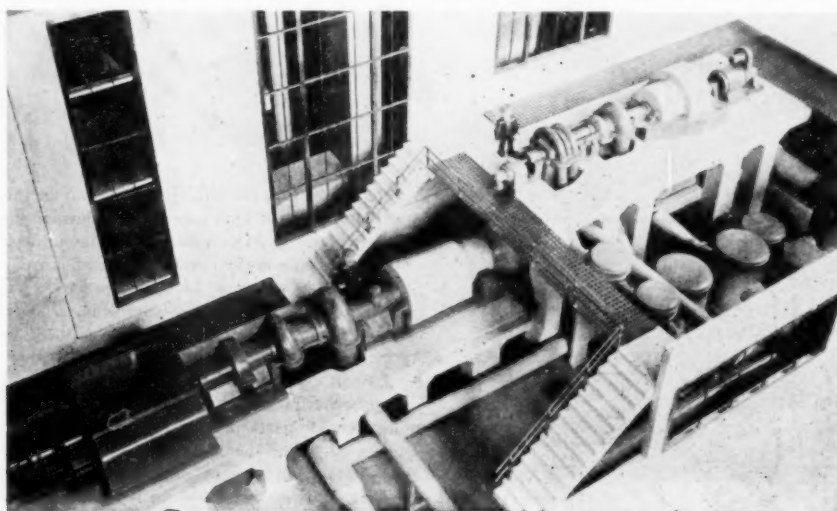


FIG. 11 IDEAL ARRANGEMENT OF MACHINE SET SHOWING FLOORS PARTIALLY REMOVED

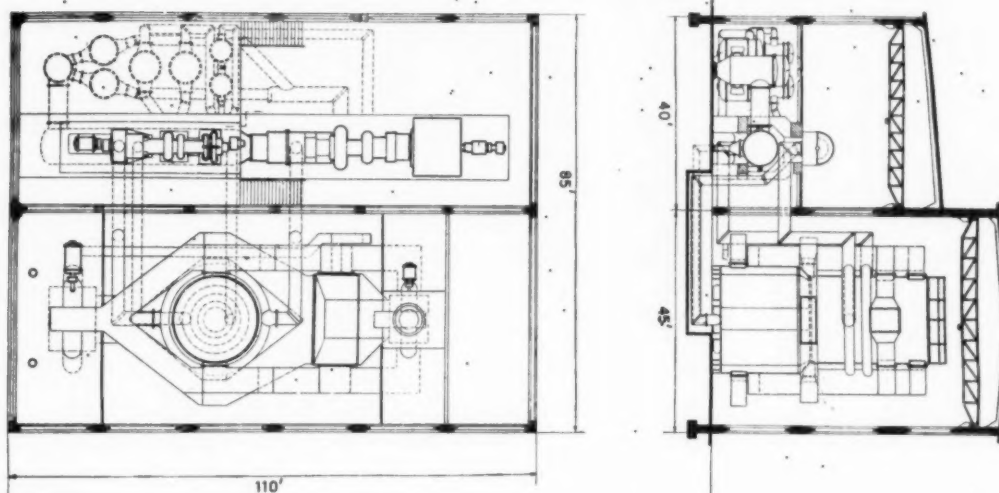


FIG. 11(a) PROPOSED LAYOUT FOR 12,000-KW COAL-FIRED PLANT

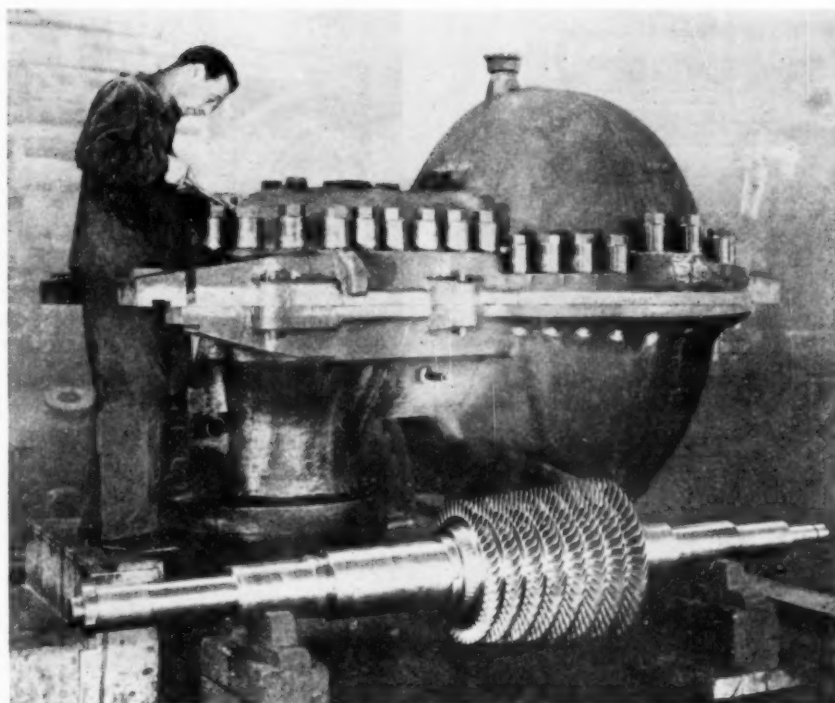


FIG. 12 HIGH-PRESSURE TURBINE CASING AND ROTOR OF PARIS SET IN ERECTION SHOP
(Rotor output 20,000 hp.)

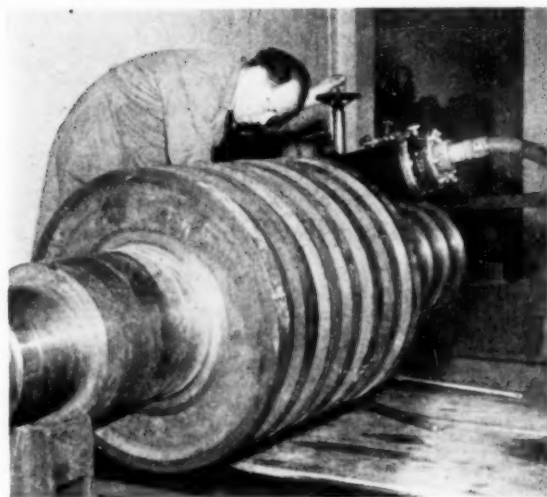


FIG. 13 ROTOR OF LOW-PRESSURE TURBINE OF PARIS SET UNDER X-RAY CHECKING
(Disks are welded on shaft. Rotor output 26,000 hp.)

tribution for the high-pressure turbine is shown in Fig. 15. All temperatures are appreciably lower than maximum temperature of working air.

An electrical analog was used to work out the temperature distribution. Similarity between differential equations for heat flow and an electric field can be used in model tests. Electrical

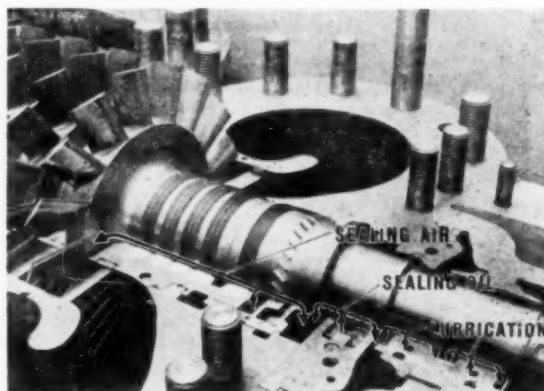


FIG. 14 COMBINED LABYRINTH—LIQUID SEALING FOR SHAFTS
(Dotted lines = pressure oil; solid lines = pressure air.)

field lines represent temperature distribution. Boundary conditions are represented by different resistances arranged along the border of the model in the electrolyte tank. Fig. 15(a) shows simple test equipment for evaluating temperature of the turbine shaft at certain working conditions.

As described previously (1), turbines and high-temperature sections of piping employ double-casing construction, with an intermediate insulating layer. This permits saving heat-resisting material. For instance, casings for both turbines are entirely of normal molybdenum steel as used for steam turbines. Fig. 16 shows the thin inner shell of the low-pressure turbine. The thin wall which leads incoming air to the first guide wheel is per-

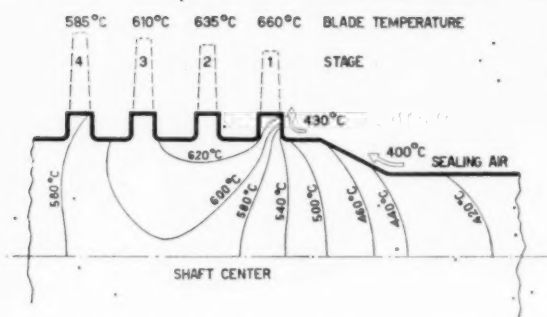
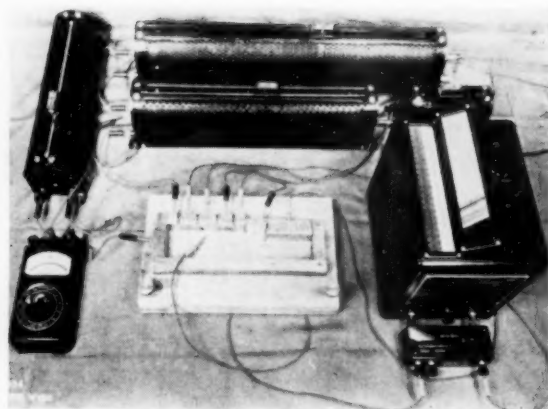


FIG. 15 (above) AND 15(a) (below) DEVICE FOR EVALUATING TEMPERATURE DISTRIBUTION IN COOLED MACHINE PARTS (Example for high-pressure-turbine shaft. Wooden model in center of Fig. 15 represents shaft.)

forated so that pressure differences on both sides do not occur when changing load. Absence of any regulating device, such as inlet valves, and lack of distributing chambers facilitate this kind of design.

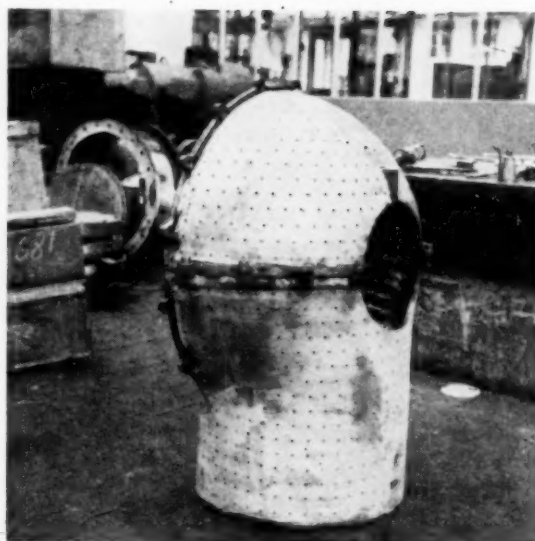


FIG. 16 INNER INLET CASING OF LOW-PRESSURE TURBINE

Compression of circuit air from 65 to 210 psig is handled in two stages by axial compressors, and from 210 to 750 psig by a centrifugal compressor, as volumes are already smaller here, Fig. 17. Three intercoolers, Fig. 18, are used. High pressures make dimensions of tube nests relatively small.

Regenerator design is basically the same as in the test plant. Fig. 19 shows the lower half of this counterflow apparatus. Test experience with the old regenerator was quite satisfactory; no soiling of the small tubes occurred. Tubes are normal mild steel. Individual tube nests are welded into conical headers from which a connecting tube of larger diameter leads to the outlet plate.

The bent flexible tubes take up differences in elongation between hot tubes and cold shell.

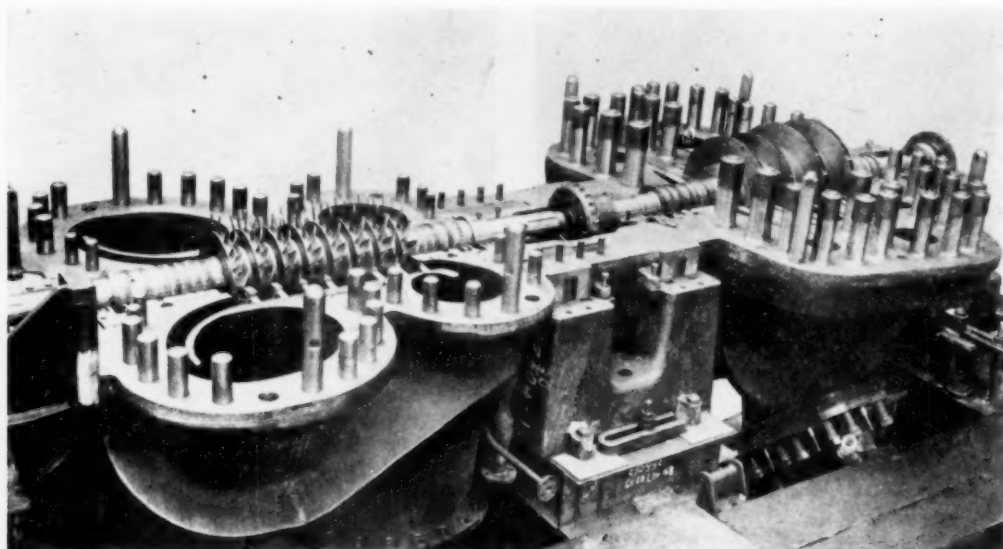


FIG. 17 SECOND AXIAL MEDIUM-PRESSURE COMPRESSOR AND RADIAL HIGH-PRESSURE COMPRESSOR FOR PARIS SET

AIR-HEATER DESIGNS

At present, the main difficulty in air-heater design is to choose the best construction out of a great variety of possible solutions, all of which have their pros and cons. In this the development resembles that of the steam boiler. Some of the basic ideas have already been discussed (mainly for oil firing) in previous papers (1). If we compare older designs with today's ideas and experience, we find that much has been gained by simplification.



FIG. 18 ONE OF TUBE BUNDLES WITH FINNED TUBES FOR INTER-COOLERS
(Tube nest is enclosed in cylindrical pressure shell.)

As a matter of fact, air-heater questions needed most re-examination in comparison with earlier projects. This is quite natural since the air heater represents an entirely new element. It is one of the most important parts of the closed-cycle plant from the economic aspect and we realize that much of the closed cycle's future depends on air-heater design. In the St. Denis plant, the air heater represents about 30 per cent of the total weight and cost.

Our studies show that great simplifications become apparent as we advance from the rather conservative layouts intentionally adopted in the first units. To appreciate the considerations leading to this choice, we should recall that, in principle, heat can be transferred from fuel to working air through heater surfaces by radiation or convection. Radiation is best in theory; it does not require any pressure drop on the gas side and results in the smallest surfaces.

This kind of heater will be the eventual solution. However, at the time of designing the first industrial plants some years ago, more exact basic information and test figures were available on convection heat transfer. The first Paris air heater is, therefore, a pure convection-type tubular heat exchanger with counterflow layout. Temperature of combustion gas entering the tube nests is only about 1000 C. Recirculated gas mixed with combustion air brings the temperature down.

Further designs based on latest heat-transfer tests have shown that a crossflow convection-type tubular heater yields a great saving in space and weight, the latter being only about 60 per cent as compared with the first type. After securing enough test figures for calculation, this later type of air heater was chosen for the Dundee plant. To reduce heat-transfer surface, pressurized firing is adopted in both cases, as convection transfer coefficient on the gas side rises sharply with pressure. Use of about 45-psia combustion pressure reduces the surface to at least one half that necessary with atmospheric pressure and no radiation. Combustion-gas volumes are also reduced, which leads to smaller piping and fans.

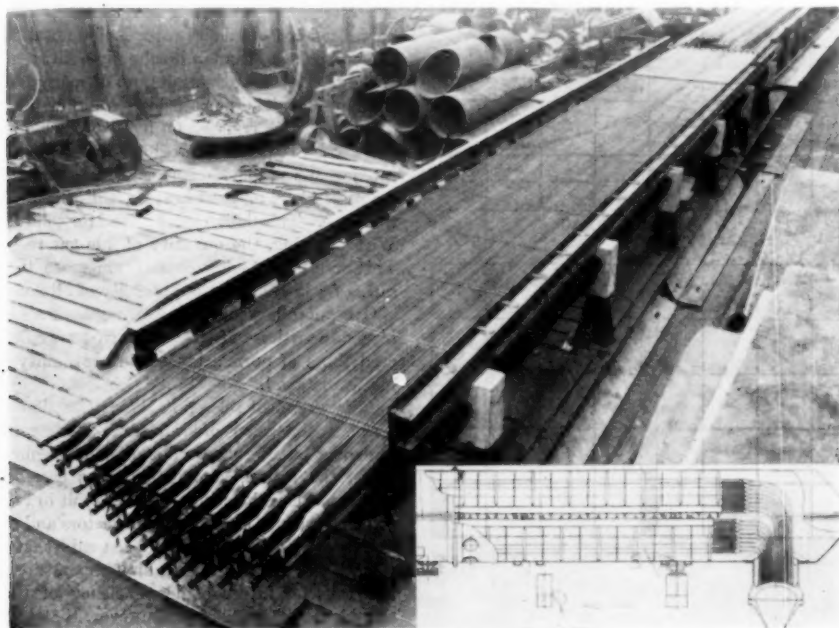


FIG. 19 TUBE BUNDLES FOR PARIS HEAT EXCHANGER
(Tube diameter $1/4$ in.)

Greater use of radiation heat permits reducing air-heater surfaces without pressurized combustion. We did not choose this system first because we needed additional information and experience on tubes directly exposed to hot flames. Tests and calculations made in the meantime show that earlier fears about deformation and temperature stresses from unequal heating were overemphasized because assumptions for initial calculations were too primitive. The test-plant air heater, the first ever built, included a radiation-tube wall and encountered none of the expected difficulties in operation, Fig. 3.

A closer study of conditions in radiation tubes with high wall temperatures revealed new phenomena (7). Normal calculations assume heat radiated from combustion space to tube wall coming in over half of the circumference, Fig. 20. Without allowance for heat transfer in a peripheral direction and interirradiation to the opposite side of the tube, a rather big temperature difference results for conditions existing in the hottest parts of air-heater tubes.

A more exact calculation shows that, because of circumferential heat flow in the relatively thick tube wall, temperature differences are appreciably smaller than they would be assuming only heat flow perpendicular to the wall. Effect of interirradiation of the inner tube surface in leveling up temperature variations can be taken into account quantitatively and proves to be considerable at temperatures above 600 C. Thus final temperature variations and resulting stresses are much smaller in actual cases than they seem at first sight, Fig. 20.

It was logical that early development of air heaters was based on ideas prevailing in boiler practice. We made many studies in

this direction but this leads to complicated and costly constructions and readily foreseeable difficulties of expansion and non-uniform temperature distribution. A symmetrical arrangement of tubes around the combustion space helps to avoid local overheating. This point need not be faced to such an extent in boilers. Their wall temperatures are comparatively low, whereas in air heaters poorer heat transfer inside tubes causes metal temperature to approach within as little as 50 C of the temperature of the working medium. Thus no large margin is left for the material.

A symmetrical arrangement which assures uniform admission to the surface is essential. Care must be taken that flame does not reach individual tubes. Many of our newer designs for oil- and gas-fired air heaters, as well as for pulverized-coal firing, are therefore of cylindrical, symmetrical type, with a central combustion chamber. For reheating, high and low-pressure tube systems can be combined suitably in one shell. This avoids losses from long pipe connections.

Figs. 21 to 23, all at the same scale, show the great influence on design and size of choice of basic heat-transfer mechanism. Starting from the conservative counterflow convection air heater, development leads to the crossflow heater. Its main advantage is absence of the many guide walls needed in the counterflow type. Accessibility is good and individual tube bundles can be replaced easily. (All heaters, Figs. 21 to 23, for 12,500-kw sets.)

Adoption of radiation transfer, with atmospheric firing, gives the simplest layout. This air heater should also prove successful for coal firing. As radiation intensity of coal flames is rather high, the mean temperature in the combustion space must be reduced. Therefore we foresee need for recirculating a rather large amount of flue gas. To keep slag-ash particles as far away from the tube wall as possible, recirculated flue gas is blown in along the whole length of the tubes and all around the circumference of the combustion chamber between the spaced tubes. This gas stream blows impurities away from the tube surface and, as it is comparatively cool (500–600 C), it has the additional effect of cooling and granulating ash particles. It can be seen that a pulverized-coal-fired air heater should not differ much in principle and components from units already built.

Cylindrical design permits use of many identical tube serpentine and headers for both high- and low-pressure systems. One design, Fig. 23, is based on figures for combustion rates (20,000 Btu per cu ft per hr) corresponding to those of modern boilers. Maximum wall temperatures and stresses are of the same order as for pressurized oil-fired heaters, and the surface per kw is about the same. This design can be used for solid fuel as well as for oil. With oil-firing, the quantity of flue gas recirculated is reduced. This results in higher combustion-space temperature, compensating for lower radiation intensity of oil flames.

Over-all dimensions of the atmospheric air heater are somewhat bigger than those of the pressurized type, but by no means exceed those of normal boilers. Accessibility and cleaning possibilities are good.

Allowable heat release in the combustion chamber largely determines dimensions of air heaters. Assumptions discussed in the foregoing paragraphs do not differ from normal steam practice. If, in the future, combustion rates can be raised by special burners, this will, as with boilers, result in reduction of size.

Temperatures in air-heater collectors and tubes are the highest in the entire plant. It has been said that these temperatures establish a limit for raising air temperature at the turbine inlet and thus for future higher efficiency of the closed cycle. It should not be overlooked, however, that temperature difference between highest tube-wall temperatures and air-inlet temperature for the turbine is not more than 30–50 C. Life of alloy steels depends on the relation of temperature and axial stress imposed.

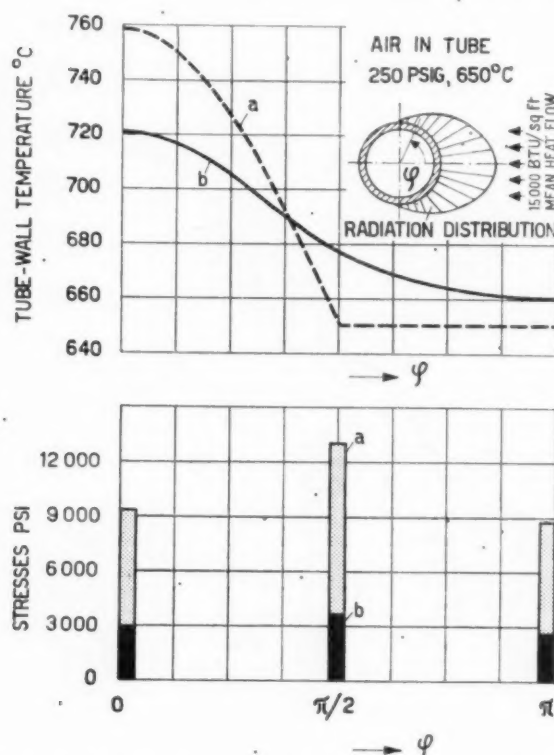


FIG. 20 EXAMPLE OF TEMPERATURE AND STRESS DISTRIBUTION IN HEATER TUBES EXPOSED TO ONE-SIDE RADIATION (Curve (a) Without circumferential heat transport in wall and without interirradiation. Curve (b) Actual conditions.)

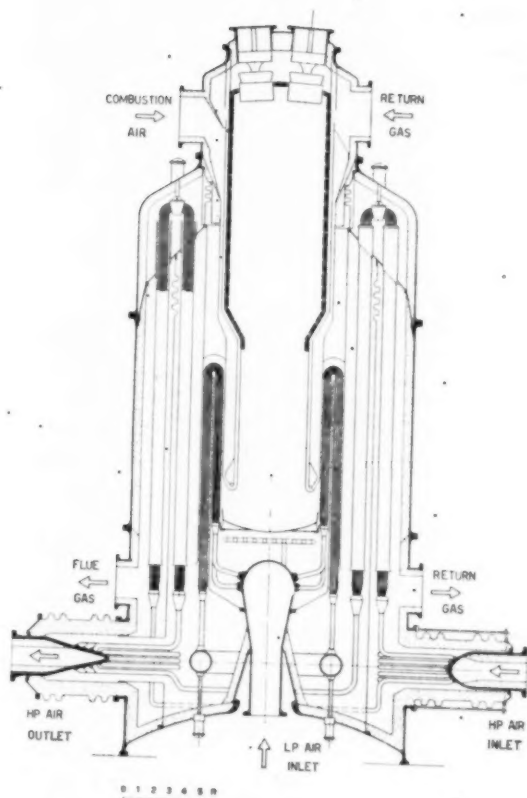


FIG. 21 COUNTERFLOW CONVECTION-TYPE AIR HEATER FOR DOUBLE HEATING
(Pressurized combustion. Individual high-pressure tube bundles are surrounded by cylinders in which combustion gases flow at elevated velocities.)

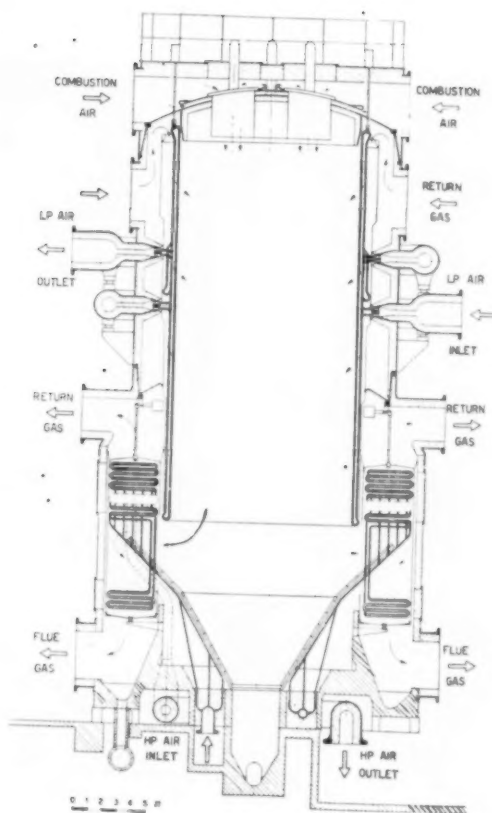


FIG. 23 RADIATION-TYPE HEATER WITH ATMOSPHERIC COMBUSTION
(Suitable for pulverized-coal or oil firing.)

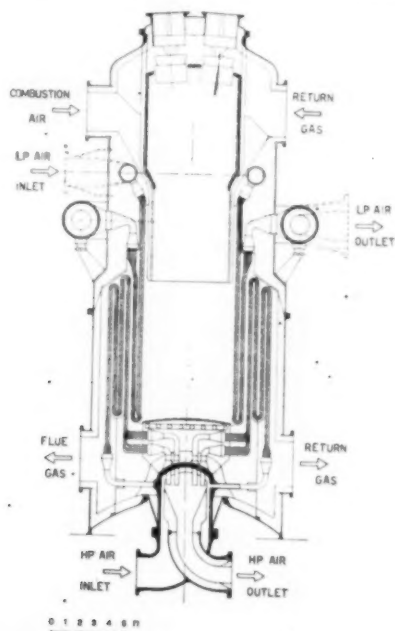


FIG. 22 CROSSFLOW CONVECTION-TYPE AIR HEATER FOR DOUBLE HEATING
(Pressurized combustion. Double-walled outlet collectors for high-pressure and low-pressure system do not need high-alloy steels.)

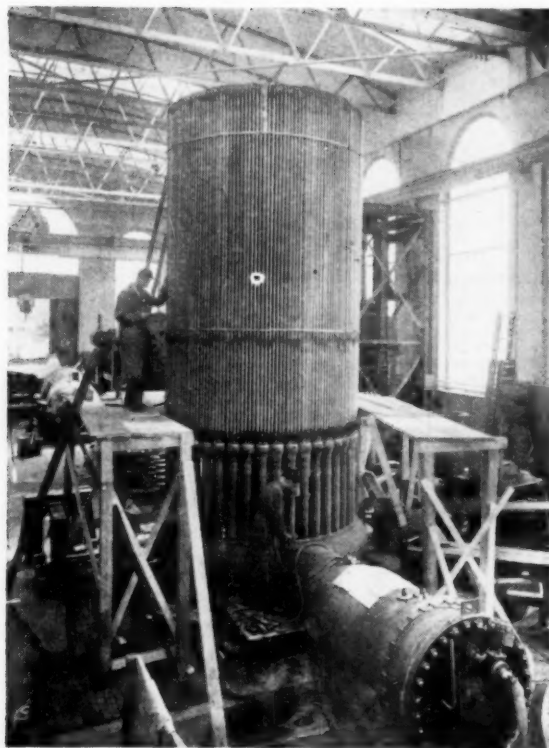


Fig. 24 Low-Pressure Tube System for Paris Air Heater in Course of Pressure Tests (Tests at Escher Wyss Works.)

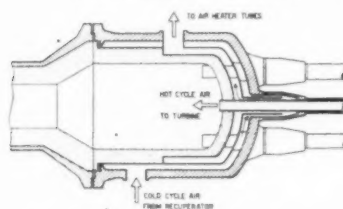


Fig. 25 Double-Shell Air-Cooled Collector for Elevated Working Pressures and Temperatures

Stresses in the air-heater surface can be kept small—between 1500 and 2000 psi. In all the gas-turbine rotors much higher stresses occur. Thus, although temperatures in some heater parts are higher, the safety margin against rupture is at least as large as in other parts of the plant. The rotors limit allowable temperature, not the air heater.

We have developed new means for reducing temperatures of collectors, which can thus be built without high-alloy heat-resisting material. Fig. 25 shows the double-shell principle used in design of the high-pressure outlet collector of the crossflow heater. Inlet and outlet collectors are combined. Relatively cold inlet air to the high-pressure heating system (about 400 C) enters a cylindrical chamber which encircles the outlet. Small pressure difference between inlet chamber and outlet corresponds to pressure drop in the high-pressure tubes. The outer casing is cooled by inlet air and takes up pressure stresses. The thin inner casing, which withstands the high temperature, is virtually not loaded.

Incoming cooling air passes first along tube inlets and produces a steady diminution between hot inlet tube wall and cooler collector shell.

Air at the pressures of these closed circuits, up to 750 psi, has a good cooling effect. Heat transfer at this pressure is 20 times as high at normal atmospheric conditions, for the same velocity. Even with a small amount of extraction air, high-temperature parts can be cooled effectively with small air velocities.

CLOSED-CYCLE TURBINES FOR INDUSTRIAL USE AND FOR SMALL OUTPUTS

In estimating future possibilities of gas turbines it is a peculiar fact that whatever their kind and size they are compared with large modern steam-turbine units. Yet only in large sizes do steam plants attain thermal efficiencies of 30 per cent or more. For smaller steam units, fuel consumption rises gradually, and for capacities below 10,000 kw an over-all efficiency of 25 per cent represents a good figure (8). It is an important but often overlooked fact that gas turbines can, even now, be built for small outputs with efficiencies nearly as high as for large outputs.

It follows that the field of small and medium-power sets is at present a promising one for gas turbines. As the closed cycle provides freedom in choosing suitable working pressures, and therefore volumes, favorable possibilities for small-output turbines exist. Units of a few hundred to a few thousand kilowatts can work with 150-250 psig top pressure. The dimensions of the machines are by no means too small for maintaining good

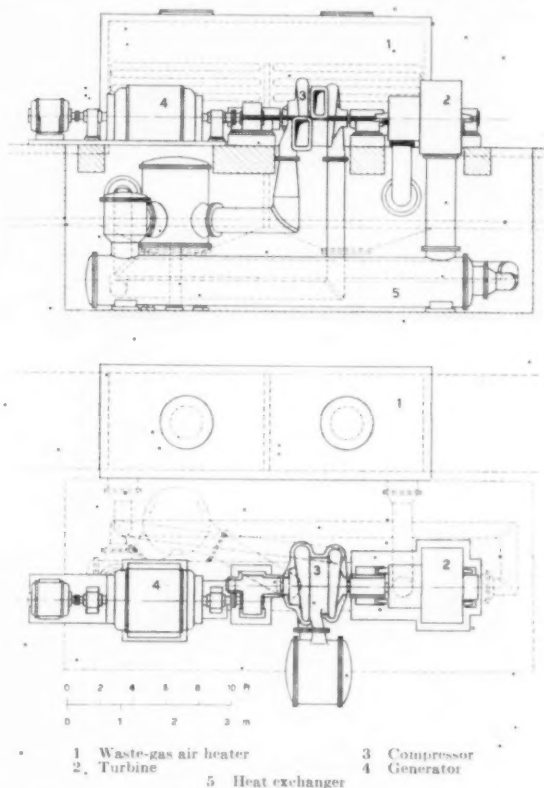


Fig. 26 LAYOUT FOR 1000-KW CLOSED-CYCLE PLANT FOR WASTE-HEAT RECOVERY

(General arrangement is same as for first 700-kw set of this kind built by John Brown & Co., Ltd., for Coventry gas works. Turbine-inlet pressure about 140 psia, counterpressure about 35 psia.)

efficiencies. The guarantee of lasting cleanliness of the circuit is essential for such small installations, which often work in dirty surroundings.

A striking example of the favorable possibilities of small closed-cycle plants is a waste-heat utilization unit of about 700 kw being built by John Brown and Co., together with Spencer Bonecourt, Ltd., London (6). It is for a gas works.

Studies have shown that a closed-cycle plant offers an economical and reliable way of utilizing heat available in waste gases such as occur in gas works, carbonizing plants, and the steel, chemical, and oil industries. It often occurs that waste heat is available at high temperatures (600–900 C) and low pressures. Heat must be supplied to the working medium of any turbine cycle in an indirect way. Up to now, waste heat was mostly used in boilers to produce steam for engines or turbines. As high-temperature service is not suitable for them and efficiencies of small sets are low, it usually does not pay to produce electrical energy.

The gas turbine changes this picture entirely. In the case just mentioned, one gets about double the electric output when choosing a closed air cycle instead of steam. The air heater can be built very simply as a counterflow tubular heat exchanger. Waste gases with a temperature of 800 C can easily heat working air to 600 C. The exhaust gases of the air heater can still be used to produce process steam.

Taking into account the favorable position of the small-output gas turbine, compared with corresponding steam sets, we have also made projects for simple coal-fired closed-cycle plants down to only 1000–2000 kw net output. The air heater may be of the cylindrical type with atmospheric combustion. Pressures in the working cycle would be 230 psia at the turbine and 60 psia at the suction side of the compressor. Simple expansion in one turbine is proposed, with maximum working temperature of 650 C. The turbine is directly coupled to a two-stage compressor and runs at about 10,000 rpm. Only one intercooler is planned. The generator connects through a reduction gear. The regenerator, of the tube-bundle type, may serve directly as a foundation for the machine set. In the arrangement shown, Fig. 27, shortness of piping is notable. The turbine would have 6 stages with a tip diameter of only 16 in. Depending upon the economic amount of heat-exchanger surface, efficiencies of from 26 to 30 per cent can be expected from this simple plant. These are over-all efficiencies, including all auxiliaries.

Necessary cooling-water quantities can be very small, one fifth to one tenth of those of corresponding steam plants. Sacrificing some fuel economy, closed-cycle plants can also run without water at all, using air cooling for compressor intercoolers.

BIBLIOGRAPHY

- 1 "The Escher Wyss-AK Closed-Cycle Turbine, Its Actual Development and Future Prospects," by Curt Keller, Trans. ASME, vol. 68, 1946, pp. 791–822.
- 2 For development of naval gas turbines which are not treated in this paper see: "The Gas Turbine as Applied to Marine Propulsion," by T. A. Crowe, *Journal of The Institution of Mechanical Engineers*, London, vol. 157, June, 1948, pp. 103–116.
- 3 "Applied Atomic Power," by S. C. Smith, A. H. Fox, R. Tom Sawyer, and H. R. Austin, Prentice-Hall, Inc., New York, N. Y., 1946, chapt. 3, p. 141.
- 4 "An Aerodynamic Thermal Power Plant," by J. Ackeret and C. Keller (in German), *Revue Polytechnique Suisse*, vol. 113, 1939, p. 229.
- 5 "Compte-Rendue des Essais de la turbine aérodynamique Escher Wyss-AK," by H. Quilby (in French), *Revue Polytechnique Suisse*, vol. 125, 1945, p. 269. English translation in *The Oil Engine*, London, England, November, 1945.
- 6 "Regulation Theory for Thermal Power Plants Employing a Closed Gas Cycle," by F. Salzmann, Trans. ASME, vol. 69, 1947, pp. 329–335.
- 7 "A Method of Calculating the Temperature Distribution in Non-Uniformly Heated Tubes," by F. Salzmann; paper presented at

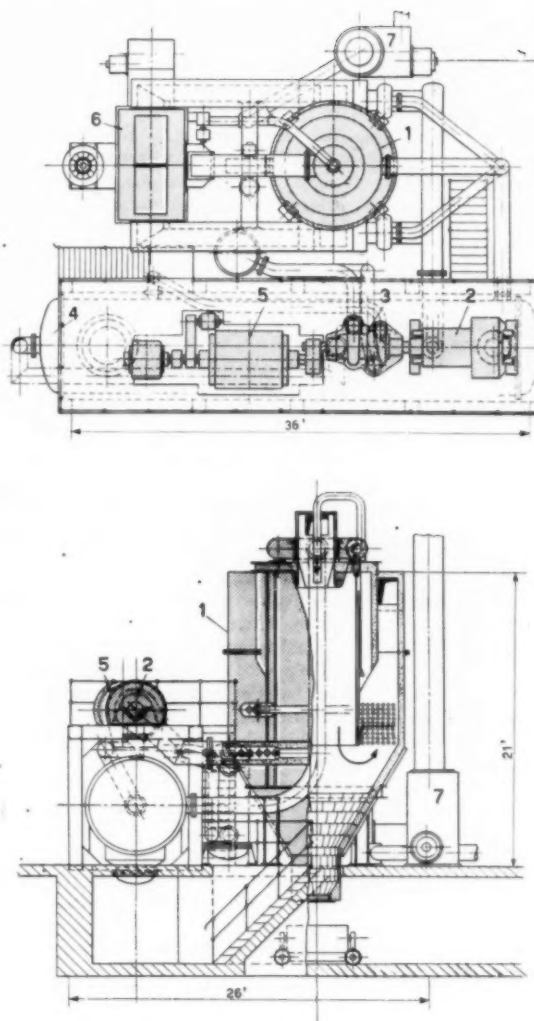


FIG. 27 PROJECT FOR 1000-KW PULVERIZED-COAL-FIRED UNIT

- | | |
|------------------|---|
| 1 Air heater | 5 Generator |
| 2 Turbine | 6 Combustion-air preheater |
| 3 Compressor | 7 Coal-handling and preparation equipment |
| 4 Heat exchanger | |

the International Congress of Applied Mechanics, London, England, September, 1948.

8 "Technische und Wirtschaftliche Aussichten von Gasturbinen," by F. Münzinger, *Schweizerische Bauzeitung*, vol. 126, 1945, p. 63; "Comparison of Gas and Steam Turbines," *Combustion*, vol. 20, September, 1948, pp. 39–42.

9 "Presidential Address," by Capt. (E) W. Gregson, *Proceedings of The Institution of Mechanical Engineers*, London, England, vol. 160, 1949, p. 58.

Discussion

P. F. MARTINUZZI.³ The author is to be congratulated on an excellent paper which reports clearly and concisely an important development in the industrial gas-turbine field. It is a great pity that Dr. Keller could not present his paper himself; not

³ Professor of Mechanical Engineering, Cornell University, Ithaca, N. Y. Mem. ASME.

only was it impossible to congratulate him and welcome him again, but also the opportunity was lost of extracting further information. The paper is full of tantalizing statements about which further details would be most welcome. The author and Escher Wyss are both to be congratulated on their courage, which is a characteristic of Swiss industry, in undertaking the whole development work described in the paper without outside financial assistance. It may surprise some American readers to learn that the whole Swiss industrial gas-turbine development work, which has been carried on in four different technical directions by four firms, the largest of which has only 8000 workmen, has been financed entirely by the firms themselves without any help from either the government, the military, or any other outside sources. Yet Switzerland is still easily in the lead in industrial gas turbines.

When in 1945 Professor Ackeret and Dr. Keller listed as an advantage of the closed-cycle turbine the fact that the air in the cycle is clean, not much importance was given to this point. Recent unfortunate experiences of other firms, as well as the author's report on compressor efficiency drops when the compressors are run with ambient air, show the importance of this point. Of course these efficiency drops become very noticeable only if the compressor efficiency is really high; if axial compressors can run in a dusty atmosphere without loss of efficiency, this might tend to indicate that the compressors are not as efficient as they should be. The extensive use of centrifugal compressors in the new plants is extremely interesting; these compressors are of course immune from efficiency drops due to impure air. This fact alone justifies their adoption in the charging sets. But it is interesting to see that the high-pressure stage of the main compressor is also centrifugal. Are these centrifugal stages designed on the Oerlikon principle? It is well known that, although Escher Wyss and Oerlikon are independent in their technical staff, they are linked financially. What is the efficiency of these centrifugal stages, and how does it compare with that of the axial stages? The fact that four centrifugal stages are used for a compression ratio of 3.6 to 1 indicates very conservative peripheral velocities; the efficiencies should be excellent. Further details on this point would be extremely welcome. Also some more information is desired on turbine-blading type and efficiency. The fact that 8-stages are used in the high-pressure section for an expansion ratio of about 3, and presumably 7 stages in the low-pressure section for an expansion ratio of 3.9, shows the desire to obtain the highest possible turbine efficiency.

The air heater is the most important component of the closed-cycle gas turbine, and the author is to be congratulated on the many details he has given. If, as is to be hoped, full test data will be published in due course about the Paris and Dundee plants, it will be most interesting to compare the performance of the counterflow and crossflow types. The fact that pressurized firing has been adopted is a distinct advantage; the complication due to the charging set does not seem excessive in view of the reduction in air-heater size (and tube stress); the more so as even the nonpressurized type must have circulation and recirculation fans. Presumably pressurization will be impossible with pulverized-coal firing.

One of the main advantages of the closed-cycle gas turbine is that it constitutes probably the only practical way of burning coal in a gas turbine; certainly the only practical way to burn coal in a high-efficiency gas turbine. At present prices of oil and coal, the cost of running a high-efficiency oil turbine might well be smaller than that of a low-efficiency coal turbine. It will be most interesting to get further details on the proposed 1000-kw pulverized-coal-fired unit described by the author. Is there any chance of its being built soon?

It is difficult to agree with the author on his contention that

the turbine blades and not the air-heater tubes represent the most delicate point in the closed-cycle turbine; 30-50 C can make a lot of difference in the creep characteristics of high-temperature alloys. One need only remember the effect that 50 F has had on the Seawaren plant as compared with the Essex plant! And the turbine of a closed-cycle installation is protected from local overheating due to uneven combustion, which sometimes gives trouble in open-cycle types; while the air-heater tubes are very much at the mercy of local overheating. The fact that the air-heater tubes are the most delicate point is implied in Professor Quiby's official test report of the experimental Escher Wyss turbine (5).⁴ In these tests the maximum temperature was increased from 687 C to 698 C, when the load was decreased from 2000 to 400 kw; these tests were of course effected at the maximum temperature the machine would stand, in order to show the highest possible efficiency. Now, a decrease in load does not affect, in practice, the turbine stresses, as the turbine peripheral velocity remained constant; but it decreases very substantially the air-heater tube stresses as the pressure in them is reduced about proportionally to the load. Hence the increase in temperature was allowed by the decrease in air-heater tube stress, which, consequently, is the critical point. This is also proved by the fact that, in the reheat turbine, the temperature is 10 C higher than in the high-pressure turbine.

There is no question that the future of the closed-cycle gas turbine depends on the development (or rather, on the lack of development) of alloys or devices which would allow very high temperatures in the turbine. If special alloys, or blade cooling, or a combination of the two should allow turbine temperatures of about 900 C in industrial use, the complication of the closed-cycle turbine and the difficulties that would arise with the air heater would not justify the use of this type of turbine. At those temperatures the efficiency and compactness of the open-cycle type would be unbeatable.

Tremendous sums of money are spent to develop very high-temperature turbines for aircraft uses. The objective is an aircraft turbine running at about 1600 C (3000 F). If such a turbine became available, it would presumably be possible to run an industrial turbine at over 1000 C, and the closed-cycle turbine would be doomed, except for special applications such as atomic energy or waste heat or coal-fired turbines. However, much of the money poured into the development of the high-temperature aircraft turbine works at very low efficiency, owing to military secrecy, changes of plan, duplication of work, and so forth, and a change in the political picture would stop very rapidly the flow of money. So it is quite possible that in the next 10 or 15 years, the temperatures of industrial gas turbines will not go above 800 C. In that event, the closed-cycle gas turbine will certainly have a vast field of application.

The waste-heat turbine described by the author at the end of his paper is a most interesting development. One is rather inclined to think of the closed-cycle turbine as a rather large unit; it is interesting to see that the cycle can be used for small and even very small powers. This is probably rendered possible by the use of centrifugal compressors which maintain their efficiencies even with small flows. This type of waste-heat closed-cycle turbine has the advantage that the efficiency drop in the waste-heat exchanger would apply equally to any other type. Test results on this type will be very interesting also because they would give indications on one of the possible types of closed-cycle turbine for atomic power.

F. NETTEL.⁵ The progress made by Escher Wyss during the last 5 years is impressive. However, while extensive information

⁴ Reference is to author's bibliography.

⁵ Consulting Engineer, Manhasset, L. I., N. Y. Mem. ASME.

was given concerning component design and arrangement, it is difficult to get a clear idea of the cycle actually employed. It would be highly desirable if a T-S diagram with pressures and temperatures at all points would be given. Lacking that, we can guess from the figures that the three intercoolers are evenly spaced over the compression range giving a fairly close approximation of isothermal compression. The plant works over a pressure range from 750 to 65 psi with top temperature 665 C. Reheating takes place to 675 C after expansion to 255 psi, which seems rather late. The high efficiency of this cycle is predicated on a heat exchanger of very high effectiveness and visibly very large dimensions. It is, however, influenced to a similar degree by the sizes of the intercoolers, the aftercooler, and the air preheater for the furnace of the air heater proper, about which hardly any information is given.

In order to compare the closed-cycle plants described with steam plants and other gas-turbine systems, it would be helpful to know the total heating plus cooling surface per kilowatt plant output of all elements involved. It seems that this figure will be found much higher than the corresponding figure for steam plants, including boiler, superheater, economizer, air heater, condenser, and feedwater heaters. This comparison will be of great import for the economic prospects of the AK plants in this country. The utilities of the United States are primarily interested in plants of from 25,000 kw upwards to 75,000 kw or more which can burn coal. For base-load application, highest efficiency is paramount, provided the installation cost remain at present levels. For peak-load plants, economic considerations often will force low installation cost and, consequently, lower efficiency. Important savings obviously can be made easiest by reducing the size of the heat exchanger and possibly the furnace air preheater.

With decreasing effectiveness (size) of the heat exchanger it remains imperative to obtain the highest cycle efficiency attainable with the chosen size of equipment. To achieve this, it will be necessary to deviate from the "double-isotherm" cycle, i.e., restrict the air intercoolers to the first half of the compression range, thus leaving the second half uncooled. It will also be important not to reheat as late during the expansion as the described plants indicate. These measures bring very substantial efficiency gains, particularly for relatively small heat exchangers, not only for thermodynamic reasons, but also because they reduce the parasitic pressure losses.⁶

While the closed-cycle plant has reached practical application for medium-sized installations using liquid fuels, new problems will arise for large coal-burning plants for which supercharged furnaces are as yet undeveloped. For such conditions, semi-closed plants may have great potentialities, and more information regarding them will help to clarify the issue.

W. T. SAWYER.⁷ The author's position as a pioneer in the field of gas-turbine engineering lends special meaning to his review of the progress of the closed-cycle gas-turbine plant during the past 5 years. He was among the very first engineers to recognize the necessity for treating rotating components from the standpoint of aerodynamic theory. The progress of this Escher Wyss plant embodying his approach is accordingly of direct interest to all of us.

It is believed the author may be accused of having been excessively modest in his reference to the effort being made by Swiss industry to bring the industrial gas turbine into being. In proportion to its size and population, Switzerland has clearly

made the greatest effort in this regard of any country in the world. Special commendation is due to Swiss industry for undertaking upon its own resources the risk involved in exploring the development of three of the major gas-turbine cycles.

At the time when the author's first paper was presented to this Society in 1945, one of the advantages claimed for the closed cycle, namely, the use of clean air under pressure in working cycles, was perhaps discounted by some of us for lack of factual information regarding the degree of compressor and turbine fouling which would be encountered in practice with other cycles. Subsequent experience which has been reported, particularly with regard to compressor fouling, lends additional weight to this feature. The writer is happy to hear that Escher Wyss considers shipboard plants among the most promising projects and is continuing to concentrate upon them along with other applications. The good full- and part-load fuel economy of this type of plant makes it very attractive for ship propulsion.

By way of emphasis, will the author reaffirm the fact implied in Fig. 1 of the paper, that an air-heater tube-wall temperature of 900 C is today a constructional possibility? Also, does the author associate a diminished operating life with the use of a temperature of this magnitude?

While not taking specific exception to the statement that the gas-turbine rotors and not the air heater limit the allowable temperature in the Escher Wyss plant, one factor in that regard deserves mention, in order to maintain our perspective. The present-day trend toward higher temperatures is clear. Many of us feel that these higher temperatures will be accommodated only by the development of adequate cooling methods. Although current progress promises considerable success with the cooling of hot turbine parts, it is extremely difficult to see how cooling can be applied to the tube walls of an air heater through which heat must be transferred. The air heater, therefore, appears destined to become, if it is not already, the limiting factor for allowable cycle temperatures in the closed cycle.

The present trend toward reduction in content of scarce and expensive materials in high-temperature parts also seems to encounter a stumbling block in the inability to cool the hottest metal parts of the closed cycle—the air-heater tubes. It will be of interest to hear the author's views on this development trend.

AUTHOR'S CLOSURE

The author unfortunately was prevented from attending the meeting and the discussion when this paper was presented. Therefore, he wishes to express his thanks to Mr. L. N. Rowley, who presented the paper. On a recent visit to the United States, the author had an opportunity to discuss many questions concerning gas turbines. On the occasion of an informal meeting of the ASME Gas Turbine Power Division, in New York on May 25, he dealt with most of the questions put forward in the paper and in the discussions. Therefore, in order to condense the closure, only the most important points will be considered.

Attention is called to the fact that the Akeret-Keller power plant bears a much closer resemblance to the steam power plant than it does to the open-cycle gas turbine. This should help in our thinking, particularly in the discussion of higher cycle temperatures.

During the recent visit mentioned, the author was greatly impressed with the practical progress in metallurgy and in the development of appropriate designs for gas and steam-turbine components. Successful developments in the chemical industry and its apparatuses for high-temperature service may have a pronounced effect on the design of future caloric machinery. This holds true at least for the closed-cycle plant with its different components such as air heaters, heat exchangers, and coolers. The advanced technical know-how of the chemical industry and

⁶ "The Universal Optimum Power Cycle for Elastic Fluid Turbine Power Plants," by J. Kreitner and F. Nettel, Paper No. 47—A-43, abstract published in *Mechanical Engineering*, vol. 70, 1948, p. 355.

⁷ Bureau of Ships, Navy Department, Washington, D. C.

its plants will lead to a marked cost reduction. When comparing the technical solution for the closed-cycle plants discussed in the paper presented 5 years ago⁸ with what can be done now, the possibility is shown of very great simplification, both in machines and apparatuses.

In answer to Professor Martinuzzi's questions: The radial-type compressor was selected for the last two stages of compression due to specific speed requirements. This is a typical high-efficiency Escher-Wyss compressor and bears no resemblance to the Oerlikon compressor referred to. This compressor has a capacity of about 8000 cfm, and an adiabatic efficiency of well above 80 per cent at a pressure ratio of slightly less than 2:1. There is a good case for design of the whole high-pressure compressor set as radial machines as we foresee the immediate possibility of achieving an efficiency of 85 per cent, and use of such a radial-flow machine for the high-pressure group will result in a saving in capital cost and space.

The author would like to attempt to clarify the thoughts that exist regarding the limitations of the cycle as governed by the air heater. It is obvious that the temperature of the working air must be lower than that of the air-heater tubes, for otherwise no heat transfer would take place. The difference in temperature between the tube wall and working air can be controlled within precise limits as it is dependent entirely upon the air-side film coefficient and the rate of heat input. It has been our practice to work with not more than 100 deg F temperature difference between tube wall and air. Considerable latitude is offered in the design of the air heater as the life of the tubes is governed by both temperature and the accompanying stress. Thus the type of steel used and the wall thickness can be varied through the heater with the type being dictated by the local temperatures, consideration being given to the oxidizing and scaling requirements and wall thickness, determined by the type of steel and the working temperatures.

Again, it should be stressed, that this is a static structure readily susceptible to analysis by anyone skilled in the art. The heater can be designed with the same high-temperature section tube material as that used for turbine blading, and the turbine-blading stress will limit the design. It must be realized that, while the turbine-blading stresses are substantially the same at all loads, due to the fact that the machines are operating at constant speed and temperature, the heater tube-wall stresses are proportional to load. Thus, assuming a load factor of 75 per cent, heater-tube operating stresses are 75 per cent of design value, while turbine-blade operating stresses are substantially 100 per cent of design value.

We will be the first to admit that the design of the air heater has constituted the greater part of our problem as we have had to work without the benefit of the experience engineers in the United States have had in the design of tube stills for the petroleum industry. Years of experience in the operation of such stills have led to a complete understanding of the problems of radiant-heat transmission and the expected life and characteristics of metals under conditions of high temperature and stress. One recent metallurgical contribution to this service is the centrifugally cast pipe for tube stills. Centrifugally cast pipe offers better creep rates at high temperature than drawn pipe, thus opening possibilities of still higher operating temperatures than those currently contemplated. The casting process of tubes also enables use in a much wider range of any desired composition of heat-resisting material which would be difficult to draw.

The position regarding the air heater can be summed up in the statement that American manufacturers can offer air heaters

to meet the required service of a 12,500-kw plant at prices of the order of \$25 per kw with 6 months delivery.

Professor Martinuzzi and W. T. Sawyer have referred to the possibility of the development of the open-cycle gas turbine to cycle temperatures of the order of 1000 C, in which case they say the closed-cycle system would be doomed. Quite naturally, we do not believe this. In fact the closed-cycle plant at 650 C cycle temperature is here, while an open-cycle plant operating at anything over 800 C is a future possibility. The efficiency of the closed-cycle plant at 650 C is currently some 20 per cent better than the higher temperature open-cycle plant. While cycle temperature is important to obtain high efficiency, it is not the only means. We prefer to trade static heat-transfer surface for high temperature to gain in efficiency and high circuit pressures for temperature in order to reduce machinery size.

It is realized that much theoretical discussion is taking place also in this country dealing with high-temperature schemes. Such schemes look quite attractive on paper, but they are far from practical realization. This is stated only from the standpoint of the power-plant engineers and operators who require a reliable plant of at least 100,000-hr service life. For the next few years 700-750 C will be the upper limit for an economical and safe gas-turbine plant. A future closed-cycle plant with this temperature range should run economically with 8500-9500 Btu-kwhr.

We do not favor the combination of high-temperature working medium with adequate cooling methods. Much complication for practical service would be involved which does not pay. Only a simple plant layout can show economical advantages compared with modern steam sets.

In reply to Mr. Nettel, the cycle arrangement and conditions within the cycle are substantially as given in the previous paper⁸ for a double heating plant.

Concerning the questions of different working cycles, mentioned in Mr. Nettel's discussion, as a means of obtaining maximum efficiency, it must be pointed out again that what may seem favorable in theory, often does not bring the expected improvement when put into design. During the last few years we calculated hundreds of different cycles with various data and came to the conclusion that not much can be gained in performance with tricky layouts, but a lot can be lost by this means in simplicity of a plant and sound operation.

With respect to heat-transfer surface, it may be said that these figures are not alone significant for the economics of the AK plant. The total surface per kilowatt depends upon various factors as wanted efficiency, cooling-water quantities, flue-gas temperature of air heater, and naturally, on the design of the various auxiliaries which may be quite manifold. Figures for different plants now under construction will be published later. As the heat exchanger plays an important role in today's gas-turbine designs, the following figures may be useful:

The savings that can be made in reducing the size of the closed-cycle heat exchanger are not as important as would appear from first glance, particularly when one realizes that the heat-exchanger surface required for the closed-cycle plant is 2.8 sq ft per kw for an 88 per cent effectiveness in contrast to about 5 sq ft per kw for existing open-cycle plants where the effectiveness is but 75 per cent. It should also be remembered that an 88 per cent effective regenerator has over 2½ times the surface of a 75 per cent effective regenerator.

For those interested in practical operation of open and closed-cycle gas turbine, attention is drawn to a recent publication by J. B. Bucher of John Brown & Company, Ltd., Clydebank.⁹

⁸ "Experimental Running of Open and Closed-Cycle Gas Turbines," by J. B. Bucher, Transactions of the Institution of Engineers and Shipbuilders, Glasgow, Scotland, vol. 93, part 5, 1949-1950.

⁹ Bibliography (1).

A Pyrometer for Measuring Total Temperature in Low-Density Gas Streams

By SIDNEY ALLEN¹ AND J. R. HAMM²

The need for improved methods of measuring total temperature in low-density moving gas streams has been emphasized by the rapidly increasing use of gas-turbine engines for aircraft propulsion at high altitudes. Recent experience with various types of pyrometers has shown that increased errors of measurement and a reduced rate of response to temperature changes become apparent as the gas density is reduced. A design of suction pyrometer is presented in which sonic gas velocity is maintained over the thermocouple element at all operating conditions, thus insuring the maximum rate of heat transfer to the thermocouple from the gas, and enabling a simple correction for impact error to be applied to the indicated reading in order to derive the total temperature of the gas stream. The rapid rate of response to temperature change obtained with this pyrometer is a fundamental necessity in any control mechanism in which gas temperature is the operating criterion.

INTRODUCTION

IN actual or simulated high-altitude testing of combustors for aircraft gas-turbine engines, the problems encountered in measuring temperatures in gas streams are greatly accentuated. In these tests the pyrometers are exposed to radiation from the flame, the wall temperatures are rather low, and the gas densities are quite low. Measurement errors of the order of 500 F have been found for bare-wire thermocouple installations in low-pressure combustor-component test rigs, and single shielded thermocouples are not appreciably better. Accurate calibration of thermocouples for this application is not possible because of the indeterminable effects of radiation from the flame and radiation to the walls. This is so because the luminosity of the flame and the temperature of the walls vary widely with location and with test conditions. Even if an approximate calibration were obtained, its application would be so difficult that it would be impractical.

In this paper a type of thermocouple pyrometer is presented in which the errors are reduced to negligible magnitudes or can be evaluated definitely. The paper deals with the reasons for the increase in error in gas-temperature measurement under these conditions, describes the development of a suction pyrometer in which sonic velocity is maintained over the thermocouple element, and presents calibration data and service performance of this instrument.

ANALYSIS OF PROBLEM

When a thermocouple, which is located in a combustor and sees

the flame, is in equilibrium with its surroundings at a given operating condition, a balance exists between the heat supplied to it by forced convection, and radiation and the heat flowing from the thermocouple to its surroundings by radiation and conduction. This may be written as follows:

$$\begin{aligned} & \text{Heat received from gas by forced convection} \\ & + \text{heat received from flame by radiation} \\ & = \text{heat lost by conduction along the leads} \\ & + \text{heat lost by radiation to surrounding walls} \\ & + \text{heat lost by radiation to surrounding gas.} \end{aligned}$$

Expressed algebraically this becomes

$$\begin{aligned} C_1 \times (G)^n \times (T_g - T_c) + C_2 \epsilon_f (\epsilon_f T_f^4 - \alpha_f T_c^4) \\ = C_3 \frac{dT}{dL} + C_4 (T_c^4 - T_w^4) + C_5 (T_c^4 - T_g^4) \quad [1] \end{aligned}$$

where C_1 , C_2 , C_3 , C_4 , and C_5 are constants for a particular installation and for a given gas, the temperature of which is required. Where also

dT/dL = temperature gradient along the thermocouple lead, deg R per ft

G = mass velocity of gas (ρV) — lb/(sec) (ft²)

n = exponent varying from, roughly, 0.5 to 0.8, depending upon size and shape of body and direction of flow of gas relative to surface, dimensionless (1)³

T_c = thermocouple temperature, deg R

T_f = flame temperature, deg R

$T_{g'} = T_{g,0} + \text{some part of temperature equivalent of gas velocity, deg R}$

$T_{g,0}$ = static gas temperature, deg R

T_w = wall temperature, deg R

V = velocity of gas, fps

α_f = absorptivity of flame, dimensionless

ϵ_c = emissivity of thermocouple, dimensionless

$\epsilon_c' = (\epsilon_c + 1)/2$, dimensionless

ϵ_f = emissivity of flame, dimensionless

ρ = density of gas, lb per cu ft

Since it is required that T_c should approach as closely as possible to $T_{g'}$, a consideration of Equation [1] shows that the error terms must be made as small as possible, and the value of G or (ρV) should be made as large as possible.

When the density of the gas stream is reduced, as in the case of gas-turbine combustors operating under simulated high-altitude conditions, where pressures as low as 1 psi may occur, it is evident that the gas velocity over the thermocouple must be increased substantially to offset the effect if the numerical value of (ρV) is to be maintained as large as possible.

Experience has shown that a thermocouple can receive only a part of the equivalent dynamic temperature ($V^2/(2gJ C_p)$) of the gas, from which it is evident that a thermocouple in the gas stream can never indicate the true total temperature of the gas (T_{t_0}). In fact, once the radiation and conduction errors in the pyrometer have been made negligible, a further increase in gas velocity may

¹ Armstrong Siddeley Motors, Ltd., Coventry, England.

² Development Engineer, Aviation Gas Turbine Division, Westinghouse Electric Corporation, Lester, Pa. Jun. ASME.

Contributed by the Gas Turbine Power, Power, and Aviation Divisions and presented at the Annual Meeting, New York, N. Y., November 27–December 2, 1949, of THE AMERICAN SOCIETY OF MECHANICAL ENGINEERS.

NOTE: Statements and opinions advanced in papers are to be understood as individual expressions of their authors and not those of the Society. Paper No. 49-A-66.

³ Numbers in parentheses refer to Bibliography at end of paper.

result in a reduced value of T_c and hence a greater divergence from the total temperature. However, no objection can be raised to this fact, provided that the error involved can be calculated for any condition under which the pyrometer is required to operate.

This impact error in pyrometry is often expressed in the form of a "temperature-recovery factor" which is given by

$$r = \frac{T_c - T_{sg}}{T_{t0} - T_{sg}} \quad [2]$$

using the same notation as previously.

The expression $(T_{t0} - T_{sg})$ represents the equivalent dynamic temperature $(V^2/2gJC_p)$ for the gas.

A number of investigators (1, 2, 3) have determined the recovery factors of various types of pyrometer, but in most cases the results are not applicable to routine experimental work because of the indeterminate nature of the actual gas conditions at the thermocouple itself.

This difficulty has been overcome by Dunning (5), who suggested that sonic gas velocity should always be maintained over the thermocouple element. Dunning has shown that under these conditions the relation:

Total temperature $(T_{t0}) = 1.02 \times$ indicated temperature of the thermocouple (T_c) is accurate to within $1/2$ per cent. (An abstract of Dunning's theory is given in the Appendix.)

Hence the use of sonic gas velocity over the thermocouple element not only enables a simple correction to be applied readily to compensate for the otherwise indeterminate impact error; but in addition, it also provides a maximum value of (ρV) for given conditions of the gas, thus insuring the maximum rate of heat transfer to the thermocouple.

Regarding the methods which can be used to minimize the losses in a pyrometer, there is a wide background of knowledge available, and in this paper only minor refinements to what is now accepted practice are suggested.

The conduction of heat along the thermocouple wire away from the junction can be reduced to a very small order, if not entirely eliminated, by arranging for the gas stream to flow over the bare wires for a certain distance after the junction.

Radiation effects on the thermocouple can be reduced to a minimum by making the thermocouple as small as is consistent with mechanical reliability, and by surrounding it with a shield, the temperature of which is maintained as near as possible to that of the thermocouple itself.

With a single radiation shield round the thermocouple, it is clear that the same arguments concerning heat transfer to the surroundings will be applicable as in the case of the thermocouple itself. Conduction of heat along the shield and radiation of heat to and from the surroundings will be present; and in addition, if the gas velocity over the outside of the shield is low, the conditions for transfer of heat from the surrounding gas to the shield by forced convection will not be optimum. These effects will make the temperature of the inner surface of the shield

different from that of the gas and hence affect the thermocouple junction temperature. If this effect is to be eliminated, the logical assumption is that an infinite number of shields will be necessary; but in actual practice it has been shown by Probert (4) that, for the conditions met with in gas-turbine combustion work, two shields are sufficient to reduce the radiation effects on the thermocouple to negligible magnitudes. If two shields are used, it is essential that the gas velocity between the shields should be maintained as high as possible and that the shields should be insulated thermally from each other.

From the foregoing discussion the following basic design features for a pyrometer may be stated:

- 1 Sonic gas velocity should be maintained over the thermocouple element, which should be made as small as is consistent with mechanical reliability.
- 2 Isothermal conditions should be maintained along the wires leading away from the junction.
- 3 Two radiation shields should be provided and be insulated from each other, and the gas velocity in the annular space between them should be maintained as high as possible.

COMMENTS ON EXISTING TYPES OF SUCTION PYROMETERS

Although several of the points mentioned in the previous discussion have been known for an appreciable period, it was not until serious attention was given to the study of combustion problems at high altitudes that the full magnitude of some of the errors involved became apparent. Previous work with high-density gas streams had shown the need for adequate radiation shielding, but with the high rates of heat transfer to the thermocouple under these conditions it was possible for comparatively large conduction losses to remain undetected. As the density of the gas stream is reduced, however, the reduced rate of heat transfer to the thermocouple by forced convection will reveal any conduction losses by an increasingly slow rate of response to change of temperature.

Several types of suction pyrometers had been constructed in which the conduction and radiation effects were considerably reduced, as shown by a more rapid response rate than ordinary stagnation thermocouples. With these pyrometers it was customary to operate with the suction adjusted to give a maximum thermocouple reading. The assumption was made that equilibrium conditions had been reached and that the resultant temperature reading was the true one. No "recovery-factor" correction could be applied since the actual gas conditions at the thermocouple junction could not be defined with certainty.

Fig. 1 shows one of these pyrometers which was developed from a design by Probert. It should be noticed that only one suction point was fitted, although double radiation shields were used. Because of this the gas-flow conditions over the thermocouple were difficult to predict over the comparatively wide range of operating conditions for which the pyrometer was required. Calibration of this pyrometer revealed that it gave substantially correct measurement of temperature down to pressures of the order

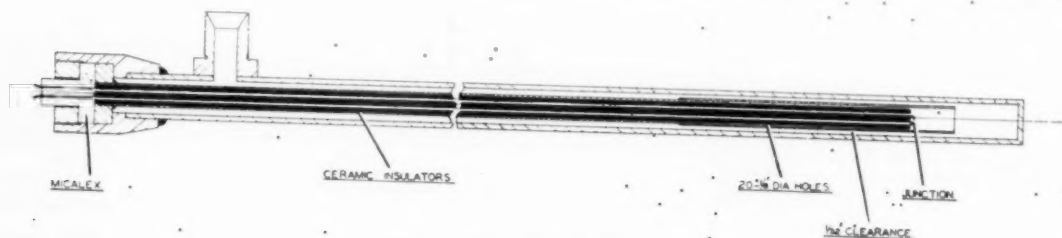


FIG. 1 PROBERT TYPE PYROMETER

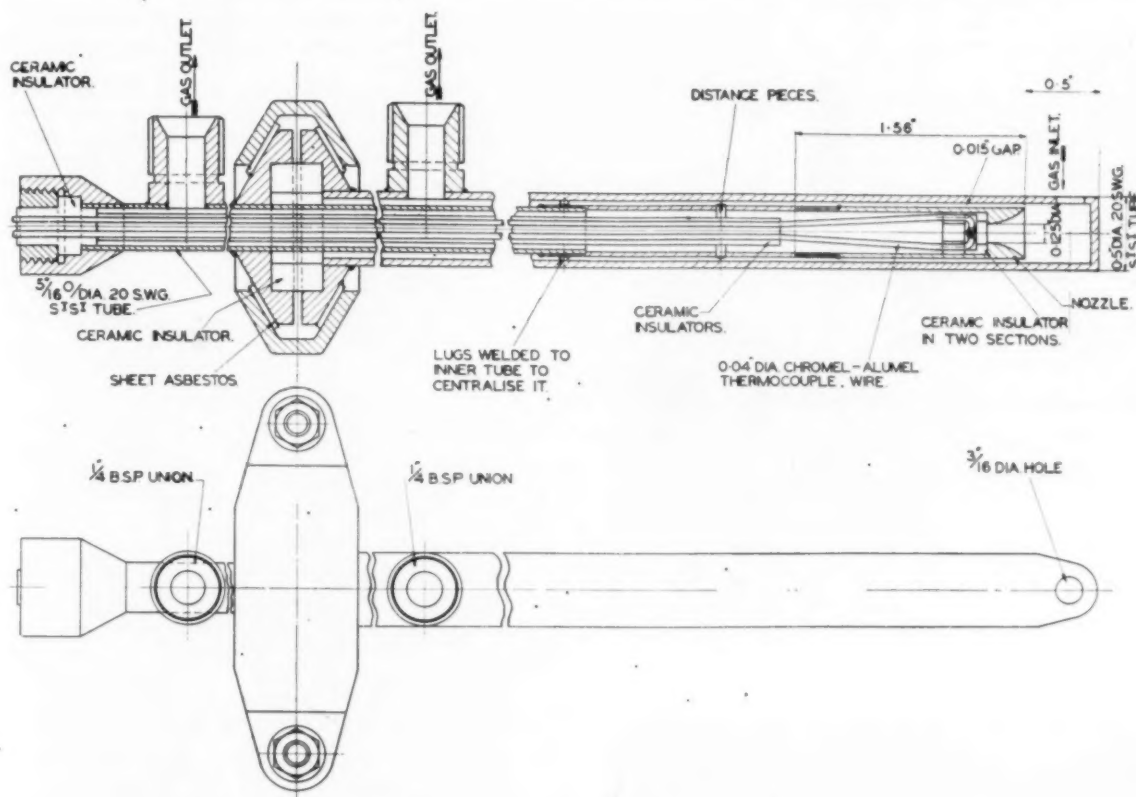


FIG. 2 GENERAL ARRANGEMENT OF SONIC SUCTION PYROMETER

of 0.75 atm. Below this pressure, errors which increased with reduction in gas density became apparent until at a pressure of 0.3 atm, an error of the order of 5 per cent was evident.

This experience emphasized the need for a pyrometer in which a known correction could be applied to the observed reading for any required operating condition, and in which the conduction and radiation effects would be negligible.

CONSTRUCTION OF SONIC SUCTION PYROMETER

Fig. 2 shows the details of a sonic suction pyrometer which was designed by Armstrong Siddeley Motors, Ltd., in an attempt to fulfill the essential requirements mentioned previously.

Sonic gas velocity over the thermocouple was obtained by placing the junction behind the throat of a convergent nozzle 0.125 in. diam, machined in the end of the inner radiation shield. Care was taken to insure that the junction was situated not more than 1 diam downstream from the nozzle throat, the location being achieved by means of two specially made ceramic insulators placed immediately behind the nozzle. A chromel-alumel butt-welded thermocouple was used, the wire being 0.040 in. diam. Flame or electric-resistance welding was used to form the junction, care being taken to remove any welding "flash" before installation in the pyrometer.

Isothermal conditions in the wires immediately next to the junction were achieved by arranging for the gas to flow over the bare wires downstream of the nozzle for a distance of about 1.5 in., after which the wires were insulated by conventional two-way porcelain insulators which were centralized in the shield by means of a suitably positioned 3-pin "spider." The gas stream

was arranged to flow around these insulators to the end of the shield where it was extracted by means of a vacuum pump. The two wires passed through a suitable gland and insulator to a small terminal block.

The outer radiation shield consisted of a heat-resisting steel tube 0.5 in. diam by 20 SWG. The annular clearance between the two shields was adjusted to 0.015 in., and a 3/16-in.-diam entry hole was used. A separate gas connection was provided at the end of the outer shield.

In order that the two shields should be insulated thermally from each other, a tapered flange was welded to each of the shields which were centered and insulated from each other by means of a ceramic bushing through which the inner shield was threaded.

The whole assembly was held together and was rendered gastight by means of a split clamping ring which compressed the two tapered flanges onto the ceramic bushing. Thermal leakage between the clamping ring and the flanges was prevented by means of two asbestos washers inserted between the ring and the flanges.

Figs. 3 and 4 show details of an actual pyrometer, and Fig. 5 shows the assembled pyrometer.

PYROMETER CALIBRATION

A detailed calibration of any type of pyrometer requires a specialized and comparatively elaborate rig. This is especially true when the investigation has to include subatmospheric gas pressures and exposure of the pyrometer to flame radiations. Since no such calibration rig has been available, it has been necessary

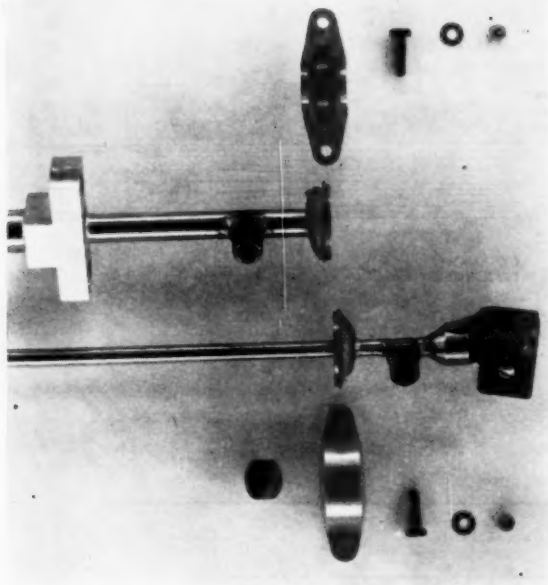


FIG. 3 SONIC SUCTION PYROMETER PARTS

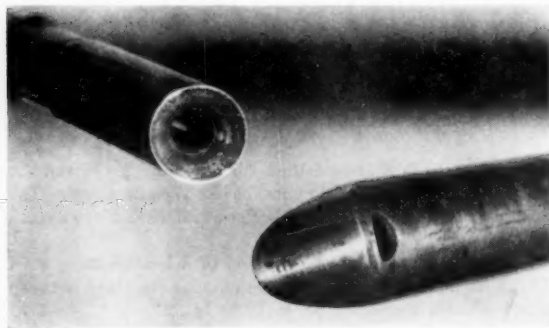


FIG. 4 SONIC SUCTION PYROMETER RADIATION SHIELDS

to use other means to obtain an absolute calibration of the pyrometer at these critical conditions.

After a consideration of various compromise methods of calibration, it was decided that an indirect method of absolute calibration against gas analysis should be adopted, especially as it would be fairly easy to apply this method at subatmospheric pressures where information on the performance of the pyrometer was particularly required.

A gravimetric technique of chemical analysis of combustion products had been developed by Macfarlane at the National Gas Turbine Establishment, England. This is described in detail by Lloyd (6). With care the over-all standard of accuracy of this technique is within 0.5 per cent when used to deduce combustion losses. If, therefore, the combustion efficiency of a combustor could be measured by both gas analysis and a heat balance under exactly reproducible conditions, an indirect assessment of the accuracy of the sonic pyrometer could be made at any desired operating condition. It is clear that this method is dependent upon the reproducibility of test conditions in the

combustor. With the standards of accuracy usually encountered in research work of this kind, it was considered that this requirement could be met satisfactorily.

The sonic pyrometer was installed in a water-cooled traversing gear fitted to the outlet end of a gas-turbine combustor which was known to maintain its performance for a considerable period of service. This combustor was being tested at simulated high-altitude engine conditions at the Royal Aircraft Establishment, Farnborough, England, and the initial development and calibration of the pyrometer were carried out there.

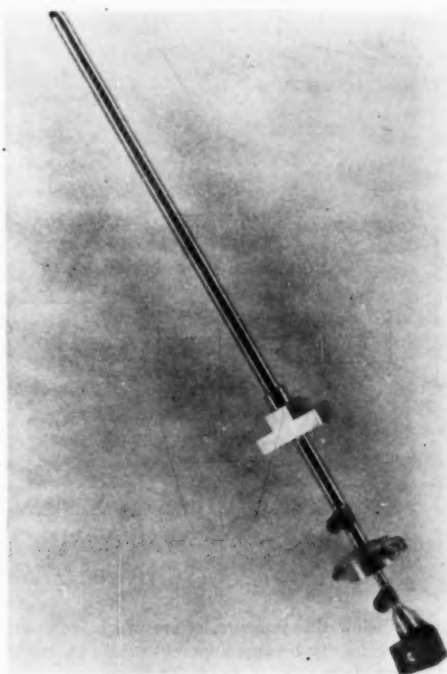


FIG. 5 SONIC SUCTION PYROMETER ASSEMBLED

Fig. 6 shows this test rig. Since the combustion-chamber pressure was always subatmospheric, the gas flow through the pyrometer was induced by means of two rotary vacuum pumps as is shown in the illustration. Pressure taps were located at the outlets of the two radiation shields in order to measure the gas-flow conditions through the pyrometer. These readings were based upon the assumption that there would be negligible pressure loss along the length of the shields. Exact measurement of the pressure drops would have required taps in the throat of the nozzle; this would have meant increased complication and a much larger instrument—a condition which could not be tolerated.

Experience with earlier types of pyrometers had shown the errors in the pyrometer readings to be of an appreciable order at pressures below 0.3 atm. Therefore all initial calibrating tests were carried out with the pressure at the entry to the combustor adjusted to 11 in. Hg abs; this pressure being of particular interest in the combustor test program then being carried out.

The fuel flow to the combustor was adjusted to give a mean gas temperature at the chamber outlet of 1090 F, and the gas flows through the pyrometer were adjusted to give a maximum thermocouple reading. While these conditions were held steady, the exposed cool end of the pyrometer was heated in a flame, but no change in reading was obtained. This indicated that there was sufficient gas flow through the pyrometer to swamp any

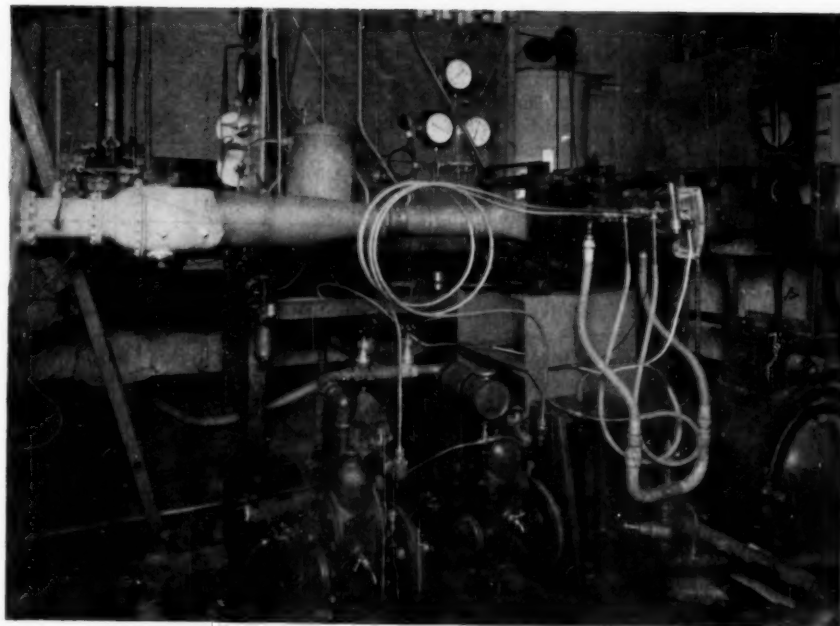


FIG. 6 PYROMETER TEST RIG

conduction losses along the leads and shields. The sensitivity to rapid changes in gas temperature was exceptionally good.

Following this, a series of response curves was obtained in order to assess the effectiveness of the radiation shields. It was assumed that the magnitude of the radiation from the thermocouple to the walls was greater than that from the flame to the thermocouple, and therefore a reduction in the radiation to and from the thermocouple would cause an increase in the thermocouple temperature. With the combustion-chamber conditions steady, the full suction available was applied to the inner shield with no gas flowing through the outer shield. The gas flow through the inner shield was then reduced progressively, the steady thermocouple reading being noted in each case, until the gas flow was reduced to zero. This enabled a curve to be drawn showing the variation of thermocouple reading with suction through the pyrometer. The suction on the outer shield was then adjusted so that there was a depression of 1 in. Hg relative to the zero-flow reading on the inner shield. A second response curve was then obtained as before, keeping this depression constant.

Further curves were obtained with increasing gas flows through the outer shield until no further effect on the thermocouple reading was evident.

The family of response curves thus obtained are shown in Fig. 7. This plot shows that all the response curves for the sonic pyrometer are similar in shape and that the maximum thermocouple reading occurs at about the critical pressure drop. Increasing the gas flow through the outer radiation shield results in a vertical displacement of the whole curve, but the difference between successive curves rapidly diminishes and no appreciable difference in reading was obtained once a relative depression of 4 in. Hg was exceeded. No significant reduction in indicated temperature was obtained once the maximum reading was reached. This was due to the fact that the maximum temperature reading was reached at near the critical pressure drop across the nozzle and, consequently, there was no change in velocity at the junction as the pressure drop was further increased. In actual practice, this factor constituted an advantage, since

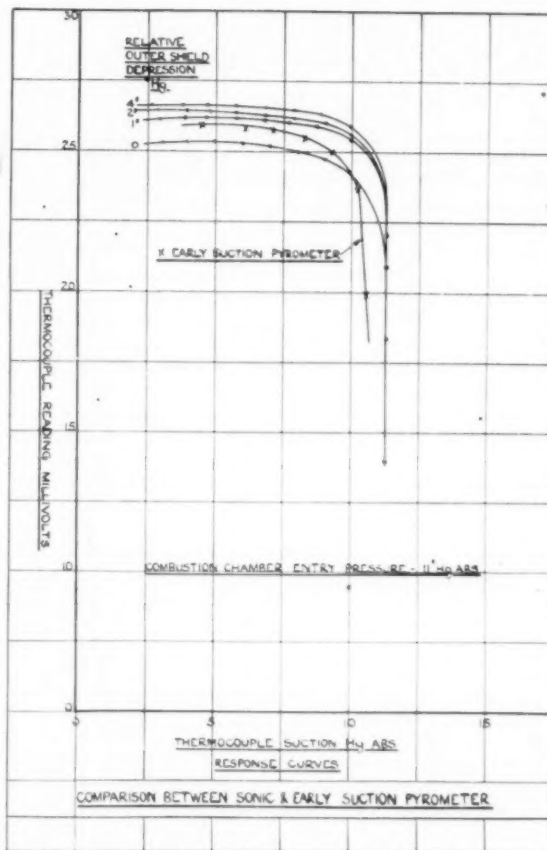


FIG. 7 RESPONSE CURVES FOR PYROMETERS

elaborate regulation of the suction on the pyrometer became unnecessary once this occurred.

The single response curve obtained with the earlier type of pyrometer under the sonic test conditions is also included in Fig. 7. Whereas the response curve for the sonic pyrometer shows the initial temperature rise to be vertical, that for the early pyrometer exhibits a definite shape. In the Appendix it is shown that the gradient of this initial portion of the curve may be interpreted as a measure of the losses existing in a pyrometer. The smaller the losses in the pyrometer, the more rapidly it reaches a maximum temperature as the gas velocity is increased from zero. Hence the response curves provide a simple qualitative method of assessing initially whether the losses in a pyrometer are appreciable. The maximum reading attained by the early pyrometer is seen to be about 2 per cent lower than that attained by the sonic pyrometer.

To check the absolute accuracy of the sonic pyrometer, a number of combustion-chamber-outlet temperature traverses were made under carefully controlled test conditions, in order to derive the combustion efficiency. Gas analyses of the combustor products were then made using the gravimetric technique mentioned previously (6). Table 1 shows a comparison among the results obtained by gas analysis, from the corrected sonic pyrometer readings, and from readings obtained with the Probert type pyrometer.

TABLE 1 COMPARISON OF TEST RESULTS

	Gas analyses		Sonic pyrometer		Probert type pyrometer	
Entry total pressure, in. Hg abs.	11	113 F	11	113 F	11	113 F
Inlet air temp, deg F	52.9	75.2	52.9	75.2	52.9	75.2
A/F ratio	95.5	94.9	95.3	95.7	90.2	92.6
Combustion efficiency, per cent						

When the standard of accuracy of the sonic pyrometer is considered, it is shown to give results which are in good agreement with those obtained by gas analysis if the correction suggested by Dunning is applied.

In order to check the thermocouple correction factor of 1.02 given by Dunning, a sonic suction pyrometer was calibrated in an atmospheric-pressure-thermocouple calibration rig at the Westinghouse Research Laboratories. In this test the gas velocity was varied from 150 to 700 fps, and the gas temperature was varied from 1000 to 2000 deg R. The average value for the correction factor for thirteen points was 1.0154. Fig. 8 shows the spread in the correction factor among these thirteen points which is about ± 0.2 per cent. Since there is no discernible trend due to velocity level, it can be assumed that this spread is due to experimental error. Spot checks on a second pyrometer gave substantially the same result.

The use of 1.0154 for the temperature correction factor in the two test points given in Table 1 gives values for efficiency of 94.7 and 94.9, respectively. These values agree with the gas-analysis results as well as do the sonic-pyrometer values which were based upon a correction factor of 1.02.

GENERAL COMMENTS

The previous discussion has shown that the design of sonic pyrometer described in this paper is capable of a high order of accuracy of temperature measurement, coupled with a rapid rate of response. These features are evident over a wide range of gas densities, tests having been made at the Armstrong Siddeley Works at pressures varying from about 100 psia down to 2 psia. So far, only laboratory versions of this type of pyrometer have been constructed. Much smaller sizes of instrument are contemplated to meet the need for a small pyrometer, having a

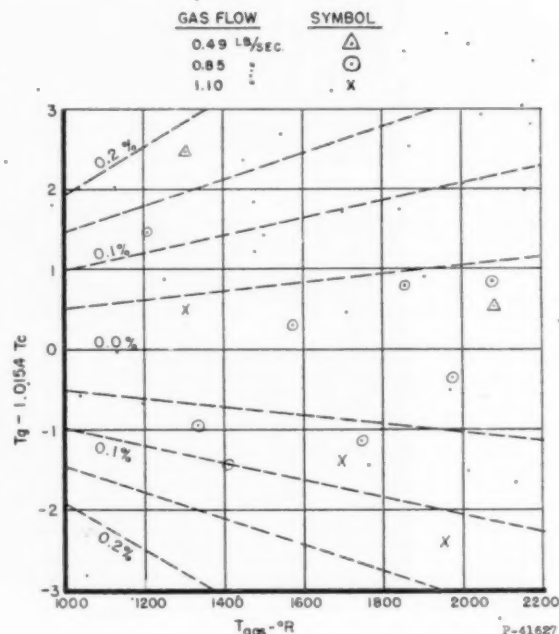


FIG. 8 CALIBRATION OF PYROMETER
(Error in sonic suction pyrometer using correction factor of 1.0154.)

rapid response rate, which exists in gas-turbine engines where a measured temperature operates the control mechanism for the engine. For this application a slow response rate may cause hunting and consequent overheating of the engine. The likelihood of this happening would be greater as the operating altitude of the engine is increased.

The mechanical reliability and the thermoelectric stability of the pyrometer design presented in this paper have proved to be very good. Sonic suction pyrometers have been used for as long as 150 hr without any mechanical problems whatsoever. The accuracy of the pyrometer after 150 hr of operation has been checked and found to be unchanged.

In laboratory tests it has been possible to use the sonic suction pyrometers in any way that ordinary bare-wire thermocouple can be used. They have been used singly for simple temperature traverses, in gangs for traverses of annular passages, and on oscillating multi-instrument rigs for obtaining average temperatures in annular passages.

In general, the need for vacuum lines to the pyrometer has not been a serious disadvantage in laboratory testing, and the relatively high cost of these pyrometers has been justified by the good accuracy and durability obtained.

CONCLUSIONS

1 The suction pyrometer employing sonic gas velocity over the thermocouple element incorporates all the essential features shown to be necessary for obtaining an accurate measurement of the total temperature of a moving gas stream for any gas density and enables a simple correction to be applied readily for impact error.

2 In the case of gases met within gas-turbine practice, the correction for impact error is theoretically:

Total temperature of gas (T_{t0}) = $1.02 \times$ indicated temperature of thermocouple (T_c). Actual calibration of two thermocouples gave a correction factor of 1.0154 which differs slightly from the theoretical figure.

3 The sonic pyrometer has a very rapid response to changes of gas temperature, and a simple qualitative check is possible to assess the magnitude of any thermal losses in the pyrometer.

4 Because of its rapid rate of response at low-density conditions, the sonic suction pyrometer has a particular application in the aircraft gas-turbine engine for any control mechanism in which a gas temperature is the operating criterion.

5 The sonic suction pyrometer has proved very satisfactory for gas-turbine combustion work, especially for temperature measurement at very low gas densities.

6 In gas-turbine combustion work the good durability and accuracy of the sonic pyrometer have justified its relatively high cost.

ACKNOWLEDGMENTS

The authors' thanks are due to Mr. R. W. O. Papworth of Armstrong Siddeley Motors, Limited, who was mainly responsible for the design of this pyrometer, to Mr. J. E. P. Dunning of the Royal Aircraft Establishment, who has greatly contributed to the successful development of the sonic pyrometer, and to the managements of Armstrong Siddeley Motors, Limited, and Westinghouse Electric Corporation for permission to publish this paper.

BIBLIOGRAPHY

- 1 "Measurement of High Temperatures in High-Velocity Gas Streams," by W. J. King, *Trans. ASME*, vol. 65, 1943, pp. 421-431.
- 2 "Temperature Measurements in High-Velocity Air Streams," by H. C. Hottel and A. Kalitinsky, *Journal of Applied Mechanics*, *Trans. ASME*, vol. 12, 1945, pp. A-25-32.
- 3 "Performance of Butt-Welded Thermocouples in High Velocity Air Streams," by L. O. Olsen, A. I. Dohl, and P. D. Freeze, National Bureau of Standards.
- 4 "The Measurement of Gas Temperatures in Turbine Engines," by R. P. Probert, *Journal of Scientific Instruments*, vol. 23, April, 1946, pp. 72-77.
- 5 Unpublished Work, by J. E. P. Dunning.
- 6 "Determination of Gas-Turbine Combustion-Chamber Efficiency by Chemical Means," by P. Lloyd, *Trans. ASME*, vol. 70, 1948, pp. 335-341.
- 7 Unpublished Paper, by P. R. Owen.

Appendix

Additional nomenclature is introduced in the Appendix as follows:

- C_p = constant-pressure specific heat, Btu/(lb) (deg F)
 C_v = constant-volume specific heat, Btu/(lb) (deg F)
 g = acceleration of gravity, ft/sec²
 J = Joule's constant, 778 (ft) (lb)/Btu
 k = ratio of specific heats, C_p/C_v
 P_r = Prandtl number, dimensionless
 R = gas constant, ft/deg F
 r = recovery factor, dimensionless
 V = gas velocity, fps

The following is an abstract from reference (5) on the theory of the sonic pyrometer, as evolved by Dunning:

Using the same notation as previously, we have

$$T_c = T_{sg} + r \cdot \frac{V^2}{2gJC_p} = T_{sg} \dots \dots \dots [3]$$

Assuming that the radiation and conduction losses are negligible, and that r is a factor depending upon the thermocouple shape and gas conditions; if V is equal to the local velocity of sound

$$V^2 = kgRT_{sg} = \frac{C_p}{C_v} \cdot gJ(C_p - C_v) T_{sg}$$

and

$$T_c = T_{sg} \left[1 + r \times \frac{(k-1)}{2} \right]$$

We require the total temperature (T_{tg}) of the gas which is given by

$$T_{tg} = \frac{(k+1)}{2} \cdot T_{sg}$$

from which

$$T_{tg} = \frac{(k+1)}{2 + r(k-1)} \cdot T_c \dots \dots \dots [4]$$

Therefore, if k and r are known, a precise correction can be applied to the thermocouple reading T_c .

German experimental work (7) has shown that the temperature of a cone in a gas stream is in very close agreement with Pohlhausen's formula

$$T_c = T_{sg} + \frac{V^2}{2gJC_p} \left[1 + \left(\frac{U}{V} \right)^2 \times (P_r^{1/2} - 1) \right] \dots \dots [5]$$

where U is the gas velocity near the surface of the cone and V is the gas velocity in the free stream. If Equation [5] can be accepted as holding at Mach number = 1, and the thermocouple is considered as a small cone, then $U \approx V$ and $r = P_r^{1/2}$.

For gases of the composition and temperature range generally met with in combustion work, P_r may be taken to have a constant value of 0.76, making $r = 0.87$.

Equation [4] shows that the nearer r approaches unity, the smaller is the effect of changes in the value of k , and with $r = 0.87$, Equation [4] becomes

$$T_{tg} = 1.021 \times T_c \text{ when } k = 1.4$$

$$T_{tg} = 1.017 \times T_c \text{ when } k = 1.3$$

Therefore, in general, the relationship

$$T_{tg} = 1.02 \times T_c$$

may be used without accepting an error greater than $1/2$ per cent.

EFFECT OF HEAT LOSSES ON PYROMETER PERFORMANCE

It is shown in reference (5) that for a given heat loss L in the pyrometer and for constant total conditions of the gas, the indicated temperature T_c will pass through a maximum value as the velocity of the gas over the thermocouple is varied, and that when T_c is a maximum, the following relationship holds

$$L = \frac{K \cdot T_{sg} \left(\frac{k}{k-1} \right) [T_{tg} - T_{sg}]^{3/2}}{\left[\frac{(k+1)}{2} \times T_{sg} - T_{tg} \right]}$$

where K is a constant.

From this it is seen that

When $L = 0$, T_c is a maximum when $T_{sg} = T_{tg}$, i.e., $V = 0$

When $L = \infty$, T_c is a maximum when $T_{sg} = 2/k + 1 T_{tg}$, i.e., V is sonic

and as L varies from zero to infinity, V increases continuously from zero to sonic to maintain T_c at a value whose locus is the envelope of maximum temperatures.

Hence it is apparent that with an ideal pyrometer, having no losses

$$\frac{dT_c}{dV} \longrightarrow \infty \text{ when } V \text{ is small}$$

Therefore the smaller the losses in a pyrometer, the more rapidly it reaches a maximum temperature as the gas velocity over the thermocouple is increased from zero.

This feature of the suction pyrometer provides a means whereby a rapid qualitative assessment can be made of the losses existing in the pyrometer.

Heat Transfer From an Air Jet to a Plane Plate With Entrainment of Water Vapor From the Environment

By MAX JAKOB;¹ R. L. ROSE;² AND MAURICE SPIELMAN³

This paper presents some experimental results, obtained by discharging hot air from a continuous slot parallel to a plane surface. A method for predicting the distribution of surface temperature, relations for the temperature and vapor pressure in the jet, a common correlation relating heat transfer and mass transfer, considering also the entrainment of environment air by the jet, and a numerical example are given.

NOMENCLATURE

The following nomenclature is used in the paper:

- a = vertical height of nozzle opening, ft
- $b_l = \dot{m}'' RT_f / (p_l - p_o) =$ local coefficient of mass transfer, ft/hr
- C = constant
- $h_l = q'' / (t_l - t_o) =$ local film coefficient of heat transfer, Btu/hr ft² F
- K = constant
- k = thermal conductivity, Btu/hr ft F
- k_f = thermal conductivity of air at temperature t_f , Btu/hr ft F
- m = an exponent
- $\dot{m}'' =$ local rate of mass flow per unit area (see note a at end of nomenclature), lb_m/hr ft²
- n = an exponent
- $N_{Nu} = h_f x / k_f =$ Nusselt number
- $(N_{Nu})_{mod} = b_l x / \delta =$ modified Nusselt number
- $N_p = (p_o - p_l) / (p_l - p_o) =$ partial-pressure ratio
- $N_{Pr} = \nu / \alpha =$ Prandtl number
- $N_{Re} = v_o x / \nu_o =$ Reynolds number
- $N_{Sc} = \nu / \delta =$ Schmidt number
- $N_t = (t_o - t_l) / (t_l - t_o) =$ temperature ratio
- $p_e =$ partial pressure of water vapor in environment air (room air), lb/sq in.
- $p_l =$ smallest observed partial pressure of water vapor measured in jet at distance x from nozzle outlet, lb/sq in.
- $p_o =$ partial pressure of water vapor in air at nozzle outlet, lb/sq in.
- $p_s =$ partial pressure of water vapor at plate surface, lb/sq in.
- $q'' =$ local rate of heat flow per unit area (see note a), Btu/hr ft²

- $R = 85.4 =$ individual gas constant for water vapor ft-lb_f/lb_m F
- r = an exponent
- $s =$ thickness of test plate, ft
- $t_b =$ temperature of bottom surface of plate, deg F (see note b)
- $t_d =$ dew-point temperature (used also with additional subscripts, e, j, o , corresponding to environment, jet, and outlet conditions), deg F
- $t_e =$ temperature of environment air, deg F
- $T_f =$ absolute temperature of air film, deg R (see note b)
- $t_f = 1/2(t_l + t_o) =$ air-film temperature, deg F
- $t_j =$ maximum jet temperature at distance x , deg F
- $t_o =$ nozzle-outlet air temperature, deg F
- $t_s =$ surface temperature of plate at distance x , deg F
- $v_o =$ air velocity at nozzle outlet, ft/sec
- $x =$ horizontal distance from nozzle outlet, ft
- $y =$ vertical distance from surface, in.
- $\alpha =$ thermal diffusivity, sq ft/hr
- $\delta =$ mass diffusivity, sq ft/hr
- $\eta_e = (t_e - t_b) / (t_o - t_b) =$ a temperature ratio
- $\nu =$ kinematic viscosity of air (used also with subscript o corresponding to outlet condition), sq ft/hr

NOTE: (a) The double prime sign in the symbol refers to unit area and the dot refers to unit time.

(b) Deg F is used for ordinary temperature, deg R for absolute temperature in the Fahrenheit scale: $F = R$ is used for the unit of temperature difference.

INTRODUCTION

The work upon which this paper is based arose from a problem submitted to the War Research Committee of Illinois Institute of Technology⁴ by the United States Army Air Forces in 1945.

Ice formation on the inside surface of aircraft windshields had become a serious problem with the introduction of high-altitude pressurized cabin bombers. One of the techniques available for preventing ice formation is that of blowing a jet of heated air over the inside windshield surface. No basic design information, however, was available.

The Republic Aviation Corporation had begun to study the problem before the authors' work started (3, 4, 5, 6).⁵ Another experimental study was published later by Zerbe and Seln (7). As in these investigations, a plane heat-flow meter was used for the present measurements. No attempt was made to duplicate frosting conditions on the test plate. It is more convenient to employ higher temperatures and to convert the results to freezing conditions using the principle of similarity.

EQUIPMENT AND OPERATION

Basically, the apparatus simulates a plane windshield by a model

¹ Research Professor of Mechanical Engineering, Illinois Institute of Technology, Chicago, Ill. Mem. ASME.

² Assistant Professor of Mechanical Engineering, Illinois Institute of Technology. Jun. ASME.

³ Associate Research Engineer, Illinois Institute of Technology. Jun. ASME.

Contributed by the Heat Transfer Division and presented at the Annual Meeting, New York, N. Y., November 27-December 2, 1949, of THE AMERICAN SOCIETY OF MECHANICAL ENGINEERS.

NOTE: Statements and opinions advanced in papers are to be understood as individual expressions of their authors and not those of the Society. Paper No. 49-A-16.

⁴ This work was also used in the MS theses of R. L. Rose (1) and M. Spielman (2).

⁵ Numbers in parentheses refer to the Bibliography at the end of the paper.

which is heated by a jet of hot air blown over one surface and cooled on the other side by a stream of water.

Figs. 1 and 2 are views of the major equipment in the laboratory. Filtered air, having passed through a refrigerating dehumidifier (Fig. 2, left background) enters the blower (Fig. 1, right background). Steam can be added to the laboratory air through perforated pipes above the door, Fig. 1, to increase the humidity difference between the jet and environment air. From

the blower, the air passes through a duct with electric heaters and baffles, to the slot, from which it is discharged over the test plate, Fig. 3. Duct air temperatures and static pressure were read from three thermocouples and a pressure tap ahead of the slot.

The slot, 17.5 in. wide, variable in height from 0 to 0.75 in. is the outlet of a nozzle having an elliptical profile. Openings 0.25 and 0.50 in. high were used in these tests. The lower edge of the

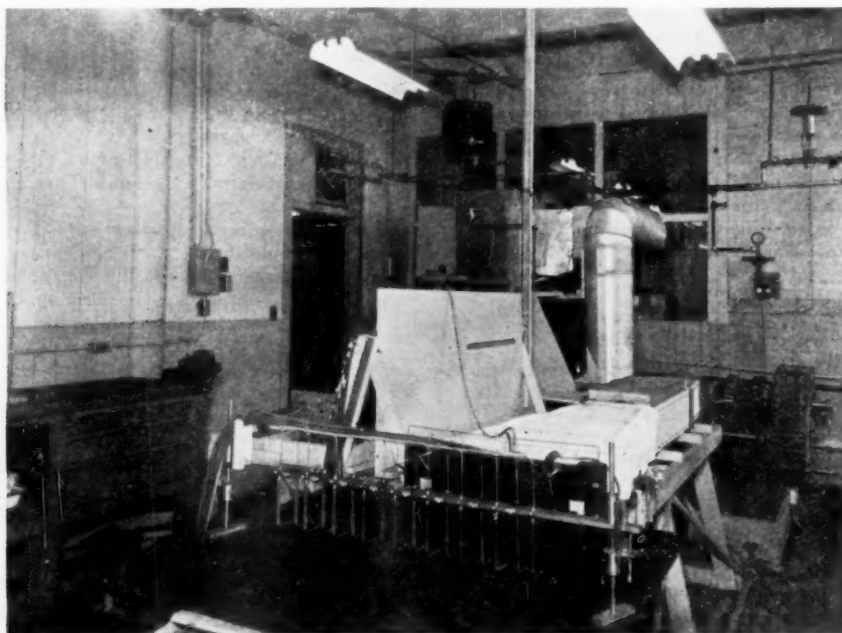


FIG. 1 VIEW OF LABORATORY, SHOWING DUCT AND TEST PLATE

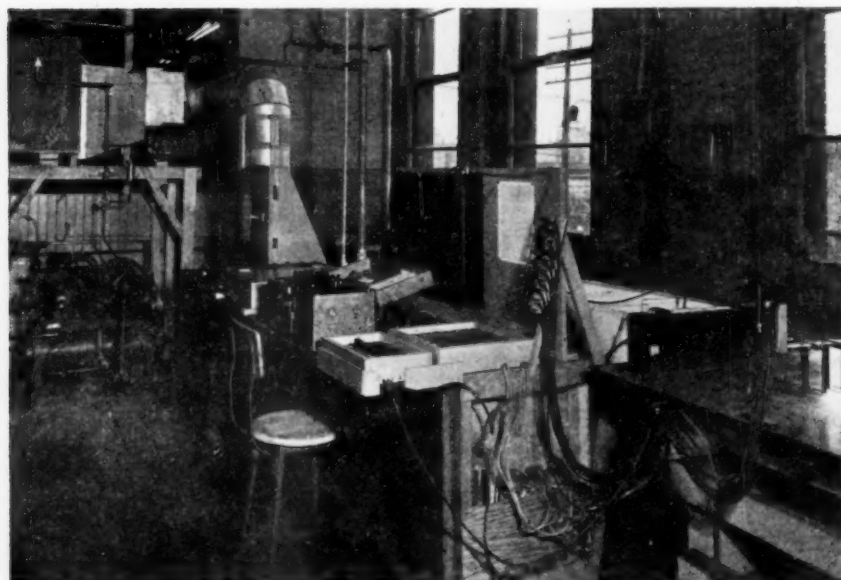


FIG. 2 VIEW OF LABORATORY, SHOWING CONTROL AND MEASURING EQUIPMENT

nozzle
plate,
stream
been d
nozzle.
of the
surface
face we
limits e

The
of John
30 in. l
the Ar
nology,

The
wide, s
Fig. 3.



FIG. 3

Thin
and ni
the pl
juncti
disks
at leas
tion al

A t
used f
mocou
across
at var
ings w
high-v
tubing
tion, t
traver

* St
enviro
This d

nozzle outlet was 0.25 in. above the starting section of the test plate, the leading edge of which was in contact with the downstream side of the nozzle plate, see Fig. 3. This arrangement has been designated by Republic Aviation Corporation as a blocked nozzle. High-velocity eddies between the jet and the surface of the starting section cause the stream to be forced against the surface, so that the jet behaves essentially as if the starting surface were even with the lower edge of the nozzle opening. This limits entrainment of environment air to one side of the jet.

The test plate, used as a heat-flow meter, is a rectangular slab of Johns-Manville asbestos ebony, 1.53 in. thick, 15 in. wide, and 30 in. long. The thermal conductivity of the plate, measured by the Armour Research Foundation of Illinois Institute of Technology, is 0.484 Btu/hr ft F at 100 deg F.

The starting section, 6 in. long, and two side extensions, 10 in. wide, as well as the outlet for the cooling water, are seen in Fig. 3.

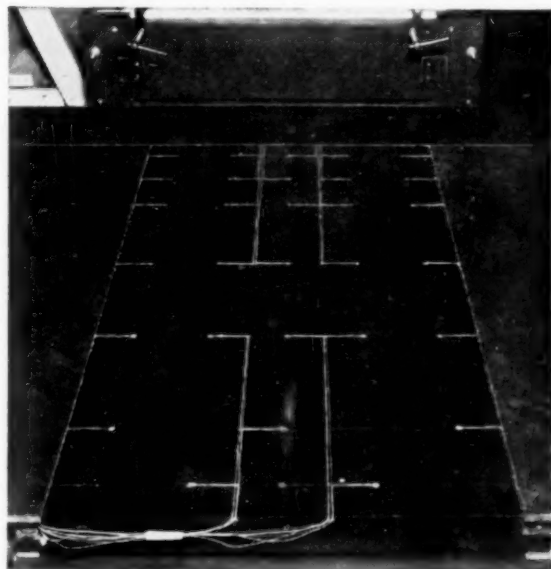


FIG. 3 TEST PLATE BEFORE FILLING THERMOCOUPLE GROOVES

Thirty surface thermocouples are on the jet side of the plate, and nine are on the water side. Fig. 3 shows the upper side of the plate before filling the grooves containing the wires. The junctions are in the center of 0.25-in.-diam by 0.020-in. copper disks recessed in the plate. The wires from the junctions run for at least 1.5 in. parallel to the nozzle outlet, to reduce heat conduction along the wires.

A traverse unit, resembling a rake (foreground, Fig. 1) was used for traverses in three dimensions throughout the jet. Thermocouples and impact tubes are spaced alternately, 1.5 in. apart, across a width of 24 in. parallel to the nozzle outlet, and can be set at various heights above the test surface. Thermocouple readings were corrected for the temperature increase encountered in high-velocity streams (8). The impact tubes, $\frac{3}{16}$ -in.-OD brass tubing, were used to measure local velocities in the jet.⁸ In addition, they were used as sampling tubes in the tests with dew-point traverses of the jet. For this purpose the tubes across the width

of the test plate were connected to a common manifold, and this was led to the dew-point meter.

Three thermocouples, one above and one at each side of the nozzle, were provided for measuring environment air temperatures. A six-point Micromax recorder served to record the duct-air and environment-air temperatures.

Fig. 4 shows details of the dew-point meter used in the jet traverses. This instrument is similar to an automatic indicating meter developed by the University of Chicago Meteorological Laboratories; simpler in design, however, because automatic indicating was not necessary. The main part is a polished silver mirror, against which samples of the air are blown. The mirror button, containing three thermocouples, is cooled from the rear until its exposed surface is clouded by condensation, which occurs at the dew point.

The finned end of the copper rod, seen in Fig. 4, was kept in melting ice. By varying the electrical input to the heating coil, a suitable range of temperatures could be maintained at the mirror surface. The temperature of clouding of the mirror was used as the dew point, because observation of clearing was less accurate.

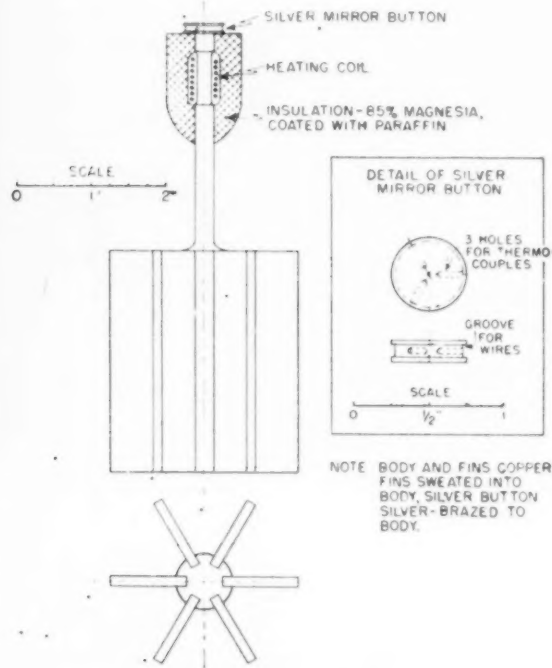


FIG. 4 DEW-POINT METER

All thermocouples used in the experiments were made of 30-gage copper and constantan wires, enameled and single-cotton covered. The cold junctions were kept in melting ice.

Equilibrium for a test was reached within 1 or 2 hr. A complete test required a full day for two observers. Such a test included velocity, temperature, and sometimes dew-point traverses, at different distances from the nozzle and heights above the plate surface, and measurement of the temperature distribution on the test-plate surface.

SCOPE OF EXPERIMENTS

A total of 19 tests are reported in this paper. Table 1 sum-

⁸ Static pressures in similar jets have been reported to exceed the environment pressure by 0.5 per cent of the dynamic pressure (9). This difference was neglected in the calculations.

TABLE 1 SUMMARY OF TEST CONDITIONS

Test no.	Initial jet vel., ft/sec	Initial jet temp., t_0 deg F	Bottom surf temp., t_b deg F	Environment temp., t_a deg F	Initial jet dew-pt temp., $t_{d,0}$ deg F	Environment dew-pt temp., $t_{d,a}$ deg F	Traverses
19	53	201	71	87			T V
18	75	202	73	91			T V
17	129	199	71	86			T V
13	129	201	52	80			T V
14	130	203	52	88			
25	132	199	36	85	20	62	T D
29	132	199	39	95	48	72	T V D
26	151	199	37	91	17	64	T D
22	167	80	80	80	49	64	D
28	167	148	38	71	31	62	T D
27	167	248	37	90	17	64	T D
24	168	202	58	94	46	70	T V D
30	169	199	43	98	55	74	T V D
9	176	200	38	75			T V
23	185	79	79	79	49	67	D
11	202	252	49	85			T V
12	203	151	49	86			T V
10	204	201	45	87			T V
21	204	201	60	98	45	77	T D

NOTES: Tests 29 and 30 were made with 0.5 in. nozzle opening, all others with 0.25 in. opening.

Transverse abbreviations:

T, jet temperature

V, jet velocity

D, jet dew point

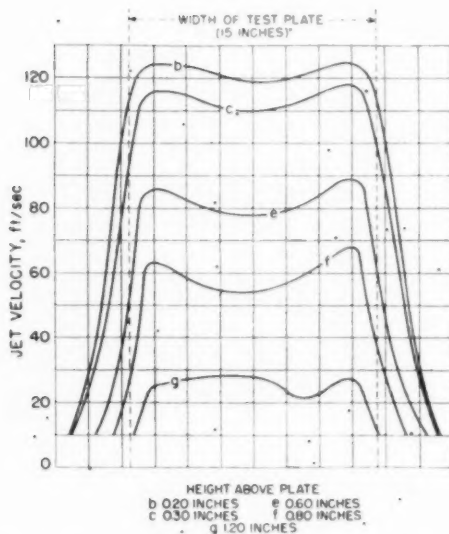


FIG. 5 VELOCITY DISTRIBUTION ACROSS JET, STATION A

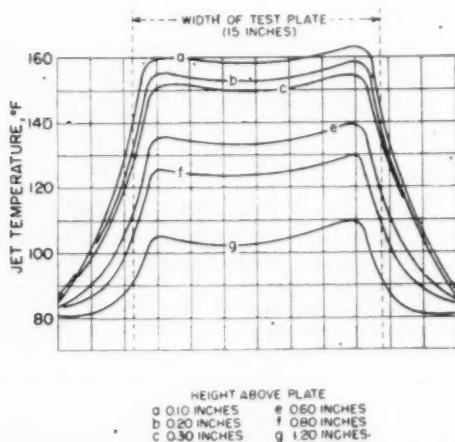


FIG. 6 TEMPERATURE DISTRIBUTION ACROSS JET, STATION A

marizes the measurements and conditions. The 6-in. starting section and the vertical distance of 0.25 in. from the plate surface to the lower edge of the nozzle opening were used in all tests.

All physical properties of air in the calculations were taken from tables of Keenan and Kaye (10).

JET CHARACTERISTICS

Results of typical velocity and temperature traverses across the width of the jet, from test No. 10, are shown in Figs. 5 to 8,

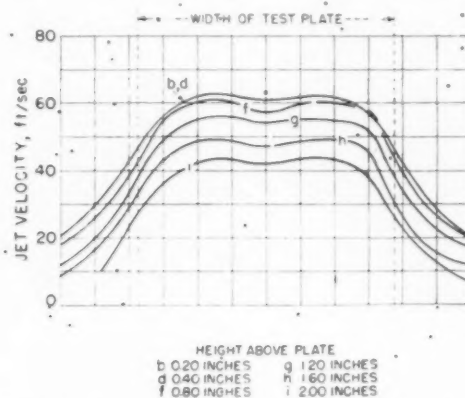


FIG. 7 VELOCITY DISTRIBUTION ACROSS JET, STATION F

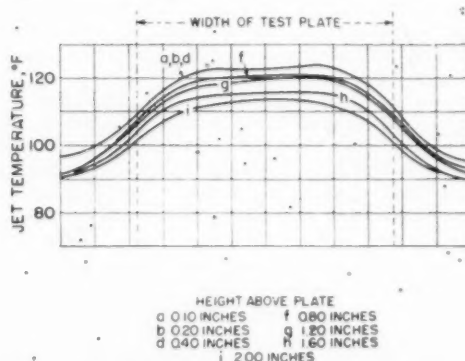


FIG. 8 TEMPERATURE DISTRIBUTION ACROSS JET, STATION F

inclusive. Distances from the nozzle to stations A and F are $x = 0.625$ and 2.625 ft, respectively.

The variations across the width of the test plate, at any height y , are not severe and therefore, in general, only average values were read in the traverses. For this purpose the thermocouples above the test plate were connected in series, and the impact tubes above the plate surface were connected to a common manifold.⁷

Using these averages at the various heights, profiles such as shown in Figs. 9 and 10 were obtained.

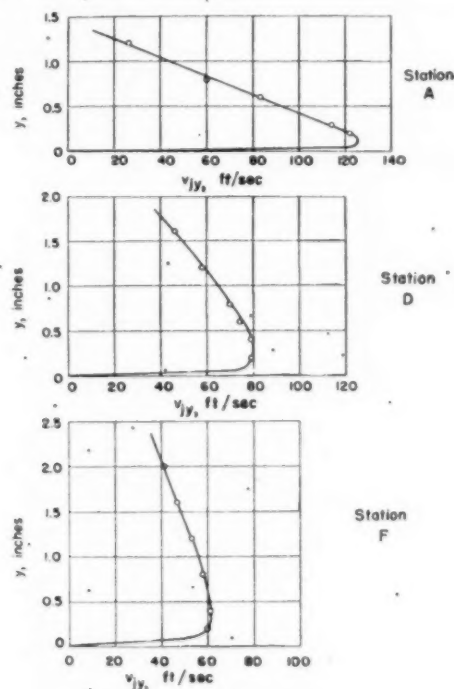


FIG. 9 JET-VELOCITY PROFILES

The average dew points measured led to vapor-pressure profiles of the type shown in Fig. 11.

It was desired to find the maximum local jet temperature t_{jy} at any distance from the nozzle because a local coefficient of heat transfer h_{jy} will be used, based on the temperature difference $t_{jy} - t_s$, where t_s is the plate-surface temperature at any distance from the nozzle. Since the greatest part of the jet cooling is caused by entrainment of environment air, the initial jet temperature t_o and the environment temperature t_e are the main factors in determining the average and the maximum jet temperature at any distance from the nozzle. Therefore a dimensionless temperature ratio may be defined as

$$N_t = \frac{t_o - t_j}{t_j - t_e} \dots \dots \dots [1]$$

This was found to be a function of the ratio of distance from the nozzle to height of the nozzle opening, x/a , independent of the initial jet temperature and velocity.

⁷ This averaging of pressures is subject to an inherent error, because the average of the square roots of the individual impact pressures should be used for the average velocity. The result of using the multiple connection was compared with the mean of individual measurements on several occasions. The difference was considered to be within the limits of accuracy of the measurements.

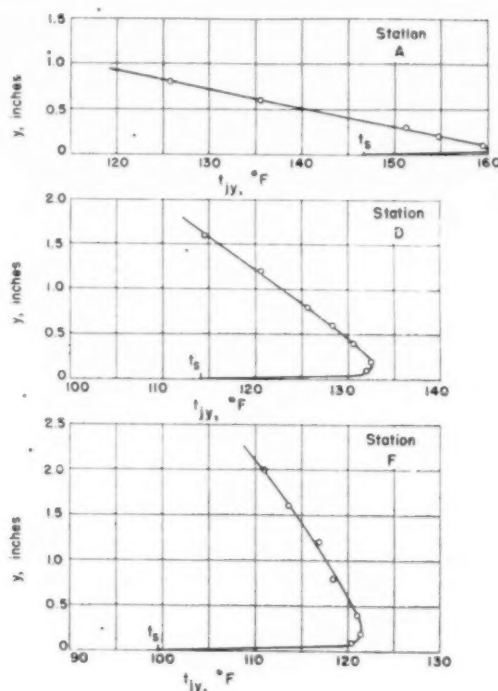


FIG. 10 JET-TEMPERATURE PROFILES

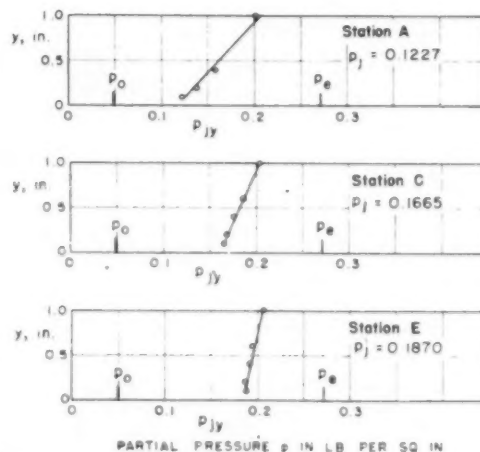


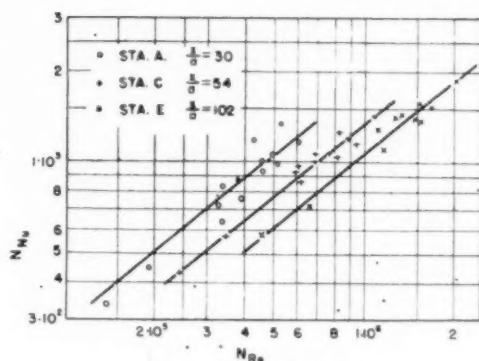
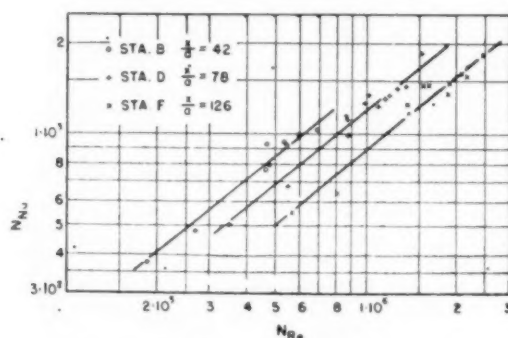
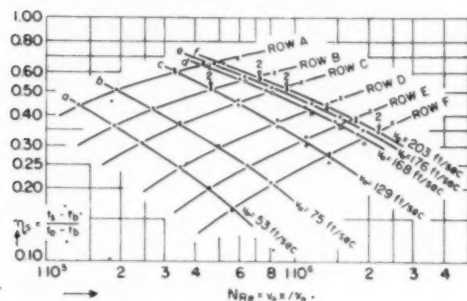
FIG. 11 JET PARTIAL-PRESSURE PROFILES

Fig. 12 illustrates the variation of N_t with x/a for all tests made with jets of hot air. The test points can be represented by a line corresponding to the equation

$$N_t = 0.055 \left(\frac{x}{a} - 12.5 \right)^{0.8} \dots \dots \dots [2]$$

This equation was determined for the following range of conditions

$53 < v_o < 205$ fps, $150 < t_o < 250$ deg F, $71 < t_e < 98$ deg F, and $15 < x/a < 126$.

FIG. 14 N_{Nu} VERSUS N_{Re} , STATIONS A, C, AND EFIG. 15 N_{Nu} VERSUS N_{Re} , STATIONS B, D, AND F

FOR ALL v_o AND x , $v_a = 203$ ft/sec
NUMERAL 2 INDICATES TWO COINCIDING POINTS

CURVE	$t_b, ^\circ F$
a	71
b	73
c	61
d	58
e	38
f	53

$t_o = 250^\circ F$
 $t_o = 200^\circ F$
 $t_o = 150^\circ F$

FIG. 16 DIMENSIONLESS REPRESENTATION OF SURFACE-TEMPERATURE PATTERN

Special Graph for Surface Temperature. A graphical representation useful for determining the surface-temperature variation is shown in Fig. 16. A ratio similar to an effectiveness, defined as

$$\eta_s = \frac{t_s - t_b}{t_o - t_b} \quad [12]$$

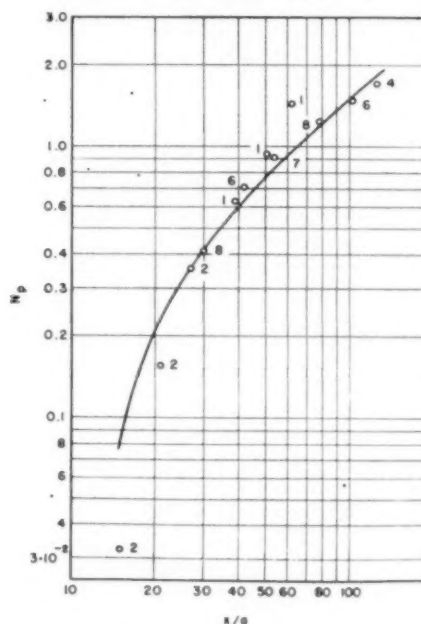
is plotted as a function of Reynolds number, defined in Equation [9]. A given plate unit conductance k/s , initial jet temperature t_o , and bottom surface temperature t_b , determine a family of curves such as Fig. 16, having x and v_o as parameters. The lines on the graph are for tests conducted with $t_o = 200$ deg F.

It will be noted that increasing v_o has a smaller effect at higher velocities. Hence little would be gained by using initial jet velocities in excess of 160 fps with this nozzle. An increase of t_o tends to shift the lines of constant v_o to the right, the lines of constant x remaining essentially the same.

The coefficient h_s would not be affected greatly by a change in surface temperature and, according to Equation [2], t_s depends only upon t_o , t_b , and x/a . Thus it would be possible to construct a similar family of curves for a different plate material and other initial conditions, using Equations [2], [4], [5], [11], and [12].

MASS TRANSFER

Corresponding to the representation of N_t in Equation [2] and Fig. 12, the results of the vapor-pressure traverses in the jet are shown in Fig. 17, with N_p , defined by Equation [3], as ordi-

FIG. 17 N_p VERSUS x/a
(Numerals at each point represent number of runs averaged.)

nate. Assuming⁹ the same influence of x/a as in Equation [2], the points in Fig. 17, are correlated by a curve according to

$$N_p = 0.042 \left(\frac{x}{a} - 12.5 \right)^{0.8} \quad [13]$$

Figs. 18-A and 18-B are sketches of typical measured profiles. Figure 18-D would represent the case of a jet becoming drier by dilution with dry air from the environment and condensation on the surface. A case similar to D, namely, Fig. 18-C, would represent entrainment of vapor from the environment, combined with evaporation on the surface, both contributing to the humidity of the jet. In the experiments, p was not measured close to

⁹ Without this assumption, a somewhat better representation of the points could be obtained.

the surface. Since no condensation or evaporation occurred at the surface, the curve in Fig. 18-B should not come to a minimum of p_j , but would proceed as a vertical line approaching the surface. This is an inherent lack of similarity.

If the experiments had been undertaken solely for checking the principle of similarity and not mainly for the practical purpose mentioned in the introduction, an arrangement yielding a profile according to C or D would have been chosen. In a continuation of the work, experiments with evaporation are being performed. In the present experiments, that partial pressure which was measured closest to the surface was called p_j , and was assumed to correspond to the maximum jet temperature t_j .

COMMON CORRELATION BETWEEN HEAT TRANSFER AND MASS TRANSFER

If heat transfer and mass transfer occur separately in geometrically similar fields, and the boundary conditions for each case are alike, the principle of similarity may be applied to predict the behavior of one field from measurements of the other.¹⁰ In the present case, heat and mass transfer, respectively, are represented by

$$N_{Nu} = C N_t^m N_{Re}^n N_{Pr}^r \dots \dots \dots [14]$$

and

$$(N_{Nu})_{mod} = C' N_p^m N_{Re}^n N_{Sc}^r \dots \dots \dots [15]$$

where $(N_{Nu})_{mod} = b_j x / \delta$ is a modified Nusselt number, a coefficient of mass transfer b_j being defined by $\dot{m}'' = b_j(p_j - p_\infty) / R T_j$ (see Nomenclature).

If the fields were perfectly similar,¹¹ the constants C , m , n , and r should be the same in Equations [14] and [15], giving

$$\frac{(N_{Nu})_{mod}}{N_{Re}^n N_{Sc}^r} = \frac{N_{Nu}}{N_{Re}^n N_{Pr}^r} \left(\frac{N_p}{N_t} \right)^m \dots \dots \dots [16]$$

To check the influence of the simplifications, two "isothermal" experiments of diffusion were performed in analogy to the heat-transfer experiments in which no humidity differences existed. The isothermal tests yielded essentially the same partial-pressure profiles as the nonisothermal diffusion tests. It was also found that the jet-temperature profiles in diffusion and mere heat-transfer tests were practically identical.

Based on this evidence of similarity, a common correlation by means of Equations [14] and [15] was attempted. Taking $n = 0.8$ from Equation [11], and assuming $r = 0.4$, $N_{Pr} = 0.72$ and $N_{Sc} = 0.63$, a trial-and-error method led to $C = 0.0242$ and $m = -0.4$, so that

$$N_{Nu} = 0.0242 N_t^{-0.40} N_{Re}^{0.80} N_{Pr}^{0.4} \dots \dots \dots [17]$$

and

$$(N_{Nu})_{mod} = 0.0242 N_p^{-0.40} N_{Re}^{0.80} N_{Sc}^{0.4} \dots \dots \dots [18]$$

Fig. 19 shows the common correlation. Either of the groups $N_{Nu} N_{Re}^{-0.8} N_{Pr}^{-0.4}$ or $(N_{Nu})_{mod} N_{Re}^{-0.8} N_{Sc}^{-0.4}$ can be considered as ordinate, depending upon whether N_t or N_p is taken as the abscissa. The straight line represents heat and mass transfer alike.

Comparing Equations [2] and [13] gives

$$N_p = 0.765 N_t \dots \dots \dots [19]$$

¹⁰ Nusselt (11) has also derived equations for both processes occurring simultaneously. Here, his simpler equations for separate fields can be used, since the concentration of water vapor in air is small.

¹¹ Nusselt mentions that there is a certain lack of similarity between heat-transfer and mass-transfer fields on a heated or cooled surface where no change of phase occurs, since heat but no mass flow crosses the surface.

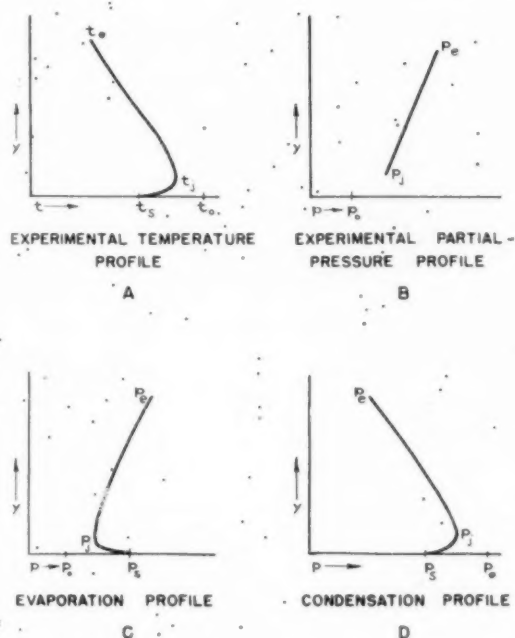


FIG. 18 COMPARISON OF SCHEMATIC PROFILES

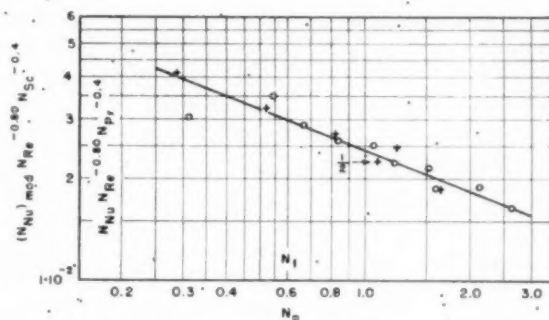


FIG. 19 A SINGLE CORRELATION FOR HEAT TRANSFER AND MASS TRANSFER

(Circles represent temperature measurements. Crosses represent partial-pressure measurements. Each point represents the average of eight experimental values except the point marked $1/3$ which represents four experimental values.)

for any x/a . Hence for any fixed value of N_{Re} and x/a

$$(N_{Nu})_{mod} = 1.05 N_{Nu} \dots \dots \dots [20]$$

The difference between N_p and N_t may be caused by the lack of similarity discussed in connection with Fig. 18. In fact, cooling of the jet by the plate, which has no equivalent in the diffusion tests; reduces t_j and therefore makes N_t larger, compared to N_p . The influence upon Equation [20] is smaller, mainly because of the exponent, -0.40 in Equations [17] and [18].

Further experiments with evaporation under experimental conditions as described in this paper are now in progress in continuation of our study for the United States Air Forces.

NUMERICAL EXAMPLE

The following example shows how the experimental results can be applied. An airplane is assumed at such an altitude and

speed that the outer windshield surface temperature is -30 deg F. A $1/2$ -in. windshield is used, having a unit conductance $k/s = 5.6$ Btu/hr ft² F. The defroster discharges air, initially at 150 deg F, 50 fps, parallel to the inner surface, from a continuous $1/4$ -in. slot. Dry air from the outside is used for defrosting. Cabin pressure is maintained at 20.6 in. Hg abs, equivalent to 10,000-ft altitude. Cabin air temperature is 45 deg F, dew point 40 deg F.

Assuming a film temperature of 40 deg F, Equation [11] reduces to

$$h_f = 4.93 (x)^{-0.6} \dots \dots \dots [21]$$

with h_f in Btu/hr ft² F and x in ft. This gives the values of h_f in Table 2. The values of N_t and N_p are found from Equations [2] and [13], respectively. Solving Equation [1] gives the values of t_f . Then Equation [6] is solved for t_s .

TABLE 2 VALUES OCCURRING IN CALCULATION OF THE EXAMPLE

x , ft	0.50	1.00	2.00	3.00
h_f from Equation [21]				
Btu/hr ft ² F	7.48	4.93	3.25	2.55
N_t from Equation [2]	0.386	0.958	1.89	2.68
N_p from Equation [13]	0.295	0.732	1.45	2.09
t_f from Equation [1], deg F	121	98.7	81.4	73.6
t_s from Equation [6], deg F	56.3	30.4	10.8	2.5
p_f from Equation [3], psia	0.0276	0.0515	0.0718	0.0822
$t_{d,j}$ from Steam Tables, deg F	8.7	20.5	27.2	30.3

From steam tables, $p_s = 0.1217$ psia. Further, $p_o = 0$. Here, with Equation [3] yields the values of p_f . The dew-point temperature $t_{d,j}$ is obtained from the steam tables, as the saturation temperature at vapor pressure p_f for the various x . Condensation or freezing is assumed to begin when $t_{d,j} = t_s$. Under the assumed conditions this occurs at a distance $x = 1.25$ ft (found by graphical interpolation).

The table shows that $(t_f + t_s)/2$ for $x = 1.25$ ft is larger than the assumed value of the film temperature $t_f = 40$ deg F. Using the correct temperature, however, would only change k_f by 2 per cent, i.e., within the accuracy of the equations.

ACKNOWLEDGMENT

The major part of the material in this paper is taken from reports submitted to the United States Air Forces (12). The authors

wish to express their appreciation to the Air Materiel Command for permission to publish these data.

BIBLIOGRAPHY

- 1 "Heat Flow From a Jet Discharged Parallel to a Plane Surface," by R. L. Rose, MS thesis, Illinois Institute of Technology, Chicago, Ill., June, 1948.
- 2 "Diffusion of Water Vapor From the Atmosphere Through a Jet of Less Humid Air," by M. Spielman, MS thesis, Illinois Institute of Technology, Chicago, Ill., June, 1947.
- 3 "Heat Transfer and Velocity Distribution Characteristics of a Free Air Jet Discharged From a Narrow Slot and Directed Parallel to a Horizontal Plate," Republic Aviation Corporation, Farmingdale, N. Y., Report ERF-3, 1945.
- 4 "Heat Transfer and Velocity Distribution Characteristics of a Free Air Jet Discharged From a Narrow Slot and Directed Parallel to a Horizontal Plate—Part II, $1/4$ Inch Deep Continuous Slot," Republic Aviation Corporation, Farmingdale, N. Y., Report ERF-3, 1945.
- 5 "Heat Transfer and Velocity Distribution Characteristics of a Free Air Jet Discharged From Individual Nozzles and Directed Parallel to a Horizontal Plate—Part I, Discontinuous Slots and Specially Designed Nozzles," Republic Aviation Corporation, Farmingdale, N. Y., Report ERF-9, 1946.
- 6 "Heat Transfer and Velocity Distribution Characteristics of a Free Air Jet Discharged From Individual Nozzles and Directed Parallel to a Horizontal Plate—Part II, Commercial Nozzle, Nozzle 'L,'" Republic Aviation Corporation, Farmingdale, N. Y., Report ERF-9, 1946.
- 7 "An Empirical Equation for the Coefficient of Heat Transfer to a Flat Surface From a Plane Heated-Air Jet Directed Tangentially to the Surface," by J. Zerbe and J. Selna, National Advisory Committee for Aeronautics, Washington, D. C., Technical Note 1070, 1946.
- 8 "Temperature Measurements in High-Velocity Air Streams," by H. C. Hottel and A. Kalitinsky, JOURNAL OF APPLIED MECHANICS, Trans. ASME, vol. 67, 1945, p. A-25.
- 9 "Turbulent Jet Expansion," by E. Forthmann, National Advisory Committee for Aeronautics, Washington, D. C., Technical Memo 789, 1936.
- 10 "Thermodynamic Properties of Air," by J. H. Keenan and J. Kaye, John Wiley & Sons, Inc., New York, N. Y., 1945.
- 11 "Heat Transfer, Diffusion and Evaporation" (Title translated), by W. Nusselt, Zeitschrift für angewandte Mathematik und Mechanik, vol. 10, 1930, p. 105.
- 12 "Aircraft Windshield Heating," Report to the Army Air Corps, Illinois Institute of Technology, Chicago, Ill., April 15, 1947.

out
not
U.
Ins
Aer
tory
nau
C
Ann
194
N
und
the

Pressure Drop and Convective Heat Transfer With Surface Boiling at High Heat Flux; Data for Aniline and n-Butyl Alcohol¹

BY FRANK KREITH² AND MARTIN SUMMERFIELD,³ PASADENA, CALIF.

Heat-transfer coefficients to commercial-grade aniline and n-butyl alcohol have been measured at high rates of heat flux. Data have been obtained for both of the liquids in the heat-flux range from 0.5 to 3 Btu/sq in. sec and in the pressure range from 50 to 400 psia at velocities from 20 to 40 fps. The test section consisted of a 1/2-in-ID stainless-steel tube which was heated electrically.

NOMENCLATURE

The following nomenclature is used in this paper:

- A = area, sq in.
- C_F = friction coefficient, $\left(\frac{\Delta H}{L} \frac{D}{V^2} \right)$
- C_p = specific heat, Btu/lb deg F
- D = inside diameter of tube, in.
- h = heat-transfer coefficient, Btu/sq in. sec deg F
- g = gravitational constant, ft/sec²
- ΔH = pressure drop in head of liquid
- j = forced-convection index, $(Nu/Re^{0.8} Pr^{1/4})$
- $C_H = (Nu/Re Pr) \cdot Pr^{1/4} (\mu_w/\mu_b)^{0.14}$
- K = thermal conductivity, Btu/ft hr deg F
- L = length, in.
- Nu = Nusselt modulus, $(hD/K) \times 12$
- P = pressure, psia
- Pr = Prandtl modulus, $(C_p \mu/K \times 3600 g)$
- ΔP = pressure drop
- q = rate of heat flow, Btu per sec
- Re = Reynolds modulus $(VD\rho/\mu \times 12)$
- T = temperature, deg F
- v or V = velocity, fps
- w = flow rate, lb per sec
- μ = absolute viscosity, lb sec/sq ft
- ρ = mass density, (lb/cu ft)/g

Subscripts:

- e = entrance
- B or F = fluid bulk
- HT = heat-transfer condition
- iso = isothermal condition
- s = saturation

v = vapor

W = wall

x = excess above saturation temperature

INTRODUCTION

This presentation is an extension of a previous paper by the same authors (1).⁴ In addition to water, the data for which were presented in the preceding paper, new data are presented for aniline and n-butyl alcohol.

EQUIPMENT AND EXPERIMENTAL TECHNIQUE

A detailed description of the experimental setup used for the study of heat transfer to liquids at high heat flux has been presented in a previous paper by the authors (1). The test section was a stainless-steel tube 17.5 in. long, 0.587 in. ID, and 0.020 in. wall thickness. This tube served also as a resistance heating element, as it was heated by electric current. The heat flux was regulated by changing the voltage potential across the tube. Measurements were taken of the liquid flow rate, the inlet and outlet temperatures, the pressure, and the frictional pressure loss in the test section. The temperature of the heat-transfer surface-to-liquid interface was calculated from the temperature of the outer tube wall, which was measured at 14 points along the tube by means of thermocouples.

The technique for installing the thermocouples and the derivation of the equation for the temperature distribution in an electrically heated cylinder has been discussed (1). However, in tests with aniline as a coolant, it was found that a deposit formed on the inner tube wall after short periods of operation. Therefore it was necessary to devise a technique for correcting the temperature measurements in order to obtain a true indication of the liquid-to-surface interface temperature.

A standard check test at a flow rate of 4.3 lb per sec, a pressure of 100 psia, and a heat flux of 1.2 Btu/sq in. sec was made with a clean and newly installed tube, and a true liquid-to-wall interface temperature was obtained. The data of this test could be reproduced within ± 5 deg F in subsequent tests after cleaning the tube with a rag saturated with clean aniline. A standard test under the foregoing specified conditions of flow, pressure, and heat flux was made before and after each series of tests, which lasted less than 10 min. During this 10-min period, a deposit formed on the inner tube wall which caused, on the average, an outer-wall temperature indication of 30–50 deg F higher than the original test on the clean tube. The build-up of the deposit for short periods of heating was found to be approximately a straight-line function of time, and by plotting temperature increase due to scale versus time for each series of tests, a temperature correction, corresponding to the time interval at which the test data had been obtained, was determined. The correction which had to be applied amounted to less than 5 per cent of the measured temperature, and the accuracy of the temperature of the liquid to surface interface

¹ This paper presents the results of one phase of research carried out at the Jet Propulsion Laboratory, California Institute of Technology, under Contract No. W-04-200-ORD-455 sponsored by the U. S. Army Ordnance Department.

² Senior Research Engineer, Jet Propulsion Laboratory, California Institute of Technology. Now, Guggenheim Fellow, Department of Aeronautics, Princeton University, Princeton, N. J. Jun. ASME.

³ Chief, Rockets and Materials Division, Jet Propulsion Laboratory, California Institute of Technology. Now, General Editor, Aeronautics Publication Program, Princeton University. Mem. ASME.

Contributed by the Heat Transfer Division and presented at the Annual Meeting, New York, N. Y., November 27–December 2, 1949, of THE AMERICAN SOCIETY OF MECHANICAL ENGINEERS.

NOTE: Statements and opinions advanced in papers are to be understood as individual expressions of their authors and not those of the Society. Paper No. 49-A-94.

⁴ Numbers in parentheses refer to the Bibliography at the end of the paper.

is believed to be at least within ± 15 deg F. Reproducible data within ± 10 deg F were obtained in tests made on different days with the same test section.

The n-butyl alcohol did not form a deposit on the heating surface, and thus the wall-temperature measurements did not require any corrections. In the test with n-butyl alcohol, the frictional pressure loss was measured with a differential mercury manometer, as well as a differential Barton pressure gage (1).

Each series of tests was made by setting the power level and flow rate, and changing the back pressure by adjusting the control valve on the downstream side of the test section. This technique made possible a maximum number of tests in a minimum time. At least five complete records of all the thermocouples mounted on the outside of the tube were obtained for each test, and steady state was assumed when three or more of the temperature records agreed within 5 deg F. In separate tests it could be shown that the time lag of the heating tube was less than 2-3 sec before coming to equilibrium. Heat balances between the electric power input and the thermal power output check within 2 to 3 per cent for all the tests.

EXPERIMENTAL RESULTS

Heat Transfer to Aniline With Bubble Formation Adjacent to Heating Surface. In the course of the experiments, data were obtained on the heat-transfer characteristics of aniline flowing upward in a stainless-steel tube 0.587 in. ID. The experiments covered the pressure range from 40 to 400 psia, and the heat-flux range from 0.3 to 3 Btu/sq in. sec at velocities of about 20 and 40 fps. The aniline, which was used in the experiments was taken from the rocket-fuel supply of this laboratory.

The data presented in this paper have been corrected for deposit build-up and are representative of heat transfer from a

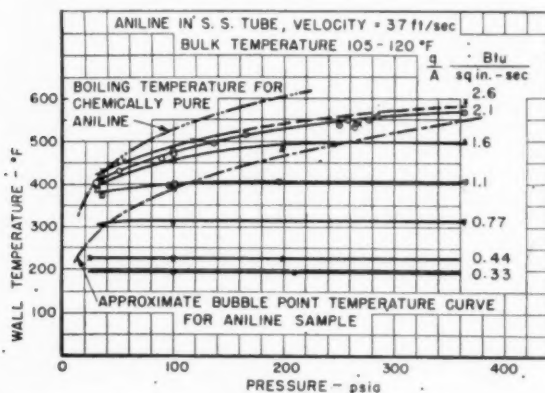


FIG. 1 WALL TEMPERATURE VERSUS PRESSURE (ANILINE)

surface of known temperature to aniline. The results of the first series of tests are shown in Fig. 1 as plots of wall temperature versus pressure at a constant aniline flow rate for various heat fluxes. It can be seen that as the pressure is reduced, the wall temperature necessary to remove a given heat flux decreases. This phenomenon has been observed previously in heat transfer to water with surface boiling. In the water experiments the decrease in wall temperature with reduction in pressure occurred initially at the saturation temperature of the liquid. The results with the commercial-grade aniline, on the other hand, show that the temperature potential necessary for the removal of a given heat flux begins to decrease at a wall temperature more than 100 deg F below the saturation temperature of pure aniline.

In the search for an explanation of the occurrence of surface-

boiling phenomena at temperatures below the saturation point of the liquid, a plot of friction coefficient C_F and heat-transfer coefficient C_H versus pressure was made at a flow rate of 16 lb/sq in. sec at a heat flux of 2.1 Btu/sq in. sec, Fig. 2. An examination of these curves shows that the friction coefficient, as well as the heat-transfer coefficient, increases as the pressure is reduced. This increase in friction coefficient was believed to be caused by the formation of gas bubbles in the heat-transfer tube. After studying the results of the aniline tests, it was assumed tentatively that some phenomenon similar to surface boiling brought about the phenomena which correspond to the surface-boiling effects in water-cooling. On the assumption that bubble formation was causing an increase in turbulence level and a corresponding increase in heat-transfer coefficient with reduction in pressure, an effective bubble-point curve was

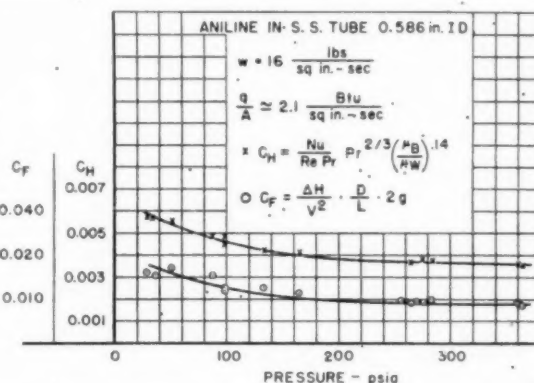


FIG. 2 HEAT TRANSFER AND FRICTION MODULI VERSUS PRESSURE (ANILINE)

estimated from the heat-transfer data presented in Fig. 1; it is superimposed on the same graph.

In order to obtain further proof of the bubble-temperature curve, estimated from the heat-transfer characteristics, a sample of the aniline which had been used in the experiments was analyzed for impurities and gas content; also the bubble temperatures were observed visually at reduced pressure in a distillation apparatus. The chemical analysis showed that about 5 per cent of water was dissolved in the aniline, and the experiments on bubble temperatures at reduced pressures indicated that bubble formation occurred at temperatures considerably below the boiling point of pure aniline. It was not feasible, without great expense and effort, to extend the visual observation of bubble temperatures to the pressure range used in the heat-transfer experiments. It was, however, possible to calculate a theoretical bubble temperature for the water-aniline solution at the critical pressure of aniline from Raoult's law.

The bubble temperatures obtained by three independent methods, (a) the visually observed bubble temperatures in the low-pressure range, (b) the calculated bubble temperature at the critical pressure, and (c) the bubble temperatures estimated from the heat-transfer experiment in the intermediate pressure range, are shown on one graph, Fig. 3, as the logarithm of the absolute pressure versus the inverse of the absolute temperature. Over a wide pressure range, all data fall on a smooth and continuous curve and thus lend additional weight to the explanation of the heat-transfer phenomena in terms of bubble formation adjacent to the heat-transfer surface.

The second series of tests was designed to determine the influence of velocity and bulk temperature on heat transfer to

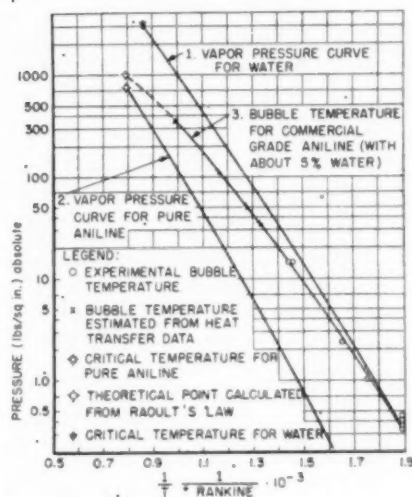


FIG. 3 BUBBLE-POINT TEMPERATURE FOR COMMERCIAL-GRADE ANILINE
(Containing about 5 per cent water.)

TABLE 1 HEAT-TRANSFER DATA* FOR TESTS WITH ANILINE
(Corrected for formation of deposit)

Test No.	Temperature Inlet	Temperature Outlet	Electric Potential (volts)	Power (watts)	Flow Rate	Heat Flux q/A	T_w	T_B	Re_B	Pressure	f_c	Nu	$\frac{\mu_B}{\mu_w}$	j	V	ΔP **	C_f
1	98	116	25.9	40.7	4.32	1.188	394	112	76270	96	0.00421	1067	7.188	0.00390	36.87	8.6	0.0105
2	103	120	25.9	40.7	4.32	1.188	375	114	78820	34	0.00455	1153	6.45	0.00385	36.98	10	0.0121
3	100	118	25.9	40.7	4.32	1.188	403	117	81570	99	0.00415	1052	7.13	0.00338	36.98	9.5	0.0115
4	103	126	31.2	54.5	4.32	1.591	460	116	80630	99	0.00462	1171	8.88	0.00367	36.98	9.5	0.0115
5	101	125	31.2	56.75	4.34	1.657	410	123	88090	34	0.00577	1463	6.78	0.00448	37.27	12	0.0143
6	100	133	36.4	70.5	4.07	2.0586	560	116	75970	284	0.00464	1176	11.92	0.00375	34.84	8	0.0100
7	101	132	36.4	70	4.37	2.044	490	116	81370	134	0.00546	1384	9.78	0.00423	37.41	10.5	0.0125
8	101	133	36.4	72.5	4.32	2.117	460	116	80630	88	0.00615	1559	8.88	0.00488	36.98	12.5	0.0152
9	105	145	36.1	74	4.32	2.161	430	116	80630	51	0.00688	1744	7.91	0.00555	36.98	14	0.0170
10	100	118	25.9	40.7	4.32	1.188	396	110	74640	96	0.00415	1052	7.46	0.00355	36.87	8.6	0.0105
11	103	120	25.9	40.5	4.10	1.183	390	103	67150	29	0.00412	1044	8.100	0.00374	36.58	9.5	0.0118
12	102	127	31.7	57.4	4.32	1.676	458	116	80630	99	0.00490	1242	8.735	0.00418	36.98	9.6	0.0117
13	107.2	133	31.5	59.2	4.32	1.729	389	118	85130	29	0.00640	1622	6.417	0.00516	37.04	12.4	0.0150
14	102	133	36.1	71	4.32	2.073	536	118	83310	265	0.00496	1257	10.795	0.00373	36.98	7.5	0.0091
15	104	136	36.1	71	4.20	2.073	470	122	87500	99	0.00596	1511	8.492	0.00452	36.96	9.7	0.0118
16	108.3	138	36.1	72	4.20	2.102	404	128	93330	29	0.00762	1932	6.209	0.00576	37.08	13.2	0.0159
17	101	118	25.9	39.12	4.32	1.142	398	118	83510	99	0.00401	1016	7.339	0.00384	36.92	8.5	0.0104
18	101	127	36.8	71.4	4.32	2.085	538	122	87690	250	0.00501	1270	10.336	0.00350	37.10	7.7	0.0093
19	103	135	36.8	74.65	4.31	2.180	476	117	84340	99	0.00617	1564	9.247	0.00488	36.90	10	0.0122
20	105	138	36.8	74.3	4.31	2.170	418	123	88140	34	0.00736	1866	6.904	0.00571	37.01	12.5	0.0152
21	101	118	25.9	39.25	4.31	1.146	390	110	74660	98	0.00409	1037	7.231	0.00352	36.78	8.4	0.0103
22	99	122	32.3	55.42	4.24	1.618	482	108	72910	199	0.00434	1100	10.549	0.00358	36.78	7.2	0.0088
23	101	126	32.3	56.42	4.32	1.647	460	118	82530	99	0.00482	1222	8.673	0.00378	36.98	8.8	0.0107
24	101	126	32.3	57.75	4.28	1.686	394	120	83740	29	0.00615	1559	6.694	0.00471	36.70	11	0.0136
25	86	103	25.9	40	4.31	1.168	401	100	64800	98	0.00389	983	8.710	0.00357	36.66	-	-
26	94	110	25.9	40.02	4.32	1.169	406	101	65570	266	0.00390	988	8.629	0.00356	36.75	8.5	0.0105
27	97	137	36.8	74	4.32	2.161	517	116	80630	165	0.00539	1366	10.357	0.00420	36.98	9.5	0.0115
28	93	110	25.9	40.5	4.32	1.183	396	104	68790	98	0.00405	1026	8.095	0.00360	36.81	8	0.0098
29	100	128	36.8	70.3	4.32	2.132	550	114	78820	275	0.00489	1239	12.027	0.00379	36.92	7.5	0.0091
30	86	103	25.9	40	4.32	1.168	398	98	63780	100	0.00389	986	8.871	0.00358	36.69	8.25	0.0102

* Cf. nomenclature for definitions of symbols and units.

** ΔP in inches of water $\times 10^{-1}$.

aniline for the heat-flux and pressure ranges covered in the tests just described, for which the entrance velocity was about 37 fps. The entrance velocities for the tests in this part of the program were held to about 20 fps, and the bulk temperature ranged from 100 to 170 F. It was found that when the surface temperature exceeds the bubble temperature, the wall temperature is determined primarily by the pressure; the effects of changes in velocity, bulk temperature, and heat flux are small.

A summary of the results of the heat-transfer tests with aniline is presented in graphical form in Fig. 4, and the basic data from the tests is given in Table 1, with important calculated results. The graph in Fig. 4 shows (for an average fluid bulk temperature of 115 deg F) the temperature difference between the surface-to-liquid interface, and the bulk of the aniline necessary to remove heat fluxes from 0.3 to 3 Btu/sq in. sec at pressures of 35, 115, and 365 psia, for velocities of 21 and 37 fps in the pure forced-convection regime, and in the bubble regime. Only a few points were obtained in the transition region, and the curves in this region were faired by comparison with the previous water tests (1). For some of the points the test pressure did not correspond exactly to the pressure ranges chosen for this presentation. In those cases the surface temperature was estimated from data which were obtained in tests at pressures slightly above and below the pressures presented in Fig. 4. For this type of presentation

TABLE 1 (Continued)

Test No.	Temperature Inlet	Temperature Outlet	Electric Potential (volts)	Power (watts)	Flow Rate	Heat Flux q/A	T_f	T_B	Re_B	Pressure	f_c	Nu	$\frac{\mu_B}{\mu_f}$	J	V	ΔP	C_F
31	92	116	31.2	55	4.32	1.606	494	108	73070	257	0.00416	1054	10.909	0.00342	36.86	7.3	0.0089
32	98	136	36.8	74	4.32	2.161	550	114	78820	256	0.00496	1257	12.027	0.00385	36.92	8.1	0.0099
33	101	117	25.9	39.8	4.32	1.162	405	106	70160	195	0.00389	986	8.197	0.00346	36.81	8.55	0.0105
34	101	119	25.9	40	4.32	1.168	398	108	73310	100	0.00403	1021	7.742	0.00348	36.98	-	-
35	99	138	40	90	4.32	2.628	540	116	81570	269	0.00620	1572	11.026	0.00475	36.98	-	-
36	106	143	40	90	4.32	2.628	500	120	84520	116	0.00692	1754	9.651	0.00525	37.10	-	-
37	110	148	40	90	4.32	2.628	457	122	87690	54	0.00784	1987	8.000	0.00596	37.10	-	-
38	112	150	40	90	4.32	2.628	430	122	87690	34	0.00853	2162	7.273	0.00657	37.10	-	-
39	107	119	20.9	28	4.32	0.7884	310	114	77940	155	0.00402	1018	4.787	0.00358	36.81	-	-
40	103	118	20.9	28	4.32	0.788	305	112	76250	34	0.00408	1034	4.742	0.00366	36.86	-	-
41	103	118	20.9	28	4.32	0.788	310	112	76250	100	0.00398	1009	4.894	0.00355	36.86	-	-
42	94	125	24.8	39.3	2.49	1.1476	417	110	43020	99	0.00374	948	8.103	0.00549	21.25	-	-
43	101	131	24.9	38.8	2.52	1.1330	500	116	47580	262	0.00295	748	9.348	0.00396	21.57	-	-
44	108	140	24.9	40.25	2.51	1.1753	375	128	54340	35	0.00476	1206	5.435	0.00631	21.59	-	-
45	100	120	20	26.1	2.49	0.7621	425	113	44920	250	0.00245	621	8.036	0.00353	21.28	-	-
46	102	124	20	26.1	2.49	0.7621	414	116	47030	115	0.00256	649	7.414	0.00360	21.32	-	-
47	104	125	20	26.4	2.50	0.7709	392	117	47020	40	0.00280	710	6.719	0.00397	21.40	-	-
48	101	139	40	85	4.32	2.5112	546	120	85550	265	0.00589	1493	10.789	0.00433	37.04	7.5	0.0090
49	103	128	32.5	55	4.32	1.606	510	120	85550	264	0.00412	1044	9.762	0.00314	37.04	6.5	0.0076
50	104	137	40	85	4.31	2.5112	508	120	85360	136	0.00647	1640	9.318	0.00488	36.96	9.3	0.0113
51	103	124	32.3	56.1	2.48	1.638	520	116	42690	252	0.00405	1026	10.610	0.00606	21.23	7.1	0.0261
52	103	146	31.2	55	2.48	1.606	450	116	42690	99	0.00481	1219	8.529	0.00742	21.23	9	0.0329
53	106	150	31.2	57	2.48	1.664	386	118	47400	31	0.00621	1574	6.439	0.00898	21.34	-	-
54	104	160	36.8	73.2	2.48	2.137	550	130	54940	291	0.00509	1290	9.733	0.00619	21.30	4.6	0.0168
55	111	163	36.8	75.0	2.48	2.190	480	126	52310	138	0.00619	1569	8.388	0.00794	21.44	-	-
56	114	171	36.8	76	2.48	2.219	435	145	62530	43	0.00765	1939	5.517	0.00943	21.37	7	0.0254
57	87	107	20.9	26.1	2.52	0.7621	432	101	38610	364	0.00230	583	9.815	0.00350	21.44	2.6	0.0094
58	92	120	24.9	38	2.47	1.1096	545	110	42680	365	0.00255	646	12.368	0.00355	21.08	2.6	0.0097
59	99	140	29.8	54	2.48	1.5768	575	120	48530	364	0.00347	879	11.857	0.00450	21.27	2.7	0.0099
60	105	160	34.9	72.3	2.48	2.111	597	122	52370	364	0.00444	1125	12.121	0.00532	21.27	-	-

it was necessary to use a common bulk temperature, and the arithmetic average for all tests of 115 deg F was chosen. Bearing in mind the limitations in the accuracy of wall-temperature measurements (± 15 deg F), the graphical presentation of the data in Fig. 4 may be used in design to determine the temperature of the liquid-to-surface interface necessary to remove heat rates up to 3 Btu/sq in. sec.

The conventional heat-transfer coefficient is defined as

$$h = \frac{q/A}{T_w - T_f} \quad [1]$$

The data presented in Fig. 4 can be evaluated in terms of the heat-transfer coefficient by dividing the ordinate (q/A) by the abscissa ($T_w - T_f$) at any desired heat flux. Calculations of this type show that heat-transfer coefficients 3 to 4 times larger than for pure forced convection can be obtained by reducing the pressure and operating at wall temperatures which permit the formation of bubbles adjacent to the heat-transfer surface.

No flow instabilities were observed in any of the tests with aniline, and no tube failure due to overheating was encountered (1). The stability of operation in cooling a surface at high heat flux with aniline containing small amounts of water is probably aided by the low vapor pressure of the major constituent of the liquid. In such a two-component system, where only a small portion of more volatile liquid is present, the bubbles formed on the heating surface may not be able to exist for any appreciable length of time in the main stream or grow to such a size as to cause violent vibrations when they collapse. Therefore the

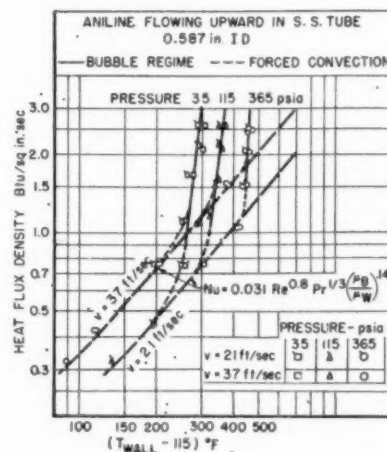


FIG. 4 HEAT FLUX VERSUS TEMPERATURE DIFFERENCE (ANILINE)

conditions of the tests were probably not as severe from a cavitation point of view as those with water, and indeed no vibrations were encountered. The maximum bulk temperature of the aniline was 170 F, which is about 100 deg F below the bubble temperature at the test pressure of 34 psia. For this test the wall temperature was about 150 deg F above the bubble point.

TABLE 1 (Continued)

Test No.	Temperature		Electric Potential (volts)	Power (watts)	Flow Rate	Heat Flux q/A	T_w	T_B	Re_B	Pressure	f_c	Nu	$\frac{\mu_B}{\mu_w}$	j	v	ΔP	C_F
	Inlet	Outlet															
61	91	102	15	15.2	2.48	0.4438	300	97	35960	116	0.00219	555	5.657	0.00379	21.03	-	-
62	93	106	15	15.2	2.48	0.4438	300	100	37290	35	0.00222	562	5.455	0.00378	21.06	-	-
63	95	102	15	15.2	4.32	0.4438	225	100	64960	200	0.00355	900	3.462	0.00370	36.69	-	-
64	94	102	15	15.2	4.32	0.4438	227	100	64960	25	0.00349	884	3.484	0.00363	36.69	-	-
65	95	102	12.6	11.2	2.48	0.3270	245	100	37290	250	0.00226	573	3.971	0.00402	21.06	-	-
66	94	100	12.6	11.2	4.32	0.3270	192	100	64960	34	0.00355	900	2.700	0.00358	36.69	-	-
67	100	120	20.9	26	2.48	0.7592	368	110	41770	34	0.00281	747	6.912	0.00433	20.63	3.5	0.0084
68	101	132	25.9	39.8	2.48	1.162	375	118	47380	34	0.00452	1146	6.159	0.00379	21.23	4.7	0.0106
69	102	145	31.2	56.1	2.48	1.638	380	120	48530	34	0.00630	1597	6.103	0.00891	21.27	5.65	0.0125
70	101	112	20.9	26.4	4.32	0.7709	315	110	74620	365	0.00376	953	5.109	0.00339	36.86	-	-
71	101	118	25.9	40	4.32	1.168	410	110	74620	364	0.00389	986	7.966	0.00330	36.86	-	-
72	103	128	31.2	54.4	4.32	1.588	500	112	76250	365	0.00409	1037	10.698	0.00329	36.92	-	-
73	103	135	36.8	72.5	4.32	2.117	573	115	79740	364	0.00462	1171	12.222	0.00354	36.92	-	-
74	103	140	40	84	4.32	2.4508	602	120	85550	364	0.00508	1288	12.813	0.00368	37.04	-	-
75	83	112	25.9	37.7	2.48	1.1096	545	100	37120	364	0.00249	631	14.211	0.00372	21.10	-	-
76	92	120	25.9	38.6	2.48	1.124	483	110	42840	212	0.00301	763	10.444	0.00425	21.16	-	-
77	97	126	25.9	39.1	2.48	1.156	430	115	45770	115	0.00367	930	8.000	0.00520	21.20	-	-
78	101	130	25.9	39.8	2.48	1.168	380	120	49130	34	0.00450	1144	5.857	0.00634	21.27	4.8	0.0108
79	98	130	36.8	72.5	4.32	2.117	560	115	79710	364	0.00476	1206	12.055	0.00366	36.92	-	-
80	93	158	40	85	2.48	2.482	545	110	42840	314	0.00571	1447	12.368	0.00754	21.16	8.1	0.0185
81	102	170	40	89	2.48	2.599	470	125	51630	115	0.00776	1917	7.959	0.01007	21.30	-	-
82	102	171	40	90	2.48	2.628	430	130	53700	34	0.00876	2221	6.818	0.01150	21.37	-	-
83	88	154	40	86	2.48	2.511	570	118	47380	364	0.00556	1409	11.972	0.00725	21.23	-	-
84	98	154	36.8	73.5	2.48	2.140	572	125	52310	367	0.00479	1214	11.000	0.00588	21.30	-	-
85	112	154	31.2	107.5	2.48	1.5695	560	135	58360	362	0.00369	935	9.452	0.00434	21.40	-	-
86	113	140	25.9	76.5	2.48	1.117	540	130	55170	362	0.00272	689	9.481	0.00331	21.37	-	-
87	95	102	-	31.5	4.32	0.4438	229	100	64960	24.5	0.00344	872	3.553	0.00359	36.69	-	-
88	94	100	-	23	4.32	0.3270	195	100	64960	250	0.00344	872	2.769	0.00372	36.69	-	-

In water tests, flow instabilities occurred when the bulk temperature approached the saturation temperature within 80 deg F, and the wall temperature exceeded the saturation temperature by about 55 deg F. In comparing results for both liquids it must be remembered that the boiling point of pure aniline is more than 100 deg F above the bubble point, and the information as to whether the saturation temperature or the bubble-point temperature is important in causing violent cavitation is inconclusive at this date.

It is expected that with pure aniline (without water) the transition from the forced convection to the boiling regime will take place at a higher wall temperature in correspondence with the vapor characteristics of the liquid. As soon as the wall temperature, at a given pressure, exceeds the boiling temperature of the coolant, it is expected that the pressure will determine the heat-transfer surface temperature and changes in flow, bulk temperature, and heat flux will have only a secondary influence similar to the results obtained for pure water and n-butyl alcohol.

The effect of dissolving a more volatile component in a liquid of low vapor pressure on the heat-transfer characteristics is somewhat similar to the effect of dissolved gases as shown by McAdams (2). Working with an electrically heated test section of annular shape, McAdams found that bubble formation and surface-boiling phenomena occurred at lower wall temperature as the air content of the water was increased. These results agree qualitatively with the observations in the present study.

Heat Transfer to n-Butyl Alcohol With Surface Boiling. A summary of the results of the heat-transfer tests with n-butyl alcohol is presented in Fig. 5, and the basic data from the tests are given in Tables 2 and 3, with important calculated results.

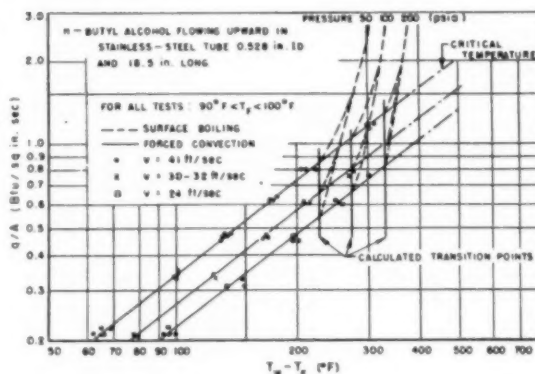


FIG. 5 HEAT VERSUS TEMPERATURE POTENTIAL FOR N-BUTYL ALCOHOL AT VARIOUS FLOW RATES

The curves show (for an average fluid bulk temperature of 95 F) the temperature potential necessary for the removal of heat fluxes up to 3 Btu/sq in. sec, at pressures of 50, 100, and 200 psia, and for entrance velocities of about 20, 30, and 40 fps. An inspection of the curves in Fig. 5 shows that when the surface temperature exceeds the boiling point of the alcohol, (a) substantial increases in heat flux result in only minor increases in the temperature of the heat transfer to liquid surface interface, and (b) the temperature of the heat-transfer surface is insensitive to variations of the coolant velocity in the surface-boiling regime.

During one test in the surface-boiling regime, the influence of

TABLE 2 HEAT-TRANSFER AND FRICTION DATA FOR TESTS WITHOUT SURFACE BOILING (n-BUTYL ALCOHOL)

Test No.	w	T_{in}	ΔT	v	q/A		T_w	T_F	h	Re_F $\times 10^{-3}$	Nu	$\frac{\mu_F}{\mu_w}$	$\left(\frac{Nu}{Re_F^{0.80} Pr^{0.33}}\right)$ $\times 10^{-2}$	ΔP *	C_{FHT}	$\frac{C_{Fiso}}{C_{FHT}}$
					Electrical	Thermal										
1	3.85	86	11.5	43.1	0.82		298	92	3.74	74.1	991	7.33	4.14			
2	3.85	85	11.4	40.9	0.80	0.77	303	88	3.59	66.1	952	8.10	4.30			
3	3.84	87	16.8	41.0	1.19	1.16	393	95	3.88	73.1	1028	11.81	4.39			
4	3.84	90	11.2	41.0	0.79	0.77	301	93	3.71	71.4	983	7.37	4.25			
5	3.84	97	11.3	40.8	0.79	0.79	314	87	3.48	65.8	922	8.66	4.17			
6	3.83	89	17.0	41.2	1.21	1.21	420	100	3.79	77.6	998	12.70	4.21			
7	3.84	97	6.2	41.2	0.44	0.46	225	100	3.66	77.6	970	4.00	4.02			
8	3.84	92	4.7	41.1	0.33	0.33	189	98	3.63	75.7	962	2.97	4.03			
9	2.79	93	6.6	29.9	0.34	0.33	224	98	2.59	55.0	686	4.10	3.71			
10	2.79	93	9.1	29.9	0.46	0.46	265	100	2.77	56.4	737	5.37	3.94			
11	2.79	94	14.9	30.0	0.78	0.79	375	104	2.91	59.4	769	9.50	4.10			
12	3.85	86	11.1	41.1	0.80	0.80	320	94	3.54	72.3	938	7.23	4.03	7.45	0.0119	1.67
13	3.85	87	16.5	41.2	1.18	1.16	405	98	3.78	75.9	1002	12.13	4.20	6.28	0.0100	1.96
14	3.85	88	11.1	41.1	0.79	0.79	320	96	3.47	74.0	920	7.06	3.91	7.58	0.0121	1.63
15	3.84	92	3.1	41.0	0.22	0.21	163	94.5	3.07	72.2	814	2.35	3.51	10.78	0.0173	1.15
16	3.84	89	4.8	41.0	0.34	0.34	192	92.5	3.39	70.6	894	3.28	3.91	10.02	0.0161	1.24
17	3.84	90	6.8	41.0	0.48	0.47	228	93.8	3.52	71.9	933	4.45	4.02	9.22	0.0149	1.34
18	3.84	94	3.0	41.1	0.21	0.21	164	96	3.09	73.9	819	2.27	3.48	10.84	0.0174	1.14
19	3.84	88	4.8	41.0	0.34	0.33	191	91.2	3.35	69.6	888	3.31	3.90	10.11	0.0162	1.23
20	3.84	91	6.6	41.1	0.47	0.46	226	94.8	3.53	72.2	936	4.34	4.03	9.28	0.0149	1.34
21	3.84	89	3.1	41.0	0.22	0.22	157	91.5	3.27	69.8	867	2.25	3.80	10.88	0.0175	1.15
22	3.84	96	4.7	41.1	0.33	0.33	196	99	3.50	76.6	928	3.12	3.87	10.01	0.0160	1.22
23	3.84	92	6.6	41.1	0.47	0.47	228	96.8	3.60	74.5	954	4.30	4.04	9.24	0.0148	1.33
24	3.84	90	3.0	41.0	0.21	0.21	158	91.8	3.24	70.0	859	2.25	3.76	10.84	0.0175	1.14
25	3.84	91	4.7	41.0	0.33	0.33	191	93.5	3.40	71.6	901	3.22	3.89	10.06	0.0161	1.24
26	3.84	93	6.4	41.1	0.46	0.46	225	97.5	3.59	75.4	952	4.12	4.00	9.30	0.0149	1.32
27	2.22	92	5.3	23.7	0.22	0.22	191	97	2.28	43.2	604	3.05	3.65	3.69	0.0177	1.26
28	2.22	92	7.9	23.8	0.33	0.33	245	95	2.19	42.2	580	5.01	3.85	3.22	0.0154	1.47
29	2.22	90	10.7	23.8	0.44	0.45	290	96	2.33	42.8	618	6.67	4.07	2.83	0.0136	1.65
30	2.22	90	14.4	23.8	0.60	0.62	350	100	2.48	44.9	657	9.09	4.14	2.40	0.0115	1.96

* The units of the frictional pressure loss in Tables 2 and 3 are: inches of mercury minus inches of n-butyl alcohol.

bulk temperature upon the temperature of the heat-transfer surface was investigated. The n-butyl alcohol was circulated at a constant flow rate and at constant pressure, but without being passed through the heat exchanger. This procedure resulted in the bulk temperature of the liquid increasing from a value of 100 deg F to a value which was higher than 200 deg F. The wall-to-liquid interface temperature was unaffected by this increase in the bulk temperature of the liquid and remained constant at 386 deg F, thus proving that in the surface-boiling regime, the temperature of the interface between the liquid and the heat-transfer surface is insensitive to changes in bulk temperature.

In reference (1), the results of the experiments on heat transfer to water, with surface boiling, were correlated by plotting the excess temperature against pressure for constant heat fluxes. The excess temperature was defined as the temperature difference between the wall-to-liquid interface and the boiling point at the pressure of the liquid during the test. The results of the tests with n-butyl alcohol are presented in the same form in Fig. 6 where the excess temperature is plotted against pressure for various heat fluxes. During these tests, the flow rate of the n-butyl alcohol was held constant at 3.85 lb per sec. It can be seen that the excess temperature required to remove a given heat flux at a constant bulk temperature decreases as the pressure increases. A corresponding relationship between excess temperature and pressure exists for water; however, the curves for water have a steeper negative slope than do those for the n-butyl alcohol.

A further comparison of the results obtained from tests using n-

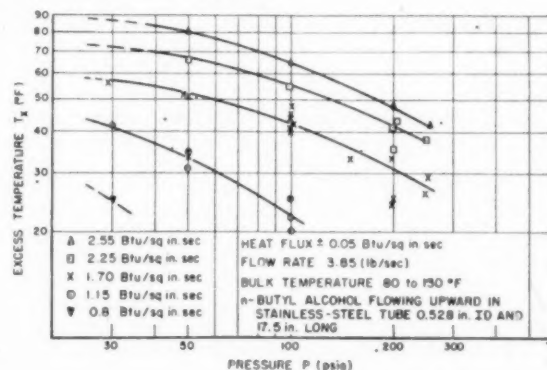


FIG. 6 EXCESS TEMPERATURE VERSUS PRESSURE AT VARIOUS HEAT FLUXES WITH SURFACE BOILING (N-BUTYL ALCOHOL)

butyl alcohol as a coolant with results obtained from tests using water as a coolant is presented in Fig. 7. In this figure the excess temperatures (from Fig. 6), are plotted against heat flux for constant pressures (100 and 25 psia). The results obtained in tests with water at corresponding pressures are superimposed on the same graph.

An inspection of Fig. 7 shows that the general trends of the curves for the n-butyl alcohol agree with trends of the curves for water. However, for the removal of the same heat flux, the n-

TABLE 2 (Continued)

Test No.	w	T_{in}	ΔT	v	q/A		T_s	T_F	h	Re_F	Nu	$\frac{\mu_F}{\mu_W}$	$\left(\frac{Nu}{Re^{0.80} Pr^{0.33}}\right) \times 10^{-2}$	ΔP	C_{FHT}	$\frac{C_{Fiso}}{C_{FHT}}$
					Electrical	Thermal										
31	2.22	89	5.1	23.7	0.21	0.21	190	93	2.21	41.3	586	3.18	3.93	3.72	0.0179	1.27
32	2.22	91	7.4	23.8	0.31	0.31	230	97	2.36	43.3	626	4.32	4.10	3.35	0.0161	1.40
33	2.22	87	10.6	23.8	0.43	0.45	298	96	2.24	42.8	594	7.00	3.90	2.82	0.0136	1.65
34	2.22	93	14.2	23.8	0.59	0.60	354	102	2.38	46.0	631	9.07	4.00	2.48	0.0119	1.86
35	2.22	92	5.1	23.7	0.21	0.21	190	95	2.23	42.2	571	3.11	3.78	3.72	0.0179	1.26
36	2.22	89	7.5	23.7	0.31	0.31	238	90	2.12	39.9	562	5.00	3.83	3.32	0.0160	1.43
37	2.22	94	10.5	23.8	0.44	0.47	294	98	2.42	43.8	640	6.72	4.16	2.88	0.0138	1.62
38	2.22	90	5.1	23.7	0.21	0.21	191	90	2.12	39.9	562	3.33	3.83	3.70	0.0178	1.29
39	2.22	90	7.8	23.7	0.32	0.33	242	92	2.19	40.6	580	5.08	3.92	3.25	0.0156	1.46
40	3.84	89	8.7	41.0	0.62	0.63	261	92	3.72	70.3	986	5.74	4.30	8.50	0.0136	1.47
41	3.85	86	9.1	41.0	0.64	0.64	265	90	3.68	69.1	975	6.04	4.29	8.36	0.0134	1.50
42	3.84	88	8.9	41.0	0.63	0.63	264	90	3.62	69.1	960	6.00	4.22	8.49	0.0136	1.48
43	3.84	95	8.7	41.1	0.62	0.63	261	98	3.86	75.7	1023	5.32	4.29	8.52	0.0136	1.45
44	3.85	86	3.2	40.9	0.21	0.21	149	86	3.40	64.8	901	2.19	4.10	10.88	0.0175	1.17
45	3.84	88	4.7	41.0	0.33	0.37	188	88	3.69	66.9	978	3.32	4.32	9.98	0.0161	1.25
46	3.84	92	6.6	41.0	0.47	0.47	221	92	3.61	70.2	957	4.25	4.18	9.25	0.0149	1.34
47	3.85	87	9.1	41.0	0.64	0.63	264	89	3.60	67.6	954	6.13	4.24	8.34	0.0134	1.51
48	2.89	95	3.1	30.9	0.21	0.21	172	95	2.75	54.8	729	2.55	3.81	6.05	0.0171	1.24
49	2.89	92	6.3	30.9	0.34	0.33	213	92	2.72	52.9	721	3.98	3.95	5.51	0.0156	1.37
50	2.89	93	8.5	30.9	0.45	0.46	257	95	2.82	54.9	747	5.43	4.01	4.96	0.0140	1.52
51	2.89	94	11.5	30.9	0.62	0.62	310	92	2.83	52.9	750	7.89	4.11	4.40	0.0125	1.71
52	3.00	92	3.8	32.0	0.21	0.21	170	91	2.72	53.9	721	2.65	3.87	6.72	0.0177	1.20
53	3.01	87	6.2	32.0	0.34	0.34	211	89	2.76	52.7	732	4.07	3.98	6.09	0.0161	1.33
54	3.00	88	8.2	32.0	0.45	0.46	253	90	2.81	53.9	745	5.56	3.99	5.48	0.0145	1.47
55	3.00	92	11.0	32.1	0.62	0.62	305	96	2.98	57.8	790	7.30	4.09	4.85	0.0130	1.61
56	3.00	91	10.9	32.1	0.61	0.61	302	94	2.96	56.4	785	7.35	4.11	4.89	0.0129	1.64
57	2.22	94	17.6	23.9	0.75	0.76	410	108	2.52	49.9	668	10.91	4.07	2.25	0.0106	2.05
58	3.00	89	13.6	32.2	0.76	0.78	353	100	3.08	60.7	816	9.20	4.12	4.40	0.0114	1.81

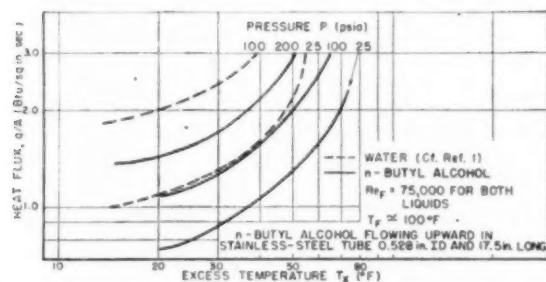


FIG. 7 HEAT FLUX VERSUS EXCESS TEMPERATURE FOR N-BUTYL ALCOHOL AND WATER

butyl alcohol requires an excess temperature which is about 25 deg F higher than that required when water is used as the coolant. The test sections used for both liquids were of similar dimensions, and the Reynolds number (evaluated at the bulk temperature) was about 75,000 for both liquids. A bulk temperature of about 100 deg F was used during the tests with both of the liquids.

The qualitative remarks presented next are pertinent to the proper use and interpretation of the data on heat transfer with surface boiling. Because the bulk temperature was nearly constant during the tests, the degree of subcooling of the bulk of the liquid was not the same in tests at different pressures. Even though the bulk temperature or degree of subcooling has no effect upon the wall temperature in the fully developed surface-boiling regime, the point of transition from the pure forced-convection regime to the surface-boiling regime is dependent upon the bulk

temperature and pressure of the liquid. Thus at a higher bulk temperature, the transition will occur at a lower heat flux, and vice versa. The heat flux at transition can be calculated for a given bulk temperature and pressure by the following equations

$$(q/A)_{trans} = 0.034 \frac{K}{D} Re^{0.5} Pr^{1/3} \left(\frac{\mu_F}{\mu_W} \right)^{0.1} (T_s - T_F) \quad \text{for n-butyl alcohol} \dots [2]$$

$$(q/A)_{trans} = 0.027 \frac{K}{D} Re^{0.5} Pr^{1/3} \left(\frac{\mu_F}{\mu_W} \right)^{0.15} (T_s - T_F) \quad \text{for water} \dots [3]$$

Before using the curves applicable only to heat transfer with surface boiling, it is necessary to determine first whether or not the surface temperature (for the pressure, flow conditions, and heat flux under consideration) exceeds the boiling temperature T_s of the coolant.

It has been shown (2) that the exact point of transition from forced-convection heat transfer to surface-boiling heat transfer is influenced by the amount of dissolved gases or impurities in the liquid. When a degassed liquid is used as the coolant, the surface temperature may exceed the boiling point by as much as 20 deg F before bubbles begin to form. On the other hand, if a large amount of gas is dissolved in the coolant, bubble formation may occur at a surface temperature below the saturation temperature. For this reason, the curves in Fig. 7 are not extended to excess temperatures of less than 10 deg F.

In previous tests with water, the heat flux that could be re-

TABLE 3 HEAT TRANSFER AND FRICTIONAL PRESSURE-LOSS DATA FOR TESTS IN SURFACE BOILING REGIME (n-BUTYL ALCOHOL)

Test No.	μ	T_{in}	ΔT	q/A		P	T_s	T_b	ΔP
				Electrical ^a	Thermal ^b				
1	3.84	93	--	1.50	--	68	371	35	--
2	3.85	78	22.5	1.59	--	200	451	26	--
3	3.85	80	16.4	1.17	--	115	348	31	--
4	3.85	86	23.5	1.66	--	168	351	34	--
5	3.86	75	23.4	1.63	--	200	450	25	--
6	3.85	86	--	2.17	--	200	460	38	--
7	3.84	89	29.7	2.17	--	250	482	35	--
8	3.83	103	29.8	2.23	--	205	470	43	--
9	3.84	91	23.1	1.66	--	250	470	26	--
10	3.84	98	23.1	1.69	--	197	448	24	--
11	3.83	103	23.5	1.66	1.74	150	432	33	--
12	3.84	90	23.0	1.67	1.66	254	476	29	--
13	3.89	99	24.7	1.72	1.73	102	407	42	--
14	3.83	99	24.1	1.74	1.77	50	376	53	--
15	3.83	101	24.1	1.74	1.77	29	340	56	--
16	3.84	92	35.3	2.52	2.58	255	489	42	--
17	3.84	96	34.9	2.59	2.57	200	473	48	--
18	3.85	81	22.2	1.60	1.58	199	457	33	5.83
19	3.85	86	30.2	2.17	2.19	200	465	41	6.55
20	3.84	92	33.5	2.52	2.45	200	472	48	7.26
21	3.85	87	16.1	1.16	1.14	100	385	22	6.92
22	3.85	87	24.0	1.69	1.72	99	405	41	7.20
23	3.85	85	31.1	2.23	2.24	99	418	55	7.91
24	3.85	85	11.2	0.79	0.79	50	319	2	7.52
25	3.84	87	16.7	1.19	1.20	50	352	35	8.35
26	3.85	87	24.3	1.72	1.74	50	364	49	9.36
27	3.84	89	31.0	2.29	2.28	50	383	66	7.68
28	3.81	79	11.2	0.82	0.78	30	310	25	8.35
29	3.85	85	16.5	1.17	1.17	30	327	42	2.81
30	2.22	90	14.7	0.62	0.62	50	318	1	2.89
31	2.22	91	10.7	0.44	0.45	30	290	5	3.20
32	2.22	90	14.5	0.64	0.63	30	296	11	4.72
33	2.80	94	11.6	0.63	0.65	30	294	9	5.02
34	3.00	90	11.5	0.64	0.63	30	296	11	2.38
35	2.22	87	26.7	1.12	1.13	199	433	9	2.62
36	2.22	90	18.2	0.74	0.77	100	370	6	2.95
37	2.22	89	27.2	1.15	1.16	100	392	28	3.10
38	2.22	86	18.8	0.78	0.79	50	328	11	3.54
39	2.22	90	27.2	1.15	1.18	50	349	32	3.51
40	2.22	88	19.0	0.79	0.80	30	300	15	3.94
41	2.22	86	28.4	1.19	1.19	30	323	38	3.96
42	3.00	89	20.2	1.14	1.14	200	434	9	4.64
43	3.00	88	20.0	1.13	1.16	100	376	12	5.01
44	3.00	90	14.0	0.78	0.78	50	320	3	5.51
45	3.00	86	20.7	1.17	1.18	50	350	33	5.60
46	3.00	89	14.0	0.78	0.79	30	290	14	6.12
47	3.00	88	20.4	1.18	1.19	30	324	39	4.30
48	3.00	90	29.3	1.66	1.64	200	456	31	5.13
49	3.00	92	29.4	1.68	1.70	100	403	39	5.66
50	3.00	98	30.1	1.75	1.70	50	372	55	3.36
51	2.27	95	39.1	1.69	1.70	100	410	46	4.16
52	2.23	102	39.6	1.73	1.74	50	377	60	5.40
53	3.02	91	14.0	0.79	0.80	30	321	36	7.59
54	3.84	99	22.2	1.67	1.63	100	404	40	7.74
55	3.84	92	--	1.79	--	100	408	44	6.98
56	3.84	94	--	1.19	--	100	389	25	7.64
57	3.84	97	--	1.72	--	100	412	40	7.00
58	3.84	93	--	1.22	--	100	384	20	7.90
59	3.84	96	--	1.70	--	100	409	45	4.88
60	3.00	95	--	2.20	--	200	470	45	5.78
61	3.00	90	39.0	2.23	2.24	100	420	56	3.27
62	2.22	93	51.1	2.20	2.20	200	473	48	3.95
63	2.22	94	51.4	2.23	2.24	100	417	53	6.82
64	3.00	95	39.3	2.26	2.28	50	384	67	7.56
65	3.82	103	34.2	2.54	2.56	200	--	--	6.62
66	3.84	89	16.3	1.17	1.16	200	--	--	6.42
67	3.84	90	22.6	1.64	1.63	200	--	--	7.51
68	3.84	89	23.1	1.67	1.66	100	--	--	8.05
69	1.84	98	24.0	1.69	1.75	50	--	--	9.92
70	3.84	99	30.6	2.27	2.27	50	--	--	10.50
71	3.82	101	35.2	2.63	2.62	50	398	81	8.84
72	3.84	90	35.1	2.60	2.57	100	429	65	3.65
73	2.22	89	59.4	2.57	2.56	200	477	52	--

^a $q/A = (k \Delta T_{in}) / (1.056 \cdot \Delta T_{in})$

^b $q/A = (c_p \Delta T) / (\Delta T_{in})$

moved by forced convection with surface boiling was limited by burnouts of the tube (1, 2). It is believed that these burnouts were caused by flow instabilities due to growth and collapse of vapor bubbles. No burnouts (such as had been encountered when water was used as the coolant) occurred in the tests with n-

butyl alcohol. However, during several tests at heat fluxes above 2 Btu/sq in. sec, the stainless-steel tubular test section developed almost invisible longitudinal cracks. These cracks are believed to have been caused by metal fatigue, possible because of vibrations induced by the growth and collapse of bubbles within the test section.

Heat Transfer by Forced Convection Without Surface Boiling (Aniline, n-Butyl Alcohol, Water). The results of the tests in which the wall temperature remained below the bubble or boiling temperature of the coolant liquid are shown in Fig. 8. The data are presented as a plot of the dimensionless index $Nu/(Re^{0.8} Pr^{1/3})$ versus the ratio of the viscosity at the bulk temperature to the viscosity at the wall temperature. This type of presentation was chosen because, at the high heat fluxes used in the experiments, a very steep temperature gradient exists adjacent to the

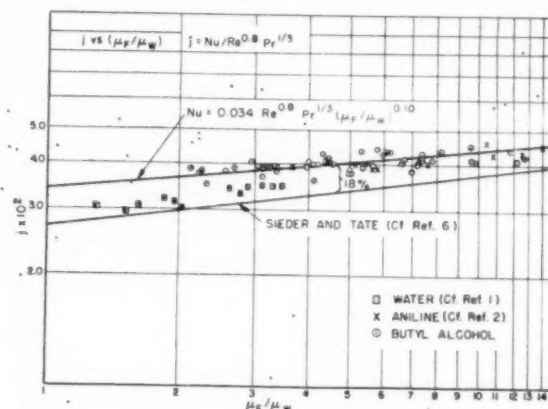


FIG. 8 CORRELATION OF PURE FORCED-CONVECTION DATA

heat-transfer surface; this temperature gradient causes an appreciable variation in the viscosity of the liquid and it is known (3, 4) that the variation in viscosity influences the heat-transfer process. The experimental results for aniline and n-butyl alcohol are correlated within ± 10 per cent by

$$Nu = 0.034 Re^{0.8} Pr^{1/3} (\mu_b/\mu_w)^{0.10} \quad [4]$$

Sieder and Tate (3) have examined the results of a large number of experiments on heat transfer to liquids at low heat fluxes and for best correlation of the experimental results derived the following equation

$$Nu = 0.027 Re^{0.8} Pr^{1/3} (\mu_b/\mu_w)^{0.14} \quad [5]$$

The results of experiments by Sherwood and Petrie on heat transfer from a tube to n-butyl alcohol (15) at heat fluxes below 0.2 Btu/sq in. sec were in agreement with Equation [5].

An inspection of Fig. 8 shows that while the data for water (1) fall within the experimental accuracy on a line representing the Sieder and Tate equation, the results for n-butyl alcohol and aniline show Nusselt moduli which are from 15 to 25 per cent higher than would be predicted by Equation [5]. However, the precision to which the forced-convection data for the latter two liquids were correlated was subject to uncertainties because no precise data for the physical properties of the liquids were available for the full range of temperature and pressure covered in the experiments. In particular, there exists some uncertainty regarding the thermal conductivity of the liquids. When more reliable information on the thermal conductivity of aniline and n-butyl alcohol becomes available, the results of the heat-transfer tests can be

re-evaluated. The physical properties for aniline and n-butyl alcohol, used in the reduction of the experimental results, were taken from the references given in the following tabulation:

	C_p	ρ	μ	P_v
Aniline	5	5	5.6	5
n-Butyl alcohol	7	8	9	10

The thermal conductivities were assumed to be independent of temperature, and the values which were used in reducing the data are given as follows:

Aniline, $K = 0.1$ (ref. 11)

n-Butyl alcohol, $K = 0.095$ (ref. 12)

It is interesting to note, Fig. 5, that the maximum heat flux which can be removed by pure forced convection with liquid n-butyl alcohol at a velocity of 24 fps is about 1.15 Btu/in.² sec. (More than twice this heat flux has been removed with surface boiling.) At this heat flux the surface temperature reaches the critical temperature. In general, the thermal conductivity of a fluid in the gaseous state is very much smaller (about one tenth) than the conductivity of the same fluid in the liquid state. Therefore the curves in Fig. 5 should not be extrapolated to temperatures and pressures higher than critical.

The heat-transfer results obtained from tests in the nonboiling forced-convection regime were also compared with the momentum transfer (as measured by the frictional pressure loss) following the technique of the von Kármán analogy theory (16). No satisfactory agreement was obtained (the experimental Nu moduli, when extrapolated to zero heat flux, were about 50 per cent higher than would be predicted by the analogy). The reason for this discrepancy is not apparent at this time.

Frictional Pressure Loss With Heat Transfer. The effect of heat transfer upon the frictional pressure loss was studied quantitatively with n-butyl alcohol only. (During the period in which the aniline tests were performed, there was no differential manometer connected across the test section, and the frictional pressure loss in the aniline tests was measured with a differential Barton pressure gage. The results are qualitatively in agreement with those presented for n-butyl alcohol in this paper.)

The frictional pressure drop as a function of heat flux is shown in Figs. 9, 10, and 11, for entrance velocities of 23, 31, and 41 fps at four different pressures. From an inspection of these curves it can be seen that the frictional pressure loss initially decreases (for a given flow rate of coolant liquid) with an increase in heat flux. This decrease continues until boiling begins adjacent to the heat-transfer surface. After surface boiling has begun, then the pressure loss increases with any increase in heat flux. In the surface-boiling regime the frictional pressure loss (at constant heat flux, bulk temperature, and flow rate) increases also with a decrease in pressure. This result appears reasonable, since boiling is more vigorous at lower pressures. In none of the tests did the pressure loss with heat transfer exceed the isothermal value at the same liquid flow rate.

In initial tests the isothermal friction factor was measured in the Reynolds-number range from 25,000 to 70,000. Friction factors were correlated within ± 1 per cent by the following equation, and are in agreement with accepted values within 2 per cent (14)

$$C_F = 0.265 Re^{-0.23} \quad [6]$$

For nonboiling heat-transfer conditions, the results on the frictional pressure drop with heat transfer are correlated by plotting the ratio of the isothermal friction coefficient to the heat-transfer friction coefficient (both evaluated at the same bulk Reynolds number) against the ratio of the viscosity at bulk temperature to the viscosity at the wall temperature, Fig. 12. These results will be studied further. However, it can be stated at this

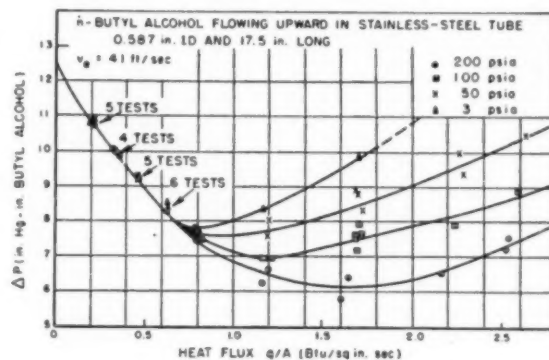


FIG. 9 EFFECT OF HEAT FLUX ON FRICTIONAL PRESSURE LOSS ($V_e = 41$ fps)

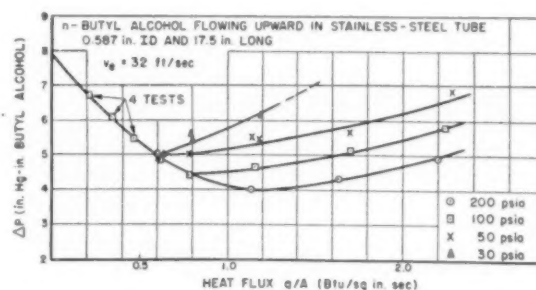


FIG. 10 EFFECT OF HEAT FLUX ON FRICTIONAL PRESSURE LOSS ($V_e = 31$ fps)

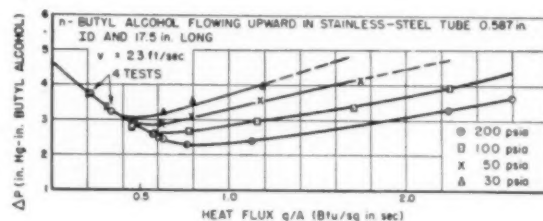


FIG. 11 EFFECT OF HEAT FLUX ON FRICTIONAL PRESSURE LOSS ($V_e = 23$ fps)

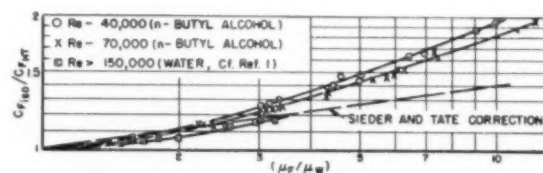


FIG. 12 RATIO OF HEAT-TRANSFER (NONBOILING) FRICTION COEFFICIENT TO ISOOTHERMAL FRICTION COEFFICIENT VERSUS RATIO OF VISCOSITY AT BULK TEMPERATURE TO VISCOSITY AT WALL TEMPERATURE

time that evaluation of the Reynolds number at a temperature equal to or slightly below the temperature of the heat-transfer surface will result in a friction coefficient under heat-transfer conditions close to the experimentally observed value.

CONCLUSIONS

1 Experimental results have been obtained on heat transfer from a stainless-steel tube to a 96 per cent aniline, 4 per cent water, solution and to n-butyl alcohol in the heat-flux range from 0.3 to 3 Btu/sq in. sec, over a pressure range from 40 to 400 psi for velocities ranging from 20 to 40 fps. The results of the tests are summarized in Figs. 5 and 6 which show (for average fluid bulk temperatures) the temperature potential necessary for the removal of given heat fluxes in the forced-convection and boiling or bubble regime.

2 The temperature of the heat-transfer surface is insensitive to changes in velocity, heat flux, and bulk temperature when it exceeds either the bubble temperature (aniline) or the boiling temperature (n-butyl alcohol) of the coolant liquid. The controlling factor of the surface temperature in the bubble or boiling regime is the system pressure. These phenomena are similar to results obtained previously in heat transfer to water with surface boiling.

3 In the pure forced-convection regime, the results for aniline and n-butyl alcohol were correlated by the following equation

$$Nu = 0.034 Re^{0.8} Pr^{1/4} \left(\frac{\mu_B}{\mu_W} \right)^{0.10}$$

4 No instabilities of flow or breakdown of the heat transfer with subsequent failure of the heating tube were encountered in any of the tests with aniline at bulk temperatures up to 170 F.

5 The beneficial characteristics of surface-boiling in heat transfer (i.e., higher heat-transfer efficiency) can be obtained with a coolant of low vapor pressure at temperatures below its boiling point by dissolving a more volatile component of low solubility in the main constituent. This technique may have application in heat-transfer devices other than rockets, especially in the chemical industry and power plants of the future.

6 The frictional pressure loss decreases (for a given flow rate of coolant liquid) with an increase in heat flux. After surface-boiling has begun, then the pressure loss increases with any increase in heat flux. Even in the bubble or boiling regime the heat-transfer pressure loss was less than the isothermal pressure loss for the same flow rate.

7 Friction coefficient for heat-transfer conditions can be approximated by evaluating the Reynolds number at a temperature slightly below the heat-transfer surface temperature. It would be desirable to predict heat-transfer friction coefficient from theoretical considerations; work along this line should be encouraged.

BIBLIOGRAPHY

- 1 "Heat Transfer to Water at High Flux Densities With and Without Surface Boiling," by Frank Kreith and Martin Summerfield, Trans. ASME, vol. 71, 1949, pp. 805-815.
- 2 "Heat Transfer at High Rates to Water With Surface Boiling," by W. H. McAdams, J. N. Addoms, and W. E. Kennel, Report ANL-4268, Argonne National Laboratory, Massachusetts Institute of Technology, Cambridge, Mass., December, 1948.
- 3 "Heat Transfer and Pressure Drop of Liquids in Tubes," by E. N. Sieder and G. E. Tate, *Industrial and Engineering Chemistry*, vol. 28, 1936, pp. 1429-1436.
- 4 "Remarks on the Analogy Between Heat Transfer and Momentum Transfer," by L. M. K. Boelter, R. C. Martinelli, and F. Jonassen, Trans. ASME, vol. 63, 1941, pp. 447-455.
- 5 "Some Studies of the Reaction of Aniline and Orthotoluidine With Red Fuming Nitric Acid," by E. W. Hough, J. M. Green, and B. H. Sage, Report No. 1-14, Pasadena, Calif., Jet Propulsion Laboratory, April 20, 1943.
- 6 "Correlating Viscosity and Vapor Pressure of Liquids," by D. F. Othmer and J. W. Conwell, *Industrial and Engineering Chemistry*, vol. 37, 1945, pp. 1112-1115.
- 7 "International Critical Tables," McGraw Hill Book Company, Inc., New York, N. Y., vol. 5, 1933, p. 108.
- 8 Ibid., vol. 3, pp. 27-33.

9 Ibid., vol. 7, p. 215.

10 Ibid., vol. 3, p. 219.

11 "Thermal Conductivities of Certain Liquids," by G. W. C. Kaye and W. F. Higgins, Proceedings of the Royal Society of London, vol. A117, 1928, p. 459.

12 "International Critical Tables," McGraw Hill Book Company, Inc., New York, N. Y., vol. 7, 1933, p. 228.

13 Eleventh Informal Monthly Report of M.I.T., Project DIC 1-6489 for period August 18 to September 18, 1947, by W. H. McAdams, Massachusetts Institute of Technology, Cambridge, Mass., Sept. 25, 1947.

14 "Friction Factors for Pipe Flow," by F. L. Moody, Trans. ASME, vol. 66, 1944, pp. 671-684.

15 "Heat Transmission to Liquids Flowing in Pipes," by T. K. Sherwood and J. M. Petrie, *Industrial and Engineering Chemistry*, vol. 24, 1932, p. 736.

16 "The Analogy Between Fluid Friction and Heat Transfer," by Th. von Kármán, Trans. ASME, vol. 61, 1939, pp. 705-710.

Discussion

O. P. BERGELIN.⁵ Local boiling can be extremely useful in certain cases of heat transfer and certainly deserves more attention than it has received in the past. In this paper, as well as in previous papers on the subject, the authors have made valuable contributions in this field. In looking over their results, the high rates of heat transfer, which are shown to be available through local boiling, appear so attractive that perhaps it would be advisable to emphasize the dangers and disadvantages that might occur when applying local boiling to the process industries. One major disadvantage is the severe conditions to which the heating surface is subjected. The vibrations caused by collapsing bubbles may cause mechanical failure of thin-walled tubes, and the rates of corrosion under local boiling conditions are as yet unknown. Until more information is available it might be wise to restrict local boiling to heavy-walled ducts, such as passages through engine blocks, or to equipment where a short life is permissible. In those cases where the upper temperature level is above the melting point of the duct wall, there is also the danger of burnout if the liquid velocity becomes so low that an insulating vapor blanket can form over the heat-transfer surface. Surface roughness may enhance vapor blanketing and must be investigated before local boiling conditions can be predicted with assurance.

The data reported for pressure drop show a relatively small increase in pressure drop due to local boiling. One might expect a much larger effect because of the increase in wall shear caused by surface "roughness," due to bubbles and to the increase in liquid velocity as a result of the volume occupied by the bubbles. Moreover, all bubbles which become detached from the surface will be accelerated to some velocity before they disappear in the liquid stream. Can it be that enough bubbles collapse away from the surface to form a relatively thick layer of high-temperature fluid near the surface and thus lower the wall shear in spite of the disturbances at the surface? Temperature and velocity traverses as well as visual observation probably will be needed to clarify the mechanism of flow near the surface during local boiling.

CLOSURE

The authors wish to acknowledge with appreciation the discussion by Professor Bergelin. The comments on the limitations of surface-boiling heat transfer are well to keep in mind when attempting to utilize this technique for practical application.

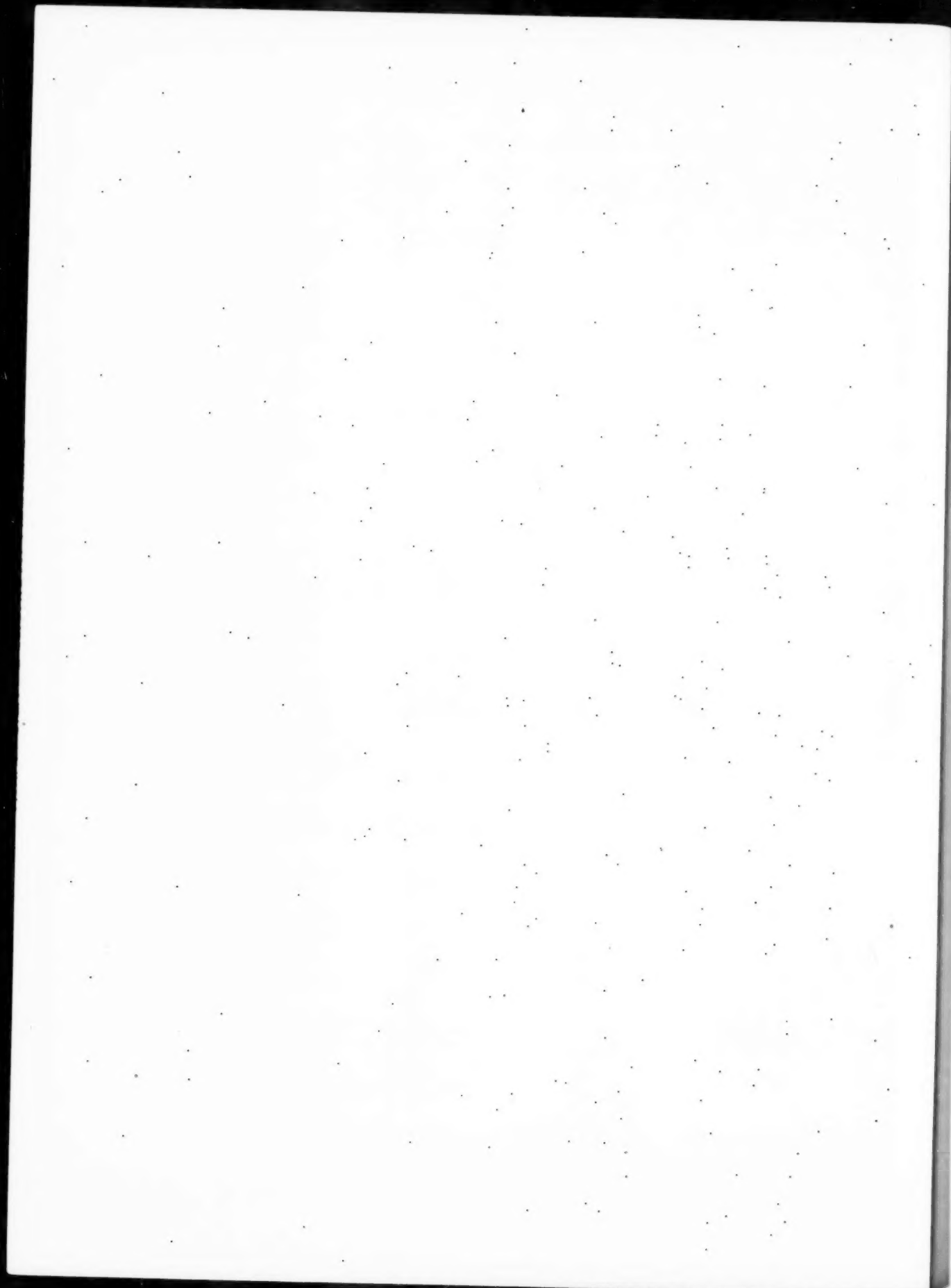
Regarding the question whether or not bubbles collapse away from the surface, the authors agree with Professor Bergelin that additional work will be necessary before a definite answer can be given. Preliminary work along the lines suggested in the discussion has been performed by means of photographic observations, and some of the results have been presented in two recent

⁵ University of Delaware, Newark, Del.

papers (17, 18). These photographic studies are being continued at present. To date no data on temperature and velocity traverses have been obtained, according to the authors' knowledge. In addition to these experiments, a determination of the increase in turbulence caused by surface boiling would help to clarify the mechanism of flow in surface boiling and aid in a quantitative analysis.

REFERENCES

- 17 "Photographic Study of Bubble Formation in Heat Transfer to Subcooled Water," by Fred C. Gunther and Frank Kreith, Heat Transfer and Fluid Mechanics Institute, June 22-24, 1949, ASME Publication.
- 18 "A Study of the Mechanism of Boiling Heat Transfer," by Warren M. Rohsenow and John A. Clark, Massachusetts Institute of Technology, 1949.



...c
f
c
a
t
a
f
r
c
v
c
p
t
f

ve
w
w
W
w
A
19
un
of

Heat Transfer and Fluid Friction During Viscous Flow Across Banks of Tubes—III

A Study of Tube Spacing and Tube Size

By O. P. BERGELIN,¹ G. A. BROWN,² H. L. HULL,³ AND F. W. SULLIVAN⁴

In the course of a research program on tubular heat exchangers, pressure-drop and heat-transfer data are reported for heating and cooling a medium-viscosity oil flowing across banks of vertical tubes in seven test exchangers. The apparatus variables include equilateral triangle, in-line square, and staggered square arrangements; tube sizes of $\frac{3}{8}$ in. and $\frac{1}{2}$ in. OD; and pitch ratios of 1.25 and 1.50. The results are shown both in simple plots of pressure drop and coefficient of heat transfer versus the rate of flow, and in generalized correlations. Tentative correlations are provided for friction and heat transfer which bring the data for these seven tube banks somewhat closer together than previous correlations. In a comparison of the heat-transfer coefficient versus pumping-power loss per unit surface area, the smaller diameter tubes at the smaller pitch ratio give the best performance.

NOMENCLATURE

The following nomenclature is used in the paper:

- \dot{A}_F = shell-side friction area, sq ft
 A_H = outside surface area of tubes, sq ft
 c = heat capacity, Btu/(lb)(deg F)
 D_s = minimum clearance between tubes, ft (except where otherwise indicated)
 D_i = inside diameter of tube, in.
 D_o = outside diameter of tube, ft (except where otherwise indicated)
 D_v = volumetric hydraulic diameter $\frac{4 \times \text{free volume}}{\text{exposed area of tubes}}$, ft
 d = tube core diameter, in.
 E = pumping-power loss per unit heat-transfer area, (ft)(lb force)/(hr)(sq ft)
 f_{C_s} = friction factor, defined by $f_{C_s} = \frac{2\Delta p g_c \rho_f D_o}{4G_m^2 L}$, dimensionless
 f_{C_t} = friction factor, defined by $f_{C_t} = \frac{2\Delta p g_c \rho}{4G_m^2 N}$, dimensionless

- f_G = friction factor, defined by $\frac{f_G}{2} = \frac{\Delta p g_c \rho D_o}{G_m^2 L} \left(\frac{\mu}{\mu_s}\right)^{0.14} \left(\frac{S_T}{D_o}\right)^{0.4} \left(\frac{S_T}{S_L'}\right)^{0.4}$, dimensionless
 G_m = mass velocity through minimum cross section, lb/(hr)(sq ft)
 g_c = conversion factor, 4.18×10^8 (mass lb)(ft)/(force lb)(hr)²
 h = surface coefficient of heat transfer based on outside surface area of tubes, Btu/(hr)(sq ft)(deg F)
 j = heat-transfer factor, $j = \left(\frac{h}{cG_m}\right) \left(\frac{c\mu}{k}\right)^{2/3} \left(\frac{\mu_s}{\mu}\right)^{0.14}$, dimensionless
 k = thermal conductivity, Btu/(hr)(ft)(deg F)
 L = length of tube bank, $L = nS_L$, ft
 m = exponent of $\frac{\mu}{\mu_s}$, dimensionless
 N = number of major restrictions encountered in flow through the bank (equivalent to n , where S_m occurs in transverse openings; equivalent to $n - 1$ where S_m occurs in diagonal openings), dimensionless
 $N_{Re} = \text{Reynolds number } \frac{D_o G_m}{\mu}$, dimensionless
 n = number of tube rows in direction of flow, dimensionless
 P = pitch, defined as minimum center-to-center distance between adjacent tubes (in case of staggered square arrangements pitch is measured along a line 45 deg from direction of flow), ft
 p = pressure, psf
 S_L = longitudinal pitch, distance between center lines of adjacent transverse rows, ft
 S_L' = longitudinal pitch, center-to-center distance from a tube in transverse row to nearest tube outside of that row, ft
 S_m = shell-side minimum flow area, sq ft
 S_T = transverse pitch, center-to-center distance between tubes in a transverse row, ft
 S_v = total annulus flow area, sq ft
 W = mass rate of flow, lb per hr
 μ = absolute viscosity at average bulk temperature, lb/(hr)(ft)
 μ_f = absolute viscosity at film temperature, lb/(hr)(ft)
 μ_s = absolute viscosity at tube-surface temperature, lb/(hr)(ft)
 ρ = density at average bulk temperature, lb per cu ft
 ρ_f = density at film temperature, lb per cu ft
 τ_0 = frictional resistance per unit tube-surface area, psf

¹ Associate Professor, Department of Chemical Engineering, University of Delaware, Newark, Del.

² Research Fellow in Chemical Engineering, University of Delaware.

³ Research Fellow in Chemical Engineering, University of Delaware. Present address, E. I. du Pont de Nemours and Company, Wilmington, Del.

⁴ Research Fellow in Chemical Engineering, University of Delaware.

Contributed by the Heat Transfer Division and presented at the Annual Meeting, New York, N. Y., November 27–December 2, 1949, of THE AMERICAN SOCIETY OF MECHANICAL ENGINEERS.

NOTE: Statements and opinions advanced in papers are to be understood as individual expressions of their authors and not those of the Society. Paper No. 49–A-87.

INTRODUCTION

It has long been known that the size and spacing of tubes in a tube bank will affect the rate of heat transfer and the friction between the fluids and the tubes. Data have been published by a number of investigators for turbulent flow of gases past

amount of water and thus increase the temperature change of the water stream. Standardized test runs, made with each unit upon installation and repeated as the final run, have shown that no appreciable fouling occurred during the period of testing. Heat balances of less than ± 5 per cent deviation were obtained for all runs reported except those at very low oil velocities when the temperature change of the water stream became too low to give reliable heat balances. The heat load was calculated from the oil stream in these cases, and it is believed that the accuracy of these data is nearly comparable to those taken at higher oil velocities.

RESULTS

The experimental results are presented graphically both as simple plots of pressure drop and coefficient of heat transfer versus rate of flow and in generalized correlations. The experimental data and calculated results are too voluminous for inclusion in this paper but are presented in a current Engineering Experiment Station Bulletin (5).

DISCUSSION OF RESULTS

Effect of Tube Spacing—Friction.

The pressure drop per row of tubes for isothermal flow at 175 F is shown in Fig. 2 as a function of the linear oil velocity through the minimum cross-sectional area for flow. It can be seen that the data fall roughly into two groups, with the upper group, as indicated by the two top lines, representing the smaller tube size and the smaller clearance between tubes. The lower band of data represents the two arrangements of smaller tubes on the 1.50 pitch ratio, and the two arrangements of larger tubes on the 1.25 pitch ratio. In the latter four cases the minimum clearance between tubes is just double that of the upper band of data, the minimum clearance being 0.188 in. as compared to 0.094 in. At the lower oil velocities the upper group of curves has a slope of unity, indicating viscous flow. The slopes of the lower group approach unity at low velocities but do not maintain this slope over any appreciable range.

The friction data are also shown in Fig. 3 as frictional resistance per unit tube-surface area which is a term more directly comparable with coefficients of heat transfer, since the latter refer to tube-surface area. The spread of data is about the same as for Fig. 2, although the order of the different models is somewhat changed.

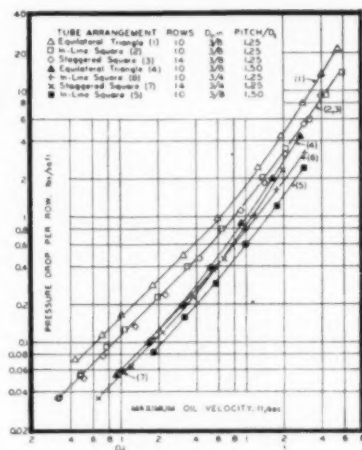


FIG. 2 PRESSURE DROP PER ROW DURING ISO-THERMAL FLOW OF OIL AT 175 F FOR SEVEN TUBE BANKS

(Flow normal to vertical tubes. Gulfcrest "E" oil, viscosity 17 centipoises at 175 F.)

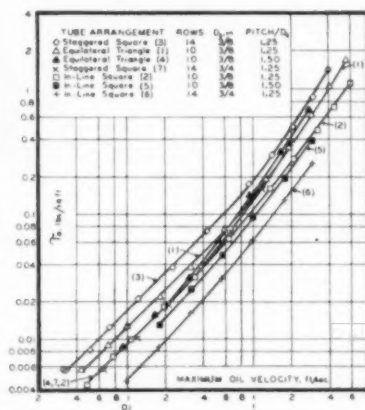


FIG. 3 FRICTIONAL RESISTANCE PER UNIT AREA OF TUBE SURFACE DURING ISO-THERMAL FLOW OF OIL AT 175 F FOR SEVEN TUBE BANKS

(Flow normal to vertical tubes. Gulfcrest "E" oil, viscosity 17 centipoises at 175 F.)

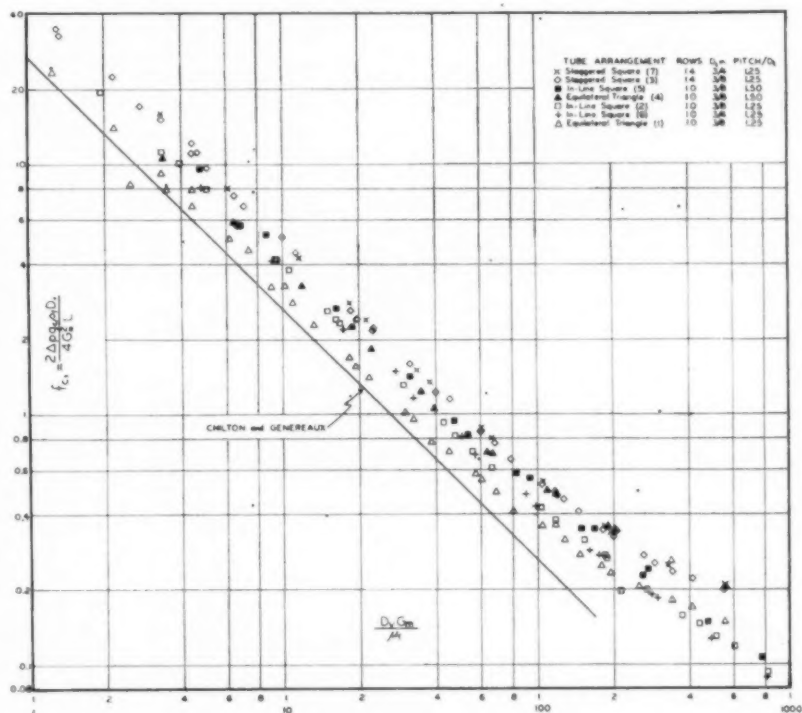


FIG. 4 FRICTION-FACTOR CORRELATION BY METHOD OF CHILTON AND GENEREAUX FOR VISCOUS FLOW

(Isothermal flow normal to vertical tubes. Average bulk oil temperatures 125, 150, 175 F. Gulfcrest "E" oil, viscosity 49 centipoises at 125 F, 28 centipoises at 150 F, and 17 centipoises at 175 F. It should be noted that the line of Chilton and Genereaux is based upon data from two equilateral-triangle arrangements with 1.25 and 1.50 pitch ratios using 3/4-in. tubes.)

Another comparison of the pressure-drop data for the two spacings is given in Fig. 4 where a friction factor is calculated and plotted versus Reynolds number in the manner proposed by Chilton and Genereaux (6). By this representation the two arrangements with the 1.50 pitch ratio lie 10 to 40 per cent above

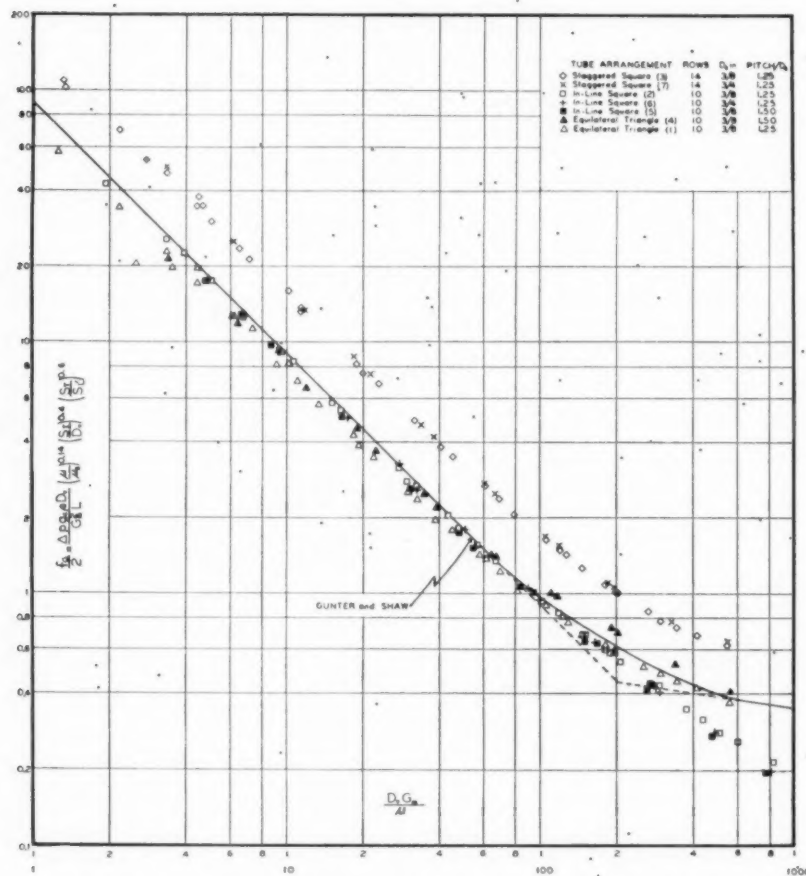


FIG. 5 FRICTION-FACTOR CORRELATION BY METHOD OF GUNTER AND SHAW
(Isothermal flow normal to vertical tubes. Average bulk oil temperatures 125, 150, 175 F. Gulfcrest "E" oil, viscosity 49 centipoises at 125 F, 28 centipoises at 150 F, and 17 centipoises at 175 F.)

their counterparts with 1.25 pitch ratio, so this representation does not allow suitably for changes in pitch. At Reynolds numbers greater than about 200, turbulence probably appears in varying degree in the different tube banks, and a clear separation of the in-line from the staggered arrangements is shown. Tube spacing does not appear to affect this separation of the data from these two general types of tube arrangements.

When the data are presented in the manner proposed by Gunter and Shaw (7), as shown in Fig. 5, there appears to be a somewhat better correlation of the effect of tube spacing, but this method does not bring the staggered square arrangement into agreement with the others. However, separate lines might be utilized for correlating the different types of arrangements.

Heat Transfer. The effect of tube spacing upon the coefficient of heat transfer, shown in Fig. 6, indicates that increasing the tube spacing results in somewhat lower heat-transfer coefficients, although the effect becomes less pronounced in the region of partial turbulence. This trend is also shown in the upper section of Fig. 7 where a j -factor with viscosity correction is plotted versus a Reynolds number based upon the tube diameter. In this figure the data represent both heating and cooling of the oil at average bulk temperature levels of 125, 150, and 175 F. The spread of the data shows that the effects of temperature variation between the tube wall and the body of the oil stream are not allowed for completely by this method of representation. It is

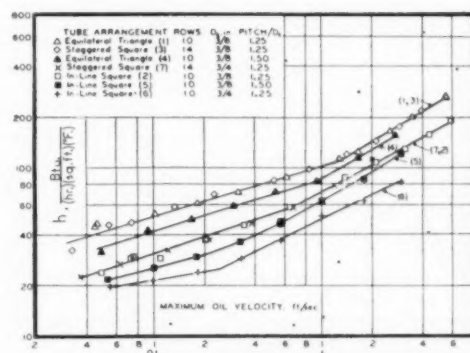


FIG. 6 OIL-FILM COEFFICIENTS OF HEAT TRANSFER FOR SEVEN TUBE BANKS

(Flow normal to vertical tubes. Average bulk oil temperature 175 F. Tube-surface temperature range 101-113 F. Gulfcrest "E" oil, viscosity 98 centipoises at 100 F, 64 centipoises at 115 F, and 17 centipoises at 175 F.)

interesting to note that the spread is greater for the in-line arrangements with the greater minimum tube clearance than for the other tube banks. This possibly may be due to free convection, but if so, a similar spread should be observed for the other arrangements with wide clearance between tubes.

Heat Transfer Versus Pumping Power. In order to show the effect of spacing upon both friction and heat transfer, the heat-transfer coefficient is shown in Fig. 8 versus the power loss per unit surface area. The triangular arrangement with the 1.25 pitch ratio has approximately 25 per cent greater heat-transfer coefficients than the same arrangement on a 1.50 pitch ratio at given power losses. The increase is not so pronounced with the in-line square arrangements where the exchangers with the smaller pitch ratio give about 5 per cent greater heat transfer than those with the larger pitch ratio. In both cases the effect of spacing tends to decrease as turbulence appears.

The Effect of Tube Size—Friction. From Figs. 2 and 3 it can be seen that doubling the tube size reduces the pressure drop per row of tubes and the surface friction, respectively, by approximately 50 per cent when the pitch ratio is maintained constant. Doubling the tube size while maintaining the same minimum clearance between tubes increases the pressure drop by about 30 per cent, probably due to the longer flow path per row. When the pressure drop is expressed in terms of friction factors, as defined by Chilton and Genereaux, Fig. 4 shows that the large-tube data agree very well with the small-tube data for both the in-line and staggered square tube banks although the two arrangements do not coincide. The same is true for the Gunter and Shaw method as plotted in Fig. 5, so it may be said that both methods adequately allow for variation in tube size, although they do not allow for changes in spacing.

Heat Transfer. Fig. 6 shows that an increase in tube size causes an appreciable decrease in the coefficient of heat transfer. When the data are plotted in Fig. 7 as j -factor versus Reynolds number, the large- and small-tube data fall together, so that, for each arrangement, a single line is justifiable for representing both tube sizes. A spreading of the data for the in-line square arrangement again is noticeable and appears to be a characteristic of the wider clearance between tubes. A definite change of slope is also noticeable in the data for the in-line arrangement in the transition zone over the range of Reynolds numbers of 60 to 150. Motion pictures (8) of flow through sections of tube banks show that flow through an in-line square bank is somewhat similar to

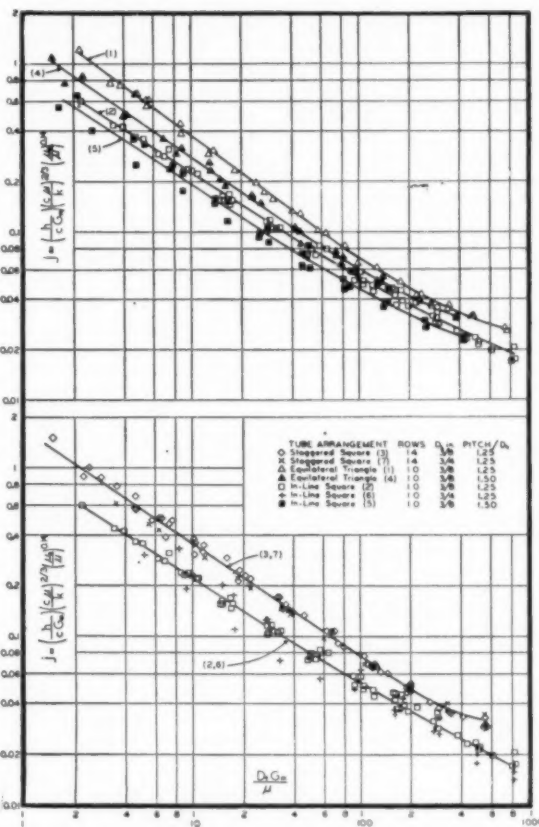


FIG. 7 HEAT-TRANSFER FACTOR j FOR SEVEN TUBE BANKS
(Flow normal to vertical tubes at average bulk oil temperatures of 125, 150, and 175 F. Both heating and cooling. Gulfcrest "E" oil, viscosity 49 centipoises at 125 F, 28 centipoises at 150 F, and 17 centipoises at 175 F.)

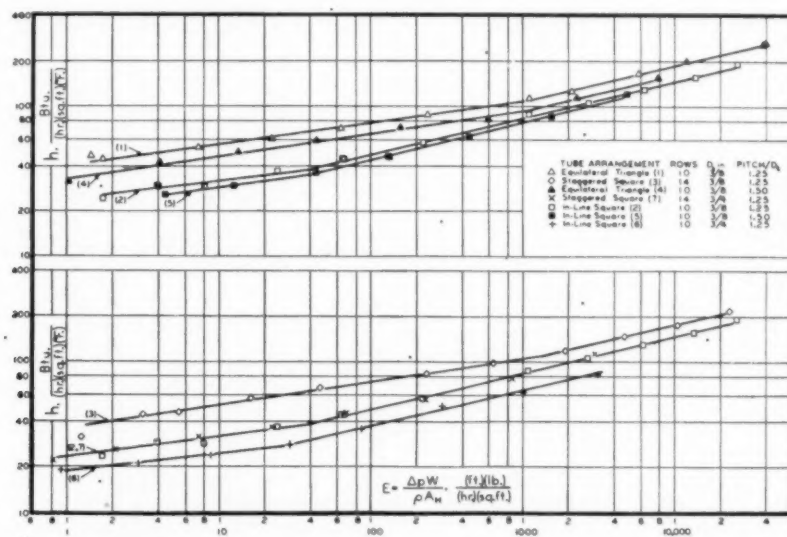


FIG. 8 COMPARISON OF HEAT-TRANSFER AND POWER REQUIREMENTS FOR SEVEN TUBE BANKS
(Flow normal to vertical tubes. Average bulk oil temperature 175 F. Tube-surface temperature range 101-113 F. Gulfcrest "E" oil, viscosity 98 centipoises at 100 F, 64 centipoises at 115 F, and 17 centipoises at 175 F.)

flow through a straight channel and therefore the increase in the rate of heat transfer which has been observed inside pipes in the transition zone may occur also to a lesser degree with in-line tube banks.

Heat Transfer Versus Pumping Power. Fig. 8, the plot of heat-transfer coefficients versus pumping power, clearly shows that when the pitch ratio is kept constant the small tubes provide from 20 to 50 per cent greater heat transfer at a given power loss per unit surface area than the large tubes.

Pressure Drop During Nonisothermal Flow. Although the foregoing discussions of pressure drop have dealt only with isothermal flow, the conclusions may be applied to flow through tube banks during heating or cooling if a suitable relation can be found to correlate the heating and cooling results with the isothermal data. A complete study of this problem has not yet been made, but it is possible that an analysis along the lines followed by Boelter and associates (9) for viscous flow inside pipes may prove successful. For the present, however, the use of an empirical factor $\left(\frac{\mu}{\mu_s}\right)^m$, similar to one proposed in a previous paper, is suggested. The extent of deviation during nonisothermal flow may be seen in Fig. 9 in which heating and cooling

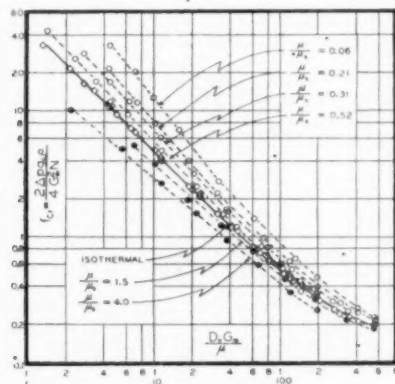


FIG. 9 VARIATION OF FRICTION FACTOR WITH HEATING AND COOLING

(Flow normal to 3/8-in.-OD vertical tubes, model 3, staggered-square tube arrangement on 15/32-in. centers. Gulfcrest "E" oil, viscosity 49 centipoises at 125 F, 28 centipoises at 150 F, and 17 centipoises at 175 F.)

pressure-drop data are plotted for model 3. While in the previous paper the data were limited to cooling conditions for three tube banks, the present study includes heating data for all exchangers except model 1, as well as cooling data for all seven exchangers. The divergence of the pressure-drop lines seen in Fig. 9 for various $\frac{\mu}{\mu_s}$ ratios in model 3 is believed to be due principally to the viscosity gradient between the oil at the tube wall and in the center of the stream, rather than nonuniformity of flow throughout the tube bank during cooling at low velocity as previously suspected. The apparent systematic trend of the data from the cooling into the heating zone indicates that the deviation is essentially a viscosity-gradient effect.

In developing a correction factor for such deviations, the exponents required for $\frac{\mu}{\mu_s}$ in order to bring the nonisothermal data in agreement with the isothermal data are plotted in Fig. 10 versus the Reynolds number. The scattering of the data is considerable but is not troublesome, since the exponent applies only a second-order correction. A straight line with the equation

$m = 0.57 N_{Re}^{-0.26}$ shown in the figure is suggested for representing the $\frac{\mu}{\mu_s}$ exponent over a range of Reynolds numbers from 1 to 300. The results of using this line to correct the data in Fig. 9 are shown in Fig. 11, and the resulting excellent agreement bears out the satisfactory nature of the correction term. This correction is equally satisfactory for the data from the other six tube banks.

Further Correlations. The isothermal pressure-drop data plotted in Figs. 4 and 5 show that neither the well-established Chilton and Genereaux method nor the more recent proposal of Gunter and Shaw allows completely for variation of tube-bank characteristics. On the whole, the Gunter and Shaw method

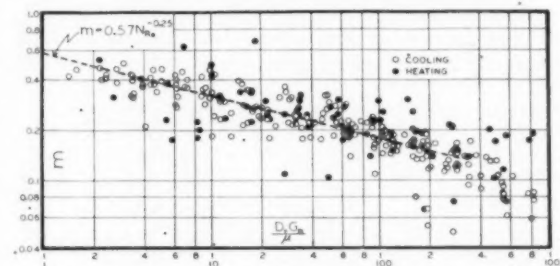


FIG. 10 EXPONENT m FOR VISCOSITY CORRECTION OF FRICTION FACTOR

(Flow normal to vertical tubes at average bulk oil temperatures of 125, 150, and 175 F. Both heating and cooling for seven tube banks. Gulfcrest "E" oil, viscosity 49 centipoises at 125 F, 28 centipoises at 150 F, and 17 centipoises at 175 F.)

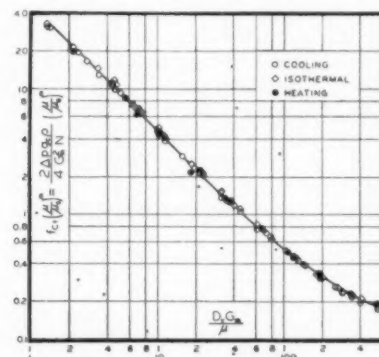


FIG. 11 FRICTION FACTORS FOR HEATING AND COOLING CORRECTED WITH VISCOSITY RATIO

(Flow normal to 3/8-in.-OD vertical tubes, model 3, staggered-square tube arrangement on 15/32-in. centers. Gulfcrest "E" oil, viscosity 49 centipoises at 125 F, 28 centipoises at 150 F, and 17 centipoises at 175 F.)

appears better in the viscous region but, in the transition region, the in-line data deviate markedly, while the staggered square arrangements deviate from the other arrangements over the entire range. This method can be utilized, however, if a separate line is used for the staggered square arrangement. It is interesting to note that for the seven tube banks under consideration a much better correlation is obtained by interchanging S_T and S_L , which places the staggered square arrangements within 5 per cent of the proposed line of Gunter and Shaw. No other data are available to check the generality of this procedure, but a similar observation was made by Jameson (10) for turbulent flow past finned tubes.

In view of the plans to obtain more experimental data, no exhaustive attempt has been made to obtain the best possible

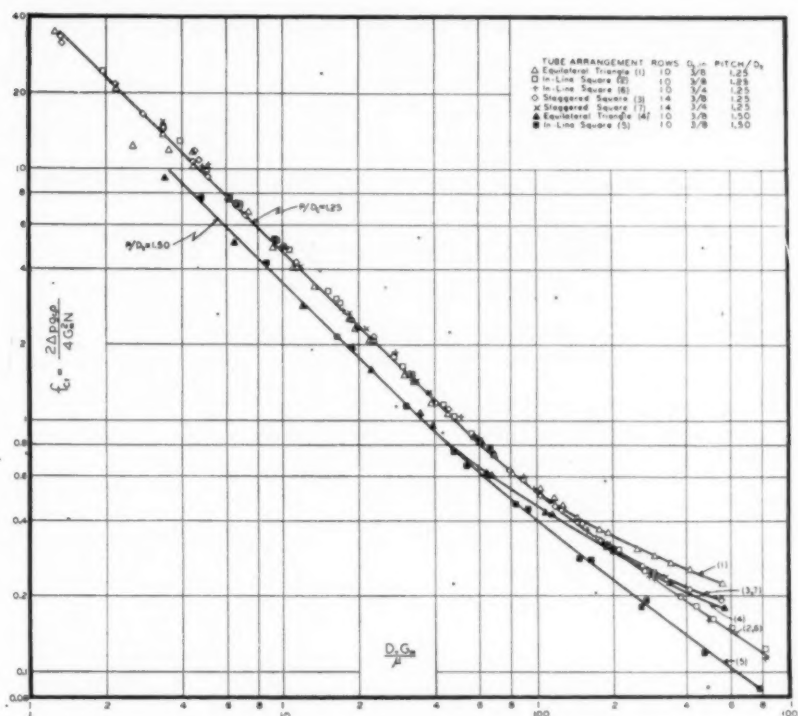


FIG. 12 TENTATIVE FRICTION-FACTOR REPRESENTATION
(Isothermal flow normal to vertical tubes. Average bulk oil temperatures 125, 150, 175 F. Gulferest "E" oil, viscosity 49 centipoises at 125 F, 28 centipoises at 150 F, and 17 centipoises at 175 F.)

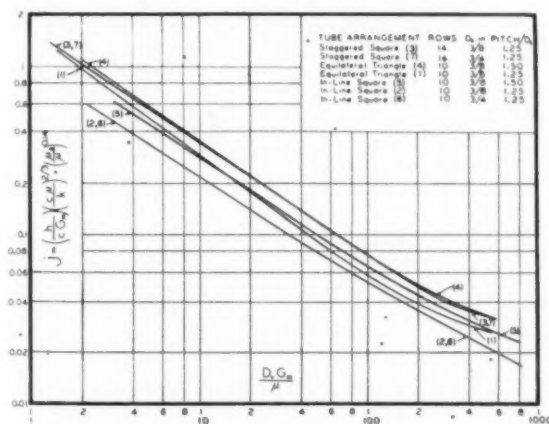


FIG. 13 TENTATIVE HEAT-TRANSFER REPRESENTATION
(Flow normal to vertical tubes at average bulk oil temperatures of 125, 150, and 175 F. Both heating and cooling. Gulferest "E" oil, viscosity 49 centipoises at 125 F, 28 centipoises at 150 F, and 17 centipoises at 175 F.)

correlation with the data now available. On the other hand, it has been found that a relatively simple form of correlation brings the friction data considerably closer together than previous methods in the literature. This method involves plotting as ordinate

$$2 \Delta P \rho D / 4 G_m^2 N$$

which was used by Chilton and Genereaux for turbulent flow versus $D_e G_m / \mu$ as shown in Fig. 12. Apparently different tube

sizes and arrangements are brought together, but pitch ratio remains a parameter.

Similarly, for heat transfer, a final correlation will await further data, but it has been found that if the j -factor is plotted versus the Reynolds number using the volumetric hydraulic diameter D_e , instead of the tube diameter D_o , the data are brought closer together as shown in Fig. 13. The correction of $\left(\frac{\mu}{\mu_s}\right)^{0.14}$ for viscosity gradient, which was originally used by Sieder and Tate (11) for flow inside tubes, is used here as an approximation until additional data permit a further refinement.

It should be kept in mind that the conclusions presented in this paper are based upon data from simple crossflow exchangers and probably cannot be expected to apply without considerable modification to baffled exchangers where leakage around baffles, parallel flow, and nonuniformity of flow are important and must be given consideration.

CONCLUSIONS

Data from the present study show the following:

1 When the pitch is increased for a given arrangement and tube size:

- (a) At constant velocity, the pressure drop is lower (Fig. 2).
- (b) At constant velocity, the coefficient of heat transfer is lower (Fig. 6).
- (c) At constant pumping-power loss, the coefficient of heat transfer is slightly lower (Fig. 8).

2 When the tube diameter is increased for a given arrangement and a constant pitch ratio:

- (a) At constant velocity, the pressure drop is lower (Fig. 2).

(b) At constant velocity, the coefficient of heat transfer is lower (Fig. 6).

(c) At a constant pumping-power loss, the coefficient of heat transfer is considerably lower (Fig. 8).

3 The highest coefficients of heat transfer were obtained with the smaller tube sizes and the smaller tube pitches in the staggered arrangements.

4 A modification of the method of Chilton and Genereaux, utilizing the volumetric equivalent diameter, gives the best correlation of the pressure drop for viscous flow across the seven tube banks tested, although separate lines are found for the two

pitch ratios. A variable exponent on the ratio of $\frac{\mu}{\mu_s}$ is suitable to correlate the nonisothermal pressure-drop data.

5 The use of the volumetric equivalent diameter in the Reynolds number gives a somewhat better correlation of the heat-transfer data than does the use of tube diameter.

ACKNOWLEDGMENT

The authors acknowledge the suggestions on design of the apparatus and on the program of study by the Special Advisory Committee of the Heat Transfer Division, which is sponsoring this co-operative research project. The committee at the time of the work was composed of W. H. McAdams, chairman; S. Kopp; W. N. McCurdy, Jr.; A. C. Mueller; B. E. Short; W. H. Thompson; T. Tinker; and P. R. Trumpler. The help of A. Wurster in the design and construction of the test units was invaluable. Assistance in interpretation and presentation of data was given by A. P. Colburn; Research Fellow W. E. Meece aided in the experimental work. Funds and equipment were kindly furnished by the Tubular Exchanger Manufacturer's Association, The American Petroleum Institute, Andale Company, Davis Engineering Company, Downingtown Iron Works, du Pont Company, Standard Oil Development Company, and

York Ice Machinery Company. The oil was provided by the Gulf Oil Company.

BIBLIOGRAPHY

- 1 "Experimental Investigation of the Influence of Tube Arrangement on Convection Heat Transfer and Flow Resistance in Cross Flow of Gases Over Tube Banks," by O. L. Pierson, *Trans. ASME*, vol. 59, 1937, pp. 563-572. See also papers by E. C. Hoge, pp. 573-581, and E. D. Grimison, pp. 583-594, and discussion, vol. 60, 1938, pp. 381-391.
- 2 "Fluid Friction at Parallel and Right Angles to Tubes and Tube Bundles," by E. N. Sieder and N. A. Scott, Jr., ASME unpublished paper No. 83, 1932.
- 3 "A Study of Tube Arrangements in Unbaffled Tubular Heat Exchangers," by O. P. Bergelin, E. S. Davis, and H. L. Hull, *Trans. ASME*, vol. 71, 1949, pp. 369-374.
- 4 "Heat Transfer and Fluid Friction During Viscous Flow Across Banks of Tubes," by G. A. Omohundro, O. P. Bergelin, and A. P. Colburn, *Trans. ASME*, vol. 71, 1949, pp. 27-34.
- 5 "Heat Transfer and Fluid Friction During Flow Across Banks of Tubes," by O. P. Bergelin, A. P. Colburn, and H. L. Hull, University of Delaware Engineering Experimental Station, Bulletin No. 2, 1950.
- 6 "Pressure Drop Across Tube Banks," by T. H. Chilton and R. P. Genereaux, *Trans. AIChE*, vol. 29, 1933, pp. 161-173.
- 7 "A General Correlation of Friction Factors for Various Types of Surfaces in Crossflow," by A. Y. Gunter and W. A. Shaw, *Trans. ASME*, vol. 67, 1945, pp. 643-660.
- 8 "Flow Across Tube Banks," a 400 ft., 16 mm. film available upon request from the Department of Chemical Engineering, University of Delaware, Newark, Del.
- 9 "Heat Transfer and Pressure Drop for a Fluid Flowing in the Viscous Region Through a Vertical Pipe," by R. C. Martinelli, C. J. Southwell, G. Alves, H. L. Craig, E. B. Weinberg, N. F. Lansing, and L. M. K. Boelter, *Trans. AIChE*, vol. 38, 1942, pp. 493-530.
- 10 Discussion by S. L. Jameson to "A General Correlation of Friction Factors for Various Types of Surfaces in Crossflow," by A. Y. Gunter and W. A. Shaw, *Trans. ASME*, vol. 67, 1945, pp. 658-659.
- 11 "Heat Transfer and Pressure Drop of Liquids in Pipes," by E. N. Sieder and G. E. Tate, *Industrial and Engineering Chemistry*, vol. 28, 1936, pp. 1429-1435.

Experimental Evaluation of Human Shape Factors With Respect to Floor Areas

By F. W. HUTCHINSON,¹ BERKELEY, CALIF.

Results are presented for the shape factor of an average standing person with respect to energy in the form of heat received from a floor area. The use of shape factors is essential in determining conditions of comfort in a heated or cooled enclosure.

INTRODUCTION

THE establishment of conditions of comfort in a heated or cooled enclosure requires realization of a stable heat balance between the occupant and his surroundings. By a stable balance is meant one which provides a practically fixed net rate of heat loss from the occupant, irrespective of his position (as standing, sitting, or reclining), and irrespective of his location within the room. If room air temperature were uniform and if all inside surfaces of the enclosure were at the same temperature, there would be no difficulty in maintaining a stable balance, but in an enclosure where some surfaces (as windows) may be warmer in summer and colder in winter whereas others (as radiant panels) may be colder in summer and warmer in winter, the difficulty of stabilizing the occupant's rate of heat loss may be very great.

As an extreme case, visualize a room with large single-glass windows heated on a cloudy midwinter day by means of a small fireplace; obviously, the occupant will be too warm if he stands very near the fireplace, and too cold if he stands very near the windows. At one or more points in such a room conditions of comfort would necessarily exist, but the heating system would be considered unsatisfactory, and the occupant would experience marked instability with respect to his rate of heat loss.

Engineering evaluation of stability requires establishing a heat balance on the occupant and investigating the manner in which individual terms of that balance vary with position or location of the occupant. Since, for any fixed-load condition that may be acting on the enclosure the air and surface temperatures normally will remain fixed with respect to time, it follows that the major factor affecting stability will be changes in the geometry of the system (consisting of occupant and surroundings) which occur as the occupant alters his position or moves around in the enclosure. All such geometrical changes appear in the equations for radiant transfer between the occupant and the various surfaces of the room, each such surface possessing a shape factor with respect to the occupant which, in itself, expresses the fraction of energy received by that surface of the total radiant energy emitted by the occupant. Conversely the fraction of radiation emitted by a surface which strikes the occupant (prior to reflection) is said to be the shape factor of the occupant F_{os} with respect to the surface; in equation form

$$F_{os} = \frac{1}{A_s} \int_{A_o} \int_{A_s} \frac{\cos \phi_o \cos \phi_s dA_o dA_s}{\pi(r_{os})^2} \dots \dots \dots [1]$$

where

F_{os} = shape factor of occupant with respect to energy received from surface A_s , or fraction of energy emitted by A_s which is received by occupant

r_{os} = distance between center of surfaces A_o and A_s

ϕ_o = angle between r_{os} and normal to center of A_o

ϕ_s = angle between r_{os} and normal to center of A_s

The mathematical problem of carrying out a double integration over the complex surface of the human body is, for practical purposes, insurmountable. Thus experimental methods must be used for evaluation of Equation [1]. The intent of this paper is to present complete results from such an experimental investigation for the particular case of an "average" occupant with respect to points, infinitesimal areas, or finite areas on the floor. A similar study² has dealt with human shape factors with respect to infinitesimal and finite areas in the wall or ceiling. The earlier study was for an occupant in either standing or sitting position whereas the present paper presents results only for the standing position.

EXPERIMENTAL PROCEDURE

The test procedure used in this research was practically identical with that which has been reported in detail in an earlier study.² The subject was a clothed dummy representing an "average" man 5 ft 10 in. in height and weighing 165 lb. The dummy was dressed in a two-piece suit, was in standing position, and had both arms at its sides. Shape factors were obtained by using a mechanical integrator of the type proposed by Hottel³ and developed by Boelter⁴ and associates.

Previous experience² had shown that the full-face shape factor of a standing subject is practically the same whether the subject is facing forward or backward, and that complete shape-factor curves for any facing direction could be readily and accurately determined by interpolation and extrapolation from experimental data for full face and for semiprofile. Accordingly, the dummy was placed in a fixed position on the test floor and a line drawn in the facing direction, another line being drawn making a 45-deg angle with the facing direction. Shape factors were then determined at intervals of 1 ft out along each of these lines to a distance of 18 ft from the dummy. In obtaining shape factors the mechanical integrator was placed at each of the designated points on the floor and a light beam from the integrator used to trace the outline of the dummy. Corresponding to each closed curve traced by the light beam, the integrator would draw a

¹ Professor of Mechanical Engineering, University of California.

Contributed by the Heat Transfer Division and presented at the Spring Meeting, Washington, D. C., April 12-14, 1950, of THE AMERICAN SOCIETY OF MECHANICAL ENGINEERS.

NOTE: Statements and opinions advanced in papers are to be understood as individual expressions of their authors and not those of the Society. Manuscript received at ASME Headquarters, November 1, 1949. Paper No. 50-S-4.

² "Optimum Surface Distribution in Panel Heating and Cooling Systems," by V. F. Raber and F. W. Hutchinson, Trans. ASHVE, vol. 50, 1944, pp. 231-257.

³ "Radiant Heat Transmission," by H. C. Hottel, *Mechanical Engineering*, vol. 52, 1930, pp. 699-704.

⁴ "A Mechanical Integrator for the Determination of the Illumination From Diffuse Surface Sources," by V. H. Cherry, D. D. Davis, and L. M. K. Boelter, Trans. Illuminating Engineering Society, vol. 34, 1939, pp. 1085-1092.

closed pencil curve; the area of the pencil curve divided by a constant of the integrator was then taken as the shape factor of the dummy with respect to energy emitted from the point on the floor at which the integrator was then located.

Shape factors were redetermined at each station at least three times and never less than the number of times necessary to assure ability to reproduce the same result.

EXPERIMENTAL RESULTS

Table 1 presents a summary of all experimental data. The maximum shape factor of the occupant with respect to a point on the floor is seen to occur when that point is 2 ft out along the line in which the occupant is facing; at this point the value of 0.0851 indicates that 8.5 per cent of the energy emitted from the infinitesimal area surrounding the point (providing this area emits diffuse radiation) will strike the occupant. The reduction

TABLE 1 EXPERIMENTAL TEST DATA

Distance from the dummy, ft.	Front view		Semiprofile view	
	Integrator reading, sq. in.	Shape factor ^a	Integrator reading, sq. in.	Shape factor ^a
1	5.10	0.065	4.65	0.0593
2	6.68	0.0851	5.45	0.0695
3	4.30	0.058	2.75	0.0350
4	2.42	0.0309	2.05	0.0261
5	1.54	0.0196	1.35	0.0172
6	1.20	0.0153	1.11	0.0140
7	0.82	0.01045	0.72	0.0092
8	0.50	0.00637	0.50	0.00636
9	0.46	0.00586	0.45	0.00572
10	0.40	0.00510	0.35	0.00445
11	0.29	0.00370	0.22	0.00280
12	0.27	0.00344	0.20	0.00235
13	0.25	0.00319	0.12	0.00153
14	0.23	0.00319	0.10	0.001265
15	0.22	0.00281	0.08	0.00102
16	0.15	0.00191	0.07	0.000892
17	0.08	0.00102	0.06	0.000765
18	0.06	0.000765	0.05	0.000637

^a The shape factor is equal to the experimentally determined integrator area divided by the area of the base circle of the integrator; for the particular mechanical integrator used in this research the constant value of the base circle area was 78.5 sq. in.

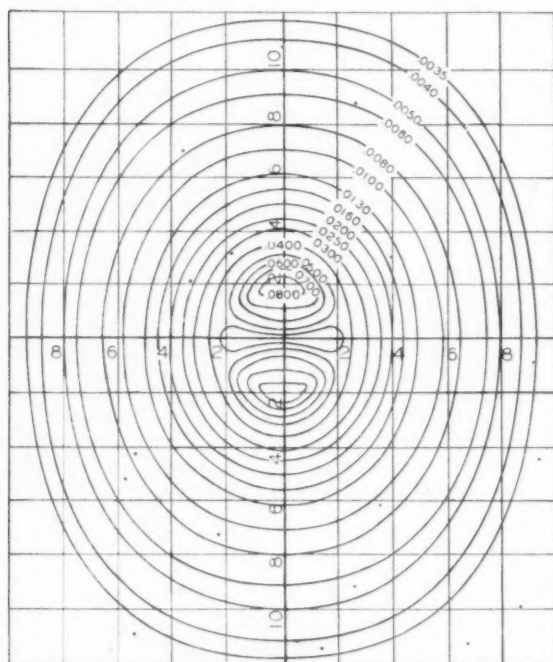


Fig. 1

in shape factor as the occupant moves closer to the point than 2 ft can be attributed to the rapid decrease in the cosine of ϕ . The decrease as the occupant moves farther from the point than 2 ft is primarily due to the increasing value of r_{001} but partially to the increase in ϕ ; these two factors far more than offset the decrease in ϕ .

The results show that floor areas more than 5 ft from the occupant emit less than 2 per cent of their energy in a direction such that it will be received by a perfectly absorbing (black body) occupant. Areas more than 7 ft away provide less than 1 per cent direct radiant transfer, whereas areas more distant than 10 ft provide less than $\frac{1}{2}$ per cent direct radiant transfer. For equal distances from the occupant, points along the semiprofile transmit 10 per cent to 15 per cent less energy to the occupant than do corresponding points (or rather infinitesimal areas) along the line corresponding to a full-face view.

Fig. 1 is a plot obtained by interpolation and extrapolation of the experimental results given in Table 1. In this figure the occupant is considered to be standing at the center of co-ordinates and facing either toward the top or the bottom (front and rear views being taken as symmetrical) of the figure. Thus the scale along the Y-axis indicates distance in feet in front of, or behind the occupant, whereas the scale along the X-axis indicates distance in feet to the right or left (again, symmetry is assumed for the full-profile views) of the occupant. Therefore the curves in Fig. 1 are iso-shape factor lines, and the number shown on each such curve is numerically equal to the fraction of energy leaving any infinitesimal floor area along that curve which would be directly absorbed by the occupant if his emissivity were unity.

For an occupant so dressed that his emissivity is less than unity, the shape factor as given would have to be multiplied by the emissivity of the occupant in order to obtain the fraction of energy that would be absorbed of that leaving the floor surface. As an example, note that from an infinitesimal floor area located 6 ft to the right and 7 ft ahead of the occupant, the shape factor would be 0.0050, hence $\frac{1}{2}$ per cent of the energy leaving such an area would be received by the (black body) occupant. Although this shape factor has been stated for an infinitesimal area, it would be equally applicable to any finite area over which the average of point shape factors had the same numerical value.

APPLICATION OF RESULTS

In practice, interest is almost wholly centered on radiant transfer between the occupant and some moderate-sized area as a window, heated panel, or an unheated but uniform surface, such as an exterior wall, floor, ceiling, or inside partition. In such cases the shape factor of the occupant with respect to energy received from the surface in question can be taken as the average (not the sum) of shape factors with respect to the small finite areas which make up the larger surface. The smaller the finite areas become the greater will be the accuracy of the averaged over-all shape factor, but the greater, too, will be the effort required to obtain an average value.

As an approximation which is adequate for usual engineering purposes, it is suggested that within a radius of 4 ft of the occupant, the unit area be taken as 1 sq ft, whereas, at greater distances, a satisfactory unit area will be one which is square and 2 ft on the side. For areas larger than 8 ft \times 8 ft, with the occupant located at the center, adequate accuracy would thus be attained by dividing the inner 4-ft \times 4-ft area of one quadrant into four unit areas of 1 sq ft each, and dividing any additional part of this one quadrant into 2-ft \times 2-ft unit areas. Note that for a centrally located occupant, the shape factor for any one quadrant (provided the occupant is facing one of the sides) will be numerically equal to the shape factor of the occupant with respect to energy received from the entire area. For arrange-

ments of occupant and panel which are nonsymmetrical, all unit areas of the panel must be used rather than those of a single quadrant.

Example. Consider a room 11 ft \times 11 ft which is to be heated and cooled by means of a 3-ft \times 3-ft floor panel which is to be centered at the center of the floor, the sides of the panel running parallel to the sides of the room. The shape factor of the occupant with respect to energy received from the panel is desired for a case in which the occupant is standing parallel with a wall at a position in the room 2 ft in from each of two walls.

Solution. Draw on tracing paper a plan of the room, with panel, to the same scale as that of Fig. 1. On this tracing divide the 3-ft \times 3-ft panel into 9 equal unit areas and indicate by point *O* the position of the occupant on the tracing. Now superimpose the tracing on Fig. 1 (refer to Fig. 2), so that point

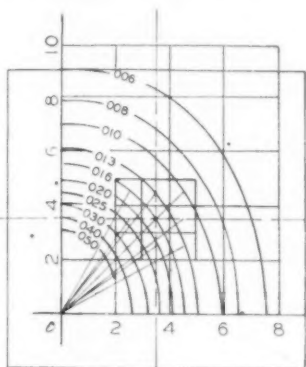


FIG. 2

O of the tracing is at the center of co-ordinates of Fig. 1, and the facing direction of the occupant corresponds on both tracing and on Fig. 1. It is now possible to read directly, or obtain by interpolation, the shape factor at the center of each of the 9 unit areas. Referring to Fig. 2, and reading these shape factors from left to right and from top to bottom, we obtain the over-all shape factor of the occupant with respect to energy received from the entire panel as

$$F_{oa} = (0.016 + 0.013 + 0.010 + 0.024 + 0.016 + 0.012 + 0.029 + 0.020 + 0.013)/9 = 0.017 = 1.7 \text{ per cent}$$

Thus 1.7 per cent of the energy emitted by the diffuse panel would be absorbed by an occupant at the stated position, provided his clothing was such that he possessed unit emissivity.

CONCLUSION

Results have been presented for the shape factor of an average standing person with respect to energy received from a floor area. Similar results for standing and sitting persons with respect to energy from wall and ceiling areas are already available in the literature.² Representations of the earlier data in a form similar to that of Fig. 1 are also available in other publications.³ The use of shape factors of this type is needed for exact studies of stability of comfort conditions in a room that is heated or cooled by radiant or partially radiant means, or for stability studies in a convection-heated room in which single-glass or other surfaces reach equilibrium temperatures lower than the room air temperature.

³ "Panel Heating and Cooling Analysis," by B. F. Raber and F. W. Hutchinson, John Wiley & Sons, Inc., New York, N. Y., 1947.

Furnace Heat Absorption in Paddy's Run Pulverized-Coal-Fired Steam Generator, Using Turbulent Burners, Louisville, Ky.

Part I Variation in Heat Absorption as Shown by Measurement of Surface Temperature of Exposed Side of Furnace Tubes

By R. I. WHEATER¹ AND M. H. HOWARD,² NEW YORK, N. Y.

This report is one of three current formal reports (1)³ covering the activities of the ASME Special Research Committee on Furnace Performance Factors in connection with the furnace-performance tests which were conducted at the Paddy's Run Station of the Louisville Gas and Electric Company in Louisville, Kentucky. The furnace heat absorption and its distribution in the furnace, as reported in this paper, were determined by the " ΔT method," which consists of using the difference in temperature between the surface of the exposed face of the tube and the mixture within the tube to measure the heat absorption at representative locations. The companion paper, Part II, covers the furnace performance as measured by a heat balance of the furnace. Part III presents a correlation of the results.

INTRODUCTION

IT IS desirable at this point to review briefly the history of the extensive test program which has been undertaken by the ASME Special Research Committee on Furnace Performance factors. This program was actually initiated in 1943 for the purpose of gaining more factual and fundamental knowledge of the various factors which affect the performance of large central-station furnaces. In order to accomplish this, it was also necessary to establish methods of measuring the amount and distribution of heat absorbed in such furnaces.

The first furnace to be tested was a completely water-cooled, dry-bottom furnace, fired tangentially by eight pulverized-coal burners which could be tilted up or down 30 deg from the horizontal. These tests were made in 1945 at the Ohio Power Company's Tidd Station, using the No. 11 boiler, which is a conventional, 3-drum, bent-tube boiler. Four papers (2) were presented in June, 1947, covering the furnace performance obtained with this design under several operating variables, as

well as the results of several different means of measuring the furnace heat absorption and its distribution in the furnace.

The subject tests were conducted at the Paddy's Run Station of the Louisville Gas and Electric Company in 1948, in order to establish the furnace performance of another completely water-cooled furnace which is fired horizontally by eight turbulent pulverized-coal burners.

The object of this paper is to establish the distribution and amount of heat absorption in this furnace, as measured by the " ΔT method" for the various operating conditions investigated, and to study the effect of these operating variables on furnace performance. The operating variables studied were (a) burner adjustments, (b) furnace rating, (c) excess air for combustion, and (d) various combinations of burners in service at 50 per cent full load.

TEST EQUIPMENT

The No. 3 unit at Paddy's Run Station is designed for a maximum continuous output of 640,000 lb of steam per hr at a pressure of 950 psig and a temperature of 900 F. It was first placed in operation on September 25, 1947, and normally has carried an output of 600,000 to 640,000 lb of steam per hr at design conditions. This unit, shown in Fig. 1, is of the single-drum bent-tube type, containing a conventional water-cooled furnace, a bare-tube pendant-type convection superheater, both a bare-tube and an extended-surface boiler section, an extended-surface economizer, a regenerative-type air preheater, and two ball-mill firing systems.

The dry-bottom furnace is approximately 31 ft in width and 24 ft in depth. The height of the furnace from the roof to the center line of the hopper throat at the bottom of the furnace is about 90 ft. The furnace walls are composed of 3-in.-OD, 0.220-in. minimum wall, carbon-steel tubes spaced on 3 1/4-in. centers. This tube spacing exists throughout the furnace. Near the top, the rear-wall tubes bend into the furnace and then extend up vertically to form the slag screen. These rear-wall tubes are bent to form four rows of slag-screen tubes on 13-in. centers. The front-wall tubes bend at the top of the furnace to form the furnace roof. Both the front and rear-wall tubes bend into the furnace to form the hopper throat at the bottom of the furnace. This throat is therefore parallel to the front or firing wall. The furnace contains 8884 sq ft total projected wall surface, which includes the outlet aperture.

This steam-generating unit is fired by eight horizontal intervane burners which are located in the lower front wall and arranged in two horizontal rows of four burners each. These burners are

¹ Assistant to the Manager, Service Department, Foster Wheeler Corporation, New York, N. Y. Mem. ASME.

² Manager, Service Department, Foster Wheeler Corporation, New York, N. Y. Mem. ASME.

³ Numbers in parentheses refer to Bibliography at end of paper.

Contributed by the Special Research Committee on Furnace Performance Factors, and the Fuels, Power, and Heat Transfer Divisions, and presented at the Annual Meeting, New York, N. Y., November 27-December 2, 1949, of THE AMERICAN SOCIETY OF MECHANICAL ENGINEERS.

NOTE: Statements and opinions advanced in papers are to be understood as individual expressions of their authors and not those of the Society. Paper No. 49-A-118.

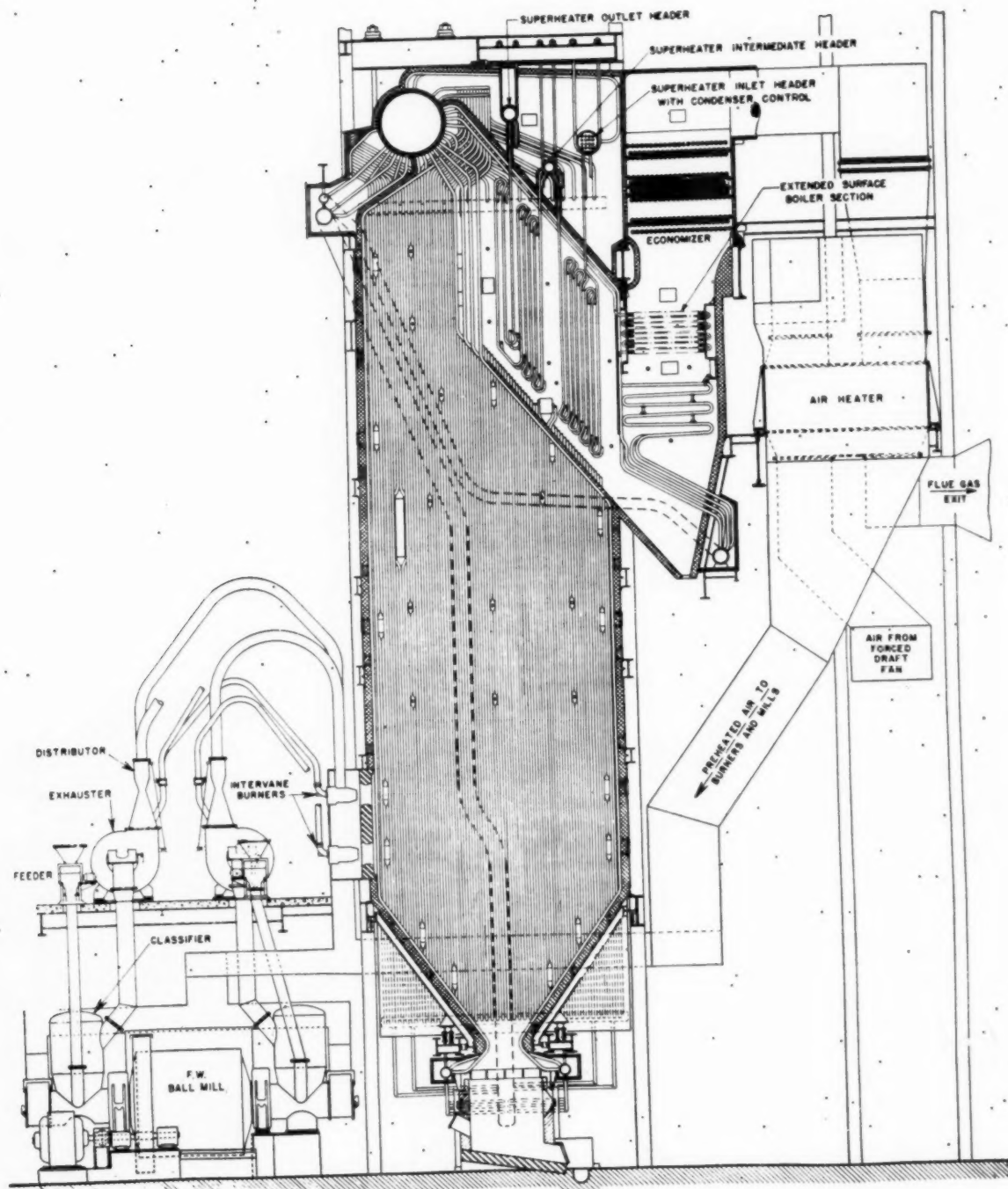


FIG. 1 GENERAL ARRANGEMENT OF BOILER No. 3

of the turbine
natural gas
was not yet
firing was
verified coal
hausters.
side burner
burners are
is equipped
to be removed

Fig. 2 shows
Each burner
smaller auxiliary
purpose of
air and coal
is created by
rotation is
of vanes to
mixture less
auxiliary air

Secondary
through ad
the second
per cent op
70 deg op
direction ad
be admitted
between the
create a rot
The burner

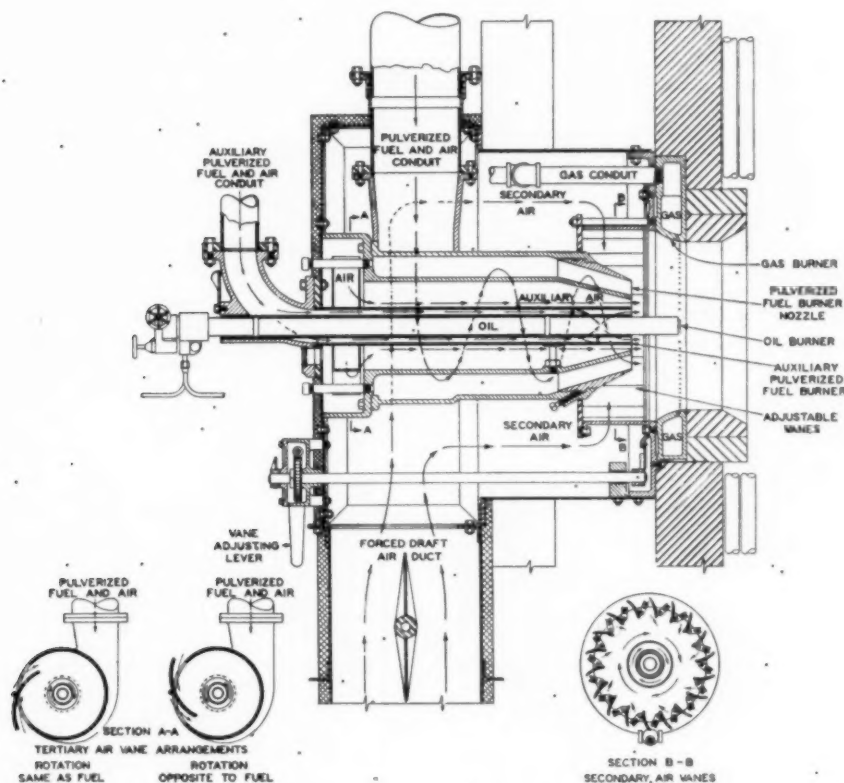


FIG. 2 GENERAL ARRANGEMENT OF HORIZONTAL INTERVANE BURNERS

of the turbulent type and may fire either pulverized coal or natural gas. However, at the time of these tests, natural gas was not yet available at the plant and only pulverized-coal-firing was investigated. The burners are supplied with pulverized coal by two ball-mill systems each containing two exhausters. The two lower inside burners and the two upper outside burners are part of one mill system, and the remaining burners are part of the other mill system. Each burner conduit is equipped with a shutoff valve which permits individual burners to be removed from service.

Fig. 2 shows the horizontal intervane burners which are used. Each burner contains two coal nozzles, a main nozzle, and a smaller auxiliary nozzle. This arrangement is designed for the purpose of extending the load range per burner. The primary air and coal leaving the main nozzle has an angular velocity which is created by the tangential inlet to the burner body. A similar rotation is given to the coal leaving the auxiliary nozzle by means of vanes located near the outlet. The velocity of the primary mixture leaving these nozzles may be varied by use of the auxiliary air dampers which are located in the exhauster inlets.

Secondary air for combustion is admitted to the burner throat through adjustable vanes which control the angular velocity of the secondary air. These vanes are adjustable from 0 to 100 per cent open, which corresponds to an actual range up to about 70 deg open. The rotation of the secondary air is in the same direction as that of the primary mixture. Tertiary air also can be admitted to the burner throat through the annular space between the coal nozzles and controlled by an adjustable vane to create a rotation either with or against the rotation of the burner.

The burner adjustments mentioned provide means of changing

the flame shape and furnace conditions. The effects of the various adjustments are as follows:

1 When the secondary-air vane opening is increased at a constant air flow, the following takes place:

- (a) The ignition zone moves away from the burner tip.
- (b) The flame is lengthened and the flame angle reduced.
- (c) The burner-box pressure is reduced.
- (d) The angular velocity of the fuel-air mixture leaving the burner throat is decreased.
- (e) The mixing of the fuel and air is changed.

When the secondary-air vane opening is decreased at a constant air flow, the following occurs:

- (a) The ignition zone moves closer to the burner tip.
- (b) The flame is shortened and the flame angle increased.
- (c) The burner-box pressure is increased.
- (d) The angular velocity of the fuel-air mixture leaving the burner throat is increased.
- (e) The mixing of the fuel and air is changed.

2 When the tertiary air is used with rotation of the burner the flame is lengthened, and conversely, when used against rotation the flame is shortened.

3 When the auxiliary air damper is opened, the burner velocities are increased and the ignition zone moves away from the burner tip.

From the foregoing it will be seen that changes in air flow can change flame shape, depending upon whether the air flow is varied at constant secondary-air vane opening, constant burner-box pressures, or by changes to both vane opening and burner-box pressure.

In order to measure the rate of heat absorption at various representative locations and thereby establish the distribution of heat absorption in the furnace, we installed 128 thermocouples on the furnace-face center line of various waterwall tubes and at various elevations throughout the furnace. This installation was made during the erection of the unit and at the locations shown in Fig. 3, which is a development of the furnace walls as viewed from the "outside" of the furnace. It can be seen that the thermocouples were installed in several bands around the furnace and arranged to give coverage of as nearly equal areas as possible. It will also be realized that it was impossible to divide the projected areas of the waterwalls into exactly equal areas due to existing interference caused by tiebacks, beams, and the like. Since it was not felt that it was possible to install thermocouples on the upper rear-wall sloped section and obtain an installation which would be reliable throughout an extended test period, these thermocouples were omitted. Therefore this section of the rear wall is not represented satisfactorily or covered by the

furnace-face thermocouples. In this particular area the tubes are backed with $2\frac{1}{2}$ in. of tile, the back of which is exposed to high-temperature gases passing through the superheater. It will also be noted that there are no thermocouples installed on the slag-screen tubes, since these tubes receive convection transfer as well as radiant transfer from the flame and furnace gases. However, aside from these areas, the furnace-face thermocouples were installed to give fairly complete coverage and relatively equal area coverage per thermocouple. Four additional thermocouples were installed on the back of individual rear waterwall tubes at approximate elevation 463 ft. These thermocouples were then used as a base indication of the temperature of the mixture within the tube.

Fig. 3 also shows the numbering of thermocouples, location of furnace observation doors, and details of the installation. The numbering shown here is the instrument numbering of the various thermocouples and is used throughout the subsequent data and curves. The thermocouples were installed substantially as

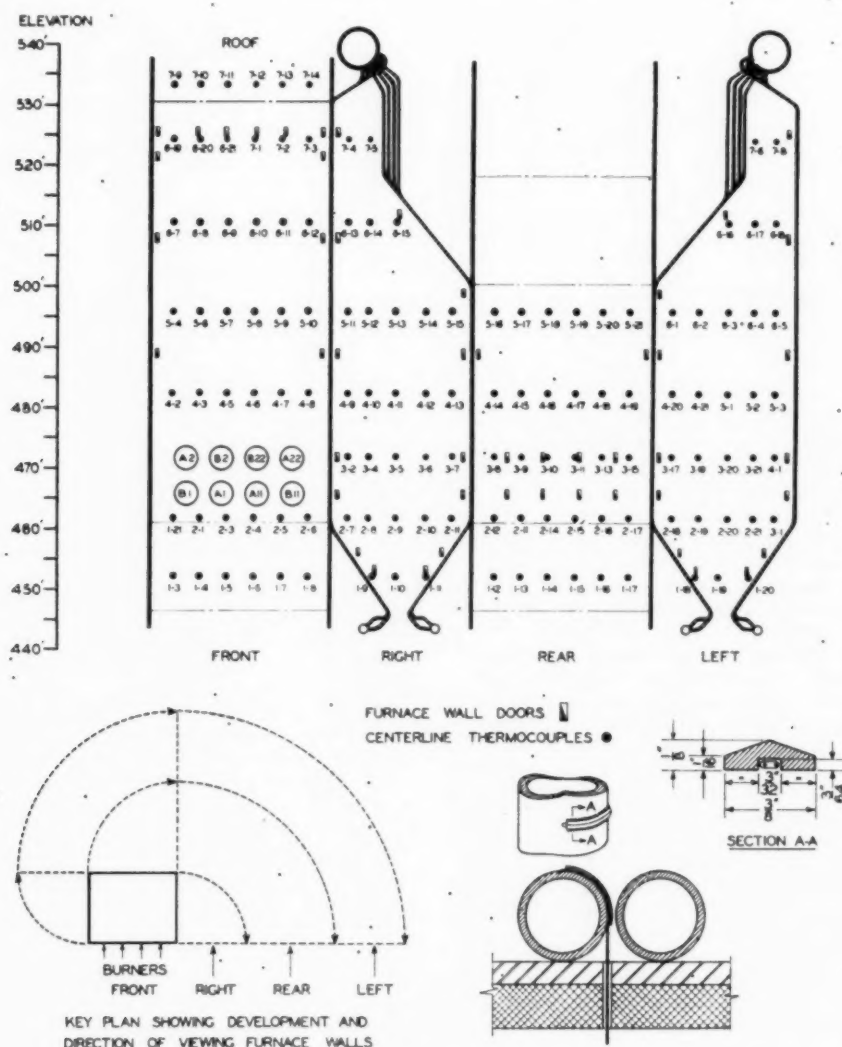


FIG. 3 KEY PLAN AND THERMOCOUPLE LOCATION IDENTIFICATION DIAGRAM

describe
factorily
thermoc
face of
sulated.

The
data was
speed po
Tidd tes
perienced
the com
corder.
has purpo
lead wire
ment was
seven gro

Thermo
groups fr
which is
chart and
time. Th
the 147 p
mately 30
it was pos
decrease
cycle with
so since t
small to w
instrumen
floor.

The te
series of
The first

FIG. 4 A

described by Humphreys (3), a method which was used satisfactorily on the previously described Tidd Station tests. The thermocouples were installed at the center line of the furnace face of the tubes and consisted of No. 22 gage, glass-fiber, insulated, chromel-alumel wire.

The instrument originally used to record the thermocouple data was the same 21-point Leeds & Northrup Micromax high-speed potentiometer-recorder which had been used during the Tidd tests. However, owing to the difficulties which were experienced with this original instrument on the first series of tests, the committee replaced the Micromax with a Speedomax recorder. The latter instrument is much more suited to our particular purpose since it has the ability to handle exceptionally high lead wire resistances at a high speed of recording. The instrument was supplemented by a switching unit which contained seven groups of 21 contacts each, or a total of 147 points.

Thermocouples were identified by numbering all of the seven groups from 1 to 21, inclusive. The group identification number, which is one of the 21 points, prints at the upper extremity of the chart and identifies the group being recorded at the particular time. The switching mechanism is entirely automatic and allows the 147 points (140 thermocouples) to be recorded in approximately 30 minutes or about 12 seconds per thermocouple. While it was possible to increase greatly the speed of recording and thus decrease the time interval required for recording a complete cycle with the latter arrangement, it was felt unnecessary to do so since the variations existing during the test period were too small to warrant the additional volume of data. Fig. 4 shows the instrument mounted in a convenient location on the operating floor.

DESCRIPTION OF TESTS

The test program at Paddy's Run Station consisted of two series of tests, each requiring about 10 days for completion. The first series of tests, containing test Nos. 1 to 14, inclusive,

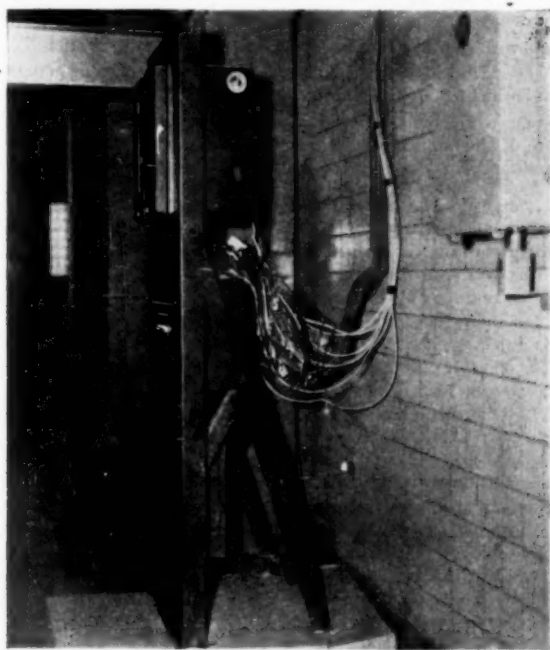


FIG. 4 VIEW OF L&N 140 POINT SPEEDOMAX RECORDING UNIT

were run in February, 1948. The second series of tests, containing test Nos. 15 to 30, inclusive, were run in October, 1948.

We are sorry to report that due to difficulties experienced with the original Micromax recorder, we did not obtain any thermocouple data of value during the first series of tests.

However, the heat-balance data taken on test Nos. 1 to 14, inclusive, did establish that flame shape has a definite effect upon furnace performance and warranted further investigation. It was also found that the effect of varying the amount of excess air for combustion on furnace performance was a very difficult factor to isolate. On this series of tests, the committee attempted to investigate the effect of changing excess air under as near to normal operating conditions as possible, which includes the adjustment of secondary-air vanes to obtain the most desirable furnace conditions. It was found that these adjustments to the secondary-air vanes affected the furnace performance obtained for various amounts of excess air. Hence it became apparent that our test program should include an investigation of the effect of flame shape on furnace performance, and also that the effect of variations in excess air, which were important, would have to be determined at constant secondary-air vane opening even though this is not normal operation. It is readily realized that it is impossible to measure flame shape, but it is possible to establish definitely the secondary-air vane opening and burner-box pressure. Since the secondary-air vanes control the flame shape over a wide range, the committee decided to investigate the effect of varying secondary-air vane opening.

The test program for the second series of tests as actually completed is shown in Table 1.

Originally, it had been hoped that it would be possible to run individual series of tests (those tests at the same load and excess air with different secondary-air vane openings) consecutively, on the same test day, in order to determine the effect of varying vane opening with a minimum change in operating conditions, such as accumulation of ash on furnace walls. However, in actually running the tests it was found that the time necessary to establish equilibrium at the desired operating conditions made it impossible to complete three tests in a reasonable test day, and it was also found that the accumulation of ash on the furnace walls did not vary greatly during the entire test period.

It was also necessary to eliminate test Nos. 20 and 23, owing to insufficient time available in the test schedule.

Prior to each test period the retractable soot blowers, located between the slag screen and the first row of superheater elements, were blown, as well as the air-heater soot blowers. No other efforts were made to clean the unit prior to tests since the furnace remained relatively clean.

TABLE 1 TEST PROGRAM FOR SECOND TEST SERIES

Test no.	Date	Heat input to furnace, per cent full load	Excess air at furnace outlet, per cent	Secondary-air vane position, per cent open	No. of burners in service	Duration of test, hr
15	10/22/48	93.2	23.0	40	8	4.0
15A ^a	10/27/48	91.6	24.8	40	8	4.5
16	10/22/48	92.2	25.0	60	8	4.0
17	10/28/48	92.3	26.2	50	8	4.0
18	10/28/48	90.6	16.9	40	8	5.0
19	10/20/48	89.5	17.0	60	8	4.0
21	10/25/48	92.8	29.7	45	8	4.0
22	10/25/48	92.3	30.2	60	8	4.0
24	10/24/48	68.7	21.4	35	8	4.0
25	10/24/48	68.9	23.4	50	8	4.0
26	10/24/48	69.0	24.5	65	8	5.0
27	10/27/48	50.2	23.6	30	8	3.75
28	10/30/48	49.3	21.7	50	4 upper	4.0
29	10/29/48	49.2	23.0	50	4 lower	4.0
30	10/30/48	49.5	21.5	50	2 upper and 2 lower	4.0

^a Test 15A was run under same conditions as test No. 15 and 5 days later as a check test.

When equilibrium was established at the desired test conditions, the instrument was placed in operation and all of the thermocouple data recorded, obtaining 8 to 11 complete cycles of temperature measurement for each test period. All board data and other pertinent data were recorded throughout the test period at regular intervals. One or two complete inspections of the furnace-wall surfaces were made during each test period to establish furnace cleanliness conditions. We also took a pulverized-coal fineness sample from each burner conduit during the test period in accordance with the ASTM Code for Pulverized Coal Sampling.

METHODS OF ANALYZING TEST DATA

Distribution of pulverized-coal flow to the various burners was determined by using the pulverized-coal fineness samples as a measure. In taking these samples, we traversed all burner conduits from two directions without changing the cyclone-vent position, once it had been set to provide the correct average recovery rate. Therefore the weight of sample collected in each conduit, divided by the total weight of sample collected from all burner conduits, was considered representative of the distribution of pulverized coal between burners. It is of interest to note how well the distribution of coal flow between mill systems, as measured by this method, checks that determined by use of the coal scales. Table 2 shows the comparison of total flow to the A-mill system by both methods.

TABLE 2 COMPARISON OF COAL FLOW TO A-MILL SYSTEM BY DIFFERENT METHODS

Test no.	Per cent of total coal flow to A mill (coal scales)	Per cent of total flow to A mill (fineness samples)
15	48.2	50.5
15A	49.4	48.6
16	49.9	49.7
17	49.6	50.1
18	47.5	47.6
19	46.2	45.8
21	47.9	47.8
22	48.5	49.1
24	50.3	51.2
25	51.0	52.5
26	50.0	50.3
27	50.0	50.3
28	50.5	47.6
29	43.3	43.6
30		

The ΔT -value referred to on these tests is the difference between the temperature of the exposed surface of the furnace-wall tube, measured on the tube center line at various locations, and the average temperature of the mixture within the tube, as indicated by the base thermocouples.

The distribution of heat absorption over the furnace walls has been represented by Figs. 5 to 19, inclusive, by use of isothermal ΔT -diagrams. Each diagram is actually a development of the furnace walls as viewed from "outside of the furnace." The ΔT -values shown on these particular diagrams use the saturation temperature at drum pressure, correcting for difference in elevation, as the average temperature of the mixture within the tube. While the base used does not affect the distribution of heat absorption, these ΔT -values may be changed to the thermocouple base by applying the correction noted under each isothermal ΔT -diagram. It has been found that the base thermocouples provide a better indication of the temperature of the mixture within the tube than is obtained by using the saturation temperature. The small arrows indicated on the circles representing burner openings in the front wall denote the rotation of the fuel mixture leaving the particular burner throat. Important test conditions are also noted on each diagram.

Ash-coverage diagrams are also included in Figs. 5 to 19, inclusive, to represent the ash conditions observed on the furnace

walls during each test period. Fig. 20 must be used in conjunction with these ash-coverage diagrams, since it describes various types of ash found and referred to on the ash-coverage diagrams. Each area, on the diagram, contains the authors' estimate of the per cent coverage, average depth of ash, and type of ash. The locations of observation doors used for these furnace observations are also shown. The small arrows represent a general indication of the direction of gas flow noted at various points throughout the furnace. We have also attempted to indicate an approximate flame angle leaving the burner throats for all tests.

The distribution of heat absorption over the height of the furnace is represented for various series of tests in Figs. 22 to 28, inclusive. This distribution is shown by plotting the average ΔT of all thermocouples located at a particular elevation against the height of the furnace in feet above the center line of the hopper throat. Average rate of heat absorption at the various elevations may be approximated by multiplying the average ΔT -value by a factor of 1060 Btu/(sq ft) (hr) (deg F).

The ΔT -values obtained for these tests do, of course, present a means of estimating the total amount of furnace heat absorption if certain assumptions are to be made. However, any such calculations are subject to many possible errors, some of which are constant and others variable. Some of the inherent errors, which must be remembered whenever considering results obtained from such calculations, are as follows:

- Possible variation of true temperature measurement with the age of the thermocouple.
- Errors due to the effect of ash accumulating at the thermocouple location and not on the surrounding surface, caused by the protective shield, and thus not giving an accurate temperature measurement of the exposed surface represented by the thermocouple.
- Variations of the internal cleanliness of the tube.
- Variations of inside-film conductance under various conditions of load and internal cleanliness.
- Errors caused by improper weighting of thermocouple data with respect to the surface represented.
- Errors due to the impossibility of covering adequately the entire projected area of the furnace waterwalls.
- Errors due to the difficulty in obtaining the true temperature of the mixture within the tube at the many thermocouple locations.

It also must be recognized that a 1-deg error in temperature measurement can result in an 8 per cent error in the furnace heat-absorption results at 50 per cent full load.

However, we have made calculations using assumptions similar to those used by Schueler (2).

The thermal conductivity of the tube metal was assumed to be 348 Btu/(sq ft-hr)/in., and by using the tube OD of 3 in. with an average ID of 2.524 in., we obtained a value for metal conductance of 1342 Btu/(sq ft) (hr) (deg F) when referred to the OD of the tube. A film conductance was assumed to be 5000 Btu/(sq ft) (hr) (deg F) when referred to the OD of the tube. The over-all conductance through the tube metal and film was then calculated to be 1060 Btu/(sq ft) (hr) (deg F). The total projected area of the furnace is 8884 sq ft, which includes the projected area of all waterwall surface in the furnace above the hopper throat and the projected area of the outlet aperture.

Total furnace heat absorption was then determined by the following equation:

$$\text{Absorption} = U_a S \Delta T, \text{ Btu per hr}$$

where

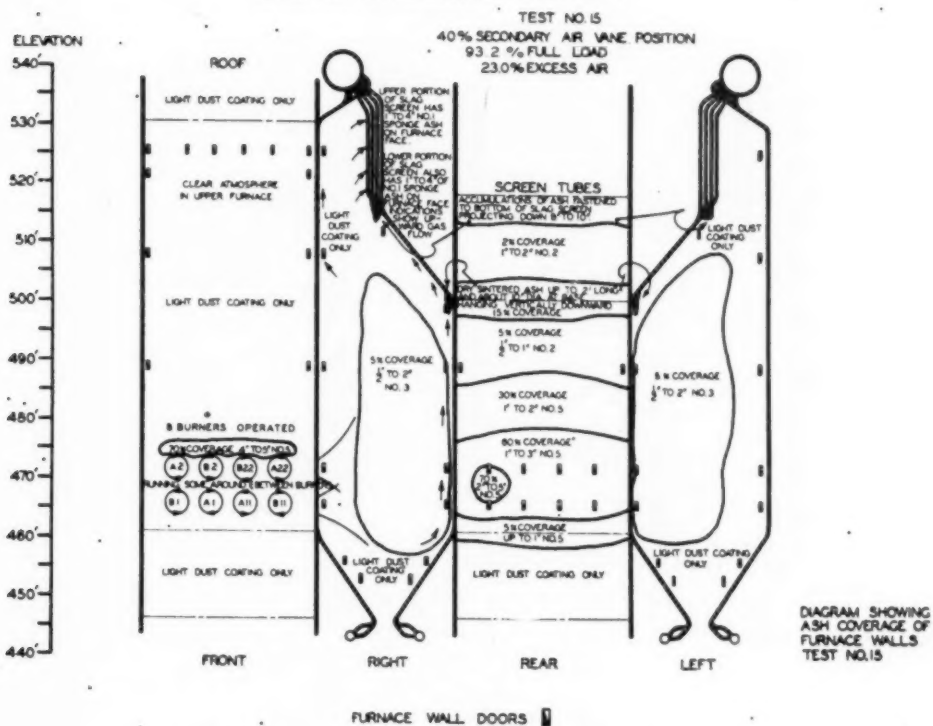
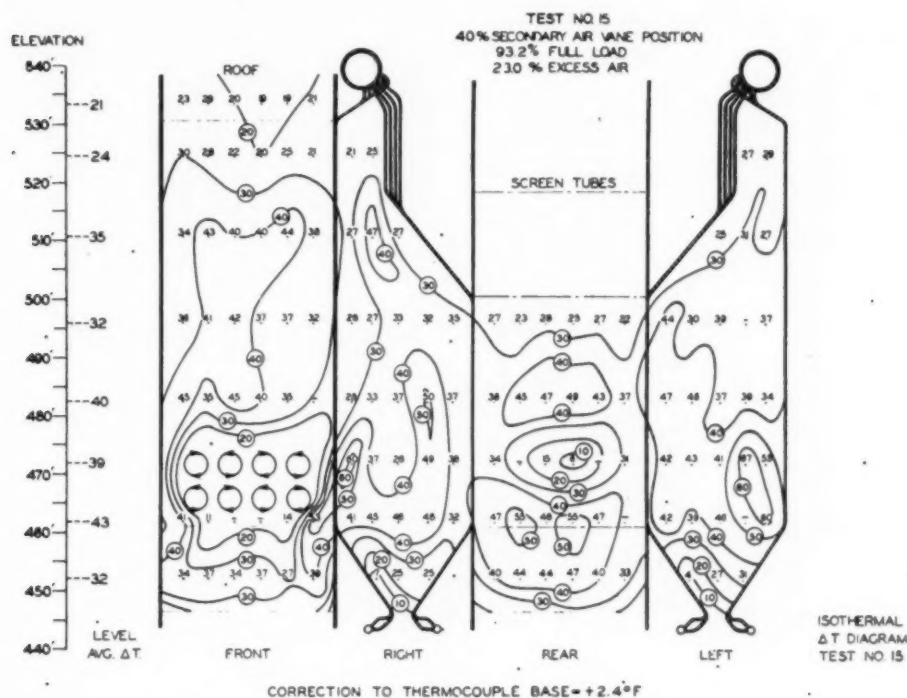
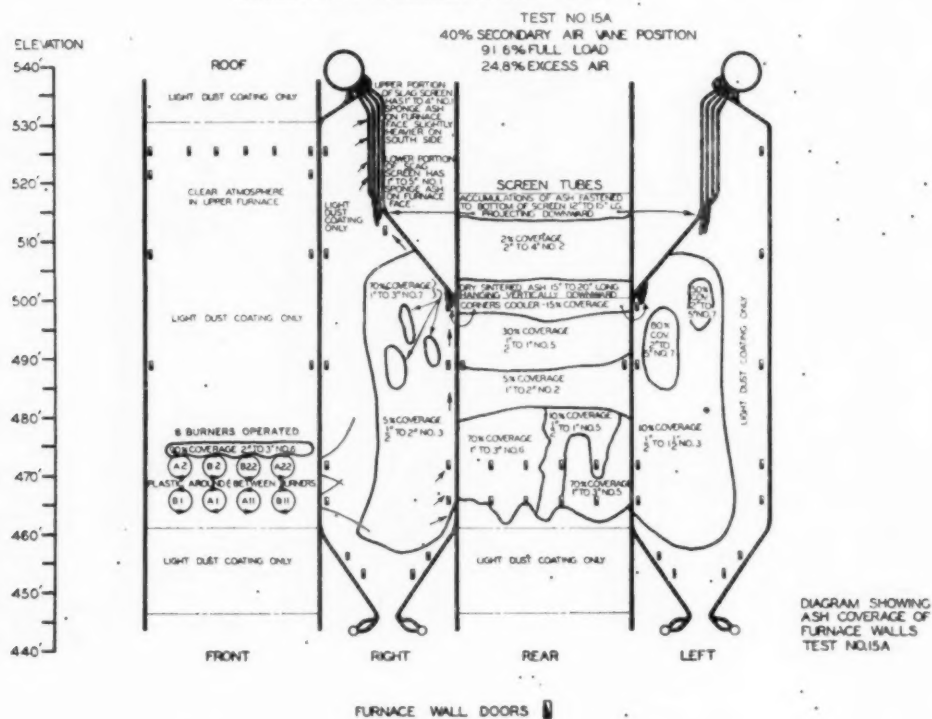
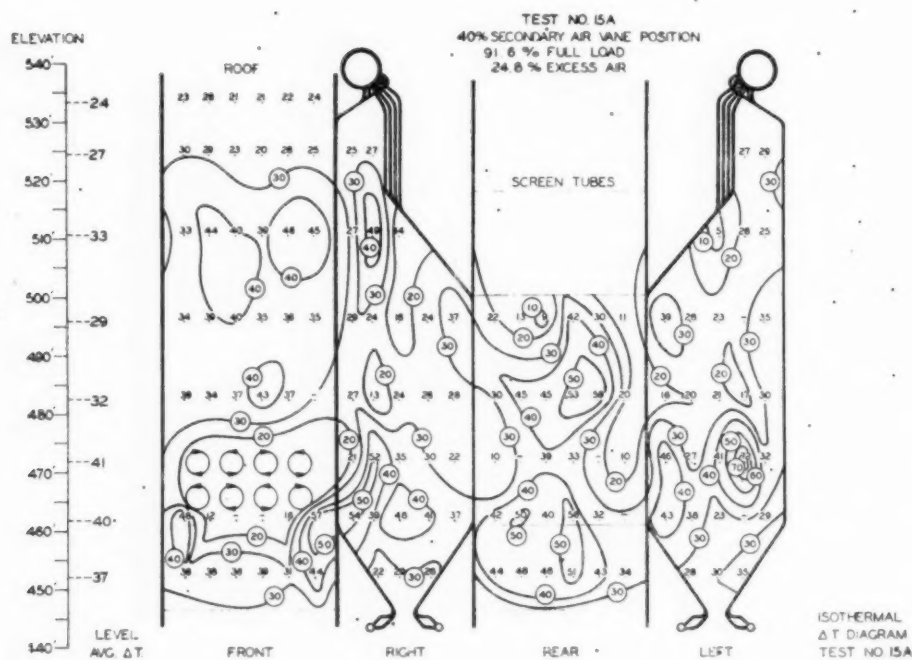
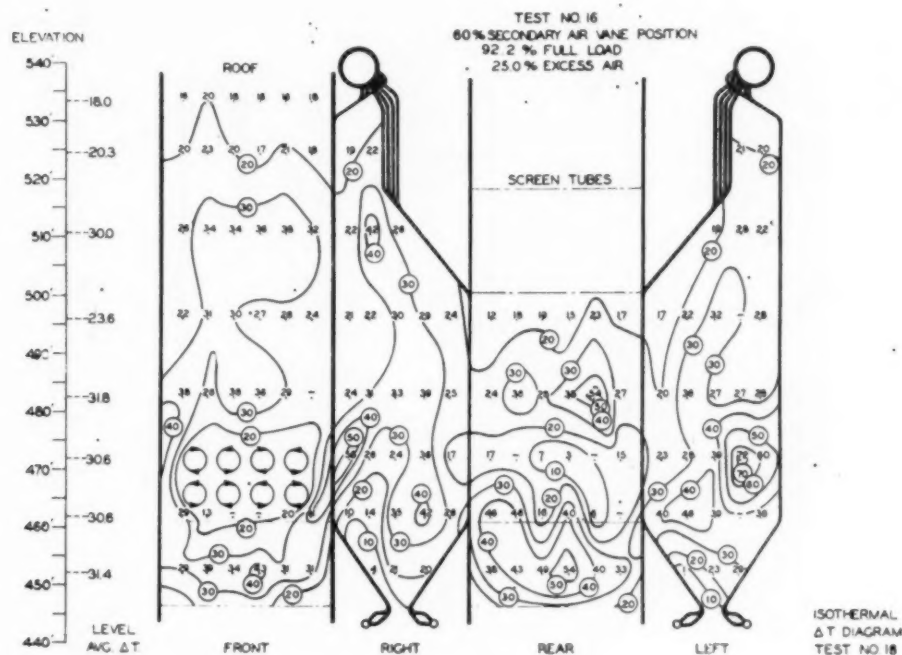


FIG. 5 ISOTHERMAL ΔT AND ASH-COVERAGE DIAGRAM TEST NO. 15

FIG. 6 ISOOTHERMAL ΔT AND ASH-COVERAGE DIAGRAM TEST NO. 15A



CORRECTION TO THERMOCOUPLE BASE = +3.0°F

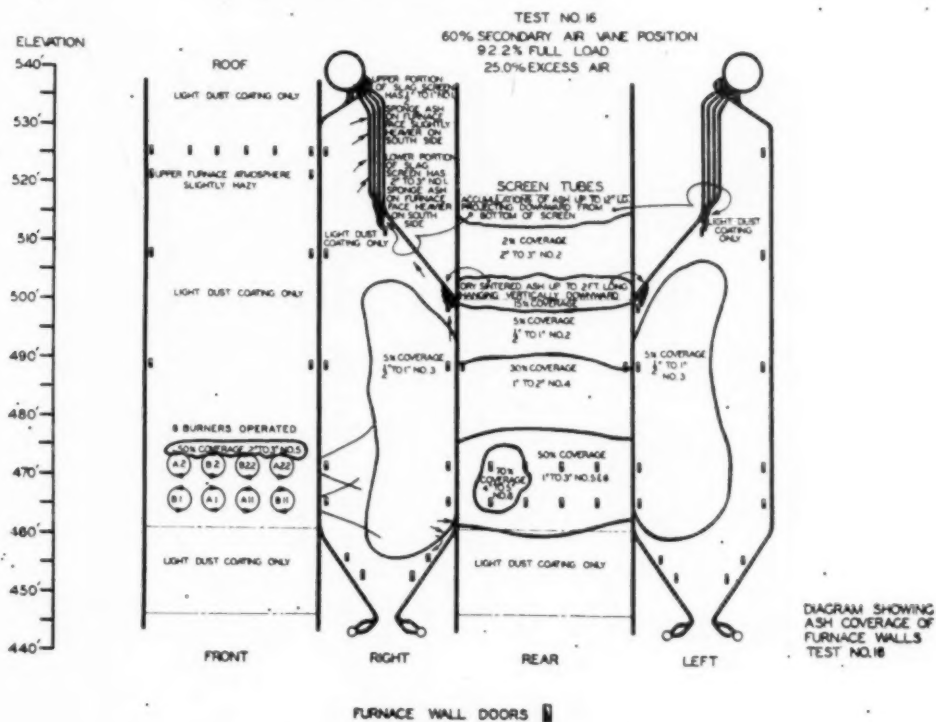
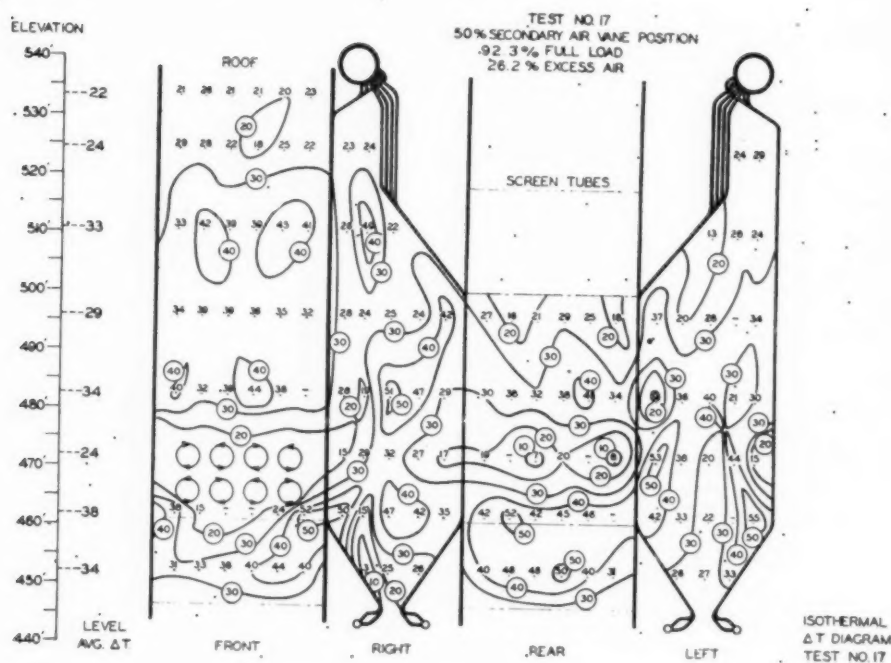
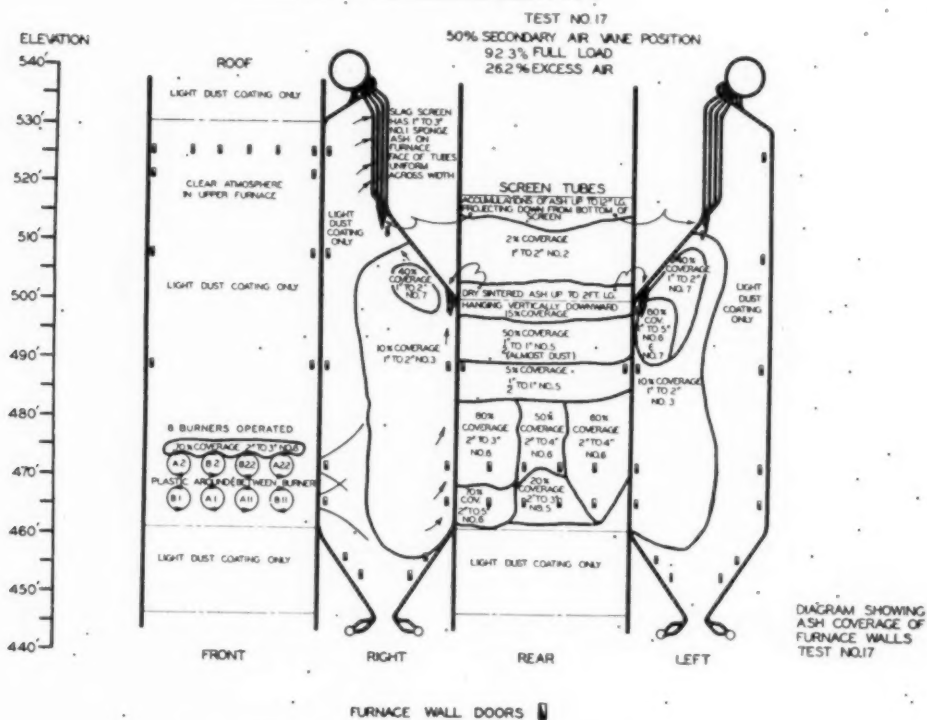
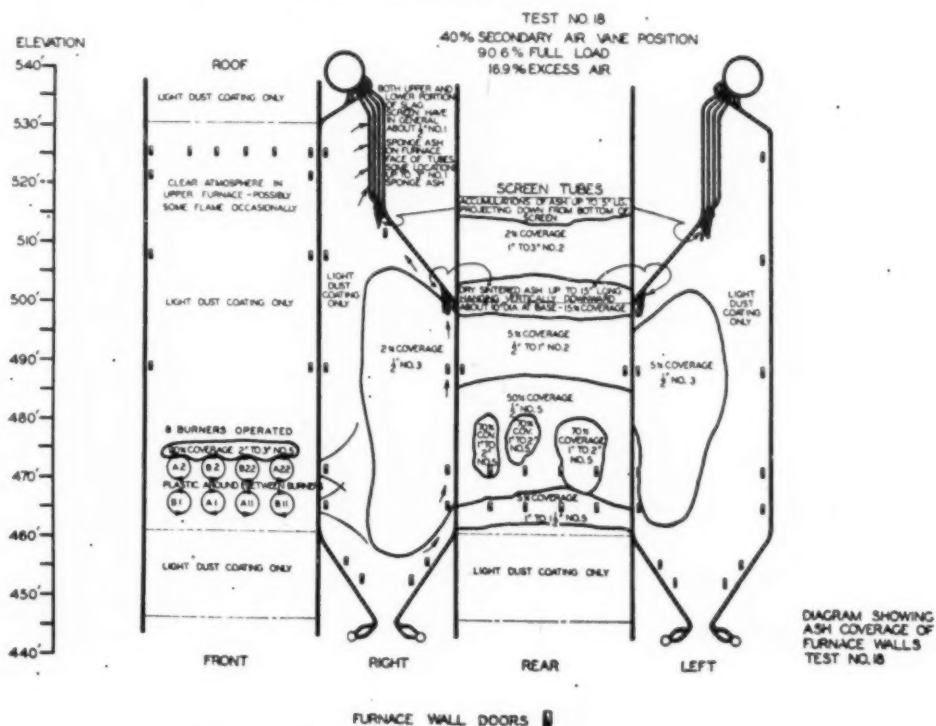
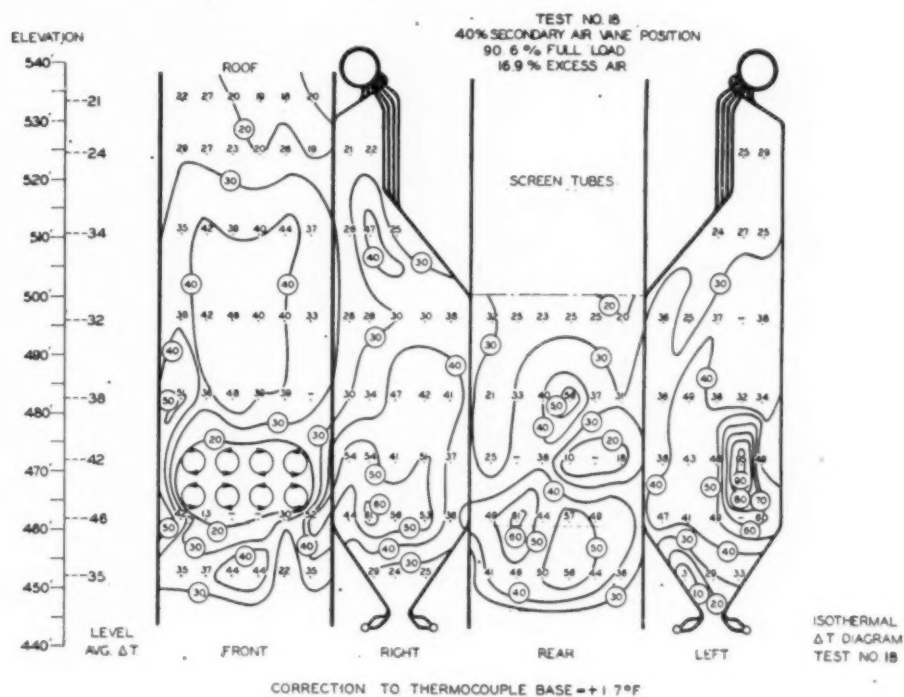


FIG. 7 Isothermal ΔT and Ash-Coverage Diagram Test No. 16



CORRECTION TO THERMOCOUPLE BASE = +1.4°F

FIG. 8 ISOTHERMAL ΔT AND ASH-COVERAGE DIAGRAM TEST NO. 17

FIG. 9 Isothermal ΔT and Ash-Coverage Diagram Test No. 18

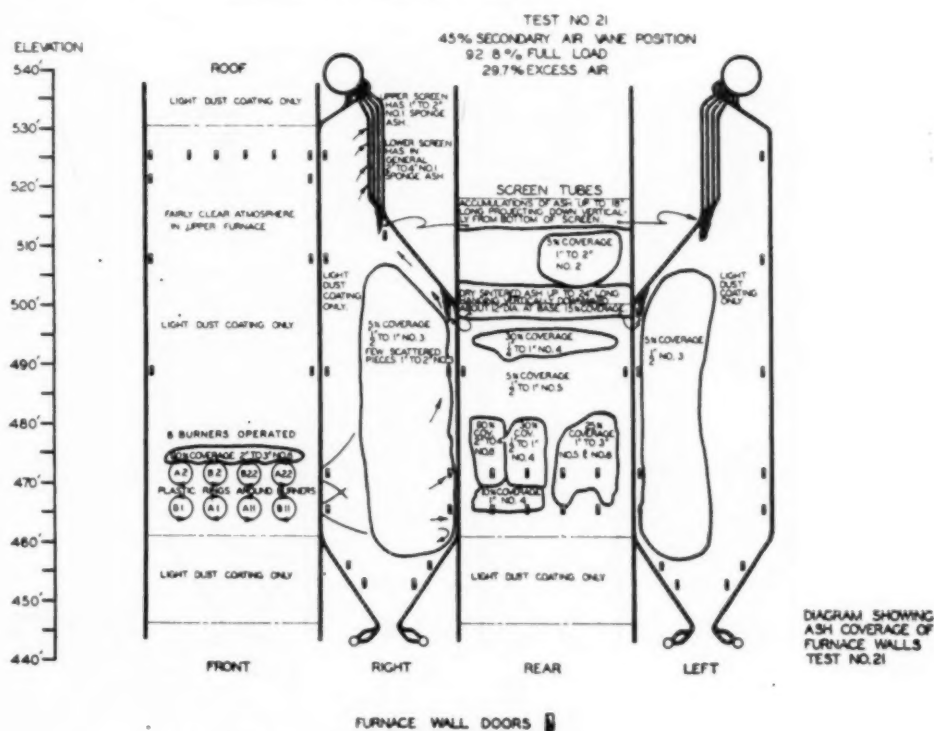
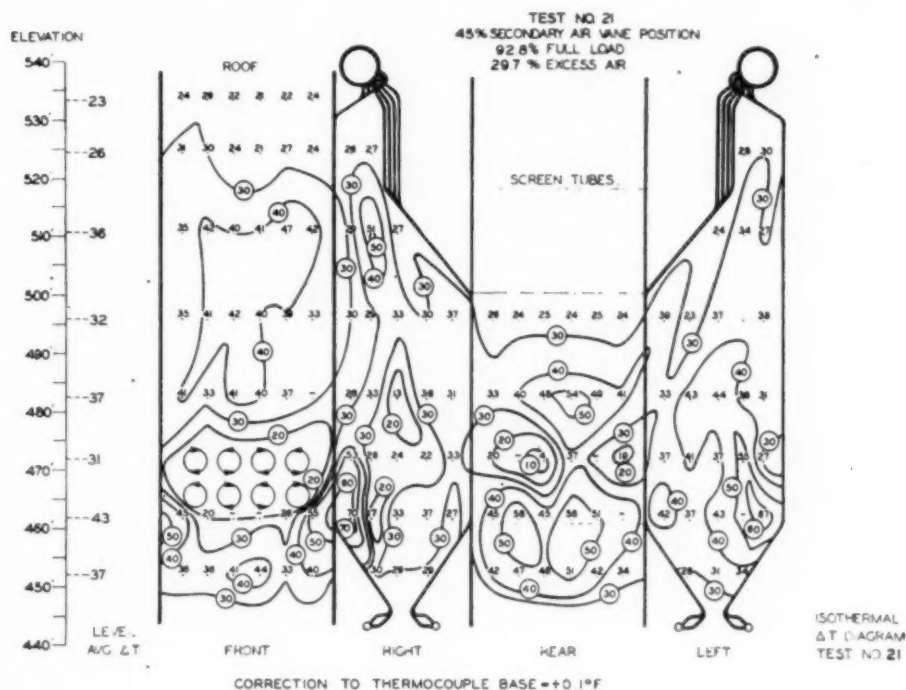
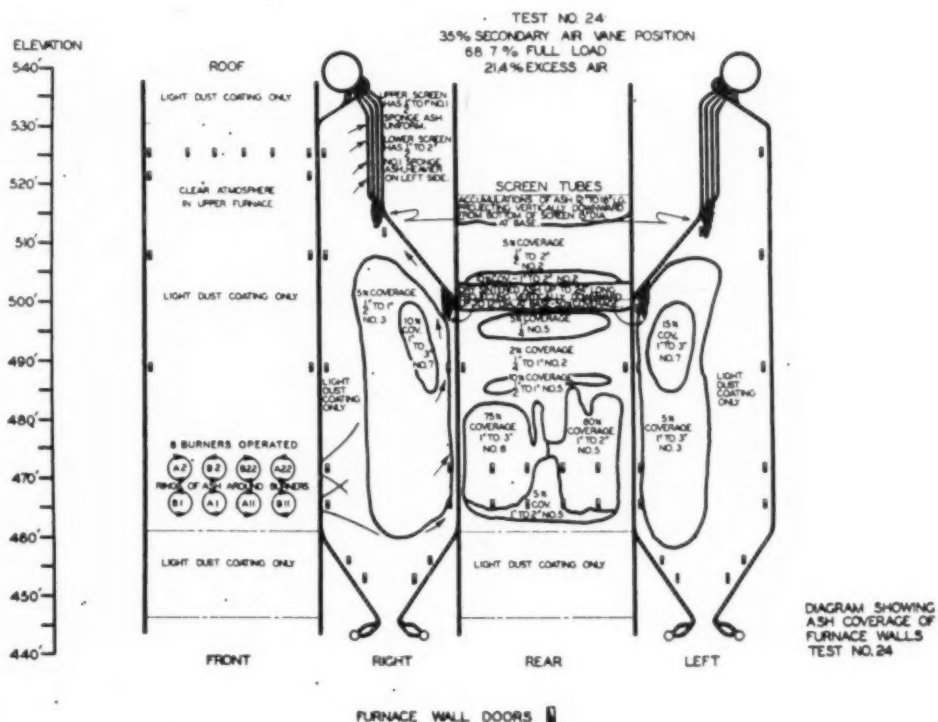
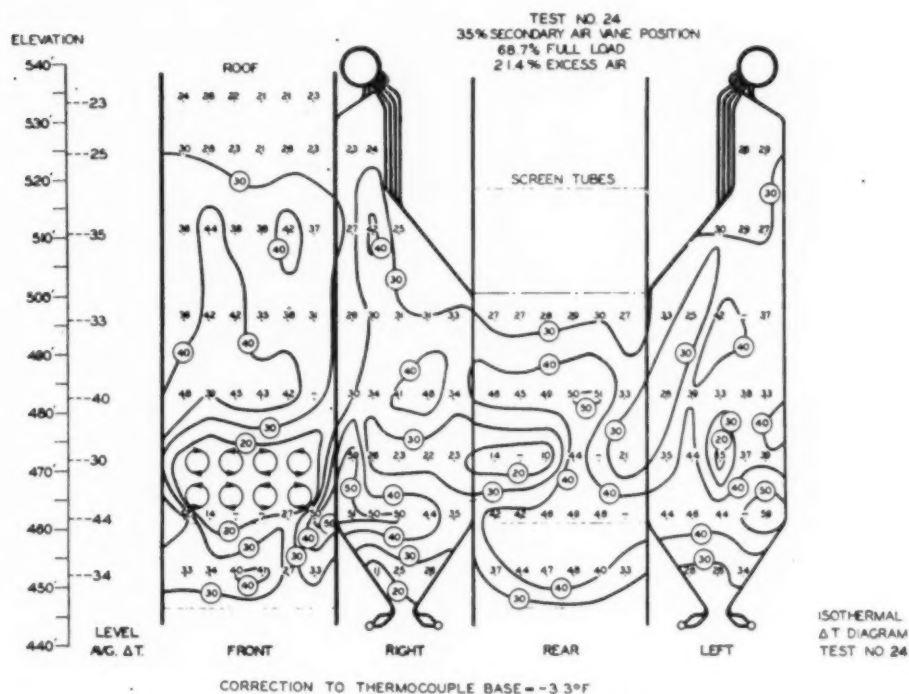
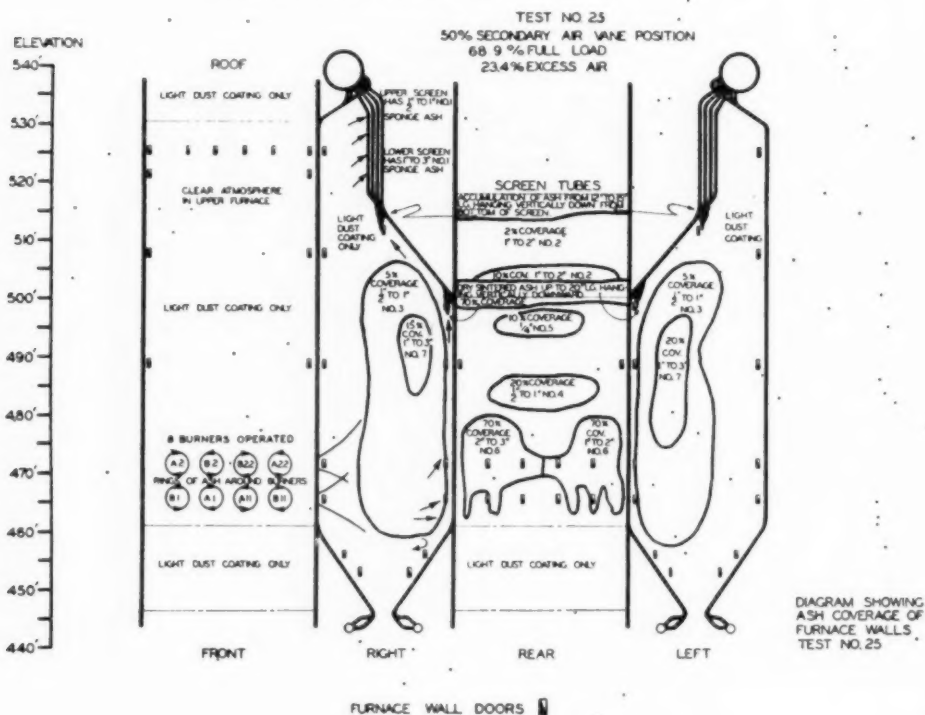
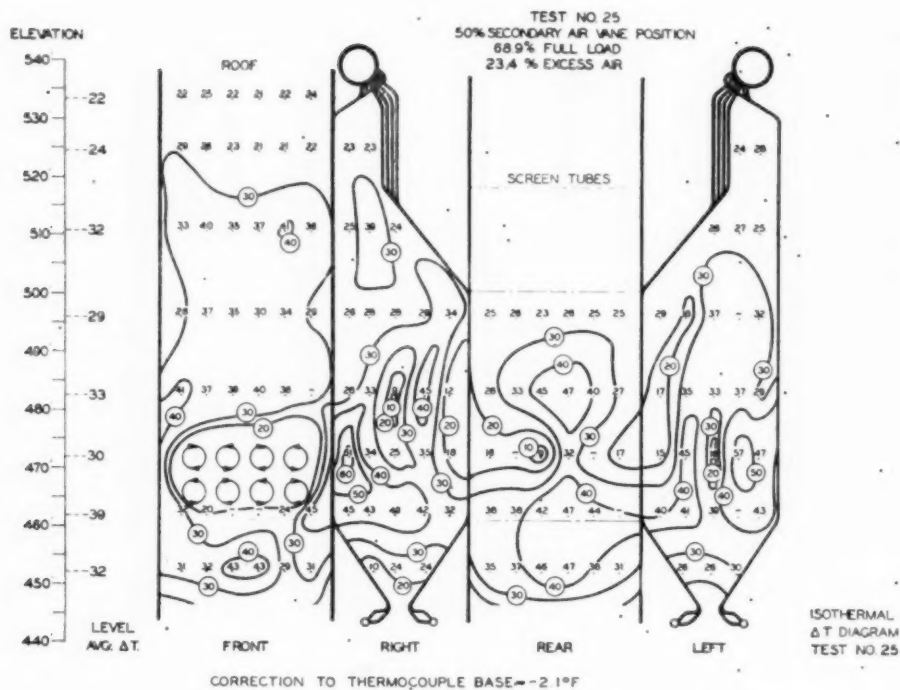
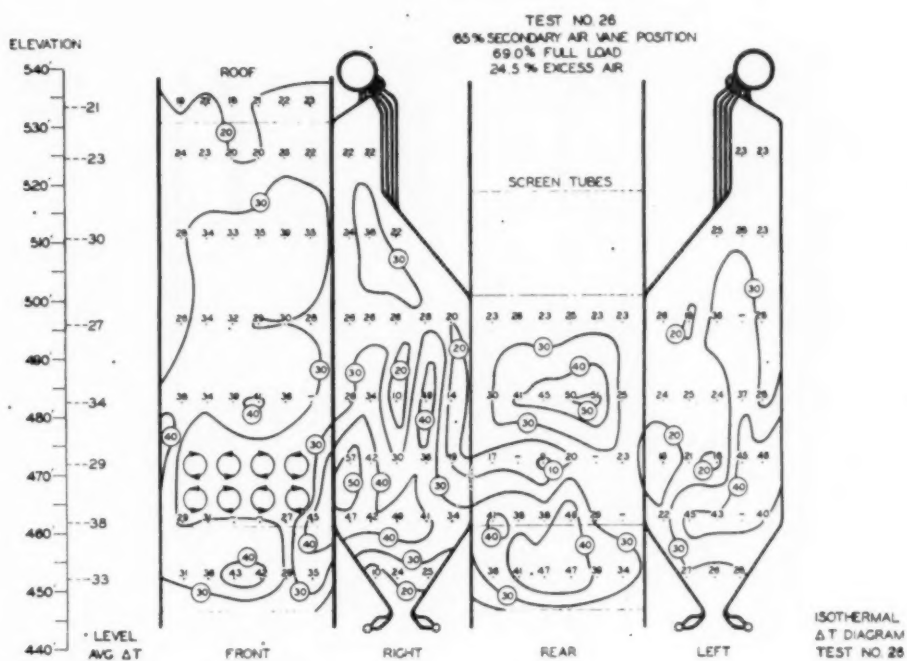
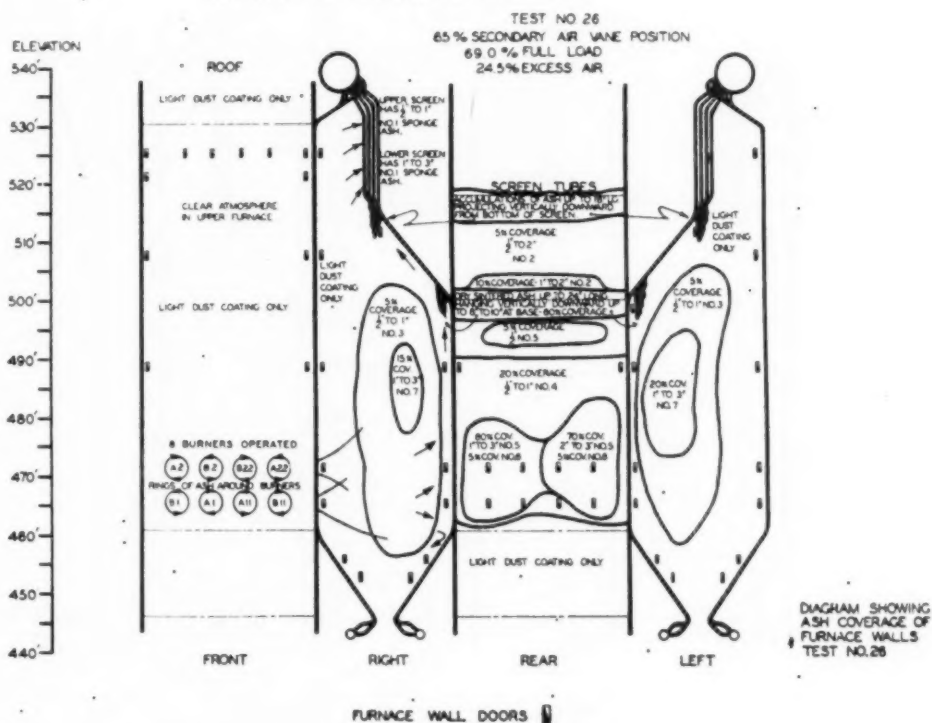


FIG. 11 Isothermal ΔT and Ash-Coverage Diagram Test No. 21

FIG. 13 ISOTHERMAL $\dot{\Delta T}$ AND ASH-COVERAGE DIAGRAM TEST NO. 24

FIG. 14 Isothermal ΔT and Ash-Coverage Diagram Test No. 25

CORRECTION TO THERMOCOUPLE BASE -10°F FIG. 15 • ISOTHERMAL ΔT AND ASH-COVERAGE DIAGRAM TEST NO. 26

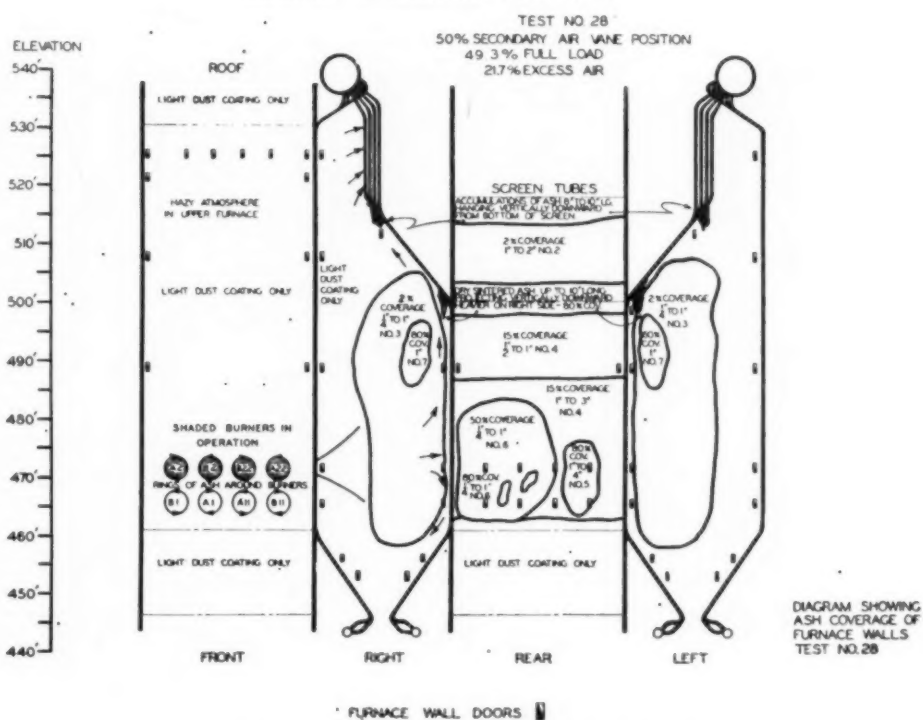
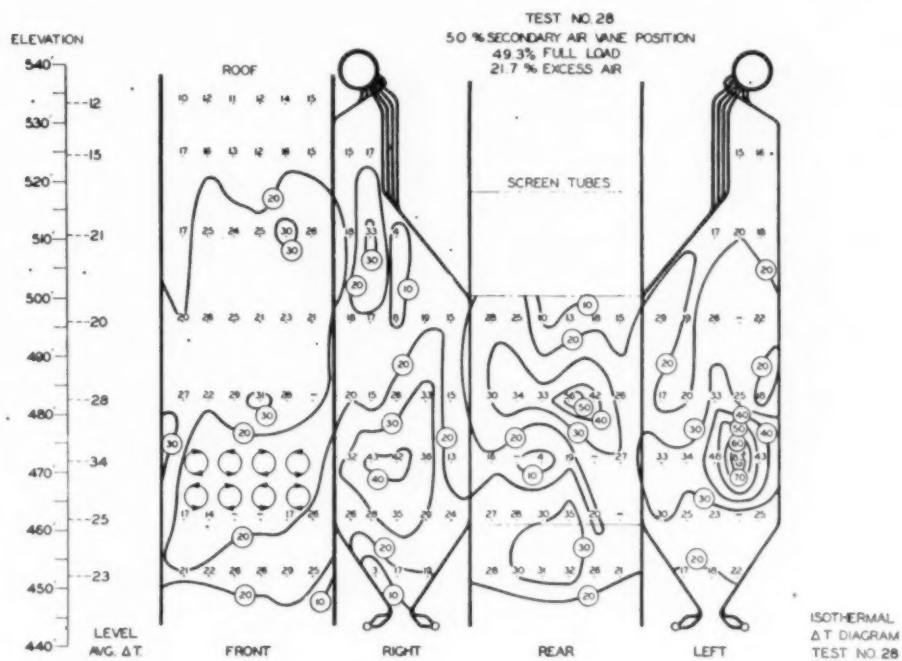
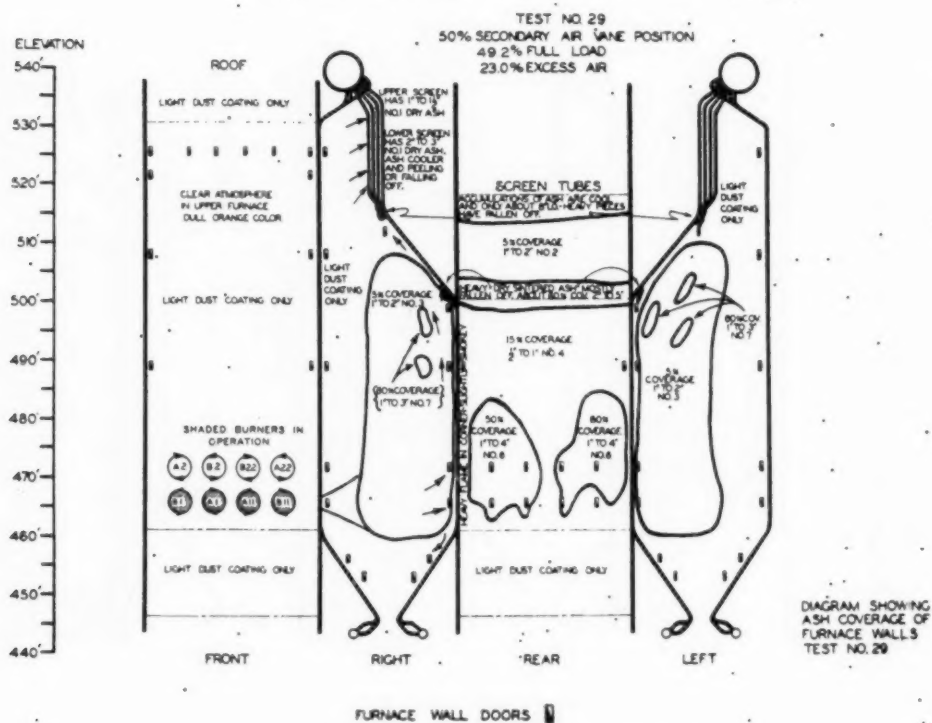
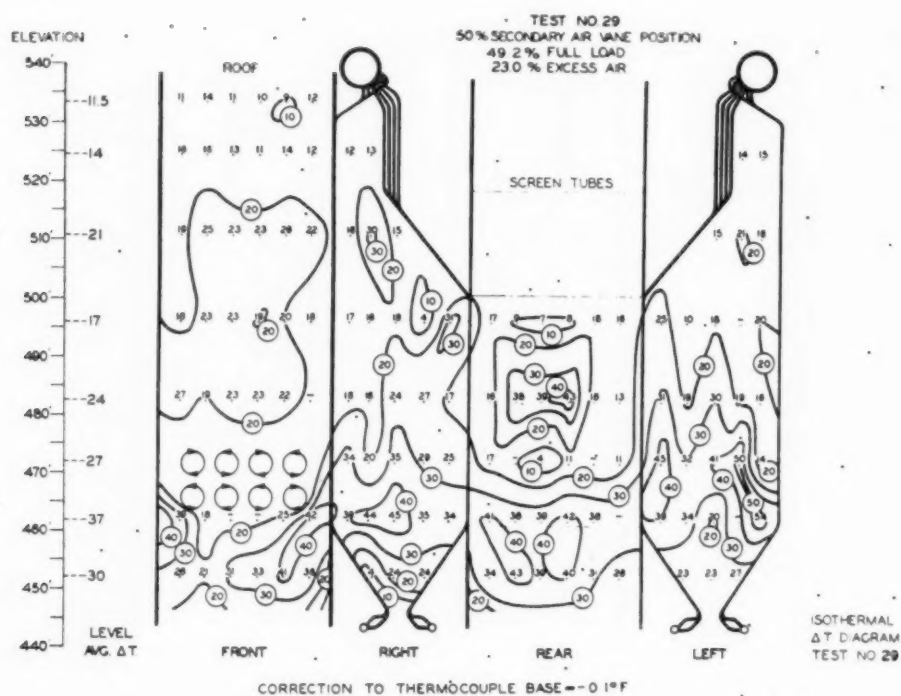


FIG. 17 Isothermal ΔT and Ash-Coverage Diagram Test No. 28

FIG. 18 ISOTHERMAL ΔT AND ASH-COVERAGE DIAGRAM TEST NO. 29

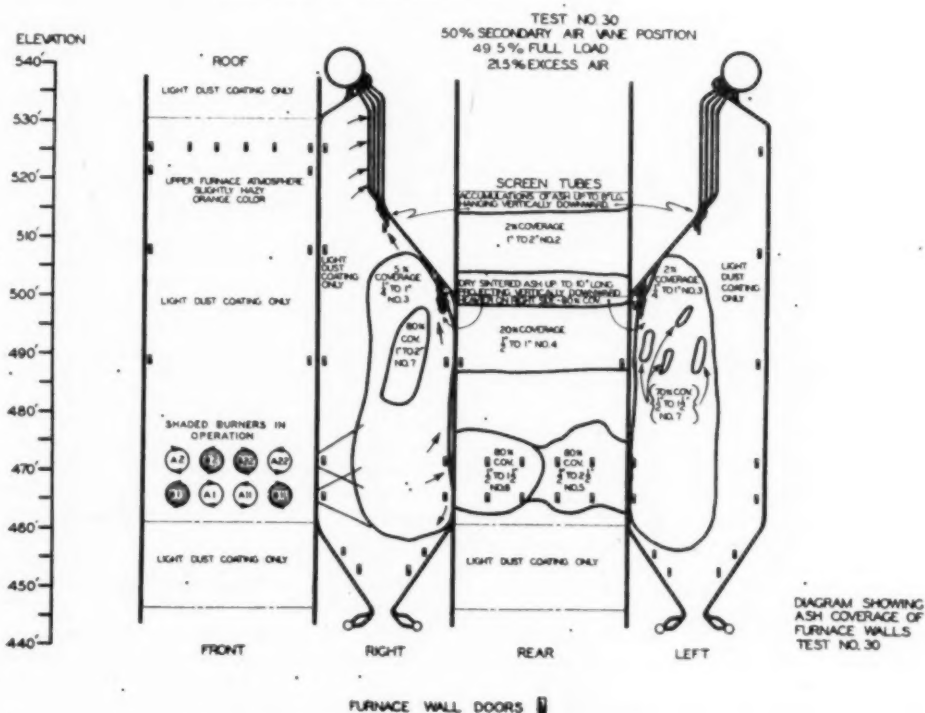
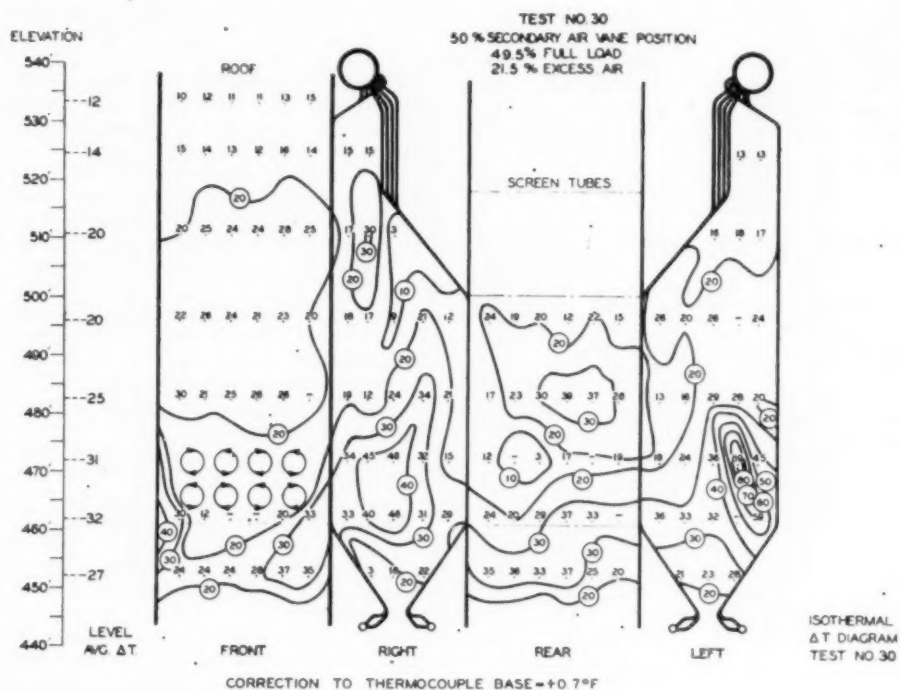


FIG. 19 Isothermal ΔT and Ash-Coverage Diagram Test No. 30

U_o = over-all conductance of metal and film = 1060 Btu/(sq ft) (hr) (deg F)

S = total projected area of furnace surface = 8884 sq ft

ΔT = average difference in temperature between surface at furnace-face center line and temperature of mixture within tube as indicated by base thermocouples

$$\begin{aligned} U_o S \Delta T &= 1060 \times 8884 \times \Delta T \\ &= 9,417,000 \times \Delta T, \text{ Btu per hr} \\ &= 9.417 \times \Delta T \text{ MKB per hr} \end{aligned}$$

Furnace heat-absorption efficiency then becomes

$$\text{Efficiency} = \frac{9.417 \times \Delta T}{\text{Net heat available to furnace}} \times 100$$

The value of heat absorption for the ΔT method has been determined for each complete test as well as furnace heat-absorption efficiency. Fig. 21 shows a comparison of the furnace heat absorption as obtained from the ΔT -results with the furnace heat absorption as determined by heat-balancing the furnace. This curve shows that, in general, a fairly good correlation is obtained between the two methods.

ANALYSIS OF RESULTS

Table 3 shows the average of all board data and all other pertinent operating data, such as burner-box pressures, burner settings, pulverized-coal fineness, etc., taken during the tests.

Table 4 shows the distribution of pulverized coal between burners on each test in per cent of total coal flow to the furnace.

Table 5 shows the average value of ΔT obtained at each furnace-face thermocouple location.

Table 6 presents a summary of the important test conditions and results for all complete tests.

Figs. 5 to 19, inclusive, show the distribution of heat absorption in the furnace and furnace-wall cleanliness for all of the operating conditions studied.

Figs. 22 to 28, inclusive, show the distribution of heat absorption over the height of the furnace for all of the operating conditions, and these curves are arranged in groups to facilitate the study of the effect of the various operating variables.

Figs. 29 to 32, inclusive, show the furnace heat-absorption efficiency, as determined by the ΔT -results for all of the operating conditions studied.

Owing to the inherent errors involved in any calculations, based upon the ΔT -values, the analysis of these data necessarily must be qualitative. The curves have been drawn to indicate trends in the distribution of heat absorption and furnace efficiency for this particular furnace under the operating conditions studied.

Referring to the ash-coverage diagrams, it is found that, in general, the furnace walls remain relatively clean under all of the operating conditions investigated. The only furnace-wall surface which accumulated any appreciable amount of ash is that surface of the rear wall located directly opposite the burners. In this location the ash coverage varies with operating conditions and the surface periodically cleans itself. The ash coverage on the side walls is negligible and is confined to small fingers which project out from between the tubes toward the direction of gas flow. The front-wall surface has no ash coverage other than a light dust coating about $1/16$ in. thick. Heavy formations of ash somewhat similar to stalactites were found hanging vertically down from the bottom of the slag-screen opening on all tests. These formations varied in size for the different tests since their accumulated weight occasionally would cause them to break away and fall to the ash pit. The average diameter of these formations at their base was 8 to 10 in. and their length approximately 12 to 18 in. They were held in place by their base, form-

ing at the location where the rear-wall tubes were bent out of line to form the slag screen. Similar ash formations were found at the bottom of the rear-wall sloped section. Here the ash appeared to be dry and sintered and again built up until the accumulated weight caused it to break away. These pieces were of the same general size as described previously and could be broken off easily. It is possible that a small eddy was located in this corner of the furnace and aided the growth of these formations.

Referring to the isothermal ΔT -diagrams, it may be seen that zones of relatively high absorption rates existed in that area of the side walls adjacent to the burners under all operating conditions. These zones, in general, indicated absorption rates in the vicinity of 50,000 to 75,000 Btu/(sq ft-hr), whereas the average absorption rate for the entire furnace is approximately 40,000 to 45,000 Btu/(sq ft-hr) at full load. The absorption rates found in these zones for some operating conditions are probably higher than those experienced in the normal operation of this furnace, since normally the secondary-air vanes are adjusted as required to obtain the optimum furnace conditions with no flame impingement. On these tests we used the vane adjustments to provide changes in flame shape so that we might study its effect upon furnace performance.

The sloping section of the rear wall which forms part of the ash hopper also showed relatively high heat-absorption rates in all cases, apparently due to the cleanliness of the surface in this area and the fact that this surface has an excellent "view" of the flames. The heat absorbed by the rear wall, where the surface is not affected by ash coverage, is generally higher than found on the other walls. The highest average absorption rates for any elevation are found in the lower part of the furnace and usually reach their maximum at the elevation just below the burners. The maximum might occur at the burner elevation if the furnace-wall surface in this area were not affected by ash accumulations.

A wide variation in absorption rate is found at the burner elevation for the various operating conditions studied, again indicating that this area is affected by ash accumulation which varies with operating conditions, or cleans itself periodically. On the curves representing the distribution of heat-absorption rates over the height of the furnace, it is found that the heat-absorption rates decrease in going to the higher furnace elevations, but that a second peak of increased absorption rates occurs in that part of the furnace where the cross-sectional area is reduced by the sloping section of the rear wall. Since this same characteristic is noted for all operating conditions, it seems that, at least partially, it is caused by an increase in convection transfer in this region due to the "scrubbing" action of the furnace gases against the wall surface as the cross-sectional area of the furnace is reduced. This is also shown by the isothermal ΔT -diagrams where zones of slightly higher absorption rates are found at this elevation on the side walls and the front wall.

The furnace heat-absorption efficiency was indicated to be approximately 41 per cent at full load, under normal operating conditions.

The effects of the various operating variables on distribution of heat absorption in the furnace and furnace efficiency are analyzed under separate headings which follow:

Effects of Varying Secondary-Air Vane Opening. Based upon our experience with these burners, we investigated this variable in the range of 40 to 60 per cent vane opening at full load and 35 to 65 per cent vane opening at 75 per cent full load. These ranges of vane opening provide sufficient variations in flame shape and still maintain satisfactory furnace conditions.

(a) 100 per cent full load—25 per cent excess air (test Nos. 15 to 17, inclusive): Under these conditions, it was found that the amount of ash accumulated on the rear wall opposite the

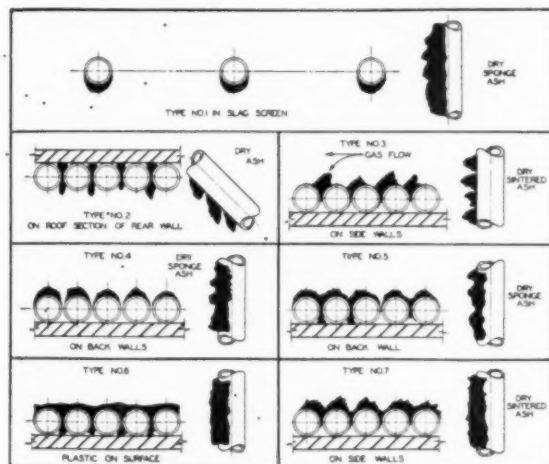


FIG. 20 KEY SHOWING VARIOUS TYPES OF ASH
(To be used with diagrams showing ash conditions on furnace-wall tubes.)

TEST NO.	HEAT-AVAILABLE		EXCESS AIR	SEC. AIR VANE POS	BURNERS
	MKB/HR	% FULL LOAD	%	% OPEN	
X 15	793.7	93.2	23.0	40	8
○ 15A	780.5	91.6	24.8	40	8
○ 16	785.2	92.2	25.0	60	6
△ 17	787.2	92.3	26.2	50	8

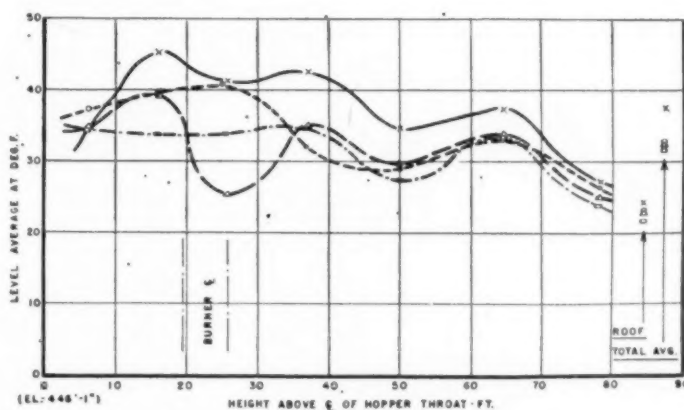


FIG. 22 FURNACE TUBE AVERAGE ΔT -VARIATION WITH LEVEL FOR THREE SECONDARY-AIR VANE POSITIONS
AT FULL LOAD AND ABOUT 25 PER CENT EXCESS AIR AT FURNACE OUTLET

burners increased slightly as the vanes were opened. This, of course, was accompanied by a decrease in absorption rate in this area. While the front-wall surface remains clean during these changes in vane opening, the heat absorbed by this surface decreased as the vanes were opened. The distribution of heat absorption in the side walls did not vary greatly, although there are some indications that the zones of relatively high absorption rates near the burners contain lower absorption rates at 50 per cent vane opening. Considering the distribution of heat absorption over the height of the furnace, it was found that at the 6-ft elevation there was little change in the average heat-absorption rates. However, between the 6-ft and 35-ft elevation, the heat absorption varied considerably for the different vane openings, apparently caused by the variations in ash coverage of the rear wall in this area. From elevation 35 ft to the top of the

furnace, the trends in absorption rates are the same for various vane openings, but the tests with the higher vane openings show lower absorption rates. The furnace heat-absorption efficiency decreased about 4 per cent as the vane openings were increased from 40 to 60 per cent.

(b) 100 per cent full load—17 per cent excess air (test Nos. 18 and 19): Again, it was found that the heat absorption in the front wall decreased as the vanes were opened, while the cleanliness in this area remained constant. The ash coverage of the rear wall did not vary appreciably between tests. The zones of relatively high heat absorption on the side walls near the burners did not change greatly as the vane openings were varied, but it did appear that the absorption rates found in these zones were reduced as the vane openings were increased. In studying the distribution of heat absorption over the height of the furnace, it

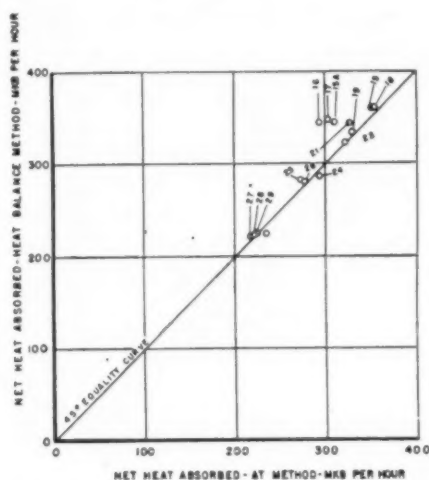


FIG. 21 COMPARISON OF FURNACE HEAT ABSORPTION COMPUTED FROM WALL TUBE ΔT -DATA WITH FURNACE HEAT ABSORPTION COMPUTED FROM FURNACE EXIT-GAS TRAVERSE

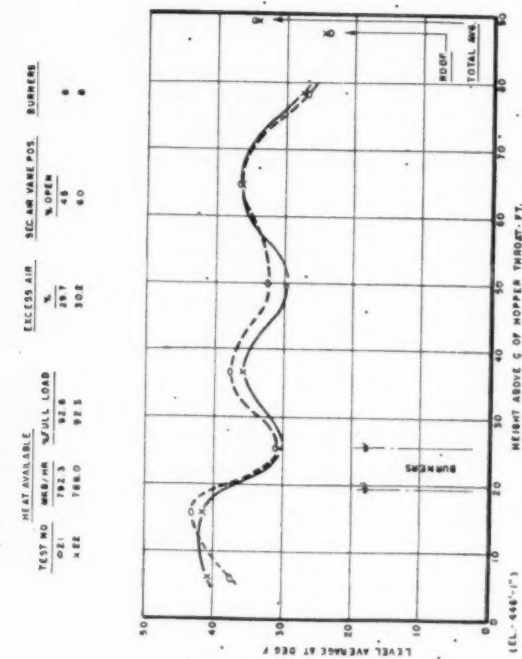


FIG. 24 FURNACE TUBE LEVEL AVERAGE ΔT -VARIATION FOR TWO SECONDARY-AIR VANE POSITIONS AT FULL LOAD AND ABOUT 30 PER CENT EXCESS AIR AT FURNACE OUTLET

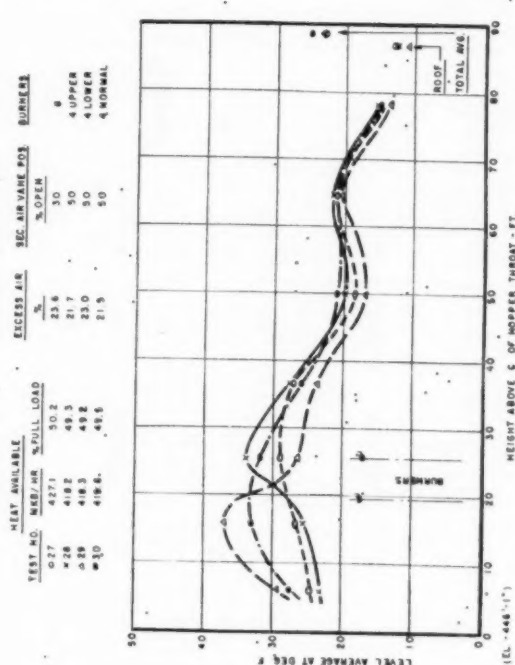


FIG. 26 FURNACE TUBE LEVEL AVERAGE ΔT -VARIATION WITH DIFFERENT BURNER FIRING ARRANGEMENTS AT 50 PER CENT LOAD AND ABOUT 25 PER CENT EXCESS AIR AT FURNACE OUTLET

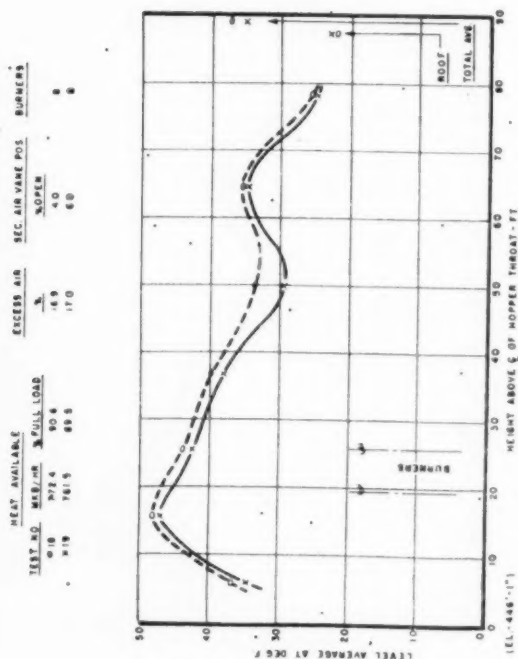


FIG. 23 FURNACE TUBE LEVEL AVERAGE ΔT -VARIATION FOR TWO SECONDARY-AIR VANE POSITIONS AT FULL LOAD AND ABOUT 17 PER CENT EXCESS AIR AT FURNACE OUTLET

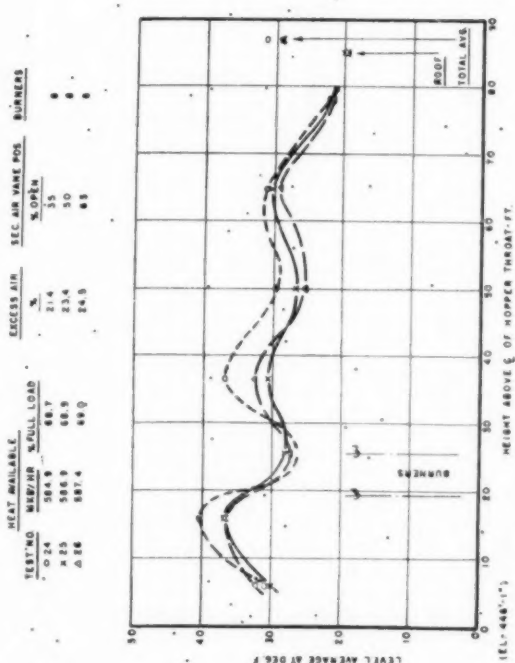
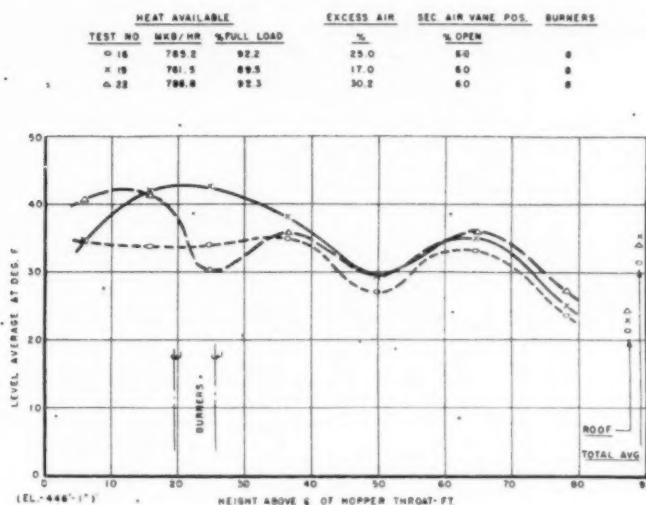
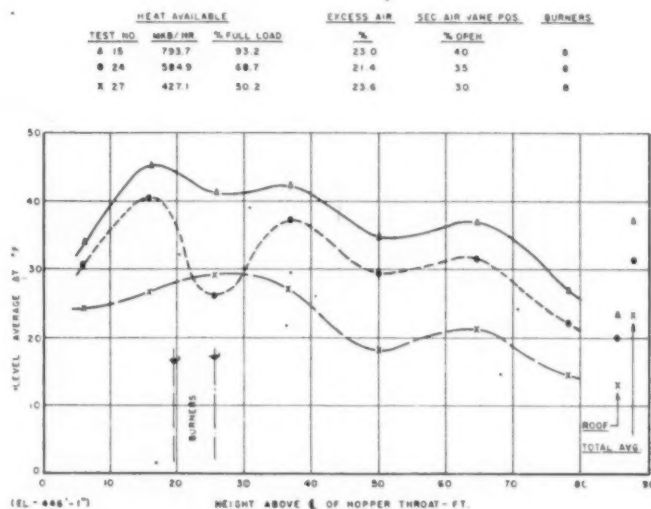


FIG. 25 FURNACE TUBE LEVEL AVERAGE ΔT -VARIATION FOR THREE SECONDARY-AIR VANE POSITIONS AT 75 PER CENT LOAD AND ABOUT 25 PER CENT EXCESS AIR AT FURNACE OUTLET

was fo
were
found
It wa
burne
this r
The f
were
(c)
21 an
the v
relati
vanes
the h
causi

FIG. 27 FURNACE TUBE LEVEL AVERAGE ΔT -VARIATION WITH EXCESS AIR AT FULL LOAD AND 60 PER CENT SECONDARY-AIR VANE POSITIONFIG. 28 FURNACE TUBE LEVEL AVERAGE ΔT WITH VARIATIONS IN NET HEAT AVAILABLE TO FURNACE FOR NORMAL SECONDARY-AIR VANE POSITIONS AND ABOUT 25 PER CENT EXCESS AIR

was found that the trends obtained for both of these vane openings were the same but that slightly lower absorption rates were found over the height of the furnace with the higher vane opening. It was noted that there was little variation in absorption at the burner elevation, which indicates that the ash accumulation in this region and its variations were small on both of these tests. The furnace efficiency decreased about 2 to 3 per cent as the vanes were opened from 40 to 60 per cent.

(c) 100 per cent full load—30 per cent excess air (test Nos. 21 and 22): The heat absorbed by the front wall decreased as the vanes were opened. The absorption rates in the zones of relatively high absorption on the side walls decreased as the vanes were opened. The ash coverage of the rear wall opposite the burners apparently increased as the vanes were opened, causing a decrease in absorption rates in this area. The dis-

tribution of the heat absorption over the height of the furnace was not changed greatly as the vane openings were varied; On both tests it is indicated that ash coverage at the burner elevations caused a reduction in heat-absorption rates in this area. The furnace efficiency remained nearly constant as the vane openings were varied, since a decrease of only 1 per cent was shown as the vane openings were increased from 45 to 60 per cent.

(d) 75 per cent full load—25 per cent excess air (test Nos. 24 to 26, inclusive): The heat absorbed by the front wall decreased when the vane openings were increased. The high absorption zones on the side walls did not appear to change significantly as the vane openings were varied. The distribution of heat absorption over the height of the furnace did not change greatly as the vane openings were varied although higher rates

TABLE 3 SUMMARY OF OPERATING AND TEST DATA FOR TEST NO. 15 THROUGH 30

TEST NUMBER	15	16	17	18	19	21	22	24	25	26	27	28	29	30
DATE - TEST	1000	1007	1008	1009	1010	1011	1012	1013	1014	1015	1016	1017	1018	1019
TIME - TEST	1000	1007	1008	1009	1010	1011	1012	1013	1014	1015	1016	1017	1018	1019
DURATION - HOURS	4	4.5	4	4	4	4	4	4	4	4	4	4	4	4
INTEGRATIONS														
COMBUSTED STEAM FLOW	K LBS PER HR	625.4	625.9	625.3	628.1	624.2	623.7	626.1	623.4	459.1	459.9	444.3	331.7	329.5
COMBUSTED FUEL FLOW	K LBS PER HR	626.4	627.1	626.5	629.8	625.7	625.2	627.6	624.9	459.1	459.9	444.3	331.7	329.5
COMBUSTED FUEL FLOW	\$ VALUE OF FLOW	23	23	23	23	23	23	23	23	23	23	23	23	23
COAL FLOW - 3A MILL	K LBS PER HR	34.23	32.50	32.27	32.06	32.26	32.12	32.31	32.46	26.41	26.32	26.18	16.98	16.81
COAL FLOW - 3B MILL	K LBS PER HR	26.54	27.13	27.13	27.13	27.13	27.13	27.13	27.13	26.09	25.97	26.18	16.98	16.81
TOTAL COAL FLOW	K LBS PER HR	70.66	69.63	70.62	69.19	69.39	69.25	69.44	69.59	52.50	52.29	52.36	33.96	33.62
TEMPERATURE RECORDING														
FINAL STEAM TEMPERATURE	°F	699	693	692	690	697	695	690	692	692	696	691	681	682
PREHEATER ENTERING ECONOMIZER	°F	400	401	400	401	400	400	398	401	375	375	378	354	353
PREHEATER LEAVING ECONOMIZER - NORTH	°F	479	478	478	478	478	478	478	478	478	478	478	478	478
PREHEATER LEAVING ECONOMIZER - SOUTH	°F	479	478	478	478	478	478	478	478	478	478	478	478	478
PREHEATER LEAVING STEAM HEATER - NORTH	°F	539	534	538	535	541	538	538	539	533	534	530	530	530
PREHEATER LEAVING STEAM HEATER - SOUTH	°F	539	532	536	533	541	538	538	539	533	534	530	530	530
GAS TEMPERATURE ENTERING ECONOMIZER	°F	663	667	667	666	660	660	669	673	790	795	791	533	530
GAS TEMPERATURE LEAVING ECONOMIZER - NORTH	°F	663	667	667	666	660	660	669	673	790	795	791	533	530
GAS TEMPERATURE LEAVING ECONOMIZER - SOUTH	°F	663	667	667	666	660	660	669	673	790	795	791	533	530
GAS TEMPERATURE LEAVING AIR HEATER - NORTH	°F	317	313	313	314	310	310	307	312	315	300	303	314	311
GAS TEMPERATURE LEAVING AIR HEATER - SOUTH	°F	313	310	310	314	314	314	313	314	312	312	314	314	314
AIR ENTERING AIR HEATER - NORTH	°F	83	83	83	83	83	83	83	83	83	83	83	83	83
AIR ENTERING AIR HEATER - SOUTH	°F	80	80	80	80	80	80	80	80	80	80	80	80	80
AIR LEAVING AIR HEATER - NORTH	°F	580	589	585	579	563	565	562	586	534	538	537	490	486
AIR LEAVING AIR HEATER - SOUTH	°F	572	584	585	579	563	565	562	586	534	538	537	490	486
AIR ENTERING 3A MILL	°F	299	453	377	365	439	439	346	430	332	332	369	370	330
AIR ENTERING 3B MILL	°F	288	440	366	346	439	439	346	430	330	330	369	370	330
PRESSURES														
UPPER MAIN OUTLET HEADER	PSIG	882	876	876	875	885	88							
DOWN	PSIG	999	993	994	992	980	980							
POLYMERIZING FUEL SYSTEM														
NUMBER OF POLYMERIZERS IN SERVICE		2	2	2	2	2	2	2	2	2	2	2	2	2
NUMBER OF POLYMERIZERS IN SERVICE		2	2	2	2	2	2	2	2	2	2	2	2	2
NUMBER OF POLYMERIZERS IN SERVICE		2	2	2	2	2	2	2	2	2	2	2	2	2
NUMBER OF POLYMERIZERS IN SERVICE		2	2	2	2	2	2	2	2	2	2	2	2	2
NUMBER OF POLYMERIZERS IN SERVICE		2	2	2	2	2	2	2	2	2	2	2	2	2
NUMBER OF POLYMERIZERS IN SERVICE		2	2	2	2	2	2	2	2	2	2	2	2	2
NUMBER OF POLYMERIZERS IN SERVICE		2	2	2	2	2	2	2	2	2	2	2	2	2
NUMBER OF POLYMERIZERS IN SERVICE		2	2	2	2	2	2	2	2	2	2	2	2	2
NUMBER OF POLYMERIZERS IN SERVICE		2	2	2	2	2	2	2	2	2	2	2	2	2
NUMBER OF POLYMERIZERS IN SERVICE		2	2	2	2	2	2	2	2	2	2	2	2	2
NUMBER OF POLYMERIZERS IN SERVICE		2	2	2	2	2	2	2	2	2	2	2	2	2
NUMBER OF POLYMERIZERS IN SERVICE		2	2	2	2	2	2	2	2	2	2	2	2	2
NUMBER OF POLYMERIZERS IN SERVICE		2	2	2	2	2	2	2	2	2	2	2	2	2
NUMBER OF POLYMERIZERS IN SERVICE		2	2	2	2	2	2	2	2	2	2	2	2	2
NUMBER OF POLYMERIZERS IN SERVICE		2	2	2	2	2	2	2	2	2	2	2	2	2
NUMBER OF POLYMERIZERS IN SERVICE		2	2	2	2	2	2	2	2	2	2	2	2	2
NUMBER OF POLYMERIZERS IN SERVICE		2	2	2	2	2	2	2	2	2	2	2	2	2
NUMBER OF POLYMERIZERS IN SERVICE		2	2	2	2	2	2	2	2	2	2	2	2	2
NUMBER OF POLYMERIZERS IN SERVICE		2	2	2	2	2	2	2	2	2	2	2	2	2
NUMBER OF POLYMERIZERS IN SERVICE		2	2	2	2	2	2	2	2	2	2	2	2	2
NUMBER OF POLYMERIZERS IN SERVICE		2	2	2	2	2	2	2	2	2	2	2	2	2
NUMBER OF POLYMERIZERS IN SERVICE		2	2	2	2	2	2	2	2	2	2	2	2	2
NUMBER OF POLYMERIZERS IN SERVICE		2	2	2	2	2	2	2	2	2	2	2	2	2
NUMBER OF POLYMERIZERS IN SERVICE		2	2	2	2	2	2	2	2	2	2	2	2	2
NUMBER OF POLYMERIZERS IN SERVICE		2	2	2	2	2	2	2	2	2	2	2	2	2
NUMBER OF POLYMERIZERS IN SERVICE		2	2	2	2	2	2	2	2	2	2	2	2	2
NUMBER OF POLYMERIZERS IN SERVICE		2	2	2	2	2	2	2	2	2	2	2	2	2
NUMBER OF POLYMERIZERS IN SERVICE		2	2	2	2	2	2	2	2	2	2	2	2	2
NUMBER OF POLYMERIZERS IN SERVICE		2	2	2	2	2	2	2	2	2	2	2	2	2
NUMBER OF POLYMERIZERS IN SERVICE		2	2	2	2	2	2	2	2	2	2	2	2	2
NUMBER OF POLYMERIZERS IN SERVICE		2	2	2	2	2	2	2	2	2	2	2	2	2
NUMBER OF POLYMERIZERS IN SERVICE		2	2	2	2	2	2	2	2	2	2	2	2	2
NUMBER OF POLYMERIZERS IN SERVICE		2	2	2	2	2	2	2	2	2	2	2	2	2
NUMBER OF POLYMERIZERS IN SERVICE		2	2	2	2	2	2	2	2	2	2	2	2	2
NUMBER OF POLYMERIZERS IN SERVICE		2	2	2	2	2	2	2	2	2	2	2	2	2
NUMBER OF POLYMERIZERS IN SERVICE		2	2	2	2	2	2	2	2	2	2	2	2	2
NUMBER OF POLYMERIZERS IN SERVICE		2	2	2	2	2	2	2	2	2	2	2	2	2
NUMBER OF POLYMERIZERS IN SERVICE		2	2	2	2	2	2	2	2	2	2	2	2	2
NUMBER OF POLYMERIZERS IN SERVICE		2	2	2	2	2	2	2	2	2	2	2	2	2
NUMBER OF POLYMERIZERS IN SERVICE		2	2	2	2	2	2	2	2	2	2	2	2	2
NUMBER OF POLYMERIZERS IN SERVICE		2	2	2	2	2	2	2	2	2	2	2	2	2
NUMBER OF POLYMERIZERS IN SERVICE		2	2	2	2	2	2	2	2	2	2	2	2	2
NUMBER OF POLYMERIZERS IN SERVICE		2	2	2	2	2	2	2	2	2	2			

TABLE 4 PULVERIZED-COAL DISTRIBUTION BETWEEN BURNER CONDUITS IN PER CENT OF TOTAL FLOW TO UNIT

Burner conduit test no.	3A1	3A11	3A2	3A22	3B1	3B11	3B2	3B22
15	12.5	13.4	12.2	12.4	13.4	11.6	12.5	12.0
15A	11.6	13.4	12.0	11.6	13.8	13.8	11.5	12.3
16	12.6	13.8	12.1	11.2	12.5	12.6	12.6	12.6
17	13.7	13.6	11.2	11.6	12.3	13.2	11.7	12.7
18	12.6	13.4	11.0	10.6	13.1	13.9	12.9	12.5
19	11.3	12.3	11.2	11.0	13.6	13.5	13.3	13.8
21	12.0	12.9	11.9	11.0	13.5	12.5	13.5	12.7
22	13.0	13.4	11.6	11.1	14.0	13.3	11.5	12.1
24	13.6	14.0	12.3	11.3	12.8	12.3	12.3	11.4
25	13.2	14.2	14.1	11.0	13.7	12.5	11.5	9.8
26	13.5	13.0	11.7	12.1	12.7	12.8	12.8	11.4
27	12.0	12.8	12.2	13.3	14.4	12.4	11.6	11.3
28			23.0	24.6			27.0	25.4
29	23.1	20.5			28.3	28.1		
30					25.6	27.0	22.9	24.5

TABLE 5 CENTER-LINE THERMOCOUPLE AVERAGE TEMPERATURE DIFFERENTIALS FOR ALL COMPLETE TESTS

TEST #	15	15A	16	17	18	19	21	22	24	25	26	27	28	29	30	TEST #	15	15A	16	17	18	19	21	22	24	25	26	27	28	29	30	
1-1	36	36	32	32	36	33	36	36	30	29	30	25	21	26	25	4-10	35	13	34	20	35	36	33	34	31	31	33	22	15	16	13	
1-2	39	38	42	34	38	38	36	42	31	30	35	24	22	21	25	4-11	39	24	36	52	48	39	13	38	7	9	25	26	24	25		
1-3	36	36	37	39	45	45	45	41	49	37	41	42	20	26	31	4-12	52	26	42	48	43	30	38	30	45	43	48	36	33	27	35	
1-4	39	39	46	41	45	44	44	49	38	41	41	27	26	33	29	4-13	39	28	28	30	42	34	31	34	31	10	13	36	15	17	22	
1-5	29	31	34	45	23	24	33	41	24	27	28	17	29	41	38	4-14	38	30	27	31	22	31	33	26	43	26	29	28	30	16	18	
1-6	41	44	34	41	36	38	40	41	30	29	34	23	25	36	36	4-15	47	45	39	39	34	39	40	47	42	41	40	27	34	38	24	
1-7	9	22	7	4	30	8	30	9	8	8	9	24	3	4	4	4-16	49	45	31	33	41	45	48	47	46	43	44	42	33	39	31	
1-8	27	29	24	26	25	25	29	27	22	22	23	18	17	24	19	4-17	51	53	41	39	57	58	54	59	47	45	49	45	56	43	40	
1-9	27	28	23	27	26	25	29	28	23	22	24	18	19	24	23	4-18	45	59	57	42	38	54	49	42	48	38	50	17	42	18	38	
1-10	42	44	41	41	42	42	42	46	34	33	35	24	18	19	24	4-19	39	20	30	35	32	36	41	35	30	25	24	25	26	13	29	
1-11	46	48	46	47	51	51	48	53	44	44	46	34	32	40	38	4-20	49	16	23	10	37	30	33	24	23	15	23	24	17	31	14	
1-12	46	48	52	47	51	51	48	53	44	44	46	34	32	40	38	4-21	48	20	39	37	50	58	43	30	36	33	24	34	20	19	17	
1-13	49	51	57	51	57	56	51	65	45	45	46	34	32	40	38	5-1	39	21	30	41	37	33	44	31	30	31	23	12	33	30	30	
1-14	42	43	43	41	45	44	42	55	37	36	38	28	26	31	26	5-2	41	17	30	22	37	38	24	35	35	36	10	25	19	29		
1-15	35	34	36	32	35	36	34	37	30	29	33	24	21	26	21	5-3	36	30	31	31	35	28	31	31	30	27	27	24	18	16	21	
1-16	6	28	4	27	4	6	28	31	25	24	26	21	17	23	22	5-4	38	34	25	35	39	29	35	30	33	26	25	24	20	18	23	
1-17	29	30	26	28	30	30	31	30	25	24	25	21	18	23	24	5-5	43	39	34	40	43	36	41	35	39	35	33	30	26	23	27	
1-18	33	35	32	34	34	32	34	34	31	28	27	24	22	27	29	5-6	44	40	33	40	47	38	42	36	39	33	31	28	25	23	25	
1-19																5-7	39	35	30	37	41	34	40	33	32	28	28	24	21	19	22	
1-20																5-8	39	36	31	36	41	35	39	35	35	32	29	23	23	20	24	
1-21	43	48	32	39	43	35	45	37	39	30	28	34	17	39	34	5-9	34	35	27	33	34	31	33	19	28	27	27	20	21	18	21	
2-1	13	12	16	16	14	13	20	24	11	18	20	11	14	18	13	5-10	30	29	24	29	29	28	30	28	26	24	25	18	18	17	19	
2-2																5-11	29	24	25	25	29	29	29	27	26	25	18	17	16	18		
2-3																5-12	35	16	33	26	31	29	33	34	28	26	25	7	8	18	10	
2-4	16	16	23	25	31	31	28	29	24	23	26	7	17	25	21	5-13	34	24	32	25	31	34	30	24	28	27	27	20	19	4	22	
2-5	55	57	44	53	53	48	55	50	47	43	44	39	26	42	34	5-14	37	37	27	43	39	34	37	40	30	32	19	6	15	31	13	
2-6	43	54	13	51	45	47	70	50	48	43	46	13	26	39	41	5-15	29	22	15	28	33	26	26	19	24	23	22	15	18	25		
2-7	47	39	17	16	62	40	17	22	47	41	41	12	28	44	41	5-16	25	13	21	17	26	25	24	19	24	24	25	18	25	9	20	
2-8	50	48	38	48	57	54	33	34	47	47	48	26	35	45	47	5-17	30	9	22	22	24	24	25	16	25	21	22	22	10	7	21	
2-9	50	41	45	43	54	53	37	37	41	40	40	30	29	35	32	5-18	27	42	18	30	26	24	24	23	26	24	5	13	8	13		
2-10	34	37	29	36	37	37	27	28	32	30	33	23	24	34	30	5-19	29	30	26	26	26	26	25	27	27	23	23	2	18	18		
2-11	49	42	49	43	50	46	45	53	39	36	40	27	27	41	25	5-20	24	11	20	19	21	22	24	24	24	23	22	15	15	16	16	
2-12	57	50	49	53	62	52	58	55	39	36	37	28	28	38	21	5-21	46	39	20	38	37	27	39	31	30	27	25	28	29	25	27	
2-13	50	40	19	43	45	45	43	40	40	37	28	30	39	30		5-22	32	28	25	21	26	23	27	22	16	17	12	19	10	21		
2-14	57	56	43	46	58	57	58	53	46	45	48	42	35	42	38	5-23	41	23	35	29	38	35	37	34	39	35	35	15	26	18	27	
2-15	49	32	9	47	50	47	51	52	45	42	28	26	20	38	34	5-24	39	35	31	35	39	33	38	33	34	30	27	26	22	20	25	
2-16																5-25	36	33	29	34	36	31	35	31	33	31	27	21	17	19	21	
2-17	44	43	43	43	48	44	42	46	41	38	21	32	29	39	37	5-26	45	44	37	43	43	39	42	40	41	38	33	26	25	25	26	
2-18	41	38	49	34	42	44	37	43	39	44	28	25	34	34		5-27	42	40	37	40	40	38	40	39	35	33	32	24	24	23	25	
2-19	48	23	42	23	50	47	43	38	41	37	42	25	23	20	33	5-28	42	39	39	40	41	42	41	41	35	35	34	24	25	23	25	
2-20																5-29	46	46	41	46	45	46	47	46	39	39	38	26	30	26	29	
2-21	62	29	41	56	61	22	67	44	56	41	39	49	25	54	58	5-30	40	45	35	42	38	40	42	40	34	34	34	24	26	22		
3-1	62	21	61	16	55	57	53	54	56	59	56	15	32	34	35	5-31	29	27	25	27	27	28	29	28	24	23	23	17	18	16	18	
3-2	39	52	29	30	55	35	26	42	23	32	41	20	43	20	46	5-32	48	49	45	50	48	49	51	48	39	37	37	29	33	30	31	
3-3	30	35	27	33	42	39	24	36	20	23	29	30	42	35	47	5-33	29	14	29	23	26	37	27	27	22	22	21	15	4	15	4	
3-4	51	30	39	28	52	32	22	32	19	33	16	16	36	29	37	5-34	27	5	22	14	25	23	24	26	27	24	24	8	17	15	17	
3-5	40	22	20	18	38	38	33	34	20	16	18	43	13	25	16	5-35	33	28	31	29	28	27	34	31	26	26	27	18	20	21	19	
3-6	36	10	20	20	26	29	20	12	11	14	16	12	16	17	13	5-36	29	25	24	25	26	24	27	26	24	23	22	16	18	16	18	
3-7	17	39	10	8	39	50	4	6	7	7	8	44	4	4	4	5-37	32	30	23	30	28	28	31	27	27	27	23	16	17	16	16	
3-8	8	33	6	21	11	10	37	24	41	30	17	41	19	11	18	5-38	30	29	26	29	28	25	30	28	25	24	22	16	14	16	15	
3-9																5-39	24	23	23	24	22	24	22	24	25	20	21	19	13	13	14	
3-10																5-40	22	20	20	19	21	22	21	23	18	19	19	11	12	11	13	
3-11																5-41	27	28	24	26	27	30	30	37	30	23	19	25	15	16	14	17
3-12																5-42	23	25	21	23	20	24	24	26	20	20	21	15	12	12	15	
3-13																5-43	23	25	22	23	22	25	27	28	21	21	21	14	17	14	1	

TABLE 6 SUMMARY OF CONDITIONS AND RESULTS OF TESTS NOS. 15 THROUGH 30

Test Number	Date	Net Heat Available to Furnace MMB/Hr.	Net Heat Input to Furnace % Full Load	Excess Air at Furnace Outlet %	Secondary Air Vane Position % Open	Number of Burners in Service	Average ΔT Deg. F.	Average Burner Box Pressure Ins. W.G.	Net Heat Absorbed in Furnace (ΔT Method) MMB/Hr.	Furnace Efficiency %
15	10-22-48	793.7	93.2	23.0	40	8	37.2	5.9	350.3	44.2
15A	10-27-48	780.5	91.6	24.8	40	8	32.9	6.3	309.8	39.7
16	10-22-48	785.2	92.2	25.0	60	8	31.2	3.1	293.8	37.4
17	10-28-48	787.2	92.3	26.2	50	8	32.3	4.6	304.2	38.6
18	10-28-48	772.4	90.6	16.9	40	8	37.4	4.6	352.2	45.4
19	10-20-48	761.5	89.5	17.0	60	8	35.0	2.8	329.6	43.3
21	10-25-48	791.0	92.8	29.7	45	8	34.7	5.9	326.8	41.3
22	10-25-48	786.8	92.3	30.2	60	8	34.1	3.5	321.1	40.8
24	10-24-48	584.9	68.7	21.4	35	8	31.3	3.0	294.8	50.4
25	10-24-48	586.9	68.9	23.4	50	8	29.1	1.7	274.0	46.6
26	10-24-48	587.4	69.0	24.5	65	8	29.4	1.2	276.9	47.2
27	10-27-48	427.1	50.2	23.6	30	8	23.1	1.4	217.5	50.9
28	10-30-48	418.2	49.3	21.7	50	4*	23.5	2.8	221.3	52.9
29	10-29-48	418.3	49.2	23.0	50	4**	24.0	2.9	226.0	54.0
30	10-30-48	419.6	49.5	21.5	50	4***	25.0	2.6	235.4	56.1

* - upper
 ** - lower
 *** - normal

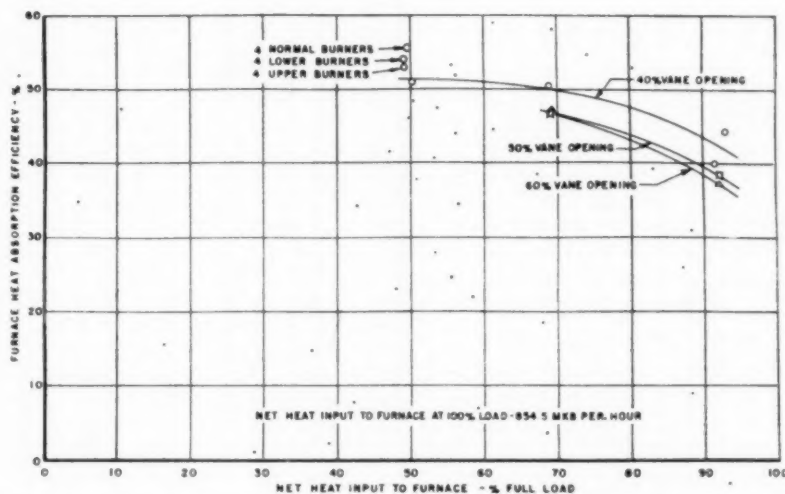


FIG. 29 VARIATIONS OF FURNACE HEAT-ABSORPTION EFFICIENCY WITH NET HEAT INPUT TO FURNACE FOR THREE DIFFERENT SECONDARY-AIR VANE POSITIONS WITH EIGHT BURNERS IN SERVICE AND APPROXIMATELY 25 PER CENT EXCESS AIR AT FURNACE OUTLET

of absorption were found on the tests at the lower vane openings. The heat-absorption rates at the burner elevations were low on all of these tests, apparently owing to the ash coverage in this area. It is also possible that this ash was deposited on some of full-load tests and that the change in furnace rating was not sufficient to allow it to clean itself. Increasing the vane opening under these conditions caused a decrease in furnace heat-absorption efficiency of about 3 to 4 per cent.

(e) General: Summarizing the foregoing results, it is found that increasing the vane opening results in decreasing the heat

absorbed in the front wall and usually causes a reduction in absorption in the rear wall owing to an increase in ash coverage. The rate of heat absorption in those zones of relatively high absorption rates on the side walls near the burners usually decreases as the vanes are opened. The distribution of heat absorption over the height of the furnace does not vary greatly in any range of elevation other than in the vicinity of the burners, but lower absorption rates are found throughout the furnace as the vane openings are increased. The effect of varying vane opening on furnace heat-absorption efficiency at full load seems

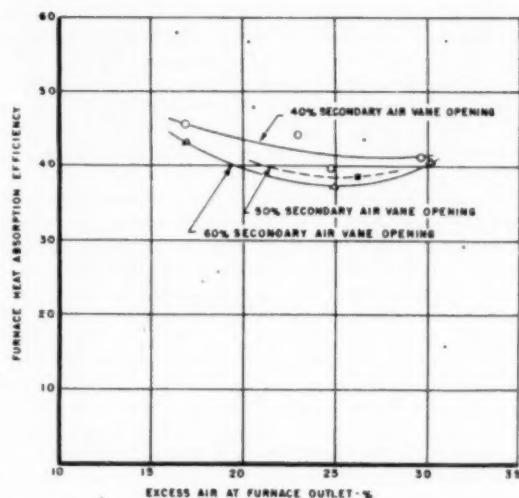


FIG. 30 VARIATION OF FURNACE HEAT-ABSORPTION EFFICIENCY WITH SECONDARY-AIR VANE OPENING AT APPROXIMATELY 100 PER CENT FULL LOAD FOR THREE DIFFERENT EXCESS-AIR VALUES AT FURNACE OUTLET

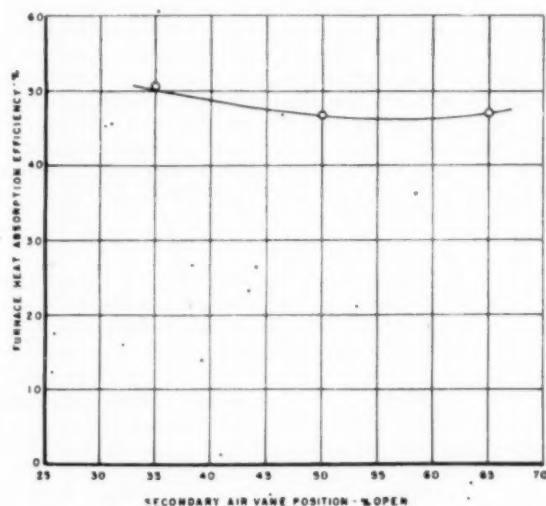


FIG. 32 VARIATION OF FURNACE HEAT-ABSORPTION EFFICIENCY WITH SECONDARY-AIR VANE POSITION FOR APPROXIMATELY 75 PER CENT FULL LOAD WITH 25 PER CENT EXCESS AIR AT FURNACE OUTLET

to change depending upon the excess air used. At 17 and 25 per cent excess air, we found a decrease of approximately 2 to 4 per cent as the vanes were opened, but found only a slight decrease in efficiency as the vane opening was increased at 30 per cent excess air. The effect of vane openings on furnace efficiency seems to be slightly reduced as the furnace rating is reduced.

Effect of Varying Heat Input to Furnace. The effect of varying heat input was studied between the approximate range of 50 to 93 per cent full load at 25 per cent excess air at the furnace outlet with eight burners in service. The effect of this variable alone is probably best shown by comparing test Nos. 15, 25, and 27, where the secondary-air vane openings were 40, 35, and 30 per cent open, respectively. Other comparisons in the range

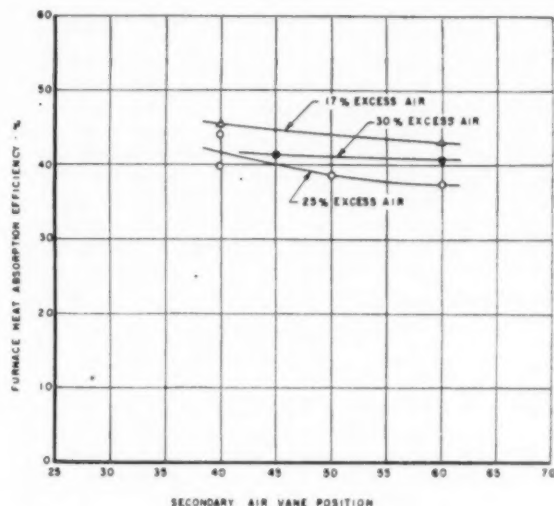


FIG. 31 VARIATION OF FURNACE HEAT-ABSORPTION EFFICIENCY WITH EXCESS AIR AT FURNACE OUTLET FOR THREE DIFFERENT SECONDARY-AIR VANE SETTINGS AT APPROXIMATELY 100 PER CENT FULL LOAD

of about 70 per cent to 93 per cent full load may also be made. Test Nos. 17 and 25 were run at 50 per cent vane opening, and test Nos. 16 and 26 were made at 60 to 65 per cent vane opening.

Comparing test Nos. 15, 24, and 27, it is found that the distribution of heat absorbed in the front wall does not vary greatly, regardless of the heat input, although, of course, it increases in amount as the heat input is increased. The location of the zones of higher absorption found on the side walls near the burners does not change greatly as the heat input is increased, but the rate of heat absorption in these zones increases. The rear wall is less affected by ash accumulation at the lower heat inputs with the result that it has a more uniform and nearly as great absorption at the lower loads as are obtained at the high load. In general, the isothermal diagrams become a little more spotted at 50 per cent full load.

Comparing the distribution over the height of the furnace, it is found that the general trends remain the same, except at the burner elevations. At full load, it is noted that there is a small reduction in the absorption in this particular area when comparing it to elevations both above and below this region. At about 70 per cent full load, there is a considerable reduction in absorption at the burner elevation, but it is felt that this is caused by ash coverage on the rear wall which was accumulated during some of the various operating conditions at full load and did not clean itself, thus distorting the true distribution at this load.

At 50 per cent load, it is found that the distribution of heat absorption over the height of the furnace is much more uniform than found under the preceding conditions and reaches a maximum at the burner elevation. This indicates that at 50 per cent load the distribution of heat absorption is not affected by ash coverage and that the ash coverage is negligible. The other tests show about the same results for the range in which they were investigated.

The furnace heat-absorption efficiency for test Nos. 15, 24, and 27 indicates that, as the heat input is increased in the range from 50 to 70 per cent full load, there is only a slight decrease in furnace efficiency, but that increasing the heat input in the range from 70 to 93 per cent causes an appreciable reduction in furnace efficiency (about 7 per cent). Comparing the other

tests at 50 and 60 per cent vane opening in the range from 70 to 93 per cent, the same results are noted.

Effect of Varying Excess Air at Furnace Outlet. The effect of varying excess air at the furnace outlet was studied at approximately full load in the range between 17 to 30 per cent. Test Nos. 15, 18, and 21 were all run with approximately 40 per cent secondary-air vane opening. Test Nos. 16, 19, and 22 were all run with 60 per cent vane opening. It is found that the distribution of heat absorption on the various furnace walls varies only a small amount as the excess air is increased, although there are some indications that the absorption rates in the rear wall are decreased as the excess air is increased, apparently due to an increase in ash coverage. The zones of high absorption on the side walls near the burners do not seem to vary significantly as the excess air is changed, although the rates of heat absorption found were a little higher at the low excess air.

In studying the distribution of heat absorption over the height of the furnace at 60 per cent vane opening, it is noted that from elevation 35 ft to the top of the furnace there is little change in distribution regardless of the amount of excess air used, but that considerable variations are found from the hopper throat up to the 35-ft elevation.

At 17 per cent excess air the heat-absorption rate reaches a maximum at the burner elevations. At 25 per cent excess air, the absorption rate is rather constant over this range of elevation. At 30 per cent excess air there is a considerable reduction in the heat absorption at the burner elevations, but the heat absorption is higher just under the burner elevations than is noted under the other conditions. These same general characteristics are noted in comparing the tests at 40 per cent secondary-air vane opening.

It was indicated that the furnace heat-absorption efficiency at 40 per cent vane opening decreased rather rapidly as the excess air was changed from 17 to 25 per cent, and then remained approximately constant as the excess air was increased from 25 to 30 per cent. It was also indicated that at 60 per cent vane opening the furnace efficiency decreased rapidly between 17 and 25 per cent excess air, and then increased slightly as the excess air was increased from 25 to 30 per cent. This indicates that, as the excess air is increased at constant vane opening from 17 to 25 per cent excess air, there is a reduction in furnace efficiency which can be recovered partially by increasing the excess air further. This might be caused by the increase in the angular velocity of the mixture leaving the burner throat. Both the study of variations of the amount of excess air and the study of variations in secondary-air vane opening seem to indicate that an increase in the angular velocity of the fuel mixture leaving the burner throats results in improving the mixing of the fuel and air and possibly increases the rate of combustion of the fuel particles. Thus it seems possible that the temperature of the flame envelope might be changed as well as its shape as the angular velocity of the fuel mixture is changed.

Effect of Various Combinations of Burners in Service at 50 Per Cent Full Load. Test Nos. 27 to 30, inclusive, were run at about 50 per cent full load with approximately 25 per cent excess air at the furnace outlet. Test No. 27 was run with all eight burners in service, Test No. 28 with only the four upper burners, Test No. 29 with only the four lower burners, and Test No. 30 with the two upper inside burners and the two lower outside burners in service. It was found that the distribution and amount of heat absorbed by the front wall did not vary greatly on any of these tests. The heat absorption by the rear wall did change considerably depending upon which burners were used. The absorption by this wall was much more uniform when all eight burners were used and also much less affected by ash coverage. It was found that the location of higher absorption rates on

the rear wall changed with the combinations of burners in service. They were located highest on the rear wall with the four upper burners in operation and lowest when the four lower burners were used. The zones of high absorption rates on the side walls near the burners did not vary greatly but yet tended to shift up and down, depending upon which burners were used. These zones contained the lowest absorption rates when all eight burners were used.

When studying the distribution of heat absorption over the height of the furnace for these tests, it was found that from the 35-ft elevation to the top of the furnace there was little change in distribution. However, from the ash-hopper throat up to the 35-ft elevation, the distribution was changed considerably for the various burner combinations. With the four lower burners in operation, the maximum absorption rates were found just below the lower burner elevations. With the four upper burners in operation, the maximum absorption rate was found at the elevation of these upper burners. When the two upper and two lower burners were used, the maximum heat-absorption rate was found to be less than those obtained with the other four burner combinations and spread over a wider range of elevation, reaching its maximum near the elevation of the lower burners. When eight burners were used, the absorption rate in this region was much lower and much more constant, reaching its maximum value at the elevation of the upper burners.

It was indicated that the lowest furnace efficiency was obtained with eight burners in operation and increased in the following order: four upper burners, four lower burners, and two upper and two lower burners. However, using the convection superheater as an indication of furnace efficiency, it was found that the four lower burner operation resulted in a higher furnace efficiency than was obtained with the two upper and two lower burner operation. It also seems that the difference in efficiency between four lower burner operation and two upper and two lower burner operation is too small to establish definitely by the ΔT -method, which is the more efficient.

CONCLUSIONS

Based upon the foregoing data and analysis of results, we have formed the following conclusions concerning the performance of this furnace under the operating conditions investigated:

1. Ash does not collect in sufficient quantities to affect the heat absorption by the furnace-wall surface at any location other than the area of the rear wall at the burner elevations, where there is a tendency to accumulate and shed ash under some of the operating conditions studied.

2. Considering the distribution of heat absorption over the height of the furnace, it is found that the average absorption rates are usually highest at the elevation just below the burners, although indications show that the maximum might be found at the burner elevations if it were not for the effect of ash coverage in this area. A second peak of higher absorption rates occurs at the elevation where the cross-sectional area of the furnace is reduced, near the top, by the rear-wall sloping section.

3. Variations in absorption rates for clean furnace surface throughout the furnace do not exceed a magnitude of 3 or 4 to 1. Zones of 60,000 to 75,000 Btu/(sq ft-hr) absorption rates exist in that area of the side walls near the burners, and relatively high rates of absorption occur in that area of the rear wall which forms part of the hopper throat at the bottom of the furnace under all of the operating conditions studied.

4. Opening the secondary air vanes, in the ranges studied, causes (a) a reduction in heat absorbed by the front walls; (b) an increase in ash accumulation on the rear wall opposite the burners, accompanied by a decrease in absorption in this area; (c) a reduction in absorption rates in the zones of higher absorption

on the side walls near the burners; (d) a decrease in absorption at the burner elevations and lower absorption rates throughout the furnace; and (e) a decrease in furnace efficiency, which varies with excess-air and heat-input conditions.

5 Increasing the excess air for combustion, in the range from 17 to 30 per cent, causes (a) a reduction in heat absorption at the burner elevations; (b) an increase in ash coverage in that area of the rear wall directly opposite the burners; and (c) a decrease in furnace heat-absorption efficiency with varying characteristics, depending upon which secondary-air vane opening is used.

6 Variations in the combination of burners in service, at 50 per cent full load, causes (a) changes in the ash coverage on the rear-wall area opposite the burners; (b) variations in the average absorption rates at the burner elevations, and the locations of higher absorption zones shift up and down, depending upon the burners used; and (c) variations in furnace heat-absorption efficiency in the range of approximately 5 per cent.

7 The ΔT -method provides a good means of determining the distribution of heat absorption in the furnace and many of its inherent errors apparently cancel themselves in the determination of the furnace heat-absorption efficiency. However, it is recommended that wherever furnace efficiency is concerned, the reader should also refer to the heat-balance data contained in Part II of the investigation at Paddy's Run Station.

The data, diagrams, and curves which have been included in this paper should be of considerable assistance to the furnace designer and operator in predicting performance characteristics of similar furnaces, although it must be recognized that other operating variables, such as different characteristics of the fuel fired, may revise or modify some of the results which have been found.

ACKNOWLEDGMENTS

The authors wish to express their appreciation for the assistance rendered by the following in making this extensive investigation possible:

The ASME Special Research Committee on Furnace Performance Factors for the opportunity of participating in this investigation.

The officials of the Louisville Gas and Electric Company, Mr. A. G. Rosenbaum, General Superintendent, and Mr. F. B. Tetzel, Superintendent of Power Production, who made the No. 3 unit at Paddy's Run Station available to the committee for testing,

and co-operated with the committee in every possible way throughout the extended test program.

Mr. John Blizzard, Mr. Martin Frisch, Mr. A. R. Mumford, and Mr. Fred Ely for their very helpful criticisms and suggestions.

The personnel of Paddy's Run Station of the Louisville Gas and Electric Company: Mr. J. D. Brecker, Plant Engineer; Mr. S. P. Connor, Assistant Plant Engineer; Mr. H. C. Scherffleus, Economy Engineer; and their assistants who gave capable and willing assistance in accomplishing the test program.

The Combustion Research Section of the U. S. Bureau of Mines whose contributions on this test project have been outstanding.

The members of the Service Department, Steam Division and Research Department of the Foster Wheeler Corporation, who gave generously of their time and experience in the running of tests and analysis of results.

BIBLIOGRAPHY

1 "Furnace Heat Absorption in Pulverized-Coal-Fired Steam Generator Using Turbulent Burners at Paddy's Run Station, Louisville, Ky."

Part I "Variation in Heat Absorption as Shown by Measurement of Surface Temperature of Exposed Side of Furnace Tubes," by R. I. Wheeler and M. H. Howard, subject paper.

Part II "Furnace Heat-Absorption Efficiency as Shown by the Temperature and Composition of Gases Leaving the Furnace," by R. C. Corey and Paul Cohen, published in this issue of the Transactions, pp. 925-935.

Part III "Comparison and Correlation of the Results of Furnace Heat-Absorption Investigation," by H. H. Hemenway and R. I. Wheeler, published in this issue of the Transactions, pp. 937-944.

2 "An Investigation of the Variation in Heat Absorption in a Pulverized-Coal-Fired Water-Cooled Steam-Boiler Furnace."

Part I "Variations in Heat Absorption as Shown by Measurement of the Surface Temperature of the Exposed Side of Furnace Tubes," by L. B. Schueler, Trans. ASME, vol. 70, 1948, pp. 553-567.

Part II "Furnace Heat-Absorption Efficiency as Shown by Temperature, Composition, and Flow of the Gases Leaving the Furnace," by W. T. Reid, Paul Cohen, and R. C. Corey, Trans. ASME, vol. 70, 1948, pp. 569-585.

Part III "Variation in Heat Absorption as Shown by Density and Velocity Measurements of the Fluid Within a Tube," by A. R. Mumford and C. G. R. Humphreys, Trans. ASME vol. 70, 1948, pp. 587-600.

Part IV "Comparison and Correlation of the Results of Furnace Heat-Absorption Investigations," by A. R. Mumford and G. W. Bice, Trans. ASME, vol. 70, 1948, pp. 601-614.

3 "Thermocouples for Furnace-Tube Surface Temperature Measurement," by C. G. R. Humphreys, *Combustion*, October, 1944, pp. 43-45.

P
Te

The
ports
tion
fired
search
The
absor
horiz
super
effici
the f
ary-a
loads
tailed
gas t
tion
and
is dis

T

condi
comp
by th
Facto
gation
Elect
dry-b
tal tu
lb of
Th

¹ S

Mine

² F

Mem

³ T

has a

Heat

Boile

1948,

Co

forma

sions

vemb

CHAN

No

under

the S

Furnace Heat Absorption in Paddy's Run Pulverized-Coal-Fired Steam Generator, Using Turbulent Burners, Louisville, Ky.

Part II. Furnace Heat-Absorption Efficiency as Shown by Temperature and Composition of Gases Leaving the Furnace

By R. C. COREY¹ AND PAUL COHEN,² PITTSBURGH, PA.

This paper is part of the second of a series of formal reports on investigations of heat absorption and distribution of heat transfer in representative pulverized-coal-fired boiler furnaces, sponsored by the ASME Special Research Committee on Furnace Performance Factors. The results are presented of fifteen determinations of heat absorption in the furnace of a 640,000 lb per hr boiler with horizontal firing, operating at 950 psig and 900 F at the superheater outlet. The effect on furnace heat-absorption efficiency is shown for variation of (a) the heat available in the furnace, (b) the excess air, (c) the setting of the secondary-air vanes of the turbulent burners, and (d), at low loads, the number and location of the burners used. Detailed data are given for the distribution of excess air and gas temperature at the furnace outlet. The heat-absorption data are analyzed in terms of radiation heat transfer, and the significance of flame location, volume, and shape is discussed.

INTRODUCTION

THIS paper presents the results of determinations of the heat-absorption efficiency of a central-station, pulverized-coal-fired, steam-boiler furnace, for a variety of operating conditions. It is a part of the report of the second³ of a series of comprehensive investigations of heat transfer in boiler furnaces by the Special Research Committee on Furnace Performance Factors of the Society. The unit studied in this second investigation is boiler No. 3, Paddy's Run Station, Louisville Gas & Electric Company, Louisville, Ky., a single-drum boiler, with a dry-bottom furnace, fired from the front wall with eight horizontal turbulent burners arranged in two rows and rated at 640,000 lb of steam per hr at 950 psig and 900 F at the superheater outlet.

The investigation of this unit by the committee consisted of

two parts, namely, determination of the total heat absorption in the furnace, which is the subject of this paper, and determination of the distribution of heat absorption in the furnace, the subject of another paper of this symposium. The furnace heat-absorption tests were made by the Combustion Research Section of the Bureau of Mines, concurrently with the other studies, as part of the Bureau of Mines co-operative research program with the committee to study the effect of ash and slag on furnace performance.

Fifteen tests were made to determine the effect on furnace heat absorption of variations of load, excess air, adjustment of the turbulent burners, and, at low loads, the number and location of the burners used. The heat absorption is defined as the heat transferred by convection to the furnace walls, not including the screen, and the heat transferred by radiation to the furnace walls, including the screen. With slight modification, the test procedure is that of Method *b* of the ASME Test Code for Stationary Steam-Generating Units. The heat absorption in the furnace is obtained as the difference between the net heat available in the furnace (the low heat value of the fuel fired, corrected for unburned combustible, plus the sensible heat in the air used for combustion) and the sensible heat in the furnace-outlet gases and the refuse, and the heat transferred from the furnace casing.

The sensible heat in the furnace-outlet gas was calculated from the temperature and composition determined by techniques appropriate for furnace testing.⁴ Measurements were made at a number of positions approximating the furnace outlet within the limitations of the available means of access to the furnace. Because of the significance of the distribution of the temperature and composition of the gases at the furnace outlet, the complete test data are tabulated in the paper.

METHODS OF TEST AND CALCULATION

Description of Furnace. Fig. 1 is a sectional side elevation of the boiler, showing the general arrangement of the components. The furnace is 78 ft high from the top of the hopper to the center line of the drum, 31 ft 0 1/2 in. wide between side-wall tubes, 24 ft 3 in. deep, and the volume is 47,100 cu ft. All furnace walls consist of 3-in.-OD tubes on 3 1/2-in. centers, backed by tile. The front portion of the furnace roof is formed by the direct continuation of the front-wall tubes, and the rear portion of the roof is formed by the back-wall tubes bent forward and covered on the outside with a tile baffle. The slag screen is formed from the back-wall tubes expanded into four rows of tubes with a 9-in. center-to-center spacing between rows and a 13-in. center-to-

¹ Supervising Engineer, Combustion Research Section, Bureau of Mines. Mem. ASME.

² Fuel Engineer, Combustion Research Section, Bureau of Mines. Mem. ASME.

³ The report on the first unit studied, Boiler No. 11, Tidd Station, has already been published: "An Investigation of the Variation in Heat Absorption in a Pulverized-Coal-Fired Water-Cooled Steam-Boiler Furnace," by L. B. Schueler, et al, Trans. ASME, vol. 70, 1948, pp. 553-619.

Contributed by the Special Research Committee on Furnace Performance Factors, and the Fuels, Power, and Heat Transfer Divisions and presented at the Annual Meeting, New York, N. Y., November 27-December 2, 1949, of THE AMERICAN SOCIETY OF MECHANICAL ENGINEERS.

NOTE: Statements and opinions advanced in papers are to be understood as individual expressions of their authors and not those of the Society. Paper No. 49-A-42.

⁴ "Methods and Instrumentation for Furnace Heat-Absorption Studies: Temperature and Composition of Gases at Furnace Outlet," by P. Cohen, R. C. Corey, and J. W. Myers, Trans. ASME, vol. 70, November, 1949, pp. 965-978.

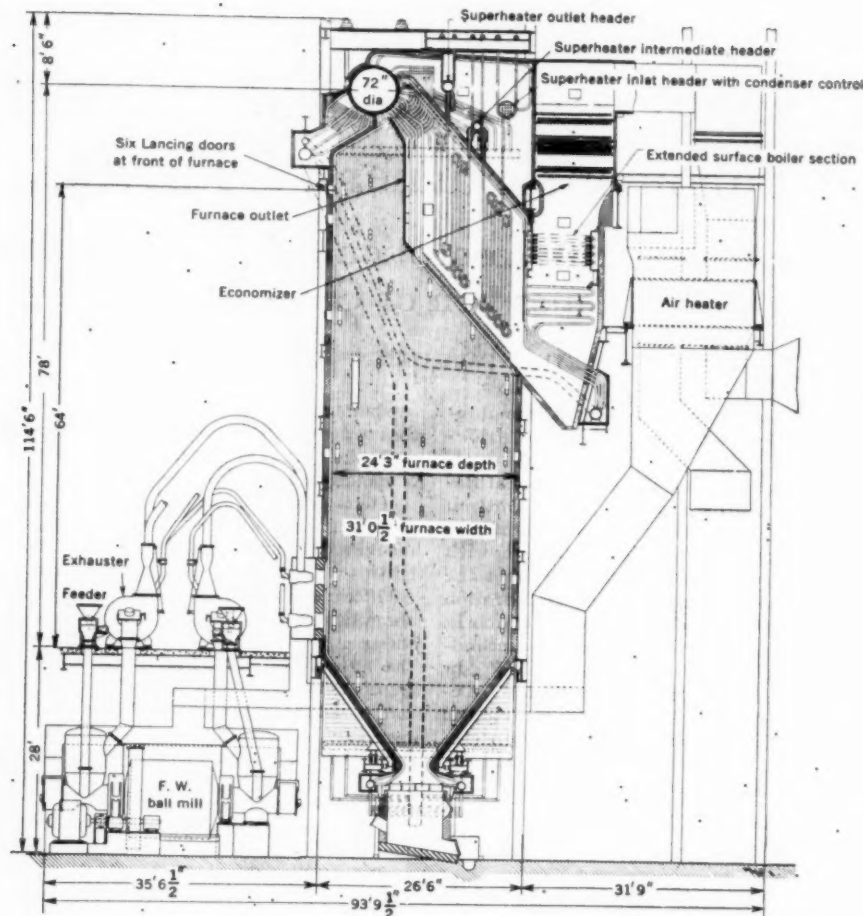


FIG. 1 SECTIONAL SIDE ELEVATION OF BOILER NO. 3, PADDY'S RUN STATION

center spacing between lanes. The front row of screen tubes is 8 ft 11 1/2 in. from the front-wall tubes, center-to-center distance. The furnace outlet is 18 ft 4 in. high and 30 ft 9 1/2 in. wide. The area of projected radiant-heating surface in the furnace is 8884 sq ft, including the developed area of the furnace outlet, 564 sq ft.

The furnace is fired with eight inter-vane burners in the front wall, arranged in two rows of four each with center lines 4 ft 4 in. and 10 ft 4 in. above the top of the hopper, respectively. Fuel is supplied by two ball-mill pulverizers equipped with two exhausters each. The north mill fires the two inner upper burners and the two outer lower burners, and the south mill, the other four burners. Forced-draft fans, induced-draft fans, and regenerative air heaters are all in duplicate and arranged at the back of the unit. Interconnecting dampers permit operation at low loads with but one set of fans and air heater, but, in the tests, both sets of auxiliaries were always used to assure the best balance in the furnace and beyond.

Location of Test Points. After consideration of the available access doors, it was decided to make all measurements from six lancing doors at the front of the furnace, 64 ft above the top of the hopper. A large proportion of the furnace outlet could be reached by inserting a 14-ft water-cooled high-velocity thermocouple probe through these doors and swinging the probe at various angles from the horizontal. Thirty sampling positions

were used in the tests, arranged in six columns (A, B, C, D, E, and F), corresponding to the location of the lancing doors in the front wall, each column having five sampling points, designated +6, +3, 0, -3, and -6, which are approximate vertical distances in feet from the midplane of the furnace outlet. The actual sampling points were 6 in. in front of the screen at the elevations shown. The resulting distribution of sampling points is shown in Fig. 2, a map of the developed furnace-outlet area, drawn to scale. The furnace outlet is also shown by the heavy line in Fig. 1.

To facilitate manipulation of the long and heavy water-cooled thermocouple holder and to provide reproducibility of the location of the sampling positions, a special insert was built for the lancing doors, which provided means for convenient and accurate manipulation of the probe and also permitted rather complete sealing of the door during sampling, with asbestos-board plates. Fig. 3 gives the general details of this special insert.

Instrumentation and Analyses. The temperature and composition of the gas at the furnace outlet were determined with instrumentation and technique previously described.⁴ The following brief review will be helpful:

(a) The temperature of the gas at the furnace outlet was determined with high-velocity thermocouples (platinum, 10 per cent rhodium-platinum elements), using two new designs of multiple shields shown as types E and G in Fig. 4. Direct compari-

son t
veloc
subje
to th
types
length
the
wire
were
becau
coupl
cord
equip
the t
from
(b)
simu
1-hr
therm
samp
calib

FIG.

FIG.

son between the shields, and the B&W MHVT (multiple high-velocity thermocouple), also shown in Fig. 4, were made in the subject furnace. The corrections of the observed temperatures, to the B&W MHVT basis were small, 30 F and 40 F for types E and G, respectively, at 2000 deg F. Because of the short length of the Pt Rh-Pt couple and the high gas-flow rates used in the probes, the temperature of the junction between the lead wire and couple in the probe exceeded the value at which the two were matched, and an additional minor correction was required because of the difference in thermoelectrical properties of the couple and lead wire. The emf of the thermocouples was recorded with a high-speed electronic potentiometer recorder equipped with a 1-hr clock, and representative average values of the temperature of the gas at a sampling point could be obtained from records of $1/2$ to 1 min duration.

(b) Gas analyses and temperature measurements were made simultaneously by connecting a Bailey oxygen recorder, with a 1-hr clock, in series with the aspirating system of the high-velocity thermocouple. Routine complete analysis of the gases being sampled by the Bailey oxygen recorder served both to check the calibration of the Bailey oxygen recorder and to correlate the

oxygen content of the furnace-outlet gas with that of the other gas constituents. As with the temperature measurements, significant average values for the oxygen content of the gas at a sampling point could be obtained from records of $1/2$ to 1 min duration.

(c) Except for analysis of the flue gas entering the air heaters, for which the technique just described was employed, all other required observations were made with plant instrumentation. The temperatures of the flue gas and air entering and leaving the air heaters were recorded at the control board by two resistance thermometers properly situated in each duct at which measurements were made. Coal feed rates were ascertained by recording at regular intervals the time and the number of the trip at each of the four coal scales (two for each mill). Increments of the coal were taken at the scales, following ASTM specifications, and were stored during the test in 10-gal milk pails. The samples were reduced to approximately 35 lb and shipped to Pittsburgh in sealed cans for analysis by the Coal Analysis Section of the Bureau of Mines.

The quantity of fly ash in the gas entering the Cottrell precipitators was determined by the staff of the Louisville Gas & Electric Company, using the methods of the Research Corporation and with equipment supplied by the latter company. The fly ash was analyzed by the Coal Analysis Section of the Bureau of Mines.

The humidity of the air was determined by sling psychrometer at the F.D. fan inlet.

General Test Procedure. The superheaters and air heaters were blown routinely before each test, and, as required, excess slag deposits on the furnace screen were removed by hand lancing. The necessary burner adjustments were made, the load was adjusted to the desired value, and the fans were balanced as closely as possible. A preliminary analysis of the furnace gas was made through door C, and the air flow was then adjusted accordingly to give the desired excess air at the furnace outlet. Because of occasional nonuniformity of the gas at the furnace outlet, this procedure involved some guesswork and did not always yield the desired excess air. Coal-scale readings were started as soon as the unit was stabilized, and the test continued for a period of about 4 hr, the time necessary to make a complete set of all the

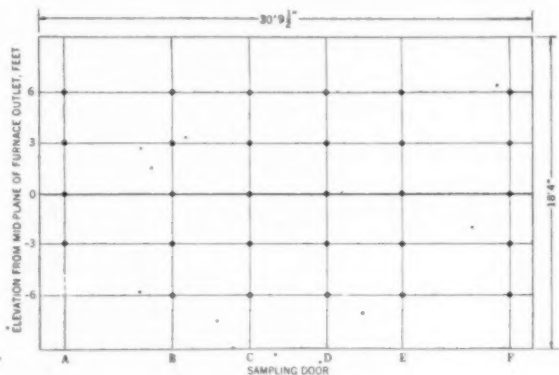


FIG. 2 DISTRIBUTION OF SAMPLING POINTS AT FURNACE OUTLET

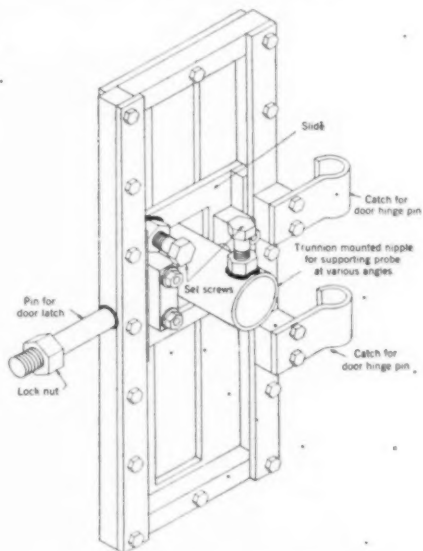


FIG. 3 LANCING-DOOR INSERT FOR SUPPORTING WATER-COOLED HIGH-VELOCITY THERMOCOUPLE PROBE

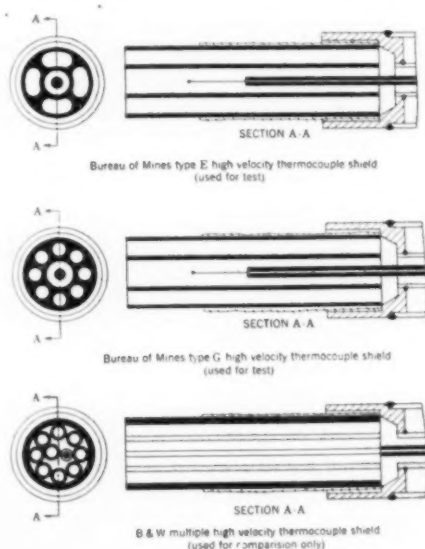


FIG. 4 RADIATION SHIELDS FOR HIGH-VELOCITY THERMOCOUPLE

measurements required for the committee's investigation. The survey at the furnace outlet usually required less than 3 hr.

Methods of Calculation. (a) *Temperature and Gas-Composition Data.* Because the sampling points are quite uniformly distributed over the furnace-outlet area, simple numerical averages were calculated of the observed temperature and oxygen-concentration data. These averages, with appropriate corrections, were then used in all subsequent calculations, as previous considerations⁴ had shown that more rigorous treatment can rarely be justified.

(b) *Furnace Heat Balance.* The heat absorption in the furnace is calculated as the difference between the net heat available in the furnace and the heat lost from the furnace in the products of combustion, and by radiation and convection from the furnace casing. The net heat available in the furnace is the sum of the low-heat value of the fuel fired (corrected for unburned combustible) and the sensible heat in the preheated air. Combustible losses were calculated from the analysis of the fly ash, the fly ash concentration, and the calculated quantities of the gases at the entrance to the Cottrell precipitator. The sensible heat in the preheated air was calculated from a heat balance on the air heaters, employing the known temperatures of the gas and air streams entering and leaving the air heaters, the average composition of the gas entering the air heater, and an assumed value for the air leakage in the preheater equal to 5 per cent by weight of the gas entering the heater.⁵

The enthalpy of the furnace-outlet gas was calculated from the quantities of the respective gases at the furnace outlet (computed from the gas composition and corrected fuel analysis), and the heat contents of the individual gases at the average temperature of the furnace-outlet gas, obtained from the tables of Heck.⁶

For the purpose of these calculations it was assumed that all the ash left the furnace at the temperature of the gases; the heat content was calculated using a mean specific heat of 0.27 Btu per lb deg F. The heat loss from the furnace casing was taken as one half that of the entire unit as given by the ABMA Standard Radiation Loss Chart.

RESULTS OF TESTS

Description of Tests. The operating data and the results obtained in the fifteen tests are summarized in Table 1. The tests are divided into three groups; group 1, consisting of eight tests at full load, numbers 15, 15A, 16, 17, 18, 19, 21, and 22, was made to determine the effect on furnace heat absorption of variations of excess air and secondary-air vane settings at the test load. Group 2, consisting of three tests at three-quarters load, numbers 24, 25, and 26, was made to determine the effect of secondary-air vane settings at the test load; and group 3, consisting of four tests at half-load, numbers 27, 28, 29, and 30, was made to determine the effect of the number and location of the burners, at the test load. The fuel burned in these tests consisted of a quite uniform mixture of high-volatile C West Kentucky coals. There was little variation in coal composition from test to test, as shown in Table 1.

Temperature and Gas Composition at the Furnace Outlet. Of considerable interest, in addition to the calculated furnace heat absorption, is the distribution of the temperature and composition of the gases at the furnace outlet. These data are given in Tables 2 and 3, respectively. The temperature data in Table 2 are the values observed with the shields used in the particular test; for the heat-absorption calculations, the averages of these values

were corrected to the B&W MHVT basis and for lead-junction errors as shown in Table 4. The gas compositions in Table 3 are expressed as per cent excess air, as possibly affording more familiar and representative values than the oxygen percentages actually observed. A recent discussion⁴ showed that these values are quite representative of the average conditions for which the tests were made, and, when plotted on a map of the furnace outlet, yield consistent and significant distribution patterns. This is illustrated in Figs. 5 and 6, which are distribution plots of the temperature and composition of the gas at the furnace outlet, respectively, for test 22.

These plots demonstrate some of the outstanding characteristics of the type of firing used in the subject boiler. One of these is the considerable spread of temperature of the gases at the furnace outlet, compared to the spread in gas composition. Thus the gas at sampling point D+6, excess air 33.7 per cent, leaves the furnace at 1920 F, whereas the gas at sampling point D-6, excess air 32.9 per cent, or practically the same as that of the gas at D+6, leaves the furnace at 2320 F. It is evident that the coal-air mixtures from which these streams of gases originated were quite similar, but had considerably different experiences in traversing the furnace volume from the burner to the furnace outlet. The gas leaving the furnace at D+6 has lost considerably more heat to the walls than the gas leaving the furnace at D-6; this is probably due to a longer residence time in the furnace, and probably a lower average velocity in the furnace. This is in accord with visual observations of the velocity of the gases leaving

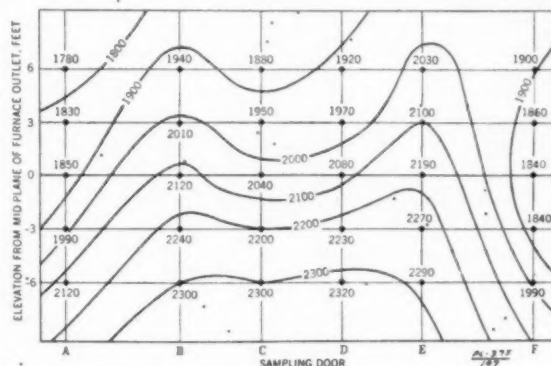


FIG. 5 DISTRIBUTION OF TEMPERATURE, DEG F, AT FURNACE OUTLET, TEST NO. 22

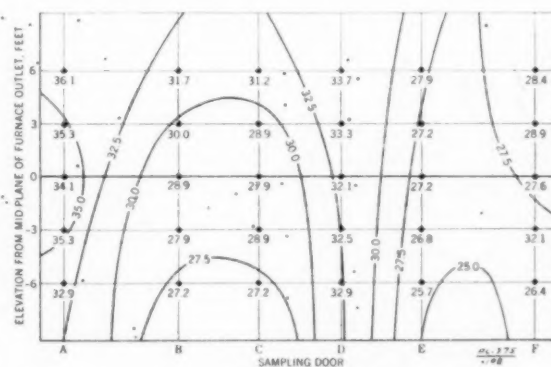


FIG. 6 DISTRIBUTION OF EXCESS AIR, PER CENT, AT FURNACE OUTLET, TEST NO. 22

⁴ "Heat Transfer and Fluid Resistances in Ljungström Regenerative-Type Air Preheaters," by Hilmer Karlsson and Sven Holm, Trans. ASME, vol. 65, 1943, pp. 61-72.

⁵ "The New Specific Heats," by R. C. H. Heck, *Mechanical Engineering*, vol. 62, 1940, pp. 9-12.

TABLE 1 SUMMARY OF DATA AND RESULTS, ASME FURNACE HEAT-ABSORPTION TESTS, BOILER NO. 3, PADDY'S RUN STATION, LOUISVILLE GAS & ELECTRIC COMPANY, OCTOBER 26-30, 1948

Test number	October 26-30, 1948									
	15	16	17	18	19	20	21	22	23	24
1 Date	10-27-48	10-27-48	10-28-48	10-28-48	10-29-48	10-29-48	10-30-48	10-30-48	10-30-48	10-30-48
2 Start of Test	9:09 A.M.	8:11 P.M.	4:09 P.M.	1:57 P.M.	6:20 P.M.	4:10 P.M.	10:02 A.M.	11:00 A.M.	6:17 A.M.	1:11 A.M.
3 End of Test	1:15 P.M.	11:42 P.M.	7:20 P.M.	5:15 A.M.	3:45 P.M.	1:12 P.M.	7:19 P.M.	1:25 P.M.	9:08 A.M.	4:03 A.M.
4 Corrected steam flow, lb per hr	635.4	625.9	628.1	624.2	628.7	628.1	628.1	628.1	628.1	628.1
5 Corrected feedwater flow, lb per hr	635.4	625.9	628.1	624.2	628.7	628.1	628.1	628.1	628.1	628.1
6 Corrected steam flow, lb per hr	635.4	625.9	628.1	624.2	628.7	628.1	628.1	628.1	628.1	628.1
7 Corrected feedwater flow, lb per hr	635.4	625.9	628.1	624.2	628.7	628.1	628.1	628.1	628.1	628.1
8 Final Steam Temperature, °F	489	489	489	489	489	489	489	489	489	489
9 Number of burners used and arrangement	4	4	4	4	4	4	4	4	4	4
10 Secondary air valve position, percent open	100	100	100	100	100	100	100	100	100	100
11 Coal feed rate, as fired weight, lb per hr	49,130	49,130	49,130	49,130	49,130	49,130	49,130	49,130	49,130	49,130
12 Coal, proximate analysis, percent as fired										
13 Moisture	10.7	10.7	10.7	10.7	10.7	10.7	10.7	10.7	10.7	10.7
14 Volatile matter	33.8	34.2	33.8	33.8	33.8	33.8	33.8	33.8	33.8	33.8
15 Ash	12.2	12.6	12.6	12.6	12.6	12.6	12.6	12.6	12.6	12.6
16 Coal, ultimate analysis, percent as fired										
17 Carbon	84.4	84.4	84.4	84.4	84.4	84.4	84.4	84.4	84.4	84.4
18 Hydrogen	8.1	8.1	8.1	8.1	8.1	8.1	8.1	8.1	8.1	8.1
19 Nitrogen	1.2	1.2	1.2	1.2	1.2	1.2	1.2	1.2	1.2	1.2
20 Oxygen	7.6	7.6	7.6	7.6	7.6	7.6	7.6	7.6	7.6	7.6
21 Sulfur	0.4	0.4	0.4	0.4	0.4	0.4	0.4	0.4	0.4	0.4
22 High heating value, as fired, Btu per lb	10,900	11,260	10,450	11,010	10,960	10,960	11,130	10,770	10,990	10,870
23 Grindability, Hardgrove index	63	62	64	62	64	64	61	67	62	64
24 Air flow rate, lb per hr	3,000	3,070	3,000	3,000	3,000	3,000	3,000	3,000	3,000	3,000
25 Air flow rate, lb per hr	3,000	3,070	3,000	3,000	3,000	3,000	3,000	3,000	3,000	3,000
26 Air flow rate, lb per hr	3,000	3,070	3,000	3,000	3,000	3,000	3,000	3,000	3,000	3,000
27 Air flow rate, lb per hr	3,000	3,070	3,000	3,000	3,000	3,000	3,000	3,000	3,000	3,000
28 Air flow rate, lb per hr	3,000	3,070	3,000	3,000	3,000	3,000	3,000	3,000	3,000	3,000
29 Air flow rate, lb per hr	3,000	3,070	3,000	3,000	3,000	3,000	3,000	3,000	3,000	3,000
30 Air flow rate, lb per hr	3,000	3,070	3,000	3,000	3,000	3,000	3,000	3,000	3,000	3,000
31 Air flow rate, lb per hr	3,000	3,070	3,000	3,000	3,000	3,000	3,000	3,000	3,000	3,000
32 Air flow rate, lb per hr	3,000	3,070	3,000	3,000	3,000	3,000	3,000	3,000	3,000	3,000
33 Air flow rate, lb per hr	3,000	3,070	3,000	3,000	3,000	3,000	3,000	3,000	3,000	3,000
34 Air flow rate, lb per hr	3,000	3,070	3,000	3,000	3,000	3,000	3,000	3,000	3,000	3,000
35 Air flow rate, lb per hr	3,000	3,070	3,000	3,000	3,000	3,000	3,000	3,000	3,000	3,000
36 Air flow rate, lb per hr	3,000	3,070	3,000	3,000	3,000	3,000	3,000	3,000	3,000	3,000
37 Air flow rate, lb per hr	3,000	3,070	3,000	3,000	3,000	3,000	3,000	3,000	3,000	3,000
38 Air flow rate, lb per hr	3,000	3,070	3,000	3,000	3,000	3,000	3,000	3,000	3,000	3,000
39 Air flow rate, lb per hr	3,000	3,070	3,000	3,000	3,000	3,000	3,000	3,000	3,000	3,000
40 Air flow rate, lb per hr	3,000	3,070	3,000	3,000	3,000	3,000	3,000	3,000	3,000	3,000
41 Air flow rate, lb per hr	3,000	3,070	3,000	3,000	3,000	3,000	3,000	3,000	3,000	3,000
42 Air flow rate, lb per hr	3,000	3,070	3,000	3,000	3,000	3,000	3,000	3,000	3,000	3,000
43 Air flow rate, lb per hr	3,000	3,070	3,000	3,000	3,000	3,000	3,000	3,000	3,000	3,000
44 Air flow rate, lb per hr	3,000	3,070	3,000	3,000	3,000	3,000	3,000	3,000	3,000	3,000
45 Air flow rate, lb per hr	3,000	3,070	3,000	3,000	3,000	3,000	3,000	3,000	3,000	3,000
46 Air flow rate, lb per hr	3,000	3,070	3,000	3,000	3,000	3,000	3,000	3,000	3,000	3,000
47 Air flow rate, lb per hr	3,000	3,070	3,000	3,000	3,000	3,000	3,000	3,000	3,000	3,000
48 Air flow rate, lb per hr	3,000	3,070	3,000	3,000	3,000	3,000	3,000	3,000	3,000	3,000
49 Air flow rate, lb per hr	3,000	3,070	3,000	3,000	3,000	3,000	3,000	3,000	3,000	3,000
50 Air flow rate, lb per hr	3,000	3,070	3,000	3,000	3,000	3,000	3,000	3,000	3,000	3,000
51 Air flow rate, lb per hr	3,000	3,070	3,000	3,000	3,000	3,000	3,000	3,000	3,000	3,000
52 Air flow rate, lb per hr	3,000	3,070	3,000	3,000	3,000	3,000	3,000	3,000	3,000	3,000
53 Air flow rate, lb per hr	3,000	3,070	3,000	3,000	3,000	3,000	3,000	3,000	3,000	3,000
54 Air flow rate, lb per hr	3,000	3,070	3,000	3,000	3,000	3,000	3,000	3,000	3,000	3,000
55 Air flow rate, lb per hr	3,000	3,070	3,000	3,000	3,000	3,000	3,000	3,000	3,000	3,000
56 Air flow rate, lb per hr	3,000	3,070	3,000	3,000	3,000	3,000	3,000	3,000	3,000	3,000
57 Air flow rate, lb per hr	3,000	3,070	3,000	3,000	3,000	3,000	3,000	3,000	3,000	3,000
58 Air flow rate, lb per hr	3,000	3,070	3,000	3,000	3,000	3,000	3,000	3,000	3,000	3,000
59 Air flow rate, lb per hr	3,000	3,070	3,000	3,000	3,000	3,000	3,000	3,000	3,000	3,000
60 Air flow rate, lb per hr	3,000	3,070	3,000	3,000	3,000	3,000	3,000	3,000	3,000	3,000

1/ Main and auxiliary burners, two mills
 2/ Two lower, two outer lower mill and auxiliary burners, north mill only
 3/ This and subsequent figures were rounded after calculation
 4/ Calculated from heat balance on air heater
 5/ One half total loss for entire boiler as given by ASME Standard
 6/ Based on total projected heat receiving surface of 1,000 ft²

7/ General standard time; time of first coal scale reading preceding period of test surveys
 8/ General standard time; time of first coal scale reading following period of test surveys
 9/ Main and auxiliary burners
 10/ Main and auxiliary burners
 11/ Main and auxiliary burners
 12/ Main and auxiliary burners
 13/ Main and auxiliary burners
 14/ Main and auxiliary burners
 15/ Main and auxiliary burners
 16/ Main and auxiliary burners
 17/ Main and auxiliary burners
 18/ Main and auxiliary burners
 19/ Main and auxiliary burners
 20/ Main and auxiliary burners
 21/ Main and auxiliary burners
 22/ Main and auxiliary burners
 23/ Main and auxiliary burners
 24/ Main and auxiliary burners
 25/ Main and auxiliary burners
 26/ Main and auxiliary burners
 27/ Main and auxiliary burners
 28/ Main and auxiliary burners
 29/ Main and auxiliary burners
 30/ Main and auxiliary burners
 31/ Main and auxiliary burners
 32/ Main and auxiliary burners
 33/ Main and auxiliary burners
 34/ Main and auxiliary burners
 35/ Main and auxiliary burners
 36/ Main and auxiliary burners
 37/ Main and auxiliary burners
 38/ Main and auxiliary burners
 39/ Main and auxiliary burners
 40/ Main and auxiliary burners
 41/ Main and auxiliary burners
 42/ Main and auxiliary burners
 43/ Main and auxiliary burners
 44/ Main and auxiliary burners
 45/ Main and auxiliary burners
 46/ Main and auxiliary burners
 47/ Main and auxiliary burners
 48/ Main and auxiliary burners
 49/ Main and auxiliary burners
 50/ Main and auxiliary burners
 51/ Main and auxiliary burners
 52/ Main and auxiliary burners
 53/ Main and auxiliary burners
 54/ Main and auxiliary burners
 55/ Main and auxiliary burners
 56/ Main and auxiliary burners
 57/ Main and auxiliary burners
 58/ Main and auxiliary burners
 59/ Main and auxiliary burners
 60/ Main and auxiliary burners

Additional data are available on fly ash analysis and distribution, and humidity of combustion air. For tests 18, 19, 24, 25, 26, the forms of sulfur and carbonate in coal were determined, as well as the ash cone softening temperatures in an oxidizing atmosphere.

TABLE 2 OBSERVED GAS TEMPERATURES DEG. F. AT FURNACE OUTLET, ASME FURNACE HEAT-ABSORPTION TESTS, BOILER NO. 3, PADDY'S RUN STATION

Test No./Door/Position	15	15A	16	17	18	19	21	22	24	25	26	27	28	29	30	
A	+6	1740	1710	1820	1730	1780	1760	1740	1780	1600	1590	1660	1510	1440	1450	1460
	+3	1880	1760	1770	1880	1960	1870	1880	1830	1890	1720	1670	1500	1610	1480	1460
	0	2060	1910	1740	2020	2210	2010	2060	1850	1930	1860	1710	1640	1710	1580	1560
	-3	2130	1960	1880	2130	2270	2040	2090	1990	1990	1980	1800	1750	1740	1660	1600
	-6	2110	1970	2060	2200	2300	2160	2140	2120	2020	1940	1970	1870	1750	1750	1800
B	+6	1990	2030	1980	1990	2040	1890	1950	1940	1850	1860	1800	1710	1570	1660	1630
	+3	2010	2070	2070	2030	2090	2000	1960	2010	1870	1880	1870	1770	1610	1680	1700
	0	2030	2150	2160	2100	2150	2100	2010	2120	1930	1940	1960	1840	1670	1750	1770
	-3	2060	2160	2280	2180	2190	2210	2070	2240	1990	2030	2010	1900	1750	1810	1840
	-6	2160	2230	2360	2170	2250	2340	2180	2300	2090	2180	2160	1980	1860	1870	1840
C	+6	1890	1970	1940	1950	1910	1900	1890	1880	1800	1760	1710	1660	1560	1590	1590
	+3	1880	1970	1980	1940	1930	1880	1880	1950	1820	1790	1760	1650	1590	1640	1630
	0	1940	2060	2060	2000	2020	2060	1970	2040	1860	1810	1810	1720	1660	1710	1680
	-3	2070	2170	2180	2070	2130	2220	2030	2200	1920	1920	1920	1790	1770	1780	1780
	-6	2190	2270	2360	2190	2240	2350	2150	2300	2000	2130	2090	1970	1900	1860	1860
D	+6	1850	1890	1770	1900	1860	1970	1830	1920	1730	1770	1690	1620	1610	1570	1620
	+3	1900	1960	1830	1940	1930	2080	1870	1970	1750	1870	1710	1650	1620	1660	1660
	0	1980	2070	1930	2010	1980	2150	1970	2080	1840	1980	1790	1700	1670	1720	1690
	-3	2090	2160	2060	2080	2060	2310	2040	2230	1910	2060	1830	1780	1800	1800	1780
	-6	2230	2230	2250	2210	2150	2330	2180	2320	2010	2180	1940	1920	1950	1860	1870
E	+6	1840	1950	1850	1870	1790	2020	1840	2030	1740	1660	1620	1630	1660	1570	1660
	+3	1880	2030	1940	1930	1860	2070	1900	2100	1810	1700	1910	1690	1720	1630	1700
	0	2010	2120	2060	2010	1920	2180	2030	2190	1910	1750	2030	1750	1790	1690	1790
	-3	2080	2220	2150	2110	2060	2270	2120	2270	1960	1820	2100	1800	1870	1730	1860
	-6	2200	2190	2260	2300	2200	2360	2190	2290	2040	1870	2120	1820	1970	1800	1870
F	+6	1740	1810	1720	1810	1710	1830	1740	1900	1630	1700	1740	1680	1620	1420	1590
	+3	1780	1790	1740	1800	1730	1810	1780	1860	1630	1710	1700	1640	1610	1480	1620
	0	1800	1810	1780	1830	1680	1800	1790	1840	1630	1690	1660	1630	1690	1490	1680
	-3	1840	1990	1880	1900	1750	1900	1830	1840	1680	1810	1760	1640	1730	1460	1610
	-6	1910	2130	2070	2060	1900	2130	1970	1990	1800	1930	1900	1620	1780	1480	1700
Average		1975	2024	1997	2011	1999	2069	1969	2046	1848	1861	1852	1715	1705	1654	1691

a/ Uncorrected; for corrections see Table 4.

b/ For test conditions, see Table 1.

c/ For location at furnace outlet, see Figure 2.

d/ Data not taken; extrapolated value

the furnace, being greatest at the bottom of the outlet and lowest at the top. The effect of this behavior on the radiation heat transfer in the furnace will be considered in a later part of this paper.

Detailed distribution data of the type shown in Figs. 5 and 6 assist in understanding ash deposition and slagging of the screen and superheater. The wide spread in temperatures at the furnace outlet demonstrates the readiness with which excessive temperatures can exist, even though the mean value is less than some assumed safe limit.

The distribution plots for the other tests are not given, but may readily be constructed from the data in Tables 2 and 3.

Furnace Heat Absorption. For reader reference, a condensed summary of the test conditions and results is presented in Table 5 in which each test is given a reference letter. In Fig. 7 the observed furnace heat-absorption efficiency has been plotted against excess air for the various combinations of the other test variables. The furnace heat-absorption efficiency is used in Fig. 7 because it is less sensitive than furnace heat absorption to the unavoidable variations in the net heat available in the tests at each particular boiler load. Lines have been drawn in Fig. 7 indicating the effect of excess air on furnace heat-absorption efficiency, for the various settings of the secondary-air vanes at full and three-quarters load; and for the various locations and number of burners used, at half-load. At full load there are enough experimental points to establish these lines, and, except for points B and C, tests 15A and 16, respectively, the relationships are quite definite. At three-quarters and half-load, the variations of furnace heat-absorption efficiency with excess air can only be inferred; these lines (dashed) have been given successively lower slopes as the load decreases, in accord with the behavior found in another furnace.³

TABLE 4 CORRECTIONS OF OBSERVED AVERAGE TEMPERATURE TO B&W MHV BASIS, ASME FURNACE HEAT-ABSORPTION TESTS, BOILER NO. 3, PADDY'S RUN STATION, LOUISVILLE GAS & ELECTRIC COMPANY, OCTOBER 20-30, 1948.

Observed average temp., deg. F	Total correction (to MHV basis and for lead-junction error), deg. F	
	Type E shield	Type G shield
1600	25	31
1700	30	37
1800	35	43
1900	41	50
2000	46	56
2100	51	62

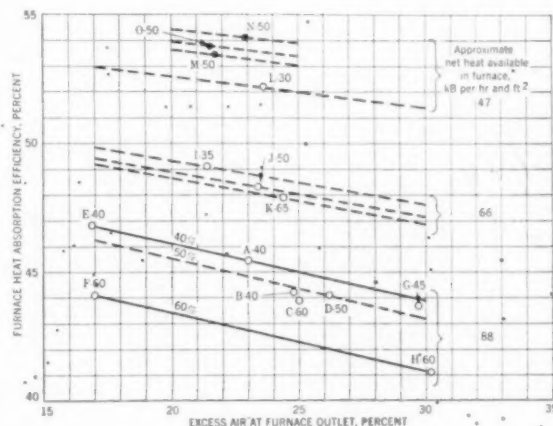


FIG. 7 FURNACE HEAT-ABSORPTION EFFICIENCY AS AFFECTED BY EXCESS AIR, NET HEAT AVAILABLE IN FURNACE, SECONDARY-AIR VANE SETTINGS, AND NUMBER AND LOCATION OF BURNERS USED (O, Eight burners, ●, four burners; letter designates test, see Table 5; number after letter is secondary-air vane opening, per cent.)

TABLE 3 OBSERVED GAS COMPOSITION AT FURNACE OUTLET, EXPRESSED AS PER CENT EXCESS AIR, ASME FURNACE HEAT ABSORPTION TESTS, BOILER NO. 3, PADDY'S RUN STATION

Test No. ^a / Door ^b / Position ^b	15	15A	16	17	18	19	21	22	24	25	26	27	28	29	30
A															
+6	31.9	30.6	28.2	36.7	23.0	25.7	39.0	36.1	29.2	34.6	36.4	31.1	31.1	33.9	25.6
+3	28.3	27.7	28.2	32.6	20.5	26.3	35.4	35.3	27.4	30.0	35.7	31.3	25.3	35.2	24.9
0	26.4	27.7	29.2	30.2	18.5	23.7	33.6	34.1	22.2	28.0	32.8	28.5	24.9	32.3	26.1
-3	27.7	28.5	29.2	28.8	23.4	24.1	30.9	35.3	22.5	27.0	31.6	28.6	24.2	28.8	27.2
-6	26.9	27.2	27.3	32.1	24.4	23.7	34.2	32.9	21.6	27.4	25.5	26.9	24.6	30.7	24.2
B															
+6	25.4	27.2	26.4	30.2	16.7	19.2	32.6	31.7	20.5	25.6	27.4	23.9	25.3	28.4	21.7
+3	24.6	25.9	25.0	27.6	16.7	17.9	28.6	30.0	21.2	24.7	26.1	23.8	26.7	26.6	22.4
0	26.8	25.5	24.1	28.3	16.4	17.4	30.0	28.9	21.2	24.4	25.0	23.0	23.1	24.8	22.8
-3	25.4	26.4	23.2	26.7	16.9	17.8	29.2	27.9	20.5	22.7	24.7	23.8	23.1	26.2	20.4
-6	26.4	26.4	23.7	27.6	17.4	17.1	27.6	27.2	19.6	20.8	23.7	23.0	23.6	25.6	21.7
C															
+6	26.9	27.2	27.3	28.6	20.0	18.1	30.9	31.2	22.6	27.4	26.5	26.4	25.6	25.5	21.0
+3	26.8	25.9	24.6	27.6	17.4	16.7	30.4	28.9	23.3	25.0	27.0	26.9	24.9	24.1	21.0
0	26.4	25.9	26.0	27.2	16.0	17.4	27.6	27.9	22.2	25.5	25.0	24.6	24.2	22.7	21.7
-3	22.8	24.3	25.0	26.4	15.7	14.4	27.6	28.9	20.5	23.6	26.0	25.0	23.1	24.1	23.6
-6	23.2	25.5	25.0	26.4	16.4	16.0	27.6	27.2	19.5	19.8	21.2	23.0	20.6	24.1	22.0
D															
+6	20.2	26.7	25.8	26.7	17.6	16.4	30.9	33.7	21.9	21.2	23.3	23.0	22.0	24.4	20.4
+3	21.5	23.9	23.7	24.7	15.7	14.6	28.8	33.3	22.6	20.8	24.0	22.2	19.9	22.0	21.0
0	19.4	22.7	22.8	23.6	15.7	13.8	28.4	32.1	20.6	18.8	22.9	21.9	21.0	22.0	22.4
-3	19.3	23.9	21.5	25.1	15.3	11.6	28.4	32.5	19.8	18.2	22.6	23.0	18.2	20.9	21.0
-6	19.9	23.1	21.5	24.3	15.0	14.6	28.8	32.9	18.9	16.9	18.8	22.7	17.1	20.6	23.6
E															
+6	20.6	23.5	25.4	23.1	15.3	15.7	28.0	27.9	19.5	22.6	19.6	22.7	22.0	19.2	19.0
+3	20.3	22.7	22.6	23.1	14.6	16.0	27.6	27.2	20.5	21.2	21.2	21.9	19.0	18.2	20.6
0	18.1	22.7	22.3	20.8	13.8	13.0	27.6	27.2	20.6	19.6	20.5	20.4	17.9	17.6	19.9
-3	20.6	21.6	24.1	21.1	14.0	14.0	26.4	26.8	18.6	18.8	19.2	20.4	17.4	14.8	19.3
-6	18.1	21.9	21.9	23.5	14.6	14.6	26.0	25.7	16.6	19.2	18.6	16.7	16.1	15.7	17.4
F															
+6	20.5	23.9	26.8	25.5	15.7	16.0	30.0	28.4	21.9	24.0	23.3	20.7	24.2	19.9	19.3
+3	20.6	22.4	25.4	23.9	14.0	16.0	29.2	28.9	21.6	24.4	22.6	21.5	20.6	17.3	18.6
0	20.6	23.1	25.8	23.1	16.7	14.6	28.2	27.5	23.6	25.5	23.6	21.5	17.9	16.6	21.0
-3	20.6	21.6	25.0	22.7	14.6	16.0	30.9	32.1	22.2	24.4	22.6	21.1	17.9	19.2	19.6
-6	20.5	18.9	24.6	19.3	16.0	14.4	26.8	26.4	21.9	23.6	18.5	21.9	17.9	15.7	16.6

a/ For test conditions, see Table 1.

b/ For location at furnace outlet, see Figure 2.

From Fig. 7 it will be noted that the effect of secondary-air vane setting is quite pronounced at full load; a change in the setting from 60 to 40 per cent open at 17 per cent excess air increases the furnace heat-absorption efficiency from 44.1 to 46.8 per cent. Also, the effect of secondary-air vane setting is considerably reduced at three-quarters load; a change in the setting from 65 to 35 per cent open, at 23 per cent excess air, increases the furnace heat-absorption efficiency by only 0.6 per cent. The effect at half-load may be presumed to be negligible. Further, the effect of secondary-air vane setting at full load appears to be quite independent of excess air, the change in furnace heat-absorption efficiency due to change in secondary-air vane setting from 60 to 40 per cent open being 2.7, 2.7, and 2.7 per cent at 17, 23, and 29 per cent excess air, respectively. Similarly, the effect of change of excess air, at constant secondary-air vane opening, appears to be independent of the opening of the secondary-air vanes. Figs. 8 and 9 are similar plots of the experimental results, showing the furnace heat absorption and the average temperature of the furnace-outlet gases, respectively.

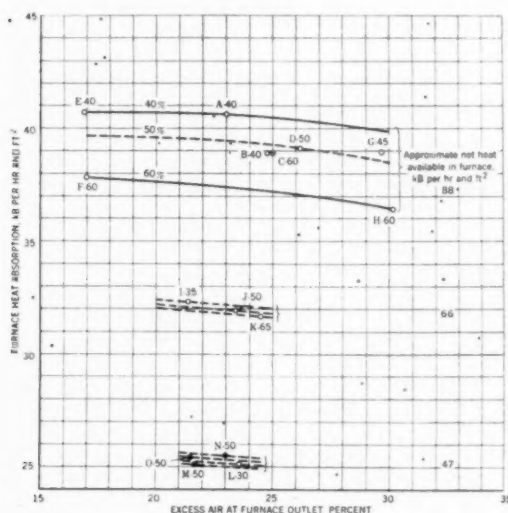


FIG. 8 FURNACE HEAT ABSORPTION AS AFFECTED BY EXCESS AIR, NET HEAT AVAILABLE IN FURNACE, SECONDARY-AIR VANE SETTINGS, AND NUMBER AND LOCATION OF BURNERS USED

(O, Eight burners, ●, four burners; letter designates test, see Table 5; number after letter is secondary-air vane opening, per cent.)

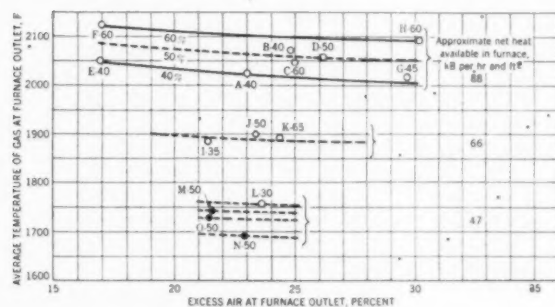


FIG. 9 AVERAGE TEMPERATURE OF FURNACE-OUTLET GAS AS AFFECTED BY EXCESS AIR, NET HEAT AVAILABLE IN FURNACE, SECONDARY-AIR VANE SETTINGS, AND NUMBER AND LOCATION OF BURNERS USED

(O, Eight burners, ●, four burners; letter designates test, see Table 5; number after letter is secondary-air vane opening, per cent.)

The rather complicated relationships between the variables cannot be represented simply, and a number of curves are required. Fig. 10 shows the effect of net heat available in the furnace on furnace heat absorption for three different values for the excess air at the furnace outlet, all at one setting of the secondary-air vanes, 40 per cent open. The curve for 23 per cent excess air is drawn with a full line, because all the necessary data are available. The effect of excess air is known only at full loads; therefore the curves for 17 and 29 per cent excess air are drawn with dashed lines.

The upper part of Fig. 10 shows the effect of secondary-air vane opening. The corrections to the furnace heat absorption for secondary-air vane settings other than 40 per cent open are plotted as a function of net heat available in the furnace for secondary-air vane openings of 50 and 60 per cent. Since the effect of secondary-air vane openings is independent of excess air, at least at high loads, Fig. 8, only one set of correction curves is required.

The relationships shown in Fig. 10 apply only to operation

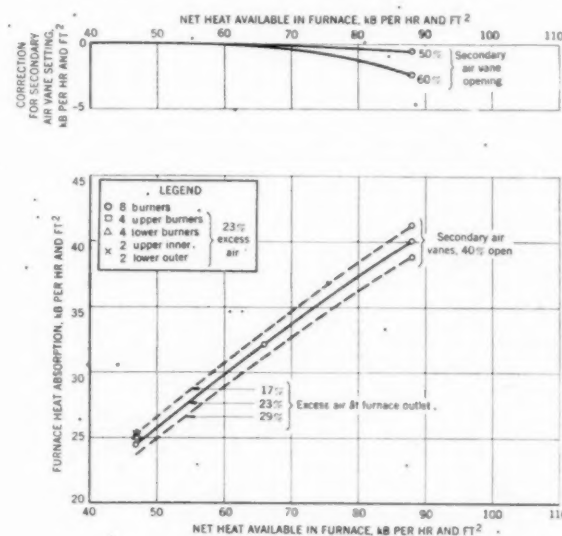


FIG. 10 FURNACE-PERFORMANCE CHARACTERISTICS

with eight burners. The effect of operation with four burners is shown on the lower part of the plot by the additional points representing the results for various combinations of the burners.

The qualitative relationship of all the variables is best conveyed by the isometric three-variable plot in Fig. 11, which readily shows the decrease in furnace heat absorption with increased excess air at all loads, the almost linear increase in furnace heat absorption with increase in net heat available in the furnace, between 47 and 88 kB per hr and ft², and the decrease of furnace heat absorption with increase in the opening of the secondary-air vanes, this effect being independent of excess air, but increasing rapidly with net heat available in the furnace, between 66 and 88 kB per hr and ft².

CORRELATION OF TEST RESULTS

The correlation of the test conditions and results so far given is purely empirical, without reference to the mechanism for heat transfer in the furnace. The information presented, though as comprehensive as the data on which it is based, nevertheless lacks generality because no account has been taken of the fundamental processes involved. Because of the complexity of the problem,

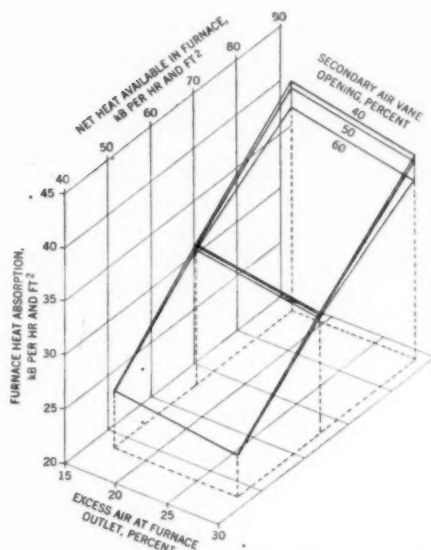


FIG. 11 THREE-VARIABLE REPRESENTATION OF FURNACE PERFORMANCE CHARACTERISTICS FOR EIGHT-BURNER OPERATION

progress in fundamental analysis has been slow, and confined largely to semiempirical correlations based either on the average temperature of the gases at the furnace outlet,^{7,8} or on a radiant mean temperature between the adiabatic temperature and the temperature of the gases leaving the furnace.⁹ Of these procedures the first is more convenient, and is applied to the data of this investigation in Fig. 12 in which the furnace heat absorption, kB per hr and ft², has been plotted against the fourth power of the average temperature of the gases leaving the furnace, deg R; the letter and point symbols correspond to Table 5. For comparison, line Z-Z shows the calculated black-body radiation from a source at the average temperature of the furnace-outlet gas, to the furnace walls at a constant temperature. In view of the cleanliness of the furnace walls, the latter temperature has been taken as 1050 R.

It will be seen that the unit heat transfer, based on the heat-receiving surface, is considerably less than that of a black body at the temperature of the furnace outlet gas, line Z-Z. Expressed in terms of an equivalent gray body at the temperature of the furnace-outlet gases, the heat transfer corresponds to that from a source with an emissivity of about 0.7, for the low-load tests and decreasing at high loads. It is further evident that if the correlation had been based on a radiation mean temperature, according to Blizard,⁹ the apparent emissivity of the source would be still lower. For one test at high load an approximate value of 0.28 was calculated for the apparent emissivity of the source on this basis. This is in sharp contrast to the high emissivities predicted from the work of Sherman¹⁰ for flames having the dimen-

sions of the subject furnace. As an example, Sherman predicted that even after combustion was essentially complete, the gas and suspended ash from Illinois coal would have total emissivities of 0.83 and 0.97 for 12 and 20-ft thicknesses, respectively.

The source of this discrepancy is found readily. The high-temperature gases do not fill the entire furnace volume, and not only is the exposed area of the radiation source less than that of the heat-receiving surface on which the unit heat transfer is calculated, but the mean beam lengths for radiation probably are considerably lower than would be calculated from the furnace dimensions. The ratio of area of flame to area of wall may be estimated as follows: As a first approximation, assuming wall emissivity of unity and flame emissivity equal to flame absorptivity, the net radiation heat transfer from flame to furnace walls, Btu per hr, may be written as

$$Q = \sigma \epsilon_F A_F (T_F^4 - T_W^4)$$

The subscripts *F* and *W* denote the flame and furnace wall, respectively, and

σ = radiation constant

A = area (of envelope for flame; of projected area for wall surface)

T = radiant mean temperature, abs

ϵ = emissivity

This equation may be rewritten as

$$Q = \sigma A_W \epsilon_F \frac{A_F}{A_W} (T_F^4 - T_W^4)$$

in which the product $\epsilon_F (A_F/A_W)$ may be considered an apparent emissivity of the flame, ϵ_F' , calculated from heat transfer per unit wall area, A_W . From an assumed value of true mean emissivity of the flame, $\epsilon_F = 0.9$, and a value of 0.28 for ϵ_F' previously calculated for one of the high-load tests, A_F/A_W may be obtained as the ratio of $\epsilon_F'/\epsilon_F = 0.28/0.9 = 0.31$. So low an indicated area of the flame, and therefore its volume, must include a significant effect of decreased true mean flame emissivity arising from smaller mean beam lengths, and the true value of A_F/A_W is undoubtedly somewhat higher than the value of 0.31 calculated. For the purposes of the present argument, no further refinement of the calculation is warranted.

Somewhat similar considerations were applied by Mumford and Bice¹¹ to the analysis of the effect of tilting the burner in a tangentially fired furnace previously studied by the committee. They concluded that multiplication of the observed rates of heat transfer for different inclination of the burners by the ratios of area of heat-receiving surface to area of flame envelope would have brought all the data into line. No estimate was made by them of the apparent emissivity of the flame, but the unit heat transfer based on the average temperature of the furnace-outlet gas was higher in the tangentially fired furnace than in the subject furnace, indicating that the apparent emissivities were higher.

This discussion has of necessity been only semiquantitative, and has undoubtedly exaggerated the true picture; for instance, the flame never achieves the adiabatic temperature. Also, only the general level of heat transfer has been considered; interpretation of the effect of burner adjustments on heat transfer at constant load is still required. So far it can only be concluded that the heat transfer in the furnace is considerably less than theoretically achievable levels.

¹¹ "An Investigation of the Variation of Heat Absorption in a Pulverized-Coal-Fired Water-Cooled Steam Boiler Furnace IV—Comparison and Correlation of the Results of Furnace Heat-Absorption Investigations," by A. R. Mumford and G. W. Bice, Trans. ASME, vol. 70, 1948, pp. 601-614.

⁷ "An Investigation of Powdered Coal as Fuel for Power-Plant Boilers," by Henry Kreisinger, John Blizard, C. E. Augustine, and B. J. Cross, U. S. Bureau of Mines, Government Printing Office, Washington, D. C., Bulletin 223, 1923.

⁸ "Evaluation of Effective Radiant Heating Surface and Application of the Stefan-Boltzmann Law to Heat Absorption in Boiler Furnaces," by H. F. Mullikin, Trans. ASME, vol. 57, 1935, pp. 517-529.

⁹ "Absorption of Heat by Walls of a Furnace," by John Blizard, ASME Furnace Performance Factors Pamphlet, May, 1944, pp. 79-82. Bound with Trans. ASME, vol. 66, 1944.

¹⁰ "Burning Characteristics of Pulverized Coals and the Radiation From Their Flames," by R. A. Sherman, Combustion, vol. 5, December, 1933, pp. 30-38.

TABLE 5 CONDENSED SUMMARY OF OPERATING CONDITIONS AND RESULTS, ASME FURNACE HEAT-ABSORPTION TESTS, BOILER NO. 3, PADDY'S RUN STATION

1 Test number	16	16A	16	17	18	19	20	21	22	24	26	27	28	29	30
2 Designation	A	B	C	D	E	F	G	H	I	J	K	L	M	N	O
3 Number and arrangement of burners	8	8	8	8	8	8	8	8	8	8	8	8	4 upper	4 lower	2 inner-upper & 2 outer-lower
4 Burner secondary air vane opening, per cent	40	40	50	50	40	40	50	45	60	36	50	56	50	50	60
5 Steam generation, M lb per hr	626.4	626.9	626.5	626.1	624.2	632.7	628.1	626.1	625.4	469.1	464.3	331.7	329.8	331.0	329.1
6 Excess air at furnace outlet, per cent	23.0	24.8	25.0	26.2	16.9	17.0	29.7	29.7	30.2	21.4	23.4	23.6	21.7	23.0	21.6
7 Net heat available in furnace, Btu per hr and ft ²	89.3	87.8	88.4	88.6	86.9	85.7	89.1	89.1	88.6	65.8	66.0	48.0	47.1	47.1	47.2
8 Heat absorption in furnace, Btu per hr and ft ²	40.6	38.9	38.9	39.1	40.7	37.8	38.9	38.9	36.4	32.1	31.7	25.1	25.1	25.5	25.4
9 Heat absorption efficiency, per cent	46.4	44.2	43.9	44.1	46.8	44.3	43.7	43.7	41.1	49.1	48.5	47.9	52.2	54.1	53.7
10 Average temperature of gas at furnace outlet, t_g , deg F	2020	2070	2045	2055	2045	2130	2016	2016	2098	1888	1890	1766	1740	1890	1750
11 t_g , deg R	2480	2530	2506	2535	2506	2590	2476	2476	2556	2345	2360	2215	2200	2150	2190
12 $(\frac{t_g}{1000})^4$	37.8	41.0	39.4	40.0	39.4	44.3	37.6	37.6	42.6	30.2	30.5	24.1	23.6	21.4	23.0

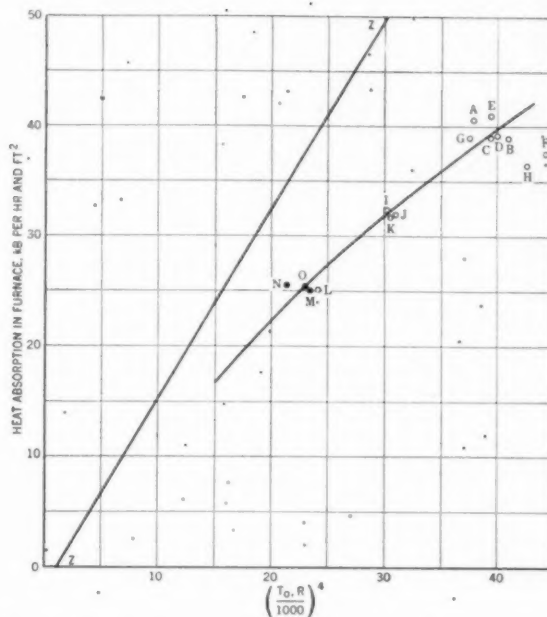


FIG. 12 CORRELATION OF HEAT TRANSFER IN FURNACE WITH FOURTH POWER OF ABSOLUTE TEMPERATURE OF GASES AT FURNACE OUTLET

(O, Eight burners; ●, four burners; letter designates test, see Table 5.)

As previously noted, the gases at the furnace outlet display a characteristic temperature distribution which has been attributed to varying velocities of the respective portions of the gas stream in traversing the furnace volume. One of the possible means by which the setting of the secondary-air vanes may affect heat transfer in the furnace is by changing the velocity-distribution patterns in the furnace. That this probably does not occur, however, is seen from examination of the temperature-distribution data. For example, in both tests 18, and 19, 17 per cent excess air, and 40 and 60 per cent secondary-air vane openings, respectively, the average deviation of the temperature of the gases at the furnace outlet from their mean is 150 F. Thus if the distribution of temperature at the furnace outlet is taken as a criterion, the change in burner vane settings does not affect appreciably the velocity distribution of the gases in the furnace. The effect of secondary-air vane settings must be sought in the delayed combustion which occurs at high secondary-air vane openings. Under these conditions heat release is delayed, and thus radiation is decreased, compared to the turbulent bushy flame conditions obtained with lower secondary-air vane openings.

At the lower burning rates, the temperature and the velocity of the gas leaving the furnace are more uniform, as would be expected, because the total residence time of the gases in the furnace is greater. Similarly, because the percentage heat absorption is greater at low loads, the effect of burner adjustments on heat absorption is less pronounced.

Another factor, which should be considered as affecting the temperature distribution at the furnace outlet, is the tendency for ash deposits to be heavier on the rear than on the front wall of the unit, due to the flame-path characteristics. Thus the insulating effect of the ash would produce higher gas temperatures along the rear than along the front wall, and any temperature gradient at the furnace outlet caused by higher gas velocity along the rear wall, which was discussed previously, would be increased further.

The unique characteristics of each of the different methods of firing pulverized coal have long been recognized and need no emphasis here. Indeed, they form an essential basis for the design of the test program of the Furnace Performance Factors Committee. The important fact brought out by the results of this investigation is that detailed consideration must be given to burner location, flame shape, and volume, and all other factors which affect flame radiation, if a rational basis is to be found for predicting the heat absorption in boiler furnaces. The problem is tremendously complicated, and special attention must be given to these details to obtain basic generalizations.

SUMMARY AND CONCLUSIONS

The absorption of heat in the furnace of the Paddy's Run boiler was measured to provide basic performance data and to determine the relationship between the rate of heat transfer and the observed temperature drop across the furnace-wall tubes. The furnace heat absorption was determined as the difference between the heat input to the furnace, corrected for losses, and the sensible heat in the furnace-outlet gas obtained from measurements of the temperature and composition employing techniques appropriate for furnace testing. The effect on furnace heat absorption of load, excess air, burner setting, and, at low loads, the number and location of the burners, was studied in a series of fifteen tests.

In all tests, the temperature of the gas at the furnace outlet varied considerably with position, being highest at the bottom and lowest at the top. At full load, the spread in temperature exceeded 500 F; at lower loads the spread was somewhat less. In contrast, the composition of the gas at the furnace outlet was considerably more uniform than the temperature. There was little variation of gas composition in any of the tests from the top to the bottom of the outlet, but occasionally nonuniform distribution from side to side. In such cases the excess air was always highest on the left or south side of the furnace. From these observations it is concluded that the variations of the temperature of the gas with position at the outlet originated from variations in the velocity of the gas streams in the furnace. Visual observations of the gas streams did indicate that the velocity of the gas was highest at the bottom of the outlet and decreased toward the top of the outlet. Because of lack of suitable access, no velocity measurements were made to check these observations.

At full load, the furnace heat-absorption efficiency decreased with both increase of excess air, and opening of the secondary-air vane settings. The effect of excess air was independent of the secondary-air vane setting, and the effect of secondary-air vane setting was independent of excess air, over the range of the variables studied. Thus the furnace heat-absorption efficiency decreased about 2.7 per cent for an increase in secondary-air vane opening from 40 to 60 per cent, and decreased about 2.8 per cent for an increase in excess air from 17 to 29 per cent. The corresponding changes in the average temperature of the gases leaving the furnace were about 75 and 30 F, respectively.

At three-quarter load, the furnace heat-absorption efficiency decreased about 0.6 per cent for an increase in secondary-air vane opening from 35 to 65 per cent. The effect of excess air was not determined at this load.

At half-load, only the effect of the number and location of the burners was studied. With eight burners, the secondary-air vanes had to be set at 30 per cent open for good operation; with four burners, the secondary-air vane settings were 50 per cent open. The furnace heat-absorption efficiency was highest when the four lower burners were used; was 0.6 per cent lower when the

four upper burners were used; 1.9 per cent lower when all eight burners were used; and about 0.4 per cent lower when the 2 upper inner and 2 lower outer burners were used. The over-all variation in the average temperature of the gases leaving the furnace for the four combinations of burners was about 75 F.

For otherwise constant conditions, furnace heat absorption increases and furnace heat-absorption efficiency decreases as the heat available in the furnace increases. With eight burners, 40 per cent secondary-air vane opening and 23 per cent excess air, the heat absorption increases almost linearly from about 24 kB per hr and sq ft, at 47 kB per hr and sq ft heat available, to about 40 kB per hr and sq ft at 88 kB per hr and sq ft heat available in the furnace. The corresponding furnace heat-absorption efficiencies are approximately 52 and 45 per cent, respectively. The corresponding average temperatures of the gases leaving the furnace were 1755 and 2020 F, respectively.

At low load, the heat transfer in the furnace corresponded to that by radiation from a body having the area of the heat-receiving surface, the average temperature of the furnace-outlet gas, and an emissivity of 0.67. At higher loads, the apparent emissivity decreased. Analysis of the test results indicates that the area of the envelope of hot gases in the furnace must be considerably less than that of the heat-receiving surfaces. A ratio of 0.31, which is probably somewhat low, was calculated for full-load conditions, on the assumption that the coal is burned instantaneously. This, however, is evidently not the case. Indeed, the effect of burner secondary-air vane settings on furnace heat absorption can best be interpreted in terms of the effect on the rate of combustion of the coal.

This investigation has provided detailed knowledge of the properties of the gas leaving the furnace, and of furnace performance for a wide range of significant operating variables. Although the heat-transfer process in the furnace has not been evaluated quantitatively, a beginning has been made toward better understanding of this basic aspect of the problem of furnace performance.

ACKNOWLEDGMENTS

The authors gratefully acknowledge, with appreciation and thanks, the contributions to this investigation made by the following:

The Special Research Committee on Furnace Performance Factors of The American Society of Mechanical Engineers, for the opportunity to participate in this work, and the individual committee members for advice and help whenever required.

Dr. A. C. Fieldner, Chief, Fuels and Explosives Division, and Dr. R. L. Brown, Chief, Coal Branch, Bureau of Mines, who authorized the work and made many helpful suggestions.

The engineers and assistants of the Combustion Research Section: Messrs. J. W. Myers, J. Jonakin, C. H. Schwartz, J. J. Pfeiffer, G. Kollar, and H. Perry, who capably made the difficult tests that form the basis for this paper.

The officials of the Louisville Gas & Electric Company: A. G. Rosenbaum, Superintendent of Steam Power, Fred Tetzl, Assistant Superintendent of Steam Power, and J. D. Brecher, Plant Engineer, Paddy's Run Station, and their staffs, for willing and able assistance in the arrangement of the tests.

The Bailey Meter Company, for the loan of a recording oxygen meter.

Mr. Fred Ely of the Research and Development Division, Babcock & Wilcox Company, for the loan of a high-speed recording potentiometer.

In
(Part
sourc
resul
data.
which
ing t
and
justn
fect o

T
tions
Resea
first p
of the
of wa
presen
uring
furnac
comp
paper
Par
dimer
meth
of tes
be re
meth
(hr) f
of Fig

¹ E
² A
³ An
Corpo
⁴ "T
of Sur
Whea
tions,
⁵ "I
Temp
by R.
action
Cor
Facto
sent
cembe
NEER
No
under
the S

Furnace Heat Absorption in Paddy's Run Pulverized-Coal-Fired Steam Generator, Using Turbulent Burners, Louisville, Ky.

Part III. Comparison and Correlation of the Results of Furnace Heat-Absorption Investigation

BY H. H. HEMENWAY¹ AND R. I. WHEATER,² NEW YORK, N. Y.

In this paper, the results of the two companion papers (Parts I³ and II⁴) are compared. Some of the possible sources of error are noted. Slightly revised calculated results are obtained by taking weighted averages of the data. The revised results are examined to determine which tests are the most dependable. An equation showing the relationship between furnace exit-gas temperature and furnace heat-absorption rate for a fixed burner adjustment is developed. From the revised results the effect of various factors on furnace performance is shown.

INTRODUCTION

THIS is the third of three papers presenting the results of investigations of furnace performance in the pulverized-coal-fired boiler No. 3 at Paddy's Run. These investigations were conducted under the sponsorship of the ASME Special Research Committee on Furnace Performance Factors. The first paper, Part I,³ of this series presents results and analyses of the data obtained by measuring the furnace face temperatures of waterwall tubes. The second paper, Part II,⁴ of this series presents the results and analyses of the data obtained by measuring the temperature and composition of the gas leaving the furnace and entering the slag screen. This paper deals with the comparison and correlation of the data presented in the first two papers.

Part I and Part II adequately describe the arrangement and dimensions of the furnace tested, the methods of testing, the methods of calculation, and the results obtained by each method of testing. By means of the two methods of testing, which will be referred to herein as the ΔT -method and the heat-balance method, the average heat-absorption rate expressed as MKB/(hr) for each test was determined. In Fig. 1, which is a copy of Fig. 21 of Part I, the results obtained by both methods of

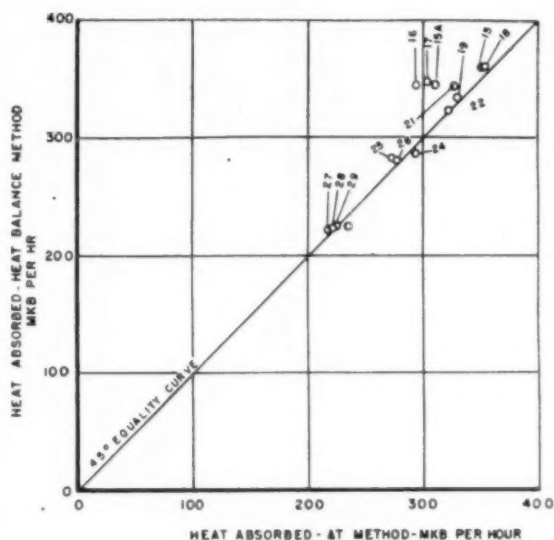


FIG. 1 COMPARISON OF FURNACE HEAT ABSORPTION, COMPUTED FROM WALL-TUBE ΔT -DATA WITH FURNACE HEAT ABSORPTION COMPUTED FROM FURNACE EXIT-GAS TRAVERSE (Number designates test.)

testing are compared, and an examination of this figure shows that except for a few of the full-load tests, the 45-deg equality line falls fairly well within the pattern of test points.

The heat-absorption rate per unit of furnace radiant projected area determined from the heat balance, divided by the average temperature difference between the furnace-tube face and saturated water temperature, ΔT , yields the average over-all heat-transfer coefficient U_o . In Fig. 2 U_o is plotted against ΔT . This figure shows that the average over-all heat-transfer coefficient of 1060 Btu/(hr) (F) (sq ft of projected area), which was assumed in Part I in the calculation of furnace heat absorption by the ΔT -method, does not differ greatly from the values obtained from the heat balance.

THE ΔT -METHOD

Some Sources of Error. The principal sources of error in the ΔT -method which are considered here are as follows:

- (a) Errors in measurement.
- (b) Errors in averaging.
- (c) Errors in the assumptions.

Errors in measurement include the errors in the instruments

¹ Executive Assistant, Foster Wheeler Corporation. Jun. ASME.
² Assistant to the Manager, Service Department, Foster Wheeler Corporation. Mem. ASME.

³ "Part I—Variation in Heat Absorption Shown by Measurement of Surface Temperature of Exposed Side of Furnace Tubes," by R. I. Wheeler and M. H. Howard, published in this issue of the Transactions, pp. 893-923.

⁴ "Part II—Furnace Heat-Absorption Efficiency as Shown by the Temperatures and Composition of the Gases Leaving the Furnace," by R. C. Corey and Paul Cohen, published in this issue of the Transactions, pp. 925-935.

Contributed by the Research Committee on Furnace Performance Factors, and the Fuels, Power, and Heat Transfer Divisions and presented at the Annual Meeting, New York, N. Y., November 27-December 2, 1949, of THE AMERICAN SOCIETY OF MECHANICAL ENGINEERS.

NOTE: Statements and opinions advanced in papers are to be understood as individual expressions of their authors and not those of the Society. Paper No. 49-A-117.

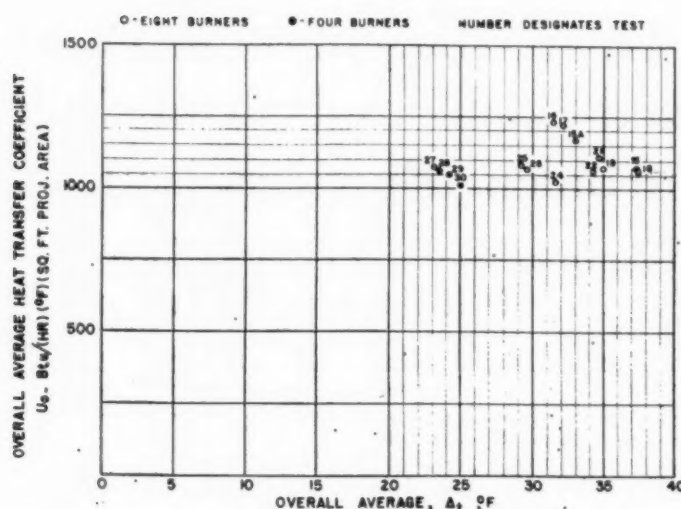


FIG. 2 CORRELATION OF FURNACE WALL-TUBE OVER-ALL AVERAGE HEAT-TRANSFER COEFFICIENT WITH ΔT

which were used in the tests. In addition, they include errors which may have been introduced in the temperature measurements of the front face of the wall tubes by the fact that the thermocouple shield probably served as a shelf for ash deposit and the resulting insulating or shading effect caused the temperature of the couple to be lower than the temperature of the wall of the tube remote from the shield.

In Part I the average over-all ΔT was assumed to be the arithmetic average of the ΔT -values for each live furnace-face thermocouple. Eight of the 128 thermocouples were dead and hence were not included in the averaging. The thermocouples could not be installed at uniform intervals, and none was installed on the rear wall roof or the slag screen. Thus there are reasons to suppose that the use of simple arithmetic averaging introduced some error in the results. In addition, since only one set of readings was taken during each 30-min period, the average value over this period may have differed slightly from the single value recorded owing to the small variations caused by operation with automatic controls.

In making the calculations it was assumed that the average tube-wall thickness at the thermocouple was 0.238 in., that the tube-wall conductivity was 348 (Btu) (in.)/(sq ft) (hr) (F), and that the heat-transfer coefficient from the tube to the water and steam mixture in the tube had a constant value of 5900 Btu/(hr) (F) (sq ft of inner surface of tube). The first two assumptions are probably tolerably accurate, but the third is subject to considerable error. It was assumed also that the heat transferred to the walls of the furnace as a whole was equal to the calculated unit rate of heat absorption multiplied by the projected area of the furnace walls. Since the walls do not have plane surfaces, this assumption, while approximate, is not exact.

In spite of all the possible errors which may have crept into the estimates of the heat absorption calculated by the ΔT -method, nevertheless the average error could not have been great because of the close agreement of the results obtained by this method and the heat-balance method.

Measurement of Saturation Temperature. It was originally assumed that the average temperature of the mixture of boiling water and steam in the tubes of all walls and at all elevations might be represented by the saturation temperature corresponding to the drum pressure. It was noted in analyzing the

results that the temperature measured by the thermocouples, peened to the backs of four rear waterwall tubes just above the hopper at elevation 463 ft did not check the temperature obtained from drum pressure readings. A review of the data indicates that the average pressure drop from the drum to the superheater outlet based on gage readings is as follows:

Evaporation (a) 1000 lb of steam per hr	Pressure drop (b), psi	(b) \times 10,000 (a) ²
625	77	1.97
460	25	1.18
330	29	2.66

From this table it is obvious that one or both pressure gages are in error. A change of 25 psi represents a change of 3.23 deg F in saturation temperature at a pressure of 950 psig. Hence a 25-psi error in pressure-gage measurement introduces in the ΔT -method an error of about 10 per cent in the calculated rate of heat absorption at full load, and of about 14 per cent at half load. With regard to the back-face thermocouple temperature measurements, differences as great as 7 F were measured between adjacent tubes in one round of measurements. Thus, while the averaging of all readings may have eliminated most of the error, some error probably still exists. After some consideration it was decided by the authors of Part I to use the thermocouple measurements to determine saturation temperature.

The assumption that saturation temperature is constant for all elevations is inexact, however, since the pressure and hence the saturation temperature is higher at the lower levels and lower at the upper levels of the furnace. Since the fluid along the length of the furnace tubes consists of saturated water and steam in varying proportions, it is necessary to know something about the circulation characteristics of the unit in order to determine the change in pressure with change in elevation. Circulation tests run in September, 1948, indicated that there was no material change in the total weight flow rate of water in the furnace tubes between half load and full load. From circulation calculations it was estimated that for all tests the saturation temperature was approximately 0.4 F higher in the hopper tubes at the lowest thermocouple elevation, and about 1.7 F lower in the roof tubes at the highest thermocouple location than in the tubes at the 463-ft elevation. The over-all correction was calculated to be plus 0.7 F.

Weighted-Average Values of ΔT . A sketch of the development of the furnace walls showing the location of thermocouples is found in Fig. 3. The dead thermocouples are underlined. The furnace is divided into several areas from A to Q, inclusive. The average ΔT for each area is the average of the ΔT -averages of the rows in the area. The sum of the products of each area by the average ΔT of the area, divided by the total area in which the thermocouples were installed, yields a weighted average ΔT . The weighted average ΔT -values thus calculated, including the $+0.7^\circ\text{F}$ correction mentioned, are tabulated in column 10 of Table 1.

As previously stated, thermocouples were not installed on the inclined rear-wall roof (K), or on the slag screen (I and J). After examination of the data it was thought reasonable to assume that, (1) the average ΔT due to radiation only in the upper screen (I) was equal to the average ΔT of roof (A); (2) the average ΔT in lower slag screen (J) due to radiation only was equal to the average ΔT of the front wall at elevation 525 ft; and (3) the average ΔT of the rear-wall roof (K) was equal to the average ΔT for the other three walls at elevation 511 ft. Applying these values of ΔT to areas (I), (J), and (K), the weighted average ΔT for each test for all furnace areas was calculated. The results, including the $+0.7^\circ\text{F}$ correction, are tabulated in column 11 of Table 1.

In column 12 of Table 1 is tabulated the difference between the final weighted average ΔT and the average ΔT taken from Part I for each test. While the differences are within the probable error of the tests and might be neglected, the weighted-

average values of ΔT should be more accurate and will be used hereafter in this paper.

HEAT-BALANCE METHOD

Some Sources of Error. Part II describes the methods of test and calculation of the heat-balance data. That paper notes that measurements of gas flow and direction were not taken and that the average gas temperature and gas composition for each test were calculated from simple numerical averages of the measurements with appropriate corrections. A possible small source of error lies in the air-leakage into the gas was equal to 5 per cent by weight of the gas entering the air heater. Probably the greatest source of error outside of the possible error in the corrections to the thermocouple measurements lies in the fact that only one traverse of the gases leaving the furnace could be made on each test. In this connection it should be noted that at full load the spread of temperature of the gas leaving the furnace was over 500 F. However, the gas composition was quite uniform, the deviation in per cent excess air rarely exceeding 10 per cent.

Weighted-Average Values of Furnace Exit-Gas Temperature. The sampling doors used for gas-temperature and gas-analysis measurements are not uniformly spaced across the boiler. For this reason simple numerical averages of the measurements where the spread is large may lead to error in the results. A method of obtaining a weighted-average furnace exit-gas temperature is shown in Fig. 4 in which isothermal lines of gas temperature for test No. 15A are drawn. Note that sampling

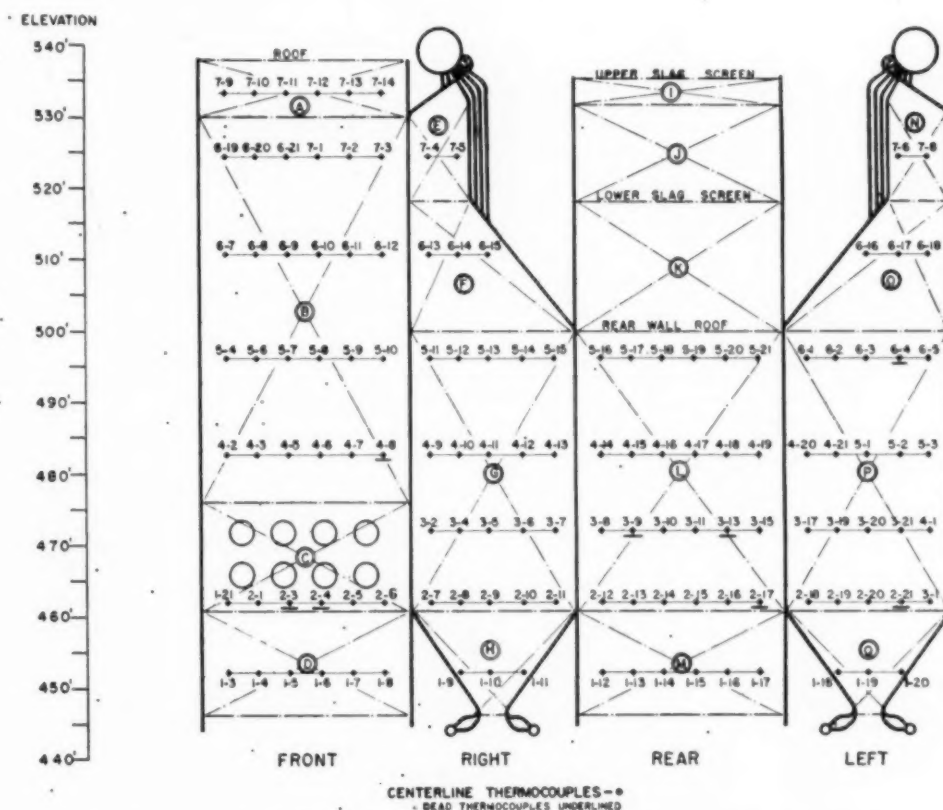


FIG. 3 DIVISION OF FURNACE WALLS INTO AREAS FOR COMPUTING WEIGHTED AVERAGE VALUES OF ΔT

TABLE 1 SUMMARY OF CONDITIONS AND RESULTS BY ΔT -METHOD

1	2	3	4	5	6	7	8
Test	Net Heat Available Above 80F In Furn. KGE/Hr.	Net Heat Available Above 80F In Furn. KB/(hr) (sq.ft.)	Excess Air At Furn. Outlet %	Secondary Air Vane Position % (open)	Number Burners In Service	Heat Abs. In Furn. from Part I KB/(hr)(F) (sq.ft.)	Furn. Heat Absorpt. Effy. from Part I Percent
15	793.7	89.3	23.0	40	8	39.4	44.2
15A	780.5	87.9	24.8	40	8	34.9	39.7
16	785.2	88.4	25.0	60	8	33.1	37.4
17	787.2	88.6	26.2	50	8	34.2	38.6
18	772.4	86.9	16.9	40	8	39.6	45.4
19	761.5	85.7	17.0	60	8	37.1	43.3
21	791.0	89.0	29.7	45	8	36.8	41.3
22	786.8	88.6	30.2	60	8	36.2	40.8
24	584.9	65.8	21.4	35	8	33.2	50.4
25	586.9	66.1	21.4	50	8	30.9	46.6
26	587.4	66.1	24.5	65	8	31.2	47.2
27	427.1	48.1	23.6	30	8	24.5	50.9
28	418.2	47.1	21.7	50	4 upper	24.9	52.9
29	418.3	47.1	23.0	50	4 lower	25.4	54.0
30	419.6	47.2	21.5	50	4 normal	26.5	56.1

1	2	10	11	12	13	14
Test	Avg. ΔT From Part I F	Weighted Average ΔT for Furn. areas not incl. I, J, & K in Fig. 3 G	Weighted Avg. ΔT for all Furn. Areas A to Q incl. in Fig. 3 G	Corr. to ΔT (Col. 11 - Col. 9) F	Corr. Heat Absorp. In Furn. from ΔT col. 11 KB/(hr)(F) (sq.ft.)	Corrected Furnace Heat Abs. Effy. from col. 13 Percent
15	37.2	38.1	37.8	+0.6	40.1	44.8
15A	32.9	33.6	33.0	+0.9	35.8	40.8
16	31.2	32.1	32.0	+0.8	33.9	38.4
17	32.3	34.0	34.2	+1.9	36.3	40.9
18	37.4	38.5	38.0	+0.6	40.3	46.3
19	35.0	36.0	35.7	+0.7	37.8	44.1
21	34.7	36.1	36.0	+1.3	38.2	42.9
22	34.1	35.8	35.6	+1.5	37.7	42.6
24	31.3	32.0	31.8	+0.5	33.7	51.2
25	29.1	30.3	30.2	+1.1	32.0	48.5
26	29.4	30.6	30.3	+0.9	32.1	48.6
27	23.1	24.0	23.5	+0.4	24.9	51.8
28	23.5	24.1	23.7	+0.2	25.1	53.4
29	24.0	24.8	24.0	0.0	25.4	54.0
30	25.0	25.1	24.6	-0.4	26.1	55.2

doors A and F are relatively close to the side walls where the gas temperatures are lower on the average than the temperatures closer to the center of the furnace.

The furnace outlet is divided into 3 vertical strips (R), (S), and (T). Center strip (S) contains temperature measurements taken through sampling doors (B), (C), (D), and (E) which are uniformly spaced. The width of strip (S) equals 4 times the uniform door spacing. Side strips (R) and (T) are equal in width. The center-line temperatures of strips (R) and (T) were determined by making an isothermal map for each test and by interpolating between the isothermals.

The sum of the average strip temperatures, each of which was multiplied by the ratio of the respective strip area to the total, yielded a weighted-average furnace exit-gas temperature. However, the calculated weighted-average temperatures vary only 5 F to 15 F from the temperatures obtained by simple arithmetic averaging in Part II. Values of furnace exit-gas temperature obtained by both methods of averaging, as well as the differences, are given in Table 2. While there are many other methods of averaging, the method just described was used, since it corrects for the lower gas temperatures measured near the walls but places a minimum of reliance on values which do not represent actual measurements.

Comparison of Furnace Exit-Gas-Temperature Data With Other Data. Inspection of furnace exit-gas-temperature data, as com-

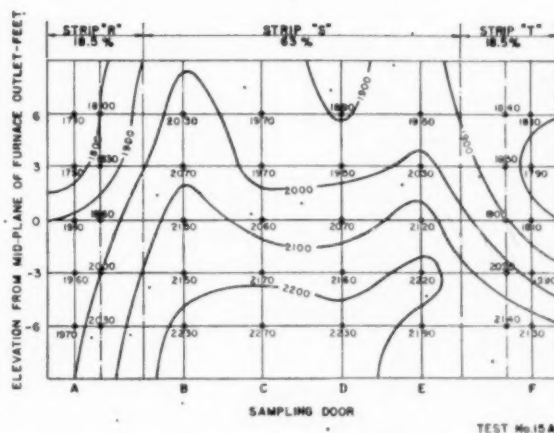


FIG. 4 DISTRIBUTION OF TEMPERATURE, DEG F, AND DIVISION OF FURNACE GAS OUTLET INTO AREAS FOR COMPUTING WEIGHTED-AVERAGE FURNACE EXIT-GAS TEMPERATURE, TEST NO. 15A

pared to other test data, indicates that there may be relatively large errors in the values of average gas temperatures of a few

TABLE 2 SUMMARY OF HEAT-BALANCE DATA WITH CORRECTIONS

1	2	3	4	5	6	7	8
Test	Heat Absorption in Furnace from Part II KB/(hr)(F) (sq. ft.)	Furnace Heat Absorption Efficiency from Part II Percent	Average Furnace Exit Temperature from Part II Op	Weighted Average Furnace Exit Gas Temperature Op	Correction to Furnace Exit Gas Temperature Op	Corrected Heat Absorption in Furnace from Gas Temperature in Column 5 KB/(hr)(F) (sq. ft.)	Corrected Furnace Heat Absorption Efficiency from Column 7 Percent
15	40.5	45.4	2020	2030	+10	40.3	45.1
15A	38.6	44.2	2070	2085	+15	38.4	43.6
16	38.8	43.9	2045	2050	+5	38.7	43.6
17	39.1	44.1	2055	2065	+10	38.8	43.8
18	40.7	46.8	2045	2055	+10	40.5	46.5
19	37.8	44.1	2120	2130	+10	37.5	43.8
21	38.9	43.7	2015	2020	+5	38.7	43.5
22	36.4	41.1	2095	2110	+15	36.0	40.7
24	32.3	40.1	1885	1890	+5	32.2	40.9
25	31.9	48.3	1900	1905	+5	31.8	48.1
26	31.7	47.9	1890	1905	+15	31.4	47.4
27	25.1	52.2	1755	1765	+10	24.9	51.9
28	25.1	53.4	1740	1750	+10	25.0	53.1
29	25.5	54.1	1690	1695	+5	25.4	54.0
30	25.4	53.7	1730	1740	+10	25.2	53.4

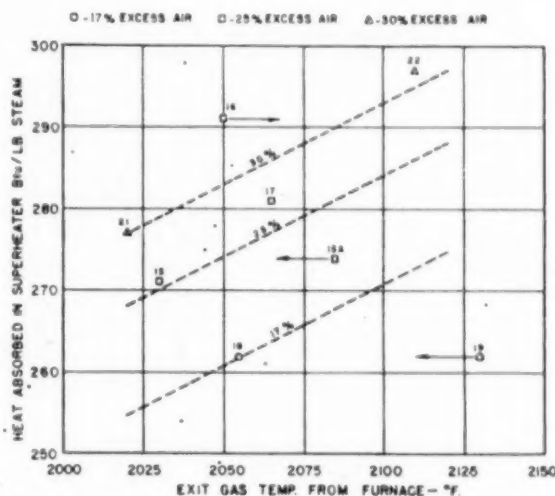


FIG. 5 COMPARISON OF SUPERHEATER HEAT DUTY AND FURNACE EXIT-GAS TEMPERATURE, DEG F, AT FULL LOAD (Number designates test.)

of the full-load tests. Several means are available to determine for which tests the temperature data appear to be the least reliable. One method of analysis is to compare gas temperature with convection-superheater duty at constant load and constant excess air. In Part I the necessary data for determining superheater duty is given except for the heat given up by the condensation of saturated steam in the inlet-superheater header to the condenser coils provided to maintain a constant final steam temperature. The rate of flow of water through the condenser coils was determined from a calibration curve of the condenser control valve. From the flow rate and the observed water-temperature rise, the heat transferred in the inlet-superheater header was estimated. Calculated superheater duty for the full-load tests is plotted against weighted-average furnace exit-gas temperature in Fig. 5.

Full-load-performance calculations were made of the rate of change of superheater duty with change in furnace exit-gas temperature at constant excess air, and of superheater duty at

constant gas temperature for three rates of excess air, namely, 17, 25, and 30 per cent. From these calculations the slope of and spacing between the lines drawn in Fig. 5 were determined. It was assumed that the 30 per cent excess-air line passes through the point for test No. 21. We may draw the tentative conclusion that values of gas temperature appear high for tests Nos. 15A and 19, and low for test No. 16.

Another method of analysis is to make plots of furnace exit-gas temperature against per cent excess air at constant secondary-air vane position, and also against secondary-air vane position at constant excess air. These plots are shown in Figs. 6 and 7 and corroborate the tentative conclusion drawn from Fig. 5 except for test No. 19. A check of ΔT and heat-balance data indicates that at 17 per cent excess air, an increase in the secondary-air vane position from 40 per cent (test No. 18) to 60 per cent (test No. 19) results in reduced heat absorption in the furnace and in a higher exit-gas temperature. It appears that the observed position of the condenser control valve for test No. 19 may have been an error.

Relationship of Furnace Exit-Gas Temperature to Furnace Heat-Absorption Rate. In predicting furnace performance, designers depend upon empirical data to calculate the rate of furnace heat absorption and the corresponding furnace exit-gas temperature. In Fig. 8 are plotted values of furnace heat-absorption rate per square foot of furnace projected area against average absolute furnace exit-gas temperature to the 4th power.

The straight line drawn in Fig. 8 represents the equation

$$Q = C \left[\left(\frac{T_a}{1000} \right)^4 - \left(\frac{T_w}{1000} \right)^4 \right]$$

where

Q = furnace heat-absorption rate, Btu/(hr) (sq ft of projected area)

C = const = 1000

T_a = average furnace exit-gas temperature, deg R

T_w = average furnace tube-wall temperature, assumed to be 1040 deg R

Note that this line passes through those points for which the secondary-air vane position was approximately 40 per cent (neglecting test No. 15A), that those points representing tests having a secondary-air vane position of 50 per cent fall below

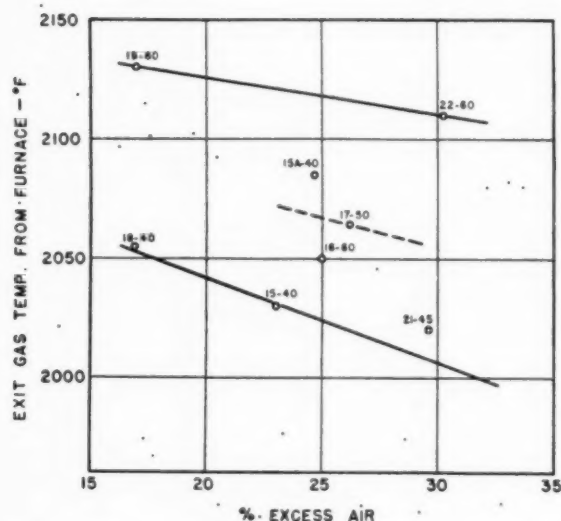


FIG. 6 RELATION BETWEEN FURNACE EXIT-GAS TEMPERATURE, DEG F, AND EXCESS AIR FOR THREE SECONDARY-AIR VANE POSITIONS AT FULL LOAD

(First number designates test; second number designates per cent opening of secondary-air vanes.)

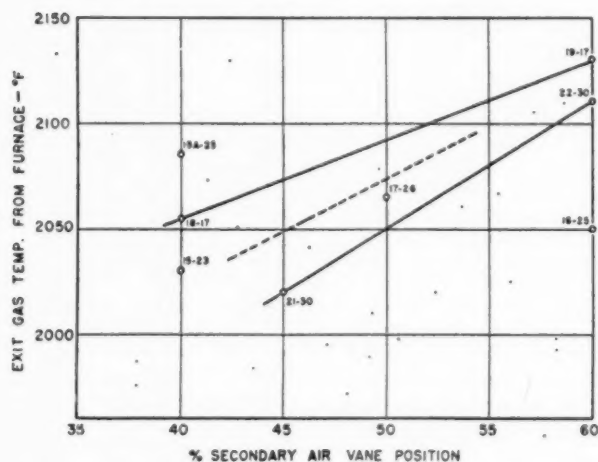


FIG. 7 RELATION BETWEEN FURNACE EXIT-GAS TEMPERATURE, DEG F, AND SECONDARY-AIR VANE POSITIONS FOR THREE VALUES OF EXCESS AIR AT FULL LOAD

(First number designates test; second number designates per cent excess air.)

the line, and those that represent tests having a secondary-air vane position of 60 per cent fall off even farther below the line. Fig. 8 shows that for eight-burner operation with the burner secondary-air vanes set for maximum heat-absorption efficiency (40 per cent open), the furnace heat-absorption rate is related to furnace exit-gas temperature by the foregoing equation. It follows that for the operating conditions given, if the furnace heat input and excess air at the furnace outlet are known, the heat-absorption rate and exit-gas temperature from the furnace may be calculated. For four-burner operation, particularly when the lower row of burners is fired (test No. 29) the value of C in the equation is greater, and may be as high as 1240. Where the vane position is 50 or 60 per cent open, the equation holds

toerably well at three-quarters load but at full load the value of C drops off to approximately 980 and 850, respectively.

CORRELATION OF ΔT AND HEAT-BALANCE DATA

In Fig. 9 furnace heat-absorption efficiency, calculated by the ΔT and heat-balance methods is plotted against excess air for the full-load tests. Note that the points for tests Nos. 15A and 16 are not in agreement with the other data, and also that the furnace heat-absorption efficiency, calculated by the ΔT -method for test No. 17 appears to be out of line. In Fig. 10 furnace heat-absorption efficiency, calculated by both methods, is plotted against secondary-air vane position for the full-load tests. Again, notice that the points for the tests previously mentioned are not in agreement.

It had previously been found that furnace exit-gas-temperature measurements for test Nos. 15A and 16 seemed less reliable than for the other full-load tests. It now appears that the ΔT -data for these tests are also less reliable and by a greater margin. The maximum deviation from the lines drawn in Figs. 9 and 10 is about 10 per cent for the ΔT -data (test No. 16) and

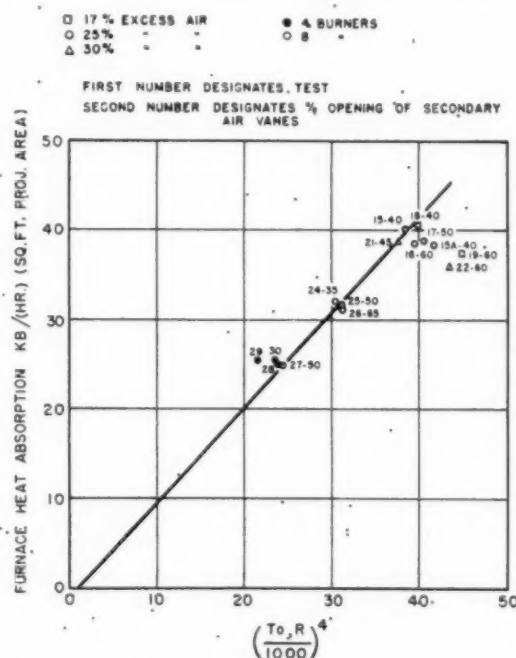


FIG. 8 RELATION BETWEEN FURNACE HEAT-ABSORPTION RATE AND FURNACE EXIT-GAS TEMPERATURE T_o , DEG R

about 3 per cent for the heat-balance data (test No. 16). These values are by no means excessive and indicate that reasonably accurate results of furnace performance may be obtained by either method of testing.

From Figs. 9 and 10 it appears:

- 1 That the furnace heat-absorption efficiency decreases as excess air is increased at constant secondary-air vane position.
- 2 That the furnace heat-absorption efficiency decreases as the secondary-air vanes are opened at constant excess air.

Statement (1) confirms past observations of the performance of radiant superheaters which give a lower steam temperature as the excess air is increased. Statement (2) applies to the adjustment of the burners used on the Paddy's Run boiler and shows

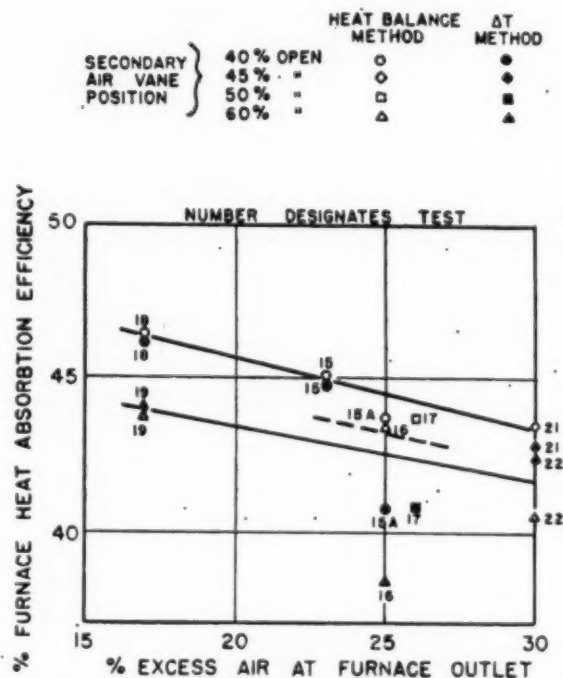


FIG. 9 RELATION BETWEEN FURNACE HEAT-ABSORPTION EFFICIENCY AND EXCESS AIR FOR THREE SECONDARY-AIR VANE POSITIONS AT FULL LOAD

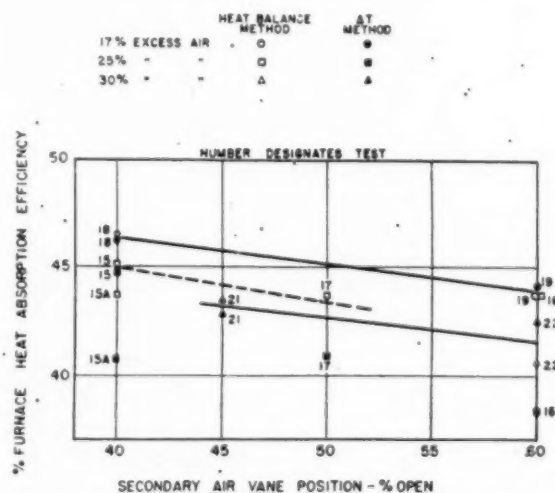


FIG. 10 RELATION BETWEEN FURNACE HEAT-ABSORPTION EFFICIENCY AND SECONDARY-AIR VANE POSITION FOR THREE VALUES OF EXCESS AIR AT FULL LOAD

that by means of burner adjustment, the heat absorption in the furnace may be varied.

In Fig. 11 the values of heat absorption obtained by both methods are compared. On the whole, the data appear to be in excellent agreement as do the data in Fig. 12 in which U_o , the over-all average heat-transfer coefficient, is plotted against ΔT . If runs Nos. 15A, 16, and 17 are neglected, Fig. 12 shows that

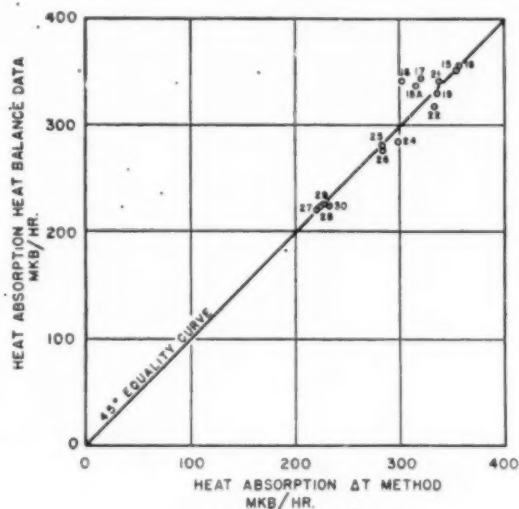


FIG. 11 COMPARISON OF CORRECTED FURNACE HEAT ABSORPTION COMPUTED BY HEAT-BALANCE AND ΔT -METHODS (Number designates test.)

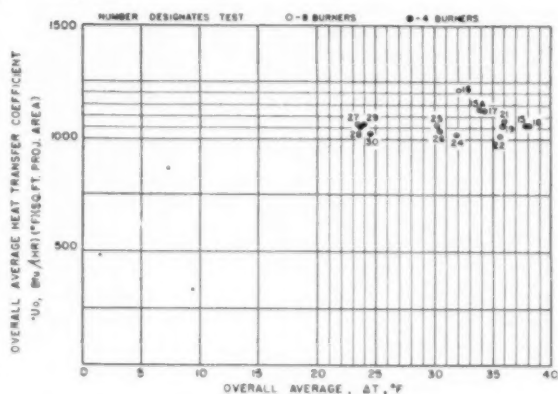


FIG. 12 CORRELATION OF CORRECTED FURNACE-WALL TUBE OVER-ALL AVERAGE HEAT-TRANSFER COEFFICIENT WITH CORRECTED VALUES OF ΔT

a fair average value of U_o for all runs would lie between 1030 and 1050 Btu/(hr) (F) (sq ft of projected area).

In Fig. 13 the furnace heat-absorption rate is plotted against the net heat available in the furnace above 80 F for the tests in which the secondary-air vanes were 40 per cent open. In Fig. 14 furnace heat-absorption efficiency is plotted against the heat available for the same tests. Only one curve is drawn in each figure showing the heat absorption at 25 per cent excess air, since only single points are available for 17 and 30 per cent excess air. It has been shown that at full load, the heat-absorption efficiencies decreased on opening the secondary-air vanes. At three-quarters load, maximum heat-absorption efficiency was obtained at a setting of 35 per cent open. At one-half load only one test was run with 8 burners and that with a vane position of 30 per cent open.

CONCLUSIONS

The following conclusions have been reached in this study.

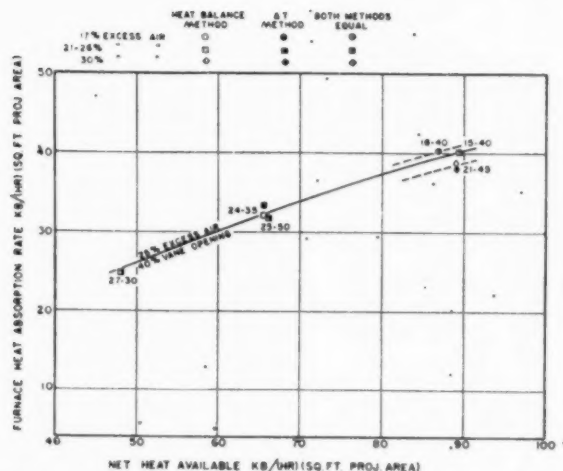


FIG. 13 RELATION BETWEEN FURNACE HEAT ABSORPTION AND NET HEAT AVAILABLE TO FURNACE
(First number designates test; second number designates per cent opening of secondary-air vanes.)

1 With care in testing, furnace performance may be determined by either the heat-balance method or by the ΔT -method with a fair degree of accuracy.

2 The over-all average heat-transfer coefficient U_o , through the tube wall and inside tube film was 1030 to 1050 Btu/(hr) (F) (sq ft projected area). From this, the calculated film coefficient is 5500 Btu/(hr) (F) (sq ft of inside tube-wall surface).

3 For eight-burner operation with secondary-air vanes 40

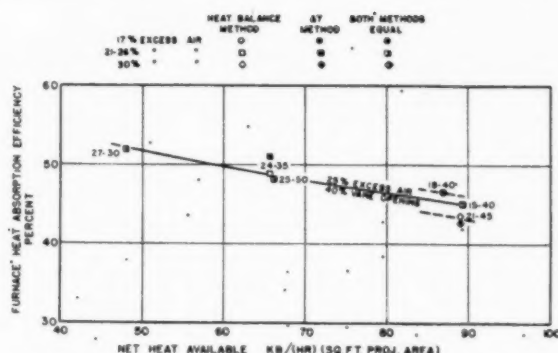


FIG. 14 RELATION BETWEEN FURNACE HEAT-ABSORPTION EFFICIENCY AND NET HEAT AVAILABLE TO FURNACE
(First number designates test; second number designates per cent opening of secondary-air vanes.)

per cent open, the average furnace heat-absorption rate Q , the average furnace exit-gas temperature T_o , and the average furnace tube-face temperature T_w , are related as follows

$$Q = 1060 \left[\left(\frac{T_o}{1000} \right)^4 - \left(\frac{T_w}{1000} \right)^4 \right]$$

4 In general, the conclusions of Part I and Part II, with some slight modifications to the calculated results found in Tables 1 and 2 of this paper are valid.

ACKNOWLEDGMENT

The authors wish to express their appreciation to Mr. John Blijard for his very helpful criticisms and suggestions.

THE for
lished
III,³ u
OLLISON C
Station dete
walls by me
measuring th
was done on
Run no doub
in the furna
of measured
close with te
One of these
fact that th
other excep
tion.

The distr
as pointed
encountered
below the
which the
exit, the te
some 300 d
planation i
the differ
openings.
at the top
for a long
heat to fun
case with
furnace ex
greater tim
completed
gases than
exit.

Slag for
the same
same furn
completed
one of the
A know
sary beca
temperat
passes of
perature
known, in

¹ Part I
ment of S
R. I. Whe

² Part
Temperat
R. C. Co

³ Part
Heat-Ab
Wheater.

⁴ Vice-
low ASM

Furnace Heat Absorption in Paddy's Run Pulverized-Coal-Fired Steam Generator, Using Turbulent Burners—Discussion

THE following discussion applies to the three papers published in this issue of the Transactions as Parts I,¹ II,² and III,³ under the subject title.

OLLISON CRAIG.⁴ The tests made on the boiler at Paddy's Run Station determine heat absorption by radiation in the furnace walls by measurement of gases leaving the furnace and not by measuring the temperatures of the boiler tubes in the furnace, as was done on a test at Tidd Station. The method used at Paddy's Run no doubt gives determination of heat absorption by radiation in the furnace more accurately. With two exceptions the average of measured temperatures leaving the furnace checks reasonably close with temperatures calculated from Orrok's modified formula. One of these exceptions is test No. 29 and is accounted for by the fact that the lower burners were used at the light load. The other exception is test No. 22, and there is no apparent explanation.

The distribution of temperature as indicated in Fig. 5 explains, as pointed out in the paper,² why, in practice, slag troubles are encountered even though the average temperature of the gases is below the slagging temperature of the ash. Due to the way in which the gases approach and flow to and through the furnace exit, the temperature of the gases at the lower part of the exit are some 300 deg higher than the average gas temperatures. An explanation is given in the paper to the effect that this is because of the difference in velocity of exit at the top and bottom of the exit openings. Actually, it would seem that those gases which leave at the top of the exit opening may have been in the entire furnace for a longer period of time and on the average may have radiated heat to furnace water tubes from a shorter distance than was the case with most of the gases which entered at the bottom of the furnace exit. In addition, there has been a greater distance and a greater time interval between the point at which combustion was completed in the furnace and the top point of exit of the gases than would be the case with the bottom point of furnace exit.

Slag formation at a furnace exit can be materially different with the same amount of coal burned with the same excess air in the same furnace, depending upon the point at which combustion is completed. This is a fact well known in stoker operation and is one of the reasons for using overfire jets in stoker operation.

A knowledge of heat absorption in a furnace envelope is necessary because, (1) it is necessary to have the gases leave under such temperature conditions that slag will not be formed in the gas passes of the boiler and in the superheater region; (2) the temperature of the gases entering the superheater region must be known, in order to determine the design of the superheater. The

results of the tests at Paddy's Run are excellent from both of these viewpoints. Similar information is desirable with other methods of burning fuels and also with other fuels than coal. The results which are obtained with other methods of firing and with other fuels are surprisingly different.

F. G. ELY.⁵ The authors^{1,2,3} have made an excellent presentation of test data dealing with a subject which involves many complexities. It is encouraging to find that their correlations are comparatively good, which may in part be attributed to improved techniques of traversing and to the circumstance that ash deposits on the furnace-wall surfaces remained generally consistent on comparative tests.

For critical appraisal of the data, the authors have made use of the superheater as a calorimeter, and from its indications find justification for considering tests Nos. 15-A and 16 less reliable than the other tests.

This procedure of cross-checking results by study of the performance of component equipment seems very proper and desirable and extends the facilities of testing beyond the limitations of the ΔT -method and the heat-balance method.

In this design of unit, the furnace boundary itself comprises the major portion of the steam-generating surface, and it is possible to draw a further comparison by calculating the steam-generating duty from enthalpy of saturation, feedwater leaving economizer, and metered steam output. In Fig. 1, herewith, the test points of

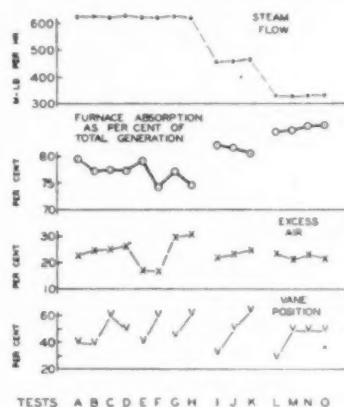


FIG. 1 FURNACE ABSORPTION AS PER CENT OF TOTAL GENERATION

furnace heat absorption by the heat-balance method are plotted as percentages of total generation and are shown to range from 74 to 86 per cent, depending upon load and operating conditions.

If it be assumed that the proportioning between furnace and convection bank is a function of excess air alone, the results for tests Nos. 19 and 21 are cast in doubt, and the influence of burner vane position is minimized. If, however, the influence of the

¹ Part I—"Variation in Heat Absorption as Shown by Measurement of Surface Temperature of Exposed Side of Furnace Tubes," by R. I. Wheeler and M. H. Howard, pp. 893-923.

² Part II—"Furnace Heat-Absorption Efficiency as Shown by the Temperature and Composition of Gases Leaving the Furnace," by R. C. Corey and Paul Cohen, pp. 925-935.

³ Part III—"Comparison and Correlation of the Results of Furnace Heat-Absorption Investigation," by H. H. Hemenway and R. I. Wheeler, pp. 937-944.

⁴ Vice-President, Riley Stoker Corporation, Worcester, Mass. Fellow ASME.

⁵ Research Engineer, Research and Development Department, Babcock & Wilcox Company, Alliance, Ohio. Mem. ASME.

burner vanes is considered primary, some question would exist for the relationship of tests Nos. 15, 16, and 17.

Discrepancies of this order may lie in the inherent errors of temperature measurement by traverse, or in the variations caused by ash deposit on the furnace walls. On the latter point it is recommended that the S-A factors as developed by Mumford and Bice⁶ be applied to observed furnace conditions to note their effect in correlation of the test points.

It is further recommended that for future programs of furnace testing, more emphasis be placed on obtaining check or repeated tests, to give statistical weight to the averaged results, and to disclose the range of performance that may occur in day-to-day operation of the equipment.

H. F. MULLIKIN.⁷ MHVT furnace outlet-gas temperatures, as obtained by Messrs. Corey and Cohen² appear low to the writer. The temperatures of 2060 F at a furnace heat-available rate of 95,000 Btu/(sq ft)(hr) and 1730 F at a furnace heat-available rate of 50,000 Btu/(sq ft)(hr), as given in Fig. 9 of the paper, are about 190 deg F and 130 deg F below values that would be expected, according to the writer's experience.⁸ Is it possible that the special design HVT thermocouples read low during the test? Platinum thermocouples tend to lose calibration rapidly. Were they checked before and after every test? Was difficulty experienced with ash plugging toward the end of a run?

The authors are to be complimented on the completeness of the test procedure.

A. A. ORNING.⁹ The statement by the authors of Part I,¹ that it is impossible to measure flame shape, merits further consideration. The inference probably intended was that flame shape is not a readily measurable quantity, while secondary-air vane opening and burner-box pressure, factors which determine flame configuration in the furnace considered, are quantities subject to measure and control. It should not be inferred that flame shape is incapable of estimation. The objective of the furnace-performance tests, to relate furnace heat absorption and its distribution in the furnace to furnace geometry and operating variables, scarcely can be accomplished without some estimate of flame configuration as the intermediate between operating conditions and heat transfer.

Since the flame originated at the burners and followed some systematic path toward the furnace outlet, the ΔT -contours at any level should have relation to those at other levels. The prevalence of ash deposits on the back wall opposite the burners accounts for low heat transfer to that surface, although it probably was blanketed by the most intense flame within the furnace. The flame became less intense or occupied a smaller cross-sectional area at higher levels in the furnace. The gas temperatures and compositions reported in Part II² indicate two flame cores entered the furnace outlet. The ΔT -contours suggest only one radiant core except near the front wall just below the furnace outlet.

The rotation imparted at each of the eight burners was of such a sense as to create a pattern of eight eddies across the furnace. However, they probably degenerated into two eddies which best filled the rectangular cross section, and each contained a maxi-

mum of radiant intensity. Placed near the center of the furnace, the two centers of maximum intensity would not be reflected in the ΔT -contours. However, the sloping back forced the flame against the front wall so that the two maxima appeared on the front wall just below the furnace outlet. Flame sweeping near the front wall would account for the third maximum generally appearing in Figs. 22-28, inclusive, of Part I.¹ It would be interesting to know whether visual observation suggested two flame cores sweeping near the front wall at that level.

The ΔT data are missing for some points indicated on the thermocouple-location identification diagram. Had the corresponding couples completely failed? Other couples appear to be faulty. The ΔT 's reported for positions 6-14 and 7-10 are generally high under all operating conditions. What criteria were used to determine that a given couple was faulty?

L. B. SCHUELER.¹⁰ The three papers^{1,2,3} presenting the test data and analytical report on the Paddy's Run boiler offer another set of complete information of interest and use to the boiler-furnace designer and user. The data appear to be well taken and have benefited from some improvement in instrumentation and technique since the Tidd boiler tests of several years ago. Favorable furnace-outlet location and profile, together with improved instrumentation, indicate that the gas-temperature and composition data should be most reliable.

A study of the furnace tube ΔT isotherms in Part I¹ indicates that the rather compact bunching of all burners in one wall is not conducive to uniform and effective heat transfer to the furnace walls. The front, or burner wall, shows only moderate absorption rates probably because the flame is traveling away from the wall, and the wall is partially screened by the cold layer of coal and air leaving the burners. The side walls show fairly good absorption rates, due to greater exposure to active flame, and a beneficial sweeping action of the flame without much slag deposition. However, these walls have less area than the front and rear so that their effect is thereby minimized. The rear wall, which should benefit most by virtue of its position opposite the burners, suffers somewhat from slag deposition by flame impact in the middle zone, although the hopper slope performs remarkably well. The upper portion of the entire furnace appears to suffer from lack of proximity and direct exposure to active flame.

All in all, it would appear that burner position, furnace shape, or both could well be changed to achieve more effective heat absorption throughout much of the furnace. The physical and operating convenience of grouping all burners in one wall at the main operating level must be weighed against the evident unfavorable flame pattern produced in a conventional furnace.

The uniformity of gas composition at the furnace outlet, as brought out in Part II,² is testimony of good coal and air distribution and combustion. The indicated effects of changing burner vane positions are interesting but not as pronounced as might be hoped for. It is possible that the extremely high pulverized-coal fineness for all tests acts to minimize the effects of vane position, and it would be interesting to determine whether the effects are greater with coal of normal fineness, say, 70 per cent through 200 mesh. Correspondingly, the present tests show virtually no carbon loss whereas vane manipulation with lower fineness and lower volatile fuels might encounter high carbon losses as a consequence.

CLOSURE BY R. I. WHEATER AND M. H. HOWARD

We agree with Mr. Ely that it would be advisable to verify the furnace-performance characteristics by incorporating additional check tests in future programs of this nature. Considera-

¹⁰ Engineer, Mechanical Engineering Division, American Gas & Electric Service Corporation, New York, N. Y. Mem. ASME.

⁶ Part IV—"An Investigation of the Variation in Heat Absorption in a Pulverized-Coal-Fired Water-Cooled Steam-Boiler Furnace," by A. R. Mumford and G. W. Bice, Trans. ASME, vol. 70, 1948, p. 601.

⁷ Head, Department of Mechanical Engineering, Montana State College, Bozeman, Mont. Mem. ASME.

⁸ "Determining Furnace Heat Transfer by Gas Temperature Measurement," by H. F. Mullikin, *Power Generation*, vol. 52, August, 1948, pp. 68-71, 116-122, Figs. 5 and 9.

⁹ Coal Research Laboratory, Carnegie Institute of Technology, Pittsburgh, Pa. Mem. ASME.

tion should be given to reducing the duration of each test, which would permit running more check tests and reduce the volume of data to be analyzed. This would also hold operating variables to a minimum.

Dr. Orning is correct in emphasizing that it is not impossible to measure flame shape. However, due to the difficulties involved in accurately measuring flame shape and duplicating it under various test conditions, burner settings, which could be duplicated and do control flame shape, were used as a reference.

The relation of the ΔT contours at various levels is not only affected by the ash accumulations on the rear wall but it is also affected by eddies in the flow path and by shielding of the emitting body. While some of the ΔT contours indicate two radiant cores existing in the upper part of the furnace, they were not visible through the available doors and no flames existed at this elevation.

On several occasions prior to the tests, the thermocouples were checked as the unit was taken off the line to assure that they indicated saturation temperature, as the pressure was reduced without fire in the furnace. The thermocouple at the location omitted from the ΔT data had either failed or consistently recorded a temperature considerably below saturation temperature.

Mr. Schueler has presented an excellent analysis of the distribution of heat absorption by the walls and its relation to the burner locations. The location of the burners and the furnace shape both affect the distribution of heat absorption by the walls but additional data is required to determine the optimum firing arrangement. Available data has however indicated that maximum furnace efficiency is obtained when the fires are located as near as possible to the bottom of the furnace.

Comparison of these results with additional heat absorption distribution data as it becomes available should enable the designer to locate the burners and shape the furnace to obtain the optimum heat-absorption distribution throughout much of the furnace.

CLOSURE BY R. C. COREY AND PAUL COHEN

Mr. Craig's explanation for the vertical temperature gradient at the furnace outlet agrees with that proposed by the authors. The gas-residence time of the stream lines leaving the top of the furnace outlet is believed to be longer, and therefore the linear velocity lower, than those leaving the lower portion of the outlet. Also considered as a possible factor was the heavier ash deposits on the rear than on the front wall, causing less net heat transfer from the gases along the rear wall. He calls attention to the need for similar investigations of furnaces fired by other methods. The Committee recognizes that all types of firing must be investigated if fundamental furnace heat-transfer relations are to be discovered. To the present time, however, it has been expedient to concentrate upon pulverized-coal-fired units, but during 1950 it is expected that a series of tests with a spreader-fired unit will be completed.

Mr. Ely makes an interesting comparison between the operating variables, excess air and vane opening, and the furnace heat absorption as per cent of total steam generation.

The question raised is whether tests 19 and 21, or tests 15A, 16, and 17 are in error, depending upon whether the relative heat-absorption efficiency of the furnace is affected by the excess air alone, or is influenced primarily by the vane opening. However, it will be noted from the three-variable plot, Fig. 11 of Part II, that each of the variables influences furnace heat absorption, the effect being greatest at full load. If it is assumed as a rough approximation that excess air and vane opening have the same relative effect in the ranges that were studied, then Mr. Ely's plot indicates test No. 15A to be somewhat low and No. 16 to be somewhat high. But it is not known definitely whether the deviations

were due to instrumental errors or to unusual ash patterns on the furnace walls for these two tests.

The authors agree with Mr. Ely that check runs should be made as often as possible in these furnace investigations. However, because of the number of independent variables that must be considered in the limited time available for such tests, it has not been possible to make as many duplicate tests as desired.

Mr. Mulliken suggests that the furnace-outlet temperatures seem low for heat-release rates of 95,000 and 50,000 Btu/(sq ft) (hr). Rigorous tests, in which direct comparisons were made in the furnace between B&W MHVT and the modified shields, showed the latter to be approximately 50 F lower. The test results were corrected accordingly and used for the enthalpy calculations. In addition, to detect possible contamination of the junctions, the test couples were calibrated frequently against a standard couple in a special electric furnace, and defective junctions were renewed.

Plugging of the shields always is a problem, particularly at full load and low excess air. However, the aspirating system was arranged so that the pressure drop across the shield was known at all times, and when it became too high the shield was replaced. Generally, the temperature at a given location in the furnace outlet was found to be the same with the new shield as with the one that was replaced, suggesting that inaccuracies due to reduction of cross section of the shield by ash were negligible. It was interesting to find that the emf of couples fitted with type E or G shields did not change noticeably, at constant mass flow of gas, even when as much as 90 per cent of the free area of the shield became plugged with ash.

Mr. Schueler's suggestion that the effect of vane setting might be more pronounced with coarser coal is probably correct. That is, for a given coal and excess air, the rate of change of flame surface with respect to vane opening may increase as the coal fineness decreases. Of course a relation of this kind would apply only within the limits of stable ignition.

CLOSURE BY H. H. HEMENWAY AND R. I. WHEATER

Mr. Craig observes that the averages of the measured temperatures leaving the furnace check reasonably with temperatures calculated from Orrok's modified formula except for test Nos. 29 and 22. General equations such as Orrok's for calculating furnace performance deal only with those few factors having the greatest influence on furnace heat absorption and are usually fairly accurate. One factor not normally considered is flame shape on which subject Mr. Orning has some very interesting comments. On the Paddy's Run unit, flame shape was varied by changing the

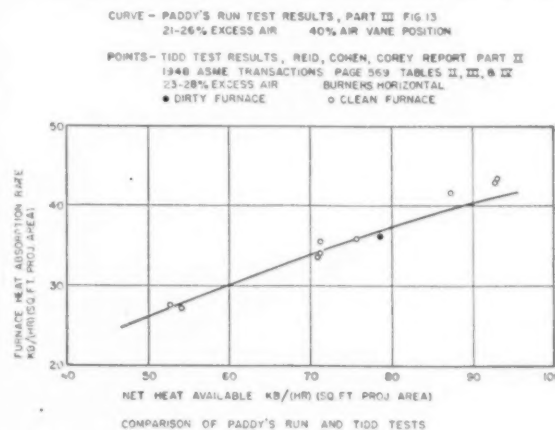


FIG. 2

position of the burner secondary-air vanes to alter the whirl imparted to the air before it entered the furnace. By opening these vanes this whirl was reduced which increased the length and reduced the spread of the flame causing a lowering of furnace heat absorption. This reduction of heat absorption on test No. 22, run with 60 per cent vane opening, probably caused the results to deviate from the results calculated by the Orrok equation.

Mr. Ely's plot of furnace absorption as per cent of total generation provides an excellent means of cross checking results. If the point for test No. 15A (B) is raised and the point for test No. 16 (C) lowered as suggested in Part III, the resulting plot will show rather well the effects of excess air and per cent vane opening on furnace heat absorption.

The authors may have been remiss in omitting the use of the S-A factors developed by Mumford & Bice⁶ and recommended by Mr. Ely but the ash deposits on the furnace-wall surfaces were so minor in nature and varied so little between tests that early ex-

amination of the data indicated little change in the correlation of the test points.

Mr. Schueler expresses the opinion that the furnace-wall surfaces might be more effectively used by making changes in burner grouping, furnace shape, or both. The relatively poor results obtained on tests with the secondary air vanes open greater than 40 per cent may have led to this observation. At Paddy's Run the vane settings were varied to study the effect of this particular factor on furnace performance. Normally the air vanes are set at the position giving optimum performance. In this case the setting is 40 per cent open. As a matter of interest a comparison was made of the results of the tests on the Tidd tangentially fired furnace when the burners are horizontal, and the Paddy's Run furnace with burner air vanes 40 per cent open, both at approximately 25 per cent excess air. This comparison is shown in Fig. 2. Note the closeness of the results obtained by the two different methods of firing.

The
by

This p
ating the
plant. E
entropy.
on a "pe
heat reje
loss can b

The fol

$G = m$
 $H = e$
 $P = P$
 $q = s$
 $Q = s$
 $s = s$
 $S = e$
 $S' = e$
 $t = e$
 $T = s$
 $v = s$

The
vantage
steam p
effect of
this, bec
from the
boiler, t
forth.

When
of entro

Conv
rated w
32 F an
sensible
at 32 F
may be
[1] from
conditi

Equ
which h

¹ Ass
Genera
Cont
Meetin
THE A
Norm
underst
of the

The Evaluation of Steam-Power-Plant Losses by Means of the Entropy-Balance Diagram

By ALLEN KELLER,¹ LYNN, MASS.

This paper deals with a method of isolating and evaluating the various cycle losses of a condensing steam power plant. Each loss in the steam cycle causes an increase of entropy. By considering each of these entropy increases on a "per hour" basis instead of a "per pound" basis, the heat rejection to the condenser caused by each individual loss can be evaluated quickly.

NOMENCLATURE

The following nomenclature is used in the paper:

G = mass flow, lb per hr
 H = enthalpy flow, 1000 Btu per hr
 P = pressure, psia
 q = sensible-heat flow, Btu per hr
 Q = sensible heat, Btu
 s = specific entropy, Btu/deg F/lb
 S = entropy flow, Btu/deg F/hr
 S' = entropy, Btu/deg F
 t = ordinary temperature, deg F
 T = absolute temperature, deg F
 v = specific volume, cu ft per lb

INTRODUCTION

The concept of a flow of entropy can, at times, be used advantageously to evaluate the different losses in a condensing steam power plant and to get quick answers as to the over-all effect of design changes. An entropy-balance diagram can do this, because entropy is a measure of the unavailability of energy from the standpoint of a complete power plant consisting of boiler, turbine, condenser, feedwater heaters, pumps, and so forth.

DEFINITION OF AN ENTROPY-BALANCE DIAGRAM

When sensible heat is added to a quantity of matter, the change of entropy is given by the equation

$$dS' = \frac{dQ}{T} \dots \dots \dots [1]$$

Conventional steam tables assume that the entropy of saturated water at 32 F is zero. For water at temperatures above 32 F and for steam, the entropy is greater than zero because the sensible-heat content is greater than that for saturated water at 32 F. For steam, water, or ice at any condition, the entropy may be obtained by making a proper integration of Equation [1] from saturated water at 32 F to steam, water, or ice at the condition specified.

Equation [1] makes no mention of the quantity of matter to which heat is added because, as a differential-equation, it may be

¹ Assistant Division Engineer, Turbine Engineering Division, General Electric Company. Mem. ASME.

Contributed by the Power Division and presented at the Annual Meeting, New York, N. Y., November 27-December 2, 1949, of THE AMERICAN SOCIETY OF MECHANICAL ENGINEERS.

NOTE: Statements and opinions advanced in papers are to be understood as individual expressions of their authors and not those of the Society. Paper No. 49-A-65.

integrated to determine the entropy of any quantity of matter. Conventional steam tables give the result of this integration for 1 lb (mass) of water. Thus the steam table lists values of "specific entropy" or entropy per pound of fluid.

If entropy per pound of fluid be multiplied by the fluid-mass flow, in pounds per hour, the product is the entropy flow per hour. An entropy-balance diagram is, then, a chart similar to a heat-balance diagram on which is represented the rate of flow of entropy throughout the entire steam cycle of a power plant. There is, however, one important difference between a heat-balance diagram and an entropy-balance diagram. On the heat-balance diagram, the boiler, turbine, feedwater pumps, and condenser are the only places where heat (or more properly enthalpy) is added to or subtracted from the thermodynamic medium itself. At all other points in the cycle, enthalpy is only transferred, as from steam to water in a feedwater heater. On the other hand, on an entropy-balance diagram the total entropy of the thermodynamic fluid is increased whenever a cycle loss takes place. For example, consider an extraction steam pipe leading from the turbine to a feedwater heater. The pressure drop in this pipe will cause an increase in the entropy of the steam flowing in the pipe, and the hourly entropy increase taking place within the pipe will be a direct measure of the cycle output loss caused by the pipe fluid friction.

CONSTRUCTION OF AN ENTROPY-BALANCE DIAGRAM

Fig. 1 is a conventional heat-balance diagram for a typical steam-turbine power plant having an 11,500-kw AIEE-ASME preferred standard turbine-generator set operating at rated load. On this diagram, the heat-radiation loss is assumed to be zero, and the power required to drive the hot-well pump and boiler feed pump is neglected. (If desired, feedwater-pumping power can be taken into account without affecting the validity of the entropy balance as a means of evaluating losses.)

The derivation of Fig. 1 is not described in this paper.

Fig. 2 is the entropy-balance diagram corresponding to Fig. 1. It is based upon the flows given on the heat-balance diagram. At each point on the diagram, the mass flow is multiplied by the specific entropy to get the entropy flow. Whenever the total entropy leaving a given piece of apparatus is greater than the total entropy entering the same apparatus, the difference between the two entropy flows is the entropy increase caused by the cycle loss taking place in the apparatus. For example, consider the steam-extraction pipe from the turbine to the No. 2 feedwater heater. The entropy flow at the pipe discharge is 9319.1 Btu/deg F/hr. This value was calculated by multiplying 5338 lb per hr flow by 1.7458 Btu/deg F/lb specific entropy.² At the pipe inlet the entropy flow is 5338 lb per hr \times 1.7344 Btu/deg F/lb or 9258.2 Btu/deg F/hr. Therefore the 10 per cent pressure drop in this pipe causes an entropy increase of 69.9 Btu/deg F/hr.

Fig. 2 shows that 143,479.2 Btu/deg F/hr is the entropy

² All properties of steam used in this paper were read from "Thermodynamic Properties of Steam," by J. H. Keenan and F. G. Keyes, John Wiley and Sons, New York, N. Y., 1936 edition.

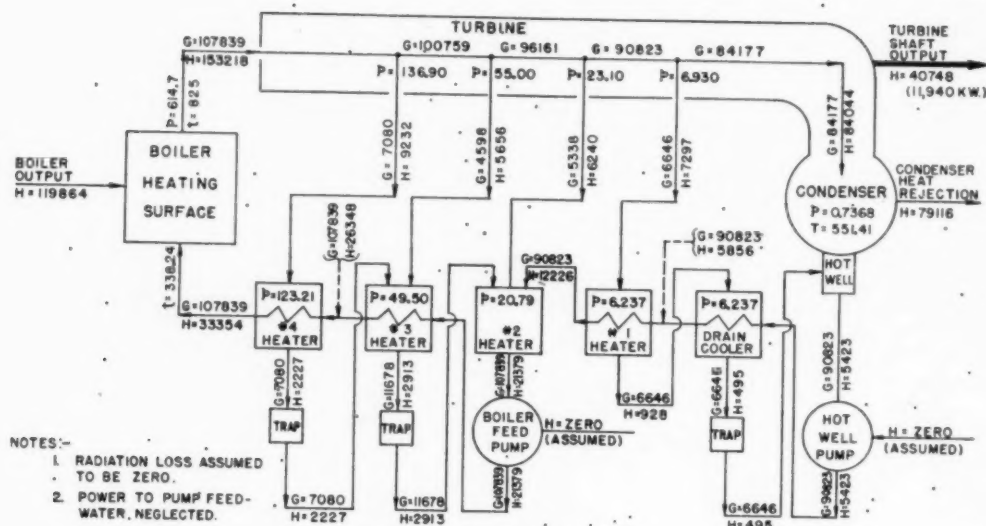


FIG. 1 TYPICAL HEAT-BALANCE DIAGRAM

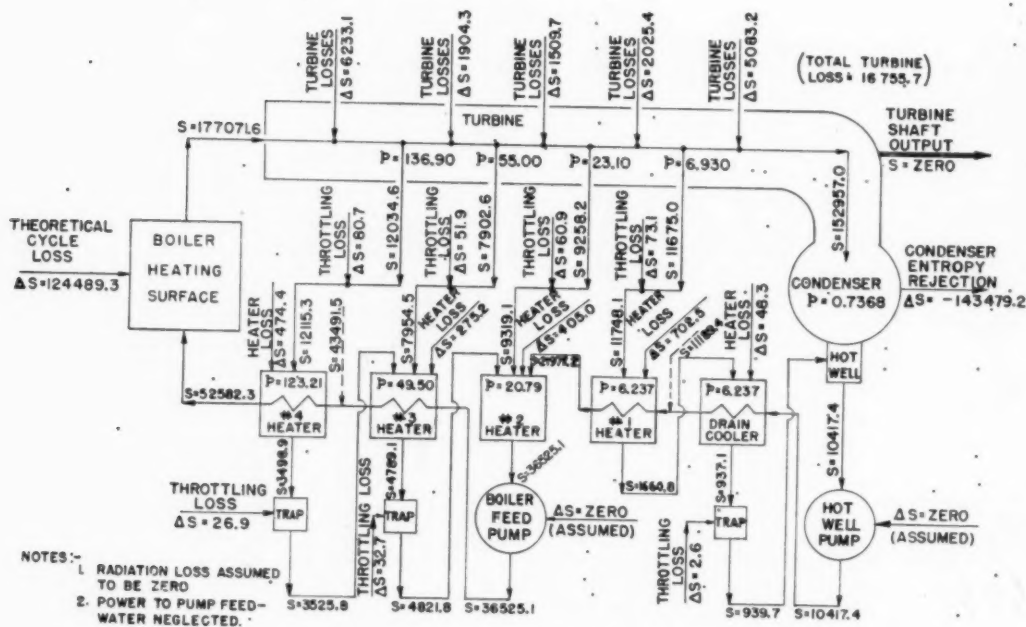


FIG. 2 TYPICAL ENTROPY-BALANCE DIAGRAM

rejection³ to the condenser circulating water. This value represents the sum of all entropy increases (ΔS) in Fig. 2. The largest single entropy increase is the 124,489.3 Btu/deg F/hr added by the boiler. This quantity represents the theoretical cycle losses for the particular flow, boiler-inlet feedwater condition, and superheated steam-outlet condition shown in Fig. 1.

³ In this paper, all values have been computed on an electrical computing machine merely to reduce the round-off errors and insure essentially perfect totals for all summations. For ordinary work such refinements usually will not be necessary.

EVALUATION OF LOSSES

Substantially all condensing power plants operate with wet steam exhausts. For such plants, the turbine-exhaust-steam temperature is a function of the exhaust pressure only. Thus when Equation [1] is applied to the heat-transfer phenomenon in the condenser, the temperature T is a constant.

Figs. 1 and 2 are based upon 1 1/2 in. Hg abs exhaust pressure. At this pressure the saturation temperature of steam is 91.72 F or 551.41 F abs ($T = t + 459.69$).

KELLI

With o
in the form

Thus the c
Btu/deg

Δq

This value
heat-balan

To illus
sider again
previous c
to be 60.
jected at
responding

This is th
pressure c
is causing
the 11,94

TABULA

Table
balance o
table is a
plant loss
of the en

Table
while ma
water he
Feedwat
Rankine
an actual
relative
This latt

The de
For ea
increase
is the en
value sh

The t
turbine-s
of 40,74
amount
of 73,89
Table 1

The 2
boiler ou
a boiler
abs tem
217,377.
equival

Colum
entropy

Kw los

Colum
the tur
each lo
The v

With constant temperature, Equation [1] may be written in the form

$$\Delta q = T \Delta S \dots \dots \dots [1a]$$

Thus the condenser heat rejection corresponding to the 143,479.2 Btu/deg F/hr condenser entropy rejection in Fig. 2 must be

$$\Delta q = 551.41 \times 143,479.2 = 79,115,866 \text{ Btu per hr}$$

This value agrees with the condenser heat rejection calculated by heat-balance methods as shown in Fig. 1.

To illustrate the method of evaluating individual losses, consider again the steam-extraction pipe to the No. 2 heater. A previous calculation has shown the entropy increase in this pipe to be 60.9 Btu/deg F/hr. This entropy increase must be rejected at the condenser at 551.41 F abs temperature. The corresponding heat rejection at the condenser is

$$\Delta q = 551.41 \times 60.9 = 33,581 \text{ Btu per hr}$$

This is the heat equivalent of 9.85 kw. Thus the 10 per cent pressure drop from the turbine shell to the No. 2 feedwater heater is causing a power output loss of 9.85 kw or 0.0825 per cent of the 11,940-kw turbine shaft output.

TABULATION OF ALL LOSSES FOR FIGS. 1 AND 2 POWER PLANT

Table 1 isolates and evaluates each loss in the Fig. 1 heat-balance diagram, and Fig. 2 entropy-balance diagram. This table is an illustration of the type of over-all picture of power-plant losses which may be prepared relatively quickly by means of the entropy-balance diagram.

Table 1 shows the losses associated with feedwater heating while many readers are accustomed to think of gains from feedwater heating. This difference is only a matter of viewpoint. Feedwater heating results in an efficiency gain relative to the Rankine cycle without feedwater heating. On the other hand, an actual feedwater-heating installation always results in a loss relative to the perfect regenerative feedwater-heating cycle. This latter is the viewpoint in this paper.

The derivation of Table 1 needs some explanation.

For each individual loss, column B of Table 2 lists the entropy increase as shown in Fig. 2. The total of all entropy increases is the entropy rejection to the condenser, which agrees with the value shown in Fig. 2.

The two asterisked entries require special explanation. The turbine-shaft power output of 11,940 kw has a heat equivalent of 40,748,235 Btu per hr. At 551.41 F abs temperature, this amount of heat flow is equivalent to 73,898.3 Btu/deg F/hr. This number has been included in Table 1 as the first asterisked quantity.

The 217,377.5 Btu/deg F/hr entropy increase shown as the boiler output in Table 1 was calculated as follows: Fig. 1 shows a boiler output of 119,864,000 Btu per hr. At 551.41 F abs temperature, this amount of heat flow is equivalent to 217,377.5 Btu/deg F/hr. This quantity represents the entropy equivalent at condenser temperature of the boiler heat output.

Column C shows the power output loss corresponding to each entropy increase. These were calculated by the formula

$$\text{Kw loss} = \left(\begin{array}{c} \text{Hourly} \\ \text{entropy} \\ \text{increase} \\ \text{Btu/deg F/hr} \end{array} \right) \times \left(\begin{array}{c} \text{temperature at} \\ \text{condenser, deg F abs} \end{array} \right) \dots [2]$$

Column D shows the percentage ratio of each individual loss to the turbine output and column E shows the percentage ratio of each loss to the boiler output.

The values in column C may be used to "capitalize" each of

TABLE 1 EVALUATION OF INDIVIDUAL LOSSES OF FIG. 1 HEAT BALANCE

(A)	(B)	(C)	(D)	(E)
Item	Entropy increase Btu/deg F/hr	Power loss Kw	Per cent of turbine power output	Per cent of boiler output
Drain cooler.....	48.3	7.8	0.065	0.022
Drain-cooler trap.....	2.6	0.4	0.003	0.001
No. 1 heater.....	702.5	113.5	0.951	0.323
No. 1 heater steam-extraction pipe.....	73.1	11.8	0.099	0.034
No. 2 heater.....	405.0	65.4	0.548	0.186
No. 2 heater steam-extraction pipe.....	60.9	9.8	0.082	0.028
No. 3 heater.....	275.2	44.5	0.373	0.127
No. 3 heater steam-extraction pipe.....	51.9	8.4	0.070	0.024
No. 3 heater trap.....	32.7	5.3	0.044	0.015
No. 4 heater.....	474.4	76.7	0.642	0.218
No. 4 heater steam-extraction pipe.....	80.7	13.0	0.109	0.037
No. 4 heater trap.....	26.9	4.4	0.037	0.012
Theoretical cycle losses.....	124489.3	20114.2	168.461	57.270
Turbine losses.....	16755.7	2707.3	22.674	7.708
Total losses.....	143479.2	23182.5	194.158	66.005
Turbine power output.....	*73898.3	11940.0	100.000	33.995
Boiler output.....	*217377.5	35122.5	294.158	100.000

* See text for an explanation of asterisked entries.

TABLE 2 INCREASE OF SPECIFIC ENTROPY CAUSED BY 10 PER CENT THROTTLING PRESSURE DROP

Extraction point	Specific entropy of steam in turbine stage, Btu/deg F/lb	Specific entropy of steam at heater entrance, Btu/deg F/lb	Change of specific entropy Btu/deg F/lb
No. 4 heater.....	1.6998	1.7112	+0.0114
No. 3 heater.....	1.7187	1.7300	+0.0113
No. 2 heater.....	1.7344	1.7458	+0.0112
No. 1 heater.....	1.7567	1.7677	+0.0110
Equation [3a].....			+0.0114

the individual losses. Again, using the No. 2 heater steam-extraction pipe as an example, if 1 kw of extra power output at constant input is worth, say, \$100, then a capital expenditure of \$980 would be justified to eliminate completely the pressure drop in this pipe, or a capital expenditure of about \$500 to decrease the pressure drop from 10 to 5 per cent.

FEEDWATER-HEATING-CYCLE LOSSES

Fig. 3 shows the cumulative loss in the feedwater-heating cycle as a function of the feedwater temperature. This shows that a perfect feedwater-heating system would improve the overall plant efficiency (at constant boiler efficiency) by about 6 per cent.

It is difficult, if not impossible, to extract superheated steam

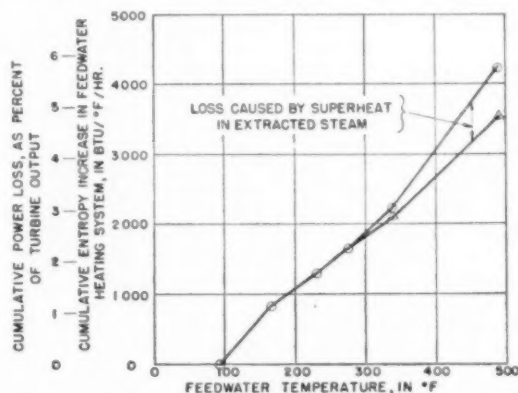


Fig. 3 CUMULATIVE LOSS IN FEEDWATER-HEATING SYSTEM

for feedwater-heating purposes without taking a loss relative to the extraction of wet steam. This results from the fact that the feedwater temperature leaving a heater usually is determined by the pressure of the extracted steam without regard to its superheat. Even when a feedwater heater is designed to use the superheat in extracted steam to decrease the heater terminal-temperature difference, the temperature of the feedwater leaving the heater is many degrees below the temperature of the extracted steam.

Fig. 3 indicates the portion of the loss in the feedwater-heating cycle that is caused by superheat in the extracted steam. This loss was evaluated by calculating the extra "entropy of superheat" that would have been extracted if the heat of superheat were available at saturation temperature. Fig. 3 shows that the loss from this source amounts to about 0.2 per cent at the 338 F feedwater temperature leaving the No. 4 heater.

To get an over-all idea of the feedwater-heating loss, the Fig. 3 curves cover the entire feedwater-temperature range from hot well to boiler saturation. To calculate the point at the 489 F boiler saturation temperature, a fictitious fifth stage of feedwater heating was assumed which delivers saturated water to the boiler at 614.7 psia pressure, heated by steam extracted from the turbine throttle. For this imaginary condition, the boiler heat output was kept unchanged from the actual 119,864,127 Btu per hr value by assuming a boiler mass flow of 126,685 lb per hr which is converted by the boiler from saturated water at 614.7 psia pressure to superheated steam at 614.7 psia pressure, 825 F temperature. Of this 126,685 lb per hr boiler flow, 18,846 lb per hr is then extracted from the turbine throttle to the imaginary heater, leaving 107,839 lb per hr to flow to the turbine first stage, the same as before. With this imaginary feedwater heater in the picture, the entire feedwater-heating system from hot well to boiler saturation temperature extracts 4244.5 Btu/deg F/hr less entropy from the turbine than it adds to the feedwater. This 4244.5 Btu/deg F/hr value represents the saving which could be made, if a perfect feedwater-heating system were available which delivered saturated water to the boiler.

REHEAT EFFECTS

The entropy-balance diagram is strictly correct for showing where cycle losses actually take place; however, it gives slightly conservative values when used to evaluate the gains which would be made if losses were eliminated or reduced.

Again, as an example, consider the No. 2 heater extraction pipe. Suppose that the pressure drop in this pipe were reduced and at the same time the extraction point in the turbine moved downstage slightly so as to maintain the same heater pressure. The state line enthalpy of the extracted steam would then be reduced slightly so that more extraction steam flow would be required to get the necessary heat for the feedwater heater. This increased extraction flow necessarily would cause less mass flow through the turbine low-pressure stages and hence less entropy flow to the condenser.

In evaluating the increased output that would result if the No. 2 heater extraction-pipe pressure drop were eliminated, it has been assumed that the decrease of entropy flow to the turbine exhaust would exactly equal the entropy increase in the extraction pipe. This is true except for one thing, namely, turbine stages are not 100 per cent efficient, and any reduction in the flow through a stage will also reduce the stage loss. Thus the entropy flow to condenser will always be decreased slightly more than any increase in the amount of entropy extracted.

At the turbine flange extracting to the No. 2 heater, the specific entropy is 1.7344 Btu/deg F/lb. At the turbine exhaust it is 1.8171 Btu/deg F/lb. Thus the "reheat factor" that must be

applied to entropy extraction at the No. 2 heater opening is approximately 1.8171/1.7344 or 1.048. The word "approximately" is used in the foregoing expression because an entropy of liquid must be subtracted from both numbers, which will make the true reheat factor more complicated than the simple quotient shown.

If a turbine were 100 per cent efficient relative to the Rankine cycle and had an isentropic expansion line, all reheat factors would be 1.00. Since all large turbines have Rankine-cycle efficiencies between 80 and 90 per cent, the reheat factors can never get appreciably above 1.00. About 1.10 to 1.15 is the highest reheat factor that will be encountered in any normal installation; thus considering it as unity will cause no great error in perspective for a given study.

SIMPLIFIED CALCULATION METHODS

It can be shown that for a throttling process

$$ds = -0.1850 \frac{pv}{T} d \log_e p \quad [3]$$

Since the value of pv/T generally changes very little along a turbine-expansion line, it may be considered as approximately a constant.

Using 0.585 as an approximate value of pv/T , Equation [3] becomes

$$\Delta s = +0.108 \log_e \frac{p_1}{p_2} \quad [3a]$$

in which p_1/p_2 is the pressure ratio of a throttling process, and p_1 is the higher pressure.

Table 2 shows the actual increase of specific entropy associated with the 10 per cent pressure drop in each of the four extraction pipes of Figs. 1 and 2, together with the values calculated by Equation [3a]. Table 2 shows that Equation [3a] is quite accurate as a means of estimating entropy increases caused by throttling.

Simple procedures also can be worked up for estimating quickly the entropy increases associated with heater terminal-temperature differences, and the like, without reference to a steam table.

CONCLUSIONS

The entropy-balance method is a fundamentally sound and easily applied method of isolating and evaluating the different losses in the steam cycle of a condensing power plant. Although a sizable amount of calculation work is required to make a complete analysis of a given installation; any one question may be answered quite quickly after a heat balance is available. Preliminary estimates of many losses also may be made prior to a heat-balance calculation by making judicious assumptions as to the mass flows involved.

The entropy-balance diagram is not a substitute for other methods of analysis. It is another way of looking at a problem which should be used when it is helpful and not used when other methods seem more straightforward to apply.

Discussion

R. E. HANSEN.⁴ The evaluation of cycle losses by calculation of entropy generation is convenient, particularly when losses under study are too small to show up in a heat-balance computation.

The author states on the second page of the paper that the entropy rejection (a better word than "loss") of the theoretical

⁴ Engineer, Elliott Company, Jeannette, Pa. Mem. ASME.

cycle is equal to the entropy received in the boiler. He does not define his theoretical cycle, but if the intention is to use as a reference the cycle defined by Selvey and Knowlton,⁵ the theoretical heat rejection would be increased by an amount given in the writer's paper⁶ of 1945.

It is not clear to the writer why, in Table 1, a fictitious entropy quantity representing turbine output is added to total entropy rejection in the cycle. This total does not appear to provide any additional information. Thermal efficiency of the turbine cycle may be found by dividing kw output by boiler output in kw, i.e., 11940/35122, or 34.0 per cent. Plant efficiency would be found by deducting auxiliary power before making this division, then multiplying the quotient by boiler efficiency.

The question of radiation loss is side-stepped by the assumption of zero. However, radiation can be handled quite readily in this type of computation. It may be of value to consider two types of entropy change, one by transfer, the other by generation. Entropy is increased by transfer in the boiler, and decreased by the same means wherever radiation or conduction losses occur. Entropy generation, as by pressure drop or internal heat transfer with a temperature difference, always results in an increase. Heat rate of the cycle becomes

$$\frac{3412.75 \Delta H_B}{\Delta H_B - (\Sigma T \Delta S)_r - (T \Delta S)_c} \dots \dots \dots [4]$$

where ΔH_B is the heat received in the boiler, $(\Sigma T \Delta S)_r$ is the summation of all entropy losses through radiation or conduction, multiplied by the temperature at which the loss occurs, and $(T \Delta S)_c$ is the entropy rejection in condenser multiplied by condensing temperature. Where radiation and pressure drop occur simultaneously, the entropy rejection due to radiation must be computed separately from the entropy generation due to pressure drop, in order to evaluate $(\Sigma T \Delta S)_r$; the net change affects $(T \Delta S)_c$.

The author's evaluation of the effect of an individual loss is substantially correct in so far as capacity value is concerned, unless capacity limitation lies in the generator. There is an additional value, however, due to fuel savings. For example, with a load factor such that 6000 kwhr can be generated annually from each kw of capacity, and where energy cost due to fuel averages 1 mill per kwhr the fuel saving amounts to \$60 annually. Assuming 12 per cent fixed charges, capitalized value of the saving becomes \$500 per kw, or \$4900 in the example cited by the author. This value is obtained regardless of capacity limitation, as fuel input may be reduced at the burner. Both values must of course be corrected to a plant value, by considering the effect of boiler efficiency and auxiliary loss, which increases the value of the savings.

⁵ "Theoretical Regenerative-Steam-Cycle Heat Rates," by A. M. Selvey and P. H. Knowlton, Trans. ASME, vol. 66, 1944, pp. 489-512.

⁶ "Irreversibility in the Theoretical Regenerative Steam Cycle," by R. E. Hansen, Trans. ASME, vol. 67, 1945, pp. 557-560.

Whenever entropy is discussed, the question arises as to what it is and why it is useful. Most forms of energy represent the product of a potential, such as force or voltage, by a quantity, such as distance or current. In the case of heat, temperature is the potential, but there is no readily perceived quantity by which to multiply it. This difficulty is solved by inferring the existence of entropy, and computing its value mathematically. There is no need to know any more than this about its nature, and no probability that we ever will.

AUTHOR'S CLOSURE

The comments of R. E. Hansen are all quite pertinent.

The theoretical cycle the author used as a reference on page 950 is the completely reversible regenerative cycle in which the feedwater is heated by extracting heat from the turbine at the same temperature as the feedwater. This could be accomplished, theoretically, by flowing the feedwater, in a counterflow direction, through a water jacket around the turbine shell and heating the feedwater by transferring heat at constant temperature through the turbine shell. The losses relative to the foregoing cycle caused by extracting superheated steam, as discussed on page 951 of the author's paper, are the same as those discussed in the R. E. Hansen paper,⁶ except that they are evaluated for an actual cycle with a finite number of feedwater heaters and a less than 100 per cent efficient turbine.

In Table 1 the fictitious entropy quantity representing turbine output was inserted for checking purposes only. The text on page 950 explains how the 217,377.5-Btu/F/hr entropy increase assigned to the boiler was calculated. By calculating a similar entropy flow value which, at condenser temperature, would be equivalent to the turbine power output, a check was established that turbine-power output plus turbine, condenser, and feedwater-heating-system losses equaled the boiler output, as expressed in entropy units.

Radiation as well as many other considerations were side-stepped to keep the paper short. For example, the entropy balance concept can be used to evaluate boiler feed-pump losses, which was also side-stepped by stating that boiler feed-pump power had been neglected. The purpose of the paper is to present a concept for isolating and evaluating different kinds of losses to which each engineer can fill in the necessary detail to adapt the concept to his own needs.

Much has already been written on the subject of steam-power-plant efficiencies and heat balances. Mr. J. K. Salisbury has given much thought to this subject, and his 1949 ASME paper⁷ presents another approach to the problem of evaluating power-plant losses. The entropy balance concept is just another tool which a power-plant designer may use in his work.

⁷ "Power-Plant Cycle Evaluation," by J. K. Salisbury, Trans. ASME, vol. 71, 1949, pp. 593-604.

T

The
 (95 per
 These
 interrup
 core res
 in a to
 sults w
 on the
 dicted
 connect
 flow ga
 low-pre
 substit

The f

$a/s =$

$A =$

$A_c =$

$A_f =$

$A_w =$

$b =$

$c_p =$

$D_e =$

$f =$

$G =$

$g =$

$h =$

¹ Chief
 Racine, W

² Proce

³ Num

the paper

Contri

sions and

vember

CHANICAL

NOTE:

understo

of the So

The Gas-to-Gas Heat Exchanger as Applied to an Oxygen Plant

Plate and Interrupted Strip-Fin Design

By CLYDE SIMPELAAR¹ AND DAVID ARONSON²

The construction and performance of high-efficiency (95 per cent) counterflow heat exchangers is reported. These exchangers are of the finned-plate type employing interrupted strip fins. Comparison is made between test-core results and performance of large-size units installed in a tonnage gaseous-oxygen plant. Heat-transfer results were in good agreement but measured pressure drops on the large-size units were considerably higher than predicted from test-core results, possibly due to losses at end connections. Successful development of the true counterflow gas-to-gas exchanger adds flexibility to the design of low-pressure gas cycles as in oxygen plants, permitting the substitution of heat exchangers for regenerators.

NOMENCLATURE

The following nomenclature is used in the paper:

- a/s = ratio of total heat-transfer surface to minimum cross-sectional area per unit of length
 A = total heat-transfer and/or friction area, sq ft ($A = A_f + A_e$). This definition of area differs from Norris and Spofford (1)³ A , which is the sum of half the direct surface plus the full indirect surface)
 A_e = minimum cross-sectional area for flow, sq ft
 A_f = surface area of fins, sq ft
 A_w = surface area of direct surface, sq ft
 b = width of strip fin (distance from leading edge to trailing edge in direction of air flow), ft
 c_p = gas unit heat capacity, Btu/(lb)(deg F)
 D_e = equivalent passage diameter, $D_e = 4r_H = 4A_e/(A/L)$, ft
 f = Fanning friction factor (see dimensionless groupings)
 G = core air-mass velocity, (lb)/(hr)(ft² of A_e)
 g = conversion factor, $g = \frac{32.2 \text{ (ft) (lb-matter)}}{(\text{sec}) (\text{sec}) (\text{lb-force})}$
 (for time in hours, $g = 4.17 \times 10^3$)
 h = surface heat-transfer coefficient referred to fin average surface temperature, not to temperature at base of fin, Btu/(hr)(ft²)(deg F). Note that for conditions of test, distinction between surface temperature and base of fin is unimportant

- j = heat-transfer factor (see dimensionless groupings)
 k = thermal conductivity of gas, Btu/(hr)(ft²)(deg F/ft)
 k_s = thermal conductivity of fin material, Btu/(hr)(ft²)(deg F/ft)
 L = length of flow passage, ft
 m = $(2h/k\delta)^{0.4}$, 1/ft
 P = gas pressure, psia
 ΔP = pressure drop, lb/in.² or lb/ft²
 t = temperature, deg F
 T = temperature, deg R
 δt = temperature change of gas from inlet to outlet, deg F
 Δt_m = temperature difference between gas and metal surface, deg F
 U = over-all heat-transfer coefficient, gas₁ to gas₂ based on total area, A
 W = mass-flow rate, lb per sec or lb per hr
 x_f = effective fin length, ft
 δ, Δ = prefixes denoting difference
 δ = thickness of fin, ft
 η = fin efficiency, dimensionless
 $\eta = (\tanh x_f m)/x_f m$, approximate⁴
 μ = viscosity, lb/(hr ft)
 ρ = gas density, lb per cu ft
 ψ = fin perimeter, ft, $\psi = 2(b + \delta)$

Dimensionless Groupings

- $St = (h/Gc_p)$, Stanton's number, a heat-transfer modulus
 $Pr = (c_p \mu/k)$, Prandtl's number, a fluid-property modulus evaluated for arithmetic-mean bulk fluid temperature
 $j = (St)(Pr)^{1/3}$ = generalized heat-transfer grouping (this factor, j versus Re , defines heat-transfer characteristic of surface)
 $Re = (D_e G/\mu)$, Reynolds number, a flow-property modulus characterizing "turbulence"
 $R\psi = (\psi G/\mu)$ modified Reynolds number based on fin perimeter
 $f = \frac{\Delta P}{G^2} \frac{2g\rho}{(A/A_e)} = \text{Fanning friction factor (the } f\text{—Replot defines friction characteristic of surface)}$
 $NTU = \delta t/\Delta t$ = number of core "heat-transfer units," a dimensionless expression of "heat-transfer size" of core;
 $NTU = (\eta)(Ah/Wc_p) = (\eta)(h/Gc_p)(A/A_e)$

Subscripts

- c refers to cooler fluid, i.e., one being heated
 h refers to warmer fluid, i.e., one being cooled

¹ Chief Research Engineer, Modine Manufacturing Company, Racine, Wis. Mem. ASME.

² Process Engineer, Elliott Company, Jeannette, Pa.

³ Numbers in parentheses refer to the Bibliography at the end of the paper.

Contributed by the Heat Transfer and Gas Turbine Power Divisions and presented at the Annual Meeting, New York, N. Y., November 27–December 2, 1949, of THE AMERICAN SOCIETY OF MECHANICAL ENGINEERS.

NOTE: Statements and opinions advanced in papers are to be understood as individual expressions of their authors and not those of the Society. Paper No. 49—A-153.

⁴ Within the accuracy of the data it is considered justifiable to apply the fin efficiency to the entire surface. The indirect surface constitutes 85 per cent of the total surface so the uncertainty of the relative effectiveness of direct and indirect surface can have only a small effect on over-all performance.

INTRODUCTION

This new type of heat-exchanger surface for gas-to-gas service is a development of the company of one of the authors.¹ The application to commercial-size heat exchangers was carried through in co-operation with the company of the second author,² for use in its oxygen pilot plant. The importance of proper heat-exchange design in the satisfactory functioning of the oxygen plant is indicated in a separate report (2) on the performance of this pilot plant.

A broad review of oxygen technology, including a consideration of heat-exchanger requirements, was featured in an AIChE symposium in December, 1946, and was later reported (3). The newer designs of oxygen plants involve heat transfer to gases at comparatively low density and require exchangers of very high efficiency. For such service as well as other applications involving gases at low density some form of extended surface is indicated from the standpoint of economy in cost, size, and weight. Tests of several types of extended surface are reported by Norris and Spofford (1), by London and Ferguson (4, 5) and by Trumpler and Dodge (3). These were all built in comparatively small size.

The present paper describes commercial-size units built around a fin pattern corresponding to sample No. 10 of the Norris and Spofford paper (1) and core J of the London and Ferguson paper (4). The core structure which is illustrative of the flat plate and strip construction is shown in Figs. 1, 2, and 3. Fin elements are built up from thin channel sections of copper which interlock into one another to give rigidity to the structure prior to soldering. The fins are formed by slitting the web of the channel at intervals corresponding to the fin width b , and then offsetting each alternate strip. This gives an arrangement of fins staggered by two's.

Somewhat different methods of construction were employed in the cores tested by the other authors. Norris and Spofford had each fin element consisting of a separate strip of copper. London and Ferguson's cores were made by folding a strip of aluminum back and forth to form a serpentine pattern of fin elements resembling the filler elements of corrugated fiberboard. These variants of fin construction result in only second-order effects in performance.

A radically different arrangement is described by Trumpler and Dodge. The cores, which were developed by Prof. S. C. Collins, consisted of a multiple-annulus tube in which each annulus was packed with closely coiled copper ribbon, soldered to the tube walls, so that a rather complex fin pattern resulted.

The methods which can be employed for assembling small core elements into large-size commercial units vary with the type of core and the intended service. For use in low-temperature plants (oxygen, liquid air, etc.), the following requirements were set for the commercial heat exchangers employing the fin pattern shown in Fig. 1:

- 1 An arrangement having a very close approach to true counterflow.
- 2 A single metallically bonded unit of reasonably large size to reduce the number of units per plant, thus eliminating excessive manifolding.
- 3 A unit capable of withstanding relatively high pressures.

After the initial units for the pilot plant under consideration were built, these parameters of design were increased by the addition of the following elements:

- 4 A structure of sufficient strength to resist operating pressures without the use of external tie rods, braces, etc.

5 A design to permit close stacking of individual units to minimize exposed surfaces.

6 A structure susceptible of being bonded into a complete unit, including end connections, in one operation.

7 A unit of relatively standardized design giving uniform performance.

8 A design eliminating all possibility of pass-to-pass leakage. The improved design is shown in Figs. 4 and 5.

DESCRIPTION OF EQUIPMENT

Core Structure—Fin Pattern. Both test cores and full-scale exchangers were built with fin elements arranged as shown in Fig. 1. Channels are nested twelve to the inch, with alternate strips offset $1/24$ in. so that a symmetrical pattern is obtained.

This fin pattern was tested with three modifications as given in Table 1.

TABLE 1 FIN PATTERNS TESTED

Core no.	Fin width, b , in.	Nominal fin length, i.e., passage height, $2x_f$, in.	Section tested
1	$1/8$	$1/4$	$3'' \times 3'' \times 3''$ core
2	$1/16$	$1/4$	$1-1/2'' \times 3''$ and full scale
3	$1/32$	$1/4$	Full scale

Test Cores and Test Equipment. Heat-transfer and pressure-drop results were obtained on test cores 1 and 2. Test core 1 was tested water to air. Description of this core is as follows:

Air side:

5 passages $1/2$ in. high and 3 in. wide \times 3 in. long
Total heat-transfer surface, $A = 4.37$ sq ft
Net open cross section, $A_c = 0.0492$ sq ft
Ratio: surface/cross section, $A/A_c = 89$

Water side: Cross-flow to air

6 passages 0.08 in. high \times 3 in. wide \times 3 in. long
Total heat-transfer surface 0.657 sq ft

This core was made up with the 3 in. \times 3 in. fin slabs soldered into individual units. These slabs were then separated with U-shaped brass strips soldered in place along the front edges so that the water passage was, in effect, a flat tube 3 in. \times 0.080 in. There was thus one water tube between each $1/2$ -in. air passage.

Test core 2 of the following description was tested steam to air:

Air side:

1 passage $1/2$ in. high \times 6 in. wide \times 3 in. long
Total heat-transfer surface, $A = 1.70$ sq ft
Net open cross section, $A_c = 0.0191$ sq ft
Ratio: Surface/cross section, $A/A_c = 89$

Steam side:

2 passages same as air side, except 3 in. wide \times 6 in. long

For heat-transfer tests, core lengths in the direction of air flow were kept small in order to maintain sufficiently high temperature differences between steam and discharge air; for example, an 18-in. length would have resulted in about 0.1 deg F temperature difference, too low for accurate interpretation.

The arrangement of the test stand is shown in Fig. 6. Air flow was measured by a special orifice chamber which had been calibrated by volumetric displacement. Inlet and discharge-air temperatures were measured with unshielded copper-constantan thermocouples inserted in the middle of wooden ducts, the walls of which were close to the air temperature. An excess of steam was passed through the core in order to insure uniformly high rates of heat transfer by condensation with absence of sub-cooling.

No mixing baffles or straightening vanes were used in the inlet or discharge connections, since the large number of fins in series

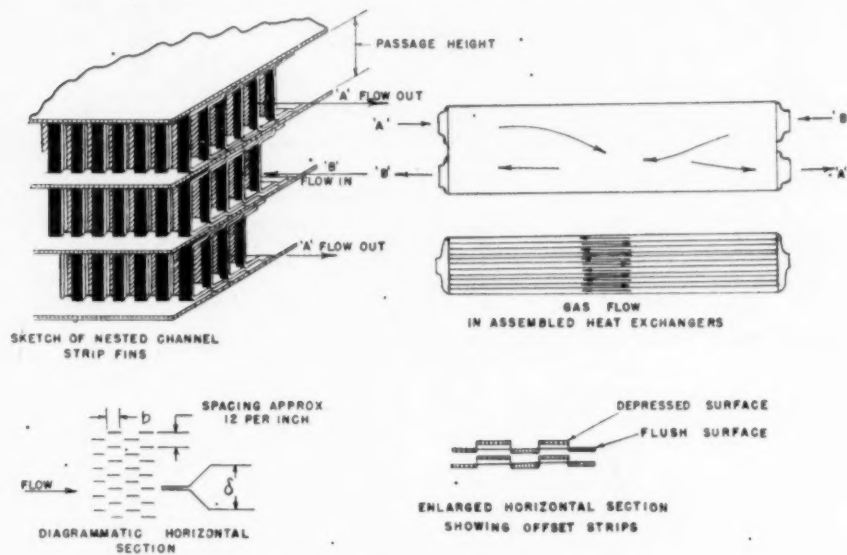


FIG. 1 CORE-STRUCTURE DETAILS

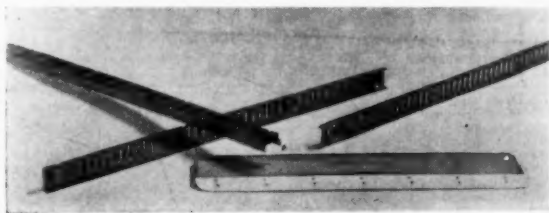


FIG. 2 FIN ELEMENTS

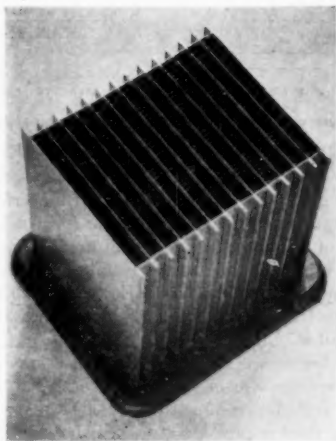


FIG. 3 CORE ASSEMBLY



FIG. 4 ASSEMBLY OF IMPROVED DESIGN OF SLAB HEAT EXCHANGERS

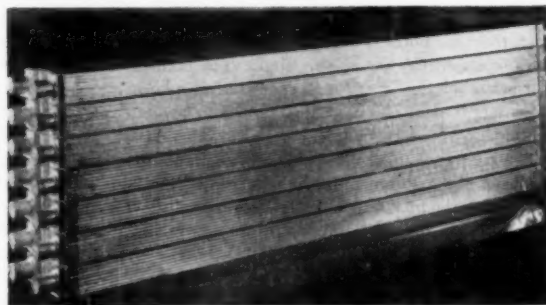


FIG. 5 IMPROVED DESIGN OF SLAB HEAT EXCHANGERS

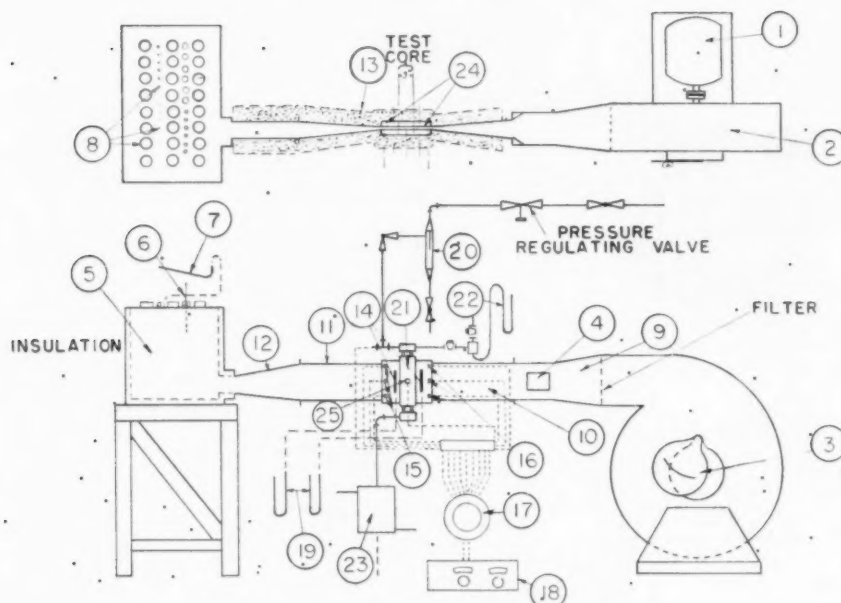


FIG. 6 EQUIPMENT FOR TESTING SMALL CORE SECTIONS

- | | |
|---|---|
| (1) Induction motor, 7.5 hp, 3470 rpm | (14) Piezometer rings |
| (2) Blower, centrifugal 1296 cfm 20 in. sp | (15) Downstream thermocouple grid |
| (3) Air-flow regulator | (16) Upstream thermocouple grid |
| (4) Air-flow by-pass | (17) Selector switch |
| (5) Orifice box | (18) Leeds & Northrop portable precision potentiometer No. 8662 |
| (6) Orifice box thermometer | (19) Draft gages |
| (7) Orifice box draft gage | (20) Moisture trap |
| (8) Orifice plugs | (21) Test core |
| (9) Transition from round to rectangular duct | (22) Mercury manometer |
| (10) Transition 6 x 3 in. to 6 x 1/2 in. duct | (23) Condenser |
| (11) Transition 6 x 1/2 in. to 6 x 3 in. duct | (24) Insulated duct |
| (12) Transition 6 x 3 in. to 3 x 3 in. duct | (25) Wall-temperature thermocouple |
| (13) Hair-felt insulation | |

effected adequate mixing. Flow was fully turbulent in all tests. Reynolds number in the ducts ranged from 4000 to 40,000. A thermocouple, attached to the separating wall of test core no. 2, was used to measure wall temperatures. These values ranged from 0.5 to 1.3 deg F lower than condensing-steam temperatures. The wall temperature in the test of core 1 was calculated on the basis of waterside coefficient being given by

$$hD/k = 0.023 (DG/\mu)^{0.8} (c_p \mu/k)^{1/4}$$

Large Units and Test Equipment. For convenience in manufacturing and subsequent handling, the finned length of the large units was made 7 1/2 ft. Two types of exchangers were built, each suited to its special application in the oxygen pilot plant. The low-pressure type has equal areas for flow of the two streams since they are both at approximately atmospheric pressure, and the flow quantities are about equal. The high-pressure type has twice as much flow area for the gas at atmospheric pressure as for the one at 6 atm. This pattern results in economy of exchanger volume.

The heat exchangers were built in sections of seven passages, and then the required number of sections were bonded together to make up the final unit. Each section consists of an outer brass plate, a layer of copper fins, a brass separating plate, another layer of fins, another separating plate, and so on, for seven layers of fins, with a final outer plate. The entire assembly was soldered together in a special oven.

For the low-pressure exchangers, the inner passages consist of 1/2-in. fins, and the two outer passages of 1/4-in. fins, as illustrated in Fig. 7(a). This results in a material balance across

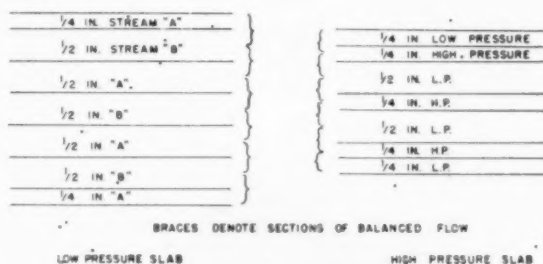


FIG. 7 ARRANGEMENT OF HEAT-EXCHANGER PASSAGES

each separating plate so that heat need be transferred only from the middle of any one passage to the separating plate. Were an even number of passages of equal height used, then, in the outer passages, the heat flow would have to take place across the full passage height which would mean a lower fin effectiveness, the length of the fin then being taken as 1/2 in. for calculating fin effectiveness instead of 1/4 in.

For the high-pressure exchangers having a smaller flow area for the high-pressure stream, there are in each slab section three passages for the high-pressure stream, each passage being 1/4 in. high; and for the low-pressure stream, two 1/2-in. plus two 1/4-in. passages as shown in Fig. 7(b).

In the later improved design, the size of the individual slab sections is larger and each slab is provided with standard sweat-solder-type end connections so that each slab becomes a complete heat exchanger. Any number of these individual exchang-

ers can be
suitable ma

A list of
changers w
Table 2.
water, car
posited on
"cleaned u

TABLE 2

Nitrogen pa
18 passag
Total hea
Net open
Ratio: s

Fin perin
 $D_o = 4.7$
Air passag
12 passag
Plus 12 r
of heat-t
passages

There
and D-2.
and D-2
There
A and B
having th

TABLE 3

Low-pres
The sam
High-pres
18 pass
Total h
Net op
Ratio:

The A
respect
the num
one thir
ratio A
Temp
couples
cury-in
of 99.5
ends of
inlet an

TABLE 4 TEST-CORE RESULTS

Run No.	Air Flow Rate, LB/HR	Air Flow Rate, (HR/FT ²)	Air Press. In, PSIA	Air Press. Out, PSIA	Air Press. Drop, PSI	Air Temp. In, °F	Air Temp. Out, °F	Air Temp. Change, °F	Avg. Water or Steam Temp., °F	h Air	h Water	f	Re	Pr
Core 1														
1	868	17,650	14.72	14.59	.13	94.2	150.7	56.5	198.5	55.6	2,000	.0104	.040	4,430
2	647	13,190	14.68	14.60	.081	100.7	160	59.3	198.7	47.5	2,000	.0119	.044	3,250
3	432	8,770	14.64	14.60	.041	102.8	168.9	66.1	198.0	37.9	2,000	.0123	.050	2,160
4	216	4,390	14.60	14.59	.014	102.1	180.1	78.0	199.5	34.1	2,000	.0180	.070	1,080
Core 2														
1	574	29,900	14.2	14.75	.47	109.3	161.0	51.7	216.4	62.3		.0062	.046	6,630
2	515	26,820	15.1	14.7	.37	113.5	166.2	52.6	216.5	59.9		.0072	.044	5,910
3	466	24,250	15.0	14.7	.32	116.0	169.2	53.2	216.6	56.9		.0076	.046	5,330
4	386	20,100	14.9	14.65	.24	112.1	172.1	60.0	216.5	52.6		.0085	.050	4,420
5	346	18,030	14.93	14.62	.30	111.4	174.2	62.8	216.7	49.8		.0089	.052	3,970
6	295	14,850	14.75	14.61	.141	109.9	177.1	67.2	216.8	44.1		.0096	.053	3,260
7	245	12,750	14.7	14.58	.109	108.0	181.1	72.3	217.5	41.5		.0105	.056	2,800
8	202	10,520	14.65	14.58	.087	107.4	184.1	76.7	217.3	37.1		.0114	.065	2,315
9	148	7,720	14.62	14.5	.090	106.5	190.1	83.5	217.5	31.3		.0131	.071	1,690
10	97.5	5,080	14.6	14.58	.031	107.2	195.7	88.5	218.7	22.6		.0144	.090	1,120
11	54.4	2,840	14.6	14.56	.043	109.0	201.9	92.9	215.6	16.1		.0184	.131	621

* f values were obtained from pressure drops measured during heating runs. Density was calculated at arithmetic average of inlet and outlet temperature.

** Based on average film temperature.

can be connected in parallel simply by connecting them to suitable manifolds. Such an assembly is shown in Fig. 5.

A list of the physical characteristics of the low-pressure exchangers which are called the "clean-up" exchangers is given in Table 2. The term clean-up is used because in operation, water, carbon dioxide, and hydrocarbons from the air are deposited on the metal surfaces as a rime and then removed or "cleaned up" with a stream of warmer nitrogen every 4 hr.

TABLE 2 PHYSICAL CHARACTERISTICS OF LOW-PRESSURE EXCHANGERS

Nitrogen passages (for a single exchanger):	
18 passages 1/4 in. high X 12 in. wide X 90 in. long	
Total heat-transfer surface, A	= 1858 sq ft
Net open cross section, A _c	= 0.70 sq ft
Ratio: surface/cross section, A/A _c	= 2655
Fin perimeter ψ	= 354 per ft of length
$D_e = 4r/f$	= 0.0166 ft
Air passages (for a single exchanger):	
12 passages 1/4 in. high X 12 in. wide X 90 in. long	
Plus 12 passages of 1/4 in. high X 12 in. wide X 90 in. long; for purpose of heat-transfer and pressure-drop calculations, set is considered as 18 passages, 1/4 in. high, i.e., identical with nitrogen passages	

There are four units of this type, identified as C-1, C-2, D-1, and D-2. Two of these units, C-1 and C-2, in one set and D-1 and D-2 in the other set, are operated in series.

There are two sets of high-pressure heat exchangers termed A and B. The B exchanger consists of two 7.5-ft units, each having the dimensions given in Table 3.

TABLE 3 PHYSICAL CHARACTERISTICS OF HIGH-PRESSURE EXCHANGERS

Low-pressure side:	
The same as the air passages of the clean-up exchangers	
High-pressure side:	
18 passages 1/4 in. high X 12 in. wide X 90 in. long	
Total heat-transfer surface, A	= 1,019 sq ft
Net open cross section, A _c	= 0.388 sq ft
Ratio: surface/cross section, A/A _c	= 3020
a/s	= 403 per ft of length

The A exchanger consists of a single 7.5 ft unit identical in every respect to the B units, except that the A unit has only one third the number of passages as the individual B units and therefore one third the surface area and net open area. The value of the ratio A/A_c is the same in both A and B exchangers.

Temperatures were measured with copper-constantan thermocouples which had been calibrated in an ice bath against mercury-in-glass thermometers and by immersion in boiling oxygen of 99.5 per cent purity. The thermocouples were soldered to the ends of thin-wall stainless-steel tubes which were inserted into the inlet and outlet ducts.

The thermocouple leads were carried without intermediate junctions to a Brown electronic indicating potentiometer, having a response time of about 4 sec. Therefore a complete record of temperature conditions in an exchanger could be taken in less than 1 min.

TEST RESULTS

Core Tests. Core-test results are given in Table 4. Values of f and j obtained with the first sample having 1/4-in-wide strip fins were slightly higher than reported by Norris and Spofford (1), as shown in Fig. 8. Tests of the second sample with 3/32-in-wide fins gave, over most of the range, lower values of j and higher values of f than predicted by the tests of Norris and Spofford (1). The results with 3/32-in. fins were confirmed by the tests of Kays and London (6) made on core sample 9 3/4 in. X 8 1/4 in. X 3.844 in. air-flow length, as shown in Fig. 9. The values of friction factor obtained by Kays and London at the low flows (hence low pressure drops) are believed to be more reliable and are the values used in the construction of Fig. 8.

The plotted values of the Norris and Spofford tests are shown lower than given in their paper. They used a surface area of the full fin surface plus one half the direct surface. In the present paper and in the work of London and Ferguson (4), the area is considered the full fin surface plus the full direct surface. Either method of representation is, of course, purely arbitrary.

The effective diameter to be employed for calculating Reynolds number is different in the two plots. Norris and Spofford proposed the fin perimeter, $\psi = 2(b + \delta)$ as a suitable correlating term. London and Ferguson pointed out that this is inadequate to cover all types of surface, and suggested that representation be made on the basis of the mean hydraulic diameter, $D_e = 4A_c/(A/L)$. There is probably no simple method of representation which will show the effect on performance of fin size, shape, passage spacing, etc.

Failure to realize improvement in j -values for the fins of reduced perimeter (as predicted by the Norris and Spofford correlation) is apparently due to the corresponding reduction in distance between in-line surfaces.

The values of friction factor f , obtained with all test cores, were higher than predicted by Norris and Spofford, as shown in Fig. 8. This may be attributed to difference in thickness of fins and condition of leading edges. Fin dies were of a preliminary nature and did not produce fin edges completely free of burr.

Performance of Assembled Heat Exchangers. The assembled heat exchangers were tested as part of the operation of the oxygen

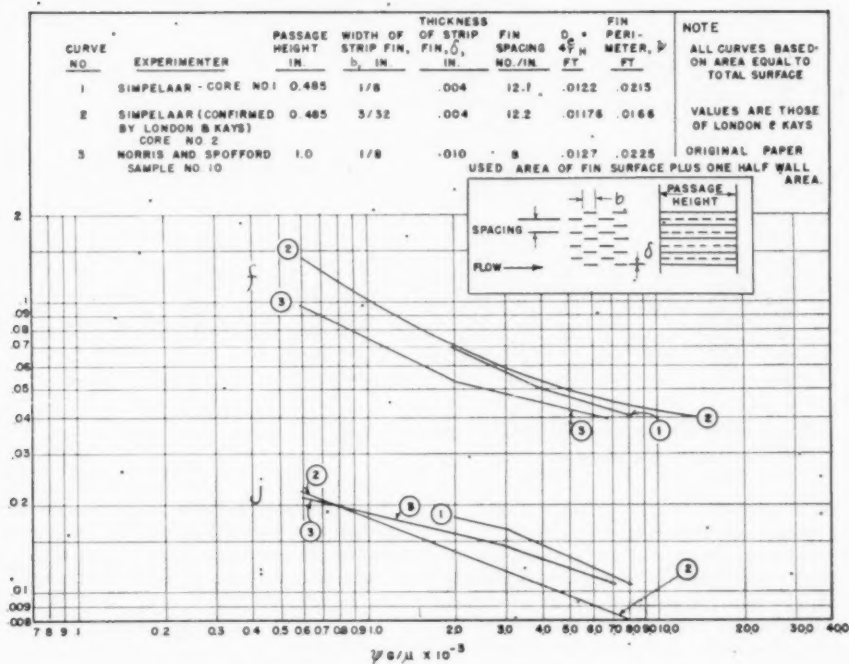


FIG. 8 COMPARISON OF PERFORMANCE OF DIFFERENT STRIP FINS
(Tests of Simpehaar and Aronson and of Norris and Spofford.)

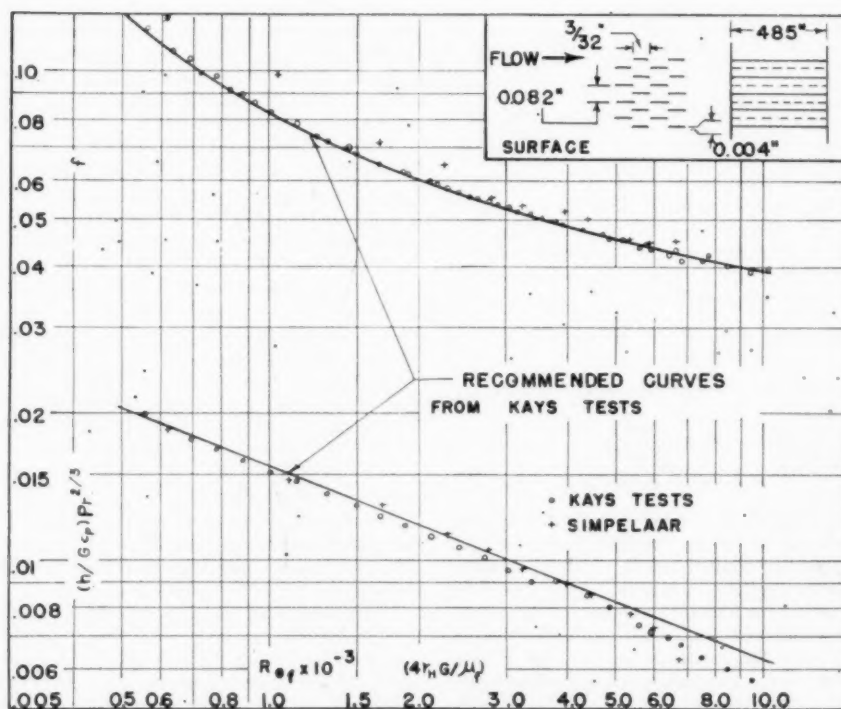


FIG. 9 PERFORMANCE OF STRIP-FIN TEST CORE
(Comparison of test results of Simpehaar and Aronson and Kays and London.)

pilot p
units a
sonably
that in
to larg
ently p
change
reading
uniform
type e
there n
sages.
exchar
tempe
much
likely
large-e
Hes
check
extre
ances
perfor

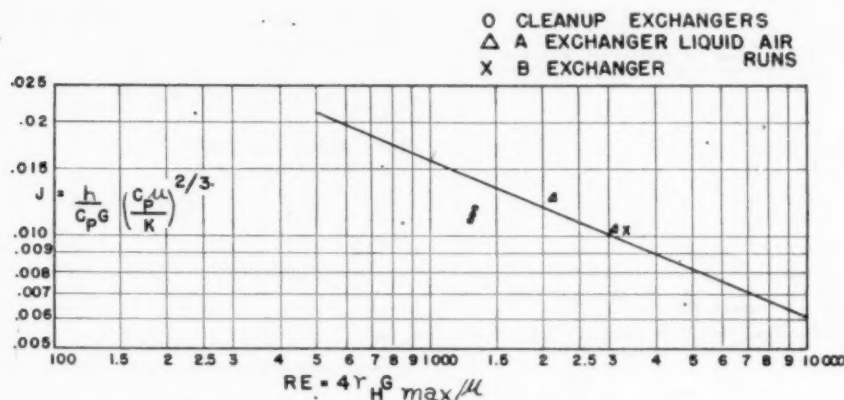


FIG. 10 HEAT-TRANSFER FACTORS FOR HEAT EXCHANGERS

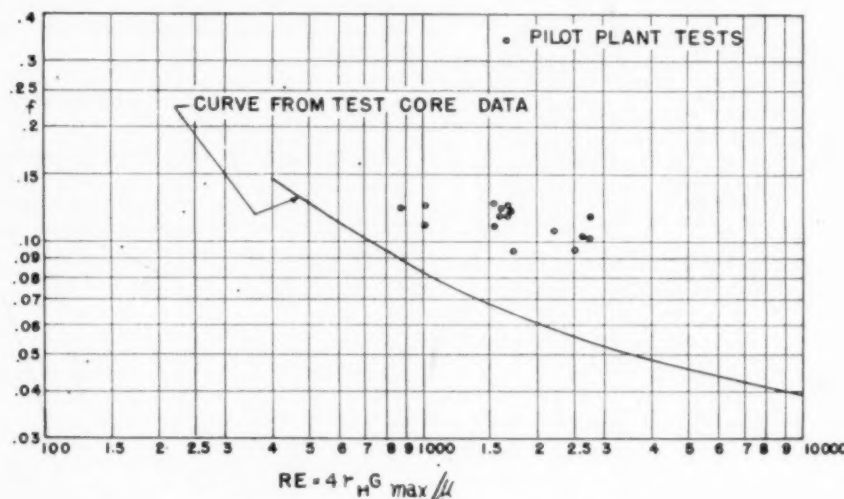


FIG. 11 FRICTION FACTORS FOR HEAT EXCHANGERS

pilot plant. Comparison of performance between assembled units and test cores is presented in Figs. 10 and 11. The reasonably good agreement of heat-transfer performance indicates that inefficiencies introduced when building up from test core to large-scale assembly are of small magnitude. The apparently poorer results indicated on the low-pressure clean-up exchangers may be attributed partly to errors in thermocouple readings and partly to a real decrease in efficiency due to non-uniform flow distribution. These exchangers have different-type end connections than the high-pressure exchangers, so that there may be a difference in the pattern of flows down the passages. An unbalance in flow of 2 per cent from one side of an exchanger passage to the other side results in an increase in end-temperature difference of 5.2 per cent, which represents just that much poorer performance. This lack of good flow balance is likely to be the only reason for poorer heat-transfer results in large-scale units.

Heat balances of the exchangers were made as part of the check of the over-all plant performance. In view of the extremely small end-temperature differences, such heat balances can only check the order of magnitude of the calculated performance.

Table 6 is a sample sheet showing the step-wise method of calculating the performance of exchanger B. A discussion of the factors involved is given in the Appendix. The variation of temperature with length of the heat exchanger is shown graphically in Fig. 12.

The over-all pressure drops measured on the assembled heat exchangers are greater than those predicted from results on test cores as may be seen from Fig. 11, showing friction factor plotted against Reynolds number. This higher pressure drop is attributed to losses in the end connections, the magnitude of which can only be estimated from the observed over-all performance. The end connections which provide for distribution of the flow from the relatively narrow inlet nozzle to the full width of the exchanger slab are built up of a number of hollow rectangular tubes placed in the form of a grid. These tubes support the separating plates, at the same time permitting flow to take place in two directions. The arrangement of these spacer tubes is shown in Fig. 13. For the clean-up exchangers, the "low-pressure-pass" arrangement is used on both air and nitrogen passes. For the high-pressure exchangers A and B, the arrangements are as indicated, respectively, for the two sets of passes.

Table 7 gives typical pressure-drop results for the pilot-plant

TABLE 7 PRESSURE DROP; PILOT-PLANT EXCHANGERS

Run	Exchanger	Flow lb/hr	Mass Flow Rate lb/(hr)(ft) ²	Ave.* Temp. °F	Ave.* Pressure psia	Pressure Drop In. Hg.	Reynolds Number N _{Re}	Friction Factor f
1/22/48 2:30 A.M.	P-1	2,080	2,970	-54	17.1	0.45	31.7	1,010
	P-2	2,080	2,970	-231	17.3	0.25	17.6	1,710
1/22/48 6:30 A.M.	P-1	2,080	2,970	-57	17.1	0.40	28.2	1,020
	P-2	2,080	2,970	-232	17.3	0.20	14.1	1,720
1/22/48 9:30 P.M.	P-1	1,730	2,470	-70	16.8	0.30	21.1	870
	P-2	1,730	2,470	-248	17.0	0.15	10.6	1,530
1/22/48 2:30 A.M.	P-1	3,420	4,880	+3	15.8	1.55	109.	1,510
	P-2	3,420	4,880	-168	16.4	0.80	56.3	2,210
2/7/48 3:30 A.M.	P-1	3,460	4,760	-40	17.2	1.15	80.8	1,570
	P-2	3,460	4,760	-211	17.6	0.55	39.3	2,450
2/7/48 6:30 A.M.	P-1	3,460	4,760	-56	17.2	1.15	80.8	1,620
	P-2	3,460	4,760	-234	17.6	0.60	42.2	2,760
2/7/48 10:30 A.M.	P-1	3,460	4,760	-60	18.3	1.0	70.4	1,650
	P-2	3,460	4,760	-232	18.6	0.5	35.2	2,730
2/7/48 3:30 A.M.	P-1	3,880	5,540	-15	16.2	1.75	123.2	1,790
	P-2	3,880	5,540	-181	16.8	0.9	63.4	2,600

* Arithmetic average of inlet and discharge conditions.

Note: Nitrogen gas used in all of the above tests.

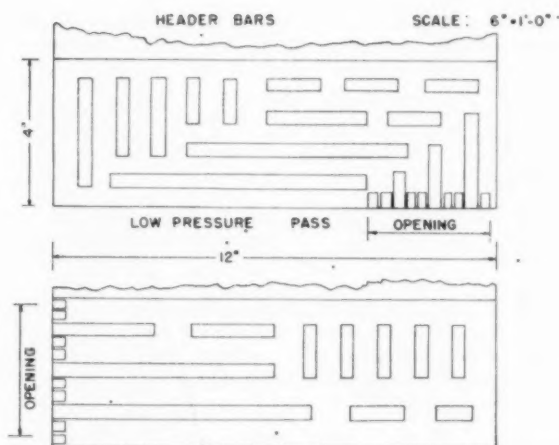


FIG. 13 PATTERNS OF SPACER TUBES IN END MANIFOLDS OF HEAT EXCHANGERS

ACKNOWLEDGMENTS

The successful construction of these heat exchangers is due largely to the untiring efforts of Mr. Don Huggins, Mechanical Engineer at Modine Manufacturing Company, who supervised exchanger assembly. Core tests were the work of Mr. Huggins and Modine laboratory technicians. Performance values on the large heat exchangers were obtained by the plant engineers responsible for the design and operation of the Elliott Company oxygen pilot plant, Messrs. Duffer Crawford, Joseph Cost, Carroll Claitor, and Mack Atcheson.

The authors also wish to express their appreciation of the contribution of Modine Manufacturing Company and the Elliott Company who underwrote this project and agreed to publication of the results.

BIBLIOGRAPHY

- 1 "High-Performance Fins for Heat Transfer," by R. H. Norris and W. A. Spofford, Trans. ASME, vol. 64, 1942, pp. 489-496.
- 2 "The Elliott Oxygen Pilot Plant," by I. Roberts, D. Aronson, M. Atcheson, L. C. Claitor, J. L. Cost, and D. B. Crawford, *Industrial and Engineering Chemistry*, vol. 41, 1949, pp. 2661-2669.
- 3 "The Design of Ribbon Packed Exchangers for Low Temperature Air Separation Plants," by P. R. Trumpler and B. F. Dodge, Trans. AIChE, vol. 43, Feb., 1947, pp. 75-84.

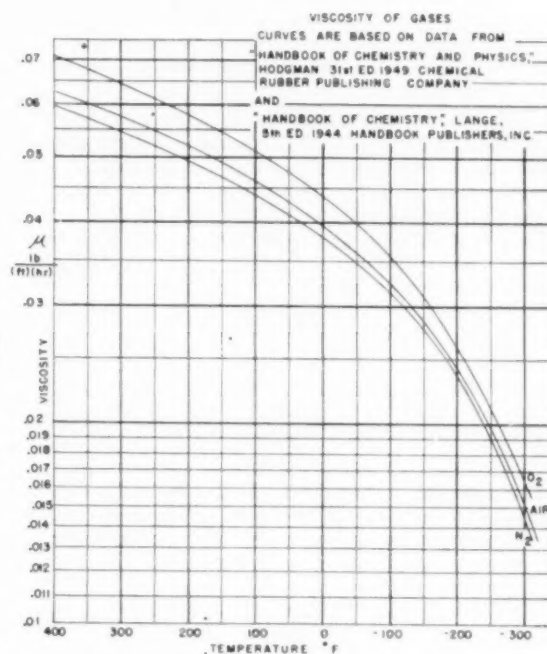


FIG. 14 CHART OF VISCOSITIES FOR AIR, NITROGEN, AND OXYGEN

4 "Gas Turbine Plant Regenerator Surfaces—Basic Heat Transfer and Flow Friction Data," by A. L. London and C. K. Ferguson, Bureau of Ships Research Memorandum no. 2-46 Navships (250-338-3), July, 1946.

5 "Test Results of High-Performance Heat-Exchanger Surfaces Used in Aircraft Intercoolers and Their Significance for Gas-Turbine Regenerator Design," by A. L. London and C. K. Ferguson, Trans. ASME, vol. 71, 1949, pp. 17-26.

6 "Tests of a Strip-Fin Heat Exchanger Surface," by W. M. Kays, Technical Report no. 4, Navy Contract N6-ONR-251 Task Order VI (NR-035-104), Department of Mechanical Engineering, Stanford University, A. L. London, Project Supervisor.

7 "Thermodynamics," by G. N. Lewis and M. Randall, second edition, McGraw-Hill Book Company, Inc., New York, N. Y., 1923, pp. 65-68.

8 "Thermodynamic Properties of Oxygen, Nitrogen, and Air," by L. C. Claitor and D. B. Crawford, Trans. ASME, vol. 71, 1949, pp. 885-895.

Appendix

CALCULATION OF EXCHANGER PERFORMANCE

The method of stepwise calculation of exchanger performance has been developed as follows:

For each set of passages of incremental length, Δl ; the incremental NTU is

$$\Delta NTU_h = \frac{\delta t_h}{\Delta t_h} = \frac{j_h (a/s)_h (\Delta l)}{0.818}$$

$$\Delta NTU_c = \frac{\delta t_c}{\Delta t_c} = \frac{j_c (a/s)_c (\Delta l)}{0.818}$$

where

δt_h = temperature change of hot fluid over length of exchanger

$\Delta t_h = t_h - t_m$ = temperature difference between hot fluid and metal wall

$\Delta t_c = t_m - t_c$ = temperature difference between metal wall and cold fluid

$t_h - t_c$ = temperature difference between two gases

a/s = ratio of total surface to net open area per unit of length

The equations for NTU are applicable over a short length for which the conditions of physical properties and temperature differences between the two gases are essentially constant. The performance for the full exchanger length is obtained by adding up the NTU for each elemental length.

The over-all NTU can be determined as a ratio of the NTU for either of the two streams:

For the hot stream

$$NTU_h = \frac{\delta t_h}{t_h - t_c} = \frac{\delta t_h}{\Delta t_h + \Delta t_c}$$

For the cold stream

$$NTU_c = \frac{\delta t_c}{t_h - t_c} = \frac{\delta t_c}{\Delta t_h + \Delta t_c}$$

Arbitrarily, the over-all NTU , based on the hot stream, will be used for calculating the exchanger performance. The final answer would be identical were the NTU based upon the cold stream. For the NTU based on the hot stream

$$NTU_h = \frac{\delta t_h}{t_h - t_c} = \frac{j_h \eta_h (a/s)_h (\Delta l) (\Delta t_h)}{(\Delta t_h + \Delta t_c) (0.818)}$$

To find the value of the ratio $\Delta t_h / (\Delta t_h + \Delta t_c)$ in terms of the known physical characteristics and temperature changes

$$\Delta t_h = \frac{\delta t_h (0.818)}{j_h \eta_h (a/s)_h (\Delta l)}$$

$$\Delta t_c = \frac{\delta t_c (0.818)}{j_c \eta_c (a/s)_c (\Delta l)}$$

$$\frac{\Delta t_h}{\Delta t_h + \Delta t_c} = \frac{\delta t_h (0.818)}{[j_h \eta_h (a/s)_h (\Delta l)] \left[\frac{\delta t_h (0.818)}{j_h \eta_h (a/s)_h (\Delta l)} + \frac{\delta t_c (0.818)}{j_c \eta_c (a/s)_c (\Delta l)} \right]}$$

which simplifies to

$$\frac{\Delta t_h}{\Delta t_h + \Delta t_c} = \frac{\delta t_h}{\delta t_h + \delta t_c \left(\frac{j_h}{j_c} \right) \left(\frac{\eta_h}{\eta_c} \right) \left[\frac{(a/s)_h}{(a/s)_c} \right]}$$

Substituting the value of this ratio in the equation for NTU

$$NTU_h = \frac{\delta t_h}{t_h - t_c} = \frac{j_h \eta_h (a/s)_h (\Delta l) (\delta t_h)}{0.818 \left[\delta t_h + \delta t_c \left(\frac{j_h}{j_c} \right) \left(\frac{\eta_h}{\eta_c} \right) \left(\frac{a/s)_h}{(a/s)_c} \right] \right]}$$

Rearranging this equation

$$\Delta l = \frac{(0.818) \left[\delta t_h + \delta t_c \left(\frac{j_h}{j_c} \right) \left(\frac{\eta_h}{\eta_c} \right) \left(\frac{a/s)_h}{(a/s)_c} \right] \right]}{j_h \eta_h (a/s)_h (t_h - t_c)}$$

The ratio of the two heat-transfer factors is a function of the modified Reynolds number to the 0.4 power (as indicated by test-core results)

$$\frac{j_h}{j_c} = \frac{0.245 / (D_e G / \mu)_h^{0.4}}{0.245 / (D_e G / \mu)_c^{0.4}}$$

The value of the effective diameter D_e for the two streams is taken as being equal.

The viscosities of the two gases, hot gas and the cold gas, within the same small increment of length, under conditions of operation, may be considered equal; hence

$$\frac{j_h}{j_c} = \left(\frac{G_h}{G_c} \right)^{0.4}$$

Then

$$\Delta l = \frac{(0.818) \left[\delta t_h + \delta t_c \left(\frac{G_h}{G_c} \right)^{0.4} \left(\frac{\eta_h}{\eta_c} \right) \left(\frac{a/s)_h}{(a/s)_c} \right] \right]}{j_h \eta_h (a/s)_h (t_h - t_c)}$$

The calculation of exchanger performance can be handled by relating the performance at any section (and any temperature) to the performance at an arbitrary temperature. This arbitrary standard temperature is taken as 100 F. The ratio of performance is given by

$$\frac{j_{100}}{j_t} = \frac{0.245 / (D_e G_{100} / \mu_{100})^{0.4}}{0.245 / (D_e G_t / \mu_t)^{0.4}}$$

Since D_e and G are constant along the length of the exchanger

$$j_{100} / j_t = (\mu_{100} / \mu_t)^{0.4}$$

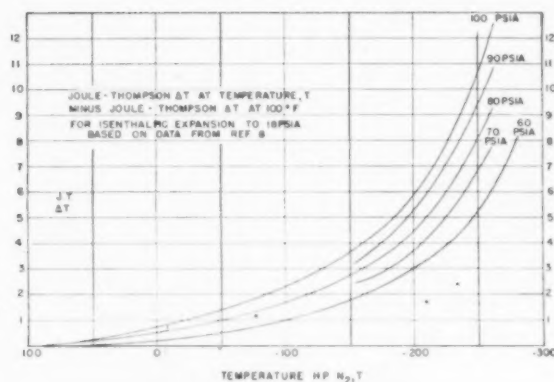
Substituting the value of $(j_h)_{100}$ in the equation for performance

$$\Delta l = \frac{0.818 \left[\delta t_h + \delta t_c \left(\frac{G_h}{G_c} \right)^{0.4} \left(\frac{\eta_h}{\eta_c} \right) \left(\frac{a/s)_h}{(a/s)_c} \right] \right]}{(j_h)_{100} \left(\frac{\mu_t}{\mu_{100}} \right)^{0.4} \eta_h (a/s)_h (t_h - t_c)}$$

From this equation the incremental length for each temperature range can be calculated and then the value of $(j_h)_{100}$ determined from the conditions in any particular interval of length. The method of calculating performance is illustrated by the following example:

Exchanger B is handling a flow of 4220 lb per hr of nitrogen in the high-pressure passages and 4270 lb per hr in the low-pressure passages. The respective average pressures are 85 psia and 18 psia. The observed end temperature conditions are as follows:

	Temperature, deg F		
	High pressure	Low pressure	Difference
Warm end.....	85	78.5	6.5
Cold end.....	-256.5	-276.7	20.2
Temperature change	341.5	355.2	

FIG. 15 NET JOULE-THOMSON ΔT

The detailed calculations are handled in tabular form as shown, in Table 6. The multiplier for the temperature change Δt_c of the cold fluid is

$$\left(\frac{G_c}{G_h}\right)^{0.4} \frac{\eta_h (a/s)_h}{\eta_c (a/s)_c} = \left(\frac{6100}{12,500}\right)^{0.4} \left(\frac{0.967}{0.922}\right) \left(\frac{403}{354}\right) = 0.896$$

The ratio of fin effectiveness for the hot fluid to that of the cold fluid at 100 F is 0.967/0.922 and is taken as being constant over the entire length of the exchanger. Variation of this ratio with temperature is negligible.

The first five columns of the table are used to calculate a heat balance over each incremental length. The balance could be made by taking enthalpy values from a temperature-enthalpy chart or table but as a practical method the scheme shown is

easier to handle. The high-pressure temperature is split into convenient intervals with the first increment taken as small as 2 deg in order to reduce the effect of averaging in using this interval for calculating the value of j_{100} . The net Joule-Thomson effect (7) is the difference between the Joule-Thomson effect at an arbitrary temperature (taken at 100 F) and the Joule-Thomson effect at the particular temperature interval. Values are plotted in Fig. 15. The adjustment for unbalance flow is calculated by allowing a higher or lower temperature change for the low-pressure stream than for the high-pressure stream, inversely proportional to the difference of the two molal flows. The column next to the last is calculated as an incremental length which is converted to actual incremental lengths in the last column.

The value of the heat-transfer factor at 100 F is then calculated by using the performance values over any increment of length

$$j_{100} = \frac{0.818 \left[\Delta t_h + (\Delta t_c) \left(\frac{G_c}{G_h} \right)^{0.4} \frac{\eta_h (a/s)_h}{\eta_c (a/s)_c} \right]}{\Delta l \left(\frac{\mu_t}{\mu_{100}} \right)^{0.4} \eta_h (a/s)_h (t_h - t_c)}$$

Substituting the values from the table for the interval 85 deg to 83 deg

$$j_{100} = \frac{0.818 [2 + 2(0.896)]}{(0.1192)(0.993)(0.967)(403)(6.5)} = 0.0104$$

Reynolds number at 100 deg F for the given conditions of flow is

$$D_s G/\mu = (0.0117)(12,500)/(0.044) = 3320$$

From the temperature and incremental length values in Table 6, the change of temperature along the length of the exchanger can be plotted, as has been done in Fig. 12.

This p
regenera
space b
the plat
maximu
regenera
plate sp
ance. M
riving a

C_2, C_3, C_4
 C_7, C_8

¹ Section
Mem. AS
Contrib
sions and
27-Dec. 2
NEERS.
NOTE:
understo
the Societ

Design of Regenerators for Gas-Turbine Service

By DAVID ARONSON¹

This paper presents a method for designing gas-turbine regenerators with particular reference to the condition of space being the principal limitation on design. For the plate-fin structure a procedure is given for arriving at maximum performance attainable in a given volume of regenerator core, and for calculating the fin patterns and plate spacings required to obtain such maximum performance. For the tubular-type regenerator a method of arriving at optimum tube spacings is presented.

NOMENCLATURE

- A = heat-transfer area, sq ft
 a = factor in determining fin effectiveness, $a = (2h/kt)^{0.5}$
 B = constant $\frac{j/(f/2)_g \eta_g R L_c^2}{(NTU)(W_g v_g)^2 (Pr)^{1/2}}$
 b = wetted perimeter, ft
 c = fraction of total length, L_c , given to cold stream:
 $L_c(c)$ = total height in no-flow direction of all cold-stream passages, ft
 $L_c(1 - c)$ = total height in no-flow direction of all hot-stream passages, ft
 c_p = specific heat at constant pressure, Btu/(lb F)
 C = air or gas capacity rate, $C = W c_p$, Btu/(hr F)
 C_2, C_3, C_4, C_5 = constants related to f, j , and $j/(f/2)$
 C_7, C_8, C_9 = constants relating performance inside to outside of tubes
 D_e = equivalent diameter of passage, for rectangular passages, ft
 $D_e = 4r_h = \frac{4S}{b} = \frac{4(D_1 D_2)}{2(D_1 + D_2)} = \frac{2D_1 D_2}{D_1 + D_2}$
 D_1 = width of rectangular passage, ft or in.
 D_2 = height of rectangular passage, ft or in.
 D_i = inside diameter of round tubes, ft or in.
 D_o = outside diameter of round tubes, ft or in.
 F = ratio of design factors, dimensionless (see text)
 f, f_g = see dimensionless groupings
 G = mass velocity, lb/(hr ft²) or lb/(sec ft²) $G = V\rho$ or V/v
 G_o = mass velocity at minimum opening between tubes, lb/(hr ft²) or lb/(sec ft²)
 g = proportionality factor, $g = 32.2$ lb ft/# sec² = 4.17×10^4 lb ft/# hr²
 h = unit conductance for thermal convection heat transfer, Btu/(hr ft² F)

- j = see dimensionless groupings
 k = thermal conductivity, Btu/(hr ft² F/ft)
 L = flow length, ft
 L_a = length of passage for flow of gas, ft
 L_b = length of passage for flow of air, ft
 L_c = length of assembly of passages in no-flow direction for crossflow plate-fin type exchanger, or length in no-flow direction for tubular exchanger, ft
 L_n = dimension in direction of stream flowing across outside of tubes, ft
 L_T = length of tubes, ft
 N = number of tubes in direction of flow across tubes, dimensionless $N = L_n/S_L$
 NTU = see dimensionless groupings
 P = pressure, #/in.² or #/ft²
 $(\Delta P/P)$ = pressure-drop ratio, dimensionless
 R = gas constant; for air $R = 53.3$ ft #/(lb F)
 r = ratio of volume flow of two streams, dimensionless
 $r = \frac{(W/\rho)_a}{(W/\rho)_g} = \frac{W_a v_a}{W_g v_g}$
 r_h = hydraulic radius, ft
 S = free flow area, sq ft
 S_T/D_o = tube-spacing ratio, center to center in direction normal to gas flow, dimensionless
 S_L/D_o = tube-spacing ratio, center to center in direction of gas flow, dimensionless
 T = temperature, R
 t = temperature, F
 Δt_{lm} = long mean temperature difference, F
 $t_{lm} = \frac{[(t_1)_g - (t_2)_a] - [(t_2)_g - (t_1)_a]}{\ln \left[\frac{(t_1)_g - (t_2)_a}{(t_2)_g - (t_1)_a} \right]}$
 Δt_m = mean-effective-temperature difference to be used in determining efficiency for crossflow heat exchangers, F
 $\Delta t_m = Y(\Delta t_{lm})$
 $\Delta t_m = (\Delta t_m)_g + (\Delta t_m)_a$
 $(\Delta t_m)_a$ = mean-effective-temperature difference between air and metal wall
 $(\Delta t_m)_g$ = mean-effective-temperature difference between gas and metal wall
 Δt_o = difference between bulk fluid temperature and temperature of metal wall at base of fin
 δt = change in temperature of fluid going through regenerator, F, $\delta t = t_1 - t_2$
 U = unit over-all thermal conductance, Btu/(hr ft² F of A)
 V = velocity of fluid, at average air or gas temperature, fps
 v = specific volume, at average air or gas temperature, ft³/lb

¹ Section Engineer, Heat Process, Elliott Company, Jeannette, Pa. Mem. ASME.

Contributed by the Heat Transfer and Gas Turbine Power Divisions and presented at the Annual Meeting, New York, N. Y., Nov. 27-Dec. 2, 1949, of THE AMERICAN SOCIETY OF MECHANICAL ENGINEERS.

NOTE: Statements and opinions advanced in papers are to be understood as individual expressions of their authors and not those of the Society. Paper No. 49-A-144.

W = flow rate, lb/sec or lb/hr

x_f = effective length of fin

Y = correction factor to apply to log-mean-temperature difference to obtain effective temperature difference, dimensionless

$$Y = \Delta t_m / \Delta t_{lm}$$

from which $NTU = \delta t / (Y \Delta t_{lm})$

Values of Y are summarized on page 147 of (15)² from report of Bowman, Mueller, and Nagle (16).

δ , Δ = prefixes denoting difference

ϵ = heat-exchanger effectiveness, a function of NTU , C_a/C_g , and flow arrangement, dimensionless (see Fig. 2)

$$\epsilon = \frac{(t_2)_a - (t_1)_a}{(t_2)_g - (t_1)_a} = X \text{ of McAdams (15)}$$

η = combined fin and metal-wall effectiveness, dimensionless

$$\eta = \eta_s \frac{D_2}{D_1 + D_2} + 1.00 \frac{D_1}{D_1 + D_2}$$

η_s = fin effectiveness, dimensionless

$$\eta_s = \frac{\tanh ax_f}{ax_f}$$

ν = absolute viscosity, lb/(hr ft)

ρ = fluid density, lb/ft³

σ = ratio of free flow to frontal area, dimensionless

Dimensionless Grouping

A/S = ratio of surface area to net open area. $A/S = 4L/D_s$

$f = \frac{(\Delta P)(\nu)}{(V^2/2g)(A/S)}$ = Fanning friction factor. The f versus Re plot defines the friction characteristic of the surface

$f_o = \frac{(\Delta P)(\nu)}{(V^2/2g)N}$ = friction factor for flow across tubes. The

f_o versus Re plot defines the friction characteristic of the tube pattern. The velocity, V , is that at the minimum opening between tubes and N is the number of such openings in the direction of flow

f_o is related to f by:

$$f_o \frac{(S_T/D_o - 1)}{\pi/4} = \phi \approx f$$

$j = (St)(Pr)^{1/4}$ = generalized heat-transfer grouping. This factor, j versus Re , defines the heat-transfer characteristic of the surface

NTU = number of core "heat-transfer units," a dimensionless expression of the "heat-transfer size" of the core. NTU is customarily based on the minimum weight flow.

$$NTU = UA/C_{min} = \frac{\delta t_a}{\Delta t_m}$$

$$= \frac{\text{Temperature change of air}}{\text{Over-all mean-temperature difference}}$$

² Numbers in parentheses refer to the References at end of the paper.

$NTU_a = NTU$ for the air side of the core. $NTU_a = \eta_a h_a A_a / C_a$

$$= j_a (Pr)^{-1/4} \eta_a (A/S)_a = \frac{\delta t_a}{(\Delta t_m)_a}$$

$NTU_g = NTU$ for the gas side of the core

$$NTU_g = \eta_g h_g A_g / C_g = j_g (Pr)^{-1/4} \eta_g (A/S)_g = \frac{\delta t_g}{(\Delta t_m)_g}$$

$Pr = (C_p \mu / k)$, Prandtl number, a fluid property modulus

$Re = (DG/\mu)$, Reynolds number, a flow property modulus characterizing the "turbulence"

$St = (h/\dot{G}c_p)$, Stanton's number, a heat-transfer modulus

$\phi = \frac{(\Delta P)(\nu)}{(V^2/2g)(A/S)}$ friction factor for flow across tubes based on ratio of surface area to minimum open area

Subscripts

a = air-side condition

g = gas-side condition

i = condition on inside of tube

o = condition on outside of tube

1 = fluid entrance condition to heat exchanger

2 = fluid condition at exit of heat exchanger

Miscellaneous

lb = pounds mass in distinction to

= pounds force

INTRODUCTION

This paper develops a design procedure for the gas-turbine regenerator. It is particularly applicable to those installations where space available for the regenerator is limited. Both the extended surface, plate-fin type, and the tubular type are considered.

In regenerator design there is an optimum ratio between the heat-transfer coefficients and surface areas on the cold side to those on the hot side which will result in the lowest over-all pressure drop $\Delta P/P$ for a given regenerator effectiveness ϵ . In the past this ratio was arrived at by tedious trial-and-error calculations. By using the relationships developed in this paper the designer may reduce the number of such trials or eliminate them completely. Further aid in design is to be found in the work of Soderberg and Smith (1) which shows the effect of regenerator thermal effectiveness on cycle efficiency, and in the paper of London and Kays (2) which is a comparison of several types of heat-transfer surfaces for regenerator application.

GENERAL DESIGN PROCEDURE

The design of a gas-turbine regenerator is simplified if one works mainly with dimensionless ratios. The two important ratios are:

$$\frac{\delta t}{\Delta t_m} = \frac{\text{Temperature change of one fluid}}{\text{Over-all mean temperature difference between one fluid and the other}}$$

$$\frac{\Delta P}{P} = \frac{\text{Pressure drop of fluid going through regenerator}}{\text{Absolute pressure of fluid}}$$

By simple for heat t relations obtains ed of the rege A balan and the fo

which can

This ratio pressed as each side the gas sid

which rea

This ratio tor j and

Substitu gives

A simila The p given by

and by the dim

and sir

For cu be tak withou Equ ship b

The v passa 5000 proxi

By simple algebraic rearrangement of the well-known expressions for heat transfer and pressure drop, it is possible to develop the relationship between these two ratios. At the same time one obtains equations relating these ratios to the physical design of the regenerator.

A balance between the quantity of heat to be transferred and the force producing the transfer is given by

$$W c_p \Delta t = U A \Delta t_m \dots \dots \dots [1]$$

which can be rearranged to

$$U A / W c_p = \Delta t / \Delta t_m \dots \dots \dots [2]$$

This ratio of temperature change to temperature difference is expressed as NTU , number of transfer units. The performance on each side of the regenerator may be expressed similarly. For the gas side

$$W_g (c_p)_g (\delta t)_g = h_g \eta_g A_g (\Delta t_m)_g \dots \dots \dots [3]$$

which rearranges to

$$NTU_g = \frac{(\delta t)_g}{(\Delta t_m)_g} = \frac{h_g \eta_g A_g}{W_g (c_p)_g} = \frac{h_g \eta_g A_g}{C_g} \dots \dots \dots [4]$$

This ratio can be calculated directly from the heat-transfer factor j and the ratio of surface to net open area A/S

$$j = \frac{h}{G c_p} \left(\frac{c_p \mu}{k} \right)^{1/4} = \frac{h}{(W/S) c_p} \left(\frac{c_p \mu}{k} \right)^{1/4} \dots \dots \dots [5]$$

Substitution of the value of j from Equation [5] in Equation [4] gives

$$NTU_g = \frac{j_g (A/S)_g \eta_g}{(c_p \mu / k)^{1/4}} \dots \dots \dots [6]$$

A similar development applies to the air side.

The pressure drop for flow in tubes or continuous passages is given by

$$\Delta P = \frac{f V^2 (A/S)}{2 g v} \dots \dots \dots [7]$$

and by dividing through both sides by the absolute pressure P , the dimensionless form is obtained

$$\Delta P / P = \frac{f V^2 (A/S)}{2 g P v} \dots \dots \dots [8]$$

and since

$$P v = R T$$

$$\Delta P / P = \frac{f V^2 (A/S)}{2 g R T} \dots \dots \dots [9]$$

For conditions in a regenerator the values of P , v , and T may be taken as the arithmetic average of inlet and outlet conditions without introducing significant error.

Equations [6] and [9] may be combined to give the relationship between NTU and $\Delta P / P$

$$NTU_g = \frac{[j/(f/2)]_g (\Delta P / P)_g g R T_g \eta_g}{V_g^2 (C_p \mu / k)^{1/4}} \dots \dots \dots [10]$$

The value of $j/(f/2)$ is a function of both Reynolds number and passage geometry. For flow through round tubes at Re from 5000 to 200,000 the values of f and j , respectively, may be approximated by

$$f = 0.046 / Re^{0.2}$$

$$j = 0.023 / Re^{0.2}$$

REGENERATOR

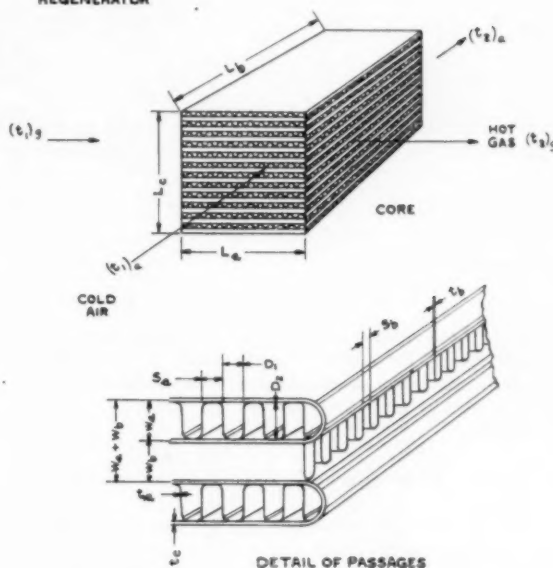


FIG. 1 ARRANGEMENT OF SURFACES IN PLATE-FIN-TYPE REGENERATOR

so that

$$j/(f/2) = 1.0$$

At values of Re less than 5000 this ratio becomes less than unity and is dependent on the length-to-diameter ratio of the passage. Test values of different types of fins are reported in (3), (4), (5), (6), and (7). For the type of construction here considered, the values of $j/(f/2)$ vary from about 0.5 to 1.0. (See Fig. 1.)

A Relationship Between Individual and Over-All Performance Values.

The reciprocals of the NTU_g and NTU_a may be added to give the reciprocal of the over-all NTU , shown as follows

$$\frac{1}{UA} = \frac{1}{h_g A_g \eta_g} + \frac{1}{h_a A_a \eta_a} \dots \dots \dots [11]$$

In a gas turbine the weight flows and the heat capacities of the two streams are approximately equal so that

$$C_g = C_a \dots \dots \dots [12]$$

Dividing Equation [11] by [12]

$$\frac{1}{UA} = \frac{1}{h_g A_g \eta_g} + \frac{1}{h_a A_a \eta_a} \dots \dots \dots [13]$$

which from Equations [2] and [4] is identical with

$$\frac{1}{NTU} = \frac{1}{NTU_g} + \frac{1}{NTU_a} \dots \dots \dots [14]$$

Where no subscript is used, NTU will be read as the over-all number of transfer units. The over-all NTU can be related to the individual pressure-drop ratios by substituting Equation [10] in [14]

$$\frac{1}{NTU} = \frac{(V_g)^2 (Pr)^{1/2}}{j/(f/2)_g \eta_g (\Delta P/P)_g gRT_g} + \frac{(V_a)^2 (Pr)^{1/2}}{j/(f/2)_a \eta_a (\Delta P/P)_a gRT_a} \quad [15]$$

The individual pressure-drop ratios can be shown by thermodynamic analysis to have an effect on the cycle proportional to their sum

$$\Delta P/P \approx (\Delta P/P)_g + (\Delta P/P)_a \quad [16]$$

This develops from the expression for the entropy gain due to pressure loss which is given by

$$-R \ln (P_2/P_1)$$

where P_1 is the pressure at the inlet to the regenerator and P_2 is the pressure at the outlet. For the small pressure ratios involved in regenerator design the logarithm of the ratio may be approximated by

$$\ln P_2/P_1 = \ln (1 - \Delta P/P_{avg}) = -\Delta P/P_{avg}$$

B Optimum Relations Between Performance in Air and in Gas Passages.

There are optimum ratios between the individual NTU and the individual $\Delta P/P$ which give the highest over-all NTU for a given $\Delta P/P$, or for a given NTU , the lowest total $\Delta P/P$. Partial differentiation with respect to the possible variables and setting the resulting partial differentials equal to zero gives the optimum conditions.

The following relationships are developed in order to arrive at equations suitable for differentiation

$$V_g = (W_g v_g)/S_g \quad [17a]$$

$$V_a = (W_a v_a)/S_a \quad [17b]$$

Let

$$r = (W_a v_a)/(W_g v_g) \quad [18]$$

and

$$L_c(c) = \text{length in ft in no-flow direction given to cold-stream passages} \quad [19a]$$

$$L_h(1-c) = \text{length in ft in no-flow direction given to hot-stream passages} \quad [19b]$$

The space occupied by metallic separating walls is neglected. The areas for flow are, respectively

$$S_g = (L_h)(L_c)(1-c) \quad [20]$$

$$S_a = (L_h)(L_c)(c) \quad [21]$$

Substituting Equations [18], [19a], and [19b], in Equations [17a] and [17b] gives

$$V_g = \frac{(W_g v_g)}{(L_h)(L_c)(1-c)} \quad [22]$$

$$V_a = \frac{(W_a v_a)}{(L_h)(L_c)(c)} = \frac{r(W_g v_g)}{(L_h)(L_c)(c)} \quad [23]$$

Inserting these values of V in Equation [15]

$$\frac{1}{NTU} = \frac{(W_g v_g)^2 (Pr)^{1/2}}{j/(f/2)_g \eta_g (\Delta P/P)_g gRT_g (L_h)^2 (L_c)^2 (1-c)^2} + \frac{r^2 (W_g v_g)^2 (Pr)^{1/2}}{j/(f/2)_a \eta_a (\Delta P/P)_a gRT_a (L_h)^2 (L_c)^2 (c)^2} \quad [24]$$

To simplify the analysis one can assume that the following terms are equalities (which is approximately true)

$$j/(f/2)_g = j/(f/2)_a$$

$$\eta_g = \eta_a$$

$$(Pr)_g^{1/2} = (Pr)_a^{1/2}$$

and that the change in value of $j/(f/2)$ in the range of possible design variations may be considered a second-order effect. Let

$$\frac{j/(f/2)_g R L_c^2}{(NTU) (W_g v_g)^2 (Pr)^{1/2}} = B$$

then Equation [24] becomes

$$B = \frac{1}{(\Delta P/P)_g T_g L_h^2 (1-c)^2} + \frac{r^2}{(\Delta P/P)_a T_a L_h^2 c^2} \quad [25]$$

Let

$$F = NTU_g/NTU_a \quad [26]$$

$$F = \frac{1/NTU_g}{1/NTU_a} = \frac{(\Delta P/P)_a T_a L_h^2 c^2}{(\Delta P/P)_g T_g L_h^2 (1-c)^2} \quad [27]$$

Substituting Equation [27] in [25] and solving for the individual values of $\Delta P/P$ gives

$$(\Delta P/P)_g = \frac{(F+1)}{B (L_h)^2 (1-c)^2 T_g} \quad [28]$$

$$(\Delta P/P)_a = \frac{(F+1)}{(F)(B)(L_h)^2 (c)^2 T_a} \quad [29]$$

Substituting Equations [28] and [29] in Equation [16] gives the general equation

$$\Delta P/P = \frac{(F+1)}{B (L_h)^2 (1-c)^2 T_g} + \frac{(F+1) r^2}{(F) B (L_h)^2 (c)^2 T_a} \quad [30]$$

The value of F and c for minimum $\Delta P/P$ are found by partial differentiation as mentioned above

$$\left(\frac{\partial(\Delta P/P)}{\partial c} \right)_F = 0 = + \frac{(F+1) 2}{B (L_h)^2 (1-c)^2 T_g} - \frac{(F+1) 2 r^2}{(F) B (L_h)^2 c^3 T_a} \quad [31]$$

$$\left(\frac{c}{1-c} \right)^2 = \frac{(r L_h/L_a)^2 (T_g/T_a)}{F} \quad [32]$$

$$\left(\frac{\partial(\Delta P/P)}{\partial F} \right)_c = 0 = \frac{1}{B L_h^2 (1-c)^2 T_g} - \frac{r^2}{F^2 (B) (L_h)^2 (c)^2 T_a} \quad [33]$$

$$F^2 = (r L_h/L_a)^2 \left(\frac{1-c}{c} \right)^2 (T_g/T_a) \quad [34]$$

Substituting the value of F obtained from Equation [34] in Equation [32] gives

$$\frac{c}{1-c} = (r L_h/L_a)^{0.5} (T_g/T_a)^{0.25} \quad [35]$$

Substituting Equation [35] in Equation [34] gives

$$F = (r L_h/L_a)^{0.5} (T_g/T_a)^{0.25} \quad [36]$$

Comparing Equation [36] with Equation [35] one notes that

$$F = \frac{c}{1-c} \quad [37]$$

Equation [27] can be rewritten as

$$F = \frac{r^2 (\Delta P/P)_g T_g L_a^2 (1-c)^2}{(\Delta P/P)_a T_a L_a^2 (c)^2} \quad [38]$$

which combined with Equation [34] gives

$$F = \frac{(\Delta P/P)_a}{(\Delta P/P)_g} \quad [39]$$

These relationships can be more readily visualized by equating them all to F .

$$F = \frac{(\Delta P/P)_a}{(\Delta P/P)_g} = \frac{c}{1-c} = \frac{(D_2)_a}{(D_2)_g} = \frac{(NTU)_g}{(NTU)_a} = \left(\frac{r L_a}{L_g} \right)^{0.5} \left(\frac{T_g}{T_a} \right)^{0.25} \quad [40]$$

$(D_2)_a$ and $(D_2)_g$ are the heights, respectively, of the cold and hot stream passages, on the basis that there is the same number of passages for both streams.

The over-all NTU can be related to the over-all pressure-drop ratio and the velocity of either stream by rearrangement of the relationships given in Equation [40]

$$NTU = \frac{(\Delta P/P)_g \eta [j/(f/2)] gRT_g}{(1+F)^2 (V_g)^2 (Pr)^{1/2}} = \frac{F^2 (\Delta P/P)_g \eta [j/(f/2)] gRT_a}{(1+F)^2 (V_a)^2 (Pr)^{1/2}} \quad [41]$$

In the foregoing analysis no allowance has been made for losses other than frictional pressure drops. These other losses are small enough as not to affect significantly the design relationships, but they should of course be included in the calculation of over-all performance.

For the general case in which

$$\begin{aligned} C_a/C_g &= Z \neq 1 \\ W_g/W_a &= M \neq 1 \\ (c_p)/(c_p)_g &= ZM \neq 1 \end{aligned}$$

the analysis is similar to that already presented, except that the ratios of the two flows must be included. The final equations so derived are

$$F = \frac{(\Delta P/P)_a}{M(\Delta P/P)_g} = \frac{NTU_g}{Z(NTU)_a} = \left[\frac{(c_p)_g}{(c_p)_a} \right]^{0.25} \left[\frac{r(L_b)}{(L_a)} \right]^{0.5} \left[\frac{T_g}{T_a} \right]^{0.25} \quad [42]$$

C Design of Exchanger Passages.

The spacings of exchanger passages can be calculated by means of Equations [6] and [40], and from plots of the j values for the particular fin design chosen. The ratio of passage heights is given by Equation [40], but the absolute value to be used is a matter of judgment on the part of the designer. He must balance high fin effectiveness against increased cost and weight as the height of individual passages is reduced. Conversely, as fin height is increased fin thickness must be maintained adequate to provide reasonable values of fin effectiveness. The fin effectiveness is given by

$$\eta_s = (\Delta t)_m/(\Delta t)_o = (\tanh ax_f)/(ax_f) \quad [43]$$

where

$$a = (hb/ks)^{0.5} = (2h/kt)^{0.5} \text{ for uniform rectangular section fin}$$

x_f = effective length of fin

This length will vary from one half the passage height to the full passage height depending on the method of assembling the individual passages. If the regenerator is built up by assembling individual flat "tubes" consisting of one gas passage and one air passage as shown in sketch B of Fig. 3, then the fin height is the full passage height. If made with one center passage for air and two half-passages for gas as shown in sketch A of Fig. 3, the fin height is taken as one half the center passage height for the air side and the height of the half-passages for the gas side. If there are an even number of passages bonded together as shown in Fig. 1, then the fin height is some value between one half and the full passage height.

The direct surface effectiveness may be taken as unity, so that the over-all effectiveness is

$$\eta = \eta_s \left(\frac{D_2}{D_1 + D_2} \right) + \left(\frac{D_1}{D_1 + D_2} \right) \quad [44]$$

The effective diameter, D_e , for smooth continuous fins may be obtained approximately by substitution in Equation [6] of the relationship between j and Reynolds number

$$NTU = j (4L/D_e) (Pr)^{-1/2} = 0.023 (Re)^{-0.2} (4L/D_e) (Pr)^{-1/2} \quad [45]$$

D Example—Over-All Performance.

The design of a regenerator for a locomotive gas turbine will illustrate the handling of the foregoing relationships:

The following are the approximate properties of the two streams (exact values not being known until the regenerator has been designed):

	Gas side	Air side
Weight flow, W , lb/sec.....	60	60
Average density, lb/ft ³	0.0333	0.166
Average specific volume, v , ft ³ /lb....	30.0	6.0
Average viscosity, μ , lb/(ft) (hr)....	0.076	0.068
Heat capacity, c_p , Btu/(lb) (F).....	0.25	0.25
Prandtl number, $c_p \mu/k$	0.67	0.67
Average temperature, T , deg R.....	1210	980
Average pressure, P , psia.....	14.9	60.0

The regenerator is to have a core of the following dimensions:

Length of flow path for hot gas, L_a , 3 ft
Length of flow path for cold gas, L_b , 7 ft
No flow direction, L_c , 6 ft

As a first step in the design one can determine the relationship between pressure-drop ratio and NTU . With this information the turbine designer can decide upon the optimum NTU for the turbine cycle.

The design parameter F is given by Equation [36]

$$F = [(0.2) (7/3)]^{0.5} (1210/980)^{0.25} = 0.72$$

(The first figure of 0.2 is obtained from $r = v_a/v_g = 6/30 = 0.2$)

Assuming that the ratio of net free area to gross cross-sectional area for the sum of the two streams ($\sigma_g + \sigma_a$) is 0.85 and that it is about proportional to the relative net free area of each, then the velocities of the gases are

$$V_a = \frac{W_a v_a}{(L_a)(L_c) \left(\frac{F}{1+F} \right) (\sigma)} = \frac{(60)(6)}{(3)(6) [(0.72)/1.72] (0.85)} = 56.2 \text{ ft/sec}$$

$$V_g = \frac{W_g v_g}{(L_g)(L_c) [1/(1+F)] (\sigma)} = \frac{(60)(30)}{(7)(6) [1/(1+0.72)] (0.85)} = 88.7 \text{ ft/sec}$$

Either of these values can be substituted in the appropriate part of Equation [41] to give the relationship between pressure-drop ratio and NTU . The following values are assumed for this preliminary study:

$$\text{Fin effectiveness, } \eta_f = 0.85$$

$$j/(f/2) = 0.75$$

The ratio of j to the half friction factor is higher than 0.75 but is reduced to allow for pressure losses at inlet and discharge and for losses or gains due to acceleration or deceleration of the fluid streams.

Based on gas stream

$$NTU_{\text{over-all}} = \frac{(\Delta P/P) (0.85) (0.75) (32.2) (53.3) (1210)}{(1.72)^2 (86.7)^2 (0.77)} = 77.2 (\Delta P/P)$$

Based on air stream

$$NTU_{\text{over-all}} = \frac{(\Delta P/P) (0.85) (0.75) (32.2) (53.3) (980) (0.72)^2}{(1.72)^2 (56.2)^2 (0.77)} = 77.2 (\Delta P/P)$$

If the $\Delta P/P$ for the cycle is limited to 3 per cent, then the maximum NTU obtainable in the given volume is

$$NTU_{\text{over-all}} = (77.2) (0.03) = 2.31$$

which for a single pass crossflow unit gives an efficiency ϵ of 64 per cent, Fig. 2.

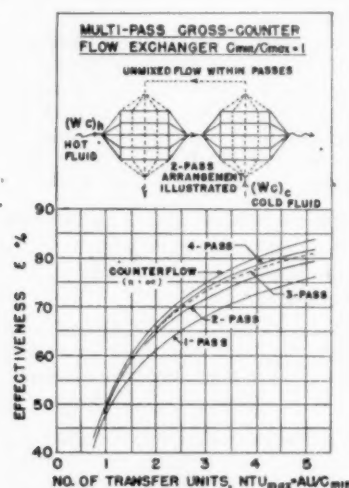


FIG. 2 PLOT OF NTU VERSUS EXCHANGER EFFECTIVENESS

E Example Design of Passages.

The calculations to arrive at passage and fin spacings for an over-all NTU of 2.31 are as follows
From Equation [40]

$$NTU_g = (1 + F) (NTU) = (1.72) (2.31) = 3.98$$

$$NTU_a = \left(\frac{1 + F}{F} \right) (NTU) = \left(\frac{1.72}{0.72} \right) (2.31) = 5.52$$

$$F = \frac{(D_2)_a}{(D_2)_g} = 0.72$$

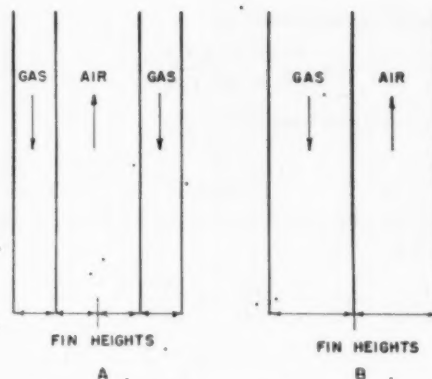


FIG. 3 HEAT-FLOW PATTERN IN FINNED SECTIONS

From Equation [45] the equivalent diameter of the two passages are found. Using the values of Pr and η assumed

$$NTU = 0.023 (0.85) (Re)^{-0.2} (4L/D_e)^{0.67} \cdot^{-1/3}$$

and assuming that $Re_g = 3000$ and $Re_a = 10,000$

$$(L/D_e)_g = (3.98) (3000)^{0.2} (0.76) / [(0.023) (0.85) (4)] = 193$$

$$(D_e)_g = 3.0/193 = 0.0155 \text{ ft} = 0.186 \text{ in.}$$

$$(L/D_e)_a = (5.52) (10,000)^{0.2} (0.76) / [(0.023) (0.85) (4)] = 343$$

$$(D_e)_a = 7.0/343 = 0.0204 \text{ ft} = 0.245 \text{ in.}$$

With these calculated values of equivalent diameter, the assumed Reynolds numbers can be checked and corrections made if there are significant differences. Calculation of passage heights and fin spacings follow customary procedure. After allowances are made for such factors as actual fin efficiencies, area occupied by metal walls, entrance and exit effects, according to the method suggested by London and Kays (2), the final predicted performance values given in Table 1 are obtained.

DESIGN OF TUBULAR REGENERATORS

From the standpoint of maximum performance for a given volume of heat-exchanger core, the use of bare tubes results in lower thermal efficiency than possible with extended-surface plate-fin construction. The foregoing analysis of extended-surface design showed that if there were no limit on the amount of surface and if the fins and separating plates could be made comparatively thin, the over-all NTU obtainable in a given volume is directly proportional to pressure-drop ratio. A similar proportion exists for tubular design but the NTU compared to extended surface is lower for the same allowable pressure-drop ratio.

The use of tubular design is often indicated on the basis of lower cost, better mechanical design, and suitability for high-pressure as well as high-temperature service. A full discussion of this subject is not within the scope of this paper.

In connection with the design of radiators and intercoolers for aircraft service, a type of heat exchanger comparable to a regenerator, a number of design charts, and methods of preparation of such charts for selecting the proper size of core have been developed (8), (9), (10), (11), (12), and (13). The procedures given usually refer to the selection of a core which has already been designed having a fixed pattern of tube spacing and diameters, or plate and fin arrangements. Tubular regenerators, on the other hand, will usually be designed for a particular model of gas turbine, so that there is a choice of both tube diameters and tube spacings. The tube length and the other dimensions will in many cases be fixed by the over-all turbine design.

TABLE 1

ϵ , per cent.	$\Delta P/P$, per
$NTU_{\text{over-all}}$	Weight, lb
Total surface	Direct surface
Indirect surface	Unit heat-transfer
Number of tubes	Outer diameter
Inner diameter	Spacing of tubes
in direction of flow	Thickness of
Gas side	
$\Delta P/P$	NTU_g
h , Btu/hr-ft ²	η , fin efficiency
Total surface	Direct surface
Indirect surface	Number of tubes
Fin thickness	Passage diameter
G , lb/hr-ft ²	V , ft ³ /hr
Re	
Air side	
$\Delta P/P$	NTU_a
h , Btu/hr-ft ²	η , fin efficiency
Total surface	Direct surface
Indirect surface	Number of tubes
Fin thickness	Passage diameter
G , lb/hr-ft ²	V , ft ³ /hr
Re	

^a The surface area is based on the total surface area of the tubes.

^b The surface area is based on the total surface area of the tubes.

^c The surface area is based on the total surface area of the tubes.

^d The surface area is based on the total surface area of the tubes.

^e The surface area is based on the total surface area of the tubes.

^f The surface area is based on the total surface area of the tubes.

^g The surface area is based on the total surface area of the tubes.

^h The surface area is based on the total surface area of the tubes.

ⁱ The surface area is based on the total surface area of the tubes.

^j The surface area is based on the total surface area of the tubes.

^k The surface area is based on the total surface area of the tubes.

^l The surface area is based on the total surface area of the tubes.

^m The surface area is based on the total surface area of the tubes.

ⁿ The surface area is based on the total surface area of the tubes.

^o The surface area is based on the total surface area of the tubes.

^p The surface area is based on the total surface area of the tubes.

^q The surface area is based on the total surface area of the tubes.

^r The surface area is based on the total surface area of the tubes.

^s The surface area is based on the total surface area of the tubes.

^t The surface area is based on the total surface area of the tubes.

^u The surface area is based on the total surface area of the tubes.

^v The surface area is based on the total surface area of the tubes.

^w The surface area is based on the total surface area of the tubes.

^x The surface area is based on the total surface area of the tubes.

^y The surface area is based on the total surface area of the tubes.

^z The surface area is based on the total surface area of the tubes.

TABLE 1 COMPARISON OF REGENERATOR DESIGNS FOR LOCOMOTIVE SERVICE

	Extended surface inconel 64	High effective- ness 64	Low effective- ness 52
ϵ , per cent.....	2.92	7.78	3.01
$\Delta P/P$, per cent.....	2.35	2.35	1.22
NTU.....	7,000	3,600	4,400
Weight, lb (core only).....	24,800	9,300 ^a	6,550 ^a
Total surface, ft ²	7,100		
Direct surface, ft ²	17,700		
Indirect surface, ft ²			
Unit heat-transfer coefficient, U , based on direct surface.....	35.8 ^b	25.5 ^c	18.8 ^c
Number of tubes.....		9,709	3,825
Outer diameter of tubes, in.....		0.280	0.500
Inner diameter of tubes, in.....		0.242	0.435
Spacing of tubes: in direction of gas flow, S_L/D_o		1.75	1.40
in no-flow direction, S_T/D_o		1.94	1.92
Thickness of separating plate, in.....	0.020		
Gas side			
$\Delta P/P$, per cent.....	1.75	3.05	1.38
NTU _g	4.01	4.05	2.09
h , Btu/(hr ft ² F).....	16.9	43.8	32.3
η , fin effectiveness.....	0.80		
Total surface, ft ²	16,000	4,990	3,500
Direct surface, ft ²	3,550		
Indirect surface, ft ²	12,450		
Number of fins per inch.....	7.7		
Fin thickness, in.....	0.010		
Passage height, in.....	0.45		
G , lb/(hr ft ²).....	10,420	10,600	10,670
V , ft/sec.....	86.7	86.5	89
Re.....	2,120	3,240	5,850
Air side			
$\Delta P/P$, per cent.....	1.17	4.73	1.63
NTU _a	5.70	5.58	2.94
h , Btu/(hr ft ² F).....	36.5	69.6	52.1
η , fin effectiveness.....	0.85		
Total surface, ft ²	8,800	4,340	3,050
Direct surface, ft ²	3,550		
Indirect surface, ft ²	5,250		
Number of fins per inch.....	4.8		
Fin thickness, in.....	0.010		
Passage height, in.....	0.337		
G , lb/(hr ft ²).....	33,600	74,400	55,000
V , ft/sec.....	56.2	121.6	92
Re.....	10,100	22,000	29,200

^a The total surface for the tubular design is given as the sum of the outside surface and the inside surface in order to give a true comparison with the total surface of the extended surface units.

^b The over-all heat-transfer coefficient U for the extended-surface design is based on one half the total direct surface to put it on a basis comparable with the tubular design.

^c For the tubular design the coefficient U is based on the outside tube-surface area.

A General Design Relationships.

The design of tubular regenerators to some extent can follow the procedure given for the extended-surface type. The ratios of NTU's for optimum performance can be expressed by a design parameter F , but it should be noted that this parameter, given in Equation [46], is independent of the over-all dimensions of the regenerator. The relationships for a tubular design are

$$F = \frac{NTU_o}{NTU_i} = \frac{h_o A_o / C_o}{h_i A_i / C_i} \quad [46]$$

For gas-turbine regenerator one may consider that

$$C_o = C_i$$

For a bare-tube design

$$A_o/A_i = D_o/D_i$$

so that Equation [46] becomes

$$F = \frac{NTU_o}{NTU_i} = \frac{h_o D_o}{h_i D_i} \quad [47]$$

The ratio of the two heat-transfer coefficients (h_o/h_i) is obtained from the ratio of the mass velocities on the two sides which will give the highest over-all conductance U for the minimum total friction power. This ratio of mass velocities when applied to the expressions for heat transfer and incorporated in Equation [47] gives

$$F = \frac{C_s}{(D_o G_o \mu_o)^{0.17}} \left[\left(\frac{D_o}{D_i} \right) \left(\frac{v_i}{v_o} \right) \right]^{0.444} \left(\frac{T_o}{T_i} \right)^{0.272} \left(\frac{\mu_o}{\mu_i} \right)^{0.111} \quad [48]$$

The constant C_s , which is a function of tube configurations, is shown in Figs. 13 and 14. Employing this ratio of the two NTU's, one can calculate the absolute values of the individual NTU's for

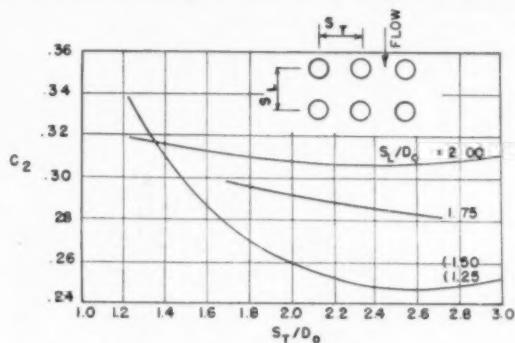


FIG. 4 CONSTANT C_2 AS A FUNCTION OF TUBE SPACING; FLOW OF AIR ACROSS IN-LINE TUBES. CHART FROM (8)

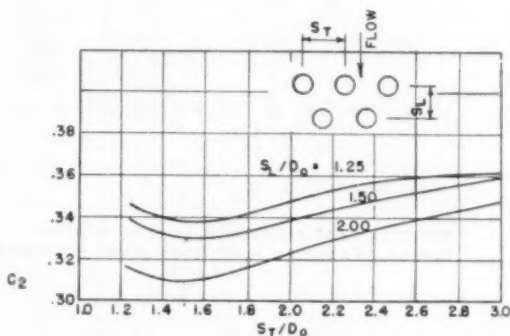


FIG. 5 CONSTANT C_2 AS A FUNCTION OF TUBE SPACING; FLOW OF AIR ACROSS STAGGERED TUBES. CHART FROM (8)

a given value of over-all NTU. From the NTU_i the L/D_i of the tube is obtained by using Equation [45a]

$$NTU_i = \frac{0.023 (4L_T/D_i)}{(Re_i)^{0.4} (Pr)^{1/4}} \quad [45a]$$

The pressure drop for flow inside the tube is given by Equation [9a]

$$(\Delta P/P)_i = f \frac{V^2}{2g} \frac{4L_T/D_i}{RT_i} \quad [9a]$$

Equation [45a] may often give a tube diameter smaller than considered practical. One can redesign the unit for multipass on the tube side so that the effective tube length is increased, or accept a design which will not give the maximum NTU/(\(\Delta P/P\)) ratio for the given volume. In the latter case more surface is required for the same NTU.

The tube spacings required for the optimum ratios of heat-transfer coefficients are given by

$$(S_L/D_o) (S_T/D_o - 1) = \frac{100 (C_2/F)^{1.25} (D_i/D_o) (L_n/L_T) (\mu_o/\mu_i)^{0.25}}{(D_o G_o/\mu_o)^{0.25}} \quad [49]$$

for the case of in-line tube arrangements and staggered tube arrangements having the minimum opening in the transverse spacings. While Equation [49] does not give the absolute values of

the spacings, one can be guided by the general principle that S_T/D_o should be made as small as mechanical design limitations permit because this results in the highest heat transfer for a given friction power as indicated roughly by the plots of Figs. 6, 7, and 8 where C_2 is related to the factor $j/(f/2)$ by

$$j/(f/2) = C_2/(D_o G/\mu)^{0.27} \quad [50]$$

and C_2 is

$$C_2 = \frac{1.10 C_3}{2C_4 (S_T/D_o - 1)} \quad [51]$$

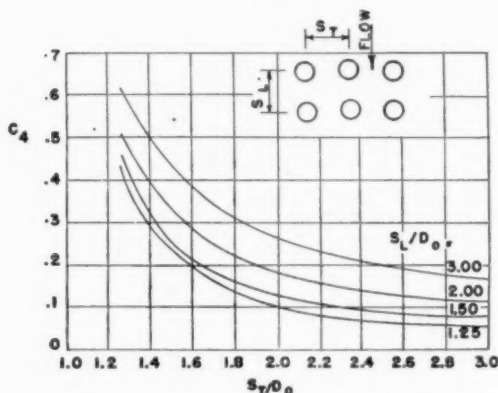


FIG. 6 CONSTANT C_4 AS A FUNCTION OF TUBE SPACING; FLOW OF AIR ACROSS IN-LINE TUBES. CHART FROM (8)

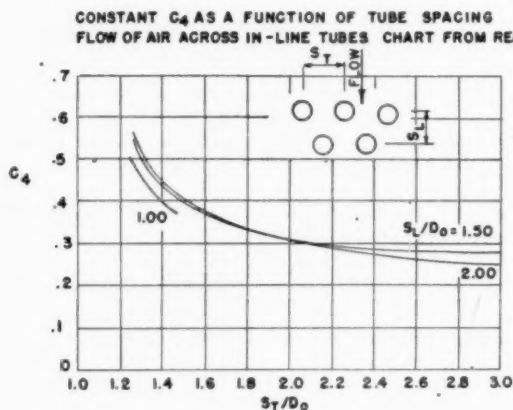


FIG. 7 CONSTANT C_4 AS A FUNCTION OF TUBE SPACING. FLOW OF AIR ACROSS STAGGERED TUBES. CHART FROM (8)

Often tube spacings will be limited by minimum ligament requirements in the tube sheet. (In the design of the regenerator for locomotive service shown in Fig. 17, close tube spacings were obtained by bending the tubes into an arc.)

The values of C_2 and C_4 are functions of Reynolds number and tube arrangement. Wood and Brevoort (8) have prepared simplified correlations, Figs. 4, 5, 6, and 7 of the data of Pierson and Huge as correlated by Grimson (14), for heat transfer and friction factors for flow across tubes. The values of the several authors are related as follows:

$C_2 = 0.31 F_a$ where F_a is the arrangement factor of Grimson and C_2 , the constant given by Wood and Brevoort in

$$hD/k = C_2 \text{Re}^{0.5} \quad [52]$$

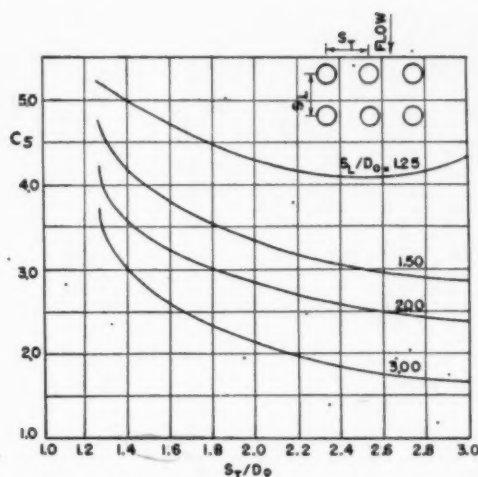


FIG. 8 CONSTANT C_3 AS A FUNCTION OF TUBE SPACING; FLOW OF AIR ACROSS IN-LINE TUBES

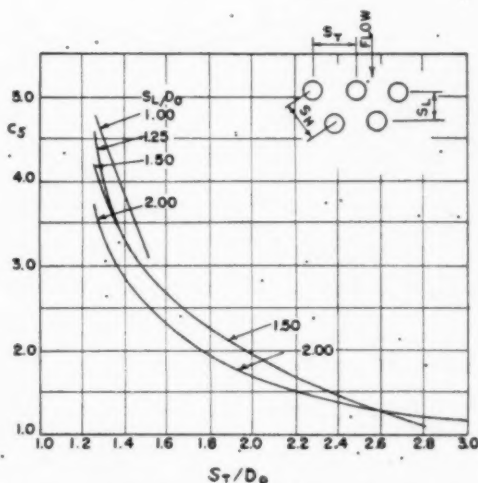


FIG. 9 CONSTANT C_3 AS A FUNCTION OF TUBE SPACING; FLOW OF AIR ACROSS STAGGERED TUBES

In the preparation of their plots Wood and Brevoort incorporated the value of Prandtl number in the constant C_2 . In order to cover a wider range of gas properties the Prandtl number is reintroduced, and in-line with the treatment followed earlier in the paper, the heat-transfer expression is transformed into the Stanton number thus

$$h/c_p G = 1.10 C_2 \text{Pr}^{-1/3} \text{Re}^{-0.4} \quad [52a]$$

The pressure drop on the outside of tubes is given by

$$(\Delta P/P)_o = \frac{4f_o NG^2 v}{2gP} = \frac{4f_o NV^2}{2gPv} = \frac{4f_o N}{RT} \frac{V^2}{2g} \quad [53]$$

where

$$f_o = C_4/(\text{Re})^{0.13} = f_{\text{Grimson}} \quad [54]$$

The value of NTU_o can be obtained from Equation [52a] by incorporating the ratio of surface to net free area

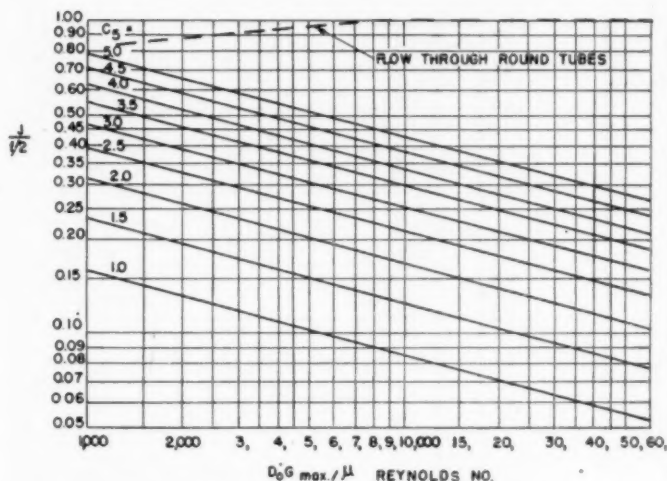


FIG. 10 VALUES OF $j/(f/2)$ FOR FLOW ACROSS TUBES FOR VARIOUS VALUES OF C_s AND OF REYNOLDS NUMBER

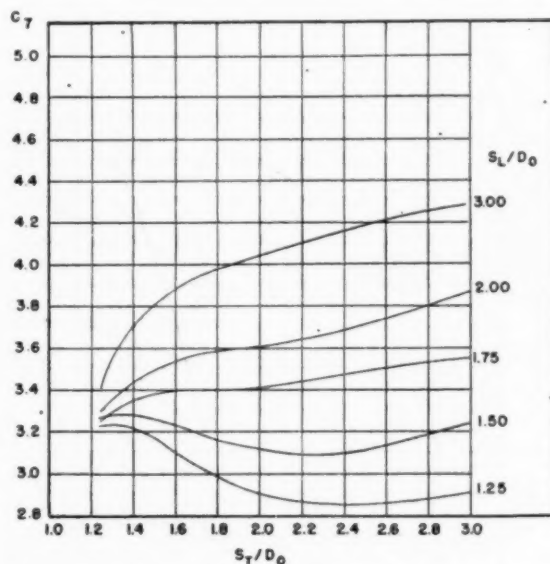


FIG. 11 CONSTANT C_1 AS A FUNCTION OF TUBE SPACING; FLOW OF AIR ACROSS IN-LINE TUBES

$$NTU_o = \frac{1.10 C_s N}{(Pr)^{1/4} (S_T/D_o - 1) (Re)^{0.4}} \dots [55]$$

The equations here presented are sufficient for the design of a tubular regenerator which will make the most effective use of the surface employed.

B Derivation of Relationship for Optimum Performance.

The analysis of tubular design for optimum performance is predicated on the thesis that the ratio of the mass velocities on the two sides is the primary variable. The effect of tube configuration on the optimum ratio of mass velocities is treated as a second-order effect.

The several design equations must be arranged to express the variation of total friction power loss and of total resistance to

heat flow with the ratio of G_o to G_i . The following are taken as equalities

$$W_o = W_i$$

$$(c_p)_o = (c_p)_i$$

The analysis will be based on the performance of a single tube in a tube bank and the length of tube to be considered will be taken as equal to the outside diameter. This does not affect the validity of the analysis since the regenerator is merely a multiple of such an elemental area with all factors in proportion.

The performance on the inside of the tube will be considered only for the case of turbulent flow for which

$$f = 0.046/Re^{0.2}$$

and

$$j = 0.023/Re^{0.2}$$

The pressure-drop ratio is then expressed as

$$(\Delta P/P)_i = \frac{0.046}{(D_i G_i / \mu_i)^{0.2}} \frac{G_i^2 v_i^2 4(D_o/D_i)}{2gRT_i} \dots [56]$$

The amount of fluid flowing is $W = GS = G(\pi/4) D_i^2$ which, substituted in Equation [56], gives

$$(\Delta P/P)_i W_i = \left[\frac{0.046 (\mu_i)^{0.2} \pi (D_o)^{1.5} v_i^{2.2}}{2g(D_o/D_i)^{0.5} RT_i} \right] G_i^{2.2} \dots [57]$$

To simplify the handling of the equations the terms inside the brackets can be called K_i

$$K_i = \frac{0.046 (\mu_i)^{0.2} (D_o)^{1.5} v_i^{2.2}}{2g(D_o/D_i)^{0.5} RT_i} \dots [58]$$

$$(\Delta P/P)_i W_i = K_i G_i^{2.2} \dots [59]$$

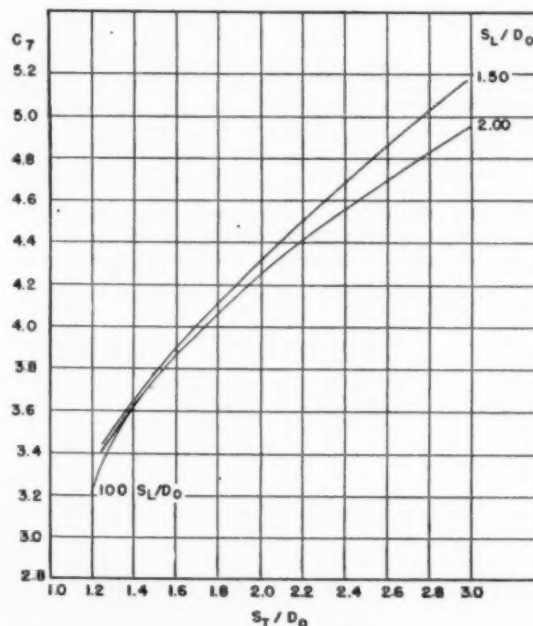


FIG. 12 CONSTANT C_1 AS A FUNCTION OF TUBE SPACING; FLOW OF AIR ACROSS STAGGERED TUBES

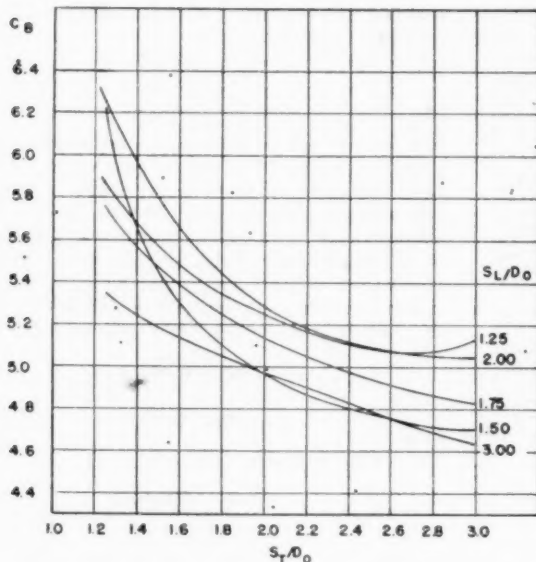


FIG. 13 CONSTANT C_8 AS A FUNCTION OF TUBE SPACING; FLOW OF AIR ACROSS IN-LINE TUBES

The heat transfer on the inside of the tube is given by Equation [45] which becomes

$$h_i A_i = \left[\frac{0.023 (\mu_i)^{0.2} D_o^{1.8} \pi (c_p)_i}{Pr^{1/3} (D_o/D_i)^{0.8}} \right] G_i^{0.8} \dots [60]$$

Let

$$H_i = \left[\frac{0.023 (\mu_i)^{0.2} D_o^{1.8} \pi (c_p)_i}{Pr^{1/3} (D_o/D_i)^{0.8}} \right] \dots [61]$$

$$h_i A_i = H_i G_i^{0.8} \dots [62]$$

For the fluid on the outside of the tube a similar rearrangement is carried through. From Equation [53]

$$(\Delta P/P)_o = 4f_o \frac{G_o^2 v_o^2}{2g RT_o} = \frac{4C_8}{(D_o G_o/\mu_o)^{0.13}} \frac{G_o^2 v_o^2}{2g RT_o} \dots [63]$$

Instead of a friction factor f_o based on the number of tubes, N , in the direction of gas flow, one can express pressure loss by a drag factor ϕ based on the ratio of surface area to net open area

$$A/S = [\pi D_o / (S_T - D_o)] = \pi / (S_T/D_o - 1)$$

$$(\Delta P/P)_o = \phi \frac{G_o^2 v_o^2}{2g RT_o} (A/S)$$

$$= \frac{C_8}{(D_o G_o/\mu_o)^{0.13}} \frac{G_o^2 v_o^2}{2g RT_o} \frac{\pi}{(S_T/D_o - 1)} \dots [64]$$

so that

$$C_8 = \frac{C_8 (S_T/D_o - 1)}{\pi/4} \quad (\text{values for } C_8 \text{ are given in Figs. 15 and 16})$$

Multiplying both sides of Equation [64] by $W = GS$

$$(\Delta P/P)_o W_o = \left[\frac{C_8}{(D_o G_o/\mu_o)^{0.13}} \right] \left(\frac{G_o^2}{2g} \right) \left(\frac{v_o^2}{RT_o} \right) (A_o) \dots [65]$$

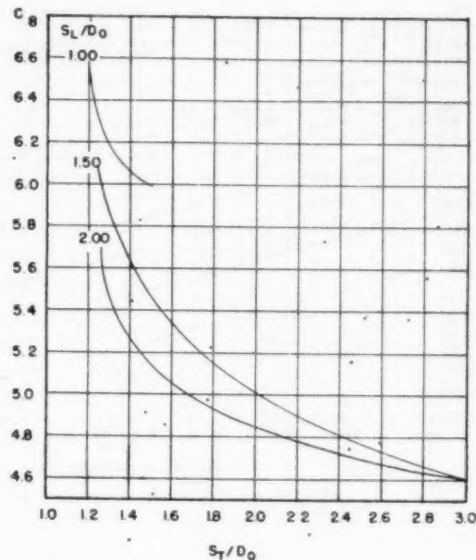


FIG. 14 CONSTANT C_8 AS A FUNCTION OF TUBE SPACING; FLOW OF AIR ACROSS STAGGERED TUBES

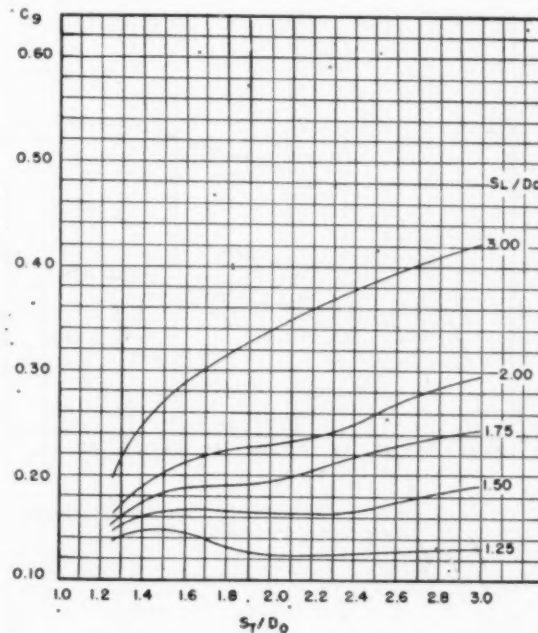


FIG. 15 CONSTANT C_8 AS A FUNCTION OF TUBE SPACING; FLOW OF AIR ACROSS IN-LINE TUBES

which simplifies to

$$(\Delta P/P)_o W_o = \frac{C_8 \pi (\mu_o)^{0.13} D_o^{1.87} v_o^2}{2g RT_o} G_o^{3.87} \dots [66a]$$

Let

$$K_o = \left[\frac{C_8 \pi (\mu_o)^{0.13} D_o^{1.87} v_o^2}{2g RT_o} \right] \dots [67]$$

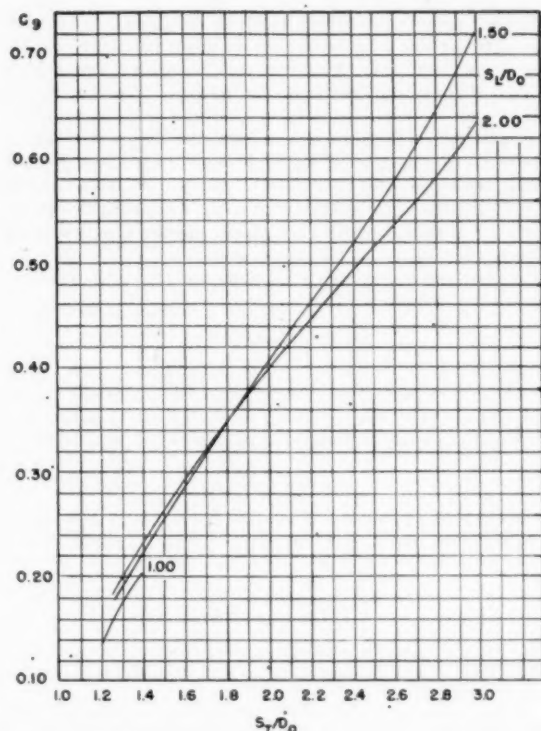


FIG. 16 CONSTANT C_g AS A FUNCTION OF TUBE SPACING; FLOW OF AIR ACROSS STAGGERED TUBES

then

$$(\Delta P/P_o)W_o = K_o G_o^{2.87} \dots \dots \dots [68]$$

The heat-transfer equation is obtained from Equation [52]

$$h_o A_o = \frac{1.10 C_2 (c_p)_o G_o}{Pr^{1/3} Re^{0.4}} A_o \dots \dots \dots [69]$$

$$= \left[\frac{1.10 C_2 (c_p)_o D_o^{1.6} (\mu_o)^{0.4}}{Pr^{1/3}} \right] G_o^{0.6}$$

Let

$$H_o = \frac{1.10 C_2 (c_p)_o D_o^{1.6} (\mu_o)^{0.4}}{Pr^{1/3}} \dots \dots \dots [70]$$

then

$$h_o A_o = H_o G_o^{0.6} \dots \dots \dots [71]$$

This completes the establishment of equations to represent performance on each side of the heat exchanger. The over-all performance is given by

$$\frac{1}{UA} = \frac{1}{h_i A_i} + \frac{1}{h_o A_o} = R \text{ (resistance)} \dots \dots \dots [72]$$

Substituting Equations [62] and [71] in Equation [72] and rearranging

$$R = \frac{1}{H_i G_i^{0.8}} + \frac{1}{H_o G_o^{0.6}} \dots \dots \dots [73]$$

or

$$\frac{1}{H_o G_o^{0.6}} = R - \frac{1}{H_i G_i^{0.8}} \dots \dots \dots [74]$$

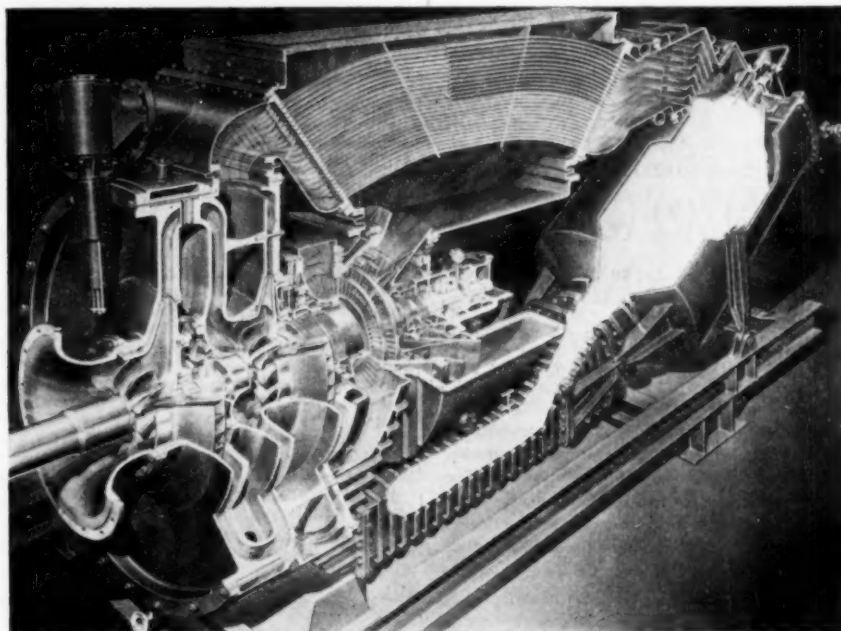


FIG. 17 TUBULAR REGENERATOR ON LOCOMOTIVE GAS TURBINE

solving for G_o gives

$$G_o = \left[\frac{1}{(H_o)(R-1)/H_i G_i^{0.8}} \right]^{1/0.6} \quad [75]$$

The total friction power loss is given by

$$(\Delta P/P)W = (\Delta P/P)_i W_i + (\Delta P/P)_o W_o \quad [76]$$

Substituting the values of the individual friction power losses from Equations [59] and [68] in Equation [76] gives

$$(\Delta P/P)W = K_i G_i^{2.8} + K_o G_o^{2.57} \quad [77]$$

Substituting the value of G_o from Equation [75] in Equation [77] gives

$$(\Delta P/P)W = K_i G_i^{2.8} + \frac{K_o}{[(H_o)(R-1)/H_i G_i^{0.8}]^{2.57/0.6}} \quad [78]$$

The optimum arrangement to obtain a given over-all heat transfer coefficient UA occurs when $(\Delta P/P)W$ is a minimum

$$\left[\frac{\partial (\Delta P/P)W}{\partial G} \right]_{UA} = 2.8 K_i G_i^{1.8} + \frac{K_o (-2.87/0.6) (0.8/H_i)}{H_o^{2.57/0.6} (R-1/H_i G_i^{0.8})^{2.57/0.6} (G_i)^{1.8}} \quad [79]$$

Setting this derivative equal to zero will give the minimum for

$$\begin{aligned} 0 &= 2.8 K_i G_i^{1.8} - \left(\frac{2.87}{0.6} \right) \frac{(K_o)(0.8)}{H_i [H_o^{2.57/0.6} (R-1/H_i G_i^{0.8})^{2.57/0.6} (G_i)^{1.8}]} \\ 0 &= 2.8 K_i G_i^{1.8} - \frac{(2.87)(0.8)}{(0.6)} \left(\frac{K_o H_o}{H_i} \right) G_i^{2.57} \\ \frac{G_i^{2.6}}{G_o^{2.57}} &= \frac{(2.87)(0.8)}{(2.8)(0.6)} \frac{K_o H_o}{K_i H_i} = 1.37 \frac{K_o H_o}{K_i H_i} \quad [79] \end{aligned}$$

Substituting the values of $K_o H_o / K_i H_i$ in Equation [79] and simplifying, results in the ratio of G values for optimum performance

$$\frac{G_i}{G_o} = \frac{1}{(D_o G_o / \mu_o)^{0.087}} \left\{ \frac{[(1.10)(C_2)(C_3)(1.37)]}{(0.046)(0.023)} \left(\frac{\mu_o}{\mu_i} \right)^{0.4} \left(\frac{D_o}{D_i} \right)^{1.0} \left(\frac{v_o}{v_i} \right)^2 \left(\frac{T_i}{T_o} \right)^{0.273} \right\} \quad [80]$$

Let $C_7 = \left[\frac{1.37(1.10)(C_2)(C_3)}{(0.046)(0.023)} \right]^{0.273}$ (the values of C_7 are given in Figs. 11 and 12)

$$\frac{G_i}{G_o} = \frac{C_7}{(D_o G_o / \mu_o)^{0.087}} \left(\frac{\mu_o}{\mu_i} \right)^{0.11} \left(\frac{D_o}{D_i} \right)^{0.444} \left(\frac{v_o}{v_i} \right)^{0.555} \left(\frac{T_i}{T_o} \right)^{0.273} \quad [81]$$

This ratio of mass velocities is seen to be largely a function of the ratio of specific volumes. The value of the constant C_7 changes only slightly with tube configuration. Reynolds number on the outside of the tubes comes in only to a low power. The viscosity, temperature, and diameter ratios have only a small effect. This optimum ratio can be used to arrive at the design parameter F given in Equation [48] or it can be used in any other design procedure to arrive at final performance values.

These equations have been used for designing a tubular regenerator for the same conditions as given previously for the extended-surface type. Predicted performance values are given in Table 1 for two alternate tubular designs. In one design the effectiveness is kept the same as for the extended surface. The much higher pressure drop for tubular design is strikingly apparent. In the other design the pressure drop is kept approximately the same as for the extended-surface type and as a result the effectiveness is considerably reduced. Offsetting this poorer thermal performance is the much smaller amount of actual metal-surface area employed in the tubular design.

Comparisons under other conditions can readily be made by means of the equations presented here.

ACKNOWLEDGMENTS

The author wishes to express his indebtedness to Mr. L. C. Claiborne who developed the relationships for optimum performance of tubular regenerators, and to the Elliott Company who supported this study and agreed to publication of the analysis.

REFERENCES

- "The Gas Turbine as a Possible Marine Prime Mover," by C. R. Soderberg and A. B. Smith, *Trans. of the American Society of Naval Architects and Marine Engineers*, vol. 51, 1943, pp. 115-155.
- "The Gas-Turbine Regenerator—The Use of Compact Heat-Transfer Surfaces," by A. L. London and W. M. Kays, *Trans. ASME*, vol. 72, 1950, pp. 611-621.
- "Gas Turbine Plant Regenerator Surfaces," by A. L. London and C. K. Ferguson, *Bureau of Ships Research Memorandum No. 2-46*, NavShips (250-338-3) July, 1946.
- "Test Results of High-Performance Heat-Exchanger Surfaces Used in Aircraft Intercoolers and Their Significance for Gas-Turbine Regenerator Design," by A. L. London and C. K. Ferguson, *Trans. ASME*, vol. 71, 1949, pp. 17-26.
- "The Basic Heat-Transfer and Flow-Friction Characteristics of Plain Plate-Fin Heat-Exchanger Surfaces," by W. M. Kays, Technical Report No. 5, Navy Contract N6-ONR-251 Task Order VI (NR-035-104), Department of Mechanical Engineering, Stanford University, Stanford, Calif.
- "High-Performance Fins for Heat Transfer," by R. H. Norris and W. A. Spofford, *Trans. ASME*, vol. 64, 1942, pp. 489-496.
- "Laminar-Flow Heat-Transfer Coefficients for Ducts," by R. H. Norris and D. D. Streid, *Trans. ASME*, vol. 62, 1940, pp. 525-533.
- "Design, Selection, and Installation of Aircraft Heat Exchangers," by G. P. Wood and M. J. Brevoort, NACA Report No. ARR-3G-31, July, 1943.
- "Generalized Equations for Selection Charts for Heat Exchangers in Aircraft," by Arthur N. Tifford and George P. Wood, NACA Report, ACR-April, 1942.
- "Generalized Selection Charts for Harrison and Tubular Intercoolers," by George P. Wood and Arthur N. Tifford, NACA Report, ARR-December, 1942.
- "Intercooler Design for Aircraft," by M. J. Brevoort, U. T. Joyner, and M. Leifer, NACA Report, ACR-September, 1939.
- "Design Charts for Cross-Flow Tubular Intercoolers," by J. George Reuter, and Michael F. Valerino, NACA Report, ACR-January, 1941.
- "The Cross-Flow Plate-Type Intercooler," by Benjamin Pinkel, J. George Reuter, and Michael F. Valerino, NACA Report, ACR-April, 1942.
- "Correlation and Utilization of New Data on Flow Resistance and Heat Transfer for Cross Flow of Gases Over Tube Banks," by E. D. Grimison, *Trans. ASME*, vol. 59, 1937, pp. 583-594.
- "Heat Transmission," by W. H. McAdams, second edition, McGraw-Hill Book Company, Inc., New York, N. Y., 1942.
- "Mean Temperature Difference in Design," by R. A. Bowman, A. C. Mueller, and W. M. Nagle, *Trans. ASME*, vol. 62, 1940, pp. 283-294.

Correlation of Plastic Deformation During Metal Cutting With Tensile Properties of the Work Material

By J. T. LAPSLEY, JR.,¹ R. G. GRASSI,² AND E. G. THOMSEN,³ BERKELEY, CALIF.

An experimental correlation of plastic deformation occurring during metal cutting with the plastic deformation in tension of the work material; an analysis permitting comparison of these two states of strain is presented. Orthogonal cutting of seamless steel tubing was employed for feeds of 0.0025–0.0085 in. per revolution (ipr), and positive rake angles of 25–45 deg. Deformation and forces of cutting were obtained from chip measurement and from a tool dynamometer employing resistance strain gages. The agreement obtained indicates that the tensile properties of the work material may offer a useful index to metal-cutting performance.

NOMENCLATURE

The following nomenclature is used in the paper:

F_T = thrust force, lb; measured in direction of motion of tool by tool dynamometer in orthogonal cutting

F_C = cutting force, lb; measured perpendicular to direction of motion of tool by tool dynamometer in orthogonal cutting

l, l_o = final and original length, respectively, in.; refers to chip length in metal cutting and gage length in tension testing

D_o, D = original and instantaneous diameter, respectively, of neck in a tension bar, in.

α = rake angle, deg; measured in plane perpendicular to cutting edge

ϕ = shear angle, deg; angle between shear plane and surface being generated, measured in plane perpendicular to cutting edge

A_s = area of shear plane, sq in.

τ_{ss} = mean shear stress on shear plane (in metal cutting) psi

γ_{ss} = shearing strain of chip during removal in metal cutting

$\bar{\sigma}_x, \bar{\sigma}_y, \bar{\sigma}_z$ = normal true stresses at a point in a deformed metal, measured parallel to three co-ordinate directions x, y, z , respectively, psi

$\tau_{xy}, \tau_{yz}, \tau_{zx}$ = shearing stresses on planes perpendicular to co-

ordinate axes of first subscript, and in direction of second subscripts, psi

$\bar{\epsilon}_x, \bar{\epsilon}_y, \bar{\epsilon}_z$ = finite plastic true strains associated with the normal stresses $\bar{\sigma}_x, \bar{\sigma}_y, \bar{\sigma}_z$, respectively

$\gamma_{yz}, \gamma_{xz}, \gamma_{xy}$ = shearing strains associated with shearing stresses $\tau_{yz}, \tau_{xz}, \tau_{xy}$, respectively

Effective true stress =

$$\sqrt{\frac{(\bar{\sigma}_x - \bar{\sigma}_y)^2 + (\bar{\sigma}_y - \bar{\sigma}_z)^2 + (\bar{\sigma}_z - \bar{\sigma}_x)^2}{2} + 3(\tau_{xy}^2 + \tau_{yz}^2 + \tau_{xz}^2)}$$

(complex stress function, psi)

Effective finite plastic strain =

$$\frac{2}{3} \sqrt{\frac{(\bar{\epsilon}_x - \bar{\epsilon}_y)^2 + (\bar{\epsilon}_y - \bar{\epsilon}_z)^2 + (\bar{\epsilon}_z - \bar{\epsilon}_x)^2}{2} + \frac{3}{4}(\gamma_{xy}^2 + \gamma_{yz}^2 + \gamma_{xz}^2)}$$

W_c = work done in cutting per unit volume of metal removed, in-lb/in.³

W_s = work done in shearing per unit volume of metal removed, in-lb/in.³

\log_e = natural logarithm

t_o = initial thickness of chip, in.

w_o = initial chip width, in.

INTRODUCTION

Tool life, the time a tool remains serviceable under a given set of conditions, is probably the most important practical index of machinability. An appreciable amount of data is now available which can be expressed by the formula $VT^n = C$, where V is cutting velocity in feet per minute, T is tool life in minutes, n and C are constants depending on the cutting conditions, nature of work material, and other factors. While this relationship between velocity and tool life is quite general, the constants n and C hold only for specific conditions. For each new condition of metal cutting for which no information is available, time-consuming and costly experiments must be performed to find the numerical values of these constants. Consequently, a correlation of tool life with physical constants pertaining to the cutting condition, similar to the correlation of friction factor with Reynolds modulus in hydrodynamics, would be an important contribution.

In order to establish a general functional relationship of tool life with physical constants of tool work, conditions in the cutting zone, such as temperature, abrasiveness of the work at this temperature, the mechanics of metal cutting, and the state of plastic deformation of the chip must be established. It is the purpose of this paper to discuss the mechanism of metal cutting and to correlate the state of plastic deformation of metal cutting with that of the tension test.

In this investigation, orthogonal cutting of seamless steel tubing was used with values of feed from 0.0025 to 0.0085 in. per revolution (ipr) and positive back-rake angles on the cutting tool of 25 deg, 35 deg, 40 deg, and 45 deg. Cutting was done dry with a high-speed-steel tool at approximately 90 fpm.

¹ Assistant Professor of Mechanical Engineering, University of California.

² Assistant Professor of Mechanical Engineering, University of California. Mem. ASME.

³ Associate Professor of Mechanical Engineering, University of California.

Contributed by the Production Engineering Division and presented at the Annual Meeting, New York, N. Y., November 27–December 2, 1949, of THE AMERICAN SOCIETY OF MECHANICAL ENGINEERS.

NOTE: Statements and opinions advanced in papers are to be understood as individual expressions of their authors and not those of the Society. Paper No. 49–A-121.

EXPERIMENTAL TECHNIQUE

Orthogonal cutting, in which a straight-edged cutting tool moved relative to the workpiece in a direction perpendicular to its cutting edge, was employed. The cutting conditions were such as to yield continuous chip formation without a built-up edge on the tool. This type of chip formation has been designated as a type-2 chip (1).⁴

The force system for orthogonal cutting, developed by Merchant (2) is shown in Fig. 1. The resultant force R may be resolved into components, the cutting force F_C , and the thrust force

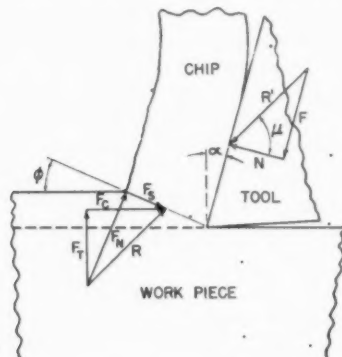


Fig. 1 FORCE SYSTEM ACTING ON CHIP DURING ORTHOGONAL CUTTING

F_T , which were measured by the tool dynamometer employed. Resolution of the force R along the shear plane, designated by the shear angle ϕ , results in F_S , the shearing force, and F_N , the force perpendicular to the shear plane. The force of friction is represented by F , and the force component perpendicular to the tool face by N . The friction angle and back-rake angle are represented by μ and α , respectively. The lack of collinearity of R and R' is not significant and has been so shown by others (2).

On the basis of Merchant's analysis, it has been shown that the work of cutting is

$$W_s = F_C/t_o w_o \dots \dots \dots [1]$$

where t_o and w_o are original chip thickness and width, respectively.

The work of shear is obtained from the relationship

$$W_s = \tau_{xz} \gamma_{xz} \text{ or } (W_s = S_s \epsilon, \text{ according to Merchant}) \dots [2]$$

where $\gamma_{xz} = \cot \phi + \tan (\phi - \alpha)$, and τ_{xz} is the shear stress on the plane designated by the angle ϕ .

The shear angle ϕ , is determined from the chip geometry by the following expression providing the chip width remains constant

$$\tan \phi = \frac{l}{l_o} \cos \alpha / \left(1 - \frac{l}{l_o} \sin \alpha \right) \dots \dots \dots [3]$$

where l_o and l are the initial and final chip lengths, respectively.

Metal cutting was done by machining the end of a short section of 6-in.-OD, 0.475-in wall thickness, seamless steel tubing. The tubing was in the "as-received" or unannealed condition. The cutting tool, of high-speed steel, was clamped in a special holder mounted on the compound rest of an engine lathe. The tool was set on center and fed perpendicularly to the end of the tube which was clamped in a four-jaw chuck. Cutting was done dry, at 57 rpm, or approximately 90 fpm. This cutting speed was selected to obtain a moderate strain rate in the chip.

⁴ Numbers in parentheses refer to the Bibliography at the end of the paper.

The tool dynamometer had as its measuring elements SR4 type A-5 electrical strain gages. The gages were mounted as shown in Fig. 2, with two active gages in adjacent legs of a conventional bridge circuit for each force determination. This arrangement increased sensitivity and also provided a means of eliminating temperature effects. Coolant was circulated through

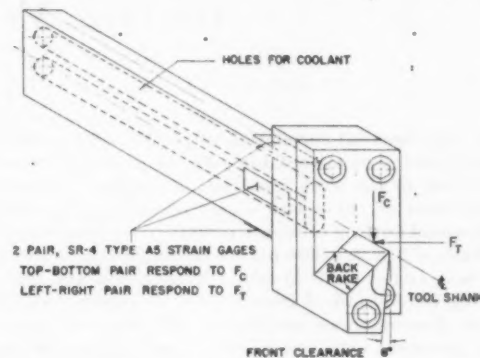


Fig. 2 SCHEMATIC DRAWING OF TOOL DYNAMOMETER USED IN MEASURING ORTHOGONAL CUTTING-FORCE COMPONENTS, F_C AND F_T

the tool shank so that heat generated during cutting did not produce a temperature differential between the strain gages. The stability of the gages was maintained by protection with wax, Ozite, and a metal shield.

The calibration of the dynamometer utilized a 5000-lb proving ring. The calibration for the thrust force F_T , was accomplished with the tool clamped in the holder used for cutting and mounted on the compound rest. Force was uniformly applied to the cutting edge through the proving ring by means of special adapters and manual carriage motion. The dynamometer calibration for the cutting force F_C , was performed with the tool mounted in its holder and clamped to the table of an upright drill press. The force was applied uniformly to the cutting edge (similar to F_T), by using manual spindle travel.

The dynamometer was designed so that the measurement of one force was independent of the other. The calibrations proved that this design criterion had been achieved. Simultaneous recording of F_T and F_C was obtained by using strain recorders. The time of cutting varied with conditions and was dependent upon attaining equilibrium values of forces and a representative number of chips. Since the chip width remained constant, the relationships previously presented are applicable. The initial conditions of chip thickness, and length, l_o and l_s , were determined from the feed and outside diameter of the tube, respectively. A reference point for measuring the final chip length, l_s , was established by cutting a shallow longitudinal slot in the outside surface of the tube. This measurement was facilitated by the fact that the chips did not curl during removal.

Specimens for the tension test were cut from the tube wall so that their axes coincided with that of the tube. The gage section was 1 1/4 in. long and 0.250 in. diam.

EXPERIMENTAL RESULTS

The experimental data of the metal-cutting tests are presented in Table 1 and are shown graphically in Figs. 3 to 6, inclusive. Although these data are not the primary objective of this investigation, they show some interesting trends which also establish their consistency.

Figs. 3 and 4 indicate the effect of back rake and feed, respectively, on the tool forces. It may be noted that the change in

Fig. 3

Fig.

TABLE 1 TABULATED TEST DATA AND CALCULATED RESULTS: ORTHOGONAL END CUTTING OF SEAMLESS STEEL TUBING

(Conditions: Dry cutting, 90 fpm, and constant chip width, i.e., 0.475 in.)

Back-rake angle, deg	Feed, ipr	Cutting ratio, l/l_0	Cutting force, F_C , lb	Thrust force, F_T , lb	Shear angle, ϕ , deg	Shear strain, γ_{ss}	Work of shear, W_s , 1000 in.-lb/in. ²	Work of cutting, W_c , 1000 in.-lb/in. ²	Effective strain, $\frac{\sqrt{3}}{3} \gamma_{ss}$	Effective stress, 1000 psi, $\frac{\sqrt{3}}{3} \tau_{ss}$
25	0.0025	0.358	380	224	20.9	2.55	209	319	1.47	143
	0.0035	0.366	475	281	21.5	2.48	180	286	1.43	126
	0.005	0.407	643	357	24.0	2.23	169	270	1.29	131
	0.006	0.345	728	398	20.1	2.65	175	255	1.53	114
	0.0085	0.383	992	551	22.4	2.38	159	246	1.37	116
35	0.0025	0.527	254	102	31.6	1.56	112	214	0.90	125
	0.0035	0.528	306	122	31.9	1.55	96.4	184	0.89	108
	0.005	0.529	433	166	32.0	1.55	96.5	182	0.89	108
	0.006	0.533	507	184	32.2	1.54	95.5	178	0.90	108
	0.0085	0.532	675	234	32.0	1.55	91.3	167	0.89	102
40	0.0025	0.585	232	71	35.7	1.32	94.0	195	0.76	124
	0.0035	0.580	296	87	35.4	1.33	87.8	178	0.77	116
	0.005	0.611	412	112	37.5	1.26	83.1	173	0.73	114
	0.006	0.606	475	127	37.2	1.27	81.1	167	0.73	111
	0.0085	0.606	634	153	37.2	1.27	78.1	157	0.73	107
45	0.0025	0.670	232	68	41.9	1.06	74.8	195	0.61	123
	0.0035	0.670	285	77	41.9	1.06	68.5	172	0.61	112
	0.005	0.649	386	94	40.2	1.10	69.6	162	0.64	110
	0.006	0.642	443	102	39.6	1.01	62.7	156	0.58	107
	0.0085	0.646	581	117	39.9	1.11	65.0	144	0.64	102

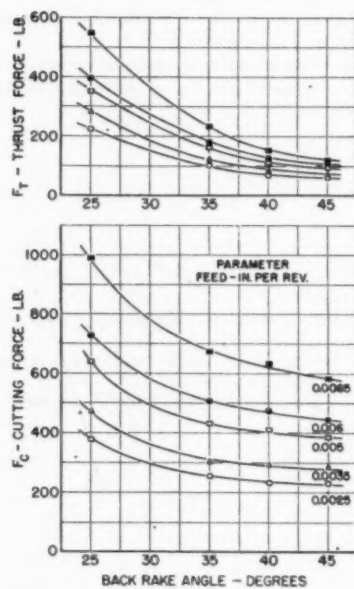


FIG. 3 EFFECT OF BACK-RAKE ANGLE ON CUTTING FORCES FOR CONSTANT FEED VALUES

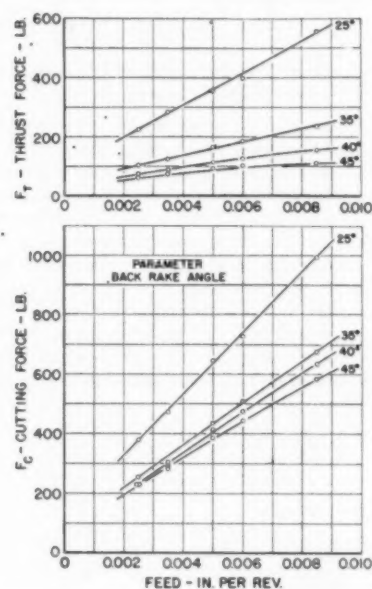


FIG. 4 EFFECT OF FEED ON CUTTING FORCES FOR CONSTANT BACK-RAKE ANGLES

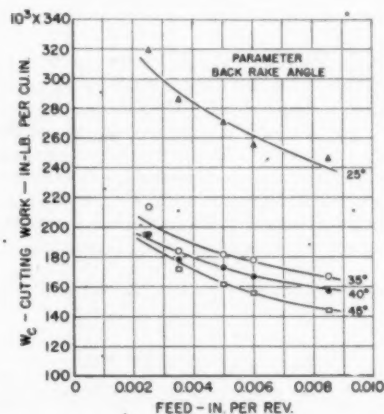


FIG. 5 EFFECT OF FEED ON WORK OF CUTTING FOR CONSTANT BACK-RAKE ANGLES

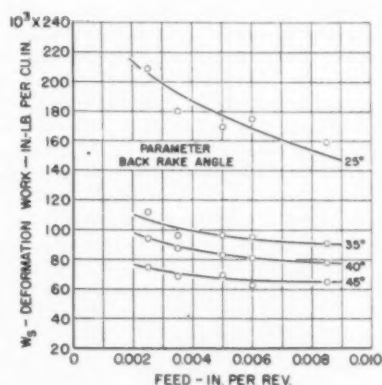


FIG. 6 EFFECT OF FEED ON WORK OF SHEAR DEFORMATION FOR CONSTANT BACK-RAKE ANGLES

feed results in a greater change in the cutting force than in the thrust force. Figs. 5 and 6 show the amount of work expended per unit volume of metal removed in cutting and in shear deformation, respectively. Examination of these figures indicates that the work expended for rake angles 45 deg, 40 deg, and 35 deg is appreciably lower than that expended for the 25-deg back-rake angle. This behavior might be attributable to the presence of a nonobserved built-up edge.

DISCUSSION

The metal of the chip during metal cutting is severely deformed and, therefore, is in a highly work-hardened state. It is possible to compare this state of work-hardening with that obtained by any other deformation process by application of a theory of plasticity (3, 4), providing the states are calculable and the metal under consideration satisfies the assumptions made in the ideal theory. The assumptions are as follows:

- (a) The metal is isotropic.
- (b) The metal is homogeneous.
- (c) The stresses are linear functions of the infinitesimal plastic strains.
- (d) Temperature, deformation rate, and hydrostatic pressure do not affect the state of plastic deformation.

While real metals do not behave ideally, it has been shown (5) that low-strength aluminum alloys, magnesium alloys, and mild steel satisfy the foregoing assumptions to a good degree of approximation when equivalent states of work-hardening in tension, compression, and torsion are compared. The following section will be devoted to the development necessary for correlation between the plastic state in a chip and in a tension bar by application of this theory of plasticity.

If the previously stated assumptions are satisfied, it can be shown that equivalent states of work-hardening can be represented on an effective stress-effective plastic strain curve. Two complex stress and strain functions utilized in the correlation are

$$\sqrt{\frac{(\bar{\sigma}_x - \bar{\sigma}_y)^2 + (\bar{\sigma}_y - \bar{\sigma}_z)^2 + (\bar{\sigma}_z - \bar{\sigma}_x)^2}{2} + 3(\tau_{xy}^2 + \tau_{yz}^2 + \tau_{xz}^2)} \dots [4]$$

Effective plastic strain =

$$\frac{2}{3} \sqrt{\frac{(\bar{\epsilon}_x - \bar{\epsilon}_y)^2 + (\bar{\epsilon}_y - \bar{\epsilon}_z)^2 + (\bar{\epsilon}_z - \bar{\epsilon}_x)^2}{2} + \frac{3}{4}(\gamma_{xy}^2 + \gamma_{yz}^2 + \gamma_{xz}^2)} \dots [5]$$

The work of plastic deformation for any particular state of deformation is given by the area under the curve from zero strain to the value under consideration.

While the stress or strain path employed does not affect the validity of the universality of the effective stress-effective plastic strain curve, it is only possible to determine the plastic state in a few simple cases. The infinitesimal plastic strains, from which the finite strains under the radical of the effective strain are constructed, are not perfect differentials. The finite strains are, therefore, path dependent and can be obtained by integration only if the stress or strain path is known. In the present investigation it is assumed that the stress ratios remain constant during the entire deformation, thus permitting the evaluation of the finite strains in terms of quantities measurable before and after the deformation. With this additional assumption, it is possible to calculate the plastic states for tension and metal cutting.

The Tension Test. Let the x -co-ordinate axis be coincident with the axis of the test bar. Therefore, $\bar{\sigma}_x$ is the true stress resulting from the applied axial load

$$\bar{\sigma}_x = \frac{\text{Axial load}}{\text{Instantaneous area}} \dots [6]$$

Since $\bar{\sigma}_x$ is the only stress, the effective stress reduces to

$$\text{Effective stress (in tension)} = \bar{\sigma}_x \dots [7]$$

The finite plastic strain $\bar{\epsilon}_x$ in the axial direction can be determined from measurements of the original gage length and the length at any stage of the deformation up to the maximum load

$$\bar{\epsilon}_x = \log_e \frac{l}{l_0} \dots [8]$$

where l_0 and l are initial and final gage length, respectively.

After the maximum load has been exceeded, the specimen necks and the deformation ceases to be uniform over the gage length. The axial strain, however, can be obtained from measurements of the minimum diameter in the neck for constant volume deformation

$$\bar{\epsilon}_x = 2 \log_e \frac{D_0}{D} \dots [9]$$

where D_0 and D are initial and instantaneous diameter, respectively, at any stage of deformation.

By use of the constant-volume relationship, the effective plastic strain can be evaluated in terms of the normal strains

$$\bar{\epsilon}_x + \bar{\epsilon}_y + \bar{\epsilon}_z = 0 \dots [10]$$

but

$$\bar{\epsilon}_y = \bar{\epsilon}_z$$

therefore

$$-\bar{\epsilon}_y = -\bar{\epsilon}_z = \frac{1}{2} \bar{\epsilon}_x \dots [11]$$

Substituting these values of strain into Equation [5] results in

$$\text{Effective plastic strain (tension)} = \bar{\epsilon}_x \dots [12]$$

Consequently, the effective stress-effective plastic strain curve

is identical with the true stress-true plastic strain curve in tension.

When necking occurs, the stress ceases to be uniform as has been shown by Bridgman (6). In general, however, the error introduced by assuming a constant stress across the section is not significant.

Metal Cutting. Merchant (7) has shown that it is possible to obtain an analysis of the metal-cutting process by assuming that the deformation is simple shear. The shearing process is visualized to take place on a plane making an angle ϕ with the original work surface, as shown in Fig. 1. The slight curvature of the shear plane observed from photomicrographs has been neglected in the analysis. The deformation stress τ_{xy} on this plane is obtainable from the measured tool forces, while the shearing strain γ_{xy} is calculable from chip-deformation measurements

$$\tau_{xy} = \frac{F_C \sin \phi \cos \phi - F_T \sin^2 \phi}{l_0 w_0} \dots [13]$$

$$\gamma_{xy} = \cot \phi + \tan (\phi - \alpha) \dots [14]$$

where l_0 and w_0 are the initial thickness and width of chip, respectively.

In addition
shear plane

Since the
strain rate

Effect

However
late the eff
 $\tau_{yz} = \tau_{xy}$
therefore
cannot be
of stress is
this condi
nated from
effective s

Effect

Correlat
the calcul
tained from
represent
extrapolat
tension,
extrapolat
may be
agreement

The fa
group al
taken in
normal s
sure in t
this may
the only
show sc
vestigat
valid an

Fig. 8
volume
metal cu
based on

FIG.
PLAST
ANAL

In addition to the shearing stress, a normal stress, $\bar{\sigma}_x$, acts on the shear plane

$$\bar{\sigma}_x = \frac{F_C \sin^2 \phi + F_T \sin \phi \cos \phi}{l_0 w_s} \quad [15]$$

Since the analysis is based only on the shear strain, the effective strain reduces to

$$\text{Effective strain (metal cutting)} = \frac{\sqrt{3}}{3} \gamma_{xz}; \quad \gamma_{xz} = \gamma_{zx} \quad [16]$$

However, a further assumption must be made in order to calculate the effective stress. Since τ_{xz} is the only shear stress acting, $\tau_{yz} = \tau_{zy} = 0$. Of the normal stresses, only $\bar{\sigma}_x$ is known; it is therefore necessary to assign values to $\bar{\sigma}_y$ and $\bar{\sigma}_z$. While values cannot be fixed, a priori, it is reasonable to assume that the state of stress is that of hydrostatic pressure on the shear plane. Under this condition, the three normal stresses are equal and are eliminated from the effective-stress expression, Equation [4]. The effective stress, therefore, reduces to

$$\text{Effective stress (metal cutting)} = \sqrt{3} \tau_{xz}; \quad \tau_{xz} = \tau_{zx} \quad [17]$$

Correlation Between Tension and Metal Cutting. Fig. 7 shows the calculated metal-cutting data and the stress-strain curve obtained from tension tests for the same material. The solid line represents the experimental data from tension tests which were extrapolated to higher values of strains than those achievable in tension, as shown by the dashed portion of the curve. Such extrapolation is not unreasonable; for example, higher strains may be obtained in torsion. It is evident that there is good agreement between the tension data and the metal-cutting data.

The fact that the effective stress values for a given rake-angle group about a particular strain value indicates that factors not taken into account are active. Merchant (7) proposes that the normal stress on the shear plane (a condition of hydrostatic pressure in the present analysis) influences the shear stress. While this may be an important factor, it is not clearly proved to be the only factor, as the experimental data, reported by Merchant, show scatter when the normal stress is considered. Further investigation is necessary to establish which assumptions are not valid and what other variables must be considered.

Fig. 8 shows a comparison of the work of deformation per unit volume of metal removed as calculated from the shear work of metal cutting and from the tension test. The deformation work based upon tension was obtained by evaluating areas under the

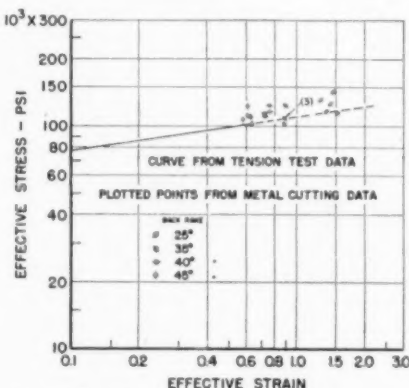


FIG. 7 CORRELATION BETWEEN EFFECTIVE STRESS-EFFECTIVE PLASTIC STRAIN VALUES AS CALCULATED FROM (1) PLASTICITY ANALYSIS OF METAL-CUTTING DEFORMATION; (2) TENSION TEST OF WORK MATERIAL

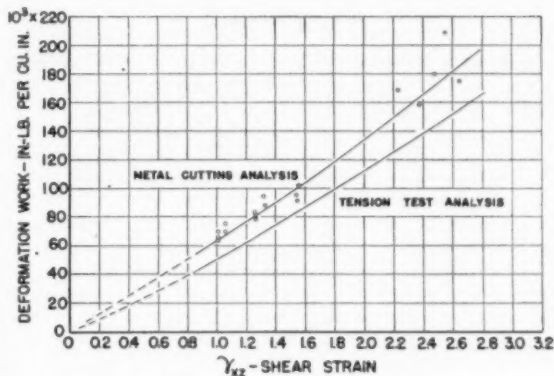


FIG. 8 WORK OF DEFORMATION AS FUNCTION OF SHEAR STRAIN, γ_{xz} , FOR (1) SHEAR STRESS-SHEAR STRAIN ANALYSIS OF METAL CUTTING AS DEVELOPED BY MERCHANT; (2) EFFECTIVE STRESS-EFFECTIVE PLASTIC STRAIN ANALYSIS BASED ON TENSION-TEST DATA

effective stress-effective plastic strain curve, presented in Fig. 7. An empirical equation was determined for this curve

$$\text{Effective stress} = 110 \times 10^3 (\text{effective plastic strain})^{0.102} \quad [18]$$

Work of deformation for given shear-strain values was determined by integration of the equation between limits of zero strain and the corresponding effective plastic-strain value.

From the comparison it is seen that the work of deformation, as determined from the metal-cutting analysis, exceeds the deformation work based upon the tension test for all cutting conditions employed in this investigation. It is felt that the present information is insufficient for an adequate explanation of this anomaly and that further investigation should be made.

CONCLUSIONS

- 1 The results of the investigation have shown that metal-cutting data can be correlated with tension data for orthogonal cutting and the test conditions employed.
- 2 The tension properties of a material may offer a useful index of cutting performance.
- 3 The work done by shear deformation, calculated from metal-cutting data, results in larger values than that determined from the tension test for equivalent states of deformation.
- 4 Further application of the plasticity theory should yield information which could give a more basic understanding of metal cutting.

BIBLIOGRAPHY

- 1 "Physics of Metal Cutting," by H. Ernst, *Machining of Metals*, American Society for Metals, 1938, p. 24.
- 2 "Mechanics of the Metal Cutting Process. I Orthogonal Cutting and a Type 2 Chip," by M. E. Merchant, *Journal of Applied Physics*, vol. 16, no. 5, 1945, p. 267-275.
- 3 "Plastic Flow of Metals," by J. J. Jelinek, A. J. Latter, E. G. Thomsen, and J. E. Dorn, OPRD Report No. W-200, May, 1945.
- 4 "The Ductility of Metals Under General Conditions of Stress and Strain," by J. E. Dorn and E. G. Thomsen, *Trans. ASM*, vol. 39, 1947, pp. 741-772.
- 5 "Investigation of the Validity of an Ideal Theory of Elasto-Plasticity for Wrought Aluminum Alloys," by E. G. Thomsen, I. Cornet, I. Lotze, and J. E. Dorn, NACA Technical Note No. 1552, July, 1948.
- 6 "The Stress Distribution at the Neck of a Tensile Specimen," by P. W. Bridgman, *Trans. ASM*, vol. 32, 1944, pp. 553-574.
- 7 "Mechanics of the Metal Cutting Process. II Plasticity Conditions in Orthogonal Cutting," by M. E. Merchant, *Journal of Applied Physics*, vol. 16, no. 6, 1945, pp. 318-324.

Discussion

M. EUGENE MERCHANT.⁶ The authors have contributed some much-needed information by carrying out cutting tests and tensile tests on the same material, and then comparing the mechanical properties of the material as calculated from the data obtained on the two types of tests. They are to be congratulated on the manner in which they have carried through the test work and analysis; such information serves to clarify further the fundamentals of the cutting process and their relation to the mechanical properties of the metal being machined.

The mathematical analysis which the authors have used to compare the metal-cutting results with those from the tensile tests provides good correlation between the two sets of data. However, this mathematical analysis is based on certain assumptions which are questionable when applied to the metal-cutting process. Therefore it appears somewhat fortuitous that such good agreement was obtained. In particular, the main basis for the mathematical theory used to compare the two sets of data is that states of work-hardening occur in the plastic deformation taking place on the shear plane in metal-cutting which are equivalent to those obtained in a normal tensile test. The fallacy here is brought out by Drucker,⁷ who points out that in the process of metal cutting virtually no work-hardening of the metal occurs on the shear plane because of the extremely high strain rates involved in the cutting process. (The "work-hardening" actually observed in hardness measurements on chips virtually all occurs after deformation on the shear plane is complete, since work-hardening is a "rate-process," like a chemical reaction!)

In the tensile test, of course, work-hardening does occur, since the rate of strain is quite low. Further, the very fact that an extremely high strain rate is involved in the cutting process, compared to the very low strain rates involved in tensile tests, will have a marked effect on the actual shear strength of the metal in the two cases; shear strength is known to increase with increasing strain rate. Therefore, in the two types of deformation in actuality there can be no comparable states of work-hardening, and so the basic premise of the authors' theory is not met.

Nevertheless, it appears from the test results reported by the authors (as well as from data obtained in the writer's laboratory, as will be shown shortly) that reasonable agreement can be obtained between mechanical properties observed from cutting tests and those observed from low-strain-rate tests. The reason for this fortunate result is not immediately evident; it appears, however, that the complicating factors involved tend to balance each other. Presumably, the "weakening" effects of the absence of work-hardening and the local heating on the shear plane in cutting offset the "strengthening" effect of the very high strain rate reasonably well. The net result apparently makes the stress values obtained from the two types of tests very nearly equal, for the range of strains and strain rates usually found in machining.

Another factor which the authors have (admittedly) neglected in making the comparison between the tensile-test data and those from metal-cutting is the effect of compressive stress (or hydrostatic pressure) on the actual values of shear strength calculated from metal-cutting data.

As pointed out previously by the writer,⁷ the shear strength of the metal on the shear plane in metal cutting is raised by the presence of a high value of compressive stress acting on that

plane. No such compressive stress acts on the slip processes occurring in the tensile tests. (In fact, the reverse is true.) Therefore the values of shear strength calculated from the authors' metal-cutting data ought, in all fairness, to be corrected to a value of zero compressive stress (at least), if they are to be compared with strength values from the tensile tests. This can be done, approximately, for the data presented by the authors, by extrapolating the shear-strength versus compressive-stress data back to zero compressive stress, making use of metal-cutting theory. When this is done, it is found that the calculated shear strength (τ_{ss}) for the steel used by the authors is approximately 60,000 psi (this value is independent of strain since no work-hardening occurs in the metal-cutting process, as previously mentioned). Thus the effective stress value ($\sqrt{3}\tau_{ss}$) is approximately 100,000 psi. This value is still in reasonable agreement with the authors' tensile-test data.

Actually, to be wholly fair, the tensile-test data ought also to be corrected to a value of zero hydrostatic pressure, which would increase the effective stress values somewhat. No effort has been made to do this, however, since the effect probably would be slight, and no provision for such correction has been made in the theory of plastic deformation used by the authors in analyzing the tensile tests.

Comparisons between metal-cutting data and data obtained from low strain-rate tests of mechanical properties, somewhat similar to the comparison reported by the authors, have been carried out in the writer's laboratory^{8,9} recently. However, these low-strain-rate tests were made by quite a different method from the tensile tests employed by the authors; a method developed by Bridgman¹⁰ was used wherein notched tubular specimens are tested in torsion while subjected to an axial compressive force. Here again, surprisingly good correlation between the metal-cutting data and those obtained from this torsion-compression type of test was obtained, even though the strain rates and corresponding work-hardening states were very different. A comparison of the values of shear strength calculated from the two types of tests at comparable values of compressive stress and shearing strain are given in Table 2 of this discussion. It may be seen that the shear-strength values calculated from the two types of tests agree surprisingly well, considering the great dif-

TABLE 2 COMPARISON OF SHEAR-STRENGTH VALUES OBSERVED FROM TORSION-COMPRESSION-TYPE TESTS WITH THOSE OBSERVED FROM METAL-CUTTING TESTS, AT EQUIVALENT VALUES OF COMPRESSIVE STRESS

Steel	Value of compressive stress at which compared, 1000 psi	(Shearing strain = 2.4 — 3.0)	
		Observed values of shear strength, 1000 psi	Metal-cutting test
SAE 1117.....	60	63	67
SAE 3150 (spheroidized).....	110	81	80
SAE 3150 (pearlitic).....	110	88	86
SAE 3450.....	110	93	88

ferences that exist between the conditions of deformation in the two cases.

In metal cutting three mechanical properties of the material being machined control the forces acting on the cutting tool.⁷ These are as follows:

- 1 Shear strength of the material.
- 2 Machining constant of the material (a property of the material, the value of which, in theory, depends upon the rate of increase of shear strength with applied compressive stress).

⁸ "Torsion-Compression Testing," by J. Kemeny, University of Cincinnati Thesis, 1947.

⁹ "Torsion-Compression Testing," by E. J. Krabacher and K. W. Whisler, University of Cincinnati Thesis, 1949.

¹⁰ "On Torsion Combined With Compression," by P. W. Bridgman, *Journal of Applied Physics*, vol. 14, 1943, pp. 273-283.

⁶ Senior Research Physicist, The Cincinnati Milling Machine Company, Cincinnati, Ohio. Mem. ASME.

⁷ "An Analysis of the Mechanics of Metal Cutting," by D. C. Drucker, *Journal of Applied Physics*, vol. 20, 1949, pp. 1013-1021.

⁸ Refer to authors' bibliography (7).

3 The co
flowing chip.

Of these
machining,
the methods
of test men
shear streng
chining cons
increasing a
specimen car
bly good co
shown by th
herewith. H
strength val
approximate

TABLE 3 CO
OBSERVED I
THOSE OBS

Steel
SAE 1117.....
SAE 3150 (sph
SAE 3150 (pear
SAE 3450.....

In conclu
their fine be
cutting. It
of the paper
beginning a
reports in th

MILTON
interesting
theorem of
sidering the
same energ
the many o
distortion-
that has be
acteristics
stress distr
effect of str

The aut
the distort
sidered bri
fact that a
period of
with the s
sults are c
continuum
the materi
For exam
tensile-tes
the same
This is no
is decreas
creases.
hardening

¹¹ Assoc
Institute o

¹² Lefte
published
V, vol. 32.

3 The coefficient of friction between the cutting tool and the flowing chip.

Of these three quantities needed to predict cutting forces in machining, only the first can be obtained from a tensile test by the methods used by the authors. The torsion-compression type of test mentioned has the advantage not only of giving values of shear strength, but also of providing theoretical values of machining constant; the increase in (torsional) shear strength as increasing axial compressive force is applied to the tubular test specimen can be observed in this type of test. Again, reasonably good correlation with metal-cutting data is obtained, as shown by the values of machining constant given in Table 3 herewith. Here the agreement is not as good as for the shear strength values (Table 2), but still serve well enough for a first approximation.

TABLE 3 COMPARISON OF VALUES OF MACHINING CONSTANT OBSERVED FROM TORSION-COMPRESSION TYPE TESTS WITH THOSE OBSERVED FROM METAL-CUTTING TESTS, AT EQUIVALENT VALUES OF SHEARING STRAIN

Steel	Value of shearing strain at which compared	—Observed values of machining constant, degrees	
		Torsion-compression test	Metal-cutting test
SAE 1117.....	2.15	85.0	77.0
SAE 3150 (spheroidized).....	3.11	84.5	76.0
SAE 3150 (pearlitic).....	3.15	74.0	70.8
SAE 3450.....	2.96	83.0	77.9

In conclusion, we again wish to congratulate the authors for their fine beginning on the exploration of fundamentals in metal cutting. It is pleasing to note from the concluding paragraph of the paper that the present work does, in truth, mark only a beginning and that we may look forward to further interesting reports in this field from the authors.

MILTON C. SHAW.¹¹ The authors have presented a most interesting discussion of the application of the distortion-energy theorem of plasticity to the cutting of metals. This idea of considering the states of stress in two bodies as equivalent when the same energy of distortion is associated with each is another of the many contributions of James Clerk Maxwell (1856).¹² The distortion-energy theorem represents the plasticity condition that has been most successful to date in relating the flow characteristics of two homogeneous bodies of different geometry and stress distribution. This method is one way of introducing the effect of strain-hardening into the theory of cutting.

The authors have listed carefully the assumptions upon which the distortion-energy theorem is based. These might be considered briefly in light of the experimental results. Despite the fact that all metals are far from homogeneous, the size or mean period of the inhomogeneity is generally very small compared with the size of the body undergoing plastic flow, and good results are obtained by treating the material as a homogeneous continuum. However, when the specimen is small, the fact that the material is actually inhomogeneous becomes more important. For example, the distortion-energy theorem indicates that all tensile-test specimens made from a given material should have the same ultimate stress regardless of diameter of the specimen. This is not the case however, for it is found that as the diameter is decreased below a particular diameter, the ultimate stress increases. This size effect is to be expected whenever strain hardening occurs in an inhomogeneous material.

¹¹ Associate Professor of Mechanical Engineering, Massachusetts Institute of Technology, Cambridge, Mass. Mem. ASME.

¹² Letter by Maxwell to William Thomson dated Dec. 18, 1856, published in *Proceedings of Cambridge Philosophical Society*, Part V, vol. 32.

In the cutting process, the depth of cut corresponds to the diameter of the tensile-test specimen, and it is apparent that in cutting we are generally dealing with small specimens. It is not surprising, therefore, that the authors' test points fall above the tensile-test data for the 1/4-in.-diam specimen in Fig. 7 of the paper, and further that the cutting-data points lie an increasing distance above the tensile curve as the chip size decreases.

The writer recently has completed work on a theory of cutting which takes strain-hardening and the inhomogeneity of the metal cut into consideration. This analysis, which will be published elsewhere, is in good agreement with the authors' data and shows quantitatively that the shear work to remove a cubic inch of material increases as the depth of cut decreases, as may be seen in Table 1, Fig. 8, of the paper. It might be remarked at this point that the reason for the increase in specific shear work with rake angle (for a given depth of cut), as shown in Fig. 8, is due to the increase in the shear strain arising in the cutting process as the depth of cut is decreased.

The assumption regarding the unimportance of temperature and the rate of strain in application of the distortion-energy theorem might also be considered. The true stress-strain curve is usually obtained under essentially static conditions, while the cutting process, on the other hand, involves a very high rate of strain. From photomicrographs it is evident that nearly all of the large strain that occurs in cutting takes place as the metal crosses the "shear plane." If this were truly a mathematical plane, we would have, in the cutting process, strain at an infinite rate. Actually, we may say the rate of strain in cutting is very high.

Since nearly all of the energy associated with the plastic-straining of metals appears in the form of heat, it is evident that a significant temperature rise is to be expected in the essentially adiabatic straining process of cutting, while a relatively small temperature rise is to be expected on the shear plane in the nearly isothermal-straining process of the ordinary true stress-strain test. The temperature on the shear plane is apt to be far more significant in the cutting process than in other processes to which the distortion-energy theorem is applied. Thus it is evident that the extreme conditions of size and rate of strain that are met in the cutting process provide a serious test of the assumed independence of strain mechanism and the temperature effect in Maxwell's distortion-energy theorem.

The authors have assumed the normal stress on the shear plane to be a manifestation of the presence of a hydrostatic pressure. This leads naturally to the result that the state of stress in cutting is independent of the normal stress on the shear plane, which, however, is in disagreement with Merchant's theory of cutting. The fact that the authors' analysis is in such good agreement with experiment (except for the afore-mentioned size effect) indicates strain-hardening and not the influence of normal stress on the shear plane to be the important item. It is therefore enlightening to examine the authors' data according to Merchant's analysis.⁷

In Fig. 9, herewith, the authors' data are shown plotted with normal stress against shear stress. According to Merchant, all of these points should be along a single straight line. Therefore we might choose either of the lines shown. According to Merchant's plasticity condition, when the observed shear angle ϕ is plotted against the quantity $(\tau - \alpha)$, where τ is the friction angle, and α the rake angle, a straight line should be obtained whose equation is

$$\phi = \frac{1}{2}(\tau - \alpha) + \cot^{-1} K \dots \dots \dots [19]$$

where K is the slope of the line in Fig. 9.

The authors' data points are shown as circles in Fig. 10 of this

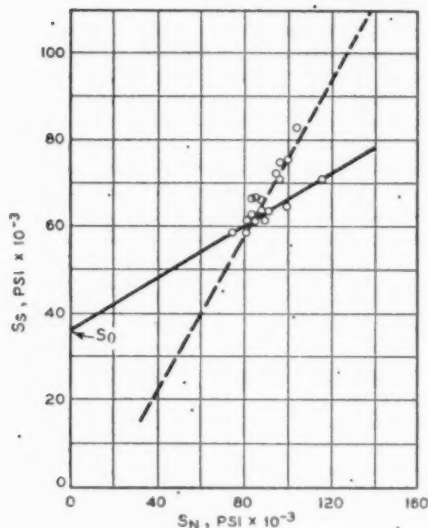


FIG. 9

discussion, while the two lines corresponding to those of Fig. 9 are shown solid and dotted. The dash line corresponds to a value of K of zero (i.e., the case corresponding to the authors' finding that shear strength is independent of normal stress on the shear plane). Most of the authors' data are seen to be in better agreement with the dash line corresponding to $K = 0$. Only those points corresponding to a rake angle of 25 deg are in agreement with the solid curve, and there is apparently no justification for the dotted curves in Figs. 9 and 10.

Actually, it would appear that the test points lie along or somewhat below the dash line in Fig. 10, the distance below the line increasing as the rake angle decreases. The increase in temperature on the shear plane which accompanies strain has not been included in the analysis leading to the upper line in Fig. 10, but if included would move the line vertically downward an increasing amount as the shear energy increased. This could account for the fact that points fall progressively farther below the upper line in Fig. 10, as the rake angle is increased, for as previously mentioned, the amount of strain, and hence the shear work required to remove a cubic inch of metal, also increases as the rake angle is decreased. It would thus appear that the authors' data are in full support of the view that strain-hardening is an important consideration in the metal-cutting process, and further that the influence of normal stress on the shear plane is relatively insignificant.

AUTHORS' CLOSURE

The authors are appreciative of the discussions submitted by Dr. Merchant and Professor Shaw. It is gratifying to note their interest in the paper as evidenced by the comments. However, there exist some areas of disagreement which we believe will be resolved only by further experimental investigations.

Merchant's comments hinge essentially upon two considerations, (1) absence of work-hardening effect during metal cutting as postulated by Drucker and (2) the effect of compression upon shear strength as reported by Bridgman. The large variation in strain rates is the basis for Merchant's comment that the

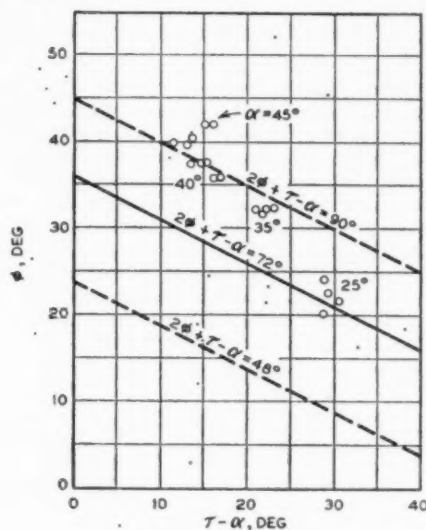


FIG. 10

two states of work-hardening (metal cutting and tension test) are not comparable. The authors' simplifying assumption (d) regarding strain rate should be modified if and when experimental data establish the order of importance of strain rate. However, in the absence of such experimental data, the authors cannot agree with the comment of Merchant based upon Drucker's theoretical analysis that work-hardening does not occur during metal cutting because of the relatively high strain rates involved.

The effect of normal stress on the shear strength or flow stress, referred to by Merchant, has been neglected by the authors because this effect has not been clearly demonstrated. The results of Bridgman cited in Merchant's paper (Bibliography 7) did not demonstrate clearly that the effect holds for all metals. In fact, Bridgman concludes that the shear stress at a definite strain value of unity increases with normal stress only for drill rod, but for SAE 1045 carbon steel the variation was within the order of experimental accuracy. If subsequent experimental work shows the normal stress factor to be appreciable, it can be incorporated in the plasticity analysis.

The authors agree in general with comments made by Shaw. The assumptions stated in the paper, such as homogeneity and isotropy of the work material, are simplifying assumptions only and should not be considered as hard and fast rules. Refinements can be applied to the plasticity theory, based on Maxwell's original hypothesis and restated by others in several ways, as certain effects not incorporated in this theory are isolated.

The authors have also applied Merchant's criteria for metal cutting as shown in the graphs of Figs. 9 and 10. In view of the hypothesis, however, that the effect of work-hardening in metal cutting is important, they have felt that insufficient data were available to isolate this effect, inasmuch as comparisons ought only to be made at equivalent states of work-hardening.

In conclusion, the authors wish to thank the discussers for their interest and to state that the approach presented in their paper should be regarded as a basis for further investigation. Additional experimental work, now in progress, indicates that the analysis correlates also for materials other than that reported.

Approximate resistance, capacity, weight, and 4-in.-long grooved nails, in design information, as influenced by steel composition, species, work presented suitable for will be issued and elapsed variables, until after study was drawn res driven at beech were

DIRECTIONS for use of the spiral binding, since products into wood perform the of wood, or ple want to portunity know-how sizes of n angular and coated, tw pered or t steel, alu loys; with bill, side countersu chandised plasterbor tion nails roofing n nails, box wagon n nails, clou

Research Polytechn Contrib Annual M 1949, of T NOTE: derstood the Societ

Improved Nails

Their Driving Resistance, Withdrawal Resistance, and Lateral Load-Carrying Capacity

By E. GEORGE STERN,¹ BLACKSBURG, VA.

Approximately 3600 tests were performed on the driving resistance, withdrawal resistance, lateral load-carrying capacity, withdrawal, and deformation of 2, 2 $\frac{1}{2}$, 3, 3 $\frac{1}{2}$, and 4-in-long plain-shank, spirally grooved, and annularly grooved nails in southern yellow pine, white oak, and beech, in order to make available comparative test and design information on these nails. Data on nail properties, as influenced by nail type, size, point, shank pilot, steel composition, heat-treatment, cement coating, wood species, wood density, and annual rings of the wood are presented to help in determining the type of nail most suitable for specific applications. At a later date a report will be issued on the effects of change in moisture content and elapsed time after driving, on the foregoing test variables, since these factors could not be investigated until after the test planks had been air-seasoned. Such a study was made possible because all nails for tests on withdrawal resistance and lateral load-carrying capacity were driven at that time of test performance when oak and beech were green and pine was partially air-dry.

INTRODUCTION

DIRECTLY or indirectly, nails are in everyday use by almost everyone. Without being in the limelight or conspicuous, they are essential to human comfort and living, since they are of fundamental importance in most wood products. Little is known about the behavior of nails once driven into wood. Experience governs their use. If one nail does not perform the job, a second one is used. If a large nail splits a piece of wood, one or two small ones are used instead. So many people want to know how to use nails properly, but few have the opportunity to collect enough experience to have the necessary know-how. To complicate matters, the number of types and sizes of nails in production and use is great. The round, triangular and square-shank nails are made as plain-shank, barbed, coated, twisted, spirally grooved, annularly grooved, nontempered or tempered nails with low or high-carbon steel, stainless steel, aluminum, copper, brass, bronze, silicon bronze, or other alloys; with short, medium, and long diamond, needle, chisel, duck-bill, side or V-points; with standard, medium or large flat, countersunk, round, oval, brad or duplex heads. They are merchandised as common nails, finishing nails, fiberboard nails, plasterboard nails, wallboard nails, sheetrock nails, cork-insulation nails, lath nails, siding nails, sheeting nails, shingle nails, roofing nails, shade nails, concrete nails, flooring brads, pallet nails, box nails, case nails, basket nails, barrel nails, boat nails, wagon nails, car nails, foundry nails, fence nails, sign nails, hinge nails, clout nails, sinkers, corks, coolers, etc.

¹ Research Professor, Department of Wood Construction, Virginia Polytechnic Institute. Mem. ASME.

Contributed by the Wood Industries Division and presented at the Annual Meeting, New York, N. Y., November 27-December 2, 1949, of THE AMERICAN SOCIETY OF MECHANICAL ENGINEERS.

NOTE: Statements and opinions advanced in papers are to be understood as individual expressions of their authors and not those of the Society. Paper No. 49-A-115.

In a recent U. S. Government publication (1),² sound and efficient nailing practices in home construction are suggested. These recommendations, although backed up by U. S. Forest Products Laboratory test data, are principally based on observed nailing practices, usually a matter of precedent, tradition, or individual judgment, however, as a rule, not fully taking into account the forces to be resisted. The use of plain-shank nails is recommended, presumably because of the unavailability of satisfactory design and test data on and field experience with relatively new nails with spirally or annularly grooved shanks, as shown in Fig. 1. Similarly, because test and design data on such improved

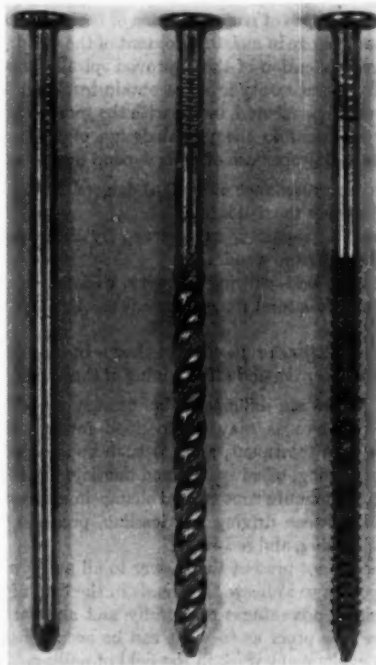


FIG. 1 PLAIN-SHANK, SPIRALLY GROOVED, AND ANNULARLY GROOVED 3 $\frac{1}{2}$ -IN-LONG NAILS

nails never have been available to the designing timber engineer, use of such improved nails for joints of timber structures has not been in the news, although such nails may have been occasionally used for such purposes. In contrast, the design of marine structures by naval architects with such spirally and annularly grooved nails has resulted in their widespread use in boat and ship construction. Automobile manufacturers have long taken advantage of these improved nails for fastening car linings to the body. Box and furniture manufacturers often have been in the position

² Number in parentheses refer to the Bibliography at the end of the paper.

to use these nails to great advantage, in many instances even in place of wood screws. Since 1939 these improved nails have found preferential acceptance for the construction of wooden pallets and were approved in recent recommendations by The National Wooden Pallet Manufacturers Association and Naval Specifications.

Annularly grooved brass, bronze, and stainless-steel nails have been used in carload quantities for butt-nailing asbestos side-wall shingles since early 1935. Lately the wood- and asphalt-shingle contractors have become convinced promoters of the use of grooved nails. Simultaneously, the building industry has become aware of the advantages of these nails for laying floors, fastening of insulation, nailing of siding and millwork. The extended use of these nails for application of metal roofing and building sheets has long been justified by their performance as convincingly exhibited in a recent treatise (2).

A considerable amount of technical information has been made available on plain-shank, barbed, and cement-coated nails. Before preliminary test and design data on spirally and annularly grooved nails had been published (3), first, cement-coated nails (4) and, later, chemically etched nails (5, 6) had been recommended for superior withdrawal resistance immediately after driving. These recommendations had been made despite the fact that these latter types of nails lose some of their holding capacity with time, and change in moisture content of the wood (5, 6).

For proper application of the improved spirally and annularly grooved nails, the necessity arose to obtain test data from which design data could be secured, in line with the generally established trend from empirical to theoretical design of wood structures. Effectiveness and proper use of nails depend upon the following:

- 1 The driving resistance offered, as determined by the energy required to hammer the nail into wood.
- 2 The holding capacity, as observed by the withdrawal resistance of the nail from wood.
- 3 The lateral load-carrying capacity, as found by the resistance of the nail to lateral forces transmitted through the nail to wood.
- 4 The nonsplitting properties, as shown by the resistance to splitting of wood during and after driving of the nail.

These properties are influenced significantly by (a) such nail-production variables as may be specified for material, design, manufacture, and treatment, and (b) such application variables as method of loading, wood species and density, member size and grain direction, moisture content and change in moisture content, time interval between driving and loading, preboring of undersized holes, clinching, and redriving.

This paper cannot present the answer to all nail problems. Its general purpose is to indicate the trends in the field of nailing, to show the special advantages of spirally and annularly grooved nails, and to give proof as to what can be accomplished by research and development work in the field of nailing. Its specific purpose is to determine proper design data for the tested spirally and annularly grooved nails,³ so they may be used to best advantage in wood structures and important wood assemblies.

The test program included evaluation of type of nail (plain-shank, spirally grooved Screwtype with a 60-deg slope of thread, and annularly grooved Stronghold with 0.060-in. spacing from

³ The nails selected for test purposes are general-purpose nails of standard design and conform to standard manufacturing procedure of the producer. Variations from these standards, to satisfy specific requirements, are numerous. Thus the test data obtained in this study may not be directly applied to other nails than those tested, although they are representative spirally and annularly grooved types of nails. Thus the presented data are only directly applicable to the spirally grooved "Screwtype" and annularly grooved "Stronghold" nails manufactured by the Independent Nail & Packing Company, Bridgewater, Mass.

center to center of grooves), size of nail (length and diameter), type of steel (low-carbon and high-carbon), treatment of nail (nonhardened and hardened), surface coating (noncoated and cement-coated), type of nail point (diamond and V), and use of pilot.

Southern yellow pine, white oak, and beech were selected for test purposes as representative for the softwood, open-porous hardwood, and closed-porous hardwood species, respectively. The test planks consisted of select, partially air-dried (20 per cent moisture content), clear, straight-grain, dressed-four-sides, structural 3 × 8-in. and 4 × 8-in. shortleaf pine from Virginia, similar green (46 per cent moisture content) white oak from Virginia, and similar green (45 per cent moisture content) beech from Indiana.

Replicate (duplicate quintuplicate) tests on each test variable were performed with different planks. The nails were spaced perpendicularly to the grain 1 1/4 in. apart, while nail spacing parallel with the grain was 1 1/2 in. In order to facilitate comparative testing with green and dry wood, the testing and matching schedules were prepared in such a way that adjacent locations in the fiber direction of the planks were used for testing with the green and, at a later date, with the dry wood. Nails for tests on withdrawal resistance and lateral load-carrying capacity were driven to 3/4 shank penetration immediately before testing, in order to eliminate any time effect on the test data. Upon completion of these tests, the second series of nails was hammered into the respective adjacent locations for performance of tests upon air-drying of the planks to uniform equilibrium moisture content.

For tests on the driving resistance of nails, a 1000-in.-lb.-capacity nail driver was employed to drive nails with uniform centric impact force into wood, in order to obtain comparative data on the depth of nail-shank penetration as a result of application of a single impact stroke.

For all tests on withdrawal resistance and lateral load-carrying capacity, an Olsen universal testing machine with 1400 and 12,000-lb.-capacity poises was provided with special jigs shown in Figs. 3 and 4.

A universal joint ascertained uniform and centric load application in the direction of the nail axis, provided the nail was driven perpendicular to the plane of the plank. Uniform rate of pulling was attained for all tests on the ultimate withdrawal resistance by the constant motion of the movable crosshead of the testing machine at 0.060 ipm. A test speed of 0.015 ipm was used for the performance of withdrawal tests for which load-deformation data were recorded.

Tests on the lateral load-carrying capacity of nails were performed by loading the projecting part of the nail shank with a free-turning, tight-fitting steel jig placed snugly between nail head and plank. The uniform rate of testing of 0.060 ipm for tests on the ultimate load-carrying capacity was reduced to 0.048 ipm for those tests for which load-deformation data were obtained.

TEST RESULTS

Nail Withdrawal Under Axial-Load Application. The relationship between withdrawal resistance in pounds and withdrawal in inches was determined experimentally in a separate test series for 2 1/2-in.-long, 0.135-in.-diam plain-shank, spirally grooved, and annularly grooved nails, as shown in Fig. 5. They penetrated for two thirds of their shank length into 3 × 8-in. southern yellow pine with a 13.9 per cent average moisture content, 0.57 specific gravity, 14 annual rings per inch, and 30 per cent summerwood.

The observed "slopes" for the three types of nails are similar, that is, 25,000, 26,800, and 22,400 lb/in., respectively. Thus the nails have a similar rigidity in withdrawal, hence cause a similar stiffness of nailed joints within the design range.

As soon as the shank friction of the plain-shank nail was exceeded, that is, upon a withdrawal of 1/10 in. at a load of 420 lb,

the nail pull applied load ing the test, only to a slip friction area tial failure. ping-where constant rate approximate

The spiral a withdrawal defined as th crease consi constant rate during conti nail was inc threaded na 25 per cent lb was obser ing, the low the surface

FIG. 2 D LARLY GRO DRAVAL-T PLAIN-SHA CARBON-S

the nail pulled for a small amount. This resulted in a decrease in applied load under the testing procedure employed. By continuing the test, the applied load could again be increased, however, only to a slightly smaller maximum, since the original friction and friction area between shank and wood were decreased by the initial failure. Further test continuation resulted in successive slipping, whereby the holding capacity decreased step by step at a constant rate, until the test was discontinued at a withdrawal of approximately $\frac{3}{16}$ in.

The spirally grooved nail showed an "initial ultimate load" at a withdrawal of approximately $\frac{1}{32}$ in., if initial ultimate load is defined as the minimum load at which deformation begins to increase considerably with no appreciable increase in load at the constant rate of withdrawal. When the nail was allowed to turn during continuation of the test, the withdrawal resistance of the nail was increased, since a firmer grip between wood fibers and threaded nail shank was attained. At a withdrawal of $\frac{11}{32}$ in., a 25 per cent increase in load beyond the initial ultimate load of 475 lb was observed. When the nail head was prevented from turning, the low-carbon-steel shank of the nail countertwisted near the surface of the plank, as shown in Fig. 2 (left), since during

withdrawal the further inserted part of the shank was forced by the wood fibers to thread itself out of the wood. The resistance offered by the wood fibers to withdrawal under this testing procedure resulted in a 33 per cent increase in withdrawal resistance beyond the initial ultimate load of 535 lb.

The annularly grooved nail attained its ultimate withdrawal

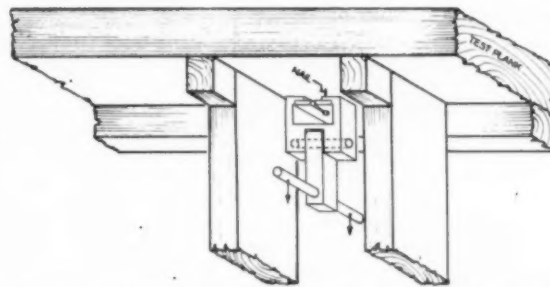


FIG. 3 DIAGRAMMATIC TEST SETUP FOR PERFORMANCE OF WITHDRAWAL TESTS

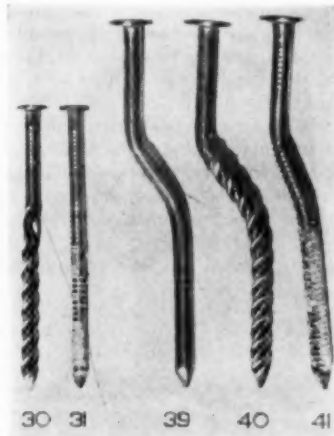


FIG. 2 DEFORMED SPIRALLY GROOVED AND WOOD-FILLED ANNULARLY GROOVED LOW-CARBON-STEEL 3-IN-LONG NAILS AFTER WITHDRAWAL-TEST PERFORMANCE ARE SHOWN AT LEFT—AT RIGHT, PLAIN-SHANK, SPIRALLY GROOVED, AND ANNULARLY GROOVED LOW-CARBON-STEEL 4-IN-LONG NAILS AFTER PERFORMANCE OF LATERAL NAIL-SHANK LOADING TESTS

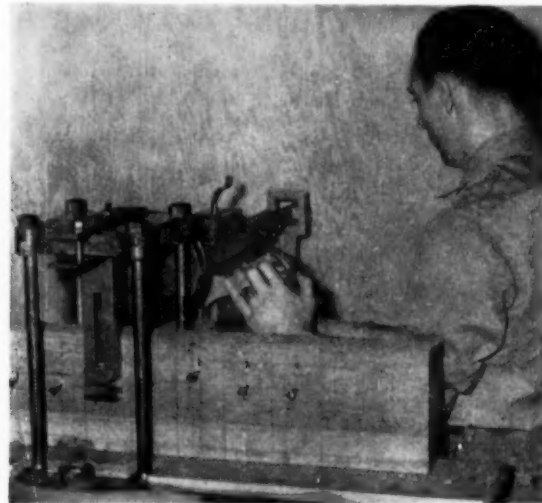


FIG. 4 TEST SETUP FOR PERFORMANCE OF LATERAL NAIL-SHANK LOADING TESTS

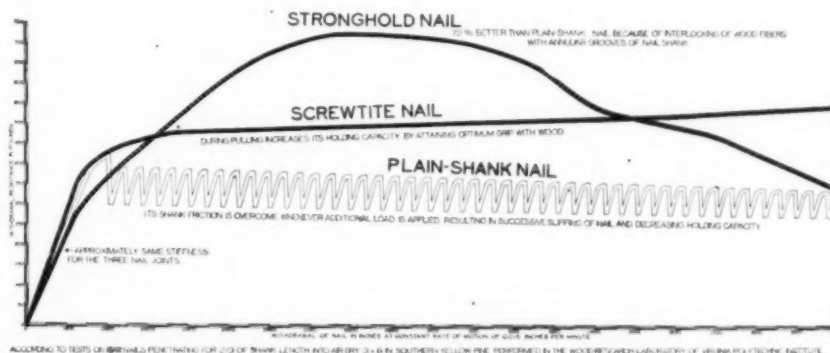


FIG. 5 LOAD-WITHDRAWAL DIAGRAM FOR AXIALLY LOADED LOW-CARBON-STEEL 2 1/2-IN-LONG PLAIN-SHANK, SPIRALLY GROOVED, AND ANNULARLY GROOVED NAILS IN PARTIALLY AIR-DRY SOUTHERN YELLOW PINE

load of approximately 700 lb at a withdrawal of $1/12$ in. Beyond this peak load, its withdrawal resistance continuously decreased with increase in withdrawal. At a withdrawal of approximately $1/8$ in., the holding capacity of this nail approximated that of the plain-shank nail. Withdrawal of such a magnitude is seldom allowable from the design viewpoint. Therefore the greater withdrawal resistance of the annularly grooved nail, as compared with that of the plain-shank nail, cannot be considered lessened by this decrease in holding capacity (beyond its ultimate) if a loading procedure is used similar to that employed in these tests.

Nail Deformation Under Lateral-Load Application. Data on nail deformation during lateral loading of the nail shank are required for the design of nailed wood structures, if the structural design is limited or influenced by the actual deformation of the structure under load. For this test series, the same test material and $2\frac{1}{2}$ -in.-long, 0.135-in.-diam nails were used as for the performance of tests on nail withdrawal. Additional data were obtained for hardened high-carbon-steel nails. The deformation of the nail shank is reported as the motion of a steel loading bar, fitting snugly around the protruding nail shank, relative to a horizontal line on the plank with the nail perpendicular to and intersecting this line. Diagrammatic test data are given in Fig. 6.

The slopes of the load-deformation curves indicate approximately the same stiffness for the three nail types within their design ranges.

The low-carbon-steel plain-shank nail deformed approximately $1/8$ in. before reaching an average maximum load of 620 lb. After having attained this peak load, the nail continued to deform. The shank finally sheared off at the loading edge nearest the plank at a total load of 325 lb and at a total deformation of $7/16$ in. The hardened plain-shank nail was too brittle to resist the shear-stress concentration along the edge of the loading bar. Thus the average ultimate load amounted to only 410 lb.

The low-carbon-steel spirally and annularly grooved nails

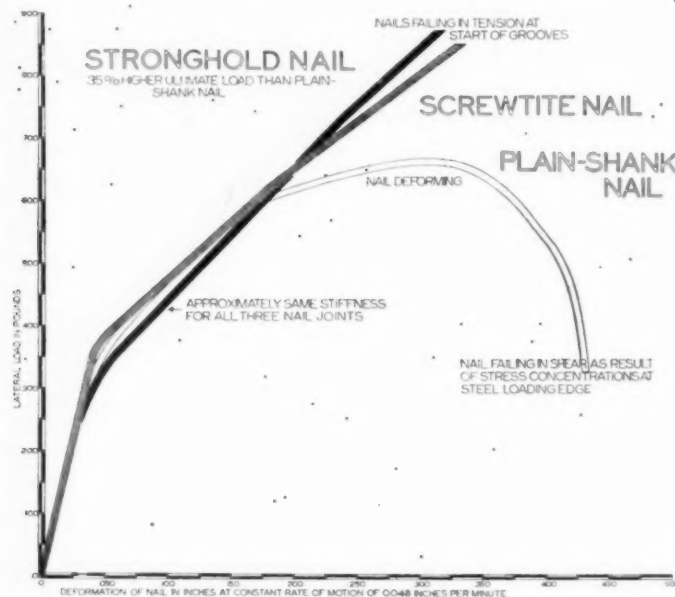
sheared off at the start of the rolled-on shape at an average maximum test load of 840 lb, and a total deformation similar to that found for the plain-shank nail at its maximum test load. Those hardened spirally grooved nails, which did not shear off along the edge of the loading bar, failed $1/2$ in. inside from the plank surface at maximum lateral loads of 820 and 1010 lb, and at a total deformation of $11/32$ in. One of the hardened annularly grooved nails similarly failed at 980 lb and at a similar amount of deformation. Thus on the basis of the limited number of tests performed, spirally and annularly grooved nails appear to have similar rigidity within their complete lateral loading range.

Ultimate Test Data. In Table 1 the driving resistance of nails is given as the ultimate penetration of the nail shank into the plank, corrected for nonuniformity, within a species, in properties of the planks used for testing.

Test data on the ultimate withdrawal resistance for spirally grooved nails are not comparable to those for plain-shank and annularly grooved nails, since the ultimate for spirally grooved nails does not occur within the same range as do the ultimates for plain-shank and annularly grooved nails. On the other hand, the "initial ultimate loads" for spirally grooved and the ultimate loads for plain-shank and annularly grooved nails are attained within a relatively similar range of withdrawal and thus may be considered of a comparable nature. In consideration of this observation, the comparative data given in Table 1 on withdrawal resistance of spirally grooved nails refer to their initial ultimate loads.

The ultimate test data, as observed during lateral loading, were limited by rupture of the nail shanks in 45 per cent of all test cases, that is, in 63 per cent for hardened and in 27 per cent for nonhardened nails. The remaining test nails failed in withdrawal or excessive flexural deformation during lateral-load application.

Both ultimate-withdrawal and lateral-loading data were also



ACCORDING TO TESTS ON NAILS PENETRATING FOR 2/3 OF SHANK LENGTH INTO AIR-DRY 3x6 IN SOUTHERN YELLOW PINE AND LOADED BY MEANS OF A 0.63 IN THICK STEEL PLATE IN THE WOOD RESEARCH LABORATORY OF VIRGINIA POLYTECHNIC INSTITUTE.

FIG. 6 LOAD-DEFORMATION DIAGRAM FOR LATERALLY LOADED LOW-CARBON-STEEL $2\frac{1}{2}$ -IN.-LONG PLAIN-SHANK, SPIRALLY GROOVED, AND ANNULARLY GROOVED NAILS IN PARTIALLY AIR-DRY SOUTHERN YELLOW PINE

TABLE 1
LATERAL

Nail
Size
Length
Wire Dia
(In Inch)

2" x 0.

2 1/2" x 0.

2 1/2" x 0

3" x 0

3" x

3 1/2" x

4" x

4" x

STERN-IMPROVED NAILS

TABLE 1. GRAND AVERAGES FOR MATCHED DECUPLE TESTS ON DRIVING RESISTANCE, WITHDRAWAL RESISTANCE, AND LATERAL LOAD-CARRYING CAPACITY FOR PLAIN-SHANK, SPIRALLY GROOVED, AND ANNULARLY GROOVED NAILS IN GREEN WHITE OAK, GREEN BEECH, AND PARTIALLY AIR-DRY SOUTHERN YELLOW PINE

Nail Size Length x Wire Dia. (In Inches)	Nail Type	Wood Species	Driving Resistance Shank Penetration (In Inches)			Withdrawal Resistance For 2/3 Shank Penetration (In Pounds)			Lat. Load-Carrying Cap. For 2/3 Shank Penetration (In Pounds)		
			Plain	Spirally Grooved	Annularly Grooved	Plain	Spirally Grooved	Annularly Grooved	Plain	Spirally Grooved	Annularly Grooved
2" x 0.120"	HC-NH-NC-D	Oak	1.04	—	—	313	—	—	604	—	—
		Beech	0.88	—	—	314	—	—	355	—	—
		SYP	1.08	—	—	205	—	—	406	—	—
	HC-H-NC-D	Oak	1.10	0.92	0.95	394	542	520	544	694	465
		Beech	0.87	0.70	0.75	419	494	416	370	342	347
		SYP	1.18	1.02	1.06	335	500	525	494	571	426
	HC-NH-NC-V	Oak	0.95	—	—	289	—	—	587	—	—
		SYP	1.06	—	—	140	—	—	383	—	—
	HC-H-NC-V	Oak	—	0.86	0.93	—	540	511	—	688	271
		SYP	—	0.91	1.05	—	455	478	—	612	280
2 1/2" x 0.120"	HC-NH-NC-D	Oak	1.01	—	—	375	—	—	625	—	—
		Beech	0.84	—	—	468	—	—	511	—	—
		SYP	1.16	—	—	198	—	—	393	—	—
	HC-H-NC-D	Oak	1.06	0.88	0.96	471	658	662	398	497	518
		Beech	0.83	0.68	0.75	520	719	688	445	464	497
		SYP	1.18	1.01	1.09	380	600	619	356	563	415
	HC-NH-NC-V	Oak	0.91	—	—	374	—	—	612	—	—
		SYP	1.01	—	—	181	—	—	357	—	—
	HC-H-CC-D	Oak	—	0.91	0.90	—	652	662	—	708	391
		Beech	—	0.73	0.71	—	711	680	—	561	328
		SYP	—	1.13	1.09	—	630	576	—	756	403
	HC-H-NC-V	Oak	—	0.87	0.90	—	657	—	—	922	213
		SYP	—	0.92	1.01	—	533	—	—	551	207
	HC-H-NC-D-P	Oak	—	0.89	0.93	—	623	668	—	591	502
		Beech	—	0.69	0.72	—	674	644	—	567	294
		SYP	—	0.99	1.00	—	535	607	—	745	275
2 1/2" x 0.135"	LC-NH-NC-D	Oak	0.93	0.73	0.72	401	645	732	700	799	597
		Beech	0.77	0.62	0.60	462	627	704	355	483	638
		SYP	1.08	0.86	0.82	264	331	644	500	751	620
	LC-NH-CC-D	Oak	0.93	—	—	515	—	—	732	—	—
		Beech	0.76	—	—	492	—	—	421	—	—
		SYP	1.12	—	—	438	—	—	638	—	—
3" x 0.135"	HC-NH-NC-D	Oak	0.85	—	—	408	—	—	773	—	—
		Beech	0.49	—	—	502	—	—	577	—	—
		SYP	1.06	—	—	243	—	—	467	—	—
	HC-H-NC-D	Oak	0.89	0.73	0.75	629	829	785	1178	1373	748
		Beech	0.53	0.35	0.40	702	841	851	685	681	742
		SYP	1.08	0.91	0.97	588	784	796	976	1252	782
3" x 0.148"	LC-NH-NC-D	Oak	0.75	0.63	0.60	541	688	866	906	1071	1080
		Beech	0.69	0.54	0.54	623	737	868	676	820	769
		SYP	0.90	0.75	0.75	366	362	825	567	830	1059
3 1/2" x 0.162"	LC-NH-NC-D	Oak	0.68	0.56	0.56	663	929	1072	1081	1178	1235
		Beech	0.61	0.47	0.47	795	946	959	630	881	925
		SYP	0.80	0.67	0.64	429	609	1015	678	994	1198
4" x 0.177"	HC-NH-NC-D	Oak	0.62	—	—	834	—	—	1741	—	—
		Beech	0.50	—	—	1061	—	—	1224	—	—
		SYP	0.70	—	—	491	—	—	214	—	—
	HC-H-NC-D	Oak	0.64	0.50	0.55	1100	1444	1397	2106	2559	1345
		Beech	0.49	0.40	0.45	1232	1291	1273	1055	1522	1513
		SYP	0.74	0.53	0.61	792	1112	1100	1634	1339	1353
4" x 0.203"	LC-NH-NC-D	Oak	0.54	0.47	0.46	815	1093	1487	1743	1989	2031
		Beech	0.44	0.38	0.34	1093	1159	1256	1215	1595	1690
		SYP	0.64	0.54	0.53	403	664	1170	949	1545	1550

LC = low-carbon steel
 HC = high-carbon steel
 NH = nonhardened

H = hardened
 NC = noncoated
 CC = cement-coated

D = diamond point
 V = V-point
 P = pilot

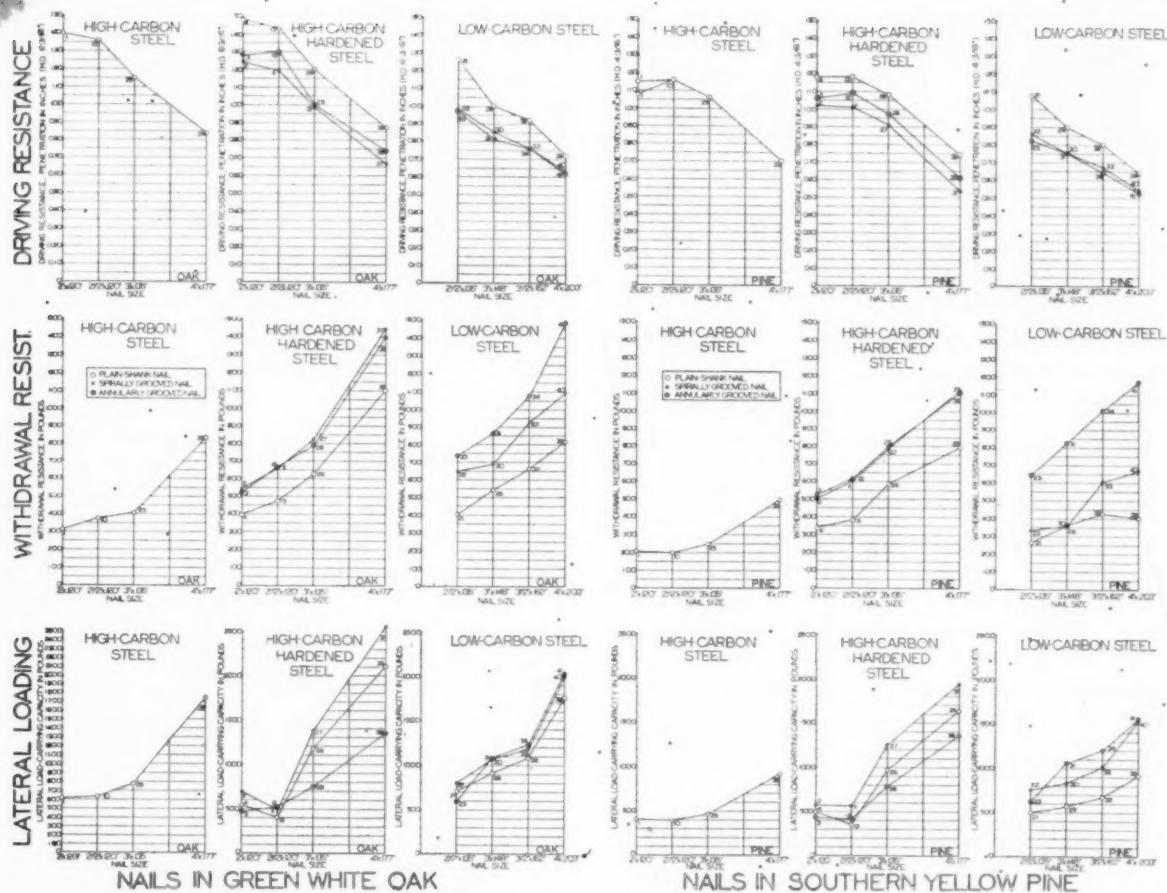


FIG. 7 INFLUENCE OF TYPE OF NAIL ON DRIVING RESISTANCE, WITHDRAWAL RESISTANCE, AND LATERAL LOAD-CARRYING CAPACITY OF 2, 2 1/2, 3, 3 1/2, AND 4-IN-LONG PLAIN-SHANK, SPIRALLY GROOVED, AND ANNULARLY GROOVED NAILS IN GREEN WHITE OAK, GREEN BEECH, AND PARTIALLY AIR-DRY SOUTHERN YELLOW PINE

corrected for nonuniformity in plank properties, if different planks within a species showed variations in their nail-withdrawal resistance and lateral load-carrying capacity.

INFLUENCE OF DESIGN VARIABLES

Nail Type. Comparative tests on driving resistance, withdrawal resistance, and lateral load-carrying capacity were performed with low-carbon-steel and hardened high-carbon-steel plain-shank, spirally grooved, and annularly grooved nails. The test results are given in Table 1 and graphically presented in Fig. 7. Because of their increased contact areas and frictional resistance between nail shank and surrounding wood, the grooved nails provided a larger withdrawal resistance and lateral load-carrying capacity than the plain-shank nails. These increases, however, were combined with an increase in driving resistance, although the latter increase proved to be somewhat smaller than those for withdrawal resistance and lateral load-carrying capacity.

The average driving resistance of the low-carbon-steel and hardened high-carbon-steel spirally grooved nails in green oak was 19 and 18 per cent, that in green beech was 20 and 21 per cent, and that in partially air-dry southern yellow pine was 19 and 16 per cent greater, respectively, than that of the plain-shank nails.

The average driving resistance of the corresponding annularly grooved nails in oak was 20 and 13 per cent, that in beech was 22 and 13 per cent, and that in southern yellow pine was 21 and 11 per cent greater, respectively. Thus the average driving resistance of spirally and annularly grooved nails tested was between 1/5 and 1/4 greater than that of the plain-shank nails.

The average withdrawal resistance of the low-carbon-steel and hardened high-carbon-steel spirally grooved nails in oak was 39 and 34 per cent, that in beech was 17 and 16 per cent, and that in southern yellow pine was 34 and 43 per cent greater, respectively, than that of the plain-shank nails. The average withdrawal resistance of the respective annularly grooved nails in oak was 72 and 30 per cent, that in beech was 27 and 12 per cent, and that in southern yellow pine was 50 and 45 per cent greater.

The average lateral load-carrying capacity of low-carbon-steel spirally and annularly grooved nails in oak was 14 and 12 per cent, that in beech was 31 and 40 per cent, and that in southern yellow pine was 52 and 64 per cent greater, respectively, than that of the plain-shank nails; that of the hardened high-carbon-steel spirally grooved nails in oak was 21 per cent, in beech was 3 per cent, and in pine was 25 per cent greater. By use of more satisfactory heat-treating procedures, considerable improvement might have been attained in the lateral load-carrying capacity of

these hard
equipment

Nail S

resistance
rectly wi
drawal r
southern
tively, th
Further
capacity
nail dian

Compa
ance, an
2 1/2, 3,
ally groo
3, and
nails, a
grooved
cally pro
vanced
This com
made of
nails.

With
which th
ally and

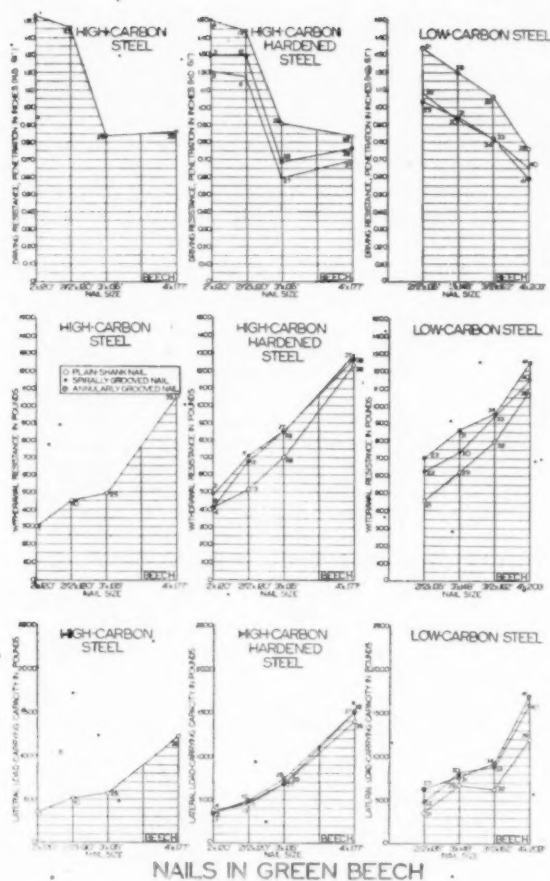


FIG. 7 (Continued)

these hardened high-carbon-steel nails. To this end, improved equipment has been installed by the nail manufacturer.

Nail Size. According to authoritative data (6), the withdrawal resistance per inch of penetration of plain-shank nails varies directly with the nail diameter. One of the exceptions is the withdrawal resistance, e.g., of $3\frac{1}{2}$ and 4-in-long plain-shank nails in southern yellow pine, which is 5 and 10 per cent smaller, respectively, than if computed according to the foregoing correlation. Furthermore, according to this reference, the lateral load-carrying capacity of plain-shank nails varies with the 1.5th power of the nail diameter.

Comparative tests on driving resistance, withdrawal resistance, and lateral load-carrying capacity were performed with $2\frac{1}{2}$, 3, $3\frac{1}{2}$, and 4-in-long low-carbon-steel plain-shank, spirally grooved, and annularly grooved nails, and with 2, $2\frac{1}{2}$, 3, and 4-in-long nonhardened high-carbon-steel plain-shank nails, and hardened high-carbon-steel plain-shank, spirally grooved, and annularly grooved nails. The test data are graphically presented in Figs. 8 and 9, in comparison with those advanced in reference (6) for low-carbon-steel common wire nails. This comparison is limited in value, since common wire nails are made of a wire with a slightly different diameter from the tested nails.

With increase in shank diameter, that is, the wire gage from which the nail was made, average driving resistance of both spirally and annularly grooved nails increased at a similar rate. This

increase, however, was slightly larger than that of the plain-shank nail driven into southern yellow pine and, especially, into oak. On the basis of the relatively uniform test data, it may be justified to assume a curvilinear relationship between shank diameter and depth of penetration for plain-shank nails, and a similar curvilinear relationship for grooved nails.

The increase in withdrawal resistance per inch of penetration with increase in shank diameter of low-carbon-steel plain-shank and grooved nails was somewhat smaller than expected, according to reference (6) for low-carbon-steel plain-shank nails. Although some of the data are somewhat erratic, a general trend of curvilinear relationship may be expected, particularly if grand average data for increase in withdrawal resistance of —2, 7, and 19 per cent for nails in oak, of 4, 8, and 22 per cent for nails in beech, and of 5, 18, and 13 per cent for nails in southern yellow pine are compared with increases in shank diameters of 10, 20, and 50 per cent.

The average withdrawal resistance per inch of penetration of the high-carbon-steel 3-in-long nails was only slightly larger, and that of the 4-in-long nails in oak 39 per cent, in beech 48 per cent, and in southern yellow pine 18 per cent larger than that of the 2 and $2\frac{1}{2}$ -in-long nails. The withdrawal resistance of some of the 3-in-long and, in particular, that of almost all 4-in-long nails should have been larger, according to the correlation suggested in reference (6), for low-carbon-steel plain-shank nails. The excessive brittleness of some of the test nails may have been of some influence on these data.

While the increase in lateral load-carrying capacity of low-carbon-steel plain-shank and spirally grooved nails in southern yellow pine, with increase in diameter, was similar to that expected, according to the general formula advanced in reference (6), the increase in capacity of these nails in oak and beech and of spirally grooved nails in oak, beech, and southern yellow pine was considerably larger. Thus with an increase in diameter of 10, 20, and 50 per cent for 3, $3\frac{1}{2}$, and 4-in-long nails, on the basis of comparison with the $2\frac{1}{2}$ -in-long nail, the respective ratios of average increases in capacity for plain-shank and spirally grooved nails in southern yellow pine were 12:34:98, in beech were 80:80:236, and in oak were 32:50:149; those for annularly grooved nails in southern yellow pine were 71:87:150, in beech were 21:45:165, and in oak were 81:107:240.

The increase in lateral load-carrying capacity with increase in diameter of most of the high-carbon-steel nails tested was also considerably larger than that expected, according to the general formula presented in reference (6) for low-carbon-steel plain-shank nails. The erratic nature of some of the test data is explained by the considerable variation in brittleness of these nails.

The relatively small increase in efficiency with increase in shank diameter of some of the grooved nails, in comparison with that of the plain-shank nails, such as in withdrawal resistance in green beech, may be explained by the uniformity in spacing of spiral and annular grooves for all nail sizes. Smaller center-to-center spacing of the grooves of the large-size nails might have increased their efficiency, although to date, no data have been obtained to substantiate such an assumption.

Nail Point. Nails tapered to and terminating in a flat point do not split wood as much as nails with a sharp or diamond point. The withdrawal resistance of nails with a tapered and flat point is equal in dense wood, though, smaller in less dense wood than that of the corresponding nail with a sharp point. Splitting of wood by a nail may also be prevented by use of a shank point with a short wedge having a blunt end, such as the V-point. Although the angle of the wedge-point axis to the wood-fiber direction may be of influence on the efficiency of this nail, all V-point nails were driven without consideration being given to the direction of the wedge axis.

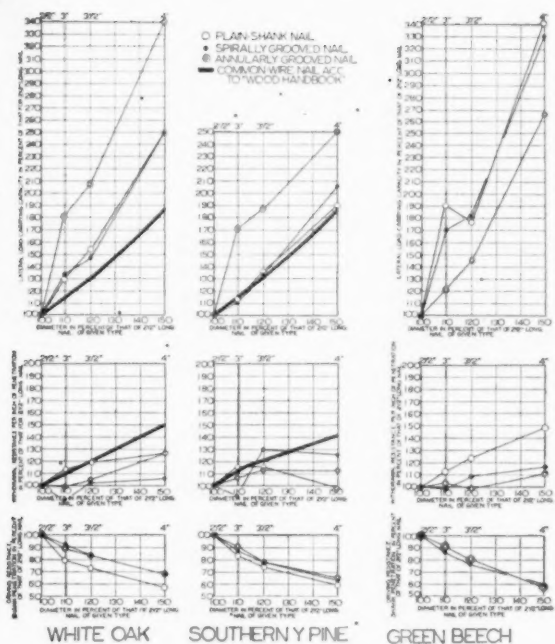


FIG. 8 EFFICIENCY DIAGRAM, WITH RESPECT TO WIRE DIAMETER OF NAIL SHANK, FOR PLAIN-SHANK, SPIRALLY GROOVED, AND ANNULARLY GROOVED LOW-CARBON-STEEL NAILS IN GREEN WHITE OAK, GREEN BEECH, AND PARTIALLY AIR-DRY SOUTHERN YELLOW PINE ACCORDING TO GRAND AVERAGES FOR DECUPLE TESTS

Comparative tests were performed with 2 and 2½-in-long diamond-point and V-point, high-carbon-steel nonhardened plain-shank and hardened spirally and annularly grooved nails, manufactured from the same wire strand, and driven into green white oak and partially air-dry southern yellow pine. The V-point, in comparison with the diamond point, resulted in a 9, 8, and 4 per cent greater average driving resistance and a 10, 5, and 5 per cent smaller average withdrawal resistance for the non-hardened plain-shank, hardened spirally grooved, and hardened annularly grooved nails, respectively. The lateral load-carrying capacity of the nonhardened plain-shank nail with V-point was 4 per cent smaller than that of the diamond-point nail. The lateral load-carrying capacity of the hardened grooved nails with V and diamond points was influenced too much by variations in nail brittleness to yield satisfactory comparative data.

With few exceptions, the effect of the V-point was consistent for all tests on the driving resistance, withdrawal resistance, and lateral load-carrying capacity. However, the influence of the V-point, in comparison with that of the diamond point, on the foregoing properties was relatively small, thus insignificant from the practical viewpoint.

Shank Pilot. For ease in initial driving of nails with grooved shanks, a pilot may be used, that is, for a short length from the nail point, the nail shank is plain and grooving starts only beyond that length. The length of the pilot may vary. For tests on the 2½-in-long hardened high-carbon-steel grooved nails with a pilot, a pilot length of ⅜ in. was used.

According to the comparative data for spirally and annularly grooved nails, the pilot resulted in a 2.5 per cent greater average driving resistance and a 5 per cent smaller average withdrawal resistance. In view of the considerable variation in brittleness of the test nails, fully comparative data could not be obtained on the

lateral load-carrying capacity of nails with and without pilots.

Thus it appears that as a short pilot was used for these comparative tests, it did not have any appreciable influence on both driving and withdrawal resistance of 2½-in-long, hardened high-carbon-steel spirally and annularly grooved nails.

Steel Composition. Both "regular" low-carbon steel, SAE 1010, and high-carbon steel, SAE 1065, were used for the manufacture of the tested nails. Comparative data were obtained on the driving resistance, withdrawal resistance, and lateral load-carrying capacity of 2½, 3, and 4-in-long plain-shank nails made from both steels, with the high-carbon-steel nails having 11.2, 8.8, and 12.8 per cent smaller diameters, respectively.

The average driving resistance of high-carbon-steel nails was 7 to 18 per cent, with a grand average of 12 per cent, smaller than that of the low-carbon-steel nails. An exception was the 3-in-long high-carbon-steel nail in beech with a 30 per cent larger driving resistance. The average withdrawal resistance of the high-carbon-steel nails was from 34 per cent smaller to 22 per cent larger, with a grand average of 10 per cent smaller, than that of the low-carbon-steel nails. Similarly, the lateral load-carrying capacity of the high-carbon-steel nails was from 25 per cent smaller to 44 per cent larger, with a grand average of 7 per cent, smaller than that of the low-carbon-steel nails.

Thus, because of the smaller diameters of the high-carbon-steel nails, as compared to the diameters of the low-carbon-steel nails of the same types and lengths, the high-carbon-steel nails were somewhat easier to drive and had a smaller withdrawal resistance and lateral load-carrying capacity than the respective low-carbon-steel nails.

Heat-Treatment. High-carbon-steel nails may be hardened to increase their buckling resistance during driving, their withdrawal resistance and lateral load-carrying capacity during use. Thus some of the high-carbon-steel nails were heat-treated at 1500 to 1600 F for 28 min, quenched in an oil bath, and tempered at 550 F for an additional 28 min. The nails thus treated varied considerably in brittleness although made from the same wire strand and issuing from the same nail batch, with some of the nails failing as a result of their brittleness and others failing only in exceeding their withdrawal resistance.

Comparative data were secured on the driving resistance, withdrawal resistance, and lateral load-carrying capacity of 2, 2½, 3, and 4-in-long high-carbon-steel, nonhardened and hardened plain-shank nails.

The average driving resistance of the hardened nails was from 2 per cent larger to 9 per cent smaller, with a grand average of 3 per cent smaller than that of the nonhardened nails. The average withdrawal resistance of the hardened nails was 11 to 142 per cent, with a grand average of 50 per cent larger than that of the nonhardened nails. The lateral load-carrying capacity of the hardened nails was from 36 per cent smaller to 109 per cent larger, with a grand average of 21 per cent larger than that of the nonhardened nails. While the driving resistance of hardened nails was almost consistently, however, from the practical viewpoint, insignificantly smaller, the withdrawal resistance of the hardened nails was consistently larger than that of the nonhardened nails. The considerable variation in brittleness is the explanation for the relatively large variation in data on both the withdrawal resistance and lateral load-carrying capacity of hardened nails. However, since as a result of heat-treatment both withdrawal resistance and lateral load-carrying capacity of some of the nails were increased more than 100 per cent, it should be possible to increase consistently to a considerable degree both withdrawal resistance and lateral load-carrying capacity by use of fully satisfactory hardening methods with equipment only lately installed by the nail manufacturer.

Cement Coating. According to information given in reference

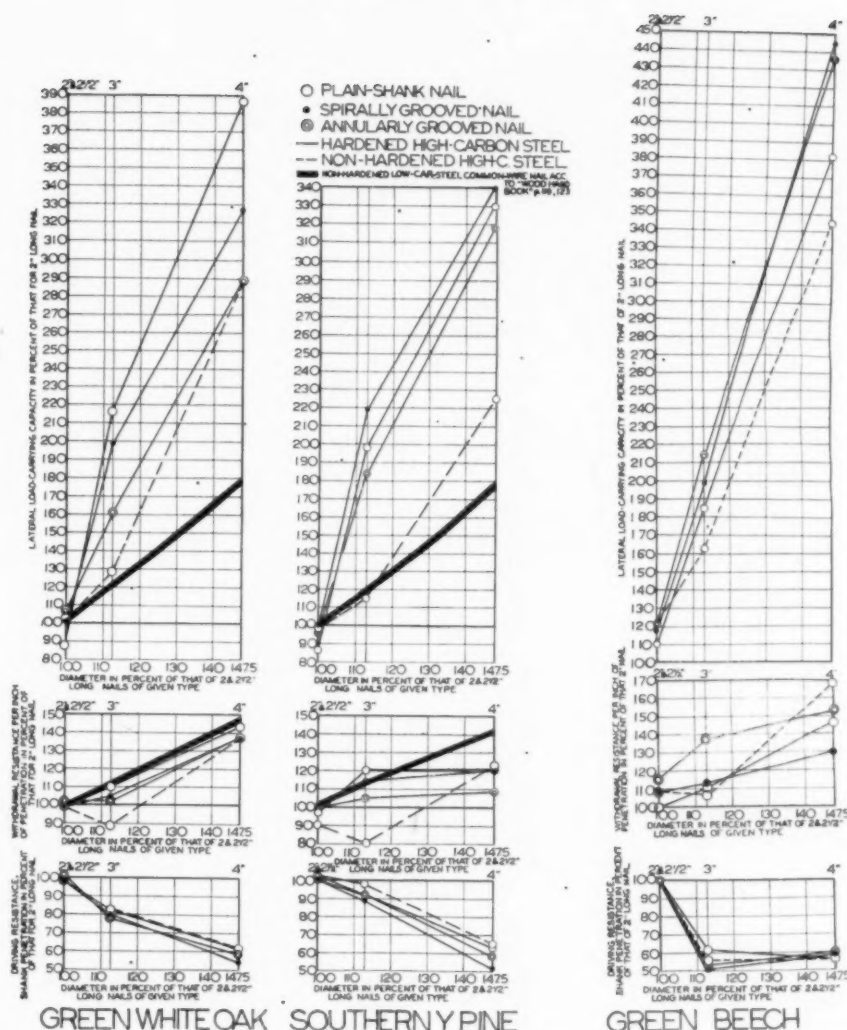


FIG. 9 EFFICIENCY DIAGRAM, WITH RESPECT TO WIRE DIAMETER OF NAIL SHANK, FOR PLAIN-SHANK, SPIRALLY GROOVED, AND ANNULARLY GROOVED HIGH-CARBON-STEEL NAILS IN GREEN WHITE OAK, GREEN BEECH, AND PARTIALLY AIR-DRY SOUTHERN YELLOW PINE ACCORDING TO GRAND AVERAGES FOR DECUPLE TESTS

(6) the withdrawal resistance of plain-shank nails immediately after driving into light wood may be 85 to 100 per cent larger if the nails are properly cement-coated, while, with increase in wood density, the benefit of cement coating decreases to practically no advantage over noncoating.

Comparative tests were performed on the driving resistance, withdrawal resistance, and lateral load-carrying capacity of 2 1/2-in-long low-carbon-steel plain-shank nails and hardened high-carbon-steel spirally and annularly grooved nails. The cement-coating compound⁴ used consisted of synthetic resin treated with linseed oil. It contained 65 per cent, by weight, petroleum naphtha as volatile carrier. It was applied in a tumbling process at normal temperature and uniformly covered the whole nail.

The average driving resistance of the noncoated and coated

⁴ No. V-5071 Elastic Nail Coating by the M. B. Suydam Division of Pittsburgh Plate Glass Company.

nails did not vary to any large extent. Cement coating increased the average withdrawal resistance of the plain-shank nail in oak 28 per cent, in beech 6 per cent, and in southern yellow pine 65 per cent. On the other hand, cement-coating of hardened high-carbon-steel spirally and annularly grooved nails was of no effect on their withdrawal resistance. The lateral load-carrying capacity of the coated plain-shank nail in oak was 5 per cent, in beech was 19 per cent, and in southern yellow pine was 28 per cent greater as a result of application of cement coating. The variation in brittleness of the hardened spirally and annularly grooved nails did not make it possible to obtain reliable data on the influence of cement coating on the lateral load-carrying capacity of these nails, although the coated spirally grooved nail showed consistently larger values than the noncoated nail. However, since the withdrawal resistance of these nails was not increased as a result of cement-coating, this increase in lateral load-carrying capacity may not be fully attributable to the coating.

The foregoing data on the withdrawal resistance of plain-shank nails are in general agreement with the information advanced in reference (6) for plain-shank nails. These data also indicate that cement-coating of spirally and annularly grooved nails may not be justified for purposes of improving their withdrawal resistance.

SUMMARY

1 With relatively small increases in driving resistance of nails, large increases can be expected in both withdrawal resistance and lateral load-carrying capacity.

2 Spirally and annularly grooved nails offer larger withdrawal resistance and lateral load-carrying capacity than plain-shank nails. Annularly grooved low-carbon-steel nails offer a larger withdrawal resistance than spirally grooved low-carbon-steel nails, while the withdrawal resistance of spirally and annularly grooved hardened high-carbon-steel nails is approximately the same.

3 Typical data on the effectiveness of spirally and annularly grooved nail shanks in comparison with plain nail shanks are presented in Table 2.

TABLE 2 COMPARISON OF PER CENT EFFECTIVENESS OF LOW-CARBON-STEEL, DIAMOND-POINT, 2 1/2-IN.-LONG, 0.135-IN.-DIAM. PLAIN-SHANK, CEMENT-COATED PLAIN-SHANK, SPIRALLY GROOVED, AND ANNULARLY GROOVED NAILS ON BASIS OF COMPARISON WITH RESPECTIVE NON-COATED PLAIN-SHANK NAIL

Wood species	Property	Plain-shank nail Non-coated	Cement-coated nail	Spirally grooved nail	Annularly grooved nail
In green	Driving resistance	100	100	122	123
	Withdrawal resistance	100	128	161	183
white oak	Lateral load-carrying capacity	100	105	114	85
In green	Driving resistance	100	101	119	123
	Withdrawal resistance	100	106	136	152
beech	Lateral load-carrying capacity	100	119	136	180
In partially air-dry	Driving resistance	100	96	120	124
southern pine	Withdrawal resistance	100	166	125	244
	Lateral load-carrying capacity	100	128	150	124

4 Both under withdrawal and lateral load, plain-shank and spirally or annularly grooved nails have similar rigidity within their design ranges; thus cause similar stiffness of nailed joints.

5 Under constant rate of withdrawal, plain-shank nails retain, within given limits, a slowly decreasing holding capacity somewhat below the ultimate holding capacity; spirally grooved nails continue to increase their holding capacity, although at a decreased rate of increase, after the "initial ultimate withdrawal resistance" has been reached; annularly grooved nails reach a considerably greater ultimate withdrawal resistance at a larger withdrawal than plain-shank and spirally grooved nails, while this withdrawal resistance decreases at a similar rate to that of increase up to the ultimate.

6 Under lateral load, the ultimate lateral load-carrying capacity of plain-shank and spirally or annularly grooved nails is reached at approximately the same amount of deformation.

7 Curvilinear relationships may be assumed between nail-shank diameter and both driving resistance and withdrawal resistance for plain-shank nails. Similar curvilinear relationships seem to exist for spirally and annularly grooved nails. The general correlation between nail-shank diameter and lateral load-carrying capacity, as presented in reference (6), seems to be somewhat conservative for plain-shank and spirally grooved nails in green white oak, green beech, and partially air-dry southern yellow pine.

8 The V-point, in comparison with the diamond point, has little effect on the driving resistance, withdrawal resistance, and lateral load-carrying capacity of plain-shank and spirally or annularly grooved nails.

9 A short pilot for grooved nails does not have any appreciable influence on either driving or withdrawal resistance.

10 High-carbon-steel nails, having smaller shank diameters

than low-carbon-steel nails of the same lengths, are, type for type, somewhat easier to drive and have correspondingly smaller withdrawal resistance and lateral load-carrying capacity than low-carbon-steel nails with their larger diameters.

11 Although the driving resistance of hardened nails is similar to that of nonhardened nails, the withdrawal resistance and lateral load-carrying capacity of hardened nails can be considerably larger.

12 Cement coating results in considerably increased withdrawal resistance of plain-shank nails immediately after driving into the low-density southern yellow pine and an almost negligible increase in withdrawal resistance for high-density beech. However, cement coating does not increase withdrawal resistance or lateral load-carrying capacity of spirally or annularly grooved nails.

13 Because of the considerable difference in moisture content, the average driving resistance, withdrawal resistance, and lateral load-carrying capacity of nails in green white oak and beech on the one hand, and partially air-dry southern yellow pine on the other hand, did not differ greatly and as much as

would be expected if the nails were tested in these species with like moisture content (7).

14 Driving resistance and withdrawal resistance increase with increase in wood density according to somewhat similar trends (7).

15 As a result of variation in physical structure of the plank, driving resistance, withdrawal resistance, and lateral load-carrying capacity may vary within the same plank cross section, even if the lumber is free of growth irregularities (7).

ACKNOWLEDGMENT

This study was performed in the VPI Wood Research Laboratory under the auspices of the VPI Research Foundation, Inc., and under the sponsorship of the Independent Nail & Packing Company of Bridgewater, Mass., manufacturer of the spirally grooved Screwite and the annularly grooved Stronghold nails.

BIBLIOGRAPHY

- "Technique of House Nailing," by U. S. Forest Products Laboratory in Cooperation with U. S. Housing & Home Finance Agency, U. S. Printing Office, November, 1947.
- "The Effectiveness of Roofing Nails for Application of Metal Building Sheets," by H. Giese and S. M. Henderson, Iowa State College Agricultural Engineering Station Research Bulletin No. 355, November 1947.
- "Influence of Depth of Penetration on Withdrawal Resistance of Nails," by E. G. Stern and A. E. Price, presented at the Annual Wood Industries Division Meeting of THE AMERICAN SOCIETY OF MECHANICAL ENGINEERS at High Point, N. C., October, 1948 (mimeographed); published in *The Journal of Southeastern Research*, vol. 1, April, 1949, pp. 14-16; also, *The Wooden Box & Crate*, vol. 11, May, 1949, pp. 21-25, and July, 1949, pp. 21-25.
- "Fibre Box Memo 11," by Fibre Box Association, 1948.
- "New Nail-Treating Process Increases Holding Power," by J. H. Gahagan and E. Beglinger, U. S. Forest Products Laboratory Report No. R970, July, 1932; also, *Barrel & Box & Packages*, vol. 37, no. 9, September, 1932.

6 "W
Governm
7 "D
Load-Car
Price, VP
vised, Ju

T. D. I
in all kin
surprising
regard to
shanks.

Excell
fication i
ject.

Simpli
expense
tions, so
duced.
to confe
this pap
casual r
stand o
cedure.

Supp
tors. I
load as
cost of
domina
strengt

H. J
nails in
point i
the str
this in
accord
Howev
power
the re
groove
It see
than t
ings sh
in the
Wh
to ext
count
other
ture.
torion
other
pair
prop
Th
finis
often
faste
to n
cost
groc
In
6
Brid

6 "Wood Handbook," by U. S. Forest Products Laboratory, U. S. Government Printing Office, 1935.

7 "Driving Resistance, Withdrawal Resistance, and Lateral Load-Carrying Capacity of Nails," by E. George Stern and A. E. Price, VPI Wood Research Laboratory Release, February, 1949; Revised, June, 1949 (typewritten).

Discussion

T. D. PERRY.⁴ The nail is one of the most common items used in all kinds of woodworking, one of our largest industries. It is surprising that so little has been investigated, technically, with regard to the gripping power of nails having different shapes of shanks.

Excellent as this paper is, there are two points which need clarification in this as well as in the author's earlier paper on the subject.

Simplify the conclusions, by emphasizing major factors at the expense of less important ones, or break the results down into sections, so that the number of variables in each bracket is much reduced. Reading technical papers is no novelty to me, but I have to confess considerable confusion, even after a careful reading of this paper. Reading rapidly or scanning would not improve the casual reader's conclusions. The facts are there but they do not stand out clearly against the background of lengthy testing procedure.

Supplement the strength data by analyzing the economic factors. If 8 lb of grooved shank nails are needed to carry the same load as 10 lb of common plain shank nails, what is the relative cost of the two lots? In other words, and in the last analysis, the dominating reason for adopting such nails would be either more strength at the same cost, or equal strength at less cost.

H. J. STONE⁵ states that with respect to the use of grooved nails in the field of building construction, the most important point is that ordinary nails are not nearly strong enough to equal the structural strength of the materials they fasten. To put this in another way, the frame used in the average home is, according to our tests, up to 5 times as strong as its fastenings. However, if properly grooved nails are used, their holding power can exceed the strength of the lumber they fasten, with the result that the frame of a house assembled with properly grooved nails will be fractured before the nails have yielded. It seems obvious that, since a house is ultimately not stronger than the fastenings which were used in its assembly, these fastenings should be as strong, if not stronger, than the lumber used in the construction of the house.

While it may be argued that most houses are never subjected to extraordinary stresses, there are in almost all sections of the country periods of high winds, extremes of temperatures, and other conditions which cause severe stresses on the house structure. These stresses often result in cracks, warpage, and distortions with resulting sticking of windows, door frames, and other comparatively minor distortions, which may result in repair bills, any one of which may exceed the additional cost of properly grooved nails.

The advantages of grooved nailing also apply to roofing, wood-finishing, door and window frames, and other elements which often deteriorate and cause trouble. An asphalt-shingle roof fastened with properly grooved roofing nails will never leak due to nail popping. Here again, a single roof leak may be more costly than the entire differential in cost between annularly grooved nails and ordinary roofing nails.

In the case of the grooved flooring nails, as compared with

conventional nails, we have experiences with spirally grooved nails going back 15 or 16 years. We have no record of failure during that period of time. On the other hand, floors nailed with either conventional cut nails or common wire brads will in time squeak, buckle, and ultimately require re-nailing and re-finishing.

Many of the cracks in walls and ceilings can be traced to failure of fastenings in the frame of a house and consequent settling of frames or distortion of walls. These conditions may be avoided with use of properly grooved nails which are proved in tests to exceed the strength of common nails as much as 1200 per cent.

If the contractor or home owner desires to offset the slight additional cost of properly grooved nails, this may be done by sheathing the house with one of several types of synthetic sheathing materials. While such materials are not as effective as boarding when common nails are used, they may safely be used if the house structure is assembled and the sheathing itself applied with the respective grooved nails. The use of these grooved nails also allows the use of lower grades of lumber without reducing the ultimate strength of the building itself.

AUTHOR'S CLOSURE

With respect to Mr. Perry's comments, it may be stated that this paper is to serve a twofold purpose. It is (a) to make available to the average engineer general information on the advantages of using improved nails; and (b) to present detailed data to the nail user concerned with a large number of variables of little interest to the average engineer. The information which may be too detailed for the former, may contain too little data for the latter. Thus a relatively large amount of information had to be crowded into a given space. For those wishing to obtain additional information, parts or complete copies of reference (7)⁷ can be made available.

Since presentation of this paper, a considerable amount of additional information on improved nails and their effects has been obtained. To those interested in this information, a supplement to the Bibliography appears at the end of this closure.

Reference (10) contains a partial summary of fully comparative information on delayed nail-holding properties, as referred to in the paper and scheduled for later presentation. Thus it shows the effect of change in moisture content and elapsed time after nail driving on the test variables under discussion.

With respect to the economic aspects created by the mass-production of grooved nails, Mr. Perry overlooked the aspect of considerably increased service at somewhat increased cost. In this case, this aspect can be combined with better service at the same cost or equal service at less cost, since the better service rendered by the individual grooved nail makes it possible to reduce, under given conditions, the number of nails hitherto required.

One of the cases in which considerably better service can be obtained at even decreased cost for grooved nails, is that of the spirally grooved Screwite flooring nails. In this particular case, 50 lb of grooved nails replace 100 lb of cut nails, with an increase in nail-holding power of 40 per cent, combined with a simultaneous saving of 28 per cent of the cost of the cut nail.

For a more complete analysis of the economic aspects of use of grooved nails, a cost analysis (Table 3) is presented which was advanced for a 50-ft X 24-ft \$10,000 five-room house with attached garage.

Thus, at a cost of \$10,000 for this house, the cost of all nails amounts to \$65.70 or 0.657 per cent if of the plain-shank type, and to \$106.25 or 1.0625 per cent if of the grooved type.⁸ In other

⁷ Reference is to Bibliography at the end of the paper.

⁸ Reference (a) Table 3 of this closure.

⁴ Engineer in Wood Work, Moorestown, N. J. Fellow ASME.
⁵ General Manager, Independent Nail & Packing Company, Bridgewater, Mass.

TABLE 3 COST ANALYSIS OF NAILS FOR TYPICAL \$10,000 HOUSE

Nail type	Nail size	Required amount lb	Quoted cost ^a	
			Plain-shank nails	Annularly grooved Stronghold nails
Framing.....	20d	110	\$ 7.98	\$13.85
	16d	75	5.44	9.44
	10d	60	4.44	7.58
	8d	130	9.75	16.51
	6d	5	0.40	0.66
Casing.....	10d	10	0.89	1.33
	6d	5	0.48	0.69
	4d	2	0.20	0.33
Finishing.....	8d	30	3.90 ^b	2.81 ^c
	7d	35	4.81	5.86
	3d	65	10.40	16.71
	4d	2	0.20	0.33
Flooring.....	8d	30	3.90 ^b	2.81 ^c
Siding.....	7d	35	4.81	5.86
Shingle.....	3d	65	10.40	16.71
Asphalt roofing.....	1 X 11	60	8.10	14.04
Lath.....	1 1/4 X 13	45	6.19	12.40

^a Based on retail quotations for products of the Independent Nail & Packing Company, Bridgewater, Mass.

^b High-carbon-steel cut flooring nails.

^c 15 lb of spirally grooved Screwwite flooring nails.

words, for an increase of \$40.55 or less than 1/2 per cent of the total cost of the house, all the following advantages can be obtained, according to data presented in the paper and in references (8, 9, 10, 11). It is not a necessity, of course, to replace all plain-shank nails with grooved nails. To date, replacement for individual applications has been more or less the case. On the other hand, with the increased amount of knowledge as to the beneficial effect of use of grooved nails, total replacement of nails must be given consideration under certain conditions. The advantages follow:

1 For the increased expenditure of \$20.03 or 0.2 per cent of the total cost of the house given as an example, the unsheathed framing can offer a 4 to 6 times greater lateral-thrust resistance, with the frame joints possibly even stronger than the framing lumber (9).

2 For a saving of \$1.09, as a result of the use of 15 lb of spirally grooved Screwwite flooring nails instead of the twice as heavy cut flooring nails, the flooring and stair treads can be more easily and quickly laid; under normal conditions do not come loose, squeaky or springy, cup or buckle; split tongues can be averted; whereby 220 and 40 per cent, respectively, greater withdrawal resistances are obtained if comparison is made with the same-size plain-shank flooring brads and cut flooring nails (11).

3 For an increased expenditure of \$1.05, all the siding may be fastened in such a way that the nails will not "creep" or "pop"; thus the siding remains firmly fastened to the structure.

4 For an increased expenditure of \$6.31, assurance may be had that none of the wood or asbestos shingles will come loose since the use of grooved nails results in a 250 per cent greater holding power than attained by use of corresponding plain-shank nails.

5 For an increased expenditure of \$5.94 for fastening asphalt-roofing shingles, assurance may be had that the nails will retain the shingles continuously tightly fastened as a result of the 50 per cent greater axial withdrawal resistance of the grooved nails in comparison with the plain-shank nails.

6 For an increased expenditure of \$6.21, the plaster lath may be fastened permanently and firmly to the framework because of the 40 per cent increased holding power of the annularly grooved nails. Thus the possibility of formation of any cracks in plaster is considerably decreased.

7 For an increased expenditure of \$2.10 for casing and finishing nails, the woodwork should never come loose. Thus a satisfactory fastening of all interior woodwork even after aging of the structure can be assured.

The cost increases cited result from the use of an equivalent number of properly grooved nails to replace plain-shank nails. In many cases, a smaller number of grooved nails may be used without detrimental effect. Thus the small increases in expenditure may even be decreased.

All the improvements in the structure immediately after erection and during its life, and the decreased cost of maintenance and repair, resulting exclusively from the use of grooved nails, can be attained for a cost amounting to less than 1/2 per cent of the total cost. This small difference in initial cost may be considered "an insurance premium of the entire value of the house for its lifetime, which will guarantee that the house will not deteriorate within its expected lifetime."

Although tables indicating the efficiency of grooved nails in comparison with plain-shank nails, as based on holding capacity per dollar value, could be presented according to the data made available in this and other papers (10, 11), it is believed that the foregoing cost analysis for nails in home construction answers the question raised by Mr. Perry as to the economic aspects of the use of grooved nails.

SUPPLEMENT TO BIBLIOGRAPHY

8 "Comparative Tests on Old and New Grooved Nails," by E. George Stern, *The Wooden Box and Crate*, vol. 11, December, 1949, pp. 21-25.

9 "Grooved Nails Strengthen House Frames," by E. George Stern, *Engineering News-Record*, vol. 144, April 6, 1950, pp. 32-34.

10 "Deterioration of Green Wood Along Steel Nail Shank and Its Influence on the Nail-Holding Properties," by E. George Stern, *Virginia Journal of Science*, vol. 1, July, 1950.

11 "Nails in End-Grain Lumber," VPI Wood Research Laboratory Release, October, 1949.

"Improved Nails for Building Construction," VPI Wood Research Laboratory Release, February, 1950. (Accepted for publication as Bulletin of the Virginia Polytechnic Institute, Engineering Experiment Station.)

Head and Flow Observations on a High-Efficiency Free Centrifugal-Pump Impeller

By W. C. OSBORNE¹ AND D. A. MORELLI,² PASADENA, CALIF.

A series of studies of the flow through the various components of hydrodynamic machinery is in progress in the Hydraulic Machinery Laboratory of the California Institute of Technology. Observations have been made on an impeller patterned after the Grand Coulee design. The impeller was operated as an isolated unit hydraulically free of the casing. The flow pattern at the discharge has been determined quantitatively for one flow rate, and a head-capacity curve for the impeller has been obtained. This paper constitutes a report on the findings up to the present.

INTRODUCTION

IN the past most of the experimental work carried on in the field of rotating machinery has dealt with the machine as a whole, and because of the technical difficulties involved, comparatively little has been done to determine the performance characteristics of the individual elements which make up the whole. As a rough classification, such a machine can be thought of as consisting of three parts, namely, (a) the stationary inlet member, (b) the rotating member, and (c) the stationary outlet member.

Some empirical work has been carried out in which various rotating members have been tested with the same stationary members and vice versa, but the test results obtained in these cases have been referred to the performance of the combination as a complete machine, and the effect of changes in the individual member has been inferred only through the effect of such changes on the over-all performance. Several laboratories, particularly those of Spannhake, Thoma, and Pfeleiderer, in Germany (1-9),³ have undertaken experimental investigations of the detailed characteristics of the flow in the rotating passages, and a few workers have explored the flow during its transition from the rotating member to the case. In practically all instances, however, the experimental machine has been greatly simplified, usually to the point of making the runner two-dimensional. The gain from such simplification has been twofold, namely, the experimental difficulties have been lessened appreciably, and the possibility of parallel analytical studies has been improved. Unfortunately, the losses accompanying the simplification have included large decreases in efficiency, lowered resistance to cavitation, and a general lack of similarity to the performance characteristics of modern hydraulic machines.

Much effort has been devoted to the development of a satisfactory analytical treatment of the flow in hydraulic machines.

¹ Research Engineer, Hydraulic Machinery Laboratory, California Institute of Technology. Jun. ASME.

² Senior Research Engineer, Hydraulic Machinery Laboratory, California Institute of Technology. Mem. ASME.

³ Numbers in parentheses refer to the Bibliography at the end of the paper.

Contributed by the Hydraulic Division and presented at the Annual Meeting, New York, N. Y., November 27-December 2, 1949, of THE AMERICAN SOCIETY OF MECHANICAL ENGINEERS.

NOTE: Statements and opinions advanced in papers are to be understood as individual expressions of their authors and not those of the Society. Paper No. 49-A-108.

Considerable progress has been made in the analysis of the axial-flow machine based upon airfoil theories, especially in the zone of efficient operation. However, for abnormal operating conditions even in the axial-flow machines, and for all conditions in the machines having appreciable components of radial flow, the presently known analytical methods leave much to be desired. If the performance of the individual elements of machines having good characteristics and high efficiencies could be obtained experimentally, and especially if the details of the flow could be determined, as well as the over-all characteristics of the elements, it would greatly enlarge the possibilities of developing a satisfactory analytical treatment and at the same time improve design possibilities through the use of more detailed empirical information.

In an effort to meet this need, a project has been initiated at the Hydrodynamics Laboratory of the California Institute of Technology under the sponsorship of the Office of Naval Research for the primary purpose of making detailed studies, both experimental and analytical, of flow through various components of well-designed modern hydraulic machines. Since the existing facilities of the Hydraulic Machinery Laboratory (10) were not readily adaptable to the type of experimental work anticipated, a smaller more suitable laboratory was constructed.

LABORATORY FACILITIES

The project is located on the mezzanine floor of the Hydraulic Machinery Laboratory. The equipment is arranged to provide a flow of water in a closed circuit which is shown schematically in Fig. 1 and which consists essentially of three principal sections. One section functions primarily as a supply reservoir and includes the necessary equipment to deliver and meter a steady flow of water at various pressures and flow rates. It includes the reservoir and service pump, the Venturi meters and the throttle valve. This part of the circuit is independent of whatever test arrangement is made.

The second section functions principally as a distribution circuit and includes an adaptable arrangement of distributing headers, valves, and piping which may be arranged in various combinations to carry the flow from the throttle valve to and from the test elements in the particular manner and direction required by the unit under observation. Fig. 1 shows two of the several flow circuits possible. The major portion of this section is expendable and may be modified as the research requires.

The test stand is the third part of the circuit. Here are provided facilities for mounting, operating, and testing hydraulic-machine elements. The principal parts are the approach piping, the test basin, and the vertical dynamometer. These components are all in duplicate and thus allow two different studies to be run alternately and effect a great saving of time. Fig. 2 shows the test equipment as arranged for the photographic studies herein reported. One of the vertical dynamometers has been removed and replaced by a centerless impeller-drive mechanism to allow a full view of the impeller. Windows have been installed in the test basin to facilitate lighting and provide additional observation points. Fig. 3 presents the parallel test setup on the opposite side of the test stand. With this arrangement over-all

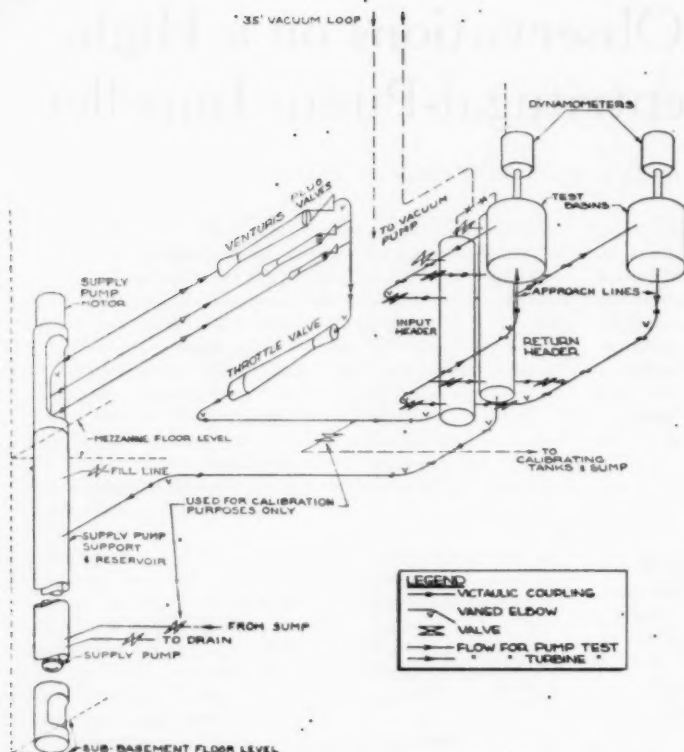


Fig. 1 DIAGRAM OF MAIN AND AUXILIARY FLOW CIRCUITS

head-capacity characteristics of the impeller were determined.

The project is a self-contained unit and can be operated independently of the other equipment in the building. However, to avoid duplication of equipment, the three Venturi meters may be connected to the main calibrating circuit of the Hydraulic Machinery Laboratory (10) and the existing facilities used for calibration. Fig. 2 shows the two points of interconnection.

The apparatus covers the following ranges:

- 1 Flow rates up to 4 cfs with a head differential of 66 ft at the test unit.
- 2 Power input or absorption up to 30 hp.
- 3 Dynamometers capable of rotative speeds of 100–2000 rpm in either direction.

The physical size of the test elements is not rigidly fixed. However, rotating channels up to 12 in. diam and diffuser or volute casings up to 30 in. diam may be accommodated.

Although the conventional opaque metal cast elements can be used in some test work, techniques have been developed at the laboratory for precision manufacture of these elements from transparent materials such as lucite. This not only makes possible the use of the various photographic techniques (12, 13) which have been developed and found to be extremely useful in observing and analyzing flow phenomena in the Hydrodynamics Laboratory (11), but it also offers advantages of controlled dimensions and guarantees symmetry and reproducibility to a degree essential for precise test work, which, ordinarily, are unattainable with standard cast elements.

OBJECT OF TESTS

The impeller of a centrifugal pump was chosen as the first

machine element to be examined. The rotating member was selected since it may be considered as the primary element of the pump; the principal interchange of energy between the machine and the fluid takes place in its rotating passages. The initial studies were confined to observations of the flow pattern at the discharge section of the impeller and to determinations of the over-all head-capacity characteristics of the impeller running free of its case. The discharge section of a modern medium-specific-speed impeller lends itself more readily to observation than does the inlet section and hence was selected as a logical starting point for a series of investigations which eventually will cover the entire impeller passage. Likewise, the head-capacity is the beginning of a series of studies designed to cover the complete over-all operating characteristics of the impeller. It is the purpose of this paper to report the findings of these initial studies and to present the tentative conclusions that have been drawn.

THE TEST IMPELLER

The test impeller used was very similar in design to the Grand Coulee pump impeller. This pump is a high-efficiency unit of medium specific speed, $N_s = 100$ (Q in cfs), and its design is representative of modern practice. The entire series of Grand Coulee model pumps was tested in the Hydraulic Machinery Laboratory and thus there is much detailed information available on the over-all performance of the pumping unit (15). Fig. 4 is a scale drawing of the impeller and presents its principal dimensions. The shroud curvature, the discharge and inlet vane angles, and the vane length were modeled to scale directly from the Grand Coulee design. However, the slight curvature or spooning of the vane in the eye was omitted and the vane was terminated along a straight line in the meridional projection. Although this alteration speeded production of the test impeller, it is not a limitation of the manufacturing technique; exact curvature of the prototype can be duplicated in the model if tests indicate the necessity. The discharge-vane tips were left blunt for the present tests.

A FREE IMPELLER

It was required that the flow through the rotating impeller be independent of external effects. The flow was delivered to the impeller eye by a nozzle which matched the eye diameter exactly, and which was designed to give a uniform velocity profile at that section (14). The impeller was mounted directly above the nozzle and was rotated about a vertical axis. When using the centerless impeller mount, Fig. 2, the large journal bearing located between the impeller and the nozzle effects the necessary seal, whereas in the setup for the head-capacity measurements a ring of $1/8$ -in.-sq packing seated in a groove in the nozzle bears against the impeller and seals the suction side against leakage. It was intended originally that the impeller should be operated with a free atmospheric discharge, Fig. 5; however, as the capacity is reduced, thus lowering the static pressure in the eye, a point of instability is reached; the water breaks away from the top shroud and air flashes back into the impeller. This results in operating with passages partially filled, Fig. 6. Operating the impeller at extremely low speeds will avoid this difficulty, but the magnitude of the head generated and the flow rate are reduced correspondingly, and measurements become exceedingly difficult.

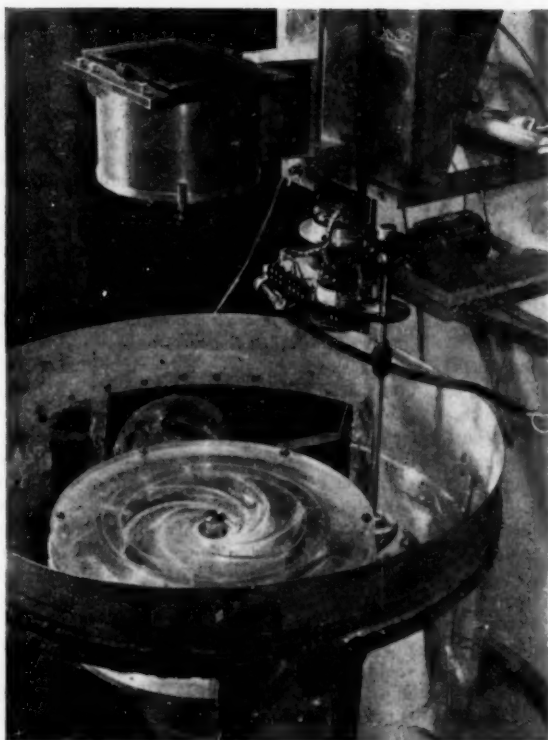


FIG. 2 EQUIPMENT FOR PHOTOGRAPHIC STUDIES OF FLOW

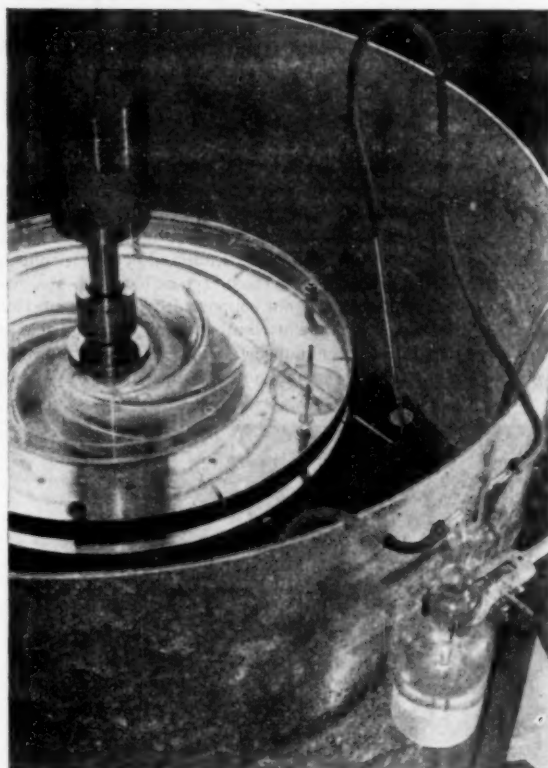


FIG. 3 EQUIPMENT FOR DETERMINING HEAD-CAPACITY CHARACTERISTICS

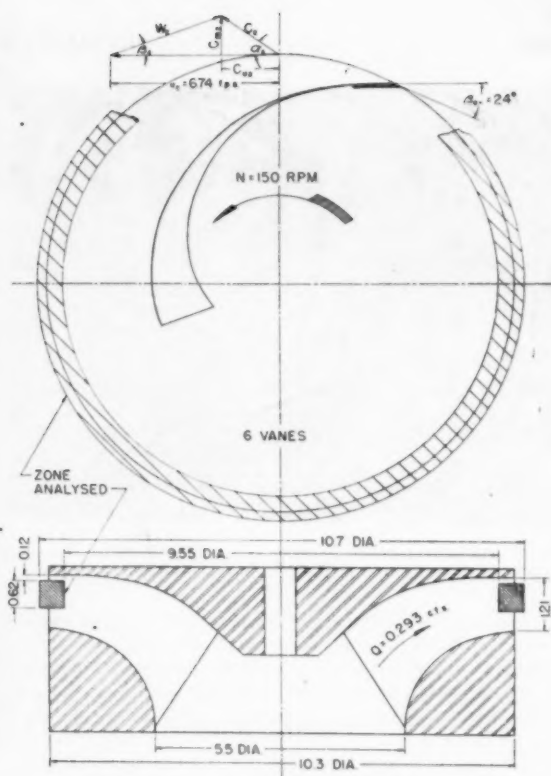


FIG. 4 PRINCIPAL DIMENSIONS OF TEST IMPELLER

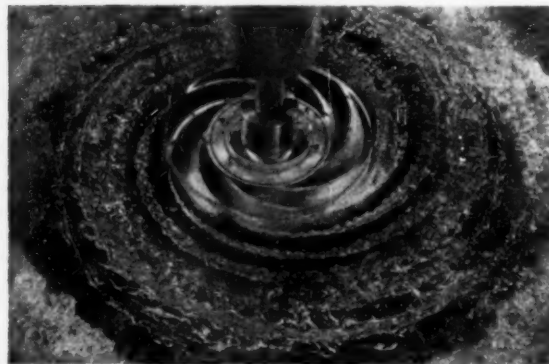


FIG. 5 AN IMPELLER DISCHARGING INTO A FREE BODY OF WATER AT HIGH CAPACITY; FULL PASSAGES

A symmetrical stationary collector about the discharge of the impeller furnished a satisfactory solution to the problem. The collector matches the impeller width at the periphery of the impeller and reduces to a smaller opening at its outer rim. A cylindrical weir is used to vary this opening and thus maintain a sufficiently high pressure in the collector and impeller to prevent flashback. The clearances between the impeller and the collector are close-running. Qualitative and quantitative studies of the flow pattern at the periphery of the impeller in the zone indicated in Fig. 4 were made with the impeller discharging freely, and also into the collector. Those showed that the latter had no perceptible effect on the pattern of flow in that zone. With the exception of the flow in the boundary layer at the pe-

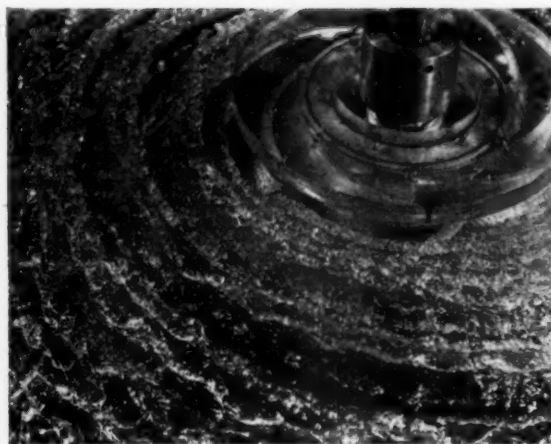


FIG. 6 AN IMPELLER DISCHARGING INTO A FREE BODY OF WATER AT LOW CAPACITY; PARTIALLY FILLED PASSAGES

riphery, it is believed that the flow pattern at the discharge and throughout the entire impeller is unaffected. The test unit so arranged is considered to be hydraulically independent of the test setup and hence is referred to as a "free impeller."

FLOW OBSERVATION

Instrumentation and Procedure. A three-dimensional photographic technique was used in making the quantitative flow studies. Thus the problems of instrument response and obstruction to the flow presented by mechanical methods were eliminated. However, photographic techniques required that the test passages be transparent and that suitable photographically identifiable particles be present in the stream. A mixture of dibutyl phthalate and kerosene proportioned to give a specific gravity equal to that of the water,⁴ colored white and observed against a black background, was found to be satisfactory. This mixture is immiscible with water and, when injected into the flow, forms small globules which retain their identity and, when illuminated properly, are photographically discernible. Unlike the more common carbon tetrachloride-benzene solution, the mixture is not injurious to lucite. The tracers were released from a series of small capillary tubes arranged in the throat of

⁴ Equality was satisfactory when globules remained suspended in a sample of the water.

the suction nozzle. Neglecting the minor surface-tension effect, the small tracers formed, $1/32$ to $1/16$ in. diam, may be considered to follow the same flow paths as the water itself.

The tracer paths were recorded with a stereoscopic camera. The stereoscopic technique was necessary to establish the axial position or third dimension of the tracers in the passages. In Fig. 2 is shown the camera located above the periphery of the test impeller. A series of exposures were made on each plate with a controlled burst of flashes of a high-speed multiflash lamp. When the flash rate was matched properly with the impeller speed, the familiar golf-ball-type pictures resulted, Fig. 7. In this manner a number of positions of a tracer were recorded. To determine the tracer velocity, the stereophotographic images were projected back into space through the same lens system, that is, the camera was used as the projector and the space positions of the tracers at each interval of time were located. In this manner the angular, radial, and axial position of the center of each tracer group, the inclination of the group to the tangent, and the displacement of the tracers within the group were obtained. Knowing the time interval, the average velocity of each group was calculated. The shaded peripheral zone in Fig. 4 indicates the region covered by the analysis. The centers of all tracer groups fell within this zone.

The test impeller was operated at 150 rpm and a capacity of 0.293 cfs. At this capacity it was possible to operate the impeller both with and without the collector and hence make the comparative studies mentioned previously. The unit capacity for this operating point is 0.165, Fig. 11. Referred to the Grand Coulee prototype performance, this represents approximately a capacity 40 per cent above the maximum efficiency point and approximately coincides with the upper operating limit of that installation.

Discussion of Results. Figs. 8 and 9 present the results of the tracer studies. The plotted points were all obtained from tracer groups selected at random, the only requirement being that they be within the zone under observation.

The wide scatter of the data is most interesting. At first it might be thought to be experimental error. However, a variation of ± 50 per cent cannot be attributed to experimental errors which did not exceed ± 2 per cent. The second explanation that might be proposed is that the scatter was caused in part by the inclusion of data at various impeller radii and depths within the zone. No correlation between these factors has been observed and hence this contention is not supported by experimental evidence. The scatter could be attributed to any asymmetry existing in the flow through the impeller. However, tracer data were recorded in one specific channel and also in channels at random,

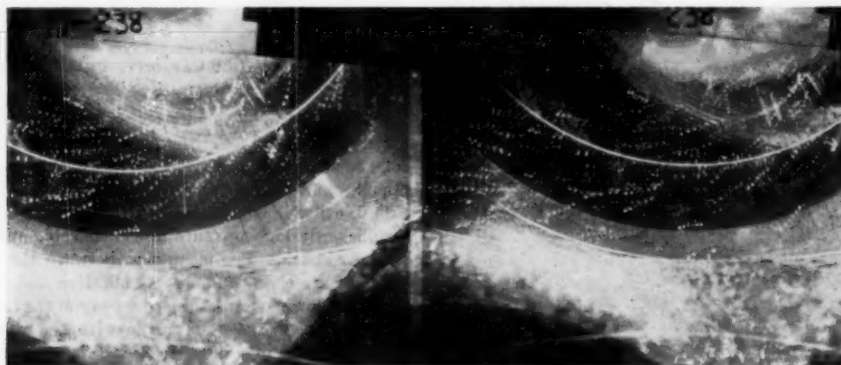


FIG. 7 STEREOSCOPIC PHOTOGRAPH OF TRACERS IN IMPELLER PASSAGES

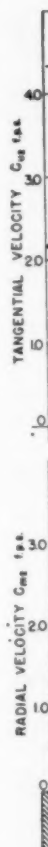


FIG. 8

and
scale
of th
in th
scale
into
that
velop
It
near
unsts
been
a lar
point
posed
expo
area.
diffic
Th
the n
 α_2 and
is to
tions
at of

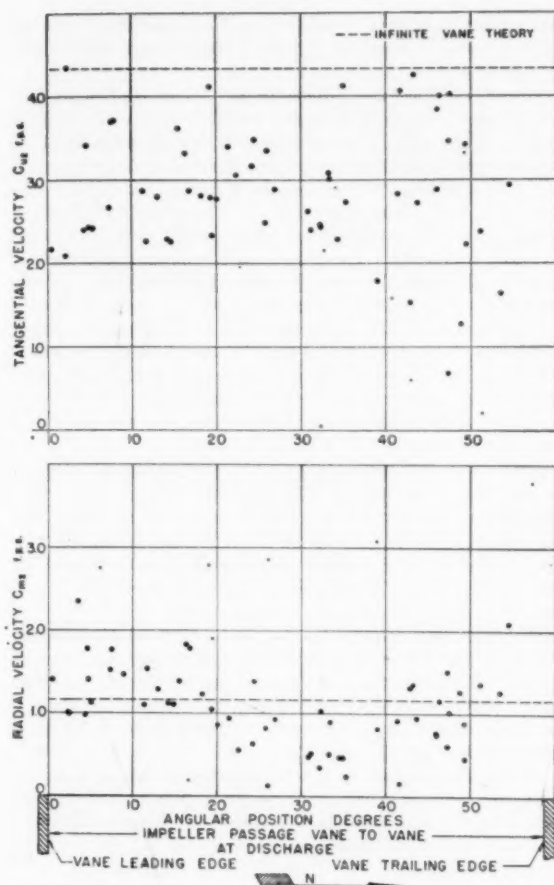


FIG. 8 RADIAL C_{m2} AND TANGENTIAL C_{u2} COMPONENTS OF ABSOLUTE VELOCITY AT DISCHARGE

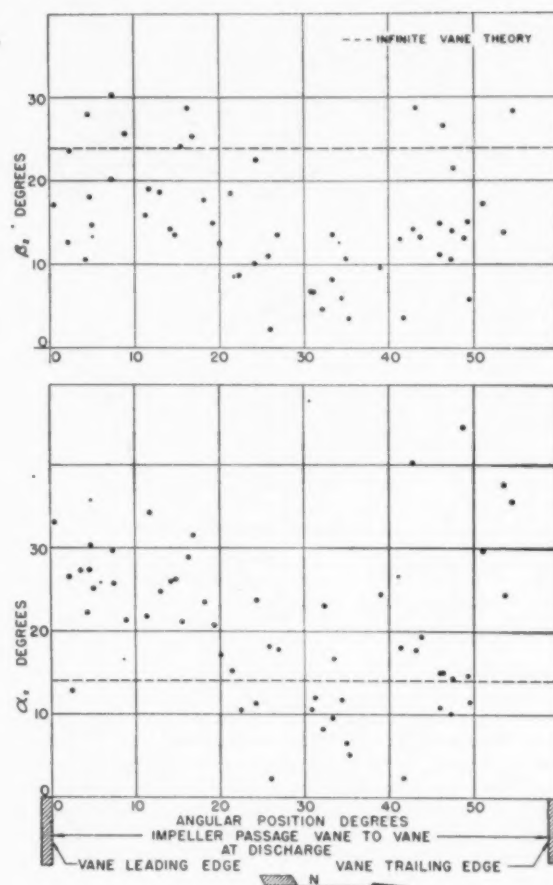


FIG. 9 RELATIVE AND ABSOLUTE ANGLES β_2 AND α_2 AT DISCHARGE

and no asymmetry could be detected. It is possible that large-scale turbulence, present in the incoming flow, might be the source of this dispersion of data. Dyestreak studies have been made in the impeller approach over a wide range of capacities. Large-scale turbulence was not observed until the dye streaks came into close proximity with the impeller passages. It is concluded that the point scatter is due to large-scale turbulence which develops within the impeller passages.

It is interesting to note the increase in the scatter in the region near the trailing edge of the vane which strongly suggests an unstable flow condition. However, although an instability has been noticed in other photographic studies recently completed, a large rolling eddy has not been observed. The scarcity of points close to the trailing edge of the vane is a limitation imposed by the photographic method employed. When a series of exposures are made on one plate, the vane images obscure that area. Stereoscopic high-speed motion pictures overcome this difficulty.

The pronounced dips at mid-passage of the radial velocity C_{m2} , the relative discharge angle β_2 , and the absolute discharge angle α_2 are the most striking features of the data. The decrease in β_2 is to be expected from theory. Likewise, theoretical considerations show that C_{m2} , β_2 , and α_2 must each be of equal magnitude at opposite sides of the vane passage, and this point is verified.

However, the C_{m2} profile is not yet substantiated by theory. Although a three-dimensional analytical solution of the problem is not available, the analysis of a two-dimensional straight radial-vane impeller indicates that, for that special case C_{m2} varies almost sinusoidally about a uniform average through-flow, being least near the leading edge of the vane and greatest near the trailing edge. The present data do not show this trend to exist in a modern three-dimensional impeller. The α_2 variation must necessarily follow the trend indicated, once C_{m2} and β_2 are established.

The obvious dip present in the other plots is noticeably absent in the C_{u2} data. The points suggest that the time-average specific energy about the periphery of an impeller is constant.

The horizontal dotted lines represent values of C_{m2} , C_{u2} , β_2 , and α_2 based upon the Euler infinite-vane theory, namely, the relative discharge flow angle β_2 equals the vane angle, and is everywhere constant, and C_{m2} is constant about the periphery. It is interesting to note that the position of this line with respect to the averages of the test data is in agreement with theoretical deductions. The Euler line must represent the average radial velocity, whereas it should lie above the mean β_2 and C_{u2} and below the mean α_2 .

The instantaneous absolute streamlines pictured in Fig. 10 were sketched from a large number of data prints. The streamlines are spaced at random and hence represent flow direction

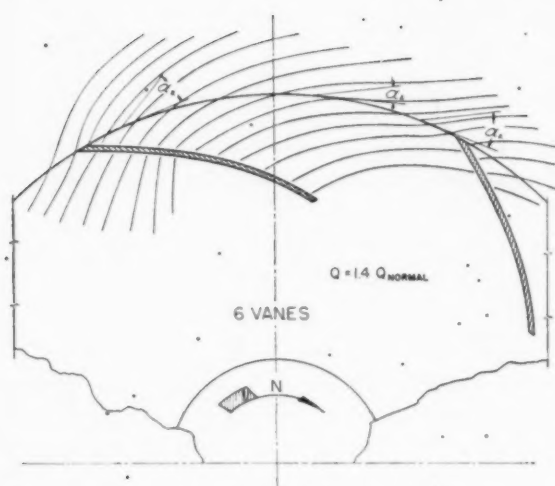


FIG. 10 INSTANTANEOUS ABSOLUTE STREAMLINES AT DISCHARGE; RANDOM SPACING

only. It is interesting to note that in the region following the vane there is no evidence of backflow.

DETERMINATION OF HEAD-CAPACITY CHARACTERISTICS

Instrumentation. The inevitable losses involved in the use of a measuring point at any distance from the impeller made it desirable to use total head tubes close to the inlet and outlet to determine the energy of the inflow and outflow from the test impeller. Although there is some doubt as to the correct reference pressure at the inlet, considerations of symmetry indicate that the total head at some point on the center line of the suction nozzle seemed to be a desirable location at which to measure the total head of the incoming flow. A total-head tube directed upstream was located at the inlet to the pump impeller at a point $7/8$ in. below the plane of the intersections of the vane leading edges with the suction shroud. The total-head tube at the outlet was mounted on a rotatable mount and was retractable through a sleeve set at right angles to the axis of rotation. By these means the inlet to the total-head tube could be set at any predetermined distance from the impeller, and its axis could be aligned with the approaching flow. The direction of the flow at the nose of the total-head tube was determined by a probe carrying a fine thread.

Since it has not been possible to obtain a pressure gage with an accuracy and frequency response sufficient to follow in detail the variations in total head, a damped water-column manometer connected directly to the metal total-head tube was used. The air side of the manometer was connected to the air space of a waterpot. The water side of the waterpot was supplied by the total-head tube at the inlet to the impeller; thus the differential head across the runner could be read directly. By adjusting the height of the water level in the pot a large range in head could be covered without great variations in the height of the water level in the manometer tube, Fig. 3.

The question always arises in applications where the measured total head fluctuates, as to the meaning of the reading obtained by the manometer. Experiments were made to determine the influence of the damping imposed on the measuring head, and it was found that a large degree of damping gave steadier readings which were fully consistent with the mean readings obtained with less damping. Since the total-head tube measures a fluctuating energy level directly, and since speed and flow control were of

such quality that the fluctuations could be considered a steady-state condition, a viscously damped system should read the true average total head.

Variation of Total Head Across Outlet. Since the flow through a radial-flow pump involves essentially a change of direction from axial to radial, it was of interest to determine the variation in total head between the lowermost streamline that emerges at the suction or lower shroud and the uppermost streamline that emerges at the back or upper shroud. This is particularly interesting in view of the velocity field observed photographically and discussed previously. A location was chosen for the total-head tube $1/16$ in. distant from the periphery of the impeller. At this location the total-head tube was aligned with the mean streamline and traversed vertically across the width of the impeller. At the chosen flow rates it was found that the energy of the lowermost streamline was approximately 5 per cent greater than the energy of the uppermost streamline. On the basis of these observations a location was chosen halfway between the two shrouds at the outlet for the subsequent work reported here.

Influence of Prerotation on Accuracy of Observations. Experimental work on complete pumps has shown that the flow conditions in the inlet pipe are in many cases highly complex. This requires that justification be provided for measuring the inlet total head with the total-head tube close to the impeller at the center line of the suction nozzle. This was done in the following manner:

The outlet total-head tube was set at $1/16$ in. from the periphery of the impeller at mid-width, and the total head change between the inlet and the outlet was recorded for a large range of flow rates. A typical run is shown in Fig. 11 which is a dimensionless head-capacity characteristic for the test impeller. Since it is reasonable to suppose that the inlet effects, if any, must decrease in intensity as one recedes further from the disturbing influence, other runs were made using the piezometer taps located after the inlet straightening vanes which are some distance upstream from the impeller inlet and guarantee a smooth velocity profile in the approach pipe.

The results of these measurements are plotted in Fig. 11, including the necessary corrections for approach-velocity head, but omitting the small loss due to the friction of the finite length of

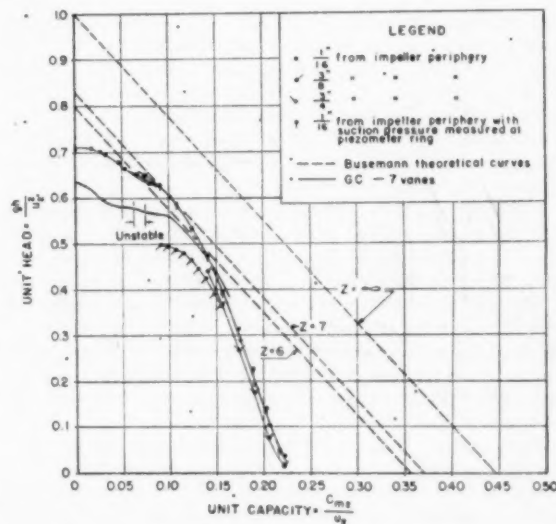


FIG. 11 DIMENSIONLESS HEAD-CAPACITY CHARACTERISTICS OF TEST IMPELLER

pipe between the piezometer taps and the impeller eye. This latter correction has not been applied to the typical run shown in Fig. 11 and would improve the agreement at the higher values of dimensionless capacity where its influence is appreciable.

It should be observed that the points plot along the same line as the points determined using the total-head tube in the inlet. This is believed to indicate that in this installation the backflows which may exist do not affect the accuracy of the total-head tube in the eye. Since total head is the measure of the energy of the fluid at the point of measurement, it seems that there has been no energy supplied by the pump to the incoming fluid at the measuring point. Visual observations with dye introduced at the eye indicate that the disturbances in the eye are localized close to the vane leading edges.

Impeller Characteristics. The type of observation discussed in the previous paragraphs may be used to study some of the detailed qualities of an impeller. Near the point of zero head, the head-capacity curve shown on the unit plot in Fig. 11 is closely linear. In the range of maximum efficiency of the prototype impeller, the linearity has disappeared and the characteristic turns smoothly without discontinuities. At a value of $C_{m2}/u_2 = 0.075$, the smooth trend of the characteristic is broken, and in this region a scatter of points was obtained which indicate that the operation of the impeller is unstable. The region of instability is indicated by the dip in the characteristic. After this region is passed, unique values are again obtained for the dimensionless head.

As a matter of interest, the unit characteristic of the prototype impeller is plotted in Fig. 11 and is marked "GC-7 Vanes." The zone of discontinuity for this impeller is marked by two vertical lines which fall in practical coincidence with the zone of discontinuity of the six-vane test impeller. Work has not yet been completed on the five-vane impeller based on the same prototype to enable definite conclusions to be drawn from this coincidence. It indicates, however, that the position of the unstable range may depend primarily on the vane shape for impellers having sufficient vane overlap.

Prerotation. It was observed very early in the experimental work that the impeller developed zero head at a flow which still showed a positive tangential component of absolute velocity at the outlet. This has been verified very carefully both by observations of the absolute flow and by measurements with the total-head tube at the outlet. Since this condition requires that the flow enter the eye with a positive prerotation, there seems to be no doubt that such a phenomenon occurs, although visual evidence indicates that this is a local effect. The absolute angle of emergence of the flow at the periphery is quite acute and cannot be attributed to experimental error in the measurement of the direction of the outflow.

Variation of Characteristic With Position of Outlet Total-Head Measurement. The type of total-head tube used in these investigations was not sensitive to yaw of the flow over the angles encountered at the outlet of the impeller except, perhaps, in the neighborhood of the vane tips. The vane tips were left wide and unsharpened. When runs are made with the Pitot head further from the outlet than has been used in the previous experiments, lower total heads are measured. Fig. 11 shows a few points taken at $1/8$ in. from the periphery and $1/4$ in. from the periphery, and they define a characteristic lower than the one obtained with the measuring point $1/16$ in. from the periphery. On the basis of present evidence it is not possible to explain this shift. Variations in instrumentation have not caused any noticeable difference in this phenomenon, and it cannot reasonably be ascribed to losses due to mixing or to the losses in the rudimentary collector ring.

The lowest curve in Fig. 11 was obtained with the measuring

point distant from the periphery of the impeller before the behavior of the total head near the impeller was noticed. This curve represents a minimum and undoubtedly contains losses due to the collector ring.

The head-capacity line, based on an infinite number of vanes and the outlet vane angle, is also shown in Fig. 11, as well as two lines for six and seven vanes, based on Busemann's (16) solution of the two-dimensional radial-flow impeller with a finite number of logarithmic spiral vanes. The displacement between the GC-7 vane characteristic and the Busemann line for seven vanes indicates that the characteristic for the test impeller is too high in relation to its corresponding Busemann line for six vanes. This indicates that the experimental data based on a measuring point very close to the outlet contain a systematic error. However, this discrepancy does not affect the experimental procedure when general characteristics of the runner are being investigated and efficiency determinations are not involved.

Influence of Collector Ring. The collector ring used in the determination of the characteristic consists of two parallel plates set apart the width of the outlet which were necessary to prevent air from striking back from the free surface. In order to throttle the outflow, one cylindrical ring was attached to the circumference of each collector-ring plate, and these could be set apart a determined amount. A systematic series of runs showed that in the range of operation there was no influence of the throttle gap on the measurements.

Affinity Relation. The data presented in Fig. 11 were obtained at a rotative speed of 225 rpm; at this speed the maximum head reading was 2.06 ft. This permitted a high accuracy of measurement of the differential head except near zero head. Flow measurements were accurate to better than 1 per cent at all flows.

With this accuracy available, another series of runs were made at 150 rpm to detect, if possible, the influence of rotative speed on the characteristic which could be significant at the low speeds used in these tests. The correspondence between the dimensionless head-capacity plots for the 225-rpm series and the 150-rpm series was complete within the accuracy of the experimental data.

ACKNOWLEDGMENTS

The authors acknowledge many suggestions of the laboratory staff, under the direction of Dr. R. T. Knapp, and particularly those of their collaborator, Mr. A. J. Acosta.

BIBLIOGRAPHY

- 1 "Untersuchung der Wasserströmung durch rotierendes Zellenkreiselrad," by H. Oertli, Rascher and Cie, Zurich, Switzerland, 1923.
- 2 "Verdrängungsströmungen bei Rotation zylindrischer Schaufeln in einer Flüssigkeit mit freier Oberfläche," by W. Barth, Mitteilungen des Instituts für Strömungsmaschinen der Technischen Hochschule, Karlsruhe, Germany, No. 1, 1930, p. 39.
- 3 "Hilfsmittel zur Beobachtung und Messung an umlaufenden Kreiselradern," by A. Closterhalfen, *Forschung auf dem Gebiete des Ingenieurwesens*, vol. 2, No. 1, 1931, p. 2; no. 2, p. 52.
- 4 "Versuche an einer Schaukreiselpumpe," by A. Closterhalfen, *Forschung auf dem Gebiete des Ingenieurwesens*, vol. 2, July, 1931, p. 252.
- 5 "Investigation of the Flow Conditions in a Centrifugal Pump," by K. Fischer and D. Thoma, *Trans. ASME*, vol. 54, 1932, p. 141.
- 6 "Über die Relativ-Strömung in einem Pumpen-Laufrad von grossem Radien-Verhältnis," by W. Stieas, Mitteilungen des Instituts für Strömungsmaschinen der Technischen Hochschule, Karlsruhe, Germany, No. 3, 1933, p. 77.
- 7 "Messungen des Druckverlaufes über Lauf und Leitschaukel einer Kreiselpumpe," by E. Hagmayer, PhD thesis, Technische Hochschule, Braunschweig, Germany, 1932.
- 8 "Wirebelbildung und Kraftwirkung an umlaufenden Kreisel-

schafeln," by E. Frietsch, *Verein deutscher Ingenieure, Forschungsheft*, 384, 1937.

9 "Die Untersuchung der Strömung durch eine Flugelradturbine bei verschiedenen Schaufelzahlen," by K. Hahn, *Mitteilungen des Instituts für Stromungsmaschinen der Technischen Hochschule, Karlsruhe, Germany*, No. 4, 1939, p. 2.

10 "The Hydraulic Machinery Laboratory at the California Institute of Technology," by R. T. Knapp, *Trans. ASME*, vol. 58, 1936, pp. 649-661.

11 "The Hydrodynamics Laboratory of the California Institute of Technology," by R. T. Knapp, Joseph Levy, J. P. O'Neill, and F. B. Brown, *Trans. ASME*, vol. 70, 1948, pp. 437-457.

12 "Laboratory Investigations of the Mechanism of Cavitation," by R. T. Knapp and A. Hollander, *Trans. ASME*, vol. 70, 1948, pp. 419-435.

13 "Special Cameras and Flash Lamps for High-Speed Underwater Photography," by R. T. Knapp, *Journal, Society of Motion Picture Engineers*, vol. 49, July, 1947, pp. 64-82.

14 "On the Design of the Contraction Cone for a Wind Tunnel," by Hsue-Shen Tsien, *Journal of the Aeronautical Sciences*, vol. 10, February, 1943, pp. 68-70.

15 "Development of the Hydraulic Design for the Grand Coulee Pumps," by C. Blom, *Trans. ASME*, vol. 72, 1950, p. 53.

16 "Das Förderhöhenverhältnis Radialer Kreiselumpen mit logarithmisch spiralförmigen Schaufeln," by A. Busemann, *Zeitschrift für angewandte Mathematik und Mechanik*, vol. 8, 1928, p. 372.

Discussion

A. J. ACOSTA.⁵ The need for a series of investigations on the individual elements of a hydraulic machine has been recognized for some time. Due to the somewhat inconclusive experimental results to date, it has been impossible to evaluate the separate effects of the components of a hydraulic machine. For that reason, the interpretation of observed phenomena and correlation with any real or perfect-fluid theory has lagged. Accordingly, the study of an impeller or volute, wherein its effects are isolated, should enable the laboratory to perform for the first time definitive tests as to the nature of flow in hydraulic machinery.

In reference to the plots of C_{m2} and C_{a2} (Fig. 8 of the paper), the authors state that there is as yet no theoretical justification for their behavior. The writer has had occasion to make an analysis of the flow of an inviscid incompressible fluid in a two-dimensional rotating-vane system. Inasmuch as an "ideal" solution offers possibilities of interpreting test data, it seems pertinent to present it now. The geometry of the chosen idealized impeller consists of eight logarithmic spiral vanes with a characteristic angle of 45 deg and a radius ratio of 0.5. The analysis involves the numerical evaluation of the differential equation governing the flow subject to appropriate boundary conditions. In the case considered, an absolute co-ordinate system (stationary with respect to the inertial reference frame) was chosen so that the differential equation to be solved is Laplace's equation in two dimensions, i.e., $\partial^2 U / \partial x^2 + \partial^2 U / \partial y^2 = 0$ where U is either the stream function or velocity potential for the flow. The boundary conditions are: (a) there is no flow through the vanes; (b) there is no flow around the tip of the vanes at exit. This latter condition is merely a statement of the Kutta-Joukowski principle for the flow around lifting surfaces. The vanes are taken to be infinitely thin, although this condition is not necessary for the solution of the problem. Finally, we require that the velocity diminish to zero at an infinitely great distance from the impeller. Then, to within an additive constant, the stream function and velocity potential for the flow are uniquely defined, and the velocities in the field may be computed from either. The flow rate through the impeller is accounted for by placing a line source at the origin. Rather than compute a number of solutions

for separate flow rates only two need be found, since the resulting velocity field within the impeller can be resolved into two parts, namely, (a) the flow due to the rotation of the vanes without any net through-flow (corresponding to shutoff head); (b) the flow from a source through a set of radially disposed stationary guide vanes. Solutions of this latter sort are available.⁶ Combined with the present work which is only for zero flow rate, the flow for any operating point on the head flow-rate diagram may be obtained by taking a linear combination of (a) and (b):

The solution itself was effected by the so-called "relaxation" method.⁷ Briefly, the method for solving Laplace's equation is as follows: The value of the function in the region of interest is approximately determined at the intersecting points of a rectangular grid. Then, to the first order, the finite-difference equation representing Laplace's equation is $\psi_1 + \psi_2 + \psi_3 + \psi_4 - 4\psi_0 = 0$, where ψ_1 to ψ_4 are the values of the function at the nearest four intersecting points to the point 0. This equation is satisfied at each point in the region by a trial-and-error process. Ways in which this is readily accomplished are discussed by Southwell.⁷

The solution was carried out by the method described, and from it the variation of the radial velocity across the impeller-exit section was determined and is shown in the accompanying diagram, Fig. 12. The value of the unit head at zero flow rate is 0.79, which is the same as that given by Busemann's theory⁸ for logarithmic vanes. Although it is unfortunate that the dimensions of the impeller chosen for analysis are somewhat different from those of the test impeller, the order of magnitude of the velocities and the general features of the flow will be the same.

Comparing Fig. 8 of the paper with Fig. 12 computed by the writer, one sees that the dip in the radial-velocity distribution is substantiated by theory. For logarithmic vanes of the angle and radius ratio used in the analysis and for the test impeller, the radial-velocity variation at the impeller exit is nearly unaffected by the flow rate; so we are justified in comparing the variation at zero flow rate with that of the experiment. The range of variation seen in Fig. 8 is about a radial velocity of 1 fps, or in a dimensionless form it is 0.15, arrived at by dividing

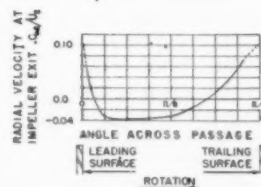


FIG. 12 PLOT OF RATIO OF RADIAL VELOCITY TO PERIPHERAL VELOCITY AT EXIT SECTION COMPUTED FOR A TWO-DIMENSIONAL IMPELLER WITH EIGHT LOGARITHMIC SPIRAL BLADES HAVING A VANE ANGLE OF 45 DEG AND A RADIUS RATIO OF 0.5 FOR ZERO FLOW RATE

by the peripheral velocity. The maximum variation computed from the two-dimensional ideal fluid case is about $\Delta C_{m2} / U_2 = 0.14$. The only noticeable departure in general trend between the two is found near the leading surface, where it is seen that the area of positive C_{m2} is much less for the computed case than for the test results. This is, however, the trend one would expect as the vane angle becomes steeper.

As the authors mentioned, the dip apparent in the C_{m2} , β_2 , and

⁵ "Diagrams for Calculation of Airfoil Lattices," by A. Betz, NACA, T.M. 1022.

⁷ "Relaxation Methods in Theoretical Physics," by R. V. Southwell, Oxford University Press, London, England, 1946.

⁸ Refer to author's Bibliography (16).

⁶ Research Fellow in Hydrodynamics, California Institute of Technology, Pasadena, Calif. *Jun. ASME*.

α_2 is not evident in the C_{u2} (absolute tangential velocity at exit) plot. For the special case analyzed, the range of variation of C_{u2} compared with the mean value was found to be 18 per cent, 12.5 per cent being positive occurring at the boundary on the vane tip. It is, then, not surprising that a variation of this order of magnitude should not be observed on the authors' plot, in view of the large point scatter.

The general trend of the data presented is seen to follow that predicted by two-dimensional perfect-fluid theory, a surprising fact considering the high level of turbulence present in the flow. However, the limitations of perfect-fluid theory for flows of this sort are as yet unknown. The writer is interested in this problem and hopes to see it explored further.

This work was supported by the Office of Naval Research.

AUTHORS' CLOSURE

The authors thank Mr. Acosta for his discussion and consider it a valuable contribution. More complete and detailed studies made on a series of impellers since the completion of the paper indicate that in the region of the design point, the total head generated by the impeller matches rather well (within 8 per cent) the ideal Busemann value, and also that the head-capacity curve of the free impeller follows very closely the ideal straight-line relationship. In this region prerotation is nil; there is no separation within the passages and the discharge flow pattern is primarily two-dimensional. Hence, in this region, the two principal parameters present in the real fluid case but omitted in the ideal case

are viscosity, μ , and the temporal velocity variations $\frac{\partial v}{\partial t}$. If through continued research the effects of these quantities on the ideal solution can be determined, an extremely powerful tool would be made available to the researcher and designer.

Unfortunately, the whole picture is not quite as simple as might be inferred. At off-design points, observations show that the flow separates from the channel walls and follows unknown and indeterminate boundaries. Cross flows develop and the discharge flow pattern does not remain two-dimensional. These elements impose serious limitations on the potential approach in the very regions where its use to predict off-design point performance would be most desirable. On top of all this, it must be remembered that the ideal situation applies only to a free impeller; an impeller operating in an infinite fluid medium with stationary boundaries only at infinity. Tests have shown that the characteristics of the complete pump, consisting of impeller and case, differ widely from those of the free impeller at all points except the design point. Hence the effect of the volute must be considered and incorporated in the final solution.

It is not meant to imply by these remarks that the potential solution is considered either impractical or impossible. The intent of the authors is to point out the long road ahead and the vast areas yet to be explored, and to underline the statement that at these early stages of the work it is most gratifying to find a good correlation between potential theory and experiment in some parts of the field.

TH

The
a three
plex r
The l
which
appro
of cer
within
gives
in the
distrib
tion a
in mi
turbine
lers an

The

$\gamma = 1$

Inde.

Other

DERIV.

The
impelle
tion.

¹ God
² Nur
the pap
Cont
nual M
of THE

NOTE
underst
of the S
April 4,

The Flow Through Centrifugal Compressors and Pumps

By H. E. SHEETS,¹ AKRON, OHIO

The flow through centrifugal compressors and pumps is a three-dimensional flow problem and is of such a complex nature that an exact solution is not obtainable. The literature (1, 2)³ shows the differential equations which the flow through an impeller must follow. An approximate solution to these equations is found by means of certain assumptions which are possible for impellers within a limited range of specific speeds. The solution gives the approximate velocity and pressure distribution in the impeller passages. The knowledge of the velocity distribution is used to analyze the phenomena of pulsation and blade stalling. The method has also been used in mixed-flow compressors and radial- and mixed-flow turbines. The application of this method for two impellers and test data are presented.

NOMENCLATURE

The following nomenclature is used in the paper:

- a = distance between 2 blades normal to flow lines
- c = absolute velocity
- f = area
- l = blade length
- m = mass
- p = pressure
- r = impeller radius
- t = blade pitch
- u = tip speed of impeller
- w = relative velocity
- z = blade number
- n_s = specific speed
- Q = total flow
- R = blade radius of curvature
- β = blade angle
- $\gamma = 1/v$ = specific weight
- ω = angular velocity
- σ = blade solidity

Indexes:

- 2 = impeller exit
- 1 = impeller inlet
- * = arbitrary point in impeller passage

Other symbols will be defined in the text.

DERIVATION OF APPROXIMATE SOLUTION—BLADE CENTER SECTION

The approximate solution of the flow problem considers the impeller-blade passage as a rotating channel for the center section. The first step is the determination of the approximate

velocity distribution in this center section, and then the solutions for the exit and inlet of the blade passage are added. The result gives the nonuniform velocity distribution throughout the entire blade passage.

This method is therefore limited to blade passages which are long enough to permit a division in three sections, and it is necessary that the center section, treated as a rotating channel, extend at least over a limited length. Therefore the proposed method is limited to a range of blade solidity

$$\sigma = \frac{l}{t} = \frac{z}{2\pi \sin \beta} \log_e \frac{r_2}{r_1} \geq 1.3 \dots \dots \dots [1]$$

or approximately

$$\sigma' = \frac{l}{l_2} = \frac{lz}{2\pi r_2} \geq 1.2 \dots \dots \dots [1a]$$

This definition for blade solidity is given in reference (3).

Fig. 1 shows a schematic drawing of an impeller. For two-dimensional flow the blade width has a constant value, $b = \text{const.}$ Considering the relative flow in the center section of the rotating channel in Fig. 1, we apply to the particle of mass dm the com-

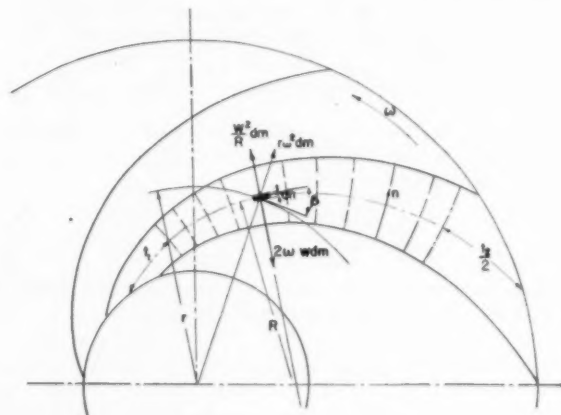


FIG. 1 FORCES IN A ROTATING CHANNEL WITH BACKWARD CURVED VANES

plementary forces $dm \, r\omega^2$ and $dm \, 2w\omega$. The normal acceleration toward the center of curvature is w^2/R , and we have the equation of motion

$$dm \frac{w^2}{R} = df(p - p^*) + dm \, 2w\omega - dm \, r\omega^2 \cos \beta \dots \dots [2]$$

for backward-curved vanes.

Since

$$dm = df \, dn \frac{\gamma}{g} = df \, dn \frac{1}{v\gamma}$$

¹ Goodyear Aircraft Corporation. Mem. ASME.

² Numbers in parentheses refer to the Bibliography at the end of the paper.

Contributed by the Hydraulic Division and presented at the Annual Meeting, New York, N. Y., November 27-December 2, 1949, of THE AMERICAN SOCIETY OF MECHANICAL ENGINEERS.

NOTE: Statements and opinions advanced in papers are to be understood as individual expressions of their authors and not those of the Society. Revised manuscript received at ASME Headquarters, April 4, 1950. Paper No. 49-A-154.

and

$$dp = p - p^*$$

and according to Fig. 1, taking dn positive from the low-velocity side of the blade to the high velocity side

$$dr = dn \cos \beta$$

we get

$$\frac{w^2}{R} = v g \frac{dp}{dn} + 2w\omega - r\omega^2 \frac{dr}{dn} \quad [3]$$

The energy equation of a streamline is

$$\frac{w^2 - w^{*2}}{2g} = - \int_p^p v dp + \frac{u^2 - u^{*2}}{2g} \quad [4]$$

For infinitely close-lying points it is with $dw = w - w^*$

$$\frac{w dw}{g} = -v dp + r\omega^2 \frac{dr}{g} \quad [5]$$

Comparing Equations [3] and [5], we get

$$\frac{w}{R} + \frac{dw}{dn} - 2\omega = 0 \quad [6]$$

for backward-curved vanes. For forward-curved vanes we get

$$\frac{w}{R} + \frac{dw}{dn} + 2\omega = 0 \quad [6a]$$

For the purpose of our approximate solution we make the assumption that the radius of curvature of the streamlines is approximately constant for each line orthogonal to the flow lines. The radius of curvature may vary from vane inlet to exit. This assumption means

$$R = \text{const.} \quad [7]$$

For the center section, Equation [7] is a good approximation, and for straight-bladed impellers it is correct.

Then Equation [6] becomes

$$\frac{dn}{R} = \frac{dw}{2\omega R - w} \quad [8]$$

For $n = 0$ the minimum velocity at the channel wall is designated as w' and the solution for Equation [8] becomes

$$w = (w' - 2\omega R)e^{-\frac{n}{R}} + 2\omega R \quad [9]$$

Developing the exponential function into a series and omitting third and higher powers of n/R we get

$$w = w' + \left(2\omega R - \frac{n}{R} w'\right) \left(1 - \frac{n}{2R}\right) \quad [10]$$

Defining the mean velocity as

$$w_m = \frac{Q}{ab} = \frac{\int_a^b w b dn}{ab} \quad [11]$$

a and b are the channel width and height, respectively.

Substitution of Equation [10] in [11] and some transformation give us the following for the extreme local velocities at the channel wall:

Minimum velocity for $n = 0$

$$w' = w_m \left[1 + \frac{a \left(1 - \frac{a}{3R}\right)}{2R - a \left(1 - \frac{a}{3R}\right)} \right] - a\omega \left[1 - \frac{a}{3R} + \frac{a \left(1 - \frac{a}{3R}\right)^2}{2R - a \left(1 - \frac{a}{3R}\right)} \right] \quad [12]$$

Maximum velocity for $n = a$

$$w'' = w_m \left[1 - \frac{a \left(1 - \frac{2a}{3R}\right)}{2R - a \left(1 - \frac{a}{3R}\right)} \right] + a\omega \left[1 - \frac{2a}{3R} + \frac{a \left(1 - \frac{a}{3R}\right) \left(1 - \frac{2a}{3R}\right)}{2R - a \left(1 - \frac{a}{3R}\right)} \right] \quad [13]$$

For straight blades $R = \infty$ these equations become

$$w'_s = w_m - a\omega \quad [12s]$$

$$w''_s = w_m + a\omega \quad [13s]$$

For forward-curved blades we get similarly

$$w' = w_m \left[1 - \frac{a \left(1 - \frac{2a}{3R}\right)}{2R - a \left(1 - \frac{a}{3R}\right)} \right] - a\omega \left[1 - \frac{2a}{3R} + \frac{a \left(1 - \frac{a}{3R}\right) \left(1 - \frac{2a}{3R}\right)}{2R - a \left(1 - \frac{a}{3R}\right)} \right] \quad [12a]$$

$$w'' = w_m \left[1 + \frac{a \left(1 - \frac{a}{3R}\right)}{2R - a \left(1 - \frac{a}{3R}\right)} \right] + a\omega \left[1 - \frac{a}{3R} + \frac{a \left(1 - \frac{a}{3R}\right)^2}{2R - a \left(1 - \frac{a}{3R}\right)} \right] \quad [13a]$$

The flow through the impeller can be divided into two parts, the "through flow" associated with w_m and the "displacement flow" associated with ω . With $w_m = 0$ we get in Equations [12] and [13] the values for the displacement flow alone.

BLADE EXIT

It is known that the relative flow through a centrifugal impeller can be expressed by a relative flow function as a sum

$$\psi = \psi_1 + \psi_2 + \psi_3$$

where

ψ_1 = flow function for through flow

ψ_2 = flow function for displacement flow

ψ_3 = flow function for circulation flow

The flow is infinite and neutralized by torsion solutions shapes

To determine that the end of the flow line between the line and the distribution of the flow line where the flow is equal to the flow line

The simple triangle from the triangle proximal of the polygon

For the straight line according to the

The channel distance is taken to the line and the line is we have separation

The axial location [12] a channel

For the frequency axial w_m element mine At case shape n ag side [2] to

The flow functions ψ_1 and ψ_2 must be of such a nature that the infinite velocity at the inlet edge caused by the through flow is neutralized. Stodola (1) has shown that the solutions of the flow function ψ_2 and ψ_3 can be found by the membrane analogy or by torsional stress analogy. In the literature (4, 5) are published solutions for the stress analogy for a large number of simple shapes.

To determine the shape of the blade-exit channel, we assume that the end effects extend a distance $t_2/2 = (D_2/2z)\pi$ from the end of the blade inward. This distance is taken along the mean flow line. A line orthogonal to the flow lines is the separation line between the center section and the blade exit. The velocity distribution up to the separation line is known according to Equations [12] and [13]. We have now to determine the variation of the velocities from the separation line to the blade exit, where the velocity on both sides of the blade must be uniform and equal to the through-flow velocity.

The shape of the blade exit thus determined is usually very simple so that the variation of velocity can be taken directly from the stress analogy for such shapes as sector of a circle, triangle, and many others. For more complex shapes, an approximate solution can be found according to the energy method of the torsional problem as proposed by Ritz and Trefftz (4). With this method the velocity distribution can be found for any polygon-shaped channel exit.

For an exit channel of nearly rectangular shape, the results of the stress analogy (5) show a velocity variation approximately according to a parabola from a known value at the separation line of the center section to zero at the blade exit.

BLADE INLET

The blade inlet can be treated like the blade exit. Therefore it becomes necessary to determine the shape of the blade-inlet channel. In this case we assume that inlet effects extend to a distance $t_1 = D_1\pi/z$ from the blade inlet inward. This distance is taken along the mean flow line. A potential line orthogonal to the flow lines is the separation line between the center section and the blade inlet. The velocity distribution at the separation line is known according to Equations [12] and [13]. In this case we have to determine the velocity distribution from the stagnation point of the blade at the inlet to the known values at the separation line with the center section.

The blade-inlet velocity distribution can be determined according to the method of Betz (6, 7), and Akeret (8) for the axial inducer-type impeller.

It is thus possible by starting with the calculation of the velocity distribution in the center section, according to Equations [12] and [13], to find the velocity distribution in the entire blade channel.

THREE-DIMENSIONAL FLOW

For three-dimensional flow the blade height is not constant and usually decreases from impeller inlet to impeller outlet. Frequently the flow turns in the vicinity of the impeller inlet from axial to radial direction. This means that the mean velocity w_m changes as a function of the blade height and must be determined.

At first we determine the absolute velocity c_m for the hypothetical case of the fluid flowing through a stationary impeller of identical shape. We designate the radius of curvature with ρ , and taking n again from the low-velocity side of the flow, i.e., the convex side in this case, we get from considerations similar to Equations [2] to [6]

$$\frac{dn}{\rho} - \frac{dw}{w} = 0 \dots \dots \dots [14]$$

A graphical solution for the velocity distribution according to Equation [14] can be found according to the method of Flugel (1).

Another method which permits direct calculation of the velocity distribution is possible if the impeller contours can be approximated by two hyperbolas following the equation

$$r^2 x = C \dots \dots \dots [15]$$

Then, the velocity calculated according to the basic equation from Durand (9) is

$$c_m = \frac{C}{2\pi} \sqrt{(2x)^2 + r^2} \dots \dots \dots [16]$$

According to either method, the absolute velocity c_m is determined for the mean streamline as well as for the inner and outer contours of the impeller, $c_{m,i}$ and $c_{m,o}$, respectively.

The relative velocity is

$$w_m = \frac{c_m}{\sin \beta} \dots \dots \dots [17]$$

where β is the local blade angle at the location of c_m . Equation [17] assumes that the mean relative velocity follows the blade contour, and this assumption is justified for the center section or rotating channel of the impeller. For impellers within the specified solidity range, Equation [17] gives also a good approximation for inlet and exit of the blade channel.

For impellers with large inducers, Equation [17] must be replaced for the blade-inlet condition by more accurate equations following the theory of axial machines (3).

Thus $w_{m,i}$ and $w_{m,o}$ can be determined for the inner and outer contour of the impeller and these velocities exist at the mean streamline between two blades.

Equation [17] cannot be used when large secondary flows occur, such as those caused by blade stalling or the impeller operating under considerably larger or smaller flow than design point.

COMPRESSIBILITY AND FRICTION

The effect of compressibility is taken into consideration by calculating the area of the impeller-flow channel for an arbitrary number of stations along the mean flow line. The velocity w_m^* is calculated from the total flow on the basis of the known area and an estimated compressibility. Later w_m^* is recalculated according to correct compressibility. The enthalpy increase from the conditions at the inlet to the compressor to an arbitrary station inside the impeller is

$$H^* - H_0 = \frac{w^{*2} - w_0^2}{2g} + \frac{w_{m1}^2 - w_{m2}^2}{2g} - \frac{c_1^2 - c_0^2}{2g} \dots [18]$$

The first two terms in Equation [18] define the enthalpy increase in the impeller, and the last term defines the inlet depression caused by the acceleration of flow from the known conditions to the impeller inlet.

Part of this total enthalpy increase is transformed into pressure and the other part into heat. The amount of enthalpy transformed into pressure is defined as

$$\Delta H_{AD} = \eta_e (H^* - H_0) = \frac{k}{k-1} RT_0 \left[\left(\frac{p^*}{p_0} \right)^{\frac{k-1}{k}} - 1 \right] \dots [19]$$

where η_e is the impeller channel efficiency, which is a function of the channel Reynolds number, turbulence, friction coefficient, and boundary-layer condition; η_e must be assumed on the basis of experience.

Equation [19] permits the calculation of the pressure rise $(p^*/p_0)_{AD}$. The temperature increase is

$$\frac{T^*}{T_0} = 1 + \frac{H^* - H_0}{c_p T_0 J} \quad [20]$$

and the volume change becomes

$$\frac{V^*}{V_0} = \frac{T^*}{T_0} \left(\frac{p_0}{p^*} \right)_{AD} \quad [21]$$

The correct volumes and velocities can be calculated according to Equations [18] to [21], and the original estimate of the compressibility is replaced by the accurate value of Equation [21]. Thus the correct values of the velocity w_m in Equations [12] and [13] are calculated. Then the following velocities are calculated, at first on the basis of incompressible flow, w_m ; w_{m0} along the inner and outer contour of the impeller and the local velocities w' , w'' ; w'_1 , w'_2 , w''_1 , and w''_2 , according to Equations [12] and [13]. If any of the foregoing velocities vary greatly from its corresponding value of w_m , the compressibility correction is calculated in the same manner.

This analysis permits calculation of the impeller-velocity distribution and gives a complete map of the velocity values for the three-dimensional compressible flow through the impeller.

The velocity distribution shall be represented as a function of the blade length and, for dimensionless representation, the values shall be divided by tip speed and impeller-tip radius, respectively.

ACCURACY OF APPROXIMATE SOLUTION

For the theoretical case of two-dimensional flow through radial-flow impellers, we can compare the results of the approximate solution with a flow analysis which has been calculated according to the relaxation method by Professor Emmons (10) for two types of impellers. In this report the velocity distribution is determined separately for the through flow and the displacement flow. The two types of impellers, which have been analyzed, are a straight radial-vane, $\beta_2 = 90$ deg, 22-blade unit, and a backward-curved $\beta_2 = 30$ deg logarithmic spiral-blade unit. Both impellers have a radius ratio $r_1/r_2 = 0.333$, constant blade width b , and a solidity of $\sigma = 3.84$.

Fig. 2 compares the velocity distributions of the displacement flow for the straight radial-vane unit. The solid line shows the velocity distribution according to the relaxation method of

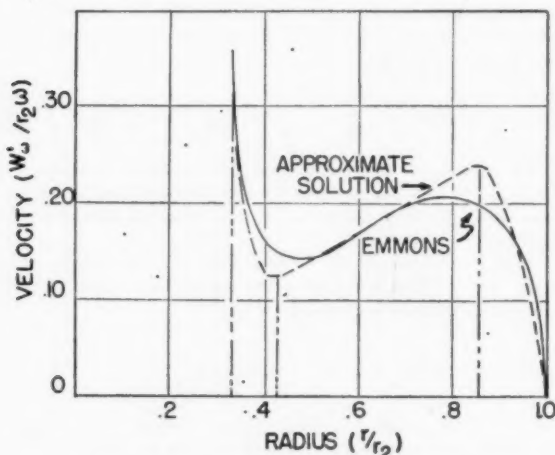


FIG. 2 VELOCITY DISTRIBUTION OF DISPLACEMENT FLOW FOR RADIAL-VANED IMPELLER, $z = 22$

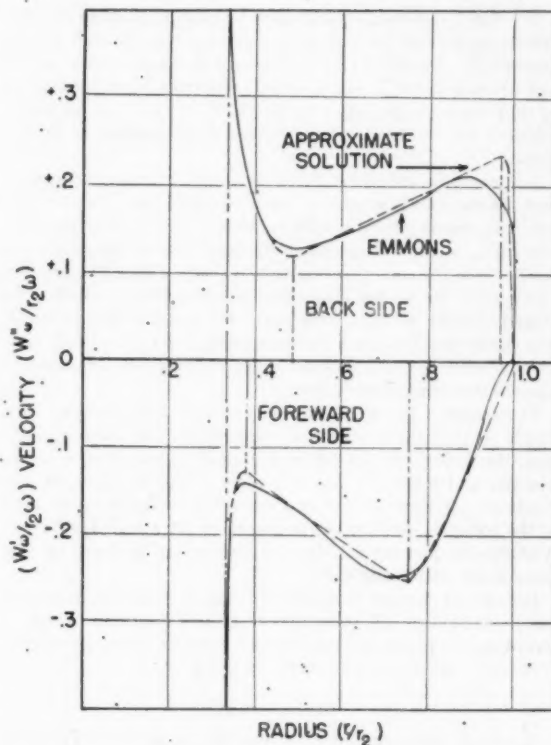


FIG. 3 VELOCITY DISTRIBUTION OF DISPLACEMENT FLOW FOR IMPELLER WITH BACKWARD-CURVED VANES, $z = 11$; $\beta_2 = 30$ DEG

Professor Emmons, and the dash line according to the approximate solution of Equations [12] and [13] with $w_m = 0$. A comparison on the basis of the displacement flow will show any discrepancies more clearly because total flow consists of the sum of displacement flow and through flow. Fig. 3 shows the velocity distribution for the displacement flow for the backward-curved unit, again with the solid line and dash line indicating the values of the relaxation method and the approximate solution, respectively. The two results indicate very good agreement for almost the entire blade passage and justify the use of the approximate solution.

We can also calculate the effect of finite blade number on the relative exit velocity. For the range of solidity under consideration this effect may be ascribed to the displacement flow only, and the influence of the circulation flow may be neglected (3). The calculation is identical with the stress or membrane-analogy methods discussed before, except that we calculate this time the velocity distribution along the impeller-exit diameter. This velocity distribution is again taken from the stress analogy. From the velocity distribution we calculate the mean value of this circumferential velocity Δw_u . This is the desired velocity correction for the finite number of blades. For nearly rectangular exit shapes, the velocity distribution is, as before, approximately a parabola, and the maximum velocities are proportionate to the width and height of the shape. The maximum velocity on the sides of the exit shape exists at the separation line between the center section and exit section and is known from the values of Equations [12] and [13] with $w_m = 0$.

The velocity Δw_u has been calculated for the two cases mentioned previously. The values are compared with the values for Δw_u

TABLE 1 RELATIVE VELOCITY CORRECTION

Relative velocity correction	Stodola ^a $\Delta w/w$	Busemann ^b $\Delta w/w$	Emmons $\Delta w/w$	This method $\Delta w/w$
Radial vanes 90 deg, $s = 22$	$0.143 \times w_2$	$0.105 \times w_2$	$0.086 \times w_2$	$0.108 \times w_2$
Backward-curved vanes 30 deg, $s = 11$	$0.143 \times w_2$	$0.137 \times w_2$	$0.136 \times w_2$	$0.137 \times w_2$

$$^a \Delta w/w = \frac{v \sin \beta_2}{s} \times w_2 \quad \text{Reference (1).}$$

$$^b \text{Reference (3).}$$

calculated according to the theories of Stodola, Busemann, and Emmons. Table 1 shows the results.

For the backward-curved impeller the theories of Busemann and Emmons agree with the results of this calculation, and, for the radial-vaned impeller, the results of this calculation agree with the theory of Busemann, but the value is somewhat above that of Emmons.

PRACTICAL APPLICATIONS

The application of the analysis will be shown for two cases. The first case relates to a compressor A which had a very narrow range of operation and pulsation outside this range of operation. An analysis of this impeller was suggested in order to find whether the range of operation could be improved. Fig. 4 shows the velocity distribution for this impeller. The vertical lines indicate the separation between the inlet, the center and exit section of the flow channel. The mean velocity w_m shows a decrease from inlet to exit of the impeller but does not permit any conclusion regarding the stability range of the unit. Backflow or pulsation of an impeller will start if the local velocity on the forward side of the blade becomes zero, and, in this impeller, the local velocity distribution indicates narrow range of operation. In this case the velocity difference $w_m - w'$ is a function of the angular velocity ω and channel width a only, according to Equation [12], with $R = \infty$, and does not change with w_m in the critical region of lowest values of w' on the forward side of the blade. Therefore a reduction in total flow of 13 per cent reduces the mean velocity in the same proportion and results in a value of mean velocity equal to $w_m - w'$ in the critical region; thus making the value of local velocity w' on the forward side zero. Backflow will occur if the flow is reduced 13 per cent.

Another item of importance is the amount of deceleration on either side of the blade per unit length. Too large an amount of deceleration causes high pressure gradients and stalling of the blades. While the velocity-distribution diagram permits predicting pulsation caused by backflow, the stalling of the blades cannot be analyzed quantitatively from the diagram, because stalling is affected by boundary-layer thickness, turbulence, and blade finish. However, on the basis of comparison of similar velocity distributions, experience can be gained indicating which velocity distributions tend to avoid stalling. The large decelerations on both pressure and velocity side of the blade of impeller A indicate a danger of stalling and thick boundary layers even under normal operation.

The second case relates to a compressor which was designed by use of the foregoing velocity-distribution method. The specifications called for a pressure ratio of 3 at 40,000 ft altitude, a wide range of stability, and a certain maximum flow capacity. Since this unit was tested under sea-level conditions, the specifications were recalculated for sea-level conditions as follows:

$$\text{Flow, } Q = 4850 \text{ cfm}$$

$$\text{Pressure ratio, } p = 2.54$$

$$Q_{\text{max}} = 5280 \text{ cfm}$$

$$\text{Speed, } n = 19,600 \text{ rpm}$$

$$n_s = \bar{n} \frac{\sqrt{Q}}{g^{1/4} H^{1/4}} = 0.096$$

In order to get the desired range of stability, the design point

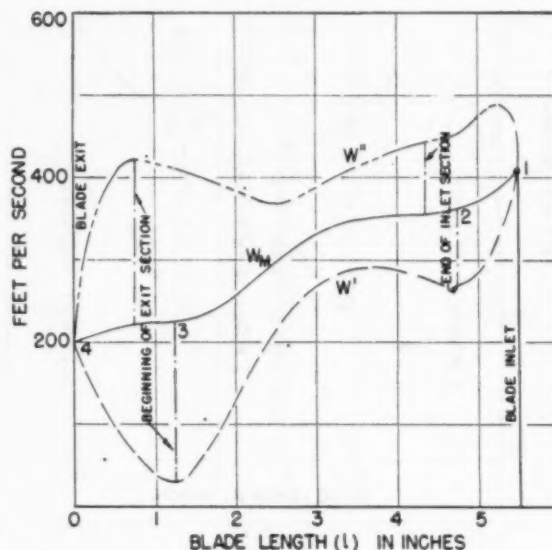


FIG. 4 UNDESIRABLE VELOCITY DISTRIBUTION IMPELLER A
($D_2 = 13.25$ in., $w_1 = 700$ fps, $n_s = 0.110$.)

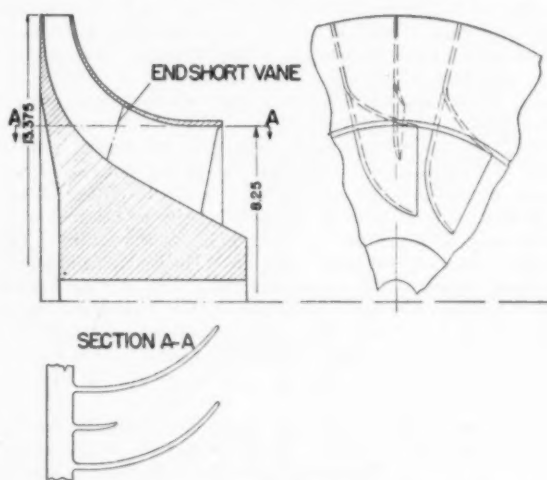


FIG. 5 IMPELLER B, 14 SHORT VANES, 14 FULL VANES

was chosen 8 per cent below the point of maximum capacity. Fig. 5 shows this compressor. This impeller has 14 full vanes and 14 short vanes. Fig. 6 shows the velocity diagram with regard to the mean relative velocity for this impeller. The various regions of the flow channel are separated by vertical lines.

The mean relative velocity shows decreasing values from inlet to exit, as well as a continuous change in decrease to the smaller

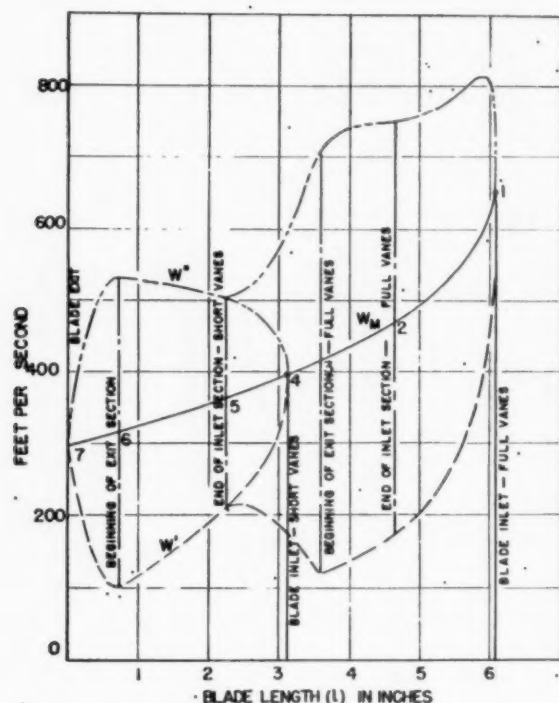


FIG. 6 VELOCITY DISTRIBUTION FOR MEAN FLOW PATH OF IMPELLER B

decelerations at the discharge end. The local velocities indicate the same characteristics on the high-pressure side of the blade, giving the largest decelerations at the blade entrance of the full and half-vanes, respectively. The low-pressure side of the blade shows little change in velocity, except at the discharge end of the blade and at the entrance into the half-vanes. The lowest value of local velocity occurs in a region where $R = \infty$; therefore, according to Equation [12], the velocity difference ($w_m - w'$) is a function of the angular velocity ω and channel width a only. Thus, reducing the through flow 33 per cent results in a value of mean velocity equal to $w_m - w'$ in the critical region, $l = 0.70$, and the value of the local velocity w' becomes zero. This means that backflow has progressed to the center of the blade channel and pulsation will occur. The beginning of pulsation can be analyzed by calculating the velocity distribution for the inner and outer contours of the impeller. From the curve, Fig. 6, it can be seen that this impeller would pulsate without the half-vane at its design flow and that half-vanes permit the extension of the operating range by reducing the value of local velocities.

Fig. 7 shows the velocity distribution of the impeller for the inner contour with the mean value w_{mi} and for the outer contour, mean value w_{mo} . All velocities have been calculated by taking into consideration an approximate value of the boundary-layer thickness. From the local velocity distribution a revised estimate of the stability range can be made. The lowest local velocity occurs on the forward side of the blade near the impeller disk. The critical value is again near the blade exit, $l = 0.70$, because in this region the value of w_{mi} is near its minimum value and $R = \infty$. Thus ($w_{mi} - w_i'$) is independent of w_{mi} , according to Equation [12]. Therefore a reduction of 27 per cent of the design capacity will result in the first local velocity value of $w_i' = 0$ initiating backflow. At a slightly larger reduction, 28 per

cent of design capacity, the local velocity w' also becomes zero in the second critical region at $l = 4.45$ near the inducer exit of the full vanes at the impeller disk. At this flow the local velocity value w' in the critical region near the impeller exit is negative at the impeller disk and backflow progresses toward the center of the flow channel.

The local velocity w'' on the back side of the blade close to the impeller shroud has the maximum value near the inducer inlet. This is the maximum value of velocity in the entire blade channel. An increase of 9 per cent above design capacity will result in the first occurrence of local sound velocity at this location. This analysis, therefore, indicates a total operating range of about 36 per cent.

Fig. 8 shows test data of the performance curve for this compressor at 1100 and 1140 fps tip speed. These performance curves indicate an operating range of 28 per cent from the design point to the beginning of pulsation, and a range of 10 per cent from the design point to maximum capacity, giving a total range of about 38 per cent at which the compressor efficiency is above 70 per cent.

Therefore the performance curve verifies the predicted result of the velocity-distribution curves. The maximum efficiency is above 79 per cent, and it should be remembered that this unit operates at an unusually low specific speed. Due to the instrumentation, flow losses in the 90-deg inlet turn are charged to the compressor efficiency. The entire performance of this compressor with regard to efficiency, pressure ratio, and stability is significant in that it was possible to calculate the performance of this unit and achieve the results shown in the curve, Fig. 8, without any modifications after tests.

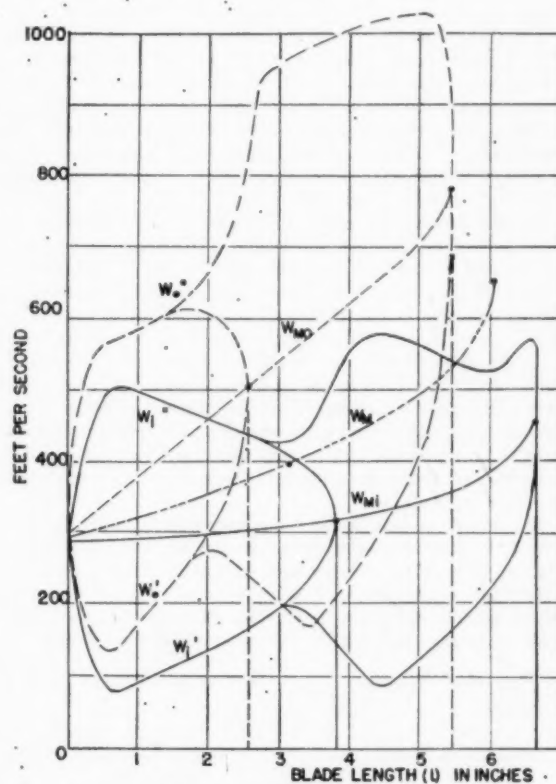


FIG. 7 VELOCITY DISTRIBUTION FOR INNER AND OUTER CONTOURS OF IMPELLER B

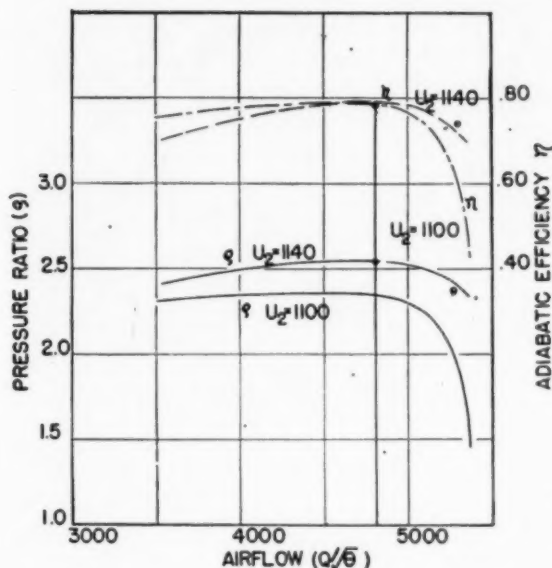


FIG. 8 COMPRESSOR PERFORMANCE CURVE IMPELLER B

CONCLUSIONS

The analysis permits calculation of the impeller velocity distribution and gives a complete map of the velocity values for the three-dimensional compressible flow through the impeller of a compressor.

The use of the velocity-distribution curves permits the prediction of pulsation of the compressor. Pulsation occurs when the local velocity reaches values of zero or below.

A qualitative analysis can be made with regard to blade stalling by comparing velocity-distribution curves for similar types of impellers. The criterion for stalling may be defined as the deceleration per unit length $(\Delta w)/(\Delta l)$, or the pressure gradient per unit length $(\Delta p)/(\Delta l)$.

In making the qualitative analysis it must be pointed out that stalling is a function of boundary-layer thickness, and the boundary layer is affected by centrifugal force which acts to remove the boundary layer from certain locations of the blade. Hence it may be stated that radially ending vanes, or vanes which easily permit complete removal of the boundary layer due to centrifugal force, can have considerably larger values of the local pressure gradients before stalling occurs. On the other hand, impellers with backward leading blades, or vane shapes which do not permit removal of the boundary layer by centrifugal force but only a relocation of the boundary layer, are much more sub-

ject to stalling, and frequently, in units with small blade exit angle, stalling occurs before pulsation (11). The analysis of the velocity distribution also leads to the conclusion that impellers of maximum efficiency should, within certain limits, have fewer blades, thus increasing the Reynolds number but decreasing stability.

Finally, the flow in any machine is not frictionless but does follow the laws of an imperfect fluid. However, with the knowledge of the local velocity and pressure gradients, it should be possible to make better predictions about the behavior of the boundary layer and secondary flows. The knowledge of pressure gradients permits the application of the analysis of flow, including friction, as shown by J. R. Weske (12) and Goldstein (13), to these impellers.

The proposed method is applicable to mixed-flow compressors and to radial and mixed-flow turbines as well.

ACKNOWLEDGMENT

The author is deeply indebted to Prof. H. W. Emmons of Harvard University and the Elliott Company, Jeannette, Pa., for their permission to show the results of the relaxation method in Figs. 2 and 3, and to the Continental Aviation and Engineering Corporation, Detroit, Mich., for their permission to publish Figs. 5 to 8. The author is also indebted to Prof. J. R. Weske of Brown University, for the derivation of, and permission to publish, Equation [16].

BIBLIOGRAPHY

- 1 "Steam and Gas Turbines," by A. Stodola, translation by L. C. Loewenstein, P. Smith, New York, N. Y., 1945.
- 2 "Die Kreiselpumpen," by C. Pfeleiderer, Verlag von Julius Springer, Berlin, Germany, 1932.
- 3 "Fluid Mechanics of Turbo-Machinery," by G. F. Wislicenus, McGraw-Hill Book Company, Inc., New York, N. Y., 1947.
- 4 "Theory of Elasticity," by S. Timoshenko, McGraw-Hill Book Company, Inc., New York, N. Y., 1934.
- 5 "Resistance of Materials," by F. B. Seely, second edition, John Wiley & Sons, Inc., New York, N. Y., 1935.
- 6 "Diagrams for Calculation of Airfoil Lattices," by A. Betz, NACA Technical Memorandum No. 1022, 1942.
- 7 "Calculation of Rotor Blades," by A. Betz and I. Flugge-Lotz, *Ingenieur Archiv*, vol. 9, 1938, p. 486.
- 8 "Zum Entwurf dichtstehender Schaufelgitter," by J. Ackeret, *Schweizerische Bauzeitung*, vol. 120, August, 1942, p. 103.
- 9 "Aerodynamic Theory," by W. F. Durand, editor in chief, Durand Reprinting Committee, California Institute of Technology, vol. 1, 1943, p. 209.
- 10 "Flow Through a Two-Dimensional Centrifugal Impeller With Backward Leading Vanes," by H. W. Emmons, unpublished report to the Elliott Company, Jeannette, Pa., February, 1945.
- 11 "Investigation of Flow in a Centrifugal Pump," by K. Fischer, NACA Technical Memorandum No. 1089, 1946.
- 12 "Investigation of the Flow in Curved Ducts at Large Reynolds Numbers," by J. R. Weske, *Journal of Applied Mechanics*, Trans. ASME, vol. 70, 1948, p. A-344.
- 13 "Modern Developments in Fluid Dynamics," by S. Goldstein, Oxford University Press, New York, N. Y., 1938.

Po

The
be real
this pa
cycle an
extract
peratur
econom
differen
This ev
character
'ciencies
paring
tures w
vided.

T
of
ti

also pres
the am
for the i
ment.³

As th
evaluate
steam t
of the v
Research
requeste
ble then
regenera
result.

The u
acterize
This ha
steam p
tures us
shown i
increase
tant is
tempera
years, to
12 F per

¹ Ther
Compan

² Eng
ment, T

³ The
Properti
& Sons,
Contr

Steam C
Temper
Transfer
N. Y., I
of Mech

NOTE
understo
of the Sc

Possibilities of the Regenerative Steam Cycle at Temperatures Up to 1600 F

By P. H. KNOWLTON¹ AND R. W. HARTWELL²

The regenerative-steam-cycle heat-rate gains that may be realized at temperatures up to 1600 F are presented in this paper. These gains are calculated for a theoretical cycle and also for a practical cycle wherein such losses as extraction-piping pressure drop, heater-terminal temperature differences, and the like, are considered. An economic evaluation of the anticipated turbine heat-rate differences for various throttle conditions is presented. This evaluation includes such factors as fuel costs, load characteristics, auxiliary-power requirements, boiler efficiencies, and annual fixed charges. A method of comparing the heat-rate gains due to higher steam temperatures with those made possible by resuperheating is provided.

THE purpose of this paper is to present the results of a study of the theoretical and practical possibilities of the regenerative steam cycle at throttle temperatures up to 1600 F. It also presents an economic evaluation of these gains which indicates the amount of capital investment which could be justified for the installation of high-temperature power-generating equipment.³

As the cost of fuel increases, it becomes more important to evaluate the savings which might be effected by increasing the steam temperatures in the power plant of the future. Because of the wide general interest in this problem, the ASME Special Research Committee on High Temperature Steam Generation requested the authors to prepare a paper covering (1) the probable thermal gains by the use of high-temperature steam in the regenerative cycle, and (2) the possible fuel savings that might result.

The use of steam for electric power generation has been characterized by a fairly steady increase in the steam temperature. This has made possible steady gains in the thermal efficiency of steam power plants. The increase in maximum steam temperatures used in power plants constructed during the past 45 years is shown in Fig. 1. This curve shows that the temperature has increased an average of 12 F per year. Perhaps more important is that the temperatures increased in steps as new high-temperature materials became available. During the past 20 years, temperatures have increased faster than the average rate of 12 F per year.

¹ Thermodynamic Engineer, Turbine Divisions, General Electric Company, Schenectady, N. Y. Mem. ASME.

² Engineer, Mechanical Engineering Division, Engineering Department, The Detroit Edison Company, Detroit, Mich. Jun. ASME.

³ The data on steam in all calculations are from "Thermodynamic Properties of Steam," by J. H. Keenan and F. G. Keyes, John Wiley & Sons, Inc., New York, N. Y., 1936.

Contributed by the Research Committee on High Temperature Steam Generation, Joint ASTM-ASME Committee on Effect of Temperature on the Properties of Metals, and Power and Heat Transfer Divisions and presented at the Annual Meeting, New York, N. Y., November 27-December 2, 1949, of THE AMERICAN SOCIETY OF MECHANICAL ENGINEERS.

NOTE: Statements and opinions advanced in papers are to be understood as individual expressions of their authors and not those of the Society. Paper No. 49-A-33.

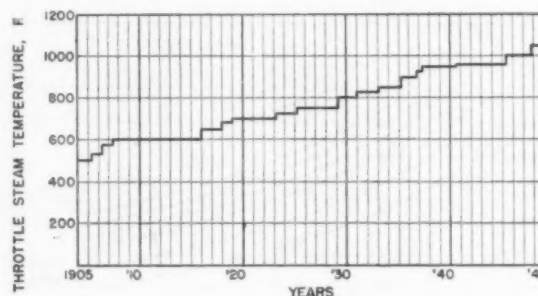


FIG. 1 MAXIMUM THROTTLE STEAM TEMPERATURES FOR PAST 45-YEAR PERIOD

THEORETICAL POSSIBILITIES AT HIGHER TEMPERATURES

Selvey and Knowlton⁴ published theoretical regenerative-steam-cycle heat rates for temperatures up to 1200 F and pressures up to 3200 psia. To facilitate a comparison over a wide range of pressure-temperature conditions, these data have been extended herein to 1600 F over the higher range of pressures, using the same theoretical cycle. As stated in the Selvey and Knowlton paper, the heat rates are for a regenerative steam cycle of the following component parts:

- 1 A turbine, having no mechanical losses, through which steam is expanded at constant entropy (engine efficiency is 100 per cent).
- 2 A regenerative feedwater system having an infinite number of bled-steam heaters heating to the saturation temperature, corresponding to the throttle steam pressure, and with zero terminal difference between the saturation temperature of the bled steam and the temperature of the feedwater leaving the heater, even when superheat is present in bled steam, and an attendant feed pump of 100 per cent efficiency with each heater to step up the feedwater pressure to the level of the next higher heater.
- 3 An electric generator of 100 per cent efficiency, which supplies, without line loss, the boiler feed pumps.
- 4 A steam generator of 100 per cent efficiency, in which blow-down, soot-blowing losses, etc., are zero.

Since energy required to drive fans, fuel equipment, general services, and so forth, is considered zero in a theoretical cycle, auxiliary-power usage other than that required for the boiler feed pumps, as described in item (2), is not included.

The theoretical heat rates are given in Table 1 and are presented in curve form in Fig. 2. This information shows that there is a steady improvement in the theoretical cycle economy with higher steam temperatures, but that the rate of improvement is diminishing as the temperatures are increased. Fig. 3 presents the theoretical heat-rate gains on a percentage basis with the 1250 psia-950 F throttle condition as a base. These curves provide a means of comparing theoretical and practical heat rates. The latter are discussed in the following section.

⁴ "Theoretical Regenerative-Steam-Cycle Heat Rates," by A. M. Selvey and P. H. Knowlton, Trans. ASME, vol. 66, 1944, pp. 489-500; discussion, pp. 501-512.

TABLE 1 THEORETICAL REGENERATIVE STEAM-CYCLE HEAT RATES IN BTU PER KWHR (1 in. Hg abs Exhaust Pressure)

Throttle pressure, psia	900 F	950 F	Throttle temperature					
			1000 F	1100 F	1200 F	1400 F	1600 F	
1000	7095		7993	6896	6802	6599	6412	
1250	6912	6867 ^a	6821	6729	6637	6457	6285	
1450	6792		6707	6620	6529	6358	6197	
2000	6542		6464	6384	6307	6156	6016	
2500	6378		6306	6232	6161	6020	5892	
3000	6246		6176	6109	6042	5912	5788	

^a Base condition assumed in Fig. 3.

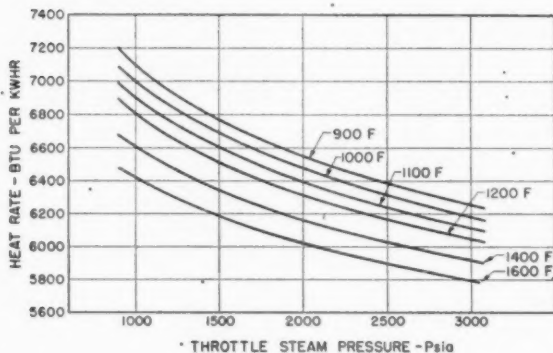


FIG. 2 THEORETICAL REGENERATIVE STEAM-CYCLE HEAT RATES

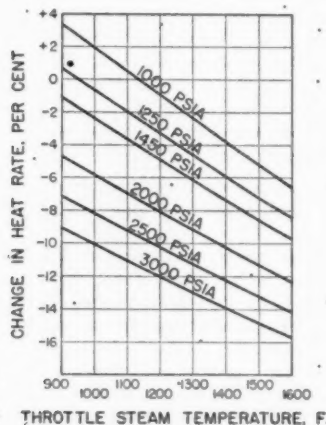


FIG. 3 PER CENT CHANGE IN THEORETICAL CYCLE HEAT RATE VERSUS INITIAL TEMPERATURE (Base condition, 1250 psia, 950 F, 1 in. Hg abs exhaust pressure.)

PRACTICAL POSSIBILITIES AT HIGHER TEMPERATURES

Fig. 4 shows comparative per cent change in regenerative-cycle heat rates which are considered practical from the design and operating standpoint. These heat-rate changes, computed for the same high-temperature and pressure range as was selected for the theoretical heat-rate calculations, include the effects of such losses as extraction-piping pressure drop, heater-terminal temperature differences, etc. From a specified heat rate for a particular turbine generator, the heat rate for any other condition may be calculated with the data included in Fig. 4.

As in Fig. 3, the base steam conditions chosen are 1250 psia, 950 F. The per cent change in heat rate from this base condition to any other condition may therefore be read directly. If it is desired to obtain correctly the difference in heat rate between any other two sets of steam conditions in terms of the heat rate at one of these conditions, the difference, as read from Fig. 4, must

be corrected for the change in base. For example, if we wish to get the difference between heat rates at 1450 psia, 1250 F and at 1450 psia, 1000 F, in terms of the heat rate at 1450 psia, 1000 F, this difference is

$$\frac{7.9 - 2.4}{1 - \frac{(2.4)}{(100)}} = \frac{5.5}{0.976} = 5.6 \text{ per cent}$$

Practical Cycle Assumptions. In making the calculations to

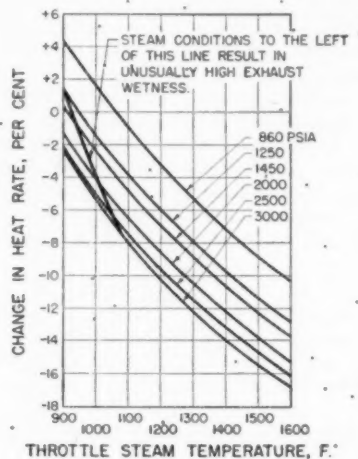
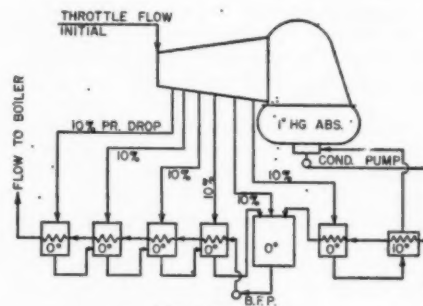


FIG. 4 PER CENT CHANGE IN PRACTICAL CYCLE HEAT RATE VERSUS INITIAL TEMPERATURE (Base condition, 1250 psia, 950 F, 1 in. Hg abs exhaust pressure.)



ASSUMPTIONS

- 1- TERMINAL DIFFERENCES AS INDICATED
- 2- 10% PRESSURE DROPS FROM STAGE TO HEATER
- 3- STEAM PRESS. 860 | 1250 | 1450 | 2000 | 2500 | 3000
- 4- B.F.P. DISCH. PRESS. 1000 | 1450 | 1700 | 2300 | 2900 | 3450
- 5- ENTHALPY RISE
- 6- NO. OF HEATERS 4 | 5 | 6 | 7 | 9 | 10
(CHANGING NUMBER OF H.P. HEATERS)
- 7- BOILER FEED TEMP, F. 380 | 434 | 456 | 516 | 556 | 590
- 8- ENTHALPY RISE IN CONDENSATE PUMP 0.6 BTU/LB.

FIG. 5 PRACTICAL CYCLE HEATER ARRANGEMENT FOR HEAT-RATE CALCULATIONS

arrive at the values plotted in Fig. 4, the following assumptions have been made:

1 The cycle arrangement and associated apparatus have been assumed to be as shown in Fig. 5 which presents the same arrange-

ment as was used by Harris and White.⁵ The present calculations have been extended to higher temperatures and pressures than those assumed by Harris and White and are based upon somewhat lower boiler feedwater temperatures. Power required to drive the boiler feed pump has been deducted from the generator terminal output.

2 As was done in the Harris and White paper, turbine and generator efficiencies have been assumed to correspond to those obtained in present-day turbine generators. The turbine-generator efficiency assumptions correspond to those made by Warren and Knowlton.⁶ This implies that at temperatures above present-day levels, new features of turbine design, or new materials, or both, must be developed if the general level of efficiency obtained in the past is to be maintained.

3 The exhaust loss from the turbine has been assumed to be a constant fraction of the turbine power output for all steam conditions.

4 It is assumed that the turbine-generator output is about 100,000 kw. This must be borne in mind particularly when comparing the heat rates at various initial pressures, since turbines of smaller capacities than 100,000 kw probably would show poorer relative performance at the higher pressures.

Steam Flows. Throttle and condenser steam rates, based on the practical cycle assumptions, have been computed to indicate the relative size of the generating equipment. The throttle and

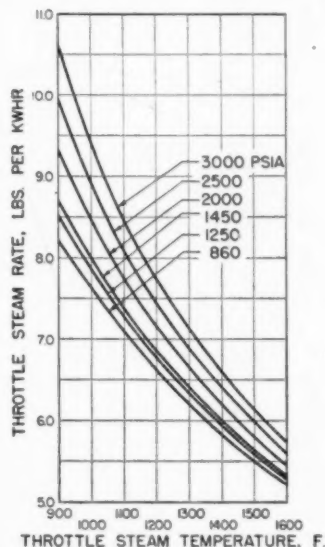


FIG. 6 THROTTLE STEAM RATE VERSUS INITIAL TEMPERATURE (1 in. Hg abs exhaust pressure.)

condenser steam rates are presented in Figs. 6 and 7, respectively. These are shown on the basis of the generator-terminal output, whereas the heat-rate change curves, Fig. 4, show the net change after deduction of boiler-feed-pump power from the generator-terminal output.

HEAT-RATE-DIFFERENCE EVALUATION

In considering the merits of one steam condition over another,

⁵ "Developments in Resuperheating in Steam Power Plants," by E. E. Harris and A. O. White, Trans. ASME, vol. 71, 1949, pp. 685.

⁶ "Relative Engine Efficiency Realizable From Large Modern Steam-Turbine Generator Units," by G. B. Warren and P. H. Knowlton, Trans. ASME, vol. 63, 1941, pp. 125-135.

it is desirable to evaluate the anticipated difference in heat rates. Because the practical heat rates represent results which at present appear possible at the higher steam conditions, these anticipated heat rates were used in this evaluation rather than the theoretical heat rates.

Basic Factors. The basic factors included in this evaluation are the cost of fuel, load characteristics, auxiliary-power requirements, boiler efficiency, turbine heat rates, and annual fixed charges on plant investment. Table 2 presents the results of an evaluation of heat-rate differences wherein a base condition of 1250 psia, 950 F has been used for comparing all of the other conditions. The figures shown in Table 2 represent the additional investment in dollars over the cost of 100,000 kw of 1250 psia 950 F capacity that is justified by the differences in heat rates. In computing the data it was assumed that plant availability and operating and maintenance personnel would be the same in all cases. No attempt was made to allow for possible differences in the extent of maintenance required.

Cost of Fuel. A 10-cent to 35-cent per million Btu fuel-cost range has been covered in the evaluation.

Load Characteristics. An annual plant-factor variation from 50 to 80 per cent has been included in the tabulation. The annual plant factor is the ratio of the kilowatthours generated on the machine in a year to the product of the kilowatt nameplate rating times 8760.

Auxiliary-Power Requirements. The following types of pulverized-coal-fired boilers were assumed in computing fan and mill power requirements:

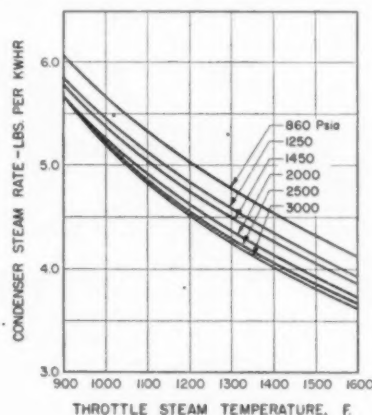


FIG. 7 CONDENSER STEAM RATE VERSUS INITIAL TEMPERATURE

(a) For throttle pressures up to and including 2000 psia; natural-circulation boilers.

(b) For 2500 psia throttle pressure; steamotive-cycle boilers with recirculating pumps which handle 130 per cent of steam flow.

(c) For 3000 psia throttle pressure; once-through forced-circulation-cycle boilers.

Allowances for miscellaneous auxiliary-power demands were included in all cases.

Boiler Efficiency. A boiler manufacturer indicated that even with feedwater temperatures approaching 600 F on these high-pressure high-temperature boilers, the exit-gas temperature could be held to about 300 F. Assuming pulverized-coal boilers operating with an average grade of coal, it was estimated that boiler efficiencies would vary from 87.7 to 88.8 per cent, depending upon the feedwater temperature.

TABLE 2 EVALUATION OF HEAT-RATE DIFFERENCES: ADDITIONAL JUSTIFIED INVESTMENT PER 100,000 KW OF CAPACITY OVER COST OF 1250 PSIA, 950 F PLANT
(Cost figures in thousands of dollars)

(Cost figures in thousands of dollars)																					
Coal Cost Cents per Million Btu		1250 Psia				1450 Psia				2000 Psia				2500 Psia				3000 Psia			
		Annual Plant Factor--Per Cent				Annual Plant Factor--Per Cent				Annual Plant Factor--Per Cent				Annual Plant Factor--Per Cent				Annual Plant Factor--Per Cent			
		50	60	70	80	50	60	70	80	50	60	70	80	50	60	70	80	50	60	70	80
900 P	10	-61	-74	-86	-98	-16	-19	-22	-25	62	74	86	98	87	116	136	155	106	137	148	169
	15	-102	-119	-147	-172	-24	-28	-33	-35	93	111	130	148	145	158	180	222	158	180	222	269
	20	-123	-147	-174	-193	-32	-38	-44	-50	103	123	143	163	158	188	222	253	188	222	253	330
	25	-153	-184	-205	-225	-39	-47	-55	-63	113	148	173	198	194	232	283	338	232	283	338	422
	30	-184	-221	-259	-295	-51	-61	-72	-83	123	168	206	247	242	290	359	422	290	359	422	507
1000 P	10	-59	-71	-83	-95	-108	-129	-151	-172	123	153	183	213	227	272	318	363	259	318	363	422
	15	-89	-106	-124	-142	-145	-174	-202	-229	153	193	233	263	267	312	358	403	312	358	403	489
	20	-118	-142	-166	-186	-165	-200	-232	-265	183	233	273	313	342	392	438	483	342	392	438	538
	25	-149	-177	-207	-237	-205	-249	-284	-317	213	263	303	343	367	417	463	508	367	417	463	569
	30	-207	-248	-290	-331	-277	-323	-368	-411	243	293	333	373	397	447	493	538	397	447	493	607
1100 P	10	-169	-203	-237	-270	-313	-355	-398	-441	289	347	405	463	342	410	478	546	357	428	499	570
	15	-254	-304	-355	-406	-438	-493	-544	-597	347	423	500	577	423	512	597	674	423	512	597	686
	20	-324	-384	-444	-504	-536	-597	-657	-717	423	500	577	654	493	582	667	744	493	582	667	753
	25	-406	-473	-541	-608	-640	-706	-773	-839	500	577	654	731	577	666	751	828	577	666	751	849
	30	-507	-582	-657	-731	-763	-839	-916	-992	577	654	731	808	654	743	828	905	654	743	828	916
1200 P	10	-259	-311	-362	-414	-458	-509	-560	-611	361	438	515	592	438	527	604	681	438	527	604	681
	15	-398	-462	-524	-586	-639	-699	-759	-819	438	515	592	669	438	527	604	681	438	527	604	681
	20	-518	-592	-664	-736	-789	-849	-909	-969	515	592	669	746	515	604	681	758	515	604	681	758
	25	-647	-727	-807	-887	-940	-1000	-1060	-1120	592	669	746	823	592	681	758	835	592	681	758	835
	30	-777	-867	-957	-1047	-1100	-1160	-1220	-1280	669	746	823	900	669	758	835	912	669	758	835	912
1300 P	10	-306	-362	-418	-474	-518	-574	-629	-685	438	515	592	669	438	527	604	681	438	527	604	681
	15	-462	-524	-586	-648	-699	-759	-819	-879	515	592	669	746	515	604	681	758	515	604	681	758
	20	-592	-664	-736	-808	-849	-909	-969	-1029	592	669	746	823	592	681	758	835	592	681	758	835
	25	-727	-807	-887	-967	-1000	-1060	-1120	-1180	669	746	823	900	669	758	835	912	669	758	835	912
	30	-857	-947	-1037	-1127	-1160	-1220	-1280	-1340	746	823	900	977	746	835	912	989	746	835	912	989
1400 P	10	-427	-513	-599	-684	-728	-794	-859	-924	515	592	669	746	515	604	681	758	515	604	681	758
	15	-642	-729	-815	-900	-944	-1010	-1075	-1140	592	669	746	823	592	681	758	835	592	681	758	835
	20	-769	-855	-941	-1026	-1069	-1135	-1200	-1265	669	746	823	900	669	758	835	912	669	758	835	912
	25	-899	-985	-1071	-1156	-1199	-1265	-1330	-1395	746	823	900	977	746	835	912	989	746	835	912	989
	30	-1029	-1115	-1201	-1286	-1329	-1395	-1460	-1525	823	900	977	1054	823	912	989	1066	823	912	989	1066
1500 P	10	-544	-630	-716	-801	-844	-909	-974	-1039	592	669	746	823	592	681	758	835	592	681	758	835
	15	-769	-855	-941	-1026	-1069	-1135	-1200	-1265	669	746	823	900	669	758	835	912	669	758	835	912
	20	-899	-985	-1071	-1156	-1199	-1265	-1330	-1395	746	823	900	977	746	835	912	989	746	835	912	989
	25	-1029	-1115	-1201	-1286	-1329	-1395	-1460	-1525	823	900	977	1054	823	912	989	1066	823	912	989	1066
	30	-1159	-1245	-1331	-1416	-1459	-1525	-1590	-1655	900	977	1054	1131	900	989	1066	1143	900	989	1066	1143

Turbine
in Fig. 4
the evalu
Annual
cent was
ments.
justed for

Invest

Exam
Throt

Assum
C
A
F
Addit

The a
1400 F
is

He

It is
higher s
heating
by comp
and W
exactly
differen
their ca
The r
made in

1 T
than w
a minor
nitude o
paper.⁸

2 T
the bas
White
reheat
machin
exhaust
The as
loss as

How
consider

(a) T
of thro
throttl
and the

(b) T
regard
centage
creases
gains i
haust l

* "Re
ASME
* Ibid

Turbine Heat Rates. Turbine heat-rate differences represented in Fig. 4, which are based on the practical values, were used in the evaluation.

Annual Fixed Charges. An annual fixed-charge rate of 10 per cent was assumed in computing the justified additional investments. The investment figures shown in Table 2 may be adjusted for other fixed-charge rates as follows:

$$\text{Investment from Table 2} \times \frac{0.10}{\text{New fixed charge rate}} = \text{adjusted investment}$$

Example. An example will illustrate the use of Table 2.

Throttle conditions to be compared: 1450 psia, 1000 F
3000 psia, 1400 F

Assumptions:

Coal cost..... 20 cents per million Btu
Annual plant factor..... 60 per cent
Fixed-charge rate..... 10 per cent

Additional investment figures from Table 2:

1450 psia, 1000 F..... \$ 259,000
3000 psia, 1400 F..... 1,503,000

The amount that could be spent for 100 mw of 3000 psia, 1400 F capacity over the cost of a 1450 psia, 1000 F installation is

$$\$1,503,000 - 259,000 = \$1,244,000$$

HIGH STEAM TEMPERATURES VERSUS RESUPERHEATING

It is of interest to compare the heat-rate gains resulting from higher steam temperatures with those made possible by resuperheating. An approximate comparison may be made directly by comparing gains shown in Fig. 4 with various charts by Harris and White, and by Reynolds.⁷ These two references do not exactly agree on the gain due to reheat, presumably because of differences in the assumptions made by the authors in setting up their calculations.

The assumptions made by Harris and White differ from those made in this paper on the following points:

1 The boiler feed temperatures are lower in the present case than were assumed by Harris and White. This difference makes a minor change in the gain due to reheat. For the order of magnitude of the effect of this on the reheat gain, refer to Reynolds' paper.⁸

2 The heat-rate gains in Fig. 4 of the present paper are on the basis of a fixed percentage exhaust loss, whereas Harris and White assumed, in calculating their reheat gain, that their non-reheat machines had a 4.5 per cent exhaust loss and their reheat machine a lesser exhaust loss obtainable from keeping the same exhaust-end size and the same rating for their reheat turbine. The assumptions made by Reynolds regarding the exhaust loss as between reheat and nonreheat are not stated in his paper.

However, we are able in the present case to show the effect of considering either two cases:

(a) The use of a "constant percentage exhaust loss," regardless of throttle-steam conditions. In this case, as we proceed to higher throttle temperatures, the exhaust size per unit rating decreases, and the gains expected are as shown in Fig. 4.

(b) The use of a "constant size of exhaust per unit rating," regardless of throttle-steam conditions. In this case, the percentage exhaust loss decreases when throttle temperature increases, and a further gain results from this, over and above the gains indicated in Fig. 4. The magnitude of this change in exhaust loss can be calculated by the use of Fig. 8, if the exhaust

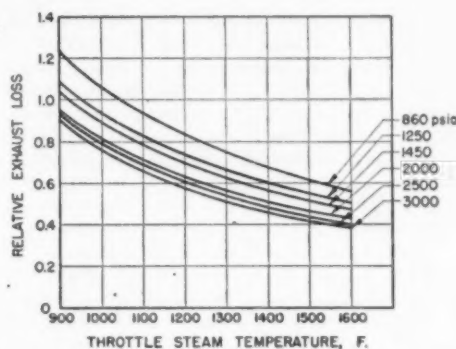


FIG. 8 RELATIVE EXHAUST LOSS VERSUS INITIAL TEMPERATURE

loss at a base condition is known. For any two sets of steam conditions shown on Fig. 8, the ratio of exhaust-loss percentage is the ratio of the ordinates therein.

An example will illustrate this point:

Assume a base condition of 1450 psia, 1000 F, and compare heat-rate gains due to the following:

- 1 Reheat to 1000 F at 450-psia reheat pressure.
- 2 Raising throttle temperature to 1250 F, nonreheat.

The answer to (1) can be read from Harris and White⁹ as 5.2 per cent gain due to reheat, on the basis of constant exhaust size per unit rating.

The answer to (2) is given here in two parts, corresponding to the foregoing items (a) and (b), as follows:

(a) For constant percentage exhaust loss from Fig. 4, the gain at 1450 psia, 1000 F is 2.4 per cent, and at 1450 psia, 1250 F is 7.9 per cent. This gives a net gain of $\frac{7.9 - 2.4}{1 - 0.024} = 5.6$ per cent.

(b) For constant size of exhaust per unit rating, the relative exhaust-loss factors from Fig. 8 are as follows:

1450 psia, 1000 F..... 0.89

1450 psia, 1250 F..... 0.66

Revised exhaust-loss percentage from the assumed 4.5 per cent

$$4.5 \times \frac{0.66}{0.89} = 3.4 \text{ per cent}$$

Additional heat-rate gain due to exhaust-loss correction

$$4.5 - 3.4 = 1.1 \text{ per cent}$$

Total gain due to temperature increase

$$5.6 + 1.1 = 6.7 \text{ per cent}$$

It will be noted that the additional gain due to a change in the exhaust loss with fixed exhaust size depends directly upon the magnitude of the exhaust loss itself.

In comparing heat-rate gains due to higher steam temperatures with those made possible by resuperheating as presented by Harris and White, an exact evaluation should include the exhaust-loss correction described in item (b).

CONCLUSION

The curves for practical performance in Fig. 4 exhibit trends similar to those for the theoretical performance in Fig. 3. However it will be seen that the practical cycle shows less improve-

⁸ Footnote 5, Fig. 11.

⁷ "Reheating in Steam Turbines," by R. L. Reynolds, Trans. ASME, vol. 71, 1949, pp. 701-706.

⁸ Ibid., Fig. 5.

ment with increasing pressure, and more improvement with increasing temperature, than the theoretical cycle. This relationship results from the fact that the practical turbine loses in efficiency with increasing pressure, and gains in efficiency with increasing temperature, while the theoretical turbine is assumed to be always 100 per cent efficient. These trends are not at all new; the only novel feature is the extrapolation of the trends to show what economies may be expected at temperatures up to 1600 F and pressures up to 3000 psia. It is believed that this has been done in a reasonable manner consistent with past practice.

Use of steam temperatures in power plants above the present maximum of 1050 F will depend on the development of suitable materials for the higher temperatures and on the design of acceptable equipment, particularly boilers and turbines, at a cost commensurate with the thermal gains to be realized. Since the costs of such materials and equipment are not presently available, this paper has presented only the total investment which could be justified on the basis of the thermal gains expected at the higher steam conditions.

ACKNOWLEDGMENT

The authors wish to express their appreciation for the advice and assistance of Mrs. Jean Harrison Higley and Mr. E. E. Harris of the General Electric Company, Mr. A. E. Raynor of the Babcock & Wilcox Company, and Messrs. H. A. Wagner and H. S. Walker of The Detroit Edison Company.

Discussion

W. E. CALDWELL.¹⁰ This paper indicates the thermal performance and evaluated savings obtainable by increasing initial steam temperature for the regenerative steam cycle. This cycle offers advantages over the reheat cycle, from the standpoint of simplicity, although it would result in more water in the exhaust stages for the same heat rate. It is indicated that an initial temperature of about 1170 F with the regenerative cycle would yield about the same heat rate as a 1000-1000 reheat cycle with the same initial pressure and heater arrangement. In the arrangement of heating stages and distribution of extraction heaters, the regenerative cycle offers more attractive thermal possibilities than the reheat cycle. The question of economic justification for the regenerative cycle above present temperature limits must await practical developments in high-temperature metallurgy.

In both the reheat and high-temperature regenerative cycles the improved performance results from utilization of a larger proportion of high-level heat than is presently employed, which aggravates surface-cleaning problems in the boiler plant, aside from metallurgical considerations.

In a 1000-1000 reheat cycle, the heat required to superheat the steam and reheat it is equivalent to a drop of about 1350 deg F in boiler gas temperature. To this must be added 600 deg F saturation temperature, 200 deg F for temperature difference or heat head between gas and steam, and 150 deg F for gas stratification, resulting in temperature zones above 2200 F in the superheater bank. With the equivalent regenerative cycle a lower gas temperature suffices, but in both cases the required gas temperature is substantially above 2000 F, which is the approximate rejection limit for some abundant low-cost coals with low-fusion ash. Improvements in design and disposition of the superheater surface should, in time, lessen the cleaning requirements and extend the range of acceptable fuels for high-temperature installations. Geographical location of plants and characteristics of available fuels will continue to be a major consideration in the choice of steam conditions.

¹⁰ Staff Engineer, Consolidated Edison Company of New York, Inc., New York, N. Y. Mem. ASME.

This paper exemplifies our dependence upon the steam tables, and some comments on their use for the higher temperatures would be of interest. The upper temperature line on Mollier charts with the 1936 tables ends at 1200 F. Was a condition curve plotted for the expansions from the various initial temperatures, or was some other procedure employed?

E. E. HARRIS.¹¹ This paper will be a very useful tool for the industry. The user will be able to compare the gains to be expected as well as the amount of additional money that may be justified for obtaining a gain in station economy.

This paper, together with the paper by E. E. Harris and A. O. White,⁶ will give the user considerable information that may be used for determining the future trend in the power-plant field.

Fig. 4 of the paper was obtained from calculations that were made for the Harris and White paper with additional calculations made for the higher pressures and temperatures. The added calculations followed the same method as was used in the original paper, correcting for volume flow, pressure, and superheat, the superheat correction taking into account the change in moisture. It was assumed, in making the calculations and arriving at the gains to be obtained with higher pressures and temperatures, that materials will be available as well as design and ability to build such turbine units without sacrificing efficiency or gain.

At 1450 psia, 1000 F initial conditions, reheating to 1000 F will show a gain of approximately 5 per cent in station heat rate. If the same gain is to be obtained by operating at a higher initial temperature without reheat, the initial temperature will be about 1175 F. The 5 per cent gain in heat rate will justify an expenditure of \$632,000 over 1450 psia, 1000 F nonreheat with a coal cost of 30 cents per million Btu and 60 per cent annual plant factor. It is felt that a reheat station will have a lower increment cost than the nonreheat plant with 1175 deg to obtain the same gain.

Sometime in the future, materials will be available as well as design and know-how for building units for the higher temperatures for nonreheat. When such information is available, reheating to the same initial temperature may be used with approximately the 5 per cent gain over the nonreheat plant.

A. E. RAYNOR.¹² The authors have made an interesting and useful survey which should be helpful to those who are looking forward to the time when they may find it desirable to go to higher pressures and higher temperatures. Dollar values have been established and given in Table 2, which indicate approximately how much may be spent economically for the higher pressures and higher temperatures.

The data are presented with the bases used in establishing the dollar values, so that corrections may be made readily by anyone wishing to modify these data and correct for conditions which may differ somewhat from those arbitrarily used by the authors. Any correction which the user may wish to make, such as a different value for fixed charges, annual plant factor, etc., can be made readily, the additional justified investment quickly determined, and proper design conditions established.

The authors have been wise in extending the pressures to 3000 psia and the temperatures to 1600 F, even though manufacturers are not now equipped with materials to satisfy, particularly, the higher temperatures. It may be that we are now in a similar situation to the designers of, say, 20 years ago, when a temperature of 1050 F appeared to be very far in the future. However, in about 20 years, temperatures have gone from something less than 800 F to 1050 F, and higher temperatures will be used when satisfactory materials are available. Inasmuch as the wall

¹¹ General Electric Company, Schenectady, N. Y.

¹² Executive Assistant, New York Proposition Division, The Babcock & Wilcox Company, New York, N. Y. Mem. ASME.

thickness of some of the present $2\frac{1}{2}$ -in. 18 Cr, 8 Ni-Cb tubes used in the hot end of superheaters designed for 2300 psia and 1050 F are 0.56 in. thick, leaving but little internal area for the flow of steam, it is quite obvious that temperatures much higher than 1050 F will call for metals with higher available stresses than those currently being used. Many engineers in the steel and allied industries are working on this problem, and time alone will tell when the better high-temperature materials will be available for use. When one considers the economies gained by the use of higher temperatures, it may be that some will find it desirable to use higher temperatures even at the risk of shorter life of the material in the hot portions of the superheater, piping, and turbines. Therefore earlier replacement of parts of the equipment than now contemplated may be economically justified.

The authors indicate that, based upon certain assumptions, \$1,244,000 more may be spent for a 100,000-kw plant designed for 3000 psia, 1400 F than for a 1450 psia-1000 F installation. Using the same assumptions, \$773,000 more may be spent for a 2500 psia-1200 F installation than a 1450 psia-1000 F unit. In either case a considerable amount of money is involved. This alternative example is used because metals are already available and being used in reheat designs for 2080 psi 1050 F and 1000 F reheat, also 1500 psia 1000 F-1000 F reheat. The latter is about equivalent in cycle efficiency to the nonreheat 2500 psia-1200 F unit.

This presumably accounts for several companies purchasing reheat units during the past few years, the steam conditions being about as follows:

1300 psia, 950 F and 950 F reheat
1500 psia, 1000 F and 1000 F reheat
2080 psia, 1050 F and 1000 F reheat

Design engineers have had and will continue to have problems where a considerable amount of judgment is required in determining the best pressure and temperature to satisfy the conditions of a given project. The data submitted in this paper should be helpful in future studies and encourage engineers and metallurgists to solve the material problem as rapidly as possible in order that higher temperature metals may be available for early use.

R. L. REYNOLDS.¹³ In this paper the authors present the thermal advantages of high pressures and temperatures and point out the additional investment which can be justified by these reductions in fuel costs. Such a comparison with what are now considered established steam conditions (1250 psia, 950 F) will serve as a valuable guide for analyzing the benefits to be derived from these increased steam pressures and temperatures. It also offers a challenge to designers of steam generators and turbines to develop equipment to meet these advanced conditions.

Of particular interest are the curves in Fig. 4, which show the change in heat rates for pressures from 860 to 3000 psia and temperatures from 900 to 1600 F. We feel that the values given on these curves are consistent with past practice and are reasonable estimates of what can be expected in the future, provided developments in design and materials keep pace with increases in steam pressures and temperatures.

At the present time the maximum operating steam temperature on central-station turbines is 1050 F. Although operation at this temperature, in general, has been satisfactory, further successful operation should be experienced before extending this limit materially. In the meantime a thermal gain equivalent to about 175 deg F increase in throttle temperature can be realized by the use of the reheat cycle.

¹³ Land Turbine Engineering, Central Station Turbine Section, Westinghouse Electric Corporation, South Philadelphia, Pa. Mem. ASME.

The authors refer to the writer's paper,⁸ and point out that values for thermal improvement derived from the reheat cycle do not agree with those given by Harris and White,⁹ due to differences in the assumptions made.

These differences in assumptions are as follows:

(a) The writer's comparisons were made upon the turbine alone. It was pointed out that additional advantages were obtained due to a reduction of from 15 to 18 per cent in boiler-feed-pump power, but this factor was not included. Power requirements for condenser and boiler auxiliaries are also reduced by the use of the reheat cycle.

(b) The writer's data were based upon 1.5 in. Hg abs exhaust pressure, as compared with 1.0 in. Hg used by Harris and White. The increased exhaust pressure results in a smaller differential in the thermal advantages of the reheat cycle.

(c) The writer's values also were based upon a constant exhaust loss expressed in Btu per pound. It was pointed out that, if constant exhaust area for a given set of initial steam conditions were used, the 7 or 8 per cent decrease in exhaust volume would result in a decrease in exhaust loss and thus increase the thermal benefits from the reheat cycle.

When reduced to the same basis, the values given by Harris and White agree quite closely with the writer's.

The evaluation figures tabulated in the authors' paper have been based upon the assumption that equal reliability can be obtained for all sets of conditions. This may at first appear unjustified and certainly would be if the increased temperatures were attempted at this time, but, when operating experiences over a long period of time are studied, it is evident that the reliability of steam turbines is now higher than ever, despite a large increase in steam pressures and temperatures. Although each new step may result temporarily in some reduction in reliability until the problems associated with this advance are solved, we feel that, if these changes are made gradually and in a fundamentally sound manner, no decrease in reliability will be suffered.

L. B. SCHUELER.¹⁴ The authors have performed an excellent service in projecting the useful data on steam-electric unit heat rates into the field of higher steam temperatures, even into the extremes where most of us will probably never see their practical realization. However they give us an important sense of direction and show that there are real possibilities if we do not accept half-way measures in many respects.

The problem of whether to adopt higher steam temperatures rapidly resolves itself into some simple but definite economic limitations. The extremely high cost of alloy materials suitable for higher temperatures is the heart of the problem. The turbine builders already have taken the big step in going to austenitic materials for the high-temperature portion of the 1050 F units. It should be possible to extend the application of these materials up to about 1200 F for turbine construction.

The superheater design, wherein maximum metal temperatures are usually about 100 deg F higher than the steam temperature, indicates a limit of about 1000 F for the lower-cost ferritic-alloy materials. Higher temperatures involve correspondingly greater quantities of costly austenitic-alloy tubing—all based upon present allowable stresses as established by the ASME Boiler Construction Code. These present allowable stresses, while presumably based on reasonably long life along with a substantial safety factor, often represent conditions of indefinite life, say, more than 40 years. In these cases, and there are many of them, an extremely high initial investment is made in materials which might be difficult to justify in the light of experience.

¹⁴ Engineer, Mechanical Engineering Division, American Gas & Electric Service Corporation, New York, N. Y. Mem. ASME.

It is proposed that designers and users give consideration to the relative merits of designing superheater and reheater materials, particularly in the extreme high-temperature zones, with the deliberate intent that they shall have a limiting life, probably somewhere between 5 and 20 years. Careful studies of this proposal appear warranted, particularly in the light of substantial experience along these very lines in oil-cracking-still units. If studies indicate possible economic merit, then it becomes necessary to establish another set of higher allowable stresses, to be used in such applications, by the appropriate regulatory bodies.

On the basis of a double-stress standard, a preselected portion of a superheater or reheater could be built to long or short-life standards, as desired, with the manufacturer and purchaser working out the best over-all arrangement, and with the user being reconciled to periodic replacement of a small portion of the superheater or reheater. If it were limited to superheater and reheater tubing materials only, and up to a limiting tube diameter, the safety element would be kept adequately under control.

The ASME Special Research Committee on High Temperature Steam Generation is embarking on a broad program of research to investigate materials which are suitable for steam temperatures up to 1500 F.

It seems advisable that an analytical study of the proposed double-stress standard be made at once so that the research work can be planned more effectively. This study can and should be made jointly by manufacturers and users to arrive at the proper relationship of physical and economic limitations.

AUTHORS' CLOSURE

The authors agree with Mr. Caldwell and Mr. Harris in their finding that the data presented show that an increase by about 175 F in initial temperature gives a gain in heat rate equivalent to that obtainable from reheat, and that at present this gain is

more economically obtained from reheat than from such a considerable increase in temperature.

The authors are grateful to Mr. Caldwell for inquiring as to how the turbine calculations were made. This point probably should have been more fully covered in the paper. The Keenan and Keyes Steam Table extends to 1600 F (the chart is plotted only to 1200 F) although very much skeletonized above 1200 F. It was necessary to extend the chart to 1600 F and fill in intermediate values between those given in the table by calculation. This was done by graphical means, using a large-scale plot of the constant-pressure specific heat to smoothly interpolate between table values. No extrapolation was necessary. The chart thus extended was used for plotting the turbine expansion lines, in accordance with the assumptions as stated in the paper.

Mr. Raynor's remarks concerning tube thicknesses presently required illustrate very well the necessity for stronger materials for very elevated temperatures. His suggestion that perhaps some parts should be considered as requiring more frequent replacement is interesting, but it is not clear that such considerations would result in any economic improvement.

The authors are also grateful for Mr. Reynolds' statements, both as to general corroboration of the findings of the present paper, and as to clarification of his own previous paper, reference 7. Further, the authors are in agreement with Mr. Reynolds' remarks concerning relative reliability.

Mr. Schueler's statements are quite to the point. The high cost of satisfactory materials, according to present knowledge, is the main reason why higher temperatures are not presently used. It seems to be too early to judge effectively whether stresses currently allowed are overconservative. However, the company with which Mr. Schueler is associated has for many years been building power plants using high temperatures and pressures, so their experience is very valuable.

Oil Holes and Grooves in Plain Journal Bearings

By S. A. MCKEE¹ AND H. S. WHITE,¹ WASHINGTON, D. C.

Data are presented showing the performance of plain journal bearings having various arrangements of oil holes and grooves operating in a four-bearing friction machine with forced-feed lubrication. Tests cover operation where the oil is fed through the bearing shell by means of five arrangements, including one, two, or four oil holes; one axial or one circumferential groove. Tests were also run with three arrangements for feeding oil from the center of a hollow shaft. These were one or two oil holes in the shaft, or one oil hole terminating in a flat on the surface of the shaft. Two clearance-diameter ratios were used with each arrangement. Test runs were made at constant speed and at a number of loads, which were unidirectional relative to the bearings. The data cover operation with one oil at one oil-inlet temperature and two speeds. In some of the tests the loads were increased until unstable lubrication was reached. The test results include the frictional characteristics, values of ZN/P at transition between stable and unstable lubrication, and data on thermal behavior and on oil flow. A summary of the general behavior of the various arrangements is given.

NOMENCLATURE

The following nomenclature is used in the paper:

- D = journal diameter, in.
- L = bearing length, in.
- C = running clearance (difference between bearing diameter and journal diameter), in.
- W = total load acting on bearing, lb.
- P = W/LD = pressure on projected area of bearing, psi
- N = speed of journal, rpm
- F = tangential frictional force, lb
- f = F/W = coefficient of friction
- Z = absolute viscosity of lubricant at atmospheric pressure and bearing temperature, centipoises (cp)
- H_t = rate of heat supplied to one bearing from both entering oil and bearing friction, in-lb per min
- ΔT_b = temperature rise above ambient of loaded side of bearing shell (average of four bearings), deg F
- ΔT_s = temperature rise above ambient of oil leaving ends of bearings (average of four bearings), deg F
- Q = rate of oil flow per bearing, cu in. per min
- ZN/P = generalized operating variable
- p = oil-feed pressure (corrected for drop between gage and bearings and for centrifugal force when oil is fed through shaft), psi

¹ National Bureau of Standards.

Contributed by the Special Research Committee on Lubrication and presented at the Spring Meeting, Washington, D. C., April 12-14, 1950, of THE AMERICAN SOCIETY OF MECHANICAL ENGINEERS.

NOTE: Statements and opinions advanced in papers are to be understood as individual expressions of their authors and not those of the Society. Manuscript received at ASME Headquarters, January 6, 1950. Paper No. 50-S-9.

INTRODUCTION

One of the problems in the lubrication of plain journal bearings is the method of admitting the oil to the bearing. The concept of the load-carrying film indicates the desirability of avoiding the use of oil holes or grooves which interfere with the normal development of hydrostatic pressure to support the load. In some bearing installations, however, it is not always possible to satisfy this requirement. With bearings where loads are fluctuating in both intensity and direction, it is sometimes impracticable to apply the oil to the unloaded side throughout the complete load cycle. Also in some cases, provision must be made for a continuous flow of oil to some other moving part.

The tests reported in this paper were made to determine the comparative performance of journal bearings having various arrangements of holes or grooves when using forced-feed lubrication under conditions where in each case the load was unidirectional on the bearing. The work comprised two separate series of tests. The first covers operation with three arrangements of oil holes and two types of oil grooves in the surface of the bearing. The second covers operation with three arrangements for feeding the oil from the center of a hollow shaft. Each of these arrangements is located at the axial center of the bearing.

This investigation was part of a research program on the lubrication of plain journal bearings which was conducted at the National Bureau of Standards with the financial support of the National Advisory Committee for Aeronautics.

APPARATUS

Four-Bearing Friction Machine. The four-bearing friction machine used in this investigation has been described in a previous publication (1).² The complete apparatus is shown in Fig. 1, and the major elements of the machine disassembled in Fig. 2. The machine consists essentially of four similar test bearings enclosed in a housing and mounted on a common shaft. Loads are applied by hydraulic jacks which form the base of the housing. The complete unit of bearings and housing acts as a cradle dynamometer. The frictional torque is measured by a dynamometer scale acting through a torque arm fitted to the housing. An automatic device is provided in the hydraulic system to release the load under the high-torque conditions occurring near bearing seizure.

In the first series of tests, oil was fed to each bearing through conventional pipe and tubing, using flexible connections to the bearing housing. In the second series, the oil was fed to the end of the hollow shaft through a rotating joint. The lubricating system was provided with a vane pump having a variable-speed drive and a relief valve. Runs could be made at constant oil-feed pressure or at a constant rate of oil flow. The oil-feed line also was fitted with a filter consisting of two layers of sheet cellulose, electric heaters for controlling the oil-inlet temperature, and a flowmeter used chiefly for control purposes. Determinations of oil flow also were made by weighing the amount of oil that flowed for a given time interval from the housing outlet into a measuring vessel.

² Numbers in parentheses refer to the Bibliography at the end of the paper.

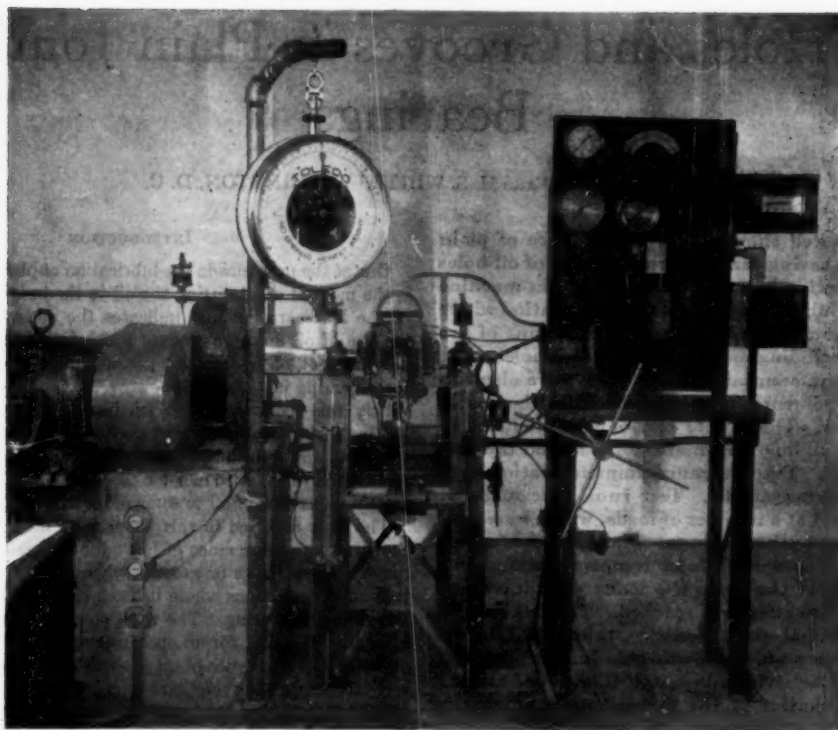


FIG. 1 FRICTION-MACHINE INSTALLATION

Operating temperatures were measured with copper-constantan thermocouples. One was fastened to the loaded side of each of the four bearings, and four thermocouples of equal resistance con-

nected in parallel, were spaced around the shaft, in the oil streams at the end of each bearing.

Shafts and Bearings. One solid test shaft was used in all of the first series of tests. It was made of SAE 3115 steel, carburized, and heat-treated to a hardness of 55 Rockwell C. The three hollow test shafts, $\frac{7}{16}$ in. inside bore, used in the second series of tests, were made of SAE 4615 steel, carburized, and heat-treated to hardnesses ranging from 58 to 61 Rockwell C. The surface roughness of each shaft was measured at 90-deg intervals at each of the four journal positions.

The averages of the observations for each shaft ranged from 4 to 5 microinches (rms profilometer). The journal diameters were measured 90 deg apart at each of the four journals on each shaft. The observations of diameters were accurate to 0.00005 in. at 68 F.

The shaft used in the first series of tests had no holes or grooves. In the second series, the shaft used with bearing sets S31, and S51 (see Fig. 3), had one radial oil hole at the mid-point of each bearing. The holes were 0.125 in. in diam and were chamfered to a diameter of approximately 0.180 in. at the shaft surface. The one used with bearing sets S32 and S52 was similar, except that two holes 180 deg apart were used for each bearing. The shaft for bearing sets S33 and S53 was similar to the shaft with one hole per bearing, except that instead of a chamfer, a flat, $\frac{5}{16}$ in. long (axially) and $\frac{3}{16}$ in. wide (depth about 0.004 in.), was located symmetrically at the end of each hole. The edges of the chamfers and flats were stoned and polished to remove sharp edges.

The test bearings were solid steel sleeves with copper-lead linings conforming to Pratt and Whitney Aircraft specification 121. They were pressed in the bearing retainers, rough-bored in a lathe, pushed in the self-aligning ball-bearing swivels, and then

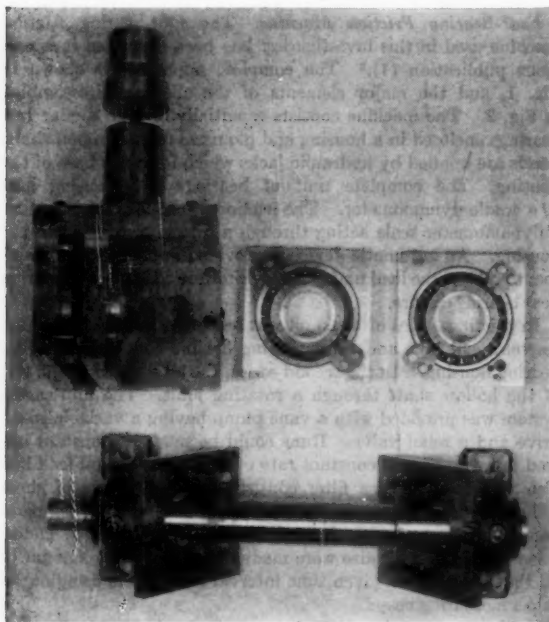
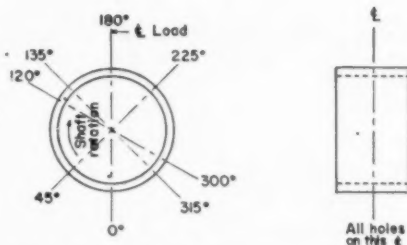


FIG. 2 FRICTION-MACHINE PARTS

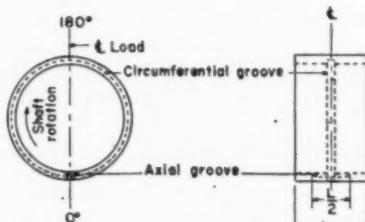
TABLE 1 ESSENTIAL DIMENSIONS OF SHAFTS AND BEARINGS

Design of oil feed	Bearing set	Length of bearing, L , inches	Avg. diam of bearing, inches	Avg. diam of shaft, D , inches	Avg. clearance, C , inches	Diameter-clearance ratio, D/C	Length-diameter ratio, L/D
1 hole in bearing	31	1.276	2.0679	2.0648	0.0031	663	0.620
	51	1.276	2.0699	2.0648	0.0051	403	0.620
2 holes in bearing	32	1.276	2.0679	2.0648	0.0031	663	0.620
	52	1.276	2.0699	2.0648	0.0051	403	0.620
Axial groove in bearing	33	1.276	2.0679	2.0648	0.0031	663	0.620
	53	1.276	2.0699	2.0648	0.0051	403	0.620
4 holes in bearing	34	1.276	2.0679	2.0648	0.0031	663	0.620
	54	1.276	2.0699	2.0648	0.0051	403	0.620
Circum. groove in bearing	35	1.125*	2.0579	2.0548	0.0031	663	0.547*
	55	1.125*	2.0599	2.0548	0.0051	403	0.547*
1 hole in shaft	531	1.276	2.0680	2.0649	0.0031	663	0.620
	551	1.276	2.0600	2.0649	0.0051	403	0.620
2 holes in shaft	532	1.276	2.0679	2.0548	0.0031	663	0.620
	552	1.276	2.0599	2.0548	0.0051	403	0.620
1 hole with flat in shaft	533	1.276	2.0677	2.0646	0.0031	663	0.620
	553	1.276	2.0597	2.0546	0.0051	403	0.620

*Allowance is made for circumferential grooves.



Sets 31 & 51, oil holes at 0°
 Sets 32 & 52, oil holes at 120° & 300°
 Sets 34 & 54, oil holes at 45°, 135°, 225°, & 315°
 All holes 0.125" diameter, chamfered to 0.18" diameter at edge



Sets 33 & 53, axial groove, 0.10" width, 0.04" depth
 Sets 35 & 55, circumferential groove, 0.150" width, 0.075" depth

FIG. 3 ARRANGEMENTS OF OIL HOLES AND GROOVES IN BEARINGS

finished to size with a special type of bearing reamer having a single cutting edge. With each bearing, determinations of four diameters 45 deg apart were made at each of three axial positions, one at the center, and one near each end. Bearings having circumferential grooves were measured on each side of the groove as well as at the ends. These measurements were accurate to 0.0001 in. at 68 F.

Bearings with one, two, or four oil holes, or with one circumferential or one axial groove were used in the first series of tests. Sketches showing the details of these arrangements are given in Fig. 3. With any of these arrangements each hole or groove was connected with the source of oil supply. In the second series of tests, the bearings had plain cylindrical surfaces. Two sets of bearings of different clearance were run for each type of oil feed.

The essential dimensions of the shafts and bearings are given in Table 1.

LUBRICANT

The oil used in these tests was an SAE 20 motor oil having an absolute viscosity of 70.8 centipoises at 100 F and 8.12 centipoises at 210 F.

FRICTION DATA

Tests at High ZN/P . With each set of bearings, tests first were made in the region of stable lubrication at the higher values of ZN/P (see nomenclature) in order to obtain characteristic data with a minimum of change in bearing surface. Each test run was made at a constant speed with a number of constant loads which were successively increased at intervals during each run. The apparatus was "warmed up" before the start of each test run and the data were obtained with the bearings in a steady state of temperature distribution.

Friction data obtained in these tests are given in Figs. 4, 5, 6, 7, 8, 9, 10 and 11 for the eight oil-feed systems. These results cover operation at an oil-inlet temperature of 200 F, two speeds, 2030 and 3040 rpm, and a range of loads from approximately 300 to 3000 psi on the projected area. In these figures f , the coefficient of friction, is plotted against the operating variable ZN/P . The values of Z used are based on temperature observations obtained with the thermocouples on the loaded side of each bearing shell.

With the bearings having a circumferential groove, the effective area of the loaded side of the bearing is reduced, and in plotting the data shown in Fig. 8, the values of P used were based on the effective area (total area minus area of groove). The slopes of the curves would be somewhat less if P were based on the total projected area of the bearing as was the case with the curves for the other designs of bearings.

Lines representing the Petroff equation for concentric running (2) for the respective D/C ratios used are also shown in the figures. The experimental data for a given bearing can be represented by a straight line roughly of the same general slope but displaced toward greater values of f than is given by the Petroff line for a given D/C ratio. This general trend of the data is similar to that obtained in an earlier investigation (3) where it was shown that the friction of a journal bearing could be represented approximately by the equation $f = k(ZN/P)(D/C) + \Delta f$, where Δf was an L/D correction and represents the difference (approximately) between the experimental data and the Petroff equation.

For purposes of comparison, values of Δf at $ZN/P = 10$ and $ZN/P = 70$ for each set of bearings tested are given in Table 2. The table also lists the average value of Δf (over the range of ZN/P from 10 to 70) for each set, and the average value for each type of bearing (two D/C ratios). The latter values are used as

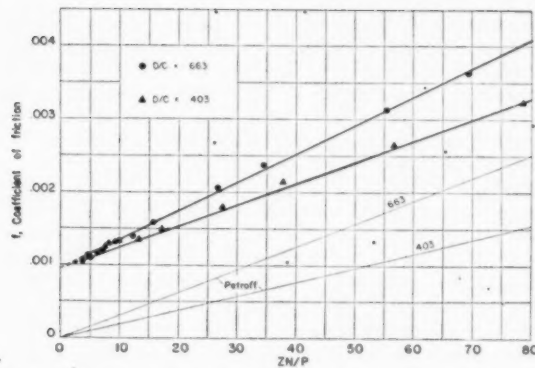


Fig. 4 FRICTION IN STABLE REGION FOR 2-IN. \times 1 1/4-IN. COPPER-LEAD BEARINGS HAVING ONE OIL HOLE IN BEARING (Operating at 2030 rpm with 15 cu. in. per min oil flow, and 3040 rpm with 22.5 cu. in. per min oil flow; SAE 20 oil at 200 F oil-inlet temperature.)

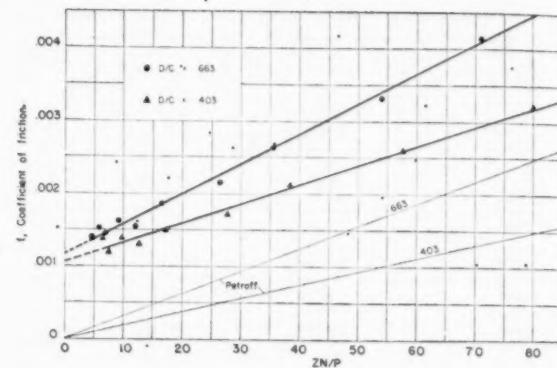


Fig. 5 FRICTION IN STABLE REGION FOR 2-IN. \times 1 1/4-IN. COPPER-LEAD BEARINGS HAVING TWO OIL HOLES IN BEARING (Operating at 2030 rpm with 15 cu. in. per min oil flow, and 3040 rpm with 22.5 cu. in. per min oil flow; SAE 20 oil at 200 F oil-inlet temperature.)

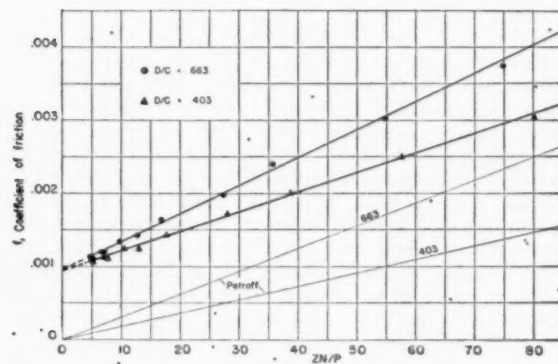


Fig. 6 FRICTION IN STABLE REGION FOR 2-IN. \times 1 1/4-IN. COPPER-LEAD BEARINGS HAVING AN AXIAL GROOVE IN BEARING (Operating at 2030 rpm with 15 cu. in. per min oil flow, and 3040 rpm with 22.5 cu. in. per min oil flow; SAE 20 oil at 200 F oil-inlet temperature.)

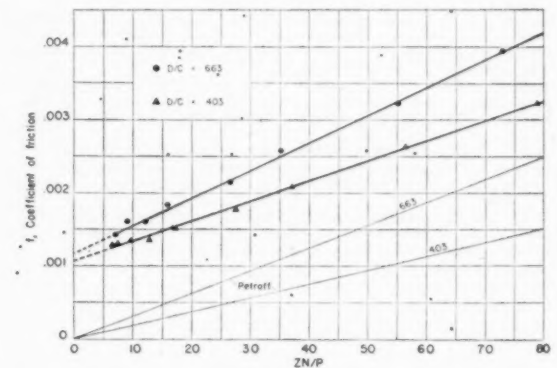


Fig. 7 FRICTION IN STABLE REGION FOR 2-IN. \times 1 1/4-IN. COPPER-LEAD BEARINGS HAVING FOUR OIL HOLES IN BEARING (Operating at 2030 rpm with 15 cu. in. per min oil flow, and 3040 rpm with 22.5 cu. in. per min oil flow; SAE 20 oil at 200 F oil-inlet temperature.)

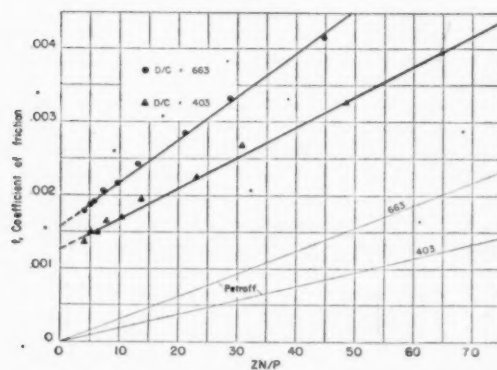


Fig. 8 FRICTION IN STABLE REGION FOR 2-IN. \times 1 1/4-IN. COPPER-LEAD BEARINGS HAVING A CIRCUMFERENTIAL GROOVE IN BEARING (Operating at 2030 rpm with 15 cu. in. per min oil flow, and 3040 rpm with 22.5 cu. in. per min oil flow; SAE 20 oil at 200 F oil-inlet temperature.)

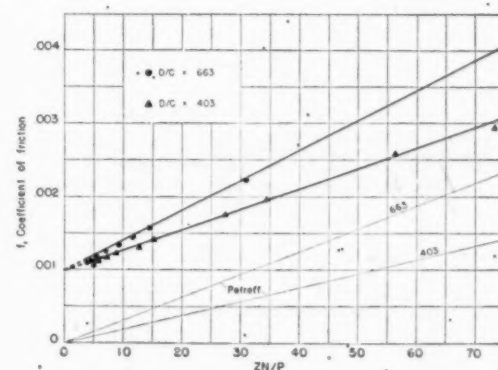


Fig. 9 FRICTION IN STABLE REGION FOR 2-IN. \times 1 1/4-IN. COPPER-LEAD BEARINGS WITH ONE OIL HOLE IN SHAFT (Operating at 2030 and 3040 rpm, 15 cu. in. per min oil flow, SAE 20 oil at 200 F oil-inlet temperature.)

Fig. 10

(Operati

a basis
point o
within
three g
tion; E
One
table i
having
two na
by Cl
lished
which
crease
of bea
area.
type
in Ta

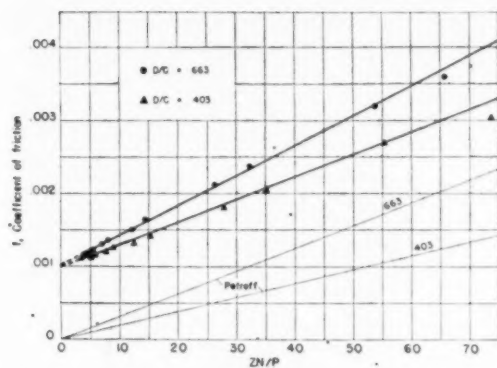


FIG. 10 FRICTION IN STABLE REGION FOR 2-IN. \times 1 $\frac{1}{4}$ -IN. COPPER-LEAD BEARINGS WITH TWO OIL HOLES IN SHAFT (Operating at 2030 and 3040 rpm, 15 cu in. per min oil flow, SAE 20 oil at 200 F oil-inlet temperature.)

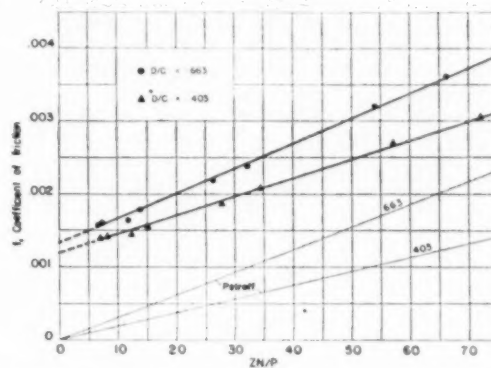


FIG. 11 FRICTION IN STABLE REGION FOR 2-IN. \times 1 $\frac{1}{4}$ -IN. COPPER-LEAD BEARINGS WITH ONE HOLE WITH FLAT IN SHAFT (Operating at 2030 and 3040 rpm, 15 cu in. per min oil flow, SAE 20 oil at 200 F oil-inlet temperature.)

a basis for rating the different types of bearings from the standpoint of friction. Since the differences between some types are within the probable experimental error, the ratings are given in three general groups: Group A, bearings of relatively low friction; B, intermediate; and C, high.

One of the most marked effects shown by the data given in this table is the relatively high friction obtained with the bearings having a circumferential groove, where the bearing is divided into two narrow bearing surfaces. This confirms the results obtained by Clayton (4). It also is in agreement with previously published data obtained at the National Bureau of Standards (3), which indicate that for L/D ratios less than unity, a decrease in L/D increases the friction. The data for this type of bearing were based on the effective area rather than the total area. If the latter is considered, the average value of Δf for this type of bearing would become 0.00217 instead of 0.00240 as given in Table 2.

The data for the bearings having two oil holes and four oil holes, of which one and two holes, respectively, were on the loaded side of the bearing, showed a slightly higher friction than for the sets having one hole or one axial groove, where the loaded side was undisturbed.

It is of interest that with the sets where the oil was fed through the shaft, there was only a relatively small increase in friction, although, during part of a revolution of the shaft, an oil hole was passing through the loaded portion of the bearing. This small increase is especially interesting with sets S33 and S53 where there was a relatively large flat on the shaft.

Tests at Low ZN/P . After the tests at high ZN/P , the range of operation with each set of bearings was extended to cover the lower values of ZN/P at and below the point of minimum f . In each test the speed and rate of oil flow were held constant and the load was increased in steps until unstable lubrication was reached.

TABLE 2 FRICTION RATINGS OF BEARINGS

Design of oil feed	Bearing set	$ZN/P=10$ Δf	$ZN/P=70$ Δf	Average Δf for each set	Average Δf for each design	Friction rating
1 hole in bearing	S1	0.00101	0.00149	0.00125	0.00130	A
	S1	0.00106	0.00164	0.00135		
2 holes in bearing	S2	0.00128	0.00187	0.00156	0.00147	B
	S2	0.00113	0.00159	0.00136		
Axial grooves in bearing	S3	0.00101	0.00143	0.00122	0.00124	A
	S3	0.00131	0.00149	0.00126		
4 holes in bearing	S4	0.00125	0.00155	0.00145	0.00143	B
	S4	0.00116	0.00136	0.00141		
Circum groove in bearing	S5	0.00186	0.00340	0.00263	0.00240	C
	S5	0.00149	0.00284	0.00217		
1 hole in shaft	S31	0.00109	0.00166	0.00136	0.00136	A or B
	S51	0.00107	0.00162	0.00134		
2 holes in shaft	S32	0.00112	0.00169	0.00140	0.00143	B
	S52	0.00111	0.00181	0.00146		
1 hole with flat in shaft	S33	0.00137	0.00183	0.00145	0.00146	B
	S53	0.00126	0.00186	0.00146		

One of the chief difficulties in obtaining representative data in the unstable region of lubrication is that the frictional characteristics of the bearings are affected by the roughness, geometry, and metallurgical features of the bearing surfaces, and, under operation, these frequently do not remain constant very long. Usually a bearing first tends to improve from the so-called running-in action (5), but when operation is continued under relatively high loads, speeds, and temperatures, the performance frequently is impaired and sometimes to a considerable degree. Accordingly, in running these tests, precautions were taken to minimize such effects by holding the bearings at a given load and speed for a relatively short time (2 min).

Friction data obtained in the first and fourth test runs when operating at 2030 rpm and with 15 cu in. per min oil flow with each of the eight designs of bearings are given in Figs. 12, 13, 14, 15, 16, 17, 18, and 19, where f is plotted against ZN/P . In Fig. 16 (as was the case in Fig. 8), the values of ZN/P used in plotting the data are based upon the effective area of the bearings.

In Figs. 12 to 19, inclusive, the differences between the curves for the first and fourth runs provide an indication of the change in bearing performance with running-in for a given set of bearings.

In these tests the bearings were operated at a given load for a period of 2 min (as was previously mentioned), and observations of the frictional torque were made at 1-min intervals. The values

of f given in the figures are based upon the second observation where conditions were more nearly in a steady state. One ex-

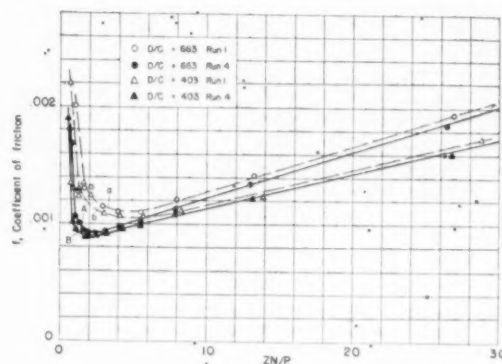


FIG. 14 FRICTION IN UNSTABLE REGION FOR 2-IN. \times 1 1/4-IN. COPPER-LEAD BEARINGS HAVING AN AXIAL GROOVE IN BEARING (Operating at 2030 rpm, 15 cu in. per min oil flow, SAE 20 oil at 200 F oil-inlet temperature.)

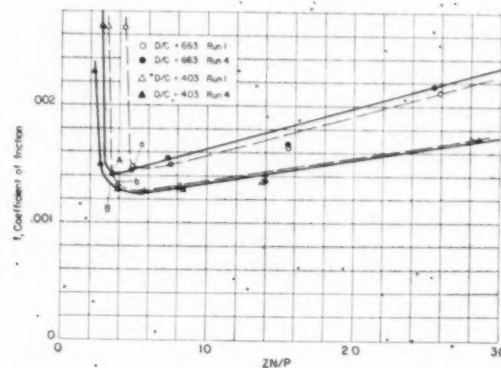


FIG. 15 FRICTION IN UNSTABLE REGION FOR 2-IN. \times 1 1/4-IN. COPPER-LEAD BEARINGS HAVING FOUR OIL HOLES IN BEARING (Operating at 2030 rpm, 15 cu in. per min oil flow, SAE 20 oil at 200 F oil-inlet temperature.)

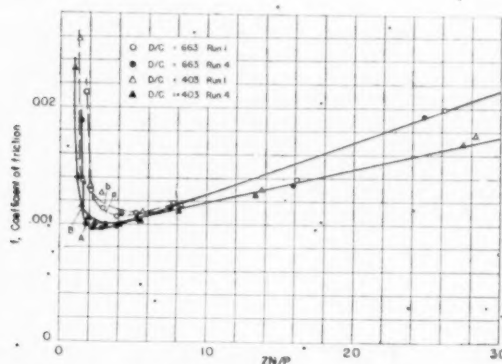


FIG. 12 FRICTION IN UNSTABLE REGION FOR 2-IN. \times 1 1/4-IN. COPPER-LEAD BEARINGS HAVING ONE OIL HOLE IN BEARING (Operating at 2030 rpm, 15 cu in. per min oil flow, SAE 20 oil at 200 F oil-inlet temperature.)

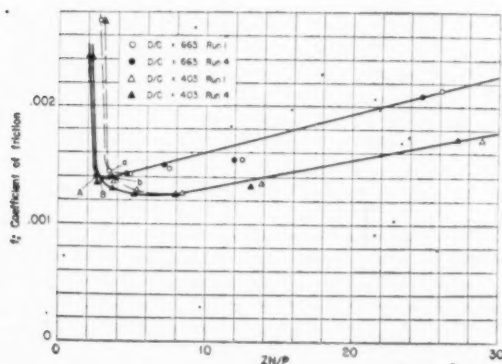


FIG. 13 FRICTION IN UNSTABLE REGION FOR 2-IN. \times 1 1/4-IN. COPPER-LEAD BEARINGS HAVING TWO OIL HOLES IN BEARING (Operating at 2030 rpm, 15 cu in. per min oil flow, SAE 20 oil at 200 F oil-inlet temperature.)

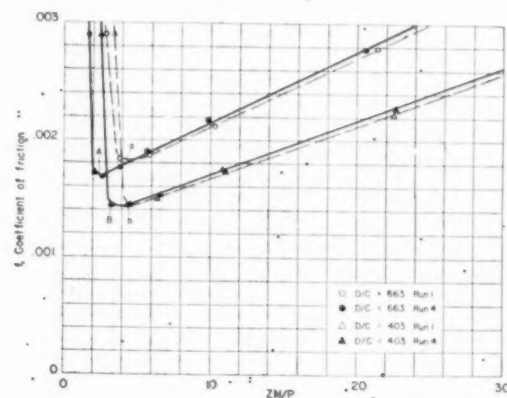


FIG. 16 FRICTION IN UNSTABLE REGION FOR 2-IN. \times 1 1/4-IN. COPPER-LEAD BEARINGS HAVING A CIRCUMFERENTIAL GROOVE IN BEARING (Operating at 2030 rpm, 15 cu in. per min oil flow, SAE 20 oil at 200 F oil-inlet temperature.)

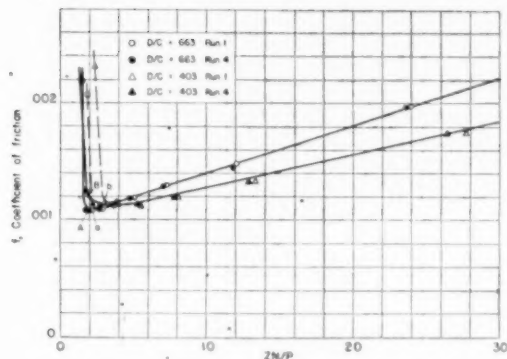


FIG. 17 FRICTION IN UNSTABLE REGION FOR 2-IN. \times 1 $\frac{1}{4}$ -IN. COPPER-LEAD BEARINGS WITH ONE OIL HOLE IN SHAFT (Operating at 2030 rpm, 15 cu in. per min oil flow, SAE 20 oil at 200 F oil-inlet temperature.)

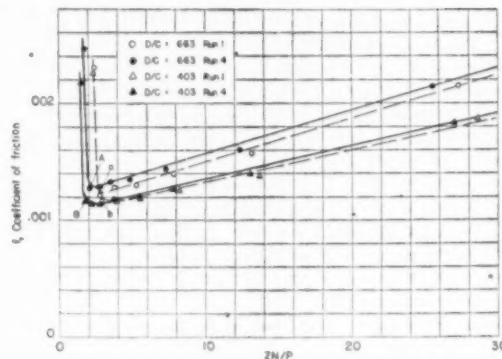


FIG. 18 FRICTION IN UNSTABLE REGION FOR 2-IN. \times 1 $\frac{1}{4}$ -IN. COPPER-LEAD BEARINGS WITH TWO OIL HOLES IN SHAFT (Operating at 2030 rpm, 15 cu in. per min oil flow, SAE 20 oil at 200 F oil-inlet temperature.)

ception to this is at the highest load in a given run where the friction rose rapidly and the automatic load release usually acted within 30 sec. When operation was in the region of stable lubrication, the second torque reading was either equal to or lower than the first, depending upon the particular rates of heating and cooling and the time required to reach a steady state.

As the loads were increased, the bearings eventually reached the unstable operating condition where the friction increased with an increase in temperature. In some of these tests this transition from stable to unstable conditions is fairly well defined by the friction curves, because the frictional torque rose rapidly and usually in a very short time reached a value high enough to trip the load release. In others, however, the change in the friction curve was more gradual, and the transition is more definitely indicated by the condition where the second torque reading is higher than the first. In Figs. 12 through 19, the approximate locations of these points of transition between stable and unstable lubrication obtained during the first test run with the bearings having a D/C ratio of 663 are indicated by the letter a and for the fourth run by A . Corresponding points obtained with the bearings having a D/C ratio of 403 are indicated by the letters b and B .

The critical values of ZN/P at which these transition points occur for the first and fourth runs with each set of bearings are given in Table 3. Also listed are the average values obtained with each type. Since the first run with each set of bearings may be significantly affected by the condition of the original surface finish, the values for the fourth run are used as a basis for rating the different types. These ratings provide an indication of the relative load-carrying capacity of the bearings when operating under the given conditions. They are indicated by letters rather than the numerical values, since (as was the case with the friction data at high ZN/P) the differences between some types are within the probable experimental error.

From the data given in Table 3 it will be noted that the values of ZN/P when unstable lubrication was reached were, in general, lower with the bearings having no holes or grooves on the loaded side (sets 31, 51, 33, and 53). In this connection, however, it is of interest that while the values obtained with the sets having one or two holes in the shaft were somewhat higher, they were sufficiently low to receive an A rating. Under the conditions of operation in these tests, the passage of an oil hole through the loaded portion of the bearing had relatively small effect on the points of transition between stable and unstable lubrication.

With the sets having a flat on the shaft, the reduction in area

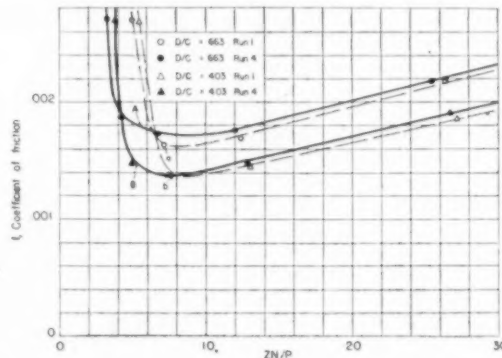


FIG. 19 FRICTION IN UNSTABLE REGION FOR 2-IN. \times 1 $\frac{1}{4}$ -IN. COPPER-LEAD BEARINGS WITH ONE HOLE WITH FLAT IN SHAFT (Operating at 2030 rpm, 15 cu in. per min oil flow, SAE 20 oil at 200 F oil-inlet temperature.)

was sufficient to cause a marked increase in the value of the critical ZN/P , and these sets have the lowest load-carrying capacity rating.

Because of the interference to the formation of a load-carrying film with the bearings having two holes, four holes, or a circumferential groove, the operation was impaired sufficiently to result in intermediate ratings. If the total area is considered for the bearings with a circumferential groove, the average critical value of ZN/P would increase from 2.8 to 3.1 and would change the rating from B to C .

The small difference between the bearings with the axial groove and with one oil hole indicates that the groove may be somewhat more effective in the distribution of the oil for maintaining the load-carrying film.

THERMAL BEHAVIOR

Data pertaining to the thermal behavior of these bearings were obtained in the tests at high ZN/P values under a steady state of temperature distribution. In the analysis of these data, consideration is given to the total heat supplied to the bearing. Since the oil-inlet temperature was higher than the ambient temperature, the temperature rise of the bearings was not only dependent upon the heat generated by shearing the oil in the bearings but also upon the heat delivered by the oil entering the bearings.

TABLE 3 LOAD-CARRYING CAPACITY RATINGS OF BEARINGS

Design of oil feed	Bearing set	First Run		Fourth Run		Load-carrying capacity rating
		Critical ZN/P for each set	Average critical ZN/P for each design	Critical ZN/P for each set	Average critical ZN/P for each design	
1 hole in bearing	31	3.2	3.2	1.7	1.6	A
	51	3.1	3.2	1.5	1.6	
2 holes in bearing	32	3.6	3.6	2.6	2.7	B
	52	3.6	3.6	2.6	2.7	
Axial groove in bearing	33	3.3	2.9	1.5	1.4	A
	53	2.6	2.9	1.2	1.4	
4 holes in bearing	34	5.0	4.4	3.4	3.4	C
	54	3.9	4.4	3.3	3.4	
Circum groove in bearing	35	4.2	4.2	2.4	2.8	B
	55	4.2	4.2	3.2	2.8	
1 hole in shaft	S31	2.2	2.6	1.9	1.8	A
	S51	3.0	2.6	1.8	1.8	
2 holes in shaft	S32	2.7	2.8	2.0	1.9	A
	S52	3.0	2.8	1.8	1.9	
1 hole with flat in shaft	S33	7.2	7.4	5.5	5.4	D
	S53	7.7	7.4	5.2	5.4	

The thermal data obtained with the two sets of bearings of different C/D ratios having a circumferential groove (sets 35 and 55) are given in Fig. 20. In this figure, H_t , the total rate of heat supply to one bearing from both the entering oil and bearing friction (expressed in in-lb per min) is plotted against the temperature rise above the ambient. The solid points indicate the rise in temperature above the ambient of the oil leaving the bearings (ΔT_o), as determined by thermocouples located in the oil streams at the ends of each bearing, while the open points represent the temperature rise of the bearings (ΔT_b) as determined by thermocouples placed in the loaded sides of the bearing shells. Since these tests were made at a steady state of temperature distribution, the data are also indicative of the rate of heat dissipation.

Analysis of the data in this figure indicates that the relation between the rate of total heat supplied to the bearings and the temperature rise above the ambient is dependent chiefly upon factors affecting the rate of heat dissipation by the oil, namely,

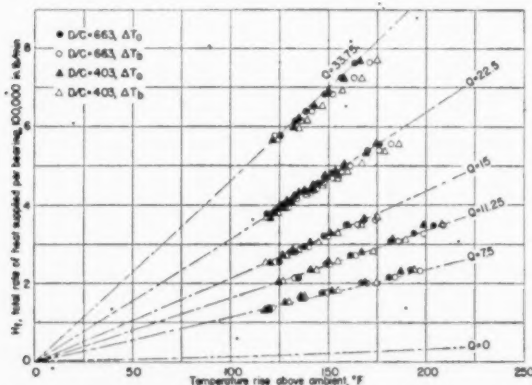


FIG. 20 THERMAL BEHAVIOR OF 2-IN. \times 1 1/4-IN. COPPER-LEAD BEARINGS HAVING A CIRCUMFERENTIAL GROOVE IN BEARING. Operating at 2030 and 3040 rpm. SAE 20 oil at 200 F oil-inlet temperature.)

rate of oil flow, specific heat of the oil, and temperature rise of the oil. This method of analysis has been outlined in detail in a previous publication (6), which also describes a method for determining from the data the rate of heat dissipation through the apparatus itself by radiation, conduction, and convection.

The lines drawn in Fig. 20 represent the H_t versus ΔT_o relationship for the indicated constant rates of oil flow (Q expressed as cu in. per min). The line $Q = 0$ represents the heat losses through the apparatus itself, and is used as a base for computing the lines representing the H_t versus ΔT_o for the different values of Q . These are obtained by computations involving the product of the rate of oil flow indicated, the temperature rise, and the average specific heat of the oil over the given temperature range. From the figure it will be noted that these computed lines are in reasonable agreement with all the experimental data based upon values of the average temperature above the ambient of the oil leaving the bearings.

In Figs. 21 and 22, H_t versus ΔT_o data are given for all sixteen sets of bearings when operating at 2030 rpm and a rate of oil flow of 15 cu in. per min. From these figures it will be noted that the data for all the bearings, having various arrangements of holes, or grooves, show the same general trend and fall reasonably well on the computed lines. This indicates that under the conditions covered, the heat-dissipation characteristics of the bearings were dependent chiefly upon the rate of oil flow through the bearings and were practically independent of clearance or the type of hole or groove used.

OIL FLOW

Measurements of the rate of oil flow at various oil-feed pressures were made also with each set of bearings when operating at a given load and speed. The flow-pressure data obtained with the bearings having a D/C ratio of 663, when operating at a load of 3008 lb per bearing ($P = 1148$ psi) and a speed of 2030 rpm, are given in Fig. 23, where Q , the rate of flow per bearing in cubic inches per minute is plotted against p the corrected oil-feed pres-

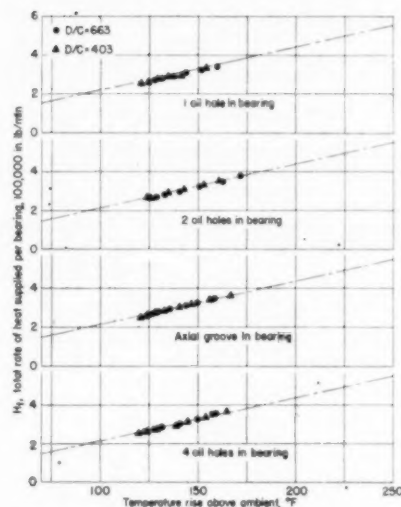


FIG. 21 THERMAL BEHAVIOR OF 2-IN. \times 1 $\frac{1}{8}$ -IN. COPPER-LEAD BEARINGS

(Operating at 2030 rpm, 15 cu in. per min oil flow, SAE 20 oil at 200 F oil-inlet temperature.)

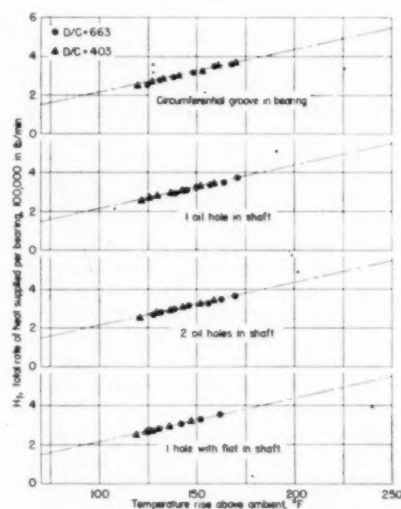


FIG. 22 THERMAL BEHAVIOR OF 2-IN. \times 1 $\frac{1}{8}$ -IN. COPPER-LEAD BEARINGS

(Operating at 2030 rpm, 15 cu in. per min oil flow, SAE oil at 200 F oil-inlet temperature.)

sure in pounds per square inch. Similar data for the bearings, having a D/C ratio of 403, are given in Fig. 24.

It should be pointed out that the data in these figures were obtained at constant load and speed but because of temperature changes caused by differences in friction and oil flow they were not obtained at constant viscosity.

The flow characteristics shown by these curves are dependent upon the particular operating conditions, hence the relative values are not necessarily applicable to other conditions. They are also dependent upon the particular dimensions of the holes and grooves used and changes in these dimensions may affect the relative values materially.

The most marked characteristics shown by these oil-flow data are the relatively high rates of flow obtained with the bearings

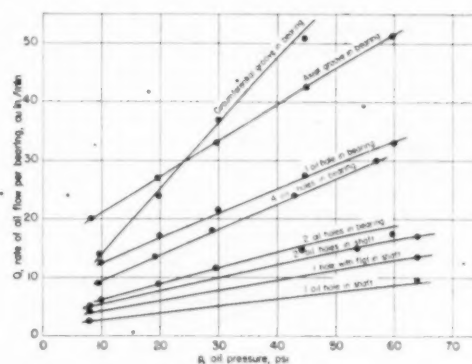


FIG. 23 OIL-FLOW VERSUS OIL-PRESSURE CURVES FOR THE DIFFERENT OIL-FEED ARRANGEMENTS WITH 2-IN. \times 1 $\frac{1}{8}$ -IN. COPPER-LEAD BEARINGS

($D/C = 663$, operating at 2030 rpm and 3008 lb load, SAE 20 oil at 200 F oil-inlet temperature.)

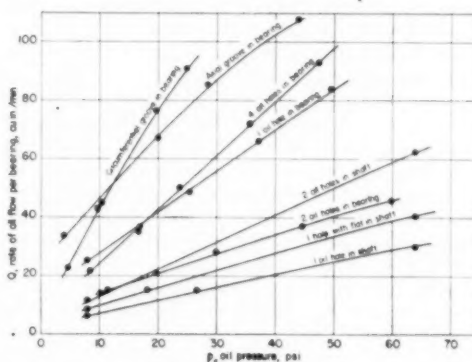


FIG. 24 OIL-FLOW VERSUS OIL-PRESSURE CURVES FOR THE DIFFERENT OIL-FEED ARRANGEMENTS WITH 2-IN. \times 1 $\frac{1}{8}$ -IN. COPPER-LEAD BEARINGS

($D/C = 403$, operating at 2030 rpm and 3008 lb load, SAE 20 oil at 200 F oil-inlet temperature.)

having the axial or circumferential oil grooves and the generally low rates obtained with the sets where the oil was fed through the shaft.

Since the rate of heat dissipation of the bearings depended chiefly upon the rate of oil flowing through the bearings, these flow data provide an indication of the relative heat-dissipation characteristics of the bearings tested under the operating conditions covered.

CONCLUSION

The influence of the various arrangements of oil holes and grooves on the behavior of bearings is as follows:

One Oil Hole in Bearing. With this arrangement, the absence of holes or grooves on the loaded side of the bearing provides for normal development of pressure in the oil film. Consequently, the bearing has relatively low friction and low ZN/P at transition between stable and unstable lubrication. While the single hole does not provide the highest oil flow, it would seem to be sufficient to provide adequate heat dissipation for most conditions.

Two-Oil-Hole Arrangement in Bearing. The single hole on the loaded side with this arrangement apparently disturbs the normal development of pressure in the film to make a measurable increase in friction and in ZN/P at the transition point. The par-

ticular location of the oil hole on the unloaded side is adverse from the standpoint of oil flow, hence the rate of heat dissipation is somewhat lower than the arrangement with one hole in the bearing.

Axial Groove in Bearing. This arrangement apparently provides a slightly better distribution of oil for the development of the load-carrying film than the arrangement with one hole in the bearing. Consequently, the bearing has low friction and lowest critical ZN/P , and the high oil flow provided is advantageous where forced cooling is necessary.

Four-Hole Arrangement in Bearing. This arrangement has two holes on the loaded side which disturbs the development of pressure in the film to a greater extent than the arrangement with two holes in the bearing, and its critical ZN/P is higher, but the friction is comparable. The two holes on the unloaded side are not in advantageous positions, and its oil flow and rate of heat dissipation is comparable to the arrangement with one hole in the bearing.

Circumferential Groove in Bearing. The groove dividing the bearing into two narrower parts increases the friction and causes a relatively high critical ZN/P . The high friction is counteracted by high oil flow and rate of heat dissipation.

One Oil Hole in Shaft. The passage of one oil hole across the loaded portion of the oil film has relatively small effect on both friction and critical ZN/P , which are only slightly higher than for the arrangement with one hole in the bearing. When the hole is exposed to some portions of the loaded area, the oil feed is practically shut off and consequently this arrangement results in the lowest oil flow and rate of heat dissipation.

Two Oil Holes in Shaft. With two oil holes for each journal, the disturbance to film-pressure development occurs twice in a revolution, resulting in slightly higher friction and critical ZN/P than with the arrangement with one hole in the shaft. The two holes also provide a greater oil flow and rate of heat dissipation. In this respect it is comparable to the arrangement with two holes in the bearing.

One Oil Hole With Flat in Shaft. The flat at the end of the oil-hole causes considerable disturbance to the development of pressure in the oil film, increases the friction, and markedly increases the critical value of ZN/P . Its oil flow and rate of heat dissipation are higher than the arrangement with one hole in the shaft without the flat but not sufficient to counteract the effect of its high ZN/P at transition from stable to unstable lubrication.

The results of these tests apply directly to unidirectionally loaded bearings for the particular range of conditions covered. The indicated differences between the various arrangements are not necessarily strictly indicative of more complex conditions where the load varies in both intensity and direction with respect to the bearings. It is believed, however, that the relative values obtained may be useful qualitatively in estimating the over-all effects of various arrangements of holes or grooves under more complex loading conditions, especially if proper consideration is given to conditions present throughout the complete load cycle.

BIBLIOGRAPHY

- 1 "Performance Characteristics of Journal Bearings With Forced-Feed Lubrication," by S. A. McKee, H. S. White, A. D. Bell, and J. F. Swindells, NACA Wartime Report ARR No. 4H15, August, 1944.
- 2 "Friction in Machines and the Effect of the Lubricant," by N. Petroff (a) in Russian, *Engineering Journal*, St. Petersburg, Russia, 1883; No. 1, p. 71; No. 2, p. 228; No. 3, p. 377; No. 4, p. 535. (b)

German translation by L. Wurzel, Hamburg, Germany, L. Voss, 1887, 187 pp.

3 "Friction of Journal Bearings as Influenced by Clearance and Length," by S. A. McKee and T. R. McKee, *Trans. ASME*, vol. 51, 1929, p. 161.

4 "Oil Grooves in Plain Bearings," by D. Clayton, *Engineering*, vol. 159, 1945, pp. 158-178.

5 "Effect of Running In on Journal-Bearing Performance," by S. A. McKee, *Mechanical Engineering*, vol. 49, 1927, p. 1335; vol. 50, 1928, p. 528.

6 "Measurements of the Combined Frictional and Thermal Behavior in Journal-Bearing Lubrication," by S. A. McKee, H. S. White, and J. F. Swindells, *Trans. ASME*, vol. 70, 1948, p. 409.

Discussion

M. D. HERSEY.³ Can the authors compare their results at any point with the work of Clayton and others, and amplify their application to engine bearings?

AUTHORS' CLOSURE

With reference to Mr. Hersey's question, the case of the bearings with 360-degree circumferential groove provides the closest approach to a direct comparison between our results and those of Clayton (4). Clayton's bearing h and our bearing set 35 are similar in diameter and length but differ in D/C ratio, that value for bearing h being 800 and for set 35 being 663. In Table 1 in his paper Clayton reports a value of the coefficient of friction of 0.0026 for bearing h when operating at a speed of 3000 rpm, a load of 1500 psi, and with the viscosity of the oil at 10.0 centipoises. Under these conditions the value of ZN/P is 20. The value of f for $ZN/P = 20$ for set 35 is about 0.00275. This is shown in Fig. 8 of our paper. An approximate correction to this value (based on the Petroff equation) to correspond to a D/C ratio of 800 would raise the value to about 0.00288. This would indicate that the value we obtained was about 10 per cent higher than that obtained by Clayton. In this connection, however, it should be pointed out that the NPL friction machine used by Clayton measures the bearing friction, whereas the NBS four-bearing friction machine measures the journal friction (see Norton's "Lubrication," 1942, p. 23). This difference in f in the two cases would seem to indicate that along a line perpendicular to the load the center of the journal was displaced from the center of the bearing about 0.00028 in., and, if it is assumed that the film thickness at the point of closest approach is somewhat smaller than the 0.0002 in. estimated by Clayton for bearing a (bottom hole), the angle between the line of the load and the point of closest approach would be of the order of 14 degrees. Since both of these values appear to be reasonable, it is believed that the friction data for the two bearings check rather closely.

Somewhat greater differences in f are shown when comparing Clayton's bearing a (one oil hole in unloaded side) with our set 31. However, this can be accounted for by the difference in L/D , which was 0.875 for bearing a and 0.620 for set 31.

Comparison of the data on oil flow is more difficult because of the complex relations between the factors involved. Rough corrections for differences in clearance, length, viscosity, and oil-feed pressure indicate that values from the two laboratories for similar types of bearings are of the same order of magnitude, but no attempt was made to evaluate the effects of differences in such factors as oil-inlet temperature, load, speed, or eccentricity.

³ U. S. Naval Engineering Experiment Station, Annapolis, Md.

This
by K. G.
1926, for
son's pro
curve for
results h
viously p
ventional
the prese
and calcu
gear-toot
tion, the
similar p
ted in te
and exte
diameter
whose vi
analytic
sented b

I T wo
ticular
paci
probable
tacting t
Three
been pub
1926 (2)
ing, tho
investig
count th
Karlson
of the lu

where Z
stant of
widely u

where 8

1 Mec
Station
1 Sch
ville, V
Station
1 Nu
Cont
sented
of the
Nort
underst
of the
Manus
Paper

Film Thickness Between Gear Teeth

A Graphical Solution of Karlson's Problem

By M. D. HERSEY¹ AND D. B. LOWDENSLAGER²

This investigation completes a solution, undertaken by K. G. Karlson in his little-known Swedish paper of 1926, for the oil-film thickness between gear teeth. Karlson's problem is characterized by the use of a parabolic curve for the viscosity-pressure relation. The numerical results here obtained are comparable with those previously published by Gatcombe, who used a more conventional viscosity-pressure formula. It is hoped that the present analysis will help to clarify the assumptions and calculations required in the hydrodynamic theory of gear-tooth lubrication. As an aid to its practical application, the relative film thicknesses found for geometrically similar pairs of gears are here shown by a chart constructed in terms of the appropriate dimensionless variables, and extending from zero to 10 microinches per in. of pitch diameter of the pinion. The limiting case of a lubricant whose viscosity is unaffected by pressure, for which an analytical solution had been given by Karlson, is represented by a straight line on this chart.

INTRODUCTION

It would be useful in studies of gear-tooth lubrication, particularly when efforts are being made to increase the load capacity of gear teeth, to be able to estimate, even roughly, the probable or possible thickness of the oil film between two contacting teeth under hydrodynamic conditions.

Three principal investigations toward this end have already been published, those of *Engineering* in 1916 (1),³ of Karlson in 1926 (2), and of Gatcombe in 1945 (3). The article in *Engineering*, though unsigned, is generally recognized as the pioneer investigation in our field. It does not, however, take into account the effect of high pressure on viscosity. The study by Karlson is based upon a parabolic equation for the viscosity, Z , of the lubricant as a function of the gage pressure p , namely

$$Z = Z_1 \left(\frac{p + k}{k} \right)^2 \quad [1]$$

where Z_1 is the viscosity at atmospheric pressure and k is a constant of the lubricating oil. Gatcombe's study is based upon a widely used exponential formula

$$Z = Z_1 (10)^{p\delta} \quad [2]$$

where δ is an empirical constant analogous to k .

¹ Mechanical Engineer, U. S. Naval Engineering Experiment Station, Annapolis, Md. Fellow ASME.

² School of Mathematics, University of Virginia, Charlottesville, Va.; Mathematics Aide, U. S. Naval Engineering Experiment Station, summer of 1949.

³ Numbers in parentheses refer to Bibliography at end of paper. Contributed by the Research Committee on Lubrication and presented at the Spring Meeting, Washington, D. C., April 12-14, 1950, of THE AMERICAN SOCIETY OF MECHANICAL ENGINEERS.

NOTE: Statements and opinions advanced in this paper are to be understood as individual expressions of their authors, and not those of the Navy Department, the Naval Service at large, or the Society. Manuscript received at ASME Headquarters, January 11, 1950. Paper No. 50-S-10.

Karlson's investigation was left unfinished, his integral for the load capacity of the film not being evaluated. Gatcombe's study was carried through and applied to a series of numerical examples. These numerical results were generalized by Hersey and Hopkins (4), in the form of a chart for the relative film thickness in geometrically similar gears. However, Blok (5) has questioned the accuracy of Gatcombe's mathematical approximations leading to the results utilized by Hersey and Hopkins. Accordingly, the present authors found it necessary to make a fresh approach to the subject, and therefore undertook a graphical solution of Karlson's problem.

BASIC ASSUMPTIONS

The physical assumptions which are customary in the theory of lubrication, and others pertinent to the gear-tooth problem, notably the following, have been made:

1 The lubricant is incompressible and without inertia; it has the same physical properties at every point and in every direction; it adheres to the solid surfaces and follows Newton's law of viscous flow.

2 The gear teeth are rigid and geometrically perfect, and therefore free from any appreciable effects of deformation, misalignment, manufacturing errors, surface roughness, or wear.

3 The gears are running at constant speeds without dynamic loading or appreciable vibration.

4 The temperature is uniform throughout the film at any moment, though it may vary greatly with operating conditions.

5 The mechanical action of the film has reached a practically steady state at every phase of contact, or angular position of the tooth; the approach process being so nearly completed that the minimum film thickness in every such position may be treated as a constant with respect to time.

These various assumptions define the scope of our investigation and limit it severely compared to what might ideally be desired (6, 7). It is hoped, however, that the present analysis may be useful in the absence of more exact knowledge, and that it may be followed by discussions which will greatly clarify the background of gear-tooth lubrication theory, thus facilitating the work that lies ahead.

INTEGRATION FOR LOAD CAPACITY

The normal tooth load F_n , which is the resultant force per unit of face width exerted by one tooth upon another at right angles to the tooth surface through the medium of the oil film, is given by

$$F_n = \int p \, dx \quad [3]$$

where p denotes the fluid pressure at any distance x measured in the direction of motion from the point of nearest approach.

Karlson's expression for the pressure distribution, derived from the usual hydrodynamic assumptions together with Equation [1] may be written

$$p = \frac{4HTk}{(1+T^2)^2 - 4HT} \quad [4]$$

Here T is the tangent of Gatcombe's angle S , and may be defined by

$$T \equiv \frac{-x}{\sqrt{2r h_0}} \quad [5]$$

where h_0 denotes the film thickness at the point of nearest approach; and r denotes the effective contact radius, defined by

$$\frac{1}{r} \equiv \frac{1}{r_1} + \frac{1}{r_2} \quad [6]$$

in which r_1 and r_2 are the radii of curvature of the pinion tooth and gear tooth, respectively. The dimensionless number H in Equation [4] is defined by

$$H \equiv \frac{Z_1 U \sqrt{2r h_0}}{k h_0^3} \quad [7]$$

where U denotes the mean tangential velocity $(U_1 + U_2)/2$ of the contacting surfaces, U_1 referring to the pinion and U_2 to the gear. It happens that H is equal to $1/12$ the ratio of Gatcombe's constant G to Karlson's constant k , both of which have the dimensions of pressure.

From Equation [4] it will be noted that $p = 0$ when $T = 0$, and, therefore, when $x = 0$. Thus the film pressure is assumed to vanish at the point of nearest approach. This assumption is known as Sommerfeld's condition, in contrast with Reynolds' condition under which both the film pressure and the pressure gradient vanish together at some point in the divergent portion of the film, appreciably removed from the point of nearest approach in the direction of motion. While the present authors subscribe to Reynolds' condition, they have tolerated the other for simplicity in completing Karlson's integration. A trial calculation indicates the difference in load capacity under the two assumptions to be of the order of 15 per cent, more or less, Reynolds' condition leading to the greater load capacity; hence our solution will be on the safe side. Both schools of thought concur for practical purposes in disregarding the region of negative pressure; hence the integration of Equation [3] need be carried out only on one side of the point of nearest approach.

Substituting from Equations [4] and [5] into [3] gives for the normal load per unit width

$$F_n = \frac{2 Z_1 U r}{h_0} \left(\frac{J}{H} \right) \quad [8]$$

where by definition

$$J \equiv \int_0^{\infty} \frac{4 H T dT}{(1 + T^2)^2 - 4 H T} \quad [9]$$

Equation [8] in conjunction with Equation [9] expresses the essential relation sought for, connecting load capacity with the minimum film thickness h_0 . Although these equations should be credited to Karlson, they have been confirmed by an independent derivation.

To evaluate the factor J/H occurring in Equation [8], we have found it sufficient to plot the integrand of Equation [9] as a function of T for five suitably spaced values of H and to measure the area under each curve. It may be shown analytically that $J/H = 2$ when $H = 0$, and that for perfectly rigid teeth, the maximum pressure p_m is infinite when $H = 0.770$. Thus by dif-

ferentiating Equation [4], the maximum pressure is found to occur when T equals $1/\sqrt{3}$. It is then given by

$$p_m = k \left(\frac{1}{1 - \frac{3}{4} \sqrt{3} H} - 1 \right) \quad [10]$$

which becomes infinite when $H = 4\sqrt{3}/9$, or approximately 0.77. The values of J/H so obtained are recorded in Table 1, and plotted against H in Fig. 1.

TABLE 1 RESULTS OF GRAPHICAL INTEGRATION

H	J/H
0.00	2.00
0.25	2.52
0.50	3.62
0.625	5.22
0.70	7.86
0.75	16.5
0.77	∞

NOTE: H and J are dimensionless; see Equations [7] and [9].

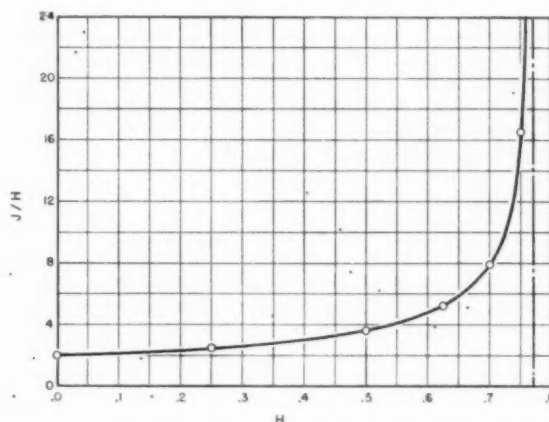


FIG. 1 PLOT OF VALUES FOUND BY GRAPHICAL INTEGRATION

To convert F_n values into the component F of tooth load per unit width acting tangentially to the pitch circle, which will be needed for computing the torque on the drive shaft, a factor C_0 , depending on the gear geometry, must be introduced, such that

$$F = C_0 F_n \quad [11]$$

where

$$C_0 \equiv k_0 L_e \cos \alpha \quad [12]$$

Here k_0 is the ratio of the average supporting action of the film at all tooth positions to its value F_n for the pitch-point phase; L_e is the average number of pairs of teeth meshing simultaneously, which governs the effective length of contact; and α the pressure angle. Gatcombe in the reference cited gave values for these constants applicable to a gear and pinion having a 5:1 reduction ratio with 24 teeth in the pinion, and to a rack and pinion described in the *Engineering* article (1) with 54 teeth in the pinion. The values of C_0 ranged from about 1.26 to 1.50.

CALCULATION OF FILM THICKNESS

Eliminating F_n between Equations [8] and [11], we obtain

for the relative film thickness, D being the pinion diameter at the pitch circle

$$\frac{h_0}{D} = C_1 \left(\frac{J}{H} \right) \quad [13]$$

where

$$C_1 \equiv \frac{2 C_0 Z_1 U r}{F D} \quad [14]$$

To find the correct value of J/H for use in Equation [13], we may solve Equation [7] for h_0 and substitute the expression so obtained into Equation [13], after which the resulting equation may be solved for J/H , giving

$$\frac{J}{H} = \frac{C_2}{H^{2/3}} \quad [15]$$

where

$$C_2 \equiv \frac{\sqrt[3]{2r}}{C_1 D} \left(\frac{Z_1 U}{k} \right)^{3/2} \quad [16]$$

Thus for any value of C_2 , representing the data of a given problem, we may plot the graph of Equation [15] in Fig. 1, or such portion as may be required to locate the intersection point. The ordinate of this point is the desired value of J/H .

It is more convenient in practice to express F in terms of P , the load per unit of projected area, this area being arbitrarily chosen as the product of the face width into the pitch diameter of the pinion. Thus

$$F \equiv P D \quad [17]$$

Similarly, it is more convenient to express U in terms of the pinion speed, or number of revolutions per unit time N . At the pitch point $U = U_1 = U_2$, where U_1 and U_2 are the tangential velocities of the tooth surfaces of pinion and gear, respectively. The effects of variations from pitch-point contact are included in the factor C_0 as shown briefly by Gatecombe (3), although a more complete exposition would be reassuring. If now ω_1 and r_1 denote, respectively, the angular velocity of the pinion tooth and its radius of curvature at the pitch point, it follows from the reference cited that U is equal to $\omega_1 r_1$. But ω_1 equals $2\pi N$, therefore

$$U = 2\pi N r_1 \quad [18]$$

Making these substitutions, the working constants become

$$C_1 = \frac{4\pi C_0 r_1 r}{D^2} \left(\frac{Z_1 N}{P} \right) \quad [19]$$

and

$$C_2 = \frac{\pi^{-1/2}}{2 C_0} \cdot \frac{D}{r_1^{1/2} r^{2/3}} \left(\frac{P}{k} \right)^{2/3} \left(\frac{Z_1 N}{P} \right)^{-1/2} \quad [20]$$

CONSTANTS OF THE LUBRICATING OIL

Evaluating Z_1 , the viscosity at atmospheric pressure, offers no difficulty aside from determining the mean effective equivalent film temperature, which has been assumed uniform—an important problem outside the scope of this paper. Evaluating Karlson's constant k requires an experimental knowledge of the viscosity-pressure curve for the lubricating oil at the temperature in question.

When the logarithm of the relative viscosity Z/Z_1 is plotted

against the gage pressure p at constant temperature, the graphs for most lubricating oils are by no means straight lines. They are commonly convex upward and can only be fitted by straight lines for a short interval near the origin, after which they bend over conspicuously. Karlson's equation takes account of this fact. From Equation [1] it will be seen that the logarithm of Z/Z_1 equals twice the logarithm of $(p+k)/k$ and approaches direct proportionality to the logarithm of p/k as the pressure approaches infinity. However, the graph of Karlson's equation falls somewhat below the true curve for the usual lubricating oil, just as the graph of Equation [2] falls too high, assuming that all three graphs have the same slope at the origin. This difficulty can be corrected to a first approximation by assigning a suitable value to the constant k , such that the graph will start out too steep, intersect the true curve near the middle of its pressure range, and drop below it at the high-pressure end, averaging about right.

Let b denote the pressure coefficient of viscosity at atmospheric pressure, elsewhere frequently denoted by b_1 . The pressure coefficient is the relative or fractional increase in viscosity per unit increase of pressure. Its value at atmospheric pressure is equal to the initial slope of the curve obtained when the natural logarithm of the viscosity is plotted against the pressure; and it may be taken equal to 2.30 times this slope when the common logarithm is plotted. Upon differentiating Equation [1], it will be seen that b is equal to $2/k$, from which

$$k = \frac{2}{b} \quad [21]$$

Now let b_0 denote the observed value of the initial pressure coefficient while b is the adjusted, or raised value, corresponding to the desired effective value of k . The adjustment ratio b/b_0 will evidently be greater, the greater the range of pressure over which a fit is required. A perfect fit at the origin would be obtained when b/b_0 equals unity. The corresponding value of k for use in Equation [1] is given by

$$k = \frac{2/b}{b/b_0} \quad [22]$$

Values of the adjustment ratio b/b_0 for two representative lubricating oils are plotted in Fig. 2 as a function of p_m , the maximum film pressure expected. These values were found by a trial fitting of Karlson's formula to the curves for petroleum oil 42 at 77 and 212 F, and castor oil at 167 F, given by Hersey and Hopkins in their paper of 1945 (4), Fig. 4. This fitting should be extended to a wider variety of oils and to higher temperatures. Equation [22] has been plotted in Fig. 3.

NUMERICAL EXAMPLES

In Tables 2 and 3 are given the results obtained by Equations [13], [15], [19], and [20], and associated procedure, for the five problems which had been solved in Gatecombe's paper (3). It is surprising what close agreement is found, considering (a) that the accuracy of his integration has been questioned, (b) that the viscosity-pressure relations used in his paper are based on a straight-line logarithmic equation, and (c) that our own adjustments for evaluating the viscosity constants are far from precise.

The symbols appearing in the tables have all been defined previously except for the abbreviations of units, most of which are familiar. The abbreviation m following the viscosity Z_1 refers to the millionth part of the pound-second per square inch, a convenient unit coming into more frequent use, equal to approximately 6.9 centipoises. This abbreviation is again employed in tabulating the values of $Z_1 N/P$, which are 60×10^4

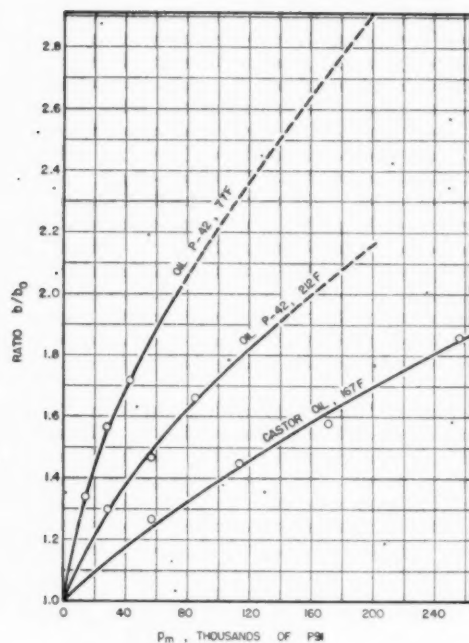


FIG. 2 ADJUSTMENT RATIO FOR PRESSURE COEFFICIENT

times as great as the values required for use in theoretical equations like [19] and [20].

In Table 3 the first two columns of h_0/D values are, respectively, those computed by Professor Gatcombe in the paper cited, and by the present authors, as explained in footnotes *a* and *b* of the table. The third column contains the limiting values for the imaginary case of zero-pressure coefficient, computed from Equation [13] with J/H set equal to 2.0, which is the value corresponding to $H = 0$ or $k = \infty$ in Equation [7]. The value 9.1 microinches per in. in problem No. 5 is recorded for comparison with the value 8.9 reported by *Engineering*. Finally, in the last column of Table 3 the influence of pressure on viscosity is plainly shown by tabulating the ratio of the film thickness, calculated for a given pressure coefficient, to that calculated for a zero coefficient this ratio varying from approximately 1 to 10.

TABLE 2 DATA FOR PROBLEMS

(Abbreviation m denotes millionths of a lb-sec/sq in.)

Problem no.	N rpm.	F lb/in.	P psi	$10^{-4} \mu_m$ psi	Temp deg F	Z_1 m	$10^{15} \mu$ psi ⁻¹	$10^{16} \mu$ psi ⁻¹
1	1750	197	98.5	56	95	5.5	8.74	20.1
2	1160	300	150	100	95	5.5	8.74	20.1
3	1750	197	98.5	206	199	0.26	4.14	9.54
4	1750	197	98.5	82	198	3.5	3.97	9.14
5	846	267	19.1	7.3	100	10.2	7.14	16.5

TABLE 3 SOLUTION OF PROBLEMS

(Mi/in. denotes microinches per inch of pinion pitch diameter; m denotes millionths of a lb-sec/sq in.)

Problem no.	b/b_0	k psi	k/P	$Z_1 N/P$ m rpm/psi	h_0/D mi/in. ^a	h_0/D mi/in. ^b	h_0/D mi/in. ^c	Pressure effect ^d
1	1.80	5530	56	97.8	8.4	8.1	1.52	5.3
2	2.13	4660	32	42.6	6.4	6.8	0.66	10.3
3	2.12	9890	100	4.6	0.7	0.7	0.7	1.1
4	1.28	17100	174	62.2	3.7	3.0	0.97	3.1
5	1.17	10500	550	456	10.4	11.4	9.1	1.3

^a From E. K. Gatcombe's paper (3).

^b By calculations of present paper.

^c For viscosity unaffected by pressure.

^d Ratio of h_0/D for the given pressure coefficient to that for zero coefficient.

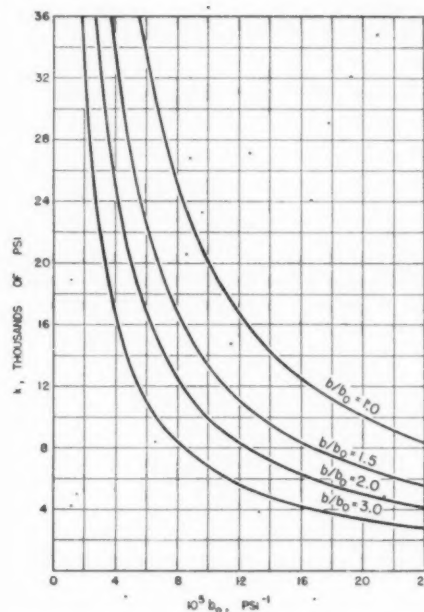


FIG. 3 KARLSON'S CONSTANT AND OBSERVED PRESSURE COEFFICIENT

FILM-THICKNESS CHARTS

Under the basic assumptions stated, dimensional analysis shows that the relative thickness h_0/D for geometrically similar pairs of gears can be plotted against the operating variable $Z_1 N/P$ and represented completely by a single family of curves, each identified by a constant value of one dimensionless parameter, provided the viscosity-pressure curve can be represented by an empirical equation containing only one constant besides Z_1 . Both Equations [1] and [2] satisfy this condition. When Equation [2] is chosen, and δ replaced by its equivalent $b_0/2.3$, the required parameter turns out to be $b_0 P$. Such a chart was given by Hersey and Hopkins in Fig. 2 of their paper (4), the notation $b_1 P$ then being used, and its value recorded as a percentage.

A chart of the same general type is now given in Fig. 4 using the parameter k/P based on Equation [2]. The value of k required in the application of this chart is that providing the best

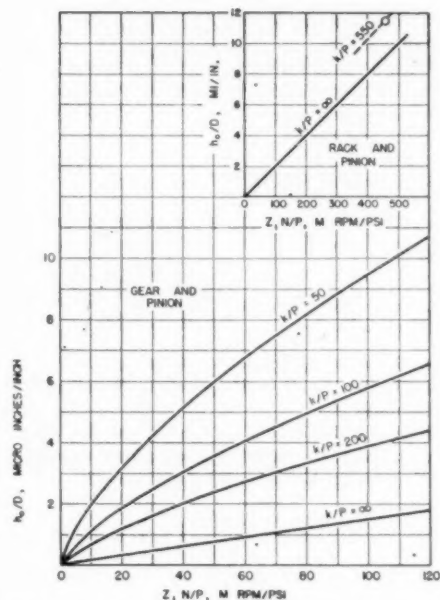


FIG. 4 FILM THICKNESS IN GEOMETRICALLY SIMILAR GEARS

fit of Karlson's formula to the experimental viscosity-pressure curve. Figs. 2 and 3 have been offered as a tentative guide in evaluating k until more systematic information can be made available.

The three curves labeled $k/P = 50, 100$, and 200 , were computed from Equations [13], [15], [19], and [20], and Fig. 1, without the aid of Figs. 2 and 3. These latter diagrams are called for only in the application, not in the construction of Fig. 4. The straight graph, identified by $k/P = \infty$, was constructed from Equation [13] in the special form corresponding to $H = 0$, namely

$$\frac{h_0}{D} = \frac{8\pi C_0 r_1}{D^3} \left(\frac{Z_1 N}{P} \right) \dots \dots \dots [23]$$

Equation [23] is equivalent to an equation published by Karlson (2), connecting the film thickness h_0 with the normal tooth load F_n . The small diagram in the upper corner of Fig. 4 shows on a compressed scale the corresponding graph for the rack and pinion described in *Engineering* (1), together with an isolated point representing our solution of problem No. 5. The h_0/D values computed for Table 3 fall exactly into place on Fig. 4 and might have been determined directly from the chart by interpolation.

The main family of curves in Fig. 4 should be found applicable not only to the gear and pinion described, but to any pair geometrically similar to these, regardless of absolute size; and to any lubricant following Karlson's equation, regardless of absolute viscosity. Moreover, it should be possible from the calculations developed in this paper to construct the appropriate charts for any pair of spur gears operating in accordance with the basic assumptions outlined. From an intercomparison of such charts the influence of the purely geometrical factors might be more clearly brought out.

ACKNOWLEDGMENTS

This brief study was undertaken as part of a survey of gear lubrication requested by the Bureau of Ships, Navy Department. The authors are indebted to Mr. H. Blok of Delft, Holland, and

to Prof. E. K. Gatzcombe of the U. S. Naval Post Graduate School, and to the ASME Research Committee on Lubrication, for information and comments that have been helpful in formulating the problem to be solved.

BIBLIOGRAPHY

- 1 "The Lubrication of Gear Teeth," *Engineering*, vol. 102, 1916, pp. 119-121.
- 2 "Kontaktproblem" (Contact Problem), by K. G. Karlson, *Teknik Tidskrift, Mekanik*, vol. 56, Jan. 16, 1926, pp. 1-6.
- 3 "Lubrication Characteristics of Involute Spur Gears," by E. K. Gatzcombe, *Trans. ASME*, vol. 67, 1945, pp. 177-188.
- 4 "Viscosity of Lubricants Under High Pressure. Co-ordinating the Data From Ten Investigations," by M. D. Hersey and R. F. Hopkins, *Mechanical Engineering*, vol. 67, 1945, pp. 820-824; vol. 68, 1946, pp. 676-683.
- 5 "Gear Wear as Related to the Viscosity of the Gear Oil," by H. Blok, *Proceedings of the Summer Conference on Mechanical Wear*, Massachusetts Institute of Technology, June, 1948 (in press); see also *De Ingenieur*, vol. 61, July 24, 1949, pp. 39-46.
- 6 "Physical Concepts of the Establishment of the Lubricating Oil Wedge and Its Associated Load Carrying Capacity for the Mating Tooth Surfaces of High Speed Gears," by E. K. Gatzcombe, *Symposium on Lubrication of High-Speed Turbine Gear Equipment*, Technical Publication No. 92, American Society for Testing Materials, Philadelphia, Pa., 1949, pp. 14-19.
- 7 "Tooth Contact Conditions in Spur and Helical Gears," by R. M. Macarthur, *Engineering*, vol. 168, 1949, pp. 654-657.

NOTATION

The following notation is used in the paper:

- C_0 = dimensionless constant depending only on the gear geometry; defined by Equation [12]
- C_1 = dimensionless constant defined by Equation [14]
- C_2 = dimensionless constant defined by Equation [16]
- D = pinion pitch diameter
- F = component of F_n tangential to pitch circle
- F_n = normal force on tooth per unit of face width due to film pressure
- H = dimensionless quantity proportional to $Z_1 U/k$ and depending also on film thickness; defined by Equation [7]
- J = dimensionless quantity proportional to tooth load; defined as a function of H in Equation [19].
- L_e = average number of teeth meshing simultaneously
- N = pinion speed in revolutions per unit time
- P = tooth load per unit of projected area formed by face width multiplied by pitch diameter; or ratio F/D , Equation [17]
- T = ratio of distance along tooth profile to square root of $2rh_0$, defined by Equation [5]
- U = mean of U_1 and U_2
- U_1 = tangential velocity of pinion-tooth surface
- U_2 = tangential velocity of gear-tooth surface
- Z = viscosity of lubricant at any point in film, as affected by pressure and temperature
- Z_1 = viscosity at atmospheric pressure but at temperature of film
- b = pressure coefficient of viscosity at atmospheric pressure, evaluated for optimum fit between theoretical and observed viscosity-pressure curves
- b_0 = observed pressure coefficient at atmospheric pressure
- h_0 = film thickness at point of nearest approach, also called minimum film thickness
- k = empirical constant in Karlson's parabola, Equation [1], expressing the viscosity-pressure relation
- k_0 = ratio of average F_n for all contact phases to value of F_n for contact at pitch point
- p = fluid pressure at any point in film as a function of x or T
- p_m = maximum value of p

- r = effective contact radius defined by Equation [6]
 r_1 = radius of curvature of pinion tooth at contact point
 r_2 = corresponding radius of curvature of gear tooth
 x = distance along tooth profile from point of nearest approach, considered positive in the direction of motion
 α = pressure angle fixed by gear geometry
 δ = empirical constant in Equation [2] proportional to pressure coefficient of viscosity
 π = as usual, 3.1416
 ω_1 = angular velocity of pinion

Discussion

H. Blok.* The paper touches upon the following important question, which forms the background to the present discussion: What are the limits inherent in the hydrodynamic lubrication of straight spur gears? Under the authors' five basic assumptions the answer doubtless is: There are no such limits, if viscosity increases quadratically with pressure according to Karlson's parabolic Equation [1]. This can easily be verified by referring to the critical cases, that is, the limiting cases where maximum oil pressure p_m becomes infinitely high (H assumes its critical value $4/3\sqrt{3} = 0.770$, as indicated by Expression [10], where H is defined by Equation [7]). In fact, it was shown by the authors that in the critical cases hydrodynamic load capacity F_n , as expressed by Equations [8] and [9], will become infinite. In this connection it is noteworthy that, in any given spur gear (given effective contact radius r ; see [7]) for any given atmospheric viscosity Z_1 , velocity U , and tolerable minimum film thickness h_0 , the critical value of H can in principle always be reached by proper choice of the empirical oil constant k , that is, of the oil. This indeed leads to the conclusion that, as long as all of the authors' basic assumptions as well as Karlson's viscosity-pressure relationship can be upheld, hydrodynamic load capacity in principle is unlimited.

It remains to be seen whether or not the basic assumptions and Karlson's relationship can be upheld, when the critical cases are approached.

In so far as Karlson's relationship is concerned, this was acknowledged by the authors to break down for the high oil pressures involved in the cases contemplated. Then, the following generalized viscosity-pressure relationship would have to be substituted for Karlson's

$$Z = Z_1(1 + p/k)^n \quad [24]$$

where n would be greater than 2; particularly, the higher the maximum oil pressure to be accounted for, the higher would n have to be.

With the foregoing generalized relationship, it is found that the critical cases, where maximum oil pressure becomes infinitely high, occur when the quantity H (see Expression [7]) becomes equal to its critical value H_c .

$$H_c = 4/3\sqrt{3}(n-1) \quad [25]$$

For instance, for $n = 8$, which the authors found to hold good for castor oil, H_c would amount to $4/21\sqrt{3} = 0.110$.

Further, it proves that, in contrast with $n = 2$ as in the paper (or more generally, $n \leq 3$), as soon as n is greater than 3; hydrodynamic load capacity in the critical cases no longer becomes infinitely high, but remains finite, notwithstanding that maximum

oil pressure continues to be infinitely high.⁵ This can be shown in the following way:

With Equation [24] instead of Karlson's relationship, Equation [1] of the paper, it can easily be deduced that the distribution of oil pressure p in the film, as a function of the variable T , is given by

$$p = k \left[\left\{ 1 - (n-1) \cdot H \cdot 4T / (1 + T^2)^2 \right\}^{-\frac{1}{n-1}} - 1 \right] \quad [26]$$

so that maximum pressure p_{max} , which occurs in the film section defined by $T = 1/\sqrt{3}$, is

$$p_{max} = k \left[\left\{ 1 - (n-1) \cdot \frac{3\sqrt{3}}{4} \cdot H \right\}^{-\frac{1}{n-1}} - 1 \right] \quad [27]$$

In fact, for $n = 2$, Equation [26] reduces to the authors' Equation [10] and, for $H = H_c$ (compare Equation [25]), p_{max} becomes infinitely high.

With Equation [26], instead of the authors' Equation [8], we now arrive at the more general expression for hydrodynamic load capacity F_n (compare Equation [3] of the paper):

$$F_n = \frac{2Z_1 U r}{h_0} \cdot \left(\frac{J_n}{H} \right) \quad [28]$$

where J_n represents the integral

$$J_n = \int_0^\infty \left[\left\{ 1 - \frac{16}{3\sqrt{3}} \cdot \frac{H}{H_c} \cdot \frac{T}{(1 + T^2)^2} \right\}^{-\frac{1}{n-1}} - 1 \right] dT \quad [29]$$

For the critical cases $H = H_c$, it now follows from analytical inspection of the singularity then occurring in the integrand of Equation [29] at $T = 1/\sqrt{3}$, that, in fact, as soon as $n > 3$, hydrodynamic load capacity remains finite, as then the Integral [29] converges.

By numerical evaluation it was found that for $n = 4$ and 6, in the critical cases $H = H_c$, the factor J_n/H amounts, respectively, to 11.9 and 7.25; this means that in these critical cases, the relative gains in hydrodynamic load capacity, as compared with the classical case where viscosity is assumed to be independent of oil pressure, are 5.95 and 3.63.⁶ It can be shown that at increasing values of n the critical J_n/H from Integral [29] monotonously decreases toward an asymptotic limit; this could be checked if the authors would communicate the critical value of the integral, Equation [29], that they computed for their value of $n = 8$.

Thus it would appear that with $n > 3$ the generalized viscosity-pressure relationship, Equation [24], in fact, results in a gain in hydrodynamic load capacity; this in contradistinction to the authors' case $n = 2$, where the gain is infinitely great. In this respect it should be noted that values of n greater than 3 (such as 8) are more representative of actual lubricating oils than the originally proposed value $n = 2$. Let us consider this point further in the light of the theory by Gatecombe,⁷ who used the same basic assumptions as the authors, but based his calculations on a viscosity-pressure relationship different from Equations [1] and [24],

⁵ By utilizing the method worked out by W. Weibull in his paper: "Glidlager teori med variabel Viskositet" (Theory of Slider Bearings With Variable Viscosity) in the Swedish journal *Teknisk Tidskrift, Mekanik*, vol. 55 (1925), pp. 164-167, it can also be shown that, if in Equation [24] the exponent n is smaller than unity, there are no critical cases at all; in other words, maximum oil pressure then could never become infinitely high.

⁶ It should be noted that for pressure-independent viscosity—the factor J_n/H from Equation [28] assumes the value 2.

⁷ Reference is to author's Bibliography (3).

* Senior Research Engineer, Koninklijke/Shell-Laboratorium, Delft, Holland.

that is, on the exponential relationship Equation [2] of the paper.

Now, the authors themselves have already compared Gatecombe's results with theirs (Table 3), but, as Gatecombe had not been able to evaluate his theory in an exact analytical way, for their purpose the authors had to confine themselves to Gatecombe's "approximate" evaluation. However, it can be shown by the following arguments that the approximation involved is no longer tolerable when a critical case is approached.

Gatecombe's exact result can be written in the form of Equation [28], if the numerical factor (J_n/H) is replaced by B

$$B = -\frac{1}{A} \int_0^{\pi} \ln[1 - A(\sin 2S + \frac{1}{2} \sin 4S)] \cdot \sec^2 S \cdot dS \quad [30]$$

where the nondimensional quantity A is defined by

$$A = \frac{1}{12} G \delta \ln 10 \quad [31]$$

if Gatecombe's notation is upheld, or, if rewritten in the authors' notation by

$$A = Z_1 U (2r)^{1/2} \cdot h_0^{-3/2} \delta \ln 10 \quad [32]$$

Gatecombe's approximation amounts to the same thing, as replacing the exact value of B Integral [30] by the approximate one

$$B \approx \frac{\pi}{120} \cdot \left[4\pi \ln 10 - \frac{27}{A} \cdot \ln \left(1 - \frac{3\sqrt{3}}{4} A \right) \right] \quad [33]$$

As was shown by Gatecombe, with the exponential viscosity-pressure relationship, Equation [2] of the paper, critical cases arise, that is, maximum pressure theoretically becomes infinitely high, when A becomes equal to its critical value⁸ of $4/3\sqrt{3}$.

Whereas, for the critical value of A , the integrand of Integral [30] shows a singularity at $S = \pi/6$, it can be shown by analytical inspection that yet this integral converges, so that the corresponding value of B or, say, hydrodynamic load capacity remains finite in the critical cases. On the other hand, Gatecombe's approximate value for B (see Expression [33]) becomes infinite for the critical value of A . This proves that, in fact, Gatecombe's approximation is no longer tolerable when a critical case is reached or approached.

In view of the background to the present discussion, we are left with the problem of computing, from Integral [30], a workable expression for B that is applicable at least to the critical and the near critical cases. Fortunately, it proves that an exact evaluation of the integral of Equation [30] is possible, so that this evaluation is even applicable to the whole physically significant range $0 \leq A \leq 4/3\sqrt{3}$. The method of exact evaluation found will now be elucidated, the more so as it is also applicable to the authors' Integral [9].

Changing to the authors' variable T , and partially integrating Integral [30], it is easily found that

$$B = 12 \int_0^{\infty} \frac{TdT}{(1+T^2)^3 - 4.4T} - 16 \int_0^{\infty} \frac{TdT}{(1+T^2)[(1+T^2)^2 - 4.4T]} \quad [34]$$

The foregoing two integrals can, in fact, be evaluated in terms of elementary functions by observing that the integrands can be re-

solved into partial fractions of no higher than the second degree, namely, as follows:

According to Descartes' well-known method of solving biquadratic equations, the form $[(1+T^2)^2 - 4.4T]$ can be resolved into the product of two quadratic forms

$$(1+T^2)^2 - 4.4T = (T^2 - uT + v)(T^2 + uT + w) \quad [35]$$

where u , v , and w are determined, for any given A , by the positive root of Descartes' "cubic resolvent"⁹

$$y^3 + 4y^2 - 16A^2 = 0 \quad [36]$$

That is, u , v , and w follow consecutively from the formulas

$$u = \sqrt{y} \quad [37a]$$

$$v = \frac{1}{2} (2 + y - 4A/\sqrt{y}) = \frac{1}{2} (2 + u^2 - 4A/u) \quad [37b]$$

$$w = \frac{1}{2} (2 + y + 4A/\sqrt{y}) = \frac{1}{2} (2 + u^2 + 4A/u) \quad [37c]$$

In this way, the integrals in Equation [34] were actually evaluated in an exact analytical way. As, however, for an arbitrary value of A , within the range $0 \leq A \leq 4/3\sqrt{3}$ to be considered, the expression for B is rather unwieldy, the expression for the critical case only of $A = 4/3\sqrt{3}$ will be given here, namely

$$B = \frac{3}{2} \cdot [(\sqrt{3} - \sqrt{2}) \cdot \pi + \ln 3 + 2\sqrt{2} \cdot \tan^{-1} (2\sqrt{2})^{-1}] = 4.588 \quad [38]$$

Thus we arrive at the conclusion that, with the exponential viscosity-pressure relationship Equation [2] of the paper, in the critical cases hydrodynamic load capacity is only $4.588/2 = 2.294$ times as high as it would be when viscosity is constant, that is, not affected by pressure. This entails, of course, that Gatecombe's approximation can no longer be upheld in those cases where it predicts a relative gain (called "pressure effect," in the last column of the authors' Table 3) in hydrodynamic load capacity that is greater than 2.294. Such cases are represented by Gatecombe's problems Nos. 1, 2, and 4; thus only to problems Nos. 3 and 5 can some significance be attached for the authors' purpose of comparing their results with Gatecombe's.

So far, the authors' and Gatecombe's basic assumptions have been upheld; it remains to be seen, however, whether these assumptions are permissible, and if not sufficiently so, when they will break down. Here we shall solely consider the question of the validity of the assumption about the perfect rigidity of the mating tooth faces. The reason that it can be made acceptable is that only the elastic distortion of the tooth faces, such as actually occurs when oil pressures in the film are sufficiently high,¹⁰ can, in conjunction with the increase in viscosity with pressure, contribute substantially to hydrodynamic load capacity; thus we might arrive at an explanation of the remarkable fact that in practice there are many cases of gears where hydrodynamic load capacity obviously is very much greater than would be predicted by Martin's anonymous paper (1)¹¹ on the elementary theory of hydrodynamic lubrication of gear teeth.

It will be evident that tooth faces may no longer be considered

⁸ It is easily demonstrated that, for $0 \leq A \leq 4/3\sqrt{3}$, which is the physically significant range of A , the cubic Equation [36] has one positive root only.

¹⁰ The type of elastic distortion meant here was called "hydrodynamic depression" in the present writer's paper: "Fundamental Mechanical Aspects of Thin-Film Lubrication," (read on March 4, 1950, before the New York Academy of Sciences); in this paper further particulars about the relevant gain in hydrodynamic load capacity can be found.

¹¹ Reference is to authors' Bibliography (1).

⁹ By sheer coincidence the critical value for A happens to be the same as the one for the authors' H in their case of $n = 2$.

to be perfectly rigid in those cases where the maximum film pressure, as calculated by the theory to be checked, attains or exceeds the order of magnitude of the Hertzian contact pressure that would obtain for the load considered if there were no oil film at all. In fact, in such cases the elastic distortions of the tooth faces under the high oil pressures must be comparable with those according to the Hertzian theory of elastic contact. This means, however, that, with the small minimum film thicknesses involved, the geometry of the film, and thereby the distribution of film pressures and hence the corresponding hydrodynamic load capacity, must be altered appreciably. Examples of the foregoing cases are provided by all of Gatecombe's problems, except No. 5 (compare the authors' Table 3).

It would also appear that the somewhat disturbing critical cases with their infinitely high maximum oil pressures would disappear automatically when the elastic distortions of the tooth faces are taken into account. Anyway, in cases representative of the beneficial effects on hydrodynamic load capacity of the increase of viscosity with pressure, the additional beneficial effects of the elastic distortions mentioned have to be accounted for simultaneously. Of course this renders the computer's task much more difficult; however, some headway has already been made and it is hoped that the results can be published in the not too distant future.

AUTHORS' CLOSURE

It is reassuring to have Mr. Blok's opinion that the effect of elastic deformation is to increase the film thickness. This confirms the authors' belief that the assumption of rigid teeth gives film thickness values on the safe side, the true values being greater than calculated. It was not the authors' desire to defend that assumption but only to treat it as a limiting case. Let us hope that new investigations will soon be available in which elastic deformation is combined with hydrodynamic action. Meldahl¹² took a long step in this direction but did not include the viscosity-pressure effect.

Mr. Blok offers constructive comment in two principal directions: first, by explaining the question he had raised (5) regarding the accuracy of Gatecombe's theory, and providing an exact analytical solution; second, by outlining a solution for rigid teeth based on a more general form of the viscosity-pressure relation, namely Equation [24].

This equation is a fairly obvious generalization of Karlson's parabola, the only change being the substitution of an empirical exponent n in place of the parabolic exponent 2. The same generalization had also been investigated by the authors, and the main results stated during the oral presentation of the paper. These are summarized below in response to Mr. Blok's inquiry regarding the critical value of the load integral in Equation [29] when $n = 8$.

Proceeding as in Karlson's paper except for the use of n in place of 2, the authors had arrived at relations identical with Equations [26] to [29] by completely analytical steps. Equation [29] was then integrated graphically for chosen values of H , leading to the round number $J_n/H = 6$ when $n = 8$ and H has the critical value $H_c = 0.110$. An analytical proof that the load integral remains finite in the critical case if n is greater than 3 had been given by Mr. Lowdenslager.

A more precise solution was then made in which the area under the pressure curve was evaluated by a semianalytical method.

¹² "Contribution to the Theory of the Lubrication of Gears and of the Stressing of the Lubricated Flanks of Gear Teeth," by A. Meldahl, *Brown Boveri Review*, vol. 28, 1941, pp. 374-382.

The tail of the diagram from T_1 to infinity, where T_1 is large compared to the value T_0 at which the formula gives infinite pressure, was computed by treating T_0/T as a negligible quantity. The peak area was evaluated by neglecting $T-T_0$ in comparison with T_0 , using a factored expression kindly suggested by Prof. J. T. Burwell, Jr., of M.I.T. The mean of both methods gave $J_n/H_c = 6.2$. This is in good agreement with a more exact value, 6.23, communicated by Mr. Blok. In fact, Mr. Blok and the authors, working independently, arrived at similar conclusions on every essential aspect of the problem.

All the values found for J_n/H_c are plotted in Fig. 5 as a function of n . Fig. 6 has been constructed with the aid of Fig. 5 and can be offered as a tentative generalization of Fig. 1. In Fig. 6 the dashed curves for $n = 3, 4, 6$, and 12 have been drawn in free-hand from $H = 0$ to their known end-points corresponding to $H_c = 0.384, 0.257, 0.154$, and 0.070 respectively, and faired by cross-plotting of H against n at constant values of the ordinate.

From Fig. 6 and its future refinements, in conjunction with Equations [13], [15], [19], and [20] of the paper it should be possible to generalize the film-thickness chart, Fig. 4, for all values of n . In the meantime, the practical use of Fig. 4, with Karlson's exponent 2, requires only that suitable values be selected for the empirical constant k with the aid of Fig. 3, as described in the paper.

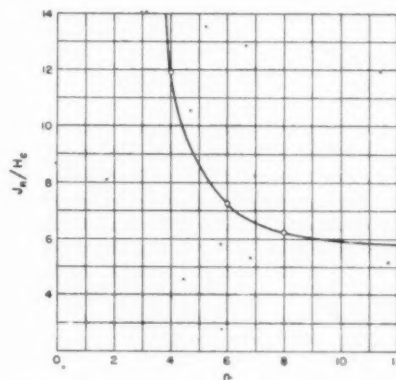


FIG. 5 CRITICAL LOAD FACTOR FOR DIFFERENT EXPONENTS n

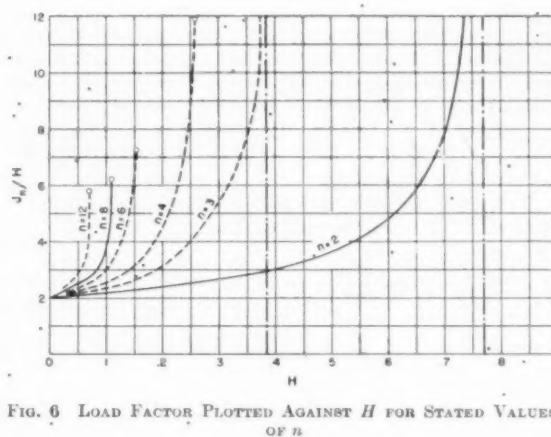


FIG. 6 LOAD FACTOR PLOTTED AGAINST H FOR STATED VALUES OF n

Thermal-Shock and Other Comparison Tests of Austenitic and Ferritic Steels for Main Steam Piping

By W. C. STEWART¹ AND W. G. SCHREITZ,¹ ANNAPOLIS, MD.

Thermal-shock tests of 6-in. pipe-and-valve assemblies, representing both austenitic and ferritic steels in 80 and 160 schedules, are described. The shock-testing procedure was devised to simulate conditions resulting from carry-over of boiler feedwater into main steam lines operating at 900 or 2000 psi pressure, 1050 F temperature. Other test procedures described include cyclic deflection tests of full-size mock-ups consisting of 160 schedule pipe and valves for simulating expansion bends. Results are reported for mock-ups of both austenitic and ferritic materials which were tested at 2000 psi pressure, 1050 F temperature. Each assembly was subjected to 4000 or more deflections corresponding to expansion cycles that would obtain on heating up a piping system from room temperature to 1050 F once every 2 days for approximately 20 years.

INTRODUCTION

DECISION to investigate the feasibility of utilizing 18-8 chromium-nickel-type steel for main steam piping for 1050 F temperature service was prompted by the superior strength properties of the material at temperatures above 1000 F. Moreover, the superior high-temperature properties of the austenitic steels over the ferritic steels for temperatures above 1000 F are reflected in the higher working stresses allowed by the ASME Boiler Code. The higher working stresses for austenitic steel should permit the use of thinner and lighter pipe which, at the higher pressures, is particularly advantageous from the standpoint of increased flexibility and weight saving. On the other hand, thermal expansion is greater for austenitic steel than for ferritic steel, and this fact must not be overlooked in considering flexibility factors.

No experience with austenitic steel for main steam piping has been reported, although the material has been used for boiler feed lines. H. Weisberg² has reported on cyclic heating tests of main steam-piping joints between ferritic and austenitic steels. Reports from the oil industry of failures of components in pipe lines used to convey charges of hot oil from cracking stills created doubt as to the suitability of austenitic steel for main steam piping.

It is reported that components in austenitic-steel pipe lines have shown much greater susceptibility to cracking as a result of thermal shock produced by the periodic flow of hot oil than have similar components of ferritic-steel pipe lines. In view of this

information it did not seem unreasonable to assume that austenitic steel might exhibit similar susceptibility in steam service under conditions of thermal shock occasioned by boiler-water carry-over. Moreover, experience has been cited which indicates strength deficiencies for austenitic-steel castings as well as for welded joints between austenitic pipe and castings.

There are numerous points of difference between pipes carrying hot oil as previously mentioned and main steam lines. In the case of oil pipe lines, the pressures are fairly low and the temperature of the oil high. For steam lines under consideration the pressure is high and the temperature intermediate by comparison. In the oil pipe lines conditions producing high thermal gradients recur regularly, while conditions producing similar gradients in steam lines occur only infrequently as a result of boiler-water carry-over. Then, there is the difference in heat-transfer characteristics for the two processes which appears to be an important factor in favor of steam applications. Hot oil on passing through a relatively cold pipe causes the inside layer to expand. This expansion is resisted by the colder outer layers with the result that the inside is stressed in compression. Cracking occurs on cooling when the inside of the pipe is in tension.

The introduction of a quantity of boiler water along with the steam flow cools the inside surface, producing a thermal gradient in the pipe wall. Contraction of the quenched layer is resisted by the outer layers of the pipe which are at higher temperature, with the result that the inside of the pipe is subjected to a tensile stress. Therefore any tendency to cracking in steam pipes under thermal shock associated with feedwater carry-over would be expected to occur on quenching.

In setting up the test program, it was decided to subject full-scale pipe-and-valve assemblies to thermal-shock conditions simulating boiler-water carry-over. It was reasoned that this procedure would produce the maximum temperature gradient in the pipe wall that could be expected in service. A second series of tests included in the program consisted of subjecting full-scale mock-ups to deflection cycles designed to simulate stress conditions produced in expansion loops on heating and cooling. At the outset, it was the intention to test only the austenitic material under thermal shock. Later, it was decided to conduct parallel tests of 2 $\frac{1}{4}$ Cr-1 Mo steel throughout.

In order that information on the strength properties of the particular test materials might be available, a laboratory test program was included as a phase of the investigation. Specimens for this purpose were fabricated from sections of 6-in., 80, and 160-schedule pipes and cast cylinders designed to simulate cast valve bodies. The same welding procedures were employed in fabricating these test sections as were used in welding the thermal-shock assemblies and mock-ups.

Welding of the original test assemblies, including the specimens for the laboratory test program, was performed by a large commercial fabricator utilizing production welding practices with regard to qualification of welders, number of welders employed on the job, shift work, and extent of supervision exercised over the welders.

¹ United States Naval Engineering Experiment Station.

² "Cyclic Heating Tests of Main Steam-Piping Joints Between Ferritic and Austenitic Steels—Sewaren Generating Station," by H. Weisberg, Trans. ASME, vol. 71, 1949, pp. 643-649.

Contributed by the Power Committee and presented at the Spring Meeting, Washington, D. C., April 12-14, 1950, of THE AMERICAN SOCIETY OF MECHANICAL ENGINEERS.

NOTE: Statements and opinions advanced in papers are to be understood as individual expressions of their authors and not those of the Society. Manuscript received at ASME Headquarters, February 27, 1950. Paper No. 50-S-23.

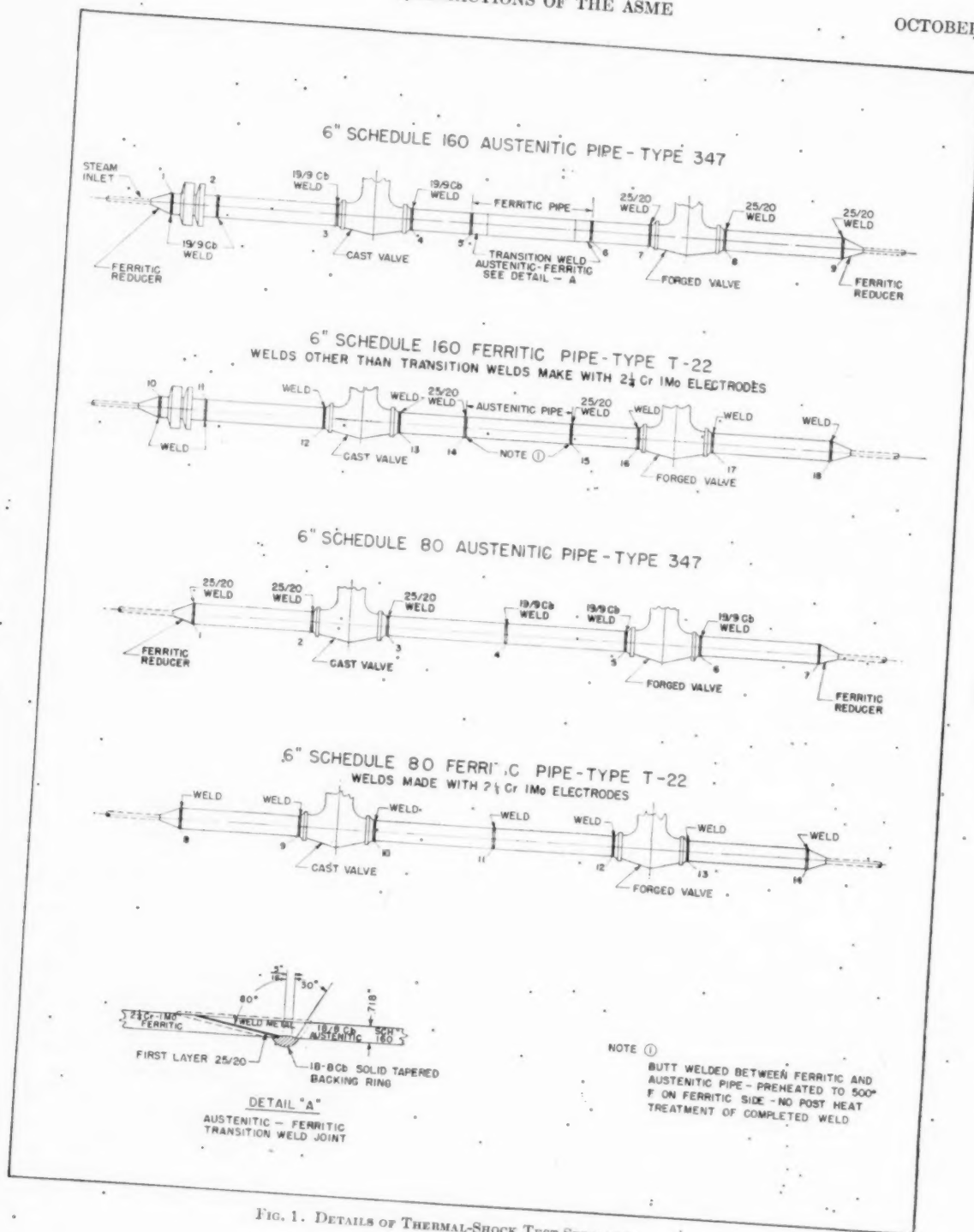


FIG. 1. DETAILS OF THERMAL-SHOCK TEST SPECIMEN

Details
Fig. 1.
steel, typ
steel, Ty
were prep
and the h
at 2000
seal bonn
forged m
160 sche
Cr-1 Mo
tains a si
permitted
similar s
welded jo
ferritic a
of the tr
metal se
shock ass
Fig. 2
the ther
assembl
tion, wer
pipes w
The V-w
made wi
trodes as

The 2
A158-46
ASTM S
The pr
All jo
tempera
maintain
welding
ferential
than 6 t
formly t
zone wa
equival
ing were
The 1
Grade P
final op
specifica
the aust
The r

DESCRIPTION OF THERMAL-SHOCK TEST ASSEMBLIES

Details of the thermal-shock test assemblies are shown in Fig. 1. Four 6-in. assemblies are shown. Two are of austenitic steel, type 347, in 80 and 160 schedules, and the other two ferritic steel, Type T-22 in the same schedules. The lighter assemblies were prepared for testing at 900 psi pressure, 1050 F temperature, and the heavier specimens for testing at the same temperature, but at 2000 psi pressure. Each assembly contains two pressure-seal bonnet gate valves, one of cast material and the other of forged material, both of similar composition to the pipe. The 160 schedule austenitic assembly contains a 36-in. length of 2½ Cr-1 Mo steel pipe at mid-length, while the ferritic assembly contains a similar length of austenitic-steel pipe. This arrangement permitted the simultaneous testing of joints between the dissimilar steels. In the austenitic assembly a transition type of welded joint was employed, while the dissimilar materials in the ferritic assembly were joined by means of V-type welds. Details of the transition-type joint are given in Fig. 1. No dissimilar metal sections were incorporated in the 80-schedule thermal-shock assemblies.

Fig. 2 shows the design of the V-type weld employed in welding the thermal-shock assemblies. The welds of the ferritic-steel assemblies, except for the welds joining the dissimilar pipe section, were made with 2½ Cr-1 Mo electrodes. The dissimilar pipes were welded with 25-20 chromium-nickel electrodes. The V-welds of the austenitic assemblies are of two types, those made with 19-9 Cb electrodes and those made with 25-20 electrodes as indicated in Fig. 1.

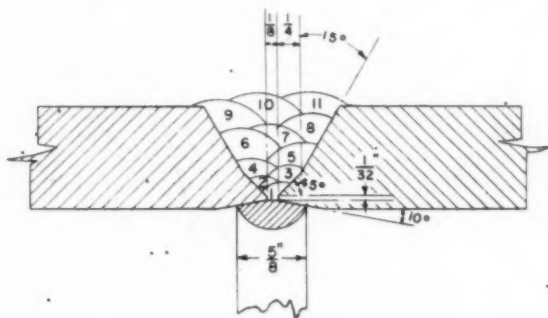


FIG. 2 DETAILS OF V-TYPE WELDED JOINT

The 2½ Cr-1 Mo steel pipe is in accordance with ASTM A158-46T, except that chemical requirements are as per ASTM Specification A213-46T for Grade T-22.

The prescribed welding procedure included the following:

All joints of 2½ Cr-1 Mo steel were preheated to a minimum temperature of 400 F for welding, and this temperature was maintained until final heat-treatment was accomplished. After welding and while the interpass temperature was held, a circumferential band on each side of the weld, having a width of not less than 6 times the section thickness of the pipe, was heated uniformly to a temperature within the range 1325-1350 F. The zone was maintained at this temperature for a period of time equivalent to 2 hr per in. of thickness. Retarded rates of cooling were employed.

The 18-8 Cb pipe is in accordance with ASTM A158-46T for Grade P8L. The pipe was stabilized at 1550 F temperature as a final operation, pickled, plus all supplementary requirements of specification. No preheat or postheat was employed in welding the austenitic-steel pipe.

The material for the cast austenitic-steel valve bodies is in

accordance with ASTM Specification A157, Grade C9, except 0.10 per cent maximum carbon and columbium stabilized. Material for the forged austenitic valve bodies is as per AISI Type 347. All bodies were given the following treatment:

Heated to 1850 F minimum, held for 4 hr, and cooled in air blast until black. Stabilizing treatment consisted of heating to 1575-1625 F, holding for 8 hr, and cooling in air.

The material of the cast ferritic-steel valve bodies is as per ASTM Specification A217, Grade WC3. The chemical composition of the forged valves is as per ASTM Specification A213-46T, Grade T-22. The valve bodies were heat-treated as follows:

Cast Bodies:

Normalizing treatment

Heated to 1775-1825 F, held for 4 hr, cooled in air

Air-quench treatment

Heated to 1675-1725 F, held for 4 hr, cooled in air

Tempering treatment

Heated to 1275-1325 F, held for 4 hr, cooled in air

Forged Bodies:

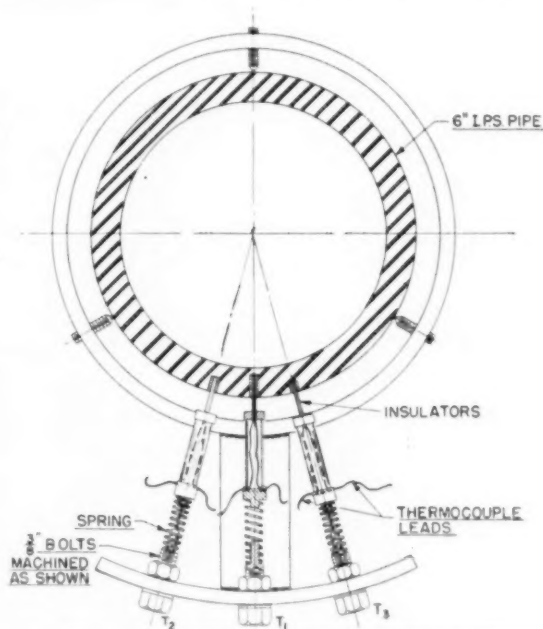
Air-quench treatment

Heated to 1550-1600 F, held for 4 hr, cooled in air

Tempering treatment

Heated to 1275-1325 F, held for 4 hr, cooled in air

Prior to welding, the thermal-shock specimens were drilled for thermocouples as shown in Fig. 3. The thermocouple holes are 0.136-in. diam and are located on the underside of the pipe about 6-in. upstream from the cast valves, where the quenching action would be most severe. The thermocouples are held against the metal at the bottom of the wells by coil springs. Drilling these



THERMOCOUPLE DESIGNATION	WALL THICKNESS AT BOTTOM OF THERMOCOUPLE HOLE—INCHES			
	18-8 160 SCH	2½ Cr-1 Mo 160 SCH	18-8 80 SCH	2½ Cr-1 Mo 80 SCH
T ₁	.032	.021	.017	.024
T ₂	.147	.146	.094	.090
T ₃	.348	.338	.179	.195
* T ₄ & T ₅	.679	.670	.412	.419

* THERMOCOUPLES PEENED IN OUTSIDE PIPE WALL

FIG. 3 THERMOCOUPLE LOCATION IN PIPE WALL

holes prior to welding permitted more accurate depth measurements to be made. Leads from the thermocouples were connected to jacks mounted in a panel board, and the circuits to the instruments were completed by plugging in on the panel.

Characteristics of the temperature recorders used in the investigation are as follows:

Four-point recorder, chart speed 8 ipm, 0 to 1200 F, minimum time between printed points 1 sec.

Continuous pen recorder, 0 to 1200 F, chart speed 8 ipm, maximum pen speed 4.5 sec for full scale travel.

Continuous pen recorder, double range 0 to 12 mv and 0 to 1200 F. Chart speed 8 ipm, maximum pen speed 2.2 sec for full scale travel.

THERMAL-SHOCK TESTS

The thermal-shock specimens were set up for test as shown in Fig. 4. Steam was supplied from a Bessler boiler and separately fired superheater, and thence through a booster superheater before entering the test assemblies. The temperature of the steam on leaving the Bessler superheater was approximately 930 F. The steam at the outlet of the booster superheater was maintained at 2000 psi pressure, 1065 F temperature, which insured steam at 1050 F at the test assemblies. The flow of steam was maintained constant by means of orifice plates in the discharge lines; about 7500 lb of steam per hr was passed through each assembly. Steam on leaving the assemblies was passed through a desuperheater, thence to a condenser.

As shown in Fig. 4, two thermal-shock specimens of the same

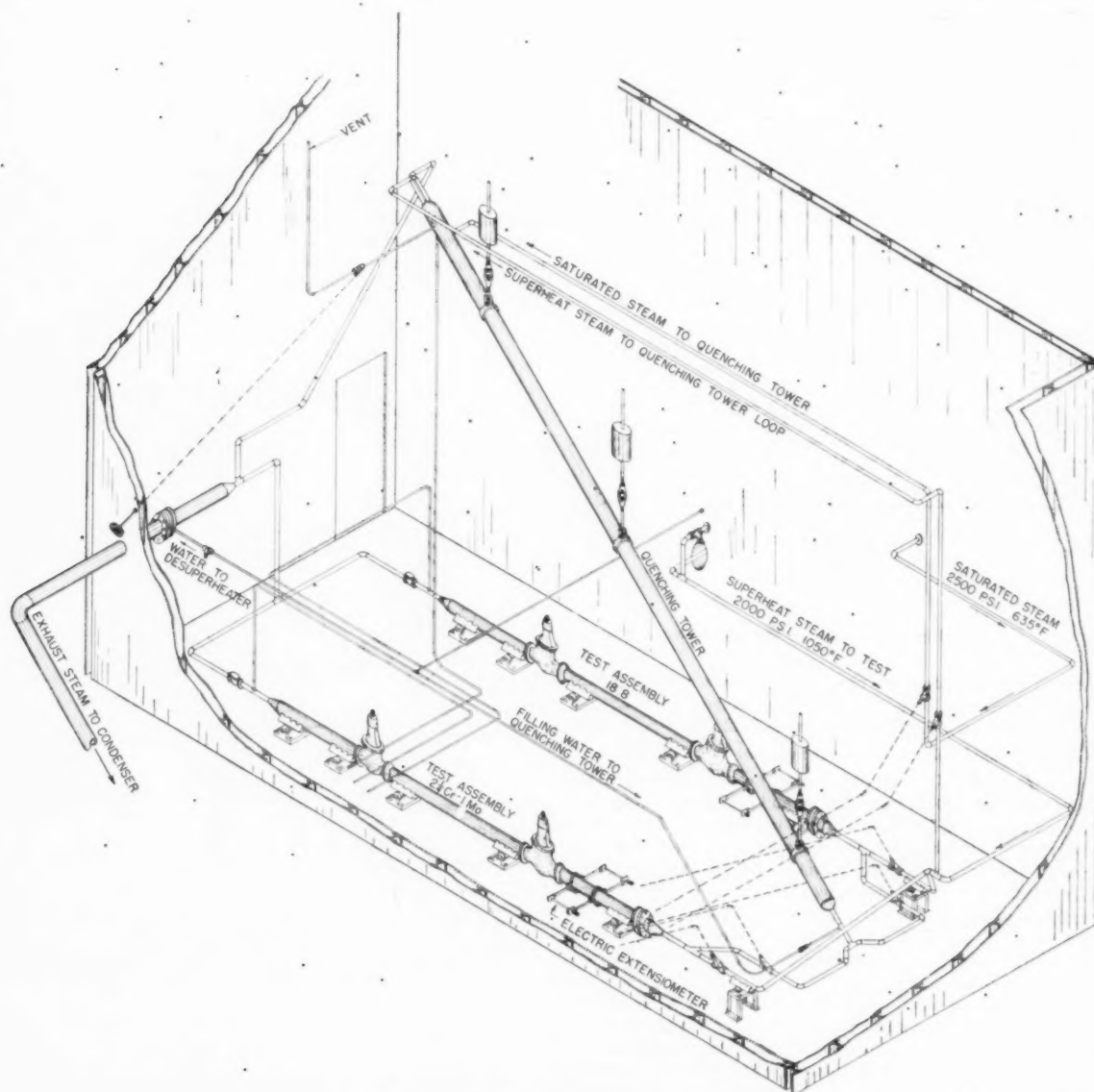


FIG. 4 LAYOUT OF THERMAL-SHOCK TEST SPECIMENS

schedule are arranged in parallel with the quenching tower suspended between them. The tower is provided with four thermocouple wells distributed over its length. Thermocouples placed in these wells indicate the water level in the tower. The test assemblies are mounted on rollers to prevent longitudinal restraint. Thermal shock is produced by introducing water at the saturated temperature into the assemblies after the latter have attained temperature equilibrium. The water is introduced along with the flow of superheated steam in order more nearly to simulate actual service conditions.

The original plan of test called for shocking the austenitic and ferritic assemblies alternately. A few preliminary runs showed that this was impracticable as the procedure caused too much fluctuation on the boiler, and besides, the main valves were difficult to operate with long rods extending outside the protective enclosure. Accordingly, one assembly was tested at a time. The assemblies were shocked with either 60 or 88 lb of water, corresponding to levels 2 and 3 of the quenching tower. The volume of quenching water, whether 60 lb or 88 lb, had no significant effect on the temperature gradients produced in the pipe walls.

A temperature record was taken for each thermal shock, the order of taking thermocouple records being varied so that all combinations of temperature differences would be obtained. For several runs, records were obtained on a multipoint recorder which gave a complete record. However, the printing speed of the multipoint recorder was not sufficient to obtain maximum temperature differentials. Temperature gradients given in the paper represent a composite of several average runs. Readings obtained with a differential recorder were not in good agreement with the corresponding temperature differentials obtained for iron-constantan thermocouples, but the records do serve to confirm a peculiar behavior observed for one of the regular thermocouples. This circumstance will be referred to later in the paper.

Test data obtained for the thermal-shock specimens are given in Table 1.

TABLE 1 TEST DATA FOR THERMAL-SHOCK TEST SPECIMENS

Condition	Ferritic assemblies quenched with 60 or 88 pounds of water		Austenitic assemblies	
	Schedule		Schedule	
Number of thermal shocks.....	80	160	80	160
Approximate time for 1 shock cycle, hr.....	100	125	100	102
Maximum temperature difference between inside and outside of pipe wall during quench, deg F..	0.5	1	0.5	1
Average time required to produce maximum temperature differ- ential in pipe wall, sec.....	225	210	115	170
Steam pressure during heating part of cycle, psi.....	2	4-5	3	17
Boiler steam pressure, psi.....	900	2000	900	2000
Temperature of pipe prior to quench, deg F.....	1020	2300	1020	2300
Temperature of quench water, deg F.....	1050	1050	1050	1050
	533	635	533	635

NOTE: All four thermal-shock assemblies withstood the 100 or more quenching cycles without failure by rupture.

Time-temperature curves for four locations in the pipe walls of the 160-schedule austenitic and ferritic assemblies are shown in Figs. 5 and 6. These assemblies were quenched with water at the saturation temperature (635 F). In Fig. 5 the curve for thermocouple T-1 is shown as crossing the curve for thermocouple T-2 at 16 sec and recrossing at 26 sec. This anomaly was observed only in the case of the austenitic assembly, as will be seen by a comparison of the time-temperature curves in Figs. 5 and 6.

Differential thermocouple readings obtained for the austenitic assembly also indicated a higher temperature for T-1 than for T-2 over a short period of time, thus confirming results obtained with regular thermocouples. Similar differential thermocouple records for the ferritic assembly showed no corresponding

anomalous behavior. Temperature differentials obtained from curves T-1 and T-4 in Figs. 5 and 6 are plotted in Fig. 7. The slow response of thermocouple T-1 of the austenitic assembly on quenching is indicated by the lower portion of the curve. No satisfactory explanation for this behavior is available.

Similar time-temperature curves for the 80-schedule austenitic and ferritic assemblies are shown in Figs. 8 and 9. During these tests, trouble developed in thermocouples T-2 and T-3 of the austenitic assembly, and in T-3 of the ferritic assembly. In view of this, results obtained for these thermocouples are not included in the paper. Temperature differentials for thermocouples T-1 and T-4 of the 80-schedule assemblies as taken from the time-temperature curves in Figs. 8 and 9 are presented in Fig. 10.

STRESS CALCULATIONS

Thermal stresses produced in the 160 schedule assemblies as a result of the quenching action were calculated from Timoshenko's thermoelastic formula. As the temperature was measured at four positions, three positions within the pipe wall and on the outside of the pipe, it was necessary to interpolate to find the temperature at points between the locations where it was actually measured. This interpolation was done under the assumption that the temperature varied linearly between successive readings, from thermocouple to thermocouple. It was possible to find the temperature of the inside wall by extrapolating the values from the first two thermocouples as these were quite near the wall.

The stresses at radii corresponding to the four thermocouples were calculated from four integrals which were added to get the corresponding integral for outside radius to inside radius. As a check the integral from outside radius to inside radius was calculated in a similar manner, assuming that the temperature varied linearly throughout the pipe wall. These yielded values are very near the values as calculated by thermocouple-to-thermocouple integration. The maximal tensile stress developed in each of the assemblies as calculated by this method was about the same, namely, 32,000 psi. The maximal tangential stress was computed using the formula,⁴ developed under the assumption that the temperature varied linearly from wall to wall. Results checked closely with the largest of the stresses computed by the method previously described.

DESCRIPTION OF MOCK-UPS

On completion of the thermal-shock tests of the 160-schedule assemblies, the valves with connecting section of pipe were removed for rewelding in mock-ups for cyclic deflection tests. In sectioning the thermal-shock specimens, one cut was made about 5 in. upstream from the cast valve, and the other 12 in. downstream from the forged valve. A 7-in-long section of pipe was welded to the pipe adjacent to the cast valve to make the assembly symmetrical. Then, S-bends were welded to the ends of the pipe and valve assemblies, producing a mock-up as shown in Fig. 11. The design of these welds differed somewhat from the original welds in that a flat split backing ring with four pins to maintain $\frac{3}{4}$ in. root spacing for the austenitic pipe and $\frac{1}{4}$ in. root spacing for the ferritic pipe was employed.

As shown in Fig. 11, one end of the loop is anchored and the other end pinned to the piston of a hydraulic cylinder having an 8-in. bore. The free end of the loop is restrained from moving in any but the horizontal direction by a 30-in-long sleeve bearing. The hydraulic cylinder is supplied with oil at the rate of 50 cu in. per min by a motor-driven pump. The direction of the piston is reversed by means of an electrically operated four-way valve, the length of the stroke being controlled by microswitches. Three

³ "Strength of Materials," by S. Timoshenko, second edition. The Macmillan Company, New York, N. Y., vol. 2, 1931, p. 261.

⁴ Ibid., p. 174.

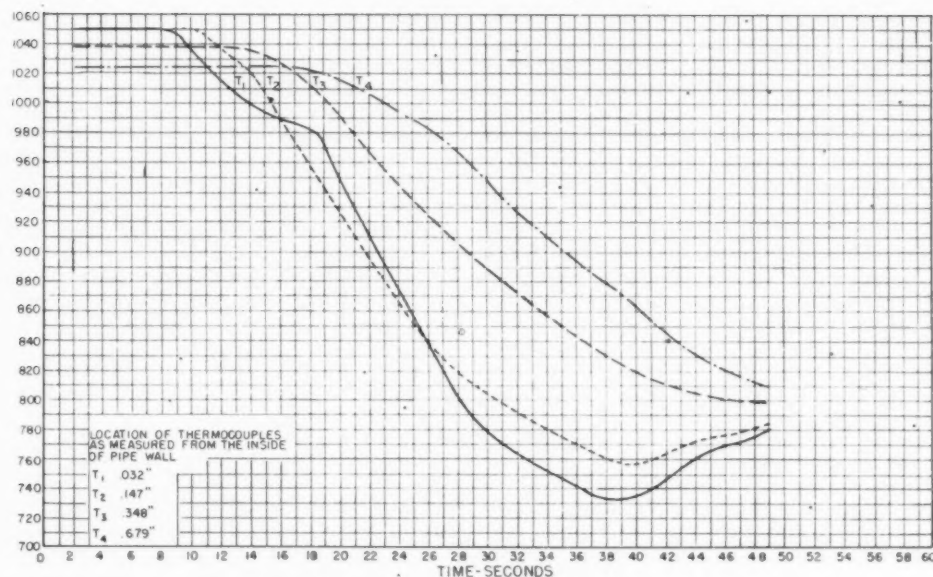


FIG. 5 THERMAL GRADIENTS FOR 18 CR-12 NI-0.8 CB 6-IN. PIPE, 160 SCHEDULE, WHEN QUENCHED WITH 635 F WATER

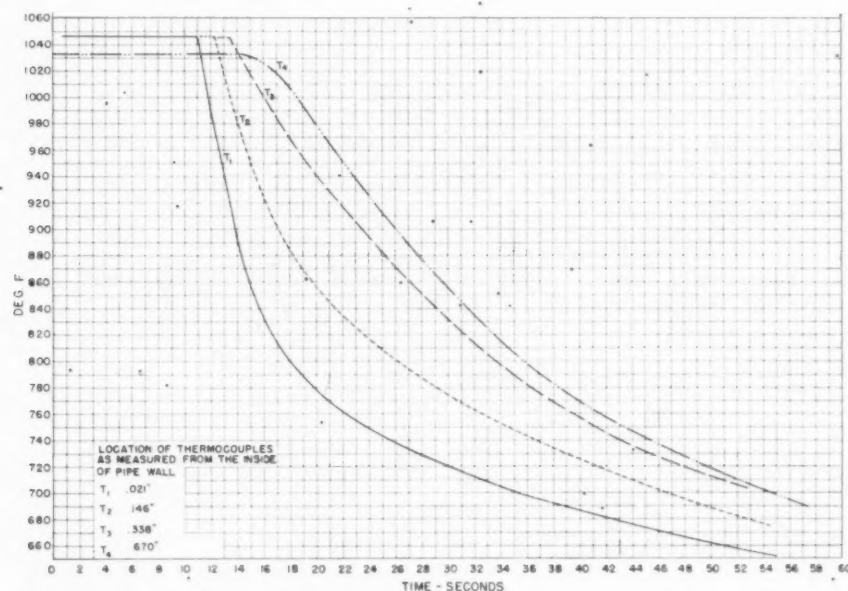


FIG. 6 THERMAL GRADIENTS FOR 2 1/4 CR-1-MO 6-IN. PIPE, 160 SCHEDULE, WHEN QUENCHED WITH 635 F WATER

safety devices are contained in the hydraulic system, i.e., (1) a pressure-relief valve set at 300 psi, (2) a pressure switch adjusted to shut-down the pump when the pressure exceeds 275 psi, and (3) a by-pass valve in a line connecting the ends of the cylinder.

RESULTS OF MOCK-UP TESTS

Deflection tests were made of the 160-schedule mock-ups at room temperature after mounting resistance-type strain gages at a number of locations as indicated in Fig. 11. Readings were taken on all gages after removing the pin from the shackle of the

piston so as to insure a free-end condition. The connecting pin was then replaced without producing appreciable change in the initial readings. Next, 2000-psi hydrostatic pressure was applied to the assembly, and another set of readings taken. Strain-gage readings were obtained for different positions of the piston while compressing the loop. Readings were taken about every 0.3-in. movement of the piston for a total movement of 2 in.

The relationship between deflection and strain or equivalent stress having been established at normal temperature, it was only necessary to multiply the normal temperature deflection by the

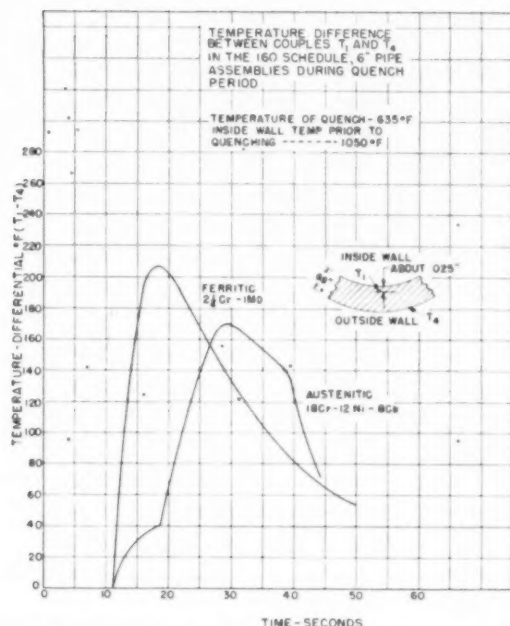


FIG. 7 TEMPERATURE DIFFERENCE BETWEEN COUPLES T-1 AND T-4 IN THE 160-SCHEDULE, 6-IN. PIPE ASSEMBLIES DURING QUENCH PERIOD

ratio of moduli of elasticity of the material at normal and 1050 F temperatures to obtain the deflection necessary to produce the corresponding stress at the elevated temperature. For the austenitic steel this ratio is $28.8/23.0 = 1.25$; and for the ferritic steel $30.4/21.0 = 1.45$.

Steam was passed through the mock-up at the rate of 5000 lb per hr, temperature equilibrium at 1050 F temperature being established after 6 hr. The unrestrained position of the free end of the assembly was determined within 0.02 in. In the case of the 160-schedule austenitic mock-up, the stroke was adjusted to produce an equivalent stress of approximately 21,500 psi for

the extreme end of the stroke, and a corresponding stress of 11,500 psi for the opposite end of the stroke, the variable equivalent stress being 10,000 psi. For the 160-schedule ferritic mock-up the corresponding stress range was 15,750 to 9750 psi, and the variable equivalent stress 6000 psi. The stroke and equivalent-stress relationships were based upon strain values obtained for gages e and f as shown in Fig. 11. In taking the strain readings on the ferritic mock-up, a rosette strain gage containing a 45-deg element was placed at location ef. This permitted evaluation of shear stress which was found to be negligible.

The principal stresses computed from the strain-gage readings for the cold condition, including the equivalent stresses, are given in Table 2. The stresses were computed from the following relationships:

$$S_x = \frac{E(\epsilon_x + \mu\epsilon_y)}{1 - \mu^2}$$

$$S_y = \frac{E(\epsilon_y + \mu\epsilon_x)}{1 - \mu^2}$$

$$S = \sqrt{S_x^2 + S_y^2} - S_x S_y$$

where

- S_x = longitudinal stress, psi
- S_y = circumferential stress, psi
- S = equivalent stress, psi
- ϵ_x = unit strain in x-direction
- ϵ_y = unit strain in y-direction
- μ = Poisson's ratio = 0.3

In setting up the test procedure for the mock-ups, it was decided to subject the members to 4000 deflection cycles. This number of cycles was selected as representing the contraction and expansion that a piping system would undergo if brought up to 1050 F from normal temperature once every 2 days for approximately 20 years.

The 160-schedule austenitic mock-up was subjected to 4100 deflection cycles, and the corresponding ferritic mock-up to 4300 cycles. Neither mock-up showed any effect of the test which could be discerned by the operating personnel. The average inlet and outlet steam temperatures for the austenitic assembly were 1055 F and 1045 F. The corresponding temperatures for the

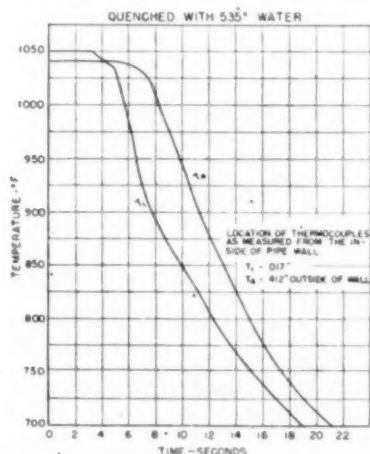


FIG. 8 THERMAL GRADIENTS FOR AUSTENITIC-STEEL 18 Cr-12 Ni-8 Cb, 6-IN. PIPE, 80 SCHEDULE, WHEN QUENCHED WITH 535 F WATER

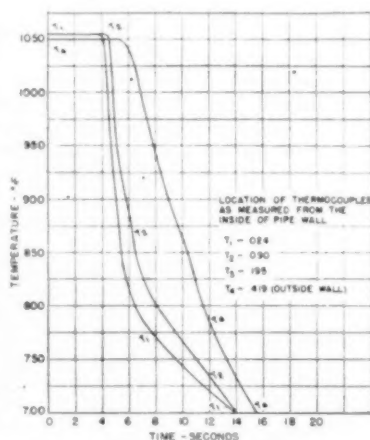


FIG. 9 THERMAL GRADIENTS FOR FERRITIC-STEEL 2 1/4 Cr-1 Mo, 6-IN. PIPE, 80 SCHEDULE, WHEN QUENCHED WITH 535 F WATER

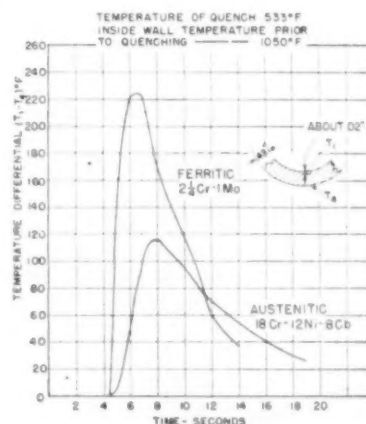


FIG. 10 TEMPERATURE DIFFERENCE BETWEEN COUPLES T-1 AND T-4 IN THE 80-SCHEDULE 6-IN. PIPE ASSEMBLIES DURING QUENCH PERIOD

TABLE 2 DATA OBTAINED FROM COLD DEFLECTION TESTS OF 160-SCHEDULE MOCK-UPS

Strain-gage location shown in Fig. 11	Direction on pipe	Principal stresses computed from— strain readings, psi				Equivalent stress, psi			
		Austenitic mock-up 160 schedule		Ferritic mock-up 160 schedule		Austenitic Mock-up 160 schedule		Ferritic Mock-up 160 schedule	
		(a)	(b)	(a)	(b)	(a)	(b)	(a)	(b)
e	Long	24500	13100	18200	11300	21900	11200	16000	9800
f	Trans	6800	6100	6100	6100				
g	Long	12500	7200	8000	5400	23800	10500	18800	9100
h	Trans	-15000	-4800	-13500	-5200				
m	Long	17800	9400	21900	13400	22800	12900	24800	15900
n	Trans	25800	14700	26800	17600				
c	Long	21800	11800	17000	10700	19400	10200	14800	9500
d	Trans	6500	6200	7600	7100				
i	Long	-16300	-6400	-11000	-3900	18500	8900	14700	8300
k	Trans	3800	3800	5700	5700				

(a) Values for maximum inward deflection of loop.

(b) Values for minimum inward deflection of loop.

ferritic mock-up were 1057 F and 1048 F. The austenitic mock-up was under test approximately 135 hr at 30.4 cycles per hr. The ferritic mock-up was under test 116 hr at 37 cycles per hr.

The next phase of the investigation will consist of similar tests of the 80-schedule mock-ups.

Following the cyclic deflection tests, zero points for the free-end condition were determined. The zero point of the free end of the austenitic assembly after 4100 deflection cycles indicated that the assembly was 0.44 in. shorter than at the start of the test. The ferritic assembly after 4300 cycles showed a corresponding shortening of 0.86 in.

It appears that shifting of the zero point was caused by yielding which tended to alter the form of the loop somewhat. At the conclusion of the test the maximum stress in the austenitic mock-up was 18,000 psi and the minimum stress 8000 psi, as compared to an initial range of 21,900 to 11,200 psi. For the ferritic mock-up, the maximum stress was 10,600 psi and the minimum stress 5500, as compared to the range 15,750 to 9750 psi at the start of the test. Inasmuch as the tests were conducted at constant deflection, the value of the variable stress would not be expected to change materially.

EXAMINATION OF THERMAL-SHOCK ASSEMBLIES AND MOCK-UP FOLLOWING TESTS

The necessity for removing the valves and connecting pipe intact from the thermal-shock specimens for rewelding in the mock-ups has precluded destructive examination of any of the welds excepting those at the ends of the assemblies. In Fig. 1 the various welds of the assemblies are numbered for convenience of reference.

Thermal-Shock Assemblies—160 Schedule. All welds contained in the 160-schedule thermal-shock assemblies were examined by an oil-powder method of flaw detection prior to the thermal-shock test. Also, transition weld No. 6 was macroetched and examined at low power for cracks. Following the thermal-shock test the welds again were examined by the oil-powder method. Those welds showing indications of defects were macroetched and examined. In addition, welds, 5, 6, and 9 were x-rayed, and welds 2 and 9 subjected to a peel test which consisted of removing the weld metal from the groove in increments ranging from 0.0075 to 0.030 in. until no indications of cracks were revealed by oil-powder inspection.

Prior to the thermal-shock test, no cracks were observed in the weldments of the 160-schedule assemblies as a result of oil-powder and macroexamination methods of inspection. Following the thermal-shock test, the oil-powder technique revealed cracks which were not evident prior to the shock treatment. The distribution of these cracks was toward the bottom of the assemblies.

The welds joining austenitic-ferritic pipe, namely, 25-20 in

V-type joints and 19-9 Cb in transition-type joints, showed the greatest tendency to develop cracks. The etched surfaces of the transition joints indicated variations as regards the deposition technique employed, in that, in some portions of the joints the weld metal was deposited stringerwise while in others in oscillations or weaves up to 1 in. in width.

The 19-9 Cb weld metal in the austenitic piping revealed the least tendency toward fissuring. Others⁵ have observed that chromium-nickel compositions of this type, which promote the formation of ferrite, are more resistant to fissuring than are the fully austenitic weld metals. Results of the peel test performed for welds Nos. 2 and 9 showed that cracks indicated on the surface were removed completely after machining to a depth of 0.023 in. for weld No. 2 (19-9 Cb), but persisted to a depth of 0.375 in. for weld No. 9 (25-20).

The welds of the 160-schedule ferritic assembly also revealed cracks following the thermal-shock test, but the number of cracks was less than in the austenitic assembly. The majority of cracks occurred in welds Nos. 10 and 15.

Thermal-Shock Assemblies—80 Schedule. The welds of the 80-schedule assemblies were examined after the manner described for the 160-schedule assemblies. No cracks were observed prior to thermal-shock treatment. Following the thermal-shock tests, cracks were revealed by the oil-powder method but were less numerous and more uniformly distributed than in the 160-schedule specimens. Of the two 80-schedule specimens, the austenitic assembly showed the greater tendency toward fissuring, the number of fissures being much greater in the 25-20 weld No. 2 which happened to be located near the inlet end of the assembly.

The welding technique employed in producing the 25-20 welds in the 80-schedule assembly was at variance with that for similar welds in the 160-schedule assembly in that deposition was stringerwise.

Austenitic Mock-Up—160 Schedule. Further examination of the welds following 4100 deflection cycles of the 160-schedule austenitic mock-up showed an increase in the number and magnitude of cracks in the 25-20 V-joint welds 7 and 8, and in the transition welds 5 and 6. In the case of joint 5, the concentration of defects was apparently on the ferritic side of the joint along the line of fusion between the layer of 25-20 weld metal and the main body of the 19-9 Cb weld metal.

Testing of the 160-schedule ferritic mock-up was not completed in time to include results of oil-powder inspection in the paper.

The fact that cracks or fissures were not revealed in the welds by the oil-powder method until after the thermal-shock treatment might indicate that the defects were potentially present as planes

⁵ "The Effect of Alloying Elements on the Tensile Properties of 25-20 Weld Metal," by H. C. Campbell and R. D. Thomas, Jr., *Welding Journal*, vol. 25, 1946, pp. 760s-768s.

TABLE 3 CHEMICAL COMPOSITION AND TENSILE PROPERTIES

Material	Type	C	S	P	Mn	Si	Cr	Ni	Mo	Cb	Temp of Test—°F	Tensile Properties			
												Tensile Strength lb per Sq Inch	Yield Strength (.2% set)	Elongation in 2 inches	Reduction of Area Percent
Percent															
Pipe, 6", 160 schedule 2-1/4 Cr- 1 Mo	T-22 ASTM (A213-46)	.12	.019	.015	.36	.35	2.23	.15	1.08	—	75	71900	37800	25.2	72.9
Cast cylinder simulating valve casting 2-1/4 Cr- 1 Mo	Grade WC9 ASTM (A217-47T)	.13	.015	.013	.57	.48	2.25	—	.89	—	1100	42100	23000	51.5	85.8
All-weld metal from longitudinal weld laid down between two quarter sections of 6" schedule 160 pipe. (2-1/4Cr-1Mo)Note(c)		.08	.036	.013	.51	.43	2.35	—	.95	—	75	77800	42300	27.0	51.5
Pipe, 6", 160 schedule 18-8 Cb Type 347	Grade p8d ASTM (A188-46T)	.08	.010	.020	1.69	.39	18.13	12.34	—	.80	75	90600	58900	40.5	65.5
Cast cylinder simulating valve casting 18-8 Cb	Grade C9 ASTM (157-44)	.06	.015	.017	.65	.83	18.82	9.03	—	.24	75	71000	28500	29.5	60.1
All-weld metal from longitudinal weld laid down between two quarter sections of 6", schedule 160 pipe 19-9 Cb. Note (b)		.06	.013	.01	1.75	.38	20.23	10.15	—	.62	1100	42600	18200	30.0	56.9
All-weld metal from longitudinal weld laid down between two quarter sections of 6" schedule 160 pipe 25-20. Note (a)		.14	.013	.013	1.78	.43	25.88	21.80	.02	—	75	91000	57500	36.7	43.7
											1100	61200	36000	33.5	38.2

Welding electrodes — (a) The 25-20 electrodes were of the lime DC type, the titania content of the coating not exceeding 2% by weight, as per N.D. Spec. 4684 (INT) Grade IV, Class 1 mod. except that Si, P and S of the deposited weld metal not to exceed the following:

Si 0.60%
P 0.02%
S 0.02%

(b) The 19-9 Cb electrodes were in accordance with N.D. Spec. 4684 (INT) Grade II except for Si, P and S contents which are the same as for the 25-20 electrodes. Columbium not less than 10 times carbon content but not more than 1%.

(c) Electrodes 2-1/4 Cr-1 Mo, coating lime-titania type.

TABLE 4 TENSILE TEST RESULTS FOR 0.505-IN. SPECIMENS TAKEN ACROSS V-TYPE WELDS

Description of Specimen	Temp. of Test °F	Tensile Strength	Yield Strength (.2% Set)	Elongation in 2"	Red. of Area	
		Lb per Sq Inch		Percent		
Specimens taken across V-type welded joints in 18-8 Cb 160 schedule 6-inch pipe - welded with 19-9 Cb electrodes.	Room	90400	59300	22.0	25.5	Failed in weld.
		85600	56900	16.5	29.5	
	900	59900	43900	18.0	41.3	Failed in weld.
		59400	42200	25.0	57.3	Broke in base metal.
	1000	59900	- - -	19.5	54.4	Broke in weld.
	1050	55000	40700	11.0	25.8	Broke in weld.
	1100	57700	41400	23.5	56.5	Broke in base metal.
		56800	42200	17.0	27.5	Broke in weld.
Specimens taken across V-type welded joints in 18-8 Cb 160 schedule 6-inch pipes - welded with 25-20 electrodes.	Room	88400	55400	18.0	28.5	Broke in weld.
		76100	53900	11.0	26.8	Broke in weld.
	1000	59400	37700*	22.0	57.3	Broke in base metal.
	1100	52400	34400	8.0	21.3	Broke in weld metal.
Specimens taken across V-type welded joints joining cast 18-8 cylinders - welded with 19-9 Cb electrodes.	Room	78700	35400	45.0	59.5	Broke in cast metal.
	550	53400	28000	23.0	59.9	Broke in cast metal.
	1000	53700	27800	23.0	49.7	Broke in cast metal.
	1050	45900	23400	22.0	52.7	Broke in cast metal.
	1100	44100	24800	22.0	64.8	Broke in cast metal.

* .1% set

of weakness from the beginning, and that the stress conditions imposed by the test caused development into fine cracks. If this is correct, it would be expected that continued stressing would further aggravate the defects as has been mentioned for the 25-20 V-joints, welds 7 and 8, and transition welds 5 and 6 of the 160-schedule austenitic assembly. These welds were subjected to both thermal shock and deflection cycles. On the other hand, fissures would not be expected to develop in sound austenitic weldments as a result of the thermal stresses imposed.

Careful and painstaking control of the entire welding process is necessary to avoid fissuring in welds of heavy sections. Opinion differs as to the relative importance of the various factors. The effect of certain residual elements for increasing the susceptibility to cracking in a number of the chromium-nickel weld metals was pointed out by R. D. Thomas, Jr.⁶ The same author observes that cracks may arise from changes in composition of the weld metal by dilution from a dissimilar base metal. O. R. Carpenter and N. C. Jessen⁷ present data to the specifying of core-wire analysis which will produce a minimum of microdefects in deposited 25-20 welds. Anton L. Schaeffler⁸ has presented

a graphical method for predicting weld-metal composition and structure in dissimilar welds. Slight deviations from the applicable technique such as a slower rate of progression, a wider weave, higher preheat, or a higher current have been mentioned by others as contributing factors to the development of fissures in austenitic welds.

LABORATORY TEST PROGRAM

The chemical composition and tensile properties at normal temperature and 1100 F for the test materials are given in Table 3. The tensile properties were determined with standard 0.505-in-diam specimens, most of the results being the average of two or more determinations.

Tensile test results obtained for 0.505-in-diam specimens taken across V-type welds in 6-in. 160-schedule austenitic assemblies are given in Table 4.

Stress-rupture test results at 1000 and 1100 F temperatures for specimens prepared from the austenitic and ferritic pipe materials and cast cylinders are presented in Fig. 12. Similar results for all-weld-metal specimens and specimens taken across V-type welds are shown in Fig. 13. The cast cylinders for simulating valve bodies were 12 $\frac{1}{2}$ -in. long with the bore tapering from mid-point, the maximum wall thickness of 1 $\frac{1}{16}$ -in. being at mid-point.

Fatigue tests were made at 1100 F temperature of conically tapered rotating cantilever specimens prepared from the 160-schedule pipes, the austenitic all-weld metals, and of specimens

⁶ "Crack Sensitivity in Chromium-Nickel Stainless Weld Metal," by R. David Thomas, Jr., *Metal Progress*, vol. 50, 1946, pp. 474-479.

⁷ "Some Factors Controlling the Ductility of 25% Cr, 20% Ni Weld Deposits," by O. R. Carpenter and N. C. Jessen, *Welding Journal*, vol. 26, 1947, pp. 727s-740s.

⁸ "Selection of Austenitic Electrodes for Welding Dissimilar Metals," by A. L. Schaeffler, *Welding Journal*, vol. 26, 1947, pp. 601s-620s.

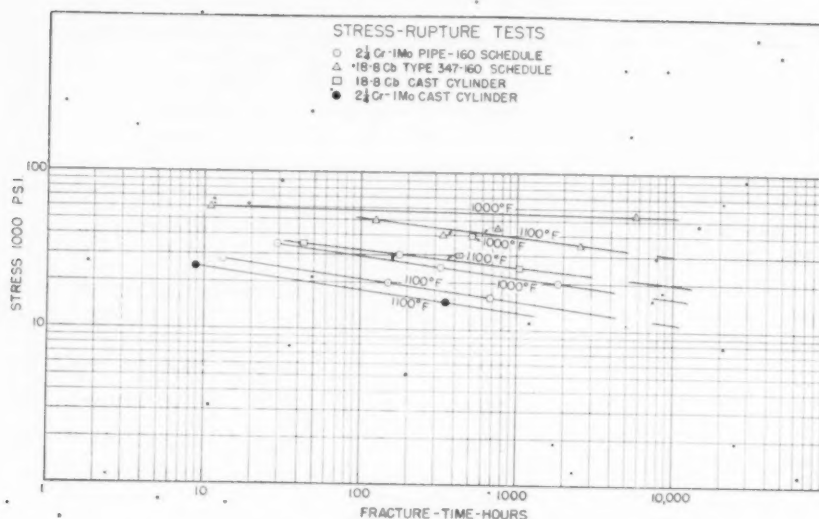


FIG. 12 STRESS-RUPTURE TESTS

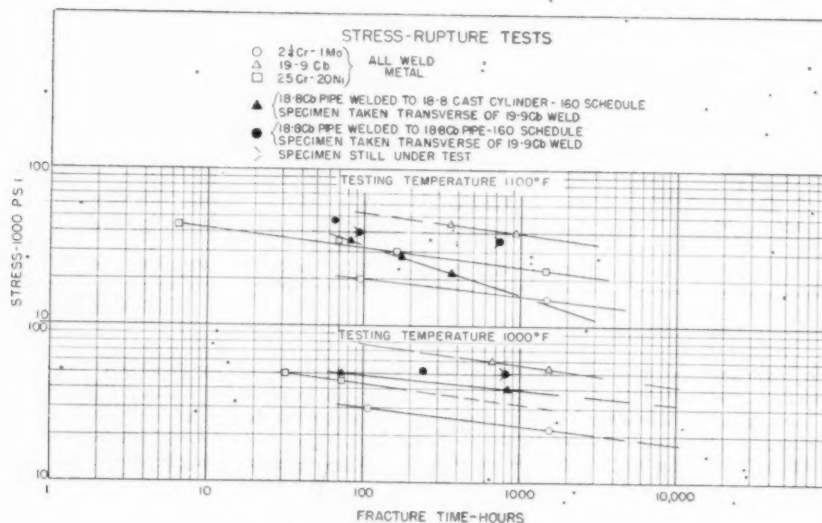


FIG. 13 STRESS-RUPTURE TESTS

taken across V-type welds. The weld zone of the latter was located in the middle of the test length of the specimen, the critical diameter of the tapered test section being 0.357 in. Results of test plotted on a semilogarithmic scale are presented in Fig. 14.

SUMMARY

Thermal-shock tests have been conducted of 6-in. pipe-and-valve assemblies representing both type 347 and 2 1/4 Cr-1 Mo steels in 80 and 160 schedules. The nominal pipe-wall thickness for 80-schedule pipe is 0.432 in. and for 160-schedule pipe, 0.718 in. Each assembly contained two valves, one cast and the other forged, of similar composition to the pipe material. The 160-schedule thermal-shock specimens contained a 36-in. length of dissimilar pipe at mid-length, the type 347 austenitic assembly being provided with a length of 2 1/4 Cr-1 Mo steel pipe, and the ferritic assembly with a length of type 347 pipe. The joints of

the austenitic assemblies were of two kinds, namely, 19-9 Cb and 25-20 chromium-nickel. Transition-type welds were employed between the dissimilar materials in the austenitic assembly. A V-type joint made with 25-20 electrodes was employed between the dissimilar materials in the ferritic assembly. Dissimilar pipe sections were not contained in the 80-schedule assemblies.

The thermal-shock tests were designed to simulate the effect of carry-over of boiler feedwater into main steam lines operating at 900 or 2000 psi pressure, 1050 F temperature. The assemblies were shocked by introducing either 60 or 88 lb of boiler water at the saturation temperature along with the flow of superheated steam. Each assembly was subjected to 100, or more shocks. Temperature differentials in the pipe walls showed that the maximum temperature difference between the inside and outside of the wall was obtained for the ferritic-steel assemblies. Moreover, the maximum temperature difference occurred in a much

shorter time in the case of the ferritic steel. All four thermal-shock specimens withstood 100 or more shocks without failure by rupture.

Measurements of the assemblies following the tests showed that the ends of the 160-schedule assemblies had been distorted upwardly about 0.10 in. at the inlet end and 0.20 in. to 0.25 in. at the outlet end. The rate of decrease in fracture stress with time at 1100 F temperature, as shown in Fig. 13, for specimens taken across welds joining a section of austenitic-steel pipe and an austenitic-steel casting was disconcerting. However, similar tests of specimens taken across welds joining two sections of austenitic-steel pipe have indicated normal behavior in this respect.

Fatigue tests at 1100 F temperature have shown considerable superiority for the 18-8 Cb pipe material. The fatigue strength for the 19-9 Cb all-weld metal is considerably lower than for the pipe material and apparently controls the fatigue strength of specimens taken across 19-9 Cb welds joining sections of pipe. Similar specimens taken across welds joining 18-8 Cb pipe to austenitic castings showed lower fatigue strength. Comparable fatigue values between 10^7 and 10^8 cycles are indicated for 25-20 weld metal and $2\frac{1}{4}$ Cr-1 Mo pipe material at 1100 F temperature.

ACKNOWLEDGMENTS

The guidance and assistance received from the Special Subcommittee under the chairmanship of Mr. N. L. Mochel throughout the course of this investigation is gratefully acknowledged. The authors also wish to express their appreciation to Capt. W. D. Leggett, Jr., U.S.N., Director of the Naval Engineering Experiment Station, and Capt. C. G. Grimes, U.S.N., Assistant Director of Laboratories, for their encouragement and support.

Discussion

M. L. IRELAND, JR.* The marine and stationary power-plant industries are both fortunate to have available the important results presented in this paper.

It is reassuring that the piping materials withstood tests of such severity with only the small amount of damage indicated. Presumably these tests correspond to the expected number of thermal shocks and normal heating and cooling cycles which will be received by similar pipe in a service life of 20 years.

Such tests are of too-short duration to give much indication of the effect of long-time exposure under sustained pressure stresses. It has been suggested that the reported cracks in the welding zone are due to enlargement of microfissures which may have been present before the test.

If this explanation is accepted then does it not appear likely that further enlargement will occur during long-time exposure at the service temperature, even if the only stresses present are those due to internal pressure?

In view of this fact, it would appear desirable to perform stress-rupture or creep tests on specimens cut from the affected areas but at moderate stress levels, corresponding to the operating conditions.

Since this program was initiated, a rational method for calculating temperature gradients in a pipe subjected to thermal shock has become available.¹⁰ However, this method requires use of a constant value for the internal surface heat-transfer coefficient. A value of 1000 Btu/hr ft² F was used in these calculations since it was expected that surface evaporation would occur.

* Engineering Department, Technical Division, Newport News Shipbuilding and Dry Dock Company, Newport News, Va. Mem. ASME.

¹⁰ "Heat Transfer," by Max Jakob, John Wiley & Sons, vol. 1, 1949, p. 270.

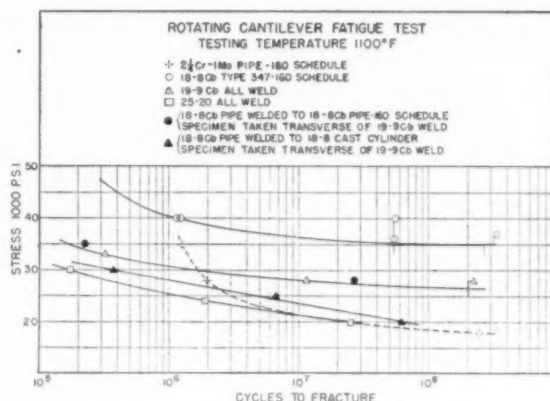


FIG. 14 ROTATING CANTILEVER FATIGUE-TEST; TESTING TEMPERATURE 1100 F

The following illustrations show how the calculated temperatures compare with the test values reported in the paper. Fig. 15 is for the ferritic schedule-160 piping and shows quite good agreement except for thermocouples T-3 and T-4.

The initial difference shown for thermocouple T-4 before start of the quench indicates that this element was subject to some error. It is possible that this was caused by heat losses due to partial exposure.

Another possibility is that wet superex insulation may have been applied over this element and the insulation insufficiently dried out before testing. The writer has recently employed thermocouples peened on the outside of a pipe to measure steam temperatures and found an error of the same order (25 F) which persisted throughout an entire one-day sea trial. Laboratory tests showed that about 24 hr at temperature were required to dry out the insulation sufficiently to give accurate readings.

Fig. 16 is a similar comparison of test and calculated values for the ferritic schedule-80 piping and shows about the same numerical difference but in the opposite direction.

The test temperatures near the outer wall are higher than the calculated values for schedule-160 pipe, but lower than calculated values for schedule-80 pipe.

Comparisons for the two thicknesses of austenitic piping are shown in Figs. 17 and 18. In both these cases the observed temperature differences across the pipe are very much less than calculated, and the discrepancy is too great to be ascribed to errors in temperature measurement.

In order to explain this discrepancy the indicated surface heat-transfer rates were computed from the test data by summing up the pipe-wall temperature changes for any interval of time. The surface temperature gradient was assumed to be the difference between thermocouple T-1 and the saturation temperature. The log-mean temperature difference was used for the initial phase when the inner pipe-wall temperature was changing rapidly. The results of these calculations are shown in Fig. 19.

These results are considerably different from the assumed surface heat-transfer coefficient of 1000, and, in general, account for the differences between observed and calculated temperatures in the pipe wall.

However, the differences in test heat-transfer coefficients still remain to be accounted for. It appears reasonable to expect some delay in establishing the full value of this coefficient, but it is difficult to understand why the 18-8 piping should have a much slower response and reach lower final values. The rapid drop in value for the schedule-80 ferritic piping is also curious.

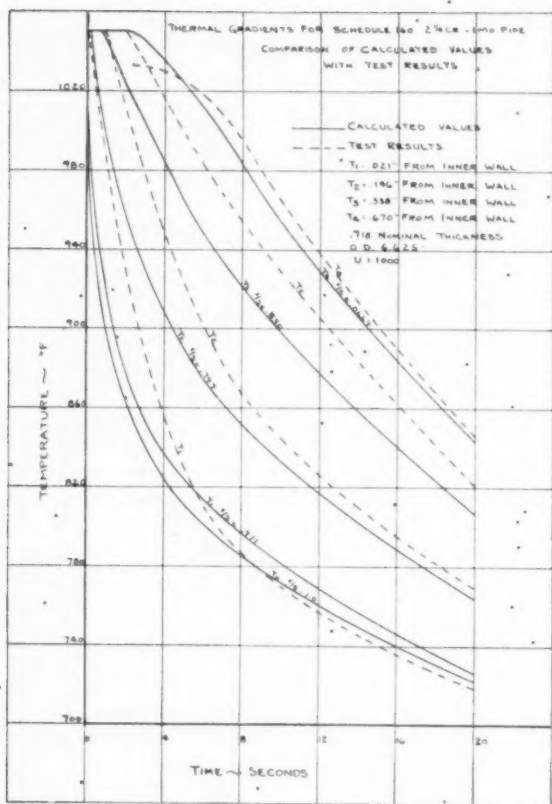


FIG. 15 THERMAL GRADIENTS FOR SCHEDULE-160 $2\frac{1}{4}$ CR-1 MO PIPE. COMPARISON OF CALCULATED VALUES WITH TEST RESULTS

It would be helpful to know just how consistent the thermocouple readings were between successive quenches of the same piping assembly, as this would indicate what variation is to be expected in the heat-transfer curves in Fig. 19.

One further item which should be established is the actual pipe-wall thickness at the points of temperature measurement. It is assumed that the piping was ordered to minimum wall specifications, in which case there is a permissible overthickness tolerance of 22 per cent.

It is hoped that this discussion has suggested some further lines of inquiry which ultimately will add to the value of the test results.

V. T. MALCOLM¹¹ AND SIDNEY LOW.¹² For many years it has been the hope of both the power-plant and refinery design engineers that they would have a sufficient amount of information with regard to this elusive condition. Due to the lack of knowledge of the conditions existing in high-temperature steam lines, flange joints were gradually abolished and replaced with welded joints.

The selection of materials for service at elevated temperatures above 900 F is a complex problem and usually results in a compromise of a number of important design and fabricating features, such as the following:

¹¹ Director of Research, The Chapman Valve Manufacturing Company, Indian Orchard, Mass.

¹² Research Engineer, The Chapman Valve Manufacturing Company. Jun. ASME.

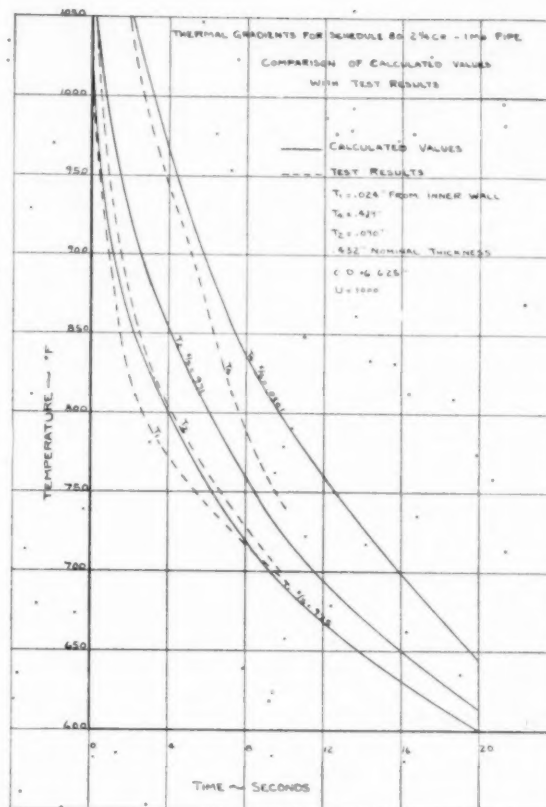


FIG. 16 THERMAL GRADIENTS FOR SCHEDULE-80 $2\frac{1}{4}$ CR-1 MO PIPE. COMPARISON OF CALCULATED VALUES WITH TEST RESULTS

- 1 Strength and ductility at operating temperatures.
- 2 Resistance to oxidation and scaling.
- 3 Resistance to corrosive attack.
- 4 Retention of satisfactory mechanical and other properties after extended exposure under operating conditions.
- 5 Resistance to thermal stresses in applications involving intermittent heating and cooling which eventually may cause deformation or cracking.
- 6 Weldability of the materials.
- 7 Structural stability.
- 8 Ease of fabrication.
- 9 Cost.

Adequacy of a given design, from a structural standpoint, requires that it be strong enough under the anticipated service conditions and that the stress imposed at the operating load and temperature be less than the strength of the material for long periods. At the same time, the imposed stress should not be much less than the strength of the material at temperature, if the design is to be practicable. Therefore all factors must be considered individually, especially such factors as consequence of failure, economic production, and degree of performance and life desired.

In the introduction we find that the authors were prompted to use the 18-8 chromium-nickel steel for 1050 F service due to the fact that it had superior high-temperature properties over the ferritic types of steel and would permit the use of thinner and lighter pipe at higher pressures. This is common practice among many design engineers who have based their designs on weight saving due to better stress values, but this thinking is

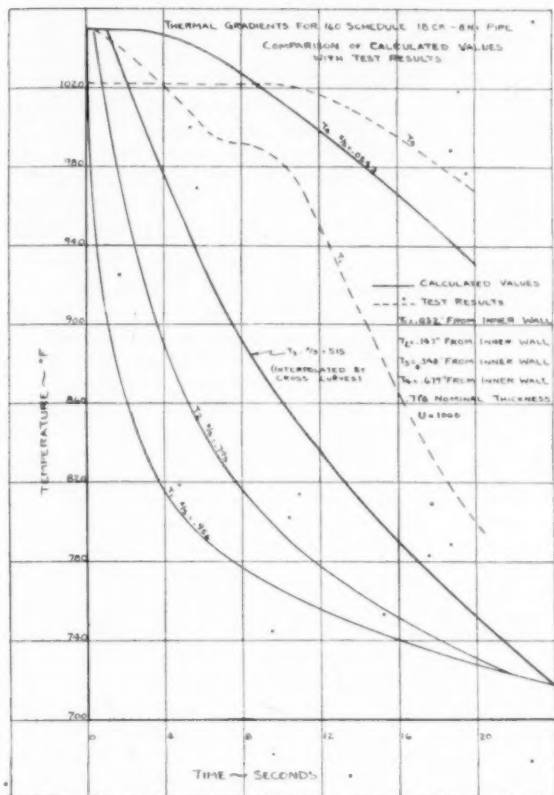


FIG. 17 THERMAL GRADIENTS FOR 160-SCHEDULE 18 CR-8 NI PIPE. COMPARISON OF CALCULATED VALUES WITH TEST RESULTS

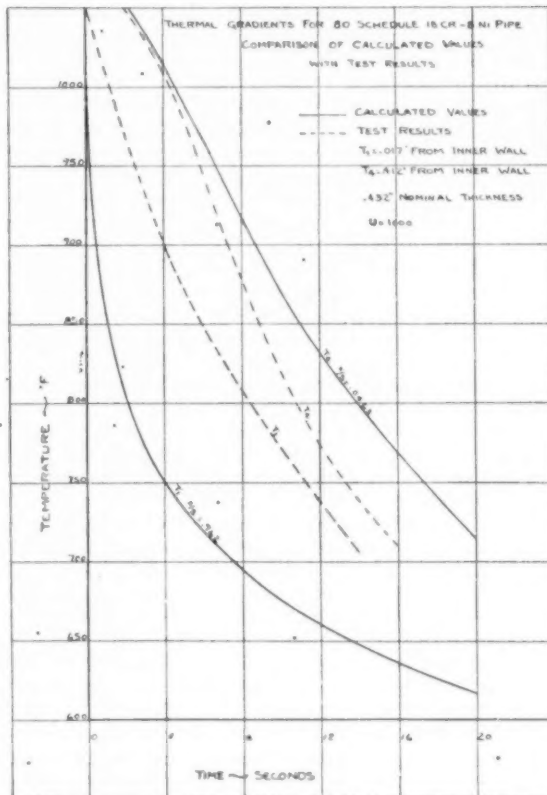


FIG. 18 THERMAL GRADIENTS FOR 80 SCHEDULE 18 CR-8 NI PIPE. COMPARISON OF CALCULATED VALUES WITH TEST RESULTS

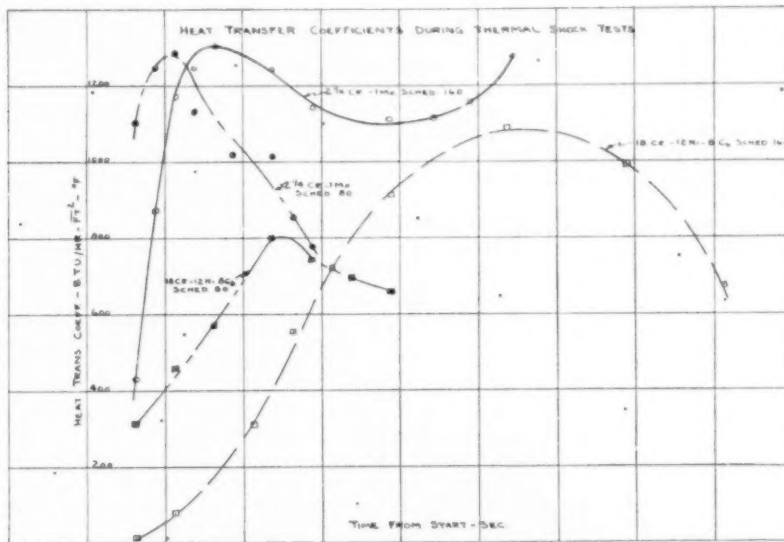


FIG. 19 HEAT-TRANSFER COEFFICIENTS DURING THERMAL-SHOCK TESTS

likely to be misleading because most of the allowable working stresses are obtained from 80 per cent of the 1 per cent creep in 100,000 hr. However, in the analysis of steels; that is, ferritic and austenitic steels, we would very likely find that at certain stress levels within indicated temperature range, the austenitic steels may be deforming at a much more rapid rate than the ferritic steels. This condition is a well-known fact in refinery work where severe oversteering may be encountered.

In 1933¹³ and in 1938,¹⁴ considerable information was given on the behavior of austenitic and ferritic steels at temperatures from 900 to 1100 F, and service hours up to 48,361 of which 38,921 had been at 1100 F. Examination of the 18-8 chromium-nickel austenitic steel showed that the material deteriorated in service due, probably, to the precipitation of chromium carbides along the grain boundaries. No stabilizing elements were present in the austenitic steel. There was no evidence of any serious reduction in physical properties when operating in steam service in the 1000-1100 F range.

It was also reported that tests of other steels of the low-alloy class disclosed no marked change in their properties in this service. Certain tubing and castings were made of a low-alloy, 4-6 per cent chromium with 1 per cent tungsten. It was reported, after a total service of nearly 11,000 hr at 1100 F, that the material did not undergo embrittlement, and that long service at high temperatures tended to increase toughness and ductility. It was also reported that "austenitic steel was growing at the average rate of 4.4 per cent per 100,000 hr, while alloy tubes were growing at a corresponding rate of 5.3 per cent. However, measurements of a 4-6 per cent chromium-tungsten tube after service of 7465 hr showed no change in dimensions." No evidence of thermal shock was reported.

The authors call attention to the fact that experience has been cited which indicates strength deficiencies for austenitic-steel castings as well as for welded joints between austenitic pipe and castings. It is a well-known fact at the present time that if the composition of austenitic steel is carefully controlled, with respect to the chromium and nickel equivalents, strength will not be lacking. This same composition balance applies to welded joints.

The writers agree there is a great difference between the use of austenitic steels in the refinery and in the power plant and also agree with the mechanism as brought out by the authors, but believe that mechanical stresses have very little to do with any damage that may be incurred, and that it is clearly one of thermal stress. However, the great question is how are we to measure these thermal stresses when they occur so rapidly and are transient in effect rather than a steady change of temperature?

One of the mistakes made by many people is that they consider the austenitic steels of 18-8 to be single-phase alloys. This is not true because we know that austenite is not thermodynamically stable at room temperature, with the result that we are likely to have a two-phase alloy, in which one portion is ferrite, while the other is undergoing transformation from austenite.

In the stress calculations the authors have assumed that the temperature varied linearly between successive readings, as shown by Timoshenko's thermoelastic formula.¹⁵ This assumption, however, may not be correct particularly in medium-heavy walls, as denoted by a valve where the stationary temperature distri-

bution is no longer a linear function of r and is represented by Equation [239].¹⁶

The tendency of the two types of austenitic weld deposits presumably to fissure during stress cycling is quite disturbing in view of the large number of similar austenitic welds currently employed in various types of piping construction.

Although if the 19-9 Cb weld metal has a calculated ferrite content of 10 per cent, coupled with a low C: Si ratio and a low P content, it is not improbable that the deposit was fissured prior to test. It has been our experience that penetrant-oil inspection of weld deposits is only 100 per cent sure if the deposit has been finely machined or ground. The oil method of inspection is particularly unsatisfactory when the weld deposit is ground manually or rough-machined. Peening of the weld deposits also has the effect of closing any fissures present and rendering the oil-inspection method ineffectual. These same remarks also apply to 25-20 weld deposits which, of course, are even more susceptible to fissuring in the as-deposited condition. The inclusion of bend-test results of both the 19-9 Cb and 25-20 welds might define more conclusively the quality of the welds.

It has always been our opinion that fissuring is essentially a high-temperature phenomenon, taking place appreciably above the maximum temperature encountered in steam service. The mechanism of fissuring is essentially the same as the mechanism of hot-tearing encountered in castings. In many cases, the formation and the propagation of these fissures may be observed during the actual welding operation, as the deposit solidifies behind the arc. This is particularly true of alloys of the 10 Cr-20 Ni type and certain high-nickel corrosion- and/or heat-resistant alloys.

If it is true that both the 19-9 Cb and the 25-20 weld deposits were fissure-free as deposited, the fact that fissures formed below 1100 F during thermal cycling is quite disconcerting. However, if macro- (or micro-) fissures were present prior to thermal cycling, it is not surprising that they would grow in width and length sufficiently to permit their detection by oil inspection (in view of the relatively high notch sensitivity of these materials).

Since the authors observed that fissuring was more severe in the 25-20 weld than in the 19-9 Cb weld, would it not be logical to presume that a 20-8 Cb deposit would have less (or perhaps no) fissures?

The presence of cracks in the welds of the 160-schedule ferritic assembly is somewhat more disconcerting than those observed in the austenitic assemblies.

Since the authors use the term fissures with respect to the austenitic welds, and cracks with respect to ferritic welds, it is presumed that their physical appearance differed, and the temperature at which they formed differed.

It is noted that a minimum preheat temperature of 400 F was maintained during welding; this relatively low preheat, coupled with a low rate of heat input during the deposition of the first pass, conceivably could result in a low ductility-transformation product susceptible to cracking. There have also been reports of root cracking using the 10-deg taper ring in a poorly "fitted-up" joint. Do the authors conclude that the cracks observed were in any way related to the welding practice, or to the "ingotism" of the initial passes?

On the basis of the S-N curves shown in Fig. 14 of the paper, and the stress calculations made by the authors, it appears that the various assemblies could be cycled 100,000 times without any fear of actual failure of the welds. Do the authors feel that it is safe engineering to extrapolate their cycling test results on the basis of the S-N curves?

¹³ "High-Temperature-Steam Experience at Detroit," by P. W. Thompson and R. M. Van Duzer, Jr., Trans. ASME, vol. 56, 1934, pp. 497-506.

¹⁴ "High-Temperature-Steam Experience at Detroit," by R. M. Van Duzer, Jr., and Arthur McCutchan, Trans. ASME, vol. 61, 1939, pp. 383-398.

¹⁵ Authors' reference (3), p. 261.

¹⁶ Author's reference (3), p. 262.

C. T.
started,
ods of in
Were

Mr. L.
ciated.
stress ru
members
It is plan
the comp

The m
cylindric
assumpti
methods
cal meth
and thes
so far as
stant be
case. I
would s
results i
factory-
operati
under ri
uniform
water,
same in
transfer
the cas
austen
cient fo
can be
fact, it
actual

The
be app
of insu
tion fi
of larg
moco
ences

The
severa
temp
160 s
. Av
therm
T-1 a

Sta
Av
therm
T-1
St
As
wells
3 in.
asse
it w
agai
the

17
18
Mc
300

C. T. EVANS.¹⁷ Were the welds cracked before the tests were started, the cracks not being detectable by conventional methods of inspection?

Were the tests abnormally severe?

AUTHORS' CLOSURE

Mr. Ireland's thorough analysis of our results is greatly appreciated. It is certainly true that it would be desirable to perform stress rupture and creep tests on samples cut from the test members and particularly from areas which show small cracks. It is planned to do this when it is decided that no further tests on the complete assemblies will be carried out.

The method for predicting unsteady-state temperatures in a cylindrical shell as referred to in the discussion is based on the assumption that the pipe wall is a flat plate. Other approximate methods are of course, available, such as the graphical or numerical method employing finite increments, and the electrical analog, and these can employ a variable coefficient of heat transfer. In so far as is known here the mathematical method based on a constant heat-transfer coefficient has not yet been applied to this case. In view of the uncertainty of necessary assumption, it would seem that the agreement between the test and calculated results indicated in Figs. 15 and 16 of the paper, is quite satisfactory. It must be remembered that these are in the nature of operating tests, rather than research experiments conducted under rigidly uniform conditions. While the test assemblies were uniform in arrangement it is possible that the flow of quench water, fairly reproducible in any one setup, was not exactly the same in all four. This might possibly account for the surface transfer coefficients being lower at the thermocouple positions in the case of the austenitic samples. It is also possible that the austenitic alloy surface has by nature a lower heat-transfer coefficient for the boiling of water.¹⁸ Figs. 17, 18, and 19 of the paper, can be interpreted, in general, by either of these explanations. In fact, if the latter be correct, the ferritic alloy in these tests is actually being shocked more severely than the austenitic alloy.

The initial temperature drop from T-1 to T-4 can be shown to be approximately what would be expected under the conditions of insulation at the location of the thermocouples, namely, radiation from the hot pipe to the room, with one intermediate baffle of larger size. Thus, it is believed that any errors in the thermocouples are considerably smaller than the temperature differences from T-1 to T-4.

The general shape of the time-temperature curves for the several thermocouples were in good agreement. The maximum temperature differentials for a number of quenches made on the 160 schedule austenitic assembly follow:

Average maximum temperature difference between T-1 and T-4 thermocouples for 27 quenches with 60 lb of water when couples T-1 and T-4 were recorded simultaneously—180 F.

Standard deviation—12.6 F.

Average maximum temperature difference between T-1 and T-4 thermocouples for 6 quenches with 88 lb of water when couples T-1 and T-4 were recorded simultaneously—179 F.

Standard deviation—10.8 F.

As shown in Fig. 3 of the paper, the thermocouples are held in wells in the pipe wall by means of coil springs. An opening about 3 in. square was left in the insulation to accommodate the spring assembly. Although this opening was a relatively dead air space, it would account for some heat loss. The writer's precaution against the use of wet insulating material is well taken. Actually, the insulation was in dry block form; first 2 in. of diatomaceous

earth, then 2 in. of 85 per cent magnesia, followed by a seal coat. Only the seal coat was put on wet, and, subsequently, this was thoroughly dried.

The pipe wall and depth of the thermocouple wells were measured carefully prior to welding.

The authors wish to thank Messrs. Malcolm and Low for their informative discussion of the paper.

The question was raised as to whether austenitic steels might not deform at a more rapid rate than ferritic steels at certain stress levels within the indicated temperature range. At certain stress levels and temperatures, transition from second-stage to very active third-stage creep may occur in austenitic steels even after thousands of hours at a fairly constant creep rate. Hence, the importance of knowing the time of transition between second- and third-stage creep. Yield-strength values at 0.2 per cent offset for the austenitic cast steel at room temperature and 1100 F, as shown in Table 3 of the paper, are lower than for the other materials. Consequently, highly stressed components of austenitic cast steel would be more likely to deform, and this observation is supported by experience. For this reason, and because of inferior high-temperature strength of welds adjacent to castings, the use of austenitic steel castings is not contemplated for main steam lines. The thermal-shock tests produced less distortion in the austenitic test assemblies than in the ferritic assemblies. However, the assemblies were of welded construction and contained no austenitic cast-steel flanges. Maximum distortion occurred in the 80 schedule ferritic assembly.

Stabilized types of austenitic chromium-nickel steel in lieu of similar types containing no stabilizing elements are indicated for the service temperatures mentioned by Messrs. Malcolm and Low. The steel they refer to as showing deterioration after a long time at temperature below 1000 F contained no stabilizing elements.

It is realized that the austenitic steels of the 18-8 type are not necessarily single-phase alloys. In fact a reference cited in the paper observed that chromium-nickel compositions which promote the formation of ferrite are more resistant to fissuring than are fully austenitic weld deposits.

At the outset of the investigation it was considered that thermal stresses might be more important than mechanical stresses when considering austenitic steel for steam piping for high-pressure, high-temperature service. It was with this in mind that the thermal-shock assemblies were fabricated and tested.

In the stress calculations presented in the paper the assumption was made that the temperature varied linearly between successive readings. While this method is not strictly valid, it was considered sufficiently accurate for the purpose.

Messrs. Malcolm and Low remark that the tendency for the two types of austenitic weld deposits to presumably fissure during stress cycling is quite disturbing in view of the large number of similar austenitic welds currently employed in various types of piping construction.

This situation is disturbing to the authors as well. The presence of fissures in the welds indicates a serious need for improved welding procedures and guidance for the welding of high-pressure, high-temperature steam piping. This need would not appear so conspicuous if the defects had been found only in the austenitic welds, for after all, the austenitic material was the subject of experiment. The development of similar defects in the ferritic welds is cause for serious consideration. This material was included in the test for comparison purposes and its suitability for the proposed service was not questioned. It is believed that sufficient technical information is available to insure sound conventional type welds in these materials provided painstaking control of the entire process is exercised.

Although oil powder and zygo methods of inspection failed to

¹⁷ Chief Metallurgist, Elliott, Company, Jeannette, Pa.

¹⁸ "Heat Transmission," by W. H. McAdams, second edition, McGraw-Hill Book Company, Inc., New York, N. Y., 1933, pp. 300-304.

reveal fissures before the tests, the defects were probably present in an incipient stage. The 19-9 weld deposits showed much less tendency toward fissuring than did the 25-20 weld deposits. It does not seem unlikely that fissures might be disclosed in austenitic welds in service if the surfaces are smoothly finished and carefully examined.

The authors did not intentionally use the term fissure with respect to the austenitic welds and crack with respect to the ferritic welds. The two terms indicate the same type of defect, that is, parting of the metal or a tear.

Root cracks observed in the welds are associated with lack of fusion at the root which points to undesirable features in the joint design. Subsequent experiments have indicated the desirability of increasing the root opening from $1/8$ in. to $3/8$ in. and employing a flat, split backing ring in lieu of the backing ring shown in Fig. 2 of the paper. It is also indicated that deposition should be

stringerwise, the thickness of each stringer not to exceed $1/8$ in.

The authors would not advise extrapolating the cycling test results for the full-scale assemblies on the basis of S-N curves obtained for laboratory test specimens. However, they do consider it advisable to continue the testing of the mock-ups at higher stress levels until failures are produced.

In answer to Mr. Evan's questions:

The oil powder and zygo methods of inspection failed to reveal the surface defects before the tests were started.

The thermal-shock test of 100 cycles might be considered rather severe but not necessarily more severe than might occur during the service life of a piping system. The 4000 deflection cycles imposed on the mock-ups represent stress conditions produced on heating up a piping system every other day for approximately 20 years, the maximum allowable stress being 25 per cent greater than that permitted by the ASME Boiler Code.

Optimum Tube Size for Shell-and-Tube-Type Heat Exchangers

By F. D. CARDWELL,¹ NEW YORK, N. Y.

The total annual cost for a shell-and-tube-type heat exchanger, which is the sum of the annual power cost plus the fixed charges or annual amortization of the initial cost of the equipment, is found to vary sharply with small changes in tube size when the heat-transfer rate is held constant. Equations are developed reducing the number of assumptions to length of tubes and diameter of tubes for fixed design conditions such as total flow rates in shell and tube and required heat-transfer rate. For a selected length as a parameter, then, the total annual cost can be calculated for each tube diameter. The optimum tube diameter is determined from a graph of these corresponding values which has a well-defined minimum value for the total annual cost. A family of these curves, each having a different length as the parameter, will each have a minimum. These minimal values will all be nearly equal. Another family of curves with standard tube diameter as the parameter will each have a minimum giving the optimum length for each diameter. Therefore only one convenient parameter need be selected from which the optimum combination can be determined from a curve. Since the required heat-transfer-surface area is now known, the number of tubes for this combination follows automatically.

NOMENCLATURE

The following nomenclature is used in the paper:

- A = area, sq ft
- A_e = area available for flow in each tube, sq ft (see Fig. 2, and text)
- A_i = surface area for heat transfer based on inside diameter of tube, sq ft
- A_o = surface area for heat transfer based on outside diameter of tube, sq ft
- A_s = total sectional area available for flow in shell outside of and parallel to tubes, sq ft
- C = constant based on fixed design conditions and defined in text
- C_{pt} = specific heat of fluid in tubes, Btu/(lb) (deg F)
- C_{ps} = specific heat of the fluid in shell, Btu/(lb) (deg F)
- D_o = diameter of circle having an area equal to area A_e , ft
- D_i = inside diameter of tube, ft
- D_o = outside diameter of tube, ft
- D_e = hydraulic diameter, ft
- D_s = inside diameter of shell, ft
- f = friction factor, function of Reynolds number, and used in Fanning formula, see text Equation [34]
- G_i = mass flow of fluid in tubes, lb/(hr)(sq ft)

- G_o = mass flow of fluid in shell, parallel to tubes, lb/(hr)(sq ft)
- g = acceleration due to gravity, 32.16 ft/sec²
- h_i = film coefficient of fluid film on inside tube wall based on mean bulk temperature of fluid, Btu/(hr) (sq ft) (deg F)
- h_o = film coefficient of fluid film on outside tube wall based on mean bulk temperature of fluid, Btu/(hr) (sq ft) (deg F)
- L = length of tube, ft
- N = number of tubes
- P = equiangular tube spacing, ft
- ΔP_i = total pressure drop for fluid inside tubes, psf
- Q = total heat required to be transferred, Btu per hr
- R = ratio of tube spacing to outside tube diameter, P/D_o
- Re = Reynolds number
- S = total annual cost, fixed charges plus operating cost, dollars
- Δt_{LM} = log-mean temperature difference, corrected for multipass
- U = over-all coefficient of heat transfer, Btu/(hr) (sq ft) (deg F)
- V = velocity of fluid in tubes, fps
- W_i = total flow of fluid in tubes, lb per hr
- W_o = total flow of fluid in shell, lb per hr
- WP = wetted perimeter, ft, used in calculating hydraulic diameter
- α = constant based on design conditions, defined in text
- β = constant based on design conditions, defined in text
- γ = constant based on design conditions, defined in text
- θ = constant based on design conditions, defined in text
- μ_i = viscosity of fluid in tubes, lb/(hr) (ft)
- μ_o = viscosity of fluid in shell, lb/(hr) (ft)
- ρ_i = density of fluid in tubes, lb per cu ft
- ρ_o = density of fluid in shell, lb per cu ft

INTRODUCTION

Heat-exchanger calculations are based upon (a) design conditions, i.e., fluid-flow rates, terminal temperatures, thermal properties of the fluids and allowable pressure drop; (b) assumptions, i.e., heat-transfer-surface area, over-all coefficient of heat transfer, or size, length, or number of tubes; (c) pressure drop across the exchanger. The design conditions are fixed by over-all plant design and determine the expected performance of the exchanger. The assumptions are more or less arbitrary with the engineer and are based upon his personal experience. Trial-and-error calculations of film coefficients are used to check the assumptions, which are also checked by an over-all heat balance. Finally, the pressure drop is calculated and compared with the allowable. If the calculated drop is too high, a new set of assumptions is made and rechecked as before.

A set of assumptions which check out and satisfy the design conditions may not be the optimum set when fixed charges and power costs are considered. Annual fixed charges is that part of the initial cost which is written off each year on the books of the owner. The actual amount written off then depends upon initial cost and company policy. In turn the initial cost depends upon

¹ Research Engineer, Chemical Construction Corporation. Mem. ASME.

Contributed by the Heat Transfer Division and presented at the Spring Meeting, Washington, D. C., April 12-14, 1950, of THE AMERICAN SOCIETY OF MECHANICAL ENGINEERS.

NOTE: Statements and opinions advanced in papers are to be understood as individual expressions of their authors and not those of the Society. Manuscript received at ASME Headquarters, December 6, 1949. Paper No. 50-8-G.

the heat-transfer-surface area and the prevailing price of steel. Analytically, then, fixed charges are primarily a function of the surface area, which includes the prevailing market price, and the accounting policy of the owner. The annual power cost depends upon pressure drop and local electric-power rates where motor-driven blowers are used, or fuel rates where steam-driven blowers are used. The total annual cost is the fixed charges plus the power cost. The optimum design, then, is the one that will result in the lowest total annual cost, and still deliver the required heat-transfer rate.

It is easily seen that a great amount of labor would be involved if one attempted to determine the optimum design by using the method of assumptions and trial-and-error calculations as outlined. Fortunately, a method of direct calculation has been found whereby the optimum design can be determined definitely in about the same time as before. Furthermore, there has been found to be not only one optimum design but several; for instance, if, say, the length of tube is chosen, an optimum design can be quickly determined for that particular length, while if some other length of tube is decided upon, the optimum design can be found for that length, and so forth, and when these optimums are compared the difference in total annual cost is negligible. Therefore the method is quite flexible in that the length of tubes is arbitrary and can be chosen independently. This is a great convenience since available space may be a factor in the design which would limit the length of the tubes. On the other hand, the size of tube may be chosen and the optimum design determined for that particular tube diameter. The development of this method follows.

HEAT TRANSFER

If we write the Newton formula

$$Q = UA \Delta t_{LM} \quad [1]$$

in the form

$$\frac{Q}{\Delta t_{LM}} = UA \quad [2]$$

we have on the left-hand side of Equation [2] the design conditions, and on the right-hand side, a product of two variables whose respective values depend upon both design conditions and the usual assumptions. These two factors must satisfy the equations for film coefficients as well as Equation [2].

Let us consider a simple gas-to-gas shell-and-tube-type heat exchanger with turbulent flow. The arrangement includes fixed tube sheets with two baffles as shown in Fig. 1. Also, to make the development as simple as possible, we will neglect the tube-wall resistance and fouling factors. The following development can be worked out for more complicated arrangements but this will not be attempted in the present paper.

Using the well-known resistance concept, we can write for the elemental areas dA_i and dA_o .

$$\frac{1}{UdA} = \frac{1}{h_i dA_i} + \frac{1}{h_o dA_o} \quad [3]$$

The elemental areas may both be expressed in terms of the elemental length dL , as follows

$$dA_i = \pi N D_i dL \quad [4]$$

and

$$dA_o = \pi N D_o dL \quad [5]$$

Substitution of Equations [4] and [5] in [3] gives upon solving for UdA

$$UdA = \frac{\pi N h_i D_i dL}{1 + \frac{h_i D_i}{h_o D_o}} \quad [6]$$

Actually, the values of the film coefficients and the overall coefficient will vary along the length of the tube because the bulk temperature of the fluids varies with the length. This will result in the variation of the conductivities and viscosities of the fluids upon which values the local coefficient will depend. However, it is reasonably safe for all practical purposes to use values of film coefficients based on the mean bulk temperatures of the fluids.

Integration of Equation [6] then gives

$$UA = \frac{\pi N h_i D_i L}{1 + \frac{h_i D_i}{h_o D_o}} \quad [7]$$

Using a mean value of 0.78 for the Prandtl number, the formula for the tube-side film coefficient as given by McAdams is

$$h_i = \frac{0.027 C_{pi} G_i^{0.8} \mu_i^{0.2}}{D_i^{0.2}} \quad [8]$$

The mass flow in the tubes, G_i , is

$$G_i = \frac{4W_i}{\pi D_i^2 N} \quad [9]$$

and substitution of Equation [9] in [8] gives

$$h_i = \frac{\alpha}{N^{0.5} D_i^{1.5}} \quad [10]$$

where

$$\alpha = 0.0327 C_{pi} \mu_i^{0.2} W_i^{0.8} \quad [11]$$

We have thus further simplified the formula for the tube-side film coefficient to the point where each factor appears only once. Furthermore, the fixed design conditions, C_{pi} , μ_i , and W_i have been separated from the usual assumptions N and D_i .

While formulas for film coefficients for fluids flowing across tube banks have been developed to a fair degree of correlation,² there is no completely satisfactory formula for the shell-side coefficient for the case of numerous baffles. Therefore the shell-side arrangement has been simplified to the point where the fluid can be considered flowing parallel to the tubes, Fig. 1. The

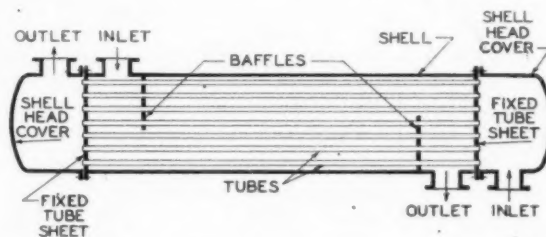


FIG. 1 TYPICAL SINGLE-PASS COUNTERFLOW, SHELL-AND-TUBE-TYPE HEAT EXCHANGER WITH FIXED TUBE SHEETS

hydraulic diameter is used as in annular spaces² and is determined as follows:

² "Heat Transmission," by W. H. McAdams, second edition, McGraw-Hill Book Company, Inc., New York, N. Y., 1942.

A typical is made, using tube sheet is excessive radii number of tubes. The graph of D_o/P and D_i is the line will result is

Equation [12] for tube space D_o/P is dimensionless. The 1.4 per cent. Writing E

and by defin

Substitutio

The section from the ge

and substit

The wette

and substit

Now, since sectional area using Equat

The mass flow the total flow

The form the hydraul

and substit simplified fo

² Standard

A typical tube-sheet layout with tubes on triangular centers is made, using the minimum spacing 1.25 tube diameters.³ The tube sheet is divided by a series of concentric circles, whose successive radii are 1, 2, 3, etc., tube spacings. The maximum number of tubes (N) in each circle is then counted. Now if a graph of D_s/P versus \sqrt{N} is made, where P is the tube spacing and D_s is the diameter of the circle containing N tubes, a straight line will result whose slope is found to be 1.09. The formula then is

$$\frac{D_s}{P} = 1.09\sqrt{N} \quad [12]$$

Equation [12] is a good approximate relationship and will hold for tube spacings up to 1.5 tube diameters. Also, since the ratio D_s/P is dimensionless, Equation [12] will hold for all sizes of tubes. The standard deviation for the range, $31 < N < 1135$, is 1.4 per cent.

Writing Equation [12] in the form

$$D_s = 1.09 P \sqrt{N} \quad [13]$$

and by definition

$$P = R D_o \quad [14]$$

Substitution of Equation [14] in [13] gives

$$D_s = 1.09 R D_o \sqrt{N} \quad [15]$$

The sectional area available for flow parallel to the tubes is from the geometry of the tube sheet

$$A_s = \frac{\pi(D_s^2 - N D_o^2)}{4} \quad [16]$$

and substitution of Equation [15] in [16] gives

$$A_s = \frac{\pi N D_o^2 (1.188 R^2 - 1)}{4} \quad [17]$$

The wetted perimeter will be

$$WP = \pi(N D_o + D_s) \quad [18]$$

and substitution of Equation [15] in [18] gives

$$WP = \pi D_o (N + 1.09 R \sqrt{N}) \quad [19]$$

Now, since the hydraulic diameter is equal to 4 times the sectional area divided by the wetted perimeter, we can write, using Equations [17] and [19] and simplifying

$$D_h = \frac{D_o (1.188 R^2 - 1)}{1 + 1.09 R / \sqrt{N}} \quad [20]$$

The mass flow of the shell-side fluid parallel to the tubes will be the total flow divided by the sectional area

$$G_s = \frac{4 W_o}{\pi N D_o^2 (1.188 R^2 - 1)} \quad [21]$$

The formula for the shell-side film coefficient is, then, using the hydraulic diameter with Equation [8]

$$h_o = \frac{0.027 C_{\rho_o} G_s^{0.8} \mu_o^{0.2}}{D_h^{0.2}} \quad [22]$$

and substitution of Equations [20] and [21] in [22] gives the simplified formula

³ Standards of Tubular Exchanger Manufacturer's Association.

$$h_o = \frac{\beta}{N^{0.5} D_o^{1.5}} \quad [23]$$

where

$$\beta = \frac{(0.026)(1 + 1.09 R / \sqrt{N})^{0.2} C_{\rho_o} \mu_o^{0.2} W_o^{0.8}}{(1.188 R^2 - 1)} \quad [24]$$

For values of N , ranging from 100 to 1000, and values of R , ranging from 1.25 to 1.50, the quantity

$$(1 + 1.09 R / \sqrt{N})^{0.2}$$

has a maximum variation of only 2.22 per cent. Therefore we can safely use the mean value of this quantity, 1.02, in order to simplify Equation [24] obtaining

$$\beta = \frac{0.0263 C_{\rho_o} \mu_o^{0.2} W_o^{0.8}}{1.188 R^2 - 1} \quad [25]$$

At this point Equation [25] can be simplified further by choosing some value for R . Further, for any particular arrangement, an optimum value for R can be found. However, Shepherd⁴ has shown that an optimum value of R is 1.45. This value will be used in our development. Substituting this value in Equation [25] we obtain

$$\beta = 0.0176 C_{\rho_o} \mu_o^{0.2} W_o^{0.8} \quad [26]$$

As a point of interest at this stage, the inside and outside film coefficients can now be compared directly by looking at Equations [26] and [11], since the two Equations [10] and [23] are identical in form. The ratio of these coefficients is found to be, when all other factors are equal

$$h_i/h_o = 1.86 \quad [27]$$

A smaller value of R or the use of baffles would naturally reduce this ratio to a point where the shell-side film coefficient would be as great as or greater than the tube-side film coefficient. However, the use of baffles has its limitations in both original cost and power cost by increasing the pressure drop on the shell side. Then, too, some stagnant areas are caused by baffles which reduce the effective heat-transfer area. The question is still open and will be neglected in this paper.

We can now substitute Equations [10] and [23] in [7] obtaining

$$UA = \frac{\pi \alpha \beta N^{0.5} L}{\beta D_i^{0.5} + \alpha D_o^{0.5}} \quad [28]$$

Equation [28] may be written

$$N^{0.5} = \frac{UA(\beta D_i^{0.5} + \alpha D_o^{0.5})}{\pi \alpha \beta L} \quad [29]$$

and substitution of Equation [2] in [29] gives

$$N^{0.5} = \frac{Q(\beta D_i^{0.5} + \alpha D_o^{0.5})}{\pi \alpha \beta \Delta T_{LM} L} \quad [30]$$

or

$$N = Q^2 \left[\frac{\beta D_i^{0.5} + \alpha D_o^{0.5}}{\pi \alpha \beta \Delta T_{LM} L} \right]^2 \quad [31]$$

The heat-transfer-surface area,⁵ based on the inside tube

⁴ "A Design Method for Counterflow Shell-and-Tube Heat Exchangers for Gas Turbines," by D. G. Shepherd, presented at the Annual Meeting, Atlantic City, N. J., December 1-5, 1947, of THE AMERICAN SOCIETY OF MECHANICAL ENGINEERS.

⁵ In the example the inside surface area is controlling. The log-mean surface area could be used but would only complicate the development unnecessarily.

diameter, then becomes from substitution of Equation [31] in $A_i = \pi D_i N L$

$$A_i = \pi D_i C^3 (\beta D_i^{0.8} + \alpha D_o^{0.8})^3 / L^4 \quad [32]$$

where

$$C = \frac{Q}{\pi \alpha \beta \Delta T L M} \quad [33]$$

It will be noted at once that the constant C is a function of the design conditions only and, for a given set of design conditions, this constant will have to be calculated only once. Moreover, it will be noted that the number of tubes N , has been eliminated from the final Equation [32]. This reduces the assumptions to only two, namely, the length and size of tubes. Of course N can always be calculated from Equation [31] for any size and length of tubes chosen, but this is supplemental to our method. The required area can always be determined directly from Equation [32].

Since we have eliminated the assumption (N) from our heat-transfer calculations, our problem now is to eliminate the same assumption from the pressure-drop calculations. There are two separate sets of pressure-drop calculations; one set is for the flow in the tubes, the other set is for the flow in the shell. For the particular design under consideration, the shell-side pressure drop is negligible and will not be considered in this paper.

Where many baffles are used, the shell-side pressure drop is quite large and should not be neglected. However, a satisfactory method of calculation of shell-side coefficients, where numerous baffles are used, has not been developed for general use as of today. As soon as some reliable method is available, the author hopes to extend this development to include pressure-drop and heat-transfer calculations for the shell side using any number of baffles.

PRESSURE DROP

The tube-side pressure drop includes the entrance and exit losses as well as the friction loss in the tubes. For convenience, all losses will be expressed in pounds per square foot. The friction loss in the tubes is found from the well-known Fanning formula

$$F = 4f \left(\frac{L}{D} \right) \left(\frac{V^2}{2g} \right) \quad [34]$$

The entrance and exit tube losses are based on the equivalent diameter ratio which is determined from the unit area in the head for each tube, which is available for flow at the tube entrance or exit. From geometry, Fig. 2, this area is

$$A_s = 0.866 P^2 \quad [35]^6$$

but by definition

$$P = R D_o \quad [36]$$

and substitution of this value in Equation [35] gives

$$A_s = 0.866 R^2 D_o^2 \quad [37]$$

The equivalent diameter corresponding to this area is

$$D_o = \sqrt{1.103 R^2 D_o^2} \quad [38]$$

and the equivalent diameter ratio becomes

$$\frac{D_i}{D_o} = \frac{D_i}{1.05 R D_o} \quad [39]$$

⁶ This is not exactly true for some of the tubes next to the shell due to the excess area in the head near the shell. However, Equation [35] is close enough for practical purposes.

Again, using Shepherd's optimum value for R , we obtain

$$\frac{D_i}{D_o} = \frac{D_i}{1.52 D_o} \quad [40]$$

Assuming a mean value for $D_i/D_o = 0.881$, substitution in Equation [40] gives

$$\frac{D_i}{D_o} = 0.58 \quad [41]$$

The entrance and exit losses may now be determined from the coefficients as given by the chart, Fig. 3, and are found to be

$$\text{Entrance loss} = 0.29 \frac{V^2}{2g} \quad [42]$$

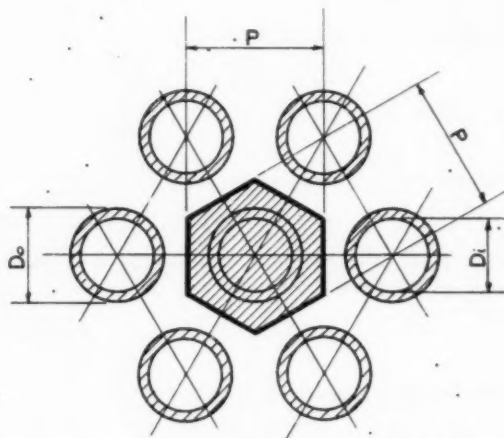


FIG. 2 TYPICAL TRIANGULAR TUBE SPACING
(Shaded area enclosed by hexagon is cross-sectional area in head, A_s , available for flow in each tube at entrance and exit.)

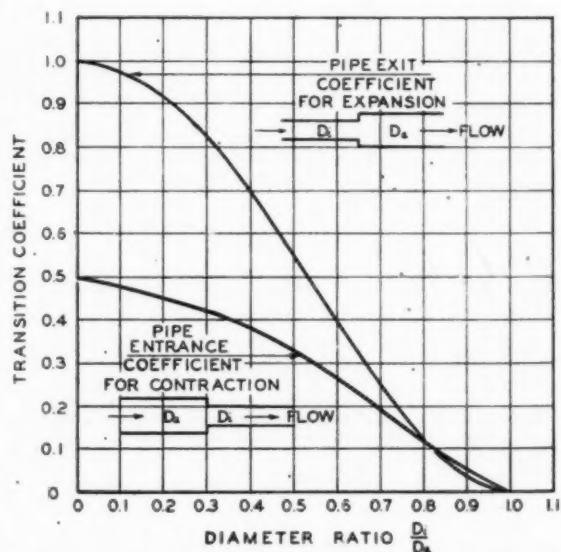


FIG. 3 CHART SHOWING VELOCITY-HEAD TRANSITION COEFFICIENTS FOR VARIOUS RATIOS OF CONTRACTIONS AND EXPANSIONS WHICH ARE USED IN PRESSURE-DROP CALCULATIONS

and

$$\text{Exit loss} = 0.44 \frac{V^2}{2g} \quad [43]$$

The total pressure drop for the tube-side fluid is, then, from Equations [34], [42], and [43]

$$\Delta P_t = \frac{V^2}{2g} \left(4f \frac{L}{D_i} + 0.73 \right) \quad [44]$$

For Reynolds numbers usually encountered in practice of from 4000 to 40,000, the friction factor f may be calculated from the expression

$$f = \frac{0.054}{R_t^{0.2}} \quad [45]$$

Substitution of the well-known expression for the Reynolds number and Equation [9] in Equation [45] gives

$$f = 0.0515 \left(\frac{ND_i \mu_i}{W_i} \right)^{0.2} \quad [46]$$

and substitution of Equation [46] in [44] gives

$$\Delta P_t = \left(\frac{0.206 LN^{0.2} \mu_i^{0.2}}{D_i^{0.8} W_i^{0.2}} + 0.73 \right) \frac{V^2}{2g} \quad [47]$$

The velocity in feet per second may be expressed by

$$V = \frac{4W_i}{3600 \pi ND_i^2 \rho_i} \quad [48]$$

Equation [47] gives the pressure drop in feet of fluid flowing. In order to obtain this loss in pounds per square foot we simply multiply by the density. Then substitution of Equation [48] in [47] gives

$$\Delta P_t = \frac{W_i^2}{5.15 \times 10^9 N^2 D_i^4 \rho_i} \left(\frac{0.206 LN^{0.2} \mu_i^{0.2}}{D_i^{0.8} W_i^{0.2}} + 0.73 \right) \quad [49]$$

The power required is the product of the pressure in pounds per square foot times the volume of fluid flowing. Therefore the tube-side hourly requirements for power are from Equations [49] and [48]

$$\text{Power} = \frac{W_i^3}{5.15 \times 10^9 N^2 D_i^4 \rho_i} \left(\frac{0.206 LN^{0.2} \mu_i^{0.2}}{D_i^{0.8} W_i^{0.2}} + 0.73 \right) \quad [50]$$

Equation [50] can be simplified by letting

$$\gamma = \frac{W_i^3}{5.15 \times 10^9 \rho_i} \quad [51]$$

and

$$\theta = \frac{0.206 \mu_i^{0.2}}{W_i^{0.2}} \quad [52]$$

Substitution of Equations [51], [52], [30], and [31] in [50] gives the final equation for power rate in foot pounds per hour

$$\text{Power} = \frac{\gamma L^{10}}{D_i^4 C^{10} (\beta D_i^{0.8} + \alpha D_o^{0.8})^{10}} \left[\frac{\theta C (\beta D_i^{0.8} + \alpha D_o^{0.8})}{D_i^{0.8}} + 0.73 \right] \quad [53]$$

The entrance and exit losses from nozzle to head are neglected in the foregoing development, since these losses are independent of tube size. Therefore the optimum tube size is not affected.

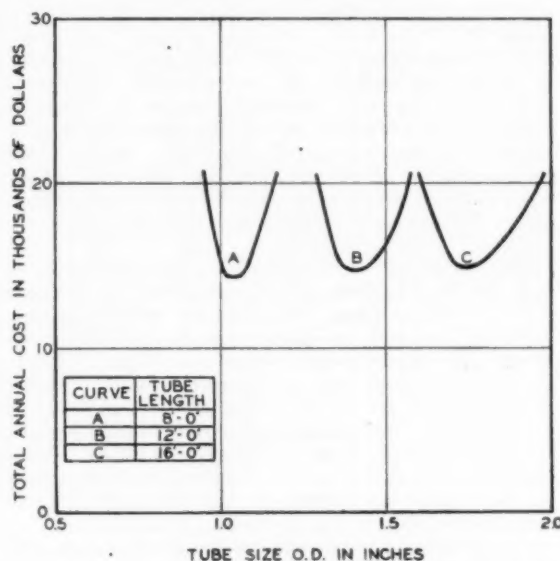


FIG. 4 CHART SHOWING VARIATION IN TOTAL ANNUAL COST WITH TUBE DIAMETER FOR VARIOUS FIXED TUBE LENGTHS AS THE PARAMETER

DESIGN PROCEDURE

It is now seen that for a given set of fixed design conditions, the required area and power can be calculated directly from Equations [33] and [53] with the use of only two variables, namely, the length and size of tube. Therefore for any convenient chosen length we can calculate directly a set of values of the area and of the power requirements for a range of tube sizes.

Fixed charges on the initial investment and annual power costs vary with the type of plant and the location. For example, the annual write-off may be, say, 0.75 dollars per square foot per year, and the annual power cost may be 30 dollars per horsepower-year. In this event, then, the total annual cost will be

$$S = 0.75 A + 30.00 \left(\frac{\text{Power}}{60 \times 33,000} \right) \quad [54]$$

Using Equations [33], [53], and [54], we can calculate and plot a curve of total annual cost versus tube size for a particular length of tube (see Fig. 4). If desired, curves can be calculated and plotted for other lengths, each of which will have a well-defined minimum, or if so desired, the optimum length of tubes can be determined for a particular size of tube. Fig. 4 has been plotted to illustrate the comparison of the minimum total annual costs for various optimum sets of tube-length and size combinations. The power cost should of course be based on output of the blower or compressor.

ACKNOWLEDGMENT

The author hereby gratefully acknowledges the helpful suggestions of the engineers of the Chemical Construction Corporation. The author also wishes to thank Mr. E. S. Roberts, chief engineer, Chemical Construction Corporation, for permission to publish this paper.

Discussion

G. M. DUSINBERRE.⁷ It is unfortunate that this paper does not include a bibliography, only three references being given in the footnotes. There is a great deal of previous work along the present line. It would be of interest if the author would show the advantages of his analysis over earlier ones, especially those which use Stanton number and L/D ratio. The author's Fig. 4 shows nearly a constant L/D , affected slightly by the entrance and exit losses which are ignored in some analyses.

D. G. SHEPHERD.⁸ This paper is a useful addition to the scanty literature available on the application of heat-transfer data to a practical design. To anyone not actively engaged in the heat-transfer field, the specific physical data available seem overwhelming and, although a considerable amount of correlation has been achieved and presented, the problem of designing the optimum form of heat exchanger for a given duty is formidable. Where the performance of the exchanger is critical with respect to the power loss, then the optimum design requires a large number of trial-and-error solutions, as initially there may be a choice of crossflow or counterflow, followed by innumerable choices of tube size, arrangement, and spacing.

Such a paper as that of the author is useful in showing how the many variables may be combined to at least direct the calculations toward an optimum design for a particular desired result. It is recognized that any such analysis will be approximate because of the simplifying assumptions which have to be made to obtain an assimilable expression. Nevertheless such analyses can be very valuable to the engineer who does not have a wealth of empirical data and experience at his command.

Inasmuch as the author has used some material from a previous paper of the writer, the latter feels bound to emphasize the limitations pertaining to their use. In Equation [25] of the paper, the author has substituted an optimum value of R of 1.45, where R is the ratio of tube spacing to outside tube diameter. As derived by the writer, this value was for a particular set of conditions pertaining to a gas-turbine heat exchanger with equal air and gas-flow rates and was intended to be illustrative only. It seems unlikely that this particular value of R has general validity.

Again, in Equation [45], a value of the friction coefficient f is given as a simple function of Reynolds number, and this too is likely to be valid only for conditions pertaining to a typical gas-turbine exchanger with small tubes of a given degree of roughness.

AUTHOR'S CLOSURE

Most of the previous work on the economical sizing of a tubular heat exchanger has been confined to topics such as the optimum velocity in the tubes⁹ and the optimum ratio of capital charges to power costs¹⁰ for a fixed tube diameter and tube pitch. The aim

⁷ Professor of Mechanical Engineering, The Pennsylvania State College, State College, Pa. Mem. ASME.

⁸ Assistant Professor, Heat Power Department, Sibley School of Mechanical Engineering, Cornell University, Ithaca, N. Y. Jun. ASME.

⁹ "Optimum Operating Conditions for Pipe Heat and Cooling Equipment," by W. K. Lewis, J. T. Ward, and E. Voss, *Industrial and Engineering Chemistry*, vol. 16, 1924, pp. 467-468.

¹⁰ "The Design of Heat Exchangers," by K. Niehus, *The Brown Boveri Review*, vol. 28, 1941, pp. 228-232.

of the present paper has been to work with fixed design conditions, over which the designer or manufacturer of the tubular exchanger has no control, and, by the development, to show the effect of the length of tube as well as the diameter of tube upon the optimum design.

If we neglect the end losses, Equation [54] of the paper may be easily differentiated and solved for the optimum L/D ratio. Thereupon substitution in Equation [32] will give the optimum area and, subsequently, the optimum over-all heat-transfer coefficient. However, since this is the subject for a future paper, the details will be omitted here.

The value of R is quite arbitrary, and any convenient value could have been used for the purpose of illustrating the method. The Tubular Exchanger Manufacturers Association gives a minimum value for R of 1.25. The maximum value in practice is around 1.5. If fouling is excessive on the shell side even a larger value may be used.

The only factors affected in the final equations by the R -value are the β -value and the numerical constant in Equation [53] which in this case is 0.73. The variation of the latter figure with $1/R$ is a straight-line relationship and may be represented by

$$E = 2 - \frac{1.84}{R}$$

where E is to be substituted in place of the constant 0.73 in Equation [53]. Any suitable R -value may then be used.

The effect of R on the β -value is given by Equation [25]. It must be remembered, however, that the numerical constant (0.0263) in Equation [25] is a purely theoretical value and that in practice, using an exchanger of the type illustrated, the actual value of this constant will be much higher due to the crossflow at the entrance and exit. This value can be calculated from operating data.

Furthermore, for the special case of a gas in the tubes and a liquid or condensing vapor in the shell, the tube-side film coefficient is controlling and Equation [32] becomes simplified to

$$A_i = \left[\frac{1}{\pi L} \right]^4 \left[\frac{Q D_i}{\alpha \Delta t_{LM}} \right]^5$$

Another point to be borne in mind is that the present paper applies only to a gas-to-gas tubular heat exchanger with triangular tube spacing. Liquid-to-liquid exchangers or in-line tube arrangements would require a similar but separate development.

Equation [45] of the paper is a direct consequence of the Reynolds analogy between heat transfer and pressure drop, i.e.

$$j = f/2$$

where

$$j = \frac{h_i}{C_{pi} G_i}$$

and h_i is defined by Equation [8], using a mean value of 0.78 for the Prandtl number. The limitations of Equation [45] of course are given in the text, but the application in this range is quite general.

In te
pact he
fer test
expansi
availab
for eval
multiple-tu
geomet
traction
tributio
ber ran
with th
the Ju
Mechan
on mu
have b
later re

The f

$A =$
 $C_c =$
 $f =$
 $g =$

$K_c =$
 $K_e =$
 $K_{eh} =$

$K_d =$

$N_R =$

$n =$

$P =$

$r_h =$

$r_o =$

$V =$

$x, y =$

$y_o =$

$\Delta =$

$\rho =$

$\rho =$

$\rho =$

$\rho =$

$\rho =$

$\rho =$

$\rho =$

Loss Coefficients for Abrupt Changes in Flow Cross Section With Low Reynolds Number Flow in Single and Multiple-Tube Systems

By W. M. KAYS,¹ STANFORD, CALIF.

In testing for the flow-friction characteristics of compact heat-exchanger surfaces concurrent with heat-transfer tests, more precise data on the flow contraction- and expansion-loss coefficients are required than are presently available in the literature. This paper presents a theory for evaluating these coefficients for both single- and multiple-tube systems for various contraction and expansion geometries. The analysis takes into account the contraction and expansion area ratio and the velocity distribution. Results of experiment for the Reynolds number range 500-20,000 are presented which compare well with the analysis. This paper was originally presented at the June, 1949, meeting of the Heat Transfer and Fluid Mechanics Institute, and included only experimental data on multiple-tube systems. Since that time experiments have been performed on single-tube systems and these later results are presented here.

NOMENCLATURE

The following nomenclature is used in the paper:

- A = cross-sectional area of flow tube, sq ft
- C_c = jet contraction-area ratio, dimensionless
- f = Fanning friction factor, dimensionless
- g = proportionality factor in Newton's second law, $g = 32.2$ (lb/#) (ft/sec²)
- K_c = contraction-loss coefficient, dimensionless
- K_e = expansion-loss coefficient, dimensionless
- K_{eb} = kinetic-energy velocity-distribution coefficient, dimensionless
- K_d = momentum velocity-distribution coefficient, dimensionless
- N_R = Reynolds number ($4r_h V \rho / \mu$), dimensionless
- n = number of small tubes in multiple-tube system
- P = static pressure, #/ft²
- r_h = flow-tube hydraulic radius, ft
- r_0 = radius of circular tube
- V = velocity, fps
- x, y = co-ordinates perpendicular to direction of flow
- y_0 = one half distance between two parallel planes
- Δ = as a prefix to P , denotes pressure difference
- ρ = density, lb/ft³

- σ = contraction and expansion area ratio, dimensionless
- μ = viscosity, lb/(hr ft)
- lb = denoting pounds mass in distinction to
- # = denoting pounds force
- \cong = denotes approximately equal

INTRODUCTION

There are many flow problems in which it is necessary to evaluate the losses of mechanical energy at abrupt changes in flow cross section. For incompressible or low Mach number flow, these losses are generally evaluated by the use of expansion and contraction coefficients K_e and K_c , which may be defined as follows, using the nomenclature in Fig. 2

$$\left(\frac{\Delta P}{\rho} \right)_{\text{(expansion loss)}} = K_e \frac{V_1^2}{2g} \dots \dots \dots [1]$$

$$\left(\frac{\Delta P}{\rho} \right)_{\text{(contraction loss)}} = K_c \frac{V_2^2}{2g} \dots \dots \dots [2]$$

(In all equations P refers to static pressure.)

The expansion coefficient K_e is generally evaluated from the Borda-Carnot equation for the pressure loss at an abrupt expansion (which may be derived from momentum considerations)

$$\left(\frac{\Delta P}{\rho} \right)_{\text{(expansion loss)}} = \frac{(V_2 - V_1)^2}{2g}$$

Then

$$K_e = (1 - \sigma)^2$$

This equation, expressing K_e as a function of the expansion-area ratio only, has been verified experimentally for fully turbulent flow ($N_R > 10,000$), by Schutt (1).²

The contraction coefficient K_c , as presented in the literature, is strictly empirical. It is also expressed as a function of the contraction-area ratio only. The K_c coefficients given in the literature are not consistent; for instance, Rouse (2) gives one tabulation of values, while McAdams (3) gives a curve for K_c which differs up to 75 per cent from the data of Rouse.

For most pipe-line problems, the pressure losses at abrupt changes in flow cross section are minor relative to the skin-friction losses. Therefore any question as to the validity of the idealizations involved in the Borda-Carnot analysis, or from the inconsistency of the data on K_c , is of minor importance. However, in testing for the flow-friction characteristics of compact heat-exchanger surfaces concurrent with heat-transfer tests, the entrance and exit losses may become a significant proportion of the total pressure drop (11). When using a gas, the Reynolds

¹ Acting Instructor of Mechanical Engineering, Stanford University. Jun. ASME.

Contributed by the Heat Transfer Division and presented at the Spring Meeting, Washington, D. C., April 12-14, 1950, of THE AMERICAN SOCIETY OF MECHANICAL ENGINEERS.

NOTE: Statements and opinions advanced in papers are to be understood as individual expressions of their authors and not those of the Society. Manuscript received at ASME Headquarters, November 9, 1949. Paper No. 50-S-7.

² Numbers in parentheses refer to the Bibliography at the end of the paper.

Combining with the definition of K_c , Equation [1]

$$K_c = 1 - 2K_{d1}\sigma + \sigma^2(2K_{d1} - 1) \dots [6]$$

This expression is perfectly general and applies for either single- or multiple-tube expansions. If the velocity distribution is uniform, K_{d1} is equal to unity and Equation [6] reduces to the Borda-Carnot relation

$$K_c = (1 - \sigma)^2$$

As will be shown later, K_{d1} is a function of Reynolds number and flow-tube geometry and approaches unity as Reynolds number is increased. For many multiple-tube expansions, Reynolds number in the large tube is very much greater than in the smaller tubes, and it is sufficiently accurate to assume uniform velocity distribution in the large tube, or K_{d1} equal to unity. Equation [6] can then be reduced to

$$K_c \cong 1 - 2K_{d2}\sigma + \sigma^2 \dots [7]$$

This equation has the advantage that, for multiple-tube systems, K_c can be plotted as a function of σ with N_R in the smaller tubes as a parameter. The error introduced in the use of Equation [7] rather than Equation [6] is $2\sigma^2(K_{d1} - 1)$. If this term is of sufficient magnitude to warrant its inclusion, it can be added to the value of K_c taken from a plot of Equation [7]. K_{d1} can be determined from N_R in the larger tube which is related to N_R in the smaller tubes, for the circular-tube system, as

$$N_{Rd}/N_{Re} = \sqrt{n}\sigma$$

Similar expressions may be derived for other geometries.

Abrupt Contraction Loss. The abrupt contraction system is described in Fig. 2 as section *a* to 3. The flow stream experiences an initial contraction to A_1 and then a re-expansion to A_2 . The losses of flow-stream mechanical energy occur in the region of flow deceleration near the stagnation point, Fig. 2, in the larger tube, and in the region of re-expansion within the smaller tube, or tubes. The former is of secondary importance, and conservation of mechanical energy is assumed in the contraction from A_1 to A_2 . The jet contraction ratio, $C_c = A_2/A_1$, is a function of σ and is evaluated for certain elementary geometries in a later section. Because of the nozzle-like flow up to the "throat" section, A_2 , the velocity distribution at A_2 is assumed to be essentially uniform. However, in applying the energy equation from A_1 to A_2 the nonuniform velocity distribution at A_1 must be taken into consideration by use of a kinetic-energy correction factor K_{e1} , similar to the momentum correction factor, K_{d1} . With the state of the stream at A_2 completely determined, the losses due to the re-expansion can be determined by a momentum analysis identical to that used for the abrupt expansion. The resulting expression for K_c for incompressible flow is

$$K_c = \frac{1 - K_{e1}\sigma^2 C_c^2 - 2C_c + C_c^2 2K_{d1}}{C_c^2} - (1 - \sigma^2) \dots [8]$$

where

$$K_{e1} = \frac{1}{A} \int_0^A \frac{V^3}{V_{av}^3} dA \dots [9]$$

Equation [8] is applicable to either single- or multiple-tube contractions. However, as was the case for the expansion coefficient, a considerable simplification is possible for many multiple-tube applications, and K_c can be expressed as a function of only two variables. Assuming uniform velocity distribution in the large tube, and thus $K_{d1} \cong 1.00$

$$K_c \cong \frac{1 - 2C_c + C_c^2(2K_{d2} - 1)}{C_c^2} \dots [10]$$

The difference between Equations [8] and [10] is $\sigma^2(K_{e1} - 1)$. If the magnitude of this term is sufficient to warrant its inclusion it can be subtracted from the value of K_c taken from a plot of Equation [10].

Evaluation of C_c , K_{d1} , and K_{d2} . Since section *a* to A_2 is a region of flow acceleration, with the exception of the immediate vicinity of the stagnation point, the flow pattern should be fairly well approximated by the pattern for an inviscid fluid flowing through an orifice. This pattern has been determined analytically for two-dimensional flow, and the resulting contraction ratio, $C_c = A_2/A_1$, is tabulated as a function of σ in reference (2).

According to this reference, C_c for the two-dimensional system can be used with good approximation for the three-dimensional circular-tube system if σ for the two-dimensional case is replaced by $\sqrt{\sigma}$ for the three-dimensional case. The extension of this coefficient to the multiple-circular-tube system needs justification. It is for the purpose of checking such assumptions that these tests were made on a multiple-circular-tube system. C_c as a function of σ , from reference (2), is given in Fig. 3 for the two-dimensional and three-dimensional circular contraction situations which approximate the heat-exchanger core contractions shown in Fig. 1.

K_{d1} may be evaluated from Equation [4], providing velocity-distribution data are known. Such data are presented here, Fig. 3, for flow in circular tubes, flow between parallel planes (infinitely wide gap), flow in equilateral-triangular tubes, and square tubes. These are the four geometries to be considered specifically in this analysis.

For laminar flow, the well-known parabolic velocity distribution in the circular tube and in the infinitely wide gap yields values for K_{d1} from the defining Equation [4] of 1.333 and 1.200, respectively. The laminar-flow velocity distribution for the square tube and the triangular tube can be determined by integration of the differential equation for laminar flow

$$\frac{\partial^2 V}{\partial x^2} + \frac{\partial^2 V}{\partial y^2} = \text{const.} \dots [11]$$

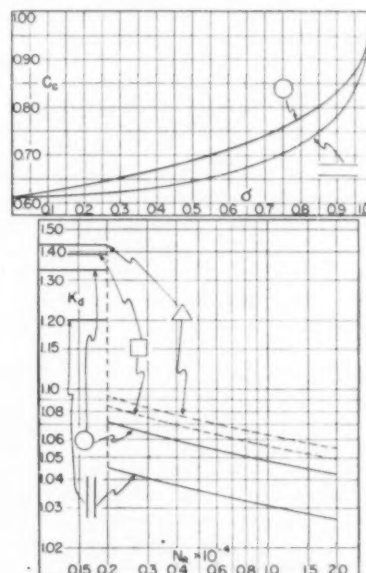


FIG. 3 C_c FOR THREE-DIMENSIONAL CIRCULAR-TUBE CONTRACTION AND TWO-DIMENSIONAL CONTRACTION AND K_{d1} VERSUS N_R FOR FOUR TYPES OF TUBE GEOMETRY

This integration has been performed by finite-difference methods in reference (5) for the square tube, and the resulting value for K_d from Equation [4] is 1.39. The solution for V is also available in algebraic form (6). For an equilateral triangle, an algebraic solution for V can be obtained (6). The differential equations for laminar-flow velocity distribution and for the stress function for elastic torsion are identical. Consequently, the solution of Saint Venant (6) is applicable.

$$V = -C \left[\frac{1}{2} (x^2 + y^2) - \frac{1}{2a} (x^3 - 3xy^2) - \frac{2}{27} a^2 \right] \quad [12]$$

C and a are constants which cancel out of the solution for K_d from Equation [4]. The resulting magnitude of K_d is $10/7 = 1.43$.

For turbulent flow, semiempirical velocity-distribution data are available for the circular tube and the infinitely wide gap as a function of the friction factor. From reference (2) the modified Kármán-Prandtl relations are as follows

For circular tubes

$$V = V_{avg} \left[\sqrt{4f} \left(2.15 \log_{10} \frac{y}{r_0} + 1.43 \right) + 1 \right]$$

For the gap

$$V = V_{avg} \left[\sqrt{4f} \left(2 \log_{10} \frac{y}{y_0} + 0.88 \right) + 1 \right]$$

Substitution of these expressions into the defining Equation [4] yields the following:

For circular tubes

$$K_d = 1.09068 (4f) + 0.05884 \sqrt{4f} + 1 \dots \dots [13]$$

For the gap

$$K_d = 0.750 (4f) + 0.024 \sqrt{4f} + 1 \dots \dots [14]$$

Equations [13] and [14], together with $f = 0.049 N_{Re}^{-0.2}$, were employed in the preparation of Fig. 3. The friction-factor relation for circular tubes was also used as an approximation for the wide-gap geometry. The coefficient 0.049 was used instead of the usual 0.046 for "smooth" tubes (3), as being more applicable to the heat-exchanger surfaces under consideration.

Also plotted in Fig. 3, are the laminar-flow solutions for K_d for all four geometries.

The turbulent flow K_d for the square and triangular cross-section geometries shown in Fig. 3 were estimated from the fact that

$$\frac{K_{d(gap)} - 1}{K_{d(circular)} - 1} \cong 0.6$$

for both laminar and turbulent flow. Therefore it was concluded that the similar ratios

$$\frac{K_{d(square)} - 1}{K_{d(circular)} - 1} = 1.17, \quad \frac{K_{d(triangle)} - 1}{K_{d(circular)} - 1} = 1.29$$

determined from the laminar-flow solutions, would also apply as an approximation for turbulent flow.

K_{e0} may be evaluated from its defining Equation [9] employing the velocity-distribution data just given. This has been worked out only for the circular-tube system. For laminar flow, $K_{e0} = 2.00$. For turbulent flow, the following equation obtains

$$K_{e0} = -1.735 (4f)^{1/2} + 3.272 (4f) + 0.0883 (4f)^{1/3} + 1 \dots [15]$$

Graphs of K_e and K_{e0} . Employing Equations [7] and [10], in conjunction with the data given in Fig. 3, the expansion and con-

traction coefficients have been evaluated for the four basic flow-tube geometries with multiple expansions and contractions, and are presented in Figs. 4, 5, 6, and 7. C_e for the two-dimensional contraction was used for the gap, square, and triangular geometries, Figs. 5, 6, and 7. Since the fins forming the square tubes, Fig. 1(b), are assumed to be very thin, the two-dimensional data are applicable. For the triangular tubes, however, there may be some question as to the validity of this assumption since the fins would be expected to interfere to a certain extent with the two-dimensional contraction.

For the single circular tube contraction and expansion, Equations [6] and [8] can be used directly. Alternatively, Fig. 4 can be used in conjunction with the corrections previously indicated relating the approximate Equations [7] and [10] to [6] and [8], respectively. Reynolds number in the large tube is always less than Reynolds number in the small tube so that the velocity distribution in the large tube must be taken into consideration. An interesting consequence arises here in that the transition from laminar to turbulent flow in the two tubes takes place at different mass-flow rates. Since there is a large change in K_e and K_{e0} at this transition (see Fig. 3), two discontinuities in K_e and K_{e0} result, corresponding to the transitions between the three possible flow conditions—both tubes laminar, one laminar and the other turbulent, and both turbulent. These two discontinuities are confirmed by the tests of a single-circular-tube contraction and expansion presented here.

Examination of Figs. 4, 5, 6, and 7 results in the following conclusions for the multiple-tube system: (a) In all cases the effect of decreasing Reynolds number is to decrease the expansion coefficient and increase the contraction coefficient, and this effect is much more marked for the flow passages with sharp corners than for the circular tubes or the infinitely wide gap. (b) In all cases there is a large change of magnitude of the coefficients from turbulent to laminar flow. (c) It is possible to have a negative "loss" coefficient K_{e0} for some cases of high σ if $K_{d0} \gg K_{d1}$, as is implied in the use of Equation [7]. This results from the fact that K_e is defined on the basis of bulk average velocities. (d) Even with area ratios of unity (which is approached as a limiting case in some types of finned-flat-tube intercooler and automobile radiator surfaces), instead of a zero loss coefficient as may be superficially expected, it is possible to have a negative loss coefficient K_{e0} for the reason given in the foregoing.

Application to Heat-Exchanger Test Cores. The curves in Fig. 7 are based on a two-dimensional contraction and velocity distribution in the smaller tubes characteristic of an equilateral-triangular flow section. These data should apply as a good approximation of flow passages such as shown in Fig. 1(c) even if the flow passages are narrow isosceles triangles. The velocity-distribution coefficient for these passages would not be expected to differ markedly from that of an equilateral triangle, and further, the fins would offer but slight interference to the two-dimensional contraction. Likewise the data in Fig. 6 should apply to rectangular flow passages such as shown in Fig. 1(b).

For most multiple-tube heat-exchanger systems, the transition from laminar to turbulent flow takes place smoothly over a range of Reynolds numbers because of the variations of tube geometry inherent in the manufacturing methods employed. This transition range can be detected from the heat-transfer performance of a test system, and then the expansion and contraction coefficients can be evaluated approximately by connecting the curves for laminar- and turbulent-flow coefficients by a smooth curve over the indicated range.

These coefficients have been evaluated for continuous non-interrupted tubes. For tubes with flow-interrupting louvers, as shown in Fig. 1(c), or with other types of discontinuous fins, the coefficients would not be expected to vary so markedly with

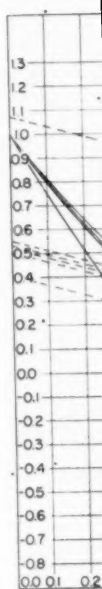


Fig. 4 C_e EFFICIENT

Reynolds
distribution
fins, or pl
= be emp

In ord
ated exp
experime

1 A
at two co
2 A
various a
3 A
one area
plate-fin
4 A
vered fin

Descri
flow me
multiple
is based
tubes, d
small ex

The t
at the t
smaller
traction
taps w
and in
as a fun

For t
metrics
manom
regulat
by adju

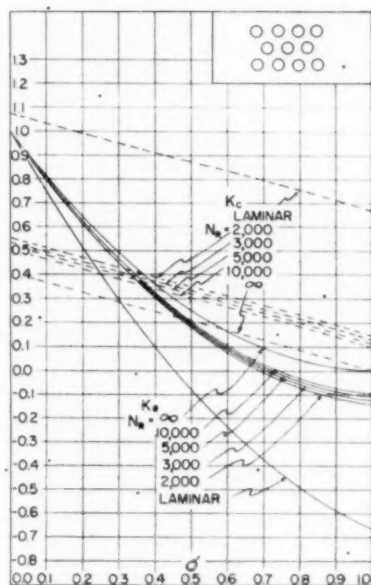


FIG. 4 CONTRACTION AND EXPANSION COEFFICIENTS FOR MULTIPLE-CIRCULAR-TUBE SYSTEM

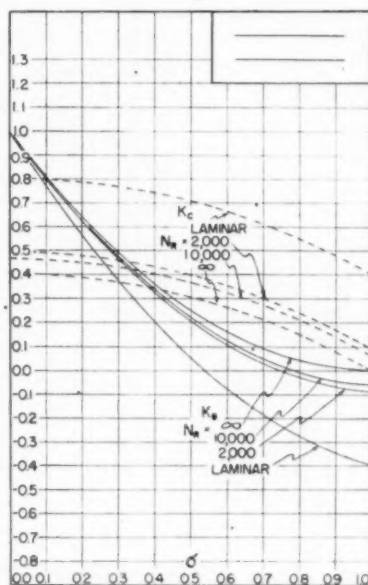


FIG. 5 CONTRACTION AND EXPANSION COEFFICIENTS FOR MULTIPLE-TUBE INFINITELY WIDE-GAP SYSTEM

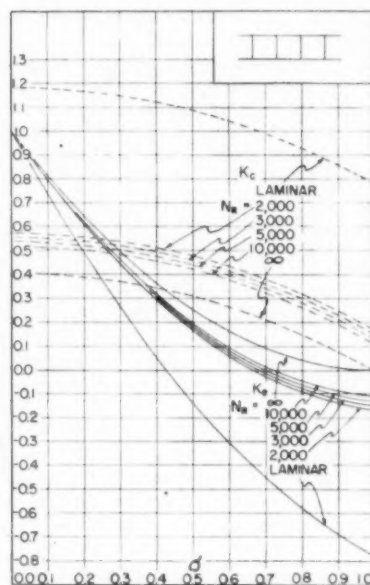


FIG. 6 CONTRACTION AND EXPANSION COEFFICIENTS FOR MULTIPLE-SQUARE-TUBE PLATE-FIN SYSTEM

Reynolds number, because marked variations in velocity distribution are prevented from occurring. For very short strip fins, or pin fins, it is recommended that the coefficients for $N_R = \infty$ be employed for all Reynolds numbers.

EXPERIMENTAL RESULTS

In order to verify the applicability of the analytically evaluated expansion and contraction coefficients to actual systems, experiments were performed on the following systems:

- 1 A single circular-tube contraction and expansion system at two contraction and expansion area ratios.
- 2 A multiple circular-tube contraction and expansion at various area ratios.
- 3 A multiple triangular-tube contraction and expansion at one area ratio. This geometry is similar to that of a typical plate-fin heat-exchanger surface, Fig. 1(c).
- 4 A system similar to that of item 3 using interrupted, or louvered fins, Fig. 1(c).

Description of Test Apparatus. Water was employed as the flow medium for the single circular-tube test system. For the multiple-tube test system air was used. Although the analysis is based on an incompressible fluid, the Mach number in the tubes did not exceed 0.2, so that compressibility effects were small except for several of the test runs of system 3.

The two test systems consisted of a brass tube cut and flanged at the test section so that cores containing the single or multiple smaller tubes could be inserted, thus forming an abrupt contraction followed by an abrupt expansion. Sufficient pressure taps were provided in both the approach and discharge ducts and in the test cores so that static pressure could be determined as a function of length, as shown in Fig. 2.

For the single-tube test system, the water was metered gravimetrically, and static pressures were measured by a bank of manometers using carbon tetrachloride under water. Flow regulation from a constant-head supply tank was accomplished by adjustment of three needle valves in parallel.

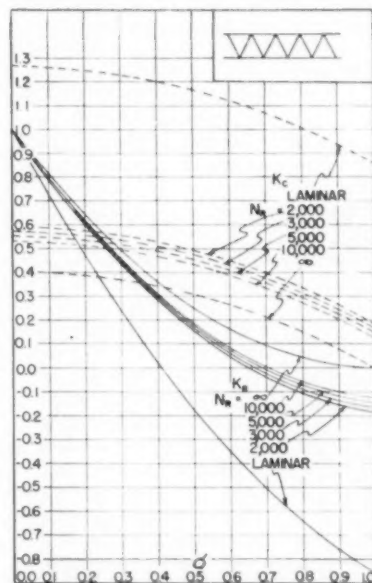


FIG. 7 CONTRACTION AND EXPANSION COEFFICIENTS FOR MULTIPLE-TRIANGULAR-TUBE PLATE-FIN SYSTEM

For the multiple-tube test system, the air was metered by a standard flat-plate orifice meter using the coefficients of reference (7). Static pressures were measured by a system of inclined draft gages and vertical single-leg water manometers. Flow-rate control from an automatic pressure regulator was accomplished by two manually controlled needle valves in parallel.

The single circular-tube test cores were constructed of brass tubing with four holes drilled and connected by a piezometer ring for each static-pressure tap.

The multiple-circular-tube test cores were constructed by drilling 19 tubes through a solid aluminum core. The static pressure taps each intersected three of the tubes. The plate-fin test core was built up of brass plates with inserts of fin material. The static pressure taps each intersected six flow tubes.

The pressure losses due to the contraction and expansion were evaluated by extrapolating the straight-line pressure variations to the point of abrupt change in flow cross section, as shown in Fig. 2. The contraction and expansion coefficients were then evaluated from Equations [1] and [2].

A more detailed description of the test systems, the original test data, and the method of analysis are contained in references (9) and (10).

Results of Tests. Figs. 8 through 13 show the experimentally determined expansion and contraction coefficients plotted as a function of Reynolds number in the smaller tube, or tubes. Denoted by dashed lines are the coefficients as predicted by the preceding analysis.

The results for the single-circular-tube system for one area ratio are shown in Figs. 8 and 9. Except for the contraction coefficients K_c at the lowest Reynolds numbers, the agreement between analysis and experiment is excellent. The poorer agreement for K_c at low Reynolds numbers is attributable to the poor experimental accuracy at low flow rates. The results of these tests illustrate clearly the double transition, especially in the case of the contraction coefficients where the effect is more pronounced.

Fig. 10 shows the expansion coefficients for four expansion-area ratios in the multiple-circular-tube system. Although there is a considerable scattering of test points, especially at the lowest Reynolds number, where the measured pressure changes were only a few hundredths of an inch of water, the analytically evaluated coefficients appear to be well substantiated by experiment. Because of the limitations of pressure-measurement accuracy, it was not possible to test at sufficiently low Reynolds numbers to substantiate completely the laminar-flow analysis, but the trend toward the laminar-flow curve is definitely evident.

Fig. 11 shows the contraction coefficients for two area ratios in the multiple-circular-tube system. Here the analytically evaluated coefficients are well substantiated for Reynolds numbers above 12,000. The behavior of the experimental coefficients at Reynolds numbers below 12,000 is believed to be due to the relatively short flow lengths in the test cores. The length-to-diameter ratio for these two test cores was 25.5 and 16.0, respectively, as compared to 100 for the single-circular-tube system. In order to evaluate the contraction coefficients it was necessary to extrapolate the pressure variation in the test core back to the entrance (see Fig. 2), and thus for accurate results, flow characteristic of long tubes would have to be established fully in at least one half the length of the core. It is evident that for the short-tube test cores, the fully developed laminar flow would never be established, and that fully developed turbulent flow would not exist until fairly high Reynolds numbers were reached.

Fig. 12 shows the results of tests of the plate-fin core with plain fins. Here the flow length was again sufficiently long to obtain good contraction-coefficient data at low Reynolds number, but below $N_R = 1000$ the experimental accuracy deteriorates rapidly. Nevertheless, the laminar-flow coefficients from Fig. 7 agree with the trend of the experimental results. At Reynolds numbers above 6000, both the contraction and expansion coefficients tend to decrease and drop away from the analytically evaluated coefficients. Here Mach number > 0.15 and the compressibility effects become significant. The coefficients K_c and K_e , since they are defined for incompressible flow, lose rigorous significance for compressible flow. However, it can be demon-

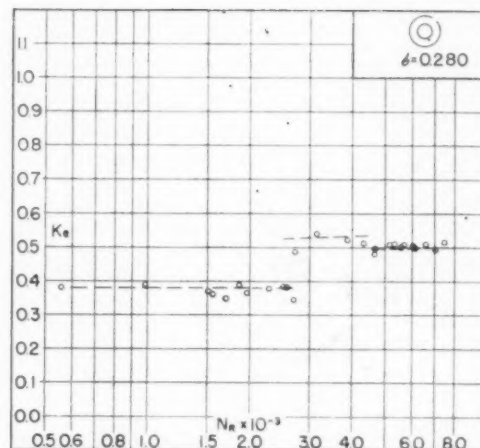


Fig. 8 EXPERIMENTALLY DETERMINED EXPANSION COEFFICIENTS FOR SINGLE-TUBE SYSTEM

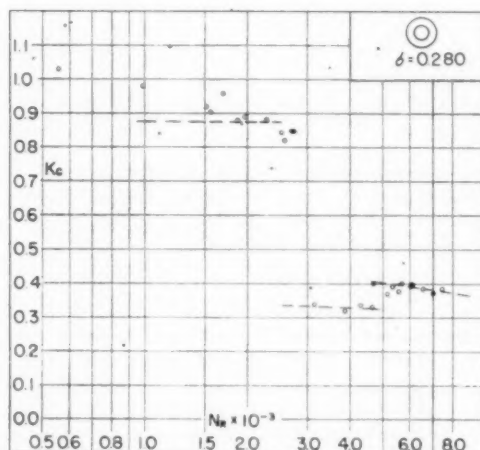


Fig. 9 EXPERIMENTALLY DETERMINED CONTRACTION COEFFICIENTS FOR SINGLE-TUBE SYSTEM

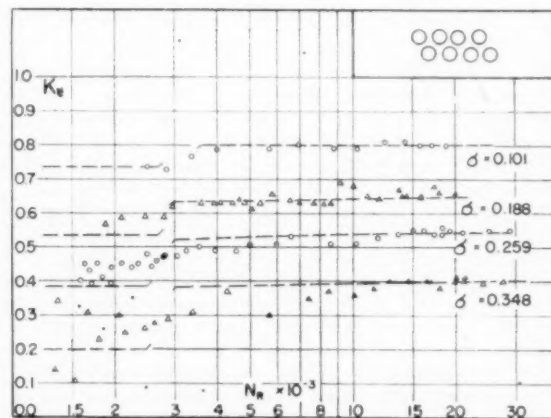


Fig. 10 EXPERIMENTALLY DETERMINED EXPANSION COEFFICIENTS FOR MULTIPLE-CIRCULAR-TUBE SYSTEM

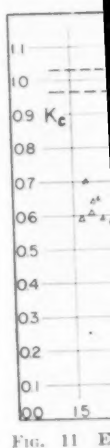


Fig. 11 EXPERIMENTALLY DETERMINED CONTRACTION COEFFICIENTS FOR MULTIPLE-CIRCULAR-TUBE SYSTEM

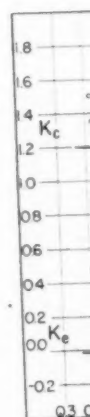


Fig. 12 EXPERIMENTALLY DETERMINED CONTRACTION COEFFICIENTS FOR PLATE-FIN CORE

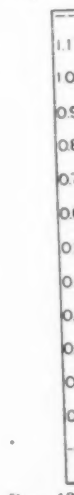


Fig. 13 EXPERIMENTALLY DETERMINED CONTRACTION COEFFICIENTS FOR PLATE-FIN CORE

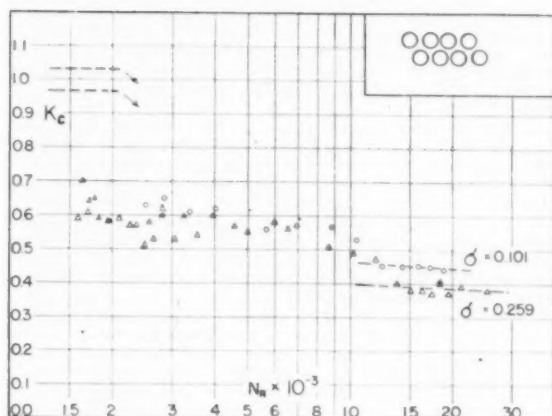


FIG. 11 EXPERIMENTALLY DETERMINED CONTRACTION COEFFICIENTS FOR MULTIPLE-CIRCULAR-TUBE SYSTEM

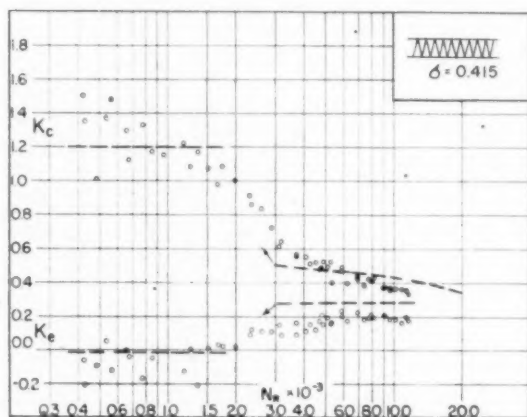


FIG. 12 EXPERIMENTALLY DETERMINED CONTRACTION AND EXPANSION COEFFICIENTS FOR A PLATE-FIN SYSTEM WITH PLAIN FINS

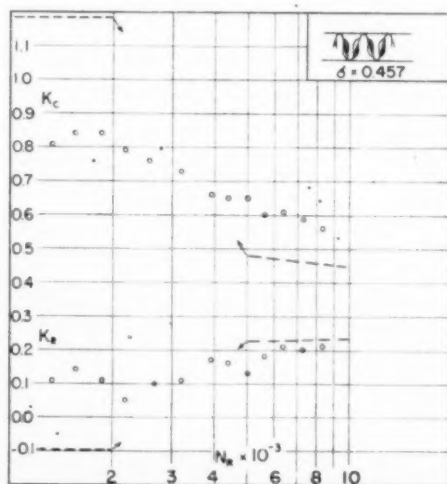


FIG. 13 EXPERIMENTALLY DETERMINED EXPANSION AND CONTRACTION COEFFICIENTS FOR A PLATE-FIN SYSTEM WITH INTERRUPTED FINS

strated on the basis of the data of reference (8) that the compressibility effect will be to decrease the "apparent" coefficients in the manner shown by the experimental results. For Mach number < 0.15 , the incompressible-flow treatment applies with good accuracy for most applications.

Fig. 13 shows the results of tests of the plate-fin core with interrupted fins. The very marked variation of the coefficients K_c and K_e with Reynolds number is no longer evident due to the tendency of the louvers to minimize large changes in velocity distribution with variations in N_R . The louvers have their greatest effect at Reynolds numbers below 2000 where the parabolic velocity distribution with a large K_d characteristic of laminar flow ordinarily would occur. The failure of the contraction coefficients K_c to approach closely the predicted curve (from Fig. 7 for smooth fins) at the higher Reynolds numbers is probably attributable to the actual system departure from the postulated two-dimensional contraction. This departure may be caused by the interference of the fins owing to curvature both in the plane of the flow and normal to the flow.

SUMMARY AND CONCLUSIONS

The results and conclusions of the foregoing analytical and experimental investigation may be summarized as follows:

- 1 A theory is developed for the prediction of contraction and expansion coefficients for essentially incompressible flow.
- 2 The theory for the expansion coefficient is an extension of the Borda-Carnot analysis allowing for nonuniformity of velocity distribution at both the upstream and downstream sections.
- 3 The theory for the contraction coefficient is an extension of the expansion-coefficient analysis. The loss of mechanical energy is considered to take place during the re-expansion after an initial contraction to a vena contracta inside the smaller tube, or tubes.
- 4 The specific application of this theory requires velocity-distribution data at both sections in question and, for the flow-contraction problem, additionally requires the area contraction ratio for the vena-contracta section.
- 5 The velocity-distribution coefficient can be obtained analytically for laminar flow in cylinders. For turbulent flow, data are available for application to the circular tube and two-dimensional flow between parallel planes. The square and triangular tubes are treated approximately.
- 6 Application of the idealized system analysis to geometries corresponding to some high-rating heat-exchanger surfaces is indicated.
- 7 Experimental results substantially confirm the predictions of the analysis. Discrepancies can be rationalized in terms of the departure of test system and idealized system geometries, and additionally in terms of experimental accuracies.

These data have been used to extract friction factors from over-all pressure-drop measurements in testing plain plate-fin heat-exchanger cores. The fact that in a typical case the friction factors are 16 per cent lower for laminar flow and 10 per cent lower at $N_R = 10,000$, when these coefficients are used in place of the conventional data, illustrates the necessity for accurate contraction and expansion coefficients for this type of work (11).

ACKNOWLEDGMENTS

This work was accomplished under the sponsorship of the Office of Naval Research on Navy Contract N6-ONR-251, Task Order VI, at Stanford University. The co-operation of the Office of Naval Research in permitting the results of this work to be presented is acknowledged.

The experimental work on the single circular tube system was accomplished by Mr. Paul G. Bissiri, who also contributed the ex-

tension of the analysis to account for the double transition in the single-tube system.

BIBLIOGRAPHY

- 1 "Losses of Pressure Head Due to Sudden Enlargement of a Flow Cross Section," by H. C. Schutt, Trans. ASME, vol. 51, 1929, pp. 83-87.
- 2 "Elementary Mechanics of Fluids," by Hunter Rouse, John Wiley and Sons, Inc., New York, N. Y., 1946.
- 3 "Heat Transmission," by W. H. McAdams, McGraw-Hill Book Company, Inc., New York, N. Y., 1942.
- 4 "The Pressure in the Annulus of Pipes With a Sudden Increase in Cross Section for High Velocity Air Flow," by W. Nusselt, *Forschung auf dem Gebiete des Ingenieurwesens*, vol. 11, No. 5, September-October, 1940, pp. 250-255.
- 5 "Heat Transfer and Pressure Drop in Heat Exchangers With Laminar Flow," by H. Glaser, MAP Volkenrode Ref.: MAP-VG 96-818 T, March 1, 1947.
- 6 "Theory of Elasticity," by S. Timoshenko, McGraw-Hill Book Company, Inc., New York, N. Y., 1934.
- 7 "Fluid Meters, Their Theory and Application," ASME Research Publication, fourth edition, 1937.
- 8 "Charts of Pressure, Density, and Temperature Changes at an Abrupt Increase in Cross Sectional Area of Flow of Compressible Air," by U. T. Joyner, NACA Wartime Report No. L-13, January, 1945.
- 9 "An Investigation of Losses of Flow Stream Mechanical Energy at Abrupt Changes in Flow Cross Section," by W. M. Kays, T.R. No. 1, Navy Contract N6-ONR-251, Task Order VI(NR-635-104), Department of Mechanical Engineering, Stanford University, Stanford University, Calif., Sept. 15, 1948.
- 10 "An Investigation of Losses of Flow Stream Mechanical Energy at Abrupt Changes in Flow Cross Section in Single Tube Systems," by P. G. Bissiri, thesis for the degree of engineer, Department of Mechanical Engineering, Stanford University, Stanford University, Calif., September, 1949.
- 11 "Heat Transfer and Flow Friction Characteristics of Some Compact Heat-Exchanger Surfaces—Parts I and II," by A. L. London and W. M. Kays; presented at the Annual Meeting, New York, N. Y., November 27-December 2, 1949, of The American Society of Mechanical Engineers. Published in this issue, pp. 1075-1097.

He
i

This
analysis
heat-tr
pact h
racy is
plate-f
the qu
perien
test m
forthc

Engl
The

A =
A_c =
A_f =
A_s =
A_w =
c_p =
D_d =
f =
f_d =
G =
g =

h =

h_s =
K_c =

K_s =

k =
k_w =

L =
l =
l_d =
l_w =
m =

1 =
Jun.
Nov.
ASM
C
sion
Nov
CHA
N
und
of t

Heat-Transfer and Flow-Friction Characteristics of Some Compact Heat-Exchanger Surfaces

Part 1—Test System and Procedure

By W. M. KAYS¹ AND A. L. LONDON,² STANFORD, CALIF.

This paper describes a test apparatus and method of analysis used for the accurate determination of the basic heat-transfer and flow-friction characteristics of compact heat-exchanger surfaces. The experimental accuracy is discussed and the results of test of a typical louvered-plate-fin heat-exchanger surface are included to illustrate the quality of data obtainable. It is hoped that the experience presented here may lead to a standardization of test methods so that more accurate design data will be forthcoming.

NOMENCLATURE

English Letter Symbols:

The following nomenclature is used in the paper:

- A = test-core total air-side heat-transfer area, ft^2
- A_c = test-core free-flow area, ft^2
- A_f = test-core extended-surface area, ft^2
- A_s = test-core total steam-side heat-transfer area, ft^2
- A_w = test-core direct-surface heat-transfer area, ft^2
- c_p = specific heat at constant pressure, $\text{Btu}/\text{lb } ^\circ\text{F}$
- D_d = hydraulic diameter of test duct, ft
- f = Fanning friction factor, dimensionless
- f_d = test-duct friction factor, dimensionless
- G = test-core mass velocity, $\text{lb}/(\text{hr ft}^2 \text{ of } A_s)$
- g = proportionality factor in Newton's second law, $g = 32.2$ (lbs/ft^3) (ft/sec^2)
- h = unit conductance for thermal-convection heat transfer, $\text{Btu}/(\text{hr ft}^2 ^\circ\text{F})$
- h_s = unit conductance for steam-side surface, $\text{Btu}/(\text{hr ft}^2 ^\circ\text{F})$
- K_c = contraction loss coefficient for flow at heat-exchanger entrance, dimensionless
- K_e = expansion loss coefficient for flow at heat-exchanger exit, dimensionless
- k = unit thermal conductivity, $\text{Btu}/(\text{hr ft}^2 ^\circ\text{F}/\text{ft})$
- k_w = unit thermal conductivity of wall material, $\text{Btu}/(\text{hr ft}^2 ^\circ\text{F}/\text{ft})$
- L = total flow length of test core, ft
- l = effective fin length, ft
- l_d = length of test duct between test core and pressure taps, ft
- l_w = wall thickness, ft
- $m = \sqrt{2h/k\delta}$, $1/\text{ft}$

- P = pressure, lb/ft^2
- r_h = flow passage hydraulic radius, ft
- T = temperature, $^\circ\text{R}$
- t = temperature, $^\circ\text{F}$
- U = unit over-all thermal conductance, $\text{Btu}/(\text{hr } ^\circ\text{F ft}^2 \text{ of } A)$
- v = specific volume, ft^3/lb
- w = air-mass flow rate, lb/hr

Greek Letter Symbols:

- Δ denotes temperature difference or, followed by P , denotes pressure difference
- δ = fin-metal thickness, ft
- ϵ_h = error in Stanton number determination, per cent
- ϵ_2 = error in core downstream temperature difference, $^\circ\text{F}$
- η_f = temperature effectiveness of fins, dimensionless
- η_o = over-all temperature effectiveness of a plate-fin surface, dimensionless
- η_s = over-all temperature effectiveness of steam-side surface, dimensionless
- ρ = air density, lb/ft^3
- σ = ratio of free-flow to frontal area of test core, dimensionless
- μ = air viscosity, $\text{lb}/(\text{hr ft})$
- μ_f = air viscosity, evaluated at a "film average" temperature, $\text{lb}/(\text{hr ft})$

Dimensionless Groupings:

- N_{St} = Stanton number, (h/Gc_p) , a heat-transfer modulus
- N_{Pr} = Prandtl number, $(\mu c_p/k)$, a fluid-properties modulus
- N_R = Reynolds number, $(Ar_h G/\mu)$, a flow modulus
- $N_{St} N_{Pr}^{1/3}$ = generalized heat-transfer grouping. This factor versus N_R defines heat-transfer characteristics of surface
- f = Fanning friction factor. This factor versus N_R defines friction characteristics of surface
- NTU = number of heat-transfer units, a heat-transfer parameter, (AU/wc_p)

Subscripts:

- O = duct conditions upstream of test core
- 1 = conditions at test-core entrance
- 2 = conditions at test-core exit
- 3 = duct conditions downstream of test core
- s = steam-side conditions
- f = film average conditions

Miscellaneous:

- lb denotes pounds mass in distinction to
- $\#$ denoting pounds force

INTRODUCTION

Until quite recently, the only accurately known basic heat-transfer and flow-friction data for application to heat-exchanger

¹ Acting Instructor, Mechanical Engineering, Stanford University. Jun. ASME.

² Professor, Mechanical Engineering, Stanford University. Mem. ASME.

Contributed by the Heat Transfer and Gas Turbine Power Divisions and presented at the Annual Meeting, New York, N. Y., November 27-December 2, 1949, of THE AMERICAN SOCIETY OF MECHANICAL ENGINEERS.

NOTE: Statements and opinions advanced in papers are to be understood as individual expressions of their authors and not those of the Society. Paper No. 49-A-95.

design was for flow through circular tubes and over banks of circular tubes. The advent of the gas turbine as a promising transportation-type prime mover, the development of portable oxygen plants, and the continued emphasis on small size and light weight in aircraft installations have pointed the need for more compact heat exchangers than are practicable utilizing these conventional tubular-type surfaces.

As a matter of definition, the term "compactness" refers to the area-to-volume ratio characteristic of the surface in question. A "compact surface," for the purpose of this paper, is one providing more than 75 ft² of transfer area per ft³ of core volume. This compares to the approximately 20 ft²/ft³ which can be realized from conventional 1-in.-diam tubes.

More compact surfaces can usually be realized by the use of fins, and higher heat-transfer coefficients can be obtained from surfaces employing various types of boundary-layer interruptions. In both cases there are few adequate basic data upon which to base even preliminary designs.

In the design of systems for the exchange of heat between liquids, accurate knowledge of the friction characteristics of the heat-transfer surface is relatively unimportant because of the low cost of pumping high-density fluids. For low-density fluids such as gases, however, the cost of friction per mass unit of flow is greatly multiplied, and thus the friction behavior of the surface becomes as important as the heat-transfer behavior. This is particularly true for the gas-turbine-plant heat exchangers—the regenerator and the intercooler, and especially the former, where the high-temperature, low-pressure exhaust gases are concerned.

It is the purpose of this paper to describe a test apparatus and testing technique which are being currently employed for the accurate determination of the basic heat-transfer and flow-friction characteristics of compact heat-exchanger surfaces in the hope that the experience gained in the design and operation of this system may be of use to others contemplating similar work. The design of this test system was based upon experience gained from a similar system at the U.S.N. Engineering Experiment Station, Annapolis, Md. (1).²

METHODS OF TESTING AVAILABLE

The heat-transfer characteristics of a surface, for application to fluids, with the exception of the liquid metals, can be expressed by the conventional nondimensional relation, $N_{St}N_{Pr}^{1/3}$ versus Reynolds number. The friction characteristics can be generalized using f (Fanning friction factor) versus Reynolds number. Air can be used as a test medium, and the relations given allow extrapolation to any fluid for which the necessary properties are known.

Since the flow-friction characteristics of a heat-exchanger surface, designed for use with gases, are equally as important as the heat-transfer behavior, it is obviously desirable for the sake of economy to have a test system capable of obtaining both characteristics from the same test core. For the compact heat-exchanger surfaces of interest, it is generally not practicable to measure pressures in the actual flow tubes, as can be seen from the typical test core, Fig. 1. Pressures must be measured in the ducting leading to and from the test core and the friction factor extracted from the total pressure drop by taking into consideration the flow losses due to the abrupt contraction and expansion at the entrance and exit to the core. Since the entrance and exit-loss coefficients for complex contractions and expansions are not known very accurately, the entrance and exit losses must be minimized by the use of long flow lengths, or in effect, as large a

² Numbers in parentheses refer to the Bibliography at the end of the paper.

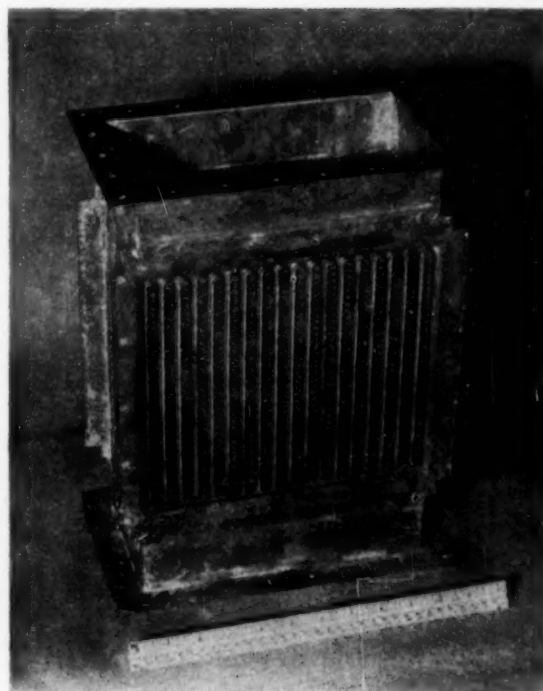


FIG. 1 TYPICAL EXTENDED-SURFACE PLATE-FIN TEST CORE

magnitude of the ratio $(L/4r_h)$, as is consistent with the requirements for accurate evaluation of the heat-transfer behavior.

Both transient and steady-state heat-transfer testing techniques have been used for this type of work. A transient technique has been developed in which it is necessary to measure only the maximum rate of change of temperature of the fluid emerging from an initially uniformly heated core, reference (2). This method has the advantage that a relatively large $(L/4r_h)$ may be employed, and thus the entrance and exit effects can be minimized. A further advantage is that it is not necessary to measure wall temperatures. This method is especially applicable to the determination of the characteristics of closely packed screens and other such surfaces as may find use in the regenerative-type heat exchanger. However, until this transient technique is further refined it is believed that the steady-state methods will yield more accurate data over the useful N_R range for the surfaces considered for this project.

One steady-state method employs a crossflow test core for which the two fluid sides are identical, and equal mass-flow rates of air are used. The over-all heat-transfer conductance can be deduced from the various average terminal temperatures. The unit film conductance of one side can be deduced from the assumption of equal conductances on both sides. The disadvantages of this method are: (a) Since the air leaving both sides has a temperature varying over the flow cross section, some kind of mixer is required. (b) A complicated ducting system is necessary. (c) Only surfaces which can be constructed into completely symmetrical test cores can be tested.

A much simpler steady-state system, without these disadvantages, uses condensing steam on one side of the test core. The steam side is at sensibly uniform temperature with a thermal resistance of generally less than 5–10 per cent of that of the air side. The temperature of the air leaving the test core is essen-

tially uniform on the steam side of the steam. The air side suffers from the same problem because of the same reasons. The methods of measurement of the NTU = UA/C are later, ten accuracy of NTU greater than the successive errors in Fig. 14).

NTU

Thus (L/4r_h) is chosen by the designer to obtain the desired magnitude of error. For example, if L/4r_h = 500 is a reasonable value. At higher values this limit

The value of L/4r_h in Figs. 2 is principally a function of the surface area placed in the flow through the test core. A steady-state steam test system is the one chosen for comparison. This error is accurate

tially uniform over the flow cross section and the type of surface on the steam side is not too important. A reasonable estimate of the steam-side resistance will suffice to determine accurately the air-side unit film conductance. However, this method suffers from definite limitations on the magnitude of $(L/4r_h)$ because of errors introduced into the computed results by limitations of temperature-measurement accuracy. For all the methods described, a dimensionless heat-transfer parameter, $NTU = AU/wc_p$, is ultimately deduced from air-side temperature measurements. For this last method, as will be shown later, temperature-measurement errors will result in maximum accuracy in the over-all conductance, U , if $NTU = 1.00$; and NTU greater than 3, or less than 0.2, will generally result in excessive error in U even with excellent instrumentation (see Fig. 14). NTU is related to $(L/4r_h)$ as follows

$$NTU = \frac{AU}{wc_p} = \frac{A}{A_c} \frac{U}{Gc_p} = \frac{A}{A_c} \frac{h}{Gc_p} = 4 \left(\frac{L}{4r_h} \right) N_{St}$$

Thus $(L/4r_h)$ is limited by the magnitude of Stanton number. However, despite this limitation, this method of testing has been chosen here because of its relative simplicity. Accurate data are obtained by using test cores constructed so that as large a magnitude of $(L/4r_h)$ as possible is employed with $NTU < 3$. For example, Stanton number for air flow in circular tubes at $N_{Re} = 500$ is about 0.010. For an NTU of 3, $(L/4r_h)$ becomes 75. At higher Reynolds numbers, Stanton number decreases so that this limitation applies to the lowest Reynolds number of interest.

DESCRIPTION OF TEST APPARATUS

The various components of the test apparatus are shown in Figs. 2 and 3, and diagrammatically in Figs. 4, 5, and 6. The principal element is an induced controllable-flow air duct with a rectangular test section, $8\frac{3}{4}$ in. \times $9\frac{3}{4}$ in. The exchanger surface under investigation is made into test cores which are placed in the test section. Air-side instrumentation is provided for metering the air, measuring the change in air temperature through the core, and measuring the air pressure drop.

A steam system is provided to supply slightly superheated steam to the test core, and instrumentation is provided so that the energy loss of the condensing steam may be measured and compared to the separately determined energy gain of the air. This energy balance provides a continuous partial check on the accuracy of the instrumentation.

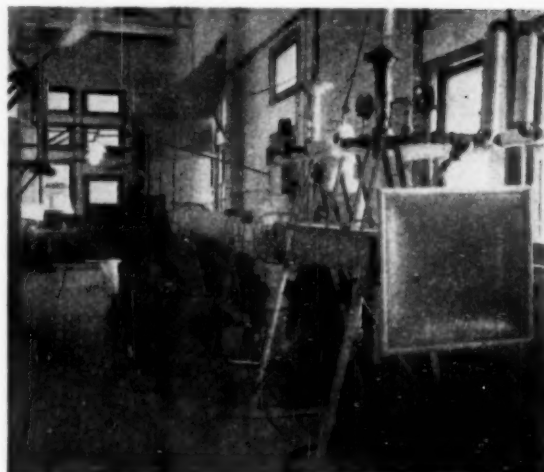


FIG. 2 TEST DUCT VIEWED FROM INTAKE END

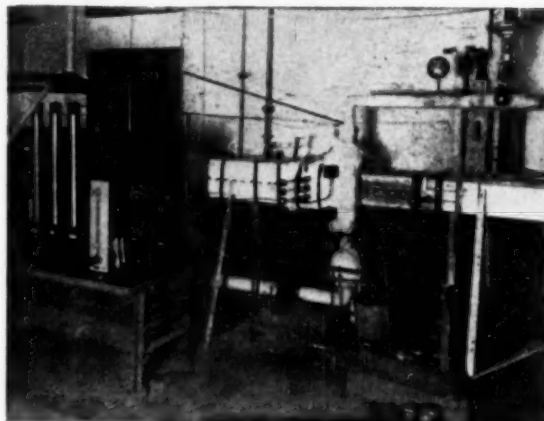


FIG. 3 CLOSE-UP OF TEST DUCT
(Installed test core and part of steam system.)

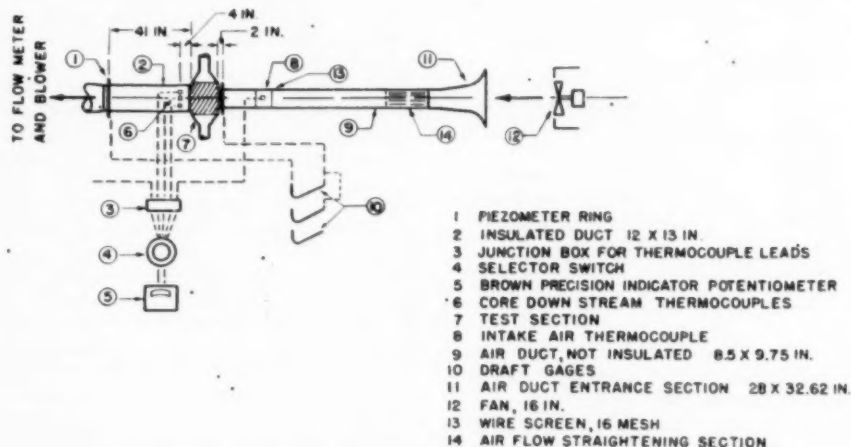
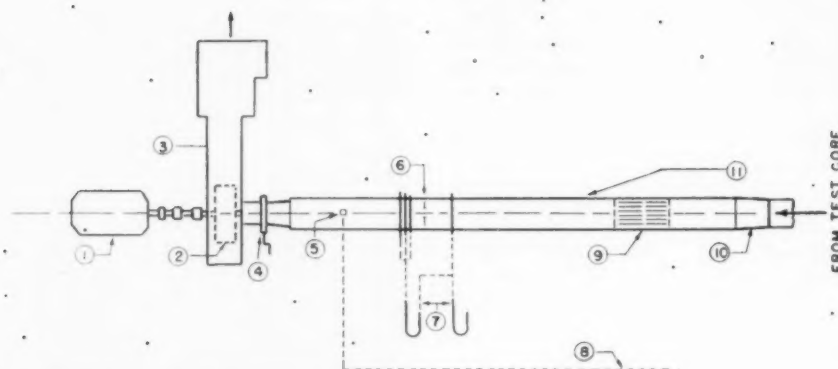


FIG. 4 DIAGRAM OF TEST DUCT
(Test section and intake section.)



- 1 INDUCTION MOTOR 75 HP 3600 RPM
- 2 BLOWER BUFFALO 7E 27 IN.
- 3 AIR DISCHARGE DUCT, SOUND INSULATED
- 4 AIR FLOW REGULATOR
- 5 ORIFICE THERMOCOUPLE
- 6 ORIFICE
- 7 ORIFICE MANOMETERS
- 8 TO THERMOCOUPLE SWITCH BOX
- 9 AIR FLOW STRAIGHTENING SECTION
- 10 TRANSITION FROM RECTANGULAR TO CIRCULAR DUCT
- 11 INSULATED DUCT, OD=15 IN., ID=12 IN.

FIG. 5 DIAGRAM OF TEST DUCT
(Air-metering section and blower.)

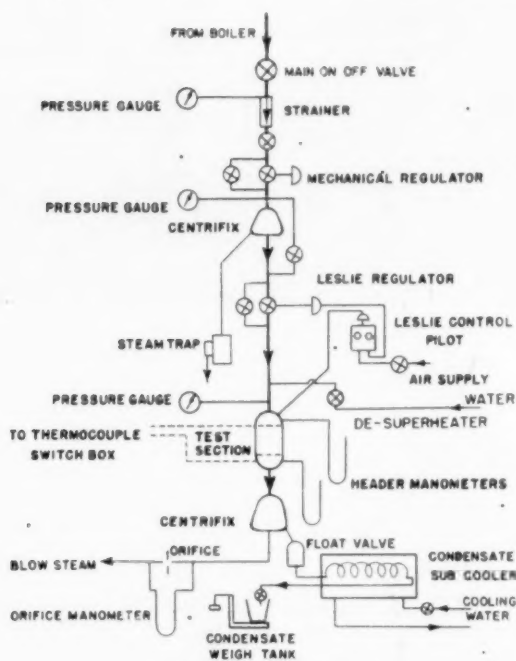


FIG. 6 STEAM SYSTEM

Air System, Figs. 4 and 5. The sheet-metal air duct consists of two sections—one rectangular which includes the test section, the other circular which includes the air-metering orifice.

Air is induced through the duct by a centrifugal blower, rated 5500 cfm at 40 in. of water static pressure. The blower is powered by a 3450-rpm induction motor. Flow regulation is accomplished by a manually operated double sliding plate which con-

stricts the flow symmetrically at the blower intake. With this intake flow control, no pulsation difficulty has been encountered, and smooth regulation is possible from wide open to shutoff. An induced-flow system was chosen to avoid the poor velocity-distribution characteristic of a forced-draft system.

Referring to Fig. 4, room-temperature air is induced into the test duct through a smoothly converging entrance section. A 16-in. axial-flow fan is placed 40 in. before the entrance section. This fan produces a hollow cone of rotating air which encloses the entrance section without blowing directly into it. This serves to mix thoroughly the intake air to a uniform temperature in spite of vertical temperature differences of 2-3 F existing in the laboratory. Following the entrance, the air passes through an "egg-crate" straightening section. The ends of the straightening section form trim tabs which were used to adjust the flow so that the velocity distribution at the test section was close to uniformity for the test range, 400 to 12,000 lb/hr. The results of Pitot-tube traverses, demonstrating this uniformity, are shown in Fig. 7.

The ducting between the entrance and the test section contains, in addition to the straightening section, two 16-mesh wire screens to standardize turbulence, a shielded thermocouple, and four pressure taps connected by a piezometer ring. The last turbulence screen is 18 in. ahead of the test core.

The ducting on the downstream side of the test section is lagged with 1 1/2-in. magnesia insulation plus a double layer of asbestos cloth to reduce radiation errors in the air-temperature measurements. The test core is clamped between 1-in.-thick plastic insulating flanges at the ends of the ducts. Three shielded thermocouples and four pressure taps connected by a piezometer ring are located in the downstream section. The final location of the upstream and downstream pressure taps was determined by a pressure survey, the results of which are shown in Fig. 8.

The air next passes through a transition section and into a circular duct lagged with 1 1/2-in. magnesia. This duct contains a straightening section constructed of 1-in. tubing and an air-

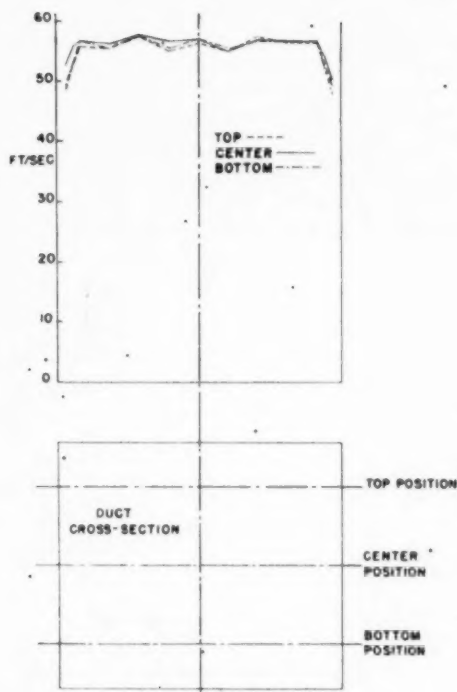


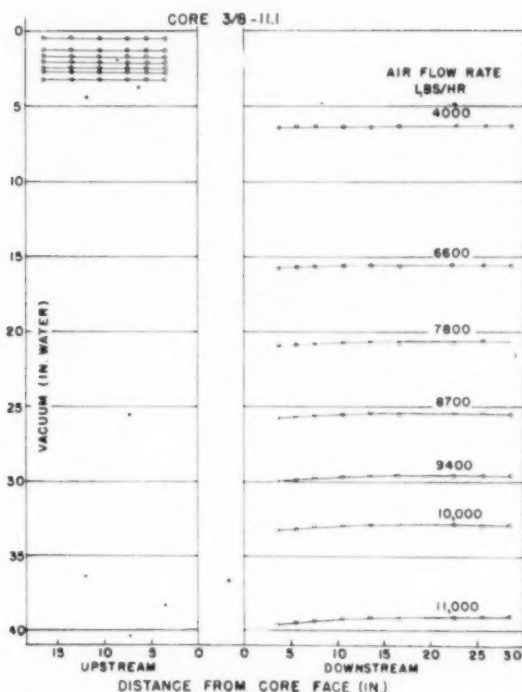
FIG. 7 PITOT-TUBE TRAVERSES UPSTREAM OF TEST CORE

metering orifice with vena-contracta taps. Three orifice sizes are used in order to cover the desired flow range. These meters are standard units, constructed and installed in accordance with the specifications of reference (3), which also provides the orifice coefficients for the flow equation. A shielded thermocouple is located downstream.

Steam System, Fig. 6. Wet steam is generated in a boiler at a pressure which can be regulated from 30 to 100 psig. Steam enters the regulatory system at boiler pressure. It is strained and then passes through a $\frac{1}{4}$ -in. automatic regulator where the pressure is reduced to between 15 and 30 psig. Most of the liquid phase is then removed in a centrifugal separator. The essentially dry vapor is further throttled in an air-operated pilot-controlled regulator to a pressure of approximately 6 psig, and about 10 F of superheat. A small amount of water may be injected at this point to provide close control on the desired 3 to 5 F superheat on entry to the top of the test core. This small degree of superheat is necessary so that the steam state can be fixed by measurements of pressure and temperature only and still maintain essentially uniform temperature conditions on the steam side. The pilot-operated regulator holds the core steam pressure within ± 0.1 in. of mercury, and the corresponding saturation temperature constant within ± 0.17 F.

A considerable excess of "blow" steam is passed through the core to prevent the build-up of a thick film of condensate on the transfer surface. The blow steam and condensate leave the test core via a header at the bottom. Copper wool in the inlet header assures an even steam distribution over the flow cross section. Pressure taps and thermocouples are located in both headers.

Directly below the exit header, the blow steam and condensate enter a centrifugal separator, and then the dry blow passes through a metering orifice before discharge to the atmosphere.

FIG. 8 PRESSURE VARIATION ON EITHER SIDE OF TEST CORE
(This diagram was used to locate piezometer rings.)

The condensate leaves the system by way of a floating-type steam trap and a subcooler where its temperature is reduced to approximately 100 F to avoid flashing during weighing. It then passes into a bucket where the flow rate is measured gravimetrically. The entire system is well insulated to minimize any extraneous heat transfer.

Pressure Instrumentation. Instrumentation is provided for measuring the test-core air-pressure differential, air-orifice pressure differential, gage pressure upstream of the test core and orifice, steam-header gage pressures, and the blow-steam orifice differential. The air pressures are all measured with vertical single-leg-type water manometers or inclined draft gages, and the steam pressures with mercury manometers.

For the steam-pressure manometers, liquid water is used to transmit the pressure to the manometer. This connection is shown in Fig. 9. Condensation and overflow in these "pots" maintain a constant water head on the manometer.

Temperature Instrumentation, Figs. 10, 11. All temperatures are measured with single-junction iron-constantan thermocouples (No. 24 gage wire). The system is designed so that temperatures may be estimated to within 0.2 F. Junctions are formed by an electrowelding process under oil, producing a clean unoxidized bead, approximately $\frac{1}{32}$ in. diam.

The five traversing-type thermocouples in the air stream are mounted in radiation shields as shown in Fig. 10. Together with the insulated duct wall, the calculated effects of thermocouple radiation are negligible.

The pencil-type steam-header thermocouples, Fig. 11, are sufficiently long, and the test-core walls well enough insulated so that the effect of steam conduction is negligible.

A reference junction at approximately 80 F is used. It is immersed in a bakelite tube filled with mercury, which is in turn immersed in a water-filled thermos bottle. The reference-

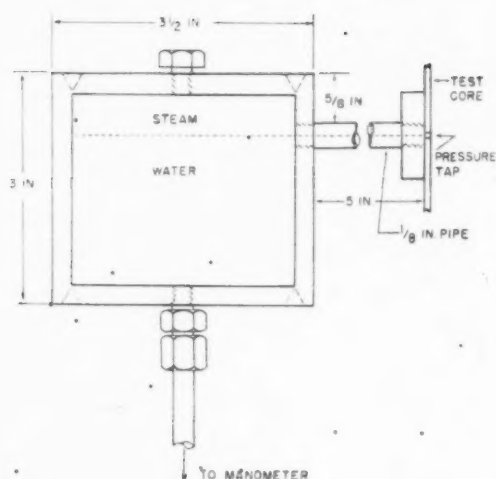


FIG. 9 STEAM-SYSTEM PRESSURE POTS
(These are used to transmit steam pressure to mercury manometers.)

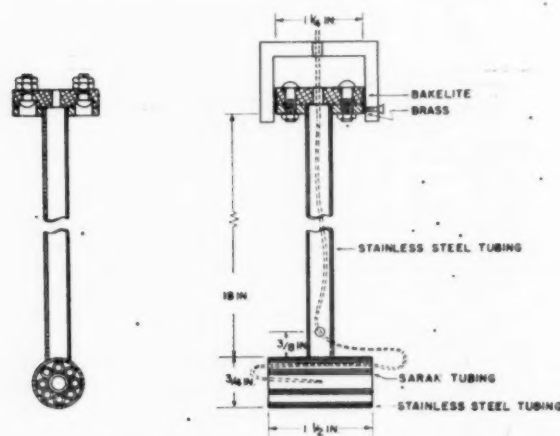


FIG. 10 RADIATION SHIELDED THERMOCOUPLES
(Used for air-temperature measurements.)

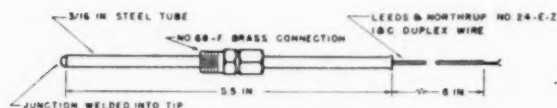


FIG. 11 STEAM-SYSTEM THERMOCOUPLES

junction temperature is obtained from a calibrated standard thermometer, 0.2 F divisions, immersed in the same mercury well.

All thermocouple leads are brought into a single zone box which is thoroughly insulated, and, in addition, two 1/4-in-thick copper plates are placed inside, sandwiching the terminal strip, for the purpose of producing an isothermal zone. Copper leads then connect the selector switch to an electronic self-balancing potentiometer. The potentiometer has a range of 5000 microvolts on a 25-in. scale. The smallest division is 10 microvolts and readings may be estimated to ± 2 microvolts (0.07 F), for the single-junction thermocouples.

The temperature which is the most difficult to measure with the desired accuracy is the bulk average air temperature leaving the test core. Nine-point traverses are made with each of three thermocouples, and Fig. 12 shows the temperature variation for two widely differing air-flow rates for a typical test core. The similarity of the temperature variations indicates that they are due to nonhomogeneity in the core construction and not to instrumentation. The variation from top to bottom can be accounted for by the build-up of steam-side resistance.

All secondary instruments were calibrated against standard

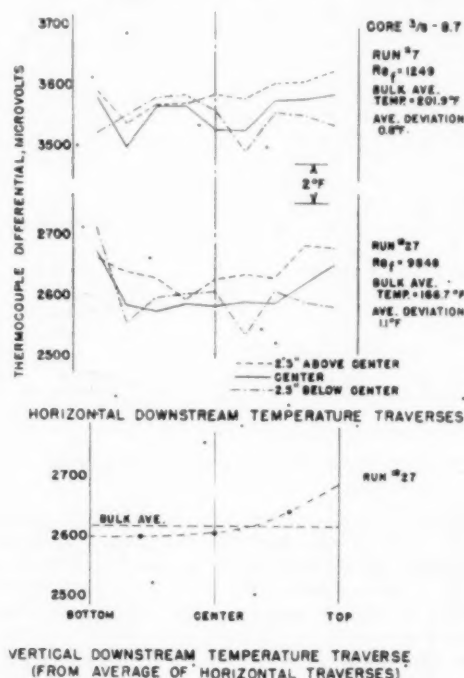


FIG. 12 TEMPERATURE TRAVERSES
(Results for downstream side of typical test core for two air-flow rates.)

instruments. In addition, three continuous checks are provided in the testing procedure, as follows:

- 1 Since the condensate plus blow steam in the bottom test-core header is in the mixed-phase region, its temperature can be determined accurately from the pressure measurement. This saturation temperature is checked against the temperature indicated by the thermocouple in the bottom header.
- 2 An energy balance has been mentioned previously.
- 3 The three orifices are checked one against another by overlapping the test air-flow rates and comparing the results. Any inconsistency in the flow measurement between orifices will then show up as jumps in the friction-factor results.

DESCRIPTION OF TEST CORES

Fig. 13 specifies the test-core dimensions with the exception of the air-flow length which must be determined separately for each surface to realize satisfactory accuracy in the determination of both N_{St} and f . The equation for evaluating the Stanton number from measurements of steam temperature and air-inlet and outlet temperatures, derived from the combination of an energy balance, and the heat-transfer-rate equation, is

The second
Since Δ_1 is
errors will

on the S
treating s
error in S
e₂, the fol

Equation
magnitud
error occu
terminati
which it i

Heat-T
superheat
tially con
average s
ture vari
order of
over-all
unit film
equation

$$\frac{(t_1 - t_2)}{(t_1 - t_3)} = \frac{\Delta_1}{\Delta_2} = e^{NTU} = e^{\frac{AU}{\dot{m}c_p}} \quad [1]$$

$$= e^{A(L/Ark)\dot{N}St} \quad [2]$$

The second equation results from the approximation, $U = h$. Since Δ_1 is always greater than Δ_2 , temperature-measurement errors will have the most pronounced effect on Δ_2 . This effect

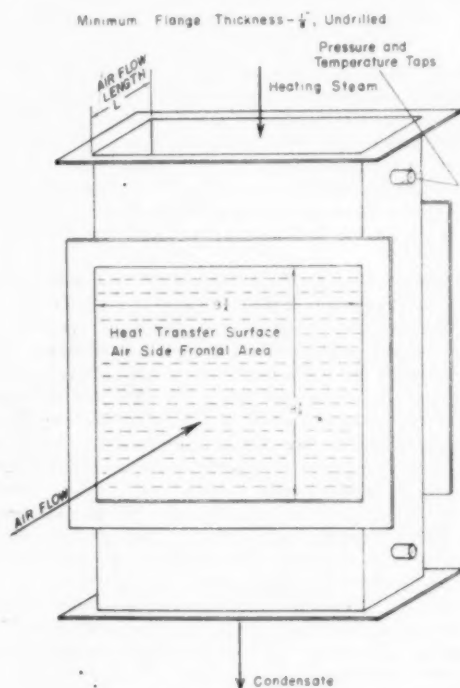


FIG. 13 TEST-CORE OUTLINE DIMENSIONS

on the Stanton-number determination can be evaluated by treating small errors as differentials. Denoting the per cent error in Stanton number as ϵ_h and the absolute error in Δ_2 as ϵ_2 , the following obtains from Equation [2]

$$\epsilon_h = \frac{\epsilon_2 e^{NTU}}{\Delta_1 NTU} \quad [3]$$

Equation [3] is plotted in Fig. 14 for $\Delta_1 = 150$ F and various magnitudes of error in Δ_2 . It should be noted that the minimum error occurs when $NTU = 1.00$. The use of this plot in the determination of the test-core air-flow length and the limitations which it imposes have already been indicated.

TREATMENT OF DATA

Heat-Transfer Calculations. The effect of the small inlet-steam superheat on the hot-side temperature is negligible. The essentially constant steam-side temperature is evaluated from the average steam-side saturation pressure (the steam-side temperature variation is 0.17 to 0.34 F due to a pressure drop of the order of 0.1 to 0.2 in. Hg). Equation [1] is used to evaluate the over-all conductance from the test data. From U , the air-side unit film conductance h can be extracted using the resistance equation

$$\left(\frac{1}{U}\right) = \frac{A}{\eta_o A_s h_s} + \frac{A}{A_w k_w} + \frac{1}{\eta_o h_o} \quad [4]$$

Over-all resistance Steam-side resistance Wall resistance Air-side resistance

The steam-side unit film conductance, h_s , is required, but as the steam-side resistance is generally less than 5-10 per cent of the total, a reasonable estimate of h_s is all that is necessary. The estimate used is based upon Nusselt's analysis given in reference (4). The other terms in the equation are system constants with the exception of η_o , the temperature effectiveness of the surface ($\eta_o = 1.00$ if there is no extended surface); η_o is related to the temperature effectiveness of the fins alone as follows:

$$\eta_o = \frac{A_w + \eta_f A_f}{A}$$

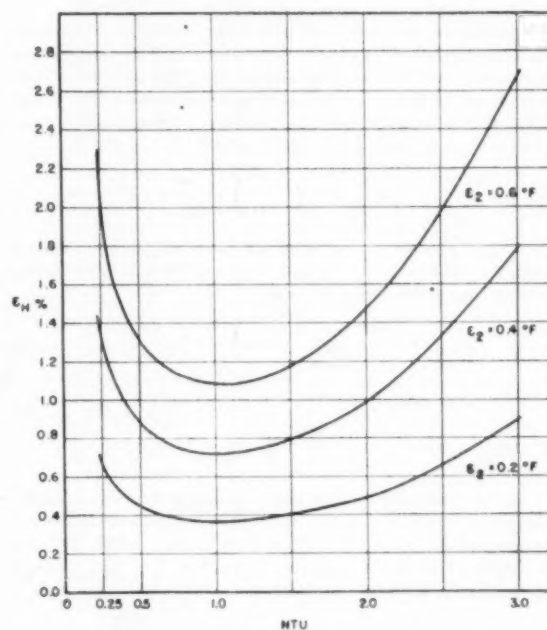


FIG. 14 ERROR IN STANTON NUMBER RESULTING FROM TEMPERATURE-MEASUREMENT ERRORS

For fins of constant conduction cross section and convection periphery

$$\eta_f = \frac{\tanh ml}{ml}$$

where $m = \sqrt{2h/k\delta}$, and l is one half the total fin length. For other fin geometries, the information of reference (5) may be used.

All the dry-air properties are taken from reference (6). N_{Pr} and μ are taken as for dry air, but for c_p used in N_{St} , as well as the density in the flowmetering calculations, an adjustment is made for atmospheric humidity.

Friction-Factor Calculations. The core pressure drop as measured is considered to consist of the following components:

- 1 A pressure drop on air-flow entrance to the core, ΔP_{a-1} .
- 2 A core-friction and flow-acceleration pressure drop, ΔP_{core} .
- 3 A pressure recovery on air-flow exit from the core, ΔP_{2-3} .
- 4 A duct-friction term allowing for the 39-in. length of duct

from the core discharge section to the downstream location of the pressure taps, and the 2-in. length of duct upstream of the core, ΔP_{duct} .

These components are related as follows

$$\Delta P = \Delta P_{0-1} + \Delta P_{\text{core}} - \Delta P_{2-3} + \Delta P_{\text{duct}} \dots [5]$$

The entrance pressure drop can be expressed, from reference (7), as

$$\Delta P_{0-1} = K_e \frac{G^2}{2g\rho_1} + \frac{G^2}{2g\rho_1} (1 - \sigma^2) \dots [6]$$

The pressure recovery at the core exit is evaluated in a similar manner.

$$\Delta P_{2-3} = -K_e \frac{G^2}{2g\rho_2} + \frac{G^2}{2g\rho_2} (1 - \sigma^2) \dots [7]$$

The entrance and exit-loss coefficients, K_e and K_a , are evaluated as a function of N_R and the flow-area contraction ratio, using the results of analysis and experiment described in reference (7). The sum ($K_e + K_a$) is considered to be accurate to ± 10 per cent.

The small duct loss, neglecting changes in density, is evaluated as follows, using a nominal magnitude of f_d

$$\Delta P_{\text{duct}} = 4 \left(f_d \frac{L}{D_d} \right) \sigma^2 \frac{G^2}{2g\rho_2} \dots [8]$$

The core pressure drop, which includes the desired friction factor, is evaluated by integration of the differential form of the dynamic equation for flow in a tube

$$\Delta P_{\text{core}} = \frac{G^2}{2g} v_1 \left[2 \left(\frac{v_2}{v_1} - 1 \right) + \frac{f}{r_h} \frac{1}{v_1} v_m L \right] \dots [9]$$

where

$$v_m = \frac{1}{L} \int_0^L v dx$$

Term v_m can be evaluated if v is known as a function of length. This integration is accomplished by using an arithmetic-average pressure, since the pressure drop is relatively small, and the temperature variation indicated by Equation [1]. The resulting equation for v_m is

$$v_m = \frac{2}{(T_1\rho_1 + T_2\rho_2)} \left[T_s - \frac{(T_2 - T_1)}{NTU} \right] \dots [10]$$

Equations [6], [7], [8], and [9] are then substituted in Equation [5] and solved for the friction factor, f .

Reynolds-Number Evaluation. A question arises as to the correct value of viscosity to use for the Reynolds number ($Ar_h G/\mu$), because the temperature, and thus the viscosity, varies with flow length and over the cross section. This problem has been partially resolved by testing for the friction factors both during the heat-transfer tests and by separate isothermal tests. In the latter case there is no question as to the correct viscosity. For the heating tests, a good correlation for turbulent flow is obtained by assuming a film average viscosity based on a temperature halfway between the wall and the arithmetic average of the air temperatures. A more rational procedure might be to use the arithmetic average of wall and logarithmic-average air temperatures, but for these tests the difference is negligible. Both the heat-transfer and friction results are then presented as a function of the "film" average Reynolds number.

ACCURACY AND ERRORS

No attempt is made to analyze rigorously for all possible

sources of error, but rather to estimate the magnitude of the more important ones and use these for arriving at an over-all estimate of the accuracy of the $N_{St} N_{Pr}^{1/3}$ and f versus N_R characteristics. The errors considered are as follows:

- (a) Errors inherent in the design and performance of the test system.
- (b) Instrument inaccuracies.
- (c) Errors introduced by virtue of the idealizations and auxiliary data used in the analysis.
- (d) Uncertainties in the determination of the test-core dimensions.

Air-Flow Metering. The air-orifice installation is made rigorously in accordance with the specifications of reference (3). Using the methods of this reference, the estimated probable error in air-flow metering is ± 0.7 per cent. The fact that no discontinuity in the test results is noted when orifices are overlapped further justifies the assumption of this small probable error, especially since the friction factor varies inversely as the square of the air-flow rate and is thus particularly sensitive to this error.

Heat-Transfer Results. It is believed that the measurements of the critical dimensions of the test cores can be made to ± 1 per cent. The maximum temperature-measurement error, is introduced in the determination of the core downstream temperature. Although the point temperatures are believed accurate to ± 0.2 F, it is probable that because of variations in temperature over the cross section of 2-4 F, Fig. 12, the 27-point traverse yields bulk average temperature results to within only ± 0.5 F. The estimated steam-side resistance is an approximation and is probably only accurate to ± 50 per cent. It should be noted, Equation [2], that the Stanton-number determination is virtually independent of the air-flow rate. A miscellaneous error of ± 1 per cent in Stanton number includes the effect of nonuniform core-entrance air velocity. According to reference (6), Prandtl number is subject to an uncertainty of ± 5 per cent, due primarily to the uncertainty for k for air.

In summary, Table 1 gives a typical estimation of uncertainties in the heat-transfer test results leading to $N_{St} N_{Pr}^{1/3}$

TABLE 1 POSSIBLE ERRORS IN HEAT-TRANSFER TEST RESULTS

	Per cent error at—	
	$N_R = 1000$	$N_R = 10000$
Temperature and dimension measurements.....	± 2.7	± 2.1
Steam-side resistance estimate.....	± 0.6	± 2.5
Miscellaneous.....	± 1.0	± 1.0
Stanton number.....	± 3.0	± 3.4
Prandtl number.....	± 5.0	± 5.0
$N_{St} N_{Pr}^{1/3}$	± 4.5	± 4.8

Friction Factors. The accuracy of the friction factors will depend to a certain extent upon the relative importance of the entrance and exit losses in the various test cores. With the pressure drop measured to ± 0.5 per cent, a ± 1 per cent probable error in the core dimensions, a ± 0.7 per cent probable error in the air-flow rate, and ($K_e + K_a$) accurate to ± 10 per cent, the probable error for a typical test core is ± 5 per cent.

Reynolds Numbers. A ± 1.0 per cent error in the test-core dimensions, a ± 0.7 per cent error in the flow rate, and a further ± 1 per cent error in the air viscosity (from reference 6), indicate a probable uncertainty of ± 1.6 per cent in the Reynolds number determination. The temperature upon which the viscosity is based is a question of interpretation of results and not of experimental accuracy.

TYPICAL RESULTS

To illustrate the quality of data obtainable from this appara-

tue, tes
surface
shown i
series of
practica
here doe
does, ho
of the fi
isotherm
plotted

Run No.	154/
5	961
6	972
7	976
12	979
9	611
10	549
13	562
14	472
15	481
16	431
17	295
18	309
19	277
20	236
21	239
22	236
23	236
24	236
25	17
26	14
27	14
28	13
29	13
30	13
31	13
32	13
33	13
34	13
35	13
36	13
37	13
38	13
39	13
40	13

Run No.	
1	
2	
3	
4	
5	
6	
7	
8	
9	
10	
11	
12	
13	
14	
15	
16	
17	
18	
19	
20	
21	
22	
23	
24	
25	
26	
27	
28	
29	
30	
31	

tus, test results for a typical louvered-plate-fin heat-exchanger surface are included here. The dimensions of the surface are shown in Fig. 15. Table 2 gives the complete test data for a series of runs covering a Reynolds number range, 400–8000, the practical range of interest for this surface. The $N_{St}N_{Fr}^{2/3}$ given here does not include the allowance for steam-side resistance. It does, however, include the effect of the temperature effectiveness of the fins, see Equation [4]. Table 3 gives the results for the isothermal friction-factor tests. The data of Tables 2 and 3 are plotted in Fig. 15. The recommended friction-factor curve is

drawn through the isothermal data. The recommended heat-transfer curve results from the correction for steam-side resistance. It should be noted that there is very little scattering of test points and that a very good correlation between hot- and cold-core friction factors is obtained. The overlapping of the flowmeters is evident by the closer spacing of the data points in the regions, $N_R = 2000$ and 4000 – 5000 . The energy balances, Table 2, are seen to be mostly on the positive side which is to be expected since 100 per cent separation of the condensate from the blow steam is not possible and thus some condensate is not

TABLE 2 HEAT-TRANSFER AND FRICTION DATA—RESULTS FOR A TYPICAL LOUVERED-PLATE-FIN TEST CORE

Air Flow Rates			Upstream Air State			Downstream			Core AP			Steam			Conversion			Friction			Reynolds' No.			Energy Bal.		
Run No.	lb/hr	Core Area Velocity lb/hr ft ²	Humidity lb/lb	Temp. °F	% H ₂ O @ 70°F	Temp. °F	Temp. °F	Core AP #H ₂ O @ 70°F	Steam Saturation °F	Temp. °F	Flow Coeff., b lb/(hr ft ² °F)	(h/ΔT) ² /°F ²	Factor f	Re	Re	Re	Re	Re	Re	Re	Re	Re	Re	Re	Re	
5	963.4	43330	.0110	87.6	404.46	179.5	33.04	229.0	66.7	.00948	8516	8516	+0.05													
6	878.7	36110	.0113	89.1	405.03	181.7	28.55	229.0	66.6	.00946	7942	7942	+1.3													
8	796.6	32650	.0109	87.5	405.19	181.7	22.80	228.9	59.9	.00946	6880	6880	+2.0													
9	764.7	31690	.0111	88.9	405.99	184.7	20.04	228.9	57.2	.00946	6021	6021	+1.8													
12	679.9	27990	.0103	84.9	406.80	181.9	17.59	229.0	50.2	.00945	5092	5092	+2.8													
13	623.7	26690	.0108	88.1	406.36	188.6	14.82	228.8	43.2	.00945	4286	4286	+1.7													
14	549.7	24880	.0110	88.5	406.42	190.0	13.00	228.8	40.9	.00942	3727	3727	+1.9													
15	567.7	26490	.0107	86.5	407.25	190.1	12.43	228.6	40.7	.00947	3727	3727	+3.6													
16	478.4	20690	.0109	87.3	407.54	193.5	9.18	228.8	45.3	.00933	3078	3078	+2.6													
17	482.5	20390	.0109	89.7	408.38	193.9	8.80	228.8	44.1	.00930	3083	3083	+1.2													
18	421.6	17990	.0103	86.8	407.32	195.7	7.22	228.4	43.2	.00943	3152	3152	+3.5													
19	390.9	15310	.0108	87.3	407.87	198.7	5.49	228.8	37.2	.00946	2522	2522	+4.5													
20	360.2	13950	.0109	89.2	407.96	203.1	4.44	228.7	34.4	.00936	2343	2343	+3.8													
21	277.8	11960	.0108	85.2	407.51	202.0	3.79	228.4	31.8	.00934	2194	2194	+3.5													
22	275.1	11340	.0110	85.7	407.56	203.1	3.21	228.3	30.1	.00946	2197	2197	+3.4													
23	230.9	10940	.0090	85.0	408.30	202.1	3.35	228.5	29.4	.00947	2184	2184	+2.6													
24	236.2	10330	.0090	83.3	408.32	203.1	2.790	228.5	28.2	.00940	2038	2038	+1.5													
25	231.1	10390	.0109	86.4	407.99	204.8	2.670	228.3	28.2	.00945	1996	1996	+4.1													
26	202.3	8834	.0109	88.9	407.63	208.7	2.170	228.3	21.9	.00946	1804	1804	+3.8													
27	202.8	8803	.0090	83.5	408.37	206.3	2.187	228.5	21.7	.00944	1777	1777	+3.8													
28	179.5	7646	.0090	84.3	408.43	208.4	1.735	228.5	21.4	.00942	1532	1532	+4.1													
29	180.3	6990	.0090	84.5	408.42	209.8	1.595	228.5	22.2	.01007	1467	1467	+4.2													
30	144.8	6324	.0090	84.6	408.44	213.2	1.290	228.5	20.8	.01073	1263	1263	+4.9													
31	138.9	5644	.0090	84.8	408.48	212.8	1.058	228.3	19.3	.01111	1197	1197	+6.2													
32	134.8	5013	.0090	81.2	408.08	214.1	.903	228.3	18.3	.01137	1035	1035	+3.6													
33	134.8	5006	.0090	85.3	408.47	214.9	.898	228.5	18.2	.01108	983	983	+2.8													
34	109.8	4480	.0090	83.8	408.56	218.0	.752	228.6	17.5	.01277	880	880	+1.0													
35	100.3	3974	.0094	82.9	408.37	219.7	.630	228.3	16.3	.01133	837	837	+1.8													
36	790.8	3453	.0119	89.7	405.88	239.9	.527	227.5	15.9	.0145	697	697	+2.9													
37	792.4	3155	.0123	89.6	405.88	240.8	.483	227.5	14.7	.0150	645	645	+2.8													
38	607.4	2652	.0123	88.9	405.80	232.5	.363	227.5	13.6	.0165	520	520	+4.1													
39	518.4	2277	.0130	87.9	405.80	233.3	.298	227.5	12.1	.0173	443	443	+3.0													
Average Deviation																							3.1			

TABLE 3 ISOTHERMAL FRICTION DATA—RESULTS FOR A TYPICAL LOUVERED-PLATE-FIN TEST CORE

Run No.	Air Flow Rates		Core ΔP H ₂ O @ 70°F	Upstream Air State			Friction Factor f	Reynolds' No. Re
	lb/hr	Core Mass Velocity lb/hr ft ²		Press. H ₂ O Abs. @ 70°F	Temp. °F	Humidity lb/hr		
1	9888	43180	28.19	405.40	80.3	.0096	.02424	9754
2	9115	39800	24.24	405.79	80.5	.0094	.02456	8991
3	8180	35720	20.00	406.23	80.9	.0095	.02530	8051
4	7006	30590	15.27	406.73	81.2	.0096	.02646	6895
5	6389	27900	12.90	406.98	81.5	.0096	.02689	6288
6	6100	26640	11.79	407.54	80.5	.0101	.02708	6018
8	5634	24600	10.28	407.26	81.6	.0099	.02766	5545
9	5200	22710	8.83	407.85	80.5	.0101	.02804	5130
7	4799	20960	7.70	407.53	81.6	.0098	.02868	4724
10	4549	19860	6.99	408.04	80.3	.0101	.02925	4486
11	3906	17060	5.36	408.22	80.6	.0101	.03043	3854
12	3561	15550	4.58	408.29	80.6	.0101	.03135	3513
13	3007	13130	3.40	408.43	80.8	.0102	.03276	2959
14	2757	12040	2.92	408.46	81.0	.0094	.03352	2714
18	2497	10900	2.469	408.10	76.7	.0087	.03505	2473
15	2454	10720	2.389	408.52	81.1	.0100	.03473	2416
19	2262	9878	2.094	408.14	77.3	.0087	.03623	2241
16	2240	9782	2.048	408.55	81.1	.0100	.03582	2205
20	2021	8825	1.740	408.17	78.0	.0089	.03786	1998
17	1981	8651	1.661	408.59	81.3	.0100	.03730	1950
21	1797	7847	1.432	408.21	78.3	.0089	.03965	1777
22	1643	7175	1.238	408.23	78.4	.0090	.04117	1624
23	1472	6428	1.033	408.24	78.6	.0089	.04309	1455
24	1323	5777	.867	408.26	78.8	.0090	.04495	1308
25	1166	5092	.712	408.28	78.9	.0090	.04787	1153
26	1007	4397	.565	408.30	79.0	.0090	.05135	995.5
27	900.6	3933	.478	408.31	79.0	.0090	.05467	890.4
28	828.1	3616	.429	408.32	79.6	.0091	.05838	816.8
29	690.1	3014	.328	408.33	79.6	.0091	.06489	680.8
30	618.5	2701	.279	408.33	79.7	.0091	.06910	610.1
31	526.8	2300	.225	408.33	79.7	.0091	.07756	519.6

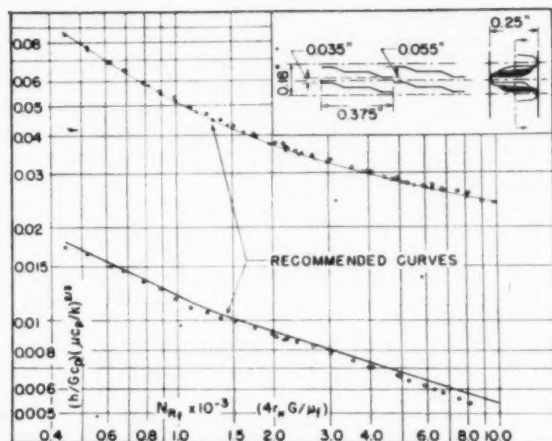


FIG. 15 TEST RESULTS FOR TYPICAL LOUVERED-PLATE-FIN HEAT-EXCHANGER SURFACE
(Circles denote results with core heating, and crosses denote results of isothermal friction-factor tests.)

metered, making $Q_{\text{sum}} < Q_{\text{air}}$. The negative unbalance at low Reynolds numbers (i.e., high NTU) is due to minor deficiencies in the steam and condensate system, since errors of this magnitude in the temperature measurements would give ridiculous $N_{St}N_{Pr}^{2/3}$ results. Introduction of a separator between the desuperheater water inlet and the core has eliminated this difficulty in later tests.

This test core was tested previously at the U.S.N. Engineering Experiment Station, Annapolis, Md., using a very similar technique to that described here, reference (1), and at the Harrison Radiator Division, General Motors Corporation, using hot water instead of condensing steam on the hot side. Fig. 16 shows a comparison of these various data. The Stanford results are seen to agree closely with those of USNEES, the difference in friction factors being due to the use of different entrance and exit coefficients. USNEES did not allow for steam-side resistance. If they had, their results would run 0-4 per cent higher than shown for N_R 3000-10,000. The maximum spread between all curves is less than 10 per cent.

SUMMARY AND CONCLUSIONS

A test apparatus and technique have been described which will yield accurate heat-transfer and flow-friction data for compact heat-exchanger surfaces. Such data may be used for preliminary design of gas-turbine regenerators and intercoolers, aircraft heat exchangers, and many other types of systems where optimum selection of surfaces will pay a premium in performance, weight, and shape. These data are not only useful for design purposes, but will be used also for a study of the basic phenomena involved in convection heat transfer and flow friction in complex flow passages. Such studies may lead to improved heat-exchanger surfaces.

The experience in the design and operation of this system has indicated that accurate results are obtainable only if the following points are given special attention:

- A method must be provided for controlling the air flow to a uniform velocity distribution at the entrance to the test core.
- Air temperatures must be measured at a large number of points over the flow cross section on the downstream side of the test core. This is preferable to using a single reading of some sort of an average temperature, obtained by flow-mixing methods or averaging types of thermometric primary elements. These

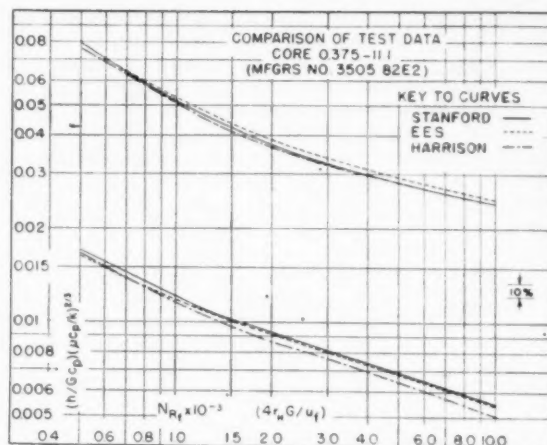


FIG. 16 COMPARISON OF TEST RESULTS WITH DATA OF OTHER INVESTIGATORS

latter methods do not allow a check on one of the basic idealizations of the analysis, namely, that of uniform outlet temperature.

(c) All air-temperature measuring devices must have radiation shields, and the duct walls must be insulated to avoid radiation errors.

(d) Small temperature-measurement inaccuracies will result in excessive error in the heat-transfer results unless the test cores are designed to operate in the limited range of NTU , 0.2-3.0.

(f) Provision must be made for the accurate control of steam pressure and steam-inlet state. A water-injection desuperheater is satisfactory if care is taken to insure essentially complete elimination of the liquid phase before entry into the core.

(g) Care must be taken to locate the air-pressure taps on the downstream side of the test core at a point allowing the maximum pressure recovery. This may amount to 20-30 in. from the core.

(h) The accuracy of the friction-factor tests should be considered in the light of the effect of entrance and exit-flow losses. Because of the limitations on NTU , the extraction of accurate f characteristics from the measurement of core pressure drop requires accurate exit and entrance-flow-loss coefficients. The generally used published data are adequate only for $N_R > 10,000$, reference (7).

(i) A continuous check on the temperature and flow instruments should be provided in the testing procedure, as by direct calibration and energy-balance comparisons.

The experience presented here may be used as a basis for establishing a standard test code for work of this character. Such standardization will have the ultimate advantage of raising the level of the accuracy of basic design data so urgently needed for new applications of existing surfaces or the development of new surfaces.

ACKNOWLEDGMENTS

The Office of Naval Research, the U.S.N. Bureau of Ships, and the U.S.N. Bureau of Aeronautics are currently sponsoring a heat-transfer research program for compact surfaces at Stanford University. The authors prepared this paper on this program and express their appreciation to the sponsoring organizations.

The U.S.N. Engineering Experiment Station, Mr. John Dinan, and Mr. A. E. Senner, have contributed materially to the development of the system described here by keeping the authors

informed of
Godfrey of
also contri

1 "Gas
and C. K.
NavShips
Test
Used in Air
Regenerator
ASME, vol
2 "Pers

informed of their experience on a similar system. Mr. John Godfrey of the Harrison Radiator Division of General Motors, also contributed generously of his experience.

BIBLIOGRAPHY

- 1 "Gas Turbine Plant Regenerator Surfaces," by A. L. London and C. K. Ferguson, Bureau of Ships Research Memorandum 2-46, NavShips (250-338-3), July, 1946.
- 2 "Test Results of High-Performance Heat-Exchanger Surfaces Used in Aircraft Intercoolers and Their Significance for Gas-Turbine Regenerator Design," by A. L. London and C. K. Ferguson, Trans. ASME, vol. 71, 1949, pp. 17-26.
- 3 "Fluid Meters, Their Theory and Application," ASME Research Publication, fourth edition, 1937.
- 4 "Heat Transmission," by W. H. McAdams, McGraw-Hill Book Company, Inc., New York, N. Y., 1942.
- 5 "Efficiency of Extended Surface," by K. A. Gardner, Trans. ASME, vol. 67, 1945, pp. 621-631.
- 6 "An Investigation of Aircraft Heaters—Part II, Properties of Gases," by Myron Tribus and L. M. K. Boelter, NACA Advanced Restricted Report, October, 1942.
- 7 "Loss Coefficients for Abrupt Changes in Flow Cross Section With Low Reynolds Number Flow in Multiple Tube Systems," by W. M. Kays, Trans. Heat Transfer and Fluid Mechanics Institute, 1949, published by ASME.
- 8 "Personal Communications," by O. A. Saunders, Imperial College, London, England, and G. L. Locke, Stanford University, Stanford, Calif.

H
te

New
ment
fer sur
flow-fr
may b
flat-tu
nondis
compa
horsep

The
Engl

$A =$

$A_e =$

$A_{fe} =$

$a =$

$b =$

$c_p =$

$E_{std} =$

$f =$

$G =$

$h =$

$h_{std} =$

$K_c =$

$K_e =$

$K_s =$

$k =$

$L =$

$l =$

$r_H =$

$V =$

Green

$\alpha =$

$\beta =$

$\rho =$

$\sigma =$

$\mu =$

$\mu_f =$

Dim

Heat-Transfer and Flow-Friction Characteristics of Some Compact Heat-Exchanger Surfaces

Part 2—Design Data for Thirteen Surfaces

New developments in prime-mover and process equipment have created a greater need for compact heat-transfer surfaces. This paper presents basic heat-transfer and flow-friction design data for thirteen such surfaces which may be described generally as the plate-fin type and finned-flat-tube type. In addition to the use of the conventional nondimensional correlations, the various surfaces are compared on heat-transfer coefficient versus flow-friction-horsepower basis. Paper No. 49—A-95.

NOMENCLATURE

The following nomenclature is used in this paper:

English Letter Symbols:

- A = transfer area, ft^2
- A_s = free-flow area, ft^2
- A_{fr} = frontal area, ft^2
- a = plate thickness for the plate-fin surface, ft
- b = plate spacing, in. , ft
- c_p = specific heat at constant pressure, $\text{Btu}/(\text{lb } ^\circ\text{F})$
- E_{std} = friction power evaluated at certain standard gas properties (see caption Fig. 9), $\text{hp}/(\text{ft}^3 \text{ of } A)$
- f = Fanning friction factor, dimensionless
- G = mass velocity based on A_s , $\text{lb}/(\text{hr ft}^2 \text{ of } A_s)$
- h = unit conductance for thermal convection heat transfer, $\text{Btu}/(\text{hr ft}^2 ^\circ\text{F})$
- h_{std} = unit conductance evaluated at certain standard gas properties (see caption Fig. 9), $\text{Btu}/(\text{hr ft}^2 ^\circ\text{F})$
- K_c = contraction loss coefficient for air flow at test-core entrance, dimensionless
- K_e = expansion-loss coefficient for air flow at test-core exit, dimensionless
- k = thermal conductivity, $\text{Btu}/(\text{hr ft}^2 ^\circ\text{F}/\text{ft})$
- L = exchanger or test-core flow length, ft , in.
- l = louver spacing, ft , in.
- r_H = flow passage hydraulic radius based on free-flow area, A_s (see Equation (1)), ft
- V = exchanger total volume, ft^3

Greek Letter Symbols:

- α = ratio of total transfer area of one side of exchanger to total volume of exchanger, ft^2/ft^3
- β = ratio of total transfer area of one side of exchanger to volume between plates of that side, ft^2/ft^3
- ρ = gas density, lb/ft^3
- σ = ratio of free flow to frontal area, dimensionless
- μ = gas viscosity, evaluated at bulk average temperature, $\text{lb}/(\text{hr ft})$
- μ_f = gas viscosity, evaluated at film average temperature, $\text{lb}/(\text{hr ft})$

Dimensionless Groupings:

- N_{St} = Stanton's number, (h/Gc_p) , a heat-transfer modulus

- N_{Pr} = Prandtl's number, $(\mu_f c_p/k)$, a fluid-properties modulus evaluated at film average temperature
- $N_{St} N_{Pr}^{1/3}$ = generalized heat-transfer grouping; this factor versus N_R defines heat-transfer characteristics of surface
- NTU = number of heat-transfer units for an exchanger
- N_R = Reynolds number, $(4r_H G/\mu)$, a flow modulus characterizing type of flow
- N_{Rf} = $(4r_H G/\mu_f)$, a tube-type-flow Reynolds number
- N_{Rl} = (lG/μ) , a flat-plate-type-flow Reynolds number
- f = Fanning friction factor based on r_H ; $f - N_R$ plot defines friction characteristics of surface

INTRODUCTION

The advent of the gas turbine as a promising transportation-type prime mover, the development of portable oxygen plants, and the continued emphasis on reduced size and weight in aircraft installations have served as strong stimuli to the development and application of lightweight compact heat-transfer surfaces.

As a matter of definition, the term compactness refers to the transfer area-to-volume ratio characteristic of the surface in question. A compact surface, for the purposes of this paper, is one providing more than 75 sq ft of transfer area per cu ft of core volume. This compares to the approximately 20 ft^2/ft^3 which can be realized at best from 1-in.-diam tubes in a shell-and-tube-type construction.

For many heat-exchanger applications, particularly those employing liquids, an accurate knowledge is not required for the friction characteristics of the surface. However, for low-density fluids such as gases, the cost of friction per unit of mass flow is greatly multiplied, and the frictional characteristics of the surface are of equal significance as the heat-transfer behavior. The flow-friction consideration is particularly important for gas-turbine-plant heat exchangers—the regenerator and the intercooler.

The purpose of this paper is to present basic heat-transfer and flow-friction design data for thirteen compact surfaces. These surfaces may prove to be useful in the gas-turbine and other applications where careful design will pay a premium in compactness and performance. Heretofore new applications have been inhibited by the lack of availability of such data.

DESCRIPTION OF SURFACES

In part, the data presented here supplement the information given in reference (1).¹ This reference reports the characteristics of seven variations of a plate-fin type of extended surface which has been extensively used in the supercharged aircraft-engine intercooler application. The general features of this surface are described in Fig. 1, which also shows the eight plate-fin surfaces considered in this paper. The scheme of designating the different surfaces in this illustration may be inferred from the following ex-

¹ Numbers in parentheses refer to the Bibliography at the end of the paper.

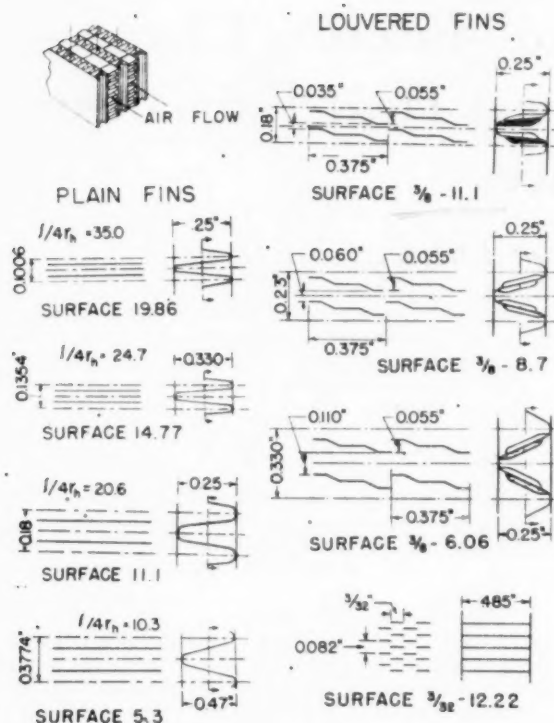


FIG. 1 DESCRIPTION OF PLATE-FIN-TYPE SURFACES
(See Tables 1 and 3 for further geometrical data.)

planation for the $3/8$ -8.7 surface. This surface has 8.7 fins per in. and the fin louvers are spaced $3/8$ in.

Two of these variations—designated as plain fins 11.1 and louvered fins $3/8$ -11.1—were reported previously (1). They were retested and their characteristics reported here for comparative purposes.

Four of the eight plate-fin surfaces described in Fig. 1 provide a systematic variation of fin spacing for the plain-fin type as indicated in Table 1. The surface designated $3/8$ -12.22, Fig. 1, Table 1, is representative of the plate-louvered-fin type with a very short fin-flow length. Although the so-called plain-fin surface cores were designed for the study of the characteristics of an uninterrupted fin, manufacturing methods required that the fin material be cut in 2.5-in. strips. Consequently, these surfaces may be considered as a louvered surface with a louver spacing of 2.5 in.

LOUVERED FINS

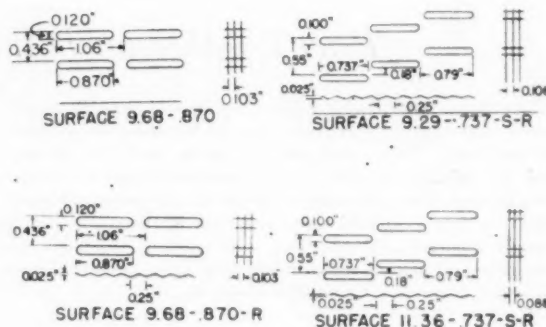
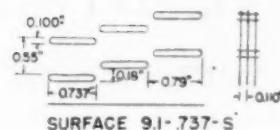
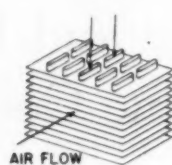
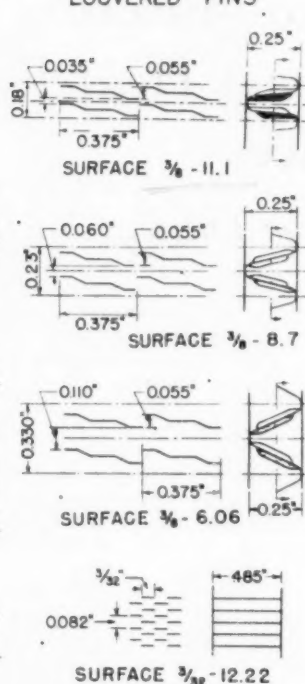


FIG. 2 DESCRIPTION OF FIN-FLAT-TUBE-TYPE SURFACES
(See Table 1 for further geometrical data.)

Fig. 2 and Table 1 describe five fin-flat-tube-type surfaces useful for gas-to-liquid heat transfer such as the automobile radiator, or the water-cooled intercooler of a gas-turbine plant, or a gas-turbine regenerator if a suitable intermediate heat-transfer fluid, such as a liquid metal, can be developed.

The surface designated 11.37-.737-S-R has 11.37 fins per in., flat tubes 0.737 in. wide, the tubes are staggered (S) and the fins are ruffled (R). The significance of the other designations may be inferred from the foregoing. The five variations considered here allow a study of the effects of staggered versus in-line tubes, ruffled versus plain fins, and staggered tubes combined with ruffled fins versus in-line tubes and plain fins. Also, the comparisons of 9.29-.737-S-R and 11.32-.737-S-R at least suggest the influence of fin spacing on a staggered-tube and ruffled-fin design.

Table 1, together with the description of Figs. 1 and 2, provides all the detailed geometrical information required for applications to heat-exchanger design. For all of these surfaces the hydraulic radius is defined relative to the flow dimension L , as

$$\frac{r_H}{L} = \frac{A_c}{A} \quad [1]$$

For cylindrical tubes of any cross-section geometry, i.e., the plate-fin surface, this definition reduces to the conventional result, r_H equals the flow cross section divided by the wetted perimeter.

TABLE 1 GEOMETRY OF THE DIFFERENT SURFACES

Surface designation	Fins per in.	Hydraulic radius, r_H , ft	Plate spacing, in.	Tube or fin thickness, in.	Extended Total area	Area (Volume between plates) δ , ft ² /ft ²	Area Core volume α , ft ³ /ft ²	Free flow Frontal area σ
Plate-fin type:								
Plain fins								
5.3	5.3	0.00504	0.470	0.006	0.719	156		
11.1	11.1	0.00253	0.250	0.006	0.730	334		
14.77	14.77	0.00212	0.330	0.006	0.831	369		
19.86	19.86	0.001495	0.250	0.006	0.833	455		
Louvered fins								
$3/8$ -6.06	6.06	0.00365	0.250	0.006	0.623	239		
$3/8$ -8.7	8.7	0.00290	0.250	0.006	0.687	288		
$3/8$ -11.1	11.1	0.00253	0.250	0.006	0.730	339		
$3/8$ -12.22	12.22	0.002941	0.485	0.004	0.862	302		
Fin-flat-tube type:								
9.68-0.870	9.68	0.00295		0.004	0.795		229	0.697
9.68-0.870-R	9.68	0.00295		0.004	0.795		229	0.697
9.1-0.737-S	9.10	0.00345		0.004	0.813		224	0.785
9.29-0.737-S-R	9.29	0.00338		0.004	0.814		226	0.788
11.32-0.737-S-R	11.32	0.00288		0.004	0.845		270	0.780

For other surfaces, however, where flow cross-section area and perimeter are variable along the flow dimension, as, for instance, the finned-flat-tube type, the definition Equation [1] is necessary.

This definition is more readily usable in heat-exchanger design. As an illustration, the nondimensional exchanger size factor directly relating to the exchanger heat-transfer effectiveness (2), is the "number of heat-transfer units"

$$NTU = \frac{U}{Gc_p} \frac{A}{A_s} = \frac{U}{Gc_p} \frac{L}{r_H}$$

where the flow mass velocity G is based on the minimum flow cross section, A_s . The Gc_pA_s product has the significance of flow stream-capacity rate.

To facilitate extension of the test results reported here to heat-exchanger-design calculations, the interrelations of the surface and the core geometrical factors are summarized. The heat-exchanger core consists of two surfaces—one for each fluid side—except for the case of the periodic-flow-type exchanger, such as the common Ljungström air preheater.

1 The following geometrical factors are given in Table 1 for each surface reported here as part of the basic data

b , r_H , and β for the plate-fin type

r_H , α , and σ for the fin-flat-tube type

2 The solution for a particular heat-exchanger core requires the following factors for each of the two sides

A , A_c , A_{fc} , L , and σ

For the complete core, V and α are also required. In the case of the plate-fin surface, the plate thickness (a , ft) between the two sides must be specified as an independent variable.

3 The foregoing surface and core factors are related as follows for one side of the exchanger: Subscript 1 refers to any one side and 2 to the other side. Factors without subscripts are common to both sides.

$$\left. \begin{aligned} \sigma_1 &= \left(\frac{A_c}{A_{fc}} \right)_1 = \left(\frac{Ar_H}{A_{fc}L} \right)_1 = \frac{(Ar_H)_1}{V} \\ \sigma_1 &= \frac{b_1\beta_1r_H}{b_1 + b_2 + 2a} \text{ (plate-fin surface only)} \end{aligned} \right\} \dots [2]$$

$$\left. \begin{aligned} \alpha_1 &= \frac{A_1}{V} = \left(\frac{A}{A_{fc}L} \right)_1 = \left(\frac{\sigma}{r_H} \right)_1 \\ \alpha_1 &= \frac{b_1\beta_1}{b_1 + b_2 + 2a} \text{ (plate-fin surface only)} \end{aligned} \right\} \dots [3]$$

$$A_{c1} = (\sigma A_{fc})_1 = \left(\frac{Ar_H}{L} \right)_1 = \left(\frac{A\sigma}{L\alpha} \right)_1 \dots [4]$$

$$\left(\frac{r_H}{L} \right)_1 = \left(\frac{A_c}{A} \right)_1 = \left(\frac{\sigma}{L\alpha} \right)_1 \dots [5]$$

The same relations of course apply to side 2 with an exchange of subscripts 1 for 2 and 2 for 1.

EXPERIMENTAL METHOD AND ACCURACY OF RESULTS

The test arrangement, method of analyzing the data, and a consideration of errors are covered in considerable detail in reference (3). Consequently, only a brief summary will be presented here for the sake of completeness.

The test system provided for condensing steam to air heat transfer with air flow on the surface of interest. The direct test data allowed determination of the over-all heat-transfer coefficient

steam to air, and the air-side-core pressure drop. The test-core dimensions were all of approximately $8\frac{3}{4} \times 9\frac{3}{4}$ in. frontal area and 5 in. in the flow length on the air side.

Allowance for the ineffectiveness of the extended surface and the steam-side condensate-film resistance permitted the evaluation of the average unit conductance for thermal convection on the air side. The friction factor was extracted from the core-pressure-drop data by allowing for entrance and exit flow-stream mechanical-energy losses (4), and for flow acceleration accompanying density changes due to both pressure and temperature variations along the flow length. Friction factors were determined from isothermal tests and also for runs with core heating.

Fig. 5 for the plate-louvered-fin surface $\beta_{12}/22$ is typical of the consistency of the test results for all the surfaces tested. The recommended friction-factor curve is based upon the data for the isothermal runs. The recommended heat-transfer factor $(h/Gc_p)N_{Pr}^{1/4}$ versus N_{Re} curve falls above the test points. The difference represents the allowance for steam-side resistance. The method used here was to fair a curve through the data points shown, and then evaluate the steam-side resistance for several test Reynolds numbers over the range to determine the correction to the faired curve to obtain the recommended curve.

The test data allowed energy balances to be made, and the average deviation for the series of tests applying to any one surface was usually less than 3 per cent. The one exception was for the low-Reynolds-number runs for the 5.3 plain-fin surface where, due to faulty operation of the condensate weighing system, poor balances were obtained. However, the air-side data used in the calculations of results are believed to be accurate. An analysis of errors similar in detail to that given in reference (3), indicates that the probable errors for the basic results presented here are less than the following indicated magnitudes:

$$\begin{aligned} N_{Re} &\pm 2 \text{ per cent} & f &\pm 7 \text{ per cent for plain-plate-fin type} \\ N_{St} &\pm 3.5 \text{ per cent} & f &\pm 5 \text{ per cent for louvered-plate-fin type} \\ N_{Pr} &\pm 5 \text{ per cent} & f &\pm 2 \text{ per cent for finned-flat-tube type} \\ N_{St}N_{Pr}^{1/4} &\pm 5 \text{ per cent} \end{aligned}$$

The difference in the estimated errors for the friction factors reflects the relative contribution of the entrance and exit flow losses to the over-all pressure drop. The properties of air—viscosity μ and N_{Pr} —used in generalizing the test results to a non-dimensional form were obtained from reference (5).

BASIC HEAT-TRANSFER AND FLOW-FRICTION DESIGN DATA

The heat-transfer and flow-friction characteristics of the various surfaces are presented as follows:

1 Figs. 3, 4, and 5 give the nondimensional correlation of friction factor f , and heat-transfer modulus, $N_{St}N_{Pr}^{1/4}$, versus Reynolds number, N_{Re} , for the eight variations of the plate-fin type of surface. Fig. 6 gives the same correlations for the finned-flat-tube type. In every case here the Reynolds number is based on the flow hydraulic-diameter dimension defined by Equation [1].

2 In contrast to the foregoing comparison, Figs. 7 and 8 present the correlations employing a Reynolds number, N_{Re} , based upon an uninterrupted flow length, or louver spacing, for the eight plate-fin surfaces.

3 Fig. 9 compares the plate-fin surfaces on a heat-transfer versus friction-power basis (1). However, unlike reference (1), the basis selected, instead of being per unit transfer area, is per unit of volume between plates, $(h_{ad}\beta)$ versus $(E_{ad}\beta)$. The gas properties used as a reference in this comparison correspond to air at 1 atm pressure and 500 F. These properties are given in

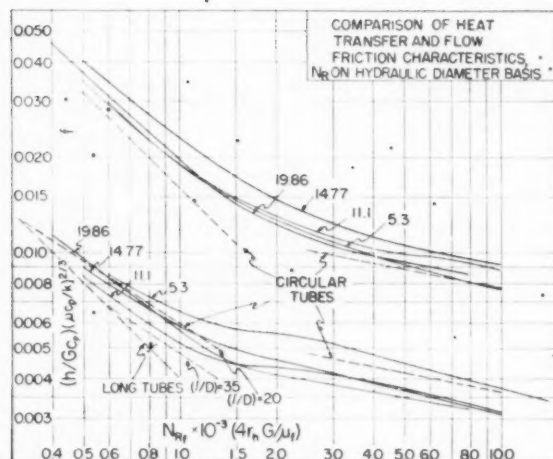


FIG. 3 PLAIN-PLATE-FIN SURFACES

(Nondimensional heat-transfer and friction characteristics compared on a tube-type Reynolds number basis; see Fig. 1, and Tables 1 and 3 for geometrical data.)

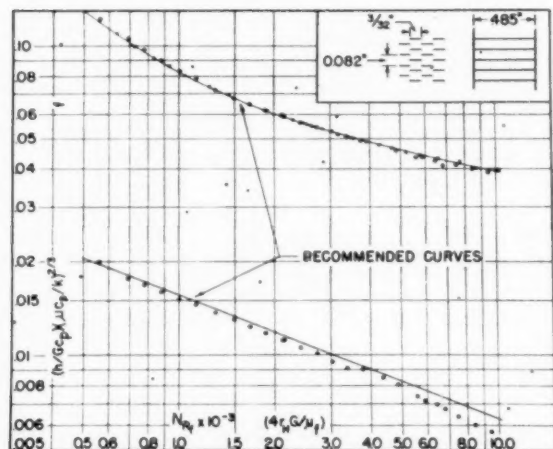


FIG. 5 SHORT-LOUVERED PLATE-FIN SURFACE

(Nondimensional heat-transfer and friction characteristics on a tube-type N_R basis; data points illustrate the typical consistency of test results; see Fig. 1, and Tables 1 and 3 for geometrical data.)

the caption of Fig. 9. Equations [6] give the extrapolation for fluid properties differing from the reference conditions.

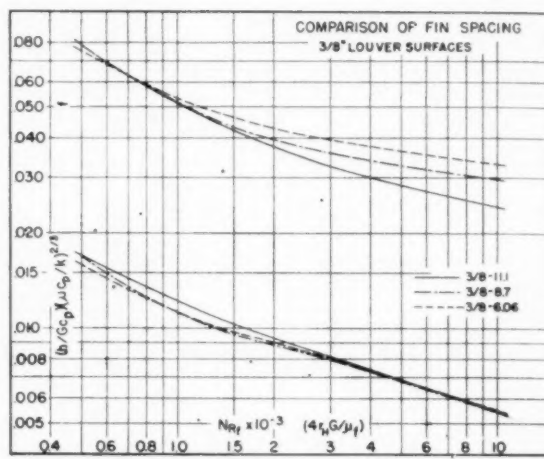
4 Fig. 10 gives a similar comparison for the finned-flat-tube-type surfaces. Here, however, the total core volume rather than volume on one side only is used, $(h_{td}\alpha)$ versus $(E_{td}\alpha)$.

5 The co-ordinates $N_{St}N_{Pr}^{1/3}$ and f versus N_{Rf} of the recommended curves are summarized in tabular form, Table 2, for all surfaces.

To avoid confusion, test-data points are given only for the 3_{32} -12.22 louvered-plate-fin surface. The test data for the approximately 30 heat-transfer and 30 isothermal runs per surface are available elsewhere (6, 7, 8, 9).

DISCUSSION AND COMPARISON OF SURFACES

Plain-Plate-Fin Surfaces, Fig. 1. The illustrations in Fig. 1 describe the roughly triangular-tube flow cross sections common to all of these surfaces. Therefore, as for the case of circular-tube flow, it may well be that a single correlation for heat-transfer and

FIG. 4 LOUVERED-PLATE-FIN SURFACES WITH $3/8$ -IN. LOUVER SPACINGS

(Nondimensional heat-transfer and friction characteristics compared on a tube-type Reynolds number basis; see Fig. 1, and Tables 1 and 3 for geometrical data.)

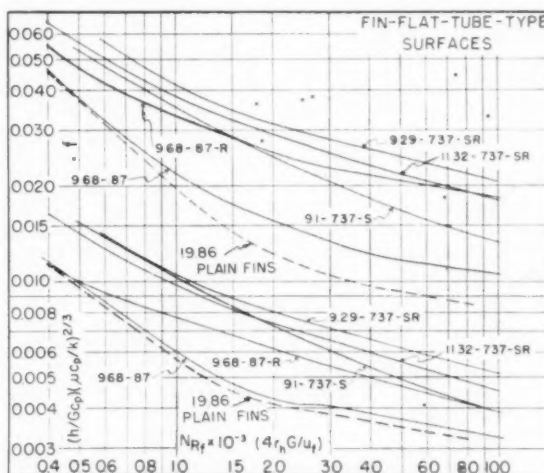


FIG. 6 FIN-FLAT-TUBE SURFACES

(Nondimensional heat-transfer and friction characteristics compared on a tube type N_R basis. Comparable characteristics of 19.86 plain-fin surface are also shown; see Fig. 2, and Table 1 for geometrical data.)

another for friction characteristics would apply for a range of plate and fin spacings. The data in Fig. 3 are not completely conclusive in this respect for the following reasons:

1 Manufacturing methods required that the test cores be constructed with a fin sheet material only 2.5 in. in flow length, resulting in the varying $l/4r_h$ magnitudes summarized in Table 3, ranging from only 10.3 for the 5.3 fins per in. surface to 35 for the 19.86 fins per in. surface.

2 Each of the four test cores had a total air-flow length of only 5 in. The effect of abrupt flow contraction at the entrance to the core will partially influence the heat-transfer and friction characteristics some distance downstream. Only for the 19.86 surface, with a core-air-flow length of 70 hydraulic diam, is this dimension considered to be great enough to yield data accurately descriptive of the long flow lengths that will be encountered in applications.

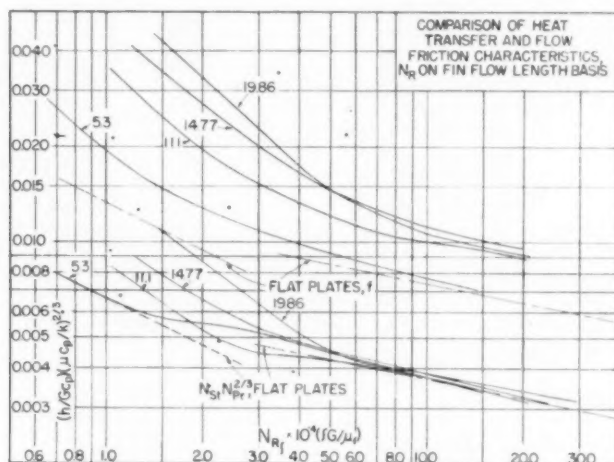


FIG. 7 PLAIN-PLATE-FIN SURFACES
(Nondimensional heat-transfer and friction characteristics compared on a flat-plate-type Reynolds number basis.)

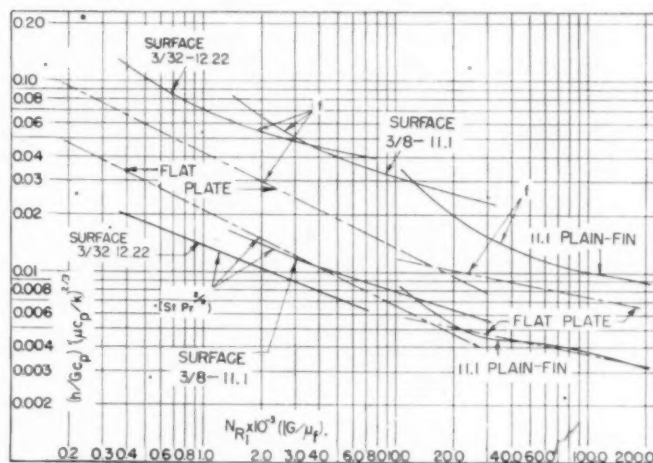


FIG. 8 LOUVERED-PLATE-FIN SURFACES
(Nondimensional heat-transfer and friction characteristics compared on a flat-plate-type Reynolds number basis.)

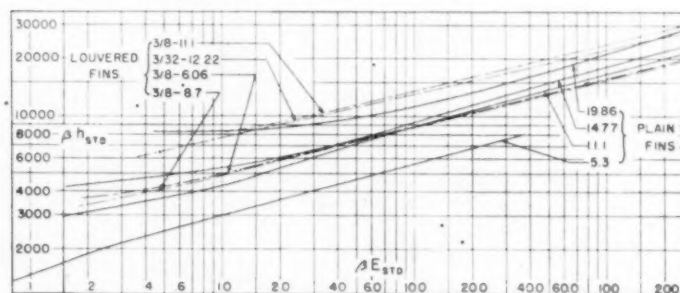


FIG. 9 HEAT-TRANSFER VERSUS FRICTION-POWER COMPARISON FOR PLATE-FIN-TYPE SURFACES

(Dimensions are [Btu/hr °F]/ft² of volume for ordinate and hp/ft² of volume for abscissa. Standard or reference fluid properties are $\mu_{std} = 0.0413$ lb/ft², $\mu_{std} = 0.0678$ lb/hr ft, $c_{p, std} = 0.2477$ Btu/(lb °F), $N_{Pr, std} = 0.671$, corresponding to air at 1 atm pressure and 500 deg F. See Equations [6] for extrapolation to other conditions.)

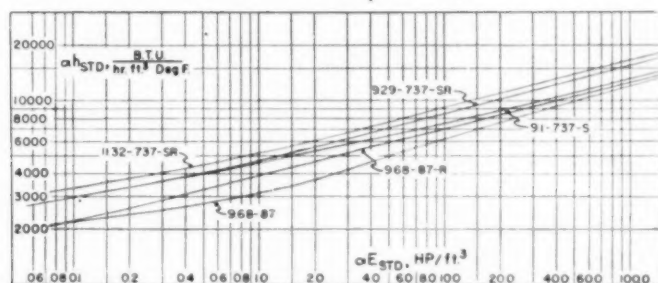


FIG. 10 HEAT-TRANSFER VERSUS FRICTION-POWER COMPARISONS FOR FIN-FLAT-TUBE-TYPE SURFACES

(Standard or reference fluid properties are used = 0.0413 lb/ft³, μ_{std} = 0.0678 lb/hr ft, $c_{p(std)}$ = 0.2477 Btu/lb °F, $N_{Pr(std)}$ = 0.671, corresponding to air at 1 atm pressure and 500 F. See Equations [6] for extrapolation to other conditions.)

3 The aluminum furnace brazing technique of core construction produced filleted corners and a somewhat roughened surface.

Fig. 3, which brings out the similarities to tubelike flow, employs a Reynolds-number abscissa based on the flow hydraulic diameter. In contrast, Fig. 7, using an N_R based on the fin flow-length dimension l , emphasizes the similarities to flow over a flat plate.

The results, with the exception of those for the 5.3 surface for heat transfer, correlate quite well on a tube-type Reynolds-number basis (within 12 per cent for heat transfer and 18 per cent for friction). A transition from laminar to turbulent flow in the approximate range $1200 < N_{Rf} < 2500$ is common to all four surfaces.

The foregoing considerations suggest that the f and $N_{St}N_{Pr}^{2/3}$ versus N_{Rf} characteristics of the 19.86 surface are the best single set of correlations to use for a variety of fin and plate spacings within the follow restrictions: (a) Fin spacing 7–25 fins per in.; (b) $l/4r_H > 25$; (c) plate-to-fin spacing 2.5–5; (d) the core flow length to hydraulic diameter greater than 50.

In distinction to the previous tube-flow-basis comparison, consider Fig. 7 which emphasizes the similarities to flat-plate flow. The flat-plate heat-transfer characteristics were derived from the friction-factor behavior using the friction-heat transfer analogy

$$N_{St}N_{Pr}^{2/3} \cong f/2$$

With respect to heat transfer, only in the fully developed turbulent-boundary-layer flow, $N_{Rf} > 50,000$, does close similarity exist between the four surfaces and the flat-plate characteristic. Unlike the tube-flow comparison in Fig. 3, the different surfaces exhibit transition flow at differing Reynolds numbers, N_{Rf} , and do not correlate at all with each other in the laminar-boundary-layer-flow regions.

The excellent agreement of the 5.3 surface behavior with that of the flat-plate-flow system, especially with respect to heat transfer, is significant. Evidently, because of the wide fin spacing and small $l/4r_H$, a fin has a relatively minor effect on the flow over a neighboring fin with the resulting similarity to flat-plate flow.

The foregoing discussion is of restricted generality because of various factors not under experimental control, primarily the uninterrupted flow length l , and the surface roughness. A more complete understanding of the behavior of these surfaces will require the testing of additional cores of a fixed $l/4r_H$ on the order of magnitude of 35 to 50.

Lowered-Plate-Fin Surface* Fig. 1. The average thickness of the laminar sublayer is reduced by interrupting the fin surface with louvers (1). Consequently, the resistance to thermal convection heat transfer is decreased and the film coefficient h , in-

creased. While the friction factor f is also made larger by this expedient, it is often possible to operate with a smaller friction power expenditure as compared to the plain-fin surface, since lower flow velocities may be used.

The interpretation of the behavior of the louvered surfaces in terms of tubelike and flat-plate-like behavior is not as valid as in the case of the plain-fin surfaces because of the more complex flow geometry. For the three $3/8$ -in. louvered surfaces, described in Fig. 1, the curvature of the fins produces minus accelerations with resulting tendencies toward flow separation and eddy formation. For all four louvered surfaces, wake effects at the leading and trailing edges and flow impingement on the blunt leading edges provide additional flow turbulence. The prime surface, accounting for 14 to 38 per cent of the total, Table I, has a markedly different geometry from the louvered fins. The junctions, louver-to-fin and fin-to-plate, introduce more flow complexities. Nevertheless, the tube-type-flow and flat-plate-type-flow comparisons employed for the plain-fin surfaces yield usable correlations, Figs. 4, 5, and 8.

The sequence of three $3/8$ -in. louvered surfaces have their characteristics presented on a tube-type N_R basis, Fig. 4. The close correlation of the heat-transfer behavior suggests that any one of these curves may be used with good accuracy for a range of fin spacings from 5 to 15 fins per in., maintaining the $3/8$ -in. louver spacing. Note that all three surfaces exhibit a flow transition in the range $1500 < N_{Rf} < 3000$ as for the case of the plain-fin surfaces.

No satisfactory explanation has been evolved to explain the poorer friction correlation, especially for $N_{Rf} > 2000$, Fig. 4. In terms of the contribution of the unlouvered prime surface one would expect a less rough-flow characteristic for the $3/8$ –6.06 surface as compared to the $3/8$ –11.1 surface, Fig. 1. This is not supported by the test results which show a higher f for 6.06-fins-per-in. surface especially for the higher N_{Rf} range. Possibly the closer fin spacing reduces flow-separation effect thereby reducing the form drag component of the friction factor without a material alteration of the heat transfer, which is associated with the skin-friction component. An additional possibility is that the closer fin spacing serves to reduce the scale and intensity of the turbulent eddies, much in the manner of a fine screen.

Until more complete data are available, it is recommended that the three f characteristics in Fig. 4 be used for interpolation and possibly a small extrapolation to other fin pitches in the range 5 to 15 fins per in.

The characteristics of the short-louvered surface $3/32$ –12.22 are given on a tube-flow Reynolds number basis, Fig. 5. No discernible flow transition appears in either the f or $N_{St}N_{Pr}^{2/3}$ characteristic. Comparison with Fig. 4 reveals that the $3/32$ –12.22

surface, as compared to the $3/8$ -11.1 surface, has a 12 to 25 per cent higher heat-transfer characteristic and 50 per cent higher f characteristic.

Fig. 8 contrasts behavior of the $3/32$ -12.22, the $3/8$ -11.1, and the 11.1 plain-fin surfaces on a flat-plate-type basis, with the louver dimension, as given in Table 3, entering into the Reynolds number, N_R . Considering the marked lack of geometrical similarity between the flat plate and the three test surfaces, the

TABLE 3 COMPARISON OF PLATE-FIN SURFACES

Designation	No. of fins per in.	Hyd. diam. $4r_H$, in.	Louver spacing, l , in.	$l/4r_H$
Plain:				
5.3	5.3	0.2419	2.5	10.3
11.1	11.1	0.1214	2.5	20.6
14.77	14.77	0.1017	2.5	24.7
19.86	19.86	0.0718	2.5	35.0
Louvered:				
$3/8$ -6.06	6.06	0.1752	0.375	2.14
$3/8$ -8.7	8.7	0.1436	0.375	2.61
$3/8$ -11.1	11.1	0.1214	0.375	3.08
$3/32$ -12.22	12.22	0.1411	0.0937	0.663

agreement with respect to heat transfer is remarkably good. This has been observed by others, notably by Norris and Spofford in their pioneer work on "high-performance fins" (10). The friction characteristics for the test surfaces, however, are only in very general agreement with each other and are substantially higher than the flat-plate characteristics. For the $3/32$ -12.22 and $3/8$ -11.1 surfaces, f is roughly twice that for the flat plate with the sharp leading edge, demonstrating that about one half the friction power expenditure is a form drag effect, not contributing to heat transfer. In spite of the higher parasitic loss, the louvered surfaces still yield a higher h , for a given friction power expenditure, E hp/ft, as compared to the plain-fin surfaces, because of the higher $N_{St}N_{Pr}^{1/3}$ characteristic. This aspect will be elaborated on shortly.

Finned-Flat-Tube Surfaces, Fig. 2. The characteristics of these surfaces are summarized in Fig. 6, using a tube-type-Reynolds number. The dotted curves give the behavior of the 19.86 plain-plate-fin surface for comparative purposes.

The close agreement of the 19.86 plain-fin and the 9.68-.87 finned tube surface emphasizes their common tubelike flow behavior. The agreement with respect to heat transfer is remarkably good, the spread being less than 5 per cent. For friction, the spread in f is not more than 25 per cent at the higher N_{Rf} range, and much less for $N_{Rf} < 1000$.

The effect of staggering the tubes but maintaining the plain-fin surfaces is striking. This is revealed by the comparison of the 9.68-.87 and 9.1-.737-S surfaces, Fig. 6. For the whole Reynolds-number range, there is an increase of N_{St} of from 15 to 50 per cent and a roughly proportional increase of f . Maintaining an in-line tube arrangement but ruffling the fins, surface 9.68-.87-R versus 9.68-.87 (see Fig. 2), produces like increases in N_{St} and f , but relative to the staggered-tube plain-fin geometry the improvement in N_{St} is less, and, in general, the friction is higher. Consequently, from a friction-heat transfer point of view, staggering alone is more advantageous than ruffling alone. In these comparisons the small difference in single-tube dimensions and the variations in fin spacing are not considered as significant.

The influence of both staggering the tubes and ruffling the fins over those expedients carried out singly can be determined by the comparison of the characteristics for surfaces 9.68-.87, 9.68-.87-R, 9.1-.737-S, and 9.29-.737-S-R. For a $N_{Rf} > 4000$, for heat transfer, the effects of staggering and ruffling are almost directly additive, giving about a 50 per cent increase in N_{St} over the in-line-tubes plain-fin arrangement. The friction curve is also higher than either the staggered or ruffled arrangement, being of the same shape as the ruffled arrangement

but 15-30 per cent higher over the whole Reynolds number range. For $N_{Rf} < 2000$ there is no significant gain of the S-R over the staggered arrangement with respect to heat transfer, and a decided loss with respect to friction.

The only significant change of fin spacing exists for the comparison 9.29-.737-S-R versus 11.32-.737-S-R, where there is a 22 per cent increase in fin pitch. The test results demonstrate both a lower friction and a lower heat-transfer performance for the closer fin spacing, on the order of 7-12 per cent over the N_{Rf} range 400 to 10,000. This relatively small difference may not be fundamental, but due, rather, to uncontrolled variations of test-core geometry, such as surface roughness introduced by the solder-dip method of fabrication.

From the point of view of moderate extrapolations to other fin spacings, say, in the range 7-12 fins per in., it is the authors' opinion that the characteristics of the ruffled and/or staggered arrangements, 9.1-.737-S, 9.68-.87-R, and 9.29-.737-S-R, will apply for the respective tube-and-fin surface geometry described in Fig. 2. A precaution to be observed, however, is that changes in the cross-sectional dimensions and spacing of the flat tubes may have a strong influence for the staggered arrangements, and that variations of the ruffled-fin geometry may also be significant for both staggered and in-line tubes.

For the plain-fin in-line-tube types, it is believed that the tube-like flow behavior of the 9.68-.87 surface may be extrapolated over a range 6-20 fins per in. within an uncertainty of ± 10 per cent on heat transfer and ± 20 per cent for friction. This recommendation arises from the agreement in behavior of this surface with the 19.86 plain-plate-fin geometry, Fig. 6.

Heat-Transfer Coefficient Friction-Power Considerations, Figs. 9 and 10. These comparisons are descriptive since, in some measure, they compare the relative sizes of exchangers incorporating the different surfaces. The abscissa is the friction horsepower per unit volume, $E\alpha$ or $E\beta$, hp/ft³, and the ordinate is the heat-transfer power per unit volume and a unit temperature potential, ah or βh , (Btu/hr)/(ft³°F). For a given friction-power expenditure these ordinates are inversely proportional to the relative volume requirements. This method of presentation evolved from the work of references (11), (1), and (12).

For the finned-flat-tube surfaces, the core volume is used as a basis and for the plate-fin surfaces the volume between plates on one side only is employed. This leads to the use of ah versus $E\alpha$, and βh versus $E\beta$ for Figs. 10 and 9, respectively. The reason for this difference in treatment results from the fact that, for the plate-fin surface, the flow geometries on each of the two sides of the core may be selected independently of one another, i.e., $3/8$ -11.1 surface with $1/8$ -in. plate spacing on one side and a plain 19.86-fins per in. surface with $1/8$ -in. plate spacing on the other side. No such freedom exists for the finned-flat-tube type.

The curves; Figs. 9 and 10, were derived for a fixed set of fluid properties corresponding to dry air at 1 atm pressure and 500 F, as given in the captions. These "standard" or reference properties and the resulting h and E magnitudes are designated by the subscript std. For any other fluid properties condition μ , c_p , ρ , N_{Pr} , the co-existing heat-transfer and friction-power coefficients may be evaluated from

$$h = h_{std} \left[\frac{c_p}{c_{p, std}} \right] \left[\frac{\mu}{\mu_{std}} \right] \left[\frac{N_{Pr, std}}{N_{Pr}} \right]^{1/3} \quad (6)$$

$$E = E_{std} \left(\frac{\rho_{std}}{\rho} \right)^2 \left(\frac{\mu}{\mu_{std}} \right)^2$$

This extrapolation is founded on keeping Reynolds number and flow geometry constant.

The advantage of louvering the fins of the plate-fin surfaces is

quite ex-
power c-
cent gr-
plain-fin
by close
shows
of this
ployed
by com-
The latt-
exchang-

It may
is not ad-
12.22 su-
power c-
suggested
vered-pl-
ings of 3

Fig. 1
tubes al-
Stagger-
higher a-
generate
improve
S-R sur-

An in-
transfer
requirem-
changer
As a co-
essary to
Figs. 9

Comp-
fin test
previou-
Annapo-
11.1 su-
are cov-
perimen-

transfer
fin core
differ b-
trance-
as 30 p-
are high

The c-
the diff-
ficients
hydrau-
to high-
mined
the imp-
tors for

The
The fac-
side res-
the EE

The
1 T
liminar
faces.
2 N
alone.

quite evident from Fig. 9. For instance, for a given friction-power expenditure the $3/8$ -11.1 surface has, roughly, a 45 per cent greater transfer coefficient per unit volume than the 11.1 plain-fin surface. Increasing the transfer area per unit volume by closer fin spacing is also advantageous. The $3/8$ -11.1 surface shows a 45 per cent greater h than the $3/8$ -6.06 surface because of this effect. The expedient of closer fin spacing can be employed instead of louvering to realize high performance as seen by comparing the 19.86 plain fin and the $3/8$ -11.1 surfaces. The latter surface, however, will produce the lighter weight heat exchanger.

It may be that decreasing the louver spacing below $3/8$ to $1/4$ in. is not advantageous as demonstrated by the comparison of $3/32$ -12.22 surface behavior with the better flow friction-heat transfer power characteristic of the $3/8$ -11.1 surface. This point is also suggested by the data of reference (1) in the comparison of louvered-plate-fin surfaces all with 11.1 fins per in. but louver spacings of $3/16$, $1/4$, and $3/8$ in., respectively.

Fig. 10 strikingly illustrates the advantage of staggering the tubes alone over ruffling the fins for the finned-flat-tube surface. Staggering and ruffling together prove advantageous only for the higher $αE_{tot}$ range, corresponding, roughly, to the air side of regenerator or compressor intercooler operation as examples. The improvement of the 11.32-737-S-R over the 9.29-737-S-R surface is due solely to the increased area per unit volume, $α$.

An important point to keep in mind when making these heat-transfer-friction power comparisons is that core "volume" requirement is only one aspect of compactness of the final heat-exchanger design and that "shape" is exceedingly important (2). As a consequence, to realize a satisfactory shape, it may be necessary to employ other than the optimum surfaces as defined in Figs. 9 and 10.

Comparison With Results of Other Experimenters. The plate-fin test cores plain 11.1, $3/8$ -11.1, $3/8$ -8.7, and $3/8$ -6.06 were previously tested at the U.S.N. Engineering Experiment Station, Annapolis, Md. The results for the plain 11.1 and louvered $3/8$ -11.1 surfaces were reported previously (1). The other surfaces are covered in reference (12). The results of the two sets of experiments agree within a maximum of 7 per cent for both heat-transfer and friction for the louvered-fin sequence. For the plain-fin core, while the heat-transfer behavior is in accord, the f results differ by 11-20 per cent. In this core, unlike the others, entrance- and exit-flow losses are substantial, amounting to as much as 30 per cent of the total pressure drop. The USNEES results are higher with respect to both N_{St} and f .

The discrepancies on f can be largely accounted for in terms of the different exit and entrance-flow loss coefficients. The coefficients used by USNEES are the conventional information in the hydraulics literature which apply with reasonable accuracy only to high N_R flow, while the Stanford treatment used test determined coefficients (3) and (4). These comparisons emphasize the importance of having accurate information on these flow factors for work of this character.

The disparity in N_{St} while not so serious, cannot be explained. The fact that the Stanford results include an allowance for steam-side resistance should tend to make them somewhat greater than the EES results for $N_{Rf} > 3000$. This is not the case.

SUMMARY AND CONCLUSIONS

The foregoing discussion leads to the following conclusions:

- 1 The data presented here are of sufficient accuracy for preliminary design calculations for new applications of these surfaces.
- 2 No optimum surface can be specified from these results alone. The designer must select the best surface for a given ap-

plication giving consideration to such factors as cleanability and fouling characteristics, weight, size, and shape.

3 The nondimensional correlation between the variations of a type of surface are sufficiently good so, as to suggest that the results reported here may be interpolated and extrapolated to some extent to other modifications.

4 Plate-fin surfaces exhibit both tubelike and platelike flow characteristics depending to some extent upon the length-to-hydraulic diameter ratio of the surface.

5 In general, the heat-transfer characteristics are more descriptive of the boundary-layer flow than f . The reason for this is the large contribution of form drag effects.

6 Since the form drag effects are largely parasitic, in that they do not contribute to the heat transfer, as more information is accumulated superior surfaces from a heat-transfer-friction power point of view may result.

7 The surfaces reported here with one exception are now being used only for relatively low-temperature applications. Design studies for such high-temperature applications as the gas-turbine regenerator (2), may reveal that an effort should be made on the part of the industry to learn how to fabricate these surfaces for high-temperature service.

ACKNOWLEDGMENTS

The Office of Naval Research, the U.S.N. Bureau of Ships, and the U.S.N. Bureau of Aeronautics are currently sponsoring a heat-transfer research program for compact surfaces at Stanford University. The authors prepared this paper as part of this program and express their appreciation to the sponsoring organizations.

The U.S.N. Engineering Experiment Station, by keeping the authors in close touch with their similar program, has contributed materially to the ideas presented here.

Mr. John Godfrey and Mr. L. P. Saunders of Harrison Radiator, Mr. C. T. Perkins and Mr. Clyde Simpelaar of Modine, Mr. H. C. Rooks of Trane, and Mr. S. K. Andersen of AiResearch, have aided this work by providing test cores of various surfaces and by their suggestions.

BIBLIOGRAPHY

- 1 "Test Results of High-Performance Heat-Exchanger Surfaces Used in Aircraft Intercoolers and Their Significance for Gas-Turbine Regenerator Design," by A. L. London and C. K. Ferguson, *Trans. ASME*, vol. 71, 1949, pp. 17-26.
- 2 "The Gas Turbine Regenerator—The Use of Compact Heat-Transfer Surfaces," by A. L. London and W. M. Kays, *ASME Paper No. 49-SA-9*, presented at the Semi-Annual Meeting, San Francisco, Calif., June 27-30, 1949, of THE AMERICAN SOCIETY OF MECHANICAL ENGINEERS.
- 3 "Heat-Transfer and Flow-Friction Characteristics of Some Compact Heat-Exchanger Surfaces Part 1."
- 4 "Loss Coefficients for Abrupt Changes in Flow Cross Section With Low Reynolds Number Flow in Multiple Tube Systems," by W. M. Kays, *Trans. Heat Transfer and Fluid Mechanics Institute*, 1949, p. 99, published by ASME.
- 5 "An Investigation of Aircraft Heaters—Part II, Properties of Gases," by M. Tribus and L. M. K. Boelter, *NACA Report ARR*, October, 1942.
- 6 "An Investigation of the Effect of Fin Spacing on the Performance of Louvered-Plate-Fin Heat Exchanger Surfaces," by W. M. Kays, *Technical Report No. 3*, Navy Contract N6-ONR-251, Task Order VI (NR-035-104), December, 1948.
- 7 "Tests of a Strip Fin Heat Exchanger Surface," by W. M. Kays, *Technical Report No. 4*, Navy Contract N6-ONR-251, Task Order VI (NR-035-104), February, 1949.
- 8 "The Basic Heat Transfer and Flow Friction Characteristics of Plain-Plate-Fin Heat Exchanger Surfaces," by W. M. Kays, *Technical Report No. 5*, Navy Contract N6-ONR-251, Task Order VI (NR-035-104), February, 1949.
- 9 "The Performance of Finned-Flat-Tube Heat Exchanger Surfaces," by W. M. Kays, *Technical Report No. 6*, Navy Contract N6-ONR-251, Task Order VI (NR-035-104), August, 1949.

10 "High-Performance Fins for Heat Transfer," by R. H. Norris and W. A. Spofford, Trans. ASME, vol. 64, 1942, p. 489.

11 "Heat Transfer by Natural and Forced Convection," by A. P. Colburn, Engineering Bulletin, Purdue University, Research Series No. 84, January, 1942.

12 "Basic Heat Transfer and Flow Friction Data . . ." by John Dinan, United States Naval Engineering Experiment Station Reports C-2171-D, C-2171-E, C-2171-F, and C-2171-G, 1947-1949.

Discussion

D. ARONSON.² The work here reported is a valuable addition to our knowledge of convective heat transfer. In the specific application of the performance data to the design of gas-to-gas heat exchangers there are some differences in viewpoints between the authors and the writer, largely as regards which factors deserve prime emphasis. Compactness is a consideration in gas-turbine design but usually is secondary to shape requirements. As a rule the compressor and turbine are first laid out roughly and then, in whatever convenient space can be found, a regenerator is fitted in. The choice to be made is then not of the most compact surface but of one which will give the balance between required NTU and pressure drop which will result in the best gas-turbine cycle.

This condition was vividly demonstrated to the writer when he first attempted to design a cross-flow regenerator for a locomotive gas turbine. At that time his company had on order heat exchangers for an oxygen plant. These exchangers used the $3/32$ -12.22 fin which is shown in Fig. 9 of the paper to be about the most compact pattern. Since space is a most important consideration in a locomotive, this particular surface appeared to offer excellent possibilities. Calculations, however, quickly revealed that such a surface would be entirely unsuitable. Amazingly enough, the 5.3 plain fin, which is indicated as the least compact surface in Fig. 9, proved to be the one which would give the required NTU of about 2 without exceeding the allowable pressure drops. The following is a comparison of the dimensions required for the two cores:

	Length, ft			Volume, cu ft
	Gas flow	Air flow	No flow	
$3/32$ -12.22 fin	$2/4$	$2/4$	80	45
Plain-5.3 fin	3	7	7	147

In terms of actual core volume the compact surface is truly more compact, but if the volume of distributing sections and inlet and outlet manifolds are added, the total volume comes out higher than for the less compact plain-fin pattern. Obviously, the compact surface cannot be used on a locomotive installation.

One can state a general rule for selection of core structures for gas-turbine regenerators. The more compact surfaces are suitable for small air flows and the less compact surfaces for large air flows; also, the more compact surfaces are the better for high values of NTU and the less compact surfaces for low values of NTU . The availability of the test data presented by the authors in this and previous papers is of considerable aid in making the optimum selection. For design work it would have been helpful to have included plots of j/f versus N_{Re} and plots of h versus E , friction power.

For oxygen plants, while compactness is important, a more significant factor is the cost. The authors mention that these surfaces have been used in portable oxygen plants. However, at present many of the companies manufacturing these extended-surface structures are interested in their use in tonnage oxygen plants where heat exchangers represent a significant part of the total cost. The most compact surfaces are probably made with pin fins or wire screening having very fine diameter wires. Such

surfaces would require fairly small passage heights in order to maintain high fin effectiveness.

However, such a design would not necessarily represent the lowest cost. A major part of the cost is in forming the fin elements and assembling them into passages between separating plates. Therefore it is desirable to have as high a passage as possible.

There are many blank spaces remaining to be filled between test-core data and large-scale performance. Future programs might include investigation of such factors as the following:

1 Effect on regenerator performance of complex flow pattern of air discharge from compressor or turbine into regenerator.

2 Effect of flow unbalance in passages which produces a material unbalance between cold fluid and hot fluid. This is of particular significance in heat exchangers of high NTU . The effect is not shown when testing with steam because of the unlimited amount of heat available from the condensing steam.

3 Effect of variations in manufacture on heat-exchanger performance—such as wear of dies.

If a test code is adopted as suggested by the authors, it might be advisable to arrange for a better check on pressure drop. This could be done by building a separate core for pressure-drop measurements. The "pressure-drop" core could be built to the same dimensions as the other core but arranged with all passages flowing in the same direction. This would give an area ratio at entrance and exit very close to unity. If such an arrangement is not possible, then a longer flow path could be used when testing for pressure drop. While there will always be some question as to whether the "heat-transfer" core and the pressure-drop core are of identical construction, the uncertainty can be reduced by suitable fabricating procedures. Also, since there are some fifteen to twenty-five individual passage sections there is a reasonably good averaging of fin variations.

J. J. DINAN.³ The information and data presented by the authors in these papers help to fill a need which exists in the field of heat-exchanger design. The paper takes the initiative in recommending a test apparatus and technique for obtaining accurate basic heat-transfer and flow-friction data for heat-exchanger surfaces. Also, it reports additional data which may be extrapolated to designs of compact heat exchangers.

Undoubtedly, the authors have put considerable thought into the design of the test apparatus reported herein. The estimated over-all accuracy of the data obtained and the excellent heat balances attest to this. Fig. 15, Part I of this paper, provides a check on the accuracy of the authors' methods. Comparison is made between data reported by the authors and that obtained by the U. S. Naval Engineering Experiment Station. Since the two test setups are, in general, similar, convincing evidence is provided for the reproducibility of test data if the authors' recommended technique is employed.

The friction-factor characteristic of the surfaces reported in this paper is defined by the friction factor f versus the Reynolds number. Evaluation of f is based upon the Fanning equation for flow in tubes. The application of this analogy to the plate-and-fin type of surface reported herein appears justifiable. One might expect the analogy to break down when applied to flow over the flat-tube type of surface. The curves in Fig. 6, Part 2 of this paper, do not bear this out since the friction-factor curves for the "finned, flat-tube" surfaces are similar in shape to the "plate-and-fin" surface designated as 1986. However, extension of the analogy to all heat-exchanger surfaces cannot logically be done. Test of a "plate and pin-fin" core at the Engineering Ex-

² Elliott Company, Jeannette, Pa. Mem. ASME.

³ U.S.N. Engineering Experiment Station, Annapolis, Md.

periment Station, showed that the analogy to flow over banks of tubés is applicable.

In comparing the heat-transfer and friction characteristics of different surfaces, the most significant comparison would seem to be a plot similar to Figs. 9 and 10, Part 2 of this paper. These figures make the comparison on a bulk or volumetric basis. Another comparison can be made purely on a heat-transfer-area basis. Possibly the plot might be extended to include the weight factor.

CLYDE SIMPELAAR.⁴ This paper, together with the individual project papers on the various surfaces tested at Stanford University laboratory, contributes materially to the literature on interrupted fin surfaces.

The authors suggest that it may not be advantageous to decrease louver spacing below $\frac{3}{4}$ to $\frac{1}{4}$ in. While certain of the data appear to bear this out, there is another directly associated condition, namely, the distance between in-line surfaces, which is not evaluated. In this it should be considered that the effect of spacing in the louvered-fin design which incorporates a surface configuration is probably different from that for a plain flat strip.

To consider then, only the uncounted strip fins such as those tested and reported in the original paper of Norris and Spofford, while the heat-transfer coefficient may increase with decrease in strip width, the coefficient may also decrease with decrease in distance between trailing and leading edges of the in-line strips so that the latter effect may substantially nullify the former. Both of these conclusions appear to be supported in the original paper mentioned, in which note should be made of the fact that without a modification of the definitive geometry (D_s), the performance of strip fins staggered by three's was substantially better than the performance of strips staggered by two's.

The strip-fin design identified as $\frac{3}{32}$ -12-22 in the present paper was tested in the Modine laboratory using a test core with a single air-side pass 6 in. high \times 3 in. in air-flow length. Heat-transfer tests of this sample correlated with those of the larger core tested at Stanford to within about 1 per cent. In order to verify what we have termed the "proximity effect" of in-line surfaces, an identical core was built except that in each channel fin alternate pairs of strips were removed at their base, increasing the distance between in-line surfaces from $\frac{3}{32}$ to $\frac{9}{32}$ in.

Tests of this core showed a gain in the Stanton-Prandtl group of 14 per cent at an N_{Re} of 1000, and 6 per cent at an N_{Re} of 10,000. Norris and Spofford showed an increase of 11 per cent in heat transfer for stagger by three's versus two's at an air flow of 1000 fpm. Other tests which were made indicated that this effect is significant over a wide range of distance between trailing and leading edges.

It appears possible, therefore, to obtain the advantage of the use of narrow strip fins if these are staggered by three's or four's so that the distance between strips is increased beyond the severely critical range. To correlate the performance, a Reynolds number based upon either the hydraulic radius or fin strip width or perimeter is not completely definitive and an "effective

Reynolds number" should be used which would take into consideration the "proximity effect" of in-line surfaces.

AUTHORS' CLOSURE

The authors' objectives in presenting this paper were to make available accurate basic heat-transfer and flow-friction data for a number of compact heat-exchanger surfaces which might find application in numerous systems where compactness is desired, including the gas-turbine heat exchangers. Whether or not any of these surfaces are suitable or desirable for the gas-turbine regenerator is for the regenerator designer to determine. The basic data presented here are not definitive and will only assist in this decision. It was not the objective of this paper to provide the designer with any criteria for the selection of an optimum surface for any particular application. In this regard the authors fail to see any "differences in viewpoints" between themselves and Mr. Aronson simply because the authors did not in this paper present any viewpoints on how gas-turbine regenerators should be designed.

Mr. Aronson's remarks regarding the shape problem when using low-density fluids are very well taken, and this aspect is discussed at some length by the authors in reference (2). However, he infers that for a given gas-turbine plant there is something of a definite physical limitation in the over-all compactness of the regenerator, and attempts to devise more compact units are doomed not to meet with success. The authors feel that such generalizations are not warranted at this time.

The effect of such things as complex flow patterns and flow unbalance in the passages can best be determined by tests of actual operating systems. It is hoped that manufacturers will make such data generally available.

A pressure-drop test core having an entrance and exit area ratio close to unity and long flow passages would be very desirable although, of course, adding considerably to the cost and time of the test program.

Mr. Dinan objects to the use of the Fanning friction factor f for other than tubular surfaces. As a matter of fact, it does not make any difference how the friction factor is defined providing that the same definition is used in the application and providing that it is applied to the same surface or to a geometrically similar surface. The only advantage of one method of presenting the friction characteristics of a surface over another occurs when attempting to generalize a correlation to cover variations in geometry. No such generalization was attempted in this paper. The friction factor and hydraulic radius were defined in the same manner for all the surfaces as a matter of convenience in applying these data. This definition was also used by Norris and Spofford in their pioneer paper, reference (10).

There are undoubtedly many improvements which can be made in the performance of heat-exchanger surfaces such as discussed by Mr. Simpelaar. The authors are presently conducting an investigation of the basic mechanisms of heat transfer and flow friction in complex flow passages with the hope that a better understanding of the basic mechanisms will lead to the development of more effective surfaces.

⁴Chief Research Engineer, Modine Manufacturing Company, Racine, Wis. Mem. ASME.

C
A

Six Bet
metric to
mine the
of the si
cients wi
were con
ther tests
ances and
of piping

THE
cuss
chan
this type of

Cross se
inclusive.
respect to
ter arrang
stallation
further det

The cali
of the main
diam tank
at the entr
laboratory
was bolted
either 4 or
of a reduc
approximat
conducted
metric tank
brated care
ing tank.
Fig. 7.

The diffe
measured w
to the press
25 ft were m
ter which v
Differential
water-and-a
side so that
differential
which the d

¹ Professor
stitute, Mo
Contribut
presented at
December 2
ENGINEERS.

NOTE: St
understood a
of the Societ

Calibrations of Six Beth-Flow Meters at Alden Hydraulic Laboratory, Worcester Polytechnic Institute

By L. J. HOOPER,¹ WORCESTER, MASS.

Six Beth-Flow tubes were calibrated by means of a volumetric tank at the Alden Hydraulic Laboratory to determine their suitability as flow-metering elements. Four of the six meters tested had practically the same coefficients with flow in either direction. The flow coefficients were constant above a Reynolds number of 100,000. Further tests are necessary to determine manufacturing tolerances and the effects of disturbed flow due to various types of piping arrangements.

THE purpose in calibrating the six Beth-Flow meters, discussed in the paper, was to determine their operating characteristics as a preliminary survey of the usefulness of this type of meter.

APPARATUS

Cross sections of the six meters tested are shown in Figs. 1 to 6, inclusive. It is noted that the meters differ from each other with respect to their upstream-throat diameter ratio and in the piezometer arrangements. Three of the meters were designed for installation in a 6-in. pipe and three in a 4-in. pipe. These and further details of the meter designs can be seen in the illustrations.

The calibration tests were performed in the lower basement of the main building of the Alden Hydraulic Laboratory. A 3-ft diam tank served as distribution center to reduce velocity effects at the entrance to the test section. The 12-in. supply from the laboratory pipe was connected near the top of the tank. To this was bolted an 8-ft length of 12-in. pipe. The test section of pipe, either 4 or 6 in. diam, was connected to this 12-in. pipe by means of a reducing flange. The approach pipe to the meter was approximately 25 ft long. The discharge from the meter was conducted to a switchway near a volumetric tank. This volumetric tank was 3 ft wide, 6 ft deep, and 22 ft long. It was calibrated carefully, immediately before the test, by means of a weighing tank. The details of the piping arrangement can be seen in Fig. 7.

The differential pressures developed by the flow meters were measured with three types of differential manometers, according to the pressure range required. Differential pressures from 2 ft to 25 ft were measured with a barometric type of mercury manometer which was calibrated by a water column prior to the test. Differential pressures from 0.2 ft to 4 ft were measured with a water-and-air manometer, which had a well connected to one side so that the deflection occurred in one manometer leg. Small differential pressures were measured with a micromanometer in which the deflection was measured in water columns 2 in. in diam.

¹ Professor of Hydraulic Engineering, Worcester Polytechnic Institute. Mem. ASME.

Contributed by the Research Committee on Fluid Meters, and presented at the Annual Meeting, New York, N. Y., November 27-December 2, 1949, of THE AMERICAN SOCIETY OF MECHANICAL ENGINEERS.

NOTE: Statements and opinions advanced in papers are to be understood as individual expressions of their authors and not those of the Society. Paper No. 49-A-38.

Point gages brought up underneath the water surface indicated the water levels in the customary manner for hook gages. The difference in elevation between the two point gages was measured with an Ames dial gage, reading to 0.0001 in. The upper limit of deflection with this manometer was approximately 4 in.

PROCEDURE

In preparing a meter for a test it was first carefully cleaned with carbon tetrachloride and clean wiping rags, to be sure that the interior surfaces were entirely free from grease. The upstream flange joint of the meter was made tight with a thin film of grease so as to avoid the possibility of a gasket sliding in the pipe and disturbing the flow in any manner. After the meter was bolted in place the line was filled with water, and all air pockets were blown out by means of suitable blowoffs both in the line and in the piezometer connections to the manometer that was in use. The proper operation of the manometer was checked by being sure that a zero deflection occurred on the manometer with zero flow. This static check was repeated frequently during the course of a test.

In preparation for a particular test the desired flow was first set and allowed to run to waste for 5 or 10 min to insure steady test conditions. When everything was in readiness, a measuring run was started on the volumetric tank by switching the discharge into the tank and simultaneously starting a calibrated stop watch. An observer on the manometer took readings of the deflection continuously throughout the discharge-measuring run. These readings were recorded on an adding machine which made it possible to secure from 40 to 100 readings of deflection for each test run. When the volumetric tank was nearly full the discharge was switched to waste, and the timer stopped. The length of the timing run varied from approximately 500 sec at the low flows to about 100 sec at maximum discharge. After the run was completed, the flow was adjusted at the next test value, and the test data were computed.

After a complete calibration curve had been obtained on the meter with the flow in the forward direction, the meter was taken out of the line and was reinserted so that the meter was in the reverse direction. A second complete calibration was then made under these conditions.

COMPUTATIONS

In computing the coefficients of the meters the actual discharge, as measured by the volumetric tank, was divided by the theoretical discharge computed from the meter deflection. The actual discharge was computed as follows:

$Q_{\text{actual}} = \text{volume divided by test time in seconds}$

The theoretical discharge for all of the meters was computed using the nominal dimensions of a meter, thus

$$Q_{\text{theoretical}} = A_1 \sqrt{2g(h_1 - h_2)} / \sqrt{R^4 - 1}$$

In the case of meter SK No. 1, the theoretical discharge was computed from the relationship

$$Q_{\text{actual}} = K \times H^{0.476}$$

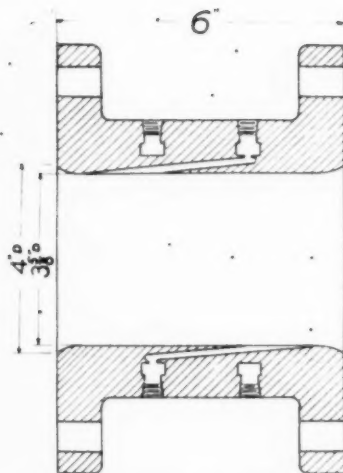


FIG. 1 SK 1 BETH-FLOW TUBE TYPE V;
 $R = 1.11:1$

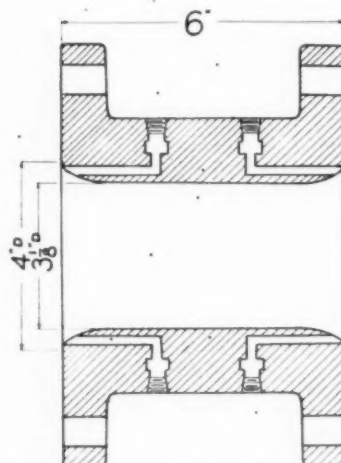


FIG. 2 SK 2 BETH-FLOW TUBE TYPE VD;
 $R = 1.28:1$

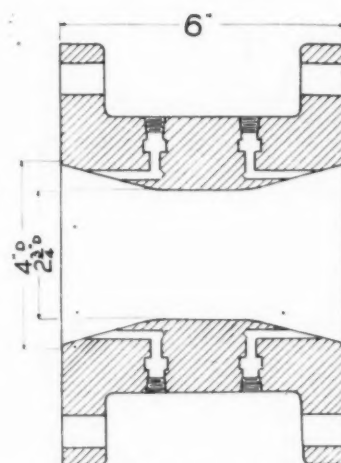


FIG. 3 SK 3 BETH-FLOW TUBE TYPE VD;
 $R = 1.40:1$

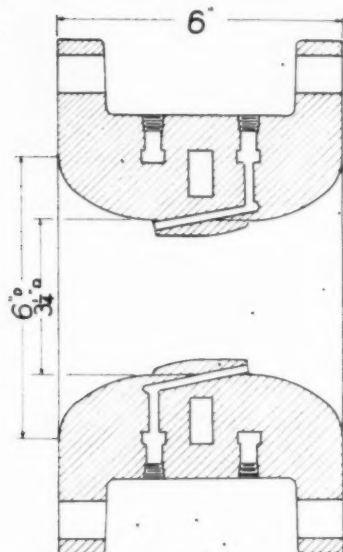


FIG. 4 SK 4 BETH-FLOW TUBE TYPE D;
 $R = 1.84:1$

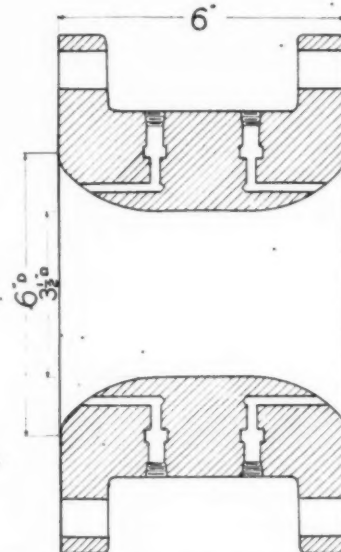


FIG. 5 SK 5 BETH-FLOW TUBE TYPE VD;
 $R = 1.72:1$

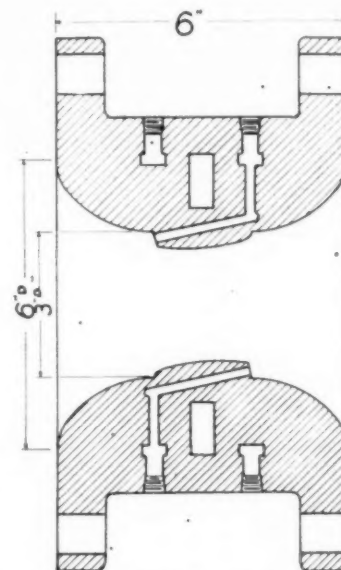


FIG. 6 SK 6 BETH-FLOW TUBE TYPE D;
 $R = 2.0:1$

where K includes the discharge coefficient as well as all constant terms.

RESULTS

The results of these tests are shown in Figs. 8 to 12, inclusive. Two of the meters, namely, No. 2 and No. 6, were not given a final calibration, and the results have not been included. These two meters did not show the same coefficients with reverse flow. Time was not taken to determine the reason for the differences inasmuch as this work could be better investigated along with other factors in a more complete investigation.

As may be seen from the curve sheets, the other four meters have practically the same coefficients for the flow in either direction. In all four cases the coefficient reaches a constant value

with a Reynolds number of approximately 100,000, based on the throat velocity. This corresponded to a throat velocity of very nearly 6 fps.

The coefficient continued constant to as high a value of throat velocity or Reynolds number as could be reached with the test setup. In the case of flow tubes No. 1 and No. 3, this was 2.3 cfs. In the case of No. 5, a discharge of nearly 3.2 cfs was reached.

In the case of flow tube No. 5, a poor set of readings was obtained on one test setup. In searching for the trouble with this particular calibration the question arose as to the stability of the point of separation in the exit tube. Two calibration curves were run, one with the entire inner surface of the tube very lightly greased by rubbing the surface with greasy hands. In the second test the inner surface was cleaned with carbon tetrachloride.

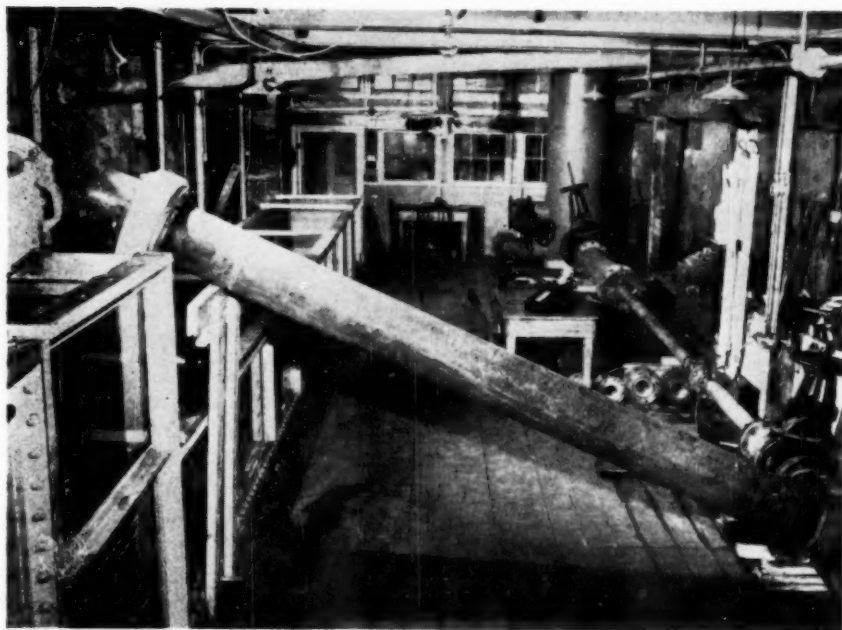
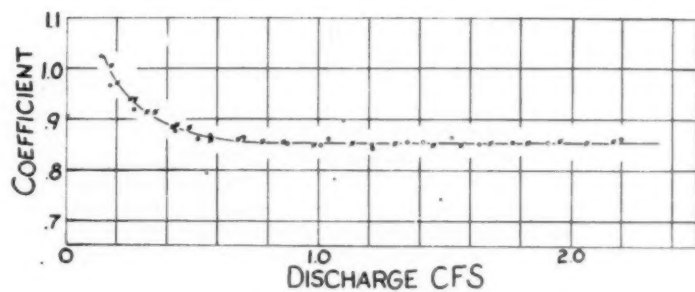
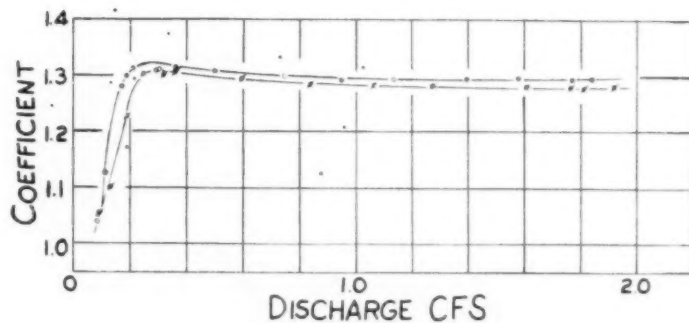
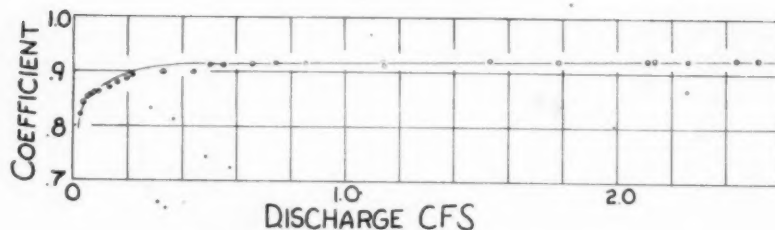
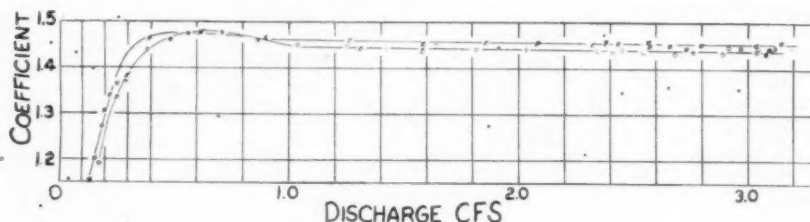
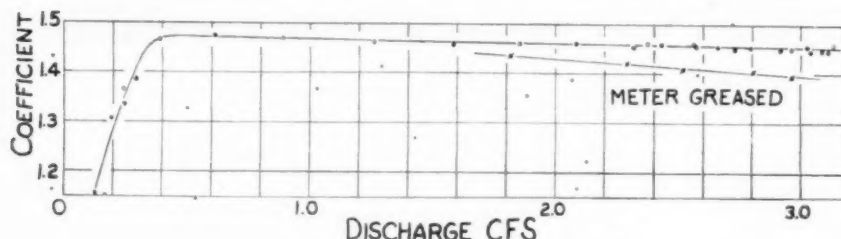


FIG. 7 ARRANGEMENT OF TEST PIPING

FIG. 8 SK 1 BETH-FLOW TUBE TYPE V; $R = 1.11:1$ FIG. 9 SK 3 BETH-FLOW TUBE TYPE VD; $R = 1.46:1$

FIG. 10 SK 4 BETH-FLOW TUBE TYPE D; $R = 1.84:1$ FIG. 11 SK 5 BETH-FLOW TUBE TYPE VD; $R = 1.72:1$ FIG. 12 SK 5 BETH-FLOW TUBE TYPE VD; $R = 1.72:1$

As may be seen in Fig. 12, the nature of the surface had a distinct effect in the higher ranges of discharge. With the greasy surface the coefficient gradually decreased from a normal value of 1.452 to 1.392, a difference of 4.1 per cent. This test was of interest in that it indicated the nature of the flow in the downstream section of the tube. In so far as accuracy of the tube is concerned, the test is undoubtedly of greater interest from a laboratory point of view than that of a commercial installation. In the laboratory the meter is normally calibrated very soon after it has been installed and the possibility of obtaining a partially greasy surface is very good. In commercial operations the tube is normally being used continually for the measuring of a single fluid, i.e., either water or oil, and the possibility of a lowered coefficient is practically negligible.

It must be remembered that the purpose of these tests was to determine the possibilities of these flow tubes as flow-measuring elements. This report therefore is of a very preliminary nature and indicates that these tubes do possess possibilities as flow-measuring devices. It is realized that considerably more research must be done with these tubes to determine the manufacturing tolerances and the effects of disturbed flow which attend various types of installations. It is presumed that the results of such a research program will be made available in the near future.

CONCLUSIONS

As a result of these calibration tests, certain designs of Beth-Flow tubes have been found to possess a constant coefficient

over a range of Reynolds numbers from approximately 100,000 to approximately 800,000. These meters were found to have the same coefficient for flow in either direction through the meter. Further research is necessary to determine manufacturing tolerances and effects of installation on the meter performance.

Discussion

M. M. BORDEN.² It may be of interest to note the differences of throat diameters for conventional Venturis (with approximate coefficient values as noted) and the Beth-Flow tubes with their coefficient values taken from the flat part of the curves in the paper.

Each tube of a given size is equated for a common (Q) quantity and differential head produced by it, as given in Table 1.

The relatively small differences of diameter of the throat constrictions given in Table 1 seem not to warrant the added cost of the Pitot bodies, as in sketch Figs. 4 and 6 of the paper, with the possible stoppage of their impact openings, or of the uncertainty of the effects of a change of velocity curve (with upstream roughness) upon the others.

The difference in head loss for a given size of constriction would

² Engineering Consultant, Simplex Valve & Meter Company, Philadelphia, Pa. Mem. ASME.

surely be
If this be
than with

It would
tion could
from the
definitely
region wi
flow.

Fig. 13
bination

The cu
tial to th
Fig. 14.
revolve 4
move it
would pr
ing both

Fig.

W. S.
author
stitute.
ideas o
author's
ment in
of Aug
Simplif

"Its
and a
Accura
avoided
or othe
interior
negligib
made,
Fig.

Labora
versity
sump,
test pi
The m
Fig.
hook g

Pr
Philad

TABLE 1 CONVENTIONAL VENTURIS AND BETH-FLOW TUBES COMPARED

SK	Assumed C_d	Size Beth-Flow, in.	β	Equivalent Venturi, in.	C_d assumed	β	Difference Venturi throat and Beth-Flow throat, in.
1	0.86	$4 \times 3\frac{3}{4}$	0.906	4×3.556	0.90	0.889	-0.069
3	1.3	$4 \times 2\frac{1}{4}$	0.688	4×3.051	0.975	0.763	+0.301
4	0.92	$6 \times 3\frac{1}{4}$	0.542	6×3.153	0.9825	0.526	-0.097
5	1.46	$6 \times 3\frac{1}{2}$	0.583	6×4.129	0.9825	0.688	+0.627

surely be favored by the action of the diverging Venturi cone. If this be omitted, the loss of head need not be seriously greater than with a belled outlet from the Venturi throat.

It would appear that the use of a Pitot opening in a constriction could be better applied by placing the Pitot opening as far from the wall of the constriction as is convenient so it would be definitely located in the flat part of the velocity curve and in a region where least affected by upstream roughness or whirling flow.

Fig. 13, herewith, illustrates a type of Venturi-Pitot combination which has been used by the writer's company.

The curve showing relation of Venturi throat—Pitot differential to the normal main and throat differential are as shown in Fig. 14. With such a Pitot combination it is also possible to revolve the Pitot tube for removal of an obstruction; or to remove it for inspection; or to rotate it through such an angle as would produce a slight change of differential—all while delivering both differential pressures from a central piece.

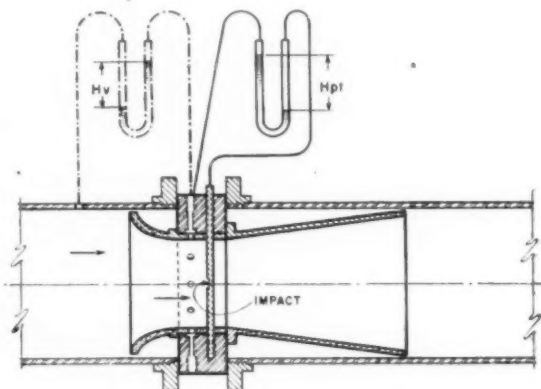


FIG. 13 VENTURI-PITOT COMBINATION

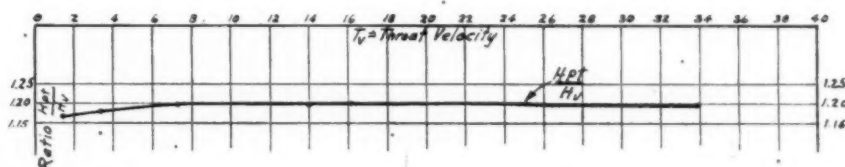


FIG. 14 CURVE SHOWING RELATION OF VENTURI THROAT—PITOT DIFFERENTIAL TO NORMAL MAIN AND THROAT DIFFERENTIAL

W. S. PARDOE.² This discussion is in no way a criticism of the author and the Alden Laboratory at Worcester Polytechnic Institute. The writer has the highest appreciation of the work and ideas of this laboratory but it is written in response to the author's suggestion of further studies and in answer to a statement in an article published in *The Engineering News-Record* of August 18, 1949, entitled, "New Flow Meter Cuts Costs, Simplifies Installation Problems," by R. E. Tarring, as follows:

"Its short length permits insertion in complicated pipe systems and at the most advantageous point on the hydraulic gradient. Accuracy is not lost and expensive revamping of the system is avoided. Straight pipe-runs before or after elbows, tees, crosses, or other fittings—are not required;" also, "The streamlined interior of the meter-Low main-to-throat (high Beta) gives negligible unrecovered pressure loss." Other claims have been made, but these will suffice.

Fig. 15 of this discussion is a schematic sketch of the Hydraulic Laboratory of the Civil Engineering Department of the University of Pennsylvania in Philadelphia, Pa. It consists of a sump, pumps, cast-iron pipe system, 5-ft 6-in.-diam stand pipe, test pipe lines, test meter, and two 16,000-lb weighing tanks. The maximum pumping and weighing rate is 12 cfs (5400 gpm.).

Fig. 16 shows the three differential gages; the first, a 3-in. hook gage measuring up to 0.6 ft reading to 0.0001 ft.

²Professor of Hydraulic Engineering, University of Pennsylvania, Philadelphia, Pa.

The second is a direct-reading air gage used from 0.6 ft to 4.5 ft.

The third is a direct-reading mercurial gage used for heads greater than 5 ft.

Fig. 17 shows the 8 × 10 in. Beth-Flow tube.

Fig. 18 is a cross section of a test of a 6-in. Gentile multiple Pitot tube showing a log-log head—(velocity in 6-in. pipe) curve the empiric equation of which is $V = 4.3 h^{0.4875}$. Note that all the points fall on the line due to the very small scale.

Fig. 19 shows the same data put in terms of C in $V = C\sqrt{2gh}$ and the velocity in the 6-in. pipe. Note the scatter of the points being plus and minus 0.6 per cent; the lost head is 21 per cent of the working head.* The laboratory has an error of plus and minus 0.1 per cent as can be seen in Fig. 20, which is a test of a 12 × 8 1/4 in. ($\beta = 0.69$) Venturi meter. Note that the lost head equals 10 per cent of the Venturi head; if β were 0.75 the lost head would be less.

Fig. 21 is a log-log throat velocity—Venturi head curve for Mr. Gentile's information. The Gentile tube shows a scatter of points six times that of the Venturi meter tested in the same setup in the presence of both the manufacturer and the customer. This must be attributed to the location of the multiple Pitot tubes which pick up fluctuations of velocity due to turbulence and minor vortexes near the wall. The manometers showed much wider fluctuations and surges than those of the Venturi meter.

Fig. 22 shows a traverse in a 4-in. pipe, and Fig. 23 shows a

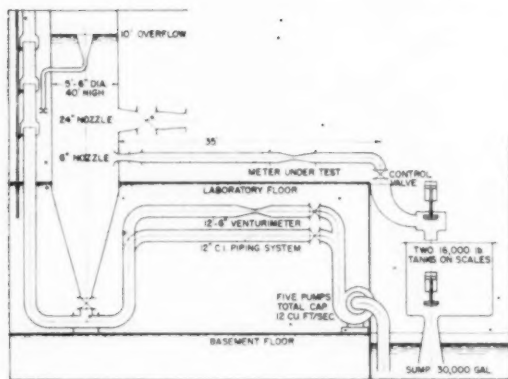


FIG. 15 SCHEMATIC ARRANGEMENTS OF HYDRAULIC LABORATORY

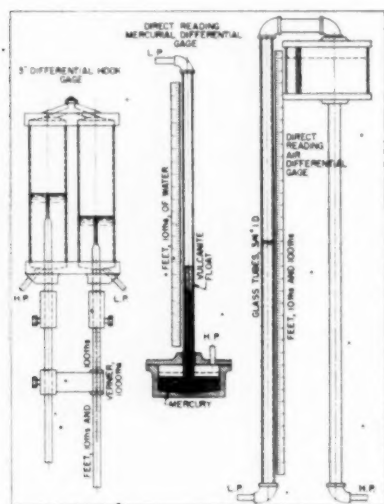


FIG. 16 DIFFERENTIAL GAGES

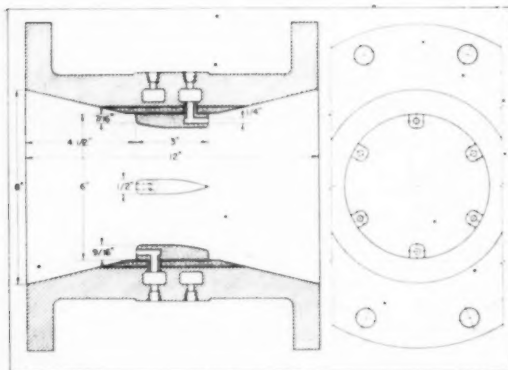


FIG. 17 TEST OF 8 X 6-IN. BETH-FLOW TUBE

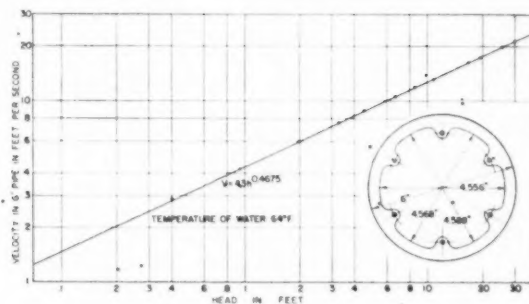


FIG. 18 TEST OF 6-IN. GENTILE MULTIPLE PITOT TUBE

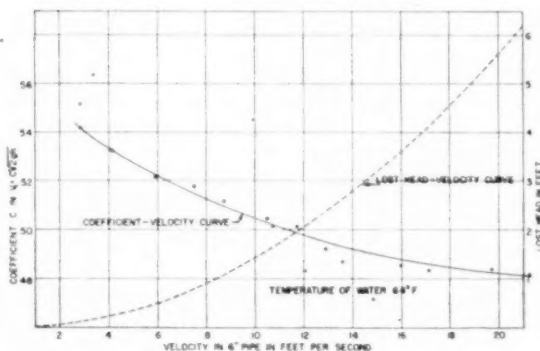


FIG. 19 TEST OF 6-IN. GENTILE MULTIPLE PITOT TUBE

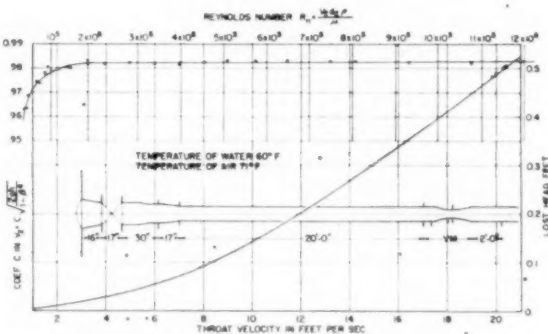


FIG. 20 TEST OF 11.956 X 8.2285-IN. VENTURI TUBE T 4349 (Leeda and Northrup Company; Philadelphia Electric Company, Richmond Station.)

traverse in an 8 in. pipe immediately following a series of flanged decreases from 24 in. to 8 in. diam. It is evident these traverses would have a profound effect on the coefficient as the Pitot tubes are acted on by the velocity near the wall. Fig. 22 should give a high coefficient due to the low head, and Fig. 23 a low coefficient due to a high working head if the mean velocities are equal.

The effect of an eccentric traverse such as occurs after elbows should increase the working head and decrease the coefficient due to the fact that the square of the mean velocity is less than the mean of the squares of the individual velocities.

With these ideas in mind the writer seized the opportunity (of the presence in his laboratory of an 8 X 6-in. Beth-Flow tube sent in for test by the city of Philadelphia) to make the following tests of the "effect of installation on the coefficient of the 8 X 6-in.

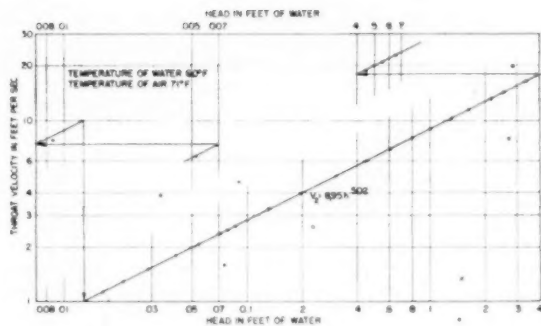


FIG. 21 TEST OF 11.596 \times 8.2285-IN. VENTURI TUBE NO. T 4349 (Leeds and Northrup Company; Philadelphia Electric Company, Richmond Station.)

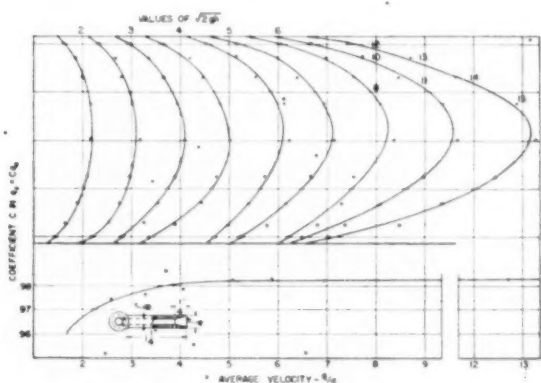


FIG. 22 TEST OF PITOT TUBE IN 4.281-IN. PIPE COUNTERSUNK POINT

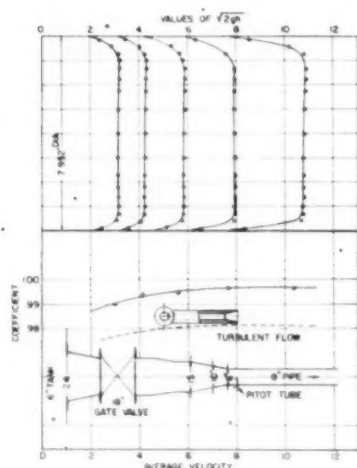


FIG. 23 COUNTERSUNK PITOT TUBE IN APPROXIMATELY SHOOTING FLOW

Beth-Flow tube," and compare them with similar data for the Venturi meter of similar proportions.

Fig. 24 is a log-log head-discharge curve for this 8 \times 6-in. Beth-Flow tube. Again, note how all the points fall on the line

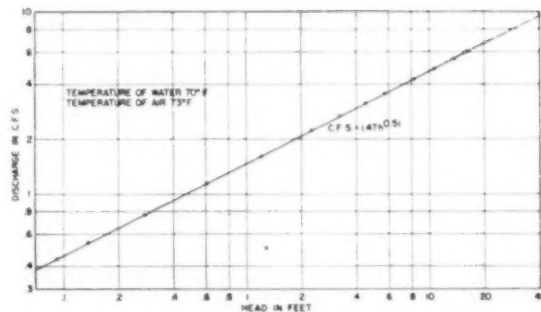


FIG. 24 TEST OF 8 \times 6-IN. BETH-FLOW TUBE FOR PHILADELPHIA

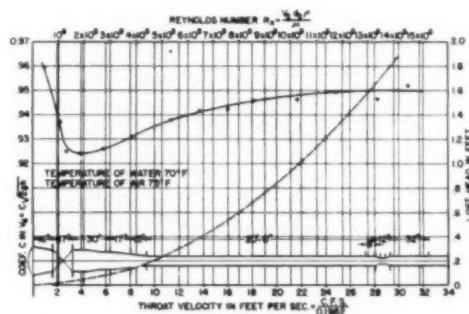


FIG. 25 TEST OF 8 \times 6-IN. BETH-FLOW TUBE FOR CITY OF PHILADELPHIA

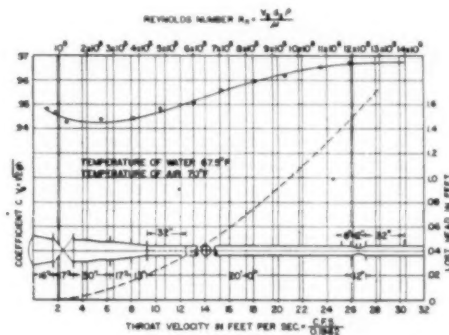


FIG. 26 BETH-FLOW TUBE WITH 32-IN-LONG CROSS-STRAIGHTENING VANE; EFFECT OF INSTALLATION

with the following equation: $cfs = 1.47 h^{0.51}$. These curves are very deceptive.

Fig. 25 gives the same data plotted as coefficient C against throat velocity. Note again the scatter of points, and the log-log curve gives no hint of the form of this coefficient curve. The lost head equals 12.1 per cent of the working head. Also, the setup has no straightening vanes. The average of ten values of the coefficient at 10, 20, and 100 per cent of the integrator range is 0.9392.

Fig. 26 shows the same setup with a 32-in-long cross-straightening vane 20 ft ahead of the Beth-Flow tube, the average coefficient being 0.9539 or 1.54 per cent above Fig. 25. This setup has been used as a basis of comparison for all the others. Note that the normal turbulence and slight vortexes always present in

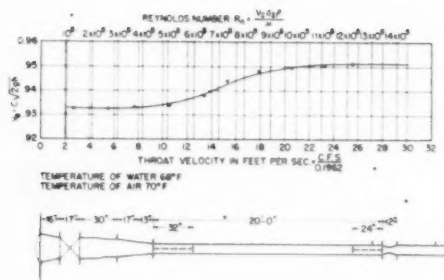


FIG. 27 TEST OF 8 X 6-IN. BETH-FLOW TUBE WITH TWO CROSS-STRAIGHTENING VANES; EFFECT OF INSTALLATION

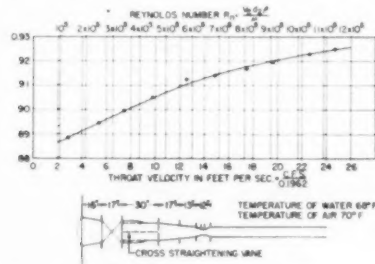


FIG. 28 TEST OF 8 X 6-IN. BETH-FLOW TUBES; EFFECT OF INSTALLATION

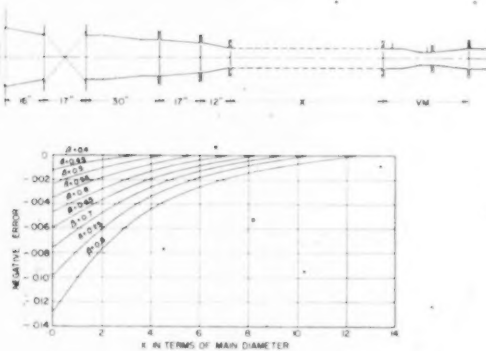


FIG. 29 EFFECT OF INSTALLATION ON VENTURI METERS

piping systems produce an error of 1.54 per cent. It looks as if this meter extends from the lower end of our pump suction through the pumps and cast-iron piping system into the stand-pipe through the 24 in. to 8 in. reducers and 20 ft (30 diam.) of 8-in. pipe, that is, it is very sensitive to the small disturbances in the flow.

Fig. 27, a cross-straightening vane 24 in. was added immediately ahead of the meter giving a coefficient of 0.9411, being 1.34 per cent less than Fig. 26. This latter vane evidently flattened the pipe traverse at the meter.

Setups in Figs. 25, 26, and 27 would all produce the same coefficient with an 8 X 6 in. Venturi meter, see Fig. 39.

Fig. 28, the Beth-Flow tube was placed immediately after the 24 in. to 8 in. flanged reducers; this gave an average coefficient of 0.9095 or minus 4.65 per cent. The coefficient of the Venturi meter under a similar setup decreased 0.098 per cent (see Fig. 29).

In Fig. 30 the Beth-Flow tube was placed after a 90-deg short-radius elbow, thus passing an eccentric traverse into the tube; the average coefficient was 0.8529 or minus 10.6 per cent. In Fig. 31 a piece of 8-in. pipe 8 in. long was placed between the elbow and the meter. The average coefficient dropped to 0.8381 or minus 12.1 per cent.

Fig. 32 indicates the 8 X 6 in. Venturi meter would be plus 1.78 and 1.09 per cent, respectively.

In Fig. 33 the Beth-Flow tube was placed immediately after two short-radius 90-deg, 8-ft elbows in planes at right angles. The average coefficient was 0.8366 or minus 12.3 per cent.

In Fig. 34 an 8-in.-long piece of 8-in. pipe was inserted between the second elbow and the Beth-Flow tube; the average co-

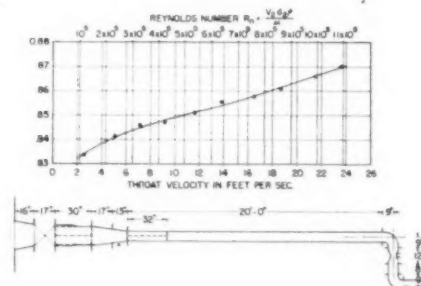


FIG. 30 TEST OF 8 X 6-IN. BETH-FLOW TUBE; EFFECT OF INSTALLATION

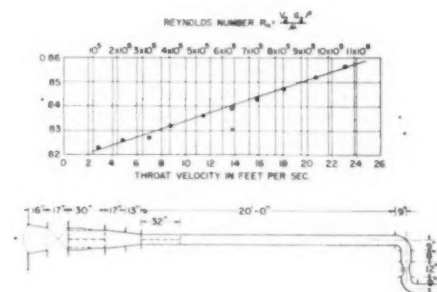


FIG. 31 TEST OF 8 X 6-IN. BETH-FLOW TUBE; EFFECT OF INSTALLATION

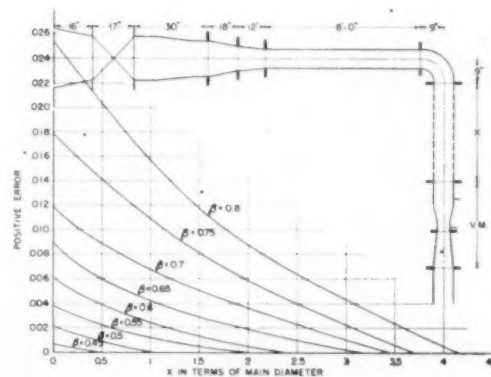


FIG. 32 EFFECT OF INSTALLATION ON VENTURI METERS

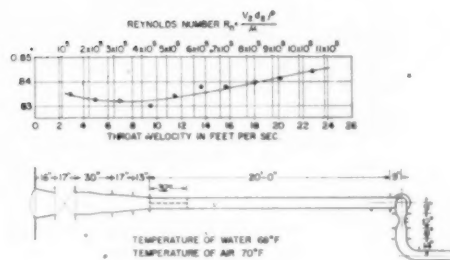


FIG. 33 TEST OF 8 X 6-IN. BETH-FLOW TUBE; EFFECT OF INSTALLATION

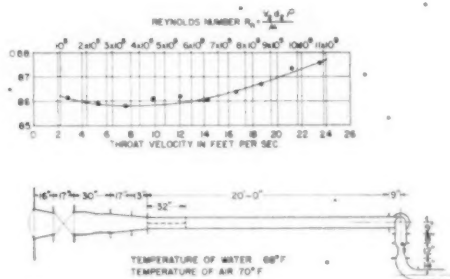


FIG. 34 TEST OF 8 X 6-IN. BETH-FLOW TUBE; EFFECT OF INSTALLATION

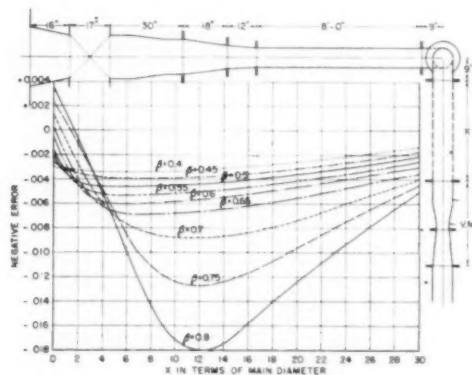


FIG. 35 EFFECT OF INSTALLATION ON VENTURI METERS

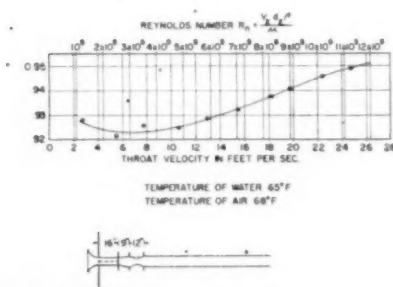


FIG. 36 TEST OF 8 X 6-IN. BETH-FLOW TUBE; EFFECT OF INSTALLATION

efficient was 0.8642 or minus 9.4 per cent. Fig. 35 shows the corresponding values for the 8 X 6 in. Venturi meter to be plus 0.22 and 0.07 per cent, respectively.

In Fig. 36 the Beth-Flow tube was placed immediately after a 6-in. to 8-in. flanged increaser. The coefficient was 0.9333 or minus 2.16 per cent. In Fig. 37 an 8-in. pipe 16 in. long was added between the enlarger and the Beth-Flow tube; the average coefficient was 0.9136 or minus 4.23 per cent. From Fig. 38 the corresponding values for the 8 X 6 in. Venturi meter were plus 7.80 and 3.75 per cent, respectively.

In order to bring out the effect of a rough upstream pipe, one layer of 1/4-in. mesh #18 wire in the form of a cylinder 8 in. OD

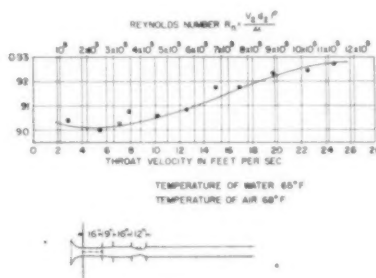


FIG. 37 TEST OF 8 X 6-IN. BETH-FLOW TUBE; EFFECT OF INSTALLATION

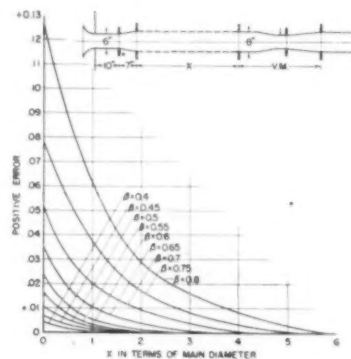


FIG. 38 EFFECT OF INSTALLATION ON VENTURI METERS

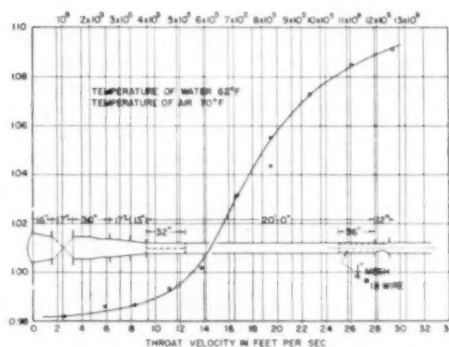


FIG. 39 TEST OF 8 X 6-IN. BETH-FLOW TUBE; EFFECT OF INSTALLATION

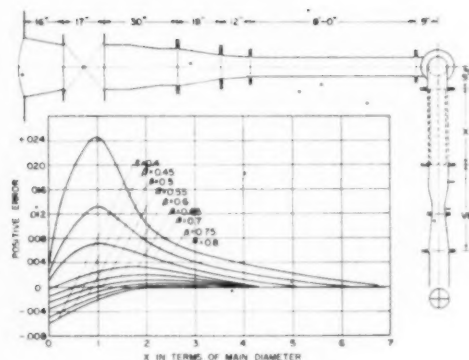


FIG. 40 EFFECT OF INSTALLATION ON VENTURI METER

and 36 in. long was placed immediately before the Beth-Flow tube as shown in Fig. 39. The average coefficient rose to 1.0297 or plus 6.9 per cent; the coefficient varied from 0.98-1.00. No similar test was made on the 8 × 6 in. Venturi meter.

Fig. 40 shows the effect on the Venturi meter of a cross-straightening vane after two elbows in planes at right angles. At six diameters we get the normal coefficient, therefore they do not affect the Venturi meter; see Fig. 27.

Fig. 41 is a collection of the foregoing data for comparative purpose.

The writer feels that if the Beth-Flow tube had been invented first what an earth-rocking invention Clemens Herschel's Venturi meter would have been.

VINCENT GENTILE, JR.⁴ Calibration of the 6 × 3½ in. type D flow tube at the Alden Hydraulic Laboratory, covered the following ranges:

Quantity.....	0.0249 cfs-2.517 cfs	(100-1)
Velocity.....	0.437 fps-44.0 fps	(100-1)
Head.....	0.0473 in. water-375 in. water	(7900-1)
Reynolds No....	7800-970,000	(124-1)

The coefficient of discharge, computed on the square-root basis, varies from approximately 0.925 at 970,000 to 0.90 at 100,000. Below that, its value drops off more rapidly.

Calibration of the 8 × 6 in. tube of the same type, at the University of Pennsylvania, covered the following ranges:

Quantity.....	0.196 cfs-6.03 cfs	(31-1)
Velocity.....	1 fps-31 fps	(31-1)
Head.....	0.203 in. water-196 in. water	(965-1)
Reynolds No....	40,000-1,300,000	(31-1)

Using the same basis as in the foregoing, the coefficient varies from 0.95 at 1,300,000 to 0.925 at 100,000, and 0.96 at 50,000. It should be noted, however, that when differentials are plotted versus capacity on log paper, all points lie on straight lines, indicating that over the entire ranges covered by these tests, the discharge coefficients remain constant if differentials are expressed to powers of velocity corresponding to slope of curves, Figs. 42 and 43 of this discussion.

Head meters, in general, do not, even for limited ranges, follow the square-root law exactly. On the other hand, practically any primary device will show a constant coefficient, if head is expressed to the proper exponent, over a range far in excess of the requirements of commercial metering, and broad enough to satisfy the most exacting demands of laboratory test work.

⁴ Brooklyn, N. Y.

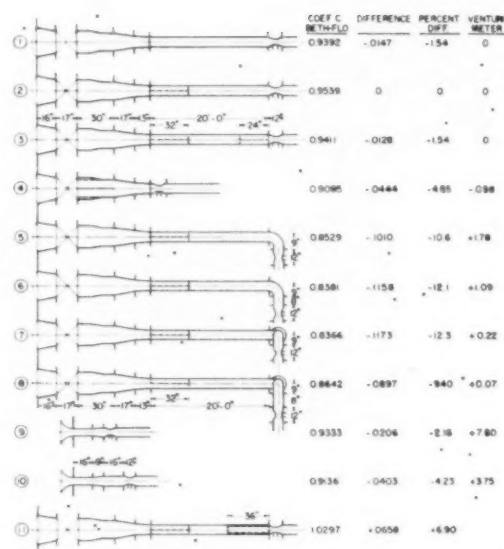


FIG. 41 SUMMARY OF TESTS ON 8 × 6-IN. BETH-FLOW TUBE FOR EFFECT OF INSTALLATION

The head developed by a primary device can be expressed by the equation

$$H = K h_v R^x$$

in which

K = calibration constant

h_v = velocity head $V^2/2g$

R = Reynolds number VD/ν

x = experimental exponent

By a simple transformation the formula for discharge becomes

$$Q = \frac{CA(2gH)^n Z^{(1-2n)}}{D^{(1-2n)}}$$

in which

C = discharge coefficient = $1/K^n$

A = area

Z = kinematic viscosity

D = diameter

$$n = \frac{1}{2 \times x}$$

For a meter of a given size, the formula can be simplified to

$$Q = C^* A (2gH)^n Z^{(1-2n)}$$

and for a given meter and fluid the expression finally reduces to

$$Q = C^* A (2gH)^n$$

The exponent n appears to vary with the type of primary device, with the D/d ratio, and probably with other factors that we know nothing at all about. It is slightly greater than $1/2$ for the type D flow tube, the nozzle, and the Venturi, and slightly less than $1/2$ for the orifice, and for the V and VD flow tubes.

If these test data are analyzed in this fashion, the type D flow tube has a demonstrated range of 30 to 1 in one case, and 100 to 1 in the other. The upper limits were governed in each case by the maximum flow capacity of the laboratory. From the direction of the log plots, it can be seen that the coefficients would have continued constant considerably beyond these ranges. It is

FIG. 42

FIG. 43

important
3 1/4 in. t
11,000 (1
the coef
numbers
is consid
head to

Logar
rational
obvious

The e
meters
static p
more di
a given
velocity
with ve
tude of
under e
ings for
the diff
tube th
ever th

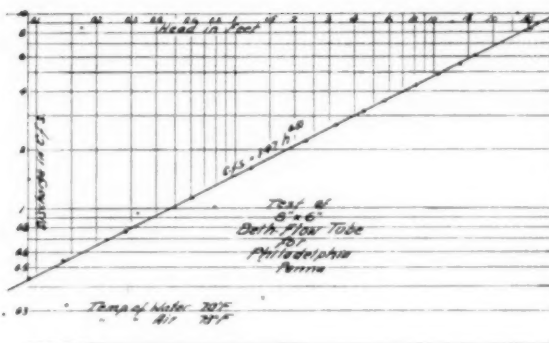


FIG. 42 TEST OF 8 X 6-IN. BETH-FLOW TUBE FOR CITY OF PHILADELPHIA

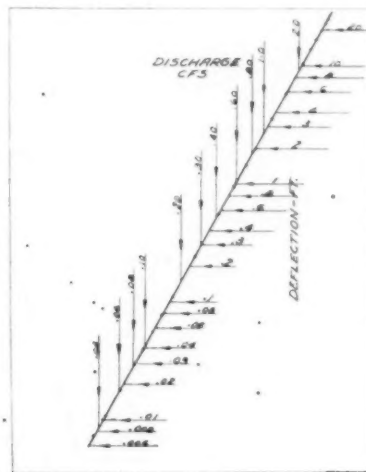


FIG. 43 LOG-LOG PLOT CALIBRATION OF 6 X 3 1/4-IN. SK 4 FLOW TUBE AT ALDEN HYDRAULIC LABORATORY

important to note that, on this basis, the coefficient of the 6 x 3 1/4 in. tube is virtually constant for all Reynolds numbers above 11,000 (lowest point on log plot), while on the square-root basis, the coefficient is only approximately constant for Reynolds numbers above 100,000. Thus the effective range of a meter is considerably increased by the simple expedient of expressing head to the proper power of velocity.

Logarithmic plots are useful, not only for furnishing a more rational basis for the study of fluid flow, but also to indicate obvious errors of measurement and observation.

The essential difference between the flow tube and other head meters is that total pressure differentials are used instead of static pressure differentials. It is submitted that this basis is more direct and less subject to error. The static pressure at a given section is equal to the total pressure minus the effective velocity pressure. But the effective velocity pressure varies with velocity distribution across the section and with the magnitude of rotative and translative components. Thus it is possible, under certain conditions, to obtain different static pressure readings for the same average flow across a section. In some cases the difference is small, in others it is appreciable. In the flow tube the static pressure cancels out whatever its value and whatever the factors contributing toward it. In the V and D tubes,

and even in modified designs of the VD tube, all readings are taken at the same section, the static pressure drops out of the equation, and the differential becomes a function of axial-velocity components, which, in turn, are proportional to mass flow. Moreover, since all readings are taken at the throat, where the velocity distribution is relatively flat, the effect of disturbed flow due to fittings is minimized. Further, since readings are taken all around the periphery, a high reading on one side will be partly compensated for by a correspondingly lower reading on the other. There is of course a theoretical error due to the fact that the average of the squares is not equal to the square of the average, but tests indicate that this is small and well within the required accuracies of commercial installations.

Tubes with a high D/d ratio will be least affected by installation. Also, the type D tube, due to straightening effect of streamlined nozzles, will perform more consistently than the others. Figs. 44 and 45, herewith, show head-capacity curves for

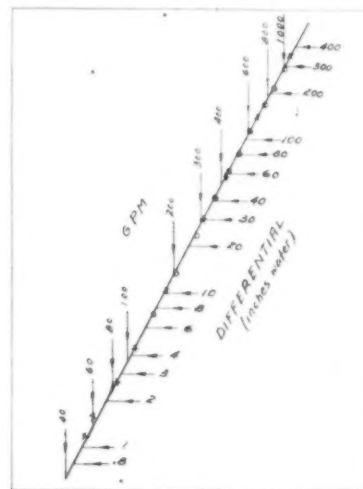


FIG. 44 CALIBRATION OF 6 X 3 1/4-IN. TYPE D FLOW TUBE FOR INSTALLATION

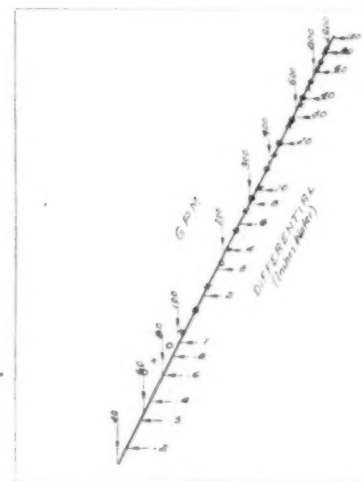


FIG. 45 CALIBRATION OF 6 X 3 1/4-IN. TYPE VD FLOW TUBE FOR INSTALLATION

the $6 \times 3\frac{1}{4}$ in. type D, and the $6 \times 3\frac{1}{2}$ in. type VD tubes (SK4 and SK5, respectively, in the paper), downstream from a compound elbow with a reducer between one elbow and the other. Even under these extreme conditions, there is no apparent change in coefficient. It is not concluded from this that straight-run calibrations can be used indiscriminately for any application, but rather that a flow tube of proper design will perform satisfactorily near an elbow or other fitting, if previously calibrated in a piping arrangement simulating the actual installation.

C. G. RICHARDSON.⁵ The writer served on the first Fluid Meters Committee. After 6 years of discussion, Part I of the committee's report was published. Later, a new committee produced Part III, dealing, in part, with the influence of installation on various types of commercial meters. It would seem that it has been amply proved that there is a great variation in the value and character of the Beth-Flow coefficients under approach conditions which have little, if any, effect on a standard Venturi tube. One does not see how the performance of the Beth-Flow can possibly be predicted unless it is volumetrically tested in a piping assembly duplicating the size, arrangement, and flow range of the final installation.

I. R. SCHWARTZ.⁶ An important criterion in evaluating any primary device of the head type is the pressure differential produced with a given flow for operating the secondary instrument. A simple analysis indicates that the Beth-Flow tube of the type with little or no contraction should produce much lower heads than any of the standard methods, viz., Venturi tube, nozzle, and orifice, for β ratios below about 0.8, and compares increasingly less favorably as the β ratio is decreased in the latter. For high enough initial velocities the Beth-Flow tube could provide adequate working-pressure differentials with almost no friction loss, but under these conditions would show little advantage over a simple Pitot meter. Both require individual calibration, in itself a rather serious drawback.

For low initial velocities it would seem necessary then to use a type with some contraction. Here the Beth-Flow tube should yield somewhat higher pressure heads than the standard device of the same contraction, but its friction loss is now comparable to that of the latter.

From these standpoints the writer fails to find wherein the Beth-Flow tube is superior, if not indeed inferior, to the usual more simple primary devices.

AUTHOR'S CLOSURE

The discussions of this paper add to the knowledge of the performance of Gentile-Flow tubes and are greatly appreciated. Professor Pardoe's test work in particular is a material contribution to the performance of one Gentile-Flow tube for flow conditions departing from the ideal. There are one or two points of his discussion that can be clarified slightly.

In Professor Pardoe's test results the performance of the two types of metering elements are compared on the basis of equal pipe diameters between the disturbing element to the inlet flange of the meter. This ignores the fact that the Gentile-Flow tube is much shorter than the Herschel Type Venturi Meter. If the comparison of performance were to take this into account the Gentile tube should be credited with the difference in length of the meters taken up with straight approach pipe between the disturbing element and the inlet flange of the meter. If this were done it would tend to reduce the magnitude of the deviations for

the Gentile Tube indicated in Professor Pardoe's table and make the comparison with the Venturi meter more favorable.

In test No. 11, the effect of pipe wall roughness on the performance of the flow tube is indicated, with a blank indicated for the performance of the Venturi. In our opinion the introduction of the screen wire along the wall of the pipe for several diameters upstream simulates to a degree the roughness effects that can be produced by tuberculation. The effect of pipe wall roughness on a Venturi coefficient was shown in one instance in a paper presented by Prof. C. M. Allen and the author, entitled, "Venturi and Weir Measurements." This paper was printed in *Mechanical Engineering* for June, 1935. It was shown at that time that the average Venturi coefficient for a 36×16 in. Herschel type meter started at .975 for a 36×16 in. Venturi meter when the penstock was clean. As the penstock and meter became more rusty the coefficient of the Venturi gradually dropped off to .954 in a period of 12 years. In 1934 a mossy growth was found developing in the penstock starting 25 ft upstream from the meter. The presence of this mossy growth dropped the coefficient from .954 to .945. Washing the moss from the penstock without disturbing the tubercles brought the coefficient back to the previously cited value of .954.

In the discussion of this paper Professor Pardoe cited the effect of tuberculation on a 12×6 in. Venturi meter in his own laboratory where the coefficient decreased from .976 with a clean pipe to approximately .962 for a tuberculated pipe after a period of approximately six years. It is seen therefore that there is some effect on a Venturi meter due to pipe wall roughness extending upstream. In this case, as in most of the other cases cited by Professor Pardoe, the effect on the Venturi coefficient is considerably smaller than the effect on the flow tube.

With respect to Mr. Gentile's use of the log-log plot of the deflection versus discharge for a flow tube, such a plot is customarily used to check an exponential formula. As Mr. Gentile points out, it is frequently found in hydraulics that by using a decimal power slightly different than a square or a square root, a formula is obtained in which the coefficient remains constant. The objection to this approach is that a formula involving a decimal power is usually less convenient to handle than one employing an even power. That, of course, is a matter of personal convenience and opinion. A log-log plot has a further advantage in that the results are presented with a constant accuracy, that is to say, a 10 per cent deviation from the curve at the lower range looks just as large as a 10 per cent deviation in the upper range which would not be true where deflection is plotted against discharge in rectilinear co-ordinates. Plotting the coefficient of the Venturi formula against throat velocity or Reynolds number also provides a curve in which deviations are shown with uniform accuracy over the range. In Professor Pardoe's presentation of coefficient values a space of one-half inch is customarily used to indicate a difference in coefficient of 1 per cent. To have a log-log plot of deflection against discharge indicate deviations with the same clarity would require a base length of 50 in. per cycle. It is seen, therefore, that where the presentation of results is to be made with a given constant accuracy the coefficient against throat velocity is a much more compact method than the log-log plot.

In closing, the valued discussions presented confirm the statement in the conclusion of the original paper that many more tests should be made before the coefficient of a Gentile flow tube can be predicted for various installation conditions. At the present time we quite agree with Mr. C. G. Richardson that the performance of a flow tube must be based upon a calibration duplicating the flow conditions of the final installation. Once calibrated, however, a Gentile-Flow tube should maintain its operating curve subject only to the effects of roughening of the pipe wall as stated above.

⁵ Vice-President, Builders Providence, Inc., Providence, R. I.

⁶ The Bristol Company, Waterbury, Conn.

The fir
ping tur
a paper
present
presentat

A TY
lo
of approx
system lo
variation
morning l
systems h
Edison Sy
maximum
necessity
there will
Waterside
Hudson A
000 kw, i
Furtherm
nightly w
lation at
F Genera
will run 2

The pr
sists of ac
or slightl
steam che
gear spee
be brought
safety in
in such a
chest me
To det
-ture duri
sections
Fig. 2 sl

¹ Mana
Company
² Gener
Company
³ Assist
solidated
⁴ "Quic
J. C. Fall
1948, pp.
Contri
Meeting,
SOCIETY
at a mee
NOTE:
understo
the Socie

Latest Technique for Quick Starts on Large Turbines and Boilers

By J. C. FALKNER,¹ D. W. NAPIER,² AND C. W. KELLSTEDT,³ NEW YORK, N. Y.

The first quick starts made on the 1200-psi 900 F topping turbines at the Waterside Station were described in a paper⁴ presented in June, 1947. The purpose of the present paper is to review the high lights of the earlier presentation and to relate the developments since then.

A TYPICAL Consolidated Edison System daily winter load cycle is represented in Fig. 1. It shows late evening winter peaks of about 2,500,000 kw, and minimum loads of approximately 700,000 kw during the 12 to 8 watch. The system load factor for 1948 was 53.1 per cent. The extreme variation in generation and also the high rate of pickup in the morning hours from 5 to 9 o'clock will be noted. While many systems have topping units similar to those on the Consolidated Edison System, few, if any, have this great difference between maximum and minimum daily loads, and are faced with the necessity of shutting down some toppers nightly. By 1952 there will be a total of ten topping units on the system; six at Waterside, two at Sherman Creek, one at Hell Gate, and one at Hudson Avenue, with a total generating capacity of over 1,000,000 kw, including the power generated by their exhaust steam. Furthermore, the number of toppers which are now shut down nightly will be greatly increased in the early 1950's by the installation at East River Station of two 120,000-kw, 1450-psi, 1000 F General Electric condensing machines, one of which at least will run 24 hr a day.

QUICK-START PROCEDURE

The principle of the quick-start procedure is simple and consists of admitting steam into a turbine at a temperature equal to or slightly higher than the metal temperature of the turbine steam chest. With the turbine generator operating at a turning-gear speed of 3 rpm, the turbine can then as a matter of routine be brought up to speed and synchronized to the bus with absolute safety in 12 to 15 min. The present practice is to load the unit in such a way that the rate of increase in the turbine steam chest metal temperature will not be over 100 F per hr.

To determine metal temperature changes in the turbine structure during the starts, thermocouples were installed over various sections of the turbine shells. The isometric sketch given in Fig. 2 shows the locations of the thermocouples installed on

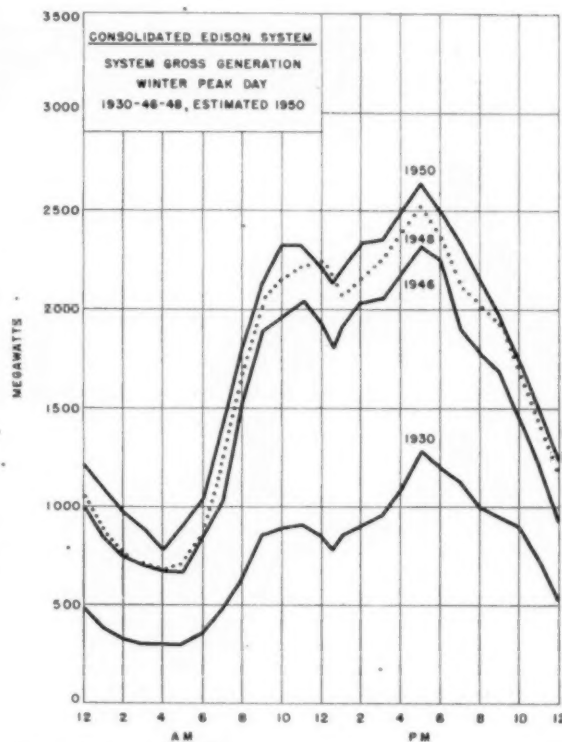


FIG. 1 CONSOLIDATED EDISON SYSTEM, GROSS GENERATION WINTER PEAK DAY FOR VARIOUS YEARS

No. 6, Westinghouse 65,000-kw unit at Waterside Station. Fig. 3 shows a comparison of steam and metal temperature changes in this machine during a quick and a normal start. Note, by observing thermocouple No. 1, how the quick start has practically eliminated the cooling which takes place during the normal or slow-start method. Fig. 4 shows another isometric sketch of No. 7 General Electric 65,000-kw unit with the locations of the thermocouples. Fig. 5 gives the comparative metal temperature change in No. 7 unit during a quick and a normal start. Again, notice in the quick start the absence of the cooling which takes place during the normal start.

Since the presentation of the first paper the practice of quick-starting topping units has been continued with improved technique, due mostly to better synchronizing of the operators' moves on the boilers, turbines, and high board. As of April 19, 1949, the number of quick starts made on the Waterside four topping units are as follows:

- 66 starts on No. 4—Westinghouse 53,000-kw unit
- 49 starts on No. 5—General Electric 53,000-kw unit
- 36 starts on No. 6—Westinghouse 65,000-kw unit
- 37 starts on No. 7—General Electric 65,000-kw unit

¹ Manager, Electric Production Department, Consolidated Edison Company of New York, Inc. Mem. ASME.

² General Superintendent, Waterside Station, Consolidated Edison Company of New York, Inc.

³ Assistant General Superintendent, Sherman Creek Station, Consolidated Edison Company of New York, Inc.

⁴ "Quick Starting of High-Pressure Steam-Turbine Units," by J. C. Falkner, R. S. Williams, and R. H. Hare, Trans. ASME, vol. 70, 1948, pp. 201-209.

Contributed by the Power Division and presented at the Spring Meeting, Washington, D. C., April 12-14, 1950, of THE AMERICAN SOCIETY OF MECHANICAL ENGINEERS. This paper was also presented at a meeting of the ASME Metropolitan Section on May 12, 1949.

NOTE: Statements and opinions advanced in papers are to be understood as individual expressions of their authors and not those of the Society. Paper No. 50—S-1.

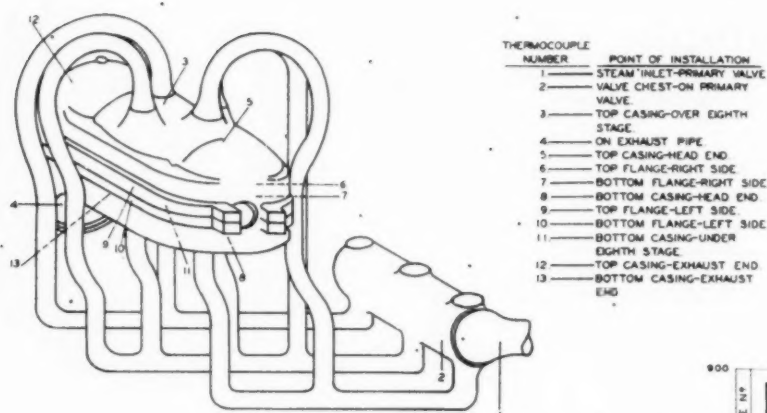


FIG. 2 (left) DIAGRAM SHOWING THERMOCOUPLES PEENED ON TURBINE CASING OF HIGH-PRESSURE UNIT NO. 6, WATERRSIDE STATION

INTERNAL CONDITION OF TOPPING UNIT AFTER 32 QUICK STARTS

Since the advent of quick-starting of topping units in April, 1946, the first opportunity which presented itself to observe the internal condition of one of these units occurred in 1948. It was brought about by an overhaul of No. 5 Unit at Waterrside, a 53,000-kw General Electric machine which, when removed from service, had had 46,000 hr of operation between November, 1942, and August, 1948. During this interval, No. 5 turbine underwent a total of 32 quick starts, 74 water washes, and 4 caustic washes. The inspection showed the spindle, buckets, nozzles, and diaphragms to be in exceptionally good condition. There was some evidence of very light spindle-shroud rubs on the leading edge, and the brightness of the rubs indicated them to be of recent origin. The thrust-bearing clearance was normal or 0.015 in., but the bearing fit which supports the thrust-bearing housing was worn and permitted an additional 0.017 to 0.020 in. axial movement of the spindle. Without a doubt, this wear together with the practice of water-washing caused the light rubs previously mentioned on the leading shroud edges. All nozzles, buckets, shrouding, and spindle were magnetically tested and no cracks were found. The spindle shaft, checked for truth, was within 0.001 in. From this inspection it was satisfactorily established to all concerned that the practice of quick starts and water-washing did not produce any detrimental effect on any part of the machine.

QUICK STARTS IMPROVE AXIAL DIFFERENTIALS

Fig. 6(a) shows the location of thermocouples on No. 5 high-pressure turbine.

Fig. 6(b), besides showing thermocouple temperature changes

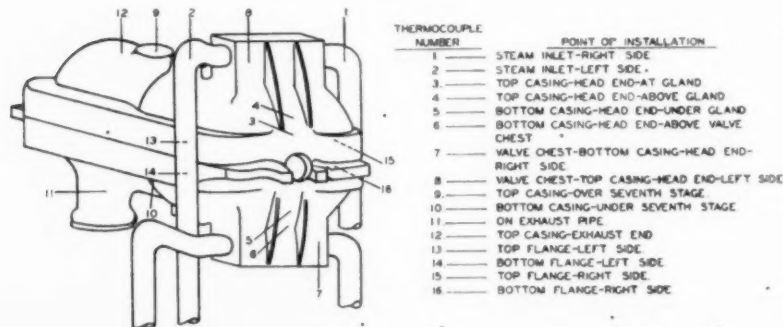


FIG. 4 (left) DIAGRAM SHOWING THERMOCOUPLES PEENED ON TURBINE CASING OF HIGH-PRESSURE UNIT NO. 7, WATERRSIDE STATION

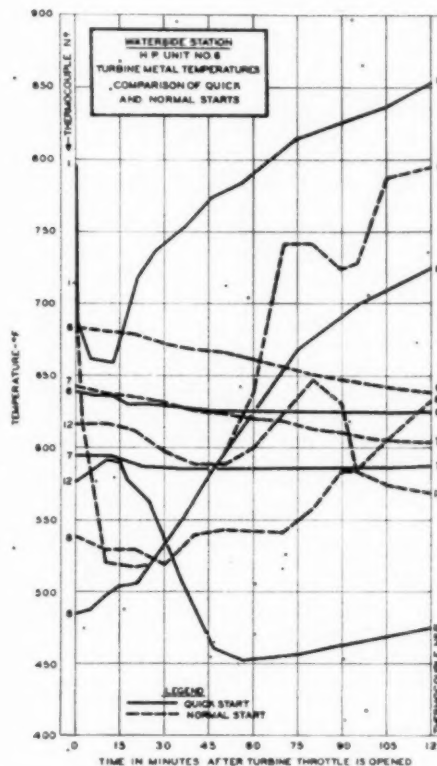


FIG. 3 COMPARISON OF QUICK AND NORMAL STARTS OF HIGH-PRESSURE UNIT NO. 6

FIG. 6 (a) THERMOCOUPLES PEENED ON TURBINE CASING

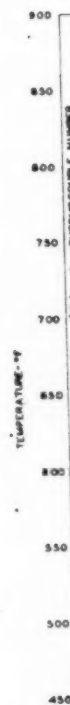


FIG. 6 (b) THERMOCOUPLES PEENED ON TURBINE CASING

during very i not be instru bine i differ strum inter pedes

FIG. 6 (a) (right) DIAGRAM SHOWING THERMOCOUPLES PEENED ON TURBINE CASING, HIGH-PRESSURE UNIT NO. 5, WATERSIDE STATION

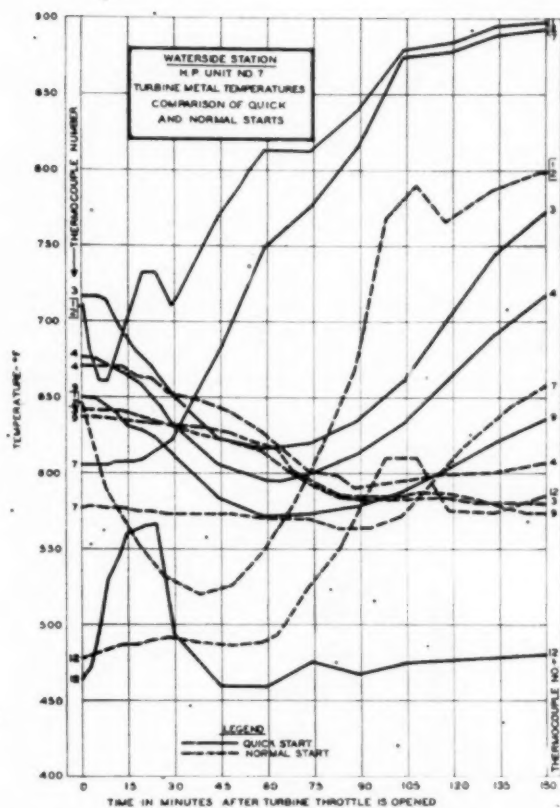
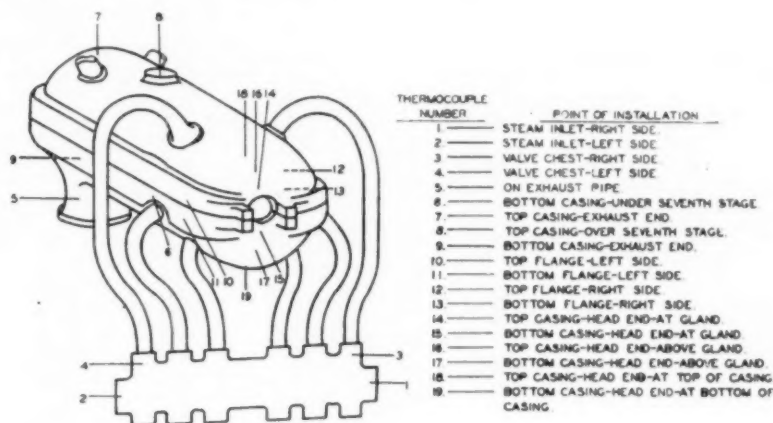


FIG. 5 COMPARISON OF QUICK AND NORMAL STARTS OF HIGH-PRESSURE UNIT NO. 7

during a recent quick start on No. 5 unit, also shows another very important factor in the quick-start procedure which could not be brought out in the initial presentation⁴ because of lack of instrumentation at the time of the earlier trials. On recent turbine installations the General Electric Company has furnished a differential-expansion recorder. The sensing element of the instrument consists of two magnetic coils mounted rigidly on the internal surface of the high-pressure-turbine exhaust-bearing pedestal with the pole faces of the coils set at given air gaps from

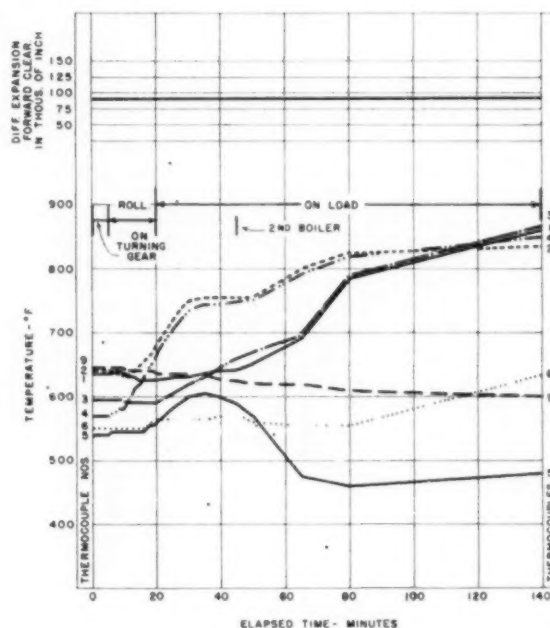


FIG. 6 (b) TURBINE METAL TEMPERATURES AND DIFFERENTIAL EXPANSION BETWEEN HIGH-PRESSURE SPINDLE AND CYLINDER DURING A QUICK START, HIGH-PRESSURE UNIT NO. 5, WATERSIDE STATION

the vertical faces of the solid coupling. With the spindle fixed axially in the front pedestal of the machine at the thrust bearing, the instrument records the relative change of internal axial clearances between spindle and cylinder during any operation. Because of its lighter mass and higher rate of heat absorption, the spindle length responds much faster to temperature change than does the heavy cylinder mass. Therefore, when a rapid cooling occurs, there is a possibility of rubbing on the entry side of the spindle blading. On No. 5 unit at Waterside Station, the differential-expansion recorder was installed in recent months and its magnetic coils were set with a governor-side air gap of 0.100 in., and a generator-side air gap of 0.150 in. With these settings the governor-side clearances of the first and last-stage wheels are 0.020 in. and 0.058 in., respectively. Note, in Fig. 6 (b), that there is absolutely no change in the axial relationship of spindle

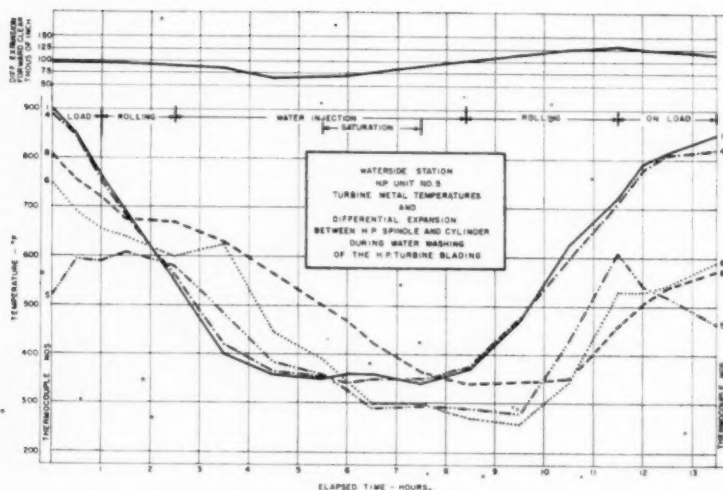


FIG. 7 (left) TURBINE METAL TEMPERATURES AND DIFFERENTIAL EXPANSION BETWEEN HIGH-PRESSURE SPINDLE AND CYLINDER DURING WATER-WASHING OF HIGH-PRESSURE TURBINE BLADING

and cylinder, thus proving beyond question that the quick-starting method of handling the turbine after an overnight shutdown is superior to the older slow-start procedure.

Fig. 7 shows what happens to the axial clearance during an overnight water wash and slow start. Note that the governor side, or forward clearance, decreases continuously as the machine cools down, and then begins to increase as the cylinder starts to cool and shrink, thereby bringing the axial clearance toward normal. The latter part of the differential expansion line shows what would happen to the clearances of the machine if it were started after an overnight shutdown with the slower-starting method, namely, the forward clearance first increases and then gradually decreases as the cylinder approaches spindle temperature.

WATER-WASHING

To digress a moment on the subject of turbine water-washing; the machines at Waterside Station foul up over a short period of time because of the large make-up needed to replace the steam sent out to the New York Steam Corporation. For several years it was the practice to shut down a topping unit on week ends when its capacity had dropped 5000 to 6000 kw, and water-wash the

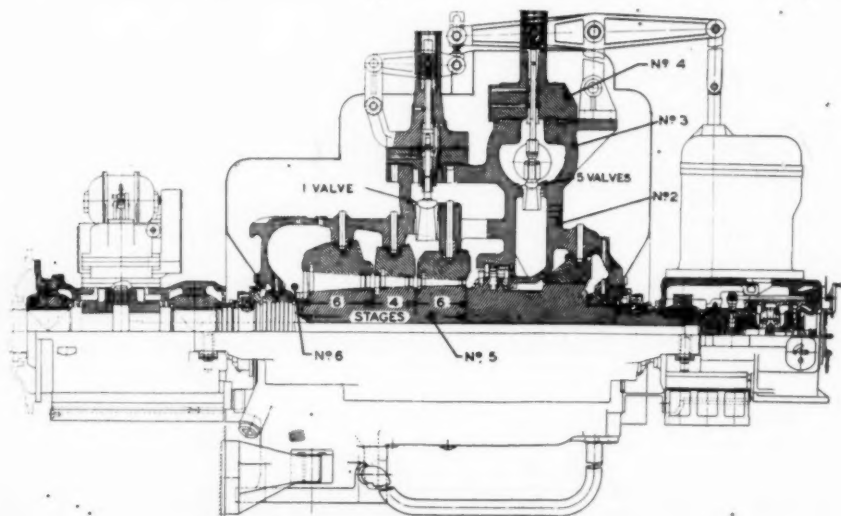
turbine blading at 400 to 500 rpm. Later it was found that a good wash result could be obtained by taking the units out of service overnight and injecting water while the machine was rolling at approximately 1000 rpm, gradually bringing the steam down to a saturation temperature, holding it saturated for 1 or 2 hr, and then gradually shutting off the water, bringing the machine up to speed, and increasing the steam temperature at a rate of 100 F per hr.

TRIALS AT SHERMAN CREEK

Success of the quick starts at Waterside Station led to further trials at Sherman Creek, where two 50,000-kw, 1600-psi, 950 F high-pressure units Nos. 9 and 10 are in operation. No. 9 unit is a Westinghouse machine which was installed in 1943, and No. 10 unit is a General Electric machine which was put in service in 1947. Each is supplied by a single boiler, rated at 1,000,000 lb of steam per hr.

All the quick starts made up to the present time at Sherman Creek have been on No. 9 unit, the first one being made on April 23, 1948. Since that time there have been 25 quick starts on this unit. No quick start has been made to date on No. 10

FIG. 8 (right) SUPERPOSED TURBINE-GENERATOR UNIT NO. 9, SHERMAN CREEK STATION (50,000-kw, 3600-rpm, 1600-psig, 950 F total temperature, 200-psig back pressure.)



unit because of boiler ignition difficulties. Experience at Waterside and the initial start at Sherman Creek indicated that it was not necessary to record any other temperatures but those of the steam temperature entering the turbine and the temperature of the outside metal of the governing valve chest ahead of the turbine nozzles. This latter point—point No. 2—is shown in Fig. 8.

Fig. 9 shows a section of No. 90 boiler. The steam passes from the superheater-outlet header to the turbine with only the turbine throttle in the circuit. Note the location of thermocouple No. 1 which gives the temperature of the steam entering the turbine and of the size of the drain line ahead of the throttle valve.

The boiler is tangentially fired with pulverized coal from three mills, each mill supplying one burner in each corner so that the four bottom burners are supplied by one mill, the four middle burners by the second, and the four top by a third.

Quick-starting of the single boiler unit at Sherman Creek introduced a different problem from that experienced at Waterside. The steam flow required to roll the topping turbines at full speed at Waterside is approximately 200,000 lb of steam per hr, and, at Sherman Creek, it is approximately 250,000 lb per hr. However, Waterside has had very little difficulty in obtaining a steam temperature at the start equal to that of the metal at the inlet of the turbine, because only one of the two boilers per unit is used at that time, and full-speed-no-load steam flow represents approximately 40 per cent of the full load rating of the Waterside boilers. However, at Sherman Creek, the full-speed-no-load steam flow is only 25 per cent of the full load rating of the boilers. This means that during the rolling period the superheater-outlet steam temperature at Sherman Creek is much lower than that obtained with the same flow on the smaller boilers at Waterside.

Fig. 10 shows the results of a slow start on No. 9 unit after a 4-hr shutdown. The rolling time after such a shutdown was 1 hr, and it can be seen that, after the throttle was opened and during the initial rolling period, the steam-chest metal temperature dropped during the first 35 min from 825 F to 570 F, or a total of 255 F, or again at a rate of 436 F per hr. It is also to be noted that the temperature fall was reversed 12 min after it had crossed the throttle-steam-temperature curve and rose from then on at approximately the same rate that it had fallen.

The quick-start procedure first used at Sherman Creek was similar to that at Waterside, but the firing of the boiler prior to

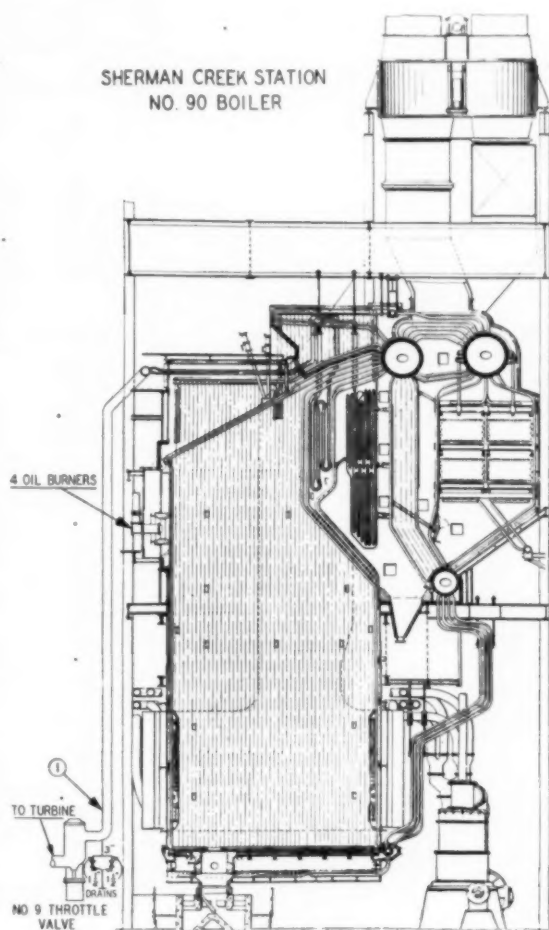


FIG. 9 NO. 90 BOILER, SHERMAN CREEK STATION

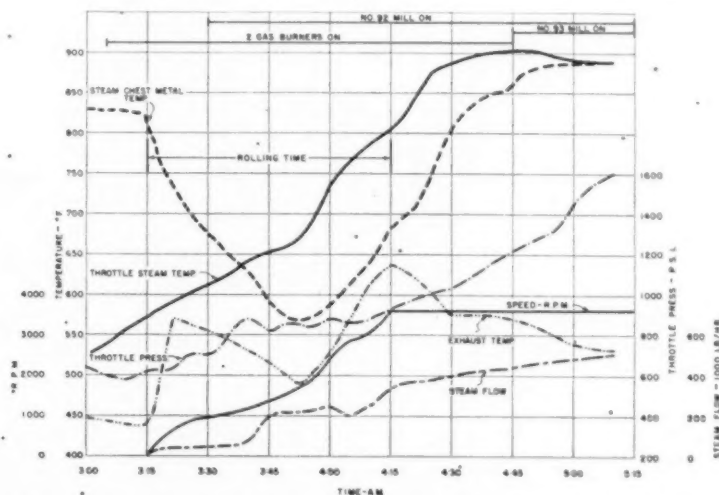


FIG. 10 SLOW START, NO OIL BURNERS, UNIT NO. 9, SHERMAN CREEK STATION, FEBRUARY 17, 1948

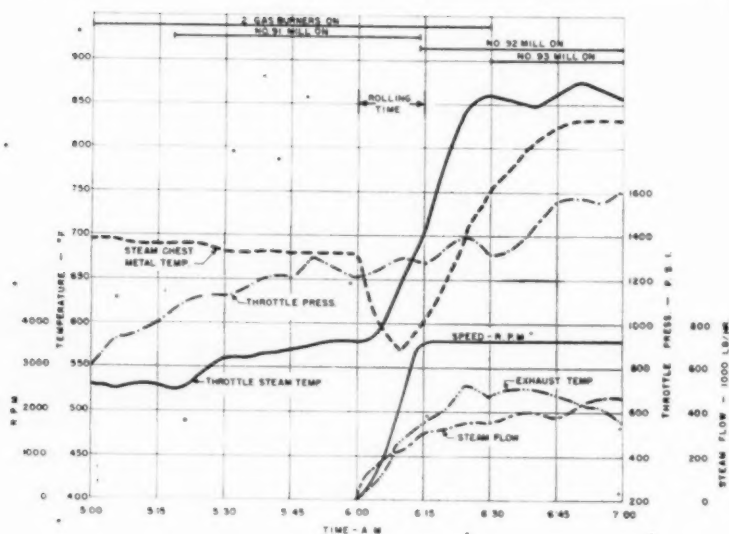


FIG. 11 (left) QUICK START USING NO OIL BURNERS, UNIT NO. 9, SHERMAN CREEK STATION, APRIL 23, 1948

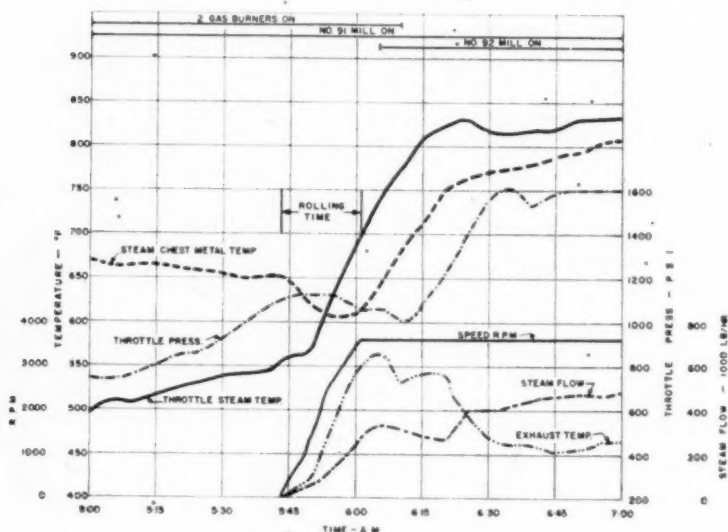


FIG. 12 (left) QUICK START USING NO OIL BURNERS, UNIT NO. 9, SHERMAN CREEK STATION, FEBRUARY 28, 1949

the rolling of the turbine was purposely made intermittent in order to avoid a sudden increase in boiler pressure, which would have resulted in a saturation-temperature rate of rise in excess of 100 F per hour which, according to the boiler manufacturers, would produce objectionable stresses in the walls of the boiler drums. The mill supplying the upper burners was used in order to obtain as high a gas temperature as possible, entering the superheater.

Results of the first quick start made on this unit are shown in Fig. 11. The steam-chest temperature dropped 106 F from 676 F to 570 F in the first 10 min of the rolling period and then increased from 255 F to 825 F in the following 35 min. This was an improvement in the magnitude of the temperature drop, partly because of the fact that the steam temperature at the start was 675 F or 150 F lower than on the afore-mentioned normal start, but there was no improvement in the temperature rise, this being still at the rate of 437 F per hr. This indicated the necessity for altering the procedure so that the steam tempera-

ture would be increased as rapidly as possible until the steam-chest temperature was on the upward trend, and then doing everything possible to keep this temperature rise at a slow rate after reaching that point. This was achieved by deliberately lowering the temperature of the steam leaving the boiler before the unit was taken off the line to obtain a lower turbine steam-chest temperature for the next start, and then using high excess air in order to obtain a larger volume of gas at a higher temperature entering the superheater before the throttle was opened. In order to slow down the temperature rise after the throttle was opened, the air flow was decreased and the mill supplying the lower burners was started, in place of the one supplying the upper burners, after the steam-chest temperature had begun its upward turn.

The improvements resulting from this procedure are shown in Fig. 12, which is the result of another start where the initial temperature of the steam chest was 650 F and the temperature reduction was only 40 F to 610 F after the throttle was opened.

Fig. 13
AUXILIARY
MATERIAL

Fig. 14

The
200
start
of th
oper
could
ture
shut
had
above
It
pend
ing t
elem
stea
mit
out
to a
resu

FIG. 13 (right) QUICK START USING FOUR AUXILIARY OIL BURNERS, UNIT NO. 9, SHERMAN CREEK STATION, MARCH 2, 1949

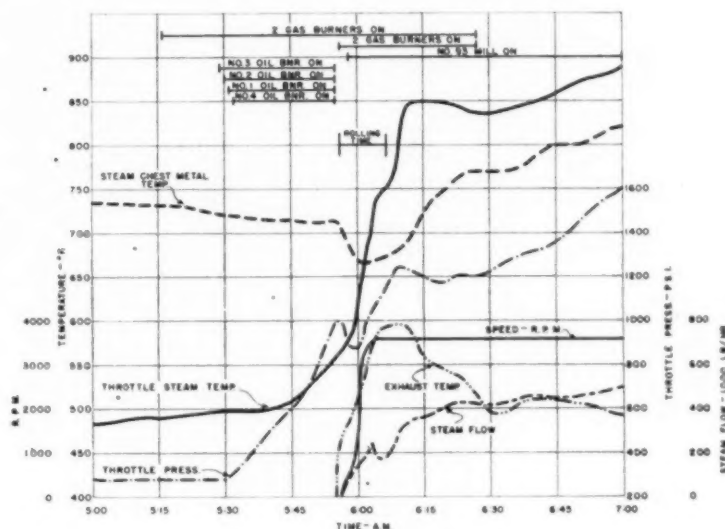
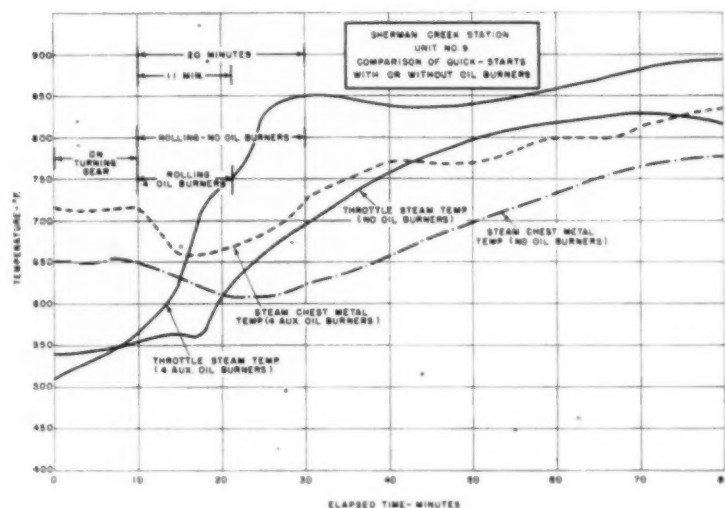


FIG. 14 (right) COMPARISON OF QUICK STARTS WITH OR WITHOUT OIL BURNERS



The temperature rise was 105 F in the first 20 min and only 200 F in the first hour. This of course was still not an ideal start, as it would have been preferable to have the temperature of the turbine at the time of its shutdown closer to its normal operating temperature. Then, if the initial steam temperature could have been brought up to this higher turbine-metal temperature at the start, the turbine-metal temperature change, from shutdown to load, would have been at a minimum. However, it had not been possible to obtain starting steam temperatures much above saturation up until this time.

It is felt that, due to the superheater design which is of the pendant type, steam condenses in the superheater elements during the bottled-up period, with the result that all but a few of the elements are full of water when it is time to start the unit. The steam drain provided in the main steam lead is too small to permit sufficient mass steam flow through the superheater to blow out the accumulated water and permit the superheater elements to act as designed, rather than as evaporating elements. As a result, the boiler pressure rose rapidly and soon reached a point

where the turbine throttle valve had to be opened, although the steam temperature was not yet equal to the turbine-metal temperature.

EXPERIMENTAL BURNERS ADDED TO NO. 90 BOILER

In an effort to increase this initial steam temperature, advantage was taken of openings which had been provided originally in the upper part of the furnace of No. 90 boiler for additional coal burners but were never used. Four oil burners were installed here, and these are shown in Fig. 9. It was thought that much higher steam temperatures would result and that the evaporation rate in the furnace walls would be cut down if the oil burners were used at the start rather than normal coal firing. Tests were made using these oil burners alone before a quick start was made and disclosed that a steam temperature of 900 F could be obtained with a steam flow of 220,000 lb per hr.

The results of a typical quick start using the oil burners are shown in Fig. 13. Here the initial steam-chest temperature was allowed to be much higher than had been the usual practice, or

720 F, and the rolling time was cut down to 10 min. The turbine metal temperature drop was from 720 F to 670 F or 50 F, and the rise was 100 F in 23 min and only 150 F in the first hour. As can be seen on the chart the steam temperature at the start was still only about 20 F above saturation, despite the use of the oil burners, and this temperature increased rapidly only after the throttle was opened, rising 105 F in the first 5 min. At the present time an additional by-pass around the turbine is being designed so that the superheater will be cleared of water, and the desired steam temperature will be obtained before opening the throttle. When this is installed the problem of steam-temperature control during starting will have been solved.

Fig. 14 shows the comparison of quick starts with and without the auxiliary front-wall oil burners.

Before closing the subject of quick starts on topping units, it must be emphasized that the rapid machine accelerations advocated in this paper apply only when the metal temperature of the high-pressure sections of the turbine have not fallen below the minimum of the range of the boiler steam-temperature control. In other words, after extended shutdowns the rolling time should be controlled by the time required to bring the temperatures of the high-pressure sections of the turbine up to the minimum steam temperature obtainable from the boiler at the rate of 100 F per hr. It is only when this condition of metal and steam temperature is fulfilled that the unit can be accelerated in approximately the same manner as practiced for quick starts. In the extreme case where a machine has been shut down for such a length of time that all its component parts have reached room temperature, this preheating must be done slowly on account of the large temperature differential existing between the turbine parts and the incoming steam. This initial heating may take several hours.

SHORTENING STARTING TIME ON LOW-PRESSURE CONDENSING UNITS

After the success of quick starts on topping units, consideration was given to shortening starting time on low-pressure condensing units all of which operate at throttle pressures between 400 psi and 200 psi.

A very complete paper⁵ on the subject of short starting of condensing units was reported in 1948, by H. P. Dahlstrand of the Allis Chalmers Company, to the Committee on Power Generation of the Association of Edison Illuminating Companies. In this paper the author summarized the requirements for short starts on condensing units as follows:

- 1 Keeping steam temperature as close to the normal as is practical during the removal of the load until the closing of the throttle valve.
- 2 Having the turning gear in operation during the whole of the shutdown period.
- 3 Maintaining temperatures of the turbine structure as close to shutting-down temperatures as practical until the unit is again started.
- 4 Checking the temperature at the inlet and the exhaust of the turbine structure.
- 5 Temperature of steam from the boiler should be about 100 F above the temperature of the cylinder at the inlet point.
- 6 Condensing equipment should be started before steam is admitted and cooling sprays in exhaust started at the same time.
- 7 Open the throttle valve and bring the turbine up to speed, synchronize, and put 10 to 25 per cent load on. During this time bring the vacuum up as fast as possible. The actual time for this operation should be determined with relation to the increase in steam temperature.
- 8 Increase the load at the specified rate and at the same time maintain the specified rate increase in steam temperature.

Mr. Dahlstrand showed actual starting time on an 80,000-kw reheat unit of 30 min and stated that this starting time was limited by the time required to obtain the necessary vacuum. The author sums up his paper with the sentence, "The starting time after short shutdowns is largely dependent upon the control of inlet steam temperature and vacuum, which means that any starting procedure for a given steam-turbine generating unit must be worked out with full consideration of the boiler and condenser characteristics."

The first Consolidated Edison Company low-pressure condensing

⁵ "Frequent Starting and Shutting Down of High-Temperature Steam Turbines," by H. P. Dahlstrand, February, 1948.

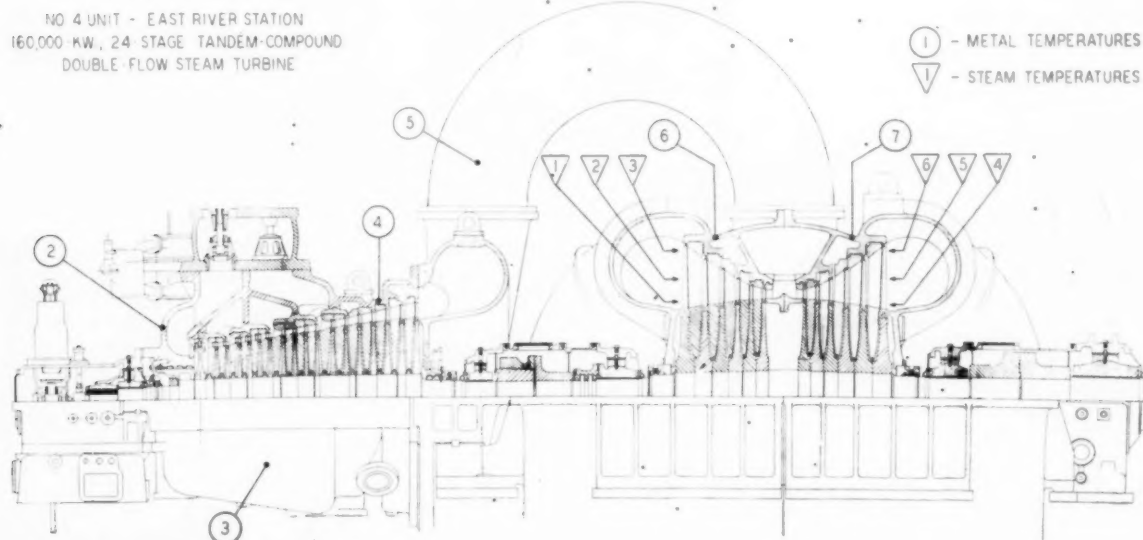
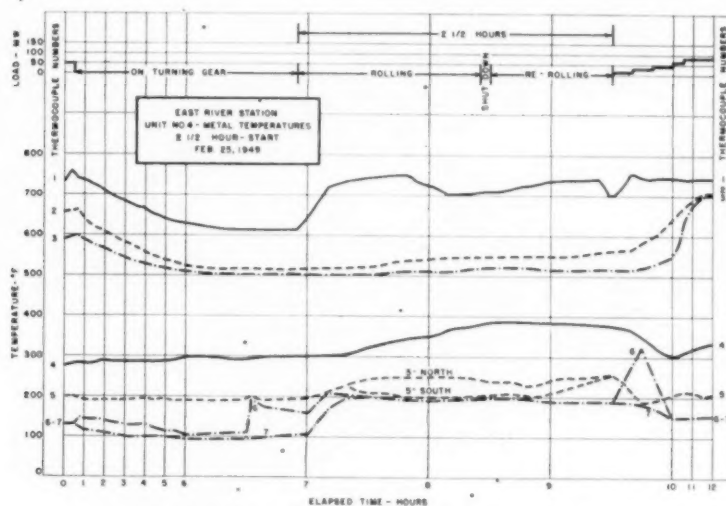
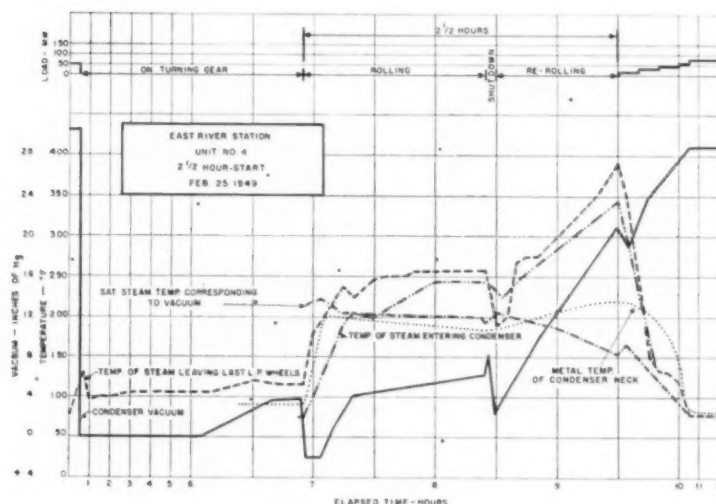


FIG. 15 160,000-KW, 24-STAGE TANDEM-COMPOUND DOUBLE-FLOW STEAM TURBINE, NO. 4 UNIT, EAST RIVER STATION

FIG. 16 METAL TEMPERATURES, $2\frac{1}{2}$ -Hr START, UNIT No. 4FIG. 17 $2\frac{1}{2}$ -Hr START, UNIT No. 4

ing machine on which quick-start trials were made was the No. 4, 160,000-kw, tandem-compound, General Electric unit at East River Station. Fig. 15 shows the location of thermocouples throughout the machine. Note particularly the thermocouples which are located in the path of the steam exhausting from the last wheels of the unit, because, in later illustrations, the temperatures recorded at these points are of considerable interest. In the early history of this machine which was initially operated in September, 1929, before the advent of turning gears, the practice was to take $2\frac{1}{2}$ hr to start, even after an overnight shutdown. While this practice is no longer in vogue since the installation of a turning gear, a test start run was made recently to learn what temperature changes took place throughout the machine during a $2\frac{1}{2}$ -hr start. Fig. 16 shows that, under this early starting method, the rates of temperature changes at the high-pressure end of the unit were very gradual. The sudden increase and decrease in temperature on point 6 while the machine is being loaded after about 10 hr of elapsed time is due to the high-pres-

sure gland leak-off being connected to the bleed piping at a point between the 21st stage bleed in the cylinder and the bleed valve. This sudden rise in temperature is due, therefore, to the pressure building up in the high-pressure packing as load increases on the machine and hot steam flowing from the packing into the bleed belt with the bleed-valve shut off. The sudden drop occurs when the bleed valve is opened, and the leak-off steam is diverted to the heater.

The shutdown indicated in the rolling period in Fig. 16 was a part of the Consolidated Edison procedure to preheat some of its generator fields before bringing these machines up to speed. During the brief shutdown period, the centrifugal force which locks the field coils is relieved and these coils are permitted to expand freely to their desired length. This has the double advantage of eliminating the possibility of stressing the coil material beyond its elastic limit in the coil sections embedded in the field slots and of reducing field end-turn distortion. Recently this procedure was changed on this machine, and the present

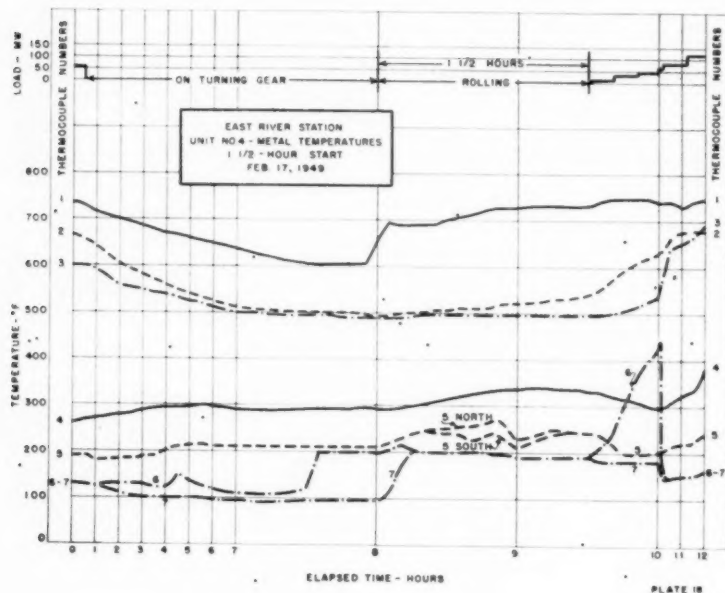


FIG. 18 (left) METAL TEMPERATURES, $1\frac{1}{2}$ -HR START, UNIT NO. 4

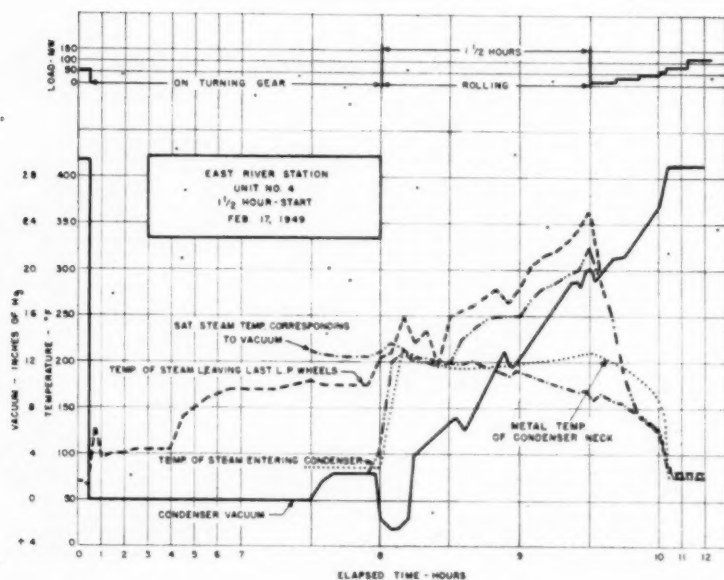


FIG. 19 (left) $1\frac{1}{2}$ -HR START, UNIT NO. 4

practice consists of doing all the preheating while the unit is on turning gear before starting.

Fig. 17 shows the extreme temperature changes which occurred during the starting cycle under the original starting procedure, due to the low vacuum and the reheating of the steam in the exhaust by windage from the large exhaust wheels, which on this machine have a tip speed of 1015 fps. In the early days it was the practice to build up the vacuum slowly as shown by the vacuum curve. Note the two sudden decreases in vacuum when steam is admitted to the turbine. As the spindle accelerates, observe that the temperature of steam entering the condenser rises rapidly, reaches a temperature corresponding to condenser vacuum, and then begins to be reheated, finally reaching a maximum temperature of 340 F. The temperature of the exhaust

steam $1\frac{1}{2}$ in. away from the last stage wheels reaches approximately a maximum of 390 F. These maximum temperatures are followed by very sudden decreases in temperature at a rate of about 800 F per hr as the vacuum is rapidly established, after the machine has been synchronized and sufficient steam flow passes through the turbine to cool the buckets. With this rapid cooling it is surprising that no casing cracking had been experienced under the induced thermal stresses, when considering that the exhaust shells are made of thin cast-iron sections and very heavy flanges. Perhaps modern-day limitations of 100 F temperature change per hr as suggested by some manufacturers are overconservative.

After a turning gear was installed on No. 4 at East River in November, 1939, to keep the spindle turning during shutdown



FIG. 18 (right)



FIG. 19 (right)

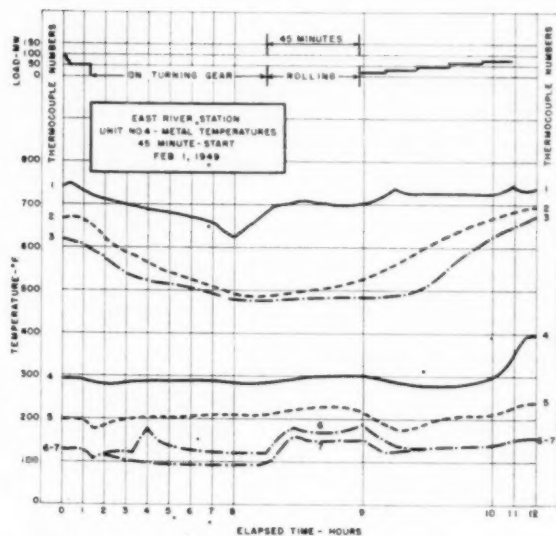


FIG. 20 METAL TEMPERATURES, 45-MIN START, UNIT NO. 4

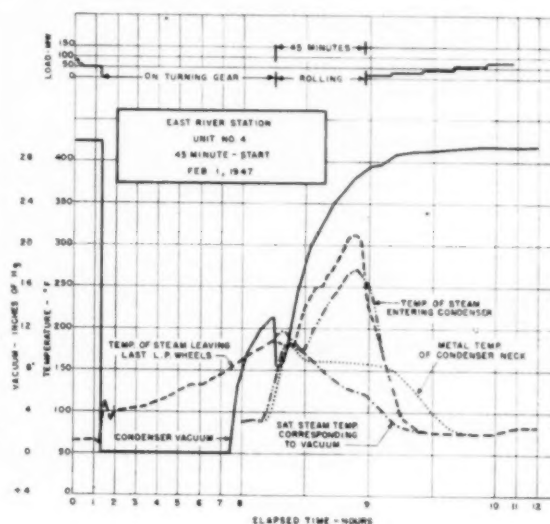


FIG. 21 45-MIN START, UNIT NO. 4

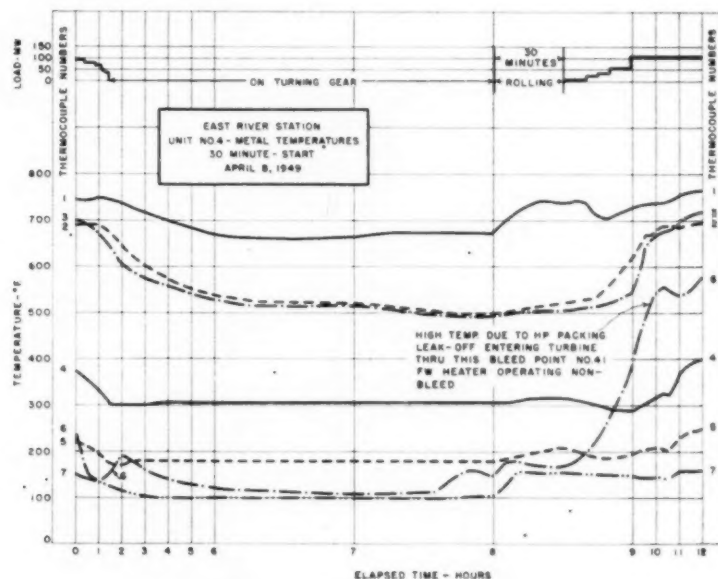


FIG. 22 METAL TEMPERATURES, 30-MIN START, UNIT NO. 4

and assure a minimum eccentricity at time of start, the starting time was reduced to $1\frac{1}{2}$ hr. Fig. 18 shows the high-pressure-cylinder temperature changes during this shorter start. Note the same occurrence of a sharp rise and fall in the bleed-belt temperature as reviewed in the figures covering the $2\frac{1}{2}$ -hr start. Points 2 and 3 show a somewhat more rapid rise in temperature at the high-pressure end of the machine than in the $2\frac{1}{2}$ -hr start, due to more rapid loading for a short period.

Fig. 19 shows the exhaust-end condition for the $1\frac{1}{2}$ -hr start. Again, note the reheating of the steam, which reaches a maximum of 365 F with the machine at full speed just prior to loading. As in the case of the $2\frac{1}{2}$ -hr start, there is cooling of the exhaust end at the high rate of 800 F per hr.

Fig. 20 shows the temperature changes which take place in the high-pressure element during a $\frac{3}{4}$ -hr start to be quite gradual. Note that point 6 shows no sudden rise and fall in temperature as in the case of the $2\frac{1}{2}$ -hr and $1\frac{1}{2}$ -hr starts, owing to the bleed heater being in service during all of the rolling and loading period.

Fig. 21 shows the temperature and vacuum changes at the exhaust end of the unit. The exhaust temperature again rises and falls rapidly but takes place during a shorter time interval. However, it is to be noted that the peak temperature reached is approximately 30 to 40 F lower than in the case of the $2\frac{1}{2}$ -hr start.

Fig. 22 shows the temperature changes in the high-pressure cylinder during a $\frac{1}{2}$ -hr start. Again, there are no excessive

rates of temperature change in the high-pressure end of the machine. Note the sharp rise in temperature of point 6 on the 21st stage bleed belt while the companion point 7 remains relatively constant. During this start, the 21st-stage heater was out of commission for repairs, and the high-pressure packing leak-off is reheating the steam in the 21st-stage bleed belt. Consideration is being given to making supplementary piping connections so that this uneven temperature condition in the low-pressure cylinder can be avoided.

Fig. 23 shows the low-pressure-end conditions during this half-hour quick start and, again, there is the pronounced rise and fall in temperature of the last-stage buckets.

Fig. 24 shows a comparison of the exhaust-end heating and cooling characteristics during all of the starts, and the gradual falling of the peak temperatures at the last-stage buckets as the starting time is shortened.

CONCLUSION

It has been calculated that if quick-starting could be reduced to 15 min or less on all topping and condensing machines on the Consolidated Edison System, an annual saving of approximately \$250,000 would result. This saving is made up of auxiliary power, stack and river losses, and fuel fed to the furnaces.

In addition to the operating saving just mentioned, there are many practical operating advantages which result from quick-starting. A notable instance occurred, on August 27, 1948, when the Manhattan Cooper Square network was de-energized because of failures of simultaneous outages in Waterside No. 2 of the four topping units in this station. As soon as the first generator cables were temporarily repaired on unit No. 4, this machine was brought up to speed and was generating power in less than 15 min, and the network re-energized. If the old original 3-hr start had still been in vogue at the time, the network would have remained out of service at least 2 1/4 hr longer.

On April 18, 1949, with simultaneous forced outages of the two topping units at Sherman Creek, No. 9 unit was restored to service in 22 min, after having been shut down for 11 hr.

To a certain extent, the short starting time relieves the problem on the turbine-room floor of each station in the early morning.

At that time it is customary to have two or three machines in the process of slow rolling preparatory to their going on load. With the quick-starting technique perfected it would be possible to put machines in service one after the other. Fewer men could

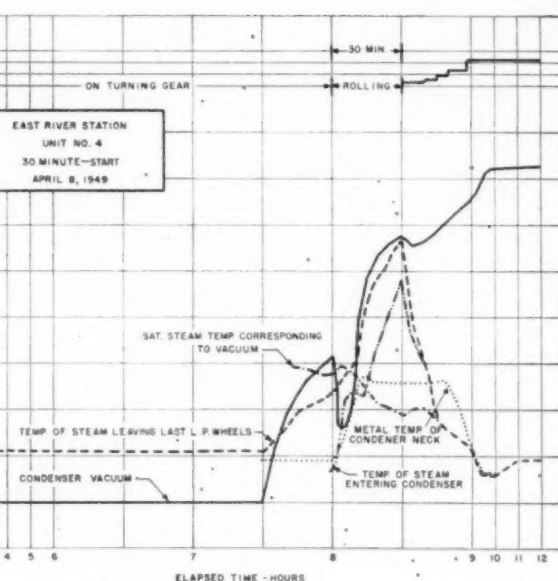


FIG. 23 30-MIN START, UNIT NO. 4

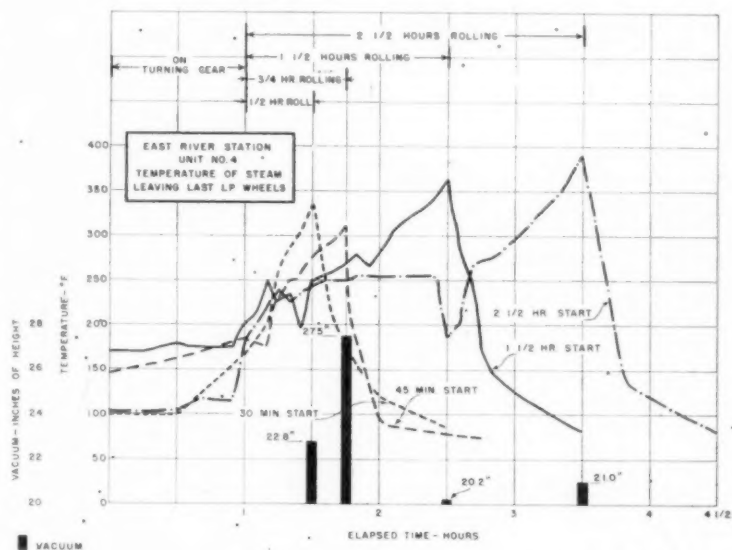


FIG. 24 TEMPERATURE OF STEAM LEAVING LAST LOW-PRESSURE WHEELS, UNIT NO. 4

focus their main attention on only one machine, instead of several.

It is fully expected that the starts discussed in this paper ultimately will be reduced to 5 min or less and will be followed by faster rates of loading in the first few minutes, thus reducing the heating and cooling of the exhaust ends. Work is now in progress on quick-starting of all the various types of condensing machines on the system.

Supplement⁶

As stated in the previous papers,⁶ the principle of the quick-start procedure is simple, and consists of admitting steam into a turbine at a temperature equal to or higher than the metal temperature of the heavy section of the machine. The purpose of matching these temperatures is to eliminate or minimize practically all of the thermal shock coincident with the start of a turbine generator. The degree of success obtained in this direction is shown in Fig. 25 of this supplement, in which the data for quick starts, transposed from Figs. 3 and 5 of the paper, are compared with the most recent data obtained on units Nos. 6 and 7 at Waterside Station. It can be seen that with experience and better co-ordination of sequential operations during the start, an even closer matching of the temperatures of the incoming steam and of the turbine shell is now realized.

The first 15-min quick start was made on No. 4 Westinghouse topping unit at Waterside on June 25, 1946. Since that time

⁶ The original paper on quick starting of boilers and turbines was delivered before the ASME Semi-Annual Meeting, Chicago, Ill., June, 1947, as paper No. 47-SA-18. (See Trans. ASME, vol. 70, 1948, pp. 201-209.) A second paper, which was a review of the progress made since the first one was written, was presented at an ASME Metropolitan Section Meeting in May, 1949, and again at the 1950 ASME Spring Meeting, as paper No. 50-S-1. The material contained in the supplement was not available for inclusion in the preprint for the 1950 ASME Spring Meeting and has been added in the final publication.

and up to March 15, 1950, over 1000 quick starts as shown in Table 1 have been performed without the slightest indication of trouble.

TABLE 1 RECORD OF QUICK STARTS ON TOPPING AND CONDENSING MACHINES

Unit	Station	Manufacturer	Description	No. of quick starts
TOPPING UNITS				
No. 4	Waterside	Westinghouse	53 Mw 1200 psi 925 F	106
No. 5	Waterside	General Electric	53 Mw 1200 psi 925 F	79
No. 6	Waterside	Westinghouse	65 Mw 1250 psi 925 F	76
No. 7	Waterside	General Electric	65 Mw 1250 psi 925 F	53
No. 9	Sherman Creek	Westinghouse	30 Mw 1600 psi 950 F	53
Total number of quick starts on topping machines.....				367
CONDENSING UNITS				
No. 14	Waterside	General Electric	60 Mw 185 psi 500 F	74
No. 15	Waterside	General Electric	60 Mw 185 psi 500 F	106
No. 1	East River	General Electric	60 Mw 400 psi 725 F	78 ^a
No. 2	East River	General Electric	60 Mw 400 psi 725 F	89 ^a
No. 4	East River	General Electric	160 Mw 400 psi 725 F	270
No. 1	Hudson Ave.	General Electric	50 Mw 265 psi 611 F	6
No. 4	Hudson Ave.	Westinghouse	80 Mw 425 psi 725 F	26
No. 5	Hudson Ave.	Westinghouse	110 Mw 425 psi 725 F	47
No. 6	Hudson Ave.	Westinghouse	110 Mw 425 psi 725 F	57
Total number of quick starts on condensing machines.....				753
Total number of quick starts on topping and condensing units.....				1120

^a In addition to the 15-min starts listed for units Nos. 1 and 2 at East River Station, there have been 617 and 552 30-min starts, respectively, since July 17, 1947.

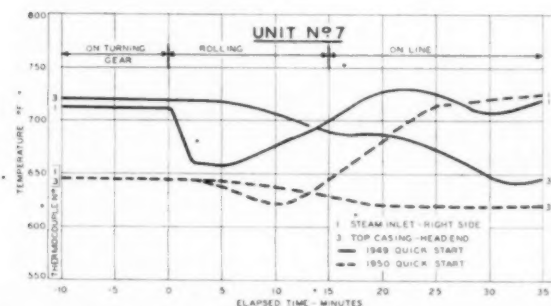
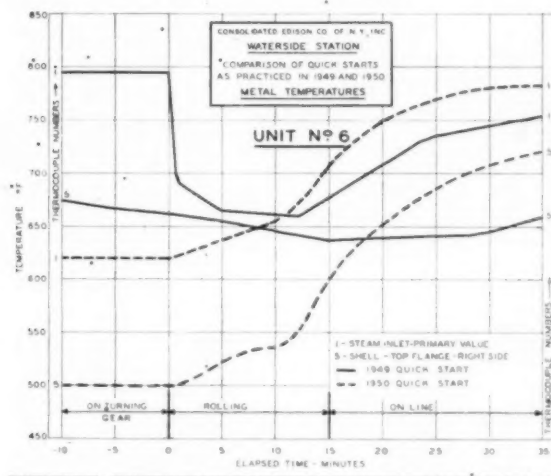


FIG. 25 COMPARISON OF QUICK STARTS AS PRACTICED IN 1949 AND 1950 AT WATERSIDE STATION

Since the 1947 paper,⁶ ten machines have been added to the list of those on routine of quick starting after overnight shut-downs. All of the units listed are started in 15 min with the exception of No. 4 tandem-compound 160,000-kw condensing unit at East River Station which is now started in 20 min. Reducing the quick-start time of this large tandem-compound unit from the 30 min, as given in the present paper, has still further improved its starting-up operation.

The decision to shorten the rolling period of a unit is not taken arbitrarily. On the contrary, data including the shell-metal temperature gradient, expansion, vacuum, and the operator's observations on the normal long-roll start are first carefully studied. If there is nothing in the data that shows it would be detrimental to shorten the starting time, instructions are issued to make the next start in 10 to 15 min less. Again, the record of the shorter start is analyzed and a second shortening of time is made. This procedure is repeated until the time is finally reduced to 15 min.

We limit the starting time to 15 min because it is felt this is the minimum which still gives the operator a comfortable period to observe the machine as it accelerates. Fundamentally, in so far as the unit is concerned, it is believed that it could be accelerated as fast as dry steam can be supplied to it.

The first application of the quick-start procedure on one of our cross-compound machines was made on No. 6 Westinghouse, 110,000-kw, 425-psi, 725 F condensing unit at Hudson Avenue early in 1950. Fig. 26 shows a cross section of each element together with the location of the test thermocouples. The machine receives its steam from a common header system, which is an ideal arrangement for quick starting because the steam temperature at the start is at all times above that of the metal parts of the front end of the high-pressure turbine, assuming, of course, that one or more boilers are operated in the station throughout the night. The high-pressure element of this unit is also well suited for quick starting because of its double-shell construction. In this type of machine only the nozzle block or steam bowl is exposed to high temperatures during starting. The main cylinder structure

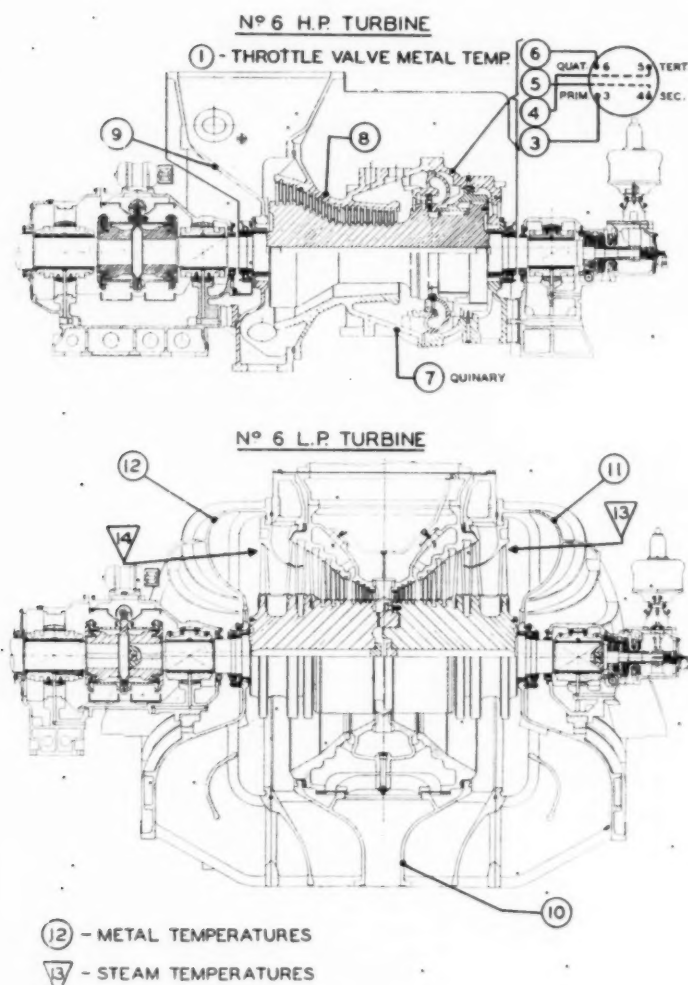


FIG. 26 110-MW CROSS-COMPOUND WESTINGHOUSE UNIT NO. 6, HUDSON AVENUE STATION
(1800 rpm, 400 psi, 730 F.)

is in contact with steam which is at a relatively low temperature after having expanded through the impulse section. Hence the temperature of the governor end of the high-pressure cylinder, as indicated by points 3, 4, 5, and 6 in Fig. 27, shows no appreciable change in the long slow roll period so that nothing is being accomplished in so far as expansion or contraction of the high-pressure cylinder is concerned. Points 11, 12, 13, and 14, the former two in the exhaust shell and the latter two in the steam path immediately adjacent to the exhaust of the last-stage wheel, indicate peak temperatures in the metal of 195 F and in the steam path of 335 F.

Fig. 28, which shows the comparative temperature conditions during the 15-min quick start, indicates even less change in high-pressure shell temperatures than occurred during the long slow roll, and the peak temperatures previously referred to in the low-pressure element have been lowered to 165 F and 290 F, respectively.

While the common header system lends itself to quick starting by delivering steam which is always hotter than the turbine shells, such is not the case on unit systems because the steam tempera-

ture leaving the superheater of our unit boilers is always lower than desired until sufficient mass gas flow and gas temperature can be attained at the superheater. In this respect it is well to remark here that one of the fallacies in the thinking of many operators is that little or no metal stress develops in the turbine when the unit is started immediately after an accidental shutdown. Test has demonstrated that even after a shutdown of a few minutes, the turbine temperature may be several hundred degrees hotter than the entering steam on restarting. Under this condition the turbine spindle with its higher rate of heat transfer cools off faster than the turbine shell, and a possible forward axial rub may result.

By the summer of 1950 we shall have installed on all of our single-boiler single-turbine topping units, turbine by-passes so that steam will be introduced into the turbine only when it reaches a temperature 50 F to 100 F hotter than the turbine shell. This design feature, besides taking care of the temperature relation on quick starting, will also handle the operating condition of restarting immediately after a brief outage of a few minutes.

In 1949 Messrs. Stanford Neal of the General Electric Com-

TEMPERATURE °F
700
600
500
400
300
200
100
0

pany
Com
mad
Stat
been
tion
strai
com
tests
give

7
Gen
72, 1

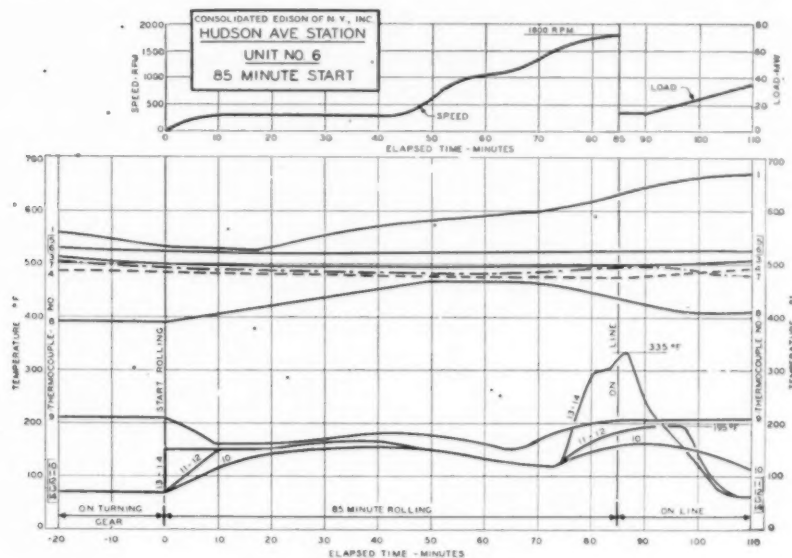


FIG. 27 85-MIN START, UNIT NO. 6, HUDSON AVENUE STATION

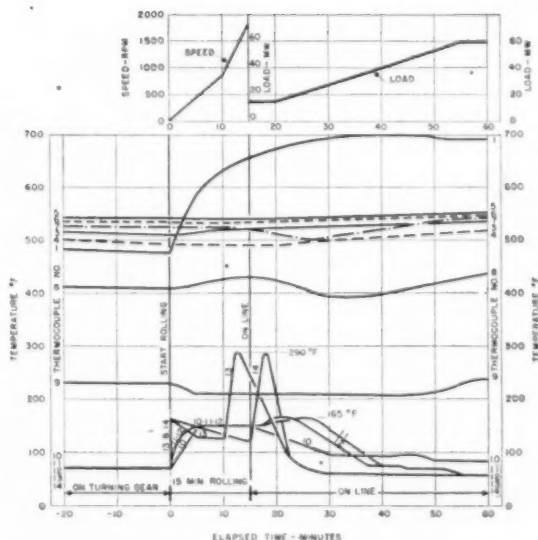


FIG. 28 15-MIN START, UNIT NO. 6, HUDSON AVENUE STATION

pany and V. S. Renton of the Public Service Electric and Gas Company of New Jersey presented⁷ the results of extensive tests made on a new 100,000-kw condensing unit installed in the Essex Station of the Public Service Company of New Jersey. It has been encouraging to find in the authors' discussion a confirmation of our belief that the quick-starting procedure imposes less strain on the turbine structure than does the starting method commonly practiced in the industry today. It is our hope that tests of this sort by other operators, as well as the endorsement given by Mr. Dahlstrand of the Allis-Chalmers Manufacturing

Company, will add to the present knowledge of quick starting and faster loading of turbines.

QUICK STARTING OF TURBINES AFTER WEEK-END SHUTDOWN

All of the turbine quick-starting investigations which we have made to date and reported in our previous papers⁴ have been based on starts after overnight shutdowns.

Recently, after a week-end shutdown we had an opportunity to observe the changes which occurred in No. 9 turbine at Waterside while quick-starting its boiler.

Fig. 29 shows a cross section of this 50,000-kw, 1600-psi, 950-F Westinghouse topping turbine, together with the locations of the thermocouples used during this quick start from cold test.

Fig. 31 shows the turbine metal temperatures, pressures, speed, and differential-expansion readings obtained. Relatively low rates of metal-temperature rise occurred in the turbine metal structure during the rolling period. However, as the load was increased at the rate of 1 mw per min above 13,000 mw, the impulse chamber pressure and temperature rose very rapidly; the latter temperature, represented by point No. 9, increased at the rate of 450 F per hr. Point No. 8, located on the outer skin of the massive horizontal flange of the main cylinder joint in line axially with point No. 9 in the impulse chamber, shows an extreme temperature lag. Very high compression stresses occur at the inner main-joint surfaces as the result of this marked temperature gradient across the joint face, and the manufacturer is studying the problem.

The differential-expansion curve shows that the axial clearances between the cylinder and spindle increased by only 50 mils during the rolling period. As the unit was loaded, the exhaust-end temperature dropped rapidly, causing the clearances to reduce gradually toward the normal running values.

SHUTTING DOWN AND STARTING OF HIGH-PRESSURE BOILERS

Now that we have the turbine and boiler procedure for quick starting after overnight shutdown satisfactorily solved, we are looking into the problem of starting boilers and turbines after shutdowns when the boiler pressure is reduced either to zero or to a very low value. This boiler-starting condition is entirely dif-

⁷ "Operating Characteristics of the 100,000-Kw Essex Turbine Generator," by Stanford Neal and V. S. Renton, Trans. ASME, vol. 72, 1950, p. 267.

3600 RPM-1600 PSI-950 °F

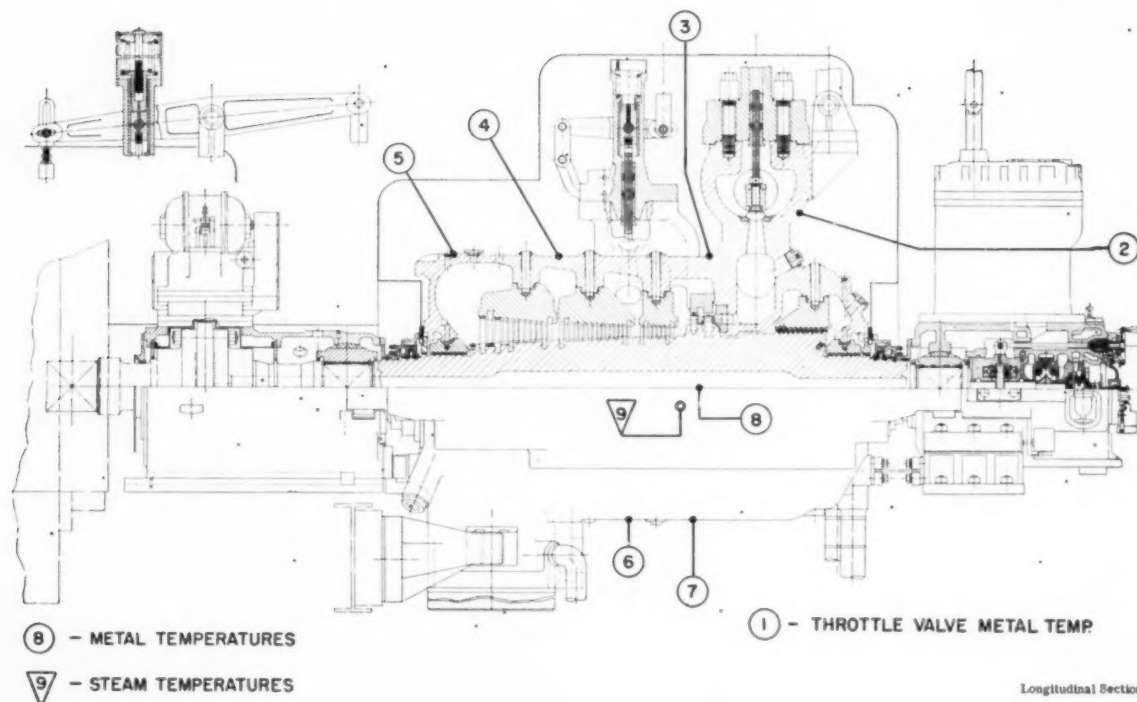


FIG. 29 50,000-Kw WESTINGHOUSE TOPPING UNIT No. 9, WATERSIDE STATION
(3600 rpm, 1600 psi, 950 °F.)

ferent from that of a boiler which has been bottled up near operating pressure for an overnight shutdown. In this latter case the boiler is brought up in only a few minutes more than the 15 min required for the turbine.

We have always felt that the present starting time from the cold condition, as recommended by the manufacturers of boilers, is much too long to fit into our operating cycle. Therefore we have made studies to determine temperature changes which occur in high-pressure boilers during such cycles and for that purpose installed thermocouples as shown in Fig. 30, on Waterside No. 90 Combustion boiler which is designed for 1,000,000 lb of steam per hr at 1800 psi and 950 F.

From the data obtained it was observed that during an overnight shutdown of No. 90 boiler when the drum pressure was purposely allowed to fall to 300 psi, a large temperature differential occurred between the top and bottom of the boiler-drum metal. In Fig. 32, which represents one of these tests, it will be noted that this differential attained 130 F for the 60-in. drum and 50 F for the 54-in. drum.

On another shutdown prior to a 3-day outage for boiler repair, during which the cooling of the boiler was accelerated by running the induced-draft fans, a spread of 170 F was noted in the metal temperatures at the top and bottom of the 60-in. drum.

However, in all our tests it was consistently observed that no appreciable drum-metal temperature differential was created during the starts of No. 90 boiler.

After reviewing these observations, the manufacturers indicated more concern about the drum stresses in shutting down than in those which might be induced by a proposed faster-starting cycle. They also agreed with our opinion that the reason the bottom of

the 60-in. drum was cooling faster than the top was due to the introduction of feedwater which is cooler by several hundred degrees than the on-line feed temperature after the mills were out out, due to loss of heat from the economizer and the turbine bleed heaters. To reduce this metal difference between the top and bottom of the drum to less than the manufacturer's recommended 100 F, it is now the practice to fill the drum immediately after firing ceases.

With the assurance that only minor drum-metal temperature differences exist in a normal start, as shown in Fig. 32, it was then decided to quick-start No. 90 boiler which had cooled to room temperature after a 3-day outage. This decision was reached after further reasoning that:

(a) There was no likelihood of rolled joint leakage in starting because the thin wall tubes expand faster than the heavier header and drum walls.

(b) There was no danger of superheater elements overheating because the nondrainable superheater tubes trap water which acts as a cushion by evaporation and keeps the superheater tubes cool during the initial period of the start.

The first quick-start test was run on February 5, 1950, and the starting time from cold was reduced from 7 hr to 3½ hr. Fig. 33 shows the pressures and temperatures obtained during this quick start.

In this test, normal firing rate was increased on the basis of raising the drum pressure at a rate that would increase saturation temperature at approximately 150 F per hr. As can be seen from Fig. 33, the maximum drum-metal temperature differential never exceeded 35 F. The superheater-metal temperatures did not reach excessive values and, as a matter of fact, the tem-

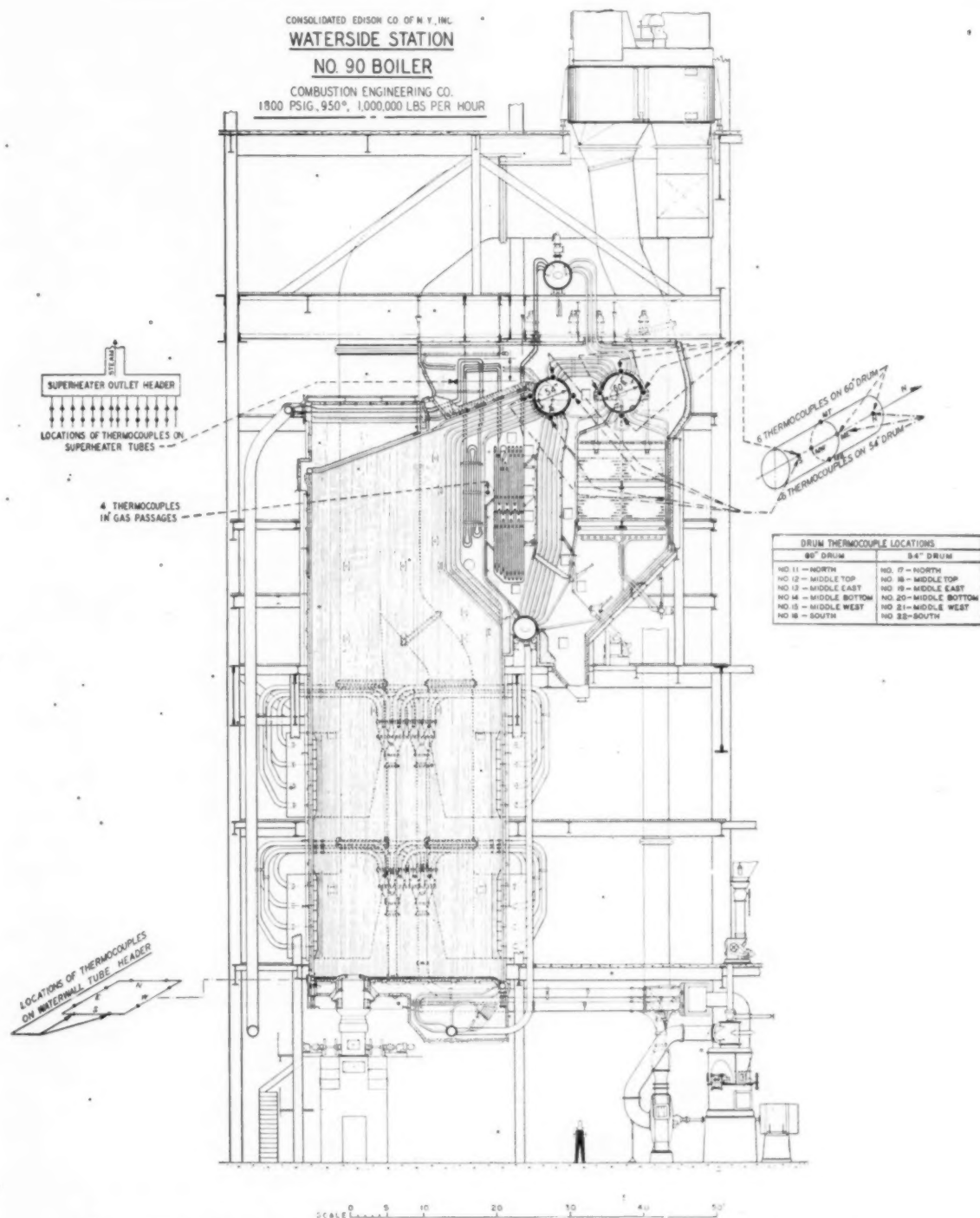


FIG. 30 1800-PSIG, 950-F, 1,000,000-LB-PER-HR NO. 90 COMBUSTION-ENGINEERING BOILER AT WATERSIDE STATION

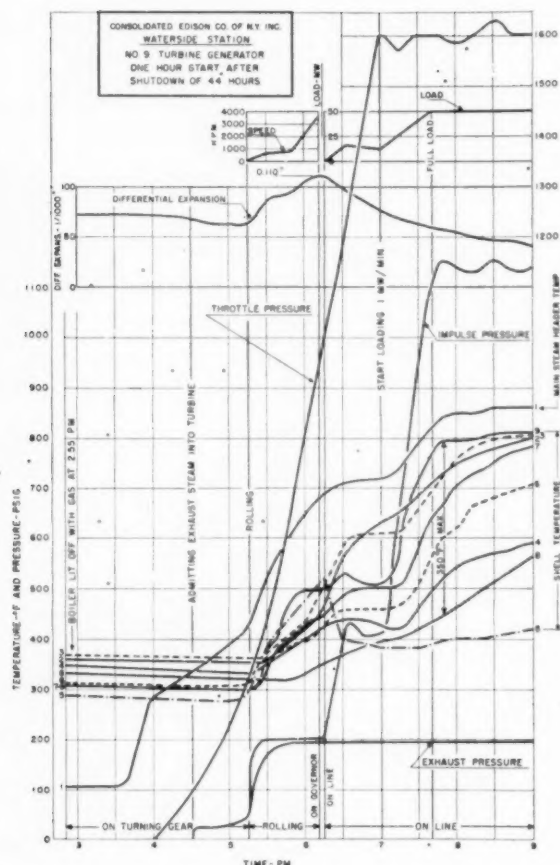


FIG. 31 ONE-HOUR START AFTER SHUTDOWN OF 44 Hr. No. 9 TURBINE GENERATOR AT WATERSIDE STATION

peratures of the hot gases (not shown on the illustration) surrounding the superheater tubes were found to average 850 F which is lower than anticipated and within safe values.

After every stop and start we are obtaining new information that leads us to believe that boilers can be started from cold much more rapidly than has been the practice in the past, and more rapidly than is at present recommended by the boiler manufacturers. We believe the quicker starts impose no greater strain in the boiler structure than the slower starts.

A potential cause of boiler extended outages ever-present in our system is due to the frequent shutting down of high-pressure units at night. As a result of these repeated shutdowns, leakages occasionally occur at the tube rolled joints in the bottom-wall header. We feel that this type of trouble could well be eliminated on new boilers by welding stub-end tubes into the header at the factory. The number of header handholes would thereby be decreased by 75 to 85 per cent and would greatly reduce the possibility of gasket leaks. This is of importance to us because one leak may cause the outage of a 1,000,000-lb-per-hr boiler for 24 to 36 hr. Additional original shop or field construction, if any, to obtain welded stub design, therefore, would amply pay for itself by preventing a few outages.

CONCLUSION

The conclusion in the present paper enumerates the benefits

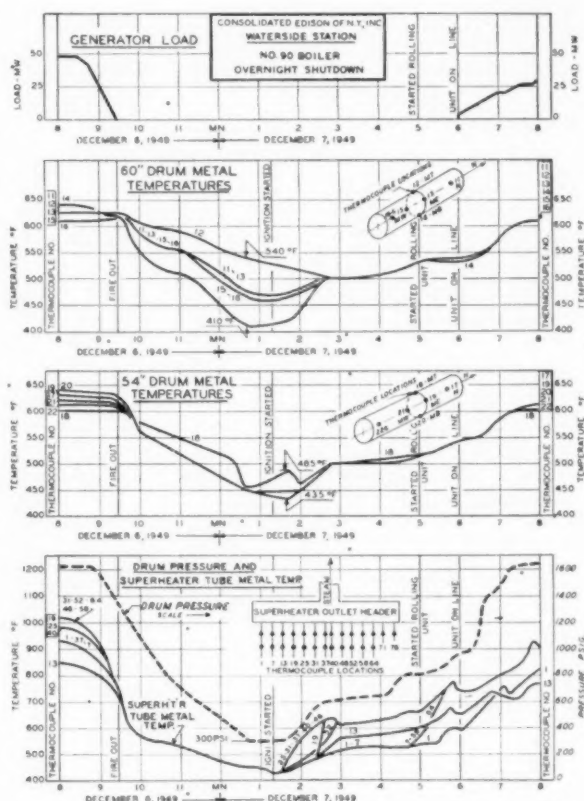


FIG. 32 OVERNIGHT SHUTDOWN, No. 90 BOILER AT WATERSIDE STATION

accruing to the Consolidated Edison System as the result of quick starting after overnight shutdowns.

There now can be added to these the time gain of 3 to 4 hr on every occasion that a high-pressure boiler is removed from service and its pressure relieved for inspection and maintenance.

Our investigation of reducing the starting time of boilers from a cold condition has been conducted for a relatively short period, but we have every reason to believe that starting can be done at a much faster rate than that now advocated by the manufacturer.

Discussion

A. A. CASEY.⁸ On the topping turbines at Waterside and Sherman Creek Stations the temperature-control problem appears to be at the head end where there was rapid cooling of the steam-chest metal by the steam admitted for rolling, and subsequent heating of the metal as the speed was increased and load was applied. In contrast, on the condensing turbine reported on at East River Station, there was little change in metal temperature at the head end during the rolling period. The problem of control of temperatures on this turbine appears to be at the exhaust end where the steam leaving the last row of blades was reheated by friction from the large exhaust wheels. As pointed out by the authors, steam leaving the last row of blades is reheated during the quick-starting, but the peak temperature is

⁸ General Superintendent of Steam Power, The Cleveland Electric Illuminating Company, Cleveland, Ohio. Mem. ASME.

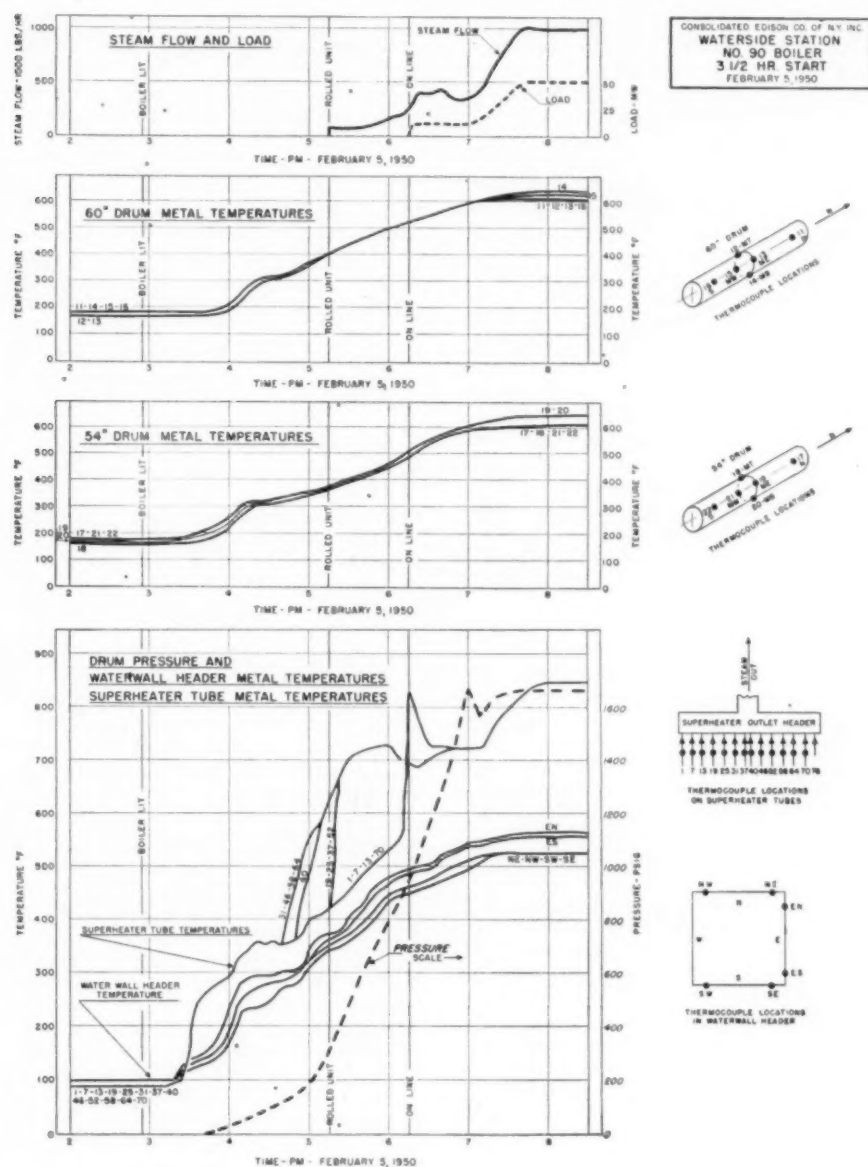


FIG. 33 3 $\frac{1}{2}$ -HR START, NO. 90 BOILER AT WATERSIDE STATION
(February 5, 1950.)

lower, and the time interval is shorter. As a result, there is less heating of metal at the exhaust end.

Of special interest is the effect of the number and size of boilers supplying the steam for starting. Low steam temperature at Sherman Creek with one boiler per turbine presented a different problem from Waterside with two boilers of smaller size per turbine. In addition, the use of oil burners at Sherman Creek and the comments on steam condensation in the pendant-type superheater emphasizes that boiler characteristics must be taken into account in developing quick-starting procedures. It would be interesting to know what the boiler-drum and superheater metal temperatures were during the quick starts.

The calculated annual savings possible with quick starting is \$250,000. Was this calculation based on operating data taken during normal and quick starts? A division of this total into the various costs would be informative.

The recent Prime Movers Committee report on Turbines, Condensers, Auxiliaries, etc., for 1946-1947 in the section on statements by operating companies shows that, in addition to Consolidated Edison Company of New York, some quick starting is used or is being tested by the following: Pennsylvania Power and Light Company; Public Service Electric and Gas Company; Wisconsin Electric Power Company.

B. J. Cross.⁹ A rate of increase in pressure, corresponding to a temperature rise of not greater than 100 F per hr has been the recommendation of boiler manufacturers in bringing a boiler in service. Actually, the concern is not so much the rate of temperature rise as the uniformity of temperature throughout the boiler as it is brought up to operating pressure.

This 100 F per hr rate is set as a safe figure that would not be expected to result in temperature differences which would produce undesirable stresses in the boiler parts, and particularly in the drum structure. It is admittedly an arbitrary figure and in the absence of reliable information was set to provide a safe margin in consideration of differences in design and operating conditions.

The observance of this limit of temperature rise would require a minimum of about 5 hr to bring a high-pressure boiler in service from a cold condition.

When boilers are taken out of service only infrequently, this time limit does not affect the operating economy of a station seriously. In fact, a similar time limit has also applied to turbines.

With a load pattern such as that of the Consolidated Edison Company, it is highly desirable that the time period be reduced. As pointed out by the authors of this paper, a substantial saving in operating expense may be effected and also by the advantage of quicker availability an improvement in customer service will result.

The greatest difference in drum temperatures occurs during the shutdown period. The cause of these large differences has been determined and corrective measures taken. In putting a boiler in service at successively shorter periods, no difficulties have developed, and a case may possibly be made for an improvement in conditions at the shorter periods.

In the start-up after a short or overnight shutdown, the critical factor is steam temperature. A supply of steam at or above the temperature of the turbine steam chest is required. Actually, this degree of superheat is required before there is any flow of steam. This dilemma will be solved by the provision of the turbine by-pass.

While the protection of the superheater elements from overheating has not proved any great problem, the turbine by-pass also will provide favorable conditions for the superheater and will permit firing rates necessary to produce the early superheat required.

The problem of leaks in rolled-tube joints and handhole-plate seats may be eliminated by the welding procedure suggested by the authors or, less expensively, by seal-welding rolled joints and handhole plates. Both techniques have been developed and used.

The authors of this paper and their co-workers are to be highly commended on their very thorough study of this problem. The progress reported in this and previous papers represents many years of hard work and intensive and systematic study.

The information they have made available will be of great value to the whole industry. Even with what may be termed a normal load pattern of a public-utility station, there are still many advantages in the quick-start procedure that has been developed. One of the major items of expense in maintenance is the loss of service of the equipment, and a few hours gained at each shutdown represents a worth-while yearly saving.

In their final conclusion the authors state that they believe the starting of boilers may be done at a much faster rate than that advocated by the manufacturer.

The writer believes that the industry will agree with that conclusion. However, because of differences in design and arrangement and also variation in operating conditions, the details of

⁹ Manager, Development and Research Division, Combustion Engineering-Superheater, Inc., New York, N. Y. Mem. ASME.

procedure in coming-off and going-on load may be different for each boiler. We would strongly recommend that the minimum starting period and the safe procedure for both shutting down and starting up be established by a program of temperature measurement such as the authors have described.

H. P. DAHLSTRAND.¹⁰ In this paper the authors have reported further studies of this vital question first reported by J. C. Falkner, R. S. Williams, and R. H. Hare in 1947. It is indeed gratifying, and the authors should be congratulated for proving the soundness of their ideas in developing a practical method for the control of the various conditions which will in all cases result in maximum reliability and economy of the equipment during the starting period.

In commenting on the original paper the writer fully agreed with the authors on the conclusions reached. The first paper covered large topping turbines only, whereas the present paper includes condensing units as well. In both cases the problem is the same, except that the control of vacuum in the latter case becomes of considerable importance in determining the length of the starting period.

Of special interest is the addition of auxiliary oil burners in the boilers for raising the steam-inlet temperature closer to the metal temperature, as well as the proposed by-pass around the turbine for draining the superheater of water. It indicates that an exhaustive study has been made in order to obtain the ideal condition which not only will shorten the starting period but also, which is more important, will add greatly to the reliability of the steam-turbine units because of the decrease in differences between the steam and metal temperatures. This will be of greater importance as higher temperatures are adopted using materials with larger coefficient of expansion and lower heat conductivity.

Commenting on the quick starting of a large condensing unit, it is shown that the shorter the starting period the lower will be the exhaust-steam temperature. There is naturally a certain limit depending upon how quickly full vacuum is established. In reducing the starting time from $2\frac{1}{2}$ hr to 45 min, the exhaust-steam temperature was materially reduced. The question might be asked, "If full vacuum had been obtained at the start of the rolling period, what would the exhaust-steam temperature have been?" It is important that this temperature does not exceed a certain limit, as stresses in the last row are higher than in any other blades of the unit. There is also the danger of loosening the blades in the grooves and breakage of shroud and lacings due to expansion of the blade structure.

All large steam-turbine units, 1800 rpm and 3600 rpm, built by our company in the past several years have been provided with steam-sealed glands only. With this type of gland, it is possible to obtain full vacuum in the condenser with the unit operating at turning-gear speed. The advantage of this type of gland has been mentioned previously.¹¹ It will also result in much lower exhaust temperature during the starting period, as indicated in the curves, Fig. 34, herewith. These curves show the conditions during the starting period when the unit is started from cold. The tip speed of the last row of blades is 1140 fps. Starting time for a cold unit is limited by how fast the various parts absorb the heat without excessive distortions, whereas units with short shutdowns, in which the metal temperature of the high-pressure elements approach that of the operating temperature, can be started relatively quickly, provided the steam-inlet temperature approaches the metal temperature and a high vacuum is obtained in

¹⁰ Director of Steam Turbine Engineering, Steam Turbine Department, Allis-Chalmers Manufacturing Company, Milwaukee, Wis. Fellow ASME.

¹¹ "1949 Port Washington Experiences," *Combustion*, vol. 21, January, 1950, pp. 45-48.

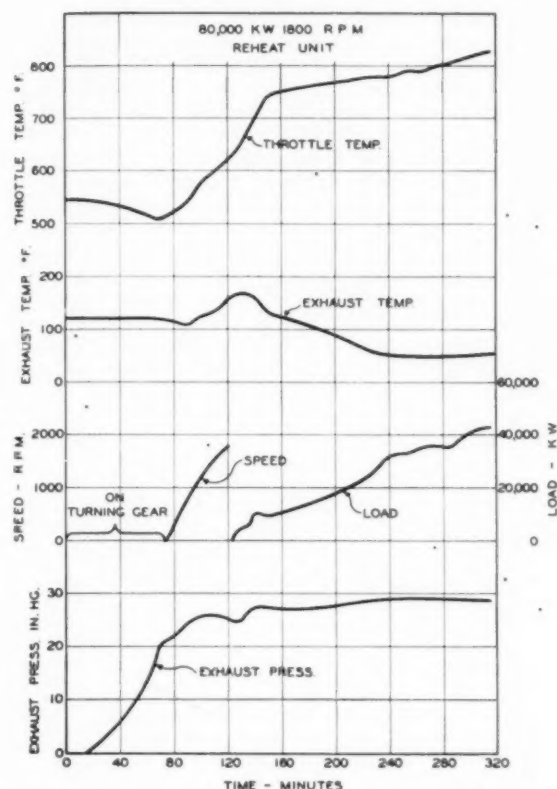


FIG. 34 CONDITIONS DURING START-UP OF 80,000-Kw 1800-Rpm REHEAT UNIT

the condenser to prevent excessive heating of the last rows of blades. In the curves shown, Fig. 34, the vacuum in the condenser is 21 in. at the start of the rolling period, resulting in a maximum exhaust-steam temperature of 170 F. This temperature would have been considerably lower if a vacuum of 29 in. had existed. Therefore, to shorten the starting period of a condensing unit after a short shutdown, both the control of the steam-inlet temperature and the vacuum is of vital importance.

W. R. LA MOTTE.¹² For years it has been the practice among conservative operators of turbine generators to require long rolling periods to "gradually warm up the machine." If a particular unit appeared to start rough, then the invariable answer was to start even more slowly.

The work at Consolidated Edison is particularly valuable for it is an effort to put the starting procedure on a rational basis and to provide the operator with a clear measure of what he is accomplishing.

Quite naturally, the writer's company is interested and has done some work along these lines, as reported in a paper by Neal and Renton.⁷

The writer would like to report on another matter, however, which may be helpful to other operators who may be contemplating experimental work on their own turbines. Last spring, when a 125,000-kw, 1250-psi, 950-F, cross-compound turbine was opened, the horizontal joint was found to be out of true and many

man-hours of labor were required to bring it back into shape. During the outage, 32 thermocouples were installed on the high-pressure cylinder and steam chests. These showed clearly that opening of the secondary and tertiary valves increased the temperature at the inner edge of the horizontal joint much more rapidly than at the outer edge or the bolts. As a result, there is a time during the loading cycle when the temperature difference across the flange is 250 to 300 F. The inner edge of the joint is crushed and there is eventual leakage.

A remedy suggested by the manufacturer is installation of a manifold through which live steam may be admitted to the annular space around each main flange bolt, thus keeping the bolts and outer portion of the flange up to temperature. Such a manifold is being built but is not yet installed, hence a report on its effectiveness cannot be made at this time.

This is brought to the authors' attention with the suggestion that the horizontal joint be included in the thermocouple installation.

R. L. REYNOLDS.¹³ Of particular importance are the discussions in this paper of the following additional aspects of the quick-starting problem which were not covered in the previous presentation:⁸

(a) Inspection of a superposed unit after having been subjected to several "quick starts."

(b) Application of the quick-start method of operation to a turbine supplied by a single boiler.

(c) Application of the quick-start method to a condensing-type turbine.

From a turbine-engineer's point of view, the determination of the proper starting cycle depends primarily upon the following conditions:

- (a) Change in axial and radial clearances between stationary and rotating parts, particularly blades and sealing strips.
- (b) Stress in bolts and flanges.
- (c) Ability of boiler to follow changes in turbine steam demand.

Inspection of one of the Waterside superposed turbines, after several quick starts and, in addition, several water and caustic washing cycles, shows that the use of this method of starting has caused no distress to the turbine. Therefore this method appears to be fundamentally sound and worthy of continued study and application.

In order to obtain more information on the effect of starting and loading units, we have installed thermocouples in the flange and bolts on a turbine quite similar to the Waterside No. 6 unit referred to in the paper.

Readings taken on these thermocouples during a start, where full-temperature steam was used for heating, indicate that in the throttle valve, where the steam sweeps past the inner wall surface at fairly high velocity, and where the covers are bolted to the body with studs, the metal temperatures in the flange and bolt follow each other quite closely and build up to nearly the steam temperature quite rapidly. In the steam chest, the flange and bolt temperatures do not build up quite so rapidly but do follow each other quite closely.

However, in the main turbine cylinder where the steam remains stagnant in some chambers during the starting cycle, the metal temperatures respond much more slowly. Of even greater importance is the fact that the temperature differential between the flange and bolt becomes quite large. This large differential re-

¹² General Superintendent of Generation, Public Service Electric and Gas Company, Newark, N. J. Mem. ASME.

¹³ Manager, Central Station Turbine Section, Westinghouse Electric Corporation, South Philadelphia Works, South Philadelphia, Pa. Mem. ASME.

sults in high compressive stresses at the sealing surfaces of the flange joint and in high tensile stresses in the bolt.

Part of this differential is probably due to the type of bolt used, this being the through-type with clearance space between the bolt and flange. With this type of bolt, heat is conducted from the flange to the bolt through the seating surface of the nut and thence through the nut into the bolt along the thread engagement. This means that heat is transmitted from the flange to the bolt along only a comparatively short length of the bolt, except for the relatively slow radiation of heat across the clearance space between the flange and bolt.

These measurements dictate the need for further study of this problem to devise means for making the bolt temperature and expansion conform more nearly to flange temperature and expansion. As an approach to this problem, means can be provided to circulate steam through the clearance space around the bolts or to coat the bolts with some material to increase heat emissivity.

During the opposite cycle of shutting down or reducing load, the flange will tend to cool at a faster rate than the bolt, thus causing the bolt tensile stress and the flange compressive stress to decrease. This reduction in stress is not harmful to the bolt and flange material but, if the temperature differential becomes great enough, it will cause the joint to leak steam. This is naturally objectionable but will not damage the joint surface, provided the leak occurs in the high-temperature region where the superheat of the steam is in excess of 100 F.

From the standpoint of blade and seal strip clearances, these must be determined on each installation to insure against rubs between stationary and rotating parts during the starting cycle. During the shutdown period the rotor is kept straight by rolling with the turning gear. However, the stationary casing tends to "hump" because of the upper half cooling off at a slower rate than the lower half. As a result, radial clearances at the bottom become smaller, and provision must be made to make these clearances sufficiently large to avoid rubs. Also, starting procedure should be arranged to straighten the casing to reduce the possibility of these radial rubs.

Axial clearances also must be determined during the starting and loading cycles to avoid rubs. The paper describes means for doing this and inspection showed that no axial rubs of any consequence had occurred.

The time required to bring a unit up to speed after a shutdown depends primarily on the following conditions:

- (a) Length of shutdown period.
- (b) Temperature of steam used for starting.

The length of shutdown will determine, to a great extent, the temperature of the metal in the throttle valve, steam chest, and turbine casing. It also will affect, to some extent, the amount of cylinder "humping" due to unequal cooling of the top and bottom halves.

As the authors have pointed out, the temperature of the steam used for rolling the unit should be only slightly higher than the metal temperature. In order to do this at times it may be necessary to make special provisions in the boiler to control the steam temperature as required.

While sufficient information is not yet available to make definite recommendations, we do know that the starting time should not be set at some fixed value, such as 15 min, under all conditions, but will be influenced by the length of shutdown and by the relation of the steam temperature to the metal temperature.

While the 15-min cycle appears to have been satisfactory for overnight shutdowns, where steam temperatures could be maintained at from 50 to 100 F above metal temperature, the safe time after a longer shutdown, where steam temperature cannot be so controlled, should be considerably more than 15 min.

Regarding the question of controlling throttle temperature

during the load-reduction and shutdown period, it has been the practice of some operating companies to reduce throttle steam temperature before starting to remove load. This accentuates the drop in turbine-stage temperatures and, therefore, may produce more severe starting conditions than if the throttle temperature could be maintained at a higher level during the load-removal period. Determination of the method of shutting down will depend upon the means for controlling steam temperature during the subsequent starting cycle. With the unit system, where the steam temperature is usually considerably lower than the metal temperature, a reduction in steam temperature during the shutdown cycle is advisable. However, if a header system is used, which is kept hot because of supplying a substantial steam flow to other units, it appears desirable not to permit the turbine to cool off more than necessary during the shutdown period. In fact, if means could be provided to increase, rather than decrease, initial steam temperatures while load is being removed, the stage temperature drop will be minimized, and the effect on metal temperature will be comparatively small. The turbine will thus be better suited to a quick start with high-temperature steam.

On condensing turbines, the problem of exhaust temperature during the starting cycle may become quite serious. Because of this, it appears advisable to maintain as high a vacuum as practicable during this starting period. In many cases, steam seals can be used to seal the glands at speeds too low for effective water sealing. The quick start helps to keep this exhaust temperature within desirable limits and thus should be beneficial in the low-pressure end of the turbine.

In conclusion, we feel that the authors have made a worth-while contribution in their studies and experiments on the starting phase of operation. Unquestionably, this not only will lead to a substantial saving in time and expense but also will subject the turbine to less severe treatment than when following the somewhat arbitrary rules applied in the past. While this has not been too important during the past few years, when it has been necessary to operate almost continuously at heavy loads to meet the load demand, the time is coming when economical operation will necessitate week-end and, in many cases, overnight shutdowns. This method of operation demands that units be returned to active service in the shortest possible time consistent with proper treatment of station equipment.

C. U. SAVOYE.¹⁴ The limitation of 100 F per hr metal-temperature change has been given, in power-plant operation, an authority which cannot be upheld. Some of us in the boiler business are responsible in a measure for this illicit development, so it seems necessary to explain our contribution and to clarify the original intent.

In the late 1930's the writer's company built its first 2200-psi boiler for an industrial power plant. The drum plate in the heaviest section was 8 5/8 in. thick. Concern over metal-temperature differentials during the starting-up and the shutting-down periods led us to the installation of thermocouples in the drum sheet at four depths. The data obtained during the early operations showed temperature differentials between the outside and the inside of the sheet to be approximately 60 F for a rise in saturation temperature of 200 F per hr, and 18 F for a rise in saturation temperature of 20 F per hr.

Consideration of these results, together with data obtained on thinner drums, led us to the following conclusions:

- 1 If each part of a drum of any thickness is held to within 100 F of any other part, the maximum stress in the drum will remain within the allowable limits.

¹⁴ Executive Assistant, Babcock & Wilcox Company, New York, N. Y. Mem. ASME.

2 With a given drum there is a loose relationship between its rate of temperature rise during starting-up and the temperature differentials between one and another parts of the drum. Past practice indicated that no overstressing of drums up to 4 in. thick was experienced when the starting-up time was extended to at least 4 hr, or to a rise in saturation temperature of approximately 100 F per hr. This 100 deg is an entirely different one from the 100-deg differential between two parts of a drum sheet. Its use as a starting-up "rate" was quite attractive, because it paralleled, roughly, the allowable limit of heat application to superheater tubes before full steam flow through them was established.

3 A high rate of temperature rise during starting-up does not dictate a high stress—unless the rate is continued long enough to produce high differentials in the metal.

For instance, a 600-deg per hr rise for 1 hr could produce a metal temperature differential of 600 F and, therefore, a damaging stress. The same 600-deg per hr rise for 10 min, however, could produce no more than 100 deg metal-temperature differential, and therefore the stress could be acceptable.

4 A starting-up rate of 100 F per hr saturation-temperature rise appeared to be good practice for the predominance of plants where the many advantages in this conservatism would not be counteracted by costly losses because of wasted time. Where rates exceeding 100 F per hr became attractive from an economic standpoint, drum-metal temperature differentials, as registered by thermocouples, were expected to be used as guides in establishing the new rates.

Suggested operating instructions issued later recommended the 100 F saturation-temperature starting-up rate—simply a rule of thumb—for standard practice in the many diversified plants throughout the country where our products were expected to go. This has become confused with the 100 F metal-temperature "differential" which, with correct premises, is a measure of stress.

Starting-up rates, therefore, have no technical standing in themselves, but only as they are reflected in temperature differentials between parts of the structure.

Separate and distinct from the problem of clarifying a misunderstanding, and simply as a matter of general information, our field data indicate that a starting-up rate of 100 F per hr rise in saturation temperature will produce a temperature gradient through a normally insulated boiler drum of approximately $4\frac{1}{4}$ F per in. of drum thickness; and (extrapolating the data) that a starting-up rate of 460 F per hr will produce a temperature gradient of approximately 10 F per in. of drum thickness.

The latter part of the authors' supplement covers some data on the starting up and shutting down of high-pressure boilers. Two explanations are given with which it is necessary for the writer to disagree.

The first deals with the reason why the bottom of the 60-in. drum cooled faster than the top. The curves indicate that the bottom followed saturation temperature very closely and dropped only 12 F below saturation at the point of maximum deviation, while the temperature at the top of the drum registered 118 F above saturation at the same time. The effect of cold feed-water might account for the 12 F subsaturation temperature at the bottom, but it cannot account for the 118 F superheat at the top.

Superheating at the top of a steam and water drum during the shutting down of a modern boiler under normal water-level conditions is a common and natural occurrence.

In starting up or in raising steam pressure, the heat absorbed by the boiler and waterwalls generates steam which collects in the drum. That portion of the steam in direct contact with the

drum metal heats it through condensation. The temperature of the inner surface of the drum in the steam space is therefore, in effect, geared directly to saturation temperature. The lower portions of the drum in contact with the boiler water are heated very close to saturation temperature by the circulating boiler water.

In shutting down, the submerged parts of the drum are maintained close to saturation temperature by the boiler water because its temperature follows saturation on falling pressure the same as it does on rising pressure. The steam in close contact with the upper part of the drum, however, does not ordinarily condense on falling pressure, because as soon as the saturation temperature drops, the drum metal with its stored heat finds itself hotter than the steam in close contact with it and it therefore superheats this steam. The rate of heat dissipated from the upper part of the drum through radiation and through conduction is usually small as compared with the cooling rate of the boiler water in the tubes and, in turn, the cooling rate of the submerged portion of the drum. The temperature of the top of the drum consequently drops at a slower rate than that of the bottom. The superheat at the top therefore increases, even though both top and bottom temperatures are falling at their different individual rates.

Filling the drum to overflowing, as recommended by the boiler manufacturer, will, of course, re-establish the direct relationship in temperature between the top of the drum and saturation and thereby make it permissible to increase the cooling-down rate to the point where it approaches the limiting starting-up rate. This filling-up procedure does demand the making of provisions for overcoming a number of important operating objections.

The second point of disagreement deals with the cooling of nondrainable superheater tubes. There may be some very special cases in which the steam resulting from the evaporation of the condensate in nondrainable superheaters contributes materially to the cooling of the tubes, or to protecting them against overheating from relatively high gas temperatures, before they are cleared of condensate and before a through-flow of cooling steam from the boiler has been established. In the overwhelming majority of cases within our experience, however, it has been necessary to consider that those portions of the superheater tubes which are above the level of the accumulated condensate, and at the same time are in the path of the heating gases, should be considered as uncooled metal which is at the mercy of the gases. Until a throughflow of steam is established, by boiling out or by blowing out the condensate, we are convinced that the temperature of the gases entering those parts of the nondrainable superheater, which might be above the level of any trapped condensate, should be kept below the point at which uncooled tubes can be damaged. Many of the nondrainable units today are placed in service successfully without any special attention given to the gas temperature at the superheater entrance. This is made feasible by a number of fortunate relationships and by the 100-F rule-of-thumb starting-up rate. The power to do damage is present, nevertheless, and those who plan to increase their starting-up rates to 200, 300, and 400-F rise in saturation temperature per hour would do well to reckon with it.

A. R. WEISMANTLE.¹⁶ The principle of the quick start is simple and consists of admitting steam into a turbine at a temperature equal to or slightly higher than the metal temperature of the steam chest, and then increasing this metal temperature at a rate of not over 100 F per hr. The descriptions of the various trials made and the expedients resorted to by the authors, in order to accomplish these ends, clearly show us that they can-

¹⁶ Assistant Manager, Steam Division, Foster Wheeler Corporation, New York, N. Y. Mem. ASME.

not be attained without considerable complexity in operation of conventional steam-generating units.

On systems where quick starts are imperative, steam-generating units considerably more flexible than conventional units as to control of steam temperature should be used. This flexibility must include not only the usual control of temperature at constant level over a wide load range but also the ability to vary steam temperature from saturation up to the full design temperature over the same range. The positive control of steam temperature provided by such a unit at any temperature level throughout the load range makes it possible to fulfill the requirements of the quick-start procedure with ease and simplicity. With such units there is no need for special starting techniques which would differ between the various power teams in the system and require revision in accordance with the length of time a turbine was shut down.

Steam-generating units which provide this flexibility of steam-temperature control have been designed and built for many years. One unit of such design, known as the Foster Wheeler twin-furnace unit, is shown in Fig. 35, herewith. This unit consists of two furnaces and gas circuits which are arranged in parallel and completely separated up to the economizer inlet. From that point on the arrangement of components is conventional. One furnace is completely water-cooled, and the gases leaving this furnace pass over the boiler surface before reaching the economizer. The other furnace is partially water-cooled and partially steam-cooled, and the gases leaving this furnace pass over the superheater before reaching the economizer. By differential firing of the two furnaces it is possible to deliver to the turbine either saturated steam or steam with any amount of superheat up to the full temperature for which the unit was designed. Thus, for a quick start, this type of unit permits delivering steam initially to the turbine at a temperature equal to or slightly above the metal temperature of the steam chest and then it allows increasing the temperature at exactly the maximum rate permissible. The control of turbine metal temperatures is positive and is very simply obtained by differentially firing the steam generator. Those engineers associated with systems where quick starts are to be made with topping turbines, straight-condensing, or even reheat units should not overlook the important advantages offered by steam-generating units of this type.

The evolution of procedures for quick starts of the No. 9 unit at Sherman Creek, as described in the paper, is quite interesting. The authors explain that a by-pass is now being designed so that the superheater will be cleared of water and the desired steam temperature obtained before opening the throttle. This undoubtedly will prove a simple means for providing steam for admission to the turbine at a temperature equal to or slightly higher than the metal of the turbine steam chest. However, unless steam-chest temperature happens to be high, it would appear that excessive rates of temperature rise could still occur during the rolling and initial loading period. In order to avoid this, a simple spray-type desuperheater, located in the circuit between the superheater outlet header and the turbine throttle, could be installed and used for control during this period. Could the authors tell us whether they have yet been able to obtain any results with the by-pass on the No. 9 unit?

Referring to Fig. 25 of the authors' Supplement, it can be seen that even though they were able to match steam and chest-metal temperatures initially, thus eliminating the initial temperature shock, the rates of temperature rise during rolling and initial loading period are still high. It appears that the metal temperature increased at the rate of 420 F per hr and 750 F per hr on Waterside No. 6 and No. 7 units, respectively. Fig. 28 shows a quick start of No. 6 unit at Hudson Avenue, from a common header system, and it appears that the throttle-valve metal temperature increased at the rate of 930 F per hr during the roll-

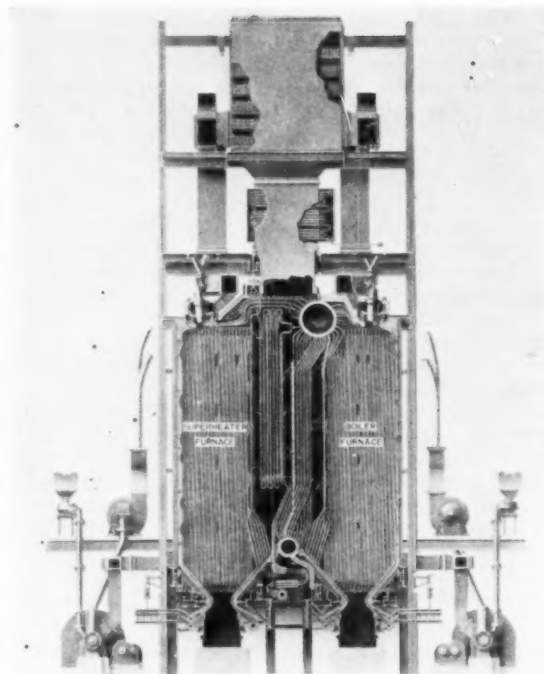


FIG. 35 FOSTER WHEELER TWIN-FURNACE UNIT

ing period, with this setup. These items only serve to emphasize further that (a) steam-generating units considerably more flexible than conventional units as to control of steam temperature should be used for quick starts of unit systems, and (b) even though steam and metal temperatures are initially matched, excessive rates of temperature rise can occur during the rolling and initial loading periods when conventional boilers are used, unless some desuperheating control is added. This latter statement also applies to quick starts of machines from a common header system.

The authors have included a section on shutting down and starting up high-pressure boilers. While the data given on this subject are not too complete, it is most gratifying to observe that they are not reducing time arbitrarily, but only on the basis of results obtained by real investigation.

The time for starting up or shutting down steam generators is usually based upon three main considerations, namely, (a) preventing excessive stresses in drums and headers, (b) avoiding the overheating of superheater-tube metals, and (c) eliminating thermal shock at joints or stresses in parts.

Excessive stresses in drums and headers can occur because of circumferential or transverse temperature differentials encountered in the start-up or shutdown procedures. It is well known that approximate heat-transfer coefficients in Btu/hr/sq ft/deg are on the order of 2000 for condensing vapors, 600 for heating or cooling water, and only about 2 for heating or superheating steam. The thermal conductivity of steel is approximately 25 Btu/hr/ft/deg. From this it is quite apparent that the inner surface of the drum plate at or below the water level will always stay substantially close to the water temperature. Also, the inner surface of the drum plate above the water level will stay close to the saturation temperature when steam is present and pressure is being raised. However, the top half of the drum will be heated only by the slow process of conduction in the period before steam pressure is raised and will be cooled slowly by con-

duction and a very low transfer rate to steam during the period after firing has ceased. It is self-evident then that greatest metal-temperature differentials circumferentially may be expected in the period after light-off has occurred and before steam is formed, and also during the cooling-off period after firing has ceased. The greatest transverse metal-temperature differentials can occur during the pressure-raising periods or during an emergency shutdown when pressure is lost practically instantaneously.

If saturation temperature, corresponding to the pressure, is plotted in Figs. 32 and 33 of the Supplement, the analysis of the data becomes easy. The circumferential temperature differential of 130 F is readily apparent in Fig. 32. One might ask the authors, however, why the drum thermocouples read as much as 30 F above saturation temperature under load conditions, and why horizontal center-line couples on the 60-in. drum are as much as 50 F above saturation temperature during the shutdown periods, unless, of course, water level was held extremely low during this latter instance. Also, it can be seen that the metal temperatures at the bottom of both the 54-in. and 60-in. drums is practically at saturation during the shutdown period. In view of this fact, it seems questionable that the bottom of the 60-in. drum is cooling faster than the top because of the introduction of feedwater. Undoubtedly, it cools faster than the top because of the fundamental heat-transfer principles involved.

To provide maximum drum safety when units are started up or shut down quickly, it is imperative that drums be practically filled with water during the initial firing period until steam is formed and also during the final firing period just before firing ceases. Special gage glasses to facilitate this operation should be applied at the top of the drums. It has been our practice to supply many units with such special glasses for these purposes, but we have found that invariably operators avoid their use. They are essential, though, for quick starts and shutdowns.

Avoiding the overheating of superheater-tube metals is of utmost importance in the start-up of any steam generator. It is well known that the tubes of nondrainable-type superheaters become practically water-filled from condensation after shutdown. This water must be removed either by evaporation or displacement before the normal cooling flow of steam through the tubes can be established. As the water is evaporated, portions of the tube become steam-trapped, in effect, and at these locations metal temperatures can become considerably higher than the steam temperature. To clear all elements of water before going on the line and to keep metal temperatures at safe values, it is necessary that the gas temperature entering the superheater be at or below 1000 F and that all the superheater surface, especially the bottom loops, be gas-swept during the start-up procedure. By reason of thermocouple location, the temperatures obtained by the authors, and included in Figs. 32 and 33, are more truly outlet steam temperature than actual heating-surface-metal temperature. Because of this fact, the data do not necessarily indicate that metal temperatures were safe.

Note the rapid change in temperatures which occurred between the hours of 4:45 and 5:15, and again at 6:15 in Fig. 33. This rapid increase occurs when loops clear themselves of water and the temperatures then read are the steam temperatures leaving the elements after cooling flow has started. Under this condition indicated temperatures are in the neighborhood of 700 F to 800 F, so it is self-evident that metal temperatures must have been considerably higher when steam was not flowing through the elements. To avoid the possibility that metal temperatures are unsafe, thermocouples should be installed on the actual heating surface during the trial quick-start periods. To best protect the superheater, the unit should be started up with lower burners,

without any superheater gas by-pass and with as much steam flow through the elements as possible. If this is done and the criterion on gas temperatures is met, there is no alternative except taking the time necessary to stay within the limits mentioned, in order to assure superheater safety.

Eliminating thermal shock at joints or stresses in parts is always important in starting up or shutting down. Too often it is found possible to establish some average circulation and temperature rise throughout a section, while local tubes which may be covered with ash, or located at corners, or entering drums above the water level still remain cool. Considering that a temperature differential of only 140 F may produce a stress of 30,000 psi, and that when circulation establishes itself in these local sections, it occurs rapidly, the possibility of trouble from this factor becomes readily apparent. The authors' comments indicate that they have experienced this trouble even with normal slow starts. The writer does not think that quick starts will improve this condition.

Properly welded joints are less susceptible to leakage than rolled joints, but the important thing is to establish circulation early and uniformly. Frequent blowdown of all lower headers during the initial heating and pressure-raising period will assist considerably in this respect, or some other means of assisting circulation during this period can be applied. The data given by the authors on this phase do not permit detailed analysis. Fig. 33 shows water-wall-header temperatures which were measured as much as 100 F lower than saturation temperature during the pressure-raising period, and even when on the line at 500,000 lb of steam per hr. The authors should account for this, and tell whether it is couple error or whether such subcooling actually exists in this unit.

The start-up and shutdown time set for a given steam generator by the manufacturer is based upon consideration of all the factors mentioned in the foregoing. There is no doubt that this time can be reduced. We have put Navy boilers into full service from cold in 8 min without catastrophe. Many of us have experienced outages in which pressure was reduced instantaneously without trouble. However, we would all agree that these practices should not be followed blindly, especially in central-station work. Any procedures for reducing the time involved should be based on full consideration of factors which can cause trouble and use of expedients available for reducing the harmful effects, in order to assure safety and long operating life of the equipment involved. The authors are to be commended for their careful and intelligent approach to this problem.

AUTHORS' CLOSURE

As Mr. Casey observes, the temperature problems to be overcome in quick starting occur at the high-pressure end of the cylinder in the case of topping units, and at the exhaust end of the condensing units. This is due, in the first case, to unit systems having a tendency to have an initial steam temperature cooler than that of the steam-chest metal temperature, while in the case of condensing units this relation is favorable because they are generally supplied by a common header system. The exhaust end of the low-pressure units, however, presents temperature problems because of windage and initial poor vacuum.

In compliance with Mr. Casey's request, we are submitting the details of the \$250,000 saving given in our paper. The computations were based on 300 days of operation in which 30 condensing units and 2 topping units were started daily. The steam normally required for starting each of these machines is 50,000 lb and 300,000 lb, respectively, for condensing units and topping units, and by quick starting, the steam saving amounts to 70 per cent. The coal rate was taken at 9 lb of steam per pound of coal. The cost of the coal was figured at \$9 per ton. The aux-

iliary power saved daily because of the shortening of the rolling time of the above 32 units was calculated to be \$100 per day. On this basis the saving was

$$300 \left[100 + 9 \times \frac{0.7}{9 \times 2000} (30 \times 50,000 + 2 \times 300,000) \right] \\ = \$250,500 \text{ per year}$$

This figure shows only the saving expected in fuel. Furthermore, at East River Station quick starting has permitted a reduction of the midnight shift to a skeleton force. This has resulted in an annual labor saving of \$130,000. When quick-start procedure is applied to all machines, further saving in personnel is expected.

Mr. Cross's comments were of particular interest to us, and his thorough endorsement of our work was most gratifying. We agreed with Mr. Cross that some variations in the operation of shutting down and quick starting of boilers may be necessary to take care of the differences in design.

As usual, we found ourselves in full agreement with Mr. Dahlstrand, and we take this opportunity for reiterating our appreciation for his contribution on quick starting of turbine generators.

By comparing thermocouple readings 8 and 9 on Fig. 30 which gives the temperature difference across the horizontal flange of No. 9 unit at Waterside, Mr. La Motte can see that this differential exceeded the 200 F set as a limit by the manufacturer and that a crushing of the inner edge of the horizontal joint could have resulted. However, this 200 F differential did not occur during the start but only after the unit had been phased in for about one hour and kept on increasing until it reached a maximum of 350 F an hour and a half after being put on the line. As the unit had been started many times previous to this test, and without the benefit of thermocouples 8 and 9 to guide us, it can be assumed that the crushing of the joint inner edge took place soon after the unit was commissioned. The possible remedy indicated by Mr. La Motte would be a valuable corrective step on existing installations. However, we believe that on new machines, double-shell construction is the practical solution so as to divide the temperature gradient between two horizontal flanges.

We have found Mr. Reynolds' discussion of our paper very informative. The possibilities of rub being caused by cylinder "humping" is, of course, one factor which continues to give us great concern, not only for the quick start but even more so for normal starts. We would like to suggest to the manufacturers for their study, the design of a new supervisory instrument which would give the operator the knowledge of, and the means of measuring this cylinder bowing. If such a tool could be devised we feel it would contribute as much toward safer operation as did the measurement of shaft deflection prior to the rolling of a unit.

Quick starting was, in fact, imposed upon us by the load characteristic of the City of New York. Our contribution was merely to demonstrate its safe possibility and evolve the procedure. Quick starting was intended to relieve the early morning rush created by the necessity of simultaneous starting of many units which had had to be shut down late the night before. Today, this objective is still the same. For longer shutdown periods,

generally over 8 hours, we do not retain the 15-minute starting cycle but adopt longer rolling periods depending, as Mr. Reynolds pointed out, upon the length of the shutdown period.

The clarification given by Mr. Savoye as to how the 100 F rule came into being and its general misinterpretation, is revealing and we suggest that every boiler operator who has the opportunity to read Mr. Savoye's clear explanation make every effort to understand and remember the valuable information given in his comments.

On the matter of divergence in the rates of cooling between top and bottom of the drum during shutdown, Mr. Savoye disagreed with our interpretation of the cause but arrived at the same conclusion, namely, that the corrective measure consists of filling the drum.

We fear that we have been misunderstood by Mr. Savoye in regard to the cooling of nondrainable superheater tubes. It has not been our intention to demonstrate that steam resulting from evaporation from the accumulated condensate in these nondrainable tubes contributed to their cooling during starting. On the contrary, we have been proposing to generate, in the quickest possible time, by accelerated firing, a large volume of steam which would establish a mass steam flow of sufficient intensity to clear the superheater tubes of the condensate. It is our belief that the proposed by-pass around topping units will accomplish this purpose successfully.

Mr. Weismantle inquires about the status of the by-pass around No. 9 unit at Sherman Creek station. As of this date, the by-pass is not in operation but all connections which could be made without a long outage of the unit are in place, and we hope that in another two or three months the by-pass will be in service.

We have no explanation to offer regarding the 30 F above saturation which was present in the 54 and 60 in. metal drum temperature when the unit was under load but about ready to be shut down, except, perhaps, that it was due to a transient condition during this unsettled period. The close agreement of the saturation temperature with that of the drum metal during the subsequent start, would indicate that the condition of the thermocouples was excellent and that this above-saturation-temperature, although not explainable, did really occur.

During the overnight shutdown test, as shown in Fig. 32, the water was held at the normal level which, in this Combustion boiler, is below the center line of the drum. Therefore the reason for the 50 F differential between thermocouples located in the middle of the drums and those at the bottom appears to be due to the slower cooling of the drum metal above the water level. Here again we are pleased to see that, regardless of the reasons for this differential, Mr. Weismantle also advocates the same curative procedure of filling the boiler drums to overflowing as soon as the boiler is taken off the line, and keeping them full until the pressure is reduced to the desired point.

At this time it is not possible to vouch for the accuracy of the thermocouple readings of the waterwall header temperatures. While we suspect that 100 F differential is greater than it should be, we are, nevertheless, satisfied that a temperature lag exists between the waterwall header temperature and the saturated temperature, with the former being lower during starting operations.

Sealing of High-Pressure Steam Safety Valves

By R. E. ADAMS¹ AND J. L. CORCORAN²

A fundamental investigation of sealing with high-pressure steam safety valves has shown that poor sealing is a result of self-induced growth of tiny initial leaks. Expansion of the leaking steam cools local areas of the valve seat, causing contraction of the seating surfaces in a manner which increases the size of the leak. A new design of valve seat was developed, incorporating thin flexible seating surfaces. The cooling effects of the leaking steam were minimized by providing better heat transfer from the high-temperature steam. The new design resulted in considerable improvement in sealing, and service tests have shown excellent performance.

INTRODUCTION

THE two primary requirements of steam safety valves are (1) that the valves open without fail and release steam efficiently when the popping pressure is reached, and (2) that the valves close at a slightly lower pressure and prevent leakage of steam at all pressures under the closing pressure. The methods of popping and closing the safety valves are well understood. However, the problem of leakage of steam safety valves has long been recognized by designers as one of the most difficult problems which they face.

The essential elements of a safety valve, in so far as sealing is concerned, are the feather and the seat bushing. The seat bushing is simply a hollow tube connected to the boiler, with a carefully finished seat on the top surface, while the feather is essentially a cover with a similar seat held against the seat bushing by pressure from a spring. When the steam pressure on the bottom of the feather exceeds the force of the spring, the design of the valve is such that the feather pops up and steam is released until the pressure drops to a predetermined value. At that point the feather is forced down by the spring, and the valve is again closed.

The reason for the difficulty of sealing with safety valves, as compared with other types of valves such as shutoff, gate, and globe valves, or the like, is that with these latter types of valves, a tremendous load can be imposed on the mating parts of the valves by simply increasing the closing force on the operating handle of the valve. In direct comparison to this, on safety valves the seating surfaces are held together only by the difference in loading between the set load of the spring and the operating pressure of the steam.

This differential load is quite small, because it is naturally desirable to operate a boiler at a pressure as close to the maximum allowable working pressure as possible. Since the maximum allowable working pressure is the setting of the safety valve, the gap between the set and operating pressure of the safety

valve is of vital interest to the designer. The economics involved in making this gap as small as possible constitutes a compelling factor of boiler design. Thus there can be no wide difference between set and operating pressure.

Many factors contribute to leakage in valves. Among the most important is distortion of the seating surfaces caused by outside influences including installation strains, piping, hook-up, and ambient temperatures, particularly on outdoor installations. Further than this, any minute amounts of dirt or foreign material lodging on the seats, together with damage caused by grit in the steam, can also be causes of safety-valve leakage.

Another serious problem in connection with safety-valve leakage is that when leakage starts, for any reason, continued operation of the pressure vessel at the normal pressure will result in continual leakage of the valve. This leads to erosion of the seating surfaces and to increases in leakage to the point where the boiler must be taken out of service in order to recondition the valve.

As the steam pressures have increased in the past 25 years the problem of safety-valve leakage has become increasingly severe. This was particularly true as pressures rose above the 600 to 900-lb class to 1500 lb and above. It was the general experience of safety-valve users that valve designs which could easily be maintained tight at 600 and 900-lb pressure proved to be a considerable problem at 1500 psi.

This problem had existed for many years with only varying degrees of success in improving sealing in various plants throughout the country. Many different techniques of seat finishing, changes in design, and the like, were tried out, with some slight improvement in the standard of tightness of the valves at 1500 psi, but without making any decided change in the over-all picture.

Because of this, it was decided that a fundamental research investigation of the cause of safety-valve leakage was essential. This would not be a study of the past efforts made toward solving the problem. Instead, it would be an approach from a fundamental basis by someone entirely separated from the problem, who would not be subject to past knowledge which might be a hampering restriction.

LABORATORY INVESTIGATION OF SEALING

Apparatus Used. Accordingly, an experimental laboratory investigation to study the sealing of safety valves was started. A standard 3-in. safety valve designed for operation at a pressure of 1500 psi was used as the test valve.

Two types of materials for the feather and the seat bushing were of interest in this investigation. One was a ferritic turbine grade of stainless steel, known as Type "T," containing about 14 per cent chromium and 0.12 per cent carbon. The other type, known as Stellite trim, had seating surfaces of Stellite welded onto an austenitic stainless-steel base.

Fig. 1 shows a schematic drawing of the steam generator designed and used for laboratory sealing tests with the valve. The boiler consisted simply of a steel pipe, capped at the lower end, with a standard 3-in. flange at the top for connection of the test valve. The boiler had a capacity of about 100 lb of water

¹ Research Engineer, Battelle Memorial Institute, Columbus, Ohio.

² Chief Engineer, Consolidated Safety Valve Division, Manning, Maxwell & Moore, Inc., Bridgeport, Conn. Mem. ASME.

Contributed by the Power Division and presented at the Spring Meeting, Washington, D. C., April 12-14, 1950, of THE AMERICAN SOCIETY OF MECHANICAL ENGINEERS.

NOTE: Statements and opinions advanced in papers are to be understood as individual expressions of their authors and not those of the Society. Paper No. 50-S-24.

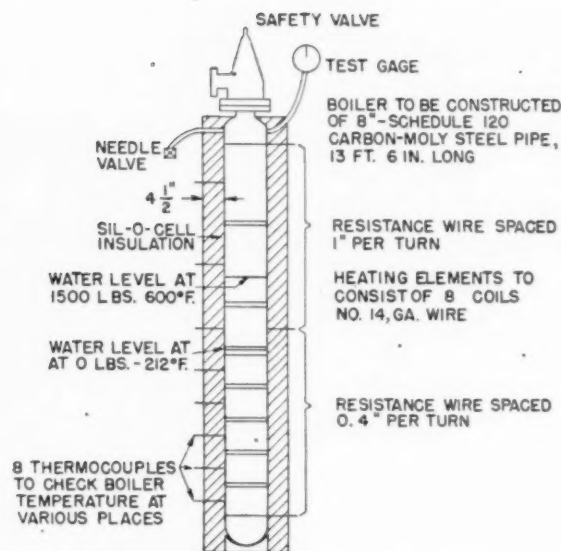


FIG. 1 DIAGRAM OF LABORATORY TEST BOILER

which was added before attaching the valve. Heat was supplied by eight separate electric resistance elements wound around the outside of the pipe, the connections so arranged that the heating elements could be connected in several different combinations to provide the desired degree of heating. Thermocouples were placed at various positions on the boiler to insure that no sections became overheated. This steam generator proved to be entirely satisfactory for the work, and pressure could be controlled easily by proper manipulation of the connections of the heating elements.

Test Technique. The valve could be made to pop with this boiler, but early tests indicated that popping was not essential to the investigation of sealing. The technique finally used for sealing tests was about as follows. The boiler pressure was raised slowly, the power being shut off as soon as rapid leakage started, so that the valve did not usually pop. With this method of testing, the valves leaked more rapidly and to lower pressures than they normally would in service. This is partly because, when a valve closes after popping, it closes with considerable impact, which assists in obtaining tightness.

The pressure at the time rapid leakage started was considered as the popping pressure; for most tests it ranged between about 1100 and 1250 psi. To facilitate comparison among various tests, pressure data are reported as per cent below the popping point.

Leakage was measured by condensing the leaking steam, an aspirator being used to pull the steam through the condenser. Leakage rates are reported as cubic feet of steam at atmospheric pressure per hour. Leakage rates ranging from about 6 to 600 cu ft per hr could be measured.

As part of the fundamental investigation, some early tests on the valves were made using tank nitrogen as a source of high-pressure gas. Leakage with nitrogen was determined by measuring the rate of displacement of known volumes of water from a burette connected to the steam outlet of the valve.

Preliminary Tests. The results of sealing tests with nitrogen indicated that misalignment of the various parts of the valve within plant tolerances had little effect on sealing. It was found that considerable improvement in sealing with nitrogen could be realized by using a higher-polished finish on the seating surfaces.

Tests with steam, however, indicated that sealing was not improved by the better finish on the seating surfaces.

Characteristics of Sealing With Nitrogen and Steam. The steam tests did reveal that sealing with steam was radically different from sealing with nitrogen. At 10 per cent below the popping point, steam leakage was found to be about 600 times greater than with nitrogen; and at the normal closing pressure of 4 per cent below the popping point, steam leakage was estimated to be several thousand times greater than the leakage obtained when testing with nitrogen. It was then realized that sealing as obtained with nitrogen was undoubtedly adequate for service requirements, and efforts were then directed toward defining the differences which existed between testing with steam and testing with nitrogen. A major difference between sealing with steam and sealing with nitrogen was noticed in leakage tests with successively increasing and decreasing pressures. This is shown graphically in Fig. 2. The upper curve, for nitrogen, shows that the rate of leakage gradually increased as the pressure increased. Only very moderate leakage occurred until the popping pressure was reached. On reducing the pressure, after leaking rapidly at the popping point, the leakage rate was only slightly greater than when the pressure was increasing.

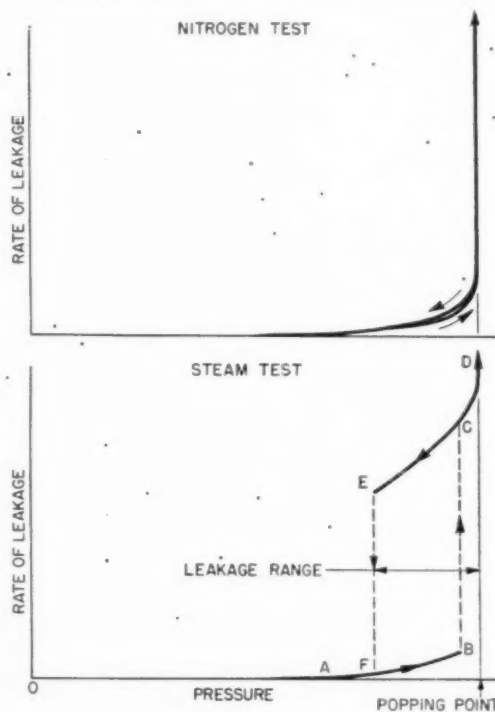


FIG. 2 LEAKAGE-PRESSURE RELATIONS WITH STEAM AND NITROGEN

With steam, a very different situation existed. As the pressure was increased from a low value, leakage at first gradually increased, as with nitrogen, along the line AB. At some pressure slightly below the popping point, such as B, the leakage suddenly increased to an enormously high value along the line BC. If pressure were still further increased, leakage increased slowly until it was sufficient to cause the valve to pop. However, if at point C the pressure were decreased, the line CB could not be retraced; instead, the leakage remained quite high to a much lower pressure, as shown by the line CE. At point E, leakage

died down suddenly to a normal value F , and if pressure were increased at that point, leakage would then retrace the line FB . The difference in behavior of the two gases was striking, and it was evident that if the reasons could be discovered, a solution to the problem of poor sealing could probably be devised.

It was first thought that the effect of the leaking steam might be to introduce thermal gradients in the valve body, causing it to distort and force the feather away from its true position. Temperature measurements of the valve body did show that temperature gradients existed. However, when these were eliminated by heating the entire valve to the steam temperature, the improvement in sealing was negligible.

Temperatures of Valve Trim. In a further effort to determine the cause of rapid leakage with steam after leaking had once started, temperatures of the valve trim were studied during a leak test. In a test with Stellite valve trim, thermocouples were welded to the side of the feather, the location of the beads being indicated in the diagram of Fig. 3(a). Although the thermocouples were not protected from the steam, good thermal contact between the thermocouple beads and the feather was assured since the beads were spot-welded to the feather. Fig. 4 shows graphically the temperatures that were recorded during a sealing test.

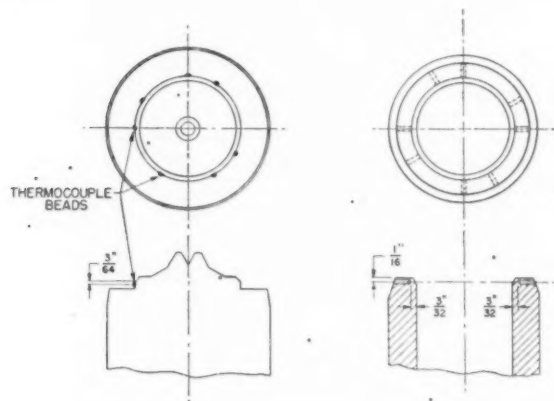


FIG. 3a (left) LOCATION OF THERMOCOUPLE BEADS ON STELLITE FEATHER

FIG. 3b (right) LOCATION OF THERMOCOUPLE HOLES IN TYPE T BUSHING

A similar test was made using the Type T valve trim. For this test, the thermocouples were spot-welded to the bottom of small holes drilled in the seat bushing, so that the thermocouples could be completely shielded from the leaking steam. Locations of the thermocouples are shown in Fig. 3(b). The temperatures at various points around the seat bushing are shown graphically in Fig. 5.

In both of these tests, the valve-trim temperatures were quite uniform up until the time leakage started. At that point, temperatures at several locations dropped considerably. When the valve was leaking badly, severe temperature gradients were observed in the valve trim, the temperature at one point of the feather being more than 200 F below the temperature at another point. As the boiler pressure dropped and leakage became less, the thermal gradients in the valve trim also decreased. When pressures dropped to the point that all leakage had ceased, the valve-trim temperatures had returned to about their original values, and the thermal gradients no longer existed.

It was thus apparent that the leaking steam was cooling the seat surfaces. The temperature differences measured in the

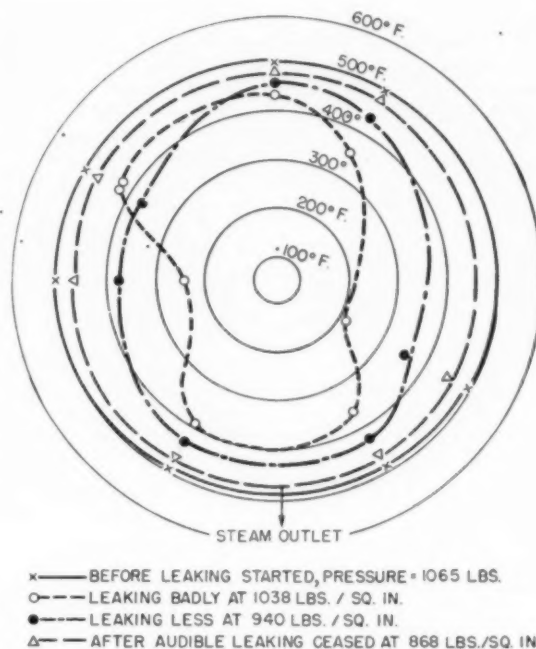


FIG. 4 TEMPERATURES OF STELLITE FEATHER DURING LEAK TEST

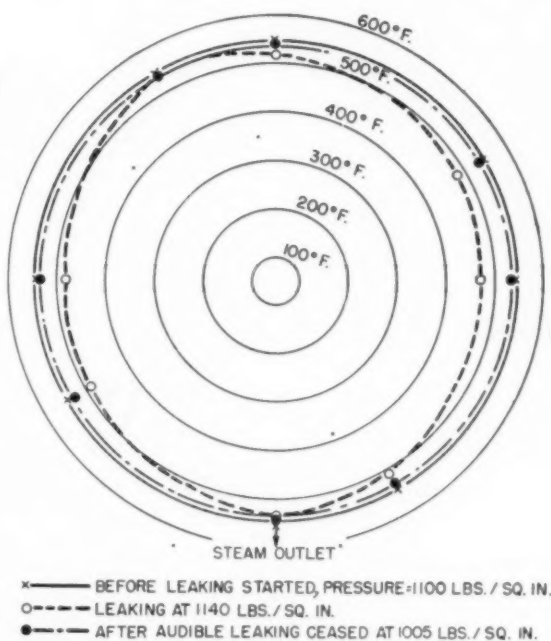


FIG. 5 TEMPERATURES OF TYPE T BUSHING DURING LEAK TEST

seat bushing were less than those noted on the feather for a number of reasons. Leakage was considerably less with the Type T trim than it was with the Stellite trim. The thermocouple beads on the Stellite feather were located practically in line with the steam flow, and would be cooled directly by contact

with the steam. In the seat bushing, the beads were well shielded from the steam, and were located essentially between the cooled area of the seat and the hot body of the bushing, the body of the bushing being maintained at a higher temperature by contact with the hot steam over the entire internal diameter. Thus it seems likely that the thermocouples on the feather measured approximately the temperature of the leaking steam, while the thermocouples in the seat bushing actually measured the temperatures of the seat bushing at a finite distance below the seat surface.

Cooling of Throttled Steam. The thermal gradients found in the valve trim were caused by the cooling of the steam as it expanded through the valve seat. When any gas is allowed to expand through a small orifice it expands in approximately a throttling process, and an imperfect gas will be cooled. The amount of cooling for steam depends upon the initial pressure and the degree of superheat. Fig. 6 shows the degree of cooling induced as steam of various qualities is allowed to expand from different pressures by the throttling to atmospheric pressure. Saturated steam at 1000 psi cools about 250 F when expanded to atmospheric pressure by a throttling process. Nitrogen, a far more perfect gas, cools only about 6 F during throttling from 1500 psi.

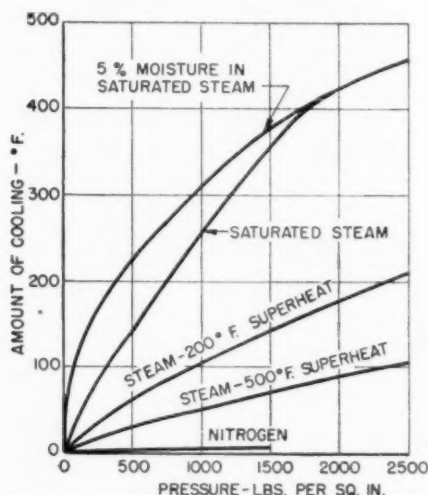


Fig. 6 COOLING OF STEAM AND NITROGEN WHEN THROTTLED TO ATMOSPHERIC PRESSURE

Mechanism of Leakage. From this information a theory of leakage of steam safety valves was developed. If a tiny steam leak exists at some point on the valve seat, the local area near that point is cooled, and the metal tends to contract. This contraction causes deformation of the valve seat in two ways, first, by direct contraction perpendicular to the seating surfaces, and second, by contraction in a direction parallel to the circumference of the seat. Both act to increase the size of the gap between the feather and the seat bushing at the local area of leaking.

Thus, once steam starts to leak through the valve seat, the size of the gap increases rapidly until the rate of leakage is extremely high. When pressure on the valve is reduced, rapid leakage does not stop until the differential force on the feather is sufficient to overcome the warpage caused by the thermal gradients. Thus the reason for the great difference in sealing with increasing pressure and decreasing pressure with steam, and the difference in sealing between steam and nitrogen is explained.

Agreement Between Theory and Experience. Many of the fac-

tors which plant experience had shown to be characteristic of sealing could be explained on the basis of this theory of leakage. Sealing was more difficult to obtain with higher pressures because the cooling effect from the expansion of throttled steam increases directly with pressure, as shown in Fig. 6. Similarly, sealing was worse for saturated steam than for superheated steam because saturated steam cools more when it expands in a throttling process. The difference in sealing between the turbine-type stainless steel and the Stellite trim could be explained by their differences in thermal expansion, the coefficient of thermal expansion for the Stellite and for the austenitic base both being about 45 per cent greater than for the Type T material.

Possible Methods for Improving Sealing. On the basis of this theory of leakage, several possible means of improving sealing could be considered. These are as follows:

- 1 Keep initial leaking low; if the amount of initial leaking could be kept nil after the valve popped, the self-increasing cycle of leakage could not start.
- 2 Use a seating material with a low coefficient of expansion, since such a material would produce less deformation with a certain degree of cooling. Consideration of various materials divulged that a high-temperature cobalt invar had an expansion coefficient of about 4×10^{-6} per deg C, about 60 per cent less than that of the turbine-type stainless. It appeared that only a limited improvement in sealing might be expected from such an attack.
- 3 Use valve-seat materials with high thermal conductivity, so that the thermal gradients induced in the valve seats would more readily equalize. However, most materials which have high thermal conductivity are not suited for use with high-pressure steam; also, only a limited degree of improvement could be expected from this attack.
- 4 Reduce thermal gradients in the valve seat by providing a short heat path between the seating surfaces and the hot steam.
- 5 Decrease the rigidity of the valve seats, so that less pressure differential would be required to overcome any distortion of the valve seat.

New Design of Valve Seat. It was soon apparent that a change in design of the valve seat offered the best means of minimizing the characteristics responsible for poor sealing. Accordingly, a new type of valve seat was designed, in which the seating surfaces were undercut to provide relatively thin seating surfaces. Fig. 7 shows a drawing of the modified valve seat. Three advantages were expected of this design; these are listed as follows:

- 1 Thermal gradients in the valve seat would be reduced. The cooling effect of the steam as it leaked would be counteracted by the hot steam on the back of the thin elements. This would provide a high rate of heat transfer, and any cool sections on the seating surfaces would be effectively heated.
- 2 The thin elements could deflect easily under very slight differential pressures, and readily accommodate any warpage or distortion of the seating surfaces.
- 3 The entire force of the steam pressure would act to hold the thin edges of the seat closed. Because of this, it was expected that sealing would be largely independent of the spring load on the valve seat.

A detailed drawing showing dimensions of the first experimental valve seat of this design is shown in Fig. 8. The seat was designed so that when the full load of the spring was on the feather, or during the impact of closing after a pop, the thin edges would deform elastically, so that the load would be carried by the thicker portions of the valve trim. However, when steam pressure was such that the spring load exceeded the gas pressure by only about a hundred pounds, the entire load would be

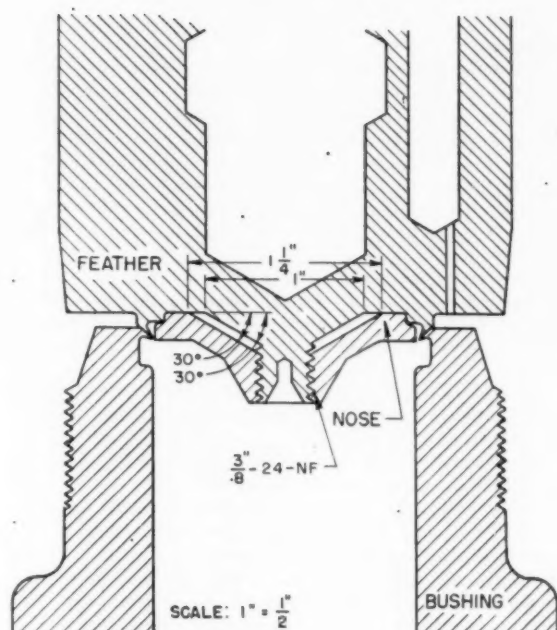


FIG. 7 ASSEMBLY DRAWING OF NEW-DESIGN VALVE SEAT

carried by the thin portions, so that the seat would be quite flexible in the range of pressure where poor sealing occurs.

Although this design has been considered from the aspect of a conical-seated valve, it should be equally applicable to designs of flat-seated valves.

Laboratory Sealing Tests With New Design of Valve Seat. Sealing tests were made with the new design of valve seat, as well as with a conventional valve seat of the Type T material. Prior to the steam tests, both types of valve trim were tested with nitrogen to insure that no serious defects existed in the seating surfaces.

The results of the sealing tests with steam are shown graphically in Fig. 9. With both types of trim, steam leakage was small at first and fluctuated considerably. The maximum values of leakage with the conventional seat were reached after the pressure had dropped to between 1 per cent and 5 per cent below the popping point. This simply indicated the finite time required for the thermal gradients and deformation of the valve trim to develop after the initial leaking started.

Characteristics of the sealing tests are discussed in the following paragraphs.

Type T Trim. With nitrogen, this set of valve trim was found to seal about as well as those which had been tested previously. The leakage curve for the Type T trim is the basis for judging the sealing characteristics of the modified design.

New Seat Design. The great improvement in sealing with the new-type valve seat is clearly indicated by the data. When tested with nitrogen, sealing with this trim was about comparable to that of the conventional seat. When tested with steam, leakage with the new design at 4 per cent below the popping point was as low as with the conventional valve seat at 12 per cent below the popping point. It had been expected that initial leakage would be lower for the new design than for the conventional trim, owing to the flexibility of the seating surfaces. However, the tests with nitrogen indicate that initial leakage with the new design was probably quite comparable to that ob-

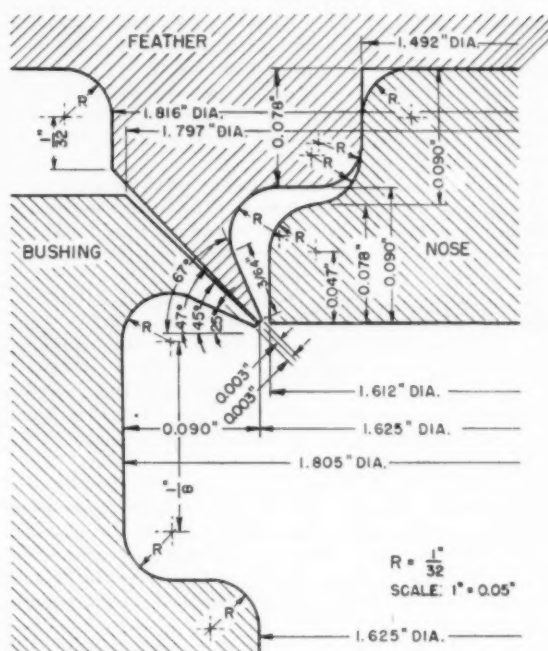


FIG. 8 ENLARGED VIEW OF NEW-DESIGN VALVE SEAT

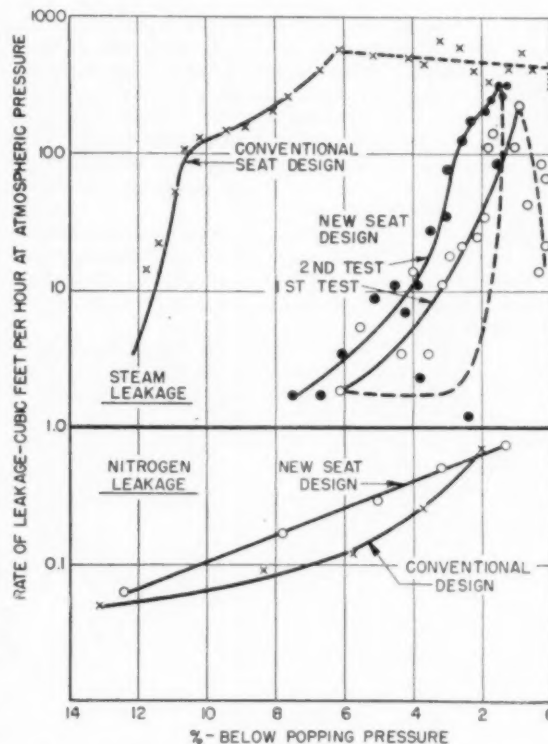


FIG. 9 SEALING TEST DATA WITH TWO VALVE-SEAT DESIGNS

tained with the Type T trim. Thus it seemed that the excellent sealing with steam must have been due in a large part to the better heat conduction to the seating surfaces.

Plant Tests With the New Design. Since such excellent results had been obtained in sealing tests with the new design of valve seat in the laboratory, it was sent to the plant for further investigation and development.

The first step in this was an exhaustive test of the valve which had been tried out in the laboratory. The valve was tested at 1200 psi steam pressure over a period of some three weeks, the valve being tested periodically by popping and then being left under loading for a period of time.

At the end of the testing, the valve having been subjected to a total of some 200 pops, the seats were examined. There were no signs of seat deformation or failure, although some wear had occurred on the seating surfaces.

This indicated that the idea embodied in the undercut seat was of a sufficiently rugged nature that it would withstand continuous service blowing, and that the research results should be developed into a practical design.

Development of the Thermosdisc Design. An analysis of expected field conditions naturally showed that it would be desirable to incorporate the design changes only in the feather, inasmuch as this part would offer the best opportunity for replacement when wear occurred. Undercutting of the bushing could be done, but slight wear might necessitate replacement of the bushing, which is a more difficult task.

Accordingly, the development was aimed at developing a design which would give the required heat conductivity and flexibility without embodying any fundamental objection in the way of field maintenance.

Further analysis of past experience showed that if the seat were made so thin as to be very flexible at the lower edge, as had been first proposed, there was more danger of potential damage to this seat from grit passing through the safety valve. This is based on experience, particularly with superheater valves, from the fact that very hard particles in the steam actually pit and abrade the noses of the safety-valve feather disks. It could easily be seen that a durable edge on the undercut seat would be desirable.

In addition to this factor, making the seat edges quite thin would result in very close tolerances in manufacture and would increase the cost of the design.

With all of these considerations in mind, a large number of variations in angles, thicknesses, and depth, were tried out, finally arriving at a thickness of 0.012 to 0.015 in. at the bottom edge of the seat, with a slightly deeper recess than had been indicated in the original design.

Plant Tests of Thermosdisc Design. Having determined the design which seemed to be most practical from the field-service viewpoint and from the manufacturing viewpoint, a series of

breakdown tests to determine the feasibility of the design were carried out.

One of these tests consisted of the continuous popping at 1200 lb of one of the seat elements over a period of time. The valve was blown rapidly and continuously for a total of 200 times and then was subjected to chatter or very rapid popping to determine whether seat damage would occur from this type of operation.

At the end of the test, the valve seat showed no damage in so far as breakdown of the seating element was concerned, although the seating surfaces showed wear, and a slight amount of leakage had developed.

A test for measuring the fatigue life of the seat element was worked out using a cam-operated weight-loaded device which dropped the seat for the distance of its normal lift with a weight of 200 lb, so the disk would strike the bushing with considerable force.

With this mechanism, the seat was subjected to a test of 80,000 cycles to determine whether or not fatigue of the seat element would develop.

At the end of the test, the disk and seat were still structurally perfect and showed no signs of fatigue failure.

Service Results With Thermosdisc Design. The first experimental Thermosdisc seats were put into service in late 1944 and initially resulted in a tightness comparable with that which had been realized experimentally during the research development phases. It was found necessary to incorporate a deflecting piece on the nose of the Thermosdisc comparable in contour to the older solid-disk design in order to eliminate a high-pitched noise which originated, apparently due to the recess in the seat.

Of the Thermosdiscs which were put into service initially in late 1944, two were later removed for examination and several are still in service at the original plant.

Following the initially successful testing of the Thermosdisc design and the checking of these after about six months' service, early in 1946 a complete change-over of a large high-pressure utility was made, all of the Thermosdiscs giving very good results as to tightness and operating characteristics during this installation.

Since that time, several hundred of the Thermosdiscs have been put into service with equally good results, at pressures ranging up to 2650 psi.

ACKNOWLEDGMENT

This research was done in co-operation with Manning, Maxwell & Moore, Inc. Their permission to publish these results is greatly appreciated.

The work at Battelle was under the direct supervision of Dr. H. W. Russell and Dr. R. W. Dayton. Their assistance throughout the work was very helpful. The idea for modification of the valve-seat design was conceived by Dr. Dayton.

New Method for Bulk-Modulus Determinations

By S. LOGAN KERR,¹ L. H. KESSLER,² AND M. B. GAMET³

The bulk modulus of fluids other than water has not been reported in engineering literature to any extent, particularly in the range of pressures and temperatures ordinarily encountered in petroleum pipe-line work. In pipe-line work it is desirable to make surge investigations in advance of construction, and this requires some knowledge of the pressure wave velocity in the system for computing the magnitude of surges which may be expected in ordinary operating or in emergency conditions. While the physical characteristics of the materials and construction of the pipe line itself are known, the same is not true of the physical characteristics of the liquid. This paper relates to a method of determining the bulk-modulus values of fluids other than water to make available the missing factor in pipe-line design considerations.

INTRODUCTION

IN any computations concerned with so-called "water-hammer" or surge conditions occurring when the flow rate of a liquid is changed in a closed conduit, the compressibility of the liquid and the elasticity of the conduit walls have a major effect upon the magnitude of the surge, as well as its distribution along the conduit.

The magnitude of the surge is directly proportional to the velocity of the surge wave and this, in turn, is affected by the diameter, thickness, materials of construction, and modulus of elasticity of the pipe walls. The character of the liquid in the pipe line also enters into the conventional equation for surge-wave velocity, with both specific gravity and compressibility affecting the values. The conventional formula for surge-wave velocity is as follows

$$a = 12 \sqrt{\frac{w}{g} \left(\frac{1}{k} + \frac{d}{Ee} \right)} \quad [1]$$

where

- a = velocity of pressure wave, fps
- w = weight of 1 cu ft of liquid, lb
- g = acceleration due to gravity, ft per sec²
- d = diameter of pipe, in.
- e = thickness of pipe walls, in.
- k = bulk modulus of compressibility of liquid, psi
- E = modulus of elasticity of material of pipe walls, psi

The specific gravity under various temperatures and pressures can be determined without great difficulty. The compressibility

factor, more commonly expressed as the bulk modulus of compressibility, is not so easily arrived at.

The bulk modulus can be calculated as follows

$$k = \frac{\Delta p}{\Delta V} V \quad [2]$$

where

- k = bulk modulus of liquid, psi
- Δp = pressure increment, psi
- ΔV = volume decrement produced by pressure increment Δp
- V = original volume in same units as ΔV

The bulk-modulus value for water at ordinary temperatures and pressures has been reported in a number of publications and is commonly taken as 300,000 psi for most surge calculations.

The bulk modulus of fluids other than water has not been reported in engineering literature to any great extent, particularly in the range of pressures and temperatures ordinarily encountered in petroleum pipe-line work (0 to 1500 psi, and 32 F to 100 F).

To make surge investigations in advance of construction of a pipe line requires some knowledge of the velocity of the pressure wave within the system for computing the magnitude of surges which might be expected due to ordinary routine operation or due to emergency conditions.

The physical characteristics of the materials and construction of the pipe line itself are fairly well known. The remaining factor relates to the physical characteristics of the liquid, and it is to these matters that attention is directed in this paper.

REVIEW OF LITERATURE

Some of the earliest work done on the determination of surge-wave velocity in liquids other than water was in connection with the studies of fuel-injection systems for Diesel engines.

Unfortunately, the investigations were carried out at fairly high injection pressures in the range from 1000 to 6000 psi, or even greater, and very little information is available for pressures below 1000 psi. The variation of compressibility or variation of bulk modulus with temperature has also been investigated to some extent, but here, too, the experiments were conducted at pressures on the order of several thousand psi and did not cover in detail the range in which petroleum pipe-line designers are primarily interested. There is included at the end of this paper a brief Bibliography listing some of the important references.

In almost every case, the determinations have been made by measuring, as accurately as possible, the quantity of additional volume of fluid required to compress the initial volume of material to various pressures. The means of measuring the increment of volume are varied, and some of the apparatus used a precision measurement of the displacement of a piston and in other cases a mercury pump was employed.

Hyde (1)⁴ measured the position of a sleeve on a plunger (8 mm bore and 12 cm long) before and after the application of pressure and determined the decrease in volume of the liquid in the small cylinder having a volume of 15.56 ml. Tyrer (2) worked at not more than 2 atm pressure with soft soda-glass and copper com-

⁴ Numbers in parentheses refer to the Bibliography at the end of the paper.

¹ Consulting Engineer, President, S. Logan Kerr & Company, Inc., Philadelphia, Pa. Mem. ASME.

² Professor, Civil Engineering Department, Northwestern Technological Institute, Evanston, Ill.

³ Associate Professor, Civil Engineering Department, Northwestern Technological Institute, Evanston, Ill.

Contributed by the Hydraulic and Petroleum Divisions and presented at the Semi-Annual Meeting, St. Louis, Mo., June 19-23 1950, of THE AMERICAN SOCIETY OF MECHANICAL ENGINEERS.

NOTE: Statements and opinions advanced in papers are to be understood as individual expressions of their authors and not those of the Society. Manuscript received at ASME-Headquarters, April 20, 1950. Paper No. 50-SA-32.

compressibility piezometers of 500 ml capacity. He attempted to change the pressure and measure the volume change before any of the heat produced in compression had been lost.

Le Mesurier and Stansfield (3) used the device shown in Fig. 1; *A* is a steel cylinder with vent plug *B* and gland *C* fitted with a slow-speed engine fuel-pump piston *D* surrounded by split washer *E* at the outer end. *E* is held tightly in place with a spiral spring *F* surrounding the groove in the halves of the washer. The inner cylinder was filled with test fluid and lowered into the outer cylinder *G*, which was filled with fluid at the same temperature as the sample. The outer cylinder was sealed by cap *H*. Pressure was applied directly to oil in *G* and to plunger *D* and hence to sample in *A*, the washer being in contact with the outer end of gland *C* moved a distance proportional to the decrease in volume of the test sample. When direct pressure was released, the plunger was forced out of the gland by the expanding sample and carried with it the washer. Measurement of movement of the washer allowed the volume change of the oil when under pressure to be calculated from known dimensions of the plunger. No dimensions of the device are given. Le Mesurier assumed no strain in the material of the test vessel, because of balanced pressures, but Davies (3) states that there is a stress present, although Le Mesurier believed it to be so small as to be negligible.

Talbott (4), Fig. 2, used a copper tube screwed to the cover of a thin sealed vessel *A*, fitted with an insulated filling cup *B* at its upper end, and a copper pot *C* at its lower end. A fine platinum wire was attached to the filling cup and passed a short distance down the center of the tube. The inner vessel was surrounded by a cylinder of adequate strength, the liquid to be tested was placed in the inner vessel, and mercury was poured into the tube and copper pot to form a mercurial seal. The space between the inner and outer vessels was filled with distilled water, and hydraulic pressure was applied. This pressure was transferred through the mercury to the test liquid so that the inner vessel contracted in volume as a solid under hydrostatic pressure until the circuit was completed when the mercury contacted the platinum wire. The entire apparatus was surrounded by a water bath.

Cap *D* was removed and mercury added or removed until the electric contact was broken at atmospheric pressure. A weighed quantity and, therefore, a known volume of mercury was added to the filling cup, and the pressure necessary to break the contact was found. The pressure was measured by an optical gage, and a lamp indicated when contact was broken. A telescope and scale were used for the pressure gage, and the lamp was placed in the field of view of the telescope.

Talbott's experimental results were corrected for decrease in volume of the containing pot, the compressibility of the mercury, and for rise in temperature due to compression, because he applied maximum pressure in 10 sec.

These experimenters used devices employing a thin-wall test chamber and balanced the internal and external pressures, but apparently did not use dead-weight testers for pressure application or to determine unit pressure applied. In all of these instances, however, the volume and pressure increments were read when the apparatus was under pressure. Some question has been raised as to the accuracy of these measurements, particularly in relation to leakage from the apparatus, leakage past a piston or stuffing box, or the displacement of the liquid within the pressure-measuring device.

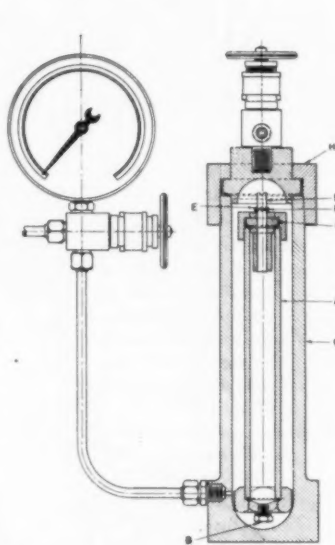


FIG. 1 LE MESURIER AND STANSFIELD'S TEST APPARATUS

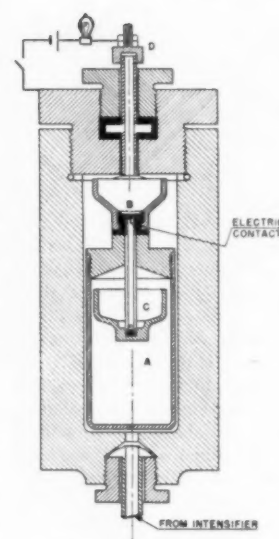


FIG. 2 TALBOTT'S TEST APPARATUS

JOINT SURGE CONFERENCE

During investigations authorized by a Joint Surge Conference, set up to study the surge conditions within petroleum pipe lines, particularly those carrying crude oil, the need for accurate data on the compressibility factor was immediately apparent.

Some determinations had been made experimentally, but it was finally agreed that an independent investigation would be desirable to check the bulk modulus for the particular oils being transported under conditions existing during the field-test work.

A conference was arranged between the three authors of this paper to conduct a program of tests⁵ in which the effect of variations of temperature and pressure on bulk modulus within ordinary ranges could be determined, using a small sample of the actual fluids flowing through test pipe lines. It was felt that certain basic-design conditions for the apparatus should be fixed to avoid the potential errors believed to be present in the methods used in other investigations.

These fundamentals of design were as follows:

- 1 The apparatus should eliminate leakage or slip in relation to the measurement of the volume increment.
- 2 The apparatus should eliminate, in so far as possible, any effect of volume change due to the pressure-measuring device.
- 3 The apparatus should incorporate a dead-weight-gage tester for basic pressure measurement and avoid the use of a Bourdon-tube-type pressure gage, except for approximate indications.
- 4 The volume change of the apparatus itself under varying pressures and temperatures was also to be kept at a minimum.
- 5 The measurement of the increment of volume (ΔV) was to be made at atmospheric pressure and under conditions whereby this increment could be read to an accuracy of 1 per cent or less.
- 6 The over-all accuracy of the bulk-modulus determination at any given temperature or pressure should be within plus or

⁵ These tests, made in 1949, were part of a program instigated by the Joint Surge Conference of individuals representing Middle East Pipelines Limited, Trans-Arabian Pipe Line Company, and Gulf-Shell Pipe Line. The test results are included in the "Final Report of Joint Surge Conference" (13), which has been made available to the national engineering societies and to interested individuals and companies.

minus 2 per cent on an individual run and within plus or minus 1 per cent on a series of runs, using an average curve through the individual test points.

It was immediately apparent that with this basis for design, none of the apparatus described in the various technical publications could be used. Therefore a new design was developed to perform these experiments in a completely different way from that described in the literature listed in the Bibliography.

Instead of measuring the quantity of liquid required to raise the pressure a given amount, by observing the displacement of a column of mercury or a piston, the new apparatus was arranged to build up the pressure to the desired value, as measured by a dead-weight-gage tester. The pressure was then constant throughout the system, and by closing a valve it was possible to trap the total volume (initial V plus ΔV) within the pressure chamber.

The pressure was relieved by gradually opening a valve connected to a precision-graduated microburette until atmospheric pressure was reached. The difference between the initial reading and the final reading on the calibrated glass tube represented the increment of volume released and thus gave the value of ΔV . The initial total volume V of the chamber was determined by dimensional measurement and also by a volumetric check to be 290 ml.

As the increment of pressure is from atmospheric up to the desired test value, the gage pressure as determined by the dead-weight tester represents Δp in Equation [2].

DESCRIPTION OF APPARATUS AND DETAILS

A thick-walled, cylindrical, steel pressure vessel A in Fig. 3 ($5\frac{1}{4}$ in. OD and 2 in. ID) was machined with the top of the cylinder containing an annular slot C or mortise of rectangular cross section to act as part of the seal for the test fluid. The inside bottom of the cap B was machined as a cone D of $2\frac{3}{4}$ in. diam with an annular V-shaped tenon E machined to fit into the mortise of the cylinder without the tenon touching the upper corners of the mortise. Hard solder wire was cut, lapped, and placed within the mortise. The V-shaped tenon was forced into the solder by tightening six $\frac{3}{8}$ -in. stud bolts F , so that a perfect fluid seal was formed. The design causes all entrapped air or gas to be forced out through the vertex of the cone.

To introduce fluid under pressure into the vessel, measure its temperature, and discharge compressed fluid upon release of pressure, suitable threaded adapters G with copper gaskets were fitted into the top of the cap with small holes extending through the cap into the pressure chamber. The small thermometer well H of stainless steel to contain thermocouple wire was first press-fitted into the cap.

A $\frac{1}{8}$ -in. steel needle valve I was screwed into the inlet adapter, and a second valve J was fitted to the relief adapter. At the top of the discharge valve there was fitted a metal-to-glass adapter, machined and ground with a tapered hole to fit precisely the male end of a standard ground-glass Pyrex tube.

Fig. 4 shows the general arrangement of the apparatus. The test vessel is mounted within a steel-encased water bath having

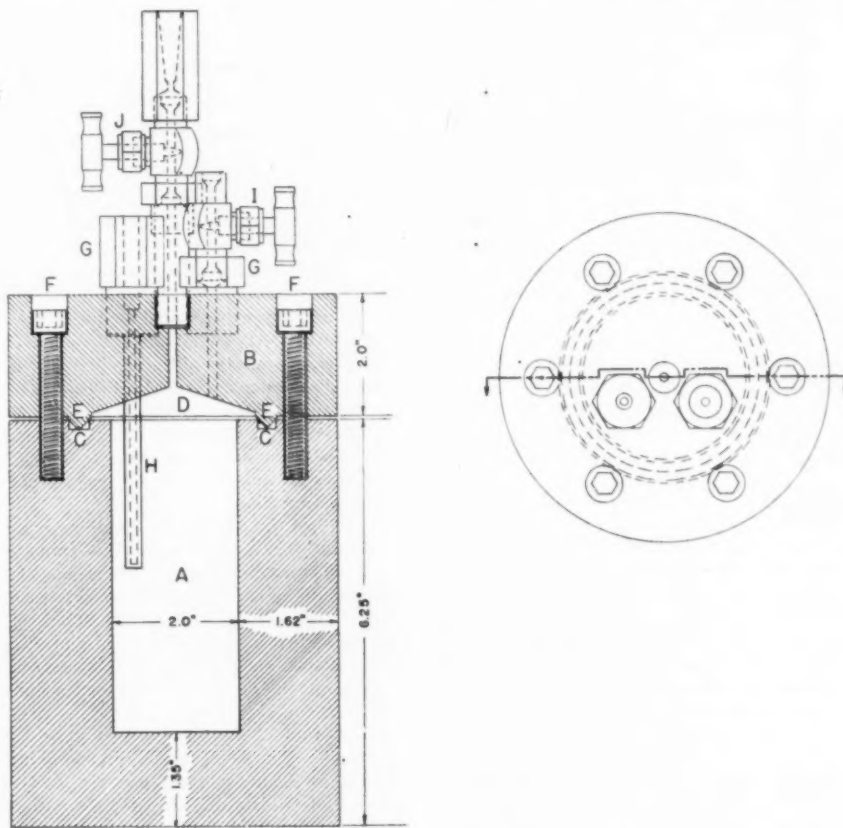


FIG. 3 CROSS SECTION OF TEST VESSEL—NORTHWESTERN UNIVERSITY

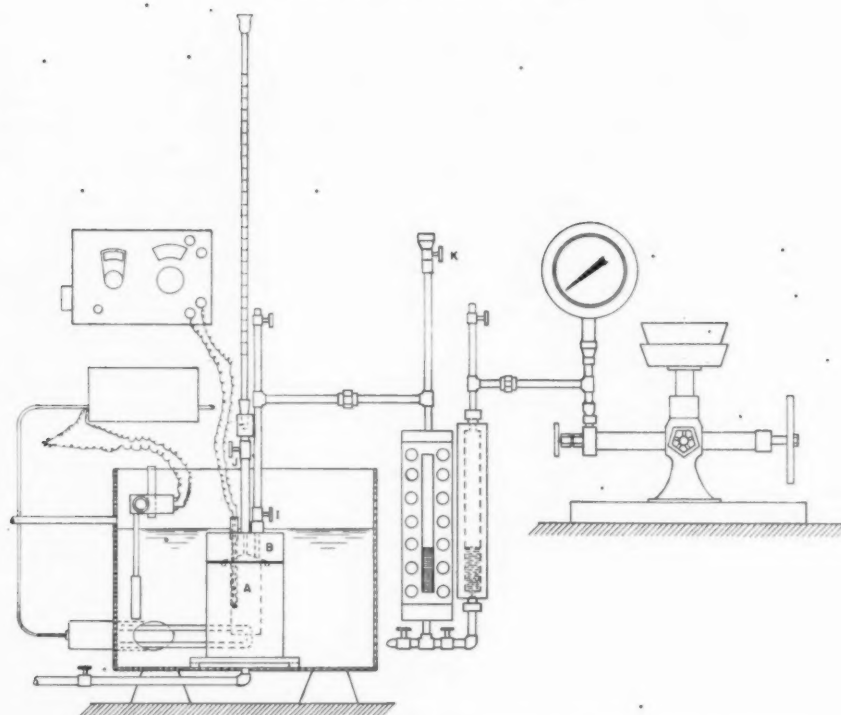


FIG. 4 ASSEMBLY OF BULK-MODULUS TEST APPARATUS AT NORTHWESTERN UNIVERSITY

inlet water and drainage connections. A 750-watt immersion heater and thermoregulator controlled the water-bath temperature. A potentiometer was connected to iron-to-constantan thermocouple leads inserted in the temperature well.

To segregate the test fluid from the fluid in the dead-weight gage tester, the inlet valve to the pressure chamber was connected by $1/8$ -in. pressure-transmission pipes to a U-tube-type mercury piston, one leg of which was a 2000-psi pressure chamber sight-gage glass, and the other leg a machined steel cylinder connected to a 5000-psi dead-weight-gage tester. Valves were used at high points of the transmission piping to release all gases or air from the system.

Three standard calibrated microburettes with Pyrex tapered adapters of 2.0, 3.0, and 5.0 ml capacity, each reading to 0.01 ml, were used to determine fluid-volume displacement from the test vessel.

In addition, the glassblower made from carefully matched serological pipettes, three other microburettes as follows: One of 0.2 ml capacity from two 0.1 ml; another of 0.4 ml capacity from two 0.2 ml; and a third of 2.0 ml capacity from two 1.0 ml. All were graduated to 0.01 ml and can be easily read to 0.001 ml. These small-capacity burettes give great accuracy in determining small volume changes as a 0.01 ml displacement causes a $5/8$ -in. rise in fluid level in the smallest-diameter burette. Calibrations of all burettes were checked by volume with mercury.

Tests proved the steel valves and pressure-transmission pipes were absolutely tight. One characteristic of all dead-weight testers is that continuous rotation of the piston is necessary and that after a 30-min period, some oil from the tester slips by the piston up into the surrounding cylinder, requiring adjustment of the handwheel to maintain weights and pan at constant level. This in no way affects the magnitude of unit pressure exerted on

the mercury piston in Fig. 4, as long as the pan is not allowed to rest on top of the fixed cylinder.

ESTIMATED ACCURACY

Using the Lamé formula as corrected by Clavarino for the determination of tangential and radial unit stresses in a thick-walled hollow cylinder under internal pressure only, theory indicates that the maximum change in total volume of the test vessel of 0.0043 per cent would be practically negligible between 25 and 1500 psi maximum internal pressure.

However, the opening of the gap between the cap and cylinder at the seal needed investigation. Seven SR-4 electric strain gages were fastened to the test vessel, in such positions that radial tangential deformations and opening of the gap were determined, in microinches per inch. According to theory, radial and tangential stresses are zero at the outside surface of the vessel, and the tests confirmed this.

At 1500 psi there is 885 lb of pull on each of the six bolts of the cap, or 16,500 psi stress in the shank, and the seal never leaked. The average increase in measured opening of the gap was 225 millionths of an inch. This is a displacement of the contents of the test vessel (290 ml) of 0.0108 ml, or 0.0037 per cent. The total calculated change in volume of the test vessel caused by all stresses is about 0.008 per cent or 0.79 per cent of the volumetric displacement in the microburette, based upon test results with gasoline.

To be sure that the test vessel could be used without placing the vessel within an equalizing pressure chamber as would be essential for higher working pressures, confirmatory tests, described in detail later in this paper, were run to check values on the bulk modulus of distilled water free from dissolved oxygen as reported by other investigators. The values of the modulus

for water came within the range of values determined by others. It is believed this new test device can be used to obtain bulk moduli with errors not exceeding 2 per cent on any liquid during an individual run at the highest test pressure which is 1500 psi.

TEST PROCEDURE

Fig. 5 shows the apparatus under simulated test conditions. Before undertaking a series of runs, the test vessel is thoroughly cleaned with carbon tetrachloride, and the lower portion of the cylinder filled with the fluid to be tested. A dry rag is used to wipe a thin film of mercury onto the surface of the V-shaped lead seal. The cap is connected to the cylinder tightly so as to withstand 2000 psi, and the remainder of the cylinder and conical dome is filled with fluid. The vessel is placed in the water bath, and transmission pipes are connected as in Fig. 4. The fluid and the test chamber are brought to uniform test temperature using either ice or heated water. It may take 30 min or more before the temperature levels off, and during this time the fluid temperature is read by the potentiometer.

Mercury is placed in the bottom of the U-tube, and pipes connecting the leg to the test vessel are filled with fluid. A medium-weight lubricating oil is used in the dead-weight tester, the connecting piping, and the leg of the U-tube away from the test vessel.

A pressure of a few pounds is placed on the system. Bleeder valves are opened to flush out all entrained air or gases and are then closed. One of the calibrated pipettes of suitable volume for the estimated displacement of test fluid is selected. The ground tapered joint is greased with a solvent-resistant stopcock grease and is heated slightly before the taper is pushed into the adapter. The fluid content of the test vessel is then placed under atmospheric pressure with the burette always open at its top.

With inlet and discharge needle valves *I* and *J* open, a slight pressure by dead-weight tester is exerted on the oil, which is

forced against the mercury U-tube, and the same pressure is transmitted by displacement of this mercury piston to the fluid in the test vessel. The test fluid rises into graduated section of the microburette for a first reading at atmospheric pressure.

Upon closure of the discharge valve a small quantity of fluid is displaced upward which increases the first reading of fluid in the burette to the exact initial value used in the test data. Opening of the valve causes a lowering of fluid in the burette equal to the quantity displaced by movement of the valve needle. The required number of weights are placed on the pan of the tester. Pressure is then applied through the tester until the pan connected to the piston of the tester is elevated about $\frac{3}{4}$ in. above the surrounding cylinder. Weights, pan, and piston are spun continuously during application of pressure to the system. The Bourdon gage is used only as an indication of the unit pressure, to keep the operator from raising the tester piston too high and forcing it out of the cylinder.

As the desired unit pressure is reached, the inlet valve is closed uniformly at a very slow rate. Unit pressure is thus locked within the test vessel. The discharge valve *J* is opened slowly, and the quantity of fluid compressed from atmospheric pressure to the applied higher test pressure is permitted to expand into the burette at atmospheric pressure to an approximate final reading. The discharge valve is then closed slowly to eliminate all error due to the volume displaced by the valve needle. The ultimate rise of fluid in the burette, as read with a magnifying glass, is taken as the true final reading. The difference between the true initial and final readings is the change in volume (ΔV) of Equation [2] caused by re-expansion of the fluid from the test pressure to atmospheric pressure.

Providing there is sufficient volume of fluid above the mercury leg of the piston, the final reading of the burette can become the initial reading for a second test. The burette need not be re-

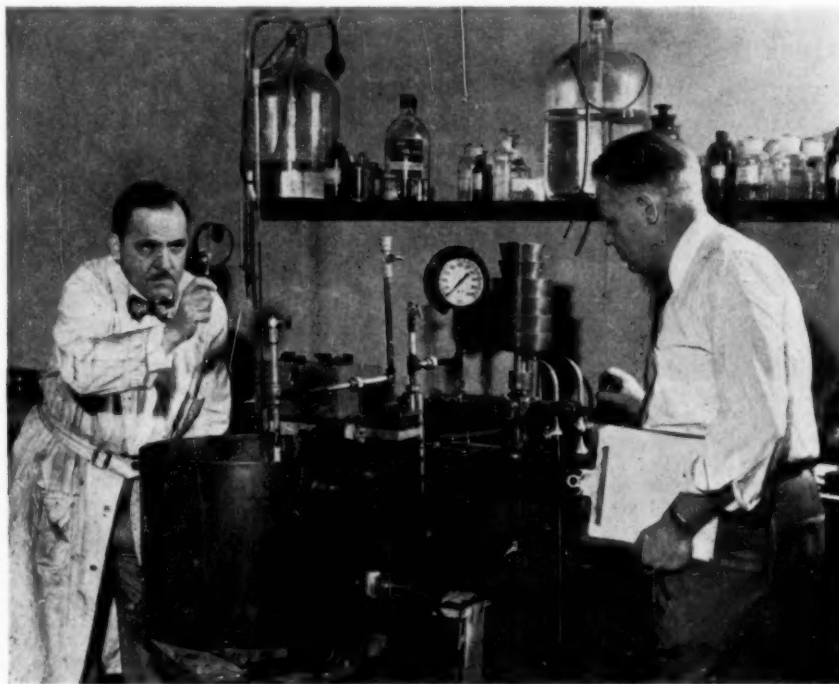


FIG. 5 TEST APPARATUS IN OPERATION

moved for cleaning until such time as the total calibrated length has been wet by the fluid. A strong Alkonox and distilled-water cleaning solution is used at about 200 F to wash test fluids from the inside of the burettes. Burettes are flushed with distilled water and dried by compressed air prior to regreasing the outside of the taper and continued use. Before the mercury in the U-tube is driven past the invert, the bleeder valve *K*, Fig. 4, is opened to atmospheric pressure. Test fluid is poured into the pipe system, and the necessary quantity of oil is removed from the dead-weight tester. Time is then allowed for the fluid in the test vessel again to arrive at the desired test temperature before further runs are made.

COMPARISON WITH PREVIOUS INVESTIGATIONS ON WATER

The experimental techniques were first worked out by preliminary runs on crude oil. These tests were then made on boiled distilled water at 68 F to check the characteristics and behavior of the apparatus on a liquid for which considerable experimental results are available on compressibility at 1 atm and at pressures above 300 psi.

Figs. 6(a and b) show the Northwestern test results, as compared with data reported by thirteen former experimenters. In

experimenters mentioned. Above 50 psi the modulus increases rapidly, until a value of about 300,000 psi is obtained in the neighborhood of 300 psi. Fig. 6(b) shows an enlarged portion of the modulus-pressure curve in the lower pressure range.

It is concluded from a careful study of the runs on distilled water, that the accuracy of the test vessel and appurtenances, and the techniques used in the Northwestern tests are comparable to that obtained with various devices or apparatus of former experimenters. This verification is important as almost all experimenters since Amagat have checked the performance of their test apparatus with distilled water as free from dissolved oxygen as is possible of attainment.

For most work on water hammer at ordinary pipe-line pressures, it is evident that a modulus of 300,000 psi for water is a valid unit, although some engineers use 294,000 and others 310,000 psi. If 300,000 psi is used and 30,000,000 psi as Young's modulus for steel in tension, the ratio of 1/10 in the formula for calculation of the speed of propagation of the water-hammer pressure wave is within experimental error. At ordinary pipe-line pressures, computations are simplified somewhat which is probably the reason for the widely adopted value of about 300,000 psi, plus or minus 3 per cent for bulk modulus of water.

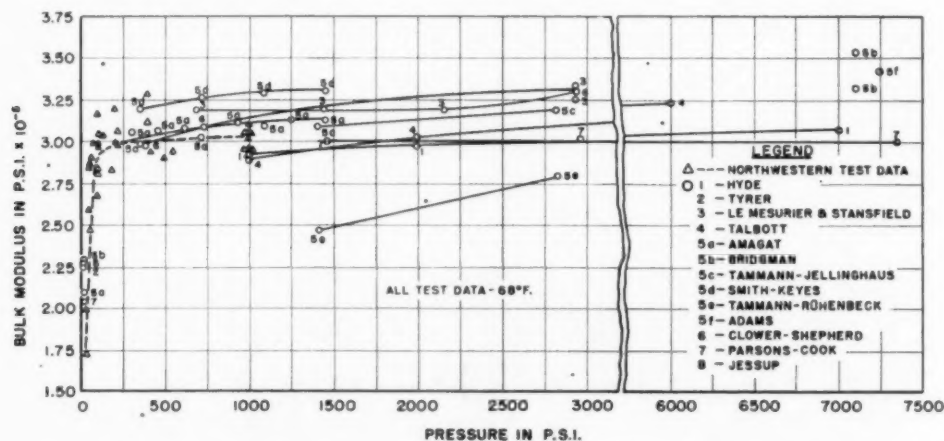


FIG. 6(a) TEST RESULTS ON BULK MODULUS OF WATER BY VARIOUS EXPERIMENTERS

some instances Equation [2] could be used directly, and in others the bulk modulus was computed as the reciprocal of the compressibility C , where C is expressed in atmospheric units, that is, the ratio of the decrease in volume per atmosphere of pressure to the volume of the liquid.

Tyrer (2) worked at 1 and 2 atm only, Amagat (5), Bridgman (5), Parsons and Cook (7), and Jessup (8) give results at 1 atm, in addition to higher pressures, none of which, however, were below 300 psi. All experimenters appeared to be interested primarily in the compressibility of water at high pressures. In most instances, where the experimenters plot data obtained at pressures above 700 psi, they extrapolate the compressibility curve as a straight line into the low-pressure range, assuming the compressibility to be independent of the change in pressure.

Parsons and Cook (7), however, are very definite in showing that water has a bulk modulus of 200,000 psi at atmospheric pressure and 4 C, and a modulus of 400,000 psi at 2000 atm. Wherein this great change takes place is not shown. Northwestern tests show that the modulus is about 200,000 psi at pressure of 25 to 50 psi which is in general agreement with the

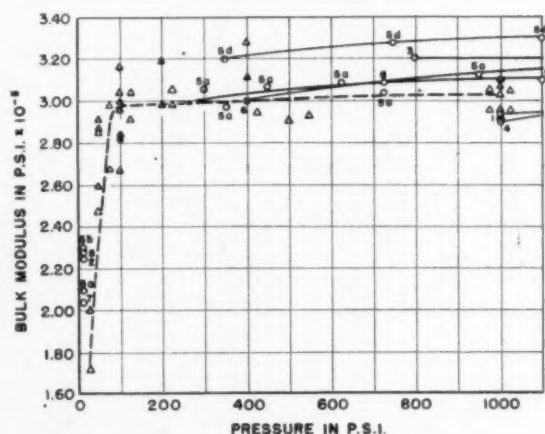


FIG. 6(b) ENLARGEMENT OF FIG. 6(a) FROM 0-1100 PSI

RESULTS ON CRUDE OILS AND GASOLINE

Figs. 7(a, b, and c) show the plotting of test results and the curves established for the two crude oils and gasoline samples taken from the test pipe sections of the field tests utilized by the Joint Surge Conference (13). Samples of 10 gal were shipped in fluid-tight metal containers to the Northwestern Technological Institute Hydraulic Laboratories for these independent bulk-modulus tests. Fig. 8 shows similar test results on G.H. No. 3 crude oil shipped from the Kuwait oil fields on the Persian Gulf.

Four temperatures, 32, 60, 100, and 130 F, were maintained for each of the pressure series for the three crude oils, but the 130 F temperature was not used in the gasoline tests. These temperatures cover the climatic and operating ranges usually experienced in oil-pipe-line work, as well as any appreciable rise in temperature caused by pipe friction. The range in pressure varied from 25 to 1500 psi, which covers the usual operating pressures of oil pipe lines.

At any given pressure the variation of bulk modulus or compressibility with temperature is pronounced. This has been found by all experimenters. No general conclusion can be reached as to the degree of variation with temperature, but in general the three crude oils and the tested gasoline seem to decrease roughly about 700 psi in bulk modulus for each degree Fahrenheit increase in temperature.

Gasoline, Fig. 7(c), at pressures above 200 psi and up to 1500 psi had a relatively insignificant change in modulus with increase in pressure. Below 200 psi, the change in modulus is more pronounced.

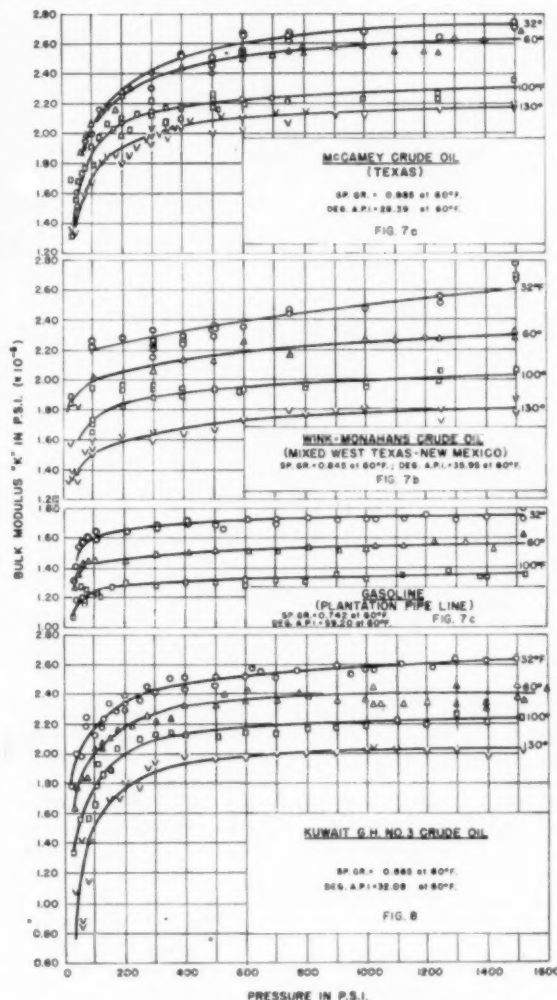
The crudes, Figs. 7(a) and (b), show that above 1000 psi the modulus remains about constant in value for any given temperature. Below 1000 psi, the modulus decreases in some degree as the pressure decreases, and below 400 psi the modulus decreases quite rapidly in some cases. Between 400 and 50 psi at 60 F, the McCamey crude shows a drop of 62,000 psi or 25 per cent; Wink-Monahans crude shows a decrease of 25,000 psi or 12 per cent; Kuwait crude, Fig. 8, shows a decrease of 53,000 or 23 per cent.

Fig. 9 shows a plot of variation of bulk modulus with temperature at a pressure of 1000 psi for the four samples tested. Until considerable additional information is available, it appears evident that petroleum products cannot be tested at just one temperature and a satisfactory conclusion arrived at for the bulk modulus at any other temperatures. In studying the test data of other experimenters, it was impossible, in most instances, to determine the compressibility or bulk modulus at temperatures other than within the range of the test. Water at 1 atm of pressure when tested by four experimenters shows that variation with temperature follows no well-defined law.

COMPARISON OF MEAN COMPRESSIBILITIES OF SAMPLES TESTED WITH WORK OF OTHERS

The test values of bulk modulus in the Northwestern tests were computed also in terms of mean compressibility in per cent from zero to 1000 psi in order to compare results with the study in the American Petroleum Institute progress report made by Jacobson (9). Values are plotted relative to API gravity at 60 F in all cases, Fig. 10. Undoubtedly, other factors than specific gravity modify this simple relationship. Viscosity is one factor as is shown by Matteson (14), where he uses the Cragoe modulus to extrapolate test data on compressibility of oils at 711 psi to values at higher pressures. The authors interpreted the data by Jacobson, et al (9), somewhat differently, and the solid-line curve shows their estimate of the reported test values. An assumed curve has been drawn for 60 F as no data existed for this temperature.

The graphical studies, Fig. 10, show close agreement between the test data used by Jacobson and the Northwestern test data at



FIGS. 7 AND 8 NORTHWESTERN UNIVERSITY TEST RESULTS ON CRUDE OILS AND GASOLINE

the higher pressure. A possible hazard exists in using data plotted in this way, because a small change in per cent compressibility means a much more significant change in the numerical value of the bulk modulus and a consequent error in the surge-wave velocity computation.

COMPARISON OF BULK MODULUS VALUES WITH WORK OF OTHERS

Fig. 11 shows a comparison of the Northwestern test data at about the median of test pressures with actual test data at 32 F and 60 F determined by other investigators. Library research disclosed that very few tests exist at lower pressures. A few tests have been found with a temperature gap as large as from 32 F to 167 F. Gravity in degrees API at 60 F is used as abscissas, as in Fig. 10, but the ordinate is the bulk modulus instead of per cent compressibility. Several experimenters used 50 kg per sq cm or 711 psi, which is the reason for selecting this apparently odd pressure value. Only the temperatures shown could be used, as these were the reported results, and no interpolation or extrapolation of test data is resorted to in the figure.

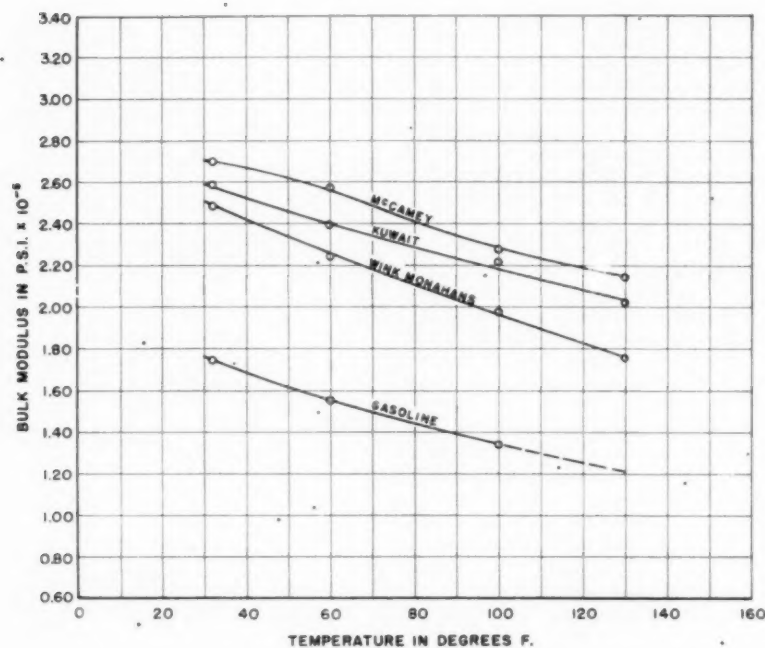


FIG. 9 VARIATION OF BULK MODULUS WITH TEMPERATURE AT 1000 PSI

Fig. 11 shows the apparent variation in bulk modulus with API gravity in a more useful light for liquid-hammer purposes than if per cent compressibility is used. It also gives an opportunity to include a few more test-data points than are shown by Jacobson (9). Curves drawn by the authors indicate that the Northwestern tests are in general agreement with the results by others, but a considerable variation in bulk modulus for a given API gravity is manifest. The graphs indicated to the authors that further investigations are needed in order to arrive at more definite conclusions as to the variation of bulk modulus with specific gravity. By interpolation and extrapolation of existing data with some risk as to accuracy of the conclusions, it is possible to show a relationship between values of bulk modulus of petroleum products and API gravity. Unfortunately, in order to do this, data must be used at pressures substantially above usual pipe-line pressures.

Fig. 12 is similar in scope to Fig. 11, but shows the Northwestern test results at a pressure of 1000 psi for 80 F and at 100 F, compared with the results by others. The points shown are in some cases actual test-data points, but in other cases they are points obtained either by interpolation or extrapolation of actual test data.

The solid-line curves in Fig. 12 are obtained from Jacobson (9), who used data by Jessup (8), Sage and Lacey, et al (12), to determine first the shape of the curve at 1000 psi and 100 F. This made it possible to determine the trend of the curves shown in Figs. 10, 11, and 12, at temperatures where only meager data are available. It appears from these comparisons that Jacobson's curves represent the "minimum" bulk-modulus values for API gravities at 60 F. The dashed-line curves drawn by the authors represent their estimate of an "average" determination of the relation of modulus to API gravity. The dot-and-dash curves show the "maximum" envelope of existing data.

DISCUSSION OF CURVES

Fig. 12 indicates that for petroleum products under a pressure of

1000 psi and with gravity above 90 API, the bulk modulus is a fairly well-defined value.

As the API gravity decreases below that of gasoline at about 60, variation in bulk modulus from the Jacobson curve is more pronounced. When the lower range in gravity is reached, in the neighborhood of the crude oils at API gravity of about 35, the variation is more significant. Fig. 11 shows that the foregoing statements are probably correct for pressures as low as 700 psi, although at that pressure no test data could be found by the authors on products having a gravity greater than 75 deg API. At the lower pressures, the variation in bulk modulus with pressure is even more significant, as shown in Figs. 7 and 8.

COMPARISON WITH FIELD RESULTS

In the field-test program carried out by the Joint Surge Conference, the actual velocity of the pressure wave could be determined, based on the synchronized pressure time recordings at various points along the test sections. The accuracy of this measurement was probably on the order of 1 per cent to 2 per cent, depending on the particular location involved.

By taking the data on the McCamey crude plotted in Fig. 7(a) and interpolating between the 32 and 60 F curves, a 45 F curve can be obtained fairly accurately. This was the temperature existing during the field tests, and the bulk modulus versus pressure is shown as the solid line in Fig. 13(a). If the assumption is made that the compressibility is uniform from zero to 1000 psi or higher, then a line tangent to the curve between approximately 800 psi and 1500 psi can be extrapolated back to zero. This is shown as the broken line in Fig. 13(a). It is believed that this particular procedure has been used in many instances to secure the bulk modulus in the lower pressure ranges.

Table 1 shows the theoretical value of the velocity of the pressure wave, based upon the 45 F Northwestern curve, and that obtained from the extrapolated line. The measured values from the field tests are given for comparison.

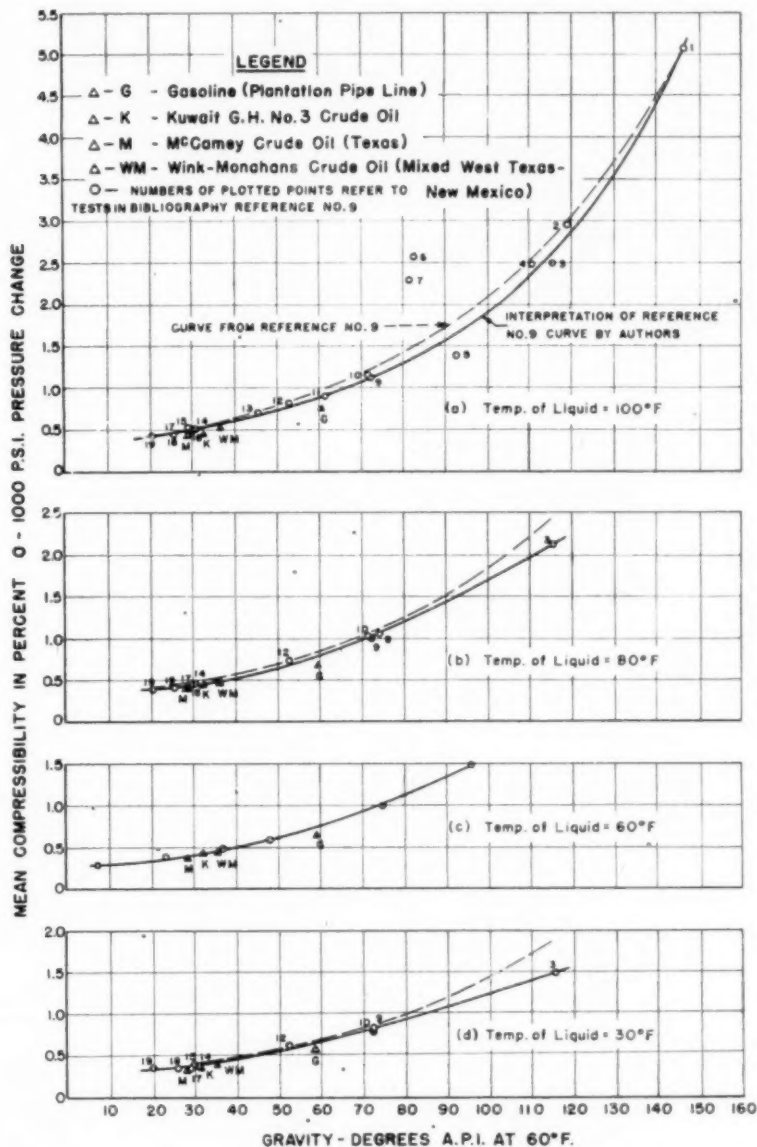


FIG. 10 COMPARISON OF NORTHWESTERN TEST RESULTS ON COMPRESSIBILITY OF PETROLEUM PRODUCTS WITH RESULTS SHOWN BY JACOBSON, ET AL.

It will be seen that the calculated value on this basis, using the 45 F Northwestern curve, is 3980 fps based upon a mean value of k equal to 218,000 psi. Ten of the field tests were examined, and the average velocity of the pressure wave was found to be 3998 fps. The maximum value was 4090 fps and the minimum 3880 fps.

Applying this same procedure to the extrapolated curve, a mean value of 256,500 psi is obtained, or about 17.5 per cent higher than the Northwestern value. When this is used in the theoretical formula for the velocity of the pressure wave, a value of 4296 fps is obtained and is nearly 8 per cent higher than the average of the field tests.

Similar comparisons were made with the tests on the Wink-

Monahans crude, shown in Fig. 13(b), and the extrapolated curve, covering pumping tests, give a value about 2 to 3 per cent higher than would the Northwestern tests.

TABLE 1 COMPARISON WITH FIELD TESTS; MCGAMEY CRUDE AT 45 F

Line pressure, psi	Bulk modulus, Northwestern tests	Extrapolated line
125.....	212000	256000
150.....	218000	256500
175.....	223000	257000
Mean value k	218000	256500
Velocity of pressure wave a :		
Calculated	3980 fps	4296 fps
Test (avg of 10)	3998 fps	

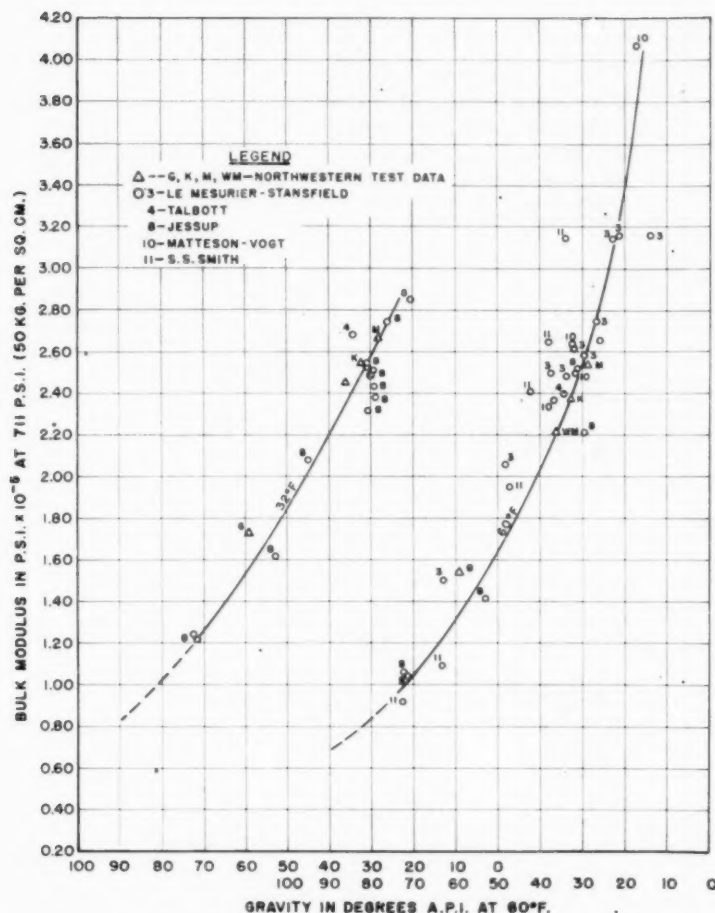


FIG. 11 COMPARISON OF NORTHWESTERN TEST DATA WITH ACTUAL TEST DATA OF OTHER EXPERIMENTERS AT 711 PSI AND AT 32 F AND 60 F

In the Plantation series the curves shown in Fig. 13(c) were obtained on gasoline at 72 F. In this case the tests in the field indicated a velocity of 3620 fps with a calculated value from the Northwestern tests of 3590 fps as compared with 3640 fps using the extrapolated curve.

It is evident that there is considerable variation from crude to crude and between crudes and refined products in the relationship between bulk modulus and pressure at a constant temperature. Where these curves do not depart by more than 5 per cent at the low pressures, an error in the velocity of the pressure wave can be quite small, probably on the order of 2 to 3 per cent.

In the case of the McCamey crude, however, the difference in the weighted mean of the bulk-modulus value was over 17 per cent and the calculated value, using this figure, is 7 to 8 per cent higher than that measured in the field.

Fig. 8 shows the results of the tests on a crude from the Middle East, and it will be noted that this material behaves more nearly like the McCamey crude and thus the possible error in determining the velocity of the pressure wave and the magnitude of surges, as well as the damping of surges would be appreciable.

CONCLUSIONS

In any surge investigation where an accuracy closer than 5 per cent is desired, in the determination of maximum surge pressures

and the degree of damping of waves, it would be highly desirable to determine experimentally the bulk modulus of the material or materials to be transported in the line.

This is particularly desirable when there is a substantial variation in temperature, as well as variations in pressure in the system, so that such effects can be taken into account in any investigation.

The means of obtaining bulk-modulus data has been greatly simplified through the use of the apparatus described in this paper, and results can be made available in a matter of a few days after a sample has been received at the laboratory.

Where there are large investments in pipe lines and particularly when low factors of safety are used in the design, it would seem highly desirable to know the bulk-modulus data in addition to the usual information concerning specific gravity, and viscosity variations with temperature, and thus provide a more accurate basis of design than if pure assumptions from meager data are relied upon.

BIBLIOGRAPHY

- 1 "On the Viscosities and Compressibilities of Liquids at High Pressures," by J. H. Hyde, Proceedings of the Royal Society of London, series A, 1920, pp. 240-249.
- 2 "Adiabatic and Isothermal Compressibilities of Some Liquids

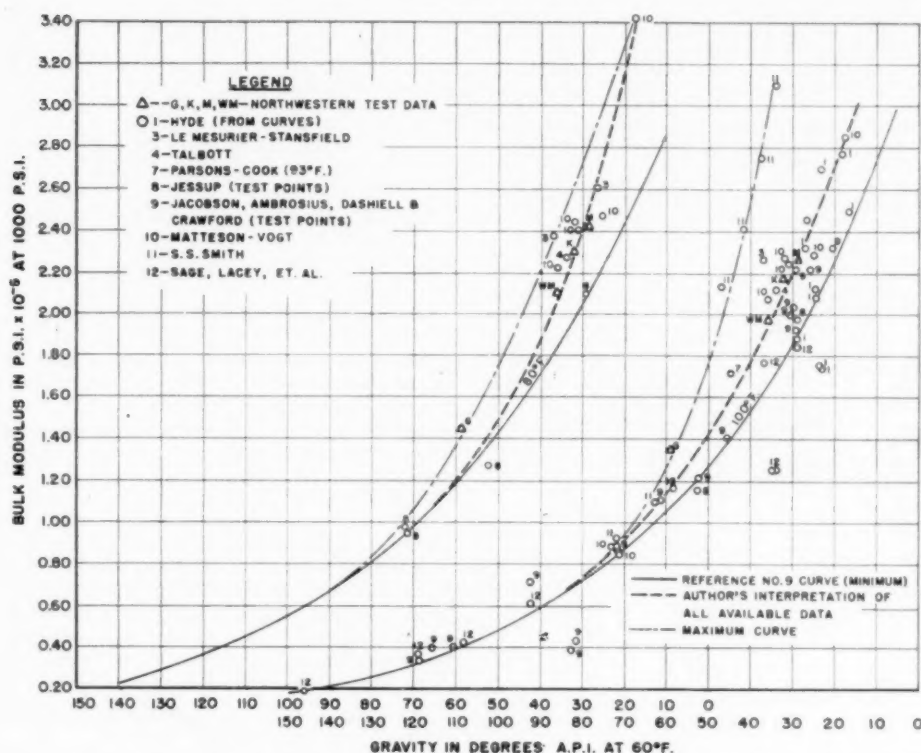


FIG. 12 COMPARISON OF NORTHWESTERN TEST DATA WITH DATA OF OTHER EXPERIMENTERS AT 1000 PSI AND AT 80 F AND 100 F

Between One and Two Atmospheres," by D. Tyrer, *Journal of the Chemical Society of London*, Transactions CHII, part 2, 1913, pp. 1675-1688.

3 "Fuel Characteristics in Relation to Pump and Sprayer Action," by L. J. Le Mesurier and R. Stansfield, Diesel Engine Users Association, 307 Abbey House, Westminster, S.W. 1, London, England, March 30, 1933, pp. 1-33.

4 "Velocity of Pressure Waves in Oil Under Pressure," by A. C. Talbott, *Philosophical Magazine*, vol. 19, 1935, pp. 1126-1141.

5 "Properties of Ordinary Water-Substance," by N. E. Dorsey, American Chemical Society Monograph Series No. 81, Reinhold Publishing Corporation, New York, N. Y., 1940, pp. 207-224.

(a) E. H. Amagat, Sections I and II, p. 207.

(b) P. W. Bridgman, Sections III and IV, p. 214.

(c) G. Tammann and W. Jellinghaus, Section V, p. 216.

(d) L. B. Smith and F. G. Keyes, Section VI, p. 219.

(e) G. Tammann and A. Ruhenbeck, Section VII, p. 222.

(f) L. H. Adams, Section VIII, p. 224.

6 "Correcting for Fluid in Hydraulics," by J. I. Clower and H. F. Shepherd, *Machine Design*, vol. 4, November, 1932, pp. 24-27.

7 "On the Compression of Liquids at High Pressures," by C. A. Parsons and S. S. Cook, Proceedings of the Royal Society of London, series A, vol. 85, no. A579, July 5, 1911, p. 332.

8 "Compressibility and Thermal Expansion of Petroleum Oils in the Range 0° to 300° C.," by R. S. Jessup, Bureau of Standards, *Journal of Research*, vol. 5, November, 1930, pp. 985-1039.

9 "Compressibility of Liquid Hydrocarbons," Second Progress Report on Study of Existing Data, by E. W. Jacobson, E. E. Ambrosius, J. W. Dashiell, and C. L. Crawford, Proceedings of the American Petroleum Institute, vol. 25 (IV), 1945, pp. 39-41.

10 "Velocity of Compressional Waves in Petroleum Fractions at Atmospheric and Elevated Pressures," by R. Matteson and C. J. Vogt, *Journal of Applied Physics*, vol. 11, October, 1940, pp. 658-665.

11 "Product Pipe Line Developments," by S. S. Smith, Proceedings of the American Petroleum Institute, vol. 23 (IV), 1942, p. 58.

12 "Pressure, Volume and Temperature Relations, and Thermal Properties of Pentane," by B. H. Sage, J. G. Schaafsma, and W. N. Lacey, *Industrial and Engineering Chemistry*, vol. 26, September, 1934, p. 1218.

"Thermal Properties of Normal Pentane," by B. H. Sage, W. N. Lacey, and J. G. Schaafsma, *Industrial and Engineering Chemistry*, vol. 27, January, 1935, p. 48.

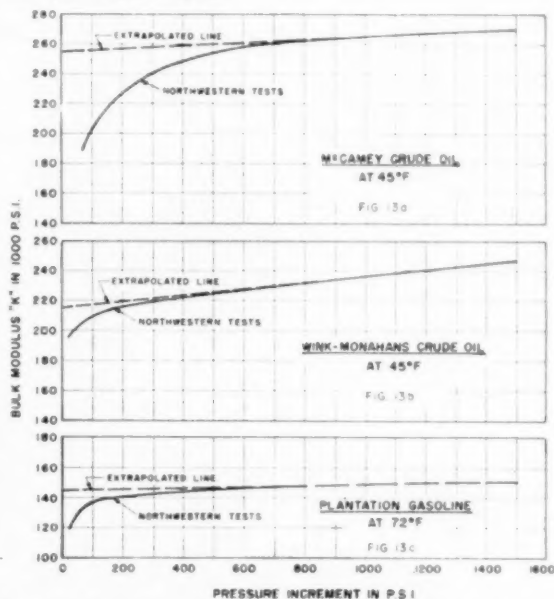


FIG. 13 COMPARISON OF BULK-MODULUS TEST VALUES AT LOW PRESSURES WITH VALUES EXTRAPOLATED FROM HIGH-PRESSURE RANGE

"Physical and Thermal Properties of Crude Oil," by B. H. Sage, W. N. Lacey, and J. G. Schaafsma, *Industrial and Engineering Chemistry*, vol. 27, February, 1935, p. 162.

"Methane-Crystal Oil System," by B. H. Sage, H. S. Backus, and W. N. Lacey, *Industrial and Engineering Chemistry*, vol. 27, June, 1935, p. 686.

"Thermo Behavior of Liquid Mixtures of N-Butane and Crystal Oil," by B. H. Sage and W. N. Lacey, *Industrial and Engineering Chemistry*, vol. 28, January, 1936, p. 106.

"Thermo Properties of Mixtures of a Crude Oil and a Natural Gas," by B. H. Sage and W. N. Lacey, *Industrial and Engineering Chemistry*, vol. 28, February, 1936, p. 249.

"Mixtures of Methane and a Crude Oil," by B. H. Sage, D. C. Webster, and W. N. Lacey, *Industrial and Engineering Chemistry*, vol. 28, August, 1936, p. 984.

"Thermo Properties of Ethane," by B. H. Sage, D. C. Webster, and W. N. Lacey, *Industrial and Engineering Chemistry*, vol. 29, June, 1937, p. 658.

"Thermo Properties of n-Butane," by B. H. Sage, D. C. Webster, and W. N. Lacey, *Industrial and Engineering Chemistry*, vol. 29, October, 1937, p. 1188.

"Thermo Properties of Iso-Butane," by B. H. Sage and W. N. Lacey, *Industrial and Engineering Chemistry*, vol. 30, June, 1938, p. 673.

"Methane-Decane System," by B. H. Sage, H. M. Lavender, and W. N. Lacey, *Industrial and Engineering Chemistry*, vol. 32, May, 1940, p. 743.

"Methane and n-Butane in the Gaseous and Liquid Regions," by B. H. Sage, R. A. Budenholzer, and W. N. Lacey, *Industrial and Engineering Chemistry*, vol. 32, September, 1940, p. 1262.

13 "Final Report of Joint Surge Conference Covering Field Investigations on Oil Pipe Lines Conducted During 1949," sponsored by Middle East Pipelines Limited, Trans-Arabian Pipe Line Company, and Gulf-Shell Pipe Line. Available on loan from Libraries of ASCE, ASME, AWWA, API, Engineering Institute of Canada, The Institution of Mechanical Engineers, and The Institution of Civil Engineers, London, England.

14 "Compressibility and Velocity of Pressure Waves in Petroleum Oils," by R. Matteson, *Journal of Applied Physics*, vol. 9, January, 1938, p. 44.

Discussion

JOHN W. DASHIELL, JR.⁵ In this paper Equation (1) might be easier to follow if written

$$a = \frac{12}{\left[\frac{w}{g} \left(\frac{1}{k} + \frac{d}{Ee} \right) \right]^{1/2}}$$

Equation [2] has an error in definition of symbols

$$K = \frac{\Delta p}{\Delta v} V$$

where Δp = pressure increment in psi

Δv = volume decrement produced by pressure increment Δp .

Figs. 7 (a, b, c) and 8 show an unexplained sudden decrease in bulk modulus as the pressure is lowered below 100 or 200 psi. Since the compressibility is the reciprocal of the bulk modulus, this would show a sudden increase in compressibility as the pressure is lowered below 100 to 200 psi. It suggests the presence of entrained air or gas coming out of solution as the pressure is reduced.

Reference to the literature shows the compressibility of a wide variety of liquids including oils to vary directly with the temperature and inversely with the pressure but it is difficult to explain any sudden deviation from a smooth curve as shown in the aforementioned figures since these curves show the bulk modulus to be approaching zero at zero pressure. This would mean that the compressibility becomes infinite at zero pressure (gage)—a condition that is exemplified by a perfect vacuum.

⁵ Gulf Research & Development Company, Pittsburgh, Pa. Mem. ASME.

Measurement of Temperatures in High-Velocity Steam¹

By J. W. MURDOCK² AND E. F. FLOCK³

The demand for more accurate values of thermal efficiencies in modern steam power plants, together with the fact that the velocity of steam is often so high that the impact effect upon temperature-measuring instruments can no longer be neglected, has created a need for improved temperature instrumentation. Studies have been made of the performance, in moving air and steam, of various total-temperature-type wells suitable for use in steam at operating conditions. The instruments recommended for such applications, constructed so that the sensing element is surrounded by nearly stagnant steam, have temperature-recovery factors above 0.9, which do not change significantly with either the medium, its temperature, or its pressure. Although additional work remains to be done on reducing their sensitivity to flow direction and pattern, these wells, when installed in straight pipes through which steam is flowing at any velocity up to 725 fps, yield total enthalpies which are accurate to within 1 Btu per lb.

NOMENCLATURE

The following nomenclature is used in the paper:

- T = temperature, deg F or deg R
- p = pressure, psia
- v = specific volume, cu ft per lb
- u = internal energy, Btu per lb
- h = enthalpy, Btu per lb
- c_p = heat capacity at constant pressure, Btu/lb deg F
- G = mass velocity, lb/sec ft²
- V = velocity = Gv , fps
- M = Mach number
- δh = heat leak between specified stations, Btu per lb
- r = recovery factor
- θ = angle of attack
- g = acceleration of gravity, ft/sec²
- R = universal gas constant, Btu/lb deg F
- J = mechanical equivalent of heat, Btu/ft lb
- $A = 1/J$, ft lb/Btu

The subscripts s , t , and i mean static, total, and indicated, respectively.

INTRODUCTION

Normal progress toward more compact and more efficient power plants involves the handling and utilization of the working

¹ The opinions or assertions contained in this paper are the private ones of the authors and are not to be construed as official or reflecting the views of the Navy Department or the Naval Service at large.

² Superintendent, Instruments Division, Naval Boiler & Turbine Laboratory, Naval Base, Philadelphia, Pa.

³ Chief, Combustion Section, National Bureau of Standards, Washington, D. C.

Contributed by the Industrial Instruments and Regulators Division and presented at the Spring Meeting, Washington, D. C., April 12-14, 1950, of THE AMERICAN SOCIETY OF MECHANICAL ENGINEERS.

NOTE: Statements and opinions advanced in papers are to be understood as individual expressions of their authors and not those of the Society. Manuscript received at ASME Headquarters, April 5, 1950. Paper No. 50-8-36.

medium at ever higher temperatures, pressures, and velocities. Simultaneously with this trend toward more severe operating conditions there is a demand for increased accuracy in values of efficiency determined experimentally. This in turn requires a better knowledge of the state of the steam at various locations throughout the power plant, which can be obtained only with improved instruments and methods of measurement.

Recognizing these facts, the Bureau of Ships is sponsoring a co-operative program of research and development at the Naval Boiler and Turbine Laboratory and at the National Bureau of Standards, aiming primarily to develop and evaluate more accurate instruments for measuring pressure, temperature, and rates of flow in steam systems. The present paper is restricted to a description of progress made to date on the measurement of steam temperatures.

The three primary sources of error in the measurement of the temperature of a flowing gas are radiation, conduction, and the effect of impact due to directed motion. In steam systems, proper insulation of pipe walls causes their temperature to approximate that of the steam and makes the loss of heat from the temperature-sensing element by radiation and conduction negligible, provided the instrument is designed properly. Thus the principal element of uncertainty, so far as most applications in steam are concerned, is the impact effect.

This effect in a flowing gas is of practical importance only when the directed velocity of the gas becomes appreciable in comparison with the mean velocity of random molecular motion. Thus, so long as steam velocities were low, there was no impact problem. However, velocities now used and those contemplated in future power plants are so high that the impact effect upon temperature-sensing devices no longer can be neglected. This becomes more apparent when it is recalled that such devices as thermocouples and resistance thermometers, either exposed directly to moving gas or sheathed in protective wells, respond only to the translational energy of the gas molecules.

THERMODYNAMIC CONSIDERATIONS

Consider that a compressed gas is allowed to expand adiabatically from a large reservoir in which its velocity is nearly zero, through a nozzle to the atmosphere. The adjective "total" and the subscript t are used to describe the quiescent state of the gas in the reservoir, while the properties of the moving gas, as they would appear to an observer moving with the gas and to whom the gas would appear to be static, are described by the adjective "static" and indicated by the subscript s .

For the adiabatic acceleration of the gas passing through the nozzle, and for the reverse process of deceleration as well, conservation of energy requires that

$$u_t + Ap_t v_t = u_s + Ap_s v_s + V^2/2gJ \dots \dots \dots [1]$$

This relation holds, even in the presence of such irreversible phenomena as friction and shock waves, which influence the distribution of energy among the three terms on the right, but not their sum.

By the definition of enthalpy, this equation can be written in the form

$$h_t = h_s + V^2/2gJ \dots \dots \dots [2]$$

which introduces the concept of two kinds of enthalpy, namely, a total enthalpy characteristic of the stagnant gas, and a static enthalpy characteristic of the moving gas, the latter being its enthalpy as it would appear to an observer moving with the gas. Obviously, it is the total enthalpy which is of interest in evaluating thermal efficiency, since this includes the kinetic energy of directed motion, along with the more familiar form characterized by temperature and pressure alone. In the adiabatic process being considered, the total enthalpy of the gas remains constant, without regard to reversibility or deviations from the perfect-gas law.

Dividing both sides of Equation [2] by c_p , which is now assumed to be independent of temperature as is the case for a perfect gas, gives

$$T_t - T_s = V^2/2gc_p \quad [3]$$

This introduces the concepts of total and static temperature, coordinate with the afore-mentioned concepts of enthalpy. Again, the total temperature is the temperature of the gas at rest, while the static temperature is that which would be indicated by an instrument moving in the same direction and at the same velocity as the gas. The two are identical in quiescent gas, but differ from one another in a moving gas, directly as the square of the velocity, and inversely as the heat capacity at constant pressure.

When a perfect gas is subjected to an adiabatic expansion of the type being considered, not only the total enthalpy but also the total temperature remains constant. However, in an adiabatic expansion of an actual gas there is usually a small change in total temperature, and such changes were observed in the present work with steam.

Obviously, it is impracticable to measure T_t directly in a moving gas. However, if an instrument designed to stop the gas adiabatically and reversibly is inserted in the stream, a temperature-sensing element located in the gas so brought to rest will indicate its total temperature. This total temperature, together with the total pressure of the stagnant gas, suffices to establish the total enthalpy of any actual gas for which tables of these properties exist.

When any device other than an idealized total-temperature probe is inserted in flowing gas, it will attain a temperature T_i intermediate between T_t and T_s , because only part of the gas impinging upon it is brought completely to rest. That part of the kinetic energy of directed motion which is converted to heat upon impact raises the temperature of the device above T_s . Friction in the boundary layer of gas around the device also makes a contribution in this same direction, so that the amount of the increase

is a function of the configuration of the device and of the rate and pattern of the flow in its immediate vicinity.

For accurate interpretation of the temperature indicated by an instrument located in a stream of high-velocity gas, the relative position of T_i with respect to T_t and T_s must be known. It is common practice to specify this position in terms of recovery factor r , defined as

$$r = (T_i - T_s)/(T_t - T_s) \quad [4]$$

These temperature relations, as influenced by velocity, are illustrated in Fig. 1 which shows the temperature which would be indicated by instruments having recovery factors of unity, 0.93, 0.65, and zero, if they were immersed in steam at various velocities, but always having a total temperature of 800 F, and a heat capacity at constant pressure of 0.5 Btu per lb deg F. These particular recovery factors were chosen for illustration because the value 0.93 is typical of the wells to be described later, and 0.65 is typical of a bare thermocouple junction.

DEVELOPMENT OF INSTRUMENTS

Characteristics Desired. The obvious advantages of using an instrument with a recovery factor close to unity are that the indicated temperature may often be taken as the total temperature, and that, in cases where higher accuracy than this is required, the small difference between T_t and T_i can be computed with ample accuracy from an approximate value of r . Stated in another way, the higher the value of recovery factor, the less is the practical importance of its actual value and of the effects of the operating variables upon it.

Instruments of the total-temperature type^{4,5} have been developed to a high degree for use primarily in high-velocity air streams such as are encountered in wind tunnels and in flight. However, these do not lend themselves to direct application in machinery containing steam at high temperatures, pressures, and velocities for the following reasons:

- 1 They are relatively large and might therefore block off more of the flow passage than is tolerable.
- 2 They would have to be made very sturdy to withstand the impact and mechanical vibrations to which they would be subjected in steam systems.
- 3 They are sensitive to the direction of flow, which may be unknown or variable within a machine.
- 4 It would be difficult to provide a pressure seal which is effective at high temperatures and yet allows ready replacement of the temperature-sensing element either during or between runs.

Instead of attempting to adapt existing devices for service in steam, it was considered more practical to develop a modification which would approximate their performance, yet be free of some of their disadvantages and possess some distinct advantages over instruments designed for other applications.

The temperatures of interest in steam systems are within the range of satisfactory performance of base-metal thermocouples, which are sufficiently accurate for the intended purpose when well-established techniques⁶ are followed. There is much to recommend the use of thermocouples in this application, for example, low cost, small size permitting measurements in a limited region

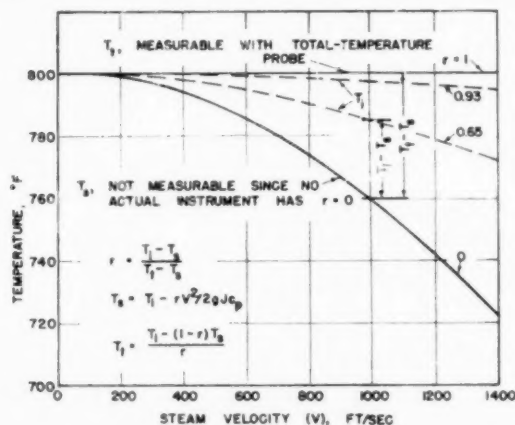


FIG. 1 EFFECTS OF IMPERFECT TEMPERATURE RECOVERY

⁴ "Temperature Measurements in High-Velocity Air Streams," by H. C. Hottel and A. Kalitinsky, Trans. ASME, vol. 67, 1945, p. A-25.

⁵ "Temperature Measurements in High-Velocity Gas Streams," by L. Malmquist, Trans. of the Royal Institute of Technology, Stockholm, no. 15, 1948.

⁶ "The Use of Thermocouples in High-Velocity Gas Streams," by E. F. Fiock and A. I. Dahl, Journal of the American Society of Naval Engineers, Inc., vol. 60, 1948, pp. 139-162.

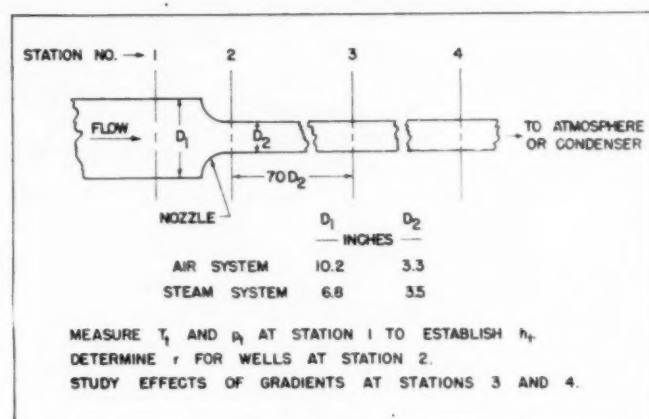


FIG. 2 SCHEMATIC DIAGRAM OF TEST SYSTEMS

as well as surveys of gradients, ruggedness, simplicity of construction and installation, rapid response to changes in temperature, and availability of indicating and recording devices which are accurate, simple to operate, and highly reliable. Therefore effort was concentrated on devices employing thermocouples as sensing elements, although the wells to be described may also be used with resistance thermometers.

Because it seemed unwise for many reasons to expose thermoelements directly to steam, the development of appropriate wells was desirable. From the thermal standpoint, the inner tube of such a well should be small and thin to promote rapid response of the measuring junction and to reduce heat loss along solid parts. If the unit is to have a high recovery factor, the inner tube must be surrounded by steam which has been brought as closely as practicable to stagnation. In addition, considerable mechanical strength is required, particularly resistance to vibration. It is highly desirable that, in case the more fragile parts should break, they be retained and prevented from passing through and damaging parts of the machinery.

The remainder of this paper describes the development of wells to meet these requirements and the results to date of studies of their performance in streams of air and of steam contained in straight pipes.

General Description of Equipment. For reasons of speed and economy, preliminary studies of the performance of wells were made in streams of air. These results were used in selecting the more promising instruments for evaluation in steam under operating conditions.

The test systems using air and steam were essentially the same. In both, the test medium was accelerated from a low velocity in a pipe of large diameter by passage through an efficient nozzle. Fig. 2 is a schematic diagram representing both systems.

The state of the medium was established accurately by measuring its temperature and pressure at station 1, in a region of low velocity. For determinations of recovery factor, the test instruments were placed in the stream at station 2 in the throat of the nozzle, where there were no significant gradients in temperature or velocity. Similar instruments also were located at stations 3 and 4. For the steam system, only those results obtained at stations 2 and 4 are presented here, because the flow pattern at station 3 was not well enough known.

Glass-insulated duplex iron-constantan thermocouples were used with both test media. The stock of wire was calibrated at frequent intervals along its length, and the thermoelectric properties were found to be sufficiently uniform that a single calibra-

tion could be used for all thermocouples in any one installation. The basic temperature of the medium was observed at station 1, and the temperatures at other stations were determined by measuring differences therefrom. Thermoelectromotive forces were measured with Brown Elektronik self-balancing potentiometer indicators, graduated to 2 microvolts, and read by estimate to the nearest microvolt. In all measurements the reference junctions were maintained at 32 F in a slush of ice. In view of the precautions taken, the probable error in a single observed value of temperature difference is believed to be ± 0.1 F or less. This estimate includes only the error in determining the temperature of the measuring junction and not that due to any difference in temperature between this junction and the medium.

Results Obtained With Air. The first tests of temperature probes were made in an air system consisting essentially of a 4000-cfm blower discharging into a 12-ft length of 10-in. pipe, thence through a nozzle having a throat diameter of 3.25 in., a diffuser with a 7-deg included angle, and into the atmosphere. This equipment is shown diagrammatically in Fig. 3. The thermocouple wells were mounted singly in the throat of the nozzle in the region of uniform velocity, and the performance of each type was evaluated in terms of recovery factor as a function of velocity or Mach number (M).

At velocities above 700 fps ($M = 0.63$), local shock waves were formed, and the observed values of recovery factor became erratic. By increasing the temperature of the air so that the dew point was not reached in the nozzle, it was demonstrated that the observed scattering was not due to condensation shocks. Therefore a similar phenomenon is to be expected in steam, but only at higher velocities, since the temperature and hence also the velocity of sound in steam is usually higher.

In later tests with air, the blower was replaced by a centrifugal compressor, and a long run of straight tubing was substituted for the exit diffuser in Fig. 3. No thermal insulation was used in either arrangement since the inlet air was only slightly warmer than the atmosphere. In both systems the loss of heat between stations 1 and 2 was negligible. However, there was sufficient heat leak between station 1 and those 50 or more diameters downstream to make the observed temperatures unreliable, so that this work must be repeated.

The nozzle used with air had been calibrated previously so that the rates of air flow could be determined from measurements of the drop in pressure across the nozzle.

In the early stages of this program the recovery factors of the following simple devices were determined: cup-type total-tem-

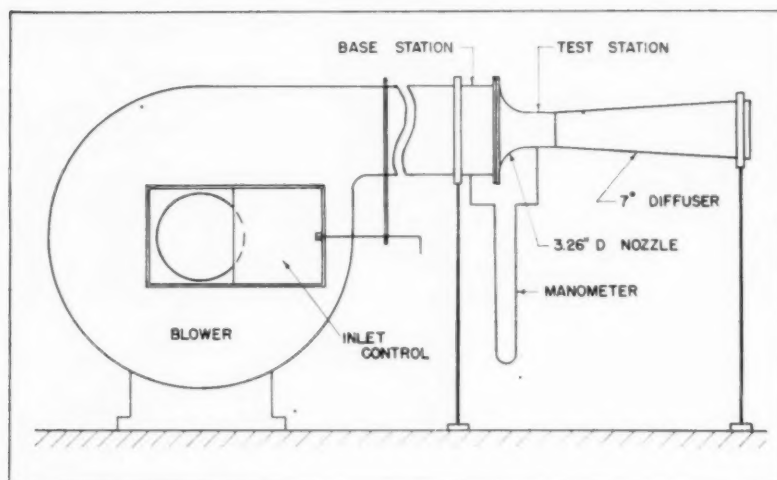


FIG. 3 DIAGRAM OF AIR SYSTEM

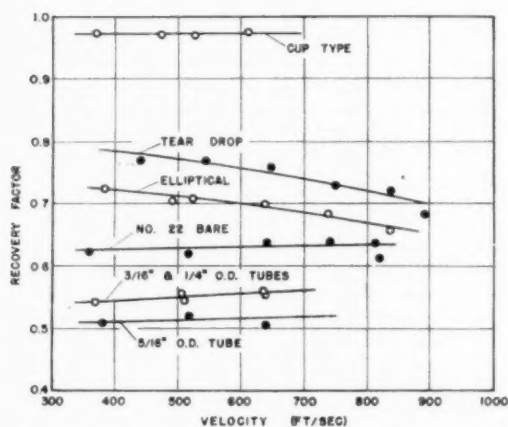


FIG. 4 RECOVERY FACTORS OF SIMPLE DEVICES

perature probes, bare junctions, cylindrical wells of various diameters, and wells of elliptical and teardrop cross section. As will be seen in Fig. 4, all of these except the cup type have recovery factors lower than was desired.

The next step was the development of devices having protecting tubes concentric with inner wells, with openings in the upstream faces of the outer tubes to admit gas to the annulus. The inner wells, containing the measuring junctions, could thus be surrounded by stagnant gas. It is well known that the outer tube can be made to approach the total temperature of the gas more closely if some of the stagnant gas is bled downstream. It was found experimentally that the recovery factor of the unit was greatest when the area of the downstream or bleed holes was approximately one tenth that of the openings upstream. This area ratio was maintained in units made and tested subsequently.

Among the various wells tried, those which seemed most promising are illustrated in Fig. 5 and shown in more detail in Fig. 6. The bleed holes in Type A Fig. 5, are not visible because the central tube obscures them. Type A can be installed in odd-shaped spaces, and Type B is to be preferred for use in pipes and in spaces where support at both ends is possible. For con-

venience these types are designated as cantilever and fixed-beam wells, respectively.

The recovery factors of wells having the dimensions shown in Fig. 6, as determined in air, are shown in Fig. 7, with the curve for the cup-type junction repeated from Fig. 4 for comparison. It will be noted that the recovery factor of the fixed-beam well is higher than that of the cantilever well, and that it changes less with velocity. Thus the use of the former is recommended wherever its installation is practicable. Due to the support at both ends, this type can be made smaller and lighter for use in a stream of given Mach number. Therefore it will block less of the flow passage and be less subject to errors from conduction. The

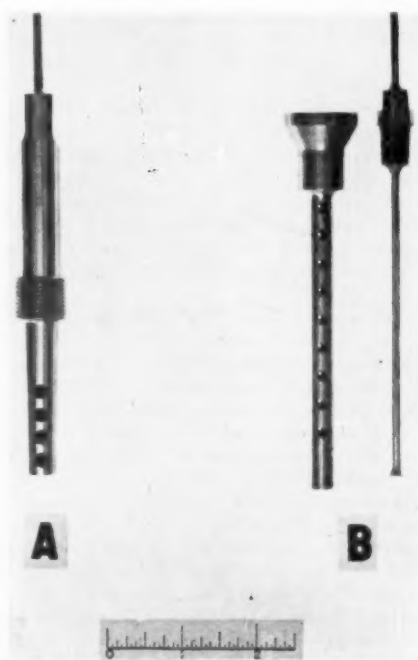


FIG. 5 CANTILEVER AND FIXED-BEAM WELLS

stagnation pressure within the well can be transmitted through a connection at either end. It is to be noted that the inner well of either type will be retained in case of breakage.

With the second air system mentioned previously, wells were installed at stations 3 and 4 in regions of fully developed pipe turbulence. Average total pressures were determined by Pitot-tube traverses at the test stations, after which the test wells were substituted and measurements were made at the same flow rates. Wells with 5, 7, and 9 holes of the size and spacing shown as Type B in Fig. 6, were used. The 5 and 7-hole wells were identical with the 9-hole well, except for the omission of holes nearest the wall. Stagnation temperatures and pressures within the wells were measured, but because of heat loss only the latter are considered significant.

All three wells were found to develop stagnation pressures which are higher than the average total pressure of the turbulent stream. As might be expected from the known form of the velocity gradient, the 5-hole well, having holes only in the region of higher velocities, attains the higher stagnation pressure, and the 9-hole well is nearest to, but still above the average total pressure. It seems probable that a well of this type can be designed to attain the average total pressure more exactly, by proper location of the holes. Further investigations are planned.

Another item of practical interest with regard to wells of this type is the effect of angle of attack θ , since the direction of flow in certain test spaces may be both unknown and variable. The effect of direction of flow upon the stagnation pressure attained in the 5-hole well was determined at station 2, and corresponding tests were made with the 9-hole well in regions of fully developed turbulence. These results are shown in the lower curves, Fig. 8, in which the position indicated by 0 deg designates that the larger holes in the well were pointed directly upstream.

High sensitivity to angle of attack is undesirable, and some modification to reduce it seemed in order. To this end a $1/8$ -in. length of tube was soldered to each of the upstream holes of the

5-hole well, at an angle of 90 deg with the axis of the well. This unit, again tested in the nozzle, gave the results shown in the uppermost curve in Fig. 8. The marked decrease in sensitivity to angle of attack indicates the desirability of using the projecting

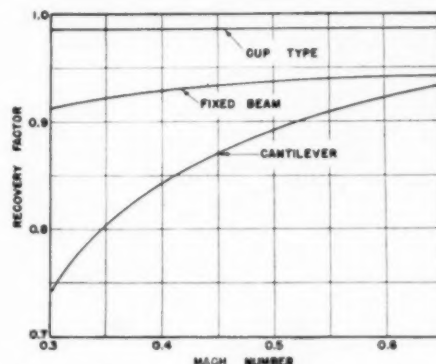


FIG. 7 RECOVERY FACTORS OF CANTILEVER AND FIXED-BEAM WELLS

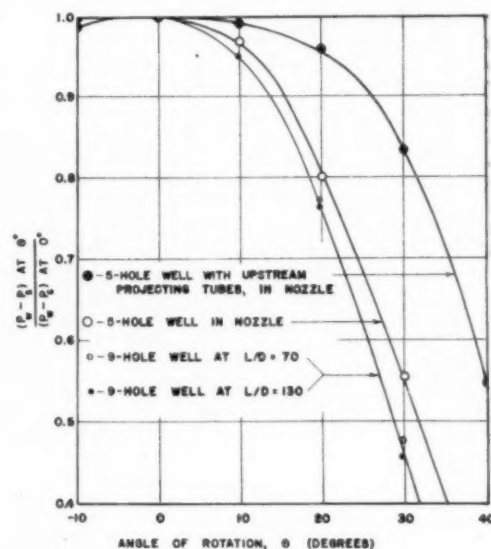


FIG. 8 EFFECT OF ANGLE OF ATTACK ON PERFORMANCE OF FIXED-BEAM WELLS

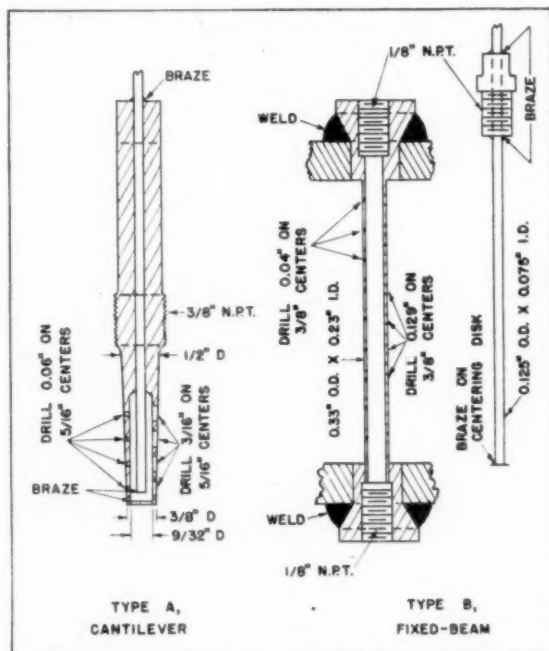


FIG. 6 DETAILS OF CANTILEVER AND FIXED-BEAM WELLS

tubes in applications where the direction of flow is uncertain. No tests have been made in steam with this type of well.

Studies of the type described, obviously, should be made on a temperature as well as a pressure basis, and this will be undertaken in the near future.

EVALUATION OF FIXED-BEAM WELLS IN STEAM

Test Equipment and Method. To date the tests in steam have been confined to fixed-beam wells in a straight run of pipe. Using the system shown diagrammatically in Fig. 9, the basic conditions of the superheated steam at station 1 were varied over the following ranges: Temperature, 450 to 625 F; pressure, 20 to 200 psia; and flow rate, 10,000 to 30,000 lb per hr.

In a system having the dimensions indicated in Fig. 2, the maximum velocity attained in the throat of the nozzle (station 2) was about 725 fps. At station 4, the average velocity across the

section had a maximum value of approximately 1150 fps.

As indicated in Fig. 9, steam produced in a superheat-control boiler passed through an appropriate sharp-edged metering orifice, a control valve V_1 , and thence through a nozzle to the test station. After passing through a second control valve V_2 , it was condensed and led to one or the other of two tanks, which were weighed alternately every 3 min. The weighing-tank data were used in calibrating the metering orifice, the pressure drop across which could then be used as an accurate measure of the flow rate at any time of specific interest.

Steam pressures were observed with a combination of 16-in. suppressed-zero Bourdon gages and high-pressure mercury manometers used differentially. Static pressures were measured at each station with a Bourdon gage connected to a sharp-edged pressure tap located flush with the inner wall and about one pipe diameter upstream. At each station a manometer was used to measure the difference between the static pressure and that inside the well. Appropriate steam traps were installed at the level of the test system in all gage and manometer lines, and corrections were applied for the water columns to the instruments located approximately 15 ft below.

The measuring junction in each thermocouple well was located at the center of the pipe. However, a limited number of traverses showed no measurable difference in temperature over the central half-diameter.

The entire test system was lagged with 4 in. of insulation suitable for service under the conditions of these tests. At each operating temperature and flow rate, one or more runs were made at high pressure and low velocity, i.e., with valve V_1 , Fig. 9, open, and valve V_2 partially closed, in order to evaluate the heat leak through the lagging. In no instance was there a measurable loss between stations 1 and 2. The loss between stations 1 and 4 was between 0.1 and 0.4 Btu per lb, depending on the temperature and the flow rate. In making the calculations for each run, the value of h_1 at station 2 was considered identical with that at station 1, and the heat leak (δh) between stations 1 and 4 was subtracted from the value of h_1 at station 1 to get the prevailing value of h_1 at station 4.

In making a run, previously selected conditions were established in the boiler, and then in the test system by operating valves V_1 and V_2 . Observations were made only after a considerable time, in which a steady state was reached throughout

the test system and its insulation. Thereafter all temperatures and pressures were read in simultaneous cycles requiring about 2 min, until changes observed in three successive cycles were insignificant. The drop in pressure across the metering orifice was read periodically in the same interval, and the weight of condensate was determined every 3 min.

Results Obtained With Steam. A great many tests with steam were required to establish the characteristics of the thermocouple wells. However, a summary of the results can be made simple, because it was found that the performance of the fixed-beam wells does not change significantly with either temperature, pressure, or flow rate, except in so far as these characteristics influence velocity. Therefore the results may be presented as a function of velocity alone, as is done in Fig. 10, for wells having the form and dimensions shown in Figs. 5B and 6B. The filled and open circles apply to wells located at stations 2 and 4, in regions of uniform and nonuniform velocity, respectively. In Fig. 10A, differences in temperature are plotted against velocity, and the same results are shown on an enthalpy basis in Fig. 10B.

The total temperatures were calculated as follows: The value of h_2 can be obtained from the known values of h_1 , p_1 , and G , because Equation [2] and the relation

$$V = Gr_s \dots \dots \dots [5]$$

must hold simultaneously, and because h_2 and v_2 are dependent variables. In the mechanics of solving Equations [2] and [5], an equation relating h_2 and v_2 may be used as suggested by Keenan.⁷ Alternatively, advantage may be taken of the relation which is implicit in the steam tables, and h_2 may be calculated by successive approximations, as was done in computing the present results. Knowing h_2 and v_2 fixes the value of entropy, which in turn has the same value at the stagnant state. The latter is fully defined by the entropy and h_1 , so that the corresponding values of T_1 and p_1 may be read from the tables.

The indicated enthalpy h_1 is that found in steam tables for the observed values of temperature T_1 and pressure p_1 . Corrections for heat leak were applied only at station 4, as explained previously.

⁷ "Friction Coefficients for the Compressible Flow of Steam," by J. H. Keenan, *Journal of Applied Mechanics*, Trans. ASME, vol. 61, 1939, p. A-11.

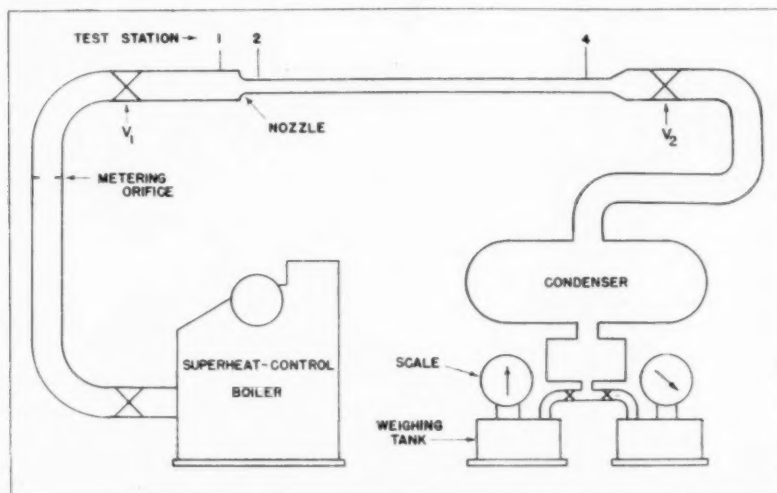


FIG. 9 DIAGRAM OF STEAM SYSTEM

The most important fact demonstrated by Fig. 10 is that every experimental value of h_i at both test stations is within less than one enthalpy unit of the value of h_i determined at station 1. Thus the observed values of T_i and p_i , without any correction for recovery, establish values of enthalpy which are correct to within better than 1 Btu per lb at velocities up to 725 fps, for both uniform flow and the velocity gradient characteristic of fully developed pipe turbulence. Therefore wells of the type described are recommended without qualification for use in steam, since these will give more accurate values of enthalpy, without correction for imperfect recovery, than wells of any other type known to have been used in steam systems.

The results obtained directly from the wells, without correction for recovery, are of the accuracy specified only because the recovery factor is high. At first it might be thought that application of corrections based upon the known recovery factor would further reduce the error. This is correct if the well is located in a region of uniform velocity such as prevailed at station 2, as will be evident from the pattern of the filled circles in Fig. 10. These are all above the base line of zero error, and they show an upward trend with velocity. In fact, recovery factors calculated from these data are in excellent agreement with values obtained in air and shown in Fig. 7.

On the other hand, when the well is located in a region of fully developed pipe turbulence, as at station 4, application of corrections for recovery, as determined in the nozzle, would increase the accuracy of the final results in the range of lower velocities and decrease it at high velocities. This is apparent from the pattern of the open circles in Fig. 10 which show a downward trend with increasing velocity and fall below the base line at high velocities.

Corrections applied for imperfect recovery would lower all of the open circles and thus increase the errors of those points already below the base line.

To date the performance of the wells has been studied only in regions of uniform velocity and of velocity gradients characteristic of fully developed pipe turbulence. Neither of these flow patterns occurs frequently in operating steam systems, so that much experimental work remains to be done on the effects of upstream disturbances created by valves, strainers, bends, etc. However, the results of such studies will serve merely to evaluate corrections which are believed to be quite small, and the interim use of the wells without correction seems to be in order.

Problems Incident to Velocity Gradients in Steam. The problems incident to proper interpretation of results determined with wells located in regions where velocity gradients exist are believed to involve the nature of the sampling accomplished by the well, and the differences between steam and a perfect gas. Present results show that the net effect of these and the imperfect recovery is very small in regions of fully developed pipe turbulence. This may not be the case in the presence of velocity gradients of other types.

An analysis of the probable effects of velocity gradients is a desirable step in planning future experiments. Such a study has led to a plausible qualitative explanation of the apparent anomalies of Fig. 10, but its presentation here would require more

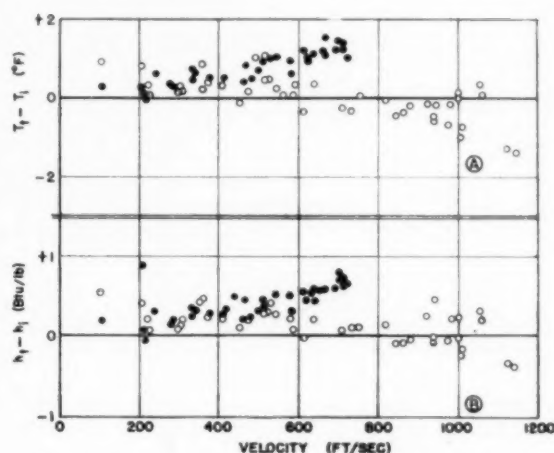


FIG. 10 PERFORMANCE OF FIXED-BEAM WELLS IN STEAM

space than is available. Hence this will be postponed, pending completion of additional experimental work.

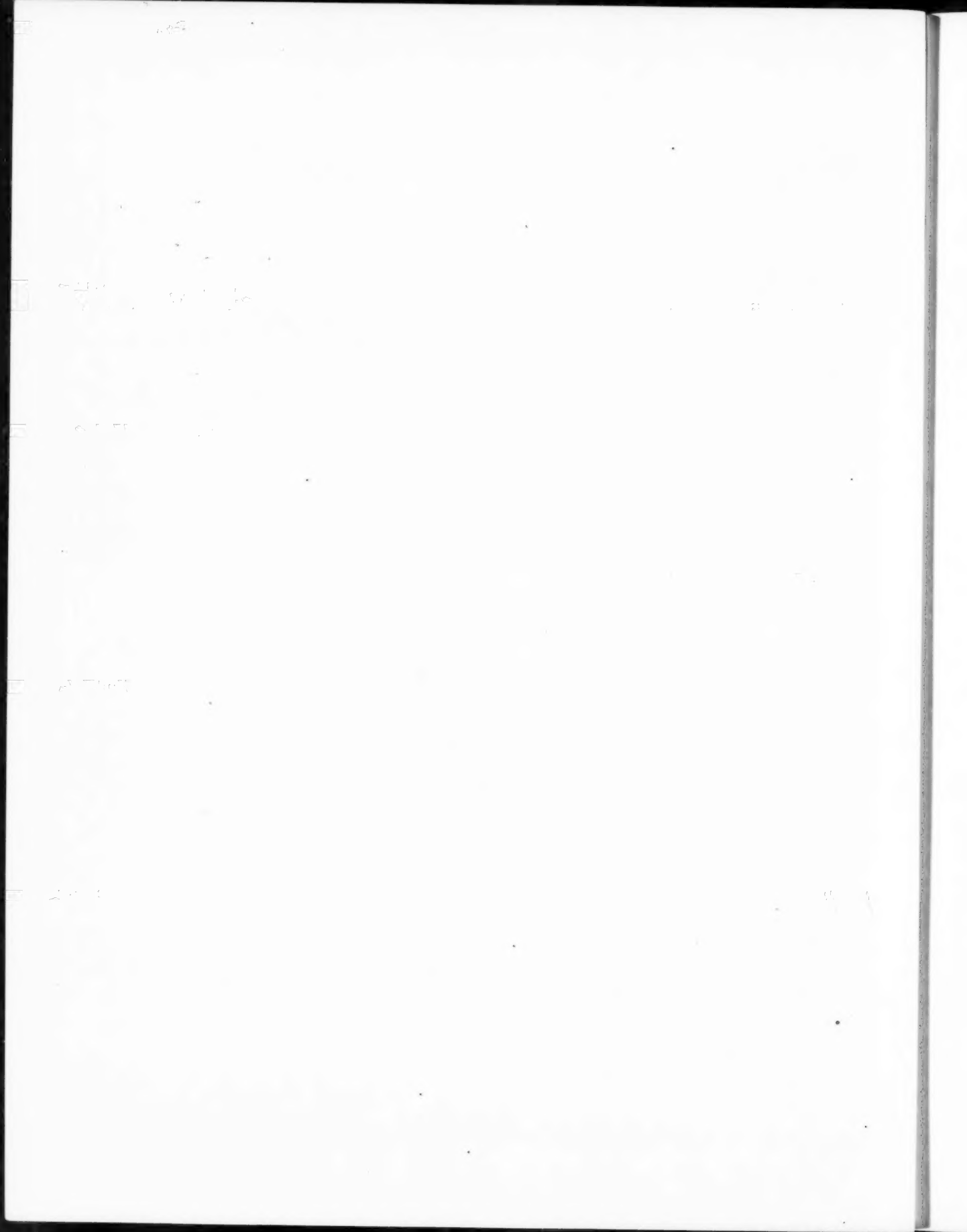
In the course of future work in steam, it is hoped to study the performance of cantilever wells, to extend the present measurements to higher velocities, to measure the effects of upstream disturbances and angle of attack, and to determine the effectiveness of tubes projecting from the upstream openings in reducing the effects of the latter.

CONCLUSION

Meanwhile, the use of wells of this type in steam is recommended without qualification, since these will, without any correction for recovery, give more accurate values of enthalpy than wells of any other type known to have been used in steam systems. The fixed-beam wells described, when installed in straight pipes, yield directly values of temperature and pressure which establish the enthalpy of steam moving at velocities up to at least 725 fps with an error of less than 1 Btu per lb, regardless of whether the flow is uniform or characteristic of pipe turbulence.

Application of corrections for recovery of the wells reduces the remaining error in regions of uniform flow. However, the application of corrections determined in uniform flow to devices used in regions of nonuniform velocity may decrease the accuracy, so that, until more is known about the effects of gradients, it is considered wise to apply no corrections at all.

Additional studies to be made in both air and steam systems are expected to yield only minor improvements in the performance of the wells and in the interpretation of results obtained therewith. These improvements may be of practical importance where highest accuracy is essential, in which case the temperature, pressure, and flow instrumentation must be highly refined and used with great care. Otherwise, some single error in measurement may be greater than that due to imperfect recovery, thus making the application of small corrections for the latter entirely futile.



Relay Servomechanisms

The Shunt-Motor Servo With Inertia Load

By T. A. ROGERS¹ AND W. C. HURTY,² LOS ANGELES, CALIF.

This paper develops the theory of the shunt-motor relay servomechanism in terms of dimensionless motor parameters. Operating curves are drawn in the phase plane illustrating the effect of parameter changes on the stability of the servo for three forms of input signal. The first two forms of input signal, a step function and a uniform variation with time, have been discussed before and are included only for completeness. The third form of input signal, a sine function, is of most interest and is treated at greater length. The phase-plane curves, obtained from a differential analyzer, show three modes of operation which have been related to the servomechanism parameters by a relatively simple expression.

INTRODUCTION

RELAY servomechanisms have been used in several applications requiring high performance with a minimum of complex apparatus. The general methods of analysis given in this paper have been discussed by Hazen (1),³ MacColl (2), and Weiss (3) in earlier papers, and the application of the phase-plane diagram has been presented in some detail by Minorsky (4), and Andronow and Chaikin (5).

The usefulness of the phase-plane diagram would be greatly increased if the motor parameters were expressed in dimensionless quantities having a limited variation about a median value of unity. In order to fulfill the requirements of dimensionless parameters, the techniques used by the electrical engineer when working with power machinery will be employed. These ideas are not new but a review of the concepts may be in order.

All electrical machines have name plates stating those values of voltage, current, speed, power output, and frequency which the manufacturers consider as nominal when designing the machine. Values deviating from name-plate values may be expressed in actual values, per cent of rated values, or as a decimal ratio of the rated value. The decimal ratio has the advantage of being dimensionless and of entering directly into the computations without the decimal-point trouble introduced by the percentage notation. Since the decimal ratio of the existing value to the rated value has as its norm unity, instead of 100, it is called the "per unit value."

If, for example, a motor is operating at 90 volts instead of the rated 120 volts and draws 1.2 amp from the line instead of 1.5 amp as rated, then it is operating at 0.75 per unit voltage and 0.8 per unit line current. The usual abbreviation for per unit values is "pu."

¹ Professor in Engineering, University of California.

² Assistant Professor in Engineering, University of California.

³ Numbers in parentheses refer to the Bibliography at the end of the paper.

Contributed by the Industrial Instruments and Regulators Division and presented at the Spring Meeting, Washington, D. C., April 12-14, 1950, of THE AMERICAN SOCIETY OF MECHANICAL ENGINEERS.

NOTE: Statements and opinions advanced in papers are to be understood as individual expressions of their authors and not those of the Society. Manuscript received at ASME Headquarters, January 30, 1950. Paper No. 50-S-13.

PER UNIT MOTOR PARAMETERS

Direct-current motors are characterized by three physical relationships as follows:

1 The torque developed on the armature is proportional to the product of the armature current, and the magnetic flux entering the armature surface.

2 The voltage generated in the armature conductors, due to their motion in the magnetic field, as a consequence of rotation, is proportional to the product of the angular speed and the magnetic flux entering the armature surface.

3 The armature-circuit relations for a motor are such that the voltage applied to the armature is composed of two components, namely, (a) the armature-circuit resistance drop; and (b) the generated, or back voltage.

These three relationships may be expressed algebraically, for a shunt motor, as follows

$$M = K_1 I_a \Phi \text{ lb-ft.} \quad [1]$$

$$E_g = K_2 S \Phi \text{ volts} \quad [2]$$

$$E = E_g + I_a R_a \text{ volts} \quad [3]$$

where

M = developed torque, lb-ft

I_a = armature current, amp

Φ = useful or active magnetic flux, webers

E_g = generated or back voltage

S = armature speed, rpm

E = applied armature voltage, volts

R_a = total motor armature-circuit resistance, ohms

K_1, K_2 = constants of proportionality

Equations [1], [2], and [3] may be rewritten in terms of per-unit quantities by expressing all terms as ratios of the motor rated values. For the problem under investigation, the motor is considered to be operating at rated field flux corresponding to full voltage on the motor field

$$m = k_1 i_a \text{ (dimensionless)} \quad [4]$$

$$e_g = k_2 \frac{d\theta_0}{dt} \text{ (dimensionless)} \quad [5]$$

$$i_a = \frac{e - e_g}{r_a} \text{ (dimensionless)} \quad [6]$$

where

$$m = \text{per unit torque} = \frac{M}{M_r} = \frac{\text{developed torque}}{\text{rated torque}}$$

$$i_a = \text{per unit current} = \frac{I_a}{I_{ar}} = \frac{\text{operating armature current}}{\text{rated armature current}}$$

$$k_1 = \text{constant (dimensionless)}$$

$$e_g = \text{per unit generated voltage} = \frac{E_g}{E_r} = \frac{\text{generated voltage}}{\text{rated voltage}}$$

$$\theta_0 = \text{per unit angle} = \frac{\Theta_0}{\Theta_r} = \frac{\text{output angle}}{\text{rated angle}}$$

θ_r = rated angle by definition, "angle the motor passes through in 1 sec at rated angular velocity"

k_2 = constant — seconds

e = per unit applied voltage = $\frac{\text{applied voltage}}{\text{rated voltage}}$

r_a = per unit resistance
= $\frac{\text{Rated armature current in amperes} \times \text{armature resistance in ohms}}{\text{Rated voltage}}$

k_1 and k_2 should be determined from test data under operating conditions.

RELAY SERVO WITH INERTIA LOAD

A relay servo with an equivalent inertia load on the motor shaft may be represented as in Fig. 1.

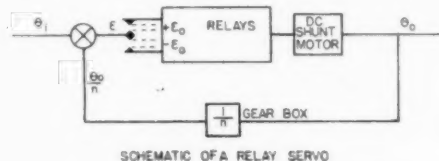


FIG. 1 SCHEMATIC OF A RELAY SERVO

The electrical connections are arranged in such a manner that, for every input angle θ_i , the relays operate the motor to make θ_o approach the value of θ_i . The difference between these two values is called the error and is defined as

$$\varepsilon = \theta_i - \frac{\theta_o}{n} \text{ per unit}$$

The term ε_0 is one half the dead space between the relay operating points and is taken to be symmetrical about the point of zero error. There are, therefore, three conditions of motor operation; (a) full voltage on the motor armature in the forward direction, (b) the motor armature short-circuited for dynamic braking, and (c) full voltage on the motor in the reverse direction. The motor performance is described by a linear differential equation, for each of these conditions of operation, as derived from Equations [4], [5], and [6].

Substitute Equation [5] in [6] and the result in Equation [4] to obtain the equation for the per unit developed torque

$$m = \frac{k_1 e}{r_a} - \frac{k_1 k_2}{r_a} \frac{d\theta_o}{dt} \text{ (dimensionless)} \quad [7]$$

The developed torque is opposed by the inertia torque if windage and friction are neglected. Then

$$M = J \frac{d^2 \theta_o}{dt^2} \quad [8]$$

where

J = moment of inertia referred to motor shaft, (lb-ft sec²) units

Equation [8] must be corrected to dimensionless units by dividing by rated M_r and then converting the angle to per unit angle. The result is

$$m = \frac{J}{M_r} \theta_r \frac{d^2 \theta_o}{dt^2} \quad [9]$$

The combination of Equations [8] and [9] produce the equation of motion under conditions of a positive error greater than the dead zone

tion of motion under conditions of a positive error greater than the dead zone

$$\frac{J}{M_r} \theta_r \frac{d^2 \theta_o}{dt^2} + \frac{k_1 k_2}{r_a} \frac{d\theta_o}{dt} = \frac{k_1 e}{r_a} \text{ for } \varepsilon > \varepsilon_0 \dots [10]$$

In order that the relay servo be correctly described in its motion, there must be two more equations corresponding to the other zones of operation

$$\frac{J}{M_r} \theta_r \frac{d^2 \theta_o}{dt^2} + \frac{k_1 k_2}{r_a} \frac{d\theta_o}{dt} = 0 \text{ for } -\varepsilon_0 < \varepsilon < +\varepsilon_0 \dots [11]$$

and

$$\frac{J}{M_r} \theta_r \frac{d^2 \theta_o}{dt^2} + \frac{k_1 k_2}{r_a} \frac{d\theta_o}{dt} = -\frac{k_1 e}{r_a} \text{ for } \varepsilon < -\varepsilon_0 \dots [12]$$

Equation [10] describes the forward motion, Equation [11] the braking action, and Equation [12] the reverse motion.

These equations are in terms of per unit angle and seconds of time. Motors may have a wide range of rated speeds and armature inertia, and it will be convenient to express time in terms of a dimensionless unit such as a "time constant." Dimensionless time is expressed as

$$\tau = \frac{t}{T}$$

where

$$T = \frac{J \theta_r r_a}{M_r k_1 k_2} \text{ sec}$$

A new velocity and acceleration are then written as

$$\frac{d\theta_o}{dt} \frac{dt}{d\tau} = \frac{d\theta_o}{d\tau}$$

$$= \dot{\phi}_0$$

hence, with the relation $(dt)/(d\tau) = T$

$$\frac{d\theta_o}{dt} = \frac{1}{T} \dot{\phi}_0 \dots [13]$$

and in a similar manner

$$\frac{d^2 \theta_o}{dt^2} = \frac{1}{T^2} \ddot{\phi}_0 \dots [14]$$

Equations [10], [11], and [12] are then written as

$$\ddot{\phi}_0 + \dot{\phi}_0 = + \frac{J r_a \theta_r e}{M_r k_1 k_2} \varepsilon > \varepsilon_0 \dots [15]$$

$$\ddot{\phi}_0 + \dot{\phi}_0 = 0 \quad -\varepsilon_0 < \varepsilon < +\varepsilon_0 \dots [16]$$

$$\ddot{\phi}_0 + \dot{\phi}_0 = - \frac{J r_a \theta_r e}{M_r k_1 k_2} \varepsilon < -\varepsilon_0 \dots [17]$$

The range of factors on the right of Equations [15] and [17] for normally designed motors may be

$$0.06 < r_a < 0.2 \text{ (dimensionless)}$$

$$0.8 < e < 1.5 \text{ (dimensionless)}$$

$$0.8 < k_1 < 1.5 \text{ (dimensionless)}$$

$$0.7 < k_2 < 2.0 \text{ sec}$$

$$0.5 < \frac{J\Theta_r}{M_r} < 2.0 \text{ sec}^2$$

and the dimensionless term $(J\Theta_r a_e)/(M_r k_1 k_2^2)$ may range from a minimum of 0.05 to a maximum of 1.5. Under actual conditions the value may cover a smaller range about 1.

The equations of motion, Equations [15], [16], and [17], are in terms of per unit motor-shaft angle and per unit time. It will be more convenient in discussing the servo performance to have the results in terms of the per unit error angle and per unit time

$$\phi_0 = n(\theta_i - \varepsilon) \text{ per unit} \dots [18]$$

In the usual case θ_i is some function of time and should be represented as $\theta_{i(t)}$; however, only three cases are of general importance and will be considered in this discussion as follows

$$\text{Case 1 } \theta_i(t) = \theta_{i(0)} \text{ radians} = \text{const} \dots [19]$$

$$\text{Case 2 } \theta_i(t) = mt + \theta_{i(0)} \text{ radians} \dots [20]$$

$$\text{Case 3 } \theta_i(t) = A \cos(\beta t + \alpha) \text{ radians} \dots [21]$$

Rewriting Equations [19], [20], and [21] in terms of τ and per unit angle

$$\text{Case 1 } \theta_i(\tau) = \theta_{i(0)} \text{ per unit} \dots [22]$$

$$\text{Case 2 } \theta_i(\tau) = \frac{mT}{\Theta_r} \tau + \theta_{i(0)} \text{ per unit} \dots [23]$$

$$\text{Case 3 } \theta_i(\tau) = \frac{A}{\Theta_r} \cos(\beta T \tau + \alpha) \text{ per unit} \dots [24]$$

From Equations [13], [14], and [18]

$$\dot{\phi}_0 = \frac{d}{d\tau} (\phi_0) = n \left(\frac{d}{d\tau} \theta_{i(\tau)} - \frac{d}{d\tau} \varepsilon \right) \dots [25]$$

$$\ddot{\phi}_0 = \frac{d^2}{d\tau^2} (\phi_0) = n \left(\frac{d^2}{d\tau^2} \theta_{i(\tau)} - \frac{d^2}{d\tau^2} \varepsilon \right) \dots [26]$$

Substituting Equations [25] and [26] in [15], [16], and [17] where

$$B = \frac{J r_a \Theta_r a_e}{M_r k_1 k_2^2 n} \dots [27]$$

then

$$\ddot{\varepsilon} + \dot{\varepsilon} = -B + \frac{d^2}{d\tau^2} \theta_{i(\tau)} + \frac{d}{d\tau} \theta_{i(\tau)} \varepsilon > \varepsilon_0 \dots [28]$$

$$\ddot{\varepsilon} + \dot{\varepsilon} = \frac{d^2}{d\tau^2} \theta_{i(\tau)} + \frac{d}{d\tau} \theta_{i(\tau)} - \varepsilon < \varepsilon < +\varepsilon_0 \dots [29]$$

$$\ddot{\varepsilon} + \dot{\varepsilon} = +B + \frac{d^2}{d\tau^2} \theta_{i(\tau)} + \frac{d}{d\tau} \theta_{i(\tau)} \varepsilon < -\varepsilon_0 \dots [30]$$

Equation [28] corresponds to Equation [15], Equation [29] to Equation [16], and Equation [30] to Equation [17].

Equations [28], [29], and [30] are general for the problem under study, and there remains only the substitution of Equations [19], [20], and [21] to formulate the equations for Cases 1, 2, and 3.

Case 1. From Equation [22] $\theta_{i(\tau)}$ is a constant, hence

$$\frac{d}{d\tau} \theta_{i(\tau)} = \frac{d^2}{d\tau^2} \theta_{i(\tau)} = 0$$

and Equations [28], [29], and [30] reduce to

$$\ddot{\varepsilon} + \dot{\varepsilon} = -B \quad \varepsilon > \varepsilon_0 \dots [31]$$

$$\ddot{\varepsilon} + \dot{\varepsilon} = 0 \quad -\varepsilon_0 < \varepsilon < +\varepsilon_0 \dots [32]$$

$$\ddot{\varepsilon} + \dot{\varepsilon} = +B \quad \varepsilon < -\varepsilon_0 \dots [33]$$

This problem has been discussed by MacColl (2) for a single value of the parameter B . Additional data are given here for a range of values of B .

Equations [31], [32], and [33] may be integrated by separation of variable. Since phase-plane diagrams are desired, let

$$\begin{aligned} \ddot{\varepsilon} &= \frac{d}{d\tau} \dot{\varepsilon} = \frac{d\dot{\varepsilon}}{d\varepsilon} \frac{d\varepsilon}{d\tau} \\ &= \frac{d\dot{\varepsilon}}{d\varepsilon} \dot{\varepsilon} \end{aligned}$$

and the equations become

$$\frac{d\dot{\varepsilon}}{d\varepsilon} \dot{\varepsilon} + \dot{\varepsilon} = -B$$

$$\frac{d\dot{\varepsilon}}{d\varepsilon} \dot{\varepsilon} + \dot{\varepsilon} = 0$$

$$\frac{d\dot{\varepsilon}}{d\varepsilon} \dot{\varepsilon} + \dot{\varepsilon} = +B$$

upon integration there results

$$\varepsilon = -B - \dot{\varepsilon} + B \ln(B + \dot{\varepsilon}) + \text{const} \quad \varepsilon > \varepsilon_0 \dots [34]$$

$$\varepsilon = -\dot{\varepsilon} + \text{const} \quad -\varepsilon_0 < \varepsilon < +\varepsilon_0 \dots [35]$$

$$\varepsilon = +B - \dot{\varepsilon} - B \ln(-B + \dot{\varepsilon}) + \text{const} \quad \varepsilon < -\varepsilon_0 \dots [36]$$

These equations completely represent the relay servo operation in the phase plane. It should be noted that the ε -curves as a function of $\dot{\varepsilon}$ are determinable to a constant and hence, once a curve is determined, any other curve may be found by shifting the first curve parallel to the ε -axis.

Fig. 2 illustrates curves for various values of B from 0 to 4, and may be used directly for design.

Case 2. The derivatives of Equation [23] are

$$\frac{d}{d\tau} \theta_{i(\tau)} = \frac{mT}{\Theta_r}$$

which is a constant D

$$\frac{d^2}{d\tau^2} \theta_{i(\tau)} = 0$$

and Equations [28], [29], and [30] become

$$\ddot{\varepsilon} + \dot{\varepsilon} = -B + D \quad \varepsilon > \varepsilon_0 \dots [37]$$

$$\ddot{\varepsilon} + \dot{\varepsilon} = +D \quad -\varepsilon_0 < \varepsilon < +\varepsilon_0 \dots [38]$$

$$\ddot{\varepsilon} + \dot{\varepsilon} = +B + D \quad \varepsilon < -\varepsilon_0 \dots [39]$$

Upon integration in the same manner as for Case 1, the equations reduce to

$$\varepsilon = -(B - D) - \dot{\varepsilon} + (B - D) \ln[(B - D) + \dot{\varepsilon}] + \text{const} \quad \varepsilon > \varepsilon_0 \dots [40]$$

$$\varepsilon = D - \dot{\varepsilon} - D \ln(-D + \dot{\varepsilon}) + \text{const} \quad -\varepsilon_0 < \varepsilon < +\varepsilon_0 \dots [41]$$

$$\varepsilon = +(B + D) - \dot{\varepsilon} - (B + D) \ln[-(B + D) + \dot{\varepsilon}] + \text{const} \quad \varepsilon < -\varepsilon_0 \dots [42]$$

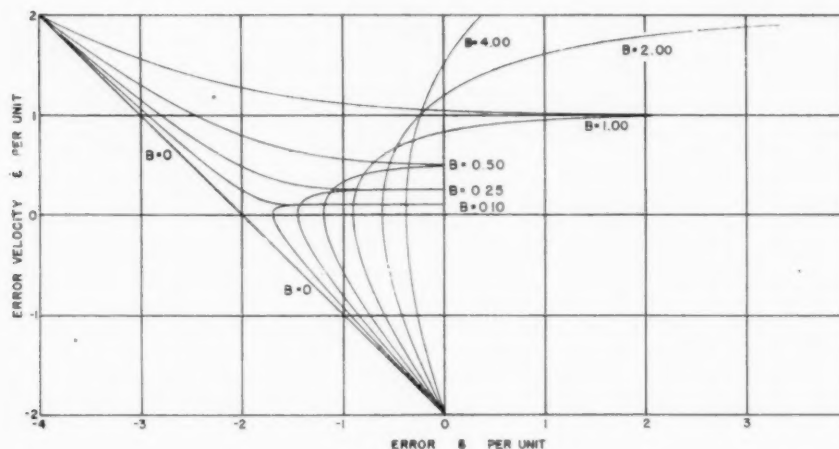


FIG. 2

These equations represent the relay operation in the phase plane. It should be noted that Equation [40] is similar to Equation [34] upon substitution of $B = (B - D)$ in Equation [40]; Equation [41] upon substitution of $B = D$ becomes Equation [36]; and Equation [42] upon substitution of $B = (B + D)$ becomes Equation [36]. Curves for design purposes may be obtained from Fig. 2.

Case 3. Case 3 is by far the most interesting in servo application because of the numerous occurrences, and the difficulty met in reducing the equations to phase-plane trajectories.

From Equation [24] the following derivatives are obtained

$$\frac{d}{d\tau} \theta_{i(\tau)} = -\frac{A}{\theta_r} \beta T \sin(\beta T \tau + \alpha)$$

$$\frac{d^2}{d\tau^2} \theta_{i(\tau)} = -\frac{A}{\theta_r} \beta^2 T^2 \cos(\beta T \tau + \alpha)$$

Substituting in Equations [28], [29], and [30] and defining

$$\frac{1}{\sqrt{1 + \beta^2 T^2}} = \cos \delta$$

and

$$\frac{\beta T}{\sqrt{1 + \beta^2 T^2}} = \sin \delta$$

then

$$\ddot{\epsilon} + \dot{\epsilon} = -B - \frac{A}{\theta_r} \beta T \sqrt{1 + \beta^2 T^2} \sin(\beta T \tau + \alpha + \delta) \quad \epsilon > \epsilon_0 \quad [43]$$

$$\ddot{\epsilon} + \dot{\epsilon} = -\frac{A}{\theta_r} \beta T \sqrt{1 + \beta^2 T^2} \sin(\beta T \tau + \alpha + \delta) \quad -\epsilon_0 < \epsilon < +\epsilon_0 \quad [44]$$

$$\ddot{\epsilon} + \dot{\epsilon} = +B - \frac{A}{\theta_r} \beta T \sqrt{1 + \beta^2 T^2} \sin(\beta T \tau + \alpha + \delta) \quad \epsilon < -\epsilon_0 \quad [45]$$

Case 3, as represented by Equations [43], [44], and [45], cannot be reduced to equations independent of time such as are necessary for phase-plane trajectories, and other methods must be used. Of course each equation is a linear differential equation with constant coefficients, and the solutions are well-known

factors of the time τ . One possible method of solving Case 3 is to compute step-by-step numerical data for each branch of the trajectory until it reaches steady state. Such a procedure is tedious, to say the least, and would not be practical for many solutions.

Since the purpose of this investigation is to determine design criteria, if possible, which would be sufficiently general to be of value to the servo user, a more efficient attack on the problem is needed. The mechanical differential analyzer is suited to this problem and was used to obtain over 50 solutions for wide ranges of the variables.

The phase-plane trajectories fell into three distinct classes as illustrated in Figs. 3, 4, and 5. Each class was characterized by a limit cycle having a period equal to that of the driving force, which in this case is the same as the period of the input angle, and having a stable motion that repeats over the same path for each successive cycle.

The limit cycle shown in Fig. 3 is somewhat analogous to resonance in linear systems in that the amplitude is large. From the point of view of the servo designer the motion appears to be unstable since the output does not follow the input with anything resembling a small error. By definition this type of motion will be called "unstable performance."

The limit cycle shown in Fig. 4 is more desirable from the operating point of view since the servo follows the input very closely in one direction, but lags the input in the other direction. By definition this type of motion shall be called "quasi-stable performance." In this motion the motor approaches one side of the dead space with approximately the velocity of the input angle and is able to follow the input for about a half-cycle. As indicated by the number of small loops, the motor-relay combination chatters about one edge of the dead space until the input angle reverses direction. At the instant of reversal the input velocity is zero, and the motor velocity is almost zero if not zero. The motor remains stationary until the input has moved sufficiently so that the error passes through zero to the other side of the dead zone. By this time the relative velocity of the input to the output is so great that the motor is unable to accelerate fast enough to overcome the input lead. The motor continues to follow without catching up until the input again reverses and the cycle repeats.

The limit cycle which is shown in Fig. 5 represents a desirable servo action in that the motor follows the input very closely by chattering about each side of the dead space. By defi-

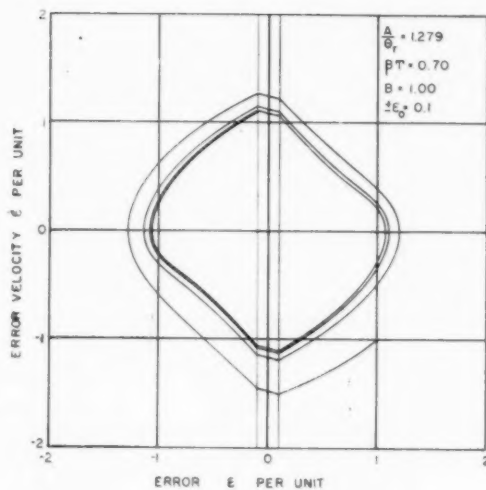


FIG. 3

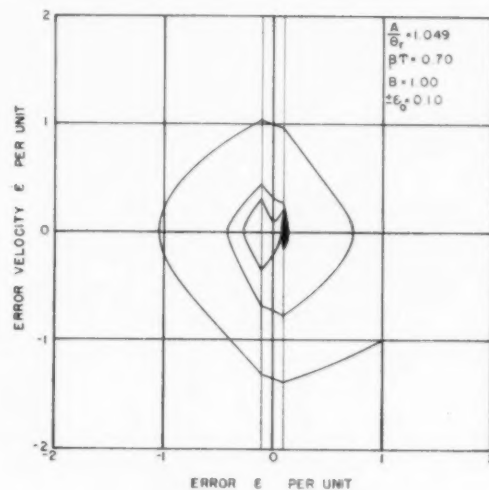


FIG. 4

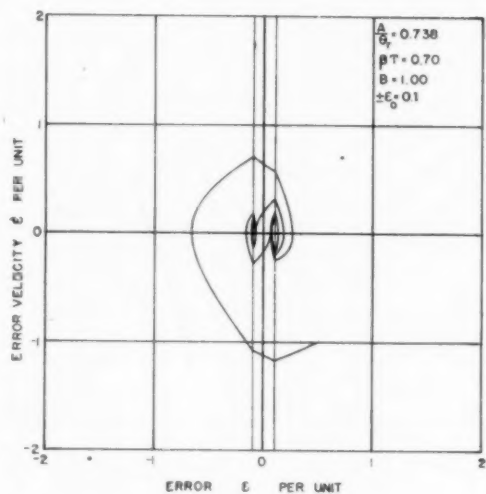


FIG. 5

nition this type of motion shall be called "stable performance."

Since the relay servo is a physical system, and the parameters may be varied uniformly over wide ranges, one might expect that the three types of motion are different phases of the same motion, and that these phases have no sharp line of separation. Results obtained from the differential analyzer show that the phases do blend smoothly without sharply defined boundaries but it is possible to predict with a reasonable accuracy the type of motion.

Most of the phase-plane trajectories were taken for a dead space of $\pm\epsilon_0 = 0.1$ per unit angle and correlations for unstable, quasi-stable, and stable performance were referred to this dead space as a base. The best correlations were obtained by use of the following empirical expression

$$N = \frac{A\beta^2 T^2 \sqrt{1 + \beta^2 T^2 \epsilon_0}}{B, B^2 0.1} \quad \left. \begin{array}{l} N < 0.6 \text{ stable performance} \\ 0.6 < N < 0.85 \text{ quasi-stable performance} \\ N > 0.85 \text{ unstable performance} \end{array} \right\} \dots\dots\dots [46]$$

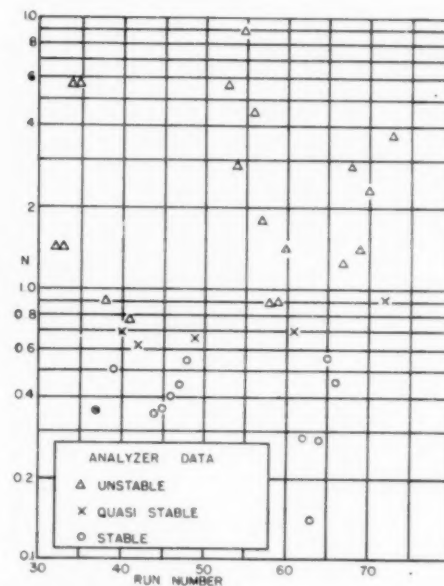


FIG. 6

Fig. 6 illustrates the type of correlation obtained. The fit is not perfect as there are two points not in the proper region but since sharp boundaries are not to be expected, the fit is sufficient for use as a design aid.

EFFECT OF DEAD-ZONE WIDTH

The empirical expression for N , Equation [46], indicates that as the dead-zone width increases, the servo becomes more unstable in performance. This is confirmed by the results shown in Figs. 7 to 11, inclusive, where the dead zone has been increased in width from zero to 0.15.

The phase-plane trajectories go from a perfectly stable performance, one that closes down on the point of zero error, Fig. 7, through successively less stable performances, Figs. 8 and 9,

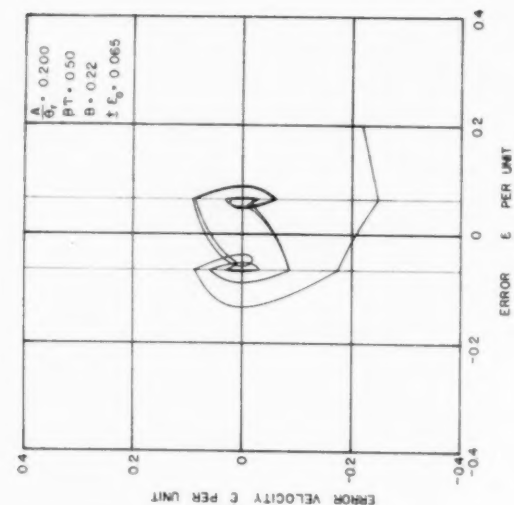


FIG. 7

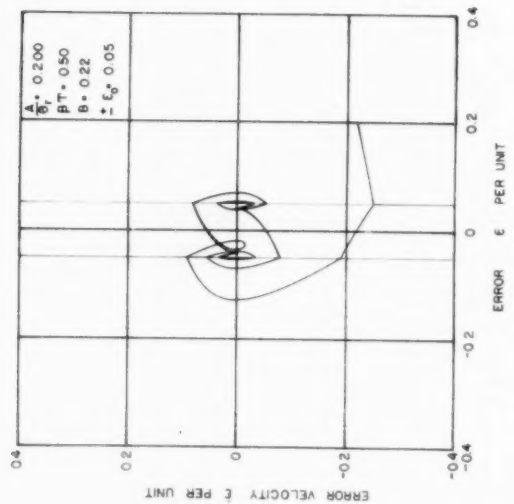


FIG. 8

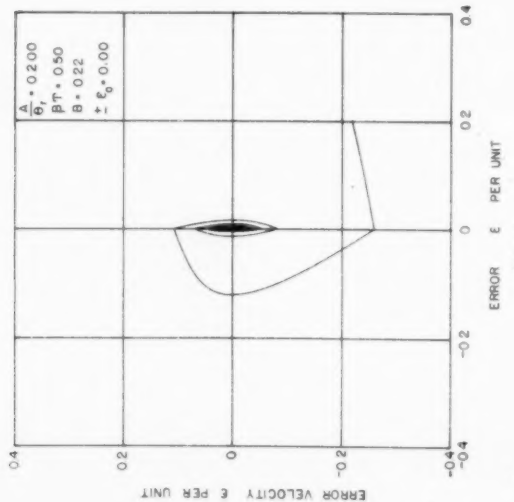


FIG. 9

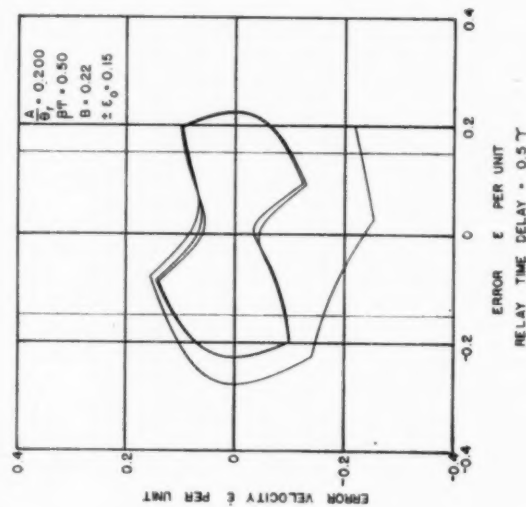


FIG. 10

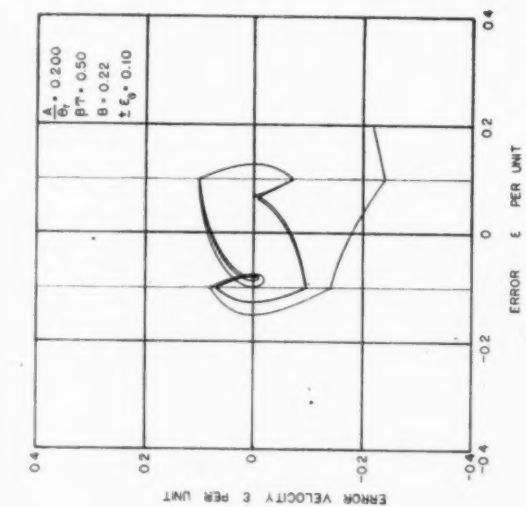


FIG. 11

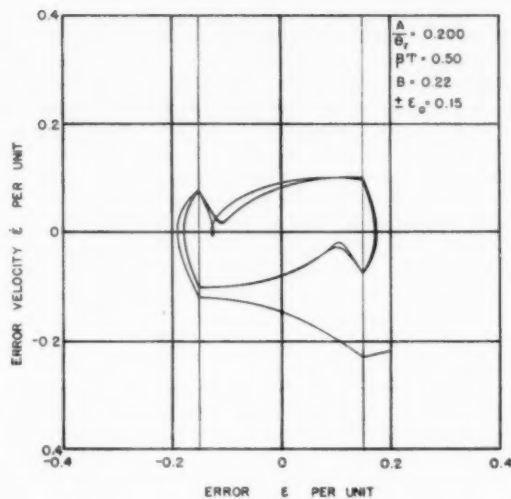


FIG. 12

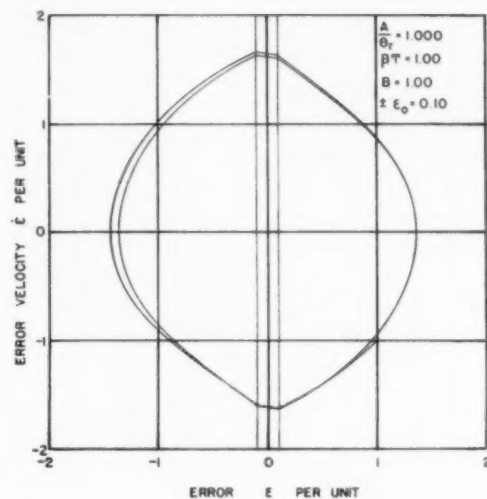


FIG. 13

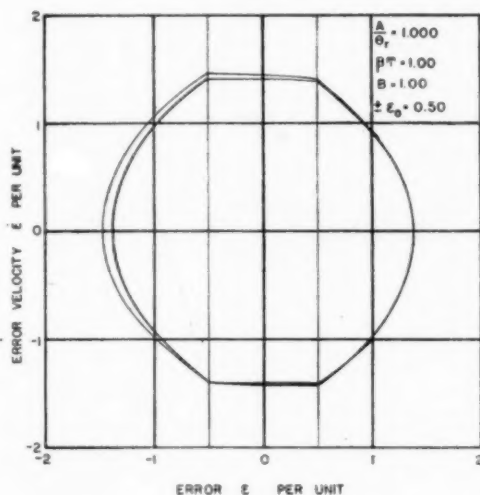


FIG. 14

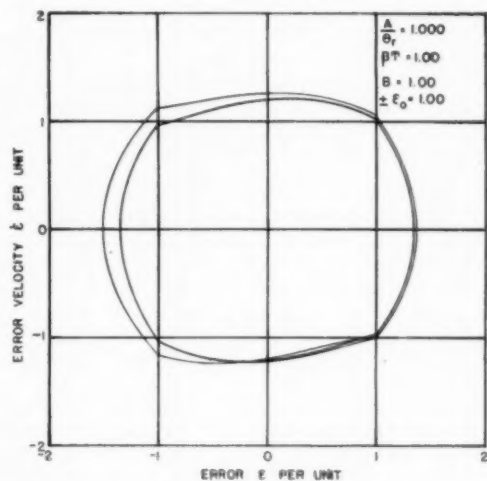


FIG. 15

to the unstable performance in Fig. 12. The quasi-stable performance lies in the upper portion of the region defined by Equation [46], as indicated by a comparison of Figs. 9 and 10. The servo has not yet reached the quasi-stable state for the conditions of Fig. 9, and has just passed through that state for the conditions of Fig. 10.

The introduction of a relay time lag always decreases the stability of the servo. A comparison of Fig. 12 with Fig. 11 indicates that with time lag the maximum errors increase, and the limit cycle becomes more open.

A similar sequence, Figs. 13, 14, and 15, shows the effect of increasing dead-zone width on a trajectory for unstable performance. As predicted from Equation [46], the unstable limit cycle does not become more stable. On the other hand, once the servo is unstable and as long as the driving amplitude, A/θ_r , is less than one half the dead-zone width, ϵ_0 , the maximum error does not change appreciably. Table 1 in the Appendix shows that

for a change of dead zone from ± 0.1 to ± 0.75 , the maximum amplitude changes from 1.362 to 1.380. When the dead zone is ± 1.0 the maximum amplitude decreases slightly to 1.345, and when the dead zone exceeds the driving amplitude, the servo motor eventually comes to rest within the dead zone at such a point that the relays are never excited. The error trajectory is then equal to the input trajectory and is a circle or ellipse.

An estimate of the maximum error may be found from the expression derived in the Appendix.

The effect of relay time lag again increases the maximum error, for the case shown in Figs. 14 and 16, from a value of 1.377 to a value of 1.500.

ARMATURE-CIRCUIT RESISTANCE

It would appear from physical reasoning that upon increasing the armature-circuit resistance, the servomotor response would be more sluggish, and possibly the performance would be more stable. This is not the case, however, since the armature-cir-

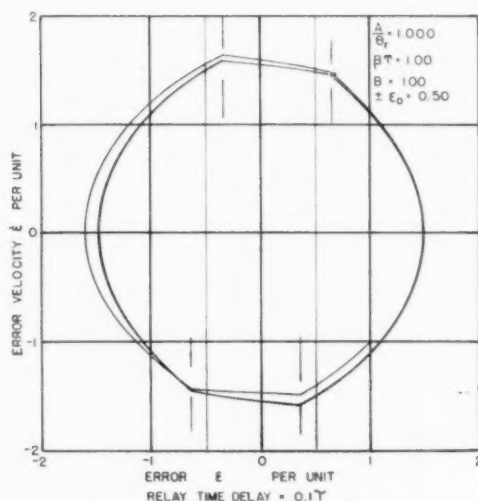


FIG. 16 RELAY TIME DELAY = 0.1T

cuit resistance enters into both the parameter B and the time constant T . With a change in the time constant T , there is an accompanying change in the size of the units of T and a change in the size of the units of error velocity $\dot{\epsilon}$.

External resistance may be included in the armature circuit, provided it is included in the armature circuit for all conditions of operation. In other words, this analysis does not account for a voltage source with an internal resistance.

CONCLUSIONS

This study has indicated the difficulties encountered in relay servo investigations whenever the input is a function of time. There appears to be no direct method of solving for phase-plane trajectories in problems of the Case 3 type where the first and second derivatives of the input functions are functions of time. In these cases, one approach to the problem seems to be by way of differential-analyzer solutions for many varied cases, and an attempt to correlate the results.

The results of this study have been sufficiently encouraging to warrant a continuation of the work for various output-load systems and various types of motors. Additional studies should be made to account for such items as relay operating lag, static friction, and Coulomb friction.

BIBLIOGRAPHY

- 1 "Theory of Servomechanisms," by H. L. Hazen, *Journal of The Franklin Institute*, vol. 218, 1934, pp. 279-331.
- 2 "Fundamental Theory of Servomechanisms," by L. A. MacColl, D. van Nostrand Company, Inc., New York, N. Y., 1945.
- 3 "Analysis of Relay Servomechanisms," by H. K. Weiss, *Journal of the Aeronautical Sciences*, vol. 13, 1946, pp. 364-376.
- 4 "Introduction to Non-Linear Mechanics," by N. Minorsky, Edwards Brothers, Ann Arbor, Mich., 1947.
- 5 "Theory of Oscillations," by H. A. Andronow and C. E. Chaikin, Princeton University Press, 1949.
- 6 "An Analysis of Relay Servomechanisms," by D. A. Kahn, Trans. American Institute of Electrical Engineers Preprint T9224, vol. 68, 1949, pp. 1079-1088.

Appendix

MAXIMUM ERROR OF A SERVO WITH UNSTABLE PERFORMANCE

Any servo, operating with a sinusoidally varying input, eventually must reach a limit cycle, on the phase plane, of a

period equal to the input period. If, for instance, the servo starts with a very large error, or error velocity, or a combination of both, the nature of the electrical connections are such as to reduce these errors to some minimum value. On the other hand, if the servomotor started from rest at the instant of both zero error and zero-error velocity, the change of input eventually would cause the relays to operate and start the motor. Once the motor has started, the amount of overshoot increases as it passes through the boundaries of the dead space until it reaches some limit such that the time for one cycle is just equal to the input period.

It is difficult to prove that these two limit cycles are identical, but mechanical solutions of the equations for the cases studied have always led to one and only one limit cycle for a given set of parameters. The limit cycle always has the same period as the servo input.

If the trajectory of the servo with unstable performance is considered, then since the input is symmetrical in its excursions about an average value, it might be expected that the servomotor and also the error would be symmetrical about some average value. For the phase-plane trajectory, the average value is the origin, and the trajectory has mirror symmetry about the origin with events occurring at the intersections of any line through the origin separated by a half-period in time.

It is proposed to solve the differential equations for each branch of the unstable trajectory, evaluate the constants of integration, the phase angle, and the time of travel over one branch, in order to have sufficient data to estimate the maximum error. The limit cycle to be investigated is shown in Fig. 17, with each branch lettered, and all points of importance numbered. The solutions are to be evaluated as if τ were zero at the beginning of each branch and the sinusoidal time functions adjusted to fit the junction points.

The period of the unstable servo is $(2\pi)/(\beta T)$ and the half-period is $\pi/(\beta T) = \Gamma$.

Reference to Fig. 17 and the condition of mirror symmetry

$$\left. \begin{aligned} \epsilon_1 &= -\epsilon_3 = \epsilon_0 \\ \dot{\epsilon}_1 &= -\dot{\epsilon}_3 \end{aligned} \right\} \dots\dots\dots [47]$$

also

$$\left. \begin{aligned} \epsilon_2 &= \epsilon_4 = \epsilon_0 \\ \dot{\epsilon}_2 &= \dot{\epsilon}_4 \end{aligned} \right\} \dots\dots\dots [48]$$

The equations for each branch of the trajectory as obtained from the differential equations [43], [44], and [45] are as follows

Branch U

$$\epsilon = P_1 + P_2 e^{-\tau} - B\tau + \frac{A}{\theta_r} \cos(\beta T\tau + \alpha) \dots\dots [49]$$

$$\dot{\epsilon} = -P_2 e^{-\tau} - B - \frac{A}{\theta_r} \beta T \sin(\beta T\tau + \alpha) \dots\dots [50]$$

Branch V

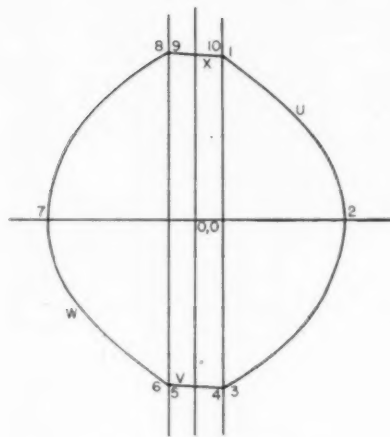
$$\epsilon = P_4 + P_5 e^{-\tau} + \frac{A}{\theta_r} \cos(\beta T\tau + \alpha) \dots\dots [51]$$

$$\dot{\epsilon} = -P_5 e^{-\tau} - \frac{A}{\theta_r} \beta T \sin(\beta T\tau + \alpha) \dots\dots [52]$$

Branch W

$$\epsilon = P_6 + P_7 e^{-\tau} + B\tau + \frac{A}{\theta_r} \cos(\beta T\tau + \alpha) \dots\dots [53]$$

$$\dot{\epsilon} = -P_7 e^{-\tau} + B - \frac{A}{\theta_r} \beta T \sin(\beta T\tau + \alpha) \dots\dots [54]$$



LIMIT CYCLE FOR A RELAY SERVO.

FIG. 17 LIMIT CYCLE FOR A RELAY SERVO

Branch X

$$\varepsilon = P_9 + P_{10}e^{-\tau} + \frac{A}{\Theta_r} \cos(\beta T\tau + \alpha) \dots [55]$$

$$\dot{\varepsilon} = -P_{10}e^{-\tau} - \frac{A}{\Theta_r} \beta T \sin(\beta T\tau + \alpha) \dots [56]$$

It can be shown by use of the symmetry condition, that

$$\begin{aligned} P_4 &= -P_1 \\ P_7 &= -P_2 \quad \tau_u = \tau_w \\ P_9 &= -P_4 \quad \tau_v = \tau_x \\ P_{10} &= -P_5 \end{aligned}$$

Also

$$\tau_u + \tau_v = \Gamma \dots [57]$$

and it is necessary to consider only Branches U and V in determining the constants, $P_1, P_2, P_4, P_5, \alpha, \tau_u$.At point 1 for $\tau = 0$ on Branch U

$$\varepsilon_1 = P_1 + P_2 + \frac{A}{\Theta_r} \cos \alpha = \varepsilon_0 \dots [58]$$

$$\dot{\varepsilon}_1 = -P_2 - B - \frac{A}{\Theta_r} \beta T \sin \alpha \dots [59]$$

At Point 3 for $\tau = \tau_u$ on Branch U

$$\varepsilon_3 = P_1 + P_2 e^{-\tau_u} - B\tau_u + \frac{A}{\Theta_r} \cos(\beta T\tau_u + \alpha) = \varepsilon_0 \dots [60]$$

$$\dot{\varepsilon}_3 = -P_2 e^{-\tau_u} - B - \frac{A}{\Theta_r} \beta T \sin(\beta T\tau_u + \alpha) \dots [61]$$

At Point 4 for $\tau = 0$ on Branch V

$$\varepsilon_4 = P_4 + P_5 + \frac{A}{\Theta_r} \cos(\beta T\tau_u + \alpha) = \varepsilon_0 \dots [62]$$

$$\dot{\varepsilon}_4 = -P_5 - \frac{A}{\Theta_r} \beta T \sin(\beta T\tau_u + \alpha) \dots [63]$$

Note that $(\beta T\tau_u + \alpha)$ is the angle that the input has at the start of Branch V.At Point 5 for $\tau = \tau_v$ on Branch V

$$\varepsilon_5 = P_4 + P_5 e^{-\tau_v} + \frac{A}{\Theta_r} \cos[\beta T(\tau_u + \tau_v) + \alpha]$$

Since $\tau_u + \tau_v = \Gamma$, and $\beta T\Gamma = \pi$

$$\varepsilon_5 = P_4 + P_5 e^{-(\Gamma - \tau_u)} - \frac{A}{\Theta_r} \cos \alpha = -\varepsilon_0 \dots [64]$$

$$\dot{\varepsilon}_5 = -P_5 e^{-(\Gamma - \tau_u)} + \frac{A}{\Theta_r} \beta T \sin \alpha \dots [65]$$

From the relations, Equations [47] and [48], and the Equations [58] through [65], the constants of integration are determined in functions of τ_u .

$$P_4 = -\frac{1}{2} B\tau_u \dots [66]$$

$$P_1 = B \left(1 + \frac{1}{2} \tau_u \right) \dots [67]$$

$$P_2 = -B \left(\frac{1 + e^{-(\Gamma - \tau_u)}}{1 + e^{-\Gamma}} \right) \dots [68]$$

$$P_5 = B \left(\frac{1 - e^{-\tau_u}}{1 + e^{-\Gamma}} \right) \dots [69]$$

Substitute Equations [47] and [48] in Equation [58] and solve for $\cos \alpha$

$$\cos \alpha = \frac{\Theta_r}{A} \left[\varepsilon_0 - B \left(1 + \frac{1}{2} \tau_u \right) + B \left(\frac{1 + e^{-(\Gamma - \tau_u)}}{1 + e^{-\Gamma}} \right) \right] \dots [70]$$

Substitute Equations [50] and [51] in Equation [62] and solve for $\cos(\beta T\tau_u + \alpha)$

$$\cos(\beta T\tau_u + \alpha) = \frac{\Theta_r}{A} \left[\varepsilon_0 + \frac{1}{2} B\tau_u - B \left(\frac{1 - e^{-\tau_u}}{1 + e^{-\Gamma}} \right) \right] \dots [71]$$

It is not possible to solve Equations [70] and [71] explicitly for α and τ_u , but values may be obtained by numerical or graphical methods.It should be observed that if ε_0 is zero, then $\tau_u = \Gamma$ and $\tau_v = 0$. For this case Equations [66] to [71] reduce to

$$P_1 = B \left(1 + \frac{1}{2} \Gamma \right) \dots [72]$$

$$P_2 = -B \left(\frac{2}{1 + e^{-\Gamma}} \right) \dots [73]$$

$$P_4 = -\frac{1}{2} \Gamma B \dots [74]$$

$$P_5 = B \left(\frac{1 - e^{-\Gamma}}{1 + e^{-\Gamma}} \right) \dots [75]$$

$$\cos \alpha = \frac{B\Theta_r}{A} \left[\left(\frac{2}{1 + e^{-\Gamma}} \right) - \left(1 + \frac{1}{2} \Gamma \right) \right] \dots [76]$$

Equation [71] reduces to Equation [76].

The point of maximum error occurs at the point $\dot{\varepsilon} = 0$ and hence an exact solution may be obtained numerically for $\tau(\dot{\varepsilon} = 0)$ upon substitution of values for Equation [48], α , and τ_u obtained from Equations [66], [70], and [71]. The value of $\tau(\dot{\varepsilon} = 0)$, together with Equation [48], α and τ_u may then be substituted in

Equation [49] for ϵ_{\max} . This procedure represents considerable numerical work that is necessary only for an exact result. In most practical cases the results will be sufficiently accurate if $\tau(\epsilon=0)$ is taken as $1/2\tau_w$. Again, if a greater tolerance is allowable in the values of ϵ_{\max} , the value obtained from the case of $\epsilon_0 = 0$ may be used, and the values from Equations [72], [73], [76], and $\tau = 1/2\Gamma$ substituted in Equation [49].

The maximum error for the case where $A/\theta_r = 1$, $B = 1$, $\beta T = 1$, and ϵ_0 varies from zero to 1 is shown in Table 1, repre-

TABLE 1 VARIATION IN ϵ_{\max} WITH VARIATION OF ϵ_0

ϵ_0	ϵ_{\max}	Deviation, per cent
0	1.359	0 (base)
0.1	1.362	+0.2
0.25	1.366	+0.5
0.50	1.377	+1.2
0.75	1.380	+1.5
1.00	1.345	-1.0

senting results from differential-analyzer curves, and is well within ± 2 per cent of the value obtained for $\epsilon_0 = 0$.

Cable-Pulley Friction¹

By W. E. SCHORR,² NEW YORK, N. Y.

The factors contributing to the friction in cable-pulley or rope systems are analyzed, and an empirical equation for calculating this friction is derived.

NOMENCLATURE

The following nomenclature is used in the paper:

- d = diameter of cable, in.
- d_g = diameter of pulley-throat groove, in.
- d_s = diameter of pulley shaft, in.
- D = effective diameter of pulley, in.
- e = misalignment of cable, deg
- f_b = coefficient of friction of bearing, based on shaft diameter
- f_b' = coefficient of friction of bearing, based on pulley diameter
- f_c = cable bending factor
- f_p = coefficient of sliding friction of cable-pulley materials
- F_B = bearing friction, lb
- F_c = cable bending friction, lb
- F_I = friction due to inertia effects, lb
- F_{max} = maximum cable bending friction, lb
- F_T = total friction, lb
- I = inertia effects
- l = length of lay of cable, in.
- n = number of strands in cable (not including core)
- N = normal load on pulley, lb
- T = cable tension, lb
- θ = angle of cable bend, deg
- θ_c = critical angle of cable bend, deg
- θ_f = angle of full cable bend, deg
- ψ = pulley design factor

The symbols are illustrated in Fig. 1.

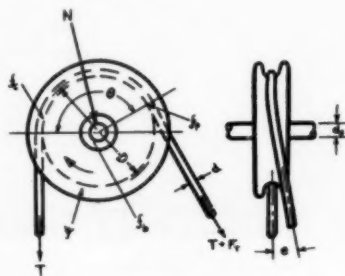


FIG. 1 ILLUSTRATING NOMENCLATURE

¹ Based on a thesis submitted to the Graduate Division of the College of Engineering in partial fulfillment of the requirements for the degree of Master of Mechanical Engineering at New York University.

² Instructor, New York University. Jun. ASME.

Contributed by the Machine Design Division and presented at the Spring Meeting, Washington, D. C., April 12-14, 1950, of THE AMERICAN SOCIETY OF MECHANICAL ENGINEERS.

NOTE: Statements and opinions advanced in papers are to be understood as individual expressions of their authors and not those of the Society. Manuscript received at ASME Headquarters, February 7, 1950. Paper No. 50-S-17.

INTRODUCTION

Cable-pulley systems or rope drives are used both for the transmission of power from one rotating shaft to another and for the transmission of a force or motion from one point to another. In the former case, much friction is desired between the pulley and the cable in order that the power of the driver pulley be transmitted undiminished to the driven pulley. Basic information is readily available on the variables involved in this application.

In the case of motion transmission, such as is experienced in control systems, hoisting, haulage and transporting services, however, the transfer of a force by means of a cable is desired. The pulleys are used merely to direct the force from the point of application to the point of action. The presence of large frictional losses in such systems has a detrimental effect upon the operation and life of the system and should be avoided.

This problem becomes especially important in control systems such as are used in aircraft where limitations of equipment and design exist, where quick and dependable action is of utmost importance, and where manual overcoming of the friction of the system may result in undue exhaustion of the pilot. In other applications, even though the problem is of lesser importance, the minimizing of the friction of the system will result in higher efficiency and more satisfactory operation.

Basic information as to the relative importance of the factors involved in these applications is lacking, however, and little data exist which will enable the energy losses of the systems to be calculated. This paper studies some of the variables involved and condenses them into a useful empirical equation as determined from experimental data.

PRELIMINARY ANALYSIS

The preliminary analysis indicates that the factors involved in cable-pulley total friction F_T are d , cable diameter; D , effective pulley diameter; θ , angle of cable bend; T , cable tension; e , cable misalignment; f_b , f_c , f_p , bearing, cable, and pulley friction factors, respectively; ψ , pulley design factor; and I , inertia factor. The coefficient of friction f_b will depend upon the type of bearing (plain, ball, or roller), and the operating conditions. The cable bending factor f_c will depend upon the design, flexibility, construction, and material of the cable. The coefficient of sliding friction f_p will depend upon the materials of the cable and the pulley. The pulley factor ψ will depend upon the material and design of the pulley, such as groove shape, groove radius, and so forth.

Moreover, the total friction arises from several sources and may be separated into (1) friction in the bearing F_B , (2) internal friction of the cable in flexing and digging into the pulley F_c , and (3) the energy expended in overcoming the inertia effects of the system, F_I

$$F_T = F_B + F_c + F_I \dots \dots \dots [1]$$

Bearing Friction, F_B . The loss due to the sliding contact of the rotating pulley on its shaft may be expressed as

$$F_B = f_b' N \dots \dots \dots [2]$$

where f_b' is the coefficient of friction at the point where F_B is applied.

The coefficient of friction f_b is usually expressed in terms of the

shaft diameter, d_s . However, since the bearing loss must be overcome by a force applied at the effective pulley diameter D , the coefficient must be expressed in terms of the pulley diameter (f_b'), or a correction ratio be applied

$$f_b' = f_b \frac{d_s}{D} \quad [3]$$

The normal load N may be expressed in terms of the cable tension T and the angle of cable bend θ as shown in Fig. 2. Thus

$$N = T (2 - 2 \cos \theta)^{1/2} \quad [4]$$

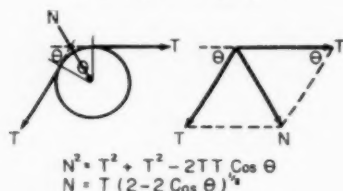


FIG. 2 RESOLUTION OF FORCES

Therefore the bearing friction may be given as

$$F_b = f_b' T (2 - 2 \cos \theta)^{1/2} \quad [5]$$

Cable Bending Friction, F_c . The wire rope used in control systems and wire drives is composed of several wires which are helically wound around another wire to form a strand. Several of these strands are then helically wound around a core (wire or fiber) to complete the cable. In bending around a pulley or sheave, the individual wires must be free to move in order to conform to the contour of the pulley. This movement expends energy, since it will result in tension in the outer wires of the bend and compression in the inner wires in contact with the pulley. Moreover, there will be sliding friction as the individual wires rub against one another and against the surface of the pulley as the cable conforms to the desired curvature. The cable bending friction F_c will be a function of d , D , θ , T , e , f_c , f_p , and ψ , as previously defined.

Friction Due to Inertia Effects, F_i . Since more initial force is required to start a system moving from rest, overcoming inertia effects, than is necessary to keep it moving, there exists both a static and a dynamic condition of friction in a cable-pulley system. The inertia effects will depend upon the weights of the moving components of the system, their moments of inertia, the velocity of the cable in moving over the pulleys, and any vibrations present in the system.

Test Conditions. The foregoing analysis indicates that the variables involved are too numerous for all to be considered in the present investigation. However, since the problem of friction is not as important where the pulleys are few and where factors such as weight and space are secondary, the actual tests will be conducted with regard to an application where the conditions are serious, for example, the control system of an aircraft. The test data obtained will therefore be directly applicable only to these systems (or to systems using identical test specimens), but the general form of the solutions will hold for all applications, except for actual values of constants and coefficients.

The components of aircraft control systems have been specified by military and governmental agencies, and thus several of the variables involved will remain constant in all such systems and need not be investigated.

Cable. Specifications require that 7×19 extra-flexible stainless-steel cable be used. The present tests were limited to the use of this type of cable, and so the cable factor f_c was not varied.

Pulley. AN 210 (AN-FFP-796) micarta pulleys with anti-

friction ball bearings (K series) were used. This limits f_p to micarta-steel, ψ to AN 210 design, and f_b to antifriction ball bearings.

Operating Conditions:

1 The combinations of cables and pulleys that may be used together are specified by AN-FFP-796, and so only these were tested.

2 Misalignment e must be avoided and kept below $1\frac{1}{2}$ deg in all acceptable systems. The effects of misalignment were kept at zero, and thus variations were not investigated in this test.

3 Since vibrations always exist in an aircraft while in flight, and since no excessive linear velocities of cable are involved, the static friction is eliminated and therefore only the dynamic friction was investigated (eliminates F_i).

The foregoing limitations reduce the variables to be investigated to d , D , θ , and T and changes the total friction to the total dynamic friction so that

$$F_T = F_b + F_c \quad [6]$$

TEST SETUP AND METHOD

Since the preliminary analysis indicated that the variables D , d , θ , and T must be investigated, a test jig was designed which would allow for the necessary variation in these factors. The test setup is shown in Fig. 3.

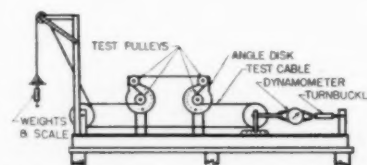


FIG. 3 SETUP USED IN CABLE-PULLEY FRICTION TESTS



FIG. 4 MOUNTING OF PULLEYS

The apparatus accommodated all standard pulleys from 1 to 6 in. diam, in combination with all cable sizes, and permitted all angles of cable bend from 0 to 180 deg at any desired cable tension. Four identical test pulleys were tested on the jig at one time, all at the same cable bend as determined by the angle disk. A close-up showing the mounting of the test pulleys is given in Fig. 4. The cable tension was adjusted by means of a turnbuckle and measured by a dynamometer. A weighted tray and small spring scale were connected by means of a cord over an idler pulley to one groove of a double-grooved guide pulley, while the test cable ran over the second groove and over the four test pulleys. A force was applied on the scale (or the scale in

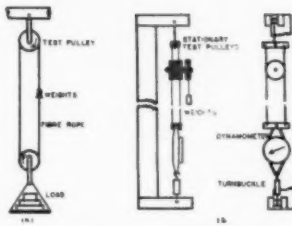


FIG. 5 SETUPS FOR MEASURING BEARING FRICTION

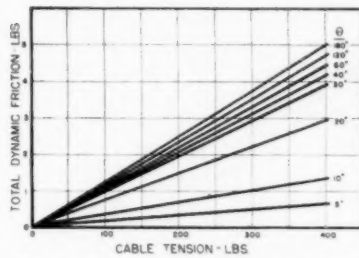


FIG. 6 TOTAL DYNAMIC FRICTION VERSUS CABLE TENSION
(4A pulley, 1/16-in. cable.)

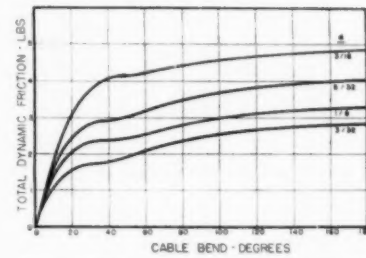


FIG. 7 TOTAL DYNAMIC FRICTION VERSUS CABLE BEND
(4A pulley, 400-lb cable tension.)

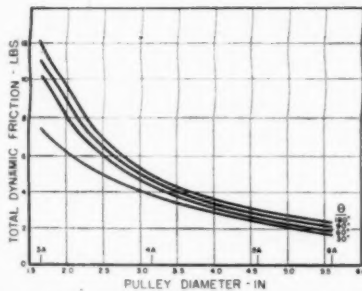


FIG. 8 TOTAL DYNAMIC FRICTION VERSUS PULLEY DIAMETER
(1/16-in. cable, 400-lb cable tension.)

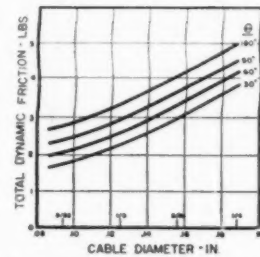


FIG. 9 TOTAL DYNAMIC FRICTION VERSUS CABLE DIAMETER
(4A pulley, 400-lb cable tension.)

conjunction with the weights in the tray), until the system moved at a constant velocity. The velocity or speed of the cable of the test was approximately 1.5 fps for a test distance of about 6 ft. The force as read on the scale plus the weights in the tray represented the friction of the entire system.

One run was taken at zero angle of cable bend. This represented the tare of the system, that is, the friction of the system minus the four test pulleys. By subtracting the tare value from the total value measured, the net friction of the test pulleys alone was determined. Since four test pulleys were involved, this net friction was divided by 4 to obtain the friction per pulley.

The pulley-cable combinations tested were as follows:

Pulley	Cable
3A	3/32, 1/8, 5/32, 3/16
4A	3/32, 1/8, 5/32, 3/16
5A	1/8, 5/32, 3/16, 1/4
6A	3/16, 1/4

The bearing-friction tests were conducted in two ways. For the light bearing loads, a very flexible fiber rope was wrapped around two identical test pulleys, and the force required to keep the system in motion at constant speed was measured. Since the fiber cord was very flexible, the cable bending friction was negligible, and the force applied merely overcame the friction present at the bearings of the two pulleys. The setup is illustrated in Fig. 5(a).

For the heavier bearings loads, a force was imposed on two stationary test pulleys by means of a cable-and-turnbuckle arrangement. The torque required to turn the shaft passing through the pulleys was then measured. The friction values resulting were divided by 2 to obtain the bearing friction per pulley. This setup is shown in Fig. 5(b).

TEST RESULTS

From the test data obtained, the following relationships were plotted for all of the pulley-cable combinations which were tested:

- Curve 1 Total friction versus cable tension (F_T vs T)
- Curve 2 Total friction versus cable bend (F_T vs θ)
- Curve 3 Total friction versus pulley diameter (F_T vs D)
- Curve 4 Total friction versus cable diameter (F_T vs d)
- Curve 5 Bearing friction versus normal load (F_B vs N)

Typical examples of Curves 1 to 4 are shown in Figs. 6 to 9, inclusive. Since the normal load N , may be expressed in terms of T and θ (see Equation [4]), the bearing-friction curves (F_B versus N) were redrawn in terms of the cable bend θ , for constant values of cable tension T .

Also, since it was determined originally that $F_T = F_B + F_c$ (see Equation [6]), the bearing friction was subtracted from the total friction, and the relationships for the cable-bending friction F_c were obtained.

The data and curves indicated immediately that F_T (F_B and F_c also) varied directly with the cable tension T within the test range, and so only the variables θ , D , and d required further consideration. Therefore the following curves were plotted:

- Curve 6 Bearing friction versus cable bend (F_B vs θ)
- Curve 7 Cable bending friction versus cable bend (F_c vs θ)
- Curve 8 Cable bending friction versus pulley diameter (F_c vs D)
- Curve 9 Cable bending friction versus cable diameter (F_c vs d)

Curves 6 to 9 are shown in Figs. 10 to 12, inclusive.

Bearing Friction, F_B . The test data indicated that the bearing friction was directly proportional to the normal load, and thus the initial analysis was substantiated. The equation for the bearing friction is therefore

$$F_B = f_b' T (2 - 2 \cos \theta)^{1/2} \dots \dots \dots [5]$$

Cable Bending Friction, F_c . The curve of cable bending friction versus cable bend (F_c versus θ) indicated that the friction increased parabolically from a zero cable bend, reached a maximum value, and then remained essentially constant at the maximum value up to a complete bend of 180 deg. This suggested that a critical angle of bend existed for every pulley-cable com-

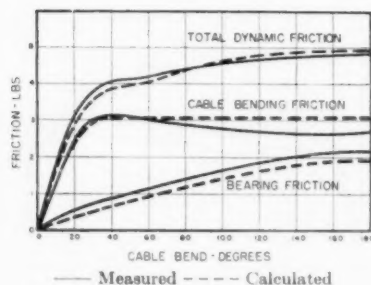


FIG. 10 Friction Versus Cable Bend
(4A pulley, 1/16-in. cable, 400-lb cable tension.)

bination, an angle above which the cable bending friction was essentially independent of increased cable wrap. This critical angle θ_c was investigated, and an empirical equation in terms of d and D was derived. This was readily done since the curves of θ_c versus d , and θ_c versus D plotted approximately as straight lines on log-log paper, within the test range, Figs. 13 and 14. The derived equation was

$$\theta_c = 161 \frac{d^{0.5}}{D^{0.5}} \quad [7]$$

The value of the cable bending friction at the critical angle F_{\max} was found to be the maximum value of friction due to this source. Curves of F_{\max} versus d , and F_{\max} versus D , also plotted

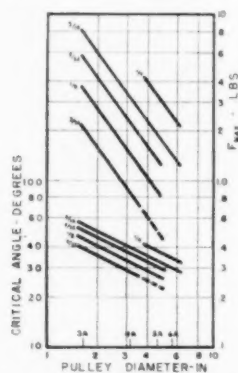


FIG. 13 F_{\max} AND θ_c VERSUS
PULLEY DIAMETER
(400-lb tension.)

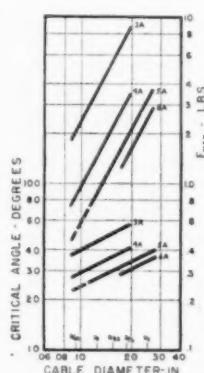


FIG. 14 F_{\max} AND θ_c VERSUS
CABLE DIAMETER
(400-lb tension.)

as straight lines on log-log paper, Figs. 13 and 14, and the following relationship was obtained

$$F_{\max} = T \frac{d^{1.92}}{D^{1.45}} \quad [8]$$

Below the critical angle, the cable bending friction is dependent upon all the variables θ , d , and D and increases parabolically with increasing cable bend. Using the values of θ_c and F_{\max} obtained, and assuming a parabolic variation, an empirical equation for the cable bending friction at subcritical angles was derived

$$F_c = T \frac{d^{0.92}}{D^{1.45}} \left[d - (\theta_c - \theta)^2 \frac{D}{(161)^2} \right] \quad [9]$$

Total Dynamic Friction, F_T . Since the total dynamic friction is the sum of the cable bending friction and the bearing friction, the derived equation for the total dynamic friction for $\theta < \theta_c$ is

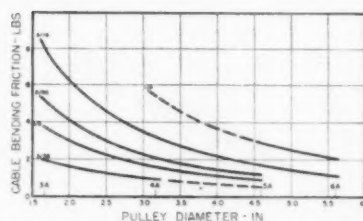


FIG. 11 CABLE BENDING FRICTION VERSUS
PULLEY DIAMETER
(Critical cable angle, 400-lb cable tension.)

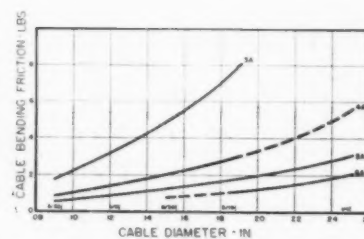


FIG. 12 CABLE BENDING FRICTION VERSUS
CABLE DIAMETER
(Critical cable angle, 400-lb cable tension.)

$$F_T = F_c + F_B$$

$$F_T = T \left\{ \frac{d^{0.92}}{D^{1.45}} \left[d - (\theta_c - \theta)^2 \frac{D}{(161)^2} \right] + f_b' (2 - 2 \cos \theta)^{1/2} \right\} \quad [10]$$

$$F_T = T \left\{ \frac{d^{0.92}}{D^{1.45}} \left[d - \left(161 \frac{d^{0.5}}{D^{0.5}} - \theta \right)^2 \frac{D}{(161)^2} \right] + f_b' (2 - 2 \cos \theta)^{1/2} \right\} \quad [11]$$

Since, in most applications, the angle of cable bend is greater than the critical value, the equation for total dynamic friction may be reduced to

$$F_T = T \left\{ \frac{d^{1.92}}{D^{1.45}} + f_b' (2 - 2 \cos \theta)^{1/2} \right\} \quad [12]$$

Examples of bearing friction, cable bending friction, and total dynamic-friction curves are shown in Fig. 10.

DISCUSSION OF TEST RESULTS

Cable Bending Friction. The existence of a critical angle of bend θ_c and a maximum value of cable bending friction F_{\max} may be explained as follows:

Internal friction in the cable is caused by the bending and unbending of the cable as it contacts and leaves the pulley. In conforming to the contour of the pulley, the individual wires and strands composing the cable must bend and rub against one another and against the pulley surface, thereby producing sliding friction. The actual bending occurs only at the points of tangency of the cable and the pulley, however, and once the cable has been bent through an angle great enough for the individual wires to reach equilibrium at the desired curvature, no further relative movement occurs until the point of unbending is reached. When an angle of cable bend greater than the critical angle is encountered, the cable sections which are bending and unbending at the points of tangency are developing friction, whereas the central section is merely fixed to the contour of the pulley and contributes nothing to the losses. A condition of maximum cable bending friction occurs, therefore, and this will exist when the critical or full bending angle has been reached.

The magnitude of the critical angle depends upon the diameters of the cable and the pulley, since these factors influence the severity of the bending required of the individual wires. Referring to available data,³ an angle of full bending is derived which depends upon the "lay" of the rope or cable. The length of lay of the cable l is defined as that distance measured parallel to the axis or center line of a cable in which a strand makes one com-

³ "Roebing Handbook," John A. Roebing's Sons Company, Trenton, N. J., 1947.

plete spiral or turn around the cable. According to the foregoing reference, once full bending is encountered, it makes no difference how great the departure (arc of contact with the pulley), the effect on the rope will be the same. The angle of full bending θ_f is given as

$$\theta_f = \frac{360}{\pi} \frac{l}{D} \quad [13]$$

This is the equation for the center angle of a circular segment whose diameter is D and whose length of arc is equal to l . For the 7×19 cable tested, the length of lay was determined to be approximately $l = 7.2 d$. Substituting this in Equation [13], we obtain

$$\theta_f = 825 \frac{d}{D} \quad [14]$$

The results of the present tests indicate, however, that within the test range, the critical angle θ_c , at least in so far as cable bending friction is concerned, is

$$\theta_c = 161 \frac{d^{0.5}}{D^{0.5}} \quad [7]$$

The constant 161 and the exponents are dependent upon f_c , f_p , n , and ψ .

Although the two equations differ, the idea of a "critical" angle is substantiated. One reason for the discrepancy may be that Equation [13] assumes that one full rope lay is necessary between the points of contact of pulley and cable before equilibrium of the individual wires occurs, whereas actual contact takes place against the sides of the pulley flanges and the actual distance between contact points may be less than one full rope lay. This would result in the critical angle θ_c being less than the calculated angle of full bending θ_f . Another factor involved is that of slippage between the cable and pulley surfaces at the points of contact. If slippage is present θ_c may be greater than θ_f , since relative movement between the wires would occur for a distance greater than one full rope lay.

Values of the critical angle θ_c (measured and calculated) and the angle of full bending θ_f are given in Table 1.

The maximum value of cable bending friction F_{\max} also depends upon d and D , inasmuch as more energy is expended in bending a given-size cable over a smaller-diameter pulley, or bending a larger-size cable over a given-size pulley. In the derived equation

$$F_{\max} = T \frac{d^{1.92}}{D^{1.48}}$$

the exponents of d and D are dependent upon the actual cables and pulleys tested. If galvanized or zinc-coated cable or less flexible cable, were used (thereby changing f_c and n), the exponent of d would increase. The use of steel or other material for the pulleys (changing f_p) would change the exponent of D . A change in pulley groove diameter or throat design (changing ψ) would result in changes of the exponents of both d and D . Regardless of the changes in materials and design, however, the general form of the equation would be similar, the actual values of the exponents being determined only by tests.

In some of the pulley-cable combinations tested, the test data indicated that the cable bending friction decreased somewhat after reaching the maximum value at the critical angle of cable bend. The results were inconclusive, however, and therefore this friction is assumed to remain constant at F_{\max} in the present analysis.

TABLE 1 COMPARISON OF CRITICAL ANGLE AND ANGLE OF FULL BENDING

Pulley diam, D , in.	Cable diam, d , in.	θ_c (measured), deg	θ_c (calculated), deg	θ_f , deg
1.656 (3A)	3/32	40	39.5	47
1.656 (3A)	1/8	42	44	62
1.656 (3A)	5/32	50	49.5	78
1.656 (3A)	3/16	62	57	101
3.156 (4A)	3/32	25	28	24.5
3.156 (4A)	1/8	30	32	33
3.156 (4A)	5/32	32	36	41
3.156 (4A)	3/16	40	39	49
4.592 (5A)	1/8	28	26.5	23
4.592 (5A)	5/32	30	29.5	28
4.592 (5A)	3/16	32	32.5	34
4.592 (5A)	1/4	38	38.5	45
5.592 (6A)	3/16	30	29.5	38
5.592 (6A)	1/4	32	33	37

Bearing Friction. According to earlier data,⁴ the loss of energy due to friction in the bearings arises from (1) the sliding contact between the balls and the separating pockets, (2) the rolling or internal friction of the steel due to deformation of the balls and races under load, (3) the slip which may occur in contact areas, and (4) the friction due to windage at the higher speeds. Since the tests were run at low speeds, friction due to windage was negligible.

The coefficients of friction for ball bearings as given in most literature range from 0.0005 to 0.0095, based on shaft diameters, depending upon the operating conditions.⁵ The actual values obtained in the present investigation, however, ranged from 0.013 to 0.032, based on shaft diameters (or 0.001 to 0.005, based on pulley diameters). The discrepancy is probably due to the fact that the literature values are for ideal, well-lubricated, new or clean conditions, whereas the test values represent actual service conditions. Qualitative tests conducted on pulleys with dusty or poorly lubricated bearings resulted in the coefficients of friction increasing to 0.032–0.075, and higher. The bearing coefficients as determined for the pulleys tested are given in Table 2.

The bearing friction was found to vary directly with the normal load, except for a slight initial sliding-contact friction which exists even at no-load conditions. In the analysis of the equation for bearing friction, this small initial friction was neglected,

TABLE 2 COEFFICIENTS OF BEARING FRICTION

Pulley no.	Pulley diam, D , in.	Shaft diam, d_s , in.	f_b	f_b'
3A	1.656	0.25	0.029	0.0044
4A	3.156	0.25	0.031	0.0024
5A	4.592	0.375	0.0147	0.0012
6A	5.592	0.375	0.0148	0.0010

and the coefficient of friction was assumed to be independent of load.

Since the bearing friction is directly proportional to the normal load, which in turn increases with the angle of cable bend (at constant cable tension), the bearing friction will increase continually with increase in cable bend.

Total Dynamic Friction. Very little data exist on the friction present in pulley-cable systems, and therefore comparative values are meager. The only data known to the author are the results given by Schorr,⁶ and Remington and Matthews.⁷ Comparison with these results are very good and are shown in Fig. 15,

⁴ "New Departure Handbook," New Departure Company, New London, Conn., vol. 11, 1939.

⁵ "Ball Bearings," by H. Heas, Trans. ASME, vol. 29, 1907, p. 371.

⁶ "Cable-Pulley Friction," by W. E. Schorr, Republic Aviation Corporation, Farmingdale, L. I., N. Y., no. 289, 1943.

⁷ "Reducing Friction in Cable Control Systems," by K. D. Remington and F. A. Matthews, *Aero Digest*, vol. 44, Feb. 1, 1944, pp. 75, et al.

together with total friction values as calculated from the derived equation.

CONCLUSIONS

The conclusions derived from this investigation are as follows:

- 1 The friction in cable-pulley systems increases as follows:
 - (a) With increase in cable tension (linearly).
 - (b) With increase in angle of cable bend.
 - (c) With increase in cable diameter.
 - (d) With decrease in pulley diameter.
- 2 An empirical equation for determining the total dynamic friction in cable-pulley systems is

$$F_T = T \left\{ \frac{d^{0.92}}{D^{1.48}} \left[d - (\theta_c - \theta)^2 \frac{D}{(161)^2} \right] + f_b' (2 - 2 \cos \theta)^{1/2} \right\} \quad \theta < \theta_c$$

For most applications, this may be reduced to

$$F_T = T \left\{ \frac{d^{1.92}}{D^{1.48}} + f_b' (2 - 2 \cos \theta)^{1/2} \right\} \quad \theta \geq \theta_c$$

- 3 A critical angle of cable-bending friction exists, above which the friction becomes independent of increased cable wrap. The value of this critical angle depends upon the cable-pulley combination involved and is related as follows

$$\theta_c = 161 \frac{d^{1.5}}{D^{0.5}}$$

- 4 A maximum value of cable-bending friction exists at angles of cable bend equal to or greater than the critical angle. This maximum value may be expressed as

- 5 The coefficients of friction for ball bearings under actual

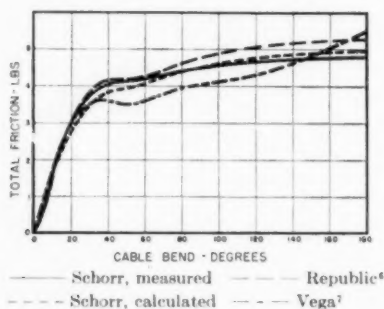


FIG. 15 COMPARATIVE TEST CURVES
(4A pulley, 1/16-in. cable, 400-lb tension.)

$$F_{max} = T \frac{d^{1.92}}{D^{1.48}}$$

service conditions are higher than those usually listed. The friction due to the bearings may therefore become a substantial part of the total friction in cable-pulley systems.

ACKNOWLEDGMENTS

The author gratefully acknowledges the helpful assistance of Prof. A. H. Church, not only as adviser, but also in obtaining the necessary equipment, space, and shop facilities for conducting the required tests. Many thanks are also due to members of the New York University Mechanical Engineering Laboratory personnel for their help in the construction of the test setup, to

Republic Aviation Corporation, and *Aero Digest* for the use of their material, and to John A. Roebling's Sons Company for supplying samples of cables and company publications.

Discussion

H. C. GUHL.⁸ The mathematical approach which has been made to evaluate design factors in cable systems is accurate and complete. Thereby the aircraft designer can select components of cable and pulleys which will permit operating loads within required design limits.

In the course of manufacture of aircraft control pulleys from phenolic laminated or macerated materials, many endurance tests have been made. With a precision bearing of low coefficient of friction, limits of endurance were established by heating and fraying of the cable. Cable friction in such cases is of predominant importance. Other cases developed where bearings were of low coefficient of friction but not precision-built, which would cause cable misalignment and thus produce high bearing and high cable friction to lower endurance limits. Certain plain bearings or those having high coefficient of friction would establish lowered endurance limits by failure from within the bearing. Again, cable failures may result from high coefficient of sliding friction of cable-pulley materials. Pulleys of semicushioning quality material, as cloth-reinforced phenolic products, provided increased endurance limits.

F. A. MATTHEWS.⁹ In his introduction the author gives as reasons for the importance of considering friction in the design of control systems, pilot fatigue and dependable action. Of equal or greater importance is the adverse effect of friction in the main flight controls on the aerodynamic stability of the airplane. Particularly in the case of control surfaces with a high percentage of aerodynamic balance does excessive friction play an extremely important part. Since, at the neutral position of the control surface in flight, forces on both sides of the surface are in balance, even small amounts of friction in the control system will upset this balance and allow sufficient surface deflection to change the attitude of the airplane without generating sufficient air load to return the surface to neutral. For example, a pilot in leveling off his ship after a maneuver has a tendency to overcorrect, due to the time lag between the movement of the surface and the response of the ship. In a good control system the surfaces, due to the lack of friction, are able to neutralize themselves, and the airplane maintains the level flight attitude. In a poor control system there is sufficient friction to prevent the surfaces from neutralizing themselves, and they must be neutralized manually. This condition results in hunting around the neutral position and instability or oscillation in the flight path.

In tests by the writer's company the apparatus used was very similar to that used by the author, with one exception: The four pulleys in the system on which the friction was being measured were mounted on a carriage which traveled on ball-bearing rollers on a machined track. Thus the cable remained stationary, and the pulleys moved along the cable. Motion was imparted to the carriage by means of a constant-speed motor which was attached to a cable connected to the carriage through a flexible bar to which a strain gage was attached. The load required to move the carriage was recorded by an SR-4 electric strain recorder. Test runs indicated that there was no appreciable variation in the load required to move the carriage through its entire travel. Inasmuch as the major concern of the tests

⁸ Manager, Micarta Division, Westinghouse Electric Corporation, Trafford, Pa.

⁹ Design Engineer, Lockheed Aircraft Corporation, Burbank, Calif.

was static friction, the carriage was moved very slowly—approximately $1/16$ ips.

In operation the carriage was placed in such a position as to allow a slight amount of slack in the operating cable, and the motor was then started. Thus, the initial stroke of the strain-recorder needle recorded the load required to overcome static friction and impart motion to the carriage, and subsequent recording was the dynamic friction at the speed previously mentioned. It was felt that this setup would result in freedom from small errors created by the necessity of determining visually the precise moment there was sufficient load to impart motion.

In conducting the tests it was found that there was some variation in friction measured in different spots in the same cable, and slightly more variation in different test specimens of the same type of cable cut from different reels made by the same manufacturer. These discrepancies were considered to be small enough to have negligible effect, since all curves resulting from the tests were the average of several test runs.

In the test conducted by the author, the effect of cable misalignment on cable-pulley friction was correctly assumed to be negligible in a properly designed control system. The writer's tests substantiate this assumption inasmuch as it was found that misalignment up to 2 deg had no appreciable effect on friction. It is interesting to note, however, that at the critical angle of cable wrap, the cable-pulley friction increased approximately 70 per cent as a straight-line function between 2 deg and 5 deg misalignment. The test conditions in this case were $3/16$ in cable on AN-210-4A pulley with a 500-lb rig load. Indications were, however, that the effects of misalignment above 2 deg were a variable function and seemed to decrease as angle of wrap of the cable on the pulley increased, within limits.

There is some disagreement with the assumption made by the author that vibration in the control system eliminates static friction and, therefore, only dynamic friction need be considered, as the assumption was not borne out in our test results. The assumption made by the writer's company was that the detrimental effects of friction in an airplane control system were due to the necessity of motion being imparted, either by the pilot or by the control surface, to a system temporarily substantially at rest.

Undoubtedly static friction is affected by vibration, and dynamic friction must also be considered in an analysis made of a control system during its design stages. However, one of the premises on which the tests at the writer's company were based is that friction in a control system being detrimental, it would be the better plan to follow a conservative course in the analysis of friction during the control-system design and use static friction in the analysis. This would allow those benefits resulting from vibration to offset the unknowns encountered in the complete system, such as congealed grease in pulley and hinge bearings, warped control-surface hinge lines, unbalanced masses in control-system elements such as quadrants, control columns, and tolerances in the balance of the control surfaces themselves.

Inasmuch as friction is most detrimental at or near the stable flight attitude of the airplane, corrections are of necessity small and usually at very low rates of speed. Therefore, it was felt that the dynamic friction would approach closely the values of static friction, and, again, using static friction would be the better course to follow.

Although there is an almost infinite number of variables to be considered in attempting to determine the effect of vibration on friction, it was decided that tests of a simple nature could be conducted and trends established, although no definite conclusions could be reached. In this test setup the entire apparatus was vibrated at varying frequencies and amplitudes. The trends established were as follows:

1 There is an over-all reduction in static friction which varies to some extent with both frequency and amplitude.

2 The reduction in friction varies in inverse ratio to the angle of wrap of the cable around the pulley.

3 The reduction in friction varies as a direct ratio of the rig load in the cable.

4 Within the scope of the tests conducted, the variation in friction appeared to be independent of the critical angle of wrap or cable bend.

5 Within the scope of the tests, the variation of friction with vibration appeared to be independent of the speed of cable travel.

It was concluded as a result of the tests that, although vibration served to reduce static friction somewhat, it did not eliminate it as a factor. In all tests conducted, both with and without vibration, it was found that the "breakaway" friction or force required to start motion between pulleys and cable was higher than the force required to maintain motion. This apparent failure to eliminate static friction may be ascribed to the fact that in most circumstances the motion of a cable in a control system under vibration is found to be perpendicular to the axis of the cable rather than along the axis. It is even conceivable to suppose that conditions of amplitude and frequency could exist which would increase the static friction of the system.

Tests of a simple nature within the scope of the test apparatus were also conducted to compare dynamic friction at slow speeds with static friction. It appeared that at the speeds possible without revising the test apparatus, there was a slight reduction of static friction once motion was started, but that up to a point there was actually a slight increase in force required to maintain motion as the speed was increased. No attempt was made to determine the cause of this increase, as a further increase in speed served to reduce the force required. Table 3, herewith, gives data typical of the results obtained.

TABLE 3 CABLE-PULLEY FRICTION IN POUNDS, AS AFFECTED BY SPEED AND ANGLE OF WRAP

($3/16$ -in-diam 7×19 zinc-coated cable on AN-210-4A pulleys at 500-lb rig load)

Angle of wrap, deg	Speed of cable travel				
	Static	0.06 ips	0.125 ips	0.25 ips	0.50 ips
10	1.6	1.5	1.8	1.8	1.75
20	3.6	3.3	3.54	3.5	3.4
30	4.3	4.2	4.74	4.6	4.25
45	5.0	4.95	5.1	4.75	4.75
90	5.4	5.0	5.31	5.4	5.5
180	5.4	5.45	6.18	6.20	6.5

It is quite apparent from these results that no definite comparison or conclusions could be reached without further testing. It was felt, however, that the decision to use static friction in control-system analysis would not be erroneous inasmuch as the speeds covered by the tests were well within the range of cable speeds encountered in the airplane in making small corrections necessary to maintain level flight.

As mentioned previously, the discrepancies between results obtained from independent tests by the writer's company and those obtained by the author in both test and mathematical analysis are small, and the over-all results corroborate one another within the accuracy necessary to conduct a satisfactory analysis of a control system where there are other elements introducing small amounts of friction in the complete system.

An indirect substantiation of the author's analytical method of determining friction may be gained in comparing the results as obtained by the analytical method and the Vega tests in Fig. 15 of the paper, and the comparison between the calculated and actual measured results obtained in using the Vega curves in calculating the friction in the flight controls on the P2V Neptune bomber which are as follows:

Aileron system, couple at rim of wheel...Calc. 3.07 lb, actual 3.1 lb
 Elevator system, force at top of column...Calc. 4.58 lb, actual 4.5 lb
 Rudder system, force at pedal pivot...Calc. 12.7 lb, actual 12.5 lb

It appears that the author's source of information on specifications covering the requirements of aircraft control systems is somewhat inaccurate; 7 X 19 extra-flexible stainless-steel cable is not required in aircraft controls, except under certain specific conditions such as resistance to corrosive fumes, liquids, etc. Government specifications allow the use of the following types of 7 X 19 extra-flexible cable:

- 1 Stainless steel uncoated to Specification MIL-C-5424
- 2 Carbon steel tin-coated to Specification MIL-C-1511
- 3 Carbon steel zinc-coated to Specification MIL-C-1511

In the writer's company tests, the difference in cable bending friction found in testing stainless-steel cable and tinned carbon-steel cable was almost imperceptible, and the same values are used for both types of cable. Tinned carbon-steel cable is used predominantly in the aircraft industry at present—the deflection characteristics of stainless-steel cable being such that it is extremely difficult to meet deflection characteristics as required by specification with the use of this material. Zinc-coated carbon-steel cable was introduced during the last war to conserve tin, a critical material, and although not generally in use at present its use is still permissible, and it probably would be required in the event of another war.

The writer's tests indicate that the cable bending friction of zinc-coated carbon-steel cable is approximately 30 per cent higher than the cable bending friction of tinned carbon-steel cable. If the maximum benefits of the analytical method introduced by the author are to be achieved, exponents should be developed for (d) in the formulas.

In conclusion it is suggested that the use of the analytical method for calculating the friction in control systems might become unwieldy and laborious, in that over a period of time the same equation would be solved repeatedly; particularly in the case of those conditions where the critical angle of wrap is not reached would this be true. By comparison it would be much simpler to develop curves or nomographs by the analytical method, which could be used repeatedly without the necessity of solving the equations.

AUTHOR'S CLOSURE

Mr. Guhl supplies interesting information regarding the endurance factors involved in cable-pulley friction. Although the simplified equations for cable-pulley friction (Equation [10] and [12]

given in this paper do not indicate the direct effects of the coefficient of sliding friction of cable-pulley materials, f_p , and the cable bending factor, f_c , a more complicated equation being developed by the author does attempt to include these factors directly in the equation.

Mr. Matthews' remarks concerning cable-pulley friction and the aerodynamic stability of the airplane are absolutely correct. Reference to the aerodynamic phase of the control system was purposely omitted since the friction present in cable-pulley systems is a general engineering problem, and the author did not wish to burden the design engineer with the aerodynamic aspects of a specific application.

The investigation conducted by the author included quantitative measurements of both static and dynamic friction, and also the qualitative effects of vibration on these frictions. The results obtained for static friction, however, were not as satisfactory as those obtained for the dynamic friction as regards the analytical treatment which was the purpose of this paper. The difference between static and dynamic friction was found to be relatively low, and to vary with pulley size, cable tension, and angle of cable bend. As noted by Mr. Matthews, the values of dynamic friction and static friction would approach each other at or near the stable flight attitude of the airplane, where friction would be most detrimental, and in the present case the more satisfactory data of the dynamic friction made it more adaptable to a mathematical analysis.

The author is in complete agreement with Mr. Matthews with regard to the many variables to be considered if vibration is to be included in this problem. Since the analytical investigation had to be kept within reasonable bounds, the quantitative effects of vibration were omitted and the qualitative tests conducted were used merely to indicate that the presence of vibration tended to reduce the static friction and to make it approach the value of the dynamic friction. The trends established by Mr. Matthews, however, are most interesting and informative.

The cables used in the tests were limited to those covered by Specification AN-RR-C-48, since this was the Government specification for the aircraft concerned (Republic XP-69) at that time, 1942. As pointed out in the paper, for coverage of all possible applications (aircraft or otherwise) the exponents of d and D and the constant of Equation [7] must be obtained for every type of cable and pulley in use.

The analytical investigation was conducted not only to supply design information for one of the more common combinations of cable pulley used, but also to indicate the basic effects of some of the variables involved in the general problem.